CONSTRUCTION MATERIALS FOR SUSTAINABLE FUTURE

Proceedings of the
1st International
Conference CoMS_2017

Zadar, Croatia, 19 - 21 April 2017

GRAĐEVINSKI MATERIJALI ZA ODRŽIVU BUDUĆNOST

Zbornik radova
1. međunarodne
konferencije CoMS_2017

Zadar, Hrvatska, 19. - 21. travnja 2017.

Proceedings of the 1st International Conference on CONSTRUCTION MATERIALS FOR SUSTAINABLE FUTURE (CoMS_2017), Zadar, Croatia, 19 - 21 April 2017

Zbornik radova 1. međunarnodne konferencije GRAĐEVINSKI MATERIJALI ZA ODRŽIVU BUDUĆNOST (CoMS_2017), Zadar, Hrvatska, 19. - 21. travnja 2017.

University of Zagreb
Faculty of Civil Engineering

University of Novi Sad
Faculty of Technical Science

Slovenian National Building and
Civil Engineering Institute

Federal Institute for Materials
Research and Testing

IMPRESSUM

Proceedings of the 1st International Conference on CONSTRUCTION MATERIALS FOR SUSTAINABLE FUTURE (CoMS_2017), Zadar, Croatia, 19 - 21 April 2017

Zbornik radova 1. međunarnodne konferencije GRAĐEVINSKI MATERIJALI ZA ODRŽIVU BUDUĆNOST (CoMS_2017), Zadar, Hrvatska, 19. - 21. travnja 2017.

Editors:
Ivana Banjad Pecur, Ana Baricevic, Nina Stirmer, Dubravka Bjegovic

Urednici:
Ivana Banjad Pečur, Ana Baričević, Nina Štirmer, Dubravka Bjegović

Translation and proofreading:
Drazen Anicic, Marina Bagaric

Prijevod i lektura:
Dražen Aničić, Marina Bagarić

Publisher:
University of Zagreb, Faculty of Civil Engineering, Zagreb, Croatia, 2017

Naklada:
Sveučilište u Zagrebu, Građevinski fakultet, Zagreb, Hrvatska, 2017

ISBN: 978-953-8168-04-8

ISBN: 978-953-8168-04-8

TABLE OF CONTENTS / SADRŽAJ

KEYNOTE LECTURES / POZVANA PREDAVANJA

TOPIC 1. INNOVATION IN MATERIALS TECHNOLOGY/ INOVACIJE U TEHNOLOGIJI MATERIJALA

TOPIC 2. MATERIALS – ENVIRONMENT INTERACTION / MEĐUDJELOVANJE MATERIJALA I OKOLIŠA

TOPIC 3. SUSTAINABLE BUILDING DESIGN/ PROJEKTIRANJE ODRŽIVIH ZGRADA

TOPIC 4. ASSESSMENT AND MONITORING / OCJENA STANJA I MONITORING KONSTRUKCIJA

TOPIC 5. PROTECTION, PRESERVATION AND REPAIR OF STRUCTURES / ZAŠTITA, OČUVANJE I POPRAVAK KONSTRUKCIJA

TOPIC 6. MODELLING AT MATERIAL AND STRUCTURAL LEVEL / MODELIRANJE MATERIJALA I KONSTRUKCIJA

TOPIC 7. SOCIAL, ECONOMIC AND HEALTH ASPECTS OF THE BUILT ENVIRONMENT / DRUŠTVENI, GOSPODARSKI I ZDRAVSTVENI ASPEKTI IZGRAĐENOGA OKOLIŠA

TOPIC 8. INNOVATIVE REUSE OF ALL TYRE COMPONENTS IN CONCRETE – ANAGENNISI / INOVATIVNA UPORABA SVIH PRODUKATA RECIKLAŽE OTPADNIH GUMA U BETONU

KEYNOTE LECTURES

POZVANA PREDAVANJA

ALTERNATIVE MATERIALS IN SUSTAINABLE CONSTRUCTION

Dubravka Bjegovic[1], Marijana Serdar[1]

[1] University of Zagreb Faculty of Civil Engineering, Department of Materials, Fra Andrije Kacica Miosica 26, 10 000 Zagreb, Croatia, email: dubravka@grad.hr, mserdar@grad.hr

SUMMARY: World population is expected to reach between 8.3 and 10.9 billion by 2050. Rapid population growth and urbanization will dramatically increase the demand for construction materials. It is estimated that, at the current rate of concrete consumption, the demand for concrete will rise to about 16 -18 billion tons a year by 2050. Therefore, construction industry, together with the building materials producers, must adopt new practices to meet the increased demand, while ensuring sustainable production. Concrete can be considered as a sustainable material if during its design all requirements of sustainable development are met. Since concrete is produced locally with short transportation routes, environmental requirements can easily be satisfied. To assure further decrease of CO_2 emissions and energy consumption, different alternative materials, mostly by-products of other industries, are used as binders instead of cement and are often called supplementary cementitious materials (SCMs). The utilization of recycled concrete aggregates, recycled tire rubber, recycled plastics and waste glass as a partial replacement for large and/or fine aggregate in structural concrete is particularly attractive. Fibres of various shapes and sizes produced from steel, plastic, glass, and natural materials are also being used. It is well accepted today that the application of such alternative materials has a different influence on concrete properties which must be studied to be proved before being used. This paper reviews the effects of different alternative materials on concrete properties. Keeping in mind that such new age materials should be available locally, potentially available quantities of SCM in the region will be presented.

ALTERNATIVNI MATERIJALI U ODRŽIVOJ GRADNJI

SAŽETAK: Očekuje se da će na svijetu 2050. godine biti između 8,3 i 10,9 milijarda stanovnika. Brzi rast stanovništva i urbanizacija dramatično će povećati zahtjeve za građevinskim materijalima. Procjenjuje se da će godine 2050. uz sadašnju brzinu potrošnje, potreba za betonom iznositi oko 16 – 18 milijarda tona godišnje. Stoga građevinska industrija i proizvođači građevinskih materijala, da bi zadovoljili povećane zahtjeve, moraju usvojiti nove postupke osiguravajući istodobno održivu proizvodnju. Beton se može smatrati održivim materijalom ako su tijekom njegova stvaranja ispunjeni svi zahtjevi održivoga razvoja. Kako se beton proizvodi lokalno uz kratke transportne putove, lako je zadovoljiti okolišne zahtjeve. Da bi se osiguralo daljnje smanjenje emisije CO_2 i potrošnje energije, kao veziva se umjesto cementa upotrebljavaju različiti materijali, najčešće nusproizvodi drugih industrija koje se često naziva dodatnim cementnim materijalima. Posebno je privlačna upotreba recikliranog agregata iz betona, recikliranih automobilskih guma, reciklirane plastike i otpadnoga stakla kao djelomične zamjene krupnog i/ili sitnog agregata u konstrukcijskom betonu. Upotrebljavaju se i vlakna različitih oblika i veličina proizvedena od čelika, plastike, stakla i prirodnih materijala. Danas je općeprihvaćeno da primjena takvih alternativnih materijala ima različit utjecaj na svojstva betona koja se prije upotrebe moraju proučiti radi provjere. U radu je dan pregled utjecaja različitih alternativnih materijala na svojstva betona. Imajući na umu da takvi materijali novoga doba trebaju biti lokalno dostupni, prikazuju se potencijalno dostupne količine dodatnih cementnih materijala u regiji.

1. INTRODUCTION

Sustainability is a way of life, an attitude that all economic activity should take care of the Earth's ecosystem, which requires a development vision [1]. Developed countries in the European Union started to create development strategies in construction at the end of the last century [2]. The basic principle of sustainable development in construction is the use of minimum natural resources and energy, and the generation of minimum waste harmful to the Earth. Environmental protection and energy saving have become the world issues in all technological areas including the production of concrete in construction industry. Large quantities of concrete will be undoubtedly used in future due to its numerous advantages and the fact that engineers and scientists have been developing technologies enhancing its sustainability. The alternative materials which can be used in sustainable concrete structures are predominantly industrial by-products in the form of finely crushed material added as a partial replacement to cement with the aim of improving particular properties and/or creating some special properties. Some of these materials have been used for years either as cement additives or as substitutes for cement, such as fly ash, arc furnace slag, silica dust and metakaolin [3,4]. Their usage is made possible by regulations and standards. Some alternative materials started to be used recently, such as sludge from waste water and rice husks ash, while some are still being researched such as ash from biomass, slag from copper and zinc, red mud, waste from the production of ferronickel, sludge from paper production, phosphor-gypsum, casting sand and sludge from scrap stone. Recycled aggregate can be produced from some types of construction waste by crushing and sorting particles into desired sizes [5,6]. Recycled materials have been increasingly used with the aim of reducing the use of natural aggregates. Some European countries, e.g. the Netherlands, Belgium and Denmark, recycle more than 80% of total construction waste resulting from demolition. Even industrial fibres in fibre reinforced concrete can be replaced with more sustainable alternatives, such as natural and recycled fibres. In the last decade, there has been a rapid growth in research and innovation in the natural fibre composite (NFC) area [7-11]. Figure 1 presents an exhaustive overview of many of possible alternative materials that can be used in concrete. Present paper covers only those materials that are researched and used as replacement for cement and/or mineral addition to concrete. The paper also indicates the materials which can be found in Croatia and neighbouring countries, in that way indicating potential research fields for future generations.

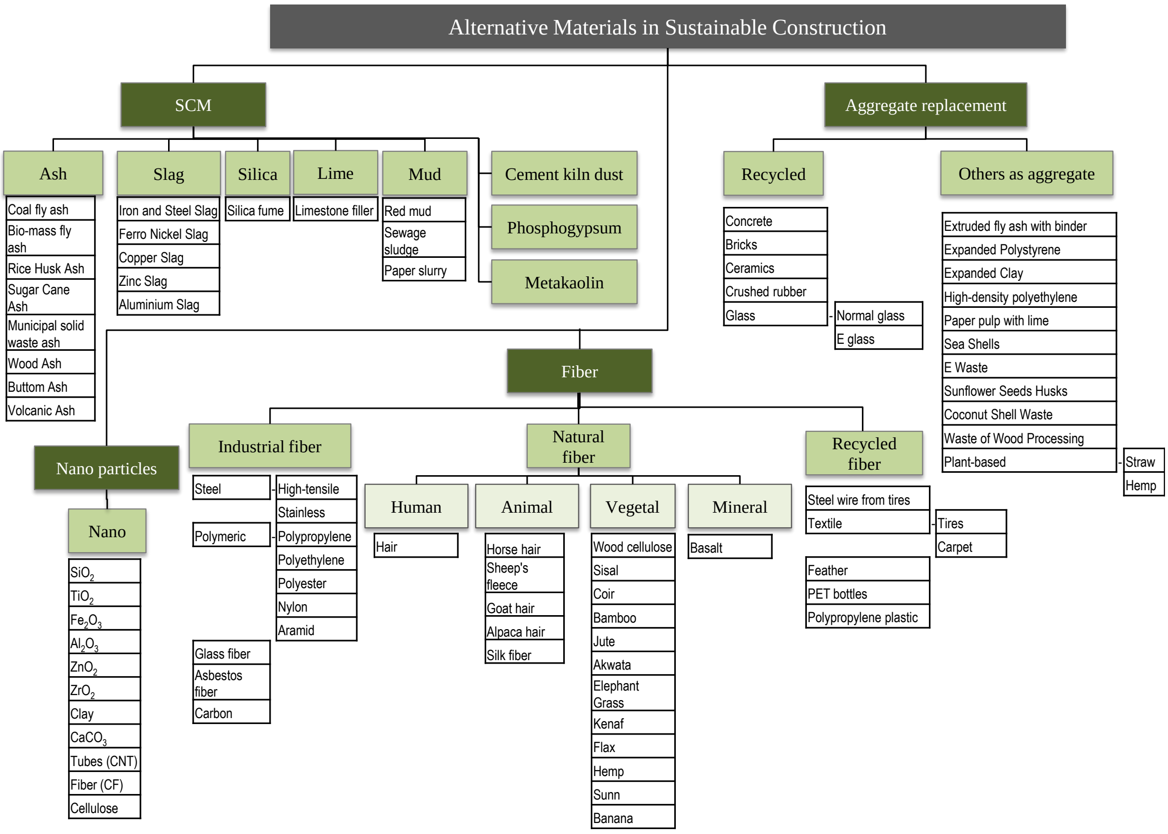

Figure 1 Comprehensive overview of possible alternative materials in concrete

2. SUPPLEMENTARY CEMENTITIOUS MATERIALS (SCMS)

Today, most concrete mixtures contain Supplementary Cementitious Materials (SCMs) which embrace a large number of materials, Figure 1. SCMs vary widely in terms of origin, chemical and mineralogical composition, and typical particle characteristics. The use of SCMs in cement blends is a well-established methodology for reducing clinker factor and imparting beneficial properties to concrete as construction material. Where does current research stand and what can be expected from SCMs in the future?

2.1. COAL ASH

Coal ash is a by-product created by burning pulverized coal or bio mass, composed of fine particles that are driven out with flue gases (Fly Ash) or particles that fall to the bottom of the furnace (Bottom Ash).

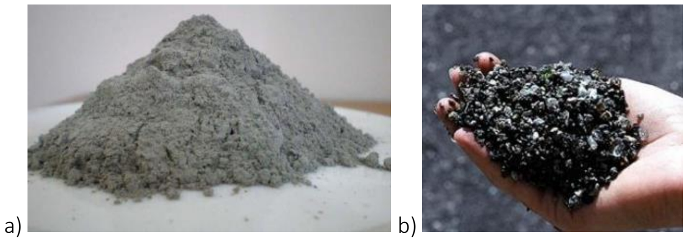

Figure 2 The look of fly ash [12] and bottom ash from burning coal [13]

2.1.1. FLY ASH

Fly ash, fine powder generated by burning coal dust in thermal power plants fired with coal, is by electrostatic filter units separated from waste gases. Particles of fly ash can be of smaller diameter than 1μm to up to 100 1μm [12,14] and as such increase the workability of concrete and thus reduce the needed amount of water in concrete [15]. Fly ash is very effective in increasing cohesiveness and in reducing the sensitivity to changes in water quantity so it is often used in the production of self-consolidating concrete [16]. Fly ash slows the release of heat of hydration so the use of this mineral additive is preferred in mass concrete [15-18]. Addition of fly ash reduces early strengths, but increase subsequent (56-90 day) strengths of concrete, Figure 3 a) [18], and reduces permeability of concrete, Figure 3 b) [19].

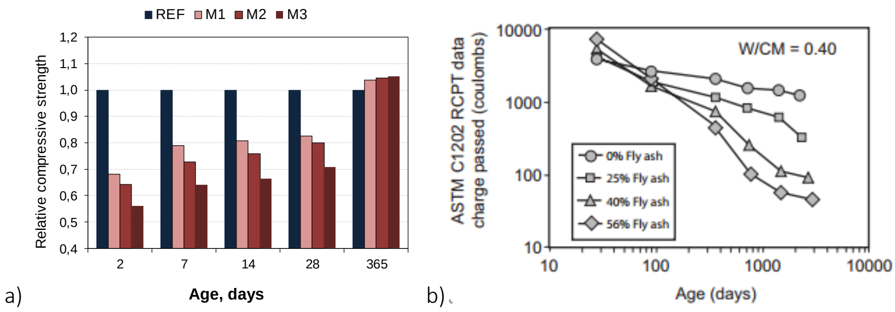

Figure 3 Influence of fly ash on the properties of concrete [18,19]

Holcim Croatia has in last ten years taken as much as million tons of waste, namely fly ash and gypsum, which has helped to improve the properties of cement in the production process at the cement factory at Koromačno in Croatia. In Slovenia, Šoštanj thermal power plant produces almost 1 million tons of coal fly ash per year and about 150 kg of slag per 1 t of steel at electric arc furnace steel (EAFS) is produced in Jesenice. In Serbia, the production of ash and slag from ash makes approximately 5.5 million tons a year, of which the largest quantity is produced at Nikola Tesla, a thermal power plant which uses Kolubara lignite [20]. Taking into consideration the overall environmental requirements of the EU the question is if in future there will be the same amount of available material as today. According to the research conducted by the *Network for Changes in Southeast Europe* [21] 13 thermal power plants are to be renewed or closed in the Balkan region countries due to the fact that they are outdated or do not comply with the standards of the European Union.

2.2. BOTTOM ASH (BA)

In the process of burning coal in thermal power plants, approx. 80% of ash is extricated through flue gases, and approx. 20% falls to the bottom of the furnace. Fractions falling to the bottom of the furnace are larger and are similar to crushed aggregate, but are lighter because they are porous and look like volcanic lava [22,13]. According to the American Coal Ash Association (ACAA) 16.9 million tons of bottom ash were produced from coal in 2006, of which 45% was used in embankments, road foundations, and in winter bottom ash is put on roads against skidding. Bottom ash is also used as lightweight aggregate in production of mortars, in cement industry, and in other areas of construction industry [23].

In the last decade, studies into bottom ash from coal thermal power plants are aimed at its application in concrete, as the replacement for the part of aggregate. According to research [24] the substitution of small aggregate up to 30% does not have a negative impact on mechanical properties of concrete. Some authors even suggest substituting 50% [25]. Andrade in [26] warns that the increased content of bottom ash in concrete reduces the properties of moisture transport.

2.3. BIOMASS ASH (BA)

Biomass is a biodegradable component of the product, the residue and waste from agriculture (including plant and animal substances), from forestry and wood industry, as well as biodegradable parts of communal and industrial waste whose energy use is allowed [27-29]. After biomass has burnt two types of ash remain, the one from fireboxes and the other from chimneys. Although ASTM C618 [30] for now prohibits the use of bio ash, the research has proved that there is a strong potential for the use of bio ash in construction industry [31-34].

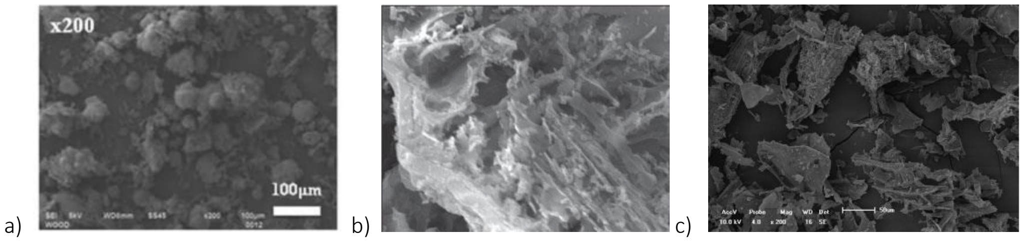

Figure 4 SEM images of particles of: a) wood ash [35], b) rice husk ash [36], c) sugar cane ash [37]

2.3.1. WOOD BIOMASS ASH (WBA)

Ash is the basic solid waste remaining after combustion of wood biomass, Figure 4 a). It comes in two forms – as ash at the bottom of the firebox and as fly ash, a fine powder structure, which is separated through filters during flue-gas processing [35]. According to the research conducted by Noviks [38], Finland annually gets million tons of biomass from ash, Sweden 0.8 million tons, the USA 3 million tons and China 2 million tons. The research on the impact of ash from biomass on concrete properties has been intensified in recent years. The published results [32,39-41] show that it is possible to achieve positive effect on concrete by applying these types of alternative materials. At the Department of Materials, at the Faculty of Civil Engineering of Zagreb University, research is being conducted into the benefits of the application of bio ash from the power plants using wood in the industry of concrete, within the national project TAREC2 funded by the Croatian Science Foundation [42].

2.3.2. RICE HUSK ASH (RHA)

Burning rice husks generates ash rich with silica [43,44], Figure 4 b). Addition of rice husk ash improves the viscosity of concrete, increases strength, reduces permeability, improves durability properties [45-47], and with self-consolidating concrete improves self-consolidating properties. Rice husk ash with a high proportion of nanoparticles of silica, $SiO_{2,,}$ significantly contributes to the decreased shrinkage of self-consolidating concrete due to drying. The substitution of cement with 12 to 15% of rice husk ash can be sufficient for the reduction of harmful expansion of aggregate caused by alkali-silica reaction in concrete, depending on the nature of aggregate. The research shown in [47] where three types of rice husk ash were investigated, states that the substitution of some part of cement with rice husk ash does not impair mechanical properties of concrete, Figure 5a), and it considerably improves durability properties, Figure 5b). Until now rice husk ash, except to replace some part of cement in concrete and/or to be added to mortar and concrete, has been used only in granular form as an insulation material, and in the production of insulation panels [48,49], but it is also used in other industrial branches [50].

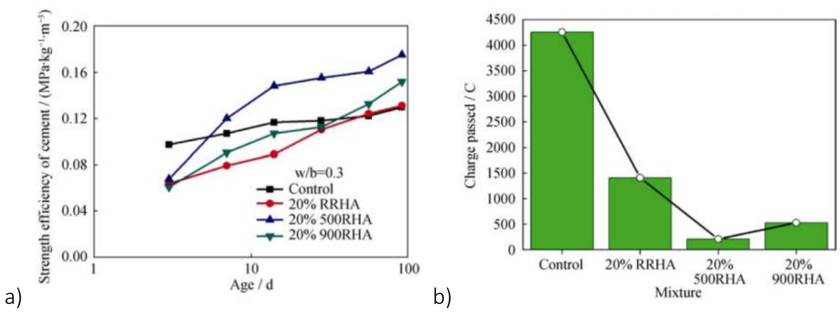

Figure 5 The impact of rice husk ash, a) on compression strength, b) on penetration of chloride ions [47]

China and India are the largest producers of rice in the world. The world annual rice production is about 600 million tons. In Croatia's neighbourhood Kočan rice fields are Macedonia's wealth and its pride. Kočan valley is situated in the eastern part of FR Macedonia. The annual production is approximately 24 000 tons, which makes rice the most important agricultural product with centuries of tradition, high yields and high quality. Therefore, it would be advisable to intensify research into the use of rice husk ash in the region.

2.3.3. SUGAR CANE BAGASSE ASH (SCBA)

Previous studies have shown that sugar cane bagasse mass, Figure 4 c), can be used in the production of both ordinary concrete and self-consolidating one which ensures safe storage of ash and prevents environmental pollution. Research at [51,52] has shown that the optimum content of the substituted part of cement in concrete is up to 10%, maximum 15%. Fly ash containing sifted sugar cane bagasse mass has a positive impact on viscosity, which results in a smaller proportion of superplasticizers than in ordinary mortar. The fineness of sugar cane ash contributes to the finer structure of pores in concrete which results in the reduced permeability and the diffusion of chloride, and subsequently in the reduction of corrosion of concrete reinforcement [53,54]. Slag and sugar cane ash activated by alkaline activator could be a potential binder for concrete, which is shown in studies in Figure 6 [55].

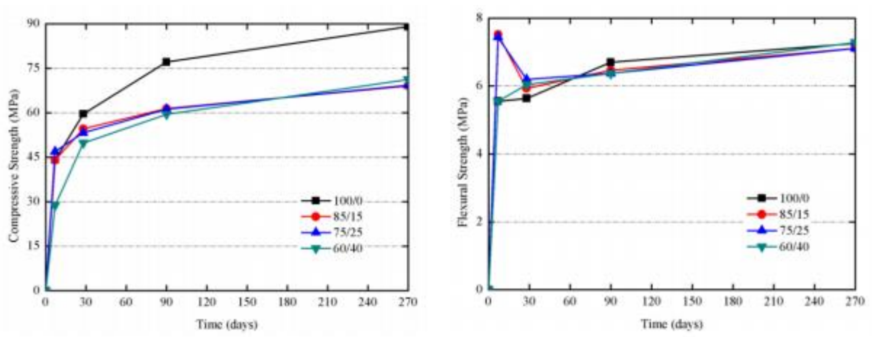

Figure 6 Mechanical properties of mortars with slag and ash from sugar cane used as binder [55]

Sugar cane ash is currently in the research phase and it is not known whether it has been used in building structures, despite highly positive research results. India, along with Brazil, is the largest producer of sugar cane in the world according to [56]. Each year India produces about 380 million tons of sugar cane which also means a large quantity of bio mass, that is, potential ash with a high proportion of silica (up to >80%).

2.4. SLAG (S)

Slag (dross) is a silicate melt, the by-product of the molten ore production and/or molten waste materials. Metallurgical industry annually generates millions of tons of various slags as secondary materials [57]. The slags should be recycled, modified and processed taking into consideration the environmental impact.

a) b) c) d) e)

Figure 7 a) Finely ground blast furnace slag [58], b) finely ground copper slag [60], c) Zinc slag [60], d) ferronickel slag [61], e) aluminium slag [62]

2.4.1. IRON AND STEEL SLAG

The two types of slag are called: blast furnace slag obtained from iron production [63] and electric arc furnace slag obtained from steel production [64]. Each produced ton of pig iron generates 150-347 kg of blast furnace slag (BFS) [65]. Granulated finely ground slag has been used in cement production for more than 100 years, and slag as a substitution aggregate fraction for concrete was used in Roman times, and it has been researched and used in the last few decades [58,66] for reasons of sustainable economic development. The substitution can go up to 50%, both in terms of properties in fresh state and in terms of properties of hardened concrete. Slag in general improves the workability and pumpability of concrete, increases strength, reduces the heat of hydration and permeability, extends durability, has positive effect on sustainability factors [17].

In the world extensive research into replacing aggregate in concrete with blast furnace slag is being carried out. Up to 50% of slag can be used as the replacement for small aggregate fractions [67-69]. Figure 8 shows the positive effect on the behaviour of concrete in fire when large aggregate has been substituted.

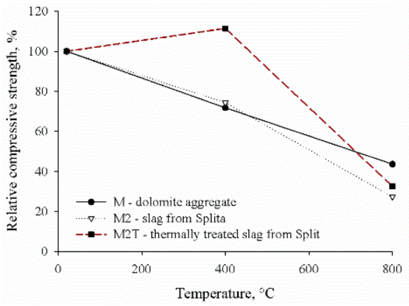

a)

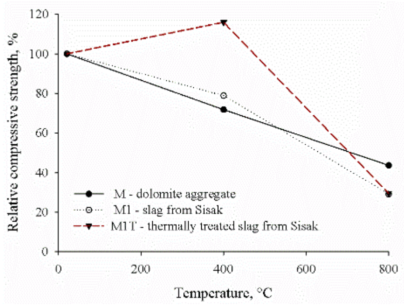

b)

Figure 8 Behaviour of concrete in fire, a) a part of aggregate has been substituted with slag from Split, b) a part of aggregate has been substituted with slag from Sisak [69]

According to the data for 2012 [70] 44.4 million tons of slag are produced annually in Europe, and 52.3 million tons are used, meaning that disposed slag has been used. In construction industry 87% is reused, of which 66% as the component of cement and/or concrete, and approx. 23% is used as aggregate in road construction. According to the data until 2009 [71,72] slag was disposed near Sisak in the Republic of Croatia over 25 hectares of land and is of mixed composition – the combination of blast furnace slag and electric arc furnace slag. The amount of disposed material in this area is estimated at 1.5 million tons. The said slag is currently used in road construction (as stabilisation layer) and agriculture (smaller fractions are used for soil improvement). Newly created quantity of 300,000 tons from the former production of seamless pipes at Sisak ironworks (located at the plant) should be taken into account. Slag from the landfill in Split comes from electric arc furnaces and its use has not been found yet. The current amount of slag thereof is estimated at 30,000 tons. The high cost of disposal of this waste material imposes the need of finding new manners of its use.

2.4.2. COPPER SLAG (CS)

Slag obtained from the production of copper is massive metallurgical waste because each produced ton of copper generates approx 2.2 to 3 tons of copper slag, which makes about 24.6 million tons of slag [73]. Finely ground copper slag [59], can replace some part of cement. The substitution of 30% of cement with copper slag reduces the 28-day compressive and tensile strength in the same manner as fly ash [59]. The research in the last two decades has proved that slag obtained from copper production could be used as the substitution for fine aggregate, whereby 20% substitution enhances the properties of hardened mortar and concrete [74-77], and the substitution of up to 40% of fine fraction could be possible [78,79]. Positive impact on the properties of gas permeability and tensile strength of concrete has been established, which means that copper slag improves the cement matrix and interfacial zone in concrete [59]. Because the effects of copper slag on the properties of concrete are still being researched, the application of said concrete in structures has not been recorded yet.

In Croatia's neighbouring countries with copper exploitation are Romania, Serbia, Macedonia and to a lesser extent Albania, while the largest copper producers are Chile, the USA, Peru and China, and in Africa Zambia, UAR and Congo. The most significant deposits of copper in Serbia are in the area of Bor and Majdanpek. In Bor surroundings, in Serbia, approx. 23 000 000 tons of smelting slag have been disposed of [80] which covers a huge area and pollutes the environment.

2.4.3. ZINK SLAG (ZS)

Slag obtained from zinc production was added as cement substitution in the amount of about 15%, Figure 9 a) and as the substitution for sand in concrete in the amount of 20%, Figure 9 b) [81]. It is obvious that compressive strengths of concrete containing cement which was partly substituted with zinc slag and the compressive strengths of concrete where also a part of sand was substituted with zinc slag were slightly lower than the compressive strengths of concrete with pure Portland cement.

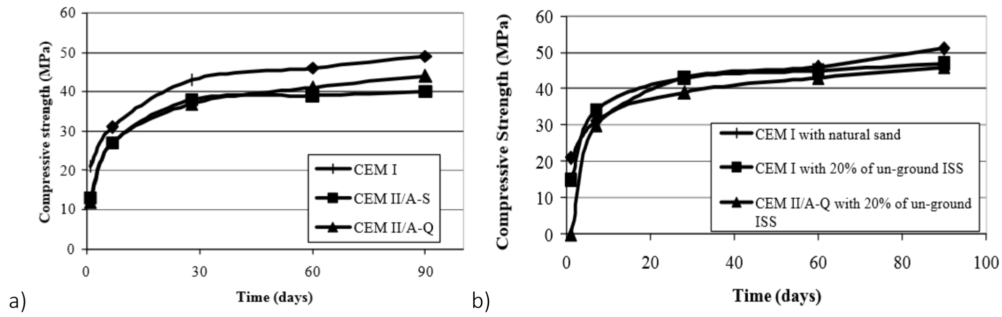

Figure 9 a) Concrete with Portland cement and with slag added to cement, b) concrete with Portland cement and with cement with the addition of zinc slag and with 20% substitution of sand with zinc slag [81].

In addition to the research on partial substitutions of cement and/or aggregate, research is conducted into the application of zinc slag in geopolymers [81-83]. The investigation carried out at BRE laboratory [84] indicates that it is possible to replace 50% and even 75% of sand with zinc slag, and only the initial strength of 1-day old concrete is going to be lower so demoulding should be done after 48 hours. Within the same investigation, conducted in 2002, a 50 m long experimental section of concrete road was built in Avonmouth.

The largest quantities of zinc ore are mined in China, Peru, Australia, Canada, the USA, Mexico and South African Republic. In Europe, active zinc mines can be found in Ireland, Poland, Finland, Bulgaria and Sweden. Total world production of zinc was 12 million tons in 2010. In Croatia's neighbouring countries zinc is produced in Bosnia and Herzegovina, Kosovo and Macedonia. As with the production of copper, here also remain large amounts of slag [60].

2.4.4. FERRONICKEL SLAG (FNS)

Ferronickel slag is iron alloy with 8% to 40% of nickel added, which is mostly used in the production of stainless steel, and it is produced in blast furnaces and electric arc furnaces [85,86]. The production of ferronickel generates slag as a by-product which, if cooled in air, looks like coarse aggregate. Fine aggregate is obtained if it is sprinkled with water in the course of cooling [61]. About 14 tons of granulated ferronickel slag (FNS) is produced as a by-product in the production process of 1 ton of ferronickel [61]. The results showed that the ferronickel slag is an excellent raw material for the production of inorganic polymers by using the geopolymerization technology. The research [87,88] has proved that concrete made from geopolymers based on ferronickel slag behaves excellently at fire temperatures with a very high (RWS curve).

The major producers of ferronickel are Russia, Canada, Australia, Indonesia, China, Cuba, Japan, South Africa, Brazil, Greece and in considerably smaller quantities Kosovo and Macedonia [89]. About 2 million tons of nickel slag are produced annually in Japan so for decades there have been attempts to solve the problem of disposal space shortage. As early as in 1994 Japan issued the recommendations for use of ferronickel slag as aggregate for concrete [90]. Macedonia and Kosovo are also facing the problem of ferronickel slag disposal and its impact on the environment [91]. There are in Kosovo more than 2.6 million m^3 of disposed ferronickel slag which makes more than 7 million tons [92]. These large available quantities of disposed material are the very reason for research into the use of ferronickel as the substitution aggregate in concrete [93,94]. The research has intensified on ferronickel slag as raw material for the production of geopolymers, a new type of binders for concretes of high mechanical and durability properties [95,96]. Still, it should be emphasized that in early investigations as well as the later ones [97,98] authors have warned about the possibility of alkali aggregate reaction and recommended the following measures: the use of low-alkali cement, addition of fly ash, and addition of ground granulated blast-furnace slag. In the last ten years the research into the application of ferronickel slag in geopolymers has intensified

2.4.5. ALUMINIUM SLAG (DROSS) (AS)

Once mined, aluminium in the bauxite ore is chemically extracted into alumina, an aluminium oxide compound, by Bayer process. The secondary material in this process is red mud (more on red mud in 6.1). Countries with a highly developed production of aluminium products also have large quantities of secondary aluminium that is recycled for production of new aluminium products. However, in the recycling process, that is, in the repeated production of aluminium, aluminium dross remains, Figure 7 e) [62]. Between 300-800 kg of salt slag is produced for every ton of secondary aluminium alloy. Worldwide secondary aluminium production stood at around 11 million tons in 2009. Taking a conservative figure of 400 kg slag/ton aluminium, salt slag arising may be estimated at 4.4 million tons worldwide. This means that about 900,000 tons of slag is generated annually in Europe, 1.2 million tons in the US and China, now the dominant player, is currently generating about 1.6 million tons of salt slag p.a. [99].

Due to its properties, salt slag is classified as toxic and hazardous waste, according to the *European Catalogue for Hazardous Wastes* specified in [100], which makes its disposal more complicated. Still, aluminium slag can be used in many ways, such as in the production of cements, in ceramic and refractory applications, as filler in concrete, in chemical and metallurgical industry.

Its utilization in such manners will reduce the cost of disposal and will also lead to fewer environmental issues [100-102]. A project, being undertaken by some of the researchers at Qatar University, aims to partially make use of aluminium slags in concrete structures [103]. The results indicate that the compressive strength value and permeability properties of concrete decrease with the increased aluminium dross content. As the substitution percentage of aluminium dross is increased, more entrapped air occurs and this causes a negative effect on strength and permeability properties.

2.5. SILICA FUME

Silica fume is the by-product generated by the production of silicon and ferrosilicon alloys in electric arc furnaces. Its granulation is very fine, ranging from light to dark grey colour [104]. Silica fume influences the properties of concrete through two mechanisms: pozzolanic reactions, leading to increase in the quantity of C-S-H gel, and small size of particles, leading to an increase in the workability and cohesion. Considering its large specific surface area, silica fume increases the need for water so it is recommended to use water in combination with a superplasticizer [17,105-107]. The dosage of silica fume should be optimized because SiO_2 binds with calcium hydroxide $Ca(OH)_2$ which can reduce pH. Since calcium hydroxide is essential for the alkalinity of concrete, its excessive binding with silica fume can have a negative effect and cause corrosion of the reinforcement in concrete. For this very effect on reinforced concrete maximum 10% of silica fume to the weight of cement in concrete should be used because then it, with its filler effect, contributes positively to the prevention of corrosion in concrete [108].

The production of a ton of ferrosilicon generates 400-600kg of SiO_2 dust which means that in the world about 1,200,000 tons of this waste material is produced annually [109]. At the end of the last century a lot of research was conducted into the application of silica fume, and scientists from Croatia were among the first to investigate the possibility of application of silica fume remaining after the production of ferroalloys in Jajce, Bosnia and Herzegovina, where 9000-10,000 tons of silica fume were produced a year. Currently the production is at a standstill because of the ownership restructuring process, but is expected to start soon.

2.6. LIMESTONE FILLER

The application of ground limestone in the production of cement originates in France about three decades back. The reasons thereof are mainly the shortage of available amount of fly ash in France which, at that time, was oriented at getting electricity from nuclear power plants. Croatian researchers have again, as with silica fume, followed the trend [110,111]. According to the data [112] between 2000 and 2010 the use of CEM II cement and limestone fillers has considerably increased in Europe.

In recent years the application of limestone as the addition to self-consolidating concrete in the production of prefabricated elements has intensified in the Netherlands. In Belgium, Canada, Germany, Italy, Poland, Sweden and the UK it is used for the production of so called easily installed concrete [113,114]. Positive effect on strength of concrete of limestone as an alternative addition to concrete was shown in [115]. Investigations conducted in Greece [116] show positive results in terms of strength and workability in concrete produced with cement containing 20% of limestone, while water and chloride permeability properties are the same as in compared concrete containing cement without limestone. In terms of durability properties, the results suggest caution about the resistance of concrete to freezing and defrosting, while the resistance to carbonization and corrosion of reinforcement is increased.

Limestone is a rock containing minimum 50% of calcite mineral (calcium carbonate). In Croatia, many mountains (Kapela, Risnjak, Velebit, Dinara), coastal Dalmatian mountains and islands are made of limestone, which means that there is enough raw material [110,112].

2.7. INDUSTRY MUD

Mud is mainly a mixture of water and some industrial residues from primary production. In the last few decades the application of mud in cement industry and the industry of concrete has been researched. The following types of mud have been researched: the mud form the production of alumina, so called red mud, the ones from waste waters, paper industry, stone cutting etc.

a)  b)  c)  d) 

Figure10 a) Sewage sludge [117], b) paper sludge ash [118], c) stone dry sludge [119], d) molding sand [120]

2.7.1. RED MUD

Red mud is the by-product of the secondary production of aluminium (see 3.5) in the amount of approx. 0.5 – 2.5 tons for the production of 1 ton of Al_2O_3. About 70% of particles of red mud are the size of 20 µm, the mud is usually rich in aluminium and iron oxides and the solution itself has a high pH value. About 77 million tons of hazardous red mud is generated annually and this makes it one of the most serious issues of waste disposal in metallurgical industry. In Europe, but also in the neighbourhood, there are a number of plants for aluminium processing and consequently a number of industrial waste landfills, in Germany, Hungary, Bosnia and Herzegovina, Montenegro, Greece. Alkali is the main pollutant in the liquid phase due to the presence of NaOH and KOH which have hazardous properties. There are two red mud landfills in Bosnia and Herzegovina. One is in Birač near Zvornik and the other is near Mostar in Dobro Selo. It is estimated that about 10 million tons of red mud are stored in Dobro Selo area. In two aluminium dumps owned by the *Kombinat aluminija* in Podgorica (KAP), Montenegro, 7 million tons of red mud have been accumulated.

In Croatia aluminium is not produced any longer, and after TGO had stopped producing it 750,000 m^3 of red mud and 100,00 m^3 of waste alkali remained in the landfill [121,122]. The pools with red mud are currently being remediated. In the small pool about 35,000 m^3 of red mud which have remained are being covered with the layer of impermeable clay 2 meters thick. The large pool with red mud has been covered with stone for about two years, currently there is an ongoing process of evaporation of about 300, 000 m^3 of alkali, which depends on the rainfall. Investigations, which have been conducted to date and available in literature, show that adding more than 15% of red mud to cement considerably reduces strength [122-124], but simultaneously has a positive effect on the durability properties of concrete [125].

During research conducted at the Faculty of Civil Engineering in Zagreb, red mud, together with fly ash and limestone was activated with a small amount of cement CEM II, with the aim of preparing concretes of high workability properties and the research also confirmed the positive effect of red mud on durability properties of concrete, Figure 11 [126].

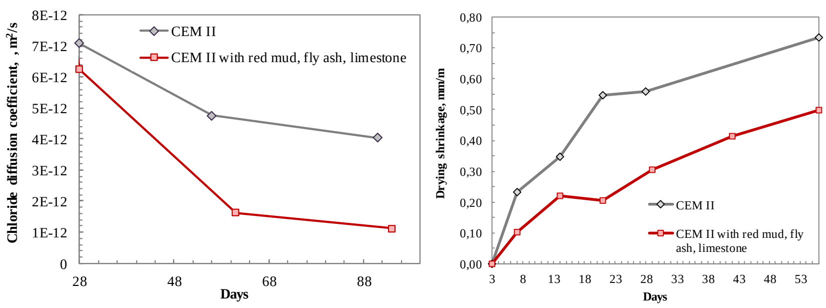

Figure 11 Diffusion coefficient of chloride ions and autogenous shrinkage of concrete prepared with cement CEM II and concrete in which a significant part of cement has been substituted with red mud, fly ash and limestone [126]

2.7.2. SEWAGE SLUDGE

For every square meter of waste water treated, about 0.5kg of sewage sludge is generated in purification systems. Burning the sludge from the waste water purifier considerably facilitates the management of newly created product, ash generated from waste water sludge. Scientific literature indicates that incinerated sewage sludge ash (ISSA), considering its chemical composition and properties, could be used in civil engineering industry, in the production of concrete, cement, bricks, asphalt and other [39,127,128].

On the surfaces next to the plant for waste water treatment in Zagreb 270,000 tons of sludge have been stored, and every following year the stored quantities will be increased by 50-80 000 ton a year [129]. Extensive research is conducted at the Faculty of Civil Engineering in Zagreb into the possibility of use of ash obtained by burning sewage sludge from purification systems in Zagreb [117,129,130]. Previous findings indicate a certain pozzolanic activity of sewage sludge ash. Also, considerable quantities of SiO_2 and Al_2O_3 found in Zagreb ash indicate the real possibility of the application of ash in this manner, Figure 12 [117,130]. However, it is essential to find the optimal method of ash activation, by mixing complementary mineral additives and finding the specific areas of application where concretes prepared with sewer sludge ash, considering their properties, would be an interesting alternative to classical concrete.

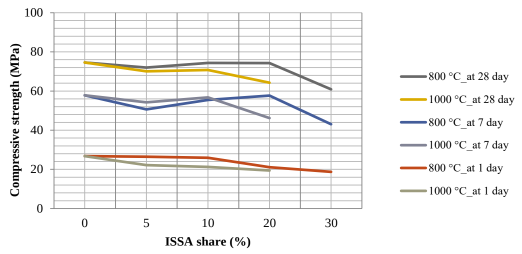

Figure 12 Influence of ISSA share and incineration temperatures on compressive strength [117]

2.7.3. PAPER SLUDGE

Paper sludge from paper industry is a solid residue from the purification of waste water in the industry of cellulose. Balwaik and Raut in [131] have reported that about 300 kg of sludge is produced for each ton of recycled paper. In EU 90 million tons of paper are produced, leaving 11 million tons of waste and 4 million tons of sludge a year. When this sludge is used as fuel it produces ash which can be used in the industry of cement and concrete [39,118,132-134] up to the quantity of 10% of cement quantity. Researchers at the Jaén University in Spain [136] combined the mixed waste from paper industry with ceramic material used in construction industry. The resuls is a brick with low thermal conductivity, meaning it is a good insulator. However, its mechanical resistance still requires further improvement.

2.7.4. STONE CUTTING SLUDGE/SLURRY

During the cutting of stone slabs, the industry produces large quantities of sludge, 346-500 tons a year in Europe – which is mostly sent to landfills [137]. Stone industry in the world disposes of large quantities of sludge which remains after cutting stone, Figure 10 c) [119].

Europe and China cover the largest part of world production of stone [119,138-141]. Since stone production is expected to grow in future, it is essential to find solutions for the application of its sludge. Current investigations are mainly aimed at the production of new artificial stone by using stone cutting sludge [142], and the research into the replacing a part of cement with the cutting stone waste and its impact on mechanical properties of concrete and mortar is rather contradictory [143-144].

2.7.5. FOUNDRY SAND

Foundry sand is a high-quality sand of different mineral origin which is used for the production of molds and cores in metallurgical industry, Figure 10 d) [120]. Foundries use sand of high-quality and purity, mostly most available quartz sand.

Foundry sand is considered as an alternative material which can substitute virgin raw materials. In modern foundry practice, sand is typically recycled and reused through many production cycles. It is estimated that approximately 100 million tons of sand are used in production annually in the USA. Of that, four to seven million tons are discarded annually and are available to be recycled into other products and in other industries [145,146]. Raw materials used in Portland cement manufacture must contain appropriate proportions of calcium oxide, silica, alumina, and iron oxide. Portland cement mixtures typically contain 10-12% silica by weight and alumina and iron oxides (2-5% by weight). These mineral components are significant components of most foundry sands, which can therefore replace virgin minerals [146]. A study by the *American Foundry Society* indicated that Portland cement manufactured with foundry sand may show higher compressive strengths than Portland cement made with conventional raw materials [147]. (Chemical consistency of foundry sands is more important than physical characteristics in determining the suitability for Portland cement manufacture. The silica content of foundry sands exceeds the 80% minimum silica content that Portland cement kilns require and the presence of other elements such as iron and aluminium is an asset. Although foundry sand can be an excellent feedstock for Portland cement manufacture, transportation distances may be an impediment to sourcing more foundry sands for Portland cement kilns [146].

In order to obtain the product with a new quality before its disposal, it is necessary to continue the production of used foundry stone as an industrially produced aggregate. After casting process the mold mixture is disposed of in piles and clusters. Because of this the material intended to be used as aggregate in civil engineering needs further mechanical processing by crushing and homogenization, and by separating small metal particles [148]. Properties of the newly produced material, used foundry sand, depend on the specificalities and types of casting production in terms of modified properties compared to raw material. In addition to the construction of embankments, and/or pavement structures where used foundry sand is added as unbound mix , the foundry sand can be used in composite materials in the mixtures of controlled low strength materials (CLSM) for subbase mass and mortars [149]. Previous research has indicated slightly poorer mechanical properties in mortar and in concrete when fine aggregate has been substituted with foundry sand. Additional research, therefore, should be conducted.

2.8. GYPSUM

Natural gypsum or plaster or calcium sulphate dyhidrate ($CaSO_4$ x 2 H_2O) is a white powder used in cement industry and in the production of mortar and plaster. Gypsum, a secondary raw material from various industries, e.g. FGD gypsum and phospho gypsum, is used in construction industry.

2.8.1. FGD GYPSUM

FGD Gypsum is a unique synthetic product derived from the emissions cleaning process known as flue gas desulfurization (FGD) systems at electric power plants. FGD gypsum is of high purity which makes it suitable for use in cement and construction industries. FGD gypsum is also commonly known as desulphogypsum (DSG) [150]. Natural gypsum and FGD gypsum have the same chemical composition; they are both calcium sulfate dihydrate ($CaSO4{\cdot}2H_2O$). Today, almost half of all gypsum used in the manufacture of gypsum boards in the United States is FGD gypsum, also known as a by-product or synthetic gypsum [151].

In Slovenia-around 400 000 tons/year of FGD gypsum is produced. In Europe, apart from its use in wallboard products, FGD gypsum markets in concrete and cement applications are being developed, such as its use as an admixture, or as a set retarder [152-154]. FGD gypsum is evaluated as a possible partial or total substitute of natural gypsum for the control of cement setting [154].

a) b)

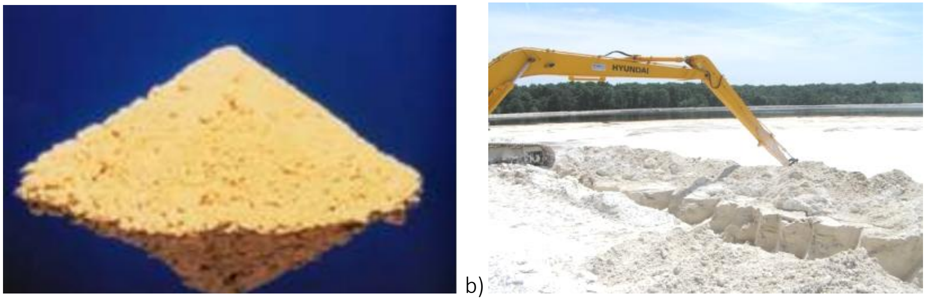

Figure 13 a) Sample of FGD gypsum [150], b) Phospho gypsum landfill owned by the fertilizer factory in Kutina [151]

2.8.2. PHOSPHO GYPSUM

Phospho gypsum is a by-product in the production of phosphoric acid. Each ton of phosphoric acid produced generates five tons of phospho gypsum which is permanently disposed of in landfills, Figure 13 b). [155]. According to the official data, 300,000 tons of phospho gypsum are disposed of in the landfill by Lonja field. The landfill with phospho gypsum is situated on the land south to the production facilities (about 5km from the plant). The land is 160 hectares in size where four “cassettes” have been built in phases. Together with the pump station of reverse flourous water it makes a unified system of phosphor gypsum disposal. The landfill is fenced with peripheral earthen embankments 6m high and 3 m wide.

Recenly, research has been conducted into the use of phospho gypsum as raw material for the production of special type cement, calcium sulphoaluminate cement (CSAC9, [156]. This type of cement is interesting because in its preparation a large quantity of waste gypsum and other waste materials (firebox ash, slag from electric arc furnace, phospho gypsum) can be used, and since synthesizing is conducted at temperature below 1500°C it requires less energy than the general use cement, i.e. Portland cement. Literature lists calcium sulphoaluminate cement (CSAC) as the cement of the 21st century [157,158]. Based on the mass and energy balances of the production process of CSAC and Portland cement it has been established that production of CSAC can significantly save raw materials and energy. The sustainable production of low energy CSA cement (with a lower emission of CO_2) contributes to the goal of reducing greenhouse gasses emission, that is, to the development of low carbon industry of concrete. However, it has to be emphasized that further research should determine long term durability and resistance to the impact of aggressive forces, freezing and defrosting cycles and the effects of high and low temperatures on concrete produced with calcium sulphoaluminate cement.

3. HOW TO EVALUATE WHAT MEASURES TO TAKE

Taking into account sustainable development as the measure of a successful project and construction business as a whole, the question arises how to evaluate planned measures. In [159] listed software for possible evaluation based on scorings that are very similar, and differ according to the proponent or originator of software. Building Research Establishment Environmental Assessment Method (BREEAM) is frequently used in the UK. It is an environmental rating scheme that awards credits based on sustainability considerations. Due to its credit-based structure, BREEAM assessment is clear and easy to understand. Clients can easily see areas in which they have either excelled or failed. The North-American software is Leadership in Energy and Environmental Design (LEED), which was inspired by BREEAM and therefore very similar to it. Japan’s most used tool for encouraging a sustainably built environment is the Comprehensive Assessment System for Built Environment Efficiency (CASBEE) rating, in which economic sustainability is not of primary importance. Envest II is a software used in preliminary design phase and has a simplified access. Company ARUP, UK has developed a fully comprehensive sustainability tool, Sustainable Project Appraisal Routine (SPeAR). SPeAR consists of four main categories: economic, societal, natural resources, and the environment. It allocates a -3 to +3 ranking for 22 sub-categories, resulting in a graphic visualization of the sustainability of a particular project at a point in time. Consequently, of two equally good construction projects the advantage will have the project which, according to the applied sustainability criteria (e.g. use of alternative materials in construction, recycled materials etc.), has more credits.

4. CONCLUSION

New types and technologies of concrete are mainly based on the use of alternative materials, either in cement or in concrete. Despite the increased cement production in the world, if the requirements of sustainable development are followed the pollution will be reduced. Both in Europe and in the west Balkans there are a lot of SCMs applicable in construction industry. But, as Karen Scrivener et all have concluded [160], for the efficient application of SCMs performance based standards for cement and concrete should be adopted. The preparation and development of such standards requires joint efforts and coordination of researchers, industry and government bodies. We can hope that also in the Republic of Croatia construction industry will consider and adopt the application of alternative materials in concrete, and use them more and more in newly built structures, as the examples of structures in the world show [161].

ACKNOWLEDGEMENTS

Sincere gratitude is expressed to the colleagues from Bosnia and Herzegovina (Merima Šahinagić-Isović, Krešimir Šaravanja), Macedonia (Meri Cvetkovska), Slovenia (Vilma Ducman) and Serbia (Ksenija Janković) for useful data on industry.

REFERENCES

[1] Bačun, D.: "E-održivost, globalna inicijativa ", ISO Forum Croaticum, 2003 06 04.
[2] Agenda 21 on sustainable construction, CIB Report Publication 237, 1999, http://cic.vtt.fi/eco/cibw82/A21text.pdf
[3] Rosković, R.; Bjegović, D.: Role of mineral additions in reducing CO2 emission, Cement and Concrete Research 35, 2005, 974– 978.
[4] Lothenbach, B.; Scrivener, K.; Hooton, R.D.: Supplementary cementitious materials, Cement and Concrete Research, Volume 41, Issue 12, 2011, 1244–1256
[5] CONWAS project, LIFE05 TCY/CRO/000114 "Development of sustainable construction and demolition waste management system for Croatia" 2006-2008, http://www2.igh.hr/conwas/index.htm
[6] Bjegović, D.; Mikulić; D.; Štirmer N.: "Proposal for construction and demolition waste management system in Croatia", Life Cycle Assessment applications: results from COST action 530, Fullana, P.; Betz, M.; Hischier, R.; Puig, R. (eds.), AENOR, 2009, 158- 165.
[7] Jain, D.; Kothari, A.; Hair Fibre Reinforced Concrete, Research Journal of Recent Sciences, Vol. 1 (ISC-2011), 128-133 (2012)
[8] Karthikeyan, S.; Elangovan, A.A.; Experimental Study of Ancient Admixture and Natural Fibre in Concrete, International Journal of Research in Engineering and Technology, eISSN: 2319-1163/pISSN: 2321-7308
[9] Bhalerao, N.; Wayal, A.S.; Patil, P.G.; Bharimalla, A.K.: A Review on Effect of Nano Cellulose on Concrete, International Journal of Civil and Structural Engineering Research, Vol.3, Issue 1, pp 251-254, www.researchpublish.com
[10] Sun, X.; Wu, Q.; Lee, S.; Qing, Y.; Wu, Y.: Cellulose Nanofibers as a Modifier for Rheology, Curing and Mechanical Performance of Oil Well Cement. Sci. Rep. 6, 31654; doi: 10.1038/srep31654 (2016).
[11] Han, B.; Yu, X.; Ou, J.: Multifunctional and Smart Carbon Nanotube Reinforced Cement-Based Materials, Chapter in Nanotechnology in Civil Infrastructure, Springer, pp 1-47
[12] Fly Ash, http://www.arthaminerals.com/fly-ash.htm
[13] [13] http://www.cewep.eu/information/publicationsandstudies/statements/ceweppublications/m_722
[14] McCraven, S.: The Future of Fly Ash Use in Concrete, Precast Inc. Magazine, 2013, http://precast.org/2013/11/the-future-of-fly-sh-use-concrete/
[15] Yijin, L.; Shiqiong, Z.; Jian, Y.; Yingli, G.: The effect of fly ash on the fluidity of cement paste, mortar, and concrete, International Workshop on Sustainable Development and Concrete Technology, Beijing, May 20-21, 2004, 339-345,
[16] Skazlić, M.; Vujica, M.: Samozbijajući ekološki prihvatljivi betoni, GRAĐEVINAR 64 (2012) 9, pp. 905-913.
[17] Bjegović, D.; Štirmer, N.: Teorija i tehnologija betona, Sveučilište u Zagrebu Građevinski fakultet, 2015., 999 str.
[18] Jelčić Rukavina, M.; Gabrijel, I.; Bjegović D.: Modifications of dolomite-based self-compacting concrete properties using mineral additives, Technical Gazzette, 2014.
[19] Thomas, M.: Optimizing the Use of Fly Ash in Concrete, http://www.cement.org/docs/default-source/fc_concrete_technology/is548-optimizing-the-use-of-fly-ash-concrete.pdf?sfvrsn=4
[20] [20] Životić, M.M.; Stojiljković, D.D.; Jovović, A.M.; Čudić V.V.: Mogućnost korišćenja pepela i šljake sa deponije termoelektrane „Nikola Tesla" kao otpada sa upotrebnom vrednošću, Hemijska industrija 66 (2012), 3, pp. 403-412.
[21] http://www.energetika-net.com/vijesti/energetsko-gospodarstvo/na-balkanu-treba-zatvoriti-13-termoelektrana-20986
[22] http://mcmbaycity.com/products.html, 31.1.2017.
[23] Coal Bottom Ash/Boiler Slag – Material Description, Recycled materials Resource Center, http://rmrc.wisc.edu/ug-mat-coal-bottom-ashboiler-slag/

[24] Soman Divya Sasi, K.; Abubaker, K.A: Strength properties of concrete with partial replacement of sand by bottom ash, International Journal of Innovative Research in Advanced Engineering (IJIRAE) Volume 1 Issue 7 (August 2014), 223-227, http://ijirae.com
[25] Aggarwal, P.; Aggarwal, Y.; Gupta, S.M.: Effect of Bottom Ash as Replacement of Fine Aggregates in Concrete, Asian Journal of Civil Engineering (Building and Housing) Vol.8, No.1 (2007) pages 49-62
[26] Andrade, L.B.; Rocha, J.C., Cheriaf, M. Evaluation of concrete incorporating bottom ash as a natural aggregates replacement, Waste Manag. 2007;27(9):1190-9.
[27] Biomasa, http://e-learning.gornjogradska.eu/energijaekologijaengleski-ucenici/4-biomasa/
[28] Zakon o energiji (NN 68/2011, 177/2004, 152/2008 i 127/2010)
[29] http://www.chinaseniorsupplier.com/Energy/Electricity_Generation/60288614351/palm_leaf_waste_to_energy_biomass_gasification_gas_genset.html
[30] ASTM C618 – 15, Standard specification for coal fly ash and raw or calcined natural pozzolan for use in concrete
[31] Chowdhury, S.; Maniar, A.; Suganya, O.M.: Strength development in concrete with wood ash blended cement and use of soft computing models to predict strength parameters, Journal of Advanced Research, Volume 6, Issue 6, November 2015, Pages 907–913
[32] Wang, S.; Baxter, L. Comprehensive study of biomass fly ash in concrete: Strength, microscopy, kinetics and durability, Fuel Processing Technology, Volume 88, Issues 11–12, December 2007, Pages 1165–1170
[33] Carević, I.; Banjad Pečur, I.; Štirmer, N.; Milovanović, B.; Baričević, A.: Potencijal biopepela i stanje u Republici Hrvatskoj, Sabor hrvatskih graditelja, 2016.
[34] Ban, C.C.; Ramli, M.: The implementation of wood waste ash as a partial cement replacement material in the production of structural grade concrete and mortar: An overview, Resources, Conservation and Recycling 55 (2011) 669–685
[35] Grau, F.; Choo, H.; Wan Hu, J.; Jung, J.: Engineering Behaviour and Characteristics of Wood Ash and Sugarcane Bagasse Ash, *Materials* 2015, *8*(10), 6962-6977; doi:10.3390/ma8105353
[36] Habeeb, G.A.; Mahmud, H.B.: Study on properties of rice husk ash and its use as cement replacement material, Mat. Res. vol.13 no.2 São Carlos Apr./June 2010, http://dx.doi.org/10.1590/S1516-14392010000200011
[37] Aparecida, M.; Schettinoa, S.; Nilson, J.; Holanda, F.: Characterization of sugarcane bagasse ash waste for Its Use in Ceramic Floor Tile, International Congress of Science and Technology of Metallurgy and Materials, SAM - CONAMET 2013
[38] Noviks, G.: Investigation of Biomass Ash Properties for Their Utilization Assesment, Environment. Technology. Resources, Proceedings of the 9 the International Scientific and Practical Conference. Volume 1, 2013, 168 – 174.
[39] Florea, M.V.A.: Secondary materials in cement-based products, Treatment, modelling and environmental interaction, Ph.D. Thesis, Eindhoven University of Technology, bouwstenen 192, the Netherlands, 2014.
[40] Wang, S.; Llamazos, E.; Baxter, L.: Durability of biomass fly ash concrete: Freezing and thawing and rapid chloride permeability tests, Fuel, Volume 87, Issue 3, March 2008, Pages 359–364
[41] Sierra Beltran, M.G.; Ukrainczyk, N.; Schlangen, E.: Development of SHCC with biomass fly ash, Proceedings of the 3rd international RILEM conference on strain hardening cementitious composites (SHCC3-Delft), Dordrecht, Netherlands, 3-5.11.2014.
[42] Štirmer, N.: Transformation of Wood Biomass Ash into Resilient Construction Composites, National Research Project, Croatian Science Foundation, 2017-2021
[43] Da Silva, F.G.; Liborio, J.B.L.; Helene, P. Improvement of physical and chemical properties of concrete with Brazilian silica rice husk (SRH), Revista Ingeniería de Construcción Vol.23 N°1, Abril de 2008 www.ing.puc.cl/ric PAG.18-25
[44] Krishnasamy, T. R.; Palanisamy, M.: Pepeo od šećerne trske i rižinih ljuski kao zamjena za cement u samozbijajućem betonu, GRAĐEVINAR 67 (2015) 1, pp. 23-31.
[45] Chopra, D.; Siddique, R.: Strength, permeability and microstructure of self-compacting concrete containing rice husk ash, Biosystems Engineering, Volume 130, February 2015, Pages 72–80
[46] Atan, M.N.; Awang, H.: The Compressive and Flexural Strengths of Self-Compacting Concrete Using Raw Rice Husk Ash, Journal of Engineering Science and Technology, Vol.6, No. 6 (2011) 720-732.
[47] Bui, L. A.; Chen,C.; Hwang, C.; Wu, W.: Effect of silica forms in rice husk ash on the properties of concrete, International Journal of Minerals, Metallurgy, and Materials 19 (2012),3, pp.252-258.
[48] Rice Husk Ash Balls, http://www.indiamart.com/nk-entps-jharsuguda/rice-husk-ash.html
[49] http://www.sandwichpanelautoline.com
[50] Pode, R.: Potential applications of rice husk ash waste from rice husk biomass power plant, Renewable and Sustainable Energy Reviews 53 (2016) 1468–1485
[51] Srinivasan, R.: Experimental Study on Bagasse Ash in Concrete, International Journal for Service Learning in Engineering Vol. 5, No. 2, pp. 60-66, Fall 2010 ISSN 1555-9033
[52] Chi, M.C.: Effect of sugar cane bagasse ash as a cement replacement on properties of mortars, Science and Engineering of Composite Materials, Volume 19, Issue 3, Pages 279-285
[53] Núñez-Jaquez, R. E.; Buelna-Rodríguez, J. E.; Barrios-Durstewitz, C. P.; Gaona-Tiburcio, C.; Almeraya-Calderón, F. Corrosion of Modified Concrete with Sugar Cane Bagasse Ash, International Journal of Corrosion, Volume 2012 (2012), Article ID 451864, 5 pages

[54] Bahurudeen, A.; Santhanam, M. Performance Evaluation of Sugarcane Bagasse Ash-Based Cement for Durable Concrete, 4th International Conference on the Durability of Concrete Structures 24–26 July 2014 Purdue University, West Lafayette, IN, USA

[55] Castaldelli, V.N.; Akasaki, J.L.; Melges, J.L.P.; Tashima, M.M.; Soriano, L.; Borrachero, M.V.; Monzó, J.; Payá, J.: Use of Slag/Sugar Cane Bagasse Ash (SCBA) Blends in the Production of Alkali-Activated Materials, Materials 2013, 6, 3108-3127; doi:10.3390/ma6083108

[56] [56] Macedo, P.C.; Pereira, A.M.; Akasaki, J.L.; Fioriti, C.F.; Payá, J.; Melges, J.L.P.; Performance of mortars produced with the incorporation of sugar cane bagasse ash, Revista ingeniería de construcción, vol.29 no.2 Santiago ago. 2014, http://dx.doi.org/10.4067/S0718-50732014000200005

[57] [57] Reuter, M.; Xiao, Y.; Boin, U.: Recycling and environmental issues of metallurgical slags and salt fluxes. VII International Conference on Molten Slags Fluxes and Salts, The South African Institute of Mining and Metallurgy, 2004, 349-356.

[58] Supplementary Cementitious Materials, http://cmcgusa.com/supplementary-cementitious-materials/

[59] http://wiredspace.wits.ac.za/bitstream/handle/10539/15369/Project%20Report.pdf?sequence=3

[60] Zinc Slag, https://www.indiamart.com/proddetail/zinc-slag-4476427791.html

[61] Ferronickel Slag, http://www.snnc.co.kr/eng/pages/02product/product_list02.php; January 2017.

[62] Aluminium Dross, http://www.am-global.com/aluminium-dross.htm, January 2017.

[63] http://www.solarnavigator.net/history/wealden_iron_industry.htm

[64] http://tehnologicaland.blogspot.com/2010/11/steelmaking.html

[65] Remus, R.; Aguado-Monsonet, M. A.; Roudier, S.; Sancho, L.D.: Best Available Techniques (BAT) Reference Document for Iron and Steel Production, Industrial Emissions Directive 2010/75/EU, http://eippcb.jrc.ec.europa.eu/reference/BREF/IS_Adopted_03_2012.pdf

[66] Aggregates - general information, http://www.euroslag.com/applications/aggregates/

[67] Kothai, P.S.; Malathy, Dr.R.: Utilization Of Steel Slag In Concrete As A Partial Replacement Material for Fine Aggregates, International Journal of Innovative Research in Science, Engineering and Technology, Vol. 3, Issue 4, April 2014 , ISSN: 2319-8753

[68] Rao, M.S.; Bhandare, U.: Application of Blast Furnace Slag Sand in Cement Concrete–A Case Study, International Journal of Civil Engineering Research. ISSN 2278-3652 Volume 5, Number 4 (2014), pp. 453-458,

[69] Netinger, I.; Jelčić Rukavina, M.; Mladenovič, A.: Improvement of Post-fire Properties of Concrete with Steel Slag Aggregate, Procedia Engineering Volume 62, 2013, Pages 745-753

[70] Euroslag Statistics, www.euroslag.org/products/statistics/2012/

[71] Netinger, I.; Jelčić Rukavina, M.; Bjegović, D.: Mogućnost primjene domaće zgure kao agregat u betonu, GRAĐEVINAR 62 (2010) 1, 35-43

[72] Sofilić, T.; Sofilić, U.; Brnardić, I.: The significance of iron and steel slag as by- product for utilization in road construction,12th International Foundrymen Conference Sustainable Development in Foundry Materials and Technologies, 2012, Opatija, Croatia

[73] Gorai, B.; Jana, R. K. ; Premchand: Characteristics and utilisation of copper slag - a review, resources. Conservation and Recycling, v. 39, n. 4, p. 299-313, 2003.

[74] Sánchez de Rojas, M.I.; Rivera, J.; Frías, M.; Marín, F.: Use of recycled copper slag for blended cements, Journal of Chemical Technology and Biotechnology, Volume 83, Issue 3, pages 209–217, March 2008

[75] Shi, C.; Meyer, C.; Behnood, A.: Utilization of cooper slag in cement and concrete, Resources, Conservation and Recycling, Volume 52, Issue 10, August 2008, Pages 1115-1120.

[76] Chavan, R. R.; Kulkarni, D.B.: Performance of copper slag on strength properties as partial replace of fine aggregate in concrete mix design, Int. J. Adv. Eng. Res. Studies/II/IV/July-Sept., 2013/95-98

[77] Mobasher, B.; Devaguptapu R.; Arino, A.M.: Effect of copper slag on the hydration of blended cementitious mixtures, Proceedings, ASCE, Materials Engineering Conference, Materials for the New Millenium, ed. K. Chong, pp. 1677-86, 1996.

[78] Patnaika, B.; Sekhar, S.; Srinivasa Rao, T.A.: An Experimental Investigation on Optimum Usage of Copper Slag as Fine Aggregate in Copper Slag Admixed Concrete, International Journal of Current Engineering and Technology, Vol.4, No.5 (Oct 2014), 3646-3648

[79] Brindha, D.; Nagan, S.: Utilization of Copper Slag as a Partial Replacement of Fine Aggregate in Concrete, International Journal of Earth Sciences and Engineering ISSN 09745904, Vol. 03, No. 04, August 2010, pp. 579585

[80] Lokalni ekološki akcioni plan opštine bor izvod (nacrt izvestaja), Bor, mart 2003., http://www.mibor.rs/projekti/leap/pdf/leap_dok.pdf

[81] Monosi, S.; Giretti, P.; Moriconi, G.; Favoni, O.; Collepardi, M.: Non Ferrous Slag as Cementitious Material and Fine Aggregate for Concrete, http://www.encosrl.it/enco%20srl%20ITA/servizi/pdf/aggiunte/18.pdf

[82] Ferrosilicate slag from zinc production as aggregates bound in cement, Aggregates Case Study, AGG0078, http://www.wrap.org.uk/sites/files/wrap/Ferrosilicate_zinc_slag_in_cement_bound_mixes.pdf

[83] Alex, T.C.; Kalinkin, A.M.; Nath, S.K.; Gurevich, B.I.; Kalinkina, E.V.; Tyukavkina, V.V.; Kumar, S.: Utilization of zinc slag through geopolymerization: Influence of milling atmosphere, International Journal of MineralProcessing, Volume 123, 2013, Pages 102–107

[84] Hughes, M.L.; Halliburton, T.A.: Use of Zinc Smelter Waste as Highway Construction Material, Highway Research Record No. 430, 1973, pp. 16-25.

[85] von Krüger, P.; Silva, C.A.; Vieira, C.B.; Araújo, F.G.S.; Seshadri, V.: Relevant Aspects Related to Production of Iron Nickel Alloys (Pig Iron Containing Nickel) in mini Blast Furnaces, The Twelfth International Ferroalloys Congress, Sustainable Future, June 6 – 9, 2010, Helsinki, Finland, 671-680.
[86] Lagendijk, H.; Jones, R.T.: Production of ferronickel from nickel laterites in a dc-arc furnace, 36th Annual Conference of Metallurgists, Sudbury, Canada, August 1997, http://www.mintek.co.za/Pyromet/Laterite/Laterite.htm
[87] Sakkas, K.; Sofianos, A.; Nomikos, P.; Panias, D.: Behaviour of Passive Fire Protection K-Geopolymer under Successive Severe Fire Incidents, Materials 2015, 8, 6096-6104; doi:10.3390/ma8095294
[88] Sakkas, K.; Nomikos, P.; Sofianos, A.; Panias, D.: Slag based geopolymer for passive fire protection of tunnels, Proceedings of World Tunnel Congress 2013, Geneva, Underground – the way to the future! G.Anagnostou& H. Ehrbar (eds), 343-349.
[89] Nickel: World Plant Production, By Country And Product, http://www.indexmundi.com/en/commodities/minerals/nickel/nickel_t12.htm, January 2017.
[90] JSCE Committee on Ferronickel Slag Fine Aggregate, Guidelines for construction using ferronickel slag fine aggregate concrete, Concrete library of JSCE No. 24, 1994, 1-16, http://www.jsce.or.jp/committee/concrete/e/newsletter/newsletter01/recommendation/recommendation/24.pdf
[91] https://zelenenovine.wordpress.com/feljton/afera-nikal/tragom-nikla-2-kavadarci-nikl-truje-zemlju-i-ljude/
[92] Ibrahimi, I.; Rizaj, M.; Ramadani, A.: Research the Possibility of Transforming the Ferronickel Slag in the Product with the Economical and Environmental Importance, J. Int. Environmental Application & Science, Vol. 5 (2): 276-281 (2010)
[93] Aba, M.; Sakoi, Y.; Shoya, M.; Tsukinaga, Y.; Nagataki, S.: Properties of Concrete Incorporating Ferronickel Slag as Coarse Aggregates, Concrete Research and Technology, Japan Concrete Institute, Vol.21, No.3, Sep 2010 (Issue 54)
[94] Sakoi, Y.; Aba, M.; Tsukinaga, Y.; Nagataki, S.: Properties of Concrete used in Ferronickel Slag Aggregate, Third International Conference on Sustainable Construction Materials and Technologies, August 18 – August 21 2013, Kyoto Research Park, Kyoto, Japan
[95] Komnitsas, K.A.; Potential of geopolymer technology towards green buildings and sustainable cities, 2011 International Conference on Green Buildings and Sustainable Cities, Procedia Engineering 21 (2011) 1023 – 1032.
[96] Maragkos, I.; Giannopoulou, I.P.; Panias, D.: Synthesis of ferronickel slag-based geopolymers, Minerals Engineering, Volume 22, Issue 2, January 2009, Pages 196–203
[97] Tomosawa, F.; Nagataki, S.; Kajiwara, T.; Yokoyama, M.: Alkali-aggregate Reactivity of Ferronickel-Slag Aggregate Concrete, Special Publication, ACI, 170, 7/1/1997,1591-1602
[98] Saha, A.; Sarker, P.: Expansion due to alkali-silica reaction of ferronickel slag fine aggregate in OPC and blended cement mortars. Construction and Building Materials. 123, 2016, pp. 135-142.
[99] Epstein, H.: A synthetic source of alumina from aluminium slags, http://www.xatico.com/weimages/pdf/valoxy-review.pdf)
[100] Tsakiridis, P.E.: Aluminium salt slag characterization and utilization – A review, Journal of Hazardous Materials, Volumes 217–218, 30 May 2012, Pages 1–10.
[101] Petavratzi, E.; Wilson, S.: Residues from aluminium dross recycling in cement, Characterisation of Mineral Wastes, Resources and Processing technologies – Integrated waste management for the production of construction material, WRT 177 / WR0115, 2007, 1-8.
[102] Dai, C.: Development of aluminium dross-based material for engineering applications, Master Thesis, Faculty of the Worcester Polytechnic Institute, January 2012.
[103] [103] Ozerkan, N.G.; Maki, O.L.; Anayeh, M.W.; Tangen, S.; Abdullah, A.M.: Effect of Aluminium Dross on Mechanical and Corrosion Properties of Concrete, https://www.rroij.com/open-access/the-effect-of-aluminium-dross-on-mechanicaland-corrosion-properties-of-concrete-.php?aid=46508
[104] Concrete Admixture Silica Fume, http://www.marginup.com/Products/55433/Concrete-Admixture-Silica-Fume-85909295-SF85-SF97.html
[105] Popović, K., Ukrainčik, V., Đureković,A.: SiO2 prašina iz proizvodnje ferolegura kao pucolanski dodatak cementu, Kemija u industriji 34 (1985), 9, pp. 575-581.
[106] Amudhavalli, N. K.; Mathew, J.: Effect of silica fume on strength and durability parameters of concrete, International Journal of Engineering Sciences & Emerging Technologies, August 2012. Volume 3, Issue 1, pp: 28-35.
[107] Kjellsen, K.O.; Wallevik, O.H.; Hallgren, M.: On the compressive strength development of high-performance concrete and paste effect of silica fume, Materials and Structures 32 (1999), 1, pp 63-69.
[108] Kayali, O.; Zhu, B.: Corrosion performance of medium-strength and silica fume high-strength reinforced concrete in a chloride solution, Cement and Concrete Composites, Volume 27, Issue 1, January 2005, Pages 117–124.
[109] Goletić, Š.; Imamović, N.; Schwarczová, H.: The Dust Emission Control in Production of Ferroalloys by Application of Best Available Technics, Acta Technica Corviniensis–Bulletin Of Engineering, Tome VI (2013), 3, pp. 21-24.
[110] http://www.kalpnaminerals.com/limestone-powder.htm
[111] Cements for a low-carbon Europe, A review of the diverse solutions applied by the European cement industry through clinker substitution to reducing the carbon footprint of cement and concrete in Europe, CEMBUREAU - The European Cement Association, http://www.cembureau.be/sites/default/files/documents/Cement%20for%20low-carbon%20Europe%20through%20clinker%20substitution.pdf
[112] http://www.sandatlas.org/limestone/

[113] Kamenić, N.; Popović, K.: Utjecaj vapnenca na svojstva cementa i betona, XIV Savjetovanje o suvremenim dostignućima u proizvodnji cementa i azbest cementa, Sarajevo, pp- 66-70, 1990.
[114] Krstulović, P.; Kamenić, N.; Popović, K.: A New Approach in Evaluation of Filler Effect in Cement I. Effect on Strength and Workability on Mortar and Concrete, Cement and Concrete Research 24 (1994), 4, pp. 721-727.
[115] http://www.cementdistribution.com/industryinfo/articles/calcium_carbonate_fines_for_sustainable_concrete.pdf
[116] Tennis, P. D., Thomas, M. D. A., Weiss, W. J.: State-of-the-Art Report on Use of Limestone in Cements at Levels of up to 15%, Portland Cement Association, 2011.
[117] Štirmer, N.; Baričević, A.; Nakić D.; Vouk, D.: Use of incinerated sewage sludge ash in concrete production, Second International Conference on Concrete Sustainability – ICCS 2016, Madrid, 2016. 1465-1475
[118] http://www.np-recycling.nl/en/industrial-residuals/paper-sludge.html
[119] Al-Joulan, N.; Salah, N.: The Stone Slurry in Palestine from Environmental Burden to Economic Opportunities—Feasibility Analysis, Journal of Environmental Protection, Vol.05 No.12(2014)
[120] [120] https://dir.indiamart.com/impcat/foundry-sand.html
[121] [121] Let HuberCrete™Calcium, Carbonate Help You Manufacture Superior Concrete, http://www.hubermaterials.com
[122] Tsivilis, S.; George, B.; Chaniotakis, E.; Theodossis, D.: Properties and behavior of limestone cement concrete and mortar, Cement and Concrete Research 30(10):1679-1683 · October 2000
[123] Uklanjanje bivše tvornice glinice Jadral u Obrovcu, GRAĐEVINAR 56 (2004) 10, 645-648.
[124] Štirmer, N.; Bjegović, D.; Baričević, A.; Carević, I. Mogućnosti primjene alternativnih materijala u proizvodnji betona, iNDiS 2015, Radonjanin, V.; Lađinović, Đ.; Folić, R. (ed.). Novi Sad : Fakultet tehničkih nauka, Departman za građevinarstvo i geodeziju, 2015.
[125] Liu, X.; Zhang, N.; Sun, H.; Zhang, J.; Li, L.: Structural investigation relating to the cementitious activity of bauxite residue — Red mud, Cement and Concrete Research 41 (2011), pp. 847–853.
[126] Serdar, M.; Biljecki, I.; Bjegović, D.: High-Performance Concrete Incorporating Locally Available Industrial By-Products, Journal of Materials in Civil Engineering 1 (2016)
[127] Cheeseman, C.R.; Virdi, G.S.: Properties and microstructure of lightweight aggregate produced from sintered sewage sludge ash. Resources, Conservation and Recycling 45 (2005, 1. pp 18-30.
[128] Chen, M.; Blanc, D.; Gautier, M.; Mehu, J.; Gourdon, R.: Environmental and technical assessments of the potential utilization of sewage sludge ashes (SSAs) as secondary raw materials in construction, Waste Management 33 (2015), pp 1268-1275.
[129] Vouk, D.; Nakić, D.; Štirmer, N.; Korištenje mulja s UPOV-a u betonskoj industriji – projekt „RESCUE“, Glasnik Hrvatskog društva za zaštitu voda, Godina 11 (2015), Broj 30;35-41,
[130] Vouk, D.; Nakić, D.; Štirmer, N.; Serdar, M.: Mogućnost zbrinjavanja mulja koji nastaje u procesu obrade otpadne vode u betonskoj industriji, Hrvatske vode, časopis za vodno gospodarstvo, 23 (2015), 94; 277-286.
[131] Bajpai, P.: Management of Pulp and Paper Mill Waste, Springer International Publishing Switzerland 2015
[132] Fava, G.; Ruello, M.; Corinaldesi, V.: Paper Mill Sludge Ash as Supplementary Cementitious Material, Journal of Materials in Civil Engineering (ASCE) 23 (2011). 6, pp. 772–776.
[133] Corinaldesi, V.; Fava, G.; Ruello, M. L.: Paper Mill Sludge Ash as Supplementary Cementitious Material, Second International Conference on Sustainable Construction materials and Technologies, Ancona, Italy, 2010.
[134] Naik, T.R.; Friberg, T.; Chun, Y.-M.: Use of pulp and paper mill residual solids in production of cellucrete, Cement and Concrete Research 34 (2004), 7, pp.1229-1234.
[135] Khan, A.S.; Panth, R.; Krishna, G.R.R, Patil, S.G.: Structural Performance of Concrete by Partial Replacement of Cement with Hypo Sludge (paper waste), International Journal of Emerging Technologies and Engineering (IJETE) Volume 1 Issue 7, August 2014,
[136] Cigle od otpadnog papira, http://znanost.geek.hr/clanak/cigle-od-otpadnog-papira/#ixzz3iPQo0JCq
[137] LIFE10 ENV/IT/000346, http://ec.europa.eu/environment/life/project/Projects/index.cfm
[138] http://www.aitemin.es/docs/piedra_natural_aprov_res/doc_e.html
[139] Al-Zboon, K.; Tahat, M.: Recycling of Stone Cutting Waste in Floor Tiles Production, International Journal of Theoretical & Applied Sciences, 1 (2009), 1, pp. 64-71.
[140] Lakhani, R.; Kumar, R.; Tomar, P.: Utilization of Stone Waste in the Development of Value Added Products: A State of the Art Review, International Journal of Innovative Science, Engineering & Technology 1 (2014), 7, pp. 180-187.
[141] Al-Joulani, N.: Utilization of Stone Slurry Powder in Production Artificial Stones, Research Journal in Engineering and Applied Sciences 3 (2014), 4,pp. 245-249
[142] Patel, A. N.; Jayeshkumar, P.: Stone Waste: Effective Replacement Of Cement For Establishing Green Concrete, International Journal of Innovative Technology and Exploring Engineering (IJITEE) 2 (2013), 5, pp. 24-27.
[143] Al-Zboon, K.; Al-Zou, J.: Recycling of stone cutting slurry in concrete mixes, Journal of Material Cycles and Waste Management, April 2015, Volume 17, Issue 2, pp 324–335
[144] Patel, A.N.; Pitroda, J.: Stone Waste Effective Replacement Of Cement For Establishing Green Concrete, International Journal of Innovative Technology and Exploring Engineering (IJITEE) ISSN: 2278-3075, Volume-2, Issue-5, April 2013, 24-27.
[145] Introduction to Foundry Sand, http://www.afsinc.org/content.cfm?ItemNumber=7075
[146] Foundry Sand as an Alternative Raw Material in the Manufacturing of Cement, https://archive.epa.gov/sectors/web/pdf/geocycle_case_study_1_31_2008.pdf

[147] Cement Manufacturing, http://www.afsinc.org/content.cfm?ItemNumber=7099)

[148] Pavlic, V.; Stipanovic Oslakovic, I.; Bjegovic, D.: Mogucnosti primjene korištenog ljevackog pijeska u gradevinarstvu, Gospodarenje otpadom, Varaždin, 2012.

[149] Monosi, S.; Sani, D.; Tittarelli, F.: Used Foundry Sand in Cement Mortars and Concrete Production, The Open Waste Management Journal 3 (2010),pp.18-25.

[150] Dunster, A.M. Flue gas desulphurisation (FGD) gypsum in plasterboard manufacture, Characterisation of Mineral Wastes, Resources and Processing technologies – Integrated waste management for the production of construction material, WRT 177 / WR0115, November 2007, 8 pp.

[151] Posejpal, B.: Lonjsko Polje – kvaliteta tla, vode i zraka, završni rad, Veleučilište u Karlovcu specijalistički diplomski stručni studij sigurnosti i zaštite, Karlovac, 2015, 53 str.

[152] EPA Concludes FGD Gypsum in Gypsum Board Contributes Significant Environmental and Economic Benefits; Affirms Environmental, Health and Safety Studies, https://www.gypsum.org/press-roomfgd-gypsum-board/

[153] Leiva, C.; García Arenas, C.; Vilches, L.F.; Vale, J.; Gimenez, A.; Ballesteros, J.C.; Fernández-Pereira, C.: Use of FGD gypsum in fire resistant panels, Waste Management 30 (2010) 1123–1129

[154] Tzouvalas, G.; Rantis, G.; Tsimas, S.: Performance criteria for the use of FGD gypsum in cement and concrete production,Measuring, Monitoring and Modeling Concrete Properties, An International Symposium dedicated to Professor Surendra P. Shah, Northwestern University, U.S.A., Springer, 2006, pp 373-378

[155] Franković Mihelj, N.; Horvat, D.: Oporaba otpada u niskougljičnom razvoju, HRVATSKA KOMORA INŽENJERA GRAĐEVINARSTVA, Dani ovlaštenih inženjera građevinarstva, Opatija, 2014.

[156] [156] Franković Mihelj, N.: Oporaba otpadnog gipsa u pripravi specijalnih cemenata, disertacija, Fakultet kemijskog inženjerstva i tehnologije, 2012.

[157] Franković-Mihelj, N.; Ukrainczyk, N.; Leaković, S.; Šipušić, J.: Waste Phosphogypsum – Toward Sustainable Reuse in Calcium Sulfoaluminate Cement Based Building Materials, Chemical and biochemical engeenering quartely 27 (2013), 2, pp. 219-226.

[158] Ukrainczyk, N.; Franković Mihelj, N.; Šipušić, J.: Calcium Sulfoaluminate Eco-Cement from Industrial Waste, Chemical and biochemical engeenering quartely 27 (2013), 1, pp.83-93.

[159] Peach, J.: Five Sustainability Tools for the Built Environment and Beyond, http://thisbigcity.net/five-sustainability-tools-for-the-built-environment-and-beyond/

[160] Scrivener, K.; John, V.M.; Gartner, E.M.: Eco-efficient cements: Potential, economically viable solutions for a low-CO2, cement-based materials industry, United Nations Environment Program (UNEP), Paris 2016.,50 pp.

[161] Bjegović, D.; Štirmer, N.; Baričević, A.: Alternativni materijali u suvremenim konstrukcijama, Zbornik radova, Društvo građevinskih konstruktera Srbije, Zlatibor, Srbija, 2016, 1084-1093.

DEVELOPMENT OF MULTI-FUNCTIONAL ENERGY-EFFICIENT STRUCTURAL MATERIALS

Kemal Celik[1], Paulo J. M. Monteiro[2], Krishnan Padmaja[3], Vanessa Rheinheimer[1], Rae Taylor[2], Yunpeng Wu[3], Liya Yu[3], Min-Hong Zhang[3]

[1] Berkeley Education Alliance for Research in Singapore, Singapore 138602, Singapore, email: kemal.celik@bears-berkeley.sg, vanessa.rheinheimer@bears-berkeley.sg
[2] Department of Civil and Environmental Engineering, University of California, Berkeley California 94720, USA, email: monteiro@ce.berkeley.edu, rae.taylor@berkeley.edu
[3] Department of Civil and Environmental Engineering, National University of Singapore, Singapore 119260, Singapore, email: kpadmaja@nus.edu.sg, wuyunpeng@nus.edu.sg, liya.yu@nus.edu.sg, mhzhang@nus.edu.sg

SUMMARY: Production and use of concrete consumes a significant amount of energy and produces large amounts of CO_2. On a global scale, in 2010 about 3.2 billion tons of CO_2 were emitted to the atmosphere from the production of 3.9 billion metric tons of cement, through fuel consumed in kiln-fired production of clinker and CO_2 emitted during calcination of carbonaceous rock. New holistic solutions are necessary to tackle such challenge. This paper summarizes our research on concrete containing high volume natural pozzolan to obtain sustainable construction materials. We also address the new challenges to produce concrete with low thermal properties and, by adding proper TiO_2 coatings, improve the air quality around to the buildings.

RAZVOJ VIŠEFUNKCIONALNIH ENERGETSKI UČINKOVITIH KONSTRUKCIJSKIH MATERIJALA

SAŽETAK: U proizvodnji i upotrebi betona troši se znatna količina energije i proizvode velike količine CO_2. Na globalnoj razini 2010. iz proizvodnje 3,9 milijarde kubičnih tona cementa u atmosferu je emitirano oko 3,2 milijarde tona CO_2 i to iz goriva utrošenog u pećima za proizvodnju klinkera i CO_2 emitiranog tijekom kalcinacije vapnenačkih stijena. Za suočavanje s takvim izazovom nužna su nova holistička rješenja. U radu su sumirani rezultati istraživanja betona koji sadržavaju veliku količinu prirodnoga pucolana kako bi se dobili održivi građevni materijali. Upućuje se i na nove izazove kako bi se proizveo beton dobrih toplinskih svojstava, a dodavanjem prikladnog premaza od TiO_2 poboljšala kvaliteta zraka oko zgrada.

1. INTRODUCTION

The U.S. National Research Council recently articulated an urgent national need for investment in the aging civic infrastructure to maintain the global competitiveness [1]. The American Federal Highway Administration Annual estimates that expenditures of $100 B are needed solely to maintain the current conditions and performance of the U.S. road system through 2028 [2]. However, the conventional means of producing such infrastructure consume substantial amounts of energy, produce large quantities of greenhouse gases, and are not ultimately sustainable. More environmental alternatives—already practiced to some extent by the construction industry—include reducing the amount of cement used or partially substituting portland cement with fly ash, a waste product of coal-fired power plants. New creative solutions are necessary to handle such challenge. In this paper we summarize on-going research on the use of natural pozzolans to enhance modern high-performance concrete.

While approximately 37% of energy consumption in the world is attributed to the building sector, about 85% of that energy is consumed when buildings are in use through cooling, heating, and lighting etc. Concrete, which has low thermal conductivity compared with other building materials, can be further enhanced by introducing air voids to resist heat flow between indoor and outdoor environments. There are several ways to introduce these air voids: (a) voids in “aggregates” of various sizes; (b) voids in cement paste; (c) packing gradation to improve the voids between coarse aggregate particles; and (d) combinations of the above. Although the introduction of voids in concrete will reduce thermal conductivity and increase insulation capacity for energy efficiency, mechanical properties, such as strength and elastic modulus, are generally compromised. Therefore, we are studying the addition of special lightweight aggregates into the cementitious matrix to improve the thermal properties while maintaining adequate structural performance.

Mitigation of airborne pollutants using *multi-functional energy-efficient* (MFEE) materials in buildings provides a cost-effective alternative to improve the ambient environment of large cities, especially when the function of degrading pollutants is integrated with energy efficiency. This enables existing and future buildings in large cities to contribute to a sustainable environment. The MFEE materials utilize solar energy to degrade three types of airborne pollutants: SOx, NOx, and particulates. The same material can also remove global warming components, such as nitrous oxide, methane, and particulates. In view of the acidic nature of airborne pollutants, TiO_2 appears to be most stable among the commonly employed photocatalysts, and a new generation of functionalized TiO_2 will be adopted and integrated with existing compatible and cost-effective building materials to maximize the resultant photocatalytic mitigation efficiencies under the humid warm tropical weather. Our research in this topic is presented at the end of the paper.

2. CHALLENGES AND OPPORTUNITIES FACING THE CONCRETE INDUSTRY

The concrete industry has both negative and positive environmental impacts. Mehta and Monteiro [3] pointed out that concrete mixtures for general construction, on the average, are composed of 12% portland cement, 8% mixing water, and 80% coarse and fine aggregate by mass. In 2010, the 33 billion tonnes yearly global concrete industry consumed nearly 3.7 billion tonnes portland-cement clinker and 27 billion tonnes of aggregate, in addition to 2.7 billion tonnes of mixing water and small amount of chemical admixtures. The mining, processing, and transport of such huge quantities of materials for making concrete, in addition to large amounts of limestone, clay and fossil fuels for portland-cement clinker manufacture, require considerable energy, and adversely affect the ecology of virgin lands.

The production of portland cement is energy-intensive (4 GJ/tonne of cement) and produces large emissions of CO_2. In average, the manufacture of one tonne of portland-cement clinker releases on the average one tonne of CO_2 into the atmosphere. The world's yearly cement production is responsible for nearly 7 percent of the total global CO_2 emissions. On the other hand, if properly designed concrete can have a positive environmental impact when industrial byproducts are incorporated into the concrete mix proportions. Many of the industrial byproducts, such as coal fly ash and iron blast-furnace slag contain some toxic metals; and disposal of these byproducts by dumping into land-fills or ponds contaminates the drinking water supply. However, if these byproducts are used as a part of the cementing materials in concrete mixtures, the toxic elements can get permanently bound in the hydration products of portland-cement. At U.C. Berkeley, intensive research is being performed on the large replacement of Portland cement with combinations of fly ash, natural pozzolan and finely ground limestone. Equally important, is the development of advanced MFEE structural materials, many included advanced concrete matrix, to increase the energy efficiency in the civil infrastructure. A summary of these two large experimental programs is described next.

2.1. DEVELOPMENT OF SUSTAINABLE CONCRETE USING HIGH VOLUME FLY ASH/NATURAL POZZOLAN

The use of supplementary cementitous materials (SCM) can reduce the carbon footprint of the concrete industry. Tomkins [4] estimated that to lessen 1 billion tons of CO_2 emission per year, almost 50% of the clinker of portland cement must be substituted with materials produced with very low carbon dioxide emissions, therefore requiring the use of 1.5 billion tons of SCM annually. The blast furnace slag and high volume fly ash mixtures have effectively used in small and large projects. Yet, the global availability of fly ash and slag is not enough to satisfy the demand for green concrete. This unsatisfied demand can create unique opportunities for the utilization of the natural pozzolan in portland cement concrete mixtures. Recently, we have performed detailed studies of portland cement-based binary and ternary blends containing various combinations of natural volcanic pozzolan (NP) and limestone filler (L) (see Tab. 1, consult [5] for details). The experimental research investigated the effect of natural pozzolan and limestone filler as cement (OPC) replacement on the properties of self-consolidating concrete (SCC). The powder materials to aggregate ratio was 1:4, and coarse aggregate to fine aggregate ratio was 1:1, and the water/powder materials ratio was hold at 0.35 along with varying amount of superplasticizers (see Figure 1a). The specimens were tested for slump flow, compressive strength (Figure 1b), chloride penetration coefficient, water absorption and gas permeability (Figure 2) as fundamental indicators of their fresh state, mechanical and durability performances. Based on the experimental data, it can be concluded that 45 wt.% replacement of OPC with NP and L can be an alternative to OPC as it generates low-cost, environment-friendly concrete with higher ultimate strength and higher resistance to chloride penetration than traditional concrete mixtures.

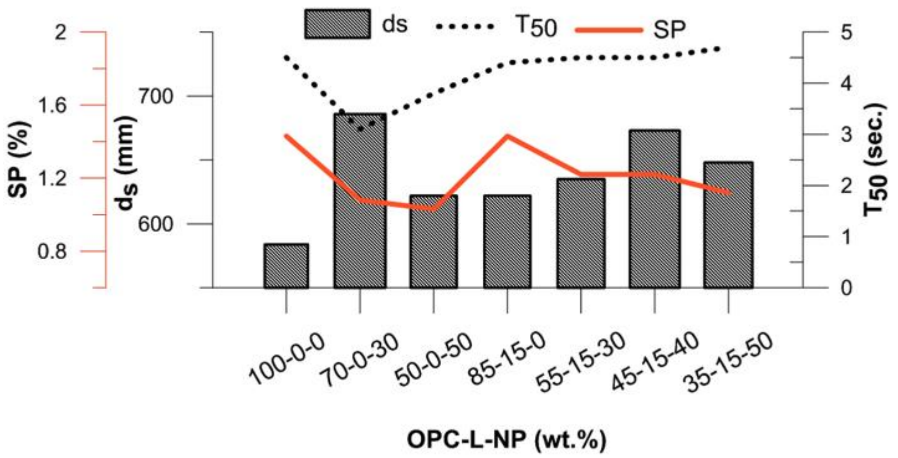

a)

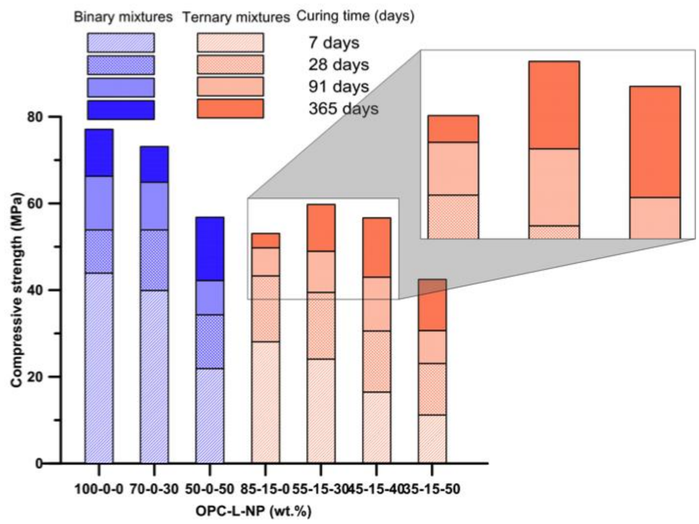

b)

Figure 1 (a) Slump flow diameter (ds) and T50 of SCC specimens, (b) Evolution of the concrete compressive strength for the studied mixture proportions

Table 1 Composition of powder materials in concrete specimens

	Materials (wt.%)		
	OPC	L	NP
OPC:100-L:0-NP:0	100	-	-
OPC:85-L:15-NP:0	85	15	-
OPC:70-L:0-NP:30	70	-	30
OPC:50-L:0-NP:50	50	-	50
OPC:55-L:15-NP:30	55	15	30
OPC:45-L:15- NP:40	45	15	40
OPC:35-L:15-NP:50	35	15	50

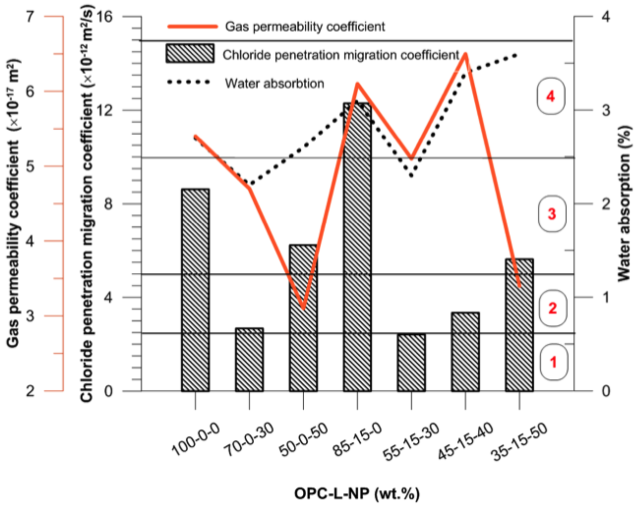

Figure 2 Gas permeability coefficient, chloride penetration migration coefficient, and water absorption of SCC specimens. Zones 1, 2, 3 and 4 indicate extremely high to moderate resistance to chloride penetration.

2.2. DEVELOPMENT OF MULTI-FUNCTIONAL ENERGY-EFFICIENT STRUCTURAL MATERIALS

The largest sector of energy consumption in the US and in the countries from Organization for Economic Co-operation and Development (OECD) is in urban buildings; these account for 40% of the total primary energy consumption, 72% of US electricity consumption, and 38% of carbon dioxide (CO_2) emissions. In tropical countries like Singapore, electricity comprises the single largest building operating expense with up to 60% of the energy going into air-conditioning. A huge fraction of this energy consumption is wasted, since studies from the United States Environmental Protection Agency (EPA) show that 30% energy savings can typically be achieved through improvements to facilities and facility management, while more aggressive measures have obtained even greater reductions. There are many efforts to improve and develop new technologies for the cement industry that can provide more durable and cost efficient materials, that are stronger and less environmentally harmful, and can reduce the energy consumption in buildings. Figure 3 describes a synergistic program to develop ecological building structures with superb thermal properties, strength and durability.

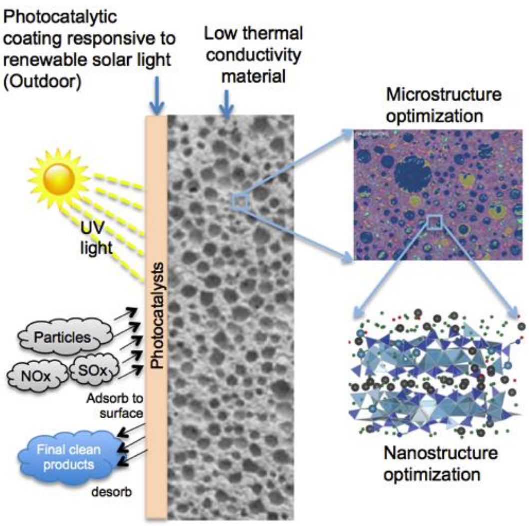

Figure 3 Integrated research to develop multi-functional energy-efficient structural materials.

Compared to other construction materials, concrete presents low thermal conductivity (TC), which can be enhanced when the material is more porous, since air voids resist the heat flow. However, increasing the porosity in concrete can compromise its strength and elastic modulus for structural applications. In this context, the use of light-weight aggregate (LWA) add pores to the paste and offer substantial decrease in the TC of the full composite material, leading to improvements in the energy efficiency of buildings. At the same time it permits the production of lightweight materials for structural purposes, with adequate strength and elastic modulus. We have been developing studies coupling thermal conductivity and mechanical parameters with microscopic investigation in order to provide insights on the behaviour of lightweight cement composites (LCC), since the optimization of the pore structure is essential for the development of such structural material. LCC and cement paste (CP) with water/cementitious materials ratio (w/cm) 0.35 were examined for density, compressive strength, and thermal conductivity. The experimental results indicate a significant decrease in the density, as well as an impressive reduction of about 50% in the thermal conductivity while no loss of compressive strength.

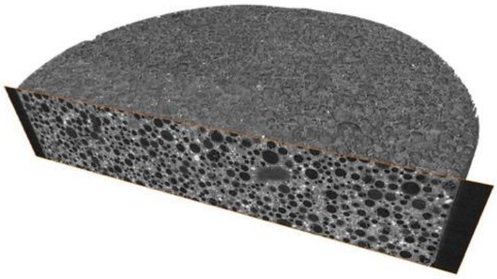

a)

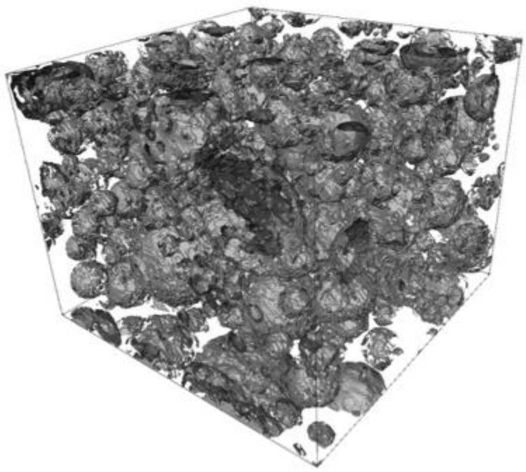

b)

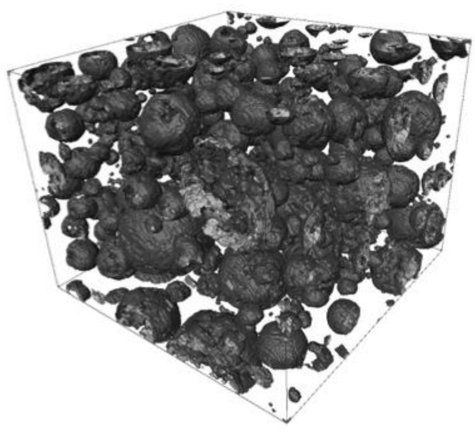

c)

Figure 4 (a) Cross section of the reconstructed volume of the LCC sample; Image segmentation of a region of interest in the LCC sample: (b) LWA (c) air voids.

LCC sample was analysed with microtomography at the Advanced Light Source (ALS) at the Lawrence Berkeley National Laboratory. This technique is extremely useful for the observation of specimens, as a non-invasive tool. A total of 1025 images were captured (~1.7 mm-thick section), reconstructed using the software Octopus®, and visualized with FIJI. The final 3D rendering and segmentation was performed with Avizo®. Reconstruction of the LCC sample in 3 dimensions is presented in

Figure 4a. Different materials with different densities can be identified by their gray scale: unreacted anhydrous cement grains are the brightest phase due to the highest density; hydrated cement paste appears in light gray; product of the reaction with LWA is shown in darker grey; unreacted LWA are represented by dark grey areas and finally the porosity is the darkest phase. Quantification of each material in the reconstructed 3D image gives a good approximation of the volume fraction of the materials in the mixing paste, as well as the pores, LWA and reaction products distribution in the volume (Figure 4b,c).

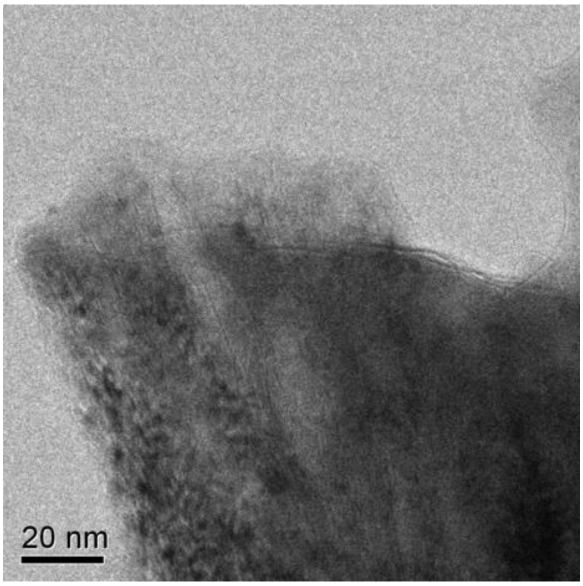

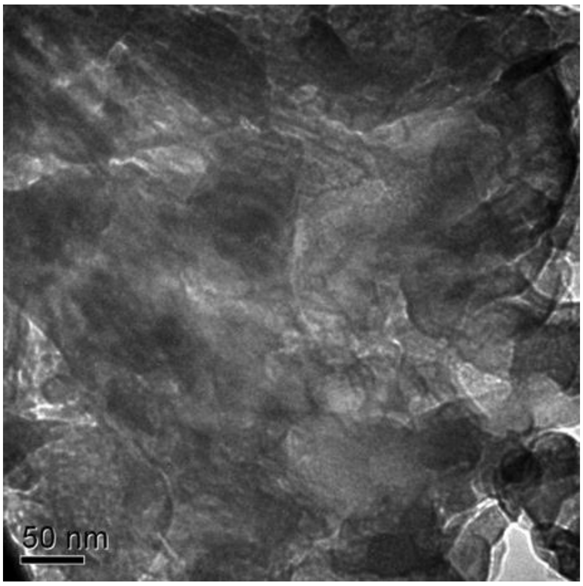

a) b)

Figure 5 (a) Large calcium hydroxide crystal (b) Nano-crystals intermixed with hydration product.

TEM was carried out on 20 months old LCC in fine powder suspended in isopropanol, examined on a JEOL-JEM 3010 TEM operating at 300kV. Images show that after 20 months the LWA present signs of large crystals (Figure 5a) and nano-crystals (Figure 5b), assumed to be calcium hydroxide, and faint indication of fibril morphology. Chemical analysis indicates a Ca/Si ratio of 1.8. This, however, includes areas known to contain nano-crystals of CH and some areas void of calcium.

2.3. DEGRADATION OF GASEOUS POLLUTANTS BY PHOTOCATALYTIC CONSTRUCTION COATING MATERIALS

Air pollution is a major concern because its adverse impacts on human health and environmental sustainability. Air pollution also incurs higher maintenance cost of building envelope. Hence, incorporation of reactive reagents in construction materials raises great interests for the possibility of enabling built structures to remove airborne pollutants and self-clean thereby contributing to cleaner and healthier environment. Most of the applications today mix compatible photocatalysts directly into construction materials, such as cement, mortars, and concretes. This can be effective for applications involving constant abrasion, such as road surface, because fresh photocatalysts mixed in can be exposed on surface to be activated once the old surface is removed. Nevertheless, for passive surface, such as building façade, where continuous abrasion is absent, challenges are to explore novel materials that can preserve the attractive appearance of buildings with low maintenance. Figure 6 shows the amounts of surface photocatalysts (titanium dioxide, TiO_2) for two samples. Although the total amount of TiO_2 used for sample (a) is much higher than sample (b), the latter provides more TiO_2 (as element Ti) on surface than sample (a) by a factor of more than 2. This demonstrates that photocatalytic coatings can be promising materials to concurrently self-clean building envelope and remove airborne pollutants.

TiO_2 is the most commonly used photocatalyst for its compatible nature with construction materials, satisfactory stability and strong reactivity compared to other catalysts, and is also one of the most economical materials available in the market. The photocatalytic capability of TiO_2 to remove of nitrogen oxides (NOx, comprises the precursors of ground-level ozone, nitric oxide (NO) and nitrogen dioxide (NO_2)), a major gaseous pollutant generated from combustion, is well studied: photocatalysis oxidizes NO_2 to form nitric acid (HNO_3). Many studies show the effectiveness of the photocatalytic removal of NOx using TiO_2 (e.g. researches from [6]–[9]), such as the study of glass panels coated with mineral silicate paint treated with 10% TiO_2, which removed more than 80% of NO and 60% of NO_2 [8]. Nevertheless, the applicability of laboratory results to actual atmospheric environment still have to be improved, because of incomparable experimental setups among published studies, complicated ambient reactions involving NOx (e.g., ozone formation), and volatility of the oxidation salt products (nitrate, NO_3^-). A few studies also examined photocatalytic removal of SO_2 and CO (e.g. [10], [11]), which are two important gaseous pollutants under close monitoring and regulation for their undesirable impacts on health and environment. It is worth to note that majority studies examining photocatalytic removal efficiencies of airborne pollutants used TiO_2 powder that, however, demands a reliable "carrier" to be applicable to construction industries. To address this need, mortar specimens coated with TiO_2-containing silicate were employed here to evaluate photocatalytic removal efficiencies of three major gaseous pollutants, CO, NO_2, and SO_2. Two TiO_2 contents, 5% and 15% of the solid weight of the silicate coating, were employed. Control specimens are coated with silicate alone without TiO_2. Effects of photolysis, physisorption, chemisorption, and overall photocatalytic degradation of the individual gaseous pollutants were successively investigated by coating the specimen' surface with epoxy, silicate, or silicate containing TiO_2. Sample preparation and experimental setup in detail are available elsewhere [12].

Carbon monoxide (CO) is one of the most stubborn gaseous pollutants. It is expected that silicate coating containing 15% TiO_2 removed negligible amounts of CO after 320 minutes of solar irradiation. This is mainly because of negligible photolysis and sorption of CO onto the specimen surface. The little removal of CO is consistent with observations of others [11], [13]. Table 2 lists the removal efficiencies of NO_2 via various processes, which were investigated using the same approach and study system. Both photolysis and physisorption play an important role of removing gaseous pollutants, in particular for NO_2 (Table 2), when photocatalysis was absent. The removal of NO_2 over epoxy coating is high because of significant photolysis converting NO_2 to NO, as reaction 1 below shows. The dynamics among reactions 1–4 together is a null cycle that, under a steady state, would result in a constant concentration of NO_2, NO, and O_3. In this study, the null cycle reactions are expected to take place concurrently with physi-chemisorption and photooxidation of NO_2 incurred by activated TiO_2. The null cycle of NO-NO_2-O_3 photochemical reactions are given below:

$$NO_2 + hv \rightarrow NO + O \quad (1)$$

$$O + O_2 \rightarrow O_3 \quad (2)$$

$$2NO + O_2 \rightarrow 2NO_2 \quad (3)$$

$$NO + O_3 \rightarrow NO_2 + O_2 \quad (4)$$

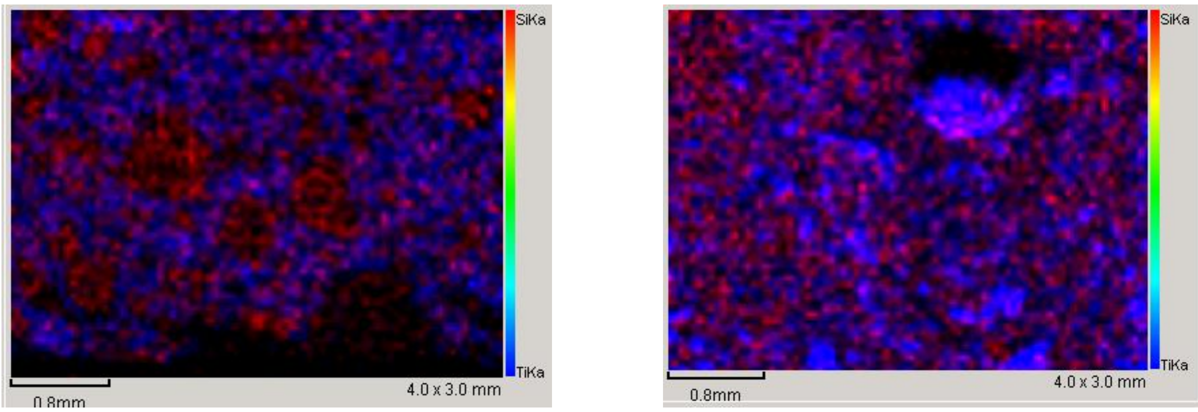

(a) (b)

Figure 6 Amounts of titanium (of TiO_2) on surface of mortar samples (a) mixed with 2% TiO_2, and (b) coated with silicate containing 15% of TiO_2 (of silicate dry weight) imaged via scanning electron microscopy with EDX measurements.

About 18% of NO_2 was removed through physisorption onto epoxy coating surface and 12% through chemisorption unto silicate coating (Tab. 2). A larger content of TiO_2 in the silicate coating was accompanied with higher removal efficiencies. While the three non-photocatalysis processes removed the majority (>70%) of NO_2, depending on the selection of loading, the presence of TiO_2 can result in little further reduction in NO_2, or provide the possibility of removing more than 90% of NO_2 (Tab. 2). Taken together, understanding the dominance among various processes enables one to evaluate cost-effective reduction of targeted airborne pollutants. For example, if a system after reducing 80% of NO_2 appears to contain a concentration of NOx above the required level, incorporating photocatalysts in the coating would be a desirable solution to further decrease the concentration of NOx. The effects of TiO_2 loading shown in Tab. 2 also suggest that a lower bound of TiO_2 content should be taken into account to employ photocatalysts with effectiveness.

Figure 7 shows the temporal concentration trend of SO_2 and NO_2 over individual specimen surfaces listed in Table 2. Individual curves represent accumulated reduction in SO_2 or NO_2. More than 50% of NO_2 was removed in 40 min, much faster than SO_2, which took more than 100 min to remove 40% of the initial concentration (Figure 7a and b). In fact, for all the processes (or all tested specimen surfaces), NO_2 was always removed more rapidly and in a larger amount than SO_2 (Figure 7a and b). Although the rapid removal of NOx through photocatalytic processes is expected, parts of the disappeared NO_2 can be converted to NO through photolysis (reaction 1), which can be later oxidized, returning back to NO_2. Hence, an exhaustive removal of NO_2 should also account for the concurrent concentration of NO. Figure 7c shows the temporal trend of NO as a fraction of initial NO_2 concentration. Without the presence of TiO_2, the amount of NO increased with time, demonstrating strong influence of converting NO_2 to NO through the null-cycle reactions that 20–50% of NO_2 actually remained in the system as NO (black and dotted red lines, Figure 7c). Nevertheless, the presence of photocatalysts decreased the NO formed from photolysis of NO_2. Over the specimens coated with silicate coating containing 5% TiO_2, the NO concentration increased during the initial 25 min, but sorption and photocatalytic degradation together dominated over the effects of the null cycle reactions, and removed around 50% of NO_2 by 40 min (Figure 7b-c).

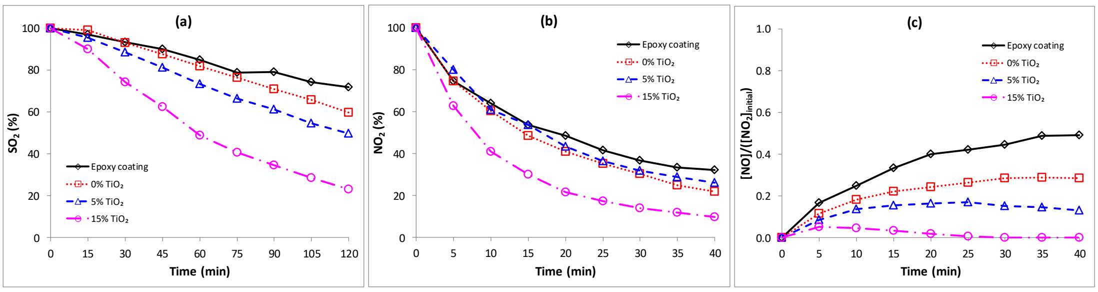

Figure 7 Temporal concentration trend during photocatalytic degradation of (a) SO_2 (Each data point represents an average of 30 values), (b) NO_2 (Each data point represents an average of 6 values for 5% TiO_2 loading, or 7 values for 15% TiO_2 loading) and (c) NO normalized by initial concentration of NO_2.

Table 2Removal of NO2 (14 ppm).

		Removed gaseous pollutant (%)
Sample surface	Process involved	NO_2 (n = 6)[1]
Epoxy coating	Photolysis & Physisorption	67.9±4.13
Silicate coating (no TiO_2)	Chemisorption	10.0±5.3
Silicate coating with 5% TiO_2	Photocatalysis	TBD4
Silicate coating with 15% TiO_2	Photocatalysis	TBD4
Overall removal by silicate coating with 5% TiO_2		77.9±5.9
Overall removal by silicate coating with 15% TiO_2		90.2±0.8

[1]Forlicate coating with 15% TiO_2, n=7; [2]Inclusive of ~10% removal through photolysis; [3]Inclusive of ~50% removal through photolysis estimated based on concentration of NO; [4]To be discussed

The dominance of sorption and photocatalytic degradation is more prominently demonstrated by the silicate coating containing 15% TiO_2. It rapidly suppressed the increasing NO within 10 min of solar irradiation. By 40 min, more than 90% of NO_2 was removed with insignificant amount of NO remaining in the system. This also demonstrates that the null-cycle reactions imposed relatively inferior impacts when a larger loading of TiO_2 in the coating was employed. Overall, laboratory accelerated studies suggest that TiO_2 incorporated in silicate coating can effectively remove acidic gaseous pollutants like NO_2 and SO_2. Depending on the targeted pollutants to be mitigated, prudent selection of TiO_2 loading is important to have cost-effective applications. Field studies are needed to investigate the long-term performance and durability of photocatalytic coating materials when they are challenged with airborne pollutants comprising both gaseous and particulate pollutants with complicated composition.

ACKNOWLEDGMENTS

This research is funded by the Republic of Singapore's National Research Foundation through a grant to the Berkeley Education Alliance for Research in Singapore (BEARS) for the Singapore-Berkeley Building Efficiency and Sustainability in the Tropics (SinBerBEST) Program. BEARS has been established by the University of California, Berkeley as a center for intellectual excellence in research and education in Singapore. The Advanced Light Source is supported by the Director, Office of Science, Office of Basic Energy Sciences, of the U.S. Department of Energy under Contract No. DE-AC02-05CH11231. The authors also thank Dr. HJ Feng for assisting the experiments of photocatalytic degradation of NO_2.

REFERENCES

[1] N. R. Council, *Sustainable Critical Infrastructure Systems*. Washington, D.C.: National Academies Press, 2009.

[2] F. H. Administration, "2010 Status of the Nation's Highways, Bridges, and Transit: Conditions & Performance," 2010.

[3] [P. K. Mehta and P. J. M. Monteiro, *Concrete Microestructure, Properties, and Material*, Third Edit. The McGraw Hill Companies, 2006.

[4] [C. D. Tomkins, "Gigaton Throwdown: Redefining what's possible for clean energy until 2020 | Renewable and Appropriate Energy Laboratory," San Francisco, 2009.

[5] [K. Celik, M. D. Jackson, M. Mancio, C. Meral, A.-H. Emwas, P. K. Mehta, and P. J. M. Monteiro, "High-volume natural volcanic pozzolan and limestone powder as partial replacements for portland cement in self-compacting and sustainable concrete," *Cem. Concr. Compos.*, vol. 45, pp. 136–147, 2014.

[6] H. Ichiura, T. Kitaoka, and H. Tanaka, "Photocatalytic oxidation of NOx using composite sheets containing TiO2 and a metal compound," *Chemosphere*, vol. 51, no. 9, pp. 855–860, 2003.

[7] [C. S. Poon and E. Cheung, "NO removal efficiency of photocatalytic paving blocks prepared with recycled materials," *Constr. Build. Mater.*, vol. 21, no. 8, pp. 1746–1753, 2007.

[8] [T. Maggos, J. G. Bartzis, P. Leva, and D. Kotzias, "Application of photocatalytic technology for NOx removal," *Appl. Phys. A*, vol. 89, no. 1, pp. 81–84, Aug. 2007.

[9] [M. M. Ballari, M. Hunger, G. Hüsken, and H. J. H. Brouwers, "NOx photocatalytic degradation employing concrete pavement containing titanium dioxide," *Appl. Catal. B Environ.*, vol. 95, no. 3, pp. 245–254, 2010.

[10] [J. Shang, J. Li, and T. Zhu, "Heterogeneous reaction of SO2 on TiO2 particles," *Sci. China Chem.*, vol. 53, no. 12, pp. 2637–2643, Dec. 2010.

[11] [A. V. Vorontsov, E. N. Savinov, E. N. Kurkin, O. D. Torbova, and V. N. Parmon, "Kinetic features of the steady state photocatalytic CO oxidation by air on TiO2," *React. Kinet. Catal. Lett.*, vol. 62, no. 1, pp. 83–88, Sep. 1997.

[12] [P. Krishnan, M.-H. Zhang, Y. Cheng, D. T. Riang, and L. E. Yu, "Photocatalytic degradation of SO2 using TiO2-containing silicate as a building coating material," *Constr. Build. Mater.*, vol. 43, pp. 197–202, 2013.

[13] [S. Hwang, M. C. Lee, and W. Choi, "Highly enhanced photocatalytic oxidation of CO on titania deposited with Pt nanoparticles: kinetics and mechanism," *Appl. Catal. B Environ.*, vol. 46, no. 1, pp. 49–63, 2003.

MULTISCALE MODELING FOR SUSTAINABLE AND DURABLE CONCRETE

Oral Buyukozturk[1], Steven D. Palkovic[1]

[1] Massachusetts Institute of Technology, Department of Civil and Environmental Engineering 77 Mass. Ave, Cambridge, MA, 02139, USA, email: obuyuk@mit.edu, spalkovi@mit.edu

SUMMARY: The ubiquity of cementitious materials in the built environment provides a significant challenge in sustainability for researchers and engineers. The environmental impact of these materials can be reduced by using locally available additives, such as volcanic ash or blast furnace slag, in lieu of ordinary Portland cement (OPC). However, a thorough understanding of the impact of additives on the performance of concrete requires a multiscale understanding of the material. Our approach uses a framework coupling experiments and computation to investigate the origin of durability based on changes in structure and properties across length scales. We emphasize the importance of translating information from the atomistic scale to continuum material behavior, necessitating the use of multiple modeling techniques including reactive molecular dynamics, coarse-grained molecular dynamics, and finite element methods. This research provides the foundation for future exploration of the role of additives in cementitious materials and we hope will enable a paradigm shift in developing the next-generation of sustainable and durable concrete.

VIŠERAZINSKO MODELIRANJE ODRŽIVOG I TRAJNOG BETONA

SAŽETAK: Sveprisutnost cementnih materijala u izgrađenom okolišu s obzirom na održivost za istraživače i inženjere predstavlja važan izazov. Opterećenje na okoliš tih materijala može se smanjiti upotrebom lokalno dostupnih mineralnih dodataka kao što su vulkanski pepeo ili zgura visokih peći kao zamjena za obični portlandski cement. Međutim, potpuno razumijevanje učinka dodataka na svojstva betona zahtijeva višerazinsko razumijevanje materijala. U ovom je radu upotrijebljeno povezivanje eksperimenata s proračunom kako bi se istražilo izvorište trajnosti osnovano na promjenama strukture i svojstva na mjerilima duljine. Naglašava se važnost prijenosa informacija od atomskog mjerila na ponašanje kontinuuma materijala, nužnost upotrebe višestrukih tehnika modeliranja uključivši reaktivnu molekularnu dinamiku, molekularnu dinamiku krupnih zrna i metodu konačnih elemenata. Istraživanje daje temelj budućih istraživanja uloge mineralnih dodataka na cementne materijale što će, nadamo se, omogućiti paradigmatski pomak u razvoju održivih i trajnih betona iduće generacije.

1. INTRODUCTION

Cementitious materials like cement paste, mortar and concrete are widely used as construction and building materials because of their low cost and availability. Due to its massive consumption, our reliance on Portland cement in mix designs creates environmental concerns related to the significant greenhouse gasses emitted during production [1]. Sustainable benefits can be realized by replacing some Portland cement with alternative natural materials and industry by-products such as volcanic ash, blast furnace slag, fly ash from coal power plants and silica fume from steel mills. The use of these additives, known as supplementary cementitious materials (SCM), can also lead to superior durability based on based on improvements in mechanical properties [2, 3] and resistance to chemical degradation [4, 5].

The design of engineered cementitious mixtures with additives is complicated by their sensitivity to the chemical composition of raw materials, volume fraction of additives, environment during hydration, and catalysts used for activation. Numerical modelling provides a computational microscope for furthering our understanding of these parameters at multiple length and temporal scales. Recent studies have focused on the hydrated gel phase, calcium-silicate-hydrate (C-S-H), a nanostructured material that provides cohesive strength to the hardened system. However, these investigations are often limited to a single length scale and cannot capture material processes that span from 10^{-10} to 10^{-3} m in a cementitious material. To address this challenge, we have developed a bottom-up multiscale framework which focuses on translating the essential physics observed at each length scales. With this framework, we will be able to study the changes in engineering properties under the influence of additives based on changes in underlying chemistry and structure.

2. BIOINSPIRED CONSTRUCTION AND BUILDING MATERIALS

Our computational framework is motivated by design strategies employed within biological materials. Nature achieves exceptional mechanical performance through hierarchical structures which are composed of simple building blocks that arrange to form larger-scale assemblies [6]. This approach allows for material designs that greatly outperform their building block constituents. One example is the deep-sea sponge shown in Figure 1, which like cementitious materials is largely composed of silica. The deep-sea sponge arranges nm sized silica particles into cylindrical rods composed of concentric rings separated by small volumes of flexible proteins [7, 8]. These rods are grouped into larger spicules that arrange to form a cage-like network that resembles a structural frame. These natural assemblies are achieved through growth mechanisms that control the interactions between nm-sized silica and protein building blocks.

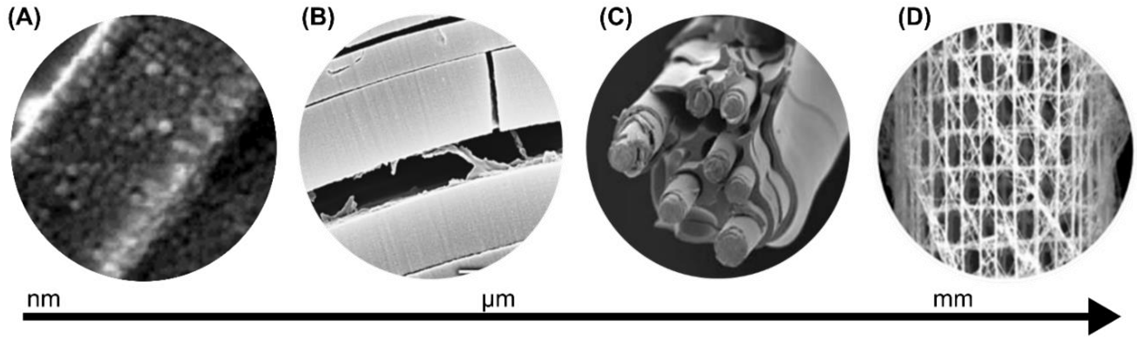

Figure 1 Hierarchical assembly of a silica-based deep sea sponge [7]. The sponge is composed of nm sized silica particles (A) which combine with a proteinaceous phase to form concentric rings within cylindrical rods (B). These rods are grouped within spicules (C) that arrange to form a structural network at the macroscale (D). Microscopy images provided courtesy of Dr. James Weaver.

Katerinal et al. have shown that structures in the hydrated C-S-H phase can also be tuned through interparticle forces [9, 10]. Their work assesses the influence of changes to the surrounding pore solution using a simple pair potential combined with long-range electrostatic repulsion as shown in Figure 2. These changes in interactions mimic the role of lime within hydrating cementitious systems as assessed through atomic force microscopy experiments (AFM) [11]. The C-S-H structure transitions from an open fibril network to large isolated clusters at different stages of hydration and with increasing amounts of lime. Although this study illustrates that simple computational models can provide new insights into cementitious materials, it provides a limited understanding of the source of these interactions and the resulting impact on macroscale properties. A multiscale framework is required to extend these structure-property relationships from the fundamental building blocks to macroscale.

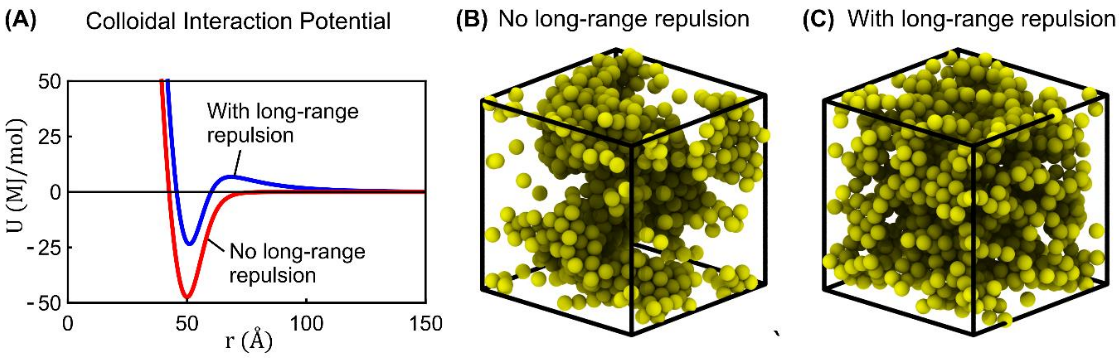

Figure 2 Influence of particle interactions on the mesoscale assembly of two hydrated system with the same solid volume fraction. (A) The potential energy (U) as a function of interparticle separation (r) can be tuned through the inclusion of long-range electrostatic repulsion. (B) Without long-range repulsion, the mesoscale structure forms large dense clusters of colloids. (C) The addition of long-range repulsion results in a more distributed solid network with smaller cluster sizes.

3. A MULTISCALE COMPUTATIONAL FRAMEWORK FOR CEMENT PASTE

Our research is focused on cement paste, the matrix phase in mortar and concrete materials which does not contain fine or coarse aggregates. Figure 3 illustrates the three distinct length scales considered, 1) hydrated building blocks, 2) assembly of hydrated building blocks into a solid-pore network, and 3) composite microstructure where the hydrated gel phase forms a composite with inclusion phases such as secondary hydration products and unreacted anhydrous phases. Macroscale strength and stiffness are largely controlled by the composite response, whereas shrinkage, creep, and permeability originate within the pore network formed from mesoscale assemblies. We select a different modelling approach for each length scale that is suitable for evaluating the essential physics. Fully atomistic models with reactive force fields are used to investigate the role of chemical composition and molecular structure. These fundamental atomistic interactions are then used as inputs to effective interactions between C-S-H colloids, where the influence of pore network and particle morphology can be assessed. Finally, each mesoscale assembly can be homogenized to a continuum finite element within a random cement paste microstructure. At this scale, connections with bulk laboratory strength experiments can be obtained. In the following sections, we describe recent and ongoing progress in computational modelling at each length scale.

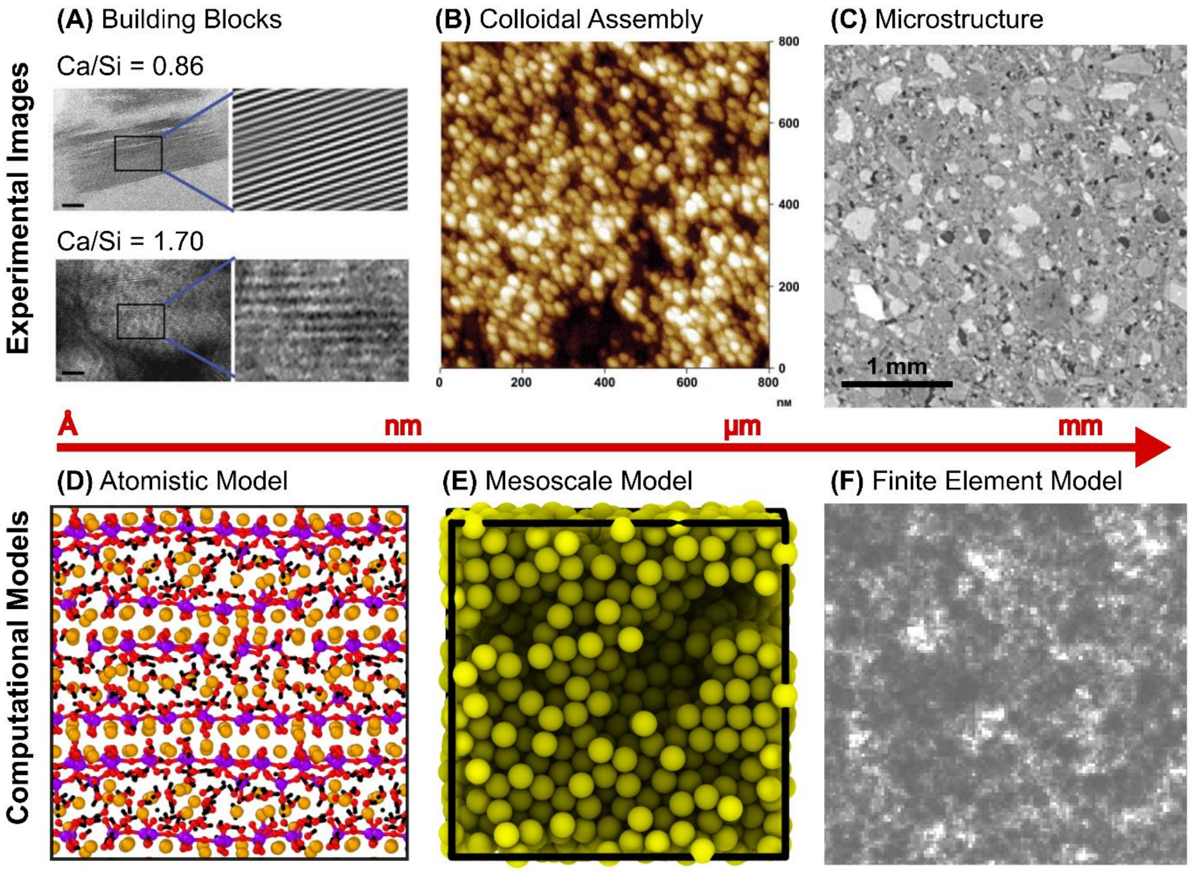

Figure 3 (A) The smallest feature within cement paste are hydrated building blocks which have a layered structure that varies with chemical composition [12]. (B) At larger scales, the layered structure forms colloidal particles which arrange to form the gel and capillary pore network [13]. (C) At the macroscale, the hydrated gel is the matrix phase in a composite microstructure [14]. The computational framework uses multiple modelling approaches to match experimental features. (D) Fully atomistic models capture the influence of chemistry and water in layered building blocks (atoms coloured by element: Si = purple, Ca = orange, O = red, H = black). (E) Mesoscale models use effective pair potentials based on fully atomistic simulations to investigate the influence of colloidal morphology and interactions. (F) Continuum finite element methods are used at the macroscale to investigate the competition between different phases. The image of the layered building block is obtained under a Creative Commons Attribution-NonCommercial-ShareAlike 4.0 International License.

3.1. BUILDING BLOCK MODELS (~1 NM)

At the molecular scale, hydrated C-S-H materials form a layered structure composed of calcium-silicate sheets separated by an interface containing water molecules and counterions. The structure and mechanical performance at this scale is strongly influenced by chemical composition. Cement paste systems composed of ordinary Portland cement (OPC) have an average Ca/Si ratio of approximately 1.7 [15]. The inclusion of additives, such as silica fume, will reduce the Ca/Si ratio of C-S-H which leads to a more crystalline structure and improved mechanical performance [16]. Our objective for building block models is to measure the role of chemistry on mechanical properties with a reactive force field capable of capturing bond formation, bond breaking and water dissociation [17, 18]. Figure 4 provides an example of a C-S-H structure with a Ca/Si ratio of 1.65 under affine shear loading. Shear strain localizes within the interface separating adjacent calcium-silicate layers, and controls the deformation and strength behaviour of the material [19, 20].

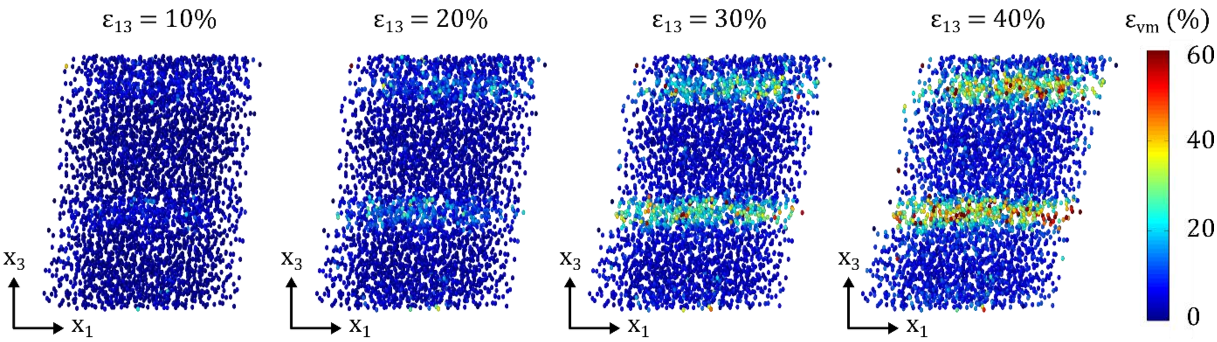

Figure 4 Local atomic shear strain (ε_{vm}) as a function of applied affine shear strain (ε_{13}) for a representative building block structure. Strain has localized within two bands associated with the water-filled interface between calcium-silicate layers.

We investigate C-S-H under combined loading that consists of a combination of compression or tension and shear. The maximum shear strength (τ) as a function of normal stress along the shearing plane (σ) can be fit to a Mohr-Coulomb linear strength envelope as shown in Figure 5(A) [21]. The atomistic structure has a coefficient of friction $\mu_P = 0.16$ and cohesion $c_P = 3.6\ GPa$. These simulations indicate that atomistic C-S-H has a strength asymmetry in compression and tension, and a normal-stress or pressure sensitivity of the maximum shear strength. We also perform uniaxial tension-compression simulations that are summarized in Figure 5(B) [22]. The uniaxial loading data can be fit to a function of the form,

$$F_n(\varepsilon) = k\varepsilon\left[1 + e^{\alpha\left(\frac{\varepsilon}{\varepsilon_u}-1\right)}\right]^{-1} \qquad (1)$$

where k defines the initial stiffness and the tensile portion of the curve is controlled by two dimensionless parameters, α and ε_u. The fit to simulations shown in Figure 5(B) is given by $k = 733$ nN/ε, $\alpha = 1.55$ and $\varepsilon_u = 9.9\%$. These mechanical loading simulations fully define the normal and tangential behaviour of the interface that controls mechanical behaviour of the layered C-S-H building blocks.

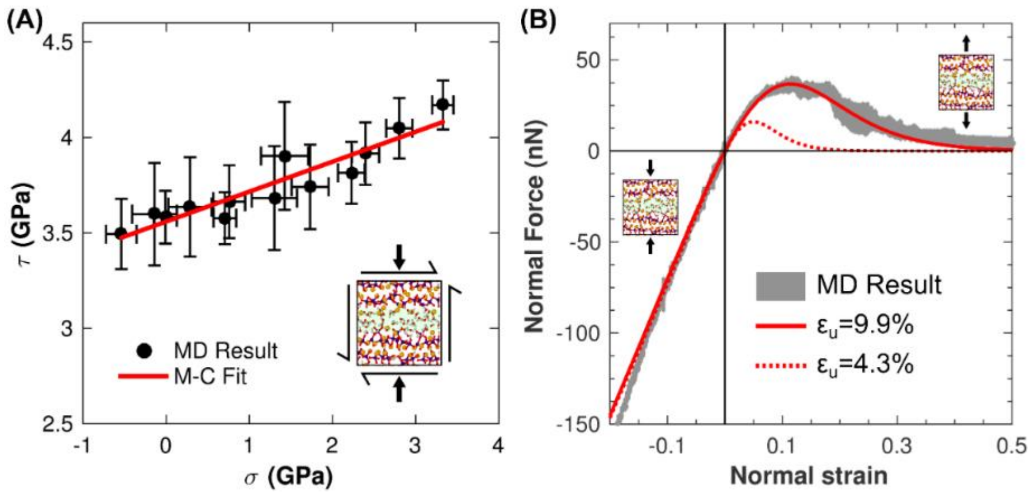

Figure 5 (A) A Mohr-Coulomb strength envelope can be fit to the results of combined loading simulations. (B) The results from uniaxial compression and tension simulations can be fit to Eq. 1, and the maximum force can be controlled by modifying the ε_u parameter. Error bars and the shaded band represent the standard deviation of 10 C-S-H samples [22].

3.2. COLLOIDAL MODELS (~100 NM)

At larger length scales, the layered molecular structure (10^3 to 10^4 atoms) forms a colloidal particle ranging from 3 to 15 nm in size [23-25]. We input the results of building block models into a cohesive-frictional force field (CFFF) that describes effective mesoscale interactions between C-S-H colloids [22]. The fundamental CFFF parameters are described in Figure 6. Normal interactions are considered through a radial pair potential by modifying Eq. 1 to consider the series interaction of spherical particles of dissimilar size. Tangential forces are implemented through friction between contacting particles using techniques from discrete element methods (DEM) [26]. This interparticle friction has been omitted in recent mesoscale models, and allows for the consideration of the Mohr-Coulomb behaviour and strength asymmetry that is fundamental to the layered building block.

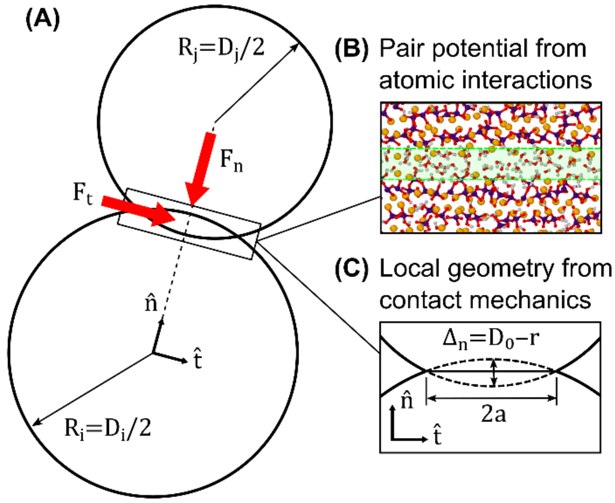

Figure 6 (A) A pair of interacting spherical particles i and j producing a normal force F_n and tangential force F_t. The CFFF considers bonded and non-bonded interactions of the atomistic interface between particles (B) as well as from physical contact between grains (C). The interface within the C-S-H layered structure is highlighted in green [22].

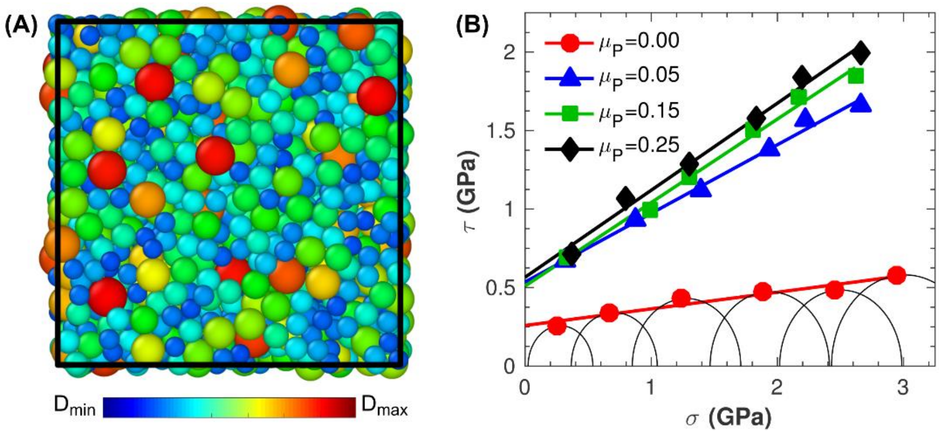

Figure 7 (A) Mesoscale structure of colloidal system with polydispersity. Particles are coloured based on relative size. (B) Mohr-Coulomb envelopes are found for C-S-H systems with varying particle friction μ_P. Solid lines represent the linear best-fit tangent to the Mohr's circles from simulations at varying initial pressure P_0. For clarity, the Mohr circles used for fitting are only shown for $\mu_P = 0$.

We generate colloidal structures, subject them to hydrostatic compression, and then measure their shear strength envelope as shown in Figure 7. Models are constructed by randomly inserting interacting particles within an initially empty simulation cell. Particle insertions are accepted according a Metropolis Monte Carlo algorithm with probability, $P_{in} = \min[1, e^{-\Delta U/(k_B T)}]$, where ΔU is the change in the system potential energy after particle insertion, k_B is the Boltzmann constant, and T is the system temperature of 300 K. After each insertion, we relax the system using a molecular dynamic simulation at constant temperature, volume, and number of particles (NVT). This procedure allows us to generate C-S-H systems of varying packing density. Polydispersity is implemented by randomly selecting the particle diameter from a uniform probability distribution that defines the minimum and maximum size considered. We consider system sizes with cubic edge lengths ranging from 35 to 78 nm and containing 500 to 7000 colloidal particles. To calculate mechanical properties, each C-S-H sample is subjected to an initial pressure ranging from 0.5 to 3.0 GPa in increments of 0.5 GPa. We then apply pure shear deformation and find the maximum shear strength and corresponding normal-stress along the shear plane. Figure 7(B) shows that the particle pair friction μ_P has a significant influence on the mesoscale bulk strength envelope, with an increase in both the system normal-stress dependency μ_B and cohesion c_B. We have used this approach to study the impact of polydispersity for solid volume fractions ranging from 0.50 to 0.74 [22]. Our results indicate that for colloidal systems neglecting particle friction μ_B ranges from 0.1 to 0.3, whereas when friction is included μ_B varies from 0.4 to 0.9. These simulation results can be compared with μ_B from macroscale triaxial loading experiments on cm scale cement paste samples [27]. We can compare with the macroscale experiments by converting experiments from the Drucker-Prager pressure sensitivity $\delta_B = 0.82$ to the Mohr-Coulomb friction coefficient using, $\mu_B = \tan\left[\arcsin(\frac{3\delta_B}{2\sqrt{3}+\delta_B})\right] = 0.70$ [28]. Therefore, colloidal assemblies with particle pair friction bound the macroscale experimental value. Microstructure models are needed to assess the influence of larger-scale mechanisms that cannot be captured in colloidal models.

3.3. MICROSTRUCTURE MODELS (~1 MM)

At the macroscale, cement paste is a random heterogeneous composite. Past studies on cementitious materials assume that the gel phase is a homogeneous matrix with embedded inclusions or voids [29]. We propose a new approach that considers the cement paste microstructure as a random field. The random field is defined by a probability density function (PDF) of local mechanical properties that can be experimentally measured through statistical nanoindentation [30]. Nanoindentation testing provides this data by probing a small volume of material to evaluate the resistance to plastic deformation during loading, and elastic stiffness during unloading. These nanoindentation values can be converted to equivalent mechanical properties by assuming a scaling relation [31] or directly through mesoscale simulations. This process is summarized in Figure 8. We test our method using published data on a cement paste mixture incorporating Portland cement and fly ash [32]. The indentation modulus was converted to an equivalent isotropic Young's Modulus by assuming a constant Poisson's ratio of 0.3 for hydrated phases and by using the elastic properties of a Berkovitch indenter. A lognormal distribution is then fit to the PDF of local Young's Moduli. Statistically equivalent two or three-dimensional realizations of the lognormal distribution can be generated using a covariance function and a discrete fast Fourier transform method [33]. We assume an exponential covariance function of the form, $B(r) = \rho^2 \exp\left(-\frac{r}{L_c}\right)$, where r is the distance between mesh points, ρ^2 is the variance of the distribution, and L_c is the correlation length. The process becomes more random for lower values of L_c, resulting in smaller isolated heterogeneities.

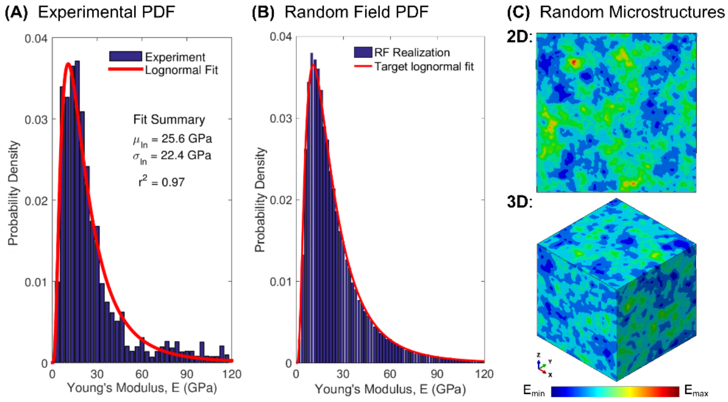

Figure 8 Procedure for generating heterogeneous cement paste microstructures. (A) The probability density function (PDF) of local mechanical properties is obtained through nanoindentation grids. We fit a lognormal distribution to data from [32]. (B) Random fields can be generated that match the experimentally measured lognormal properties. (C) These realizations can be two-dimensional or three-dimensional random fields, which become the inputs to finite element models.

We use this procedure to study the influence of correlation length on two-dimensional random microstructures with the same lognormal distribution, as well as a homogeneous control. For all models, we approximate the plastic properties by assuming a constant cohesion of 0.5 GPa and coefficient of friction of 0.6 in agreement with results from mesoscale simulations. Representative results are shown in Figure 9 for Young's Modulus and plastic strain fields under uniaxial compression. The heterogeneous stiffness distribution results in strain localization within shear bands that form through low stiffness regions, whereas a homogeneous deformation mode is observed for the sample with uniform elastic properties. We also observe that a smaller correlation length results in a more diffuse plastic strain field because the more random structure makes it harder to form a system spanning shear band. The qualitative results agree with inclined shear failures that have been reported for uniaxial experiments on macroscale cement paste samples. This failure mode is also expected for concrete samples subjected to hydrostatic compression. The results emphasize the importance of considering the gel phase as a heterogeneous material to capture localization processes.

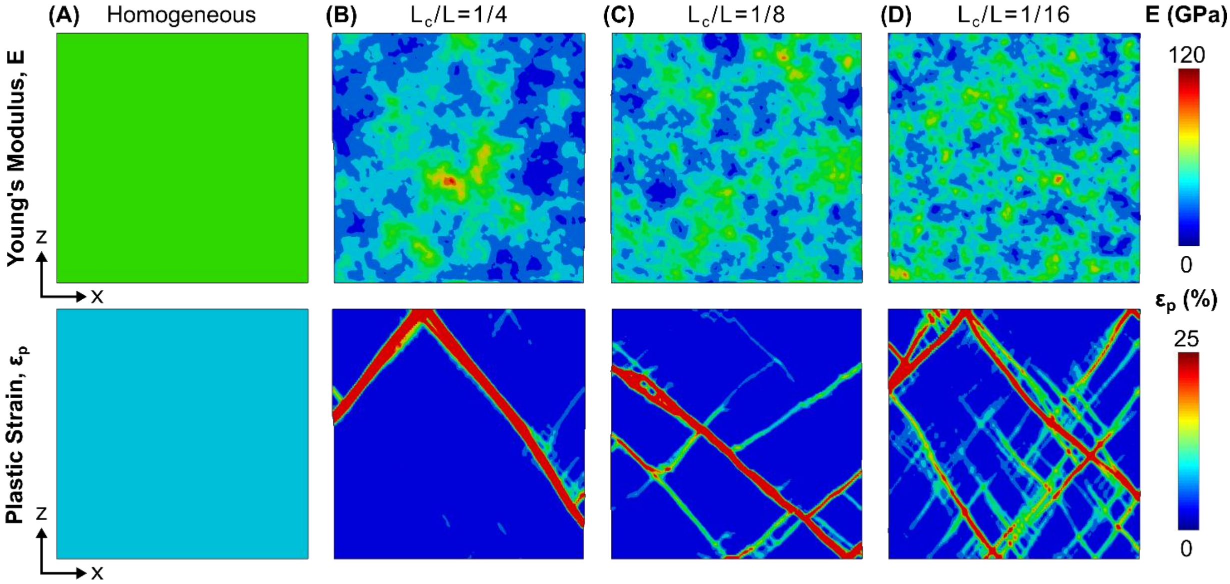

Figure 9 Results of 2D models under a uniaxial compression strain applied along the z-axis. A homogeneous control is compared to random fields with varying normalized correlation lengths, L_c/L. The plastic strain fields at 5% compressive strain are shown in the bottom row. For heterogeneous samples, plastic strain localizes within narrow inclined bands.

4. CONCLUSIONS

Our multiscale framework captures the molecular structure, colloidal assembly, and random microstructure within a cementitious material. We focus on translating information between these scales to allow for establishing structure property relationships that span from atomistic details to macroscale continuum. This bridge is critical because the macroscale is where material properties are measured by engineers for design through traditional laboratory experiments. Our initial study focuses on mechanical strength and elasticity, but future work can investigate additional parameters such as thermal properties and creep. When combined with experiments, our computational framework will enable a greater understanding of the role of additives in modifying macroscale properties of cementitious materials, and identifying the origin of these properties at different length scales. This can be used to identify the relative importance of many complex parameters, including changes to the gel phase building block chemistry, mesoscale pore network, and microstructural morphology. Computational models are also suitable for parametric studies, to investigate changes in chemistry, structure and geometry that promote durability. We believe that applying our framework to study cement paste behaviour across orders of magnitude in length scales will enable the development of novel engineered cements incorporating sustainable additives and with increased durability.

ACKNOWLEDGMENTS

This project was sponsored by the Kuwait Foundation for the Advancement of Sciences as part of the Kuwait-MIT signature project on sustainability of Kuwait's built environment. We also thank Markus Buehler and the Laboratory for Atomistic and Molecular Mechanics (LAMM) for many insightful discussions and access to computational resources.

REFERENCES

[1] Marland, G., et al.: Global, regional, and national fossil fuel CO2 emissions, *Trends: A Compendium of Data on Global Change*. (2007), pp. 37831-6335,

[2] Chindaprasirt, P., et al.: Effect of fly ash fineness on compressive strength and pore size of blended cement paste, *Cement and Concrete Composites*. (2005); 27 4, pp. 425-8, 0958-9465

[3]] Qing, Y., et al.: Influence of nano-SiO 2 addition on properties of hardened cement paste as compared with silica fume, *Construction and Building Materials*. (2007); 21 3, pp. 539-45, 0950-0618

[4] Chindaprasirt, P., et al.: Resistance to chloride penetration of blended Portland cement mortar containing palm oil fuel ash, rice husk ash and fly ash, *Construction and Building Materials*. (2008); 22 5, pp. 932-8, 0950-0618

[5] Chindaprasirt, P., et al.: Sulfate resistance of blended cements containing fly ash and rice husk ash, *Construction and Building Materials*. (2007); 21 6, pp. 1356-61, 0950-0618

[6] Fratzl, P., Weinkamer, R.: Nature's hierarchical materials, *Progress in Materials Science*. (2007); 52 8, pp. 1263-334, 0079-6425

[7] Aizenberg, J., et al.: Skeleton of Euplectella sp.: structural hierarchy from the nanoscale to the macroscale, *Science*. (2005); 309 5732, pp. 275-8, 0036-8075

[8] Cha, J.N., et al.: Silicatein filaments and subunits from a marine sponge direct the polymerization of silica and silicones in vitro, *Proceedings of the National Academy of Sciences*. (1999); 96 2, pp. 361-5, 0027-8424
[9] Ioannidou, K., et al.: Controlling local packing and growth in calcium–silicate–hydrate gels, *Soft Matter*. (2014); 10 8, pp. 1121-33,
[10] Ioannidou, K., et al.: The crucial effect of early-stage gelation on the mechanical properties of cement hydrates, *Nature Communications*. (2016); 7, pp.,
[11] Plassard, C., et al.: Nanoscale experimental investigation of particle interactions at the origin of the cohesion of cement, *Langmuir*. (2005); 21 16, pp. 7263-70, 0743-7463
[12] Qomi, M.A., et al.: Combinatorial molecular optimization of cement hydrates, *Nature communications*. (2014); 5, pp.,
[13] [13] Nonat, A.: The structure and stoichiometry of CSH, *Cement and Concrete Research*. (2004); 34 9, pp. 1521-8, 0008-8846
[14] Kupwade-Patil, K., et al.: Examination of Pore- and microstructure in Hardened Cement Pastes prepared with Natural Volcanic Ash, Silica Fume and Ordinary Portland Cement *Materials Characterization*. ((Submitted)), pp.,
[15] Allen, A.J., et al.: Composition and density of nanoscale calcium–silicate–hydrate in cement, *Nature materials*. (2007); 6 4, pp. 311-6, 1476-1122
[16] Hou, D., et al.: Reactive molecular simulation on water confined in the nanopores of the calcium silicate hydrate gel: structure, reactivity, and mechanical properties, *The Journal of Physical Chemistry C*. (2015); 119 3, pp. 1346-58, 1932-7447
[17] Van Duin, A.C., et al.: ReaxFF: a reactive force field for hydrocarbons, *The Journal of Physical Chemistry A*. (2001); 105 41, pp. 9396-409, 1089-5639
[18] Manzano, H., et al.: Hydration of calcium oxide surface predicted by reactive force field molecular dynamics, *Langmuir*. (2012); 28 9, pp. 4187-97, 0743-7463
[19] Manzano, H., et al.: Shear deformations in calcium silicate hydrates, *Soft Matter*. (2013); 9 30, pp. 7333-41,
[20] Palkovic, S.D., et al.: Mechanical behavior of a composite interface: Calcium-silicate-hydrates, *Journal of Applied Physics*. (2015); 118 3, pp. 034305, 0021-8979
[21] Palkovic, S.D., et al.: Constitutive Response of Calcium-Silicate-Hydrate Layers Under Combined Loading, *Journal of the American Ceramic Society*. (2016), pp., 1551-2916
[22] Palkovic, S.D., et al.: A cohesive-frictional force field (CFFF) for calcium-silicate-hydrates, *Soft Matter*. ((Submitted)), pp.,
[23] [Jennings, H.M.: Refinements to colloid model of CSH in cement: CM-II, *Cement and Concrete Research*. (2008); 38 3, pp. 275-89, 0008-8846
[24] [Skinner, L., et al.: Nanostructure of calcium silicate hydrates in cements, *Physical review letters*. (2010); 104 19, pp. 195502,
[25] [Chiang, W.-S., et al.: Microstructure determination of calcium-silicate-hydrate globules by small-angle neutron scattering, *The Journal of Physical Chemistry C*. (2012); 116 8, pp. 5055-61, 1932-7447
[26] Cundall, P.A., Strack, O.D.: A discrete numerical model for granular assemblies, *geotechnique*. (1979); 29 1, pp. 47-65, 0016-8505
[27] Heukamp, F., et al.: Mechanical properties of calcium-leached cement pastes: triaxial stress states and the influence of the pore pressures, *Cement and Concrete Research*. (2001); 31 5, pp. 767-74, 0008-8846
[28] Chen, W.-F. *Plasticity in reinforced concrete*: J. Ross Publishing; (2007), 1932159746
[29] Lilliu, G., van Mier, J.G.: 3D lattice type fracture model for concrete, *Engineering Fracture Mechanics*. (2003); 70 7, pp. 927-41, 0013-7944
[30] Ulm, F.J., et al.: Statistical indentation techniques for hydrated nanocomposites: concrete, bone, and shale, *Journal of the American Ceramic Society*. (2007); 90 9, pp. 2677-92, 1551-2916
[31] Ganneau, F., et al.: Dual-indentation technique for the assessment of strength properties of cohesive-frictional materials, *International journal of solids and structures*. (2006); 43 6, pp. 1727-45, 0020-7683
[32] Zadeh, V.Z., Bobko, C.P.: Nanoscale mechanical properties of concrete containing blast furnace slag and fly ash before and after thermal damage, *Cement and Concrete Composites*. (2013); 37, pp. 215-21, 0958-9465
[33] Fenton, G.A.: Simulation and analysis of random fields: Princeton University Princeton, NJ; 1990.

SELF-HEALING CONCRETE IN AGGRESSIVE ENVIRONMENTS

Nele De Belie[1], Kim Van Tittelboom[1], Mathias Maes[1], Bjorn Van Belleghem[1,2], Philip Van den Heede[1,2]

[1] Ghent University, Department of Structural Engineering, Magnel Laboratory for Concrete - Research, Tech Lane Ghent Science Park, Campus A, Technologiepark Zwijnaarde 904, B-9052 Ghent, Belgium, Tech Lane Ghent Science Park, Campus A, Technologiepark Zwijnaarde 904, B-9052 Ghent, Belgium,
email: nele.debelie@ugent.be, kim.vantittelboom@ugent.be, mathias.maes@sanacon.be
[2] Strategic Initiative Materials (SIM vzw), project ISHECO within the program 'SHE' Tech Lane Ghent Science Park, Campus A, Technologiepark 935, B-9052 Ghent, Belgium, email: bjorn.vanbelleghem@ugent.be, philip.vandenheede@ugent.be

SUMMARY: Although certain crack widths are allowed in reinforced concrete structures, without having immediate effects on the structural stability, they may impair the durability and service life of the structure in the long term. Cracks wider than 10 µm will result, for instance, in a faster penetration of chlorides into the crack and from there onwards into the concrete matrix. Fortunately, the autogenous healing ability of concrete may close cracks of up to 100 µm completely. The further hydration of binder particles, will be supplemented by the deposition of calcium carbonate crystals in case of wet/dry cycles. In case of marine infrastructures in tidal zones, the presence of magnesium sulfates may enhance the crack sealing by means of brucite precipitation. These processes will result in reduced chloride penetration rates. If the cracks are larger than 100 µm or the conditions are not favourable for autogenous healing, autonomous healing mechanisms can be incorporated. In this case, healing is obtained through encapsulated polymeric healing agents, superabsorbent polymers, microbial agents, expansive additives, etc. With encapsulated polyurethane based healing agents, a reduction of the chloride concentration by 75% or more was obtained in a zone with a 300 µm wide crack after chloride diffusion tests, relative to the case in which cracks were not healed. As a result, the service life of reinforced concrete elements in marine environments could be increased with a factor of about 10. Neutron radiography images obtained during a capillary sorption test indicated that release of encapsulated polyurethane in wet conditions was favourable for the polyurethane reaction. As an alternative to the autonomous healing with encapsulated polyurethane, also the incorporation of encapsulated water repellent agents and corrosion inhibitors, has proven to effectively delay reinforcement corrosion during electrochemical measurement campaigns. Accelerated corrosion tests on cracked, manually treated mortar samples, allowed to rapidly screen different agents for their efficiency.

SAMOZACJELJUJUĆI BETON U AGRESIVNIM OKOLIŠIMA

SAŽETAK: Iako je u armiranobetonskim konstrukcijama dopuštena određena širina pukotina koja nema neposredne učinke na konstrukcijsku stabilnost, one mogu dugoročno utjecati na trajnost i uporabni vijek konstrukcije. Pukotine šire od 10 µm prouzročit će, primjerice, brži prodor klorida u pukotinu a onda dalje u betonsku matricu. Na sreću, sposobnost autogenog zacjeljivanja betona može pukotine do 100 µm u cijelosti zatvoriti. Daljnja hidratacija čestica veziva dopunit će se odlaganjem kristala kalcijeva karbonata pri ciklusima mokro/suho. Kod morske infrastrukture u zoni plime prisutnost magnezijeva sulfata može poboljšati brtvljenje pukotina taloženjem brucita. Ti procesi dovest će do smanjenja brzine prodora klorida. Ako su pukotine veće od 100 µm ili uvjeti nisu povoljni za autogeno zacjeljenje moguće je ugraditi mehanizme autonomnog zacjeljenja. Tada do zacjeljenja dolazi s pomoću ugrađenih polimernih tvari za zacjeljenje, superapsorbirajućih polimera, mikrobnih sredstava, ekspanzivnih dodataka itd. S ugrađenim sredstvima za zacjeljenje na osnovi poliuretana dobiveno je smanjenje koncentracije klorida za 75 % ili više u području s pukotinama širim od 300 µm nakon ispitivanja difuzije klorida, u usporedbi sa slučajem u kojem pukotine nisu zacijeljene. Posljedica toga je da se u morskom okolišu uporabni vijek armiranobetonskih elemenata može produljiti s faktorom oko 10. Slike neutronske radiografije dobivene tijekom ispitivanja kapilarnog upijanja pokazuju da je otpuštanje ugrađenog poliuretana u vlažnim uvjetima bilo povoljno za reakciju poliuretana. Druga mogućnost umjesto autonomnog cijeljenja s ugrađenim poliuretanom jest ugradnja vodoodbojnih sredstava i inhibitora korozije koji dokazano učinkovito odlažu koroziju armature tijekom izvođenja elektrokemijskih mjerenja. Ubrzana ispitivanja korozije na raspucalim ručno obrađenim uzorcima morta omogućuju brzo ocjenjivanje učinkovitosti različitih tvari.

1. INTRODUCTION

Cracks in concrete need to be repaired as soon as possible to avoid concrete deterioration and reinforcement corrosion. Maintenance and repair works impose high direct and indirect costs to society and some structures are even not accessible for inspection and repair. In marine structures, crack formation will accelerate the penetration of chlorides, which will induce rebar corrosion. Fortunately, small cracks in concrete have the ability to heal autogenously. For this process, the presence of water is crucial to stimulate hydration of unhydrated binder particles and carbon dioxide presence will enhance calcium carbonate precipitation. However, the influence of the seawater on this healing process is yet uncertain [1].

In addition, to increase the self-healing capacity of concrete elements, different methods have been explored to obtain autonomous crack healing [2]. In this case, healing is obtained through encapsulated agents, superabsorbent polymers, microbial agents, expansive additives, etc. One promising approach is the embedment of brittle capsules filled with polymeric healing agents inside the concrete. Crack formation leads to capsule breakage and release of the polymeric healing agent, which fills up the crack and forms a barrier which prevents fluid ingress through the cracks. An option further explored currently is the use of encapsulated corrosion inhibitors. Generally, corrosion inhibitors are applied by adding them to the fresh concrete mix or by applying them on the hardened concrete to impregnate the matrix from the surface. Adding the inhibitor into the concrete with the mixing water is a user friendly technique, but concrete properties such as setting time or compressive strength may be affected unfavourably. For application on the concrete surface, the penetrability is mostly an issue leading to an insufficient molar concentration ratio between inhibitor and chlorides [3]. The aim of the current study was to combine the advantages of both water repellent agents (WRA) and corrosion inhibitors (CI). The WRA and/or CI are contained inside capsules which are located close to the reinforcement bar, to provide a high concentration of the inhibitor at the location of the steel reinforcement without influencing the properties of the concrete. At the moment of crack formation, the capsules break and release their content in the vicinity of the rebar leading to a reduced corrosion risk for the steel reinforcement [4].

2. MATERIALS AND METHODS

To investigate the influence of marine environments on autogenous crack healing in cementitious materials, ordinary Portland cement mortar samples and blast-furnace slag mortar samples containing 100 µm and 300 µm wide cracks were permanently immersed in chloride solutions as well as in combined chloride and sulphate solutions, as explained more in depth in [1]. Another part of the samples were exposed to wet-dry cycles in the same solutions. Autogenous crack healing was evaluated by means of microscopic measurements over time. The resistance against chloride penetration was measured and evaluated by means of colorimetric measurements and chloride profiles.

Secondly, accelerated chloride diffusion tests on (un)cracked and self-healing concrete with encapsulated polyurethane based healing agents were performed, as explained in [5]. Concrete samples with self-healing properties contained cylindrical borosilicate glass capsules (length: 35 mm, internal diameter: 3.00 ± 0.05 mm, wall thickness: 0.175 ± 0.030 mm) filled with a one component polyurethane based healing agent. Artificial cracks of 300 µm width were created. Chloride profiles were obtained after 49 and 133 days exposure. The self-healing efficiency at multiple depths i below the exposed surface (SHE_i) was defined as the difference between the chloride concentration in cracked concrete and the concentration in healed concrete, divided by the difference in concentration between cracked and uncracked concrete [5].

Furthermore, the effectiveness of an encapsulated low viscosity (150-250 mPas at 25 °C) polyurethane based healing agent has been investigated by means of capillary water absorption tests on mortar while monitoring the time-dependent water ingress with neutron radiography (facility NEUTRA of the Paul Scherrer Institute in Switzerland), as explained in [6]. Standardized cracks were created in prisms with dimensions of 40 × 40 × 160 mm^3 by positioning 300 µm thick metal plates in the molds up to a depth of 20 mm. For the samples without self-healing properties, the metal plates were removed from the mortar at the moment of demolding. For samples with self-healing properties, the metal plates were removed after the curing period of 28 days. For some additional samples, cracks were only created (and triggering of the self-healing process occurred) just before exposure to the water absorption test.

Finally, to test the efficiency of (combinations of) WRA and CI, accelerated corrosion tests were performed on standard mortar prisms (sand:cement:water = 3:1:0.5; 40 x 40 x 160 mm^3). One smooth reinforcement bar with a diameter of 8 mm was placed centrally along the length of the molds (Figure 1). Artificial cracks were introduced by placing brass plates of 300 µm thickness in the mold up to the mid-level of the reinforcement bars. These plates had a width of around 40 mm and had a half sphere drilled out at the bottom with the same radius as the reinforcement bar for positioning onto the rebar (Figure 1.A). Samples were demoulded after 24 hours and the brass plates were removed at the same time. Finally, samples with a targeted thickness of 12 mm were sawn from the prismatic mortar specimens after the trowelled surface was smoothened (Figure 1.B). For the accelerated corrosion test, the edges of the samples were covered 10 mm high on the sides with aluminum butyl tape to ensure that only the cracked surface was exposed to the chloride solution. Furthermore, an electrical connection was made with the reinforcement bar by means of a copper wire. An overview of the different test series with their corresponding code is given in Table 1. The cracks were repaired by injecting the WRA and/or CI, which were not admixed (Table 1), into the crack by means of a syringe with a needle. For every specimen, a volume of 0.43 ml was injected.

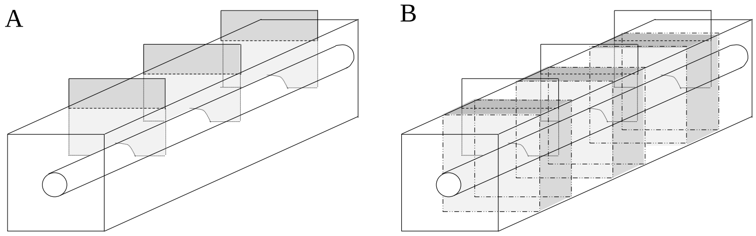

Figure 1 Preparation of the reinforced mortar samples used for the accelerated corrosion test.

Table 1. Test series used for the accelerated corrosion test (mortar)

Code	State	Injected products	Admixed products
UN	Uncracked	-	-
CR	Cracked	-	-
B	Cracked	CI / WRA, silanes (MasterProtect 8000 CI)	-
S	Cracked	CI, amino alcohols (Ferrogard 903 Plus)	-
SF	Cracked	WRA, silanes (Sikagard 705 L)	CI, amino alcohols (Ferrogard 901 S)
N	Cracked	CI, sodium nitrite	-

To evaluate the performance of the different WRA and CI in a short time-span, an accelerated corrosion test was performed. The mortar prisms were positioned inside a plastic box on two line supports with the crack facing downward and a stainless steel mesh in between the supports as shown in Figure 2. The mesh and the bottom of the specimen were submerged into a 165 g/l NaCl solution. The copper wire of the specimen and the stainless steel mesh were respectively connected to the positive and the negative terminal of a power supply. An electric potential of 12 V was imposed between the rebar and the mesh The imposed voltage on the reinforcement steel increased the velocity of chloride ion movement in the sample, hence accelerating the corrosion process together with the higher concentration of NaCl solution. During the test, every 1.5 hours the current was monitored and a visual observation of all specimens was performed.

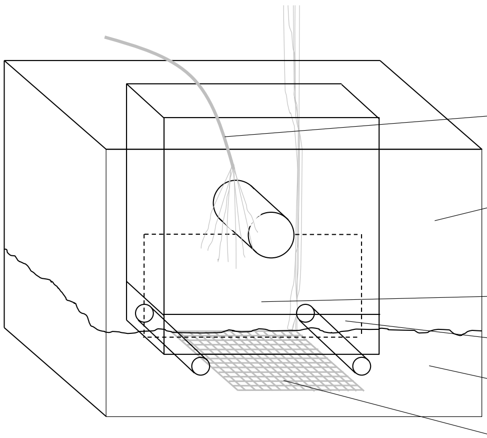

Figure 2 Test setup used for the accelerated corrosion test

3. RESULTS

As explained more in detail in [1], autogenous crack healing occurs quite fast by means of calcium carbonate precipitation and ongoing hydration when mortar is cyclically exposed to wet/dry conditions. In case of continuous immersion, autogenous crack healing occurs much slower and mainly by means of ongoing hydration. The composition of the environmental solution, with or without chlorides, has no significant influence on the healing mechanism. However, the presence of magnesium sulphate results in the formation of a brucite layer, sealing the cracks (Figure 3). Crack widths lower than 105 µm are able to heal autogenously. Crack widths larger than 105 µm will also heal but not completely. As a result, crack healing in these larger cracks will not much improve the resistance against the penetration of aggressive substance such as chlorides.

It appears that 10 µm is the critical crack width for chloride penetration, and at lower crack widths the mortar behaves as being uncracked (Figure 4).

In case of autonomous crack healing of artificial cracks (width 300 µm) with encapsulated polyurethane, the experimentally obtained chloride profiles at the two exposure periods of 49 and 133 days were positioned in between the profiles of the uncracked and the cracked specimens, except for the outer layer (0-4 mm) [5]. From a depth of 6 mm onwards, the SHE was always above 75%. It was shown that this reduction of chloride concentration in the zone around the crack will increase the service life of the structural element with a factor of about 10.

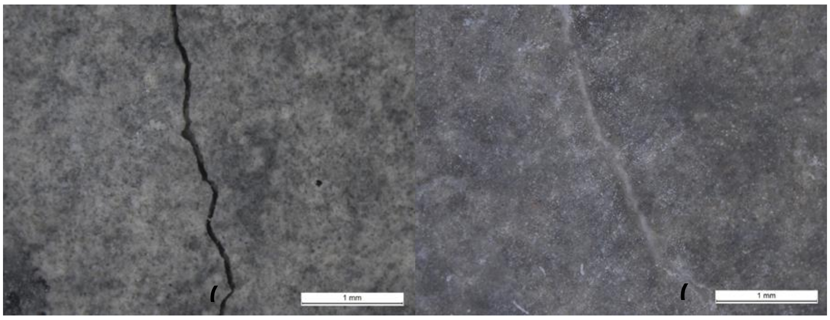

Figure 3 Crack with initial width of ~ 100 µm in OPC mortar before (left) and after (right) 196 days immersion in 165 g/l NaCl + 42.5 g/l $MgSO_4$ [1]

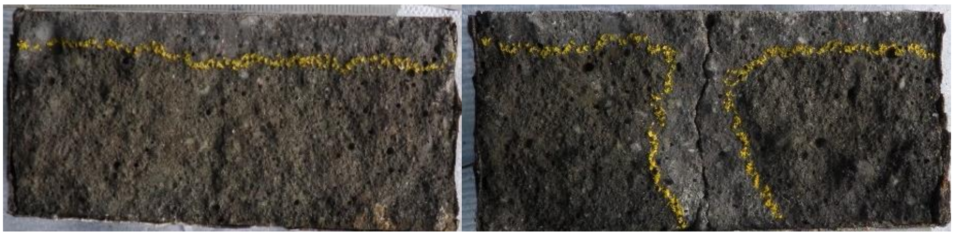

Figure 4 Chloride penetration in autogenously healed mortar with a remaining crack width < 10 µm (left) and > 10 µm (right) [adapted from 1]

In the previous experiments, the healing agents were allowed to harden 24 h before bringing them in contact with water. However, in real structures, contact with water may occur immediately after crack formation. This effect was investigated in [6] by taking neutron radiography images of specimens where exposure to water started immediately after formation of the standardized crack through removal of the thin metal plates which triggered the release of the healing agent. In contrast with the specimens where the polyurethane in cracks had already hardened (Figure 5, left), these specimens (Figure 5, right) show an enhanced healing efficiency. It appears that the immediate contact of the moisture-curing polyurethane with water creates the optimal conditions for its reaction.

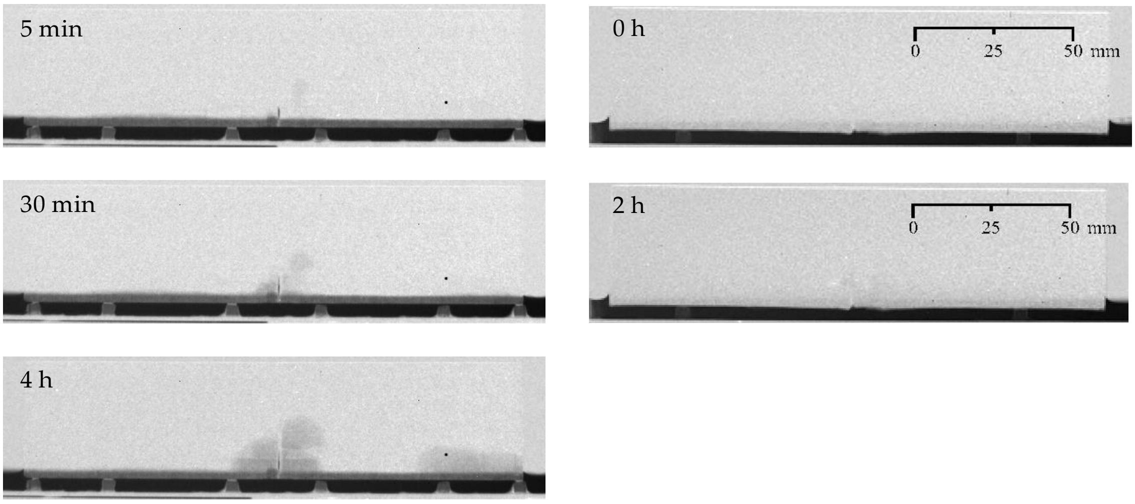

Figure 5 Water uptake in cracked mortar as a function of exposure time using neutron radiography: (left) crack healing before contact with water; (right) immediate contact with water after crack formation (adapted from [6])

Regarding the accelerated corrosion tests on mortars with WRA and/or CI, the current evolution was measured and the status of the rebar and surrounding mortar matrix was observed from the side of the samples. The current was recorded every 1.5 hours for a total of 31.5 hours. The mean current measured for all samples of each test series is plotted in Figure 6. Between

12 hours and 23 hours no current was measured due to the manual recording of these data points. If a current with a value of zero was recorded, it is assumed that no corrosion took place. Higher values indicated a higher probability of the corrosion reaction occurring. Comparing series UN and CR in Figure 6, shows that obviously higher current values were obtained for the latter. The evolution shows the increase to a peak, after which the current decreases again which can be explained by the hindering of transport of chlorides to the reinforcement due to the formed corrosion products which are acting as a barrier and due to the formation of horizontal cracks in the mortar matrix. The small peak noticed for the UN series around 7 hours was caused by one sample starting to show an unexpected behavior (see further), which later on stabilized again. The measured currents for the samples with admixed or injected WRA and/or CI are constrained by the cracked reference samples as an upper boundary, except for the second measuring period where series S resulted in the highest current with a peak around 25 hours. Samples treated with sodium nitrite (series N) showed a steady increase of the current at first after which a small decrease occurred, leading to a stable rate. For the SF series no current was measured during the entire test. Based on this accelerated corrosion test, one can conclude that the combination of Sikagard 705 L and Ferrogard 901 S (series SF) seems very promising to efficiently halt the corrosion initiation.

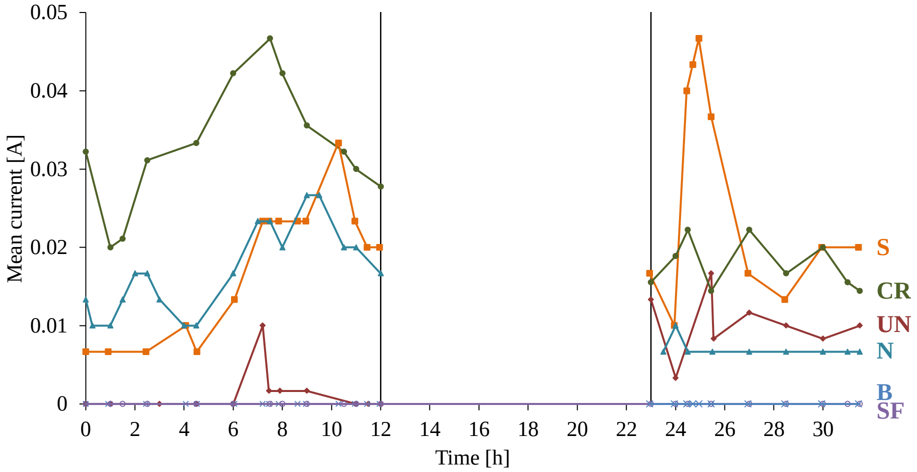

Figure 6 Evolution of the mean current over time for the different test series.

Together with the current recordings, pictures were taken of the specimens every 1.5 hours in order to monitor visual changes on a regular base. Figure 7 shows the different stages of deterioration which were noticed. The first stage corresponded to the point where the moisture front, caused by NaCl ingress through the artificial crack, reached the reinforcement level. The second stage corresponded to the point at which the corrosion process had started, resulting in tensile stress formation and leading to a horizontal crack through the mortar at the reinforcement level. The last stage was represented by the formation of a vertical crack above the reinforcement bar.

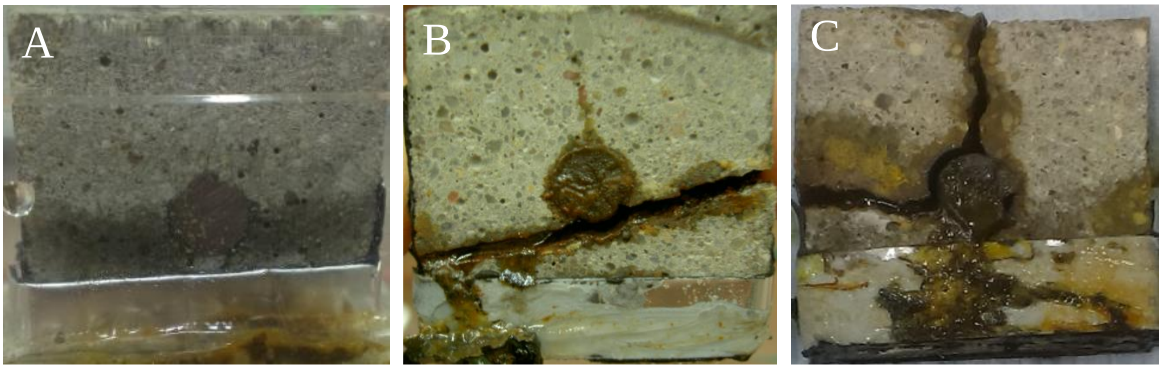

Figure 7 Observed stages within the corrosion process: A. Moist matrix up to the reinforcement level; B. Horizontal crack formation in the mortar matrix; C. Vertical crack formation in the mortar matrix.

In Figure 8 the time at which one of the three above mentioned stages was observed is shown. In agreement with the outcome of the current evolution, samples of the UN, B and SF series performed very well and exhibited none of the three aforementioned stages. After completion of the test, it appeared that for one sample of the UN series a small transverse crack at the bottom surface was present in one of the samples. This was probably present from the start which could explain the higher current measured at 7 hours compared to the other samples of this series. In general, the samples of the CR series showed a faster evolution in deterioration compared to the less performing treated samples. In less than 10 hours of exposure to the accelerated corrosion test all samples of the CR series showed moisture ingress, followed by horizontal and vertical crack formation in the mortar matrix due to formation of expansive corrosion products. Also for the samples of the S and the N series, moisture ingress and horizontal crack formation was noticed. However, it seemed that due to the treatment the damage due to corrosion was less severe compared to the series with untreated cracks (CR) and vertical cracking could be prevented. Moreover, for the series treated with sodium nitrite only two out of the three samples showed some degradation.

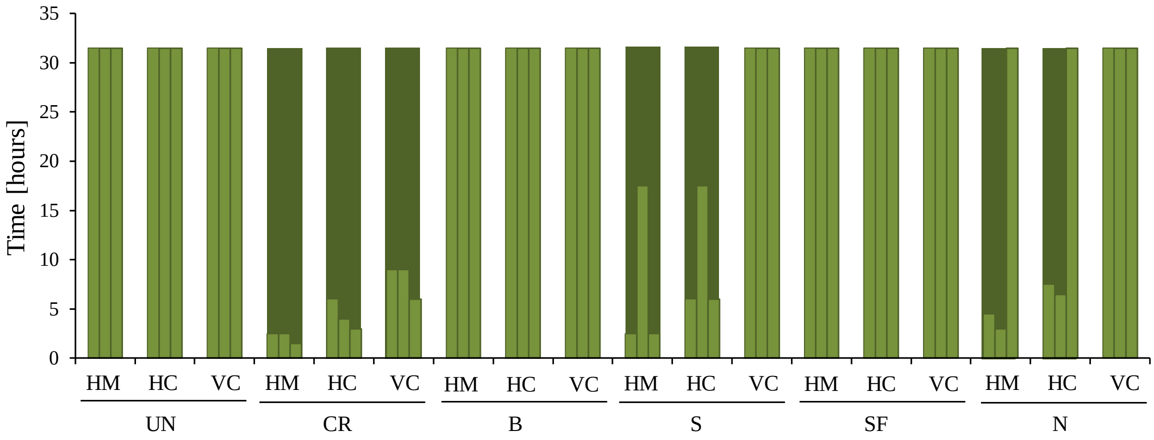

Figure 8 Time of appearance of the different degradation stages for the samples of all test series (light green colour indicates that the degradation stage was not yet noticed; as soon as a certain degradation mechanism was noticed, the colour changes to dark green, HM = horizontal moisture front, HC = horizontal crack and VC = vertical crack).

4. CONCLUSIONS

The autogenous healing property of concrete, a mechanism that includes further binder hydration and calcium carbonate precipitation, may close cracks of up to 100 µm completely. In marine infrastructure, the presence of magnesium sulfates may aid the crack sealing through brucite precipitation. However, as soon as the remaining crack width is above 10 µm, chlorides will penetrate faster through these cracks into the matrix, impairing the service life of reinforced concrete structures. Incorporation of autonomous healing mechanisms can then provide a solution. Self-healing by encapsulated polyurethane based agents, is characterised by a self-healing efficiency above 75% towards chloride diffusion in the presence of 300 µm wide cracks. Neutron radiography images obtained during a capillary sorption test indicated that in-situ healing in wet conditions was favourable for the polyurethane reaction and improved the crack sealing. Finally, also the incorporation of water repellent agents and/or corrosion inhibitors, effectively delayed reinforcement corrosion during accelerated corrosion tests on cracked, manually treated mortar samples.

ACKNOWLEDGEMENTS

Part of this research was carried out under the program SHE (Engineered Self-Healing materials), project ISHECO (Impact of Self-Healing Engineered materials on steel COrrosion of reinforced concrete), funded by SIM (Strategic Initiative Materials in Flanders) and VLAIO (Flanders Innovation & Entrepreneurship). Kim Van Tittelboom is a postdoctoral fellow of the Research Foundation – Flanders (FWO). Mathias Maes has obtained funding from IWT for his PhD.

REFERENCES

[1] Maes, M.; Snoeck, D.; De Belie, N.: Chloride penetration in cracked mortar and the influence of autogenous crack healing, *Construction and building materials*, Vol. 115 (2016), pp. 114-124.

[2] Van Tittelboom, K.; De Belie, N.: Self-healing in cementitious materials – A review. *Materials*, Vol. 6 (2013), No. 6, pp. 2182-2217.

[3] L. Bertolini, B. Elsener, P. Pedeferri, E. Redaelli, R. Polder: *Corrosion of steel in concrete: Prevention, diagnosis, repair*, Wiley-VCH Verlag GmbH & Co. KGaA, (2013)

[4] Van Tittelboom, K.; Van Belleghem, B.; Dhaene, J.; Van Hoorebeke, L.; De Belie, N. Preventing reinforcement corrosion in cracked concrete by self-repair. Proceedings of the second International Conference on Concrete Sustainability (ICCS16), Galvez, J.C. et al. (eds.), pp. 787-796, ISBN: 978-84-945077-7-9, Madrid, June 2016.

[5] Van Belleghem, B.; Van den Heede, P.; Van Tittelboom, K.; De Belie, N.: Quantification of the service life extension and environmental benefit of chloride exposed self-healing concrete, *Materials*, Vol. 10 (2017) No. 5, 22 p.
[6] Van den Heede, P.; Van Belleghem, B.; Alderete, N.; Van Tittelboom, K.; De Belie, N.: Neutron radiography based visualization and profiling of water uptake in (un)cracked and autonomously healed cementitious materials, Materials, Vol. 9 (2016) No. 5, 28 p.

USE OF ROBOTICS IN AUTOMATED AND COMPREHENSIVE NDE OF RC STRUCTURES

Nenad Gucunski[1], Basily Basily[1], Ali Maher[2], Jinyoung Kim[3] and Trung Duong[2]

1 Rutgers University, Department of Civil and Environmental Engineering, 96 Frelinghuysen Road, Piscataway, NJ 08854, USA, email: gucunski@rci.rutgers.edu, basily@soe.rutgers.edu
2 Rutgers University, Center for Advanced Infrastructure and Transportation 100 Brett Road, Piscataway, NJ 08854, USA, e-mail: mmaher@soe.rutgers.edu, duonghuytrung@gmail.com
3 Ajou University, Department of Architectural Engineering Sanhakwon 712, 206 Worldcup-ro, Yeongtong-gu, Suwon-si, Gyeonggi-do 16499, Republic of Korea, e-mail: jinyoungkim@ajou.ac.kr

SUMMARY: Economical management of bridges primarily depends on the objective assessment of their condition. This is especially true for reinforced concrete bridge decks that deteriorate faster than other bridge components due to their direct exposure to traffic and environmental loads. The current practice of concrete bridge deck evaluation in the greatest part relies on visual inspection, and use of simple evaluation tools. Non-destructive evaluation (NDE) technologies provide more accurate and comprehensive condition assessment and enable accurate monitoring of deterioration progression. However, the manual NDE data collection is often limited to a single NDE technology and in many cases is slow. The system RABIT (Robotics Assisted Bridge Inspection Tool) overcomes the problems of manual NDE through implementation of multiple NDE technologies on a fully autonomous robotic platform that collect data at a significantly higher speed. Use of multiple technologies implemented in RABIT: impact echo, electrical resistivity, ground penetrating radar and ultrasonic surface waves provides comprehensive assessment of three elements of primary concern: deck delamination, corrosion, and concrete quality. The RABIT platform and its components, the data collection process and typical results from the RABIT data collection, and benefits stemming from a periodical data collection, are presented.

UPOTREBA ROBOTIKE U SVEOBUHVATNOM I EKONOMIČNOM OCJENJIVANJU STANJA ARMIRANOGA BETONA

SAŽETAK: Ekonomično gospodarenje mostovima prvenstveno ovisi o objektivnoj ocjeni njihovog stanja. To se naročito odnosi na armiranobetonske ploče mostova koje uslijed direktne izloženosti prometnom opterećenju i opterećenju iz okoliša propadaju znatno brže u odnosu na ostale elemente mosta. Trenutna praksa ocjene stanja betonskih ploča mostova se u najvećem dijelu oslanja na vizualni pregled i korištenje jednostavnih alata za ocjenu stanja. Nerazorne tehnologije ocjene stanja (NDE) osiguravaju točniju i obuhvatniju ocjenu stanja te omogućuju precizno praćenje procesa degradacije. Međutim, ručno prikupljanje NDE podataka je vrlo često ograničeno pojedinom NDE tehnologijom te je u mnogim slučajevima vrlo sporo. Sustav RABIT (eng. Robotics Assisted Bridge Inspection Tool) nadilazi ograničenja ručne NDE tehnologije kroz implementaciju višestrukih NDE tehnologija u potpuno autonomnu robotiziranu platformu koja prikuplja podatke značajno većom brzinom. Sustav primjenjuje sljedeće višestruke nerazorne tehnologije vrednovanja: električnu otpornost (impedanciju), odziv na udar, georadarsko ispitivanje i ultrazvučne površinske valove; što sigurava opsežnu ocjenu tri primarna faktora: ocjenjivanje korozije, raslojavanje i kvalitetu betona. U radu su prikazani primjeri koristi od takva nadzora i prednosti pred tradicijskim pregledom kolnika mosta. Oni su u prvom redu povezani sa sveobuhvatnim ocjenjivanjem uvjeta i razvojem realističnijih modela degradacije, predviđenih troškova i troškova životnoga ciklusa.

1. INTRODUCTION

Economical management of bridges primarily depends on the objective assessment of their condition. This is especially true for reinforced concrete bridge decks that deteriorate faster than other bridge components due to their direct exposure to traffic and environmental loads. As a result, implementation of preventive maintenance, rehabilitation, repair or replacement actions on bridge decks is far more frequent and requires significantly higher financial resources. The current practice of concrete bridge deck evaluation in the greatest part relies on visual inspection and use of simple evaluation tools. While limited physical sampling is used in some cases, there are justified reservations regarding how representative the results from those samples are of the overall bridge condition. Consequently, there are limitations in the accuracy of the obtained information for the purpose of assessment and deterioration and predictive modelling of a deck condition. Equally important, there are reservations regarding the objectivity of comparison of the condition of bridges on the network level.

Results from application of non-destructive evaluation (NDE) technologies in the past twenty to thirty years have shown that NDE provides far more accurate and comprehensive condition assessment, and that it enables accurate monitoring of deterioration progression [1]. However, there were also obstacles related to their wide option for two primary reasons. The first reason was too frequent reliance on the results from a single NDE technology. Each of the technologies, as described later, has its strengths and limitations and, thus, is best suited for detection and characterization of a particular property or deterioration. The second reason is a relatively low speed of NDE data collection for many technologies that led to more expensive inspections and longer traffic interruptions. The NDE system named RABIT (Robotics Assisted Bridge Inspection Tool) overcomes the above problems through implementation of multiple NDE technologies on a fully autonomous robotic platform that collects data at a significantly higher speed than manual data collection approaches. The following sections describe the RABIT platform, typical results from the RABIT data collection, and benefits stemming from a periodical NDE data collection.

2. DESCRIPTION OF RABIT AND IMPLEMENTED NDE TECHNOLOGIES

The robotic system RABIT, shown in Figure 1, fully autonomously assesses the condition of a bridge deck by deploying multiple NDE technologies. In particular, the RABIT implements four NDE technologies: electrical resistivity (ER), impact echo (IE), ground-penetrating radar (GPR), and ultrasonic surface waves (USW). There are two main reasons the four technologies are implemented. The first reason is the ability to detect and/or characterize corrosion, delamination and concrete quality, while the second is the speed and simplicity of data collection. In addition, the four technologies enable the description of the deck condition at any point in its life, from the earliest signs of corrosive environment development, to formation of fully developed delamination. In particular, the ER is used to evaluate the concrete's corrosive environment, which is influenced by presence of moisture chloride, salts and other, by measuring concrete’s electrical resistivity. Previous studies have shown a close correlation between the electrical resistivity and reinforcement corrosion rates [2]. The IE test is used to detect and characterize the stage of development of deck delamination [3]. The GPR provides multiple information about the deck, including the reinforcement position, concrete cover thickness, and qualitative assessments of the bridge deck's corrosive environment and its overall condition [4]. Finally, the USW test is used to assess the concrete quality by measuring its elastic modulus [5]. Previous results have shown that the changes in concrete modulus from the USW are minor and, thus, are lesser indicators of deterioration progression than measures from other NDE technologies [1]. Finally, three cameras deployed on RABIT complement visual inspection by creating permanent records of the deck surface condition (two cameras on the front end of the platform), and wider bridge deck areas (panoramic camera on the mast).

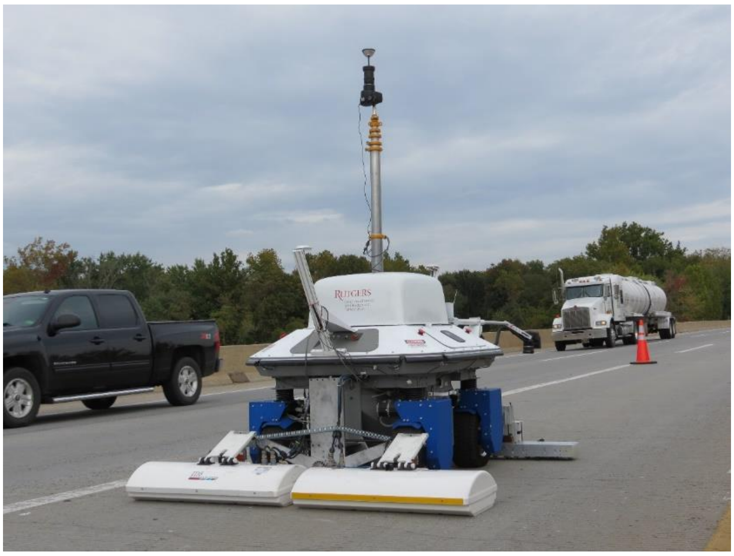

Figure 1 RABIT system during data collection

The details of the RABIT system and deployed NDE technologies are depicted in Figures 2 and 3. There are two acoustic arrays on the front end of RABIT to conduct IE and USW testing, as shown in Figure 2. Each of the arrays has four solenoid type impact sources and seven sensors (accelerometers), marked by red and blue circles in the figure, respectively. As such, each of the arrays is enabling up to eight IE and six USW tests. Attached to the two acoustic array boxes are four Wenner type electrical resistivity probes. To ensure electrical contact between the probes and deck surface, the ER probes' electrodes are continuously moistened using a spraying system. Also visible in Figure 2 are two cameras for high-resolution imaging of the deck surface. Two GPR arrays on the rear end of RABIT are shown in Figure 3. Each of the arrays has sixteen GPR antennas, or eight pairs of antennas of dual polarization, as illustrated in the antenna schematics. Two acoustic and GPR arrays combined are 1.8 m wide, providing data collection over a half width of a typical driving lane during a single RABIT pass.

The RABIT is collecting data in a fully autonomous mode. For the autonomous motion, the system relies on a fusion of data from three positioning systems or devices: differential global positioning system (DGPS), on board inertial measurement unit

(IMU) and a wheel encoder, or a distance measurement instrument (DMI). The DGPS consists of two GPS antennas mounted on the robot's front and rear ends, and the third GPS antenna, the base station, on a tripod. The tripod is typically placed on a side of the bridge within a 100 m distance from the robot. Three GPS coordinates on the deck and the GPS coordinate of the base station are sufficient to fully define the data collection path. The RABIT collects data at a significantly higher speed than it is done using manual NDE equipment. It can collect data at rates of about 300 to 350 m2 per hour.

Figure 2 Front end of RABIT with acoustic arrays, Wenner probes and cameras.

The RABIT is transported to the bridges to be surveyed by a van, The van also serves as a command center, where the robot movement and data collection are being monitored. All the data during the data collection is streamed to the van, where it is presented on one of multiple displays for quality control. As an illustration, positions of all locations for which the IE data were successfully collected on a bridge approximately 35 m long and 14 m wide, are presented by blue dots in Figure 4. The spatial resolution of the RABIT data is significantly higher than the one from typical manual data collection.

3. BENEFITS OF NDE AND ROBOTIC DATA COLLECTION

The results from bridge deck surveys are presented in terms of condition maps, and summarized in terms of condition indices. Condition maps describe spatial distribution of severity of deterioration, or of certain material property, like concrete modulus. This is illustrated in Figure 5 by delamination, concrete modulus and corrosion condition maps from a survey of a bridge in the State of Oregon. In all maps, hot and warm colors (red and yellows) are indications of deterioration or lower material quality, while cold colors (greens and blues) are indications of the opposite. For example, the small red areas in the IE map describe delamination in its final stage of the development, while orange to red zones in the ER map describe zones of a highly corrosive environment and, thus, anticipated high corrosion rates.

Figure 3 Rear end of RABIT with GPR arrays.

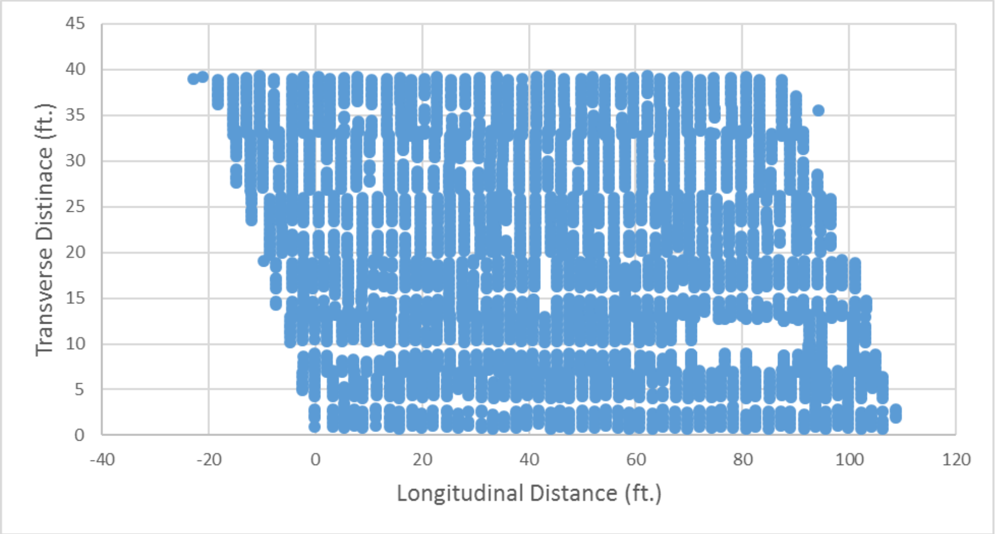

Figure 4. Plot of accepted IE test locations based on GPS data.

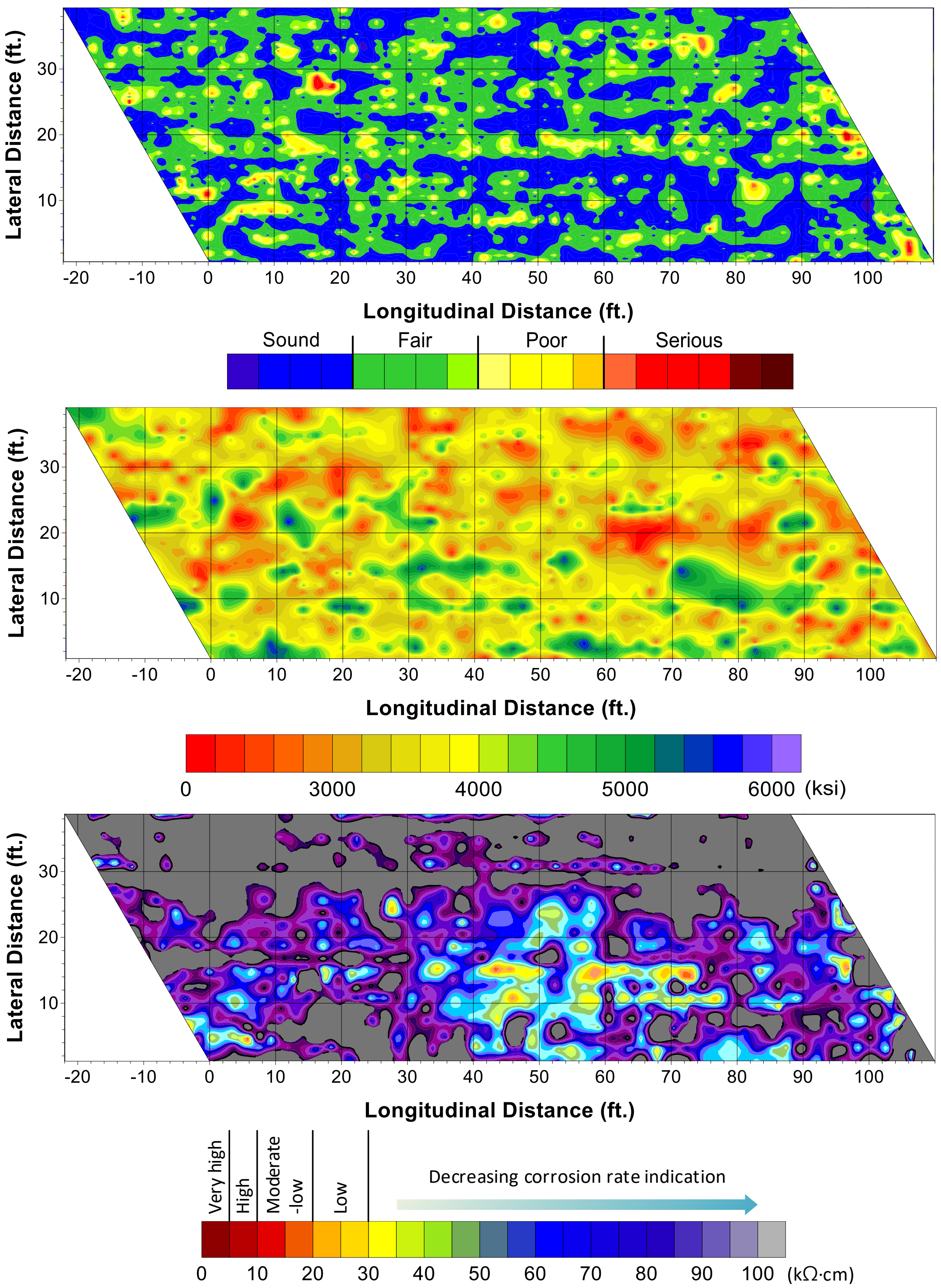

Figure 5 Condition maps for a bridge deck in State of Oregon: delamination map from IE (top), concrete modulus map from USW (middle), and corrosion map from ER (bottom).

NDE based condition indices (Cis) were introduced to describe the overall condition of a bridge deck. A CI for a particular NDE technology represents a weighted average of percentages of areas of the deck in various states of deterioration or condition. The CI is on a scale of 0 to 100, where 0 represents the worst, and 100 the best possible condition. For example, the delamination CI for the Oregon Bridge was 68.2, while the ER corrosion CI was 97.2. The description of deck condition in terms of CIs is essential for modelling of deterioration progression and objective comparison of bridges on the network level. This is illustrated in Figure 6 for a bridge in Haymarket, Virginia. While the bridge was surveyed four times during the 2009 to 2015 period using manual NDE technologies, it is illustrative of the ability of NDE technologies to capture deterioration progression through periodical surveys. The condition indices in the figure are for ER, GPR and IE. In addition, a combined CI was calculated, which in this case was a simple average of the individual NDE technology CIs. In contrast, the results from visual inspection quantified through a National Bridge Inventory (NBI) condition rating, did not indicate any change during the same period. In fact, the NBI condition rating for the Haymarket Bridge of 6, on a scale 0 (worst) to 9 (best), did not change from 1992 to 2015.

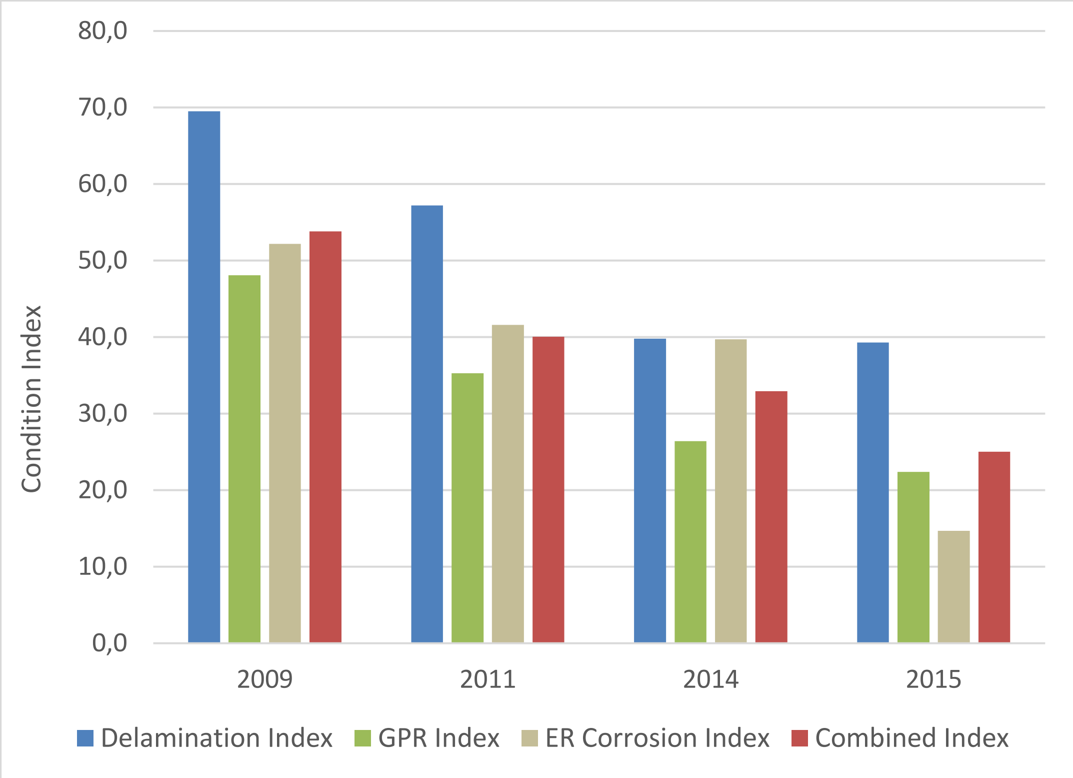

Figure 6 Condition indices for Haymarket Bridge for the 2009 to 2015 period.

4. CONCLUSIONS

Rapid NDE data collection using robotics will be essential for effective management of transportation infrastructure in the future. As illustrated by the RABIT platform for concrete bridge decks, rapid and fully autonomous data collection is significantly reducing both the required workforce and risks associated with inspections in bridge work zones due to the passing traffic. RABIT's ability to simultaneously deploy multiple NDE technologies, and the use of a significantly larger number of sensors, enables detection and characterization of deterioration with higher spatial resolution and higher confidence of problem detection than single manual NDE technologies. In addition, the quantitative nature of NDE data, enables monitoring of deterioration progression through periodical surveys, and more objective comparison of bridges for prioritization on the network level. Equally important, the data collection at higher speeds and with support of a smaller crew, reduced time needed for traffic management, reduces the cost of bridge deck inspection both directly and indirectly.

ACKNOWLEDGMENTS

The RABIT development was supported by a subcontract from Rutgers University, Center for Advanced Infrastructure and Transportation (CAIT), under DTFH61-08-C-00005 from the U.S. Department of Transportation – Federal Highway Administration (USDOT-FHWA). The authors are especially grateful to Dr. Hamid Ghasemi, the former manager of FHWA's Long Term Bridge Performance (LTBP) Program.. A large number of individuals from Rutgers' School of Engineering working within the Center for Advanced Infrastructure and Transportation (CAIT) have contributed to various aspects of the robotic system development, construction and implementation. The authors gratefully acknowledges contributions of Professors Kristin Dana, Hung La and Seong-Hoon Kee, Research Associate Kien Dinh, and Research Engineers Ronny Lim and Hooman Parvardeh.

REFERENCES

[1] Gucunski, N., Pailes, B., Kim, J., Azari, H., and Dinh, K.: Capturing and quantification of deterioration progression in concrete bridge decks through periodical NDE surveys. ASCE Journal of Infrastructure Systems, ASCE, Vol. 23 (2016), No. 1,.

[2] Whiting, D.A. and M.A. Nagi (eds.): Electrical Resistivity of Concrete – A Literature Review. PCA R&D Serial No. 2457, 2003, PCA, Skokie, IL.

[3] Barnes, C., Trottier, J. F., and Forgeron, D. Improved concrete bridge deck evaluation using GPR by accounting for signal depth-amplitude effects. NDT & E International, Vol. 41 (2008), No. 6, pp. 427-433.

[4] Sansalone, M. J.: Detecting delaminations in concrete bridge decks with and without asphalt overlays using an automated impact-echo field system", NDT in Civil Engineering, Proceedings of Intl. Conference of British Institute of Non-Destructive Testing, Liverpool, U.K., April 14-16, 1993, pp. 807-820.

[5] Nazarian, S., Baker, M.R. and Crain, K. Development and Testing of a Seismic Pavement Analyzer. Report SHRP-H-375, Strategic Highway Research Program, NRC, Washington, D.C. (1993)

DEVELOPMENTS IN THE PERFORMANCE APPROACH FOR DURABILITY AND SERVICE LIFE PREDICTION FOR CONCRETE STRUCTURES

Mark G. Alexander[1], Gladwell Nganga[1]

[1] University of Cape Town, Department of Civil Engineering, Concrete Materials and Structural Integrity Research Unit (CoMSIRU), Cape Town, South Africa, email: mark.alexander@uct.ac.za,
ngngla001@myuct.ac.za

SUMMARY: The paper reviews the performance-based approach for durability design and specification in reinforced concrete structures. It shows that such an approach requires the development of service life prediction (SLP) models for concrete structures, based on durability considerations. Taken together, these two aspects permit rational quantification of durability. Associated concepts also covered in the paper are performance testing and durability indicators. Typical applications of SLP models in different countries are discussed, as well as practical examples of performance-based approaches. Finally, developments in code approaches to service life modelling and prediction are reviewed.

RAZVITAK PRISTUPA PREMA PONAŠANJU POVEZANOG S TRAJNOŠĆU I PREDVIĐANJEM UPORABNOG VIJEKA BETONSKIH KONSTRUKCIJA

SAŽETAK:U radu je dan pregled pristupa zasnovanog na ponašanju pri projektiranju trajnosti i specifikacijama za armiranobetonske konstrukcije. Pokazano je da je za takav pristup potreban razvoj modela predviđanja uporabnog vijeka betonskih konstrukcija koji se zasniva na razmatranjima trajnosti. Ta dva aspekta uzeta zajedno omogućuju racionalno kvantificiranje trajnosti. Tomu pridružene ideje obuhvaćene u radu jesu ispitivanje ponašanja/svojstava i pokazatelji trajnosti. Raspravljene su tipične primjene modela predviđanja uporabnog vijeka u različitim zemljama i praktični primjeri pristupa zasnovanog na ponašanju/svojstvima. Na kraju je dan pregled razvoja u propisima za modeliranje uporabnog vijeka i predviđanja.

1. INTRODUCTION

Durability of reinforced concrete structures depends largely on the resistance to penetration of the concrete cover by aggressive agents that initiate and propagate deterioration processes, specifically reinforcement corrosion [1]. The protective nature of the concrete cover depends on: i) its penetrability, which is influenced by concrete mix properties and materials used, ii) execution of construction practices such as compaction and curing, and, iii) actual thickness of concrete cover of the finished structure. In current standards e.g. EN 206-1 [2], provisions for durability include a minimum cement content, maximum water/cement ratio and minimum strength class, for a given exposure condition. Significantly, the quality control measure is based on compressive strength. These provisions are described as ‘prescriptive’ and have several limitations. Firstly, the quality of the concrete cover is not only dependent on the material parameters (cement content and water/cement ratio) but is also dependent on proper placing, compaction and curing [3]. Secondly, the quality control measure of strength is a bulk property which does not provide any indication of the resistance to penetrability[1] of the concrete cover. Also, it is difficult if not impossible to actually check the provisions on the finished structure, which makes the specifications rather meaningless.

Due to the limitations present in the current prescriptive approach, a shift to performance-based approaches is now favoured. This approach to durability design and specification is quantitative, in the sense of actually being able to measure specified concrete parameters. Also, deterioration mechanisms are considered through the use of suitable mathematical models that are based on the rate of transport of aggressive substances that cause deterioration [4]. From the application of mathematical models for a pre-defined working life, output parameters such as material properties (e.g. a diffusion coefficient) and geometric properties (cover depth) are determined, which can be verified using suitable performance tests.

This paper provides a brief review of the performance-based approach and selected service life prediction models that have been developed and used in different countries. An example is also provided of the application of performance-based specifications for quality control. The paper ends with an overview of developments in the codes to consider service life modelling.

[1] Penetrability is the ability of the concrete to be penetrated by gases, liquids and ions under different transport mechanisms.

2. PERFORMANCE-BASED DESIGN APPROACH

Durability should be considered as a material performance concept for a structure in a given environment, and as such, it cannot easily be assessed through simple mix parameters [5]. As indicated earlier, a performance approach focuses on measurement of relevant properties of the concrete, in particular transport-related properties for durability. Consequently, robust and industry-accepted test methods are required in this approach, with test results that can be shown to be accurate, reliable and reproducible. In the past, this issue of acceptable test methods, which are 'proven' to represent the relevant durability properties of concrete, has been the major stumbling block to more rapid and general adoption of performance-based methods.

In practice, performance approaches can represent either a partial approach (termed 'hybrid'), or a full performance-based approach [6]. Both encompass key elements such as: tests by which to characterise the desired performance; definition and specification of performance limits by which to judge acceptable performance; and, importantly, integration of durability requirements and durability design through service life models in order to estimate service life of the RC structure [7, 8]. Crucially, in a full performance approach, specified concrete properties should be measurable in situ to ensure as-built quality is actually achieved. This leads to questions of performance testing and performance specifications.

2.1 PERFORMANCE TESTING AND LIMITS

Performance testing requires the development of reliable and representative test methods and the imposition of suitable performance limits. In some cases, the appropriate limit may come from service life models – e.g. deriving a chloride diffusion coefficient such as from the Life-365 model [9]. In other cases, particularly where service life models are not well developed, the limits may come from best judgment and experience, with the intent to modify or improve these limits as better models are developed. Further, performance tests may be used in different ways. Typically they are used for pre-qualification of mixes prior to construction, where the concrete producer conducts trials to show that the concrete produced meets the specified performance limits; in this case, it is obvious that only the material 'potential' (in the sense of the ability of the material to potentially be durable) is proved, since the mixes are pre-construction mixes that are usually tested in a laboratory. The other use for performance testing is for quality control (QC) during construction, where two possible options exist: firstly, tests on concrete mixes as supplied or delivered before actually being placed in the structure, similar to current routine concrete strength testing; secondly, tests on the actual structure, using in-situ tests, or samples that are removed from the structure and tested in a laboratory; in both these cases the object is to assess the actual as-built quality of the structure. For actual in-situ testing, there is a more direct link between the test result and the expected performance of the structure.

Further, the tests used for these different purposes may themselves be different, although they may assess the same basic performance aspect. For example, a diffusion coefficient may be measured on 'laboratory' concrete used for pre-qualification purposes, while a resistivity/conductivity test may be used in-situ for QC purposes. Also, various performance-based test methods have been developed in different parts of the world (reviewed in chapter 4 of the State-of-the-Art Report of RILEM TC-230 PSC [10]). RILEM TC-PSC also makes the point that, in some instances, deterioration modelling may not be necessary for a performance-based approach to be implemented. For example, in freeze-thaw resistance evaluation, the performance test leads to the acceptance of the concrete mix if the loss of mass is lower than a certain value. There is currently no appropriate model to integrate the result, and essentially long-term experience is the 'criterion' against which the test results are evaluated. This does not preclude development of reliable models for, say, freeze-thaw in the future – it simply speaks to the limitation of our current knowledge and the need to move forward practically.

2.2 PERFORMANCE SPECIFICATIONS

In any methodology, the performance parameters and criteria for the structure must be explicitly described and quantified, and a conformity scheme must be set up to verify these parameters in practice and ensure the criteria are met. According to the US National Ready Mixed Concrete Association (NRMCA), "A performance specification is a set of instructions that outlines the functional requirements for hardened concrete depending on the application. The instructions should be clear, achievable, measurable and enforceable. Performance specifications should avoid requirements for means and methods and should avoid limitations on the ingredients or proportions of the concrete mixture" [11, 12].

Features of performance specifications are: (i) the functional requirements should be clearly defined to ensure that the parties involved in their implementation (concrete producers and contractors) do not interpret them differently; (ii) compositional and proportioning requirements of the concrete mix are not given but the concrete producer and constructor work together in the design of the concrete mix, allowing for flexibility in materials selection and ensuring that the concrete produced and supplied will meet the performance requirements; (iii) verification of compliance using tests that are reliable, repeatable, accurate and preferably easily applicable on site; and (iv) a means to enforce compliance with the specifications, e.g. through penalties when specifications are not met.

While the above requirements are laudable, in current practice a mix of performance and prescriptive requirements is more useful, particularly while fully performance-based approaches are being developed. This is called the 'hybrid' approach, mentioned above and further discussed below.

2.3 HYBRID PERFORMANCE-BASED APPROACHES

In any 'hybrid' approach, greater emphasis should be placed on the performance criteria. The client and/or specifier decide on the desired level of performance in the given exposure conditions and propose relevant 'durability indicators' or other durability parameters which are used to prepare specifications [13]. In the hybrid approach, the durability parameters are chosen based on technical recommendations without necessarily or explicitly defining a design service life period, although it may be possible to incorporate a notional service life requirement. Generally, both approaches – full performance-based and hybrid – should aim at achieving the relevant durability parameters that demonstrate the suitability of the concrete, including its composition, in relation to the exposure conditions.

2.4 DURABILITY INDICATORS

Recently, durability indicators or durability indexes have been proposed and developed. These comprise physical, chemical, or electro-chemical parameters that characterise the concrete at an engineering level. Therefore, they must a) be easily interpreted in an engineering context, such as being linked to a notional service life or rate of deterioration; b) be easily measurable and reliably quantifiable so as to give engineers confidence in their use in construction specifications; and c) be sensitive to processing and environmental factors such as binder type, influence of SCMs, mix proportions, placing and compaction, and type and degree of curing.

Durability indicators provide a powerful means of characterising concrete in terms of its potential to be durable, which is largely a function of the constituent materials and how these are processed to produce a concrete of the desired properties [14, 15]. Durability indicators may be conventional durability-related parameters such as a direct measure of permeability, conductivity or the like; in other cases they may be indirect measures of durability such as a permeability or porosity index, or a chemical property of the concrete that provide an indication of potential durability. It is critical that the relevant deterioration mechanism be taken into account: durability, however described or characterised, relates to a governing deterioration mechanism. Consequently, durability parameters must be closely related to the relevant mechanism, which in many cases will also relate to a transport property of the concrete.

3. SERVICE LIFE PREDICTION MODELS

The service life prediction (SLP) models used for durability design are based on the appropriate deterioration mechanism affecting a concrete structure and the rate of deterioration [4]. The corrosion of reinforced concrete structures is mainly influenced by transport of aggressive agents into and through the concrete cover. Understanding the rate at which these transport mechanisms occur forms the basis of mathematical modelling used in SLP models. An example of a SLP model is LIFE365 which is a software used to determine time of initiation of corrosion for a reinforced concrete structure [9]. The input parameters in this model are the type of structure, its location, depth of concrete cover and material parameters. The approach of SLP and design for durability differs in various countries. A brief overview of these approaches is provided below.

3.1 APPLICATION OF SERVICE LIFE PREDICTION MODELS

In Spain, service life models (SLM) for the initiation and propagation period of corrosion in reinforced concrete structures have been developed based on the use of electrical resistivity [16, 17]. The input parameters in the SLM are: i) reaction or retarder factor of chlorides (rcl) for different cement types, which accounts for the amount of chlorides that are immobilized by cement phases through binding, ii) environmental factors (kcl,CO2) based on exposure classification as provided in EN 206-1 [2], iii) service life required, iv) cover depth and, v) the aging factor (ρt). From these input parameters, the resistivity is obtained which is used as a corrosion indicator (or durability indicator) that can be applied to assess performance of a structure. Alternatively, the cover thickness can be calculated and used for performance specifications where the actual resistivity is known.

In Switzerland, a model (Ref-Exp) to estimate service life was proposed by Torrent [18]. This model is a function of two key characteristics, both measured on site: cover depth and air permeability, kT, measured using the Torrent air permeability test [19]. The model considers the provisions in EN Standards of maximum water/cement ratio and minimum cover depth, for an expected service life of 50 years. On selection of the maximum water/cement ratio for a given environment, the CEB-FIP Model Code 1990 Equation 2.1-107 is applied to convert w/c ratio into a reference value of gas permeability (kTref). If the value of kT measured on site is smaller than kTref and/or the cover depth (measured in the same place) is larger than the specified value, a service life longer than 50 years is predicted by the model. The Ref-Exp model is based on a reference condition (50 year service life) and on experimental values measured non-destructively on site.

In the Netherlands, the DuraCrete model for chloride-induced corrosion is used [20]. Three options can be considered when selecting the performance-based approach: i) a full probabilistic approach based on specified input parameters that consider mean values and variability, ii) semi-probabilistic approach, which uses a safety margin for the cover depth, and iii) a range of cover depths adapted to binder type and exposure class. The chloride diffusion coefficient of the concrete is determined using the Rapid Chloride Migration Test, RCMT (NT Build 492) [21] which has a good linear correlation with diffusion coefficients from pure (immersion) diffusion tests [22]. The RCMT has been applied for many concrete mixtures in association with service life design for large infrastructure projects. For regular production control, the Two Electrode Method (TEM) for measuring resistivity is used which enables a quick, simple and non-destructive test on any regularly shaped specimen. A correlation has been established between resistivity and chloride transport in concrete. The test samples used for TEM are standard concrete cubes for compressive strength testing after wet curing at an age of 28 days. The performance specifications for a given service life provide a maximum RCMT value, and mean cover depth (reinforcing or prestressing steel) for a given binder type and exposure conditions.

In Norway, the probability-based DURACON Model has been used as a basis for durability design, quality assurance and operation of a number of new concrete structures in recent years. In principle, the DURACON Model is a simplified and modified version of the DuraCrete Model. Based on the combination of a modified Fick's Second Law of Diffusion and a Monte Carlo Simulation, a basis is obtained for calculating the probability of corrosion during a certain "Service period" for the given concrete structure in the given environment [23]. For such a calculation, a special software (DURACON) is applied, where the following input parameters are needed [24]: a) environmental loading: chloride loading (CS), age at chloride loading (t´) and temperature (T), b) concrete quality: chloride diffusivity (D), time dependence of the chloride diffusivity (α) and critical chloride content (CCR), c) concrete cover: nominal concrete cover (X). In the DURACON Model, the overall durability requirement is based on the specification of a certain "Service period" before the probability for onset of steel corrosion exceeds an upper serviceability level of 10%, which is in accordance with current standards for reliability of structures. Based on the above calculations, a proper combination of concrete quality and concrete cover can be selected which will meet the specified "Service period".

In South Africa, SLP models for carbonation-induced and chloride-induced corrosion have been developed. The input parameters in these models are empirically related to the South African durability index tests, i.e. the chloride conductivity index (CCI) and oxygen permeability index (OPI). Ballim [25] evaluated the relationship between 28 day OPI values and carbonation depth of 10 month old concrete samples and established a strong correlation between the two. Mackechnie [26] carried out further investigations on this relationship by comparing 28 day OPI values with carbonation depth of cores from concrete samples exposed to outdoor conditions for a period of 1, 4 and 6 years. A strong correlation was observed between OPI and carbonation depth, and based on this relationship, a carbonation prediction model was proposed. Mackechnie and Alexander [27] further developed a chloride ingress model for use in marine environments. This model considers material properties (effect of different binders), construction processes (e.g. curing methods) and environmental processes and their effect on chloride ingress. The model is based on the modified solution to Fick's second law of diffusion. The CCI values were found to have a good correlation with diffusion coefficients when binding effects are taken into account.

4. PRACTICAL EXAMPLES OF THE APPLICATION OF PERFORMANCE-BASED APPROACHES

4.1 IMPLEMENTATION OF THE DURABILITY INDEX PERFORMANCE-BASED APPROACH

The South African durability index performance-based approach has been implemented practically in various infrastructure projects in the country. For structures located inland, a limit OPI value is provided, while for structures in the marine environment, a limit CCI is provided [14]. An assessment of the practical implementation of the DI performance-based specifications was undertaken [28]. In this study, the variability in OPI test values for different sub-projects of a large construction project was determined, and the level of compliance with the set limit value of 9.70 (log scale) was determined. The variability for the OPI results was observed to be high for in situ structures and lower for precast elements - see Figure 1. This indicates that with a proper level of control of construction practices (proper placing, curing and compaction), the required durability properties of a structure can be obtained.

4.2 PERFORMANCE-BASED APPROACH FOR STRUCTURES IN MARINE EXPOSURE

The use of performance testing and predictive models for marine exposure, and validation of this approach using data from a North American marine-exposure site, is provided in Alexander and Thomas [29]. Results from the performance tests were used in the predictive model, and data from the exposure site was collected over a long period of time. The predictive model used was the "apparent-diffusivity model" [30] which is similar to the Life-365 Model [9]. Chloride transport is assumed to be governed by Fick's second law and the initial (28-day) diffusion coefficient, D28, is estimated from the mixture proportions (w/cm) and the type of binder (cementing material). The diffusion coefficient changes with time and is also temperature dependent. Details of these predictive equations are provided in Alexander and Thomas [29].

The algorithms used to predict D28 in the models described above were based on results from "bulk-diffusion tests" such as ASTM C1556 [31] and Nordtest Method NT Build 443 [22]. The bulk diffusion is too time-consuming and laborious to be used as a rapid index for quality control and/or quality assurance for most projects. A number of rapid indices such as the accelerated migration test, e.g. NT Build 492 [21], the rapid chloride permeability test, e.g. ASTM C 1202 [32] and various measures of electrical resistivity (or conductivity) have been found to correlate reasonably well with the results of the bulk-diffusion test [31]. Such tests may offer a suitable substitute to diffusion tests for quality control purposes.

A study from site samples was obtained from Treat Island, which lies off the coast near Eastport, Maine in the US. Studies on this site were established in 1936 by the U.S. Army Corps of Engineers to evaluate the performance of concrete in marine conditions representative of the North Atlantic. In 1978, Malhotra and Bremner [33] commenced an extensive investigation into the durability of concrete containing supplementary cementitious materials (SCM) in a marine environment with the placement of the first series of concrete blocks (305 x 305 x 915 mm) at the mid-tide level at Treat Island. In 2003, a program was launched to retrieve one block from each mixture as it reached the age of 25 years for a comprehensive investigation in the laboratory. It was found that the chloride profiles determined for selected mixtures at 25 years were very similar to the predicted profiles from the diffusivity model developed by Riding [34]; very similar profiles are also produced by Life-365, giving confidence in the use of these prediction models.

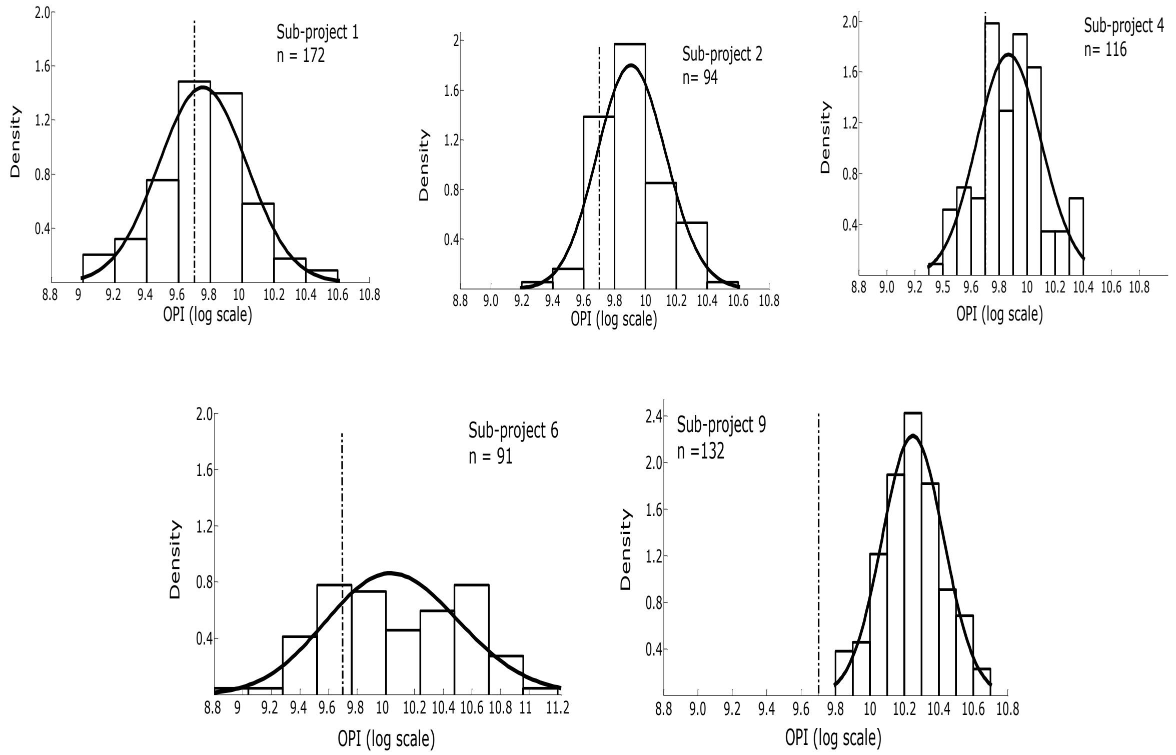

Figure 1 Illustration of variability in OPI values for different sub-projects. Variability is high for in situ structures (sub-projects 1, 2, 4 and 6) and low for precast structures (sub-project 9).

5. DEVELOPMENTS IN CODE APPROACHES FOR SERVICE LIFE MODELLING

A quantitative approach to the design of structures for durability was proposed by Somerville already in 1997, similar to that adopted in structural design [35]. He described it as an 'engineering approach' to durability design, and maintained that there were five aspects to be considered: the predominant deterioration mechanisms which could be quantified using environmental 'loads'; performance criteria for a structure, e.g. notional service life or avoidance of deterioration; prediction models that consider the type and rate of deterioration; factors of safety that consider variability in environmental loads and the precision of models; and lastly specifications and quality assurance systems that verify compliance with the required performance.

Somerville was essentially proposing a 'performance-based' approach to durability design and specification, which should be based on quantitative predictions for durability from exposure conditions and measured material parameters. Such 'quantitative predictions' in effect imply the ability to determine a 'Service life'. The resistance of the structure against deterioration, measured through durability parameters of the actual concrete used, is compared against the environmental load. Deterioration of a structure is quantified using appropriate deterioration models. The concrete properties from a durability perspective are thus critical. What Somerville proposed in 1997 has led to developments in performance-based approaches to durability design and service life quantification, and has also spurred code developments for the same. This is further discussed below.

5.1 LIMIT STATES FOR DURABILITY, AND SERVICE LIFE DESIGN APPROACHES

Walraven suggested that the practical application of a performance-based approach for service life assessment and codification requires the following elements [1]: (i) limit state criteria; (ii) a defined service life; (iii) deterioration models; (iv) compliance tests; (v) a strategy for maintenance and repair; and (vi) quality control systems.

Limit state criteria for concrete durability should be quantifiable, with clear physical meaning. The deterioration models are generally mathematical, and should include parameters that are directly or indirectly linked to the performance criteria.

Different levels of sophistication may be applied to performance-based design for durability, such as use of durability indicators, the application of deterioration models, and full probabilistic approaches. Depending on the sophistication, tools for performance-based design may incorporate service life models with end of service life criteria, and test methods for verifying concrete material properties.

Engineers mostly work to codes of practice, making it essential that any usable approach be codified. Structural codes, which include durability provisions, are often slow in being updated, so that new knowledge from research and practice takes a long time to find its way into the standards. However, as an example of implementation of performance-based durability design, ISO 13823 [36] outlines a limit-state methodology which is related to different service life design approaches.

These ideas from ISO 13823 [36] have been taken up in the 2010 fib Model Code [37], with a number of approaches to durability design, or more broadly service life design. The approaches used are:

- Full probabilistic approach
- Partial safety factor approach
- Deemed-to-satisfy approach
- Avoidance of deterioration approach

The Model Code approach has much merit in moving away from the current simplistic approaches. Note that for many if not the majority of RC structures, a minimalist approach may be adequate – since many structures are not exposed to severe environments that threaten their longevity. For example, EN 206-1 [2] has an exposure category of XO, described as: "Concrete with reinforcement or embedded metal: Very dry", i.e. "Concrete inside buildings with very low air humidity", which represents a large proportion of concrete construction in very mild or benign environments. For such exposures, simple attention to good construction practices, which should include good mix design, compaction and curing, should help to ensure adequate durability.

tab

6. CLOSURE

Durability of reinforced concrete structures most often depends on quality of the concrete cover. This quality depends on material properties and proper execution of construction practices (placing, compaction and curing). In a performance-based approach, service life prediction models are used, where depending on the environmental conditions; measurable properties of concrete cover are obtained. These properties are used in performance specifications where limit values are established and used for the control of quality of the concrete cover.

From the practical examples on implementation of the performance-based approach, it was observed in the first example that the required quality can be obtained where proper execution of construction practices is carried out. The second example illustrates the significance of modelling in predicting the service life of a structure where good correlations were obtained between values from a model and measured chloride profiles on site elements. The application of the performance-based approach should be formalised in codes of practice where different approaches to durability design can be given.

REFERENCES

[1] Neville. 'Consideration of durability of concrete structures: Past, present and future'. Materials and structures. 34(2): 2001,114-118

[2] EN 206-1: 'Concrete - Part 1: Specification, performance, production and conformity'. British Standards Institution. 2013

[3] Bentur and D. Mitchell, 'Material performance lessons'. Cement and concrete research. 38(2): 2008.259-272.

[4] M.G. Richardson, Fundamentals of durable reinforced concrete. First ed. London: Spon Press. 2002

[5] J. Walraven, 'Design for service life: how should it be implemented in future codes', International Conference on Concrete Repair, Rehabilitation and Retrofitting, Proceedings ICCRRR 2008, Cape Town, 24-26 November 2008, pp. 3-10, 2008.

[6] J.G. Kessy, M.G. Alexander and H. Beushausen, "Concrete durability standards: international trends and the South African context". SAICE, Journal of the South African Institution of Civil Engineering, Vol 57 No 1, March 2015, pp. 47–58.

[7] H. Beushausen, and M. G. Alexander, "Application of durability indicators for quality control of concrete members – a practical example". Proceedings of the International RILEM TC-211 PAE Final Conference, Toulouse, June 2009, Bagneux: RILEM Publications S.A.R.L., 2009, 548-555.

[8] M.G. Alexander and M. Santhanam, "Achieving durability in reinforced concrete structures: durability indices, durability design and performance-based specifications", Keynote, International Conferences on Advances in Building Sciences & Rehabilitation and Restoration of Structures, Feb 2013, IIT Madras, Chennai, India, 2012, 21pp.

[9] B.Violetta, 'Life-365 Service life prediction model', Concrete International, 24(12), 2002, pp. 53-57

[10] RILEM TC 230-PSC, "Performance-Based Specifications and Control of Concrete Durability", State-of-the-Art Report. Springer Netherlands, 2016.

[11] J. Bickley, R.D. Hooton, and K.C. Hover, “Preparation of a Performance-based Specification for Cast-in-Place Concrete“. RMC Research Foundation, 2006b

[12] Lobo, L. Lemay, and K. Obla, “Performance-based specifications for concrete“, The Indian Concrete Journal, 79(12), 2005, pp. 13-17

[13] P. Taylor, “Performance-Based Specifications for Concrete“, Concrete International, 8(2004), pp. 91-93.

[14] M.G., Alexander, Y., Ballim, and K., Stanish, “A framework for use of durability indexes in performance-based design and specifications for reinforced concrete structures“. Materials & Structures, 41(5), June 2008, pp. 921-936.

[15] V. Baroghel-Bouny, T. Q. Nguyen, M. Thierry, P. Dangla, and P. Belin, “Evaluation and prediction of reinforced concrete durability by means of durability indicators. Part II: Multi-level predictive modelling“. In International RILEM-JCI seminar on concrete durability and service life planning. K. Kovler, ed. France: RILEM publications S.A.R.L., 2006, pp. 270–280

[16] Andrade, ‘Calculation of initiation and propagation periods of service life of reinforcements by using the electrical resistivity’. In International Symposium: Advances in Concrete through Science and Engineering. Evanston, Northwestern University, USA, 2004. p. 8.

[17] Andrade, C. and R. d’Andrea. “Electrical resistivity as microstructural parameter for modelling of service life of reinforced concrete structures“. In 2nd International symposium on service life design for infrastructure. 2010. pp. 379–388.

[18] R. Torrent, "Exp-Ref: A Simple, Realistic and Robust Method to Assess Service Life of Reinforced Concrete Structures", Concrete 2015, 30 August - 2 September, 2015, Melbourne, Australia

[19] R.J. Torrent, “A two-chamber vacuum cell for measuring the coefficient of permeability to air of the concrete cover on site“. Materials and structures. 25(6):1992, 358-365.

[20] G. van der Wegen, R.G. Polder and K. van Breugel ‘Guideline for service life design of structural concrete - A performance based approach with regard to chloride induced corrosion’. HERON, 57(3), 2012. pp.153–166.

[21] NT Build 492, “Concrete, mortar and cement based repair materials: Chloride migration coefficient from non-steady state migration experiments“, 8pp. Nordtest. Finland. 1999

[22] NT Build 443. ‘Concrete, hardened: Accelerated chloride penetration‘. 5 pp. Nordtest. Finland. 1995

[23] R.M. Ferreira, O.E. Gjørv and S. Jalali “Software for Probability-Based Durability Design of Concrete Structures”, In: B. H. Oh, K. Sakai, O. E. Gjørv and N. Banthia, ed., Proceedings from 4th International Conference on Concrete under Severe Conditions – Environment and Loading, Seoul National University and Korea Concrete Institute, Seoul, 2004, pp. 1015-1024.

[24] O.E. Gjorv, ‘Durability of Concrete Structures’. Arab Journal of Science and Engineering, 36, 2011. pp.151–172.

[25] Y. Ballim, ‘Towards an early-age index for the durability of concrete‘. International Conference Concrete 2000 Economic and Durable Construction through excellence. Dhir, R.K. and Jones, M.R., Ed. London: E & FN SPON. 1993. 1003-1012.

[26] J.R. Mackechnie, ‘Prediction of carbonation in concrete‘. University of Cape Town, Department of Civil Engineering. 1999

[27] J.R. Mackechnie and M.G. Alexander, ‘A pragmatic prediction model for chloride ingress into concrete‘. 3rd RILEM Workshop on Testing and modelling the chloride ingress into concrete. 9 - 10 September, 2002. C.Andrade and J.Kropp, Ed. France: RILEM. 65-76.

[28] G. Nganga, M.G. Alexander and H. Beushausen, “Practical implementation of the durability index performance-based design approach”. Construction & Building Materials, Published online: 6-May-2013. Construction and Building Materials. Vol 45 .2013. pp. 251-261.

[29] M. Alexander and M. Thomas, “Service Life Prediction and Performance Testing – Current Developments and Practical Applications”. Cement & Concrete Research, Vol 78, 2015, pp. 155-164.

[30] K. Riding, M.D.A. Thomas, and K.J. Folliard, “Apparent Diffusivity Model for Concrete Containing Supplementary Cementitious Materials“, ACI Materials Journal, 110(6), November-December 2013, pp. 705-714.

[31] ASTM C1556, “Standard Test Method for Determining the Apparent Chloride Diffusion Coefficient of Cementitious Mixtures by Bulk Diffusion.” American Society for Testing and Materials, West Conshohocken, PA. 2005.

[32] ASTM C1202, “Standard test method for electrical indication of concrete's ability to resist chloride ion penetration“ American Society for Testing and Materials, West Conshohocken, PA. 2005.

[33] V. Malhotra, and T. Bremner, “Performance of Concrete at Treat Island, USA: CANMET Investigations”, Performance of Concrete in Marine Environment, Third CANMET/ACI International Conference SP-163, St. Andrews by-the-Sea, Canada, 1996, pp. 1-52.

[34] K. Riding, “Early Age Concrete Thermal Stress Measurement and Modeling“, PhD Dissertation, the University of Texas at Austin, Austin, TX, 2007.

[35] G. Somerville, “Engineering design and service life: a framework for the future“. In Prediction of concrete durability: Proceedings of STATS 21st Anniversary Conference. Glanville, J.A.N., Ed. London. E & FN SPON 58-76, 1997

[36] ISO 13823-1, “General Principles on the design of structures for durability“. Geneva. International Organization for Standardization, 2008.

[37] fib Model Code. “Model code for concrete structures“, Ernst & Sohn, 402 p. 2010.

TOPIC 1.

Innovation in materials technology

Inovacije u tehnologiji materijala

ECO-CONSTRUCTION MATERIALS THROUGH INNOVATIVE USES OF CO_2

Zhenjun Tu[1], Caijun Shi[1], Xiaoying Pan[1], Jianlan Zheng[2]

[1] College of Civil Engineering, Hunan University, Changsha, Hunan, 410082, China,
email: cshi@hnu.edu.cn, xiaoyingpan@hnu.edu.cn
[2] School of Engineering, Fujian Jiangxia University, Fuzhou, Fujian, 350116, China, email: jianlan@fzu.edu.cn

SUMMARY: Carbon capture, storage and utilization are recently receiving strong attention world widely due to its potential environmental and socio-economic negative consequences. This paper summarizes the innovative uses of CO_2 for the curing of concrete products, surface treatment of concrete and performance enhancement of recycled concrete aggregates. Using carbon dioxide for concrete curing, surface treatment and performance enhancement was essentially based on the chemical reactions between CO_2 and cement particles in the presence of water or water evapour. This technology can be used to replace steam curing to produce environmentally-friendly concrete with rapid curing, desirable mechanical properties, good dimensional stability, low energy consumption, CO_2 capture and store in the uphill battle of combating climate change. CO_2 curing treatment can be used to improve the properties of recycled concrete aggregates (RCAs) so as to get better quality concrete made with RCAs. Through this treatment process, CO_2 can be captured and recycled aggregates can be produced with good performance due to the formation of calcite and silica gel resulting from the reaction between carbon dioxide with calcium hydroxide and calcium silicate hydrate. Moreover, compared with the mortars made of un-carbonated recycled concrete aggregates (RCAs), the mortars made with carbonated RCAs showed reduced water absorption and chloride migration coefficient. CO_2 surface treatment can increase the compressive strength, and effectively reduce the water absorption and chloride migration of cement mortars at one day age. Lower Ca/Si ratio and calcite-rich products in the carbonated surface layer was responsible for the performance enhancement.

EKOLOŠKI GRAĐEVNI MATERIJALI UZ INOVATIVNU PRIMJENU CO_2

SAŽETAK: Danas se širom svijeta velika pozornost polaže na prikupljanje, spremanje i upotrebu ugljika zbog njegovih mogućih negativnih posljedica na okoliš i društveno-gospodarske odnose. U radu su prikazane inovativne upotrebe CO_2 za njegu betonskih proizvoda, površinsku obradu betona i poboljšanje svojstava recikliranog betonskog agregata. Upotreba ugljičnoga dioksida za njegu betona, površinsku obradu i poboljšanje svojstava zasniva se u biti na kemijskog reakciji CO_2 i čestica cementa uz prisutnost vode ili vodene pare. Ta se tehnologija može primijeniti kao zamjena njege parom kako bi se proizveo beton prikadan za okoliš uz brzu njegu, poželjna mehanička svojstva, dobru dimenzijsku stabilnost i malu potrošnju energije, prikupljanjem CO_2 u napornoj bitci s klimatskim promjenama. Njega uz pomoć CO_2 može se upotrijebiti za poboljšanje svojstava oporabljenog betonskog agregata i dobivanje bolje kvalitete betona s tim agregatom. U tom se procesu CO_2 može prikupiti a reciklirani agregat može se proizvesti s dobrim svojstvima zbog formiranja kalcita i silicijskog gela koji nastaju iz reakcije ugljičnoga dioksida s kalcijevim hidroksidom i kalcijevim silikatnim hidratom. Štoviše, u usporedbi s mortovima pripremljenim s nekarbonatiziranim recikliranim betonskim agregatom, mortovi izrađeni s karbonatiziranim recikliranim agregatom pokazali su smanjenu apsorpciju vode i koeficijent migracije klorida. Obrada površina pomoću CO_2 može povećati tlačnu čvrstoću i učinkovito smanjiti apsorpciju vode i migraciju klorida u cementnim mortovima starim jedan dan. Manji omjer Ca/Si i proizvodi bogati kalcitom u karbonatiziranom površinskom sloju imaju učinak poboljšanja svojstava.

1. INTRODUCTION

In 2015, the United Nations Framework Convention on Climate Change was signed by over 200 countries, agreeing in principle to hold the increase in global average temperature below 2oC above pre-industrial levels of less than 2 oC in this century, and that Parties should take urgent action to meet this long-term goal. Thus, carbon capture, storage and utilization are receiving strong attention world widely [1]. Since the cement industry contributes to about 7% of the total global CO_2 emissions [2, 3], innovative development is required to promote more effective use of CO_2 in cement industry. CO_2 curing as a fast curing technology for eco-efficient concrete blocks may hold the key to capturing and storing CO_2 emissions from cement industry for the production of value-added concrete products [4, 5].

Using carbon dioxide for concrete curing which was based on the chemical reactions between CO_2 and the main silicate phases, such as tricalcium silicate and dicalcium silicate, in the presence of water or water vapor. Castellote et al. [6] observed that the amount of C3S and C2S decreased due to these constituents with CO_2 in the presence of water or water vapor. This is because the formation of hydration products was rare within a short time of hydration prior to carbonation. Similar results were reported by Kashef-Haghighi et al. [7] in which only approximately 14% of

C3S and 25% of C3A were transformed to CH, C-S-H and AFt after 4 h of hydration. CO_2 curing technique was beneficial to many aspects of the cured concrete blocks, such as rapid compressive strength development [8-10], considerable sequestration of CO_2 [11, 12] and improved dimensional stability [13].

Surface treatment is one of the effective protection methods to improve the durability of concrete [14-16]. It has been widely used for marine structures and bridge decks. The most common commercial surface treatment techniques include polymer coatings and hydrophobic impregnation. Calcium carbonate precipitation has been adopted recently for concrete surface treatment due to its good stability. CO_2 surface treatment based on the fact that CO_2 can react with dry cement particles and generates calcium carbonate, which may engender important changes of microstructure, such as porosity, pore size distribution, connectivity, etc., and hence significant changes transport properties of cement-based materials [17, 18]. This presentation investigated the effects of CO_2 surface treatment on properties of cement mortars at one day age, including the changes of precipitated calcium carbonate, compressive strength, water absorption and chloride migration coefficient of cement-based materials by CO_2 surface treatment.

With rapid development of economy and construction of infrastructure, many construction and demolition (C & D) wastes are generated and need to be reused. However, it needs to improve the properties of RCAs so as to get better quality concrete made with RCAs. With CO_2 curing treatment of recycled concrete aggregates, CO_2 can be captured and reused, and recycled aggregates can be produced with good performance [19]. Hydration products in hardened cement pastes and concrete, such as Ca(OH)2, calcium silicate hydrate (C-S-H), ettringite (AFt) and monosulphate (AFm) can react with CO_2 as follows [20-22]:

$$Ca(OH)_2+CO_2 \rightarrow CaCO_3+H_2O \tag{1}$$

$$C\text{-}S\text{-}H+CO_2 \rightarrow CaCO_3+SiO_2\ nH_2O \tag{2}$$

$$\begin{gathered} 3CaO\ Al_2O_3\ 3CaSO_4\ 32H_2O+3CO_2 \\ \rightarrow Al_2O_3\ xH_2O+3CaCO_3+3(CaSO_4\ 2H_2O)+(26-x)\ H_2O \end{gathered} \tag{3}$$

$$\begin{gathered} 3CaO\ Al_2O_3\ CaSO_4\ 18H_2O+3CO_2 \\ \rightarrow Al2O_3\ xH_2O+CaSO_4\ 2H_2O+3CaCO_3+(16-x)\ H_2O \end{gathered} \tag{4}$$

The carbonation of calcium hydroxide and C-S-H increased the solid volume by 11.5% and 23.1%, respectively. Thus, carbonation can reduce the porosity of the adhered mortar [20]. This work attempted to improve the quality of RCAs through carbonation of the attached cement paste.

2. USE OF CO2 AS A FAST CURING AGENT FOR CONCRETE BLOCKS

2.1. COMPRESSIVE STRENGTH

Figure 1 shows the compressive strength development of the concrete blocks after CO_2 curing, and steam-cured samples were tested for comparison. It can be seen from Figure 1 that the concrete samples after CO_2 curing displayed almost similar strength to that of steam-cured ones. This means that no significant different in strength between the CO_2-cured and the steam-cured blocks. Furthermore, as shown in Fig.1, the strength of blocks after CO_2 curing continued to develop in a moist environment, which was similar to the steam-cured blocks. It was suggested that carbonation may not hinder the further hydration of calcium silicates and thus allow the carbonated concrete to gain more strength during subsequent moist curing process, which was perhaps due to the formation of C-S-H gel and ettringite crystals resulting from the uncarbonated or partially carbonated cement particles [23].

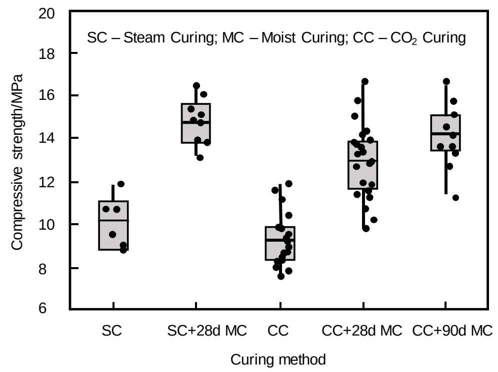

Figure 1 Compressive strength development of the concrete blocks after steam and CO_2 curing [13]

2.2. CO_2 CURING DEGREE

CO_2 curing technique are generally used for dry plain concrete because the diffusion rate of CO_2 in saturated capillary pores is about 10,000 times slower than that in unsaturated capillary pores [24]. So, it was no doubt that the water-to-binder ratio had a very important factor that influenced the CO_2 curing of concrete blocks. Since concrete needs a water-to-cement ratio of 0.35~0.6 to facilitate the mixing and to maintain its workability [9], pre-conditioning before CO_2 curing was necessary for CO2 curing of concrete [9, 10, 13]. Selection and optimization of pre-conditioning curing conditions (e.g. relative humidity and temperature) is a critical step for the production of carbonated concrete with high CO_2 consumption and excellent properties [9]. Figure 2 shows the effect of pre-conditioning time on CO_2 curing degree of concrete samples pre-conditioned in both dry environment (T = 22 ± 3°C, RH = 55 ± 10%) and moist environment (T = 22 ± 3°C, RH > 95%). It can be seen from Fig.2 that, under the dry environment, the CO_2 curing degree of concrete sharply increased with the pre-conditioning time within 4 h of pre-conditioning. However, under the moist environment, the CO_2 curing degree of the concrete decreased with the increase of the pre-conditioning time (Figure 2).

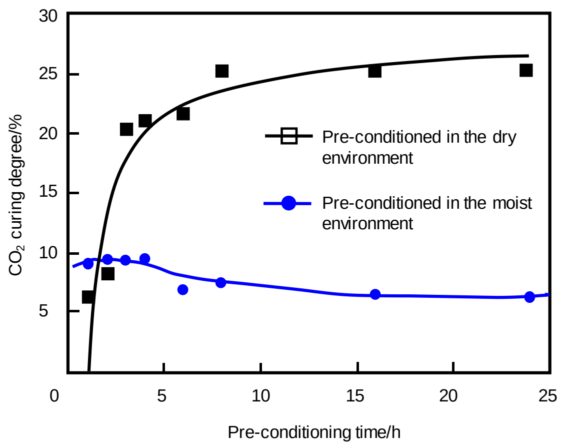

Figure 2 Effect of pre-conditioning time on CO_2 curing degree of concrete [25]

2.3. DIMENSIONAL STABILITY

Dimensional stability is one of the most important weathering properties of CO2 cured concrete blocks. Figure 3 shows the drying shrinkage of CO2-cured concrete blocks after 180 days of winter weathering exposure and compared it with those of steam curing. It can be seen that the CO2 curing treatment can decrease the drying shrinkage of concrete blocks, and thus improve the dimensional stability of concrete [13]. The CO2-cured cement mortar had excellent dimensional stability was due to significant productions of CaCO3, which is a well crystallized product and exhibits a better dimensional stability than the main hydration products, C-S-H, in steam-cured concrete blocks [26].

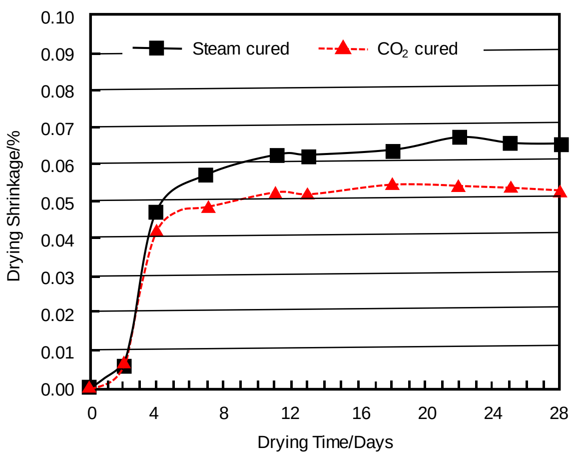

Figure 3 Drying shrinkage of concrete blocks after 180 days of winter weathering exposure [13]

3. USE OF CO_2 FOR PERFORMANCE ENHANCEMENT OF RECYCLED CONCRETE AGGREGATES

3.1. EFFECT OF CO_2 TREATMENT ON PHYSICAL PROPERTIES OF RECYCLED CONCRETE AGGREGATES

The physical properites of recycled concrete aggregates (RCAs) before and after CO2 treatement were given in Table 1. The recycled gravel concrete aggregate (G-RCA) was retrieved from concrete beams with the compressive strength of 30MPa, and the recycled crushed stone concrete aggregate (C-RCA) was retrieved from concrete beams with the compressive strength of 50MPa. G-CI and R-CI represented the carbonated recycled gravel concrete aggregate and carbonated recycled crushed stone concrete aggregate, respectively. It can be seen from Table 1 that the apparent density of both RCAs increased after CO2 teatment, and the water absorption and crushing value decreased significantly. As mention in previous section, carbon dioxide reacts with the hydration products and unhydrate cement particles to form calcium carbonate and silica gel, which fill the capillary pores in the hardened cement paste.

Table 1 Physical properties of recycled concrete aggregates before and after CO_2 treatment [27]

Physical properties	Un-carbonated aggregate		Carbonated aggregate	
	G-RCA	C-RCA	G-CI	R-CI
Water absorption (%)	8.06	8.70	5.78	6.73
Apparent density (kg/m3)	2.53	2.49	2.65	2.63
Crushing value (%)	18.6	17.1	16.9	15.8

3.2. COMPRESSIVE STRENGTH

Figure 4 provides the compressive strength of the hardened mortar samples. It can be seen from Fig.4 that the compressive strength of the recycled aggregate mortars was lower than the natural sand mortars at all ages. After CO_2 treatment, the compressive strength significantly increased at all ages for all the mortars. It was notice that the strengths of carbonated recycled aggregate mortars were more close to the natural sand mortars, indicating that carbonation improved both physical and mechanical properties of the recycled aggregates.

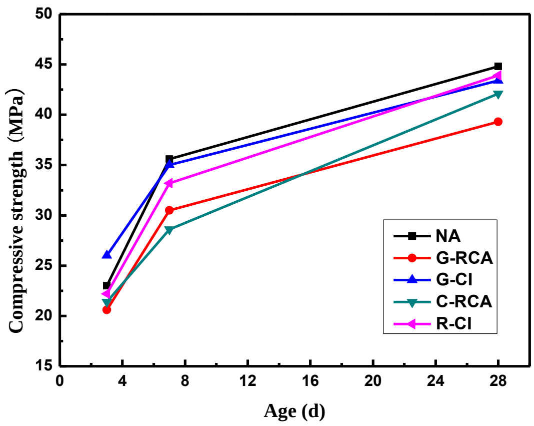

Figure 4 Effect of carbonation treatment of recycled concrete sands on compressive strength [27]

3.3. CHLORIDE DIFFUSION COEFFICIENT OF RECYCLED AGGREGATE MORTAR

Table 2 presented the results of chloride diffusion coefficient from rapid chloride migration tests. It was found that the poor ITZ and high porosity of the recycled aggregates caused the mortars unable to resistant chloride effectively [28]. After carbonation treatment, the chloride diffusion resistance was increased for all the mortars, which might be due to the increase of the density of the attached paste and the original ITZ. For example, the chloride diffusion coefficient of the G-CI and C-CI mortar was 11 and 6 times lower than their corresponding un-carbonated mortars respectively.

Table 2 Chloride diffusion coefficient of mortars (10-12 m/s^2) [27]

Sand-cement ratio	Un-carbonated mortar		Carbonated mortar	
	G-RCA	C-RCA	G-CI	C-CI
2.25	18.8	14.7	1.7	2.1

4. USE OF CO_2 FOR SURFACE TREATMENT OF CONCRETE

4.1. PRECIPITATED CALCIUM CARBONATE CONTENT AT DIFFERENT DEPTHS

To understand how the CO_2 treatment influences the early-age cement mortars, the amount of $CaCO_3$ in the outer layer ranged from 0 to 2.0 mm was measured by an interval of 0.2 mm as shown in Figure 5. As expected, CO_2 surface treatment resulted in the increase of $CaCO_3$ contents for Series 0.4 and 0.3 carbonated samples were found in 0.2 mm surface layer. For a given depth, a higher content of CaCO3 was measured in the w/c = 0.4 sample, probably due to its larger pores, allowing CO_2 to penetrate more easily into the inner parts for carbonation. It was clear that the content of $CaCO_3$ decreased with the increase of depth, indicating that the CO_2 treatment on the early-age mortars only occurred in the surface layer with maximum depth of 2.0 mm, depending on the w/c ratio. Thus, influence depth of CO_2 surface treatment might not cause great damage on cover layer of the reinforced steel bars [20, 29]. The reacted depth of CO_2 surface treatment increased with the prolongation of treatment time period and w/c ratio. The influence depth of 3 h and 6 h CO_2 surface treatment on cement mortar with w/c = 0.4 were 1.0 mm and1.6 mm respectively. For cement mortar with w/c = 0.3, the influence depth of 3 h and 6 h CO_2 surface treatment were 0.8 mm and1.2 mm.

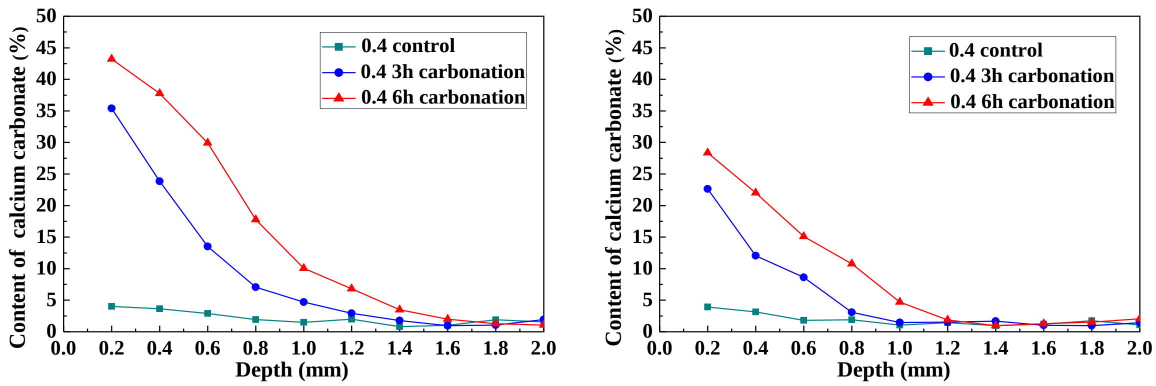

(a) w/c = 0.4 (b) w/c = 0.3

Figure 5 Effect of CO_2 surface treatment on $CaCO_3$ content at different depths in surface layers[30]

4.2. COMPRESSIVE STRENGTH

Figure 6 shows the influence of CO_2 surface treatment on the compressive strength of cement mortars. After CO_2 surface treatment, the compressive strength of all the mortars increased significantly as compared with the corresponding uncarbonated ones. For both series of cement mortars, the strength increased with the increase of treatment time. The increase in strength probably results from the higher strength and elasticity modulus of $CaCO_3$ than those of C-S-H [31]. It is obvious that CO_2 surface treatment had greater effect on the compressive strength of series 0.4 than that of series 0.3.

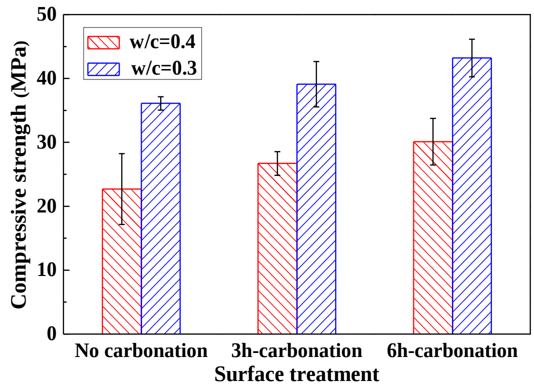

Figure 6 Effect of CO_2 surface treatment on compressive strength of cement mortars [30]

4.3. CHLORIDE MIGRATION COEFFICIENT

Figure 7 presents the results of RCM coefficient of mortars without and with surface treatment cement. It was obviously that the RCM coefficient of mortars decreased after CO_2 surface treatment and continued to decrease with treat time. As previously discussed, the CO_2 treatment could reduce the pore voids and consequently reduced the total porosity of the surface layer upon carbonation. However, the CO_2 surface treatment had effects on very limited surface layer, but greatly reduced the diffusion of chloride ions.

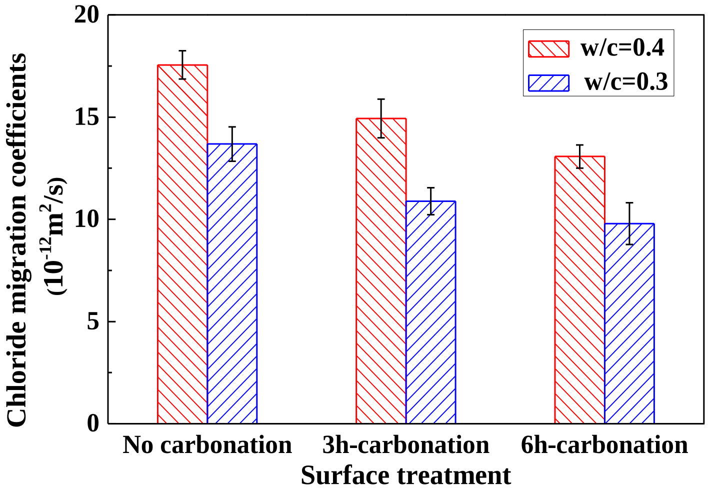

Figure 7 Effects of CO_2 surface treatment on the chloride migration coefficient of cement mortars [30]

5. CONCLUSIONS

CO_2 curing can be used to produce Eco-construction materials with environmentally-friendly, low energy consumption, CO_2 capture and store in the uphill battle of combating climate change. The main conclusions drawn from this study are:

1) CO_2 curing as a fast curing technique for concrete blocks was beneficial to many aspects of the cured concrete blocks, such as rapid compressive strength development, considerable sequestration of CO_2 and improved dimensional stability.

2) During CO_2 curing treatment process, carbon dioxide reacted with calcium hydroxide and calcium silicate hydrate to form calcite and silica gel, which filled the pores in the attached cement paste. Compared with the mortars made of un-carbonated RCAs, the mortars made with carbonated RCAs showed decreased water absorption, and chloride migration coefficient.

3) CO_2 surface treatment can increase the compressive strength, and effectively reduce the water absorption and chloride migration of cement mortars at one day age perhaps due to the produced lower Ca/Si ratio and calcite-rich products in the carbonated surface layer, which resulting in the performance enhancement of cement-based materials.

ACKNOWLEDGEMENT

The authors would like to acknowledge the financial supports from Specialized Research Fund for the Doctoral Program of Higher Education (SRFDP) (20130161110019) and National Natural Science Foundation of China under contract U1605242.

REFERENCES

[1] Olajire, A.A.: A review of mineral carbonation technology in sequestration of CO2. Journal of Petroleum Science and Engineering, Vol. 109 (2013), pp.364-392

[2] Zhang, J.K. et al.: Performance Enhancement of Recycled Concrete Aggregates through Carbonation. Journal of Materials In Civil Engineering, Vol. 27 (2015) No. 11, pp. 04015029

[3] Shi, C. et al.: New cements for the 21st century: the pursuit of an alternative to Portland cement. Cement and Concrete Research, Vol. 41 (2011) No. 7, pp. 750-763

[4] Kashef-Haghighi, S. and S. Ghoshal: Physico-chemical processes limiting CO2 uptake in concrete during accelerated carbonation curing. Industrial & Engineering Chemistry Research, Vol. 52 (2013) No. 16, pp. 5529-5537
[5] Hossain, M.U. et al.: Evaluation of environmental friendliness of concrete paving eco-blocks using LCA approach. The International Journal of Life Cycle Assessment, Vol. 21 (2016) No. 1, pp. 70-84
[6] Castellote, M., et al.: Chemical changes and phase analysis of OPC pastes carbonated at different CO2 concentrations. Materials and Structures, Vol. 42 (2009) No. 4, pp. 515-525
[7] Kashef-Haghighi, S. et al.: Mathematical modeling of CO2 uptake by concrete during accelerated carbonation curing. Cement and Concrete Research, Vol. 67 (2015) No. 0, pp. 1-10
[8] Shi, C.J., et al.: Factors affecting kinetics of CO2 curing of concrete. Journal of Sustainable Cement-Based Materials, Vol. 1 (2012) No. 1-2, pp. 24-33
[9] Shi, C.J. et al: Effect of pre-conditioning on CO2 curing of lightweight concrete blocks mixtures. Construction and Building Materials, Vol. 26 (2012) No. 1, pp. 257-267
[10] Shi, C.J. and Y.Z. Wu: Studies on some factors affecting CO2 curing of lightweight concrete products. Resources Conservation and Recycling, Vol. 52 (2008) No. 8-9, pp. 1087-1092
[11] Goodbrake, C.J. et al: Reaction of beta-dicalcium silicate and tricalcium silicate with carbon-dioxide and water-vapor. Journal of the American Ceramic Society, Vol. 62 (1979) No. 3-4, pp. 168-171
[12] Goodbrake, C.J. et al: Reaction Of Hydraulic Calcium Silicates with Carbon-Dioxide And Water. Journal Of the American Ceramic Society, Vol. 62 (1979) No. 9-10, pp. 488-491
[13] Shi, C.J., et al.: Weathering properties of CO2-cured concrete blocks. Resources, Conservation and Recycling, Vol. 65 (2012), pp. 11-17
[14] Basheer, P.A.M., et al.: Surface treatments for concrete: assessment methods and reported performance. Construction and Building Materials, Vol. 11 (1997) No. 7, pp. 413-429
[15] Jia L, et al.: Effects of inorganic surface treatment on water permeability of cement-based materials. Cement & Concrete Composites, Vol. 67 (2016), pp. 85-92
[16] Pan X, et al: Effect of inorganic surface treatment on air permeability of cement-based materials. Journal of Materials In Civil Engineering, Vol. 28 (2015) No. 3, pp. 04015145
[17] Morandeau, A et al.: Investigation of the carbonation mechanism of CH and CSH in terms of kinetics, microstructure changes and moisture properties. Cement and Concrete Research, Vol. 56 (2014), pp. 153-170
[18] De Belie, N et al.: Influence of pozzolans and slag on the microstructure of partially carbonated cement paste by means of water vapour and nitrogen sorption experiments and BET calculations. Cement and Concrete Research, Vol. 40 (2010) No. 12, pp. 1723-1733
[19] Shi, C. et al.: Performance enhancement of recycled concrete aggregate–a review, Journal of Cleaner Production, Vol.112 (2016), pp.466-472
[20] Thiery, M. et al: Investigation of the carbonation front shape on cementitious materials: Effects of the chemical kinetics. Cement and Concrete Research, Vol. 37 (2007) No. 7, pp. 1047-1058
[21] de Juan, M.S.; Gutiérrez, P.A.: Study on the influence of attached mortar content on the properties of recycled concrete aggregate. Construction and Building Materials, Vol. 23 (2009) No. 2, pp. 872-877
[22] Šauman, Z.: Carbonization of porous concrete and its main binding components. Cement and Concrete Research, Vol. 1 (1971) No. 6, pp. 645-662
[23] He, P.P. et al.: Effect of further water curing on compressive strength and microstructure of CO2-cured concrete. Cement and Concrete Composites, Vol. 72 (2016), pp. 80-88
[24] He, P.: The effect of subsequent moist curing on the hydration of cement in concrete after CO2 curing, Hunan University,Changsha, (2014)
[25] ZOU, Q.Y et al.: Effect of pre-conditioning on CO2 curing of block concretes. Journal of the Chinese Ceramic Society, Vol.11 (2008) No. 1, pp. 116-120
[26] Shi, C.J. and Y.Z. Wu: CO2 curing of concrete blocks-research toward greener production. Concrete international, Vol. 31 (2009) No. 02, pp. 38-43
[27] Zhang, J. et al.: Influence of carbonated recycled concrete aggregate on properties of cement mortar. Construction and Building Materials, Vol. 98 (2015) No. 15, pp. 1-7
[28] Song, H. et al.: Factors influencing chloride transport in concrete structures exposed to marine environments. Cement & Concrete Composites, Vol. 30 (2008) No. 2, pp. 113-121
[29] Villain G et al.: Measurement methods of carbonation profiles in concrete: thermogravimetry, chemical analysis and gammadensimetry. Cement and Concrete Research, Vol. 37 (2007) No. 8, pp. 1182-1192
[30] Pan, X. et al.: Effects of CO2 surface treatment on strength and permeability of one- day-aged cement mortar (Under review). Construction and Building Materials, (2017)
[31] Xiao J et al.: Experimental study on strength and ductility of carbonated concrete elements. Construction and Building Materials, Vol. 16 (2002) No. 3, pp. 187-192

ENVIRONMENTAL IMPACT OF CARBONATED CALCIUM SILICATE CEMENT-BASED CONCRETE

Nicholas DeCristofaro[1], Vincent Meyer[2], Sada Sahu[1], Jason Bryant[1], Fabrizio Moro[2]

[1] Solidia Technologies, 11 Colonial Drive, Piscataway, NJ 08854, USA, email: ndecristofaro@solidiatech.com, ssahu@solidiatech.com, jbryant@solidiatech.com
[2] LafargeHolcim Research Centre, 95, rue du Montmurier, BP 15, 38291 Saint-Quentin Fallavier, France,
email: vincent.meyer@lafargeholcim.com, fabrizio.moro@lafargeholcim.com

SUMMARY: Solidia Technologies and LafargeHolcim have collaborated on the development and commercialization of an innovative process allowing mineral sequestration of CO_2 through the carbonation of calcium silicate-based cement (CSC). In advancing international efforts to meet CO_2 emissions reduction goals, the success of this technology is predicated on three major components: (1) the extent of CO_2 emission reductions in cement manufacturing, (2) the capacity of CSC materials to efficiently store CO_2 during concrete curing, and (3) wide-scale adoption of this technology within the concrete industry. The potential for emissions reductions and CO_2 storage have already been demonstrated. The production of CSC, as a replacement for Portland cement (PC), can reduce CO_2 emissions at a cement plant by decreasing energy and limestone consumption. Reductions in CO_2 emissions up to 30% (~250 kg per tonne of cement clinker) have been predicted and measured. CSC carbonation during the curing of concrete occurs extremely rapidly. Full hardness in CSC-based concretes can be achieved within 24 hours, during which CO_2 is permanently and safely sequestered in the form of calcium carbonate. Sequestration of up to 300 kg of CO_2 per tonne of CSC in the concrete have been predicted and measured. Taken together, these two factors enable the CO_2 footprint associated with the production and use of cement to be reduced by up to 70%.

KORIST ZA OKOLIŠ OD SUSTAVA OSNOVANIH NA KARBONATIZIRANOM KALCIJ-SILIKATU

SAŽETAK: Tvrtke Solidia Technologies i LafargeHolcim surađivale su na razvoju i komercijalizaciji inovativnog procesa koji omogućuje daljnje vezivanje CO_2 putem karbonatizacije cementa na osnovi kalcij-silikata (engl. CSC). U međunarodnim naporima postizanja smanjenja emisije CO_2 uspjeh ove tehnologije određen je trima glavnim komponentama: (1) količinom smanjenja CO_2 u proizvodnji cementa, (2) sposobnošću CSC materijala da učinkovito zadrže CO_2 tijekom njege betona i (3) općim usvajanjem te tehnologije u industriji betona. Potencijal smanjenja emisije CO_2 i njegova daljnjeg vezivanja već su dokazani. Proizvodnja CSC-a kao zamjene portlandskog cementa može smanjiti emisiju CO_2 već u tvornici cementa smanjenjem energije i potrošnjom vapnenca. Predviđena su i izmjerena smanjenja emisije CO_2 do 30 % (oko 250 kg po toni cementnog klinkera). Karbonatizacija CSC-a tijekom njege betona nastupa izuzetno brzo. Puno očvršćivanje betona na osnovi CSC-a može se postići unutar 24 sata, a tijekom tog vremena CO_2 je stalno i sigurno vezan u obliku kalcijskog karbonata. Predviđeno je i izmjereno vezivanje do 300 kg CO_2 po toni CSC-a u betonu. Uzevši zajedno, ta dva faktora omogućuju da se količina CO_2 povezana s proizvodnjom i upotrebom cementa smanji do 70 %.

1. INTRODUCTION

Concrete is the most consumed man-made material in the world. A typical concrete is made by mixing Portland cement (PC), water, and aggregate (e.g., sand and crushed stone). PC is a synthetic material made by burning a mixture of ground limestone, clay and corrections materials, or materials of similar composition, in a rotary kiln at a sintering temperature of 1450°C. PC manufacturing releases considerable quantities of greenhouse gas (CO_2). The cement industry accounts for approximately 5% of global anthropogenic carbon dioxide (CO_2) emissions.

A modern cement plant releases ~810 kg of CO_2 per tonne of cement clinker produced. More than 60% of this CO_2 comes from the chemical decomposition, or calcination, of limestone ($CaCO_3 \rightarrow CaO + CO_2$). The balance comes from the combustion of fossil fuel to heat the kiln. A small amount of additional CO_2, approximately 90 kg per tonne of cement, is associated with the electricity required to operate the clinkering process, to grind and transport materials throughout the process, and is not considered in this paper.

The International Energy Agency (IEA) has created a roadmap to guide the long-term sustainability efforts of the cement industry. As per this roadmap, the cement industry must reduce its total CO_2 emissions from 2.0 Gt in 2007 to 1.55 Gt by 2050. Nevertheless, over this same period, cement production is projected to grow from 2.6 Gt to 4.4 Gt [1].

With the implementation of energy-efficient production technologies, the use of alternative fuels, the development of new, low-lime cement chemistries, and the reduction of clinker factor in cement through addition of supplementary cementitious materials, the cement industry has tried to attain the IEA objective. However, even the combined effect of these initiatives is likely to fall far short of the IEA goals.

Solidia Cement™, a new calcium silicate-based cement (CSC) product developed by Solidia Technologies®, is poised to address this unanswered challenge [2,3]. Solidia Cement is a reduced-lime, non-hydraulic calcium silicate cement capable of significantly reducing the energy requirement and CO_2 emissions at the cement plant. The Solidia Cement manufacturing process is adaptable and flexible, allowing it to be produced under a variety of raw materials formulations and production methods across the globe. It offers cement manufacturers considerable savings in CO_2 emissions and energy consumption. Additionally, this CSC cures via a reaction with gaseous CO_2, thus offering the ability to permanently and safely sequester CO_2.

2. ENERGY REQUIREMENTS AND CO_2 EMISSIONS DURING CEMENT MANUFACTURING

Both PC and CSC manufacturing require significant amounts of energy and emit significant quantities of CO_2. Heat energy is needed to dry the raw meal, calcine the limestone, react the oxide components, and form the cement clinker. The electrical energy needed to crush and grind the raw materials, to operate the clinkering process, to comminute the clinker, and to transport materials throughout the process will not be considered in this analysis. To illustrate the benefits associated with the processing of CSC, the differences in energy consumption and CO_2 emissions are discussed below.

2.1. PORTLAND CEMENT

2.1.1. ENERGY REQUIREMENTS

In modern cement plants, the production of one tonne of PC clinker requires heat energy totalling 3.2 GJ [4]. From a theoretical perspective, the thermal energy consumed in producing one tonne of PC clinker is about 1.757 GJ. The breakdown of that enthalpy into the various pyro-processing steps is provided in Table 1 [5]. While the overall process is endothermic, note that the process step in which the cement phases are formed is exothermic. The difference between the actual and theoretical heat requirements is due to heat retained in clinker, heat losses from kiln dust and exit gases, and heat losses from radiation. As can be seen from Table 1, the pyro-processing step that consumes the most heat energy is the endothermic decomposition of calcium carbonate (calcination).

Table 1 Theoretical enthalpy of formation of 1 tonne of clinker. PC clinker values are from [5]; CSC clinker values are based on a model clinker and may vary slightly depending on the phase composition.

Reaction	PC Clinker ΔH (GJ)	CSC Clinker ΔH (GJ)
Calcination	+2.138	+1.514
Decomposition of clay	+0.063	+0.075
Formation of cement phases	-0.377	-0.538
Total	1.757	1.051

2.1.2. CO_2 EMISSIONS

EPA's historical estimates indicate that 900 to 1,100 kg of CO_2 is emitted for every tonne of PC clinker produced in the US. The exact quantity depends on the raw ingredients, fuel type, and the energy efficiency of the cement plant [6]. Even the most efficient Portland cement facilities report CO_2 emission ~810 kg/tonne of clinker [7].

There are three sources of CO_2 emission in cement production:

1. the chemical decomposition of the calcium carbonate within the limestone

2. $CaCO_3 \rightarrow CaO + CO_2$;

3. the combustion of fossil fuel to heat the kiln for pyro-processing the raw meal; and, the generation of electricity needed to drive the kiln, the grinding mills and materials transportation systems.

As stated earlier, the CO_2 associated with the generation of electricity are not considered here.

The CO_2 emissions from chemical decomposition of calcium carbonate depend on the lime content of the clinker product (~70% for PC). The CO_2 emissions from pyro-processing depend on the fossil fuel type (for example, ~3.0 tonnes of CO_2 per tonne of coal consumed). The carbon footprint from electricity consumption for cement production is about 90 kg/tonne in the US. Table 2 compares the sources of CO_2 emission in the production of cement clinker.

2.2. CALCIUM SILICATE CEMENT

2.2.1. ENERGY REQUIREMENTS

The total lime content of CSC clinker is in the range of 45-50 wt.%, representing approximately a 30% reduction from that required for PC. This reduction in lime concentration translates directly into a 30% reduction in the major component of the theoretical enthalpy, i.e., the calcination step. CSC and PC are roughly equivalent in terms of the enthalpy required to decompose the clay component of the raw meal and the exothermic reaction associated with the formation of the cement phases. Dominated by the large difference in calcination step, the total enthalpy of formation of CSC clinker is expected to be about 1.051 GJ/t, almost 40% lower than that of PC clinker (see Table 1).

From a practical perspective, CSC clinker is burned at temperatures approximately 200°C lower than those used in PC manufacturing, and with the potential for significantly reduced system-wide heat losses than that experienced in PC manufacturing. This is expected to translate into a reduction in fossil fuel consumption by as much as 30%. This may translate into additional savings in the electrical energy required for clinker grinding.

2.2.2. CO_2 EMISSIONS

The unique, low-lime content of CSC clinker enables two separate opportunities to reduce the CO_2 emissions associated with cement production.

The first opportunity can be traced to the chemical decomposition of the calcium carbonate in limestone. Reduction in the lime content of the cement from approximately 70% (for PC) to approximately 50% (for CSC) enables a proportionate reduction in this form of CO_2 emission. Thus, the CO_2 released from the chemical decomposition of limestone will be reduced from 540 kg per tonne of PC clinker to about 375 kg of CO_2 per tonne of CSC clinker.

The second opportunity, also enabled by the low-lime chemistry of CSC, allows the reaction between lime and silica to occur at a clinker temperature of 1250°C, which is 200°C lower than the temperature required for PC clinker formation. During the production of CSC, the CO_2 emissions associated with the burning of fossil fuel to heat the kiln are expected to be 190 kg per tonne of clinker, compared to 270 kg per tonne for PC clinker.

The total CO_2 emissions associated with PC and CSC manufacturing are compared in Table 2. Note that CSC clinker production offers the potential to reduce CO_2 release associated with cement manufacturing by as much as 30%.

Table 2 CO2 emissions during the production of PC and CSC clinker (Note: The CO2 associated with the electrical energy usage in the cement making process is not considered.)

CO_2 emissions from:	Per tonne of PC clinker	Per tonne of CSC clinker
Limestone decomposition	540 kg	375 kg
Fossil fuel combustion	270 kg	190 kg
Total CO_2 emissions	810 kg	565 kg

2.2.3. ENERGY REQUIREMENTS AND CO_2 EMISSIONS DURING PRODUCTION OF SOLIDIA CEMENT CLINKER.

Recently, the first, industrial Solidia Cement production campaign was performed in a North American plant of the LafargeHolcim group. This campaign sought to prove the production feasibility in a modern industrial preheated kiln. Approximately 5000 tonnes of Solidia Cement clinker were produced based on raw materials available in the quarry of the plant. The raw mix was adapted to meet the chemical specifications and the wollastonite (CS) and rankinite (C_3S_2) clinker phases of Solidia Cement. This was accomplished by reducing the limestone content and favouring the silica source

During the production campaign, CO_2 emissions and energy consumption (specific heat consumption) were tracked in order to assess the relevance of the theoretical numbers indicated above. In order to adequately compare the production of PC and Solidia Cement clinker, stable production periods were taken into account for each cement type--not only in the same plant, but in the same kiln. . The measurements, highlighted in Table 3, confirm the predicted energy and CO_2 savings.

In terms of energy, a 20% savings was measured for the specific heat consumption (SHC). This SHC savings is slightly lower than expected because the production rate of Solidia Cement clinker in the kiln was not yet equal to that of PC clinker. It was noted that the Solidia Cement clinker behaviour in the kiln is different than that of PC clinker. Room for considerable improvement in Solidia Cement clinker production remains.

Table 3 Industrial Solidia Cement clinker trial measurements

		PC clinker	Solidia clinker
Period		Normal production	Stable production period
Specific heat consumption (SHC)	GJ/t ck	3.89	3.16
Stack CO_2	%	24.4	14.2
CO_2 emissions	Nm^3/h	25350	15004
CO_2 emissions	Nm^3/t ck	474	334

It should also be noted that the typical plant fuel utilization was modified for the Solidia Cement clinker production. Only the main burner, fed with petcoke, coal and recycled plastic, was used during Solidia Cement production. PC production used the main burner in the same manner, but tires were also fed into the back end of the kiln.

The reduction in CO_2 emissions during Solidia Cement clinker production is in accordance with expected values. Measurements at the stack of the plant confirmed that conversion from PC production to Solidia Cement production resulted in CO_2 emission savings of more than 30%.

In conclusion, measured reductions in the SHC and CO_2 emissions during the first industrial Solidia Cement clinker production campaign match predictions. Further improvements of these parameters are expected as clinker production is optimized.

3. CONCRETE MIXING, FORMING AND CURING PROCESSES

PC- and CSC-based concretes are manufactured using the same basic mixing and forming processes. Concrete production typically begins by mixing the dry (cement, sand and crushed stone) and the liquid (water and chemical additives) components of the concrete. The water and chemical additive control the flow behavior of the concrete mix while it is in the plastic stage.

Both PC- and CSC-based concretes can be mixed in standard concrete mixers. Similarly, they can be formed into the final concrete part shape by the same processes and equipment. These processes include casting, extrusion, rolling and pressing.

PC- and CSC-based concrete differ in the chemical process by which they set and harden. These processes are collectively referred to as “curing.”

3.1. PC-BASED CONCRETE CURING

When PC is exposed to water, a series of hydration reactions initiate with a release of a significant amount of heat. These hydration reactions are responsible for the setting and hardening of PC-based concrete. In a very simplistic way, the curing process involves reactions between:

- C_3A, gypsum and water, to produce ettringite;
- C_3S and water, to produce a complex calcium silicate hydrate and calcium hydroxide; and,
- C_2S and water, which also yields calcium silicate hydrate and calcium hydroxide.

The complex calcium silicate hydrate is an amorphous phase wherein the Ca:Si ratio can vary during the hydration period.

The hydration of the calcium silicate components of Portland cement begins as soon as the PC is exposed to water, but proceeds at a relatively slow pace. The maturity of PC-based concrete is only reached after up to 28 days, when the required performance is achieved. Under normal curing conditions, and without chemical accelerators, roughly 70% of the cement particles are hydrated.

The microstructure of hydrated PC paste shows that two distinct types of calcium silicate hydrate form in the system: an “inner product” and an “outer product.” The outer product forms early in the curing process, is highly porous, and precipitates in the open spaces within the concrete structure. The inner product forms late in the curing process, is denser than the outer product, and forms near the original cement particles.

3.2. CALCIUM SILICATE CEMENT-BASED CONCRETE CURING

The low-lime, CS and C_3S_2 components of CSC do not hydrate when exposed to water during the concrete mixing and forming processes. Formed CSC-based concrete parts will not cure until they are simultaneously exposed to water and gaseous CO_2. CSC-based concrete curing is a mildly exothermic reaction in which the low-lime calcium silicates in the CSC react with CO_2 in the presence of water to produce calcite ($CaCO_3$) and silica (SiO_2) as follows:

$$CaSiO_3 + CO_2 \rightarrow CaCO_3 + SiO_2$$

The above reaction processes require a CO_2-rich atmosphere. However, the process can be conducted at ambient gas pressures and at moderate temperatures (~ 60°C). These parameters are well within the capabilities of most precast concrete manufacturers.

Unlike the hydration reaction in PC-based concrete, the carbonation reaction in CSC-based concrete is a relatively speedy process. Full curing of CSC-based concrete is limited only by the ability of gaseous CO_2 to diffuse throughout the part. Thin concrete products such as roof tiles (~10 mm thick) can be cured in less than 6 hours. Larger concrete parts, such as those in railroad sleepers (~250 mm thick), can be cured within a 24-hour period. This rapid curing process can potentially enhance the productivity of an existing precast operation.

A microstructural evaluation of CSC-based concrete shows the reaction products calcite ($CaCO_3$) and amorphous silica (SiO_2) as well as un-carbonated cement particles. A typical microstructure of CO_2-cured CSC-based concrete is illustrated in Figure 1. The calcite fills the pore space within the concrete, creating a dense microstructure. As the silica is relatively insoluble in the prevailing conditions of the carbonation process, it forms at the outer surface of the reacting cement particle.

Unlike PC-based systems, concrete products hardened with CO_2-cured CSC do not consume water. In fact, up to 90% of the water used in the CSC-based concrete formulation can be recovered during the CO_2-curing process. The remaining water is retained in the cured concrete and may be additionally recovered, if necessary. Assuming a water to cement ratio of 0.4, this implies that, if the 30 billion tons of concrete that was produced in 2011 was cured using CSC in place of PC, them the amount of water consumed or lost during the production of concrete could be reduced from an estimated 2.6 billion tons [8] to 0.45 billion tons.

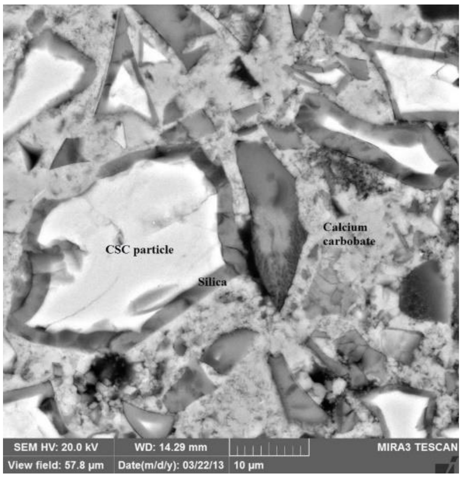

Figure 1: Microstructure of CO_2-cured CSC (light grey area is calcite ($CaCO_3$), dark grey area is amorphous silica (SiO_2), and white area is unreacted CSC ($CaO{\cdot}SiO_2$).)

3.3. CO_2 SEQUESTRATION IN CALCIUM SILICATE CEMENT-BASED CONCRETE

The unique ability of CSC to avoid hydration and cure via a reaction with gaseous CO_2 opens the possibility for the permanent sequestration of CO_2 in cured concrete structures. The curing processes, described in Section 3.2, enables CSC-based concrete to sequester up to 300 kg of CO_2 per tonne of CSC used in the concrete formulation. The CO_2 used in the curing process and captured within CSC-C is industrial-grade CO_2 sourced from waste flue gas streams.

CO_2 sequestration in two fully-cured, CSC-based concrete forms was studied:

- Pavers of dimensions 6 cm thick x 15 cm wide x 23 cm long paver, with a dry concrete formulation of 14.7 wt. % CSC, 41.6 wt. % aggregate, 0.2 wt. % pigment, and 43.5 wt. % sand; and,
- A hollow core slab of dimensions 20 cm thick x 115 cm wide x 10 m long, with a dry concrete formulation of 15 wt. % CSC, 44 wt. % aggregate, and 41 wt. % sand.
- Small core specimens, representative of the overall concrete microstructure, were drilled from the concrete forms and exposed to the procedure described below.

To calculate the amount of CO_2 sequestered within a CSC-based concrete sample, the test specimen is oven dried at 105°C for 72 hours to remove any residual moisture and placed in a furnace at 550°C for 4 hours to remove any remaining bound water or organic material. Once fully dried, the specimen is heated to 950°C at a ramp up rate of 10°C/min. After 3 hours at 950°C, the specimen is returned to 105°C and mass loss was recorded. This mass loss was then corrected to account for mass loss from the sand and aggregate, exposed to the same procedure. The remaining mass difference represents the amount of CO_2 sequestered during the curing process and is attributed to the thermal decomposition of $CaCO_3$, which is the primary reaction product of CSC carbonation.

The specimens taken from the CSC-based concrete paver exhibited an average mass gain of ~3.4% due to CO_2 sequestration. This translates to 236 kg of CO_2 sequestered per tonne of CSC in the paver concrete formulation. The specimens from the concrete hollow core slab exhibited an average mass gain of ~3.3%. This translated to 220 kg of CO_2 sequestered per tonne of CSC in the slab concrete formulation.

4. CONCLUSIONS

The unique, low-lime content of CSC clinker enables two separate opportunities to reduce the CO2 emissions at the cement plant. The CO2 released from the chemical decomposition of limestone will be reduced from 540 kg per tonne of PC clinker to about 375 kg of CO2 per tonne of CSC clinker. Additionally, the low-lime chemistry of CSC allows the reaction between lime and silica to occur at temperatures 200°C lower than that required for PC clinker formation, reducing the CO2 emissions associated with the burning of fossil fuel from 270 to 190 kg per tonne. This makes it possible to reduce the CO2 emissions from ~810 kg/tonne of PC clinker to ~565 kg/tonne of CSC clinker. A 30% CO2 emissions saving was measured during a first worldwide industrial Solidia clinker production, as predicted. Energy savings of 20% were measured (with only SHC taken into account). Production improvements remain to be done to reach the value assessed theoretically (30%). Nevertheless for a first industrial trial, these values remain extremely promising.

The unique ability of CSC to avoid hydration and cure via a reaction with gaseous CO_2 opens the possibility for the permanent sequestration of CO2 in cured concrete structure. It has been demonstrated that the curing process enables CSC-C to sequester over 230 kg of CO2 per tonne of CSC used in the concrete formulation. The CO_2 used in the curing process and captured within CSC-based concrete is industrial-grade CO2 sourced from waste flue gas streams.

Depending on the specific ratios of sand, aggregate and CSC used in the concrete mix, the final CSC-based concrete part may contain in excess of 3 wt.% of sequestered CO2.

The combined effects of 1, 2, and 3 above, replacement of PC by CSC offers the potential to reduce the carbon footprint associated with the production and use of cement by up to 70%.

Unlike PC-based, concrete products hardened with CO_2-cured CSC do not consume water. Thus, if necessary, the process water used in the CSC-based concrete formulation can be recovered during the CO_2-curing process.

ACKNOWLEDGMENTS

This paper deals with cement and concrete production done in North America.

In June 2016, the European LIFE program provided the award grant N° LIFE15 CCM/FR/000116 to the Solid LIFE project This grant will fund the Solid LIFE partners (LafargeHolcim, Solidia Technologies® and Building Research Establishment) efforts to develop and deploy this technology within Europe. The authors acknowledge the European Union for this funding.

Additional data will be available with the actions foreseen in Solid LIFE project, to continue to prove the environmental benefits reached by the technology.

REFERENCES

[1] Barcelo, L. et al : Cement and Carbon Emission, Materials and Structures 47 (2013) 6, pp. 1055-1065, 1871-6873

[2] Riman R.E. & Atakan V.: Systems and methods for carbon capture and sequestration and compositions derived therefrom. US Patent 8,114,367 (2012)

[3] Riman R.E. et al : Bonding element, bonding matrix and composite material having the bonding element, and method of manufacturing thereof. US Patent Application Publication US 2013/0122267., May 16 (2013).

[4] Madlool, N.A. et al : A critical review on energy use and savings in the cement industries, Renewable and Sustainable Energy Reviews 15 (2011) 4, pp. 2042-2060, ISSN 1364-0321

[5] Taylor H.F.W.: Cement Chemistry, 2nd Edition, Thomas Telford, ISBN 978-0727725929, (1997)

[6] Environmental Protection Agency, Washington, DC : AP42 - Compilation of air pollutant emission factors, Vol. 1; Stationary point and area sources (2005). Available from https://nepis.epa.gov/ Accessed: 2017-03-24

[7] Marceau M.L. et al : Life Cycle Inventory of Portland Cement Manufacture, PCA R&D Serial No. 2095b, Available from https://www.nrmca.org/ Accessed: 2017-03-24

[8] U.S. Geological Survey (2012) USGS Mineral commodity summaries 2012, ISBN 978-1-4113-33499.

PROPERTIES OF NEW CEMENT FROM CERAMIC WASTE

Vincenzo Perugini[1], Matthias Schwotzer[2]

[1] School of Science and Technology, Geology Division, University of Camerino, Via Gentile III da Varano, 62032 Camerino (MC), Italy, email: vincenzo.perugini@unicam.it
[2] Karlsruhe Institute of Technology (KIT), Institute of Functional Interfaces, Hermann-von-Helmholtz-Platz 1, 76344 Eggenstein-Leopoldshafen, Germany, email: matthias.schwotzer@kit.eduINTRODUCTION

SUMMARY: Since thousands of years, ancient civilities produced primitive concretes using ceramic waste, thanks to the increasing of mechanical strength and water resistance due to their pozzolanicity. Today, hot topics as the necessity to reduce greenhouse gas from clinker portland production, the reduction of quarrying activity and, in many cases, the needs of higher durability through Pozzolanic cements, make eligible ceramic waste as supplementary cementitious material (SCM). In this study, new experimental pozzolanic cements, produced through ceramic waste from different sources, are tested in comparison with commercial cements containing fly ashes, natural pozzolans and blast furnace slag, in order to assess the actual level of pozzolanicity. These new cements were also tested about the capability to reduce the damage from alkali silica reaction (ASR) using the accelerated test with mortar bars. The same experimental cements were also compared in concrete production, in order to check the behaviour on the fresh concrete, the mechanical performances and the hydraulic shrinkage. The results indicate that, ceramic waste properties match perfectly those of the currently used materials in the most common Pozzolanic cements, or SCM used in concrete. The possibility to use these kind of waste, allows to increase the circular economy in industrial sectors of quarrying and building construction, assuring economic benefits and better environmental sustainability of the related industrial sectors.

SVOJSTVA NOVOG CEMENTA IZ KERAMIČKOG OTPADA

SAŽETAK: Prije više tisuća godina stare civilizacije proizvodile su primitivne betone primjenom keramičkog otpada zbog njihove pucolanske aktivnosti koji povećava mehaničku čvrstoću i vodootpornost. Danas je keramički otpad prikladan kao dodatni materijal uz cement, uz aktualna pitanja o nužnosti smanjenja stakleničkih plinova vezanih uz proizvodnju portlandskog klinkera, smanjenje količina iskopa sirovina i potrebu povećane trajnosti dodatkom pucolanskih cemenata. U radu su prikazana ispitivanja novih pokusnih pucolanskih cemenata proizvedenih iz keramičkog otpada iz različitih izvora i uspoređena s komercijalnim cementima koji sadržavaju leteći pepeo, prirodni pucolan i zguru visoke peći s ciljem ocjenjivanja stvarne razine pucolanske aktivnosti. Za te nove cemente njihova sposobnost smanjenja oštećenja prouzročenih alkalnosilikatnom reakcijom ispitana je ubrzanim ispitivanjem na prizmicama morta. Eksperimentalni cementi ispitani su također pri pripremi betona kako bi se provjerilo ponašanje svježega betona, mehanička svojstva i skupljanja pri očvršćavanju. Rezultati pokazuju da se svojstva keramičkoga otpada odlično slažu sa svojstvima danas upotrebljavanih materijala u većini običnih pucolanskih cemenata ili dodatnih cementnih materijala upotrijebljenih u betonu. Mogućnost upotrebe takve vrste otpada omogućuje porast kružnog gospodarstva u industrijskim sektorima iskopa sirovina i građenja, osiguravajući gospodarske dobitke i bolju održivost okoliša odgovarajućih industrijskih sektora.

1. INTRODUCTION

The necessity of higher environmental sustainability, which requires lower greenhouse gas emission and landscape safeguard, leads to increase the Portland cement replacement through every possible kind of supplementary cementitious materials (SCM), in order to reduce the use of clinker Portland in the cement production. The use of SCM requires to assure the required mechanical performances in concrete allowing the saving of clinker Portland in the cement, or Portland cement in the concrete [1,2]. In many cases, the use of SCM determines higher durability due to the chemical characteristics as well as an improved physical performance, resulting from to specific properties, as the lower hydraulic shrinkage, the lower hydration heat, or ASR mitigation. Due to economic reasons as transport costs and low sustainability of the transfer, not everywhere the natural pozzolan, fly ash from burned coal, or blastfurnace slag, allow to fulfil the above-mentioned scopes. Consequently, new SCM, as calcined clays or ashes from different sources, could become essential in order to increase the Portland cement replacement in the concrete, or clinker Portland use in cement production [3, 4, 5]. In this regard, the use of ceramic waste, due its pozzolanic behavior, may become a feasible opportunity, providing an alternative for the currently used SCM. This holds in particular for building demolition, that consists to large extent of bricks and tiles. Usually, the SCM assessment is based on the testing of the Strength Activity Index (SAI), considering it as an indirect demonstration of pozzolanicity, while, more correctly, it is a demonstration of contribute to the hardening [6, 7]. This study is pointed to assess the eligibility of two samples of ceramic waste as pozzolanic material for cement production, including the verification of the pozzolanicity of two experimental Pozzolanic cements containing them. After that, the experimentation is pointed to verify mechanical properties, linear shrinkage in concrete and capability to mitigate of Alkali-Silica Reaction (ASR) of those cements, in comparison to several types of commercial cements.

2. MATERIALS AND METHODS

2.1. MATERIALS

Two different sample of ceramic waste containing brick and roof tiles, from demolition works in Umbria (CW2) and Emilia Romagna (CW8), are involved in the experimentation. Two experimental cements were prepared through the adding of 20% of them, grinded at specific surface of 6000 cm^2/g, to the Portland cement base, type I 52,5 R. The same Portland cement, which is produced in central Italy, was also used as reference cement in the experimentations. Experimental cements were compared to two commercial Pozzolanic cements containing 20% of natural pozzolan, from Borghetto (Italy), and fly ash from Brindisi (Italy), respectively classified as type IV/A (P) 42,5 R and type IV/A (V) 42,5 R (EN 197-1). The study involves comparison also with a Composite Portland cement, type II/A-LL 42,5 R, containing about 20% of limestone and a Blast furnace cement, type III/B 42,5 N, containing about 70 % of slag. Concretes containing those cements were prepared in order to verify their properties and technological behaviour in final applications.

2.2. METHODS

The characterization of the chemical composition of the CW samples was performed accordance to EN 196-2. The pozzolanicity was assessed through the reference methods EN 196-5. These results were compared to the common pozzolanic cements made through natural pozzolan (from Borghetto, Italy) and fly ash (from Brindisi, Italy). The impact on the hardening of the investigated CW samples, was tested by means of the Strength Activity Index (SAI), in accordance to EN 450-1, after grinding at 6000 cm^2/g. The reference Portland cement used in the SAI tests is a type I class 52,5 R (in accordance EN 197/1, ASTM C618 and EN 450-1), which was also used as reference cement in other tests. Moreover, considering that pozzolanicity, also were specifically detected and not infer from the SAI, isn't an ultimate indication of the auspicated chemical and physical behaviour, these two experimental cements were also tested about linear shrinkage in concrete and capability to mitigate ASR. The comparison of the ASR mitigation was tested in accordance to UNI 8520-22 in accelerate way (comparable to ASTM C1567), using a reactive aggregate having expansions over 0,3 % if tested in accordance to ASTM C1260, using the same reference Portland cement containing more than 1% of alkali (1,02 %). The new experimental cements, containing 20% of ceramic waste (CW2 and CW8) pre-ground at finesses of 6000 cm^2/g, were compared with the mentioned commercial Pozzolanic cements, type IV/A (P) and IV/A (V) as well as three not-pozzolanic cements types, about mechanical strength in standard mortar, in accordance to EN 196-1, workability and mechanical strength in concrete, in accordance to EN 12390 and 12350. Mechanical strength in standard mortar (EN 196-1) was detected at 2, 7, and 28 days. Assessment of cement performance in concrete was carried using the same mix design, limestone aggregates, cement dosage (400 kg/m^3), PCE admixture (4 lit/m^3), workability class (slump 18 ± 2 cm). Water/cement ratio was in all cases close to 0,42, due to very little differences of water demand. The mechanical strength of the concrete was detected after 2, 7, 28, 60, and 180 days. Moreover, the linear shrinkage of the concrete was tested for all types of cement involved in the experimentation in accordance to UNI 11307. The measurement was started while removing of the moulds, after 24 h of storage in an environment at 20° C with humidity of 90%. The following drying period was performed in environment at temperature of 20°C and constant humidity of 50 %. Due to the rapid hardening of the reference Portland cement, type I 52,5 R, which shows an early strength 10 MPa higher than the other cements, for this cement the measurement was retaken, removing the moulds after 15 h, when it reaches a compressive strength close to the other blended cements at 24 h, which is about 30 MPa.

3. RESULTS AND DISCUSSION

The chemical composition of the ceramic waste samples containing brick and roof tiles from demolition are shown in Table 1. The results match the limits prescribed in the ASTM C 618 for SCM, and EN 450-1 regarding fly ash, about the sum of silica + alumina + iron oxide, being in all cases over 70 % (sample CW 2 = 84,1%; sample CW 8 = 87,6%). In the same way, they match the prescribed limits of the EN 197-1 and EN 450-1 about the reactive silica content, showing values higher than 25 % (sample CW2 = 25,4%; sample CW8 = 30,1%). In Figure 1 shows the results of the determination of pozzolanicity of the experimental Pozzolanic cements containing 20% of ceramic waste, in accordance to EN 196-5, in comparison to the Pozzolanic cements containing 20% of natural pozzolan IV/A (P) and 20% of fly ash IV/A (V). The results show a marked pozzolanicity of the investigated ceramic waste. In fact, the sample named CW2 shows after 15 days a pozzolanicity comparable to the natural pozzolan from Borghetto (Italy) and fly ash from Brindisi (Italy). Instead, pozzolanicity of sample CW8 is clearly higher, assuring the positive results of pozzolanicity after only 8 days. The investigation of the Strength Activity Index (SAI) of the ceramic waste, in accordance to EN 450-1, allows the comparison with the SAI of the natural pozzolan and fly ash used in the commercial Pozzolanic cements involved in the experimentation. The results indicate a very good contribute to the hardening, especially for the sample of ceramic waste named CW8, which shows a SAI clearly higher to the natural pozzolan and fly ash, both at 28 days (0,98) that 90 days (1,06) of maturation, as shown in Table 1. In all cases the SAI values match the EN 450-1 limits, being higher than 0,75 at 28 days and higher than 0,85 at 90 days.

Table 1 Compressive strength in standard mortar (EN 196-1) and concrete (EN 12390 and 12350) of the cements with different SCM. Activity index (EN 450-1), reactive SiO2 (EN 197-1 and EN 450-1) and sum of silica+alumina+iron oxide (ASTM C618 and EN 450-1)

	Compressive Strength (MPa)								Activty Index SAI (EN 450-1)		Reactive SiO_2 (%)	SiO_2+ Al_2O_3 + Fe_2O_3 (%)
	Standard Mortar			Concrete								
CEM Maturation age (days)	2	7	28	2	7	28	60	180	28	90		
I 52,5 R	38	48	58	51,8	66,7	80,1	84,5	90,2				
II/A-LL 42,5 R (Limestone 20%)	29	39,7	49,5	42,2	57,0	66,0	71,2	81,6				
III/B 42,5 N (Slag 70%)	13,2	41,1	53,4	37,9	55,0	66,4	70,3	75,5				
IV/A (P) 42,5 R (Natural Pozzolan 20%)	26	37,3	51,7	43,2	53,5	65,0	73,5	83,7	0,78	0,9	37,2	76,6
IV/A (V) 42,5 R (Fly Ash 20%)	25	40,1	50,8	41,0	52,2	64,4	74,4	84,9	0,78	0,89	38,1	81,9
IV/A (CW) 42,5 R (Ceramic Waste n.2 20%)	23,3	38,5	51,4	43,5	60,6	69,5	72,9	89,2	0,80	0,91	25,4	84,1
IV/A (CW) 42,5 R (Ceramic Waste n.8 20%)	27,5	41	57,5	41,5	59,7	71,1	77,4	85,7	0,98	1,06	30.1	87,6

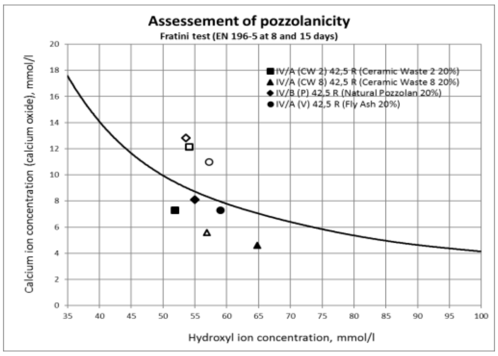

Figure 1 Pozzolanicity tests (EN 196-5) of the Pozzolanic cements containing 20% of respectively ceramic waste CW2 and ceramic waste CW8, natural pozzolan and fly ash; empty symbol 8 days, full symbol 15 days

Compressive strength in mortar (EN 196-1), confirming the indication of the SAI tests, indicate a good contribute to hardening of the ceramic waste used in the experimental production of the new cements, as shown in Figure 2.

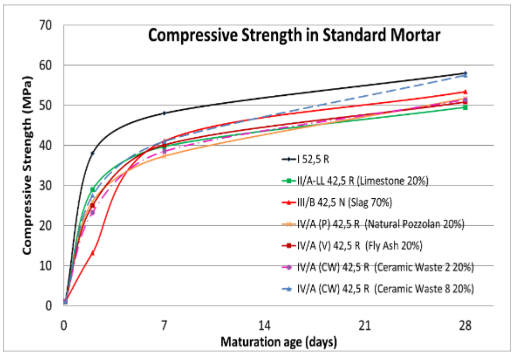

Figure 2 Compressive strength in mortar (EN 196-1) of the Pozzolanic cements containing 20% of respectively ceramic waste CW2 and ceramic waste CW8, natural pozzolan, fly ash and limestone, in comparison to reference Portland cement type I 52,5 R.

The results show, in both cases, compressive strength in standard mortar, at 28 days, equivalent or higher than common cements containing the same percentage of natural pozzolan or fly ash, being 51,4 MPa for the cement containing 20% of ceramic waste sample CW2 and 57,5 MPa for the cement containing 20% of ceramic waste sample CW8.

These results are higher than compressive strength of cement II/A-LL 42,5 R, III/B 42,5 N, IV/A (P) 42,5 R and IV/A (V) 42,5 R, commonly used in the most important building infrastructure works. Compressive strength of the concrete containing ceramic waste are closer to the reference Portland cement type I class 52,5 R than other commercial blended, as shown in Figure 3. Very interesting is the behavior at long term, which indicates at 180 days of maturation a continuous trend to increase, as commonly occurs for good pozzolanic materials. Considering the use of only 320 Kg/m^3 of Portland cement with 80 Kg/m^3 of ceramic waste, as addition, the compressive strength of 89,4 MPa at 180 days, as in the cases of ceramic waste CW2, and 85,7 MPa in cases of ceramic waste CW8, is higher than the better expectations.

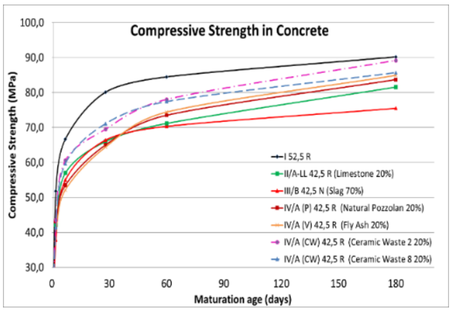

Figure 3 Compressive strength in concrete, at equivalent workability (in accordance to EN 12390 and EN 12350) of the Pozzolanic cements containing 20% of respectively ceramic waste CW2 and ceramic waste CW8, natural pozzolan, fly ash and limestone, in comparison to reference Portland cement type I 52,5 R.

The linear shrinkage in concrete of the experimental Pozzolanic cements containing ceramic waste, carried out in dried environment, at constant temperature of 20°C and 50% of humidity (UNI 11307), show changing of length in perfect matching with the other Pozzolanic cements containing equivalent percentage of pozzolan or fly ash. Nevertheless, taking in account the higher compressive strength, which allows lower cement dosage for concrete at same mechanical performance, the experimental cements made through ceramic waste show better performances about linear shrinkage.

Due to the timing of measurement of the initial dimension, taken for the count of the changing of length, which the standard method indicates at 24 h, the early hardening of the concrete containing the reference Portland cement type I 52,5 R determines the apparent lower shrinkage. Thus, considering the faster progression of the shrinkage due to the rapid reactions, for that cement the measurement of initial length was replicated at earlier time, removing the moulds and starting the measurement at 15 h from the casting. In fact, at this age of maturation, Portland cement, type I 52,5 R shows mechanical strength of 30 MPa, which is very close to the values of the Pozzolanic cements involved in the experimentation at 24 h (Figure 4). In this way, thanks to the early starting of measurement, which allows to count an initial measurement of about 70 μ/m longer, the linear shrinkage of that cement appears very higher at any maturation ages. Thus, considering the matching of the compressive strength at 180 days between cement containing ceramic waste (CW2 = 89,4 MPa and CW8 = 85,7 MPa) and Portland cement (90,2 MPa), the new experimental cements assure, at equal strength, a better performance regarding linear shrinkage.

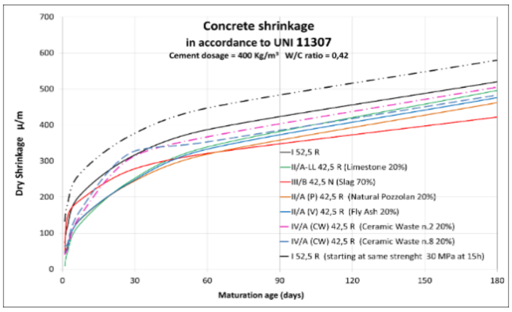

Figure 4 Linear shrinkage in concrete (μ/m) in accordance to UNI 11307, starting the measurement after 24 h from the casting and storage at 20°C and over 90% of humidity. Replication of measurement for Portland cement type I 52,5 R starting after 15 h from the composition and casting, at the maturation age corresponding to strength of 30 MPa.

The tests about ASR mitigation, in accordance to UNI 8520-22 in accelerated way (or ASTM C1567/C1260), using reactive aggregate having expansion over 0,337 %, if tested with the same reference Portland cement containing over 1% of Na_2O equivalent, show positive results, indicating the marked reduction of expansion (Figure 5). The results indicate expansion of 0,072 % at 14 days for the sample of ceramic waste CW2 and 0,047 % for the sample of ceramic waste CW8. These values match perfectly the fixed limit of 0,1 % as maximum expansion at 14 days. They show a reduction of expansion very similar, or higher to the Pozzolanic cement IV/A (P) and IV/A (V) involved in the experimentation, which indicate 0,082 % for the type IV/A (P) containing natural pozzolan and 0,086 % for the type IV/A (V) containing fly ash.

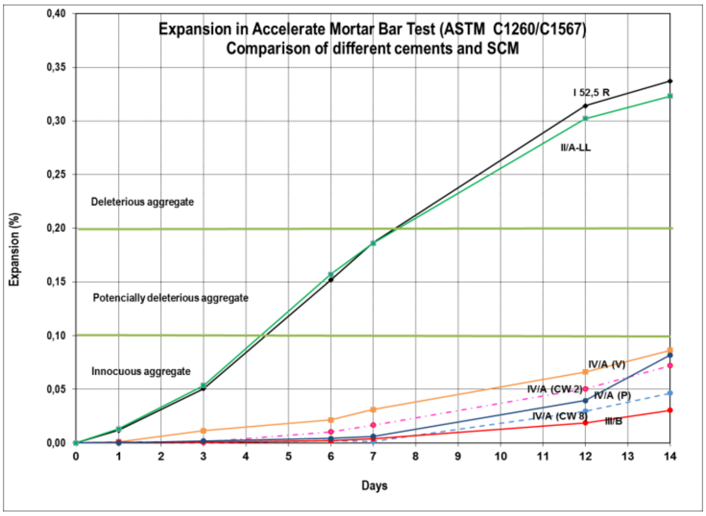

Figure 5 ASR mitigation in accordance to UNI 8520-22 in accelerated way (or ASTM C1567/C1260), using reactive aggregate and Portland cement type I 52,5 R containing 1% of alkali as reference cement.

4. CONCLUSIONS

The chemical and physical properties of the investigated samples of ceramic waste indicate the eligibility of such a material as pozzolanic component for cement, or SCM for concrete production. It allows to save clinker Portland maintaining the equivalent mechanical performances, or replace Portland cement in the concrete, in the same way of the currently used SCM. Its contribute to the hardening is even higher than the most used pozzolanic materials. Concrete prepared with these experimental cements containing ceramic waste, shows compressive strengths that are even higher than the compressive strength of concrete prepared using Pozzolanic cement based on natural pozzolans and fly ashes. They are also higher than Composite Portland cement, type II/A-LL containing limestone, and Blastfurnace cement, type III/B, containing slag, sometimes used alternatively to the Pozzolanic cement. Regarding the chemical assessment, the cements containing ceramic waste shows a strong pozzolanicity, lower linear shrinkage and a strong mitigation of alkali-silica reaction (ASR). This make it very adapt to be used, in the same way of the common Pozzolanic cements, in structures exposed to severe environments, which require high sulphate resistance or leaching resistance. In case of ASR risk, cement containing ceramic waste assures strong mitigation of this deleterious reaction, being comparable to the other well known types of Pozzolanic cement and Blastfurnace cement containing high percentage of slag.

In conclusion, the use of ceramic waste provides an opportunity for the production of new eco-sustainable cements, having very high performances, which depending from distance of other Pozzolanic cement, or materials, from transport cost and its availability, could be economically convenient, but, above all, increase sustainability and circular economy, indicating the possibility of a new eco-friendly scenario.

REFERENCES

[1] Naceri, A. et al.: Physico-Chemical Characteristics of Cement Manufactured with Artificial Pozzolan (Waste Brick). World Academy of Science, Engineering and Technology. 52, 2009.

[2] Lavat, A. E. et al.: Characterization of ceramic roof tile wastes as pozzolanic admixture. Waste Management, Vol. 29, pp. 1666–1674 (2009).

[3] Rehan, R. & Nehdi, M.: Carbon dioxide emissions and climate change: policy implications for the cement industry, Environmental Science & Policy, Vol. 8, pp. 105–114, (2005)

[4] Madlool, N.A. et al.: Critical review on energy use and savings in the cement industries, Renewable and Sustainable Energy Reviews, Vol. 15, pp. 2042–2060, (2011)

[5] Justnes H.: Alternative Low-CO2 "Green" Clinkering Processes, Reviews in Mineralogy & Geochemistry, Vol. 74, pp. 83-99, (2012)

[6] Perugini, V. et al.:The use of urban ceramic wastes in eco-sustainable durable cement. 34th Cement and Concrete Science Conference. Paper N. 223 14-17 September 2014, University of Sheffield

[7] Baronio, G. & Binda, L.: Study of the pozzolanicity of some bricks and clays, Construction and Building Materials, 11, No. 1, pp. 41-46, (1997)

RECYCLING CERAMIC WASTE TO PRODUCE GREEN CONCRETE

Elsa Lasseuguette[1], Shane Burns[1], Dan Simmons[1], Erik Francis[1], Hwa K. Chai[1], Vasileios Koutsos[1], Yuner Huang[1]

[1] University of Edinburgh, School of Engineering, Robert Stevenson Road, Edinburgh EH9 3BF, United Kingdom, email: E.Lasseuguette@ed.ac.uk, s.burns@ed.ac.uk, s1269176@sms.ed.ac.uk, s1235215@sms.ed.ac.uk, hwakian.chai@ed.ac.uk, vasileios.koutsos@ed.ac.uk, yuner.huang@ed.ac.uk

SUMMARY: Concrete is the most consumed construction material in the world. The cement production contributes around 5 % of CO_2 emissions globally. Due to this substantial production, conventional resource supplies are in decline. This unsustainable supply has prompted a paradigm shift towards alternative raw materials to reduce the consumption of conventional concrete constituents and produce "green concrete". One of the most effective ways is to replace cement with pozzolans derived from industry wastes, such as ceramic. Ceramics are the single largest contributor to construction and demolition waste globally, 54 % in 2014 alone. There are approximately 68 million tonnes of ceramic waste sent to landfills annually in the UK. Current research into utilizing ceramics waste as a potential pozzolanic material in the production of 'green concrete' has had promising results. This study investigates the feasibility of using recycled ceramic waste in order to produce high performance concrete, while simultaneously reducing the consumption of cement. In this project, the mechanical performance of cement mortar samples, with a 15 % ceramic-cement replacement by weight was analysed and discussed. Further, the chemical properties of the concrete samples were determined using X-ray Powder Diffraction and the results were correlated with the mechanical strength tests. This study shows that ceramic waste of UK source can be a promising cement replacement to produce "green concrete".

RECIKLIRANI KERAMIČKI OTPAD ZA PROIZVODNJU ZELENOGA BETONA

SAŽETAK: Beton je najviše upotrebljavani građevni materijal u svijetu. Na svjetskoj razini proizvodnja cementa sudjeluje s oko 5 % emisije CO_2. Zbog tako velike proizvodnje, konvencionalnih izvora sirovina sve je manje. Takva neodrživa dobava sirovina pokrenula je pomak ka alternativnim sirovinama kako bi se smanjila upotreba konvencionalnih sastojaka betona i proizveo "zeleni beton". Jedan od najučinkovitih načina jest zamjena cementa pucolanima dobivenim iz industrijskih otpada kao što je keramika. Keramika na svjetskoj razini ima najveći pojedinačni udio u građevnom otpadu i otpadu pri rušenju i čini 54 % otpada samo u 2014. godini. U Ujedinjenom Kraljevstvu godišnje se oko 68 milijuna tona keramičkog otpada šalje na odlagališta. Sadašnja istraživanja upotrebe keramičkog otpada kao potencijalno pucolanskog materijala u proizvodnji 'zelenoga betona' pokazuju obećavajuće rezultate. U radu je istražena prikladnost upotrebe recikliranog keramičkog otpada za proizvodnju betona visokih svojstava uz istodobno smanjenje potrošnje cementa. Analizirana su i raspravljena mehanička svojstva uzoraka od morta sa zamjenom 15 % mase cementa keramikom. Kemijska svojstva betonskih uzoraka određena su primjenom difrakcije praha X-zrakama, a rezultati su uspoređeni s ispitivanjem mehaničke čvrstoće. Pokazano je da upotreba keramičkog otpada iz Ujedinjenog Kraljevstva može biti obećavajuća zamjena cementa pri proizvodnji "zelenoga betona".

1. INTRODUCTION

A large amount of ceramic waste ends up in landfill causing severe worldwide environmental and economic burden. Around 100 million tons of construction and demolishing wastes are generated in the EU yearly, amongst which 54% are ceramic materials (i.e. tiles, walls, floors). In the UK, ceramic wastes consist of around 20% of construction materials and 12% of demolishing wastes for housing buildings [1, 2]. In developing countries like China, large amounts of ceramic powder waste are generated in cutting and polishing process for the furnishing industry. Around 10 million tonnes of ceramic waste powder are generated per year [3]. Due to dwindling natural resources, it is also a necessity to find a replacement for the cement content in concrete. The cement constituent within concrete is by far the most environmentally impactful material, as the process of mining raw materials (calcium carbonate, silica, alumina and iron ore), calcining to clinker form and then grinding to cement powder consumes considerable energy, requiring 850kcal/kg [4]. As well as being an energy intensive manufacturing process which emits high levels of CO_2, it also produces by-products in the form of mining waste. During the mining stage of cement production approximately 1.7 tonnes of material is extracted for every tonne of necessary minerals [5]. In order to address the high emissions and inefficient manufacturing process it is a necessity to reduce the consumption of cement within concrete production.

An innovative solution for the concrete mix is to replace a portion of cement with ceramic powder as a chemical reactive material. It has been stated in research that ceramics are in fact pozzolanic and provide the feedstocks required for secondary hydration to occur, forming a greater number of bonds in the ITZ [6]. Unlike most other pozzolanic materials being implemented today, ceramics are not a by-product of a manufacturing process (although a lot of ceramic waste is created during production and installation). As such, waste streams must be utilised in order for ceramics to be sensibly considered.

Despite needing processing in order to attain adequate particle size, ceramics undergo calcination during manufacture and so already possess the required microstructure in order to be reactive. As such they are a potentially pozzolanic material in ample supply with no current reuse, and so should be investigated. This will provide comparable mechanical properties, hence suggesting that ceramics could be used as a suitable supplementary cementitious material (SCM) for Portland cement. The commonly used Portland cement concrete mainly consists of aggregates, cement and water. When the dry cement is mixed with water, calcium silicates (C_3S and C_2S) in cement react with water and produce calcium silicate hydrate (C-S-H) and hydrated lime (CH). This chemical reaction process is primary hydration. C-S-H is primarily responsible for providing concrete strength by binding with aggregates. More C-S-H can be generated in concrete if a portion of cement is replaced by constituents with active silicates (S) to facilitate secondary hydration with CH, as given below:

Hydration (mix cement with water): $C_3S + 3H \rightarrow C\text{-}S\text{-}H + 2CH$; $C_2S + 2H \rightarrow C\text{-}S\text{-}H + CH$

Secondary hydration (mix S containing constituents with CH from cement hydration): $CH + S \rightarrow C\text{-}S\text{-}H$

A typical example of secondary hydration is found though the use of metakaolin, which is the derivative from kaolin in heat treatment [7]. Hence, it is highly possible for ceramic powder to be chemically reactive in hydration processes. Heidari and Tavakoli [8] indicate that ceramic waste powders will participate in secondary hydration, and thus it should be added into concrete as cement substitute for enhancing performance. It is also suggested that 20% of cement can be replaced by ceramic powders.

In this study, we investigate the properties of a cement mortar mix design with a 15% ceramic-cement replacement by weight at different ages after casting, with the aim of correlating the mechanical strength with the mineralogy properties to evaluate the effectiveness of ceramic as a pozzolan for concrete.

2. EXPERIMENTAL WORK

2.1. MATERIALS

Type 1 Portland cement was selected as the primary binding agent. This is the most commonly used cement in the UK, and as such has a substantial production (contributing large portions of CO2 emissions). The ceramic source used in this study was a Johnson-Tiles glazed white ceramic wall tile, produced in Stoke, UK. This source was chosen as it is commonly used in the UK.

The ceramic tiles were initially broken using a hammer and then ground to a diameter of 1 – 2 mm using a jaw crusher. The ground pieces were then ground further to a fineness of less than 100 microns using an Orbital Mill. Details of the chemical composition and size distribution of raw materials are given in Table 1 and Figure 1.

Table 1 Chemical composition of the main components given by XRF (Top part) and crystalline composition by XRD-Rietveld (Bottom part) of the ceramic and the cement

Oxide Composition (%)	Cement	Ceramic
SiO_2	18.87	68.92
Al_2O_3	4.28	19.78
Fe_2O_3	2.89	0.89
MgO	2.12	0.31
CaO	64.78	7.03
Na_2O	0.08	0.33
K_2O	0.449	1.734
TiO_2	0.181	0.694
MnO	0.102	0.005
P_2O_5	0.112	0.173
LOI	5.93	0.15
Main crystalline composition (Rietveld) (%)	Cement	Ceramic
C_3S	85.7	3.1
C_2S	3.66	0.3
Quartz	0	47

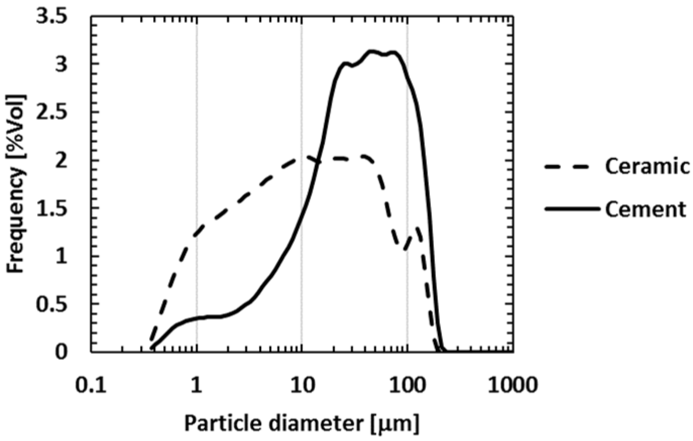

Figure 1 Particle size distribution of the raw materials.

2.2. MIXING, CASTING AND CURING

All constituents were carefully measured out (to the nearest gram) before a motorised hand mixer was used to homogeneously blend the mortar mixture in accordance with Eurocode 6: EN 1015-2 [9] before the mortar was poured into the moulds. The mortar was mixed using an Evolution Twister Mixer for a controlled mixing time of 2 minutes. The formulations investigated are given in Table 2. Mortars were cast at a cement/sand ratio of approximately 1:3 according EN 998-2 [10]. The water to binder ratio was empirically fixed at 0.581 to ensure constant and reasonable workability. The moulds selected were to Eurocode 6: EN 12390-1 [11] standard 40x40x160mm prims in 3-gang moulds. The specimens were then left to autoclave cure for 24 hours in the moulds, before being demoulded. Once demoulded the specimens were placed in a heated, circulating curing tank. The first compressive strength tests were carried out when the samples were demoulded (at 24hrs), at which point all other replicates were moist cured until the required testing age (7, 29 and 56 days). The specimens were carefully removed from the curing tank and dried before testing began. The water is temperature controlled and maintained at a constant ambient room temperature, and the curing room is humidity controlled.

Table 2 Mix design

Mix	Water [kg/m^3]	Sand [kg/m^3]	Cement [kg/m^3]	Ceramic [kg/m^3]
Control	292.969	1477.214	503.418	0
15% White	292.969	1477.214	428.059	75.521

2.3. ANALYSIS AND TESTING TECHNIQUES

The compressive strengths of the specimens at different curing ages were determined using an Instron 4505 Universal Test Machine with a maximum capacity of 100 kN. The testing procedure and data interpretation follow the European Code 6: EN 1015-11 [12]. At least three samples were conducted for each mix. The specimen strength was calculated by using the measured loading plate dimension. Once the specimen had failed (when the maximum load was reached), the failure cracks were recorded photographically before the samples were broken by hand, such that the failure mode could be better observed (Figure 2).

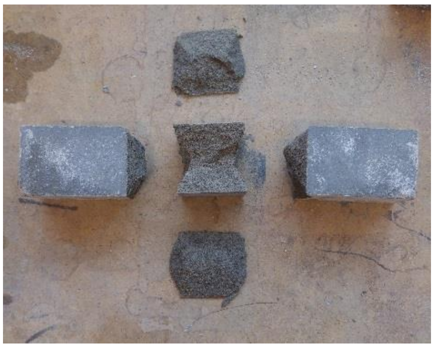

Figure 2 Failure mode of a 15% white ceramic at 29 days (after compressive testing)

The particle size analysis was performed by laser granulometry using a Beckmann Coulter LS100. The chemical and mineralogical composition of the samples were studied by XRF and XRD analysis respectively. XRF was performed on a Panalytical PW2404 wavelength-dispersive sequential X-ray spectrometer. For the XRD analysis, pastes with the same mix design as concretes were prepared without sand and cured under the same conditions. The samples were immersed in isopropanol to stop the hydration process after being crushed, dried at 110°C for 2 h and stored in a desiccator. The samples were characterized by using Bruker D8 Advance with Sol-X Energy Dispersive detector with CuKα source (1.54Å) (Figure 3). Samples were scanned on a rotating stage between 2 and 65 [°2θ] using a time per step of 5 s. Quantitative analysis was carried out by using TOPAS 3.0 Rietveld analysis software.

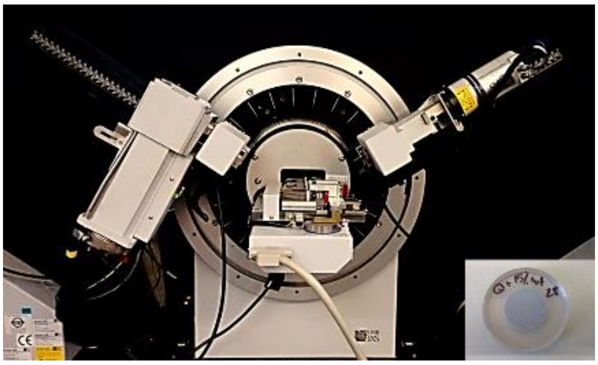

Figure 3 Bruker D8 Advance and XRD tested sample.

3. RESULTS

3.1. XRD ANALYSES

Figure 4 shows the XRD patterns of hydrated cement pastes control (without ceramic) and with 15%wt cured at 1, 7, 28 and 56 days. Using these patterns, it is possible to identity the main peaks characterising the hydration process, such as SiO2, calcium silicates (C_2S/C_3S) and the hydrated products, CH, CSH, and Ettringite. The two samples present similar XRD patterns. The patterns show that C_2S and C_3S still exist up to 56 days. Their peak intensities decrease with the curing times (Figure 5), as a result of their hydration. The decrease is similar for the control and ceramic specimens. We notice a stabilization of the consumption of C_2S/C_3S after 10 days of curing.

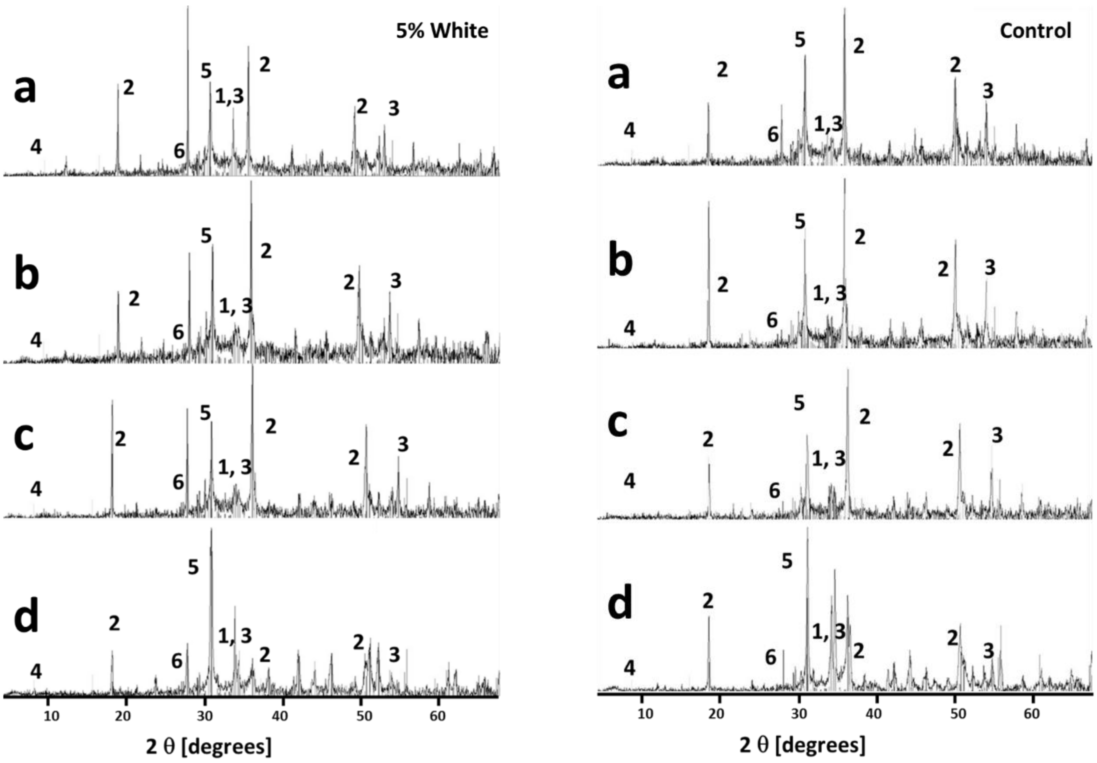

Figure 4 XRD pattern of hydrated cement pastes Control (Right) and 15% White ceramic (Left) cured at 1 (d), 7 (c), 28 (b and 56 (a) days. (1: C_2S/C_3S, 2: CH, 3: CSH, 4: Ettringite, 5: $CaCO_3$, 6: SiO_2).

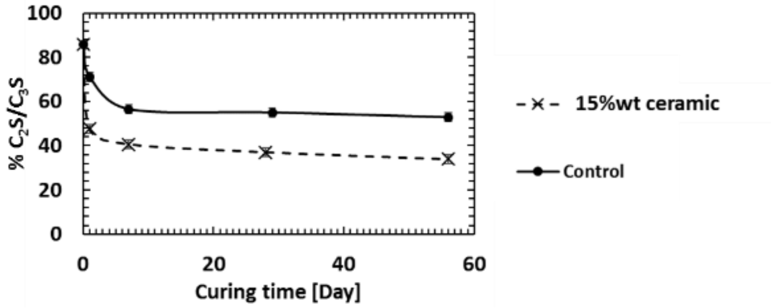

Figure 5 Variation of C_2S/C_3S with the curing time for the control specimen (black dots) and for 15%wt ceramic specimen (cross dots).

The presence of the hydration is also demonstrated by the formation of CH and CSH (Figure 6). After 1 day of curing, we notice the presence of CH and CSH in the control and in the ceramic specimen.

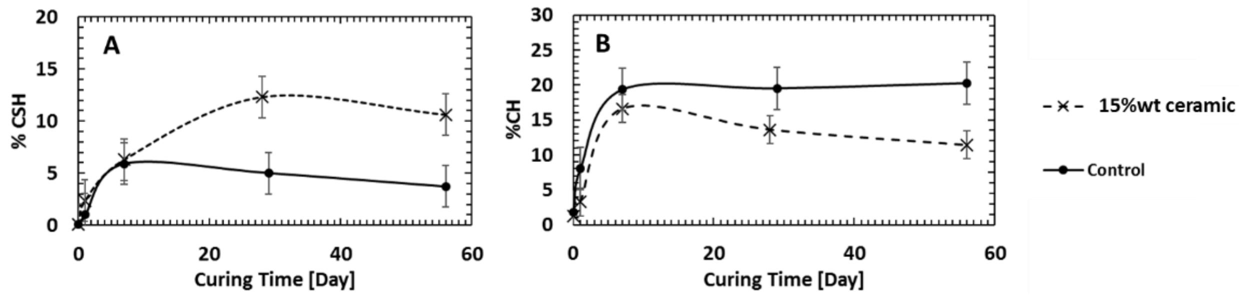

Figure 6 Variation of CSH (A) and CH (B) with the curing time for the control specimen (black dots) and for the 15%wt ceramic specimen (cross dots).

Until 7 days, the two samples present the same evolution for CH and CSH. The content of CH and CSH is increasing with the curing time (Figure 6), due to the primary hydration of silicate phases of cement with the liberation of CH and the formation of CSH. The hydration is very fast for both specimens. Lavat et al. [13] showed also that during the first 7 days, the samples were highly reactive. After 7 days, the behaviour differed noticeably between the two mixes. For the control specimen, the %CH content stabilizes whereas for the specimen with ceramics, it decreases with the curing time, indicating the presence of the secondary hydration. Further, with the ceramic, a pozzolanic reaction occurs between silicate and aluminates compounds and the CH produced by the first hydration of the cement. The variation of the CSH content indicates also the presence of the secondary hydration. Indeed, after 7 days, the sample with ceramic presents a higher content of CSH, which are produced during the secondary hydration. Others researchers reported also that the pozzolanic reaction takes place at longer curing times (over 7 days) [14-16].

3.2. COMPRESSIVE STRENGTH

Compressive strength values of the control mortar and 15%wt ceramic mortar are given in Figure 7. The behaviour of the two mixes is identical at 24 hours after casting. The compressive strength values are similar and are increasing with the curing time. The greatest growth in strength is experienced in the initial 7 days after casting, which is consistent with the XRD analysis. Further, a large increase in strength indicates occurrence of substantial hydration.

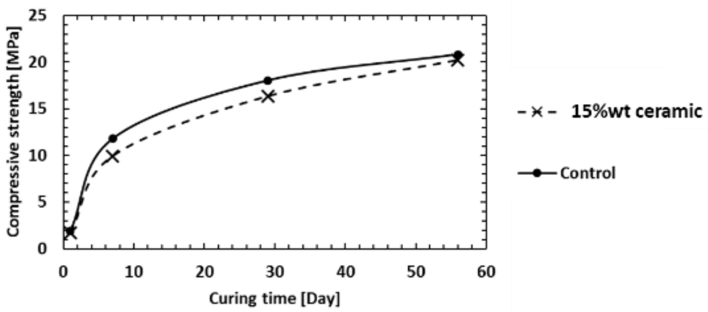

Figure 7 Compressive strength of control mortar (black dots) and 15%wt ceramic mortar (cross dots) at 1, 7, 28 and 56 days.

Between 28 and 56 days of curing, the compressive strength of the control sample stabilises whereas for the15%wt ceramic replacement sample, it is still increasing. If this trend continues, it would exceed the strength of the control. Steiner [17] and Naceri [18] noticed the same trend, after 90 days of curing specimens with ceramic replacement levels of 10% exceeding the strength of ordinary Portland cement concrete. The increased rate of growth is an indication of secondary hydration. Actually, the secondary hydration process has been reported to be beneficial at long curing times [19].

4. CONCLUSIONS

The short-term performance of 15%wt ceramic replacement cement was investigated, in terms of mechanical and physical-chemical properties. The presence of the first and secondary hydration has been proved using XRD analysis. The secondary hydration, corresponding to the pozzolanic reaction, occurs after 7 days. The compressive strength values of the cement with 15% ceramic replacement is similar to the control sample until 56 days. However, at longer curing times, the trend indicates that the sample with ceramic would exceed the strength of the ordinary Portland cement.

These results show the feasibility of using recycled ceramic waste as cement replacement. They demonstrate the potential of achieving structural grade concrete whilst simultaneously reducing the consumption of cement and providing a novel end-use of ceramic wastes.

ACKNOWLEDGMENTS

The authors would like to thank Dr Nicholas Odling for his help for the XRD and XRF analysis, Mr Jim Hutcheson for his support for sample preparation and mechanical testing. The research work described in this paper was supported by a grant from the EPSRC Institutional Sponsorship (Project No. J27318).

REFERENCES

[1] Zakar, S. Overview of demolition waste in the UK, Construction Resources and Waste Platform, Building Research Establishment (BRE), www.bre.co.uk, (2008).
[2] Hobbs, G. Developing a strategic approach to construction waste – 20 year strategy, Building Research Establishment (BRE), www.bre.co.uk, (2006).
[3] Hou, L.; Zeng, L., Current situation on reusing ceramic wastes, Chinese Ceramic Industry 12 (2005) 41 – 44.
[4] Meyer, C. The Greening of the Concrete Industry, Cement and Concrete Composites 31 (2009) 601-605.
[5] Pacheco-Torgal, F. and Jalali, S. Reusing ceramic wastes in concrete. Construction and Building Materials 24(5) (2010) 832-838.
[6] Mas, M., Monzó, J., Payá, J., Reig, L. and Borrachero, M. (2016). Ceramic tiles waste as replacement material in Portland cement. Advances in Cement Research, 28(4), pp.221-232.
[7] Lavat, A.E.; Trezza, M.A.; Poggi, M. Characterization of ceramic roof tile wastes as pozzolanic admixture, Waste Management 29 (2009) 1666-1674.
[8] Heidari, A.; Tavakoli, D., A study of the mechanical properties of ground ceramic powder concrete incorporating nano-SiO2 particles, Construction and Building Materials 38 (2013) 225 – 264.
[9] European committee for standardization. Methods of test for mortar for masonry. Bulk sampling of mortars and preparation of test mortars. EN 1015-2:1999
[10] European committee for standardization. Specification for mortar for masonry. Masonry mortar. EN 998-2:2016.
[11] European committee for standardization. Testing hardened concrete. Shape, dimensions and other requirements for specimens and moulds. EN 12390-1:2012
[12] European committee for standardization. Methods of test for mortar for masonry. Determination of flexural and compressive strength of hardened mortar. EN 1015-11:1999
[13] Lavat, A.E.; Trezza, M.A.; Poggi, M. Characterization of ceramic roof tile wastes as pozzolanic admixture, Waste Management 29 (2009) 1666-1674.
[14] Li, Q.; Geng, H.; Shui, Z.; Huang, Y. Effect of metakaolin addition and seawater mixing on the properties and hydration of concrete, Applied Clay Science 115 (2015) 51–60.
[15] Frias, M.; Cabrera, J.; Influence of MK on the reaction kinetics in MK/lime and MK-blended cement systems at 20 degrees C, Cement Concrete Research 31 (2001) 519–527.
[16] Cheng, S.; Shui, Z.; Li, Q.; Sun, T.; Yang, R. Properties, microstructure and hydration products of lightweight aggregate concrete with metakaolin and slag addition Construction and Building Materials 127 (2016) 59–67.
[17] Steiner, L.R.; Bernardin, A.M.; Pelisser, F. Effectiveness of ceramic tile polishing residues as supplementary cementitious materials for cement mortars, Sustainable Materials and Technologies 4 (2015) 30-35.
[18] Naceri, A.; Hamina, M.C. Use of waste brick as a partial replacement of cement in mortar, Waste Management 29 (2009) 2378-2384.
[19] O'Farrel, M.; Wild, S.; Sabir, B.B. Pore size distribution and compressive strength of waste clay brick mortar, Cement and Concrete Composites 23 (2000) 81-91.

LOW DENSITY FLY ASH: AN EFFICIENT BY-PRODUCT FOR LOWER THERMAL CONDUCTIVITY MORTARS

Siyimane Mohaine[1], Frederic Grondin[1], Mohamed Rougui[2], Ahmed Loukili[1]

[1] Ecole Centrale de Nantes, Institut de Recherche en Génie Civil et Mécanique (GeM) UMR-CNRS 6183 1 rue de la Nöe, 44300 Nantes, France, email: siyimane.mohaine@ec-nantes.fr, frederic.grondin@ec-nantes.fr, ahmed.loukili@ec-nantes.fr
[2] Ecole Supérieure de Technologie de Salé, Université Mohamed V, Avenue le Prince Héritier, 11060 Salé, Morocco, email: rougui93@yahoo.fr

SUMMARY: Low density fly ashes (LDFA) are a by-product (1-2%) of fly ash from the coal burning process. Some of their distinctive properties (low bulk density, high mechanical strength, spherical shape, low porosity and thermal conductivity) make their use in various industry areas –particularly in construction materials - interesting as recycled waste. Therefore, their recovery process can add important value to the coal fired power plant activity. In this work, we tried to look into the possibility of using LDFA as a partial replacement of cement in mortars in order to have structural materials with a lower thermal conductivity. For a better evaluation of their effect, an investigation on mechanical properties (compressive strength), thermal properties (thermal conductivity) with a microstructural study (apparent porosity, SEM imaging) was carried with different water/cement ratios, two particle size distributions of LDFA and replacements up to 23%.

LETEĆI PEPEO MALE GUSTOĆE: UČINKOVIT NUSPRODUKT ZA MORTOVE MALE TOPLINSKE PROVODLJIVOSTI

SAŽETAK: Leteći pepeli male gustoće nusprodukt su (1 do 2 %) letećeg pepela pri izgaranju ugljena. Zbog njihovih naročitih svojstava (mala obujamska masa, velika mehanička čvrstoća, sferičan oblik, mala poroznost i toplinska provodljivost) upotrebljavaju se u više industrijskih područja, posebno u građevnim materijalima kao zanimljiv reciklirani otpad. Stoga proces njihove oporabe može imati važnu vrijednost u radu energana pogonjenih ugljenom. U radu se pokušala ustanoviti mogućnost upotrebe takvog pepela u mortovima kao djelomične zamjene cementa kako bi se dobio građevni materijal manje toplinske provodljivosti. Za bolje vrednovanje njihova učinka provedena su istraživanja mehaničkih svojstava (tlačne čvrstoće), toplinskih svojstava (toplinske provodljivosti), mikrostrukturno ispitivanje (prividna poroznost, slikovni prikaz skeniranja elektronskim mikroskopom) za različine omjere voda/cement, dvije raspodjele veličina čestica pepela i njegove zamjene do 23 %.

1. INTRODUCTION

With the increase in environmental concern, solid waste management has gained significant importance, especially with the increasing quantities of industrial wastes. Concrete and cement mortars, which are the most used construction materials, have a high potential of recycling wastes into improving existing products. Low density fly ashes (LDFA) are inert hollow alumina-silicates spheres obtained from fly ash from coal burning power plants. They constitute a small (1-2%) but important fraction of the fly ash production process [1-2]. They are formed from cooling and solidification of inorganic molten coal residues around trapped gas. The typical sizes of LDFA range from 5 to 500µm. They have hollow interior with a wall thickness constituting 5 to 10% of their diameter. Interest in introducing these by-products in cementitious materials has grown in the last decade due to their low particle density (bulk density up to $800\ kg/m^3$), perfectly spherical shape and low thermal conductivity. Many studies have used LDFA as primary aggregates to produce lightweight concrete [3-4-5]. Some authors reported good acoustic insulation when developing absorbent structural materials [4], good resistance against alkali-silica reactions at ambient temperatures [6] and excellent thermal insulation in ultra-lightweight cement composites [7]. However, low density fly ashes are often used with other mineral additions in the studied mixes and their isolated impact on the improvement of the studied properties is uneasy to discern. In this work, therefore, different mortar mixes incorporating only LDFA as partial replacement of cement have been studied in order to have structural materials with a lower thermal conductivity in terms of compressive strength, apparent porosity and thermal conductivity. Observations with SEM were also made to observe potential reactivity of the low density additions.

2. MATERIALS AND METHODS

2.1. MATERIALS AND MIXING

CEM II/A-LL42.5R cement was used as a hydraulic binder. Siliceous washed sand with particle size distribution ranging from 0 to 4 mm was used as aggregates. Two particle size distributions of LDFA were used for the study: LDFA-500 $(5-500\mu m)$ and LDFA-180$(5-180\ \mu m)$. LDFA are lightweight, free flowing, glass hard, inert hollow silicate spheres. They contain a high percentage of CO_2 (70%). The physical and chemical properties of LDFA as given by the manufacturer are summarized in Table 1.

Table 1: Chemical and physical properties of FAC

Chemical composition		Content (wt. %)	Physical properties	Values
Shell composition	SiO_2	55.0 - 65.0	Loose bulk density (ISO 787/11)	0.35 – 0.48
	Al_2O_3	27.0 – 33.0	Average wall thickness of sphere diameter	5 – 10%
	Fe_2O_3	≤ 6	Thermal Conductivity	0.11 W/m.K
Gas content in the spheres	CO_2	70	-	-
	N_2	30	-	-

In all the mix proportions, the volumetric fraction of sand was kept the same. LDFA was used as a partial substitute to cement. Two main mix proportions were adopted with LDFA/Cement mass ratios of 6% and 23% with the same water content.

The mixing procedure consisted of dry mixing all the powders for two minutes followed by continuously adding water while mixing for three minutes so that to obtain a homogeneous and consistent matrix. The moulds were first half filled with the mortar mixes and compacted for a few seconds on a vibrating table to enable removal of entrapped air. The same operation was carried out with the moulds full. A special attention had been paid to non-excessive vibration due to the very low density of LDFA. Specimen of 4x4x16 cm^3 (compressive strength), 30x30x8 cm^3 (thermal conductivity) and cylinders of Ø11x22cm were casted for each mix. The specimens were covered with plastic film and kept sealed after casting in a 100% relative humidity chamber for 24h and demoulded. The specimens were then stored in tap water in the same room for 28 days.

2.2. TESTING METHODS

2.2.1. COMPRESSIVE STRENGTH

Compressive strength tests were carried at 28 days. The specimens were cut in half using a diamond blade saw. The test was then carried on a 4x4 cm² surface and a height of 4cm. The specimens were placed sideways to guarantee parallel faces. The compression rate was of 2.4kN/s until failure.

2.2.2. APPARENT POROSITY

Two Ø11x5cm cylinders were cut from each Ø11x22cm mortar specimen at 28 days. The cylinders were then vacuum saturated and immersed for 48h. The apparent – or water – porosity was measured with ratio of volume of voids per the dry mass of the mortars. Hydrostatic and saturated weights of the mortars were measured. The specimens were then oven-dried at 80°C for two weeks then at 105°C until achieving a constant weight. The porosity was then calculated from the formula where M_w, M_h, M_d are respectively the saturated weight, the hydrostatic weight and the oven dried weight.

$$p = \frac{M_w - M_h}{M_w - M_d}\ (\%)$$

2.2.3. THERMAL CONDUCTIVITY

Thermal conductivity of the specimens was measured using a heat flow meter (HFM). Mortars have rough surfaces which can lead to a significant thermal resistance in any air gaps between the instrument plates and sample surfaces. Therefore, an additional instrumentation kit was used during the measurements. Thin silicone interface sheets with small diameter thermocouples were placed between the plates and sample surfaces (**Error! Reference source not found.**) to accurately measure the temperature difference across the sample and correct the interface thermal resistance.

Figure 1 HFM arrangement for sample surface thermocouples

At 28 days, the samples were oven-dried at 80°C for one month and then at 105°C until achieving constant weight in order to be tested. Thermal conductivity of mortars was measured at $10 \pm 1°C$ as mean temperature and the temperature difference across the two plates was also set to 10°C.

3. RESULTS

3.1. SEM OBSERVATION

SEM micrographs of mortars with LDFA at age 28 and 120 days respectively are shown in **Error! Reference source not found.** and **Error! Reference source not found.**. The low density additions are easily recognisable in the samples due to their perfectly spherical shapes. Some of the LDFA were broken due to the polishing process while others were still intact. The same results were reported in [8] where fewer than 10% of LDFA exposed to the polished surface of the mortars where fractured. The thin shells of LDFA seem to have close physical bounding with the surrounding matrix. Only limited hydration products were found at the surfaces of the additions at both ages. This can be explained by the fact that LDFA are inherently alumina silicate spheres of very low reactivity with the products they are used in, slightly pozzolanic and neutral in pH. There was no evidence of potential reactivity of LDFA at these ages.

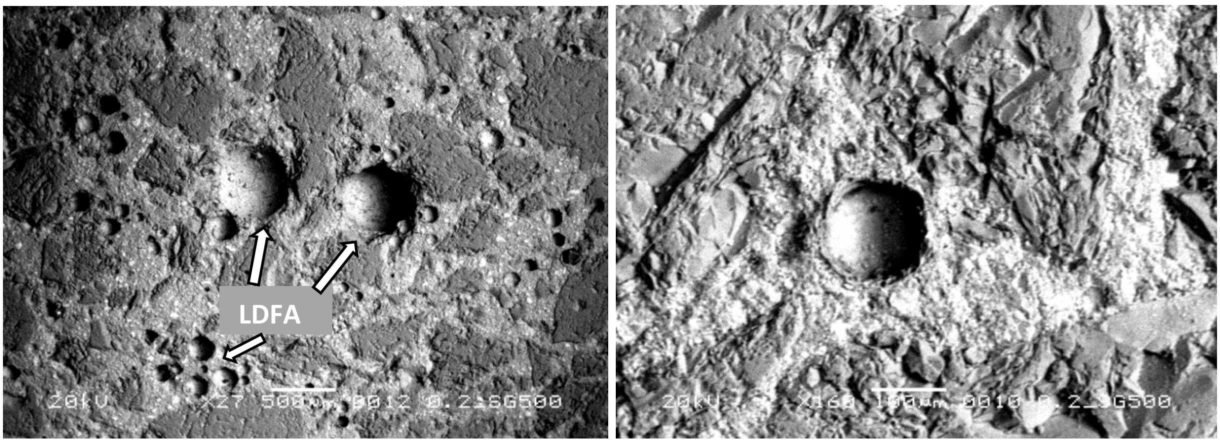

Figure 2 SEM image of polished LDFA-mortars at 28 days

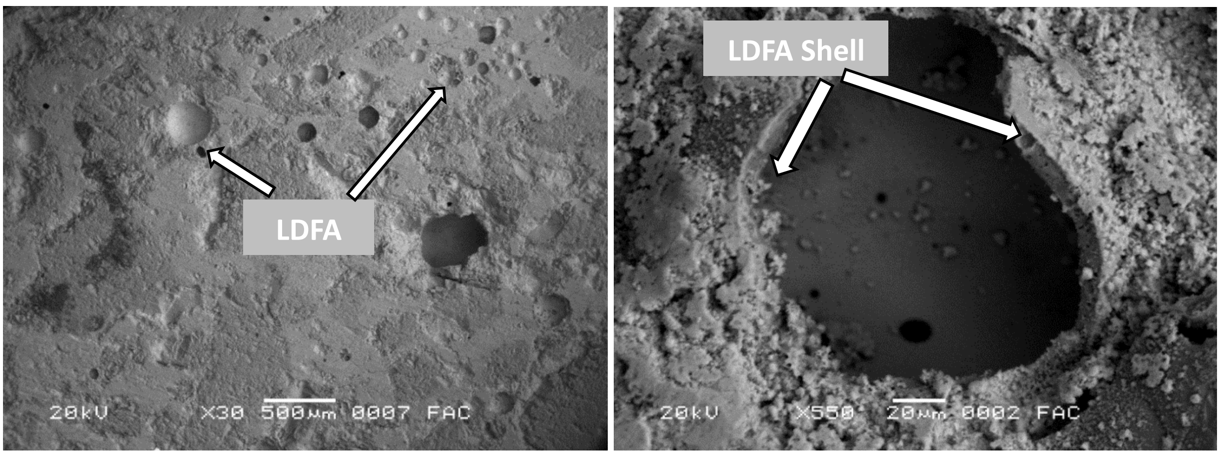

Figure 3 SEM image of polished LDFA-mortars at 120 days

3.2. COMPRESSIVE STRENGTH

Compressive strengths at 28 days for the studied mortars are shown in **Error! Reference source not found.** and **Error! Reference source not found.**. Both LDFA induced a drop of compressive strength at all rates of replacements. However, LDFA-180 showed a better performance, with a decrease of 1.5% and 21% against 20% and 30% for LDFA-500, for 6% and 23% replacement rates respectively. An isothermal calorimetry was carried on the mortars and has shown that the heat of hydration of the mixes decreases with the incorporation of LDFA, which can explain the drop of compressive strength. Other authors [9-10] reported similar results for replacements of 20-30% of cement with ordinary fly ash. Compressive strengths of those mortars showed a drop up to 30% compared to control specimens with the same water/cement ratio at 28 days and were better at 120 days. It would be interesting to investigate the compressive strength of LDFA-mortars at that age to see if the same pattern is followed.

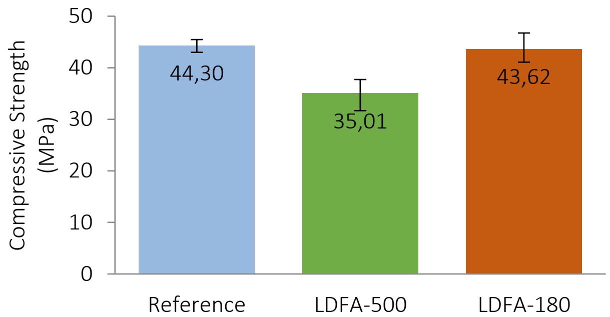

Figure 4 Compressive strength of mortars with E/C=0.56 and LDFA/Cement=6%

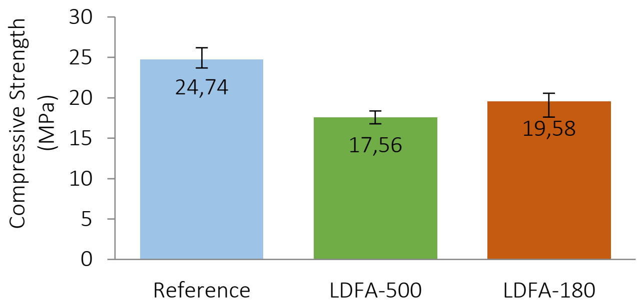

Figure 5 Compressive strength of mortars with E/C=0.9 and LDFA/Cement=23%

3.3. APPARENT POROSITY

Apparent porosity at 28 days of LDFA-mortars and their respective control specimens are shown in **Error! Reference source not found.** and **Error! Reference source not found.**. The apparent porosities of all LDFA-mortars were found to be 2-3% less than the mixes without additions. This can be explained by the fact that apparent porosity does not include sealed pores. A study of µ-tomography reconstruction of cement mortars with low density additions has shown that internal pores of LDFA are less connected to exterior areas compared to other additions like expanded perlite and expanded glass[11].

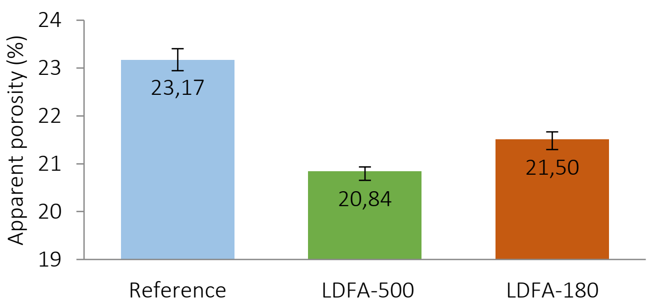

Figure 6 Apparent porosity of mortars with E/C=0.56 and LDFA/Cement=6%

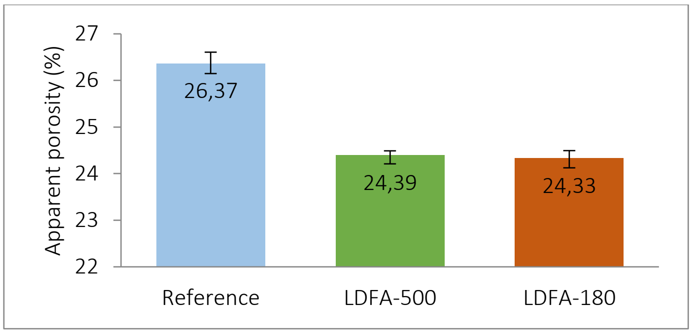

Figure 7 Apparent porosity of mortars with E/C=0.9 and LDFA/Cement=23%

3.4. THERMAL CONDUCTIVITY AND UNIT WEIGHT

As it can be seen in **Error! Reference source not found.** and **Error! Reference source not found.**, thermal conductivity as well as oven dried density of mortars decrease with the increase of LDFA replacements. Oven-dried density and thermal conductivity were respectively 2% and 6% less than control sample for 6% LDFA, and respectively 9% and 20% for 23% LDFA. One of the distinctive effects of the LDFA is its ability to decrease the weight unit and thermal conductivity without additional open porosity. Others studies [5-7] have reported lower thermal conductivities for their designed cement composites using LDFA. This is due to the fact that no aggregates whatsoever except LDFA – considered as micro-aggregates - were used in the mixes. This is an important parameter knowing that the thermal conductivity of sand is not negligible ($\approx 2-3\, W/m.K$) and that it constitutes 47% of the volume of the studied mortars. Samples in [7] showed good insulation behaviour but poor Young modulus due to absence of aggregates.

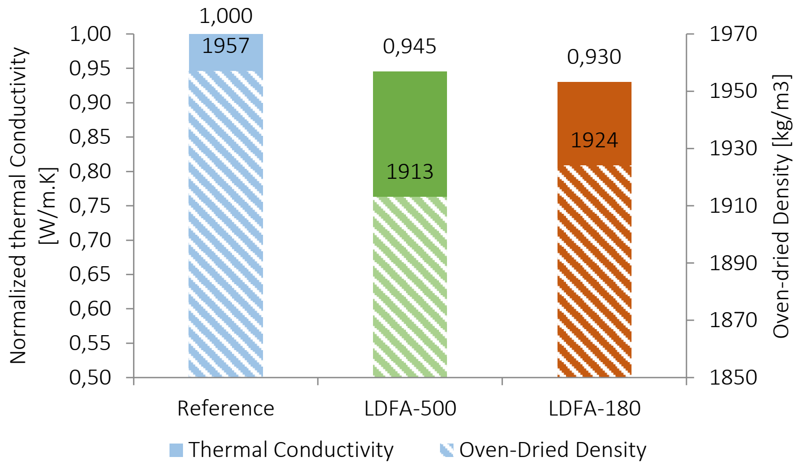

Figure 8 Normalized Thermal Conductivity and ODD of mortars with E/C=0.56 and LDFA/Cement=6%

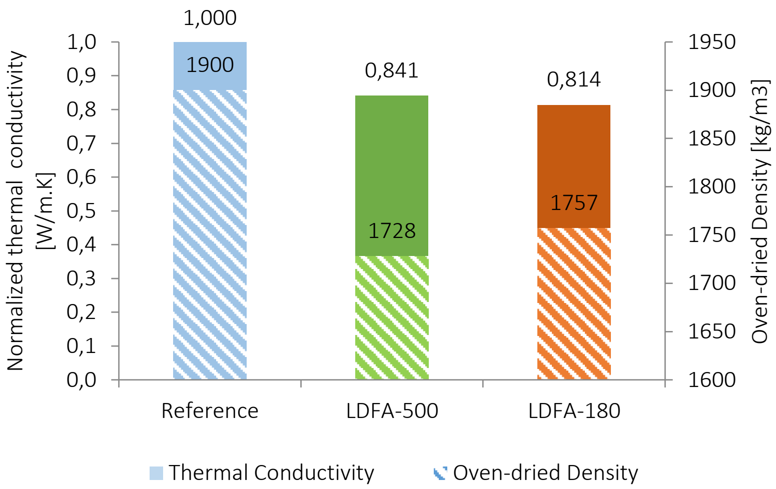

Figure 9 Normalized Thermal Conductivity and ODD of mortars with E/C=0.9 and LDFA/Cement=23%

4. CONCLUSIONS

The valorisation of by-products like low density fly ash through improvement of construction materials seems promising. Good mechanical and thermal properties along with a reduced environmental impact are some of the benefits expected of the use of such products. Partial replacement of cement with LDFA led to a good compromise of mechanical and thermal properties. Thermal conductivity of LDFA-mortars was decreased while maintaining acceptable compressive strength and open porosity, and decreasing oven dried density even at low rate replacements. Better performances were found for LDFA-180.

ACKNOWLEDGMENTS

Authors would like to acknowledge the EU METALIC II Project funded by the Erasmus Mundus Program of the European Union and coordinated by Cardiff Metropolitan University.

REFERENCES

[1] Siddique, R.: Utilization of coal combustion by-products in sustainable construction materials, Resources, Conservation and Recycling, vol. 54, no. 12, pp. 1060–1066, 2010, 09213449.

[2] Zyrkowski, M. et al : Characterization of fly-ash cenospheres from coal-fired power plant unit, Fuel, vol. 174, pp. 49–53, 2016, 00162361.

[3] Blanco, F. et al : Characteristics and properties of lightweight concrete manufactured with cenospheres, Cement and Concrete Research, vol. 30, pp. 1715–1722, 2000, 00088846.

[4] Tiwari, V; Shukla, A. & Bose, A. : Acoustic properties of cenosphere reinforced cement and asphalt concrete, Applied Acoustics, vol. 65, pp. 263–275, 2004, 0003-682X.

[5] Hanif, A. et al: Green lightweight cementitious composite incorporating aerogels and fly ash cenospheres - Mechanical and thermal insulating properties, Construction and Building Materials, vol. 116, pp. 422–430, 2016, 09500618.

[6] Wang, J.Y. et al : Stability of cenospheres in lightweight cement composites in terms of alkali-silica reaction, Cement and Concrete Research, vol. 42, no. 5, pp. 721–727, 2012, 00088846.

[7] Wu, Y. et al : Development of ultra-lightweight cement composites with low thermal conductivity and high specific strength for energy efficient buildings, Construction and Building Materials, vol. 87, pp. 100–112, 2015, 09500618.

[8] Montgomery, D.; & Diamond, S. : The influence of fly ash cenospheres on the details of cracking in flyash-bearing cement pastes, Cement and Concrete Research, vol. 14, no. c, pp. 767–775, 1984, 00088846.

[9] Demirboğa, R. : Influence of mineral admixtures on thermal conductivity and compressive strength of mortar, Energy and Buildings, vol. 35, no. 2, pp. 189–192, Feb. 2003, 03787788.

[10] Lam, L. ; Wong, Y. & Poon, C. : Effect of Fly Ash and Silica Fume on Compressive and Fracture Behaviors of Concrete, Cement and Concrete Research, vol. 28, no. 2, pp. 271–283, 1998, 00088846.

[11] Lanzón, M. et al : X-ray microtomography (μ-CT) to evaluate microstructure of mortars containing low density additions, Cement and Concrete Composites., vol. 34, no. 9, pp. 993–1000, 2012, 09589465.

LADLE SLAG CONTROVERSY

Vesna Zalar Serjun[1], Ana Mladenovic[1]

[1] Slovenian National Building and Civil Engineering Institute, Dimiceva ulica 12, 1000 Ljubljana,
email: vesna.zalar@zag.si, ana.mladenovic@zag.si

SUMMARY: The recycling of ladle slag from the steelmaking industry has become a global need and challenge. The utilization of such slag in cementitious materials is, on the one hand, promising due to its hydraulic properties (it can be used as a supplementary cementitious material), but on the other hand it could be problematical due to its phase composition and possible volumetric instability. This paper presents the results of some experimental investigations and of a microstructure study which were carried out in order to evaluate the possibility of using ladle slag as a partial replacement for cement in the preparation of mortars. Ladle slag blended cement composites were also investigated, and compared to limestone filler blended cement composites, as well as to reference cement composites. The results showed that the investigated slag did not represent an environmental hazard, and that it contained several hydraulic phases. Volume instability of the slag is not expected to occur. In the case of the slag cement composites, a larger proportion of hydration products were observed than in the case of the limestone cement composites, as well as a higher rate of strength increase.

KONTROVERZA O BIJELOJ ZGURI

SAŽETAK: Recikliranje bijele zgure (sekundarne rafinirane zgure) u industriji proizvodnje čelika postalo je globalna potreba i izazov. Upotreba takve zgure u cementnim materijalima obećavajuća je zbog njezinih hidrauličkih svojstava (može ju se upotrijebiti kao dodatak cementnom materijalu) ali može biti i problematična zbog njezina faznog sastava i moguće volumenske nestabilnosti. U radu se prikazuju rezultati nekoliko eksperimentalnih istraživanja i studija mikrostrukture provedenih radi ocjene mogućnosti upotrebe bijele zgure kao djelomične zamjene cementa pri pripremi mortova. Ispitani su kompoziti od mješavine cementa i zgure i uspoređeni s mješavinama cementa i vapnenačkog filera kao i s referentnim cementnim kompozitima. Rezultati pokazuju da istražena zgura ne predstavlja opasnost za okoliš i da sadržava nekoliko hidrauličkih faza. Ne očekuje se da će doći do volumenske nestabilnosti zgure. Kod cementnih kompozita sa zgurom opažen je veći udio produkata hidratacije nego li kod kompozita s vapnencem a i veća brzina povećanja čvrstoće.

1. INTRODUCTION

Globally, the management of steelmaking slags has become an issue of growing importance. According to recently adopted European regulations, conventional management methods involving dumping are now being replaced by methods which lead to waste stabilization and safe recycling. These methods may also lead to the recovery of valuable raw materials from potentially dangerous materials, in order to enable their cascade utilization and proper final use. However in many EU states steelmaking slags have already been declared as a by-product or a product. Different types of slag have different potentials for recycling, and ladle slag (LS) has the lowest such potential. Due to its fine grain size and adverse properties with regard to leaching, ladle slag has a low potential for recycling. For this reason about 80 % of it is currently landfilled, taking into account the whole of the EU [1].

The ideal sector for the consumption of the slag is the building industry. In the construction sector two synergetic effects are achievable: large amounts of material can be consumed, and hazardous elements and components can be permanently immobilized. An additional benefit lies in the fact that LS has latent hydraulic components, and may be considered as a cementitious material. Steelmaking slags could be either low-cost materials in applications where low demands are expected, or products with a high-added value that could improve the properties of the final products. At present, LS is still an innovative option, being less extensively used in the building sector than other steelmaking slags. The possible applications of LS are diverse, and could be extended to any field where their use is permitted, advised or even recommended by imagination, common sense, and/or good practice.

Each type of LS has its own characteristics, so accurate knowledge about the chemical, mineralogical and morphological properties of steel slags is essential because their cementitious and mechanical characteristics, which play a key role in their possible re-use, are closely linked to these properties. Further, the reaction mechanisms of secondary metallurgical slags as supplementary cementitious materials (SCM) in cement composites are not yet well understood, which is true also for the hydration products which are formed over longer time intervals. More detailed knowledge is needed in this field in order to boost the commercialization and beneficial use of slags of this type in the building and construction industry.

The aim of this work was to provide a study of the compositional, microstructural, and activity characteristics of secondary metallurgical slag obtained from refining processes of stainless steel production, and of its influence as a SMC on the properties of cement composites. Ladle slag was used at a 30 % substitution rate. In order to compare the effect of ladle slag to that achieved by conventional supplementary cementitious material, the properties of cement composites made with the ladle slag were compared to those in which a limestone filler was used as a SCM. The blended cement composites were then compared to the reference cement composites. In order to verify the utilisation potential of the investigated ladle slag as manufactured, directly after industrial recycling, the slag was not laboratory pre-treated in any way. In order to enhance the recycling of this kind of slag in the construction and civil engineering sector, we investigated its possible usage as a cement supplement precisely in the form as it was received from the producer.

2. MATERIALS AND METHODS

Ladle slag (LS) from secondary metallurgical processes, generated at the Acciaierie Bertoli Safau (ABS) steelworks, Italy was used for the investigations. It consisted of a mixture of slag derived from a vacuum oxygen decarburization process and ladle furnace slag. Limestone filler (LF), obtained from the dust collection systems during aggregate production, and Portland cement CEM I (PC) was also used. Pastes and mortars in which 30% of cement by mass was replaced by slag were prepared. In order to establish a basis for comparisons, pastes and mortars in which 30% of the cement by mass was replaced by a limestone filler were also prepared, as well as reference 100% PC based pastes and mortars. The water/binder ratio in all of the investigated pastes and mortars was selected to be 0.5. The aggregate in the mortars was crushed dolomite, with a gradation of 0/4 mm.

A chemical analysis of the LS was performed by means of inductively coupled plasma mass spectrometry. In order to estimate the leachability of elements from the LS, a compliance test for the leaching of granular waste materials and sludges [2] was followed. The phase analysis was performed by X-ray diffraction Rietveld refinement quantitative analysis (XRD QPA). The amorphous phase and mono-sulphoaluminate were not quantified since the Rietveld refinement was performed in terms of a semi-quantitative analysis, and because of a lack of data with respect to the structure of the Ms. In order to emphasize the quantities of potentially expansive mineral phases in the LS, thermogravimetric (TG-DTG) analyses was applied as a complementary method. SEM/EDS of the LS was also carried out. Since activity is an important characteristic of slag when used as a SCM in blended cement composites, this property, too, was evaluated. As no standard exists for the determination of an activity index for this type of slag in the case of applications in cement-based materials, it was decided to apply the standard SIST EN 15167-1 [3] for ground granulated blast furnace slag (GGBFS). The particle size distribution was determined by a combination of dry sieving according to SIST EN 933-1 [4], and laser diffraction analysis. The Brunauer, Emmet, and Teller (BET) surface area, sorption isotherms and pore size distribution of the slag and the limestone filler, were determined by nitrogen gas sorption. The mechanical properties of the mortars were tested after 2, 7, 28 and 90 days of hydration. The compressive and flexural strengths at these ages were determined according to the standards SIST EN 1015-11/A1 [5] and SIST EN 196-1 [6].

3. RESULTS AND DISCUSSION

3.1. CHEMICAL AND MINERALOGICAL COMPOSITION OF THE LS

The chemical composition of the investigated slag revealed that the major elements of LS were Ca (22.6 wt. %), Fe (18,5 wt. %) and Al (6,8 wt. %), followed by Si (3,5 wt. %) and Mg (1,9 wt. %). Since ladle slag is a by-product of the steel-making industry, it contains small quantities of Cr (0,3 wt. %), Mn (3,8 wt. %), Ti (0,1 wt. %) and Ni (0,1 wt. %), in the form of minor elements. All the other constitutional components represent trace elements. In order to estimate the possible release of elements from the LS, a leaching test was applied, and the results were compared to the maximum permitted values set by the Slovenian legislation for inert waste. The results showed that all concentrations of the defined elements (Cr, Cu, Zn, Ni, Pb, Ba, Cd, Mo, As, Sb, Se, Hg) in the LS leachates were within the limits set by the presently valid legislation.

The XRD QPA showed that the most abundant phases in the ladle slag were calcium aluminates (tricalcium aluminate, mayenite) and metallic mineral compounds (wüstite, spinels, Fe alloy, hematite) followed by calcium silicates, portlandite, periclase, gehlenite, calcite and brownmillerite. The dicalcium silicates (C_2S), which occur in two allotropic forms (reactive β form and weakly reactive γ form), prevailed over the C_3S.

The presence of βC_2S, CaO and MgO as mineral phases in the slag microstructure can cause long-term instability (disintegration and swelling) of the slag. Except for the γC_2S, all the other forms of C_2S in slag are metastable at room temperature; whereas CaO and MgO tend to react rapidly with water and CO_2 [1, 7]. The quantity of βC_2S in LS is about 5 wt. %. Beta C_2S is known as a hydraulic phase, which can be considered as a stable form when its size is less than the critical size [7].

TG-DTG analysis was applied as a complementary test method in order to define more precisely the quantities of MgO and CaO. The results were then compared to the only determined limiting values of MgO and CaO which were defined for a conventional SCM (fly ash) [8]. Figure 1 shows the results of the TG-DTG analysis of the LS. It illustrates several mass losses. The TG-DTG values up to 400 °C show several maxima, which could not be used to determine the individual phase components due to the overlapping of DTG maxima. In this temperature range mass losses can be associated with the removal of moisture and loosely bound water (Chen et al., 2011), and also with the dehydration of different hydration products [9]. Since the significant maxima at 381°C can be correlated with microcrystalline $Ca(OH)_2$ [10], $Mg(OH)_2$ [11], and C_3AH_6 [9], this change in mass could not be defined in greater detail. The mass loss with a maximum at 429 °C was attributed to the dehydroxylation of the portlandite, whereas the maxima at 675 °C reflected the CO_2 which was released during the decomposition of calcium carbonate. The weight losses, defined by the TG-DTG analysis, with observed maxima at 429 °C and 675 °C, indicate that 8.2% and 2.7% of the total CaO content occur in the form of Ca $(OH)_2$ and $CaCO_3$ respectively. According to SIST EN 450-1 [8], the threshold content of reactive MgO and CaO in fly ash is 4 and 10 wt.%, respectively. The results of the TG-DTG analyses, in comparison with those obtained by XRD QPA, revealed a 0.9% and 0.5% higher content of portlandite and calcite, respectively. Nevertheless, the calculated primary total free CaO content in the slag (7.76 wt.%), which was later hydrated and carbohydrated, did not exceed the limit value of CaO prescribed in the European standard for fly ash. The content of MgO in the investigated slag exceeded the prescribed limit by less than 2.0 wt.%.

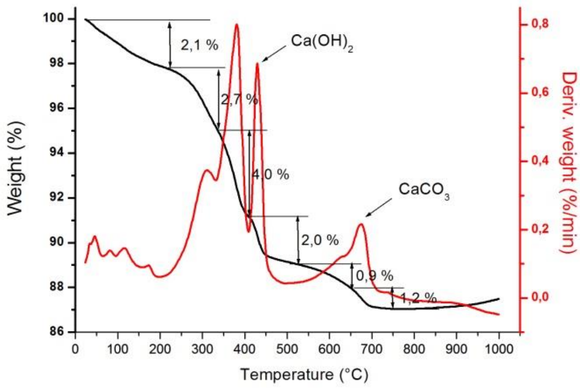

Figure 1 The TG-DTG results of the investigated LS

The results of SEM/EDS analysis are in agreement with the results obtained by the XRD and TG/DTA. Some other minor phases were further defined by SEM/EDS, such as: calcium aluminate, calcium ferrite, rankinite, merwinite, akermanite, forsterite, lime and oldhamite. Furthermore, mainly on the edges of the calcium aluminate phases, it was possible to observe hydration reaction products. Based on the results of the EDS analysis, the phases of these products were assigned to calcium aluminate hydrates (C-A-H). The SEM/EDS also revealed that the chromium in the LS is present mainly in the form of a highly insoluble chromite mineral, which belongs to the spinel group. This explains the low concentrations of Cr in the LS leachate.

Evaluation of slag activity showed that, at an age of 7 days, the activity index was relatively low, i.e. 35%. Furthermore, at an age of 28 days it was still very low, a value of 38% being measured in comparison with the values prescribed for GGBF slag in EN 15167-1 [3], which are a minimum of 45% and 70% at 7 and 28 days, respectively. The measured activity index of the LS showed that it cannot be used as a conventional slag SCM (GGBFS) as the prescribed values were not fulfilled (Figure 2). Nevertheless, since the activity index of the slag increases during curing, a comparison of the values prescribed for GGBF slag with the activity index of the LS in the cement composite investigated further in the research, i.e. mortar with the ratio PC : LS of 70 : 30, was performed. At an age of 7 days the hydraulic activity of the LS in the mortar in which 30 wt. % of cement was replaced by LS exceeded the limit value prescribed in the standard by 18%, whereas at an age of 28 days the activity index was below the prescribed values, but only by less than 4%. Such a comparison indicates that the activity of the LS in cement composites in which 30 wt. % of PC is replaced by LS is very comparable to the values in the standard, which specifies a 50% replacement of PC with GGBFS (Figure 2).

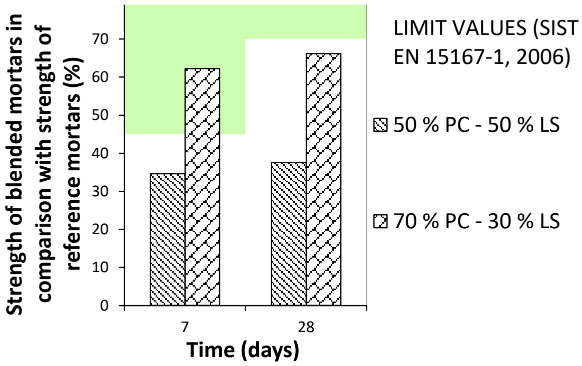

Figure 2 Measured indices of the hydraulic activity of the ladle slag cement mortars, showing the limits set for GGBFS

3.2. PHYSICAL PROPERTIES OF THE LS AND LF

The results of the particle size distribution analysis show that, in comparison with the limestone filler, the slag consisted of coarser grained particles, and had a wider particle size distribution, as 90% of the grains were smaller than 480 µm for the slag, but only 60 µm for the limestone powder. Almost half of the grains of the slag and only about 16% of the limestone particles were bigger than 45 µm. The mean particle size value was six times greater in the slag than in the limestone. The particle size distribution of the slag and the limestone was shown to be non-uniform, with a more or less bi-modal distribution. Measurements of the nitrogen sorption isotherms of the slag and the limestone filler were also performed (Figure 3 A).

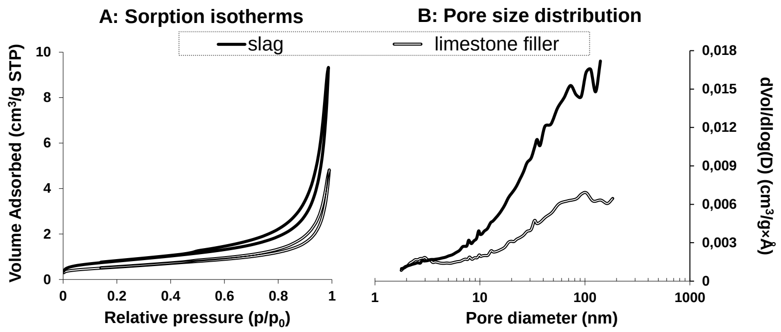

Figure 3 Sorption isotherms (A) and pore size distribution curves (B) of the investigated slag and the limestone filler, determined by nitrogen adsorption analysis

The profiles of the slag and limestone isotherms exhibit a type IV isotherm according to the ISO 15901-2 [12] classification, with narrow hysteresis loops of type H3. This type of isotherm is generally associated with porous solids consisting of particle aggregates [12, 13]. The low gas uptake at a relative pressure of < 0.2 indicates the absence of micro porosity and, since the adsorption limit is not well defined at a relative pressure dosage up to one, this points to the presence of macroporosity in both of the investigated materials [13, 14]. This is even more evident from the curves showing the nitrogen sorption pore size distributions (Figure 3 B), where macropores (which mainly fall within the range 60-150 nm) are the most abundant. The BET specific surface area was found to be almost 1.5 times higher in the case of the slag than in the case of the limestone filler, the corresponding measured values being equal to 2.8 and 1.9 m^2g^{-1} respectively.

3.3. MINERALOGY OF THE CEMENTITIOUS PASTES

The hydration products of the cement pastes incorporating LS (S) were determined and compared to those of the cement pastes incorporating the LF (L), and those of the reference cement pastes (R). The influence of the hydration time (1, 2, 7, 28 or 90 days) on the hydration products was monitored. A significant difference in the newly formed hydration products of all three of the investigated pastes was observed, when the S and F pastes were compared to the R pastes. Whereas in the R paste mono-sulphoaluminate could be observed, no monocarboaluminate could be detected. On the contrary, mono-carboaluminate occurs in the S and F pastes, whereas monosulphoaluminate could not be identified. Such an observation can be attributed to the fact that, in the presence of limestone, AFm-carbonates are formed rather than sulphate-containing AFm phases. The evolution of the quantified hydration phases over time can be seen in Figure 4.

Since the proportion of replacement of PC in the two different blends of the cement composites was the same, and since the investigated slag contained both calcium aluminates and calcium silicates, it was to be expected that, in general, all of the hydration products would be more abundant in the slag pastes than in the limestone filler pastes. Whereas calcium silicates constituted the prevailing phases in the R pastes, C-S-H and portlandite were the most abundant in these pastes. The quantity of all the hydration products in the pastes increased over time, except for ettringite. The progress of ettringite formation in the S pastes differed from that in the F pastes but was comparable to that in the R pastes. As has already been highlighted by several researchers, the decrease in the amount of ettringite during the hydration of PC may be attributed to the formation of mono-sulphoaluminate or a hydroxy-AFm phase hydrocalumite solid solution.

As the presence of limestone (calcite) affects the hydration of PC by reacting, primarily, with the C3A to form carboaluminates [15], Mc started to appear in both of the two different blends. Katoite was present in the largest quantities in the S pastes, since the slag contained a large quantity of calcium aluminates and thus presented a stabilized form of some of the metastable AFm phases.

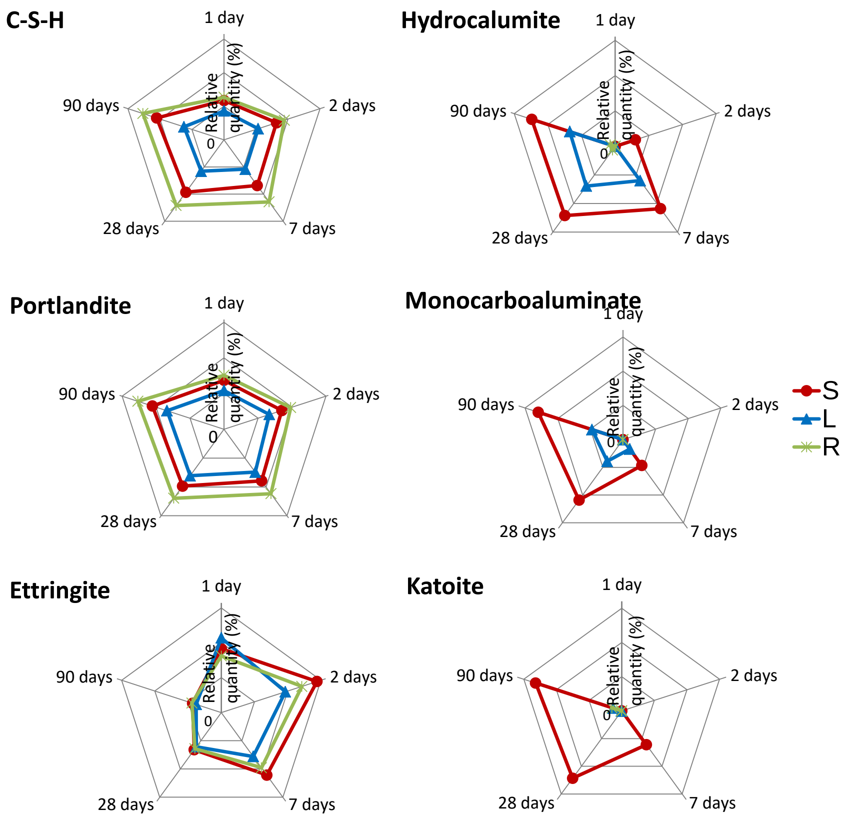

Figure 4 Evolution over time of the quantified hydration phases in the cement pastes incorporating the ladle slag (S), the limestone filler (L), and in the reference cement pastes (R)

3.4. MECHANICAL AND PHYSICAL PROPERTIES OF THE CEMENTITIOUS MORTARS

The mechanical strength of the cementitious mortars was tested after 2, 7, 28 and 90 days of hydration. The development of compressive strength over time (f_t), was defined by empirical constants defining the initial strength (A in MPa) and the rate of strength increase (B in MPa/(ln days)) [16]. Although the initial strength (A) of the slag-containing mortars was lower than that of the mortars containing the limestone filler, the rate of strength increase (B) of the former was higher than that of the latter (Figure 5). This can be attributed to the larger amount of hydration products formed in the case of the slag cement composites compared to the limestone filler cement composites. produced in colour in the book.

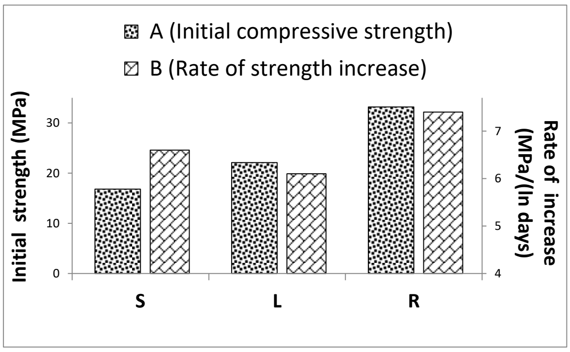

Figure 5 The development of compressive strength over time of LS mortars (S), LF mortars (L) and reference mortars (R)

Based on the measured compressive strengths, the slag mortar can be classified as masonry mortar of class M35, according to the criteria prescribed by the standard SIST EN 998-2 [17].

4. CONCLUSIONS

The results of the research showed that the studied slag is a crystalline reactive material which contains about 50 wt. % of hydraulic phases and it does not represent an environmental hazard due to low mobility of toxic elements. The volume instability of investigated slag is not expected to occur. The results of the tests showed that the activity of the ladle slag was, despite its observable hydraulic activity, rather weak in comparison with the values prescribed for conventional slag SCM. In the case of the slag mortar, a larger degree of strength development was observed in comparison with the mortar which contained the added limestone filler. This was attributed to the larger proportion of hydration products which were formed in the slag cement composites. The investigated slag mortars can be classified as mortars of class M35. In various civil engineering applications, materials with different levels of quality are needed, so it is best if they satisfy the requirements for the selected application, neither more nor less. Only in this way will the substantial resources be used optimally.

ACKNOWLEDGMENTS

The authors acknowledge the financial support from the Slovenian Research Agency (research core funding No. P2-0273).

REFERENCES

[1] Serjun, V.Z., Mirtič, B., Mladenovič, A.: Evaluation of ladle slag as a potential material for building and civil engineering, Materials and Technology, 47 (2013) 5, pp. 1580-2949, 543-550
[2] SIST EN 12457-2, 2004. Characterisation of waste – Leaching – Compliance test for leaching of granular waste materials and sludges. Part 2, One stage batch test at a liquid to solid ratio of 10 L/kg for materials with particle size below 4 mm (without or with size reduction)
[3] SIST EN 15167-1: 2006. Ground granulated blast furnace slag for use in concrete, mortar and grout- Part 1: Definitions, specifications and conformity criteria
[4] SIST EN 933-1:2012. Tests for geometrical properties of aggregates - Part 1: Determination of particle size distribution - Sieving method
[5] SIST EN 1015–11: 2001/A1: 2007. Methods of test for mortar for masonry. Part 11, Determination of flexural and compressive strength of hardened mortar
[6] SIST EN 196-1:2005. Methods of testing cement - Part 1: Determination of strength
[7] Barnes, P. & Bensted, J.: Hydration of Portland cement, In Structure and Performance of Cements, Taylor and Francis, 0-419-23330-X, London; New York, (2002), pp. 57-113
[8] SIST EN 450-1:2013. Fly ash for concrete- Part 1: Definition, specifications and conformity criteria
[9] Antonovič, V. et al.: The Effect of Temperature on the Formation of the Hydrated Calcium Aluminate Cement Structure, Procedia Engineering, 57 (2013), pp. 99-106, Y506-4252. - 1877-7058
[10] Medveššek, S. et al.: Hydration Products in Water Suspension of Portland Cement Containing Carbonates of Various Solubility, Acta chimica Slovenica, 53 (2006) 2, pp. 172-179, 1318-0207

[11] Zhang, F. et al.: Attack of limestone cement-based material exposed to magnesium sulfate solution at low temperature. Journal of Wuhan University of Technology-Material Science Eddition, 29 (2014) 3, pp. 507-512, 1000-2413

[12] ISO 15901-2: 2006. Pore size distribution and porosity of solid materials by mercury porosimetry and gas adsorption. Part 2: Analysis of mesopores and macropores by gas adsorption

[13] Navarro, C., Díaz, M., Villa- García, M.A.: Physico-chemical characterization of steel slag. Study of its behaviour under simulated environmental conditions, Environmental Science & Technology, 44 (2010) 14, pp. 5383-5388, 0013-936X

[14] IUPAC: Manual of symbols and terminology, Appendix 2, Part 1, Colloid and Surface Chemistry, The Journal of Pure and Applied Chemistry Research, 31 (1972), pp. 579-638

[15] Ramezanianpour, A.M., Hooton, R.D: A study on hydration, compressive strength, and porosity of Portland-limestone cement mixes containing SCMs, Cement and Concrete Composites, 51 (2014), pp. 1-13, 0958-9465

[16] Abd elaty, M.: Compressive strength prediction of Portland cement concrete with age using a new model, HBRC Journal, 10 (2013) 2, pp.145–155, 1687-4048

[17] SIST EN 998-2: 2010. Specification for mortar for masonry- Part 2: Masonry mortar

TRANSFORMATION OF WOOD ASH WASTE INTO CONSTRUCTION MATERIALS

Neven Ukrainczyk[1], Eduardus A.B. Koenders[1], Nina Stirmer[2]

[1] Technische Universität Darmstadt, Institute of Construction and Building Materials, Franziska-Braun-Straße 3, 64287 Darmstadt, Germany, email: ukrainczyk@wib.tu-darmstadt.de, koenders@wib.tu-darmstadt.de
[2] University of Zagreb, Faculty of Civil Engineering, Department of Materials, Fra Andrije Kacica Miosica 26, 10 000 Zagreb, Croatia, email: ninab@grad.hr

SUMMARY: This work investigates partial replacement of cement with fly ash waste generated by burning forest residues and waste wood from the timber industry. The ash has minerals complementary to Portland cement with a relatively high amount of free CaO and MgO that might exert significant expansion. The ash exhibits hydraulic and pozzolanic activity that initially increases and subsequently decreases the amount of portlandite in the hydrated material. With ash addition the rate of hydration, strength and workability are decreased. Optimum dosage showed 15 % of ash, where it replaces 5 % of cement and 3.33 % of sand, which can still produce a structural grade cementitious material with acceptable workability and mechanical properties.

PRETVORBA PEPELA IZ DRVNOG OTPADA U GRAĐEVNI MATERIJAL

SAŽETAK: U radu je istražena djelomična zamjena cementa otpadnim letećim pepelom dobivenim izgaranjem šumskih ostataka i otpadnog drva iz drvne industrije. Pepeo sadržava minerale komplementarne portlandskom cementu s relativno velikim udjelom slobodnoga CaO i MgO koji bi mogli prouzročiti znatno širenje. Pepeo pokazuje hidrauličku i pucolansku aktivnost koje u početku povećavaju, a potom smanjuju količinu portlantida u hidratiziranom materijalu. Dodatkom pepela smanjuju se brzina hidratacije, čvrstoća i obradivost. Pokazalo se da je optimalno doziranje 15 % pepela koji zamjenjuje 5 % cementa i 3,33 % pijeska čime se može proizvesti cementni materijal konstrukcijske kvalitete uz prihvatljivu obradivost i mehanička svojstva.

1. INTRODUCTION

Woody and agricultural biomass are among the highest biomass potentials for energy production as a sustainable fuel. This will lead to the production of a foresee amount of 15.5 million tons of biomass ash in the EU-28 [1], which will double its current amount. Presently, most ashes in Europe are landfilled, causing financial and material losses as well as an environmental burden. In general, biomass ash composition and properties are highly variable depending on: 1) type of base-biomass feed stock, 2) geographical location, 3) combustion technology (e.g. fixed bed, or pulverized fuel boilers). Further classification of ashes is done by type of collection from a boiler: 1) Bottom ash, 2) Relatively coarse fly ash, and 3) Fine fly ash. A possible application for biomass ash is as a cement and/or sand replacement in cementitious materials [2-4]. However, some standards (e.g. EN 450-1) prohibit use of biomass ash in concrete. This results in rising costs for the biomass ash waste management that forces power plant owners to search new opportunities to recycle ashes.

2. EXPERIMENTAL

Materials used are: 1) Commercial cement CEM II/A-M(S-V) 42.5N. Blended cement was chosen for possible synergy with biomass ash, namely an activation of the pozzolans in the cement by alkalies in ash. 2) Fly ash produced by 1MWe co-generation plant Lika Eko-Energo d.o.o., Udbina, Croatia: with a fixed bad (moving grate) furnace fuelled by forest residues and waste wood from timber industry in Croatia. TGA was done with NETZSCH STA409, 10 K/min, 50mg Pt crucible with N_2 flow of 30 cm^3/min. The hydration was stopped by grinding the sample with addition of acetone in agate mortar (exposure to CO_2 was minimized). Scanning electron micrographs (SEM) were obtained using a SEM-TESCAN VEGA TS5236LS scanning microscope. Samples were placed over a graphite strip and coated with gold. Specific surface area of cement and fly ash was measured by a BET method using Micromeritics ASAP 2000. Mortar mixtures M, M10F10, M15F15, M20F20, M5F15 are designated by M (reference: 450g cement and 1350g sand, w/b=0.5), followed by the number representing the percentage of mass ratio between wood ash and cement. Paste mixtures are prepared with w/b=0.5, where P is a reference (45g cement), P10 has 10 % cement replacement with wood ash, P15, P20, P30, and WA (only woody ash). By Le Chatelier tests (cylinders H=D=30mm), the paste expansion value is obtained as a difference (d_2-d_1) between distance of the Le Chatelier needle tips before (d_1) and after boiling (d_2).

Table 1 Experimental plan for mortars (for pastes see text).

Sample name	Stand. Sand, g	Cement, g	Wood ash (WA), g	WA/binder, %	Sand replace-ment, %	Cement replace-ment, %	Workability, mm
M	1350	450	0	0	0	0	
M10	1317	438	45	10	2.5	2.7	
M15	1301	432	67.5	15	3.7	4.1	155±5
M20	1284	426	90	20	4.9	6.4	

3. RESULTS AND DISSCUSION

3.1. WOOD ASH CHARACTERISATION

Chemical composition of wood ash obtained by XRF (on pressed tablets, mass. %) was: 15% SiO_2, 55.5% CaO, 10.7% K_2O, 2.59% Al_2O_3, 2.66% MgO, 3.98% Fe_2O_3, 1.4% SO3, 0.64% Na_2O, 0.51% TiO_2, 0.9% P_2O_5, 0.037% Cr_2O_3, 0.045 ZnO, 0.63% MnO, 0.127% BaO, 0.073% SrO, 0.032% CuO, 0.053% SnO_2, 0.056% Rb_2O, 0.1% ZrO_2, 0.01% Y_2O_3. It shows a relative high level of CaO, MgO and K_2O. Total alkali oxides may be considered acceptable in amounts up to 2% in cement and up to 5% in fly ash (EN 450-1). Alkali content in woody ash was around 10% which contributes with 1.5% for 15% replacement of the cement. However, higher additions of ash were investigated here as well, because the alkalies in biomass ash are were expected to activate the pozzolans in the blended cement, and subsequently combine with pozzolanic calcium-silicate hydrates in the long term. Besides alkalies, the ash also didn't meet the following EN 450-1 requirements: reactive CaO less than 10%, reactive SiO_2 greater than 25%, MgO less than 4%, the sum of (SiO_2 + Al_2O_3 + Fe_2O_3) greater than 70%. Moreover, the ashes might require attention on the amounts of Cr, Cd and Zn. Chloride content of the ash was below 0.1% limit: 0.037% for water soluble, and 0.054% for acid soluble. The amount of unburned carbon (EN15104) was 1.87%.

Analysis of wood ash by X-ray diffraction (Figure 1) determined the main mineral phases of the sample as being: lime (free CaO, 4.5%), MgO (2%), larnite (β-C_2S), calcium carbonate ($CaCO_3$), quartz (SiO_2), Brownmillerite (C_4AF) and calcium aluminosilicate (C_2AS). Excessive amounts of free CaO and MgO (above 1%) must be avoided as this may cause expansion, cracking and strength loss of the hydrated material.

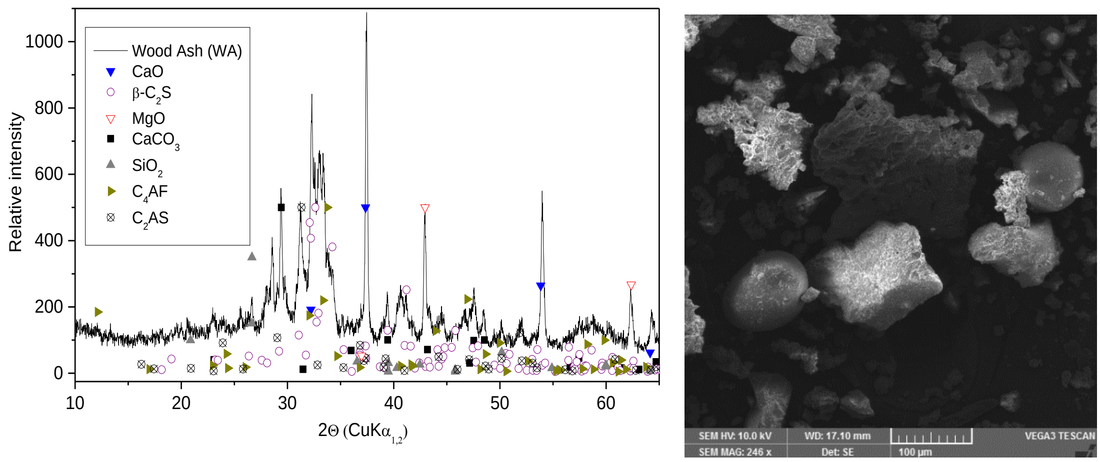

Figure 1 left: XRD analysis of fly ash; right: SEM micrographs showing the morphological diversity of woody ash particles

SEM-SE micrographs (Figure 1 right) shows the morphological diversity of woody coarse fly ash, ranging from spherically fused to irregularly shaped and porous particles. The specific surface area obtained by BET for cement (1.66 $m^2 g^{-1}$) is higher than for woody fly ash (0.58 $m^2 g^{-1}$). This is in agreement with results obtained from the particle size distribution (Fig 1) where 50 vol. % of the fly ash particles were bigger than 146 µm, while for cement this was 24.5 µm with a maximal particle size of 40 µm.

3.2. EFFECT OF WOOD ASH ON CEMENT HYDRATION

The analysis of calorimetric results (Figure 2 left) shows that the end of the induction period occurred after 2, 5, 6 and 7 hours respectively for samples with an increased content of woody ash. The hydration of pure cement achieved the highest and narrowest first heat maximum in the shortest time, i.e. the reaction quickly moved into the induction period. Contrarily to this, woody ash had an elongated first hydration maximum, and had not a visibly expressed induction period, but the reactions of dissolution and precipitation overlapped. With addition of woody ash, two initial maximums were expressed. The first, earliest one (at 0.1 hrs) was reduced, while the second (at 1 hrs) was increased (Figure 2 left). The addition of ash showed a retardation of setting time, a lower main maximum of the reaction rate reached at later times (11, 15, 16 and 17h), while demonstrating the extensive retardation of cement hydration by ash. Due to the retardation of the hydration reactions the final heat evolved after 45 h significantly decreased with (10, 20 and 30%) ash addition: by -6%, -13% and -25% of the reference cement, respectively. The hydration of ash alone exhibited a significant hydration heat development, attributed to hydration reactions of CaO and MgO, as well as larnite and aluminate phases.

Results of volume stability (soundness) tests (Figure 2 right) show that addition of more than 15% of ash results in unacceptable expansions (the limit value is 10mm) which increases very rapidly with further ash dosage. It is interesting that the 10% addition shows lower expansion than plain cement paste, as confirmed by three mixing repetitions of the test, with a total of 9 replicates. For hydration of plain ash the expansion of 70 mm was observed already after 24 h of curing, even without boiling. The effect of this detrimental expansion could be minimized/avoided by washing (pre-hydration and carbonation) and mechanical (grinding) pre-treatments.

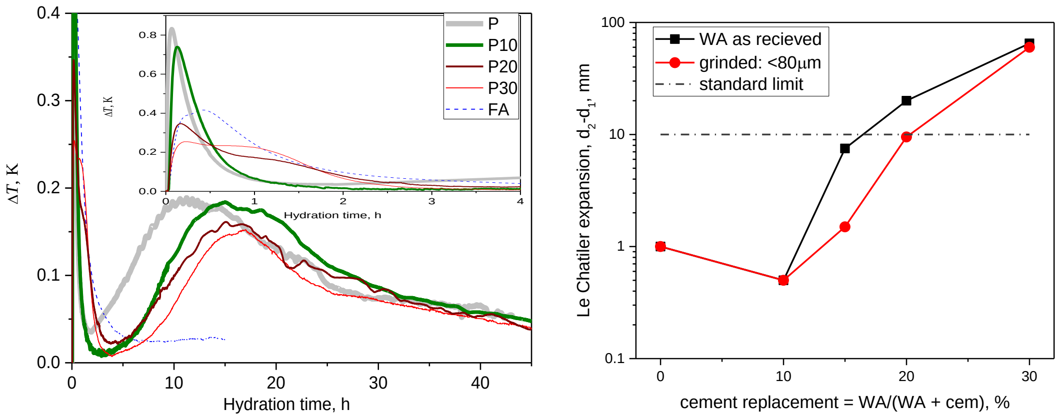

Figure 2 left: isothermal calorimetry; inset: of the first 4 hours. right: Le Chatilier expansion

XRD results (Figure 3) shows the effect of ash addition. Beside clinker phases, also the following hydration products were identified: $Ca(OH)_2$, ettringite, AFm (anionic clay) phases, namely C_4AH_x and Monosulphate aluminate. With elapse of hydration time there was a relative increase in diffraction peaks of the hydration products, predominantly $Ca(OH)_2$, $CaCO_3$ and calcium-silicate hydrate (CSH), as well as ettringite and AFm phases. Unfortunately, overlap of $CaCO_3$ and amorphous CSH diffraction lines (at around 29.3 degrees two theta) made their separation and semi-quantitative analysis impossible. Hydration of ash alone showed the development of C_4AH_x, $CaCO_3$ and/or CSH. The main effect of ash on hydration visible by semi-quantitative XRD analysis was in production of the C_4AH_x phase, which increased with ash addition and with hydration time. This demonstrates that ash had a reactive form of aluminate phases, namely C_4AF and C_2AS (Fig 1 left), which contributed to a pozzolanic reaction that reduced the content of the most soluble $Ca(OH)_2$. Moreover, very interestingly was the hydration of ash alone, showing formation of a very stable, desirable and durable hydration product stratlingite (C_2ASH_8), whose origin may be attributed to a combined hydration of C_4AF and C_2AS [5].

The thermogravimetric analysis (Figure 4) of investigated binders shows a gradual loss of mass during temperature increase. The mass loss is the consequence of the release of water from the hydration products until approx. 400 °C and decarbonization after approx. 600°C. The breakdown of Ca(OH)2 occurs at around 430 °C. The loss of mass until 400°C is the result of the breaking down of CSH gel, AFm phases and ettringite. Based on the loss of mass (water) at 430 °C and stoichiometry of Ca(OH)2 decomposition, the amount of Ca(OH)2 per mass of powder has been calculated by employing a tangential approach [6] and is shown in Fig 5 up. In the case of pure cement hydration, the Ca(OH)2 content reaches its maximum on the 7th day. In wood ash hydration, the maximum Ca(OH)2 content is achieved at day 3, which points to pozzolanic activity. By adding the ash, the reduction of Ca(OH)2 content occurs after 28 days of hydration. This can be explained with the pozzolanic activity of the biomass fly ash and/or the activation of pozzolanic ingredients in the cement.

Specimens mixed with a constant water-to-cement ratio showed a decrease in workability by increasing ash content (samples with 10, 15 and 20 % cement replacement). This can be attributed to a coarser size distribution of ash than cement only. With increasing cement replacement level the strength reduced. However, with a 15% dosage of ash, which replaced only 5% of cement, but 3.33% of the sand, still a good structural grade mortar (or concrete) with acceptable mechanical properties was produced. The results (Fig 5 down) also show that the compressive strength of all mixtures reduced once cured in a heated water bath at 100 °C.

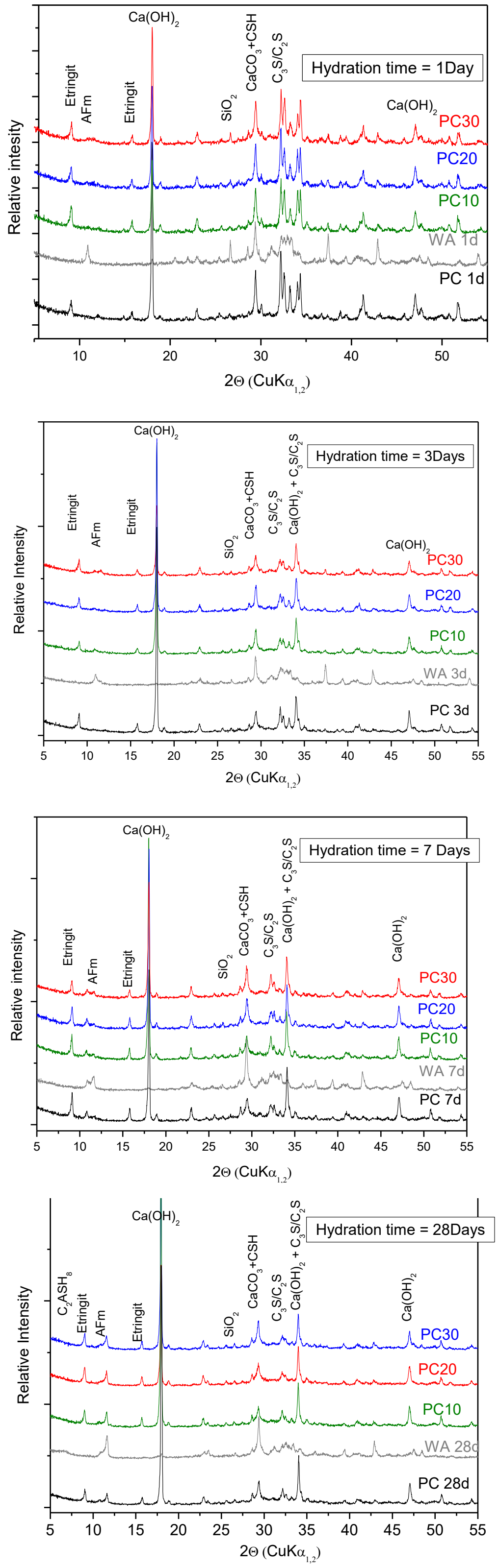

Figure 3 X-ray powder diffraction of pastes hydrated 1, 3, 7 and 28 days: effect of woody ash addition

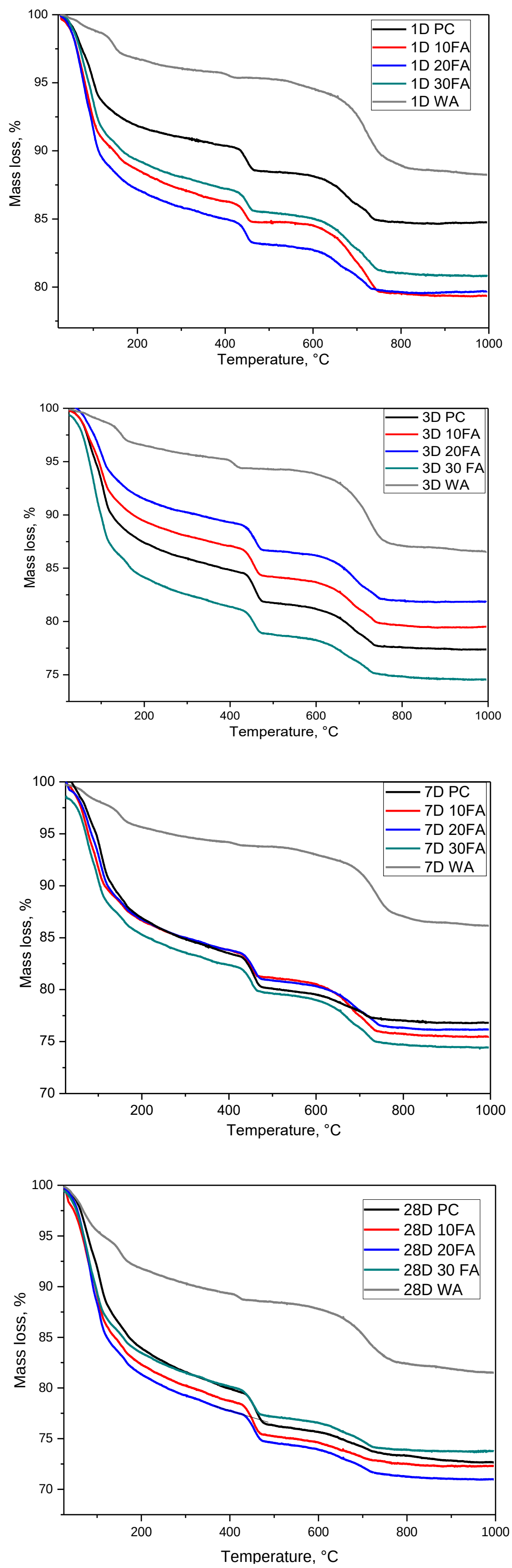

Figure 4 TG analysis of pastes hydrated 1, 3, 7 and 28 days: effect of woody ash addition

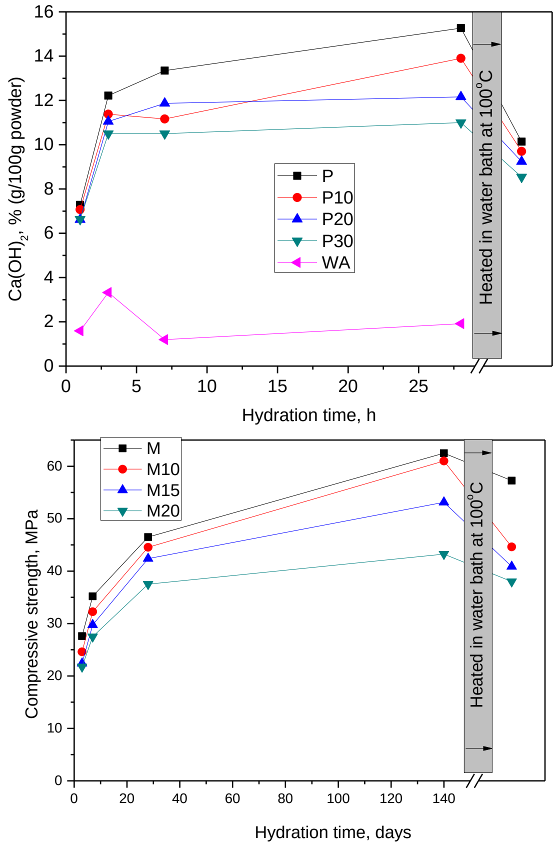

Figure 5 Development of Ca(OH)2 during hydration quantified by TG analysis

Results show that wood ash is broadening the particle size distribution (PSD) of cement as it comprises particles smaller than 1 µm and larger than 100 µm. An extended De Larrard's model [7] was implemented in Matlab and used for calculating packing density of a mixture of polydisperse constituent materials: cement, wood ash and sand. The aim of particle packing modelling was optimization of mixture of cement, wood ash and sand to obtain perfect fractions of these components to achieve the best packing density. In mortar mixture optimisation, fine fraction of ash was taken as a partial replacement of cement (3 - 6.5%), while ash coarse fraction was partially replacing sand (2.5 – 5%). Particle packing density and PSD of each constituent material was measured and used to calculate the mixture packing densities (Fig 6). The calibration of the packing model with the experimental results provided that the maximum packing density is achieved with 70% sand, 25% cement and 5% biomass fly ash.

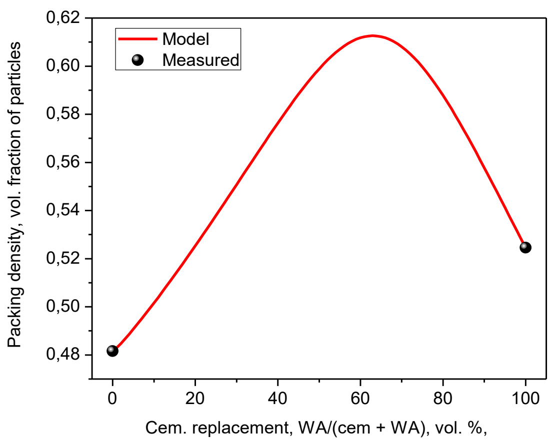

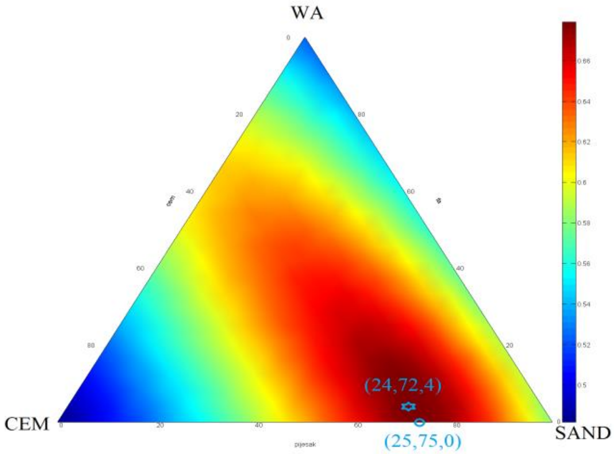

Figure 6 Modelling of particle packing density of mixtures

4. CONCLUSIONS

Chemical requirements for woody ash use in concrete by EN 450-1 (year 2012) were not met due to coarse particle size distribution, an insufficient amount of pozzolanic oxides (SiO2, Al2O$_3$ and Fe2O$_3$) and an excessive amount of alkalies, reactive CaO and MgO. However, the ash was broadening the particle size distribution of cement as it comprised particles smaller than 1 µm and larger than 100 µm. This showed the potential of woody ash to improve the packing density of blends where both sand and cement were partially replaced by ash. Moreover, presence of clinker minerals showed potential as cement replacement material. Addition of 20% ash resulted in unacceptable expansions which increased rapidly with further ash dosage. This expansion was due to a delayed hydration of free and dead burned CaO and MgO.

Plain ash hydration produced a maximal Ca(OH)2 quantity at 3 days and decreased with further hydration demonstrating the pozzolanic activity of the ash. With increasing ash addition more Ca(OH)2 was produced initially than for plain cement due to hydraulic properties of the ash with a relatively high content of reactive CaO, but at 28 days, inversely, there was less Ca(OH)2 due to activated pozzolanic reaction.

Hydration of ash alone showed a development of C4AHx, stratlingite (C2ASH8), $CaCO_3$ and/or calcium-slilicates hydrates. The main effect of ash on hydration, visible by semi-quantitative XRD analysis, was in production of C4AHx phase, which increased with ash addition.

With increase of cement replacement level, hydration kinetics, workability, compressive and flexural strength significantly reduced. However, the optimum dosage of 15% woody ash, where it replaces 5% of cement, but 3.33% of the sand, still produced structural grade mortar (or concrete) with acceptable workability and mechanical properties. Thus, potential reuse of ash could reduce landfilling and at the same time improve the sustainability perspective of cement production, reducing energy needs for cement production, cutting back in CO_2 emissions, and preserving natural resources (i.e. limestone) with no concern for depletion of biomass ash supplies.

ACKNOWLEDGMENTS

Authors acknowledge the support of HRZZ project ''Transformation of wood biomass Ash into REselient Construction Composites - TAREC^2''. Credit is given also to *Lika Eko-Energo* d.o.o., Udbina, Croatia (Mr. Zeljko Lovrak) for supply of the woody ash samples.

REFERENCES

[1] Carrasco-Hurtado, B; et al., Addition of bottom ash from biomass in calcium silicate masonry units for use as construction material with thermal insulating properties, Constr. Build. Mater. 52 (2014) 155.

[2] Berra M., Mangialardi T., Paolini A. E., Reuse of woody biomass fly ash in cement-based materials, Constr. Build. Mater. 76 (2015) 286.

[3] Cheah B. C.., Ramli M., The implementation of wood waste ash as a partial cement replacement material in the production of structural grade concrete and mortar: An overview, Resour. Conserv. Recycling 55 (2011) 669.

[4] Ukrainczyk, N., Vrbos, N., Koenders, E. A. B.: Reuse of Woody Biomass Ash Waste in Cementitious Materials, Chemical and Biochemical Engineering Quarterly 30 (2015) 137-148.
[5] Gosselin C., Gallucci E., Scrivener K., Influence of self heating and Li2SO4 addition on the microstructural development of calcium aluminate cement, Cem. Concr. Res. 40 (2010) 1555.
[6] Marsh B. K. and Day R. L., Pozzolanic and cementitious reactions of fly ash in blended cement pastes, Cem. Concr. Res. 18 (1988) 301-310.
[7] Fennis, S. A. A. M., Walraven, J. C., UIJL, J. A. den, Compaction-interaction packing model: regarding the effectof fillers in concrete mixture design, Materials and Structures, 46 (2013) 463 - 478.

POTENTIAL OF USE WOOD BIOMASS ASH IN THE CEMENT COMPOSITES

Ivana Carevic[1], Nina Stirmer[1], Ivana Banjad Pecur[1], Bojan Milovanovic[1], Ana Baricevic[1], Marija Jelcic Rukavina[1]

[1] University of Zagreb, Faculty of Civil Engineering, Department of Materials, Fra Andrije Kacica Miosica 26, 10000 Zagreb, Croatia, email: icarevic@grad.hr, ninab@grad.hr, banjadi@grad.hr, bmilovanovic@grad.hr, abaricevic@grad.hr, jmarija@grad.hr

SUMMARY: Due to high energy dependency, the European Union´s policy is turned to promotion of the use of renewable energy throughout directives with culmination with the agreement at the 21st Conference of the Parties (COP21) in Paris. Within, European Union (EU) has put forward the share of renewable energy increasing to at least a 27 % until 2030. Among these resources, biomass as forestry and agricultural waste, and power plants fuelled by them are a promising source of renewable energy. As one of the consequences of development and investment in the biomass renewable energy is increasing the amount of ash, including wood biomass ash (WBA). During the bioenergy production, ash as a by-product is a major environment pollutant and health hazard in the absence of emission controls, most of which are very expensive. Therefore, it is necessary to establish the sustainable ash management, which is major challenge in the bioenergy production. One of possible solution for its management is utilization of WBA in the construction. This paper describes the process in the biomass power plants which affects on the WBA properties, problems regarding WBA management and the possibility of its application in construction industry, particularly with regard to the concrete industry.

POTENCIJAL UPOTREBE PEPELA OD DRVNE BIOMASE U CEMENTNIM KOMPOZITIMA

SAŽETAK: Zbog velike ovisnosti o energiji politika Europske unije usmjerena je na promidžbu upotrebe obnovljive energije u direktivama što je doseglo vrhunac u sporazumu na 21. konferenciji (COP21) sudionika u Parizu. Prema sporazumu, cilj je da se u Europskoj uniji udio obnovljive energije poveća do najmanje 27 % do 2030. godine. Obećavajući izvori obnovljive energije su, između ostalih, biomasa iz šumskog i poljoprivrednog otpada i energane koje kao gorivo koriste te materijale. Jedna od posljedica razvoja i investiranja u obnovljivu energiju iz biomase povećana je količina pepela, uključujući pepeo iz drvne biomase (engl. wood biomass ash, WBA). Tijekom proizvodnje bioenergije pepeo je kao nusproiuzvod glavni onečišćivač okoliša i zdravstvena opasnost ako nema kontrole emisije od kojih je većina vrlo skupa. Stoga je nužno uspostaviti održivo upravljanje pepelom koji je glavni izazov u proizvodnji bioenergije. Jedno od mogućih rješenja za upravljanje njime upotreba je pepela u gradnji. U radu se opisuje proces u pogonu energane na biomasu koji utječe na svojstva pepela, problemi koji se odnose na upravljanje pepelom i mogućnost njegove primjene u građevinskoj industriji, posebno u industriji betona.

1. INTRODUCTION

In the current years, the concern of our global environment and increasing energy insecurity has led to an increasing demand in renewable energy and their sources [1]. According to European policy, under EU Renewable Energy Directive [1] the European Union (EU) has set the goal to reach a 20% renewable energy share by 2020 where each Member State has set national legally binding targets as well as provisions and measures to reach this ambitious objective. Moreover, an European Council and Commission, within 2030 framework for climate and energy [2], agreed on EU´s long-term commitment target of at least 27% for the share of renewable energy consumed in the EU in 2030. Among these resources, biomass resources (forestry and agricultural wastes) and power plants fueled by them are a promising source of renewable energy with an economically low operational cost and continuously regeneration of the fuel. Wood biomass is considered as a carbon neutral fuel as it absorbs the same amount of carbon dioxide while growing as released by burning it [3]. For that reason, combustion of biomass for electricity production is increasing worldwide. Consequently the amount of ash derived from biomass combustion is also increasing, including wood biomass ash (WBA). According to the European regulations to increase the 20% of RES by 2020 assumes that the amount of ash will growth on 15.5×10^7 t [4]. According to existing data [5], it is considered that the use of forest biomass resulted in production of 1.6×10^7 - 3×10^7 tons of WBA in Europe for the 2005., respectively from 5% to 15% (by weight) of biomass processed [6]. These significant quantities of ash requires its sustainable management causing financial and environmental burden. Currently, 70% of WBA is landfilled, 20% tends to be used as a soil supplement in agriculture and 10% is used for miscellaneous application [3, 7, 8].

On the other hand, in the EU-28 construction accounts for 10% of the GDP, 20 million jobs (30% of the industrial employment), and 3 million enterprises [9]. Furthermore, the European construction sector is a major contributor to exports, realizing over 50% of the major international contracts. In a recent communication [10], the European

Commission (EC) has established that the construction sector plays an important role in the delivery of the Europe 2020 Strategy on smart, sustainable and inclusive growth [11]. There is a pressing need for innovation in sustainable construction, particularly in cement based materials so as to ensure EU's long term objective of 80 - 95% reduction of greenhouse gas emissions, but also to contribute to the preservation of natural resources and use of renewable materials.

Following, the utilization of WBA in construction is an environmentally motivated choice for saving disposal costs but also for conserving natural resources and reducing greenhouse gas emissions. This supports the Waste Framework Directive (2008/98/EC) [12] in which a waste hierarchy is established giving a higher priority to prevention, then reuse or recycling and finally to disposal. The Roadmap to a Resource Efficient Europe (COM 2011, 571) [13] and the Eco-Innovation Action Plan (COM 2011, 899) [14] also promotes recycling and reuse over landfilling. The Directive of Waste Management (2006/12/EC) [15] even prohibits landfilling of waste in Europe and encourages recovery. Also there is an exponential increase in the demand of cement, which is the primary constituent in the production of mineral composites in construction industry. Researchers have shown that for every 1000 kg of cement, approximately 850 kg of CO_2 is released into the atmosphere [16, 17]. Therefore, application of WBA in construction composites is a promising solution of the disposal problem.

This paper describes problems regarding WBA management, the process in the biomass power plants which effects on the WBA properties and the possibility of its application in construction industry, particularly with regard to the concrete industry.

2. WBA MANAGEMENT

When land filling is carried out in the EU, it has to be done according to the regulations set in the Landfill Decree [18] in order to minimize the effects of adverse environmental impacts of the landfill of waste, particularly due to the effects of pollution caused by emissions of substances in surface water, groundwater, soil and atmosphere, and in the context of global environmental pollution to reduce greenhouse gas emissions and prevent risks to human health. This decree sets limiting values for concentrations of certain elements and components in the waste (i.e. ash) as well as in the leachate. In most cases, taxes need to be paid for each ton of waste disposed. Regarding the biomass ash waste management, most of the biomass ash generated in thermal plant is either disposed of in a landfill or recycled in open agricultural fields without any control. The costs of the biomass ash waste management are between 200 and 500 EUR/ton, while in future, increase of costs of landfill in the form of waste tax or deposit fee, as well as the difficulties in acquiring new landfill sites, and stricter EU landfill directives, may be expected [6]. Several studies performed that WBA from the combustion of natural solid biomass contains valuable plant nutrients such as K, P, Mg and Ca [6, 19, 20]. Some of the European country with a long history of using biomass for energy production, such as Finland, Sweden, Denmark, Austria, Germany, Netherlands, have established legal frameworks that allows and control the re-use of ash from biomass power plants. For example, the German Fertilizer Decree (Düngemittelverordnung) [21] enables the use of biomass ashes as fertilizer but different conditions (limit values for heavy metals) are set based on different types of fertilizer. In the Netherlands, there are no specific regulations for the use of biomass ash or WBA in forestry. This means that the use in forestry should be qualified as spreading of waste, which is forbidden [22]. Even though the idea of sustainability of biomass power plants is to return the minerals from the ash back into the soil from which they originated during biomass growth, relatively high heavy metal content of the ash restricts such a practice [23]. Additionally, in recent days, land filling is becoming limited due to scarcity of waste land, increasing environmental concerns and the ever increasing volume of ash. Contamination of ground water resources is a major problem due to leaching of heavy metals from the ash or by seepage of rain water in case of land filling. Moreover, the use of biomass ash as a soil supplementary material is getting increasingly restrictive due to significantly high metal content in ashes, especially biomass ash, which may cause hazards in case of groundwater contamination and infertility of agricultural fertile land, Figure 1.

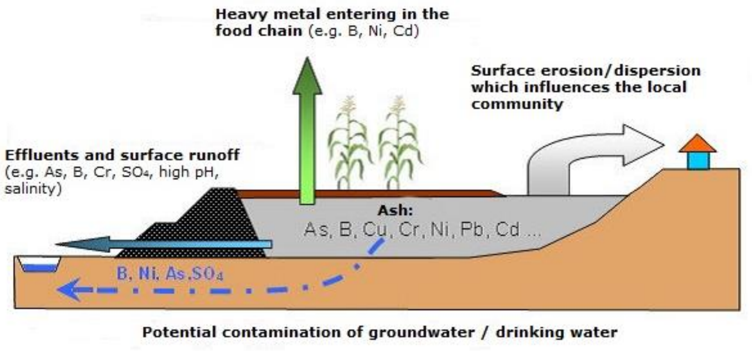

Figure 1 Inadequate methods of disposing of ash with pollution possibilities [24]

Today supplementary cementitious materials (SCMs) are widely used in concrete either in blended cements or added separately in the concrete mixer. The use of SCMs such as blast-furnace slag, a by-product from pig iron production, or fly ash from coal combustion, represents a viable solution to partially substitute Portland cement (PC) [25]. The fraction of coal fly ash (FA) that qualifies under the interpretation of EN 450-1 [26] for use in mortars or concretes is in rapid decline due to issues such as co-firing fuels with coal and injecting a variety of materials for emissions control [27]. WBA may be considered as its possible replacement, depending to a large extent on gained chemical characteristic.

3. COMPOSITION OF WOOD BIOMASS ASH

In order to establish beneficial application of WBA, it is necessary to understand technology processes in biomass power plants and composition of WBA as by-product of this processes. The characteristics of WBA may differ and chiefly depend on:

(1) tree species – type and source of wood

(2) combustion technology (especially combustion temperature)

(3) and the location where collection of ash is done [3].

Among the technologies available for power and heat production, biomass combustion is a proven technology in which technologies of fluidized bed and grate furnace combustion are mainly used [28, 29, 30]. In plants with efficient fluidized bed furnaces, ash produced is predominantly fine fly ash with only a small fraction of coarse ash retained within the combustion chamber but when grate fired furnaces are used, wood ash produced is coarser in nature and tend to settle inside the combustion chamber as bottom ash [31]. Bottom ashes (the coarser ash fraction) can usually be used as fertilizing agent on fields as it contains valuable elements for soils and plants and only minor concentrations of heavy metals. Fly ashes (the finer ash fraction) are in most cases disposed as their heavy metal concentrations are too high for a usage as soil enhancer [32, 33]

The chemical characteristics of WBA, which govern its credibility to be used as a replacement for cement or other SCMs, such as silica (SiO_2), alumina (Al_2O_3), iron oxide (Fe_2O_3) and quicklime (CaO) differ significantly from one species of trees to another, Table 1. Factors such as an origin of the biomass, location of ash collection, as well as combustion conditions, strongly affect chemical and mineralogical composition(s) of ashes.

Table 1 Chemical composition of WBA from various species of timber and from different origins [3]

Ash type	Timber species	SiO_2	CaO	K_2O	P_2O_5	Al_2O_3	MgO	Fe_2O_3	SO_3	Na_2O	TiO_2
Fly (coarse and fine)	Birch bark	4.38	69.06	8.99	4.13	0.55	5.92	2.24	2.75	1.85	0.13
	Forest residue	20.65	47.55	10.23	5.05	2.99	7.2	1.42	2.91	1.6	0.4
	Pine bark	9.2	56.83	7.78	5.02	7.2	6.19	2.79	2.83	1.97	0.19
	Pine chips	68.18	7.89	4.51	1.56	7.04	2.43	5.45	1.19	1.2	0.55
	Poplar	3.87	57.33	18.73	0.85	0.68	13.11	1.16	3.77	0.22	0.28
	Poplar bark	1.86	77.31	8.93	2.48	0.62	2.36	0.74	0.74	4.84	0.12
	Sawdust	26.17	44.11	10.83	2.27	4.53	5.34	1.82	2.05	2.48	0.4
	Spruce bark	6.13	72.39	7.22	2.69	0.68	4.97	1.9	1.88	2.02	0.12
	Spruce wood	49.3	17.2	9.6	1.9	9.4	1.1	8.3	2.6	0.5	0.1
	Wood residue	53.15	11.66	4.85	1.37	12.64	3.06	6.24	1.99	4.47	0.57
	Average [26]	**26.5**	**16.0**	**5.00**	-	**9.00**	**3.00**	**5.40**	**4.80**	-	**0.51**
Bottom	Ground wood ash (GWA) [13]	69.5	8.10	3.60	-	4.18	1.24	1.99	< 0.1	1.40	-
	Average [25]	**42.3**	**11.40**	**1.30**	-	**17.90**	**2.50**	**12.60**	**0.40**	-	-

4. USE OF WBA IN CONCRETE INDUSTRY

In concrete industry there is a high potential for substitution of certain components by adequate alternative materials, and in that context the use of WBA has been examined. Depending on the physical and chemical characteristic WBA may be used in manufacturing of concrete products as active pozzolanic material [34; 35], partly substituting cement [36], or as mineral additive [37], i.e. inert filling replacing sand and/or fine aggregate.

Based on performed research high calcium WBA can be used as a supplementary cementitious material for the production of structural grade concrete of acceptable strength and durability and even self-compacting concrete [31]. Pozzolanic activity for ground coarse bottom WBA is negative, thus confirming that ground WBA cannot be considered a Type II addition based on requirements set in HRN EN 206 [38] and should therefore be considered as filler [31]. The pozzolanicity of biomass ash can be significantly less than coal fly ash depending on their chemical composition (especially SiO_2 and Al_2O_3 contents) [34].

The option of combining WBA with blended cements, is the most interesting option due to synergic advantages of individual main constituents, and thus for developing these blends into even more robust systems. High alkali content of the biomass ashes will activate the hydration of CEM II (i.e. clinker and pozzolanic admixtures) [25, 35]. Studies shown that the strength (both compressive and flexural) of cementitious mixtures is lowered at early and late ages after incorporating WBA, with a correlation between increasing ash content and lower strength [34]. Such results have prompted the suggestion that WBA, depending on its composition, can be used at low percentages of replacement or as a filler material. Others report the marginal decrease in strength with increasing WBA percentage in concrete, but increased with age due to increased pozzolanic reactions.

The preliminary result of use of WBA in the concrete mixtures produced by partial replacement of cement binder were made at the Laboratory of materials, Faculty of Civil Engineering University of Zagreb in order for better understanding of WBA use in concrete. WBA is collected from electrostatic precipitator of a biomass co-generation plant located in Croatia that uses forest waste as fuel resulting from wood processing activities, mostly red oak. For laboratory testing, different concrete mixtures were prepared by replacement PC with different amounts of WBA (5 % as M2-5, 10 % as M3-10 and 15 % as M4-15 per mass of cement).

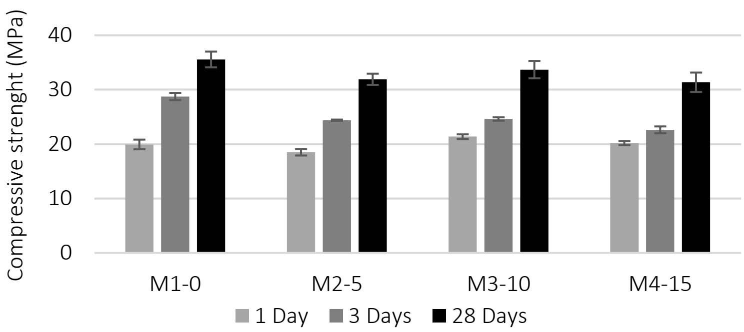

Figure 2 Compressive strength of concrete mixtures with WBA

From the results of compressive strength testing (Figure 2), it can be seen that all concrete mixtures have achieved compressive strength of 30 MPa in age 28 days with its slightly decrease with the levels of cement replacement. Compressive strength was tested according to HRN EN 12390-3:2009 [39] on the cubes 15×15×15 cm at ages of 1, 3 and 28 days.

5. CONCLUSION

The growing trend of using biomass as a renewable energy source results also in a growth of the produced ash, including the amount of WBA. As the amount of WBA and the price of its landfill grows, it is necessary to establish the sustainable ash management, which is major challenge in bioenergy production. Currently, 70% of WBA is landfilled, 20% tends to be used as a soil supplement in agriculture and 10% is used for miscellaneous application. Reviewing the available knowledge in the field of research there is great potential of WBA utilization in concrete industry and therefor the possibility of its successful and sustainable management. Using WBA as a new form of raw material in the construction industry offers an interesting alternative to today's materials. Benefits of using coal fly ash have already been repeatedly demonstrated at commercial scale. For WBA, the same approach is not fully demonstrated yet. Results of worldwide research show considerable differences of WBA composites in solid state. As shown, several factors influence on physical and chemical composition of WBA and consequently on produced composites. These factors include combustion temperature, types and hydrodynamics of the furnace and the species of trees from which the wood is derived. Given the number of variables that effect on the mineralogical and chemical compositions of WBA, additional researches are required for its reuse in the concrete industries. In case of application in the agriculture, it is necessary to transparently monitoring of the chemical composition of the WBA in order to ensure the appropriate use of WBA and to prevent the risk on the environment.

ACKNOWLEDGMENTS

This research was performed within research project: “Transformation of Wood Biomass Ash into Resilient Construction Composites”, IP-06-2016, funded by Croatian Science Foundation.

REFERENCES

[1] Directive 2009/28/EC of the European parliament and of the Council of 23 April 2009 on the promotion of the use of energy from renewable sources and amending and subsequently repealing Directives 2001/77/EC and 2003/30/EC, OJ L 140, 5.6.2009, pp. 16–62

[2] Communication from the Commission to the European Parliament, the Council, the European Economic and Social Committee of the Regions, A policy framework for climate and energy in the period from 2020 to 2030, COM/2014/015 final

[3] Chowdhury, S; Mishra, M.; Suganya, O.: The incorporation of wood waste ash as a partial cement replacement material for making structural grade concrete: An overview, Ain Shams Engineering Journal, Volume 6, Issue 2, June 2015, pp. 429–437

[4] Obernberger, I., Supancic, K.: Possibilities of ash utilization from biomass combustion plants, Proceedings of the 17th European Biomass Conference and Exhibition, Hamburg, Germany, 29 June–3 July 2009

[5] James A.K., Thring R.W., Helle S., Ghuman H.S.: Ash Management Review - Applications of Biomass Bottom Ash, Energies 2012, 5, pp. 3856-3873

[6] James, A.K, Thring, R.W., Helle S., et al.: Ash Management Review—Applications of Biomass Bottom Ash, Energies 2012, 5, pp. 3856-3873

[7] Campbell, A.G.: “Recycling and disposing of wood ash”, Tappi J, 73 (9) (1990), pp. 141–143

[8] Ban, C.C; Nordin, N.S.A.; Ken, P.W.; Ramli, M. et al.: The high volume reuse of hybrid biomass ash as a primary binder in cement less mortar block“, American Journal of Applied Sciences 11 (8), 2014, pp. 1369-1378

[9] Commission staff working document: State of the Industry, Sectoral overview and Implementation of the EU Industrial Policy (SWD/2014/014 final)

[10] Communication from the Commission to the European Parliament and the Council Strategy for the sustainable competitiveness of the construction sector and its enterprises (COM (2012) 433 final)

[11] Communication from the Commission EUROPE 2020 A strategy for smart, sustainable and inclusive growth, Brussels, 3.3.2010, COM(2010) 2020

[12] Directive 2008/98/EC of the European Parliament and of the Council of 19 November 2008 on waste and repealing certain Directives, OJ L 312, 22.11.2008, pp. 3–30

[13] Communication from the Commission to the European Parliament, the Council, the European Economic and Social Committee and the Committee of the regions: Roadmap to a Resource Efficient Europe (COM/2011/0571 final)

[14] Communication from the Commission to the European Parliament, the Council, the European Economic and Social Committee and the Committee of the regions: Innovation for a sustainable Future - The Eco-innovation Action Plan (Eco-AP) (COM/2011/899 final)

[15] Directive 2006/12/EC of the European Parliament and of the Council of 5 April 2006 on waste, OJ L 114, 27.4.2006, pp. 9–21

[16] Štirmer, N.: Influence of Construction Material on the Environment, Institute for Scientific and Artistic Work of the City Požega, 1 (2012), pp. 293-311

[17] Štirmer, N.: Sustainable construction - selection of materials and influence of environmental characteristics, Požega i Požeština kroz stoljeća / Jakobović, Snježana (ur.). - Požega: Croatian Academy of Sciences and Arts, 2010., pp. 45.

[18] Council Directive 1999/31/EC of 26 April 1999 on the landfill of waste, Official Journal L 182 , 16/07/1999 pp. 0001 – 0019

[19] Ingerslev, M., Skov, S., Sevel, L., et al.: Element budgets of forest biomass combustion and ash fertilisation - A Danish case-study, Biomass and Bioenergy 35 (2011), pp. 2697 – 2704

[20] Pitman, R. M.: “Wood ash use in forestry – a review of the environmental impacts, Forestry (Lond) (2006) 79 (5), pp. 563-588.

[21] Verordnung über das Inverkehrbringen von Düngemitteln, Bodenhilfsstoffen, Kultursubstraten und Pflanzenhilfsmitteln, Düngemittelverordnung vom 5. Dezember 2012 (BGBl. I S. 2482)

[22] Eijk, van R.J, Obernberger, I., Supancic K.: EA Bioenergy Task 32 Deliverable D4, Options for increased utilization of ash from biomass combustion and co-firing, Arnhem, March, 2012
[23] Scheider, D. R.: Ecological aspects of energy utilization of forest biomass, ECE, 2012
[24] RECOAL: Reintegration of coal ash disposal sites and mitigation of pollution in the West Balkan Area, Handbook on treatment of coal ash disposal sites, INCO-WBC-1-509173, 2008
[25] Lothenbach, B.; Scrivener, K.; Hooton, R.D.: „Supplementary cementitious materials“, Cement and Concrete Research, Volume 41, Issue 12, December 2011, pp. 1244–1256
[26] EN 450-1 Fly ash for concrete. Definition, specifications and conformity criteria
[27] Maschio, S.; Tonello, G.; Piani, L.; Furlani, E.: "Fly and bottom ashes from biomass combustion as cement replacing components in mortars production: Rheological behaviour of the pastes and materials compression strength", Chemosphere, Volume 85, Issue 4, October 2011, pp. 666-671
[28] Yin, C.; Rosendahl, L.A.; Kær, S.K.: „Grate-firing of biomass for heat and power production“, Progress in Energy and Combustion Science, Vol. 34, No. 6, 2008, pp. 725-754.
[29] Loo S.V.; Koppejan J.: "Handbook of Biomass Combustion and Co firing", Twente University Press, The Netherlands, 2003.
[30] Lončar, D.; Krajačić, G.; Vujanović, M.: "Support to the developers - Best practices in biomass combined heat and power (CHP) in wood industry and forest sector ", Centar for Technology Transfer, Zagreb, 2009.
[31] Garcia, M.L.; Sousa-Coutinhob, J.: „Strength and durability of cement with forest waste bottom ash“, Construction and Building Materials, Volume 41, April 2013, pp. 897–910
[32] Biedermann, F., Obernberger, I: Ash-related Problems during Biomass Combustion and Possibilities for a Sustainable Ash Utilisation, www.bios-bioenergy.at
[33] Kröppl, M.; Lanzerstorfer, C.: „Acidic extraction and precipitation of heavy metals from biomass incinerator cyclone fly ash“, E3S Web of Conferences 1, 16007 (2013)
[34] Shearer C.R.: „The productive reuse of coal, biomass and co-fired fly ash“, Dissertation Georgia Institute of Technology, August, 2014
[35] Naik, T.R.; Kraus, R.N.; Kumar, R.: Wood ash: a new source of pozzolanic materials, Center for By-Products Utilization, ACI Maharastra Chapter, Mumbai, India, July 2001
[36] Ban C.C.; Ramli M.: Mechanical strength, durability and dryinf shrinkage of structural mortar containing HCWA as partial replacement of cement, Construction and Building Materials 30 (2012) pp. 320-329
[37] Wang S., Miller A., Llamazos E., Fonseca F., Baxter L.: Biomass Fly Ash in Concrete: Mixture Proportioning and Mechanical Properties, Fuel, 2008, Volume 87(3), pp. 365–71
[38] CSI, Croatian Standard Institute: Concrete -- Specification, performance, production and conformity (HRN EN 206:2016)
[39] CSI, Croatian Standard Institute: Testing hardened concrete -- Part 3: Compressive strength of test specimens (HRN EN 12390-3:2009)

APPLICATION OF ASH FROM AGRICULTURAL BIOMASS IN CONCRETE

Krunoslav Cosic[1], Ivanka Netinger Grubesa[1],

[1] Josip Juraj Strossmayer University of Osijek, Faculty of Civil Engineering, Department for materials and structures, Vladimira Preloga 3, 31000 Osijek, Croatia, email: kcosic@gfos.hr, nivanka@gfos.hr

SUMMARY: The production of cement, the main component of concrete, leads to high energy consumption and emissions of the greenhouse gas CO_2. Acting in accordance with the principles of sustainable construction, the building industry is trying to find new alternative concrete materials. In relation to binders, various powder materials are being studied that are able to partially or completely replace cement in concrete. One of these materials is ash from biomass. The term biomass refers to all organic matter produced by plant and animal activity. Eastern Croatia is traditionally oriented toward the cultivation of various agricultural crops, which generate large quantities of agricultural waste and requires proper handling. One of the effective methods of handling the waste from agricultural biomass is using it in industries as fuel. The remaining ash from the burning of biomass could be used as a partial replacement for cement in concrete. This paper provides an overview of the global research on the use of ash from biomass as a binder in concrete. It also presents the results of a preliminary research on the use of ash, produced by the utilization of agricultural biomass as fuel by the local industries of eastern Croatia, as a partial replacement for cement in concrete.

PRIMJENA PEPELA IZ POLJOPRIVREDNE BIOMASE U BETONU

SAŽETAK: Prilikom proizvodnje cementa, glavnog sastojka betona, dolazi do velike potrošnje energije i emisije stakleničkog plina CO_2. Nastojeći djelovati u skladu s principima održive gradnje, građevinska struka teži iznalaženju uvijek novih alternativnih materijala za ugradnju u beton. U području veziva istražuju se različiti praškasti materijali koji su u mogućnosti djelomično ili potpuno zamijeniti cement u betonu. Jedan od trenutno aktualnih materijala te vrste je i pepeo iz biomase. Pojam biomase odnosi se na svu organsku tvar nastalu rastom bilja i životinja. Istočna Hrvatska tradicionalno je orijentirana na uzgoj različitih ratarskih kultura od kojih nastaju velike količine poljoprivrednog otpada koji je potrebno zbrinuti. Jedan od učinkovitih načina zbrinjavanja poljoprivredne biomase njezina je uporaba u industriji kao goriva. Spaljivanjem biomase preostaje pepeo koji bi se mogao upotrijebiti kao djelomična zamjena za cement u betonu. U radu se daje pregled svjetskih istraživanja o primjeni pepela iz biomase kao veziva u betonu. Također, prikazani su i rezultati preliminarnih istraživanja pepela iz poljoprivredne biomase s područja istočne Hrvatske kao zamjene dijela cementa u betonu a koju lokalna industrija upotrebljava kao gorivo.

1. INTRODUCTION

Concrete is the most widely used building material in the world [1]. The production of cement, the main ingredient of concrete, implies large CO_2 emissions and high energy consumption. Hence, the construction sector occupies a leading position on the scale of activities that result in significant emissions of CO_2 to the atmosphere and promote the greenhouse effect. Cement is a widely used building material in the world, and the rise of global infrastructure development demands actions to reduce its negative environmental impact to the lowest possible level [2].

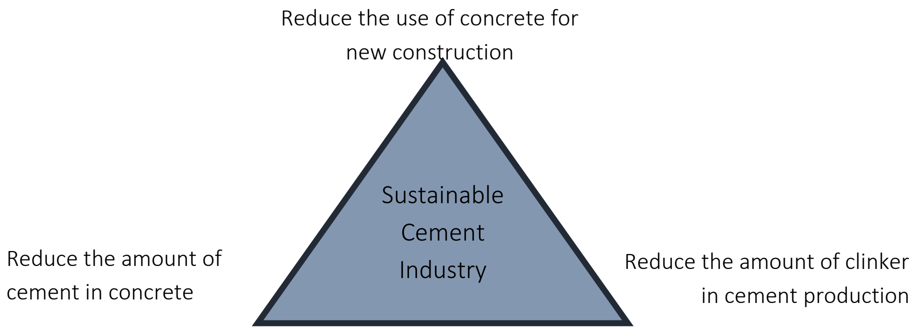

Figure 1 The possibilities of reducing CO_2 emissions in the cement industry [3]

To act in accordance with the principles of sustainable construction, new materials for the production of concrete are being studied. One of the solutions is using local materials of vegetable, animal, or mineral origin in industrial processes, with minimal previous processing, and the use of recycled or waste materials, such as fly ash from agricultural biomass, a powder material that partially or completely replaces the cement in concrete. Biomass is an organic material formed by the growth of plants and animals and is effectively used in industries as a fuel. Globally, there are numerous studies that have investigated the use of agricultural biomass ash in concrete, such as ash from straw, rice husk, coconut shell, bamboo stalks, sunflower husk, jute fibers, and fibers of sugar cane. The utilization of agricultural biomass as fuel forms ash, which can be used as a partial replacement for cement in concrete.

2. SUSTAINABILITY

One of the biggest problems faced today is climate change, to which greenhouse gas emissions make a significant contribution. In addition to the production and transformation of energy and road transportation, the construction sector produces significant CO_2 emissions and is responsible for 40% of the total energy consumption in Europe [4]. Natural resources are being used in an irrational, non-organic, and incomplete way, and most likely in the near future, global energy needs cannot be met with expensive fossil fuels. An example is the production of cement, where the use of expensive fossil fuels consumes considerable amounts of energy and causes pollution.

Natural resources are limited and must be constantly renewed. The production process of construction materials should become as friendly as possible to the environment and the people, without harmful effects. Consequently, alternative materials are being investigated that do not result in harmful phenomena during the production and utilization phases, thus minimizing the use of non-renewable resources and the emission of harmful substances throughout their life cycle. An example is the ash obtained by burning agricultural biomass as a fuel. Biomass is considered a CO_2 neutral fuel, as the amount of CO_2 absorbed by the plant during its life and the quantity released during its thermal decomposition are equal [5].

In accordance with the regulations of the European Union, individual member states, such as Austria, Sweden, and Finland, are already producing up to 20% of their energy from biomass, [6]. The continuous increase in the use of agricultural biomass as a fuel poses a challenge, which is the utilization of its waste in the construction industry.

3. BIOMASS

Biomass is a renewable energy source, which refers to a living or recently living substance, of plant or animal origin, that can be used as fuel or for industrial production activities. It represents the main product of the biological processes in the biosphere, a part of which have a very short life span, such as the single-celled organisms, and the other a very long span, such as wood. The use of biomass energy has a positive impact on the local and national economy and provides considerable opportunities for the creation of new jobs, particularly in rural areas outside the major cities. The impact of these and other socioeconomic aspects that are difficult to observe, represents the biggest advantage of using biomass. To guarantee the use of biomass in the long run, it must be produced and used in a sustainable way, and it must demonstrate certain environmental and social benefits compared to fossil fuels. Of all the processes in the renewable supplies industry, the conversion of biomass into heat, electricity, or cooling energy generates the greatest number of jobs and has a significant impact on environment and specifically climate protection at the global level. The development of the bioenergy sector contributes to energy security, creates new jobs, improves industrial competitiveness, and contributes to regional development [7].

Biomass is mainly used as final consumption for the production of hot water, heat, and electricity, and particularly for the production of biofuels. It is often referred to as a carbon neutral fuel. The carbon in the atmosphere is stored in plants; during burning, it is again released into the atmosphere as carbon dioxide. Biomass can be divided into wood biomass, which is the most commonly used (from waste generated by sawing, for instance), agricultural biomass (straw, stems, seeds, shells, corn, etc.), animal biomass (excrement and carcasses), and biomass from waste (green fractions of household waste and sludge from sewage treatment plants) [8].

The quality of the ash depends on the origin and quality of the burned biomass, which is mainly related to particle size, moisture content, density, chemical composition, and calorific value [5]. The application of ash from agricultural biomass in the construction industry mainly depends on the concentration of the major inorganic elements and their mineral form. The content of the various types of agricultural waste mostly includes similar concentrations of carbon, hydrogen, and oxygen. However, it shows significant differences in the concentrations of the main elements that form the ash (Si, Ca, Mg, K, Na, P, S, Cl, Al, Fe, Mn), in the concentrations of heavy metals (Cu, Zn, Co, Mo, As, Ni, Cr, Pb, Cd, V, Hg), and in the concentration of nitrogen [9]. Ash is an inorganic, uncombusted fuel, generated by combustion, and contains most of the mineral substances originated from biomass. The ash content depends on the type of biofuel, which may have from 1% up to 40% of biomass by weight. Moreover, it is important to distinguish between ash that comes from the bottom of the boiler and fly ash [5].

4. GLOBAL RESEARCH

Biomass is relatively cheap, renewable, and available throughout the world. The main advantages of the use of biomass as a building material is its low density, good insulation properties, low cost, reduced energy consumption, less use of non-renewable resources, and protection of the environment. Agriculture generates large amounts of byproducts, such as dry sugar cane fiber (bagasse), rice husk, cotton stalk, coconut shell, straw, and stalks and husks of sunflower. Previous research has shown justification for the use of this agricultural waste, which enables the safe handling of ash and prevents environmental pollution.

Studies have shown that the biomass of olive can be used as a filler in self-compacting concrete [10], while adding ash from rice husks improves the viscosity of this type of concrete [11]. The physical and chemical composition of these ashes is responsible for the subsequent process of hydration [12]. By applying the ashes of sugar cane in concrete, a lower degree of hydration has been achieved in comparison to ordinary concrete, while the fineness of the ash from cane contributes to the creation of a fine pore structure in concrete [13]. The preparation, compaction, and curing of concrete in which the cement is partially replaced with ash from agricultural biomass is generally the same as that for ordinary concrete. Tests of the properties of concrete made with ashes from agricultural biomass have proved that such concrete has a low density in the hardened state [14], high tensile strength and ductility [15], and good insulation and acoustic properties [16], obviously depending on the type of biomass used.

Figure 2 Concrete with shell of coconut: a) concrete cylinder, b) concrete panel, c) house built with concrete with shell of the coconut [17]

Researchers from the Polytechnic University of Hochiminh City (Vietnam) investigated the use of coconut shells in concrete (Figure 2) [17]. The average size of the ash particles from agricultural biomass ranges from 9,6 to 85 µm, which is typical for cement materials. Tests of the size and shape of the particles of ash from cane and rice husks with an electron microscope (SEM) showed that it is formed by irregular particles (the ash particles observed are less than 45 µm). The chemical composition of the listed ashes is in accordance with the properties of the cement materials standard [12]. A morphological analysis of the ash from sunflower shell using an electron microscope showed the presence of very small particle sizes, of several microns, as well as clusters of particles.

Studies have also shown that the optimum ash content for partial replacement of cement with ashes from sugar cane and rice husks is up to 8%, without affecting the workability requirements. The slump flow test of a self-compacting concrete with a mixture of 8% of ash from rice husks, combined with ashes from sugar cane and rice husks, showed good results. Similarly, V-funnel, J-ring, L-box, and U-box tests revealed satisfactory results [12]. With respect to the concrete workability properties, it was found that the the optimum ash content for partial replacement of cement with ash from stalks of wheat, corn, and sunflower, is 5% [18].

According to a study, the compressive strength of concrete with partial replacement of cement with ashes from sunflower stalks is lower than that of the reference, ordinary concrete [18]. Beltran et al. also investigated a concrete with partial replacement of cement with ash from biomass (remains of olives) and concluded that the compressive strength and density in such concrete was reduced in comparison to the reference concrete [19].

5. PRELIMINARY OBSERVATIONS

Eastern Croatia traditionally cultivates various field crops that produce large quantities of agricultural waste. One of them is the sunflower seed husk, which is generated in the production of oil as a by-product of the oil factory Čepin. It is used as a renewable energy source in the production of thermal energy for processing steam. The sunflower seed husk has a fibrous layer of oil seed, with less oil and protein content, and is mainly made of cellulose and hemicellulose materials (Figure 3). Burning sunflower husk produces ash (Figure 4) that can be used as a partial replacement for cement in concrete.

Figure 3 Sunflower seeds husk [20]

The oil factory Čepin deals with the production of crude and refined oil. It is the largest producer in Croatia in this sector, with a processing capacity of 500 t / 24 h of processed raw materials, and 100 t / 24 h of produced refined oil [20]. Considering that its existing boiler has been recently modernized and that it uses renewable energy sources, in particular shell sunflower seeds, accurate and current data on the amount of ash resulting from the burning of biomass is unknown. However, considering the processing capacity of the factory, it is a large amount with growth potential.

Figure 4 The ash generated by burning sunflower shell

At the Faculty of Civil Engineering in Osijek, a preliminary research on ash from sunflower husk from the oil factory Čepin as a partial replacement for cement in concrete has been conducted. Two mixtures were prepared, the reference mixture (M1) and a mixture with partial replacement of cement with ash from the sunflower husk (M2) amounting to 7.5%, which is the optimal proportion according to the above mentioned international studies. The total amount of binder was 400 kg / 1m^3 of concrete for both mixtures.

For the preparation of concrete, a mixture with a water-cement ratio of 0,50 was used with a dolomite aggregate in fractions of 0–4 mm, 4–8 mm, and 8–16 mm, with a sieve grade GF 85 (fraction 0–4 mm), GC 85/20 (fraction 4–8 mm), and GC 90/15 (fractions 8–16 mm). The density of the dolomite aggregate was 2,75 kg/dm^3, the density of the ash from sunflower husk was 2,15 kg/dm^3, and the cement used was CEM I 42,5R, with a density of 3,0 kg/dm^3.

The test results in the fresh state are shown in Figures 5 and 6, while the compressive strength test results are shown in Figure 7.

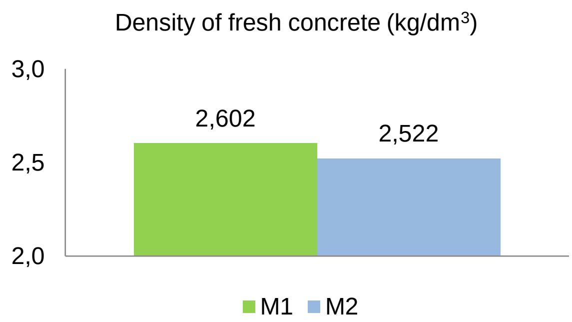

Figure 5 Results of the density of fresh concrete

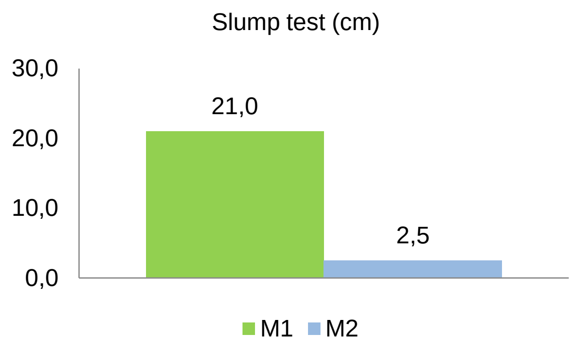

Figure 6 Results of the consistency test of fresh concrete

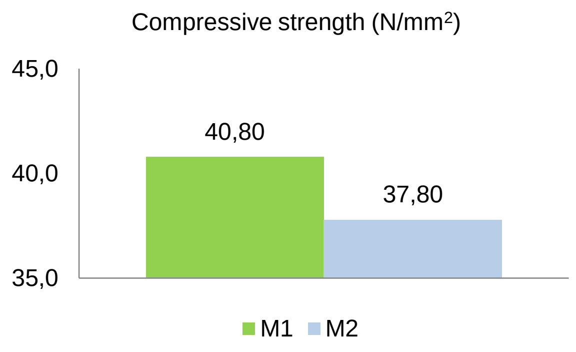

Figure7: Results of the compressive strength test of concrete

The tests for fresh concrete showed that the density of mixture M2 with the ash from the sunflower husk is less than that of the reference mixture M1. The slump test showed that the mixture of concrete with ash from sunflower husk has a significantly lower consistency value, 2.5 cm in mixture M2, compared to the reference mixture in which the consistency was 21.0 cm. The results of compressive strength tests showed that mixture M2 has 7,4 % lower compressive strength than the reference mixture M1.

6. CONCLUSION

This paper presents an overview of the preliminary investigation on the use of the ash from sunflower husk (agricultural waste), from an oil factory in eastern Croatia, as partial replacement for cement in concrete. It also presents a review of global research on the application of ash from biomass as a binder in concrete, which showed the justification for its application. A partial replacement of cement with ash from the sunflower husk reduces the consumption of cement. It also contributes to effective waste management, thereby reducing greenhouse gas emissions, negative impacts on human health and the environment, and environmental protection with economic feasibility. The ash generated by burning biomass creates a new and valuable application, which is one of the ways to use the energy potential of the sun and raise environmental awareness in eastern Croatia. Results of the preliminary research on partial replacement of cement with ash from sunflower husk from the oil factory Čepin have shown that there is potential for its application. Further research is needed to demonstrate its possibilities and for a full review of its use in concrete.

REFERENCES

[1] Mehta, P. K., Monteiro, P. J. M.: Concrete: Microstructure, Properties and Materials, Third ed. ed, McGraw-Hill, New York, 2006.

[2] Jozić, D. Studija utjecaja letećeg pepela iz termoelektrane na fizikalno-kemijska svojstva i ponašanje cementnog kompozita. Kemijsko-tehnološki faultet Sveučilišta u Splitu; 2008 (In Croatian)

[3] Mehta, P., Kumar. Sustainable cements and concrete for the climate change era – a review. Second International Conference on Sustainable construction materials and technologies. Ancona: Milwaukee: UWM Center for By-Products Utilization; 2010.

[4] Giudice, G. M. L., Asdrubali, F., Rotili, A.: Influence of new factors on global energy prospects in the medium term: comparison among the 2010, 2011 and 2012 editions of the IEA's World Energy Outlook reports, Economics and Policy for Energy and Environmental 3 (2013), pp. 67-89.
[5] Radojević, A., Repić, B., Dakić, D., Erić, A.: Analiza i ispitivanje pepela poljoprivredne biomase i potencijalnih aditiva, Savremena poljoprivredna tehnika 36 (2010) 4, pp. 357-365. (In Croatian)
[6] Gierulski, K., Marcin, P.: Utilisation of solid biomass for energy, porposes in Poland, Mechanisation and Electrification of Agriculture (2001), pp. 4.
[7] Domac, J., Risović, S., Šegon, V., Pentek, T., Šafran, B., Papa, I.: Može li biomasa pokrenuti energijsku tranziciju u Hrvatskoj i jugoistočnoj Europi, Šumarski list 11-12 (2015), pp. 561-569. (In Croatian)
[8] Biomasa, https://hr.wikipedia.org/wiki/Biomasa
[9] Obernberger, I., Biedermann, F., Widmann, W., Riedl, R.: Concentracions of inorganic elements in biomass fuels and recovery in the different ash fractions, Biomass and Bioenergy 12 (1997) 3, pp. 211-224.
[10] Cuenca, J., Rodríguez, J., Martín-Morales, M., Sánchez-Roldán, Z., Zamorano, M.: Effects of olive residue biomass fly ash as filler in self-compacting concrete, Construction and Building Materials 40 (2013), pp. 702–709.
[11] Memon, S., Shaikh, M., Akbar, H.: Utilization of rice husk ash as viscosity modifying agent in self compacting concrete, Construction and building materials 25 (2011), pp. 1044-1048.
[12] Krishnasamy, T. R., Palanisamy, M.: Pepeo od šećerne trske i rižinih ljuski kao zamjena za cement u samozbijajućem betonu, Građevinar 67 (2015) 1, pp. 23-31.
[13] Ganesan, K., Rajagopal, K., Thangavel, K.: Evaluation of bagasse ash as supplementary cementitious material, Cement and concrete composites 29 (2007), pp. 515-524.
[14] Alengaram, U., Jumaat, M.: Comparison of mechanical and bond properties of oil palm kernel shell concrete with normal weight concrete, International Journal of Physical Sciences 5 (2010), pp. 1231-1239.
[15] Kundu, S. P., Chakraborty, S., Roy, A., Adhikari, B., Majumder, S. B.: Chemically modified jute fibre reinforced non-pressure (NP) concrete pipes with improved mechanical properties, Construction and Building Materials 37 (2012), pp. 841-850.
[16] Sivaraja, M., Kandasamy, Velmani, N., Pillai, M. S.: Study on durability of natural fibre concrete composites using mechanical strength and microstructural properties, Bulletin of Materials Science 33 (2010), pp. 719-729.
[17] Vo, L. T. T., Navard, P.: Treatments of plant biomass for cementitious building materials – A review, Construction and Building Materials 121 (2016), pp. 161-176.
[18] Aksogan, O., Binici, H., Ortle, E.: Durability of concrete made by partial replacement of fine aggregate by colemanite and barite and cement by ashes of corn stalk, wheat straw and sunflower stalk ashes, Construction and Building Materials 106 (2016), pp. 253-263.
[19] Beltrán, M. G., Agrela, F., Barbudo, A., Ayuso, J., Ramírez, A.: Mechanical and durability properties of concretes manufactured with biomass bottom ash and recycled coarse aggregates, Construction and Building Materials 72 (2014), pp. 231-238.
[20] Oil factory Čepin, http://www.uljara.hr/

MECHANICAL AND DURABILITY PROPERTIES OF CEMENT MORTARS WITH BUILT-IN SEWAGE SLUDGE ASH

Domagoj Nakic[1], Ana Baricevic[2], Nina Stirmer[2], Marijana Serdar[2], Drazen Vouk[1]

[1] University of Zagreb Faculty of Civil Engineering, Water Research Department, Fra Andrije Kacica Miosica 26, 10000 Zagreb, Croatia, email: dnakic@grad.hr, dvouk@grad.hr
[2] University of Zagreb Faculty of Civil Engineering, Department of Materials, Fra Andrije Kacica Miosica 26, 10000 Zagreb, Croatia, email: abaricevic@grad.hr, ninab@grad.hr, mserdar@grad.hr

SUMMARY: Sewage sludge is being generated as a by-product of nearly all technological processes on wastewater treatment plants. Its disposal, in accordance with the current legislation, is expensive and environmentally and socially sensitive process. In accordance with the principles of sustainable development and circular economy, special emphasis is put on the possibilities of recycling and/or use of the sewage sludge or ash obtained as by-product of sludge thermal treatment. Due to the chemical composition based on oxides of calcium, silicon, aluminium and iron and possible pozzolanic properties of sewage sludge ash, there is a possibility of its use as a replacement for part of the cement in mortars and concrete. Results of previous research conducted on mortars and concrete point to significant potential for the use of sewage sludge ash in the concrete industry, from the standpoint of preserving mechanical properties. In this study, ash generated by combustion of sludge from the wastewater treatment plant Varazdin, in laboratory conditions in an electric furnace at temperatures 800 – 1000 °C, was used for the preparation of mortar samples. The paper analyses the influence of incineration temperature and ash replacement ratio on the properties of the mortars in the fresh state, mechanical (compressive and flexural strength) and durability (gas permeability) properties of mortar, as well as the impact on the corrosion resistance of steel during exposure to 3.5% NaCl solution. Results indicate that the addition of ash causes decrease in workability of mortars, as well as its strength. It is also found that it tends to reduce resistance to corrosion of reinforcing steel during exposure to 3.5% NaCl solution, while at the same time, because of the so-called "filler effect" occurs partially reduced permeability, which is confirmed by lower values of the gas permeability coefficient for some of the tested mortars.

MEHANIČKA I TRAJNOSNA SVOJSTVA CEMENTNIH MORTOVA S PEPELOM OD MULJA OTPADNIH VODA

SAŽETAK: Kao nusproizvod gotovo svih tehnoloških procesa na uređajima za pročišćavanje otpadnih voda nastaje mulj, čije je zbrinjavanje u skladu s važećom zakonskom regulativom skup te ekološki i socijalno osjetljiv postupak. Danas se u skladu s načelima održivog razvoja i kružnoga gospodarstva, poseban naglasak stavlja na mogućnost recikliranja i/ili korištenja mulja, odnosno pepela dobivenog kao nusproizvoda postupcima toplinske obrade mulja. S obzirom na kemijski sastav mulja koji sadržava okside kalcija, silicija, aluminija i željeza te rezultirajuća pucolanska svojstva pepela dobivenog spaljivanjem mulja, javlja se mogućnost njegove upotrebe kao zamjene za dio cementa u mješavinama morta i betona. Dosadašnja istraživanja provedena na cementnim mortovima i betonu ukazuju na značajne mogućnosti upotrebe pepela u proizvodnji betona, sa stajališta očuvanja mehaničkih karakteristika (tlačna čvrstoća i čvrstoća na savijanje). U ovom radu se za pripremu uzoraka morta upotrijebio pepeo dobiven spaljivanjem mulja s uređaja za pročišćavanje otpadnih voda u Varaždinu, u laboratorijskim uvjetima, u električnoj peći pri temperaturama od 800 – 1000 °C. Analiziran je utjecaj temperature spaljivanja mulja i udjela pepela na svojstva morta u svježem stanju, mehanička (tlačna i vlačna čvrstoća) i trajnosna svojstva morta (plinopropusnost), te utjecaj na korozijsku otpornost čelika tijekom izloženosti 3,5 %-tnoj otopini NaCl. Provedena istraživanja ukazuju da dodatak pepela utječe na smanjenje čvrstoće, smanjenje korozijske otpornosti armaturnih čelika u mortu s dodatkom pepela tijekom izloženosti 3,5 %-tnoj otopini NaCl, dok istovremeno zbog tzv "efekta filera" dolazi do djelomično smanjene propusnosti što se za ispitane mortove očituje manjim vrijednostima koeficijenta plinopropusnosti.

1. INTRODUCTION

Adequate management of wastewater belongs to priority activities of water management. It implies collecting, transport and treatment of wastewater, but also adequate management of waste substances generated by treatment. Treatment of wastewater and management of by-products generated in the process has become a very important problem on the global level, in particular in the last twenty years. This is particularly important for Croatia where the number of wastewater treatment plants (WWTP) is increasing to meet EU requirements. Construction of WWTPs has resulted in another problem – production of enormous quantities of sludge. The sludge generated at WWTP is a by-product of accumulation of dry matter during physical, biological and chemical processes. The sludge texture is composite; a mixture of organic and non-organic substances dispersed in water, and may contain pathogen microorganisms, parasites, viruses and also potentially toxic elements and compounds (heavy metals, etc.). Adequate management of sewage sludge is a challenge for all municipal utilities and other participants dealing with sewerage and wastewater treatment. Disposal of sewage sludge is a costly and ecologically sensitive procedure, a problem faced by almost all developed countries. So far, the practice offers several possible solutions for handling of sludge as the by-product of wastewater treatment [1]: landfilling (which is becoming more and more restricted and in some cases even forbidden), use in agriculture, use for soil improvements and filling trenches, incineration and further management of ash and others. The EU Directive 91/271/EEC requires that sludge management involves efficient recycling of resources without influencing public health or contaminating the environment. Across the EU, incineration has become an alternative approach to sewage sludge disposal which provides water utilities a great deal of stability and control over sludge management. Currently ~22 % of sewage sludge in EU is incinerated [2]. Thermal processing (incineration) of sewage sludge considerably facilitates further sludge management, first of all due to significantly reduced mass and volume. Thermal processing reduces the total mass of sludge by 85% [3], while the volume is reduced even by 90%; thermal processing destroys toxic organic components, minimizes unpleasant odours and facilitates further sludge management, with additional possibility of power generation [4]. Sewage sludge incineration generates major quantities of sewage sludge ash (SSA) as the main by-product. SSA also needs to be properly managed. The majority of SSA generated worldwide is currently landfilled.

The construction industry is an important consumer of natural resources and materials, and has significant potential to use selected wastes Possibilities of using and recycling of SSA greatly depend on the chemical composition, which is related to the sludge origin and the wastewater and sludge treatment technology. One possible solution is the use of SSA in the concrete industry as a partial cement replacement because the main chemical elements present in Portland cement (Ca, Si, Al and Fe) are also present in SSA [5]. Crystal forms of these elements are stable quartz (SiO_2), $Ca_3(PO4)_2$ and hematite (Fe_2O_3). SSA is primarily a powdery material with some particles sized as sand, with negligible share of organic matter and moisture [6]. The particle sizes of SSA are within the range from 1 to 100 µm, with mean diameter value of about 26 µm [7][8]. SSA consists of irregular particles with large specific area, which results in higher water requirements in cement mortars and concretes. The texture of SSA is porous, with irregularly shaped particles [9], it is a non-plastic, powdery material. SSA may be used in cementitious materials as a pozzolanic material, partly substituting for cement or as a filler replacing or partly replacing sand. When replacing cement with SSA in mortars and concrete, longer setting times [9], [10] increased total porosity [8], reduced workability [9], [11] [12] and increased water requirements [5][11] were observed. A reduction in flexural and compressive strength has also been reported [5][13][14]. Some of these problems could be overcome by using various chemical additives, such as superplasticizer for improving workability [1]. The main aim of the presented research is to examine the possibility and feasibility of building in of SSA, as the by-product from incineration process of sewage sludge, in cement mortars with special emphasis on, so far less investigated, durability properties of such mortars. This primarily refers to the tests of gas permeability and corrosion resistance of reinforcing steel.

2. MATERIALS AND METHODS

2.1. MATERIALS

For the purposes of this study stabilized and dehydrated sewage sludge was collected from WWTP Varazdin, Croatia and subjected to drying at 105°C to reach 90 % of dry matter. To produce SSA, sludge was incinerated in the electric laboratory furnace at temperatures ranging from 800°C to 1000°C. During exposure to high temperatures in the furnace, sewage sludge is transformed to the porous but hardened ash granules. Further grinding was required to obtain a powdery material, suitable for a cement replacement. The grinding was carried out by hand, using laboratory grinder with volume of 150 - 200 g, for about 30 sec per batch. An additional sieving through a fine sieve with mesh size of 0.5 mm was carried out. The remaining clumps were returned to the mill, grinded again and re- screened. Obtained ash was subjected to multiple tests to obtain detailed information on its physical and chemical composition and subsequently used as a partial cement replacement in mortars.

For preparing of cement mortars, cement CEM II/B-M (S-V) 42.5N, dolomite sand 0/4 mm and ordinary tap water were used, with water-binder ratio of 0.50. Seven different mixes were prepared. Reference mix (without added SSA) and six mixes with incorporated SSA obtained at 800, 900 and 1000°C (replacing 10 and 20% of cement by mass). Samples were thoroughly mixed for 4 minutes. To test the corrosion resistance corrugated steel reinforcement in the length of 10 cm and with a diameter of 12 mm was used.

2.2. EXPERIMENTAL METHODS

The density of obtained ashes was determined according to the ASTM C-188, using representative sample of homogenous mass equal to 65 g. Particle size distribution of SSA was determined by air jet sieving, according to the standard EN 933-10: 2009, after the ash was dried to the constant mass.

The workability of fresh mortar samples was determined using standard cone samples on a flow table using 15 drops. Flow table spread (FTS) was calculated from the average value of the maximum and minimum diameters of the spread cone in accordance with HRN EN 1015-3:2000/A2:2008.

Specimens for strength testing were prepared as 4 cm x 4 cm x 16 cm prisms. Nine specimens of each mix were made using steel moulds. Three specimens were tested at each curing age (1, 7 and 28 days). Specimens for gas permeability testing were 100 mm diameter and 50 mm high cylinders. All the specimens were demoulded after 24 hours and cured in a humidity chamber (relative humidity >95%, temperature 20±2°C). Mechanical tests were performed according to HRN EN 1015-

11:2000/A1:2008. Specimens were first tested for flexural strength and then the two resulting pieces were tested in compression.

The gas permeability tests were performed on three specimens for each mix (each specimen represents 1/3 of initially prepared 160 mm high cylinder). Specimens were oven dried for 24 hours and tested in accordance to RILEM Cembureau method [15] to give gas permeability coefficients.

Testing of corrosion resistance was also conducted on the 4 cm x 4 cm x 16 cm prisms with built-in reinforcement bars. The exposed length of the reinforcement was 80 mm with the total free surface area of 69.33 cm^2. On the upper side of the sample is connected insulated copper wire, enabling the electrical connection, which served for monitoring of corrosion parameters. The compound of copper wire and the specimen was protected by a two-component adhesive impermeable. Three samples were prepared for each mix, so that the steel reinforcement is centered in the middle of the specimen (Figure 1). The specimens were demoulded after 24 hours and cured in a humidity chamber (relative humidity >95%, temperature 20±2°C) for 90 days. After 90 days, the specimens were immersed to 2/3 into the 3.5% NaCl solution, which simulates sea water. The penetration of oxygen was expected from the upper half of the specimen, and the saline solution from the bottom half of the specimen [16]. Investigation of chloride induced corrosion inhibition of steel in mortar was performed by measuring changes in corrosion potential during 6 months.

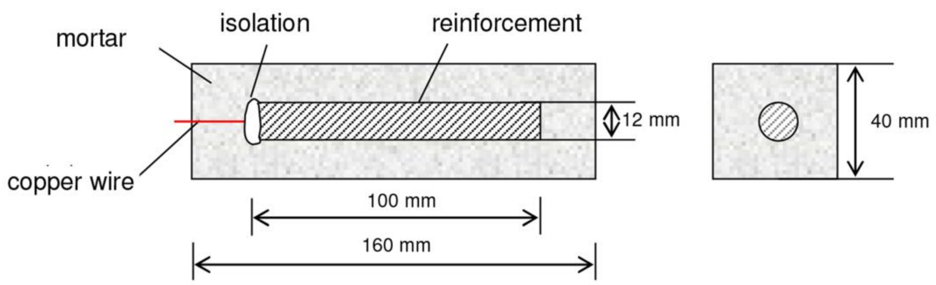

Figure 1 Schematic representing the embedding of reinforcing steel bars in cement mortar prisms

3. RESULTS AND DISCUSION

3.1. PHYSICAL AND CHEMICAL CHARACTERISTICS OF PRODUCED SSA

The density of SSA samples produced at different temperatures was found to increase with increasing combustion temperature. SSA obtained at 800°C had a density of 2.52 g/cm^3, SSA obtained at 900°C of 2.66 g/cm^3, whilst SSA obtained at 1000°C had a density of 2.94 g/cm^3.

Chemical composition (in terms of oxides) of SSA samples produced at different combustion temperatures shows dominant share of CaO (55-62%), followed by P_2O_5 (10-12%), SO_3 (around 10%), SiO_2 (7-8%) and Al_2O_3 (less than 2%).

SSA has a low organic and moisture content. The results, based on 6 samples of analysed SSA, showed that there are no significant differences in particle size distribution relative to the combustion temperature. Most of the particles are between 20 and 63 µm.

3.2. EFFECT OF SSA ON PROPERTIES OF MORTARS

Fresh state properties are important for future application of developed materials and have major influence on the behaviour of cementitious materials in hardened state. Incorporation of large percentage of very fine particles causes higher water demand and without additional corrections of mix design it implicates lower consistency of mix. The FTS tests indicate that the workability of mortars decreases when SSA is used, to an average of about 5% decrease in FTS results with the addition of 10% of SSA. It was also observed that the decline in workability is less expressed when SSA obtained at 800 °C was used, while the drop in FTS tests was most significant when SSA obtained at 1000 °C was used. The trend of an increase in the temperature of fresh mortars when increasing the share of added SSA was also noticed.

The values of flexural and compressive strength increase with time of hydration for all the samples as a sign that certain reactions occur in the mortars with the added SSA. However, it is evident that with the increasing share of the added SSA, strengths (both flexural and compressive) decrease. Mixture containing 10% of SSA obtained at temperature of 1000°C showed the best results in terms of flexural and compressive strength when compared to the reference mix (Figure 2). However, on the basis of these results, can hardly be drawn conclusions on the influence of incineration temperature of sludge on the mechanical characteristics of mortars with built-in SSA.

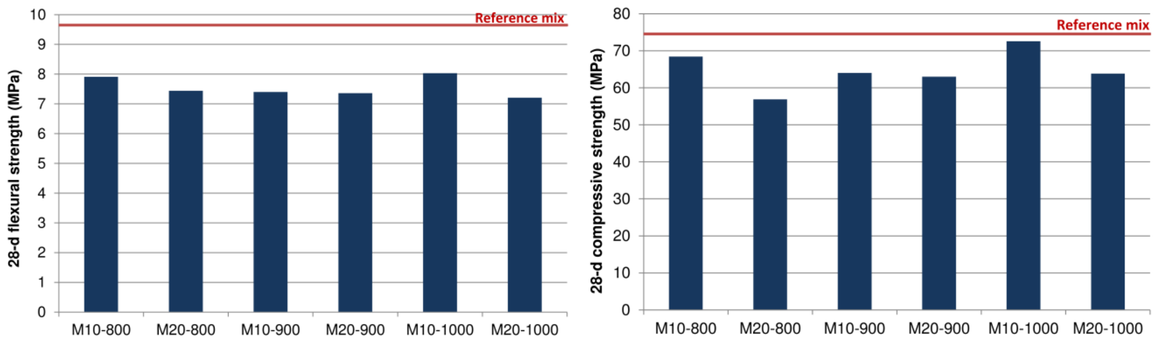

Figure 2 28-d flexural and compressive strength of analysed samples

The average decrease of 28-d compressive strength was around 8% with the addition of 10% of SSA and around 18% with the addition of 20% of SSA. The average decrease of 28-d flexural strength, with the addition of 10% of SSA was ~19%, while with the addition of 20% of SSA was on average ~24% lower when compared to the reference mix.

Analysing the obtained results of permeability tests one can see there is no clear trend of changes in the values of permeability coefficient with increasing SSA content (Figure 3). However, it can be seen that there is an obvious difference between a mixtures with equal proportions of SSA obtained at different temperatures. The poorest results were obtained with ash generated at 800°C, and in this case there is even deterioration of the mortar resistance in relation to the reference one. The reason for this could be the fact that the temperature of 800°C is possibly insufficient for complete breakdown of the SSA. Results obtained using the SSA obtained at 1000°C represent the best improvement of the resistance of the mortar when compared to the reference mixture by partially reduced permeability which is probably because of the so-called "filler effect" of the SSA. However, it should be noted that for most of the analysed samples class of mortar resistance remained the same as for the reference mixture. Also, it should be warned to the sensitivity of the permeability test procedure and therefore emphasizes the need for further research in this area.

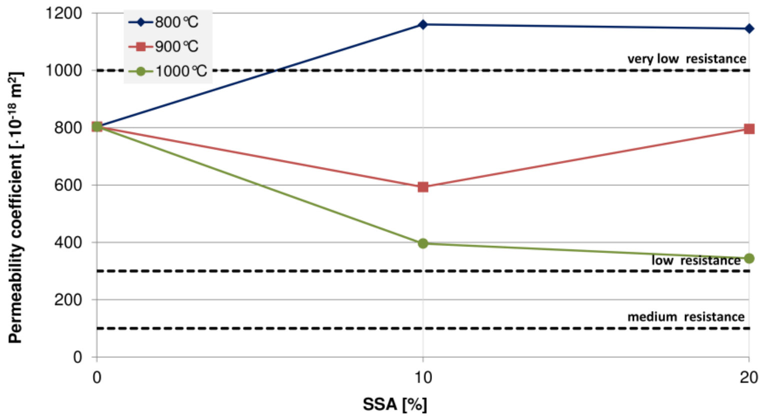

Figure 3 Gas permeability coefficient and classification of samples by mortar resistance

The results of corrosion potentials (E) as a function of the exposure period obtained from both steel bars embedded in mortars containing various levels of SSA and reference mortar are presented in Figure 4. During first 50 days of curing, the steel bar embedded in reference mortar and mortar with 10% SSA obtained at temperature of 800°C exhibited a stable E values (from -100 to -200mV versus SCE). The addition of 10% SSA obtained at temperature of 900°C and 1000°C exhibited E values more negative than -300mV. However, after 100 days of exposure, the E values gradually became less negative and shifted towards the passive state region. The E values continued to move toward less negative values and exhibited less negative potentials for steel bar embedded in SSA mortar compared to E values of those steel bars embedded in reference mortar.

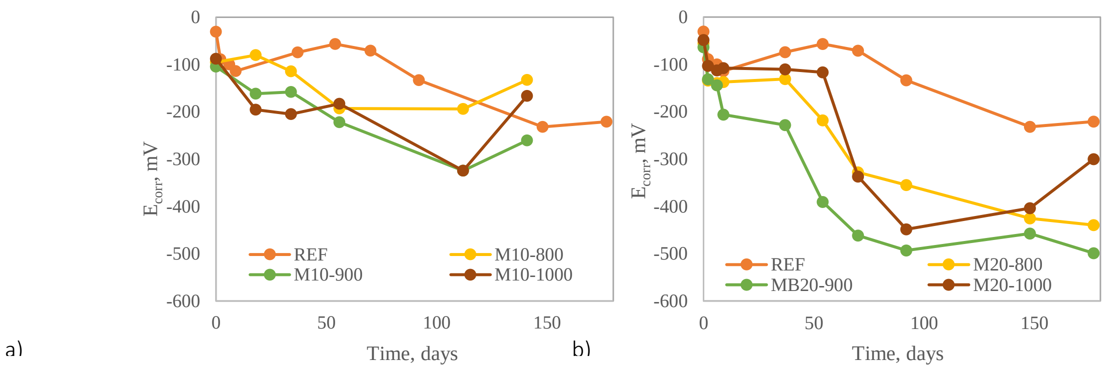

Figure 4 The change of the open-circuit potential for reinforcing steel embedded in the mortar with addition of: a) 10 %SSA, b) 20% SSA obtained by incineration at 3 temperatures (800, 900 and 1000 °C) and exposed to 3.5% NaCl solution during 6 months

From the potential change for mixes with 20% SSA it is evident that after 100 days of exposure, values of corrosion potential are moving towards negative values indicating a destabilization of passive film and the possible initiation of corrosion; reported values range from -350 to -500 mV.

From the measurement of the corrosion potential can be concluded that the reinforcing steel has a greater tendency to corrosion when embedded in mortar with addition of 20% SSA and exposed to 3.5% NaCl solution as compared to the steel in mortars with addition of 10% SSA. In addition, the tendency to corrosion of reinforcing steel increases in both mortars groups with SSA in relation to reinforcing steel in the reference mortar.

4. CONCLUSIONS

The environmental and economic benefits from the recycling of SSA in concrete industry, including conservation of raw materials and production of “green products”, can also be very significant depending on the end uses and production scale. The process of incineration of sewage sludge and the use of resulting ash in concrete industry requires a high degree of control and application of strict environment protection measures. Considering the obtained results, use of SSA in cement based materials is conceivable, but with certain limitations and this could present a good alternative to landfilling. Although there are some negative impacts when part of cement is replaced by SSA, it is likely that these could be overcome by changing the process or the addition of additives. Nevertheless, other technological and environmental tests should be performed, taking into account different SSA from multiple sources (WWTP).

ACKNOWLEDGMENTS

This work has been fully supported by Croatian Science Foundation under the project "7927 - Reuse of sewage sludge in concrete industry: from microstructure to innovative construction products".

REFERENCES

[1] Vouk, D., Nakic, D. & Stirmer, N.: Reuse of sewage sludge – problems and possibilities. Proceedings of the International Conference IWWATV 2015, Athens, Greece. Available from http://iwwatv.uest.gr/proceedings/pdf/Vouk_et_al.pdf Accessed: 2016-10-20

[2] Lynn, C.J., Dhir, R.K., Ghataora, G.S. & West, R.P.: Sewage sludge ash characteristics and potential for use in concrete. Construction and Building Materials, 98 (2015), pp. 767-779, 2015.

[3] FHWA-RD-97-148, User Guidelines for Waste and Byproduct Materials in Pavement Construction: Sewage Sludge Ash – Material Description (2012).

[4] Tantawy, M.A., El-Roudi, A.M., Abdalla E.M. & Abdelzaher, M.A.: Evaluation of the pozzolanic activity of sewage sludge ash. *ISRN Chemical Engineering*, (2012), Article ID 487037.

[5] Donatello, S. & Cheeseman, C.R.: Recycling and recovery routes for incinerated sewage sludge ash (ISSA): A review. *Waste Manage,* 33 (2013), pp 2328-2340.

[6] Al-Sharif, M.M. & Attom, M.F.: A geoenvironmental application of burned wastewater sludge ash in soil stabilization. *Environ. Earth Sci*., 71 (2014), DOI 10.1007/s12665-013-2645-z.

[7] Coutand, M.; Cyr, M. & Clastres, P.: Use of sewage sludge ash as mineral admixture in mortars. *Construction Materials*, 159 (2006), pp. 153-162.

[8] Yusuf, R.O.; Moh'd Fadhil, M.D. & Ahmad, H.A.: Use of sewage sludge ash (SSA) in the production of cement and concrete – a review. *Int. J. Global Environmental Issues,* 12 (2012), pp. 214-228.

[9] Cyr, M.; Coutand & M.; Clastres, P.: Technological and environmental behavior of sewage sludge ash (SSA) in cement-based materials. *Cem. Concr. Res*. 37 (2007), pp. 1278-1289.

[10] Lin, K.-L. & Lin, C.Y. Hydration characteristics of waste sludge ash utilized as raw cement material. *Cement and Concrete Research*, 35 (2005), pp. 1999-2007.

[11] Monzo, J.; Paya, J.; Borrachero, M.V. & Girbes, I.: Reuse of sewage sludge ashes (SSA) in cement mixtures: the effect of SSA on the workability of cement mortars. *Waste Manage*., 23 (2003), pp. 373-381.

[12] Garces P.; Perez-Carrion, M.; Garcia-Alcocel, E.; Paya, J.; Monzo, J. & Borrachero, M.V.: Mechanical and physical properties of cement blended with sewage sludge ash. *Waste Manage*., 28 (2008), pp. 2495-2502.

[13] Donatello, S.; Tyrer, M. & Cheeseman, C.R.: Comparison of test methods to assess pozzolanic activity. *Cem. Concr. Compos*., 32 (2010), pp. 63-71.

[14] Pan, S.C.; Tseng, D.H.; Lee, C.C. & Lee, C.: Influence of the fineness of sewage sludge ash on the mortar properties. *Waste Manage*., 33 (2003), 1749-1754.

[15] Geiker, M., Grube, H., Luping, T., Nilsson, L.O. & Andrade, C.: Laboratory test methods. Rilem Report, No 12 (1995), pp.144-147.

[16] C. Andrade, C. Alonso, R. Polder, R. Cigna, O. Vennesland, M. Salta, et al.: Recommendations of RILEM TC-154-EMC: “Electrochemical techniques for measuring metallic corrosion” Test methods for on-site corrosion rate measurement of steel reinforcement in concrete by means of the polarization resistance method, *Mater Struct*., 37 (2004), pp 623-643.

AWASO BAUXITE REDMUD-CEMENT BASED COMPOSITES: PROCESSING, CHARACTERISATION, DESIGN AND APPLICATIONS

David Dodoo-Arhin[1], A.R. Nuamah[1], B, Agyei-Tuffour[1], D. Obada[2], A. Yaya[1]

[1] University of Ghana School of Engineering Sciences, Department of Materials Science and Engineering, Annie Jiaggie Road, P.O.Box Lg 25 Legon-Accra, Ghana, email: ddarhin@yahoo.com, afianuamah@yahoo.com, bagyeituffour@gmail.com, abuy95@yahoo.com
[2] Ahmadubello University, Faculty of Engineering, Department of Mechanical Engineering, Zaria, Nigeria, email: obadavid4@gmail.com

SUMMARY: The behaviour of Ghanaian bauxite residue (red mud) – Portland cement based composites have been investigated for their applicability in the pavement construction as a means of recycling the bauxite waste. The experimental techniques considered include the structural, thermal, morphological and microscopy analysis of the raw bauxite and red mud samples calcined at 800 °C. Composite mortar blocks of different batch formulations were produced and their physicochemical properties were investigated. The results show that the compressive strength of the as-prepared composites increased by ~40% compared to the type M mortar strength of ~2500psi. The load bearing applications of the composites are discussed to influence the adoption of the calcined red mud as supplement in the production of low-cost Portland cement composite mortar blocks for the construction industry.

KOMPOZITI IZ AWASOA OD BOKSITNOG CRVENOG MULJA I CEMENTA: PROIZVODNJA, ODREĐIVANJE ZNAČAJKI, PRORAČUNI I PRIMJENE

SAŽETAK: Istraživano je ponašanje kompozita od ostataka boksita (crvenoga mulja) iz Gane i portlandskog cementa sa svrhom oporabe boksitnog otpada i utvrđivanja njegove primjenjivosti u izgradnji kolnika. Eksperimentalni postupci obuhvaćaju strukturnu, toplinsku, morfološku i mikroskopsku analizu uzoraka sirovog boksita i crvenoga mulja kalciniranoga pri 800 °C. Istražena su fizičko-kemijska svojstva izrađenih mortova različitih sastava. Rezultati pokazuju da se tlačna čvrstoća pripremljenih kompozita povećala za približno 40 % u usporedbi s mortom tipa M čvrstoće oko 2500 psi (oko 17,5 MPa). Raspravljeno je o primjeni kompozita od kalciniranog crvenog mulja kao dodatka u proizvodnji jeftinih portlandcementnih kompozitnih ploča morta u građevinskoj industriji.

1. INTRODUCTION

The search for recycling alternatives of several industrial wastes has become a very common practice aimed at reducing cost of industrial waste disposal and protection of the environment. One of such industrial waste is bauxite red mud; an alkaline leaching waste with typical pH of 10-13 [1-4] which is generated during the Bayer process or bauxite calcination method for alumina production [5-7]. During the treatment of the bauxite ore by the Bayer process, it is initially crushed and digested with a hot solution of sodium hydroxide (NaOH), and lime liquor at ≈175 °C and subjected to attack at high pressure and temperature. This condition makes it possible to convert the hydrated alumina into sodium aluminate solution (Eq. (1)), while the impurities remain in a solid state.

$$Al(OH)_{3(aq)} + NaOH_{(aq)} \xrightarrow[pressure]{Heat} AlO_2Na_{(aq)} + 2H_2O_{(l)} \qquad (1)$$

The impurities are separated from the aluminate solution by decantation and filtration, followed by washing. The solid residues thus obtained are called red mud and are mainly made up of oxides of iron, aluminium, silicon and titanium. However, despite being washed and considered as an inert solid waste, red mud remains strongly alkaline and highly corrosive. It is usually discharged as highly alkaline slurry (pH 10-13.5) with 15-40 % solids, which is pumped away for appropriate disposal. This strong alkaline character (Na2O + NaOH = 2.0-20.0 wt.%), restricts the disposal conditions of red mud in order to minimize environmental problems such as soil contamination and ground water pollution. Its chemical and mineralogical composition may however slightly vary, depending on the source of bauxite, the technological processing conditions (Bayer process or bauxite-calcination method) and storing ages. It is composed of six major oxides (Al2O3, Fe2O3, Na2O, SiO_2, CaO, and TiO_2), and a large variety of other minor elements. It has been estimated that 66 million tons of red mud [8] is produced annually across the world and it is considered to be "hazardous" according to the Brazilian NBR 10004 standard [9]. Over the years the disposal of red mud by methods such as sea water discharge, lagooning and dry- stacking has been a major challenge to alumina companies and environmentalist. It is expensive, requires lot of land and poses numerous environmental and health hazards. As a result of these challenges, lots of research has been carried out to device means of economically utilizing this highly alkaline waste as a raw meal for the production of Portland cement clinker, as a partial substitute for clay in the production of bricks [10], in the preparation of special cements [11] and pozzolanic pigment.

Portland cement happens to be one of the most popular and widely used building materials across the world due to the availability of raw materials over the world, easy processing and its amenability to conceivable shapes [12]. However, there are two major drawbacks with respect to sustainability in the use of Portland cement which are:(1) about 1.5 tons of raw materials is needed in the production of every ton of PC, at the same time also about one ton of carbon dioxide (CO_2) is released into the environment which means that the production of Portland cement is a resource and energy intensive process. (2) Concretes made of Portland cement deteriorate when exposed to severe environments and this affects the service behaviour, design life and safety of structural constructions [13]. Studies have shown that utilization of red mud in the production of construction and building materials has the potential of consuming the red mud waste in higher quantities. For instance, it was reported that 2.5 million tons of red mud was consumed by the cement industry during 1998-1999 in India and researchers found that the hydration reaction of Portland cement is favoured by a highly alkaline environment which red mud is noted for [14]. The high alkalinity of red mud which is of environmental concern serves as a major asset in the attempt of inhibiting corrosion in reinforced concrete rebar and reducing sulphur build-up in the kiln system of cement plants. Tsakiridis et al., [11] in Greece studied the addition of red mud residue by 1% in the raw mix for the production of Portland cement and found that the red mud can be utilized as a raw material in cement production, at no cost to the producer thus, contributing in the reduction of the process cost. It has also been found out that the maximum potential strength developed by cement is never fully utilized as about half of the amount of Portland cement consumed in building construction is used in masonry and plastering whose strength requirement is about 4.0 MPa whiles Portland cement is suited for applications with strength requirements exceeding 15.0 MPa [15]. Materials with pozzolanic characteristics may thus be used to partially replace the cement in those applications and red mud is tested here for this purpose. This study investigates the physico-mechanical and economic influence of calcined Bayer red mud addition in Portland cement based pavement blocks.

2. EXPERIMENT

In a typical red mud production via the Bayer process, ball milled bauxite with particle sizes < 355 µm were slurred with hot (135°C - 140 °C) 2M concentration of NaOH and digested in a 1L pyrex beaker at atmospheric pressure under constant stirring for ~30 minutes to enable dispersion of particles. After digestion, the homogenous mixture was allowed to cool to room temperature for 24 hours and the liquid aluminous is filtered off leaving the residue on a filter paper. The chemical and mineralogical composition of the samples was determined using a Thermo Fisher ARL9400 XP+ Sequential XRF equipped with a WinXRF software for analyses. The samples were milled in a tungsten-carbide milling pot to achieve particle sizes < 75µm and dried at 100°C.After drying, the samples were roasted at 1000°C to determine loss on ignition (LOI) values. 1g of the sample was mixed with 6g lithium tetraborate flux (Li2B4O7) and fused at 1050°C to make a stable fused glass bead. For trace element analyses, the sample was mixed with a PVA binder and pressed into a pellet using a 10-ton press. X-ray powder diffraction (XRD) patterns were collected on an XPERT-PRO diffractometer (PANalytical BV, Netherlands) with theta/theta geometry, operating a cobalt tube at 35 kV and 50 mA. The goniometer is equipped with automatic divergence slit and a PW3064 spinner stage. The X-ray diffraction patterns of all specimens were recorded in the 10°- 70° 2θ range with a step size of 0.017° and a counting time of 14s per step. Qualitative phase analysis was conducted using the X'Pert Highscore plus search match software. The morphology of the samples was studied on a FEI XL 30 Environmental Scanning Electron Microscope equipped with an Energy Dispersive X-ray Spectroscopy system based on a nitrogen cooled Si-Li detector. The samples were metalized and analyzed at 30 kV and 93 µA.

Table 1 Batch formulation

Sample	Red Mud replacement (%)	Fine Aggregate (sand) Kg	Cementitious materials (Kg)		Remarks
			Portland cement	Red mud	
BRC-0	0	2.000	1.000	0.000	Reference
BRC-1	5	2.000	0.950	0.050	5%RM
BRC-2	10	2.000	0.900	0.100	10%RM
BRC-3	15	2.000	0.850	0.150	15%RM
BRC-4	20	2.000	0.800	0.200	20%RM
BRC-5	25	2.000	0.750	0.250	25%RM

The thermal stability of the various phases in the samples was studied on a standard SDT Q600 (V20.9 Build 20) TG/DTA instrument under air flow of 50 mL/min. Prior to analysis A sapphire standard was used to calibrate the thermal response due to heat flow as well as the temperature. 25 mg of the specimens were placed in an alumina (Al2O3) crucible (100mg capacity), subjected to a linear heating ramp between 15 °C and 1200 °C at a rate of 10°C/min and a cooling rate of 50 °C/min. The test measurements were made for the mass change (loss) of the sample as a function of the temperature and the phase changes by the adsorption or the emission of energy. The mortar was prepared using a Ghanaian limestone Portland cement (Diamond class 42.5 N), calcined red mud, fine aggregates (river sand) and laboratory tap water. The red mud from the Bayer process was calcined for 2 hours at 800°C in a gas test kiln in order for the aluminium hydroxides (boehmite and gibbsite) to develop some pozzolanic behaviour [16,17]. The control mix proportion for the mortar preparation was Portland cement, sand and 0.5 water/cement ratio according to the BS EN196-1: 1995 standard. The materials were weighed into the mixer bowl which mixes the materials into a homogenous mixture whiles a measured amount of water is poured into the mix simultaneously to form the paste.

The quantity of the sand and water were kept constant while that of the cement was varied with red mud in the percentages of 5, 10, 15, 20 and 25. Table 1 gives an illustration of the design mix proportion and the batch formulation respectively. Four 7.5 cm x 7.5 cm cubes, 6 cm x 3 cm x 2 cm briquettes and 20cm x1cmx 1cm bar samples were made from each mix batch. The standard consistency, the initial and final setting times of the fresh red mud – Cement based mortar of the various batches were determined using the Vicat needle apparatus (Controls, L28) according to the British and European Standards BS EN 196-3:1995. The water of absorption characterisation was conducted to estimate the final products' (mortar blocks) susceptibility to seepage of water through its pores when immersed in water. ASTM C830-09 and ASTM D6111-09 standard tests were followed in the determination of the porosity and bulk density respectively. The apparent and bulk density tests were carried out by making briquettes of 6 cm x 3 cm x 2 cm samples. The apparent porosity and bulk density was determined using the Archimedes principle. Using three-point bending testing (ASTM C99/C99M-09 standard protocols), the flexural strength of the test bars was determined. Monotonic loading was done at 1.85 kg/min till point of fracture.

3. RESULTS AND DISCUSSION

3.1. XRF AND XRD ANALYSIS

The mineralogical composition as well as physical and chemical properties has a critical influence on the industrial applications of ceramic materials. From Table 2 it can be seen that the dominant oxide in the Awaso red mud is Al_2O_3. It is also worth stating that the dominant red colour of both the red mud and bauxite is attributed to the well dispersed particles of iron oxide (Fe_2O_3) in both samples. Other oxides found with weight percentages less than 1% are for Awaso bauxite: MgO (0.08%), P_2O_5 (0.15%), SO_3 (0.13%), K_2O (0.04%), MnO (0.01%); for Awaso red mud: MgO (0.22%), P_2O_5 (0.15%), SO_3 (0.10%), K_2O (0.04%), and MnO (0.01%).

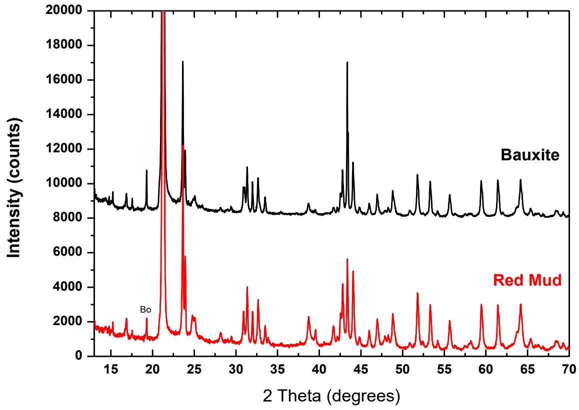

Figure 1 XRD pattern of Awaso bauxite and red mud

From the XRD data (Figure 1), the main mineral phases identified in the Awaso red mud sample using the X'Pert Highscore plus software are hematite (Fe_2O_3, card no.33-0664), rutile (TiO_2, card no. 21-1276), perovskite ($CaTiO_3$, card no. 22-1053), quartz (SiO_2, card no. 18-1166), sodalite ($Na_2O.Al_2O_3.SiO_2$, card no. 16-0612), boehmite {AlO(OH), card no. 21-1307}, goethite {FeO (OH), card no. 26-0792}, gibbsite {$Al(OH)_3$, card no. 33-180}, calcium alumina silicate {$Ca_2Al_2(SiO_4)(OH)_8$, card no. 03-0798}.

Table 2 Chemical composition of bauxite and red mud estimated by XRF

Major oxides	Awaso Bauxite (%)	Awaso red mud (%)
Al_2O_3	65.15	51.07
SiO_2	2.75	2.15
Fe_2O_3	6.99	7.15
Na_2O	1.05	2.84
TiO_2	1.93	1.77
CaO	0.06	1.07
L.O.I	23.08	33.9

3.2. THERMAL ANALYSIS (TG-DTA) AND MICROSCOPY

The main mineral phases of dried red mud at room temperature are calcite ($CaCO_3$), dicalcium Silicate (Ca_2SiO_4), hematite (Fe_2O_3), perovskite ($CaTiO_3$), gibbsite ($Al(OH)_3$), and CaO. The TG-DTA thermograms (Figure 2) show a continuous weight loss distributed in the range of 25–1200ºC. The figure shows two main portions of mass loss as the rise of temperature. The first one is during the heating temperature interval of 50–550°C when the physically absorbed water and chemically bound water is off. Before the temperature gets up to 500ºC, the sample loses ≈8.26% of its total weight. The proportion of physically absorbed water is small. Comparing this result with the results of the XRD analysis, the lost chemically bound water could be mainly attributed to the decomposition of gibbsite ($Al(OH)_3$) to alumina (Al_2O_3) and H_2O which can combine with the CaO to form tricalcium aluminate or Gehlenite. The more rapid decline in the range of 550–900ºC with a mass change of ≈ 21.81% could be attributed to the release of CO_2 [18]. The release of CO_2 is due to the decomposition of Calcite ($CaCO_3$) into CaO. The chemical equations during this phase transformation are as follows:

$$CaCO_3 \rightarrow CaO + CO_2,\ 3CaO + Al_2O_3 \rightarrow Ca_3Al_2O_6, \quad (6)$$

$$2CaO + 2Al_2O_3 + SiO_2 \rightarrow 2Ca_2Al_2SiO_7. \quad (7)$$

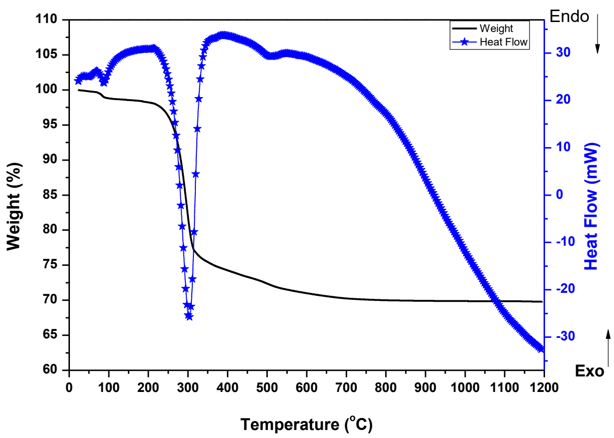

Figure 2 Tg (Wt%)-DTA (Heat flow) thermographs of Awaso Red mud

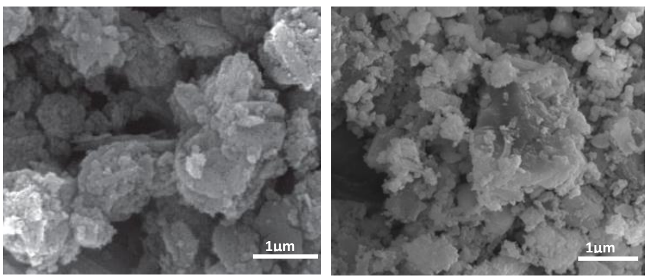

(a) (b)

Figure 3 SEM images of (a) Calcined Red Mud and (b) Red Mud-Cement composite

The phases of tricalcium aluminate ($Ca_3Al_2O_6$) and gehlenite ($Ca_2Al_2SiO_7$) start to develop in the 800–900ºC range. There is no obvious mass change or phase change above 900ºC.

The SEM micrographs (Figure 3) of the red mud and red mud-cement composites show particles with plate-like shapes and agglomerates on the microstructure scale which could be attributed to the processing of the powders via ball milling. Homogeneous blend of the red mud and cement for the various batches were physically observed.

3.3. PHYSICAL AND MECHANICAL PROPERTIES OF RED MUD CEMENT MORTAR BLOCKS

From the Table 3, it is observed that both the initial and final setting times of the Portland cement mortar decreases with increase in red mud additions thus, the addition of red mud tends to accelerate the setting process. This result can be attributed to the high alkalinity of the red mud and the presence of aluminium and sodium hydroxides (known as curing accelerators).

Table 3 Physical and Mechanical Properties of RMC mortar and blocks

Sample	Standard consistency	Initial setting time (mins)	Final setting time (mins)	Flexural strength (Kg/cm²)	Compressive strength (N/mm²)	Bulk density (g/cm³)	Apparent Porosity (%)	Water absorption (%)
BRC-0	24.00	176	379	55.84	43.20	2.18	2.65	0.96
BRC-1	25.00	134	364	57.85	43.00	2.22	0.45	1.11
BRC-2	27.00	132	335	43.48	35.98	2.22	1.13	2.20
BRC-3	30.00	126	201	43.66	32.65	2.19	1.36	2.60
BRC-4	32.00	100	172	39.17	31.88	2.15	2.74	3.57
BRC-5	36.00	95	212	34.87	27.90	2.15	4.04	7.70

The standard consistency of the mortar samples increases as the amount of calcined red mud increases.as shown in Table 3. This observation can be attributed to the fact that the red mud particles are lighter, finer and occupy large volume hence the amount of water needed to obtain the same standard paste as compared to the reference mortar increases. Also, as the red mud content increases, the workability of the mortar decreases and more water is needed for the wetting and kneading of the paste. It can be seen from Table 3 that the flexural strength value decreases for as-prepared mortar blocks with red mud percentages of 10, 15, 20 and 25 and value increases for 5% red mud replacement in cement with respect to the reference mortar block. This decrease in strength could be attributed to the fact that as the red mud content increases the workability decreases and the packing effect reduces thereby causing the material to be porous and having reduced strength. However, for 5% red mud replacement it could be seen from the table that the flexure strength was higher than that of the reference cement mortar block and this could be attributed to the fact that the bonding between the particles was very strong due to better backing hence the increase in strength.

It can be observed from Figure 4 that as the red mud content increases the compressive strength decreases whiles the water absorption increases. The strength of the blocks is affected by the workability and the porosity and as deduced earlier, the increase in red mud content tends to decrease workability and increase porosity. From these inference it can be said that the more the red mud content the less the strength. It is also observed from Table 3 that for 5%, 10% and 15% red mud replacement, the bulk density increases as compared to the reference cement block. This is due to the fact that with these replacements, the fine nature of red mud increased mortar block compactness thus producing high density. However, for subsequent increase in red mud, because of the decrease in workability, the mortar block compactness is less hence decreases density.

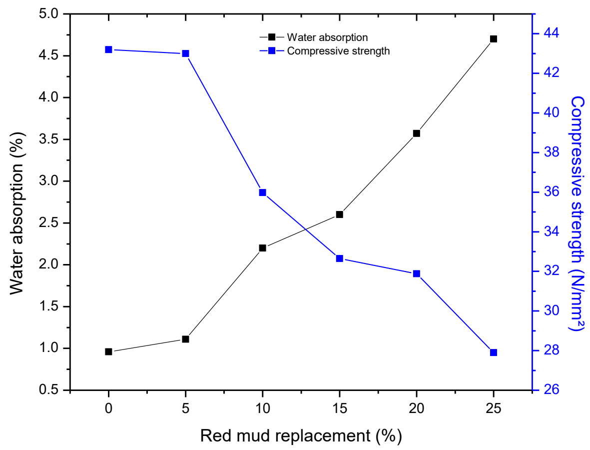

Figure 4 Relationship between water absorption and compressive strength with red mud replacement

It can also be seen that as the density increases, porosity decreases and as porosity increases density decreases. Furthermore, as the red mud content increases in the as-prepared mortar blocks, the water absorption also increases. This observation can be attributed to the fact that as the RM content increases the workability decreases and as the workability decreases the porosity increases, hence the amount of water that is able to seep through the pores increases. For water of absorption to increase, it means a material is porous and from our observation, increasing red mud addition to the initial cement mortar mixtures increases the porosity due to reduced workability and increase porosity and water absorption degrades the strength of the final block. This also increases the standard consistencies of the mortars before the formation of the blocks. Mortars for paving applications are more likely to be in a saturated condition than those for walls. In view of this, the mortar typically must be more durable to resist the harsher exposure. Type M mortar is recommended with Type S as the alternate. In general, comparing the compressive strengths of the various compositions of red mud mortar with ASTM C 270 classification of mortar, the red mud based mortars can be classified as a type M (high strength and for load bearing applications) mortar [19, 20].

4. CONCLUSIONS

Generally, increase in calcined red mud content decreases the compressive as well as flexural strength. However, 5% red mud additions tend to have superior or equal qualities to the reference cement mortar blocks. Workability of mortar generally is decreased with the increase in red mud content and both the initial and final setting times are accelerated mostly due to the presence of aluminium and sodium hydroxides (curing accelerators). The addition of calcined red mud at 800°C tend to increase bulk density and decrease porosity for red mud percentages of 5, 10 and 15. The rate at which water seep through the pores (water of absorption) of mortar also tends to increase with the increase in red mud addition and this has a negative influence on the strength of the mortar. The replacement of Portland cement with RM up to 25% in mortar preparation for pavement blocks as achieved in this study would help reduce cost, reduce the impact of the Bayer red mud waste on the environment and also reduce the depletion of the raw materials needed to produce cement which will in turn reduce the amount of CO2 released into the environment. To improve the workability of the red mud mortar, super plasticizers such as polycarboxylate ether and melamine sulfonate may be added.

ACKNOWLEDGMENTS

Authors acknowledge the University of Ghana, University of Pretoria and the Ghana Standards Authority for support.

REFERENCES

[1] Amritphale, S.S.; Patel, M.: Utilisation of red mud, fly ash for manufacturing bricks with pyrophyllite. *Silicates Ind.* 1987; 2: 31-35.
[2] Building Code Requirements for Masonry Structures (ACI 530/ASCE 5/TMS 402) and Specification for Masonry Structures (ACI 530.1/ASCE 6/TMS 602), The Masonry Society, Boulder, CO, (2005).
[3] Habashi, F.: Bayer's process for alumina production: a historical Perspective. *Bull. Hist. Chem.* 1995; 17:18.
[4] Hind, A.R. et al.: The surface chemistry of Bayer process solids: a review. *Colloids Surf. A.: Physicohem. Eng.Aspects*. 1999; 146[1-3]: 359-347.
[5] Lin, C.; et al.: Acid neutralizing capacity of two bauxite residues and their potential applications for treating acid sulphate soil and water. Aust. J. Soil Res. 2004; 42 [5&6]: 649-657.

[6] Liu, D.Y.; Wu, C.S.: Stockpiling and comprehensive utilization of Red Mud. *Mat.* 2012; 5: 1232-1246.
[7] Li, Z. et al.: Development of Sustainable Cementitious Materials. Proceedings of the International Workshop on Sustainable Development and Concrete Technology, Beijing, China. 2004:55-76.
[8] Mahadevan, H.et al.: An appraisal of the methods for red mud disposal under Indian conditions. New Delhi: Allied Publishers. 1996:337-347.
[9] Mehta, P.K.: Advancements in Concrete Technology. Conc. Inter. 1999;21[6]: 69-76.
[10] Mehta, P.K.; Aïtcin, P.C.: Principles Underlying the Production of High-Performance Concrete. *Cement, Concrete, and Aggregates*, ASTM, 1990;12[2]: 70-78.
[11] Menzies, N.W.et al.: Seawater neutralizing of alkaline bauxite residue and implications for revegetation. *J. Environ. Qual.* 2004; 33: 1877-1884.
[12] Pascale, V.; et al.: Chemical and biological leaching of aluminum from red mud. *Environ. Sci. Technol.* 1994;28 [1]: 26-30.
[13] Pera, J.; Motazi, A.: Pozzolanic activity of calcined red mud. Proceedings of the 4th CANMET/ACI International Conference on Fly Ash. Silica fume, Slag and Natural Pozzolans in Concrete. Istanbul, Turkey, V.M Malhotra, (ed.) SP 1992; 132[749]:132.
[14] Pera, J. et al.: Development of a Pozzalanic Pigment from Red Mud. *Cem. Conc. research*, 1997;27[10]:1513-1522.
[15] Summers, R.N.; Pech, J.D.: Nutrient and metal content of water, sediment and soils amended with bauxite residue in the catchment of the Peel Inlet and Harvey Estuary. Western Australia. *Agr. Ecosyst, Environ.* 1997; 64: 219-232.
[16] Tsakiridis, P.E. et al.: Red mud addition in the raw meal for the production of Portland cement clinker. *J. of Haz. Mat.* 2004; B116: 103-110.
[17] Technical Notes on Brick Construction-8B: Mortars for Brickwork - Selection and Quality Assurance, Brick Industry Association, Centennial Park Drive, Reston, Virginia. 2006: 1-6.
[18] Vincenzo, M.S.; et al.: Bauxite red mud in the ceramic industry, Part 2: production of clay based ceramics. *J. Euro. Ceram. Soc.* 2000;20: 245-252.
[19] Yogananda, M.R.; Jagadish, K.S.: Pozzolanic properties of rice husk, burnt clay and red mud. *Buil. and Env.* 1998; 23[4]: 303-308.

EFFECT OF SILICA FUME ON WASTE BASED GEOPOLYMER COMPRESSIVE STRENGTH AND EFFLORESCENCE

Jinbang Wang[1], Fangshu Li[2], Zonghui Zhou[1], Peng Du[1], Ning Xie[1], Xin Cheng[1]

[1] Shandong Provincial Key Laboratory of Preparation and Measurement of Building Materials, Engineering Center of Advanced Building Materials of Ministry of Education, University of Jinan, Jinan 250022, China, email: wjbo344@126.com, mse_zhouzh@ujn.edu.cn, mse_dup@163.com, mse_xien@ujn.edu.cn, ujn_chengxin@163.com
[2] The United States resource pro (Jinan) Co. Ltd. Jinan 250022, China, email: Lifangshu109@foxmail.com

SUMMARY: Geopolymer has been a research hot spot in recent years in the field of building materials owing to its wide range use as raw material, low energy consumption, less pollution and superior performances. Geopolymer materials were activated with alkali, so soluble alkali can be dissolved out from geopolymer material surface and reacts with carbon dioxide in the air to form carbonate, which is called efflorescence and hinders the practical application of geolpolymer materials. The effect of silica fume on the compressive strength and efflorescence of waste based geopolymer were studied and efflorescence inhibition mechanisms was analyzed with XRD and SEM in this paper. The results show that the compressive strength of the waste based geopolymer is the best when the content of silica fume is 10%, and it can reach 125MPa in 60 days. However, when a threshold (10%) is surpassed, strengths could be hurt; the compressive strength is decreased with the increase content of silica fume. Besides, the efflorescence of waste based geopolymer has inhibited best when silica fume content was 10%. Carbonate ions concentration of geopolymer leaching solution showed a decreasing trend with increasing content of silica fume.

UČINAK SILICIJSKE PRAŠINE NA TLAČNU ČVRSTOĆU I ISCVJETAVANJE GEOPOLIMERA

SAŽETAK: U području građevnih materijala geopolimer je posljednjih godina opsežno istraživan zbog svoje široke upotrebe kao sirovine, kao materijal male potrošnje energije, manjeg onečišćenja i odličnih svojstava. Geopolimerni materijali aktivirani su alkalijama. Topljive alkalije mogu se izdvojiti s površine geopolimernog materijala i reagirati s ugljičnim dioksidom iz zraka te formirati karbonat. To se naziva iscvjetavanje i otežava praktičnu upotrebu geopolimernih materijala. U radu je istražen utjecaj silicijske prašine na tlačnu čvrstoću i iscvjetavanje geopolimera, a mehanizmi sprečavanja iscvjetavanja analizirani su difrakcijom X-zrakama i skeniranjem elektronskim mikroskopom. Rezultati pokazuju da se najbolja tlačna čvrstoća s geopolimerom dobiva uz sadržaj silicijske prašine od 10 % i da može dostići 125 MPa nakon 60 dana. Ako se prijeđe granica od 10 % to utječe na smanjenje tlačne čvrstoće koja je sve manja s povećanjem sadržaja silcijske prašine. Osim toga, iscvjetavanje na uzorcima s geopolimerom najbolje je spriječeno kad je sadržaj silicijske prašine 10 %. Koncentracija iona karbonata izluženih iz geopolimera bila je to manja što je sadržaj silicijske prašine bio veći.

1. INTRODUCTION

Research on the effectively use of industrial waste in alkali-activated technology, which were initialy reported by Davidovits [1], has been a hot spot in recent years in building materials field. Geopolymers can be synthesized from aluminosilicate waste materials such as steel slag [2-4], blast furnace slag [5–7] and fly ash [8-10] under strong alkaline condition. Compared with cements, ceramics and metals, geopolymer materials have many advantages, such as high early age strength [11-13], low permeability [14-16] and good fire resistance behaviour [17-18]. However, there were some disadvantages which can not be ignored such as efflorescence. It is well known that geopolymer materials were activated with alkali such as sodium hydroxide (NaOH), potassium hydroxide (KOH). So soluble alkali can be dissolved out from geopolymer material surface and react with carbon dioxide in the air to form carbonate, which hinders the practical application of geolpolymer materials.

Efflorescence is a very crucial problem that should be reduced in the development of geopolymer materials. Few studies on the efflorescence of geopolymer materials were reported, in addition to that most of them were based on fly ash-based geopolymer material. Najafi et al reduced efflorescence in a geopolymer binder by adding Aluminium rich mineral admixtures and curing at elevated temperatures [19]. Minfang Han et al. found that the efflorescence extent of fly ash-based geopolymeric specimen decreased with 5A zeolite addition and lead to the lesser pore volume of macropores [20]. Zuhua Zhang [21] et al. discussed the relationship between composition, slag addition and curing temperature.

In this work, the study aims to investigate silica fume content, compressive strength, carbonate ions concentration, PH and pore size distribution of geopolymer prepared using steel slag and blast furnace slag as resource material and activated by sodium hydroxide after curing for 3, 28 and 60 days when silica fume was partially replaced with waste powder at levels ranging from 0% to 20% with an intervals of 5%.

2. MATERIALS AND METHODS

2.1. MATERIALS

The steel slag and blast furnace slag used in the experiment were from Shandong Steel Group, and their specific surface area were 376m^2/kg and 436m^2/kg, respectively. The silica fume was from Tianjing winitoor company and its specific surface area was 1750m^2/kg. The sodium hydroxide was used as activator to prepare the geopolymer specimens and its content was 5%. The chemical composition of raw materials was determined and shown in Table 1.

Table 1 Chemical composition of raw materials（wt%)

Component	CaO	MgO	Fe_2O_3	Al_2O_3	SiO_2	TiO_2	MnO	Loss	Others
Steel slag	38.91	7.61	23.11	1.57	13.20	1.11	0.30	1.20	0.23
Slag	36.99	9.70	0.46	15.22	31.87	0.82	0.15	1.31	4.45
Silica fume	2.10	1.02	3.00	3.89	79.48	2.10	1.38	1.02	3.93

2.2. PREPARATION OF SPECIMENS

Silica fume was used as the substitute of waste powder such as steel slag and blast furnace slag at levels ranging from 0% to 20% with an intervals of 5% in this experiment. Geopolymer material samples were molded to 4cm×4cm×16cm under pressure of 20MPa with the water to solid ratio of 0.1 and cured in standard condition for 3, 28 and 60 days. The raw material ratio of geopolymer mortar adding silica fume was as illustrated in Table 2.

Table 2 Raw material ratio of geopolymer mortar adding silica fume

Sample	Solid materials ratio（wt%）		Sodium hydroxide（wt%）	Water to solid ratio
	Silica fume	Steel slag + slag + sand		
B0	0	100	5	0.1
B1	5	95	5	0.1
B2	10	90	5	0.1
B3	15	85	5	0.1
B4	20	80	5	0.1

2.3. TEST PROCEDURES

The compressive strength of geopolymer specimens were tested according to GB/T17671 -1999 (Method of testing cement--determination of strength). The efflorescence was characteristized by measuring the concentration of carbonate ions of geopolymer mortar specimens leaching liquid which curing for 60 days. The procedures were as follows: the specimen was placed in 250ml distilled water for 48h in order to make the efflorescence products which mainly was carbonate dissolve in water completely. Then, 10 ml leaching liquid was taken and diluted to 100 ml which can be determined by hydrochloric acid standard solution titration. The efflorescence inhibition mechanism was analyzed by measuring the pore size distribution and PH value. Scanning electron microscopy was used to characterize the geopolymer and to investigate the micro-structure of the geopolymer specimens with different silica fume contents. The mineralogical compositions of geopolymer specimens curing for 3 days and 60 days were assessed by X-ray powder diffraction (XRD).

3. RESULTS AND DISCUSSION

3.1. EFFECT OF SILICA FUME ON WASTE BASED GEOPOLYMER COMPRESSIVE STRENGTH

The compressive strength of geopolymer specimens with different silica fume contents cured for 3, 28 and 60 days is presented in Figure 1. It can be seen that the compressive strength increases with the prolong of curing period, and its value is largest when the dosage of silica fume is 10wt.%, and it can reach 125MPa in the 60 days, which is improved by 92% compared with the samples without silica fume. However, when a threshold (10%) is surpassed, strengths could be hurt; the compressive strength of the waste based geopolymer is decreased with the increase content of silica fume.

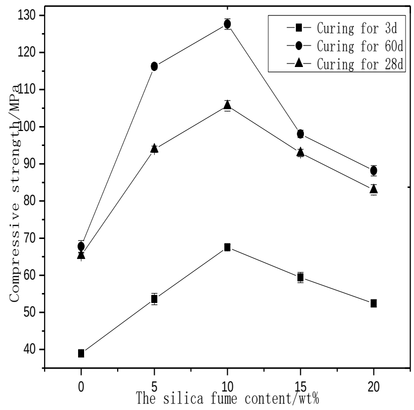

Figure1: Effect of silica fume on geopolymer compressive strength

Activated silica is the main component of silica fume, which promoted condensation reaction of $SiO(OH)_3$ and $Al(OH)^-$ that from depolymerization by the amorphous structure in steel slag and slag, contributing to the formation of multimers[22]. On the one hand, the activated SiO_2 under strong alkaline condition offers more precursor to produce multimers. On the other hand, the activated SiO_2 in silica fume also benefit to the polymerization according to the chemical equilibrium principle. Furthermore, the silica fume with high specific surface area is able to fill the internal pore and improve geopolymer pore structure that can be seen from firure 3, which makes the geopolymer more compact, that is another reason why compressive strength of geopolymer can be improved by adding silica fume.

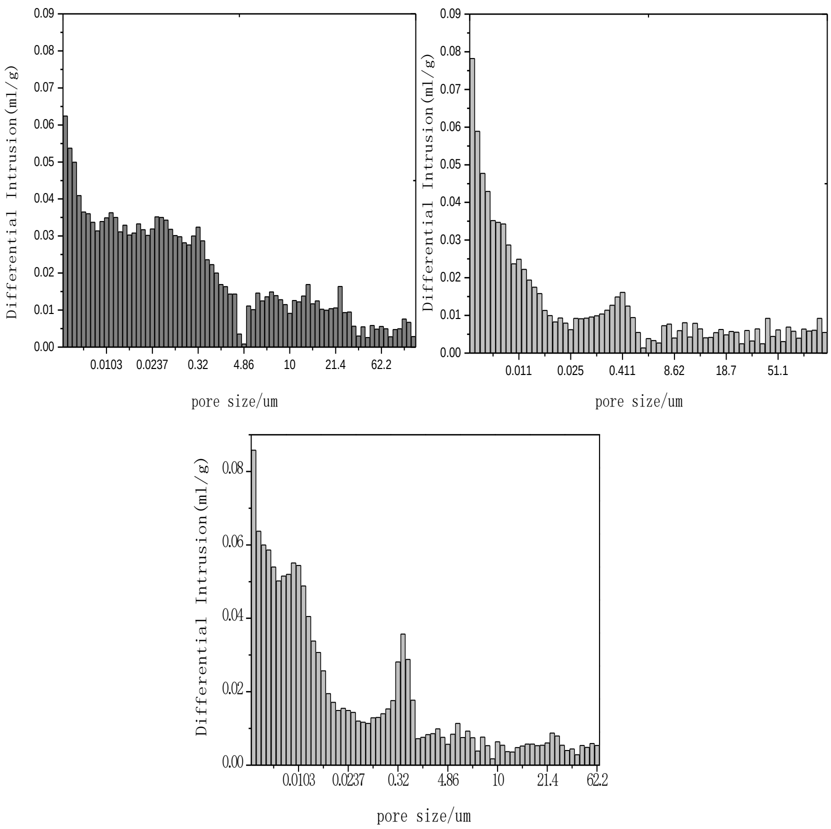

0wt% silica fume, (b) 10wt% silica fume, (c) 15wt% silica fume

Figure 2 Pore size distribution of geopolymer samples curing for 60 days

From Figure 2, it is found that for the sample without silica fume, the pore size are larger than 0.02um make up the largest percentage, which indicates that the average pore diameter is larger in the internal pore structure. For the sample with 10wt% silica fume, the proportion of pore size smaller than 0.02um is the largest, the pore size is smaller and the sample is more compact compare with the sample without silica fume, which accorded with the compressive strength results. The pore size of sample with 15wt% silica fume is larger than that the sample with 10wt% silica fume, the reason maybe that the water-solid ratio is constant and the water is adsorbed by silica fume for its high specific surface area when silica fume content added too much, which reduce the water participate in polymerization reaction and hinder the reaction to continue, the pore structure of geopolymer sample become loose and the pore size larger. Insufficient water amount will reduce the condensation/polymerization rate, which will further decrease geopolymer compressive strength [23].

3.2. EFFECT OF SILICA FUME ON WASTE BASED GEOPOLYMER EFFLORESCENCE

From Figure 3 and Figure 4, respectively, it is evident that the carbonate ions concentration of leaching liquid decrease with the increase of silica fume content up to 10%, and slight increase with the increase of silica fume content when silica fume content is more than 10%. Adding the moderate amount of silica fume has inhibitory effect on geopolymer efflorescence for that the smallest carbonate ions concentration of leaching liquid is 1181.2 mg/L when silica fume content is 10wt%, which decreased obviously compared with carbonate ions concentration of 2510.3 mg/L when silica fume content is 0wt%. It can be seen that from Figure 4, the PH value of leaching liquid significantly decrease with increasing of silica fume content, which implied the sodium hydroxide in geopolymer is consumed by the silica fume and produce more C-S-H gel that can be seen from XRD patterns.

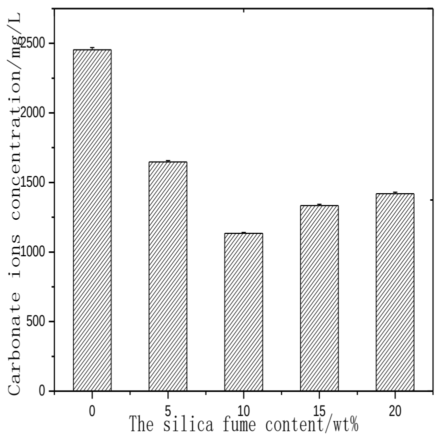

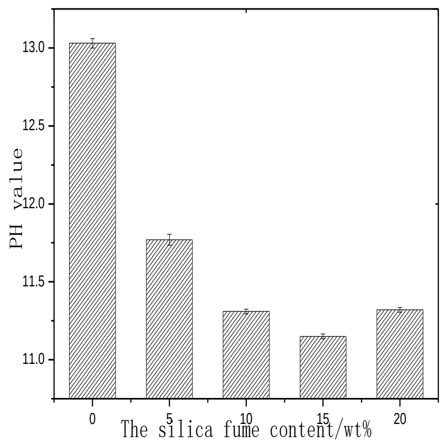

Figure 3 Carbonate ions concentration of leaching liquid. Figure 4 PH value of leaching liquid

Efflorescence inhibition mechanism is that, the activated SiO_2 in silica fume is easy stimulated to participate in the geological polymerization reaction under strong alkaline condition, which produce more polymer and compact polymer structure. The silica fume with high specific surface area as micro-aggregates is able to fill the internal pore and improve geopolymer pore structure, which blocks the channels of alkali solution dissolving out. Moreover, the redundant sodium hydroxide in geopolymern is consumed by the silica fume in later stage and produce more C-S-H gel.

3.3. MICRO-STRUCTURE ANALYSIS

It can be seen from Figure 5 and Figure 6 that, the types of reaction products no obvious change after adding the silica fume according to the comparison of Figure 5 and Figure 6. However, the intensity of the diffraction peak increase with the adding silica fume content and the diffraction peak intensity is the strongest when silica fume content is 10wt%, then the intensity of the diffraction peak decrease with the adding silica fume content when silica fume content surpass 10wt%, which is in coincide with the mechanical properties of samples.

By comparing with the same sample curing for different days, more C-S-H gel, rankinite and gonnardite were produced in the geopolymer curing for 60 days than curing for 3 days, which can be confirmed that, the redundant sodium hydroxide in geopolymer is consumed by the silica fume in later stage and produce more C-S-H gel.

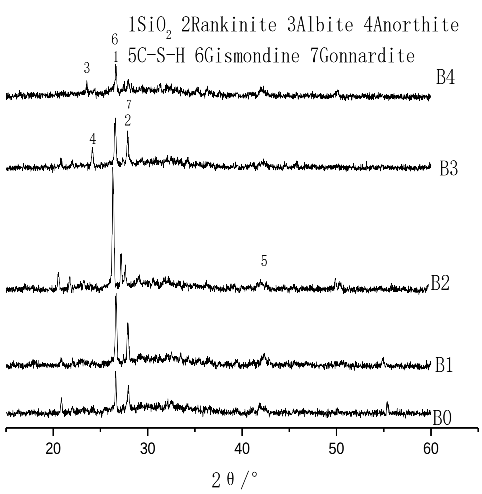

Figure 5 XRD patterns of samples curing for 3 days

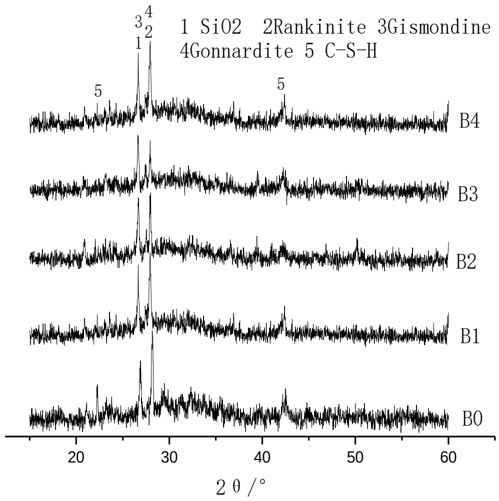

Figure 6 XRD patterns of samples curing for 60 days

(a) B0 sample without silica fume (b) B2 sample with 10wt% silica fume (c) B3 sample with 15wt% silica fume

Figure 7 SEM pictures of geopolymer curing for 60 days.

The SEM pictures of geopolymer with different silica fume contents curing for 60 days were stated in Figure 7. It can be seen from the picture that, there were so many pores and incompact micro-structure in SEM picture of B0 sample, B2 sample with 10wt% silica fume had more compact micro-structure than that of B0 and B3 sample, more amorphous coherent micro-structure were rest in SEM picture of B3 sample. From the SEM pictures, it can be confirmed that, silica fume as micro-aggregates is able to fill the internal pore and improve geopolymer pore structure.

4. CONCLUSIONS

To investigate effect of silica fume on waste based geopolymer compressive strength and efflorescence, a set of tests were conducted. The experiment results led to the following conclusions:

a). The compressive strength of the waste based geopolymer is the best when the content of silica fume is 10%. However, when a threshold (10%) is surpassed, strengths could be affected: the compressive strength of the waste based geopolymer is decreased with the increase content of silica fume.

b). The carbonate ions concentration of geopolymer leaching liquid decrease with the increase of silica fume content when silica fume content is less than 10%, and slight increase with the increase of silica fume content when silica fume content is more than 10%.

c). The silica fume with high specific surface area as micro-aggregates is able to fill the internal pores and improve geopolymer pore structure. The redundant sodium hydroxide can be consumed by the silica fume in later stage and produce more C-S-H gel.

ACKNOWLEDGMENTS

This research work has been made possible through using finance obtained from National Hightech R&D Program of China (863program) (2015AA034701), Shandong Province Science and Technology Major Project (new industry) (2015ZDXX0702B01) and Shandong Province Science and Technology Development Plan (2014GSF117017). It could not have gone ahead without the materials supplied by Zonghui Zhou, thanks a lot for the help.

REFERENCES

[1] Davidovits, J.: Geopolymers, Thermal Analysis and Calorimetry, 37. (1991),pp. 1633–1656.
[2] Huang, F.H., Zhou, Z.H., & Zhang, J.H.: Preparation of Geopolymer Materials using Steel Slag and Fly Ash by Pouring Process, Proceedings of the 8th International Symposium on Cement &Concrete, Yao,Y., pp. 935-938, China, September and 2013, Nanjing.
[3] Huang, F.H.et al.: Properties of waste-based geopolymer building blocks, Applied Mechanics and Materials, Vol. 357-360 (2013), pp. 935-938.
[4] M.S.H. Khan, A. Castel.: Utilisation of steel furnace slag coarse aggregate in a low calcium fly ash geopolymer concrete, Cement and Concrete Research, Vol. 89 (2016), pp. 220–229.
[5] Yang, T., et al.: Quantification of chloride diffusion in fly ash-slag-based geopolymers by X-ray fluorescence(XRF), Construction and Building Materials, Vol. 69 (2014), pp. 109–115.
[6] Xu, H., et al.: Effect of blast furnace slag grades on fly ash based geopolymer waste forms, Fuel, Vol. 133 (2014), pp. 332–340.
[7] Gao, X., et al.: Properties of alkali activated slag-fly ash blends with limestone addition, Cement and Concrete Composite, Vol. 59 (2015), pp. 119–128.
[8] Huang, Y., Han, M.: The influence of α-Al2O3 addition on microstructure, mechanical and formaldehyde adsorption properties of fly ash-based geopolymer products, Hazardous Materials, Vol.193 (2011), pp. 90–94.
[9] Sindhunata, J.et al.: Effect of curing temperature and silicate concentration on fly-ash-based geopolymerization, Industrial & Engineering Chemistry Research, Vol. 45(2006), pp. 3559–3568.
[10] Škvára, F.et al.: Microstructure of geopolymer materials based on fly ash, Ceramics-Silikáty, Vol. 50 (2006), pp. 208–215.
[11] Assi, L.N. et al.: Investigation of early compressive strength of fly ash-based geopolymer concrete, Construction and Building Materials, Vol. 112 (2016), pp. 807–815.
[12] Zhang, Y. J. et al.: Mechanical performance and hydration mechanism of geopolymer composite reinforced by resin, Materials Science and Engineering, Vol. 527 (2010), pp. 6574–6580.
[13] Chi, M. C. et al.: Strength and drying shrinkage of alkali-activated slag paste and mortar, Advanced Engineering Materials, Vol. 212 (2012), pp. 980-989.
[14] Davidovits, J.: 30 years of successes and failures in geopolymer applications, Market Trends and Potential Breakthroughs, Proceedings of Geopolymer Conference, pp. 56-62, Australia, October and 2002, Melbourne.
[15] Ma, H. et al.: Mineral polymer: current developments and prospects, Earth Science Frontiers, Vol. 196 (2002),pp.397–407.
[16] Duxson, P. et al.: Geopolymer technology: the current state of the art, Material Science, Vol. 42(2006), pp. 2917–2933.
[17] Kupwade-Patil, K. et al.: Multiscale modeling and experimental investigations of geopolymeric gels at elevated temperatures, Computers & Structures, Vol. 122 (2013), pp. 164–177.
[18] Temuujin, J. et al.: Preparation and thermal properties of fire resistant metkaolin-based geopolymer-type coatings, Non-Crystalline Solids, Vol. 357(2011), pp. 1399-1407.
[19] Kani, N. et al.: Efflorescence control in geopolymer binders based on natural pozzolan, Cement & Concrete Composites, Vol. 34 (2012), pp. 25–33.
[20] Huang, Y. et al.: Microstructure and properties of fly ash-based geopolymeric material with 5A zeolite as a filler[J], Construction and Building Materials, Vol.33 (2012), pp. 84–89.
[21] Zhang, Z. H.et al.: Fly ash-based geopolymers: The relationship between composition, pore structure and efflorescence, Cement and Concrete Research, Vol. 64 (2014), pp. 30–41.
[22] Reddy, M. S.et al.: A review of the influence of source material's oxide composition on the compressive strength of geopolymer concrete, Microporous and Mesoporous Materials, Vol. 234 (2016), pp. 12-23.
[23] Provis, J.L. et al.: The role of mathematical modeling and gel chemistry in advancing geopolymer technology. Chemical Engineering Research and Designs, Vol. 83 (2005), pp. 853-860.

KOSJERIC DIABASE AS BUILDING STONE

Ivana Delic-Nikolic[1], Lidja Kuresevic[1], Olivera Vusovic[1]

[1] Institut IMS, Laboratory for stone and aggregate, Bul. vojvode Misica 43, 11 000 Beograd, Srbija,
email: ivana.delic@institutims.rs, lidja.kuresevic@institutims.rs, olivera.vusovic@institutims.rs

SUMMARY: Diabase is an old name for a magmatic effusive and vein rock, which is regarded a highly-prized building material due to its good technical properties. It has high values of compressive strength and abrasion resistance, small water absorption and it is resistant to frost impact. Despite all this, in Serbia, diabase did not receive the deserved attention as a building material. Thorough geological exploration performed in the period from 2003 to 2009 in six locations in the territory around Kosjerić (western Serbia) aimed to prove geological reserves and quality of diabase rocks, mostly for use as an aggregate in road-construction. All explored localities are situated on Maljen Mt. and belong to diabase-chert formation (ophiolitic melange) of the Mesozoic age. Ophiolitic melange is situated within the chain of Podrinje-Valjevo mountains, formed in the unstable geologic structure together with other basic and ultramafic rocks, and contemporaneous with surrounding sedimentary formations. Most often, diabase forms large masses of submarine effusions, up to several hundred meters thick. These masses most often are trending NW-SE. Conducted exploration works found that the rock mass is homogeneous and sound in all localities, although with dense joint networks filled with white quartz veins, or rarely with calcite veins. The exploration works included numerous laboratory examinations of petrological and technical properties. These have shown that the main minerals belong to plagioclase and pyroxene groups. Subordinate components are opaque minerals and, rarely, quartz. Chlorite, epidote and calcite have formed as secondary minerals in various alteration processes. Rock texture is most often ophitic, and the structure homogeneous. Testing of the technical properties has proved high quality of the stone from these localities and its possibility of use as a building material. The presence of two colour varieties is detected: dark grey and dark green. However, no differences in the technical properties of the two varieties have been found.

DIJABAZ IZ KOSJERIĆA KAO GRAĐEVNI KAMEN

SAŽETAK: Dijabaz je staro ime za magmatsku efuzivnu stijenu i stijenu u obliku žila koja se smatra skupocjenim građevnim materijalom zbog svojih dobrih tehničkih svojstava. Ima veliku tlačnu čvrstoću i otpornost na abraziju, malu vodoupojnost a otporan je na zamrzavanje. Unatoč tome dijabaz kao građevni materijal u Srbiji nije dobio zasluženu pozornost. Geološkim istraživanjima provedenim u razdoblju od 2003. do 2009. na šest lokacija na području u okolici Kosjerića (zapadna Srbija) željelo se utvrditi geološke rezerve i kvalitetu dijabazne stijene, ponajviše radi upotrebe kao agregata za gradnju cesta. Svi istraženi lokaliteti nalaze se na planini Maljen i pripadaju formaciji dijabaza – čerta (ofiolitička mješavina) iz razdoblja mezozoika. Ofiolitička mješavina nalazi se u lancu gorja Podrinje – Valjevo. Nastala je kao nestabilna geološka struktura uz druge bazične i ultramafične stijene i suvremene sedimentne formacije koje ih okružuju. Najčešće dijabazi tvore veliku masu podmorskih tvorevina debelih više stotina metara. Smjer tih masa najčešće je u pravcu SZ-JI. Provedenim istražnim radovima utvrđeno je da je stijenska masa homogena i zdrava na svim lokalitetima iako postoji gusta mreža ispunjena kvarcnim ili rjeđe kalcitnim žilama. Istražni radovi obuhvatili su brojna laboratorijska ispitivanja petroloških i tehničkih svojstava. Pokazalo se da glavni minerali pripadaju skupinama plagioklasa i piroksena. Podređene komponente su minerali opala a rjeđe kvarc. Tijekom različitih procesa pretvorbe formirani su sekundarni minerali kao klorit, epidot i kalcit. Tekstura stijene najčešće je ofitička a struktura homogena. Ispitivanje tehničkih svojstava potvrdilo je visoku kvalitetu kamena s tih lokaliteta i mogućnost njegove upotrebe kao građevnog materijala. Utvrđena je prisutnost dva varijeteta boje: tamno siva i tamno zelena. Između dva varijeteta nisu utvrđene razlike u tehničkim svojstvima.

1. INTRODUCTION

Diabase is an effusive and vein rock from the gabbro group, mostly fine-grained or medium size-grained, dark-grey to dark-green in colour. Most often, this rock has very good technical properties and durability, and for this reason, it is considered a high-quality building material, especially for production of aggregate for road-construction, and namely for wearing courses.

Until 2003, there was no active exploitation of diabase deposits in Serbia, not even the explored deposits of this material. Dacite and dacite-andesite have been used in road-construction works instead. As the process of traffic infrastructure renewal began, detailed geologic exploration works have begun on diabase occurrences. In Kosjerić municipality, these explorations have included six locations, over the area of around 10 km^2. These have included numerous petrologic examinations and testing of technical properties.

2. GENERAL DATA ON EXPLORATION AREA

Studied area is in the western Serbia, north of Kosjerić and it belongs to Zlatibor district. It includes the SW slopes of Bukovi massif, i.e. the western part of Maljen mountain massif. This area is woody, scarcely inhabited, with mountainous relief and elevation range between 650 and 850 m. Figure 1 shows the geographic position of the studied area, with schematic markings of the explored deposits.

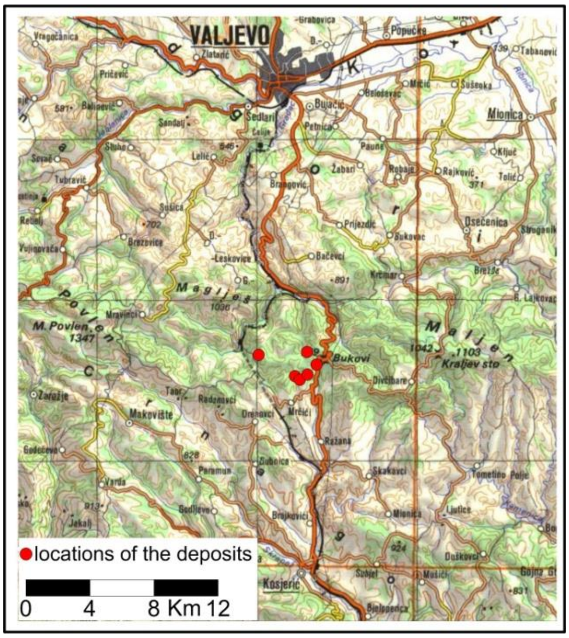

Figure 1 Geographic position of the area with schematic markings of the explored deposits

The first written data on geology of this area originates from 19th century; it can be found in the papers of Žujović (1889,1893), describing porphyrite, diabase, serpentinite and giving the basic data on genetic processes of Palaeozoic and Mesozoic formations. Geomorphology, stratigraphy and tectonics of this area have been in later times examined and described in the papers of Cvijić (1924), Loczy sen. (1924), Ampferer and Hammer (1924), Simić (1931-1939), Milovanović (1941), Pejović (1957), Pašić (1957), Stevanović (1957), Anđelković (1961) and others (cited in: Mojsilović et al., [1]).

In the time period from 1959 to 1965, area of Kosjerić has been included in field examinations for the purpose of the basic geology map, section Valjevo, scale 1:100000 [1].

Dimitrijević [2] defines the examined area, the Maljen-Suvobor ultramafic unit, as a part of the extremely complex regional geotectonic unit – the Vardar zone. Large ultramafic bodies accompanied with gabbro and ophiolitic melange mark the boundary between the Vardar zone and the Dinaride unit to the west.

The first examination of diabase as an industrial raw material has been performed for its use for production of mineral wool, in locality ''Tavani'' during 1981. In 1986, additional examinations have been performed in order to determine the possibility of its use as a technical building stone. The latter have shown that diabase from this deposit is a good quality raw material for production of aggregate for road-construction [3,4].

In the time period between 2003 and 2009, thorough geologic explorations have been performed in six spatially near locations to determine the amount of geological reserves and the technical properties of diabase as a technical building stone: ''Tavani", "Mali Bašinac", "Mrčići", "Tavani-Markovići", "Drenovački kik“ and "Veliki Bašinac" (Figure 2).

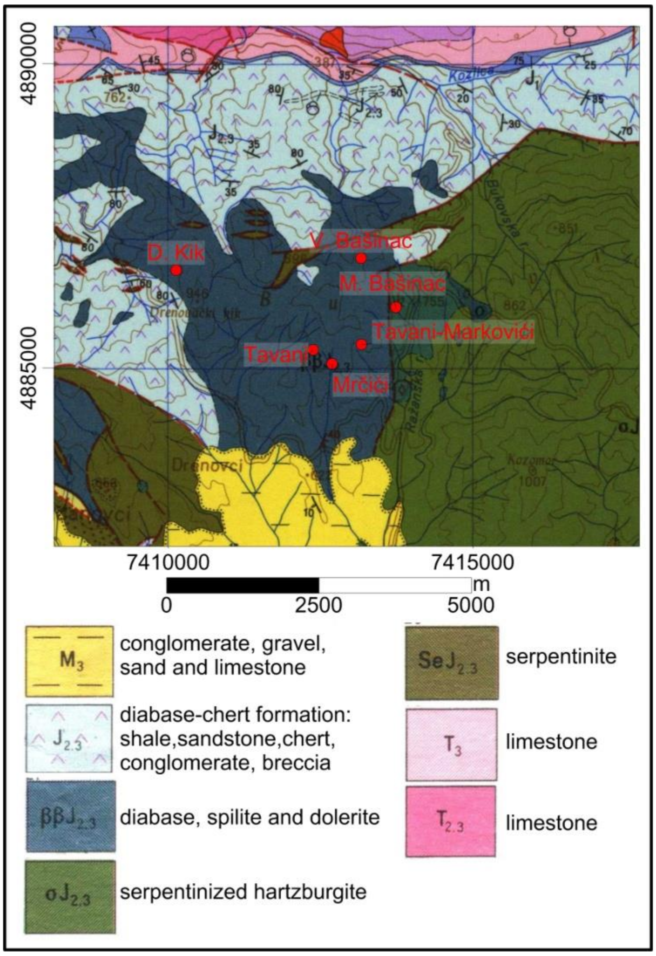

Figure 2 Part of the basic geologic map with markings of examined deposits

3. GEOLOGY OF THE EXAMINED AREA

In the area of the western Serbia and in the wider surroundings of the examined area, based on the lithology, stratigraphy and tectonic characteristics and palaeogeographic evolution, three basic geotectonic units have been recognized: Drina area in the SW, Jadar area in the north and NE, and the zone of Mesozoic ultramafic rocks and diabase-chert formation (ophiolitic melange), between the first two.

Drina area is characterized by the presence of sandy-shaly Palaeozoic complex in Drina river and Seča Reka basins, and Mesozoic complex of Tornik Bobija. Jadar area includes widely spread Palaeozoic sediments in Jadar and Kolubara river basins, and Mesozoic, mostly carbonate rocks in the area of Medvednik-Lelići-Bačevci [1]. Peridotite-gabbroid rock association includes serpentinized peridotite, serpentinite, troktolite and gabbro (Figure 3).

Diabase-chert formation is of Jurassic age and it covers a wide area. It is outcropping in the NW-SE trending zones from Zvornik, over Medvednik and Povlen to Čačak. It is made up of various sedimentary, magmatic and metamorphic rocks: diabase (sometimes brecciated), spilite, porphyry, gabbro, dolerite, melaphyre; shale, limestone, sandstone, conglomerate, chert. This formation has a faulted contact with other units. Its age is determined based on typical micro-fauna, found in numerous sites in oolitic limestone appearing as small lenses and intercalations in chert, shale, sandstone and other surrounding rock types. Various rock types interchange each other often vertically and horizontally. There are also large terrain parts where only one or two rock types are present at the surface [5].

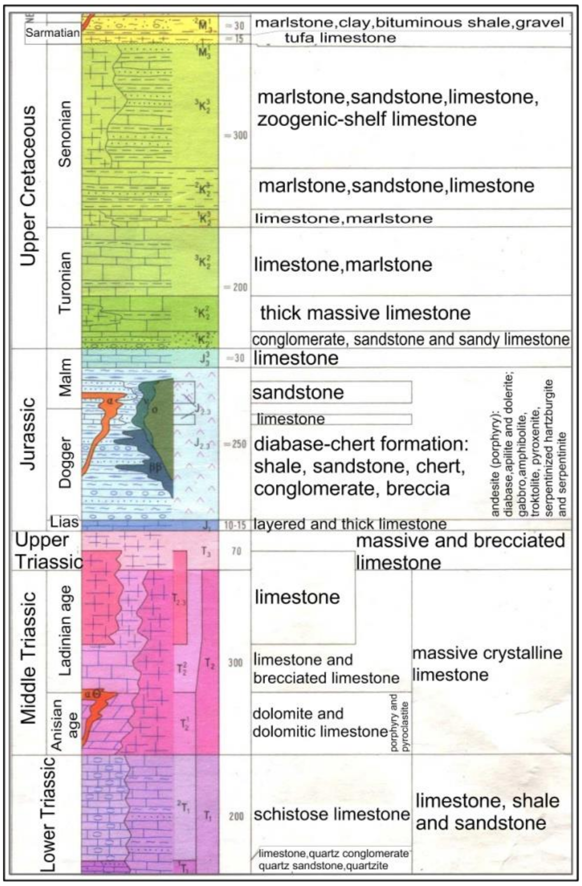

Figure 3 Fragment of geologic column of explored area with position of diabase-chert formation (basic geologic map, section Valjevo 1:100 000)

Diabase most often appears as submarine effusion, synchronistic with surrounding sediments, as large masses. In marginal parts, it includes cherty and shaly zones. Diabase masses can be up to several hundred meters thick. Also, it appears as small sheeted dikes and veins in lower parts of the formation. In all localities, two colour varieties are present: dark grey and dark green. Both are sound, compact and homogeneous, with irregular, rough break-surfaces and sharp edges.

In all localities, joints appear as singular or, more often, joint networks in dm-cm length spans. Their orientation mostly conforms the regional tectonic elements' orientation, dominated by linear structures trending NW-SE, and NE-SW. Joints are most often filled by secondary minerals, white, or rarely dark grey to green in colour. No clay infillings have been found [4].

Diabase is made up of plagioclase (mostly altered) and monoclinic pyroxene (mostly altered into amphibole). According to the grain size, it can be fine-grained to coarse-grained. Texture is mostly ophitic or poikilitic. It is often cataclased, brecciated and mylonited. Tectonic crushing is often accompanied by strong chloritization. Common property of these rocks is the complete transformation of pyroxene to amphibole, saussuritization, albitization and partial prehnitization of plagioclase. Primary augite is rarely preserved, and so is the primary plagioclase of labrador-bytownite composition.

4. LABORATORY EXAMINATION RESULTS

Petrologic examinations have shown that there is no significant difference between the samples taken from different deposits. All diabase samples are dark grey to dark green in colour, with fine-grained ophitic texture and homogeneous structure. They are made up of mafic and salic minerals, with grain size up to 2 mm, but most often smaller than 1 mm. On flat-cut surfaces, irregular lath-like to round forms of salic minerals can be observed. Mafic minerals appear in prismatic and irregular forms. Thin linear joints are rare, and filled by white precipitate, 0.5 to 5 mm thick. Sporadically, there are zones of the same minerals composition within the main mass, with grain size up to 0.5 mm, forming irregular masses. Main constituents of the rock are plagioclase and monoclinic pyroxene.

Subordinate and secondary minerals are chlorite, actinolite and rarely opaque mineral (Figures 4 and 5). Almost all grains have etched edges and are intensely altered (saussiritization and chloritization).

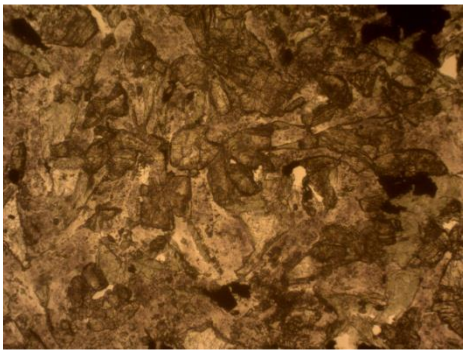

Figure 4 Photomicrograph of Kosjerić diabase, view field width 3 mm, parallel Nicol prisms

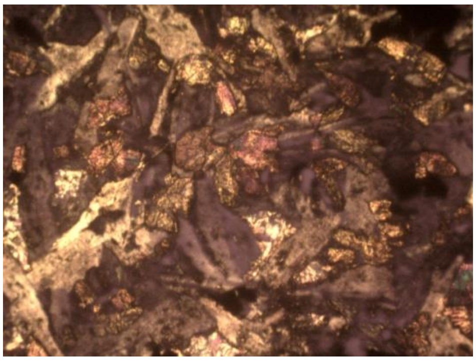

Figure 5 Ibid., crossed Nicol prisms

Plagioclase grains have elongated, needle-like, lath-like or irregular forms, most often up to 0.5 mm long. Albitization and epidotization of these grains are present with varying intensity, commonly strong. These grains are irregularly crossbred and intertwined, forming a grid. Pyroxene grains are round to angular, up to 0.2 mm in size, commonly altered into amphibole and chlorite. Occasionally, these form small accumulations. Chlorite grains are often allotriomorphic to angular, depending on the way they were formed. Magnetite is present as small grains. Volcanic glass in present as inter-granular masses, commonly completely altered into chlorite. Micro-joints and micro-cavities are filled with silicate or carbonate matter.

Synthetic display of basic technical properties obtained through testing of 140 samples from all six deposits is shown in Table 1 [6].

Table 1 Technical properties of tested diabase samples

Property, testing method SRPS		Tavani	Mali Bašinac	Mrčići	Tavani Markovići	Drenova-čki kik	Veliki Bašinac
Apparent density (g/cm^3), B.B8.032		2.82	2.85	2.82	2.81	2.81	2.84
Porosity, (%),B.B8.032		1.1	0.8	0.7	1.5	1.2	0.2
Compre-ssive strength (MPa) B.B8.012	dry	179	200	163	146	160	162
	water-saturated	158	174	133	125	129	131
	after 25 freeze-thaw cycles	136	205	158	109	153	167
Water absorption (%), B.B8.010		0.17	0.24	0.21	0.28	0.24	0.21
Abrasive resistance ($cm^3/50\ cm^2$), B.B8.015		11.45	9.7	11.90	8.45	11.84	11.07
Abrasive resistance ''Los Angeles'' B.B8.045	Grade "B"	11.65	10.5	8.6	10.6	12.80	10.6
	Grade "C"	13.4	12.6	-	15.1	11.4	12.7
Resistance to freezing B.B8.002		stable	stable	stable	stable	stable	stable

The technical properties shown in Table 1 form a clear picture of raw material quality. Based on the shown results, it can be concluded that the deposit Mali Bašinac has the best quality (low porosity and abrasion, high values of compressive strength) and deposit Tavani Markovići the poorest (higher porosity and abrasion, lower compressive strength). Analysis of variation coefficient (Table 2) however, shows that the variations are very small, except for the value of porosity. Thus, the results are very consistent.

Table 2 Analysis of variation coefficient for the results shown in Table 1

Property	Appar. density	Porosity	Comp. strength (dry)	Comp. strength (wet)	Comp. strength (frost)	Water absorp.	Abras. resist.	''Los Angeles" "B"	''Los Angeles" "C"
Average value	2.82	0.9	168	142	155	0.22	10.74	10.8	13.0
Standard deviation	0.01643	0.4535	18.7261	19.6943	32.0416	0.03728	1.37798	1.39514	1.36034
Coefficient of variation	0.00582	0.49473	0.11124	0.13902	0.20717	0.1657	0.12836	0.12928	0.10426

Apparent density has the greatest homogeneity degree, since it has the lowest variation coefficient. The obtained average value classifies the tested stone as heavy. Porosity value determines the stone as compact (<1%) according to the limits given in [7]. Compressive strength in dry state is considered high (>150 MPa). Decrease of compressive strength value in water-saturated state compared to the dry-state value is 15 %, while the decrease after 25 freeze-thaw cycles is 8 % (possibly due to the considerably smaller number of samples tested). Water absorption with average value of 0.22 % is considered very small (<0.5%). Abrasive resistance value classifies this stone as hard (hard stone has values between 10 and 20 $cm^3/50\ cm^2$), although its value is on the lower limit for this class. All tested samples (total of 140) are resistant to frost impact, tested via Na_2SO_4.

According to the European standards EN 12620 Aggregates for concrete and EN 13043 Aggregates for bituminous mixtures and surface treatments for roads, airfields and other trafficked areas, the aggregate obtained by crushing of the stone from these deposits can be declared as category LA_{15} (≤15%); according to the standard EN 13450 Aggregates for railway ballast as category LA_{RB} 12 (≤ 12%); according to EN 13242 Aggregates for unbound and hydraulically bound materials for use in civil engineering work and road construction as category LA_{20} (≤20%).

5. CONCLUSION

Diabase deposits near Kosjerić in western Serbia have not been evaluated as a raw material for use in building industry until around 15 years ago. The first explorative works have been performed in 2003, in locality "Tavani". After these first explorations, thorough explorative works have ensued in five near-by localities: "Mali Bašinac", "Mrčići", "Tavani-Markovići", "Drenovački kik" and "Veliki Bašinac".

After processing the results of laboratory examinations of technical properties of 140 samples originating from all six deposits, it can be concluded that the rock mass has excellent characteristics, and is satisfying the extant technical requirements for its use as a raw material for production of aggregate for concrete and asphalt-concrete, for all categories of traffic load, both according to the Ordination on obligatory certification of the fractioned stone aggregates which is still valid in Serbia, and according to the European standards, regarding the tested technical properties of the aggregate particles.

ACKNOWLEDGMENT

This exploration is performed under the grant of Ministry of education and science of the Republic of Serbia, through the scientific-explorative project III 45008.

REFERENCES

[1] Mojsilović, S. et al.: Tumač za list Valjevo 1:100 000 OGK, Zavod za geološka, hidrogeološka, geofizička i geotehnička istraživanja – Geozavod, Beograd, OOUR Geološki institut, 1976.
[2] Dimitrijević, M.D.: Dinarides and the Vardar zone: a short review of the geology. Acta vulcanologica (2001), vol. 13, no. 1-2, p. 1-8.
[3] Ilić, B.: Elaborat o rezervama dijabaza kao tehničkog građevinskog kamena u ležištu Mali Bašinac kod Kosjerića, Geo explorer, Beograd, 2006.
[4] Ilić, B.: Elaborat o rezervama dijabaza kao tehničkog građevinskog kamena u ležištu Veliki Bašinac kod Kosjerića, Geo explorer, Beograd, 2008.
[5] Aleksić, V. et al.: *Geologija Srbije III-1, Magmatizam.* Zavod za regionalnu geologiju i paleontologiju Rudarsko-geološkog fakulteta, Univerzitet u Beogradu, Beograd, 1981.
[6] Laboratory for stone and aggregate of the IMS Institute archives.
[7] Bilbija, N.; Matović, V.: Tehnička petrografija, Svojstva i primene kamena, Građevinska knjiga, Beograd, 2009

ZEOLITES - SUSTAINABLE BUILDING MATERIAL

Todorka Samardzioska[1], Milorad Jovanovski[1], Sonja Lepitkova[2]

[1] Ss Cyril and Methodius University, Faculty of Civil Engineering, blvd Partizanski odredi 24, 1000 Skopje, Macedonia, email: samardzioska@gf.ukim.edu.mk, jovanovski@gf.ukim.edu.mk
[2] University of Goce Delcev in Shtip, Faculty of Natural and Technical Sciences, Krste Misirkov No.10-A, 2000 Shtip, Macedonia, email: sonja.lepitkova@ugd.edu.mk

SUMMARY: Zeolites are natural porous volcanic tuffs that represent hydrated crystalline aluminosilicates minerals with alkaline and earth-alkaline metals. Their chemical properties, a large percentage of porosity, ability of adsorption of the material define high specific surface and low specific weight. Many experimental studies confirm zeolites' excellent mechanical properties that include this material in the group of building materials for structural elements. Another use of zeolite is as an additive in cement, as an active mineral supplement and binder component for silicate concrete and as gypsum cement pozzolatic binder component and concretes based on them. A mixture of cement and zeolite is used for the production of high-strength concrete with greater compression resistance than that of Portland cement. Primary objective of this paper is to investigate the field of application of zeolites found near Probishtip in Macedonia. Properties of the individual zeolites strongly depend on the location of the site. Therefore, experimental testing has been performed in order to define mechanical properties of the local zeolites. Water absorption, porosity, specific weight and mechanical properties have been determined. Additional testing of the physical and mechanical properties of the zeolites can open new horizons in the industry of building materials in Macedonia. This newly discovered material is feasible, easily mined from quarries and easily processed. It contributes to greener and safer environment in many ways or plays a significant role in reducing toxic waste and energy consumption. In fact, almost each application of zeolites has been introduced because of environmental concerns. The results of the parameters obtained from laboratory tests will provide guidance on opportunities for the proper application of local zeolite, in terms of both natural stone and as filler for obtaining a light mortars and concretes.

ZEOLITI – ODRŽIVI GRAĐEVNI MATERIJALI

SAŽETAK: Zeoliti su prirodni porozni vulkanski tufovi sastavljeni od hidratiziranih kristaliničnih alumosilikatnih minerala s alkalnim i zemnoalkalnim metalima (engl. alkaline earth metals). Njihova kemijska svojstva, velik postotak poroznosti i sposobnost adsorpcije materijala određuju veliku specifičnu ploštinu, a malu specifičnu težinu. Mnoge eksperimentalne studije potvrđuju izvanredna mehanička svojstva zeolita koja taj materijal svrstavaju u skupinu građevnih materijala za konstrukcijske elemente. Druga je upotreba zeolita kao dodatka u cementu, kao aktivnog mineralnog dodatka i vezivne komponente za silikatni beton i kao pucolanske komponente veziva cementa s gipsom i betona izrađenih s takvim sastojcima. Za proizvodnju betona s većom tlačnom čvrstoćom od betona s portlandskim cementom upotrijebljena je mješavina cementa i zeolita. Glavni cilj ovog rada bio je istražiti mogućnost primjene zeolita iz nalazišta kraj Probištipa u Makedoniji. Svojstva pojedinih zeolita znatno ovise o lokaciji. Stoga su provedena ispitivanja radi definiranja mehaničkih svojstava lokalnih zeolita. Određeni su vodoupojnost, poroznost, specifična težina i mehanička svojstva. Dodatna ispitivanja fizičkih i mehaničkih svojstava zeolita mogu otvoriti nove vidike industriji građevnih materijala u Makedoniji. Taj novootkriveni materijal je prikladan, lako se vadi u nalazištu i lagano prerađuje. On doprinosi zelenijem i sigurnijem okolišu na više načina i ima značajnu ulogu u smanjenju otrovnoga otpada i potrošnji energije. S obzirom na okolišne aspekte moguća je gotovo svaka primjena zeolita. Rezultati parametara dobivenih laboratorijskim ispitivanjima smjernica su za mogućnosti odgovarajuće primjene lokalnoga zeolita kako kao prirodnog kamena tako i kao ispunskog materijala za dobivanje laganih mortova i betona.

1. INTRODUCTION

Zeolites are natural porous volcanic tuff with high adsorptive ability, high specific surface and low specific weight, which, by their chemical structure, represent hydrated alumina-silicate structured minerals that contain alkaline and earth-alkaline metals.

As a material, the zeolites are characterized with a high open porosity. Throughout their endless three-dimensional crystal structure, the zeolites have uniformly sized pores, called windows, which is actually an effective open porosity directly connected to the open specific surface, i.e. the surface in the interface of the material with the surrounding medium.

All naturally occurring zeolites are hydrophilic (having affinity for polar molecules, such as water). Therefore, they can act as adsorbers, adsorbing the contaminants and pollutants in their surface.

Due to their ability for water adsorption, exchange of cations, dehydration - rehydration, zeolites are considered as the environmentally cleanest materials and they are widely used in agriculture, medicine, construction and environmental protection, especially for treatment of urban wastewater and decontamination of radioactive waste water. The natural zeolites can remove different heavy metals from drinking water and therefore they are widely used as a suitable technical and economic solution for water treatment. Also, zeolites they can be used for commercially successful applications to separations of mixtures, especially for supercritical or close-boiling liquid mixtures that are poor candidates for separation by distillation.

The use of zeolite in construction dates back a long time ago, primarily due to its excellent mechanical properties, Chmielevska, [1]. Namely, its absorption of water, porosity, specific weight and mechanical properties are parameters that impose application of the zeolite in constructions. There are a number of studies in the world, related to the mechanical properties of volcanic tuffs pertaining to its use in construction, Hudymaa at al., [2], Marcari at al., [3] as a foundation basis, Price, [4] or as masonry blocks in buildings, Marcari, [5].

Furthermore, this research shows that characteristics of individual zeolites depend on the location of the site itself. The tests made on samples of tuff from multiple sites in Turkey in terms of the compressive strength, abrasion, porosity, water absorption and density, recognize the zeolite as a material with high porosity, large capacity of water absorption and high compressive strength, whose characteristics change depending on the site, Yasar et al., [6]. Comparison of mechanical properties of zeolite tuff in Çanakkkale, Turkey, used to build the Temple of Apollo and the tuff situated in close proximity, Ergenç, [7], confirmed its excellent properties as a building stone.

Exploitation of zeolite in Republic of Macedonia was carried out for the first time in 2013 at the site Slavishko Pole near the village of Vetunica, from "Strmosh AD" – Mines for non-metals. In order to start application of this type of zeolite, and starting from the fact that the properties of the individual zeolites depend on the location of the site [7], it is necessary to do extensive research on defining its characteristics and properties.

This paper represents the experimental tests for determination of the mechanical properties of natural zeolite obtained from the Strmosh Mine. The procedure of examination performed on two series of cubes of zeolite is illustrated, in dry condition and in saturated condition. As a result of the procedure, the compressive strength and the ability of water absorption of the material have been determined.

2. EXPERIMENTAL METHODS

The experimental testing for determination of the mechanical properties of the zeolites has been performed in the geotechnical laboratory at the Faculty of Civil Engineering in Skopje. The testing was conceptualized in two parts: determination of the percentage of water absorption and determination of the compressive strength. The compressive strength, one of the essential mechanical properties of any material, was determined by specimens in dry condition and by specimens in saturated condition, in order to check the manner by which the water in the pores in the material affects the compressive strength. In order to obtain reliable results, the experimental testing was performed in accordance with the standards EN 13755:2008 [8] and EN 14617-15:2005 [9]. Specimens are with cubical shape, extracted from a zeolite block with larger dimensions, and all damaged and loose parts are removed from them, according to the standard EN 14617-15:2005 [9].

In order to get smooth and parallel surfaces for application of the compressive forces, they were flattened by gridding until traces of cutting were removed from the samples. The specimens, i.e. cubes, are with standardized dimensions of 50±1mm, Figure 1, and mass between 180 and 200 gr, depending on the sample, Table 1. The specimens tested in dry condition were marked with a mark M-S, while the specimens in saturated condition are marked with a mark M-W. Numbers 1, 2 and 3, after the mark, indicate the appropriate testing specimen.

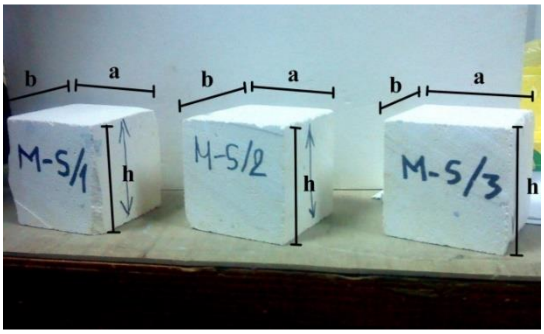

Figure 1 Geometrical characteristics of the specimens

Both series of the experimental specimens are firstly dried to temperature of 105°±5°C. Afterwards, they have been cooled and weighed on a scale with an accuracy of ± 0,01g. In that way, the mass of each specimen in dry condition was determined respectively, Table 1.

Table 1 Geometrical characteristics and mass of the specimens

Specimen	Dimensions			Mass in dry condition
	a	b	h	m_{dry}
	[cm]	[cm]	[cm]	[g]
M-S/1	5,17	5,18	5,16	185,41
M-S/2	5,16	5,20	5,13	189,42
M-S/3	5,17	5,18	5,16	191,91
M-W/1	5,16	5,17	5,18	188,54
M-W/2	5,20	5,16	5,15	193,34
M-W/3	5,18	5,18	5,16	189,16

The second series of specimens for determination of the compressive strength in saturated condition is used for determining the percentage of water absorption, also. The experimental testing for obtaining the percentage of water absorption of the zeolite is carried out according to the method of gradual immersion under atmospheric pressure. The testing was initiated by immersion of the test samples to ¼ of their height in a container with distilled water. The container is gradually filled with water up to ½ of the height of the specimens after 1 h and after 2 h to ¾ of the height of the specimens. The specimens are completely submerged in water after 22 hours. The specimens are accessed for weighing of their mass after 24 h from the initiation of immersion. Before each measurement, the samples are dried with a soft cloth, in order to prevent evaporation of the absorbed water, according to EN 13755: 2008. Weighing of the mass of each sample was repeated every 24 hours, until the sample has reached complete saturation, Table 2.

Table 2 Mass of the testing specimens in saturated condition

Specimens	Mass in saturated condition m_{sat} [g]
M-W1	232,48
M-W2	236,55
M-W3	232,69

The experimental testing of the compressive strength has been performed using testing machine type 102/3000 HK-4, with capacity of 3000 kN. The specimens were set in a way that the compressive force was applied perpendicular to the material layers. The compressive force was gradually increased by 0,5 MPa/sec, until failure of the specimen, when the force at failure F and respective stress were registered, Figure 2.

a) b)

Figure 2 Experimental testing: a) machine for testing compression strength, b) specimen

3. RESULTS AND DISCUSSION

3.1. WATER ABSORPTION

For the first series of three test samples, the percentage of water absorption was determined before defining compressive strength in saturated condition. The obtained results of the experimental testing are presented in Table 3.

The results in the Table 3 lead to conclusion that the quantity of absorbed water in each of the tested specimens is almost same, having the average water absorption of 23%.

Table 3 Experimentally obtained results for percentage of water absorption

Specimens	Water absorption
	U [%]
M-W1	23,31
M-W2	22,35
M-W3	23,01
Average value	22,89

3.2. COMPRESSIVE STRENGTH

The second part of the experiment, determination of the compressive strength of the zeolite in dry and saturated condition, was conducted on six specimens in total, i.e. on two sets of three specimens.

Experimentally obtained results for the compressive strength of zeolite in dry condition are presented in Table 4, while the results for the compressive strength in saturated condition are presented in Table 5.

Table 4 Mechanical properties of zeolite cubes in dry condition due to compressive stresses

Specimen	Bulk mass	Force at failure	Compressive strength
	ϒ=ms/V (kg/m3)	F (kN)	σp (MPa)
M-S1	1341.72	76.18	28.5
M-S2	1376.12	114.60	43.0
M-S3	1388.76	128.03	47.9
Average values	1369.87	106.27	39.8

Table 5 Mechanical properties of zeolite cubes in saturated condition due to compressive stresses

Specimen	Force at failure	Compressive strength
	F (kN)	σp (MPa)
M-W1	63.29	23.7
M-W2	90.87	33.9
M-W3	107.39	40.1
Average values	87.18	32.6

According to the standard EN 14617-15:2005, [9], the compressive strength of the zeolite is determined as an average of the compressive strengths of all three test specimens. In this case, the compressive strength of the zeolite cubes in dry condition is almost 40 MPa. From the conducted experimental testing, it can be concluded that the compressive strength of the tested specimens ranged from 28,5 MPa to 47,9 MPa.

As it was expected, the results shown in Table 5 of the tested specimens in saturated condition are lower than the results obtained from the experimental testing of the specimens in dry condition, presented in Table 4. Although the material is very porous and absorbs a large amount of water up to 23%, Table 3, the average compressive strength in saturated condition is 33 MPa. Comparing the results presented in Table 4 and Table 5, it can be concluded that the compressive strength of the zeolite decreases by 22% when the material is saturated with water.

The shape of fracture of the samples depends on the size of the friction that occurs at the interface between the sample and the plates through which the axial compressive force is applied. Inner friction prevents transverse deformation of the specimen and additional shear occurs, causing fracture in inclined planes, Figure 3a. This type of fracture is registered in four of the tested specimens. Practically, the compression testing system rather develops a complex system of stresses due to the end restraints by steel plates of the testing machine. Namely, due to the Poisson's effect, these four specimens undergo lateral expansion. However, the zeolite and the steel plates have different lateral expansions and as a result, tangential forces are induced at the contact between the zeolite cube and the steel plates of the machine. Therefore, as an addition to the compressive stresses, additional shear stresses are active in the zeolite specimen. The effect of the shear stresses decreases towards the centre of the cube, and the cracks at the centre are nearly vertical.

Fracture in the remaining two samples occurs in vertical planes parallel to the sides and approximately parallel to the applied load, Figure 3b. This type of fracture is registered in samples M-S/1 and M-W/1. The influence of shear stresses in these two specimens was smaller and they may failed by lateral splitting. They exhibit much lower compressive strength than the first four samples, both for dry and saturated condition. The compressive strength for these two samples is lower about 60% than the compressive strength of the first four samples, Table 4 and Table 5.

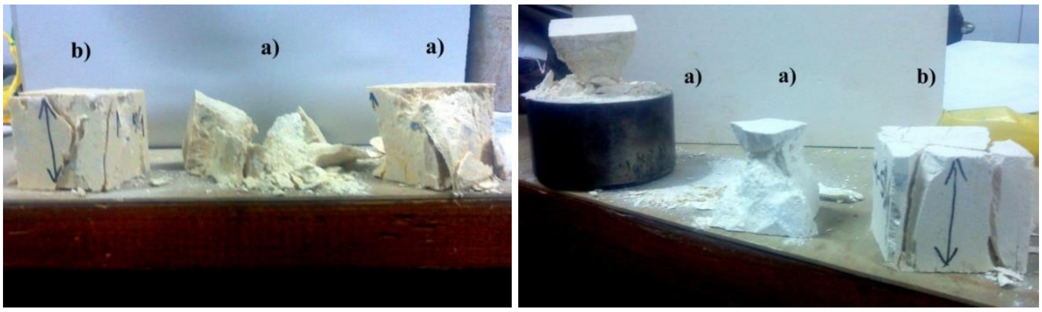

Figure 3 Type of failure in the tested specimens: a) failure in inclined planes, b) failure in planes parallel to the surfaces

The obtained results of the tests show a high value of compression strength of the material. From the comparison of the compression strength on both test series, it can be concluded that the series of samples in saturated condition have lower strength. This is due to the high porosity of the material that is accompanied by a large percentage of water absorption, which reduces the bearing capacity of the material.

4. CONCLUSIONS

The experimental research of two series of specimens of natural zeolite has been presented in this paper. The obtained results for the strength characteristics of the zeolite in dry and saturated condition, as well as its ability for water absorption, are main parameters for definition of its properties and suitable use.

This emphasizes the justification for application of this type of zeolite in structures. The obtained results of the tests show a high value of compressive strength of the material. As a result of the high porosity of the material, followed by a rate of water absorption, the compressive strength of samples in series in saturated condition is lower than the compressive strength of samples in dry condition.

Presented results lead to conclusion that the type of failure plays a major role in the compressive strength of the material. In the two specimens fractured in vertical planes parallel to the sides of the cubes, the compressive strength is much lower than in the specimens with inclined cracks. They exhibit much lower compressive strength than the first four samples, both for dry and saturated condition.

However, the results indicate a possible use of the zeolites not only in dry conditions, but also in conditions where the humidity is very high. Additional testing of the physical and mechanical properties of the zeolites can open new horizons in the industry of building materials in Macedonia. This newly discovered material in Eastern Macedonia is feasible, easily mined from quarries and easily processed. It contributes to greener and safer environment in many ways and plays a significant role in reducing toxic waste and energy consumption. In fact, almost each application of zeolites has been introduced because of environmental concerns. The results of the parameters obtained from laboratory tests will provide guidance on opportunities for the proper application of local zeolite, both, as a natural stone and as an agreggate for obtaining light mortars and concretes.

ACKNOWLEDGMENTS

The authors would like to express their gratitude to the members of the measurement team in the Laboratory of Geotechnics, at the Faculty of Civil Engineering in Skopje.

REFERENCES

[1] Chmielevska, E.: Zeolites – Materials of sustainable significance (short retrospective and outlook), *Environment Protection Engineering*, vol.36, No.4, pp. 129-135, (2010)

[2] Hudymaa, N.; Avarb, B.B. & Karakouzian, M.: Compressive strength and failure modes of lithophysae-rich Topopah Spring Tuff specimens and analog models containing cavities, *Engineering Geology* No. 73, pp. 179–190, (2004)

[3] Marcari, G.; Fabbrocino, G. & Lourenço, P.B.: Mechanical properties of tuff and calcarenite stone masonry panels under compression, 8th International Masonry Conference in Dresden, pp. 1083-1092, (2010)

[4] Price, R.H.: Analysis of Rock Mechanics Properties of Volcanic Tuff Units from Yucca Mountain, Nevada Test Site, Sandia National Laboratories, Albuquerque, (1983)

[5] Marcari, G.; Fabbrocino, G. & Lourenço, P.B.: Investigation on compressive behaviour of tuff masonry panels, University of Minho, (2010)

[6] Ergenç, D.: Investigation of tuff quarries around the Tample of Apollon Smitheus (Çanakkale, Turkey), Middle East Technical University, (2011)

[7] Yasar, E.; Tolgay, A. & Teymen, A.: Industrial Usage of Nevsehir-Kayseri (Turkey) Tuff Stone, *World Applied Sciences Journal* Vol. 7 No.3, pp. 271-284, (2009)

[8] EN 13755:2008, Natural stone test methods - Determination of water absorption atmospheric pressure, CEN/TC 246 -Natural stones.

[9] EN 14617-15:2005, Agglomerated stone - Test methods - Part 15: Determination of compressive strength, CEN/TC 246 -Natural stones.

APPLICATION OF CONSTRUCTION AND DEMOLITION WASTE AND OTHER BY-PRODUCTS IN CONSTRUCTION

Emanuela Manolova[1], Yatchko Ivanov[1]

[1] European Polytechnical University, Civil Engineering Department, 23 Sv. sv. Kiril i Metodiy str., Pernik, 2300 Bulgaria, email: amymanolova@yahoo.com, yadir_1@abv.bg

SUMMARY: European Commission and European Parliament adopted documents regarding solving the problems of environmental protection during the production of the building materials in construction as well as during the management and utilization of construction and demolition waste. This report analyzes the situation in implementation of the Bulgarian legislation for the management of construction wastes, their recycling and re-use as a building material. Furthermore the possibilities for reducing the impact on the ecology with the use of some recycled waste and by – products from the industry (metallurgical slag, phosphogypsum, iron-silicon powder, etc.) are shown. It is shown that the use of high performance concrete can be with remarkable effect on the sustainable future of building industry.

PRIMJENA GRAĐEVNOG OTPADA I DRUGIH NUSPROIZVODA U GRADNJI

SAŽETAK: Europska komisija i Europski parlament usvojili su dokumente koji se odnose na rješavanje problema zaštite okoliša tijekom proizvodnje građevnih materijala i na upravljanje i upotrebu građevnog otpada i otpada pri rušenju. U radu se analizira situacija pri primjeni bugarskoga zakonodavstva u upravljanju građevnim otpadom i njegova oporaba kao građevnog materijala. Također su prikazane mogućnosti smanjenja ekoloških opterećenja pri upotrebi nekih oporabljenih otpada i industrijskih nusproizvoda (metalurška zgura, fosfogips, ferosilicijska prašina itd.). Pokazano je da upotreba betona visokih svojstava može imati znatan učinak na održivu budućnost građevne industrije.

1. INTRODUCTION

Nowadays the humanity is faced with a number of difficulties concerning climate change. These changes are a result of human activity which leads to the emission greenhouse gasses, excessive waste production and irresponsible use of natural resources. One of the sectors of the economy which contributes greatly to environmental pollution is construction, including the production of building materials, construction work itself, reconstruction and modernization of buildings and facilities, as well as their destruction at the end of their life cycle.

In order to minimize the harmful effects of construction on the environment, the European Parliament and Council have adopted a number of documents during the past several years:

- Directive 2008/98/EC of the European Parliament and of the Council on waste;
- Regulation (EC) 2150/2002 of the European Parliament and of the Council of 25 November 2002 on waste statistics;
- Regulation (EU) 305/2011 of the European Parliament and of the Council of 9 March 2011 laying down harmonised conditions for the marketing of construction products and repealing Council Directive 89/106/EEC Text with EEA relevance

A goal has been set to reach a utilization of construction waste of at least 70% by 2020.

Measures have been taken in Bulgaria to create a national legislation, which guarantees the reduction of the harmful impact of construction on the environment. Among the laws and regulations passed are:

- The Law on Territory Planning (which has undergone numerous changes in the last decade);
- The Waste Management Act (2012);
- The Technical Requirements Towards Products Act (2013).

A special Regulation on Management of Construction Waste and Use of Recycled Materials (04.07.2014) has been passed, which emphasizes on the use of recycled materials for projects with public funding.

Based on the aforementioned documents of the national legislation, this report analyses their implementation, as well as the results of the studies on the reduction of the harmful effect on the environment by utilizing a particular class of industrial waste in construction.

2. ASSESSMENT OF THE IMPLEMENTATION OF THE NATIONAL LEGISLATION FOR ACHIEVING SUSTAINABLE CONSTRUCTION

According to the data [1] the annual **global** production of concrete amounts to 25 million tons and requires 20 million tons of raw materials (sand and coarse aggregates), 3 million tons of cement, 2 million tons of drinking water. This means that the production of raw materials from rivers and mountain quarries greatly damages the environment. Meanwhile, the production of 1 ton of cement requires the use of 7000 MJ of energy (electricity and fuel) and the emission of 1 ton of CO2 which amounts to 3 – 8% annual CO2 emissions.

Because of this effect of construction on the ecology and in order to implement the decision of the European Council from March 2007 to increase energy efficiency and achieve a decrease in electricity consumption of 20% by 2020, a drastic change must be made in the policy of production and use of materials for construction. To guarantee the sustainable development of construction, the main focus should be on:

- Processing and use of recycled construction waste and water;
- Utilizing waste products from industrial production.

The fulfilment of these measures will result in protecting the environment, reduction of energy consumption and CO2 emissions.

2.1. ASSESSMENT OF THE IMPLEMENTATION OF THE REQUIREMENT OF USE OF RECYCLED BUILDING AND DEMOLITION MATERIALS

The data for Bulgaria [2] shows that the total quantity of construction waste is 3 041 300 tons, including 300 000 tons from repairs, 700 000 tons from demolitions, 778 500 tons from the roads sector, 100 000 tons from rail infrastructure.

Our studies show that 93 – 97% of the mass of construction waste can be reused in construction. Table 1 presents the requirement of the national Regulation on Management of Construction Waste and the amounts which should be used after recycling [3].

Table 1 Goals for utilization of construction and demolition waste

Remainder	Dimension	2016	2017	2018	2019	2020
Concrete	%	85	85	85	85	85
Bricks	%	43	50	57	63	70
Roof tiles, tiles, faience; ceramics	%	43	50	57	63	70
Timber	%	67	70	73	77	80
Glass	%	44	53	62	71	80
Plastic	%	58	63	69	74	80
Iron, steel	%	90	90	90	90	80
Copper, bronze, brass	%	90	90	90	90	90
Aluminium	%	90	90	90	90	90
Lead		90	90	90	90	90
Zink	%	90	90	90	90	90
Asphalt mixes	%	62	67	71	77	80
Road section	%	67	70	73	77	80
Railroad section	%	67	70	73	77	80

The use of the quantities of recycled materials specified in Table 1 would guarantee that:

- By 1 January 2018 at least 50% of the total mass of construction waste is reused;
- By 1 January 2020 at least 70% of the total mass of construction waste is reused.

As of today 13 installations for recycling construction waste have been built in the country. Their locations and capacities do not yet provide the conditions needed to fulfil the set goals. A relatively good progress has been made in the use of recycled materials in road construction. The building of modern depots for newly incoming construction waste also leaves a lot to be desired.

Bulgaria is lagging behind other EU member states considerably despite the fact that the possibility of the effective use of recycled concrete waste in construction has been proven by the studies undertaken in the past decade /4/.

2.2. STATUS OF THE USE OF WASTE PRODUCTS FROM INDUSTRIAL PRODUCTION (METALLURGY AND CHEMICAL INDUSTRY)

The first positive attempt in this regard was made in the 1980s.

During the construction of parts of the Maritsa and Hemus motorways slag from the Kremikovtsi Steel Complex was used for the wearing course [5]. This product also is used for the production of mixed (Slag Portland) cements in which contain of finely ground slag is up to 50%.

The next attempt at the using a waste product from the chemical industry was made in the Central Laboratory of Physico-Chemical Mechanics, which is a part of the Bulgarian Academy of Sciences, where the applications of phosphogypsum in the production of elements for barrier walls were studied [6]. The results from these promising studies were not developed further and applied in practice.

In 1991 a composition of a binder containing phosphogypsum and expanded perlite for materials for thermal insulation was patented [7], but these materials were not study enough and their thermal insulation properties were unsatisfactory.

As of today, data from the studies on the applications of phosphogypsum in construction are patented [8] as a building material called gypsumperlite, which is used for building elements. Gypsumperlite as a binding agent utilizes processed ground to size of 5 to 40 micrometres mechanically activated phosphogypsum (active gypsum) and hydrophobized expanded perlite sand and superplasticizer Melflux (0.2 % by mass).

The proportions of the components are as follows:

- active gypsum– 84.8 – 93.8 % by mass;
- perlite sand – 6 – 15 % by mass;

The properties of the resulting gypsumperlite are described in Table 2.

Table 2 Composition and properties of different compositions of gypsumperlite [8]

Sample	Active gypsum, wt.%	Perlite, wt.%	Plasticizer, wt %	Density, kg/m3	Compressive Strength, MPa	Thermal conductivity V/mK
1	84,8	15	0,2	0,45	0,78 – 0,98	0,09
2	86,8	13	0,2	0,65	3,43 – 3,92	0,13
3	93,8	6	0,2	0,80	5,88 – 6,86	0,15

As evident from the data in Table 2, gypsumperlite can guarantee considerably better strength indicators compared to silicate bricks (compressive strength – 16,5 MPa; density – 1,67 g/ cm^3). A 30 cm bearing wall made from this gypsumperlite is up to 6 times less thermally conductive. As a comparison, the same thermal conductivity can be achieved with a silicate brick wall with a width of 1, 5 m. This composition of gypsumperlite has a higher strength than the widely available foam concrete (in the range of 1,18 – 3,49 MPa). Additionally, because of the fast solidification (about 20 min when using a retarder) the speed of construction is increased up to 10 times.

2.3. UTILIZATION OF WASTE BASED MATERIALS IN HIGH PERFORMANCE CONCRETE

The utilization of high performance concretes offers one possibility for decreasing the CO_2 emissions and the energy consumption during the production of cement and increasing the amount of industrial waste materials used. Defined in 1990 [9, 10], these concretes have three main characteristics – high workability, high strength and high durability. Compared to ordinary concrete, their special features are:

- Decreased size of the components used (mainly coarse aggregate);
- Using mineral additives with high dispersity – waste products from industrial production;
- Using modern chemical additives;

The studies [11] show that they fulfil the six criteria for sustainable development in the construction sector:

- Reduction in the amount of energy used in the production of the materials;
- Reduction in the amount of water used for production;

- Improvement of the quality of the air in the buildings;
- Reduction in CO_2 emissions;
- Increase in the amount and types of waste products used;
- Improved thermal effect.

Therefore they are in line with the requirements for “green materials”, because they possess the following characteristics:

- Low environmental impact;
- Prices comparable with the natural materials, used in ordinary concrete;
- Produced in substantial quantity;
- Easily produced;
- Easily repaired.

The experimental results for a class of high performance concretes are shown in Table 3.

Table 3 Various compositions and indicators of high performance concretes [11]

Sample	Cement, kg	Water, l	W/C	Slump, mm	Compressive strength, MPa
Standard sample	330	183	0,55	80	35
Standard sample +superplasticizer	310	158	0,54	80	35

The data in Table 3 shows that the supplement use of 0,7 % of superplasticizer in high performance concretes has several effects: ensuring high workability, reducing the water and cement quantity, guaranteeing the required compressive strength and lowering the price of the concrete. Moreover, the reduction in the cement quantity will result in lowering the CO_2 emissions and the energy required for its production.

The experience from the application of high performance concretes thus far shows that the following materials with grain size in the range micrometers of 0.3 can be used as fine dispersion materials:

- Silica fume
- Zeolites;
- Metakaolin;
- Reactive aluminium silicate filler derived from aluminium oxide and silicon oxide;
- Fly ash from coal combustible
- Ground Granulated Blast-Furnace Slag;
- Iron-silicate fines from copper production.

A considerable effect can be achieved by combining two or three mineral additives with different proportions of the mass of the cement.

During the past 20 years high performance concretes of the type Ultra High Performance Concrete (UHPC) have been developed globally and in Bulgaria. They possess not only extremely high strength (compression strength exceeding 150 MPa and flexural strength of 40 MPa), but also unparalleled durability and the ability to partially withstand plastic deformations [12]. That is why they are used in heavily loaded constructions as well as constructions under aggressive impact in combination with dynamic impact. Their composition contains various active mineral additives from the aforementioned ones. One of the most often used additives is silica fume because of its fine size and its impact on the heightened strengths. One of the features of these concretes is the additional thermal treatment using an autoclave or heat treatment. Figure 1 shows the change in compressive strength of UHPC with reduction of the maximum amount of the aggregate added. As smaller is the size of the Dmax, as higher is the compressive strength, due to better compaction and absent of weak zones.

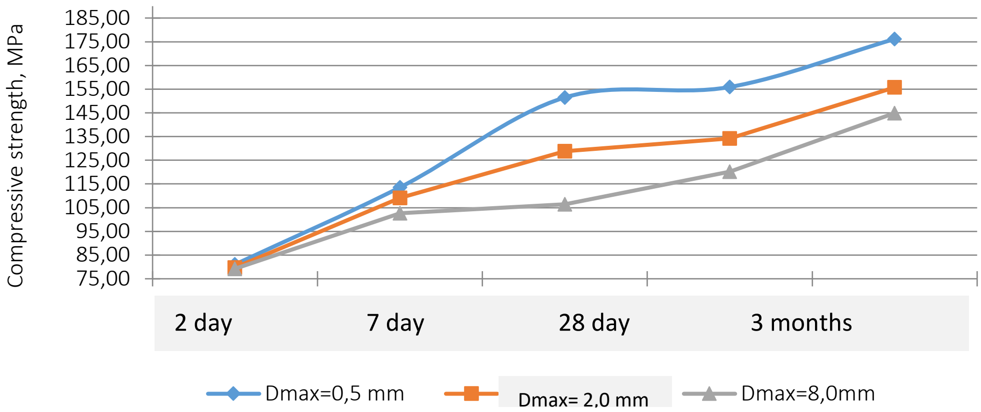

Figure 1 Compressive strength of UHPC, according to Dmax in time

One of the comparatively newer waste based materials, which has got increasingly wider application in construction, is iron-silicon powder, resulting from a flotation process in copper metallurgic plants. Because of its fine particle size (75% particles between 50 µm and 38 µm) and high specific density (3.8 g/cm³) when added in concretes, the main mechanical characteristics of the elements increase and the behaviour of the fresh concrete mix is improved [13]. The presence of pozzolanic activity when interacting with $Ca(OH)_2$ forms additional hydration products, which have a favourable effect on the compaction of the structure of the material as a whole and its increased durability.

3. CONCLUSION

The successful realization of the paradigm of sustainable development in construction in combination with the fulfilment of the European and Bulgarian legislative requirements can guarantee the sustainable future of Bulgaria. The latter can be accomplished by:

- The effective use of mineral additives (natural and recycled waste products) in the production of the most common building material – concrete;
- The use of effective chemical additives to reduce the water content while maintaining good workability of the concrete mix;
- The use of recycled construction and demolition waste in the form of recycled aggregates.

The further detailed study of the processes of formation of the structure with the increase in the quantity and types of the mineral additives replacing a portion of the cement is in progress.

REFERENCES

[1] Ivanova M., Ya. Ivanov, V. Stoyanov, Concrete and the demand of sustainable development, Pros. ESI'2013, p. 37 – 49.

[2] Bulgarian Institute of statistics, 2010, n.2. 146 p.

[3] www3moew.government..bg/file/.../ NAREDBA_CAN.pdf.

[4] Boden P., et al., Le beton avec des materiaux dechets de constrictions. Artois, 2000, 248 p.

[5] Babachev G. , Izpolzvane na metalurgicna shlaka v patnoto stroytelsvo, Tehnika, Sofia, 1989, 320 p.

[6] Cheshkov V., Phosfogipce kato material za stroytelni elementi, PHCHM, BAS, v. 53, 1996, p. 39 - 51

[7] Kotenkov A., Invention RU 2 519 146 C1.

[8] Invention RU 1650 640

[9] Ivanova M., M. Mironova, Analysis of the demands for the high performance concrete, Proc. VSU'2013.

[10] Roshavelov T., DSc Thesys, VSU, Sofia, 2003, 264 p.

[11] Ivanov Ya., M. Ivanova, V. Stoyanov, High technological concrete, Proc. VSU' 2013, 145 p.

[12] Graybeal B. Characterization of the behaviour of Ultra-high performance concrete, dissertation, University of Maryland, 2005;

Manolova E, Stoyanova V. Utilization of iron-silicate fines as replacement of fine aggregates in cement concrete pavements, Slag Valorisation Symposium, Leuven, 2017 /under print

USE OF WASTE GLASS AS AGGREGATE IN CONCRETE

Todorka Samardzioska[1], Vesna Grujoska[1], Jasna Grujoska[2], Darko Moslavac[1]

[1] Ss Cyril and Methodius University, Faculty of Civil Engineering, blvd Partizanski odredi 24, 1000 Skopje, Macedonia, email: samardzioska@gf.ukim.edu.mk, vesna.grujoska@gf.ukim.edu.mk, moslavac@gf.ukim.edu.mk
[2] FON University in Skopje, Faculty of Architecture, Kiro Gligorov, bb, 1000 Skopje, Macedonia, email: jasna.grujoska@fon.edu.mk

SUMMARY: The environmental and economic concerns are the biggest challenge that concrete industry is facing nowadays. Use of renewable materials instead of natural resources is one of the best approaches in sustainability of the concrete industry. Glass, being non-biodegradable, is not suitable for addition to landfill. On the other hand, 18% of the total waste in Macedonia is waste glass. Primary objective of this paper is to investigate the feasibility of utilizing recycled glass as aggregate concrete. Four different mixtures have been made. The glass is used as partial (50 %) or entire replacement (100 %) of the fine aggregate (0-4mm) in concrete, with and without admixtures. Couple of samples were prepared for each mix design and properties of fresh concrete and hardened concrete were tested at 3, 7, and 28 days. The most important physical and mechanical properties of the concrete made with variable quantity of processed waste glass aggregates and possibilities of its application are presented in the paper. The density, porosity, compressive strength and tensile strength, water absorption of the concrete with different percentage of glass aggregate have been tested. Few disadvantages due to the using recycled glass exist, as well. They relate to impurities that may occur in the raw material, the price for purchase of scrap glass, the quality of the new material etc. Nevertheless, due to the fact that the glass is one of the few materials in the nature which can be endlessly recycled, the purpose of this paper is to demonstrate a sustainable development of the industry for recycling glass and natural impacts on the Macedonian economy.

UPOTREBA OTPADNOG STAKLA KAO AGREGATA U BETONU

SAŽETAK: Najveći izazovi s kojima se industrija betona danas susreće jesu pitanja okoliša i ekonomije. Upotreba obnovljivih materijala umjesto onih iz prirodnih izvora jedan je od najboljih pristupa održive industrije betona. Staklo koje nije biorazgradivo nije prikladno za deponiranje. S druge strane, 18 % ukupnog otpada u Makedoniji čini otpadno staklo. Glavni cilj ovog rada istraživanje je prikladnosti upotrebe recikliranog stakla kao sitnog agregata za beton u obliku finog staklenog praha. Izrađene su četiri različite mješavine. Staklo je upotrijebljeno kao djelomična zamjena (50 %) ili potpuna zamjena (100 %) sitnoga agregata (0 do 4 mm) u betonu s dodacima i bez njih. Serije uzoraka izrađene su za svaku mješavinu te su ispitana svojstva svježega betona i očvrsnuloga betona nakon 3, 7 i 28 dana. U radu su prikazana najvažnija fizička i mehanička svojstva betona pripremljenih s različitim količinama pripremljenog staklenog agregata i mogućnosti njegove upotrebe. Ispitani su gustoća, poroznost, tlačna i vlačna čvrstoća i vodoupojnost betona pripremljenih s različitim postotcima staklenoga agregata. Pri upotrebi recikliranog stakla postoje neki nedostatci. Oni se odnose na nečistoće kojih može biti u sirovini, u cijeni nabavke lomljenog stakla, kvaliteti novoga materijala itd. Međutim, s obzirom na činjenicu da je staklo jedan od malobrojnih materijala u prirodi kojeg je moguće neograničeno reciklirati, svrha je ovog rada dokazati mogućnost održivog razvoja industrije s recikliranim staklom i njezin učinak na makedonsko gospodarstvo.

1. INTRODUCTION

Concrete is one of the most used and most important building materials and with the increased development of the civil engineering, necessity of it increases daily. Huge amounts of concrete that are produced require large amounts of aggregate. Aggregate used for concrete production is mostly of natural origin (sand, gravel, crushed stones, etc.). However, the continued exploitation of these natural resources, which are non-renewable, leads to destruction of the nature.

For these reasons, many countries restrict or completely prohibit the exploitation of natural aggregate for concrete and they are oriented towards finding new alternatives for obtaining artificial aggregates. Processing and application of certain waste materials as a substitute for natural aggregate is one of the best ways to make the concrete industry sustainable. With this procedure, the problem of excessive waste is solved on one hand, while on the other hand the possibilities for recycling are increased. One of the materials that are suitable for such processing is glass.

Huge amounts of waste glass are created every day. Although it is known that glass is not naturally degradable material, the biggest part of the waste glass ends up in landfills. In most European countries, the total amount of waste glass can be recycled only about 20% in the glass industry. Because of its structure, the glass can be recycled many times without losing its properties. Recycling only applies to glass containers (bottles and jars) that satisfy specific criteria of purity. On the other hand, windows, mirrors, glasses, lamps etc. are mainly not recycled. In Macedonia, the entire glass waste from different sources (around 18 % of the total waste according to the Strategy for Waste in Republic of Macedonia) is deposited or exported. It is very important to find a solution to this waste, both in terms of preserving the environment and in terms of solving the problem of excessive waste. The processing of waste glass and its use as aggregate for concrete provides major economic and environmental savings: prevents the exploitation of natural resources, saves energy, reduces the amount of waste material, reduces the price of concrete etc.

Research with laboratory experiments were conducted at the Faculty of Civil Engineering in Skopje to further explore the use of waste glass as fine aggregates for concrete. Both, properties of fresh and hardened concrete were tested. This paper presents mainly the latter properties: different strengths of the concrete with various percentage of waste glass as a fine aggregate. Results demonstrate that the use of waste glass as aggregate facilitates the development of concrete towards a high structural level.

2. STATE-OF-THE-ART

Many researchers around the world have performed aggregate replacement studies using waste glass. The general aim was to define a quantity of glass that will provide optimal strength properties of the concrete.

The influence of the waste glass on the mechanical properties of concrete has been researched by many researchers, including Du and Tan (2014), [1], Multon et al. (2008), [2], Newes and Zsuzsanna (2006), [3], Xie and Xiang (2003), [4], Johnson (1974), [5]. Their results show that the aggregate of waste glass decreases the concrete strength, in general. They attribute this behaviour to a strong chemical reaction between the quartz from the glass and the alkalis in the cement paste, which can lead to expansion and cracking of concrete.

Recently, there have been experimental investigations of Rubaie and Fouad, [6], which evaluate the properties of the concrete mixture containing waste glass up to 20% of the sand volume. The results show that the concrete mixture containing waste glass shows a very slight decrease in the compressive strength and tensile strength compared to reference classic mixtures.

Ling and Poon, [7], have been investigating the alkali-silica reaction in concrete with waste glass and the influence on the properties of fresh and hardened concrete, as well as on decorative concrete in civil engineering and architecture.

Following results were obtained in a survey conducted by Malik et al, [8]: 20% replacement of fine aggregate indicates increased compressive strength for 15% at 7 days and 25% increased strength for 28 days. The fine aggregate can be replaced with glass up to 30% of its weight, with the compressive strength at 28 days increased by 9.8% compared to standard concrete.

Gautam et al., [9], found that waste glass can effectively be used as fine aggregate replacement, but the optimum replacement level of waste glass as fine aggregate is 10%. Marginal decrease in the compressive strength is observed at 30 to 40% replacement level of waste glass with fine aggregate.

Therefore, different studies show various results and conclusions on the use of waste glass as fine aggregate in the concrete. However, almost none of them suggest replacement of the fine aggregate with glass for more than 30%.

3. EXPERIMENTAL METHOD

This study shows the opportunities for using waste glass in concrete industry. Performed work, presented in this paper, is a part of a larger on-going project, which examines the influence of different types of waste glass as an aggregate in concrete on the concrete's properties. The front glass from CRT monitors is used for this purpose. The glass is used as partial (50%) or entire replacement (100%) for the fine aggregate (0-4mm) in concrete. Four recipes have been made:

- normal concrete (0% glass),
- concrete containing 50% waste glass as fine aggregate,
- concrete containing 100% waste glass as fine aggregate, and
- concrete with admixtures (air entrainers and superplasticizers) containing 50% waste glass as fine aggregate.

The mixtures have water to cement ratio of 0,45. Couple of samples were prepared of each recipe and the properties of fresh concrete and hardened concrete.

The following samples were made out of each recipe for concrete mixture:

- 9 cubes (15/15/15 cm) for testing of compressive strength
- 3 cylinders (15/30 cm) for testing of slitting tensile strength (Brazilian test)
- 3 prisms (10/10/50 cm) for testing of flexural strength
- 6 cubes (15/15/15 cm) for testing waterproofing.

Porosity, density and consistency of the fresh concrete were measured for all recipes. Afterwards, the cube moulds were fixed and oiled, i.e. prepared for filling with fresh concrete. The fulfilment of the molds was carried out by compacting with vibration, ensuring the shape of the samples. De-moulding of the samples was carried out after 24 hours, after the hardening of the concrete, with utmost care to prevent any damage to the samples. The samples were stored in standardised laboratory conditions, and tested at 3, 7 and 28 days.

4. RESULTS AND DISCUSSION

4.1. COMPRESSIVE STRENGTH

Tested samples were cubes with dimension 15/15/15 cm. They were tested in testing machine – press, according to the standard EN 12390-4, Figure 1. The specimens were set centrally to the lower plate of the press; therefore the applied load is in direction normal to the sample. The load has been applied gradually with constant step of 10%, until a greater load was achieved than the range selected for application. The compressive strength was tested in series of three cubes each, at 3, 7, 28 days, as it is presented at Figure 2.

Figure 1 Press for testing compressive strength

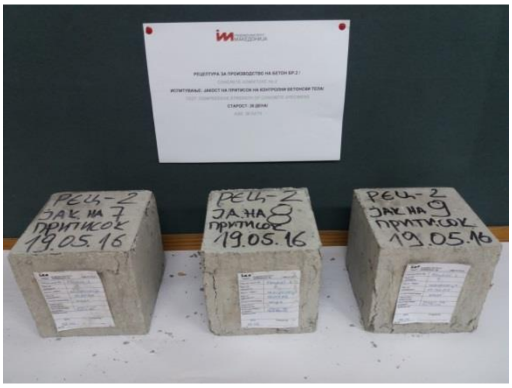

Figure 2 Tested cubes of recipe 2 for compressive strength at 28 days

By increasing the proportion of glass in the concrete, mechanical properties of the concrete at 7 days were improved, Figure 3a. Values of the compressive strength of the concrete with 50% and 100% glass as fine aggregate are greater than the ones of the standard concrete. The best compressive strength exhibits the concrete with 100% glass in the first fraction (f_c = 39,7 MPa). Comparing to the strength of standard concrete (f_c = 35,1 MPa), the increase in the strength is 13%.

Similar results appear for testing at 28 days. The compressive strength for the concrete with 50% glass as a fine aggregate is f_c = 46,4 MPa, while for the concrete with 100% glass is f_c = 46,8MPa. Standard concrete in this case showed compressive strength of 44 MPa. Replacement of 50% of the fine aggregate with waste glass shows 5% increase in the compressive strength, while replacement of 100% of the fine aggregate with glass aggregate shows 6% increase in the compressive strength comparing to the standard concrete. Best results were obtained for the fourth recipe (50% glass with admixtures), where the increase in the compressive strength is 12% compared to the standard concrete, see Figure 3b.

Using glass as a substitute for the fine aggregate, higher values of the compressive strength are obtained, both at an early stage and later stage of hardened concrete. Best values for the compressive strength are obtained at full replacement of the fine aggregate with glass. The range between companion samples from the same set and tested at age of 7 days is from 0,2% to 2,8% of the average strength. Error margins for the companion samples tested at age of 28 days range from 0,8% to 3,6% of the average strength.

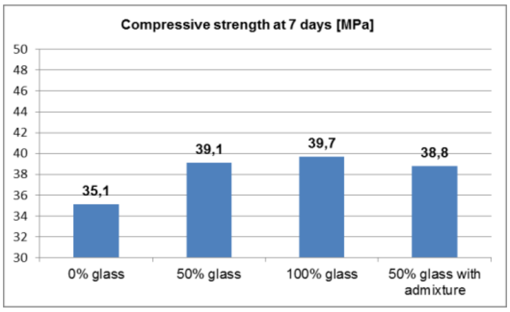

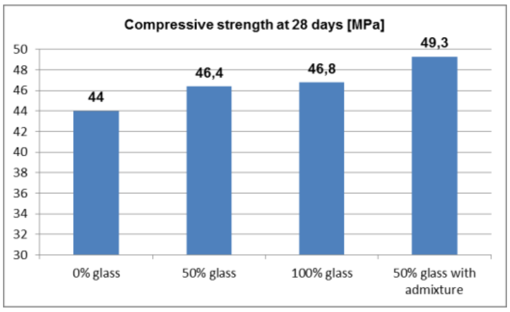

Figure 3 Diagrams of compressive strengths at: a) 7 days and b) 28 days for different recipes

4.2. SPLITTING TENSILE STRENGTH

The testing of tensile strength was performed according to the standard MKS EN 12390-6. Tested samples were cylinders with dimensions 15/30 cm. The testing of the samples was carried out in an appropriate machine (press) according to MKS EN 12390-4, according to the so-called Brazilian method. During the test, the samples are set centrally in the machine, and load was applied while the upper and lower rollers were placed parallel to each other. The load was applied gradually with step of 10%, until a fracture of the sample under the indicated maximum load.

Figure 4 Testing of specimen with splitting test – Brazilian method

In general, tensile strength of the concrete is much lower than its compressive stress. For usual concretes, the ratio between them is 1:10. Testing of the tensile strength with splitting is performed at age of 28 days on three cylindrical samples. Fractured samples are presented in Figure 5. The concrete of the recipe 2 (with 50% glass), shows best values for the splitting tensile strength, f_{zc} = 3,54 MPa. With increasing the proportion of glass (above 50%), the tensile strengths decrease. Therefore, the concrete recipe 3 (100% of glass for the first fraction) has the weakest splitting tensile strength f_{zc} = 2,90 MPa, as it can be seen in Figure 6.

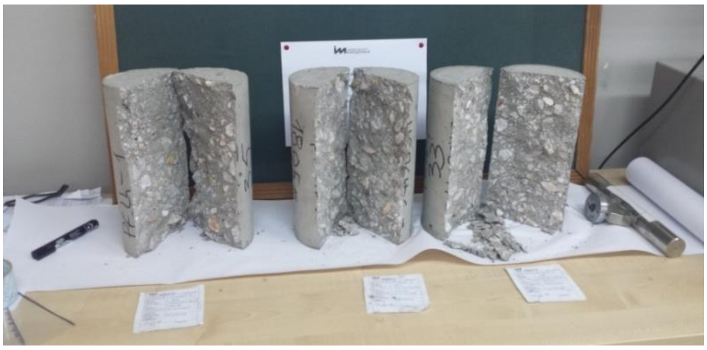

Figure 5 Tested specimens – Brazilian method

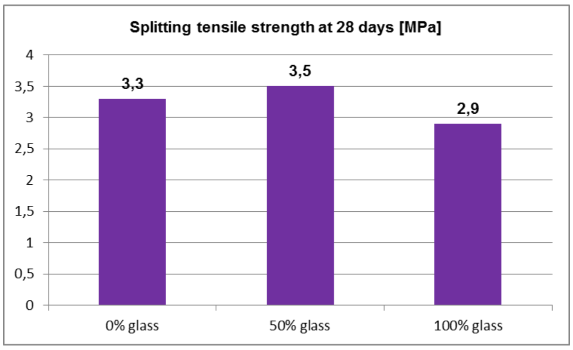

Figure 6 Diagram of splitting tensile strengths at 28 days

The results lead to conclusion that the difference in the values of tensile strengths for various concrete recipes is low. Reason for such a small difference is that the splitting tensile strength of the concrete depends on the relationship between cement stone and grains of the coarse aggregate, rather than on the properties of fine aggregates.

4.3. FLEXURAL STRENGTH

Even though flexural strength is not used for field control and the engineers generally find the use of compressive strength convenient and reliable to judge the quality of the concrete as delivered, still the designers of pavements use a theory based on flexural strength. The results of this test method may be used to determine compliance with specifications or as a basis for mixture proportioning, evaluating uniformity of the mixture, and checking placement operations by using sawed beams. It is used primarily in testing concrete for the construction of pavements and slabs.

This test method is used to determine the flexural strength on prismatic specimens with dimensions 10x10x40 cm и 10x10x50 cm, prepared and cured in accordance with the standard MKS EN 12390-4. The testing device comprises: a load roller (which can be rotated and bends) and supporting rollers that can be rotated and pivoted, Figure 7. Rollers are made of steel with a circular cross-sectional diameter of 10 to 20 mm. Rollers are placed in a way that they can freely rotate around their axes. The test is actually a simulation of a simple beam loaded with a concentrated force in the middle, as it is shown in Figure 7.

Figure 7 Prisms tested to bending

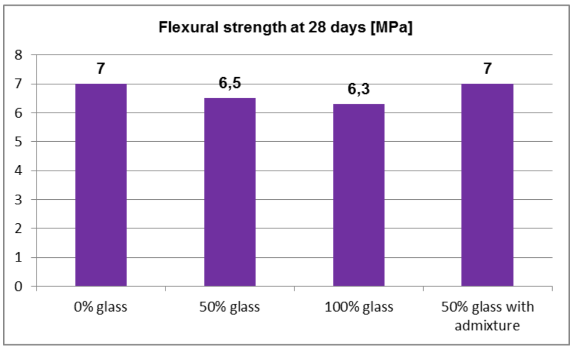

Figure 8 Diagram of flexural strengths at 28 days

The concrete according to the second recipe (50% glass in the first fraction) and the concrete of recipe 3 (100% glass in the first fraction), have almost same values for the tensile strength due to bending. For the second recipe f_s = 6,5 Mpa, while for the third f_s = 6,3 MPa. Both of these concretes show lower values of flexural strength compared to the normal concrete (f_s = 7 MPa) and to the concrete of recipe 4 (concrete with admixtures), where f_s is 7 Mpa again (Figure 8).

5. CONCLUSIONS

The research in this paper contributes to new opportunities for using waste glass. Namely, an experimental laboratory study of concrete containing a partial or total replacement of the fine aggregate with glass has been conducted. Results on the properties of hardened concrete are analyzed. A comparison of samples of concrete containing glass with samples of standard concrete has been made. The results of these laboratory tests are compared with previous similar experiences in the world.

The compressive strength increases in concrete with used waste glass instead of gravel aggregate. Both mixtures made with 50% replacement of the fine aggregate with waste glass and with 100% replacement showed improved compressive strengths (up to 12%) in comparison to the standard concrete. As for the tensile strength due to splitting and bending, concrete containing waste glass has almost identical properties as the standard concrete.

The idea in this research is to show that the proper use of waste materials can produce a concrete with same or even better properties than the standard concrete and great economic and ecological savings. The recommendations in the world literature for this type of concrete are that it can be used for making non-structural members, mostly for paving large surfaces, curbs, pavements, etc., but not for structural bearing members in structures. However, according to the properties obtained in this experimental study, this type of concrete possesses the same properties as the concrete used for the manufacture of bearing structural members. The concrete containing waste glass as fine aggregate satisfies the requirements for achieving compressive strength of 30 Mpa at age of 28 days, which corresponds to the widely used type of concrete for most of the structural members in buildings. Validation of the physical and mechanical properties of concrete which contains variable amounts of waste glass as an aggregate enables the use of this material for production of environmental material with sustainable significance. This approach solves the problem of excessive waste, contributing to greener and safer environment.

Having opened new opportunities and horizons for application of concrete with aggregate of waste glass, new fields are opened for their further study as well. Use of waste glass as coarse aggregate in concrete presents a potential for new studies. Such a concrete with visible larger fractions of glass in different colours would have a wider use as a decorative material in the civil engineering and architecture. An interesting phenomenon in this material is an alkali - silica reaction that develops over time and its impact on the properties of fresh and hardened concrete. Further tests on concrete with glass waste should be carried out for this purpose, in long periods of time that will allow development of such reaction.

ACKNOWLEDGMENTS

The authors express their gratitude to the members of the measurement team in the Laboratory of the Civil Engineering Institute Macedonia, as well as to Cementarnica Usje AD and Nulaotpad, all from Skopje, for continuous support of this research.

REFERENCES

[1] Du, H. & Tan, K. H.: Concrete with Recycled Glass as Fine Aggregates, *Materials Journal*, Vol. 111 (2014), No. 1, pp. 47-58.

[2] Multon, S.; Barin, X.; Godart, B. & Toutlemende, F.: Estimation of The Residual Expansion of Concrete Affected by Alkali Silica Reaction, *Journal of Materials in Civil Engineering*, Vol.20 (2008), No.1, 2008, pp. 54-62.

[3] Newes R. & Zsuzsanna: Strength of light weight glass aggregate concrete, *Journal of Materials in Civil Engineering*, Vol. 18 (2006), No. 5, pp. 710-714.

[4] Xie Z.; Xiang W. & Xi, Y.: ASR Potentials of glass aggregate in water glass activated fly ash and Portland cement mortar, *Journal of Materials in Civil Engineering*, Vol. 15 (2003), No. 1.

[5] Johnson, C. D.: Waste glass as coarse aggregate for concrete, *Journal of testing and evaluation*, Vol. 2 (1974), pp. 344-350.

[6] Rubaie, A. & Fouad, M.: Properties of concrete building units containing crushed waste glass, M.Sc. Thesis, The University of technology, 2007.

[7] Ling, T.C.& Poon, C.S.: Utilization of recycled glass derived from cathode ray tube glass as fine aggregate in cement mortar, *Journal of Hazardous materials*, Vol. 192 (2011), No.1, pp.451-456.

[8] Malik, M. et al.: Study of concrete involving use of waste glass as partial replacement of fine aggregates, *IOSR Journal of Engineering*, Vol. 3 (2013), No. 7, pp. 8-13, ISSN: 2278-8719.

[9] Gautam, S.P.; Srivastava, V. & Agarwal, V.C.: Use of glass wastes as fine aggregate in Concrete, *J. Acad. Indus. Res.*, Vol. 1 (2012), No. 6, ISSN: 2278-5213.

POTENTIAL USE OF WASTE FROM PAPER INDUSTRY IN THE CLAY BRICK SECTOR

Selena Bosnjak[1], Vilma Ducman[1]

[1] Slovenian National Building and Civil Engineering Institute, The Department of Materials, Laboratory for Cements, Mortars and Ceramics, Dimiceva ulica 12, 1000 Ljubljana, Slovenia, email: selena.bosnjak@zag.si, vilma.ducman@zag.si

SUMMARY: Alongside the production of paper, a certain amount of waste is generated, like papermaking sludge and biomass ash. Such waste materials can be usefully applied in the clay brick sector. Paper sludge can be used as a pore-forming agent that can improve the thermal insulating properties of bricks by increasing the porosity of the ceramic body. An additional benefit of using papermaking sludge is that it reinforces the clay body structure during drying, thus preventing cracking. Biomass ash, i.e. ashes that remain after firing of paper sludge, can be added to the ceramic body to enhance the process of sintering by creating a liquid phase. Laboratory tests were carried out on brick making clay with the addition of different proportions of papermaking sludge and biomass ash in order to assess the influence of a single additive on the final properties and to determine the optimal mixture for a pilot production. The influence of the addition of both types of additives on drying and firing shrinkage was determined, as well as the water absorption, bulk density, frost resistance, bending and compressive strengths of fired samples. It was found that all three additives (one paper sludge, two different biomass ashes) required a higher amount of water for moulding but depending on their properties, all three could be used in the clay based industry in different proportions. Promising results regarding the technological parameters as well as the properties of the final products, such as compressive strength and water absorption are to be expected with additives of ashes in the quantities of up 10 mass %, while paper sludge could be added even up to 20 mass %.

POTENCIJALNA UPOTREBA OTPADA IZ INDUSTRIJE PAPIRA U OPECI

SAŽETAK: U proizvodnji papira nastaje određena količina otpada poput papirnog mulja i pepela iz biomase. Takvi se otpadni materijali mogu korisno primijeniti u proizvodnji opeke. Papirni mulj može se upotrijebiti kao sredstvo za formiranje pora koje može poboljšati toplinsko-izolacijska svojstva opeke zbog povećane poroznosti keramičkoga tijela. Dodatna je korist primjene toga mulja što on pojačava strukturu glinenoga tijela tijekom sušenja pa tako sprečava raspucavanje. Pepeo iz biomase tj. pepeo koji ostaje nakon paljenja papirnog mulja može se dodati keramičkom tijelu radi poboljšanja procesa sinteriranja stvaranjem tekuće faze. Provedena su laboratorijska ispitivanja na opeci načinjenoj iz gline s dodatkom različitih omjera papirnog mulja i pepela iz biomase kako bi se ocijenio učinak pojedinog dodatnog sastojka na konačna svojstva i odredila optimalna mješavina u pokusnoj proizvodnji. Određen je učinak dodavanja dodatnog sastojka obiju vrsta na skupljanje pri sušenju i paljenju te vodoupojnost, obujamska masa, otpornost na zamrzavanje, tlačna čvrstoća i čvrstoća na savijanje paljenih uzoraka. Utvrđeno je da sva tri dodatka (papirni mulj i dva različita pepela iz biomase) zahtijevaju veću količinu vode pri oblikovanju u kalupu ali da se, ovisno o njihovim svojstvima, sva tri mogu upotrijebiti u opekarskoj industriji u različitim omjerima. Mogu se očekivati obećavajući rezultati tehnoloških parametara i svojstava konačnih proizvoda i to tlačne čvrstoće i vodoupojnosti uz količinu dodatka pepela do 10 % mase i papirnoga mulja do čak 20 % mase.

1. INTRODUCTION

The growing trend in recycling is also reflected in the construction industry; many waste materials can be successfully implemented as additives or secondary raw materials in the production of concrete products or clay bricks. In the clay brick sector the most commonly used waste materials are different sludge like incinerator sludge, sludge waste from water treatment plants, sewage sludge [1,2,3] marble residue [4], and different ashes, like biomass ashes [5],municipal incinerator ashes [6, 7, 8], fly ash and bottom ash [9]. But, the most widely used waste in clay brick production is paper sludge and ashes from paper sludge incineration [5, 10].

The paper industry produces a large amount of waste sludge which represents, in the case of inappropriate disposal, a serious load on the environment [10]. Paper sludge has a high content of clay (kaolin) and a high proportion of interstitial water, and it is therefore not so suitable for energy recovery, due to its low calorific value [11]. But such sludge can be successfully implemented in the ceramic sector as a secondary raw material as reported in many studies[12, 13, 14, 15, 16], etc. The presence of organic fibres increases the porosity of the matrix, as proven by study [17]. Increasing the content of the paper sludge in a clay mixture reduces the mechanical strength, but improves its properties with regard to thermal and acoustic insulation.

Summarising, clay products that are manufactured with paper sludge exhibit the following advantages [17]:

- acceptable mechanical properties of the new material,

- improvement in thermal and acoustic insulating properties of the material,
- as a result of leaching tests, no restrictions on its use as a building ceramic,
- the final ceramic product is of similar quality to conventional ceramics.

When paper sludge possesses a calorific value high enough for energy recovery then during the firing ash is created which is again waste. Ashes can differ greatly in chemical compositions, mineralogical compositions and particle size, depending mainly on the raw materials which enter the process, but also on the process itself. Researchers Merino et al. [7] and Lin [8] showed ash produced with the incineration of sewage sludge can be used for the production of ceramic material. Also, Anderson [18] investigated the production of bricks by mixing ash and clay and found that even 5 mass % of ash had benefits in brick production. Recently Perez-Villarejo et al. [5] have shown that the inclusion of up to 20 wt. % of biomass ash obtained from incineration in wood plants in the clay is still adequate and that the final products meet the standard requirement for compressive strength.

The use of waste in the production of clay based products could, on the one hand, represent a significant decrease in costs due to the replacement of basic raw materials by waste, and in some cases, such an addition can significantly improve the quality of the final product, and on the other hand, such application would help the waste holder to use these materials instead of disposing them in a landfill and paying taxes.

The aims of the study were therefore to verify the usability of locally available paper sludge and paper sludge ashes (biomass ash) regarding their usability as additives in the production of clay bricks, helping in solving the problem of waste disposal on the one hand and reduce the production cost on the other hand.

2. EXPERIMENTAL

2.1. RAW MATERIALS AND TEST MIXTURES

2.1.1. BRICK MAKING CLAY

Clay was taken from a production of masonry bricks. The chemical composition and mineralogical composition are given in Tables 1 and 2, respectively. As seen from Tables 1 and 2, clay can be classified as chlorite illitic type. Particle size distribution D50: > 6 µm.

2.1.2. PAPERMAKING SLUDGE

Papermaking sludge consists of the following inorganic components: calcite, kaolinite and illite (Table 1 and 2). Loss on ignition at 500°C is 3.40 mass % and at 950°C is 5.09 mass %.

2.1.3. BIOMASS ASHES

Biomass ashes (the chemical composition is given in Table 1) arise from incineration of paper sludge and the one designated as K4 contains quartz, lime, hematite, periclase, brown millerite, calcite, gehlenite, magnetite, portlandite, anhydrite and plagioclase, and a sample designated as K5 (ash mixed with bottom ash) contains calcite, lime, portlandite, larnite, quartz, mayenite, talc and gehlenite as seen from Table 2. Particle size distribution for K4 D50: > 30 µm and for K5 D50: > 30 µm.

Table 1 Chemical composition of clay, paper sludge, biomass ashes K4 and K5

	Clay	Paper sludge	Biomass ash- K4	Biomass ash - K5
Na_2O	0.89	0.06	1.04	0.25
MgO	1.67	1.69	9.79	2.14
Al_2O_3	15.42	9.77	9.01	9.35
SiO_2	59.21	11.26	27.84	13.53
P_2O_5	0.10	0.18	0.72	0.23
K_2O	2.47	0.03	2.18	0.31
CaO	3.41	28.89	25.92	53.02
TiO_2	0.74	0.23	0.97	0.21
MnO	0.17	/	0.40	0.02
Fe_2O_3	6.10	0.39	13.92	0.42
LOI	8.62	46.34	3.99	18.60

Table 2 Mineralogical composition of clay, paper sludge, biomass ashes K4 and K5

Sample	Mineralogical composition
Clay	Montmorillonite, illite/muscovite, feldspar, clinoclorite, quartz, calcite
Paper sludge	Calcite, tac/talcum, kaolinite
Biomass ash – K4	Quartz, lime, hematite, periclase, brown millerite, calcite, gehlenite, magnetite, portlandite, anhydrite, plagioclase
Biomass ash – K5	Calcite, lime, portlandite, larnite, quartz, mayenite, talc, gehlenite

2.2. TEST METHODS

The chemical compositions were determined by XRF spectrometer ARL 8480 S.
The mineral phases of all samples were determined by X-ray diffractometer using a PANalytical Empyrean apparatus in the following conditions: CuKα radiation was in the range of 2θ from 4-70 °.
The particle size distribution of the tested clay was determined by a Cilas 920 laser analyser.
Linear shrinkage, ceramic body density, water absorption (by boiling test specimens in water for 2 h), and compressive strength were determined on fired samples with dimensions of 150x50x25 mm.

2.3. MOULDING, DRYING AND FIRING OF TEST SPECIMENS

The design of the mixture is given in Table 3. Test specimens were moulded in a laboratory de-airing extruder at a vacuum of about 20%, i.e. 84 kPa. During extrusion, a proper amount of water was added to the mixtures to avoid surface cracks on test specimens and to maintain a Pfefferkorn number of 1.7 (±0.1) –the results are given in Table 4. Test specimens were dried for 7 days at ambient room conditions, followed by 6 h at 40°C and 12 h at 110°C in a dryer. Dried samples were then fired in a laboratory kiln at a selected temperature - 950°C using heating rates of 150°/h.

Table 3 Mixture design and conditions at moulding of samples based on clay, paper sludge, and biomass ashes K4 and K5 (* moulding was practically impossible on the extruder with 20 mass % of K4)

Designation	S0	S1	S2*	S3	S4	S5	S6	S7	S8
Clay content (mass %)	100	90	80	95	95	90	95	90	80
Paper sludge(mass %)	0	0	0	0	0	0	5	10	20
Biomass ash – K4 (mass %)	0	10	20	5	0	0	0	0	0
Biomass ash – K5 (mass %)	0	0	0	0	5	10	0	0	0
Moulding									
Water content based on dry mass (mass %)	25.2	30.0	34.4	29.8	32.1	35.7	27.6	30.5	37.7
Water content based on wet mass (mass %)	20.1	23.1	25.6	22.9	24.3	26.3	21.6	23.4	27.4

3. RESULTS

The results of testing after drying and firing are given in Table 4.

In the case of ash the mixtures were workable up to 10 mass % of addition; with a higher amount of addition of ashes moulding was impossible because many cracks appeared within the structure during the moulding process. Additions of ashes require a higher amount of water for moulding which, from a technological point of view, is not beneficial since this water should be removed during drying. As can be seen from Table 4 the addition of ash K4 in the amount of 10 mass % practically does not influence the drying shrinkage while the addition of ash K5 decreases the drying shrinkage.

Body density after firing at 950°C decreased in all samples when compared to sample containing only clay - S0, where it is 1.93 kg/dm^3. The biggest drop of body density was observed with the addition of 10 mass % of biomass ash K5 when body density after firing was reduced to 1.50 kg/dm^3

As expected, bending and compressive strength decreased in almost every case of additives, only in the case of S6 with 5 mass% of paper sludge did compressive strength increase. With the addition of a higher amount of ash, the strength continued to decrease. A certain decrease in mechanical properties on a laboratory level can be tolerated because in the regular production, a hollow clay brick made of mixture S0 reaches a compressive strength of approx. 30 MPa and the declared value is a minimum 20 MPa.

Table 4 Properties of specimens of different mixture designs after drying and firing

Designation	S0	S1	S3	S4	S5	S6	S7	S8
Shrinkage after drying measured along the prism length(%)	8.2	8.3	7.6	7.4	5.6	8.4	8.3	9.5
Shrinkage after drying measured across the prism width(%)	6.7	6.6	5.7	5.4	5.4	7.7	7.7	10.3
Firing at temperature (°c) (±15)	950	950	950	950	950	950	950	950
Shrinkage after firing measured along the prism length (%)	0.7	0.6	0.7	1.1	2.1	0.4	0.5	0.5
Shrinkage after firing measured across the prism width(%)	1.1	1.3	1.5	1.9	2.2	0.5	0.7	0.7
Body density after firing (kg/dm^3)	1.93	1.71	1.77	1.64	1.50	1.78	1.74	1.66
Water absorption (%)	9.2	19.0	16.5	21.7	27.3	12.2	14.2	21.2
Clinker point								
Temp. of firing where water absorption amounts to 6 wt.%	1081	1130	1118	1131	/	1112	/	/
Bending strength measured on prisms(MPa)	13.8	8.8	9.8	9.0	4.0	13.8	11.8	9.5
Compressive strength measured on prisms (MPa)	68.1	48.5	56.4	30.7	17.3	73.9	46.9	38.5

From the technological parameters shrinkage and water absorption during firing is important to properly regulate the process and set the final firing temperature. In Figures 1, 2 and 3 shrinkage and water absorption upon firing are presented for the mixtures with the addition of paper sludge, ash K4 and ash K5, respectively.

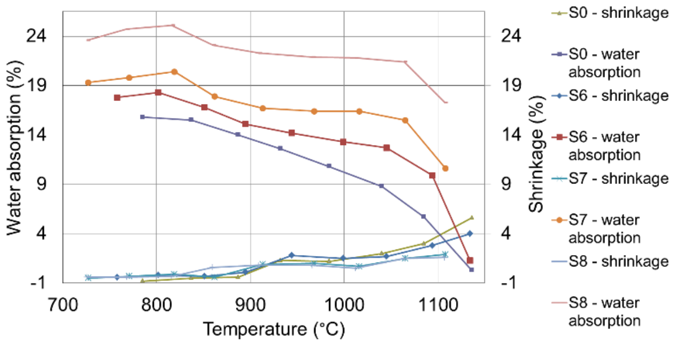

Figure 1 Influence of paper sludge additives on shrinkage and water absorption

As seen from Table 4 and Figure 1, paper sludge addition has a positive impact on shrinkage after firing. Shrinkage from 0.7% (result of shrinkage along the prism length in designation S0 – 100% clay) was lowered to 0.4%with 5 mass % of paper sludge (the result of shrinkage along the prism length in designation S6 – with 5% paper sludge). With the higher addition of paper sludge (10 mass% and 20 mass%) the shrinkage was even lower. On the other hand, it can be seen from Figure 2 (and Table 4) that paper sludge has an impact on water absorption. In every mixture with the addition of paper sludge water absorption rises due to the combustion of organic matter in the paper sludge which creates additional open pores. As expected more mass % of paper sludge addition increases water absorption. For example, mixture S0 (100 mass% of clay) had water absorption of 9.2%, while with 20 mass % of paper sludge (S8)water absorption increased to21.2%.

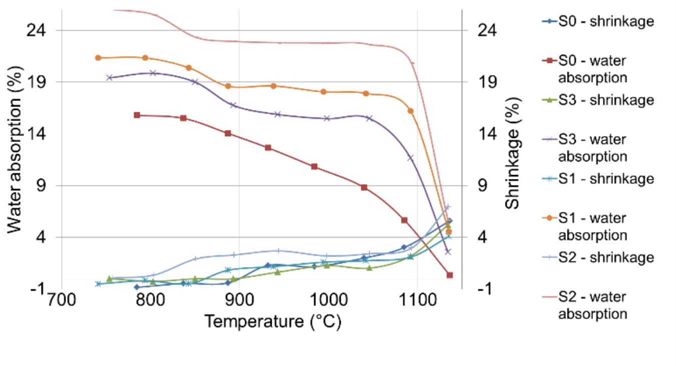

Figure 2 Influence of biomass ash K4 additives on shrinkage and water absorption

Biomass ash K4 has a negative impact on shrinkage after firing and on water absorption in general (Table 4, Figure 2). With a 5 mass% of K4 ash, shrinkage along the prism length was the same as S0, but shrinkage along the prism width increased from 1.1% to 1.5%, which is unexpected when compared with the designation of 10 mass % where we had 1.3% shrinkage along the prism width. Biomass ash K4 had an even bigger impact on water absorption than paper sludge; with increasing mass% of biomass ash K4, water absorption also increased – from 9.2% S0 to 16.5% S3 and 19.0% S2 (10 mass % of ash).

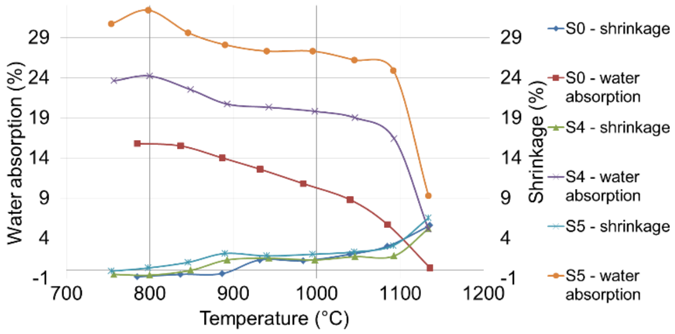

Figure 3 Influence of biomass ash K5 additives on shrinkage and water absorption

Biomass ash K5 has the biggest impact on shrinkage and water absorption of all additives (Table 4 Figure 3). Shrinkage along length with only 5 mass% rises from 0.7% S0 to 1.1% S4 and shrinkage along width from 1.1% S0 to 1.5% S4.Water absorption increased with increasing mass% of biomass ash K5 as we see from Fig 3 and Table 4. In S0 (100 mass% of clay) water absorption was 9.2%, in mixture S4 with only 5 mass% of biomass ash K5 it was 21.7% and for the mixture S5 with 10 mass % of K5 ash it was 27.3%. Biomass ash K5 exhibit quite a high amount of loss on ignition at 900°C (18.6%; Table 1) which is ascribed to the organic matter as well as to the carbonates; both can contribute to the increase in porosity in fired specimens. An increase in water absorption by adding biomass ashes to the clay mixture was also reported in the literature [19] but it could be lowered by increasing the firing temperature.

4. CONCLUSIONS

From the results obtained so far it can be concluded that:

- All three additives exhibited a higher demand for water to enable proper moulding which would require more energy during the drying process;

- Ash K4 can be added only up to approx. 10 mass%, while ash K5 already in the quantity of 5 mass% significantly reduces mechanical properties; and

- Paper sludge has the most favourable effect on the properties of fired specimens; based on the laboratory results it seems that even up to 20 mass% could be added.

In further steps pilot production at the clay bricks producer premises are foreseen to definitely confirm the usability of investigated secondary materials for the clay sector.

ACKNOWLEDGMENTS

The work was carried out within the RDI project Cel.Cycle: "Potential of biomass for development of advanced materials and bio-based products", co-financed by the Republic of Slovenia, Ministry of Education, Science and Sport, and the European Union under the European Regional Development Fund, 2016-2020.

REFERENCES

[1] Jordan, M.M. et al.: Application of sewage sludge in the manufacturing of ceramic tile bodies, Appl. Clay Sci., 30 (2005), 219–224, 0169-1317.

[2] Devant, M., Cusidó, J.A. and Soriano, C.: Custom formulation of red ceramics with clay, sewage sludge and forest waste, Appl. Clay Sci., 53 (2011), 669–675, 0169-1317.

[3] Demir, I., Serhat Baspinar, M. and Orhan, M.: Utilization of kraft pulp production residues in clay brick production, Build.Environ., 40 (2005), 1533–1537, 0360-1323.

[4] Montero, M.A. et al.: The use of sewage sludge and marble residues in the manufacture of ceramic the tile bodies, Appl. Clay Sci., 46 (2009), 404–408, 0169-1317.

[5] Pérez-Villarejo, L. et al.: Recycling of ash from biomass incinerator in clay matrix to produce ceramic bricks, Journal of Environmental Management, 95 (2012), S349-S354, 0301-4797.

[6] Ferreira, C., Ribeiro, A. and Ottosen, L.: Possible applications for municipal solid waste fly ash, J. Hazard. Mater., B 96 (2003), 201-216, 0304-3894.

[7] Merino, I., Arévalo, L.F. and Romero, F.: Characterization and possible uses of ashes from wastewater treatment plants, Waste Manag., 25 (2005), 1046-1054, 0956-053X.

[8] Lin, K.L.: Feasibility study of using brick made from municipal solid waste incinerator fly ash slag. J. Hazard. Mater., B 137 (2006), 1810-1816, 0304-3894.

[9] Monteiro, R.C.C. et al.: Characterization of MSWI bottom ashes towards utilization as glass raw material, Waste Manag. 28 (2008), 1119-1125, 0950-0618.

[10] Vieira, C.M.F. et al.: Clay bricks added with effluent sludge from paper industry: Technical, economical and environmental benefits, Appl. Clay Sci., 132–133 (2016), 753–759, 0169-1317.

[11] Council Directive 99/31/EC of 26 April 1999, Official Journal L 182, Available from http://eur-lex.europa.eu/legal-content/en/TXT/?uri=CELEX%3A31999L0031. Accessed: 2016-12-23.

[12] Zani, A., Tenaglia, A. and Panigada, A.: Re-use of papermaking sludge in brick production, Ziegelind. Int./Brick and Tile Ind. Intl., 43 (1990) 12, 682–690.

[13] Ducman, V., Kopar, T.: Sawdust and paper-making sludge as pore-forming agents for lightweight clay bricks, Ind. Ceram, 21 (2001) 2, 81–86.

[14] Smith, A.S.: Alternative materials in brick making – UK perspective, Brickyard Road, 5 (2006) 4, 24–27.

[15] Ismail,M. et al.: Fabrication of bricks from paper sludge and palm oil fuel ash, Concr. Res. Lett., 1 (2010) 2, 60–66.

[16] Chemani, B. and Chemani, H.: Utilization of paper sludge in clay bricks industry to obtain lightweight material: evidence from partial replacement of feldspar by paper sludge, Int. J. Phys. Sci., 8 (2013) 9, 335–342, 1992-1950.

[17] Cusidó, J.A. et al.: Incorporation of paper sludge in clay brick formulation: ten years of industrial experience, Appl. Clay Sci., 108 (2015), 191–198, 0169-1317.

[18] Anderson, M.: Encouraging prospect for recycling incinerated sewage sludge ash (ISSA) into clay-based building products, J. Chem. Tech. Biotechnol., 77 (2002) 3, 352-360, 0268-2575.

[19] Fernandez – Pereira, C. et al.; Application of biomass gasification fly ash for brick manufacturing, Fuel, 90 (2011), 220-232, 0016-2361.

REDUCING THE RISK OF THERMAL CRACKING IN CEMENTITIOUS MATERIALS BY MEANS OF ENCAPSULATED PHASE-CHANGE MATERIALS

Didier Snoeck[1], Nele De Belie[2]

[1] Ghent University, Faculty of Civil Engineering and Architecture, Magnel Laboratory for Concrete Research, Tech Lane Ghent Science Park, Campus A, Technologiepark-Zwijnaarde 904, 9052 Ghent, Belgium,
email: didier.snoeck@ugent.be, nele.debelie@ugent.be

SUMMARY: Nowadays, when building new sustainable constructions with cementitious materials, energy efficiency becomes of larger significance especially in terms of global warming. The thermal insulation is hereby of utmost importance and the end-user wants a high and efficient thermal comfort. Concrete, having a high thermal mass, should and can be optimized in terms of heat capacity. Encapsulated Phase-Change Materials (PCMs) could be used for this purpose. PCM-mortars expand the thermal comfort in buildings. They store the heat during hot periods and release their stored heat during colder periods. This leads to a more gradual temperature feeling in buildings, increasing the experienced thermal comfort. PCMs can reduce energy consumption in buildings due to their thermal energy storage capability. In this paper, the effects of PCMs on the fresh properties, strength and thermal properties of mortar were studied. PCMs do not impair workability but they delay setting and reduce the strength, especially when high amounts (more than three mass percentage of cement weight) are added to the mortar. But the strength suffices for most concrete applications. Furthermore – as a proof of concept – the influences on the thermal properties and thermal cracking of insulated concrete sandwich panels were studied. Different PCMs with varying melting points of paraffin were hereby studied. PCMs reduce thermal strains due to their heat storage and thus counteract thermal cracking. They are innovative and promising materials to be used in future applications of civil constructions to promote thermal comfort and to reduce the risk of thermal cracking.

SMANJENJE RIZIKA TOPLINSKOG RASPUCAVANJA CEMENTNIH MATERIJALA S POMOĆU FAZNO PROMJENJIVIH MATERIJALA

SAŽETAK: Danas, kad se grade nove održive građevine, energetska učinkovitost postaje sve važnija, posebno u svjetlu globalnog zagrijavanja. Toplinska izolacija ima najveću važnost, a krajnji korisnik želi visok i učinkovit toplinski komfor. Beton koji ima veliku toplinsku masu treba se i može se optimirati na toplinski kapacitet. U tu svrhu mogu se upotrijebiti fazno promjenjivi materijali (engl. phase-change materials, PCM). Mortovi s PCM-om povećavaju toplinski komfor u zgradama. Oni zadržavaju toplinu u toplim razdobljima, a otpuštaju ju u hladnijim razdobljima. To rezultira u stupnjevitom osjećaju temperature u zgradama povećavajući doživljeni toplinski komfor. PCM-i mogu smanjiti potrošnju energije u zgradama zbog svoje sposobnosti zadržavanja ("skladištenja") toplinske energije. U radu su istraženi učinci PCM-a na svojstva svježeg i očvrsnulog morta i njegova toplinska svojstva. PCM-i ne utječu na obradivost, ali usporavaju vezivanje i smanjuju čvrstoću, posebno ako se mortu dodaju veće količine (više od tri masena postotka na težinu cementa). No čvrstoća zadovoljava za većinu primjena u betonu. Nadalje, radi dokazivanja ove ideje proučavan je utjecaj na toplinska svojstva i toplinsko raspucavanje izoliranih betonskih sendvič panela. Proučeni su različiti PCM-i s različitim talištima parafina. PCM-i smanjuju toplinske deformacije zbog zadržane topline i stoga smanjuju toplinsko raspucavanje. To su inovativni i obećavajući materijali za buduće primjene u građevinarstvu, jer nude poboljšani toplinski komfor i smanjenje rizika od toplinskog raspucavanja.

1. INTRODUCTION

Energy-efficient building technologies are becoming more and more important and focus on increasing the energy efficiency and optimizing the thermal comfort. Construction materials with a large thermal mass, such as concrete, can and should be optimized to increase the energy efficiency and the overall thermal comfort. Outdoor heat can be used and its ingress can be delayed in time by using so-called Phase-Change Materials (PCMs) [1-6]. In this paper, we studied encapsulated PCMs, spherical in form and size. By using these PCMs, the thermal comfort can be increased.

Encapsulated PCMs are made by stirring an emulsion of hot water and paraffin. In next step, monomers and a possible reaction initiator are added. In this way, particles with a paraffin core and polymer shell from polymethylmethacrylate (PMMA) or melamine formaldehyde (MF) are made. By spray-drying these particles, a dry powder is produced. The paraffin plays an important role in the thermal behavior of the PCM. It is able to absorb and release a high amount of thermal energy upon solid-liquid and liquid-solid phase change, respectively. It thus may delay and flatten the increase in temperature during hot periods and may release its stored heat upon cooling during colder periods of time. The general principle is to use a PCM with a phase-change temperature of 1 - 3 °C above the average room temperature, which should be ideal to obtain optimal thermal comfort with possible direct energy savings of 5 - 20% [7].

Aside from this very interesting and positive feature of PCMs, they also possess a negative influence. They may decrease the overall mechanical properties of cementitious materials [8, 9]. In the latter research [9], two different techniques of PCM addition are studied. One is by replacing part of the small aggregates by the same mass of PCMs and the second by addition of PCMs on top. Replacing part of the sand led to less influence on the mechanical properties, as could be expected. They found reductions of 9, 15, 17 and 26% in compressive strength with respectively 5, 10, 15 and 20 % by volume (v%) of encapsulated PCM when using the replacement method. In case of the addition method 24, 40, 38 and 42% reductions in compressive strength were obtained, respectively. The higher decrease is due to the higher amount of small particles and partially due to the decrease in relative amount of cement per cubic meter of concrete. Hunger et al. [8] found a decrease of 29.5 % for 1 weight percentage of total weight (w%) of encapsulated PCM added and an additional 13% for each additional w% of encapsulated PCM added on top.

In this paper, commercially available encapsulated PCMs are studied on their influences on the mechanical properties. The effects on the fresh properties are studied as well as they are interesting from practical point of view. The PCMs were also applied in a practical case with insulated concrete sandwich wall panels. Here, due to differences in temperature, the wall elements tend to bend which causes high tensile stresses and thus also possible cracks in the outer panels. This is not desired and should be overcome as potentially harmful substances may start to deteriorate the concrete [10-12]. PCMs could be used to limit the thermal strains due to temperature variations as they may store part of the heat in their phase-change system.

2. MATERIALS AND METHODS

2.1. TYPES OF PHASE-CHANGE MATERIALS (PCMS)

Five commercial types of encapsulated PCMs were studied. These included Micronal DS 5039 X, Micronal DS 5040 X, Mikrathermic D18, Mikrathermic D24 and Mikrathermic D28. The Micronal PCMs were received from BASF (Germany) and had a PMMA shell and the Mikrathermic PCMs with a MF shell from Devan Chemicals NV (Portugal). All encapsulated PCMs are micro-encapsulated paraffin: 85 - 90 w% PCM and 10 - 15 w% polymer shell. The Micronal DS 5039 X microcapsules were dispersed in water and the other PCMs were powders. Their size, melting point and heat of fusion as found by means of Differential Scanning Calorimetry (DSC) are shown in Table 1. Differential Scanning Calorimetry (DSC) with a DSC Q2000 was used to verify the melting points and to determine the latent heat storage capacity within the encapsulated PCMs around the melting point.

Table 1 Different encapsulated PCMs with their size, melting point and heat of fusion

PCM	Size [µm]	Melting point [°C]	Heat of fusion [J/g]
Micronal® DS 5039 X	50-300	23.3	88.1
Micronal® DS 5040 X	50-300	23.3	88.1
Mikrathermic D18	17-22	18.1	177.2
Mikrathermic D24	17-22	23.3	134.3
Mikrathermic D28	17-22	28.3	161.3

2.2. MIXING PROCEDURE, CASTING AND MECHANICAL PROPERTIES

A mortar with a water-to-cement ratio of 0.50 by mass was used and composed of Portland cement (CEM I 52.5 N) (510 kg/m³), silica sand 0/2 (1530 kg/m³) and water (255 kg/m³). The ingredients were mixed according to the EN 196-1 Standard. A varying mass percentage (m%), in terms of the cement mass, of encapsulated PCM was added on top to the composition at the end of the mixing process, in order not to damage the capsules too much. After mixing, the flow value was determined following the EN 12350-5 Standard. After casting, the specimens were stored at 20 ± 2°C and a relative humidity of 95 ± 5%. At an age of 28 days, the mechanical characteristics were determined by means of a three-point-bending test and a compressive strength test following the Standard EN 196-1 on three specimens (40 × 40 × 160 mm³).

2.3. PRACTICAL APPLICATION: INSULATED SANDWICH PANELS

The temperature profiles in small insulated mortar sandwich panels were studied. They had an interior cladding of 90 mm, PU insulation of 50 mm and an external cladding of 60 mm. The width and the length of the tested samples were approximately 200 and 300 mm. Reinforcements were placed in the inner and outer panel (Ø 8 mm and mesh size 150 mm), as can be seen in Figure 1. Encapsulated PCMs were added in an amount of 3 kg per square meter encapsulated PCM. This amount is typically used in thermal applications [1]. This corresponds to approximately 5 m% encapsulated PCM. Thermocouples were put at the outer surfaces and the boundaries with the insulation. The strains in horizontal and vertical direction were also monitored in time at the interior and exterior surface. The specimen was put in an oven as replacement of the oven door and insulation was put around the specimen to ensure a uniform heat transfer through the specimen. The oven was put at 50°C. The dimensions and setup are shown in Figure 1.

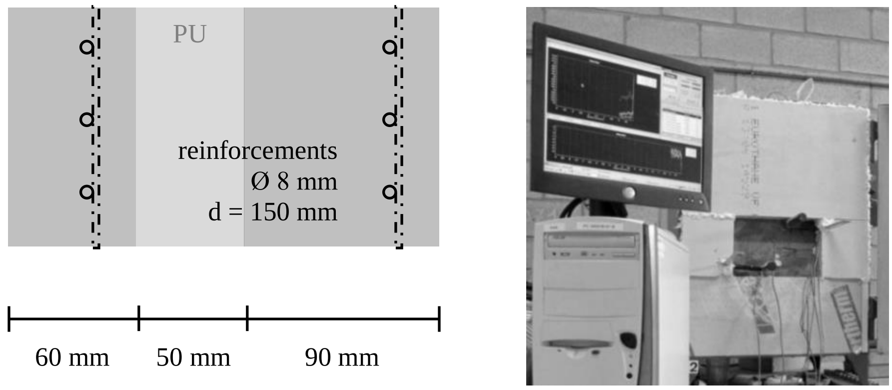

Figure 1 Dimensions (left) and test setup (right) of the insulated sandwich panel test

3. RESULTS

3.1. FRESH PROPERTIES

When investigating the workability upon casting (Figure 2), it is obvious that the addition of encapsulated PCMs reduces the flow values. The reduction, however, is acceptable up to 5 m% of encapsulated PCM addition. From practical point of view, one should limit the amount of PCMs to this value. Additional mixing water could be added to maintain the workability of mortar with PCM addition. However, by doing so, one would change the water-to-cement ratio, which is unwanted in consideration of the strength tests and microstructural properties. Another solution would be to use a superplasticizer, but this would influence the setting properties. Therefore, in this study, no alteration was made in the amount of used mixing water.

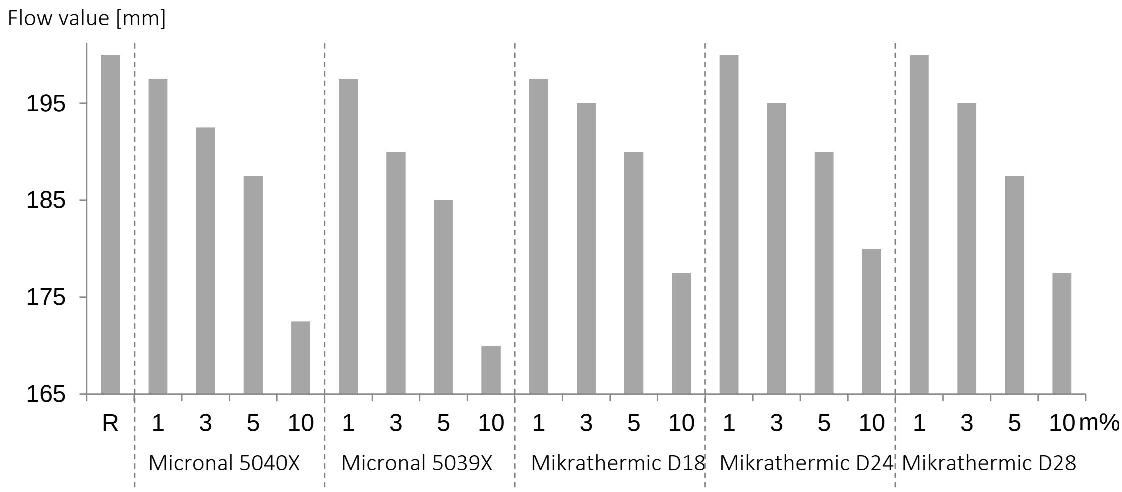

Figure 2 Workability (flow values) of samples with and without encapsulated PCMs

If one used a dispersed PCM, i.e. the Micronal DS 5039X, the workability was lower. As the amount of mixing water was reduced to counteract the fact that the dispersed solution also had water included, the overall workability was lower. This is due to the clogging of PCMs upon mixing due to the high viscosity of the Micronal DS 5039X. Part of the dispersion water is therefore trapped in between different PCM particles. In practical point of view, one should always use dry PCMs for their good dispersion in the cementitious matrix. This dispersion was also verified by breaking open the samples. Single PCMs were found and in case of the dispersed PCMs, some cluster formation of the PCMs was seen. This is unwanted as the interior PCMs will not be exposed to the heat as efficiently as the exterior PCMs. This may lead to a less positive influence of the PCMs in terms of absorbing the heat and thus the overall thermal comfort.

3.2. MECHANICAL PROPERTIES

The mechanical properties, especially flexural and compressive strength were studied, as can be seen in Figure 3. The overall trend in flexural strength is a reduction upon addition of PCMs. As the effective cross-sectional area of the samples is reduced, the flexural strength is lower. But, overall, it was found that the results were not significantly different from one another. In case of the compressive strength, the decrease is significant and larger when higher amounts of encapsulated PCMs are added. Again, the dispersed PCM proved to be less practical as a high reduction in strength was found. Furthermore, compared to the larger Micronal DS 5040X, the smaller Mikrathermic D PCMs behaved better considering the compressive strength of the mortar. The smaller PCMs are less influencing the strength due to their size. Furthermore, the reduction in compressive strength is in accordance with the results found in literature [8, 9]. For example, Hunger et al. [8] found a decrease of 29.5 % for 1 w% versus total weight (7.8 m% versus cement mass) of encapsulated PCM added and an additional 13 % for each w% of encapsulated PCM added on top. This value (29.5 % for 7.8 m%) seems to be of the same order of magnitude as the result found in this research (27 % for 5 m%).

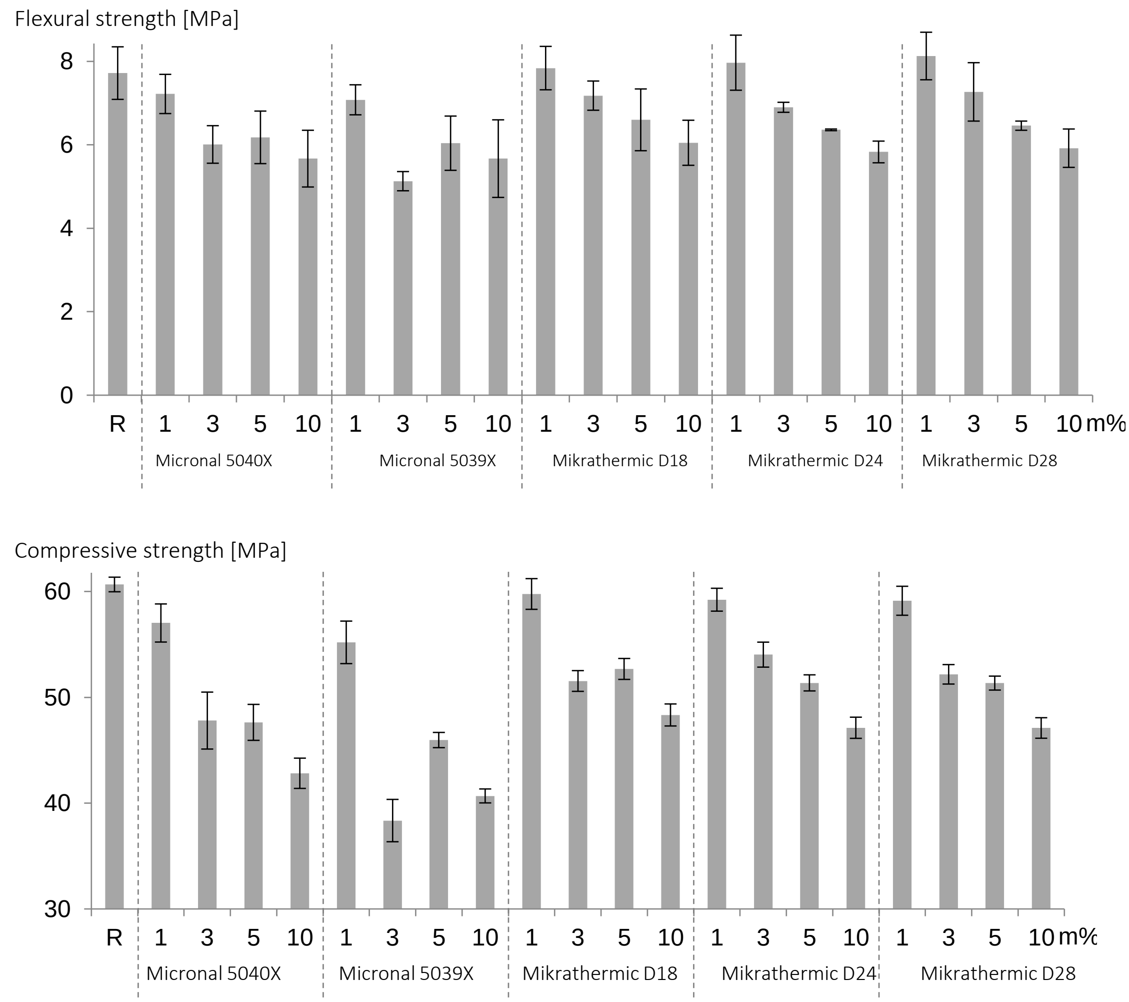

Figure 3 Mechanical properties of samples with and without encapsulated PCMs, with averages and standard deviations on single results

3.3. THERMAL PROPERTIES AND INSULATED SANDWICH PANELS

Generally, when heating and cooling mortar samples with and without PCMs, a typical thermal behavior was obtained. The delay upon cooling due to the encapsulated PCMs was clearly visible and the energy stored in the prisms was released more slowly if cooling is applied. Upon heating, it was the other way around; a delay in increase of temperature as could be expected. The biggest effect was seen with Mikrathermic D18, followed by Micronal DS 5039X, Mikrathermic D24, Micronal DS 5040X and Mikrathermic D28 which showed the smallest effect upon heating. Upon cooling the samples behaved inconsistently. There, in order of decreasing influence can be listed: Mikrathermic D28, Micronal DS 5040X, Mikrathermic D24, D18 and Micronal DS 5039X.

The insulated sandwich panels were heated till 50°C, and the temperature profiles at different times are shown in Figure 4. Again, it was found that encapsulated PCMs delayed the temperature changes. They also increased the heat capacity as they lowered the thermal conductivity. As this is only the case for PCM specimens, the heat in reference panels increased considerably, especially the temperature between the outer panel and the insulation itself. There were no significant temperature differences for the temperatures at the exterior of the inner panel, as was expected. But, as the average temperature gradient in the reference samples was higher compared to the specimens with PCMs, one can expect higher failure probability when using the reference panels. The reference wall elements tend to bend which causes high tensile stresses and thus also possible cracks in the outer panels. This cracking should be counteracted and the use of PCMs seems promising.

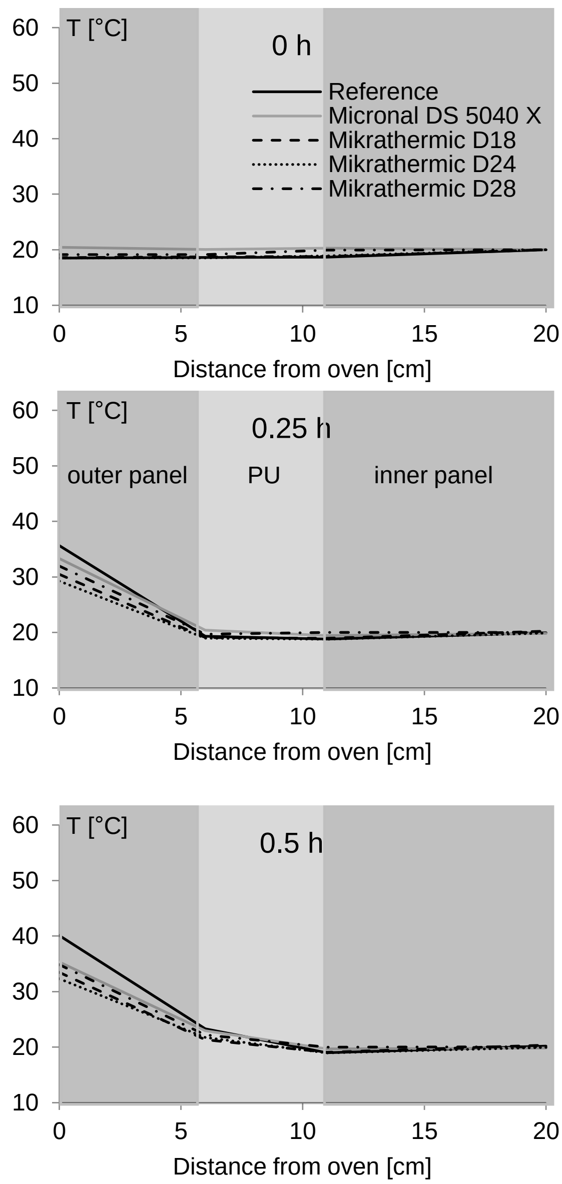

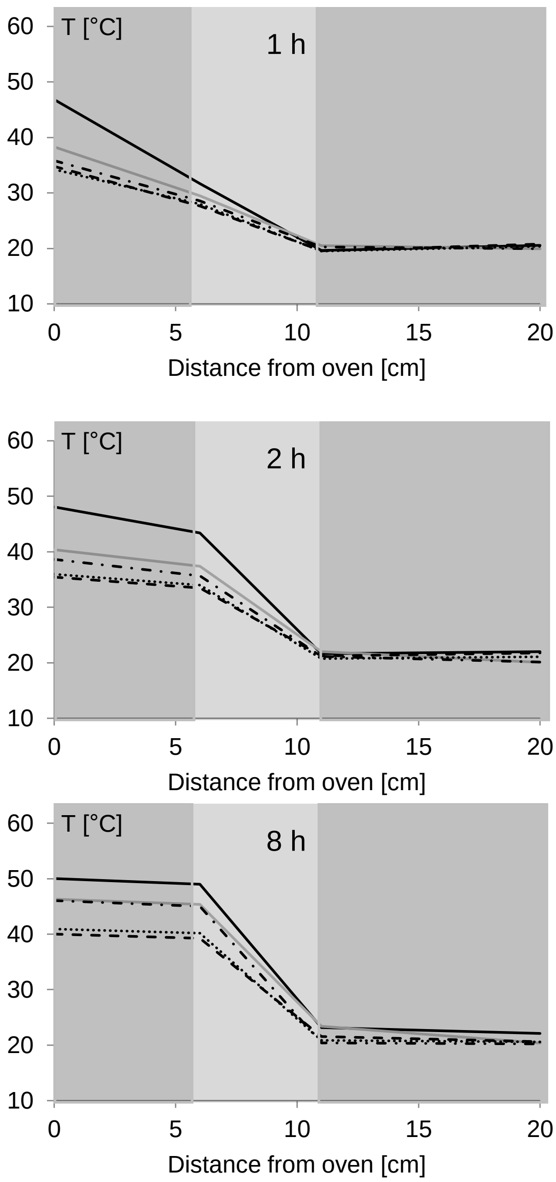

Figure 4 Temperature distribution in insulated sandwich panels with and without encapsulated PCMs

The best performance is found with Mikrathermic D18, followed by Mikrathermic D24 and Mikrathermic D28 and Micronal DS 5040X. As the melting temperature of Mikrathermic D28 particles is higher, they only become active after a certain period, and thus have a limited effect in terms of thermal properties. They can, however, be interesting in other countries or practical applications where the ambient temperature is expected to be higher. The high heat storage of Mikrathermic D18, as shown in Table 1, explains the best behavior. The reason why the Micronal DS 5040X behaves less in a larger specimen could be explained by the difference in particle size. As the particles are bigger compared to the Mikrathermic D type PCM, the heat flow may run in between the less well-distributed encapsulated PCMs, thus not decreasing the thermal conductivity as good as compared to the Mikrathermic types. The latter thus are better distributed in the matrix and can store the heat in an efficient way. Furthermore, when using small encapsulated PCMs, the overall surface area of PCM exposed to the cementitious matrix is higher, explaining the overall better behavior in terms of heat storage transfer and capacity. The heat is stored more quickly in the small PCMs compared to the larger ones.

The same trend as for the thermal behavior is found when simultaneously measuring the strains both in the vertical and horizontal directions at both faces of the sandwich panel. The directions of strain measurement did not show any differences in strains. This was expected as the panels are able to move and deform freely in every direction. The measurement therefore served as proof of concept of the measurement itself. During heating, a reference panel showed 140 µm/m strain, the panel with Micronal DS 5040X 117 µm/m, the panel with Mikrathermic D28 106 µm/m, the panel with Mikrathermic D18 84 µm/m and panel with Mikrathermic D24 only 80 µm/m strain. The accuracy of the strain gauges was approximately 1 µm/m. As expected, this confirms the previous conclusions.

4. CONCLUSIONS

The encapsulated PCMs were homogenously dispersed in mortar and the reduction of workability is acceptable up to 5 m% of PCM addition. Practically, dry PCMs are preferred for adding to mortar.

The mechanical properties and especially the compressive strength decreased significantly. The amount of PCM addition should be limited to 5 m% not to reduce the strength too much.

Encapsulated PCMs are suitable for increasing the thermal comfort in buildings if cooling happens daily, thus giving the encapsulated PCMs the opportunity to release their stored heat. Encapsulated PCMs lead to lower thermal conductivity and increased heat capacity of a concrete structure. They improve the thermal performance of concrete and therefore may save energy.

Encapsulated PCMs are promising materials to use in sandwich panels as they delay the temperature rise and, by doing so, decrease the resulting stresses and strains. They thus may reduce thermal cracking.

ACKNOWLEDGMENTS

As a Postdoctoral Research Fellow of the Research Foundation-Flanders (FWO-Vlaanderen), D. Snoeck wants to thank the foundation for the financial support. The authors would also like to thank BASF and Devan Chemicals NV for providing the PCM samples.

REFERENCES

[1] Baetens, R.; Jelle, B.P.; Gustavsend, A.: Phase change materials for building applications: A state-of-the-art review, *Energy and Buildings*, 42 (2010) 9, pp. 1361-1368, 0378-7788

[2] Bentz, D.P.; Turpin, R.: Potential applications of phase change materials in concrete technology, *Cement and Concrete Composites*, 29 (2007) 7, pp. 527-532, 0958-9465

[3] Delgado, M.; Lázaro, A.;Mazo, J.; Zalba, B.: Review on phase change material emulsions and microencapsulated phase change material slurries: Materials, heat transfer studies and applications, *Renewable and Sustainable Energy Reviews*, 16 (2012) 1, pp. 253-273, 1364-0321

[4] Mehling, H.; Cabeza, L.F.: *Heat and cold storage with PCM: An up to date introduction into basics and applications*, Springer, 978-3-540-68557-9, Berlin, (2008)

[5] Snoeck, D.; Priem, P.; Dubruel, P.; De Belie, N.: Encapsulated Phase-Change Materials as additives in cementitious materials to promote thermal comfort in concrete constructions, *Materials and Structures*, 49 (2015) 1, pp. 225-239, 1359-5997

[6] Zalba, B.; Marín, J.M.; Cabeza, L.F.; Mehling, H.: Review on thermal energy storage with phase change: materials, heat transfer analysis and applications, *Applied Thermal Engineering*, 23 (2003) 3, pp. 251-283, 1359-4311

[7] Peippo, K.; Hauranen, P.; Lund, P.D.: A multicomponent PCM wall optimized for passive solar heating, *Energy and Buildings*, 17 (1991) 4, pp. 259-270, 0378-7788

[8] Hunger, M.; Entrop, A.G.; Mandilaras, I.; Brouwers, H.J.H.; Founti, M.: The behavior of self-compacting concrete containing micro-encapsulated phase change materials, *Cement and Concrete Composites*, 31 (2009) 10, pp. 731-743, 0958-9465

[9] Meshgin, P.; Xi, Y.: Effect of phase change materials on properties of concrete, *ACI Materials Journal*, 109 (2012) 1, pp. 71-80, 0889-325X

[10] Snoeck, D.: *Self-Healing and Microstructure of Cementitious Materials with Microfibres and Superabsorbent Polymers*, Ghent University, 978-90-8578-845-4, Ghent, (2015)

[11] Snoeck, D.; Steuperaert, S.; Van Tittelboom, K.; Dubruel, P.; De Belie, N.: Visualization of water penetration in cementitious materials with superabsorbent polymers by means of neutron radiography, *Cement and Concrete Research*, 42 (2012) 8, pp. 1113-1121, 0008-8846

[12] D. Snoeck, K. Van Tittelboom, S. Steuperaert, P. Dubruel, N. De Belie, Self-healing cementitious materials by the combination of microfibres and superabsorbent polymers, *Journal of Intelligent Material Systems and Structures*, 25 (2014) 1, pp. 13-24, 1045-389X

NEWLY DEVELOPED NCC BASED THERMAL INSULATION BRIMEE

Sabina Jordan[1], Mihael Ramsak[1]

[1] Slovenian National Building and Civil Engineering Institute, Department for Building Physics, Dimiceva ulica 12, 1000 Ljubljana, Slovenia, email: sabina.jordan@zag.si, mihael.ramsak@zag.si

SUMMARY: A new thermal insulation material based on a Nano-Crystalline Cellulose (NCC) foam derived from renewable resources has been developed as a part of the research project BRIMEE. The source for the NCC material is industrial waste from pulp and paper production. The construction products have to meet basic requirements for construction works. Therefore, it is of great importance to carry out the characterisation of the material already in stage of its development. In BRIMEE project the early categorization includes basic thermal and noise protection performance testing. The analyses of the conducted measurements have shown good results and the potential for the usage of this material in the construction sector. However, more tests will be needed to demonstrate compliance with all requirements.

NOVORAZVIJENA TOPLINSKA IZOLACIJA NA OSNOVI NANOKRISTALNE CELULOZE U OKVIRU PROJEKTA BRIMEE

SAŽETAK: U okviru istraživačkog projekta BRIMEE stvoren je novi toplinskoizolacijski materijal na osnovi nanokristalne celulozne pjene iz obnovljivih izvora. Izvor tog materijala je industrijski otpad iz proizvodnje pulpe i papira. Građevni proizvodi moraju ispuniti temeljne zahtjeve za građevinu. Stoga je od velike važnosti provesti karakterizaciju materijala već u fazi njegova razvoja. U projektu BRIMEE rana kategorizacija obuhavaća ispitivanje osnovnih toplinskih svojstava i svojstava zaštite od buke. Analize provedenih mjerenja pokazale su dobre rezultate i potencijal upotrebe tog materijala u području gradnje. Međutim, za dokazivanje sukladnosti sa svim zahtjevima bit će potrebno više ispitivanja.

1. INTRODUCTION

One of the main challenge of nowadays research and development activities in the field of construction sector lies in the achievement of low-energy buildings with the goal of being at the same time also sustainable. Sustainable buildings are focusing on energy, economic and environmental aspect with the main aim to provide healthy, comfortable, accessible and safe indoor environment for the users. Therefore, the reduction of the energy demand of the buildings through the use of materials with excellent thermal properties remains an important task for European designers and the producers.

Nevertheless the market-oriented product for thermal insulation of buildings should demonstrate also the durable thermal performance. Equally important are its other properties such as degradation or shrinkage and safety during handling and installation. Today's product must necessarily also be cost effective and must not pollute the indoor environment when installed into the building. Its environmental impact has to be proven through Life Cycle Assessment (LCA) analysis. Therefore, the successful development of new insulation materials based on renewables will be a significant step towards the realisation of healthy, environmentally friendly and energy efficient buildings. These materials must demonstrate better performances compared to the currently available insulation products.

2. DEVELOPMENT OF NEW MATERIAL

2.1. RESEARCH WORK IN PROJECT BRIMEE

In European research project BRIMEE [1] a new thermal insulation material derived from renewable resources has been developed. BRIMEE is a project co-funded by the 7th framework programme of the European Union under Grant Agreement 608910 (2013-2017). The consortium involves 14 partners from 10 European countries (**Error! Reference source not found.**).

Figure 1 BRIMEE consortium of 14 partners from 10 European countries

The main objective of the BRIMEE project was the development of a new generation of insulation material to improve energy performance of the buildings without emitting harmful substances. The material solutions developed within BRIMEE are based on a Nano-Crystalline Cellulose (NCC) foam, which can be strengthened with different bio-based resins. The source for the NCC material is industrial waste from pulp and paper production (**Error! Reference source not found.**), available across EU-27 and being today an environmental issue for paper mills. BRIMEE product is applicable for the envelope and interior partitions of both new and existing buildings. Thus most of the impact is represented by buildings requiring retrofitting.

Figure 2 Industrial waste from pulp and paper production, serving as resource material for BRIMEE NCC foam

Process for producing NCC foam insulation panel of BRIMEE is based on three steps: mechanical and chemical process of industrial streams carrying cellulose to obtain NCC. The second step includes processing the NCC in aqueous solution with the functional resins. The last step, which is structured from particular phases (**Error! Reference source not found.**), represents foaming and consolidation process of the mixture for achieving the insulation panel.

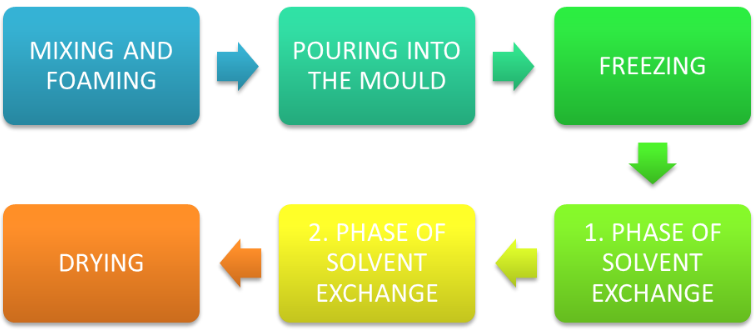

Figure 3 Individual phases of the third step of process for producing the BRIMEE NCC foam insulation panel

2.2. REQUIREMENTS FOR CONSTRUCTION PRODUCTS

Construction products must be fit for their intended use, taking into account in particular the health and safety of persons involved through its entire life cycle. To be used in constructional sector, the construction products have to meet basic requirements for construction works [2], which are: 1. Mechanical resistance and stability, 2. Safety in case of fire, 3. Hygiene, health and the environment, 4. Safety and accessibility in use, 5. Protection against noise, 6. Energy economy and heat retention and 7. Sustainable use of natural resources. Only construction products which are in compliance with these requirements can be placed on the market. Therefore, all these materials and products have to be tested according to methods set up in the prescribed standards. The certificate of the test result and in specific cases also the classification provides a basis for the use of the material or product. However, the first thing that needs to be done already in the phase of development of the construction material or product is the characterisation of the samples according to standard measurement methodologies.

According to intended use of BRIMEE NCC foam these activities among others involve the measurement of thermal conductivity and the testing and analysis of acoustic characteristics. For BRIMEE project the above mentioned measurements, testing and analyses were performed in the Laboratory for Thermal Performance and Acoustics of the Department for Building Physics, at Slovenian National Building and Civil Engineering Institute (ZAG), in Ljubljana. The procedure comprises measurement of thermal conductivity and the measurement of sound absorption coefficient, the analysis of the results and the assessment of the performance. The activities were performed on two types of samples developed throughout the project (**Error! Reference source not found.**).

Figure 4 Different BRIMEE samples developed in the project and prepared for the laboratory testing

3. CHARACTERISATION OF BRIMEE MATERIAL

3.1. THERMAL PERFORMANCE CHARACTERISATION

The testing of thermal conductivity of the BRIMEE samples was done according to standard measurement methodology described in SIST EN 12667: 2002, the heat flow method type. The experimental setup here was a heat flow meter (HFM) apparatus with the single specimen configuration (**Error! Reference source not found.**).

Figure 5 Heat flow meter (HFM) apparatus with the single specimen configuration for measuring medium sized samples

The apparatus is intended to establish a unidirectional constant and uniform density of the heat flow rate. It is therefore divided into a central metering section in which the measurements are taken, and a surrounding guard section. It has the fluid tempered hot and cold side and operates at small temperature difference across the specimen with the mean temperature approximately 10-12 °C. The full size of the specimen in this setup can be 800 x 800 mm. Due to sample size, which was roughly 250 X 350 mm, the HFM apparatus was not fully covered with the sample. The metering area itself was, however, fully covered with the sample and the sufficient guard was provided. During the test the specimen was installed horizontally. Temperature difference was measured with T-type thermocouples. The heat flux was measured with 2 calibrated heat flux meters, installed in the machine and placed against the specimen. The thermal resistance of specimen is calculated from measured density of heat flow rate, the metering area of specimen and the temperature difference. The thermal conductivity of the measured specimen is then calculated from the thermal resistance and the thickness of the specimen.

The measurements were conducted in the laboratory under controlled air temperature and humidity conditions. Samples were subjected to laboratory conditioning more than 7 days. Measurements for determining the thermal conductivity were carried out on five samples from the first batch and three samples from the second batch delivered to the laboratory. The samples were in form of small sized lightweight plates. The apparent density of the first batch of the samples was 89.9 kg/m^3, while the second was 55.8 kg/m^3. The averaged thickness was 9.1 mm and 8.8 mm, respectively.

For the first BRIMEE samples the measurements results showed quite diversified thermal conductivity; their calculated average was 0,041 W/mK. Though, the results of the measurements on the next batch of the BRIMEE samples were much better: the average for the measured thermal conductivity was 0,035 W/mK (**Error! Reference source not found.**).

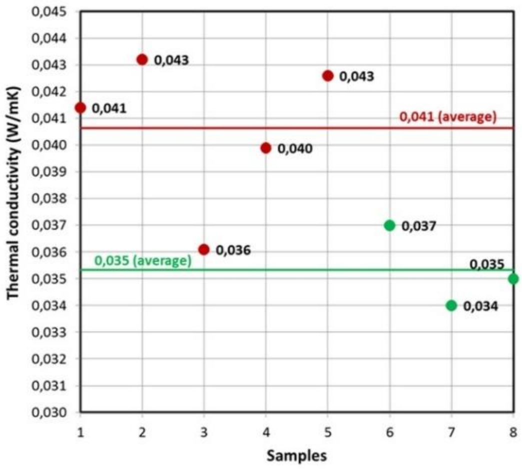

Figure 6 Graphical presentation of the measured values for thermal conductivity on two batches of BRIMEE samples and the calculated averages

3.2. CHARACTERISATION OF NOISE PROTECTION

Testing and analysis of the acoustic characterisation of the samples was done according to standard measurement methodology SIST EN ISO 10534-1: 2002. This comprises laboratory measurement of sound absorption coefficient on the pre-treated samples, the round pieces with the diameter 88 mm and 36 mm that were cut from the delivered BRIMEE plates (**Error! Reference source not found.**).

Figure 7 Round samples for laboratory measurement of sound absorption coefficient

Measurement method, the determination of sound absorption coefficient in impedance tube using standing wave ratio, is as follows: the samples are inserted into the impedance tubes in such a way that there is no air gap between the base surface of cylindrical samples and the bottom of the tube.

Two impedance tubes, made of 4 mm thick steel, were used. The first one is the 100 cm long impedance tube with a diameter of 88 mm for measuring in the frequency region between the third-octave band 250 Hz and the third octave band 1000 Hz. With the 28 cm long impedance tube and the diameter of 36 mm the measurement in the frequency region between the third-octave band 1250 Hz and the third-octave band 5000 Hz can be done. Additionally, the microphone with the probe tube was used. A correction for tube attenuation has not been applied.

The measurements of sound absorption coefficients were performed on 3 samples of diameter 88 mm and 3 samples of diameter 36 mm for each batch of the material. These were the same two batches of the BRIMEE samples delivered to the laboratory for measuring the thermal conductivity. The measured values were basis for calculation of averaged sound absorption coefficients that are graphically presented on the graphs below (**Error! Reference source not found.**, **Error! Reference source not found.**).

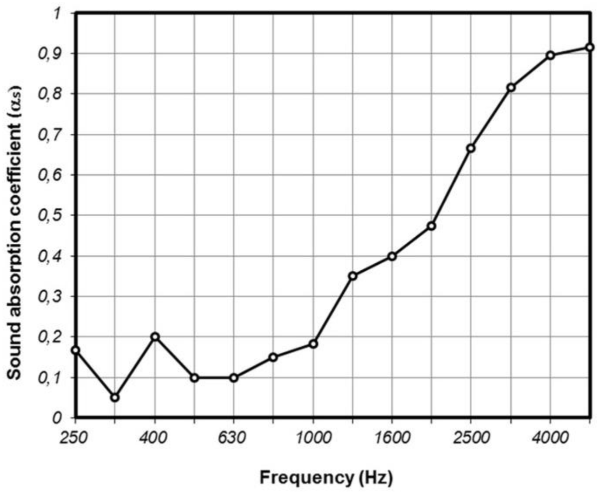

Figure 8 Graphical presentation of averaged sound absorption coefficients measured on the first batch of BRIMEE samples

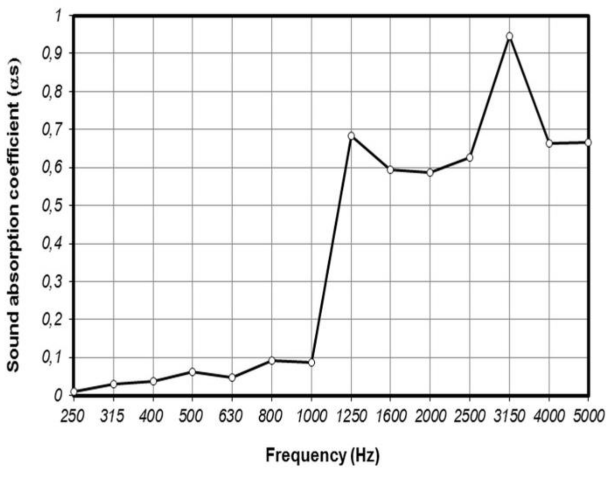

Figure 9 Graphical presentation of averaged sound absorption coefficients measured on the second batch of BRIMEE samples

The measurements of sound absorption coefficient carried out on the first batch of BRIMEE samples showed following results (**Error! Reference source not found.**): at low frequencies (between 250 and 1000 Hz) this material has quite low sound absorption coefficient, less than 20 %. The results of the measurements also showed that between 1000 and 3150 Hz the sound absorption coefficient increases strongly and reaches almost 100 % at 3150 Hz. The measurements on second batch of the BRIMEE samples showed similar results (**Error! Reference source not found.**): at low frequencies (between 250 and 1000 Hz) this material has very low sound absorption coefficient, less than 10 %. The results of the averaged acoustic measurements between 1000 and 1250 Hz showed that the sound absorption coefficient increases strongly and reaches around 60 %; at 3150 Hz the sound absorption coefficient is almost 100 %, but at higher frequencies it is again between 60 and 70 %.

4. CONCLUSIONS

Early analyses in the development of the material are extremely important. They can contribute in directing the research and can help to lead into the optimisation of the product. In this research the analysis of the results of thermal conductivity measurements on BRIMEE NCC samples showed that this material can be classified as thermal insulation product in the range of thermal insulation materials that are available on the market. In the field of protection against noise in buildings the results of sound absorption coefficient measurements indicate that BRIMEE NCC insulation material can be used in partition walls as a sound absorber in the high frequency region only.

According to the intended use of the final product and the necessity to arrive to a trade-off between the different performances, these results are representing a basis for the further development of the product, which will be compliant to all other necessary requirements, including those that fulfil the safety in case of fire.

ACKNOWLEDGMENTS

The authors are grateful for the financial support provided by the EU for the FP7 project BRIMEE (grant agreement N°608910).

REFERENCES

[1] BRIMEE, Cost-effective and sustainable Bio-Renewable Indoor Materials with high potential for customisation and creative design in Energy Efficient buildings (FP7, 2013-2017), http://www.brimee.eu/

[2] REGULATION (EU) No 305/2011 OF THE EUROPEAN PARLIAMENT AND OF THE COUNCIL laying down harmonised conditions for the marketing of construction products and repealing Council Directive 89/106/EEC, Official Journal of the European Union, (2011)

INFLUENCE OF COMPACTION PROCESS ON DENSITY AND MICRO-STRUCTURE OF HEMP SHIV PACKING

Jean-Francois Camenen[1], Vincente Picandet[1], Thibaut Lecompte[1]

[1] Université Bretagne sud, Faculty of Sciences, FRE CNRS 3744, IRDL, F-56100 Lorient, France,
email: jean-francois.camenen@univ-ubs.fr, vincent.picandet@univ-ubs.fr, thibaut.lecompte@univ-ubs.fr

SUMMARY: About 10 % of global carbon dioxide anthropogenic emissions are due to the building materials' sector in Europe. Taking into account this environmental impact, alternative materials such as bio-based materials like hemp shiv, a byproduct of hemp industry, are experiencing a quick development. In particular the use of lime and hemp concrete is increasing thanks to its thermal performances induced by the high porosity of hemp shiv. It is lighter than conventional concrete but with a low compressive strength probably due to the high flexibility of aggregates and to the particle arrangement properties. However, several methods allow improving the strength of the materials by the use of an admixture or by compaction of the fresh mixture during molding. Indeed, it is crucial to achieve a uniform solid fraction but it is difficult to identify the cause of heterogeneity induced during this process. We have to understand compressibility, friction and stress transmission mechanisms. In order to investigate this issue, the influence of several compaction methods (vibration, uniaxial compaction) on density and micro-structure properties are studied through discrete numerical simulation using the Non Smooth Contact Dynamics (NSCD) simulation platform LMGC90 (https://git-xen.lmgc.univ-montp2.fr/lmgc90). After describing the sample preparation and the simulation procedure, the present study explores their micro-mechanical properties. Thus, in order to get insight into particles arrangement, geometric anisotropy, relative mobility and orientation of the particle in the initial poured sample and during the compaction process are investigated for the various studied assemblies.

UTJECAJ PROCESA ZBIJANJA NA GUSTOĆU I MIKROSTRUKTURU PAKIRANJA ULOMAKA KONOPLJE

SAŽETAK: Oko 10 % globalnih emisija ugljičnog dioksida ljudskog podrijetla posljedica su građevinskoga sektora u Europi. Uzimajući u obzir takvo opterećenje okoliša očekuje se brzi razvoj alternativnih materijala kao što su materijali biljnoga podrijetla poput ulomaka konoplje, nusproizvoda u industriji konoplje. Posebno je u porastu upotreba betona od vapna i konoplje zahvaljujući toplinskim svojstvima prouzročenim velikom poroznošću konopljinih ulomaka. Taj je beton lakši od uobičajenoga ali ima mali tlačnu čvrstoću vjerojatno zbog velike savitljivosti agregata i granulacije čestica. Međutim, neke metode omogućuju poboljšanje čvrstoće materijala primjenom dodatnih sastojaka ili zbijanjem svježe mješavine tijekom ugradnje. Zapravo je važno postići jednolikost krute frakcije a teško je prepoznati uzrok heterogenosti tijekom tog procesa. Moraju se shvatiti mehanizmi stlačivosti, trenja i prijenosa naprezanja. Da bi se ta pitanja istražila, proučavan je utjecaj raznih metoda zbijanja (vibracijama, jednoosnim zbijanjem) na gustoću i svojstva mikrostrukture putem diskretne numeričke simulacijske platforme (programa) LMGC90 (https://git-xen.lmgc.univ-montp2.fr/lmgc90) pod nazivom Non Smooth Contact Dynamics (NSCD). Nakon opisa pripreme uzoraka i simulacijskog postupka, u radu su istražena njihova mehanička svojstva. Za različite proučavane mješavine istraživani su geometrjska anizotropija, relativna pokretljivost i orijentacija čestica u početno izlivenom uzorku i tijekom procesa zbijanja kako bi se dobio uvid u granulaciju.

1. INTRODUCTION

About 10% of global carbon dioxide anthropogenic emissions are due to the building materials' sector in Europe [1]. Taking into account this environmental impact, alternative materials such as bio-based materials like hemp shiv, a byproduct of hemp industry, are experiencing a quick development. In particular the use of lime and hemp concrete (see Figure 1) is increasing thanks to its thermal performances induced by the high porosity of hemp shiv.

It is lighter than conventional concrete but with a low compressive strength probably due to the high flexibility of aggregates and to the particle arrangement properties [2]. However, several methods allow improving the strength of the materials by the use of an admixture or by compaction of the fresh mixture during moulding. Indeed, it is crucial to achieve a uniform solid fraction but it is difficult to identify the cause of heterogeneity induced during this process: amongst them, compaction method (vibration, uniaxial compaction) and particle size distribution have an important influence. In this contribution, density and micro-structure properties are investigated in the sample whereas particles are poured in the mould. In this first step of compaction process, the intention is to focus on particles arrangement, geometric anisotropy, relative mobility and orientation of the particle. Details of numerical simulation and control parameters are given first, followed by the study of the influence of polydispersity.

Figure 1 hemp concrete sample

2. NUMERICAL MODEL

2.1. PARTICLE

Hemp shiv particles are modelled by convex rigid polyhedra of mass density 100 Kg/m^3 [3] comprised of eight vertices, fourteen edges and eight faces as shown on Figure 2. As explained elsewhere [4, 5], this geometry has three planes of symmetry and is determined by four parameters, length L, width G, height E (L ≥ G ≥ E) and angle α set to 60°. Alternatively, it may be determined by its characteristic dimension d such as $d^2 = G^2 + L^2$, corresponding to the diameter of its circumscribed sphere, supplemented with its aspect ratios L/G and G/E. Hemp shiv particles diameter d follows log-normal distribution. The large range between d_{min} and d_{max} is difficult to handle for detection algorithm. Therefore, in the present study, monodisperse sample containing the particle configuration with L/G=4 and G/E=6 mimicking the needle shape of hemp shiv particles is considered. Nevertheless, in order to highlight possible effect of polydispersity, bidisperse sample is built with 10%, 25% and 50% (proportion by number) of particles with L/G=2 and G/E=6, modelling the presence of blade shape particle [11].

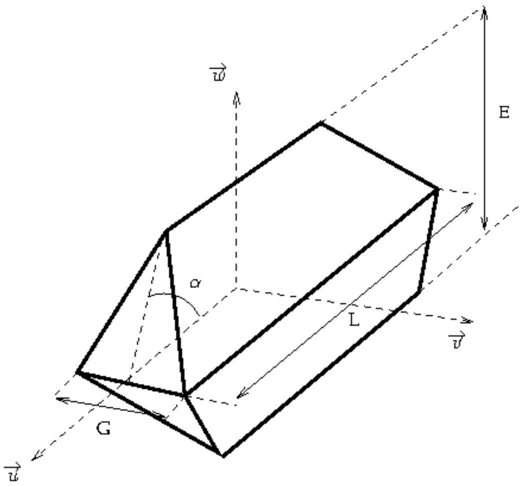

Figure 2 model polyhedron characterised by its length L, width G, height E and angle α. This polyhedron has three symmetry planes, each perpendicular to an inertia axis u , v , or w

2.2. SIMULATION PROTOCOL

The simulated systems are dense assemblies of 3000 rigid particles, interacting with each other through totally inelastic collisions. Samples have been prepared following a pluviation protocol inspired from [6] and described with details in [4, 5]: spherical shells, each circumscribed to a randomly oriented particle, are first randomly dropped inside a vertical parallelepiped container (square base, dimension 7Lx7L) and subsequently moved to the closest local minimum of potential energy; finally, the spherical shells are removed, bi-periodic boundary conditions are substituted for the container vertical walls, and gravity g is applied (see Figure 3). All simulations were performed using the Non Smooth Contact Dynamic method (NSCD) [7], which is especially convenient for large collections of rigid particles. This distinct element method (DEM), implemented in the LMGC90 Software platform [8], was successfully applied to a number of physical problems ranging from dense inertial flows [4] to quasi-static deformable packings [5]. Basically, the equations of motion of a collection of rigid particles interacting through unilateral contacts with dry friction are integrated over one time step, thus allowing to substitute velocity unknowns for acceleration, and percussion unknowns both for collisions and lasting contact forces. Percussions are parametrized using normal (e_N) and tangential (e_T) restitution coefficients as well as a sliding friction coefficient (μ).

In the present study, friction coefficient is equal to 0.75 [3]. Upon substituting complementarity relations between relative velocities and percussions for usual Signorini-Coulomb conditions, and describing each potential contact in terms of location and normal unit vector, the equations of motion are then solved at each time step by an iterative process using a non-linear Gauss-Seidel like method.

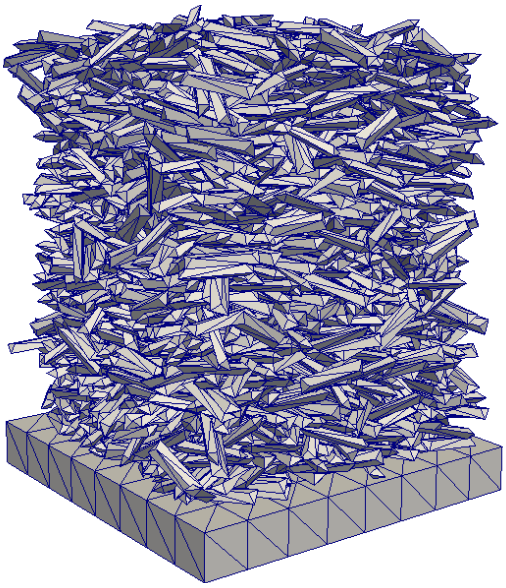

Figure 3 3D snapshot of monodisperse packing. Bi-periodic boundary conditions applied in x and y horizontal directions

3. COMPACTION PROCESS BY PLUVIATION

3.1. PACKING DENSITY AND ORIENTATION OF THE PARTICLE

Figure 4(a) illustrates density time evolution within the monodisperse and bidisperse samples. Density reaches a constant value, roughly the same at about 0.4 for both. The monodisperse sample achieves this value at 1.5 seconds, bidisperse (50%) sample at 1.25 seconds. It seems that polydispersity frustrates particle arrangement. Given their symmetry properties, particles may potentially adopt the same orientation upon aligning one or more of their inertia axes, thus conferring orientational order to the packing and influencing arrangement. To detect such an orientational order, the nematic order parameter Q^2_{00} is computed [9, 10]. Q^2_{00} assesses the highest level of alignment of a given inertia axis between all particles, either u ,v , or w (see Figure 2). This value range between 0 (no alignment) and 1 (perfect alignment). Figure 4(b) depicts time evolution of Q^2_{00} for monodisperse and bidisperse packings.

During pouring process, particle alignment is always more important within the bidisperse (50%) sample, Q^2_{00} reaching 0.725 (0.589 within the monodisperse sample). It means that the latter is more randomly packed whereas the blade shape particles (flat particles) allow the sample finds more quickly the arrangement which minimizes their potential energy.

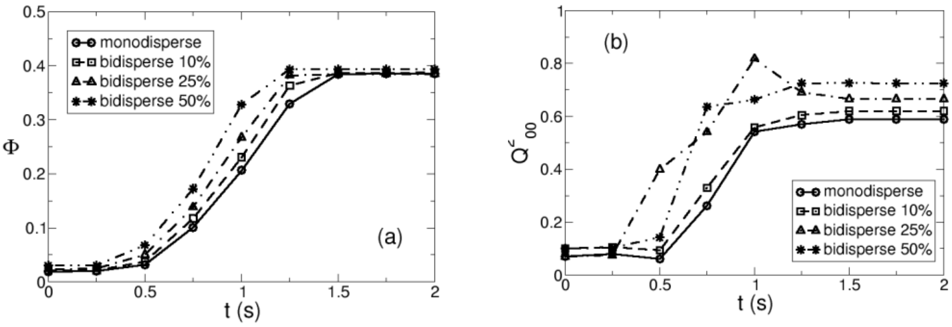

Figure 4 (a) density Φ and (b) nematic parameter order Q^2_{00} time evolution within the monodisperse and bidisperse samples

3.2. RELATIVE MOBILITY AND GEOMETRIC ANISOTROPY

In order to detect relative mobility during pouring due to particle re-arrangement, time evolution of the contacts network in the sample is investigated. Figure 5 shows time evolution of the coordination number.

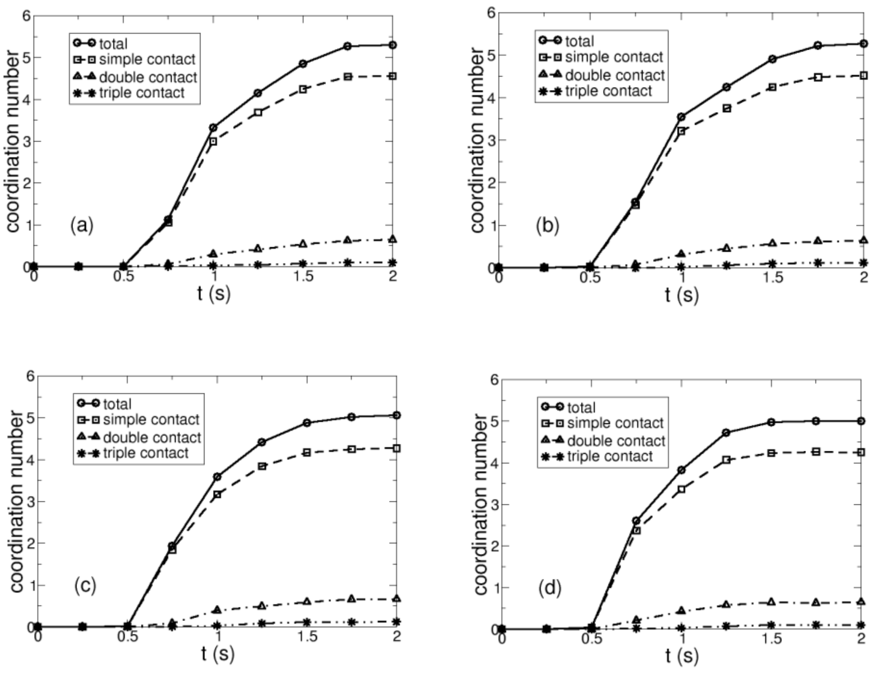

Figure 5 Coordination number time evolution within the (a) monodisperse, (b) bidisperse 10%, (c) bidisperse 25% and (d) bidisperse 50% sample

The total number reaches values between 5.3 in the monodisperse sample and 5 in the bidisperse 50%. However, this value amalgamates diverse contact types corresponding to different numbers of constraints. Indeed, upon assigning 1 constraint to each vertex-face or edge-edge contact (simple contact), 2 constraints to each edge-face contact (double contact) and 3 constraints to each face-face contact (triple contact) [20,22,32], one can define Ns, Nd and Nt as respectively, the numbers of simple, double and triple contacts. Whatever the sample and type of contact, evolution is monotonous. It doesn't allow interpreting any dynamic accident such as sudden displacement or jamming of group of particles in the sample.

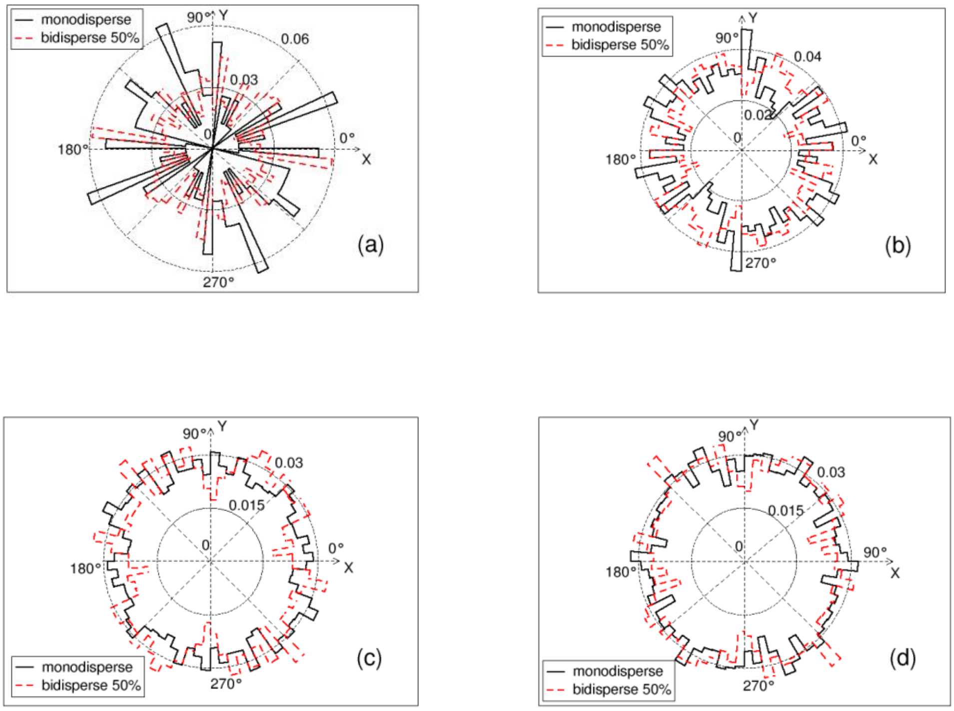

Figure 6 2D polar histogram representations of the distribution of the normal contacts for all the particles over horizontal (x–y) plane during pouring process (a) t=0.75s, (b) t=1.0s, (c) t=1.25s, and (d) t=2.0s.

Anisotropy of the distribution of contact orientations is visible at the beginning of the pluviation process and almost disappears after 1.25 seconds in the monodisperse sample (Figure 6(c)). Though we observe the same evolution in the bidisperse sample, anisotropy is weaker at the beginning (Figure 6(a)).

4. CONCLUSIONS

Monodisperse and bidisperse packings have been built by pouring rigid polyhedra into a container with periodic boundary conditions. The total inelastic collisions and friction interaction between particles were taking into account. The polydispersity effect is exhibited: on density by improving the dynamic of the compaction process; on particles arrangement by increasing orientational order within the sample which it tends towards to a less random close packing. Since size distribution is more complex, closer than a log-normal distribution, polydispersity should have been taken into account. Moreover even if other studies suggest that cubical sample of 3000 particles are relevant, we have a lack of statistics and need to investigate a possible size effect.

REFERENCES

[1] Brand, R. et al.: European pollutant emission register, Final Report, 2004
[2] Bouloc P.; Allegret, S. & Arnaud L.: Le chanvre industriel: production et utilisations, France Agricole, Paris, 2006
[3] Tronet, P. et al.: Study of lime hemp composite precasting by compaction of fresh mix — An instrumented die to measure friction and stress state, Powder Technology, Vol. (2014) No 258, pp 285-296
[4] Azéma, E. et al.: Discrete simulation of dense flows of polyhedral grains down a rough inclined plane. Phys. Rev. E, (2012) page 031303
[5] Camenen, J.F. et al.: Effect of Confinement on Dense Packings of Rigid Frictionless Spheres and Polyhedra. Phys. Rev. E, Vol. (2012) No 86, page 061317
[6] Laniel, R.: Modélisations et Caractérisations Numériques, à Différentes Echelles, d'un Géomatériau Renforcé par un Fil. PhD thesis, 2007
[7] Jean, M.: The non-smooth contact dynamics method. Computer Methods in Applied Mechanics Engineering, Vol. (1999) No 177, pp. 235–257
[8] Dubois, F. & Jean, M.: Lmgc90 : Une Plateforme de Développement Dédiée à la Modélisation des Problèmes d'Interaction. Actes du sixième colloque national en calcul des structures CSMA-AFM-LMS, Vol. 1, pp. 111–118, (2003)

[9] John, B.S.; Stroock, A. & Escobedo, F.A.: Cubatic Liquid Crystalline Behavior in a System of Hard Cuboids. Journal of Chemical Physics, Vol (2004) 120

[10] Camp, P.J. & Allen M.P.: Phase Diagram of The Hard Biaxial Ellipsoid Fluid. J. Chem. Phys., Vol. (1997) 106, pp. 6681–6688

[11] Picandet, V., Tronet, P. & Baley, C.: Caractérisation granulométrique des chènevottes. Actes des XXXème Rencontres AUGC-IBPSA, Chambéry-Savoie, (2012)

INVESTIGATION OF THE ADDITIVES ON THE PROPERTIES OF EPS MORTAR USING RESPONSE SURFACE METHODOLOGY

Mingxu Chen[1], Lingchao Lu[1], Shuxin Zhang[1], Wenlong Zhang[1], Shoude Wang[1], Wen Zong[1], Piqi Zhao[1], Chenchen Gong[1]

[1] Shandong Provincial Key Lab. of Preparation and Measurement of Building Materials, University of Jinan, Jinan 250022, China, email: 15806612606@163.com

SUMMARY: As the essential part of mortar, the influences of the additives on the on the compressive strength, water absorption and dry density of EPS mortar are investigated by using response surface methodology (RSM), in which R2 and p-value are important evaluation parameter. In this experiment, the additives are focused on air-entraining agent (AEA), water reducing agent (WRA) and hydroxypropyl methyl cellulose ether (HPMC). The results show that every additive has significant influence on the compressive strength, water absorption and dry density of EPS mortar, which proved that RSM is effective method to optimize EPS mortar components. Based on RSM, the optimal addition range of HPMC, WRA and AEA in EPS mortar is 0.25%~0.28%, 0.5%~0.55% and 0.5%~0.55%, respectively.

ISTRAŽIVANJE UTJECAJA DODATAKA NA SVOJSTVA MORTA S EKSPANDIRANIM POLISTIRENOM PRIMJENOM METODE ODZIVNIH POVRŠINA

SAŽETAK: Kako su dodatci bitni dio morta, istraživani su njihovi utjecaji na tlačnu čvrstoću, vodoupojnost i gustoću u suhom stanju mortova s ekspandiranim polistirenom, primjenom metode odzivnih površina (engl. response surface method, RSM) u kojoj su R2 i vrijednost p važni parametri vrednovanja. U provedenim eksperimentima dodatci su bili sredstvo za uvlačenje zraka, sredstvo za smanjivanje količine vode i hidroksipropil-metil-celuzozni-eter. Rezultati pokazuju da svaki dodatak ima znatan utjecaj na tlačnu čvrstoću, vodoupojnost i gustoću u suhom stanju morta s ekspandiranim polistirenom. To dokazuje da je metoda odzivnih površina učinkovita za optimiranje sastojaka morta s ekspandiranim polistirenom. Na osnovi ispitivanja utvrđeni su optimalni rasponi svojstava takvoga morta i to 0,25 % do 0,28 % za hidroksipropil-metil-celulozni-eter, 0,5 % do 0,55 % za sredstvo za smanjenje vode i 0,5 % do 0,55 % za sredstvo za uvlačenje zraka.

1. INTRODUCTION

In recent years, the world is facing a grim situation of energy conservation and emission reduction. The building sector is known to contribute largely in total energy consumption and CO_2 emissions [1] and the external insulation technology has become one of the most direct and scientific way of energy saving [2-3]. So, the energy conservation in the preparation of insulation mortars and insulation panels with better properties (water resistance and dry density) has occurred. The cement-based insulation material can be divided into four categories (cement-based polyurethane foam insulation materials, redispersible latex powder of polystyrene insulation mortar [4-5], cement-based foam insulation materials [6], cement-based EPS/VM insulation mortar [7-8]). This case could be produced by the use of many kinds of materials, such as additives, fly ash [9], rice straw [10], wood shavings [11], paper sludge ash [12], sunflower [13], polymers electric wires [14] and rice husk ash [15]. These materials, in some cases, can improve the properties of EPS mortar to a large extent in durability, strength and dry density.

The additives in EPS mortar or concrete have become an indispensable part of production, which can improve the properties effectively. Schackow et al [16] investigated the effect of AEA on the properties of lightweight concrete with EPS and vermiculite, showing lower amount of AEA and smaller amount of lightweight aggregate provided higher compressive strength for lightweight concretes and the air entraining also influenced the decrease in density. Dong et al [17] researched the polymer modifiers on the properties of EPS mortar. It presented that the performances of water resistance and dry shrinkage for insulation mortar with redispersible latex powder were inferior to insulation mortar with emulsified asphalt. Chen et al [18] studied matrix components with low thermal conductivity and density on performances of EPS mortar using several additives, showing the HPMC can be used to improve adhesion stress between EPS particle and cement paste, and WRA was obtained to reduce water consumption.

In this paper, the EPS mortar is prepared by SAC, paper sludge, small aggregate of VM with size of several millimeters and big aggregate of EPS with high porosity consisting essentially of 98% air. Three kinds of additives were investigated to improve the properties in EPS mortars and achieve reasonable application. Also, effect of some mix design parameters (i.e., HPMC, WRA and AEA) on the performance of EPS mortar had been analyzed to employ response surface methodology, which chooses the Box–Behnken experimental design [19-20].

2. EXPERIMENTAL

2.1. MATERIALS

Sulphoaluminate cement (SAC, 42.5-grade, Shanshui Cement, CHN) was used as the cementitious material in EPS mortar, which is a type of special rapid-hardening cement. Its initial and final setting times were 9 min and 15 min, respectively. The EPS particles (Dingtai Company, CHN) were used as the coarse aggregates, with particle sizes ranging from 1.5 mm to 3.0 mm. Vitrified microsphere (Dingtai Company, CHN), with the particle size distribution of 0.15 mm to 0.5 mm, was used as the fine aggregate. The detailed properties of EPS and VM are shown in Table 1. Figure 1 shows the SEM of the insulation mortar between EPS and the cement paste. Additionally, some additives was used to improve the properties, HPMC (its viscosity was 2000Pa·s) was used to improve adhesion stress between EPS particle and cement paste, AEA (sodium dodecyl sulfate) was used to decrease the dry density of EPS mortar and WRA was obtained to reduce water consumption.

Table 1 Properties of insulation aggregate

Insulation aggregate	Particle size (mm)	Bulk Density (kg/m3)	Apparent density (kg/m3)	Thermal conductivity (W/m·K)	Water Absorption (%)
aEPS	1.5 to 3.0	17.1	4.69	0.041	—
bVM	0.15 to 0.50	120	71	0.048	38.5

[a] Expanded polystyrene (EPS), [b] Vitrified microsphere (VM)

2.2. SPECIMENS PREPARATION

The EPS mortar was prepared as follows. First, additives and water were stirred well-distributed by mortar mixer for 4min. Then, SAC was mixed with HMPC and AEA, which was added in the paste above. EPS and VM particles were added to the mortar when the mixture stirred evenly. After that, the mixture was put into 40*40*160 mm^3 moulds. It was cured at 20℃ for 24 h, and its relative humidity was 95%. At last, EPS mortar was demoulded and cured in water at 20℃ till the curing time was up to the specific age.

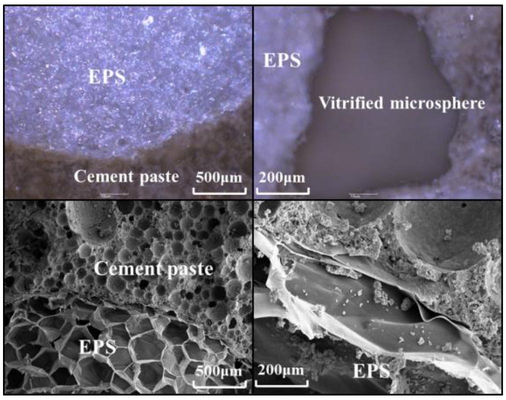

Figure 1 The SEM of insulation mortar between EPS and the cement paste

2.3. TESTING METHODS

The mechanical properties (compressive and pressure-off ratio) of CEP mortar were performed using a flexural and compressive testing machine, with a loading speed of 0.3 kN/s (CDT1305-2) and a maximum load of 300 kN. The water absorption of the EPS mortar was carried out according to JC/T 1042 [21]. The EPS mortars were kept in a vacuum drying oven at 60 °C until no changes in weight were detected. The dry specimens were completely immersed in water for 48 h until a constant weight was obtained. As a result, the softening coefficient was measured, which was the ratio of the compressive strength for the saturated mortar to the dried mortar and reflected the water resistance of the insulated mortar. Scanning electron micrograph images from a field emission scanning electron microscope (Quanta FEG 250, FEI company, USA) were used to observe the morphology of EPS mortar. The images were produced in FEI, with a resolution smaller than 1.0 nm.

3. RESULTS AND DISCUSSION

Effect of three mix design parameters (i.e., HPMC, WRA and AEA) on the properties of EPS mortar has been analyzed employing RSM, which chooses the Box–Behnken experimental design. The coefficient of determination, R^2 and R^2 adjusted, of responses are shown in Table 2, presenting that optimal R^2 values of compressive strength, softening coefficient and dry density were 90%, 97% and 86%, respectively. So, the model of quadratic was used to investigate the influence of additives on the EPS mortar. It also presents that a good degree of correlation between the measured values and predicted values of these responses has been built. In addition, parameter estimates of the model for compressive strength, softening coefficient and dry density are tabulated in Table 3. It shows that B and C (i.e. AEA and WRA) have the p-value of 0.1009 and 0.1099 for softening coefficient, A and C (i.e. HPMC and WRA) have the p-value of 0.6968 and 0.8668 for dry density, showing that these factors are not statistically significant. But, the p-value of A, B and C are found to be statistically significant for compressive strength. Therefore, A, B and C are all kept in the model.

Table 2 Coefficient of determination for the responses investigated

Response	Model	Compressive strength	Softening coefficient	Dry density
R2	Linear	0.852	0.213	0.603
	2FI	0.900	0.285	0.732
	Quadratic	0,921	0.967	0.859
R2 adjusted	Linear	0.818	0.031	0.511
	2FI	0.840	0.144	0.571
	Quadratic	0.821	0.924	0.678

Table 3 Parameter estimates of the model to compressive strength, softening coefficient and dry density

Sources	Compressive strength		Softening coefficient		Dry density	
Factor	Estimate	p-value	Estimate	p-value	Estimate	p-value
Intercept	0.92	0.004	0.8	0.0002	296.8	0.0262
A-HPMC	0.04	0.0033	0.033	0.0005	-0.87	0.6968
B-AEA	-0.06	0.0003	-0.01	0.1009	-11.75	0.0010
C-WRA	0.034	0.007	1.00E-02	0.1009	-0.37	0.8668
AB	-0.024	0.1117	-0.015	0.0852	0.75	0.8127
AC	-1.75E-03	0.896	-0.02	0.032	-2.50	0.4391
BC	0.013	0.3654	-0.015	0.0852	-7.25	0.0490
A^2	5.03E-03	0.7017	-0.065	<0.0001	-1.15	0.7101
B^2	-5.23E-03	0.6906	-0.035	0.0021	-6.90	0.0532
C^2	-0.016	0.2451	-0.04	0.001	2.85	0.3693

3.1. COMPRESSIVE STRENGTH

The relation between additives and compressive strength is shown in Figure 2 in order to investigate the effect of the single factor on the performances of EPS mortar. It can be seen from Figure 2, the compressive strength of EPS mortar added HPMC and WRA shows positive influence and EPS mortar added AEA shows negative influence. So, less addition of AEA and more addition of HPMC and WRA present the favorable effects on the compressive strength. Both of these factors have significant influence in the compressive strength of EPS mortar. The normal plot of residuals for model shows the difference value of actual and fitted value in Figure 2 d, presenting that the error of different plots are extremely small.

Response surface of compressive strength for EPS mortar is shown in Figure 3. In Figure3 (a), the WRA content of 0.5, the compressive strength of mortar almost has no obvious change with HPMC content increasing at higher content of AEA and it also increases with increasing HPMC content at lower content of AEA. The reason is that the addition of HPMC can improve adhesion stress between EPS particle and cement paste, which results in compressive strength increasing sharply. In addition, as a whole, compressive strength gradually decreases as the increase of AEA content, the reason is that a large number of tiny bubbles (originating from AEA) are introduced in EPS mortar to decrease the content of cement paste, which results in a low mechanical strength. SEM of EPS mortar with pores introduced by AEA has been shown in Figure 4. In Figure 3 (b), the HPMC content of 0.5, it is obvious that compressive strength increases with increasing WRA content at any AEA content and the results for AEA is similar to Figure 3 (a). The smallest AEA content of 0.2 is corresponding to its highest value in both of Figure 3 (a) and (b). But, the addition of AEA can improve the thermal conductivity and decrease the dry density for EPS mortar effectively due to the introduction of bubbles. Therefore, the addition level of additives should be controlled by others properties due to the compressive strength of linear growth and reduction.

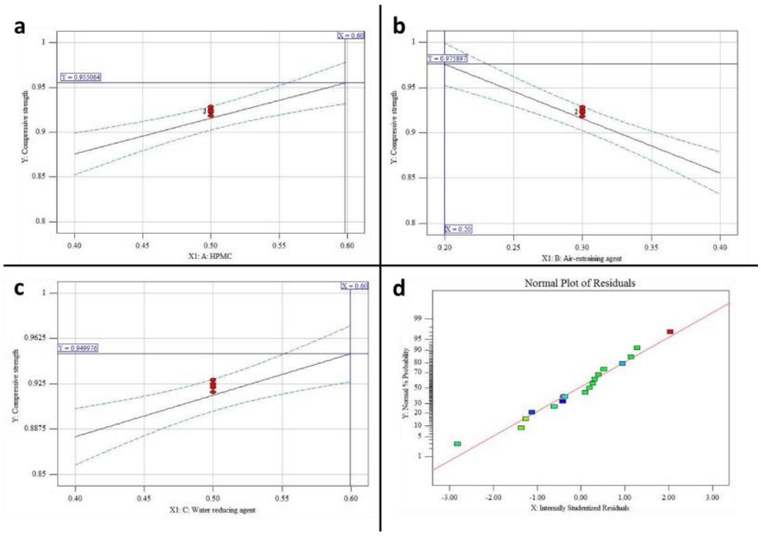

Figure 2 (a) The relation between HPMC and compressive strength (b) The relation between AEA and compressive strength (c) The relation between WRA and compressive strength (d) Normal plot of residuals for model

3.2. SOFTENING COEFFICIENT

The softening coefficient is an important index for representing the water resistance in EPS mortar, which is influenced by additives. The resolution loss of $Ca(OH)_2$ and C-S-H gel in the mortar will lower the mechanical performance. Moreover, the capillary pore in the mortar is filled with water and migrates to the capillary under the compressive load producing extra pressure on the partition of pores and impairing the compressive strength of EPS mortar [22].

Figure 5 shows the relation between additives and softening coefficient, presenting that softening coefficient of EPS mortar only for single additive all increases first and then decreases with the content of additives increasing. The optimal range of addition level for HPMC, AEA and WRA is 0.49%~0.55%, 0.26%~0.3% and 0.49%~0.53%, respectively. Both of these factors have significant influence in the softening coefficient of EPS mortar. The normal plot of residuals for model shows the difference value of actual and fitted value in Figure 5 (d), presenting that the error of different plots are extremely small.

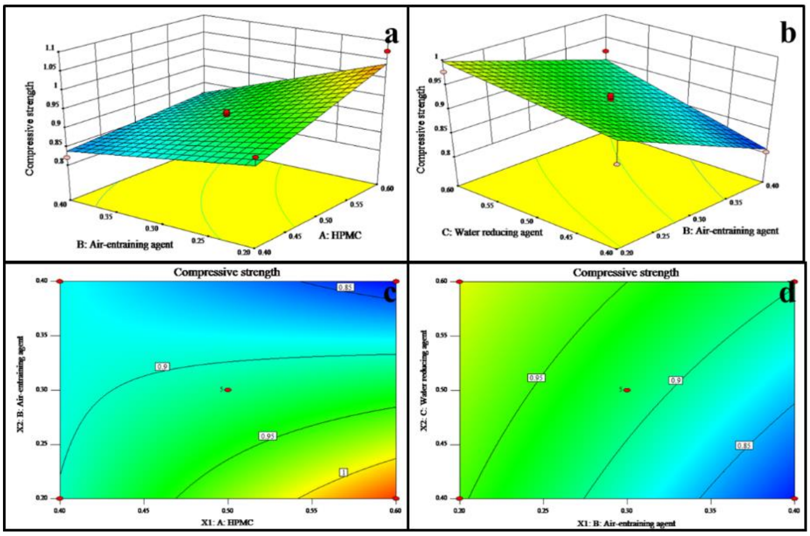

Figure 3 (a) response surface plots of compressive strength, WRA = 0.5 (b) response surface plots of compressive strength, HPMC = 0.6 (c) contour line of compressive strength, WRA = 0.5 (d) contour line of compressive strength, HPMC = 0.6

Response surface of softening coefficient for EPS mortar is shown in Figure 6. As shown from Figure 6 (a), the softening coefficient shows the trend of increases first and then decreases with increasing the addition of HPMC and AEA under the WRA content of 0.5. In addition, Figure 6 (b) shows the results are similar to Figure 6 (a), presenting that the optimal value is smaller than that of Figure 6 (a). So, the addition of HPMC, AEA and WRA can be controlled in the range of 0.5~0.55%, 0.25~0.3% and 0.5~0.55% respectively.

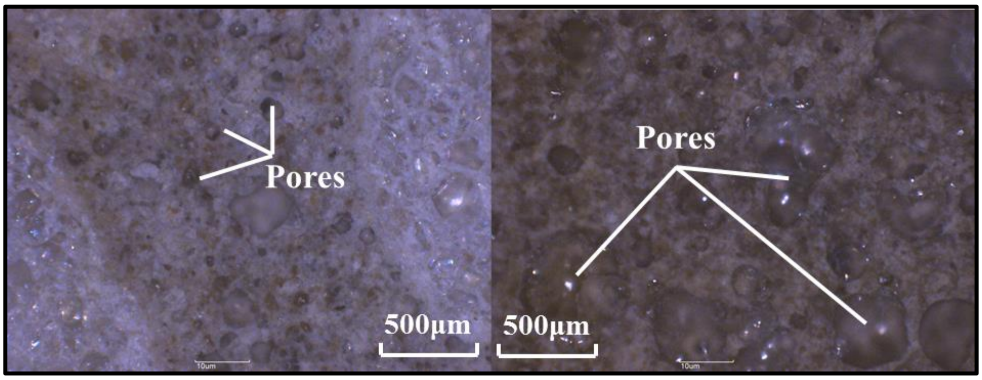

Figure 4 SEM of EPS mortar with pores introduced by AEA

3.3. DRY DENSITY

The dry density of CEP mortar is an important index for evaluating its practicability. Overall, the dry density exhibited an inverse relationship with the compressive strength of CEP mortar.

Figure 7 shows the relation between additives and dry density, presenting that dry density of EPS mortar mainly remains unchanged with the increase of HPMC and WRA. It means that HPMC and WRA have no effect on the dry density of EPS mortar. The dry density of EPS mortar added AEA decreases gradually with the addition of AEA increasing and it has significant influence, except HPMC and WRA, in the dry density of EPS mortar. The normal plot of residuals for model shows the difference value of actual and fitted value in Figure 5 (d), presenting that the error of different plots are extremely small similar to previous.

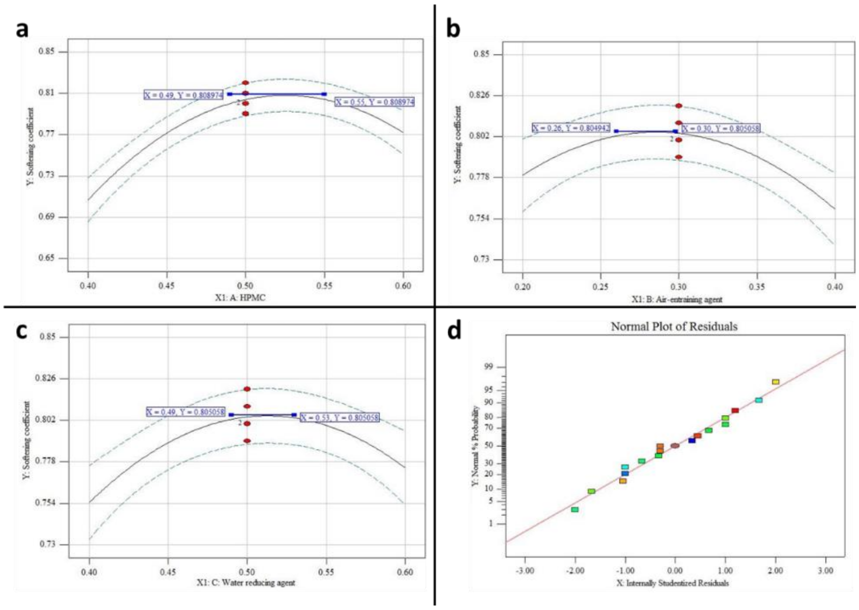

Figure 5 (a) The relation between HPMC and softening coefficient (b) The relation between AEA and softening coefficient (c) The relation between WRA and softening coefficient (d) Normal plot of residuals for model

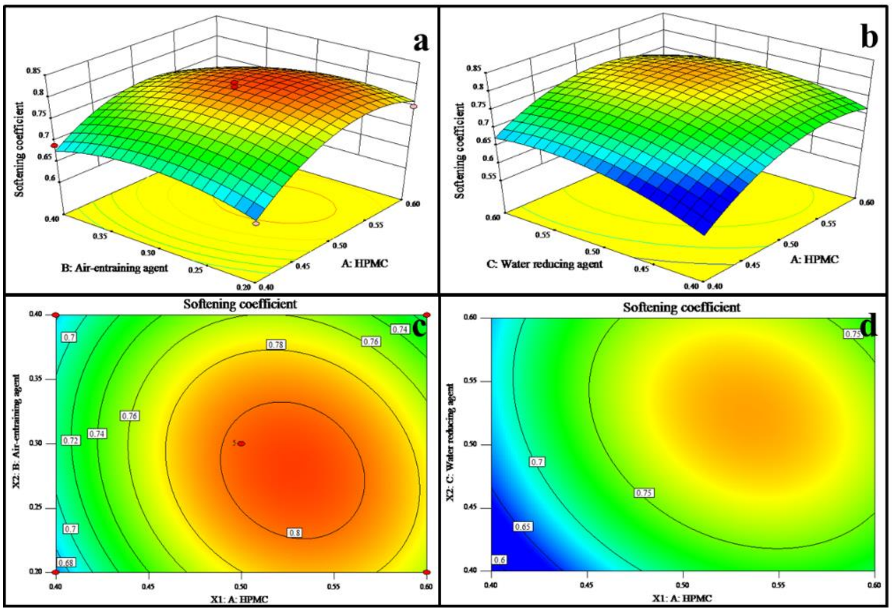

Figure 6 (a) response surface plots of softening coefficient, WRA=0.5 (b) response surface plots of softening coefficient, AEA=0.4 (c) contour line of softening coefficient, WRA=0.5 (d) contour line of softening coefficient, AEA=0.4

Figure 8 shows the response surface and contour lines under different addition of additives. It can be from Figure 8 (a) and (c), the addition of WRA is 0.5, the dry density of EPS mortar added AEA decreases sharply in the range of 0.28%~0.4% and keeps unchanged in the range of 0.2%~0.28%. But, this result must be controlled under high addition of HPMC. From Figure 8 (b) and (d), it can be seen that HPMC and WRA mainly have no effect on the dry density of EPS mortar.

So, it can be concluded that the optimal addition range of HPMC, WRA and AEA in EPS mortar is 0.25%~0.28%, 0.5%~0.55% and 0.5%~0.55% comprehensive comparison to these properties, respectively.

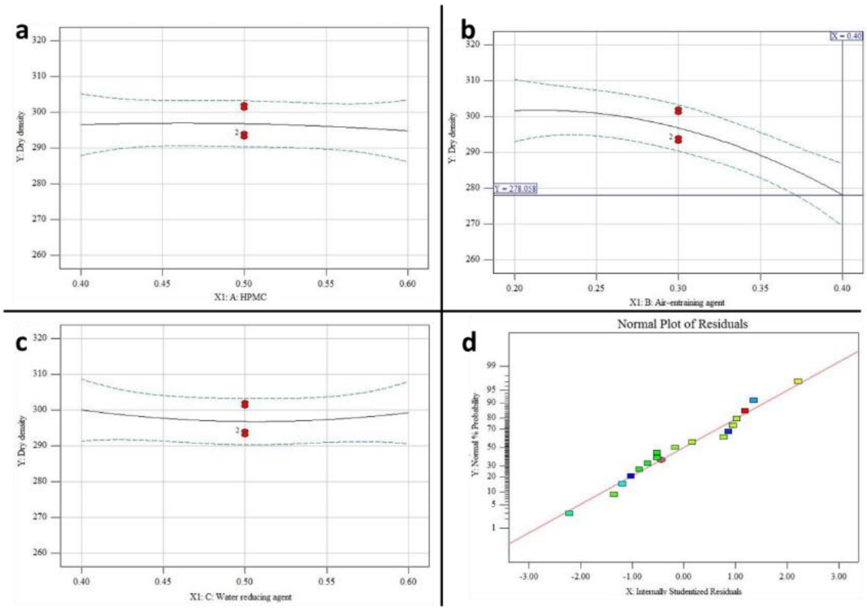

Figure7 (a) The relation between HPMC and dry density (b) The relation between AEA and dry density (c) The relation between WRA and dry density (d) Normal plot of residuals for model

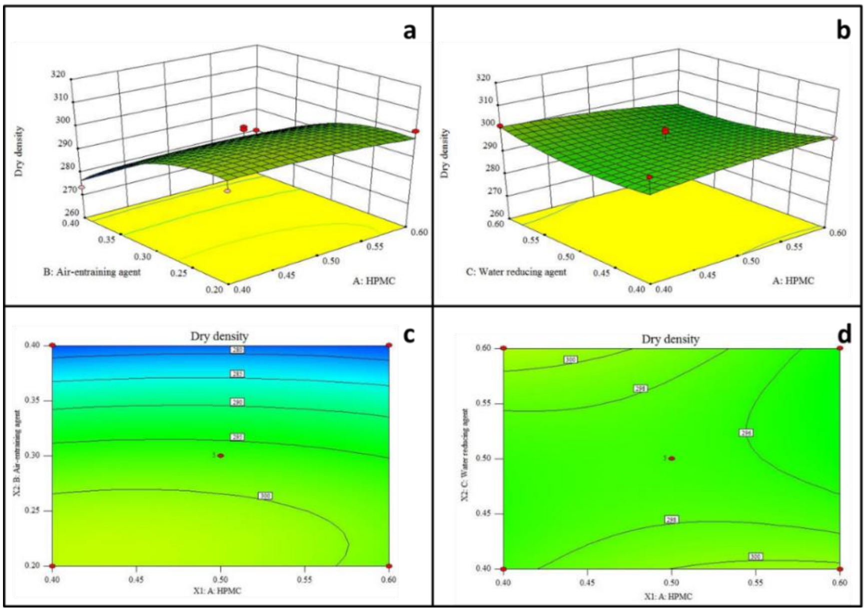

Figure 8 (a) response surface plots of dry density, WRA=0.5 (b) response surface plots of dry density, AEA=0.4 (c) contour line of dry density, WRA=0.5 (d) contour line of dry density, AEA=0.4

4. CONCLUSIONS

(1) By the comparison of different models, the method of response surface methodology is effective to optimize the components of EPS mortar.

(2) The optimal additive range of HPMC, WRA and AEA in EPS mortar is 0.25%~0.28%, 0.5%~0.55% and 0.5%~ 0.55%, respectively.

ACKNOWLEDGEMENTS

This work is supported by Natural Science Foundations of China (51472109), 13th Five-Year the state key development program (2016YFC0701001), Shandong Province Technological Development Program (2014GGB019N) and Bold Talent Program (ZR2015EM002). We also thank Program for Scientific Research Innovation Team in Colleges and Universities of Shandong Province.

REFERENCES

[1] Ji, R., Zhang, Z. T., Liu, L. L., and Wang, X. D. (2014). "Development of the random simulation model for estimating the effective thermal conductivity of insulation materials." Build. Enviro., 80, 221-227.

[2] Stazi, F., Di Perna, C., and Munafò, P. (2009). "Durability of 20-year-old external insulation and assessment of various types of retrofitting to meet new energy regulations." Energ. Buildings., 41(7), 721–731

[3] Kolaitis, D. I., Malliotakis, E., Kontogeorgos, D. A., Mandilaras, I., Katsourinis, D. I., and Founti, M. A. (2013). "Comparative assessment of internal and external thermal insulation systems for energy efficient retrofitting of residential buildings." Energ. Buildings., 64, 123–131.

[4] A. Laukaitis, R. Zurauskas, J. Keriene. The effect of foam polystyrene granules on cement composite properties[J]. Cement and Concrete Composites, 2005, 27: 41-47.

[5] D. Bouvard, J.M. Chaix a, R. Dendievel, et al. Characterization and simulation of microstructure and properties of EPS lightweight concrete[J]. Cement and Concrete Research, 2007, 37: 1666-1673.

[6] Keun-Hyeok Yang, Kyung-Ho Lee, Jin-Kyu Song, et al. Properties and sustainability of alkali-activated slag foamed concrete[J]. Journal of Cleaner Production, 2014, 68(1): 226-233.

[7] Qiangshan Jing, Linxia Fang, Hongyan Liu, et al. Preparation of surface-vitrified micron sphere using perlite from xinyang, China[J]. Applied Clay Science, 2011, 53(4): 745-748.

[8] E.M. Saucedo-Salazar, Y.A. Perera-Mercado, F.R. Rodríguez-Ruiz, et al. Production of glass spheres from blast furnace slags by a thermal flame projection process[J]. Ceramics International, 2014, 40(1): 1177-1182.

[9] Ganesh Babu, K., and Saradhi Babu, D. (2004). "Performance of fly ash concretes containing lightweight EPS aggregates." Cem. Concr. Compos., 26(6), 605-611.

[10] Wei, K. C., Lv, C. L., Chen, M. Z., Zhou, X. Y., Dai, Z. Y., and Shen, D. (2015). "Development and performance evaluation of a new thermalinsulation material from rice straw using high frequency hot-pressing." Constr. Build. Mater., 87, 116-122.

[11] Belhadj, B., Bederina, M., Montrelay, N., Houessou, J., and Quéneudec, M. (2014). "Effect of substitution of wood shavings by barley straws on the physico-mechanical properties of lightweight sand concrete." Constr. Build. Mater., 66, 247-258.

[12] Ferrándiz-Mas, V., Bond, T., García-Alcocel, E., and Cheeseman, C. R. (2014). "Lightweight mortars containing expanded polystyrene and paper sludge ash." Constr. Build. Mater., 61, 285-292.

[13] Binici, H., Eken, M., Dolaz, M., Aksogan, O., and Kara, M. (2014). "An environmentally friendly thermal insulation material from sunflower stalk, textile waste and stubble fibres." Constr. Build. Mater., 51, 24-33.

[14] D'Alessandro, F., Asdrubali, F., and Baldinelli, G. (2014). "Multi-parametric characterization of a sustainable lightweight concrete containing polymers derived from electric wires." Constr. Build. Mater., 68, 277-284.

[15] Sadrmomtazi, A., and Sobhani, J. (2012). "Properties of multi-strength grade EPS concrete containing silica fume and rice husk ash." Constr. Build. Mater., 35, 211-219.

[16] Schackow A, Effting C, Folgueras M V, et al. Mechanical and thermal properties of lightweight concretes with vermiculite and EPS using air-entraining agent[J]. Construction & Building Materials, 2014, 57(9):190-197.

[17] Dong X, Wang S, Gong C, et al. Effects of aggregate gradation and polymer modifiers on properties of cement-EPS/vitrified microsphere mortar[J]. Construction & Building Materials, 2014, 73(73):255–260.

[18] Chen M, Wang S, Lu L, et al. Effect of matrix components with low thermal conductivity and density on performances of cement-EPS/VM insulation mortar[J]. Journal of Thermal Analysis & Calorimetry, 2016, 126(3):1-10.

[19] Bektas, F., Bektas, B. A. (2014). "Analyzing mix parameters in ASR concrete using response surface methodology." Constr. Build. Mater., 66, 299–305.

[20] Cai, L. C., Wang, H. F., Fu, Y. W. (2013). "Freeze–thaw resistance of alkali–slag concrete based on response surface methodology." Constr. Build. Mater., 49, 70–76.

[21] JC/T 1042 (2007). "Expanded vitrified microsphere," Building Materials Standardization Administration of China, Beijing, China.

EFFECT OF RHEOLOGICAL PARAMETERS ON RICE HUSK ASH BLENDED PASTES WITH VARIOUS SUPERPLASTICIZERS

Nsesheye Msinjili[1], Wolfram Schmidt[1], Sarah Leinitz[1], Hans-Carsten Kühne[1], Andreas Rogge[2]

[1] Bundesanstalt für Materialforschung und – prüfung (BAM), Division 7.4 – Technology of Construction Materials, Unter den Eichen 87, 12205 Berlin, Germany, email: nsesheye.msinjili@bam.de, wolfram.schmidt@bam.de, sarah.leinitz@bam.de, hans-carsten.kuehne@bam.de
[2] Bundesanstalt für Materialforschung und – prüfung (BAM), Department 7 – Safety of Structures, Unter den Eichen 87, 12205 Berlin, Germany, e-mail: andreas.rogge@bam.de

SUMMARY: Rice husk ash (RHA) is a low-energy efficient material with high pozzolanic characteristics compared to other supplementary cementitious materials (SCMs). The replacement of cement with RHA has extensive improvement on the mechanical properties of concrete. However due to the porous nature of the RHA particles, it requires a higher water demand when replaced with Portland cement. Therefore, superplasticizers (SPs) are essential to reduce the water demand and improve the workability of the mixes. There is very little information about the effect of RHA with added SPs in its fresh state. Hence, this paper investigates the interaction of RHA pastes with three types of SPs, i.e. one polycarboxylate-based SP and two different types of lignosulphonates. This paper presents results of the investigation related to the flow behaviour of blended mixes with increasing percentage of RHA. The yield stress for the pastes with and without the addition of SPs is investigated over time as well as the plastic viscosity.

UTJECAJ REOLOŠKIH PARAMETARA NA PASTE S PEPELOM OD RIŽINIH LJUSAKA UZ RAZLIČITE SUPERPLASTIFIKATORE

SAŽETAK: Pepeo rižinih ljusaka niskoenergetski je učinkovit materijal s visokim pucolanskim značajkama u usporedbi s drugim dodatnim cementnim materijalima. Zamjena cementa pepelom rižinih ljusaka dovodi do velikog poboljšanja mehaničkih svojstava betona. Zbog poroznosti tih čestica, kad ih se zamjenjuje za portlandski cement, zahtijevana je veća količina vode. Stoga su, radi smanjenja potrebne vode i poboljšanja obradivosti mješavine, bitni superplastifikatori. O utjecaju pepela rižinih ljusaka s dodanim superplastifikatorima na svježi beton ima vrlo malo informacija. Stoga je u ovom radu istraženo međudjelovanje pasta od pepela rižinih ljusaka s trima vrstama superplastifikatora, tj. s jednim na osnovi polikarboksilata i s dvama različitim od vrstama na osnovi lignosulfonata. Rezultati istraživanja prikazani u radu odnose se na ponašanje tečenja mješavina s postupnim povećavanjem postotka pepela rižinih ljusaka. Istražena je granica tečenja pasta s dodatkom superplastifikatora i bez njega tijekom vremena, kao i plastična viskoznost.

1. INTRODUCTION

The demand for cement is increasing and the global CO_2 emissions resulting from its production is one of the major hazards to the environment in this current century [1]. The promotion of supplementary cementitious materials (SCMs) as cement replacement in concrete production is a reasonable solution to counteract this effect. The use of SCMs lead to a reduction in CO_2 emissions as well as a reduction in costs due to the relatively low costs of production of the SCM compared to clinker.

Rice husk ash (RHA) is an artificial pozzolan, which can contain a high amorphous silica content (ca. 85 – 95 %) when it is produced by combustion of rice husks between 600 – 650 °C [2]. The pozzolanic reactivity of the ash significantly depends on the combustion temperature and duration [3], as well as the fineness of the material after grinding [4]. RHA has a large surface area, which is governed by the porous nature of the particles [5]. The large surface area causes a high demand for water, which adversely affects the flowability of the concrete [6]. The addition of superplasticizers (SPs) to cementitious systems allows for a better workability in the fresh state without altering the water/cement (w/c) ratio [7]. Cement can be replaced with SCMs in substantial volumes, thus reducing the overall clinker factor whilst possibly enhancing the performance of the cement systems [8]. Nevertheless, the adsorption of SP polymers generally depends on the properties of the SCM, type of SP as well as the interaction between the SP and the SCM, among others. Due to the porous nature of RHA particles, it is likely that some SP polymers get trapped in the pores, where they cannot contribute to the dispersion. This compromises the efficiency of the SP to enhance the workability. Hence, the inclusion of SCMs as cement replacements in concrete generally affects the rheological parameters.

Rheology is a key tool in understanding the behaviour of fresh properties and this can be done through the application of various tests. Generally, the slump flow test is used as a measure to determine the properties of the cement-based systems in terms of its flow characteristics. However, cement-based systems are non-Newtonian fluids, and slump flow test alone is inadequate to determine the behaviour of cement-based systems in their fresh state [9]. Therefore, further rheological parameters such as yield stress and plastic viscosity are essential in determining the flow behaviour. The yield stress is the stress threshold above which flow is initiated, and this is mainly influenced by inter-particle attractive forces in the systems [10]. Yield stress and plastic viscosity are strongly affected by the addition of SPs as well as replacement of cement with SCMs, which affects the water demand, the overall surface area as well as the particle's morphology [11, 12].The flow behaviour of cementitious systems can be determined by many non-Newtonian models, however the simplest model is the Bingham model presented in Equation 1, whereas more complex models include the Herschel-Bulkley model presented in Equation 2 [9].

$$\tau = \tau_o + \eta_{pl} \cdot \dot{\gamma} \qquad (1)$$

$$\tau = \tau_o + \mathrm{K} \cdot \dot{\gamma}^n \qquad (2)$$

In these equations, τ is the shear stress (Pa), τ_o the yield stress (Pa), η_{pl} is the plastic viscosity (Pa·s); and $\dot{\gamma}$ is the shear rate (1/s). The parameters K and n in Equation 2 are constants related to the material properties, determining the consistency index and flow index, respectively. Depending on the value of n, the flow of the paste can behave as shear thinning i.e. when n<1, or as shear thickening i.e. when n>1.

Extensive research has been focussed on the strength properties of cement systems blended with RHA, especially at later ages [13-15], however, limited research is directed at the fresh properties i.e. workability and rheological behaviour of RHA-blended systems with the addition of SP. This paper aims to study the workability and rheological parameters of RHA-blended systems with three types of SPs. This is done through experimental observations of the spread flow of the fresh RHA-blended paste with various additions of the SPs, and a selected spread flow for all pastes is measured to determine the yield stress and plastic viscosity over time.

2. MATERIALS AND METHODS

2.1. MATERIALS

The powders used in this research were ordinary Portland cement CEM I 42.5 R (CEM I), limestone filler (LSF) and RHA. Both CEM I and LSF originated from Germany, whereas RHA originated from Tanzania. The dry rice husks were incinerated in a furnace at 600 °C for 6 hours and left to cool naturally to room temperature for 24 hours. The coarse ash produced was then ground in a disc mill for approximately 1 minute. The properties of the powders are provided in The chemical admixtures used in this research were commercially obtained SPs, namely a polycarboxylate ether (PCE SP), a lignosulphonate with retarding effects (LS SP1) and a lignosulphonate with accelerating effects (LS SP2). Both, PCE SP and LS SP1 were liquid-based SPs with a concentration of 20 % solids. LS SP2 was a powder-based SP, which was made into a solution in the laboratory with distilled water, and a concentration of 20 % by mass of the powdered polymer.

. The density and surface area (Blaine) was determined by He-pycnometry and a Blaine apparatus according to DIN EN 196-6:2010, respectively. The particle size distribution of the powders presented in **Error! Reference source not found.** was determined by laser granulometry.

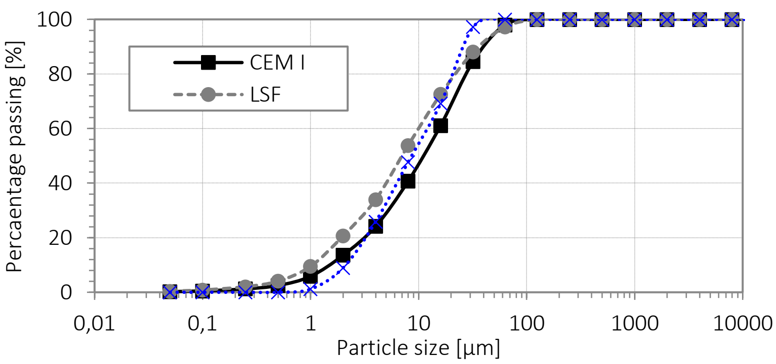

Figure 1 Particle size distribution of powders used

The chemical admixtures used in this research were commercially obtained SPs, namely a polycarboxylate ether (PCE SP), a lignosulphonate with retarding effects (LS SP1) and a lignosulphonate with accelerating effects (LS SP2). Both, PCE SP and LS SP1 were liquid-based SPs with a concentration of 20 % solids. LS SP2 was a powder-based SP, which was made into a solution in the laboratory with distilled water, and a concentration of 20 % by mass of the powdered polymer.

Table 1 Properties of powders

Property	CEM I	LSF	RHA
SiO_2 (%)	20.56	1.47	88.84
Al_2O_3 (%)	4.36	0.46	0.80
Fe_2O_3 (%)	2.27	0.40	0.39
TiO_2 (%)	0.20	0.05	0.04
CaO (%)	62.80	90.68	1.78
MgO (%)	2.14	0.61	0.92
Na_2O (%)	0.28	3.27	1.10
K_2O (%)	0.95	0.54	2.80
SO_3 (%)	3.45	0.34	0.35
P_2O_3 (%)	0.00	2.19	0.61
LOI (%)	2.40	-	2.02
d_{50} (µm)	11.75	7.38	8.30
Density (g/cm^3)	3.12	2.74	2.31
Blaine (cm^2/g)	4110	5130	9040

2.2. METHODS

The mixtures were divided into 4 blended pastes, consisting of RHA replacement ratios varying from 0 – 15 % by weight of binder (bwob). LSF was kept constant at 10 % in all mixtures. The pastes were prepared with a water/binder (w/b) ratio of 0.4 using a mortar mixer in a controlled temperature of 21 ± 2 °C and relative humidity of 55 ± 5 %. All four pastes were experimented against the three types of SPs and compared with the reference pastes without SP. The composition of the pastes is shown in

. The SP was added to the pastes to attain a slump flow of 230 ± 20 mm without segregation immediately after mixing. The mixing procedure is described in Table 3.

Table 2 Mixture composition of paste systems including spread flow

Type of SP	Mixture	CEM I [g]	LSF [g]	RHA [%bwob]	w/b	SP dosage [%bwob]	Spread flow [mm]
No SP	RHA0	540	60	0	0.4	-	135
	RHA5	510	60	5	0.4	-	125
	RHA10	480	60	10	0.4	-	125
	RHA15	450	60	15	0.4	-	120
PCE	RHA0	540	60	0	0.4	0.3	230
	RHA5	510	60	5	0.4	0.3	230
	RHA10	480	60	10	0.4	0.3	220
	RHA15	450	60	15	0.4	0.3	215
LS-ret	RHA0	540	60	0	0.4	0.9	215
	RHA5	510	60	5	0.4	0.9	210
	RHA10	480	60	10	0.4	1.2	210
	RHA15	450	60	15	0.4	1.5	210
LS-acc	RHA0	540	60	0	0.4	1.2	220
	RHA5	510	60	5	0.4	1.2	215
	RHA10	480	60	10	0.4	1.2	210

	RHA15	450	60	15	0.4	1.5	210

2.2.1. . SPREAD FLOW

The spread flow test was done by using a Haegermann cone and flow table. The cone has a lower diameter of 100 mm, an upper diameter of 70 mm, and a height of 60 mm. The method for determining the spread flow was done according to DIN EN 1015-3:2007. The spread flow for each paste was calculated as the average of the perpendicular distances of the spread and determined immediately after the mixing time for increasing dosages of SP. For each dosage, a new mixture was prepared.

2.2.2. RHEOMETER TEST

Rheometer measurements were done for all SP systems attaining a spread flow of 230 ± 20 mm and compared to the systems without SP. The investigation was done with a Viskomat NT Couette types rotational rheometer, using a double gap coaxial cylinder with a basket probe (Vogel cell). The pastes were subjected to a step-wise pre-shear for 1 minute, then a constant shearing at a rotational speed of 100 rpm for another minute. Then the rotational velocity was reduced in a downward ramp of 6 steps to 0.1 rpm. Each step lasted 20 seconds and only the last 8 measurements were deduced from each step of the downward ramp.

Table 3 Mixing procedure of the pastes

Time [min:sec]	Description step
-00:30 – 00:00	Mixing of all binders manually
00:00 – 00:05	Addition of water
00:05 – 00:35	Mixing at low speed
00:35 – 01:05	Mixing at high speed
01:05 – 01:35	Stop mixing and scraping of the walls of the mixing bowl
01:35 – 02:35	Continue mixing at high speed
02:35 – 02:40	Addition of SP
02:40 – 02:45	Mixing at low speed
02:45 – 03:30	Mixing at high speed

3. RESULTS

3.1. EFFECT OF SP ON THE WORKABILITY OF RHA-BLENDED PASTES

The results of the spread flow measurements of the pastes are presented in **Error! Reference source not found.**. The figure elements (a) through (d) show an increase in the spread diameter for all pastes with increasing dosages of SP and replacement ratios of RHA. When SP is added to a cementitious system, a dispersion of agglomerates occurs, thus causing the water trapped in the agglomerates to be free, resulting in a more flowable mix. A similar trend is observed for all PCE SP curves. With the addition of small dosages of PCE SP, there is an immediate improvement of the slump. In the presence of small amounts of RHA, i.e. 5 %, the spread flow is attained at the same PCE SP dosage, whereas at higher amounts of RHA, i.e. 10 – 15 % the spread flow only decreases slightly at the same PCE SP dosage. Hence, the slump reaches a spread of 230 ± 20 mm at very low dosages of the SP. The improvement of the slump flow with PCEs is more significant, which could indicate more precipitation of ettringite. Ettringite is critical for workability in the presence of PCE due to the availability of large surfaces of the ettringite crystals for the adsorption of the PCE [12]. Hence higher slump flows were evident for the pastes with PCE (Table 2) than pastes with both LS SP and pastes without SP. On the contrary, for LS SPs, the precipitation of ettringite crystals is less relevant than for PCEs. The addition of LS SPs to the pastes show a slow and steady increase in the spread flow, requiring higher dosages to attain a spread flow of 230 ± 20 mm. The highest dosages are required with replacement of CEM I with 15 % RHA as observed in **Error! Reference source not found.** (d). At replacement ratios of 0 – 5 % RHA (**Error! Reference source not found.** (a) and (b)), there exhibits no change in the spread flow for pastes with LS SP1, however a higher dosage of LS SP2 is required to obtain the same spread flow. At higher replacement ratios of RHA i.e. 10 – 15 % RHA (**Error! Reference source not found.** (c) and (d)), both LS SPs require the same dosage to obtain the same spread flow, which is higher than the dosage of the PCE systems. Therefore, the higher the replacement of CEM I with RHA, the more LS SP required. Although higher dosages of SP can lead to a high degree of segregation, no segregation was observed with the LS SPs used. LS SPs also show to retain the workability at later ages [12], and similar results were observed with such pastes and presented in [16]. This may be a result of the higher dosages required for flowability.

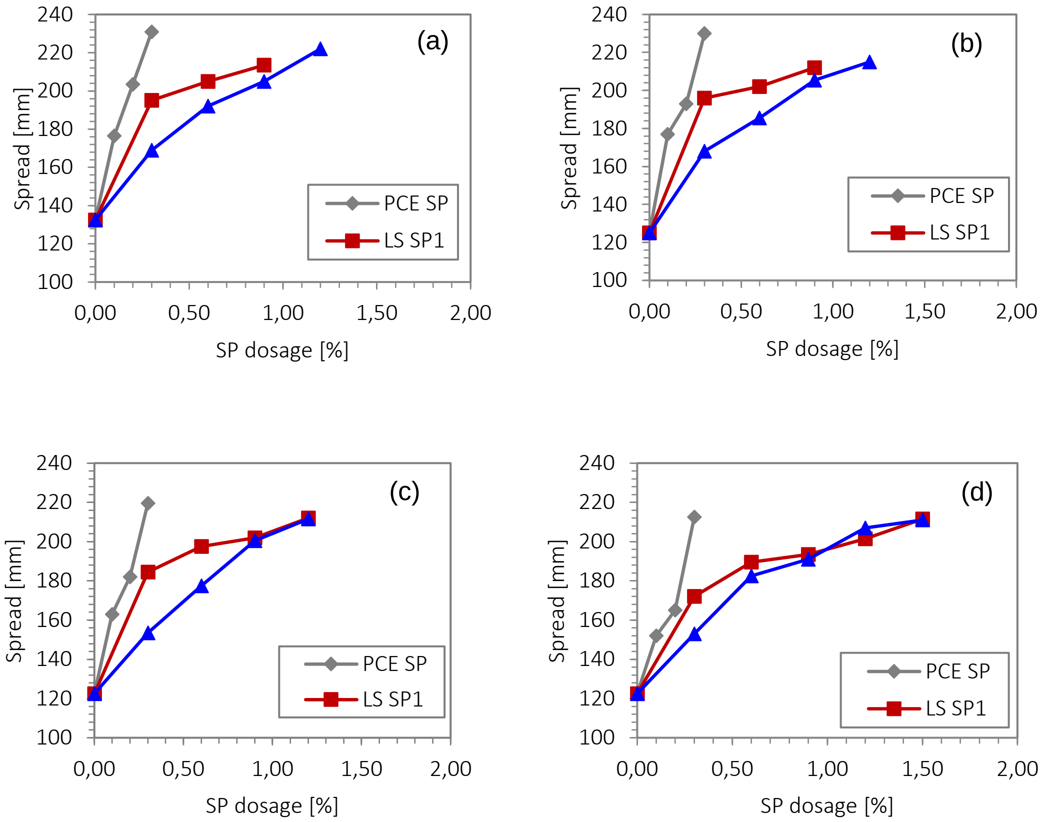

Figure 2 Spread flow with increasing dosage of SP for (a) RHA0 (b) RHA5 (c) RHA10 and (d) RHA15

3.2. EFFECT OF SP ON THE WORKABILITY OF RHA-BLENDED PASTES

The rheometer measurements were done over a period of 35 minutes. The data collected from the measurements were made to fit either the Bingham or Herschel Bulkley model after applying the closest approximation. For negative yield stresses obtained the latter was achieved. **Error! Reference source not found.** (a) to (d) shows a representation of the yield stress over time for all pastes with increasing percentage ratios of RHA calculated after the pre-shearing. In the absence of SP, the blended pastes without RHA is observed to have the highest yield stress as shown in **Error! Reference source not found.** (a). When RHA is added to such systems, the yield stress is initially reduced (**Error! Reference source not found.** (b) – (d)) but tends to increase with time. The degree of reduction of yield stress immediately after mixing is similar regardless of the replacement ratio of RHA. The reduction of the yield stress may be related to a number of factors related to the particle size and shape of the RHA and the surface effects induced by ions from the solution [17]. However, with time, and at lower replacement ratios of RHA i.e. 5 – 10 % the yield stress increases and exhibits a similar yield stress to systems without RHA and SP. With higher percentage ratios of RHA i.e. at 15 % RHA, the yield stress increases significantly over time. This may be related to the agglomeration of particles in the system as well as the high water demand of the RHA particles causing a stiffer mix in the system.

The addition of SP creates a dispersion of particles, thus causing the water trapped in the former agglomerates to be free for further mixing, resulting in a more flowable mix, and therefore a lower yield stress. The degree of reduction of the yield stress depends on the adsorption of the SP on the RHA particles as well as its particle size [18]. All pastes with RHA and addition of PCE SP displayed a shear thickening behaviour with relatively low yield stresses. The systems with PCE SP and LS SP1 exhibit the lowest yield stress immediately after mixing and with higher percentage ratios of RHA, PCE SP systems tend to slightly increase the yield stress over time whereas LS SP1 systems decreases the yield stress. This indicates that one can retain the workability over time slightly better with LS SP1 rather than PCE SP. The pastes with LS SP2 have a higher yield stress than other SPs but lower yield stress than pastes without SP. In the presence of RHA, LS SP2 systems increase the yield stress slightly over time, except for the paste with 15 % RHA (**Error! Reference source not found.** (d)), where the yield stress varies but tends to show an increase over time.

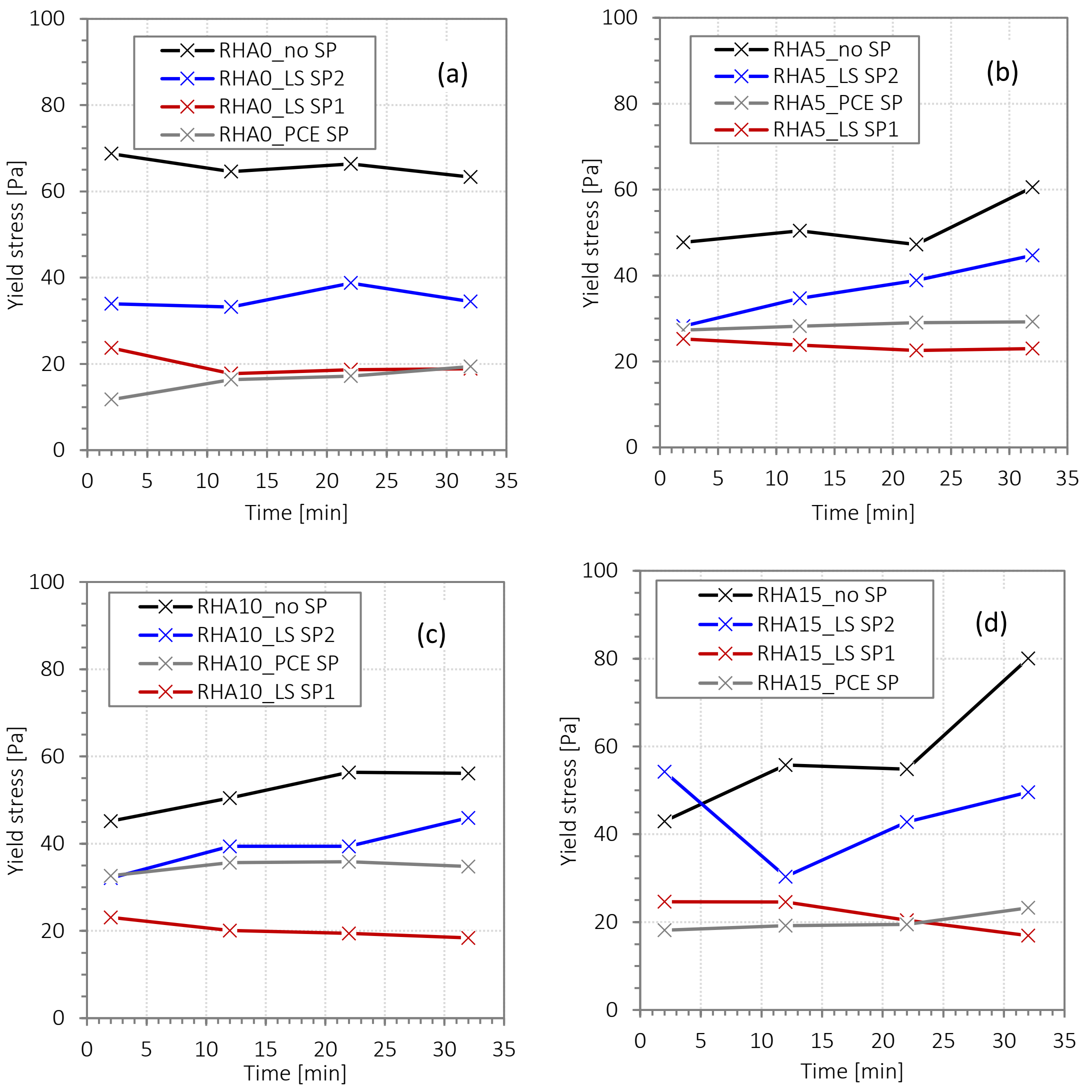

Figure 3 Effect of yield stress vs time on RHA blended pastes with addition of various SPs for (a) RHA0 (b) RHA5 (c) RHA10 and (d) RHA15, calculated 2 minutes after pre-shearing

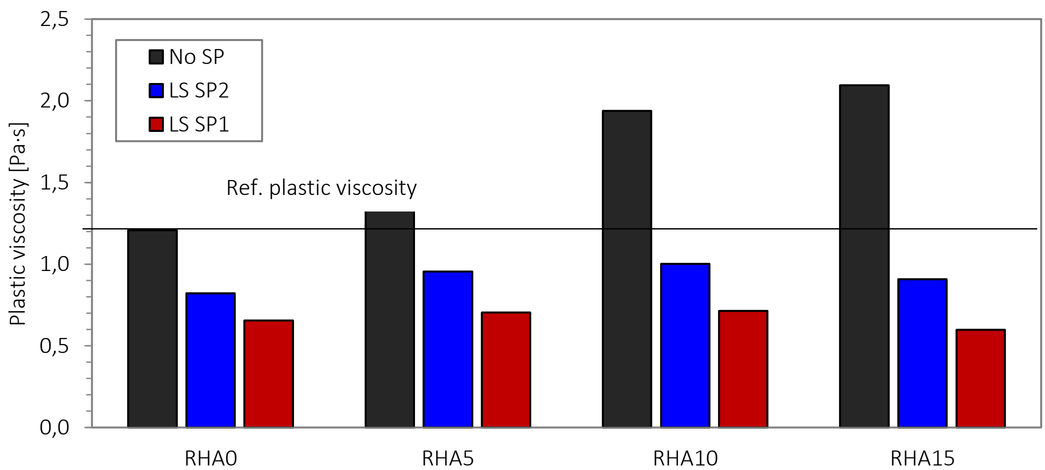

Figure 4 Influence of plastic viscosity on blended pastes with SPs except PCE SP

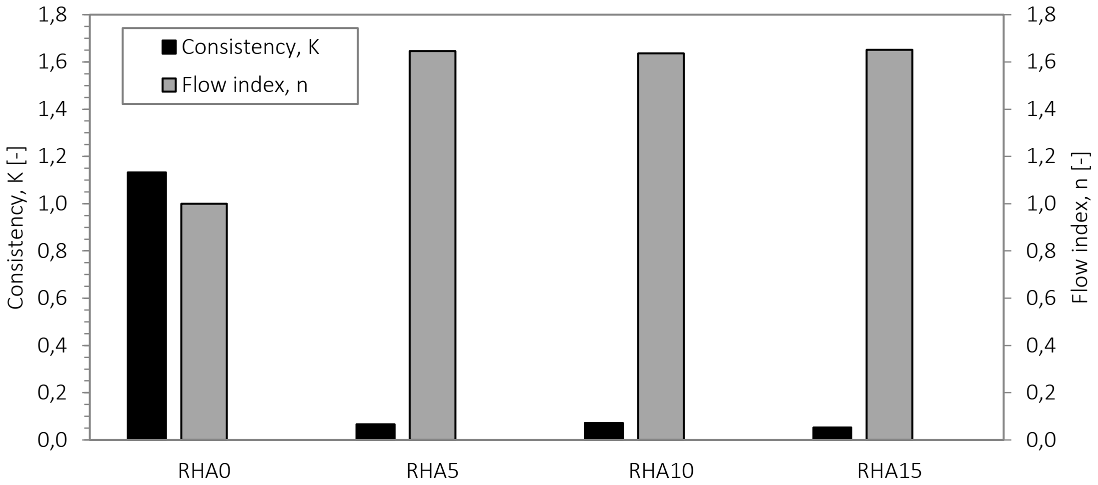

Figure 5 Influence of consistency and flow index on blended pastes with PCE SP

The plastic viscosity of the pastes was observed to not change significantly over time. However, a lower plastic viscosity was observed with the addition of the LS SPs. **Error! Reference source not found.** shows the influence of the plastic viscosity of the pastes immediately after mixing. In the absence of SP, the plastic viscosity increases as the replacement ratios of RHA increase. This may be a result of the reduction of available water in the system for mixing influenced by the porous nature of the RHA particles [18]. A lower spread flow is also observed for pastes with high replacement ratios of RHA. With the addition of LS SPs to the pastes, the plastic viscosity does not change in the presence of RHA. Nevertheless, the lowest plastic viscosity is observed with LS SP1 systems. The plastic viscosity of PCE SP systems with RHA addition is dependent on the shear rate due to its shear thickening behaviour (Equation 2). **Error! Reference source not found.** shows the consistency and flow index for the pastes with PCE SP with increasing ratios of RHA. In the absence of RHA, the pastes behave as Bingham (Equation 1) having a flow index of 1 and a consistency is assumed to be the plastic viscosity. In the presence of RHA, the flow index and consistency do not significantly change according to the increment of RHA.

4. CONCLUSIONS

The results of this paper showed that the workability of RHA blended pastes can be improved with the addition of SPs. PCE SP systems show the highest slump flow which could be attributed to the precipitation of more ettringite in the system causing better SP adsorption. With the replacement of CEM I with RHA, there is shown to be no significant change in the spread and only changes slightly at higher replacement ratios of RHA. Nevertheless, minimum dosages of PCE SP are required to attain a good workability. With LS SP systems, more dosages are required to reach a similar spread flow, which could lead to a high degree of segregation or delay in setting of the pastes. In addition, the higher the replacement ratio of RHA, the higher the dosage of SP. This could also explain the workability retention for LS SPs.

Within the experimental analysis, a lower yield stress was observed when small amounts of RHA are added to the pastes without SP. Larger amounts show no further effect in the decrease of the yield stress, and over time the yield stress increases. This could be attributed to the inter-particle forces in the solution. The addition of SP further reduces the yield stress due to the release of trapped water from agglomeration. Immediately after mixing, PCE SP and LS SP1 pastes showed low yield stresses, and over time the PCE SP systems slightly increase the yield stress whereas the LS SP1 reduces. The pastes with LS SP2 showed a lower yield stress than pastes without SP however over time the yield stress significantly increases. In addition, the plastic viscosity of the pastes with SP is reduced however does not change with further replacement ratios of RHA. The contrary is observed for the pastes without SP.

This paper helps to understand the behaviour of varied SPs with the different RHA blended mixtures. Depending on the SP and amount of RHA in the mixture, there are a number of factors that can change the behaviour of the system. Further studies in the interactions and inter-particle effects between the SP polymers and the RHA particles are required to understand the rheological behaviour of the systems.

REFERENCES

[1] Tyrer, M., *et al.*: Potential for carbon dioxide reduction from cement industry through increased use of industrial pozzolans, *Advances in Applied Ceramics*, Vol. 109 (2010), pp. 275-279.

[2] Mehta, P.K., Folliard, K.J.: Rice Husk Ash--a Unique Supplementary Cementing Material: Durability Aspects, *ACI Materials Journal Special Publication*, Vol. 154 (1994), pp. 419-444.

[3] Siddique, R.: Rice Husk Ash. A. Loeb, A. Ferrara, and R. S. Ellis (Ed), *First Light in the Universe*, Springer, 978-3-540-74294-4, Vol. 16 (2008) pp. 235-264.

[4] Bui, D.D., *et al.*: Particle size effect on the strength of rice husk ash blended gap-graded Portland cement concrete, *Cement and Concrete Composites*, Vol. 27 (2005), pp. 357-366.

[5] Cook, D.J.: Rice Husk Ash. R. N. Swamy (Ed), *Cement Replacement Materials, Concrete Technology and Design*, Surrey University Press UK, Vol. 3 (1996) pp. 171 - 196.

[6] Van Tuan, N., *et al.*: Hydration and microstructure of ultra high performance concrete incorporating rice husk ash, *Cement and Concrete Research*, Vol. 41 (2011), pp. 1104-1111, 0008-8846.

[7] Schmidt, W., *et al.*: Admixture Concepts for the sub-Saharan African Environment with Indigenous Raw Materials, Proceedings of the Eleventh International Conference on Superplasticizers and Other Chemical Admixtures in Concrete, V. M. Malhotra, P. R. Gupta, and T. C. Holland (Ed), pp. 491-505, 9781942727224, Ottawa, American Concrete Institute (ACI) (2015).

[8] Flatt, R.J., *et al.*: The Rheology of Cementitious Materials, *Materials Research Society Bulletin*, Vol. 29 (2004), pp. 314-318.

[9] Banfill, P.F.G., "Rheology of Fresh Cement and Concrete," in *Rheology Reviews*, ed: The British Society of Rheology, 2006, pp. 61-130.

[10] Vance, K., *et al.*: The rheology of cementitious suspensions: A closer look at experimental parameters and property determination using common rheological models, *Cement and Concrete Composites*, Vol. 59 (2015), pp. 38-48, 0958-9465.

[11] Khayat, K.H., *et al.*: Effect of Supplementary Cementitious Materials on Rheological Properties, Bleeding, and Strength of Structural Grout, *Aci Materials Journal*, Vol. 105 (2008), pp. 585-593.

[12] Schmidt, W., *et al.*: Influences of superplasticizer modification and mixture composition on the performance of self-compacting concrete at varied ambient temperatures, *Cement and Concrete Composites*, Vol. 49 (2014), pp. 111-126, 0958-9465.

[13] Wada, I., *et al.*: Strength properties of concrete incorporating highly reactive rice-husk-ash, *Transaction of Japan Concrete Institute*, Vol. 21 (1999), pp. 57-62.

[14] Ganesan, K., *et al.*: Rice husk ash blended cement: Assessment of optimal level of replacement for strength and permeability properties of concrete, *Construction and Building Materials*, Vol. 22 (2008), pp. 1675-1683, 0950-0618.

[15] Antiohos, S.K., *et al.*: Rice husk ash (RHA) effectiveness in cement and concrete as a function of reactive silica and fineness, *Cement and Concrete Research*, Vol. 61–62 (2014), pp. 20-27, 0008-8846.

[16] Msinjili, N.S., *et al.*: Obtaining optimum workability using rice husk ash in a modified cementitious system, Proceedings of the Eleventh International Conference Sustainability Conference, L. Lemay (Ed), pp. Washington D.C., National Ready Mix Concrete Association (2016).

[17] Lowke, D., Gehlen, C.: Effect of Pore Solution Composition on Zeta Potential and Superplasticizer Adsorption, Proceedings of the Eleventh International Conference on Superplasticizers and Other Chemical Admixtures in Concrete, V. M. Malhotra, P. R. Gupta, and T. C. Holland (Ed), pp. 253-264, 978-1-942727-22-4, Ottawa, American Concrete Institute (2015).

[18] Le, H.T., *et al.*: Effect of macro-mesoporous rice husk ash on rheological properties of mortar formulated from self-compacting high performance concrete, *Construction and Building Materials*, Vol. 80 (2015), pp. 225-235, 0950-0618.

THE IMPACT OF STRESS INTENSITY ON SETTING TIME AND POROSITY OF CEMENT-BASED MORTARS OF DIFFERENT SIZES

Tayfun Uygunoğlu[1], İsmail Hocaoğlu[1], İlker Topçu[2]

[1] Afyon Kocatepe University, Engineering Faculty, Civil Engineering Department, 03200, Afyonkarahisar, Turkey, email: uygunoglu@gmail.com, afyonbeton@hotmail.com
[2] Eskişehir Osmangazi University, Engineering Faculty, Civil Engineering Department, 26480, Eskişehir, Turkey, email: ilkerbt@ogu.edu.tr

SUMMARY: Thanks to developing industry, concrete gains strength at an early time and it can be used in a shorter time. Through applying different methods, concrete gains early strength. Accelerated curing method through applying electrical stress is one of the main curing techniques. In this study, the relations between setting time and stress intensity as a result of applying 7.5 V, 15 V, 22.5 V stress to 250 dosaged cement-based mortars at 5 x 5 x 10, 5 x 5 x 15, 5 x 5 x 20, 5 x 5 x 25 (cm x cm x cm) sizes have been investigated. Through measuring the temperature of the specimens to which stress has been applied in every 2 minutes, relation between temperature and setting time has been established. Moreover, the porosities of specimens to which stress has been applied and to which stress hasn't been applied have been compared. It has been concluded that setting time can be shortened and porosity can be decreased as a result of applying electrical current to mortars.

UČINAK INTENZITETA (ELEKTRIČNOG) NAPONA NA VRIJEME VEZIVANJA I POROZNOST CEMENTNIH MORTOVA NA RAZLIČITIM VELIČINAMA ISPITNIH UZORAKA

SAŽETAK: Zahvaljujući industrijskom razvoju beton postiže čvrstoću sve ranije pa se može upotrijebiti nakon kraćeg vremena. Beton postiže ranu čvrstoću primjenom različitih metoda. Jedna od glavnih je metoda ubrzane njege primjenom električnog napona. U radu su istraženi odnosi vremena vezivanja i intenziteta napona primjenom napona od 7,5 V, 15 V i 22,5 V na 250 cementnih mortova na uzorcima dimenzija 5x5x10, 5x5x15, 5x5x20 i 5x5x25 (cm x cm x cm). Mjerenjem svake dvije minute temperature ispitnih uzoraka izloženih električnom naponu utvrđen je odnos temperature i vremena vezivanja. Dodatno je uspoređena poroznost ispitnih uzoraka koji su bili izloženi i onih koji nisu bili izloženi djelovanju napona. Zaključeno je da se vrijeme vezivanja može skratiti a poroznost smanjiti zbog djelovanja električne struje na mortove.

1. INTRODUCTION

The importance of mass production and industrialization enhances in order to meet the increasing demand in building sector in a short time and in an economical way. Concrete's gaining strength at an early time and it's being used immediately are the results of developing industry [1]. In order to reach these results, there are several cure methods and through these methods, the concrete can get early strength. Main cure methods are hot water cure method, boiling water cure method, autogeneous cure method, changed hot water cure method, microwave cure method, steam curing in prefabricate structure and accelerated cure method Nevertheless, almost all these cure methods are used for preproduction concrete. The accelerated cure methods which are applied during pouring the concrete is very limited. Depending upon the hydration time, accelerated cure at the buildings in which ready mixed concrete used is important in terms of the project's predicted time since concrete compressive strength reaches the target level in a short time. Moreover, the prediction of the level of strength in an early time is very crucial in terms of building's both performance and economy.

Concrete is not conductive but it can show a conductive feature until its final setting time since it includes water.. Furthermore, additive minerals in concrete can change in terms of electrical resistivity of concrete. Different methods have been developed to measure electrical conductivity of morters and various researches and applications which examine cement's microstructure development have been carried out [1-2].

Electrical conductivity of concrete in cement based systems can be explained through the ion movement in space. It is considered that electrical conductivity is related with both porosity and conductivity of space amount. Free space water which is in the gaps of the mixture is used in the chemical reactions for producing hydration products and in hydrolysis for conducting electric current. Therefore, by increasing water and binder amount, hydrolysis reaction is accelerated [3]. Previous researches indicate that cement paste and cement based mortars show electrical conductivity till setting time and after setting time electrical resistivity reaches its maximum value. According to theory of Levita et. al., when porosity increases, conductivity increases, too and thus they concluded that it is in relation with hydration degree [4]. The variation of conductivity as function of time can indeed reflect internal changes of the pore solution of cement paste with time [5]. As it is well-known, the hydration process in cement paste and mortar results in the formation of C–S–H, calcium hydroxide, ettringite and other compounds. During hydration, the capillary pores in hardening cement paste are gradually filled up with hydration products and the solid phases form a rigid microstructure with increasing strength. Then, electrical resistivity of cement paste increases with time [6]. In [2] water/cement ratio of cement pastes, the effect of alkali on cement hydration and fluency on cement paste are investigated. Electrical resistivity and water/binder ratio are compared and when electrical resistivity increases, it is predicted that temperature of morter also increases. Topcu et al. [7] applied current to cement pastes which have different water/cement ratio (0.40, 0.45, 0.50, 0.55), different mineral admixtures (fly ash, silica fume, and blast furnace slag) and different ratio by weight (0%, 10%, 20%, 30%). As a result, applying electric current can be used for obtaining rapid setting time on the cement paste with high volume mineral admixture. Backe et al. [8] studied the relation between conductivity, porosity, cement chemistry and ion content. According to their theory when porosity increases, conductivity increases too and thus they concluded that it is in relation with hydration degree. As a result, when setting time becomes shorter to take mould time becomes shorter too. This research is important for the structures which require rapid repair or fast production such as prefabricate.

2. EXPERIMENTAL STUDY

In experimental study crushed sand have been used in order to show the impact of electrical resistivity on mortars. Specific gravity of crushed sand is 2.7 and the maximum grain size is 4 mm. In the experiments, CEM I 42.5 R cement which is suitable to TS EN 197-1 standarts have been used.

2.1. PRODUCTION OF SPECIMEN

250 dosage mortars whose water/cement ratio is 0.50 are produced. The 5 lt capacity mixer is used. Then the mortars put in electrically isolated wooden moulds whose sizes are 5 x 5 x 10, 5 x 5 x 15, 5 x 5 x 20 and 5 x 5 x 25 (cm x cm x cm). Unit volume component of 250 dossage mortar has shown in Table 1.

Table 1. Unit volume component of 250 dosage mortar

Serial	Cement kg/m3	Water lt/m3	Crushed Sand, kg/m3
M1	250	125	2104

Initially for the mixture of mortars, aggregate and cement were mixed for 1 minute in order to have dry mixture. Then almost 2/3 of mixture water were added to the dry mixture. Finally the rest (1/3) of water were put into the mixture and the process of mixing were continued for 3 minutes. Prepared mortars were put into wooden moulds which has different sizes as 5 x 5 x 10, 5 x 5 x 15, 5 x 5 x 20 ve 5 x 5 x 25, cm x cm x cm. Then some of mortars were applied to 7.5 V, 15 V, 22.5 V stress by direct current (DC) power- supply source during 24 hours and some of them were used to control specimen at laboratory conditions. For applying stress intensity to specimens, two copper electrodes were used.

2.2. PREPARATİON OF EXPERİMENT SET UP

For applying stress intensity to the specimens a DC power-supply source Hioki mark which has 30 canal and 60 V capacity has been used. Firstly, power supply was connected to a port (+ pole and – pole separately), then data logger was connected to the port. Then direct connection from the port to the specimens was made to apply DC current. In order to measure the temperature of specimens to which stress was applied, K type termocopel were connected. A view of mortar which electrical current applied to has shown in Figure 1.

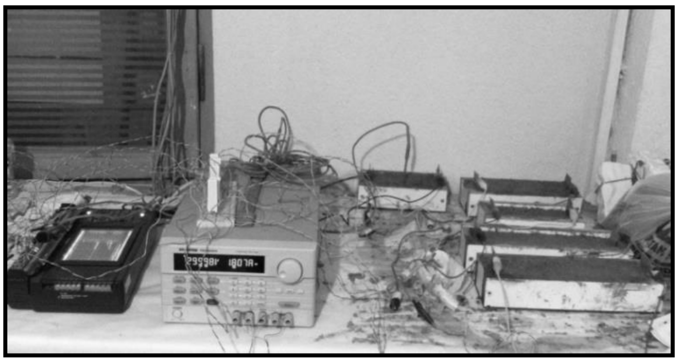

Figure 1 A view of mortar which electrical current applied to

3. DISCUSSION AND CONCLUSION

For measuring temperature of mortars, K type termocopel was used and in every 2 minutes the temperature values were recorded by data logger. For measuring setting time of mortars where stress has been applied, penetration device was used. Setting time test was made according to ASTM C 807 standards. Consequently the final setting time (28 Mpa in setting time standart) and maximum value of temperature of mortar are almost at the same minute. This point is mortar's final setting time. The comparison of 250 dosage specimen to which 7.5 V, 15 V and 22.5 V stress are applied in terms of the relation between temperature and setting time is shown Figure 2, Figure 3 and Figure 4. As an example, when 7.5 V, 15 V and 22.5 V stress are applied to 250 dosaged mortars, final setting times are measured as 146, 144 and 138 minute by penetration experiment device. Through temperature measurement, final setting times of the same sized mortars to which same stress intensity are applied are measured as 148, 144 and 140 minute.

3.1. THE RELATION BETWEEN TEMPERATURE AND SETTING TIME OF THE MORTARS TO WHICH ELECTRICAL CURRENT IS APPLIED

From the beginning of hydration time, temperature of cement based mortars have been measured and saved. When temperature reaches maximum value, this minute is thought as final setting time. In order to compare initial and final setting time of the mortars to which stress is applied and not applied, Table 2 is prepared. This table is prepared for the mortars whose sizes are 5 x 5 x 10 (cm x cm x cm). The mortars whose sizes are 5 x 5 x 10 (cm x cm x cm) are chosen because setting time is considered as shorter when it is compared with other size of mortars. When Table 2 is examined, it is seen that initial setting time of the mortars to which stress is applied and not applied are almost same but final setting time of the mortars to which stress is applied is shorter than the ones to which stress is not applied. It is observed that as the stress intensity increases, final setting time gets shorter. When the superposed graphics are examined, it is seen that when the stress intensity is increased and the sizes of specimens are made smaller (5 x 5 x 10 ve 5 x 5 x 15, cm x cm x cm), setting time of the specimens are getting shorter.

Table 2. Duration of Initial and Final Setting Time of 250 Dossage Mortars Whose Sizes are 5 x 5 x 10

		With stress			Without stress		
Dosage	Stress intensity (V)	Initial setting time (min)	Final setting time(min)	Upper-Lower Error (min)	Initial setting time (min)	Final setting time(min)	Upper-Lower Error (min)
250	7.5	124	146	2-4	128	185	2-4
250	15	122	144	4-6	130	180	2-4
250	22.5	125	138	6-8	132	178	2-4

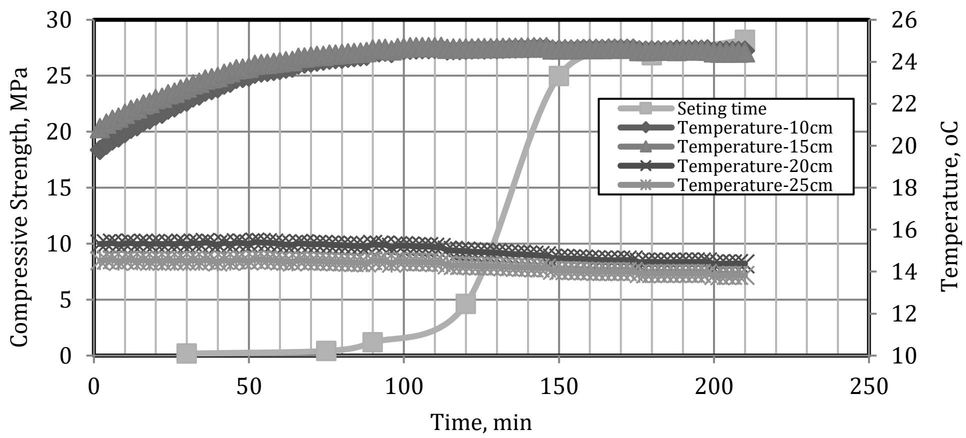

Figure 2. The relation between temperature and setting time of the Mortars to which 7.5 Voltage stress is applied

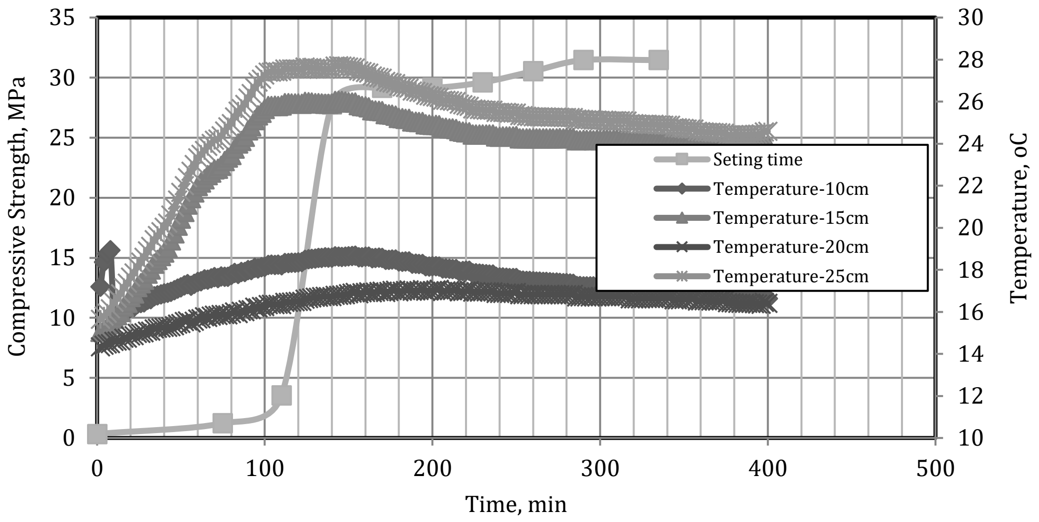

Figure 3. The relation between temperature and setting time of the Mortars to which 15 Voltage stress is applied

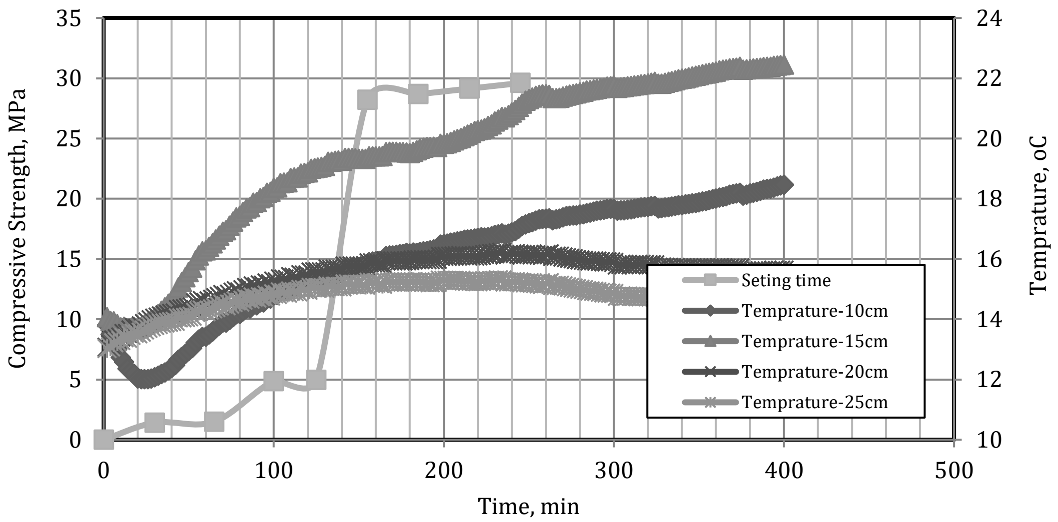

Figure 4. The relation between temperature and setting time of the Mortars to which 22..5 Voltage stress is applied

3.2. POROSITY OF THE MORTARS TO WHICH STRESS IS APPLIED AND NOT APPLIED

For investigating porosity of mortars to which stress is applied and not applied 6 specimens at each size were produced. Stress was applied to 3 of them and other 3 specimens were used to control specimen. Then all the specimens were cured for 28 days in laboratory conditions. Porosity tests were made appropriate to TS 3624 Standards. Porosities of the mortars whose sizes are 5 x 5 x 10 and 5 x 5 x 15 (cm x cm x cm) have low values than the morters whose sizes are 5 x 5 x 20 and 5 x 5 x 25 (cm x cm x cm) (Figure 5). It is observed that generally porosities of specimens to which stress is applied are lower than the specimens to which stress is not applied (Figure 5). Hence, it can be said that stress application to mortars can decrease porosity In general the mortars whose sizes are 5 x 5 x 10 (cm x cm x cm) and with 15 Volt stress application, porosity takes lower value than the other sizes of mortars and other application of stress intensity to mortars. At the mortars which have 22.5 Volt stress application, porosity takes higher values. For this reason 22.5V stress application is not available for decreasing porosity. As it shown in Figure 5 at the mortars whose sizes are 5x 5 x 25 (cm x cm x cm), porosity takes higher values than the other sizes of mortars.

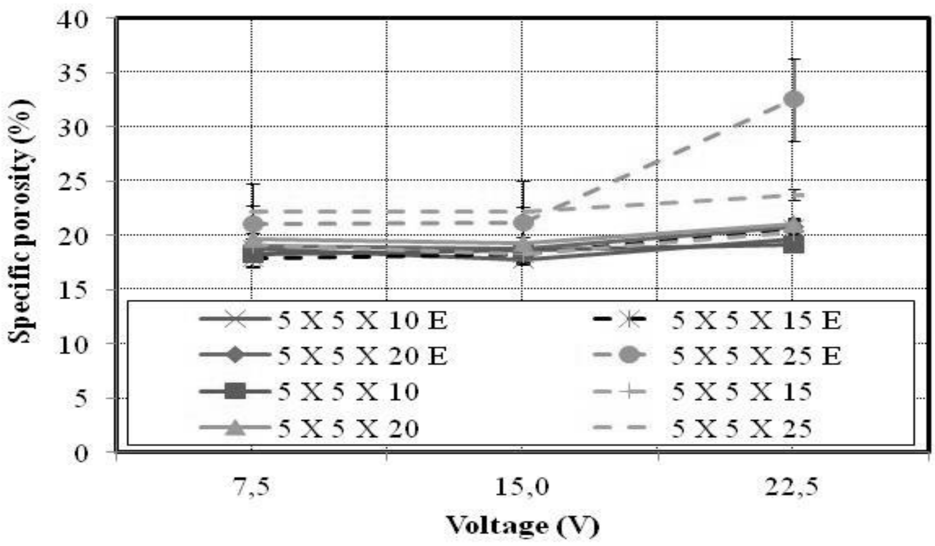

Figure 5. The relation between stress intensity and porosity of 250 dosage mortars to which stress is applied (E) and not applied

4. CONCLUSION AND SUGGESTIONS

In this study, the relations between setting time and stress intensity as a result of applying 7.5 V, 15 V, 22.5 V stress to 250 dosaged cement-based mortars at 5 x 5 x 10, 5 x 5 x 15, 5 x 5 x 20, 5 x 5 x 25 (cm x cm x cm) sizes have been investigated. Several conclusions can be drawn from this study:

- When the stress intensity applied to mortars increase (7.5 V to 22.5 V), setting time becomes shorter.
- When 22.5 volt stress is applied to mortars whose sizes are 5 x 5 x 10 (cm x cm x cm), initial setting time is almost the same whereas final setting time becomes 40 minutes shorter than the mortars to which stress are not applied.
- There is relationship with hydration temperature and final setting time.
- It is concluded that for minimum porosity 15 Volt stress application is the best intensity.
- As electrods approach each other, setting time becomes shorter.

It is thought that this research can be developed to apply different stress intensity and put in electrodes at different size of the mortars.

ACKNOWLEDGEMENTS

Authors thank Afyon Kocatepe University, Institute of Natural and Applied Sciences and Coordinatorship of Scientific Research Projects for their support to this study as both a part of doctoral thesis and 16th Science Project with number of 43.

REFERENCES

[1] McCarter, W. J.; Chrisp, T. M.; Starrs. G.; Blewett, J.: Characterization and monitoring of cement-based systems using intrinsic electrical property measurements, Cement and Concrete Research, 33. (2003)., pp.197-206.

[2] Whittington, H. W.; McCart, J.; Forde, M. C.: *The conduction of electricity through concrete, Mag Concr Res,* 33. (1981)., pp. 48–60.

[3] Topçu, İ.B.; Uygunoğlu, T.; Hocaoğlu, İ.. *Electrical resistivity of fly ash blended cement paste at hardining state. Materials Science,* 22.(2016)., pp. 458-462.

[4] Levita, G.: Marchetti, A.: Gallone, G.: Princigallo, A.: Guerrini, G. L.: Electrical Properties of Fluidified Portland Cement Mixes in the Early Stage of Hydration, Cement and Concrete Research, 30. (2000)., pp. 923-930.

[5] Rajabipour, F.: Weiss, J.: Electrical Conductivity of Drying Cement Paste, Materials and Structures, 40. (2007)., pp.1143-1160.

[6] Koleva, D. A.: Copuroglu, O.: Breugel, K. V.: Ye, G.: Wit, J. H. W. de.: Electrical Resistivity and Microstructural Properties of Concrete Materials in Conditions of Current Flow, Cement and Concrete Composites, 30. (2008)., pp. 731-744.
[7] Topçu, İ.B.; Uygunoğlu, T.; Hocaoğlu, İ.. Electrical conductivity of setting cement paste with different mineral admixtures. Construction and Building Materials, 28. (2012)., pp. 414-420.
[8] Backe, K. R.; Lile, O.B.; Lyomov, S.K.: Characterizing curing cement slurries by electrical conductivity, SPE Drilling and Completion, 16.(2001)., pp. 201-207.

INFLUENCES OF INTERNAL TEMPERATURE AND HUMIDITY CHANGE ON THE HYDRATION AND MICROSTRUCTURE OF MASS CONCRETE

Shuai Nie[1], Pan Yuan[1], Fazhou Wang[1], Shuguang Hu[1], Yunpeng Liu[1]

[1] State Key Laboratory of Silicate Materials for Architecture, Wuhan University of Technology, Wuhan, PR China, email: nieshuai@whut.edu.cn, fzhwang@whut.edu.cn, hsg@whut.edu.cn

SUMMARY: The mass concrete also shows the similar heat damage phenomena as heat-cured concrete. It was found that when the maximum temperature of internal mass concrete and heat curing were both 55 °C, the mass concrete also has a worse microstructure and performance, such as much lower compressive strength, degree of hydration, content of portlandite and a higher porosity, degree of polymerization of C-S-H gel than standard curing samples as it ages. But the negative of internal temperature and humidity change of mass concrete on microstructure and performance was not so serious than heat curing at later stage, which may be caused by the lower heating and cooling rate of mass concrete. No obvious ettringite peak was observed in mass concrete at 28 days, which may be caused by cured at elevated temperature and low relative humidity for a long time. Moreover, the subsequent high relative humidity curing can decrease the heat damage in mass concrete.

UTJECAJI UNUTARNJE TEMPERATURE I PROMJENE VLAŽNOSTI NA HIDRATACIJU I MIKROSTRUKTURU MASIVNOGA BETONA

SAŽETAK: Masivni beton pokazuje slična toplinska oštećenja kao beton njegovan toplinom. Utvrđeno je da kada maksimalna temperatura u unutrašnjosti masivnog betona i pri toplinskoj njezi dostigne 55 °C taj beton ima lošiju mikrosturkturu i svojstva tj. mnogo manju tlačnu čvrstoću, stupanj hidratacije, sadržaj portlantida, veću poroznost i stupanj polimerizacije C-S-H gela od standardno njegovanih uzoraka tijekom starenja. Ipak, negativnosti unutarnje temperature i promjene vlažnosti masivnog betona na mikrostrukturu i svojstva nisu bili toliko ozbiljni od učinka toplinske njege u kasnijoj fazi što može biti prouzročeno manjom brzinom zagrijavanja i hlađenja masivnoga betona. U masivnom betonu pri 28-dnevnoj starosti nije opažen etringit što može biti prouzročeno njegom pri povišenoj temperaturi i malom relativnom vlagom kroz dulje vrijeme. Štoviše, naknadna njega uz veliku relativnu vlagu može smanjiti toplinsko oštećenje masivnoga betona.

1. INTRODUCTION

In recent years, the rapid development of society raises the demand for bigger and bigger concrete infrastructures. Mass concrete has been widely used in civil engineering, bridge construction and dam. While the early rapid hydration of cement and relatively small conductivity of concrete would lead to the temperature easily rises in the internal of mass concrete. This would cause temperature gradients between the core and surface of the concrete member. This temperature gradient can cause a thermal crack through tensile stress due to the concrete's expansion and contraction [1]. And it can also affect the structural performance, serviceability and durability of the concrete structures.

Many studies [2~5] have been done about how to control the temperature gradient and crack of mass concrete. But very few research has studied the influences of internal temperature and humidity change of mass concrete on cement hydration. According to previous research, temperature and humidity change have a significant impact on cement hydration and the microstructure. And at present, the vast majority studies [6~9] of cement hydration are carried out at constant high or low temperature curing. These are very different from internal temperature and humidity change of mass concrete. The internal temperature and humidity change of mass concrete is affected by many factors [1], e.g., cement types, mix proportion, ambient temperature and so on. But the early rapid exothermic of cement hydration and small conductivity of concrete determine the overall trend [10]: temperature rises quickly at early age (general reaches 0.4℃/h, finish at 3~4 days); reaching maximum temperature (easily reaches 60~65℃ and even 80℃ in some environment) at 3~5days and lasting about 20h; slow cooling after maximum temperature (no more than 2℃/d). Even if adopting the pipe cooling method, it can only reduce the maximum temperature to some extent and accelerate the cooling rate [11]. But the overall trend of temperature change won't be changed. The internal temperature change of mass concrete is a long-term process. And it is also different from heat curing. The temperature change of heat curing is completed within a day. It has a negative effect on the subsequent cement hydration and microstructure formation. So, the influence of internal temperature and humidity change of mass concrete on cement hydration and its microstructure is worth exploring. And it is necessary to figure out the difference of heat curing and the internal temperature and humidity change of mass concrete on cement hydration.

It can also provide guidance for construction and the improvements of service performance and life prediction of mass concrete.

According to the research results of monitoring temperature and relative humidity of mass concrete, considering the pipe cooling method, we simulate the temperature and relative humidity curves shown in Figure 1: reaching the maximum temperature at 80h; the maximum temperature is 55℃, lasting 20h; the mean cooling rate is 1.45℃/d. The relative humidity begins to decline at 50h and finally decreases to 78% at 28d. Besides, we set a controlled trial to explore the impact of humidity change. As shown in Figure 1, MC-97%RH, the temperature change is the same with abovementioned, but the humidity decreases to 97% at 130h and remains unchanged till to 28 days. The detailed heat curing regime is also shown in Figure 1, HC, the preheating duration is 3h; the heating rate is 15℃/h; the treatment temperature is 55℃, lasting 4h; the cooling rate is 15℃/h. After heat curing, samples are placed in the standard curing condition. Compared with standard curing and heat curing, explore the internal temperature and humidity change of mass concrete on cement hydration and its microstructure.

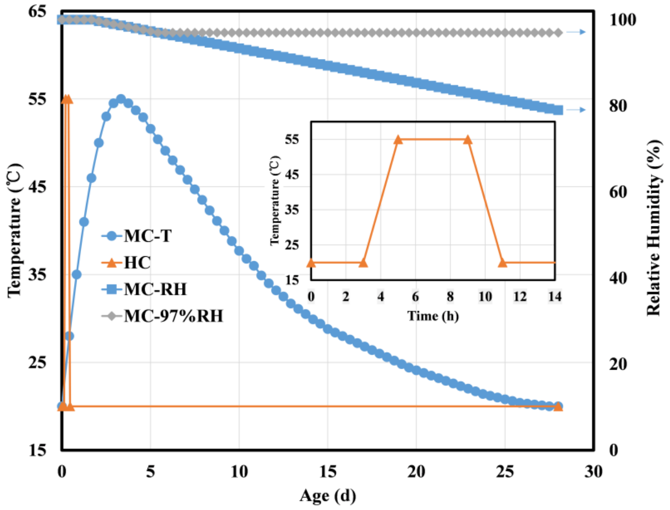

Figure 1 Curing regimes of Mass Concrete (MC), Mass Concrete with subsequent 97% RH curing (MC-97%RH) and Heat Curing (HC)

2. RAW MATERIALS AND EXPERIMENTAL METHODS

2.1. RAW MATERIALS

The chemical and mineralogical composition of the PI 52.5cement used was determined by X-ray fluorescence (XRF) (Table 1). According to the mix design requirements of mass concrete that the water binder ratio is no more than 0.50, we set the water binder ratio is 0.35. All cement pastes were prepared to China Standard GB/T 50080—2002, using deionized water, cast in 40mm×40mm×160mm prismatic moulds. The specimens were divided into four groups. The first group was placed in programmable temperature and humidity chamber (detailed temperature and humidity was shown in Figure 1) immediately after molding. The second group was placed in another programmable temperature and humidity chamber (detailed temperature and humidity was also shown in Figure 1) immediately after molding. The third group was placed in heat curing box (detailed heat curing regime was shown in Figure 1) immediately after molding. The last group was cured at standard curing room(20±1 ℃, relative humidity＞95%). After 24h, the specimens were demoulded and compressive strength tests were conducted at each predetermined curing time (1, 3,7 and 28 days).

The fragments obtained after failure were crushed and immersed in alcohol to interrupt hydration, dried at 40℃ in the vacuum oven and then used for the tests of X-ray diffraction(XRD), thermogravimetric analysis(TGA), mercury intrusion porosimetry(MIP) and nuclear magnetic resonance(NMR). Besides, the hydration was stopped by cutting the sample from the central of cement pastes at each age, immersed in alcohol and also dried at 40℃ in the vacuum oven. Subsequently, the samples were impregnated with epoxy-resin and polished with 600, 800, 1200 and 2500grit polishing papers and then polished using diamond abrasives of sizes 3, 1 and 0.25μm, no water being used.

Table1. PI 52.5 Cement chemical and mineralogical composition (% by weight)

Composition	SiO_2	Al_2O_3	Fe_2O_3	CaO	MgO	K_2O	Na_2O	SO_3	Loss
Content	21.72	4.92	3.01	62.14	2.27	0.65	0.22	2.20	1.78

C_3S = 48.48%, C_2S = 25.78%, C_3A = 7.95%, C_4AF = 9.15%, determined by Bogue calculation.

2.2. TEST METHODS

2.2.1. DEGREE OF HYDRATION

The degree of hydration was determined based on the measurement of non-evaporable water. The preconditioning of sample involved oven drying at 105℃ for 24h to remove the evaporable water. Then the sample was transferred to a resistance furnace at 1050℃ for 3h. The amount of non-evaporable water was determined as the mass loss of the sample between 1050℃ and 105℃. The cement loss on ignition was also taken into account in the calculation and the Loss of cement had been measured as 1.78%. Typically, the non-evaporable water content for well hydrated cement was considered to be 0.23 g of water by 1 g of cement. The degree of hydration can be estimated proportionally [12].

2.2.2. X-RAY DIFFRACTION TEST

The X-ray diffraction patterns of the powdered samples were recorded on a Bruker D8 Advance diffractometer. The machine settings were: wavelength = 1.5046 A ˚ (λCuKα), scanning range = 5° 2θ~60° 2θ, and scanning rate = 5°/min.

2.2.3. THERMOGRAVIMETRIC ANALYSIS(TGA)

TGA was carried out with a STA449F3 thermogravimetry analyzer in N_2 on about 250mg of powdered cement pastes at 10 ℃/min up to 1000℃. The content of portlandite was determined by the weight loss in the temperature intervals 400~500 ℃.

2.2.4. NUCLEAR MAGNETIC RESONANCE(NMR) TEST

A Bruker AVANCE III 400M working at resonance frequencies of 79.49MHz was used to obtain the solid sample ^{29}Si NMR spectra, which were recorded following onepluse with 5s relaxation delays. The scan numbers were 2048 for ^{29}Si, sample spin rates were 6 kHz, respectively. The ^{29}Si chemical shifts were recorded against tetramethylsilane (TTMS).

2.2.5. MERCURY INTRUSION POROSIMETER (MIP) TEST

Porosity was determined with an AutoPore IV 9500 mercury intrusion porosimeter on prismatic samples taken from the specimens. Total porosity and pore size distribution were found over a range of 348–0.003μm.

2.2.6. BACKSCATTERED ELECTRON (BSE) IMAGES

An FEI QUANTA FEG 450 ESEM was used to capture the backscattered electron (BSE) images, with acceleration voltage of 15 KV, and performed at low vacuum (60 Pa), so no sample coating was required to avoid charging effect.

3. RESULTS AND DISCUSSION

3.1. COMPRESSIVE STRENGTH

Compressive strength is an important parameter of cement paste. The pastes cured at different curing regimes were tested for compressive strength at ages 1, 3, 7 and 28 days. The results obtained are plotted in Figure 2.

Compared with the standard curing sample (abbreviated to SC sample), Figure 2 showed a positive influence of elevated temperature on the early compressive strength. Sample cured under the temperature and humidity match the condition inside the mass concrete (abbreviated to MC sample) was 10MPa higher than SC sample at 1day. And the heat curing sample (abbreviated to HC sample) was 17.5MPa higher than SC sample. These results concurred with the findings of other authors who reported rises in compressive strength with temperature in early age cement. While the increases of compressive strength of MC sample and HC sample were much slower than SC sample. The higher the early compressive strength was, the more obvious of this phenomenon. SC sample overtook MC sample 6.1MPa and HC sample 10.1MPa at 28 days. Compared with MC sample, the compressive strength of controlled trial sample (abbreviated to MC-97%RH sample) increased a little bit more during 3~28 days.

Above results indicate that the internal temperature and humidity change of mass concrete had a negative effect on the later development of compressive strength of cement pastes. It was the same with heat curing, but the negative effect of internal temperature and humidity change of mass concrete was slightly smaller. And the increase of late humidity of internal mass concrete can improve this adverse effect at some degree.

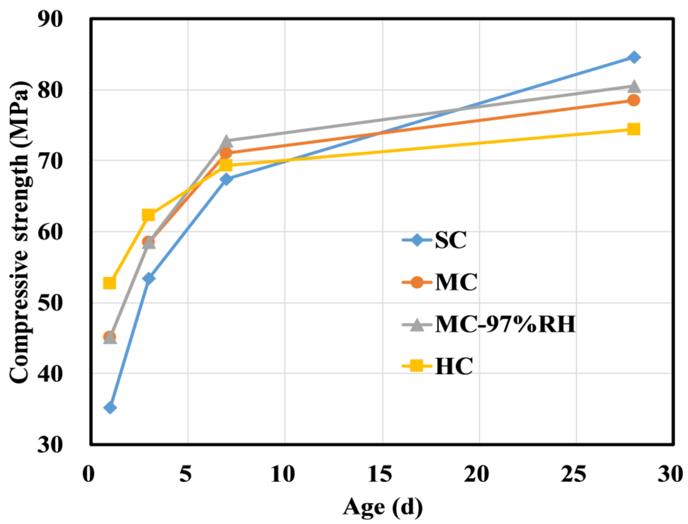

Figure 2 Compressive strength of cement pastes cured at different curing regimes

3.2. DEGREE OF HYDRATION

The degree of hydration was an important indicator of the cement hydration process. Figure 3 showed the degree of hydration of cement pastes cured at different curing regimes. The degree of hydration of MC sample and HC sample was much higher than SC sample at 1day. These huge differences of degree of hydration at 1day can explain the greater differences of compressive strength found at 1day. These illustrated that the rate of cement hydration was significantly affected by the temperature within 1day after molding. During the 1~3day, the hydration rate of SC sample was far faster than MC sample, reaching the minimum gap of degree of hydration. With the development of age, the gap between MC sample and SC sample had increased at 7d and slightly decreased at 28d. While the hydration rate of HC sample was always slower than SC sample after 1day. The gap of degree of hydration between HC sample and SC sample decreased with ages. Compared with MC sample, the hydration rate of MC-97%RH sample was a little faster after 3day.

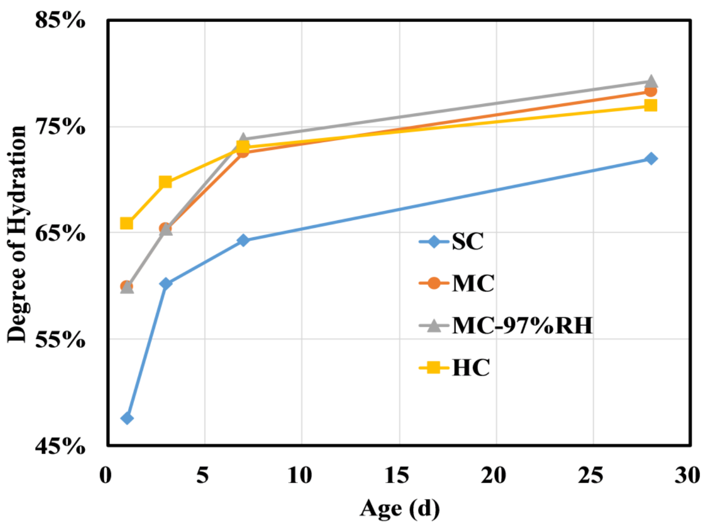

Figure 3 Degree of hydration of cement pastes cured at different curing regimes

The results of degree of hydration showed that elevated temperature within a day after molding would greatly promote cement hydration. The higher the temperature was, the more obvious of this phenomenon. The gap of degree of hydration between MC sample and SC sample got smallest at 3day. Because the degree of hydration of MC sample was 59.86% at 1d, due to the quantity limit of tricalcium silicate(C3S) and tricalcium aluminate(C3A)(occupied 56.43wt% of cement) which had a rapid hydration rate. The vast majority of C3S and C3A had been consumed in MC sample at 1d, resulting in a small increase of degree of hydration during 1~3d. While the degree of hydration of SC sample was 47.53% at 1d, although there was no temperature promoting, the rest C3S and C3A still kept a rapid hydration rate during 1~3d. The degree of hydration reached 60.18% at 3d. Along with the age, the ambient temperature of MC sample reached peak temperature and began to slowly decrease. promoted by the high temperature, the degree of hydration of MC sample got faster than SC sample during 3~7d. After 7d, due to the decrease of environmental humidity, the gap of degree of hydration between MC sample and SC sample got slower during 7~28d, consisting with the result of compressive strength. And the degree of hydration of MC-97%RH sample was higher than MC sample at 7 and 28 days, indicating that the increase of later humidity of internal mass concrete can promote the cement hydration. For HC sample, it was not promoted by elevated temperature after 1day. The internal hydration products around cement grains that had hydrated at early age would hinder subsequent hydration. Leading to that its hydration rate was always slower than the SC sample after 1day.

3.3. . CONTENT OF PORTLANDITE

Portlandite was an important material to maintain the high alkaline environment of cement paste. Figure 4 showed the portlandite content, determined by means of TGA. For each age, portlandite contents in MC sample, MC-97%RH sample and HC sample were compared to the reference SC sample.

The variations in portlandite with different curing regimes found with TGA showed significant difference in the formation rate of portlandite during first 1day of curing. Compared with SC sample, the portlandite data showed that rise in the curing temperature spurred the chemical reaction and early stabilization of the hydrated cement paste. It was the same with result of degree of hydration and compressive strength. But the formation rate of portlandite of samples promoted by elevated temperature at early age was all slower than SC sample at later period, especially for HC sample.

The slower formation rate of portlandite after 7days of MC sample related to slow down of hydration rate. Besides, the accumulation of dense internal hydration products around cement grains that had hydrated at early ages would hinder subsequent hydration. This phenomenon was more significant in HC sample. The formation rate of portlandite of HC sample gradually slow down after 1day. And the increase of portlandite content was nearly zero in HC sample during 7~28 days. While the formation rate of portlandite of MC-97%RH sample was a little bit faster than MC sample. But it was still slower than SC sample. These indicating that the early faster hydration rate would delay the formation of further hydration products. The faster of early hydration rate, the more significant of later adverse effects. But the increase of later curing humidity can improve this adverse effect at some degree.

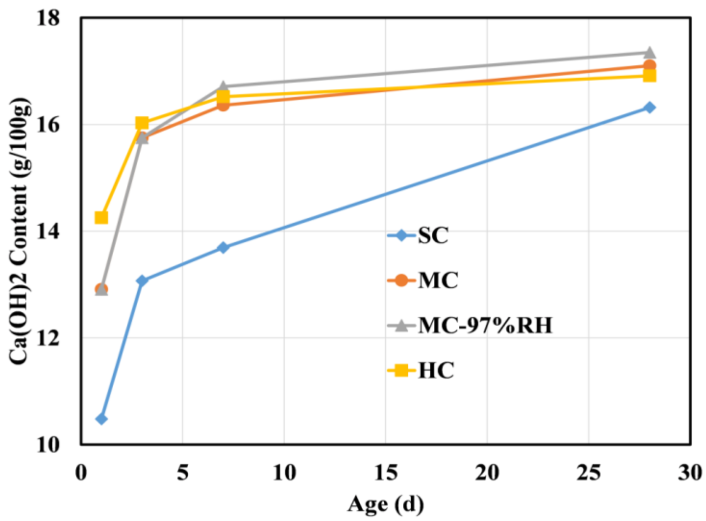

Figure 4 Variations in portlandite with different curing regimes

The relationship between compressive strength and degree of hydration for different curing regimes were shown in Figure 5. There were good linearity between compressive strength and degree of hydration, while the SC paste obtained a greater increase of strength than MC and HC pastes for a given decrease of degree of hydration. The MC paste has a slightly increase of strength than HC paste even though they have the same maximum curing temperature. The results show that the curing temperature dramatically affected compressive strength, the higher temperature the paste was cured, the lower compressive strength would be obtained, and with the same maximum curing temperature, the higher heating rate and cooling rate of HC sample also caused the lower compressive strength. The microstructure of cement paste is easily affected by the process of heat curing, the higher temperature and rapid process of heat curing would cause the cement paste has higher porosity and worse microstructure, which may be the reason for lower compressive strength.

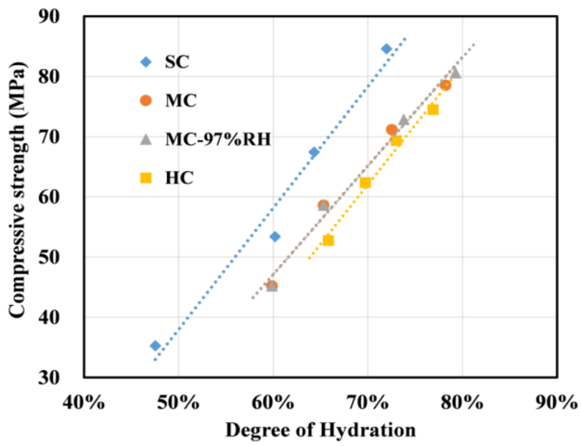

Figure 5 Compressive strength versus degree of hydration for different curing regimes

3.4. POROSITY

The evolution of the total porosity of pastes with different curing regimes were shown in Figure 6. At 1 day the SC sample has the highest total porosity, after which it declined sharply through the end of the test period. And the other three sets of samples followed the same pattern. While the decline rate of total porosity of the other three sets of samples was much slower than SC sample. Especially for the HC sample, the total porosity was smallest at 1day. When came to 28 days, the total porosity was highest. Compared with MC sample, the total porosity of MC_97%RH sample had been reduced at 7day and 28 days.

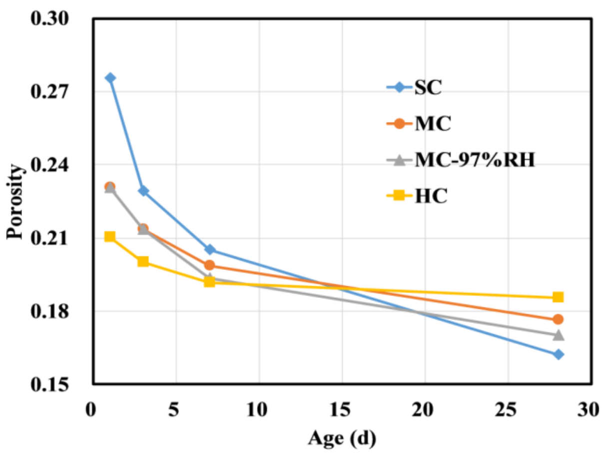

Figure 6 Evolution of the total porosity with different curing regimes

Further to the compressive strength test results and the portlandite content determined by TGA, curing at elevated temperature after molding accelerated initial hydration and raised early age compressive strength. But it had an adverse effect on the later mechanical performance development. The higher the temperature was, the more obvious of this effect. The explanation for these developments was when hydration took place too rapidly lying in insufficient time and space available for the hydration products to separate from the cement grains and precipitate evenly into the interstitial space [13]. It generated more porous structures in the late. By contrast, lower initial hydration rates (such as SC sample) provided sufficient time for hydration products to separate from the cement grains and precipitate evenly into the interstitial space. Compared with the total porosity of MC sample, porosity result of MC-97%RH sample showed that the increase of later curing humidity can alleviate the adverse effects caused by the early rapid hydration.

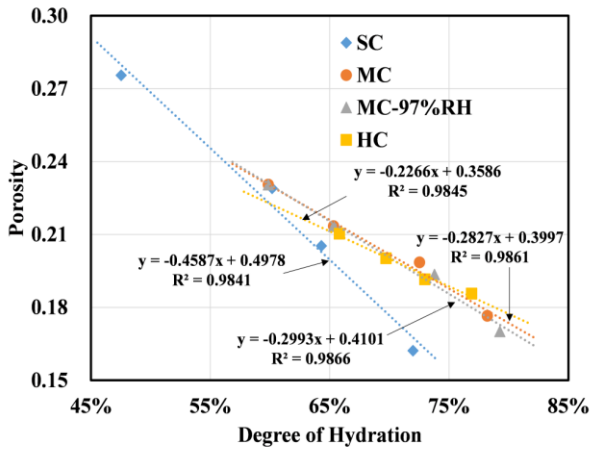

Figure 7 Porosity versus degree of hydration for different curing regimes

The porosity of cement paste shows a good linear relationship with the degree of hydration, as shown in Figure 7. However, pastes cured at different temperature present different tendency, when cured at elevated temperature, the paste has a much higher porosity for a given degree of hydration. Moreover, the paste cured at different curing regimes, with the same maximum temperature, also has different porosity for a given degree of hydration. Lower heating rate, cooling rate and higher subsequent relative humidity can slightly decrease the heat damage.

The relationship between compressive strength and porosity for different curing regimes were shown in Figure 8. Porosity is an important factor affecting the compressive strength of cement paste, there were also good linearity between compressive strength and porosity, while different curing regimes show different slopes. The HC paste has the steepest slope, and MC paste has a steeper slope than SC paste, thus for a given increase of porosity, the greatest decrease of compressive strength is obtained by HC paste, and MC get a greater decrease of compressive strength than the SC paste. MC-97%RH paste has a slightly gentler slope than the MC paste, which indicate that the subsequent higher relative humidity curing has good influence on porosity and compressive strength. The lines of four paste intersect at about the 0.19 porosity, above 0.19 porosity SC paste has a much greater strength than paste cured at elevated temperature. The same result was also reported by Feldman, the lines intersect at 0.27 porosity with water to cement ratio is 0.45. The same porosity has different compressive strength with different curing regimes, which show that curing by different regimes the pastes has different hydration products.

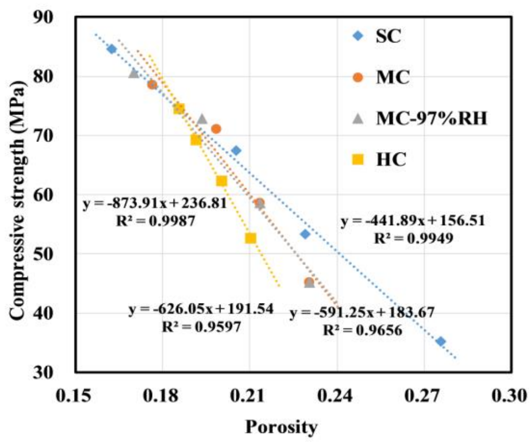

Figure 8 Compressive strength versus porosity for different curing regimes

3.5. BSE IMAGES

BSE images is a direct way to observe the microstructure of cement paste. The BSE images of cement pastes with different curing regimes are shown in Figure 9. As can be seen in Figure 9, at 1 day the standard curing sample has a more porous structure than the paste cured at elevated temperature, as a much lower degree of hydration. However, the microstructure of standard sample became much denser as it aged. And the microstructure of MC and HC samples didn't become much better, even worse after 7 days, which may be caused by the denser hydration products formed around anhydrous clinker particles at elevated temperature inhibited the hydration of cement paste. The subsequent high relative humidity curing can form a more compact structure, as seen the images of MC_28d and MC_97%RH_28d.

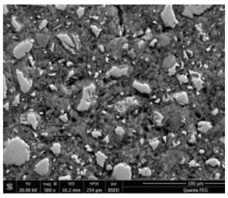
SC_1d

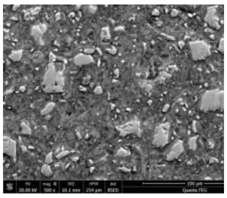
MC_1d

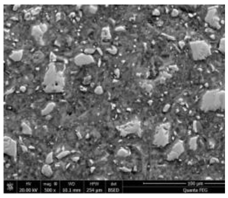
MC_97%RH_1d

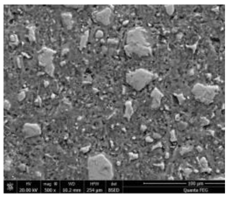
HC_1d

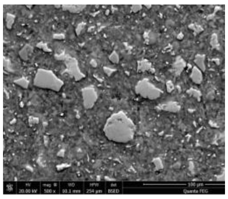
SC_3d

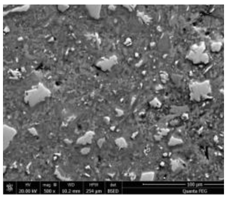
MC_3d

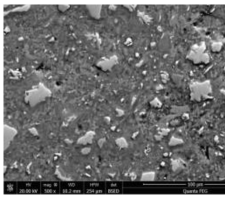
MC_97%RH_3d

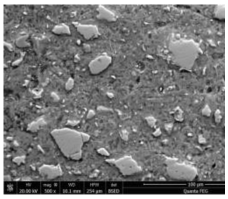
HC _3d

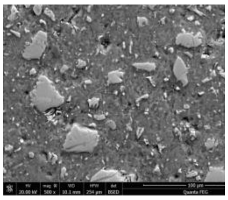
SC_7d

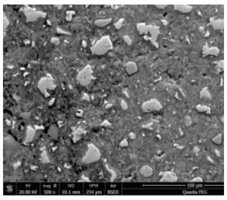
MC_7d

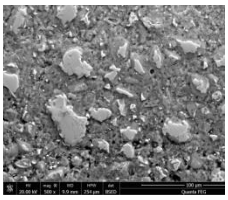
MC_97%RH_7d

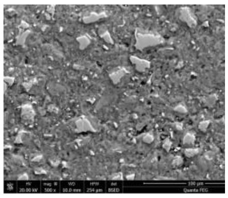
HC _7d

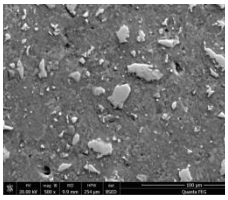
SC_28d

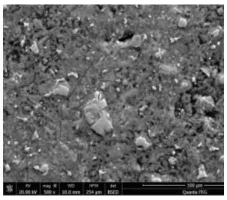
MC_28d

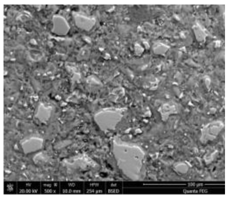
MC_97%RH_28d

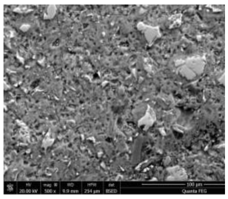
HC _28d

Figure 9 BSE micrographs of cement pastes cured at different regimes for 1,3,7 and 28 days

3.6. CHARACTERIZATION OF HYDRATION PRODUCTS

3.6.1. X-RAY DIFFRACTION

Figure 10 showed details of the XRD patterns of samples cured at different systems for 1,3,7 and 28 days. In addition to anhydrous cement, the diffractograms of four sets of samples showed the formation of portlandite and ettringite. No differences in paste composition were observed in the diffractograms. The mainly difference was the formation of ettringite.

Ettringite existed in SC sample in all age. While it only existed in MC sample at 1day and 3day. Then it disappeared at 7days and 28 days. In MC_97%RH sample, the diffraction peak intensity of ettringite diminished with the age. And it was nearly undetectable at 28 days. In HC sample, the diffraction peak intensity of ettringite gradually increased with the age. And it was nearly undetectable at 1day.

These results showed that the rapid enhance of temperature internal mass concrete was not conducive to the growth and existence of ettringite. Especially when the temperature reached 55℃ at 80h which was slightly away from the decomposition temperature of ettringite (around 70 ℃). But the increase of later curing humidity would be benefit to the existence of ettringite. On the other hand, the heat curing would delay the formation of ettringite. It was very different from the influence of internal temperature and humidity changes of mass concrete. The formation of ettringite is easily affected by the temperature, when cured at elevated temperature, even lower than 70 ℃, the crystal size of ettringite is dramatically smaller than cured at lower temperature. Moreover, when cured at elevated temperature, the Al and S ions in the pore solution are more easily absorbed by C-S-H gel, thus inhibit the formation of ettringite. And after heat curing, the Al and S ions absorbed by C-S-H gel at elevated temperature would be released into the pore solution, then the ettringite would be formed again. The long time at elevated temperature and low relative humidity in mass concrete caused no obvious ettringite peak was observed at 28 days.

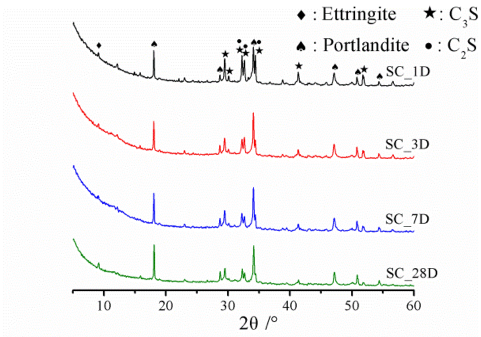

SC

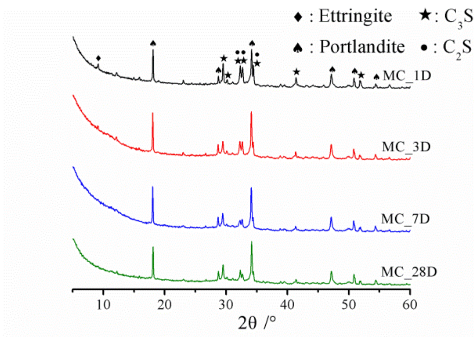

MC

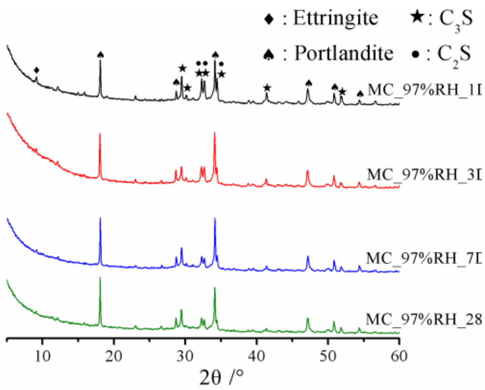

MC-97%RH

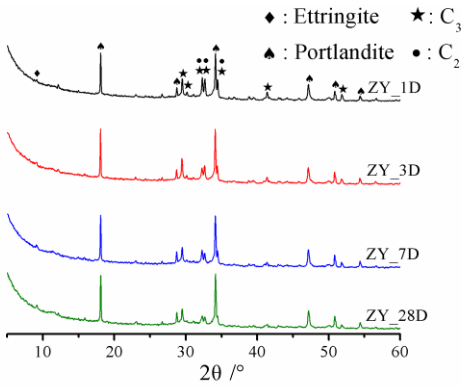

HC

Figure 10 XRD patterns of cement paste hydrated under different conditions

3.6.2. ANALYSIS OF C-S-H GEL

^{29}Si magic angle spinning (MAS) NMR spectroscopy was a technique used to characterize the state of polymerization of the silicates (i.e., tetrahedral $SiO4^{4-}$) in the cement paste. It was used to monitor cement hydration kinetics at different curing regimes. The spectra in Figure 11 represented the ^{29}Si findings, respectively, for cement pastes hydrated at different curing regimes for 1,3,7 and 28 days.

According to the deconvolution data shown in Table 2, there was obvious difference of Q^2 units in four samples. Compared with SC sample, there were more Q^2 units in MC sample, MC-97%RH sample and HC sample at each curing age. This was consistent with the results of degree of hydration and portlandite content. Indicating the conversion of the anhydrous Q^0 species to Q^1 and Q^2 units was promoted by elevated temperature. In addition, the mean chain length (MCL) was calculated from the relative fractions of the different Q-species by substituting the deconvolution data for the ^{29}Si NMR spectra into the following equation [14, 15]:

$MCL=[Q^1+Q^2+3/2Q^2(1Al)]/0.5Q^1$.

The results (Table 2) showed that the elevated temperature at early age would promoted the increase of MCL. The faster of early age temperature rose, the more obvious of this phenomenon. And the high degree of polymerization of C-S-H gel can also explain the greater compressive strengths found at 1day in MC sample, MC-97%RH sample and HC sample. While the early age formation of C-S-H gel with long chains may hinder the uptake of further hydration products. This in turn generated more porous and heterogeneous and consequently less cohesive structures. And it can be observed from BSE image [16]. Besides, the MCL of all samples rose with time. But after 7day, the growth was very slow. It may attributed to content restriction of Q^{0H} (hydrated silicate monomer) which can polymerize with protonated C-S-H gel dimer to form C-S-H gel high-mer.

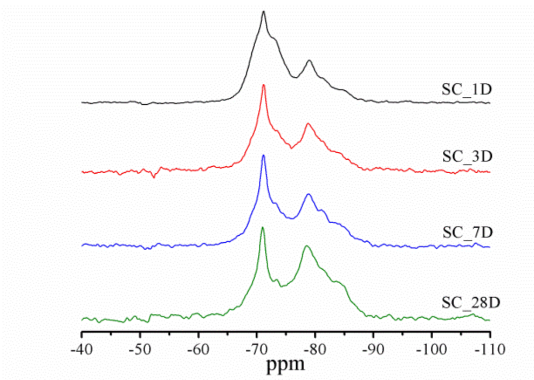

SC

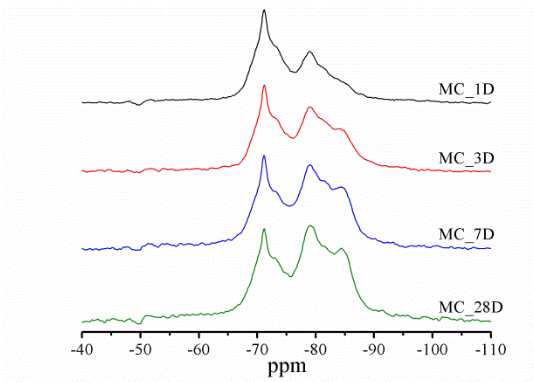

MC

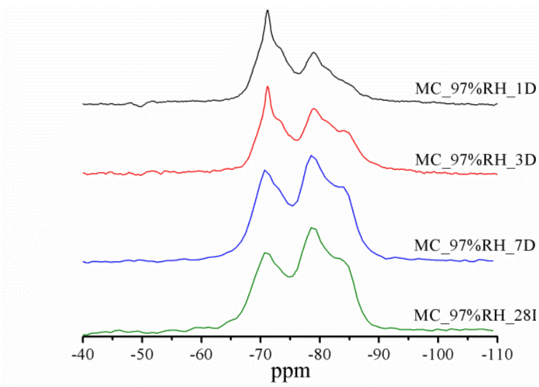

MC-97%RH

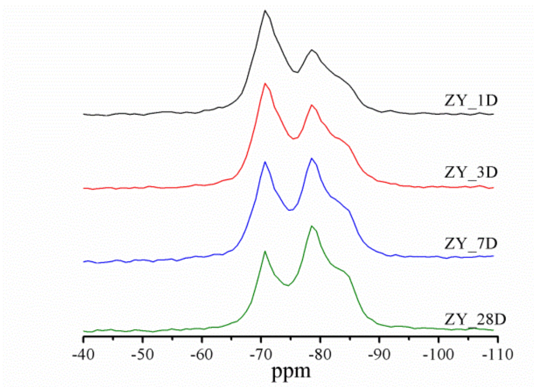

HC

Figure 11 ^{29}Si NMR spectras for cement pastes hydrated at different conditions

Table 2 Deconvolution data of 29Si NMR spectra of cement paste

Sample	Age/d	$Q^0(C_3S,C_2S)$	Q^1	Q^2(1Al)	Q^2(0Al)	MCL
SC	1	69.61%	19.91%	6.25%	4.19%	3.36
	3	59.12%	22.43%	9.20%	9.25%	4.06
	7	54.95%	23.26%	10.24%	11.55%	4.31
	28	45.58%	27.70%	12.72%	14.00%	4.39
MC	1	60.11%	20.12%	10.75%	9.02%	4.50
	3	48.31%	22.80%	12.20%	16.69%	5.07
	7	43.78%	24.33%	13.09%	19.31%	5.20
	28	40.84%	25.20%	13.93%	20.03%	5.25
MC-97%RH	1	60.11%	20.12%	10.75%	9.02%	4.50
	3	48.31%	22.80%	12.20%	16.69%	5.07
	7	40.78%	24.89%	14.73%	19.58%	5.35
	28	38.55%	25.73%	15.61%	20.10%	5.38
HC	1	58.50%	19.54%	8.05%	13.91%	4.66
	3	51.66%	20.64%	10.42%	17.28%	5.19
	7	46.76%	22.79%	14.91%	15.54%	5.32
	28	39.06%	26.08%	16.42%	19.45%	5.40

4. CONCLUSIONS

In comparison to standard curing and heat curing, this study showed the effect of internal temperature and humidity change of mass concrete on cement hydration, microstructure and hydration products. When the maximum temperature of internal mass concrete and heat curing was both 55℃. The promotion of internal temperature and humidity change of mass concrete on cement hydration was less than heat curing at early age. It was attributed to the slower temperature rose of internal mass concrete. While the thermal damage on cement paste was also present in mass concrete. It can be seen from the results of porosity and microstructure. But the negative of internal temperature and humidity change of mass concrete on compressive strength and microstructure was weaker than heat curing at late stage. And the increase of later curing humidity can improve this adverse effect at some degree. This finding can be explained as follows:

1. Internal high temperature of mass concrete decreased the compressive strength, degree of hydration and increase the porosity as it ages, which is similar to heat-cured concrete, while the heat damage of mass concrete is slightly lower than the heat-cured concrete and the subsequent higher relative humidity curing can decrease the heat damage.
2. The relationships between compressive strength and porosity, as well as degree of hydration and porosity of paste with different curing regimes, are in linearity. However, when paste cured at elevated temperature has a much lower compressive strength for a given porosity, and a much higher porosity for a given degree of hydration.
3. The internal temperature and humidity change of mass concrete was not conducive to the growth and existence of ettringite. While the heat curing would delay the formation of ettringite.
4. Drying damage was also present in mass concrete, and increased the later curing humidity of internal mass concrete can improve the adverse effect of thermal damage and drying damage, which can be seen from the results of porosity, microstructure and portlandite content.

REFERENCES

[1] MH Leea., and BS Khilb. (2014). "Influence of cement type on heat of hydration and temperature rise of the mass concrete." Indian Journal of Engineering and Materials Sciences, 21:536-542

[2] Riding K A., and Poole J L. (2014). "Statistical Determination of Cracking Probability for Mass Concrete." Journal of Materials in Civil Engineering, 26(9):148-148.

[3] Corporation H P. (2014). "Experimental Study on Early-Age Crack of Mass Concrete under the Controlled Temperature History." Advances in Materials Science and Engineering, 12(3):352-358.

[4] Lawrence A M., and Tia M. (2014). "Considerations for Handling of Mass Concrete: Control of Internal Restraint." Aci Materials Journal, 111(1):3-11.
[5] Lawrence A M., and Tia M. (2014). "Effect of Early Age Strength on Cracking in Mass Concrete Containing Different Supplementary Cementitious Materials: Experimental and Finite-Element Investigation." American Society of Civil Engineers, 24(4):362-372.
[6] Escalante-Garcıa J I., and Sharp J H. (1998). "Effect of temperature on the hydration of the main clinker phases in Portland cements." Cement and Concrete Research, 28(9): 1259-1274.
[7] Martínez-Ramírez S., and Frías M. (2009). "The effect of curing temperature on white cement hydration." Construction and Building Materials, 23(3): 1344-1348.
[8] Zain M F M., and Radin S S. (2000). "Physical properties of high-performance concrete with admixtures exposed to a medium temperature range 20℃℃ to 50℃℃." Cement and concrete research, 30(8): 1283-1287.
[9] [9] Elkhadiri I., and Palacios M. (2009). "Effect of curing temperature on hydration process of different cement." Ceramics-Silikáty, 53(2): 65-75.
[10] Ha J H., and Jung Y S. (2014). "Thermal crack control in mass concrete structure using an automated curing system." Automation in Construction, 45:16–24.
[11] Zhou Y., and Bai L. (2012). "Simulation Analysis of Mass Concrete Temperature Field." Procedia Earth and Planetary Science, 5(32):5–12.
[12] Wang F Z., and Yang J. (2016). "Influence of superabsorbent polymers on the surrounding cement paste." Cement and Concrete Research, 81:112-121.
[13] Lothenbach B., and Winnefeld F. (2007). "Effect of temperature on the pore solution, microstructure and hydration products of Portland cement pastes." Cement and Concrete Research, 37(4):483-491.
[14] Richardson I G, Brough A R, Brydson R, et al. Location of Aluminium in Substituted Calcium Silicate Hydrate (C–S–H) Gels as Determined by 29Si and 27Al and EELS[J]. Journal of the American Ceramic Society, 2005, 76(9):2285-2288.
[15] Richardson I G. (1999). "The nature of C-S-H in hardened cements." Cement and Concrete Research, 29(8):1131–1147.
[16] Elkhadiri I., and Puertas F. (2008). "The effect of curing temperature on sulphate-resistant cement hydration and strength." Construction and Building Materials, 22(7):1331–134

POTENTIAL FOR APPLICATION OF WASTE MATERIALS AS MINERAL ADMIXTURE FOR MAKING OF SELF-COMPACTING CONCRETES

Nenad Ristic[1], Zoran Grdic[1], Gordana Toplicic-Curcic[1], Dusan Grdic[1], Dejan Krstic[1]

[1] University of Nis, Faculty of Civil Engineering and Architecture, Aleksandra Medvedeva 14, 18 000 Nis, Serbia, email: nenad.ristic@gaf.ni.ac.rs, zoran.grdic@gaf.ni.ac.rs, gordana.toplicic.curcic@gaf.ni.ac.rs, dusan.grdic@gaf.ni.ac.rs, dejan.krstic@gaf.ni.ac.rs

SUMMARY: The basic principle of sustainable construction is usage of building materials which will not have negative effects on the environment, as well as proper management of waste materials generated during construction or demolishing of structures. Rapid technological and industrial development in the recent decades caused big environmental problems, and one of the most significant is, undoubtedly, disposal and recycling of waste materials and by-products of industrial production. Since concrete is a composite material, waste materials can suitably be used in its composition. Waste materials in concrete can be used as partial substitution of cement, partial substitution of aggregate or as reinforcement of concrete composite. In this paper, the research of effects of milled recycled glass from cathode tubes, flotation tailings from a copper mine, fly ash, red mud and limestone filler as mineral admixtures on properties of fresh and hardened self compacting concrete was presented. The test results indicated that addition of such materials does not cause a drop in performance quality of self-compacting concretes in fresh and hardened states, and they even improve certain properties of concrete. Waste materials such as fly ash and recycled glass of cathode tubes exhibit a pozzolanic activity, so the performances of the concretes with these admixtures proved to be better after ageing than the concretes with other admixtures.

POTENCIJAL PRIMJENE OTPADNIH MATERIJALA KAO MINERALNOG DODATNOG SASTOJKA PRI IZRADI SAMOZBIJAJUĆIH BETONA

SAŽETAK: Osnovno načelo održive gradnje upotreba je građevnih materijala koji neće imati negativne učinke na okoliš i odgovarajuće upravljanje otpadnim materijalima koji nastaju pri gradnji i rušenju građevina. Brzi tehnološki i industrijski razvoj posljednjih desetljeća prouzročio je velike probleme za okoliš. Jedan od najvažnijih bez sumnje je odlaganje i recikliranje otpadnih materijala koji su nusproizvodi industrijske proizvodnje. Kako je beton kompozitni materijal prikladno je u njegovu sastavu upotrijebiti otpadne materijale. Otpadni se materijali u betonu mogu upotrijebiti kao djelomična zamjena cementa, djelomična zamjena agregata ili za armiranje cementnoga kompozita. U radu je prikazano istraživanje učinaka reciliranog mljevenog stakla iz katodnih cijevi, jalovine nakon flotacije iz rudnika bakra, letećeg pepela, crvenoga mulja i vapnenačkog filera kao mineralnih dodataka na svojstva svježega i očvrsnuloga samozbijajućeg betona. Rezultati ispitivanja pokazuju da dodavanje takvih materijala ne uzrokuje pad kvalitete samozbijajućih betona u svježem i očvrsnulom stanju nego da su neka svojstva betona čak i poboljšana. Otpadni materijal kao što su leteći pepeo i reciklirano staklo iz katodnih cijevi pokazuju pucolansku aktivnost pa će svojstva betona s tim dodacima biti bolja tijekom vremena nego li kod betona s drugim dodacima.

1. INTRODUCTION

The basic principle of sustainable construction is usage of building materials which will not have negative effects on the environment, as well as proper management of waste materials generated during construction or demolishing of structures. Increasing attention is paid to the rapid technological and industrial development in the recent decades which caused big environmental problems, and one of the most significant is, undoubtedly, disposal and recycling of waste materials and by-products of industrial production. On the other hand, concrete, being a composite and frequently used building material is fitting for usage of waste materials as components in its composition. Waste materials in concrete can be used as partial substitution of cement, partial substitution of aggregate or as reinforcement of concrete composite. Exactly integration of those materials into concrete itself can, to a considerable extent, contribute to solving the problem of their disposal. However, in order to achieve this goal, it is important to establish how these materials affect the concrete properties, and what quantities of them can be added without compromising strength and durability of concrete which make it such a suitable building material.

In this paper, the research of effects of milled recycled glass from cathode tubes, flotation tailings from a copper mine, fly ash, red mud and limestone filler as mineral admixtures on properties of fresh and hardened self compacting concrete was presented. The composition of self-compacting concrete can be designed in multiple ways, but one must take care to achieve certain adequate rheological properties of fresh concrete, such as fluidity, viscosity, resistance to segregation [1]. Each of the mentioned materials has a characteristical impact on concrete, so it is necessary to individually examine each one prior to making concrete.

Fly ash is very frequently used as admixture when making self-compacting concrete. The research established that addition of fly ash reduces slump time T_{500} [2], porosity [3] as well as shrinking and creeping [4]. The spherical shape of ash particles increases mobility and workability of concrete. Presence of fly ash retards alite reaction, so early concrete strengths are lower in comparison with the usual values of SCCs without mineral admixtures. However, in time the strength increases and after 90 days, it is equal to the corresponding reference concrete. Because of the reduced porosity, concretes with the admixture of fly ash achieve, in general, higher terminal strengths [5], but this impact considerably depends on the amount of added ash. Excessive quantity of fly ash in concrete can lead to reduction of its strength [6-8].

In the copper production process, large quantities of waste material are generated whose disposal represents large environmental issue. Flotation tailings, as one of the by-products of copper production, are rich in iron oxides and silicates, and thus it is suitable for production of concrete and mortar. Depending on its chemical composition, they can be used either as an admixture to ordinary Portland cement, or as a replacement of fine aggregate particles. This method may solve this large metallurgical environmental issue and bring a great financial benefit, while simultaneously leading to reduction of gases emission and energy consumption related to production of the same quantity of materials whereby natural resources remain preserved [9]. Onuaguluchi and Eren in their researches demonstrated that concretes with admixture of flotation tailings possess improved mechanical characteristics in comparison to vibrated concrete. Compressive, tensile shear and flexural strengths of SCCs with the mineral admixture of flotation tailings are increased. Also, an increased resistance to abrasion and lower chloride penetration depth were observed. Such improved characteristics are more prominent in cases when 5% of flotation tailings are used and when water/cement ratio is high (water absorption is increased, when flotation tailings are used) [10]. They also tested chemical action on concretes comprising flotation tailings, and on their basis they determined that the increase of presence of flotation tailings in concrete increases acid action resistance, but simultaneously reduces resistance to destructive sulphate expansion [11].

In the Bayer alumina production process, red mud created as a waste is composed mostly from hematite, goethite, quartz, boehmite, calcite, tricalcium aluminate, zinc and magnesium oxide, sodium hydroxide etc. What makes red mud a a dangerous polluter of land, ground and surface waters is alkaline liquid phase which filters down from disposal sites into ground waters carrying with it a still high content of sodium [12-13]. A large number of studies done in the world relate to the various aspects of implementation of red mud as a composite element of mortars and concretes: as cement replacement, partial replacement of fine aggregate in mortars, integral part of geopolymers, etc. On the basis of the tests performed on SCC, it was established that red mud admixture increases viscosity, reduces fluidity and considerable reduces segregation and concrete bleeding, i.e. water separation. On the other hand, porosity of SCC increases, but shrinking reduces [14]. Density of hardened concrete also reduces with the admixture of red mud. Compressive strength yields higher values in relation to the reference SCC after 90 days. Flexural and tensile splitting strengths are considerably higher in comparison with the reference self-compacting concrete made without red mud [14-15].

Limestone filler in SCC contributes to increase of fluidity and viscosity and to reduction of concrete porosity [16-17]. Fluidity of SCC made with milled limestone increases with the fineness of the admixture particles. In comparison to the SCC wit fly ash, concrete with milled limestone has a higher water permeability and lower frost resistance [18]. Limestone contributes to creation of large pores in concrete which are formed around larger particles, which acts as hydration inhibitor in an early hardening stage [17].

There were numerous tests of application of recycled glass as a partial replacement of fine aggregate for making of SCC. [19-20]. The test results showed that with the increase of recycled glass content in concrete, fluidity and air content increase, but mechanical strengths and static elasticity model are reduced. When SCC with limestone filler was tested, it was established that compressive strength and ultrasound velocity increase with the increase of recycled cathode ray tube glass content [21].

2. EXPERIMENTAL RESEARCH

2.1. USED MATERIALS

The cement used for making of concrete mixtures was manufactured by „CRH“ CEM I 42,5 R, whcih complies with all the quality requirements prescribed by SRPS EN 197-1 standard. Three fractions of river aggregate used (0/4 mm, 4/8 mm i 8/16 mm) originate from the South Morava river, and they comply with all the quality requirements prescribed by SRPS EN 206-1 and EN 12620 standard. Limestone filler was obtained by milling stone from the „Babin Kal“ quarry near Bela Palanka, fly ash is from the Kostolac B coal-fired power plant, flotation tailings are from the Mining and Smelting Combine Bor, red mud is from the Aluminum Plant Podgorica created in the Bayer process of aluminum production. Recycled cathode ray tube glass was taken from the company „E-reciklaža“ Niš and milled in the laboratory mill. The superplasticizer Sika Viscocrete 5380 was used as chemical admixture in the mixtures.

2.2. CONCRETE MIXTURE COMPOSITION

A total of five different mixtures of SCCs were made for the requirements of the experimental research, those being: mixture with the mineral admixture of limestone filler (mixture designated LF), mixture with te admixture of powdered recycled glass of cathode ray tubes (RS), mixture with the admixture of fly ash (EP), mixture with the admixture of flotation tailings (FT) and mixture with the admixture of red mud (RM). Concrete mixtures differ only in terms of the implemented powder admixtures type. All these admixtures are finer than 0,125 mm, because they were passed through an adequate sieve. The percentage share of component volume in 1 m^3 of concrete is the same for all the concrete mixtures. All the concrete mixtures were made so as to have a similar spreading (around 650 mm) when concrete fluidity is tested. This condition is met by varying the superplasticizer quantity. Compositions of concrete mixtures for 1 m^3 of concrete are given in Table 1.

Table 1 Composition of 1m^3 of concrete mixtures used in the experiment

<table>
<tr><th colspan="3">Kinds of materials</th><th colspan="2">Percentage of volume in 1m³ [%]</th><th>Volume in 1m³ [m³]</th><th>Density [kg/m³]</th><th>Mass in 1m³ [kg]</th></tr>
<tr><td colspan="3">Cement</td><td colspan="2">12.7</td><td>0.127</td><td>3150</td><td>400</td></tr>
<tr><td colspan="3">Water</td><td colspan="2">18.15</td><td>0.1815</td><td>1000</td><td>181.5</td></tr>
<tr><td colspan="2">Fine aggregate</td><td>0/4 mm</td><td colspan="2">29.62</td><td>0.2962</td><td>2620</td><td>776</td></tr>
<tr><td colspan="2" rowspan="2">Coarse agregat</td><td>4/8 mm</td><td rowspan="2">31.69</td><td>11.58</td><td>0.1158</td><td>2650</td><td>307</td></tr>
<tr><td>8/16 mm</td><td>20.11</td><td>0.2011</td><td>2650</td><td>533</td></tr>
<tr><td colspan="3">Assumed air content</td><td colspan="2">2.0</td><td>0.02</td><td>–</td><td>–</td></tr>
<tr><td rowspan="10">Designation of the mixture</td><td rowspan="2">LF</td><td>Limestone filler</td><td colspan="2">5.5</td><td>0.055</td><td>2720</td><td>150</td></tr>
<tr><td>Superplasticizer</td><td colspan="2">0.45</td><td>0.0045</td><td>1100</td><td>4.95</td></tr>
<tr><td rowspan="2">RG</td><td>Recycled glass</td><td colspan="2">5.5</td><td>0.055</td><td>2840</td><td>156</td></tr>
<tr><td>Superplasticizer</td><td colspan="2">0.40</td><td>0.0040</td><td>1100</td><td>4.40</td></tr>
<tr><td rowspan="2">FA</td><td>Fly ash</td><td colspan="2">5.5</td><td>0.055</td><td>2130</td><td>117</td></tr>
<tr><td>Superplasticizer</td><td colspan="2">0.50</td><td>0.0050</td><td>1100</td><td>5.50</td></tr>
<tr><td rowspan="2">FT</td><td>Flotation tailings</td><td colspan="2">5.5</td><td>0.055</td><td>3150</td><td>173</td></tr>
<tr><td>Superplasticizer</td><td colspan="2">0.43</td><td>0.0043</td><td>1100</td><td>4.68</td></tr>
<tr><td rowspan="2">RM</td><td>Red mud</td><td colspan="2">5.5</td><td>0.055</td><td>2710</td><td>149</td></tr>
<tr><td>Superplasticizer</td><td colspan="2">0.80</td><td>0.008</td><td>1100</td><td>8.80</td></tr>
</table>

2.3. TYPES OF TESTS INVESTIGATED ON THE FRESH AND HARDENED CONCRETE

The following tests were conducted on the fresh concrete: density according to SRPS EN 12350-6:2010 standard, air content in concrete according to SRPS EN 12350-7:2010, slump flow test and T_{500} spreading test according to SRPS EN 12350-8:2012 standard, workability using L-box test according to SRPS EN 12350-10:2012 standard and the segregation test using sieves according to SRPS EN 12350-11:2012 standard.

The tested physical properties of the hardened concrete were the density of water saturated concrete according to SRPS EN 12390-7:2010 standard, using the specimen cubes having sides of 15cm at the age of 2, 7, 28 and 90 days. Also tested were mechanical properties of concrete, the most important being compressive strength. This characteristic was tested according to SRPS EN 12390-3:2010 standards, on cube shaped specimens having sides of 15cm at the age of 2, 7, 28 and 90 days. The flexural strength test was performed on the prism shaped specimens, having dimensions 10×10×40 cm at the age of 28 and 90 days according to SRPS EN 12390-5:2010 standard. Also, the splitting tensile strength test (Brazilian test) was performed on cylindrical specimens having diameter Ø15 cm and length 30 cm at the age of 28 and 90 days according to SRPS EN 12390-6:2012 standard. „Pull-off" strength test was performed on the cubes having sides 15 cm at the age of 28 and 90 days according to SRPS EN 1542:2010 standard.

The primary goal of this research is testing potential for application of waste materials as mineral admixture for making of SCC. For that reason, the concrete mixture with limestone filler (LF) can be considered a reference mixture used for comparison with other mixtures which contain admixtures of recycled cathode ray tube glass, fly ash, flotation tailings and red mud.

The previous tests according to SRPS B.C1.018 standard established that only fly ash and pulverized recycled ray tube glass exhibit puzzolanic activity. Other powder admixtures can be considered inert.

3. RESULTS OF EXPERIMENTAL RESEARCH

The test results of fresh and hardened concrete are provided in Tables 2 and 3. The tables provide mean values of the obtained test results.

Table 2 Characteristic concrete in fresh state

Properties	Unit	Test results				
		LF	RG	FA	FT	RM
Density	kg/m^3	2375	2390	2340	2385	2365
Air content	%	2.0	0.8	2.9	2.8	2.6
Test T_{500} time	s	3.5	4.5	7.0	6.0	6.5
Slump flow test	mm	650	660	640	660	640
Tests using the L - box H_2/H_1	(mm/mm)	0.94	0.95	0.91	0.92	0.87
Testing segregation using sieves	%	14.0	12.8	5.6	6.8	6.0

Table 3 Characteristic concrete in hardened state

Properties	Unit	Age of samples	Test results				
			LF	RG	FA	FT	RM
Density of water saturated specimen	kg/m^3	2 days	2375	2390	2340	2385	2365
		7 days	2372	2388	2338	2382	2363
		28 days	2370	2385	2336	2380	2359
		90 days	2370	2383	2335	2378	2356
Compressive strength	MPa	2 days	39.6	38.7	44.6	36.6	41.2
		7 days	49.1	47.7	51.0	46.2	45.0
		28 days	56.3	59.0	59.6	59.7	54.0
		90 days	65.1	72.2	69.3	64.7	57.0
Flexural strength	MPa	28 days	6.3	6.4	5.6	5.3	7.3
		90 days	7.0	7.7	7.8	6.3	8.4
Tensile splitting strength	MPa	28 days	4.4	4.2	4.8	4.0	4.0
		90 days	4.7	5.5	5.1	4.2	4.3
Bond strength by Pull-off test	MPa	28 days	3.7	4.2	4.4	4.0	3.8
		90 days	4.0	4.9	4.8	4.3	4.1

4. DISCUSION OF RESULTS AND CONCLUSION

Based on the test results of fresh concrete density, Table 2, it can be concluded that it primarily depend on the specific mass of the used mineral admixture, but also on the air content in concrete which is noticeable in the case of concrete mixture with cathode ray tube glass admixture (the mixture designated with RG). The highest density is demonstrated exactly by the mixture having the RG designation, which has 15 kg/m^3 more than the reference concrete with limestone filler, and the least density is demonstrated by the mixture with fly ash having FA designation, which has 35 kg/m^3 less than the reference concrete.

In terms of air content in fresh concrete, the mixture designated with RG had the lowest value, i.e. 0,8%, and the mixture designated with FA had the highest value (2,9%). Almost all concrete mixtures with the exception of RG have the approximately same air content and they have similar values to the reference LF, Table 2.

As it was already said, all the concrete mixtures were made to have approximately same spread (around 650 mm) on the event of testing concrete fluidity, Table 2, which was achieved by implementing superplasticizer. T_{500} test indicates viscosity of concrete mixture, and represents the time in which the concrete achieves the spread of 500 mm when testing fluidity. Based on the test results in the Table 2, it can be concluded that all concrete mixtures with the admixture of waste materials have higher values of T_{500} test than the reference concrete. The FA mixture had the highest spread time for 500 mm, the mixtures RM and FT were similar, while the RG mixture had a similar value as the LF reference concrete.

Filling ability was determined using L-box test, and other methods can be implemented as well: U – box, J – ring and Kajima box. On the basis of the test results from the Table 2, it can be concluded that RG mixture has the best filling ability while the RM mixture has the lowest ability in comparison to the other mixtures. FA and FT mixtures had mutually similar values, but lower than the reference, LF mixture.

Segregation resistance is expressed as the percentage of the amount of concrete which passed through the sieve with 5 mm openings in comparison with the total mass. Based on the results from the Table 2, it can be concluded that all the mixtures with waste materials have a higher resistance in respect to the reference concrete LF, whereby the best resistance was demonstrated by the FA mixture, followed by RM, FT and RG mixtures, respectively.

As for the properties of hardened concrete, densities of water saturated concrete at the age of 2, 7, 28 and 90 days are coordinated with the density of fresh concrete, Table 3. As well as in the case of fresh concrete, differences occur due to the various specific masses of mineral powder admixtures and air content in concrete.

Compressive strengths of concretes, as one of the most important characteristics of concrete, are mutually similar at corresponding age of concrete, Table 3. At the age of 2 days, the highest strength was exhibited by the FA mixture which is 12,6% higher than LF reference concrete, and the lowest by the FT mixture which is 7,6% lower than LF. At the age of concrete of 7 days, the highest strength was demonstrated by the FA mixture which is 3,9% higher than the LF reference, and the lowest was demonstrated by the RM mixture which is 8,4% lower than LF. At the age of 28 days, the highest compressive strength increase was demonstrated by the FT mixture. It simultaneously had the highest compressive strength, as well, which is 6,0% higher than the LF, while the lowest value was exhibited by the RM which was 4,1% lower than the LF. At the age of 90 days, the highest increase and highest value of compressive strength was exhibited by the RG mixture, while the FA mixture exhibited a slightly lower increase, followed by the LF and FT mixtures, while the lowest mixture was exhibited by the RM mixture. Compressive strength of the RG mixture was 10,9% higher than LF, while compressive strength of the RM mixture is 12,4% lower than the LF. This was expected, since among all the mineral admixtures, only fly ash and pulverized recycled glass demonstrated puzzolanic activity.

The highest value of flexural strength at the age of 28 days was demonstrated by the RM mixture which contained red mud admixture, which was 15,9% higher than the LF reference value, and the lowest value was demonstrated by the FT mixture which contained flotation tailings, which was 15,9% lower than EF. The mixture containing recycled glass from cathode ray tubes had a flexural strength similar to the LF mixture, while the mixture containing fly ash admixture had 11,1% lower value than the LF reference. At the age of 90 days, the highest increase of flexural strength was exhibited by the RM mixture, whose value is 20,0% higher than the LF mixture. The FT mixture had the lowest value of flexural strength, which was 10,0% lower than the LF, while the RG and FA mixtures had 10,0% and 11,4% higher flexural strength, respectively, than the LF mixture.

In terms of tensile splitting strength at the age of 28 days, all the concrete mixtures had the similar strength values. All the concrete mixtures made with waste materials, except the FA mixture with fly ash had the lower tensile split values than the LF reference. The highest value was exhibited by the FA mixture which is 9,1% higher than the LF, and the lowest by the FT and RM mixtures, 9,1% lower than the LF. At the age of 90 days, the highest tensile splitting strength increase was exhibited by the RG mixture, whose value was 17,0% higher than the LF mixture. The lowest value of tensile splitting strength was exhibited by the FT mixture which was 10,6% lower than the LF. The RM mixture had a s similar value, while the FA mixture had 8,5% higher tensile splitting strength than the LF mixture.

In case of the bond strength Pull-off tests, all the concrete mixtures had the similar strength values. At the age of 28 and 90 days, all the concrete mixtures made with waste materials, had the higher bond strengths in comparison with the LF reference. At the age of 28 days, the highest value was exhibited by the FA mixture which was 18,9% higher than the LF reference, and the lowest value of all the waste material mixtures by the RM mixture which was 5,4% higher than the LF. At the age of 90 days, the highest value was exhibited by the RS which was 22,5% higher than the LF reference. The FA mixture had the similar value, while the lowest value was shown by the RM mixture which was 2,5% higher than the LF.

Based on the test results of SCC with the admixture of waste materials, it can be concluded that addition of these materials does not considerably reduce the quality of fresh and hardened concrete performances. It can be said that they even contribute to the increase of certain concrete properties presented in this paper. A special attention must be paid to the durability of concrete mixtures containing admixture of waste materials such as cathode ray tube recycled glass, fly ash, flotation tailings and red mud. Further research should be focused on that aspect, since proofs of unaffected durability would complete the study of potential application of these materials for making of concrete.

ACKNOWLEDGMENTS

The work reported in this paper is a part of investigation within the research project TR 36017 „Utilization of by – products and recycled waste materials in concrete composites in the scope of sustainable construction development in Serbia: investigation and environmental assessment of possible applications“ supported by Ministry for Science and Technology, Republic of Serbia. This support is gratefully acknowledged.

REFERENCES

[1] Nina Štirmer N.; Banjad Pečur I.: Mix design for self compacting concrete, Gradjevinar 4 (2009), pp. 321-329

[2] Ahari R.S.; Erdem T.K.; Ramyar K.: Effect of various supplementary cementitious materials on rheological properties of self-consolidating concrete, Construction and Building Materials 75 (2015), pp. 89–98

[3] Mnahoncakova E.; Pavlıkova M.; Grzeszczyk S.; Rovnanıkova P.; Cerny R.: Hydric, thermal and mechanical properties of self-compacting concrete containing different fillers, Construction and Building Materials 22 (2008), pp. 1594–1600

[4] Despotović I.: Uticaj različitih mineralnih dodataka na osobine samougrađujucih betona, Doktorska diertacija, Građevinsko-arhitektonski fakultet u Nišu (2014)

[5] Hannesson G.; Kuder K.; Shogren R.; Lehman D.: The influence of high volume of fly ash and slag on the compressive strength of self-consolidating concrete, Construction and Building Materials 30 (2012), pp. 161–168

[6] Siddique R.: Properties of self-compacting concrete containing class F fly ash, Materials and Design 32 (2011), pp. 1501–1507

[7] Khatib J.M.: Performance of self-compacting concrete containing fly ash, Construction and Building Materials 22 (2008), pp. 1963–1971

[8] Sukumar B.; Nagamani K.; Srinivasa Raghavan R.: Evaluation of strength at early ages of self-compacting concrete with high volume of fly ash, Construction and Building Materials 22 (2008), pp. 1394–1401

[9] Shi C.; Mayer C.; Behnood A.: Utilization of copper slag in cement and concrete, Resources, Conservation and Recycling 52 (2008), pp. 1115–1120

[10] Onuaguluchi O.; Eren O.: Copper tailings as a potential additive in concrete: Consistency, strenght, and toxic metal imobilizator, Indian Journal of Engineering & Materials Sciences 19 (2012), pp. 79-86

[11] Onuaguluchi O.; Eren O.. Cement mixtures containing copper tailings as an additive: durability properties, Materials Research 15 (2012), pp. 1029-1036

[12] Zlatičanin B.; Vukčević M.; Krgović M.; Bošković I.; Ivanović M.; Zejak R.: Karakteristike geopolimera na bazi crvenog mulja kao komponente sirovinske mješavine, Zaštita Materijala 53 (2012) broj 4, pp. 292-298, UDC:669.712.1.068-03.6.8.

[13] Kadović M.V.; Klašnja M. T.; Blagojević N.Z.; Rajko Vasiljević R.; Jaćimović Ž.K.: Tretman tečne faze sa deponije crvenog mulja u kombinatu alumunijuma Podgorica, Hemijska industrija 58(4) 2004, pp. 186-190

[14] Liu R.X.; PoonC.S.: Utilization of red mud derived from bauxite in self-compacting concrete, Journal of Cleaner Production 112 (2016), pp. 384-391.

[15] Shetty K.K.; Nayak G.; Vijayan V.: Effect of red mud and iron ore tailing on the strength of self compacting concrete, European Scientific Journal, July 2014 edition vol.10, No.21 ISSN: 1857 – 7881 (Print) e - ISSN 1857- 7431.

[16] Gomez-Soberon J.: Porosity of recycled concrete with substitution of recycled concrete aggregate: An experimental study, Cement and Concrete Research 32 (2002), pp. 1301-1311

[17] Persson B.: Internal frost resistance and salt frost scaling of self-compacting concrete, Cement and Concrete Research 33 (2002), pp. 373-379

[18] Levy S.M.; Helene P.: Durability of recycled aggregates concrete: a safe way to sustainable development, Cement and Concrete Research 34 (2003), pp. 1975-1980

[19] Ali E.E.; Al-Tersawy S.H.: Recycled glass as a partial replacement for fine aggregate in self compacting concrete, Construction and Building Materials 35 (2012), pp. 785–791

[20] Kou S.C.; Poon C.S.: Properties of self-compacting concrete with recycled glass aggregate, Construction and Building Materials 31 (2009), pp. 107–113

[21] Sua-Iam G.; Makul N.: Use of limestone powder to improve the properties of self compacting concrete produced using cathode ray tube waste as fine aggregate, Applied Mechanics and Materials Vols. 193-194 (2012), pp. 472-476

PROPERTIES OF FRESH SELF-COMPACTING CONCRETE WITH RECYCLED CONCRETE FILLER

Aleksandar Savic[1], Snezana Marinkovic[1], Dragica Jevtic[1], Dimitrije Zakic[1], Marina Askrabic[1]

[1] University of Belgrade, Faculty of Civil Engineering, Department of Materials and Structures,
Bulevar kralja Aleksandra 73, 11 000 Belgrade, Serbia, email: sasha@imk.grf.bg.ac.rs, sneska@imk.grf.bg.ac.rs, dragica@imk.grf.bg.ac.rs, dimmy@imk.grf.bg.ac.rs, amarina@imk.grf.bg.ac.rs

SUMMARY: The investigation of recycling waste concrete as recycled aggregate for production of new concrete gave positive results in many cases. Sources from literature indicate that the finest, powder component of recycled concrete can be successfully used, also. The paper presents the results of the fresh properties of self-compacting concrete (SCC), made with the addition of three different fillers (originated from ground waste/recycled concrete). Besides the reference, made with the limestone filler, three more SCC mixtures were made, containing 50% of ground recycled concrete in relation to the total mass of the mineral filler. The study included investigation of the following properties: density, slump flow, slump flow time (t500), V-funnel flow time (tv), the ratio of the heights in L-box test, sieve segregation resistance and the content of entrained air. Generally, all the SCC mixtures with ground recycled concrete filler showed a very similar behavior in fresh state.

SVOJSTVA SVJEŽEG SAMOZBIJAJUĆEG BETONA S RECIKLIRANIM BETONSKIM FILEROM

SAŽETAK: Istraživanja recikliranog otpadnog betona upotrijebljenog kao agregat u proizvodnji novoga betona u mnogim je slučajevima dalo pozitivne rezultate. Izvori iz literature naznačuju da se uspješno može upotrijebiti i najfinija praškasta komponenta recikliranog betona. U radu su prikazani rezultati ispitivanja svojstava svježeg samozbijajućeg betona izrađenog s dodatkom triju različitih punila (filera) (čiji je izvor drobljeni otpadni/ reciklirani beton). Osim referentnog betona izrađenog s vapnenačkim filerom, načinjene su još tri mješavine samozbijajućeg betona s 50 % drobljenoga recikliranog betona u odnosu na ukupnu masu mineralnog filera. Istraživanjem su obuhvaćena ova svojstva: gustoća, slijeganje rasprostiranje, vrijeme rasprostiranja slijeganjem (t500), vrijeme punjenja s pomoću V-lijevka (tv), omjer visina u ispitivanju s pomoću L-posude, otpornost na segregaciju sijanjem i sadržaj uvučenoga zraka. Općenito, pokazalo se da su sve mješavine samozbijajućeg betona s drobljenim recikliranim betonskim filerom u svježem stanju imale vrlo slično ponašanje.

1. INTRODUCTION

Building industry traditionally presents a conservative area, where principles of sustainable development are not easily implemented. Nevertheless, due to the climatic changes and serious depletion of natural resources, environmental awareness is increased. In the building industry, owing to the results of research and practice, a substantial research in the sphere of recycling various building materials is taking place.

The principles of sustainable development and the effects of recycling have been studied in self-compacting concrete (SCC) for a while now [1]. SCC is often defined as a concrete that can be compacted into every corner of a formwork, purely by means of its own weight and without the need for vibrating [2]. This material shows many qualities, including: ease of placement with limited access in a complex structure or shape, higher in-place quality and aesthetics, faster speed of construction, labor and time savings and improved worker safety and noise reduction [3]. There are also several disadvantages regarding SCC, which are constraining its wider use in precast and ready-mix concrete production: difficulties in design, higher initial costs (due to use of higher quantities of admixtures and mineral additions), possible problems regarding its robustness, and general resistance of the people involved to the unknown materials and techniques. SCC is being researched and practiced worldwide, also providing a fertile ground for the research concerning incorporation of different recycled materials.

Most of the investigations on the topic of using recycled concrete aggregate (RCA) in SCC were made with partial or complete replacement of coarse natural aggregate [4,5,6]. Use of the fine recycled concrete aggregate (which is always present as a result of the grinding process in concrete recycling) is usually avoided, like in conventional concrete, due to the inferior properties of such aggregate.

There is a consensus in the researcher community about the higher potential for the use of secondary materials as fines or fillers in SCC, than in conventional concrete [7]. For instance, Swedish guidelines identify materials suitable as fillers for SCC [8]. Limestone filler, dolomite filler, finely ground recycled packing glass, condensed silica fume and ground granulated blast furnace slag are recognized in these guidelines as main fillers for SCC production. Fines from crushed general construction and demolition (C&D) waste are often contaminated, but there is a small portion of the fines from reclaimed building materials. This potential use has to be made with careful control.

Holton [7] suggested that up to 10% replacement of fine aggregate with uncontaminated sources of material may be achieved from reclaimed hardened and crushed concrete both in the pre-cast and in ready-mix industry. The categorization of recycled concrete fines originating from these industries is, by Hanson et al. [9], as follows:

1. Wash-out fines include particles of the recycled concrete obtained when any of the concrete handling equipment (e.g. trucks and mixers) is washed out. The water containing these fines has to be treated in a suitable way in order to be purified prior to its release in the sewage system.

2. Grinding fines include the particles obtained through the process of diamond grinding of concrete pavements, that also represent waste material which must be properly disposed of. These particles include lower amounts of hydrated cement particles than in the case of wash-out-fines.

3. Recycled concrete dust is produced during recycling of Portland cement concrete by crushing, which results in a substantial amount of particles including hydrated cement paste. Generally, this is considered to be less of a waste disposal problem than the previous two types of waste, since some fine material is allowed to be present in base course materials (most common use for recycled concrete).

Corinaldesi and Moriconi [10] concluded that the use of recycled concrete filler can result in acceptable fresh self-compacting concrete properties (and increased segregation resistance) providing acceptable offset of compressive strength and excellent surface finishing. Janssen et al. [11] demonstrated that the use of recycled concrete fines could offset some or all of the delayed strength gain effects from cement-ground granulated blast furnace slag blends. Current work is conducted with the aim of increased cement replacement rates with no additional reduction in early strength gain.

It has been noticed that finely-ground particles of hydrated Portland cement have accelerating effect on the hydration rate of Portland cement concrete [9]. One of the possible explanations for this effect is that the hydrated cement particles act as nucleation centers, enabling easier hydration reaction. Secondary acceleration effects lie in the presence of the calcium hydroxide and alkalis in the hydrated Portland cement.

Possibility of utilizing ground fine recycled concrete aggregate (RCA filler) as filler component in SCC was investigated in this study. RCA fillers in question do not fall in any of the above mentioned groups, owing to the fact that additional process of grinding was applied on fine recycled concrete aggregate. Investigation was aimed towards higher filler replacement amount, and the recording of its impact on fresh SCC properties. Different recycled concrete fine aggregates (0/4 mm) were ground to the same output filler size, in order to estimate the possible differences in their behavior in SCC.

2. MATERIALS AND MIXTURES

In this paper properties of fresh SCC made with RCA filler as partial replacement of mineral filler are presented. The influence of RCA filler on these properties was evaluated through experiments conducted on four mixtures. Three mixtures (R0, R50 and R100) were designed by replacing 50% of limestone filler, used as filler component in the reference mixture (E), with RCA filler originating from three different concrete composites – „parent" mixtures (NVC, RAC50 and RAC100). Content of all the other components in the mixtures was held constant (cement, water, river sand, coarse aggregate).

Original mixtures had following properties:

- Normally vibrated concrete (NVC) made with natural aggregate. This concrete was crushed and then fractioned. The finest fraction (0/4 mm) was ground to filler component named mineral filler A;
- Normally vibrated recycled concrete (RAC50), made with river sand and coarse aggregate that presented combination of 50% of river aggregate and 50% of recycled aggregate (originated from demolished concrete). The concrete was crushed and then fractioned. The finest fraction (0/4 mm) was ground to filler component named mineral filler B;
- Normally vibrated recycled concrete (RAC100), made with river sand and coarse recycled aggregate (originated from demolished concrete). The concrete was crushed and fractioned. The finest fraction (0/4 mm) was ground to filler component named mineral filler C.

2.1. COMPONENT MATERIALS

Natural river aggregate (separated in three standard fractions) originated from Danube river, Belgrade region. Granulometry of this aggregate was tested according to [13] and presented in the Figure 1 (semi logarithmic plot). Modulus of fineness of the fine aggregate (0/4 mm) was 2.92 and satisfied conditions defined in the standard [14] (limit values 2.3-3.6). Moduli of fineness of second (4/8 mm) and third (8/16 mm) fraction were 6.04 and 6.99

respectively. Content of fine particles in the first fraction was 0.59% for particles smaller than 0.063 mm, and 1,68% for particles smaller than 0.09 mm. In the coarse aggregate this content was close to zero. Based on the previous tests granulometry of the mixture consisted of 31.8% of the fine aggregate, and 32.5% of both second and third fraction of the coarse aggregate.

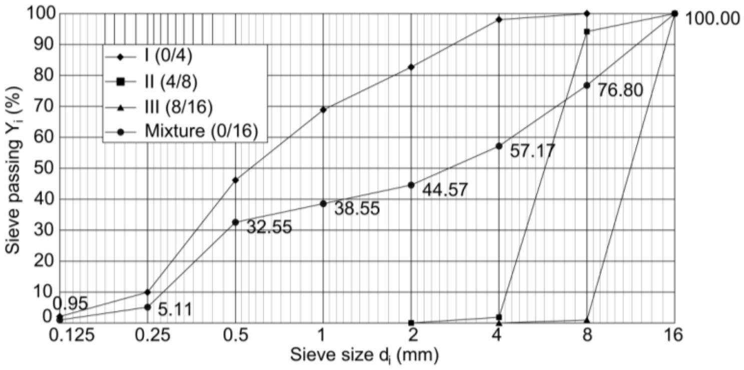

Figure 1 Granulometry of the used fractions of aggregate (together with the granulometry of the mixture)

Portland cement of the type CEM I was used, declared as PC 42.5, produced by Lafarge, Beočin. Specific surface of the cement, according to Blaine, was 4240 cm^2/g, while its density was 3040 kg/m^3.

Basic filler component for all of the mixtures was limestone filler produced by "Granit Peščar" Ljig, with average particle diameter of 250 µm. Specific surface of limestone filler was 3800 cm^2/g, while its density was 2720 kg/m^3. Chemical content of this filler together with chemical content of RCA powders are presented in Table 1.

Table 1 Chemical composition of the used mineral fillers

Parameter	Limestone filler	Mineral filler A	Mineral filler B	Mineral filler C
SiO_2 (%)	0.21	67.13	60.55	61.31
Al_2O_3 (%)	0.5	6.58	6.84	6.65
CaO (%)	54.86	12.94	17.77	16.06
Fe_2O_3 (%)	0.09	1.33	1.32	1.32
MgO (%)	1.10	0.76	0.94	0.86
K_2O (%)	0.05	0.86	0.83	0.79
Na_2O (%)	<0.005	1.27	1.13	1.05
TiO_2 (%)	<0.005	<0.17	<0.17	<0.17
LOI (%)	43.64	9.11	10.59	11.93

RCA powders named mineral fillers A, B and C originated from three types of fine aggregate from three different concrete mixtures with declared content, as explained above. Granulometry of these fillers was similar, while their specific surface was 4400 cm^2/g.

The greatest differences in chemical content were as expected in higher content of SiO_2 and Al_2O_3 and lower content of CaO in the RCA filler than in the limestone filler. The content of SiO_2 was the highest in the mineral filler A, due to the exclusive use of river aggregate as coarse aggregate in its „parent” concrete.

Water from city water supplay system was used for concrete mixtures. Temperature of water was measured before each mixing and it ranged between 19 and 22°C. Superplasticizer Glenium Sky 690, produced by BASF Italia (density 1060 kg/m^3) was dosed in amount of 2%.

2.2. MIXTURES

Final recipes for reference SCC mixture (E) and mixtures where 50% of limestone filler was replaced with mineral filler A (R0), B (R50) or C (R100) were adoped based on the previous trials and presented in Table 2.

Table 2 Composition of tested SCC mixtures

Mixture	E	R0	R50	R100
Water W (kg/m^3)	183	183	183	183
Cement (kg/m^3)	380	380	380	380
Limestone filler (kg/m^3)	220	110	110	110
Mineral filler A (kg/m^3)	0	110	0	0
Mineral filler B (kg/m^3)	0	0	110	0
Mineral filler C (kg/m^3)	0	0	0	110
Fine aggregate(0/4mm) (kg/m^3)	840	840	840	840
Coarse aggregate (4/8mm) (kg/m^3)	430	430	430	430
Coarse aggregate (8/16mm) (kg/m^3)	430	430	430	430
Superplasticizer (kg/m^3)	7.6	7.6	7.6	7.6

3. TESTING OF FRESH SCC MIXTURES

Fresh SCC mixtures were tested according to standard methods in order to investigate the influence of the partial filler replacement on their passing and flowing ability, as well as their segregation resistance. These methods included: slump flow test (measuring both the final diameter and time t_{500}), V-funnel test, L-box test and measurements of segregation factor (sieve analysis), bulk density and entrained air determination [15,16,17,18]. Results of slump flow tests (mean values based on three measurements for each mixture) are presented in Figure 2, while the values of the segregation factors (mean values based on two measurements for each mixture) are presented in Figure 3. Ambient temperature during mixing of the concrete ranged between 20.6°C and 22.6°C.

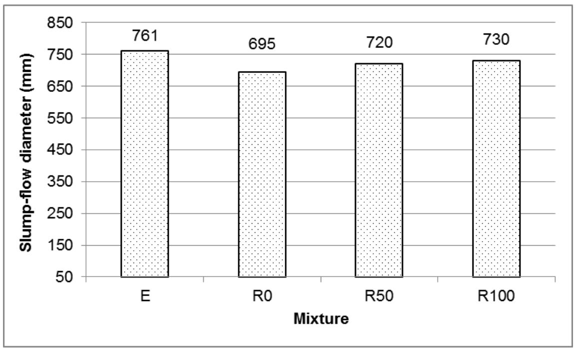

Figure 2 Slump flow test results for all concrete mixtures

Generally, with slump flow diameters ranging between 695 mm and 761 mm all SCC mixtures can be placed in the SF2 category according to European recomendations [12], with exception of the reference mixture E whose result overstepped the upper limit for this category (750 mm). It was noticed that flowing ability of the concrete was reduced with application of RCA powders as mineral filler. Based on the presented results this effect was smallest in the case of mixture R100 with mineral filler C (with the highest amount of coarse recycled aggregate in the original concrete).

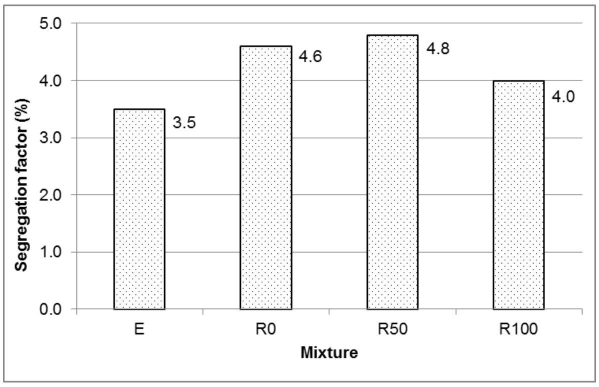

Figure 3 Segregation factor for all concrete mixtures

When comparing segregation factor of tested mixtures several effects can be noticed. There has been an increase of segregated material (decrease in segregation resistance) in all of the mixtures containing RCA filler when compared with reference mixture. This increase amounted to 31.4% (for mixture with mineral filler A), 37.1% (for mixture with mineral filler B) and 14.3% (for mixture with mineral filler C). These effects can be explained by the fact that mineral filler originating from normaly vibrated recycled concrete (marked as RAC100) had higher level of fine particles with higher density and lower porosity. Still, all of the measured values were within the allowed limits (segreggation factor was lower than 20%).

When it comes to measuring the passing ability of tested mixtures through the L-box results, independantly on the origin of the RCA filler, the decrease of the measured values was noticed in all of the mixtures where limestone filler was replaced in the amount of 50%. Value measured for reference mixture was 0.97, while values measured on three other mixtures was 0.95. These values were obtained as a mean of three measurements for each mixture. All of the concrete mixtures can be placed in the PA2 category according to European recommendations.

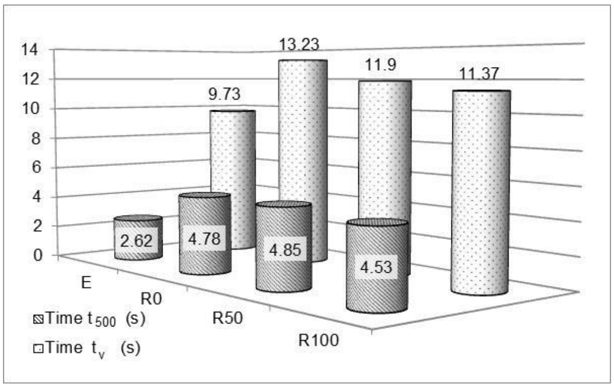

Figure 4 Times t_v and t_{500} for tested mixtures

Measured times t_{500} and t_v, for all of the series, are presented in Figure 4, as mean values based on three measurements for each mixture. In general, all of the series satisfy category VS2/VF2 of European recomendations with measured time t_{500} longer than 2 s, and t_v longer than 9 s. Values measured for reference mixture were closest to the upper limit for this category. Mixtures containing RCA filler showed prolongation of both t_{500} and t_v time when compared to reference mixture, although their final slump flow diameters were smaller than the reference one. This indicates that the flowing ability of the SCC was reduced with partial replacement of limestone filler, regardless of the origin of the mineral fillers A, B and C. On the other hand measured time t_v was decreasing (becoming closer to the reference mixture) with increase of the amount of coarse recycled aggregate in the „parent" concrete composites.

Figure 5 represents relation between time t_v measured in the V-funnel test and time t_{500} measured during the slump flow test. It can be noticed that all of the mixtures with RCA filler as limestone filler replacement have similar behaviour, regardless of the origin of the recycled agregate filler. Still, their results are positioned away from the reference mixture values. It is also noticed that usage of different filler types had higher influence on the time t_v than on the time t_{500}.

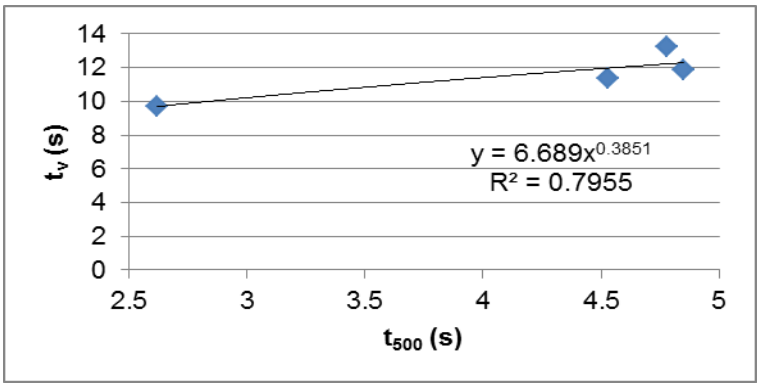

Figure 5 Relation between measured time t_{500} and tv for tested mixtures

When comparing flowing and passing ability of different mixtures it can be noticed that partial replacement of mineral filler has different effects. Although the measured values from slump flow tests were similar for all of the series, which indicates similar flowing ability, results measured in the V-funnel test indicate that type of mineral filler affects concrete's flowing ability. This also shows that comparing different mixtures only by results of the slump flow tests is insuficient and can lead to an overall inappropriate conclusions.

Bulk densities of fresh SCC mixtures with filler partially replaced with recycled aggregate filler are very similar to bulk density of the reference mixture, as presented in Table 3. Decrease of measured bulk density for the mixtures containing ground recycled concrete filler was lower than 1%. These differences can be explained by the slightly greater entrained air content, as well as by the presence of lighter grains of mortar origin that can be found within recycled aggregate filler. These values were obtained on the basis of five measurements for each mixture.

Table 3 Results of the entrained air content measurements

Mixture	E	R0	R50	R100
Entrained air content (%)	1.9	2.3	2.2	2.4
Bulk density (kg/m^3)	2397	2387	2389	2391

Results of the entrained air content measurements (mean values based on two measurements for each mixture) are shown in Table 3. The greater amount of entrained air is noticed within all of the mixtures with partial raplacement of limestone filler. In average, this growth was around 20%, and it was the highest for the mixture with mineral filler C.

It has to be noted here that the addition of recycled concrete as partial replacement of mineral filler did not affect mechanical properties of tested concretes. After 28 days, compressive strength of reference mixture amounted to 62 MPa, while compressive strengths of mixtures R0, R50 and R100 were 60.0 MPa, 59.2 MPa and 61.6 MPa, respectively [19]. Five 10 cm cube specimens were tested for each mixture.

4. CONCLUSION

This paper focuses on the influence of RCA fillers, as a partial replacement of limestone filler in SCC mixtures, on fresh concrete properties. Behavior of mixtures with recycled concrete fillers originating from different concretes (original concrete with natural aggregate R0, concrete with partial replacement of coarse aggregate with recycled concrete aggregate R50 and concrete with recycled concrete coarse aggregate R100) was compared. All of the fillers were produced by grinding of the first fraction of the recycled concrete aggregates in question.

Flowing ability of tested SCC mixtures measured through slump flow diameter, as well as passing ability measured through L-box height ratio, was reduced with partial replacement of limestone filler when compared with reference mixture. This reduction, however, did not lead to change of category of the SCC and was not influenced by the origin of the recycled concrete filler used.

Segregation factor was increased in comparison with the reference mixture. The SCC mixture with mineral filler C showed the highest segregation resistance among the mixtures where limestone filler was partially replaced, with 14.3% lower segregation factor. Mineral filler C, used in this mixture, had the highest amount of fine particles originating from both coarse recycled aggregate and cement stone.

Measured time t_{500} was longer for all of the mixtures containing partial replacement of mineral filler with no reference to the origin of the RCA filler. In addition to the conclusion that the slump flow diameter was reduced in the mixtures with RCA filler, this confirmes reduction in flowing ability of these concrete mixtures. V-funnel tests gave similar results, as the longer time t_v was also measured for mixtures with partial replacement of limestone filler. Still, these values depended on the origin of the mineral filler in question. Best results were recorded on the mixture containing mineral filler C (filler obtained from the concrete with the recycled concrete coarse aggregate).

Bulk densities of all tested mixtures were very similar, with differences not exceeding 1%, compared to the reference mixture. Entrained air content increased with the partial replacement of limestone filler, but with no reference to the origin of the filler used.

Generally, all of the fresh SCC mixtures with RCA filler showed similar behavior, and the effect of this replacement can be attributed to the amount of the filler used rather than to the type of the filler (A, B or C). It can also be concluded that although the addition of these mineral fillers did lead to the reduction of almost all tested abilities, these reductions were not substantial, and in most cases did not change the category of the SCC according to European recommendations.

Future investigations in this area could address systematic testing of the different factors of influence of SCC mixtures. This regards, especially, the properties of “parent” concrete mixtures of the filler (compressive strength, aggregate/cement paste ratio, age, origin, etc.).

ACKNOWLEDGMENTS

The work reported in this paper is a part of the investigation within the research project TR 36017 "Utilization of by-products and recycled waste materials in concrete composites in the scope of sustainable construction development in Serbia: investigation and environmental assessment of possible applications", supported by the Ministry of Education, Science and Technological Development, Republic of Serbia. This support is gratefully acknowledged.

REFERENCES

[1] Jevtić D.; Savić A.: Impact strength evaluation of rubberized fiber reinforced SCC, Proceedings of the RILEM International workshop on performance-based specification and control of concrete durability, Proceeding PRO 89, Edited by Dubravka Bjegović, Hans Beushausen, Marijana Serdar, pp. 641-646, Zagreb, Croatia, 11-13. Publisher: RILEM Publications S.A.R.L., (2014)

[2] Okamura, H.; Ouchi, M., Self-Compacting Concrete, Development, Present Use and Future, Proceedings of the First International Symposium on Self-Compacting Concrete, pp. 4-11, Stockholm, Sweden, (1999),

[3] Daczko, J.A.: *Self-Consolidating Concrete: Applying what we know*, Spon Press, UK, (2012)

[4] Modani, P. O.; Mohitkar, V. M.: Recycled Aggregate Self Compacting Concrete: A Sustainable Concrete for Structural use, *International Journal of Engineering Research & Technology*, pp. 116-120 (2015)

[5] Tang, W. C.; Ryan, P. C.; Cui, H. Z.; Liao, W.: Properties of Self-Compacting Concrete with Recycled Coarse Aggregate, *Advances in Materials Science and Engineering*, pp. 1-11 (2016)

[6] Boudali, S; Kerdal, D.E.; Ayed, K.; Abdulsalam, B.; Soliman, A.M.: Performance of self-compacting concrete incorporating recycled concrete fines and aggregate exposed to sulphate attack, *Construction and Building Materials* 124, pp. 705–713 (2016)

[7] Holton, I.: *DTI Project Report: A review of the potential use of secondary and recycled aggregates in self-compacting concrete*, Department of Trade and Industry, Building Research Establishment, UK, (2003)

[8] Skarendahl, A.: Self-compacting concrete in Sweden. Research and application. Proceedings of the International Workshop on Self-Compacting Concrete, pp. 60-71, Kochi, Japan, 23-26 August, 1998, (1998)

[9] Hanson, E. M.; Connolly N. J.; Janssen D. J.: Evaluating and Optimizing Recycled Concrete Fines in PCC Mixtures Containing Supplementary Cementitious Materials, Final Report, TNW2010-03, Department of Civil and Environmental Engineering, TransNow (2010)

[10] Corinaldesi, V.; Moriconi, G.: Self-compacting concrete: A Great Opportunity for Recycling Materials, International RILEM Conference on the Use of Recycled Materials in Buildings and Structures, pp. 600-609 (2004)

[11] Janssen, D. J.; Vandenbossche, J. M.; Koubaa, A.: Optimizing the use of recycled concrete fines in slag-cement, Materials Science, pp. 1-8 (2007)

[12] European Guidelines for Self-Compacting Concrete: Specification, Production and Use, European Project Group, (2005)

[13] SRPS EN 933-1:2009 Tests for geometrical properties of aggregates - Part 1: Determination of particle size distribution - Sieving method, ISS, (2009)

[14] SRPS B.B2.010:1986 (withdrawn): Aggregate for concrete - Technical requirements, ISS (1986)
[15] SRPS EN 12350-8:2012 Testing fresh concrete - Part 8: Self-compacting concrete - Slump-flow test, ISS, (2012)
[16] SRPS EN 12350-9:2012 Testing fresh concrete - Part 9: Self-compacting concrete - V-funnel test, ISS, (2012)
[17] SRPS EN 12350-10:2012 Testing fresh concrete - Part 10: Self-compacting concrete - L box test, ISS, (2012)
[18] SRPS EN 12350-11:2012 Testing fresh concrete - Part 11: Self-compacting concrete - Sieve segregation test, ISS, (2012)
[19] Savić, A: Investigation Of The Properties Of Fresh And Hardened Self-compacting Concrete With Mineral Additions Based On Industrial By-Products, Doctoral thesis, University of Belgrade, Faculty of Civil Engineering, Beograd, mentors: prof. dr Dragica Jevtić, prof. dr Tatjana Volkov Husović (2015)

EFFECT OF WATER TO BINDER RATIO AND GROUND GRANULATED BLAST FURNACE SLAG ON MATURITY AND PROPERTIES OF SELF-COMPACTING CONCRETE USED FOR PRE-STRESSED SLABS AND BEAMS

Mohammed Sonebi[1], Peter Deegan[2], Gavin Kelly[2], Su Taylor[1], Liberato Ferrara[3], and Andrea Pattarini[4]

[1] Queen's University of Belfast, BT9 5AG Belfast (Northern Ireland), e-mail: m.sonebi@qub.ac.uk, s.e.taylor@qub.ac.uk
[2] Banagher Precast Concrete Ltd., Co. Offaly (Republic of Ireland), e-mail: PeterD@bancrete.com, GavinK@bancrete.com
[3] Politecnico di Milano, Milan (Italy), e-mail: liberato.ferrara@polimi.it
[4] Azichem Ltd, Goito, Mantova, (Italy), e-mail: a.pattarini@azichem.it

SUMMARY: The maturity method is a technique to account for the combined effects of time and temperature on the strength development of concrete. The method provides a relatively simple approach for making reliable estimates of in-place strength during construction. The prediction of concrete strength at an early age is very important in the concrete industry. This will help in accelerating the construction process, determining the safe time for de-tensioning of pre-stressed concrete and for stripping of formwork or the proper time to conduct any construction activity. The maturity concept has gained increasing interest as a scientific way to evaluate in-situ strength of concrete in a very accurate way. This paper reports on an investigation of the effect of water-to-binder ratio (w/b) and the percentage of ground-granulated blast furnace slag on fresh properties, the hardened properties and the maturity of mixes to be used in pre-stressed structural elements. The filling ability, flowability and passing ability of SCC mixes were measured using slump flow and J ring. The compressive strength 1, 3, 7 and 28 days were determined. The maturity index was measured using maturity box apparatus at Banagher precast concrete. The results of this investigation show that w/b and the replacement of cement by GGBS had a significant effect on the maturity index. As expected, the reduction of w/b from 0.45 to 0.40 led to an improvement of compressive strength and the increase in percentage of GGBS resulted in a reduction of compressive strength. The relationship between the maturity index and compressive strength has been established for several SCC mixes for releasing the pre-stressed tendons used in precast elements and the prediction of Eurocode is not good in the experimental results.

UTJECAJ VODOVEZIVNOG OMJERA I FINO MLJEVENE ZGURE VISOKE PEĆI NA ZRELOST I SVOJSTVA PREDNAPREGNUTIH PLOČA I GREDA OD SAMOZBIJAJUĆEG BETONA

SAŽETAK: Metoda zrelosti postupak je kojim se utvrđuju sjedinjeni učinci vremena i temperature na razvijanje čvrstoće betona. Metoda se sastoji od razmjerno jednostavnog postupka kojim se pouzdano procjenjuje čvrstoća betona na mjestu ugradnje. U industriji betona važno je što ranije predvidjeti čvrstoću betona. Time se ubrzava postupak izgradnje, određuje se koje je sigurno vrijeme za opuštanje prednapregnutog betona, za skidanje oplata ili za određenu fazu graditeljske aktivnosti. U znanosti pojam zrelosti dobiva sve veću važnost kod točnog određivanja čvrstoće betona na licu mjesta. Ovaj se rad bavi istraživanjem utjecaja vodovezivnog omjera (v/v) i postotka fino mljevene zgure visoke peći na svojstva svježega betona, na svojstva očvrsloga betona i na zrelost mješavina koje će se rabiti u prednapregnutim konstrukcijskim elementima. Viskoznost, sposobnost tečenja i obilaženja prepreka samozbijajućih betona mjerene su pomoću ispitivanja rasprostiranja slijeganjem i J prstena. Mjerena je tlačna čvrstoća nakon 1, 3, 7 i 28 dana. Mjerio se indeks zrelosti pomoću uređaja za određivanje zrelosti na predgotovljenom betonu tvrtke Banagher. Rezultati istraživanja pokazuju da vodovezivni omjer (v/v) i zamjena cementa fino mljevenom zgurom imaju znatan utjecaj na indeks zrelosti. Kako se i očekivalo, smanjenje omjera vode i veziva od 0,45 do 0,40 dovelo je do poboljšanja tlačne čvrstoće a povećanje postotka fino mljevene zgure rezultiralo je manjom tlačnom čvrstoćom. Odnos između indeksa zrelosti i tlačne čvrstoće odredio se za nekoliko vrsta samozbijajućih mješavina, a u cilju predviđanja pogodnog trenutka za otpuštanje prednapregnutih nateznih kablova korištenih u predgotovljenim elementima i u analizu eksperimentalnih podataka i predviđanja Eurokoda koje nije u skladu s eksperimentalnim rezultatima.

1. INTRODUCTION

Self-compacting concrete (SCC) is a concrete type that meets a unique combination of performance and uniformity requirements [1-4], it flows under its own weight, maintaining its homogeneity without any vibration. The filling ability of SCC (unconfined flowability) can be described by the ability of the concrete to flow into and to fill all spaces of the formwork under its own weight.

SCC has a low water-to-binder ratio, incorporating high quantities of fillers (cement and mineral additives such as ground granulated blast furnace slag (GGBS), fly ash (FA), limestone powder (LSP), an effective superplasticiser (SP), increasing the sand-to-aggregate ratio, and if needed, using a stabilising agent [1-4]. The use of SP can disperse cement grains, reduces inter-particle friction and enables the reduction in water content while maintaining the required levels of flowability [1-4].

These are more sensitive to temperature than those made only with Portland cement. This investigation focused on establishing whether maturity functions could be used to monitor early age strength development for precast elements. These could be used to control the temperature of the casting bed to obtain the early age strengths needed for lifting the units and also to be used for quality control assurance ensuring the strengths required are achieved to release the pre-stressed tendons in W-beams, slabs, etc.

The concept of estimating concrete strength in terms of curing time and temperature has been well developed, and a maturity function has been proposed by Saul and Nurse [5]. The Saul–Nurse maturity function took the following simple form:

$$M = \sum_{0}^{t} (T - T_0)\Delta t \tag{1}$$

where M is the maturity value at age t, T_0 is the datum temperature (=-10°C), and T is the average curing temperature of the concrete during the interval Δt.

The simplicity of using the Saul–Nurse maturity equation is shown. It has received much attention and found wide use in engineering practice as a proper method for in-situ strength determination in concrete structures. Freiesleben Hansen and Pendersen [6, 7] proposed a new expression for the maturity function based on the well-known Arrhenius equation, as follows:

$$M = \sum_{0}^{t} k(T)\Delta t \tag{2}$$

where k(T) is the rate constant of hydration at temperature T.

The rate constant of hydration, k (T), can be calculated using the Arrhenius equation as:

$$k\ (T) = Ae^{-E/RT} \tag{3}$$

where A is a proportionality constant (day-1), R is the gas constant (8314 J/mol K), E is the activation energy (J/mol) and T is the absolute temperature (K).

The prediction of maturity of compressive strength with Eurocode 2 at an age t depends on the type of cement, temperature and curing conditions (Eq. 4). The model of compressive strength is:

$$f_{cm}(t) = f_{cm} \times \beta_{cc}(t) = f_{cm} \times exp\left\{s\left(1 - \sqrt{\frac{28\,d}{t}}\right)\right\} \tag{4}$$

Where:

f_{cm} = average compressive strength at 28 d standard curing at 20°C

t is the age of concrete in days

S is the coefficient which depends the type of cement

S = 0.20 for cement of strength classes CEM 42.5 R, CEM 52.5 N and CEM 52.5 R

S = 0.25 for cement of strength classes CEM 32.5 R, CEM 42.5 N

S = 038 for cement of strength classes CEM 32.5 N.

The objective of this study is to investigate the effect of w/b ratio and dosage of GGBS on the relationship between the maturity index and the compressive strength of various SCC mixes.

2. EXPERIMENTAL PROGRAMME

2.1. MATERIALS

Cement class CEMI 42.5R and GGBS were used as constituents of the binder. The average particle size of the GGBS was 13.8 microns. Limestone powder (LSP) was also used as a filler, with an average particle size was 9.1 microns. The chemical composition of these materials is shown in Table 1. A polycarboxylate ether-based superplasticiser

(SP) was used, its specific density being 1.06 and with a water content of 65%. In addition to the sand, two coarse aggregates with different maximum size (8 and 14 mm) were used, all of them crushed.

Table 1 Chemical composition of cement, LSP and GGBS.

	Cement	LSP	GGBS
SiO_2	19.61	1.74	35.65
TiO_2	0.336	0.011	0.735
Al_2O_3	5.02	0.09	11.53
Fe_2O_3	3.14	0.11	0.96
MnO	0.097	0.048	0.210
MgO	2.67	0.54	7.22
CaO	63.79	55.24	41.26
Na_2O	0.22	<0.003	0.26
K_2O	0.469	0.026	0.396
P_2O_5	0.077	0.132	0.008
SO_3	3.04	<0.002	2.33

2.2. MIX COMPOSITIONS

Five different mixes were considered, differing in terms of their water-to-binder (w/b) ratio and their GGBS content and reference mix. Binder is cement and GGBS. They are summarized in Table 2. The w/b ratio was considered at the levels of 0.40 and 0.45. In all cases, the total binder content (total weight of cement and GGBS) was kept constant at 450 kg/m^3. The relative amount of GGBS was considered at two different dosages: either 25% or 50% of the total binder weight. Ref mix was made with 100% cement and w/c is 0.42. The SP dosage was adjusted in each case after some trial mixes to achieve a maximum spread between 570-770 mm in the slump flow test. Fuller's theoretical curve was assumed when proportioning the aggregates, seeking the relative volumes that optimised the fit between the actual and the theoretical curve. The total aggregates content was 1600 kg/m^3 or 1650 kg/m^3 for the mixes with w/b of 0.45 and 0.40 respectively. The sand/coarse ratio was kept to 1.0 in all cases in order to ensure a reasonably good degree of cohesion. The LSP content was kept constant at 150 kg/m^3 in all cases.

Table 2 Mix compositions of all mixes tested

Mix	Ref	SSC-A25	SCC-A50	SSC-B25	SSC-B50
w/b	0.42	0.40	0.40	0.45	0.45
Cement	475	337	225	337	225
LSP	--	150	150	150	150
GGBS	--	112	225	112	225
Water	190	180	180	202	202
Sand	841	825	825	800	800
AG4/8	--	611	611	592	592
AG8/14	900	400	215	215	208
SP	3	2.2	2.9	2.5	2.5

2.3. MATURITY INDEX TEST

The computer measured the temperature and time through the four thermo-coupling leads placed into the concrete product and connected to the computer (Figure 1). The information contained within the computer prior to testing are: The C-value (constant related to type of cement); Test period; Time/Date settings.

The test period specified how long the test will run for. The test was carried out for a long period of time in order to get good results and readings. The computer linked to apparatus was set for a period of 75 hours which enabled us to take a reading every 10 minutes. The maximum period of time possible for testing is 1800 hours (75 days). The maturity apparatus measured temperature between -10°C to 110°C with a measurement accuracy of 0.5°. The thermocouple leads supplied with the computer are 25 metres in length and are sacrificial meaning we cut the lead flush with the surface of the concrete when the test is complete. The leads require a rubber cap to be fitted to the exposed thermocouple wires. This cap is applied with a heat gun.

Figure 1 Apparatus of maturity used at Banagher Precast Concrete

The formula according to CIMEJ is given by equation (5):

$$Rg = \Sigma\ t.\ T\ C^n \quad (5)$$

Rg the weighted maturity (ºCh)

t temperature (ºC); T: time in hours; C-value is taken 1.3 (with cement 42.5R used by Banagher)

n numbers of test specimens.

The slump flow and V-funnel tests were used to evaluate the filling ability and deformability of SCC, respectively. The passing ability of SCC mixes was assessed by J ring test. Standard 100-mm cubes were demoulded one day after casting and covered with wet burlap and plastic sheeting. Specimens were then cured in lime water at 20 ± 2 °C until testing at ages of 1d, 3d, 7d, and 28d.

3. RESULTS AND DISCUSSSION

3.1. FRESH PROPERTIES

The experimental results obtained for the slump flow, J ring spread and V-funnel are presented in Table 3. According to SCC guidelines [8], all SCC mixes can be classified for slump flow SF2 (660-750 mm) except SCC-B50. As expected, the values of J ring spread were lower than the slump flow. It can be seen that most J ring spread values were more than 600 mm a part mix SCC-B50 which the initial slump flow was the lowest one (570 mm). This is due to the lower dosage of SP (SP = 1.7 L/m^3). All results of V-funnel values showed that SCC mixes were classified as VF2 (V-funnel time between 9 to 25 s). The V-funnel time less than 15 s can be considered as a good flow-ability and deformability of SCC. In this case, SCC-A25 had the highest V-funnel time (21 s). This may due to the high dosage of SP of 2.9 L/m^3 used in this mix, which can lead to more inter-friction between aggregates at the orifice, thus resulted in a high flow time.

Table 3 Results of fresh properties

Mix	Slump flow (mm)	Jring (mm)	V-funnel (s)
Ref	770	710	10
SSC-A25	700	665	21
SCC-A50	660	595	15
SSC-B25	720	705	13
SSC-B50	570	500	15

3.2. COMPRESSIVE STRENGTH

The results of compressive strength at 1d, 3d, 7d and 28d are presented in Figure 2. The replacement of cement by 25% or 50% GGBS for both w/b radio 0.40 and 0.45 led to lower results of compressive strength at 1d and 7d compared to reference mix containing only cement. However, the compressive strength results at 7d and 28 d of SCC-A25, SCC-A50, SCC-B25 and SCC-B50 were higher than those of ref mix particularly at 28 d with SCC mixes incorporating only 25% GGBS. As expected, the increase of w/b from 0.40 to 0.45 resulted in a reduction of compressive strength at all ages. Additionally, the increase of GGBS from 25% to 50% led a reduction on compressive strengths at 1d, 3d, 7d and 28 d.

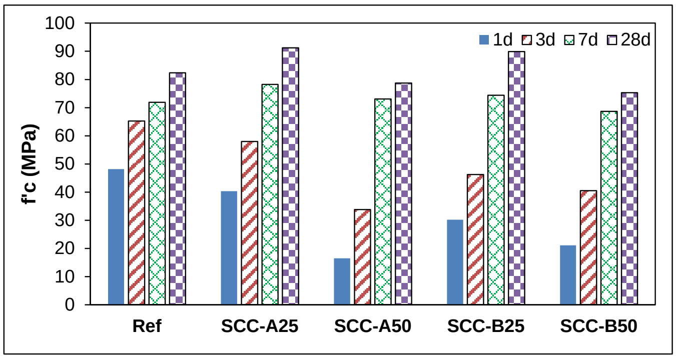

Figure 2 Development of compressive strength of all mixes.

3.3. MATURITY INDEX

Figure 3 presents the variation of compressive strength with maturity index. It can be observed that the maturity index increased with the increase in compressive strength. For any given maturity index, the reduction of percentage of GGBS from 50% to 25% led to an increase of compressive strength for both w/b ratios of 0.40 and 0.45. For any fixed maturity index, the reduction of w/b from 0.45 to 0.40 resulted in an increase of compressive strength. Additionally, for any given maturity, the ref mix demonstrated the highest compressive strength.

For example, at fixed maturity index of 1000 ºCh and w/b of 0.40, the increase in GGBS percentage from 25 to 50% led to a marked reduction of the compressive strength from 38 to 23 MPa. Similarly, in case of w/b of 0.45, the reduction of compressive strength was from 48 to 30 MPa. This attributed to the change in w/b and percentage of GGBS. With ref mix without GGBS and w/b of 0.42 and cement content of 425 kg/m^3, for similar maturity index of 1000 ºCh, the predicted compressive strength was 57 MPa.

Figure 3 can be used also to determine the maturity index for any fixed compressive strength. This figure is very useful for Banagher for releasing pre-stressing cables when the maturity is measured, the early compressive strength can be estimated for these curves in Figure 3. For example, for a compressive strength of 20 MPa, SCC mix made with w/b of 0.45 and 50% GGBS had a maturity index of 540 Ch which is lower than 840 °Ch for similar made with 0.40. Therefore, the reduction of w/b led to an increase in maturity index. For a target compressive strength of 30 MPa, the maturity index was 640 Ch. There were two options either increasing w/b to 0.45 or increasing GGBS to 50%. In these cases, the maturity index was 1000 °Ch for mix made with w/b = 0.45 and 50% GGBS and 1490 °Ch for made lower w/b of 0.40 and incorporating 50% GGBS. For w/b of 0.45 and fixed a compressive strength of 40 MPa, the maturity index was almost tripled increasing from 740 to 1910 °Ch. For similar compressive strength, the maturity index was lower for ref mix (w/b = 0.42 and C = 475 kg/m^3) having value of 500 Ch.

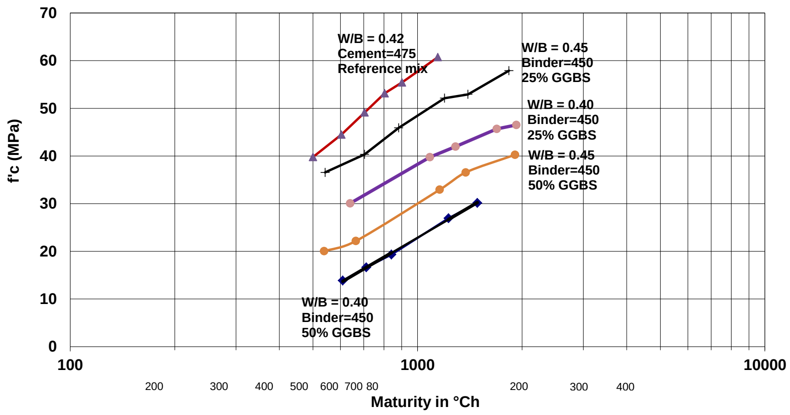

Figure 3 Variation of maturity index.

The Eurocode 2 does not state how to take into account the use of mineral additions such as ground granulated blast furnace slag, fly ash, silica fume, etc. The comparison between Eurocode 2 models and experimental results of compressive strength showed the difference varied in range of 2% to 50% by using s = 0.20, therefore there is need to revise the EC model prediction when supplementary cementitious materials used as replacement such as GGBS.

4. CONCLUSIONS

The effects of binder type and content (GGBS) and w/bon the filling ability, passing ability, the concrete compressive strength at 1 d, 7 d, 3d and 28 d and maturity index were investigated in this study. Based on the results, the following findings can be stated:

- In general, all SCC mixes demonstrated a good filling ability and passing ability. They were classified as SF1 for SCC-B50 and SF2 for other SCC mixes. SCC-A25 was classified VF2 for V-funnel time, and other SCC mixes were VF1.
- Increase in w/b and GBBS led to a reduction of compressive strength at all ages.
- The increase in w/b significantly affects the maturity index. For any given compression strength, the reduction in w/b led to an increase in maturity index for a similar percentage of GGBS.
- The increase of GGBS from 25 to 50% caused a significant increase in the maturity index.
- The relationship between maturity index and the predicted compressive strength is very useful for Banagher in order to establishing detensioning times for pre-stressing cables in precast elements.

For the module of Eurocode, it seems to be a need for more accurate models especially when supplementary cementitious materials is used.

ACKNOWLEDGMENTS

The authors wish to acknowledge the financial support and funding received from the European Union, as this research is part of the FP7-PEOPLE-2012-IAPP project "EiroCrete: Development of sustainable, lower carbon, pre-cast concrete infrastructure".

REFERENCES

[1] Sonebi, M., Bartos, P.J.M., “Hardened SCC and its Bond with Reinforcement,” Proceedings of the First International RILEM Symposium on Self-Compacting Concrete, Stockholm, Sept. 1999, pp. 275-289.
[2] Sonebi, M., Bartos, P.J.M., ‘Hardened SCC and its Bond with Reinforcement’, Proceedings of the First International RILEM Symposium on Self-Compacting Concrete, Stockholm, Sept. 1999, pp. 275-289.
[3] Sonebi, M. (2004), ‘Medium strength self-compacting concrete containing fly ash : modelling using factorial experimental plans’, Cement and Concrete Research 2004; 34(7):1199-1208.
[4] Sonebi, M., Tamimi, A., Bartos, P.J.M. ‘Performance and cracking behaviour of reinforced beams cast with self-compacting concrete’, ACI Materials Journal 2003; 100(6):492-500.
[5] Saul, A. G. A., (1951)’Principles Underlying the Steam Curing of Concrete at Atmospheric Pressure,’ Magazine of Concrete Research, Vol. 2, No. 6, March, pp. 127-140.
[6] Carino, N.J. and Tank, R.C. (1992) ‘Maturity Functions for Concrete Made with Various Cements and Admixtures’, ACI Materials Journal, Vol. 89, No. 2, March-April, pp. 188- 196.
[7] Freiesleben Hansen, P. and Pedersen J., (1977) ‘Maturity Computer for Controlled Curing and Hardening of Concrete’, Nordisk Betong, 1, pp. 19-34.
[8] EFRNARC (2005), “The European Guidelines for Self-Compacting Concrete Specification, Production and Use”.

PROPERTIES OF LOW STRENGTH SELF-COMPACTING CONCRETE WITH RECYCLED BRICK AS AGGREGATE

Ana Jakumetovic[1], Damir Markulak[1], Ivana Milicevic[1]

[1] University of Osijek, Faculty of Civil Engineering Osijek, Department of Materials and Structures, Vladimira Preloga 3, 31 000 Osijek, Croatia, email: ana.jakumetovic@gmail.com, dmarkulak@gfos.hr, ivana.milicevic@gfos.hr

SUMMARY: Clay brick waste is usually delivered to the landfill sites for disposal. The utilisation of recycled brick aggregate (RB) in self-compacting concrete (SCC) has the potential to reduce both the environmental impact and financial cost. Due to increasing charges of landfill and scarcity of natural coarse aggregate (NA), recycled brick aggregate (RB) derived from masonry waste is of increasing interest in construction industry. In the presented study, RB is used as full re-placement of natural aggregate (NA) to produce low strength self-compacting concrete (SCC). Nine different SCC mixes were produced. The water to binder ratio and water to powder ratio were kept the same for all concrete mixtures. The impacts of RB on the key fresh properties such as filling ability and passing ability of SCC, and on the properties in his hardened state were investigated. Based on experimental results, conclusions are made about usage of crushed bricks as partial replacement of natural aggregate in SCC for precast concrete blocks which will serve as steel and R/C frame infill. It is well-known fact that common masonry infill significantly affects the structural behaviour of frames. This type of structures is still considered as 'earthquake risk' structural systems so our intention is to improve the structural behaviour of these systems by applying an infill which may possess beneficial characteristics from the aspect of frame-infill interaction. This puts a new perspective on the use of crushed clay bricks as SCC aggregate with the additionally benefit of providing a sustainable management of such material.

SVOJSTVA SAMOZBIJAJUĆEG BETONA MALE ČVRSTOĆE S AGREGATOM OD RECIKLIRANE OPEKE

SAŽETAK: Otpadna opeka obično se odvozi na odlagališta. Upotreba recikliranog opečnog agregata u samozbijajućem betonu ima potencijal smanjenja utjecaja na okoliš i konačni trošak. Za građevnu industriju povećano zanimanje predstavljaju povećani troškovi odlaganja i manjak prirodnoga krupnog agregata. U radu je prikazana upotreba reciklirane opeke kao cjelovita zamjena prirodnoga agregata u proizvodnji samozbijajućeg betona male čvrstoće. Načinjeno je devet različitih mješavina samozbijajućeg betona. Za sve je mješavine vodovezivni omjer i omjer voda – prah bio isti. Istraženi su učinci reciklirane opeke na svojstva svježe mješavine i to s obzirom na sposobnost punjenja i sposobnost prolaska kao i na svojstva očvrsnuloga betona. Na osnovi ispitivanja donijeti su zaključci o upotrebi drobljene opeke kao djelomične zamjene za prirodni agregat u samozbijajućem betonu za predgotovljene betonske blokove koji će se upotrijebiti kao ispun čeličnih i armiranobetonskih okvirnih konstrukcija. Poznato je da obično ziđe znatno utječe na konstrukcijsko ponašanje okvira. Ova vrsta konstrukcija još se uvijek smatra konstrukcijskim sustavom podložnim potresnom riziku pa je namjera da se ponašanje konstrukcija toga sustava poboljša primjenom ispune koje bi imalo povoljne značajke pri međudjelovanju okvir – ispun. To otvara novu perspektivu za uporabu drobljene opeke kao agregata u samozbijajućem betonu uz dodatnu korist ostvarivanja održivog upravljanja takvim materijalom.

1. INTRODUCTION

The application of self-compacting concrete (SCC) increases the quality and durability of construction, [1]. Because of all its benefits, the use of SCC as an innovative concrete has gained a wider acceptance in recent years, [2]. Enormous quantities of construction and demolition wastes are produced every year and it represents a huge problem that exists worldwide. Most of the waste materials are left as a landfill material or illegally dumped. Consequently, the waste storage disposals are becoming a serious environmental problem, especially for large cities that lack disposal sites [3]. Environmental impact can be reduced by making more sustainable use of this waste. Clay brick waste is usually delivered to the landfill sites for disposal. The utilisation of recycled brick aggregate (RB) in SCC has the potential to reduce both the environmental impact and financial cost. A number of studies were conducted to evaluate the potential of using crushed bricks as aggregates. Singh et al. found that the brick dust and marble powder can be efficiently used to produce good quality self-compacting concrete with satisfactory slump and setting times, [4]. Under certain conditions, replacement of fine aggregate by brick dust and marble powder appears to increase the strength of self compacting concrete. Abib et al. investigated the effect of clay fines on the behaviour of SCC, [5]. They found that the addition of 5% of a waste crushed brick has helped not only to improve the strength (tensile and compression), but also to foster a better rheological behaviour in terms of fluidity and stability, with a low heat of hydration compared to control mixture. Kamal et al. evaluated the properties of fresh self-compacting concrete incorporating crushed red brick and crushed ceramic as aggregates over time, [6]. Recycled materials were used to replace the dolomite used as coarse aggregate in control mixes. The results indicated that the long fresh duration reduced by 48% for the mixes with crushed red brick compared to the mixes with crushed ceramic. Styrofoam was widely used as packaging material to absorb vibration during handling and transportation process. After this process, the styrofoam normally is disposed as waste. This leads to a large amount of waste, which is not biodegradable [7]. Application of styrofoam as a material for artificial replacement for coarse aggregate will help to reduce the environmental problems associated with waste styrofoam. Using styrofoam in concrete will result with lightweight aerated concrete, because it has a very low density as styrofoam forms airspaces. Mandlik et al. found that increase in the expanded polystyrene (EPS) beads content in concrete mixes reduces the compressive and tensile strength of concrete, [8]. Obtained results suggest that expanded polystyrene concrete has scope for non-structural applications, like wall panels, partition walls, etc. Taking into account conclusions from literature review, in this study the usage of RB and combination of RB and styrofoam as full replacement of natural aggregate (NA) was investigated.

2. MATERIAL PROPERTIES

In total, nine mixtures were made. The cement used was Portland composite cement CEM II/B-M(V-L) 32.5 N. Four mixtures were made with hydrate calcium lime CL 90-S as a binder. Hydrate calcium lime was manufactured according to EN 459-1:2015 (HRN EN 459-1:2015). Recycled crushed clay bricks, obtained as industrial waste product, were used as a recycled aggregate (in this paper referred as recycled brick (RB)). The bricks were crushed at the factory 'Opeka d.d.' Osijek and delivered to the concrete-mixing location. Styrofoam is obtained by mechanical recycling of EPS packaging at the factory 'Plastform Ltd.' and was also delivered to the concrete-mixing location. The usage of RB as an aggregate for concrete causes high porosity and water absorption of the concrete. Water absorption of crushed-brick aggregate is several times higher than those of natural aggregate. Aggregate was saturated surface dry before the mixing. By using the RB as an aggregate in concrete it is possible to design concrete mixtures in the same way as the mixtures for commonly used aggregates. The usage of styrofoam as aggregate produced concrete that behaves very similarly to lightweight concretes containing traditional aggregates. Compared to the natural aggregates, especially RB, which are porous materials, styrofoam is a non-absorbent material. In three mixtures RB is used as a full replacement of natural aggregate and in the other six mixtures RB is combined with styrofoam. Particles size of 0-4 mm and 4-8 mm have been used for both, crushed bricks aggregate and styrofoam aggregate. The grading curves of RB and styrofoam are shown in Figure 1.

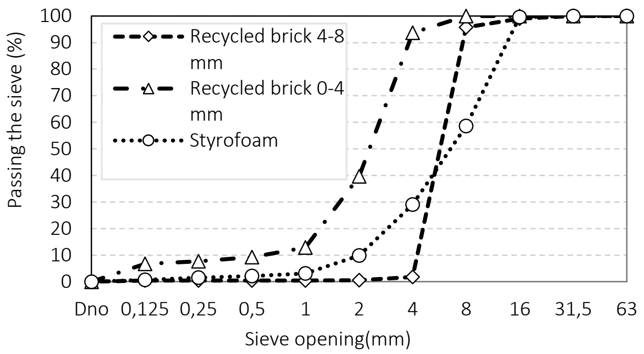

Figure 1 Grading curves for RB and Styrofoam

Brick dust and dolomite powder were used as fillers in SCC mixtures. Fillers are all fine particles smaller than 0,125 mm. It is desirable for at least 70% of particles to pass a 0,063 mm sieve because it can significantly improve the workability of self-compacting concrete. The filler addition also regulates the cement content in order to reduce the heat of hydration and thermal shrinkage. The particle size distribution, shape and water absorption of mineral fillers may affect the water demand and therefore suitability for using in the manufacture of SCC. In all mixtures was used brick dust, obtained by sieving of crushed clay bricks, and in three mixtures dolomite powder combined with brick dust was used. Mix designs often use volume as a key parameter because of the importance to fulfil the voids between the aggregate particles. Some methods attempt to fit available constituents to an optimised grading envelope. Another approach is to evaluate and optimise the flow and stability of first the paste and then the mortar fractions before the coarse aggregate is added and the whole SCC mix tested. In this study, all mixtures were designed in accordance with the recommendation of 'The European Guidelines for Self Compacting Concrete', [9]. The compositions of all mixtures are shown in Table 1. All mixtures were designed to achieve low strength self-compacting concrete. As defined by ACI, controlled low-strength material (CLSM) usually has a compressive strength of 8.3 N/mm^2 or less.

Table 1 Mixture proportions

Composition of SCC mixtures for 1 m^3	SCC1 (kg)	SCC2 (kg)	SCC3 (kg)	SCC4 (kg)	SCC5 (kg)	SCC6 (kg)	SCC7 (kg)	SCC8 (kg)	SCC9 (kg)
CEM II/B-M(V-L) 32.5 N	200	0	0	200	0	0	175	200	200
CL 90-S	255	455	455	255	455	455	280	255	255
Water	210	210	210	210	210	210	210	210	210
w/b ratio	0,46								
Sika ViscoCrete 20 Gold	1% mb								
BASF - RheoMatrix 110	1% mb								
Brick powder	137	68	137	137	68	137	137	68	68
Dolomite powder	-	-	68	-	-	68	-	-	68
0-4 mm - RB	553	553	554	503	503	502	556	558	552
4-8 mm - RB	479	479	480	373	373	372	407	430	425
0-4 mm - styrofoam	-	-	-	6	6	6	-	-	-
4-8 mm - styrofoam	-	-	-	-	-	-	3	2	2
w/p ratio	0,96								

In all mixtures the following chemicals were used: the viscosity modifying admixtures (VMA) and a superplasticiser. As VMA high performance viscosity modifying admixture MasterMatrix SDC 100 was used, produced by 'Badische Anilin & Soda-Fabrik' (BASF). The superplasticizer used was high rang water reducer Sika ViscoCrete - 20 Gold, produced by Sika Group, and its purpose was to improve the workability of the mixtures.

3. EXPERIMENTAL INVESTIGATION

The impacts of RB on the key fresh properties such as filling ability and passing ability of SCC, as well as the properties in its hardened state were investigated. The aim of this experimental investigation was to obtain a lightweight self-compacting concrete mixture with low-strength properties which will be used as precast concrete blocks. Properties of SCC in the fresh state were tested in accordance with the standards HRN EN 12350. The mean values of the tested properties are presented in Table 2.

Table 2 Properties of SCC in the fresh state

Mixture	SCC1	SCC2	SCC3	SCC4	SCC5	SCC6	SCC7	SCC8	SCC9
Density (kg/m3)	1986	1996	2003	1700	1600	1770	1620	1960	1930
Air content (%)	4.8	4.6	4.2	7.0	5.5	6.4	11.0	6.1	8.0
Slump-flow test T500 (s)	1.8	2.0	7.1	14.6	9.3	8.6	11.8	5.0	7.0
L-box test	0.88	0.97	0.89	0.93	0.85	0.92	0.86	0.82	0.87
J-ring test	10.75	11.00	22.50	7.50	2.50	8.75	7.50	10.00	1.25

Density of SCC in the fresh state was determined in accordance with the standard HRN EN 12350-6:2009. According to the results shown in Table 2, the density of SCC with RB as an aggregate is higher than the density of the mixtures with the addition of styrofoam. It was expected because styrofoam has lower density than the recycled brick, 70 kg/m^3 and 1850-1960 kg/m^3, respectively. Air content was determined in accordance with the standard HRN EN 12350-7:2009. As it can be seen in Table 2, the lower density mixtures have higher air content and vice versa, which was also expected. Actually, in the combination of RB and a styrofoam aggregate, due to their specific shape, more air was entrained by the mixing so the air content was higher. The slump-flow test was conducted in accordance with the standard HRN EN 12350-8:2010. The slump-flow and T_{500} time is used to estimate the flow ability and the flow rate of self-compacting concrete in the absence of obstacles. In this study the T_{500} time was measured. The T_{500} time test showed that the slowest mixture was SSC4 with the value of 14.6 s. Since its value exceeded 2 s, as was also the case with the mixtures SCC3, SCC5, SCC6, SCC7, SCC8 and SCC 9, they all are classified as VS2 according to the viscosity classes defined in the HRN EN 206:2014. The mixtures SCC1 and SCC2 had values below 2 s so that are classified as VS1. A higher T_{500} value indicates a more viscous mixture which is more suitable for concrete in applications with congested reinforcement or in deep sections. A lower T_{500} value may be appropriate for concrete that has to travel long horizontal distances without much obstruction. A lower value of T_{500} time results in better fluidity. The recommended values are ranging between 2 s and 5 s. The L-box test was carried out in accordance with the standard HRN EN 12350-10:2010. The L-box test examines the passing ability of a self-compacting concrete to flow through narrow spaces between reinforcing bars without segregation or blocking. According to the HRN EN 206:2014, L-box passing ability values should be greater than or equal to 0.80. For the L-box with three reinforcement bars values are classified as PL2 if H2/H1 is greater than or equal to 0.80. The recommended values are ranging between 0.8 and 1.0. As it is shown in Table 2 all mixtures were classified as PL2. The J-ring test was carried out in accordance with the standard HRN EN 12350-12:2010. The J-ring test is of the same purpose as the L-box. According to the HRN EN 206:2014, a J-ring passing ability values should be lower than or equal to 10 mm. For J-ring with 16 steel bars values were classified as PJ2. The recommended values are ranging between 0 and 10. Figures 2 to 4 show the J-ring test for mixtures SCC1, SCC4 and SCC 7. From Table 2 and Figure 3 is visible that SCC3 mixture does not satisfy the passing ability value in range 1 to 10 mm, while all the other mixtures satisfied given criteria. In the case of further using the SCC3 mixture there will be a need to increase a superplasticizer from 1% to 1,5% of the binder mass.

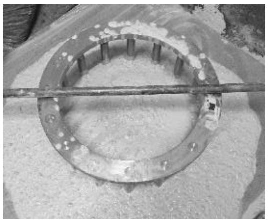

Figure 2
J-ring test for mixture SCC1

Figure 3
J-ring test for mixture SCC3

Figure 4
J-ring test for mixture SCC7

Properties of SCC in hardened state were tested in accordance with the standards HRN EN 12390. The tested properties were: compressive strength, flexural strength, density of hardened concrete and modulus of elasticity. The prism moulds 100x100x400 mm in size along with the cube moulds of size 150x150x150 mm were filled with fresh concrete in one layer. After placing the concrete into moulds the top surface of the fresh concrete specimens was finished off with a trowel. The moulds were covered with a plastic film and left 24 to 72 hours (i.e. 24 h the mixtures with the cement and 72 h the mixtures without cement) at room temperature of 20°C ± 5 °C. The specimens were demoulded after 48 hours and afterwards cured in the lab at controlled temperature of 20°±5°C, until they were tested. Compressive strength was determined in accordance with the HRN EN 12390-3:2009. The compressive strength was tested after 28, 56, and 91 days. Three specimens per each mixture were tested at each selected age. The mean values are presented in Figure 5. It can be seen that the mixtures based only on a lime as a binder have lower compressive strengths compared to the mixtures based on cement and lime as binders. The mixtures with fraction 0-4 mm of styrofoam as an aggregate have lower compressive strengths compared to the mixtures made with recycled brick, but the mixtures with fraction 4-8 mm of styrofoam have a higher compressive strengths. A compressive strength depends primarily on the strength, stiffness and density of an aggregate. The compressive strength increased with the longer curing time for all mixtures, as expected. Once the cubes reached failure, the shape of the cubes altered due to the compression stresses. The failure shape can indicate whether a failure is satisfactory or unsatisfactory. Figure 6 shows the shape of the cubes after failure, so it can be seen that the all cube failures are satisfactory in accordance with the HRN EN 12390-3:2009. It can be concluded that all mixtures have low strength as it was our intention in the first place, so that the concrete composition was designed well. Also, the mixtures SCC1, SCC7, SCC8 and SCC9 have the compressive strength acceptable for production of precast concrete blocks with the vertical compressive strength of minimum 2.5 MPa.

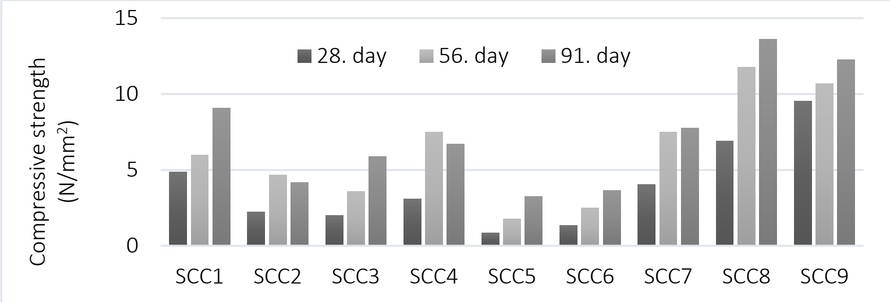

Figure 5 Compressive strengths of SCC Concrete

Figure 6 SCC shape of the cubes after failure

Flexural strength was tested on prisms of size 100x100x400 mm in accordance with the HRN EN 12390-1:2009. The flexural strength was tested after 28, 56, and 91 days of curing. Three specimens per each mixture were tested at each selected age and the mean values are presented in Figures 7 and 8. Similar to the compressive strength, the mixtures based only on a lime as a binder have lower flexural strengths compared to the mixtures based on cement and lime as binders. The mixtures with fraction 0-4 mm of styrofoam as an aggregate have lower flexural strengths compared to the mixtures made only with recycled brick, but with styrofoam fraction 4-8 mm the flexural strength is higher. The flexural strength increases with the increasing of a curing time for the all mixtures.

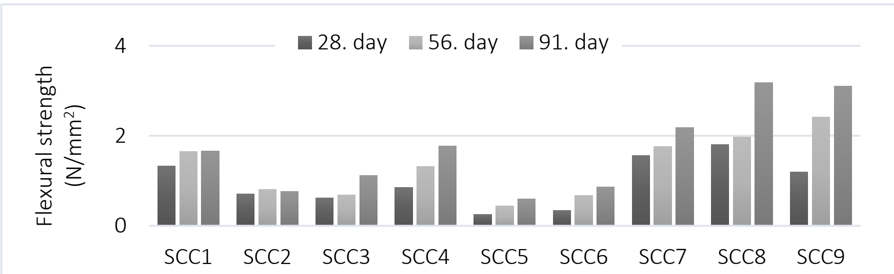

Figure 7 Flexural strengths of SCC Concrete

Figure 8 SCC after flexural strength test

Density of the hardened concrete was tested in accordance with the standard HRN EN 12390-7:2009. Three specimens per each mixture were tested at each selected age and the mean values are presented in Figure 9. According to the results, the density of SCC made only with the recycled brick as an aggregate is higher than the density of the mixtures with the addition of styrofoam. All mixtures have densities lower than 2000 kg/m^3 and therefore are classified as the lightweight concretes. According to the density classes of the lightweight concrete defined in the HRN EN 206:2014, the values of the mixtures SCC1, SCC2, SCC3 and SCC9 after 28th day were between

1600 and 1800 kg/m^3, so that they were classified as D1.8. The other five mixtures had lower values (between 1400 and 1600 kg/m^3) and were classified as D1.6. The densities of the hardened concretes decrease with the increasing of the curing time for all mixtures.

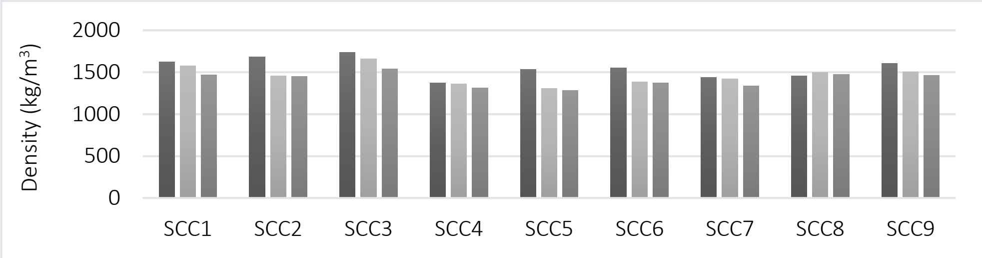

Figure 9 Densities of SCC Concrete

Modulus of elasticity was determined according to the standard HRN EN 12390-13:2013. The obtained values are shown in Figure 10. Modulus of elasticity of concrete is a function of the modulus of elasticity of aggregate, cement matrix and their relative proportions. The modulus of elasticity of the concrete with crushed brick as an aggregate is about 30 % lower than the one of a normal concrete, [10]. It is important to take into consideration the lower modulus of elasticity when designing precast construction elements by using concrete with RB as an aggregate, since the lower modulus of elasticity reduces the stiffness of a structure. In the case of infilled frames, this fact, along with lower strengths of precast blocks, may be even useful, taking into account possible detrimental effects of common masonry infill to the frames, especially to the steel frames, [11].

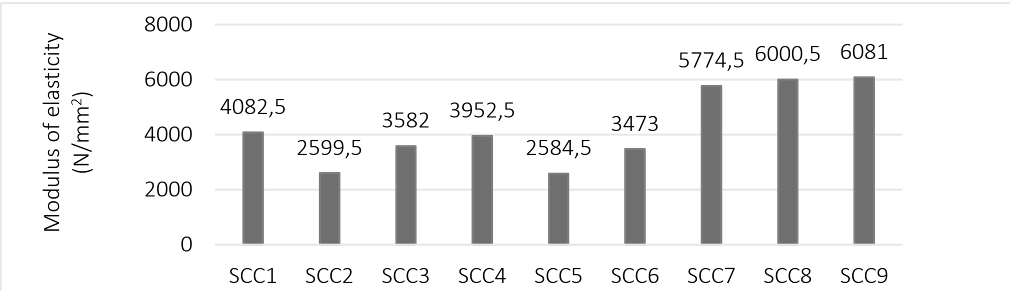

Figure 10 Modulus of elasticity

Consequently, well-known equations given in most standards for estimating a concrete elastic modulus for conventional concretes may not be applicable for the concretes incorporating recycled aggregates.

4. CONCLUSION

Since the application of the concrete with crushed clay bricks is not widespread, it is important to investigate the possibility of applying it in areas where such concrete may show better properties than concrete with a natural aggregate. Recycling of the crushed clay bricks as a new raw material is not only economically viable but it is also considered as an environmental friendly approach. This paper presents the possibility of usage of crushed bricks and styrofoam as a replacement of the natural aggregate in self-compacting concrete used for precast concrete blocks. It is well-known fact that common masonry infill significantly affects the structural behaviour of infilled frames, so our basic idea is to make an attempt to improve observed detrimental effects caused by common masonry infill, [11]. Nine different SCC mixtures were produced in this experimental study. RB is used as a full replacement of the natural aggregate, and in the six mixtures it is combined with a styrofoam. The water to binder (W/B) ratio and the water to powder (W/P) ratio were kept the same for all concrete mixtures. The mixtures of SCC were designed to achieve different concrete classes with the low compressive strength. Properties of SCC in fresh and hardened state were tested. The results of this study confirmed that the mixtures of SCC used are classified as lightweight concretes with low-strength, which was our first aim. The conducted laboratory testing also indicates that SCC with RB aggregate shows reasonable potential for use in precast concrete blocks which may serve as a frame infill. A further research will be carried out to investigate the properties of precast concrete blocks, wallets as well as masonry made of SCC with RB aggregate, in order to fully investigate their potential as a frame infill.

ACKNOWLEDGMENTS

The research presented in this full paper is a part of the internal research project "Controlled seismic behaviour of masonry infilled steel frames", supported by University of Osijek, Faculty of Civil Engineering, Croatia, and its support is gratefully acknowledged.

REFERENCES

[1] Okamura, H. & Ouchi, M.: Self-compacting concrete, Journal of Advanced Concrete Technology, Vol. 1, No. 1, 5-15, April 2003

[2] Ouchi, M.; Nakamura, S.; Osterson, T; Hallberg, S.; Lwin, M.: Applications of Self-Compacting Concrete in Japan, Europe and the United States, ISHPC, 2003, pp.1-20

[3] Batayneh, M.; Marie, I.; Asi, I. Use of selected waste materials in concrete mixes, Waste Management, 27(2007),pp 1870-1876.

[4] Singh, R.; Kaushik, R.; Singh, G.: Study of Self Compacting Concrete Using Brick Dust and Marble Powder, International Journal of Engineering Research and Applications (IJERA), May-Jun 2013, Vol.(3) No. 3, pp.1283-1286, ISSN: 2248-9622

[5] Abib, Z.; Gaher-Abib, H.; Kharchi, F.: Effect of Clay Fines on the Behavior of Self-Compacting Concrete, Engineering, 2013, Vol. (5) No. 2, pp. 213-218

[6] Kamal, M.; Safan, M. A.; Etman, Z. A.; Eldaboly, E.: Evaluating the Prolonged Properties of Fresh Self-Compacting Concrete Incorporating Recycled Aggregates, International Journal of Current Engineering and Technology, June 2013, Vol.(3) No 2, pp. 436-446, ISSN 2277 - 4106

[7] Ahmad, M. H.; Lee, Y. L.; Mohd Noor, N.; Adnan, S. H.: Strength development of lightweight styrofoam concrete, International Conference on Civil Engineering (ICCE08), May 2008, Hyatt Regency Kuantan Resort, Kuantan, Pahang.

[8] Mandlik, A.; Sood, T.S.; Karade, S.; Naik, S.; Kulkarni, A.: Lightweight Concrete Using EPS, International Journal of Science and Research (IJSR), March 2015, Vol.(4) No. 3, pp. 2007-2010, ISSN: 2319-7064

[9] FNARC:Specification and Guidelines for Self-Compacting Concrete, Farnham, February 2002.

[10] Akhtaruzzaman, A.A. & Hasnat, A.: Properties of concrete using crushed brick as aggregates, ACI Concrete International, 1983, Vol.(5) No. 2, pp. 58–63.

[11] Markulak, D.; Radić, I.; Sigmund, V.: Cyclic testing of single bay steel frames with various types of masonry infill, Engineering Structures, Vol.(51), June 2013, pp. 267-277, ISSN 0141-0296

SELF-COMPACTING CONCRETE SHRINKAGE MEASUREMENT

Donka Würth[1], Ivana Banjad Pecur[2]

[1] Zagreb University of Applied Science, Vrbik 8, 10 000 Zagreb, Croatia, email: dwurth2@tvz.hr
[2] University of Zagreb Faculty of Civil Engineering, Department of Materials, Fra Andrije Kacica Miosica 26, 10 000 Zagreb, Croatia, email: banjadi@grad.hr

SUMMARY: Shrinkage of self-compacting concrete is the volume deformation that occurs in concrete during the phase of cement hydration, and continues after hydration. Greater shrinkage results with cracking of concrete. The shrinkage rate of self-compacting concrete is influenced by several factors such as: dimensions of the structural element, concrete components, environmental conditions in which the element is located, as well as casting and curing period. This paper describes the shrinkage measurement of self-compacting concrete incorporated in the structure. Measurements were conducted on prism shaped samples in laboratory controlled conditions, all in accordance with the Croatian standard HRN U.M1.029 – Determination of volume deformation. The other two measurements were conducted on the construction site. The first measurement started in the fresh concrete phase, and the test specimens were stored at construction site in the real ambient conditions as the structure itself. Second measurement was carried out directly on reinforced concrete elements, i.e. wall and column, immediately after the removal of formwork. The paper presents the results of shrinkage measurements of self-compacting concrete.

MJERENJE SKUPLJANJA SAMOZBIJAJUĆEG BETONA

SAŽETAK: Skupljanje samozbijajućeg betona volumenska je deformacija koja se pojavljuje u betonu već u fazi hidratacije cementa, a traje i nakon hidratacije. Posljedica većeg skupljanja betona pojava je pukotina. Na veličinu skupljanja samozbijajućeg betona utječe nekoliko čimbenika a to su: dimenzije konstrukcijskog elementa, sastavni materijali betona, uvjeti okoliša u kojoj se nalazi armiranobetonski element, te način i vrijeme njege. U radu je prikazano mjerenje skupljanja samozbijajućeg betona ugrađenog u konstrukciju. Mjerenja su provedena na uzorcima prizmi koje se nalaze u laboratorijskim kontroliranim uvjetima prema normi HRN U.M1.029 – Određivanje volumenskih deformacija. Ostala dva mjerenja provedena su na gradilištu. Prvo mjerenje započeto je u fazi svježeg betona, te su ispitni uzorci prizmi ostavljeni na gradilištu u uvjetima okoliša konstrukcije. Drugo mjerenje skupljanja provedeno je izravno na armiranobetonskim elementima, odmah nakon uklanjanja oplate. Skupljanje betona na gradilištu mjereno je na armiranobetonskom zidu i stupu. U radu su prikazani dobiveni rezultati mjerenja skupljanja samozbijajućeg betona.

1. UVOD

Samozbijajući beton SZB („self compacting concrete“ – SCC) pripada grupi posebnih betona. Sam naziv govori o tome da je to beton koji svojom vlastitom težinom teče i ugrađuje se i popunjava oplatu, zaobilazeći armaturu. Svojom tekućom konzistencijom i manjim zrnom agregata (D 16mm), izuzetno lako popunjava prostor oko armature i na nedostupnim mjestima, kao što su gusto armirani presjeci, te tanki i geometrijski zahtjevni presjeci.

Dobar samozbijajući beton mora biti tekuć ali i dovoljno viskozan, kako bi se sam ugrađivao bez zahtjeva za vibriranjem. Nakon skidanja oplate površina ostaje glatka, bez šupljina i zadovoljava estetske kriterije – vidljive betone, a očvrsli beton ima svojstva običnog betona. Uslijed povećane količine sitnih čestica, samozbijajući beton je osjetljiviji na povećano skupljanje, a sami time i na pojavu pukotina [1]. Osim samih sastavnih sastojaka betona, na skupljanje samozbijajućeg betona utječe sastav betona, te njega betona nakon ugradnje (temperatura, relativna vlaga zraka), a isto tako značajan utjecaj ima duljina vremena njegovanja betona.

Skupljanje je deformacija betona tijekom vremena i to na neopterećenom uzorku. Do skupljanja dolazi uslijed promjene vlažnosti u betonu i fiziklalno – kemijskih promjena u betonu. Skupljanje se izražava kao bezdimenzionalna deformacija u mm/m u uvjetima stalne i određene relativne vlažnosti i temperature.

Ukupno skupljanje betona može se prikazati kroz nekoliko faza, a to su: plastično skupljanje, koje nastaje evaporacijom vode uslijed početka hidratacije, autogeno skupljanje nastaje nakon 1 dana (promjena vlažnosti u očvrslom betonu), uslijed hidratacije cementa, povećava se temperatura betona, te na kraju nastaje skupljanje betona uslijed sušenja (nakon završetka hidratacije) koje je manje [3], ali može trajati godinama [4].

Mjerenja skupljanja samozbijajućeg betona koja su opisana u ovom radu, izvedena su u svrhu promatranja ponašanja betona u dijelu podzemnih garaža Poslovnog kompleksa HEP-a. Podzemni dio garaža izveden je metodom top-down, te princip izolacije zgrade je na principu vodonepropusnih elemenata. Zidovi podzemne garaže izvedeni su od samozbjajućeg betona prema zahtjevu projektanta

2. ZAHTJEVI ZA SAMOZBIJAJUĆI BETON

Vrsta samozbijajućeg betona C30/37, SF2, VS2, PL2, D16 ugradila se u zidove i stupove garaže Hrvatske elektroprivrede u Zagrebu. Prije same ugradnje provedena su ispitivanja svojstava svježeg samozbijajućeg betona prema normama HRN EN 12350-8 do12, ispitana je tlačna čvrstoća pri starosti od 28 dana i provedena su mjerenja skupljanja samozbijajućeg betona. U Tablici 1 dat je sastav samozbijajućeg betona koji je projektiran prema Europskim smjernicama EFNARC [2].

Tablica 1: Sastav samozbijajućeg betona C30/37, SF2, VS2, PL2, D16

Sastavni materijali	Opis	Masa (kg) po m^3
Cement	CEM II/A-S 42,5R	340
Voda	Vodovod	175
Filer	Vapnenački - Dalmacija	130
Agregat	Prirodni – riječni D16	1730
Dodatak	Superplast. na bazi polikarboksilata (1,3%)	4,42
Vodo/praš. omjer (maseno)	Praškaste komponente (cement+ filer)	0,37
Vodo/praš. omjer (volumno)	Preporuka EFNARC (0,95-1,05)	1,13

3. MJERENJA SKUPLJANJA SAMOZBIJAJUĆEG BETONA

U radu su obrađena 3 različita mjerenja skupljanja samozbijajućeg betona i to: prvo mjerenje je bilo u trenutku betoniranja, na uzorku svježeg betona, a druga dva mjerenja na betonu s početkom u očvrslom stanju. Svrha ispitivanja bila je da se usporede mjerenja skupljanja betona prema normi HRN U.M1.029, s ispitivanjima na istim uzorcima ali prvo početno mjerenje u svježem stanju, te na samim betonskim elementima, stupu i zidu, nakon uklanjanja oplate.

3.1. MJERENJE SKUPLJANJA NA SVJEŽEM BETONU

Na gradilištu su izrađene prizme dimenzija 100x100x400mm sa mjernom bazom od 200mm (Slika 1). U trenutku kada je beton mogao primiti repere i mjerni uređaj (cca 4 sata) izvršeno je prvo nulto mjerenje. Mjerenja su provedena do 28 dana starosti uzorka, tako da se prvih 7 dana mjerilo skupljanje svaki dan, a kasnije svakih 2 dana. Izmjerena temperatura zraka u trenutku betoniranja je 15ºC i relativna vlažnost zraka 72%, koja se iz dana u dan mijenjala s obzirom na meteorološke uvjete. (nije se mjerila temperatura i relativna vlaga zraka nakon prvog dana)

Slika 1: Mjerenje skupljanja na svježem betonu

3.2. MJERENJE SKUPLJANJA SAMOZBIJAJUĆEG BETONA NA UZORCIMA U LABORATORIJU

Prema normi HRN U.M1.029 izrađeni su uzorci na gradilištu, te se čuvaju 24 sata u kalupu, koji su prekriveni najlonom. Slijedeći dan uzorci se voze u laboratorij i narednih 48h drže se u vodi temperature 20 ± 4ºC. Uzorci se nakon 72 ± 0,5h starosti vade iz vode, ostavljaju u prostoru termo-higrometrijskih uvjeta sličnim na gradilištu 20 ºC i 70±5% relativne vlage (Slika 2). Za mjerenje deformacija koristio se prijenosni mjerni instrumenti s mjernom bazom 200 mm. Početno mjerenje je pri starosti od 72 ± 0,5h, a zatim se nastavlja mjeriti skupljanje betona pri starosti od 4,5,6,7,14 21 i 28 dana.

Slika 2: Uzorci za ispitivanje skupljanja na očvrslom betonu u laboratoriju

3.3. MJERENJE SKUPLJANJA SAMOZBIJAJUĆEG BETONA NA TERENU

Na elementima probnog stupa i zida, nakon uklanjanja oplate (nakon 2 dana) započeto je mjerenje skupljanja betona sa mjernom bazom od 300 mm (Slika 3a i 3b). Mjerenja su provedena do 28 dana starosti betona, tako da se prvih 7 dana mjerilo skupljanje svaki dan, a kasnije svaka 2 dana. Reperi za mjerenje skupljanja ugrađeni su nakon 2 dana. Površina betona je očišćena, osušena, te su reperi zalijepljeni brzovezujućim ljepilom na udaljenosti baze 300mm. Kod prvog mjerenja zabilježena je temperatura zraka 15ºC i relativna vlažnost zraka 72 %.

Slika 3a i 3b Stup i zid– mjesto na kojem su postavljeni reperi

4. REZULTATI MJERENJA SKUPLJANA SAMOZBIJAJUĆEG BETONA

Nakon 28 osam dana starosti uzorka samozbijajućeg betona prema normi HRN EN 12390-3 ispitana je tlačna čvrstoća betona koja iznosi 57,5 N/mm^2. Na samim armiranobetonskim elementima zida i stupa, nema pojave pukotina, a izgled površine ukazao je na nedostatke i prednosti načina ugradnje betona. Upumpavanjem betona u oplatu, postigla se prekrasna vidljiva površina betona (što je bio zahtjev projektanta). U probnom dijelu zida ugradnja betona bila je odozgora, a na površini su se pojavili mjehurići zraka, što je bilo nepovoljno. Također moramo naglasiti da tijekom ispitivanja na uzorcima na gradilištu nije bilo njegovanja betonske površine, što se tijekom izvođenja zahtijevalo, prekrivanjem i vlaženjem geotekstila koji je bio pričvršćen na zidove i stupove buduće garaže. Rezultati skupljanja samozbijajućeg betona dati su u Tablici 2., a prikazani su na Slici 4.

Tablica 2: Rezultati mjerenja skupljanja samozbijajućeg betona

starost betona t (dani)	def. skupljanja svježi beton $e_{skup}(t)$ (mm/m)	def. skupljanja stup $e_{skup}(t)$ (mm/m)	def. skupljanja zid $e_{skup}(t)$ (mm/m)	def. skupljanja očvrsli beton – labor. $e_{skup}(t)$ (mm/m)
0	0,000	-	-	-
1	0,275	-	-	-
2	0,275	0,000	0,000	-
3	0,045	0,000	0,033	0,000
4	0,400	0,000	0,067	0,038
5	0,450	0,067	0,167	0,050
6	0,500	0,067	0,167	0,100
7	0,457	0,067	0,167	0,125
12	0,525	0,067	0,167	0,200
14	0,574	0,067	0,167	0,288
17	0,599	0,067	0,167	0,225
19	0,724	0,067	0,167	0,263
21	0,724	0,067	0,200	0,313
28	0,724	0,100	0,200	0,375

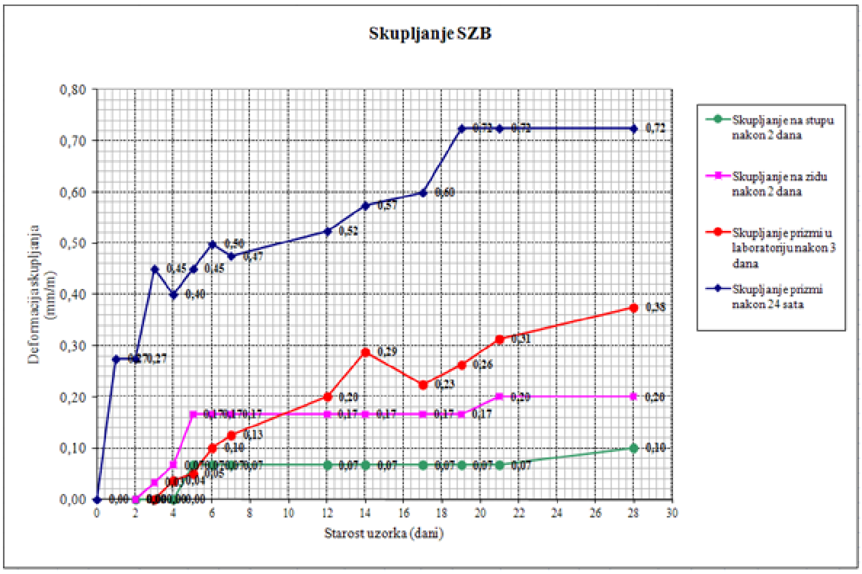

Slika 4: Grafički prikaz rezultata skupljanja

5. ZAKLJUČAK

U radu su prikazana mjerenja skupljanja samozbijajućeg betona prema normi HRN U.M1.029 koja je važeća u Hrvatskoj. Provedena su dodatna mjerenja na gradilištu kako bi se uvidjele volumne deformacije samozbijajućeg betona u različitim klimatskim uvjetima, te na stvarnim elementima. Rezultati mjerenja skupljanja nakon 24 sata pokazala su najveće skupljanje betona, što objašnjava da su uzeta u obzir i ona rana skupljanja betona u trenutku hidratacije cementa, plastično i autogeno skupljanje. Nedostatak mjerenja je da nije evidentirana svakodnevna temperatura zraka i relativna vlažnost koji zasigurno imaju utjecaj na rezultate mjerenja. Mjerenja na armirano betonskih elementima (zid i stup) pokazala su manje vrijednosti skupljanja s obzirom da su elementi bili 2 dana u oplati (nema evaporacije s površine betona), a i armatura koja se nalazi u ab elementima smanjuje vlačna naprezanja uslijed skupljanja betona. Vrijednosti rezultata ispitivanja na uzorcima koji su izrađeni i ispitani prema normi HRN U.M1.029, nalaze se između vrijednosti mjerenih na terenu.

Možemo zaključiti da mjerenje skupljanja prema normi HRN U.M1.029 pokazat će vrijednosti skupljanja veće nego što će biti na stvarnom objektu, te armatura sudjeluje u smanjenju vrijednosti skupljanja samozbijajućeg betona na ab elementima. Ako se prihvati metoda mjerenja skupljanja i u samoj fazi plastičnog i autogenog skupljanja, vrijednost skupljanja bit će veća, te bi se na gradilištu uz pomoć optičkih vlakana ili nekih drugih mjernih pomagala uz nove metode, može promatrati skupljanje u samoj fazi hidratacije.

Ovo su preliminarna mjerenja za buduća ispitivanja skupljanja samozbijajućeg betona mjerenog na gradilištu (na stvarnim elementima), te mjereno na uzorcima betona, no već u fazi hidratacije cementa. Također kod ovakvih mjerenja trebalo obratiti pozornost na svakodnevno mjerenje promjene temperature zraka i relativne vlažnosti zraka, a isto tako uključiti njegovanje uzoraka na gradilištu, kao mogućnost smanjenja skupljanja samozbijajućeg betona.

LITERATURA

[1] Schutter G., Bartos P.J.M., Domone P., Gibbs J.: Self-compacting concrete, Scotland UK, (2008). pp 115-121

[2] ERMCO; EFNARC; EFCA; CEMBUREAU; BIBM : The European Guidelines for Self-Compacting Concrete, Specification, Production and Use, 2005.

[3] Šahinagić-Isović M.,. Markovski G, Ćećez M.: Deformacije skupljanja betona - uzroci i vrste, Građevinar 64 9 (2012), str. 727-734

[4] EL-Khoury R.D.: Creep and Shrinkage behavior of SCC, Dissertation Rutgers, The State University of New Jersey, New Brunswick, New Jersey, October, 2010.

[5] HRN U.M1.029 : Beton - Određivanje volumnih deformacija

ASSESSMENT OF CONCRETE CHARACTERISTICS DURING THE DELIBERATE DEFORMATION OF A FLEXIBLE MOULD AFTER CASTING

Roel Schipper[1], Steffen Grunewald[1,2], Sergiu Troian[3], Raghunath Prashanth[4], Erik Schlangen[5], Oguzhan Çopuroğlu[5]

[1] Delft University of Technology, Department of Structural and Building Engineering, Stevinweg 1, 2628 CN Delft, Netherlands, email: H.R.Schipper@tudelft.nl
[2] Ghent University, Laboratory Magnel for Concrete Research, Technologiepark-Zwijnaarde 904, 9052 Ghent, Belgium, email: s.grunewald@tudelft.nl
[3] Institute of Geology and Seismology, Academy of Sciences of Moldova, 60/3 Gh. Asachi str., 2028 Chişinau, Republic of Moldova, email: troian.sergiu@gmail.com
[4] VS-A.HK, W2, 9/F, The Bedford, No. 91-93 Bedford Road, Tai Kok Tsui, Kowloon, Hong Kong, e-mail: prashanthprefabs@gmail.com
[5] Delft University of Technology, Department of Materials and Environment - Microlab, Stevinweg 1, 2628 CN Delft, Netherlands, email: H.E.J.G.Schlangen@tudelft.nl, O.Copuroglu@tudelft.nl

SUMMARY: Expensive CNC (computer numerical controlled)-milled formwork is required for the production of double-curved precast concrete elements for cladding or shell structures. The innovative flexible mould method for economically efficient and sustainable production of such elements, developed at Delft University of Technology, comprises the use of a flexible, CNC-controlled formwork, which is filled with self-compacting concrete (SCC). This paper describes how curved precast concrete elements can be manufactured in this open and reusable flexible mould. The proposed method reduces formwork costs of architectural freeform elements made with concrete. First, the method is described briefly, then tests are discussed, demonstrating that by measuring the rheological parameters of the concrete during the process, the right moment of deformation can be determined. The measurements show that thixotropic behaviour of concrete for this manufacturing method is very helpful, since it leads to a quick increase of the yield strength of the fresh concrete, but still leaves concrete deformable in order to prevent cracking caused by the deformation of the mould. The change of the rheological behaviour of concrete in the period between mixing and deformation of the mould was assessed; an additional study was executed in order to assess the integrity of the concrete after the deformation of the mould.

OCJENJIVANJE ZNAČAJKI BETONA TIJEKOM NAMJERNOG DEFORMIRANJA SAVITLJIVE OPLATE NAKON UGRADNJE

SAŽETAK: Za oplatu pri proizvodnji dvostruko zakrivljenih predgotovljenih betonskih elemenata za obložne ili ljuskaste konstrukcije zahtijeva se skupa brušena oplata kontrolirana pomoću računala. Inovativna metoda savitljive oplate za ekonomično učinkovitu i održivu proizvodnju takvih elemenata razvijena na Tehnološkom sveučilištu u Delftu sadržava upotrebu savitljive oplate kontrolirane pomoću računala punjene samozbijajućim betonom. U radu se opisuje kako se mogu proizvesti zakrivljeni predgotovljeni betonski elementi u toj otvorenoj i višekratno upotrebljivoj savitljivoj oplati. Predloženom metodom smanjuju se troškovi oplate za arhitektonske slobodno oblikovane betonske elemente. Na početku metoda je ukratko opisana, zatim su raspravljena ispitivanja koja su pokazala da se mjerenjem reoloških parametara betona tijekom procesa može odrediti pravi trenutak deformiranja. Mjerenje pokazuje da je tiksotropno ponašanje betona u toj proizvodnoj metodi vrlo korisno jer dovodi do brzog porasta čvrstoće tečenja svježega betona ali ujedno ostavlja beton deformabilnim kako bi se spriječilo raspucavanje prouzročeno deformiranjem oplate. Ocijenjeno je vrijeme promjene reološkog ponašanja betona u vremenu između miješanja i deformiranja oplate. Dodatno, provedeno je istraživanje radi ocjenjivanja cjelovitosti betona nakon deformiranja oplate.

1. INTRODUCTION

Curvature offers a beautiful shape language for architecture, a language that would not exist if only straight lines and rectangular, flat surfaces made up the architect's vocabulary. Double-curved structures in general, and monolithic concrete shell structures more specifically, can transfer forces very efficiently. Two famous examples of prefabricated shell structures are the Palazzetto dello Sport [1] and the Heydar Aliyev Cultural Centre [2]. In practice, however, the number of shell structures is still limited because of higher costs of curved buildings due to both the extra efforts needed for handling complex geometry during the design and productions stages and the need for unconventional construction methods on the building site or in the factory. The flexible mould method is an alternative method for economically efficient and sustainable production of curved and double-curved elements. Renzo Piano [3] described the principle of producing deformed plastic cladding elements, using a pneumatic formwork. Based on Piano's principle, Vollers and Rietbergen [4] developed a computer-driven set of actuators, which by changing their position on their top could form a curved surface. The flexible mould system for the production of double-curved prefabricated concrete elements was further developed and studied at Delft University of Technology [5]; the up-scaling of the mould system is an ongoing project. The production comprises casting of an element in horizontal position and, after a waiting period, the mould is deliberately deformed and positioned on pre-arranged mould supports. The element hardens in the deformed mould, which can be re-used for the production of elements having the same or a different geometry. Casting of concrete in general takes place in a wide variety with regard to mixture consistency, placement and compaction methods. The deformability of concrete in the plastic stage is an important characteristic, which contributes to its widespread utilisation. In the period between mixing and de-moulding, the concrete behaviour changes from a plastic to a solid state with changing contributions to the yield strength in time of thixotropic structural build-up and progress of hydration. Roussel [6] defined three categories of flocculation rate dependent on the increase of yield stress in time: 1) Non-thixotropic SCC: A_{thix}<0.1 Pa·s, 2) Thixotropic SCC: A_{thix}=0.1-0.5 Pa·s and 3) Highly thixotropic SCC: A_{thix}>0.5 Pa·s. The element geometry and applied mix design determine whether the criteria can be fulfilled and if so, the duration of the open window for adequate deformation. Especially, the early phase before setting is very important for the production with the flexible mould system:

1) In the horizontal position, effective casting is realized by the use of self-compacting concrete. Placement does not require compaction, since the yield stress is very low.

2) During deformation, the yield stress of concrete has to be a) sufficiently high to prevent that concrete flows over the wall of the mould and b) sufficiently low to prevent that the elongation of the concrete localises in (large) cracks (Figure 1).

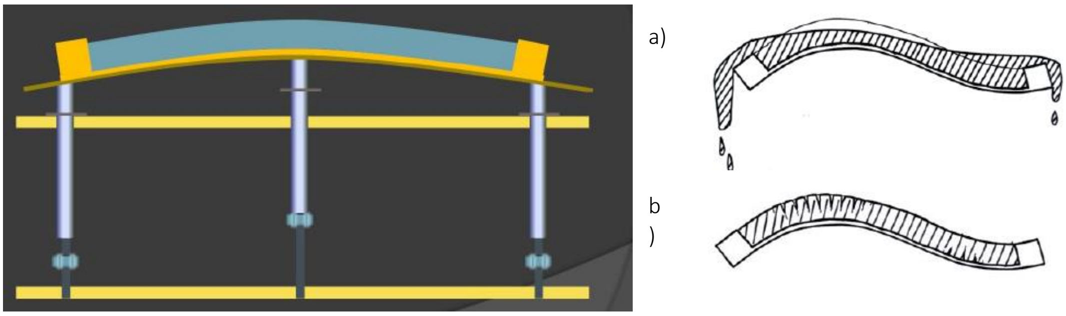

Figure 1 Flexible mould system during deformation, with two governing criteria – a) maintaining stability and b) prevention of significant cracking provide boundary conditions with regard to yield strength

2. EXPERIMENTAL SET-UP

A reference self-compacting mixture was applied for the tests; the mix design took into account that within one hour sufficient yield strength had to be gained to deform the mould. The combination of applied powders and superplasticizer was adjusted for a short workability retention period. Slump flow [7] and slump [8] testing took place in parallel to the deformation of the mould; the workability decreased from a slump flow of 700 mm 7 min after mixing to a slump of only 5 cm 61 min after mixing. The dosage of superplasticizer was varied in the research. The rheological characteristics yield strength and plastic viscosity were determined directly after mixing with the BML-viscometer and were about 5 Pa and 40 Pa·s, respectively.

Table 1 Mixture components, dosage and characteristics

Mixture component	
Cement CEM I 52,5 R	400 kg/m^3
Fly ash	160 kg/m^3
Superplasticizer Premia 196	variable
Water	172 kg/m^3
Sand 0.125/4 mm	1046 kg/m^3
Gravel 4/8 mm	563 kg/m^3
Mixture characteristics	
Compressive strength (cube; 1/7/28 days)	45/65/80 MPa
Splitting tensile strength (cube; 1/7/28 days)	3.5/4.0/5.5 MPa
Flexural strength (prism; 1/7/28 days)	6.0/9.5/10.5 MPa
Slump flow / slump measurement at	7/30/45/61 min
Slump flow (7 min) - Slump (30/45/61 min)	700 mm - 20.2/16.8/5.2 cm

In order to determine the effect of different parameters on the risk of cracking as a result of the deformation of the mould a simple test system was developed [9], which consisted of three main components: (1) the casting surface (Figure 2a), (2) a flexible mould (Figure 2b) and (3) the deformation surface (Figure 2c). Two deformation stages are shown by Figures 2d and 2e.

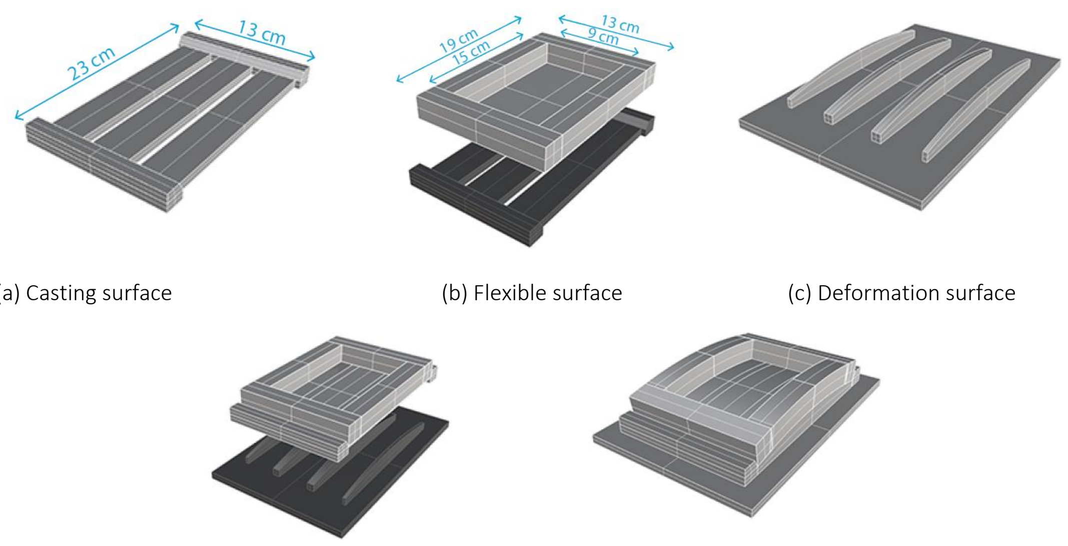

(a) Casting surface (b) Flexible surface (c) Deformation surface

(d) Complete mould (e) Deformed mould

Figure 2 Mould construction in five different steps

Several moulds were filled in parallel in order to deform the moulds at different moments after casting. In order to prevent evaporation a plastic foil was placed to cover the cast elements; the plastic foil was not in direct contact with the concrete surface. A flexible mould consists of polyether-mattress foam (ρ=25 kg/m^3) glued to co-polyester sheets. The inner surfaces of the mould were treated in advance with bi-component silicone rubber P58510 (produced by Poly-Service) in order to avoid direct contact of the co-polyester sheets with cement paste. The aforementioned materials were selected in order to assure proper flexibility. The dimensions of the specimens were 15 cm in length and 9 cm in width, which were selected to allow placing specimens in the vacuum machine during specimen preparation. The casting and deformation surfaces (Figure 2) were built from 4 mm thick MDF(Medium-Density Fibreboard)-panels and cut using a laser cutter, which assured that the shape and dimensions were highly accurate. Four arc-shaped ribs with the required curvature were arranged on the deformation surface. The flexible mould was fixed during production to the casting surface. The supports of the deformation surface fit in the openings of the casting surface. The deformation of the mould can be quickly executed by positioning the casting surface and flexible mould on the deformation surface (Figure 2e).

After 7 days of hardening under normal room conditions the specimens were de-moulded and prepared for the assessment of cracks by epoxy impregnation. The specimens were placed one by one in a vacuum installation. Under vacuum conditions the elements were impregnated with a mix of liquid epoxy resin and hardener. The aim of the impregnation process is to fill the micro-cracks and micro-pores with the epoxy mixture, which has a high fluorescence under UV light. After the elements were impregnated, characteristic sections of the specimens were selected and cut; the element was cut in half using a diamond saw with a thickness of 3 mm, thus obtaining two very similar impregnated surfaces. The section surfaces were ground and polished to obtain high quality images. A stereo-microscope was applied to investigate micro-cracking on the top surface of the specimens (magnifications: 6.3x & 12.5x); under the UV light the epoxy-impregnated areas become fluorescent and are clearly visible. The images were studied and analysed with the stereo microscope. Each sample was investigated separately and the cracks were counted and measured. It is important to mention that only the cracks formed on the exterior curved surface of the deformed concrete element were inspected, those being the ones most responsible for limiting concrete's service life.

3. RESULTS AND DISCUSSION

3.1. YIELD STRENGTH DEVELOPMENT

Concrete has to support its own weight after the deformation of the mould. Equation 1 (Figure 3), proposed by De Larrard [10], was applied in this research and relates the geometry of the mould after deformation (slope θ) and the required yield strength. The thickness and the curvature of an element determine how high the yield strength has to be during the deformation of the mould. As the discussion in this paper will show, not for all cases the two criteria with regard to yield strength and prevention of cracking can be balanced. The main parameters studied by Schipper [5] were concrete mix design, time of deformation as well as curvature, height, geometry and scale of elements.

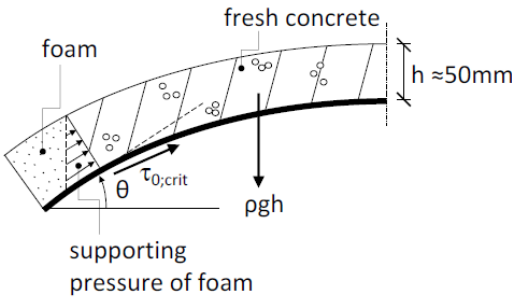

$$\tau_{0;crit} = \rho \cdot g \cdot h \cdot \sin(\theta) = \rho \cdot g \cdot h \cdot \frac{L}{2R} \qquad \text{(Equation 1)}$$

$\tau_{0;crit}$	Critical yield strength of concrete under slope [Pa]
ρ	Density of the concrete [kg/m^3]
g	Acceleration of gravity [kg·m/s^2]
h	Height of concrete [m]
θ	Slope angle [rad]
L	Length of element [m]
R	Radius of element [m]

Figure 3 Critical shear yield strength $\tau_{0;crit}$ of concrete under a slope

Table 2 indicates how the critical yield strength of an element is affected by differences in height and curvature (radius).

Table 2 Critical yield strength $\tau_{0;crit}$ required for casting under a slope θ, depending on the mould radius R, the element length L and the element height h (for ρ = 2 400 kg/m^3)

Slope θ and critical yield strength $\tau_{0;crit}$		R =1.5 m		R =2.5 m		R =5.0 m	
Horizontal length L	Element height h	θ	$\tau_{0;crit}$	θ	$\tau_{0;crit}$	θ	$\tau_{0;crit}$
[m]	[m]	[°]	[Pa]	[°]	[Pa]	[°]	[Pa]
0.80	0.025	15.5	157	9.2	94	4.6	47
0.80	0.050	15.5	314	9.2	188	4.6	94
0.80	0.100	15.5	628	9.2	377	4.6	188
2.00	0.025	41.8	392	23.6	235	11.5	118
2.00	0.050	41.8	785	23.6	471	11.5	235
2.00	0.100	41.8	1570	23.6	942	11.5	471

The development of the yield strength in time was assessed by Slump flow and Slump testing. The yield strengths were calculated with Equations 2 and 3 (Table 3).

Table 3 Empirical equations for the calculation of the yield strength

Empirical formula	Equation for	Reference
$\tau_0 = \frac{225 \cdot \rho \cdot g \cdot V^2}{128 \cdot \pi^2 \cdot R^5}$	Slump flow (Equation 2) (V: Concrete volume; R: Spread radius)	[11]
$\tau_0 = \frac{\rho}{17.6} \cdot (25.5 - S)$	Slump (Equation 3) (S: Measured slump [cm])	[12]

With a desired deformation time in production after 30-60 minutes (1800-3600 s) the required structural build-up rate A_{thix} can be in the range of 0,01 Pa·s (R = 5 m, h = 0.025 m, L = 0.8 m & waiting period = 60 min) up to 0.87 (R = 1.5 m, h = 0.1 m, L = 2 m & waiting period = 30 min) dependent on the boundary conditions (Table 2). The yield strength increased from almost zero directly after mixing to more than 550 Pa·s after a rest period of 45 minutes during a reference test with the BML-viscometer; the thixotropic increase A_{thix} was about 0,2 Pa/s, which is an intermediate thixotropic behaviour according to the definition of Roussel [6]. When a relatively high yield strength is required the risk of cracking should also be assessed by experimental testing. The curved elements produced in this research had a length of L = 0.80 m and a height of h ≤ 0.05 m; dependent on the radius the critical yield strength is in the range of 94 to 314 Pa (Table 2). Figure 4 shows that already in the first hour the yield strength significantly increased. The yield strengths were determined with empirical formulae given in Table 3. The test results show that a significant yield strength was build up in the period between 15 and 45 minutes after mixing, which is in agreement with the deformation experiments (the concrete did not flow out of the mould). It can also be concluded that the applied mixture shows a clear change of workability in the first hour from being self-compacting to a very low-slump state.

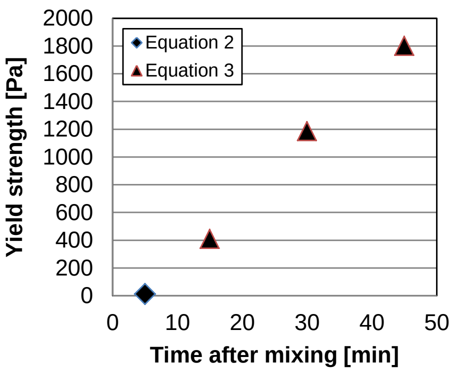

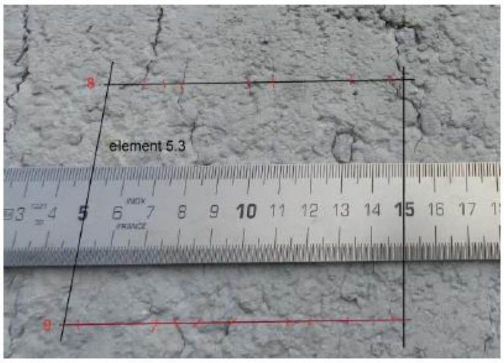

Figure 4 (left): Development of the yield strength during the first 45 minutes; calculation of yield strength for slump flow with Equation 2 and for slump with Equation 3; (right) cracked element deformed after 60 minutes

When the concrete was too stiff to deform, cracks appeared. In a number of deformation tests, this was indeed observed. Figure 4b shows the surface of an element which was deformed after 60 minutes; the yield strength, calculated with Equation 3, at this moment determined with the slump test (zero slump), was at least 3000 Pa according to Equation 3. The resulting cracks had a width of 0.05-0.20 mm and were found at a distance of 30 to 40 mm.

3.2. CONCRETE DEFORMABILITY

The required yield strength of concrete depends on different parameters, as was elaborated in Section 3.1, among which are the geometrical parameters of an element (height, length and curvature). The occurrence of cracks is discussed in the following paragraphs in detail. This paper focusses on the number and frequency of cracks; the maximum and average crack widths are also presented. A more detailed analysis of the results is provided by Troian [9].

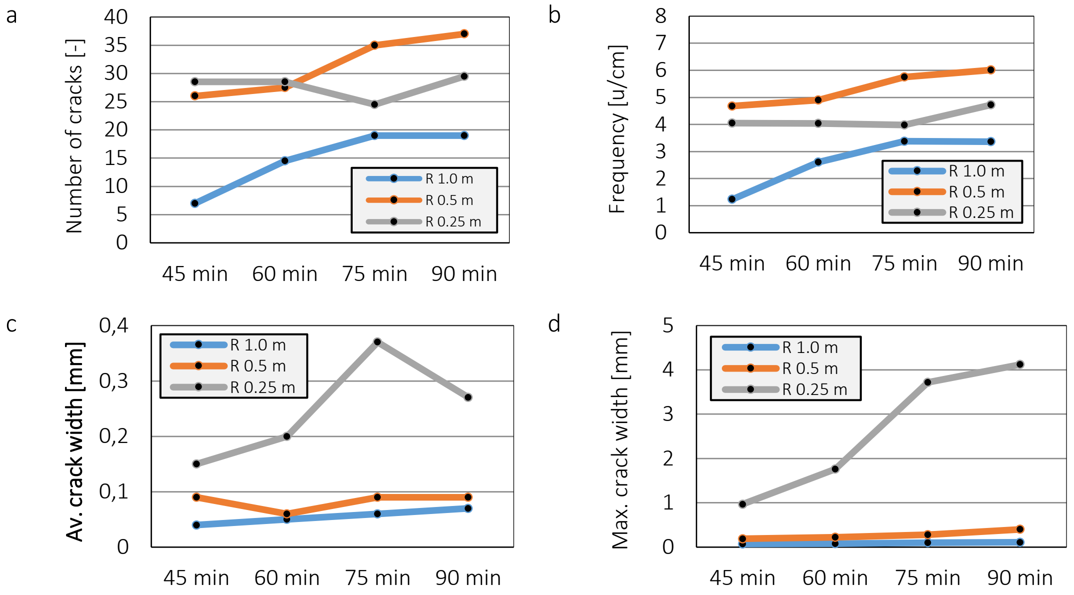

Figure 5 Effect of curvature (panel thickness: 25 mm): (a) number of cracks, (b) crack frequency, (c) average crack width and (d) maximum crack width

<u>Effect of the radius of deformation:</u> At increasing curvature and decreasing panel radius the maximum strain of the concrete increases. The total strain is composed of strain of plastically deformed concrete and strain that is located in cracks. In time, the plastic deformability of concrete decreases and more and wider cracks are expected. The results with regard to the effect of the radius of deformation are shown in Figure 5 for a panel thickness of 25 mm. The radius has an important influence on the number of cracks propagating from the surface of the bend concrete. A high number of cracks and the largest maximum and average crack widths are obtained for a radius of 0,25 m. The increase of crack widths in time was especially pronounced for the 0.25 m radius, whereas for the radii of 0.5 and 1.0 m the maximum crack widths even after 90 min were smaller than 0.1 mm. Radii of 0.5 and 1.0 m caused very similar outcomes with regard to crack widths.

<u>Effect of the panel thickness:</u> Two types of panels having a thickness of 25 or 50 mm were investigated; the results are presented in Figure 6.

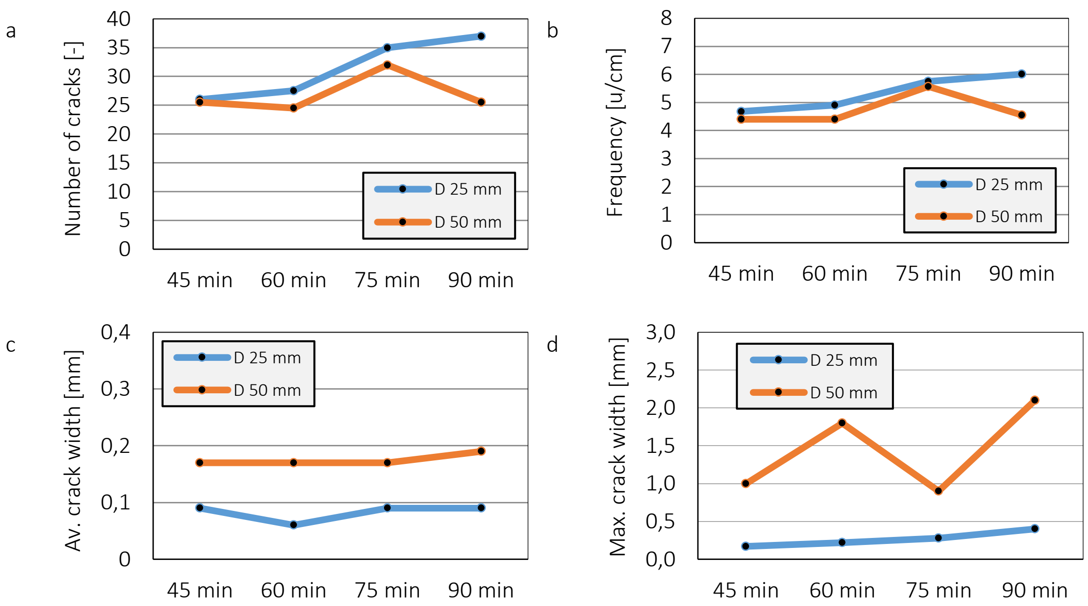

Figure 6 Effect of the panel thickness (radius: 0,5 m): (a) number of cracks, (b) crack frequency, (c) average crack width and (d) maximum crack width

Until 75 minutes, the panel thickness had a relatively small effect on the frequency of cracks formed on the surface of the element. The strain during deformation is larger for thicker panels. However, this effect is not reflected in the number of cracks; the number of cracks was slightly higher for the thinner panel. In contrast, larger crack widths were found for the thicker panel which were in most cases significantly larger (about twice the crack width). As expected, with a thicker panel wider cracks were obtained, but the number of cracks was lower.

4. CONCLUSIONS

High quality facades, roofs and precast shuttering for buildings and infrastructure with complex geometry can be produced with the flexible mould method. In an experimental study the effect of mixture characteristics and geometrical boundary conditions were assessed and the following conclusions can be drawn:

(1) Under consideration of the geometry of an element and a rheological analysis the right moment of deformation can be determined;

(2) The strain of concrete is the sum of the contributions of plastic deformation, and the localised deformation in cracks if cracks appear. With an optimized mix design and production conditions that take into the rheological behaviour of concrete in time, curved or double-curved elements can be produced without any cracks or with very small crack widths.

REFERENCES

[1] Bucur-Horvath, I.; Saplacan, R.: Force lines embodied in the building: Palezzetto dello sport, IASS Journal, Vol. 54 (2013), pp. 179–187.

[2] Zaha Hadid Architects: http://www.zaha-hadid.com/architecture/heydar-aliyev-centre/, (2016).

[3] Piano, R.: Progettazione sperimentale per strutture a guscio-experimental project of shell structures. Casabella, 335 (1969), pp. 38–49.

[4] Vollers, K.; Rietbergen, D.: Adjustable mould for annealing freely curved glass panes. In: Glass Processing Days, (2007), pp. 105–107.

[5] Schipper, H.R.: Double-curved precast concrete elements: Research into technical viability of the flexible mould method, PhD-thesis, Delft University of Technology, ISBN: 978-94-6299-154-5, doi:10.4233/uuid:cc231be1-662c-4b1f-a1ca-8be22c0c4177, (2015).

[6] Roussel, N.: A thixotropy model for fresh fluid concretes: Theory, validation and applications. Cement and Concrete Research, 36(10) (2006), pp. 1797–1806.

[7] NEN-EN 12350-8:2010: Testing fresh concrete – Part 8: Self-compacting concrete – Slump flow test, ICS-Code 91.100.30, (2010).

[8] NEN-EN-12350-2: 2009: Testing fresh concrete - Part 2: Slump-test, ICS-Code 91.100.30, (2009).

[9] Troian, S.: Crack evaluation in double-curved concrete elements, Delft University of Technology, Master thesis, http://repository.tudelft.nl, (2014).

[10] De Larrard, F.: Why rheology matters, Concrete International, 8 (1999), pp. 79–81.

[11] Roussel, N.; Coussot, P.: Fifty-cent rheometer' for yield stress measurements: From slump to spreading flow, Journal of Rheology, 49(3) (2005), pp. 705-718.

[12] Roussel, N.: Correlation between Yield Stress and Slump: comparison between numerical simulations and concrete rheometer results, Materials and Structures, 39 (2006), pp. 501-509.

APPLICATION OF SELF COMPACTING CONCRETE IN BOSNIA AND HERZEGOVINA

Hamdo Mesic[1], Marijan Skazlic[2], Ivana Banjad Pecur[2]

[1] GP-Plan d.o.o., 77 000 Bihac, Bosnia and Herzegovina, email: hamdo.mesic@hotmail.com
[2] University of Zagreb, Faculty of Civil Engineering, Department of Materials, Fra Andrije Kacica Miosica 26, 10 000 Zagreb, Croatia, email: skazle@grad.hr, banjadi@grad.hr

SUMMARY: Self-compacting concrete (SCC) is concrete that has excellent performances, and it is easy to cast it in the structure with absence of vibrations. This concrete type is very useful for areas with congested reinforcement. Self-compacting concrete has some other features, such as fluidity, good resistance to segregation etc. According to the many authors, self-compacting concrete is one of the best materials technology which is developed at the end of 20th century. The advantages of self-compacting concrete include speed of construction, less workers on site, quality final surface of the concrete elements, improved durability parameters, easier concrete casting, freedom in structural design of bearing elements, the absence of vibrations at the construction site, and much healthier environment for workers. The main objective of this work are case studies of typical application of self-compacting concrete in Bosnia and Herzegovina.

UPOTREBA SAMOZBIJAJUĆEG BETONA U BOSNI I HERCEGOVINI

SAŽETAK: Samozbijajući beton beton je koji ima dobra uporabna svojstva, lako i brzo se ugrađuje u oplatu pod djelovanjem vlastite težine i bez potrebe za zbijanjem. Ova vrsta betona može lako popuniti oplatu koja sadržava čak i veliku količinu armature. Samozbijajući beton ima svojstva kao što su fluidnost, dobra otpornost segregaciji i mogućnost ugrađivanja bez vibriranja tijekom ugradnje betona, te se na taj način eliminira buka na gradilištu. Prema mnogim autorima samozbijajući je beton jedno od najrevolucionarnijih otkrića dvadesetog stoljeća u području tehnologije materijala. Prednosti samozbijajućeg betona u odnosu na običan beton uključuju bržu gradnju, manji broj radnika, bolji završni izgled površine betonskih elemenata, lakše ugrađivanje, poboljšanje trajnosti konstrukcije, veću slobodu u projektiranju različitih nosivih elemenata, elimininiranje buke od vibriranja na gradilištu te zdravije radno okruženje. U radu su prikazani karakteristični primjeri primjene samozbijajućeg betona u Bosni i Hercegovini u različitim područjima graditeljstva.

1. UVOD

Samozbijajući beton se u osnovi bazira na modifikaciji klasičnog betona sa dodacima koji smanjuju potrebnu količinu vode, a povećavaju pokretljivost svježe betonske mješavine. Samozbijajući beton posjeduje dobra mehanička i trajnosna svojstva. Kombinacija sa dodatkom filera i smanjenjem zrna agregata proizvodi tečni beton.Procjenjuje se da se uporabom samozbijaćeg betona umjesto običnog betona smanjuje potreba za radnom snagom za 10%uz istovremenu uštedu uvremenu gradnje za oko 20%. Nedostaci samozbijajućeg betona uključuju veću cijenu materijala, strožije zahtjeve za kontrolu kvalitete pri proizvodnji i ugradnji i veći pritisak na oplatu u odnosu na obični vibrirani beton.

Sam početak razvoja samozbijajućeg betona datira iz osamdesetih godina prošlog stoljeća u Japanu. Principe dobivanja samozbijajućeg betona objasnio je Okamura. Prema Okamuri [1], osnovni principi projektiranja sastava samozbijajućeg betona odnose se na:

- Ograničenje količine krupnog agregatai veličine maksimalnog zrna agregata;
- Mali vodocementni omjer;
- Uporaba superplastifikatora.

Samozbijajući beton se u pojedinim primjenama proizvodi sa niskim vodocementnim omjerom kako bi se što prije postigla potrebna čvrstoćaza skidanje oplate, te brzo korištenje elemenata i konstrukcije[2]. Osnovni razlog razvoja samozbijajućeg betona bio je taj što je dolazilo do ubrzanog propadanja armiranobetonskih konstrukcija, posebno onih blizu mora i obalnih područja, te nedostatak dovoljnog broja stručne građevinske radne snage. Razumljivo je bilo što je u tom pravcu bio usmjeren najveći broj istraživanja, koje je predvodio Haime Okamura sa Sveučilišta u Tokiju. On je prvi istaknuo i ukazao na potrebu za razvojem samozbijajućeg betona. Međunarodno udruženje laboratorija i eksperata za materijale i konstrukcijepod nazivom RILEM je bila prva institucija koja je shvatila važnost razvoja tehnologije samozbijajućeg betona i u Europi. Zaključivši da postoji veliki potencijal samozbijajućeg betona, RILEM je 1996. osnovao Odbor za ispitivanje samozbijajućeg betona. U sklopu rada, stručnjaci iz više zemalja su koristili japanske ideje kao polaznu točku za istraživanje samozbijajućeg betona.

Tehnički odbor (TC 174-SCC) je 1999. godine organizirao prvu međunarodnu konferenciju o samozbijajućem betonu u Stockholmu. Na konferenciji je bilo ukupno 70-ak znanstvenih i stručnih radova iz ukupno13 zemalja.

Europsko udruženje proizvođača građevinskih materijala (EFNARC) je osnovano 1989. EFNARC je formirao svoj Tehnički odbor za samozbijajući beton, u čijem su radu sudjelovali svi vodeći proizvođači građevinskih materijala, proizvoda i sustava, te su kao rezultat rada nastale preporuke za samozbijajući beton[3], koje će postati osnova za donošenje europskih normi za proizvodnju samozbijajućeg betona (HRN EN 206-9)i metode ispitivanja u svježem stanju (serija HRN EN 12350). Sve do 2007. godine samozbijajući beton nije spomenut ni u jednom standardu od CEN-a (The European Committee for Standardization).

U nedostatku standarda, otežana je i njegova veća primjenau pojedinim europskim državama.Tako, npr. u Njemačkoj je sve do 2004. godine trebalo tražiti posebnu dozvolu za primjenu samozbijajućeg betona, jer sadržaj ukupnih sitnih čestica u betonu nije bio u skladu sa nacionalnim standardima.

2. UPOTREBA SAMOZBIJAJUĆEG BETONA U BOSNI I HERCEGOVINI

Kada je Bosna i Hercegovina u pitanju, samozbijajući beton se pojavljuje dosta ranije u odnosu na mnogo razvijenije europske zemlje. Samozbijajući beton u Bosni i Hercegovini se pojavljuje početkom 2003. godine. Tvrtka Integral Inžinjering iz Banja Luke u svojoj redovnoj proizvodnji od 2003. godine ima recepturu SCC 30 br. 56 i SCC 40 br.58.[4]

Ove recepture se koriste za nosive betonske konstrukcije koje imaju gusto armirane presjeke. S obzirom da su pravilnici za beton i važeći standardi u Bosni i Hercegovini izostavili ovu vrstu betona, jer je njegova pojava kao konstruktivnog materijala novijeg datuma, to se pri izradi ove vrste betona koristila pozitivna praksa stručnjaka i eksperata iz Japana (Ouchi, Nakamura), preporuke udruženja EFNARC, pozitivna iskustva laboratorija za beton korporacija Mapei, Degussa, Sika, kao i stručni radovi eminentnih profesora. Do tada u Europi i svijetu su se uglavnom upotrebljavali slijedeće podvrste samozbijajućeg betona:

- SLC(eng. Self-Levelling Concrete) je praktičan za primjenu betoniranja gusto armiranih betonskih elemenata
- PSCC(eng. Precast Self-Compacting Concrete) je primjenljiv u industriji montažnih betonskih elemenata
- HSSCC(eng. High-Strength-Self Compacting Concrete) je namijenjen za izradu betona visokih zlačnih čvrstoća (≥60 N/mm2).

Dosadašnja upotreba samozbijajućeg betona u Bosni i Hercegovini može se podijeliti u tri grupe:

- Hidrotehnički projekti: izgradnja vodobazena tvornice vode u Banjoj Luci, kanalizacijski sustavi-betoniranje kanalizacijskih cijevi promjera većeg i jednakog 1,5 m, kolektor u Banjoj Luci i drugi manji objekti.[4]
- Projekti niskogradnje: izgradnja cestovnih i željezničkih mostova i nadvožnjaka (npr. predgotovljeni prednapeti betonski nosači za objekt Pasarela 1 duljine 33 metra, predgotovljeni armirani betonski nosači za objekt Pasarela 2 duljine 33 metra,betonska ploča mosta u Klašnicama,glavni nosači mosta na Vrbasu u Banjoj Luci,armirano betonska ploča željezničkog mosta u Banja Luci,mostovi u Modriči i Doboju itd. [4]
- Privredni objekti: predgotovljene betonske T grede za pivovaru u Banja Luci, predgotovljene betonske T grede u punionici vode u Banja Luci, armaturni čvorovi na fermentoru banjalučke pivovare kao i nizu drugih privrednih objekata.[4]

Na Slici 1. prikazana je armirano betonska ploča vodobazena koja je izrađena od samozbijajućeg betona. Slika 2. prikazuje izgled kanalizacijske cijevi velikog promjera koja se proizvodila u Bosni i Hercegovini.

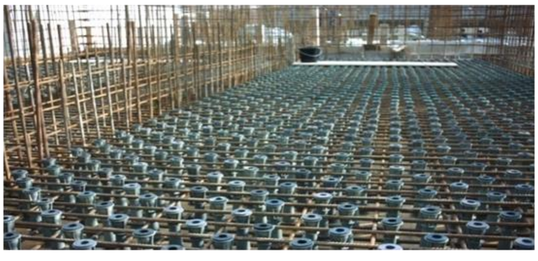

Slika 1: Ploča vodobazena [4]

Slika 2: Kanalizacijska cijev od samozbijajućeg betona [4]

Na Slici 3. prikazano je betoniranje korištenjem samozbijajućeg betona za objekt Pasarela. Slika 4. prikazuje završen objekt Pasarela, koji je izveden od samozbijajućeg betona.

Slika 3: Betoniranje nosača [4]

Slika 4: Izgrađeni objekat Pasarela [4]

Na Slici 5. je prikazana izbetonirana predgotovljena betonska T greda od samozbijajućeg betona, dok je na Slici 6. prikazana armirano betonska ploča fermentora pivovare pripremljena za betoniranje samozbijajućim betonom.

Slika 5: Izbetonirana montažna T nosiva greda [4]

Slika 6: Ploča fermentora banjalučke pivovare[4]

Bitno je napomenuti da su prethodna eksperimentalna ispitivanja samozbijajućeg betona i njegovih komponenti u laboratoriju i ispitivanja uzoraka uzetih tijekom građenja prilikom betoniranja navedenih objekata pokazala usklađenost rezultata ispitivanja. Ispitivanja probnim opterećenjem navedenih konstrukcija pokazala su da su progibi i deformacije elemenata od samozbijajućeg betona manji od projektom predviđenih. Ponašanje pojedinih elemenata od samozbijajućeg betona ocijenjeno je kao dosta prihvatljivo, jer nisu uočena oštećenja na elementima uzrokovana trajnosnim opterećenjima.

3. ANALIZA REZULTATA ISPITIVANJA BETONA NA MOSTOVIMA U DOBOJU I MODRIČI

U ovom radu bit će posebno obrađeni radovi betoniranja samozbijajućim betonom na mostovima u Doboju i Modriči u Republici Bosna i Hercegovina. U okviru poslijeratne obnove u Bosni i Hercegovini, studija Master plana za transport ukazala je na važnost izgradnje dva mosta koji se nalaze u Doboju i Modriči. Financiranje Master plana i izgradnje ova dva mosta je preuzela Vlada Japana.

Kompletan projekt konstrukcije mostova uradili su investitori iz Japana. Dužina mosta u Modriči je 240 m, a mosta u Doboju je 200m. Za potrebe betoniranja glavnih nosača mosta, ukazala se potreba za betonom koji će moći udovoljiti zahtjevima projekta. Zahtjevi iz projekta odnose se na osobine svježeg betona kao što su: ugradnja betona, obrađivanje betona, svojstva betona u pogledu postizanja ranih čvrstoća, te svojstva očvrslog betona i kvalitete betoniranog nosača.

3.1. IZBOR TEHNOLOGIJE IZGRADNJE

Ugradnja samozbijajućeg betona zahtijeva da se u kraćem vremenskom periodu uradi betoniranje kompletnog elementa. Razlog je u rasprostiranju betona na većoj površini od uobičajene, te se ne smije desiti prekid betoniranja. U slučaju malog kapaciteta betonare, potrebno je u proizvodnju uključiti i rezervnu betonaru. Betoniranje se obavlja sa mjesta koje će omogućiti daljnje potiskivanje betona premamjestima gušće armature. Ubacivanje u oplatu može biti iz miksera, auto-pumpe, lijevka ili cjevovoda. Na izradi svakog od mostova, prvo su konstruirane po dvije metalne oplate za izradu glavnih nosača, te je nakon toga izvršeno i postavljanje armature za cijeli element. Proizvodnja betona provođena je u dvije betonare. [5]

Kod izrade prvog nosača, radio je samo prvi pogon za proizvodnju betona (0,25m^3), betonska pumpa i tri auto-miješaliceod 7,9 i 10 m^3. Proces same ugradnje betona odvijao se bez oplatnih vibratora, samo ubacivanjem betonske mješavine sa visine od 2,5m. Volumen ugrađenog betona za jedan nosač bio je 56m^3. Samo vrijeme ugradnje betona moglo se smanjiti da je kojim slučajem izvođač imao betonskih pogon većeg kapaciteta od 0,25m^3.

3.2. ZAHTJEVI ZA BETON I PRETHODNA ISPITIVANJA BETONA

Konstruktivni elementi koji su betonirani korištenjem samozbijajućeg betona su slijedećih karakteristika:

- Gredni nosač statičkog sistema proste grede raspona 40 m;
- Poprečni presjek nosača je I profil;
- Visina nosača je 2,5 m;
- Dužina nosača je 40 m;
- Rebro nosača na srednjem, najužem dijelu 0,25 m.

Prema ovom projektu,pored gustog klasičnog armiranja, predviđeno je da se vrši prednaprezanje nosača sa 6 prostorno vođenih kablova, što se vidi na Slici 7.

Slika 7: Detalj spoja nosača mosta [5]

Može se zaključiti da je zbog gustoće armiranja i prednaprezanja u srednjem dijelu nosača prolaz betona omogućen samo kroz zaštitni sloj sa strane. Prema specifikaciji, projektanta za beton, su zahtijevana slijedeća svojstva:

- Marka betona MB60, koja odgovara razredu tlačne čvrstoće betona C50/60;
- Potrebna količina uvučenog zraka u beton od 2 do 4,5%;
- Uvjet za otpornost betona na djelovanje mraza u trajanju od 250 ciklusa (M-250).

Prije izrade prethodnih proba, a na osnovu gornjih zahtijeva, pristupilo se obilasku i upoznavanju materijala koji je na raspolaganju u području gdje se rade mostovi. Utvrđeno je da na betonskom pogonu nije moguća ugradnja silosa za filer i leteći pepeo koji su sastavne komponente samozbijajućeg betona, a ručno dodavanje ovih komponenti bi veoma usporilo izradu samozbijajućeg betona. Alternativa je bila da se poveća količina cementa, te se tako zadovolji potreba za sitnijim česticama i visokom razredom tlačne čvrstoće betona C50/60.

Pregledom kompletne dokumentacije došlo se do sljedećih zaključaka o svojstvima samozbijajućeg betona u svježem stanju [5]:

- Konzistencija rasprostiranja slijeganjem (HRN EN 12350-8) > 65 cm
- Odnos visina kod L kutije (HRN EN 12350-10) > 0,9
- Visina penjanja u U kutiji > 31 cm

Nakon završetka prethodnih ispitivanja, usvojene su slijedeće komponente za izradu betonske mješavine:

- Cement CEM I 52,5 Našice cement: 560 kg/m3
- Vodocementni omjer (količina vode):v/c =0,34 (190kg/m3)

- Superplastifikator, aerant): DYNAMON SX, META AIR MAPEI…ukupno 4kg/m3
- Sitni prirodni agregat (savski): 754kg/m3
- Krupni agregat, drobljeni riječni: 923kg/m3

Ova receptura je pokazala sljedeće rezultate ispitivanja u svježem stanju:

- Konzistencija rasprostiranja slijeganjem (HRN EN 12350-8): 67,0 cm
- Odnos visina kod L kutije (HRN EN 12350-10): 0,92cm
- Visina penjanja u U kutiji: 31,50cm

3.3. ANALIZA REZULTATA ISPITIVANJA

Ispitivanje skupljanja betona provedeno je prema normi HRN U.M1 029, a određivanje puzanja betona prema HRN U.M1 027. Na Slikama 8.,9. i 10 prikazani su dijagrami izmjerenih deformacija samozbijajućeg betona. U Tablicama 1., 2. i 3. su brojčano prikazane vrijednosti izmjerenih deformacija.

Tablica 1: Prikaz srednjih vrijednosti skupljanja samozbijajućeg betona [5]

Starost (dani)	4	7	9	14	21	28	35	42	49	56	63	70	77	84	91
Srednja vrijednost skupljanja (mm/m')	0.0333	0.0697	0.1023	0.1367	0.1557	0.1830	0.1967	0.2147	0.2270	0.2423	0.2620	0.2683	0.2717	0.2730	0.2730

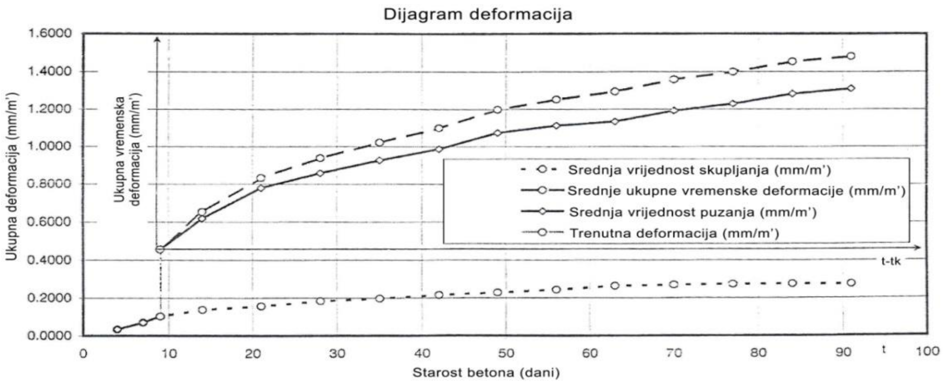

Slika 8: Dijagram ukupnih deformacija samozbijajućeg betona [5]

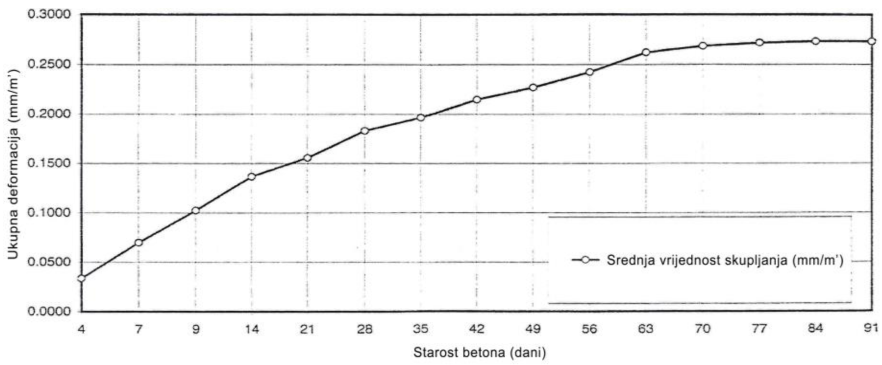

Slika 9: Dijagram srednjih vrijednosti skupljanja samozbijajućeg betona [5]

Tablica 2: Izmjerene vrijednosti puzanja samozbijajućeg betona [5]

Starost (dani)	9	14	21	28	35	42	49	56	63	70	77	84	91
Srednja vrijednost puzanja (mm/m')	0.0000	0.1617	0.3233	0.4017	0.4703	0.5303	0.6173	0.6563	0.6783	0.7357	0.7730	0.8260	0.8537

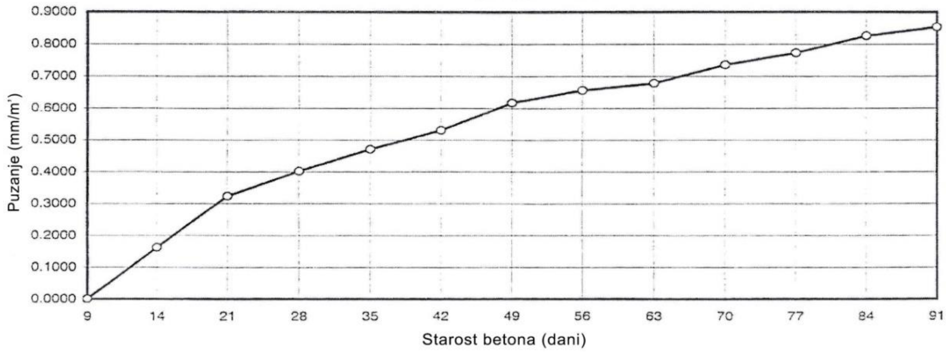

Slika 10: Dijagram puzanja samozbijajućeg beton [3]

Tablica 3: Prikaz trenutne deformacije i koeficijenta puzanja samozbijajućeg betona [5]

Trenutna deformacija $\varepsilon_{tren,sr}$ (tk)

$\varepsilon_{tren,sr}$ (tk) 0.3537

Trenutna deformacija	0.3537

Koeficijenti puzanja Φ(t,tk)													
Starost (dani)	9	14	21	28	35	42	49	56	63	70	77	84	91
Koeficijenti puzanja Φ(t,tk)	0.000	0.457	0.914	1.136	1.330	1.500	1.746	1.856	1.918	2.080	2.186	2.336	2.414

Ukupna izmjerena vrijednost skupljanja betona pri starosti od 28 dana je 0,27 mm/m, a što je u skladu s predloženim vrijednostima prema EC2 za beton (za C60/75, relativna vlažnost okoline od 60 %, 0,30 mm/m). Prema važećem PBAB-u koeficijent puzanja za obični beton kod nanošenja opterećenja pri starosti od 7 dana, za relativnu vlažnost okoline od 70 % i srednju debljinu presjeka od 200 mm iznosi 2.9. Dobivene vrijednosti puzanja (2.414) su unutar dopuštenih vrijednostiu skladu s propisima Bosne i Hercegovine.Rezultati ispitivanja tlačne čvrstoće samozbijajućeg betona tijekom izvođenja radova prikazani su u Tablici 4. i na Slici 11.

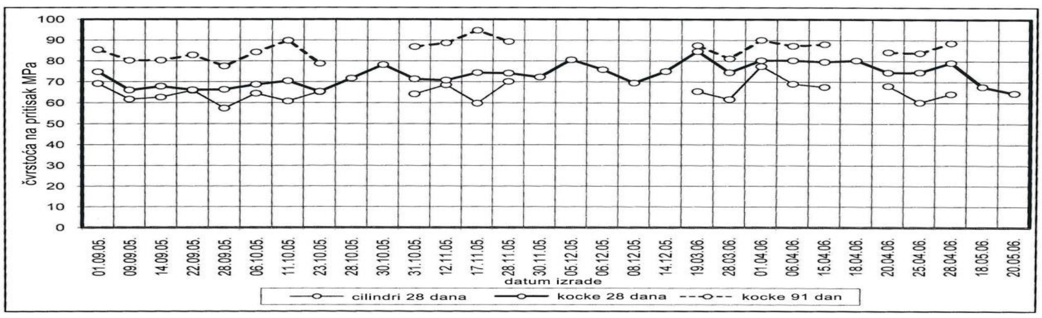

Slika 11: Vrijednosti tlačne čvrstoće samozbijajućeg betona tijekom vremena [5]

Tablica 4: Vrijednosti tlačnih čvrstoća samozbijajućeg betona [5]

datum izrade	pripadajuća oznaka	Element	kocke 7 dana	kocke 28 dana	kocke 91 dan	valjci 28 dana	f_7/f_{28} %	f_{91}/f_{28} %	f_{cyl}/f_{cube}
01.09.05.	BD-36	Glavni nosač G3, raspon A1-P1	73,1	74,8	85,4	69,2	97,7	114,2	0,925
09.09.05.	BD-37	Glavni nosač G2, raspon A1-P1	59,7	66,1	80,2	61,7	90,3	121,3	0,933
14.09.05.	BD-38	Glavni nosač G1, raspon A1-P1	60,1	67,9	80,3	62,7	88,5	118,3	0,923
22.09.05.	BD-39	Glavni nosač G4, raspon A1-P1	58,4	66,2	82,8	65,9	88,2	125,1	0,995
28.09.05.	BD-40	Glavni nosač G3, raspon P1-P2	58,5	66,4	77,5	57,4	88,1	116,7	0,864
06.10.05.	BD-41	Glavni nosač G2, raspon P1-P2	64,2	68,8	84,2	64,5	93,3	122,4	0,938
11.10.05.	BD-42	Glavni nosač G1, raspon P1-P2	69,3	70,5	89,8	60,8	98,3	127,4	0,862
23.10.05.	BD-46	Glavni nosač G4, raspon P1-P2	65,4	65,4	78,7	65,2	100,0	120,3	0,997
28.10.05.	BD-49	Kraj nosača G1, G2 (A1-P1)	68,4	71,7			95,4		
30.10.05.	BD-50	Kraj nosača G3, G4 (A1-P1)	67,4	78,2			86,2		
31.10.05.	BD-51	Glavni nosač G2, raspon P2-P3	66,7	71,4	86,8	64,2	93,4	121,6	0,899
12.11.05.	BD-52	Glavni nosač G3, raspon P2-P3	64,2	70,8	88,6	68,6	90,7	125,1	0,969
17.11.05.	BD-54	Glavni nosač G1, raspon P2-P3	64,5	74,4	94,7	59,8	86,7	127,3	0,804
28.11.05.	BD-55	Glavni nosač G4, raspon P2-P3	67,7	74,2	89,3	70,2	91,2	120,4	0,946
30.11.05.	BD-56	Kraj nosača G1,2,3,4 (P1-P2) iznad P1	62,9	72,3			87,0		
05.12.05.	BD-57	Kraj nosača G1,2 (P2-P3)	65,9	80,6			81,8		
06.12.05.	BD-58	Kraj nosača G1,2 (P1-P2) iznad P2	65,0	75,9			85,6		
08.12.05.	BD-59	Kraj nosača G3,4 (P1-P2) iznad P2	59,4	69,5			85,5		
14.12.05.	BD-60	Kraj nosača G3,4 (P2-P2)	64,9	75,0			86,5		
19.03.06.	BD-62	Glavni nosač G3, raspon P4-A2	72,1	84,6	87,4	65,5	85,2		0,774
28.03.06.	BD-65	Glavni nosač G2, raspon P4-A2	69,0	74,5	81,1	61,7	92,6	108,9	0,828
01.04.06.	BD-66	Glavni nosač G1, raspon P4-A2	74,1	80,3	90,0	77,5	92,3	112,1	0,965
06.04.06.	BD-70	Glavni nosač G4, raspon P4-A2	74,0	80,3	87,2	69,1	92,2	108,6	0,861
15.04.06.	BD-73	Glavni nosač G2, raspon P3-P4	69,6	79,6	88,0	67,6	87,4	110,6	0,849
18.04.06.	BD-75	Kraj nosača G (P-P)	70,3	80,3			87,5		

Iz prikazanih dijagrama postignutih vrijednosti tlačnih čvrstoća samozbijajućeg betona vidi se da je prirast tlačne čvrstoće nakon 90 dana u odnosu na 28 dana od 8,6 % do 27,4 %. Tlačna čvrstoća samozbijajućeg betona nakon 7 dana u odnosu na 28 dnevnu čvrstoću iznosila su od 81,8 % do čak 100 %.

Kompletna ispitivanja samozbijajućeg betona rađena su jednim dijelom na gradilištima, a drugi dio ispitivanja u laboratoriju Instituta IMS AD u Beogradu uz pomoć Institutagrađevinarstva iz Banja Luke.

4. ZAKLJUČAK

Može se reći da je samozbijajući beton našao mjesto u svakodnevnoj inženjerskoj praksi. Za primjenu samozbijajućeg betona kod nosivih armirano-betonskih konstrukcija još se provode razna istraživanja.

S pravom se može reći da je samozbijajući beton donio prosperitet industriji betona omogućivši da gradnja bude brža, kvalitetnija, te prihvatljivija kako sa ekološkog, tako i sa aspekta zdravstvene zaštite radnika i radnog okruženja. Samozbijajući beton je postao nezamjenljiv kod gusto armiranih presjeka što je potvrđeno i u ovom radu.Najčešći praktični razlozi primjene samozbijajućeg betona su gusto armirani presjeci,nemogućnost vibriranja,kompliciran geometrijski oblik elementa,pojeftinjenje radova ili skraćenje roka izgradnje. Kod izrade konstruktivnih elemenata betoniranih na licu mjesta samozbijajući beton se zbog svoje jednostavnosti kod ugradnje sve više nameće kao rješenje. Sve veća primjena iskustva i teorijska napredovanja, kao i znanstveno istraživački rezultati omogućit će konstruktorima da budu slobodniji u izboru i primjeni samozbijajućeg betona.

Samozbijajući beton je postao inovacija čiji se financijski udio u građevinarstvu mjeri u milijardama dolara. Rijetko koji je inovativni proizvod postigao toliki uspjeh na svjetskoj razini.

LITERATURA

[1] Okamura,H., Ouchi, M.:Self-Compacting Concentrate, Journal of Advanced Concentrate Technology,1 (2003) 1, pp. 5-15
[2] FBI Task Group 3.3 (2004): Environmental Design, International Federation for Structural Concrete, FIB, Laussane , Switzerland, pp. 74.
[3] EFNARC,ERMCO,EFCA,CEMBUREAU, BIBM: The European Guidelines for EFNARC: Specification, Productionand Use; 2005, pp. 68.
[4] Reference izgrađenih objekata od samozbijajućeg betona tvrtke Integral-Inžinjering doo
[5] Laboratory Test Results Report NO: 03-R-01-06, INSTITUT IMS AD, Beograd
[6] Khrapko M.: SCC-A Solution for Technology Hungry Concrete Construction; CBE Consultancy, Ltd
[7] V.Ramasamy, S.Biswas: Mechanical properties and durability of rice husk ash concrete, International Journal of Applied Engineering Research, December 1, 2008, pp. 206-212.

ARCHITECTURAL PRECAST CONCRETE ELEMENTS

Danica Jelenic[1], Suzana Hozmec[1], Marijan Skazlic[2]

[1] Beton Lucko d.o.o., Puskariceva 1b, 10 250 Lucko, Hrvatska, email: jelenic@betonlucko.hr, shozmec@betonlucko.hr
[2] University of Zagreb, Faculty of Civil Engineering, Department of Materials, Fra Andrije Kacica Miosica 26, 10 000 Zagreb, Croatia, email: skazle@grad.hr

SUMMARY: Architectural decorative concrete is a kind of concrete, used by architects to express their creativity and by contractors to express their performing ability, which makes that our surroundings is made of functional, innovative and very nice concrete elements. Demands by designers for this kind of concrete are primarily based on the final appearance of precast elements. Today's concrete can be produced in different colours and with different surface treatments, without any post-treatments. Optimal production of architectural concrete is made in controlled environment, in plants for production of precast elements. Such way of production provides efficient production, in both economical and speed segment, with uniformed quality of produced elements. Lately, the architectural concrete is made of recycled building materials. In this paper are shown examples of different kinds of architectural concrete in precast concrete elements.

PRIMJENA ARHITEKTONSKOG BETONA U PREDGOTOVLJENIM BETONSKIM ELEMENTIMA

SAŽETAK: Arhitektonski ili dekorativni beton vrsta je betona kod kojeg arhitekti svojom kreacijom te izvođači svojim umijećem izvedbe omogućuju da nas okružuju funkcionalni, inovativni te vrlo lijepi betonski elementi. Projektantski zahtjevi na ovu vrstu betona su u prvom redu završni izgled površine predgotovljenih elemenata. Današni se betoni mogu proizvoditi u različitim bojama i površinskim obradama, a bez potrebe za naknadnom (završnom) obradom. Optimalna proizvodnja arhitektonskih betona odvija se u kontroliranim uvjetima u pogonima za proizvodnju predgotovljenih betonskih elemenata. Na taj se način osigurava brza i ekonomski učinkovita proizvodnja uz postizanje ujednačenosti kvalitete proizvoda. U posljednje vrijeme arhitektonski betoni proizvode se i upotrebom recikliranih građevnih materijala. U radu su prikazani primjeri primjene različitih vrsta arhitektonskih betona u predgotovljenim betonskim elementima.

1. UVOD

Arhitektonski beton je vrsta betona koja se koristi u vanjskim i unutarnjim betonskim elementima zbog kvalitetnog i estetski prihvatljivog izgleda površine. Razvoj tehnologije betona doveo je do toga da je danas moguće napraviti arhitektonske betone najrazličitije površinske obrade, boje ili teksture. Arhitektonski betoni su posebno učinkoviti u primjeni kada se koriste kod izrade predgotovljenih betonskih elemenata. Predgotovljenim načinom gradnje postiže se smanjenje vremena i cijene gradnje, te je u tvorničkim uvjetima moguće izraditi i arhitektonski zahtijevne elemente. [1]

U ovom radu su prikazani primjeri primjene arhitektonskih betona u predgotovljenim betonskim elementima. Zajedničko za sve projekte navedene u radu jest da je izvođač pregotovljenih betonskih elemenata bila tvrtka Beton Lučko d.o.o. Tvrtka Beton Lučko se već više od 20 godina bavi proizvodnjom predgotovljenih betonskih elemenata za primjenu u svim područjima graditeljstva.

2. PRIMJERI PRIMJENE PREDGOTOVLJENIH ELEMENATA OD ARHITEKTONSKOG BETONA

2.1. VIDLJIVI BETONI

Vidljivim betonima nazivaju se betoni koji imaju vanjsku površinu strukturirane oplate i/ili ako je beton tako oblikovan da može ostati vidljiv bez naknadnih obrada. Tipičan primjer izrade predgotovljenih betonskih elemenata od vidljivog betona odnosi je pristupna staza za spomen obilježje naziva „Slomljeni pejzaž“ na brdu Čukur kod Hrvatske Kostajnice. Ovo spomen obilježje je napravljeno 2015. godine i predstavlja jedan od najljepših spomenika Domovinskog rata. Napravljen je u znak sjećanja na poginulog ratnog snimatelja Hrvatske radiotelevizije Gordana Lederera. Pristupna staza izvedena je od ploča iz lijevanog betona različitih dimenzija, koje simboliziraju razmotanu filmsku traku. Staza se sastoji od 33 ploče različitih dimenzija, ali jednakog principa oblikovanja (vidi Slike 1 i 2). Svaka ploča se sastoji od dva glavna elementa, a to su čelična oplata koja služi kao kalup u koji se lijeva beton. Dimenzija svake ploče iznosi oko 2 m^2, a dubina čeličnog kalupa je 15 cm. Svaka ploča u svojem lijevom donjem kutu ima otisnutu godinu. Elementi su proizvedeni kao predgotovljeni u tvornici betona i transportirani na lokaciju. Postavljeni su na betonski temelj uz potrebnu nivelaciju i poravnavanje sa mortom.


Slika 1: Izgled betonskih ploča za spomen obilježje Gordanu Ledereru na brdu Čukur kod Hrvatske Kostajnice


Slika 2: Izrada i montaža ploča za pristupnu stazu za Spomen obilježje Gordanu Ledereru

Kalup je izveden od čeličnih ploča debljine 5 mm koje su međusobno varene na način da oblikuju kutiju sa žlijebom preko kojeg element sjeda na kontinuirani čelični profil. Kalup se pri ugradnji sidrio pomoću čeličnih sidara u armiranobetonsku ploču. Presjek kalupa nepravilnog je oblika ukupnih dimenzija cca 900 mm/150 mm.

Antikorozivna zaštita čelika provedena je vrućim cinčanjem te antikorozivnim premazom u 3 sloja, namijenjen za korištenje u C5 kategoriji korozivnosti. Završni sloj premaza izveden je u crnoj boji. Sve mjere provjeravane su u naravi.

Beton za pristupne staze je razreda čvrstoće C30/37 te je ugrađen u kalup lijevanjem u dva sloja. Donji nosivi sloj betona debljine je 10 cm sa maksimalnim zrnom agregata od 16 mm. Gornji habajući sloj je sitnozrni beton, maksimalnog zrna agregata od 4 mm, otporan na habanje (XM2), te otporan na mraz i sol (XF4). U gornji sloj su utisnute šablone (brojevi), sa dubinom otiska od 1,0 cm.

Poseban zahtjev u ovom projektu odnosio se na vidljivi beton, koji je trebao biti izveden besprijekorno glatko, bez ikakvih nepravilnosti na betonskoj površini. Površinska obrada gornjeg sloja ploče je glatka te naknadno impregnirana. Beton je izveden u natur sivoj boji. [2]

2.2. BOJANI BETONI

Bojani betoni postižu se korištenjem različitih pigmenata za boju i/ili uporabom različitih vrsta agregata. Prilikom dodavanja pigmenata u beton potrebno je voditi računa o ujednačnosti površine betona, te utjecaju prigmenta na mehanička i trajnosna svojstva betona. Neki od primjera građevina koje je tvrtka Beton Lučko izvela korištenjem bojanih betona su arheološki park Principij te fasadni paneli za shopping centar West Gate kod Zaprešića, stambeno naselje Rab, poslovni objekat Zadar i druge.

U projektu arheološkog parka Principij koji je završen 2014. godine korištene su armiranobetonske predgotovljene lamele malog, složenog poprečnog presjeka različitih dužina. Lamele su proizvedene u glatkoj čeličnoj oplati s uredno izvedenim rubovima od bijelog betona. Beton je razreda tlačne čvsrtoće C30/37 i razred izloženosti XS1, a za njegovu proizvodnju korišten je bijeli cement i posebni bijeli agregat (vidi Sliku 3).

Slika 3: Arheološki park Principij i okolni javni prostor

Lamele su izvedene u pjeskarenoj površinskoj obradi, te su naknadno zaštičene od utjecaja soli iz zraka transparentnom antigrafitnom impregnacijom. Vertikalne lamele montirane su pomoću inox pričvrsnih veza u pripremljene šliceve, u prethodno izvedenim monolitnim nadtemeljnim gredama.

U ovom projektu su po zahtjevu projektanta izrađeni uzorci različite površinske obrade radi odabira površinskog izgleda, i to: pjeskareni, prani i brušeni. Na temelju izvedenih probnih modela projektant je odabrao pjeskarenu obradu. [2]

U projektu izgradnje shopping centra West Gate kod Zaprešića korišteni su betonski fasadni paneli crne boje (Slika 4). Dvostruki predgotovljeni armiranobetonski zidovi proizvedeni su od dviju međusobno spojenih ploča ukupne debljine 30 cm, sa dodatkom 4 % pigmenta crne boje u svježu betonsku mješavinu, sa glatkom obradom obostrano vidljivih crnih površina. Treba istaknuti da je upravo crni pigment jedan od pigmenata koji najviše utječe na smanjenje tlačne čvrstoće betona. [2]

Slika 4: Crni fasadni paneli na shoping centru West Gate kod Zagreba

2.3. BRUŠENI BETONI

Brušeni betoni dobivaju se završnim strojnim brušenjem površine betona te se na površini betona umjesto cementne skramice vide zrnca agregata. Uslijed brušenja i poliranja površina betona je vrlo glatka. Brušeni betoni se najviše koriste u proizvodnji opločenja.

Prilikom izgradnje bazenskog kompleksa Svetice u Zagrebu, koji je završen 2016. godine, za izradu objekta i uređenje okoliša korišten je veliki broj elemenata od brušenog betona (Slika 5).

Slika 5: Predgotovljeni betonski brušeni elementi u bazenskom kompleksu Svetice u Zagrebu

Bazenski kompleks Svetice je smješten na jednoj od najstarijih sportskih lokacija u Zagrebu, te je zbog svog položaja u kontaktu s maksimirskom šumom i zatečenim prirodnim ambijentom sportskog parka. U sklopu bazenskog kompleksa nalazi se olimpijski bazen (50×25 m), bazen za rasplivavanje (25x13.7 m) i mali bazen za učenje plivanja (8x6 m), te vodeno igralište, prostor wellnessa sa toplim i hladnim bazenom i vanjskim drvenim atrijem pod nebom.

Rubni dijelovi parcele ograđeni su i izgrađeni sa istoka i zapada masivnim uzdužnim servisnim traktovima dužine 120 m, a središnji prostor velike bazenske dvorane natkriven je filigranskom bijelom čeličnom konstrukcijom, osvjetljen bazilikalno te otvoren u smjeru sjevera i juga prema okolnoj prirodi, sportskim borilištima i stambenim neboderima. Uzdužni su zidovi bazenske dvorane tretirani u potpunosti eksterijerski. Njihova je površina kontinuirano obložena predgotovljenim brušenim betonskim elementima sa agregatom dravskog šljunka i ista je kao i obloga vanjskih zidova servisnih traktova.

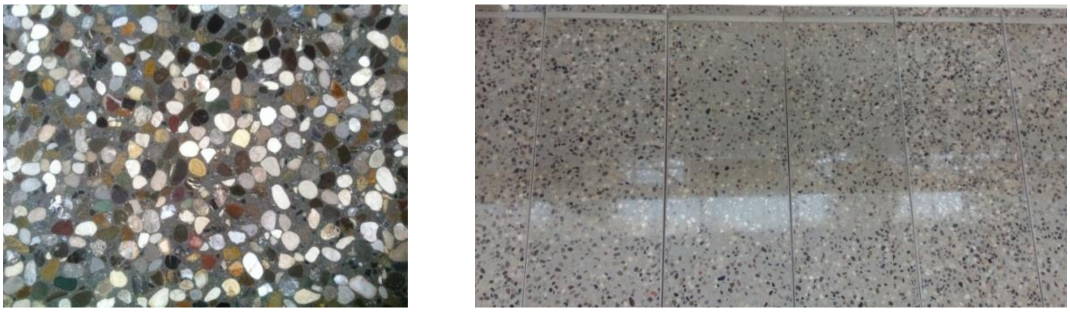

Slika 6: Izgled predgotovljenih betonskih elemenata sa završnom brušenom obradom

Montažni betonski elementi za oblaganja vanjskih pročelja su pravokutni. Maksimalne dimenzije elemenata su 200 x 350 cm i 402 x 150 cm. Elementi su proizvedeni u pogonu za proizvodnju predgotovljenih betonskih elemenata, na vibrostolovima u metalnim kalupima. Element se sastoji od nosivog sloja, izvedenog od armiranog mikrobetona razreda tlačne čvrstoće C30/37. Agregat je riječni oblutak maksimalne veličine zrna od 16 do 32 mm. Završna obrada betonskog elementa izvedena je brušenjem (Slika 6), i to sloj debljine 16 mm po čitavoj širini, visini i debljini elementa te se dobiva završna brušena obrada betonskih elemenata. Završni sloj izveden je sa dodacima za vodoodbojnost, poboljšanje prionjivosti za podlogu, kao i dodacima za poboljšanje elastičnosti i ugradljivosti betona. Pored betonskih brušenih elemenata za oblaganje pročelja u istoj obradi proizvedene su i isporučivane ploče za vanjsko uređenje i opločenje terasa. [2]

2.4. PRANI BETONI

Arhitektonski prani betoni dobivaju se na način da se na unutarnju stranu oplate stavljaju premazi koji sprečavaju vezanje cementa, te se nakon raskalupljivanja površina betonskog elementa obrađuje vodom pod pritiskom da se ispere cementna skramica. Ovakvom obradom betona zrna agregata postaju vidljiva. Na Slici 7 prikazane su različite varijante izvedbe elemenata od pranog betona.

Tipični primjer primjene pranih betona odnosi se na stepenište izvedeno na Građevinskom fakuktetu u Osijeku (Slika 8). Posebitost ovog projekta jest da je vanjsko stepenište izvedeno od pranog, a unutarnje stepenište od brušenog betona u žutoj boji.

Fasadni paneli od pranog betona se često koriste kod izgradnje različitih tipova poslovnih ili stambenih objekata (Slika 9). Fasadni paneli su obično izvedeni kao troslojni elementi od unutarnjeg nosivog betona, sloja ekspandiranog polistirena kao izolacije te vanjskog arhitektonskog betona. Fasadne površine obrađuju se kao prani kulir granulacije 4/8 ili 8/16 mm. [2]

Slika 7: Različite varijante izvedbe elemenata od pranog betona

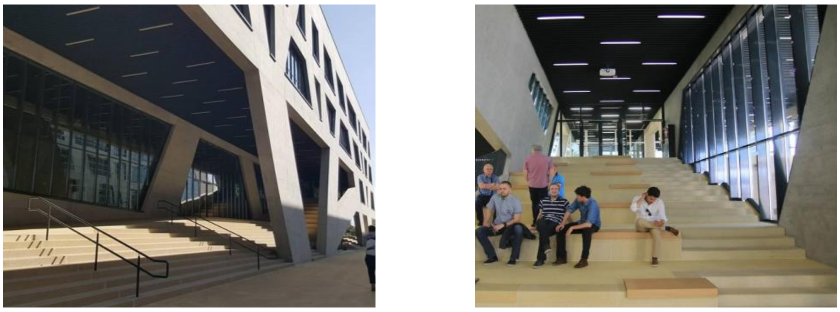

Slika 8: Stepenište od žutog pranog betona (lijevo) i unutarnje stepenište od brušenog žutog betona na Građevinskom fakultetu Sveučilišta u Osijeku

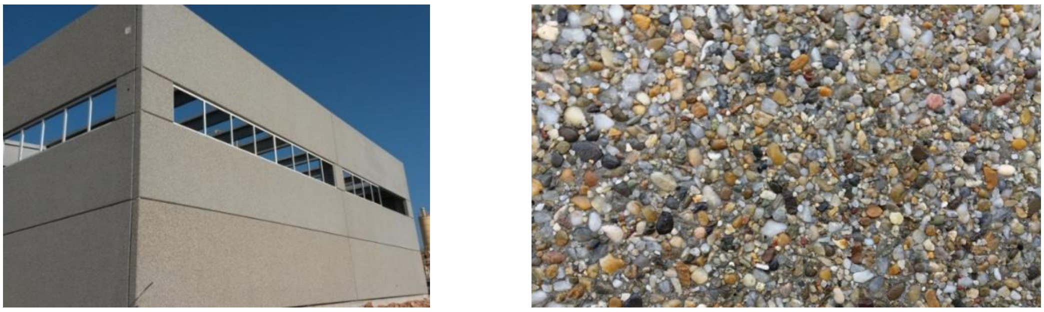

Slika 9: Izgled objekta s fasadnim panelima od pranog betona (lijevo) i detalj elementa od pranog betona (desno)

2.5. PJESKARENI BETONI

Pjeskareni betoni dobivaju se obradom površine pjeskarenjem pomoću zrnaca kvarcnog pijeska ili čeličnim kuglicama, koji obrađuju površinu, oslobađaju je cementne skramice te tako ostaju vidljiva zrna agregata. Prilikom primjene metode pjeskarenja potrebno je da beton posjeduje dostatnu čvrstoću da ne bi došlo do njegovog oštećenja. Jedan od niza projekata gdje je tvrtka Beton Lučko primijenila arhitektonski pjeskareni bijeli beton jest trg u Pušći (Slika 10.).

Slika 10: Bijeli pjeskareni beton na trgu u Pušći

2.6. BETONI S NALIČJEM OD DRUGOG MATERIJALA

Jedinstven primjer primjene predgotovljenog betona za izvođenje cijelog objekta uključujući i fasadnih elemenata jest sportska dvorana u Balama (Slika 11). Bale su malo istarsko mjesto s oko 1000 stanovnika, većinom poljodjelaca. Projekt nove sportske dvorane se suočio s bogatim povijesnim, kulturnim i društvenim mediteranskim kontekstom. Rješenje je nađeno u interpretaciji tradicionalnih načina gradnje uz pomoć novih tehnologija u proizvodnji predgotovljenih betonskih elemenata. Tradicionalni lokalni motiv suhozida je iskorišten kao uzorak i motiv čitavog oplošja.

Slika 11: Sportska dvorana Bale

Dvorana je kompletno predgotovljena, tako da su svi nosivi i fasadni elementi izvedeni sa armiranobetonskim predgotovljenim elementima. Fasadni nosivi zidovi za vertikalno opterećenje proizvedeni su u dva sloja ukupne debljine 25 cm. Unutarnji nosivi armiranobetonski sloj debljine 15 cm proizveden je od betona razreda tlačne čvrstoće C30/37, a vanjski fasadni sloj je debljine 10 cm proizveden od prirodnog kamena utopljenog u svježu betonsku masu. Koncept dvorane je potpuno prilagođen traženoj brzini projektiranja i izvedbe od 11 mjeseci, što je bilo moguće izvesti samo sa armiranobetonskim predgotovljenim betonskim elementima. Nova dvorana izgrađena je 2005.godine. Izgled sagrađene dvorane je namjerno prilagođen okolišu, postavljanjem što manjeg mjerila, korištenjem krajolika, ali i fasadne obloge iz lokalnog kamena koja je približena izgledu starih kuća. [2]

Jedan od posljednjih dostignuća u ovom području jest razvoj održivih predgotovljenih panelnih sustava od recikliranog agregata pod nazivom ECO-SANDWICH. Ovaj proizvod je razvijen u sklopu znanstveno istraživačkog projekta u okviru programa CIP-EIP-Eco-Innovation 2011. Nositelj projekta je Građevinski fakultet Sveučilište u Zagrebu, Zavod za materijale. Jednan od prvih objekata koji je izveden ovom tehnologijom od strane Beton Lučko je prikazan na Slici 12.


Slika 12: Montaža predgotovljenih fasadnih panela razvijenih u projektu Eco Sandwich

Zidni panel ECO-SANDWICH sastoji se od dva sloja betona koji su međusobno povezani rešetkastim nosačima od nehrđajućeg čelika. Od ukupne količine agregata potrebnog za izradu betona, 50 % je zamijenjeno s recikliranim agregatom dobivenim iz građevinskog otpada. Unutarnji, nosivi sloj betona izrađen je agregatom od recikliranog betona, dok je vanjski fasadni sloj izrađen od reciklirane opeke kao agregata u betonu. Kao toplinsko izolacijski materijal koristi se novorazvijena reciklirana vuna. Unutarnji sloj betona je povezan s nosivom konstrukcijom zgrade (stupovima, zidovima) pomoću sustava priključaka od nehrđajućeg čelika. Inovativno rješenje betoniranja vanjskog sloja predgotovljenog zidnog panela ECO-SANDWICH razlikuje opisani od sličnih proizvoda. Nakon očvršćivanja unutarnjeg sloja, postavlja se sloj toplinske izolacije, zatim se oba sloja okrenu za 180° oko uzdužne horizontalne osi, te se utapa u prethodno izliveni vanjski sloj betona na način da se između ostavi ventilirajući sloj zraka.

U cijelom životnom ciklusu (od proizvodnje sirovina, izrade, ugradnje, korištenja i recikliranja panela) ECO-SANDWICH paneli troše 43 % manje energije od sličnih fasadnih sustava. U istom životnom ciklusu ECO-SANDWICH paneli ispuštaju u okoliš oko 34 % manje CO_2 plinova. [2]

3. ZAKLJUČAK

U radu su prikazani uspješni primjeri primjene arhitektonskog betona u predgotovljenim betonskim elementima. Može se ustvrditi da je arhitektonski beton tijekom zadnjih 10-20 godina postao materijal koji posjeduje svojstva za kvalitetnu završnu obradu predgotovljenih betonskih elemenata.

Mnoge bi vrste fasada bile preskupe za izvedbu na licu mjesta. Zbog toga predgotovljeni betonski fasadni elementi omogućuju izvedbu fasada najraznovrsnijih boja, detalja, profila i tekstura uz prihvatljive cijene. Glavne prednosti primjene arhitektonskih predgotovljenih betonskih elemenata su brzina, kvaliteta i cijena gradnje te mogućnost izvedbe širokog spektra fasada.

LITERATURA

[1] Precast Prestressed Concrete Institute: *Architectural Precast Concrete*, editor S. Freedman, ISBN 978-0-937040-78-3, Chicago, (2007)
[2] Arhiva tvrtke Beton Lučko d.o.o.

INFLUENCE OF NATURAL FIBRES ON MECHANICAL PROPERTIES AND DURABILITY OF CEMENTITIOUS MORTARS

Ildiko Merta[1], Aljosa Sajna[2], Bojan Poletanovic[1], Ana Mladenovic[2]

[1] TU Wien, Faculty of Civil Engineering, Karlsplatz 13/206/4, 1040 Vienna, Austria, email: ildiko.merta@tuwien.ac.at, bojan.poletanovic@gmail.com
[2]Slovenian National Building and Civil Engineering Institute, Dimiceva ulica 12, 1000 Ljubljana, Slovenia, email: aljosa.sajna@zag.si, ana.mladenovic@zag.si

SUMMARY: In this paper preliminary results of an ongoing bilateral joint research project between TU Wien and Slovenian National Building and Civil Engineering Institute dealing with durability of natural fibre cementitious composites in Alpine regions are presented. At this stage, the research concentrates on the influence of different natural fibres on the mechanical properties of mortars when exposed to severe environmental conditions present during winter in the region. Mortars reinforced with hemp and flax fibres were cast and exposed to accelerated aging under freeze/thaw cycles in the presence of de-icing salts. On macro level, the influence of fibres on the composites mechanical properties before/after accelerated aging was quantified by means of its compressive strength, flexural strength and flexural toughness. The preliminary results show a marked beneficial effect of natural fibres on the mortars' freeze/thaw resistance.

UTJECAJ PRIRODNIH VLAKANA NA MEHANIČKA SVOJSTVA I TRAJNOST CEMENTNIH MORTOVA

SAŽETAK: U radu su prikazani preliminarni rezultati dvostranog zajedničkog istraživačkog projekta koji je u tijeku između Tehničkog sveučilišta Beč i Zavoda za građevinarstvo Slovenije o trajnosti cementnih kompozita s prirodnim vlaknima u alpskim područjima. U ovoj fazi istraživanje je usredotočeno na utjecaj različitih prirodnih vlakana na mehanička svojstva mortova izloženih oštrim uvjetima okoliša tijekom zime u tom području. Izrađeni su mortovi pojačani vlaknima konoplje i lana i izloženi ubrzanom starenju u ciklusima zamrzavanja i odmrzavanja uz prisutnost soli za odleđivanje. Na makrorazini utjecaj vlakana na mehanička svojstva kompozita prije i nakon ubrzanog starenja određen je iz tlačne čvrstoća, čvrstoće na savijanje i žilavosti pri savijanju. Preliminarni rezultati pokazuju povoljan učinak prirodnih vlakana na otpornost mortova na zamrzavanje i odmrzavanje.

1. INTRODUCTION

The majority of traditional building materials in infrastructures belong to the category of so-called cement based materials, like concrete and mortars. Their major ingredients are non-renewable natural resources, such as aggregate, sand, Portland cement and various types of steel or synthetic reinforcement. Consequently, traditional cementitious materials are extremely resource and energy intensive to manufacture, their production contributes to high pollution, resulting in greenhouse gas emissions, global warming, and climate change. Growing environmental awareness and need for reducing raw material consumption and carbon emissions forces intense research in area of sustainable cementitious materials.

Recently natural plant fibres, such as sisal, coir, flax, etc. have been considered as promising substituent fibers for steel, synthetic or glass fibres in cementitious materials [1-5]. The results so far demonstrate that the mechanical and fracture mechanical properties of these fibre cementitious composite are comparable to those of conventional composites reinforced with synthetic or metallic fibres [5, 6]. However, the major challenge is still ensuring the durability of natural fibres in the cementitious matrix as well as the long-time performance of the composite itself under various environmental conditions. Under the influence of common outdoor conditions such as moisture, carbonation, snow and action of de-icing salts, degradation of the composite accompanied with loss of its mechanical properties were reported [7-9].

An ongoing joint research project between TU Wien (Austria) and the Slovenian National Building and Civil Engineering Institute (Slovenia) aims to contribute to bridge this gap and to reduce the barriers for the possible application of natural fibre composites in Alpine regions. The objective is first to fundamentally understand the mechanisms involved in the aging and degradation of natural fibre composites (i.e. fibres degradation, fibre/matrix interface degradation, etc.) under severe environmental conditions common in Alpine regions, and second – with some modifications of the cement matrix – to substantially improve the material's durability. In this paper, the first preliminary results dealing with the influence of natural fibres on the durability and mechanical properties of the composite when exposed to severe environmental conditions of freeze/thaw cycles with de-icing salts are presented.

Mortars reinforced with plant fibres of hemp and flax were cast and exposed to accelerated aging conditions of freeze/thaw/de-icing salt cycles. On macro level the influence of fibres on the composites mechanical properties before/after accelerated aging was quantified by mean of compressive strength, flexural strength and flexural toughness measurement.

2. MATERIALS AND METHODS

2.1. MORTAR MATRIX

The mortar mix design of cement/sand/water was 1:1:0.4 by weight, with a water-cement-ratio of 0.4. The grain size of sand was 0.4 - 0.8 mm and cement CEM II/B-M (S-L) 32,5R was used. The mortar was mixed in a laboratory drum-mixer and compacted on a vibrating table. The specimens were demoulded 24 hours after casting and stored in water until testing at age of 28 days.

2.2. FIBRE REINFORCEMENT

As reinforcement for the mortar matrix two types of locally available natural fibres were used: industrial hemp (Cannabis sativa L) and flax (Linum usitatissimum), cultivated and processed in Hungary. These are so called primary bast fibres in the range of microfibers with a diameter of 16 – 50 μm and have extremely high tensile strength between 300 - 1100 N/mm^2. Natural fibres are highly hydrophilic, absorbing water several times their weight. If they are mixed in a cementitious matrix in dry condition they will absorb a part of the water that is needed for cement hydration. To counter this, the fibres were first soaked with water and then added to the matrix in saturated surface dry condition. The fibre bundles were cut to an average length of 10mm and added to the mortar matrix in the volume percentages of 1 %vol. The density of fibres was 1.5 g/cm^3.

Additionally, polyacrylonitrile (PAN) synthetic micro fibres of Type Binder+ produced by Fisipe Fibras Sintéticas de Portugal, S.A. were used as reference fibre reinforcement for a comparison with natural fibres. The density of PAN fibres is 1.17 g/cm^3, the tensile strength 685 N/mm^2, and the elastic modulus 13400 N/mm^2. The geometry and morphology of fibres under Scanning Electron Microscope (SEM) is shown in Figure 1.

2.3. ACCELERATED AGING

The durability of the mortars under severe environmental conditions present in Alpine regions was determined by imposing the specimens to accelerated aging of freeze/thaw/salt (FTS) cycles in controlled laboratory environment according to CEN/TS 12390-9 [10]. The samples were completely submerged in 3% NaCl solution and then exposed to 56 freeze/thaw cycles. In regular intervals the amount of scaling per unit surface area was weighed.

2.4. THREE POINT BENDING TEST (3PBT) AND COMPRESSIVE TEST

Three point bending- (3PBT) and compressive tests were conducted on both aged (56 FTS cycles) and unaged specimens and the materials' flexural strength, flexural toughness and compressive strength were measured. The tests were carried out on the mechanical testing machine Schenck RSA with a load capacity of 100 kN and a rigidity of 8×10^{-3} mm/kN at a room temperature of 21°C and relative humidity of 50 %. In the bending tests, the load was applied at the middle of the specimens with a span length of 100 mm. The compression tests were carried out on one half of the split specimens by applying the compressive force on 40x40 mm^2 area. All tests were accomplished on 6 identical specimens.

From the load-displacement curves of the 3PBT the flexural strength and flexural toughness of the specimens were calculated as the peak stress as well as the area under the curve up to a mid-span deflection of 4.5 mm (in case of natural fibres) respectively.

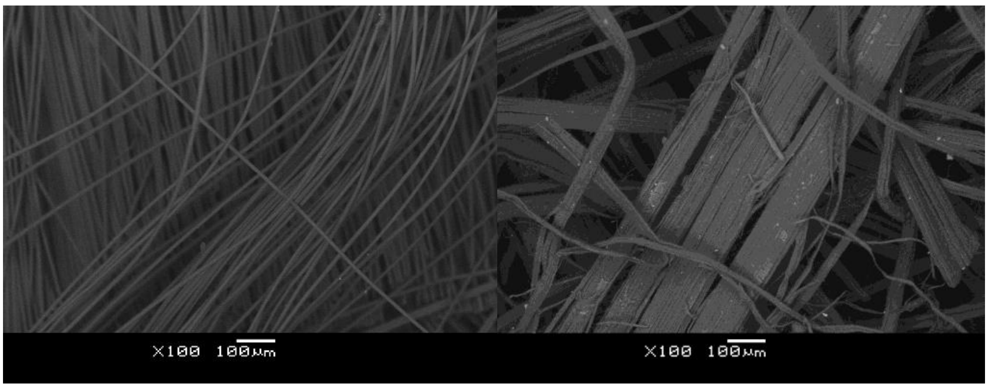

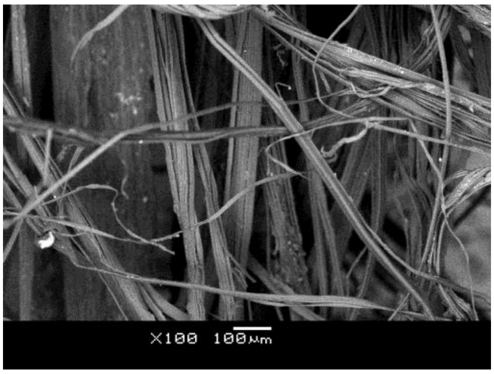

Figure 1 Morphology of hemp, flax and PAN fibres under Scanning Electron Microscope

3. RESULTS AND DISCUSSION

3.1. DURABILITY OF MORTARS

The durability of mortar specimens under accelerated aging when exposed to FTS cycles is presented in Figure 2 by means of the cumulative scaling mass. Significant differences in the performance of the mortars can be observed. Plain mortar and synthetic fibre mortar exhibit a significant mass loss with increasing number of FTS cycles and consequently exhibit the least resistivity in severe environmental conditions. In contrast, the addition of hemp and flax fibres significantly improves the FTS resistivity of plain mortar. The surface scaling of natural fibre mortars after 56 FTS cycles is up to 5 times lower than that of plain mortar. This is believed to be the consequence of the beneficial effect of uniformly distributed micro fibres within the materials volume, acting as a stabilising mesh, preventing the scaling of the specimens surface layer (Figure 3).

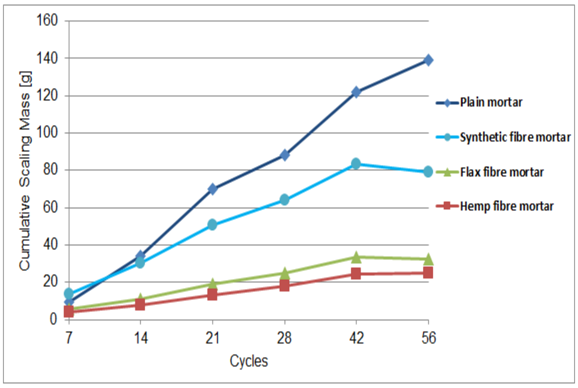

Figure 2 Cumulative scaling mass of mortar specimens during FTS test

Figure 3 Plain mortar (left) and hemp fibre mortal (right) specimens before and after accelerated aging

3.2. COMPRESSIVE STRENGTH OF MORTARS

Figure 4 shows the compressive strength of the mortar specimens tested at the age of 28 days and after exposure to accelerated aging under severe environmental conditions of freeze/thaw cycles including de-icing salts. The mean compressive strength of unaged plain mortar specimens was 49.6 N/mm². Generally with the addition of fibres, the compressive strength of mortar decreases on average by 25 %. The most significant decrease of compressive strength occurs in flax fibre mortars (36 %), whereas mortars reinforced with hemp and synthetic fibres show a significantly lower compressive strength loss of 16 % and 18 % respectively.

Both plain mortars and mortars reinforced with synthetic fibres exhibit a marked compressive strength loss after accelerated aging under severe environmental conditions. The residual compressive strength of these specimens is solely at 40 % of their compressive strength before aging. On the contrary, mortars containing natural fibres of hemp maintain 75 % of their compressive strength after aging. The most beneficial effect is observed in flax fibre mortars where the compressive strength remained unchanged after accelerated aging. Thus although the addition of natural fibre reinforcement to mortars reduces the compressive strength on average by 30 %, natural fibres markedly help in retaining the material's compressive strength when it is exposed to severe environmental conditions of freeze/thaw combined with the action of de-icing salts.

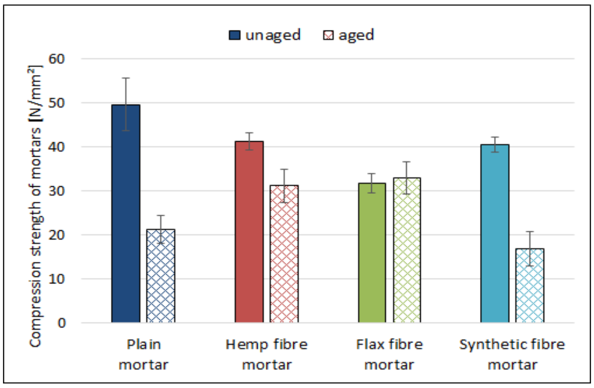

Figure 4 Compressive strength of mortar specimens before and after accelerated aging of 56 FTS cycles

3.3. FLEXURAL STRENGTH OF MORTARS

The flexural strength of mortars before and after accelerated aging is shown in Figure 5. Generally, the addition of fibre reinforcement to the mortar matrix does not have any influence on the composite's flexural strength. This is because the flexural strength is basically determined by the strength of the cementitious matrix itself and the fibres becoming active in carrying stresses after the matrix is cracked.

With exposure to accelerated aging conditions of FTS cycles, the flexural strengths of the mortars decreases. Here, however, the type of fibres has an influence on the flexural strength. Plain mortars or mortars reinforced with synthetic fibres exhibit a pronounced flexural strength loss after aging, i.e. up to 33 % and 48 % respectively. Natural fibre mortars, on the contrary, preserve their flexural strength better and show only a minor strength loss, 13 % for hemp fibres and 23 % for flax fibres.

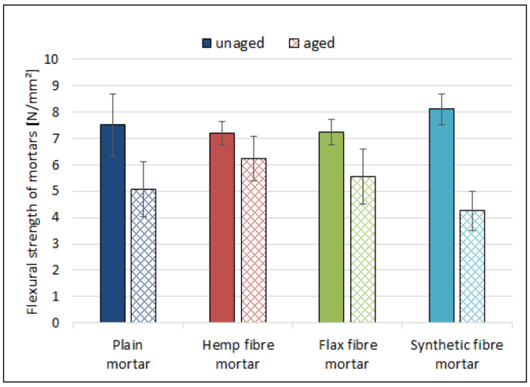

Figure 5 Flexural strength of mortar specimens before and after accelerated aging of 56 FTS cycles

3.4. FLEXURAL TOUGHNESS OF MORTARS

The flexural toughness of mortar specimens before and after accelerated aging is shown in Figure 6. The addition of fibre reinforcement to mortars distinctively improves the energy absorption capacity or toughness of the material. The most significant improvement of the mortars' flexural toughness is observed in the case of hemp fibre reinforcement. The toughness of hemp fibre mortar is 4.5 times higher than that of plain mortar. In the cases of flax and synthetic fibres, the increase in toughness is somewhat lower, up to 3 and 2 times respectively compared to plain mortar.

After exposure of the material to FTS conditions, the flexural toughness of natural fibre reinforced mortars significantly decreases compared to values before aging. Hemp fibre reinforced mortars lose up to 57% of their flexural toughness whereas flax fibre mortars up to 43 %. Synthetic fibre reinforced mortars exhibit the least toughness loss, i.e. up to 25 %. Plain mortars, in contrast, remain completely their flexural toughness after accelerated aging. However, although natural fibre mortars lose a significant portion of their flexural toughness, their residual flexural toughness is still up to 70 % and 40 % higher than that of plain- and synthetic fibre mortars respectively. This indicates that the aging process under FTS conditions most dramatically influences the fibre/matrix interface, i.e. the bond properties between the fibres and cement matrix.

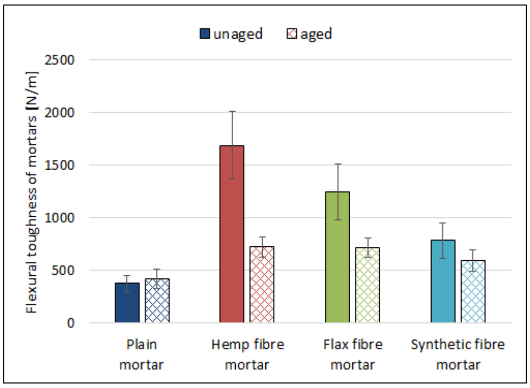

Figure 6 Flexural toughness of mortar specimens before and after accelerated aging of 56 FTS cycles

4. CONCLUSIONS

In this research, mortars reinforced with hemp and flax fibres were cast and exposed to accelerated aging conditions of freeze/thaw cycles combined with the action of de-icing salts. The influence of fibres on the composites mechanical properties before/after accelerated aging was quantified by means of compressive- and flexural strength as well as flexural toughness of the material. Based on the tested specimens the following conclusions can be drawn:

Natural fibres significantly improve the freeze/thaw resistivity of plain mortar. The surface scaling of natural fibre mortars after 56 FTS cycles is up to 5 times lower than that of plain mortar.

Although the addition of natural fibre reinforcement to mortars reduces the compressive strength on average by 30 %, natural fibre mortars maintain their compressive strength almost entirely after exposure to severe environmental conditions of FTS cycles.

Natural fibre mortars exhibit only a minor flexural strength loss compared to plain mortars after exposure to severe environmental conditions of FTS cycles.

The flexural toughness of natural fibre mortars exposed to accelerated FTS conditions significantly decreases. However, their residual flexural toughness is still up to 70 % higher than that of plain mortars.

ACKNOWLEDGEMENTS

This research was carried out within the bilateral international cooperation project: *Durability of sustainable natural fibre cementitious composites in Alpine regions*, between the TU Wien (TUW) and the Slovenian National Building and Civil Engineering Institute (ZAG) funded by the Federal Ministry of Science, Research and Economy (BMWFW) in Austria under the grant nr. SI 18/2016. The authors greatly acknowledge the support of Fisipe Fibras Sintéticas de Portugal, S.A. for providing the synthetic fibres for the research.

REFERENCES

[1] Silva, F.A. et al.: Physical and mechanical properties of durable sisal fiber–cement composites. Constr Build Mater 2010; 24(5): 777–85.

[2] Agopyan, V. et al.: Developments on vegetable fibre–cement based materials in São Paulo, Brazil: an overview. Cem & Concr Composites. 2005; 27: 527-36.

[3] Savastano, Jr. H. et al.: Fracture and fatigue of natural fiber-reinforced cementitous composites. Cem & Concr Composites. 2009; 31: 232-43.

[4] G. Di Bella, G. et al.: Effects of natural fibres reinforcement in lime plasters (kenaf and sisal vs. Polypropylene), Construction and Building Materials, Volume 58, 15 May 2014, Pages 159-165, ISSN 0950-0618
[5] Merta, I.; Tschegg, E.K.: Fracture energy of natural fiber reinforced concrete, Original Research Article Construction and Building Materials, Volume 40, March 2013, 991-997
[6] Merta I.: Hemp Fibre Reinforced Foam Concrete: Discussion of the Wedge Splitting Test Method, International Journal of Research in Engineering and Technology, 0X (2014), pp. 1 -5.
[7] Wei, J.; Meyer, C.: Degradation mechanisms of natural fiber in the matrix of cement composites, Cement and Concrete Research, Volume 73, July 2015, Pages 1-16, ISSN 0008-8846
[8] Almeida, A.E.F.S. et al.: Improved durability of vegetable fiber reinforced cement composite subject to accelerated carbonation at early age, Cement and Concrete Composites, Volume 42, September 2013, Pages 49-58, ISSN 0958-9465
[9] João de Almeida, M. F. et al.: Degradation kinetics and aging mechanisms on sisal fiber cement composite systems, Cement and Concrete Composites, Volume 40, July 2013, Pages 30-39, ISSN 0958-9465
[10] CEN/TS 12390-9:2016 Testing hardened concrete - Part 9: Freeze-thaw resistance with de-icing salts - Scaling, Ch. 6

INFLUENCE OF STEEL FIBRE REINFORCEMENT ON THE PROPERTIES OF CONCRETE

Darko I. Nakov[1], Goran R. Markovski[1], Toni P. Arangjelovski[1]

[1] University "Ss. Cyril and Methodius", Faculty of Civil Engineering, Department of Conrete and Timber Structures Bul. Partizanski odredi 24, 10 00 Skopje, Republic of Macedonia, email: nakov@gf.ukim.edu.mk, markovski@gf.ukim.edu.mk, arangelovskitoni@gf.ukim.edu.mk

SUMMARY: To find out the influence of different fibre dosages on the mechanical and time-dependent properties of concrete, an experiment was carried out at the Faculty of Civil Engineering Skopje. The experiment consists of 126 specimens in total, all manufactured with concrete class C30/37, but reinforced with different amount of fibres (0, 30 and 60 kg/m^3). According to the experimental results up to age of 400 days, addition of steel fibres has influence on most of the mechanical properties: around 4% increase of the compressive strength, around 14 % increase of the splitting tensile strength, around 19% increase of the flexural tensile strength and almost no influence on the modulus of elasticity. The addition of steel fibres has almost no influence on the free drying shrinkage (decrease of 2 %), while for the considered compressive stress level, steel fibres have a bigger influence on the creep (decrease of 12 %).

UTJECAJ ARMIRANJA ČELIČNIM VLAKNIMA NA SVOJSTVA BETONA

SAŽETAK: Na Građevinskom fakultetu u Skopju provedena su ispitivanja kojima se željelo utvrditi utjecaj različitih količina vlakana na mehanička i vremenski ovisna svojstva betona. Ispitivanjem je obuhvaćeno ukupno 126 ispitnih uzoraka proizvedenih od betona razreda C30/37 armiranih različitim količinama vlakana (0, 30 i 60 kg/m3). U skladu s rezultatima ispitivanja do starosti od 400 dana dodavanje čeličnih vlakana ima utjecaj na većinu mehaničkih svojstava: tlačna čvrstoća povećala se za oko 4 %, vlačna čvrstoća cijepanjem povećala se oko 14 %, vlačna čvrstoća pri savijanju povećala se oko 19 %, a na modul elastičnosti vlakna nisu imala utjecaj. Dodavanje čeličnih vlakana gotovo nije imalo utjecaj na slobodno skupljanje pri sušenju (smanjenje 2 %) dok su za razmatranu razinu tlačnog naprezanja čelična vlakna imala veći utjecaj na puzanje (smanjenje 12 %).

1. INTRODUCTION

When steel fibre reinforcement is added in concrete, it is assumed that the fibres are uniformly randomly oriented in the concrete matrix. However, after placing and vibrating, no one can be sure that this is true. This often leads to a large scatter in the test data and high variability in measured values due to the direction of loading in relation to the direction of casting.

When table vibration or excessive internal vibration is used, fibres tend to become horizontally aligned. They also show preferential parallel alignment close to the bottom and sides of the moulds. With electromagnetic measurements and X-ray photographs of the fibre distribution, it was proven that fibres showed not only preferential alignment, but also non-uniform distribution along the length of the steel fibre reinforced concrete (SFRC) beam. Therefore, small amounts of fibre reinforcement, less than 30 kg/m^3, should not be used because they lead to more non-uniform distributions. On the other hand, the preferential alignment can be good, if the fibres can be oriented in the direction of the acting stress. However, if all recommendations for mix design, mixing, handling, placing and finishing are followed, it is possible to produce SFRC with acceptably low variability in the fibre distribution and orientation [1].

The effectiveness of the fibres in improving the characteristics of concrete is dependent on the fibre matrix interactions, which are governed by the closer zone around the fibres, called interfacial transition zone (ITZ). This zone, just around the fibre, is significantly different from the other zones of the matrix. When fibres are added to the concrete, they act like special long aggregates that are preventing the aggregate to fulfill the spaces between other aggregates. In this way, there is more cement paste around the fibres to fill the empty space (wall effect) [2]. The three main fibre matrix interactions are [1]: physical and chemical adhesion, friction, and mechanical anchorage induced by deformations on the surface or by overall complex geometry.

Physical and frictional bondings between a steel fibre and a cementitious matrix are very weak and therefore mechanical anchoring is required. Fibres actually act through stress transfer from the matrix to the fibre by some combination of interfacial shear and mechanical interlock between the deformed fibre and the matrix. Up to the point of matrix cracking, the load is carried by both the matrix and the fibres. When cracking occurs, the fibres carry the entire stress by bridging across the cracked concrete until they pull out completely. Actually, the energy is dissipated as the fibre undergoes plastic deformation while being pulled out.

2. STATE OF THE ART

2.1. PHYSICAL AND MECHANICAL PROPERTIES OF STEEL FIBRE REINFORCED CONCRETE (SFRC)

When the volume percentage of fibres is less than 2%, the Modulus of Elasticity and the Poisson's ratio of SFRC can be taken as equal to those of plain concrete [3].

The compressive strength is only slightly affected by the presence of fibers. The observed increases range from 0-15% for up to 1.5% fibers by volume, as reported in [3], or from 0-25% for up to 2% fibers by volume [1]. Although strength is not significantly increased, the energy absorption (post-cracking ductility) of the material under compression is improved [1].

The direct tensile strength is significantly increased for 30-40% with the addition of 1.5% fibres by volume [3]. This is valid for more or less randomly distributed fibres, while for fibres aligned in the direction of the tensile stress, the increase can be 133% for 5% smooth straight steel fibres by volume [1].

The flexural strength is much more improved by the addition of steel fibres. 50-70% increase has been reported using the usual fibre volume and standard third-point bending test [3]. The increase can be 100% or even 150% if bigger fibre volumes are used, if center-point bending test is performed or if smaller specimens are used. Except the fibre volume, the shape of the fibers and the aspect ratio also plays a crucial role, with deformed fibres and bigger aspect ratio being more effective [1].

The improvement in the residual strength of the concrete elements with the addition of steel fibres leads to an increase of shear capacity. For 1% steel fibres by volume, the shear strength was increased for 0-30% [3]. There is not much data about torsional strength, but different studies show an increase up to 100% [1].

The biggest improvement that is achieved by addition of steel fibres to plain concrete is in the energy absorption capacity or in the toughness. The flexural toughness can be defined as the area under the complete load-deflection curve or it is the total energy needed for a fracture. It increases with bigger fibre dosage, bigger aspect ratio and with the use of deformed fibers.

For normal strength concrete under flexural impact load, the peak loads for SFRC were about 40% higher than those for plain concrete. The fracture energy, which is the second most important parameter when observing impact loading, was increased for 2.5 times [3].

As fibres do not increase significantly the static compressive strength, there is also no significant improvement in the fatigue strength under compressive loading. On the other hand, as it is the case with the static tensile strength, fibres increase the fatigue strength under tensile loading. Steel fibres enable higher endurance limits, finer cracks and more energy absorption to failure [1].

2.2. TIME-DEPENDENT DEFORMATION PROPERTIES OF SFRC

The Report on FRC published by ACI [3] shows that, according to limited test data on creep and shrinkage of SFRC, if fibres are used to the amount of less than 1% of the volume, there is no significant improvement in creep and shrinkage strain. Edgington et al. have reported that shrinkage of concrete over a period of three months is unaffected by the presence of steel fibres [4].

Balaguru and Ramakrishnan found that 0.5% of steel fibres slightly increase the creep of concrete and lead to less shrinkage strains [5]. Houde et al. found that 1.0% of steel fibres increase the creep strain by 20-40%. On the other hand, Chern and Chang found that steel fibres reduce the creep strain [1]. Swamy and Theodorakopoulos have reported that inclusion of 1% fibres results in improved creep properties of concrete under flexure [6].

Swamy and Stavrides have reported that drying shrinkage is reduced by about 15-20% due to the addition of 1% fibres [7]. Hannant has reported that steel fibres have no significant effects on both creep and shrinkage properties of concrete [8]. Malmberg and Skarendahl, have reported that Steel fibre concrete with a fibre content of up to 2% undergoes less shrinkage than plain concrete [6].

Similar conclusion was reported by Young and Chern. They found out that the optimal volume fraction of steel fibres to reduce shrinkage is not more than 2%. Another conclusion from their research is that the larger aspect ratio of fibres leads to smaller shrinkage strains. They also proposed a modification of the BP model for calculation of the shrinkage of SFRC. The parameters that they included in the modification were the volume fraction and the aspect ratio of the steel fibres [9].

One of the most important researches in this field was done by Mangat and Azari [10,11]. They proposed theories of creep and shrinkage of SFRC based on experiments and knowledge about the behaviour of the material. At the end of their research, they gave simple equations for predicting creep and shrinkage of SFRC related to ordinary plain concrete According to their expressions, the decreasing of creep and shrinkage of SFRC, compared to plain concrete, ranges from 0 to 40 %.

3. EXPERIMENTAL PROGRAM

As a part of large experimental program that involved full scale beams from three types of concrete, control specimens were cast in order to test the compressive strength, flexural tensile strength, splitting tensile strength, elastic modulus and deformations due to creep and shrinkage.

In order to find out the influence of different fibre dosages on the properties of concrete, the investigated parameter in this research was the fibre dosage. The used steel fibres were hooked-end HE1/50, manufactured by Arcelor Mittal, produced of cold-drawn wire, with a diameter of 1mm, length of 50mm and tensile strength of 1100 N/mm^2. The shape of the used fibres is presented in Figure 1.

The three types of concrete were denoted as:

- Reinforced concrete (C30/37);
- SFRC with 30 kg/m^3 steel fibres (C30/37 FL1.5/1.5);
- SFRC with 60 kg/m^3 steel fibres (C30/37 FL2.5/2.0).

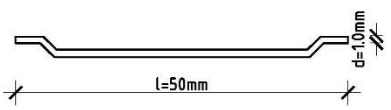

Figure 1 Hooked-end steel fibre HE1/50

The mixture proportioning was the same for the three types of concrete and is presented in Table 1.

Table 1 Mixture proportions for C30/37, C30/37 FL1.5/1.5 and C30/37 FL2.5/2.0

Mixture proportions	(kg/m^3)
Cement CEM II/A-M 42.5N	410
Water	215
Water/Cement ratio, w/c	0.524
Aggregate: 0-4 mm (river sand), 50% 4-8 mm (limestone), 20% 8-16 mm (limestone), 30%	 875 350 525
Fibres: C30/37 C30/37 FL 1.5/1.5 C30/37 FL 2.5/2.0	 0 30 60

3.1. TESTING OF CONTROL SPECIMENS

For each concrete type, 42 control specimens were cast for testing of the mechanical and time-dependent properties of concrete at the age of 40 and 400 days. After 8 days of curing the specimens were transported to the Laboratory at the Faculty of Civil Engineering – Skopje, where they were kept under almost constant temperature with an average of 19.5°C and constant relative ambient humidity with an average of 60.2%, regulated with special humidifiers and dehumidifiers.

The mechanical properties at the age of 40 days were tested on 3 specimens for compressive strength, splitting tensile strength and Modulus of Elasticity and 6 specimens for flexural tensile strength. The mechanical properties were also tested at the age of 400 days on 3 specimens for compressive strength, splitting tensile strength and Modulus of Elasticity and 3 specimens for flexural tensile strength. The compressive strength, splitting tensile strength and Modulus of Elasticity were tested by use of hydraulic jack HPM3000, produced by ZRMK - Ljubljana, Slovenia.

The most specific testing was the testing of the flexural tensile strength (Figure 2a), which was performed according to RILEM TC 162-TDF [12]. The deflection controlled testing was done on notched prisms with cross section dimensions of 15/15cm, length of 70cm and span of 50cm. Beams were notched by wet sawing with width of notch of 5mm and depth of 25mm. The application of the deflection was at a constant rate of 0.2mm/min by use of Wykeham Farrance, England, which is a 50kN machine with a big stiffness. During the tests, the load and the midspan deflection were recorded continuously by the data acquisition system produced by Hottinger Baldvin-HBM, Germany.

Compression creep was applied in creep frames (Figure 2b) whereat the stress level of the 12x12x36cm prism specimens was 7.5MPa. The drying shrinkage was measured immediately after the opening of the moulds of the control specimens. The measurements were performed with mechanical deflection meter, type Hugenberger, Switzerland, with base of 250mm.

Figure 2 Testing of: a)flexural tensile strength and b) concrete creep

3.2. RESULTS FROM TESTING

The mixture proportioning was done according to all recommendations, [13] and [3], in the up to date literature, so the slump of the concrete without fibres was 120mm. Since fibres decrease workability, the slump was decreased to 75mm and 50mm with addition of 30 and 60 kg/m^3 (Table 2).

Table 2 Slump of C30/37, C30/37 FL 1.5/1.5 and C30/37 FL 2.5/2.0

Type of concrete	Slump (mm)
Reinforced Concrete (C30/37)	120
Steel fibre reinforced concrete with 30 kg/m^3 (C30/37 FL 1.5/1.5)	75
Steel fibre reinforced concrete with 60 kg/m^3 (C30/37 FL 2.5/2.0)	50

The average results for the mechanical properties with the corresponding standard deviations, as well as, the increase in the mechanical characteristics with time, are presented in Table 3.

The testing of the flexural tensile strength at the age of 40 and 400 days resulted in force – deflection relations for the three concrete types. In Figure 3, the result only for the concrete type C30/37 FL 1.5/1.5 is presented. In the case of plain concrete, sudden brittle failure occurred, manifested by a sudden drop in force. From the force – deflection relations, stress – strain relations in tension were obtained where the biggest difference between plain and fibre concretes can be noted.

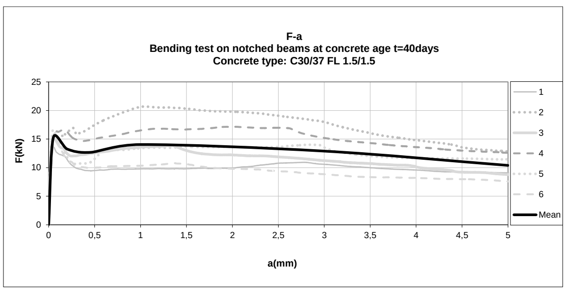

Figure 3 Bending test on notched beams at the age of 40 days for C30/37 FL 1.5/1.5

The time-dependent creep and shrinkage strains were measured on four sides of each prism, which means that for each type of concrete, the presented results in the Table 4, Figure 4 and Figure 5 are mean value of 12 measurement points. The obtained values of the time-dependent deformation properties for the three concrete types and the decrease for the SFRC types are presented in Table 4.

Table 3 Mechanical properties at age of 40 and 400 days of C30/37, C30/37 FL 1.5/1.5 and C30/37 FL 2.5/2.0

Mechanical properties	Age at test. t(days)	C30/37	σ (st.dev)	C30/37FL 1.5/1.5	σ (st.dev)	C30/37 FL 2.5/2.0	σ (st.dev)
Compressive strength (MPa) (cubes 15/15/15cm)	40	42.89	0.18	41.63	4.79	44.59	1.83
	400	45.70	5.742	47.41	1.07	46.15	1.69
Increase (%)		6.55		13.88		3.50	
Splitting tensile strength (MPa) (cubes 15/15/15cm)	40	3.51	0.10	3.22	0.14	4.00	0.31
	400	4.17	0.02	4.58	0.13	4.24	0.13
Increase (%)		18.80		42.23		6.00	
Flexural tensile strength (MPa) (beams 15/15/70cm) -σ_1(stress at δ_L=0.05mm) -σ_2(stress at $\delta_{R,1}$=0.46mm) -σ_3(stress at $\delta_{R,4}$=3.00mm)	40	5.18	0.56	4.95 1.80 1.53	0.34 0.44 0.40	5.30 2.83 2.33	0.66 0.67 0.73
-σ_1(stress at δ_L=0.05mm) -σ_2(stress at $\delta_{R,1}$=0.46mm) -σ_3(stress at $\delta_{R,4}$=3.00mm)	400	5.00	0.66	4.40 1.38 1.15	1.32 0.28 0.47	5.95 2.90 2.38	0.13 0.44 0.32
Increase σ_1 (%)		-3.5		-11.11		12.26	
Modulus of Elasticity (MPa) (cylinders 15/30cm)	40	26956	127.2	26771	93.2	26120	423.2
	400	27041	811.4	30809	618.2	28224	674.2
Increase (%)		0.32		15.08		8.06	

Table 4 Decrease of time-dependent deformation properties of C30/37 FL 1.5/1.5 and C30/37 FL 2.5/2.0

Time-dependent properties	Age t(days)	C30/37	C30/37 FL1.5/1.5	decr. % ↓	C30/37 FL2.5/2.0	decr. % ↓
Drying shrinkage ε_{ds} [μs]	400	808.0	805.0	0.4	794.9	1.6
Instantaneous strain ε_e [μs]	40	286.3	254.0	11.3	241.3	15.7
Creep strain ε_{cc} [μs]	400	429.7	374.7	12.8	385.0	10.4
Total strain $\varepsilon=\varepsilon_{ds400}+\varepsilon_e+\varepsilon_{cc}$ [μs]	400	1524.0	1433.7	5.9	1421.2	6.8

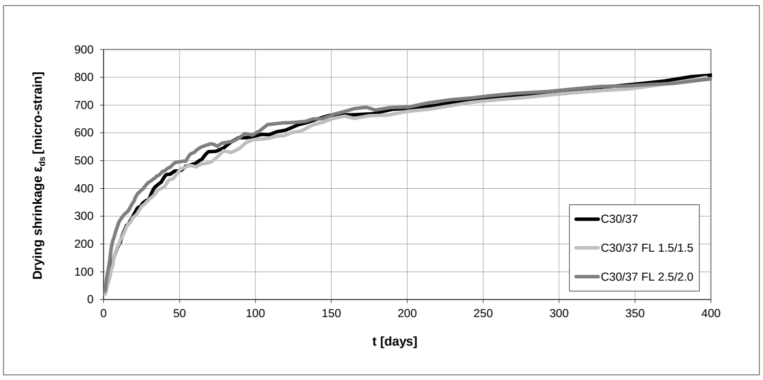

Figure 4 Drying shrinkage strain for the three concrete types

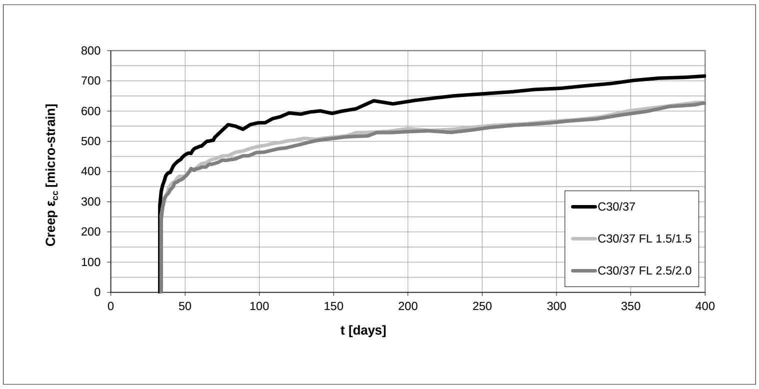

Figure 5 Creep strain for the three concrete types

4. CONCLUSIONS

From the experimental results, the following conclusions can be drawn:

- The addition of steel fibres has small influence on most of the mechanical properties: around 4% increase of the compressive strength, around 14% increase of the splitting tensile strength, around 19% increase of the flexural tensile strength and almost no influence on the Modulus of Elasticity. The increase of the mechanical properties was noted in the case of the concrete with 60 kg/m^3, while in the one with 30 kg/m^3 due to the fact that there is no uniform distribution because of the smaller amount of fibres, there is even a decrease in the mechanical properties. Usual increase of the mechanical properties with time was observed, as in the case of plain concrete.
- The biggest difference in the mechanical properties between the concrete without and with steel fibres is the appearance of residual tensile strengths.
- According to the experimental results at the age of concrete of 400 days, the addition of steel fibres has almost no influence on the free drying shrinkage (decrease of 2%). For the considered compressive stress level, steel fibres have a bigger influence on the creep (decrease of 12%).

REFERENCES

[1] Bentur, A.; Mindess, S.: Fibre Reinforced Cementitious Composites, Taylor and Francis, (2007)
[2] Dupont, D.: Modelling and experimental validation of the constitutive law (σ-ε) and cracking behaviour of steel fibre reinforced concrete, Doctoral dissertation, Catholic University of Leuven, Belgium, (2003)
[3] Report on Fiber Reinforced Concrete, Reported by ACI Committee 544, (1996, Reapproved 2002)
[4] Edgington, J., et al, Steel Fibre Reinforced Concrete, Current Paper CP69/74, Building Research Establishment, Garston, Watford, (1974)
[5] Balaguru, P.; Ramakrishnan, V., Properties of Fiber reinforced concrete: Workability, Behaviour under long-term loading and Air-void characteristics, ACI Materials Journal, (05-06.1988)
[6] Tan, K.H.; Saha, M.K., Ten-year study on Steel fiber-reinforced concrete beams under sustained loads, ACI Structural Journal, (05-06.2005)
[7] Swamy, R.N.; Stavrides, H., Influence of Fiber reinforcement on restrained shrinkage and cracking, ACI Journal, (03.1979)
[8] Tan, K.H. et al, Long term deflections of Steel fiber-reinforced concrete beams, ACI Structural Journal, (08-09.1994)
[9] Young, C.H.; Chern, J.C., Practical prediction model for shrinkage of Steel fibre reinforced concrete, Materials and Structures 24, (1991)
[10] Mangat, P. S.; Azari, M. M., A theory for the creep of steel fibre reinforced cement matrices under compression, Journal of Materials Science 20, (1985)
[11] Mangat, P. S.; Azari, M. M., A theory for the free shrinkage of steel fibre reinforced cement matrices, Journal of Materials Science 19, (1984)
[12] RILEM TC 162-TDF: Test and design methods for steel fiber reinforced concrete, σ-ε design method, Final recommendation, Materials and structures, Vol. 36, (10.2003)
[13] Measurement of Properties of Fiber Reinforced Concrete, Reported by ACI Committee 544, (1989, Reapproved 1999)

PERFORMANCE OF FIBRE CONCRETE WITH REGARD TO TEMPERATURE

Alan Richardson[1], Rhys Ovington[1]

[1] Northumbria University, Faculty of Engineering and Environment, Department of Mechanical and Construction Engineering, Tyne & Wear, NE1 8ST, UK, email: alan.richardson@northumbria.ac.uk

SUMMARY: The effect of temperature variation on concrete properties with steel and synthetic fibre additions was examined. The range of performance characteristics were determined at room temperature (20 °C) and ± 40 °C of room temperature. Standard test methods were carried out in order to determine the flexural strength, bond strength and toughness of fibre reinforced concrete at varying temperatures. A significant increase in the performance of concrete was observed at a temperature of -20 °C as well as a minor decrease in performance at temperatures of 60 °C. Synthetic fibres provided the optimal performance when compared to the control and steel fibre samples.

SVOJSTVA BETONA S VLAKNIMA S OBZIROM NA TEMPERATURU

SAŽETAK: Istražen je utjecaj promjene temperature na svojstva betona s dodatkom čeličnih i sintetičkih vlakana. Raspon svojstava određen je pri sobnoj temperaturi (20 °C) i pri temperaturi ± 40 °C od sobne temperature. Za određivanje čvrstoće pri savijanju, čvrstoće prianjanja i žilavosti betona armiranog vlaknima pri promjenjivim temperaturama upotrijebljene su normirane ispitne metode. Opaženo je znatno povećanje svojstava betona pri temperaturi od -20 °C i manje smanjenje svojstava pri temperaturi od 60 °C. Sintetička vlakna imaju optimalno svojstvo u usporedbi s kontrolnim uzorcima s čeličnim vlaknima.

1. INTRODUCTION

There are large fluctuations in temperature Worldwide. In Russia, Greenland and Canada, the temperature varies massively over the four seasons. It is therefore crucial to effectively predict the thermal behaviour of building materials in order to properly design structures which are capable of withstanding such extreme variations in temperature. The temperature parameters used in the research represent the effect of real world temperatures, such as those recorded in the Middle-East and Canada [1].

This research examines two fibre types, namely steel and polypropylene Type 2 macro synthetic fibres. Polypropylene has a high resistance to the flow of electrons, leading to a low rate of heat transfer within the material. At ambient to high temperatures, polypropylene is a ductile material and shows qualities of a plastic/elastic nature. At temperatures below freezing, polypropylene tends to become brittle. Hall [2] states that the brittle nature of polypropylene is a serious disadvantage and can become problematic, especially in certain applications when mechanical performance is concerned.

Research carried out by Lau et al [3] investigated the effect that elevated temperature had on steel fibre concrete. The steel fibre concrete was subject to temperatures ranging between 105°C and 1200°C. These temperatures are extreme and beyond maximum air temperature, but they do provide an understanding of the performance of steel fibre concrete under high temperatures. Lau *et al's* [3] research reported a decrease in elastic modulus as the temperature increased as well as a small, but not significant, reduction in strength at temperatures below 400°C. It was concluded that the use of steel fibres in concrete continues to be beneficial even at temperatures of 1200°C and that steel fibre concrete can provide a greater resistance to the effects of heating.

Mirzazadeh *et al* [4] found that concrete beams tested at -25°C demonstrated an increase in strength and ductility of 13% and 34% respectively, compared to those tested at room temperature. Neville [5] suggests that, within wet specimens, the compressive strength of cooled/frozen concrete can reach values up to three times the strength at room temperature. This is believed to be due to water freezing within the pores and thus providing the increased strength.

Possibly the most beneficial effect of fibre additions in concrete is the ability to absorb energy [6,7 & 8]. This is the main reason for the use of fibre reinforcements within floor slabs. If toughness is reduced with an increase in temperature, this could be considered a major disadvantage when designing structural elements for hot climates, such as the Middle East, where it is not unheard of for air temperatures to rise above to and beyond 40°C. This research has investigated this physical property further in order to determine whether fibre reinforced concrete should be designed with temperature induced mechanical degradation in mind. According to Bakis et al. [9] there is a linear relationship between temperature and pull out force, tested between the values –20 ºC and 60 ºC and this research has influenced parameters of this series of tests. Temperature fluctuations between the limits of –20 and 60ºC influence nominal bond strength and this influence was not dominated by changes in elastic properties of the material properties of the fibres tested.

Despite the widespread use of fibre reinforced concrete, there is still debate within the industry as to the benefits they offer. Steel and type 2 synthetic fibres are currently used to good effect in many engineering applications however temperature changes the physical characteristics of the fibres and the composite matrix of fibres and concrete. This paper examines the relationship between fibre performance and temperature.

2. MATERIALS

2.1. CONCRETE SPECIFICATION

The concrete used for this research is specified within Eurocode 2 as strength class C28/35 at 28 days of curing. The specifications for both synthetic and steel fibres are detailed in BS EN 14889 Parts 1 and 2 [10].

2.2. FIBRE SPECIFICATION

Synthetic fibre specification is detailed in BS EN 14889-2: 2006 [10] and the steel fibre classification is covered in BS EN14889-1[10]. The adopted steel fibres have a hooked end profile, which provide additional bond strength [11] and the overall fibre dimensions were 50mm x 1mm with a tensile strength of 1050 N/mm^2. Steel fibres were added to the concrete mix at 40kg/m^3. Type 2 synthetic fibres, had nominal dimensions of 40 x 0.95mm and were incorporated into the mix design. Previous research shows that these fibres are generally more effective in supplying an increase in residual strength [11] when compared to similar synthetic fibres used commercially. The fibre type used was a 90% polypropylene and 10% polyethylene mix with known high performance values [12] and is referred within the text as simply “polypropylene”. Synthetic fibres were added to the concrete mix at a dosage of 4kg/m^3.

3. METHODOLOGY

The test methodology was designed to determine how the mechanical properties of plain and fibre reinforced concrete vary with respect to temperature changes, at -20°C and 60°C. An environmental chamber was used to heat the specimens and a walk-in freezer was used for freezing the specimens. The specimens were left in the respective heat and cold appliances for 24 hours prior to testing. To ensure the temperature change was minimised during the test, bubble wrap was used to insulate the test specimens during the test period when the specimens were removed from their storage areas. The samples as tested were surface dry at -20°C and 60°C, in addition the frozen samples were free from any surface ice.

Flexural and bond strength of concrete with the addition of steel and synthetic fibre types was established using test methods BS EN 12390-5: [13] and BS EN 1542: [14] for three point flexural and bond strength. The energy absorption capacities of both steel and synthetic fibre reinforced was established using the area under the load deflection curve

The flexural toughness and the total energy absorption of each beam was to be determined using the load/deflection curves which were established during the testing of flexural strength. Vellore *et al*. [6] states that most standards are comparable and that ACI 544 uses the ratio of the load/deflection curve to determine concrete toughness. The load/deflection curve was first used to determine toughness, then in order to further evaluate the post crack toughness of the beam specimens, the test methodology specified within BS EN 14651:2005+A1:[15] was used. This method requires the use of the load/deflection graphs which were established during the flexural strength tests. Values of flexural strength were determined using equation [1] at varies crack mouth openings. The results measured and calculated using this method are therefore more useful to designers within industry when attempting to control cracking within concrete structures [16].

The points of crack mouth opening displacement (CMOD) which the flexural strength is to determined are as follows: $CMOD_1$ = 0.5mm from the limit of proportionality (LOP), $CMOD_2$ = 1.5mm from (LOP), $CMOD_3$ = 2.5mm from (LOP), $CMOD_4$ = 3.5mm from (LOP).

$$\text{Flexural strength} = \frac{3}{2}\frac{\text{FL}}{\text{bd}^2} \qquad (1)$$

Where:

F = maximum load
L = Span between the roller supports
b = beam width
d = beam depth

4. RESULTS

Results were obtained for a range of tests as compressive strength, flexural strength, pull out force and toughness.

4.1. COMPRESSIVE STRENGTH

The average compressive strength of the concrete was 37N/mm^2 and the characteristic strength using a 5% defective was 35N/mm^2. The test was undertaken at ambient room temperature in accordance with BS EN 12390-3 (2009) at 28 days after batching.

4.2. FLEXURAL STRENGTH

The flexural strength was determined using Equation 1 and the average values of the results are displayed in Table 1. Each beam tested was subject to a central loading mechanism which extended at a speed of 2.2mm/min and the span between the rollers was 300mm.

Table 1 The average flexural strength for each beam classification and temperature.

Concrete Type	Average Flexural Strength (N/mm^2)		
	-20°C	Ambient	60°C
Plain	11.63	5.84	3.78
Polypropylene fibre	11.47	4.58	4.01
Steel fibre	11.74	6.29	3.85

The results show that Type 2 polypropylene fibres reduce the flexural strength of concrete beams at ambient temperature compared to plain concrete beams. This is a characteristic of Type 2 fibres which has been well research by Richardson *et al.* [11].

All beams suffered from a flexural strength reduction when comparing ambient temperature to a temperature of 60°C. The plain beam showed an average 35% reduction, the polypropylene fibre beam showed an average a 12% reduction and the steel fibre beam showed an average a 49% reduction. However, at temperatures of 60°C a lesser decrease in flexural strength can be observed when polypropylene fibres are used and compared to plain concrete, which could suggest that polypropylene fibre concrete can be beneficial in providing improved performance within concrete that experiences elevated temperatures. All beams tested at -20°C displayed a significant increase in flexural strength when compared to the same beam tested at ambient temperatures.

The plain beam showed an average 99% increase in flexural strength, the polypropylene fibre beam showed an average a 150% increase in flexural strength and the steel fibre beam showed an average a 79% increase in flexural strength. Polypropylene fibre concrete displayed the most improved performance at higher and lower temperatures.

The beams which featured steel fibres showed improvements across the entire tested temperature range when compared to plain concrete beams. This observation was expected as steel fibres have been proven to supply increased concrete strength [3]. The flexural strength tests also show that steel fibre concrete supplied a slightly greater strength at temperatures of 60°C when compared to plain concrete. This is backed up by Lau *et al* [3] and, who state that steel fibre reinforced concrete continues to be beneficial to concrete after exposure to high temperatures.

The most notable trend observed from the results of the flexural strength test are that beams stored at temperatures of -20°C had the ability to withstand much larger loads before failure occurred, leading to a significant increase in flexural strength with a subsequent decrease in temperature, for all concrete types. This outcome concurs with Mirzazadeh *et al* (2016) who found an increase in strength of concrete specimens tested at -25°C. A large increase in flexural strength is believed to be due to the formation of ice within the pores of the concrete [1 & 5].

4.3. PULL OUT RESULTS

Table 2 displays the results from the pull out tests for both polypropylene and steel fibres. The results show that as temperature decreases from 60°C to -20°C, there is a 50% increase in force required to pull out or snap the polypropylene fibres. This could be due to the fact that as concrete is cooled; it shrinks around the fibres, causing an increase in bond strength between concrete and polypropylene fibre. The synthetic fibres clearly have an improved performance at lower temperatures.

Table 2 The average pull out force of each fibre type

Type of Fibre	Average Pull Out Force (N)	
	-20°C	60°C
Polypropylene	196.6	131.0
Steel	768.9	841.4

As temperature decreases, the force required to pull out the steel fibres saw a decrease by 8.6%. This value is negligible within the interpretation of these results. The reason for such a small variation in pull out force within steel fibre concrete may be due to the fact that there is a natural affinity between steel and concrete, in that their coefficient of thermal expansion is near identical [11]. This could be the reason that bond strength is retained as temperature changes, as both materials will deform similarly due to change in temperature. There is also aa statistical degree of scatter within any results and this could be another possibility of this observation.

4.4. TOUGHNESS

The energy absorption capacities of both steel and synthetic fibre reinforced was established using the area under the load deflection curve and the results are displayed in Figure 1. The values shown are indices without any units and the calculations are based on ASTM 1018 [17].

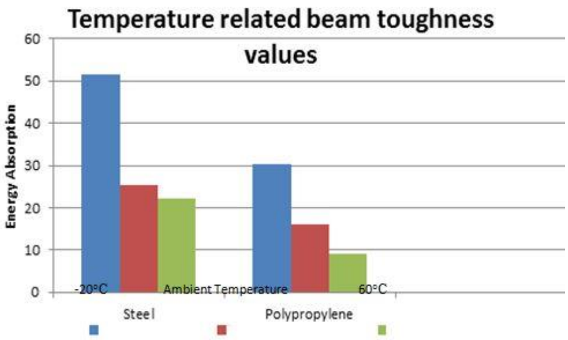

Figure 1 The average total energy absorption of each type of beam after three point bending (the area under the load/deflection curve).

From examination of Figure 1 is can be taken that steel fibres outperform synthetic fibres at all temperatures. It is also apparent that a reduction in temperature equates to an improvement in performance irrespective of the fibre type. At the relative fibre dosage and fibre type, this result is predictable as the cut off point for the test is 10.5 times the initial displacement up to the point of rupture. This does not take account of the tendency for polypropylene fibre concrete to transfer loads at very high deflections.

5. CONCLUSION

This research was carried out in order to determine the effects that temperature has on various types of fibre reinforced concrete. The study has illustrated that temperature does affect the properties of fibre reinforced concrete. Both steel and synthetic fibre reinforcement were tested extensively in order to draw comparisons between the various fibre reinforced concrete types as well as plain concrete. The following outcomes were established:

Regardless of the reinforcement type, concrete which is stored at -20°C for 24 hours prior to being tested has the ability to withstand a significantly higher load before failure occurs when compared to concrete at ambient temperature. This leads to a much greater flexural strength exhibited by concrete at temperatures below freezing point of water. In contrast, concrete stored for the same length of time in conditions of 60°C, can be observed to fail at lower loads and the overall flexural strength will deteriorate due to the elevated temperature, when compared to ambient temperatures.

The average force required to snap or pull out synthetic fibres increases with a decrease in temperature, possibly as a result of a stronger frictional grip generated as concrete shrinks around the fibre, as temperature is reduced. By reducing the specimen temperature, the bond strength is increased within synthetic fibre reinforced concrete at temperatures of -20°C.

Having used various methods to analyse the toughness of each concrete type, the conclusion that decreasing temperature, increases the toughness of fibre reinforced concrete has to be drawn. This outcome concurs with past research which states the reason for increase in performance of concrete at temperatures below freezing is due to the formation of ice within concrete pores, which decreases porosity and hence improves stiffness and strength.

The deterioration in mechanical properties of fibre reinforced concrete, which this research observed at temperatures of 60°C, is a potential cause for concern as world temperatures continue to rise. Recommendations for future research would be to investigate the performance of structures which feature fibre reinforced concrete elements at 60°C and beyond in order to determine whether the loss in performance may harm the fibre concrete structures within the built environment.

REFERENCES

[1] DeRosa, D. (2012). “Thermal Effects on Monitoring and Performance of Reinforced Concrete Structures”. Published MSc Thesis, Ontario, Canada.
[2] Hall C, (1981), Polymer Materials, Macmillan Press, London, pp 177 –145.
[3] Lau, A. and M. Anson. "Effect Of High Temperatures On High Performance Steel Fibre Reinforced
[4] Concrete". Cement and Concrete Research 36.9 (2006): 1698-1707.
[5] Mirzazadeh, M., Noël, M. and Green, M. (2016). Effects of low temperature on the static behaviour
[6] of reinforced concrete beams with temperature differentials. Construction and Building Materials,
[7] 112, pp.191-201.
[8] [5] Neville, A.M. (2006). Properties of concrete, 5th edition. Pearson Education Limited, Malaysia.
[9] pp. 53-61.
[10] Vellore S, Golpalaratham V.S.and Gettu R, (1995), “On the Characteristics of flexural toughness in
[11] fibre reinforced concrete”, Cement and Concrete Composites, Vol 17, Issue 3, pp 239-254
[12] Richardson A, Coventry K, Lamb T, Mackenzie D, (2016), “The addition of synthetic fibres to
[13] concrete to improve impact/ballistic toughness”, Construction and Building Materials, Vol 121,
[14] September, pp 612 - 621
[15] Richardson A E, Coventry KA, (2015), “Dovetailed and hybrid synthetic fibre concrete – Impact,
[16] toughness and strength performance, Construction and Building Materials, January, pp 439 – 449.
[17] Bakis C E, Uppuluri V S, Nanni A & Boothby T E, 1998, “Analysis of Bonding Mechanisms of Smooth and Lugged Fibre Reinforced Plastic Rods Embedded in Concrete”, Composites Science and Technology,
[18] Vol 58, Elsevier Science Ltd, GB, pp 1307 1319
[19] BS EN 14889 Parts 1 and 2.Fibres for concrete (2006), BSI, London
[20] Richardson, A., Coventry, K. and Landless, S. (2010). Synthetic and steel fibres in concrete with
[21] regard to equal toughness. Structural Survey, 28(5), pp.355-369.
[22] Richardson, A. (2005). Bond characteristics of structural polypropylene fibres in concrete with
[23] regard to post-crack strength and durable design. Structural Survey, 23(3), pp.210-230.
[24] British Standards Institute, BS EN 12390 - 3. (2009), Testing hardened concrete. Compressive
[25] strength of test specimens, BSI, London
[26] British Standards Institute, BS EN 1542: (1999), Products and systems for the protection and repair
[27] of concrete structures. Test methods. Measurement of bond strength by pull-off, BSI, London
[28] British Standards Institute, BS EN 14651:2005+A1 (2007), Test method for metallic fibre concrete.
[29] Measuring the flexural tensile strength (limit of proportionality (LOP), residual, BSI, London
[30] Richardson, A. and Jackson, P. (2011). Equating steel and synthetic fibre concrete post crack
[31] performance. INTERNATIONAL CONFERENCE ON CURRENT TRENDS IN TECHNOLOGY, ‘NUiCONE – 2011’.
[32] American Society for Testing and Materials, ASTM C 1018. (1997), Standard test method for flexural toughness and first crack strength of fibre reinforced concrete, ASTM

EXPERIMENTAL CHARACTERIZATION OF THE FRACTURE BEHAVIOR OF UHPFRC

Götz Hüsken[1], Stephan Pirskawetz[1], Dietmar Meinel[1]

[1] Federal Institute for Materials Research and Testing (BAM), Unter den Eichen 87, 12205 Berlin, Germany, email: goetz.huesken@bam.de, stephan.pirskawetz@bam.de, dietmar.meinel@bam.de

SUMMARY: Ultra-high performance fiber-reinforced concretes (UHPFRCs) are most suitable for applications with extreme mechanical loads. These extreme conditions require ductile behavior under tensile loading, which is obtained solely by the working mechanism of steel fibers. Profound knowledge on the working mechanism of the steel fibers is necessary to optimize this material. Usually, this knowledge is obtained by means of classical destructive measuring techniques. Adopting measuring techniques from non-destructive material testing helps to analyze and to identify the different stages of the fracture mechanism of UHPFRC in detail. The application of different non-destructive measuring techniques is shown exemplary on tensile tests conducted on an UHPFRC mix and its applicability for analyzing the fracture behavior of such concretes is discussed. The main focus is on the characterization of the relevant failure modes under tensile loading by the different measuring techniques and the comparison with classical measuring techniques (e.g. extensometer). The tensile tests have been analyzed by optical deformation measurements using digital image correlation (DIC), acoustic emission analysis (AE), and 3D computed tomography (CT).

EKSPERIMENTALNO ODREĐIVANJE ZNAČAJKI PRI LOMU BETONA ULTRAVISOKIH SVOJSTAVA ARMIRANIH VLAKNIMA

SAŽETAK: Betoni ultravisokih svojstava armirani vlaknima najprikladniji su za primjene za izuzetna mehanička opterećenja. Ti izuzetni uvjeti zahtijevaju duktilno ponašanje pri vlačnom opterećenju koje se postiže isključivo radnim mehanizmom čeličnih vlakana. Za optimiranje tog materijala nužno je produbljeno znanje radnog mehanizma čeličnih vlakana. Obično se ono utvrđuje klasičnim razornim mjernim postupcima. Usvajanje mjernih postupaka iz područja nerazornih ispitivanja materijala pomaže analiziranju i detaljnom prepoznavanju različitih faza mehanizma loma takvih betona. Na primjeru vlačnih ispitivanja provedenih na takvim mješavinama betona pokazana je primjena različitih nerazornih postupaka, a raspravljena je i njihova primjena u analizi ponašanja pri lomu takvih betona. Glavna pozornost usmjerena je na određivanje značajki odgovarajućih oblika loma pri vlačnom opterećenju pomoću različitih mjernih postupaka i na usporedbu s klasičnim mjernim postupcima (npr. pomoću ekstenziometra). Vlačna ispitivanja analizirana su optičkim mjerenjem deformiranja primjenom digitalne slikovne korelacije (engl. digital image correlation), analizom akustičke emisije i 3D kompjutoriziranom tomografijom.

1. INTRODUCTION

The utilization of ultra-high performance fiber-reinforced concretes (UHPFRCs) is an alternative to reinforced concrete for practical applications with extreme mechanical loads. Here, the more advantageous crack and post-cracking behavior is of vital importance [1]. The brittle fracture behavior of the unreinforced high-strength matrix is improved by adding suitable fibers and results in an increase in strength and the potential for energy dissipation [2]. Likewise, a quasi-ductility of the material is obtained by the addition of steel fibers. Besides steel fibers, synthetic fibers (e.g. polyethylene or polyvinyl alcohol) can be used [3].

The major benefit of the fibers (both synthetic and steel fibers) results from their crack bridging mechanism in the concrete matrix. For doing so, the fibers need sufficient tensile strength and stiffness in order to restrain the formation of cracks and the opening of micro cracks with increasing loading [1]. Likewise, steel fibers can connect the crack faces tightly and will take over the tensile stresses in the cracked concrete. The crack bridging mechanism of the steel fibers depends to a large extent on the bond length and bond strength between steel fibers and surrounding matrix. Under extreme loadings, the large tensile forces that have to be carried by the steel fibers cannot be transmitted by the bonding zone between steel fibers and matrix and, therefore, the steel fibers are pulled out of the matrix. This process is also controlling the energy dissipation at large plastic deformations. In addition to the pull-out of the fibers, the failure of the matrix as well as the failure of the steel fibers due to tension or shear characterizes the three main failure mechanism of fiber reinforced concretes. However, steel fiber reinforced concretes do not show failure of the fibers at normal temperature. This is caused by the high tensile strength of the steel fibers compared to the low matrix strength and the high elasticity of the fibers [1].

The different damage mechanism of steel fiber reinforced concretes illustrate that the failure process is characterized by diverse parameters that have to be considered when analyzing the fracture behavior. Classical test methods that are used for destructive material testing are restricted to the measurement of the applied force and the related overall deformation measured by extensometers or strain gauges. Information on the strain distribution at the sample surface or the local and time depending formation of matrix cracks and fiber pull-out cannot be obtained by these classical destructive test methods. For this purpose, methods adopted from non-destructive materials testing are suitable.

The analysis of the crack formation and propagation using methods adopted from non-destructive materials testing is discussed exemplary for tensile test of UHPFRC. In this study, optical deformation measurement by means of digital image correlation (DIC) for determining the strain distribution at the sample surface, acoustic emission (AE) for the local and time depending characterization of the crack forming processes and 3D-computed tomography (CT) for analyzing the fiber distribution (fiber orientation, fiber agglomerates and crossing of fiber/fiber bundles) as well as spatial orientation of the resulting cracks are applied.

2. TEST PROGRAMME

2.1. SPECIMENS

The tensile tests have been performed on dumbbell-shaped tension bars. The dimensions of the specimen depicted in Figure 1 (left) is based on the geometry suggested by Mechtcherine and Schulze [3]. Mix design as well as mechanical properties of the UHPFRC mix used for the tensile tests are listed in Table 1. All specimens were stripped from the mold after 24 hours and stored underwater until testing at an age of 28 days. Detailed information on the mix design can be found in [5].

Table 1 Mix design of the concrete mixture used and mechanical properties [6]

Material	Amount [kg/m³]	Parameter	Value
CEM I 42,5 R-SR/LA	625.0	Flexural strength (DIN EN 196-1) [N/mm²]	17,1 ± 2,5
CEM I 52,5 R-SR/LA	125.0	Compr. strength (DIN EN 196-1) [N/mm²]	165,2 ± 5,3
Microsilica	37.5	Compr. strength (Cube 100 mm) [N/mm²]	131,1 ± 2,3
Metakaolin	75.0	Young's modulus [N/mm²]	50290 ± 1175
Basalt (0.125/2.0)	916.7	σ_{max} tension bar [N/mm²]	6,3 ± 0,5
Basalt (2.0/5.0)	550.0	σ_{crack} (first crack) [N/mm²]	6,0 ± 1,0
Water	180.0		
Steel fibers (13/0.2)	76.9		
Superplasticizer (PCE)	20.25		

2.2. TEST SETUP

The tensile tests have been conducted displacement-controlled on a servo-hydraulic universal testing machine with a displacement rate of 0.15 mm/min and total displacement of 1.5 mm. The tension bars were glued into the rigid loading device of the test machine in order to ensure an equal stress distribution over the cross section of the specimen and parallel opening of the cracks in the post-critical region (see Figure 1 right). The glue was a 2-component polyurethane resin. The instrumentation comprises 1 extensometer (measuring length 100 mm); 4 AE-sensors; 1 flat surface with stochastic pattern for the optical deformation measurement and 1 loading cell for recording the applied tensile force. The extensometer used for measuring the overall deformation was fixed at the rear side of the tension bar in the region with constant cross section. The 4 AE-sensors were coupled closed to the upper and lower supports using viscoelastic adhesive pads BostikPrestik® (see Figure 1 right). A stochastic pattern on the front side of the specimen was used for the optical deformation measurement. The force and displacement data of the test machine were recorded continuously with a rate of 50 Hz. The photogrammetric system recorded a picture of the front side of the specimen every 3 seconds triggered by the testing machine. The optical deformation measurement was performed using an ARAMIS 5M system supplied by GOM – Gesellschaft für optische Messtechnik mbH.

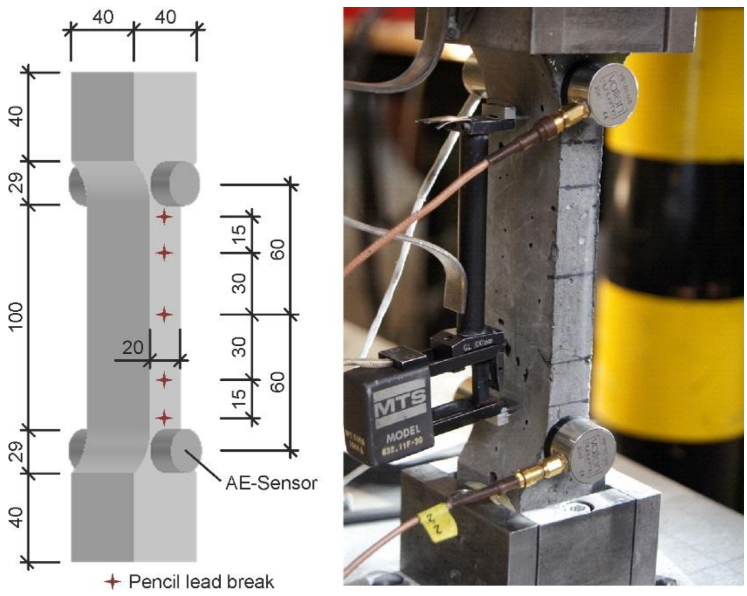

Figure 1 Schematic illustration of the tension bar [6] (left). In the test machine fixed tension bar with extensometer on the rear side and AE-sensors (right)

2.3. INSTRUMENTATION

2.3.1. OPTICAL DEFORMATION MEASUREMENT

Optical deformation measurement is a photogrammetric technique for contact-free measurements of surface deformations. Displacement fields and resulting strains are determined by digital image correlation (DIC) from a series of pictures of a deformed sample under load. The analysis of the pictures using grayscale correlation requires reference points or stochastic pattern rich in contrast at the surface of the specimen. The stochastic pattern was realized by a chalk coating of the specimen's surface and the subsequent placing of a stochastic dot pattern using graphite spray.

2.3.2. ACOUSTIC EMISSION

Acoustic emission testing is a passive non-destructive testing method for detecting evolving or propagating (active) cracks. Formation and propagation of cracks causes small, rapid structural changes (displacements) at the crack tip and crack face. These disturbances propagate within the material as elastic waves –so called ultrasonic waves– that can be detected by piezo-electric sensors. In addition to the precise arrival time of the acoustic events at the sensors, further signal parameters such as amplitude, energy and duration can be determined. This allows for locating the source of the acoustic event and conclusion on the fracture process can be drawn [7].

2.3.3. 3D-COMPUTED TOMOGRAPHY

The formed crack and the distribution of the steel fibers can be analyzed non-destructively after testing the specimen by means of 3D X-ray computed tomography (CT). Therefore, the tension bar is placed on a rotating table, which is located between X-Ray tube and detector, and continuously radiographed while rotating by 360 degrees. The numerous radiographic pictures taken from different angles are processed by a computer aided image reconstruction in order to obtain a volume based data set. A 3D-µCT installation developed in cooperation with BAM was used. The device uses a 225 kV micro focus X-ray tube with a 2k x 2k flat detector. The maximum resolution of the setup used is 24 µm (side length of a voxel). Every voxel of the 3D data set represents the X-ray absorption by a corresponding gray value. Steel fibers are segmented from the reconstructed volume picture by defining a corresponding threshold value. Furthermore, the spatial orientation of the steel fibers can be determined by using special software tools (see Figure 5).

3. RESULTS

3.1. OPTICAL DEFORMATION MEASUREMENT

The data (force, extensometer displacement) recorded by the test machine are depicted in

Figure 2 as stress-strain curve for the region of the specimen with constant cross section. The run of the stress-strain curve corresponds to the typical stages of uniaxial tensile tests as described in [1] and [8]. Stress and strain are increasing proportional in the linear-elastic region. The slope of the stress-strain curve in the linear-elastic region gives the Young's modulus under tensile loading, which amounts to 56.200 MPa in this case, and which is slightly larger than the Young's modulus determined on cylinders under compression (see Table 1).

Figure 3a shows the strain distribution determined by optical deformation measurement. A direct comparison with the extensometer data shows a good agreement. The absolute deviation of the strains is less than 0,08 ‰. Strains are equally distributed along the surface (see step 17 in Figure 3a). Furthermore, the displacement of the single facets is increasing equally in y-direction (see step 17 in Figure 3b) and is corresponding to the Young's modulus. Starting with step 18, 2 cracks are formed that are located oppositely, whereas the left, above the middle located crack, is dominating at later steps. This main crack is formed about 20 mm above the middle and becomes clearly visible in **Error! Reference source not found.** at step 18. At this stage, a peak in the strain distribution located at the left side is indicating the later crack before the ultimate load is obtained. Besides, no relevant deformations are verifiable by the optical deformation measurement at this loading rate in the middle section of the specimen (see step 18 in Figure 3b).

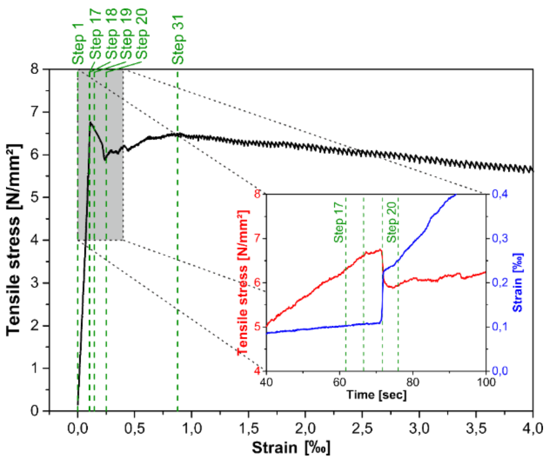

Figure 2 Stress-strain curve of the tensile test.

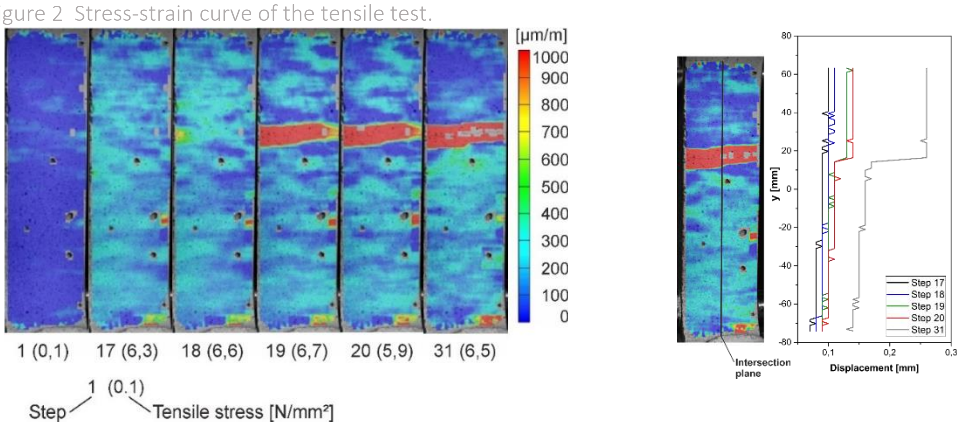

a)

b)

Figure 3 Results of the optical deformation measurement: a) strain distribution of the specimen under tensile loading; b) Displacement in y-direction in the middle section.

The formation of the main crack involves an instantaneous decrease of the tensile stress as well as a clear increase of the strain determined by the extensometer (see detail in Figure 2). Picture 19, taken close to the formation of the main crack, shows that the front side of the specimen cracked completely. At this stage, tensile stresses are carried only by the steel fibers with their crack bridging mechanism. It becomes clear from the analysis of the sample's deformation that the strain increase is concentrated to the region close to the formed crack (see step 19 to 31 in Figure 3b). The main crack opens with increasing load and further cracks are verifiable by the results of the optical deformation measurement. After the main crack is formed in the sample and the related instantaneous decrease of the tensile stress, a slight strain hardening effect can be identified until the loading level of step 31 is reached. Further loading results in softening of the specimen and the tensile stresses decrease continuously (Figure 2). This ductile behavior and the observed softening is caused by the gradual bond failure and the related loss of the frictional bond between steel fibers and matrix. According to [1], this behavior can be observed in materials with a fiber content that is below the critical fiber content. Therefore, the load carrying behavior of the specimen corresponds to the softening behavior with slight increase in the mechanical properties (level 1) as described in [8].

3.2. ACOUSTIC EMISSION

Pencil-lead breaks have been performed at the position marked by the crosses in Figure 1 in order to proof the function of the sensors and to determine velocity of sound of the specimen. A velocity of sound of about 4 200 m/s was determined by adjusting the results of localized artificial acoustic events generated according to ASTM E976 [9] with the known position of the acoustic source. The average of the localized pencil-lead breaks is marked by yellow dots in Figure 4.

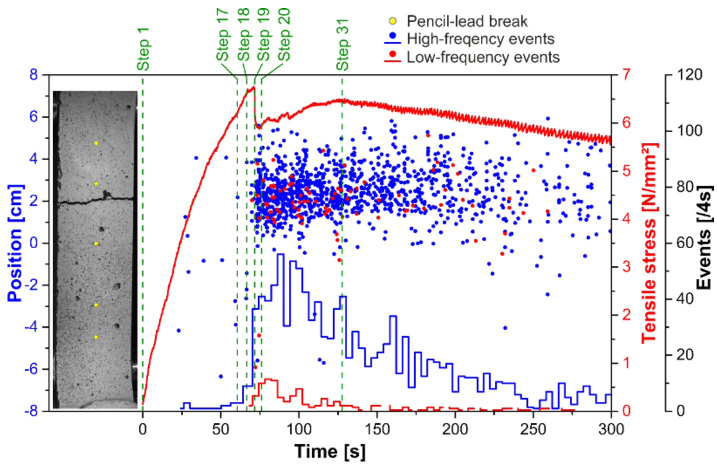

Figure 4 Results of the acoustic emission analysis.

The time period until the maximum tensile stress is obtained in the specimen is characterized by only view localized acoustic events. These acoustic events with average frequencies of about 120 kHz can be attributed at this loading level only to the formation of micro cracks in the brittle matrix. The failure of the specimen is indicated by an accumulation of acoustic events just before the ultimate load is obtained. The activity of the acoustic events increases with increasing load and decreases only slightly after the formation of the main crack. Most of the events are high-frequency events, which is an indication for further cracking of the matrix. However, also acoustic events with lower average frequencies between 30 and 70 kHz have been detected after the main crack was formed. These low-frequency events can be attributed to the pull-out of single fibers from the matrix. This assumption has to be confirmed by pull-out tests performed on single steel fibers. The localized acoustic events scatter around the macroscopically visible crack. The relatively large scatter cannot be attributed only to the formation of micro cracks along the fiber length (± 13 mm). Furthermore, the accuracy of the localization of the acoustic events is influenced by the velocity of sound and damping that both changes with increasing crack width.

3.3. 3D-COMPUTED TOMOGRAPHY

The reconstructed volume picture shows that most of the steel fibers are aligned in longitudinal direction. The orientation of the steel fibers is influenced by the casting process of the tension bars, as the molds have been filled along the narrow long side of the mold (W = 20 mm). Considering the load, which is also acting in longitudinal direction, it can be expected that the steel fibers are aligned beneficially in the loading direction. Due to the high absorption difference between UHPRFC and air, pores in the specimen can be detected easily by 3D X-ray computed tomography. Similar holds also for cracks formed due to tensile loading and the voids formed at the end of the steel fibers in consequence of the fiber pull-out (see Figure 5 right). The length of these voids can be determined quantitatively from the CT data. Furthermore, the bond length of the crack bridging steel fibers can be determined.

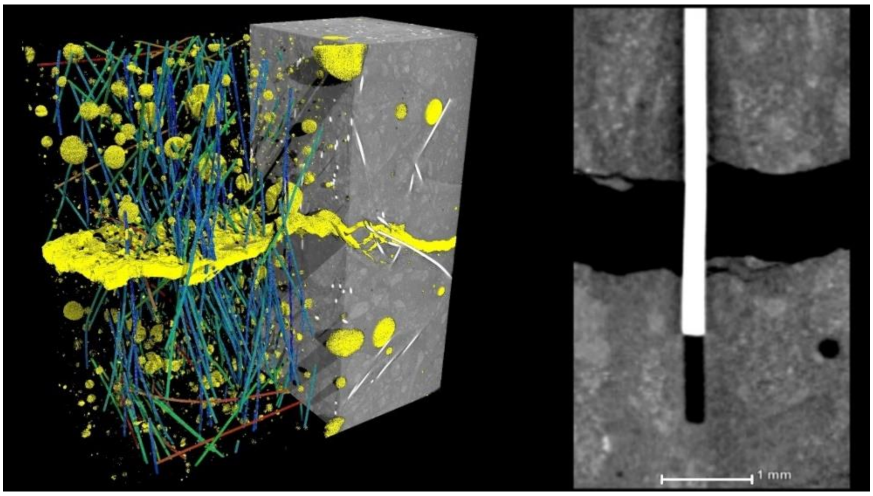

Figure 5 Color-coded illustration of the fiber distribution including segmented fracture crack and pores (left). Detail of a vertical cross section with fiber pull-out (right).

4. CONCLUSIONS

The fracture behavior of ultra-high performance fiber-reinforced concrete (UHPFRC) under tensile loading was investigated adopting measuring techniques from non-destructive material testing. The strain distribution on the sample's surface was analyzed by means of optical deformation measurements using digital image correlation (DIC). Useful conclusions regarding the load bearing behavior before and after the formation of the first cracks can be drawn from the DIC results. Analyzing the events of the acoustic emissions (AE) allows for an additional characterization of the crack formation. Combining both measuring techniques, DIC and AE, offers further insights into the interaction of steel fibers and concrete matrix and their influence on the crack formation, which can be used for optimizing these concrete mixtures. After testing the tension bars, the damage of the cracked samples was examined by 3D X-ray computed tomography (CT). The results of CT measurements facilitate quantitative assessment of the fiber orientation, fiber pull-out and bond length of the crack bridging fibers. Therefore, the CT measurements form the basis for analyzing the structure of the concrete matrix and the fibers embedded therein, before and after tensile testing. The ex-post results of the CT measurements have been verified by the in-situ results of the DIC and AE measurements.

REFERENCES

[1] Bergemeister, K.; Fingerloos, F.; Wörner, J.-D.: Beton-Kalender 2011, Ernst & Sohn 2011, ISBN: 978-3433029541, Berlin, 2011

[2] Banthia, N.; Nandakumar, N.: Crack growth resistance of hybrid fiber reinforced cement composites, Cement & Concrete Composites, Vol. 25 (2003), pp. 3-9, http://dx.doi.org/10.1016/S0958-9465(01)00043-9

[3] Curosu, I.; Mechtcherine, V.; Millon, O.: Effect of fiber properties and matrix composition on the tensile behavior of strain-hardening cement-based composites (SHCCs) subject to impact loading, Cement and Concrete Research, Vol. 82 (2016), pp. 23-35, http://dx.doi.org/10.1016/j.cemconres.2015.12.008

[4] Mechtcherine, V.; Schulze, J.: Testing the behaviour of strain hardening cementitious composites in tension, Int. RILEM Workshop on HPFRCC in Structural Applications, Fischer, G.; Li, V. C. (Eds.), pp. 37-46, Honolulu, May 2005, RILEM Publications S.A.R.L., Bagneux, France, (2005)

[5] Babski, V.; Hüsken, G.; Pirskawetz, S.; Ehlers, N.; Kühne, H.-C.; Brouwers, H.J.H.: Characterisation of ultra-high performance fibre reinforced concrete (UHPFC) under tensile loading by acoustic emission and optical deformation analysis, Proceedings of the 4th International Symposium on Ultra-High Performance Concrete and High Performance Construction Materials, Fehling, E.; Middendorf, B.; Thiemcke, J. (Eds.), pp. 1-9, ISBN: 978-3-7376-0095-8, Kassel, Germany, March 2016, Kassel university press GmbH, Kassel, (2016)

[6] Ehlers, N.: Experimentelle Untersuchung des Bruchverhaltens von faserverstärkten ultrahochfesten Betonen unter quasistatischer Belastung mittels innovativer Prüftechnik, Master Thesis, Hochschule für Technik und Wirtschaft Berlin, Berlin, (2015)

[7] Grosse, C. U.; Ohtsu, M.: Acoustic Emission Testing, Springer, ISBN: 978-3-540-69895-1, Berlin, (2008)

[8] Wille, K.; El-Tawil, S.; Naaman, A. E.: Properties of strain hardening ultra high performance fiber reinforced concrete (UHP-FRC) under direct tensile loading, Cement and Concrete Composites, Vol. 48 (2014), pp. 53-66, http://dx.doi.org/10.1016/j.cemconcomp.2013.12.015
[9] ASTM E976: Standard Guide for Determining the Reproducibility of Acoustic Emission Sensor Response, ASTM International, West Conshohocken, PA, 2010

STRAIN RATE EFFECT ON THE MECHANICAL PROPERTIES OF FIBER REINFORCED CEMENT COMPOSITES

Min Jae Son[1], Gyu Yong Kim[1], Gyeongcheol Choe[1], Hongseop Kim[1], Sangkyu Lee[1]

[1] Chungnam National University, Department of Architectural Engineering, 99 Daehak-ro, Yuseong-gu, Daejeon 305-764, Korea, email: minjae931226@naver.com, gyuyongkim@cnu.ac.kr, oliver-kahn12@nate.com, lsg2357@naver.com, gyuyongkim@cnu.ac.kr

SUMMARY: This study evaluated the strain rate effect on the mechanical properties of high performance fiber reinforced cement composites (HPFRCC) reinforced with hooked-end steel fiber and polyamide fiber. The compressive and tensile properties of HPFRCC were evaluated. As a result of compressive properties, the compressive strength and strain at peak stress were improved as the strain rate increased. And the effect of fiber types on the compressive properties at static and high strain rates was not significantly different. However, strain rate effect on the tensile properties was clearly different according to the fiber types. HPFRCC reinforced with hooked-end steel fiber indicated high tensile strength as the strain rate increased. On the other hand, polyamide fiber reinforced HPFRCC showed greater strain capacity than hooked-end steel fiber. Therefore, it is considered that the interfacial bonding between fiber and matrix affects the tensile properties. Evaluation results of the strain rate effect on the mechanical properties of HPFRCC indicated that tensile properties were highly sensitive to strain rate according to the fiber types.

UTJECAJ BRZINE DEFORMACIJE NA MEHANIČKA SVOJSTVA CEMENTNIH KOMPOZITA ARMIRANIH VLAKNIMA

SAŽETAK: U studiji je vrednovan utjecaj brzine deformacije na mehanička svojstva cementnih kompozita armiranih vlaknima visokih svojstava i to čeličnim vlaknima sa zakrivljenim krajevima i poliamidnim vlaknima. Istražena su tlačna i vlačna svojstva. Utvrđeno je da se s povećanjem brzine naprezanja povećala tlačna čvrstoća i deformacija pri vršnom naprezanju. Vrsta vlakana nije imala znatnog učinka na tlačna svojstva pri statičkim deformacijama i pri velikoj brzini deformacije. Međutim, brzina deformacije imala je znatan učinak na vlačna svojstva ovisno o tipovima vlakana. Kompozit amiran čeličnim vlaknima sa zakrivljenim krajevima imao je veliku vlačnu čvrstoću kako je brzina deformacije rasla. S druge strane, kompozit armiran poliamidnim vlaknima imao je veću sposobnost deformacije od kompozita s čeličnim vlaknima sa zakrivljenim krajevima. Stoga se smatra da na vlačna svojstva utječe prianjanje na sučeljku između vlakana i cementne matrice. Rezultati pokazuju da su vlačna svojstva vrlo osjetljiva na brzinu deformacije ovisno o tipu vlakana.

1. INTRODUCTION

Generally, concrete is a material with excellent impact resistance. However, it exhibits vulnerable performance against extreme loads such as earthquake, explosion and impact. Therefore it has a high possibility of causing extreme damage of human life and property.

High performance fiber reinforced cement composites (HPFRCC) are attention as materials that can effectively resist from extreme loads, because reinforced fiber in matrix exhibit a cross-linking action at the cracks. The cross-linking action of fiber affects the stress distribution and crack expansion inhibiting. Therefore, HPFRCC have high tensile resistance and excellent energy absorption capacity based on strain-hardening and multiple cracks. However, HPFRCC should be aware of the mechanical properties by strain rate, because their performance depending on the type of matrix, reinforcing fiber and the fiber volume fraction. Thus, many researchers have been conducting experiments to evaluate the mechanical properties of HPFRCCs by the type of reinforcing fiber.

And recently, some researcher has reported that the behavior of HPFRCC for high strain rates is different from static rate condition. So, to analysis and design of structures for extreme loads, using the data that evaluated under quasi-static rate conditions is difficult. Therefore, the evaluation and understanding of the strain rate effect on the mechanical properties of HPFRCCs under dynamic rate conditions are very important and necessary.

It is the aim of this study to evaluate the strain rate effect on the mechanical properties of HPFRCCs according to the fiber type and fiber volume fraction. The compressive and tensile properties were evaluated according to the strain rate.

2. EXPERIMENTAL PROGRAM

2.1. MATERIALS AND SPECIMEN PREPARATION

Table 1 shows the details of specimen. Fiber reinforced cement composite specimens are HSFRCC1.0, HSFRCC2.0, PAFRCC1.0, PAFRCC2.0, using the hooked steel fiber and polyamide fiber. Fiber volume fractions were 1.0 and 2.0vol%.

The mechanical properties of the fiber used in this study are shown in Table 2. Figure 1 shows the fiber shape. The hooked steel fiber was a length of 30mm, a diameter of 0.5mm, an aspect ratio of 60, a tensile strength of 1140MPa, and a density of 7.85g/cm^3. The polyamide fiber was a length of 30mm, a diameter of 0.5mm, an aspect ratio of 60, a tensile strength of 597MPa, and a density of 1.14g/cm^3. Table 3 shows the mixing proportions of the cement composites, and the W/B was set to 0.4. Table 4 shows the mechanical properties of the materials that were used.

Table 1 Detail of specimens

ID.[1)]	Fiber type	Volume fraction (V_f.%)
HSFRCC1.0	Hooked steel fiber	1.0
HSFRCC2.0		2.0
PAFRCC1.0	Polyamide fiber	1.0
PAFRCC2.0		2.0

1) HSFRCC : Hooked steel fiber reinforced cement composite
PAFRCC : Polyamide fiber reinforced cement composite

Table 2 Mechanical properties of fibers

Type	Length (mm)	Diameter (mm)	Aspect ratio (L/D)	Density (g/cm^3)	Tensile Strength (MPa)
Hooked steel fiber	30	0.5	60	7.85	1140
Polyamide fiber	30	0.5		1.14	597

Table 3 Mix proportion of cement composites

W/B	S/a (%)	Unit weight(kg/m^3)				Fiber		
		Cement	Fly-ash	Water	Silica sand	Type	V_f.%	Kg
0.4	100	850	150	400	350	HSF	1.0	78.5
							2.0	156.0
						PA	1.0	11.4
							2.0	22.8

Table 4 Mechanical properties of matrix materials

Materials	Mechanical properties
Cement	Ordinary portland cement, Density : 3.15g/cm^3, Fineness : 3200cm^2/g
Fly-ash	Density : 2.20g/cm^3, Fineness : 3000cm^2/g
Silica sand (Type 7)	Density : 2.64g/cm^3, Absorptance : 0.38%
Super plasticizer	Polycarboxylic acid type

2.2. TEST SET-UP AND METHOD

The cylinder specimen of Ø100×200mm size was prepared for static compressive test. And the geometry of tensile specimen and test set-up for static tests are shown in Figure 2. Two layers of steel wire mesh were reinforced at both ends of the specimen for tensile tests to avoid failure outside of the gauge length. The cross section of tensile specimen was 25mm by 50mm, and the gauge length was maintained as 100mm.

Figure 3(a) shows the quasi-static compressive and tensile test equipment. In the case of the compressive test, the compressive stress was measured using a load cell attached to the load plate. And, compressive strain was measured by the strain gauge (PL-60) attached to the specimen. In order to tensile test, it was manufactured in a tensile jig that can give a tensile load to the specimen. The tensile stress was measured using a load cell attached to the top of the tensile jig. And, tensile strain was measured by LVDT installed the specimen. Figure 3(b) shows the middle~high strain rate compressive and tensile test equipment. The compressive stress is measured by a load cell installed on the test stand and tensile test is performed using the tensile jig.

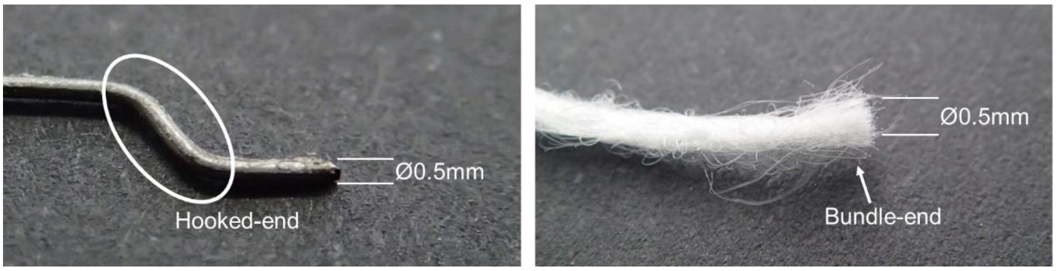

Figure 1 End shape of fibers: (a) Hooked steel fiber, (b) Polyamide fiber

In this study, the strain rate is determined by the slope of the time-strain curve. And dynamic increase factor (DIF) is the ratio between dynamic and static properties for above parameters. DIF obtained by experiment were compared with the following calculated values of the proposed formula of CEB-FIP model code and ACI-349.

3. RESULTS AND DISCUSSION

3.1. STRESS-STRAIN CURVE BY STRAIN RATE

Figure 4 shows the compressive stress-strain curve of HPFRCC under the strain rate of 10^{-5}, 10^{1} and 10^{0}/s. Compressive strength and strain at the peak stress were increased with increase the strain rate. The compressive stress-strain curve of the strain rate 10^{-5}/s and 10^{-1}/s were substantially similar. But, compressive strength and strain at the peak stress of strain rate 10^{-1}/s were increased compared with that of 10^{-5}/s. On the other hand, under the strain rate 10^{0}/s, the initial compressive stress-strain curve was rapidly increased, and the compressive strength and strain at the peak stress was improved.

Figure 5 shows the tensile stress-strain curve of HPFRCC by strain rate. Under static loading condition (strain rate 10^{-6}/s), the tensile strength was improved with the increase the fiber volume fraction. In the fiber volume fraction of 2.0%, the tensile strength was significantly increased, and strain hardening behavior, stress was gradually increased with the increase the strain, was observed.

Tensile strength was increased with increasing strain rate, regardless of fiber type and fiber volume fraction. In the case of the fiber volume fraction 1.0%, strain-hardening was not observed under static loading condition. However, strain-hardening was clearly occurred with increasing strain rate. But, under the strain rate 10^{1}/s, the decrease of stress was significantly occurred after the peak stress. In the fiber volume fraction of 2.0%, strain-hardening was observed under static loading condition and strain-hardening was clearly occurred with increasing strain rate. However, under the strain rate 10^{1}/s, stress was rapidly decreased after the peak stress.

In static loading condition, HSFRCC was generated a single fracture, and PAFRCC1.0 was observed two~three cracks. PAFRCC2.0 was generated the multiple cracks. In addition, the number of cracks was increased with increasing the strain rate, because fiber was not pulled out from the matrix and other cracks was derived by the increase of bonding strength of fiber and the matrix. On the other hand, the tensile strength of PAFRCC was small compared with the tensile strength of HSFRCC. However, the number of multiple-crack was most numerous. This is explained that PAFRCC is greater the cross-linking of fiber and dispersion of stress, because the number of fiber is numerous.

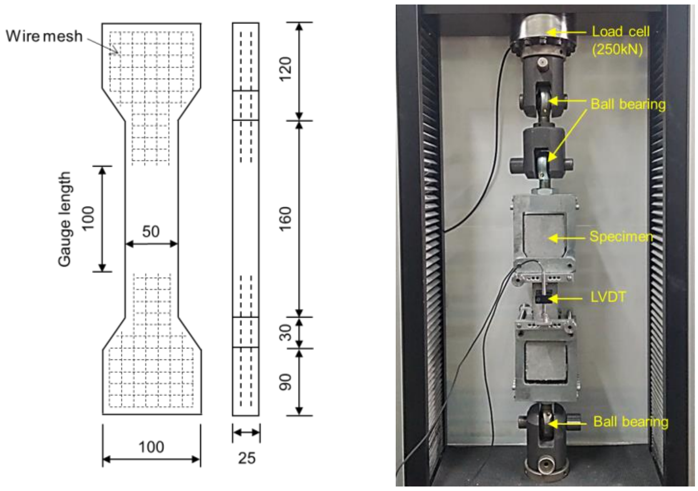

(a) Tensile specimen (Unit : mm) (b) Static tensile test

Figure 2 Geometry of tensile specimen and test set up for static test

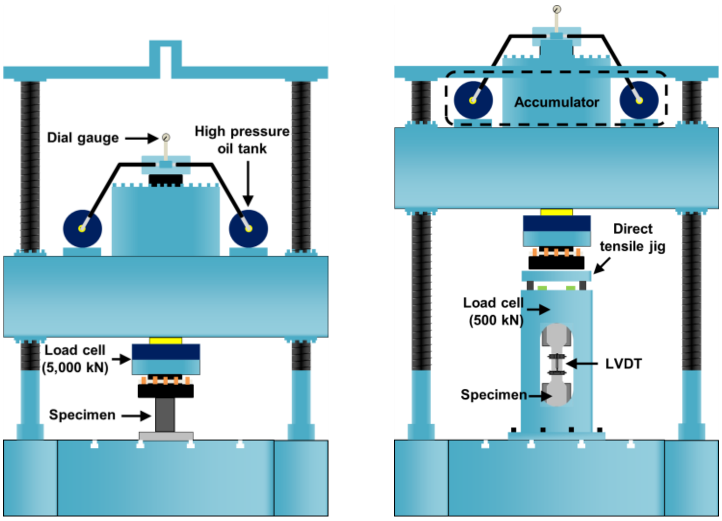

(a) Quasi-static (strain rate : 10^{-1}/s, loading velocity : 0.1m/s)

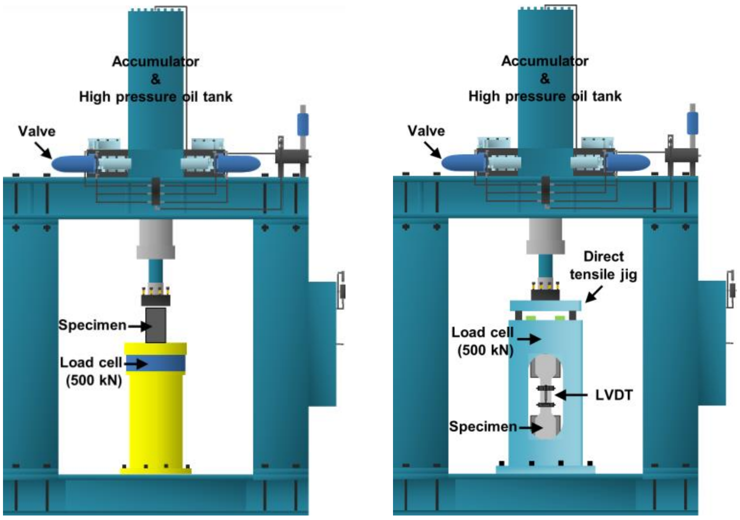

(b) Middle (strain rate : 10^{1}/s, loading velocity : 5m/s)

Figure 3 Test set up for dynamic test

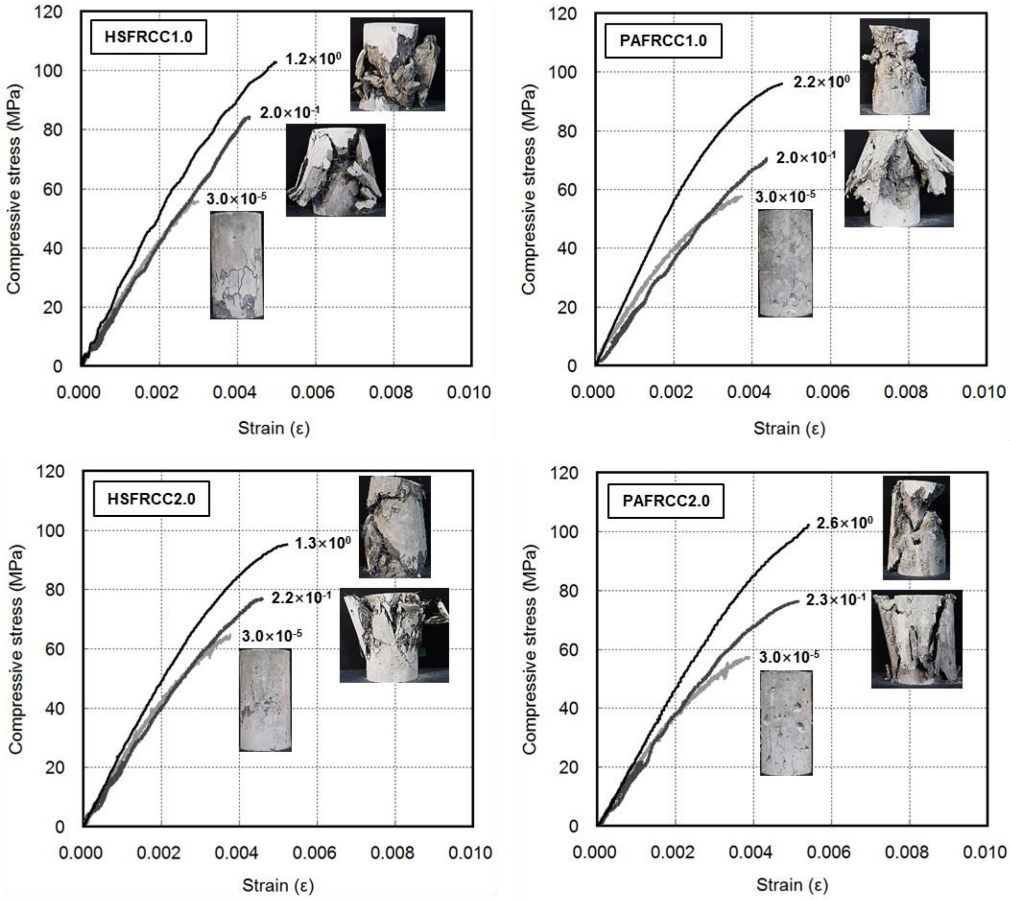

Figure 4 Compressive stress-strain curve and fracture shape by strain rate

3.2. DYNAMIC INCREASE FACTOR OF COMPRESSIVE AND TENSILE

Figure 6 shows the compressive strength DIF by strain rate. As the strain rate increases, tendency to increase the compressive strength was verified regardless of the fiber type and the volume fraction. The DIF of compressive strength was also increased with increase strain rate, regardless of the fiber type and the volume fraction. Estimated DIF of compressive strength by the CEB-FIP model code was lower than that of the experimental results. And the DIF of compressive strength by the experiments have shown a similar trend with the ACI-349.

Figure 7 shows the tensile strength DIF by strain rate. DIF of tensile strength of fiber reinforced cement composite was exceeding the value of CEB-FIP code. In the same fiber volume fraction and strain rate condition, tensile DIF of PAFRCC was larger than that of the HSFRCC, because the strain rate sensitivity of polyamide fiber tensile strength was greater than the bonding strength between hooked steel fiber and the matrix.

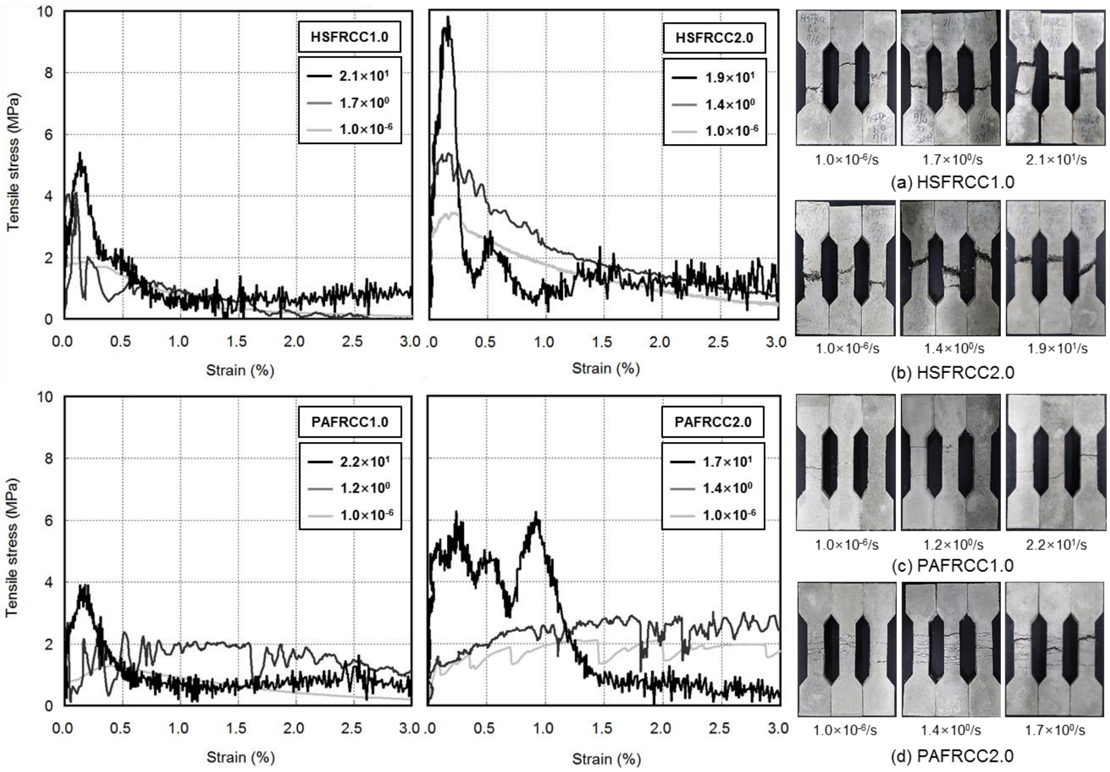

Figure 5 Tensile stress-strain curve and fracture shpae by strain rate

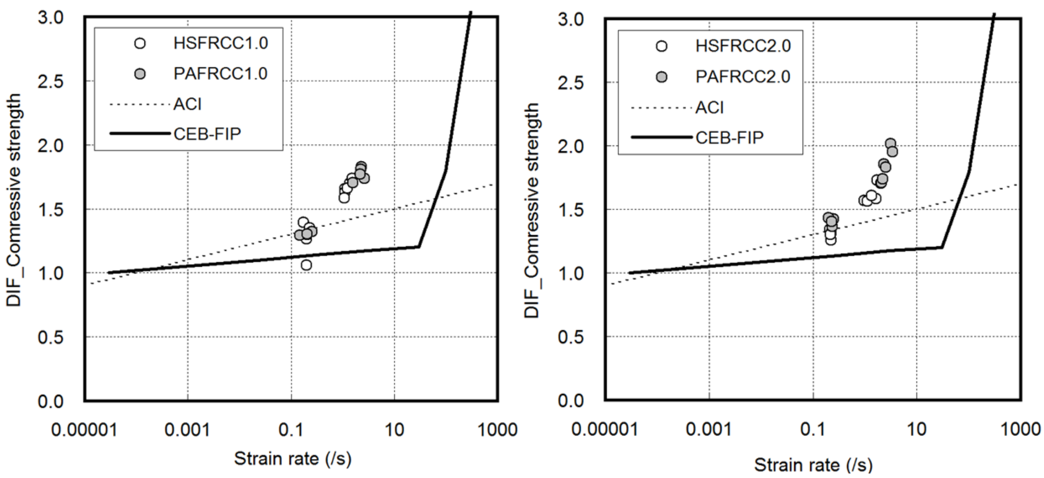

(a) V_f = 1.0% (b) V_f = 2.0%

Figure 6 Compressive strength DIF by strain rate

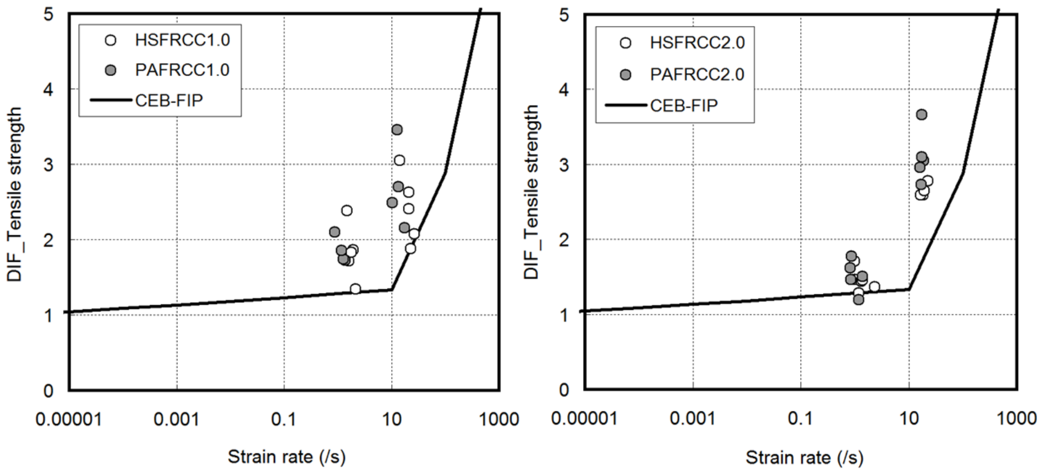

(a) V_f = 1.0% (b) V_f = 2.0%

Figure 7 Tensile strength DIF by strain rate

4. CONCLUSIONS

The following conclusions were drawn from the results of strain rate effect on the mechanical properties of HPFRCC.

1) In the case of compressive strength, tendency to increase the compressive strength was verified regardless of the fiber type and the volume fraction. However, in the case of tensile strength, the tendency to increase the tensile strength of polyamide fiber was higher than hooked steel fiber. Especially, as the fiber volume fraction increases, strain rate effect on the DIF of tensile strength and strain capacity was increased.

2) The pull out behavior of hooked steel fiber and tensile fracture of polyamide fiber has a great influence on the static and dynamic tensile fracture properties. HSFRCC occurred macro crack behavior, whereas PAFRCC occurred multiple crack behavior. Thus, the mechanical properties of reinforcing fiber have a great influence on the tensile fracture properties according to the strain rate.

3) As a result of evaluating the strain rate effect on the mechanical properties of HPFRCC, compressive properties were improved with increase the strain rate regardless of the reinforcing fiber. However, tensile properties showed high sensitivity of strain rate effect according to the reinforcing fiber. The reason of high sensitivity is the difference interfacial bonding strength between fiber and matrix by mechanical properties of the fiber.

ACKNOWLEDGMENTS

This research was supported by a grant from a Construction Technology Research Project (Development of impact/blast resistant HPFRCC and evaluation technique thereof, 13SCIPS02) funded by the Ministry of Land, Infrastructure, and Transport.

REFERENCES

[1] Tuan Kiet Tran, Dong Joo Kim (2014), High strain rate effects on direct tensile behavior of high performance fiber reinforced cementitious composites, Cement&Concrete Composites, 45, 186–200

[2] Kazunori Fujikake, Katsutoshi Uebayachi, Tomonori Ohno, katsuhiko Emori (2001), Study on Dynamic Tensile Softening Characteristic of Concrete Material under High Strain-Rate, Japan Society of Civil Engineers, 669(50), 125-134

[3] Viktor Mechtcherine, Flávio de Andrade Silva, Marko Butler, Deju Zhu, Barzin Mobasher, Shang-Lin Gao and Edith Mäder (2011), Behaviour of Strain-Hardening Cement-Based Composites Under High Strain Rates, Journal of Advanced Concrete Technology, 9(1), 51-62

[4] Kazunori Fujikake, Yoshikazu Shinozaki, Tomonori Ohno, Jun Mizuno and Atsushi Suzuki (1999), Post-peak and strain-softening of conrete materials in compression under rapid loading, Japan Society of Civil Engineers, 627(44), 37-54

[5] Tuan Kiet Tran, Dong Joo Kim (2013), Investigating direct tensile behavior of high performance fiber reinforced cementitious composites at high strain ratesCement and Concrete Research, 50, 62–73

[6] Jung Jin Kim, Gi-Joon Park, Dong Joo Kim, Jae Heum Moon, Jang Hwa Lee (2014), High-rate tensile behavior of steel fiber-reinforced concrete for nuclear power plants, Nuclear Engineering and Design, 266, 43-54

[7] Jeongsoo Nam, Yasuji Shinohara, Toshiyuki Atou, Hongseop Kim, Gyuyong Kim (2016), Comparative assessment of failure characteristics on fiber-reinforced cementitious composite panels under high-velocity impact, Composites Part B, 99, 84-97

[8] Hongseop Kim, Gyuyong Kim, Nenad Gucunski, Jeongsoo Nam, Joongkyu Jeon (2015), Assessment of flexural toughness and impact resistance of bundle-type polyamide fiber-reinforced concrete, Composites Part B, 78, 431-446

[9] ACI Committee 349. Code requirements for nuclear safety related concrete structures. Report No. ACI 349.01; 2001.

[10] Fib Bulletin 55, 2010, Model code 2010 - first complete draft, vol. 1; 2010. 153-155 pages ISBN 978-2-88394-095-6

STRAIN HISTORY ON THE REAR SIDE OF CONCRETE SUBJECTED TO HIGH-VELOCITY IMPACT

Sangkyu Lee[1], Gyu Yong Kim[1], Hongseop Kim[1], Min Jae Son[1], Jeongsoo Nam[2]

[1] Chungnam National University, Department of Architectural Engineering, 99 Daehak-ro, Yuseong-gu, Daejeon 305-764, Korea, email: lsg2357@naver.com, gyuyongkim@cnu.ac.kr, oliver-kahn12@nate.com, minjae931226@naver.com
[2] Tokyo Institute of Technology, Laboratory for Materials and Structures, 4259 Nagatsuta, Midori, Yokohama 226-8503, Japan, nam.j.aa@m.titech.ac.jp

SUMMARY: This study evaluated the fracture properties and strain behaviour on the rear side of concrete panels subjected to high-velocity (983J, 170m/sec) projectile (66.8g, 25mm) impact for application on the protection wall. It was confirmed that the compressive stress generated in the front side of concrete panel due to high-velocity projectile impact, transformed into the tensile stress on the rear side. It was found that the tensile strain on the rear side was restrained by the reinforcement of the hooked steel fiber. In addition, it was improved the tensile strain capacity and impact resistance performance rather than normal concrete. Therefore, reinforcing the hooked steel fiber to reduce the local fracture of the concrete is considered to be more effective than increasing the concrete thickness. And also, it is useful to evaluate the strain history of fiber reinforced concrete for verifying the safety performance of protection wall against impact load.

POVIJEST DEFORMACIJA NA STRAŽNJOJ STRANI BETONA IZLOŽENOG UDARU VELIKE BRZINE

SAŽETAK: U radu su vrednovana svojstva pri lomu i deformacije na stražnjoj strani betonskih panela izloženih udaru projektila (66,8 g, 25 mm) velike brzine (983 J, 170 m/s) za primjenu na zaštitnom zidu. Potvrđeno je da se tlačno naprezanje nastalo na prednjoj strani betonskoga panela zbog udara projektila velike brzine pretvorilo u vlačno naprezanje na stražnjoj strani. Utvrđeno je da je vlačna deformacija na stražnjoj strani ograničena armaturom od čeličnih vlakana sa zakrivljenim krajevima. Osim toga, poboljšala se sposobnost za preuzimanje vlačnih deformacija i otpornost na udar u odnosu na obični beton. Stoga se smatra da je armiranje čeličnim vlaknima sa zakrivljenim krajevima radi smanjenja lokalnoga loma učinkovitije od povećanja debljine betona. Vrednovanje povijesti deformacije betona armiranog vlaknima radi provjere sigurnosti zaštitnog zida na udarno opterećenje pokazalo se također korisnim.

1. INTRODUCTION

Concrete subjected to high-velocity projectile impact has local fracture behaviour unlike under static loading condition. When concrete is impacted by high-velocity projectile, a compressive wave is propagated on the front side, and then reflected as tensile stress on the rear side. If tensile stress exceeds the dynamic tensile strength of concrete, cracks and fractures were occurred, as shown in Figure 1 [1].

Local fracture of concrete caused by this mechanism can be classified in to penetration, scabbing, perforation [1-3]. If the scabbing or perforation were occurred in the structure by projectile impact, the damage of life and property inside the structure due to the fragment of the concrete and the perforation of projectile is considerably large. So, it is necessary to suppress the scabbing of concrete on the rear side and perforation of projectile for prevent such damage. Therefore, to increase the flexural tensile strength which greatly affects the fracture of concrete, fiber reinforced concrete has been actively studied [4-8]. It is known that fiber reinforced concrete absorbs and disperses stress by the bridging action of fiber and it reduce deformation [9-11]. And, the improvement of the tensile performance of the fiber reinforced concrete is related to the impact resistance performance.

In this study, fracture property and strain behaviour on the rear side of normal and hooked steel fiber reinforced concrete by projectile impact were evaluated. Through this evaluation, the influence of the reinforcing fiber and strain behaviour of concrete on the rear side was investigated.

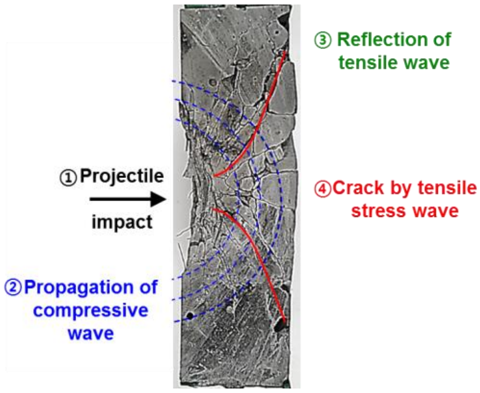

Figure 1 Propagation of the stress wave in the concrete by projectile impact

2. EXPERIMENTAL DESIGN AND METHOD

2.1. MATERIALS AND MIX PROPORTION

Table 1 shows the experimental design. The diameter and mass of projectile were 25mm and 66.8g. Projectile nose shape was spherical type. Impact velocity was controlled 170m/s. The size of the Concrete panel was 700×600mm (W×H), and thickness were 50, 60mm.

Table 2 shows the mix proportions of concrete. The water/binder (W/B) ratio was set to 40%.

Table 1 Experimental design

Impact condition				Specimen condition	
Projectile nose shape	Projectile diameter (mm)	Projectile mass (g)	Velocity (m/s)	Size (W×H)	Thickness (mm)
Spherical type	25	66.8	170	700×600	50, 60

Table 2 Mix proportions of concrete

ID.[1)]	W/B (%)	S/a (%)	Unit weight (kg/m^3)					Hooked steel fiber	
			Water	Cement	Fly-ash	Sand	Gravel	(V_f.%)	(kg)
NC	40	55	220	850	150	350	655	1.0	78
HSFRC1.0									

1) NC : Normal Concrete, HSFRC 1.0 : Hooked Steel Fiber Reinforced Concrete(V_f=1.0%)

Table 3 Mechanical properties of the used materials

Materials	Mechanical properties
Cement	Ordinary portland cement, Density : 3.15g/cm^3, Fineness : 3,200cm^2/g
Fly-ash	Density : 2.20g/cm^3, Fineness : 3,000cm^2/g
River sand	Density : 2.61g/cm^3, Absorptance : 0.81%
Gravel	Crushed gravel, Maximum size : 20mm, Density : 2.65g/cm^3, Absorptance : 0.76%
Super plasticizer	Polycarboxylic acid type
Hooked steel fiber	Length : 30mm, Diameter : 0.5mm, Aspect ratio : 60, Density : 7.80g/cm^3, Tensile strength : 1,140MPa

And, the fiber volume fraction was 1.0%.

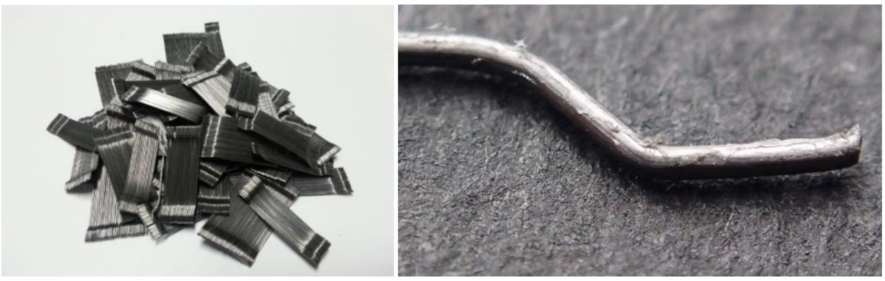

Figure 2 Hooked steel fiber

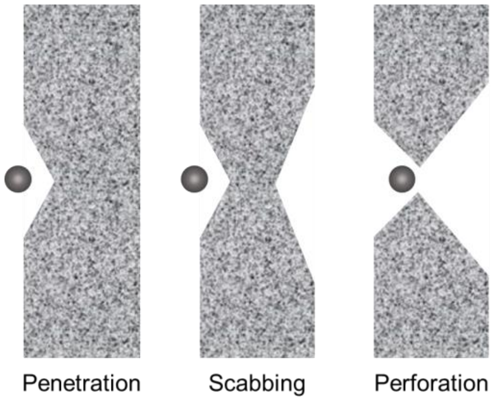

Figure 3 Fracture mode of concrete

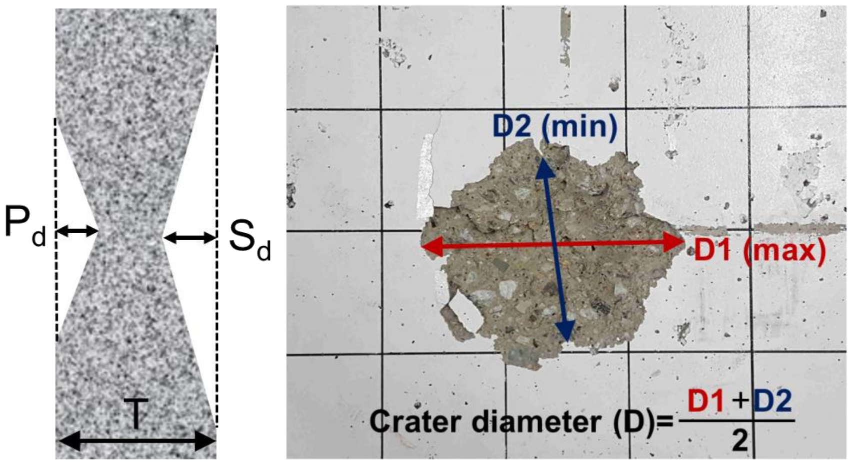

(a) Fracture depth (b) Crater diameter

Figure 4   Measurement method of fracture depth and crater diameter

Table 3 shows the mechanical properties of the used materials. The hooked steel fiber has a length of 30 mm, a diameter of 0.5 mm, an aspect ratio 60, a density of 7.80 g/cm^3, and a tensile strength of 1,140 MPa. Figure 2 shows the shape of hooked steel fiber.

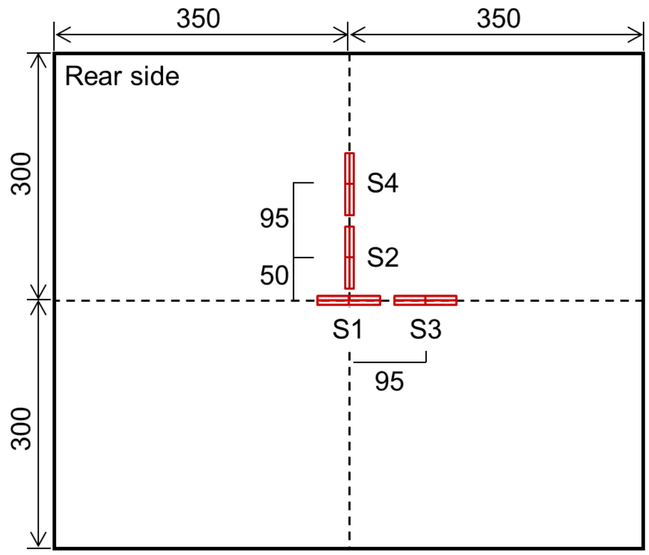

※S0 : Center of front side (Impact point), ※Sampling rate : 200,000Hz

Figure 5 Position of the gauge

2.2. TEST METHOD

Figure 3 shows the fracture mode of concrete by projectile impact. When the projectile was only penetrated on the front side of concrete, it is classified into the penetration grade. If the fragment is occurred on the rear side, it is classified into the scabbing grade. When the projectile perforated through the concrete, it is classified into the perforation grade.

Figure 4 shows the test methods of fracture depth and crater diameter. Fracture depth was determined as maximum depth and crater diameter was determined as the average of the maximum and minimum diameters.

Figure 5 shows the position of strain gauge (PL-60) used to measure the strain history on the rear side. One gauge was attached at the projectile impact point (S0) on the front side of the concrete panel to check the initial impact time. Four gauges (S1–S4) were attached to the rear side of the concrete panel at distances of 0–145 mm from the center. The sampling rate for the strain measurements was set to 200,000 Hz.

Figure 6 (a) shows a gas pressured high-velocity projectile impact test device. This impact test device uses a temporary spray method; the gas chamber is filled with nitrogen gas at a pressure of 1.5 MPa. The concrete specimen is fixed with using clamps on the left and right side of concrete specimen and projectile is launched with a velocity of 170 m/s. The impact velocity was measured using the velocity measurement system. The shape of projectile is shown in Figure 6b).

Figure 3 shows the fracture mode of concrete by projectile impact. When the projectile was only penetrated on the front side of concrete, it is classified into the penetration grade. If the fragment is occurred on the rear side, it is classified into the scabbing grade. When the projectile perforated through the concrete, it is classified into the perforation grade.

Figure 4 shows the test methods of fracture depth and crater diameter. Fracture depth was determined as maximum depth and crater diameter was determined as the average of the maximum and minimum diameters.

Figure 5 shows the position of strain gauge (PL-60) used to measure the strain history on the rear side. One gauge was attached at the projectile impact point (S0) on the front side of the concrete panel to check the initial impact time. Four gauges (S1–S4) were attached to the rear side of the concrete panel at distances of 0–145 mm from the center. The sampling rate for the strain measurements was set to 200,000 Hz.

Figure 6 (a) shows a gas pressured high-velocity projectile impact test device. This impact test device uses a temporary spray method; the gas chamber is filled with nitrogen gas at a pressure of 1.5 MPa. The concrete specimen is fixed with using clamps on the left and right side of concrete specimen and projectile is launched with a velocity of 170 m/s. The impact velocity was measured using the velocity measurement system. The shape of projectile is shown in Figure 6(b).

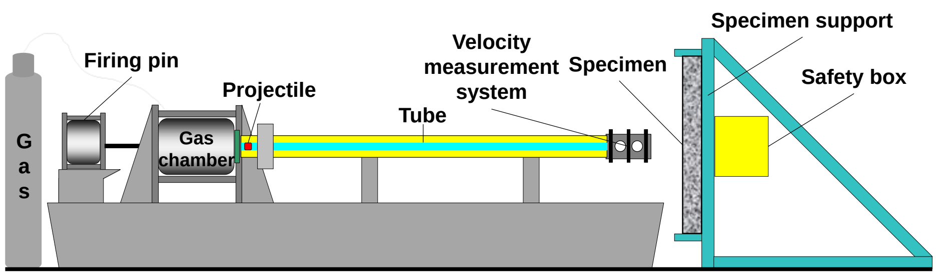

(a) Gas-pressured high-velocity impact test device

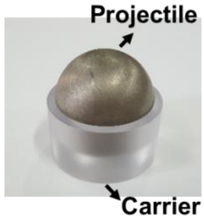

(b) Projectile

Figure 6 Scheme of the impact test set up

3. RESULTS AND DISCUSSION

3.1. FRESH PROPERTIES AND COMPRESSIVE STRENGTH

The slump values of the NC and HSFRC 1.0 were all within the target range (150 ± 30 mm) regardless of fiber reinforcement. Compressive strengths were all found to be above 50 MPa. And, flexural strength was 6.42 MPa on NC, 12.32 MPa on HSFRC 1.0. It was found that flexural strength of HSFRC1.0 was improved by the bridging action of hooked steel fiber.

3.2. FRACTURE PROPERTIES BY PROJECTILE IMPACT

Table 4 shows the fracture shape of concrete panels. For the 50mm thickness specimen, both NC and HSFRC 1.0 showed the scabbing grade, but the crater of HSFRC 1.0 was smaller than that of NC. For the 60mm thickness specimen, NC showed a scabbing grade, whereas HSFRC 1.0 showed a penetration grade. It was confirmed that the fiber reinforcement inhibited the scabbing.

Figure 7 shows the fracture depth as proportion of the specimen thickness. In specimen thickness 50mm and 60mm, the penetration depth of HSFRC1.0 was deeper than that of NC. Whereas the scabbing depth of NC was deeper than HSFRC1.0. In specimen thickness 60mm, scabbing was not occurred in HSFRC1.0.

Figure 8 shows the crater diameter. Crater diameter of HSFRC1.0 on the front and rear side was smaller than that of NC. It is considered that detachment of fragment was suppressed by bridging action between the hooked steel fiber and matrix.

Table 4 Fracture on the concrete panels

ID.	Thickness 50mm		Thickness 60mm	
	Front side	Rear side	Front side	Rear side
NC	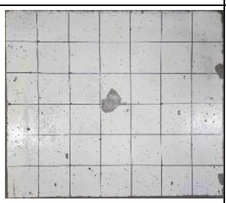	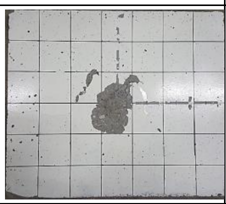	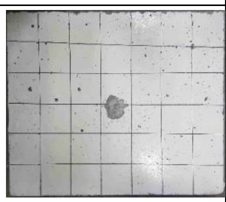	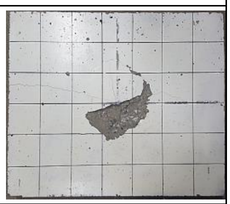
	Scabbing		Scabbing	
HSFRC 1.0	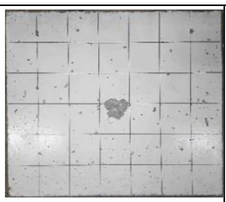	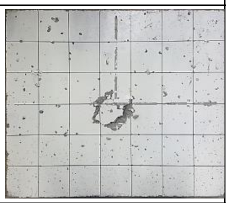	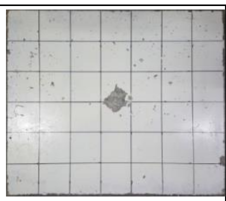	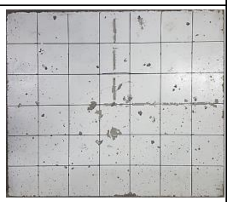
	Scabbing		Penetration	

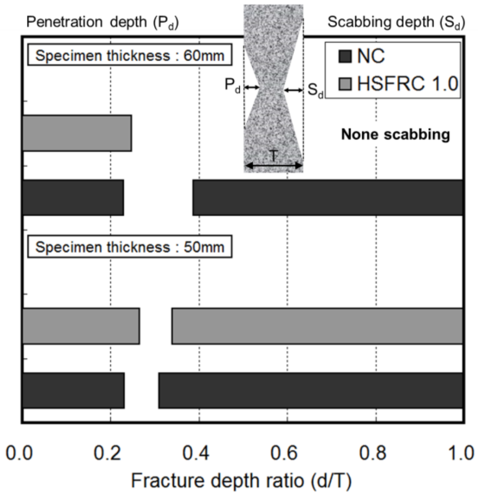

Figure 7 Fracture depth ratio

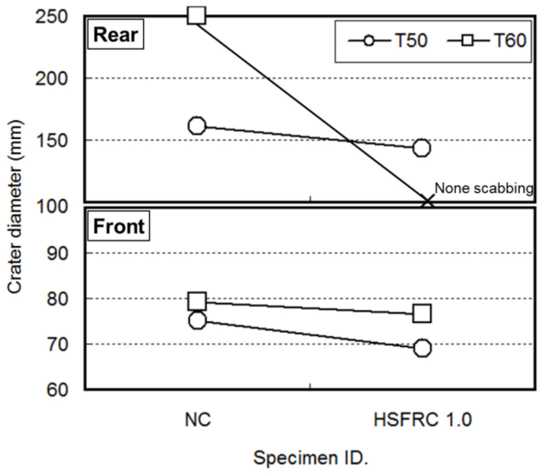

Figure 8 Crater diameter

3.3. STRAIN HISTORY

Figure 9 shows the strain history on the rear side in specimen thickness 50mm. S1 gauges (Center on the rear side) were all broken by scabbing regardless of the fiber reinforcement. In case of the NC, the S2 gauge was broken due to high tensile strain. The S3 gauge showed a large tensile strain and the scabbing was occurred. In case of the HSFRC1.0, the S2 gauge did not break because the tensile strain was decreased by fiber reinforcement. The tensile strain did not occur in the S3 gauge and scabbing was not occurred. For the S4 gauge, both NC and HSFRC1.0 showed very small tensile strain.

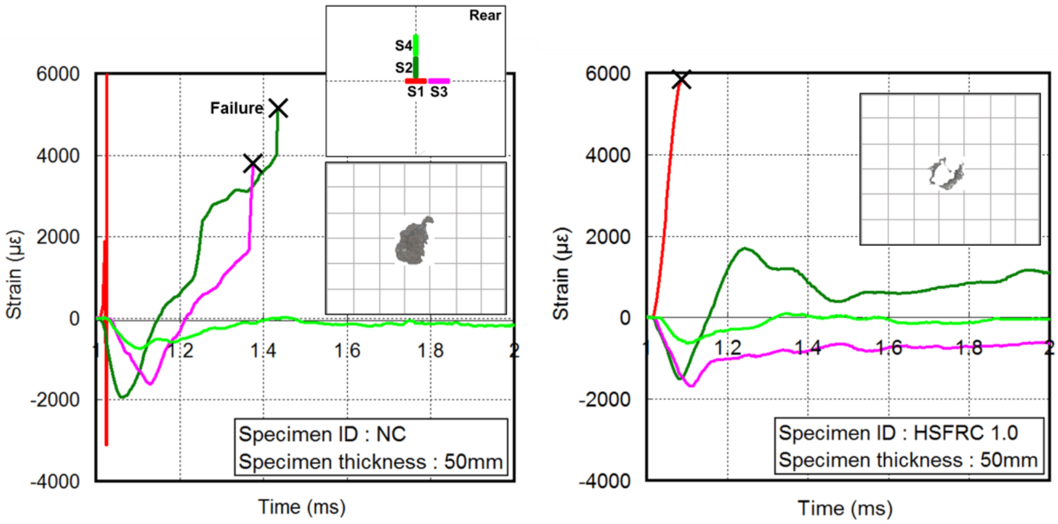

Figure 9 Strain history on the rear side of concrete

Figure 10 shows the peak tensile strain on the rear side, in the specimen thickness 60mm. The peak tensile strain of the NC was larger than that of HSFRC1.0 in all gauges. In the HSFRC1.0, small crack was occurred in S1 due to high tensile strain. But in the S2 gauge, the tensile strain was decreased to less than 2,000με. From the next gauge (S3, S4), tensile strain were very small so scabbing were not occurred. This results are considered to be influenced by absorption and dispersion action of impact stress by steel fiber reinforcement.

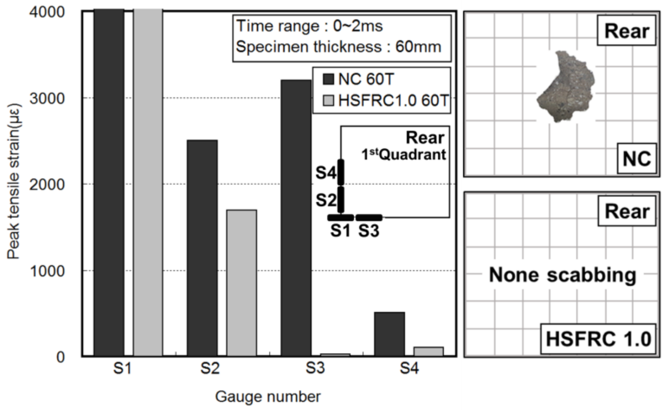

Figure 10 Peak tensile strain on the rear side of concrete

4. CONCLUSIONS

As a result of the evaluation of the strain history of the normal concrete and hooked steel fiber reinforced concrete, the following conclusions were obtained.

1) It was confirmed that the compressive stress wave was generated by projectile impact on the front side, and then it is transformed to the tensile stress at the free end of the rear side. In addition, it was confirmed that fracture and cracks were occurred on the rear side of concrete by tensile stress and strain.

2) The flexural strength and tensile deformable capacity of fiber reinforced concrete was improved, compared with normal concrete due to the bridging action of the reinforced fiber. It was also shown that the fracture on the rear side of concrete was suppressed by reduction of tensile strain on the rear side.

3) It is effective to improve the impact resistance by the reinforcement of the hooked steel fiber, and it is expected that the efficient design of protection wall is possible. Evaluation of the strain history of fiber reinforced concrete by projectile impact is useful for verifying the safety performance of protection wall against impact load.

ACKNOWLEDGMENTS

This work was supported (in part) by the Collaborative Research Project (CRP) of Materials and Structures Laboratory, Tokyo Institute of Technology (International CRP 2016ーCategory B 227) and Mid-career Researcher Program through NRF (NRF-2015R1A2A2A01007705) grant funded by the MEST.

REFERENCES

[1] James, R.: Penetration resistance of concrete: A Review, National Bureau of Standards Special Publication, ISBN B0006E76U2, Washington DC, (1982)
[2] Mohamed, A. & Ahmed, F.: Effect of reinforcement on the response of concrete panels to impact of hard projectiles, International Journal of Impact Engineering, Vol. (2014) 63., pp. 1-17, ISSN 0734-743X
[3] Zhang, M., et al.: Resistance of high-strength concrete to projectile impact, International Journal of Impact Engineering, Vol. (2005) 31(7)., pp. 825-841, ISSN 0734-743X
[4] Almusallam, T., et al.: Response of hybrid-fiber reinforced concrete slabs to hard projectile Impact, International Journal of Impact Engineering, Vol. (2013) 58., pp. 17-30, ISSN 0734-743X
[5] Hrynyk, T. & Frank, J.: Behavior of Steel Fiber-Reinforced Concrete Slabs under Impact Load, ACI Structural Journal, Vol. (2014) 111(5)., pp. 1213-1224, ISSN 0889-3241
[6] Kanda, T. & Li, V.: Interface property and apparent strength of high strength hydrophilic fiber in cement matrix, Journal of materials in Civil Engineering, Vol. (1998) 10(1)., pp. 5-13, ISSN 1943-5533
[7] Bolat, H., et al.: The effects of macro synthetic fiber reinforcement use on physical and mechanical properties of concrete, Composites Part B: Engineering, Vol. (2014) 61., pp. 191-198, ISSN 1359-8368
[8] Bencardino, F., et al.: Implications of test methodology on post-cracking and fracture behaviour of Steel Fibre Reinforced Concrete, Composites Part B: Engineering, Vol. (2013) 46., pp. 31-38, ISSN 1359-8368
[9] Kim, H., et al.: Assessment of flexural toughness and impact resistance of bundle-type polyamide fiber-reinforced concrete, Composites Part B: Engineering, Vol. (2015) 78., pp. 431-446, ISSN 1359-8368
[10] Kim, H., et al.: Static mechanical properties and impact resistance of amorphous metallic fiber-reinforced concrete, Composite Structures, Vol. (2015) 134., pp. 831–844, ISSN 0263-8223

[11] Nam, J., et al.: Comparative assessment of failure characteristics on fiber-reinforced cementitious composite panels under high-velocity impact, Composites Part B: Engineering, Vol. (2016) 99., pp. 84-97, ISSN 1359-8368

IMPACT RESISTANCE OF AMORPHOUS METALLIC FIBER REINFORCED CEMENT COMPOSITE PANELS

Gyu Yong Kim[1], Hongseop Kim[1], Sangkyu Lee[1], Min Jae Son[1], Jeongsoo Nam[2]

[1] Chungnam National University, Department of Architectural Engineering, 99 Daehak-ro, Yuseong-gu, Daejeon 305-764, Korea, email: gyuyongkim@cnu.ac.kr, oliver-kahn12@nate.com, lsg2357@naver.com, minjae931226@naver.com
[2] Tokyo Institute of Technology, Laboratory for Materials and Structures, 4259 Nagatsuta, Midori, Yokohama 226-8503, Japan, email: nam.j.aa@m.titech.ac.jp

SUMMARY: This study evaluated the flexural properties and impact resistance performance of thin plate shape amorphous metallic fiber reinforced cement composites. The flexural strength of amorphous metallic fiber reinforced cement composite was greater than that of the hooked steel fiber reinforced cement composite. However, after peak load, flexural load was rapidly decreased in the strain-softening section, because the amorphous metallic fiber reinforced cement composite was cut-off without pull-out from the matrix. For perpendicular deposition, the fiber are arranged parallel to the direction of the shockwave, thus causing the cracks to be concentrated in the center of the specimen when transferred to the rear. However, for parallel deposition, the fiber are arranged perpendicular to the direction of the shockwave, allowing cracks to be dispersed away from the center, and they are distributed perpendicularly, but not radially.

UDARNA OTPORNOST KOMPOZITNE PLOČE OD CEMENTA ARMIRANOG AMORFNIM METALNIM VLAKNIMA

SAŽETAK: U radu su ispitana svojstva pri savijanju i udarna otpornost tankih ploča – kompozita od cementa armiranog amorfnim metalnim vlaknima. Čvrstoća pri savijanju takvih kompozita bila je veća od cementnih kompozita armiranih čeličnim vlaknima sa zakrivljenim krajevima. Međutim, nakon postizanja najvećeg opterećenja, opterećenje pri savijanju ubrzano se smanjilo u presjeku omekšanja deformacija, jer je cementni kompozit armiran amorfnim metalnim vlaknima bio presječen bez izvlačenja iz matrice. Kad je uzorak bio lijevan okomito na smjer djelovanja udara, vlakna su raspoređena usporedno sa smjerom udarnog vala zbog čega su se pukotine koncentrirale u središtu uzorka, a zatim su nastale na stražnjoj strani. Međutim, kad je lijevanje uzroka bilo usporedno sa smjerom djelovanja udara, vlakna su raspoređena okomito na smjer udarnoga vala što je omogućilo da se pukotine rasprše dalje od središta, a raspoređene su okomito, a ne radijalno.

1. INTRODUCTION

The improvement in the flexural and tensile strength of the fiber reinforced cement composites (FRCC) is largely influenced by the type, aspect ratio(L/d), tensile strength, volume fraction of fiber, the type, strength of the matrix, fiber-matrix bonding strength and pull-out properties [1-3]. Therefore, various short fiber have been developed for concrete reinforcement, and their applicability is being evaluated. Generally, steel fiber reinforced concrete (SFRC) is most commonly used because it is very effective for increasing the tensile strength, deformability, and crack propagation resistance and impact resistance performance of concrete [4-11].

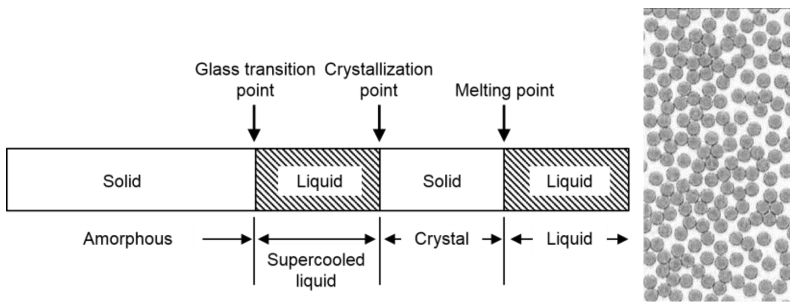

Figure 1 Overview and structure of amorphous metal

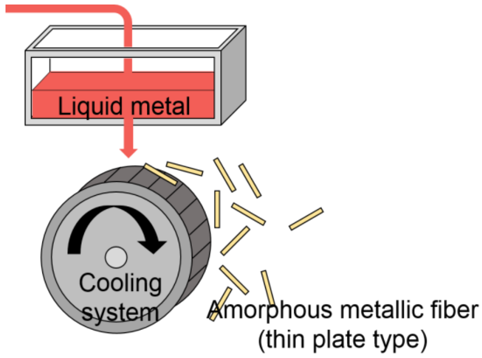

Figure 2 Manufacturing process of amorphous metallic fiber

An amorphous metallic fiber has recently been developed. Amorphous metal has an amorphous (non-crystalline) structure, unlike common metals with crystalline structures, because amorphous metal is manufactured through a melt-spinning process, as shown in Figure 1. Therefore, it has a higher tensile strength and corrosion resistance than common metal. In addition, the amorphous metal is formed into a thin plate as part of the manufacturing process of quenching liquid metal, as shown in Figure 2. Thus the surface area and bonding performance are increased. In addition, because it is ultralight, the number of amorphous metallic fiber is large in the matrix for the same volume fraction. Therefore, by using amorphous metallic fiber as a concrete reinforcement material, the crack resistance, flexural/tensile strength of concrete are expected to improve.

This study evaluated the flexural properties and impact resistant performance of thin plate shape amorphous metallic fiber reinforced cement composites. The flowability, compressive strength and flexural strength were evaluated, and the impact resistance performance by projectile impact was also evaluated according to the arrangement of the thin plate shape amorphous metallic fiber.

2. EXPERIMENTAL DESIGN AND METHOD

2.1. MATERIALS AND MIX PROPORTION

Table 1 shows the mechanical properties of the amorphous metallic fiber and hooked steel fiber used in this study. The amorphous metallic fiber had a length of 30 mm, a width of 1.6 mm, a thickness of 29 µm, a density of 7.2 g/cm^3, and a tensile strength of 1,400 MPa, and had a shape akin to a thin plate. The hooked steel fiber had hook-shaped ends, with a length of 30 mm, a diameter of 0.5 mm, a density of 7.85 g/cm^3, and a tensile strength of 1,140 MPa. Figure 3 shows the shapes of the amorphous metallic fiber and hooked steel fiber. The amorphous metallic fiber bonded to the matrix by friction originating from the rough surface of the thin plate, while the hooked steel fiber relied on friction from the hooked end of the fiber.

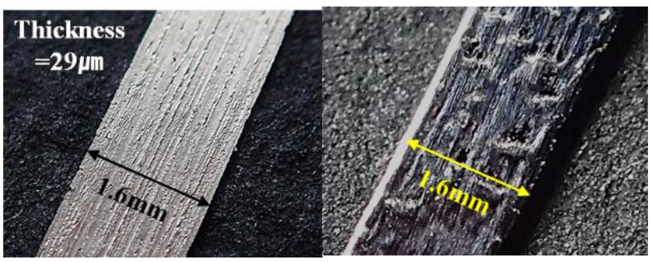

(a) One side (b) The other side

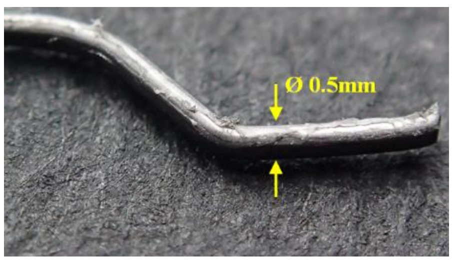

Figure 3 Hooked steel fiber

Table 2 shows the experimental conditions under which the flexural strength and impact resistance of the fiber reinforced cement composite were evaluated. The volume fraction of amorphous metallic fiber and hooked steel fiber were 2.0 vol.%. Meanwhile, to evaluate the impact resistance performance by arrangement of thin plate amorphous metallic fiber, the amorphous metallic fiber reinforced cement composite was cast perpendicular to the direction of the projectile's impact, as shown in Figure 4(a), and parallel as in Figure 4(b).

Table 1 Mechanical properties of the used fiber

Type	Length (mm)	Diameter (mm)	Width (mm)	Thickness (um)	Aspect ratio	Density (g/cm^3)	Tensile strength (MPa)
Amorphous metallic fiber	30	-	1.6	29	18.75(L/W) 1034.48(L/T)	7.2	1,400
Hooked steel fiber	30	0.5	-	-	60(L/D)	7.8	1,140

Table 2 Details of fiber reinforced cement composite

ID.[1)]	Details of fiber	
	Type	Volume fraction (vol.%)
NCC	-	0
AFRCC2.0	Amorphous metallic fiber	2.0
HSFRCC2.0	Hooked steel fiber	

1) NCC : Normal Cement Composite, AFRCC : Amorphous metallic Fiber Reinforced Cement Composite
HSFRCC : Hooked Steel Fiber Reinforced Cement Composite

Table 3 Mix proportions of concrete and cement composite

W/B	S/a (%)	Unit weight (kg/m^3)				Fiber	
		Cement	Water	Fly-ash	Silica sand	(V_f.%)	(kg)
0.4	100	850	400	150	350	2.0	144.0 (AF)
							156.0 (HSF)

Table 4 Mechanical properties of the used materials

Materials	Mechanical properties
Cement	Ordinary portland cement, Density : 3.15g/cm^3, Fineness : 3,200cm^2/g
Fly-ash	Density : 2.20g/cm^3, Fineness : 3,000cm^2/g
Silica sand (Type 7)	Density : 2.64g/cm^3, Absorptance : 0.38%
Super plasticizer	Polycarboxylic acid type

Table 3 shows the mixing proportions of the cement composites, and the W/B was set to 0.4. Ordinary Type I Portland cement was used, and fly ash was used as the admixture. Type-7 silica sand was used for the cement composite. Table 4 shows the mechanical properties of the materials that were used.

2.2. TEST METHOD

The flexural strength of the fiber reinforced concrete beam was tested according to ASTM C 1609 "Standard Test Method for Flexural Performance of Fiber Reinforced Concrete (Using Beam with Third-Point Loading)".

The projectile impact test was done using a high velocity projectile impact test device, as shown in Figure 5(a). The steel ball used in the test had a diameter of 20 mm (mass of 31.8 g) and, by adjusting the pressure of the nitrogen gas, the projectile was launched at 170 m/s. The shape of projectile is shown in Figure 5(b). After the impact test, the failure mode, fracture depth and crater diameter were measured.

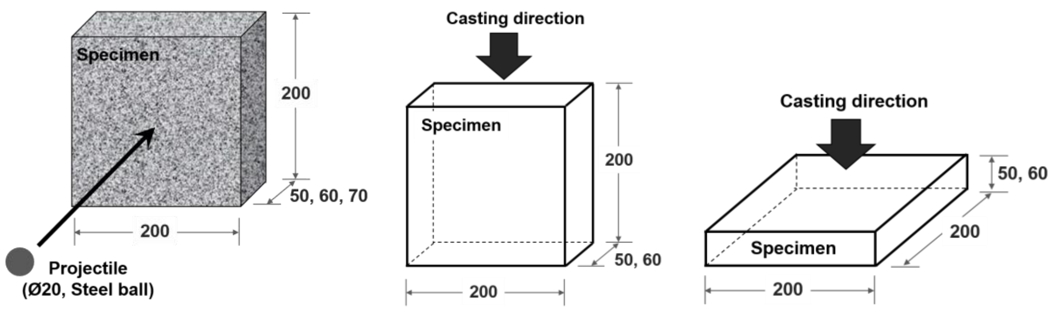

Figure 4 Specimen preparation (unit : mm): (a) Casting of perpendicular to the direction of the projectile's impact, (b) Casting of parallel to the direction of the projectile's impact

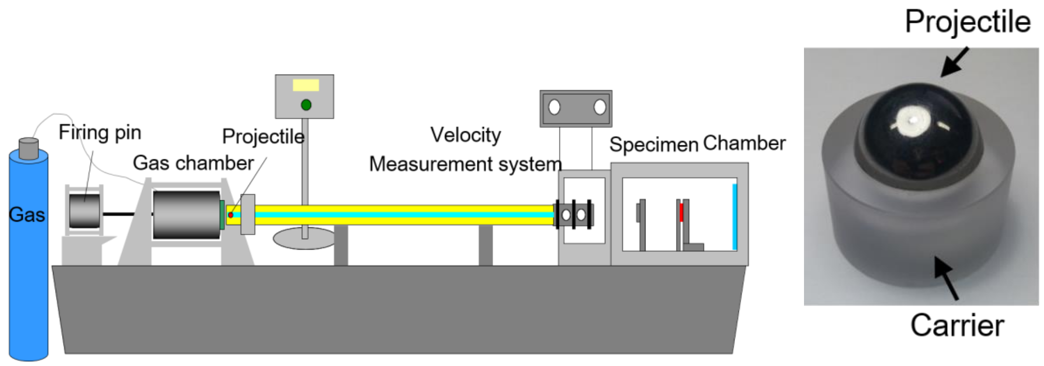

Figure 5 Scheme of the impact test set up: (a) Gas-pressured high-velocity impact test device, (b) Projectile

3. RESULTS AND DISCUSSION

3.1. FRESH PROPERTIES AND COMPRESSIVE STRENGTH

Table 5 shows the slump, air content, and compressive strength after aging for 28 days. The slump-flow values of the FRCC were all within the target range (210 ± 30 mm), regardless of fiber reinforcement. And the compressive strengths were all found to be above 40 MPa.

Table 5 Fresh properties and compressive strength

ID.	Slump -flow (mm)	Air (%)	Compressive strength (MPa)
NCC	210	4.1	45.36
AFRCC2.0	205	4.2	46.48
HSFRCC2.0	225	3.8	44.32

3.2. FLEXURAL PROPERTIES

Figure 6 shows the flexural load-deflection curve. A brittle fracture occurred in the NCC. For the FRCC, the flexural load and deflection were significantly improved due to the stress dispersion by the cross-linking of reinforcing fiber. Both the amorphous metallic fiber reinforced cement composite and hooked steel fiber reinforced cement composite exhibited strain hardening up to the peak flexural load. The maximum flexural load of the amorphous metallic fiber reinforced cement composite was greater than that of the hooked steel fiber reinforced cement composite. However, after peak load, flexural load was rapidly decreased in the strain softening section, because the amorphous metallic fiber reinforced cement composite was cut-off without pull-out from the matrix. Meanwhile, the maximum flexural load of the hooked steel fiber reinforced cement composite was found to be smaller than that of the amorphous metallic fiber reinforced cement composite. However, decrease of flexural load was a smaller than that of amorphous metallic fiber reinforced cement composite, because the hooked steel fiber was pulled out from the matrix in the strain-softening section.

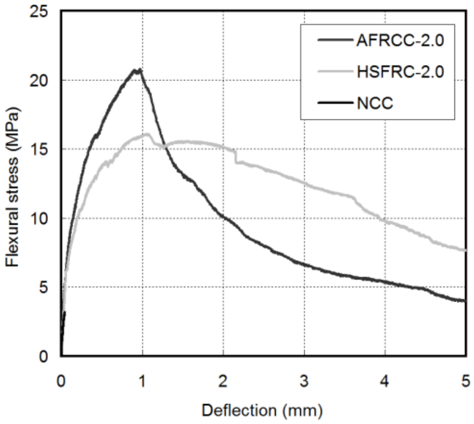

Figure 6 Flexural load-deflection curve

Table 6 shows the failure modes of cement composites after being impacted by a 20 mm projectile at the impact velocity of 170 m/s. With the NCC specimen, perforation occurred for the 50, 60 mm specimens. However, for the FRCC, scabbing was significantly decreased, but a few cracks formed around the center of the rear side. Scabbing of the 50 mm specimen occurred in HSFRCC2.0, but the cross-linking between the fibers and matrix prevented fragmentation scabbing. Meanwhile, scabbing did not occur for the AFRCC2.0 specimens in the all specimens. And the amount of cracking on the rear side clearly decreased as the specimen thickness increased.

Table 6: Failure mode of cement composite after impact test. (Projectile diameter 20mm, Impact velocity 170m/s)

ID.	Specimen thickness 50mm		Specimen thickness 60mm	
	Front side	Rear side	Front side	Rear side
NCC	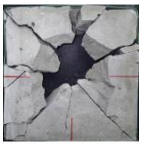			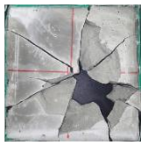
AFRCC2.0 (perpendicular)				
AFRCC2.0 (parallel)				
HSFRCC2.0 (perpendicular)	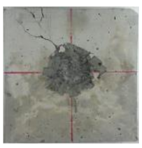	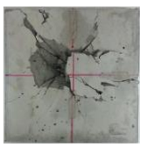		

Figure 7 shows the cracking patterns of the hooked steel fiber reinforced cement composite, as observed in a cross-section. Generally, concrete subjected to the projectile impact exhibited radial cracks inside the specimen. However, in the case of FRCC, the cracking patterns were affected by the arrangement and distribution of the reinforcement fibers. For the HSFRCC cross-section, large radial cracks and slight fragmentation scabbing were observed in the 50 mm specimen, but scabbing was prevented by the increase of specimen thickness. For the AFRCC, it was recognized that there is a correlation between the direction of the projectile impact and the fiber deposition, because the amorphous metallic fibers have a thin plate shape.

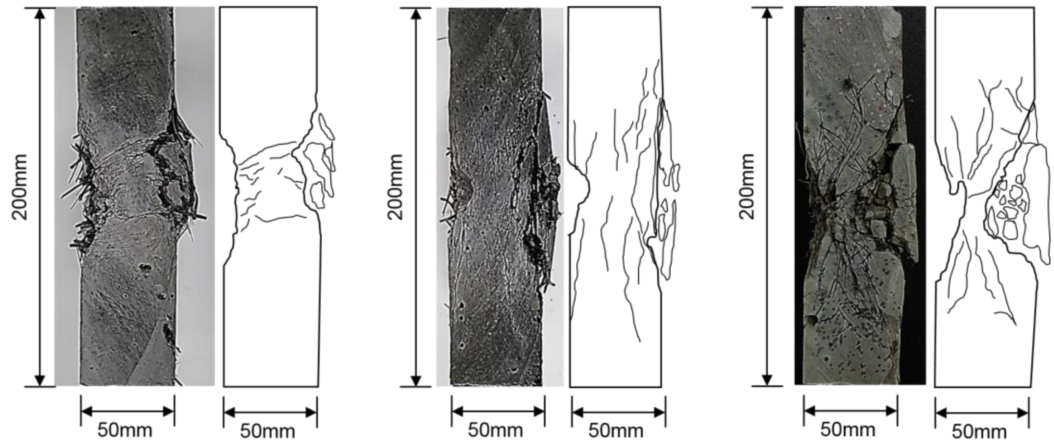

(a) AFRCC2.0 (perpendicular) (b) AFRCC2.0 (parallel) (c) HSFRCC2.0 (perpendicular)

Figure 7 Cracking patterns on the cross section

For the amorphous metallic fiber, the directions of the fibers themselves were greatly influenced by the casting direction, causing a clearly different crack pattern in a cross-section of the specimen. For perpendicular deposition, the fibers are arranged parallel to the direction of the shockwave, thus causing the cracks to be concentrated at the center of the specimen when transferred to the rear. However, for parallel deposition, the fibers are arranged perpendicular to the direction of the shockwave, allowing cracks to be dispersed away from the center, and they are distributed perpendicularly, but not radially.

4. CONCLUSIONS

The following conclusions were drawn from the results of comparing and evaluating amorphous metallic fiber and hooked steel fiber reinforced cement composite, in terms of their static mechanical properties and impact resistance.

1) The amorphous metallic fiber reinforced cement composite has a greater flexural strength than the hooked steel fiber reinforced cement composite. However, in the amorphous metallic fiber reinforced cement composite, the fiber was not pulled out from the matrix. Instead a cut-off occurred in the strain-softening section after crack initiation, so there was a greater decrease in the load than that of the hooked steel fiber reinforced cement composite.

2) The effects of the fiber shape on the fracture by projectile impact were also observed. The amorphous metallic fiber reinforced cement composite was found to be more effective at resisting impact-caused cracking than the hooked steel fiber reinforced cement composite. This is thought to be a result of the amorphous metallic fiber having more fiber for the same fiber volume fraction, thus making it better able to resist the initiation and propagation of cracks upon an impact. Furthermore, because of the thin plate shape, the direction of the fiber has an effect on the crack patterns, such that the concrete's casting and member (panel) directions must be considered.

3) Based on these results, it can be concluded that amorphous metallic fiber could be used in fiber reinforced cement composite materials and structures, for structural materials and protection panels. To attain a superior level of protection, therefore, the application of thin plate shape amorphous metallic fiber should be considered, with sufficient attention being given to the design of the precast concrete member.

ACKNOWLEDGMENTS

This work was supported (in part) by the Collaborative Research Project (CRP) of Materials and Structures Laboratory, Tokyo Institute of Technology (International CRP 2016ー Category B 227) and Mid-career Researcher Program through NRF (NRF-2015R1A2A2A01007705) grant funded by the MEST.

REFERENCES

[1] Kanda T, Li Victor C. Interface property and apparent strength of high strength hydrophilic fiber in cement matrix. J Mater Civ Eng 1998;10: 5-13.

[2] Bolat H, S¸ ims¸ ek O, Çullu M, Durmus¸ G, Can €O. The effects of macro synthetic fiber reinforcement use on physical and mechanical properties of concrete. Compos Part B: Eng 2014; 61: 191-198.

[3] Bencardino F, Rizzuti L, Spadea G, Swamy RN. Implications of test methodology on post-cracking and fracture behaviour of Steel Fibre Reinforced Concrete. Compos Part B: Eng 2013; 46: 31-38.

[4] Avraham N. Dancygier, Amnon Katz, David Benamou, David Z. Yankelevsky , Resistance of double-layer reinforced HPC barriers to projectile impact, International Journal of Impact Engineering 2014; 67: 39-51.

[5] Petr Máca, Radoslav Sovják, Petr Konvalinka, Mix design of UHPFRC and its response to projectile impact, International Journal of Impact Engineering 2014; 63: 158-163.

[6] Mohamed Abdel-Kader, Ahmed Fouda, Effect of reinforced on the response of concrete panels to impact of hard projectile, International Journal of Impact Engineering 2014; 63: 1-17.

[7] Trevor D. Hrynyk and Frank J. Vecchio, Behavior of Steel Fiber-Reinforced Concrete Slabs under Impact Load, ACI Structural Journal 2015; 111(5):

[8] Tarek H. Almusallam, Nadeem A. Siddiqui A. Iqbal, Husain Abbas, Response of hybrid-fiber reinforced concrete slabs to hard pojectile impact, International Journal of Impact Engineering 2013; 58: 17-30.

[9] Hongseop Kim, Gyuyong Kim, Nenad Gucunski, Jeongsoo Nam, Joongkyu Jeon, Assessment of flexural toughness and impact resistance of bundle-type polyamide fiber-reinforced concrete, Composites Part B 2015; 78: 431-446

[10] Hongseop Kim, Gyuyong Kim, Jeongsoo Nam, Junghyun Kim, Sanghyu Han, Sanggyu Lee, Static mechanical properties and impact resistance of amorphous metallic fiber-reinforced concrete Composite Structures 2015; 134: 831–844

[11] Jeongsoo Nam, Yasuji Shinohara, Toshiyuki Atou, Hongseop Kim, Gyuyong Kim, Comparative assessment of failure characteristics on fiber-reinforced cementitious composite panels under high-velocity impact, Composites Part B 2016; 99: 84-97

X-RAY MICROTOMOGRAPHIC ANALYSIS OF POROUS BUILDING MATERIALS

Lidija Korat[1], Vilma Ducman[1]

[1] Slovenian National Building and Civil Engineering Institute, The Department of Materials, Laboratory for Cements, Mortars and Ceramics, Dimiceva ulica 12, 1000 Ljubljana, Slovenia, email: lidija.korat@zag.si, vilma.ducman@zag.si

SUMMARY: Recent innovations in the construction industry have led to the development of various types of porous building materials, which are formed by the addition of different foaming agents to waste material matrix. Within the present study, samples such as lightweight foamed aggregates (LWAs), alkali-activated foam (AAF) and autoclaved aerated concrete (AAC) were selected for porosity determination by X-ray computed microtomography (micro CT). Such porous materials are produced with different foaming processes. During these processes, foaming agents release gasses and the resulting gasses remain trapped within the material structure. This study presents the results of the internal sample structure and porosity development of LWAs, AAF and AAC obtained by X-ray computed microtomography. The micro CT investigation gives results on overall porosity, as well as pore size distribution, connected pore space and volume of isolated pore space, depending on the elevated temperature and foaming process. Highly porous structures were obtained, with overall porosities ranges from 37.9 to 42.5% of LWAs, up to 54% for AAF and up to 77% for AAC. Finer pores occurred in the structure, whereas somewhat larger pores (some had diameters greater than 4 mm for AAC) also occurred. The results showed the usefulness of such technique for a wider range of various types of porous building materials with different pore ranges, especially those with larger pores with diameters greater than a few mm.

MIKROTOMOGRAFSKA ANALIZA POROZNIH GRAĐEVNIH MATERIJALA S POMOĆU X-ZRAKA

SAŽETAK: Novijim istraživanjima u građevinskoj industriji razvijene su različite vrste poroznih građevnih materijala nastalih dodatkom različitih sredstava za pjenjenje u matricu otpadnoga materijala. Za određivanje poroznosti s pomoću računalne mikrotomografije s pomoću X-zraka u ovom su radu odabrani uzorci od laganih agregata dobivenih pjenjenjem, alkalno aktivirane pjene i porastoga betona. Ti porozni materijali proizvedeni su različitim procesima pjenjenja. Tijekom procesa sredstva za pjenjenje otpuštaju plinove koji ostaju zarobljeni u strukturi materijala. U radu se prikazuju rezultati dobiveni računalnom mikrotomografijom s pomoću X-zraka o unutarnjoj strukturi uzorka i razvoju poroznosti za tri navedena materijala. Istraživanje računalnom mikrotomografijom daje podatke o ukupnoj porozonosti i raspodjeli veličine pora, obujmu spojenih pora i obujmu izoliranih pora što ovisi o veličini temperature i procesu pjenjenja. Dobivene su vrlo porozne strukture s ukupnom poroznošću između 37,9 i 42,5 % za lagani agregat, do 54 % za alkalno aktiviranu pjenu i do 77 % za porasti beton. U strukturi su nastale finije pore, ali je bilo i nešto većih pora (kod porastoga betona neke su imale promjer veći od 4 mm). Rezultati pokazuju korisnost takvih procesa za dobivanje širokoga raspona različitih vrsta poroznih građevnih materijala s različitim rasponima veličine pora, posebno onih s većim porama promjera većeg od nekoliko milimetara.

1. INTRODUCTION

In the construction industry, different porous building materials are frequently used, mainly for the purposes of improved thermal and/or acoustic insulation properties. Among such porous building materials are lightweight foamed aggregates (LWAs), alkali-activated foams (AAFs) and autoclaved aerated concrete (AAC). Such materials can be used for application in acoustic panels, in lightweight pre-fabricated components for thermal insulation purposes and as an aggregate in concrete which decreases the deadweight of structures [1-3].

LWAs are produced from glassy matrices at different, mainly elevated temperatures (above 900 °C) by a foaming process [4]. Foaming of such expanded material depends on the firing temperature, as well as the initial composition of the raw material, and/or dwelling time. During this process, foaming agents release gasses and the resulting gasses remain trapped within the glassy structure [5]. Different foaming agent(s) can be selected from sulphides, carbonates, water-glass, Fe_2O_3, MnO_2, SiC [6-8].

AAFs are inorganic systems, consisting of reactive solid component (SiO_2 and Al_2O_3) in reactive form (fly ash, clays), alkaline activation solution (contains alkali hydroxides and silicates) and foaming agents, such as H_2O_2, NaOCl, metal powders such as aluminium or zinc powder, or a silica fume [3, 9-12]. AAFs are formed at temperatures below 100 °C [3,10].

AAC is a widely-used building material because of its insulation properties obtained with hardening the mortar. Generally, it is produced from a mix of raw materials (quartz sand, fly ash, Portland cement, lime, gypsum), water and foaming agent (aluminium powder) [13-15].

Such porous constructions materials consist of different raw waste (fly-ash, paper sludge, slag etc.) based matrix and differ due to the foaming processes and foaming agents used. Foaming agent(s), and the previously mentioned parameters, greatly influence the density, especially the development of porosity within the material structure. The maximum density of LWAs could reach 2 g/cm^3 [16] and those reported in the literature vary from 0.3 to 1 g/cm^3 [17]. Density of AAFs reported in the literature varies from 0.6 to 1.4 g/cm^3 [2, 10] and of AAC from 0.3 to 1.8 g/cm^3 [14]. As Pehlivanlı [14] said, the thing that provides the feature of high thermal insulation and the feature of being the most lightweight material is dry air tucked into these tiny pores. Porosity of LWAs ranges around 70% [1, 18] and of AAFs between 30 to 70% [2, 19, 20]. 60–80% of the AAC structure consists of pores including stagnant air [14, 15]. Due to the material structure, such porous building materials usually have closed porosity. If the porosity is of the closed type, then conventional techniques for the porosity determination, such as water absorption or mercury intrusion porosimetry (MIP) are not suitable because the medium cannot reach the pores. In such cases only X-ray computer microtomography is an adequate technique.

X-ray computed microtomography (micro CT) is a user-friendly non-destructive technique for the evaluation of various porous building materials within the maximum resolution of about 1 µm; the size of the specimens has an impact on the final resolution, where X-ray absorption is an exponential function of the sample thickness and scanning time is highly dependent on sample size. It is an X-ray based imaging technique that can provide 3D images of the internal sample structure. Its main advantages are that the specimens of different building materials do not require special pre-treatment or preparation and can be analysed several times using different sample exposures. Regarding that, the size of the specimens has an impact on the final resolution. With X-ray computed microtomography and its absorption factors of different phases, it is easy to detect special features, especially voids or pores. With further special image analysis, it is possible to determine pore-size distribution, overall porosity and other 2D and 3D information on each pore, where such parameters are crucial for a good understanding of the material's properties. Also with an appropriate software programme permeability and thermal conductivity of the material could be determined, which is one of the very important parameters for thermally resistant materials.

Within the present study, samples such as lightweight foamed aggregates (LWAs), alkali-activated foams (AAFs) and autoclaved aerated concrete (AAC) were selected for porosity determination by X-ray computed microtomography.

2. EXPERIMENTAL

2.1. MATERIALS

Lightweight foamed aggregates (LWAs) were prepared by a foaming process with waste glass, silica sludge (containing mostly quartz and some feldspar), and MnO_2 [21]. The LWAs were heated up to the selected temperatures (1060, 1070, 1080) at a heating rate of 10 °C/min, with a dwelling time of 0 min.

Alkali-activated foam (AAF) was prepared also by a foaming process using fly ash, H_2O_2 foaming agent, water-glass activating solution and NaOH, where the foaming agent was first added to the solution of water glass, NaOH and fly ash. A more detailed foaming process is reported in Ducman et al. [2]. Autoclaved aerated concrete was taken from the market.

2.2. TECHNIQUE

Samples of LWAs, AAF and AAC were analysed by "Xradia 400" X-ray computed microtomograph (XRadia, Concord, California, USA). Using a high precision rotating stage, a larger number of projection images was taken from different view-points with different exposure times per projection. The transmitted images were detected by an X-ray image detector, which consisted of a CCD camera equipped with a 0.39X magnification optical objective. More detailed scanning parameters and pixel resolution under these conditions are reported in Table 1, depending on the sample.

Table 1 X-ray computed microtomography scanning parameters.

Sample	Size of the sample (cm)	Energy	Number of projection	Exposure times (s)	Pixel resolution (µm)
LWAs	diam. ~ 2.0	80 kV, 125 µA	1000	5	12
AAF	2.0 x 2.0 x 2.0	80 kV, 125 µA	1000	2	32
AAC	3.0 x 3.0 x 5.0	80 kV, 125 µA	1600	2	34

Samples of LWAs, AAF and AAC were analysed later by Avizo Fire 3D image analysis software, which was used to obtain 3D representations of the pore structure of the material, following the process for pore segmentation, object separation and quantification described by Korat et.al. [1] and Ćosić [22].

3. RESULTS

3.1. LIGHTWEIGHT FOAMED AGGREGATES (LWAS)

X-ray computed microtomography was used for 3D representations of the pore structure and for the determination and evaluation of the number of pores and 3D volume of LWAs. From Figure 1 it can be seen that the distribution of pores is uniform throughout the material structure and enlarged by the heating temperature, which is expected since a higher temperature promotes the foaming agent's decomposition.

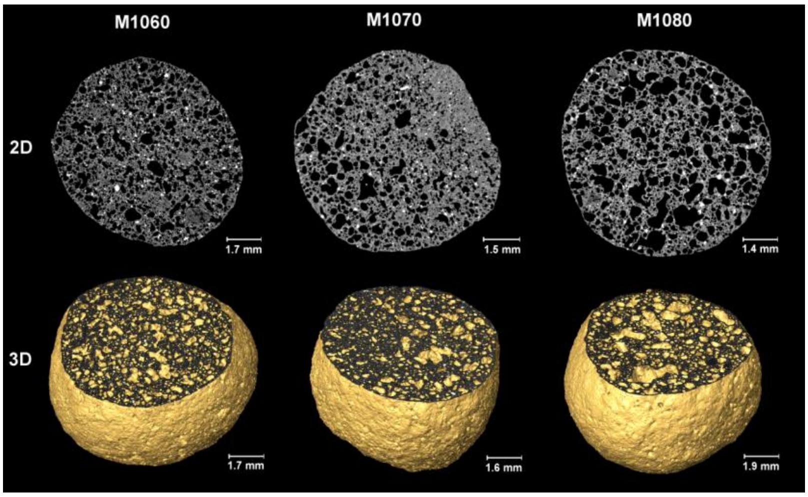

Figure 1 Lightweight foamed aggregates (LWAs) fired at 1060, 1070 and 1080 °C, grayscale images and 3D pore shape images obtained by X-ray computed microtomography.

Avizo Fire 3D image analysing software programme was used for quantitative analysis of LWAs, and the results are presented in Figure 2 and Table 2. Due to the pixel resolution of the materials, the results can be obtained for pores above 40 µm. As expected, overall porosity increased with temperature (Table 2), and ranges from 37.9 to 42.5%, depending of the sample. It can be further seen from Figure 2 (a), the pore size distribution is calculated and presented as the "number of pores" versus the "pore size", that the largest number of pores is in the range of 50–100 µm, and seen from Figure 2 (b), calculated and presented as the "volume of pores" versus "pore size", confirmed that the volume of the pores enlarge upon heating temperature, where approximately 97% of the pores volume lies in the range above 250 µm (Table 2).

a)

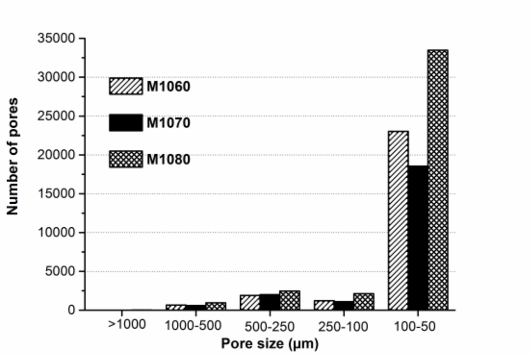

b)

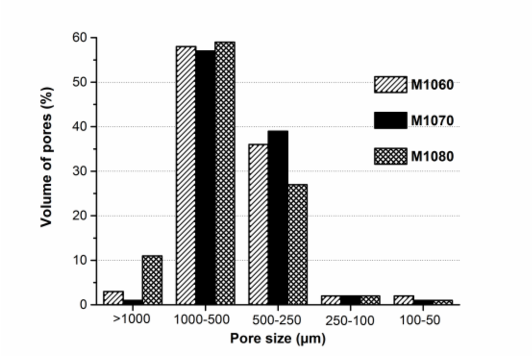

Figure 2 Pore size distribution determined by means of X-ray computed microtomography for the lightweight foamed aggregates (LWAs) fired at 1060, 1070 and 1080 °C, presented as (a) the number of pores with regards to pore size, and (b) as the volume of pores with regard to pore size.

3.2. ALKALI-ACTIVATED FOAM (AAF)

Pore structure of AAF is presented in Figure 3 (a) and the results of quantitative analysis of AAF, volume of pores with regard to pore size, are presented in Table 2 and Figure 3 (b). Two-dimensional (XZ orientation) cross-section of AAF, Figure 3 (a), shows a fine porous structure, with the average pore size 0.3 mm and dimensions of larger pores up to 1 mm. From Table 2 it can be seen that overall porosity is 54% of the total volume, where approximately 79% of the pores volume lies in the range above 1 mm (Table 2). With Avizo Fire 3D image analysing software programme, beside the overall porosity, the volume of connected pore space (pores that are connected to others and to external surface), and the volume of isolated pore space (pores that are not connected to the external space) were evaluated. The volume of connected pore space of AAF was 25.3% and the volume of isolated pore space of AAF was 28.7%.

Table 2 Overall porosity and share of pores for the LWAs, AAF and AAC, determined by X-ray computed microtomography.

Samples	Overall porosity (%)	Share of pores within the range of pore size (%):				
		40-100 μm	100-250 μm	250-500 μm	500-1000 μm	≥ 1000 μm
M1060	37.9	2	2	36	58	3
M1070	39.7	1	2	39	57	1
M1080	42.5	1	2	27	59	11
AAF	54.0	<1	<1	<1	21	79
AAC	77.2	<1	<1	<1	2	98

3.3. AUTOCLAVED AERATED CONCRETE (AAC)

The pore structure of AAC is also presented in Figure 3 (a), and the results of quantitative analysis of AAC are presented in Table 2 and Figure 3. (b). From Figure 3 (a), the cross-section in YZ orientation of AA shows a very porous structure, with the average pore size 2 mm and dimensions of larger pores up to 6 mm. The AAC structure is much more porous than the structure of AAF, where overall porosity is around 77% of the total volume, where approximately all (98%) of the pores volume lies in the range above 1 mm (Table 2). If we divide this area into more detail, still 64% of the pores volume can be attributed to the larger pores, which lies in the range above 4 mm, 27% of the pores volume lies in the range between 2-4 mm and 9% of the pores volume between 1 and 2 mm. Also, the volume of the connected pore space of AAC was 34.5% and volume of isolated pore space was 42.7%.

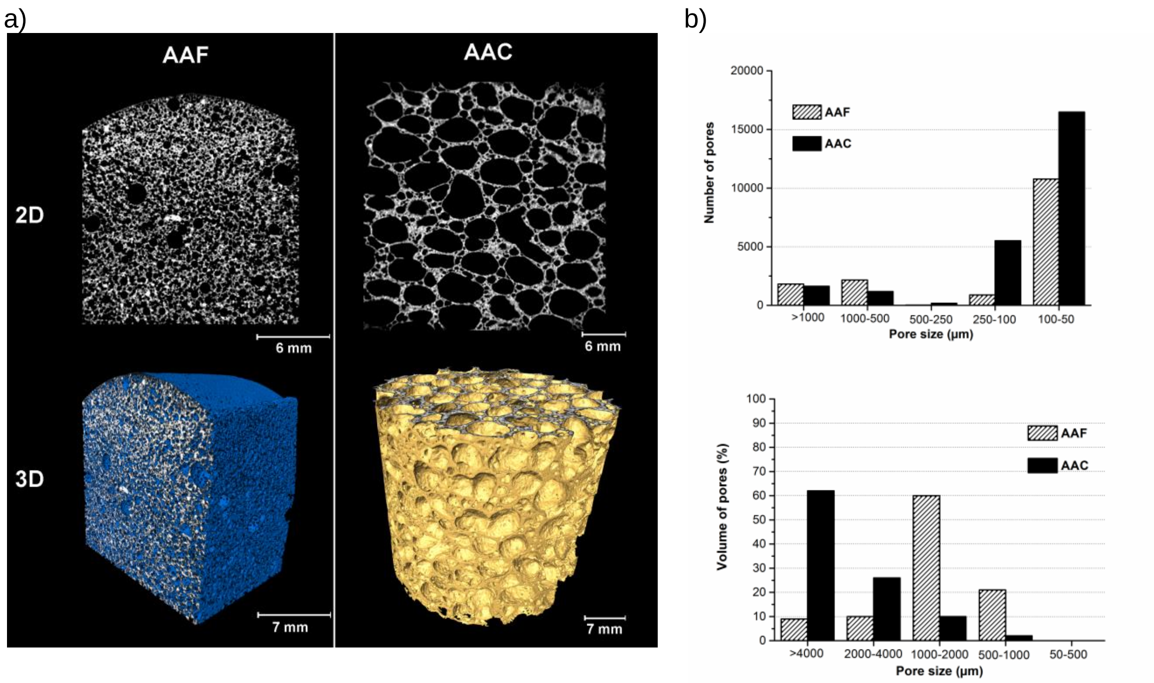

Figure 3 (a) Slice images (XZ for AAF and YZ for AAC) and 3D images, (b) Pore size distribution (as the number of pores with regards to pore size, and as the volume of pores with regard to pore size), of AAF and AAC obtained by X-ray computed microtomography.

4. CONCLUSIONS

The internal sample structure and porosity development of LWAs, AAF and AAC were evaluated by means of X-ray computed microtomography. In the case of all samples, the pores were found to be uniformly distributed throughout the sample structure and their number and size depends on the foaming process, agent or temperature. The results of microtomography have shown the usefulness of such technique for a wider range of various types of porous building materials. X-ray computed microtomography is a powerful and important technique due to its non-destructive three-dimensional characterization, where samples could be used several times and also compared with other techniques. Supported with appropriate 3D image analysing software programme beside overall porosity, pore size distribution, connected pore space and volume of isolated pore space can be determined. As seen from the results, X-ray computed microtomography seems to be an appropriate methodology for the study of various types of porous building materials (Figure 4) and provides much wider possibilities for the graphic presentations of the results.

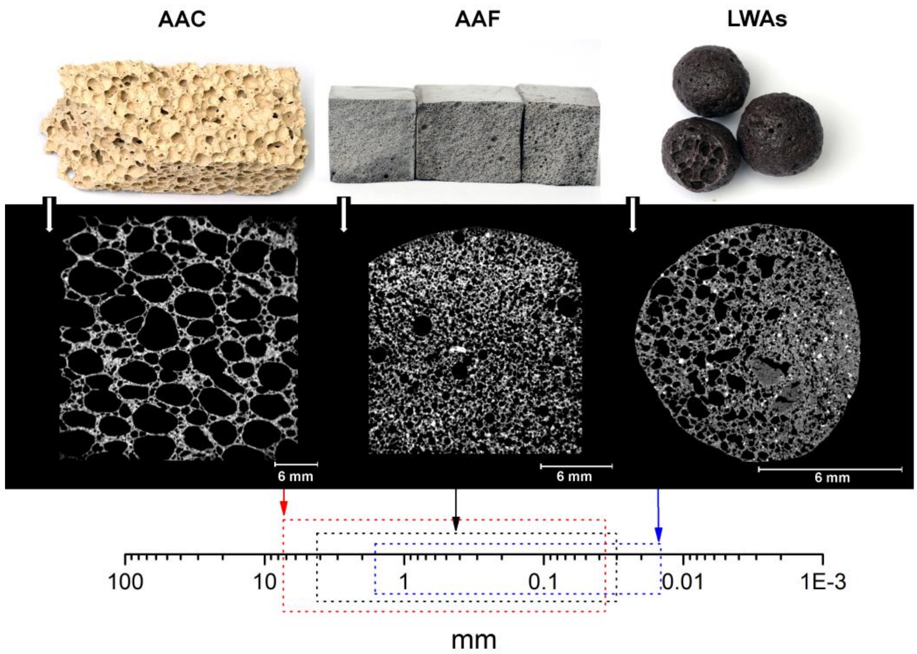

Figure 4 Macro images and slice images, obtained by X-ray microtomography, of investigated samples

ACKNOWLEDGMENTS

This work has been financially supported by the Slovenian Research Agency (ARRS) through the programme P2-0273: Building structures and materials and J1-7148: 3D and 4D microscopy - development of new powerful tools in geosciences.

REFERENCES

[1] Korat, L.; Ducman, V.; Legat, A.; Mirtič, B.: Characterisation of the pore-forming process in lightweight aggregate based on silica sludge by means of X-ray micro-tomography (micro-CT) and mercury intrusion porosimetry (MIP), Ceramic International, Vol. 39 (2013), pp. 6997–7005, ISSN 0272–8842.

[2] Ducman, V.; Korat, L.: Characterization of geopolymer fly-ash based foams obtained with the addition of Al powder or H2O2 as foaming agents, Materials characterization, Vol. 113 (2016), pp. 207–213, ISSN 1044–5803.

[3] Łach, M.; Kornjiejenko, K.; Mikuła, J.: Thermal insulation and thermally resistant materials made of geopolymer foams, Procedia Engineering, Vol. 151 (2016), pp. 410–416, ISSN 1877–7058.

[4] Bremner, T.W.; Ries, J.P.; Wolf, W.H.: Environmental friendly uses of lightweight aggregates, Proceedings of the International Sustainable Development of Cement, Concrete and Concrete Structures, Malhotra, V.M.; Sakai, K. (Ed.), October 5-7 2005, pp. 201–210.

[5] Köse, S.; Bayer, G.: Schaumbildung im System Altglas-SiC und die Eigenschaften derartiger Schaumgläser, Glastechn. Ber. 55, Vol. 7 (1982), pp. 151–160.

[6] Bernardo, E.; Cedro, R.; Florean, M.; Hreglich, S.: Reutilization and stabilization of wastes by the production of glass foams, Ceramics International, Vol. 33 (2007), pp. 963–968, ISSN 0272–8842.

[7] Ducman, V.: Foaming process of waste glass using CaCO3, MnO2 and water-glass as foaming agents, In: Limbachiya, Mukesh, C.; Roberts, J. J. (Ed.). pp. 59–66. Sustainable waste management and recycling, Glass waste. London: Thomas Telford,

[8] Bernardo, E.; Scarinci, G.; Hreglich, S.: Foam glass as a way of recycling glasses from cathode ray tubes, Glass. Sci. Technol. 78, Vol. 1 (2005), pp. 7–11, ISSN 0946–7475.

[9] Abdullah, MMB.; Hussin, K.; Bnhussain, M.; Ismail, KN.; Yahya, Z.; Razak, RA.: Fly Ash-based Geopolymer Lightweight Concrete Using Foaming Agent. Int. J Mol. Sci. (2012), pp. 13:7186–7198, ISSN 1422–0067.

[10] Masi, G.; Rickard, WDA.; Bignozzi, MC.; Riessen, A: The influence of short fibres and foaming agents on the physical and thermal behaviour of geopolymer composites, Advances in Science and Technology, Vol. 92 (2014), pp. 56–61, ISSN 0272–8842.

[11] Hlavaček, P.; Šmilauer, V.; Škvara, F.: Alkali-activated fly ash foams – synthesis, chemo-physical properties and microstructure modelling, Advances in Science and Technology, Vol. 92 (2014), pp. 14–19, ISSN 1662–0356.

[12] Sanyan, JG.; Nazari, A.; Chen, L.; Nguyen, H.: Physical and mechanical properties of lightweight aerated geopolymer, Construction and Building Materials, Vol. 79 (2015), pp. 236–244, ISSN 0950–0618.

[13] Rozycka, A.; Pichór, W.: Effect of perlite waste addition on the properties of autoclaved aerated concrete, Construction and Building Materials, Vol. 120 (2016), pp. 65–71, ISSN 0950–0618.

[14] Pehlivanlı, Z.O.; Uzun, I.; Yücel, Z.P.; Demir, Z.: The effect of different fiber reinforcement on the thermal and mechanical properties of autoclaved aerated concrete, Construction and Building Materials, Vol. 112 (2016), pp. 325–330, ISSN 0950–0618.

[15] Narayanan, N.; Ramamurthy, K.: Structure properties of aerated concrete: a review. Cement and Concrete Composites, Vol. 22 (2000), pp. 321–329, ISSN 0958–9465.

[16] EN 13055-1:2002, Lightweight aggregates. Lightweight aggregates for concrete, mortar and grout, BSI.

[17] The Concrete SOCIETY, Lightweight aggregates, Available from: http://www.concrete.org.uk/fingertips-nuggets.asp?cmd=display&id=849, Accessed:2016-01-10.

[18] Volland, S.; Brötz, J.: Lightweight aggregates produced from sand sludge and zeolitic rocks, Construction and Building Materials, Vol. 85 (2015), pp. 22–29, ISSN 0950–0618.

[19] Hlavaček, P.; Šmilauer, V.; Vorel, J.: Engineering Properties of Alkali Activated Fly Ash Foams 21st International Conference ENGINEERING MECHANICS 2015, pp. 90–91, Svratka, Czech Republic, May 11 – 14, 2015 Paper #227.

[20] Dembovska, L.; Bajare, D.; Ducman, V.; Korat, L.; Bumanis: The use of different by-products in the production of lightweight alkali activated building materials, Construction and Building Materials, Vol. 135 (2017), pp. 315–322, ISSN 0950–0618.

[21] Ducman, V.; Korat, L.; Legat, A.; Mirtič, B.: X-ray micro-tomography investigation of the foaming process in the system of a waste glass - silica mud - MnO2. Materials characterization, Vol. 86 (2013), pp. 316-321, ISSN 1044–5803.

[22] Ćosić, K.; Korat, L.; Ducman, V.; Netinger, I.: Influence of aggregate type and size on properties of pervious concrete, Construction & building materials, Vol. 78 (2015), pp. 69–76, ISSN 0950-0618.

IN-SITU BEND TESTS ANALYZED BY X-RAY TOMOGRAPHY AND DIGITAL VOLUME CORRELATION

Amine Bouterf[1], Benjamin Smaniotto[1], François Hild[1], Stéphane Roux[1]

[1] ENS Paris-Saclay / CNRS / Université Paris-Saclay, Laboratoire de Mécanique et Technologie (LMT), 61 avenue du Président Wilson 94230 Cachan, France, email: bouterf@lmt.ens-cachan.fr, smaniotto@lmt.ens-cachan.fr, francois.hild@lmt.ens-cachan.fr, stephane.roux@lmt.ens-cachan.fr

SUMMARY: In-situ three- and four-point bend tests on lightweight plasterboard samples were carried out inside a tomograph. Global and regularized digital volume correlation was used to follow the kinematics of the tests. Cracking of plaster in the tensile face of the sample was detected as the first event in the sequence leading to failure. Yet the paper is able to withstand the transfer of stress, which leads to a progressive degradation of the stiffness of the plate by multi-cracks of the core. The analysis of the tests leads to conclude that the mechanical behaviour of plasterboard in bending is essentially governed by the mechanical properties of the paper and the quality of the paper-plaster interface.

ISPITIVANJA NA SAVIJANJE IN-SITU ANALIZIRANA TOMOGRAFIJOM I DIGITALNOM VOLUMENSKOM KORELACIJOM

SAŽETAK: U uređaju za tomografiju provedeno je ispitivanje uzoraka od gipskartonskih ploča ispitivanjem na savijanje opterećenjem u tri i četiri točke. Za određivanje kinematike ispitivanja upotrijebljena je globalna i regularizirana digitalna volumenska korelacija. Kao prva pojava u nizu koja dovodi do sloma otkriveno je raspucavanje gipsa na vlačnom licu uzorka. Ipak se potom papir odupire prijenosu naprezanja što dovodi do progresivne degradacije krutosti ploče s višestrukim pukotinama jezgre. Analiziranjem ispitivanja dolazi se do zaključka da na mehaničko ponašanje gipskartonske ploče pri savijanju bitno utječu mehanička svojstva papira i kvaliteta sučeljka papir – gips.

1. INTRODUCTION

Economic and technological developments have given rise to increasingly demanding requirements in terms of safety, comfort, functionality and energy consumption. They ask for the development or improvement of new concepts. It is in this context that plasterboard was invented by A. Sackett in 1894. Since its invention, the manufacturing process of this product has steadily improved to meet new standards. The current trend is on the one hand towards lightening the gypsum board in order to minimize energy consumption while optimizing the mechanical properties, and on the other hand towards the multi-functionality of materials combining, for example, good mechanical characteristics with properties such as thermal and acoustic insulation.

Plasterboards are sandwiches composed of a plaster foam core cast between two paper linings. They are now the most widely used interior finish in construction. Plaster is a material particularly suitable for indoor use thanks to its thermal and acoustic insulation properties and its fire resistance. However, the energy consumption represents about 25% of the production costs of the gypsum board. Sustainable development leads to lighten the gypsum board with lighter and lighter foam. This alleviation unfortunately leads to a weakening of the mechanical properties of the plate. In addition to the fire resistance to be checked, a lightweight plate must meet mechanical requirements, the most severe of which is resistance to bending, a crucial mechanical property for transport, handling and installation of the plate. The fine understanding of mechanical behaviour and the physics of damage of the gypsum board during loading is a key element in the definition of the optimum microstructure of plasterboard compatible with the current standards.

Modern plasterboard has a core of controlled porosity, dense plaster layers at the paper-plaster interface. The original work on this subject was carried out by Bruce et al. [1] by demonstrating that light gypsum boards with good mechanical properties can be obtained by controlling the distribution of foam. It should be noted that, although the weight of the plate is an important factor for its mechanical properties, there are few (if any) published results on the mechanical behaviour of lightweight gypsum board. Moreover, very little information is available concerning the mechanical connection between paper and plaster. The latter will be sought by performing in-situ tests. Contrary to in-situ compressive or tensile tests, bending tests are rarely discussed in the literature.

In order to evaluate the performance of clay barriers that constitute radioactive waste, Nakano et al. [2] carried out in-situ equibiaxial bend tests on compacted clay. The tomographic observations show that the cracks were generated from the tensile face of the specimen and propagated towards the upper face with increasing load. Forsberg et al. [3] carried out a three-point bend test on wood. The sample was imaged at different loading levels up to final failure. The authors exploited the reconstructed volumes via local Digital Volume Correlation (DVC). The inception of compressive and tensile bands, respectively in the upper and lower regions, separated by a neutral fibre in the medium are in agreement with what is expected for a sample subjected to three-point bending. This study showed the feasibility of measuring three-dimensional displacements fields on wood at a microscopic scale. Recently, Brault et al. [4] developed an experimental in-situ bend device. They carried out three-point bend tests on carbon / epoxy composites. In order to increase the contrast in the structure of the composite, copper particles were added, which served as markers. According to the authors the measurement uncertainty is of the order of 0.04 voxel, and it can increase in the vicinity of the supports. The use of tomographic acquisitions coupled with DVC revealed the transverse shear effects that occur during the bend test in composite materials.

DVC is an extension of digital image correlation [5, 6, 7]. The first implementations consisted in registering small volumes of interest (or sub-volumes) in order to determine their mean translation [8]. Local rotations were added later on [9]. The warping distortion of the sub-volume was also introduced [10]. All these approaches are called "local" since each analysis is local (i.e. on the scale of the interrogation volume) and no kinematic constraints are enforced with neighbouring sub-volumes. The average displacement of each sub-region is assigned to its centre. Hence the resulting displacement field will not be continuous [11] but consists of a cloud of points. In order to give a certain consistency to the measurement over the whole region of interest (ROI) an estimated (discrete) motion field interpolation is carried out. This interpolation, and the corresponding filtering, takes place in a second step unrelated to the analysed images. This is a weakness of this approach because it prohibits a proper evaluation of the quality of the obtained result. However, it is the most used approach today. It has the major advantage of being parallelised very easily and does not require very large storage in memory.

The global approach was subsequently introduced [12]. Contrary to local approaches, the sought displacement field is defined over the whole ROI. For example, a kinematics is imposed by projecting the sought displacement field on a (continuous) finite element basis [12]. If cracks are to be analysed, enriched kinematics have also been introduced [13,14]. Another step is to regularise the registration problem by requiring the measured displacement field to be mechanically admissible locally [15, 16]. In particular, in areas where the texture of the image is not sufficiently contrasted, regularisation is used to extrapolate the displacement field [17]. The spatial integration of the difference between the deformed configuration corrected by the estimated displacement field and the reference configuration is called the global residual. It is of the order of a few percent in the usual cases. It gives indications on the non-satisfaction of kinematic hypotheses on which the determination of the sought displacement field has been carried out and on the noise level.

The above bibliographic study showed that in-situ bend tests are very seldom carried out. Previous works have shown that local DVC was feasible to estimate displacement and strain fields. In the remainder of this paper, a complete methodology for the analysis of in-situ three- and four-point bend tests is proposed. The aim is to: (i) perform in-situ bend experiments in order to better understand the mechanism of failure of plasterboard, and (ii) confirm the proposed failure scenario from surface observations [18]. After a description of the different experiments, the failure scenario of the studied plates will be discussed according to the tomographic observations coupled with DVC analyses.

2. METHOD

The samples are prepared from industrial plasterboard. The tested specimens are cut to a size of 200 × 13 × 15 mm^3. They are tested in-situ in three- and four-point bending. The distance between the external supports is 150 mm. In four-point bending, the distance between the two central supports is 40 mm. The supports are machined PMMA cylinders 16 mm in diameter. The bend assembly used in this study is shown in Figure 1. It gives the possibility to test two specimens at the same time. The central part of the device is clear from any obstruction in order to allow X-ray transmission. Loading is applied manually by turning the two wing screws symmetrically.

The samples were imaged in the initial state (i.e. without loading) and at several loading levels. The experiments were carried out on the LMT tomograph (NSI X50+) with the following acquisition parameters: the tension of the beam is 90 kV and the electron current 200 µA, the physical size of the voxel is 25 µm. 900 radiographs are acquired in a 360 -rotation for each scan. The total duration of an acquisition is 60 minutes.

Figure 1 In-situ bend test device

3. RESULTS

3.1. THREE-POINT BEND TEST

The sample was imaged in the initial state and then at four load levels (i.e. scans (a), (b), (c) and (d)) at a resolution of 25 µm. It was chosen to analyse only one half of the specimen in order to demonstrate the appearance of delamination cracks between the tensile paper and the core of the plate. The volume of interest analysed by DVC has a size of $840\times444\times348$ voxels^3. The size of the 8 noded cubes (i.e. C8 elements) was chosen to be equal to 12 voxels. The regularisation length is equal to 20 voxels. Figure 2 shows 3D renderings of the measured fields for the fours scans. For scans (a) and (b), Figure 2(a-b), the elastic regime predominates and no cracks have been detected. For scan (c), Figure 2(c), the first crack appeared in the core of the plate. The longitudinal displacement field, U_x, has a pronounced discontinuity around x = 100 voxels. This crack is also detected on the residual field. For the last scan, Figure 2(d), the sample shows, just before failure, multiple cracks most of which have been shielded (i.e. closed). The dominant crack, which leads to the final failure of the sample, is also observed. It is important to note that the core of the plate has variable crack shapes in the width of the sample. There is a transition from a single crack with a very pronounced delamination to coalescence of multiple cracks where the delamination between the paper and the plaster is less developed.

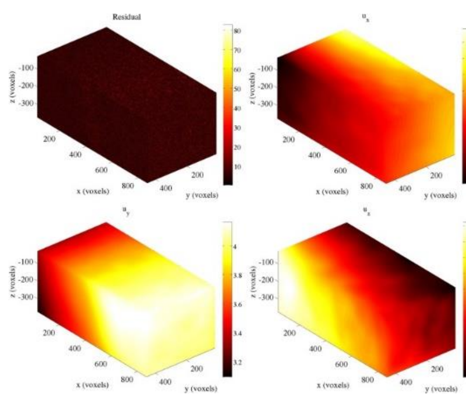

(a) Scan (a)

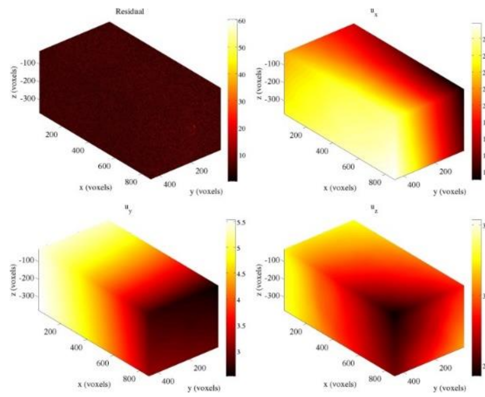

(b) Scan (b)

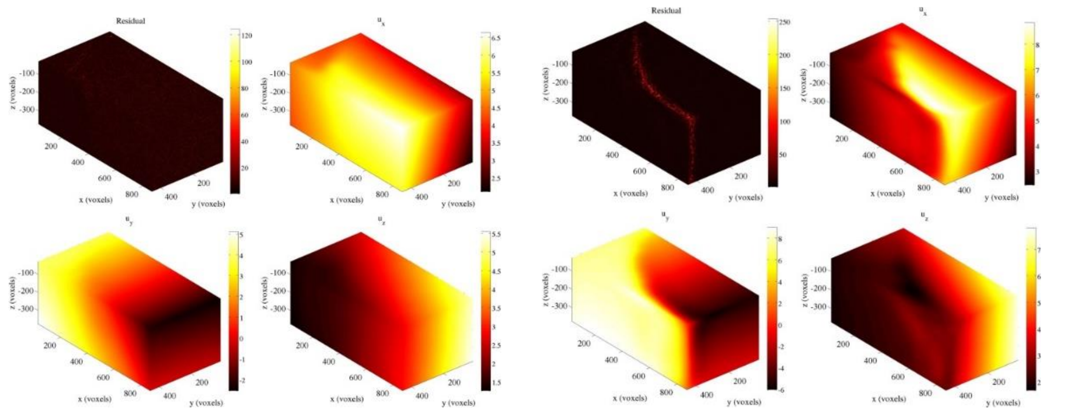

(c) Scan (c) (d) Scan (d)

Figure 2 DVC analyses of 3-point bending. 3D renderings of displacement fields measured by DVC corresponding to scans (a), (b), (c) and (d). The displacement fields are expressed in voxels (1 voxel ↔ 25µm). The correlation residuals are expressed in grey levels

3.2. FOUR-POINT BEND TEST

The sample was imaged at initial state and then at three levels of loading. Figure 3 shows the analysed volumes by DVC. The ROI after voxel aggregation has a size of 792 × 192 × 192 voxels^3. The size of the C8 elements was chosen to be equal to 12 voxels. The regularization length is 30 voxels. The physical voxel size becomes 50 µm.

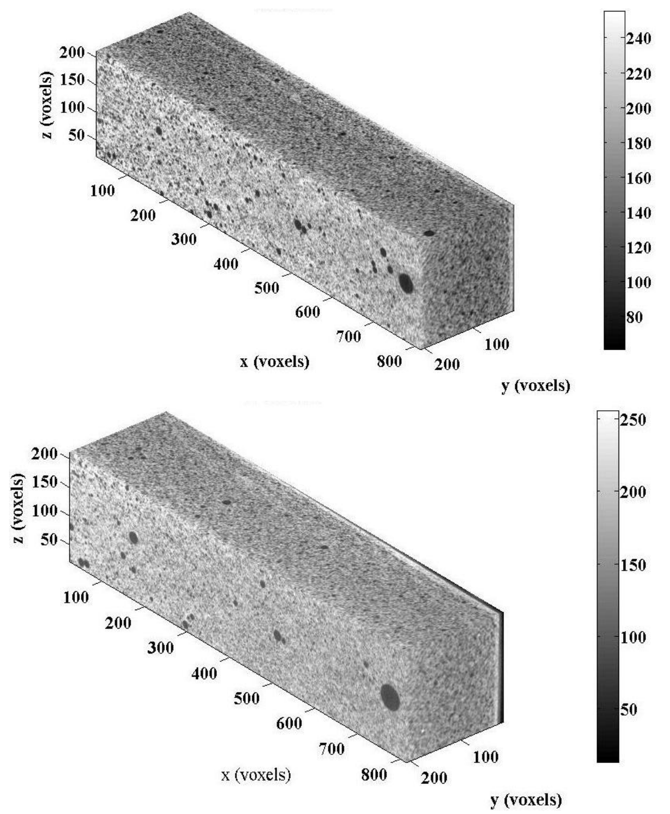

(a) Reference configuration (b) Scan (a)

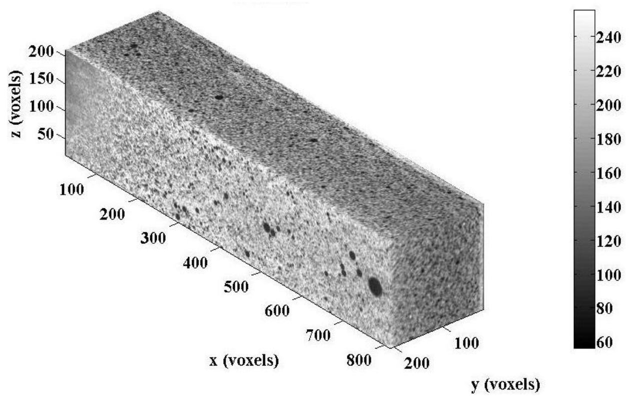

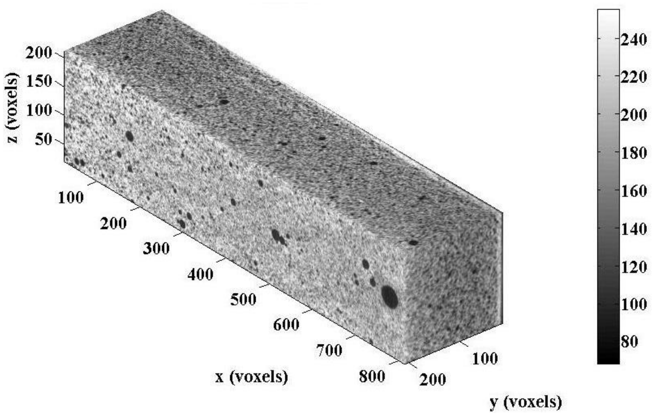

(c) Scan (b)   (d) Scan (d)

Figure 3 3D renderings of the microstructure of foamed gypsum subjected to 4-point bending (1 voxel ↔ 50 µm)

The DVC results are shown in Figure 4. For scan (a), Figure 4(a), the sample is stressed in the elastic domain. No sign of discontinuity on the measured displacement fields and the correlation residual field is homogeneous throughout the volume (mean correlation residual = 2.57 % of the dynamic range of the reference scan). For scan (b), Figure 4(b), the longitudinal displacement field (U_x) presents multiple discontinuities along the specimen length. These discontinuities are more pronounced for scan (c), Figure 4(c). The correlation residual fields of scans (b) and (c) are homogeneous throughout the analysed volume. The mean correlation residual for the last scan is equal to 2.65 % of the dynamic range of the reference scan (i.e. virtually identical to the level observed when no cracks were present). The crack network estimated from the longitudinal strain fields is illustrated in Figure 4(d). The development of the crack network is clearly observed. The sample presents multiple cracks before failure perpendicular to the longitudinal axis of the sample. It is also observed that the crack spacing is of the order of the thickness of the plate.

It should be noted that in the two experiments discussed herein the correlation residual fields (with the exception of Figure 4(d)) show no traces of cracks because they are not very open. Discontinuities on the displacement fields are also less visible; this is related to the effect of mechanical regularization on the displacement fields (i.e. smoothing effect). Conversely, the strain fields give very clear indications of the presence of numerous cracks. Let us insist on the fact that the tomographic observations alone would not allow to deduce the mechanism of failure of plasterboard in bend tests. The contribution of DVC is crucial in order to finely analyse the tests.

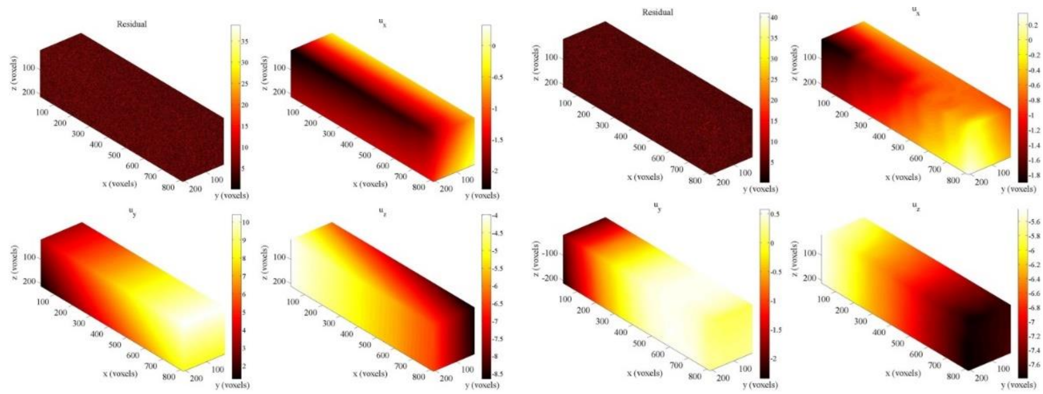

(a) scan (a) (b) scan (b)

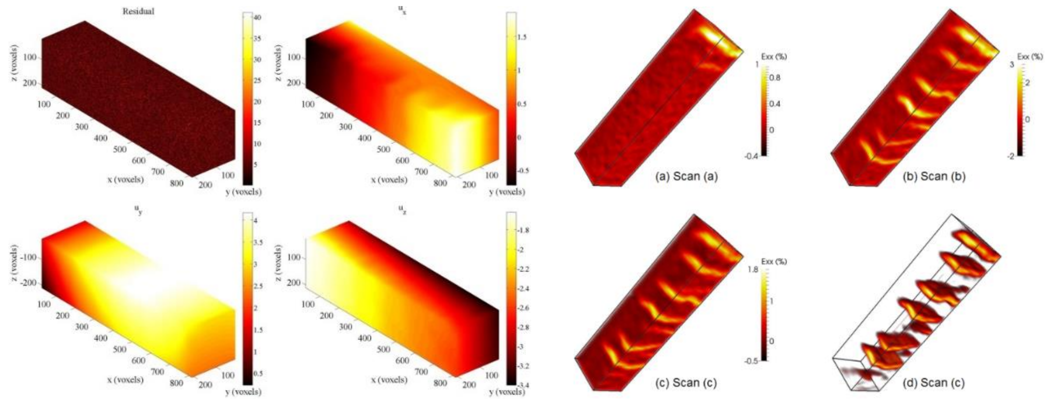

(c) scan (c) (d) ε_{xx}

Figure 4 DVC results in 4-point bending. 3D renderings of the measured fields corresponding to scans (a), (b) and (c). (d) 3D renderings of the measured longitudinal strain ε_{xx} in (%) for all scans. The displacement fields are expressed in voxels (1 voxel ↔ 50 µm). The correlation residuals are expressed in grey levels

4. CONCLUSIONS

In-situ three-point and four-point bend tests were performed on plasterboard samples up to failure. Thanks to the association of tomographic observations, global and regularized digital volume correlation, the mechanisms of failure of the plate in bending was identified. Cracking of the core is detected as the early phenomenon in the failure scenario. The presence of paper linings allows for a gradual degradation of the rigidity of the plate by multiple cracking of the core. The present results confirm in particular the initiation and propagation of mode II cracks (i.e. delamination) between the tensile paper face and the core of the plate. These observations lead to the conclusion that the mechanical behaviour of plasterboard in bending is essentially governed by the mechanical properties of the paper and the quality of the paper-plaster interface.

In this paper it has been shown that in order to analyse finely the different tests the use of digital volume correlation as experimental tool is priceless. In some tests discussed in this paper (i.e. four-point bending), the detection of cracks via correlation residual fields alone is not possible. The fine analysis of the displacement fields, in particular along the direction of opening of the cracks, provides valuable information on the development of the crack network. The latter is also observable on the strain fields.

ACKNOWLEDGMENTS

For the completion of this work, AB has been supported by a CIFRE PhD fellowship from ANRT and Saint-Gobain. The authors are thankful to E. Maire, S. Meille, J. Adrien, R. Gy and X. Brajer for stimulating discussions. This work has been financially supported by the French Agence Nationale de la Recherche through the ‘‘Investissements d’avenir” program (ANR-10-EQPX-37 MAT-MECA grant).

REFERENCES

[1] Bruce, R & Mitakidis, D.: Improved Gypsum Board. U.S. Patent No. 5,085, 929, 1992.
[2] Nakano, T. et al.: Development of a Bending Test Apparatus for Quasi-dynamical Evaluation of a Clayey Soil Using X-ray CT Image Analysis. Visualization using industrial x-ray CT scanner. Advances in Computed Tomography for Geomaterials : GeoX 2010 Edited by Khalid A. Alshibli and Allen H. Reed 2010 ISTE Ltd. Published 2010 by ISTE Ltd.
[3] Forsberg, F. et al.: Full Three-Dimensional Strain Measurements on Wood Exposed to Three-Point Bending: Analysis by Use of Digital Volume Correlation Applied to Synchrotron Radiation Micro-Computed Tomography Image Data. Strain, 46, 47-60, 2010.
[4] Brault, R. et al.: In-situ Analysis of Laminated Composite Materials by X-ray Micro-Computed Tomography and Digital Volume Correlation. Exp.l Mech., 53, 1143-1151, 2013.
[5] Sutton, M.A. et al.: Determination of displacements using an improved digital correlation method. Image Vision Comput., 1(3), 133-139, 1983.
[6] Chu, T.C. et al.: Applications of digital image-correlation techniques to experimental mechanics. Exp. Mech, 3(25), 232-244, 1985.
[7] Besnard, G.; Hild, F.; & Roux, S.: "Finite-element" displacement fields analysis from digital images: application to Portevin-Le Châtelier bands. Exp. Mech, 46, 789-803, 2006.
[8] B.K., Bay, B.K. et al.: Digital volume correlation: three-dimensional strain mapping using x-ray tomography. Exp. Mech., 39, 217-226, 1999.
[9] Smith, T.S.; Bay, B.K. & Rashid, M.M.: Digital volume correlation including rotational degrees of freedom during minimization. Exp. Mech, 42, 272-278, 2002.
[10] Verhulp, E.; van Rietbergen, B. & Huiskes, R.: A three-dimensional digital image correlation technique for strain measurements in microstructures. J. Biomech, 37, 1313-1320, 2004.
[11] Bornert, M. et al.: Mesure tridimensionnelle de champs cinématiques par imagerie volumique pour l’analyse des matériaux et des structures. Instrum. Mes. Métrol., 4(3-4), 43-88, 2004.
[12] Roux, S. et al.: Three dimensional image correlation from X-ray computed tomography of solid foam. Comp. Part A, 39, 1253-1265, 2008.
[13] Réthoré, J. et al.: Extended threedimensional digital image correlation (X3D-DIC). C. R. Mécanique, 336, 643- 649, 2008.
[14] Rannou, J. et al.: Three dimensional experimental and numerical multiscale analysis of a fatigue crack. Comp. Meth. Appl. Mech. Eng, 199, 1307-1325, 2010.
[15] Leclerc, H. et al.: Voxel-scale digital volume correlation. Exp. Mech, 51(4), 479-490, 2011.
[16] Leclerc, H. et al.: What are the limits to the spatial resolution? Mech. Indus., 13, 361-371, 2012.
[17] Roux, S. et al.: Digital Volume Correlation from Tomographic Images: Results and Challenges. IUTAM Symposium on Advances of Optical Methods in Experimental Mechanics, 2012.
[18] Bouterf, A. et al.: Damage law identification from full-field displacement measurement: Application to four-point bending test for plasterboard. Europ. J. Mech., Part A: Solids, 49, 60-66, 2015.

ADVANCED METHODS FOR ASSESSING THE NUCLEATION AND GROWTH KINETICS AND MICROSTRUCTURAL DEVELOPMENT OF CONVENTIONAL AND ALTERNATIVE CEMENTITIOUS BINDERS

Luca Valentini[1], Maria Chiara Dalconi[1], Gilberto Artioli[1]

[1] University of Padua, Department of Geosciences, Via Gradenigo 6, 35131 Padua, Italy,
email: luca.valentini@unipd.it, mariachiara.dalconi@unipd.it, gilberto.artioli@unipd.it

SUMMARY: Currently, much effort and enthusiasm are being devoted to research into alternative, environmental friendly, low-carbon binders, with the aim of devising the most viable solutions for cutting greenhouse gas emissions without dampening the drivers of infrastructural development, especially in the developing countries. The design of optimal alternative binders will require a bottom-up, knowledge-based approach, by which the basic physical and chemical processes associated with the reaction of precursor materials and formation of reaction products could be quantitatively assessed. Here, we review a series of advanced, non-destructive methods based on in-situ real-time X-ray powder diffraction, kinetic modelling and tomographic imaging methods, which successfully provided quantitative insight into the kinetics and mechanisms of nucleation and growth, and microstructural development in ordinary Portland cement. Possible applications to alternative binders, based on calcined clay soils, will be discussed.

NAPREDNE METODE OCJENJIVANJA NUKLEACIJE I KINETIKE RASTA I MIKROSTRUKTURNOG RAZVOJA KONVENCIONALNIH I ALTERNATIVNIH CEMENTNIH VEZIVA

SAŽETAK: Danas se ulažu veliki napori i strast u istraživanje alternativnih niskougljičnih veziva prijateljskih za okoliš s ciljem utvrđivanja najpovoljnijih rješenja za smanjenje emisije stakleničkih plinova bez gušenja pokretača infrastrukturnog razvoja, posebno u zemljama u razvoju. Iznalaženje optimalnih alternativnih veziva iziskivat će vrhunski, na znanju utemeljen pristup u kojem bi temeljni fizički i kemijski procesi povezani s reakcijom prethodno predviđenih materijala i formiranje proizvoda reakcije mogli biti kvantitativno ocijenjeni. U radu je dan pregled niza naprednih nerazornih metoda osnovanih na ***in situ*** difrakciji praha s pomoću X-zraka u realnom vremenu, metoda kinetičkog modeliranja i metoda tomografskog slikovnog prikaza koje uspješno daju kvantitativni uvid u kinetiku i mehanizme nukleacije i rasta te mikrostrukturni razvoj običnog portlandskog cementa. Raspravljene su i moguće primjene alternativnih veziva osnovanih na vapnenastim glinastim tlima.

1. INTRODUCTION

Although the basic formulation of Ordinary Portland Cement has remained the same as that standardized at the end of the 19th century, there is still much to be learned about the processes by which dry cement reacts with water to give a hardened material having excellent mechanical performance and durability.

If cement chemistry has to be included among those “high-tech” fields within the realm of materials science, then it is necessary to deploy innovative techniques with the aim of focussing research towards the basic mechanisms associated with hydration and reconcile the macroscopic properties with the behaviours observed at the smallest scales.

At the same time, it is necessary to plan a sustainable future for the construction industry by defining appropriate productive processes and raw materials that may mitigate the environmental footprint associated with cement production. Of course, we cannot envisage a “singularity point” where the production of Ordinary Portland Cement is suddenly shut off in favour of that of alternative binders. Therefore, research into conventional and alternative cements should run in parallel in the near future and knowledge acquired into OPC should be transferred to alternative systems.

In this context, some advanced methods for investigating the details of the kinetics of nucleation and growth of OPC hydrates and of microstructural development will be presented. Finally, it will be briefly discussed how such methods, based on a combination of in-situ X-ray diffraction and mathematical models, and on tomographic techniques, could be applied to the study of the basic processes associated with the reaction of calcined clays in alkaline solutions.

2. GETTING THE MOST OUT OF X-RAY DIFFRACTION

X-ray diffraction (XRD) is now routinely used as a method for determining the mineralogical composition of dry cement powders. However, much more information can be obtained when XRD measurements are performed in-situ, i.e. by acquiring sequential signals from a single hydrating cement sample. Data processing based on Rietveld analysis provides a time-dependent mineralogical composition, which is in turn dependent on the kinetics of cement dissolution and hydrate precipitation. Of course, it has to be taken into account that the dataset obtained from Rietveld analysis is incomplete, since it contains no information about C-S-H and pore water, due to the X-ray amorphous nature of these phases. Methods for the quantification of the X-ray amorphous phases include the use of external or internal standards, or methods by which the diffuse scattering contribution associated with C-S-H is described by specific peak functions [1-3]. Otherwise, the time-dependent amount of C-S-H and pore water can be quickly estimated, without the need of any previous calibration, by mass balance calculations (Figure 1), which proved to return reliable results [4, 5].

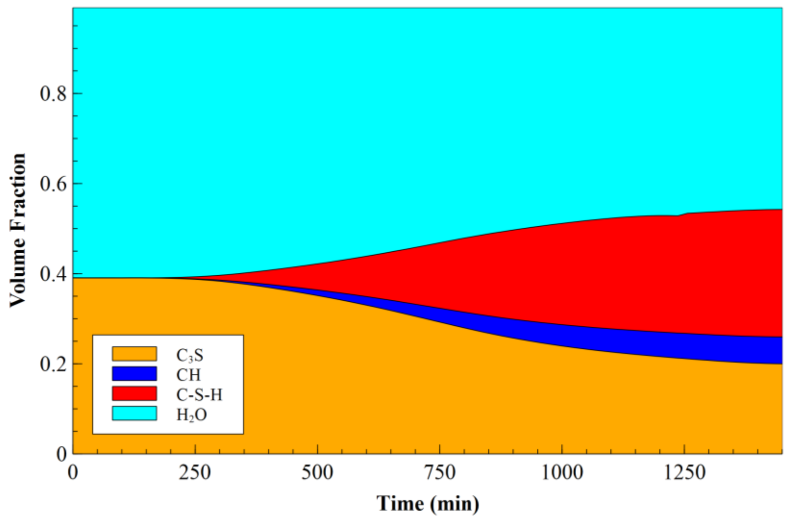

Figure 1 Time-dependent phase composition for a hydrating alite system, obtained by combining in-situ XRD measurements and mass balance calculations using the software RieCalc [4].

Fitting the curves of time-dependent C-S-H amount by appropriate kinetic equations can provide the rates of C-S-H nucleation and growth. Recently, it has been shown that such kinetic models provide information about the mode of C-S-H nucleation in the presence of PCE superplasticizers, suggesting a switch to homogeneous nucleation [6].

3. NON-DESTRUCTIVE PROBES INTO CEMENT MICROSTRUCTURE

The use of tomographic imaging represents a non-destructive, 3D alternative to methods based on electron microscopy for the analysis of cement microstructure [7]. However, one limitation of conventional X-ray tomography is the lack of full phase selectivity, resulting from poor attenuation contrast. Recently, fully phase-selective phase maps (Figure 2) have been obtained by an alternative method that combines tomography with synchrotron X-ray diffraction (XRD-CT) [8].

Time-dependent phase maps can be obtained by performing sequential measurements on the same sample and provide a direct visualization of the locations where dissolution and precipitation occur. Such maps can be quantitatively analysed by means of radial distribution functions, by which the degree of spatial correlation between different phases can be calculated. This method has been used to show that precipitating C-S-H loses correlation with clinker surfaces in the presence of PCE superplasticizers [9].

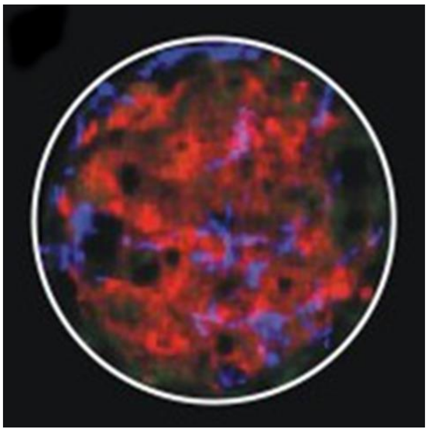

Figure 2 XRD-CT Selective phase map of a hydrating OPC paste (only hydration products are displayed) enclosed in a 300 μm glass capillary. Colour encoding: C-S-H (red), ettringite (green), portlandite (blue).

4. APPLICATIONS TO CALCINED CLAY SYSTEMS

Much effort and enthusiasm is being devoted by researchers to devising formulations alternative to OPC, with the aim of cutting CO_2 emissions associated with cement production. Fly ash and ground granulated blast furnace slag are widely used clinker-replacing materials having no intrinsic embodied CO_2 (in contrast to calcined limestone), although their worldwide availability is not homogeneous and will probably decrease in the medium to long term. Recently, low-grade calcined clays are being studied as a possible replacement for clinker. Clay soils are widely available worldwide (particularly in the developing countries) and also represent an economically viable alternative to pure metakaolin, which has a strong demand in other markets. Pilot projects for large-scale production of alternative cements comprising 50% OPC and a blend of low-grade clay and raw limestone are currently ongoing [10]. Such a recipe can significantly cut CO_2 emissions, however an even more drastic reduction of the environmental footprint can be envisaged if formulations without clinker are used. Preliminary tests, performed in this Institution, of the mechanical performance of binders obtained from low-grade calcined kaolinitic and smectitic clays, blended with limestone and activated in alkali solutions, provided encouraging results, with values of the mechanical strength as high as 30 MPa after three weeks at ambient temperature. Knowledge of the basic processes associated with the reactions occurring in such systems will contribute to optimizing the formulation of such alternative binders. In order to do so, specific protocols must be devised to adapt the methods outlined in the previous sections to such systems. For such systems, the study of the reaction kinetics by in-situ XRD becomes even more complicated due to the X-ray amorphous nature of both the thermally treated clay and the reaction product. Attempts to quantify the degree of reacted material have been performed by using the PONCKS method [11], by which the diffuse scattering hump (Figure 3) occurring at 2θ values close to 25° (for Cu-kα radiation) was described using a Le Bail fit [12]. Specific mass balance equations will have to be devised in order to estimate the time-dependent amount of reaction product formed.

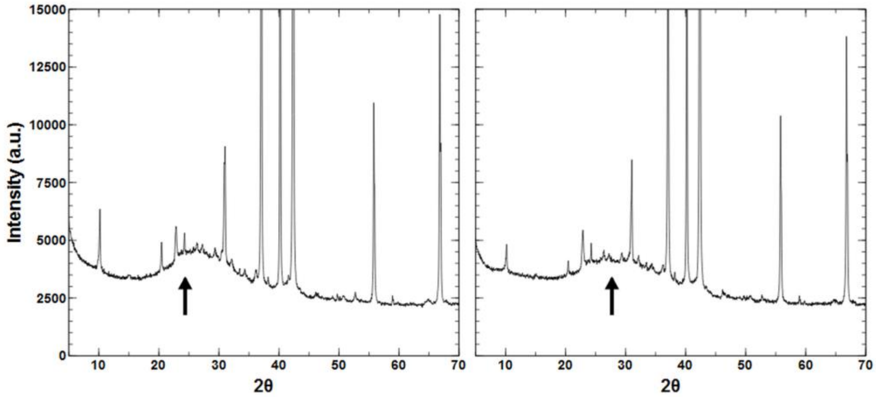

Figure 3 XRD patterns (Cu-Kα) of calcined clay: dry (left) and hydrated in the presence of an alkaline solution (right).

Issues associated with the X-ray amorphous nature of the main phases must also be tackled for microstructural analysis based on the tomographic imaging method outlined in the previous section. Nonetheless, it has been previously shown that even phases characterized by diffuse X-ray scattering can be correctly imaged if appropriate 2θ ranges are selected [13]. Therefore, unreacted calcined clay and its reaction product can in principle be discriminated based on the different 2θ ranges that characterize their diffuse scattering (Figure 3).

5. CONCLUSIONS

The design of alternative, sustainable and eco-efficient building materials obtained from widely available raw materials, having no embodied CO_2 and reasonable prices will represent one of the fundamental societal and scientific challenges for the near future. Research into the basic physical and chemical processes associated with the reaction and microstructural development of such materials will play a fundamental role. Calcined low-grade clays, without the addition of OPC, may represent an ideal candidate as binders for a sustainable future, as testified by good mechanical properties measured during preliminary tests using impure kaolinitic and smectitic clays.

Methods based on in-situ X-ray diffraction and tomographic imaging may help shade light on the reaction kinetics and microstructural development, allowing a knowledge-based design of sustainable binders.

REFERENCES

[1] Jansen, D. et al.: The Hydration of Alite: A Time-Resolved Quantitative X-ray Diffraction Approach Using the G-Factor Method Compared with Heat Release, Journal of Applied Crystallography, 44 (2011), pp. 895-901

[2] Bergold, S.T. et al.: Quantitative Analysis of C–S–H in Hydrating Alite Pastes by In-Situ XRD, Cement and Concrete Research, 53 (2013), pp. 119-126

[3] De la Torre, A.G. & Aranda, M.A.G.: Accuracy in Rietveld Quantitative Phase Analysis of Portland Cements, Journal of Applied Crystallography, 36 (2013), pp. 1169-1176

[4] Valentini, L.: RieCalc: Quantitative Phase Analysis of Hydrating Cement Pastes, Journal of Applied Crystallography, 46 (2013), pp. 1899-1902

[5] Valentini, L. et al.: In-Situ XRD Measurement and Quantitative Analysis of Hydrating Cement: Implications for Sulfate Incorporation in C–S–H, Journal of the American Ceramic Society, 98 (2015), pp. 1259-1264

[6] Valentini, L. et al.: Kinetic Model of Calcium-Silicate Hydrate Nucleation and Growth in the Presence of PCE Superplasticizers, Crystal Growth and Design, 16 (2016), pp. 646-654

[7] Parisatto, M. et al.: Examining microstructural evolution of Portland cements by in-situ synchrotron micro-tomography, Journal of Materials Science, 50 (2015), pp. 1805-1817

[8] Valentini, L. et al.: Towards three-dimensional quantitative reconstruction of cement microstructure by X-ray diffraction microtomography, Journal of Applied Crystallography, 44 (2011), pp. 272-280

[9] Artioli, G. et al.: Direct Imaging of Nucleation Mechanisms by Synchrotron Diffraction Micro-Tomography: Superplasticizer-Induced Change of C-S-H Nucleation in Cement, Crystal Growth and Design, 15 (2015), pp. 20-23

[10] Bisnoi, S. et al.: Pilot scale manufacture of limestone calcined clay cement: the Indian experience, Indian Concrete Journal, 88 (2014), pp. 22-28

[11] Scarlett, N.V.Y. & Madsen, I.C.: Quantification of phases with partial or no known crystal structures, Powder Diffraction, 21 (2006), pp. 278-284

[12] Le Bail, A.: Whole powder pattern decomposition methods and applications: A retrospection, Powder Diffraction, 20 (2015), pp. 316-326

[13] Voltolini, M. et al.: Understanding cement hydration at the microscale: new opportunities from 'pencilbeam'synchrotron X-ray diffraction tomography, Journal of Applied Crystallography, 46 (2013), pp. 142-152

ANALYSIS OF CONCRETE STRUCTURES USING LASER-INDUCED BREAKDOWN SPECTROSCOPY

Nina Sankat[1], Cassian Gottlieb[1], Steven Millar[1], Tobias Günther[1], Gerd Wilsch[1]

[1] BAM Federal Institute for Materials Research and testing, Unter den Eichen 87, 12205 Berlin, Germany,
email: nina.sankat@bam.de, Cassian.Gottlieb@bam.de, steven.millar@bam.de, gerd.wilsch@bam.de

SUMMARY: The Laser-Induced Breakdown Spectroscopy (LIBS) is a laser spectroscopic method which allows a time efficient, minor-destructive, chemical analysis of materials. In principle all elements on the periodic table can be simultaneously analysed by using LIBS, regardless of the state of aggregation. LIBS offers numerous applications in the field of civil engineering; most importantly the analysis of building materials. This work will focus on the evaluation of concrete structures and harmful substances which can penetrate the concrete. A variety of information can be collected through LIBS. Determining the concentration of harmful substances like chloride, sodium or sulphur, the examination of the carbonation depth and the distinction between varying layers of materials (e.g. aggregates, cement paste, metals, etc.) are possible applications. All this information can be provided through one LIBS measurement in the form of a high resolution 2D element map, with resolutions up to 0.1 mm x 0.1 mm. To scan a concrete surface only an optical access is needed. To create a depth profile of an intruding substance the extraction of a drill core is necessary. Onsite measurements via LIBS can be conducted by using a mobile version of the LIBS system. Through using calibration curves LIBS allows not only the qualitative but also quantitative analysis of element concentrations. All those prospects make LIBS a trendsetting method to secure the integrity of infrastructures in a sustainable manner. A variety of examples which show the performance and results of LIBS analysis will be presented.

ANALIZA BETONSKIH KONSTRUKCIJA UPOTREBOM LASERSKE SPEKTROSKOPIJE

SAŽETAK: Laserska spektroskopija (engl. laser-induced breakdown spectroscopy, LIBS) je metoda koja omogućuje učinkovitu kemijsku analizu materijala uz manje razaranje. Načelno se svi elementi periodnog sustava elemenata mogu simultano analizirati primjenom LIBS-a, neovisno o agregatnom stanju. LIBS omogućuje brojne primjene u građevinarstvu, a najvažnija je analiza građevnih materijala. U radu je težište na vrednovanju betonskih konstrukcija i štetnih tvari koje mogu prodrijeti u beton. S pomoću LIBS-a moguće je prikupiti raznolike informacije. Moguće primjene su određivanje koncentracije štetnih tvari poput klorida, natrija ili sumpora, ispitivanje dubine karbonatizacije i razlikovanje različitih slojeva materijala (npr. agregata, cemente paste, metala itd.). Sve se te informacije mogu dobiti jednim mjerenjem s pomoću LIBS-a u obliku 2D slike (mape) velike rezolucije sve do rezolucije od 0,1 mm x 0,1 mm. Za skeniranje površine betona dovoljan je optički pristup. Za stvaranje profila tvari koja je prodrla po dubini nužno je izvaditi valjak. Mjerenja na terenu mogu se izvesti upotrebom mobilne verzije sustava LIBS. Upotrebom kalibriranih krivulja LIBS omogućuje ne samo kvalitativnu nego i kvantitativnu analizu koncentracije pojedinih elemenata. Sve te prednosti čine LIBS trendovskom metodom osiguranja cjelovitosti infrastrukture na održiv način. U radu su prikazani raznoliki primjeri koji pokazuju svojstva i rezultate analize s pomoću LIBS-a.

1. INTRODUCTION

Most infrastructures suffer damages throughout their lifetime. A high number of those detriments originate from harmful substances like chlorine or sulphur entering the concrete structure. Other defects occur due to the interaction of intruding substances with components of the building material, for example carbonation or the alkali-silica reaction (ASR). Those damage processes shorten the lifetime of the infrastructure. A structure suffering from pitting corrosion (induce though chlorides) for instant needs to be heavily reconstructed or even be rebuild. Reconstructions require a high amount of time, money and resources. Hence preventing reconstruction saves time, money and favours the environment. To counteract the shortening of a structures lifetime the ingress of potentially harmful substances is monitored. Those monitoring processes are ordinarily conducted by coring, time consuming sample preparation and chemical analysis like potentiometric titration. Those chemical cannot represent the heterogeneity of concrete structures or the subsequently heterogeneous distribution of harmful substances. An alternative is the Laser-induced Breakdown Spectroscopy (LIBS).

LIBS is a spectroscopy method that allows the analysis of building materials. The LIBS method uses a focused laser pulse to generate a plasma on the surface of a specimen. The plasma of the vaporised material emits a specific light depending on the element composition. Intruding, potentially harmful substances like e.g. chlorine [1] and sulphur [2] can be detected.

The LIBS analysis allows to create a 2D map of the element distribution on the surface of the scanned specimen. This is achieved by scanning the surface in a horizontal and vertical grid, moving the laser on the specimen surface. Those scans can have a resolution up to 0.1 mm². Such high resolutions allow to distinguish thin layers of varying materials or find chloride carrying cracks (view Figure 5b). LIBS is a surface measurement and thereby can only provide information about the surface of an object. Surface measurements only require an optical access. To acquire a depth profile a drill core needs to be extracted and cut in half. The cross section of this drill core can be used for the analysis without any further specimen preparation. Scanning the relevant area of a drill core's cross section (view Figure 1), while using a typical resolution (0.5 mm x 0.5 mm) takes approximately 30 minutes which makes LIBS much faster than classic chemical methods. In principal LIBS can analyse every chemical element on the periodic table during one measurement, which makes LIBS a multi element analysis.

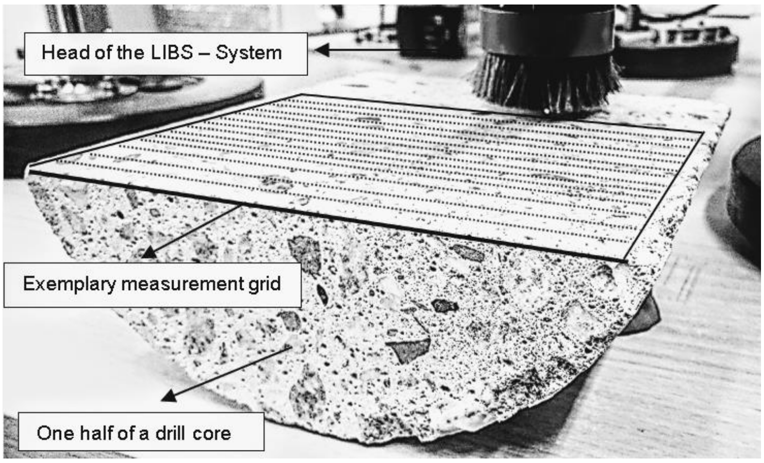

Figure 1 Half of a drill core with an exemplary measurement grid on the cross section (grid is magnified) and the head of the mobile LIBS-system

Typical applications of LIBS in the field of civil engineering are: analysing chloride and sulphur distribution to prevent pitting corrosion and concrete corrosion respectively; detecting alkalis (e.g. sodium, potassium) to detain ASR; providing information regarding the carbonation depth; differentiating between materials like e.g. aggregates and the cement matrix in a concrete specimen [3], verifying the penetration depth of hydrophobicity systems [4].

2. MEASUREMENTS

A typical laboratory LIBS set-up (as seen in Figure 2a) consists of a laser, a system of lenses and mirrors to focus the laser beam, an optical fibre that collects and guides the light emitted by the plasma to the measuring object, a spectrograph which disperses the light according to the wavelength, a detector (here a CCD camera) which detects the intensity of the radiated light according to its wavelength and thereby creates the typical LIBS spectrum (view Figure 2b) and finally a PC that collects the data and is used to operate the LIBS system, including the translation stage which moves the specimen and allows the generation of a 2D element map. To increase the signal intensity and lower the limit of detection (LOD) for the quantitative analysis, helium (or other gases like argon) can be added to the LIBS set-up and be used to purge the ambient atmosphere. [5]

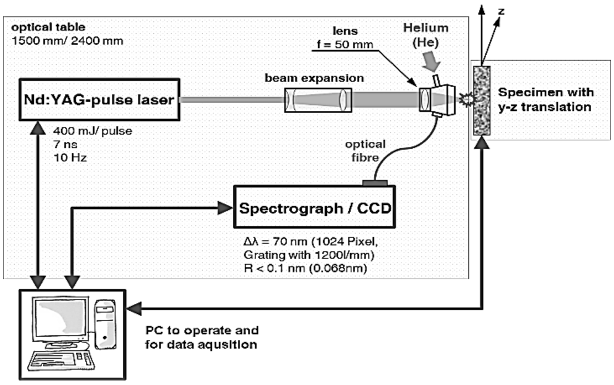

Figure 2a: A typical LIBS laboratory set-up [2]

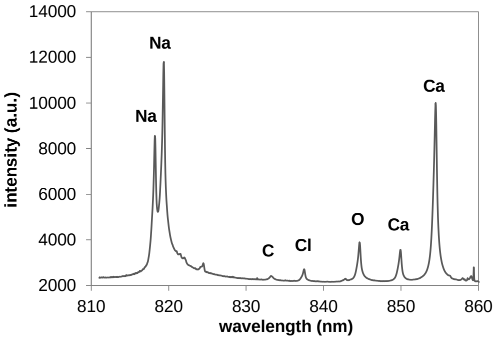

Figure 2b: Spectrum of a concrete measurement in the near infrared range (NIR)

A regular LIBS measurement has following steps: collecting a drill core; cutting the core in half; deciding on the elements that will be analysed and choosing the relevant LIBS parameters (e.g. spectrograph; purging gas; measurement area, etc.); calibrating the LIBS-System (if quantitative results are necessary); position one core half on the translation stage; entering the measurement parameters into the operating PC; measuring the relevant area of the drill core and finally analysing the data. Examples for LIBS results follow in paragraph 3.

Mobile LIBS set-ups that allow onsite LIBS measurements are available (view Figure 3). Onsite measurements on freshly drilled cores can help to adjust the drill plan according to the directly available results. Onsite LIBS measurements of the infrastructure surface can furthermore help to find contamination hot spots and thereby minimized the amount of extracted drill cores. Extracting less drill cores means less damage to the infrastructure and saving time and money.

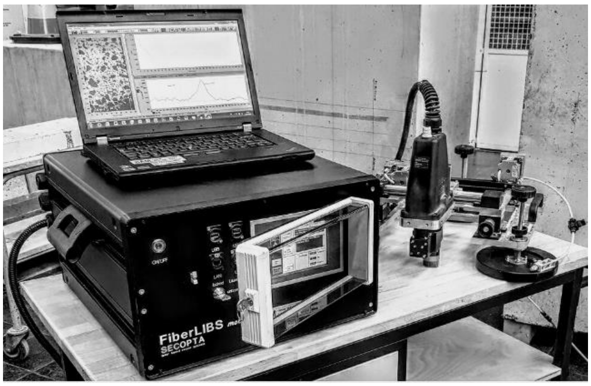

Figure 3 Mobile LIBS System for onsite measurements

3. RESULTS

The following paragraph presents a selection of LIBS results relevant for the field of civil engineering.

3.1. CHLORIDE INGRESS

The ingress of chlorides in a reinforced concrete structure can lead to chloride induced corrosion. To prevent this type of corrosion the chloride concentrations of structures are measured and compared to critical values (based on e.g. EN 206) which are used to estimate the risk of corrosion. This critical value can vary due to the high complexity of the corrosion process and its high amount of influencing factors.

In Figure 4a the measured cross section of a drill core is shown. This cross section was analysed by the mobile LIBS system (view Figure 3). The objective of the measurement was to determine the penetration depth of chloride. A 2D element map of the chloride distribution was created (view Figure 4b). To retain quantitative chloride concentrations a calibration of the LIBS system was implemented. To gain relevant results the heterogeneity of the concrete needs to be taken into account. For chloride induced corrosion the chloride concentration of the cement matrix, without the aggregates, is relevant. Therefore the aggregates need to be excluded. As long as the chemical composition of the aggregates differs from the composition of the cement matrix an elimination of most of the aggregates via LIBS is viable. Aggregates smaller than the laser spot (≈ 0.08 mm) cannot be fully exclude yet. Still a high accuracy can be achieved (limit of detection for chloride ≈ 0.1 wt %). The excluded aggregates are represented by the white areas in Figure 4b (left). Those areas are not taken into account for the calculation of the mass percentage of chloride. Consequently LIBS provides the chloride content based on the cement matrix which is necessary to estimate the risk of chloride induced corrosion reliably.

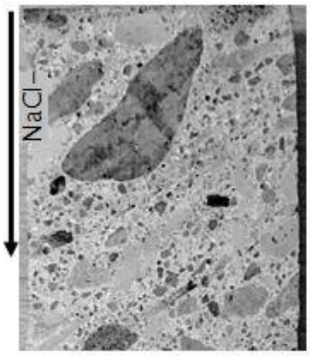

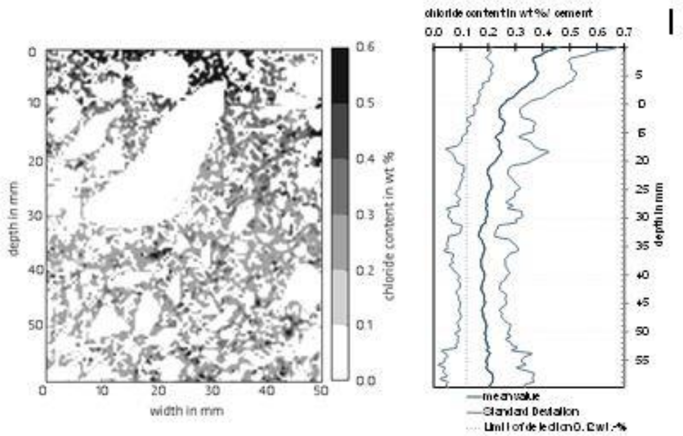

Figure 4a: Image of the measured cross section of a drill core (area = 50 x 60 mm) Figure 4b (left): Chloride distribution of the specimen shown in Figure 4a (white space represents excluded aggregates) (right): Depth profile for chloride including the standard deviation and the limit of detection

Additionally to the 2D map a depth profile of the chlorine content is shown (Figure 4b right). The depth profile is the standard visualisation of the chloride content in concrete specimens. Depth profiles can easily provided by LIBS. This type of visualisation lacks information like chloride hot spots (view Figure 5a), chloride carrying cracks (view Figure 5b) or any information about the heterogeneity of the specimen.

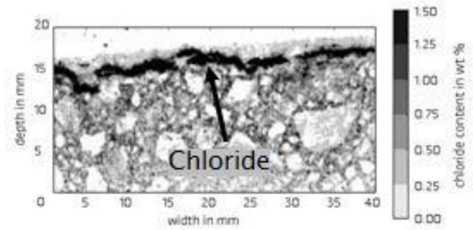

Figure 5a: Accumulation of chloride under the specimen surfaces due to a cathotic system

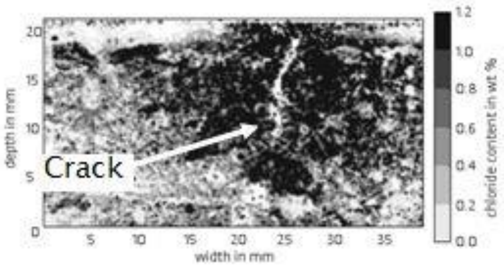

Figure 5b: Chloride distribution surrounding a crack in a concrete specimen

3.2. SODIUM CONTAINING AGGREGATES

Sodium and other alkalis, in combination with reactive aggregates, can result in an alkali-silica reaction (ASR). To prevent ASR the alkali contents of a concrete structure are monitored. Sodium can enter concrete structures e.g. through de-icing salts. Some aggregates naturally contain sodium. Immobile sodium inside the aggregates will not result in ASR-damages. Therefore immobile sodium inside the aggregates needs to be separated from mobile sodium in the cement matrix. LIBS allows a separation of both types of sodium with a high reliability. By excluding measurement points with a low calcium to sodium ratio sodium containing aggregates can be eliminated. Figure 6a shows a concrete specimen with sodium containing aggregates. In Figure 6b (right) the depth profile for sodium while including and excluding aggregates are compared to each other. The depth profile that includes the aggregates is misleading and should be avoided.

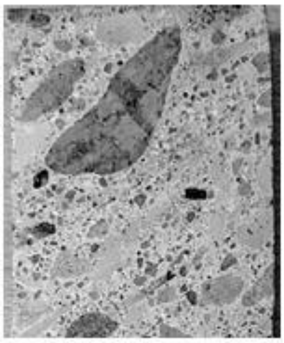

Figure 6a: Image of the measured cross section surface of a drill core (area = 50 x 60 mm)

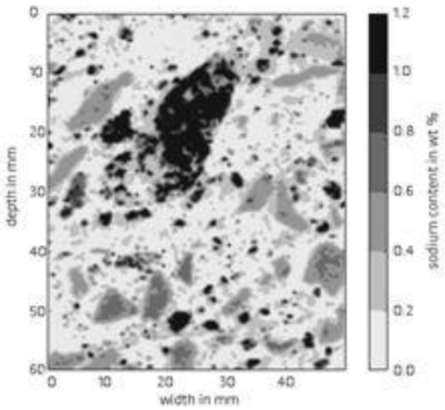

Figure 6b (left): Element Map of the sodium distribution of the specimen shown in Figure 6a; sodium containing aggregates recognisable; (right): sodium depth profile with included and excluded aggregates

3.3. CARBONATION

The carbonation of concrete and the linked decline of the pH-value can lead to corrosion of the reinforcement. Once the area surrounding the reinforcement is carbonated, and lost its alkaline ambience, the reinforcement loses its passive coating and thereby becomes vulnerable to corrosion. The most common way to check for carbonation is to test the pH-value of the concrete by using a phenolphthalein solution (view Figure 7a). Phenolphthalein creates a pink/magenta discolouration on the concrete surfaces if the pH-value is higher than 8.2. Carbonated concrete has a pH-value below 8.2 and the carbonation front can therefore be recognise by its missing discolouration. The carbonation of concrete can be monitored through LIBS by analysing the carbon intensity. A rise of the carbon content (compared to the mean value of carbon in the cement matrix) is a sign of carbonated concrete. The carbon content of the aggregates can be disregarded since aggregates don't influence the carbonation of the concrete. The results of a phenolphthalein test and LIBS analysis are compared in Figure 7a and 7b. The results are equivalent to each other.

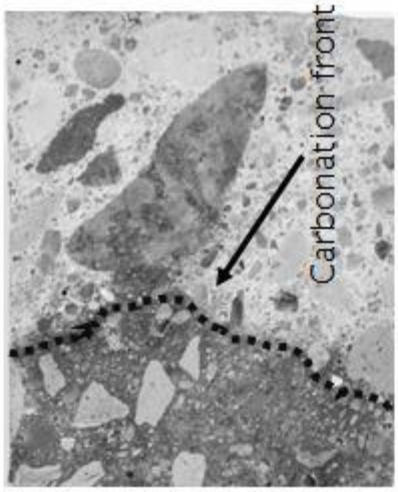

Figure 7a: Image of the measured cross section surface of a drill core treated with phenolphthalein

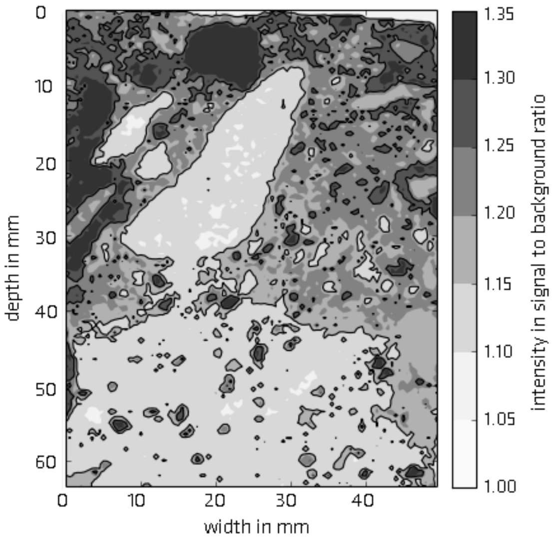

Figure 7b: Element Map of the carbon distribution of the specimen shown in Figure 7a; including contour lines to outline varying carbon concentrations

The presented results (determination of the chlorine/sodium content, separation of aggregates, analysis of the carbonation depth) can all be provided though one single LIBS measurement. Other questions like intruding sulphur, verifying the penetration depth of hydrophobicity systems or separating different of layers materials are further applications of LIBS in the field of civil engineering.

4. CONCLUSION

With rising construction costs and receding resources the preservation of infrastructures is a vital part of civil engineering. The preservation of already existing infrastructures requires an efficient and accurate monitoring method.

LIBS is an alternative to the classic monitoring methods that provides many advantages. The sample preparation for example is simple and sometimes even unnecessary. This makes LIBS more efficient and faster than classic methods. The main advantage of LIBS is the possibility of multi element analysis. Typical applications in the field of civil engineering like determination of the chloride, sulphur and sodium content as well as the examination of the carbonation depth can be evaluated in one LIBS measurement and used to generate a 2D element map. Those maps not only improve the visualisation of the results but also represent the genuine condition of the concrete specimen and thereby increase the accuracy of monitoring methods immensely. Which helps civil engineers to make the right decision when planning the reconstruction of an infrastructure. LIBS is also able to represent the heterogeneity of building materials like concrete. The high resolution of LIBS not only makes is possible to distinguish between aggregates and cement matrix but also allows to find contamination hot spots. Sodium containing aggregates or chloride carrying cracks can be detected, an issue classic chemical methods cannot handle.

The applications shown in this paper are a selections of the results LIBS provides in the field of civil engineering. More practical examples for the use of LIBS are shown in [6] and [7]. Other uses of the LIBS like the classification of cement or aggregate types are under investigation. But LIBS already is an alternative to classic methods.

REFERENCES

[1] Wilsch. G. et al: *Determination of chloride content in concrete structures with laser-induced breakdown spectroscopy*, Construction and building materials, 19. (2005) 10., pp. 724–730, 0950-0618

[2] Weritz. F. et al: *Detailed depth profiles of sulfate ingress into concrete measured with laser induced breakdown spectroscopy*, Construction and building materials, 23. (2009) 1., pp. 275–283, 0950-0618

[3] Weritz. F. et al: *Effect of heterogeneity on the quantitative determination of trace elements in concrete*, Analytical and Bioanalytical Chemistry, 385. (2006) 2., pp. 248–255, 1618-2642

[4] Bienert. K. et al: Quality control of hydrophobic coatings with an integrated marker element by laser-induced breakdown spectroscopy (LIBS), Proceedings of Concrete Solutions, Grantham, M., pp. 805-811, 978-0-415-61-622-5, Dresden, September 2011, Taylor and Francis, London (2012)

[5] Noll, R.: *Laser-Induced Breakdown Spectroscopy - Fundamentals and Applications*, Springer Verlag, 978-3-642-20667-2, Berlin Heidelberg, (2012)

[6] Wilsch. G. et al: Imaging Laser Analysis of Building Materials – Practical Examples, Proceedings of AIP Conference, Thompsom, D.; Chimenti D., pp. 1315 – 13322, 978-0-7354-0888-3, San Diego, July 2010, AIP, College Park, (2011)

[7] Millar. S. et al*: Laser Induced Breakdown Spectroscopy (LIBS) in civil engineering - innovative analysis of building materials*, Beton- und Stahlbetonbau, 110. (2015) 8., pp. 501-U10, 0005-9900

TOPIC 2.

Materials – Environment interaction

Međudjelovanje materijala i okoliša

OVERVIEW OF DURABILITY PROPERTIES OF RECYCLED AGGREGATE CONCRETE

Nina Stirmer[1]

[1] University of Zagreb, Faculty of Civil Engineering, Department of Materials, Fra Andrije Kacica Miosica 26,
10 000 Zagreb, Croatia, email: ninab@grad.hr

SUMMARY: Use of recycled aggregate concrete (RAC) for structural purposes is still limited in spite of extensive research projects that have been done worldwide. The reasons are impurities in recycled aggregates, lower density and higher water absorption in comparison to natural aggregates that influence on concrete mechanical and durability properties. Only in EU, there is around 850 million tons of construction and demolition (C&D) waste per year. It is estimated that approximately 90 % of C&D waste could be reused or recycled, depending on the structure and local market of waste materials. Researchers identified various influencing aspects related to the use of recycled aggregates, such as replacement level, size and origin, as well as the influence of curing conditions, use of chemical and mineral admixtures on carbonation, resistance to chloride ion penetration, freeze-thaw resistance, capillary water absorption and water permeability. This paper gives overview of durability properties of RAC produced with different amounts of recycled concrete aggregate.

PREGLED TRAJNOSNIH SVOJSTAVA BETONA S RECIKLIRANIM AGREGATOM

SAŽETAK: Unatoč tome što su širom svijeta provedeni opsežni istraživački projekti, upotreba betona s recikliranim agregatom za konstrukcijske svrhe još je uvijek ograničena. Razlozi su tome nečistoće u recikliranom agregatu, manja gustoća i veća apsorpcija u usporedbi s prirodnim agregatom koji utječu na mehanička i trajnosna svojstva betona. Samo u Europskoj uniji godišnje nastaje oko 850 milijuna tona građevnog otpada i otpada od rušenja. Procjenjuje se da bi se oko 90 % tog otpada moglo ponovno upotrijebiti ili reciklirati, ovisno o konstrukciji i lokalnom tržištu otpadnih materijala. Istraživači su prepoznali različte aspekte koji utječu na upotrebu recikliranog agregata kao što su razina zamjene, veličina i podrijetlo te utjecaj uvjeta njege, upotreba kemijskih dodataka i mineralnih dodataka na karbonatizaciju, otpornost na prodor klorida, otpornost na zamrzavanje i odmrzavanje, kapilarna apsorpcija i vodopropusnost. U radu je dan pregled trajnosnih svojstava betona s recikliranim agregatom proizvedenim s različitim količinama betonskog recikliranog agregata.

1. INTRODUCTION

Use of recycled aggregate concrete (RAC) for structural purposes is still limited in spite of extensive research projects that have been done worldwide. The reasons are impurities in recycled aggregates, lower density and higher water absorption in comparison to natural aggregates that influence on concrete mechanical and durability properties. However, by combining recycled and natural aggregate and with proper mixing procedure, properties of recycled aggregate concrete could be satisfactory for many purposes. Some properties of recycled aggregate concrete could be improved with chemical and/or mineral admixtures, but it depends of its cost and availability. Use of recycled aggregate in concrete will tend to increase because of limited natural resources and decreased landfill sites on the one hand and large production of concrete for new structures and large quantities of construction and demolition waste (C&D) obtained at the end of structure lifetime. Only in EU, there is around 850 million tons of C&D waste per year [1]. This represents 31% of the total waste generation in the EU. It is estimated that approximately 90 % of C&D waste could be reused or recycled, depending on the structure and local market of waste materials. It is also estimated that between 40 to 60% of the C&D waste arising at the European level is made of concrete [2]. Problems to obtain higher percentage of C&D waste recycling are relating to lack of standards, low awareness on importance of using recycling materials for environment protection as well as heterogeneity of recycled aggregate which requires most frequent quality control. It is of great importance to separate C&D waste on site to minimize amount of mixed waste and to obtain high quality of recycled aggregate wherever possible.

Recycling has a positive influence on the production of materials as the production from waste is less burdening for the environment. Increasing recycling rates, for some materials in particular, substantially decrease the environmental impacts from their production regardless of the development in their total consumption by the construction industry [3]. The EU27 consumed between 1.200 - 1.800 million tonnes of construction materials per annum for new buildings and refurbishment between 2003 and 2011. Data and information collected on use of construction materials suggests that concrete, aggregate materials (sand, gravel and crushed stone) and bricks make up to the 90% (by weight) of all materials used. The biggest fraction is aggregate materials, which represent about 45% of the total materials by weight, even when the amount of aggregates used in concrete are excluded. Concrete, with 42% is the second next fraction by weight, then bricks with 6.7%. According to Waste Framework Directive [4], Member States shall take the necessary measures designed to achieve the following target: by 2020, the preparing for re-use, recycling and other material recovery, including backfilling operations using waste to substitute other materials, of non-hazardous construction and demolition waste excluding naturally occurring material defined in category 17 05 04 in the list of waste shall be increased to a minimum of 70% by weight. Production of recycled and reused aggregates increased to 228 mil. t. in 2014, representing 8.6% of the total output of 2.65 billion tonnes, this also representing around 40% of total demolition materials available. In EU, Germany led with 73 mil. t. of recycled materials, followed by UK, the Netherlands, France, Belgium, Poland and Switzerland, the leaders supplying over 20% of national demand through recycling (Figure 1).

The ability to use these products in construction applications is heavily dependent on their compliance with MS/EU standards relating to the aggregates applications they are being produced for [5].

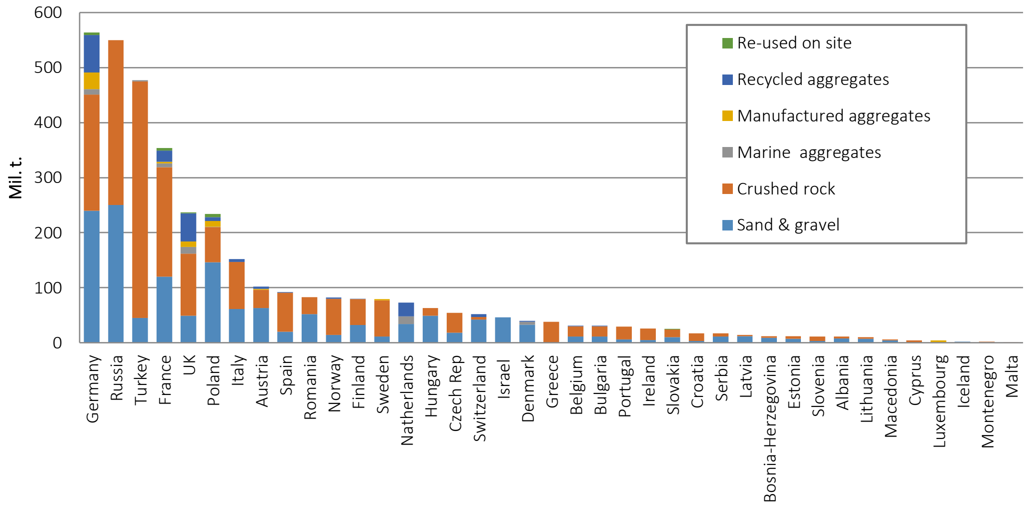

Figure 1: The aggregates production 2014. (in millions of tonnes by country and type) [6]

This paper gives overview of durability properties of RAC produced with different amounts of recycled concrete aggregate.

2. REQUIREMENTS FOR RECYCLED AGGREGATE

Composition of recycled concrete aggregate, especially amount of residual mortar has large influence on durability properties of RAC. In most cases, natural coarse aggregate is replaced with 20 to 30 % of recycled aggregate. The most often use of recycled aggregate is in precast production (especially in production of non-structural elements) where there is always some amount of defected concrete elements which could be recycled and used again in concrete production. The advantage of this type of recycled aggregate is that it has no impurities and its quality is known and relatively uniform. On the other hand, recycled aggregate from demolition waste is of lower quality and should be tested most frequently.

Annex E of the European standard EN 206 [7] gives recommendations for the use of coarse recycled aggregates (d ≥ 4 mm) conforming to EN 12620 [8]. No recommendations for the use of fine recycled aggregate are given in this standard. Maximum percentage of replacement of coarse aggregates is given in Table 1. Type A recycled aggregates from a known source may be used in exposure classes to which the original concrete was designed with a maximum percentage of 30 %. Type B recycled aggregates should not be used in concrete with compressive strength classes > C30/37.

Main categories for constituents of coarse recycled aggregates according to EN 12620 are: Rc (concrete, concrete products, mortar, concrete masonry units); Ru (unbound aggregate, natural stone, hydraulically bound aggregate); Rb (clay masonry units – bricks and tiles, calcium silicate masonry units, aerated non-floating concrete); Ra (bituminous materials); FL (floating material in volume), X (other – gypsum plaster, cohesive material – clay and soli, metals, plastic, rubber, non-floating wood) and Rg (glass). The proportion of constituent materials in coarse recycled aggregate shall be determined in accordance to EN 933-11 and then declared with the relevant category specified in EN 12620. Standard EN 206 also recommends to consider drying shrinkage, creep and modulus of elasticity when using concrete containing recycled aggregates.

Table 1 Maximum percentage of replacement of coarse aggregates (% by mass) according to EN 206

Recycled aggregate type	Exposure classes			
	X0	XC1, XC2	XC3, XC4, XF1, XA1, XD1	All other exposure classes
Type A	50%	30%	30%	0%
Type B	50%	20%	0%	0%

Recommendations for coarse recycled aggregates according to EN 12620 are shown in Table 2.

Table 2 Recommendations for coarse recycled aggregates according to EN 12620

Property	Type	Category according to EN 12620
Fines content	A + B	Category or value to be declared
Flakiness index	A + B	≤ Fl_{50} or ≤ SI_{55}
Resistance to fragmentation	A + B	≤ LA_{50} or ≤ SZ_{32}
Oven dried particle density ρ_{rd}	A	≥ 2100 kg/m^3
	B	≥ 1700 kg/m^3
Water absorption	A + B	Value to be declared
Constituents	A	R_{C90}, R_{Cu95}, R_{b10-}, R_{a1-}, FL_{2-}, X_{Rg1-}
	B	R_{C50}, R_{Cu70}, R_{b30-}, R_{a5-}, FL_{2-}, X_{Rg2-}
Water soluble sulphate content	A + B	$SS_{0.2}$
Acid-soluble chloride ion content	A + B	Value to be declared
Influence on the initial setting time	A + B	≤ A_{40}

[a] category NR (no requirements) applies for all other properties not stated in this table for which a category NR can be declared according to EN 12620
[b] for special applications requiring high quality surface finish the constituent FL should be limited to category $FL_{0.2-}$

3. DURABILITY PROPERTIES OF RECYCLED AGGREGATE CONCRETE

Durability of recycled aggregate concrete is strongly related to amount of recycled aggregate, w/c ratio and water absorption which influence on porosity of concrete. In general, the use of recycled aggregate is detrimental to the quality of hardened concrete in terms of its durability [9, 10].

4. CARBONATION

Many researchers reported that carbonation depth increased with an increase in the replacement ratio of natural aggregate by recycled aggregate [9-13]. In this case, the addition of fly ash to RAC shows a negative response towards carbonation resistance [14]. Bravo et. al. [9] tested 33 concrete mixes with recycled aggregate from different C&D waste recycling plants and concluded that the carbonation resistance is the property most affected by the use of recycled aggregate, leading to increases in the carbonation depth between 22.2% and 182.4% for the various recycled aggregate types. However, the most influencing factor is by far the recycled aggregate composition. Pedro et al. [15] also shown that the carbonation depth increased with the replacement of natural aggregate by recycled aggregate and with the decrease of the concrete's target strength. This research included three strength ranges of the concrete 15–25 MPa, 35–45 MPa and 65–75 MPa and total replacement of coarse natural aggregates by coarse recycled concrete aggregates. Xiao et. al. [16] concluded that the carbonation depth of the recycled aggregate concrete decreases with the increase in the strength grades of the original concrete. Regarding percentage of replacement, they concluded that when the replacement of the recycled coarse aggregate is less than 70%, the carbonation depth of the recycled aggregate concrete increases with the increase of the recycled coarse aggregate and when it exceeds 70%, the carbonation depth of the recycled aggregate concrete decreases with the increase of the recycled coarse aggregate (Figure 2). Figure 2 shows two different effects of recycled aggregate: negative and positive. Porous recycled aggregates result in a much higher porosity of recycled aggregate concrete than that of a similar mix of normal concrete, and leads to a reduction in the carbonation resistance of recycled aggregate concrete (negative effect). On the other hand, recycled aggregate concrete may have a higher total binder content, and then a higher alkaline reserve that can be carbonated due to the attached mortar of the recycled coarse aggregates, which is in favour of carbonation resistance (positive effect).

Silva et al. [13] identified various influencing aspects related to the use of recycled aggregates, such as replacement level, size and origin, as well as the influence of curing conditions, use of chemical admixtures and additions, on carbonation. Based on statistical analysis, the authors concluded that mixes made with 100% coarse RA content have a 95% probability of exhibiting carbonation depths up to almost 2.5 times greater than that of a corresponding NAC and for the same incorporation ratio of fine RA, this value increased to 8.7 times. This is explained with the fact that fine RA normally exhibit greater water absorption than coarse RA and thus increase the permeability of the resulting concrete. However, it was also concluded that RAC mixes meeting the recommended limiting values for conventional concrete mixes exhibit carbonation resistance performances adequate to accomplish the target service life.

Singh et al. [17] investigated SCC mixes with recycled aggregate concrete and metakaolin and also concluded that carbonation resistance decreases with the increasing of RCA content. They found that the carbonation depth of SCC mix containing 100% RCA increases nearly by 58% compared to that of SCC mix made with 100% NA as well as that the addition of 10% metakaolin to some extent compensates the loss in the carbonation resistance.

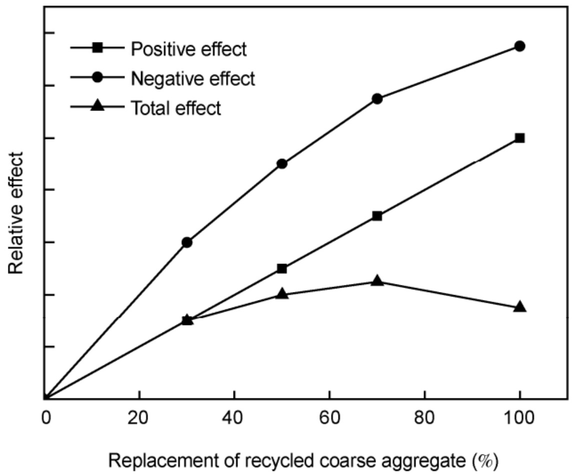

Figure 2: The effects of the RCA replacement on the carbonation performance of RAC [16]

4.1. RESISTANCE TO CHLORIDE ION PENETRATION

Based on the results of testing concrete produced with 40, 50 and 60 % recycled aggregate as replacement for natural aggregate, Banjad Pecur et al. [18] concluded that resistance to chloride penetration is unsatisfactory and that tested concrete types would not be suitable for structural elements in marine environment or it should be additionally protected. Pedro et al. [15] concluded that, when producing concrete with low w/c ratios and with recycling aggregate of average/high quality, it is possible to obtain a performance similar to that of the reference concrete (without recycled aggregate). It should be mentioned that this research included recycled aggregate from rejected products from the precasting industry and concrete produced in laboratory. Soares et al. [19] also made research with recycled aggregates from crushed elements produced by the precasting concrete industry and concluded that recycled concrete aggregates, from high-strength concrete elements, does not significantly affect this property.

Kou and Poon [14] shown that the resistance to chloride ion penetration decreased as the recycled aggregate content increased. However, they suggested that at the same recycled aggregate replacement level, the use of fly ash as a partial replacement and addition of cement can increase the resistance to chloride ion penetration.

Vázquez et. al [20] studied possibility of improvement of the durability of concrete with recycled aggregates in chloride exposed environment. They tested concrete with 0%, 20%, 50% and 100% coarse aggregates replacement and detected chloride binding phenomenon in RAC which may compensate the recycled concrete aggregates (RCA) higher permeability. This phenomenon is explained by chemical reaction between chlorides and hydrated cement aluminates, or by physicochemical adsorption in the CSH. Chlorides, coming from an external medium, could be bound by the new cement paste of the RAC and the old mortar which is adhered to the RCA.

4.2. FREEZE-THAW RESISTANCE

The results of testing frost resistance of recycled aggregate concrete is quite different and there are not unified conclusion until now [12, 21]. Zaharieva et. al [22] concluded that frost resistance of saturated RAC is not satisfying, and their use in structures exposed to severe climate is not recommended. This is explained with high total w/c, inducing higher porosity and lower mechanical characteristics of RAC, as well as the frost resistance of RA themselves. Banjad Pecur et al. [18] carried out testing of concrete specimens with recycled brick and recycled concrete with proportions of 40 % and 60 %. From the results obtained, it was concluded that concrete with coarse aggregate from recycled brick and recycled concrete are resistant to freezing and thawing with de-icing salts and that concrete satisfy requirements for exposure classes XF2 (28 cycles) and XF4 (56 cycles). It should be mentioned that in this research, concrete mixtures were prepared with air entraining admixture.

Bogas et al. [23] investigated freeze-thaw resistance of concrete produced with partial or total replacement of fine natural aggregate by fine recycled concrete aggregate (0%, 20%, 50% and 100% replacement) and concluded that contrary to high-strength concrete, normal strength concrete was not frost resistant, regardless the type of aggregate used. The w/c ratio had a greater influence on the freeze-thaw resistance than the type of aggregate. However, it was concluded that the incorporation of fine recycled concrete aggregate is not detrimental to the freeze-thaw resistance of concrete. Only the total replacement led to lower residual mechanical strengths after freeze-thaw action than those obtained in reference mixes.

4.3. CAPILLARY WATER ABSORPTION

Kou and Poon [14] reported that water absorption of recycled aggregate concrete was significantly greater than that of the natural aggregate concrete. They also shown that use of fly ash as a partial of cement and an addition of cement significant decrease the water absorption of recycled aggregate concrete. Soares et al. [19] evaluated the effect of incorporating recycled concrete aggregates from precast concrete elements on new concrete's properties and concluded that the incorporation ratio should be limited to 25% for water absorption by immersion and by capillarity to remain unaffected. They also recommended to use superplasticizers to improve performances of recycled aggregate concrete.

4.4. WATER PERMEABILITY

Water permeability increases with the w/c ratio and with the percentage of incorporated RA [24]. For the maximum penetration of 50 mm, compressive strength of the RAC with 100% recycled coarse should be greater than 40 MPa. Thomas et al. also shown that for values of compressive strength larger than 60 MPa, the RA incorporation has no appreciable effect on the water penetration depth (Figure 3).

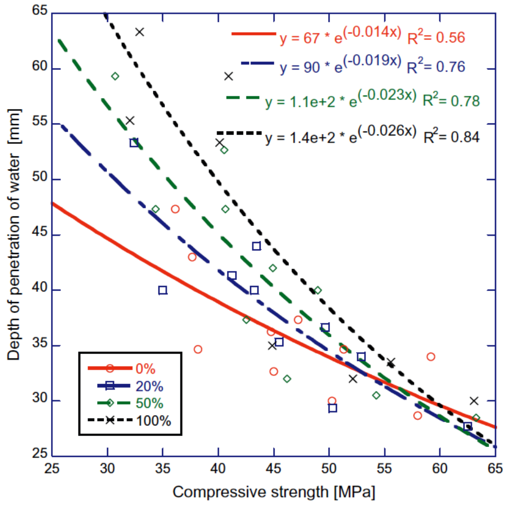

Figure 3: Maximum water penetration under pressure versus the compressive strength of the RAC [24]

5. CONCLUSIONS

Properties of recycled aggregate concrete depend on many factors. Recycled aggregates obtained by crushing a high strength original concrete will usually have a lower absorption. However, in the case of C&D waste, quality of original concrete is usually unknown. In general, carbonation depth of the recycled aggregate concrete increases with an increase in the replacement ratio of natural aggregate by recycled aggregate and with a decrease in the strength of the original concrete. Resistance to chloride ion penetration also decreases as the recycled aggregate content increases and that can be improved with the use of fly ash. Regarding frost resistance of recycled aggregate concrete, the results are not unified. Some authors concluded that frost resistance of saturated RAC is not satisfying. This can be improved with addition of air entraining admixture. Also, it was concluded that fine recycled concrete aggregate is not detrimental to the freeze-thaw resistance of concrete, only the total replacement led to lower residual mechanical strengths after freeze-thaw action than those obtained in reference mixes. Water permeability of RAC depends on w/c ratio and amount of recycled aggregate. For compressive strength larger than 60 MPa, RA incorporation has no appreciable effect on the water penetration depth. However, it is not ease to achieve large compressive strength with some types of recycled aggregate, especially from C&D waste. It should be emphasised that recycled aggregate should be used for the most appropriate application on the place of use [25] and that relatively poorer durability properties of recycled aggregates concrete can be adequately compensated by the use of fly ash which can be acceptable based on economic and environmental point of view [14, 26].

REFERENCES

[1] Fischer, C.; Werge, M.: EU as a Recycling Society Present recycling levels of Municipal Waste and Construction & Demolition Waste in the EU, April 2009

[2] Management of construction and demolition waste – SR1 Final Report Task 2, February 2011, http://ec.europa.eu/environment/waste/pdf/2011_CDW_Report.pdf

[3] Resource efficiency in the building sector, Final report, ECORYS Nederland BV, 2014, http://ec.europa.eu/environment/eussd/pdf/Resource%20efficiency%20in%20the%20building%20sector.pdf

[4] Directive 2008/98/EC of the European Parliament and of the Council of 19 November 2008,

[5] Workshop "Improving management of construction and demolition waste" 25 May 2016, Background paper, http://ec.europa.eu/environment/waste/studies/cdw/Improving%20management%20of%20CDW%20-%20Workshop%20-%20Background%20paper.pdf

[6] Annual Review 2015 - 2016, European Aggregates Association, http://www.uepg.eu/publications/annual-reviews

[7] HRN EN 206:2016 Concrete -- Specification, performance, production and conformity (EN 206:2013+A1:2016)

[8] HRN EN 12620:2008 Aggregates for concrete (EN 12620:2002+A1:2008)

[9] Bravo, M. et. al.: Durability performance of concrete with recycled aggregates from construction and demolition waste plants, Construction and Building Materials 77 (2015) 357–369

[10] Thomas, C. et. al.: Durability of recycled aggregate concrete, Construction and Building Materials 40 (2013) 1054–1065

[11] Behera, M. et. al:: Recycled aggregate from C&D waste & its use in concrete – A breakthrough towards sustainability in construction sector: A review, Construction and Building Materials 68 (2014) 501–516

[12] Rao, A.; Jha, K. N.; Misra, S.: Use of aggregates from recycled construction and demolition waste in concrete, Resources, Conservation and Recycling 50 (2007) 71–81

[13] Silva, R. V. et. al.: Carbonation behaviour of recycled aggregate concrete, Cement & Concrete Composites 62 (2015) 22–32

[14] Kou, S. C.; Poon, C. S.: Enhancing the durability properties of concrete prepared with coarse recycled aggregate, Construction and Building Materials 35 (2012) 69–76

[15] Pedro, D.; de Brito, J.; Evangelista, L.: Influence of the use of recycled concrete aggregates from different sources on structural concrete, Construction and Building Materials 71 (2014) 141–151

[16] Xiao, J. Z., Lei B.; Zhang, C. Z.: On carbonation behavior of recycled aggregate concrete, Science China Technological Sciences, September 2012 Vol. 55 No. 9: 2609–2616

[17] Singh, N.; Singh, S. P.: Carbonation and electrical resistance of self compacting concrete made with recycled concrete aggregates and metakaolin, Construction and Building Materials 121 (2016) 400–409

[18] Banjad Pečur, I.; Štirmer, N.; Milovanović, B.: Durability properties of recycled aggregate concrete, Proceedings of the RILEM International workshop on performance-based specification and control of concrete durability, Bjegović, D.; Beushausen, H.; Serdar, M. (ed.), Zagreb: RILEM Publications S.A.R.L., 2014., 191-198

[19] Soares, D. et. al: Use of coarse recycled aggregates from precast concrete rejects: Mechanical and durability performance, Construction and Building Materials 71 (2014) 263–272

[20] Vázquez, E. et. al.: Improvement of the durability of concrete with recycled aggregates in chloride exposed environment, Construction and Building Materials 67 (2014) 61–67

[21] Progress of Recycling in the Built Environment, Final report of the RILEM Technical Committee 217-PRE, Vázquez, Enric (ed.), RILEM State of the Art Reports 8, RILEM 2013

[22] Zaharieva, R.; Buyle-Bodin, F.; Wirquin, E.: Frost resistance of recycled aggregate concrete, Cement and Concrete Research 34 (2004) 1927–1932

[23] Bogas J. A.; de Brito, J.; Ramos, D.: Freeze-thaw resistance of concrete produced with fine recycled concrete aggregates, Journal of Cleaner Production 115 (2016), pp. 294–306

[24] Thomas, C. et. al.: Durability of recycled aggregate concrete, Construction and Building Materials 40 (2013) 1054–1065

[25] James, B.: Supporting the recycled materials market, Workshop on Resource Efficient Use of Mixed Wastes, Brussels, 2016
[26] Kou, S.-C.; Poon, C.-S.: Long-term mechanical and durability properties of recycled aggregate concrete prepared with the incorporation of fly ash, Cement & Concrete Composites 37 (2013) 12–19

THE EFFECT OF COARSE CRUSHED CONCRETE AGGREGATE ON THE DURABILITY OF STRUCTURAL CONCRETE

Wayne Dodds[1], Chris Goodier[1], Simon Austin[1], Christian Christodoulou[2], David Dunne[2], E. Wingrove[1]

[1] Loughborough University, School of Civil and Building Engineering, Centre for Innovative and Collaborative Construction Engineering, Leicestershire, UK, LE11 3TU, email: W.J.Dodds@lboro.ac.uk, C.I.Goodier@lboro.ac.uk, S.A.Austin@lboro.ac.uk
[2] AECOM, Colmore Plaza, 20 Colmore Circus Queensway, Birmingham, UK, B4 6AT, email: Christian.Christodoulou@aecom.com, David.Dunne@aecom.com

SUMMARY: The use of crushed concrete aggregates (CCA) (formerly referred to as recycled concrete aggregate (RCA)) is increasing, particularly for low-grade applications, where quality is of less importance. In higher value applications, such as structural concrete, further research has been required to understand the effect of coarse CCAs on the mechanical properties and durability performance. This research investigated the effect of coarse CCA in CEM I and CEM III/A structural concretes. The resistance to water and chloride ion ingress in terms of surface resistivity, sorptivity and rapid chloride migration were evaluated in this study, together with compressive strength to determine compliance with characteristic and target mean strengths. From this limited study - which forms part of a wider research project - results indicate that a higher proportion of CCA is detrimental to the resistance to water and chloride ion ingress, possibly due to the higher water absorption characteristics of the aggregates as suggested in literature. The incorporation of GGBS however, significantly improves the durability performance, possibly due to the reduced porosity of the cement matrix, improved quality of the interfacial transition zone (ITZ) between the recycled aggregates and cement matrix and an increased chloride binding effect. From the results it is recommended that a structural CEM III/A concrete incorporating coarse CCA up to 60% may be a viable option for future sustainable construction projects.

UTJECAJ KRUPNOG DROBLJENOG BETONSKOG AGREGATA NA TRAJNOST KONSTRUKCIJSKOG BETONA

SAŽETAK: U porastu je upotreba drobljenog agregata iz betona (ranije zvanog reciklirani betonski agregat), posebno za upotrebe manje zahtjevnosti gdje kvaliteta ima manju važnost. Za primjene s većim zahtjevima kao što je konstrukcijski beton zahtijevaju se daljnja istraživanja kako bi se ustanovio učinak takvog krupnog agregata na mehanička svojstva i trajnost. U radu je istražen učinak krupnog agregata iz betona na konstrukcijske betone s CEM I i CEM III/A. U radu su istraženi otpornost na prodiranje vode i klorida izraženi otpornošću površine, sorpcija i migracija klorida i tlačna čvrstoća kako bi se odredila sukladnost s karakterističnom i ciljanom srednjom čvrstoćom. Na osnovi tog ograničenog istraživanja koje je dio opsežnijeg istraživačkog projekta rezultati pokazuju da je za otpornost na prodiranje vode i klorida štetan veći udjel drobljenog agregata iz betona, moguće zbog veće apsorpcije agregata nego što se navodi u literaturi. Uključivanje mljevene granulirane zgure visokih peći, međutim, znatno poboljšava svojstvo trajnosti, moguće zbog smanjene poroznosti cementne matrice, poboljšane kvalitete zone sučeljka između recikliranog agregata i cementne matrice i povećanog učinka vezivanja klorida. Na osnovi rezultata preporučeno je da konstrukcijski betoni s CEM III/A koji sadržavaju krupni drobljeni betonski agregat do 60 % mogu biti prihvatljiva opcija u budućim projektima održive gradnje.

1. INTRODUCTION

Recycled aggregates (RA) and crushed concrete aggregates (CCA/RCA) have become an increasingly popular construction material to replace virgin aggregates since the 1980's. Approximately 18.8 and 21.2 million tonnes of hard demolition arisings were produced in the UK in 2014 and 2015 respectively, and the quantity is predicted to continue to increase annually [1]. CCA is primarily specified as low-grade unbound aggregates in general fill, capping layers and as drainage materials, as the quality requirements for aggregates in these applications are generally less [2,3].

The Waste and Resources Action Programme (WRAP), in the UK, provides a framework of quality controls for the production of CCA for use in structural concrete, and all aggregates produced must conform to the European standard for aggregates in concrete [4,5]. Utilising CCA in lower grade applications has its advantages economically as it enables the inclusion of fine aggregates (0/4mm). This eliminates the need for aggregate screening, and in turn helps to reduce any potential waste being produced. Recycled aggregate producers however are looking to improve the quality and performance of CCA to allow specification in higher grade applications such as sub-base materials and pipe bedding as this has a higher market value [3,6]. The use of CCA in structural concrete is currently limited due to uncertainty regarding performance [6].

With a large quantity of hard demolition arisings becoming available, and an industry shift towards incorporating CCA into a wider variety of higher value applications [6], certain situations may arise where CCA may be a suitable replacement material in structural concrete, such as: a specific project/client requirement, improved project sustainability credentials, a good quality, consistent source of CCA is available on-site, and/or where there is a short supply of natural aggregates (NA) [7,8,9].

The European standard for concrete specification states that *'Type A aggregates from a known source may be used in exposure classes to which the original concrete was designed with a maximum percentage of replacement of 30%'* [10]. The British standard permits the inclusion of CCA, up to 20% replacement by mass, in concrete up to strength class C40/50, except when the structure is to be exposed to chlorides [11,12]. The British standard also states that *'these aggregates may be used in other exposure classes provided it has been demonstrated that the resulting concrete is suitable for the intended environment'*, which is an ambiguous statement as no performance criteria or limits are included to determine suitability. This highlights uncertainty with respect to incorporating coarse CCA into structural concrete [13]. Further research is therefore required to understand the true effects of coarse CCA on the mechanical and durability properties, if a more robust framework for the use of coarse CCA is to become a possibility in the future.

A review of existing research has highlighted that the effect of CCA on the mechanical properties of structural concrete has been investigated [14-18]. The effect of CCA on long-term durability performance however, is less well established, particularly in relation to chloride ingress and corrosion initiation. The durability of reinforced concrete is primarily influenced by the connectivity, continuity and tortuosity of its pores, as this is how gases, liquids and other substances penetrate the concrete cover to reinforcement [19-21]. The majority of published research on the effect of coarse CCA on concrete durability has focused on rapid migration and absorption test methods to determine acceptable levels of replacement of NA. The general consensus is that 25-30% coarse CCA can be successfully incorporated without detrimentally affecting the transport properties of concrete [22-27]. Quantities up to 75% have been shown to produce structural concrete of adequate quality, however it was noted that higher amounts also increased the variability of durability performance compared to the control concretes [24]. Limbachiya *et al* (2000) established that a replacement level of up to 100% may not have a significant effect on the durability performance of high strength Portland cement (CEM I) concretes, provided the CCA source is obtained from high quality precast concrete sources [18].

Supplementary cementitious materials (SCMs) have latent hydraulic and pozzolanic properties which can improve the durability performance of CCA concrete, due to the reduced porosity of the cement matrix, improved quality of the ITZ and improved chloride binding capacity [28-32]. Dodds *et al* (2016) also established that inclusion of SCMs; pulverised fuel ash (PFA 30% - CEM IIB-V) and ground granulated blast furnace slag (GGBS 50% - CEM III/A), can improve the resistance of concrete to water and chloride ingress even when up to 60% coarse CCA replaced NA [33]. Berndt (2009) found that CEM III/A (at 50%) concrete was found to perform best when compared against other replacement levels of SCMs when 100% CCA was used [31].

The aim of this limited study therefore, was to examine one source of coarse CCA, in varying amounts in structural concrete, in order to determine its resistance to water and chloride ion ingress. GGBS was also incorporated to replace CEM I by 50% (to produce a CEM III/A concrete) to quantify the potential beneficial effects on durability performance. The compressive strength was tested to determine compliance with the characteristic and target mean strength.

2. METHODOLOGY

Structural concretes were designed to achieve characteristic ($f_{c,cube}$) and target mean strengths of 39MPa and 53MPa respectively by the BRE mix design method [34]. CEM I and CEM III/A (50%) concrete mixes were tested at a free water-binder ratio of 0.5. The concretes were produced in accordance with BS 1881-125 [35] and all specimens were cured in water at a temperature of (20±2°C) until the date of testing. The free water-binder ratio and cement content of 390kg/m³ were chosen to comply with the recommendations for XD3/XS3 exposure classes in accordance with BS8500-1 [11]. Coarse CCA (4/20mm) was incorporated at increments of 20%, up to 100%, to replace coarse NA by mass, denoted as 'CCA' followed by the replacement percentage. Additional water was added to account for the higher aggregate absorption characteristics of the coarse CCA in accordance with the BRE mix design method [34]. No admixtures were used in production and no additional cement was added to compensate for the inclusion of CCA. All CCA concretes were compared against a control concrete made with 100% NA (rounded quartzite river gravel and sand). Table 1 details the test method justification.

Table 1: Test method justification

Test	Standard	Justification
Compressive cube strength	BS EN 12390-3 [36]	To determine compliance of mixes with characteristic ($f_{c,cube}$) and target mean strengths and to analyse the effect of coarse CCA on compressive strength.
Surface resistivity	AASHTO T358-15 [37]	To determine the effect of coarse CCA on electrical resistivity of concrete, which provides an indication of its ability to resist chloride ion penetration.
Absorption by capillary action	BS EN 13057 [38]	To determine the effect of coarse CCA on the sorptivity of concrete with no external pressures applied. This is the key transport mechanism of water and chloride ingress when concrete is initially in a dry state.
Rapid Chloride Migration [39]	NT BUILD 492 [39]	To determine the effect of coarse CCA on the chloride migration coefficient in concrete. The results cannot be directly compared to natural diffusion tests; however it provides a rapid indication of durability performance, and is comparative.

Statistical analysis was undertaken using t-tests to determine the effect on sample means when coarse CCA was added based on a 10% decrease in performance. A 10% decrease in performance is considered to be significant as this is greater than any expected human or batch reproducibility error. The results of concrete produced with CCA were compared against the results of the control concrete for each binder type to calculate a probability of a significant detrimental effect. A statistical result of 0.999 relates to a 99.9% confidence of a significant detrimental effect.

3. CCA COMPOSITION

BS EN 206-1 states that a quality source of CCA, of known composition, should be obtained to produce sustainable structural concrete. This is to prevent possible contamination and reduce any detrimental effects [10]. The CCA obtained for this study was from the demolition of a 1970's office building structure in Leicester, UK. Three randomly selected samples were sent for petrographic analysis [40,41] to determine concrete composition and type (Figure 1). Randomly selected samples of coarse CCA were also tested for water absorption properties, and concrete cores from larger sections were obtained to determine compressive strength [42-45].

The 30 minute and 24 hour water absorption values for the coarse CCA are shown in Table 2 and compared against that of the NA used in this study. The 24 hour water absorption of the coarse CCA has been reported elsewhere between 3.60% and 11.57%, dependent on the original source of concrete [22-27,29-32], and is similar to the results obtained in this study. The results of compressive strength testing from cored specimens are shown in Table 3.

Table 2: Water absorption properties of CCA and NA

	CCA		NA	
	30 minutes [%]	24 hour [%]	30 minutes [%]	24 hour [%]
10/20mm (Coarse)	5.57	5.93	0.63	0.89
4/10mm (Coarse)	9.72	9.92	1.07	1.15

Table 3: Determination of equivalent in-situ characteristic strength from cored specimens

Sample	Compressive strength of cored specimen [MPa]	Correction Factor [$K_{is,cyl}$]	Corrected compressive strength [MPa]	Equivalent in-situ characteristic strength [$f_{ck,is}$] [MPa]
A	52.8	0.998	52.7	40.8
B	47.5	0.991	47.1	
C	43.1	1.009	43.5	

Figure 1 Thin section of demolition concrete for petrographic analysis [46]

The key findings of the petrographic analysis were:

- The concrete was produced with partly-crushed gravel typical of East/South-East England (sandstone, limestone, quartzite and chert), quartz-dominated sand and ordinary Portland cement.
- No evidence of cement replacements or admixtures was detected.
- Estimated water-cement ratio, slump and 28 day strength were 0.58, 30-60mm and 38.5MPa respectively; the latter is similar to that of the determined equivalent in-situ characteristic strength.
- Estimated cement content was 325kg/m^3, 13.8% of total weight of concrete.
- There was no obvious segregation, excessive voids, honeycombing or visible microcracking.
- Junctions between aggregates and enclosing binder were tightly sealed, indicative of good quality ITZ.
- Phenolphthalein indicator solution suggests maximum carbonation from the surface was 20-25mm.

4. ANALYSIS OF RESULTS

4.1. COMPRESSIVE CUBE STRENGTH

Tests were conducted on 100mm cube samples at 28 and 56 days. The results show that the inclusion of coarse CCA does have an increasingly detrimental effect on compressive strength at both 28 and 56 days for both CEM I and CEM III/A concretes (Figures 2 and 3 respectively). In the majority of cases the characteristic strength ($f_{c,cube}$ - 39MPa, indicated by the horizontal line) at 28 days was achieved, except for the CEM III/A concretes made with 80% and 100% coarse CCA. At 56 days the characteristic strength was met for all concrete mixes.

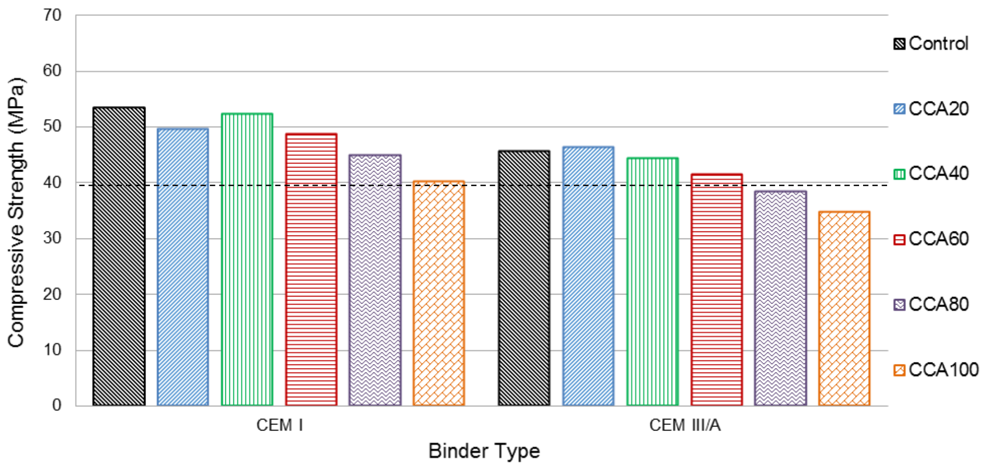

Figure 2 28 day compressive cube strengths

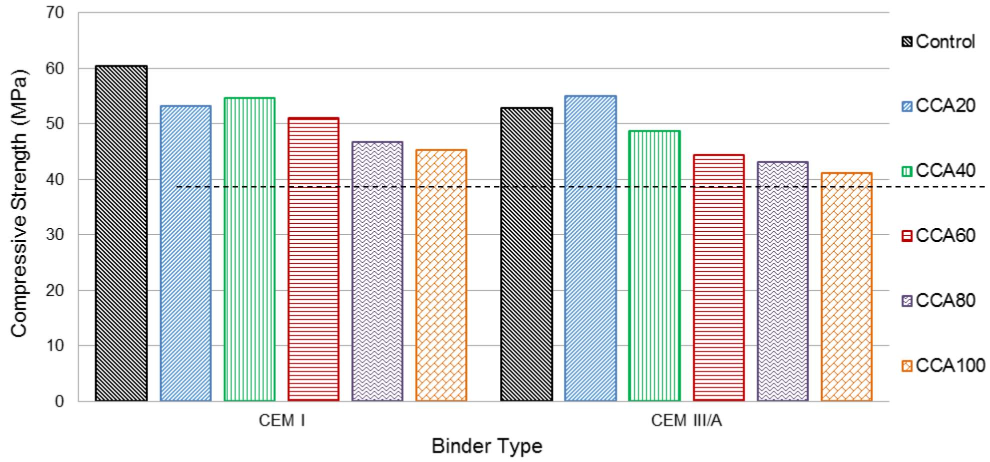

Figure 3 56 day compressive cube strengths

A left-tailed t-test was used to determine if the addition of CCA had a detrimental effect (10% decrease) on sample means, compared to the control concretes for each binder type. The results are shown in Table 4. Higher probabilities (highlighted in bold) of a detrimental effect were observed for coarse CCA contents above 60%, for both CEM I and CEM III/A concretes at 28 days. At 56 days a higher probability was observed for lower coarse CCA contents, which suggests that coarse CCA had a greater detrimental effect on compressive strength at later ages.

Table 4: Probability of a detrimental effect on compressive cube strength

	Coarse CCA content (%)				
	20	40	60	80	100
CEM I – 28 days	0.249	0.107	0.389	**0.876**	**0.939**
CEM III/A – 28 days	0.002	0.010	0.304	**0.980**	**0.997**
CEM I – 56 days	0.216	**0.455**	**0.951**	**0.989**	**0.993**
CEM III/A – 56 days	0.017	0.284	**0.862**	**0.944**	**0.979**

4.2. SURFACE RESISTIVITY

The surface resistivity of cylindrical specimens (200mm × 100mm diameter) was measured at 28 days (Figure 4). This is a relatively quick method of assessing the microstructure and subsequent transport properties of different concretes [47]. The results are commonly interpreted following the recommendations in Table 5. Lower resistivities indicate a more porous concrete microstructure as it allows a higher current to pass between the probes at the surface.

Table 5: Interpretation of four-point Wenner probe readings [37,48]

Concrete Society Technical Report 60		AASHTO T358	
Resistivity [kΩcm]	Interpretation	Resistivity [kΩcm]	Interpretation
<5	Very high corrosion rate	<12	High chloride ion penetration
5-10	High corrosion rate	12-21	Moderate chloride ion penetration
10-20	Low to moderate corrosion rate	21-37	Low chloride ion penetration
>20	Low corrosion rate	37-254	Very low chloride ion penetration
-	-	>254	Negligible chloride ion penetration

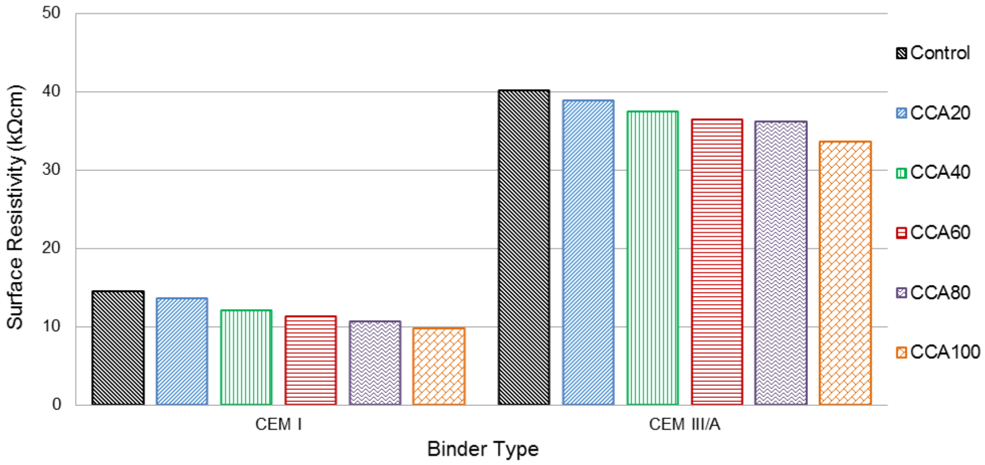

Figure 4 Concrete surface resistivity at 28 days

The results show that the CEM I concretes had a lower surface resistivity than CEM III/A concretes, by a factor of 3 to 4. A structural CEM III/A concrete incorporating up to 100% CCA performed better than the control CEM I concrete. The addition of coarse CCA had an increasingly detrimental effect on the surface resistivity of both concrete types. The results for the CEM I concretes indicate a 'moderate' corrosion rate/chloride ion penetration. In contrast, the results for CEM III/A concretes indicate a 'low' corrosion rate/chloride ion penetration.

The results of statistical analysis are shown in Table 6. Higher probabilities (highlighted in bold) of a detrimental effect against the control concretes for each binder type were observed for coarse CCA contents above 20% and 60%, for both CEM I and CEM III/A concretes respectively. This suggests that GGBS has reduced the detrimental effect of coarse CCA on surface resistivity.

Table 6: Probability of a detrimental effect on surface resistivity

	Coarse CCA content (%)				
	20	40	60	80	100
CEM I – 28 days	0.099	**0.961**	**0.997**	**0.998**	**0.999**
CEM III/A – 28 days	0.066	0.209	0.377	**0.462**	**0.899**

4.3. ABSORPTION BY CAPILLARY ACTION

Kropp *et al* describe sorptivity as the *'transport of liquids into porous solids due to surface tension acting in capillaries'* [19]. The sorptivity is influenced by the characteristics of the liquid and solid material it is in contact with, particularly the radius, tortuosity and continuity of the capillaries. The concrete specimens (60mm × 100mm diameter slices) were sealed on the side to ensure uni-directional ingress of water. Cumulative absorption was measured at 28 days for CEM I and CEM III/A concrete mixes (Figure 5a and 5b respectively) and the sorption coefficients were determined from the gradients at 12 minutes and 24 hours (Table 7).

Table 7: 28 day sorption coefficients for all concretes tested

	CEM I						CEM III/A					
CCA Content (%)	0	20	40	60	80	100	0	20	40	60	80	100
12 mins Sorption Coefficient [$kg/m^2.h^{0.5}$]	1.15	1.36	1.14	1.14	1.63	1.75	1.19	1.15	1.21	1.21	1.72	1.86
% change	-	18	-1	-1	42	52	-	-3	2	2	45	56
24 hour Sorption Coefficient [$kg/m^2.h^{0.5}$]	0.41	0.42	0.34	0.30	0.57	0.61	0.28	0.25	0.29	0.24	0.43	0.45
% change	-	2	-17	-27	39	49	-	-11	4	-14	54	61

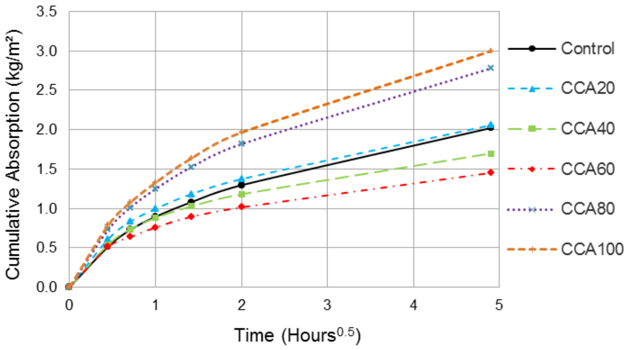

a)

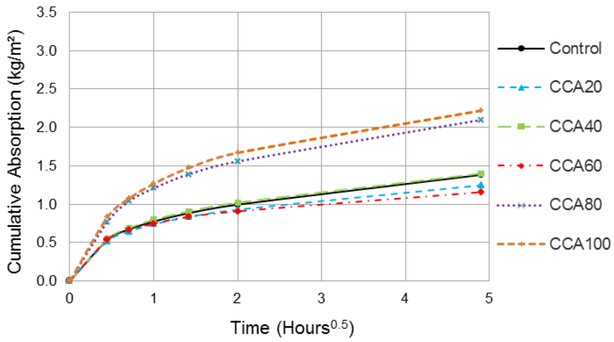

b)

Figure 5 Cumulative absorption at 28 days for a) CEM I, and b) CEM III/A concrete

Some anomalies were observed in this test method. In the instances of 40% and 60% coarse CCA content in CEM I concrete, and 20% and 60% coarse CCA content in CEM III/A concrete, the cumulative absorption at 24 hours was lower than the respective control concretes. As this apparent improvement in durability has not been observed in other test methods it is difficult to determine the exact cause for the reduced absorption. One possibility is that the combination of rounded NA and angular coarse CCA for these mixes reduced the continuity of the capillaries in the cement matrix. In any case there was a significant increase in the cumulative absorption for CCA contents above 60% for both CEM I and CEM III/A concretes, and the inclusion of GGBS reduced the sorption coefficients at 24 hours. This can be further clarified from the results of statistical analysis comparing CCA concretes against the control concretes for each binder type, with the higher probabilities highlighted in bold (Table 8). A structural CEM III/A concrete incorporating up to 60% CCA performed better than the control CEM I concrete.

Table 8: Probability of a detrimental effect on 24 hour sorption coefficients

	Coarse CCA content (%)				
	20	40	60	80	100
CEM I – 28 days	0.073	0.009	0.003	**0.983**	**0.996**
CEM III/A – 28 days	0.014	0.051	0.010	**0.994**	**0.995**

4.4. RAPID CHLORIDE MIGRATION

Migration of chloride ions occurs when an electric field is applied across a concrete specimen (50mm × 100mm diameter slice), causing the negatively charged chloride ions to move towards an anode [49]. The non-steady state chloride migration coefficients in Figure 6 have been calculated from average penetration depths.

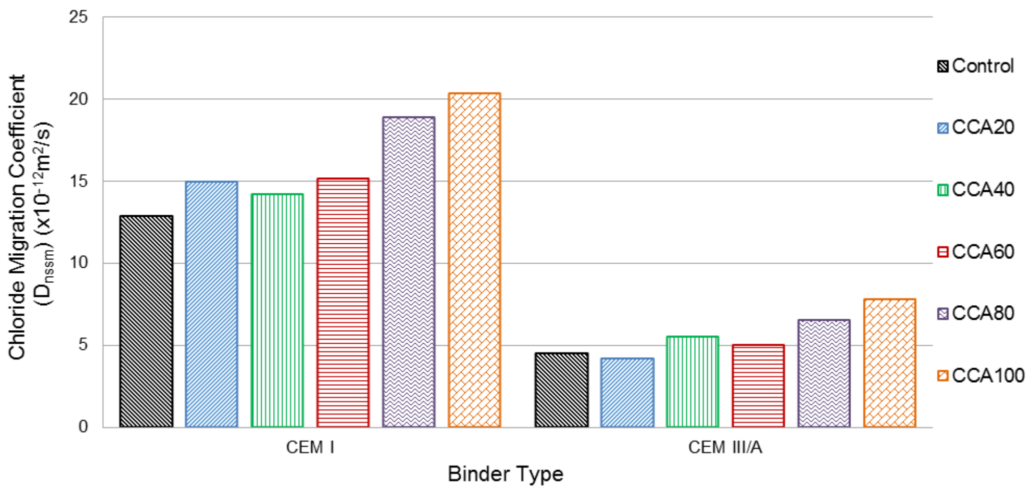

Figure 6 Chloride migration coefficients at 28 days

The results show that the inclusion of coarse CCA content had an increasingly detrimental effect on the chloride migration coefficient of concrete. CEM III/A concretes were found to provide enhanced resistance to chloride ion penetration compared to CEM I concrete, by a factor of 2 to 3. A structural CEM III/A concrete incorporating up to 100% CCA performed better than the control CEM I concrete. Statistical analysis shows a relatively high probability (highlighted in bold) that the chloride migration coefficient will increase by more than 10% for all CCA contents compared to the control concretes for each binder type; except for the 20% content in CEM III/A concrete (Table 9).

Table 9: Probability of a detrimental effect on chloride migration coefficients

	Coarse CCA content (%)				
	20	40	60	80	100
CEM I – 28 days	**0.831**	**0.520**	**0.835**	**0.976**	**0.993**
CEM III/A – 28 days	0.135	**0.756**	**0.508**	**0.914**	**0.981**

5. DISCUSSION

5.1. COMPRESSIVE CUBE STRENGTH

In the majority of cases, the characteristic strength ($f_{c,cube}$ - 39MPa) at 28 days was achieved, except for the CEM III/A concretes made with 80% and 100% coarse CCA (Figure 2). The characteristic strength however, was met for all concrete mixes at 56 days due to the latent hydraulic effects of GGBS (Figure 3) [28-32]. This suggests that the BRE method of mix design [34] is suitable for designing structural concrete produced with up to 100% coarse CCA. It should be noted that a large margin of 14MPa was used in this study to determine the target mean strength. This ultimately allowed some variability to occur in the compressive strength results when higher quantities of CCA replacement was used [24].

The results confirm previous research that the inclusion of coarse CCA has a detrimental effect on the compressive strength of concrete. The statistical analysis shows that a higher probability of a detrimental effect was observed for coarse CCA contents above 60% when compared against the control concretes for each binder type, for both CEM I and CEM III/A concretes at 28 days (Table 4). This suggests that 60% coarse CCA inclusion is acceptable for CEM I and CEM III/A concretes without increasing the risk of a non-compliant concrete (i.e. not achieving the specified characteristic strength).

5.2. SURFACE RESISTIVITY

Figure 4 shows that an increase in the coarse CCA content generally reduced the surface resistivity of concrete. This is possibly due to the increased porosity of the CCA [22-27]. In all cases, the GGBS had a beneficial effect on surface resistivity, by a factor of 3 to 4, reducing the potential chloride ion penetration from a 'moderate' to 'low' level (Table 5). A structural CEM III/A concrete incorporating up to 100% CCA performed better than the control CEM I concrete.

The results of the statistical analysis indicate that a detrimental effect against the control concrete occurs for coarse CCA contents above 20% and 60% for CEM I and CEM III/A concretes respectively (Table 6). This highlights the beneficial effect of incorporating GGBS to reduce the porosity of the cement matrix as a higher quantity of coarse CCA can be utilised. This finding is in agreement with other research on SCMs and CCA concrete [28-33].

5.3. ABSORPTION BY CAPILLARY ACTION

The cumulative absorption, sorption coefficients and statistical analysis indicate that higher quantities of coarse CCA (>60%) have a large detrimental effect when compared against the control concretes for each binder type (Figures 5a and 5b, Tables 7 and 8). Some anomalies exist for the lower quantities of CCA replacement for both CEM I and CEM III/A concretes as the cumulative absorption at 24 hours was lower than the respective control concretes. One possibility for the reduced cumulative absorption is that the combination of rounded NA and angular coarse CCA for these mixes reduced the continuity of the capillaries in the cement matrix. In any case, there was a significant increase in the cumulative absorption for CCA contents above 60% for both CEM I and CEM III/A concretes, and the inclusion of GGBS reduced the sorption coefficients at 24 hours due to a reduced porosity of the cement matrix and improved ITZ [28-33]. A structural CEM III/A concrete incorporating up to 60% CCA performed better than the control CEM I concrete, which suggests that up to 60% coarse CCA inclusion is acceptable which is higher than previously reported values [22-27].

5.4. RAPID CHLORIDE MIGRATION

Figure 6 shows that an increase in the coarse CCA content generally increased the chloride migration coefficient of concrete, primarily due to its own increased porosity [22-27]. Although the statistical analysis (Table 9) shows that CCA contents as low as 20% can increase the probability of a detrimental effect (by 10% increase) when compared with the control concrete for each binder type, the results clearly show that the inclusion of GGBS reduced the chloride migration coefficient by a factor of 2 to 3, most likely due to a reduced porosity of the cement matrix, improved ITZ and an increased chloride binding effect [28-33]. The chloride migration coefficient for 100% CCA content in CEM III/A concrete was 39% lower than that of the control CEM I concrete with 100% NA. This suggests that higher proportions of coarse CCA can be adopted when CEM III/A concrete is to be exposed to chloride environments.

6. CONCLUSIONS

From this limited study of CCA, which is part of a wider research project, the results show that the inclusion of coarse CCA generally has a detrimental effect on the transport mechanisms in the resultant concrete, as well as the compressive strength.

The compressive strength testing showed that the characteristic strength ($f_{c,cube}$) of the majority of concretes tested was met at 28 days, with the remaining mixes achieving it by 56 days. This suggests that the BRE method of mix design can be suitably applied for designing structural concrete produced with up to 100% coarse CCA. From the results of the statistical analysis it is recommended that the coarse CCA inclusion is limited to 60% to reduce the risk of a non-compliant concrete (i.e. not achieving the specified characteristic strength).

The tests conducted into the durability have highlighted that the inclusion of coarse CCA can have an increasingly detrimental effect on water and chloride ion ingress. A detrimental effect (of 10% decrease in performance) can be observed, even for coarse CCA quantities as low as 20% for CEM I concrete, and as low as 40% for CEM III/A concretes, when compared against the control concretes for each binder type. Moreover, the inclusion of GGBS significantly increased the concretes resistance to water and chloride ion ingress compared to CEM I concretes due to the reduced porosity of the cement matrix, improved ITZ and the increased chloride binding capacity of the material. A structural CEM III/A concrete incorporating up to 60% CCA performed better than the control CEM I concrete for all durability test methods adopted. From these results, it is recommended that up to 60% coarse CCA can be adopted in structural concrete, provided that GGBS (50%) is also incorporated; as it has been demonstrated that the resulting concrete is suitable when exposed to chloride environments. This is a positive finding for the increased incorporation of CCA into a wider variety of higher-value structural applications.

ACKNOWLEDGMENTS

The authors thank the Engineering and Physical Sciences Research Council (EPSRC), Loughborough University's Centre for Innovative and Collaborative Construction Engineering (CICE) and AECOM for the funding of this research. The authors would also like to acknowledge DSM Demolition Group for helping to obtain the CCA source and Hanson Limited for the cementitious materials.

REFERENCES

[1] National Federation of Demolition Contractors (NFDC), 2016. *Waste returns spreadsheet 2013, 2014 and 2015*, personal communication, 14th October 2016.

[2] Waste and Resources Action Programme (WRAP), 2009. *Delivering higher recycled content in construction projects* [pdf]. Accessed: 1st July 2016.

[3] Waste and Resources Action Programme (WRAP), 2003. *A strategy for construction, demolition and excavation waste as recycled aggregates* [pdf]. Accessed: 1st July 2016.

[4] Environment Agency and WRAP, 2013. *Quality protocol: Aggregates from inert waste* [pdf]. Accessed: 1st July 2016.

[5] British Standards Institution (BSI), 2013a. *BS EN 12620:2013, Aggregates for concrete*. London: BSI.

[6] Barritt, J, 2015. *An overview on recycling and waste in construction*. Proceedings of the ICE, Construction Materials, Volume 169, Issue 2, pp1-5.

[7] Hassan, K.E. *et al*, 2016. *Recycled aggregates in structural concrete – a Qatar case study*. Proceedings of the Institution of Civil Engineers, Construction Materials, Volume 169, Issue CM2, pp72-82.

[8] Yehualaw, M. Woldesenbet, A, 2016. *Economic Impacts of Recycled Concrete Aggregate for Developing Nations: A Case Study in the Ethiopian Construction Industry*. Construction Research Congress 2016, pp250-259.

[9] Filho, R.D.T. *et al*, 2013. *Rio 2016 sustainable construction commitments lead to new developments in recycled aggregate concrete*. Proceedings of the Institution of Civil Engineers, Civil Engineering Special Issue, Volume 166, Issue CE6, pp28-35.

[10] British Standards Institution (BSI), 2013b. *BS EN 206-1:2013, Concrete: Specification, performance, production and conformity*. London: BSI.

[11] British Standards Institution (BSI), 2015a. *BS 8500-1:2015+A1:2016, Concrete - Complementary British Standard to BS EN 206 – Part 1: Method of specifying and guidance for the specifier*. London: BSI.

[12] British Standards Institution (BSI), 2015b. *BS 8500-2:2015, Concrete – Complementary British Standard to BS EN 206 - Part 2: Specification for constituent materials and concrete*. London: BSI.

[13] Saffiuddin, M. *et al*, 2013. *Use of recycled concrete aggregate*. Journal of Civil Engineering and Management, Volume 19, Issue 6, pp796-810.

[14] Silva, R.V. *et al*, 2016. *Design of reinforced recycled aggregate concrete elements in conformity with Eurocode 2*. Construction and Building Materials, Volume 105, pp144-156.

[15] Collery, D.J. *et al*, 2015. *Establishing rational use of recycled aggregates in concrete: a performance-related approach*. Magazine of Concrete Research. Paper 1400206.

[16] Exteberria, M. *et al*, 2007. *Influence of amount of recycled coarse aggregates and production process on properties of recycled aggregate concrete*. Cement and Concrete Research, Volume 37, pp735-742.

[17] Ajdukiewicz, A. Kliszczewicz, A, 2002. *Influence of recycled aggregates on mechanical properties of HS/HPC*. Cement and Concrete Composites, Volume 24, pp269-279.

[18] Limbachiya, M.C. *et al*, 2000. *Use of recycled concrete aggregate in high strength concrete*. Materials and Structures, Volume 33, pp574-580.

[19] [19] Kropp, J. *et al,* 1995. *Chapter 2: Transport mechanisms and definitions,* In: Kropp, J. Hilsdorf, H.K. *RILEM Report 12 - Performance criteria for concrete durability*, E&FN Spon.

[20] Ollivier, J. *et al*, 1995. *Chapter 4: Parameters influencing transport charcteristics*, In: Kropp, J. Hilsdorf, H.K. *RILEM Report 12 - Performance criteria for concrete durability*, E&FN Spon.

[21] Tuutti, K, 1982. *Corrosion of steel in concrete*. Swedish Cement and Concrete Institute (CET) no. 4–82. Stockholm.

[22] Bravo, M. *et al*, 2015. *Durability performance of concrete with recycled aggregates from construction and demolition waste plants*. Construction and Building Materials, Volume 77, pp357-369.

[23] Lofty, A. Al-Fayez, M, 2015. *Performance evaluation of structural concrete using controlled quality coarse and fine recycled concrete aggregate*. Cement and Concrete Composites, Volume 61, pp36-43.

[24] Pedro, D. *et al*, 2014. *Influence of the use of recycled concrete aggregates from different sources on structural concrete*. Construction and Building Materials, Volume 71, pp141-151.

[25] Soares, D. *et al*, 2014. *Use of coarse recycled aggregates from precast concrete rejects: Mechanical and durability performance*. Construction and Building Materials, Volume 71, pp263-272.

[26] Zega, C.J. *et al*, 2014. *Influence of natural coarse aggregate type on the transport properties of recycled concrete*. Journal of Materials in Civil Engineering, Volume 26, Issue 6, pp04014006-1-04014006-9.

[27] Limbachiya, M. *et al*, 2012. *Use of recycled concrete aggregate in fly-ash concrete*. Construction and Building Materials, Volume 27, pp439-449.

[28] Bapat, J.D, 2013. *Mineral admixtures in cement and concrete*, CRC Press.

[29] Hwang, J.P. *et al*, 2013. *Enhancing the durability properties of concrete containing recycled aggregate by the use of pozzolanic materials*. KSCE Journal of Civil Engineering, Volume 17, Issue 1, pp155-163.

[30] Somna, R. *et al*, 2012. *Effect of ground fly ash and ground baggase ash on the durability of recycled aggregate concrete*. Cement and Concrete Composites, Volume 34, pp848-854.

[31] Berndt, M.L, 2009. *Properties of sustainable concrete containing fly ash, slag and recycled concrete aggregate*. Construction and Building Materials, Volume 23, pp2606-2613.

[32] Ann, K.Y. *et al*, 2008. *Durability of recycled aggregate concrete using pozzolanic materials*. Waste Management, Volume 28, pp993-999.
[33] Dodds, W. *et al*, 2016. *Durability performance of structural concrete made with coarse recycled concrete aggregates*. fib Symposium 2016, Performance-based approaches for concrete structures, Cape Town, South Africa, 21-23 November 2016.
[34] Building Research Establishment (BRE), 1997. *Design of normal concrete mixes: Second edition*. Watford, UK.
[35] British Standards Institution, 2013c. *BS 1881-125:2013, Testing concrete – Part 125: Methods for mixing and sampling fresh concrete in the laboratory*, London, BSI.
[36] British Standards Institution, 2009a. *BS EN 12390-3:2009, Testing hardened concrete. Part 3 – Compressive strength of test specimens*, London, BSI.
[37] American Association of State Highway and Transport Officials, 2015. *AASHTO T358-15, Standard test method for surface resistivity indication of concretes ability to resist chloride ion penetration*, Washington, USA.
[38] British Standards Institution (BSI), 2002. *BS EN 13057:2002, Products and systems for the protection and repair of concrete structures – Test methods – Determination of resistance of capillary absorption*. London: BSI.
[39] NordTest, 1999. *NT-Build 492, Chloride migration coefficient from non-steady state migration experiments*, NordTest Project No. 1388-98, Espoo, Finland.
[40] American Society for Testing and Materials (ASTM), 2014. *ASTM C856-14, Standard practice for petrographic examination of hardened concrete*. ASTM International, West Conshohocken, PA, USA.
[41] Concrete Society, 2010. *Concrete Society Technical Report 71: Concrete petrography*. The Concrete Society, Surrey, UK.
[42] British Standards Institution (BSI), 2013d. *BS EN 1097-6:2013, Tests for mechanical and physical properties of aggregates. Part 6: Determination of particle density and water absorption*. London: BSI.
[43] British Standards Institution, 2010. *BS 6089:2010, Assessment of in-situ compressive strength in structures and precast concrete components – Complementary guidance to that given in BS EN 13791*, London, BSI.
[44] British Standards Institution, 2009b. *BS EN 12504-1:2009, Testing concrete in structures. Part 1: Cored specimens – Taking, examining and testing in compression*, London, BSI.
[45] British Standards Institution (BSI), 2007. *BS EN 13791:2007, Assessment of in-situ compressive strength in structures and precast concrete components*. London: BSI.
[46] Aston Services, 2015. *Petrography report: New Walk Centre, Leicester City Council Building, In-situ demolition waste RCA.* Report number LU/PA/101215, 10th December 2015.
[47] Angst, U.M. Elsener, B, 2014. *On the applicability of the Wenner method for resistivity measurements of concrete*. ACI Materials Journal, Volume 111, Issue No 6, pp661-672.
[48] Concrete Society, 2004. *Concrete Society Technical Report 60: Electrochemical tests for reinforcement corrosion*. Cromwell Press Ltd.
[49] Claisse, P. A, 2014. *Transport properties of concrete – Measurement and applications*. Woodhead Publishing.

AGGREGATE SELECTION TO IMPROVE DURABILITY OF CONCRETE EXPOSED TO SEVERE ENVIRONMENTAL CONDITIONS

Josee Duchesne[1], Benoit Fournier[1], Andreia Rodrigues[1], Benoit Durand[2], Patrice Rivard[3], Medhat H. Shehata[4]

[1] Université Laval, Dep. of geology and geological enginnering, Québec, QC, Canada,
email: josee.duchesne@ggl.ulaval.ca, benoit.fournier@ggl.ulaval.ca, andreia.de-almeida-rodrigues.1@ulaval.ca
[2] IREQ, 1800 Boulevard Lionel-Boulet, Varennes, QC J3X 1S1, email: durand.benoit@ireq.ca,
[3] Université de Sherbrooke, Faculty of Engineering, Department of Civil Engineering, 2500, boulevard de l' Université, Sherbrooke, QC, Canada, J1K 2R1, email: patrice.rivard@USherbrooke.ca
[4] Ryerson University, Faculty of Engineering and Architectural Science, Depratment of Civil Engineering
350 Victoria St, Toronto, ON, Canada, M5B 2K3, e-mail: mshehata@ryerson.ca

SUMMARY: Concrete is the most widely used building material worldwide. The great popularity of concrete is explained by the fact that it is inexpensive, easy to produce, very versatile and it is produced and used locally. In many countries, concrete structures suffer from premature degradation. This is an important problem since the costs of repair are important in addition to harming the activities of users. The concrete is often exposed to very severe exposure conditions characterized by significant fluctuations in temperature (freeze-thaw cycles, extreme temperatures), in addition to the contact with aggressive solution such as deicing salts, and often coupled with other problems as the alkali-silica reaction or the presence of sulfide-bearing aggregates. A more durable concrete is the first step towards sustainable material. Aggregates account for 60 to 75 percent of the total volume of concrete and their selection is an important process to ensure the quality of the material. Any deleterious reaction causing swelling and cracking of the concrete such as alkali-silica reaction, or the presence of sulfide-bearing aggregates should be avoided. As soon as the concrete cracks, water and other contaminant could penetrate into the material and resulting in premature deterioration related to freezing and thawing. Different case studies will be presented to illustrate the degradation caused by a deficient selection of aggregates for concrete making. A testing protocol recently develop to enable the identification of potentially deleterious sulfide-bearing aggregates prior to their use in concrete will be presented along with a performance approach developed to assess the alkali-silica reactivity potential of concrete aggregates.

ODABIR AGREGATA ZA POBOLJŠANJE TRAJNOSTI BETONA IZLOŽENOG OŠTRIM UVJETIMA OKOLIŠA

SAŽETAK: Beton je u svijetu najviše upotrebljavan građevni materijal. Njegova se velika popularnost objašnjava činjenicom da je jeftin, da se lagano proizvodi, da je svestran i da se proizvodi i upotrebljava lokalno. U mnogim zemljama betonske konstrukcije pate od prerane degradacije. To je važan problem, jer su troškovi popravka veliki uz to što škode aktivnostima korisnika. Beton je često izložen vrlo oštrim uvjetima koje karakteriziraju znatne oscilacije temperature (ciklusi zamrzavanja i odmrzavanja, ekstremne temperature) uz kontakt s agresivnim otopinama kao što su soli za odleđivanje, a često i povezanošću s drugim problemima kao što su alkalnosilikatna reakcija ili prisutnost agregata koji sadržavaju sulfide. Prvi je korak ka trajnijem betonu održivi materijal. Agregat čini 60 do 75 posto ukupnog obujma betona pa je njegov odabir važan za osiguranje kvalitete materijala. Treba izbjeći svaku štetnu reakciju koja dovodi do bubrenja i raspucavanja betona kao što je alkalnosilikatna reakcija ili prisutnost agregata sa sulfidima. Čim se beton raspuca, u materijal mogu prodrijeti voda i drugie štetne tvari što dovodi do preranog gubitka svojstava povezanih sa zamrzavanjem i odmrzavanjem. U radu je obrađeno više istraživanja kojima se ilustrira degradacija prouzročena manjkavim odabirom agregata za izradu betona. Prikazuje se i protokol ispitivanja koji je nedavno razvijen i koji omogućuje prepoznavanje potencijalno škodljivog agregata sa sulfidima prije njegove upotrebe u betonu i ocjenjivanje potencijala alkalnosilikatne reakcije agregata za beton.

1. INTRODUCTION

Concrete is the most widely used construction material worldwide with an average of about one cubic meter of concrete produced per person per year. Extending the service life of concrete infrastructures is one of the ways to save natural resources and improving sustainability in construction. Aggregates account for 60 to 75 percent of the total volume of concrete and their selection is an important process. To ensure the quality of concrete, aggregates should comply with compulsory regulations. Aggregates have to be clean, hard, strong, and free of deleterious substances. These properties are well evaluated in several standards such as the ASTM C33 specifications for concrete aggregates in which the physical testing of aggregates takes a very considerable part [1]. Unfortunately, the good physical properties of the aggregates are not a guarantee of good chemical properties and often aggregates are considered as inert material within a concrete mix.

Deficient selection of aggregates may lead to premature degradation of concrete structures. This is the case, for example, of aggregates susceptible to the alkali-aggregate reaction (AAR), a chemical reaction between some aggregates and the alkali hydroxides of the concrete pore solution causing expansion and cracking of concrete. Since the last decades, AAR reaction has received a lot of attention and the reaction mechanisms are better understood. Laboratory tests are available to evaluate the performance of aggregates or to evaluate performance of concrete mixtures to prevent excessive expansion.

More recently, cases of early deterioration of concrete have been observed in presence of sulfide-bearing aggregate in the Trois-Rivières area, Québec, Canada. Concrete damages were reported in structures 3 to 5 years after construction. A large number of concrete samples were investigated. In all cases, the aggregate material was an intrusive igneous rock containing various proportions of sulfide minerals including pyrite (FeS_2) and pyrrhotite ($Fe_{1-x}S$). No repair and rehabilitation methods are available at this time and structures must be demolished and replaced (Figure 1). The signs of concrete deterioration observed in the distressed concretes mainly consist of map cracking on the surface of the walls, yellowish and brownish discoloration often observed surrounding these cracks. Pop-outs are observed on the walls showing the presence of oxidized and rusted aggregate particles. Some of these deterioration features are illustrated in Figure 2.

Pyrrhotite is well known as an unstable mineral in the presence of oxygen and humidity [2-3]. A deleterious process involving the oxidation of sulfide minerals and the sulfate attack of the cement paste is thought to have caused the swelling and cracking of the affected concrete elements [4]. In fact, the presence of secondary reaction products including iron oxyhydroxide, gypsum, ettringite, and thaumasite was observed and support this hypothesis [5]. A testing protocol recently develop to enable the identification of potentially deleterious sulfide-bearing aggregates prior to their use in concrete is presented.

2. RESEARCH WORK GOAL AND SCOPE

Iron sulfide minerals are common minor constituents in many rock types. Several studies have already identified the risks of sulfide oxidation for engineering works [6], but no precise guideline is available for the quality control of the aggregate materials. As part of an extensive investigation carried out in Canada, a global evaluation protocol was developed [7]. The goal of this paper is to highlight the main lines of the proposed protocol to identify potentially deleterious sulfide-bearing aggregates prior to their use in concrete.

Figure 1 Replacement process of residential concrete foundations in the Trois-Rivières area

3. MATERIALS AND METHODS

3.1. MATERIALS

The main material used in this study is the anorthositic gabbro (problematic aggragate) from the Trois-Rivières area, Québec, Canada. Aggregate materials without sulfide minerals are used as control specimen. A total of 8 aggregates were studied including 6 sulfide-bearing aggregates and 2 control aggregates.

3.2. METHODS

3.2.1. CHEMICAL APPROACH – TOTAL SULFUR CONTENT AND IDENTIFICATION OF SULFIDE MINERALS

The chemical approach, using a measurement of the total sulfur content is a tool used for the rapid detection of the presence of sulfide minerals. The total sulfur content of aggregate material is determined by an infrared absorption method using an Eltra CS 800 carbon/sulfur analyzer. The petrographic examination, using reflected polarized light microscopy is a rapid way for sulfide identification (Figure 3).

Figure 2 Examples of concrete deterioration features including map-cracking, cracks filled up with sealant materials, large open cracks, and pop outs showing oxidized aggregates particles surrounded by whitish secondary products

Figure 3 Samples of the anorthositic gabbro including thin sections selection (top). Photomicrograph of the anorthositc gabbro viewed under reflected light. (Py: pyrite; Po: pyrrhotite; Pent: pentlandite; Chalco: chalcopyrite)

3.2.2. CHEMICAL APPROACH - OXYGEN CONSUMPTION TEST

In the approach proposed, the oxidation potential of the aggregate is assessed directly by an oxygen consumption test (Figure 4). In fact, in the sulfide oxidation reaction, the oxygen is one of the reactants and the monitoring of its concentration can be used to determine if sulfide-bearing aggregates are potentially harmful. This test consists in the monitoring of the oxygen consumption resulting from the iron sulfides oxidation based on the studies of Elberling et al. [8]. The rate of oxygen consumption is measured in the headspace at the top of a cylinder containing the aggregate material placed in favorable oxidizing conditions (presence of moisture and oxygen). When oxygen is consumed, its concentration decreases in the closed volume. The method can thus provide a quantitative assessment of the potential "reactivity" of the aggregate material through the measurement of the reactants necessary for the oxidation reaction.

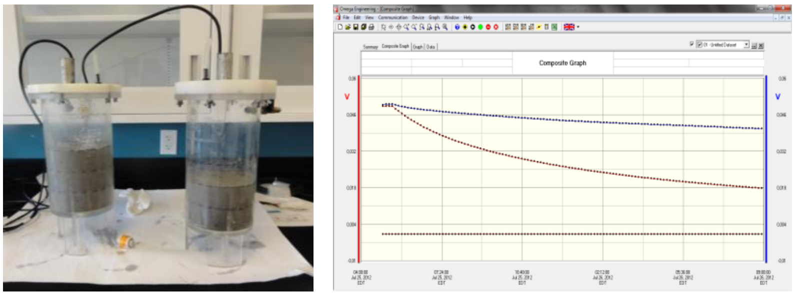

Figure 4 Oxygen consumption set up with an example of the concentration of oxygen monitored in the headspace of the cylinder of known volume.

3.2.3. MORTAR BAR EXPANSION TEST

A newly-developed mortar bar expansion test is proposed where the bars are subjected to a cyclic exposure conditioning regime involving wetting and drying cycles in an oxidizing agent followed by extended storage under temperature and humidity conditions promoting the oxidation reaction. The goal of this test is to establish favorable conditions that will reproduce, in the laboratory, the expansive process responsible for the damage of the concrete incorporating sulfide-bearing aggregates.

4. RESULTS AND DISCUSSION

4.1.1. CHEMICAL APPROACH – TOTAL SULFUR CONTENT AND IDENTIFICATION OF SULFIDE MINERALS

Until now, the chemical approach, via a measurement of the total sulfur content, is a tool used for the rapid detection of the presence of iron sulfide minerals in an aggregate sample. The measurement of the total sulfur content is used to calculate the sulfide content using iron sulfide minerals stoichiometry. For example, pyrite (FeS_2) contains 53.45% of S and pyrrhotite ($Fe_{1-x}S$) contains 37.67 % S. To determine the content of iron sulfide minerals, some assumptions must be made. First, almost all sulfide minerals contain sulfur, whether it is pyrrhotite, pyrite, chalcopyrite, ... so you cannot redistribute sulfur in different minerals unless data on the mineralogical distribution of the different phases is known. Petrographic examination is a rapid tool for the identification of sulfide minerals but quantitative assessment is more difficult.

The total sulfur content is often determined by a carbon/sulfur analyzer on a sample of 0.3 to 1 g required for the analysis. Because of the very small amount material used for testing, a rigorous sample preparation method is required to ensure sample representativity. For aggregate evaluation, we proposed to start with a minimum initial sample of 4 kg, with particle size ranging between 5 and 20 mm. This sample is split in two representative subsamples containing more than 300 particles each. A portion of 2 kg is then crushed to reduce all particles to a size less than 5 mm. The sample is again split until a sub-sample of 500 g is obtained (2 splits). The sub-sample of 500 g is then pulverized so that all particles are less than 300 microns. The sample is then split until a mass of 50 g is obtained (3 splits). The sample, with a weight of about 50 g, is entirely pulverized until all particles are less than 80 microns in size. The resulting sample is split is used for the different chemical analyses.

4.1.2. CHEMICAL APPROACH - OXYGEN CONSUMPTION TEST

The oxygen consumption method seems of great interest to assess the potential of oxidation of aggregates containing iron sulfide minerals because the method is quantitative and based on the direct measurement of the reactants necessary for the oxidation reaction.

Parametric testing was carried out that resulted in the optimized testing conditions described hereafter. Rodrigues et al. [9] presented in detail the development of this new test. The aggregate material, ground to < 150 µm grain size, is prepared to a controlled degree of saturation (40%) and then placed in the cylinder in two layers. Each layer is compacted to a thickness of 5 cm. The volume of material used for each layer of 5 cm is calculated based on its density. A 10-cm headspace is maintained in the closed container above the compacted aggregate material. When oxygen is consumed, its concentration decreases in the closed volume. The duration of the test is 2 hours.

4.1.3. MORTAR BAR EXPANSION TEST

The oxidation of iron sulfide minerals generates secondary reaction products such as iron oxyhydroxides (goethite, limonite) products. This reaction also generates sulfuric acid that reacts with the cement paste components producing internal sulfate attack in the form of gypsum, ettringite and thaumasite. All these secondary minerals have a higher volume than the reactants and are responsible for the swelling and cracking of the concrete. The objective was to develop a performance test on mortar bars that would reproduce in the laboratory the expansion observed on the affected concrete caused firstly by the oxidation of the sulfide-bearing aggregate followed by the sulfate attack of the cement paste.

Mortar bars, 25x25x28.5 mm in size, were manufactured using a w/c of 0.70 and a cement-to-aggregate ratio of 1:2.73. A high w/c was chosen to reproduce the characteristics of concrete used in the damaged housing foundations in the Trois-Rivières area. The grading requirement for aggregate used was the same as that used in the standard test method for potential alkali reactivity of aggregates. All the bars were prepared with a general use (GU) portland cement.

Parametric testing was carried out that resulted in the optimized testing conditions described hereafter [10]. The expansion test was divided into two phases, i.e. Phase 1 involving iron sulfide oxidation, sulfuric acid formation, and its subsequent reaction with calcium hydroxide to form gypsum, and Phase 2 involving the formation of thaumasite. Phase 1 consists in exposing mortar bars to high temperature (80˚C) and RH (80%) conditions for 90 days with two 3-hour immersion period in a 6% bleach solution per week. Obtaining an expansion value greater than 0.10% at 90 days shows an oxidation potential of the aggregate. However, this limit was established on the basis of limited tests and will need to be validated through the evaluation of a larger number of aggregate sources. After Phase 1, the test can be continued to determine the potential for thaumasite formation. For this, the mortar bars subjected to Phase 1 are transferred to low temperature (4˚C) at a relative humidity of 100% for an additional testing period up to 90 days with, once again, two 3-hour immersion period in a 6% bleach solution per week.

Figure 5 presents the expansion curves obtained for different aggregates tested. The control aggregate (A) was not affected by the very severe exposure conditions. MSK aggregate (the problematic aggregate from the Trois-Rivières area) shows a moderate expansion in the Phase 1 followed by an acceleration of the expansion following the transfer to low temperature (thaumasite formation). The B, C and D aggregates present a different behaviour, when compared with MSK, with a very rapid onset of expansion followed by a plateau after about 100 days of testing, i.e. upon transfer to 4˚C. This behavior is associated to the fact that those three aggregates contain sulfide minerals but are also alkali-silica reactive. Additional work should be carried on to understand this phenomenon and possibly find a way to discriminate the effect of the sulfide oxidation from the effect of the ASR. Also, for these 3 aggregates, there is no further expansion following the transfer to low temperature.

4.1.1. PROTOCOL FOR THE IDENTIFICATION OF POTENTIALLY DELETERIOUS SULFIDE-BEARING AGGREGATES

A three-step evaluation protocol test for the evaluation of sulfide-bearing aggregates prior to their use in concrete is proposed. In the first step, the aggregate total sulfur content (S_T, % by mass) is measured. The values obtained and existing standards lead to proposing: (1) a $S_T > 1\%$ as the value for rejecting the aggregate, (2) $0.10\% \geq S_T < 1\%$ as the interval value for proceeding to the second step, and (3) the $S_T < 0.10\%$ as the limit value of acceptance. The aggregates that are directed to step 2 are then exposed to an oxygen consumption test. Taking into account the limited number of aggregates tested, the tentative acceptance limit was lower than 5% of consumed oxygen, while aggregates inducing values equal or higher than 5% should be tested in the step 3. Step 3 consists of a two-part mortar bar test. In Part I, mortar bars are subjected to a 90-day storage period at 80°C and 80% RH with two 3-hour soaking periods in a 6% bleach solution. The aggregate can be immediately rejected if the expansion value is higher or equal to 0.10% at 90 days. If the values are lower than 0.10%, the samples should be transferred to 4˚C and 100% RH for another 90 day-period. If, at the end of those 90 days, the samples expansion remains stable, the aggregates could be accepted. However, if the expansion continues, the aggregate should be rejected. The proposed protocol and preliminary test limits will need to be further validated through the testing of a larger number of aggregates.

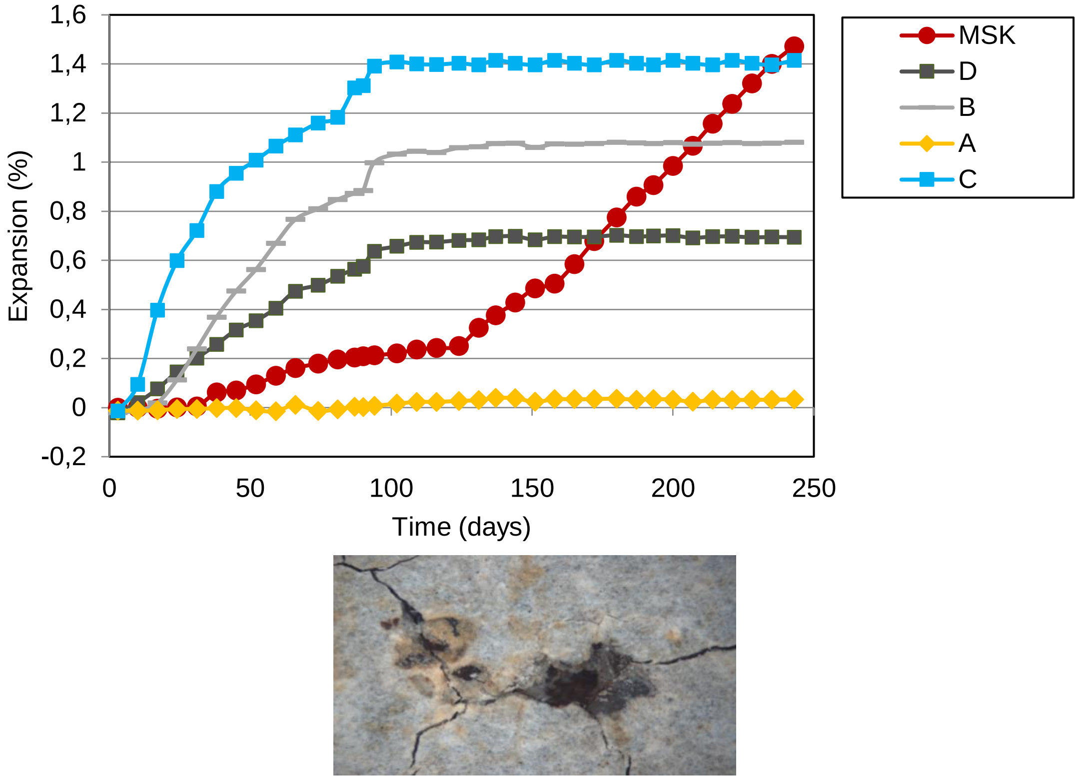

Figure 5 Expansion of mortar bars kept at 80°C and 80% RH for 90 days and then transferred to 4°C and 80% RH with immersion (twice per week) in bleach (6%) solution.– Signs of degradation of the bars subjected to the expansion test.

5. CONCLUSION

The goal of this study was to present a global evaluation program of concrete aggregate to identify potentially deleterious sulfide-bearing aggregates prior to their use in concrete in order to improve the quality and durability of materials. The approach proposed begins with the measurement of the total sulfide content of the aggregate. After that, the oxidation potential of the aggregate is directly assessed through the oxygen consumption test. Finally, the aggregate is evaluated by a newly-developed mortar bar expansion test. Mortar bars are kept at 80°C and 80% relative humidity for 90 days with two 3-hour wetting and drying cycles a week in a 6% sodium hypochlorite solution (bleach). At 90 days, the bars are transferred at 4°C to promote thaumasite formation. The performance approach developed will be extended to a broader range of aggregates to validate the threshold values at each step of the protocol.

ACKNOWLEDGMENTS

This study has been supported by the National Science and Engineering Research Council of Canada (NSERC). A. Rodrigues benefits from a PhD scholarship financed by FCT-Fundação para a Ciência e Tecnologia, Portugal, Ref.: SFRH/BD/71203/2010.

REFERENCES

[1] ASTM C33 / C33M-16e1, Standard Specification for Concrete Aggregates, ASTM International, West Conshohocken, PA, 2016.

[2] De Villiers, J.P.R, & Liles, D.C.: The crystal-structure and vacancy distribution in 6C pyrrhotite, American Mineralogist, Vol. 95 (2010) No.1, 148-152.

[3] Belzile, N., Chen, Y.W., Cai, M.F. & Li,Y.: A review on pyrrhotite oxidation, Journal of Geochemical Explororation, Vol. 84 (2004) No. 1, 65-76.

[4] Rodrigues A., Duchesne J., & Fournier B.: Microscopic analysis of the iron sulfide oxidation products used in concrete aggregates. Proc. 34th Int. Conf. on Cement Microscopy, ICMA ed, Halle, Germany, (2012).

[5] Rodrigues A. et al.: Mineralogical and chemical assessment of concrete damaged by the oxidation of sulfide-bearing aggregates: Importance of thaumasite formation on reaction mechanisms, Cement and Concrete Research, Vol. 42 (2012) No. 10, 1336–1347.

[6] Hawkins, A.B.: Implications of pyrite oxidation for engineering works, Springer 2014, VII 307 p.

[7] Rodrigues, A. et al.: Evaluation protocol for concrete aggregates containing iron sulfide minerals. ACI Materials Journal, Vol. 113, (2016) No. 3, 349-359.

[8] Elberling, B. et al.:. Evaluation of sulphide oxidation rates: a laboratory study comparing oxygen fluxes and rates of oxidation product release, Canadian Geotechnical Journal, Vol. 31 (1994) No. 3, 375-383.

[9] Rodrigues A., Duchesne J., & Fournier B.: Quantitative assessment of the oxidation potential of sulfide-bearing aggregate in concrete using an oxygen consumption test, Cement and Concrete Composites, Vol. 67 (2016) 93-100.

[10] Rodrigues A., Duchesne J., & Fournier B.: A new accelerated mortar bar test to assess the potential deleterious effect of sulfide-bearing aggregate in concrete, Cement and Concrete Research, Vol. 73 (2015) No. 7, 96-110.

EXPERIMENTAL STUDY ON THE EFFECTS OF AGGREGATES IN CEMENTITIOUS MATERIALS SUBMITTED TO DRYING

Marie Malbois[1], Aveline Darquennes[1], Caroline De Sa[1], Farid Benboudjema[1]

[1] ENS Paris-Saclay / CNRS / Université Paris-Saclay, Laboratoire de Mécanique et Technologie (LMT), 61 avenue du Président Wilson 94230 Cachan, France, email: malbois@lmt.ens-cachan.fr, darquennes@lmt.ens-cachan.fr, de-sa@lmt.ens-cachan.fr, benboudjema@lmt.ens-cachan.fr

SUMMARY: The drying of concrete induces surface microcracking due to hydric gradients, and internal microcracking due to drying shrinkage incompatibilities between cement paste and aggregates. The difficulty of separating each phenomenon on concrete cracking makes it hard to quantify aggregates effects with classical experiments. An ongoing parametrical experimental study aims at quantifying the impact of drying and of concrete components by using morphologically controlled materials where the aggregates size and volume fraction are set. The samples are then submitted to drying and tested to assess the evolution of mechanical properties. The first results highlight the significant impacts of both parameters. The study is to be enhanced of several results: different formulations and tests to assess the evolution of mechanical and transport properties at several ages are currently undertaken.

EKSPERIMENTALNO ISTRAŽIVANJE UTJECAJA AGREGATA U CEMENTNIM MATERIJALIMA IZLOŽENIM SUŠENJU

SAŽETAK: Sušenje betona uzrokuje površinsko mikroraspucavanje zbog hidrauličnih gradijenata i unutarnje mikroraspucavanje zbog nekompatibilnosti skupljanja pri sušenju cementne paste i agregata. Zbog teškoće odvajanja učinka svake od pojava na raspucavanje betona klasičnim je ispitivanjima teško kvantificirati učinke agregata. Eksperimentalno parametarsko ispitivanje koje je u tijeku ima za cilj kvantificirati utjecaj sušenja i komponenti upotrebom morfološki kontroliranih materijala pri čemu je određena veličina agregata i volumen frakcije. Izrađeni uzorci izloženi su sušenju i ispitani radi ocjenjivanja razvoja mehaničkih svojstava. Prvi rezultati objašnjavaju znatan učinak obaju parametara. Istraživanje će se proširiti s više rezultata različitih sastava i ispitivanja kako bi se ocijenio razvoj mehaničkih svojstava i svojstava propusnosti pri različitim starostima.

1. INTRODUCTION

ANR MOSAIC. The French project ANR MOSAIC (MesoscOpic Scale durAbility Investigations for Concrete) is a collaboration between four French laboratories all recognized for their expertise within the field of cement-based materials durability: LML (Lille, France), LMT Cachan (Cachan, France), LMDC (Toulouse, France) and IFSTTAR (Champs-sur-Marne, France). This project investigates, experimentally and numerically, the effect of drying and delayed ettringite formation on the mechanical and transport properties at a mesoscopic scale.

First, this project plans to set up an experimental methodology based on studying the two types of pathologies on two classes of materials:

– Materials where the mesoscale morphology is completely controlled : “morphologically controlled” materials

– Materials where the mesoscale morphology is uncertain : “real” materials

The study of the morphologically controlled materials aims at easily uncoupling the influent parameters (as aggregates size or aggregates distribution) on the global concrete behaviour. In order to assess the role of the morphology within the pathologies development, but also to allow the gathering of results of all the members of the project, these materials must be built from the same components: cement, aggregates, water to cement ratio.

In a second time, the MOSAIC project aims at developing a predictive way of modelling the consequences of the two phenomena at a mesoscopic scale.

Drying. The drying phenomenon is inherent to the life of concrete structures. It is triggered by the hydric imbalance of the structure with its environment and consists in water departure from the structure. The water loss leads to internal strains and stresses gradients that may lead to superficial micro-cracking, perpendicular to the surface of the structure. Besides under drying, the cement paste tends to contract while the aggregates are generally inert.

Therefore, a restraint of the cement paste shrinkage by the aggregates can appear, leading to strains and stresses gradients between cement paste and aggregates. This last phenomenon induces the debonding at the cement paste - aggregates interfaces (circumferential cracks) and the development of inter-granular cracks (radial cracks) as displayed ([1], [9], [10], [15]). This cracking may impact significantly mass transfer properties, which are of major importance for civil engineering structures durability.

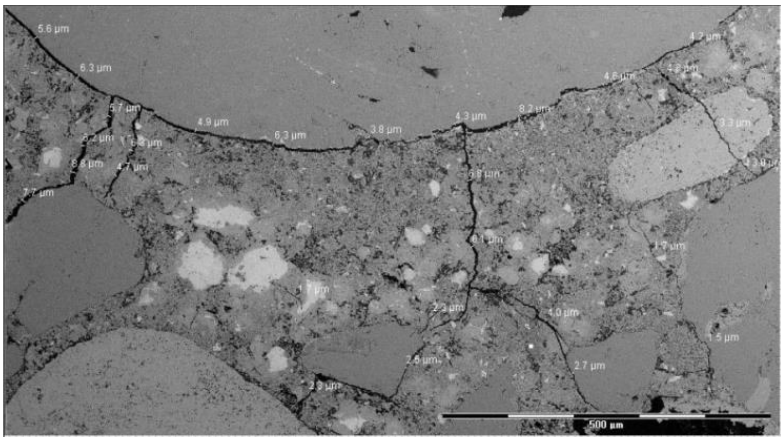

Figure 1 Low magnification image of a sample after drying at 105°C, displaying cracking induced by aggregates restraint. Microcracks widths: 0.5-10 µm. (1182 x 655 µm) [13]

Many papers deal with the structural effects of drying, reporting qualitative and quantitative experimental ([4], [5], [9], [12]) and numerical studies ([5], [7]). Few works have been devoted to cement paste and aggregates strain incompatibilities ([1], [2], [13]). The difficulty of studying this heterogeneity effect lies in, on one hand, the problem of separating each size effect on concrete cracking, and on the other hand, assessing the effects of the numerous parameters linked to aggregates (e.g. shapes, size distribution, aggregates type, surface rugosity and interfacial transition zone).

Some recent works have investigated the experimental decoupling of macroscopic and mesoscopic effects, studying more particularly the influence of concrete heterogeneity on cracking due to drying ([10], [13]). The preliminary work of Lagier et al. [10], based on 2D digital image correlation experiments on morphologically controlled materials, has shown the ability of quantifying cracking due to drying and the impact of the heterogeneities (Figure 2). Numerically, several strategies can be considered to study drying effects. The literature ([3], [6], [8], [10], [11], [13]) has already underlined the interest of working at mesoscopic scale to describe the effects of heterogeneity. Yet, those works have not demonstrated the entire predictive feature of mesoscopic models.

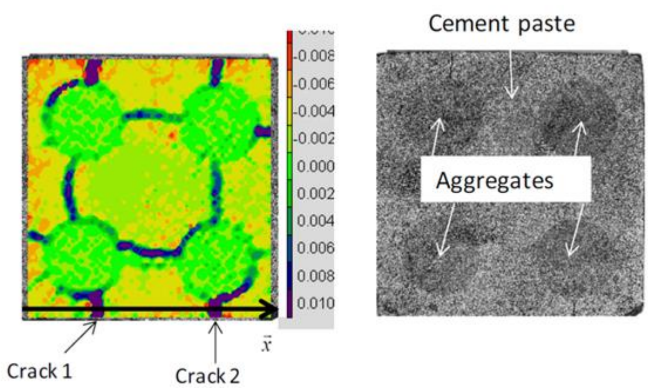

Figure 2 2D digital image correlation study on morphologically controlled materials investigating cracking due to drying incompatibilities between cement paste and aggregates. [10]. Trace of the strain tensor.

In this paper we will focus on the ongoing experimental study led in the LMT Cachan dealing with the drying phenomenon and its impact on morphologically controlled materials. First, we will present the different materials studied. Next we will take interest in the different technics to assess the macroscopic effects of drying and the morphology impact. We will finally present and discuss the results.

2. EXPERIMENTAL APPROACH

2.1. MATERIALS

The main objective of this study is to perform a parametric study on drying of cementitious morphologically controlled materials. In order to stay representative of the interactions between aggregates and cement paste, the inclusions are real calcerous aggregates (Boulonnais aggregates). Calcia cement CEM II (42.5 MPa) is used in Water-Cement Ratio of 0.57.

- The two parameters selected for this parametric study are:
- Inclusions sizes: aggregates diameter between 6.3 and 8mm and between 10 and 12.5mm.
- Inclusions volume fractions: 30% and 50% of the total volume.

As these morphologically controlled materials lack most of the granular skeleton that would have insured a homogeneous distribution of the aggregates in the sample, the risks of segregation are significant. Thus an optimization of the composition was performed by the use of a viscosity modifying admixture. Then, the first three compositions that will allow us to assess the impacts of the two selected parameters were made:

- Cement paste with 6-8 mm inclusions in a 50% volume fraction
- Cement paste with 10-12.5 mm inclusions in a 50% volume fraction
- Cement paste with 10-12.5 mm inclusions in a 30% volume fraction
- We will now see by which means we will assess the different effects of drying and of aggregates.

2.2. PROCEDURE

2.2.1. DRYING

Drying is studied on 70*70*280 mm prismatic specimens. For each formulation, 3 samples are made. They are removed of their mold after 24h and immediately protected against drying with two layers of aluminum foil. They are kept during 28 days under sealed conditions. Then, they are unwrapped to begin a drying phase, in a room controlled in temperature, 25 ± 1°C, and relative humidity, 35± 5%HR, until 200 days. To guarantee a unilateral drying, layers of aluminum foil are applied on the superior and inferior square faces of the prisms. The samples are regularly controlled for mass loss and shrinkage via an embedded apparatus made of brass, allowing the positioning of sample between a fixed support and a comparator. 3 prisms of each composition are also studied under sealed conditions.

2.2.2. MECHANICAL TESTING: 3 POINTS FLEXURAL TESTS

3 points flexural tests are performed at 200 days, on 70*70*280 mm prims which have followed the same preservation conditions than detailled before. For each composition and for each conservation condition, 3 samples are charge operated at a 0,5mm/s speed.

3. RESULTS AND DISCUSSION

3.1. MORPHOLOGY EFFECTS: IMPACT OF SIZE AND VOLUME FRACTION OF AGGREGATES

Figure 3 displays the mass loss of the different formulations express in function of the root of time on the average radius (Rm) of the samples followed, in order to be exonerated from samples size effects.

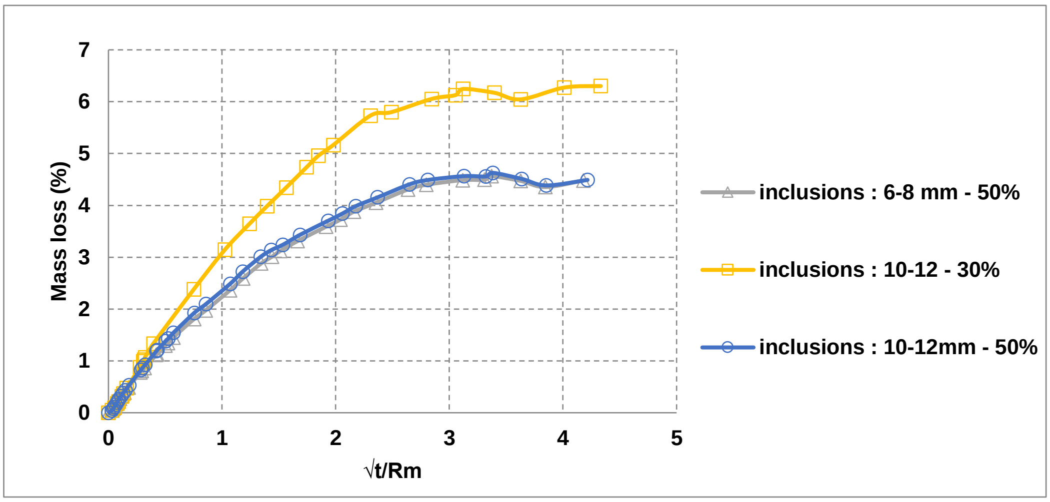

Figure 3 Mass loss evolution of different compositions with time under drying conditions

First these curves reveal that the drying phenomenon seems stabilized after 200 days. In order to more clearly observe the effect of the aggregates on the diffusion phenomenon, Figure 4 shows the mass loss of the samples, normed by the volume fraction of cement paste. The curves are surimposed on each other, which can raise the question of the role of the interfacial transition zone and of cracking on mass transport.

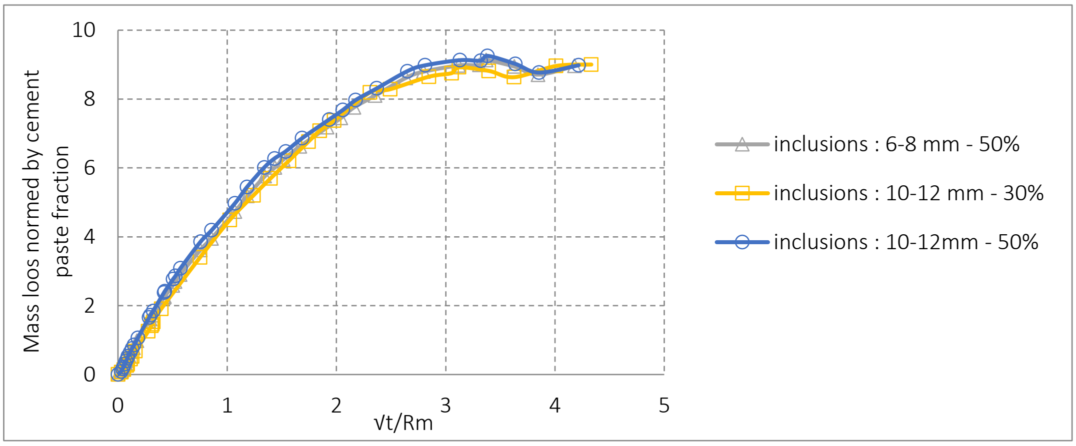

Figure 4 Evolution of mass loss normed by cement paste volume fraction with time under drying conditions

Total shrinkage of the different compositions is displayed on Figure 5. As expected under drying conditions, a decrease of apparent shrinkage with the increase of the volume fraction of aggregates can be observed. Besides it can also be noticed that, at the same volume fraction, the formulations with smaller inclusions have an apparent shrinkage more important than the ones with bigger inclusions, meaning that the size of inclusions has an influence.

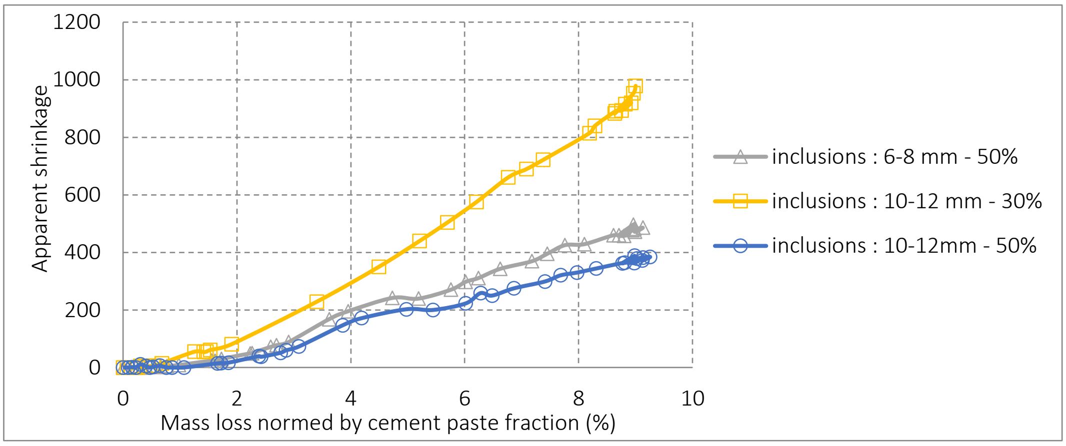

Figure 5 Total shrinkage of different mesostructures versus relative mass loss percentage under drying conditions

3.2. MACROSCOPIC EFFECTS OF DRYING: EVOLUTION OF FLEXURAL STRENGTH

Flexural strength results are gathered in Table 1. It can be first noticed that comparing the results in autogenous conditions, the aggregates size or volume fraction have a very low impact. Also, submitting samples to drying induces a significant decrease of the strength compared to the autogenous state, but this decrease varies depending on the composition as indicated in the third column of the table.

These results reveal that aggregates size has a considerable impact on the damaging of samples whereas it seems that the volume fraction has a limited effect.

Table 1 Flexural resistances

Composition Inclusions	Drying conditions	Autogenous conditions	Decrease of strength
6-8mm – 50 %	3,3 MPa	5,1 MPa	34 %
10-12mm – 50 %	2,3 MPa	5,1 MPa	54 %
10-12mm – 30 %	2,1 MPa	4,8 MPa	57 %

Comparing the failure characteristics, different observations could be made between samples in drying conditions and the ones in autogenous conditions.

- In autogenous conditions: most of the aggregates are ruptured and some are ripped off.
- In drying conditions: most of the aggregates are ripped off and few are ruptured.
- The difference could reveal a debonding phenomenon at the aggregate – cement paste interface.

4. CONCLUSIONS

The results gathered so far highlight the significant effects of aggregate parameters on the delayed deformations and the evolution of mechanical properties.

The first results evidence several phenomena:

- Aggregate size and volume fraction don't affect the mass loss
- Aggregate volume fraction has a significant impact on the delayed deformations. The more aggregates there are in the samples; the less it will be subjected to delayed shrinkage due to the substitution of the cement paste (responsible for the shrinkage) by rigid inclusions.
- Aggregate size also has an impact on the delayed formations. The samples with 10-12 mm aggregates tend to shrink less than the ones with 6-8 mm aggregates, due to the different restraints induced.
- Finally, the aggregate size seems to influence the damaging induced by drying, with leads to different behavior when assessing the mechanical performances. The samples with 10-12mm aggregates display a bigger loss of flexure resistance than the ones with 6-8mm aggregates, which could result from a more important internal cracking induced by drying.

The experimental study presented in this paper is to be enhanced with more results : compressive tests, several tests to conclude on the evolution of the transport properties (after potential drying cracks) and a visualisation and quantification of the cracking by tomography.

Besides, three other formulations are to be tested: cement paste, mortar and "real" concrete, which will allow us to conclude more precisely on the effect of aggregates in a classical concrete.

ACKNOWLEDGMENTS

This research was achieved in the framework of the French research Project ANR MOSAIC. The authors would like to extend their appreciation and gratitude for the financial support provided by the French National Research Agency.

REFERENCES

[1] Bisschop, J. and van Mier, J.G.M., Effect of aggregates on drying shrinkage microcracking in cement-based composites, Materials and Structures, Vol.30, September-October 2002, 453-461

[2] Bisschop, J. and van Mier, J.G.M., How to study drying shrinkage microcracking in cement-based materials using optical and scanning electron microscopy, Cement Concrete Res, 32 (2002), 279-287

[3] Bissonette, B., Pierre , P., Pigeon P., Influence of key parameters on drying shrinkage of cementitious materials, Cement Concrete Res, 32 (1999), 279-287

[4] Burlion, N., Yurtdas, I., Skoczylas F., Comportement mécanique et séchage de matériaux à matrice cimentaire, (In French), Revue Française de Génie Civil, Vol.7(2) (2003), 145-165

[5] Burlion, N., Bourgeois F., Shao J.-F., Effects of desiccation on mechanical behaviour of concrete, Cement Concrete Compos, 27 (2005), 367-379

[6] De Sa, C., Etude hydro-mécanique et thermo-mécanique du béton (In French), PhD thesis, Ecole Normale Supérieure de Cachan, France (2007)

[7] De Sa, C., Benboudjema F., Thiery M., Sicard J., Analysis of microcraking induced by differential drying shrinkage, Cement Concrete Compos, 30 (2008), 947-956.

[8] Grassl, P., Wong, H.S., Buenfeld, N.R., Influence of aggregate size and volume fraction on shrinkage induced micro-cracking of concrete and mortar, Cement Concrete RES 40(1) (2010), 85-93

[9] Hearn, N., Effect of shrinkage and load-induced cracking on water permeability of concrete, ACI Mater , 96(2) (1999), 234-241

[10] Lagier, F., Jourdain, X., De Sa, C., Benboudjema F., Colliat J.-B., Numerical strategies for prediction of drying cracks in heterogeneous materials: Comparison upon experimental results, Engineering Struct., 33(3) (2011), 920-931

[11] Pickett, G., Effects of aggregates on shrinkage of concrete and a hypothesis concerning shrinkage, Proceedings, 1 (1956), 581-590

[12] Torrenti, J.-M., Comportement multiaxial du béton : aspects expérimentaux et modélisation (In French), PhD thesis, Ecole Nationale des Ponts et Chaussées, France (1987)

[13] Wong, H.S., Zobel, M., Buenfeld, N.R., Zimmerman R.W., Influence of interfacial transition zone and microcracking on the diffusivity, permeability and soptivity of cement-based materials after drying, Concrete Res, 61 (8) (2009), 571-589

COLD TECHNOLOGIES RELATED TO SUSTAINABLE ROADS – EXPERIENCE IN FRANCE

Philippe Chifflet[1]

[1] COLAS, Central Europe Directorate, Operngasse 17-21, 1040 Wien, Austria, e-mail: philippe.chifflet@colas.com

SUMMARY: In France, during the last 10 years, the environemental assessment of the pubic works in different aspects (aggregates saving, emission of CO2, recycling, energy consumption...) became of great importance. The impact of the public works on the environnement, was introduced in the public tender as a optional criteria to attribute the tender. In the same time a special common tool open to all the companies was developped, a software called SEVE. This presentation deal with the contents and use of SEVE software calculation to compare traditional solution for road construction with the cold techniques using bitumen emulsion. First the software and its parameters will be exposed. Then a focus will be made on few examples of the environnemental impact of cold techniques and cold recycling techniques.

HLADNE TEHNOLOGIJE I ODRŽIVE CESTE – FRANCUSKO ISKUSTVO

SAŽETAK: Tijekom posljednjih deset godina u Francuskoj je ocjenjivanje javnih radova s različitih aspekata (ušteda agregata, emisija CO_2, recikliranje, potrošnja energije…) postalo vrlo važno. Utjecaj radova na okoliš uvedeno je u javne natječaje kao dodatni kriterij. Istodobno je razvijen posebni opći alat za sve kompanije, softver pod nazivom SEVE. U radu se prikazuje sadržaj i upotreba tog sofvera radi usporedbe tradicijskih rješenja za gradnju cesta s hladnim postupcima primjenom bitumenske emulzije. Na početku će biti objašnjen softver i pripadajući mu parametri. Zatim će se prikazati nekoliko primjera o utjecaju na okoliš hladnih postupaka i hladnih postupaka koji uključuju recikliranje.

1. INTRODUCTION

After many years of climatic warming and ecologic disaster affecting the world, the environmental issues became of big importance. All countries are concern by this topic and many government had participate at the last world climate change summit, COP21, in Paris in 2015. To face to the climate changes the French road construction industry was engaged in drastic reduction of energy consumption and CO2 footprint. To support this action, in 2009, an agreement was signed between this federation and the French Ministry of Transportation and Ecology. One of its aims was to they create a software called SEVE in order to evaluate the environmental impact of road construction. In this paper are presented the results for cold techniques and cold recycling techniques used in road construction.

2. SEVE SOFTWARE

SEVE software (environmental evaluation of variant solution) was created by French road federation in 2010 to get a common tool to compare basic solutions with alternative solutions through some environmental indicators. Obviously, to be able to compare the offer, all the basic parameters like the quantity of energy to produce aggregates were fixed and are coming from French or European official sources. SEVE software can help the road industry to decrease its environmental impact with same technical performance or better.

Through this tool local authorities will be able to evaluate the environmental impact between different design solutions first before the tender was launched, and after that, in the part of adjudication. By limiting the impact of industrial activities on climate change, the use of this tool will enable to help National authorities to reinforce the legislation and challenge enterprises in the environmental aspect.

The life cycle analysis is partially made by this way, including only environmental impacts during the construction stage, that is to say production of different materials or products used in road construction, like unbound material, concrete, hot mix asphalt, pipes, and the delivery of those materials, application on site and use of recycled materials or recycling techniques. The general principles for that are defined in the European standards EN ISO 14040: 2006 and EN ISO 14044:2006. The software is apply only to the construction stage. It cannot include maintenance of road that is subject to variation.

List of parameters: the evaluation of environmental impact is made through five indicators which are process energy, CHG emission, natural resources, recycled material, transportation. Hereafter in more detailed description for asphalt road construction:

- Process Energy: it is the primary energy which is the sum of non renewable and renewable energies used during the road construction process. It doesn't take into account the energy of the material itself but the energy to produce it.
- CHG emission in equivalent tons of C02: this indicator is the sum of all CHG emissions for all the process including production, delivery, and applications. The C02 N2O CH4 emissions are converted into CO2 equivalent.
- Aggregates; this item is the consumption of aggregates from the quarries
- RAP: This is the consumption of reclaimed asphalt pavement reuse in the formulation of asphalt mixes.
- Transport: This indicator is the sum of the kilometres made by truck during the construction works, first for the delivery of primary materials to the asphalt plant, then from the production site to the jobsite and multiplication by the weight they load.

This software is in French language and available at the public French institute for road, streets, and infrastructures called IDRRIM. It is certified by independent auditor. We are now in the third version of it.

In European level a project called LIFE SustainEuroRoad was launched in 2013. This project aim to assess and promote on European level a software in order to be used by all the European countries with different technical requirements and meteorological conditions but same basic data. The SustainEuroRoad LIFE Project proposes to create, validate and implement an innovative software to evaluate and reduce the environmental impact of road construction and maintenance in Europe. [1]

3. COLD IN PLACE RECYCLING TECHNIQUES

3.1. PRINCIPLES

Cold in-situ recycling process consists in milling or crushing the old pavement, up to 20 cm depth and incorporate in the same time in the fragmented material a bituminous emulsion, to stabilize the recycled layer in order to give back to it rejuvenation and cohesion. This technic is used on old road which present cracks related to the meteorologic events (temperatures, rains, snow, frozen..etc) and fatigue damages link to the traffic conditions. The recycled layer is protected by a new wearing course that can be, depending on the traffic, surface dressing, micro surfacing, cold asphalt concrete, hot mix asphalt. The thickness of the recycled layer and wearing course depend on the bearing capacity of the soils, the deflectivity of the pavement and other mechanical properties of materials.

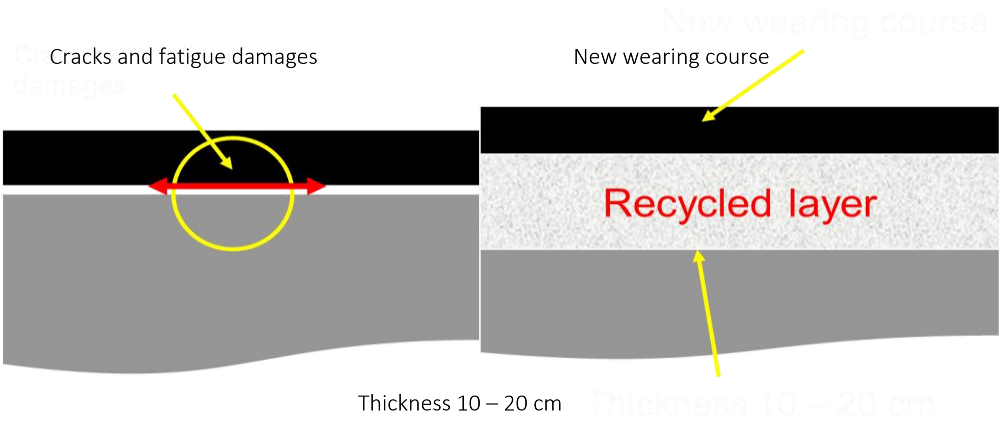

Figure 1 Schematic view of road before and after cold recycling

3.2. EQUIPEMENT

After a tack coat application, the mixture is laid with a finisher and compacted with high weight roller to reconstitute the binder course

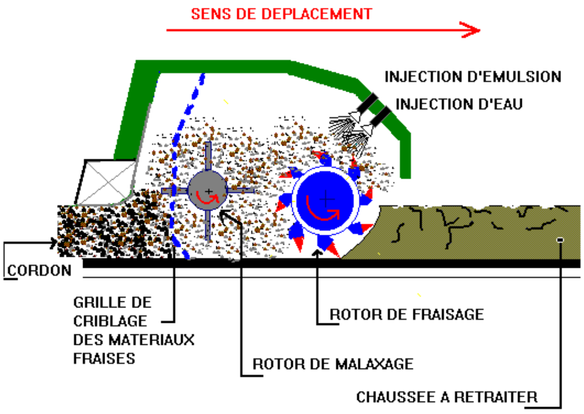

Figure 2 Crushing and Milling room

4. RESULTS

4.1. COLD RECYCLING

As a first example we made a calculation for the work site of the first class road RD703 located in St Livrade in south of France. The initial solution in the tender is to mill the existing road which present thermal and fatigue cracks and apply then two layers of hot mix asphalt. The tender is open to alternative solutions. COLAS propose the Novacol technique [2][3], asphalt cold recycling in place, that consist in milling the existing road (wearing and base courses) together with mixing a emulsion with special properties, in this case incorporating rejuvenating component. After NOVACOL use as binder course, a cold wearing course was applied. The main indicator we follow is C02 equivalent emission.

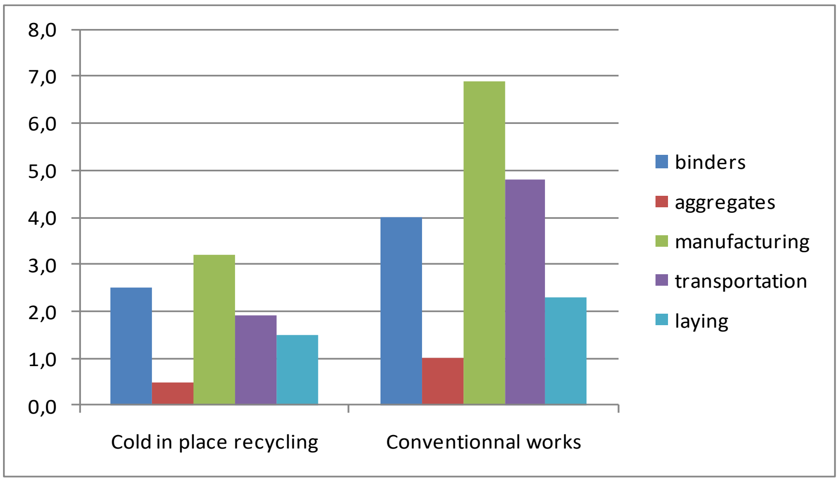

Figure 3 kg C02 equivalent by type of task for 1m^2

The Figure 3 above shows very systematic differences in C02 équivalent emission between the conventional work with hot mix asphalt and the cold in place recycling technique.

The binder amount is of course less in cold recycling techniques because there is a fully use of the binder contained in the existing asphalt layer. The emulsion that is added in the mix allow to create new fresh link between the coated aggregate and mortar of the milled mix. The C02 footprint of the rejuvenating agent is also take into account.

The aggregates consumption is obviously less in cold recycling techniques due to the fact that the existing road is totally reuse. The consumption of aggregates become only from the cold wearing course

One main difference is the manufacturing indicator Even if the cold recycling techniques use energy to manufacture emulsion but ten times less than hot mix asphalt plant and very heavy and powerful equipment for milling and mixing in place, there is a great gap compare to the conventional works. This is directly linked to the consumption of the burner of the asphalt plant who produces more than 5 kg/C02 per ton of hot mix asphalt

Another noticeable difference is in the transportation. Because cold recycling is an in place techniques there is no delivery of the aggregate from quarry neither hauling on the work site.

The laying step cost also a little bit less energy because the cold asphalt application need a little less powerful engine. If we sum up the CHG emission saving, and, directly correlated to this, the energy consumption, we obtain the results below:

Table 1 Life cycle analysis: energy consumption and CHG emission for 1 m2 recycled pavement

Criteria	Hot mix asphalt	Cold recycling	Difference
Energy consumption (MJ)	226.1	118.3	-52%
CHG emission (kg $CO_{2eq.}$)	19.3	9.9	-51%

That means that for each square meter of NOVACOL the CHG emission is one half the one obtained in the conventional work.

4.2. COLD MIXES

The second example of the cold techniques is a French comparative study with SEVE software of two road pavements wearing course of 7 cm thickness: one with conventional hot mix asphalt and one with cold mix asphalt. All the parameters like the distance between the quarry and the asphalt plant or the aggregate composition of the mix and the asphalt paving work are the same. That's why the aggregate consumption and transport have also the same value. In the Figure 4 therefore are exposed the comparison for Energy consumption in MJ per m2 and CHG emission for this work site.

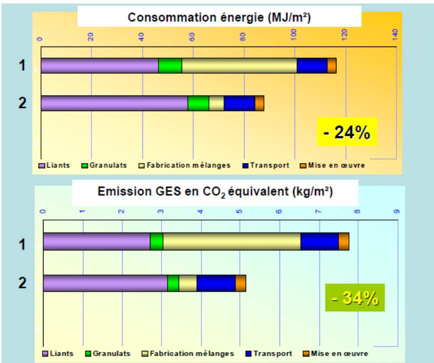

Figure 4 Energy consumption and CHG emission for 1m² of pavement

The two main points to underline are:

- The binder for cold asphalt mix is a bituminous emulsion. In that case, although the energy to produce it is less than for a bitumen, the quantity inside the mix is one third high, that explain the little more energy for binder for cold techniques than for hot mix asphalt.
- The big difference when we compare the techniques is that for the manufacturing of cold asphalt there is no need to heat and dry the aggregates in the drum of the asphalt plant. This point make the energy and cHG emission decrease at 8 times less for cold mixes.

Finally, the sum of the retained criteria obtained with Seve software give the results below in Table 2

Table 2 Life cycle analysis: energy consumption and CHG emission for 1 m² recycled pavement

Criteria	Hot mix asphalt	Cold mix asphalt	Difference
Energy consumption (MJ)	118.5	84.7	-24%
CHG emission (kg C02eq.)	7.8	5.1	-34%

The energy saving during the manufacture of cold mix asphalt provide a high decrease of energy consumption and CHG emission, respectively 24 and 34 percent. Of course this technology allow an even more big advantage when the cold asphalt plant is located close to the work site.

5. CONCLUSIONS

Through the calculation we made with ALIZE software design by the French federation of public works and certified by the French institute of road, we have shown that the development of two cold techniques, one with in place recycling technique and the other with cold mix asphalt in plant can generate a very big economy of energy and can decrease drastically the CHG emission. If each year we can renovated 30000 km of road in France with this techniques we could save about 500,000 Tons of C02 equivalent.

This software SEVE will be soon available in the European Union and we wish that the better knowledge of the potential of energy savings that are demonstrate for cold techniques will promote their use in every country.

REFERENCES

[1] Cavagnol, I.;Life+Sustaineuroroad software, 6th Eurobitume congress, PRAGUE; June 2016.: www.eecongress2016.org

[2] Prades, F.: BTP Magazine, vol 285, ISSN 0299-1905, FRANCE, (2015), pp. 22-25

[3] ROAD NEWS, vol. 224, ROUTE ACTUALITE, 1215T 85265, France (2015), (pp24-25)

LONG-TERM RELEASE OF HEAVY METALS FROM FOAM GLASS AND RECYCLED CONCRETE AGGREGATES USED IN ROAD CONSTRUCTION

Christian Engelsen[1], Gordana Petkovic[2]

[1] SINTEF Building and Infrastructure, Forskningsveien 3B, 0314 Oslo, Norway,
email: christian.engelsen@sintef.no
[2] Norwegian Public Roads Administration, Department for Traffic Safety, the Environment and Technology, P.O.Box 8142 Dep, 0033 Oslo, Norway, email: gordana.petkovic@vegvesen.no

SUMMARY: Applying recycled aggregates in road construction may contribute significantly to a more sustainable development of the infrastructure. The key incentives for such practice are many and may include the following; local scarcity of natural aggregates, utilisation of waste materials instead of disposal at landfill, economical benefits, certain material properties required (e.g. thermal insulation) and environmental goals at European and national levels (e.g. waste recovery criteria in Waste Framework Directive). However, the extent of using recycled aggregates in road construction varies across Europe. In Norway, relatively small volumes are used today. The main reasons are the lack of access to alternative materials, challenges with providing relevant documentation of technical properties in a cost-effective way and risk adversity among end-users, because of the lack of information regarding technical and environmental properties of waste-derived aggregates. In the present study, glass based recycled aggregates (foam glass) was used in the road sub-base together with crushed concrete and asphalt. The release of chemical substances has been monitored for more than 6 years. The results regarding the release of inorganic constituents from foam glass and crushed concrete showed in general low concentrations of heavy metals in the collected infiltration water samples. The study showed that the relatively high total contents of Cr and Pb in the foam glass compared to crushed concrete, did not pose any increased environmental risk, as the released concentrations where below 3 µg/L and 15 µg/L, respectively.

DUGOTRAJNO OTPUŠTANJE TEŠKIH METALA IZ PJENASTOG STAKLA I RECIKLIRANIH BETONSKIH AGREGATA UPOTRIJEBLJENIH U GRADNJI CESTA

SAŽETAK: Primjena recikliranog agregata u gradnji cesta može znatno pridonijeti održivijem razvoju infrastrukture. Ključnih poticaja za takvu praksu ima mnogo, a mogu obuhvatiti sljedeće: lokalnu nestašicu prirodnih agregata, upotrebu otpadnih materijala umjesto njegovo odlaganje na odlagalištima, gospodarske koristi, neka zahtijevana svojstva materijala (npr. toplinska izolacija) i ciljeve povezane s okolišem na europskoj i nacionalnoj razini (npr. kriterije ponovne upotrebe otpada prema Okvirnoj direktivi za otpad). Međutim, opseg upotrebe recikliranog agregata u gradnji cesta različit je diljem Europe. U Norveškoj danas se upotrebljava relativno mali obujam. Glavni je razlog nedostatak pristupa alternativnim materijalima, izazovi osiguravanja odgovarajuće dokumentacije o tehničkim svojstvima na troškovno učinkovit način i neprihvaćanje rizika kod krajnjih korisnika zbog nedostatka informacija o tehničkim svojstvima i svojstvima povezanih s okolišem za agregat dobiven iz otpada. U ovom istraživanju za posteljicu ceste upotrijebljen je reciklirani agregat od stakla (pjenasto staklo) s drobljenim betonom i asfaltom. Otpuštanje kemijskih tvari praćeno je dulje od šest godina. Rezultati praćenja otpuštanja anorganskih sastojaka iz pjenastog stakla i drobljenog betona u prikupljenim uzorcima infiltrirane vode pokazuju općenito male koncentracije teških metala. Istraživanje je pokazalo da relativno veliki ukupni sadržaj Cr i Pb u pjenastom staklu u usporedbi s drobljenim betonom ne predstavlja nikakvo povećanje rizika za okoliš, jer su otpuštene koncentracije bile manje od 3 µg/L za pjenasto staklo i 15 µg/L za drobljeni beton.

1. INTRODUCTION

Potential environmental impact of recycled aggregates to soil and groundwater are of great concern in countries trying to achieve high levels of recycling. One relevant way to judge such impact is to assess the potential release of chemical constituents from the recycled aggregates by leaching characterisation.

In the present study, the leaching from recycled concrete aggregates (RCA) and foam glass aggregates (FGA) was studied in a full scale demonstration project. The recycled materials were applied as sub-base materials of a road and have been exposed to weather and precipitation for more than 6 years. The temperature, pH and heavy metal leaching were measured. Full-scale studies of a similar type are scarcely represented in the literature and have not been reported for recycled aggregates of concrete and foam glass used in the sub-base. The present study was developed under the Norwegian Roads Recycling R&D program [1].

2. EXPERIMENTAL

2.1. MATERIAL AND FIELD DESCRIPTION

The materials studied at the field site were recycled concrete aggregate (RCA) and foam glass aggregate (FGA). The RCA originated from a demolished section of the highway E6 (25 km south of Oslo), which was constructed with concrete pavement in the beginning of 1980. The demolished concrete was crushed and fractionized into a grain size of 20-120 mm and applied in test segments of the road base in the entrance lane to the north-bound lane of E6, see Figure 1. The crushing and fractioning of the old road pavement was conducted only weeks after demolition. Further details can be found in [2]. The FGA, with a grain size of 10-50 mm, was applied in the same way as the RCA. In addition, a test section with the road base consisting of natural aggregates (NA), with grain size of 20-120 mm, was also included.

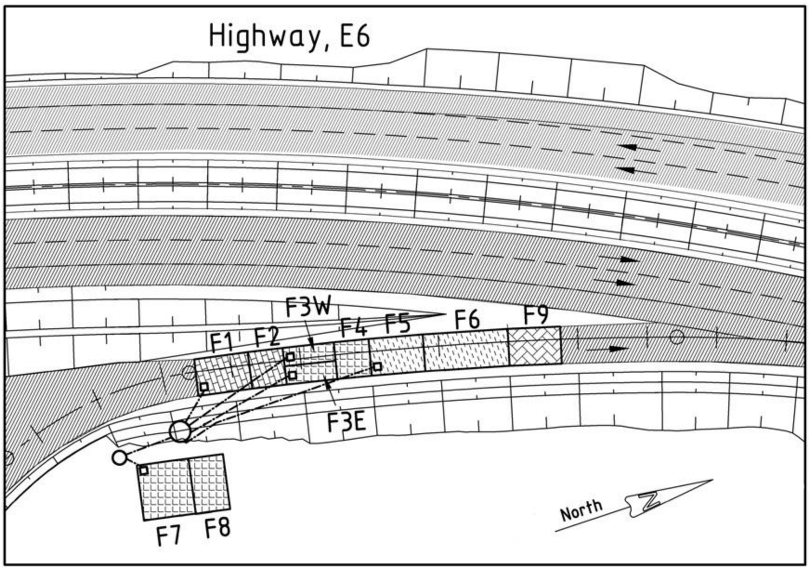

Figure 1 Schematic presentation of the field site located 20 km south of Oslo, Norway. The test field was divided into sections F1–F9 where the following materials were used: foam glass aggregate, FGA (F1 and F2), recycled concrete aggregate, RCA (F3W, F3E, F4, F7 and F8), natural aggregates, NA (F5 and F6) and a mixture of RCA and recycled asphalt (F9). All test sections except F7 and F8 were covered with asphalt pavement. The drains (open squares) were connected to the two sampling collection stations (open circles). Test sections F2, F4 and F8 were constructed without a watertight HDPE membrane to avoid cross contamination.

2.2. MONITORING

The drainage water from the different test sections was led in PE pipes to the collection well where it was automatically sampled in separate closed systems, see Figure 2. The outlet of each sampling system was connected to Tipping Bucket Flow Gauge (ITAS, Norway), in order to measure the volume collected from each drain. The pH, air temperature, water flow and the precipitation were determined online by using the logging system PC Logger 3100i (Intab Interface-Teknik, Sweden). Temperature and moisture content in the road base were also determined online by connecting the sensors to a Hewlett Packard Logging system. Only the temperature and pH were shown in the present study.

Figure 2 Collection of infiltration water from sub-base were conducted in separate sampling lines inside a collection well

2.3. CHEMICAL ANALYSES

ICP-OES was used to determine major elements (Al, Ca, Si, Fe, S, Ba, Na, K), typical metal cations (Cd, Cu, Ni, Pb, Zn) and elements that, under certain conditions, form oxyanions (Cr, As, Sb, Se, B, V, Mo). The anions Cl^-, Br^-, SO_4^{2-} and F^- were analyzed by ion chromatography (IC) and the dissolved organic carbon (DOC) and dissolved inorganic carbon (DIC) were measured by a Shimadzu carbon analyzer. In the present study, the results regarding heavy metals are shown. pH measurements were conducted on the computerized titration system Metrohm Basic Titrino 794 and the conductivity was measured with the Hach Sension analyzer. For determination of total element concentrations, FGA and RCA material were pulverised to < 125 µm and decomposed by a mixture of HF and HNO_3.

3. RESULTS

3.1. TEMPERATURE DIFFERENCE

The temperature will greatly influence the quantity of infiltration water, due to temperatures being well below 0 °C during winter season in Norway. However, it was observed that the daytime temperatures in the winter seasons often rose above 0 °C and the snow started to melt on top of the test field. In addition, there was a vertical upward thawing process from the deepest layers in the test sections, due to the higher temperatures in the bottom layer and beneath it. This was confirmed by the measurements of the temperature depth profiles in F1 and F3, as shown in Figure 3. The recorded temperatures were always above 0 °C in the bottom layer of F1. In addition, due to the high insulation property of foam glass, the temperatures were higher in the bottom layer of F1 than in F3.

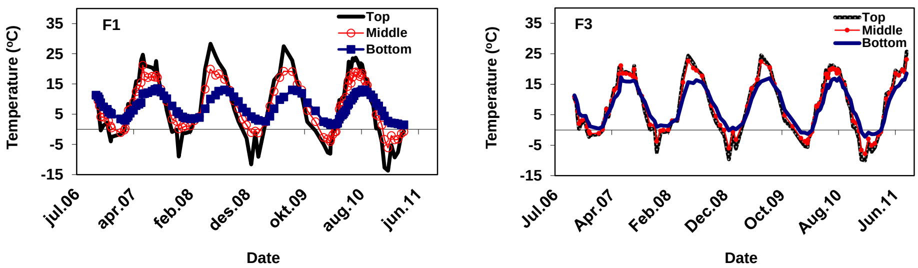

Figure 3 Temperatures measured at three depths (bottom, middle and top) in F1 (FGA) and F3 (RCA, average of F3W and F3E). Each data point represents the average value determined in the 4 sensors per depth in F3 and the values determined in one sensor per depth in F1

3.2. TOTAL CONTENT

The total concentrations of heavy metals in the water samples are shown in Table 1. It is emphasised that the concentrations always vary and that the results in Table 1 were therefore considered as indications. However, the FGA used in this study usually contained higher concentrations of As, Cr, Cu and Pb than RCA. This is also clearly indicated in Table 1. The total contents of Cr and Pb, in particular, were higher than recommended concentrations. For instance, the criteria for soil categorised in Class 1 (no health and environmental risk) in Norway are 50 mg/kg and 60 mg/kg for Cr and Pb, respectively.

Table 1 Concentration of heavy metals given in mg/kg

Element	RCA	FGA
As	< 10	32
Cr	69	234
Cd	< 0.7	1.3
Cu	12	163
Ni	14	19
Pb	31	841

3.3. ACID NEUTRALISATION CAPACITY AND PH MEASURED AT FIELD SITE

The acid neutralisation capacity (ANC) and the pH measured at field site are shown in Figures 4a and 4b, respectively. The ANC expresses the ability of the material to resist pH changes and was measured in the laboratory according to CEN/TS 14429. The ANC was found to be high for RCA and low for FGA, as expected, since the material pH of RCA and FGA is 12.6 and 10.3, respectively. This indicated that only RCA (not carbonated) would significantly dictate the pH of the external infiltration water. This is confirmed in Figure 4b, where it can be seen that a pH above 12 was obtained for F3 and F7 the first months in the monitoring period, whereas a pH between 7 and 8 was measured for F5 (natural aggregates). The pH for F1 was measured to be 8-9 (not shown in the Figure 4). This reflects the large difference between RCA and FGA concerning ANC.

Differences in pH have large impacts on the release of chemical substances, as have been demonstrated in several earlier studies [3-6]. This is important for RCA, in particular, since the pH changed from around 12.6 to a pH between 8-9, as shown in Figure 4b. The pH change was due to the carbonation of the concrete, which is a well-accepted natural aging process, where calcium hydroxide in the concrete pore water reacts with the dissolved CO_2 absorbed from the air and forms calcium carbonate (equilibrium pH of 8.3). The carbonation speed is, among other parameters, dependent on the access to air. This was clearly seen for the open RCA-section, F7, since the pH decreased significantly faster than in the case of the paved test sections (F3).

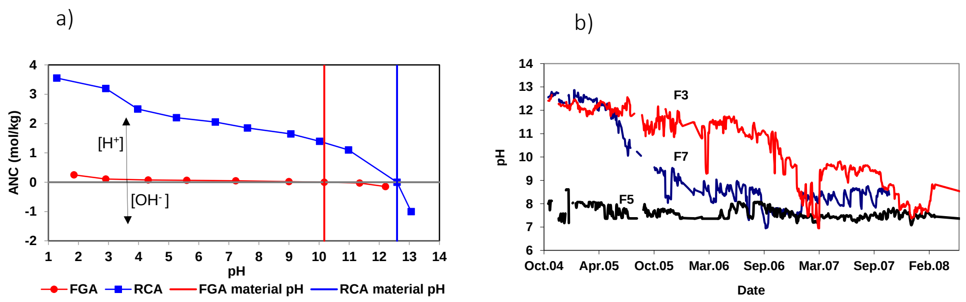

Figure 4 a) Acid Neutralisation Capacity (ANC) determined in laboratory for FGA and RCA b) pH determined on-line for the collected infiltration water from test sections F3, F5 and F7 [2]. F1 contains FGA and F3 contains RCA (average of F3W and F3E). F5 contains natural aggregates (reference test section). These sections were covered with asphalt pavement. F7 contains RCA not covered with asphalt pavement. pH data for infiltration water are given as daily average values and discontinuities in the curves occurred when the logging system was inoperative.

3.4. LEACHING OF HEAVY METALS

The measurements of the total concentrations (Section 3.2) revealed that the content of Cu, Cr and Pb in FGA was significantly higher than in RCA. The leaching of these elements at field site are shown in Table 2. A comparison of the results for F1 and F3 leads to some interesting observations. The leaching of Cr from F1 was significantly lower than F3, which indicated that Cr-binding in the foam glass was different from the binding in the concrete material. Regarding Cu-leaching, the released amounts from F3 seemed to decrease after the first monitoring period (2004/2005). It seemed that some of the high values obtained for F1 in the second monitoring period (2006/2010) might be related to the seasonal effects (e.g. de-icing salts). The leaching of Pb was in general low for F1 and F3, and only slightly higher concentrations were measured for F1. Thus, the leachability of Pb from the FGA material was considered to be low.

Criteria for groundwater and fresh surface water are also given in Table 2. It is emphasised that comparing pore water concentrations directly with acceptance criteria for the recipient does not give a realistic picture. The infiltration water normally penetrates the underlying soil before it mixes with the groundwater. This mixing process dilutes the released substances in the pore water, and further dilution can also be expected if the groundwater is flowing into a nearby river. A dilution factor of 0.07 was calculated earlier by mixing of the pore water with groundwater [2]. When this factor was applied, all concentrations complied with the acceptance criteria for groundwater and nearly all concentrations complied with the criteria for surface water. It can also be noted that without considering the dilution processes, the released concentrations from F5 (natural aggregates) also exceeded the criteria for fresh water.

Table 2 Lowest and highest concentrations in the collected leachates at field site during the monitoring period (2004 – 2010)

Test section[a]	Year	Concentration (µg/L)		
		Cr	Cu	Pb
F1	2004/2005	< 0.5 -1.9	11 - 81	< 1.4 - 15
F1	2006-2010	< 0.5 – 2.7	17 - 154	< 1.4 - 13
F3	2004/2005	11 - 156	7.2 - 237	< 2.5 - 5.3
F3	2006-2010	2.0 - 241	< 0.2 - 28	< 2.5 - 2.7
F5	2004/2005	< 0.3 - 4.1	0.8 - 6.9	< 2.5
F5	2006-2010	0.6 - 3.2	0.2 - 26	< 2.5 - 4.2
F7	2004/2005	7.9 - 187	0.8 - 156	< 2.5
F7	2006-2010	1.6 - 13	0.4 - 3.0	< 2.5
Acceptance criteria				
Groundwater[b]		50	100	10
Fresh water[c]		3.4	7.8	1.2

[a] F1 contains FGA covered with pavement. F3 (merged data from F3W and F3E) contains RCA covered with pavement. F5 contains natural aggregates covered with pavement (reference test section). F7 contains RCA unpaved. [b] Norwegian drinking water limits are used as guideline criteria. Value for Cu applies for the water that exits the waterworks before entering the water main. The limits given for Pb are also used as classification of good quality groundwater given in Norwegian water regulation. [c] Norwegian fresh water Class II: represents good quality water (Norwegian Climate and Pollution Agency, 2016) and the criteria are in accordance with the annual average-environmental quality standard (AA-EQS) in The EU Water Framework Directive.

4. CONCLUSIONS

The constituent leaching from recycled concrete aggregates (RCA) and foam glass aggregates (FGA) have been studied at field site over a period of 6 years. A low acid neutralisation capacity (ANC) was shown for FGA, which also could be seen in the pH measurements at field site. The initial pH in the infiltration water from the test sections with RCA and FGA was around 12.6 and 8.5, respectively.

Due to relatively high total contents of Cr, Cu and Pb in FGA compared to RCA, the leaching of these heavy metals was shown. Low leachability was in general found for the FGA material, particularly the leaching of Cr and Pb. The leached concentrations comply with the pre-defined acceptance criteria for ground water, when one takes into account the dilution effects due to the mixing of the pore water with groundwater.

ACKNOWLEDGMENTS

This study has been supported by Norwegian Public Roads Administration.

REFERENCES

[1] Petkovic, G.; Engelsen, C.J.; Haoya, A.-O. & Breedveld, G.D.: Environmental impact from the use of recycled materials in road construction: method for decision-making in Norway, *Resources, Conservation and Recycling,* 42. (2004), pp. 249-264.

[2] Engelsen, C.J.; Wibetoe, G.; van der Sloot, H.A.; Lund, W. & Petkovic, G.: Field site leaching from recycled concrete aggregates applied as sub-base material in road construction, *Science of the Total Environment*, 427. (2012), pp. 86-97.

[3] Butera S.; Hyks J.; Christensen T.H.; Astrup T.F.; Construction and demolition waste: Comparison of standard up-flow column and down-flow lysimeter leaching tests, Waste Management, 43. (2015), pp. 386-397.

[4] Engelsen, C.J.; van der Sloot, H.A.; Wibetoe, G.; Petkovic, G.; Stoltenberg-Hansson, E. & Lund, W. (2009). *Cement and Concrete Research* 39. (2009) 446-459.

[5] Engelsen C.J.; van der Sloot H.A.; Wibetoe G.; Justnes H.; Lund W. & Stoltenberg-Hansson E.: Leaching characterisation and geochemical modelling of minor and trace elements released from recycled concrete aggregates, *Cement and Concrete Research* 40. (2010), pp. 1639-1649.

[6] Galvin, A.P.; Ayuso J.; Garcia I.; Jimenez J.R. & Gutierrez F.: The effect of compaction on the leaching and pollutant emission time of recycled aggregates from construction and demolition waste, *Journal of Clean Production*, 83. (2014), pp. 294-304.

PROPERTIES OF BITUMEN MODIFIED WITH WASTE COOKING OIL AND HIGH DENSITY POLYETHYLENE FOR APPLICATIONS IN FLEXIBLE PAVEMENT

Bamidele Ibukunoluwa Dahunsi[1], Peter Ayobami Adesina[1]

[1] University of Ibadan Faculty of Technology, Department of Civil Engineering, Egbogah Building, Ibadan, Nigeria, email: bio.dahunsi@ui.edu.ng, P.A.Adesina@liverpool.ac.uk

SUMMARY: Commercial modifiers such as fillers, extenders, polymers, fibre, antioxidants, etc. have been incorporated in bitumen for improved performance. Though commercial modifiers could be effective in improving the performance of bitumen, the cost of asphalt mixes could increase as a result of their application. This made it imperative to develop alternative low-cost modifiers, hence, the use of wastes as modifiers for bitumen modification as in this research. These wastes have proven to modify bitumen yielding several benefits including improved rutting resistance, fatigue cracking and durability, while mitigating environmental hazards accrued from their increasing disposal to the environment. This research investigates the properties of bitumen modified with wastes such as Waste Cooking Oil (WCO) and High Density Polyethylene (HDPE) for applications in flexible pavements. Base bitumen was partially replaced with WCO at 5 % replacement level to develop WCO-modified bitumen. HDPE was then added at 2.5 %, 5 % and 7.5 % of binder weight to the WCO-modified bitumen to form WCO-HDPE modified bitumen. Empirical tests such as specific gravity, penetration and softening point were investigated to determine the behaviour of the modified bitumen. It was found that the replacement of bitumen with WCO reduces the specific gravity and softening point of the resulting binder while the penetration is increased. However, the addition of HDPE reduces the penetration and increases the specific gravity and softening point of the binder. HDPE added at 2.5 %, 5 % and 7.5 to the WCO modified bitumen results in lower penetration and higher specific gravity and softening point when compared to the base bitumen. It can be concluded that incorporating WCO blended with HDPE in bitumen results in increased performance.

SVOJSTVA BITUMENA S DODATKOM OTPADNOG ULJA ZA KUHANJE I POLIETILENA VELIKE GUSTOĆE ZA PRIMJENE U FLEKSIBILNIM KOLNICIMA

SAŽETAK: Za poboljšanje svojstava bitumena dodaju se trgovački modifikatori kao fileri, produživači, polimeri, vlakna, antioksidansi itd. Iako oni mogu biti učinkoviti za poboljšanje svojstava bitumena, zbog njihove primjene može se povećati trošak izrade asfaltnih mješavina. To onda postavlja kao obvezu razvoj alternativnih jeftinih modifikatora odnosno upotrebe otpadnih materijala kao modifikatora bitumena, što je učinjeno u ovom istraživanju. Ti otpadni materijali dokazano modificiraju tečenje bitumena i daju više koristi kao što su poboljšana otpornost na kolotrage, raspucavanje zbog zamora i trajnost, a ublažavaju okolišne opasnosti zbog njihova sve većeg odlaganja u okoliš. U ovom istraživanju ispituju se svojstva bitumena modificiranog s otpadnim materijalima poput otpadnog ulja od kuhanja (engl. waste cooking oil, WCO) i polietilena velike gustoće (engl. high density polyethylene, HDPE) za primjene u fleksibilnim kolnicima. Bitumen je djelomično zamijenjen s 5 % WCO-a. HDPE je dodan u količinama od 2,5 %, 5 % i 7,5 % težine veziva u bitumen modificiran s WCO-om čime je dobiven bitumen s WCO-HDPE-om. Za određivanje ponašanja modificiranog bitumena provedena su ispitivanja specifične težine, penetracije i točke omekšanja. Ustanovljeno je da se zamjenom bitumena s WCO-om smanjuje specifična težina i točka omekšanja nastalog veziva dok se povećava penetracija. Međutim, dodatak HDPE-a smanjuje penetraciju i povećava specifičnu težinu i točku omekšanja veziva. Dodatkom HDPE-a s tri navedene količine u bitumen modificiran s WCO-om postiže se manja penetracija i veća specifična težina i točka omekšanja u usporedbi s osnovnim bitumenom. Zaključeno je da dodavanje WCO-a uz HDPE u bitumen daje poboljšana svojstva.

1. INTRODUCTION

Bitumen is a viscoelastic material possessing suitable rheological and mechanical properties and has been used as the binder in asphalt for applications in road pavements [1-3].

Bitumen properties greatly influence the performance of road pavements as it is the binding and only deformable component of the asphalt mixture [4]. However, conventional bitumen is not often able to withstand the harsh conditions of heavy traffic loading, chemical attacks, ingress of water and widely fluctuating temperatures that it is frequently subjected to. Though, selecting the proper starting crude to make bitumen offers some benefits, it is unfortunate that only a few crudes capable of producing bitumen suitable for paving applications exist [2, 4]. It is therefore necessary to modify the properties of bitumen to improve its performance in pavement applications.

Modifying the properties of bitumen has been achieved using various means [5]. Some of these include the incorporation of commercial modifiers such as fillers, extenders, polymers, fibre, anti-stripping agents, antioxidants, etc. in asphalt mixes [6]. Though commercial modifiers could be effective in improving the performance of bitumen, the cost of asphalt mixes could increase as a result of their application [7, 8]. This made it imperative to develop alternative low-cost modifiers, hence, the use of wastes as modifiers for bitumen modification as in this research.

More so, wastes such as waste cooking oil (WCO), plastic wastes including high density polyethylene (HDPE), used motor oil (UMO) etc. exists in great quantities and their disposal pose threats to a sustainable environment. About 3 billion gallons of WCO were annually amassed from restaurants and fast food businesses in the United States only [9]. Incorporating these wastes in asphalt mixes is an effective means for their disposal as they have proven to modify bitumen yielding improved performance while mitigating environmental hazards accrued from their increasing disposal. In other to encourage and drive the application of wastes in bitumen modification, it is essential to investigate their properties and provide relevant information on their suitability and the benefits they offer to stakeholders of the highway construction industry.

This study aims to investigate the properties of wastes such as WCO and HDPE in the modification of bitumen properties for applications in road pavements. In order to achieve the aim of the study, WCO modified bitumen was developed by replacing base bitumen with WCO at 5% binder weight and test for properties including specific gravity penetration and softening point were conducted on the modified bitumen. WCO-HDPE modified bitumen were then developed by adding HDPE to the developed WCO modified bitumen at 2.5%, 5% and 7.5% binder weight with the properties (specific gravity, penetration and softening point) of these binders tested to determine the optimum proportions. The properties of the base bitumen, WCO modified bitumen and WCO-HDPE modified bitumen were then compared in other to determine the best performing binder. It is expected that this study will encourage the highway construction industry to consider the effective management and application of the wastes for the delivery of road pavements with longer life and better serviceability.

2. MATERIALS AND METHODS

2.1. MATERIALS

Penetration grade bitumen which formed the base bitumen used in this study is of grade 60-70 and was sourced from the material lab of a construction company in Nigeria. The bitumen specification is presented in Table 1 below. Figure 1 shows the penetration grade bitumen used in the study. The base bitumen was black in colour.

Table 1 Specification of base bitumen (Bitumen 60/70)

Property	Grades	Method
Specific Gravity @ 25˚C	1.00 - 1.05	D-70
Penetration @ 25˚C	60/70	D-5
Softening Point ˚C	49 min -56 max	D-36
Ductility @ 25˚C CMS	100 min	D-113
Loss On Heating (Wt)%	0.2 max	D-6
Drop In Penetration After Heating %	20 max	D-6 & D-5
Flash Point ˚C	250 min	D-92
Solubility In CS @ (Wt) %	99.5 max	D-4
Density @ 25 ˚C	1.00/1.05	D-70

The waste cooking oil used for the study was sourced from households in Ibadan, Nigeria. Figure 2 shows the WCO used in the study. The colour of the WCO was yellowish-brown. HDPE plastic wastes sourced from households in Ibadan and shredded into powdery form for an effective blend was used in the research. Figure 3 shows the HDPE used.

Figure 1 Penetration grade bitumen 60/70

Figure 2 Waste Cooking Oil

Figure 3 HDPE

2.2. MIX PROPORTIONS

Firstly, as shown in Table 2 below, the base bitumen was replaced with WCO at 5% percentage to form WCO modified bitumen. Then, HDPE was added at different percentages to the WCO modified bitumen to form WCO-HDPE modified bitumen. Tests including specific gravity, penetration and softening point were conducted on the modified bitumen.

Table 2 Mix Proportions for the Modified Bitumen

Bitumen 60/70 (%)	WCO Replacement (%)	HDPE addition (%)
100	0	0
95	5	0
95	5	2.5
95	5	5.0
95	5	7.5

2.3. METHODS

2.3.1. BLENDING OF WCO AND HDPE IN BITUMEN IN PREPARATION FOR TESTS

To develop the different blends of the modified bitumen, the base bitumen which was initially in semi-solid form was melted by placing it in the oven until it was sufficiently fluid to pour. The temperature of the oven was maintained at a maximum temperature of 135°C for about 30 minutes. Melting the bitumen was in a bid to make it mix effectively.

After the bitumen has been melted, blending of the WCO and HDPE was manually done by placing the mix on a hot plate with temperature at 192°C, and a stirring of the mix was done using a metal rod until a homogenous mix is formed. The mix was considered to have blended homogeneously by visual inspection when a uniform colour of the blend has been achieved. During blending, the modified bitumen mixes were observed to produce frying sound which was due to the WCO present in the mix.

The modified bitumen samples were thereafter poured into the softening point test and penetration test moulds and left to solidify under cool air. The moulds had been initially greased for easy removal of the specimens after the tests. It was observed that WCO modified bitumen took longer time to solidify when compared to the base bitumen. This is because the replacement of bitumen with WCO in the mixes led to softer blends (as apparent in the reduction in the viscosity and an increase in the flow of the WCO modified bitumen) which needs longer time to solidify. WCO-HDPE modified bitumen was however found to solidify earlier than the WCO modified bitumen and the base bitumen as the addition of the HDPE resulted in harder blends. WCO modified bitumen was also found to shrink more than the base bitumen and the WCO-HDPE bitumen because of the softness brought about by the WCO.

2.3.2. PENETRATION TEST

The penetration test was carried out in accordance to ASTM D5 [10]. Penetration is the consistency of a bituminous material expressed as the distance in tenths of a millimeter that a standard needle vertically penetrates a sample of the material under known conditions of loading, time, and temperature. To carry out the test, the sample which has been allowed to cool in the mould as initially explained is mounted in the penetrometer. The penetration is measured by means of a standard needle applied to the sample under specific conditions in the penetrometer. The penetration test is used as a measure of consistency. Higher values of penetration indicate softer consistency.

2.3.3. SOFTENING POINT TEST

The softening point test was carried out using the ring and ball apparatus in accordance to ASTM D36 [11]. In summary, two horizontal disks of bitumen, cast in shouldered brass rings, are heated at a controlled rate in a liquid bath while each supports a steel ball.

The softening point is reported as the mean of the temperatures at which the two disks soften enough to allow each ball, enveloped in bitumen, to fall a distance of 25 mm (1.0 in.). The softening point is useful in the classification of bitumens, as one element in establishing the uniformity of shipments or sources of supply, and is indicative of the tendency of the material to flow at elevated temperatures encountered in service.

2.3.4. SPECIFIC GRAVITY OF BITUMEN

The specific gravity of the base bitumen and the modified bitumen was done in accordance to ASTM D70 [12]. Specific gravity also known as relative density is the ratio of the mass of a given volume of a material to the mass of the same volume of water at the same temperature. It is used to indicate how dense the bituminous material is. For the test, the sample was placed in a calibrated pycnometer. The pycnometer and sample are weighed, and then the remaining volume is filled with water. The filled pycnometer is brought to the test temperature, and weighed. The density of the sample is calculated from its mass and the mass of water displaced by the sample in the filled pycnometer.

3. RESULTS AND DISCUSSIONS

3.1. SPECIFIC GRAVITY OF THE MODIFIED BITUMEN

Figure 4 below shows the specific gravity of the modified bitumen. It was observed that the replacement of bitumen with WCO reduces the specific gravity of the resulting binder. The reduction in the specific gravity of the WCO modified bitumen can be attributed to the lower density of WCO when compared to the base bitumen. Replacement of bitumen with WCO led to softer blends (as apparent in the reduction in the viscosity and an increase in the flow of the WCO modified bitumen) with lower specific gravity. However, the addition of HDPE increases the specific gravity of the binder. This can be attributed to the higher density of the HDPE coupled with the fact that HDPE was added to the WCO modified bitumen and not used to replace any component. HDPE added at 2.5%, 5% and 7.5% resulted in modified bitumen with higher specific gravity when compared to the base bitumen. Modified bitumen B95-WCO-5-HDPE7.5 was found to be of the greatest specific gravity.

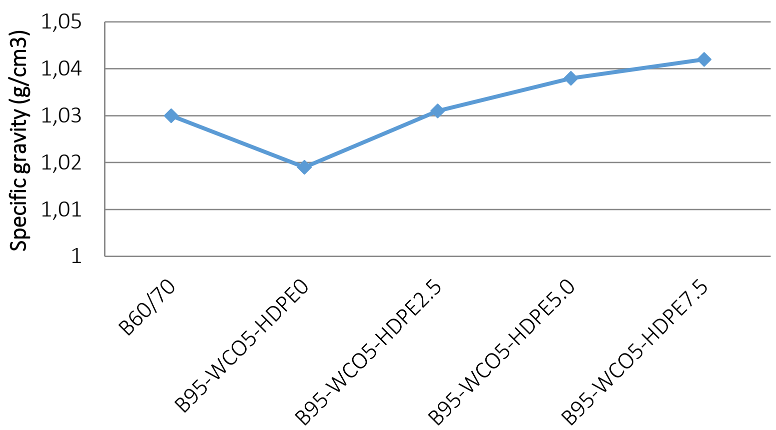

Figure 4 Specific Gravity of WCO-HDPE modified bitumen

3.2. PENETRATION BEHAVIOR OF THE MODIFIED BITUMEN

Figure 5 shows the effect of WCO and HDPE on the penetration behaviour of modified bitumen. It can be seen from the figure that the replacement of bitumen with WCO increases the penetration of the resulting binder. The increase in penetration also discovered by [13] can be attributed to softening brought about by WCO. However, the addition of HDPE to the WCO modified bitumen resulted in a reduction of the penetration values of the modified bitumen. The reduction in penetration can be attributed to a change in phase in the binder upon the addition of HDPE which resulted in increased internal resistance [14]. Modified bitumen with 2.5%, 5% and 7.5% HDPE addition to the WCO modified bitumen were found to be of lower penetration value when compared to the base bitumen, hence, WCO-HDPE bitumen has a higher consistency.

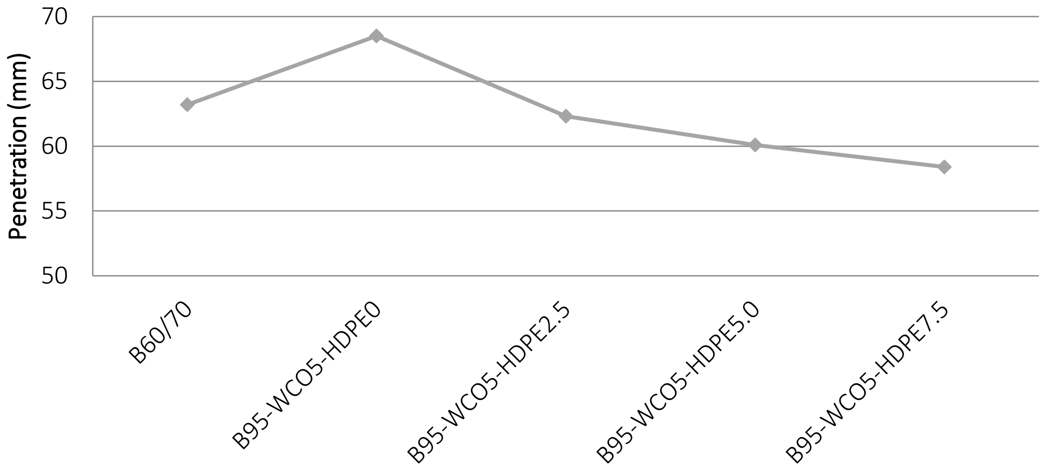

Figure 5 Penetration behavior of WCO-HDPE modified bitumen

3.3. SOFTENING POINT BEHAVIOUR OF THE MODIFIED BITUMEN

Figure 6 shows the softening point behaviour of WCO-HDPE modified bitumen. The figure shows that the softening point of WCO modified bitumen reduces upon the replacement of the base bitumen with WCO. Just as suggested for the penetration behaviour, the reduction in the softening point brought about by WCO can be attributed to the softening of the binder by WCO. The reduced softening point also reflects that the viscosity of the binder reduced as was observed during blending. This is in accordance with the findings of [13]. It was however observed that increasing amount of HDPE added to the WCO modified bitumen increased the softening point of the modified bitumen. This is also in accordance to the findings of [14]. Modified bitumen with 2.5%, 5% and 7.5% addition of HDPE to the WCO modified bitumen were found to be of higher softening point when compared to the base bitumen.

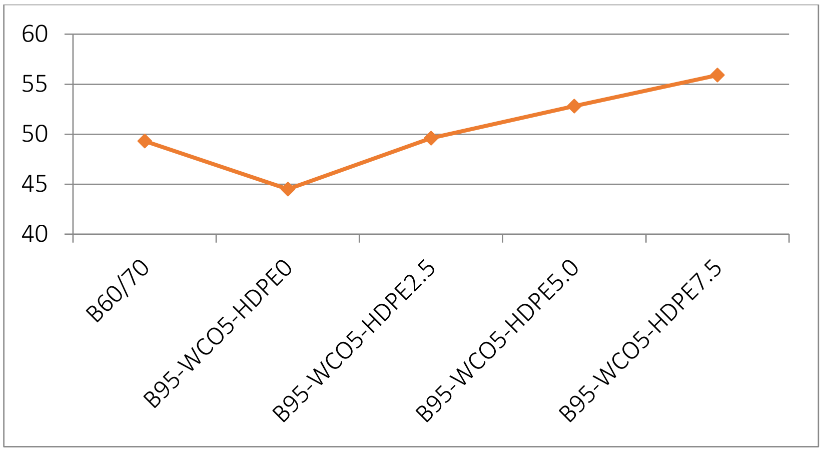

Figure 6 Softening Point behaviour of WCO-HDPE modified bitumen

3.4. RELATIONSHIP BETWEEN THE PENETRATION BEHAVIOUR AND THE SPECIFIC GRAVITY OF THE MODIFIED BITUMEN

The relationship between the penetration behavior and the specific gravity of WCO-HDPE modified bitumen is represented in Figure 7 below. The figure shows that increasing specific gravity of the modified bitumen caused by the addition of HDPE results in modified bitumen with reduced penetration, the higher the specific gravity, the lower the penetration. Increased specific gravity brought about by the addition of HDPE built up higher internal resistance in the resulting binder thereby reducing penetration.

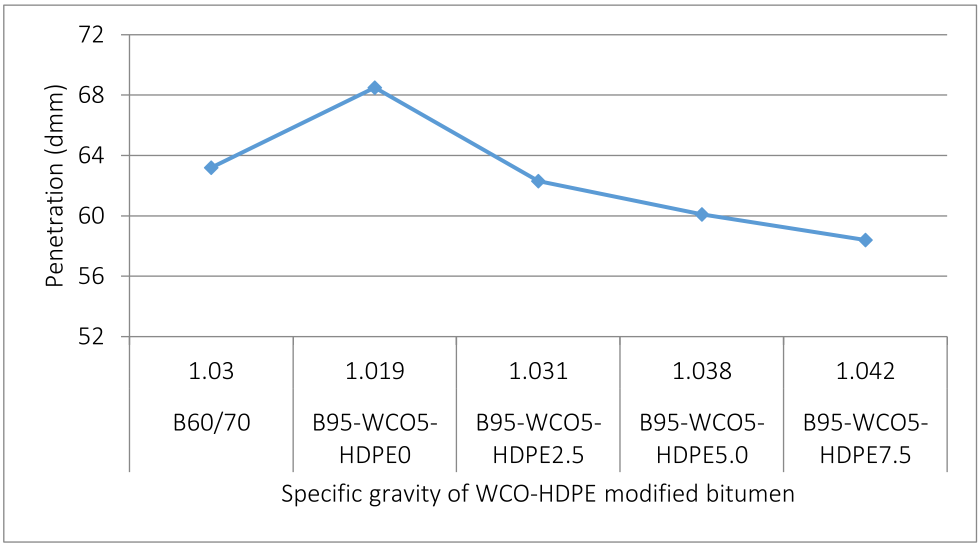

Figure 7 Penetration vs Specific gravity of WCO-HDPE modified bitumen

3.5. RELATIONSHIP BETWEEN THE SOFTENING POINT BEHAVIOUR AND THE SPECIFIC GRAVITY OF THE MODIFIED BITUMEN

Figures 8 present the relationship between the softening point behaviour and the specific gravity of WCO-HDPE modified bitumen. It was observed as in the figure that increasing specific gravity of the modified bitumen caused by the addition of HDPE results in modified bitumen with increased softening point, the higher the specific gravity, the higher the softening point. Therefore the increase in softening point of the WCO-HDPE modified bitumen can be attributed to the increased specific gravity brought about by the addition of HDPE.

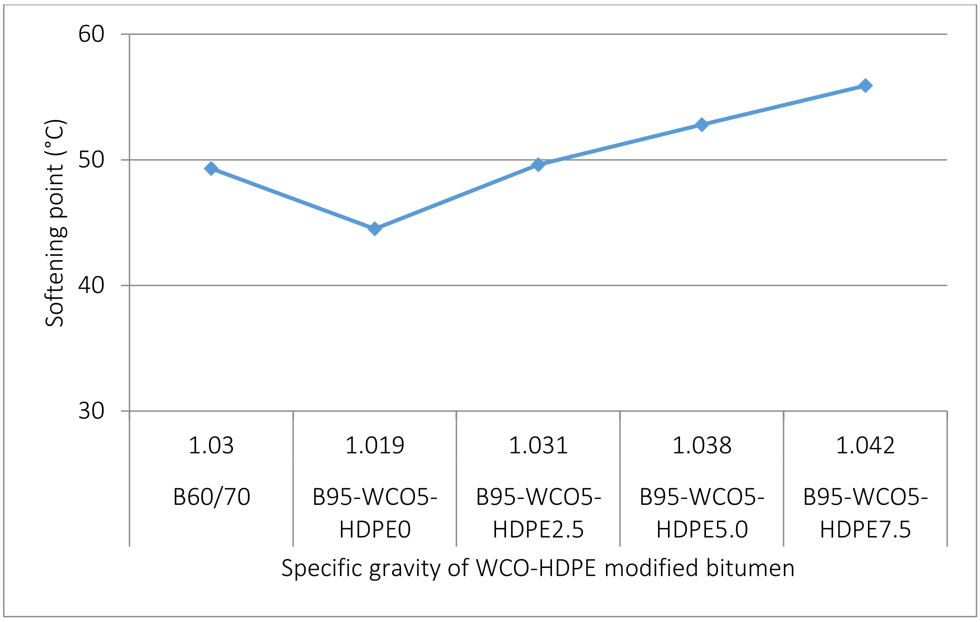

Figure 8 Softening Point vs Specific gravity of WCO-HDPE modified bitumen

4. CONCLUSION

Properties of bitumen modified with blended waste cooking oil and high density polyethylene for applications in flexible pavements was investigated in this research. The properties investigated include the specific gravity, penetration and softening point of the modified bitumen. The following are the conclusions made from the research:

(1) The replacement of bitumen with WCO reduces the specific gravity and the softening point of the resulting binder. The penetration value of bitumen was however found to increase upon replacement with WCO.

(2) The addition of HDPE reduces the penetration and increases the specific gravity and softening point of WCO-HDPE modified bitumen. HDPE added at 2.5%, 5% and 7.5% to the WCO modified bitumen results in lower penetration and higher specific gravity and softening point when compared to the base bitumen.

(3) A relationship was found to exist between the specific gravity and both the penetration and softening point of the modified bitumen investigated in the research. Increase in specific gravity results in an increase in the softening point and a decrease in the penetration of the modified bitumen.

ACKNOWLEDGEMENTS

Appreciation goes to the head and staff members of the Federal Ministry of Works, Lagos, Nigeria and the staff of Julius Berger Asphalt testing laboratory who provided the facilities and the enabling environment to carry out this research.

REFERENCES

[1] Polacco, G. et al., (2006) 'Relation between polymer architecture and nonlinear viscoelastic behavior of modified asphalts.', Current Opinion in Colloid and Interface Science.11, pp. 230-245.
[2] Garcia-Morales, M. et al., (2005) 'Effect of waste polymer addition on the rheology of modified bitumen', Fuel. 85(11), pp. 936-943.
[3] Navarro, F. et al., (2009) 'Bitumen modification with reactive and non-reactive (virgin and recycled) polymers: A comparative analysis', Journal of Industrial and Engineering Chemistry 15(4), pp. 458-464.
[4] Yuonne, B. & Yajaira, R. (2001) 'Polymer Modified Asphalt', Vision technologica. 9(1): 39.
[5] Shashidhar, S. et al., (1995) 'Rheological properties of Chemically Modified Asphalts', 74th Transportation Research Record.
[6] Roberts, F. et al., (1996) 'Hot Mix Asphalt Materials, Mixture Design, and Construction.', (National Asphalt Pavement Association Education Foundation. Lanham, MD.).

[7] Widyatmoko, I. (2008) 'Mechanistic-empirical mixture design for hot mix asphalt pavement recycling.', Constr Build Mater, 22(2), pp. :77-87.
[8] Su, K., Hachiya, Y. and Maekawaa, R. (2009;) 'Study on recycled asphalt concrete for use in surface course in airport pavement.', Resour Conserv Recycl, 54(1):, pp. 37-44.
[9] EPA. (2011) Available at: http://www.epa.gov/region9/waste/biodiesel/questions.html (Accessed: 2016).
[10] ASTM D5/ D5M-13: Standard Test Method for Penetration of Bituminous Materials
[11] ASTM D36/D36M: Standard Test Method for Softening Point of Bitumen (Ring-and-Ball Apparatus)
[12] ASTM D70: Standard Test Method for Density of Semi-Solid Bituminous Materials (Pycnometer Method)
[13] Meizhu, C. et al. (2014) 'Physical, chemical and rheological properties of waste edible vegetable oil rejuvenated asphalt binders ', Construction and Building Materials, 66, pp. 286-298.
[14] Fernandes, S. et al., (2013) 'Can oil, plastic and RAP wastes have a new life in novel asphalt mixtures? ', *Portuguese Foundation for Science and Technology.*

GEOCELL-REINFORCED PAVEMENT

Samo Peter Medved[1], Stanislav Lenart[2], Bojan Zlender[3]

[1] Lineal d.o.o., Jezdarska ulica3, 2000 Maribor, Slovenija, email: samo.medved@lineal.si
[2] Slovenian National Building and Civil Engineering Institute (ZAG), Dimičeva ulica 12, 1000 Ljubljana, Slovenija, email: stanislav.lenart@zag.si
[3] University of Maribor, Smetanova ulica 17, 2000 Maribor, Slovenija, email: bojan.zlender@um.si

SUMMARY: Unbound bearing layers have a distinct weakness that they are not capable of bearing tensile stresses in a horizontal plane. This results in plastic deformations that transmit on the surface of the pavement as cracks and ruts as a consequence. Despite the transformation of natural gravel and sand materials and added binders, vertical deformations of the pavement cannot be avoided. These are the consequence of excessive horizontal tensions in detached layers of the pavement construction, especially when overloading, or in the case of deteriorated hydro-geologic conditions of the natural ground. Bound, deformed defensively-supporting layers combined with geocell reinforced unbound bearing layers of earth represent an effective system of pavement structure with its structure that guarantees permanent elasticity, flexibility and adequate bearing strength of the construction itself. Recent research has shown the advantage of using rigid geocells, which was also confirmed by the results of numerical modeling. Rigid geocells were also used in the test field. Numerical modelling and experimental analysis showed a crucial improvement of the bearing strength and reduction of deformation when geocells are used.

KOLNIK ARMIRAN GEOĆELIJAMA

SAŽETAK: Nevezani nosivi slojevi imaju svojstvenu slabost, jer ne mogu prenositi vlačna naprezanja u horizontalnoj ravnini. To dovodi do plastičnih deformiranja koja se na površinu kolnika prenose kao pukotine i kolotrazi. Unatoč zamjeni prirodnoga šljunka, pješčanih materijala i dodanih veziva, vertikalna se deformiranja kolnika ne mogu izbjeći. Ona su posljedica prekomjernih horizonalnih vlačnih naprezanja u pojedinim slojevima konstrukcije kolnika, posebno pri preopterećenju ili degradaciji hidrogeoloških uvjeta prirodnoga tla. Učinkovit sustav konstrukcije kolnika čija konstrukcija jamči stalnu elastičnost, fleksibilnost i primjerenu čvrstoću konstrukcije jesu povezani, deformirani nosivi slojevi pojačani geoćelijama u kombinaciji s nepovezanim nosivim slojevima zemlje pojačanim geoćelijama. Novija istraživanja pokazala su prednosti upotrebe krutih geoćelija, a to su potvrdili i rezultati numeričkoga modeliranja. Krute geoćelije upotrijebljene su i u terenskom ispitivanju. Numeričko modeliranje i analiza eksperimenta pokazali su da se pri upotrebi geoćelija bitno poboljšava nosivost i smanjuju deformacije.

1. INTRODUCTION

Unbound bearing layers of pavement structure have a distinct disadvantage in that they are not able to resist tensile stresses in the horizontal plane. This leads to a plastic deformation, which is subsequently passed on to the track surface in the form of cracks and ruts. Despite the transformation of the natural stone material and the addition of a binder especially in the stone material of lower quality (eg. gravel), the overload, and in the case of unfavourable hydrogeological conditions of the foundation soil, one cannot avoid the vertical deformation of the roadway, which are caused by exceeded horizontal tension in unbound layers of road structure. In practice, this problem can be solved with crushing [1] of these materials and improving the structure of the fractions in composition, suitable for use. For the manufacture of high load-bearing pavements cement and bitumen binder should be added to provide a corresponding increase in capacity. In the past, strips and meshes were used for the reinforcement of soils. Meshes and strips made of steel or synthetic material were arranged in a horizontal direction. Ribbons have improved capacity mainly through the mechanism of friction between the strip and the soil. Using strips and reinforcement in the horizontal level of unbound bearing layers resulted in the increase of bearing capacity, while it did not give the desired results in pavement deformations. In case of larger dynamic effects (e.g. traffic loads), such reinforcement of roadway structure has been proven to be not effective enough. In the substructure, or in the embankment, where the dynamic effect is much smaller, a geogrid reinforcement is sufficient.

Therefore, the use of different inclusions to improve the capacity of an unbound base layer was studied. Pavement reinforced with geocells is indicated as a suitable structure. Geocells as a spatial lattice structure of vertically arranged strips represent an upgrade to the development of the conventional methods for reinforcing soil materials.

Thus, studies and research in the field of soil reinforcement with geocells have been performed. The vast majority of studies were based on laboratory experiments. Some researchers [2-4] have focused on the impact of geocells on reinforcing the soil and improving soil bearing capacity or embankments. It was found that the geocells with appropriate geometry were effective in improving the load capacity. Some other researchers [5-9], have studied the effect of geocells to reduce the deformability of the ground and the impact of a change in the modulus of the soil, under static and dynamic load. Research has shown that the use of geocells can improve the capacity of the base material for 40 to 100%, depending on the load, the mode of application of geocells and forms load. Mengelt, et al. [7] found that the use of geocells increased elastic modulus coarse materials to 1.4-3.2% and 16.5-17.9% for fine-grained materials. The above-mentioned studies were specifically focused on testing single geocell structures. The results have generally changed mainly due to the type of selected geocells, and the means of the load. Rajagopal [6] and Wasseloo [8] also carried out research on strain properties of the structure reinforced with several layers of geocells. In this research, geocells with thicknesses of 100 and 200 mm were used, and the results showed that the use of geocells effectively prevent or reduce the occurrence of ruts in the road surfaces. Al-Qadi, et al. [10] investigated the effect geocells with a height of 100 mm in the project of reconstruction of roads in Pennsylvania, where they used geocells from non-woven geo-synthetic with ground bearing capacity CBR 4. Subsequent analysis of the Falling Weight Deflectometer (FWD) found that is in the construction of reinforced geocells of geo-synthetic over a period of three years that modules load increased by factor of 2. Latha, et al. [11] conducted a field study to evaluate the improvement of soil bearing capacity and the reduction of the occurrence of ruts on unpaved roads. Different types of geocells were used. It has been found that the use thereof is a much more effective form of reinforcement than in the case of using geosynthetics. Pokharel, et al. [9] investigated the use of polymer geocells as reinforcements of unpaved roads constructed over fundamental ground bearing capacity CBR <3. The survey was conducted at a small, busy road. They used the geocell height of 15 cm from the nonwoven geosynthetic as a separator between the ground and the fundamental carrier layer. The study showed that the use of geocells increase the life of the macadam road between 1.5 and 3.5 times compared to untough pavement.

Figure 1 3D mesh structure; a) rigid geocells, b) soft geocells [7]

2. RESISTANCE DEVELOPMENT MECHANISM

To understand the functioning of geocells as reinforcements of unbound bearing layers, it is necessary to know the mechanisms of action. Based on a detailed analysis and review of the literature [12-14], it can be concluded that, in principle, there are three main mechanisms by which geocells have an effect on increasing the capacity of reinforcement layers. For both main types of geocells (soft and rigid) we can indicate the mechanism limiting the lateral creep of the soil, which is implemented through friction contact between geosynthetic and soil. In this case, the shear stress in the earth is efficiently transmitted via friction to the tension in geosynthetics. Another mechanism represents distribution of vertical stress in the foundation ground, similar to the principle of the foundation. The third mechanism is a membrane mechanism that increases the bearing capacity, which occurs when the reinforced soil has already developed a certain deformation.

a) 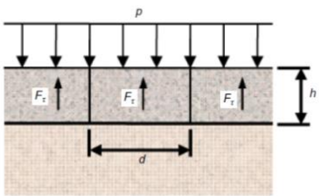

b) 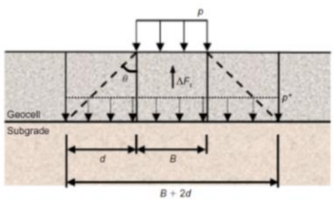

c) 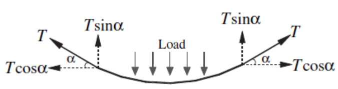

Figure 2 Capacity increase mechanisms a) confinement mechanism [12], b) stress dispersion [12], c) membrane mechanism [14]

2.1. CONFINEMENT EFFECT

When load appears, horizontal tension between infill walls and geocells is mobilized as shear stress. The effect of partitioning the filler manifested by improving the geotechnical characteristics of the filling soil (strength and deformability), which increases the load capacity and the increased absorption of loads via the horizontal tension in geocells. Such tensions are transmitted between adjacent cells in the mobilization of passive pressures (passive resistance) in the earth (filler) and shear resistance (shear stress) of soil (filler) and geocell walls. The effectiveness of the mechanism depends on the intermediate friction between the filler and individual geocell.

Based on observations and laboratory tests [11, 15, 16], if h means the height and d means the cell diameter, it is noted that the increase in the ratio (h / d) beyond 1, results in a change of the geocell behaviour. In summary, the geocell with a smaller ratio (i.e. h / d <1), bend (deform) as the central load slim fundament on the elastic basis, which is deformed as a function of increasing contact tension below by the mobilization of shear stress in the underlying soil. A higher ratio (i.e. h/d > 1) leads to increased stiffness whereby geocell structure begins to behave more like a base plate, which allows a more even distribution of pressure and vertical loads on the foundation ground [11, 15, 16].

2.2. STRESS DISPERSION EFFECT

Stress dispersion effect can also be called the effect of the foundation plate. Also, this does not require the displacement of the activation. This is the basic principle, which can be described as stress distribution to a lower layer due to the 3D structure of the cell and the filler which forms a connected structure which is able to provide strength and resistance to bending, compressive, tensile and shear stress, similar to the rigid base plate. Geocells transferred the load to the underlying ground, and the load is redistributed to the increased area of a lower level of tension.

This way of taking account of the Spreading loads can be used on the ground cellular structure of the reinforcement layer and mainly due to the effect of cell restriction in each cell, assuming that the nose has tension trapped in the walls of neighbouring cells. Such even-distribution brings a relatively large angle (Θ) in relation to the use of traditional concepts of soil mechanics and foundation. It will be appreciated that the nose intersects the wall of the neighbouring cells; the nose is prevented due to the rigidity of the cell wall, and the discontinuity of materials, even if it is lower than the normal values are set for the mechanics of the soil and the foundation.

2.3. MEMBRANE EFFECT

The membrane effect is the result and consequence of the vertical displacements in the foundation ground under a layer reinforced with geocells [12], forming a concave shape and tension in geosynthetics. On account of the compressibility and lateral anchoring curved reinforcement causes the opposite vertical force which acts on an increase in the load in terms of the membrane, which are activated by a tensile stress and reduce the load on the substrate [13] . Activating this effect requires the occurrence of significant vertical displacement, high strength of geosynthetics and minimal roughness between the reinforcement and soil for activating the anchoring force or friction. Among other things, this effect requires a separation between the two layers of the soil (above and below the reinforcement) to mobilize capacity.

As we can see, the mechanism is amplification of geocells' complexity of the mechanism of geogrid reinforcement, because the increase in the load sum of the effects of different mechanisms.

3. NUMERICAL MODELING

Effectiveness of geocells in the pavement structure is analyzed with parametric stress-strain analysis, using program, FEM Everstress [17]. The purpose of the analysis was to examine the effect of reinforcing the capacity of geocells on the pavement with a focus on the impact of the tangential stress in the asphalt layers.

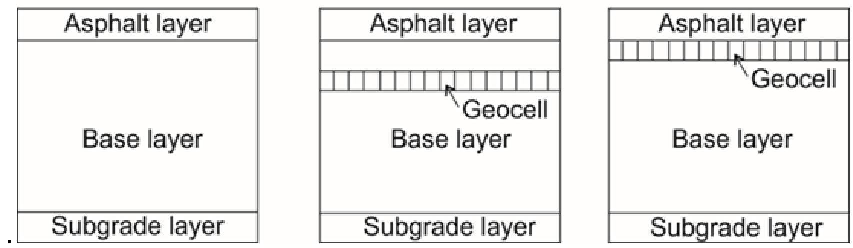

Figure 3 Geocell position concept

The analysis applied transport axle load of F = 100 kN, the pressure in the wheel p = 690 kPa. Two different models were made: (1) the basic model, without reinforcement; and (2) model, where the support layer is reinforced with geocells. In the second model, position of the geocells in the unbound supporting layer was changed. This paper presents the reinforcing effect of the geocells on the tangential stress in the asphalt layer.

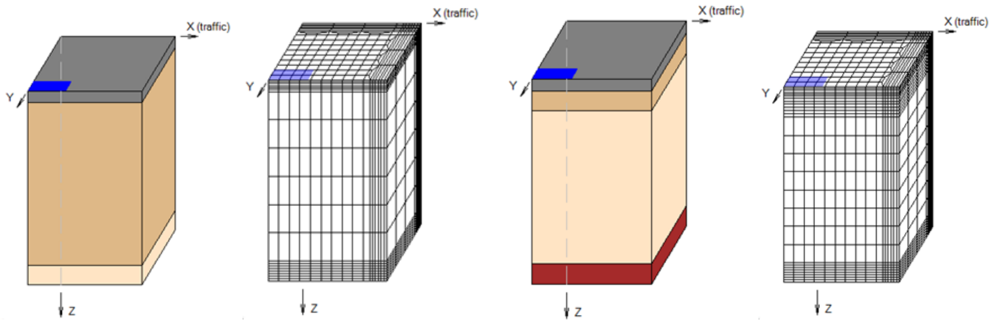

Figure 4 Numerical models: a) without geocell, b) with geocell

3.1. BASIC MODEL

Basic numerical model consists of asphalt layer thickness D_a, unbound bearing layer thickness D_b and subgrade with modulus E_{sg}. The analysis was performed on variable thicknesses of the asphalt layer (10, 20 and 30 cm), as well as the thickness of the unbound bearing layer, which has been changed in the thicknesses of 20, 40 and 60 cm. As a subgrade, the calculations applied a constant value E_{sg}. Thickness of the layers and properties of materials used:

an asphalt layer (E_a = 3000 MPa, v = 0.40, D_a = 10, 20, 30 cm)

unbound bearing layer (k_1 = 110-300 MPa, k_2 = 0.5, k_3 = 0, v = 0.35, D_b = 20, 40, 60 cm)

subgrade (E_{sg} = 14,7 MPa, v = 0.45)

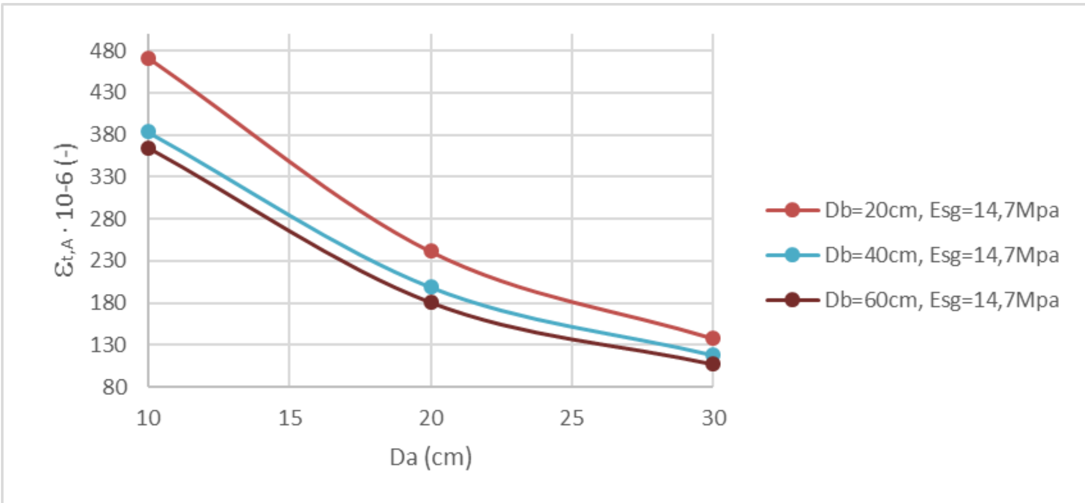

Figure 5 Transverse strains in the asphalt depending on the thickness of the asphalt, unbound bearing layer and flexibility of the subgrade.

From the results it can be concluded that the transverse deformation of asphalt is most affected by the thickness of the asphalt layer, its thickness also contributes unbound bearing layer, which decreases with increasing thickness. The graph shows the details of the effects of varying the thickness.

3.2. GEOCELL REINFORCEMENT MODEL

Geocells thickness variation

The model consists of asphalt layer thickness D_a, geocells D_{cel}, unbound supporting layer thickness D_b and substrates with modulus E_{sg}. In this analysis, a constant thickness of the asphalt layer of 10cm, a constant thickness of unbound bearing layer 40 cm, and constant property of subgrade are assumed. Thickness of the geocells was varied through the thickness of 5, 10 and 15 cm. The modulus of the geocell elasticity was changed and the impact of different geocell stiffness on the tangential deformation of asphalt layers was analysed. Layer thickness and properties of these materials are:

Asphalt layer (E_a = 3000 MPa, ν = 0.40, D_a = 10 cm)

geocells (E_{cel} = 200 - 3000 MPa, ν = 0.20, D_{cel} = 5, 10, 15 cm)

unbound bearing layer (k_1 = 110-300 MPa, k_2 = 0.5, k_3 = 0, ν = 0.35, D_b = 40 cm)

subgrade (E_{sg} = 14,7MPa, ν = 0.45)

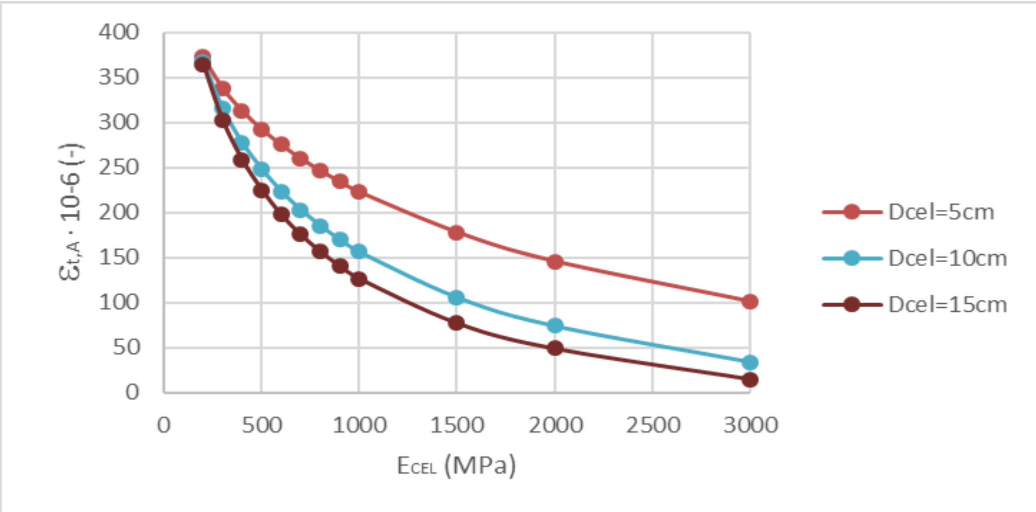

Figure 6 Transverse strains in the asphalt depending on the stiffness of geocells and different thicknesses geocells at constant subgrade deformability - Location geocells beneath the asphalt

It was found in the analysis that the stiffness of the geocells significantly affects the shear deformation in the asphalt, while the effect of increasing the rigidity of the geocells with module greater than 2500 MPa did not contribute significantly to the reduction of deformation. Also, the thickness of the geocells had a significant impact on the size of the transverse deformation, where it is reasonable to increase the thickness of the geocells up to approximately 10 cm. Thus, it can be concluded that the rigidity and thickness of the geocells is essential for reducing horizontal deformations in the asphalt.

Variation of geocells position in the unbound bearing layer

The influence of the geocell position to horizontal deformation of asphalt was tested. Geocells were initially placed just below the asphalt. In subsequent trials, geocell positions lower in unbound supporting layer were tested.

It was found that the position of the geocells in the unbound bearing layer have significant impact on the horizontal tension in the asphalt, and the location of the geocells just below the asphalt was advantageous and contributes significantly to reducing deformation in the asphalt. Contribution of the geocells decreases with the depth installation. It can be concluded that the installation of geocells (particularly of rigid type) can reduce deformation of asphalt wages and thereby rationalize them. Therefore, geocells increase capacity and usability of pavements.

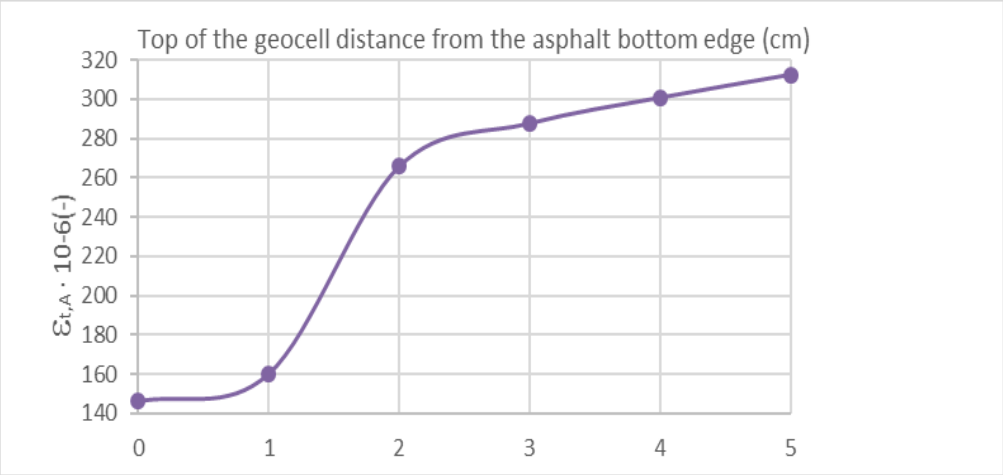

Figure 7 Transverse strains in the asphalt depending on the geocell location in unbound bearing layer at a geocell constant stiffness E_{cel} = 2000 MPa

4. TEST FIELD

A field test using both the presence and absence of geocells in similar locations using numerical modelling was conducted. The length of the test field was 24 m. Objectives of this were to examine the feasibility of using geocells; a practical example of real use to test the technology implementation of the pavement using geocells, gain initial experience with installing, perform basic measurements of elastic moduli and determine the effect of geocells, measurements of pliability of roadway construction (FWD) before carrying out remedial action and beyond, and to determine the effect that geocells have on the pavement deflection. In addition, the field was tested to monitor the long-term behaviour of reinforced roadway construction.

4.1. TEST FIELD CONCEPT

The completed test field is a total length of 24 m, where there are three 8-metre-long pavement sections with altered conditions, namely:

section – top geocells positioned 5cm below the asphalt layers

section – without geocells

section – geocells installed just under the asphalt

Given the projected rehabilitation of a section of the road, monitoring of the test field with the non-destructive testing was proposed.

4.2. THE CONSTRUCTION OF THE TEST FIELD

Geocells were placed in a built-in separated gravel material. Blocks are linked to the carrier via a shear contacts. This was followed by the execution of filling cells with gravel material, to be incorporated in a working machine with manual spreading out. After the execution of spreading out, the material is first vibrated by facilitating a compactor plate. At the pre-prepared base, dynamic and static compacting with several compactors was implemented. The trial showed that the planned installation technology was fully effective and unproblematic.

After completing the installation of the wear layer, it can be ascertained that the technology works smoothly, quickly and without complications. In the implementation phase measurements, compacting rate unbound supporting layer confirmed previous suspicions that there is a problem of compacting the material into rigid geocells as lower current thickness when using geocells were expected. Findings after measurements have shown that geocells affect the measurements in a manner to reduce the module E_{VD}. Reduction of the module was measured at the level geocells greater than when it was geocell upgraded by 5 cm gravel material.

4.1. RESEARCH AND MEASUREMENTS ON THE TEST FIELD

Falling Weigh Deflectometer (FWD) measurements

Measurements on the test field were carried out with FWD. Measurements were carried out longitudinally on each meter of the test field.

Figure 8 Implementation of the test field

Figure 9 Falling Weigh Deflectometer on the test field [18]

In this way, the results of measurements evaluated were at a temperature of 25°, to allow for a proper comparison of the measurement results. The results presented show a comparison of modules asphalt layers on, namely when measuring a few days after the execution and measurement 4 months after completion of the test field.

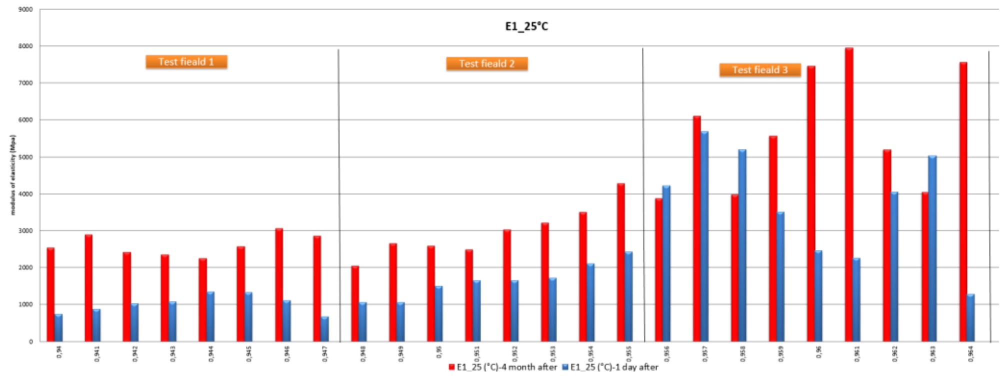

Figure 10 Module E1 and the average module across the field, calculated at 25 °C

The findings based on measurements performed

Based on the completed measurements it can be stated that measurements have shown a positive effect on the geocell stiffness asphalt layer (E1_25O) if they are installed just below the asphalt, which was based on the previously performed numerical modelling also expected. It was partly surprising that the results in the case of lower embedded geocells were worse than in the field without geocells.

Table 1 Module E1_25°C (MPa) and ratio between measurements 0 and 1

	Box 1 $E_{1\_25}{}^{o}{}_{C}$	Box 2 $E_{1\_25}{}^{o}{}_{C}$	Box 3 $E_{1\_25}{}^{o}{}_{C}$	$E^{3}{}_{1\_25}{}^{o}{}_{C}/ E^{2}{}_{1\_25}{}^{o}{}_{C}$	$E^{1}{}_{1\_25}{}^{o}{}_{C}/ E^{2}{}_{1\_25}{}^{o}{}_{C}$
0. measurement	1019	1645	4051	2,46	0,62
1. measurement	2633	2988	5762	1,93	0,88
$\Delta\%$	258	182	142		

It should be noted that geocells installed directly below the asphalt significantly increase the capacity of the asphalt layers, comparing to geocells installed deeper into the decoupled support layer. It is interesting to observe the trend, as the increment of the modulus of elasticity is the largest in test field 1 and the lowest on the test field 3. There has been a significant increase of stiffness in the field without reinforcements.

Based on the results of deflection, minimum deflection on the spot with reinforcements geocells implanted just under the asphalt layers is commonly observed. This supports the results of performed experimental and numerical analysis and can thereby confirm the favourable impact of rigid geocells installed just under the asphalt pavement deformation.

Deviation from expected deflection of the carriageway in the event of installation in unbound supporting layer in the case of deeper installation, which is different from the numerical analysis and laboratory tests. Cause still needs to be further explored and clarified with further measurements.

It is also interesting what is displayed by modules E_2, which measured the stiffness of unbound bearing layers. Here it can be noted that geocell rigidity does not impact favourably on what we have already confirmed by measurements E_{vd}, where a similar correlation was observed.

5. CONCLUSIONS

Geocells increase the capacity of the asphalt layers of pavement structures and reduce permanent deformation in asphalt. Therefore, using geocells could reduce the use of asphalt layers. The results show that the load and deformation of the pavement depends on the location of the geocells in the base layer. Geocells installed just below the asphalt greatly reduces the deformation of asphalt. In the case that they are arranged so that the asphalt and geocell layer are then followed by the unbound supporting layer, then this effect is significantly reduced. Geocells installed on the bottom of unbound carrier layer significantly improve the capacity of the surface and replace unbound road bases as improvement of ground (Bear, 2016). The permanent vertical deformation of the base layer is not significantly affected by the location of geocells within the base layer. (Medved 2016). Geocells affect the reduction of the shear deformation in the base layer directly at the site of the reinforcement. Usability of the geocells' reinforcement of pavement structures such as decoupled bound pavements shows an example of the potential usability, but will require additional research and experience in the application. Given the magnitude of the road network, it shows great potential in the use of recycling waste materials in construction and reconstruction of roads. Thus, in addition to the mechanical effects, there is the need to explore the ecological and economic effects of the geocell application in practice.

REFERENCES

[1] Ficko, G., Žlender, B., 2005. The analysis of permanent deformations of repeatedly loaded gravels from the Mura region. Acta geotechnica Slovenica, vol. 2, no. 2, pp. 24-37.
[2] Cowland, J. & Wong, S., 1993. Performance of a Road Embankment on Soft Clay Supported on a Geocell Mattress Foundation. Geotextiles and Geomembranes, pp. 687-705.
[3] Dash, S. K., Sireesh, S. & Sitharam, T., 2003. Model studies on circular footing supported on geocell reinforced sand underlain by soft clay. Geotextiles and Geomembranes 21, pp. 197-219.
[4] Yang, X., Han, J., Pokharel, SK, Manandhar, C., Parsons, RL., Leshchinsky, D., 2011. Accelerated pavement testing of unpaved roads with geocellreinforced sand bases. Geotextiles and Geomembranes.
[5] Bathurst, R., Blatz, J. & Burger, M., 2003. Performance of instrumented largescale unreinforced and reinforced embankments loaded by a strip footing to failure. Canadian Geotechnical Journal 40, pp. 1067-1083.
[6] Rajagopal, K., Krishnaswamy, N. R. & Madhavi Latha, G., 1999. Behavior of sand confined in single and multiple geocells. Geotextiles and Geomembranes, p. 171–184. 154
[7] Mengelt, M., Edil, T. & Benson, C., 2006. Resilient modulus and plastic deformation of soil confined in a geocell. Geosynthetics International No.5.
[8] Wasseloo, J., Visser, A. & Rust, E., 2009. The stress–strain behaviour of multiple cell geocell packs. Geotextiles and Geomembranes 27, pp. 31-38.
[9] Pokharel, S.K., Letchkinsky, D., Parsons, R.L., Halahmi, I., 2010. Investigation of factors influencing behaviour of single geocell-reinforced bases under static loading. Geotextiles and Geomembranes 28, pp. 570-578.
[10] Al-Quadi, I. & Hughes, J., 1999. Geocell subgrade stabilization, Washington DC: US Department of Transportation.
[11] Latha, G. M., Dash, S. & Rajagopal, K., 2009. Numerical simulation of the behavior of geocell reinforced sand in foundations. International Journal of Geomechanics ASCE, 9 No. 4, p. 143–152.
[12] Avesani, N., Bueno, B., Futai, M., 2013. A bearing capacity calculation method for soil reinforced with a geocell. Geosynthetics International No. 3.
[13] Zhou, H. & Wen, X., 2008. Model studies on geogrid- or geocell-reinforced sand cushion on soft soil. Geotextiles and Geomembranes 26, pp. 231-238.
[14] Ling, Z., Zhao, M., Shi, C. & Zhao, H., 2010. Bearing capacity of geocell. Geotextiles and Geomembranes 28, pp. 475-482.
[15] Dash, S., Rajagopal, K. & Krishnaswamy, K., 2007. Behaviour of geocell reinforced sand beds under strip loading. Canadian Geotechnical Journal 44, pp. 905-916.
[16] Han, J., Yang, X., Leshchinsky, D. & Parsons, R., 2008. Behavior of geocell-reinforced sand under a vertical load. Transportation Research Record, 2045(95–101).
[17] Everstress Pavement Analysis Programs, Washington State Department of Transportation, s.l.:Oylimpia, WA., 1999
[18] Želodec, D. & Jurgele, M., 2016. Deflection measurements and capacity analysis on pavement test field - regional road Sotina R3-720/5624, Ljubljana: DRI.

CHLORIDE PENETRATION THROUGH CONCRETE COVER UNDER PRESSURE OF SALTY WATER

Damir Zenunovic[1], Nesib Residbegovis[1], Radomir Folic[2]

[1] University of Tuzla, Faculty of Mining, Geology and Civil Engineering, Univerzitetska 2, 75 000 Tuzla, Bosnia and Herzegovina, email: damir.zenunovic@gmail.com
[2] University of Novi Sad, Faculty of Technical Sciences, Trg Dositeja Obradovica 6, 21000 Novi Sad, Serbia, email: r.folic@gmail.com

SUMMARY: A part of the laboratory investigations was presented in the paper, conducted in order to define the behaviour of the concrete cover submerged in salty water. Samples from three different concrete mixes were made in order to analyze the penetration of chloride. The profiles of chloride penetration for specific concrete mix were determined. The comparative analysis of the chloride penetration process through the concrete cover submerged in salty water (Bulk Diffusion Test - BDT) and concrete submerged in salty water under various pressures (Pressure Penetration Test - PPT) was performed. At the end of the paper BDT diffusion coefficients and PPT permeation coefficients relation was discussed and recommended for further research.

PRODOR KLORIDA KROZ ZAŠTITNI SLOJ BETONA PRI TLAKU SLANE VODE

SAŽETAK: U radu je prikazan dio laboratorijskih istraživanja provedenih kako bi se definiralo ponašanje zaštitnog sloja betona uronjenog u slanu vodu. Izrađeni su uzorci od triju različitih mješavina betona kako bi se analizirao prodor klorida. Određeni su profili prodora klorida za određenu mješavinu betona. Provedena je usporedna analiza procesa prodora klorida kroz zaštitni sloj betona uronjenog u slanu vodu (engl. bulk diffusion test, BDT) i betona uronjenog u slanu vodu pri određenim tlakovima (engl. pressure penetration test, PPT). Na kraju rada raspravljeni su koeficijenti difuzije za BDT i odnos s koeficijentima zasićenja u PPT-u. Dane su preporuke za daljnje istraživanje.

1. NTRODUCTION

Concrete is the most widely used construction material in the world. This is because of its availability in the market and competitive price compared to other materials. Over the years, the type and quality of concrete materials, methods of construction and design methods have improved considerably. The concept of safety of concrete structures has been defined and elaborated in standards [1]. Also, there has been an increased understanding of the chemical behaviour and performance of concrete. It is an unfortunate fact that all concrete structures deteriorate with time. The challenge for researchers and engineers in engineering practice is how to ensure a rational durability of concrete structures. This issue is treated by the literature that deals with modelling the service life of concrete structures, which is a result of intensive research over the last thirty years. Thus, there are some important references from this period [2] - [8].

It is well known that reinforcement corrosion is the main cause of reduction of service life of concrete structures. The chemical process of corrosion is described in a large number of references. Here, we can mention the book [9] which explains the process of corrosion and describes the methods of monitoring and preventing the corrosion process. The two main causes of reinforcement corrosion are carbonation and contamination of concrete by chlorides. Since this paper is dedicated to the effects of chlorides, the analysis of the effects of the presence of chloride in concrete has been carried out. Here is presented a part of experimental research from the research project called "Modelling the service life of concrete structures in industrial zones", conducted at the Faculty of Mining, Geology and Civil Engineering at the University of Tuzla. Chloride diffusion coefficients through the concrete surface layer exposed to salted water with and without pressure were analyzed. Three concrete mix formulas were used. The samples were tested by immersing them into salty water (Bulk Diffusion Test - BDT) and pressuring them with salted water (Pressure Penetration Test - PPT). The term permeation coefficient was introduced, which represent a difference of the transport mechanisms during BDT and PPT. The paper concludes with overview for ratios of diffusion coefficients and permeation coefficients through the surface layer of concrete, as determined based on BDT and PPT.

2. CHLORIDE TRANSPORT THROUGH A CONCRETE MATRIX

The parameter concrete permeability is vital for most deterioration processes affecting durability of reinforced concrete. Aggregates have usually low permeability and thus transport mechanisms occur essentially through the pore system of the cement paste, the interfacial transition zone and cracks or fissures in the concrete [10, 11].

Chloride ions penetrate through concrete via different mechanisms depending on the driving force involved. Capillary suction, migration, diffusion, and permeation are the most well known chloride transport mechanisms through concrete. Capillary suction is usually the dominant mechanism for concrete exposed to wetting and drying cycles [12]. During these cycles capillary water uptake occurs in the wetting stage, while the drying period allow the capillaries to be partly emptied, which enhances capillary suction in the next wetting cycle [11]. The depth to which capillary suction influences moisture condition in concrete is limited. It is due to the limited interconnectivity of the capillary pore system. Migration or electromigration of chloride ions occurs in the presence of an electric field. The velocity of the migration ions depends on the ionic mobility and the strength of the electric field [13]. In the case of water-saturated concrete diffusion is the main transport process. Diffusion is the mechanism that is capable of bringing chlorides to the level of the reinforcing steel, thereby accelerating the corrosion of the rebar. The driving force for diffusion of dissolved chloride ions is the presence of concentration gradients. A common method of determining the chloride diffusion in concrete is to expose saturated samples to a chloride solution for a known period of time. Diffusion coefficients and surface chloride concentrations are determined by fitting the chloride profiled data to the non – linear Fick's second law of diffusion [14]. The simplest solution of Fick's second law is Crank's solution [15]. Chloride ions are also introduced by hydrostatic pressure or by standing water, which causes the permeation of chloride ions through the matrix. Permeability is the movement of a liquid under hydrostatic pressure and can be described by Darcy's law, explained in [16].

The examples of significant amounts of chloride in engineering practice include buildings near the sea, maintenance of roads and bridges in winter, and buildings in industrial zones. The chloride ions accelerate the chemical process that leads to corrosion of reinforcement. Chloride ions have a small influence on the pH of the pore solution, but can destroy the passive layer when the chloride content in the pore solution exceeds a critical value (chloride threshold). In modelling the service life of concrete structures, the key parameters for forecasting the structure's service life (diffusion coefficient and surface concentration) are derived based on the established chloride profile. Because of that, testing techniques have been designed primarily for measurements of diffusivity of chloride ions. The investigation of chloride ions transport mechanism under salty water pressure was presented in [17]. The authors pointed out two mechanisms active during the transport of salt solutions into concrete under pressure. First the dissolved ions are filtered out of the solvent and the solvent migrates much deeper into the pore space. This leads to an increased difference of chloride concentration, which than acts as a driving force for accelerated diffusion of chloride. Interactions of the two mechanisms have still to be quantified in detail. The report [18] gives an overview of methods for determining the resistance of concrete against chloride penetration. The BDT and PPT test procedures are explained in details.

3. PART OF THE EXPERIMENTAL RESEARCH REFERRING TO RESISTANCE OF THE SURFACE LAYER OF CONCRETE AGAINST CHLORIDE PENETRATION

The objective of this part of the experimental research was to specify relation between diffusion coefficient obtained by BDT and permeation coefficient obtained by PPT. In the research, tests were performed on three concrete mixes, designated as CM1, CM2 and CM3. Table 1 provides the basic information about the mixes, while Figure 1 shows the measured rate of settlement and the appearance of CM1 samples. The samples were kept in laboratory conditions 28 days, and then exposed to the test regime. Part of the samples is immersed into salty water (BDT) (Figure 1), and the other part of the sample is exposed to internal pressure in the chamber, which was compiled specifically for the testing (PPT) (Figure 2). In both test (BDT and PPT) pure industrial salt concentration in the water was 16.5%. The BDT was performed according to NordTest NTBuild 443. The test was executed in a period of 90 days. For the concrete mixes CM1 and CM2 level of water pressure 2 bars was chosen. The pressure was applied for five periods of 2, 4, 6, 8 and 10 days. For the concrete mix CM3 three levels of water pressure were chosen, namely 1 bar, 2 bars and 2,5 bars with applied periods of 1, 2 and 4 days. Table 2 presents the sampling regime. After removing the samples from salty water, the surface layer of concrete was sampled on the saturated, dry-surface sample. At the same time, two types of sampling were conducted: sampling by grinding for the purpose of determining the concentration of chloride along the depth (Figure 3a) and sampling by tearing for the purpose of determining the depth of chloride penetration (Figure 3b).

The chloride concentration was determined by the Mohr's argentometry method, that is titration using solution of standard silver nitrate (AgNO3) with potassium chromate (K2CrO4) as an indicator, while the depth of chloride penetration was determined using the colorimetric approach by spraying the tear-up samples with silver nitrate of 0.1 M concentration.

Table 1 Concrete mixes

CM1	CM2	CM3
Cement: CEM 42.5N - 320kg Aggregate: 0-4mm – 840kg 4-8mm – 300kg 8-16mm – 340kg 16-32mm – 500kg Water-cement ratio: w/c = 0.50 Rate of settlement 8.0cm.	Cement: CEM 42.5N –440kg Aggregate: 0-4mm – 850kg 4-8mm – 284kg 8-16mm – 416kg 16-32mm – 378kg Water-cement ratio: w/c = 0.50 Rate of settlement 9.5cm.	Cement: CEM 42.5N –265kg Aggregate: 0-4mm – 700kg 4-8mm – 304kg 8-16mm – 384kg 16-32mm – 580kg Water-cement ratio: w/c = 0.60 Rate of settlement 17.0cm.

a) 
b) 

Figure 1 Concrete mix CM1: a) rate of settlement, b) CM1 samples - BDT

a) 

b) 

Figure 2 Concrete mix CM1: a) test chamber, b) concrete samples in the chamber

Table 2 Sampling regime

BDT (CM1, CM2, CM3)	PPT (CM1, CM2)	PPT (CM3)
3 samples after 30 days	3 samples; 2 days, 2 bars	3 samples; 2 days, 2 bars
3 samples after45 days	3 samples; 4 days, 2 bars	3 samples; 2 days, 1 bar
3 samples after 60 days	3 samples; 6 days, 2 bars	3 samples; 4 days, 1 bar
3 samples after 75 days	3 samples; 8 days, 2 bars	3 samples; 1 day, 2,5 bars
3 samples after 90 days	3 samples; 10 days, 2 bars	

a) 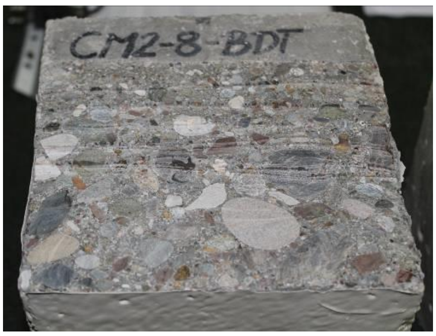

b) 

Figure 3 Concrete mix CM2; a) sample grinding by layers, b) sample tearing

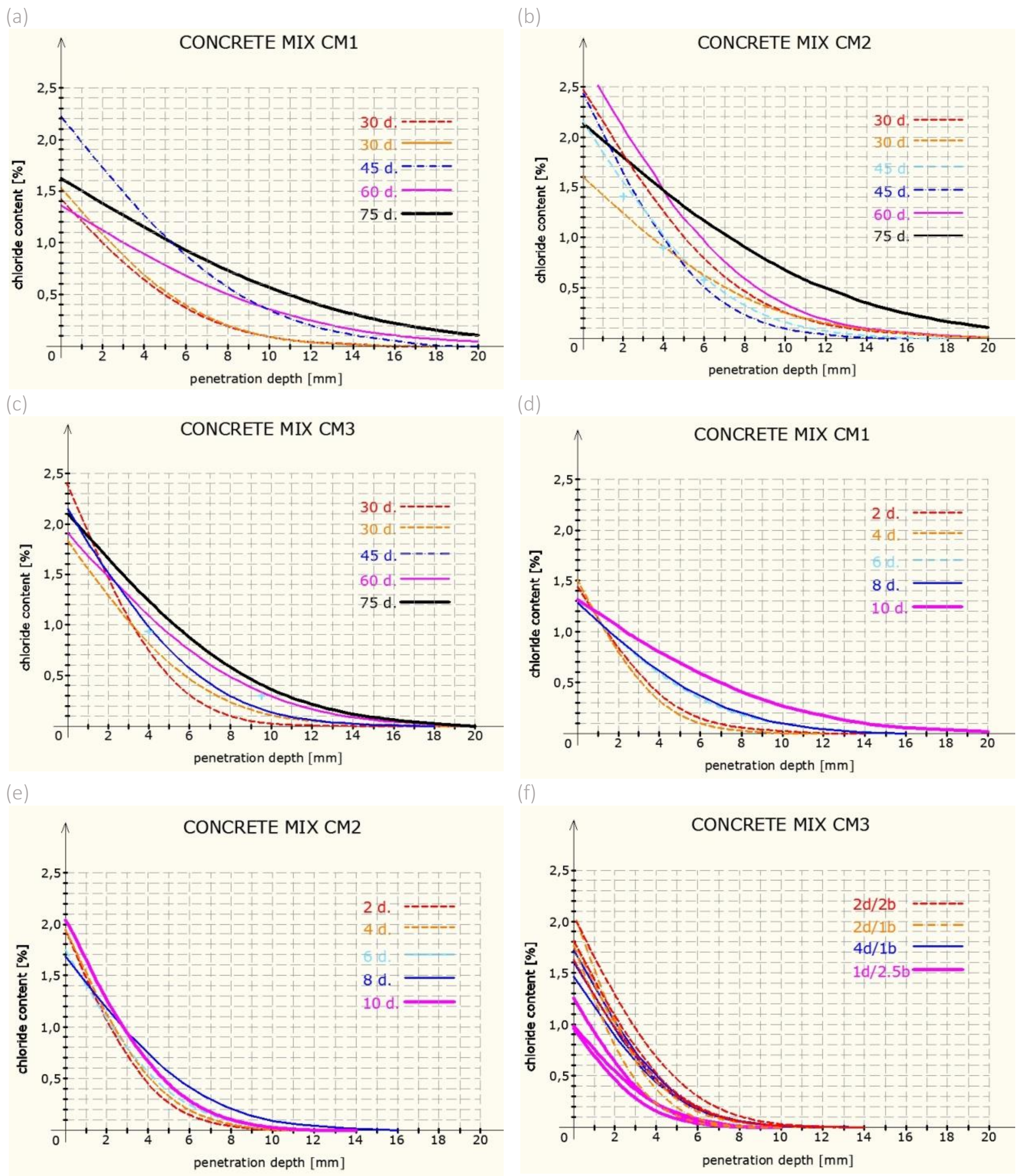

Figure 4 Chloride profiles: (a)BDT CM1; (b)BDT CM2; (c)BDT CM3; (d)PPT CM1; (e)PPT CM2; (f)PPT CM3

4. EXPERIMENTAL RESULTS AND DISCUSSION

Based on the above sampling, chloride penetration profiles were fitted using genfit function with three inputs explained in [19].

The first is an array relating the chloride concentration to the depth of the samples. The second is an array of guesses to start the curve fitting process, and the third is an array of three equations: the solution to Fick's Second Law, the partial derivative of the solution with respect to the surface concentration parameter and the partial derivative of the solution with respect to the diffusion coefficient.

From the fitted chloride profiles the diffusion coefficients and the permeation coefficients were determined as basic parameters for the development of a model of the concrete's service life which were intended to further research activities. Figure 4 shows the profiles of chloride penetration into concrete surface layers in BDT tests and PPT tests. Comparative BDT and PPT chloride profiles are presented in Figure 5 and 6.

An overview of identified average diffusion coefficients (BDT) and average penetration coefficients (PPT) is presented in Table 3.

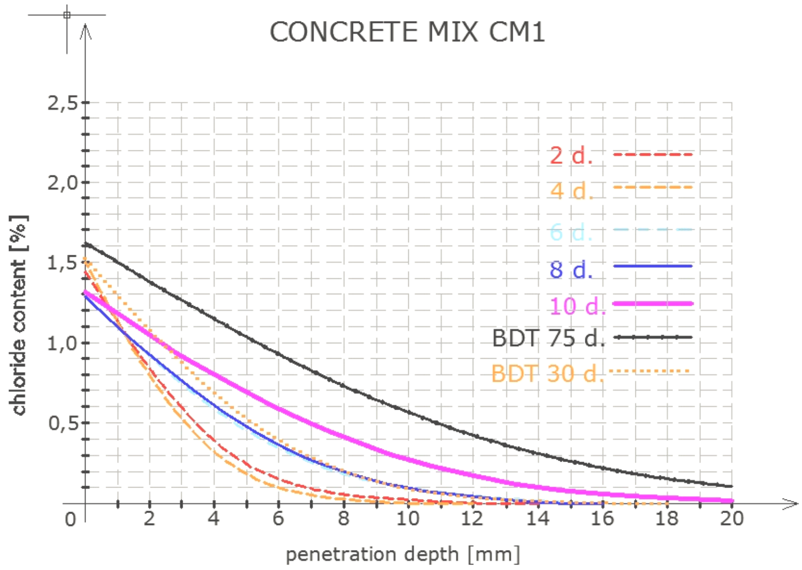

Figure 5 Comparative profiles of chloride penetration in CM1 concrete samples immersed in 16.5% salted water – BDT and samples immersed in 16.5% salted water exposed to pressure - PPT

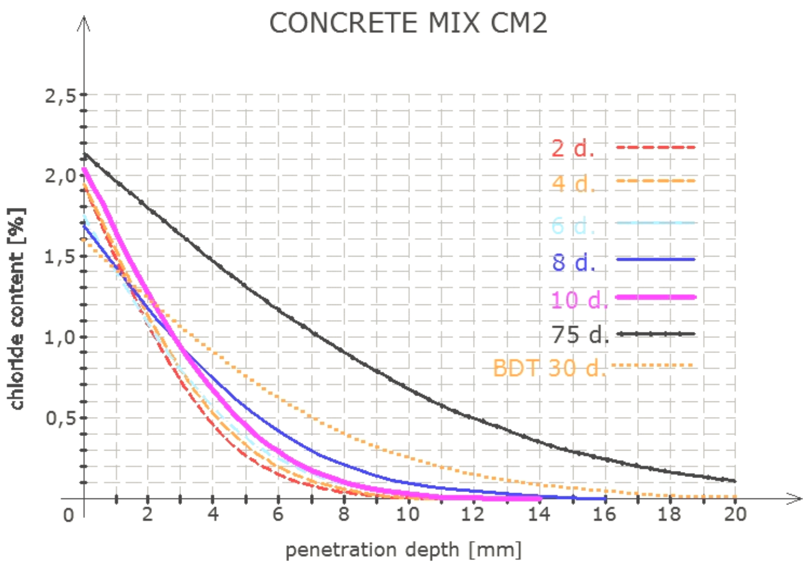

Figure 6 Comparative profiles of chloride penetration in CM2 concrete samples immersed in 16.5% salted water – BDT and samples immersed in 16.5% salted water exposed to pressure - PPT

The values for average permeation coefficients (PPT) are larger compared to the values for average diffusions coefficients (BDT). Values show a drop during the PPT tests, with two days water pressure samples having the highest values and drop depending on duration of the PPT test. The PPT/BDT ratio values vary: 5.88 – 1.84 for the CM1, and 4.24 - 1.27 for the CM2. Values during the PPT test for the CM3, with different level of the pressure and duration of the test, show that permeation coefficients values depend on the level of the pressure and drop depending on duration the PPT test. The lowest values are for PPT 10 days test. The values are close to the diffusion coefficients values obtained by BDT test.

Table 3 Ratios of average diffusion coefficients (BDT) and average permeation coefficients (PPT)

Concrete Mix	CM1		CM2		CM3	
	dif. or per. coeff. (10^{-12} m^2/s)	**PPT/BDT ratio**	dif. or per. coeff. (10^{-12} m^2/s)	**PPT/BDT ratio**	dif. or per. coeff. (10^{-12} m^2/s)	**PPT/BDT ratio**
BDT	6.102		7.468		4.177	
PPT 1d/2.5b					54.55	**13.06**
PPT 2d/2b					43.73	**10.47**
PPT 2d/1b					26.28	**6.29**
PPT 4d/1b					20.22	**4.84**
PPT 2d	35.89	**5.88**	31.67	**4.24**		
PPT 4d	10.33	1.69	18.56	**2.49**		
PPT 6d	27.43	**4.50**	15.68	4.50		
PPT 8d	22.17	**3.63**	18.74	**2.10**		
PPT 10d	11.25	**1.84**	9.51	**1.27**		

5. CONCLUSIONS

Based on the presented research results it can be concluded:

The results of chloride permeation through the concrete cover during PPT 2 days test show a significant increased difference of chloride concentration which leads to the higher values of permeation coefficients compare to BDT diffusion coefficients. The reason is filtering of the solvent and spreading into the pore space [18].

The values of the permeation coefficients vary depending on duration of the PPT test, with the highest values obtained in PPT test in duration of 2 days, with a downward trend as the test duration increases.

The values of the PPT/BDT ratios for PPT 10 days test are 1.84 (CM1) and 1.27 (CM2), close to the diffusion coefficients values obtained by BDT test. These results indicate that after the first few days of samples´ exposure to pressure, diffusion has gradually become the dominant mechanism of transport of chloride ions in this case as well. This fact allows description of the transport of chloride ions at PPT test in the same manner as in the BDT test, which permits the use of faster PPT test instead of the long BDT test for determining the resistance of the protective layer of concrete to chloride penetration.

In further research, it is necessary to check the previous findings at higher intensities of pressure.

REFERENCES

[1] EN 1990-Eurocode- Basis of structural design, CEN, Brussels, 2002.
[2] CEB: Durable of Concrete Structures, Design Guide, T. Thelford, London, 1992. p. 112.
[3] Durability Design of Concrete Structures- RILEM Report 14:(Ed. A. Sarja and E. Vesikari), Spon, London,1996. p.155.
[4] FIB (CEB-FIP), Bulletin 3 – Structural Concrete – Textbook on behaviour, Design and Performance (Updated knowledge of the CEB/FIP Model Code 1990), Vol. 3, December 1999.
[5] ACI Committee 365. 1R-42: Service-Life Prediction-State of the Art report, 2000. pp. 44.
[6] FIB (CEB-FIP), Bulletin 34 – Model Code for Service Life Design, fib, Lausanne, Switzerland, 2006, p. 116
[7] FIB (CEB-FIP): Concrete structure management: Guide to ownership and good practice, TG 5.3, February 2008.
[8] ACI 201.12R-08: Guide to durable concrete, ACI, 2008.
[9] Bohni H. (Ed.): Corrosion in reinforced concrete structures, Woodhead Publishing Limited, Abington Hall, Abington Cambridge CB1 6AH, England, 2005.
[10] Neville, A.M.: Properties of Concrete, 4th ed, Longman Ltd, 1995.
[11] Rostam, S. et al.: Durable Concrete Structures, 2nd ed., Comite Euro-International du Beton, Laussane, Switzerland/ Thomas Telford Services Ltd., 1989.
[12] Bioubakhsh, S.: The penetration of chloride in concrete subject to wetting and drying: measurement and modelling, Doctoral thesis, UCL (University College London), 2011.
[13] Bockris, J.O.M.; Reddy, A.K.N.: Modern electrochemistry, Vol 1: Ionics, 2nd ed., Plenum Press, New York, 2000.
[14] Hamilton, H.R. et al.: Permeability of concrete – Comparison of conductivity and diffusion methods, UF Project no. 00026899, University of Florida, 2007.

[15] Crank, J.: The mathematics of Diffusion, 2nd ed., Clarendon Press, Oxford, 1975.
[16] Basheer, L. et al: Assessment of the durability of concrete from its permeation properties: a review, Construction and Building Materials, V, 15, Issues 2-3, (2001), pp.93-103.
[17] Zhao, Y. et al: Penetration of Water and Chloride Dissolved in Water into Concrete under Hydraulic Pressure, Restoration of Buildings and Monuments, Vol.20, No.2 (2014), pp.117-126, DOI 10.12900/RBM 14.20.2-0012
[18] Stanish, K.D. et al.: Testing the Chloride Penetration Resistance of Concrete: A Literature Review, Research project, FHWA Contract DTFH61-97-R-00022 “Prediction of Chloride Penetration in Concrete”, University of Toronto, Toronto, Ontario, Canada, 1997.
[19] Gergely, J. et al.: Concrete diffusion coefficients and existing chloride exposure in North Carolina, North Carolina Department of Transportation, Research Project No. HWY-2004-12, 2006.

CORROSION IN CONCRETE UNDER SULPHATE AND CHLORIDE ATTACKS

Naser Kabashi[1], Cene Krasniqi[1], Anita Sadikaj[1], Skender Bublaku[1], Ali Muriqi[1], Hysni Morina[2]

[1] University of Prishtina, Faculty of Civil Engineering and Architecture, Department of Materials, Suny Hill p.n, 10 000 Prishtina, Kosovo, email: naser.kabashi@uni-pr.edu, cene.krasniqi@uni-pr.edu, anitasadikaj@hotmail.com, skender.bublaku@uni-pr.edu, ali.shmuriqi@uni-pr.edu
[2] Institute of Building Materials and Structures "IBMS", str."A.Ramadani" nr 74/2, 10000 Prishtine, Kosovo, email: hmorina@gmail.com

SUMMARY: Concrete durability continues to be a subject of challenges for design professionals and concrete specialiste. The presence of many degradation of concrete in structures lead to the changes or modifications in codes or application rules in each country. The paper is based on the actual testing data in the existing structure in cement factory, and in the laboratory using analyses of chemical effects of concrete degradation during the more than 50 years. Effects of other key factors contributing to concrete durability, in particular properties of concrete hardening, steel cover and cement layer deposit during the time were analyzed in this paper. To identify other factors in the real situation non-destructive methods were applied to structure. In scope of existing conditions solutions for repairing the existing structures were proposed, using the adequate materials and methods according the EN 1504.

KOROZIJA BETONA IZLOŽENOG DJELOVANJU SULFATA I KLORIDA

SAŽETAK: Trajnost betona i dalje je izazov za projektante i stručnjake za beton. Nazočnost mnogih degradacija betona u konstrukcijama uzrokuje promjene ili prilagodbe propisa ili pravila u svakoj zemlji. Rad se zasniva na rezultatima ispitivanja postojeće konstrukcije tvornice cementa i laboratorijskim ispitivanjima kemijskih učinaka degradacije betona tijekom više od pedeset godina. U rad su uključeni i drugi ključni faktori koji doprinose trajnosti betona, posebno svojstva očvršćivanja betona, i zaštitni sloj. Za određivanje čimbenika u stvarnoj situaciji betonskih konstrukcija upotrijebljene su nerazorne metode. Predložena su rješenja za popravak postojećih konstrukcija uz primjenu odgovarajućih materijala i metoda sukladno normi EN 1504.

1. INTRODUCTION

Concrete corrosion is the chemical, colloidal or physicochemical deterioration and disintegration of solid concrete components and structures, due to attack by reactive liquids and gases. Concrete structures are under the different several conditions in different time period which will be caused the deterioration and damages in structures. In this paper we will be focused in the effect of sulphates and chlorides in concrete corrosion.

The sulphates attack, such the more common type and typically occurs where water containing dissolved sulphate penetrates the concrete. A fairly well-defined reaction front can often be seen in polished sections; ahead of the front the concrete is normal, or near normal. Behind the reaction front, the composition and microstructure of the concrete will have changed. These changes may vary in type or severity but commonly include:

- Extensive cracking
- Expansion
- Loss of bond between the cement paste and aggregate

The chloride attack leads to corrosion of the reinforcing steel and a subsequent reduction in the strength, serviceability, and aesthetics of the structure. The affects the time for chlorides to reach the reinforcing bars and, consequently, the corrosion initiation time.
The concrete structure, in fact the low permeability and dense microstructure proved to extend the time needed for corrosion to occur.

2. SULPHATE ATTACK AND CHLORIDE PENETRATION IN CONCRETE

2.1. .SULPHATE ATTACK IN CONCRETE

The sulphate attack on concrete might show itself in different forms depending on:

- The chemical form of the sulphate
- The atmospheric environment which the concrete is exposed

When sulphates enters into concrete:

- It combines with the C-S-H, or concrete paste, and begins destroying the paste that holds the concrete together. As sulphate dries, new compounds are formed, often called ettringite.
- These new crystals occupy empty space, and as they continue to form, they cause the paste to crack, further damaging the concrete.

Developing the sulphate attack is divided in two different sources:

- Internal Sources
- External Sources

The internal Sources- are more rare but, originates from such concrete-making materials as hydraulic cements, fly ash, aggregate, and admixtures. The presence of this type is focused on the:

- Portland cement might be over-Sulphated.
- presence of natural gypsum in the aggregate.
- Admixtures also can contain small amounts of sulphates.

The external Sources- are more common and usually are a result of high-sulphate soils and ground waters, or can be the result of atmospheric or industrial water pollution.

- Soil may contain excessive amounts of gypsum or other Sulphate.
- The water be transported to the concrete elements, retaining walls, and other structure elements
- Industrial waste waters.

2.1.1. PHYSICAL PROCESS OF SULPHATE ATTACK

Developing the Sulphate Attack will result with the physical degradation of the concrete and will be presented with: The complex physicochemical process of "Sulphate attack" are interdependent as is the resulting damage.

- physical sulphate attack, often evidenced by bloom (the presence of sodium sulphates
- Na_2SO_4 and/or $Na_2SO_4.10H_2O$) at exposed concrete surfaces.
- It is not only a cosmetic problem, but it is the visible displaying of possible chemical and
- microstructural problems within the concrete matrix.

Both chemical and physical phenomena observed as sulphate attack, and their separation is inappropriate.[1],[4],[11].

2.2. CHLORIDE PENETRATION IN CONCRETE

Chloride attack is one of the most important aspects for consideration when we deal with the durability of concrete. Chloride attack is particularly important because it primarily causes corrosion of reinforcement. Statistics have indicated that over 40 per cent of failure of structures is due to corrosion of reinforcement. Due to high alkalinity of concrete a protective oxide film is present on the surface of steel reinforcement. The protective passivity layer can be lost due to carbonation. This protective layer also can be lost due to the presence of chloride in the presence of water and oxygen. In reality the action of chloride in inducing corrosion of reinforcement is more serious than any other reasons. One may understand that Sulphates attack the concrete whereas the chloride attacks steel reinforcements.

The amount of chloride required for initiating corrosion is partly dependent on the pH value of the pore water in concrete. At a pH value less than 11.5 corrosion may occur without the presence of chloride. At pH value greater than 11.5 a good amount of chloride is required.

2.2.1. PHYSICAL PROCESS OF CHLORIDE ATTACK

The presence of the chloride in real structures shows that the surface chloride content is different in different structures, but may also vary in time .For structures exposed like capillary absorption and diffusion, depending on the relative position with respect to the mean water level, wave height, tidal cycle and so on Moreover the cyclic wetting and drying (with different cycle lengths for tidal and splash zones) may cause accumulation of chloride; exposure to prevailing wind and precipitation may wash out previously absorbed chloride, and carbonation will release bound chloride. Most of these factors also depend on the concrete composition (cement type, chloride binding, absorption, permeability for water vapour). The effect is that chloride penetration is a complex function of position, environment and concrete.

3. CASE STUDY- CEMENT FACTORY "SHARR CEM"

The concrete element during the long period of the explorations time are in different condition. One of the important thing is the deposition the cement and cement powder in concrete elements, in our case the deposit in concrete support under the Rotary Kiln. The situation is presented in Figure 1.

Figure 1 Rotary Kiln-Concrete Support

The concrete elements in middle support was inspected and results with some part of presence of corrosion, more presented in corners and under the edge of concrete slab. Inspection of leg support was checked and evidence just small cracks, presented in Figure 2.

Figure 2 Cracks and corrosion in edge of slab

The effect of long period of deposition of the cement under several environmental conditions results the effect of carbonization under effect of steel corrosion. In moist environments, carbon dioxide present in the air forms an acid aqueous solution that can react with the hydrated cement paste and tends to neutralize the alkalinity of concrete (this process is known as carbonation). Also other acid gases present in the atmosphere, such as SO_2, can neutralize the concrete’s alkalinity, but their effect is normally limited to the surface of concrete.

$CO_2 + Ca(OH)_2 \xrightarrow{H_2O, NaOH} CaCO_3 + H_2O$ (1)

The carbonation reaction starts at the external surface and penetrates into the concrete producing a low pH front. The rate of carbonation decreases in time, as CO2 has to diffuse through the pores of the already carbonated outer layer. The penetration in time of carbonation can be described by equation:

d = K x t 1/n, where (2)

d- Depth of carbonization

t- Time (years)

K- Carbonization coefficient (mm/y1/2)

In our case, presence of the CO_2 content in the air increases and the carbonation rate increases drastically because the other present factors: Sulphates and chlorides present in deposit of cement, speed the degradation of the steel and in same time degradation the concrete. One of the parameter is the humidity presence in environment. The carbonation rate, and also the K-coefficient, will change passing from a wet or humid climate to a dry one. The carbonation rate may be correlated to the humidity of the environment as shown in Figure 3 [2],[5],[10],[11].

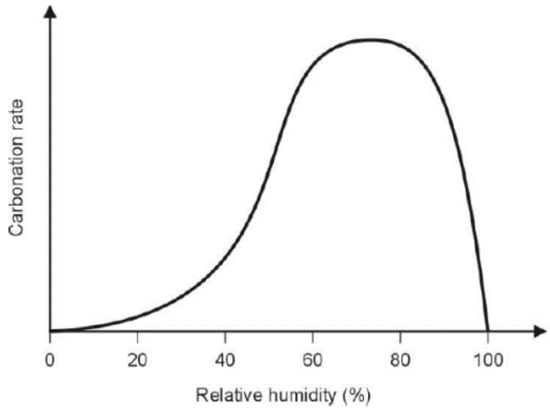

Figure 3 Schematic representation of the rate of carbonation of concrete as a function of the relative humidity of the environment [2]

The concentration of carbon dioxide in the atmosphere may vary from 0.03% in rural environments to more than 0.1% in urban environments. Comparatively high concentrations can be reached under specific exposure conditions, such as in Cement Plant. As the CO2 content in the air increases, the carbonation rate increases depend of the high humidity area.

3.1. ASSESSMENT OF THE CONCRETE IN STRUCTURE

During the visual assessment of the concrete we found just small cracks in concrete, but using the additional acoustic method with hammer impact results with some of defects in concrete. After we remove the cover layer of concrete and the results was very unsatisfactory. The corrosion of steel was in very high stage, presented in Figure 4.

Figure 4.The removing the concrete layer and corrosion of the steel

The calculation of carbonation depth using the formula d = $K \text{ x } \sqrt{t}$,

When K=9.(medium porosity),[2]; and t=50 years , result the d= 63 mm. In this way we are on the interval from previous researchers according to the Figure 5.

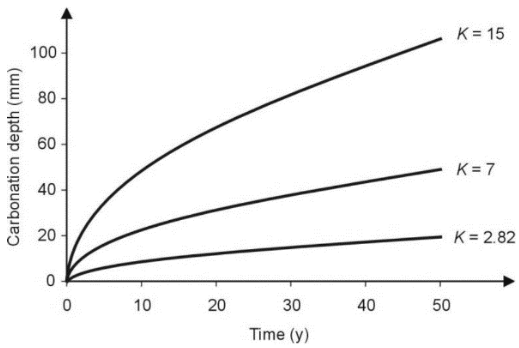

Figure 5 Carbonation induced Corrosion [2]

The situation in this case is much more serious than the one described above if chlorides are present in the concrete. The presence of a small amount of chlorides in concrete may be due to the use of raw materials (water, aggregates) containing these ions or to the penetration of chlorides from the external environment (rain, de-icing salts, etc).The presence of chlorides initiate pitting corrosion and will take place when the chloride content at the surface of the reinforcement reaches a threshold value. The concrete structures is submerged in water, or in any case the moisture content of concrete is near the saturation level, the transport of oxygen to the steel is low and the reinforcement reaches very negative potentials, and In this case, the chloride threshold is much higher, sometimes even reaching values. [1],[2],[3],[7].

4. REPAIRING THE CONCRETE STRUCTURE

Concrete spalling is usually caused by corrosion of the steel reinforcement bar embedded in the concrete, but can be caused by other ferrous elements either fully or partially embedded in the structure. Corrosion is the cause of spalling and splitting in older concrete structures.

In this case corrosion is typically caused by carbonation (which lowers the pH in the concrete) and chloride ions from salt-laden air combined with water, moisture and oxygen which creates a corrosive environment (Figure 6)

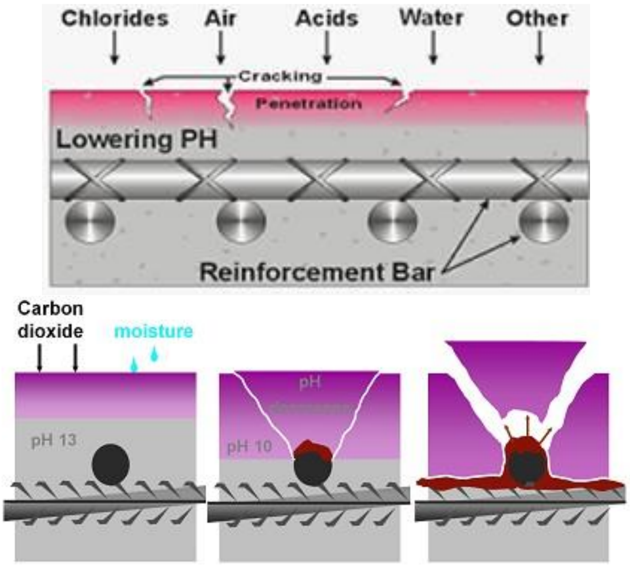

Figure 6 Factors that indicate the corrosion

Chloride induced corrosion is more common around ocean front structures (show in pink). Carbonation-induced corrosion tends to develop later and proceeds at slower rates than chloride-induced rust. In this process carbon dioxide penetrates the concrete through pores, cracks, and imperfections in the concrete. In addition by the time visible corrosion damage is noticed, structural integrity is already compromised.[2],[6],[8].

4.1. THE RETROFIT OF THE EXISTING STRUCTURE

The retrofit of the existing in this case needs the emergency repairing, and we use the two main steps;

- protecting the corrosion of reinforcement steel
- repairing the damage concrete with repairing materials

Corrosion of reinforcing steel in concrete structures, when exposed to chlorides, is a common occurrence. It is a complex phenomenon related to structural, physical, chemical and environmental considerations and in our case we used the protection with coating with MAPEFER, in this way create the protective layer (Figure 7 & Figure 8)[2][4][6].

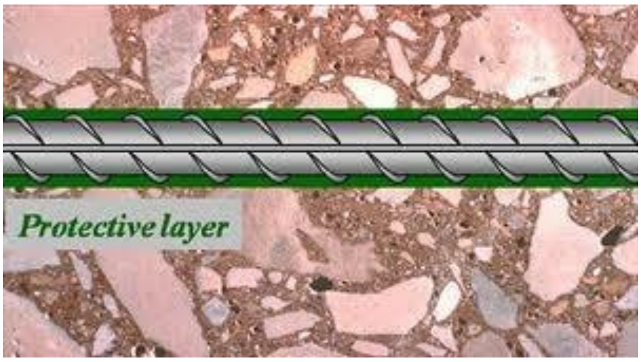

Figure 7 Protective layer of corrosion

Figure 8 Protective layer of corrosion with MAPEFER

Repairing, such second step will be applied in two layers:

- The first layer, such main layer will cover the damages in concrete including the reinforcement steel, depend of the positions is applied in thickness from 25-30 mm. The temperature was very high under the rotary kiln, about 50-60 ^{0}C and we follow eventually the presence of cracks in period of 24 hours.
- The second layer such final layer is applied in thickness about 25 mm and also we used the same methodology to follow the cracks in repairing mortar.

The repairing is done using Mapegrout T 40, and execution process is presented in Figure 9 & 10.

Final or protection layer is apply with Mapelastic, to ensure the penetration of Chlorides, Sulphates and CO_2 in repairing structures.[7],[8][9].

Figure 9 First layer of mortar

Figure10 Finalizing the repairing

4.1.1. TESTING THE REPAIRING MORTAR LAYER IN STRUCTURE

Execution of repairing works is the challenge: is the new layer or repairing layer will be in functions of repairing. In this case we use the usually method: Pull-of test and results are presented in Table 1.

Table1: Results of examinations of repairing surface

Positions-point	"1"	"2"	"3"	Criteria
Pull-of tests (kN)	1.85	2.23	2.15	> 1.5 kN

According to the EN 1542 we tested the adhesion between the new layer and existing concrete layer, and full filling the requested conditions, based on the Standards. [13].

5. CONCLUSIONS

The concrete structure or elements under the different aggressive environmental conditions will attacked from different factors and frequently in combinations of the aggressive factors. In our case study the concrete structure was very long time under different environmental conditions and no maintenance during this time. Probably the corrosion was very active and arrived in critical stage.

- Based on the research and factors we can conclude:
- Concrete in similar structures is under the various aggressive influences, the most common being:
- Atmospheric pollution- Levels of carbon and sulphur dioxide in the atmosphere have increased, and directly will attack the concrete
- Use of de-icing salts -containing chlorides has increased dramatically in the past 20 year will decrease the life time of structures

Temperature extremes. Exposed concrete may have to endure a wide range of weather conditions and temperature variations, because the temperature under Rotary Kiln is very high.

Loss of passivity – on the steel surface allows rust to form if the steel is in the presence of water and oxygen. The volume of this rust can increase by up to 12 times that of the original steel, resulting in progressive expansive stresses.

For the long-term protection, our basic approach for the typical structure must include the following:

- Any corroding reinforcement should be cleaned and then protected, preferably in an impervious alkaline environment;
- A strong homogeneous bond should be created between the repair materials and the existing concrete;
- Where necessary, repair materials should have a similar thermal expansion coefficient to the original concrete (especially at extremes of temperature):
- Water vapor diffusion resistance should be similar to that of the common concrete;
- The treatment should offer a high resistance to future carbon dioxide and chloride ion ingress;
- materials should be physically compatible with structural requirements; and
- All of the repair materials should be designed for on-site application.

REFERENCES

[1] [Raupach, M.; Buttner, T.; Concrete Repair to EN 1504-Diagnosis, Design, Principles and Practice, CRS Press,London, New York, 2014
[2] Betolini,L.;at al; Corrosion of steel in Concrete-Prevention, Diagnosis, Repair;
[3] Wiley-VCH,Weinheim,Germany,2013
[4] Campbell,P.;Learning from Construction Failures-Applied in Forensic Engineering; New York,2001
[5] Mladenovic,S.;at.al: Korozija I Zastita Betona I Armiranog Betona;SISZAM, Beograd,2008
[6] Polder,R; Peelen, W.; Use of advanced corrosion monitoring for risk based management of concrete structures; HERON Vol. 52 No. 4, 2007
[7] J.L.Smith;Y.P.Virmani; Materials and methods for corrosion control of reinforced and presstresed concrete structure in new construction; USA,2000;
[8] Kabashi,N,; at.al ; The Repairing of Concrete Walls in Structure for Water Treatment in Thermo Power Plant; Journal of Civil Engineering and Architecture, ISSN 1934-7359, USA Feb. 2013, Volume 7, No. 2 (Serial No. 63), pp. 147-152
[9] Concrete Repair Guide, ACI 546R-04, USA, 2004, p. 53
[10] Causes, Evaluation and Repair of Reapproved 1998, Cracks in Concrete Structures,

[11] ACI 224.1R-93, USA, 1998.
[12] B. Elsner, Corrosion inhibitors for steel in concrete; International Congress on Advanced Materials, Hawaii, 2000.
[13] P.H. Emmons; Concrete Repair and Maintenance, ACI Bookstore, USA, 1993.
[14] Building Code Requirements for Structural Concrete, ACI 318-05, USA, 2011, p. 503.
[15] Pull of Test Method-EN 1542, MAPEI International, UK, 2005.

THE DECISIVE ROLE OF ACIDOPHILIC BACTERIA ON MICROBIAL INDUCED CONCRETE CORROSION IN SEWERS

Cyrill Grengg[1], Florian Mittermayr[2], Guenther Koraimann[3], Mate Szabò4, Attila Demeny4, Martin Dietzel[1]

[1] Graz University of Technology, Institute of Applied Geosciences, Rechbauerstraße 12, 8010, Graz, Austria, email: cyrill.grengg@tugraz.at, martin.dietzel@tugraz.at
[2] Graz University of Technology, Institute of Technology and Testing of Building Materials, Inffeldgasse 24, 8010 Graz, Austria, email: f.mittermayr@tugraz.at
[3] University of Graz, Institute of Molecular Biosciences, Humbldstraße 50, 8010 Graz, Austria, email: guenther.koraimann@uni-graz.at
[4] Hungarian Academy of Science, Institute for Geologicaland Geochemical Research, Budarösi Street 45, H-1112 Budapest, Hungary, email: szmatez@gmail.com, demeny@geochem.hu

SUMMARY: The efficient, safe and cost-effective collection and transport of sewage is a key criteria maintaining expected sanitary standards of modern society. Within the last century microbial induced concrete corrosion (MICC) has been recognized as one of the main processes for degradation of concrete based sewer networks worldwide, triggering high economic expenses, as well as severe health and environmental concerns. This work describes a novel model intertwining biological, mineralogical and hydro-chemical factors, which in combination are ultimately controlling corrosion propagation within strongly deteriorated sewer networks. Additionally, the first location bound analyses of microbial distribution in MICC environments and its impact and interaction regarding chemical, mineralogical and material related aspects will be discussed. Arising new insights are central for the understanding of the process mechanisms of MICC and key for further technological advancements regarding material design and durability, as well as sewer network sustainability.

ODLUČNA ULOGA ACIDOFILSKIH BAKTERIJA NA KOROZIJU BETONA PROUZROČENU MIKROBIMA U KANALIZACIJI

SAŽETAK: Uspješno, sigurno i troškovno učinkovito prikupljanje i transport otpadne vode ključni su kriteriji održavanja očekivanih sanitarnih standarda modernoga društva. U prošlom je stoljeću korozija betona prouzročena mikrobima prepoznata kao jedan od glavnih procesa degradacije betonskih kanalizacijskih mreža širom svijeta iziskujući velike gospodarske troškove i pokrećući ozbiljna zdravstvena i okolišna pitanja. U radu se opisuje novi model isprepletenih bioloških, mineraloških i hidrokemijskih faktora koji u kombinaciji bitno utječu na napredovanje korozije u jako degradiranim kanalizacijskim mrežama. Dodatno, raspravlja se o prvim analizama vezanim za lokaciju mikrobiološke raspodjele u okolišu korozije betona prouzročene mikrobima i međudjelovanju kemijskih, mineraloških i materijalnih aspekata. Novi pogledi na problem bitni su za razumijevanje procesa korozije betona prouzročene mikrobima i ključ daljnjeg tehnološkog napretka vezanog za projektiranje i trajnost materijala te održivost kanalizacijske mreže.

1. INTRODUCTION

Degradation of sewage systems due to microbial induced concrete corrosion (MICC) is a frequently observed issue worldwide [1,2]. In certain cases, it can reduce the service life from expected 100 down to less than 10 years [3]. Required remediation are costly and challenging. Additionally, hazardous and odorous gas production, always associated with MICC environments, are raising civil adversity and represent a potential origin of danger for community workers. The general process mechanisms can be described as a succession of coupled redox reactions, where initial sulfate reduction proceeds within the anaerobic sediments deposited along the walls of slow flowing sewer pipes and power mains [4–6]. There, various species of sulfate reducing bacteria (SRB) steer hydrogen sulfide (H_2S) production, which is accompanied by fermentation processes producing carbon dioxide (CO_2) together with various volatile organic compounds (VOC's) [7]. H_2S and CO_2 produced emit into the atmosphere of the concrete pipes and manholes and subsequently diffuse into the condensates within the pore structure of the concrete. Due to the strongly alkaline conditions of hardened concrete (~13) initial pH reduction is caused by acid base reactions of H_2S and CO_2. Starting from pH ~9.5 H_2S re-oxidation by a succession of sulfur oxidizing bacteria (SOB) results in biogenic sulfuric acid (H_2SO_4) production and associated concrete corrosion [1,8]. This study aims to investigate the distribution of microorganisms within a strongly deteriorated sewer system that was recently described by Grengg et al. [9]. Understanding the succession, distribution and interaction of microbes involved, in combination with the chemical, mineralogical and material related aspects of concrete degradation is central for MICC control. Therefore, in situ nucleic acid staining in combination with fluorescence microscopy was applied in order to determine the distribution of microorganisms in the up to 4 cm thick corrosion layers. Cell accumulations obtained were linked to element distributions of the same areas in order to acquire extensive information. Associated mineral dissolution and precipitation were monitored using high-resolution spot analyses of mineralogical compositions throughout the corrosion fronts, together with mineralogical bulk analyses. This dataset was integrated into a new model describing the dynamic processes of advanced MICC propagation.

2. METHODS

Concrete samples from strongly deteriorated sewer manholes were extracted during remediation works. A detailed description of the system, including the mineralogical characterization of applied concrete, wastewater and pore fluid chemistry, relevant pH levels and microbes involved, has been recently described in Ref. [9]. In short, representative mineralogical compositions and hydro geochemical data of the system are shown in Table 1.

Table 1 Representative mineralogical characterization of the implemented concrete and expressed interstitial fluids within this system. Showing the mineralogical composition of non-deteriorated (CM 1 and CM 2) and strongly corroded (CM_c 1 and CM_c 2) concrete samples in wt. %, containing quartz (Qz), plagioclase (Pl), alkali feldspar (Kfs), calcite (Cal), muscovite (Ms), portlandite (Port), hornblende (Hbl), clinochlore (Clc), gypsum (Gp), bassanite (Bs), anhydrite (Anh) and X-ray amorphous phases (Amph), together with the analytical error (R_{wp}). Additionally, chemical compositions of expressed interstitial solutions (IS1, IS2 and IS3) from strongly deteriorated concrete manholes are shown together with pH and electrical conductivity (EC) (modified from [10]). For a complete dataset see Grengg et al. [9].

concrete composition														
	Sample ID	Qz	Pl	Kfs	Cal	Ms	Port	Hbl	Clc	Gp	Bs	Anh	Amph	R_{wp}
Intact	CM 1	41.3	20.2	6.7	5.4	5.2	1.8	0.0	0.7	0.9	0.0	0.0	17.9	5.79
	CM 2	42.2	19.4	4.9	6.8	4.8	2.4	1.4	1.0	0.0	0.0	0.0	17.1	5.54
Corroded	CM_c 1	27.2	6.6	2.8	0.0	0.0	0.0	0.0	0.0	25.5	1.5	15.2	11.6	7.02
	CM_c 2	31.4	14.5	0.0	0.0	0.0	0.0	0.0	0.0	43.0	0.0	0.0	10.8	7.14
interstitial fluid chemistry		pH	EC	Na^+	NH_4^+	K^+	Mg^{2+}	Ca^{2+}	Fe	Zn	Al	Cl^-	NO_3^-	SO_4^{2-}
			mS cm^{-1}	mg l^{-1}	mg l^{-1}	mg l^{-1}	mg l^{-1}	mg l^{-1}	mg l^{-1}	mg l^{-1}	mg l^{-1}	mg l^{-1}	mg l^{-1}	mg l^{-1}
	IS 1	0.9	64.2	91	152	266	243	584	2080	3.47	540	168	15.0	18139
	IS 2	1.0	102.0	2978	2994	1383	4322	551	15693	152	5720	1648	6.58	104210
	IS 3	0.7	101.0	573	210	330	990	567	2818	23	998	376	5.35	40818

The cutouts with the dimensions of several 10's of cm were embedded in a two-component epoxy resin in order to guarantee the stability of the 3.5 to 4.0 cm thick corrosion layers for further analytics. Quantitative elemental distribution images of aluminium (Al), calcium (Ca), iron (Fe), magnesium (Mg), silicon (Si) and sulfur (S) were recorded by electron probe microanalysis (EPMA) using a JEOL JXA-8200 Superprobe (JEOL, Tokyo, Japan). The wavelength-dispersive analytical mode with 15 kV acceleration voltage and a beam current of 30 nA was used. 1024 x 1024 point analyses and a step size of 3 µm yielded elemental distribution mappings of 3072 x 3072 µm. Figure 1 is stitched from 3 such images, with an overlap of 100 pixel between each mapping, resulting in a 9016 x 3072 pixel graphic. The quantification of the individual mappings in wt. % was performed against mineral standards from SPI (Pyrope for Al, Si and Fe; Anhydrite for Ca and S (SPI) (Figure 1).

Point mineralogical analyses on flat cut surface of the samples were carried out using a Rigaku DMAX-Rapid II micro diffraction system with a rotating Cu anode and micro-focus optics. X-rays were generated at 50 kV and 0.6 nA and collimated to 800 micrometres on the samples surface according to the textural and mineralogical characteristics of the analysed spots with a dwell time of 600 seconds. Corresponding spot areas were ~0.5 mm^2 as calculated from collimator sizes and incident angles. Diffraction patterns were collected onto a 2D detector and transformed to conventional intensity vs. 2theta patterns using the Rigaku 2DP data processing software and subsequently analysed using PANalytical X'Pert HighScore software (version 2.2e) and pdf-2 crystal structure database.

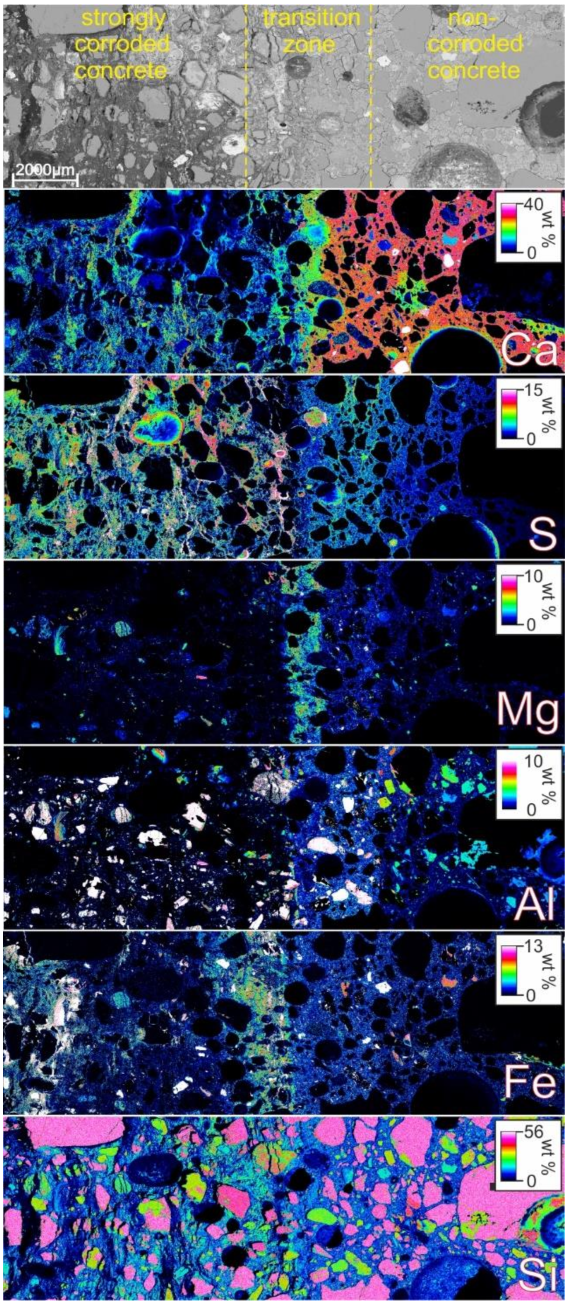

Figure 1 Displaying the element distributions throughout the corrosion front from non-corroded (right side) and strongly corroded concrete (left side). Notice the succession of S, (up to 15 wt.%), Mg (up to 10 wt.%), Al (up to 10 wt.%), and Fe (up to 13 wt.%) accumulation areas throughout the transition zone, which is characterized by decreasing Ca concentrations and massive crack formation. No decrease in Si (up to 56 wt.%) concentrations could be detected throughout the entire corrosion front.

A mixture of two dyes that show fluorescence when bound to nucleic acids (DNA and/or RNA) was applied in order to directly visualize the distribution of microbial activity. The dye consisted of SYTO9 (green fluorescence, 480 nm excitation, 500 nm emission) and propidium iodide (PI, red fluorescence, 490 nm excitation, 635 nm emission) which are components of the LIVE/DEAD BacLight bacterial viability kit (Molecular Probes). Epifluorescence microscopy images were obtained from the stained surface of the concrete sample block using a Nikon Eclipse Ti microscope with a 10x objective (Plan Fluor 10x DIC L N1). For each position three images with three different filter sets (blue 360/460 DAPI, green 480/535 FITC, red 559.5/645.5 Texas Red) and identical exposure times of 100 ms were taken. Images were analysed using NIS-Elements software (Figure 2). 1 g of deteriorated concrete was suspended in 1 mL of 0.9% NaCl solution. 0.5 mL was used to inoculate a 100 mL Erlenmayer flask containing 20 mL growth medium for the enrichment of Acidithiobacillus ferrooxidans (according to ATCC Medium 2039 and [11]). The growth medium was prepared by combining 4 volumes of sterile solution A (800 mL containing 1 g $(NH_4)_2SO_4$, 1 g $MgSO_4$ x 7 H_2O, 0.5

g KH_2PO_4, 0.1 g KCl; adjusted to pH 2.3 with H_2SO_4) and 1 volume of freshly prepared sterile solution B (200 mL containing 20 g $FeSO_4$). Microorganisms growing aerobically in this medium in a shaker-incubator (180 rpm) at 25°C for five to seven days were transferred to fresh medium to allow further enrichment of At. ferrooxidans.

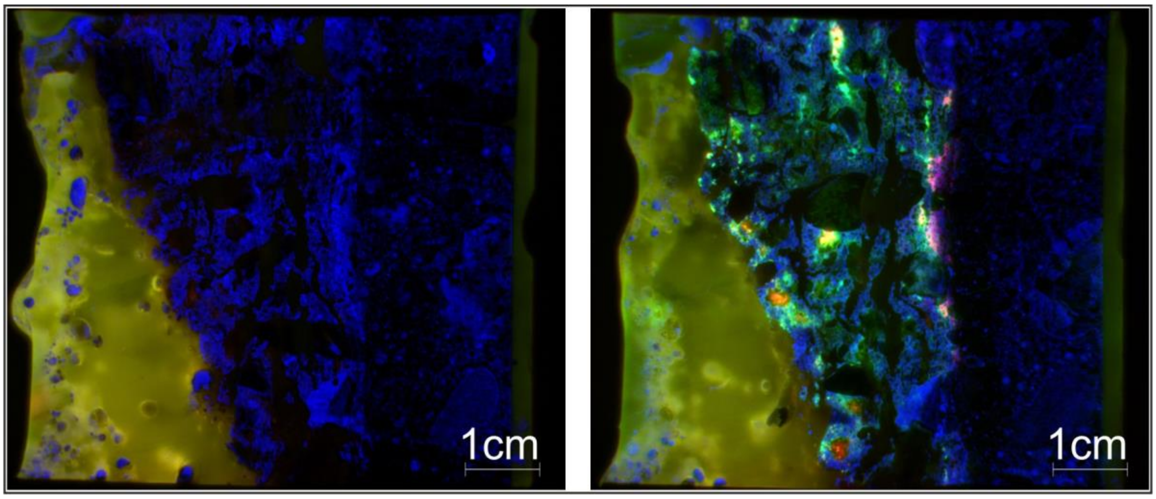

Figure 2 Fluorescent images taken from unstained (left image) and stained (right image) concrete sample block. No background fluorescence could be observed before staining (left image). Fluorescence, indicating presence of microorganisms and microbial activity is visible throughout the entire corrosion layers of the stained concrete sample block (right image) [10]

Bacterial cells from 10 mL of the cultures were harvested by a two-step centrifugation protocol. Precipitates present in the medium were removed by a 2 min centrifugation at low speed (180 x g). Cells present in the supernatant were harvested by centrifugation for 15 min at 4500 x g and washed several times with phosphate buffered saline (PBS). DNA was extracted from the cells using the Meta-G-Nome DNA Isolation Kit following to the manufacturer´s protocol (Epicentre, Madison, Wisconsin). The extracted DNA was used as a template for amplification and sequence determination of a 298 base pair 16S rDNA fragment covering variable regions V5 and V6 as recently described [9,10].

3. RESULTS

Although high sulfate resistant concrete precast elements with a compressive strength class of C30/37, C_3A free cement and a water/cement ratio of ~0.35 to withstand severe aggressive environments according to standard regulations was implemented, high corrosion rates of >1 cm yr-1 were observed (for detail see [9]).

Non-corroded concrete displayed typical pattern of silicate and carbonate aggregates of various sizes, which were embedded in a fine grained, greyish cementitious matrix. The transition to strongly deteriorated concrete was marked by a sharp horizon of a width of 2 to 3 mm at a depth of up to 3 ± 1 cm, followed by a sequence of shifting reddish/brownish and whitish layers, accompanied by massive crack formations. Element mappings of Al, Ca, Fe, Mg, S and Si throughout these corrosion fronts revealed a clearly defined element succession path controlled by diffusion and pH (Figure 1). Element accumulations were unequivocally correlated with responding pH levels, associated dissolution and precipitation of solids and with the spatially resolved distribution of microbes ([10]). The cementitious matrix of non-corroded concrete was dominated by Ca and Si rich phases like portlandite ($Ca(OH)_2$) and calcium silicate hydrates (C-S-H phases), framing siliceous and carbonatic aggregates. The transition zone (TZ) between non-corroded and strongly affected concrete was characterized by a drop in pH from 13 to below 1 (see IS, Table 1), causing dynamic dissolution and precipitation, determined by single mineral stability ranges which could be observed in element distributions and high resolution spot analyses of the mineralogical compositions. The inner border of the TZ was marked by decreasing Ca concentrations and first S incorporation, mainly along grain boundaries and cracks. Subsequently, an accumulation zone of predominately Mg, linked to brucite ($Mg(OH)_2$) precipitates established which was cut off by a sharp (< 0.1 mm) Al rich layer, consisting mainly of gibbsite ($Al(OH)_3$), followed by the first Fe accumulation zone (Figure 1). Ferric iron (Fe^{3+}) containing precipitates were identified as goethite (α-FeO(OH)), lepidocrocite (γ-FeO(OH)) and parabutlerite ($Fe(SO_4)(OH)\cdot 2H_2O$) by high resolution Micro-XRD analyses (Figure 3) [10]. The outermost 2-3 cm of the deterioration layer were characterized by alternating filamentary S and Ca accumulation zones, representing sulfate salts, e.g. gypsum, anhydrite and bassanite, and Fe accumulation zones, while complete depletion of Mg and Al was observed (Figure 2; Table 1). Throughout the entire corrosion front, no change in Si abundances within the aggregates could be observed, while partly depletion of Al, Mg and Fe occurred within smaller mineral aggregates, e.g. feldspar and muscovite, indicating the resistivity of quartz against acid corrosion [10].

Opposed to current hypothesis [12,13], microorganisms were not limited to the uppermost layers of the deteriorated concrete, but were distributed throughout the entire corrosion front. Three areas of high microbial activities could be subcategorized using epifluorescence imaging: (i) clusters of high intensities within the first 0.5 cm from the surface, (ii) clusters at an average depth of about 2.0 to 2.5 cm and, (iii) clusters located directly at the transition zone to non-corroded concrete at a depth of about 3.5 to 4.0 cm (Figure 2). Bacteria, enriched from the deteriorated concrete were identified as At. Ferrooxidans and At. thiooxidans by DNA extraction, amplification and subsequent comparison to a template for amplification and sequence determination of a 298 base pair 16S rDNA fragments, encompassing V5 and V6 variable regions [9,10].

Sample ID	Qtz	Fsp	Cal	Ms	Port	Ett	Gp	Anh	Lpdc	Pbl	Gth	Gbs	Clc
P4_1	x	x	x	x	x	x	x						
P4_2	x	x		x			x		x		x	x	
P4_3	x						x			x	x		
P4_4	x	x					x			x			
P4_5	x	x		x			x						
P4_6	x	x		x			x			x			
P4_7	x	x		x			x	x					x
P4_8	x	x		x			x						
P4_9	x	x					x						
P4_10	x	x					x						

Figure 3 High resolution spot analyses of mineralogical composition throughout a corrosion front from intact concrete (left side) to strongly deteriorated concrete (right side) [10]

While At. thiooxidans are widely approved as one of the central species within advanced MICC [14–16], the role and impact of At. ferrooxidans on concrete corrosion is still under debate. Those autotroph SOB bacteria have a growth optimum between pH 1.5 and 2.5 and the ability to switch between an aerobic and an anaerobic metabolism. Under aerobic conditions oxygen is used as electron acceptor and energy is obtained by the oxidation of ferrous iron to ferric iron or reduced sulfur compounds to sulfuric acid. Under anaerobic conditions reduced sulfur compounds are used as the electron donor, while ferric iron serves as the electron acceptor [17]. These flexible metabolisms could favor the growth of At. ferrooxidans within the deeper corrosion layers in which oxygen support is expected to be limited [12], while At. thiooxidans dominate the outermost regions. Additionally, corresponding zones of high microbial activity and iron accumulation zones within the interior of the corrosion layers support this model. There, iron was utilized by At. ferrooxidans, which used ferric iron as the electron acceptor to form ferrous, iron during oxidation of reduced sulphur speciation and associated in situ acid production.

4. CONCLUSION

The novel model described in this study, intertwined biological, mineralogical and hydro geochemical factors, which resulted in a dynamic micro-system, dominated by ongoing mineral dissolution and re-precipitation and subordinated microbial distribution, ultimately controlled by pH and aqueous diffusion (Figure 4) [10]:

- Opposed to current opinion, microbial activity was not limited to the surface near, oxygen rich corrosion layer, but expanded throughout the entire deterioration layer up to a depth of 4 cm. No decrease in microbial activity with depth was identified, but high cell density at and close to the corrosion front was detected.
- At. ferrooxidans was isolated from the deteriorated concrete and could be linked with Fe accumulation zones within the deeper, anoxic to anaerobic corrosion layers, thereby proving in

situ H_2SO_4 production at and close to the corrosion front thus strongly affecting corrosion dynamics. Accordingly, the central role of iron regarding bioreceptivity and associated durability of concrete affected by MICC should be emphasized.

- Single element distributions were controlled by pH and diffusion of dissolved components, creating a dynamic system of ongoing dissolution and precipitation of solids throughout the progressing corrosion front.
- Ultimately, we propose a model where At. thiooxidans dominated the oxygen rich zone close to the surface, while At. ferrooxidans adopted the pore spaces within deeper, anaerobic, corrosion layers. In fact, described in situ acid production at and close to the corrosion front has to be recognized as one central factor, steering high corrosion rates of about 1 cm yr-1 and associated failure of great parts of the sewer system after a service life of 10 years.

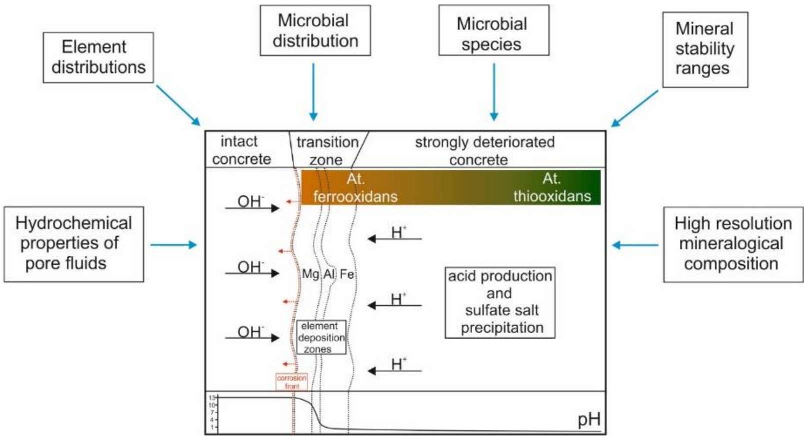

Figure 4 pH and diffusion controlled model showing the succession of element accumulations together with associated microbiological activity within a progressive corrosion front (from the left to the right side), together with the relevant mineralogical, biological and material related inputs. The transition zone is characterized by strongly decreasing pH levels from 13 to below 1 and associated element accumulation zones. Mg accumulations indicate pH >9, while Al deposition is associated with a strong pH decrease from 9 to 4. Fe deposition zones can be linked with the anaerobic metabolism of At. ferrooxidans within the deeper corrosion layers, where Fe^{3+}, present in iron hydroxides and sulfates, e.g. Lpdc, Gth, Pbl, gets reduced to Fe^{2+} during oxidation of reduced sulfur compounds at strongly acidic conditions (modified after [10])

ACKNOWLEDGMENTS

The authors gratefully thank the Graz University of Technology (Austria) scientific grant program for financial support, as well as the scientific input of Josef Tritthart and Florian Konrad. Special thanks to Peter Rappold and the Department of Water Resources Management, Styria, as well as to Heinz Lackner and the Department of Energy, Residential Constructions and Technology, Styria, for their financial support. Mineralogical and chemical analyses were carried out at the NAWI Graz Central Lab for Water, Minerals and Rocks.

REFERENCES

[1] B.R.L. Islander, J.S. Devinny, A. Member, F. Mansfeld, A. Postyn, H. Shih, Microbial ecology of crown corrosion in sewers, J. Environ. Eng. 117 (1991) 751–770.

[2] C. Grengg, M. Kiliswa, F. Mittermayr, M. Alexander, Microbially-induced Concrete Corrosion- A worldwide problem, in: Microorg. Mater. Interact., 2016: pp. 1–19.

[3] H.S. Jensen, PhD thesis; Hydrogen sulfide induced concrete corrosion of sewer networks, Aalborg University, 2009.

[4] A. Jayaraman, F.B. Mansfeld, T.K. Wood, Inhibiting sulfate-reducing bacteria in biofilms by expressing the antimicrobial peptides indolicidin and bactenecin, J. Ind. Microbiol. Biotechnol. 22 (1999) 167–175. doi:10.1038/sj.jim.2900627.

[5] J. Herisson, E.D. van Hullebusch, M. Moletta-Denat, P. Taquet, T. Chaussadent, Toward an accelerated biodeterioration test to understand the behavior of Portland and calcium aluminate cementitious materials in sewer networks, Int. Biodeterior. Biodegradation. 84 (2013) 236–243. doi:10.1016/j.ibiod.2012.03.007.

[6] M. Alexander, A. Bertron, N. De Belie, Performance of Cement-Based Materials in Aggressive Aqueous Environments, 1st ed., Springer, Ghent, 2013. doi:10.1007/978-94-007-5413-3.

[7] T. Hvitved-Jacobsen, J. Vollertsen, A.H. Nielsen, Sewer Processes - Microbial and Chemical Process Engineering of Sewer Networks, 2nd ed., CRC Press, London, 2013.
[8] M. O'Connell, C. McNally, M.G. Richardson, Biochemical attack on concrete in wastewater applications: A state of the art review, Cem. Concr. Compos. 32 (2010) 479–485. doi:10.1016/j.cemconcomp.2010.05.001.
[9] C. Grengg, F. Mittermayr, A. Baldermann, E. Böttcher, M, A. Leis, G. Koraimann, et al., Microbiologically induced concrete corrosion: A case study from a combined sewer network, Cem. Concr. Res. 77 (2015) 16–25.
[10] C. Grengg, F. Mittermayr, G. Koraimann, M. Szabo, A. Demeny, M. Dietzel, The decisive role of acidophilic bacteria in concrete sewer networks: A new model for advanced microbial concrete corrosion, Rev. (2016).
[11] M.P. Silverman, D.G. Lundgren, Studies on the chemoautotrophic iron bacterium ferrobacillus ferrooxidans, J. Bacteriol. 77 (1959) 642–647.
[12] S. Okabe, M. Odagiri, T. Ito, H. Satoh, Succession of sulfur-oxidizing bacteria in the microbial community on corroding concrete in sewer systems, Appl. Environ. Microbiol. 73 (2007) 971–980. doi:10.1128/AEM.02054-06.
[13] H. Satoh, M. Odagiri, T. Ito, S. Okabe, Microbial community structures and in situ sulfate-reducing and sulfur-oxidizing activities in biofilms developed on mortar specimens in a corroded sewer system., Water Res. 43 (2009) 4729–39. doi:10.1016/j.watres.2009.07.035.
[14] A.L. Ling, C.E. Robertson, J.K. Harris, D.N. Frank, C. V Kotter, M.J. Stevens, et al., High-resolution microbial community succession of microbially induced concrete corrosion in working sanitary manholes, PLoS One. 10 (2015). doi:10.1371/journal.pone.0116400.
[15] A. Yousefi, A. Allahverdi, P. Hejazi, Accelerated biodegradation of cured cement paste by Thiobacillus species under simulation condition, Int. Biodeterior. Biodegradation. 86 (2014) 317–326. doi:10.1016/j.ibiod.2013.10.008.
[16] A.L. Ling, C.E. Robertson, J.K. Harris, D.N. Frank, C. V Kotter, M.J. Stevens, et al., Carbon Dioxide and Hydrogen Sulfide Associations with Regional Bacterial Diversity Patterns in Microbially Induced Concrete Corrosion, Environ. Sci. Technol. 48 (2014) 7357–7364. doi:10.1021/es500763e.
[17] D.E. Rawlings, T. Kusano, Molecular Genetics of Thiobacillus ferrooxidans, Microbiol. Rev. 58 (1994) 39–55.

RELATIVE IMPORTANCE OF CORROSION RATE AND EXPOSURE CONDITION ON THE PRACTICAL USE OF NEW ENVIRONMENTALLY FRIENDLY BINDERS

Matteo Stefanoni[1], Ueli Angst[1], Bernhard Elsener[1,2]

[1] ETH Zurich Faculty of Civil Engineering, Institute for Building Materials, Stefano-Franscini-Platz 3, CH-8093 Zürich, Switzerland, email: matteost@ethz.ch, uangst@ethz.ch, elsener@ethz.ch
[2] University of Cagliari, Department of Chemical and Geological Science, I-09100 Cagliari

SUMMARY: Lowering the clinker content of concrete using SCMs can contribute significantly to reduce the energy consumption and the CO_2 emissions of concrete. Uncertainty about long-term durability, especially carbonation induced corrosion, is the main factor limiting the practical use: containing less CaO they have less capacity to neutralize CO_2 and thus higher carbonation rates, which may lead to premature corrosion of steel reinforcement. Results in literature concerning corrosion of steel in carbonated concrete are rare and refer mostly to ordinary Portland cement. Generally, a trend to higher corrosion rates at higher relative humidity was found. To estimate the service life of concrete structures made with new blended cements, corrosion rate data are urgently needed, because the so called "corrosion propagation stage" might significantly contribute to the total service life. Corrosion rate has to be measured for different blended cements, w/c ratios and exposure conditions. To collect data of corrosion rates in a reasonable time, a new experimental set up has been designed. The new test setup consists of small (8 x 8 cm) and thin (6 mm) mortar samples instrumented with reference electrode, 5 steel wire electrodes and a stainless steel grid counter electrode. The thin sample allows full carbonation within 3 weeks (4% CO_2). Parameters that can be measured are electrical resistivity, corrosion potential, corrosion rate and oxygen diffusion. These results should allow to investigate the mechanism, particularly the kinetics, of carbonation induced corrosion. The first results show that new blended cements could be more susceptible to corrosion in certain exposure conditions. Depending on the environment the steel dissolution rate can vary by a factor of 200, from < 0.1 µm/year at 50 % RH, to 20 µm/year in wet conditions. To define the application limits of new binders, the interaction with variable exposure conditions has to be carefully evaluated.

RELATIVNA VAŽNOST BRZINE KOROZIJE I UVJETA IZLOŽENOSTI NA PRAKTIČNU UPOTREBU NOVIH VEZIVA PRIJATELJSKIH ZA OKOLIŠ

SAŽETAK: Smanjenje sadržaja klinkera u betonu uz upotrebu upravljanja opskrbnim lancem (engl. supply chain management, SCM) može znatno pridonijeti smanjenju potrošnje energije i emisije CO_2. Glavni faktor ograničenja u praktičnoj upotrebi nesigurnost je povezana s dugoročnom trajnošću, posebno pri koroziji prouzročenoj karbonatizacijom: što je manje CaO betoni imaju manju sposobnost neutralizacije CO_2 i stoga imaju veću brzinu karbonatizacije što može dovesti do prerane korozije čelične armature. U literaturi su rezultati o koroziji čelika u karbonatiziranom betonu rijetki i uglavnom se odnose na obični portlandski cement. Općenito, utvrđen je trend većih brzina korozije pri većoj relativnoj vlažnosti. Da bi se procijenio uporabni vijek betonskih konstrukcija izvedenih s novim mješavinama cemenata nužno su potrebni podatci o brzini korozije jer bi tzv. stupanj napredovanja korozije mogao znatno doprinijeti određivanju ukupnog uporabnog vijeka. Brzina korozije mora se mjeriti za različite mješavine cemenata, vodocementne omjere i uvjete izloženosti. Da bi se podatci o brzini prikupili u prihvatljivom vremenu projektiran je novi eksperimentalni sklop. On se sastoji od malih (8 x 8 cm) i tankih (6 mm) mortnih uzoraka opremljenih referentnom elektrodom, 5 čeličnih žičanih elektroda i mreže elektroda brojača od nehrđajućeg čelika. Tanki uzorci omogućuju da do pune karbonatizacije dođe unutar tri tjedna (4 % CO2). Mogu se mjeriti parametri kao što su električna otpornost (impedancija), korozijski potencijal, brzina korozije i difuzija kisika. Ti rezultati trebaju omogućiti istraživanje mehanizma, posebno kinetike korozije prouzročene karbonatizacijom. Prvi rezultati pokazuju da su nove mješavine cemenata podložnije koroziji u nekim uvjetima izloženosti. Ovisno o okolini, brzina raspada čelika može se kretati u rasponu od < 0,1 µm/godina pri 50 %-tnoj relativnoj vlažnosti do 20 µm/godina u vlažnim uvjetima, tj. mijenjati se s faktorom 200. Da bi se odredile granice primjene novih veziva mora se brižljivo vrednovati međudjelovanje s različitim uvjetima izloženosti.

1. INTRODUCTION

In the past years environmental issues in the building industry have become an increasingly hot topic. According to *Trends in global CO_2 emissions: 2015 Report* [1] cement production accounts for roughly 8% of global CO_2 emissions. On the raw materials side lowering the clinker content of cements using supplementary cementitious materials (SCM) can contribute significantly to reduce the energy consumption and the CO_2 emissions of building materials, thus they become more environmental friendly. Uncertainty about durability, especially carbonation-induced corrosion, is the main factor limiting the practical use of these blended cements. As a matter of fact, the carbonation rate is faster for blended cements [2] due to their inherent chemical properties, in particular the reduced pH buffering capacity (lower calcium hydroxide content):

- Lower amount of calcium hydroxide formed during the hydration reaction [3], as consequence of a reduced amount of CaO with respect to Ordinary Portland Cement (OPC 65% CaO), variably down to 40% [4-6], depending on the type and amount of substituents;
- Consumption of calcium hydroxide [3,7,8] in presence of SiO_2-rich components by the pozzolanic reactions.

The carbonation rate, viz. the penetration of the carbonation front in the concrete matrix, is faster in case of blended cements as documented in comprehensive reviews of data collected since 1968 for ground granulated blast-furnace slag (GGBS) [9] and for fly ash concrete [10].

Carbonation also influences differently the microstructure properties depending on the type of binder. Carbonation leads to a reduction in total porosity [11-15] which is ascribed to the positive difference of molar volume between the calcium carbonate formed and the initial hydration products. However at lower clinker contents a shift of the capillary porosity to coarser distribution was reported [15-19], possibly due to the disappearance of the clusters of CH crystals replaced by a packing of calcium carbonate crystals leaving new voids. These changes in the material pore size distribution can be of major importance in defining the adsorption and diffusion properties of water and oxygen in the concrete matrix, influencing the corrosion rate as a consequence.

Considering the schematic representation of the service life (Figure 1), increasing addition of SCMs leads to a shorter induction period for the onset of corrosion (depassivation) and it becomes obvious that the corrosion rate of steel in carbonated concrete becomes a critical factor for reaching the expected service life of a structure. However, results in literature on the corrosion rate of steel in carbonated concrete are rare and refer mostly to ordinary Portland cement.

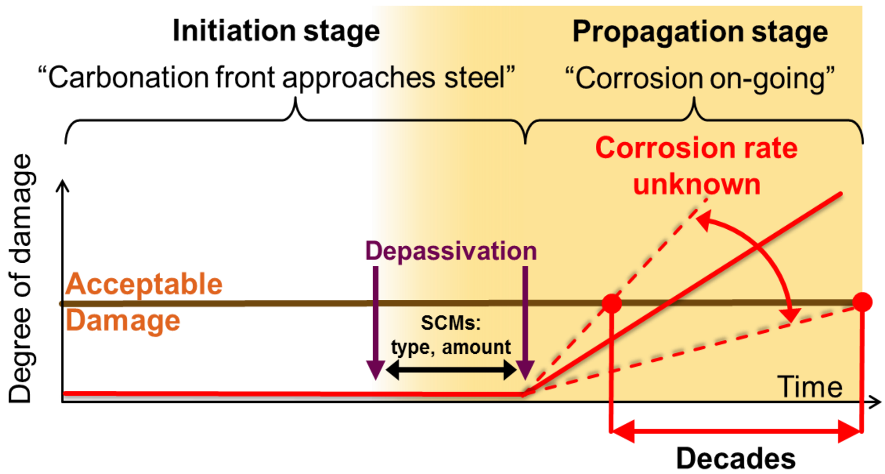

Figure 1 Schematic representation of the service life of a reinforced concrete structure (Tuutti diagram) showing the importance of the propagation-stage of corrosion in carbonated concrete.

For service life prediction of concrete structures with new, blended cements, corrosion rate data are urgently needed because the so-called "corrosion propagation stage" might be a significant part of the total service life. Being the corrosion process a system property, influenced both by the material and the environment, the combination of different materials (composition and mix design) together with different exposure conditions (constant RHs and wet-dry cycles) have to be studied.

The final objective is to evaluate the application limit, case by case, and develop guidelines for the use of new blended cements. In this paper an approach for carbonated mortars is presented, aiming to achieve fast testing of corrosion properties, thanks to an innovative sample setup. The relative importance of type of binder, w/c ratio and exposure condition, with respect to corrosion propagation rate, is evaluated.

2. MATERIALS AND METHODS

2.1. SAMPLE DESIGN

To be able to collect data of corrosion rate of steel in carbonated mortar in a reasonably short time, a new experimental set up has been designed. The new test setup consists of small (8 x 8 cm) and thin (6 mm) cement mortar sample instrumented with a reference electrode, 5 steel wire electrodes and a stainless steel grid counter electrode (Figure 2). The thin sample allows rapid full carbonation (max 3 weeks in 4% CO_2) and rapid equilibration of environmental humidity (checked by the sample weight). Parameters that can be measured are electrical resistivity of the mortar, corrosion potential and corrosion rate (LPR measurements) of the steel wires, oxygen diffusion and consumption rate. From these data the mechanism of steel corrosion in carbonated concrete made of different blended cements can be evaluated.

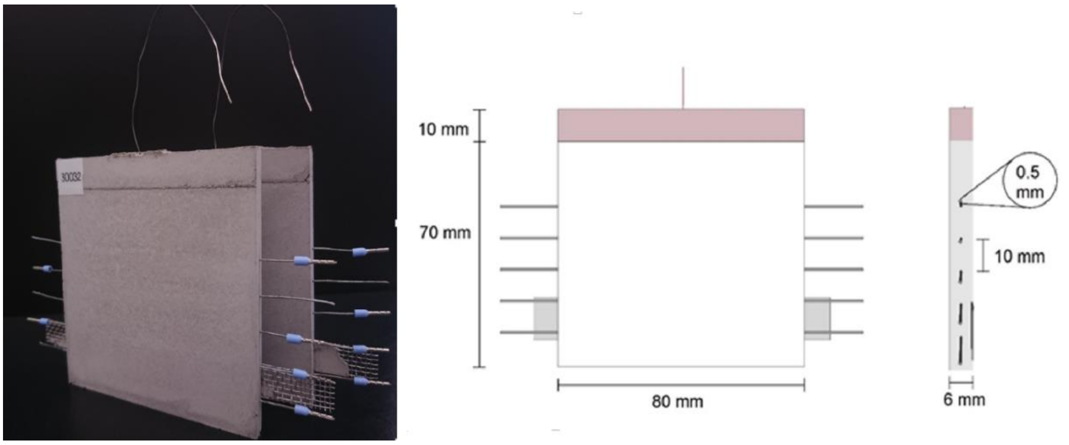

Figure 2 Sample after casting and hardening (left) and schematic representation of dimensions (right).

2.2. MATERIALS

For the realization of the mortar samples Holcim Optimo 4 cement (CEM II/B-M (T-LL) 42,5) and Holcim Normo 5R (CEM I 52,5 R) were used. The mix design was chosen to allow the best fluidity while maintaining a high stability of the cementitious suspension. The w/b ratios tested were 0.4, 0.5 and 0.6; the sand/binder ratio was 2 and the sand had a maximum particle diameter of 1mm. A poly-carboxylate ether superplasticizer with de-foaming agent was added to the mix in order to increase the fluidity and be able to fill the mould, the amount was chosen in order to achieve a visually similar fluidity of the mortars.

2.3. CARBONATION PROCEDURE

The samples were carbonated in a carbonation chamber at room temperature, 65% relative humidity and 4% CO_2 concentration in the controlled atmosphere. The time required for complete carbonation was:

- 2 weeks for CEM II mortars;
- 3 weeks for CEM I mortars.

Complete carbonation was ensured by the phenolphthalein test.

2.4. EXPOSURE CONDITIONS

The corrosion behavior of the carbonated samples was studied in different exposure conditions. The first tests were performed in controlled and constant environments (50% and 95% relative humidity and 20 °C). Another series of experiments studied the response to wet and dry cycles, samples have been provided with a silicon sealed wall for the ponding solution (Figure 3). The cycles have been carried out by placing 3 mm of water on the samples and let it adsorb, the parameters have been monitored over time from the water adsorption to the drying of the sample.

2.5. ELECTROCHEMICAL TESTS

All the electrochemical experiments were performed using a potentiostat Metrohm Autolab PGSTAT30. The embedded Ag/AgCl sensor was always used as reference electrode and its reference potential was checked by means of an external Ag/AgCl reference electrode. One steel wire was used as working electrode and the stainless steel grid was used as counter electrode depending on the test performed. The measurements were repeated over time for each exposure condition.

Corrosion rate: the instantaneous corrosion current density was determined by polarization resistance measurements. The polarization resistance Rp of the single steel wires was measured with the stainless steel grid as counter electrode at ± 10 mV around the open circuit potential with a scan rate of 0.1 mV/s. The IR-drop in the mortar was taken into account indirectly. Impedance measurements were performed right before each polarization resistance test, and the ohmic resistance obtained was subtracted from the result each time at the end of the tests.

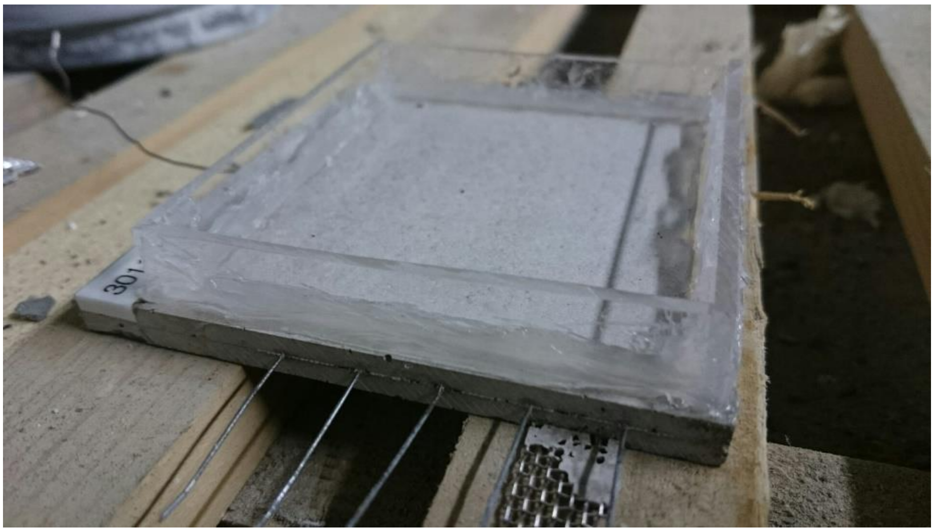

Figure 3 Samples used for wet and dry cycles.

Linear polarization measurements allowed the determination of an electrical resistance R_p' that is the sum of the polarization resistance R_p of the steel wires and the ohmic resistance R_Ω between working electrode and counter electrode. Electrochemical impedance spectroscopy tests were performed in order to measure R_Ω. The values of R_Ω were subtracted from the total resistance R_p' to get the real polarization resistance values.

The corrosion rate was then calculated using the Stern Geary relation (1):

$$i_{corr} = \frac{B}{R_p} \tag{1}$$

Where R_p is the polarization resistance and B is a parameter depending on the electrochemical properties of the considered system; for iron in actively corroding state a value of 26 mV is commonly used.

3. RESULTS

At 50% RH the corrosion rate both of CEM I and CEM II at all w/c ratios was lower than 0.01 µA/cm^2 (lower than 0.1 µm/year) (Figure 4). Initially the corrosion rate slightly increased over time, together with the corrosion potential shifting to slightly more negative values for both cement types.

At 95% RH corrosion rates were higher for samples made with blended cement and at higher w/c ratio, but overall found to be lower than 0.1 µA/cm^2 (ca. 1.2 µm/year) (Figure 4). Also in this case, in the first period of exposure, the corrosion rate increased with time and the corrosion potential decreased, for both cement types.

Samples exposed to wetting showed a very rapid decrease of the open circuit potential and of the polarization resistance (Figure 5), the maximum value of the corrosion rate after wetting was 1.7 µA/cm^2 (ca. 20 µm/year) (Figure 4). The process of drying out took much more time, at the end the corrosion potential and polarization resistance reached values similar to 50% RH (Figure 5). The maximum corrosion rate in the wet state was not influenced by the w/c ratio. On the contrary, the type of binder did play a role: for CEM II higher corrosion rates were measured in the wet phase and it was also noticed that CEM II showed a faster drying.

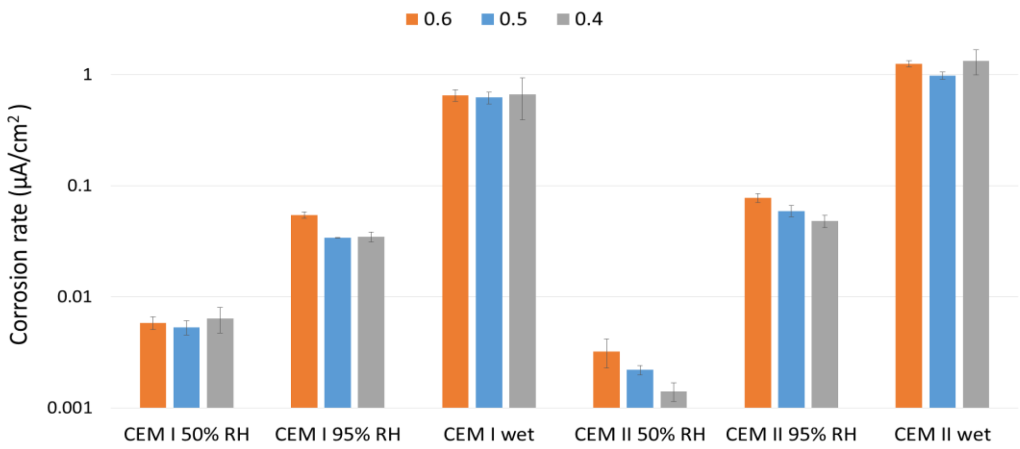

Figure 4 Corrosion rates measured for every exposure condition, w/c ratio and type of binder (for wet-dry cycles the maximum value for each cycle was taken).

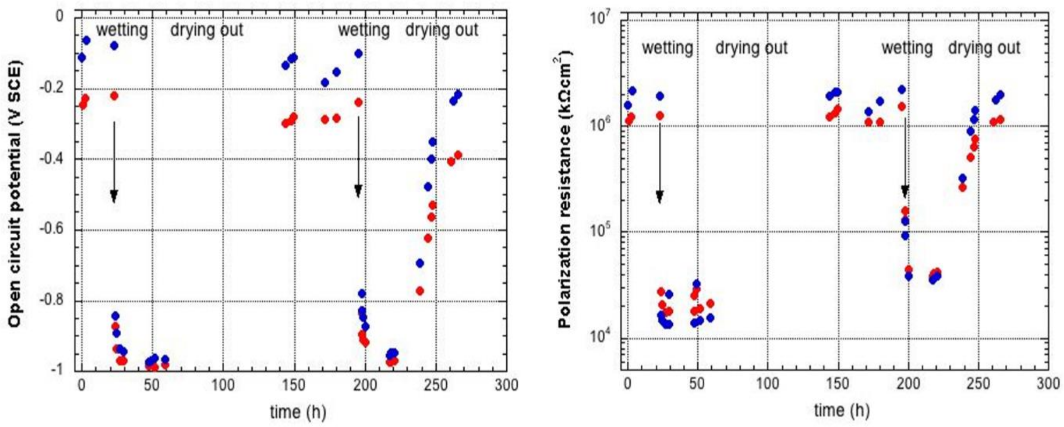

Figure 5 Variation of the open circuit potential and the corrosion rate during wet-dry cycles (measurements on two steel wires per sample).

4. DISCUSSION

The influence of the cement type and w/c ratio on the corrosion rate could be influenced by the pore size distribution of the carbonated mortars (see introduction section). Being corrosion an electrochemical process that needs an electrolyte layer, on the steel surface, to take place, the condensation behaviour of water could be a possible limiting factor in non-saturated conditions. At 50% RH CEM I samples show a higher corrosion rate than samples made with blended cement (Figure 4) in agreement with data presented in the literature [20]. One possible explanation could be found in the finer pore structure of CEM I carbonated mortars that would allow some water condensation also at such low relative humidity. At 95% RH the dissolution rate is higher in CEM II mortars (Figure 4). Also this fact might possibly be attributed to the pore structure, if it is coarser in carbonated blended cement: a higher amount of large pores would increase the amount of free water present at high relative humidity and increase the corrosion rate as a consequence.

The highest corrosion rates were found during wet and dry cycles (exposure class XC4). In the wet periods maximum values as high as 1.7 µA/cm^2 were measured (Figure 4). The corrosion rate in the wet phase is up to 20 times higher than at constant 95% RH. Such high corrosion rates of about 20 µm/year can be critical and markedly limit the service life of a structure. At the end of the drying phase, which seems to be faster in the case of CEM II mortar, perhaps due to a more open pore structure, the dissolution rate turns back to negligible values.

The better durability performance claimed for blended cements (associated to a finer pore structure and lower permeability [11, 21-23]) is perhaps relevant only in a non-carbonated state. After carbonation blended cements have been found to develop a coarser pore size distribution that might be influencing the corrosion behaviour of the embedded steel, leading to higher dissolution rates in a humid/wet environment (Tab. 1). In wet conditions (XC4) steel in carbonated mortars made of CEM II showed a corrosion rate higher by a factor up to 2 compared to mortar made of CEM I. Note that the reasoning regarding the limiting mechanism is only based on from literature data, as no porosity data of the tested samples are available yet. Further research is therefore needed, and currently ongoing.

Keeping in mind that depassivation of steel in blended cements occurs at shorter times (Figure 1), the total amount of corrosion in the propagation state becomes important. As shown in this work, the dissolution rates vary between < 0.1 µm/y and 20 µm/y (factor 200) and the maximum values are up to 2 times higher in carbonated mortar made of CEM II. Thus for a safe, long-term durable application of blended cements not only the general exposure class (XC3 or XC4) has to be considered, but a careful evaluation of the site specific climatic conditions (number of wet/dry cycles, average relative humidity etc.) is necessary. From this study it can also be concluded that corrosion in carbonated concrete at a given exposure condition is influenced to a greater extent by the binder type than by the w/c ratio.

Table 1 Averaged corrosion rate values for each binder in each exposure condition (average over minimum 6 measurements). Ratio of dissolution rate of the steel embedded in the two binders for each exposure.

Corrosion Rate (µA/cm^2)	CEM I	CEM II	CEM II / CEM I
50% RH	0.0058 ± 0.0011	0.0023 ± 0.0005	0.39
95% RH	0.0410 ± 0.0025	0.0617 ± 0.0067	1.50
WET	0.6436 ± 0.1416	1.1842 ± 0.3116	1.84

5. CONCLUSIONS

The corrosion rate of steel in carbonated mortar made of CEM I and blended cement (CEM II) has been studied for w/c ratios from 0.4 to 0.6 and different exposure conditions. Comparing CEM I and blended cement (CEM II) at a given exposure condition, the corrosion rate in carbonated mortar made of blended cement is about twice as high compared to mortar made of CEM I. However, the corrosion rate varies between ca. 0.1 µm/y at 50% RH, ca. 1 µm/y at 95% RH and 20 µm/y in wet conditions, thus the influence of exposure conditions is crucial. In terms of service life, both the time to depassivation and the total amount of corrosion of the steel (in µm) in the propagation period have to be considered.

From the results it is obvious that major concern for the application of blended cements in atmospheric exposure conditions is related to wet/dry cycles (exposure class XC4). The use of blended cements in a specific structure in exposure class XC4 can be recommended only after a careful evaluation of the site-specific climatic conditions (number of wet/dry cycles, average relative humidity etc.) showing that the total steel corrosion does not lead to spalling or cracking during the required service life.

ACKNOWLEDGMENTS

Research supported by the Swiss National Foundation for Research (SNF) project no. 154062 entitled “Formulation, use and durability of concrete with low clinker cements” is gratefully acknowledged.

REFERENCES

[1] OLIVIER, J. G. J. et al.: Trends in global CO_2 emissions: 2015 Report, PBL Netherlands Environmental Assessment Agency, The Hague, 2015.

[2] LEEMANN, A. et al.: Relation between carbonation resistance, mix design and exposure of mortar and concrete. *Cement and Concrete Composites*, 2015, 62, 33-43.

[3] LOTHENBACH, B. et al.: Supplementary cementitious materials, *Cement and Concrete Research*, 2011, 41(12), 1244-1256.

[4] YOUNSI, A. et al.: Accelerated carbonation of concrete with high content of mineral additions: effect of interactions between hydration and drying, *Cement and concrete research*, 2013, 43, 25-33.

[5] Papadakis, V. G.: Effect of supplementary cementing materials on concrete resistance against carbonation and chloride ingress. Cement and concrete research, 2000, 30(2), 291-299.

[6] SASATANI, T. et al.: Five-Year Exposure Test on Long-Term Properties of Concretes Containing. In Fly Ash, Blast-Furnace Slag, and Silica Fume in Concrete, Proceedings, Fifth International Conference, Milwaukee, 1995, WI Vol. 1, 283-296.

[7] Wang, S.: Quantitative kinetics of pozzolanic reactions in coal/cofired biomass fly ashes and calcium hydroxide (CH) mortars, *Construction and Building Materials*, 2014, 51, 364-371.

[8] KOLANI, B. et al.: Hydration of slag-blended cements, *Cement and Concrete Composites*, 2012, 34(9), 1009-1018.

[9] LYE, C. Q. et al.: Carbonation resistance of GGBS concrete, *Magazine of Concrete Research*, 2016, 1-34.

[10] LYE, C. Q. et al.: Carbonation resistance of fly ash concrete. *Magazine of Concrete Research*, 2015, 67(21), 1150-1178.

[11] PAPADAKIS, V. G. et al.: Physical and Chemical Characteristics Affecting the Durability of Concrete, *ACI Materials Journal,* 1991, 88, no. 2, 186–96.

[12] Pihlajavaara, S. E.: Some Results of the Effect of Carbonation on the Porosity and Pore Size Distribution of Cement Paste, *Matériaux et Construction 1*, 1968, no. 6, 521–27.

[13] PIHLAJAVAARA, S. E. et al.: Effect of Carbonation on Microstructural Properties of Cement Stone, *Cement and Concrete Research*, 1974, no. 2, 149–54.

[14] AUROY, M. et al.: Impact of carbonation on unsaturated water transport properties of cement-based materials, *Cement and Concrete Research*, 2015, 74, 44–58.

[15] NGALA, V. T., et al.: Effects of carbonation on pore structure and diffusional properties of hydrated cement pastes, *Cement and Concrete Research,* 1997, 27, no. 7, 995–1007.

[16] THIERY, M., et al.: Investigation of the Carbonation Front Shape on Cementitious Materials: Effects of the Chemical Kinetics, *Cement and Concrete Research,* 2007, 37, no. 7, 1047–58.

[17] BIER, T. A. et al.: Carbonation and Realcalinisation of Concrete and Hydrated Cement Paste, *Durability of Construction Materials*, Chapman and Hall, London-New York, 1987, pp. 927–934.

[18] HOUST, Y. F. et al.: Influence of Porosity and Water Content on the Diffusivity of CO_2 and O_2 through Hydrated Cement Paste, *Cement and Concrete Research,* 1994, 24, no. 6, 1165–76.

[19] Borges, P.H.R.: Carbonation of CH and C–S–H in composite cement pastes containing high amounts of BFS, *Cement and Concrete Research,* 2010, 40, 284–292.

[20] ALONSO, C. et al.: Relation between resistivity and corrosion rate of reinforcements in carbonated mortar made with several cement types, *Cement and Concrete Research*, 1988, 18(5), 687-698.

[21] MCCARTER, W. J. et al.: Electrical conductivity, diffusion, and permeability of Portland cement-based mortars, *Cement and Concrete Research*, 2000, 30.9, 1395-1400.

[22] MARSH, B. K. et al.: Pore Structure Characteristics Affecting the Permeability of Cement Paste Containing Fly Ash, *Cement and Concrete Research,* 1985, 15, no. 6, 1027–38.

[23] LI, S. et al.: Investigation of Relations between Porosity, Pore Structure, and C1– Diffusion of Fly Ash and Blended Cement Pastes, *Cement and Concrete Research,* 1986, 16, no. 5, 749–59.

CHLORIDE BINDING CAPACITY OF SYNTHETIC C-(A)-S-H TYPE GELS IN ALKALI-ACTIVATED SLAG SIMULATED PORE SOLUTIONS

Xinyuan Ke[1], Susan A. Bernal[2], John L. Provis[1]

[1] Department of Materials Science and Engineering, The University of Sheffield, Sheffield S1 3JD, United Kingdom, email: xke2@sheffield.ac.uk, j.provis@sheffield.ac.uk
[2] Department of Civil and Structural Engineering, The University of Sheffield, Sheffield S1 3JD, United Kingdom, email: s.bernal@sheffield.ac.uk

SUMMARY: The ingress of chloride from the environment towards the interface between steel reinforcement and a cementitious matrix is one of the main factors causing degradation in reinforced concretes. The permeation of free chloride is controlled by its diffusion into a hardened concrete, and the chloride ionic binding capacity of the cementitious phases present in the binder. In this study, the chloride binding capacity of synthetic C-(N)-A-S-H gels (Ca/Si=1 and 1.4, Al/Si=0 and 0.1), the main reaction product forming in alkali-activated slags, were determined in simulated pore solutions with varying [Cl-]/[OH-] ratios. The results showed that both the chemical composition of C-(N)-A-S-H gel and the [Cl-]/[OH-] ratio in the solutions influence the chloride binding capacity of these synthetic gels. The surface adsorption seems to be the main chloride binding mechanism, however changes in lattice parameters of the disordered layered silicate phases within the gels were observed, suggesting that replacement of the interlayer hydroxyl groups by chloride ions might also be possible.

SPOSOBNOST SINTETIČKIH GELOVA TIPA C-(A)-S-H ZA VEZIVANJE KLORIDA U PORNOJ VODI BETONA S ALKALIJAMA AKTIVIRANOM ZGUROM

SAŽETAK: Unos klorida iz okoliša na sučeljak čelične armature i cementne matrice jedan je od glavnih čimbenika koji uzrokuju degradaciju armiranoga betona. Prodor slobodnih klorida kontroliran je njihovom difuzujom u očvrsnuli beton i sposobnošću cementne faze u vezivu da veže ione klora. U radu je određena sposobnost vezivanja klorida za sintetičke gelove C-(N)-A-S-H (Ca/Si=1 i 1,4, Al/Si= 0 i 0,1), proizvod glavne reakcije koja nastaje u alkalno aktiviranoj zguri, u simuliranim pornim otopinama betona s promjenjivim omjerima [Cl-]/[OH-]. Rezultati pokazuju da i kemijski sastav gela C-(N)-A-S-H i omjer [Cl-]/[OH-] u otopinama utječu na sposobnost vezivanja klorida tih sintetičkih gelova. Čini se da je površinska adsorpcija glavni mehanizam vezivanja klorida iako su opažene promjene u parametrima rešetke neuredno uslojenih silikatnih faza u gelu što upućuje da bi bila moguća zamjena međusloja hidroksilnih grupa ionima klora.

1. INTRODUCTION

Alkali-activated slag (AAS) cements often exhibit low chloride permeability compared with Portland cement [1-3], which might be attributed to the reduced capillarity identified in these materials [4, 5]. A potentially high chloride binding capacity of the AAS cement binder, as postulated in some studies, might also contribute to the higher resistance to chloride ingress [1, 2], although detailed studies of chloride binding in AAS have not yet been carried out. The chloride binding capacity of AAS cements will be largely dependent on the chloride binding capacities of the individual phases forming in these systems, including Mg-Al hydrotalcite-like phases, the Ca-Al AFm phase strätlingite, and (Al,Na)-substituted calcium silicate hydrate (C-(N)-A-S-H) type gels, whose composition and relative quantities forming are governed by the chemistry of both the slag [6] and the alkali-activator used [7, 8]. Understanding the ionic binding capacity for chlorides of each individual phase forming in cementitious matrices is crucial in determining the rate of chloride transport, as this underpins the correct prediction of the long term performance of concretes based on these cements [9].

It is widely accepted that the interactions between Cl^- ions and C-(A)-S-H gel in portlandite saturated OPC/blended cementitious binders are mainly governed by surface adsorption due to an ionic pairing effect (≡Si-O-Ca-Cl), as expressed in Eq. 1 toEq. 3 [10]. The $[CaOH]^+$ dissociated from portlandite has also been reported to have adsorption capacity (Eq. 4), which could also be interpreted as an ion-exchange process (Eq. 5). Adsorption of Cl^- onto the diffusion layer of positively charged C-(A)-S-H type gel surface is also a possible mechanism for binding of chloride ions [11].

$$-Si\text{-}OH \leftrightarrow -Si\text{-}O^- + H^+ \quad (1)$$

$$-Si\text{-}O^- + Ca^{2+} + Cl^- \leftrightarrow -Si\text{-}OCaCl \quad (2)$$

$$-Si\text{-}OH + OH^- \leftrightarrow SiO^- + H_2O \quad (3)$$

$$[CaOH]^+ + Cl^- \leftrightarrow CaOHCl \quad (4)$$

$$Ca(OH)_2 + Cl^- \leftrightarrow CaOHCl + OH^- \quad (5)$$

In the case of AAS systems, the C-(N)-A-S-H gel will precipitate before forming portlandite and consuming the free Ca^{2+} in the pore solution [12, 13]. Therefore, the reactions Eq. 4 and Eq. 5 are not likely to take place in AAS cement. The overcharging properties of the C-S-H phase, as observed by Labbez et al. [11], suggests that adsorption of Cl^- onto the diffuse layer of positively charged C-S-H gel surface would be more plausible. In AAS cement, the C-(N)-A-S-H has a varying Al/Si ratio depending on the source of slag used, which might lead to a decreased positive charge density [14]. There is also evidence that the surface charge density of C-(N)-A-S-H gel is mainly determined by the bulk Ca/Si ratio of the gel [11], which is dependent on the source of slag and type of activator used [15]. The different features in C-(N)-A-S-H type gel will then lead to different interactions with chloride ions, as well as different binding capacities. Also, with excess alkali in the pore solutions (mostly Na^+ and OH^-), more Na^+ would bind with substituted Al. The surface adsorption might decrease as a result of reduced Ca^{2+} availability and end of chain Q^1(II) sites (-Si-O-Ca^{2+}) of the C-(N)-A-S-H type gel in AAS cement, reducing the chance of binding chlorides through Eq. 2. The high OH^- concentration in pore solutions might also reduce the surface charge density or/and compete with Cl^- as co-ions [16]. Evaluation of the ionic interactions between chlorides and C-(N)-A-S-H considering the pore solution chemistry of alternative cementitious materials is important, however there is not sufficient information related to this aspect available in the literature.

The chloride binding capacities and changes in mineralogy of hydrotalcite-like phase and strätlingite, phases which typically form as secondary reaction products in AAS systems, when exposed to chloride-rich simulated pore solutions with varying $[Cl^-]/[OH^-]$ ratios are reported in detail in a previous study [7]. In this study, the same chloride-rich simulated pore solutions with varying $[Cl^-]/[OH^-]$ ratios were used, and the chloride binding capacities of three types of synthetic C-(N)-A-S-H type gel (with Ca/Si ratio 1.0 and 1.4, Al/Si ratio 0 and 0.1) have been determined. Changes in chemistry and mineralogy of the synthetic phases studied here were determined using X-ray diffraction (XRD).

2. MATERIALS AND SAMPLE PREPARATION

2.1. SYNTHETIC C-(N)-A-S-H TYPE GELS

CaO was obtained by calcination of calcium carbonate ($CaCO_3$, Sigma-Aldrich, ≥ 99.0%, powder) at 1000 °C for 12 hours. Fumed silica, AEROSIL® 200, with a Brunauer-Emmett-Teller (BET) surface area of 200 ±25 m^2/g was used as the silica source. $CaO{\cdot}Al_2O_3$ (CA) was chosen as the aluminium source due to its high reactivity [17]. The CA used in this research was synthesised by heating homogenised $CaCO_3$ and Al_2O_3 [18] following the sintering schedule shown in Figure 1.

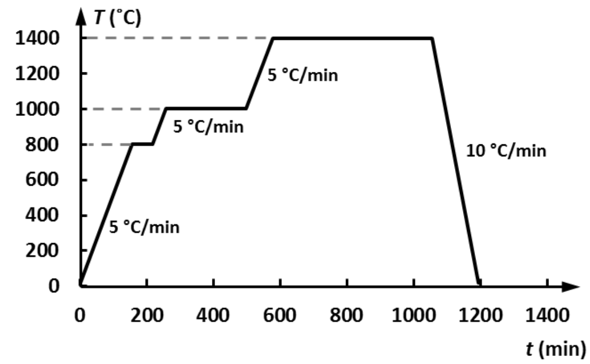

Figure 1 Sintering curve showing heating times applied for synthesis $CaO{\cdot}Al_2O_3$ (CA).

The C-(N)-A-S-H samples were prepared according to the procedure described by L'Hopital et al. [18], mixing 2 g of CaO, CA and SiO_2 powder mixtures with 100mL of 1.0 mol/L sodium hydroxide in 125 mL HDPE bottles. C-(A)-S-H samples with different Ca/Si and Al/Si ratios were produced according to the formulations shown in Table 1. The synthesis of all samples was conducted in a nitrogen filled glovebox to minimise possible CO_2 contamination. All the HDPE bottles were stored in an environmental chamber at 60 °C, regularly shaken (kept in rolling mixer for 1 hour at a time) twice a week for 10 weeks. Then the HDPE bottles were moved to an environmental chamber at 20°C for three days, until reaching room temperature prior to separation.

Table 1 Formulation of C-(N)-A-S-H gel-forming mixes for each batch prepared

Sample ID	Molar ratio		Mass (g)			
	Ca/Si	Al/Si	CaO (40 g/mol)	$CaO-Al_2O_3$ (142 g/mol)	SiO_2 (60 g/mol)	0.5 M NaOH (1.02 g/mL)
CNASH-A	1.0	0	0.800	0.000	1.200	100.0
CNASH-B	1.0	0.1	0.723	0.135	1.142	100.0
CNASH-C	1.4	0.1	0.892	0.117	0.991	100.0

2.2. CHLORIDE-RICH SIMULATED PORE SOLUTION

Chloride rich simulated pore solutions with a constant total Na^+ concentration and total ionic strength, but with varying $[Cl^-]/[OH^-]$ ratios, were produced according to the formulations shown in Table 2. In order to study the interaction of chloride-rich simulated pore solution with the synthetic C-(N)-A-S-H type gels, 40 g of pre-prepared solutions (Table 2) were weighed in 50 mL centrifuge tubes, and 0.4 g of solids were added to each tube, under a nitrogen atmosphere in a glove box. Each formulation was prepared in duplicate. All tubes were sealed with Parafilm to minimise water evaporation and sample carbonation, stored at 20 ± 3 °C, and manually shaken for 3 min every day until the mixtures reached equilibrium.

Table 2 Stoichiometric compositions of the simulated chloride-rich pore solutions studied

Carbonate-free solutions	Concentration (mol/L)				$[Cl^-]/[OH^-]$	Total ionic strength, I (mol/L)
	NaCl	NaOH	Na_2CO_3	Total Na^+		
CH-1	0.10	0.90	0	1.00	0.1	1.00
CH-2	0.25	0.75	0	1.00	0.3	1.00
CH-3	0.50	0.50	0	1.00	1.0	1.00
CH-4	0.75	0.25	0	1.00	3.0	1.00

2.3. TESTING METHODS

The solids mixed/reacted with the different Cl-rich solutions, were separated from the chloride-rich solution using a centrifuge (Heraeus Biofuge Primo, at 4000 rmp for 6 min). Prior to analysis, the separated supernatant solutions were filtered through 0.45 µm PVDF filter membranes. The pH values of the supernatants were determined using a digital pH meter (Oakton Acorn Series). The chloride ionic concentration was obtained using an ion selective electrode (Cole-Parmer Epoxy solid-state chloride electrode, accuracy ± 2%) according to ASTM D512 – 12 [19]. The chloride binding capacity of C-(N)-A-S-H type gels was calculated.

$$Q_e = (C_e - C_0) \cdot V / m_{input} \quad (6)$$

Q_e - Chloride binding capacity of solid, mg/g (by dry mass of initial solid).

C_e - Chloride concentration of the supernatant solution, mol/L.

C_0 - Initial chloride concentration, mol/L.

V - Volume of solution, mL.

m_{input} - Initial mass of solid, g.

The remaining solids were separated from chloride-rich simulated pore solutions, and then dried in a desiccator with controlled relative humidity (by saturated $CaCl_2$ salt) prior to further analysis. The dried solids were then powdered and analysed via X-ray diffraction (XRD) using a Bruker D2 Phaser instrument with Cu-Kα radiation and a nickel filter.

A step size of 0.02° and a counting time of 0.5 s/ step was applied, and diffraction patterns were recorded from 5° to 50° 2θ.

3. RESULTS AND DISCUSSION

3.1. CHLORIDE BINDING CAPACITY

The total chloride uptake values in chloride-rich pore solutions with different $[Cl^-]/[OH^-]$ ratios were measured and calculated using a similar method to that described for synthetic LDHs (e.g. hydrotalcite and strätlingite) in [20], and the results are shown in Figure 2. The chloride binding capacities of C-(N)-A-S-H with different Al/Si ratios increase when exposed to solutions with higher $[Cl^-]/[OH^-]$ ratios. However, the increase in Q_e values for each type of C-(N)-A-S-H assessed was not significant when the initial $[Cl^-]/[OH^-]$ ratios were lower than 1.0. Instead, the chemistry of the synthetic C-(N)-A-S-H type gel appears to be the main factor governing the overall chloride uptake. The C-(N)-A-S-H type gel 'C' with a Ca/Si ratio around 1.4, and 0.1 Al-substitution ratio (Al/Si=0.1), showed the lowest chloride uptake at a lower $[Cl^-]/[OH^-]$ ratio (<1.0), but the highest chloride uptake was identified when immersed at a $[Cl^-]/[OH^-]$ ratio around 3.0. C-(N)-A-S-H type gel 'B', with a bulk Ca/Si ratio of 1.0 and the same Al-substitution (Al/Si=0.1) compared with C-(N)-A-S-H gel 'C', showed the highest chloride uptake at a low $[Cl^-]/[OH^-]$ ratio, but the lowest at highest $[Cl^-]/[OH^-]$ ratios.

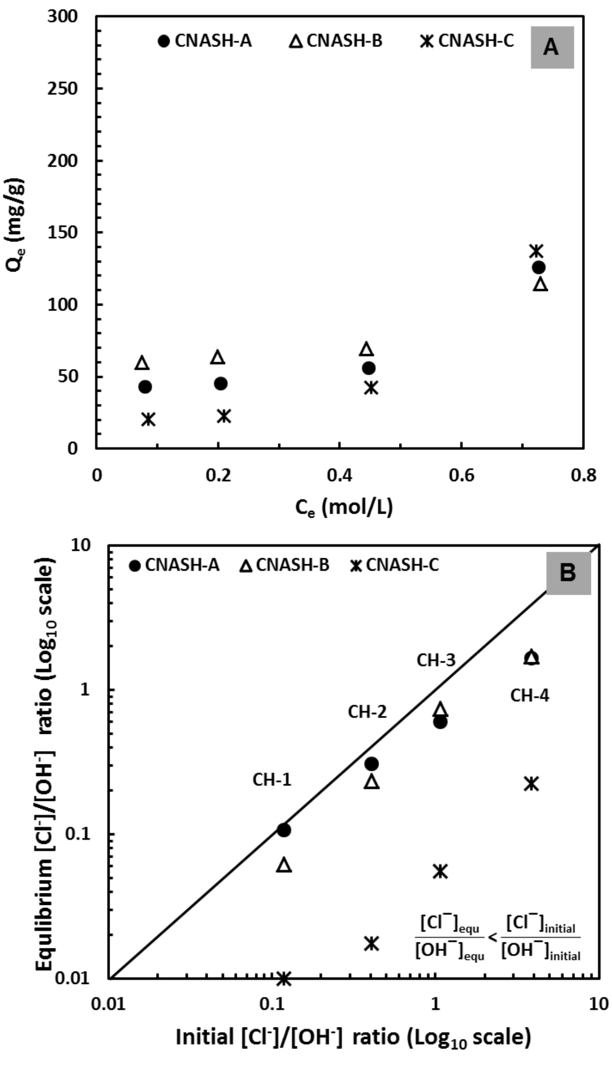

Figure 2 (A) Chloride binding capacity of three types of synthetic C-(N)-A-S-H type gels in various chloride rich simulated pore solutions. Q_e calculated using [20]. The error of the measurement is lower than 1.0%. (B) Correlation of the $[Cl^-]/[OH^-]$ ratios measured at equilibrium as a function of their initial values

The uptake of chloride ions by C-(N)-A-S-H type gels mostly takes place in the diffuse layers surrounding the gel surface, and no significant chemical binding has been observed between chloride ions and C-(A)-S-H phases [21-23].

The C-(N)-A-S-H type gels present a positively charged surface in alkaline solutions [11], and a more positively charged surface will most likely result in a higher uptake of counter-ions, including both OH^- and Cl^-. A higher bulk Ca/Si ratio increases the positive charge density at the C-(N)-A-S-H type gel surface [11, 22], while increased Al-substitution (higher Al/Si ratio) decreases the overall surface charge density [14, 24]. The presence of excess Na^+ might also balance the charge of substituted Al in the C-(N)-A-S-H gel [25, 26]. However, only when chloride ions are the dominant anions (e.g. the initial $[Cl^-]/[OH^-]$ ratio>1), less OH^- is competing with Cl^-, therefore the overall chloride uptake by C-(N)-A-S-H gels is positively correlated with its positive surface charge density.

3.2. X-RAY DIFFRACTION

Figure 3 shows the XRD patterns of C-(N)-A-S-H type gels with varying compositions after immersion in chloride-rich solutions. Crystallised NaCl was identified in the solid phase after the first filtration, as a result of the retention of Na^+ and Cl^- ions in the diffuse layer. Reduced intensities of the NaCl reflections were seen in samples exposed to solutions at lower initial $[Cl^-]/[OH^-]$ ratio. The reduced $[Cl^-]/[OH^-]$ ratio (lower chloride concentration but higher NaOH content) results in a lower surface charge density and probably a thinner diffuse layer [16], reducing the amount of chloride retained in the diffuse layer upon filtration.

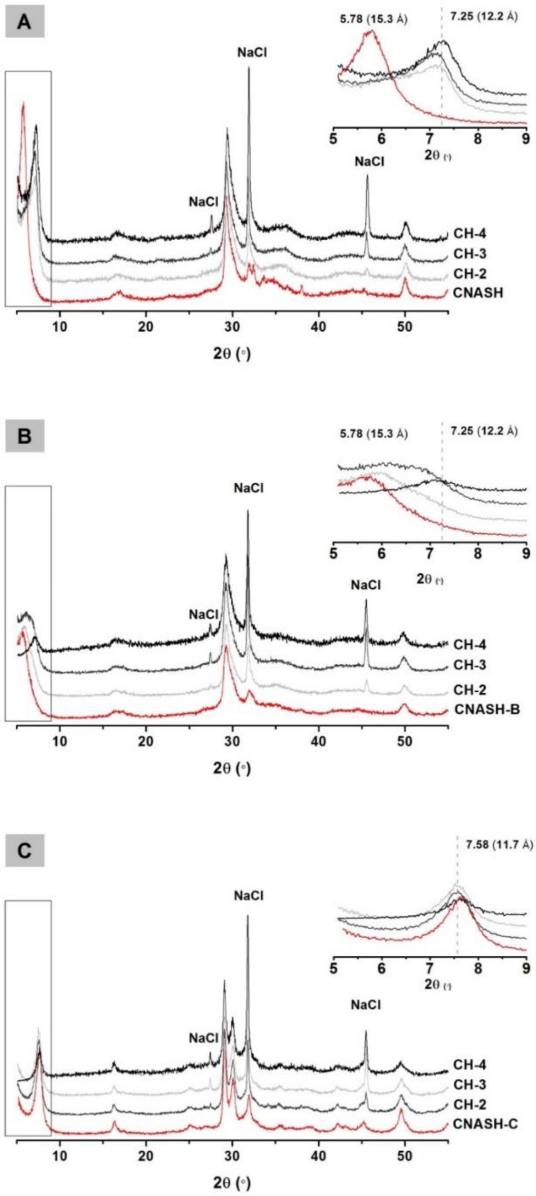

Figure 3 XRD patterns of C-(N)-A-S-H type gels after interaction with chloride rich simulated pore solutions, (A) Ca/Si=1, Al/Si=0, (B) Ca/Si=1, Al/Si=0.1, (C) Ca/Si =1.4, Al/Si=0.1.

The d_{002} peak of C-(N)-A-S-H type gels 'A' and 'B' shifted to higher diffraction angles (shorter *d*-spacings) after interacting with sodium chloride, while the d_{002} peak in C-(N)-A-S-H type gel 'C' stayed unchanged even after binding of chloride. The d_{002} peak at higher diffraction angle correlates to a lower basal spacing. The results shown here are contrary to the outcomes of studies using pH-neutral NaCl solution as the chloride source [22]. The presence of excess Na^+ and the high alkalinity in the aqueous phase might be responsible for the differences, however further analysis is needed before coming to a definitive conclusion.

4. CONCLUSIONS

This study reports for the first time the chloride binding capacities of synthetic C-(N)-A-S-H type gels with different chemical compositions determined under high alkalinity conditions. The preliminary results shown in here indicate that, apart from the chemical compositions of C-(N)-A-S-H gels, the [Cl-]/[OH-] ratio in the solutions also strongly influence the chloride binding capacity of the synthetic gel. Conversely to observations in OPC binders, the high alkalinity in the pore solutions of AAS cement strongly influenced the ionic interactions between chlorides and C-(N)-A-S-H gel, not only in the capacities but also in the mechanism of binding. Changes observed in lattice parameters from XRD suggests that the surface adsorption might be the main chloride binding mechanism, however, replacement of interlayer hydroxyl groups by chloride ions might also be possible in AAS binders.

ACKNOWLEDGEMENTS

This research was funded by the European Research Council under the European Union's Seventh Framework Programme (FP7/2007-2013) / ERC Grant Agreement #335928 (GeopolyConc). XK thanks the China Scholarship Council (CSC) for sponsoring her PhD studies. The participation of SAB in this research was partially funded by the UK Engineering and Physical Sciences Research Council through grant EP/M003272/1. This study was performed in part at the MIDAS Facility, at the University of Sheffield, which was established with support from the UK Department of Energy and Climate Change.

REFERENCES

[1] .Ismail, I., et al., Influence of fly ash on the water and chloride permeability of alkali-activated slag mortars and concretes. Construction and Building Materials, 2013. 48: p. 1187-1201.

[2] Ma, Q., et al., Chloride transport and the resulting corrosion of steel bars in alkali activated slag concretes. Materials and Structures, 2015. 49: p. 3663-3667.

[3] .Shi, C., Strength, pore structure and permeability of alkali-activated slag mortars. Cement and Concrete Research, 1996. 26(12): p. 1789-1799.

[4] .Bernal, S.A., et al., Effect of binder content on the performance of alkali-activated slag concretes. Cement and Concrete Research, 2011. 41(1): p. 1-8.

[5] .Shi, C.J., Effect of mixing proportions of concrete on its electrical conductivity and the rapid chloride permeability test (ASTM C1202 or ASSHTO T277) results. Cement and Concrete Research, 2004. 34(3): p. 537-545.

[6] .Bernal, S.A., et al., MgO content of slag controls phase evolution and structural changes induced by accelerated carbonation in alkali-activated binders. Cement and Concrete Research, 2014. 57(0): p. 33-43.

[7] .Ke, X., S.A. Bernal, and J.L. Provis, Controlling the reaction kinetics of sodium carbonate-activated slag cements using calcined layered double hydroxides. Cement and Concrete Research, 2016. 81: p. 24-37.

[8] .Ben Haha, M., et al., Influence of activator type on hydration kinetics, hydrate assemblage and microstructural development of alkali activated blast-furnace slags. Cement and Concrete Research, 2011. 41(3): p. 301-310.

[9] Andrade, C., et al., Testing and modelling chloride penetration into concrete. Construction and Building Materials, 2013. 39(0): p. 9-18.

[10] .Elakneswaran, Y., T. Nawa, and K. Kurumisawa, Electrokinetic potential of hydrated cement in relation to adsorption of chlorides. Cement and Concrete Research, 2009. 39(4): p. 340-344.

[11] .Labbez, C., et al., Experimental and theoretical evidence of overcharging of calcium silicate hydrate. Journal of Colloid and Interface Science, 2007. 309(2): p. 303-307.

[12] .Lothenbach, B. and A. Gruskovnjak Hydration of alkali-activated slag: thermodynamic modelling. Advances in Cement Research, 2007. 19, 81-92.

[13] .Chen, J.J., et al., Solubility and structure of calcium silicate hydrate. Cement and Concrete Research, 2004. 34(9): p. 1499-1519.

[14] .Schneider, J., M.A. Cincotto, and H. Panepucci, ^{29}Si and ^{27}Al high-resolution NMR characterization of calcium silicate hydrate phases in activated blast-furnace slag pastes. Cement and Concrete Research, 2001. 31(7): p. 993-1001.

[15] .Winnefeld, F., et al., Influence of slag composition on the hydration of alkali-activated slags. Journal of Sustainable Cement-Based Materials, 2015. 4: p. 85-100.

[16] .Trefalt, G., S.H. Behrens, and M. Borkovec, Charge regulation in the electrical double layer: ion adsorption and surface interactions. Langmuir, 2016. 32(2): p. 380-400.

[17] .H.F.W, T., Cement chemistry. 1990, London: Academic Press.
[18] L'Hôpital, E., et al., Incorporation of aluminium in calcium-silicate-hydrates. Cement and Concrete Research, 2015. 75: p. 91-103.
[19] .International, A., ASTM D512-12, in Standard test methods for chloride ion in water 2012, ASTM International.
[20] .Ke, X., S.A. Bernal, and J.L. Provis, Uptake of chloride and carbonate by Mg-Al and Ca-Al layered double hydroxides in simulated pore solutions of alkali-activated slag cement. submitted to Cement and Concrete Research, 2017.
[21] .Plusquellec, G. and A. Nonat, Interactions between calcium silicate hydrate (C-S-H) and calcium chloride, bromide and nitrate. Cement and Concrete Research, 2016. 90: p. 89-96.
[22] .Yoon, S., et al., X-ray spectromicroscopic study of interactions between NaCl and calcium silicate hydrates. Magazine of Concrete Research, 2014. 66(3): p. 141-149.
[23] .Beaudoin, J.J., V.S. Ramachandran, and R.F. Feldman, Interaction of chloride and C-S-H. Cement and Concrete Research, 1990. 20(6): p. 875-883.
[24] .Sun, G.K., J.F. Young, and R.J. Kirkpatrick, The role of Al in C–S–H: NMR, XRD, and compositional results for precipitated samples. Cement and Concrete Research, 2006. 36(1): p. 18-29.
[25] .Hong, S.-Y. and F.P. Glasser, Alkali sorption by C-S-H and C-A-S-H gels: Part II. Role of alumina. Cement and Concrete Research, 2002. 32(7): p. 1101-1111.
[26] .Myers, R.J., et al., The role of Al in cross-linking of alkali-activated slag cements. Journal of the American Ceramic Society, 2014. 98(3): p. 996-1004.

CORROSION INITIATION OF STEEL REINFORCEMENT IN SIMULATED ALKALI-ACTIVATED SLAG PORE SOLUTIONS

Shishir Mundra[1], Susan A. Bernal[2], John L. Provis[1]

[1] Department of Materials Science and Engineering, The University of Sheffield, Sir Robert Hadfield Building, Mappin Street, Sheffield S1 3JD, United Kingdom, email: smundra1@sheffield.ac.uk, j.provis@sheffield.ac.uk
[2] Department of Civil and Structural Engineering, The University of Sheffield, Sir Fredrick Mappin Building, Sheffield S1 3JD, United Kingdom, email: s.bernal@sheffield.ac.uk

SUMMARY: The alkaline nature of the pore solution in Portland cement based concretes allows the embedded reinforcement steel to be protected from the action of aggressive species by a passive film, composed of a complex solid assemblage of iron oxides and hydroxides. However, in the case of non-Portland cements, such as alkali-activated binders, there exists limited evidence on the nature of the passive film and its role in the protection of the reinforcement from corrosion initiation. This study investigated the effect of different species of relevance to redox and steel passivation chemistry (such as sulfide and hydroxide) which are present in simulated alkali-activated slag (AAS) pore solutions, on the initiation stage of chloride induced reinforcement corrosion, by electrochemical techniques. AAS pore solutions with varying concentrations of hydroxide, chloride and sulfide were produced to determine the chloride content which induces loss of passivity as a function of overall solution composition. In sulfide free solutions, corrosion initiation was found to be driven by the localised breakdown of the passive film, followed by metastable/stable pit growth. The complex nature of corrosion initiation in such systems cannot be described only by the chloride content, or the concept of chloride 'threshold' ([Cl-]/[OH-]) ratio, and is sensitive to various other parameters. Conversely, localised pitting due to chlorides was not observed in sulfide containing pore solutions. Electrochemical measurements reveal that the presence of S^{2}- in simulated AAS pore solution alters the mechanism of corrosion initiation and is highly dependent on the concentration of S^{2}- at the steel/solution interface and the time of exposure.

INICIJACIJA KOROZIJE ČELIČNE ARMATURE U SIMULIRANOJ PORNOJ OTOPINI ALKALNO AKTIVIRANE ZGURE

SAŽETAK: Alkalna priroda otopine u porama betona na osnovi portlandskog cementa omogućuje da je ugrađeni čelik za armiranje zaštićen od djelovanja agresivnih sastojaka pasivnim filmom koji se sastoji od složenog skupa oksida i hidroksida željeza. Međutim, kod cemenata koji nisu portlandski, kao što su alkalno aktivirana veziva, postoje ograničeni podatci o prirodi pasivnoga filma i njegovoj ulozi u zaštiti armature od početka korozije. U radu je elektrokemijskim postupcima istražen učinak različitih vrsta na redukcijsko-oksidacijsku reakciju i kemiju pasivizacije čelika (kao što je sulfid i hidroksid) koji postoje simuliranoj pornoj otopini alkalno aktivirane zgure na početno stanje korozije armature prouzročeno kloridima. Proizvedene su porne otopine alkalno aktivirane zgure s promjenjivom koncentracijom hidroksida, klorida i sulfida da bi se odredio sadržaj klorida koji uzrokuje gubitak pasivnosti ovisno o općem sastavu otopine. Za sulfidne otopine utvrđeno je da na početak korozije utječe lokalizirani proboj pasivnoga filma nakon čega slijedi metastabilni / stabilni točkasti rast korozije. Složena priroda početka korozije u takvim se sustavima ne može opisati samo sadržajem klorida ili omjerom "praga" klorida ([Cl-]/[OH-]), a osjetljiva je na različite druge parametre. Nasuprot tomu, lokalizirana točkasta korozija prouzročena kloridima nije opažena u pornim otopinama koje su sadržavale sulfid. Elektrokemijska mjerenja pokazuju da prisutnost S^{2}- u simuliranoj pornoj otopini alkalno aktivirane zgure mijenja mehanizam početka korozije i da je on znatno ovisan o koncentraciji S^{2}- na području sučeljka čelik – otopina i o vremenu izlaganja.

1. INTRODUCTION

When steel is embedded in cement binders, the highly alkaline nature of the pore solution in the cement matrix allows the growth of a stable passive film that protects the steel from the action of aggressive species such as chloride. The composition of this film has been found to be a complex solid assemblage of iron oxides such as α-Fe_2O_3, γ-Fe_2O_3, Fe_3O_4; and iron hydroxides and oxy-hydroxides such as $Fe(OH)_2$, $Fe(OH)_3$ and α-FeOOH, γ-FeOOH and β-FeOOH, in layers [1]. In the case of Portland cement (PC) based concretes, the breakdown of the passive layer due to the action of chloride has been explained previously using the concept of a chloride 'threshold' value [2]. This chloride 'threshold' value can be defined as the minimum amount of chloride required for the breakdown of the passive film. For PC based systems, the chloride threshold value has been reported to be in the range of 0.04 to 8.34 wt.% of the binder, and between 0.01 and 45 in terms of $[Cl^-]/[OH^-]$ ratio [2].

Alkali-activated materials (AAMs) are a new class of cementitious binders that are produced by reaction between solid aluminosilicate powders (generally industrial by-products such as fly ash or slag) and alkaline activators (generally an aqueous solution of alkali metal silicate or hydroxide) [3]. AAMs can be broadly divided into high-Ca systems such as alkali-activated slags where the phase assemblage is dominated by a calcium-aluminosilicate hydrate (C-A-S-H) type gel; and low-Ca systems such as alkali-activated fly ashes or metakaolin, where the main reaction product is a three dimensional hydrous alkali-aluminosilicate (N-A-S-H) type gel [3]. The composition of the pore solution at the steel-concrete interface in AAMs is significantly different from that of PC-based concretes, due to differences in the bulk composition and hydration product chemistry of these cements. It is therefore imperative to understand the interaction between steel reinforcement and these different matrices, to elucidate how durable reinforced AAMs will be, during their service life.

Pore solutions of alkali-activated slags (AAS) possess significant amounts of dissolved sulfur as S^{2-} [4,5]. The presence of sulfide in an electrolyte solution has been reported to alter the nature of the passive film formed on the steel surface during immersion in that electrolyte [6], and this could directly impact the mechanism of chloride induced corrosion. This study investigated the corrosion initiation of steel reinforcement due to the action of chlorides in highly alkaline simulated pore solutions representative of AAS, with the aim of determining whether the chloride 'threshold' value is a useful concept for such materials. This was approached using electrochemical techniques such as open circuit potential (OCP), electrochemical impedance spectroscopy (EIS), linear polarisation resistance (LPR) and anodic polarisation (AP).

2. EXPERIMENTAL METHODS

2.1. MATERIALS

Mild steel rebars (ϕ = 12 mm) were obtained from a local supplier, with a chemical composition of – Fe: 97.91 wt.%, C: 0.21 wt.%, Cr: 0.13 wt.%, Ni: 0.20 wt.%, Cu: 0.47 wt.%, Si: 0.23 wt.%, Mn: 0.76 wt.%, S: 0.03 wt.%, Mo: 0.02 wt.%, P: 0.04 wt.%. The rebars were sectioned into small discs with thicknesses ranging between 5.5 mm and 6.5 mm. Before electrochemical testing, the pellet surfaces were polished using SiC abrasive paper with 240 to 600 grit sizes and degreased using acetone.

To investigate the initiation of chloride induced corrosion in AAS, three classes of simulated pore solutions were formulated using hydroxide concentrations of 0.80 M, 1.12 M and 1.36 M. The rationale behind selecting three different $[OH^-]$ concentrations was to investigate the role of the chloride 'threshold' value (C_{crit} or $[Cl^-]/[OH^-]$) in corrosion initiation. Table 1 shows the chemical compositions of the simulated AAS pore solutions considered in this study, which are designed to replicate those reported in the literature [5,7]. The Cl^- concentration was varied with respect to the $[OH^-]$ concentration, and the ratio of $[Cl^-]/[OH^-]$ ranged between 0 and 3 to 4 for all the solutions. Synthesis of the pore solutions was carried out using reagent grade NaOH (Sigma Aldrich), commercial grade NaCl (EMD Chemicals), Na_2SiO_3 (Sigma Aldrich), $Ca(OH)_2$ (Alfa Aesar), $NaAlO_2$ (Fisher Scientific) and $Na_2S{\cdot}9H_2O$ (Sigma Aldrich).

Table 1 Composition of the simulated AAS pore solutions.

OH (M)	Ca (mM)	Si (mM)	Al (mM)	S (M)	$[Cl^-]/[OH^-]$
0.80	0.475	0.90	10.00	0.45	0-4
1.12	0.475	0.90	10.00	0.45	0-3
1.36	0.475	0.90	10.00	0.45	0-3

Initial tests were conducted with the electrolyte containing all species mentioned in Table 1, however, the Al, Ca and Si were found to be electrochemically redundant when studying corrosion initiation. Tests were then conducted on solutions containing species relevant to the passivation and depassivation of the steel rebar (OH^-, S^{2-} and Cl^-). The simulated pore solutions are referred according to the concentration of OH^- throughout the text.

2.2. ELECTROCHEMICAL TECHNIQUES

Electrochemical testing was conducted using a PGSTAT 204 Potentiostat/Galvanostat (Metrohm Autolab B.V.). All measurements were carried out in a 400 mL corrosion cell using a conventional three-electrode setup (electrolyte volume: 250 mL), comprising stainless steel counter electrodes, an Ag/AgCl (filled with 3 M KCl) reference electrode, and the steel surface (0.287 cm^2 area) acting as the working electrode. The reference electrode was positioned near the surface of the working electrode using a Luggin capillary. All measurements were conducted at room temperature (22 ± 2 °C) on duplicate samples. The following electrochemical techniques were used:

Open circuit potential – measurement of the natural potential of the steel immersed in the electrolyte, when no applied current/potential bias exists. OCP was measured for 30 min or until dV/dT ≤ 1 µV/s.

Electrochemical impedance spectroscopy – electrical properties of the system were analysed between 10^4 and10^{-2} Hz, with a logarithmic sweep of 5 points per decade. The measurements were conducted in the galvanostatic mode where the net current of the cell was 0 A, and the amplitude of the current was set to 10^{-5} A.

Linear polarisation resistance – the current response of the system was measured by variation of the potential from -20 mV to 20 mV vs. OCP. The polarisation resistance (R_p) values were calculated using the modified Stern-Geary equation:

$$R_p = \frac{\Delta \mathrm{E}}{\Delta \mathrm{I}}_{(\Delta \mathrm{E} \to 0)} \qquad \text{(Eq. 1)}$$

According to Eq. 1, the slope of the E vs I plot was used to measure the R_p for each specimen.

Anodic polarisation – the potential was varied from OCP to 1.00 V vs OCP and the current response of the system was recorded, to observe passivation and pitting of steel in electrolytes with and without chloride additions.

3. RESULTS AND DISCUSSION

3.1. SIMULATED PORE SOLUTIONS WITHOUT SULFIDE

Figure 1 shows the OCP and R_p (obtained through LPR) measurements obtained for steel immersed in pore solutions with varying concentrations of OH^- and Cl^-, in the absence of sulfide. The OCP and R_p values remained fairly constant until a particular concentration of chloride, indicating the steel being in its passive state below this chloride concentration. This concentration of chloride at which both the OCP and R_p exhibited a sudden decrease in value is indicative of the critical chloride concentration, C_{crit}, required for initiation of chloride induced corrosion. The C_{crit} was observed to be dependent on the concentration of OH^- in the electrolyte: the critical chloride concentrations in terms of $[Cl^-]/[OH^-]$ ratios were found to be 0.90, 1.70 and 2.40 for electrolytes with 0.80 M, 1.12 M and 1.36 M OH^- respectively.

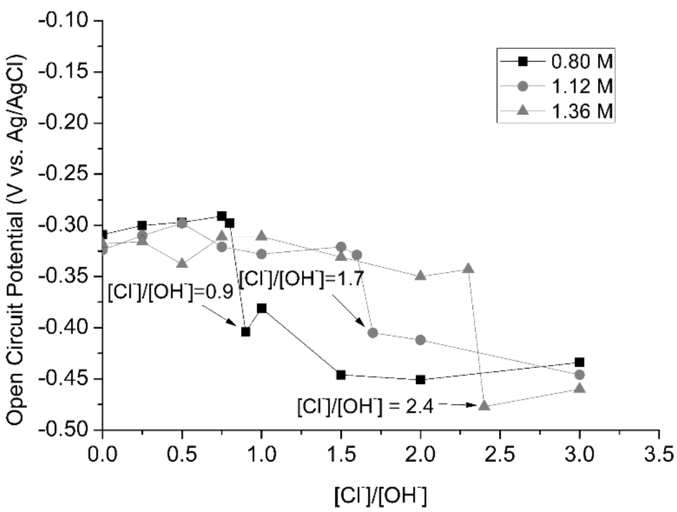

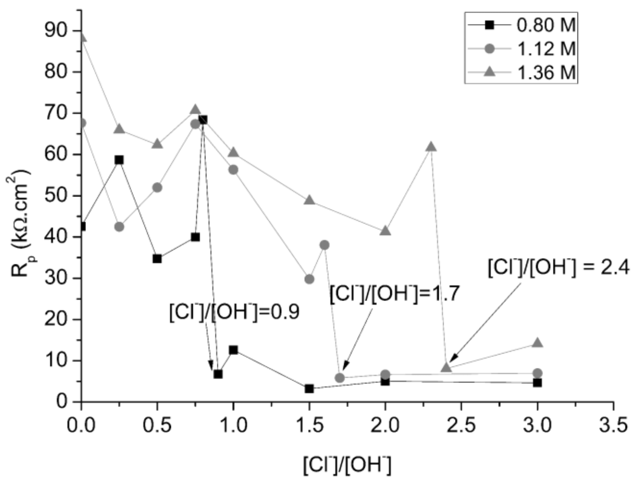

Figure 1 OCP and R_p measurements for steel rebars in electrolytes with varying concentrations of OH^- and Cl^-. The critical chloride concentrations in terms of $[Cl^-]/[OH^-]$, were 0.90, 1.70 and 2.40 for pore solutions with 0.80 M, 1.12 M and 1.36 M OH^- respectively.

The observations from Anodic Polarisation and EIS, were also found to be in complete agreement with the critical chloride concentrations found using OCP and R_p measurements [8].

3.2. SIMULATED PORE SOLUTIONS WITH SULFIDE

In the case of steel immersed in sulfide containing simulated pore solutions, the OCP measurements were found to be fairly constant in the range of -0.550 to -0.618 V; -0.543 to -0.613 V; and -0.556 to -0.629 V for 0.80 M, 1.12 M and 1.36 M NaOH solutions (for all chloride concentrations) respectively. The OCP values were more negative than those observed for steel immersed in simulated pore solutions without sulfide. Unlike the trend for OCP values observed in sulfide free pore solutions with respect to chloride concentrations, no apparent correlation could be identified between the chloride concentration and the OCP values. This can be explained by the reducing nature of the sulfide present in the pore solution. According to the Pourbaix diagram for the Fe-S system, in the presence of S^{2-}, iron has a tendency to form $Fe_{1-x}S$ instead of iron oxide/hydroxide. Therefore, it is highly likely that a complex iron sulfide layer exists on the surface at such negative potentials [6].

Figure 2 shows the anodic polarisation curves obtained for steel immersed in 0.80 M sulfide containing pore solution with $[Cl^-]/[OH^-]$ ratios varying from 0 to 4.00. Similar polarisation curves were obtained for 1.12 M and 1.36 M NaOH simulated pore solutions. The presence of S^{2-} in the pore solution dramatically changed the shape of the polarisation curves, when compared to those obtained for sulfide free pore solutions [8].

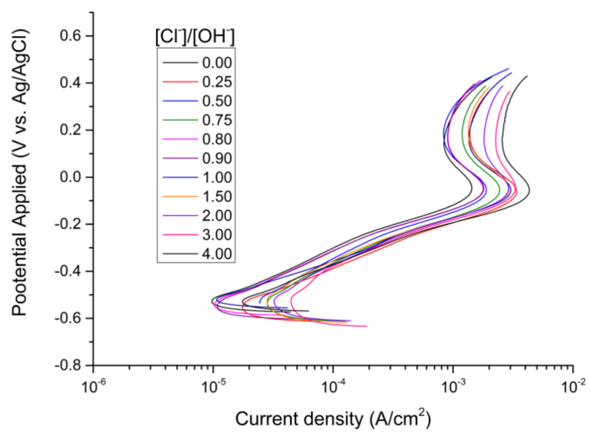

Figure 2 Anodic polarisation curves obtained for steel immersed in 0.80 M sulfide containing pore solution with [Cl]/[OH-] ratios varying from 0 to 4.00 as indicated

Unlike sulfide free pore solutions, passivation regimes and pitting were not detected for any concentration of chloride in the presence of sulfide. The current densities for steel specimens in the presence of 0.45 M S^{2-} are considerably higher than those observed in steel immersed in sulfide free pore solutions. As seen in Figure 2, on increasing the potential from the OCP towards the positive side, a sharp decrease in the current density (until -0.52 V) was identified. The polarisation curves were characterised by a constant increase in current density for potentials between -0.52 and -0.02 V. At values above -0.02 V, the current density decreased until a potential of 0.25 V was achieved, beyond which point the current density increased steadily. Even at $[Cl^-]/[OH^-]$ ratios as high as 4.00, no detectable pitting was observed. This was also true for steel immersed in 1.12 M and 1.36 M pore solutions. The observations from anodic polarisation measurements can be attributed to the inhibition of anodic dissolution of iron due to the reducing nature of sulfide in the pore solution. Therefore, the behaviour of the current density upon polarisation from OCP to +1 V vs OCP could possibly be related to the oxidation of sulfide in the pore solution, leading to electrodeposition of sulfur on the steel surface.

EIS and LPR tests also did not show any signs of localised pitting on the steel surface due to chloride and no apparent correlation could be defined between the concentration of chloride and the initiation of corrosion. From the above results, one could possibly say that in the presence of sulfide species at concentrations of 0.45 M and for short durations of exposure, the chloride ion does not seem to play a role and no localised corrosion occurs. Therefore, the role of sulfide and time in the initiation of corrosion were investigated by keeping the concentrations of OH^- and Cl^- constant.

For these tests, steel specimens were exposed to solutions containing 0.80 M OH^- and 0 M, 0.001 M, 0.01 M, 0.09 M and 0.45 M S^{2-} for 0, 5 and 12 days, prior to electrochemical testing in vacuum to avoid any interaction with air. The electrochemical tests were carried out in electrolytes that matched the compositions of the exposure solutions and with the addition of 2.4 M Cl^- to ensure a $[Cl^-]/[OH^-]$ ratio of 3, which was found to be sufficient to initiate pitting in sulfide free pore solutions. Table 2 gives a brief overview of the results obtained through these tests.

Table 2 An overview of the results obtained when steel specimens were exposed to varying concentrations of S^{2-} for 0, 5 and 12 days, with constant $[OH^-]$ = 0.80 M and $[Cl^-]$ = 2.4 M.

Exposure solution	Duration of Exposure before testing		
	0 days	5 days	12 days
0.80 M OH^- + 0 M S^{2-}	Pitting	Pitting	Pitting
0.80 M OH^- + 0.001 M S^{2-}	Pitting	Pitting	Pitting
0.80 M OH^- + 0.01 M S^{2-}	Metastable Pitting	Pitting	Pitting
0.80 M OH^- + 0.09 M S^{2-}	No Pitting	No Pitting	Metastable Pitting
0.80 M OH^- + 0.45 M S^{2-}	No Pitting	No Pitting	No Pitting

From the results mentioned in Table 2, it can be clearly seen that the concentration of sulfide in the pore solution and the time of exposure play a critical role in the initiation of chloride induced pitting on the surface of steel rebar. The dependency of chloride induced pitting on time and concentration of sulfide can possibly be due to the alteration of the passive film in the presence of a highly reductive agent like sulfide. However, further research is required to conclusively comment on the relationship between the alterations in the passive film due to sulfide and its effect on the initiation of chloride induced corrosion.

4. CONCLUSIONS

In sulfide free solutions, corrosion initiation was found to be driven by the localised breakdown of the passive film, followed by metastable/stable pit growth. The complex nature of corrosion initiation in such systems cannot be described only by the chloride content, or the concept of chloride 'threshold' ([Cl-]/[OH-]) ratio, and is sensitive to various other parameters. Conversely, localised pitting due to chlorides was not observed in sulfide containing pore solutions. Electrochemical measurements reveal that the presence of S2- in simulated AAS pore solution alters the mechanism of corrosion initiation and is highly dependent on the concentration of S2- at the steel/solution interface and the time of exposure.

ACKNOWLEDGEMENTS

The research leading to these results received funding from the European Research Council under the European Union's Seventh Framework Programme (FP/2007-2013) / ERC Grant Agreement #335928. The authors would like to acknowledge the technical support provided by Dr Oday Hussein.

REFERENCES

[1] M. Jayalakshmi, V.S. Muralidharan, Passivation and hydrogen evolution studies on iron in alkali solutions, Corros. Rev. 12 (1994) 305–320.

[2] U. Angst, B. Elsener, C.K. Larsen, Ø. Vennesland, Critical chloride content in reinforced concrete - A review, Cem. Concr. Res. 39 (2009) 1122–1138.

[3] J.L. Provis, S.A. Bernal, Geopolymers and related alkali-activated materials, Annu. Rev. Mater. Res. 44 (2014) 299–327.

[4] [A. Gruskovnjak, B. Lothenbach, L. Holzer, R. Figi, F. Winnefeld, Hydration of alkali-activated slag: Comparison with ordinary Portland cement, Adv. Cem. Res. 18 (2006) 119–128.

[5] R.J. Myers, S.A. Bernal, J.L. Provis, A thermodynamic model for C-(N-)A-S-H gel: CNASH_ss. Derivation and validation, Cem. Concr. Res. 66 (2014) 27–47.

[6] D.W. Shoesmith, M.G. Bailey, B. Ikeda, Electrochemical formation of mackinawite in alkaline sulphide solutions, Electrochim. Acta. 23 (1978) 1329–1339.

[7] R.R. Lloyd, J.L. Provis, J.S.J. van Deventer, Pore solution composition and alkali diffusion in inorganic polymer cement, Cem. Concr. Res. 40 (2010) 1386–1392.

[8] S. Mundra, M. Criado, S.A. Bernal, J.L. Provis, Chloride-induced corrosion of steel rebars in simulated pore solutions of alkali-activated concretes, Cem. Concr. Res. (2016) Submitted.

ENHANCED SERVICE LIFE OF REINFORCED METALS FOR CONCRETE IN A CHLORIDE ENVIRONMENT

Erwin W. Baumgartner[1], Andreas Kammersberger[2], Martin Schneider[3]

[1] Ingenieurbüro Dr. Erwin Baumgartner, Ringstraße 19, 9330 Althofen, Austria,
email: e.baumgartner@fh-kaernten.at
[2] Amt der Steiermärkischen Landesregierung, Abteilung 16, Verkehr und Landeshochbau, Stempfergasse 7, 8010 Graz, Austria, email: andreas.kammersberger@stmk.gv.at
[3] Carinthian University of Applied Sciences, Department of Construction Materials, Villacherstraße 1, 9800 Spittal/Drau, Austria, email: m.schneider@fh-kaernten.at

SUMMARY: Corrosion of reinforced steel has a great influence in reducing the lifetime of reinforced concrete structures. Corrosion is caused by the following two factors: carbonation of concrete pore solution resulting in pH drop to below 9, followed by de-passivation initiating corrosion on the steel surface and penetration of chloride-ions through the capillary system of the concrete cover causing pitting corrosion on the steel surface. Since corrosion of metals is highly dependent on the environmental conditions, exposure to chloride ions can be critical to the service life of reinforced steel structures exposed to deicing salt or marine environment. In this paper methods for corrosion diagnostics will be outlined on the basis of non-destructive and destructive test procedures. The potential mapping applied on the concrete surface is discussed as a standard method for corrosion detection and will be explained including application parameter of this method. The economic aspects of corrosion of reinforced concrete structures will be discussed, as well as preventive measures to reduce corrosion reactions by electrochemical methods. The last part consists of a practical case study of corrosion protection on the basis of principles and methods based on EN 1504 part 9. The decision was made between the conventional repair method of removing the chloride contaminated concrete and substitute with fresh concrete vs. cathodic protection, CP of steel in concrete. CP is introduced as a method to increase the service life of concrete structures exposed to salt environment without mechanical taking off the chloride containing concrete cover of the structure. This principle is successfully applied for parking garages, infrastructure buildings exposed to deicing salts like bridges, tunnels, retaining walls and structures exposed to marine environment.

POBOLJŠANJE UPORABNOG VIJEKA ARMATURE ZA BETONSKE KONSTRUKCIJE U KLORIDNOM OKOLIŠU

SAŽETAK: Korozija čelika za armiranje ima velik utjecaj na smanjenje životnoga vijeka armiranobetonskih konstrukcija. Koroziju prouzročuju dva faktora: karbonatizacija u porama betona koja dovodi do smanjenja pH ispod 9 koju slijedi depasivizacija koja dovodi do korozije na površini čelika i prodora klorida kroz kapilarni sustav zaštitnoga sloja betona uzrokujući točkastu koroziju površine čelika. Kako korozija metala znatno ovisi o okolišnim uvjetima, izloženost kloridima može biti biti kritična za uporabni vijek armiranobetonskih konstrukcija izloženih solima za odleđivanje ili morskom okolišu. U radu su obrađene metode dijagnosticiranja korozije na osnovi nerazornih i razornih ispitnih postupaka. Raspravljena je mogućnost mapiranja površine betona kao normirane metode otkrivanja korozije, a objasnit će se parametri za primjenu te metode. Raspravit će se gospodarski aspekti korozije armiranobetonskih konstrukcija i preventivne mjere smanjenja korozije elektrokemijskim metodama. U posljednjem dijelu rada prikazan je praktični slučaj istraživanja zaštite od korozije na osnovi načela i metoda danih u normi EN 1504-9. Odlučivalo se između konvencionalne metode popravka uklanjanjem betona zagađenog kloridom i zamjene svježim betonom i katodne zaštite čelika u betonu. Katodna zaštita predstavljena je kao metoda povećanja uporabnog vijeka betonskih konstrukcija izloženih slanom okolišu bez mehaničkog uklanjanja klorida iz zaštitnog sloja konstrukcije. Načelo je uspješno primijenjeno na garaže za parkiranje, infrastrukturne građevine izložene solima za odleđivanje kao što su mostovi, tuneli, potporni zidovi i konstrukcije izložene morskom okolišu.

1. INTRODUCTION

The reduction of service life of road infrastructure is mainly caused by corrosion of reinforcement steel in concrete. In recent decades a lot of research was done to understand corrosion and to develop sustainable repair methods in order to increase service life of such structures [1]. The presented study explains the normative approach to detect corrosion and establish a sustainable repair strategy for the side walls of a 341 m long railway underpass near the city of Feldbach in the south-east of Styria, Austria. The 25 years old structure was built as watertight tray made of reinforced concrete and was exposed to the application of de-icing salt in winter during its lifetime. Diagnostic checks in 2012 unveiled intense cracks, spalling and delamination in part of concrete due to ongoing corrosion of the steel reinforcement. A repair project was set up from the road authorities of the province of Styria, Austria with the objective for an economic and sustainable execution of the project.

To better understand the corrosion phenomena which occur when reinforcement steel is exposed to Chloride environment, causal relation of electrochemical corrosion reactions are explained in the following chapter. Knowledge of the corrosion phenomena in combination with results from corrosion diagnostics are the basis for sound decisions for a sustainable repair strategy and notable increase in lifespan of a structure. The decision at hand is either a conventional repair method based on the removal of Chloride containing concrete and embedding the steel reinforcement with fresh concrete, simultaneously increasing the concrete cover or an electrochemical method of corrosion protection, where the removal of concrete can be omitted.

In the presented study the decision for a sustainable repair strategy was based on existing data from visual inspections, which were made available from the road authorities, together with the investigation of the concrete quality by compression tests, a detailed corrosion diagnostics based on potential mapping and two series of Chloride profile analysis. The results of these comprehensive diagnostics led to the decision for the economically optimal repair strategy, which in this case turned out to be a conventional repair method. Material test applications and results were discussed in detail as well as the repair process, which was implemented to give best results with respect to durability and additional lifespan in accordance with optimal economic results.

2. CORROSION OF STEEL IN CONCRETE

Corrosion of steel in concrete is the main reason to reduce the service life of steel reinforced concrete structures. Based on EN ISO 8044:1999 corrosion is defined as *"physicochemical interaction between a metal and its environment that results in changes in the properties of the metal and which may lead to significant impairment of the function of the metal, the environment, or the technical system, of which these form a part"*. This interaction is often of an electrochemical nature. [2] Thus, corrosion is a property of the system metal – environmental media – design, as depicted in Figure 1.

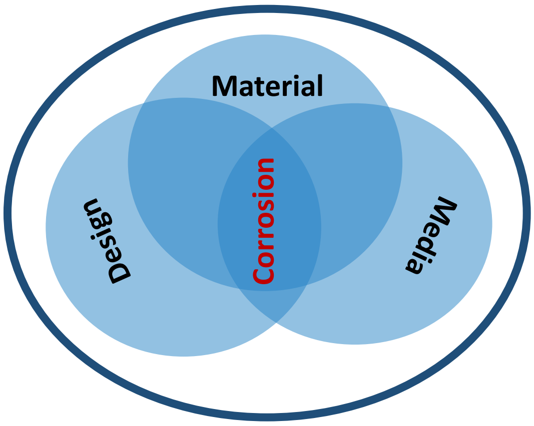

Figure 1 Corrosion system

As reinforcement steel is imbedded in concrete, a necessary overlay is applied to protect the steel from penetrating compounds through the porous system in the concrete. In fresh concrete the pore solution is strongly alkaline due to the hydration of the cement, at which besides the hardened phase of $C_3H_2S_3$, Calcium – Hydrate, $Ca(OH)_2$ is formed. The soluble part of this alkaline compound is increasing the pH to a value of 12.6 and above. The extreme alkaline environment is responsible for the formation of a passive layer of a few nanometre of iron oxide, Fe_2O_3 on the steel surface. This dense and pore free layer protects the steel from the initiation of the anodic dissolution of steel by corrosion.

2.1. CORROSION INITIATION OF STEEL IN CONCRETE

Two processes are known for the breakdown of the protective passive layer on the steel surface [3]:

- Reduction of the pH – value of the pore solution by carbonation
- Penetration of Chloride-ions through the passive layer of the steel surface

The former reaction is triggered by the diffusion of CO_2 through the capillary system of the concrete which in the presence of humidity reacts to Carbonic acid. The acid reacts further in an acid – base reaction with Calcium – Hydrate to form the insoluble salt Calcium-Carbonate, followed by the drop of the pH to a value below 9. When the carbonation front has reached the surface the steel is de-passivated. At this point the passivating layer on the steel is spontaneously destroyed and corrosion can occur.

Chloride containing salts like Sodium or Calcium Chloride are highly soluble in water and therefore also soluble in the pore solution present in the porous system of the concrete under humid conditions. Chloride ions can partially react with Calcium – Aluminates to form the insoluble complex Friedel-salt, 3 $CaO \cdot Al_2O_3 \cdot CaCl_2 \cdot 10\ H_2O$ [4]. If the concentration of Chloride-ions near the steel surface exceed a threshold value the protective layer will be locally destroyed due to the highly negative charge density of the Chloride-ions. This is inducing the anodic dissolution of iron and start the corrosion.

As already stated, the corrosion reactions are of electrochemical nature, which implies the formation of an active anodic reaction centre and a passive cathodic one on the metal surface to enable the transfer reactions of electrons. Electrons emerge from the metal surface to be absorbed from a reducing compound in the presence of water molecules. Under neutral conditions oxygen, diffusing through the porous system of concrete is acting as reducing compound. Hydroxide-ions, $(OH)^-$ are formed as reaction products and released in the pore solution. These reactions are depicted in equations (1) and (2):

Anodic oxidation: $Fe \longrightarrow Fe^{2+} + 2e^-$ (1)

Cathodic reduction: $\frac{1}{2} O_2 + H_2O + 2e^- \longrightarrow 2\ (OH)^-$ (2)

These corrosion reactions result in the dissolution of iron and end up after additional oxidation steps by the formation of rust, as shown in Figure 2.

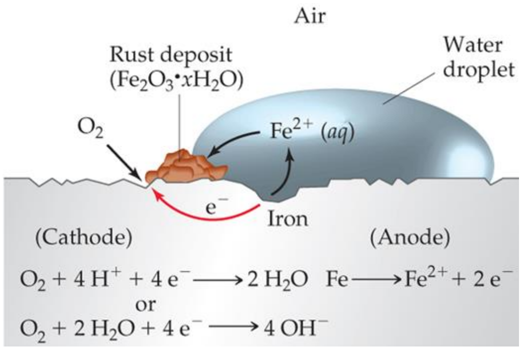

Figure 2 Cathodic and anodic corrosion reactions of iron

During carbonation-induced corrosion after de-passivation of the steel anodic and cathodic areas are formed next to each other, resulting in a steady loss in cross section of the reinforcing steel. Besides general reaction conditions like temperature, humidity the corrosion rate is highly influenced by concrete compositions like water/cement ratio or type of cement. The change in climatic conditions especially with respect to alternating dry and wet cycles have a great influence on the corrosion rate. For typical conditions of relative humidity, R. H. at 70-80% the maximum corrosion rate ranges between 5 and 50 µm/y, whereas at maximum values with R. H. of near 100% the corrosion rate can reach up to 100 – 200 µm/y instead [1].

More critical to the lifespan of reinforcing steel is Chloride induced corrosion. In that case a pit is formed, where the anodic dissolution of iron takes place. The emerging electrons can use the large surface area of the steel as cathode, to be attached to oxygen molecules in the presence of water thus forming a macrocell corrosion. Corrosion rates can easily reach up to 1 mm/y leading to a considerable reduction in the cross section of the steel rebar. Reinforced concrete structures can lose their structural soundness in short time as can be seen in Figure 3.

2.2. COST AND ECONOMIC ASPECTS OF CORROSION AND CORROSION PROTECTION OF STEEL

In industrial countries the yearly loss of value due to metal corrosion is around 3% of GDP. For Germany figures of € 50 billion annually are reported. According to a detailed NACE study in 2002 on *Corrosion Costs and Preventive Strategies in the United States* direct and indirect cost of metal corrosion is $ 276 Billion each, $ 552 billion in total. Extrapolated by inflation and growth the total corrosion costs in USA reached $ 1 trillion per year in June 2013, 6.1% of GDP [5]. Today, corrosion is one of the biggest unseen costs to society. The amount of corrosion costs in construction is estimated between 4 – 6% of total costs.

K. Tuutti published a simple model on the time depending penetration depth of corrosion [6]. In Figure 3 a recently published expanded model can be seen. During the initiation phase aggressive compounds like CO_2 or Cl^- diffuse through the capillary system of the concrete overlay. As soon as these compounds reach the steel surface, the electrochemical corrosion reactions begin their destructive process. On the time axis, the increase of corrosion rate can is presented, leading to cracking, spalling, finally to the collapse of the structure. In the same time the repair costs to reduce the corrosion rate down to an acceptable value proceed exponential. This reveals, that the decision to implement a repair project is greatly influenced by the corrosion process. From this model, the conclusion can be drawn, as to when the best economic moment in time is to start a repair project. In any case, it is necessary to start the repair project as long as the static of the structure is still sound.

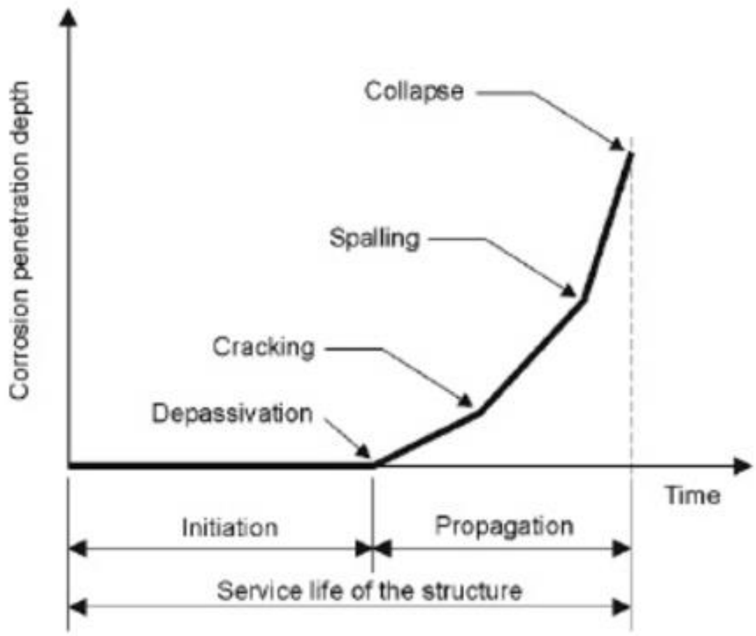

Figure 3 Corrosion of reinforcement steel vs. service life of a structure [1]

3. REPAIR OF A 340 M WATERTIGHT TRAY CONSTRUCTION OF A RAILWAY UNDERPASS

3.1. CASE DESCRIPTION

Along the bypass of the city of Feldbach in the Austrian province of Styria on the highway B66 a 341 m railway underpass was built in 1988 as watertight trough. Pictures of the construction can be seen in Figure 4a. The open frame construction built in reinforced concrete consists of 15 blocks either side. The length of the block No. 1 is 12 m, the other blocks No. 2 - 15 have a lengths of 23.5 m each, thus the total construction lengths is 341 m. The height of the blocks starts from ground level at the beginning to a maximum of 2.70 and 2.90 m resp. at block 8. The railway crosses transverse, the side walls of the underpass are attached to the abutments of the railway bridge. Typical damage situation due to corrosion can be seen in Figure 4b.

After more than 25 years in service the vertical block walls showed extensive spalling and delamination of up to 6 cm in depths caused by corrosion products of the reinforcement steel in combination with deficient concrete cover. Vertical cracks and damaged coatings from former local repair procedures were detected. The obvious reason for the damages was the penetration of salt used in winter for de-icing through the concrete overlay.

A detailed investigation of the damage in combination with a repair project was initiated by the road authorities in second half of 2015. The aim of the investigation was to find out the cause and degree of damage at different blocks. Based on that information, a repair concept was developed with the criteria of minimum intervention in the construction and maximum extension of the life span of the construction, thus leading to a sustainable repair process.

Figure 4a: B66 – railway underpass near Feldbach

Figure 4b: Typical damage caused by corrosion of steel

3.2. CONCEPT FOR THE ASSESSMENT OF THE STRUCTURE

The procedure for the assessment of the described structure consisted of the following mix of destructive and non-destructive test methods to obtain parameters which allow the experts to decide on the optimal repair strategy. All tests were performed on the basis of European and Austrian standards by accredited Austrian test laboratories:

Concrete properties:
compressive strength, f_c from concrete core samples, Ø 10 cm in N/mm²

Corrosion diagnostics:
potential mapping: non-destructive method to obtain corrosion probabilities of the reinforcement of all 30 blocks comprising an area of 1,194 m² in total

Chloride profile analysis, overview with 1st series of drill dust samples on block No. 2, 3, 5, 8, 11, 13, 14 left and right resp., total 22 test positions, comprising of 66 individual samples
depths profile, three depths levels: 0 – 1.5 cm, 1.5 – 3.0 cm, 3.0 – 4.5 cm

height profile: 0.10 m, 0.40 m, 0.70 m above concrete base level depending on block height

Chloride profile analysis, 2nd series of drill dust samples on Block No. 8 and 11 left and right resp., total 20 test positions and 96 individual samples
depths profile: 0 – 1.5 cm, 1.5 – 3.0 cm, 3.0 – 4.5 cm, 4.5 – 6.0 cm, 6.0 – 7.5 cm, 7.5 – 9.0 cm
height profile: 0.40 m, 0.70 m, 1.10 m, 1.50 (1.60) m, 2.0 (2.20) m above base level depending on block height

Carbonation depth in mm, performed from the concrete core samples, with no anomalies found.

The tests positions for each method were statistically spread over all blocks on both sides, the number of tests on different blocks depended on block height.

3.3. TEST RESULTS

Compressive strength of concrete core samples:

On both sidewalls of the concrete tray 6 core samples were drilled with Ø 10 cm and length of 25 cm. The length of the samples allowed to receive two test results with 1:1 length to width ratio. The results of the compressive strength of 6 concrete samples from the left (eastern) side blocks gave a calculated average value of f_c = 61.8 N/mm² corresponding to the concrete class of C 45/55 (based on EN 206). The result of the 6 concrete samples from the right (western) side blocks gave a calculated average value of f_c = 64.5 N/mm² corresponding to the concrete class of C 50/60 (EN 206). The result lead to the conclusion that the quality of the concrete after more than 25 years is in good agreement with the required concrete quality. No damage can be attributed to the concrete quality.

Corrosion diagnostics, potential mapping:

Potential measurements were performed on the entire surface area of 1,194 m² [7]. Each of the 15 blocks were tested on both sides. For the measurements a grid of 25 x 25 cm was assessed. Each measuring spot delivered a potential value in mV, positive or negative depending on the condition thereunder, which was transported as equipotential line to the concrete surface. In case of corrosion products were exposed on the steel surface the potential values dropped towards negative values, indicating a corrosion reaction to occur on the steel surface. The probability of corrosion increases from values below - 350 mV of up to 90%. For better understanding the columns of digits obtained from the potential measurement, a graphic display of the results is performed in segments of 50 mV. Green colour means low corrosion probability, red colour indicates high corrosion probability. At – 350 mV a yellow line is displayed as borderline. As example in Figure 5 the test results of block 8, left side and in Figure 6 block 11, left side are shown as potential mapping.

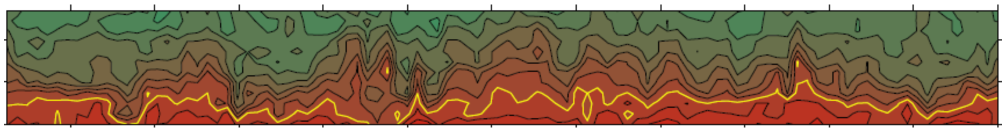

Figure 5 block 8, left side, open area

Figure 6 block 11, left side, under the railway bridge

Corrosion diagnostics, Chloride profile analysis, 1st and 2nd series:

The first series of Chloride profile analysis was performed to obtain an overview of the Chloride penetration through the capillary system of the concrete. The Chloride-ions originate from the use of Sodium Chloride as de-icing salt in winter due to the climate conditions in this area. An additional problem to create corrosion was the low concrete cover of in some parts < 1.0 cm, which made it possible for the Chloride-ions to reduce the initiation period to reach the metal surface to a short time and start the corrosion reaction. From the results it can be seen, that the Chloride content at the reinforcement level reached values up to 3.7% Chloride based on cement content in concrete. The tolerated Chloride content based on Austrian regulations is equal or below 0.6% Chloride based on cement content [8]. In block 2, right side a Chloride content of 6.4% Chloride based on cement content in the 1.5 – 3.0 cm probe at 10 cm above ground level was found as the highest value.

The 3.0 – 4.5 cm samples in different blocks indicated a content of up to 2.8% Chloride based on cement content. Therefor a 2nd series of Chloride samples was examined on blocks higher than 2.0 m on each side. Samples from block 8 and 11 were taken, the first being outside, the latter being inside the railway bridge. The results from the height and depth profile analysis of the right side of these blocks can be seen in Table 1 and 2.

Table 1 Block 8, right side

Height	Block 8, right side, % Chloride		
	0 – 3 cm	3 – 6 cm	6 – 9 cm
0.4 m	2.25	1.88	0.93
0.7 m	0.95	1.28	0.58
1.1 m	0.88	0.56	0.20
1.5 m	0.71	0.44	0.17
2.0 m	0.44	0.24	0.12

Table 2 Block 11, right side

Height	Block 11, right side, % Chloride		
	0 – 3 cm	3 – 6 cm	6 – 9 cm
0.4 m	2.80	1.67	0.78
0.7 m	2.40	1.52	0.39
1.1 m	0.73	0.89	0.26
1.6 m	0.95	0.55	0.13
2.2 m	0.90	0.29	0.04

The data show Chloride content above the threshold value of 0.6% at 0.4 m up to a depth of 6 – 9 cm. At a depth of 3 – 6 cm the Chloride content almost reached the threshold value at 1.6 cm in block 11. It is worth highlighting that in block 11 the Chloride content reaches 0,90% at a height of 2.2m at 0 – 3 cm, while in block 8 at 2.0 m in the 0 –

3 cm probe the value is at 0,44% distinctly below. Reason for that is, that block 11 is covered from the railway bridge, the Chloride containing spray mist is hindered to escape and is circulating to reach the concrete wall from the top. Due to the much lower concentration of Chloride in the spray mist the Chloride penetration does not reach further than 3 cm into the concrete.

3.4. REPAIR AND CORROSION PROTECTION STRATEGY

From the available visual assessment and the results of the corrosion analysis performed, the road authority being responsible for the structure gave the order for a reliable and sustainable repair method with an additional lifespan of 50 or more years. According to the non-harmonized part 9 of EN 1504 two repair principles were suitable to be applied:

– Principle No. 7: Preserving or Restoring Passivity using Mortar or fresh concrete

– Principle No. 10: Cathodic Protection by Application of an External Potential.

The project team consisting of the consultant for planning and a contractor for the material testing had to make the decision between the two repair strategies shortlisted by the representative of the road authority. After a discussion on the pros and cons, a unanimous decision was made for Principle No. 7: Preserving or Restoring Passivity using Mortar or fresh concrete. On the basis of the results of the corrosion diagnostics a concept was developed including the following five repair steps as the basis for the tender for the project:

– Removal of 8 cm Chloride contaminated concrete including removal of corrosion products of the steel surface: high pressure water jetting was applied at 1,000 to 1,400 bar

– Supplement of corroded vertical reinforcement and placement of additional horizontal reinforcement for the limitation of the crack-width as designed, the restoration of passivity on the steel surface was achieved by the concrete applied

– Installation of formwork, 9.5 cm ahead of new concrete surface, thus enlarging the concrete cover to around 4 cm

– Transit-mixed concrete of the quality C30/37/XC4/XD2/XF3/XA2/GK16/RRS/SCC, 16 mm aggregate was used for the concrete walls of the 15 blocks on either side, curing time of at least 3 days was applied

– Application of a hydrophobic layer on the concrete surface to retain the ingress of humidity.

The tender was announced by the consultant firm early 2016, the order was awarded few months later. One of the leading Austrian construction companies, Porr Bau GmbH won the tender. Work started in June 2016 and was completed in November of the same year. In Figure 7 the repair process of the left (eastern) wall of the tray under the railway bridge is shown at different construction stages. Starting from the left, block 11 can be seen with the contaminated concrete removed to behind the reinforcement in a depth of 8 cm in total, further to the right a finished segment with the formwork already taken off and at far right a segment with construction formwork can be seen.

Figure 7 Repair of the reinforced walls under the railway bridge at different stages

4. CONCLUSIONS

Corrosion of steel in concrete is one of the most limiting factors in the service life of Chloride exposed reinforced concrete structures. The presented paper deals about finding the best sustainable repair strategy for a corrosion induced infrastructure building on the basis of an increase in service life of 50 years plus. A case study of a 341 m tray construction for a railway underpass is discussed. Based on destructive and non-destructive corrosion diagnostics the decision had to be made between a conventional repair method and an electrochemical method like cathodic protection, CP. As a result of the tests applied, a conventional repair method turned out to be the best approach for a sustainable and long lasting rehabilitation of the structure. The consecutive steps performed during the repair process are discussed in detail.

ACKNOWLEDGMENTS:

The principal author would like to express thanks to the Styrian Government, Department of Road Authorities for supplying necessary data and pictures. The firm Kupsa & Morinaz consulting, Graz, Austria is greatly acknowledged for providing plans and discussions on the repair project at B66, Feldbach bypass in south-east Styria, Austria.

REFERENCES:

[1] Bertolini, L.; Elsener, B.; Pedeferri, P.; et al: *Corrosion of Steel in Concrete: Prevention, Diagnosis, Repair,* 2nd Edition, Wiley-VCH Verlag GmbH, 978-3-527-33146-8, Weinheim, Germany, (2013)

[2] EN ISO 8044: *Corrosion of metals and alloys – Basic terms and definitions,* CEN, Brussels, (1999)

[3] Raupach, M; Orlowsky, J.: *Schutz und Instandsetzung von Betontragwerken,* Verlag Bau + Technik GmbH, 978-3-7640-0475-0, Düsseldorf, Germany, (2008)

[4] Birnin-Yauri, U. A.; Glasser, F. P.: Friedel's salt, Ca2 · Al(OH)6 · (Cl, OH) · 2H2O: its solid solutions and their role in chloride binding, *Cement and Concrete Research*, Vol. (1998) No. 28 (12), pp. 1713–1723

[5] Available from http://www.nace.org/Publications/Cost-of-Corrosion-Study/ Accessed: 30.01.2017

[6] Tuutti, K.: Corrosion of Steel in Concrete, In: *CBI Research, No. FO 4/82,* Swedish Cement and Concrete Research Institute, Stockholm, (1982)

[7] Merkblatt B 03, Hrsg.: Deutsche Gesellschaft für Zerstörungsfreie Prüfung e. V., Berlin: *Elektrochemische Potential-messungen zur Detektion von Bewehrungsstahlkorrosion,* (2014)

[8] Baumgartner, E.: Bewehrungskorrosion und Kathodischer Korrosionsschutz, KKS-B, In *3. Grazer Betonkolloquium,* Verlag der Technischen Universität Graz, ISBN 978-3-85125-480-8, (2016), pp

APPLICATION OF Cr-Ni STEELS IN CONSTRUCTION AND OUTFITTING OF BUILDINGS

Ivan Juraga[1], Vinko Simunovic[1], Vesna Alar[1], Ivan Stojanovic[1], Marin Kurtela[1]

[1] University of Zagreb Faculty of Mechanical Engineering and Naval Architecture, Department of Welded Structure, Chair of Materials Protection, Ivana Lucica 5, 10 000 Zagreb, Croatia, email: ivan.juraga@fsb.hr, vinko.simunovic@fsb.hr, vesna.alar@fsb.hr, ivan.stojanovic@fsb.hr, marin.kurtela@fsb.hr

SUMMARY: From the time of their invention at the beginning of the past century high alloys corrosion resistant Cr-Ni steels have found their application in various fields, for example in food, drink and pharmaceutical production, water treatment, power production, medicine, shipbuilding, in building nuclear power plants, etc. From the start of their practical use these structural materials have been successfully used in civil engineering and architecture and for construction of various sculptures. In this paper properties of Cr-Ni steels which have found application in civil engineering and architecture are presented with review of their weldability and corrosion resistance properties, as well as their fields of application. Problems of their use, regarding corrosion in marine atmosphere are also presented.

PRIMJENA KROM-NIKALSKIH ČELIKA U GRADNJI I OBLAGANJU ZGRADA

SAŽETAK: Od vremena izuma visokolegiranih čelika otpornih na koroziju na početku prošlog stoljeća ti su čelici našli svoju primjenu u različitim područjima, primjerice u proizvodnji hrane, pića i farmaceutici, obradi vode, proizvodnji energije, medicini, brodogradnji, gradnji nuklearnih elektrana itd. Od početka njihove praktične primjene ti konstrukcijski materijali uspješno su upotrijebljeni u građevinarstvu i arhitekturi i za izradu različitih skulptura. U radu su prikazana svojstva krom-nikalskih čelika koji su našli primjenu u građevinarstvu i arhitekturi uz pregled njihove zavarljivosti i korozijske otpornosti te područja primjene. Također su prikazani problemi njihove upotrebe s obzirom na koroziju u morskom okolišu.

1. INTRODUCTION

High-alloyed Cr-Ni steels or as they are more often called, corrosion resistant steels or even stainless steels have been continuously evolving for over a century and surely belong to structural materials that marked significantly many areas of human needs in the past hundred years. These steels notably change and improve the standard and quality of human life. Alloying the steel with 12% Cr, a material resistant to the loss of gloss in moisture environment and respectively the material resistant to mild corrosive medium is achieved. Also, by more complex alloying procedure with more chromium, and other alloying elements (Ni, Mo, N), produced steels contain substantially improved properties of corrosion resistance in highly aggressive environments, improved mechanical properties, and also good mechanical properties from very low to very high temperatures. At the beginning of the last century due to needs for development and implementation of better materials, in Britain and in Germany steels with austenitic, ferritic and martensitic structure were developed. Already at that time, H. Brearly introduces the term "stainless steel", and the first serious application of these steels is realized in the production of cutlery. Later, that same steel on the market was called "Staybrite" for a long time [1]. Dependence on oil, and encouragement of research and exploitation of oil in the North Sea, lead to intensive research and development of materials resistant to aggressive marine environments. In Europe, a whole series of new so-called super-austenitic steel start developing. For example, Avesta developed steel 254SMO or even steel 654SMO containing 7% Mo intended to become a substitute for titanium. High-alloyed Cr-Ni steels are used in power plants, petrochemical industry - refining plants, as well as in the construction and equipping of oil and gas drilling/production offshore platforms. Thanks to good maintenance of "hygienic surfaces", they are used for the construction of plants for the production of medicines, food, beverages, and also in water management systems and desalination of sea water. Furthermore, they are used in architecture and construction, in production of implants, marine and nautical equipment, automotive parts, and tableware and household appliances. Cr-Ni steels are extremely valuable as scrap material because they are completely recyclable. From the earliest beginnings of the development and their application, high-alloyed Cr-Ni steels are used in civil engineering and architecture. It is estimated that the use of these structural materials in civil engineering and architecture will further intensify. A few examples of the use of these steels are given in Figure 1 and 2.

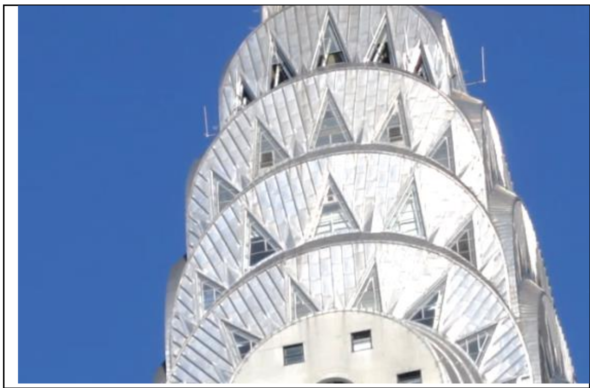

NEW YORK, 1929, Chrysler building. Six levels high dome made from austenitic steel AISI 302 (18% Cr - 8% Ni), manufacturer Krupp, Germany. Since it was built, the dome has been cleaned only few times, in excellent condition. The building is one of New York's landmarks.

LOS ANGELES, 2004, Walt Disney Concert Hall, also called the "Symphony in Steel", detail of building shell, the outer structure is made from steel AISI 304 (18% Cr - 8% Ni) and AISI 316 (18% Cr - 8% Ni - 2% Mo), architect Frank Gehry. Highly polished surfaces were subsequently sandblasted, because due to the reflection of the sun there was an increase of temperature in the surrounding buildings (about 5°C).

DUBLIN, Ireland, 2002., "Monument of Light", 125 m high, marking the new millennium, 130 t of steel AISI 316 (18% Cr - 8% Ni - 2% Mo) wall thickness 35-20 mm, the diameter at the bottom 3 m, and at the top 15 cm, welded at the site in sections of 12-18 meters. It looks like it's in one piece

[2].

STOCKHOLM, sculpture "God, our Father, on the Rainbow", 1995., 23 m high, steel quality EN 1.4547, trademark of the manufacturer Avesta – now Outokumpu 254SMO, extremely high corrosion resistance in the marine atmosphere,

architect Carl Milles [3].

SINGAPORE, Helix Bridge, 280 meters, 250 tons of duplex (austenitic-ferritic) steel EN 1.4462, rounded shape symbolizes the DNA molecules [4].

Figure 1 Examples of Cr-Ni steel application in the construction and equipping of buildings and sculptures in the world

	
ZAGREB, University of Zagreb, Academy of Music, 2015, "needle" quality AISI 312, height 29 m, 4 t. Architect Milan Šosterič, made by company Bastal, Zagreb.	**ZAGREB**, National and University Library, new building opened in 1995, the interior of the library is largely made from Cr-Ni steels, architects Neidhardt, Hržić Krznarić, Mance.

Figure 2 Examples of Cr-Ni steel application in the construction and equipping of buildings and sculptures in Zagreb

The properties of these steels substantially depend on their structure, which is a result, primarily, of their chemical composition. Regards their structure, austenitic, ferritic, martensitic and austenitic-ferritic (duplex steels) steels are known. It is also known, that 70% of the total production of stainless steels, only two austenitic steels, the steel alloyed with 18% Cr and 8% Ni (AISI 304) and the steel which in addition to 18% of Cr and 8% Ni has a 2% Mo, (AISI 316), are most common used today.

In this paper, steel designations are in accordance with EN 10088-1:2005 and ASTM/UNS standard (AISI designation). It should be noted that, due to the more frequent use of the code according to American standards, the AISI system was designed in the mid-20th century and has not been changed since the 1960s. Therefore, steels that have no AISI designation incurred after that period, which means that they are "younger" than 50 years. Despite of these facts, because of its simplicity, AISI/ASTM designation system is still widely used in factories and workshops today. Very often steelmakers use their own registered trademark designation, which is again an additional complication.

2. CLASSIFICATION, PROPERTIES AND APPLICATION OF CR-NI STEELS IN CIVIL CONSTRUCTION AND ARCHITECTURE

AUSTENITIC STEELS

Austenitic steels form the largest and most used group of stainless steels. They are not magnetic what often in the practice creates expectations that all the other stainless steels are nonmagnetic. Also the fact that the austenitic steels by cold working become magnetic can sometimes confuse their users. These materials are corrosion resistant, weldable, with good deforming properties and good ductility and toughness even at low temperatures, thus ensuring a wide application. In welding they are particularly prone to deformations due to high heat ductility and reduced thermal conductivity. The best-known austenitic steel 18% Cr and 8% Ni makes about 50% of total world production of stainless steels, and if it is added austenitic steel 18% Cr, 8% Ni and 2% Mo (steel alloyed with molybdenum), then those two steels make up almost three quarters of total world production. Austenitic steel experts share a number of ways of their classification, which can sometimes cause confusion, but in any case it is important to know the alloying elements and their content, because they predominantly determine the properties of those steels. They are used a lot in architecture and construction due to their good weldability, corrosion resistance and easy maintenance.

FERRITIC STEELS

Ferritic steels most often contain 11-26 %Cr; generally do not have, or can have very low nickel content, and the 2% molybdenum can be added in order to enhance corrosion resistance. They are stabilized with niobium or titanium if weldability is to be improved. Ferritic steels are magnetic and do not retain the toughness at low temperatures. They are relatively cheap, and their price in the market is stable. According to their physical properties, ferritic steels show more similarities to the carbon ("black") steels than austenitic steels, which of course affect the conditions and behaviour during welding. Their corrosion stability significantly depends on the degree of alloying, thus ferritic steels with higher proportions of chromium have resistance to the pitting corrosion and crevice corrosion equal to austenitic steels, and also a bit better resistance to stress corrosion cracking. It's harder to shape them by deformation so they are mainly used as thin sheets, for example for, household equipment - washing machines, stoves, lining surfaces, elevators, handrails, interior decoration etc.

DUPLEX STEELS

Duplex stainless steels have ferritic - austenitic microstructure in approximately the same proportion of about 50% ferrite and 50% austenite. The development of these steels in good measure succeeds to achieve the combination of good properties of both, ferritic and austenitic steel. Chrome proportion has increased and is around 20-25%, and nickel is reduced to 1-7%, which significantly contributes to the stability of steel prices in the market. The carbon content is generally below 0.03% for good weldability. Molybdenum is added in the proportion of 0.3% to 4%, and contributes to the improvement of corrosion resistance and structural stability. With duplex - austenitic ferritic structure, increase in steel strength and stress corrosion cracking resistance is obtained.

Today, with the most common duplex steel marked as 2205 (22% Cr, 5% Ni and 3% Mo) increasingly is being given attention, especially in construction and architecture, to so called "Thin" (lean) duplex steel, marked as 2101 (21% Cr and 1% Ni). It is cheaper, and by its properties it is closer to austenitic steel 18% Cr, 8% Ni and 2% Mo. A wide range of applications of these materials in various environmental conditions resulted in its subtypes development, which sometimes when it comes to their selection can be a particular problem. The opinion of experts that "there are no bad stainless steel, only a bad choice can happen", warns on unpredictable serious problems (especially when it comes to corrosion) which may occur in service.

Table 1 Designations and some properties important for the use of steel in civil engineering constructions and architecture [3, 5, 6]

EN 10088-1	ASTM/ UNS	PRE_N	%C	%Cr	%Ni	%Mo	Rest	Str.
1.4301 - X5CrNi 18-10	304	18	<0,07	18,5	8,5			A
1.4307 - X2CrNI 18-9	304 L	18	<0,03	18,5	8,5			A
1.4401 - X5CrNiMo 17-12-2	316	24	<0,07	17	10,5	>2		A
1.4404 – X2CrNiMo 17-12-2	316 L	24	<0,03	17	11,5	>2		A
1.4016 - X6Cr 17	430	18	<0,08	17,5				F
1.4062 – X2CrNiN 22-2	2205	24	<0,02	22	2		0,2 %N	A/F
1.4521 – X2CrMoTi 18-2	444	27	<0,025	17-20		1,8-2,5		F
1.44438 – X2CrNiMo 18-15-4	317 L	29	<0,03	18,5	14	>3		A
1.4462 – X2CrNiMoN 22-5-3	2205	>33	<0,03	22	5,3	2,8	0,16 %N	A/F
1.4439 – X2CrNiMoN 17-13-5	317 LMN	35	<0,03	18	14	>4	0,15 %N	A
1.4539 – X1NiCrMoCu 25-20-5	904 L	37	<0,02	20	25	>4	0,13 %N and 1,5 %Cu	A
1.4410 – X2CrNiMoN 25-7-4	327	>40	<0,03	25	7	3,5	0,25 %N	A/F
1.4547 – X1CrNiMoCu 20-18-7	S31254	42	<0,03	20	18	>6	0,2 %N and 0,5-1 %C	A
1.4529 – X1CrNiMoCuN 25-20-7	N08926	43	<0,02	20	25	>6	0,2 %N and 1 %Cu	A
1.4652 – X1CrNiMoCuN 24-22-8	S32654	50	<0,02	24	22	7-8	0,5 %N and 0,3-0,6 %Cu	A

PRE_N – Pitting resistance equivalent number
PRE_N= Cr + 3.3 %Mo + 16 %N; the data obtained according to equation, determined by accelerated laboratory experiments.
If austenitic steels contain more than 3 %Mo than the equation is PRE_N= Cr + 3.3 %Mo + 30 %N.
In practice PRE_N number is shown to be very useful and if it is greater than 27 than stainless steel has increased resistance to pitting and crevice corrosion.

For the selection of stainless steels for the construction or equipping of civil buildings and various civil engineering structures as well as execution of architectural solutions which primarily characterize the atmospheric conditions of exploitation, the factors that could jeopardize their corrosion resistance and should be primarily taken into account are:

- Atmospheric environment conditions (e.g. rural, urban, and industrial, etc.).
- Maritime atmosphere is specially analysed, this refers also to the area that is treated with salt for de-icing of roads, or even a combination of both areas. This includes also the consideration of the wide range of impact factors which occur in e.g. the splash zone or the areas which are several kilometres away from the coast.
- Local atmospheric conditions - considering microclimate, characteristic temperatures, humidity, frequency and intensity of rain, fog and the like.
- Structural design - concerning the construction, availability for cleaning and maintenance, surface features: vertical – horizontal position, roughness, whether the surface is electro-polished, etched, way of connection, gaps and the like.
- Cleaning - maintenance of the surfaces: no special maintenance, annual, monthly, weekly or daily.

If it is a highly corrosive - aggressive environment, consulting with experts in the field of corrosion and material protection is recommended. Consider the use of Tables 1 and 2.

Table 2 Selection of Cr-Ni steel, depending on the corrosivity of the atmosphere

Corrosivity category	Corrosivity	Examples indoor	Examples outdoor	Appropriate steel	
				EN	ASTM/UNS
C1	Very low	Heated indoor spaces: offices, schools, museums, etc.	Central Artic/Antarctica and certain deserts	1.4016 1.4307 1.4372 1.4521 1.4162	430 304L 201 444 S32101
C2	Low	Unheated storages and sport halls	Rural areas and small towns. Deserts and subarctic areas	1.4016 1.4307 1.4372 1.4521 1.4162	430 304L 201 444 S32101
C3	Medium	Food processing plants, laundries, breweries and dairies	Urban areas and coastal areas with low deposition of chlorides. Subtropical and tropical zones with low pollution	1.4307 1.4521 1.4404 1.4162 1.4362	304L 444 316L S32101 S32304
C4	High	Enclosed spaces with volatile aggressive substances. Industrial processing plants and indoor swimming pools	Polluted urban areas, industrial areas, coastal areas without spray and exposure to de-icing salts. Subtropical and tropical zones with medium pollution.	1.4404 1.4438 1.4439 1.4539 1.4547 1.4565 1.4362 1.4462 1.4410 1.4501	316L 317L 317LMN 904L S31254 S34565 S32304 S32205 S32750 S32760
C5	Very high	Mines, caverns for industrial purposes. Unventilated sheds in subtropical and tropical zones.	Highly polluted industrial areas. Coastal areas and sheltered positions on coast line.	1.4539 1.4547 1.4565 1.4652 1.4462 1.4501 1.4410	904L S31254 S34565 S32654 S32205 S32750 S32750
CX	Extreme	Unventilated sheds in humid tropical zones with penetration of outdoor pollution	Subtropical and tropical zones, extreme industrial areas, coastal and offshore areas.	1.4547 1.4565 1.4652 1.4501 1.4410	S31254 S34565 S32654 S32760 S32750

Table 1 presents the chemical composition, designation according to European and American standards, microstructures, and PREN number of major stainless steels which are widely used in civil engineering constructions and architecture. This data of course does not exclude the possibility to choose some other construction materials.

3. WELDABILITY AND CORROSION RESISTANCE OF CR-NI STEELS

Welding technology is widely used in building structures and parts of Cr-Ni steel, but it has to be noted that the welded joint is often a critical spot of such structures when it comes to corrosion. The corrosion resistance of high-alloyed Cr-Ni steels is the result of their natural properties, which is reflected in the formation of compact and homogeneous chromium oxide passive layer on the steel surface (for steels with Cr > 12%). Damage or irregularity on the stainless steel surface, such as, e.g. heat tints formed by heating, formation of mill scale, slag residues, scratches, undercutting, welding spatter formed by welding, the use of inappropriate tools and devices, endanger their expected corrosion resistance. Today's stage of development of welding technology made it possible to perform once unimaginable technological solutions in the building of the structures by welding. It is believed that welding of corrosion resistance steels is a solved technological problem, but the concern that the area of welded joints can become in certain exploitation conditions critical place is still present. This is affected by welding conditions, so it is necessary that the welding conditions and technology are prescribed by authorized experts in the field of welding. Specifics of weldability of stainless steels such as roughness and sensitization of the structure in the heat-affected zone, creation of brittle intermetallic compounds, cold or hot cracks appearance, the share of delta ferrite, will not be discussed further, because those are the issues related to welding metallurgy, however it is necessary to be noted that all these changes and phenomena may significantly affect corrosion resistance of welded joints. It is an unpalatable fact that these steels are particularly prone to local corrosion phenomena (intergranular corrosion, pitting corrosion, stress corrosion cracking, as well as galvanic and crevice corrosion), which often destroy material even in a few days. The condition of the material surface significantly affects the corrosion resistance, so it is important to point out that the welding is completed only when the surface treatment of welded joint area after welding is completed. Problems in the use of Cr-Ni steels are shown in Figure 3 and 4.

Table 2 shows the classification of atmosphere corrosivity according to ISO 9223 and selection of appropriate Cr-Ni steel.

The pictures show a very frequent problem in the use of stainless steel structures close to the sea, Dalmatia. In both cases the stainless steel stairs were attached with screws made from “black” steel. Galvanic corrosion threatens the structural bearing capacity and significantly ruins the aesthetic appearance of the stairs. Use of suitable Cr-Ni steel screws is also needed.

The bus stop, highly exposed to splashing due to the traffic, Cr-Ni steel, corrosion after only a few months.

Light pole is made of Cr-Ni-Mo steel, which has increased corrosion resistance in the marine atmosphere, however due to improper surface treatment of the welds, corrosion processes initiated and disrupt the aesthetics of lighting poles, Dalmatia. After cleaning welded joints should be passivated.

Figure 3 Problems in the use of Cr-Ni steels

The pipeline in the part of the plant for preparation and purification of water in the swimming pool, steel Cr-Ni, the Croatian North Coast. Aggressive atmosphere in the plant (high concentration of chlorides). Steel with higher resistance is needed (PRE_N above 27).

The balcony fence, Cr-Ni steel tubes, rural atmosphere, Zagreb surroundings. Surface defects are the result of inhomogeneity in the material, which were found by metallographic tests.

Suspended ceilings collapse in indoor pools (Switzerland, Netherlands, Finland, etc.), is the result of wrong selection of steel from which supporting bars were made. Austenitic stainless steels are prone to stress corrosion cracking when tensile stressed in corrosive atmosphere with high chloride content [7].

Figure 4 Problems in the use of Cr-Ni steels

4. CONCLUSIONS

Especially important for professionals, particularly designers in the field of civil engineering and architecture, but also for artists, is a proper choice of corrosion resistance Cr - Ni steels, for which, beside a variety of factors, the corrosivity of the environment in which the facility will be built should be taken into account. Finally it is important to point out that in case of welded structures, it is certainly necessary to conduct a proper surface treatment after welding. Today, the mechanical, chemical and electrochemical surface treatment after welding are equally used, depending on the type of material, a corrosive environment and aesthetic requirements.

REFERENCES

[1] Dulieu D.: Stay Bright, A History of Stainless Steels in Britain, Outokumpu Stainless Ltd, UK, (2013)
[2] A Spire to Inspire, Nickel, Vol. (18), pp. 16, Nickel Development Institute, London, (2002)
[3] Atmospheric Corrosion of Stainless Steel, in Corrosion Hanbook, 11th edition, Outokumpu Oyj, Finland, (2015)
[4] Chater, J.: A Steel for all seasons: duplex expands its range, Stainless Steel World, Vol. (26), pp. 26-30, KCI, Zuthapen (2014)
[5] IMOA: Which Stainless Steel Should Be Specified for Exterior Applications, International Molybdenum Association, London, (2000)
[6] Industeel, Stainless steels, alloys and cladding grades, ArcelorMittal, rev.10., (2010)
[7] Heselmans, J. M., Van Dujin, J. E. H.: Stress corrosion cracking of stainless steels in swiming pools, Stainless Steel World, Vol. (13), KCI, Zuthapen, (2001)

MOULD PROOFNESS PROPERTIES OF CIRCULATING FLUIDIZED BED COAL COMBUSTION ASHES AS NEW ADDED PERFORMANCE VALUE

Július Strigáč[1], Pavel Martauz[1]

[1] Považská cementáreň a.s. Ladce (Povazska cement plant), Department of Quality and Strategy, Ul. Janka Krala, 018 63 Ladce, Slovakia, email: strigac.j@pcla.sk, martauz.p@pcla.sk

SUMMARY: The article deals with studying the anti-mould effect of circulating fluidized bed coal combustion (FBC) fly ash and bottom ash in comparison with the effect of fly ash from pulverized coal combustion (PCC) arised from coal-fired power plant boilers. Mould proofness properties were tested on the model fungi using the procedure given in the Czech national standard ČSN 72 4310 – Testing the mould proofness properties of building products and materials. A mixture of the model fungi Aspergillus niger, Chaetomium globosum, Penicillium funiculosum, Paecilomyces variotii and Gliocladium virens was used for testing. The scale for evaluating mould proofness properties according to ČSN 72 4310 is from 0 to 5 in degree of fungi growth, where a value of 0 means that no growth of fungi occurs and the building products and materials possess fungistatic properties. The study confirms the fungistatic propeties of FBC fly ash and FBC bottom ash, contrary to the effect of PCC fly ash, which is their new added performance value. The results of the PCC fly ash have demonstrated no mould proofness properties because of the PCC fly ash sample surfaces were fully 100 % covered by fungi and so the value of 5 of fungi growth degree was reached. However, no fungicide effect of FBC ashes was measured. The addition of fungistatic FBC ashes can increase the antimicrobial properties of the building materials and products and to ensure achieving fungistatic environment.

SVOJSTVA OTPORNOSTI NA PLIJESAN PEPELA NASTALIH IZGARANJEM UGLJENA U POSTUPKU KRUŽNOG FLUDIZIRANOG LOŽIŠTA

SAŽETAK: Proučen je učinak otpornosti na plijesan letećeg pepela dobivenog izgaranjem ugljena u postupku kružnog fluidiziranog ložišta (engl. circulating fluidized bed combustion, FBC) i pepela s dna u usporedbi s učinkom letećeg pepela dobivenog iz praškastog izgaranja ugljena (engl. pulverized coal combustion, PCC) nastalog u kotlovima energana pogonjenih ugljenom. Otpornost na plijesan ispitana je na modelima gljivica prema postupku u češkoj nacionalnoj normi ČSN 72 4310 – Ispitivanje otpornosti građevnih proizvoda i materijala na plijesan. Za ispitivanje uzeta je modelska mješavina gljivica Aspegillus niger, Chaetomium globosum, Penicillium funiculosum, Paecilomyces variotii i Gliocladium virens. Mjerilo vrednovanja otpornosti na plijesan su prema normi ČSN 72 4310 ocjene od 0 do 5 ovisne o rastu gljivica, pri čemu vrijednost 0 znači da ne dolazi do rasta gljivica i da građevni proizvodi i materijali imaju svojstvo otpornosti na gljivice. Istraživanje je potvrdilo da su leteći pepeo dobiven postupkom FBC i pepeo s dna otporni na gljivice dok leteći pepeo dobiven iz praškastog izgaranja ugljena (PCC) to nije, što je nova dodana vrijednost tog proizvoda. Rezultati letećeg pepela dobivenog postupkom PCC-a pokazali su da on nema svojstvo otpornosti na plijesan jer je površina tih uzoraka bila 100 % prekrivena gljivicama pa im je dodijeljena ocjena 5 za rast gljivica. Međutim, fungicidni učinak pepela iz postupka FBC nije mjeren. Dodatak pepela iz postupka FBC otpornog na gljivice može povećati antimikrobna svojstva građevinskih materijala i proizvoda i osigurati postizanje okoliša otpornog na gljivice.

1. INTRODUCTION

Bioactivity of living microorganisms on building materials is a serious problem because of reducing the utility properties and shortening the service-life of building materials and building structures by biocorrosion and subsequent biodeterioration [1, 2]. Conventional combustion of pulverized coal, which is the most common burning method used in coal-fired power and heating plants, carries out at high temperatures around 1200-1500 °C [3] resulting in high NO_X emissions and solid residues such as fly ashes from pulverized coal combustion (PCC). However, the high NO_X emissions connected with PCC fly ash formation have to be decreased by ammonia-based post combustion NO_X reduction systems [4]. There are the strict NH_3 limits for ammonia contamination of PCC fly ashes 50 mg/kg. On the other hand to PCC, the circulating fluidized bed combustion (FBC) takes place at much more lower temperatures only 800 – 900 °C [5]. This results in reduced NO_X emissions and in both a fine FBC fly ash and a coarse FBC bottom ash product. FBC technology is much more environmental than PCC technique in regard of the NO_X and SO_2 emissions, it does not need the ammonia-based post combustion NO_X reduction systems, therefore in the future FBC technology could be favourable and preferred combustion technique. However FBC technology brings additional problems with FBC fly and botton ashes. FBC fly ash differs from PCC fly ash as it is not fused or spherical, has lower content of melt and it is high in crystalline phases, in free lime CaO and calcium sulphate $CaSO_4$. Although this FBC fly ash is outside of the ASTM C-618 specification and European standards EN 197-1 and EN 450-1 [5], it contains also glassy silicates, has a relatively high surface area and has the potential to be both pozzolanic and cementitious [6]. While the PCC fly ash is commonly used as the component for production of cements according to standard EN 197-1 and concretes according to standards EN 450-1 and EN 206, the FBC fly ash and FBC bottom ash have considerably higher content of reactive calcium oxide CaO, usually from 15.0 to 35.0 % by mass and sulphur trioxide SO_3 from 7.0 to 18.0 % by mass. FBC ashes have usually lower content of glassy phase and a higher loss of ignition in comparison to PCC fly ashes. In regard to the chemical and mineralogical composition relating to the high content of reactive calcium oxide CaO and high content of calcium sulphate $CaSO_4$, the FBC fly ash and FBC bottom ash are characterized by the volume instability, undefined setting times and overall undefined setting and hardening process. FBC fly ash and FBC bottom ash have only limited practical utilization in building industry. However, construction applications have been identified as one of the major uses for FBC ashes [6]. In spite of these solutions of FBC ashes utilization, the global applying of FBC ashes in building construction industry is minimal and great amounts of FBC ashes are disposed in land-filling. It would be very advantageous to extend application purposes of FBC ashes in the field of building materials productions. Therefore this article deals in the antimicrobial potential of FBC ashes with focusing in the mould proofness properties of FBC ashes according to the method given in the Czech national standard ČSN 72 4310 [7].

2. EXPERIMENTAL

2.1. MATERIALS

Following samples were tested: circulating fluidized bed combustion (FBC) fly ash and bottom ash as well as fly ash from pulverized coal combustion (PCC) arised from coal-fired power plant boilers.

Table 1 Chemical composition of FBC fly ash (FBCFA), FBC bottom ash (FBCBA) and PCC fly ash (PCCFA)

wt.%	FBCFA	FBCBA	PCCFA
CaO total	25.86	32.99	4.43
SiO_2	40.99	36.23	54.44
Al_2O_3	21.24	17.05	27.38
Fe_2O_3	7.80	5.49	6.71
MgO	3.22	2.74	2.43
K_2O	0.99	1.21	3.49
Na_2O	0.31	0.11	0.08
SO_3 total	9.07	16.36	1.00
Cl^-	0.02	0.01	0.007
TiO_2	2.93	1.60	1.19
CaO free*	6.59	18.53	0.08
L.O.I.**	3.11	0.93	1.49
pH***	12.3	12.5	11.8

The chemical composition (semi-quantitative XRF analysis) of the tested samples was performed by X-ray fluorescence analysis (XRF) according to EN 196-2 using apparatus SPECTRO X-LAB 2000. The FBC and PCC ashes were ground to the specific surface area of 400 m^2/kg. The semi-quantitative XRF chemical composition of FBC fly ash (FBCFA), FBC bottom ash (FBCBA) and PCC fly ash (PCCFA) is given in Table 1 (* free lime CaO; ** L.O.I. – loss of ignition; *** pH of ash water leaches).

The mineralogical composition of the constituents is as follows: FBCFA is composed of quartz SiO_2, anhydrite $CaSO_4$, free lime CaO, anorthite CAS_2, hematite Fe_2O_3, magnetite Fe_3O_4; FBCBA is composed of quartz SiO_2, anhydrite $CaSO_4$, free lime CaO, calcite $CaCO_3$, hematite Fe_2O_3, magnetite Fe_3O_4; PCCFA is composed of quartz SiO_2, mullite $3Al_2O_3.2SiO_2$, hematite Fe_2O_3, magnetite Fe_3O_4.

2.2. METHOD OF TESTING THE MOULD PROOFNESS OF BUILDING PRODUCTS AND MATERIALS

The antifungal activity of the materials such as FBC fly ash, FBC bottom ash and PCC fly ash was tested using the procedure given in the Czech national standard ČSN 72 4310 [7]. The mould proofness properties expressed as the intensity of fungi growth on building products and materials are determined by both artificial and natural contamination, with exposure to the selected testing moulds under the prescribed conditions presented in [7]. The testing method is described in English [8], in detail. The scale of evaluation of the mould proofness properties of building products and materials according to [7], by which the degree of the fungi growth is expressed by a value from 0 to 5. The value 0 means that no growth of fungi occurs and the building products and materials possess fungistatic properties; in some cases fungicide properties also occured after the formation of an inhibiting zone in the broth around the sample. The building products and materials are not mould-proof, when the intensity of mould growth on the sample surface itself is from 1 to 5.

The testing has been realized in the accredited microbiological laboratory of Testing Institute for Textiles (Textilní Zkušební Ústav, s.p.) in Brno, Czech Republic. A mixture of fungi *Aspergillus niger* (CCM 8155), *Chaetomium globosum* (CCM 8156), *Penicillium funiculosum* (CCM F-161), *Paecilomyces variotii* (CCM F-566) and *Gliocladium virens* (CCM 8042) – cultures delivered from the Czech collection of microorganisms, has been used for the testing. The tested samples have been exposed to the contamination by the chosen microorganisms in the broth medium according to exactly defined conditions given in ČSN 72 4310 during the incubation period of 3 months, after which their mould proofness has been evaluated.

3. RESULTS AND DISCUSSION

After the 3 months incubation period, the mould proofness properties of the tested samples were evaluated; the results are given in Table 2.

Table 2 Test results of the mould proofness properties of FBC fly ash (FBCFA), FBC bottom ash (FBCBA) and PCC fly ash (PCCFA) according to ČSN 72 4310 [7].

Degree of fungi growth	Products with the mould proofness properties
0	FBCFA, FBCBA
5	PCCFA

The FBC fly ash, FBC bottom ash and PCC fly ash possess a different mould proofness properties, tested according to standard ČSN 72 4310 [7], depending on the amount of free lime CaO. The results imply that the higher the amount of free lime CaO in the ash, the more antimicrobially active the particular ash becomes. The mould proofness properties of the FBC fly ash and FBC bottom ash reach 0 degree of fungi growth. The results for the mould proofness properties of PCC fly ash reach 5 degree of fungi growth i.e. PCC fly ash does not have a fungistatic effect and the sample surface is fully covered by fungi (fungi colonies cover 100% of the sample surface). The inhibiting zone did not form on the agar around all of the tested samples. This means that the FBC fly ash and FBC bottom ash as well as PCC fly ash do not have a fungicidal effect. However, the results did show that the FBC fly ash and FBC bottom ash have a fungistatic effect. Moulds did not develop on the samples, but the mould growth on the agar was not affected. Generally speaking, the FBC fly ash and FBC bottom ash are suitable for reaching 0 degree of fungi growth according to standard ČSN 72 4310 [7]. On the basis of the results, it can thus be stated that the FBC fly ash and FBC bottom ash are defined as fungistatic building materials according to ČSN 72 4310 [7]. The fungistatic effect of FBC fly ash and FBC bottom ash is declared on the basis of reference testing, which was carried out in an accredited microbiological laboratory at the Textile Testing Institute (Textilní Zkušební Ústav, s.p.) in Brno, Czech Republic, which is an approved certification body. FBC fly ash and FBC bottom ash satisfying the requirements of ČSN 72 4310 [7] can be used for the production of fungistatic building materials and products.

However, FBC fly ash and FBC bottom ash increases pH values of the leaches up to 12.3 and 12.5, which affects the viability of microorganisms. This effect is similar to the effect of lime during sanitisation (hygienisation). Disinfection by lime at a wastewater treatment plant reduces the number of microorganisms extensively when operated at pH 11.2 [9]. Lime enables the destruction of all pathogens due to the pH effect it provides (alkaline hydrolysis), combined with the temperature increase that quicklime hydration brings (thermolysis) [9]. Of course, the thermolysis effect can be excluded in the case of FBC fly ash and FBC bottom ash in comparison with lime, but alkaline hydrolysis can be considered as an antimicrobial potential of FBC fly ash and FBC bottom ash. Alkaline hydrolysis (OH^-) results in the destruction of protein-based cellular walls and of enzymes, the destruction of proteins at polypeptide bonds to amino acids and oligopeptides, the destruction of nucleic acids RNA/DNA, the destruction of carbohydrate cell constituents and lipids and the denaturing of enzymes [10]. However, the mechanism of the antimicrobial effects of FBC fly ash and FBC bottom ash should be the subject of further study.

According to the results, the addition of fungistatic FBC fly ash and FBC bottom ash is suitable for achieving fungistatic protection. From a practical point of view, fungistatic FBC fly ash and FBC bottom ash are suitable for achieving a mould-free environment. FBC fly ash and FBC bottom ash potentially offer wide application possibilities from preventive use to the purposes of repairing and reconstruction. The application of FBC ashes reduces the overall costs for creation of microbially uncontaminated environment, which is their new added performance value.

4. CONCLUSIONS

The main conclusions that can be drawn from this experimental study may be summarized as follows: FBC fly ash and FBC bottom are fungistatic building materials according to the requirements of ČSN 72 4310; no growth of fungi is observed in FBC fly ash and FBC bottom ash; fungistatic FBC fly ash and FBC bottom ash are suitable for use in a wide scope of applications aimed at eliminating fungal growth, starting with preventive purposes and ending with repairing and reconstruction works; PCC fly ash does not have a fungistatic effect; FBC fly ash and FBC bottom ash as well as PCC fly ash do not have a fungicidal effect.

REFERENCES

[1] Cwalina, B.: Biodeterioration of concrete, Archit. Civ. Eng. Environ., Vol. 1 (2008) No. 4, pp. 133-140, ISSN 1899-0142

[2] George, R.P. & et al: Current understanding and future approaches for controlling microbially influenced concrete corrosion: a review, Concr. Res. Lett., Vol. 3 (2012) No. 3, pp. 491-506, ISSN 2180-1371

[3] Shen, X.: Coal combustion and combustion products, Chapter 3 Coal Technology (II), In Coal, Oil Shale, Natural Bitumen, Heavy Oil and Peat - Volume 1, ECUST China, Gao Jinsheng (Ed.), ISBN: 978-1-84826-467-0, China, (2009), pp. 1-21

[4] Higgins, B. & et al: ROFA and Rotamix System Reduced NOX below 200 mg/Nm3 at Elektrownia Opole, Proceedings of the 35th International Technical Conference on Clean Coal & Fuel Systems, Sakkestad, B.A. (Ed.), pp. 1-12, ISBN 9781617388040, Clearwater, June 6-10, 2010, Coal Technologies Associates, Clearwater, Florida, USA, (2010)

[5] Chindaprasirt, P. & Rattanasak, U.: Utilization of blended fluidized bed combustion (FBC) ash and pulverized coal combustion (PCC) fly ash in geopolymer, Waste Management, Vol. 30 (2010) No. 4, pp. 667–672, ISSN 0956-053X

[6] Stevens, W.; Robl, T. & Mahboub, K.: The cementitious and pozzolanic properties of fluidized bed combustion fly ash, Proceedings of the 2009 World of coal ash (WOCA) conference, pp. 1-13, Lexington, May 4 – 7, 2009, Lexington, KY, USA, (2009), Available from http://www.flyash.info/2009/042-robl2009.pdf; http://www.flyash.info/2009/196-stevens2009.pdf

[7] Czech national standard ČSN 72 4310: 1977 – The testing of mould proofness of building products and materials, 1977

[8] Strigáč, J. & Martauz, P.: Fungistatic properties of granulated blastfurnace slag and related slag-containing cements, Ceramics-Silikáty, Vol. 60 (2016) No.1, pp. 19-26, ISSN 0862-5468

[9] Grabow, W.O.K.; Middendorf, I.G. & Basson, N.C.: Role of lime treatment in the removal of bacteria, enteric viruses and coliphages in a wastewater reclamation plant, Applied and Environmental Microbiology, Vol. 35 (1978) No. 4, pp. 663–669, ISSN 0099-2240

[10] Remy, M.: Scientific evidence on the effectiveness of lime, Proceedings of the conference Animal health & welfare: a sustainable solution from industry, European Lime Association (EuLA) (Ed.), pp. 11-21, Brussels, 18th February 2009, EuLA c/o IMA-Europe, Brussels, Belgium, (2009), Available from http://www.eula.eu/; http://www.ima-europe.eu/

INVESTIGATION OF WEATHERING RESISTANCE OF HEMP CONCRETE

Yoann Castel[1], Sofiane Amziane[1], Mohammed Sonebi[2]

[1] Université Blaise Pascal, Institut Pascal, Polytech Clermont-Ferrand, 63174, Aubière, France, email: yoann.castel.12@gmail.com, sofiane.amziane@gmail.com
[2] Queen's University Belfast, School of Natural and Built Environment, Belfast, BT7 1NN, UK,
email: m.sonebi@qub.ac.uk

SUMMARY: Hemp concrete is relatively new, multi-facetted, sustainable construction material. It has a high porosity, which leads to it exhibiting mechanical behaviour different to that of more conventional building materials. Its thermal and acoustic properties, coupled with its ability to absorb carbon dioxide make it an exciting and interesting new material. Hemp concrete is used for about twenty years in France, and it is increasing, but its use stays minor compared to other materials, despite many research have been carry out to optimize its composition and determine its characteristics. This material being relatively new, it is still problematic to predict its durability through time. The aim of this paper is investigated the durability performance of hemp concrete, particularly the effect of the weathering on mechanical performance. In first stage, the study was focused on the investigation of the transport properties of hemp concrete, which have an impact on the attitude of the concrete under rainfall to absorb water. Therefore, the capillary absorption and full immersion tests were performed on hemp concrete. Different mix composition of concrete were tested to several weathering cycles, alternating full immersion and drying, while monitoring the evolution of volume and mass. This led to evaluate the consequence of rainfall on the mechanical performance of hemp concrete. These tests were carried out with different compositions already used in construction, and with different binders. The results of durability performance were discussed in this paper.

ISTRAŽIVANJE OTPORNOSTI NA OKOLIŠNA DJELOVANJA BETONA S KONOPLJOM

SAŽETAK: Beton s konopljom relativno je nov, mnogostrani održiv građevni materijal. Ima veliku poroznost zbog čega ima mehanička svojstva različita od većine konvencionalnih građevnih materijala. Njegova toplinska i akustička svojstva povezana s njegovom sposobnošću apsorpcije ugljičnog dioksida čine ga uzbudljivim i zanimljivim novim materijalom. Beton s konopljom upotrebljava se u Francuskoj oko dvadeset godina, njegova upotreba je u porastu, ali još uvijek vrlo mala u usporedbi s drugim materijalima unatoče tomu što su radi optimiranja njegova sastava i određivanja njegovih značajki provedena mnoga istraživanja. No još je uvijek upitno predviđati njegovu trajnost tijekom vremena. Svrha ovog rada istraživanje je trajnosti betona s konopljom, a posebno učinka okolišnih opterećenja na mehanička svojstva. U prvom koraku istraživanje je usredotočeno na svojstva betona s konopljom koji ima svojstvo da pri kiši upija vodu. Stoga su na betonu s konopljom provedena ispitivanja kapilarne apsorpcije i ispitivanje potpunog uranjanja. Ispitane su različite mješavine betona uz više ciklusa izlaganja naizmjenično potpunom uranjanjanju i sušenju pri čemu se opažala promjena obujma i mase. To je omogućilo vrednovanje posljedica djelovanja kiše na mehanička svojstva betona s konopljom. Ispitivanja su provedena s različitim sastavima koji se upotrebljavaju pri gradnji i s različitim vezivima. U radu su raspravljeni rezultati povezani s trajnošću.

1. INTRODUCTION

The construction of hemp into building materials is relatively new which had been introduced in the early 1990's in some European countries. In fact, there are now several hundred hemp buildings in France and Canada, the materials carrying out for hemp building. They are non-load bearing materials which have its advantages on a low environmental friendly used in building construction of high embodied energy and CO_2 emission [1]. Hemp is a very good natural insulation material and it has thermal conductivity, λ is very low. Comparisons between thermal conductivity and density were reported in literature [2]. Values were found to vary between 0.055 and 0.095 W/m K for densities between 240 and 440 kg/m^3 [2]

One of the most interesting renewable materials is hemp shiv. It is not only used for construction purposes, also for rope and cloth making. Again, Hemp can be used for wall, floors and roofs which can be mixed with lime or other binders to build an insulating, breathing composite.

It was reported that 60% of a hemp particle's volume is made up of air [3], and estimate the dry density ranged between 50 kg/m^3 and 100kg/m^3 [4]. This high porosity leads to a hemp fibre being able to absorb up to 4 times its own dry mass in water over 48 hours [5]. This ability to absorb may result in competition for water, between the binder - which requires it for hydration, and the shives, which could disrupt the mechanical abilities of the hemp concrete. Consideration must be given to this process when designing mixes. At present there is no standard for mix designs to serve as a guide for expected compressive strength results, but some researchers have reported their mix proportions for their results [6].

Concerning its durability, limited literature was reposted. Furthermore, The first hemp concrete house in France being approximately 20 years old, few observations and conclusions can been made on its long term durability. It seems that hemp concrete is quite resistant to freezing and salt damage and bio deterioration [7]. But this conditions are not the most commons, and the reaction of this concrete towards classic climatic condition are not obvious in the long run. Because of its open porosity and the high absorption capacity of the hemp shiv, hemp concrete is sensitive to water absorption and can absorb up to 300% of its mass in water [1, 2]. This absorption could have consequences on its cohesion between binder and fibres.. First, the absorption capacity was quantified with a capillary test on different formulations. Then, the hemp concrete was submitted through a weathering test, consisting of the alternation of drying and wetting cycles. Finally, the compressive strengths were measured to evaluate the influence of the weathering test on the mechanical performance of hemp concrete.

2. MATERIALS, MIX PROPRTIONS AND TEST METHODS

2.1. MATERIALS USED

Two different binders have been tested: the Tradical PF70 and the Prompt Natural Cement Vicat. The Tradical is a binder mainly made from aerial lime (75%) but also with some hydraulic binder (15%) and pozzolan (10%). It is a lime binder commonly used by professionals to realise hemp concrete. On the other hand, the Vicat Prompt Cement has properties closer to hydraulic binder. It is made by heating limestone mixed with clay, but at a lower temperature than Portland cement, thus allowing energy saving and a quicker hardening.

The aggregate used is the industrial hemp Tradical HF. The hemp shiv have been extracted from the hemp stem by grinding, sieving and refining, in order to guaranty similar granulometry and properties for each sample. It is also a product commonly used by professionals.

2.2. MIX PROPORTIONS AND MIXING METHOD

Three different formulations were selected. These formulations are similar to the ones used for hemp concrete houses and are from the professionals rules made by the French association "Construire en Chanvre" [8]. The formulations correspond to different uses of the concrete: rendering (mix A), shuttered wall (mix B), floor (mix C).

The binder used in each mix is the Tradical PF70 (TPF). But a forth mix, called mix A', similar to the rendering mix, will be realised with the Vicat Prompt Cement (VPC) to compare the binder.

Table 1. Mix proportions of all mixes

Component	Mix A	Mix A’	Mix B	Mix C
Binder type	TPF	VPC	TPF	TPF
Hemp shiv (H)	17 %	17 %	23 %	22 %
Binder (B)	36 %	36 %	31 %	41 %
Water (W)	47 %	47 %	46 %	37 %

The samples are made with a method implying a pre-soaking of the hemp shiv to reduce the problem of water absorption by the aggregate. The mixing procedure was:

- Hemp shiv is placed in a blender, then mixed during 2 minute 30, while adding 65% of the total amount of water
- The binder is added and the mixing continue for 30 seconds
- The rest of the water (35%) is added in the preparation, then mixed for another 2 minutes, for a total of 5 minutes
- The hemp concrete is then cast into the moulds, in which we previously apply a non-reactive release agent.

The samples 100x100x100 mm were made, and 50x50x200 mm for the swelling measurement. To optimize the mechanical resistance of the specimen, the hemp concrete is cast in three layers (two for the prism mould) and manually compacted [9]. Also, it is important to ensure the cohesion of each layer by scratching the surface of contact between each layer. The samples were left after 72 hours to ensure the solidity, then stored in a room at 21°C and 55% relative humidity until the tests.

2.3. TEST METHODS

2.3.1. CAPILLARY ABSORPTION

The capillary test is made on the 100x100x100 mm cubes. It is was carried out at 28 days after casting. The purpose of this test is to simulate a capillary rising in a wall. This method is based on EN 13057 standard relating to the determination of capillary absorption of concrete structures. A waterproof tape was applied around the circumference of the test piece. Test pieces were then placed in a plastic container on two steel bars (to ensure a water absorption only on the underside of the specimen). Finally, the container was filled with water until obtain an imbibition front of 8 mm. Water level was maintained to 8 mm during the time of the experiment (Figure 1).

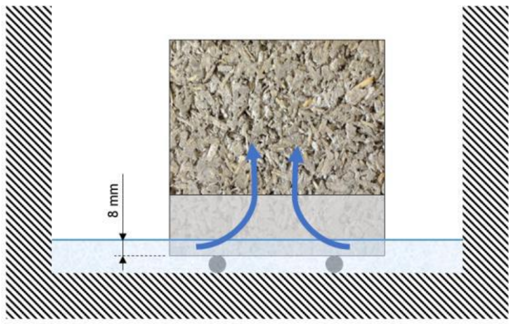

Figure 1. Capillary absorption test

2.3.2. WEATHERING TEST

This test begin 21 days after casting of the cubes. Its goal is to measure the variation of volume and mass of hemp concrete under large variations of humidity. To simulate this variation, the samples are placed in an oven at 50°C during 48 hours. Then they are immerged in water at 20°C for 48 hours. This 2 cycles are then repeated at least 10 times, and the mass and length of the samples are monitored between each cycle.

2.3.3. COMPRESSIVE STRENGTH TEST

The compressive resistance is measured before the weathering test started, as well as the end of these cycles, on the tested samples and on reference samples. It is measured with a mechanical press Zwick, with a loading speed of 3 mm/min. The samples are placed under the press with the compacted layers perpendicular to the base, which allowed to achieving the maximum strength [2].

3. RESULTS AND DISCUSSION

The results include first capillary absorption of the absorption following the mix and then a discussion about the impact of the weathering on the volume and mass change of the material and more important on the mechanical performance after several cycles.

3.1. CAPILLARY ABSORPTION OF HEMP CONCRETE

Following the absorption test described above, the variation of the mass of the cubes can be determined while the cube is plunged in 8 mm of water, therefore, the mean water absorbed by each mix can be calculated (Figure 2). Two phenomenon’s can be noticed. First there was a rapid absorption of the water, which leads to a mass rise between 14% and 16% in the first minutes, depending on the formulation. Then the absorption rate decreased over time. This absorption followed a logarithmic law, from which the sorption coefficient (Figure 3) was determined by quantifying the importance of the capillary action.

It can be noticed that the absorption capacity of the hemp concrete is very high. This is due to the open porosity of the concrete and to the hemp shiv, which have a high absorption capacity: it can absorb up to 300% of its mass in water [9].

From the results of capillary absorption test, two behaviours can be identified. The samples of mixes A and A' had a low initial absorption but a high sorption coefficient, in opposite to the mixes B and C which they had a high initial absorption and a low sorption coefficient. This behaviour is linked to density of the concrete and to the capillary action principle. The mixes A and A', containing less hemp shiv aggregate, is thus denser (around 400 kg/m^3) and less porous, and led in consequence to absorb less water when they were immersed in water. Contrary to mixes B and C, they were less dense (between 300 and 350 kg/m^3) and more porous, which were more able to absorb water.

But after this initial absorption, the sorption coefficient become more important and it can be seen that it was higher for mixes A and A' compared to mixes B and C. This can be explained by the nature of porosity in the hemp concretes. A high sorption coefficient shows a high capillary action, which can be attributed to a lower pore capillary diameters. Indeed, the capillary action is greater when the pore capillary diameter are very fine which led to more capillary tension. Thus, mixes A and A' are less porous with a thin capillary while the mix B and C are more porous with large capillary.

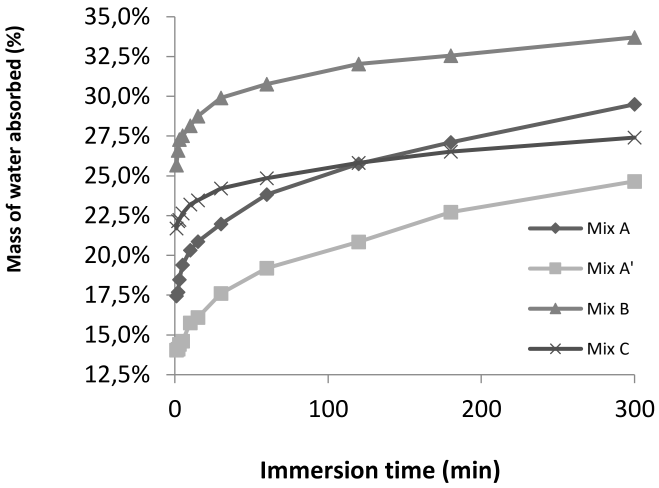

Figure 2. Capillary absorption of the samples

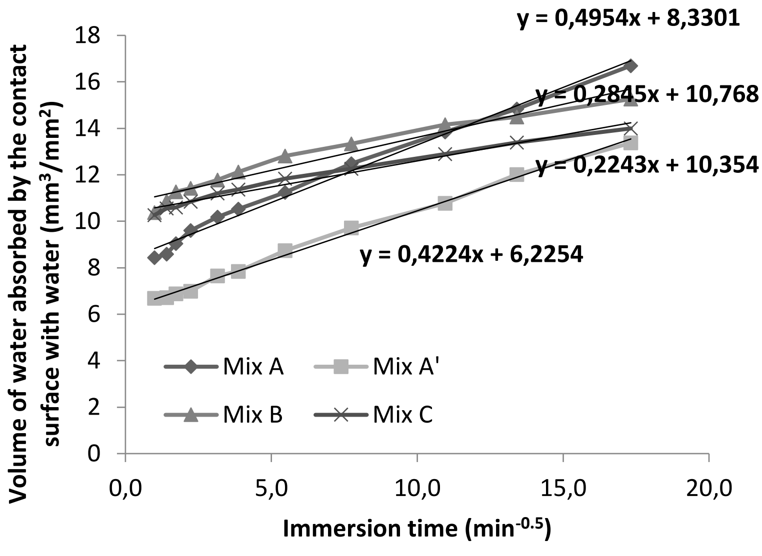

Figure 3 Capillary absorption as a function of square root of time (Sorption coefficient = slope)

3.2. WEATHERING CYCLES RESULTS

3.2.1. VOLUME VARIATION

Figure 4 presents the variation of length of sample after each cycle of dry and wet of wreathing cycle of 3 mixes A, A’ and C.

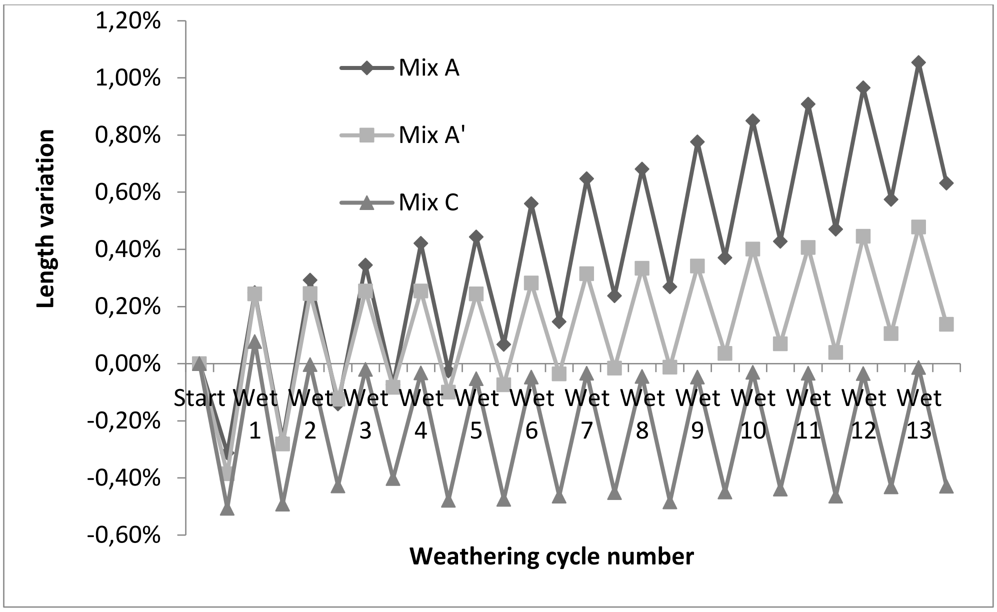

Figure 4 : Length variation of the samples after each cycle (There is no result for mix B, since the samples were broken during the first wetting cycle because of their low resistance)

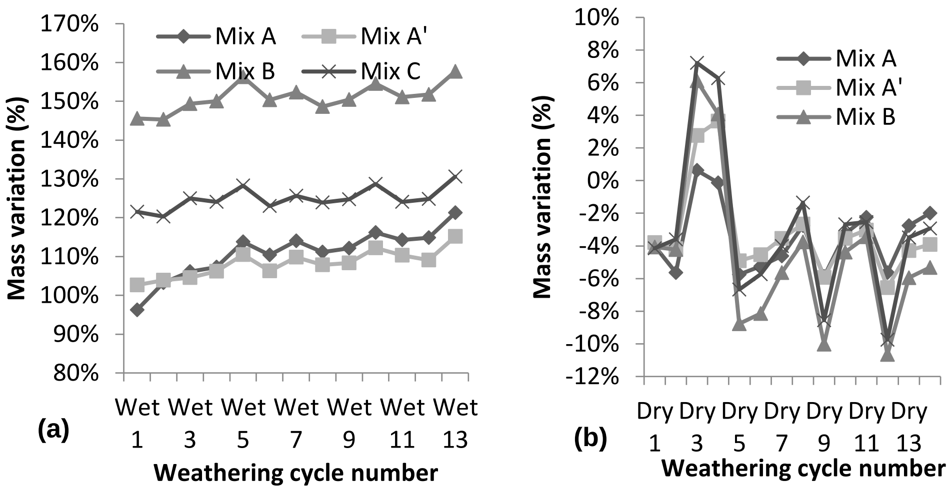

Figure 5 Mass variation of the samples after each immersion (a.) and drying cycle (b.)

The diagram above shows the variation of samples of 200 mm after each cycle. It can be observed that all mixes have the same pattern changes: the hemp concrete swelled after absorbing water and swelled after drying. But it can be noticed the variation of length are increased differently of the 3 mixes. The variations of volume of mixes A and A' kept increasing after each cycle of wreathing test, which seems to submit to irreversible deterioration of the samples, while the mix C always returned to initial volume after each cycle of weathering.

3.2.2. MASS VARIATION

As the same time as the variation of volume, the evolution of the mass is monitored at each cycle. Figure 5 presents the variation of mass during the weathering cycles of mixes A, A’, B and C. It can be observed that the dry mass stayed stable after each drying (Figure 5b.), the variation observed being rather due to measure imprecision, and that the mass after each wetting slightly increase slowly (Figure 5a.), especially for mixes A and A'.

These observations show that the water absorption can have a direct effect on the structure of the hemp concrete. Indeed, for mixes A and A', the volume increased after each cycle while the dry mass stayed stable, which implied a decrease of the density and an increase of the porosity. During the wetting phase, the hemp shiv absorbed the water and swelled, thus increasing the volume of the sample and deteriorating the binder matrix. And during the drying, the plant aggregates lost their water and shrinked, but the binder matrix stayed damaged, with new pores

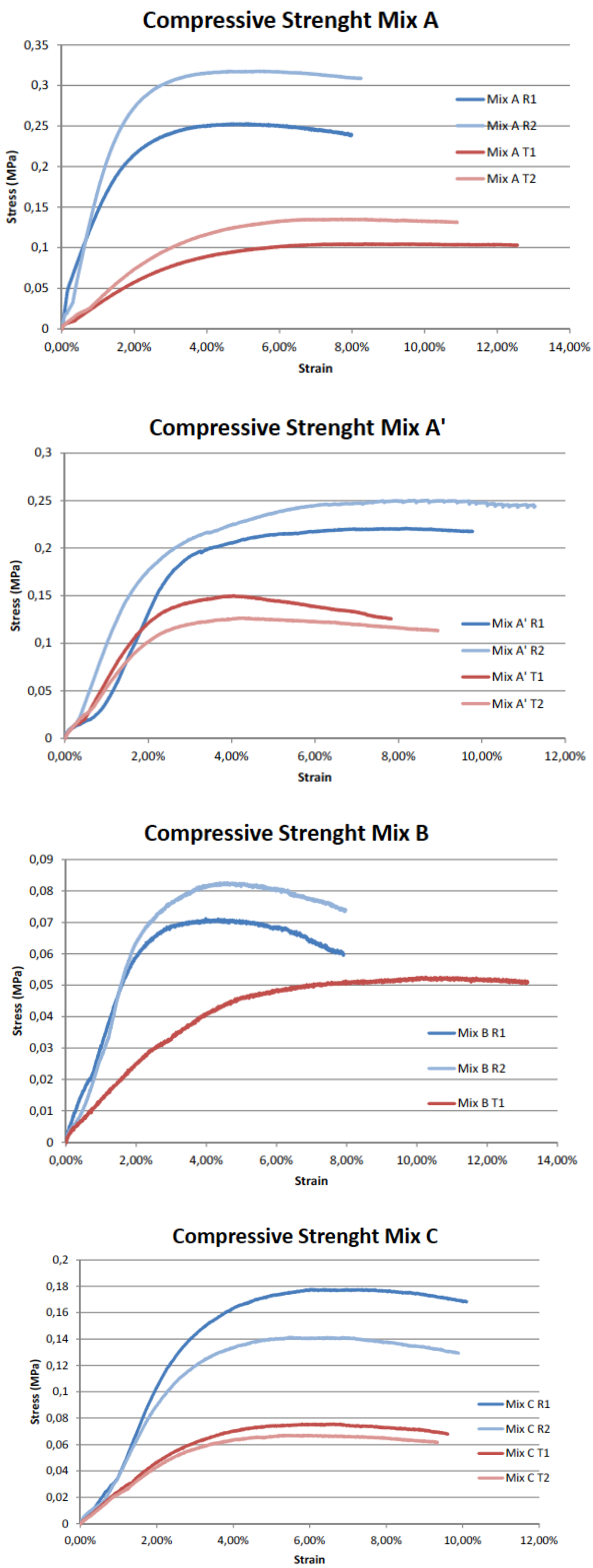

Figure 6 Compressive resistance of samples after the weathering test

open, hence the density dropped. This phenomenon is called capillary rupture. This also explained why after each immersion the mass of water absorbed increased, because of the newly open porosity.

In case of mix C, which had a constant volume after each drying, it was less affected by this phenomenon. It can be explained by the lower density and sorption coefficient, thus decreasing the risk of new pores appearing during the weathering cycles. It can be noticed that mix A' seems more resistant to the variation of volume than mix A, while they have the same formulation. Thus, the binder has a major effect on the resistance of the hemp concrete towards the water absorption.

3.1. MECHANICAL PROPERTIES BEFORE AND AFTER DETERIORATION

The diagrams show the compressive resistance of the samples that went through the weathering test (indicated by mix T1 or T2) and of the references samples (indicated by mix R1 or R2) in Figure 6.

The hemp concrete has behaviour close to conventional concrete, with an elastic phase followed by a plastic phase. However, it can be noticed a difference between the test samples and the reference sample. The samples tested had a maximum compressive resistance between 30 and 50% smaller compared to the reference samples, and the Young modulus is greatly decreased too.

This loss of resistance can also be explained by the water absorbed by the hemp shiv. When the hemp shiv aggregates were soaked with water, they swelled and deteriorated the binder matrix but also the adhesion at the interface zone between the binder and the hemp particles. The degradation of these adhesions, which contributed largely to the mechanical resistance of the hemp concrete, had thus direct and significant consequences on the compressive resistance. It can be observed that mix C, even if it did not show irreversible volume variation through the weathering cycles, lost significantly the compressive strength than the other mixes. This demonstrated that the binder matrix was affected. This is not due to the variation of the density, but the interfacial transition zone between the hemp shiv aggregate and the binder was certainly weaker after the weathering cycles.

4. CONCLUSION

In conclusion, the hemp concrete appears to be a material really sensitive to water damage. Because of the high absorption capacity of the hemp shiv and the open porosity of the concrete, it is a material sensitive to the capillary action. And when the water absorb is too important, the aggregate swell and cause a capillary rupture in the concrete, leading to volume variations and, above all, a drop of the compressive resistance, up to 50%, due to the degradation of the binder matrix. This is particularly true for dense and less porous concrete.

It is important to point out that the weathering test is exaggerated compared to real climatic condition, where the absorption of hemp concrete cannot be similar to lab weathering cycle test. But it gives us an overview of the behaviour of the hemp concrete in the long term, after suffering many cycles of weathering.

Thus, to limit the deterioration, it is important to protect the construction in hemp concrete from extreme capillary absorption, like rinsing damp. One way to protect the hemp concrete would be to use a hydrophobic product during the fabrication on the concrete, to prevent the absorption of water by the hemp shiv. The Vicat binder seems also, in lower proportions, less sensible to these water damages. Finally, the use of a different plant aggregate, with a lower absorption capacity, should also limit the deterioration cause by water absorption.

REFERENCES

[1] Amziane, S., Sonebi, M., “Overview on Biobased Building Material made with plant Aggregate”, RILEM Technical Letters, Vol. 1, 2016, pp. 31-38.

[2] Page, J., Sonebi, M., Amziane, S. “Experimental Investigation on the Performance of Hybrid Hemp-Flax Composite Materials”, Proceedings of the First International Conference on Bio-Based Building Materials, Ed. Amziane, S., Sonebi, M., Clermont-Ferrand (France), RILEM Publications s.a.r.l., pp. 243-250.

[3] Nguyen, T.T.; Picandet, V.; Amziane, S.; Baley, C.; Influence of compactness and hemp hurd characteristics on the mechanical properties of lime and hemp concrete. European Journal of Environmental and Civil Engineering, 2009, Vol. 13, No. 9, pp. 1039-1050.

[4] Elfordy, S.; Lucas, F.; Tancret, F.; Scudeller, Y.; Mechanical and thermal properties of lime and hemp concrete (“hempcrete”) manufactured by a projection process. Construction and Building Materials, 2008, Vol. 22, No. 10, pp. 2116-2123.

[5] Nozahic, V.; Amziane, S.; Torrent, G.; Saïdi, K. et al. “Design of green concrete made of plant-derived aggregates and a pumice–lime binder”. Cement & Concrete Composites, 2012, Vol. 34, No. 2, pp. 231-241.

[6] Amziane, S., Sonebi, M., Proceedings of the First International Conference on "Bio-Based Building Materials", ICBBM-2-15, Proceedings PRO 99, Ed. Amziane, S., Sonebi, M., Clermont-Ferrand (France), 21-24 June 2015, RILEM Publications s.a.r.l., 746 p.
[7] Walker, R.; Pavia, S.; Mitchell, R.; An assessment of the physical properties. Construction and Building Materials, 2014, Vol. 61, No. 30, pp. 340-348.
[8] Association Construire en Chanvre; FFB ; Règles professionnelles d'exécution d'ouvrages en béton de chanvre, Ed. SEBTP, 2007.
[9] Nguyen TT., Picandet V., Carre P., Lecompte T., Amziane S., Baley C., Effect of compaction on mechanical and thermal properties of hemp concrete, Eur. J. Environ. Civ. Eng. 14 (2010) 545–560.

WATERPERMEABILITY OF CONCRETE – MECHANISM, METHODS, EXPERIENCE

Nikola Uzunov[1]

[1] ADING AD Skopje, Novoselski Pat bb. 1000 Skopje, Macedonia, email: uzunov@ading.com.mk

SUMMARY: Main topic of these article is testing the resistance of concrete with different strength class, produced using different admixtures, to penetration of water under pressure. For these reason, comparative testing is conducted with four different types of concrete with strength class C25/30 and C30/37, produced using different admixtures – Plasticizers and Superplaticizers. Furthermore, for concrete with strength class C25/30, different water-resisting admixtures were used – based on sulfate and silane siloxane. All concretes are produced at industrial batching plant, in order to demonstrate admixtures effect in real conditions. Testing is conducted according to European standards EN 12390-8 Depth of penetration of water under pressure, as well as EN 480-5 Determination of capillary absorption. Finally, review is given to the construction of the concrete arch dam „Sv.Petka" build at the Treska river, near Skopje, as a positive example how adequate technology for production, transportation and curing of concrete can provide excellent results.

VODOPROPUSNOST BETONA – MEHANIZAM, METODE ISPITIVANJA I PRAKTIČNA ISKUSTVA

SAŽETAK: U radu je prikazano ispitivanje otpornosti na prodor vode pod tlakom kod različitih tipova betona različitih razreda čvrstoće, izrađenih primjenom različitih vrsta dodataka za beton. Provedeno je usporedno ispitivanje četiriju različitih vrsta betona razreda čvrstoće C25/30 i C30/37 proizvedenih primjenom dodataka iz skupine plastifikatora ili superplastifikatora. Dodatno, kod betona razreda C25/30 upotrijebljeni su i specijalni dodaci za vodonepropusnost na osnovi sulfata i silana-siloksana. Svi su betoni proizvedeni industrijski u tvornici betona s ciljem da se sagleda učinkovitost dodataka u realnim uvjetima. Ispitivanje je provedeno sukladno europskim normama EN 12390-8 Dubina prodora vode pod tlakom i EN 480-5 Određivanje kapilarnog upijanja. Dodatno je prikazano iskustvo pri izvođenju betonske lučne brane Sv. Petka na rijeci Treski u blizini Skopja. Pokazano je kako se pravilnom primjenom adekvatne tehnologije za proizvodnju, transport i njegu betona mogu postići vrhunski rezultati.

1. UVOD – MEHANIZMI PRODORA VODE U BETONU I METODE ISPITIVANJA

Po svojoj prirodi, beton je *hidrofilni* materijal i ne može da bude 100% otporan na prodor vode. Struktura cemntnog maltera (a time i samog betona) je porozna – u malteru neminovno postoje mikro prsline i pore kroz koje voda može da prodre u beton. Prodiranje vode može da bude posledica hidrostatskog pritiska, ili kapilarnih pojava.

Prodor vode u strukturu betona kako posledica aktivnog hidrostatskog pritiska je slučaj na koji su izloženi hidrotehnički objekti (brane, prelivnici, pristanišni objekti), bazeni i rezervari, temelji i drugi ukopani delovi konstrukcije koji se stalno ili povremeno nalaze ispod nivoa podzemne vode. Otpornost betona na prodor vode pod pritiskom (VDP betona), zavisi prvenstveno od čvrstoće betona i načina njegovog ugrađivanja i nege. Beton visoke čvrstoće, koji je homogen, dobro ugrađen, vibriran i negovan, ima zatvoreniju strukturu i monogo manju mogućnost za prodor vode. Evropski standard *EN 12390-8 Depth of penetration of water under pressure* [1] definiše način ispitivanja nepropusnosti betona na prodor vode pod priskom. Standard predviđa izlaganje betona na konstantni vodeni pritisak od 5,0 Bar, u trajanju od 72 sata (Slika 1). Projektantima ostaje da sami odrede koja otpornost na prodiranje vode zadovoljava uslove na određeom projektu – naravno, uzimajući u obzir stepen izloženosti betona u datoj konstrukciji.

Slika 1: Ispitivanje otpornosti betona na prodor vode pod pritiskom

Drugi način na koji voda može da uđe u beton je kapilarno upijanje – prenos vode kroz sistem kapilarnih prslina prisutnih u betonu. Da bi došlo do pojave kapilarnog upijanja nije potrebno da postoji značajan hidrostatski pritisak - dovoljno je da beton bude u kontaktu sa vodom ili vlagom. Kapilarna vlaga u betonu često se "penje" i prodire u delove konstrukcije koji nisu direktno u kontakt sa vodom (Slika 2).

Slika 2: Efekt kapilane apsorpcije vode u betonu

Smanjenje mogućnosti za pojavu kapilarne apsorpcije vode u betonu postiže se na način što se proizvede beton visokih performansi, koji je pravilno ugrađen i ima zatvoreniju strukturu. Dodatno, primenom specijalizovanih aditiva za beton (Hidrofob-T) postiže se formiranje vodo-nerastvorljivih kristala koji (delimično) zatvaraju strukturu betona.

Najefikasniji način za sprečavanje kapilarnog upijanja vode u betonu je upotreba aditiva na bazi *silana-siloksana* (Hidrofob-21), koji utiču na površinski napon betona, praveći da betonska površina odbija molekule vode koji ne mogu da prodru u kapilare u betonu. Na taj način postiže se da površina betona postane visoko hidrofobna, odnosno *Vodorepelentna* (Slika 3). Isti materijali (najčešče prilikom sanacija) mogu da se koriste i kao premazi za površinsku impregnaciju betona (*EN1504-2, metoda 1-hidrofobna impregnacija*).

Slika 3: Vodo-repelentna betonska površina

Evropski standardi predviđaju više metoda kako da se utvrdi stepen otpornosti na kapilarnu apsorpciju vode kod betona i drugih građevinskih matrjala koji imaju otvorenu stukturu. Prema standardu *EN480-5 Determination of capillary absorbtion [2]*, ispituje se količina apsorbirane vode nakon 7 dana (ispitivanje se vrši na standardni malter, i ispituje se u odnosu na etalon). Uzorci se čuvaju u zatvorenoj komori, postavljeni na rešetku, konstantno potopljeni u vodi visine 2-4mm (Slika 4). Nakon 7 dana meri se masa uzoraka i određuje količina apsorbirane vode. Naša su laboratoriska ispitivanja pokazala smanjenje kapilarne apsorpcije vode kod uzorka maltera sa dodatkm Hidrofob-21 (dozaža 0,7%) za oko 75% u odnosu na etalon (po standardu mora da bude više od 50%). Drugi deo ispitivanja vrši se testiranjem kapilarne apsorpcije na 90 dana star uzorak, tretiran u vodi 28 dana. Naša su laboratoriska ispitivanja pokazala smanjenje kapilarne apsorpcije vode kod uzorka maltera sa dodatkom Hidrofob-21 (dozaža 0,7%) za oko 70% u odnosu na etalon (po standardu mora da bude više od 40%). Ova se ispitivanja vrše se redovno, a rezultati su objavjeni i dostupni u Izveštaju za kontrolno ispitivanje gotovog proizvoda br.KI-08/16 materijala HIDROFOB-21, Ading AD Skopje [6], kao i u Izjavi za svojstva materijala HIDROFOB-21, Ading Ad Skopje [7]).

Slika 4: Ispitivanje otpornosti betona na kapilarnu apsorpciju

Druga metoda za određivanje kapilarne apsorpcije koju smo primenili je *Karsten tubes* metoda. Prema ovoj metodi ispituje se volumen vode koji se apsorbovao - "upio" u neki medium za određeno vreme. Aplikacija vode vrši se preko cevi - *Karsten tube* (Slika 5), koja se fiksira na površinu poroznog mterijala. Ovim metodom se ispituju i različiti materijali koji su površinski impregnirani (beton, malter, prirodni kamen, opeka).

Slika 5: Karsten tube metoda

2. EKSPERIMENTALNO ISTRAŽIVANJE OTPORNOSTI BETONA NA PRODOR VODE POD PRITISKOM

Sa ciljem da se utvrdi kako različiti performansi betona i aditivi utiču na otpornost betona na prodiranje vode pod pritiskom (*EN 12390-8)*, sproveli smo uporedno ispitivanje vodo-nepropusnosti na tri klase betona. Beton je proizveden na fabrici betona koristeći standardne recepture za proizvodnju – samo je dodatak za vodonepropusnost bio dodat naknadno u mikser. Korišćen je cement TITAN "Usje" – Skopje, CEM II/A-V 42.5 R. Agregat je krečnjaćkog porekla, drobljeni, osim frakcije 0-4mm koja je mešana sa 20% peska rečnog porekla. Betoni su 4-frakciski, sa maksimalnom frakcijom do 32mm. Konzistencija betona je visoke klase S3 i S4. Ispitivanja su izvršena u nezavisnoj akreditovanoj laboratoriji GIM – Skopje [4].

Tablica 1: Uporedno istraživanje otpornosti betona na prodor vode pod pritiskom

Klasa betona	Količina cementa [kg/m³]	Plastifikaor / Superplastifikator	Aditiv za vodonep.	Konz. *Slump*	Zapreminska masa betona [kg/m³]	Čvrsoća betona [MPa]	Prodor vode [mm]
C25/30	360	Fluiding-M	/	S3	2364	43,6	35
C25/30	360	Fluiding-M	Hidrofob-T (1%)	S3	2353	46,8	21
C30/37	390	Superfluid-21M EKO	/	S4	2413	58,2	19

Rezultati pokazuju da na otpornost betona na prodiranje vode pod pritiskom utiču čvrstoća betona, kvalitet ugradnje, zbijenost i homogenost betona. Svi ovi činioci doprinose da struktura betona bude zatvorenija i da smanji procenat mikroprslina kroz koje voda može da prode u beton. Postižu se upotrebom aditiva za beton od grupe Superplastifikatora, koji omogućuju redukciju vode u betonu, veće čvrstoće i kvalitetniju ugradnju betona. Dodatno, upotrebom specijalizovanih aditiva za VDP beton, postiže se zatvaranje pora u betonu i dodatno smanjuje se mogućnost za prodiranje vode (Tablica 1).

Ispitivanja kapilarne apsorpcije *Karsten tubes* metodom obuhvatila je dve klase betona sa različitom čvrstoćom koji su tretirani materijalom za hidrofobnu impregnaciju na bazi Slana-siloksana Hidrofob-21. Ispitivanje se vrši u odnosu na etalon - beton koji nije tertian materijalom za hidrofobnu impregnaciju. Prvo je testiranje izvršeno na 4-frakciski beton, proizveden u labaratoriji, klase *C30/37, dmax=32mm,* proizveden sa *350kg/m³ CEM I (Cementara TITAN "Usje" – Skopje).* Konzistencija betona je klase S4. Ova klasa betona je izabrana je jer se taj beton najačešče upotrebljava za izvođenje objekta u okruženju gde je visok stupanj izloženosti (Tablica 2).

Tablica 2: Uporedno istraživanje kapilarne absorbcije vode u betonu klase C30/37

Etalon	t (min)	0	10	25	100	160	225	245
	V(ml)	0	0,5	1	2,3	3,1	3,7	4
Beton tertian Hidrofob-21	t (min)	0	36	113	153	240	/	/
	V(ml)	0	1	2	2,3	3	/	/

Drugo testiranje izvršeno je na Beton klase *C 0.70 (EN 1766) sa 275kg/m³ CEM I i čvrstoćom na pritisak od 25-35MPa.* Ova klasa betona je izabrana zbog relativno niske količine cementa (i relativno niskih čvrstoća na pritisak), tako da su ovi betoni više podložni na kapilarnu absorbciju u odnosu na beton klase C30/37 (Tablica 3).

Tablica 3: Uporedno istraživanje kapilarne absorbcije vode u betonu klase C 0,70 (EN 1766)

Etalon	t (min)	0	12	26	42	62
	V(ml)	0	1	2	3	4
Beton tertian Hidrofob-21	t (min)	0	60	120	240	480
	V(ml)	0	0	0	0	0

Velika razlika u efektu površinske impregnacije betona je posledica različitog kvaliteta, odnosno različite otvorenosti strukture i poroznosti materijala za dve klase betona. Slabiji beton klase C 0.7 ima otvoreniju strukturu i u njemu lakše prodire aditiv

Hidrofob-21. Zbog toga je i efekat površinske hidrofobne impregnaciji bolji – dobijena je kompletno vodo-repelentna površina betona.

3. ISKUSTVO – TEHNOLOGIJA IZVOĐENJA LUČNE BRANE "SV. PETKA"

Veliki hidrotehnički objekti - pre svega betonske brane, zahtevaju beton koji ima izuzetne performance u pogledu otpornosti na prodor vode. Dodatno, vakvi objekti se po pravilu izvode u masivne betonske kampade gde su od prvenstvenog značaja temperaturni efekti koji se javljaju kao posledica hidratacije cementa.

Jedan takav primer je brana u okviru Hidrosistema "Sv. Petka" na reci Treska, u blizini Skopja. *Sv.Petka* [5] je tanka lučna brana sa dvojnom zakrivenošču – po horizontalnom i vertikalnom pravcu (Slika 6). Visina brane je 64m, a debjina u osnovi 10m, koja se postpeno umanjuje da bi na kruni brane dostigla 2m širine. Dužina luka u kruni brane je 115m, dok je u osnvi 25m. Na desnom bregu izveden je gravitacioni blok za premošćivanje slabijih zona u stenskom masivu. Po vertikali, brana ja podeljena na 10 lamela, sa 9 vertikalnih radijalnih dilatacija (fuga), koje se injektiraju cementnim materijalom nakon maksimalnog otvaranja (završenog procesa skupjanja betona i hlađenja konstrukcije u zimskom periodu). Injektiranje vertikalnih dilatacija se vrši pomoću dva nezavisna sistema čeličnih cevi i zatvarača. Sama kontaktna površina je nazubjena sa ciljem da se obezbedi bolji kontakt i monolitizacija betonskih blokova. Širina otvorenih radijalnih fuga je 2-4mm, a pritisak u toku injektiranja dostiže do 5Bar. Kroz telo brane prolaze dve čelične cevi – povezane sa dve zahvatne konstrukcije – kojima se voda iz akumulacije uvodi u hidro-elektranu koja je postavjena neposredno uz nizvodnu stranu brane. Sama akumulacija je dužine 11km, i ukupnog volumena vode $9,1x10^6$ m^3.

Slika 6: Brana "Sv.Patka"

Tehnologija betona je predviđala je ipunjivanje više uvjeta sa ciljem da se obezbedi monolitnost i vodonepropusnost konstrukcije. Sam je beton dizajniran da bude 6-frakciski, sa maksimalnom granulacijom agregata do 100mm. Sa ciljem da se što više umanji oslobođena hidrataciona toplota, korišćen je specijalno proizveden nisko-kalorični cement TITAN "Usje" Np35p 35 – količina maksimalno 280 kg/m^3. Zahtevana marka betona je bila MB30, ali je tražena i čvrstoća na savijanje od 4-4,5MPa (da bi se samnjila mogućnost pojave pukotina u betonu), zbog čega je proizvedeni beton imao približno W/C=0,465 i čvrstoće na pritisak mnogo veće od zahtevanih (iznad 50MPa). Zbog krupnoće adregata (100mm), čvrstoće betona su ispitivane na uzorcima dimenzija 300x300x300mm i grede 300x300x900mm. Proizvedeni beton je u potpunosti ispunio i zahtevane performance u pogledu vodonepropusnosti V-8 i otpornost na mraz M-100.

Konzistencij betona bila je S1, a transport i ugrađivanje vršeni su kiblama. Vibriranje ja vršeno paketom od 4 "boca" – pervibratora. Tehnologija ugrađivanja betona u telo brane predviđala je betoniranje u blokovima visine 2m, u slojevima debljine ~50cm (Slika 7). Svaki je novi sloj morao da bude ugrađen na predhodni sloj kd kog još nije počelo vezivanje cementa (u roku od 2-3 sata) tako da su dva sloja mogli da budu zajedno revibrirani i homogenizirani.

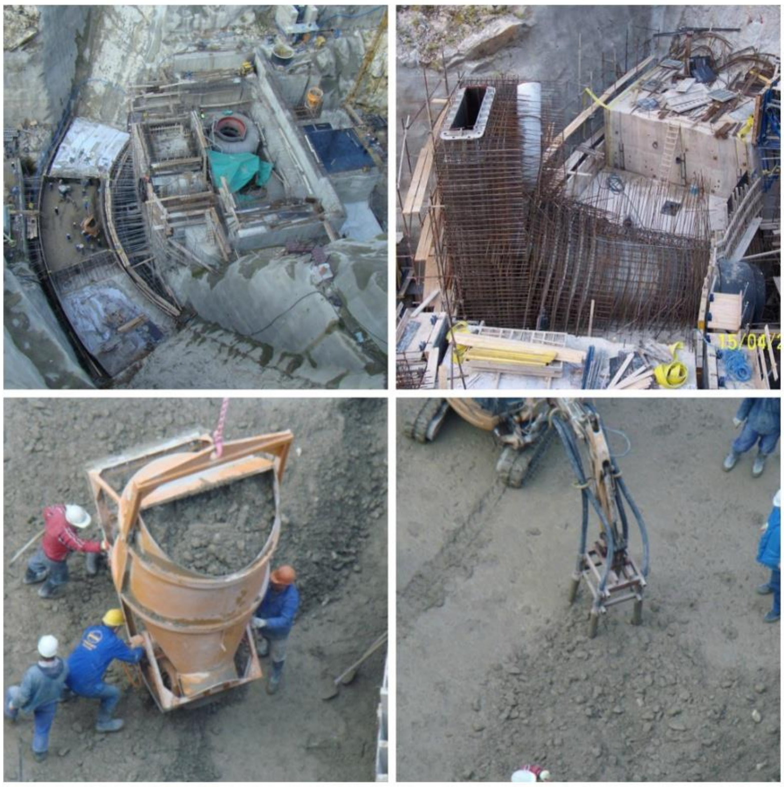

Slika 7: Brana “Sv.Patka”, Ugradnja betona

Da bi mogao da se proizvede i pravilno ugradi beton traženih performansi korišćen je SUPERFLUID-M1 (proizvodnja ADING AD Skopje) - Aditiv Superplastifikator-Retarder vezivanja betona, u saglasnosti sa EN 934-2 T11.1 i T11.2, proizveden na bazi naftalin-lignosulfonata. Dozaža aditiva je iznosila od 1,2-1,6% u odnosu na masu cementa u zavisnosti od pozicije i ambientalnih uvjeta (temperature). Temperatura betona je bila ogrničena na +40ºC i praćena je u toku vezivanja betona preko ugrađene opreme za monitoring gradnje i eksploatacije.

Veza između horizontalnih blokova ostvarena je direktnom ugradnjom starog na novi beton, pri čemu površina starog betona-bloka je obrađivana u roku od 5-6 sati nakon ugradnje pranjem cementnog mleka vodom pod pritisak dok se ne izloži krupni agregat. Pre ugrađivanja novog betonskog bloka, podloga se još jednom pere vodom, pri čemu se i stari beton način “zasiti” vodom i obespraši. Na kontaktu, kao prvi sloj novog betona predvеđeno je ugrađivanje sitnozrnog betona (Slika 8).

Slika 8: Brana “Sv.Patka”, Veza između horizontalnih i vertikalnih betonskih blokova

Glavni izvođač hidrosistema “Sv.Petka” je kompanija RIKO Inžinjering, Slovenija, podizvođač za konstukciju brane je kompanija GRANIT Skopje, podizvođač za mašinska postrojenja je BETON Skopje, dok je injektiranje izvršio Građevinski Institut MAKEDONIJA, Skopje. Korišćeni aditivi za beton su iz proizvodnog programa kompanije ADING AD Skopje.

4. ZAKLJUČAK: ADEKVATNA TEHNOLOGIJA PROIZVODNJE I UGRAĐIVANJA BETONA - KLJUČNI FAKTOR VISOKE OTPORNOSTI NA PRODOR VODE

Sva izvršena ispitivanja, kao i praktična iskustva ukazuju da je kvalitet betona ključni factor za obezbeđivanje visoke otponosti betona na prodor vode. Beton visoke klase čvrstoće, koji je kvalitetno ugrađen i negovan ima zatvoreniju strukturu i visoku otpornost na prodiranje vode. Dodatno, upotrebom specijalizovanih aditiva za vodonepropusnost betona može da se postigne dodatno smanjenje propustlijvosti betona na prodor vode pod pritiskom I kapilarne absprbcije. Kod već izvedenih betonskih konstrukcija, sa ciljem da se smanji-spreči kapilarna absorbcija vode, može da se primeni hidrofobna impregnacija materijalom na bazi Silana-Siloksana koji obezbeđuje vodorepelentnost površine betona.

LITERATURA

[1] Evropski standard EN 12390-8 Depth of penetration of water under pressure
[2] Evropski standard EN480-5 Determination of capillary absorbtion
[3] Uzunov, N. Jancev, D: Trajnost betona izloženog na dejstvo vode,atmosferskih uticaja i hemisku koroziju, Simopzium DGKS, Zlatibor, R.Srbija, Septembar 2016
[4] Gradežen Institut Makedonija – Skopje, Izveštaj za ispituvanje Br. ABK-06/15/370 – 1/2/3 Juni 2015
[5] Slavevski, M. Izgradba na branata “SV.Petka”, 16 Megunaroden Simpozium DGKM Ohrid, R,Makedonija, Oktobar 2015
[6] Izveštaju za kontrolno ispitivanje gotovog proizvoda br.KI-08/16 materijala HIDROFOB-21, Ading AD Skopje
[7] Izjava svojstva materijala HIDROFOB-21, Ading Ad Skopje

TOPIC 3.

Sustainable building design

Projektiranje održivih zgrada

ENERGY EFFICIENT BUILDINGS IN PRACTICE

Silvio Novak[1]

[1] Knauf Insulation d.o.o., Varazdinska 140, 42220 Novi Marof, Croatia, email: silvio.novak@knaufinsulation.com

SUMMARY: With the aim of reducing energy consumption in the building sector, the obligation of all EU member states is to embrace the new standards of construction - low-energy and nearly zero energy buildings (nZEB). Energy efficient buildings, in addition to the criteria of significantly reduced energy consumption, they must also meet the requirements of healthy and comfortable indoor climate. Design of these buildings is a complex, multidisciplinary field that requires mutual cooperation of various technical professions. Low-energy and nZEB buildings can be theoretically calculated, but the question is whether they can be built to perform as designed, and most importantly, will they ensure the highest standards in terms of good and healthy indoor air. There is a gap between the ''calculated'' and ''real'' consumption which can be the result of, among other things, quality of construction works and conditions of use. The calculations assume, depending on the type and use of the building and climate, conditions of use that differ from the actual user behavior. User behavior is difficult to predict. This paper presents a system for monitoring energy consumption and domestic hot water in 6 apartments in a multi-family house (energy class A) in city of Varazdin. Conditions of external and internal temperatures in apartments were monitored to gain an insight into occupant's behavior and the resulting consumption. The analysis of results reveled the deviations between ''calculated'' and ''real'' consumption of each observed apartment. Deviations can be explained as a result of different apartment orientations and boundary conditions of envelopes, but also as a result of the user behaviour. A significant reduction of energy consumption in December 2016 was noticed compared to the same month in 2015, and it was noticed in apartments whose occupants have accepted the system of monitoring consumption.

ENERGETSKI UČINKOVITE ZGRADE U PRAKSI

SAŽETAK: S ciljem smanjenja potrošnje energije u sektoru zgradarstva, obveza svih zemalja članica EU usvajanje je novih standarda gradnje – niskoenergetskih zgrada i zgrada gotovo nulte energije. Energetski učinkovite zgrade, osim kriterija znatno smanjene potrošnje energije moraju također zadovoljiti kriterije zdrave i ugodne unutarnje klime. Projektiranje takvih zgrada predstavlja složeno multidisciplinarno područje koje zahtijeva međusobnu suradnju različitih tehničkih struka. Proračunima je moguće „izvesti" takve zgrade, no postavlja se pitanje hoće li one i u stvarnosti biti takve te ono što je najbitnije, hoće li osigurati najviše standarde vezane za povoljnu i zdravu mikroklimu unutarnjih prostora. Prisutan je raskorak između "proračunske" i „stvarne" potrošnje što može biti posljedica, između ostaloga, kvalitete gradnje i uvjeta upotrebe zgrade. Proračunima se pretpostavljaju, ovisno o tipu i namjeni zgrade te klimi, uvjeti upotrebe od strane korisnika čije ponašanje je u stvarnosti teško predvidjeti. U radu je prikazan sustav praćenja potrošnje energije za grijanje i pripremu potrošne tople vode za 6 stanova u jednoj višestambenoj zgradi (energetskog razreda A) u Varaždinu. Također su praćeni uvjeti vanjske i unutarnje temperature u promatranim stanovima, kako bi se dobio uvid u ponašanje korisnika i rezultirajuću potrošnju. Analizom rezultata, ustanovljena su odstupanja između ''proračunske'' i ''stvarne'' potrošnje svakog promatranog stana, što je posljedica različitih orijentacija i rubnih uvjeta ovojnica stanova, ali i ponašanja stanara. Uočeno je značajno smanjenje potrošnje u prosincu 2016. godine u usporedbi s istim mjesecom 2015. godine, i to u stanovima u kojima su stanari prihvatili sustav praćenja potrošnje.

1. UVOD

Republika Hrvatska kao punopravna članica EU, u obvezi je pridržavati se svih europskih direktiva, pa tako i direktiva vezanih uz energetsku učinkovitost. U svjetlu toga, valja posebno spomenuti Direktivu 2010/31/EU europskog parlamenta i Vijeća o energetskoj učinkovitosti [1]. Zgrade su odgovorne za 40 % ukupne potrošnje energije u Uniji. Sektor se širi, što će neupitno povećati potrošnju energije. Stoga su smanjenje potrošnje energije i korištenje energije iz obnovljivih izvora u zgradarstvu važne mjere koje su potrebne kako bi se smanjila energetska ovisnost Unije i emisije stakleničkih plinova. Ta Direktiva vrlo često se „eksploatira" na način da se prvenstveno naglašava energetska učinkovitost u vidu uštede energije, ali prvenstveno kroz uštedu financijskih sredstava, odnosno prikazivanja povratnog perioda uloženih sredstava („cost-optimal level"). Međutim, sa stanovišta struke, definitivno je izuzetno važno istaknuti rečenicu sljedećeg sadržaja: *„Energetsku učinkovitost zgrada trebalo bi izračunati na temelju metodologije koja se može razlikovati na nacionalnoj i regionalnoj razini. To, uz toplinske značajke uključuje i druge faktore kojima pripada sve važnija uloga, kao što su postrojenja za grijanje i klimatizaciju, primjena energije iz obnovljivih izvora, elementi pasivnoga grijanja i hlađenja, zaštita od sunca* ***, kvaliteta unutarnjeg zraka****, odgovarajuća* *prirodna rasvjeta i oblik zgrade. Metodologija za izračunavanje energetske učinkovitosti ne bi se smjela temeljiti samo na sezoni u kojoj je potrebno grijanje, već bi trebala obuhvatiti godišnju energetsku učinkovitost zgrade [1].“*

Upravo tom rečenicom definiran je pojam građevinske fizike (ili fizike zgrade) kojom se naglašava važnost projektiranja i izvedbe „zdravih“, ili kako često znamo spomenuti „zelenih“ zgrada. No, u praksi se to vrlo često ili zanemaruje, ili nema dovoljno znanja i iskustva izvesti takve zgrade. Dio te rečenice je na neki način i sadržan u članku 43, Tehničkog propisa o racionalnoj uporabi energije i toplinskoj zaštiti u zgradama [2], koji definira uvjete za osiguranje ugodnosti unutarnjeg prostora te preporučene proračunske vrijednosti pojedinih mikroklimatskih parametara koji se vežu uz ugodnost unutarnjeg prostora (kvaliteta zraka, toplinska ugodnost, osvjetljenje i akustika).

2. ENERGETSKI UČINKOVITE ZGRADE

Izvedba energetski učinkovitih zgrada u današnje vrijeme predstavlja sve veći izazov za projektante i izvoditelje, tim više što sada izvedba takvih zgrada više nego ikada predstavlja multidisciplinarni pristup, posebno kada je uvjet izvedbe zgrada približno ili gotovo nulte energije (eng. nearly zero-energy Buildings – nZEB), vrlo blizu. Prema Direktivi, a u skladu s time i Tehničkim propisom, određeno je da: (a) do 31. 12. 2020. sve nove zgrade budu zgrade približno (gotovo) nulte energije*; (b) nakon 31. 12. 2018. nove zgrade u kojima su smještena tijela javne vlasti odnosno koje su u vlasništvu tijela javne vlasti budu zgrade gotovo nulte energije [1].

* *„zgrada gotovo (približno) nulte energije” znači zgrada koja ima vrlo visoku energetsku učinkovitost. Ta približno nulta odnosno vrlo niska količina energije trebala bi se u vrlo značajnoj mjeri pokrivati energijom iz obnovljivih izvora**, uključujući energiju iz obnovljivih izvora koja se proizvodi u krugu zgrade ili u blizini zgrade [1].*

** *Energija iz obnovljivih izvora jest energija iz obnovljivih nefosilnih izvora, tj. energija vjetra, sunčeva energija, aerotermalna, geotermalna, hidrotermalna energija i energija mora, hidroenergija, biomasa, deponijski plin, plin iz postrojenja za pročišćavanje otpadnih voda i bioplinovi [1].*

Teoretski, proračunima se mogu „izvesti“ takve zgrade, no postavlje se pitanje hoće li one i u stvarnosti biti takve te ono što je najbitnije, hoće li osigurati najviše standarde po pitanju povoljne i zdrave mikroklime unutarnjih prostora?

Europski projekt PROF/TRAC [3] („*Professional multi-disciplinary Training and Continuing Development in skills for nZEB principles - Multidisciplinarna izobrazba i trajno stručno usavršavanje profesionalaca u vještinama za zgrade približno nulte energije*“) se upravo bavi problematikom međusobnog povezivanja struka direktno uključenih u izvođenje takvih zgrada što se pokazalo jednim od najvećih, ako i najvećim izazovom prilikom projektiranja (i izvedbom) takvih zgrada. Naime, osim što postoje velike razlike između procijenjenih (proračunskih) i realnih (stvarnih) potrošnji, „sve više“ se javlja, do nedavno nepoznat pojam *sindroma bolesnih zgrada.* Spomenuta razlika između procijenjene i realne potrošnje najbolje je vidljiva na Slika 1

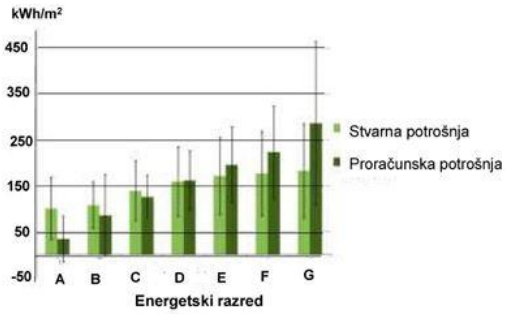

Slika 1: Stvarna i proračunska potrošnja po m^2 samostojećih zgrada po pripadnim energetskim razredima [4]

Uzorak je i više nego respektabilan (230.000 obiteljskih kuća na kojima je izvršen detaljan energetski pregled [4]), a ono što najviše zabrinjava je raskorak potrošnje upravo u segmentu *niskoenergetskih* zgrada (pojam i definicija niskoenergetske zgrade varira u literaturama, tako da se najčešće pojmovi vežu uz količinu korisne energije za grijanje koja se kreće do najviše 25 kWh/m^2, a po nekima čak i do 49 kWh/m^2. Bez obzira na to, današnja regulativa praktički “prisiljava” već uz zadovoljenje minimalnih zahtjeva izvedbu “niskoenergetskih” zgrada).

Zašto je tome tako i kako u praksi ispraviti, odnosno „poravnati“ grafove?

Razloga za razlike je mnogo. Uz pretpostavku da su korištene veće debljine toplinske izolacije, svaka i najmanja greška u projektiranju/ izvođenju detalja uzrokuje značajnija odstupanja. Ako smo ranije „podrazumijevali“ da je utjecaj toplinskih mostova oko 10%, u slučaju loše toplinske zaštite, taj utjecaj nije bio toliko primjetan kao sada kada utjecaj od 10% može direktno značiti prijelaz u viši, nepovoljniji energetski razred. No, u tom slučaju, svaki loše riješen toplinski most, zahvaljujući visokoj zrakonepropusnosti, uzrokuje dodatne probleme – razvoj plijesni, gljivica, mikroorganizama i sl. što direktno utječe na kvalitetu unutarnjeg zraka. Nedišući slojevi građevnih dijelova, nedišuća toplinska izolacija i otvori, uzrokuju nedostatak svježeg zraka, što rezultira neophodnošću uvođenja kvalitetnih sustava ventilacije unutarnjih prostora. To je posebno važno kod prostora u kojima boravi veliki broj korisnika, posebno kod prostora kod kojih je količina svježeg zraka izuzetno bitna za normalno funkcioniranje (bolnice, dječji vrtići, škole...). Pametni sustavi upravljanja i rasvjete također mogu doprinijeti velikim uštedama, bez narušavanja, u ovom slučaju udobnosti stanovanja. Iz svega nabrojenog vidljiva je važnost povezivanja građevinske, arhitektonske, strojarske i elektro struke.

Može se bez ustručavanja reći da je, bez međusobnog istovremenog rada i suradnje teško izbjeći mnogobrojne probleme koji se kasnije, u fazi korištenja javljaju i uzrokuju spomenuta odstupanja. S arhitektonsko-građevinskog aspekta spominju se važnosti morfologije, tipologije, toplinske, zvučne i protupožarne izolacije, razrade detalja toplinskih mostova, sa strojarskog aspekta kvaliteta ventilacijskih sustava, termotehničkih sustava, korištenih energenata, a s aspekta instalacija sustavi i tip rasvjete, vođenja sustava itd. Pod prizmom niskoenergetskih zgrada i današnjih standarda ne može se više govoriti što je važnije. Sve je važno i mora biti savršeno usklađeno. Samo u tom slučaju možemo postići željene rezultate sa stanovišta struke.

Prije svega, potrebno je definirati osnovne vrste energija koje se spominju uz pojam energetske učinkovitosti zgrada [2]:

Godišnja potrebna toplinska energija za grijanje, $Q_{H,nd}$ (kWh/a), jest računski određena količina topline koju sustavom grijanja treba tijekom jedne godine dovesti u zgradu za održavanje unutarnje projektne temperature u zgradi tijekom razdoblja grijanja zgrade;

Isporučena energija jest energija, izražena po nositelju energije, **E_{del} (kWh/a),** koja se dovodi u tehnički sustav u zgradi kroz granicu sustava kako bi se zadovoljile promatrane potrebe (za grijanjem, hlađenjem, prozračivanjem, toplom vodom za kućanstva, rasvjetom, uređajima itd.) odnosno kako bi se proizvela električna energija;

Primarna energija jest energija iz obnovljivih i neobnovljivih izvora koja nije podvrgnuta niti jednom postupku pretvorbe, **E_{prim} (kWh/a);**

Shematski prikaz spomenutih energija na zgradi prikazan je na Slika 2.

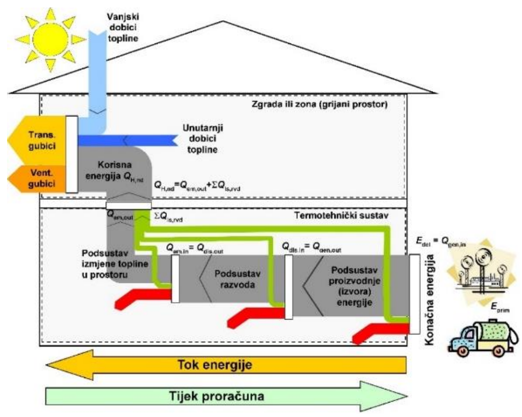

Slika 2: Shema energetske bilance u zgradama i energija za zadovoljenje potreba zgrade [6]

Godišnja potrebna toplinska energija za grijanje, $Q_{H,nd}$ (kWh/a) pojednostavnjeno predstavlja razliku svih gubitaka i dobitaka na zgradi [5]:

$$Q_{H,nd,cont} = Q_{Tr} + Q_{Ve} - \eta_{H,gn}\left(Q_{int} + Q_{sol}\right) \quad [\mathrm{kWh}] \tag{1}$$

gdje su:

Q_{Tr} – izmjenjena toplinska energija transmisijom za proračunsku zonu (kWh);

Q_{Ve} – potrebna toplinska energija za ventilaciju/klimatizaciju za proračunsku zonu (kWh);

$\eta_{H,gn}$ – faktor iskorištenja toplinskih dobitaka (-);

Q_{int} – unutarnji toplinski dobici zgrade (ljudi, uređaji, rasvjeta) (kWh);

Q_{sol} – toplinski dobici od Sunčeva zračenja (kWh).

Dakle, toplinski gubitak ovisi o koeficijentima prolaska topline pojedinih građevnih dijelova (s pripadnim ploštinama), ali **i utjecaju toplinskih mostova te točkastih gubitaka.** Upravo ti gubici se vrlo često zanemaruju, a mogu imati presudni utjecaj na povećanje realne potrošnje . Prema definiciji, toplinski most predstavlja manje područje u ovojnici grijanog dijela zgrade kroz koje je toplinski tok povećan radi promjene proizvoda, debljine ili geometrije građevnog dijela.

Potrebna toplinska energija za ventilaciju ovisi o potrebnoj toplinskoj energiji radi infiltracije vanjskog zraka, potrebnoj toplinskoj energiji radi prozračivanja otvaranjem prozora te potrebnoj toplinskoj energiji radi mehaničke ventilacije (ukoliko je ona prisutna). Kod sustava prisilne ventilacije, naglasak je na sustavima s rekuperacijom zraka bez kojih je, slobodno se može reći, teško postići najviše standarde energetske učinkovitosti svih, a posebno nestambenih zgrada javne namjene. **Ventilacijski gubici su značajni gubici i ono što je najbitnije prilikom razmatranja je činjenica da na njih direktan utjecaj mogu imati (i imaju) korisnici zgrada, odnosno ponašanje samih korisnika.**

3. PONAŠANJE KORISNIKA

Ponašanje korisnika i njihov utjecaj na potrošnju u niskoenergetskim zgradama je tema koja je na neki način u drugom planu prilikom edukacije stručnjaka s područja energetske učinkovitosti, a s pravom se može reći da bez pravilne i kvalitetne edukacije svih korisnika zgrade ne možemo očekivati rezultate kakve smo dobili proračunima i procjenama. Iz tog razloga svaki projektant i investitor moraju razmišljati o namjeni zgradi, ali i uvjetima pod kojima će se zgrada koristiti. To će u konačnosti imati i presudan utjecaj na ukupnu potrošnju svih energija i energenata u zgradi.

Prilikom proračuna koriste se unutarnje postavne temperature određene Algoritmom [5] i u skladu s time se definiraju i režimi rada termotehničkih sustava. No, u određenim slučajevima stvarni uvjeti korištenja objektivno ne mogu biti takvi i neminovno dolazi do odstupanja u rezultatima procijenjene i stvarne potrošnje energije.

Ako promatramo samo na primjeru višestambene zgrade za koju se proračunom određuje unutarnja temperatura od 20°C, jasno je da već od jednog do drugog korisnika (stana) dolazi do izvjesnih razlika. Unutarnje temperature mogu se razlikovati doslovno od prostorije do prostorije (iako je intencija kvalitetne toplinske zaštite što ujednačenija unutarnja temperatura), odnosno namjene i načina korištenja pojedinih prostora (aktivnosti u prostoru). Tome u prilog dijagram prikazan na Slika 3.

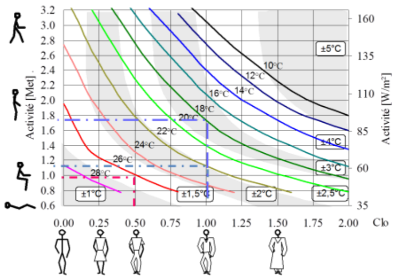

Slika 3: Utjecaj aktivnosti i odjevenosti korisnika na unutarnju temperaturu prostora [9]

Tablica 1: Kvantitativne vrijednosti odjevenosti i aktivnosti [7]

I - Clothing Insulation (toplinska izolacija odjeće) (m^2K/W); 1 clo=0,155m^2K/W)				
				
clo < 0,5	0,6 – 1,2		> 3,5	
M - Metabolic Rate (metabolizam) (m^2K/W); 1 Met = 58,15 W/m^2				
			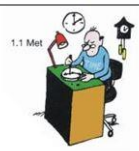	
2,5 Met	6,5 Met		1,1 Met	

Slika 3 prikazuje idealnu temperaturu kao funkciju odjevenosti i metabolizma (crne linije). Radna (operativna) temperatura je ponderirani prosjek temperature zraka i zračenja. Grafikon se odnosi na relativnu vlažnost između 30 i 70% i brzinu strujanja zraka manju od 0,1 m/s. Osjenčana i bijela područja predstavljaju toleranciju zadovoljstva 90% korisnika. Plave crte prikazuju osobu u unutarnjem prostoru zimi (1 clo) s određenom aktivnošću (npr. kućanski poslovi). Ta osoba će se bolje osjećati na temperaturi 18 ± 3 °C, odnosno između 15 i 21°C. Linije ispod, naprotiv, pokazuju temperaturu od 22 ± 2 (20 do 24 °C) za osobu s istom odjećom, ali manjom aktivnošću (čitanje). Temperatura raste na 26 ± 1,5 °C za jednaku aktivnost u ljetnim mjesecima (crvena linija).

Osim aktivnosti, veliku ulogu ima i relativna vlažnost unutarnjeg prostora. Tu ovisnost najbolje prikazuje tzv Mollier-ov dijagram prikazan na Slika 4.

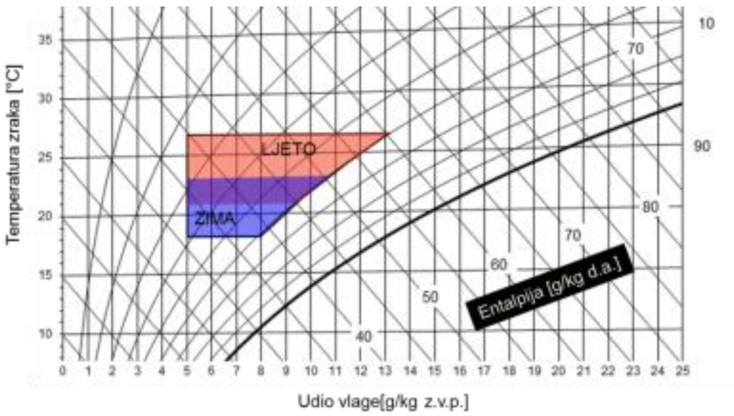

Slika 4: Mollierov dijagram [8]

Drugim riječima, „ugodna relativna vlažnost“ se kreće u granicama od 30% do 50% zimi, odnosno 60% u ljetnom periodu, odnosno, možemo zaključiti da se unutarnje ugodne temperature kreću zimi u granicama između 20 i 24°C, odnosno, između 22 i 26°C u ljetnim mjesecima. Visoka relativna vlažnost u zimskim mjesecima pridonosi lakšem razvoju plijesni, gljivica i mikroorganizama u unutarnjim prostorima što svakako treba izbjeći. Osim spomenutih čimbenika, na ugodnost, odnosno na ambijetalnu (osjetilnu) temperaturu velik utjecaj mogu imati i vertikalni temperaturni gradijenti, strujanje zraka, asimetrično zračenje topline, temperatura poda itd. Dakle, kada sve to zajedno promotrimo, jasno je da na konačnu, stvarnu potrošnju energije postoji „bezbroj“ čimbenika koje na neki način moramo uzeti u obzir.

Primjer „raspodjele“ energije može se vidjeti iz ovog opsežnog ispitivanja u Austriji za slučaj jednog prosječnog stana (Slika 5) i za slučaj jednog stana u niskoenergetskoj zgradi kod koje je prisutna bitno drugačija raspodjela potrošnje (Slika 6).

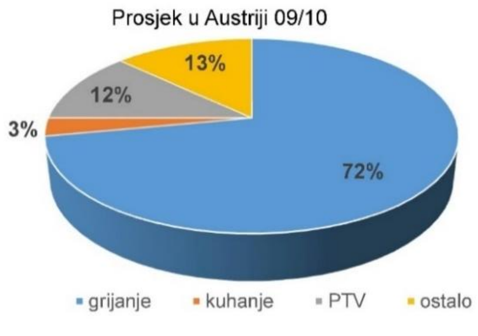

Slika 5: Raspodjela potrošnje u prosječnom stanu [9]

Iz ovog je vidljivo da je potrošnja električne energije dominantna, gotovo jednako kao potrošnja energije za grijanje i PTV. Iz tog razloga vrlo je važna stalna edukacija korisnika zgrade čemu uvelike može pomoći mogućnost stalnog praćenja potrošnje energije i po mogućnosti regulacija i korigiranje potrošnje kod korisnika koji odstupaju od prosjeka.

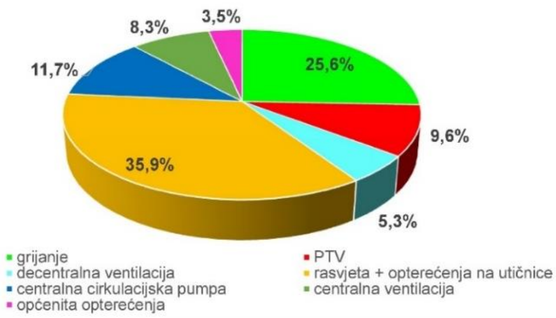

Slika 6: Raspdjela potrošnje u niskoenergetskom stanu [9]

4. STUDIJA SLUČAJA – PRAĆENJE PONAŠANJA KORISNIKA I POTROŠNJE ENERGIJE U VIŠESTAMBENOJ NISKOENERGETSKOJ ZGRADI

Najbolji primjer i dokaz uspješnosti sustava stalnog praćenja potrošnje energije je višestambena zgrada u Varaždinu,

Slika 7-lijevo, (*Investitor: Teming Nova d.o.o. Kućan Marof, direktor Miroslav Težak, d.i.s., Izvoditelj: Teming d.o.o.Varaždin, projektant: Arhia d.o.o. Varaždin*), kod koje je investitor ujedno i izvoditelj, ali i upravitelj zgrade. Vanjski zidovi ovojnice toplinski su izolirani lamelama kamene vune za kontaktne fasade FKL debljine d=16 cm, proizvođača Knauf Insulation d.o.o. (

Slika 7-desno). Time je osigurana paropropusnost, negorivost i zanemarivi toplinski rad bez korištenja mehaničkih pričvrsnica (izbjegnuti točkasti gubici). Podgledi stropova iznad garaže toplinski su izolirani s 12 cm kamene vune, a ravni krov sa 20 cm (također proizvođač Knauf Insulation d.o.o.). Izvedeni su tipski prekidi toplinskih mostova i djelomična RAL ugradnja prozora.

Slika 7: Lijevo – Promatrana višestambena zgrada; Desno – korištene lamele kamene vune za izolaciju vanjskih zidova zgrade

Svi proračuni fizike zgrade izvedeni su u računalnom programu KI Expert2013, u skladu s tada važećom regulativom. Budući da proračun isporučene i primarne energije u vrijeme projektiranja nije bilo potrebno računati, E*del* je izračunat s pretpostavkom 85%-tne iskoristivosti sustava. Zgrada je izvedena 2015. godine. Izvršen je energetski pregled i zgrada je svrstana u energetski razred A, što je potvrđeno izdavanjem energetskog certifikata. Osnovni geometrijski parametri zgrade i rezultati proračuna prikazani su u tablici 2.

Tablica 2: Geometrijske karakteristike i rezultati proračuna potrošnje energije promatrane višestambene zgrade

Oplošje grijanog dijela zgrade – A [m^2]	2254,33
Obujam grijanog dijela zgrade – V_e [m^3]	3870,00
Obujam grijanog zraka – V [m^3]	3096,00
Faktor oblika zgrade - f_0 [m^{-1}]	0,58
Ploština korisne površine – A_K [m^2]	1238,40
Ukupna ploština pročelja – A_{uk} [m^2]	1689,10
Ukupna ploština prozora – A_{wuk} [m^2]	274,21

Rezultati proračuna potrebne potrebne toplinske energije za grijanje i toplinske energije za hlađenje prema poglavlju VII. Tehničkog propisa o racionalnoj uporabi energije i toplinskoj zaštiti u zgradama, za zgradu grijanu na temperaturu 18°C ili višu:	
Godišnja potrebna toplina za grijanje	$Q_{H,nd}$ = 25145,55 [kWh/a]
Godišnja potrebna toplina za grijanje po jedinici ploštine korisne površine (za stambene i nestambene zgrade)	$Q''_{H,nd}$ = 20,30 (max = 56,03) [kWh/m^2 a]
Godišnja potrebna toplina za grijanje po jedinici obujma grijanog dijela zgrade (za nestambene zgrade prosječne visine etaže veće od 4.2m)	$Q'_{H,nd}$ = - (max = -) [kWh/m^3 a]
Godišnja potrebna energija za hlađenje	$Q_{C,nd}$ = 25711,02 [kWh/a]
Koeficijent transmisijskog toplinskog gubitka po jedinici oplošja grijanog dijela zgrade	$H'_{tr,adj}$ = 0,32 (max = 0,56) [W/m^2 K]
Koeficijent transmisijskog toplinskog gubitka	$H_{tr,adj}$ = 719,39 [W/K]
Koeficijent toplinskog gubitka provjetravanjem	$H_{ve,adj}$ = 510,84 [W/K]
Ukupni godišnji gubici topline	Q_l = 357129,66 [MJ]
Godišnji iskoristivi unutarnji dobici topline	Q_i = 195270,91 [MJ]
Godišnji iskoristivi solarni dobici topline	Q_s = 226172,58 [MJ]

Rezultati proračuna potrošnje i cijene energenata temeljem godišnje potrebne topline za grijanje.

Parametri proračuna	Formule	Vrijednosti	Jedinice
Korisna toplina za grijanje ($Q_{H,nd}$)		25.145,55	kWh/a
Konačna toplina za grijanje ($Q_{H,del}$)	$Q_{H,del} = Q_{H,nd} / \eta$	29.583,00	kWh
Odabrani energent		Prirodni plin	m3
Iskoristivost sustava grijanja (I)		85,00	%
Ogrijevna vrijednost (Ov)		9,71	kWh/m3
Godišnja potrošnja energenta (Pe)	$Pe = Q_{H,del} / Ov$	3.046,65	m3
Cijena energenta (C)		3,5	kn/m3
Ukupna cijena za grijanje (Uc)	$Uc = Pe \cdot C$	10.663,28	kn

Dakle, prema isporučenoj energiji, stanovi bi u prosjeku trebali trošiti oko **23,90 kWh/m^2 energije za grijanje prostora (prosječno godišnje).** Interesantan podatak je da je investitor ujedno i dobavljač energenta/energije za grijanje (prostora i PTV), te mu je time izuzetno značajan podatak realne potrošnje u zgradi, kako bi mogao odrediti što točniji paušal za „izgubljenu“ energiju, odnosno sve lokalne gubitke vođenjem instalacija kroz grijane i negrijane prostore. Iz tog razloga je vrlo bitno u najvećoj mogućoj mjeri voditi računa o pravilno izvedenim detaljima, te u isto vrijeme „stajati“ iza deklarirane potrošnje energije. Grijanje i sustav opskrbom toplom vodom je izvedeno centralno (izbjegavanje naknadnih troškova oko servisiranja protočnih bojlera) i s prvobitnog energenta peleta, radi izuzetno niske potrošnje, odlučeno je da će osnovni energent ipak biti prirodni plin. U svim stanovima je uveden sustav podnog grijanja, te solarni kolektori za pripremu PTV, ali i sustava grijanja. Sustav rekuperacije nije izveden, što se pokazalo da ipak ima utjecaj na konačnu potrošnju energije.

Uz prethodnu suglasnost stanara, u svaki stan je uveden sustav praćenja potrošnje energenata, te unutarnje postavne temperature (tek nekoliko stanara je odbilo tu mogućnost) za svaki sat tijekom dana. Princip rada regulacije stanova je sljedeći: svaki stan ima ugrađen kontroler koji je povezan na internu kompjutersku mrežu od cijele zgrade; korisnik u svakom trenutku može sa bilo kojeg mjesta preko mobilnih uređaja ili kompjutera pristupiti aplikaciji za nadzor sustava i praćenje potrošnje grijanja (aplikacija Teming sh izrađena je isključivo za potrebe ovog sustava),

Slika 8. Navedeno omogućuje namještanja parametara grijanja baš kada korisnik to treba (npr. može pojačati ili smanjiti grijanje u nekoj od prostorija u stanu 30 min prije dolaska kući ili pak odgoditi početak grijanja ukoliko kasni). Svi stanovi imaju multizonsku regulacije temperature te je moguće pojačati temperaturu samo od nekih prostorija u stanu (svaka prostorija ima ugrađen indikator temperature te radijatorske glave kojima se upravlja bežično). Svi elementi regulacije rade na z-wave protokolu tako da nije potrebno dodatno ožičenje izvršnih elemenata, što omogućuje i naknadnu ugradnju. Mjerenje potrošnje toplinske energije omogućeno je preko kalorimetara koji su ugrađeni u toplinskim podstanicama ispred svakog stana. Kalorimetri su preko Mbus kabla povezani sa centralnim uređajem koji je smješten u kotlovnici. **Očitanje potrošnje radi se svakih 15 min**. Kotlovnica je u potpunosti automatizirana te je investitoru omogućeno praćenje svih parametara potrošnje i stanja pojedinih izvršnih elemenata

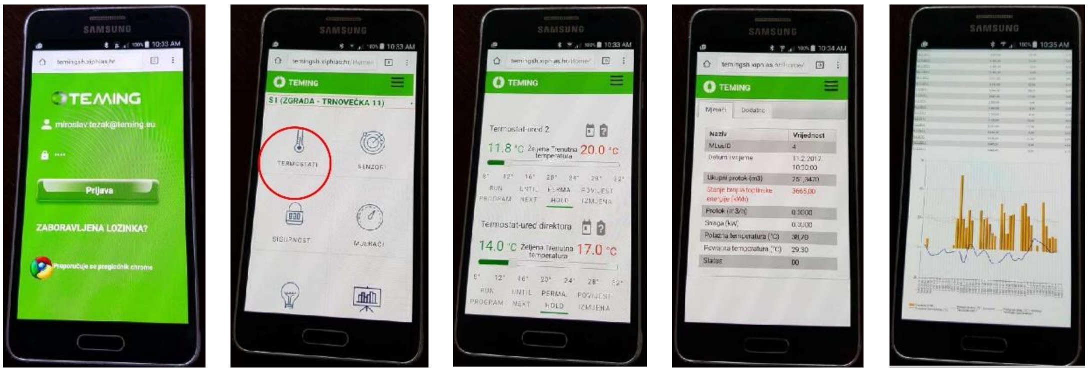

Slika 8: Prikaz aplikacije TEMING na mobilnom uređaju za praćenje potrošnje energije i temperature prostorija

Niže u tekstu dani su rezultati mjerenja 6 „karakterističnih" stanova, te rezultati stvarne potrošnje energije za grijanje i PTV čime se pokušalo „odvojiti" količine posebno za grijanje prostora, a posebno za grijanje PTV.

4.1. ANALIZA POTROŠNJE KARAKTERISTIČNIH STANOVA

U Tablica 3 prikazani su karakteristični stanovi s pripadnim opisom.

Tablica 3: Opis promatranih karakterističnih stanova

Stan	Oznaka	Etaža	Orijentacija	Ukupna površina	Broj članova kućanstva	Specifičnost	Slika
Stan 5	S5	Prizemlje	Sjever	42,52 m^2	2	Ispod negrijana garaža, jug i zapad negrijano stubište (hodnik)	Slika 9
Stan 10	S10	1. kat	Sjever	42,52 m^2	1	Ispod je stan S5, jug i zapad negrijano stubište (hodnik)	Slika 10
Stan 12	S12	2. kat	Jug	52,65 m^2	2	Sjever negrijano stubište (hodnik)	Slika 11
Stan 13	S13	2. kat	Jug i istok	66,56 m^2	2	Sjever negrijano stubište (hodnik)	Slika 11
Stan 18	S18	3. kat	Jug i istok	63,83 m^2	2	Sjever negrijano stubište (hodnik)	Slika 12
Stan 19	S19	3. kat	Sjever i istok	58,89 m^2	1+1(povremeno)	Jug negrijano stubište (hodnik)	Slika 12

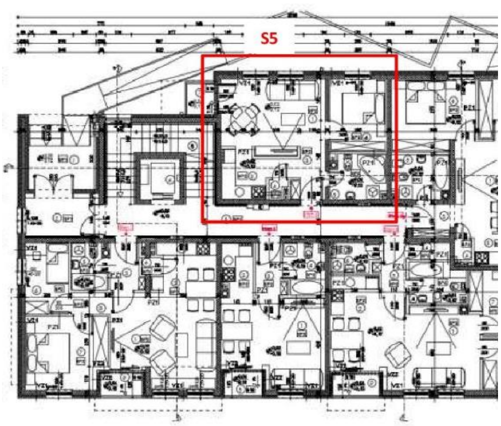

Slika 9: Stan S5 u prizemlju

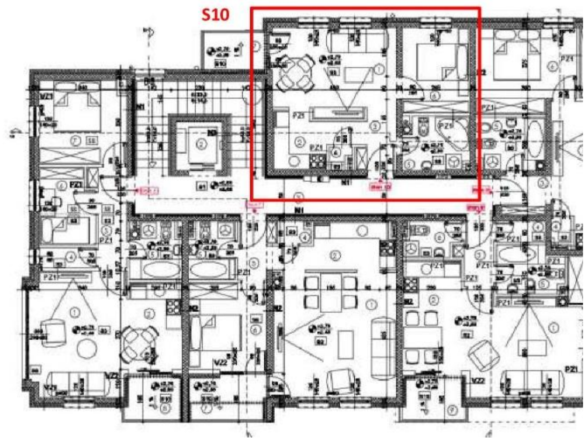

Slika 10: Stan S10 na 1.katu

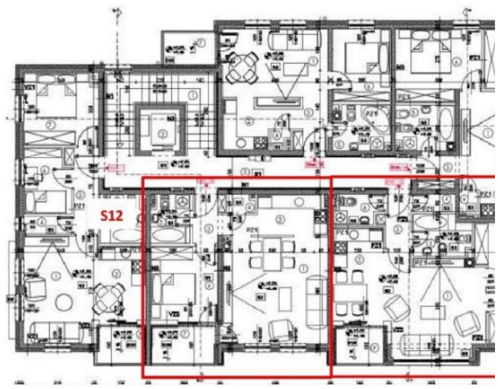

Slika 11: Stanovi S12 i S13 na 2. katu

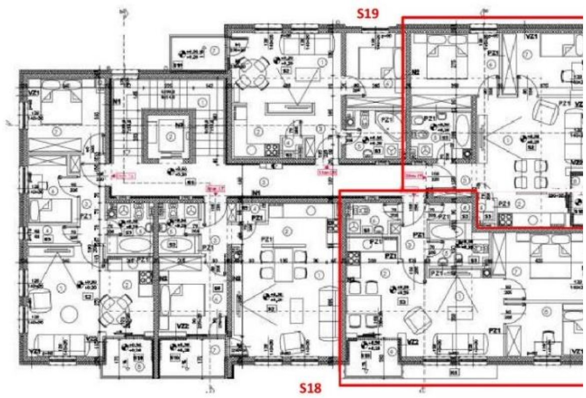

Slika 12: Stanovi S18 i S19 na 3. katu

U nastavku rada će se prikazati rezultati praćenja potrošnje karakterističnih stanova, i to detaljno za stan S12 a za ostale stanove samo ''konačni'' rezultati.

4.1.1. STAN S5

Tablica 4: Pregled potrošnje i temperature po mjesecima stana S5 (prizemlje, orijentacija sjever) za 2016. godinu

Mjesec	Prosječna dnevna temperatura (°C)	Ukupna potrošnja toplinske energije (kWh)	Toplinska energija za PTV (kWh)	Toplinska energija za grijanje (kWh)
SIJEČANJ/2016	0,73	610,00	58,50	551,50
VELJAČA/2016	6,33	434,00	58,50	375,50
OŽUJAK/2016	7,16	447,00	58,50	388,50
TRAVANJ/2016	12,92	150,00	58,50	91,50
SVIBANJ/2016	16,37	100,00	58,50	41,50
LIPANJ/2016	21,46	70,00	70,00	0,00
SRPANJ/2016	23,58	59,00	59,00	0,00
KOLOVOZ/2016	19,28	39,00	39,00	0,00
RUJAN/2016	18,04	66,00	66,00	0,00
LISTOPAD/2016	9,70	209,00	58,50	150,50
STUDENI/2016	5,80	279,00	58,50	220,50
PROSINAC/2016	-0,46	539,00	58,50	480,50
	UKUPNO 2016:	3002,00	702,00	2300,00
			23,38%	

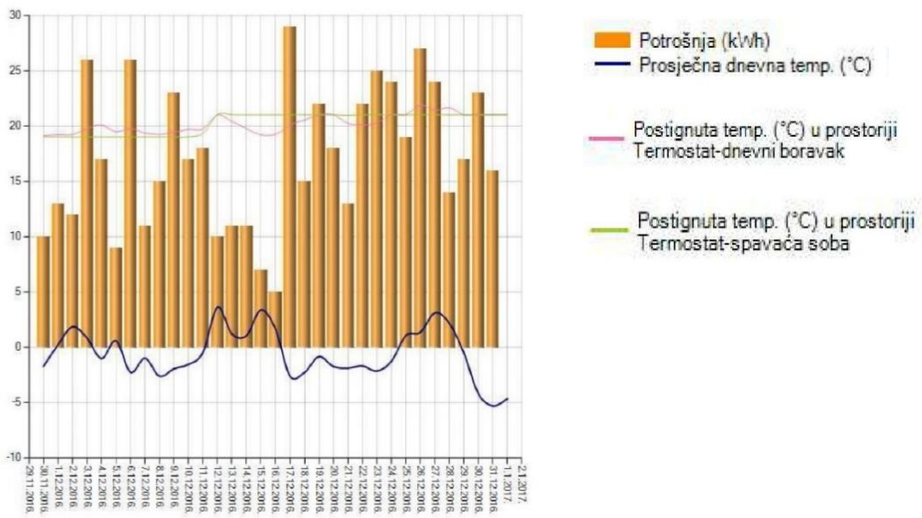

Slika 13: Potrošnja energije u stanu S5 u periodu od 29.11.2016. do 02.01.2017.

Osim što je primjetan osjetno veći udio potrošnje energije za PTV, primjetna i manje racionalna uporaba energije. Međutim, činjenica je da je stan iznad još uvijek neuseljen, te se radi toga dio energije troši „neplanirano“. Karakteristično za ovaj stan je i to da korisnici nisu uveli „kontroler“ unutarnje temperature, te stoga nije moguće utvrditi unutarnju temperaturu prostora. Prema ovome, prosječna potrošnja za grijanje iznosi 49,20 kWh/m2 (što je ipak manje nego za stan ispod), ali s energijom za PTV je značajno viša potrošnja.

4.2. STAN S12

Za stan S12 će se, kako je prethodno naglašeno, detaljnije prikazati rezultati praćenja potrošnje. U Tablica 5 usporedno je dan pregled potrošnje i temperature po danima za prosinac 2015. godine te za prosinac 2016. godine. Zatim je dan pregled potrošnje i temperature po satima za karakteristični dan mjeseca prosinca, i to i za 2015. i za 2016. godinu (tablica 6).

Tablica 5: Ukupna potrošnja toplinske energije za stan S12 za prosinac 2015. i 2016. godine (pregled potrošnje i temperature po danima)

DATUM		STANJE BROJILA		POTROŠNJA (kWh)		PROSJEČNA TEMP. (°C)	
		12/2015	12/2016	12/2015	12/2016	12/2015	12/2016
30.11.2015.	30.11.2016.	313,00	4.055,00	17,00	4,00	6,20	-1,75
01.12.2015.	01.12.2016.	330,00	4.061,00	17,00	6,00	10,08	0,21
02.12.2015.	02.12.2016.	349,00	4.063,00	19,00	2,00	7,74	1,81
03.12.2015.	03.12.2016.	374,00	4.069,00	25,00	6,00	3,29	0,82
04.12.2015.	04.12.2016.	399,00	4.083,00	25,00	14,00	3,96	-1,06
05.12.2015.	05.12.2016.	426,00	4.087,00	27,00	4,00	4,37	0,57
06.12.2015.	06.12.2016.	461,00	4.090,00	35,00	3,00	3,42	-2,29
07.12.2015.	07.12.2016	487,00	4.105,00	26,00	15,00	3,86	-1,02
08.12.2015.	08.12.2016.	518,00	4.115,00	31,00	10,00	2,93	-2,65
09.12.2015.	09.12.2016.	541,00	4.121,00	23,00	6,00	3,81	-1,97
10.12.2015.	10.12.2016.	565,00	4.136,00	24,00	15,00	4,50	-1,58
11.12.2015.	11.12.2016.	602,00	4.148,00	37,00	12,00	0,35	-0,50
12.12.2015.	12.12.2016.	631,00	4.151,00	29,00	3,00	0,94	3,59
13.12.2015.	13.12.2016.	662,00	4.155,00	31,00	4,00	0,18	1,17
14.12.2015.	14.12.2016.	690,00	4.160,00	28,00	5,00	1,08	1,02
15.12.2015.	15.12.2016.	717,00	4.173,00	27,00	13,00	2,97	3,36
16.12.2015.	16.12.2016.	749,00	4.178,00	32,00	5,00	3,95	1,61
17.12.2015.	17.12.2016.	775,00	4.181,00	26,00	3,00	3,55	-2,63
18.12.2015.	18.12.2016.	808,00	4.200,00	33,00	19,00	2,85	-2,31
19.12.2015.	19.12.2016.	843,00	4.218,00	35,00	18,00	2,78	-0,88
20.12.2015.	20.12.2016.	872,00	4.242,00	29,00	24,00	2,06	-1,77
21.12.2015.	21.12.2016.	901,00	4.257,00	29,00	15,00	2,15	-1,91
22.12.2015.	22.12.2016.	922,00	4.269,00	21,00	12,00	2,99	-1,72

23.12.2015.	23.12.2016.	942,00	4.285,00	20,00	16,00	4,03	-2,18
24.12.2015.	24.12.2016.	970,00	4.302,00	28,00	17,00	3,00	-1,30
25.12.2015.	25.12.2016.	995,00	4.320,00	25,00	18,00	0,94	1,03
26.12.2015.	26.12.2016.	1.029,00	4.323,00	34,00	3,00	1,46	1,32
27.12.2015.	27.12.2016.	1.069,00	4.341,00	40,00	18,00	0,26	3,08
28.12.2015.	28.12.2016.	1.101,00	4.346,00	32,00	5,00	-0,43	2,14
29.12.2015.	29.12.2016.	1.132,00	4.359,00	31,00	13,00	2,14	-0,57
30.12.2015.	30.12.2016.	1.171,00	4.373,00	39,00	14,00	0,77	-4,22
31.12.2015.	31.12.2016.	1.202,00	4.380,00	31,00	7,00	-4,96	-5,34

Tablica 6: Prikaz potrošnje i temperature za karakteristični dan mjeseca prosinca (08.12.2015. i 08.12.2016.) za stan S12

VRIJEME	STANJE BROJILA		POTROŠNJA (kWh)	
	2015.	2016.	2015.	2016.
1:00	487,00	4.105,00	0,00	0,00
2:00	487,00	4.105,00	0,00	0,00
3:00	487,00	4.105,00	0,00	0,00
4:00	487,00	4.105,00	0,00	0,00
5:00	487,00	4.105,00	0,00	0,00
6:00	487,00	4.105,00	0,00	0,00
7:00	492,00	4.105,00	5,00	0,00
8:00	494,00	4.105,00	2,00	0,00
9:00	494,00	4.105,00	0,00	0,00
10:00	494,00	4.105,00	0,00	0,00
11:00	494,00	4.105,00	0,00	0,00
12:00	494,00	4.105,00	0,00	0,00
13:00	494,00	4.105,00	0,00	0,00
14:00	494,00	4.105,00	0,00	0,00
15:00	494,00	4.105,00	0,00	0,00
16:00	494,00	4.105,00	0,00	0,00
17:00	499,00	4.105,00	5,00	0,00
18:00	502,00	4.106,00	3,00	1,00
19:00	505,00	4.107,00	3,00	1,00
20:00	508,00	4.111,00	3,00	4,00
21:00	511,00	4.111,00	3,00	0,00
22:00	513,00	4.111,00	2,00	0,00
23:00	518,00	4.115,00	5,00	4,00
0:00	518,00	4.115,00	0,00	0,00
UKUPNO:			31,00	10,00

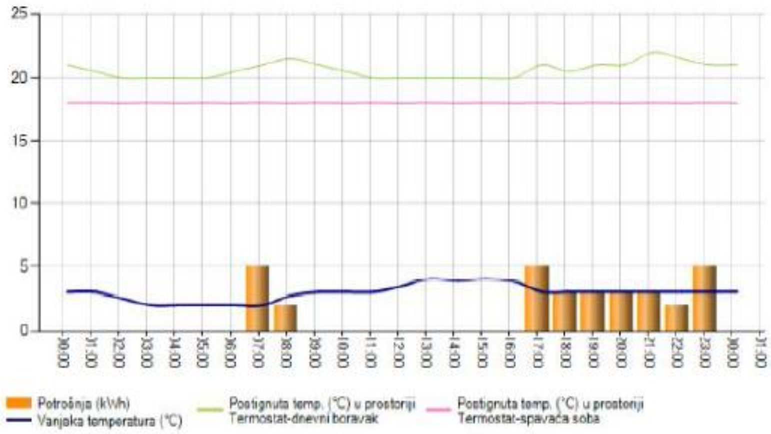

Slika 14: Prikaz potrošnje i temperature za stan S12 za karakteristični dan 08.12.2015.

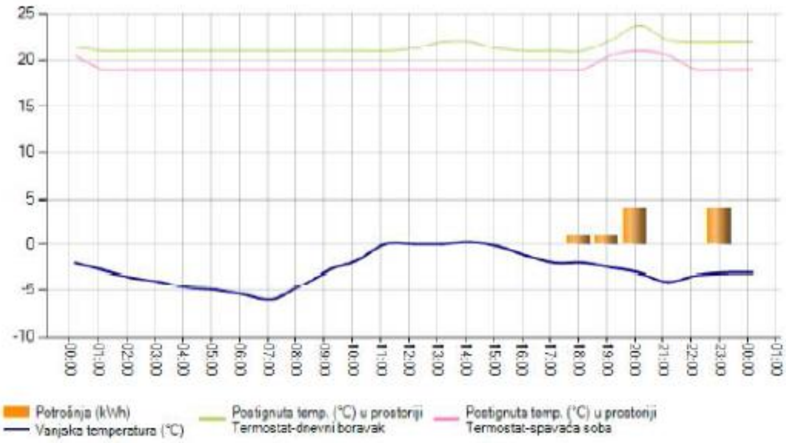

Slika 15: Prikaz potrošnje i temperature za stan S12 za karakteristični dan 08.12.2016.

Usporedbom potrošnje energije stana S12 u prosincu 2015. i u prosincu 2016. godine, vidljivo je da potrošnja u prosincu 2016. godine iznosi čak manje od polovice potrošnje u istom mjesecu prošle godine (i to uz značajno niže vanjske temperature nego što su bile u prosincu 2015. godine). Valja naglasiti da je vidljiva razlika u potrošnji rezultat kvalitetne edukacije stanara kako koristiti sustav praćenja potrošnje i prednosti koje donosi. Također, iz

Tablica 6 tablice 6 vidljivo je da je stanar potrošnju karakterističnog dana (08.12.) u 2016. godini smanjio na trećinu potrošnje iz 2015. godine.

4.2.1. STAN S13

Tablica 7 Pregled potrošnje i temperature po mjesecima stana S13 (2. kat, orijentacija jug i istok) za 2016. godinu

Mjesec	Prosječna dnevna temperatura (°C)	Ukupna potrošnja toplinske energije (kWh)	Toplinska energija za PTV (kWh)	Toplinska energija za grijanje (kWh)
SIJEČANJ/2016	0,73	611,00	66,25	544,75
VELJAČA/2016	6,33	386,00	66,25	319,75
OŽUJAK/2016	7,16	383,00	66,25	316,75
TRAVANJ/2016	12,92	110,00	66,25	43,75
SVIBANJ/2016	16,37	110,00	66,25	43,75
LIPANJ/2016	21,46	78,00	78,00	0,00
SRPANJ/2016	23,58	50,00	50,00	0,00
KOLOVOZ/2016	19,28	67,00	67,00	0,00
RUJAN/2016	18,04	70,00	70,00	0,00
LISTOPAD/2016	9,70	128,00	66,25	61,75
STUDENI/2016	5,80	234,00	66,25	167,75
PROSINAC/2016	-0,46	633,00	66,25	566,75
	UKUPNO 2016:	2860,00	795,00	2065,00
			27,80%	

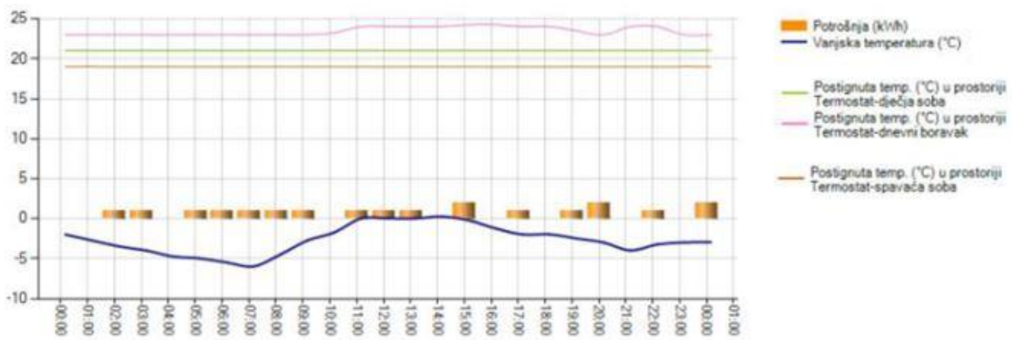

Slika 16: Prikaz potrošnje u stanu S13 po satima tokom karakterističnog dana 08.12.2016.

Prosječna potrošnja za grijanje u ovom stanu iznosi oko 32,9 kWh/m² (što je otprilike prosječna realna potrošnja zgrade). Povoljna orijentacija, ali i više temperature u unutarnjim prostorima (osobito dnevna soba). Više-manje kontinuirano grijanje tokom čitavog dana. Udio potrošnje energije za PTV cca 28%.

4.2.2. STANOVI S18 I S19

Iako stan 18 ima daleko bolju orijentaciju u odnosu na stan 19, u konačnici je potrošnja po m² podjednaka. Stan iznad stana 18 se još uvijek ne koristi (!) i to ima određeni utjecaj, ali i uvjeti korištenja također. Kod stana 18 je primjetno kontinuirano grijanje bez prekida i višom temperaturom korištenja u odnosu na projektiranu, dok se kod stana 19 vidi da se grijanje aktivira u određenim vremenskim intervalima. Unutarnja temperatura je većinu vremena niža od projektirane. Potrošnja stana 18 iznosi 33,6 kWh/m², dok za stan 19 iznosi 32,6 kWh/m².

Tablica 8: Pregled potrošnje i temperature po mjesecima stanova S18 (3. kat, orijentacija jug i istok) i S19 (3. kat, orijentacija sjever i istok)

Mjesec	Prosječna dnevna temperatura (°C)		Ukupna potrošnja toplinske energije (kWh)		Toplinska energija za PTV (kWh)		Toplinska energija za grijanje (kWh)	
	STAN S18	STAN S19	STAN S18	STAN S19	STAN S18	STAN S19	STAN S18	STAN S19
01/2016	0,73	0,73	642,00	543,00	134,25	39,25	507,75	503,75
02/2016	6,33	6,33	315,00	367,00	134,25	39,25	180,75	327,75
03/2016	7,16	7,16	328,00	307,00	134,25	39,25	193,75	267,75
04/2016	12,92	12,92	176,00	79,00	134,25	39,25	41,75	39,75
05/2016	16,37	16,37	172,00	65,00	134,25	39,25	37,75	25,75
06/2016	21,46	21,46	132,00	42,00	132,00	42,00	0,00	0,00
07/2016	23,58	23,58	132,00	44,00	132,00	44,00	0,00	0,00
08/2016	19,28	19,28	122,00	33,00	122,00	33,00	0,00	0,00
09/2016	18,04	17,46	151,00	38,00	151,00	38,00	0,00	0,00
10/2016	9,70	9,70	253,00	203,00	134,25	39,25	118,75	163,75
11/2016	5,80	5,80	427,00	255,00	134,25	39,25	292,75	215,75
12/2016	-0,46	-0,46	787,00	378,00	134,25	39,25	652,75	338,75
	UKUPNO 2016:		3637,00	2354,00	1611,00	471,00	2026,00	1883,00
					44,29%			

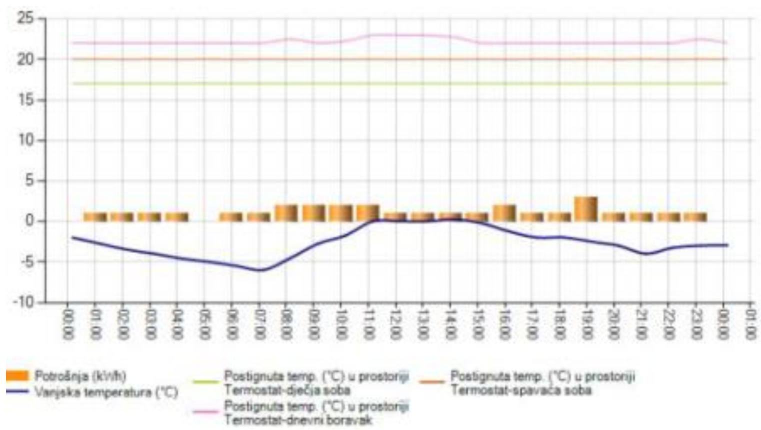

Slika 17: Prikaz potrošnje u stanu S18 po satima tokom karakterističnog dana 08.12.2016.

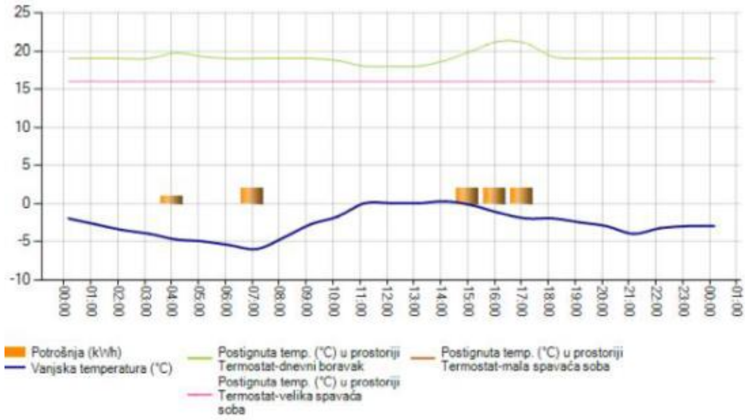

Slika 18: Prikaz potrošnje u stanu S19 po satima tokom karakterističnog dana 08.12.2016

5. ZAKLJUČAK

Prosječna potrošnja energije za grijanje na razini čitave zgrade tijekom 2016. godine iznosi 32,8 kWh/m^2 što je definitivno više u odnosu na procijenjenu potrošnju za stvarnu lokaciju (E_{del}) na razini 23,90 kWh/m^2. Primjetan je značajan udio energije za grijanje potrošne tople vode, ali o određeni gubici u sustavima. Gubici u mreži i kotlovnici iznose oko 20% - procijenjeno 15%. Prema raspoloživim podacima, od ukupno potrošenih 51.280,10 kWh prirodnog plina godišnje (za grijanje i PTV), doprinos solarnih kolektora je iznosio 7.381,90 kWh, odnosno 13%, dok su istovremeno gubici iznosili oko 10.614,00 kWh. Drugim riječima, investitor je veći dio gubitaka uspio pokriti obnovljivim izvorima energije, što će biti dobra smjernica prilikom projektiranja i izvođenja (u tijeku) sljedeće takve zgrade pored.

Razliku između procijenjene i stvarne potrošnje treba tražiti i u ventilacijskim gubicima koje je ipak teško kontrolirati, tim više što nije uveden sustav rekuperacije zgrade. Bez obzira na to, može se konstatirati da je zgrada prema korisnoj energiji opravdala dodijeljeni energetski razred.

Ono što je vrlo važno naglasiti, jest činjenica da je potrošnja u prosincu 2016. godine značajno niža u odnosu na isti mjesec 2015. godine, unatoč tome što je prosječna temperatura bila niža. Razlog definitivno leži i u činjenici stalne edukacije korisnika zgrade što je konačno vidljivo na konkretnoj potrošnji stanova koji su prihvatili sustav praćenja (primjer stana S12).

Izvedba zdravih, i za stanovanje ugodnih (udobnih) zgrada mora postati prioritet i krajnji cilj energetske učinkovitosti i energetske efikasnosti u cjelini. Pri tome projektanti moraju biti dobro upoznati s materijalima koje koriste na zgradama, posebno o kvaliteti toplinske, zvučne i protupožarne izolacije kojima zadovoljavaju temeljne zahtjeve za građevine. Svi bitni parametri fizike zgrade moraju biti u sinergiji i nikada niti jedan od parametara ugodnog i sigurnog stanovanja ne smije isključiti drugi.

Osim zadovoljenja svih uvjeta vezanih uz pravilno projektiranje i izvođenje zgrada, nedovoljno računa se vodi o ponašanju i potrebama korisnika što je još uvijek područje kojem se ne pridaje dovoljno pozornosti prilikom projektiranja, a posebno ne prilikom eksploatacije zgrada.

LITERATURA

[1] DIREKTIVA 2010/31/EU EUROPSKOG PARLAMENTA I VIJEĆA od 19. svibnja 2010. o energetskoj učinkovitosti zgrada, Dostupno na http://www.mgipu.hr/doc/Propisi/Direktiva_2010_31_19052010.pdf Pristupljeno: 2017-01-17

[2] Tehnički propis o racionalnoj uporabi energije i toplinskoj zaštiti u zgradama, Narodne novine br. 128/2015, dostupno na http://narodne-novine.nn.hr/clanci/sluzbeni/full/dodatni/438515.pdf ; Pristupljeno: 2017-01-17

[3] PROF/TRACK Open Training and Qualification Platform on NZEB construction and renovation, dostupno na http://proftrac.eu/open-training-platform-for-nzeb-professionals.html

[4] Heiselberg.P: Specifics of nzeb at the design, realization, commissioning, operation, financing, TtT course Prag, February 15-17,2016

[5] Soldo.V.; Novak, S; Horvat.I. : Algoritam za proračun potrebne energije za grijanje i hlađenje prostora zgrade prema HRN EN ISO 13790, Sveučilište u Zagrebu, Fakultet strojarstva i brodogradnje, Zagreb, ožujak 2015.

[6] Lenić.K.: Poglavlje 11. Metodologija proračuna toplinske energije; Priručnik za energetsko certificiranje, Program Ujedinjenih naroda za razvoj - UNDP, Zagreb, 2010.

[7] IDES-EDU-IEQ; LECTURE N° 2 - Thermal comfort; LECTURE N° 7 - User´s behavior and interaction; dostupno na http://proftrac.eu/training-materials.html

[8] EN 15251 Indoor environmental input parameters for design and assessment of energy performance of buildings addressing indoor air quality, thermal environment, lighting and acoustics(1.12.2007)*

[9] ROTH, K., ENGELMANN, P. (2010): Impact of user behavior on energy consumption in high-performance buildings – Results from two case studies, Fraunhofer USA, Denver*

''GREEN'' SYSTEM SOLUTIONS FOR BUILDING ENVELOPES

Marina Hlap[1], Domagoj Sojat[2]

[1] University of Zagreb, Faculty of Economics and Business, University Specialist Postgraduate Study Programme of Marketing and Communications Management, email: hlap@caparol.hr
[2] Zagreb University of Applied Sciences, Specialist graduate professional study in Civil Engineering, Specialization Civil Engineering, Avenija Veceslava Holjevca 15, 10 010 Zagreb, Croatia, email: sojat@caparol.hr

SUMMARY: This paper deals with protection and safety provided by new innovative combination of environmentally friendly materials with the highest Impact resistance category and their properties and main characteristics. Façade system Capatect consists of hemp insulation boards and mineral finishing reinforced with carbon fibres. Combination of hemp and finishing layers reinforced with carbon fibres achieves the highest Impact resistance category 1 and Resistance to hailstorms class 4. According to the experimental testing conducted by German Institute for Certified Safety (Institut für geprüfte Sicherheit, IGS), façade system Capatect withstand the impact of hailstorm size of a golf ball without any damage, thus providing the maximal safety to investor. More than 90% of façade systems available on the market are classified only as Impact resistance category 2. Hemp as a material is thermally stable and therefore eliminates thermal stresses regardless of the colour shade of finishing layer. Fibres give porous structure which provide additional insulation effect due to air enclosed in the pores, and by its thermal conductivity coefficient hemp is equal to classic thermal insulation materials. High water vapour permeability is responsible for great indoor climate. Besides all of that, hemp acts as good acoustic insulation and it reduces noise up to 13 dB. This paper presents a detailed overview of certified solution of thermal façade system supported by testing conducted by independent Austrian Institute for Fire Protection and Safety (Institut für Brandschutztechnik und Sicherheitsforschung, BIS). BIS has specifically for this testing developed a special testing machine for simulating the impact of hailstorm with ice balls as big as 40 mm in diameter. All products presented in this paper fulfil strict requirements for building envelopes with strong emphasis on ecology and sustainability.

„ZELENA" SISTEMSKA RJEŠENJA FASADNIH OVOJNICA

SAŽETAK: U radu se obrađuje sigurnost i zaštita koju pruža nova inovativna kombinacija ekološki prihvatljivih materijala koji imaju najviši razred izolacije kategorije korisnosti 1 i njihova svojstva i osnovne značajke. Fasadni sustav Capatect sastavljen je od izolacijskih ploča od industrijske konoplje s mineralnim armiranim slojem ojačanim ugljičnim vlaknima. U kombinaciji konoplje s proizvodima ojačanim ugljičnim vlaknima postiže se najviši razred izolacije kategorije korisnosti 1 te otpornost na tuču razreda 4. Prema ispitivanjima njemačkog instituta za dokazanu sigurnost (njem. Institut für geprüfte Sicherheit, IGS) fasadni sustav Capatect bez ikakvih znakova oštećenja podnosi udarce tuče veličine loptica za golf te tako investitoru donosi maksimalnu sigurnost. Više od 90 % fasadnih sustava za toplinsku izolaciju na tržištu postiže samo kategoriju korisnosti 2. Konoplja kao materijal osigurava izostanak toplinskih naprezanja bez obzira na nijansu boje završnog sloja fasade. Zatvaranjem zraka između vlakana konoplje stvara se dodatni izolacijski učinak, izuzetna paropropusnost daje izvrsnu klimu prostora a svojim toplinskim koeficijentom materijal stoji uz bok klasičnim izolacijskim materijalima te je uz sve to odličan zvučni izolator smanjujući buku i do 13 dB.

U radu se daje detaljan prikaz certificiranog rješenja fasadnog sustava za toplinsku izolaciju potkrijepljenog ispitivanjima koja je proveo neovisni austrijski Institut za protupožarnu zaštitu i sigurnost (njem. Institut für Brandschutztechnik und Sicherheitsforschung, BIS) koji je za tu priliku razvio poseban stroj za simulaciju udara tuče ledenim kuglama promjera 40 milimetara. U radu prikazani proizvodi zadovoljavaju stroge zahtjeve za fasadne ovojnice s velikim naglaskom na ekologiju i održivost.

1. UVOD

Princip toplinske izolacije temelji se na činjenici da su izolacijski materijali loši toplinski vodiči te stoga sprječavaju izlazak toplinske energije iz interijera prema van, ali isto tako za vrijeme ljetnih vrućina sprječavaju ulazak vrućeg zraka unutra. Ugradnjom fasadnog sustava za toplinsku izolaciju građevni materijal od kojeg je izrađen zid na koji se sustav aplicira, služi kao termo stacionarno skladište koje osigurava ugodnu klimu životnog prostora.

Kao najčešći izolacijski materijal obično se koriste ploče od polistirena, poznate i kao EPS ploče odnosno bijeli stiropor koji sve više zamjenjuju Dalmatiner izo-ploče koje spajaju prednosti bijelog i grafitnog stiropora. Također postoje i druge mogućnosti kao što je na primjer upotreba aero gela, no nije svaka izolacija pogodna za korištenje u fasadnim sustavima za toplinsku izolaciju. Kao što je poznato iz tehnologije završnih slojeva, pogrešan odabir materijala može dovesti do mekanog unutarnjeg sloja i tvrdog završnog sloja što će s vremenom zbog naprezanja dovesti do stvaranja pukotina na fasadnoj površini. Dakle, fasadni sustav za toplinsku izolaciju bit će funkcionalan samo ukoliko su rubovi izolacijske ploče čvrsto zalijepljeni za podlogu kako ne bi došlo do „efekta jastuka" koji bi u konačnici uzrokovali pukotine. Zbog malene mase armirnog i završnog sloja na površini fasade dolazi do brzog mijenjanja temperature na površini fasadnog sustava, no prolaskom te toplinske energije do izolacijskog sloja fasadnog sustava ona se pretvara u mehaničku i raspoređuje po izolacijskom sloju. Uzimajući u obzir ranije navedene razloge industrijska konoplja se pokazala kao idealan materijal koji eliminira gore navedene probleme kod fasadnih sustava za toplinsku izolaciju.[1]

Izolacijski sloj sam po sebi nije dovoljan za postizanje dobre izolacije, već ga je potrebno povezati s odgovarajućim ostalim slojevima kako bi se ostvarila maksimalna zaštita objekta. Upravo iz tog razloga se za armiranje i završni sloj koriste proizvodi ojačani karbonskim vlaknima koji brinu o tome da vanjski utjecaji nikada ne dođu do izolacijskog sloja fasadnog sustava. Ujedinjeni u fasadni sustav za toplinsku izolaciju, industrijska konoplja i karbonski ojačani proizvodi postižu najvišu klasu izolacije, kategorije korisnosti 1 te otpornosti na tuču klase 4.

2. INDUSTRIJSKA KONOPLJA - EKOLOŠKI IZOLACIJSKI MATERIJAL [2]

Konoplja raste iznimno brzo, od 0 do 4 metra u samo 100 dana. Raste brže od bilo kojeg korova te joj stoga nisu potrebni pesticidi niti umjetna gnojiva. Uz sve to jako je otporna te nema problema s nametnicima. Konoplja je najstarija kultivirana biljka na svijetu. Nekada se 80% svih konopa, užadi i jedara izrađivalo od konoplje. Izuzetno je vodootporna i elastična te stoga i otporna na pucanje. Obrađuje se i koristi čak 97% biljke: vlakna, slama i sjeme, što ne ostvaruje niti jedna druga poljoprivredna kultura. Ekološki gledano, konoplja na sebe veže više CO_2 nego šuma, a kalorijska vrijednost peleta ista je kao ona u mrkog ugljena i sve to bez efekta staklenika.

Zahvaljujući značajnom vezanju CO_2, niti emisije tijekom uzgoja i proizvodnje ne utječu bitno na sliku CO_2 bilance industrijske konoplje kao materijala. Tome svakako pridonose i kraće udaljenosti transporta od polja do pogona za preradu te korištenje domaćih obnovljivih izvora energije kod prerade. U usporedbi s klasičnim izolacijskim materijalima, konoplja predstavlja vidljivo poboljšanje u vidu izolacijskih materijala kada su u pitanju ekološke izvedbe fasadnih sustava za toplinsku izolaciju.

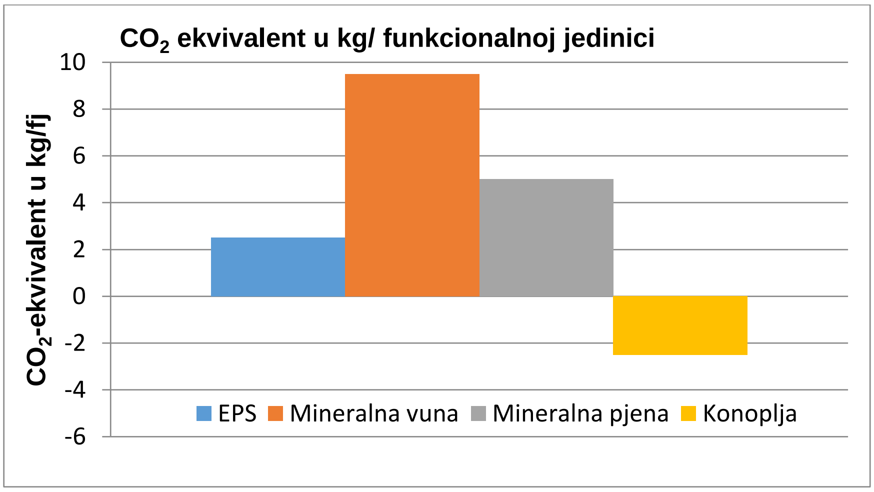

Slika 1: CO_2 bilanca izolacijskih materijala za fasadne sustave [3]

Na ekološki otisak pojedinog materijala također djeluje i potrošnja neobnovljivih izvora energije koja je prikazana na sljedećoj slici. Visina stupca predstavlja potrošnju energije iz neobnovljivih izvora energije tokom čitavog životnog ciklusa materijala uključujući zbrinjavanje. S obzirom da se s nekim materijalima značajan dio utrošene energije može nadoknaditi, linijom je naznačena potrošnja energije iz neobnovljivih izvora na kraju životnog ciklusa materijala.

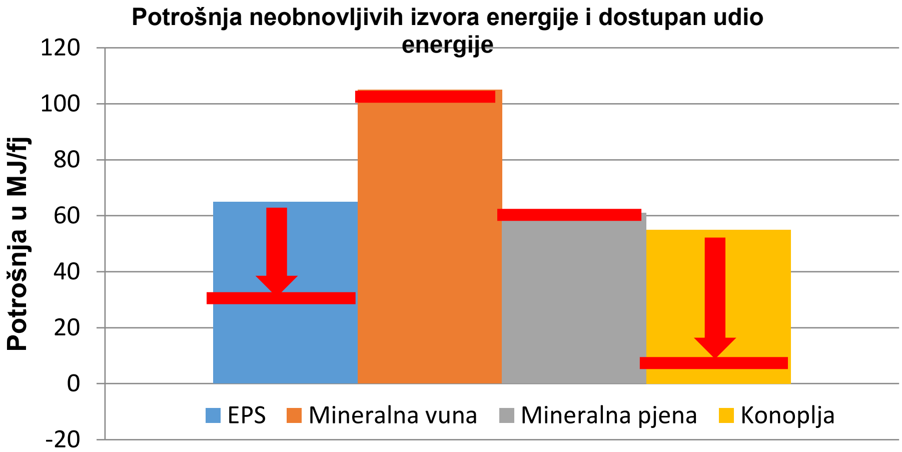

Slika 2: CO_2 bilanca izolacijskih materijala za fasadne sustave [3]

Najnoviji rezultati ispitivanja eko bilance izolacijskih materijala Instituta za građevinsku biologiju (IBO - Institut für Baubiologie) prema ekološkom otisku svrstavaju izo-ploče od industrijske konoplje na prvo mjesto. Bečki Institut određuje ekološku ravnotežu iz najnovijih podataka koji se odnose na uzgoj konoplje te proizvodnju izo-ploča od konoplje. Za točan izračun potrebni su podatci o potrošnji svih stadija procesa proizvodnje od berbe do završnog proizvoda. Dobroj eko-bilanci značajno pridonosi preseljenje proizvodnih pogona bliže poljima konoplje, smanjujući tako transportnu udaljenost na manje od 25 km, ali i korištenje zelene električne energije u samom procesu proizvodnje. [3]

Za izradu ekološkog otiska materijala korišteni su sljedeći kriteriji:

- potrošnja neobnovljivih izvora primarne energije,
- CO_2 bilanca prema funkcionalnoj jedinici,
- potencijal povećanja kiselosti tla i vode,
- fertilizacijski potencijal,
- potencijal stvaranja troposferskog ozona i
- potencijal stvaranja stratosferskog ozona

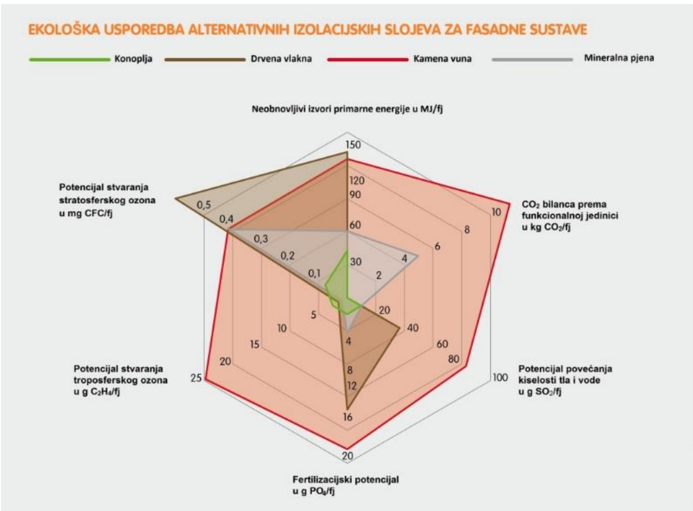

Slika 3: Ekološka usporedba alternativnih izolacijskih slojeva za fasadne sustave [4]

Šest ekoloških osnovnih vrijednosti postavljeni u mrežu čitaju se kao ekološki otisak. Što je manji ekološki otisak to se izolacijski materijal smatra ekološki osvještenijim. Zahvaljujući svojstvima, konoplja zauzima posebno mjesto među izolacijskim materijalima te konkurira konvencionalnim izolacijskim materijalima. Izolacijske ploče sastavljene su od vlakana konoplje povezanih termičkom metodom ne-tkanog vlakna uz pomoć biopolimera odnosno kukuruznog škroba te je na taj način tehnički zaokružena priča izolacije koja se u potpunosti može kompostirati.

Porastom korisnosti industrijske konoplje ova kultura ponovno se popularizirala te je njena sjetva značajno porasla u posljednjih nekoliko godina.

3. PROIZVODI OJAČANI KARBONSKIM VLAKNIMA [5]

Karbon je vrhunski tehnološki razvijen materijal izuzetno lagan, ali istovremeno elastičan i iznimno robustan. Već godinama je prepoznat u robotici, auto-moto i zrakoplovnoj industriji gdje se uspješno koristi budući da već kod neznatnih debljina sloja pokazuje najveći stupanj otpornosti. Caparol je odlučio iskoristiti prednosti karbonskih vlakana u armirnom i završnom sloju svog fasadnog sustava kako bi dugotrajno zaštitio izolacijski sloj od vanjskih vremenskih utjecaja.

3.1. ARMIRNI SLOJEVI OJAČANI KARBONSKIM VLAKNIMA

Armirni sloj desetljećima mora štititi izolaciju od zalutalih lopti, naslonjenih bicikala i prije svega od vremenskih nepogoda. Nadalje, osim mehaničkih tu su i termička naprezanja do kojih dolazi kod temperaturnih razlika od vrlo niskih temperatura zimi do iznimno visokih temperatura ljeti kada se fasadna površina može ugrijati i iznad 50°C stupnjeva. Obično se koristi armirni sloj debljine 3 mm koji bi trebao podnijeti predviđena opterećenja, no za pojačani fasadni sustav preporuča se i 5 mm armirnog sloja. [6]

Najveće prirodno mehaničko opterećenje koje može zadesiti fasadni sustav zasigurno je tuča. Kako bismo simulirali snagu udarca tuče u suradnji s neovisnim austrijskim institutom za protupožarnu zaštitu i sigurnost – IBS (Institut für Brandschutztechnik und Sicherheitsforschung) razvijen je poseban stroj kako bi simulirao udarce tuče o fasadu, ledenim kuglama promjera 40 milimetara. Uz pomoć komprimiranog zraka, uređaj ispaljuje kuglice leda koje postižu brzinu i do 100 km/h i udaraju o metu pod kutom od 45 stupnjeva. Dakle, realno se može prikazati mehaničko opterećenje kojem je izložena fasadna površina u slučaju stvarne vremenske nepogode te usporediti ponašanje klasične fasade u usporedbi s onom ojačanom karbonskim vlaknima. Naime kod klasičnog fasadnog sustava završni sloj puca već kod prvog udarca i na taj način ostavlja slobodan put do izolacije koja biva oštećena. Kod fasadnog sustava ojačanog karbonskim vlaknima, završni sloj uspješno amortizira i odbija kugle leda bez tragova na površini fasade. Zahvaljujući rezultatima švicarski institut za istraživanje i razvoj, EMPA, prvi puta je proizvode nekog proizvođača nagradio najvišom ocjenom za otpornost na tuču HW 5. [7]

Slika 4: Ispucavanje ledenih kuglica na fasadnu površinu pod kutom od 45° [7]

Od armirnih slojeva ojačanih karbonskim vlaknima u testu su korištene sljedeće armirne mase:

- praškasti bijeli mineralni armirni sloj
- disperzivno vezana masa za armiranje
- armirni sloj s dodatkom posebno lakih materijala
- dvokomponentni armirni sloj

Tablica 1: Otpornost fasadnog sustava na udarce tuče u ovisnosti na armirni sloj [7]

Klasa otpornosti	HW1	HW2	HW3	HW4	HW5
Promjer tuče	Ø 10 mm	Ø 20 mm	Ø 30 mm	Ø 40 mm	Ø 40 mm
Masa tuče	0,5 g	3,6 g	12,3 g	29,2 g	56,9 g
Brzina tuče	> 49,7 km/h	> 49,7 km/h	> 70,2 km/h	> 86,0 km/h	> 111 km/h
Energija	> 0,04 J	> 0,7 J	> 3,5J	> 11,1 J	> 27,0 J
Fasadni sustav-korišteni armirni sloj		Prosječan sistem	Dobar sistem	Minera Carbon – mineralni armirni sloj	CarbonSpachtel, CarbonSpachtel Easy, CarboNit

3.2. ZAVRŠNI SLOJEVI OJAČANI KARBONSKIM VLAKNIMA

Uz prije navedenu mehaničku i termičku otpornost, karbonskim vlaknima ojačana žbuka te fasadna boja zaštiti fasadne ovojnice dodaju i sljedeće karakteristike:

- aktivno samočišćenje fasadnih površina zahvaljujući efektu fotokatalize
- suhe fasade zahvaljujući tzv. Hydroperlefektu koji omogućuje grupiranje vode u kapljice i njihovo nestajanje s fasadne površine
- visoki koeficijent difuzije koji osigurava suhe fasadne površine zahvaljujući niskom koeficijentu upojnosti vode
- dugotrajna zaštita od pojave algi i gljivica zahvaljujući suhim površinama

4. EKOLOŠKA ALTERNATIVA: CAPATECT ECOLINE FASADNI SUSTAV [8]

Capatect EcoLine fasadni sustav predstavlja alternativu zelene tehnologije u odnosu na već dobro poznate izolacijske materijale. Jedinstvena simbioza konoplje i karbona predstavlja jedinstveno inovativno i održivo rješenje u ponudi konvencionalnih fasadnih sustava za toplinsku izolaciju.

4.1. PREDNOSTI I KOMPONENTE ECOLINE FASADNOG SUSTAVA

Kvalitetne te međusobno usklađene komponente fasadnog sustava osiguravaju sigurnost prilikom ugradnje navedenog fasadnog sustava, a neke od osnovnih prednosti su:

- mehanička otpornost
- dobra izolacijska svojstva, $\lambda = 0{,}039$ W/mK [9]
- zaštita od buke i do 13 dB [10]
- dugotrajno čista fasada postojanih boja
- dobra eko bilanca

Komponente EcoLine fasadnog sustava čini:

1. Izolacijska ploča od industrijske konoplje - Zahvaljujući svom izolacijskom svojstvu industrijska konoplja ($\lambda = 0{,}039$ W/mK) svrstava se u prirodne izolacijske materijale te po svom učinku stoji uz bok konvencionalnim izolacijskim umjetnim materijalima. Također uz toplinsku izolaciju, konoplja pridonosi i odličnoj zvučnoj izolaciji čime raste komfor stanovanja pojedinca. Ukoliko se ugrađuje u kombinaciji s proizvodima razvijenim na karbonskoj tehnologiji, znatno se povećava otpornost na tuču i ostala mehanička opterećenja.

2. Ljepilo - Za brzo i dobro prianjanje koristi se posebno razvijeno ljepilo, za vrhunske izolacijske komponente kako bi se dodatno povećao životni komfor.

3. Mineralni armirni sloj ojačan karbonskim vlaknima brine za otpornost i dugotrajnost fasadnog sustava za toplinsku izolaciju, u debljini od 5 mm kod testa otpornosti na tuču zadovoljava klasu otpornosti razreda 4. Upotrebom pastoznog armirnog sloja varijante ili dvokomponentne verzije armirnog sloja s armirnim slojem od 5 mm postiže se klasa otpornosti na tuču razreda 5.

4. Ekstremno difuzivna i vodoodbojna strukturna žbuka ojačana karbonskim vlaknima brine za suhu površinu fasade te sprječava prianjanje čestica prljavštine zahvaljujući Hydroperl efektu koji ubrzava sušenje fasade.

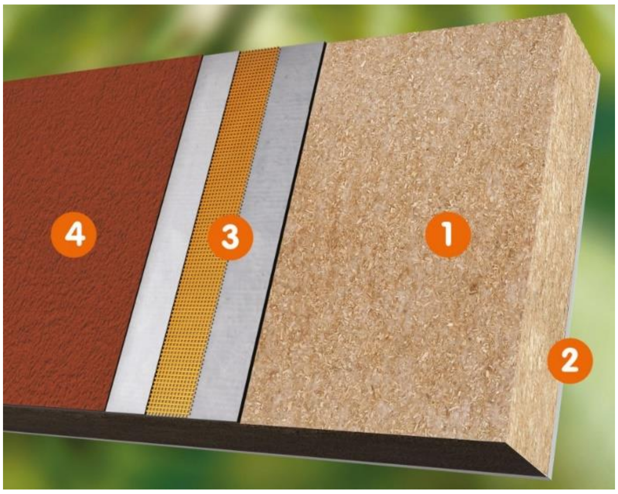

Slika 5: EcoLine fasadni sustav za toplinsku izolaciju [2]

5. ZAKLJUČAK

U radu je predstavljena nova inovativna kombinacija ekološki prihvatljivih materijala koji donose najvišu klasu izolacije kategorije korisnosti 1, sa svojim svojstvima i osnovnim karakteristikama.

Capatect EcoLine fasadni sustav sastavljen od izolacijskih ploča od industrijske konoplje s mineralnim armirnim slojem ojačanim karbonskim vlaknima. U kombinaciji konoplje s proizvodima ojačanim karbonskim vlaknima postiže se najviša klasa izolacije, kategorije korisnosti 1 te otpornosti na tuču klase 4, dok se korištenjem pastoznog disperzivnog ili dvokomponentnog armirnog sloja postiže klasa otpornosti na tuču 5 što do sada nije uspjelo niti jednom proizvođaču građevinskih materijala.

Konoplja kao materijal osigurava izostanak toplinskih naprezanja bez obzira na nijansu završnog sloja fasade. Zatvaranjem zraka među vlaknima konoplje generira se dodatni izolacijski učinak, izuzetna paropropusnost brine se za izvrsnu klimu prostora, svojim toplinskim koeficijentom materijal stoji uz bok klasičnim izolacijskim materijalima te je uz sve to odličan zvučni izolator smanjujući buku i do 13dB.

U radu prikazani proizvodi zadovoljavaju stroge zahtjeve glede primjenskih svojstava kod fasadnih ovojnica s velikim naglaskom na ekologiju i održivost.

LITERATURA

[1] Enzenberger, G.: Sympathischer Dämmstoff Hanf, Technikforum – Farben Lacke Bautenschutz, interna publikacija, Caparol Farben Lacke Bautenschutz GmbH, Ober-Ramstadt, Njemačka, 01/2015

[2] Skupina autora: Hanf dämmt grüner, interna brošura, Capatect Baustoffindustrie GmbH, Perg, Austrija,(2016)

[3] Baubook Deklarationszentrale: Capatect Hanffaserdämmplatte / NAPOROwall - ab Juni 2016 Dostupno na: http://www.baubook.info/m/PHP/Info.php?SI=2142722541&SW=5&SBT_open=57055&win=y Pristupljeno: 2016-11-23

[4] Top Ökobilanz für die Capatect Hanfdämmplatte, Dostupno na http://www.hanfdaemmung.at/%C3%B6kobilanz/ Pristupljeno: 2016-11-23

[5] Skupina autora: Die unschlagbare Carbon-Edition, interna brošura, Synthesa Chemie Gesellschaft m. b. H., Perg, Austrija,(2013)

[6] Skupina autora: Hier hagelt's Sicherheit!, interna brošura, Capatect Baustoffindustrie GmbH, Perg, Austrija,(2016)

[7] IBS- Institut für Brandschutztechnik und Sicherheitsforschung, Prüfbericht Nr.: 134_1004_001, Labortechniche Simulation von Hagelschlag mittels Eiskugeln, Datum: 22.08.2013, Sachbearbeiter: Ing. Mag. Robert Brenner/MarR, DW:886

[8] Izjava o svojstvima: Leistungserklärung S13-013/V02 ETA-05/0052 Capatect ÖKO Line ETA-05/0052, Perg, 01.07.2016.

[9] Österreichisches Institut für Bautechnik: Europäische technische Zulassung: ETA 13-0147 Hanffaserdämmplatte

[10] HTL- Baulabor- Luftschallprüfstand: Schalldämmaß nach ÖNORM EN ISO 140-3, Messung der Luftschalldämmung von Bauteilen im Prüfstand, 12.01.2012.

STRUCTURALLY GLAZED TIMBER CURTAIN WALL

Nebojsa Buljan[1], Adriana Bjelanovic[2], Hrvoje Turkulin[3]

[1] RI ISA d.o.o. Permasteelisa Group, Delta 5, 51000 Rijeka, Croatia, email: n.buljan@permasteelisagroup.com
[2] University of Rijeka Faculty of Civil Engineering, Department of Structural Engineering, Radmile Matejcic 3, 51000 Rijeka, Croatia, email: adriana.bjelanovic@gradri.uniri.hr
[3] University of Zagreb, Faculty of Forestry, Svetošimunska cesta 25, 10000 Zagreb, Croatia, email: hrvoje@sumfak.hr

SUMMARY: TimberCW is an innovative structurally glazed timber curtain wall system entirely comprised of glued laminated timber profiles incorporated in a fully prefabricated unitised curtain wall design. The system eliminates aluminium elements whilst maintaining a high weathertightness performance. Specialised corner connections and stainless steel bracketry has been developed and laboratory tested. The target in the research of the TimberCW was to apply the current state of the art technology in aluminium to wooden based frames and to improve the energy performance of the building envelope. The developed system is an environmental friendly, with physical, structural and aesthetic performance equal to or better than equivalent aluminium systems.

STAKLENO-DRVENA KONSTRUKCIJA OVJEŠENE FASADE

SAŽETAK: Drvena ovješena fasada inovativni je sustav stakleno-drvene ovješene fasade koji se u cijelosti sastoji od lijepljenih uslojenih drvenih profila uključenih u projekt potpuno predgotovljenog fasadnog panela. U sustavu su izostavljeni aluminijski elementi, a postignuto je visoko svojstvo brtvljenja. Razvijeni su i u laboratoriju ispitani posebni uglovni spojevi i spojnice od nehrđajućeg čelika. Cilj istraživanja drvene fasade bio je primijeniti postojeće stanje tehnološkog znanja od aluminijskih na drvene okvire i poboljšati energetsko svojstvo ovojnice zgrade. Razvijeni sustav prijateljski je za okoliš a fizička, konstrukcijska i esetetska svojstva jednaka su mu ili bolja od istovrijednih aluminijskih sustava.

1. INTRODUCTION

In recent years, an ever increasing awareness in energy efficiency and sustainablility has lead to the introduction of wood as a suitable framing material for building envelopes. Presently, the technology of exterior building envelopes is dominated by the curtain wall based on the aluminium framing, which can be divided in two families: unitised systems and stick systems. Unitised systems are completely prefabricated (frames and infill) and more technologically advanced, providing the better overall quality and performance than stick systems, which are assembled on site, but offer the economical advantage, in particular for low-rise buildings. Unitised systems are often structurally glazed, and this technology provides aesthetically pleasing flush appearance, but also some perfomance advantages (bomb blast resistance, f.e.).

The scope of this research is to prove that the technologically advanced concept of the curtain wall system can also be applied using innovative wooden frames:

- Unitised wooden frames in lieu of the stick system
- Glass units structurally sealed directly to the wooden substrate

By achieving the scope the additional advantage will be brought to the unitised technology:

Improved energy performance - TimberCW system effectively increases the energy efficiency during the lifetime of the building due to the difference in the thermal transmittance between aluminium and wood systems.

0% aluminium content - Aluminium is a material with the large carbon footprint, having C02 net emissions in the production and processing of 26 t/m3 (whereas wood sequesters 1 t/m3, CEI-Bois 2013).

Hygrotechnical (rot) and mechanical (thermal dilatation) interaction problems between aluminium and the wood are eliminated.

2. CURRENT STATE OF THE ART

Due to the nature of wood, the current state of the art wood based curtain wall systems are composite stick system designs whereby wood sections are combined with aluminium elements which provide weathertighness and glass retention. Stick systems are assembled on site from individual frame elements which form a lightweight grid that supports the infill (glass, cladding panels and insulation). While stick systems are simple and efficient, there are known limitations of such systems:

They are installed from the outside, so the scaffolding or an external platform is required, which is impractical and costly for high-rise construction,

assembly on site is detrimental to the quality of the execution, in particular when the structural silicone is used, which is not recommended to be applied on site,

limited capacity for the accomodation of differential vertical movements between floors. These are caused by live loads, but also by long term effects as the creep and settlement. High rise buildings usually feature thin metal deck slabs, whose low stiffness will highlight this problem.

Further, there are interaction problems between aluminium and the wood itself:

Differential temperature elongation between aluminium and wood, which may lead to the defect in fixings of the aluminium to the wood. Usually, countersunk head screws are used to fix the aluminium (or inox) profile to the wood, which prevents the differential thermal elongation. Typical 3600 mm high unit will experience thermal elongation of the aluminium profile:

On the yearly basis the temperature of the aluminium profile will vary between approximately 0 °C and 40-50 °C, depending on the type of the glass and of the construction of the frame, resulting in 3,3 – 4,1 mm differential dilatation between the aluminium and wood, or 1,6 – 2,0 mm at screws located near profile's ends.

On the daily basis in the summer the temperature of the aluminium profile will vary between approximately 20 °C and 40-50 °C, depending on the type of the glass and of the construction of the frame, resulting in 1,6 – 2,5 mm differential dilatation between the aluminium and wood, or 0,8 – 1,2 mm at screws located near profile's ends.

Since the movement capacity at screws is limited or prevented, this elongation will cause the searing load in screws and and over time this will lead to the deterioration of the connection and eventually to the failure of the metal-wood assembly, which has been observed in the practice. If stainless steel is used instead of the aluminium, the differential movement will be reduced to 40% of those of the aluminium, but still, over a number of cycles, detrimental effects may be observed.

Figure 1: Countersunk head screws fixing the inox profile with limited movement capacity

Screws that fix the aluminium to the wood have the same temperature as the aluminium section, which may create thermal sinks at low temperatures, thus leading to the risk of condensation and the onset of the rot localised at screws holes with subsequent failures of the connections.

3. DESIGN CONCEPT

TimberCW is a system entirely comprised of glued laminated wood profiles, using spatial lamination – longitudinal, lateral and layered gluing of wood lamellae, incorporated in a fully unitised curtain wall design. Glass units are fixed to the frame by the structural sealing, which avoids the direct exposure of wood elements to the weather. Unitised systems feature split mullions; conveniently slim in typical aluminium framing design, that provide aesthetic narrow sight lines.

3.1. EQUIVALENT ALUMINIUM SYSTEM

In typical curtain wall applications, spanning between floors, the main limiting structural property of frame members is stiffness, rather than resistance. The allowed lateral deflection d under the design load is, according to EN 13830:

- d ≤ L /200, if L ≤ 3000 mm;
- d ≤ 5 mm + L /300, if 3000 mm < L < 7500 mm;
- d ≤ L /250, if L ≥ 7500 mm.

Frame elements of TimberCW have the same stiffness of the equivalent aluminium system. The chosen comparable aluminium system is series 180 by Permasteelisa. The width of the frame is maintained the same for both systems, 90 mm. TimberCW system features:

- Split wood mullions and stack joints,
- 0% aluminium content,
- Same sight lines (width of the frame) as the equivalent aluminium system,
- Structural properties and loadbearing capacity not lower than the equivalent aluminium system,
- Same or better weathertightness performance as the equivalent aluminium system,
- Better energy performance than the equivalent aluminium system and adequate durability.

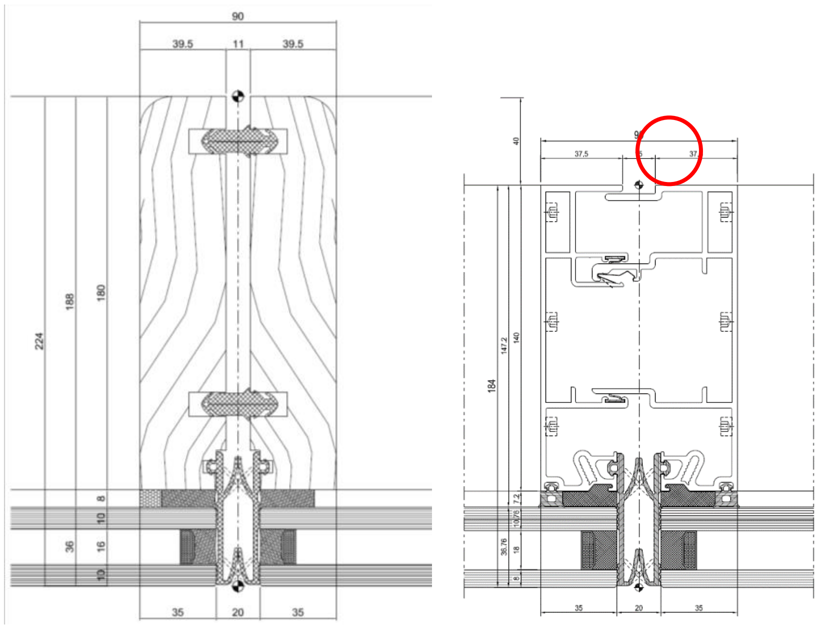

Figure 1: Wood frame and equivalent 180 series aluminium frame

The Young's module of elasticity in bending of the wood is 4-7 times lower than that of the aluminium. Also the limiting bending stress is much lower, depending on the used wood species and grade. The system depth has to be increased approximately 30% in order to match the structural performance of the aluminium frame. The depth of the wood profile is 180 mm and of the aluminium profile 140 mm, i.e. 28,6% more for the nearly equal lateral stiffness.

The material used for the sample was fir wood for the core and siberian larch for the ridges, Marine grade plywood stiffened the internal lateral face. The choice of the wood material was based on its availability, moderate cost and adequate structural properties. The choice of the material is, in the end, project driven and a number of other species, including hardwood, may be used.

3.2. CORNER CONNECTIONS

A vertical row of curtain wall units structurally forms a Gerber beam. The horizontal reaction from the upper unit is transferred to the lower unit through the stack joint using bespoke spigots at the corners of the unit. Mullion sections in unitised system are very narrow, for 90 mm of the frame width, the mullion width is only 39,5 mm and specialised bespoke corner connections are required to form the corners of the frame and enable the load transfer the load in limited space. Connection corners and brackets in stainless steel 1.4404 have been developed for this. The transfer of the shear load through the corner connection (joint of the gerber beam) until the failure has been successfully tested at Faculty of Civil Engineering of University in Rijeka. 3 corner samples were successfully tested. The observed range of results was homogeneous. The increase of the deformation was approximately linear and it did not show any significant plastic deformation after the load release at 5 kN. The breakage pattern was through the splitting of the wood at fixings of the stainless steel connection joint. The resulting loadbearing capacity (~15 kN) is superior to the loadbearing requirements of the joint (2,5-4,0 kN).

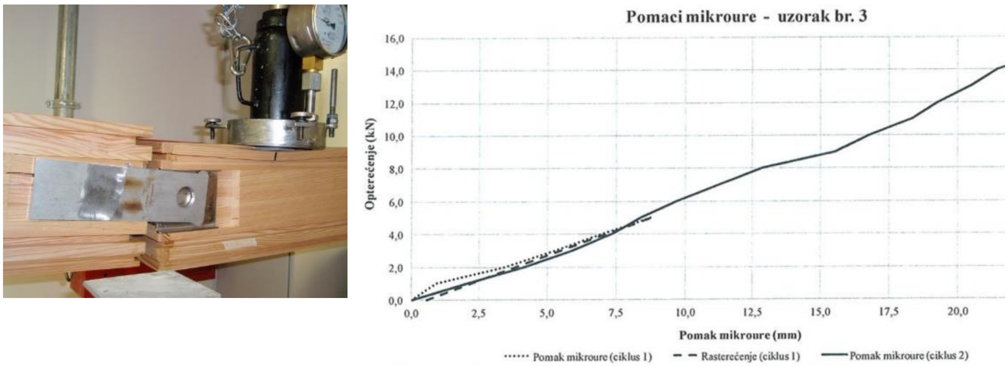

Figure 3: Structural test of the corner connection and Deformation / Load diagram of tested sample

3.3. STRUCTURAL GLAZING

The mechanical glazing with external retaining clips was not preferred, as it would expose wood elements to adverse exterior weathering conditions. Glass units are fixed directly to the wood frame by structural sealing. The structural silicone used is two component Sikasil SG500. The silicone joint and the process of the application has been developed with the collaboration of the company Sika and tested for adhesion in their laboratory, tensile strength tested by Permasteelisa.

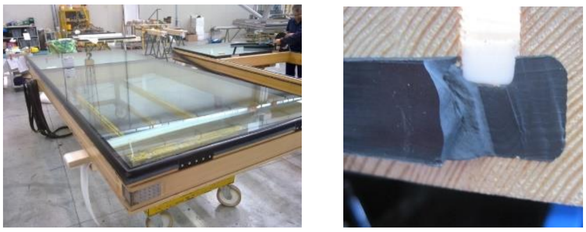

Figure 4: Glazed unit, Peel test – pure cohesive failure

3.3.1. PEEL TEST

The adhesion of 3 silicones were tested (peel test according to EN 13022-2: A.3.2 and C.3.1):

- Sikasil SG-500 – two component structural silicone sealant
- Sikasil SG-20 - one component silicone sealant for structural glazing
- Sikasil WS-605 - one component silicone weather sealant

The silicone was applied to the:

- non treatad surface,
- surface of the sample that was painted with water based transparent finish (the surface in contact with the silicone was protected by adhesive tape)
- and to the surface of samples impregnated with fire retardants. Surfaces in all combinations both treated and not with the primer. Samples were also conditioned up to 21 days in the water saturated atmosphere (90% RH) and high temperature (55 °C).

#	Sample:	1st Pretreatment Step:	Sealant / Adhesive:	7d 23°C		7d 55°C / 90% r.h.		14d 55°C / 90% r.h.		21d 55°C / 90% r.h.	
1.		-	Sikasil® SG-500	1	-	1	-	1	-	1	-
2.	Sample A:	Sika® Primer-210		1	-	1	-	1	-	1	-
3.	Timber, natural Surface completely natural - untreated	-	Sikasil® SG-20	1	-	5	-	5	-	5	-
4.		Sika® Primer-210		1	-	1	-	1	-	1	-
5.		-	Sikasil® WS-605S	1	-	1	-	1	-	1	-
6.		Sika® Primer-210		1	-	1	-	1	-	1	-

#	Sample:	1st Pretreatment Step:	Sealant / Adhesive:	7d 23°C		7d 55°C / 90% r.h.		14d 55°C / 90% r.h.		21d 55°C / 90% r.h.	
1.		-	Sikasil® SG-500	1	-	1	-	1	-	1	-
2.	Sample B:	Sika® Primer-210		1	-	1	-	1	-	1	-
3.	Timber	-	Sikasil® SG-20	1	-	2	RA	3	RA	4	-
4.		Sika® Primer-210		1	-	1	-	1	-	1	-
5.	Surface painted, except SG side	-	Sikasil® WS-605S	1	-	1	-	1	-	1	-
6.		Sika® Primer-210		1	-	1	-	1	-	1	-

No	Sample:	1st Pretreatment Step:	2nd Pretreatment Step:	Sealant / Adhesive:	Results:	
1.	Wood – Timber Finishing: impregnated (all side)	Sika® Aktivator-205	-	Sikasil® SG-500	1	-
2.		Sika® Aktivator-205	-	Sikasil® SG-550	1	-

Figure 5: Peel test results – adhesion

The results of the adhesion test were positive, meaning that the silicone peels through the cohesive failure, proving that the adhesion to the substrate is higher than the cohesive strength (denominated by "1"). Only samples of Sikasil SG-20 (not used for the project) on non-primed surface showed partial adhesive failure ("2" through "5") and separation od edges ("RA").

3.3.2. TENSILE STRENGTH TEST

Tensile strength test of silicone (EN 13022-2: A.3.1 and C.5 and EN 15434) on 10 "H" samples. The results of the adhesion test were positive. No adhesion failure was observed. All samples broke through cohesive failure in the silicone within known material strength limits. At 4 samples the breakage of the wooden substrate was observed, caused by the small thickness of the wooden lamella used (between 5,6 and 5,8 mm), but this did not invalidate the test results.

SAMPLE N.	TYPE OF RUPTURE	Tot. Kg	Kg/cm2	Mpa
1	100 % cohesive	58	9.66	0.948
2	100 % cohesive	71	11.83	1.16
3	100 % cohesive	56	9.33	0.915
4	100 % cohesive	60	10	0.98
5	100 % cohesive	65	10.83	1.06
6	100 % cohesive	56	9.33	0.915
7	100 % cohesive	64	10.66	1.04
8	100 % cohesive	62	10.33	1.01
9	100 % cohesive	56	9.33	0.915
10	100 % cohesive	53	8.33	0.866

Figure 6: Samples and results of tensile strength testing

4. PERFORMANCE MOCK-UP TESTING

Successful full scale laboratory testing (according to EN 13830[1]) of a two-storey high and three units wide sample (4500mm x 7200mm high) has been undertaken in Permasteelisa's laboratory in Vittorio Veneto, Italy, in 05/2013.

The sample has been certificated for constructability, air permeability, watertightness, serviceability, thermal cycling, accommodation of building movements, impact and structural resistance, proving the TimberCW concept suitable for the project application. Test sequence and performance:

Air permeability	±600 Pa surface pressure
Static watertightness	600 Pa surface pressure
Wind resistance	±2 kPa surface pressure
Air permeability	±600 Pa surface pressure
Static watertightness	600 Pa surface pressure
3 temperature cycles	-20 ºC / +50 ºC External temp., 20 ºC internal temp., no adverse effects observed
Air permeability	600 Pa (chamber only) surface pressure
Air permeability	±600 Pa surface pressure
Static watertightness	600 Pa surface pressure

Vertical movements ±10 mm -1 cycle, vertical movement of the upper row of units
Horizontal racking ±7 mm - 2 cycles in the plane of the façade at the stack joint
Air permeability ±600 Pa surface pressure
Static watertightness 600 Pa surface pressure
Dynamic watertightness 600 Pa (airplane engine moving over the façade)
Water hose test 1 vertical and 1 horizontal joint
Safety test ±3 kPa surface pressure
Impact load, external 3 points, 45 kg falling from 950 mm height
Impact load, internal 3 points, 45 kg falling from 950 mm height

Figure 7: Installed sample: internal view

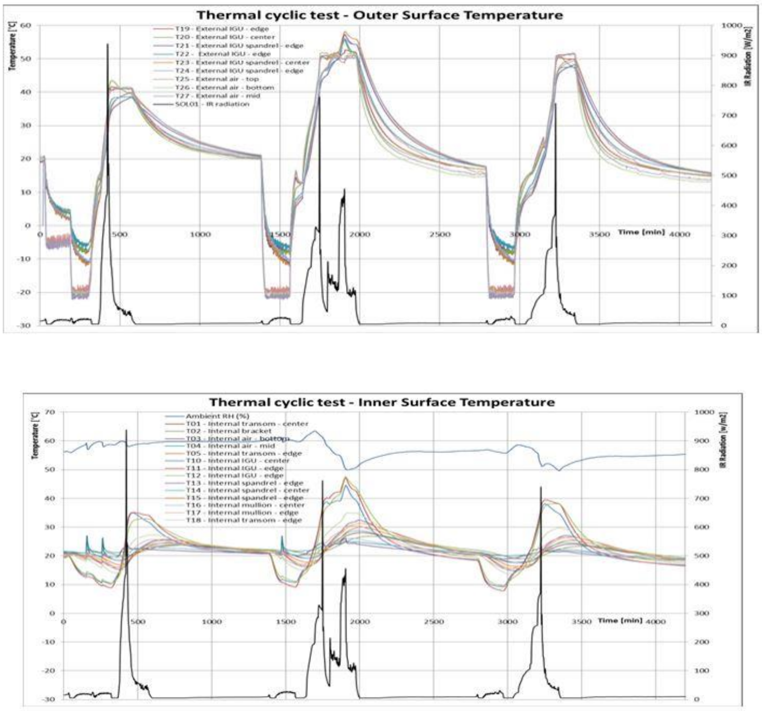

Figure 8: Thermal Cycling: -20 ºC / +50 ºC external temperature, 20 ºC internal temperature

Figure 9: Installed sample: external view

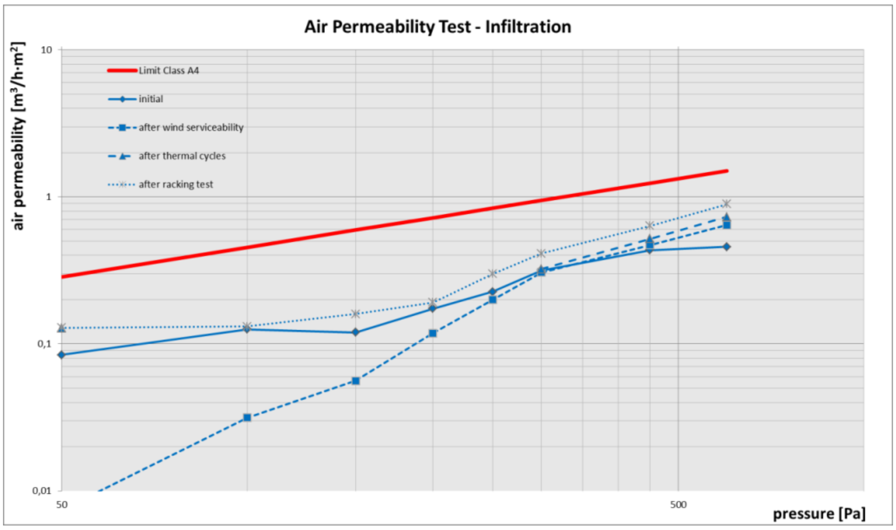

Figure 10: Measured air permeability: max 0,89 m³/(h·m²) at 600 Pa

5. ENERGY PERFORMANCE

In order to evaluate the thermal performance of the Timber CW, a comparative analysis of 4 different systems is made for a typical unit, characteristic for unitised curtain wall projects. The modular width of a unit is 1500 mm and the height 3600 mm, of which 2400 mm is the visual area and 1200 mm is the insulated shadowbox. It has been assessed the thermal transmittance characteristic for winter conditions, using 2 different glass configurations: a double glazed unit (DGU, $U_g = 1{,}1$ W/m²K) and a triple glazed unit (TGU, $U_g = 0{,}6$ W/m²K).

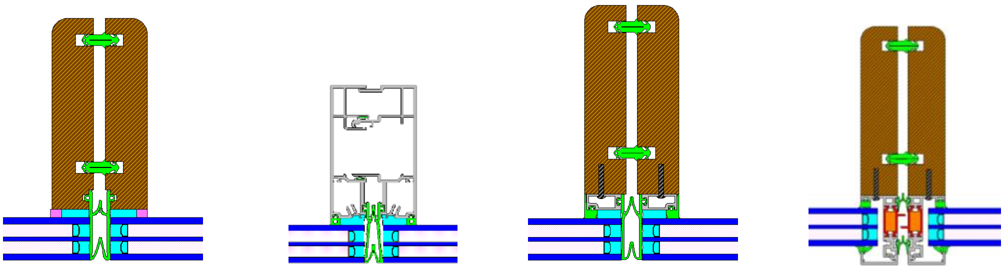

TimberCW structurally glazed | Aluminium system structurally glazed | Composite wood/alu structurally glazed | Composite wood/alu mechanically (dry) glazed

Figure 11: 4 framing systems for the thermal transmittance assessment

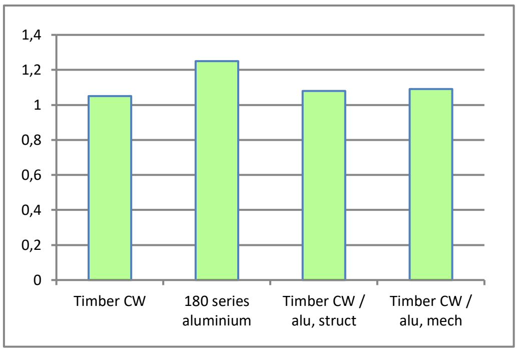

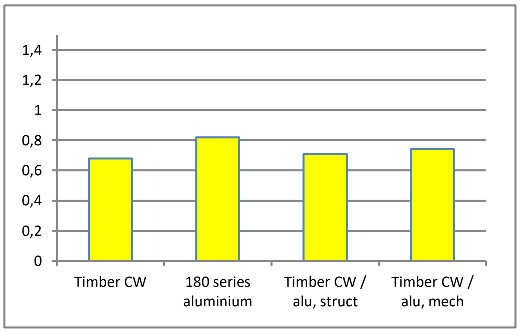

Figure 12: Overall U [W/m2K], DGU

Figure 13: Overall U [W/m2K], TGU

TimberCW has 84% of the overall thermal transmittance of the aluminium system for the option with DGU (U = 1,05 vs 1,25 W/m^{2}K) and 83% for the option with TGU (U = 0,68 vs 0,82 W/m^{2}K). Composite systems fall in between.

6. CONCLUSIONS

The development of the TimberCW system has proven to be a successful innovative technical solution in meeting the proposed targets:

- Spatially laminated wood frames with specifically developed fittings proved applicable for a fully unitised prefabricated façade system, featuring advantages over wood stick façade systems and aluminium constructions.
- The structural glazing directly to the wooden frame proved to be feasible and functional after the extensive testing.
- Energy performance of the wood-based framing system is better than of the equivalent aluminium curtain walling, resulting in ca 35-41 % better thermal transmittance of the frame alone (for the warm glass edge technology) and up to 20 % better overall thermal transmittance of the building envelope. The carbon footprint and heating costs are demonstrated to fall below the standard aluminium prefabricated façade elements. 0% aluminium content contributes to the reduction of the embedded energy in the system.
- The structural properties, weathertightness and transparency of the TimberCW building envelope are equal or better then the aluminium solutions. Standard testing of the TimberCW system proved that all the high end requirements according to EN 13830 are fullfilled, rendering the system suitable for high-rise buildings and adverse climatic conditions.

TimberCW demonstrates that the structurally glazed unitised systems using innovative wooden frames is the feasible technology that provides better energy performance than aluminium based systems. At the same time it is advantageous to composite alu-wood stick systems, being suitable for high-rise buildings and avoiding some stick related constraints (poor movement accomodations and alu to wood fixing problems).

REFERENCES

[1] “Tackle Climate Change: Use Wood”, CEI-Bois, 2013
[2] Prof. Dr Hrvoje Turkulin, “Technical Report - Technical Design of the Wooden Prototype Members of The Curtain Walling System”, Nr LDG HT - 18/2013, Laboratory for Wood in Construction (LDG) of the Faculty of Forestry - University of Zagreb, Croatia, 06/2013
[3] EN 13830:2003 “Curtain Walling – Product Standard“
[4] doc.dr.sc. D. Grandić, T. Franković, prof.dr.sc A. Bjelanović, „Izvještaj o ispitivanju lameliranih drvenih greda“, Faculty of Civil Engineering of University in Rijeka, 07/2012
[5] doc.dr.sc. D. Grandić, T. Franković, prof.dr.sc. A. Bjelanović, „Izvještaj o ispitivanju drvenog priključka greda“, Faculty of Civil Engineering of University in Rijeka, 01/2013
[6] Sika Services AG, “Adhesion test – P.ISA 105/2012 S“, 00077-CTS2-00004, 12/2012

[7] Sika Services AG, “Wood Façade – P.ISA 04/2013 S“, 00077-CTS2-00005, 03/2013
[8] Permasteelisa, “Wood Façade – Laboratory test report“, QCR SG, 12/2012
[9] T. Willmott, „Report 48942W – Timber Curtain Wall – Façade Performance Test“, Sandberg Consulting Engineers, 07/2013
[10] N.Buljan, A.Bjelanović, H.Turkulin, M.Zobec, „Comparing the energy efficiency of a timber curtain wall with an aluminium system“, Conference proceedings, 10th Energy Forum: Advanced Building Skins, Bern, 11/2015, ISBN 978-3-98120538-1

EXPERIMENTAL TESTING OF COMPOSITE MATERIALS AND SANDWICH PANELS WITH COMPOSITE FACE SHEETS WITH POLYESTER AND EPOXY MATRIX

Ana Trombeva-Gavriloska[1], Marijana Lazarevska[2], Meri Cvetkovska[2]

[1] Ss. Cyril and Methodius University in Skopje, Faculty of Architecture, Partizanski odredi 24, 1 000 Skopje, Macedonia, email: gavriloska@arh.ukim.edu.mk
[2] Ss. Cyril and Methodius University in Skopje, Faculty of Civil engineering, Partizanski odredi 24, 1 000 Skopje, Macedonia, email: marijana@gf.ukim.edu.mk, cvetkovska@gf.ukim.edu.mk

SUMMARY: This paper presents the experiment test for the tensile properties of two series of composite materials and two series sandwich panels with composite face sheets, which differed according to the type of matrix. The ultimate tensile strength and the initial module of the elasticity of the composite materials were experimentally determined. Sandwich panels in the experimental tests were subjected on three points bending by linear load in the middle of their span. The analysis was performed in order to evaluate the influence of the matrix type on the ultimate mechanical characteristics of the sandwich panels. Influence of the matrix type used in the composite face sheets was evaluated by analysis of F – δ behavior of series of sandwich panels, as well as by analysis of F – σ behavior of the composite face sheets.

EKSPERIMENTALNO ISPITIVANJE KOMPOZITNIH MATERIJALA I SENDVIČ PANELA S KOMPOZITNIM OBLOGAMA OD POLIESTERSKE I EPOKSIDNE MATRICE

SAŽETAK: U radu se prikazuje ekperimentalno ispitivanje vlačnih svojstava dvije serije kompozitnih materijala i dvije serije sendvič panela s kompozitnim oblogama koje se razlikuju po vrsti matrice. Vlačna čvrstoća i početni modul elastičnosti kompozitnih materijala određeni su eksperimentalno. Sendvič paneli u eksperimentalnim ispitivanjima slobodno su oslonjeni i opterećeni linijskim opterećenjem u sredini raspona. Provedenim proračunima ustanovljen je utjecaj vrste matrice na krajnje mehaničke značajke sendvič panela. Taj je utjecaj utvrđen analizom ponašanja F – δ za seriju sendvič panela i analizom ponašanja F – σ za kompozitne obloge lica.

1. INTRODUCTION

Sandwich structures are being often used as constructive elements in the civil engineering. The usage is mostly based on their high performance, such as high stiffness and high strength compare with their weight. Based on the concept of increasing the bending bearing capacity and stiffness sandwich panels are defined as structures that have low weight. They are multi layered composites formed of two thick, but strong and stiff face sheets, and lower core. Depending on the specific application of the final product different materials could be used for fabrication of sandwich panels.

Any constructive product available as a thin plate could be used for the face sheets [2]. Material are chosen so that face sheets will have high bending stiffness, high tensile and compressive strength and excellent resistance to external influences. Composite materials, as anisotropic materials, especially as materials with high strength to weight ratio, high stiffness to weight ratio and as non-corrosiveness easy handling material that offer many options in the design process, are very often used as materials for the face sheets.

Lingaiah and Suryanarayana [7] in their work present experimental research of sandwich panels with composite face sheets and aluminum honeycomb core subjected on bending, while the Alias [1] did experiments on sandwich panel with steel face sheets and polyvinylchloride core statically loaded with concentrated force. The fracture mechanism should be well-known in order to determine the mechanical characteristics of sandwich panels. Fracture types of sandwich panels in linear part are studied and discussed by Allen [2], Ashby and Gibson [3] and Plantema [10]. In order to simplify the mathematical operations numerous analyses of sandwich panels are being performed on beam model. Swanson and Kim [11] and Mines and Alias [9], focused on analyses of sandwich beam fracture. Fracture of the sandwich elements could occur as a result of reaching the ultimate compressive or tensile strength of the face sheets or as a result of reaching the ultimate shear strength of the core [8, 6]. According to the available literature the mechanical characteristics and the fracture type of the sandwich panels depend on the used materials. Mechanical characteristics of sandwich panels with composite face sheets depend also on the components used for the composite material.

Many papers that concern composite materials present the excellent mechanical characteristics of the composite materials. Many experimental research work show that the mechanical characteristics of the composite materials depends on the matrix and fiber reinforcement selection. The strength and stiffness of the composite materials according to Barbero [5] depend on the matrix choice, while the strength of the composite material to compression and tension, in a direction normal to the reinforcement fibers, depend on the matrix strength, on the strength of the contact surface between the matrix and the reinforcing fibers and from the defects in the matrix such as holes and micro fractures. Despite the fact, that the mechanical characteristics of the composite materials could be estimated from previous gained knowledge, the experimental testing should be performed if new composite product is developing, in order to obtain precise mechanical characteristics. Furthermore, the experimentally obtained results could give clear view on the behaviour of the mechanical characteristics due to changes of components or changes of environmental conditions, and help the designer to analytically predict behaviour of a complex structure.

This paper presents an experimental tests performed on two series of composite materials and two series of sandwich panels with composite face sheets differed by the type of the used matrix. Two types of matrix material-polyester and epoxy based resins are used for these experiments. In order to analyse the influence of the different components on the final mechanical characteristics of the composite materials the basic mechanical characteristics from experimentally obtained σ-ε diagrams, such as ultimate tensile strength and module of elasticity, were determined. Sandwich panels in the experimental tests were subjected on three points bending. The analysis was performed in order to evaluate the influence of the matrix type on the ultimate mechanical characteristics of the sandwich panels. Influence of the matrix type used in the composite face sheets was evaluated by analysis of F-δ behavior of series sandwich panels, as well as by analysis of F-σ behavior of the composite face sheets.

2. SPECIMENS PREPARATION AND EXPERIMENTAL PROCEDURE

2.1. COMPONENTS OF COMPOSITE MATERIALS AND SANDWICH PANELS

For the purpose of the experiment the testing was performed in two parts: testing of the composite materials and testing of the sandwich panels. For the experimental testing of the composite materials two different series of thin laminates were fabricated, using two types matrix and fiber glass reinforcement in two plies. The laminates were fabricated using rowing with density 0,535 kg/m^2 for fiber glass reinforcement and polyester resin and two-component epoxy resin for matrix. The examined sandwich panels were fabricated of polyurethane core and thin composite face sheets, same as the previously experimentally tested composite materials. The core of sandwich panels is 60 mm hard foam polyurethane with density of 30 kg/m^3. Actually, the sandwich panels' series differ by type of matrix used for the thin composite face sheets.

Marking of the laminates and sandwich panels was according to the components used for the production of composite materials: the symbol (S) refers to the sandwich panel, the symbols (P or E) refers to the type of the matrix, the symbol (2) refers to the number of reinforcement plies and the last symbol (R) denotes the type of used reinforcement. The materials types used for production of the laminates and sandwich panels are summarized in Table 1.

Table 1: Components of series tested sandwich panels

Laminate	Sandwich panels	Core	Composite face sheet		
			Matrix	Reinforcement plies	Reinforcement
P2R	SP2R	Polyurethane	Polyester resin	2	Rowing
E2R	SE2R	Polyurethane	Epoxy resin	2	Rowing

2.2. SPECIMEN GEOMETRY

Test specimens for the first part of the experiment were cut from fabricated laminates. Their geometry was defined according to American test standard ASTM D 3039 [4], Figure 1. All test specimens had a constant rectangular cross section and tabs on each side. These tabs were made form G11 laminate, epoxy material reinforced with E glass rowing under high temperature. In order to avoid different surface stresses, the bond between tabs and specimen was made by araldite, epoxy and polyurethane based adhesive with high extensive properties.

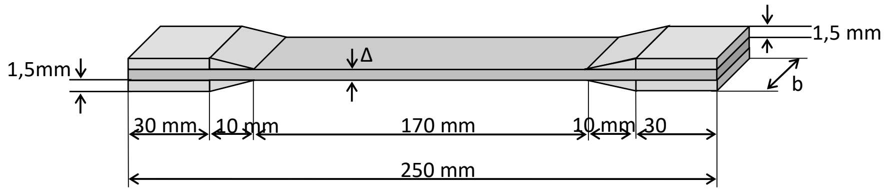

Figure 1: Geometry of composite test specimens

For the second part of the experiment test specimens were fabricated by hand lay-up of the composite face sheets on the hard foam polyurethane. Their geometry was defined by the properties of the test machine, Figure 2. All test specimens had a constant length of 1000 mm and rectangular cross section with width of 300 mm. The depth of each sandwich panel differs depending on the depth of the composite face sheets. For precise determination of the relative strain of each composite face sheet of the tested sandwich panel, strain gages in longitudinal direction were used.

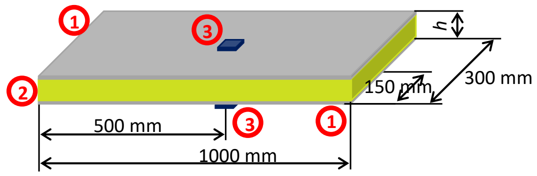

Figure 2: Geometry of sandwich panel specimens 1) composite face sheets; 2) core; 3) strain gages

2.3. EXPERIMENT TEST SETUP

Test procedure for the composite material was defined in accordance with American test standard ASTM D 3039 [4]. Prior to the tension tests the final surface preparation was carefully examined for each test specimen. The dimensions of the specimens were measured before tension testing and the specimens' area were determinate at three places in order to record the average area.

Experiments were performed by using testing machine SCHENCK HYDROPLUS-PSB, with capacity of 250 kN. Tests were made in range up to 25 kN. Pressure controllable hydraulic grips were used. Initial trails were made in order to determinate the most appropriate pressure on the hydraulic grips. The speed of the testing machine was set to 1 mm/min in order to obtain constant strain rate in the gage section, which was observed with trail tests. The specimens were inserted in the grips of the testing machine taking care of alignment of the ripped specimen with the test direction.

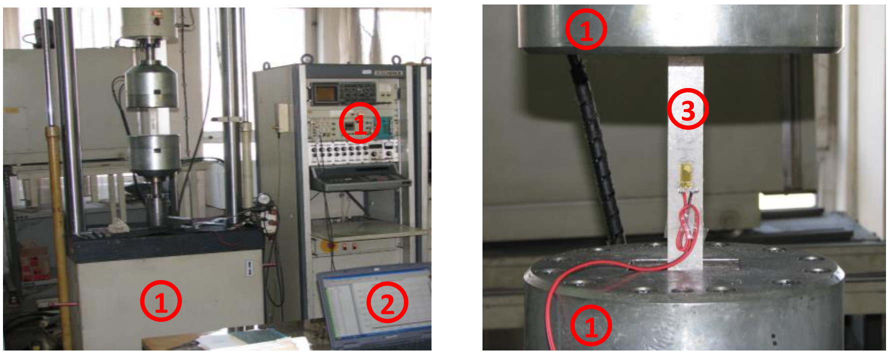

Figure 3: Testing machine and equipment for tensile test of FRP specimens: 1) testing machine; 2) computer; 3) test specimen

The final surface preparation of the sandwich panels was carefully examined for each test specimen prior to the flexural tests. The dimensions of the specimens were measured before flexural testing. In order to record the average area of the specimens' their area was measured at three places.

The tests specimens were subjected on three point bending. Additional device was set on the test machine in order to test the flat beams loaded on flexure. The specimens were carried by steel supports with 50 mm width set on 50 mm diameter steel cylinders which permit slip and deformation of the sandwich panels during the experiments. Slip on the contact surface was avoided by using of 2 mm neoprene layers between sandwich panels and a steel support. Line load was applied through 100 mm width steel beam mounted on steel cylinder with diameter of 50 mm. A 40 mm square hole was made in the middle of the steel beam in order to set a strain gage on the top face sheet of the sandwich panel in the middle of the span. By placing a 4 mm thick neoprene layer between steel beam and sandwich panel the local fracture of the top layers of the composite face sheet was avoided. The actual span of the sandwich beam was 800 mm and the load was applied with constant speed of 5 mm/min.

Tension force and flexural force was determined with force transducer integrated in the testing machine. The full bridge strain gage type force transducer was used. Head displacement of the testing machine was determined by displacement transducer of inductive type. Strain data were determinate using strain gage in longitudinal direction. The strain gage with resistant of 350 Ω, type HBM 10/350LY11 were selected in order to reduce the heating effects due to the low conductivity of the used composite materials. The surface preparation and the selection of bonding agent for the strain gage installation was done in consultation with the strain gage producer. The temperature compensation was done by a passive strain gage, connected in half-bridge. The force versus head displacement and the force versus strain were continuously recorded with sampling rate of 50 Hz. The HBM Spider 8 and software HBM CATMAN 4.0 were used for data acquisition.

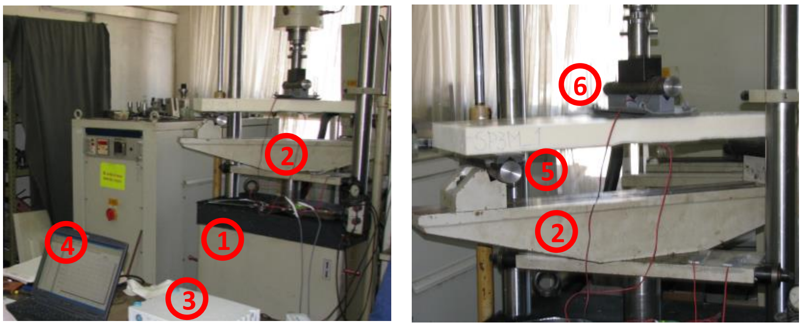

Figure 4: Testing machine and equipment for flexural test of sandwich specimens: 1) testing machine; 2) additional device for testing flat beams; 3) acquisition unit; 4) computer; 5) steel support lay on cylinder; 6) loading steel beam on cylinder

3. EXPERIMENTALLY OBTAINED RESULTS AND DISCUSSION

3.1. COMPOSITE MATERIALS

The tensile testing has been performed on two different series of specimens. For the purpose of the experiment three specimens of each serial were tested. Geometry and experimentally obtained results for tested FRP specimens are summarized in Table 2.

Table 2: Geometrical and mechanical properties of tested composite specimens

Specimen	*b* [mm]	Δ [mm]	Tensile strength [MPa]	Module of elasticity [MPa]	Average tensile strength [MPa]	Average module of elasticity [MPa]
P2R_1	25	1,5	87,33	12200	86,02	11445
P2R_2	25,1	1,6	81,77	10850		
P2R_3	25,2	1,6	88,96	11285		
E2R_1	25,1	1,4	91,66	12160	92,01	12170
E2R_2	25,2	1,3	85,41	12150		
E2R_3	25,2	1,3	98,96	12200		

In order to observe the influence of the components on the mechanical properties of the composite materials, comparative analyses of the experimentally obtained results were carried out. From the σ-ε diagrams shown on Figure 5 and results summarized in Table 2 could be concluded that tensile strength and module of elasticity are slightly higher for the composite materials with epoxy matrix. From Figure 5 could be seen that composite materials with polyester matrix have more distinct transitional boundary on the bilinear σ-ε diagram in comparison with the composite materials with epoxy matrix.

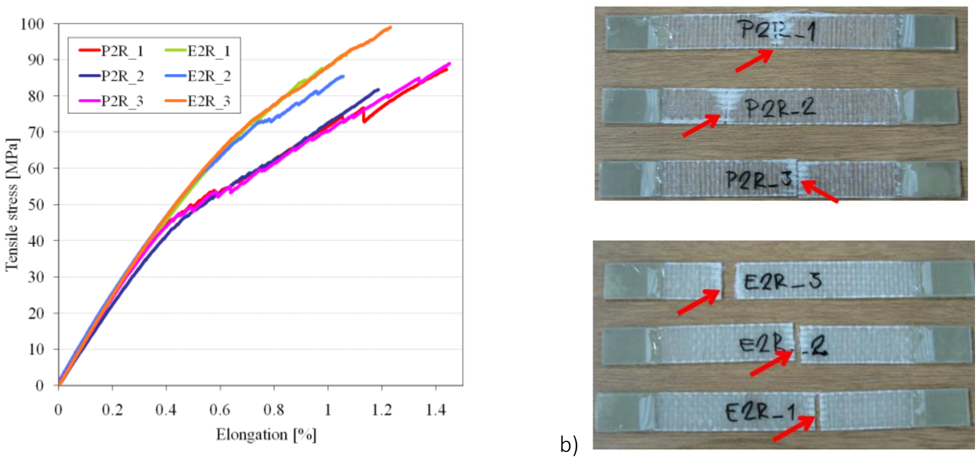

a) b)

Figure 5: Experimentally tested specimens of the series P2R and E2R: a) σ-ε diagrams; b) failure modes

The failures of all tested FRP specimens were sudden and brittle. Standard description of the failure modes was chosen using the three-part failure mode code, according to American standard ASTM D 3039 [4]. The failure mode for the test specimens was denoted as LGM (Lateral Gage Middle), Figure 5b). Actually, the type of the failure mode depends on the type of the used reinforcement and it doesn't depend on the type of the used matrix.

3.2. SANDWICH PANELS

The flexural testing has been performed on two different series of specimens. Two specimens of each serial were tested for the purpose of the experiment. The geometry and the experimentally obtained results for tested sandwich specimens are summarized in the Table 3.

Table 3: Geometrical and mechanical properties of tested sandwich specimens

Sandwich specimen	Face sheet thickness, *t* [mm]	Sandwich panel thickness, h [mm]	Load [N]	Deflection [mm]	Tensile strength [MPa]
SP2R_1	1,5	62	3340	30,67	34,65
SP2R_2	1,7	63	3367	29,08	29,18
SE2R_1	1,3	62	3538	32,27	41,48
SE2R_2	1,2	63	3511	32,58	45,07

From the performed tests can be concluded that the behavior of the tested sandwich panels subjected on three points bending can be divided in three characteristic parts. Behavior of the sandwich panels is linear up to the point where cracking of the polyurethane foam occurs reducing their stiffness. In the nonlinear part, by increasing the load, new micro cracks appear and spread through the depth of the core, while the composite face sheets are still in elastic part caring out the applied load. In the last stage crash of the top composite face sheet and core occur followed by a considerable drop in the stiffness of the sandwich panels.

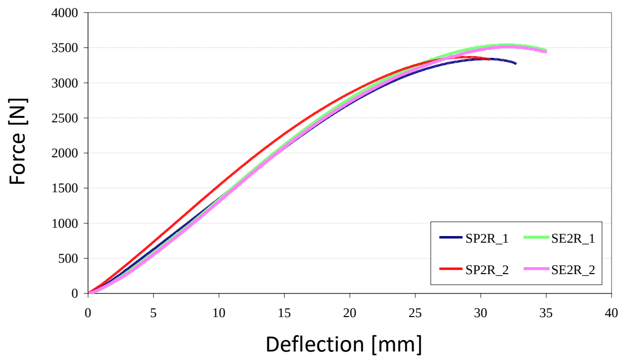

Figure 6: F-δ diagrams for specimens SP2R and SE2R subjected on three point bending

The F-δ behaviour of the tested sandwich panels SP2R and SE2R in the middle of the span is similar, as can be concluded from the Figure 6. The ultimate strength of the series sandwich panels SE2R is minimally higher in comparison to the series of sandwich panels SP2R. In particular, the behaviour of the both series of sandwich panels is in the linear part with the approximately equal stiffness and minor differences observed in the ultimate deformations.

In order to observe the influence of the used matrix on the mechanical properties of the sandwich panels, comparative analyses of the experimentally obtained results for the stress on the bottom face sheet were carried out, Figure 7. The analysis of the results summarized in Table 3 lead to conclusion that the deflections and ultimate tensile strength in the bottom face sheets in each series of sandwich panels are approximately equal under the ultimate load. Under the equal loading, the series of sandwich panels SE2R have minimal higher stress in the bottom face sheet in comparison to series sandwich panels SP2R, as can be seen in Figure 7. Nevertheless, it should be mentioned that the stresses in the composite face sheets are very small in comparison with the strength of the composite material, and the properties of the composite material are not completely used.

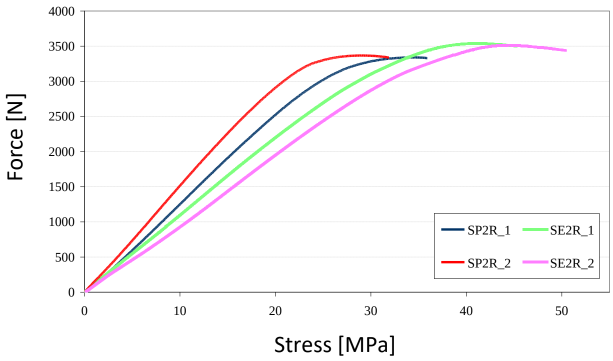

Figure 7: F- σ diagrams for specimens SP2R and SE2R subjected on three point bending

Figure 8: Fracture of the sandwich panels SP2R and SE2R subjected on three points bending

The results of the performed experiments state that the fracture of the sandwich panels was followed by fracture of the top composite face sheet and fracture of the polyurethane foam core in the top of the sandwich panel, while the bottom composite face sheet remained undamaged with no visible cracks, Figure 8.

4. CONCLUSIONS

This paper presents results from the experimental tests of two series of composite materials, subjected on axial tension and two series of sandwich panels subjected on three points bending.

The basic mechanical characteristics from σ-ε diagrams, ultimate tensile strength and module of elasticity, were determined in order to analyse the influence of the type of matrix on the final mechanical characteristics of the composite materials. Strains of the composite materials depend on the matrix characteristics, before the appearance of the first micro cracks. It could be concluded that the matrix selection has influence on the strain of the composite material, but it has no influence on composite material ultimate mechanical properties. The experiments show that the failure mode doesn’t depend on the choice of the matrix used for the material.

Analyzing the experimentally obtained results it can be concluded that the type of used matrix in the composite face sheets of the sandwich panels doesn't have a great influence on the initial strength of the sandwich panels and on their deformation. Similarly, the type of the used matrix in the composite face sheets doesn't have an influence on the stress in the bottom face sheet, on the stiffness of the sandwich panel and on their ultimate bearing capacity. Experiments show that the fracture of the sandwich panels is driven by the characteristics of the polyurethane foam core. Its low strength and deformation characteristics have great influence on the fracture of the sandwich panels. It does not permit an utilization of the characteristics of the composite materials used for the face sheets.

REFERENCES

[1] Alias, A.; Nor, N.A.A.; Said, M.R.: The Behaviour of Square Sandwich Panel. Part I: Under Static Loading, *Journal Teknologi*, Vol. 47 (2007), pp. 1-18, E-ISSN 2180-3722

[2] Allen, H. G.: *Analysis and Design of Structural Sandwich Panels*, Pergamon Press, ISBN 9780080128702, Oxford, 1969

[3] Ashby, M. F.; Gibson, L. J.: *Cellular Solids-Structure and Properties*, Cambridge University Press, ISBN 0521495601, Oxford, UK, 1997

[4] ASTM D3039/D 3039M-08: Standard Test Method for Tensile Properties of polymer Matrix Composite Materials, ASTM International, USA 2008

[5] Barbero, E. J.: *Introduction to Composite Materials Design*,Taylor & Francis, ISBN 1560327014, USA 1999

[6] Li, Q. M.; Mines, R. A. W.; Birch, R. S.: The Crush Behaviour of Rochacell-51 WF Structural Foam, *International Journal of Solids and Structures*, Vol. 37 (2000) No. 43, pp. 6321-6341, ISSN 0020-7683

[7] Lingaiah, K.; Suryanarayana, B. G.: Strength and Stiffness of Sandwich Beams in Bending, *Experimental Mechanics*, Vol. 31 (1991) No. 1, pp. 1-7, ISSN 0014-4851

[8] Mines, R. A. W. et al: On the Measurement of the Crush Behaviour of Structural Foams, 11th International Conference on Experimental Mechanics, pp. 287-292, ISBN 9058090140, Oxford, August 1998

[9] Mines, R. A. W.; Alias, A:, Numerical Simulation of The Progressive Collapse of Polymer Composite Sandwich Beam under Static Loading, *Composites Part A: Applied Science and Manufacturing*, Vol. 33 (2002) No. 1, pp. 11-26, ISSN 1359-835x

[10] Plantema, F.: Sandwich Construction, The bending and buckling of Sandwich Beams, Plates and Shells, John Wiley & Sons inc., ISBN 9780471691068, New York, USA 1966

[11] Swanson, S. R.; Kim, J.: Design of Sandwich Structure under Contact loading, *Composite Structures*, Vol. 59 (2003) No. 3, pp. 403-413, ISSN 0263-8223

TOPIC 4.

Assessment and monitoring

Ocjena stanja i monitoring konstrukcija

QUANTITATIVE ESTIMATION METHOD OF REBAR CORROSION RATE OF RC STRUCTURES

Hideki Oshita[1], Konosuke Kanemoto[1]

[1] Chuo University, Department of Civil and Environmental Engineering, 1-13-27 Kasuga, Bunkyo-ku, Tokyo, 112-8551 Japan, email: oshita@civil.chuo-u.ac.jp, k-kanemoto@civil.chuo-u.ac.jp

SUMMARY: A very promising NDE technique for the corrosion of reinforcing steel-bar in RC is presented by applying thermography. The corrosion characteristics of rebar in RC could be evaluated on the basis of temperature history at concrete surface, which would vary due to heat conduction from reinforcement heated by electromagnetic-induction.

METODA KVANTITATIVNE PROCJENE BRZINE KOROZIJE ŠIPKI U ARMIRANOBETONSKIM KONSTRUKCIJAMA

SAŽETAK: Prikazana je vrlo obećavajuća nerazorna tehnika procjene korozije armaturnih čeličnih šipki u armiranom betonu primjenom termografije. Značajke korozije šipki u armiranom betonu mogle bi se ocijeniti na osnovi tijeka temperature betonske površine koja bi se mijenjala zbog vođenje topline iz armature zagrijane elektromagnetskom indukcijom.

1. INTRODUCTION

In concrete structures, the corrosion of reinforcing steel-bar (rebar) is well-known to not only initiate cracks due to the expansion of corrosion products, but also to decrease the ultimate strength with the decrease in the effective cross section of rebar. Moreover, the delamination in cover concrete could lead the remarkable decline of the durability and the ultimate strength as the accelerated degradation with the exposure of rebar to atmosphere. Consequently, it is very important to quantitatively estimate the characteristic of the corrosion of rebar in RC structures. The most accurate technique currently available for the estimation of the corrosion is to remove the rebar and to measure visually. It is, however, realistically difficult to take rebar in existing structures, and thus non-destructive evaluation (NDE) techniques have been applied. NDE techniques, which are currently applied to the estimation of rebar corrosion, is the half-cell potential method [1] and the polarization resistance method [2]. It is known that both methods are marginally successful to predict the occurrence or not of rebar corrosion, and that there exists one problem that a damage is inevitably exerted by chipping covered concrete to set the electrode in rebar directly. That is, it seems that any NDE techniques currently available could not predict the rate of corrosion or the thickness of corrosion products in rebar accurately.

In this paper, one promising NDE technique is presented by applying thermography. The corrosions of rebars are estimated from the temperature history at the concrete surface, which would vary due to heat conduction from reinforcement heated by electromagnetic-induction.

2. OUTLINE OF PROPOSED TECHNIQUE

2.1. GENERAL

Evaluation technique for the characteristic of rebar corrosion in concrete structures is developed under such conditions as perfectly non-destructive and non-contact at the surface of concrete. Based on the characteristics of rebar with high heat conduction and easy magnetization, heat applied to rebar by an electromagnetic induction heating is diffused to the surface of concrete as shown in Figure 1. When the corrosion product exists on the rebar surface, the temperature on the surface of concrete over rebar could shift from that of non-existence of the corrosion product. Thus, the temperature on the surface is dependent on thickness and distribution of the corrosion products. It is known that thermal characteristics of the corrosion product are similar to that of air, as a specific heat is relatively large and a thermal conductivity is inversely small as shown in Figure 2. The effect of the corrosion product is illustrated in same figure. Since heat conduction is prevented by a layer of the corrosion product, the temperature at the concrete surface over non-corroded rebar is quite different from that of corroded rebar.

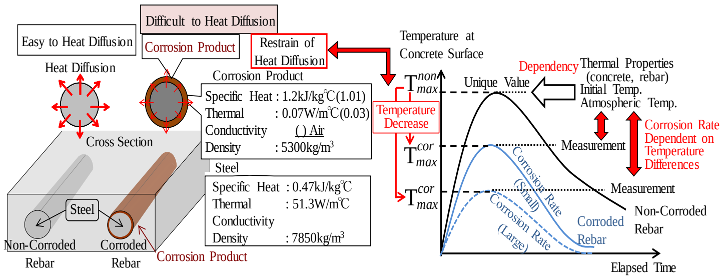

Figure 1 General of Proposed System Figure 2 Detailed Proposed System

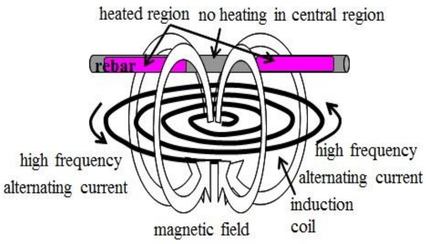

Figure 3 Circle Coil

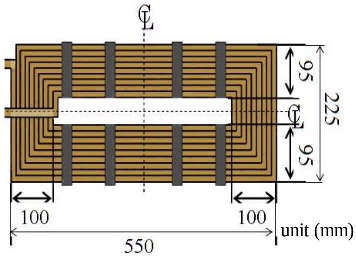

Figure 4 Developed Coil

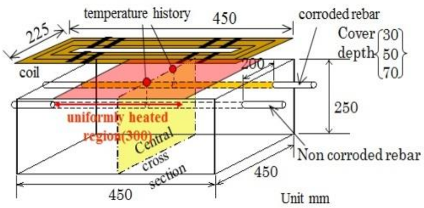

Figure: 5 Specimen

2.2. ELECTROMAGNETIC INDUCTION HEATING

As non-contact heating, an electromagnetic induction is applied. By charging a high-frequency electric current on an electromagnetic induction coil, an alternating field is generated around the coil and thus an eddy current is driven in a steel bar located in that field. As a result, rebar is heated. In the case of a circular coil, an electromagnetic induction generates an alternating magnetic field concentrically as shown in Figure 3. At the center and the edge of the coil, the magnetic flux density becomes smaller than that in between. Therefore, for a rebar set in the alternating magnetic field, non-uniform heating areas are generated as the temperature around the center and the edge of the coil becomes lower, while that of the other region becomes higher.

In the proposed procedure, it is very important to heat a rebar uniformly in the longitudinal direction. To this end, various experiments for the characteristics of heating were performed in which the coils were investigated on the shape, the size of steel tube for the coil and the diameter of steel tube. It is found that a rectangular coil shown in Figure 4 is of the most suitable shape to heat the rebar uniformly so that no heating gradients exist in the range of 60 mm x 300 mm. The electromagnetic induction coil developed is equipped with a copper pipe of 10 mm diameter, inside which cooling is performed with water to reduce heat of the coil due to radiofrequency current. The coil temperature becomes about 30 ºC at the time of radio frequency current charge, even if cooling is performed. Therefore, it is necessary to set a styrene foam of about 10 mm of thickness as an insulator at the concrete surface when heating is conducted.

Table 1 Specimen's Parameters

Specimen's Name	Cover Depth (mm)	Diameter of Rebar	Corrosion Rate (%)	Coil Power (kW)	Heating Time (s)
K30-C0-1	30	16	0.00	2.0	320
K30-C0.66			0.66		
K30-C0-2			0.00	1.8	90
K30-C1.0			1.00		
K30-C5.0			5.00		
K50-C0-1	50		0.00	6.0	540
K50-C0.82			0.82		
K50-C0-2			0.00	1.8	420
K50-C1.0			1.00		
K50-C5.0			5.00		
K70-C0	70		0.00	6.0	780
K70-C0.70			0.70		

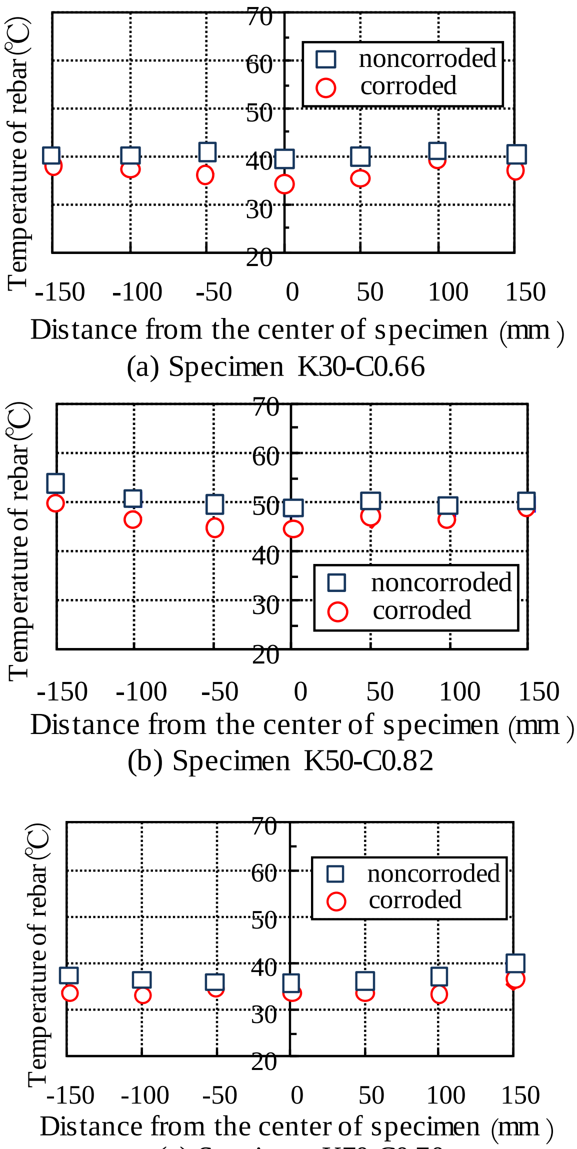

(a) Specimen K30-C0.66

(b) Specimen K50-C0.82

(c) Specimen K70-C0.70

Figure 6 Temperature Distribution of Rebar

3. THERMAL CHARACTERISTIC AT CONCRETE SURFACE RELATED WITH RATE OF CORROSION

3.1. EXPERIMENTAL OUTLINE

Concrete specimens are of a cubic with the height of 250 mm, the width of 450 mm, the length of 450 mm as shown in Figure 5. Two rebars with the diameter of 16 mm are arranged with 200 mm interval of 30, 50, and 70 mm cover-thicknesses. One is non-corroded and another is corroded, where uniform corrosion was confirmed along the axial direction. Charging electric current into a coil for fixed time, the temperature of rebar was controlled by the electromagnetic induction heating and then the coil was removed. Here, the region of rebar uniformly heated is the 300 mm as shown in Figure 5 due to the restrictions of coil size. Both lengths of the coil and the specimen are 450 mm, but extended regions of the rebar outside the concrete specimen were actually heated due to the formation of magnetic field.

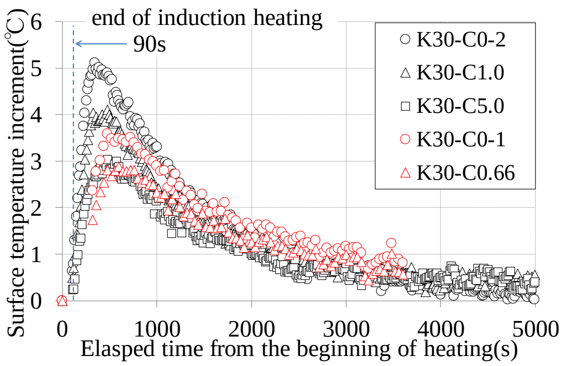

(a) Cover depth 30mm

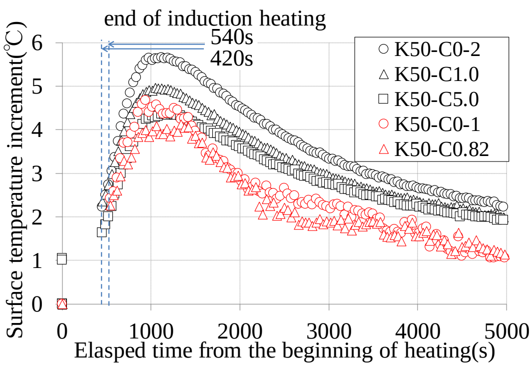

(b) Cover depth 50mm

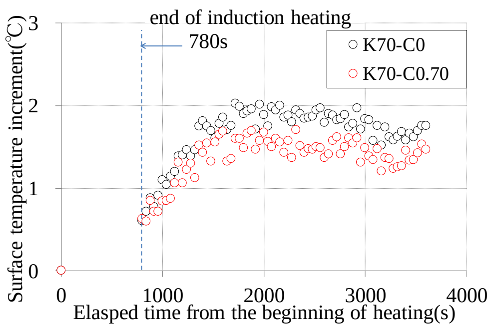

(c) Cover depth 70mm

Figure 7 Temperature History at Concrete Surface

In the measurement, the temperature on the surface of concrete was measured by infrared thermography. Initially, the surface temperature was measured before installing the electromagnetic induction coil. Then, the temperature was measured for 90 minutes, during 5 sec. after termination of electromagnetic induction heating. Experimental parameters are the cover depth of concrete and the rate of corrosion. Details of all specimens are listed in Table 1. Thus, the specimen's name is classified with the cover depth as K30, the rate of corrosion as C0.66. The electric powers applied are also shown in Table 1.

The rate of the corrosion is defined as a mass ratio of the corrosion product to the non-corroded rebar. The corrosion product was removed by soaking the corroded rebar into citric acid di-ammonium solution of 10 % concentration with temperature of 20 ºC for twenty-four hours. The thickness of the corrosion product was calculated from the rate of the corrosion and the density of steel and corrosion product given in Figure 2.

3.2. THERMAL CHARACTERISTIC ON REBAR EMBEDDED IN CONCRETE

Figure 6 shows the distribution of temperature on the surface of the rebars for representative specimens K30-C0.66, K50-C0.82 and K70-C0.70. Here the rate of corrosion in rebars are appended as K30-C0.66, of which the rate is 0.66 %. As seen, the temperature of the corroded rebar is lower than that of non-corroded rebar. This thermal behavior shows converse compared with that of a rebar putting in an air. These differences are caused by that the corrosion product restrains the heat diffusion to concrete from non-corroded cross-section of the reinforcing bar.

3.3. THERMAL CHARACTERISTIC AT CONCRETE SURFACE

Figure 7 shows the incremental temperature history at the concrete surface over the rebars at the middle point of the rebar shown in Figure 5. It is observed that temperature over the corroded rebar is 0.5-1.0 ºC lower than that of non-corroded.

4. PREDICTION MODEL FOR RATE OF CORROSION OF REBAR

The rate of corrosion of a reinforcing bar is greatly dependent on such characteristics of the temperature at the concrete surface, as the maximum temperature and the rate of the temperature rise. As mentioned above, the presence of the corrosion product causes the decrease in the maximum temperature at the concrete surface and then the decreasing value is corresponding to the rate of the corrosion. Hence, the rate of the corrosion will be predicted by the comparison between the value measured in corroded RC structure and the prescribed value, which is in case of the non-corroded bar.

4.1. TEMPERATURE AT CONCRETE SURFACE

To predict the rate of the corrosion of rebar, the information of the temperature at the concrete surface T_{max}, where the non-corroded rebar is arranged, is essential. One empirical estimation is known as the solved value by the non-steady heat conduction problem.

Now, the non-steady heat conduction as an axisymmetric problem shown in Figure 8, in which the center of rebar is origin and the radius is the length from the center of the rebar to the surface of the concrete, can be expressed as a following equation.

$$\frac{1}{\kappa}\frac{\partial u}{\partial t} = \frac{\partial^2 u}{\partial r^2} + \frac{1}{r}\frac{\partial u}{\partial r} \quad , \ \kappa = \frac{\lambda}{\rho c} \tag{1}$$

where, u is a temperature, t is a time, γ is a coordinate from an origin, ρ is a density and λ is a heat conductivity.

The initial temperature of concrete and rebar can be expressed as Equation (2) and the boundary condition on the surface of concrete is heat transfer as Equation (3).

$$u(r,0) = \delta(r) \tag{2}$$

$$\frac{\partial u}{\partial r}_{r=d} = h(u - u_\infty) \tag{3}$$

where, u_∞ is an atmospheric temperature, h is a coefficient of heat transfer and d is cover depth.

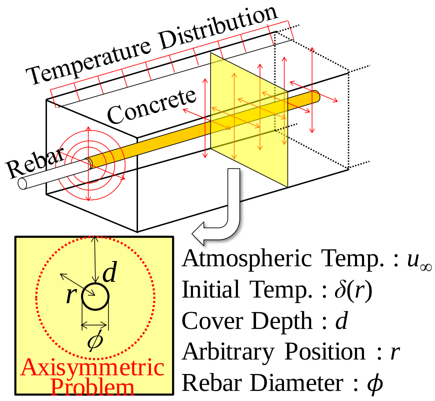

Figure 8 Axisymmetric Problem

Solving Equation (1) under the condition of Equation (2) and (3) and discretizing the exact solution to the rebar and concrete region, the temperature at arbitrary position and time can be derived as follows.

$$u(r,t) = u_\infty - \left\{ \frac{2(u_{con}-u_\infty)h^2}{d} \sum_{i=1}^{\infty} \frac{J_0(k_i r) e^{-\kappa k_i^2 t}}{(k_i^2+h^2) k_i J_1(k_i d)} + \frac{(u_\phi - u_\infty)\phi}{d^2} \sum_{i=1}^{\infty} \frac{k_i J_1\left(\frac{k_i \phi}{2}\right) J_0(k_i r) e^{-\kappa k_i^2 t}}{(k_i^2+h^2) J_0^2(k_i d)} \right\} \tag{4}$$

where, u_{con} and u_ϕ are an initial temperature of concrete and rebar, respectively and ϕ is a diameter of rebar. J_0 and J_1 are 0 order and 1order Bessel function and k_i is a solution of the Bessel's equation.

$$hJ_0(k_i d) - k_i J_1(k_i d) = 0 \tag{5}$$

Finally, the temperature on the surface of concrete just above where the rebar is arranged can be derived substituting the position of concrete surface d into r. Regarding to the initial temperature of rebar, its value was defined as the adiabatic temperature rise of only rebar by the magnetic induction heating dependent on the diameter and cover depth of rebar.

4.2. RATE OF CORROSION OF REBAR

The corrosion product at the surface of rebar restrains the heat conduction from the non-corroded section inside steel to concrete and thus the heat restrained is dependent on the rate of the corrosion, as shown in Figure 8. In conclusion, the rate of the corrosion is able to be estimated, if the heat restrained is obtained from the difference between the temperature at the surface over corroded rebar and that of non-corroded.

The temperature rise at the concrete surface is dependent on the heat flux conducted which is predominated by the thermal characteristics of constitutive material, i.e. the thermal conductivity, specific heat, density, thickness and the thermal gradient. One empirical estimation is known as the coefficient of overall heat transmission (K value) which is defined the heat flux passing unit area under the differences of unit temperature.

Namely, it is an index expressing the heat transfer and is similar to the heat conductivity. However, the heat conductivity is an index as the material characteristic, but the coefficient of overall heat transmission is heat flux transferring per unit area taking the thickness of the material into account.

$$\bar{K} = \frac{1}{\sum_{i=1}^{n} \frac{\ell_i}{\lambda_i}} \tag{6}$$

where, $\bar{K}$ is the coefficient of overall heat transmission, ℓ_i and λ_i are the thickness and the heat conductivity of each material, respectively.

Applying Equation (6) into the non-corroded state and corroded state of the rebar, the coefficient of overall heat transmission can be obtained as follows.

$$\bar{K}_{sc} = \frac{1}{\frac{\frac{\phi}{2}}{\lambda_{stl}} + \frac{d}{\lambda_{con}}} \text{ non-corroded state,} \quad \bar{K}_{src} = \frac{1}{\frac{\frac{\phi}{2}o}{\lambda_{stl}} + \frac{\frac{\phi}{2}m}{\lambda_{cor}} + \frac{d}{\lambda_{con}}} \text{ corroded state} \tag{7}$$

where, ϕ is a diameter of rebar, d is a cover depth. λ_{con}, λ_{stl} and λ_{cor} are coefficient of heat conductivity of concrete, steel and corroded product, respectively. o and m are the rate of the thickness of non-corroded region and corroded region to the radius of the rebar before occurring of corrosion and then o and m are called as "non-corroded ratio" and "corroded ratio".

The heat flux transferring the covered concrete can be expressed as follows.

$$\bar{Q}_{sc} = \frac{\bar{K}_{sc}}{\bar{\rho}_{sc}\bar{c}_{sc}} \quad \text{non-corroded state,} \qquad \bar{Q}_{src} = \frac{\bar{K}_{src}}{\bar{\rho}_{src}\bar{c}_{src}} \quad \text{corroded state} \tag{8}$$

where, $\bar{\rho}_{sc}$ and $\bar{c}_{sc}$ are an average density and specific heat of the rebar and covered concrete for RC member before occurring the corrosion. After occurring the corrosion, $\bar{\rho}_{sc}$ and $\bar{c}_{sc}$ are expressed as $\bar{\rho}_{src}$ and $\bar{c}_{src}$ which are an average value of the non-corroded rebar, corroded rebar and covered concrete. These are expressed as follows.

$$\bar{\rho}_{sc} = \frac{\frac{\phi}{2}\rho_{stl}+d\rho_{con}}{d+\frac{\phi}{2}} \quad \bar{\rho}_{src} = \frac{\frac{\phi}{2}o\rho_{stl}+\frac{\phi}{2}m\rho_{cor}+d\rho_{con}}{d+\frac{\phi}{2}(m+o)} \quad \bar{c}_{sc} = \frac{\frac{\phi}{2}\rho_{stl}c_{stl}+d\rho_{con}c_{con}}{\frac{\phi}{2}\rho_{stl}+d\rho_{con}} \quad \bar{c}_{src} = \frac{\frac{\phi}{2}oc_{stl}\rho_{stl}+\frac{\phi}{2}mc_{cor}\rho_{cor}+dc_{con}\rho_{con}}{\frac{\phi}{2}o\rho_{stl}+\frac{\phi}{2}m\rho_{cor}+d\rho_{con}} \tag{9}$$

where, ρ_{stl}, ρ_{cor} and ρ_{con} are a density of rebar, corrosion product and concrete, respectively. c_{stl}, c_{cor} and c_{con} are a specific heat of rebar, corrosion and concrete, respectively.

Therefore, according to the accumulate heat in the rebar by the magnetic induction heating to be almost similar between rebar with non-corroded state and corroded state, the ratio ΔQ of Equation (8) as follows is dependent on the degree of corrosion of rebar.

$$\Delta Q = \bar{Q}_{src}/\bar{Q}_{sc} \tag{10}$$

In other words, ΔQ can be defined as the ratio of the temperature increment from the initial value to the maximum value at the concrete surface of the state with non-corroded and corroded rebar as follows.

$$\Delta Q = \Delta T_{src}/\Delta T_{sc} \tag{11}$$

where, ΔT_{sc} and ΔT_{src} are corresponding to the state of non-corroded and corroded rebar, respectively.

According to Equation (8), (10) and (11) and assuming the average heat capacity $\bar{\rho}_{src}\bar{c}_{src}$ with the corroded rebar to be almost similar to that of $\bar{\rho}_{sc}\bar{c}_{sc}$ with the non-corroded rebar in case of the relatively small rate of corrosion of rebar, the following equation can be obtained.

$$\Delta T_{src}/\Delta T_{sc} = \bar{Q}_{src}/\bar{Q}_{sc} = \bar{K}_{src}/\bar{K}_{sc} \tag{12}$$

Substituting Equation (7) into Equation (12), the corroded ratio m can be obtained as a following equation.

$$m = \frac{\beta}{\gamma}(\Delta T - 1) - \alpha\gamma \tag{13}$$

$$\alpha = \frac{\lambda_{con}}{\lambda_{stl}} \;, \beta = \frac{\lambda_{cor}}{\lambda_{con}} \;, \gamma = \frac{\phi}{2d}, \Delta T = \frac{\Delta T_{sc}}{\Delta T_{src}}, \nu = \frac{\rho_{cor}}{\rho_{stl}}$$

Now, applying the mass conservation law to the non-corroded rebar and corroded rebar, the following equation can be obtained.

$$o^2 + (m^2 + 2om)\nu = 1 \tag{14}$$

The rate of corrosion of rebar defined as the ratio of the mass decreasing can be expressed as follows.

$$n = \left\{\pi\left(\frac{\phi}{2}\right)^2\rho_{stl} - \pi\left(\frac{\phi}{2}o\right)^2\rho_{stl}\right\} / \left\{\pi\left(\frac{\phi}{2}\right)^2\rho_{stl}\right\} = 1 - o^2 \tag{15}$$

Finally, substituting the non-corroded ratio o solved in Equation (14) into Equation (15), the rate of corrosion of rebar n can be obtained as follows.

$$n = 1 - \left\{\sqrt{1 - m^2\nu(1-\nu)} - m\nu\right\}^2 \tag{16}$$

5. APPLICABILITY OF PROPOSED MODEL

The applicability of the proposed model is examined in comparison with experimental results. Values estimated of the rate of corrosion, which are predicted by the temperature increment at the concrete surface shown in Figure 7 and Equation (16), are shown in Table 2. For specimens with the relatively shallow the cover depth, it can be seen that the proposed model shows a good agreement with the values measured. On the other hand, for relatively deeper the cover depth i.e. the specimen K70-C0.70, the estimated value is fairly large compared with the values measured. due to the small differences between the temperature increment at the concrete surface for specimens with the non-corroded and corroded rebar.

An example of on-site measurement is shown in Figure 9. A bridge pier of RC structure has been deteriorated by salt attack and then the corrosion of rebars occur in wide ranges. The values estimated of the rate of corrosion in the direction of the axis of rebars, which are predicted by the temperature increment at the concrete surface and Equation (16), are compared with the measured values in Figure 10. The distribution of the rate of corrosion estimated by the proposed model is in reasonable agreement with that of measured.

Table 2 Corrosion Rate

Specimen	Corrosion Rate (%)	
	Measurement	Prediction
K30-C0.66	0.66	0.67
K30-C1.0	1.00	1.13
K30-C5.0	5.00	3.23
K50-C0.82	0.82	0.81
K50-C1.0	1.00	0.81
K50-C5.0	5.00	5.23
K70-C0.70	0.70	1.61

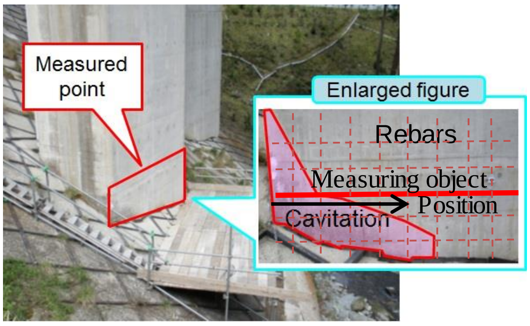

Figure 9 Bridge Pire

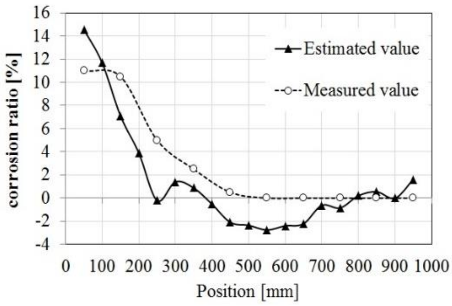

Figure 10 On-site Measurement

6. CONCLUSIONS

One promising NDE technique, which can estimate quantitatively the rate of corrosion of rebar in RC structures, is presented. The technique is based on the temperature history at the concrete surface, which could change due to the heat conduction from the rebar stored by electromagnetic induction heating.

The temperature at the concrete surface over the rebar increases uniformly due to the heat conduction from the rebar, in the case where the heat is applied and stored by electromagnetic heating. If the corrosion product exists on the rebar, the temperature at the concrete surface just over the corroded region of rebar becomes lower than that of the non-corroded region by the effect of the thermal property of the corrosion product.

The model to predict the rate of the corrosion of rebar was presented on the basis of the temperature at the concrete surface. It can be seen that the proposed model was applicability for the full-length corrosion of rebar.

REFERENCES

[1] ASTM C876, Standard test method for half-cell potentials of uncoated reinforcing steel in concrete, Annual Book of ASTM Standards, (2001), pp.452-457

[2] ASTM G59, Standard Test Method for Conducting Potentiodynamic Polarization Resistance Measurements, Annual Book of ASTM Standards, (2009)

PROBABILISTIC ASSESSMENT OF REINFORCED CONCRETE SLAB BRIDGES WITH LOW AMOUNT OF SHEAR REINFORCEMENT

Roland Trummer[1], Markus Vill[1]

[1] Vienna University of Applied Sciences, Faculty of Building and Design, Favoritenstraße 226, 1100 Vienna, Austrian, email: roland.trummer@fh-campuswien.ac.at, markus.vill@fh-campuswien.ac.at

SUMMARY: The resistance of reinforced concrete slab bridges without shear reinforcement has not been completely investigated to the present day. Therefore, probabilistic recalculations on three different bridge structures with the use of three different international standards are conducted. For these probabilistic recalculations the limit state function is defined and explained. The most important parameters of the tested bridge constructions are summarized. The results of the recalculation are compared with the calculated results according to Eurocode 0.

PROBABILISTIČKA OCJENA ARMIRANOBETONSKIH GREDNIH MOSTOVA S MALOM KOLIČINOM POPREČNE ARMATURE

SAŽETAK: Do danas nije potpuno istražena posmična sposobnost i ocjenjivanje posmične nosivosti armiranobetonskih konstrukcija bez poprečne armature. Tijekom desetljeća znanstvenici su nastojali istražiti to pitanje i pronaći rješenje problema. Radi provjere stanja znanja istraženo je više nacionalnih i međunarodnih norma koje koriste probabilistički pristup proračunu. Proračuni na temelju tri različita međunarodna propisa provedena su za tri mosta i uspoređena s rezultatima proračuna prema Eurocode 0.

1. GENERAL DEFINITION OF THE PROBLEM

The shear capacity of reinforced concrete structures without shear reinforcement (stirrups) has not been completely investigated to the present day. For decades, scientists have been trying to explore this topic and find a solution for this problem. During the last century, the design methods that are used in standards have changed and this development has taken a more conservative approach in terms of the design of shear force resistance. Therefore, recalculations of aged railway bridges consisting of concrete slabs show lower values of safety. For the design of shear resistance in the past according to previous standards, only a small amount of shear reinforcement was necessary for bridge structures. Consequently, only a small amount of shear reinforcement ratio was considered for the purposes of construction in the form of bent up bars.

As a result, evidence for the verification of shear resistance cannot be provided, in some cases by the majority of single beam slab bridges with up to 20 meters span, by recalculating in accordance with the current Eurocode 2. According to the recalculation, these structures have to be strengthened or even completely replaced.

In this focus, and further considering that no generally accepted mechanical shear assessment method exists, the present contribution investigates and verifies the multiple state-of-the-art national and international standards using probabilistic calculation methods.

2. STANDARDS AND INTERNATIONAL CODES

Several standards for the verification of the shear reinforcement are compared; among them ÖNORM EN 1992-2: 2012 as well as ÖNORM B 1992-2: 2008 focusing on shear reinforcement, the ACI 318-14 detailed procedure, and the fib model code 2010 using the level of approximation II. Further examinations are conducted and published [2] for the assessment of reinforced concrete slab bridges without web reinforcement from the 1940s to the 1990s by using probabilistic calculation methods For this verification at a probabilistic level, it is necessary to define the limit state function for each standard.

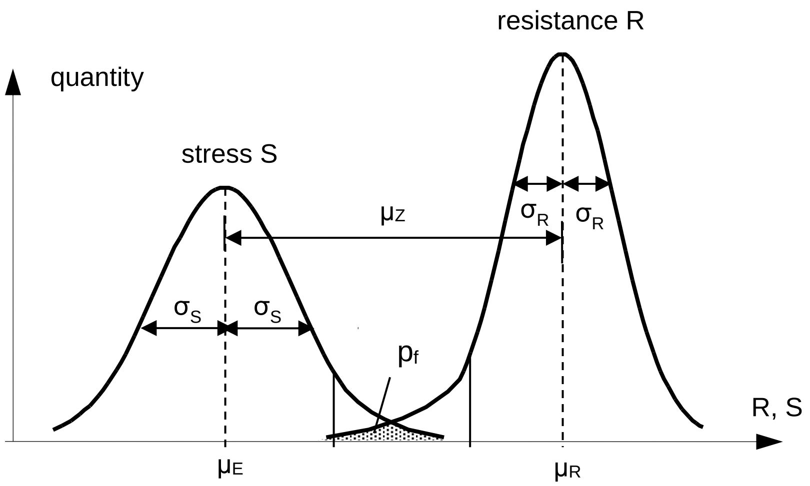

Figure 1 Definition of the reliability of structures

There are two fundamental parameters for a probabilistic assessment. Firstly the limit state function (LSF) and secondly the reliability index β. The limit state function separates the area of the sample space into two sections, as you can see in the Figure 1 axis "R,S". S represents the Loading and R represents the resistance. The reliability index β is a measurement of the failure probability p_f of a structure. The general definition of the limit state function is defined in the following equation [3].

$$G(x) = R - S = U_R * V_R - U_S * V_S$$

The coefficients of model uncertainties (U_S, U_R) are random variables to cover imprecision and incompleteness of the relevant theoretical models for the resistance and the load effects.

2.1. LSF ACCORDING TO ÖNORM EN 1992-2:2012 [4] AND ÖNORM B 1992-2:2008 [5]

The following equation represents the limit state function of the shear capacity and consists of 8 different parameters. Figure 2 represents the distribution of the model uncertainty for the resistance. In Table 1, the individual parameters explained are exemplary for the bridge construction B03.

$$G(x) = U_R \times \left(C_m \times \left(1 + \sqrt{\frac{200}{d}}\right) \times \left(100 \times \frac{A_s}{b_w \times d} \times f_{cm}\right)^{\frac{1}{3}} + 0{,}15 \times \frac{N_{E,m}}{b_w \times d - A_s} \right) \times b_w \times d - (U_E \times V_{Em})$$

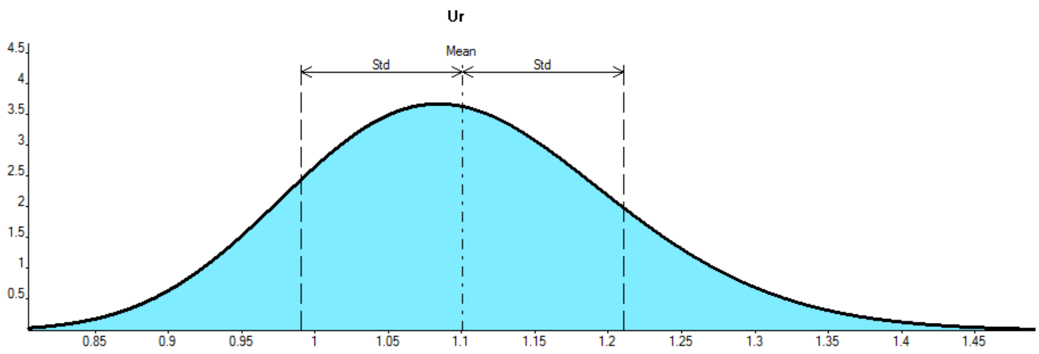

Figure 2 Distribution of the model uncertainty resistance

Table 1 Parameters of the limit state function exemplary for the bridge construction B03 according to the to ÖNORM EN 1992-2:2012 and ÖNORM B 1992-2:2008

Variable	Name	Distribution (Type in FReET) [8]	Unit	Mean value	Standard deviation
U_R	Model uncertainty resistance	Lognormal (2par)	-	1.1	0.11
U_E	Model uncertainty load effect	Lognormal (2par)	-	1	0.1
V_{Em}	Mean value of the shear force at the defined cross section	Lognormal (2par)	MN	1.587	0.1587
N_{Em}	Mean value of the normal force at the defined cross section	Lognormal (2par)	MN	-	-
f_{cm}	Mean value of the cylinder strength of the concrete	Normal	MN/m²	25.6	3
d	Statically effective height	Normal	m	0.65	0.005
b_w	Width of the cross section	Normal	m	3.5	0.005
A_s	Reinforcement Area	Deterministic	m²	0.0137	
cm	Pre-exponential factor for the shear capacity without shear reinforcement	Normal	-	0.26	0.052

2.2. LSF ACCORDING TO FIB MODEL CODE 2010 LOA II [6]

The level II approximation is based on a generalized stress field approach. The difference to the level III of approximation is that the concrete's contribution is considered. According to the equation form the fib Model Code LoA II, 12 different parameters influence the limit state function:

$$G(x)=U_R\times\frac{0{,}4}{1+750\times\frac{\left(\frac{M_{Em}}{0{,}9\times d}+V_{Em}+N_{Em}\times\left(\frac{1}{2}\mp\frac{\Delta e}{0{,}9\times d}\right)\right)}{E_s\times A_s}}$$
$$\times\frac{1300}{1000+\frac{32}{16+d_g}\times 0{,}9\times d}\times\sqrt{f_{cm}}\times 0{,}9\times d\times b_w$$
$$-(U_E\times V_{Em})$$

Table 2 Explanation of the parameters of the limit state function according to the fib model code 2010 LoA II

Variable	Name
U_R	model uncertainty resistance
U_E	model uncertainty load effect
M_{Em}	mean value of the normal force at the defined cross section
V_{Em}	mean value of the shear force at the defined cross section
N_{Em}	mean value of the normal force at the defined cross section
f_{cm}	mean value of the cylinder strength of the concrete
d	statically effective height
b_w	width of the cross section
A_s	Reinforcement Area
Δe	distance between the load application point of the normal force and the center of gravity
dg	diameter of aggregate
E_s	elastic modulus of the longitudinal reinforcement

2.3. LSF ACCORDING TO ACI 318-14 (DETAILED) [7]

The detailed definition of the ACI 318-14 consists of two different equations. The first equation represents the upper limit of the resistance. The second equation represents the limit state function which consists of 10 different parameters:

$$G(x) = \mathrm{U_R} \times 0{,}29 \times \sqrt{\mathrm{f'_{cm}}} \times \mathrm{d} \times \mathrm{b_w} \times \sqrt{1 + \frac{0{,}29 \times \mathrm{N_{um}}}{\mathrm{b_w} \times \mathrm{h} - A_s}} - (\mathrm{U_E} \times \mathrm{V_{um}})$$

$$G(x) = \mathrm{U_R} \times \left(0{,}16 \times \sqrt{\mathrm{f'_{cm}}} + 17 \times \frac{\mathrm{A_s}}{\mathrm{b_w} \times \mathrm{d}} \times \frac{\mathrm{V_{um}} \times \mathrm{d}}{\mathrm{M_{um}} - \mathrm{N_{um}} \times \frac{(4 \times \mathrm{h} - \mathrm{d})}{8}} \right) \times \mathrm{b_w} \times \mathrm{d} - (\mathrm{U_E} \times \mathrm{V_{um}})$$

Table 3 Explanation of the parameters of the limit state function according to the ACI 318-14 (detailed)

Variable	Name
UR	model uncertainty resistance
UE	model uncertainty load effect
M_{um}	mean value of the normal force at the defined cross section
V_{um}	mean value of the shear force at the defined cross section
N_{um}	mean value of the normal force at the defined cross section
f_{cm}	mean value of the cylinder strength of the concrete
d	statically effective height
b_w	width of the cross section
A_s	Reinforcement Area
h	slab depth

3. BRIDGE STRUCTURE

Three case studies, existing bridges structures, are recalculated at a probabilistic level. Previous research has shown that probabilistic assessment of reinforced concrete beams considering shear loads provide a satisfactory solution.

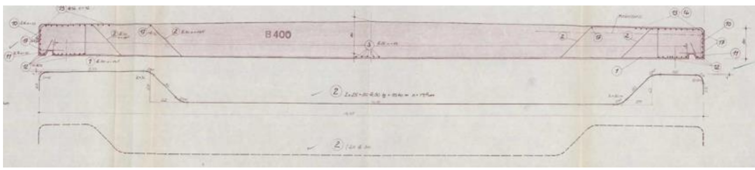

Figure 3 Exemplary cross section of the bridge structure B05

The most important parameters concerning these objects are:

- the static system is in each case a single span girder with a span width from ten to nearly thirteen meters
- the statically effective height varies between 69cm and 87cm
- steal types B500A and B550A are used
- shear reinforcement between 39.1cm²/m and 72.75cm²/m is used

4. RESULTS OF THE PROBABILISTIC RECALCULATION

The probabilistic recalculation of the first bridge construction which was tested, B03, has shown a reliability index □ for the load bearing capacity of 3.15, the prescribed reliability index □□according to the Eurocode 0 for the reliability class RC2 for a 50 year period of consideration is 3.80. The prescribed reliability index of the reliability class RC3 4.3

[3]. Compared with the benchmark of the Eurocode 0, the verification of the load bearing capacity has a negative result. The assessment of the second bridge construction which was tested, B04, resulted in a reliability index β for the load bearing capacity of 3.61, which is also, compared to RC2 of β=3.80, a negative result. The third bridge construction which was tested, B05, shows a β index of 5.68 which is sufficient for RC2 structures as well as for RC3 structures. The following chart illustrates the results for the probabilistic assessment of the limit state function of the shear capacity of these three different bridge constructions. These three bridges were recalculated with three different standards and compared to the reliability index of RC2 and RC3 of the Eurocode 1, which are again 3.80 and 4.30.

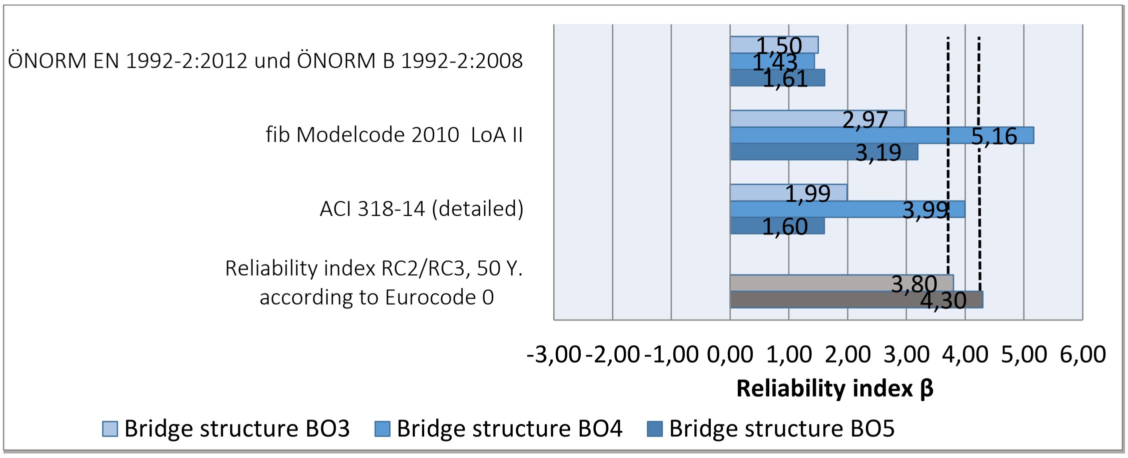

Figure 4 Results of probabilistic recalculation of three different bridge constructions

Figure 5 shows the limit state function of the bridge construction B03 according to the ÖNORM EN1992-2:2012 with an reliability index β=1,50.

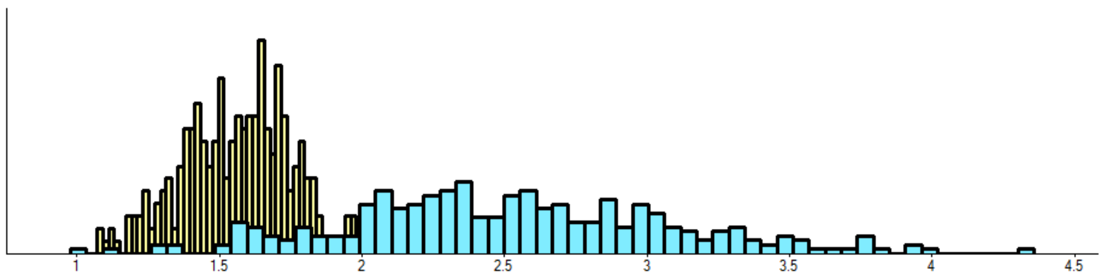

Figure 5 Results of the limit state function exemplary for the bridge construction B03

As a comparison Figure 6 shows the limit state function of the bridge construction B04 according to the ACI 318-14 (detailied) with an reliability index β=3,99.

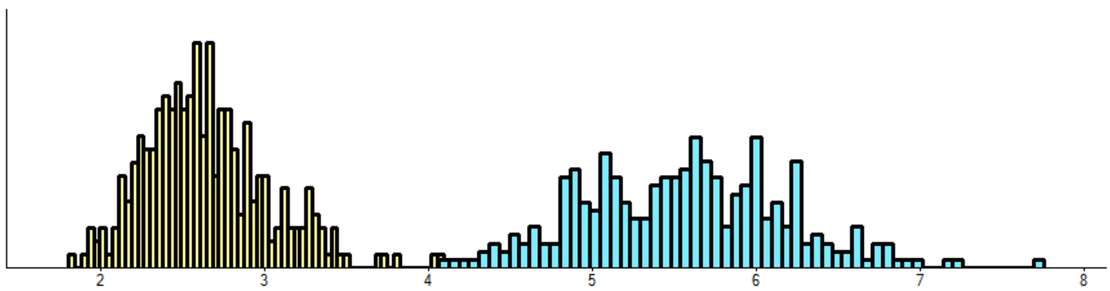

Figure 6 Results of the limit state function exemplary for the bridge construction B03

The probabilistic recalculation indicates that no valid assessment is possible for the limit state function of the shear capacity, as long as the reliability class RC2 is required. One reason for the low reliability index of the shear capacity compared to the load bearing is that within the empirical verification model coefficient, additional partial safety coefficients have been implemented on the loads as well as in the resistance sphere which result in a higher reliability at a semi-probabilistic verification. The fib model code, especially, provides acceptable results because the target value of 3.80 is close to the calculated results. The results of the ACI 318-14 are less favorable. Whereas the ACI at the semi-probabilistic recalculation had provided the highest values of results, the results of the probabilistic calculation shows a high failure probability. Therefore two reasons can be found. Firstly the ACI 318-14 shows a very low reliability level. Secondly in this standard several deterministic parameters are included for which the mean value should be calculated. However there are no fundamentals concerning the distribution function and the variation coefficient available. Therefore the result of the probabilistic recalculation is less meaningful. For this purpose further fundamental investigations ought to be conducted.

As a conclusion, the results of the probabilistic recalculation of the limit state function of the shear capacity on basis of the Eurocode assessment equations provide no satisfactory degree of reliability.

The results are basically higher than the results of the semi-probabilistic recalculation, because the mean value of the resistance is higher than the mean value of the loads. Nevertheless, in the assessment of the resistance according to the Eurocode model-uncertainty-factors, strengths and size factors are combined and each of them enlarged with a partial safety factor, which is defined as an empirical factor generated and added according to examinational data.

With a probabilistic recalculation, a verification of the shear resistance on the basis of the current Eurocode resistance model provides a negative result. If the pre-exponential factor were a deterministic factor with the size of the indicated mean value shown in the literature, the probabilistic calculation could lead to a satisfactory reliability index. But in reality there are distributions which could be embedded after a focused evaluation of test results with a small distribution in the assessment.

REFERENCES

[1] Austrian Standard Institute.: ÖNORM EN 1990:2013.: Basis of structural design, Vienna, (2013)

[2] Dornetshumer, Franz.; Methods for the assessment of reinforced concrete slab bridges without web reinforcement form the 1940s to the 1990s by using probabilistic calculation methods, Master´s thesis, Vienna University of Applied Science Campus Vienna, (2015)

[3] Schneider, Jörg.: Sicherheit und Zuverlässigkeit im Bauwesen, Hochschulverlag AG an der ETH Zürich, ISBN: 3-7281-2167-3, Zürich, (2007)

[4] Austrian Standard Institute.: ÖNORM EN 1992-1-1.: Design of concrete structures, General rules and rules for buildings, Vienna, (2015)

[5] Austrian Standard Institute.: ÖNORM B 1992-1-1.: Design of concrete structures, General rules and rules for buildings, National specifications concerning ÖNORM EN 1992-1-1, national comments and national supplements , Vienna (2011)

[6] International Federation for Structural Concrete (fib).: fib Model Code for concrete Structures 2010, Wilhelm Ernst & Sohn Verlag für Architektur und technische Wissenschaften GmbH &Co KG, ISBN: 987-3-433-03061-5, Lausanne, (2013)

[7] American Concrete Institute.: ACI 318: Building Code Requirements for Reinforced Concrete, ISBN: 9780870319303, Washington, (2014)

[8] Novák, Drahomir et a.: FReET Programm documentation, Cervenka Consulting, Brno, (2016)

STRUCTURAL ASSESSMENT USING ULTRASONIC PULSE ECHO IMAGING

David Corbett[1], Felix Gattiker[1]

[1] Proceq SA, Ringstrasse 2, 8603 Schwerzenbach, Switzerland, email: david.corbett@proceq.com, felix.gattiker@proceq.com

SUMMARY: Due to its inhomogeneous nature and composite structure, concrete has always been a very difficult material to assess. Imaging of concrete elements cannot be compared with imaging of homogeneous materials such as metals. Each of the commonly used technologies such as ground penetrating radar, ultrasonic pulse echo, impact and magnetic eddy current have their limitations. Nevertheless there is a real need for imaging for assessment purposes. This can be to determine the installed rebar structure which is not always well documented or installed as specified. It can also be to accurately locate and assess deeper lying objects such as tendon ducts. These are objects which belong in the structure, but it is also necessary to be able to locate and determine the extent of internal defects such as voids, delaminations and honeycombing. Continual research and technological developments have led to gradual improvement in the commercially available instruments that are able to provide useful images of the internal structure of concrete elements. This paper deals with recent advances in ultrasonic pulse echo technology and in particular its application in notoriously difficult assessment problems such as the location of grouting defects in tendon ducts, investigation of steel fibre reinforced concrete and the location of second layer rebars.

OCJENA STANJA KONSTRUKCIJE VIZUALIZACIJOM ULTRAZVUČNOG ODJEKA

SAŽETAK: Zbog svoje nehomogene prirode i kompozitne strukture beton je uvijek bio materijal težak za ocjenjivanje. Slikovni prikaz betonskih elemenata ne može se usporediti sa slikovnim prikazima homogenih materijala kao što su metali. Sve uobičajeno upotrijebljene tehnike kao što su georadarsko mjerenje (engl. ground penetrating radar), ultrazvučni ehoimpuls, udarne i magnetske edijeve struje imaju ograničenja. Unatoč tomu pri ocjenjivanju postoji stvarna potreba slikovnoga prikaza. Slikovni prikaz može poslužiti za određivanje ugrađenih šipki što nije uvijek dobro dokumentirano ili one nisu ugrađene kako je specificirano. Slikovnim prikazom može se također točno locirati i ocijeniti položaj dublje postavljenih predmeta kao što su cijevi natega. To su predmeti koji pripadaju konstrukciji, ali je nužno locirati i odrediti opseg unutarnjih nedostataka kao što su šupljine, raslojavanje i segregacija betona. Kontinuirana istraživanja i tehnološki razvitak doveli su do postupnog poboljšanja komercijalno dostupnih instrumenata koji mogu proizvesti korisne slike unutarnje strukture betonskih elemenata. U radu je prikazan suvremeni napredak u tehnologiji refleksije ultrazvučnog impulsa, a posebno njegova primjena u općepoznato teškom ocjenjivanju položaja nedostataka pri injektiranju morta u cijevima natega, istraživanju betona armiranog čeličnim vlaknima i lociranju šipki u drugom sloju.

1. INTRODUCTION

Ultrasonic pulse echo technology has proven itself to be very useful applications such as determination of the thickness of concrete structures and detection of internal defects such as honeycombing, voids and delaminations. [1] This is due to the fact that that ultrasonic signals are totally reflected at a concrete / air boundary. This is also true for impact echo signals, but the major advantage of ultrasonic pulse echo technology is the capability to create images which are much easier to interpret. Pulse velocity measurements where access is limited to a single side have also been used for correlation to compressive strength, although the current European standard EN 12504-4 does not strictly allow this. It refers to the use of longitudinal waves only. However as the determination of compressive strength is based on a correlation to core strength, there is no practical reason why this could not be done with shear waves as well as longitudinal waves. The major drawback of pulse echo technology when compared with other imaging techniques such as ground penetrating radar (GPR) is the slow scanning speed recent advances in pulse echo technology

The instrument used to carry out the ultrasonic pulse echo scans used in this paper can be seen in Figure 1. It is an 8 channel instrument with 8 x 3 rows of 50 kHz shear wave, dry point contact transducer elements. The major advances in this instrument is that it is able to display a B-scan in real time and it is also capable of stitching B-scans together in real time to produce large scale images of concrete structures directly on site.

Figure 1 Pundit 250 Array ultrasonic pulse echo instrument and transducer contact arrangement

2. STRUCTURAL ASSESSMENT

The following example shows how a typical structural assessment can be carried out. In this particular example there is a relatively thick section of concrete. The transmission range of pulse echo instruments depends on the quality of the concrete and the amount of reinforcement steel. Research carried out in Germany with large aperture systems have achieved measurements up to 4m in depth [2]. That being said, the current practical range of commercially available instruments is typically around 1m. It can be seen that the structure here is close to that limit.

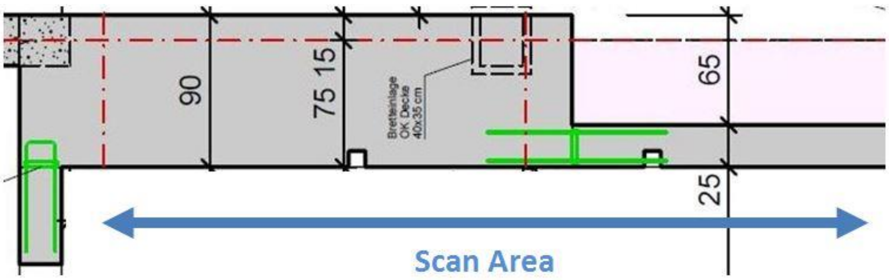

Figure 2 Detection of second layer rebars

As the B-scan is displayed in real time, the first step is to do simple spot checks to establish whether or not it is even possible to see the back wall echo in the thick section of the structure. The same procedure would be used if the task was to locate objects such as pipes, tendon ducts, delaminations or honeycombing within the structure. Rapid spot checks to locate anomalies then more detailed scans in the areas of interest.

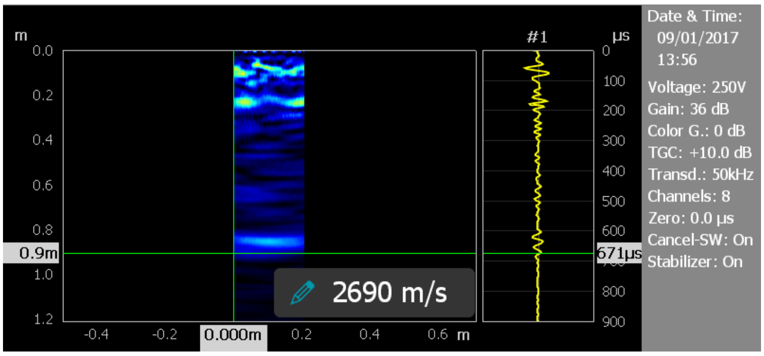

Figure 3 Initial B-scan of 90 cm

In Figure 3 the back wall echo can be seen at a depth somewhere between 0.8m and 0.9m. For ultrasonic pulse echo measurements, depth information is determined by the pulse velocity. For this scan the pulse velocity (2690 m/s) was estimated by measuring the velocity at the surface over a known distance. This is often the case when access is only available from one side and there is no accurate documentation available on the structure. However, it is well known that the pulse velocity at the surface of a concrete structure can differ significantly from the pulse velocity when measured directly through the structure. According to the literature this difference can be as much as 20%. Better results can be obtained if the pulse velocity is calibrated at a point on the structure where the actual thickness is known.

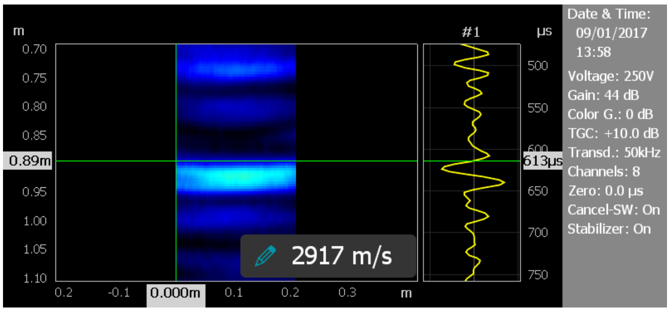

Figure 4 B-scan after pulse velocity calibration and gain adjustment

Figure 4 shows a B-scan at the same location after the pulse velocity has been calibrated by measuring at an area of the structure where the thickness is known. The A-scan to the left of the B-scan is used to align the cursor to the beginning of the echo. The difference in pulse velocity from the surface velocity measurement is 227 m/s which resulted in a measured thickness error of about 7cm or 8% in this case. So if accurate depth information is required it is clear that pulse velocity calibration is necessary. The gain has also been optimised to give a clear back wall signal. These settings can then be used to generate wide area scans.

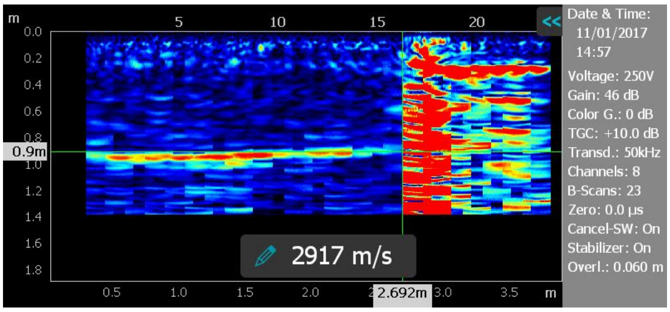

Figure 5 Wide area scan of structure showing step change in wall thickness

Figure 5 shows a scan of around 3.5m. It consists of 23 separate B-scans stitched together. It took less than 2 minutes to generate this scan. The location of the scan be seen in Figure 2. After 2.7m from the beginning of the scan there is a step change in the wall thickness. From here on there are multiple back wall reflections due to the short path length. Figure 6 shows how this scan was created and blends out the superfluous information to highlight the back wall reflections.

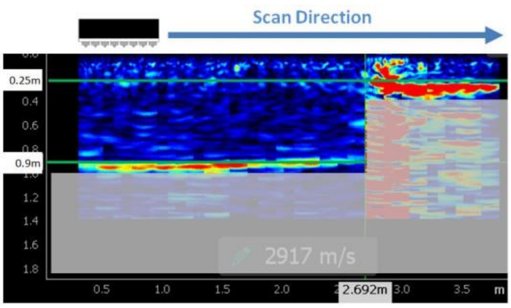

Figure 6 Wide area scan with structural information superimposed

The wall thickness after the step change is 25cm which corresponds very well with the information on the structural drawing in Figure 2.

3. DIFFICULT APPLICATION AREAS

Tests carried out with the prototype instrument prior to its launch in late 2016 have produced some interesting case studies on traditionally challenging applications. The results shown below are very promising and definitely further investigation into these applications is warranted.

3.1. GROUTING DEFECTS IN TENDON DUCTS

Past research has shown that ultrasonic pulse echo testing is possibly the most promising technology for locating grouting defects in tendon ducts [3, 4].Testing on samples with known grouting differences were carried out at the Japan Construction Machinery and Method Research Institute (JCMMRI) A clear differentiation could be made in areas filled with grout and areas without grouting as can be seen in Figure 7. This application is of major interest in the industry and further testing is planned.

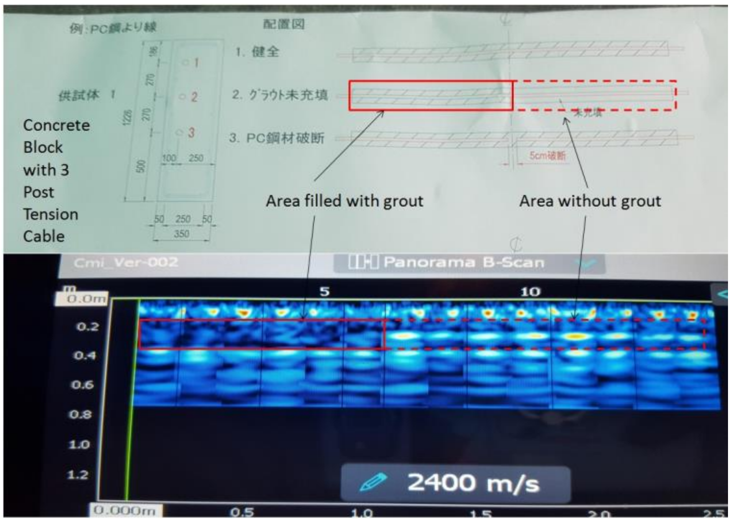

Figure 7 Grouting defects in tendon ducts

3.2. DETECTION OF 2ND LAYER REBARS

Generally speaking the best NDT technologies for detecting rebars are ground penetrating radar (GPR) and eddy current. Eddy current instruments are limited to detecting the first layer rebars. What makes GPR so good for detecting rebars is that there is a total reflection of the transmitted signal at a concrete / steel boundary. This can be a problem in cases where the first layer rebar structure is quite dense and it is desirable to detect objects beyond the upper rebar layer. Figure 8 shows a scan carried out by MAEK Consulting in Singapore on such a structure. Known good and bad areas were tested and could be differentiated. Further to this, the detection of 2nd layer rebars was of particular interest as they had been unable to detect the second layer rebars using GPR equipment in this structural element. The reason this was possible is that ultrasonic signals are only partially reflected at a concrete / steel boundary. Typically about 50-60% of the signal will be reflected. This means that detection is possible, but also sufficient signal passes through to be able to detect objects deeper in the structure.

3.1. NDT OF FIBRE REINFORCED CONCRETE

This testing was carried out a Rapperswil Technical High School in Switzerland. Three identical concrete slabs containing rebars of varying thickness and pipes were constructed. The slabs differed only in the steel fibre content. Testing showed that GPR and Eddy current instruments were more or less blind on the blocks containing steel fibres. The ultrasonic pulse echo instrument was largely unaffected by fibre content. Only the pulse velocity was affected with varying fibre content. Accurate detection of the back wall and resolution of individual rebars and pipes was the same on all three blocks.

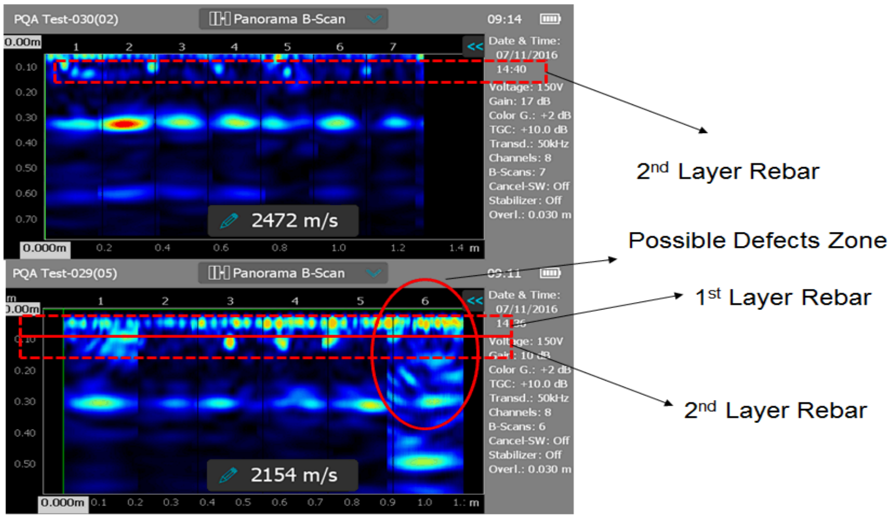

Figure 8 Detection of second layer rebars

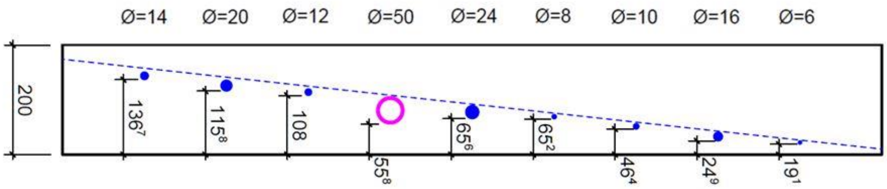

Figure 9 Fibre reinforced concrete test block

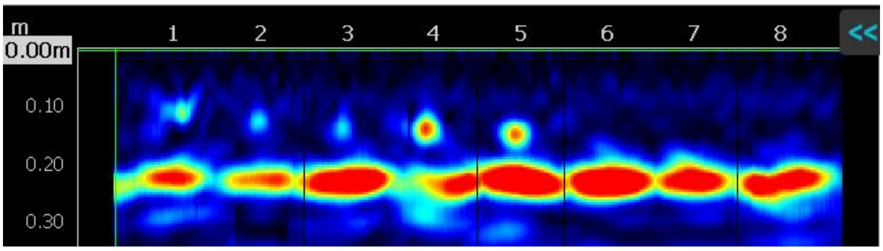

Figure 10 Fibre reinforced concrete test block (no fibre content)

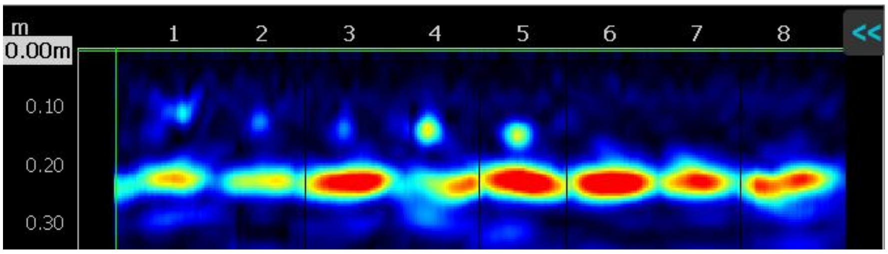

Figure 11 Fibre reinforced concrete test block (60 kg/m3 fibre content)

4. CONCLUSIONS

Ultrasonic pulse technology has established itself as a useful technology for imaging of concrete structures. It is able to detect and display defects such as delaminations, voids and thickness variations which. In the past its practical use has been compromised by the time and effort required to make comprehensive scans. The advent of real time B-scan technology and the possibility to create wide area scans in a very short time will have a very positive effect on the widespread use of this technology. Further to this, new application areas for difficult NDT problems such as the detection of grouting defects, detecting objects beyond dense rebar layers and the assessment of fibre reinforced concrete structures are opening up. Further research will certainly develop these applications further.

REFERENCES

[1] Mähner D., Sodeikat C., Maack S., "ZfPBau-Verfahren an Elementwänden – Fallbeispiel und vergleichende Untersuchungen", Fachtagung Bauwerksdiagnose, 2016 – Vortrag 10, Berlin, Germany.

[2] Mayer K., Krause M., Wiggenhauser H., Milmann B., "Investigations for the Improvement of the SAFT Imaging Quality of a Large Aperture Ultrasonic System", International Symposium Non-Destructive Testing in Civil Engineering (NDT-CE), 2015, Berlin, Germany pp 1026-1034.

[3] Mayer K., Langenberg K-J., et al., "Characterization of Reflector Types by Phase-Sensitive Ultrasonic Data Processing and Imaging", J Nondestruc Eval (2008) 27: 35-45, DOI 10.1007/s10921-008-0035-3

[4] Krause M., Gräfe B, Mielentz F., Milmann B., Friese M., Wiggenhauser H., Mayer K., "Ultrasonic imaging of post-tensioned concrete elements: New techniques for reliable localization of grouting defects", Concrete Repair, Rehabilitation and Retrofitting II – Alexander et al (eds), 2009, London, ISBN 978-0-415-46850-3

IDENTIFICATION OF FAILURE PATTERN IN CYLINDRICAL GROUTED CONNECTION FOR WIND STRUCTURES – A PILOT STUDY

Md Shamsuddoha[1], Matthias Baeßler[1], Götz Hüsken[1], Stephan Pirskawetz[1], Hans-Carsten Kühne[1], Marc Thiele[1]

[1] Federal Institute for Materials Research and Testing (BAM), Unter den Eichen 87, 12205 Berlin, Germany, email: Md.Shamsuddoha@bam.de, Matthias.Baessler@bam.de, Goetz.Huesken@bam.de, Stephan.Pirskawetz@bam.de, Hans-Carsten.Kuehne@bam.de, Marc.Thiele@bam.de

SUMMARY: At present, Wind Turbine Generators (WTGs) operating in onshore and offshore wind farms are primary sources of renewable energy around the world. Cylindrical grouted sleeve connections are usually adopted in these WTG structures to connect the upper structure and foundation for ease of installation. These structures including grouted connections experience considerable adverse loading during their lifetimes. Settlements were reported inside similar connections used in energy structures especially oil and gas platforms, which were installed in last three decades. Thus, repair and rehabilitation of such connections in existing wind structures should also be planned ahead to keep them operating in the future. The nature of failure and crack generation in grouted connections are crucial prior to adopt a strengthening strategy. This pilot study is carried out to actualize the failure mechanism in the grouted connection, when subjected to axial loading. A novel reusable scaled cylindrical grouted connection with shear keys was designed and tested for its load bearing behaviour. The mechanical test was accompanied by classical measuring techniques (e.g. displacement transducer) as well as non-destructive measuring techniques (e.g. digital image correlation (DIC), acoustic emission analysis (AE)). The failure mechanism incorporating slippage of the shear keys and cracking of the grout was investigated. The capacity and applicability of such test mould were also discussed. The knowledge is expected to pave way towards repair of deteriorated grouted connections with similar geometry and failure pattern.

PREPOZNAVANJE OBLIKA SLOMA VALJKASTIH INJEKTIRANIH PRIKLJUČAKA ZA VJETRENE KONSTRUKCIJE – PILOT-STUDIJA

SAŽETAK: Danas su generatori vjetrenih turbina koji rade na priobalnim i odobalnim vjetrenim poljima primarni izvori obnovljive energije širom svijeta. Valjkasti injektirani naglavni priključci radi lakše ugradnje obično u tim konstrukcijama generatora služe za spajanje gornje konstrukcije s temeljem. Te konstrukcije i injektirani priključci izloženi su znatnim nepovoljnim opterećenjima tijekom svoj životnog vijeka. U konstrukcijama za proizvodnju energije, posebno na naftnim i plinskim platformama građenim posljednja tri desetljeća kod sličnih su priključaka opažena slijeganja. Stoga popravak i obnovu takvih priključaka u postojećim vjetrenim konstrukcijama treba planirati unaprijed kako bi one u budućnosti bile u funkciji. Prirodu sloma i razvoj pukotina u injektiranim priključcima važno je poznavati prije usvajanja strategija pojačanja. Ova pilot-studija provedena je da bi se ostvario mehanizam sloma u injektiranom priključku izloženom osnom opterećenju. Projektiran je i ispitan u mjerilu izrađeni novo oblikovan i ponovno upotrebljiv valjkasti injektirani priključak s posmičnim moždanicima. Ispitana je njegova nosivost. Mehaničko ispitivanje popraćeno je klasičnim mjernim instrumentima (npr. mjeračima pomaka) i nerazornim ispitivanjem (npr. digitalnim slikovnim prikazom i analizom akustičke emisije). Istražen je mehanizam sloma koji obuhvaća proklizavanje posmičnih moždanika i raspucavanje injektiranog morta. Raspravljena je i sposobnost i primjenjivost takve pokusne oplate. Očekuje se da će postignutim znanjem utrti put za popravak degradiranih injektiranih priključaka sličnog geometrijskog oblika i oblika sloma.

1. INTRODUCTION

About 30% growth is expected in energy demand worldwide by the year 2040 [1]. Although, oil and gas (O&G) sector may well dominate the global primary energy supply for the rest of this century, energy security issues are directing countries towards renewable energy choices, which can reduce their dependency on fossil fuels as well as achieving sustainable energy future [2]. Hence, a future of sustainable energy demands substitution of fossil fuels by renewable energy sources around the world. The contribution of renewable energy sources in primary energy use, suggested by the New Policies Scenario, is raised to 18% in 2035 compared to 13% in 2011, where wind energy is expected to provide major share, limiting the rapid growth of traditional fossil fuels [3]. In fact, investments towards annual wind energy in 27 European Union member states (EU-27) will reach almost €20 billion with 60% towards offshore productions by 2030 [4]. In the year 2015 alone, there was 108.3% increase in offshore wind power capacity compared to that of 2014 [5]. Therefore, growing energy demand and advancement of technology lead to explore both onshore and offshore locations using wind structures, which are susceptible to adverse loading conditions and costly maintenance.

There are three common types of piles that are used for fixed offshore wind turbine generators (WTG) structures, namely: Main and Skirt piles, Cluster piles and Monopiles. Monopile structures are currently the most preferred option for WTG structures. These tubular towers occupy the wind turbine market due to their suitability in terms of economy, aesthetic and safety. By 2014, 78.8% of the total 2488 offshore wind turbines substructures installed in Europe were monopiles, which had even higher (91%) popularity in the year 2014 alone [6]. The connections between the superstructure and the substructure can be either ring welded and bolted in the flanges. However, fabrication of flanges is very costly and takes a long delivery time along with the disadvantages of fatigue damage over time [7]. Besides, the transition between the monopile or foundation member, and tower or upper structure poses challenges, which can be addressed using infilled sleeved connection. As a result, grouted or infill connections are often sought for the wind and offshore energy structures all over the world. Figure 1 shows typical grouted connections between upper structures to the foundations or piles in the offshore O&G platforms, and monopile in WTG towers, which are usually cylindrical in shape. These connections are formed by filling the annulus with grout between two members with dissimilar dimensions, where the infill acts as a load transfer medium. These grouted joints have been effectively used in the offshore drilling and production platform jackets and wind turbine structures.

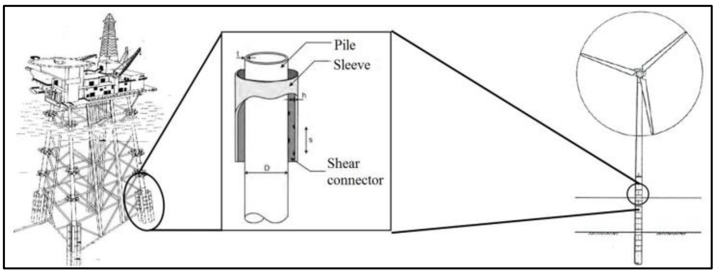

Figure 1 Grouted connections in offshore platform and wind turbine tower [8]

In general, the grouted connections are susceptible to degradation due to repetitive adverse bending moments in conjunction with axial loading including fabrication challenges [9, 10]. In last three decades, grouted joints have been installed in offshore wind energy structures especially monopiles using plain steel sections with no additional mechanical interlock. However, vertical displacements have been noticed at these connections. Therefore, repair of existing grouted connections provides considerable challenge. In pursuit of solutions, Schaumann et al. [11] had indicated that this movement might be resulting from a loss of bond between steel and mortar suggesting a repair option for the joints by applying a number of bearing mechanisms. In another study later, Schaumann et al. [12] concluded that higher flexibility in response to bending loads lead to gap openings and relative sliding motion between adjacent material surfaces causing abrasive wear of the grout, which can considerably reduce the service life of the hybrid connection. Besides, increase in wear rate for various conditions including presence of water at an order of 2 – 18 times higher than for the equivalent dry condition, which may reduce the coefficient of friction below that currently recommended [13]. Hence, potential repair options should be sought after for any degradation in these structures especially the infill itself. To achieve this goal, it is necessary to characterise the failure patterns for selection of any repair option. The aim of this study is to conduct a feasibility study of producing failure patterns similar to degraded structures under axial load. This study is a preliminary stage of actualizing the failure pattern of such grouted connection. Feasibility of using a novel reusable mould connection is also investigated. These defects can then be repaired using various methods, from which further research can continue.

2. CONNECTION GEOMETRY, MATERIALS AND TEST DETAILS

In all jointing methods, the transition piece from the superstructure encircles the foundation pile or vice versa. Generally, there are two types of grouted connection systems in terms of load transfer mechanism – ‘plain’ connection and ‘with shear key’ connection that are intensively applied in the industry. The plain grouted joint is the earliest form of connection for joining foundation with superstructure. However, the geometry of the joint can be either tubular or conical in shape depending on the suitability in various structures [14]. Mechanical connectors can be introduced to increase bond strength of these joints. Mechanical connectors are shear keys in the form of welded beads or bars. Shear keys are advantageous over plain connections [15]. There can be different combinations of geometries and shear key provisions applicable to the tubular connections. However, according to DNV OS J101 [16], a grouted joint in wind energy monopile should not combine conical shape with shear keys. This standard also provides design guidelines of grouted joints in monopile structures based on different geometries and shear key provisions. In this study, a cylindrical connection geometry with shear key was selected. A scaled grouted connection, which can be used in the laboratory for producing control cracks or defects, was manufactured.

The sizes of the members vary depending on type of structures, purpose and locations. A detailed range of geometries used by previous researchers are given by Dallyn et al. [17]. Due to simplicity of testing, a scaled test set-up was used. Besides, the loading for this preliminary test was planned to be below 1 MN. However, it is to be noted that a more realistic grout layer was adopted, since the prime aim was to observe the crack pattern in the infill layer. This also implied that size of the pile and sleeve would be scaled down slightly disproportionately. For this study, a joint geometry was chosen after Chivato et al. [18] as a reference. Details of the geometry are given in Figure 2a. For ease of understanding, connection components are named as Pile (p), Grout (g) and Sleeve (s). The pile was one piece cylindrical core. The sleeve was built up from equal two parts and externally clamped with five external clamps with bolts. The clamps were 30 mm wide and 20 mm thick. Bolted flanges of two of the clamps were kept along the sleeve split, whereas three of them were aligned at a 90° with the previous group at an alternating sequence. Clamps were bolted with Class 8.8 M18 bolts, whose minimum tensile strength was 800 MPa. The sleeve was split into half for two reasons: firstly, for ease of creating shear keys inside sleeve interior with precise dimensions, and secondly, to make the mould reusable since the sleeve would not have to be cut to see internal cracks similarly to previous studies. The length of the joint is chosen such that three shear key pairs are accommodated to observe the failure criteria. The comparison of the selected size and the actual size is shown in Table . The reason for such scaling is that, after scaling down of the members, grout layer will still remain closely representative of full scale grout thickness similar to that adopted earlier in Dallyn et al. [19]. The guidelines by current DNV OS J101 [16] for geometric parameters were adhered to where possible. However, the size of the shear key is kept 2.5 mm, which is less than DNV practice. However, it was done so to be proportional to other reduced dimensions of components of the connection.

Table 1. Symbols and scaling factors for the geometry

Symbols	Definition	Reference	Adopted	Factor
D_s (mm)	Sleeve outer diameter	1800	216	8.33
ts (mm)	Wall thickness of sleeve	60	16	3.75
D_p (mm)	Pile outer diameter	1050	70	12.73
t_p (mm)	Wall thickness of pile	50	16	3.13
D_g (mm)	Grout outer diameter	1680	184	9.13
t_g (mm)	Thickness of grout	315	50.75	6.21
h (mm)	Shear key outstand	12	2.5	4.80
s (mm)	Shear key spacing	300	50	6.00
w (mm)	Shear key width	20	5	4.00

The mould was manufactured using steel with yield strength of 355 MPa. A commercial grout material was applied. A summary of the properties of the fresh and hardened grout is given in Table . Specimens were removed from moulds after one day and cured underwater at 23.5°C before determining hardened grout properties after 28 days. It is to be noted that 40x40x160 mm prismatic specimens were used conforming European Standard EN 196-1 [20] to determine compressive strength, whereas current DNV [16] practice suggests for 75 mm cube specimen. This reason for choosing prismatic samples is due to the fact that prism strength were found closely align with cube specimens earlier [21]. No sand blasting or surface treatment was applied on the specimen. The test specimen was filled up with grout and kept at 23°C with a relative humidity of 50% for 28 days prior to testing.

The test was carried out after 28 days of casting the connection using a 1000 kN MTS servo-hydraulic testing machine. Static axial loading was applied at a rate of 0.1 mm/min. It was decided that the loading will continue until cracks are generated or a plateau in loading response is observed. Data acquisition was carried out using Linear Transducers (LT), Digital Image Correlation (DIC), and Acoustic Emission (AE). Figure 2b shows the set-up and equipment used for testing. To identify small cracks in the specimen after testing, liquid resin was poured at the top of the specimen to flow inside those cracks under atmospheric condition. This process allowed the resin to penetrate cracks and hardened over time. These cracks were then seen under ultraviolet (UV) light.

Table 2. Summary of grout properties

Properties	Standards	Values
Workability (mini cone)	[22]	305 mm
Compressive strength	[20]	112 MPa
Flexural strength	[20]	13 MPa
Modulus	[23]	40 MPa
Drying shrinkage	[24]	0.73%

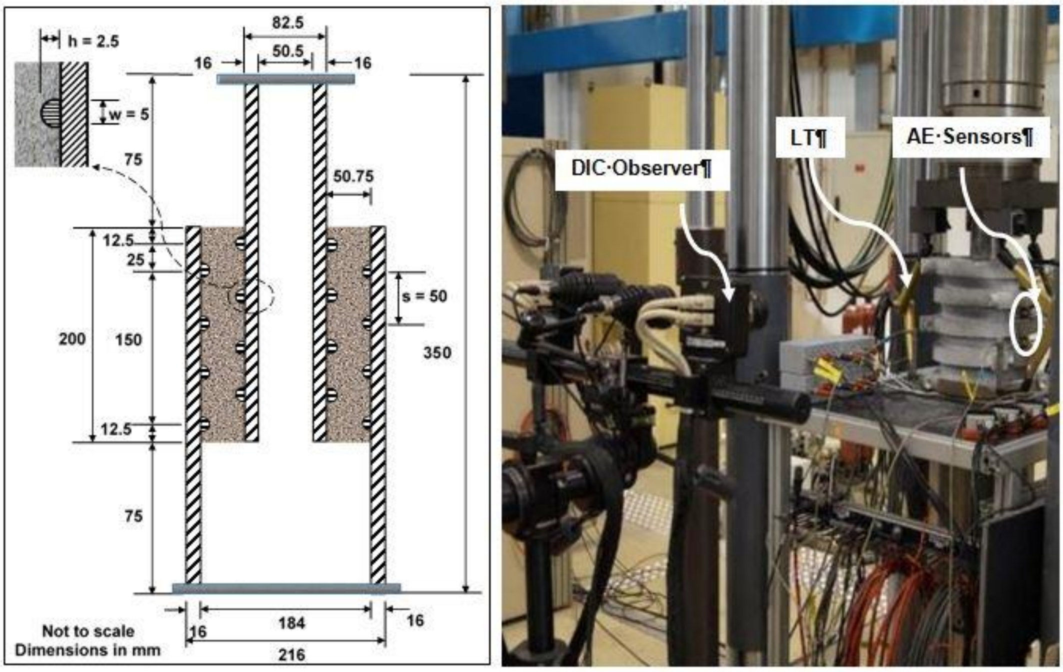

a) b)

Figure: 2a) Details of the connection geometry; 2b) Set-up

3. RESULTS AND DISCUSSION

This investigation is divided in two steams: loading behaviour with associated displacements, and failure patterns in grout infill.

3.1. LOADING RESPONSE

Figure 3 shows the load-displacement plot of the connection under static axial load. The displacement represents average of the four transducers readings. The acoustic response is also plotted in this figure. The loading response can be divided into four primary segments. Firstly, the initial instrumental adjustment under loading occurred until about 0.125 mm, beyond which the loading response is straight in nature up to about 500 kN at a displacement of about 0.50 mm. To draw a comparison, according to DNV-OS-J101 [16], the characteristic interface shear capacity considering a monopile structure without factor of safety was about 280 kN. This load calculation assumes that the grout layer will fail before the failure of pile or sleeve, assuming the sleeve is homogeneous without any split. It should be noted that there can be deviation between this experiment and DNV guideline due to the variation in stiffness for adopting external clamps for split sleeves. Since the load-displacement is relatively straight up to 500 kN, it can be considered as maximum load that the connection can undergo without any permanent onset. Since this capacity is higher than the calculated characteristic interface shear capacity of 280 kN, the connection can be considered safe for engineering applications. Further loading beyond 500 kN generated relatively higher undulations and the load-displacement plot is no longer straight with a peak load of 635 kN at about 0.75 mm. Finally, beyond peak, the curve drops gradually and remained almost plateau at about 550 kN after 1.125 mm until about 1.5 mm, where test was terminated. The test was terminated at 1.5 mm total displacement of the testing machine due to the fact that AE activity reduced considerably at this point without any significant increase in load, which is discussed later in this section.

The comparison of loading and acoustic emission indicates that cracks observed by non-destructive technique relate well with the readings of transducers. The AE activity is minimum at the adjustment stage with a small peak at about 0.075 mm. The activity increases gradually after 0.25 mm up to about 1.125 mm, which falls within the plateau stage beyond peak load. Beyond this load plateau, the AE plummets down although the loading is almost flat. However, the AE response shows a plateau between 0.375 mm – 0.50 mm, which also correlates with small undulations in load response in this region. The response reduces significantly between displacements of 1.375 mm – 1.50 mm, which indicates that larger cracks have formed in the grout layer.

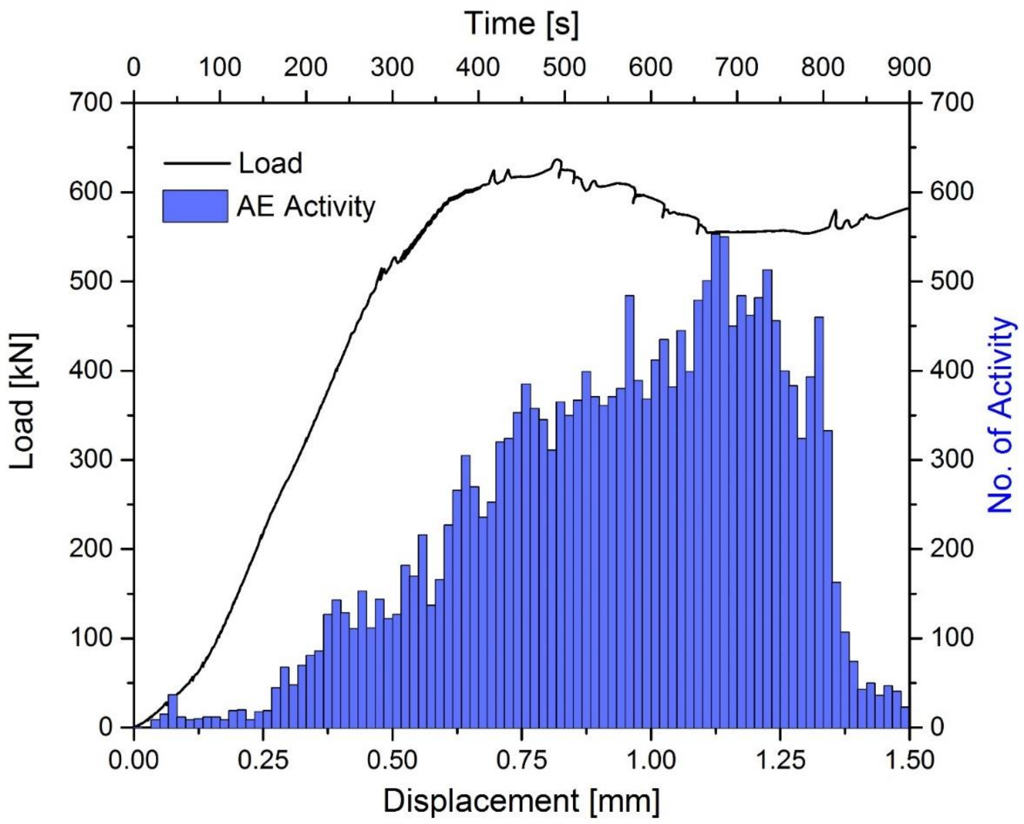

Figure 3 Load-displacement behaviour

Figure 4 shows the relative displacements on the surface at the start and ultimate loading conditions. It is obvious that the sleeve and external clamps are expanded. There is about 1 mm circumferential extension in the sleeve. Although, the sleeve and clamps deformed concurrently, the deformation is more pronounced near the split-line compared to the middle part of the sleeve. This suggests that stiffer clamps are necessary.

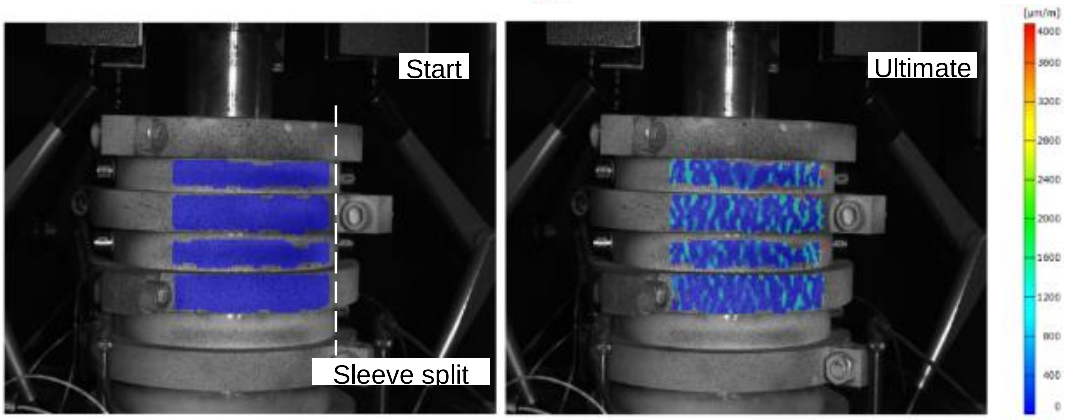

Figure 4 Relative displacements on surface

3.2. FAILURE MECHANISM

At first, cracks are observed externally. Figure 5a shows four visible cracks on the top of the connection. The largest crack is about 0.4 mm wide. Figure 5b shows a magnified view of the crack at location 1 and the gap in the sleeve. The wider cracks at location 1 and location 2 occurred at almost perpendicular with cracks at location 3 and location 4. It is to be noted that wider cracks formed close to the dashed line showing sleeve split. This suggests that the infill was more prone to circumferential cracks near the split sleeve due to peripheral expansion. This can also lead to a requirement of higher circumferential stiffness in future experiments. This can be achieved by using larger clamps and by realignment of clamps. There are no external cracks at the bottom surface. However, there are small cracks at the top of the connection, which are only visible under ultraviolet light after using resin penetration. These small cracks are often interconnected among themselves suggesting localised crushing. There is a vertically extended small crack in location 2 only.

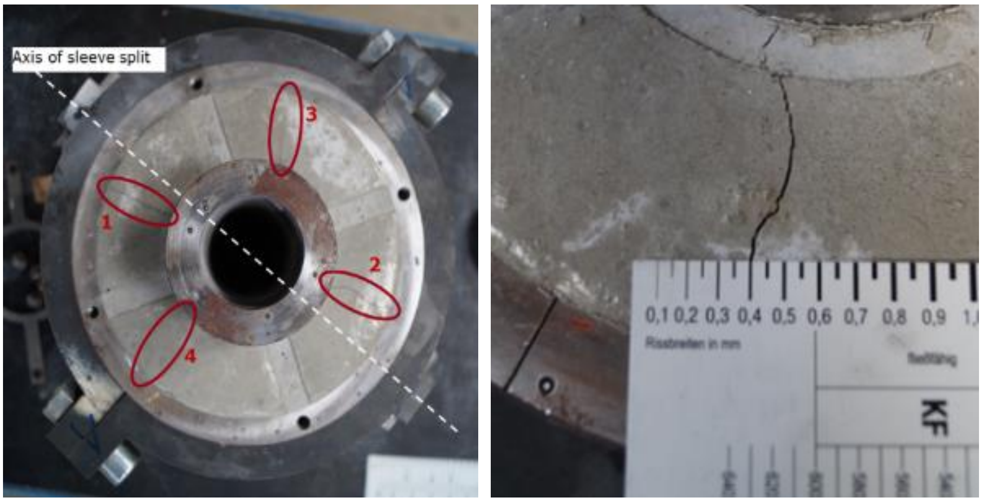

(a) Location of external

(b) Detail of external crack near

Figure 5 External cracks and observations from cut cores

Cracks, which are visible in separated parts of the connection are shown in Figure 6. Two larger cracks are distinctly visible in the lower part of the connection. The bottom crack is extended from the lowest shear key of the sleeve and the pile. However, the longer second crack on top is extended between the lowest key of the sleeve to the immediate upper shear key. There was no significant slippage near shear keys probably due to the high strength grout used. This is evident from the compressed grout with dark appearance below the top shear keys. This failure pattern and condensing in grout phenomenon are exactly similar to the cracks observed by Anders [25]. These cracks are, however, not perfectly extended between successive diagonal keys as seen in earlier studies [26, 27]. The reason, again, can be due to the use of low strength grouts in these past studies. Small cracks at the top connection are also found to be similar in alignment, however less distinct compared to bottom ones.

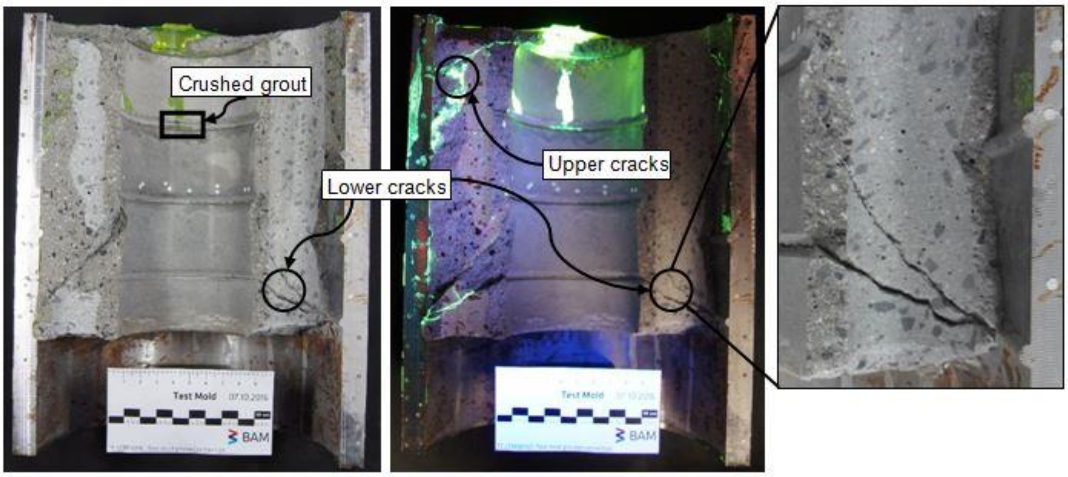

Figure 6 Internal cracks in the specimen

4. CONCLUSIONS

A reusable grouted connection with steel sleeve and pile, and grouted infill was manufactured and tested under axial static load to study the feasibility of producing failure pattern so that a repair strategy can be adopted. The load-bearing behaviour and failure patterns were observed. The load-bearing capacity of the connection exceeded the predicted characteristic interface shear capacity suggesting the fact that similar connection can be used in the future. The failure pattern was representative of results reported previously in the literature. However, radial expansion in the sleeve in the specimen indicates a necessity of increasing the circumferential stiffness for future test specimens.

ACKNOWLEDGMENTS

This study was undertaken under the LeBeWind project carried out in Federal Institute for Materials Research and Testing (BAM) and funded by the Federal Ministry for Economic Affairs and Energy (BMWi), Germany.

REFERENCES

[1] World Energy Outlook, *International Energy Agency*, Paris, (2014)

[2] Larsen, H.; Petersen, L.S.: Non-fossil energy technologies in 2050 and beyond, *Risø National Laboratory for Sustainable Energy, Technical University of Denmark*, Denmark, (2010)

[3] World Energy Outlook, *International Energy Agency*, London, (2013)

[4] Morthorst, P.-E.; Awerbuch, S.: The Economics of Wind Energy, *European Wind Energy Association*, Denmark, (2009)

[5] Ho, A., Mbistrova, A. & Corbetta, G.: The European offshore wind industry - key trends and statistics 2015, *The European Wind Energy Association*, Brussels, Belgium, (2016)

[6] Corbetta, G., et al.: The European offshore wind industry - key trends and statistics 2014, Brussels, Belgium, (2015)

[7] Verma, A.: Adhesive Bonded Towers for Wind Turbines: Design, Optimization and Cost Analysis, Delft University of Technology, The Netherlands, MSc, (2011)

[8] Jiang, S.C., Wang, Z. & Zhao, X.L.: Structural Performance of Prestressed Grouted Pile-to-Sleeve Connections, *Procedia Engineering*, 14 (2011), pp. 304-311

[9] Faulkner, P.; Hassell, M.: *EWEA Wind Energy Event 2013*, European Wind Energy Association, Vienna, Austria, 3-7 February 2013

[10] [10] Hassanzadeh, M.: Cracks in onshore wind power foundations: Causes and consequences, *Elforsk*, Stockholm, (2012)

[11] Schaumann, P., et al.: Durchrutschende Grout-Verbindungen in OWEA – Tragverhalten, Instandsetzung und Optimierung, *Stahlbau*, 79 (2010) 9, pp. 637-647

[12] Schaumann, P., et al.: *The Twenty-third International Offshore and Polar Engineering*, International Society of Offshore and Polar Engineers, Anchorage, Alaska, USA, 30 June - 5 July 2013

[13] Dallyn, P., et al.: Experimental investigation on the development of wear in grouted connections for offshore wind turbine generators, *Engineering Structures*, 113 (2016), pp. 89-102

[14] Schaumann & Keindorf Ingenieurges. mbH: Offshore Wind Energy: Transition Piece, Available from http://www.ski-consult.de/1/erneuerbare-energien/offshore-wind-energy/transition-piece.html, Accessed: 2015-12-19

[15] Ingebrigtsen, T., Loset, Ø. & Nielsen, S.G.: *Offshore Technology Conference*, The Society of Petroleum Engineers, Houston, Texas, 7 May 1990

[16] DNV-OS-J101, Design of Offshore Wind Turbine Structures, *DNV*, Norway, 2014

[17] Dallyn, P., et al.: Experimental testing of grouted connections for offshore substructures: A critical review, *Structures*, 3 (2015), pp. 90-108

[18] Chivato, R., Kougioumtzoglou, M. & Sanchez, N.: Industrial Case Study: Finite Element Model, Available from http://www.esru.strath.ac.uk/EandE/Web_sites/13-14/Jacket_Substructures/grouted/modfinitelement.html, Accessed: 2016-03-11

[19] Dallyn, P., et al.: Development of a Numerical Model to Predict Wear in Grouted Connections for Offshore Wind Turbine Generators, *International Journal of Civil, Environmental, Structural, Construction and Architectural Engineering*, 9 (2015) 2, pp. 122-131

[20] BS EN 196-1:2005, Methods of testing cement - Part 1: Determination of strength, *Deutsches Institut für Normung*, Berlin, 2005

[21] Schaumann, P., Raba, A. & Bechtel, A.: *35th International Conference on Ocean, Offshore and Arctic Engineering*, ASME, Busan, South Korea, 19-24 June 2016

[22] DIN EN 1015-3:2007, Methods of test for mortar for masonry – Part 3: Determination of consistence of fresh mortar (by flow table), *Deutsches Institut für Normung*, Berlin, 2007

[23] DIN EN 12390-13:2014-06, Testing hardened concrete - Part 13: Determination of secant modulus of elasticity in compression, *Deutsches Institut für Normung*, Berlin, 2014

[24] DIN EN 12617-4:2002, Products and systems for the protection and repair of concrete structures; Test methods Part 4: Determination of shrinkage and expansion, *Deutsches Institut für Normung*, Berlin, 2002
[25] Anders, S.: Betontechnologische Einflüsse auf das Tragverhalten von Grouted Joints, Leibniz Universität Hannover, Hannover, PhD, (2007)
[26] Billington, C.J.; Lewis, G.H.G.: *Offshore Technology Conference*, The Society of Petroleum Engineers, Houston, Texas, 8-11 May 1978
[27] Sele, A.B., Veritec, A.S. & Kjeóy, H.B.: *Offshore Technology Conference*, The Society of Petroleum Engineers, Houston, Texas, 1 May 1989

CONDITION ASSESSMENT OF TORPEDO LAUNCH PAD STATION STRUCTURE IN RIJEKA

Davor Grandic[1], Paulo Sculac[1], Adriana Bjelanovic[1], Tomislav Frankovic[1]

[1] University of Rijeka Faculty of Civil Engineering, Department of Load-bearing Structures, Radmile Matejcic 3, 51 000 Rijeka, Croatia, email: davor.grandic@gradri.uniri.hr, paulo.sculac@gradri.uniri.hr, adriana.bjelanovic@gradri.uniri.hr, tomislav.frankovic@gradri.uniri.hr

SUMMARY: The world's first torpedo has been manufactured in Croatia, in the city of Rijeka in 1866, where the production of torpedoes continued until 1966. Before shipment, each torpedo had to pass very complex testing, including the test-launch in order to confirm the regularity of its direction. The current reinforced-concrete launch pad station was built between 1928 and 1942 in three phases and therefore has highly heterogeneous properties regarding the shape of the structure and quality of the materials. In order to perform condition assessment of the launch pad structure detailed structural investigation has been performed on a large number of test locations and samples, where mechanical and durability properties of concrete have been tested and chloride content measured. A 3D laser scanning survey has also been conducted in order to obtain the cross-section dimensions and the overall form of the structure. Based on the gathered data a structural reanalysis of the bearing capacity of the current launch pad structure has been made. The heterogeneous material properties have been analysed together with their influence on the bearing resistance of the current structure.

OCJENJIVANJE STANJA KONSTRUKCIJE PLATFORME ZA LANSIRANJE TORPEDA U RIJECI

SAŽETAK: Prvi torpedo na svijetu proizveden je u Rijeci u Hrvatskoj 1866. godine a proizvodnja torpeda nastavljena je do 1966. Prije isporuke svaki torpedo mora proći kroz vrlo složena ispitivanja koja uključuju pokusno lansiranje kojim se potvrđuje pravilnost njegova usmjerenja. Današnja armiranobetonska platforma za lansiranje izgrađena je između 1928. i 1942. u tri faze. Zbog toga ima vrlo heterogena svojstva s obzirom na oblik konstrukcije i kvalitetu materijala. Provedena su detaljna istraživanja s ciljem ocjene stanja konstrukcije lansirne platforme na velikom broju ispitnih mjesta i velikom broju uzoraka. Ispitana su mehanička i trajnosna svojstva betona i izmjeren sadržaj klorida. Provedeno je i lasersko 3D skenersko snimanje radi utvrđivanja dimenzija poprečnih presjeka i sveukupnog oblika konstrukcije. Na osnovi dobivenih podataka načinjen je ponovljeni proračun nosivosti konstrukcije postojeće lansirne platforme. Analizirana su heterogena svojstva materijala i njihov utjecaj na nosivost postojeće konstrukcije.

1. INTRODUCTION

Launch pad station structures are often situated on very attractive locations, such as the sea or lake coasts. Due to their monumental appearance they are sometimes called the sea cathedrals [1]. In this work we will analyse the launch pad station structure in Rijeka, which is one of the oldest of this type in the world. Torpedo has its origin from an idea of Ivan Lupis, an Austro-Hungarian naval officer from Rijeka, who designed a floating weapon operated by ropes from the land in 1860 [2]. In 1864 he formed a partnership with Robert Whitehead, an English engineer and factory manager, who has developed the torpedo as an underwater device with an explosive warhead. In the process of torpedo creation, some new devices have been developed, like the device that kept the torpedo at a constant depth or the gyroscopic stabilisation of the torpedo's direction which was used for the first time at the torpedo factory in Rijeka. The production of torpedoes in Rijeka continued for exactly 100 years, until 1966 [2].

Before shipment, each torpedo had to pass very complex testing, including the test-launch in order to confirm the regularity of its direction. The first launch pad station was built already around 1870 as a wooden stilt-house [2]. The current reinforced-concrete launch pad station was built between 1928 and 1942 in three phases [2] and therefore has highly heterogeneous properties regarding the shape of the structure and quality of the materials. The launch pad is located partly on the shore and partly on columns in the sea (some of them are more than 10 meters deep). Due to the aggressive marine environment exposure (marine chlorides induced reinforcement corrosion) and mechanical action of the waves the reinforced-concrete structure is severely damaged. The wooden roof structure and the watchtower are partially collapsed. In order to perform condition assessment of the launch pad structure detailed structural investigation has been performed on a large number of test locations and samples, where mechanical and durability properties of concrete have been tested and chloride content measured. A 3D laser scanning survey has also been conducted in order to obtain the cross-section dimensions and the overall form of the structure [3]. Finally, based on the gathered data a structural reanalysis of the bearing capacity of the current launch pad structure has been made. In this work we present the structural investigation program conducted and provide the field and laboratory test results. The heterogeneous material properties have been analysed together with their influence on the bearing resistance of the current structure. Finally, guidelines for future retrofitting of the torpedo launch pad structure are given.

2. ABOUT THE STRUCTURE

The launch pad station is situated in very specific conditions: one part of it rests on coastal foundations, while the rest of it is supported by the concrete columns in a way that most of the structure lies just above the sea level (Figure 1). The structure is severely damaged due to the long-time maritime conditions, including mechanical action of the waves and chemical (corrosion of reinforcing steel), which due to the lack of maintenance caused a progressive decay of the structure.

Figure 1 Current state of the launch pad structure

The reinforced-concrete structure may be divided into three main parts: a) columns below the working floor level, b) structure at the working floor level and c) frame structure above the working floor level.

3. STRUCTURAL INVESTIGATION

Detailed structural investigation included: overview of the existing documentation, visual inspection of the structure, laboratory and in-situ material property testing and geotechnical survey. A 3D laser scanning survey has also been conducted in order to obtain the cross-section dimensions and the overall form of the structure (Figure 2).

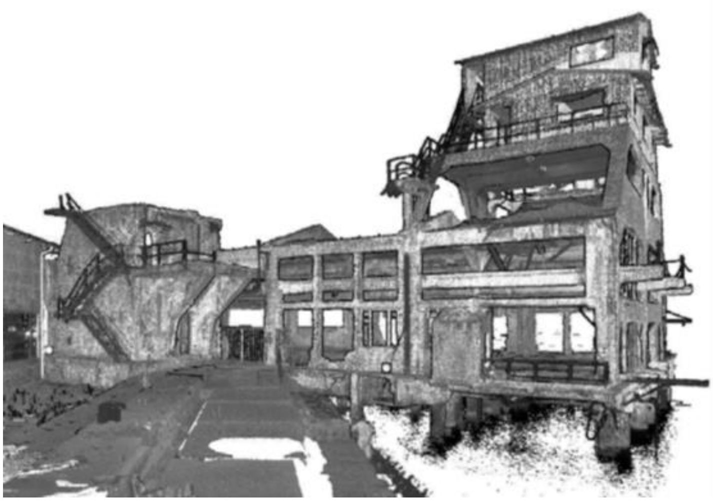

Figure 2 3D model - point cloud created by 3D scanners (view from northwest) [3]

Visual inspection has been conducted on all members of the launch pad structure, including underwater inspection of the columns (Figure 3). As a general conclusion, parts of columns that are permanently in water are considerably less damaged than parts above the water.

Visual inspection led to the conclusion that the reinforced-concrete structure has been constructed in three phases (Figure 4). Figure 5 shows typical damage of a column (column 4.3 - see Figure 4) caused by corrosion of reinforcement and atmospheric action. Note that the column on the figure is composed of two parts – there is a vertical joint indicating parts made in the 2nd and in the 3rd phase, and it can be clearly seen that the concrete colour at the left and right side of the joint is different.

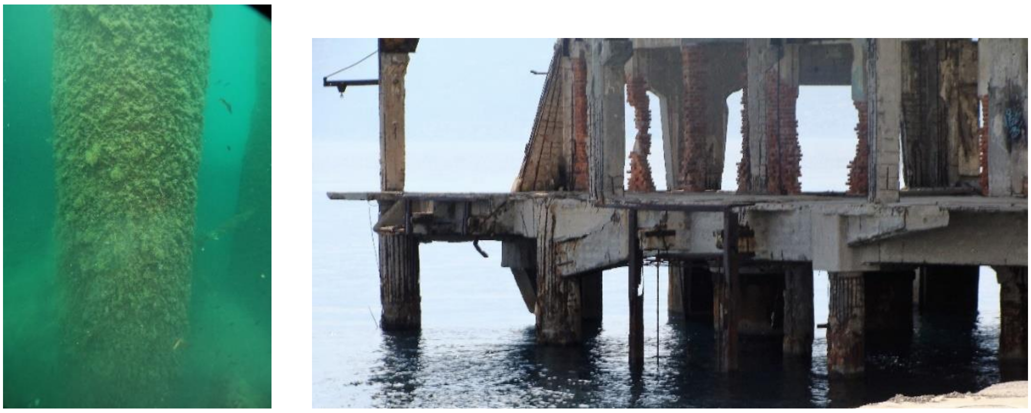

Figure 3 Parts of columns permanently in water (left) and above sea level (right)

The bearing structure of the roof consists of a truss system (so-called Queen post) typical for classical\traditional wooden roof ranges up to 10 m, architecture of that era and the Mediterranean region. Part of the roof has collapsed, while the rest is affected by biological processes of decay.

Results of the visual inspection are summarised in Table 1, by using the damage levels according to CEB Bulletin 162 [4]. If the damage level is C or D, an urgent repair of structural elements is required. When the damage level is either A or B it is recommended to start the repairing - if this is not done then the recommendation is to conduct a corrosion monitoring. Level E indicates that the structural element or a part of it is fully damaged and has to be urgently replaced or reconstructed since its bearing capacity is questionable.

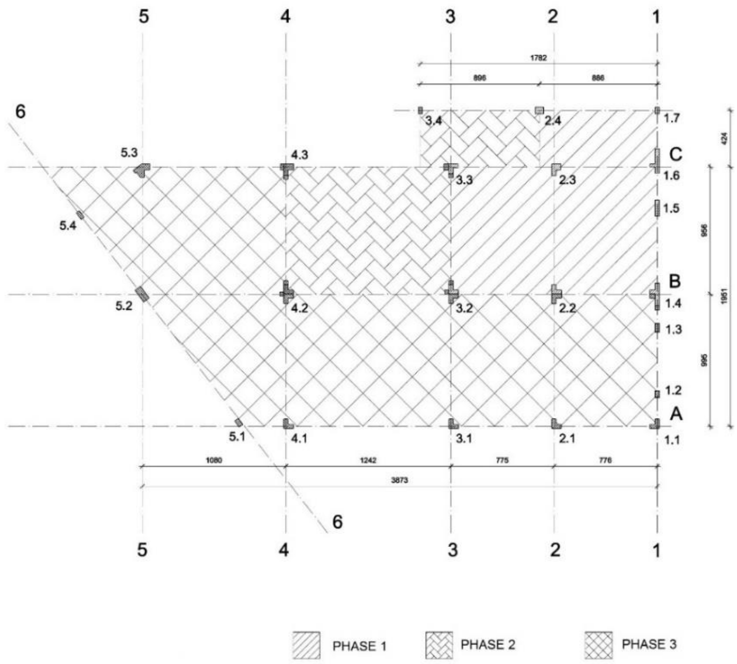

Figure 4 Construction phases [5]

Figure 5 Column 4.3 with visible distinction between different construction phases

Mechanical and durability properties of concrete have been investigated. First, preliminary tests were carried out in the Materials testing laboratory of the Faculty of Civil Engineering in Zagreb, while the second tests were conducted by Ascon Institute from Zagreb [6].

Table 1 Damage levels of reinforced-concrete members

Structural member	Position	Exposure class according to EN 206	Damage level	Percentage of damage
Frame columns in the first row next to the sea	1-1	XS3	D E	15% 85%
Frame beams in the first row next to the sea	1-1	XS3 XS1	D E	40% 60%
Frame columns in the second row next to the sea	2-2	XS3	D E	25% 75%
Frame beams in the second row next to the sea	2-2	XS1	C D	25% 75%
Frame columns in the third row next to the sea	3-3	XS3	C D E	50% 15% 35%
Frame beams in the third row next to the sea	3-3	XS3	B C E	50% 10% 40%
Frame columns in the fourth row next to the sea	4-4	XS3	D E	25% 75%
Frame beams in the fourth row next to the sea	4-4	XS1	D E	50% 50%
Structure at the working floor level	ABRP	XS3	D E	80% 20%
Columns under the working floor level	SIRM	XS2 XS3	A B D E	40% 20% 10% 30%

Preliminary tests of compressive concrete strength were performed on cylinders extracted from 14 different locations. Since there was a very large scatter of results of compressive strength, these preliminary tests have later been complemented by more extensive testing on a much greater number of cylinders (28) extracted from the entire launch pad station structure. Characteristic concrete compressive strength was determined individually for each building phase and for columns in water (Table 2) according to approach B of HRN EN 13791-1 [7] (all available testing results have been used).

Table 2 Characteristic concrete strength fck

Part of structure (phase)	fck (MPa)
Phase I	14,5
Phase II	12,3
Phase III	9,8
Columns in water	16,8

Chloride ion content in concrete has been determined through chemical analysis of concrete powder extracted from the structure. First the free chloride ion content soluble in water was determined (according to [8]), and then the total chloride content soluble in acid was determined [9]. Figure 6 shows chloride ion concentration in dependence on depth from the surface [6].

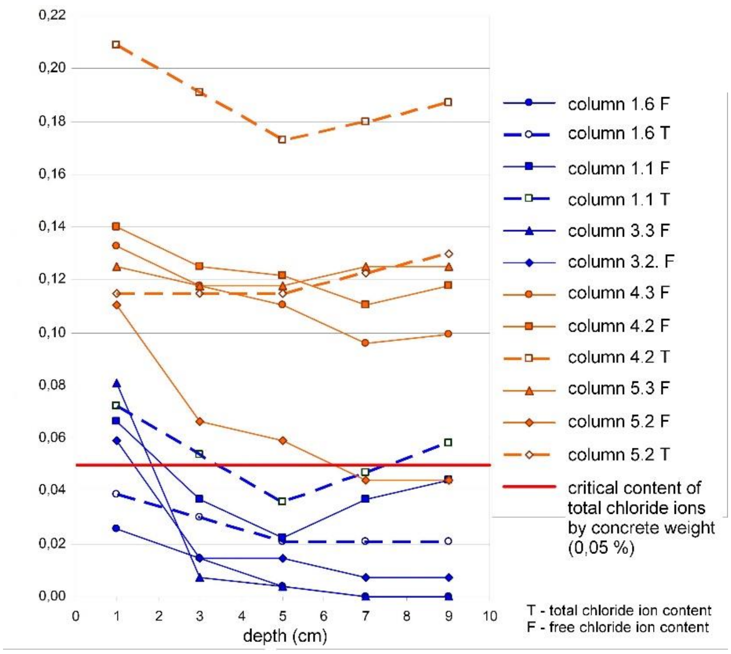

Figure 6 Chloride ion content (% by concrete weight) in dependence on depth from the surface

Permeability to gases was conducted according to EN 993-4 [10] on three samples. Coefficient of permeability to gases was obtained as $>10^{-16}$ m^2, meaning that the quality of concrete is very poor with regard to permeability to gases [11]. On other samples the test failed because the samples were too permeable and porous. Diffusion coefficient of chloride ions was obtained as $> 5\times10^{-12}$ [5]. Steel reinforcement is considerably damaged by corrosion, its bearing capacity and ductility is reduced, and on many elements the bond is entirely lost. The results obtained by testing of the reinforcement are: minimum yield strength of 255 MPa, minimum tensile strength of 362 MPa (regarding net cross-section surface area) [5].

4. STRUCTURAL REANALYSIS AND FINAL STRUCTURAL ASSESSMENT

Structural analysis of the current bearing capacity and serviceability of the reinforced-concrete launch pad station has been conducted using material properties and geometry data obtained through structural investigation. More details may be found in [5]. The following actions have been taken into account: dead load, imposed load, snow load, wind load, mechanical action of the waves and seismic action (with peak ground acceleration of 0,2g). Working floor level structure and columns underneath were analysed using the full structural model, while some parts of the structure (construction phases) above the working floor level were modelled and analysed separately since there is no connection between them (Figure 7). Further, the bearing capacity of the critical elements was calculated. On the basis of the structural investigation and structural analysis it can be concluded that due to insufficient bearing capacity of the critical elements there is high probability of collapsing a portion or even the entire launch pad station structure. Hence, an urgent retrofitting of the torpedo launch pad station structure is needed.

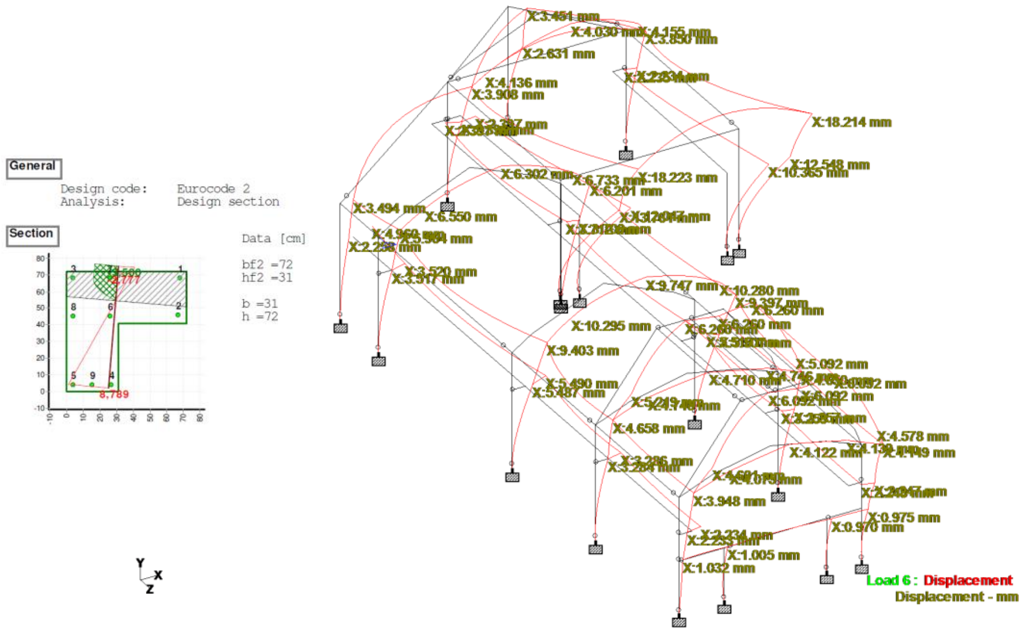

Figure 7 Structural model (phase 3) – displacements from seismic actions; strain and stress diagram in column 3.2

5. GUIDELINES FOR FUTURE RETROFITTING

All parts of the structure and the structural elements which originate from different construction phases and are currently separated should be connected into a single unit. In this way the bearing capacity of individual members (columns) and the structure as a whole will considerably increase. This connection is especially important due to the extremely low strength of existing concrete. This connection may be obtained by making an outer shell using repair mortar with high strengths which covers all parts of the element (e.g. part of columns from different construction phases), reinforced with stainless (ribbed steel 1.4462) or plain steel, depending on the environment exposure conditions (Figure 8). The outer shell should be made within the original dimensions, after the damaged material has been removed from the member surface and should be connected through stirrups with the element core. The original appearance and dimensions of the elements should be preserved, since the building is a heritage monument.

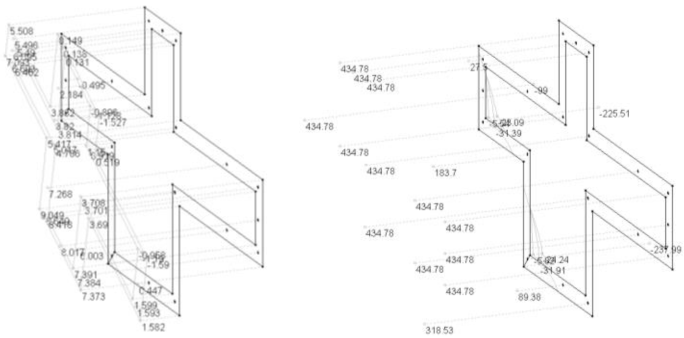

Figure 8 Column 3.2: strain (left) and stresses in MPa (right). Existing concrete in the core $f_{ck,core}$ = 12,2 MPa, outer layer $f_{ck,out}$ = 50 MPa, reinforcement f_{yk} = 500 MPa – recquired reinforcement: 19 bars of d=14 mm

6. CONCLUSIONS

Port areas along the coast worldwide include many industrial heritage monuments. The torpedo launch pad station structure in Rijeka is one of the oldest of this type in the world and, therefore, deserves special attention. Since that the first world torpedoes have been manufactured in Rijeka, the launch pad structure analysed in this paper is an important monument of technical culture at the world level. According to all the criteria that apply to regular buildings the design working life of the launch pad structure is near its end since the vast majority of the structural elements is classified in the highest damage levels (D and E), mechanical and durability properties of concrete are very poor, reinforcement is severely damaged by corrosion and results of the structural analysis indicate that there is a direct risk of collapse. However, given the exceptional value of the building the Ministry of Culture and the local community recognised the need of preserving it for the future generations. Therefore, in this and in similar situations it is necessary to find appropriate methods for structure retrofitting in spite of their poor condition. Only on the basis of a detailed structural investigation and an appropriate structural analysis essential properties of the structure may be identified and the way of improving them in the process of restoration of the structure.

REFERENCES

[1] Calzolaio, F.: Cattedrali dell'archeollogia industriale costiera, Etigraf, ISBN 8889447052, Venice, Italia, (2006)
[2] Smokvina, M: Testing of Torpedoes and the Evolution Rijeka's Torpedo Launch Pad Station, Proceedings of 5th International Conference on Industrial Heritage, Palinić, N. (Ed.), pp. 315-336, ISBN 978-953-56132-2-0, Rijeka, Croatia, May 2012, Pro Torpedo, Rijeka, (2014)
[3] Report on geodetic survey of the torpedo launch pad station in Rijeka and 3D laser scanning creating georeferenced 3D models in the form of a cloud of points, Vektra Ltd., Varaždin, Croatia, (2012), in Croatian
[4] CEB Bul. No. 162, "Assessment of Concrete Structures and Design Procedures for Upgrading (Redesign)". Bulletin D'Information, Comité euro-international du béton, Paris, (1983)
[5] Condition state study of the of the torpedo launch pad station in Rijeka, University of Rijeka, Faculty of Civil Engineering, Rijeka, Croatia, (2012), in Croatian
[6] Materials testing report No. 003/12, Ascon Institute, Zagreb, (2012), in Croatian
[7] EN 13791:2007, Assessment of in-situ compressive strength in structures and precast concrete components, CEN, Brussels, (2007)
[8] Chaussadent, T.; Arliguie, G: AFREM test procedures concerning chlorides in concrete: Extraction and titration methods, RILEM – Materials and structures, Vol. 32 (1999) No. 3, pp. 230-234, ISSN 1359-5997
[9] EN 14629:2007, Products and systems for the protection and repair of concrete structures - Test methods - Determination of chloride content in hardened concrete, CEN, Brussels, (2007)
[10] EN 993-4:1995, Methods of test for dense shaped refractory products - Part 4: Determination of permeability to gases, CEN, Brussels, (2007)
[11] Ukrainczyk, V.; Bjegović, D.: Examination of the materials in the insurance system durability of concrete structures, Civil engineering yearbook 1995, Croatian Society of Civil Engineers, ISBN 953-96085-1-1, Zagreb, Croatia, (1995) pp. 209-286, in Croatian

AGGRESSIVE IMPACT OF SEAWATER ON CONCRETE STRUCTURES, THE REPAIR THEREOF AND THE EXAMPLE OF THE REHABILITAION OF THE PIER IN BAR HARBOUR

Radenko Pejovic[1], Miodrag Bujisić[1], Nina Serdar[1], Ivana Tesović[2], Olga Lukovic[3]

[1] University of Montenegro, Faculty of Civil Engineering, Cetinjski put b.b., 81000 Podgorica, Montenegro, email: radenko@ac.me, zile87@yahoo.com, nina_serdar@yahoo.com
[2] Civil Engineering Institute, Sima Barovića 14, 81000 Podgorica, Montenegro, email: ivanatesovic90@gmail.com
[3] Port of Adria Bar, Obala 13 jula bb,85 000 Bar, Montenegro, email: olga.lukovic@portofadria.me

SUMMARY: The paper presents the aggressive impact of seawater on concrete structures. It describes the corrosion process which leads to structural damage and the causes for the rapid progression of damage. It presents the outline and the causes of damage on the cofferdam in Bar harbour, which has been in use for 40 years. The concrete structure of the cofferdam has suffered serious damage which is seriously threatening its safety. The paper concludes with the guidelines for the manner of repair and reinforcement of the cofferdam structure, which is treated as a specific issue.

AGRESIVNO DJELOVANJE MORSKE VODE NA BETONSKE KONSTRUKCIJE I NJIHOVA SANACIJA NA PRIMJERU GATA U LUCI BAR

SAŽETAK: U radu je prikazano agresivno djelovanje morske vode na betonske konstrukcije. Opisan je proces korozije koji dovodi do oštećenja konstrukcije i glavni uzroci ubrzanog napredovanja oštećenja. Za gat u Luci Bar, koji se nalazi u eksploataciji oko 40 godina, dan je prikaz i uzroci oštećenja. Betonska konstrukcija ovog gata pretrpjela je ozbiljna oštećenja koja su takva da je njena sigurnost u velikoj mjeri ugrožena. Na kraju prikazan je način sanacije i ojačanja konstrukcije gata, kao veoma specifičan problem.

1. INTRODUCTION

All structures which are built near the sea, above the sea surface or in the sea, are exposed to aggressive actions of sea salt. Salt effects are transferred to the structures near the sea over atmosphere including these products and it is the least form of action. Structures which are above the sea are exposed to effects of sea waves. These structures are either periodically submerged, or out of sea water that is they are exposed to wetting or drying and they suffer the strongest form of sea water effects while the structures which are permanently submerged in the sea are in more favorable position.

It should take into consideration that reinforced-concrete structures in these conditions have less durability, especially if during their design and construction it did not care about their durability. Life span of these structures can be extended with adequate maintenance.

2. REASONS OF DAMAGE

Reinforced-concrete structures in the sea water, specially those above sea surface, are exposed to certain aggressive effects. Firstly, it is the aggressive effects of the sea salt, wetting and drying of the structure during oscillation of the sea level, (tide and falling tide) or washing by waves, abrasive effects of waves, but in some climatic zones freezing and defrosting.

Penetration of salt in concrete is expressed in the strongest way during cyclic action of wetting and drying of the structure, which can cause large concentration of salt in the surface parts of concrete and corrosion of reinforcement. Corrosion of reinforcement is the main reason of damages and failure of reinforced concrete structures. It causes falling of a protective layer of concrete and decreasing of cross section of reinforcement.

Damaging process will be faster if the concrete is not compact or if it has a large permeability and if the conventional cements are used for concrete fabrication. Often, reasons of damages of these structures is small thickness of protective layer,- either it is designed with small thickness or designed thickness is not realizes during construction. Beside that, often reasons of damage are inadequate compactness and waterproofing of concrete during construction. Beside that, these structures are not maintained well during exploitation, so their life span is decreased in that way.

3. MEASURES FOR DURABILITY IMPROVEMENT

Basic measures for improvement durability of the structure is using of high quality concrete which is compact and has little permeability, with the usage of the adequate cement. High quality concrete gives to the reinforcement good anticorrosive protection which makes tightly bound layer of steel oxide on the reinforcement surface. This implies adequate thickness of protective layer. Generally, in order to improve durability of the structure, engineers should take care about it during designing, construction works and maintenance. The most important factors for durability of the structures in sea water are adequate thickness of protective layer, concrete compactness with little degree of permeability, and adequate technology for concrete works which means usage of cement which is resistant to the salt effects.

4. SHORT PRESENTATION OF JETTY STRUCTURE IN PORT BAR

The structure of the south shore Jetty 1 was built of reinforced concrete in 1976. The structure is situated above sea level with the distance ranging from 85 cm to 35 cm (tide and ebb tide).

The length of Jetty structure is 360 m and its width is 19,50 m and it consisted of four lamellas length 90 m each. Lamellas are mutually dilated. RC structure of Jetty is the system of grill girders with the longitudinal and transversal girders over which is RC slab. Cross girders are the main bearing elements and they are placed at the axle distance of 4,60 m. Dimensions of these girders are width 80 cm and 197 cm height 197 (including the slab). Longitudinal girders are placed asymmetrically in order to meet the needs of crane rails. The width of these girders is 60 cm, and the height is 164 including the slab.

RC grill, over cross girders, relies on piles which are places in four rows. Piles are made by steel pipes ø 508/8 m which are filled by reinforced concrete. For this jetty, previously has been designed cathodic protection to prevent piles corrosion.

Cross section of the Jetty is shown below.

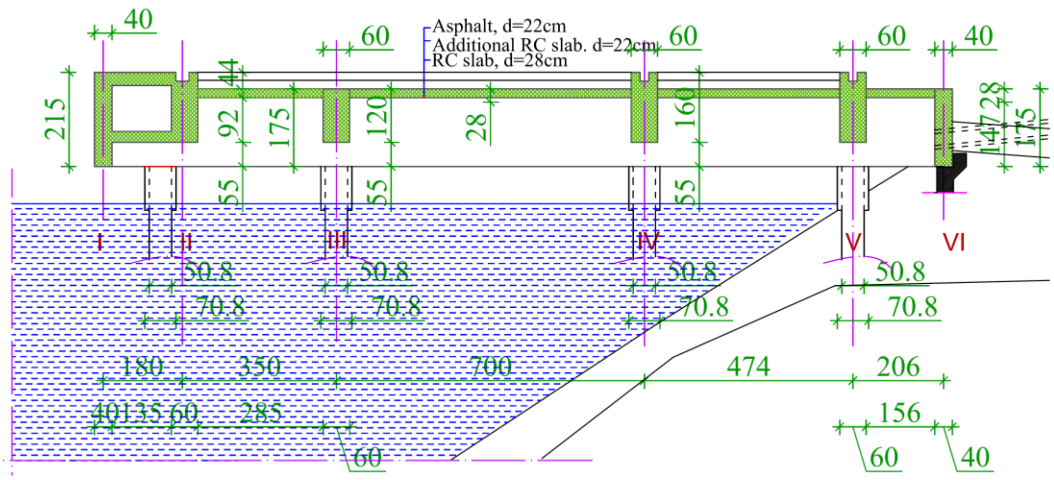

Figure 1 Cross section of the Jetty

5. EXISTING STRUCTURE, INSPECTION AND AND REALIZED TESTS

The designed concrete class is MB 30. The existing concrete quality is established by pulling out and testing of cylindrical concrete samples, diameter and the height of about 10 cm. According to the results of tests, it is concluded that the existing structure satisfy the designed concrete class MB 30.

It was also done testing of the chloride and sulphate content per the depth of structural elements. Quantity of sulphate and chloride is determined with hypothesis that cement quantity in $1m^3$ of concrete is 350 kg. Testing was executed at the surface and at the depth 12-15 cm. The test results are given in the Table 1. Reviewing of test results, it can be realized that value of content of chloride and sulfate is more than permitted, and it reduces greatly along the depths of the structural elements. Permitted contents of chloride ranges from 0,2% to 0,4%.

Also, samples were taken from the surface of steel pipes in order to check the grade of pipes corrosion. It was concluded that the pile surface taken by corrosion does not go over 1 mm.

Table 1 Content of chlorides and sulphates

Structural element	Place of taking	Chloride (%)		Sulfate (%)	
		In concrete	Related to the cement mass	In concrete	Related to the cement mass
Cross girder	At the surface of girder	0.14	0.92	1.38	2.5
	At depth (12-15)cm	0.08	0.53	0.19	1.25
RC slab	At girder surface	0.04	0.27	0.37	2.48
	At depth (12-15)cm	0.04	0.27	0.19	1.27

Figure 2 Damage Type 1 – Longitudinal and transversal reinforcement of cross girders was totally corroded and it fell out from its initial position. The reinforcement diameter has been significantly reduced.

Figure 3 Damage Type 2 – The appearance of fractures of cross girders in the zone of reinforcement in lower zone

6. EXISTING STATE OF THE STRUCTURE

Except piles, all structural elements of the Jetty have been significantly damaged. Registered damages are divided in two categories (Types) according to the degree of damage.

Type 1 – the strongest damaged elements

Type 2 – less damaged elements

The Strongest damaged elements where concrete parts of element fell down or are prone to fall down are classified as damage Type 1. Reinforcement is visible and it is strongly corroded. Cross section of main piles is significantly reduced because of corrosion, and some piles were significantly cracked. Stirrups have fallen and are separated from concrete surface.

Less damaged elements where protective layer partially fell or cracked are classified as damages Type 2. Reinforcement is visible and its surface corroded. Cracks are registered in RC slabs and its width is about 0,3 mm.

Characteristic damages of Type 1 and Type 2 are shown at Figures No 2 and No 3.

Recording of dameges has been done for all lamellas. The most damaged lamella is shown at Figure 4.

Type 1 damages are presented as red and Type 2 damages as blue color.

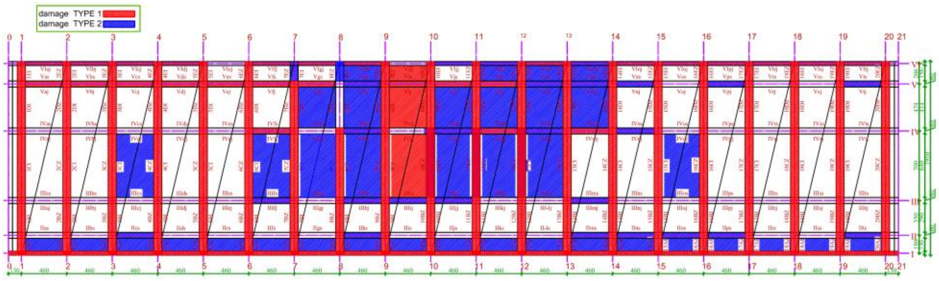

Figure 4 Damages in Lamella No.2

7. CAUSE OF DAMAGES

Basic cause of damages of reinforced concrete structure is very aggressive area, because this structure is closely above the sea level and it is exposed to constant impacts of the sea water. Special issue is permanent wetting and drying of the lowest parts of concrete structure of cross and end longitudinal girders which are the closest to the sea water and which are very damaged.

When compare to the structures in non-aggressive areas, protective layer has been increased, but conditions in exploitation are not favorable for these structures.

In relation to the basic features of concrete and its resistance to the aggressive sea effects, the designer did not provide any conditions or limits.

Beside the aggressiveness of the area, quite fast failure of this structure was caused by omissions which happened in the phase of construction of reinforced concrete structure. The largest omission was made during placing of reinforcement for which designed protective layer was not obtained. At the site inspection it is stated that all protective layers of concrete on all damaged places are executed with lower thickness that it is designed, and at some places reinforcement was placed close to the formwork, and reinforcement was practically left without any protective layer. Beside that, taking cylindrical concrete is proved insufficient completeness of concrete in the structure. Insufficient completeness of concrete in the structure was established by taking cylindrical concrete samples. Insufficient compactness of concrete is confirmed by low volume mass which is established by testing.

Static calculation of the structure on the more real model it was stated some deviations in relation to the effects from the basic project. The reason was in the fact that in previous calculation piles are taken as fixed supports, which is not real, because it is about thin and deformable elements.

By the control of limit state of cracking it was stated that their width for this level of aggressiveness is higher than it is permitted. The control was done for characteristic sections and the following results are received: for plates au=0,12 – 0,49 mm, for longitudinal girders au=013-0,20 mm and for cross girders au=0,06 - 0,17 mm. According to the Rulebook for concrete for this level of aggressiveness the permitted width of fracture is au max=0,1 mm. This state of cracking with the little protective layer accelerated the corrosion of the reinforcement.

In exploitation period RC structures of Jetty had big damages. The degree of damages is so that in large measure their safety is damaged, that is it does not have adequate safety in the existing exploitation state.

Pile structure of this Jetty is quite in a good state and its bearing is not endangered.

8. REVIEW OF EXISTING STATE OF THE STRUCTURE

In exploitation period RC structure had large damages. The level of damage is that in a large measure its safety is endangered.

Pile structure of this Jetty is in a quite good state and its bearing is not endangered.

9. REHABILITATION SOLUTION

During the choice of the repair solution, we started from the following assumptions:

- RC structure of Jetty suffered extremely large damages and its safety is endangered.
- Unfavourable exploitation conditions i.e. it is about aggressive area.
- It is necessary to obtain adequate static safety of the Jetty structure.
- It is necessary to obtain adequate durability, that is to prolong the life of this structure as long as possible.
- It is necessary to strengthen the Jetty structure so it can receive increased useful loads.

- Suggested solution must be accepted from the economic point of view.

10. PREPARATION FOR RECONSTRUCTION AND REHABILITATION

Because of the specifications of the Jetty structure and difficult conditions of repair (confined space above sea water) it is necessary to do the following preparatory activities:

- In RC plate of the Jetty among the transversal girders should be made one opening 60x60 cm for the access to the structure.
- To install hanging steel scaffold which is hung for the RC structure and it serves for execution of repair work.
- To do the blasting of all concrete areas by water under the high pressure.

Rehabilitation of damages of the Type 1

Two repair solutions are chosen for this type of damage. One is consisted in extending the cross section in the zone where the damages are registered. The thickness of new-added concrete is adopted 10 cm from the lower side and 8 cm from lateral sides. This thickness is dimensioned in a way that it can place the necessary reinforcement and to obtain the adequate protective layer. The height of the extension is dependant on the height of damages and at transversal girders it ranges from 20 to max 55 cm, and at longitudinal girders this height is 25 cm. Detail of the repair is given in the Figure 5.

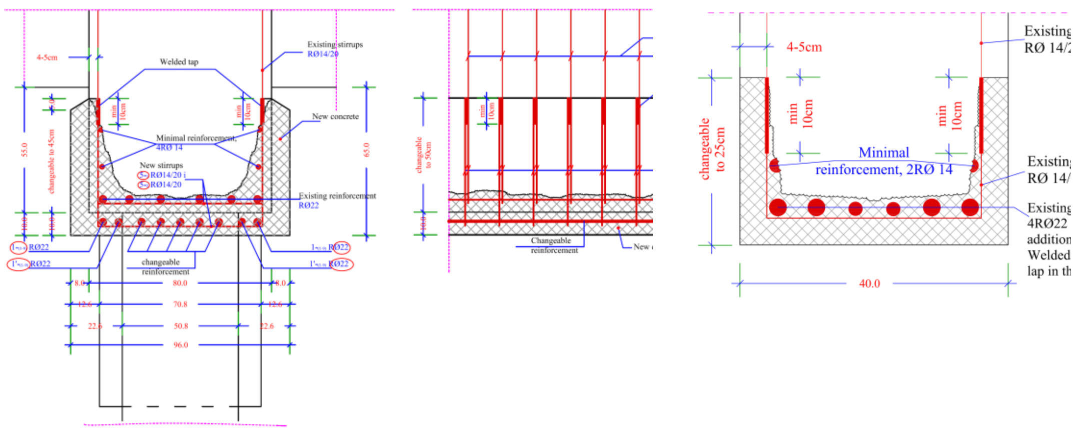

a) with the increase of cross section

b) without increase of cross section

Figure 5 Detail of the repair of the type 1

The second repair solution is performed in the existing dimensions of the girder according to the details given in the Figure 6.

Rehabilitation of damages of the Type 2

In this type of the damage, as it is stated above, there are local damages of concrete of all structural elements which depth is different, surface corrosion of the concrete and reinforcement and fracture.

Other rehabilitation measures

Other repair measures include the repair of fractures by injecting, repair of the piles head, establishing of the cathode protection of piles and surface anticorrosion protection of all concrete surfaces of Jetty (repaired and non-repaired), as well as strengthening of RC plates by carbon strips which do not have adequate bearing capacity.

11. CONCLUSION

Issue of durability of RC structures in the sea is very complex. In order to achieve the adequate durability through all phases of design and construction of structure, all requests must be met in that sense, that is in the sense of design, technology and construction. The important factor for durability improvement is regular maintenance with the removal of samples of failure and certain repairs on the structure.

In any case ,it should have in mind that durability of RC structures in these cases is significantly decreased.

LITERATURE

[1] “Detailed design of rehabilitation of the South Jetty in Port of Bar”, Civil Engineering Institute Ltd Podgorica, July 2016;

[2] Pejovic R, Mijuskovic O, Kapor V: “Rehabilitation of the bridge across river “Pcinja” at motorway Podgorica – Kolasin, International Conference “Civil Engineering – Science and Practice”, Proceedings ISBN 86-82707-13-6 (Book No 2), pg. 669-676, University of Montenegro – Faculty of Civil Engineering Podgorica, Zabljak 20-24 February, 2006;

[3] Pejovic R, Kapor V: “Rehabilitation of the bridge across river “Lim” near Marsenica river”, Fifth advising “Ocena stanja, odrzavanje i sanacija građevinskih objekata i naselja”, Proceedings ISBN 987-86-904089-3-1 (Book No 2), pg. 91-96, IT Savez inzenjera i tehnicara Srbije, Zlatibor, 29th May – 1st June, 2007;

[4] Pejovic R, Blagojevic J, Blagojevic R, Matijasevic S, Prasecevic V. “Rehabilitation of the bridge “Mojkovac””, International Conference “Civil Engineering – Science and Practice”, Proceedings ISBN 978-86-82707-18-9 (Book No 1), pg. 365-370, University of Montenegro – Faculty of Civil Engineering Podgorica, Zabljak 15-19 February, 2010;

[5] Pejovic R. ,,Rehabilitation of the Branko Zezelj's bridge across river Moraca in Podgorica”, International Conference “Istrazivanja, projekti i realizacije u gradjevinarstvu, povodom stogodisnjice rodjenja Akademika profesra Branka Zezelja”, Proceedings ISBN 978-86-8208-116-6, pg. 261-266, Institute IMS Belgrade, Belgrade 28-29 October, 2010;

[6] Pejovic R. ,,Examples of rehabilitation of bridges”, Advising “Savremeni materijali i postupci sanacije građevinskih objekata”, Proceedings ISBN 978-86-82307-21-1, pg. 125-143, Udruženje inzenjera gradjevinarstva, geotehnike, i urbanizma ,,Izgradnja”, University of Belgrade – Faculty of Civil Engineering, Belgrade 2013;

[7] Pejovic R, Mijuskovic O.: “Rehabilitation of the silo which capacity is 30 t in Port of Bar”, Advising “Savjetovanje, Evaluacija, održavanje i sanacija objekata u gradjevinarstvu”, Tara, 1999.

CONDITION ASSESMENT OF COLLECTION CENTER AND RAWHIDE LEATHER WAREHOUSE STRUCTURE

Donka Würth[1], Slavica Cosovic Bajic[1]

[1] Zagreb University of Applied Science, Vrbik 8, 10 000 Zagreb, Croatia, email: dwurth2@tvz.hr, sbajic@tvz.hr

SUMMARY: Collection center and a warehouse of rawhide leather is a place where the rawhide leather, impregnated with salt solution (NaCl), is brought in and driven away on daily basis. Rawhide leather is palletized and salted and at the same time, drained from water, blood and remains of meat and feces in combination with salt solution. The salt affects the concrete structure by penetrating into the concrete pores, aggregate and crystallizing there. However, the biggest problem occurs when salt comes into contact with reinforcement causing corrosion of the reinforcement, i.e. it starts the process of “pitting” which, over the time, can cause a reduction in cross-section of the bars. Such aggression is said to be among the most aggressive and complex chemical undesired media where reinforced concrete structure can be. This paper gives an overview of assessment of this kind of structure.

OCJENA STANJA KONSTRUKCIJE SABIRALIŠTA I SKLADIŠTA SIROVE KOŽE

SAŽETAK: Sabiralište i skladište sirove kože prostor je u kojem se svakodnevno dovozi i odvozi sirova koža impregnirana solju (NaCl). Koža se slaže na palete i soli se, u isto vrijeme iz kože se procjeđuje voda, krv, ostatci zaostalog mesa te izmet u kombinaciji s otopinom soli. Utjecaj soli na strukturu betona je takav da otopljena sol ulazi u pore betona, agregata i kristalizira. No najveći problem nastaje kada sol dođe u dodir s armaturom. Tada započinje korozija koja ju oštećuje, tj. započinje „točkasta“ korozija, koja može tijekom vremena uzrokovati smanjenje poprečnog presjeka armature. Takva vrsta agresije spada u skupinu najagresivnijih i kompleksnih kemijski nepoželjnih medija u kojima se nalazi armiranobetonska konstrukcija. U radu je dan prikaz ocjene stanja konstrukcije.

1. UVOD

Objekt skladišno poslovnog prostora (sabiralište/ skladište sirovo-slane kože) u Varaždinu sastoji se od dva dijela. Stari dio skladišta izgrađen je 1984 godine, a novi, dograđeni dio, izveden (nadograđen) je 2004 godine. U području skladišnog dijela radnici preuzimaju, sortiraju, impregniraju sirovu kožu sa soli, skladište je do određene starosti i kasnije se koža prosljeđuje na daljnju preradu. Pod skladišta je uglavnom pod utjecajem vode, soli za soljenje kože, ostataka sirovog mesa, krvi, urina i izmeta. U skladištu dovoz i manipulacija kože odvija se viličarima, te koža stoji ili na podu ili na paletama (slika 1).

Slika 1 Skladište sirove kože

Objekt je izveden kao ab montažna konstrukcija, koja ima 12 armirano betonskih montažnih stupova visine 5,5 m, na njima su montažne glavne grede raspona 10,0m i montažni krovni nosači tipa „M“. Svi armiranobetonski montažni elementi proizvedeni su u tvornici G.K. „Međimurje“ iz Čakovca. Temelji stupova su ab čašice – stope koje su se izvodile monolitno na gradilištu. Isto tako trakasti temelji izvedeni su monolitno, na koje su položene zidne ispune od siporeksa ili blok opeke. Podovi su izvedeni s dvije dvoslojne ab. ploče s hidroizolacijom u sredini. Donja betonska podloga izvedena je na tamponskom sloju šljunka. Hidroizolacija je jednostruka ljepenka, koja je položena na najlon. Prvotno, 1984. godine završni sloj poda bila je cementna glazura, ali nakon dogradnje, gornja glazura je maknuta, a na novo izvedenoj gornjoj ploči završna površina izvedena je do crnog sjaja, na koju je nanešen epoxidni završni protuklizni premaz [1]. Spoj vertiaklnog zida i horizontalne ploče izvedeni su zaobljeno (holker). Zidovi skladišta ožbukani su grubom i finom produžnom žbukom. Samo zidovi i ab stupovi u skladišnom prostoru premazani su epoxidnim vodonepropusnim premazom do visine cca 2m. Hidroizolacija zgrade i skladišta završava kroz vanjske zidove van do fasade [2].

Kako bi se proveo postupak ocjene stanja konstrukcije potrebno je razraditi sljedeće postupke [3]:

a) ocijeniti postojeće stanje betonske konstrukcije

b) proučiti izvorni projekt

c) proučiti okoliš, uključujući razred izloženosti u kojoj se konstrukcija nalazi

d) proučiti uvjete tijekom građenja – građevinski dnevnik

e) zahtjeve u budućoj uporabi betonske konstrukcije

2. POSTOJEĆE STANJE BETONSKE KONSTRUKCIJE

Na temelju preliminarnog pregleda skladišta kože, određen je program istražnih radova u cilju ocjene postojećeg stanja konstrukcije. U samom početnom pregledu vidi se da je uzrok svih oštećenja procjeđivanje otpadne vode iz skladišta preko hidroizolacije kroz zidane zidove skladišta sirove kože van na fasadu (slika 2, slika 3).

Slika 2 Dio fasade – curenje otpadne vode

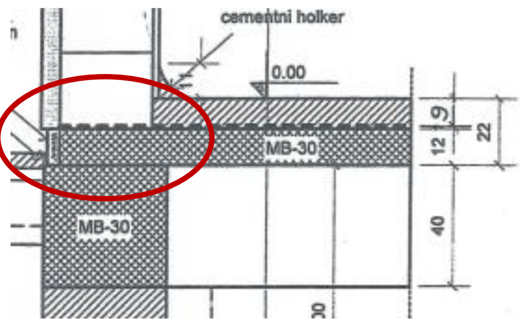

Slika 3 Nacrt –detalj hidroizolacije

Popucala cementna glazura koja je izvedena na hidroizolaciji, ne usmjerava vodu u odvodne slivnike, već se voda procjeđuje do hidroizolacije, te odlazi kroz zidove do fasade. Također vidljivo je da se voda zadržava na površini poda, što ukazuje na loše izvedene nagibe završne površine prema odvodima. Procjeđivanje vode odvija se tako da u starom dijelu, dio vode koji ne ode u slivnike, ulazi u podnu ploču kroz izrezane i popucale fuge pa se djelomično procjeđuje vjerojatno u tlo, a dio vode slijeva se prema novom dijelu zgrade i izlazi kroz zidove na fasadu. Evidentno je da se sva voda koja dođe u kontakt sa ožbukanim zidovima, zbog efekta kapilarnog upijanja, penje po žbuci i po ab elementima. Otpadna slana voda kemijski je agresivna za dijelove čelika, tj. armature u betonu.

Kako bi se dala ocjena stanja konstrukcije pristupilo se istražnim radovima sa sljedećim planom [4]:

1. Vizualni pregled - stanje površine betona
2. Terenska ispitivanja - stanje betona po dubini (uzimanje uzoraka za laboratorijska ispitivanja)
3. Terenska ispitivanja - stanje armature u betonu

2.1. VIZUALNI PREGLED

Vizualnim pregledom ustanovljeni su nedostaci nastali tijekom izvedbe građevine (loše izveden detalj hidroizolacije) i oštećenja nastala tijekom eksploatacije kretanjem viličara (pukotine, ljuštenja oštećenih podnih površina).

Slika 4 Vidljiva oštećenja površine poda

Na podnoj ploči u starom dijelu vidljivo je ljuštenje epoxi premaza (3 mm). Također je vidljivo da je ploča imala pukotine, koje su sanirane lijepljenjem epoxi traka, koje su se ponovo aktivirane uslijed kretanja viličara, te dolazi do ponovnog otvaranja postojećih saniranih pukotina. Ispune između ab stupova i vertikalnih serklaža su zidovi od opečarskih blokova i siporeks blokova, za koje znamo da imaju veliki koeficijent kapilarnog upijanja, te na taj način su kapilarno povukli klor ione, pa žbuka otpada, a vlaga je vidljiva u zidova.

2.2. TERENSKA ISPITIVANJA - STANJE BETONA PO DUBINI (UZIMANJE UZORAKA ZA LABORATORIJSKA ISPITIVANJA)

2.2.1. TLAČNA ČVRSTOĆA BETONA

Mjesta uzimanja valjaka iz konstrukcije za utvrđivanje tlačne čvrstoće, određena su na način da je izražena sumnja u kvalitetu betona, a to su najugroženiji stupovi i podna ploča. Uzorci valjaka uzeti su bušenjem s dijamantnom krunom Ø 100mm i Ø 50mm. Na ab stupovima malih dimenzija od cca 40 cm, bušeni su valjci Ø 50mm, dok su u podnoj ploči izbušeni valjci Ø 100mm. Rezultati ispitivanja tlačne čvrstoće prema HRN EN 12390-3 prikazani su u tablici 1.

Tablica 1 Rezultati ispitivanja tlačne čvrstoće na valjcima

Oznaka uzorka Oznaka naručitelja	Volumna masa (kg/dm^3)	Tlačna čvrstoća (MPa)
Stup S4 i S14		
S4/1	2,26	39,6
S4/2	2,29	40,1
S14	2,26	39,7
Pod S (stari dio) i N (novi dio)		
PS1	2,36	65,6
PS2	2,27	31,6
PN1	2,36	54,0

Temeljem ispitivanja tlačne čvrstoće valjaka gornje podne ploče (d= 135mm) dobivene su vrijednosti od 65,6 MPa i 54,0 MPa, dok donja ploča (d=160mm) (vizualno loše strukture betona), ima tlačnu čvrstoću 31,8 MPa. (projektirane tlačne čvrstoće betona su za gornju i donju ploču MB30, što odgovara današnjem razredu C 25/30). Kao što vidimo rezultati tlačne čvrstoće betona donje ploče pokazali su nižu vrijednost, dok rezultati tlačne čvrstoće betona gornje ploče veći su nego projektirani.

2.2.2. ODREĐIVANJE SADRŽAJA UKUPNIH KLORIDA KAO CL-

Količina sadržaja ukupnih klorida u betonu, ispitana je na način da su uzeti uzorci betona (prah) bušenjem u zidu do dubine armature. Određivanje sadržaja ukupnih klorida ispitano je prema normi HRN EN 14629. Rezultati ispitivanja prikazani su u tablici 2.

Tablica 2: Količina klorida s obzirom na dubinu uzimanja uzoraka

Oznaka	Položaj u konstrukciji (mm)	Sadržaj Cl^- na kol. betona (%)	Sadržaj Cl^- na kol. cementa (%)
Stup S4	0-20	0,03	0,004
	20-30	0,03	0,004
Stup S14	0-20	0,68	0,10
	20-35	0,23	0,03

Jedan od razloga depasiviziranja čelika jest prisutnost određene količine klorida otopljenih u pornoj tekućini u blizini armature. Rizik od korozije postoji ako je količina klorida 0,4% na masu cementa [5]. Stupovi koji su u skladištu, a na površini su premazani vodonepropusnim premazom, nisu ugroženi penetracijom klorida uz pomoć difuzije, već kroz pukotine koje se nalaze u dnu stupova, kloridi su kapilarnim upijanjem penetrirali u površinski dio betona cca 20 mm.

2.3. TERENSKA ISPITIVANJA - STANJE ARMATURE U BETONU

Prilikom otvaranja pojedinih dijelova ab konstruktivnih elemenata (slika 5), kako bi se vizualno vidjelo stanje armature u elementima, vidljiva je bila prisutnost otopine NaCl, vlažnost betona, te korozija armature u dijelovima stupova koji su ožbukani (slika 6). Zbog agresivnog medija koji penetrira u beton, potrebno je odrediti stanje armature u ab elementima kod kojih nije bila vidljiva korozija. Kako bi se locirala i odredila moguća pojava korozije armature, a da se ne razara konstrukcija, koristi se metoda polućelijskog potencijala. Njom se određuje pad potencijala između odabrane točke na ispitnoj armaturi (koja je obično otvorena, kroz malu, izbušenu, rupu) i pokretne, referentne ćelije na samoj površini ab elementa. Mjerna pozicija i odgovarajuća vrijednost potencijala Ec se iskazuju u vrijednosti (mV) i boji, kako bi se odredila vjerojatnost pojave korozije.

Slika 5 Armatura ab zida bez žbuke

Slika 6 Armatura ožbukanog ab zida

Rizik od korozije raste sa većim negativnim padom potencijala. Za određivanje nivoa rizika od pojave korozije armature, uzeta je američkia norma ASTM/C876, koja daje podjelu dobivenih vrijednosti potencijala Ec vrijednosti u tri "razreda" (tablica 3).

Tablica 3: Vrijednosti potencijala Ec mjera pojave korozije

Vrijednost Ec	Opis pojave korozije	Vjerojatnost pojave korozije
Ec ≈ 200 mV	nema opasnosti od korozije	10%
350 < Ec <-200 mV	moguća korozija	50%
Ec <−350 mV	velika mogućnost pojave korozije	90%

Nakon izmjerenih elektopotencijala tabelarno je dato stanje pojedinih elemenata s obzirom na vjerojatnost pojave korozije (tablica 4).

Tablica 4: Prikaz vjerojatnosti pojave korozije armature s obzirom na dimenziju elementa

KONSTRUKTIVNI AB ELEMENT	POVRŠINA ZAHVAĆENA ODGOVARAJUĆOM VJEROJATNOŠĆU POJAVE KOROZIJE ARMATURE (%) iz mjerenja polućelijastog potencijala u odnosu na Ag/AgCl elektrodu		
	VJEROJATNOST POJAVE KOROZIJE ARMATURE		
	10% MALA (%)	50% SREDNJA (%)	90% JAKA (%)
Stup S1 ulaz	Više od 110 cm 36	80-110 cm 9	0-80 cm 55
Stup S2 podest	Više od 230cm 47	210-230 cm 27	0-210 cm 26
Greda G1	0	0	Cijela duljina grede 100
Stup S4 skladište	Više od 100 cm 80	20-100 cm 20	0-20 cm 0
Stup S14 skladište	Više od 100 cm 20	20-100 cm 60	0-20 cm 20

3. OCJENA STANJA KONSTRUKCIJE

Nakon vizualnog pregleda, terenskih i laboratorijskih ispitivanja može se dati ocjena stanja konstrukcije po pojedinim konstruktivnim elementima. Tlačna čvrstoća betona armirano betonskih stupova i poda je veća nego što je projektirano (projektirano C25/30 dobiveno C35/45), što znači da je otopina NaCl koja je ušla u pore betona i agregata kristalizirala, te je na taj način povećana tlačna čvrstoća betona (ispitivanje u suhom stanju). U praksi provedena ispitivanja tlačne čvrstoće betona elemenata koji su stalno pod morem, također su potvrdila teoriju o rezultatima koji pokazuju veću tlačnu čvrstoću betona [6]. Kako kristalizacijske soli imaju veću provodljivost vode, armatura ove konstrukcije je ugrožena uslijed difuzije klorida u betonu. Rezultati ispitivanja količine klorida u betonu na stupovima u skladištu koji su premazani epoxidnim vodonepropusnim premazom pokazali su manje vrijednosti, jer je premaz spriječio, na dijelovima gdje je oštećen usporio penetraciju klorida. Armiranobetonski stupovi koji su ožbukani vapnenom žbukom, a to su stupovi u upravnoj zgradi, zbog žbuke koja ima veliki koeficijent kapilarnog upijanja, kloridi su penetrirali i proces korozije armature je započeo. U zidovima koji su izvedeni od opeke i siporeksa, otopina soli ušla je u zidove, te su vidljivi dijelovi natopljeni vodom i oštećenja od ljuštenja same žbuke i boje zida. Kada je suho i nema doticaja vode u zidovima, opeka i siporeks se prosuše, te vlažne mrlje nestanu. Najveća opasnost za konstrukciju su oštećenja koja se nalaze na podnoj ploči, a to su pukotine (do 5-10 mm), koje omogućuju otpadnoj vodi da curi do hidroizolacije i tada agresivni medij izlazi preko hidroizolacije van kroz zidove. U unutarnjem dijelu skladišta također su loše izvedeni „holkeri“ spojevi vertikalnog i horizontalnog dijela zida i ploče, te uzduž dna zida vidljive su pukotine, koje otvaraju slobodan put vodi da uđe u elemente konstrukcije.

4. ZAKLJUČAK

Krv, ostaci sirovog mesa, izmet u kombinaciji sa sol za kondicioniranje, čine medij koji je vrlo agresivan u pogledu ab konstrukcije. Životinjska krv i urin imaju vrijednost pH oko 7,4, tako da agresija samih sastojaka tijela i izmeta životinja nije značajno agresivna za beton i armaturu. Međutim sol (NaCl) s kojim se provodi postupak kondicioniranja kože nekoliko dana, vrlo je agresivan medij. Nakon odvoza odstajale kože dolazi i postupak čišćenja, koji se provodi s HCl (solnom kiselinom) i vodom pod pritiskom. Kada se spoje svi navedeni reagensi, tada možemo reći da je konstrukcija izložena jakoj kemijskoj agresiji. Projektant je konstrukciju predvidio projektiranjem nepropusnog epoxi premaza na podu i vertikalnim zidovima, međutim, pojavile su se pukotine duž cijelog skladišta u „holkerima“ te je otvoren put agresivnoj vodi da penetrira u tijelo konstrukcije. Bez obzira na vodonepropusne premaze na bazi epoxida kojim su premazani svi unutrašnji dijelovi skladišta, potrebno je predvidjeti dodatno osiguranje od procurivanja vode, na način da se hidroizolacija izvede iz poda na zidove, tako da tvori jednu cjelinu - „kadu“. Nakon ocjene stanja konstrukcije potrebno je izraditi projekt sanacije, kako bi se zaustavila daljnja degradacija cijele konstrukcije.

LITERATURA

[1] „Glavni projekt otkupne stanice“ Projekt biro Zagreb iz 1984
[2] „Glavni projekt Poslovne dogradnje“ ART FILIPAŠIĆ d.o.o. Varaždin iz 2004
[3] Radić J. i suradnici, Dani betona 4 – Sanacije, Hrvatska sveučilišna naknada, Zagreb, 2010, pp 469-471
[4] Izvještaj o istražnim radovima ocjene stanja ab konstrukcije u skladišno – poslovnom prostoru (sabiralište/skladište sirovo, slane kože) u Varaždinu, Tehničko veleučilište u Zagrebu, ‚Izvj. Br. 003/2016 od 13.04.2016.
[5] Radić J. i suradnici, Dani betona 4 – Sanacije, Hrvatska sveučilišna naknada, Zagreb, 2010, pp 362-365

[6] Bjegović D., Serdar M, Baričević A., Jelčić Rukavina M.: Ocjena stanja betonskog obalnog zida izloženog djelovanju morske vode više od 30 godina, Građevinar 67, (2015) 12, pp 1155-1164

CONDITION ASSESSMENT OF TRADITIONAL POST-REVIVAL RURAL BUILDINGS IN MOUNTAIN REGIONS IN BULGARIA

Marina Traykova[1], Tanya Chardakova-Nackova[1]

[1] University of Architecture, Civil Engineerong and Geodesy, Faculty of Structural Engineering, Department of Reinforced Concrete Structures, 1 Hristo Smirnenski Blvd., 1046 Sofia, Bulgaria, email: marina5261@abv.bg, tanq_chardakova@abv.bg

SUMMARY: In the Post-Revival period in Bulgaria (late XIX and early XX century) the construction in rural regions, unlike city regions, was still dominated by traditional methods of construction. The buildings and structures were non-engineered, but were built by craftsmen, well-learned in the accumulated for centuries knowledge. In mountain regions the traditional construction methods were defined by the difficult terrain conditions, including very inclined sides and landslides. In the paper condition assessment of an early XX century residential building in a village in the Rodopi Mountain is presented. Given the history of the building, the causes of recent structural damages are analyzed. Using the Dutch standard, condition assessment of the main structural components of the house is made. The “diagnosis” of the structure is the result of investigation (the complexity of which depends on the degree of damage to the members/structure) and represents the basis for adopting intervention measures. Finally, based on the analysis of the presented structure, some general conclusions, concerning the preservation of such type of buildings, part of the Bulgarian architectural heritage, are given, and also general conclusions, concerning the application of condition assessment.

OCJENJIVANJE STANJA TRADICIJSKIH POSTOBNOVITELJSKIH SEOSKIH ZGRADA U PLANINSKIM PODRUČJIMA BUGARSKE

SAŽETAK: U postobnoviteljskom razdoblju u Bugarskoj (razdoblje od kraja 19. do početaka 20. stoljeća) u građenju u seoskim područjima, za razliku od gradskih područja, prevladavale su još tradicijske metode gradnje. Zgrade i konstrukcije bile su neinženjerske, ali su ih gradili dobro obučeni obrtnici sa znanjem prikupljenim tijekom stoljeća. U planinskim područjima tradicijske metode gradnje bile su određene teškim terenskim uvjetima s vrlo nagnutim padinama i klizištima. U radu se prikazuju uvjeti ocjenjivanja stambene zgrade s početka 20. stoljeća u selu u planinskom lancu Rodopi. Analizirani su uzroci sadašnjeg oštećenja konstrukcije uz poznatu povijest zgrade. Ocjena stanja glavnih dijelova konstrukcije kuće provedena je prema nizozemskoj normi. Dijagnoza konstrukcije rezultat je istraživanja (čija složenost ovisi o stupnju oštećenja elemenata odnosno konstrukcije) i predstavlja osnovu usvojenih mjera zahvata. Na kraju, na osnovi analize postojeće konstrukcije dani su opći zaključci povezani sa zaštitom takve vrste zgrada koje su dio bugarskog arhitektonskog nasljeđa, a dani su i opći zaključci koji se odnose na primjenu ocjenjivanja stanja.

1. INTRODUCTION

According to Arya [1], “the term non-engineered building is defined as buildings which are spontaneously and informally constructed in the traditional manner with-out intervention by qualified architects and engineers in their design, but may follow a set of recommendations derived from observed behaviour of such buildings during past earthquakes and trained engineering judgement.” On one side the lack of integrity on building’s structural elements, improper detailing on building’s structural elements, low quality of material’s construction are typical problems found on many sites, but on the other side - the changes related to some contemporary infrastructure solutions and the climate changes are very often reasons for serious damages and degradation of the building components. A building survey consists of an investigation and assessment of the structure and condition of a building, which generally include the structure, finishes etc. A thorough assessment of a building condition is a technically complex task, requiring knowledge, time and equipment.

The buildings in Bulgaria from the period of the National Revival and the Post-Revival period, which are important part of the architectural heritage of Bulgaria, are typical representative of the non-engineered buildings. The preservation of such buildings is particularly difficult in mountain regions, where the terrain conditions are severe. The correct assessment of their structure is very important for the maintenance planning of the buildings, performance control and the possibility to extend their durability and working life. Conditions change the physical and operational impact on the buildings. Capturing of the significant changes and damages and quantifying their rate are required before they impact the performance of the structure.

In several countries the condition of a building is assessed on the basis of a diagnosis of the extent of deterioration in the building elements. Apart from some differences in the objectives, the assessment methods and development processes in the various countries are very similar. The condition of a building is assessed by systematic registration of the entire building, divided into elements. Despite variations in the classification of these elements, the aim is to provide a comprehensive assessment. Any defects detected in an element are assessed on pre-defined criteria. The assessment is carried out by means of visual inspections performed by qualified surveyors. Different assessment methods are in current use: methodology of South Africa [2], Portuguese method [3], Dutch standard [4], etc.

This paper is focused on the condition assessment of the main structural component of a typical Post-revival building from the region of the Rodopi mountain in Bulgaria.

2. APPLIED METHODOLOGY FOR CONDITION ASSESSMENT

The paper considers the basic concepts of the Dutch standard [4]. Condition assessment according to the standard should be used as a strategic management tool. The standard is a tool to assess the technical status of the properties to underpin the long-term maintenance expectations. Supplementary information is needed in the phase of preparing the execution of remedial work. Supplementary information might be the precise location of the defects and causes of defects to take adequate maintenance actions. A six-point scale for condition assessment is adopted – the condition of the building components is rated as excellent, good, fair, poor, bad, or very bad. The rating is based on the importance, intensity, and extend of the defects. The standard classifies the importance of defects of distinct building components into minor, serious and critical. The intensity is classified as low (hardly visible defect), middle (progressing defect), or high (defect, that cannot progress any further). The extend of the defects is classified, based on the occurrence of the defect or the percentage of defected elements: <2% (incidentally), 2-10% (locally), 10-30% (regularly), 30-70% (frequently), >70% (generally).

The condition assessment process starts with the assessment of the defects. The extent and the intensity of a defect combined with the importance of the defect lead to a condition rating. Building components may show more than one defect.

Based on the matrix on resulting condition ratings for defects (see Table VI, VII, VIII in [4]) the maintenance performance level can be determined. Maintenance performance levels can be based on the minimum condition of building components after executing maintenance work. The risks of defects of building components that are not solved are rated on a three-point scale. The risk categories are rated with a risk-priority matrix [4]. As this paper is focused on the condition assessment of structural components only, these further steps are not in the scope of the paper.

3. CONDITION ASSESSMENT OF A BUILDING IN THE RODOPI MOUNTAIN

A typical representative of the Post-Revival architecture in mountain rural regions is considered. The house is situated in Ugovo village, near the famous Bachkovo monastery in the Rodopi mountain. The region had been well-known for its skilled builders for centuries.

3.1. HISTORY OF THE HOUSE AND CHANGES IN ITS BUILT AND NATURAL ENVIRONMENT

The house was built in the very beginning of XX century – probably around 1904. The traditional construction techniques for the region were used. The terrain (with inclination from 1:1 to 1,5:1) was terraced (Figure 1), using stone masonry retaining walls. Parts of it were also used as outer wall of the house. The first floor of the house, used for agricultural purposes, is with stone masonry outer walls, while the second residential floor (with the exception of the retaining wall) is with outer walls from local type of poured limestone, that is very light and with very good heat insulation properties (Figure 2). All inner walls are half-wooden. The timber roof was originally covered with stone roof tiles, traditional for the region, but these were later changed with ceramic tiles.

The stone masonry is with very good quality and detailing, and originally provided box-behaviour of the structure. However, there were two events that diminished the global behaviour of the structure. First, around 1966 the west wing (almost 2/3 of the house) was demolished, and the building materials were used for another house. The new outer west masonry wall was originally tied to the north outer wall, but not to the south one. Second, around 1985, the existing road north of the house was widened, so trucks can pass trough. The original stone masonry retaining wall was demolished, and new higher reinforced concrete retaining wall was built closer to the house. In the process the north-west corner of the house was cut (see Figure 2 and 3). Thus, nowadays there is no longer box-behaviour of the structure, as it now has only two tied masonry corners – the south-east and the north-east ones. Also, the connection between the structure and the new retaining wall means that the house is practically bearing part of the loads from the road, as well as from a new 3-storey building with reinforced concrete structure across the road.

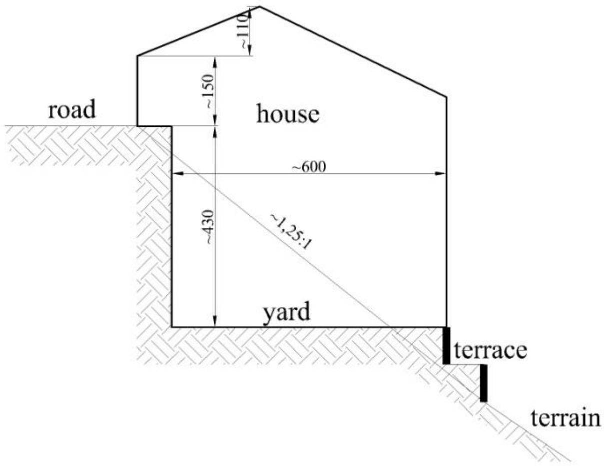

Figure 1 Terracing of the terrain nowadays

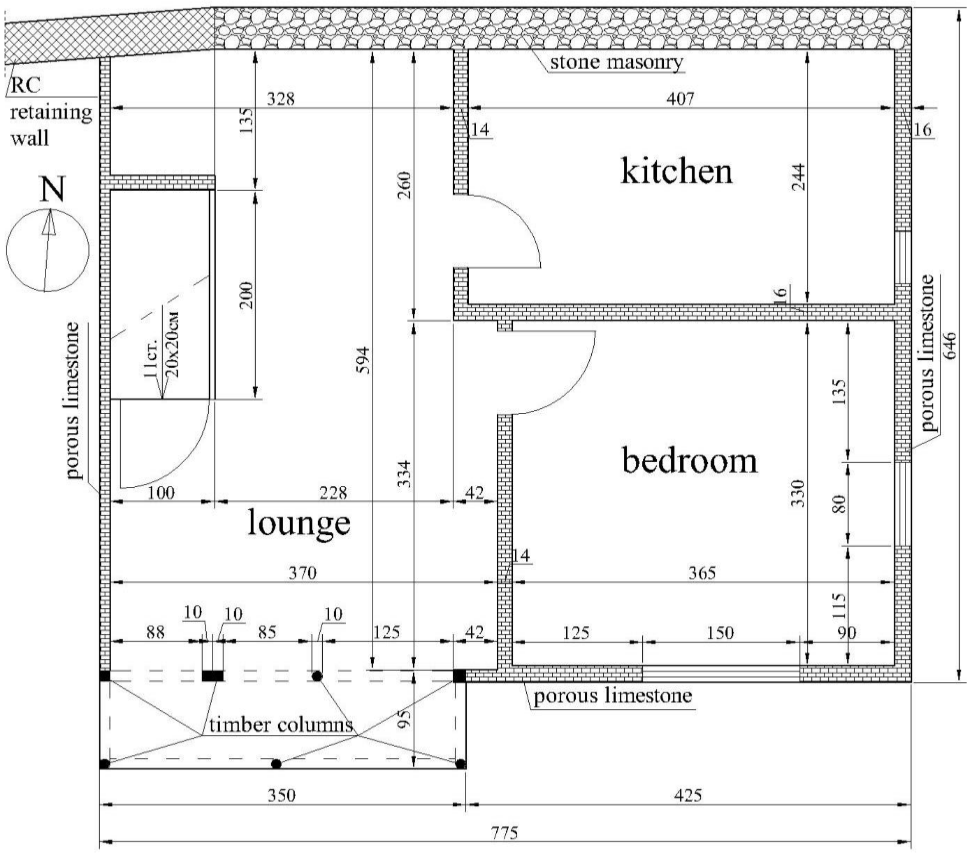

Figure 2 Architectural plan of the house nowadays

Figure 3 North-west corner of the building and connection with RC retaining wall

Additionally, climate changes worsen the already heavy terrain conditions. In recent years there were a few episodes of extreme weather in the region. Strong winds uprooted several old trees, both above and below the house. Also, there were a few very rainy years. The data, presented in Table 1, shows, that in 10 of the last 13 years the annual precipitation for the region was up to 67% higher than the average, and for the last 5 years the average increase is 26%. These change in conditions activated landslides, which are typical for the region.

Table 1 Annual precipitation (AP), station Kardjali (Data source: National Institute of Meteorology and Hydrology – Bulgarian Accadamy of Science [5])

year	2004	2005	2006	2007	2008	2009	2010	2011	2012	2013	2014	2015	2016
AP, [mm]	744	736	601	760	373	701	818	467	727	760	1089	870	658
% of average AP*	114%	113%	92%	117%	57%	108%	126%	72%	112%	117%	167%	134%	101%

*Average annual precipitation for the period 1961-1990 is 651mm.

3.2. RESULTS FROM VISUAL INSPECTION ON SITE

It is found by visual inspection on site that:

1) All structural and non-structural elements on the western facade have deformed visibly. There are considerable horizontal displacements at the level of the level of the floor structure (Figure 4a). The drift of the timber column, marked in Figure 5 is larger than 1:25. The absolute displacements are probably much larger than the measured relative ones, as there is also horizontal displacement at the base of the column (Figure 4b).

2) The southern column at the western facade is shear damaged due to the great displacement (there is no base displacement here, so the relative displacements are larger) – Figure 5.

3) There are cracks at the western facade half-wooden wall at the first floor. They correspond to the places of the timber frame elements. The in-plane deformation of the wall is obvious (Figure 6).

4) The southern stone masonry wall is inclined at its western end, while the eastern stone masonry wall is in good condition (Figure 7).

6) At the southern (lower) end of the yard some of the stone masonry retaining walls are heavily damaged, there are fallen handrails, inclined and cleaved stairs (Figure 8).


a) b)

Figure 4 Timber column at western facade: a) horizontal relative displacement; b) base displacement


a) b) c)

Figure 5 Timber column on western facade: a) general view; b) shear damage; c) column base.


a) b)

Figure 6 Cracks and in-plane deformation of half-wooden wall: a) outside; b) inside.

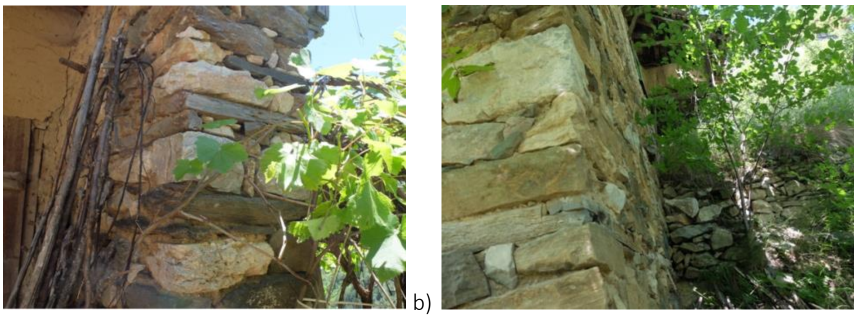
a) b)

Figure 7 Stone masonry walls: a) southern – inclined; b) eastern – in good condition.

a)  б) 

Figure 8 Southern end of the yard: a) heavily damaged retaining wall; b) inclined and cleaved stairs.

3.3. CONDITION ASSESSMENT

Based on the results from the visual inspection, the condition of the defected structural components is assessed in accordance with [4]. The results are shown in Table 2.

Table 2 Condition assessment of the house

structural component	importance of defect	intensity of defect	extend of defect	condition rating
stone masonry walls	critical	high	10-30%	Poor
timber columns	critical	high	30-70%	Bad
half-wooden walls	serious	middle	30-70%	Fair
retaining walls	critical	high	30-70%	Bad
stairs	serious	middle	30-70%	Fair

It may be concluded that, due to the changes in built and natural environment, lateral loads from earth pressure have increased and critical structural components are in bad condition, which means that remedial actions should be taken immediately. Steps should be taken towards the design of adequate rehabilitation of the house itself and the retaining walls on site. The addition of draining systems and reforesting may prevent future damages of the same type.

4. CONCLUSIONS

The condition assessment of a Post-Revival building from a mountain rural region in Bulgaria, presented in this paper, shows that sometimes the degradation of the existing old non-engineered structures and the construction materials is an effect of changes in the climate, the environment or the development of some contemporary infrastructure projects. Therefore, for the preservation of such buildings, it is necessary to:

- adjust modern infrastructure (roads, retaining walls) and new buildings in this regions to the design features of the traditional building – the height of new buildings should be limited, and the infrastructure changes should not affect critical elements and details of the existing buildings;
- react to the dynamic changes in environment – provide better draining systems in this regions, take steps to reforest regions where trees have become scares, etc.

The following general conclusions, concerning condition assessment, can also be made:

- The condition assessment is a powerful tool for evaluation of the real state of existing buildings.
- The service life prediction based on condition assessment is directly related to the sustainable development of existing buildings.
- Despite the results of the different assessment procedure and their accuracy, for the structural safety, a detailed structural analysis is mandatory.

REFERENCES

[1] rya, A., Boen, S., Ishiyama, Y.: *Guidelines for Earthquake Resistant Non-Engineered Construction*, United Nations Educational, Scientific and Cultural Organization, ISBN 978-92-3-000032-5, Paris, 2014

[2] Abbott, G.R.: Mc Duling, J.J.; Parsons, S.; Schoeman, J.C.: Building condition assessment: A performance evaluation tool towards sustainable asset management, Proceedings of CIB World Building Congress, Cape Town, South Africa, May 2007.

[3] Pedro, B., Paiva, V., Vilhena, A: Portugise method for building condition assessment, *Structural Survey*, Vol. 26, No. 4, 2008 pp. 322-335, ISSN: 0263-080X

[4] Straub, A: Dutch standard for condition assessment of buildings, *Structural Survey*, Vol. 27, No. 1, 2009 pp. 23-35, ISSN: 0263-080X

[5] http://www.stringmeteo.com, accessed 12.01.2017

ASSESSMENT AND PROPOSAL OF REPARATION OF EARTH DAM MESIC NEAR VRSAC

Goran Jeftenic[1], Slobodan Kolakovic[1], Milos Seslija[1], Srdan Kolakovic[1]

[1] University of Novi Sad Faculty of Technical Sciences, Department of Civil Engineering and Geodesy Sime Milosevica 12, 21 000 Novi Sad, Serbia, email: goran.jeftenic@uns.ac.rs, kolakovic.s@uns.ac.rs, sele@uns.ac.rs, kolak@uns.ac.rs

SUMMARY: There is a severe problem with entering and conducting external water through the city of Vršac primarily because of its inconvenient location, hydrologically speaking. With this in mind, an earth dam with outbuildings was built in the year of 1980. Thirty years after being built, changes which might have caused instability of the structure have occurred. These changes have been manifested in a form of damages of concrete structure as well as the appearance of sliding plane on downstream slope of the dam. This paper will show several activities including assessment of the dam and proposal of reparation measures with the goal of returning complete function of the structure i.e. defence against torrential waters.

OCJENJIVANJE I PRIJEDLOG POPRAVKA ZEMLJANE BRANE MESIĆ KRAJ VRŠCA

SAŽETAK: Prvenstveno zbog nepovoljne hidrološke lokacije postoji velik problem vođenja oborinske vode kroz grad Vršac. Stoga je godine 1980. izgrađena zemljana brana s pomoćnim građevinama. Trideset godina nakon gradnje pojavile su se promjene koje bi mogle prouzročiti nestabilnost konstrukcije. Te su se promjene očitovale u obliku oštećenja betonske konstrukcije i pojave klizne ravnine na nizvodnoj kosini brane. U radu je prikazano više aktivnosti uključujući ocjenjivanje brane i prijedlog popravnih mjera s ciljem da se konstrukciji vrati cjelovita funkcija tj. obrana od bujičnih voda.

1. INTRODUCTION

On the slopes of Vršac Hill, the city of Vršac is permanently confronted with surface waters which are, even with the lightest rainfall, pouring down the slopes of Vršac Hill and freely overflow the streets going to natural recipients of Mesić stream, Jovan stream, Malorit canal, Crni Jovan canal, Keveriš stream and Vršac canal, flooding the urban area as well as agricultural planes near the city.

Mesić stream springs below the Kulmea Mare summit and has a predominantly torrential character. Since its slope is steep, during rainfall and snowmelt, water level of the stream is very high in the matter of hours. The catchment area of Mesić stream has mainly mountainuous character and it belongs to a category of small torrential rivers.

The width of the trough and conditions dominating in it, have caused several floods in the city of Vršac by torrential water of Mesić stream. Recorder floods happened in 1941, 1942, 1946, 1954, 1956, 1975 and 1978, which were the cause of great material damage. Since the dam was built with belonging accumulation in 1980, there was no major flood activity in the city, therefore the dam proved its function. By regular inspection of the dam, possible process of sliding has been established in 2013. Sliding of defended slope could be very dangerous because the flood wave can cause breach of the dam itself [1-4]. This paper shows various damages of the dam and gives a proposal of its reparation.

2. BASIC CHARACTERISTICS OF MESIĆ DAM

Earth dam has been put on Mesić stream in 7+250 km. Its cross-section is homogenous with a maximum height of h= 6,68 meters. Width of the dam crest is B = 4,00 meters with inclinations of slopes: upstream 1:2,5, downstream 1:2,0. For the purpose of flood wave protection there was built a reinforced concrete wall with height of 1,00 meter on upstream inclination of the slope. Because of dam profile's heterogeneous surroundings, and because of the possibility of unfavourable impact of filtration through lentil below the foundation of Mesić dam on its stability, prevention of protruding water has been made through the lentil with a clay-concrete diaphragm.

Evacuation of heavy waters is performed by transverse reinforced concrete spillway, with the width of B = 9,00 m. For the purpose of draining the accumulation, bottom outlet was built Ø 800 mm. Based on structural elements of the dam, hydrological and hydraulic parameters and geometrical characteristics of upstream bottom land, the accumulation contains following elements:

- total volume of accumulation at normal level, at altitude of 108,30 m.a.A.s. is 700.000,00 m^3,
- total volume of accumulation at $Q_{1\%}$ water, at altitude of 109,52 m.a.A.s. is 1.250.000,00 m^3,
- total volume of accumulation at $Q_{0,1\%}$ water, at altitude of 110,02 m.a.A.s. is 1.515.000,00 m^3,
- altitude of normal level of backwater is: 108,30 m.a.A.s.,

- altitude of 100-years water level is: 109,52 m.a.A.s.,
- altitude of 1000-years water level is: 110,03 m.a.A.s.,
- transformed flood wave intensity $Q_{1\%}$ = 29,90m^3/sec,
- maximum flow for dimensioning the spillway = 47,00 m^3/sec,
- crest length of the dam L = 420,00 m,
- height of the dam h_{max} = 6,68 m,
- volume of earth dam with foundations VB = 40.252,00 m^3.

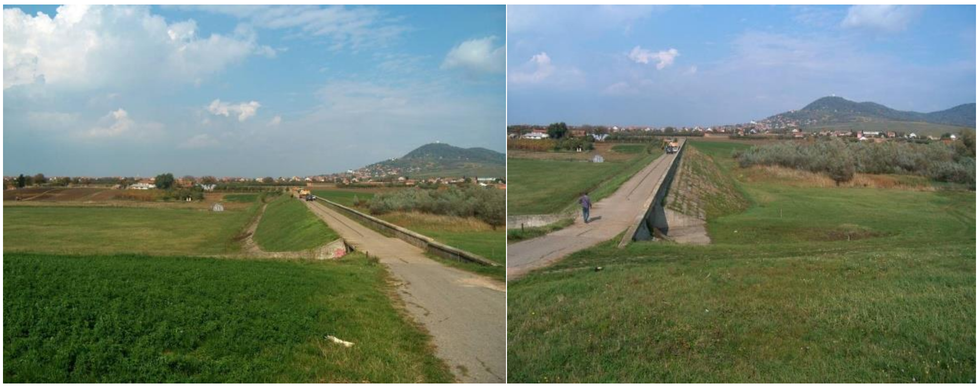

Figure 1 Upstream slope of the dam (left); downstream slope of the dam (right)

The dam is a part of Republic operational plan for flood defence. Dam with accumulation 'Mesić' on the Mesić stream belongs to a category of higher dams having in mind the volume of accumulative space for $Q_{0.1\%}$ over 1.500.000 m^3.

3. VISUAL INSPECTION

Visual inspection of the dam has established the presence of a large number of cracks on downstream slope. Damages on downstream slope occurred in relatively shallow surface area of the embankment from base of the crest, downstream to the rock cover which is placed in the pin area. The dam crest is protected by concrete plates which are cracked and settled toward downstream slope area of the dam. Damaged part with length of about 150 meters, is located between lateral spillway and bottom outlet. At the same location of the dam body, settlement of defended slope has been registered, as well as a large number of transverse cracking along cross-sections of soil fill of the dam that indicates possible appearance of a sliding plate all the way to the rock cover in the pit area. On the surface of downstream slope, damages are manifested as widespread net cracks. Considering the dam by length and height, the cracks repeat at every 2 - 5 meters, and are more or less visible. Generally speaking, cracking appears throughout the downstream slope, so the whole slope should be repaired, not just partial areas. Almost every crack has a cavity (Figure 2). Width of open parts of the cracking at the dam surface is usually between 2 - 5 cm, but locally may be even wider.

Figure 2 Cavities registered in downstream slope

Based on the aforementioned, it is concluded that for further investigation, performing excavation alongside of visible cracking is the most rational proceeding. To this end, there has been made an exploration pit 3.2 meters deep (Figure 3). Excavation has been done carefully with intermissions and detailed charting – examination of the pit from every side. Special attention and occasional cleaning of the slope is performed along visible cracks with cavities which were followed during the excavation.

Inside the deep excavation, it was established that the width of open part of the cracking decreases in depth and that cracks are 2,25 meters deep. It was clear that some cracks are sub-vertical, and others are arched, which implies a certain movement - sliding of embankment in 2,25 meters deep surface area. Design of the dam predicts an inclination value of the slope 1:2, and that rainwater flows uncontrollably from concrete plate in the crest to a humus slope. That uncontrolled water drainage is the main cause of the movement - sliding. These movements are also the reason of cracking and displacement of concrete plates (Figure 4). [5-6]

Figure 3 Exploration excavation

Figure 4 Damages of a concrete plate on the dam crest

By overview of the embedded clay soil in the dam body, it was found that embedded layers of clay soil appear in shades of yellow and red. After deformation - sliding, those layers in moving area are bent in some parts and mixed altogether. The deepest movement - sliding found is 2,25 meters deep (Figure 3). Shear cracks appear in this area. In the pin area of downstream slope, a cover made of large rocks was built in. According to geodetic measuring and visual overview, there was no deformation of the covered part of the dam. Therefore, it can be considered that the whole downstream slope (except for the part covered in rock in the pin) has embankment displacement depth of 1,5 – 2,5 meters.

Figure 5 Damages of concrete trough of the chute caused by uneven soil subsidence (left); and caused by pore pressure in the soil behind the cover (right)

Figure 6 Damages of the bottom outlet drain canal

4. PROPOSAL OF REPARATION

Although now there are shallow displacements along downstream slope which do not endanger stability of the dam, it does not necessarily mean that reparation activity will not be needed. Namely, damages of downstream slope are manifested as cracking in concrete plates which are embedded along the crest and as displacements of the shallow surface area of embankment. The cracking occurred partly due to overload by vehicle movement and partly due to deformation in the dam embankment. Also, wide cracks contribute to the flow of rainwater directly into them, more so jeopardizing dam's stability. If the cracks are not sealed and corresponding reparation activities of concrete structures are not done, it is certain that overall stability of the dam will be jeopardized.

Within this paper, two possibilities are proposed for reparation of negative occurrences on downstream slope. The first contains inclination value of downstream slope 1:2 with rock covering, and the second one excludes existing inclination of downstream slope i.e. considers softening of inclination by adding new soil mass.

First proposal includes activities with permanent removal of humus. After that, there should be removed and rebuilt displaced - sliding parts of the embedded dam. This would assure continuity and compactness of displaced soil mass on downstream slope. After that, slope should be covered with large rocks as it was done in the pin area of downstream slope. This part of the slope, now covered, along with the canal would be in good condition and would not require any intervention.

Removing of displaced soil mass would mean indentation of slope, directly above the existing covering rocks in width of about 2.5 meters. Removed material would be deposited closely so that it can be embedded in the finishing layers afterwards. After forming first horizontal indentation along the entire length of the dam, subsoil would be compacted and then, new indentation of displaced mass would be made, which would be embedded in horizontal layers 30 cm thick. It means that digging would secure the material for only one layer and that same layer would be compacted. New indentation 2,5 meters wide and 30 cm high, would be made for every layer until summit of the slope. Optimum moisture and compactness of the material would be measured during embedding layers of soil.

After part of embankment up to the crest is repaired, concrete plates should be reconstructed at the crest of embankment. Beside reconstruction of concrete plates, longitudinal collective concrete canal should be designed along the dam. From that canal, transverse channels would control the flow of rainwater, draining it to the flat area behind the dam. This kind of controlled flow of rainwater has not existed yet.

Second proposal includes groundwork on removing humus along the entire downstream slope and embedding new soil supports. Soil support basically means softening the inclination to 1:2,5 and it would demand removing displaced layers, bringing new clay materials from borrow pit and embedding it, and reconstruction of concrete plates in the crest and controlled flow of rainwater as it was mentioned in the first proposal.

First proposal is considered as more favourable because the second one implies embedding of relatively small soil mass and necessity for destruction of existing rock cover and canal in the pin of downstream slope.

5. CONCLUSION

The biggest isue of 'Mesić' dam is deformation, swelling of downstream slope followed by deep cracking. The cracks are wide enough (up to 5 cm) to collect all rainwater flowing from the crest and slope, thus causing softening of downstream slope down to a considerable depth. The cycles of drying and drenching will further widen the cracks and intensify process of degradation. Weakened and often drenched slope slides, causing settlement of downstream edge of the crest, inclination of concrete plates of crest cover and finally cracking.

Also a great isue is represented through damages of following concrete elements, structures of the dam. The connection of drain canal of bottom outlet with the lower weir is ruined. Bottom outlet is constantly opened, meaning that water flowing to accumulation is discharged without holding to the drain canal of bottom outlet without holding back. The canal is not covered with watertight material so important amount of water is absorbed in the right slope and the level of groundwater is kept high. That same water flows toward downstream trough of the stream Mesić. However, the cover of lower weir does not drain it from the ground making pore pressure higher i.e. increasing the load for undrained cover. By destruction of the cover, springing is intensified causing further retrograde erosion of unprotected slope.

Uncontrolled drain away of rainwater and inadequate draining of groundwater caused damages at the chute of safety spillway so severe, that longer part of lateral wall on the left side of chute is dislocated. Damage is considerable in concrete elements caused by frosting and differential subsidence. Due to neglection, vegetation is contributing to degradation process.

Considering everything mentioned above, conclusion is that current state of deformation and damages of downstream slope and the crest, as well as degradation of following structures does not allow safe filling of accumulation and therefore proposals of series of reparation measures are made, which would give the structure its full function - defence of the city of Vršac from torrential flood water.

ACKNOWLEDGEMENTS

The work reported in this paper is a part of the investigation within the research project TR 37003 "Development of hydro-information system for monitoring and early drought warning", supported by the Ministry for Science and Technology, Republic of Serbia. This support is gratefully acknowledged.

REFERENCES

[1] Pravilnik o tehničkom osmatranju visokih brana, Službeni list SFRJ br. 7, 1966.
[2] Pravilnik o sistematskom tehničkom osmatranju vodoprivrednih objekata, Sl. Gl. Srbije br. 53, 1983.
[3] Pravilnik o tehničkim normativima za seizmičko osmatranje visokih brana, Sl. list SFRJ br. 6, 1988.
[4] Pravilnik o sadržini i načinu osmatranja tla i objekta u toku građenja i upotrebe, Službeni glasnik RS, br. 13, str. 296, 1998.
[5] Srđan Kolaković, Kritika objekata za evakuaciju velikih voda u Vojvodini i predlozi za buduća rešenja, Doktorska disertacija, Univerzitet u Novom Sadu, Građevinski fakultet, Subotica, 1993.
[6] Uputstva i smernice za unifikaciju tehničke dokumentacije za osmatranje i ocenu stanja osmatranja i bezbednosti visokih brana, Institut za vodoprivredu "Jaroslav Černi", RJ Zavod za konstrukcije i geotehniku, Beograd, 1996.

DURABILITY OF CEMENT-BASED MATERIALS IN DRINKING WATER STORAGE - TOWARDS AN INTEGRAL PERFORMANCE ASSESSMENT

Matthias Schwotzer[1], Jens Heinrichs[2], Monjur ul Islam[2], Vincenzo Perugini[3], Andreas Gerdes[1,2]

[1] Karlsruhe Institute of Technology (KIT), Institute of Functional Interfaces, Hermann-von-Helmholtz-Platz 1, D-76344 Eggenstein-Leopoldshafen, Germany, email: matthias.schwotzer@kit.edu, andreas.gerdes@kit.edu
[2] University of Applied Sciences Karlsruhe, Institute for Prevention in Construction, Moltkestr. 30, D-76133 Karlsruhe, Germany, email: jens.heinrichs@partner.kit.edu, monjur.islam@partner.kit.edu
[3] University of Camerino, Geology Division, Via Gentile III Da Varano, I-62032 Camerino, Italy, email: vincenzoperugini.phd@gmail.com

SUMMARY: In order to promote a sustainable development in construction, a significant increase of the durability of cement-based materials is mandatory, resulting in a reduction of the total life cycle costs. To improve the materials and adjust their properties to the requirements, a detailed understanding of the damaging reactions is just as necessary as sophisticated methods to assess the performance of the materials. This contribution evaluates the applicability of an accelerated degradation test that takes advantage of the impact of electrical fields on the stability of cement-based materials in permanent contact to aqueous environments. Laboratory experiments show, that such tests are suitable to compare the resilience against reactive transport processes of materials and to draw conclusions regarding their performance. In this context, it is essential to investigate material changes in terms of depth and time. This approach appears suitable for performance assessment in material development as well as for quality control in practice.

TRAJNOST MATERIJALA NA OSNOVI CEMENTA U SPREMNICIMA PITKE VODE - INTEGRALNI PRISTUP OCJENI SVOJSTAVA

SAŽETAK: Za promicanje održivog razvoja u gradnji obvezno je znatno povećanje trajnosti materijala na osnovi cementa što dovodi do smanjenja troškova ukupnog životnog vijeka. Da bi se materijali poboljšali, a njihova svojstva prilagodila zahtjevima nužni su detaljno poznavanje procesa oštećivanja i usavršene metode ocjene svojstava materijala. U radu se ocjenjuje primjenjivost ubrzanog ispitivanja degradacije s pomoću djelovanja električnih polja na stabilnost materijala na osnovi cementa koji su u stalnom dodiru s vodom. Laboratorijski pokusi pokazuju da su takva ispitivanja prikladna za usporedbu otpornosti na procese reaktivnog transporta materijala i donošenje zaključaka o njihovim svojstvima. U tom smislu bitno je istražiti promjene materijala po dubini i tijekom vremena. Taj se pristup čini prikladnim za ocjenu svojstava pri razvoju materijala i kontrolu kvalitete u praksi.

1. INTRODUCTION

The continued performance of infrastructure is of utmost importance for continued societal development. Nonetheless, the condition of the technical infrastructure is far from perfect. In this regard, major attention has to be paid to the durability of cement-based materials, as concrete is, by far, the most widely used infrastructure material. In their various application fields, cement-based materials are subject to a number of environmental and operational loads. Especially, the detrimental impact of aggressive aqueous environments on the stability of cementitious systems is among the most important factors that affect durability. Resulting damages lead to n cost intensive repair measures as well as increased life-cycle costs and are further associated with an ecological burden. Apparent examples are concrete structures of the transport infrastructure exposed to the impact of de-icing agents or offshore buildings and wastewater treatment plants that are permanently exposed obviously harsh aqueous environments. In such cases, chemical attacks can endanger the continued functionality by means of structural damages. However, in the case of the drinking water supply infrastructure, the distinguishing features of the functionality are more differentiated, as e.g. surface properties of the materials determine the performance regarding hygienic aspects in water storage. Thus, drinking water reservoirs have been coated with mineral mortar linings in all epochs of European history, in order to promote a hygienic water storage. Nowadays, due to their high alkaline characteristics, cement-based materials are commonly considered as most suitable for this purpose. They are frequently used because flat "easy-to-clean" surfaces showing a low biorecepitvity can be produced with them. Furthermore, they are used to provide an efficient sealing of the concrete structures, e.g. in repair measures. As tap water is commonly not considered particularly harmful for cement-based materials [1], concerns regarding the durability of these systems were not present in the past decades. Thus, only minor attention has been payed to the material performance of such mortar linings. As a result since the 1990ies, a noteworthy number of cases has been reported in which "modern" cement-based materials, subjected to the special operational environment of tap water storage, showed an inadequate durability (e.g. [2, 3]). The material degradation showed up particularly unusual damage symptoms and was denoted as hydrolytic corrosion (e.g. [4]). The hydrolytic corrosion becomes visible by coloured spots (Figure 1a). In these areas, the cementitious binder is completely disintegrated (Figure 1b). This chemical degradation is featured by an extensive depletion of the $Ca(OH)_2$-inventory concomitant to a significant increase of the $CaCO_3$-content (Figure 1c) and an attack on the C-S-H phases. The velocity of this reaction is remarkably high. In some cases, the degradation reaches a depth of several mm after a service life of a few months.

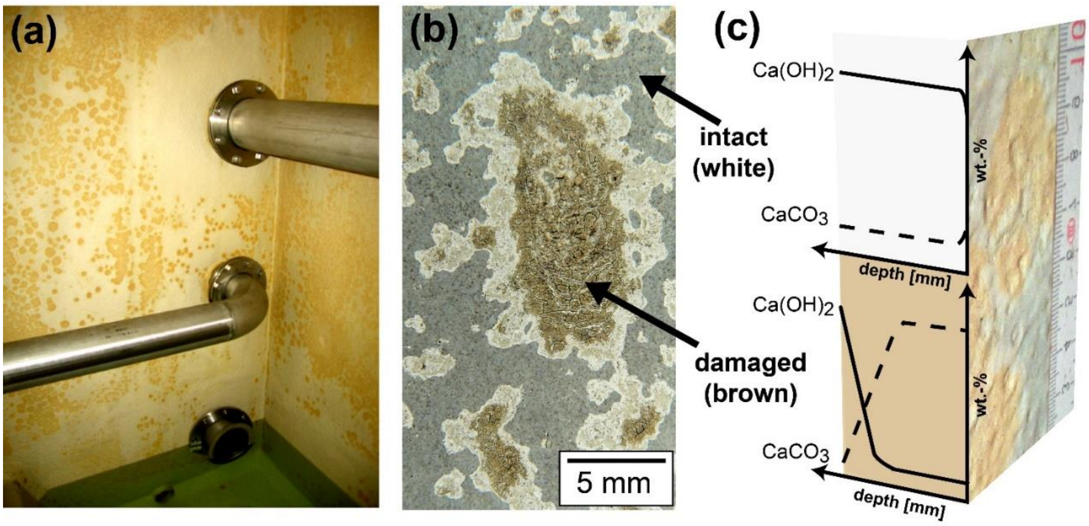

Figure 1 Characteristic appearance of the hydrolytic corrosion on the wall of a tap water reservoir showing up as coloured areas (a), with a strictly local manifestation of a degradation of the binder (b), and resulting in significant chemical and mineralogical changes (c)

The fundamental reaction mechanism was recently elucidated, comprehending it as a two-step reaction [5]. The process starts with an initial damage resulting from the impact of condensate on the materials surface at a young material age. It is followed by an extensive degradation due to an “underwater carbonation” resulting from a permanent exposure to tap water during the operational phase of the tap water reservoir. Generally, the fundamentals of the hydrolytic corrosion are transport processes of dissolved ionic species, resulting in changes of the chemical equilibria between the solid phases and the pore solution. This is commonly referred to as reactive transport [6]. Particularly in this case, a wide range of characteristics of the use scenario has been investigated regarding their potential impact on the deterioration process. Among them topics such as the influence of electrical effects present on the reinforcement and stainless steel installations in the reservoirs [4] and the relevance of microbiological activities for the material degradation have been discussed [7]. These manifold aspects are suspected to contribute to reactive transport processes and therefore promote deterioration processes. To cope with this issue in practise the design of more durable materials and application techniques is mandatory. For this, performance-oriented approaches are essential to improve durability. Indeed, a comprehensive understanding of the load scenario including the underlying physical, chemical as well as biological processes has to be targeted by fundamental research. However, just as important is applied research focussing on a reliable assessment of the material performance. In this context, it is the aim of this study to investigate and establish an adequate methodology to characterize the resilience of cement-based materials against reactive transport processes and therefore aggressive aqueous environments. This test takes advantage of the accelerating impact of electrical fields on material degradation due to reactive transport processes (e.g. [8]). This approach appears admissible, because the causes for the chemical stresses, which the cement-based materials in tap water storage have to withstand (e.g. the hydrolytic corrosion), are essentially reactive transport processes. Such accelerated degradation tests were investigated in the past decades in order to study the long-term behaviour of cement-based materials (e.g. [9, 10]). Thus, this study will provide proof of concept of a performance assessment by means of a comparative study adapting such an accelerated degradation test. In this regard, the impact of the electrical fields on the chemical composition and relevant material properties as porosity and pore size distribution was investigated. In particular, a monitoring of the material changes as a function of depth and time-resolved over the duration of the experimental procedure was integrated. In order to investigate the applicability, mortar samples differing in the water/cement ratio (w/c) and, therefore, in the porosity and pore size distribution, have been subjected to this testing procedure. This contribution presents selected results from this research activity.

2. MATERIALS AND METHODS

2.1. EXPERIMENTAL SETUP

The experimental setup for the accelerated degradation test is schematically shown in Figure 2. The test chamber consisted of two polyvinyl chloride (PVC) tubes, capped with PVC disks. A PVC disk placed in the centre of the setup is dividing the two tubes in separate chambers. The mortar sample is placed in a hollow cylinder with a diameter of 9 cm in this middle disk, pasting it into the PCV frame using a silicone adhesive compound. Water of two different supply cycles flows through the two separated chambers in order to simulate the continuous exchange of water in a tap water reservoir. The outer capping disk is equipped with a feedthrough for electrodes. In each of the chambers, stainless steel electrodes are located equidistant (4 cm) to the surface of the mortar sample. The electrode setup is comparable to parallel-plate capacitor. A constant d.c. voltage is applied to the electrodes by an electronically controlled voltage supply system.

The mortar samples were prepared using a commercially available dry mix mortar based on white Portland cement with carbonate and quartz aggregates, containing as well a minor amount of silica fume. The samples were prepared applying w/c ratios of 0.43 and 0.52, respectively. After an initial curing for one day with a plastic foil, the samples were demolded and stored for further curing for 28 days in hard tap water (17°dH). Cores with a diameter of 90 mm were drilled from the slabs, adapted to be introduced in the middle PVC-frame of the test chambers.

The mortar samples were exposed to a continuous flow of hard tap water over a time period of 70 days. Samples were taken after 28 days and 70 days from the cathode side of the mortar disk. The samples were cut in mm steps by means of a precision saw. The experiment was conducted in two different modes, one with an applied d.c. voltage of 5 V, another without a connection to the voltage supply (0 V).

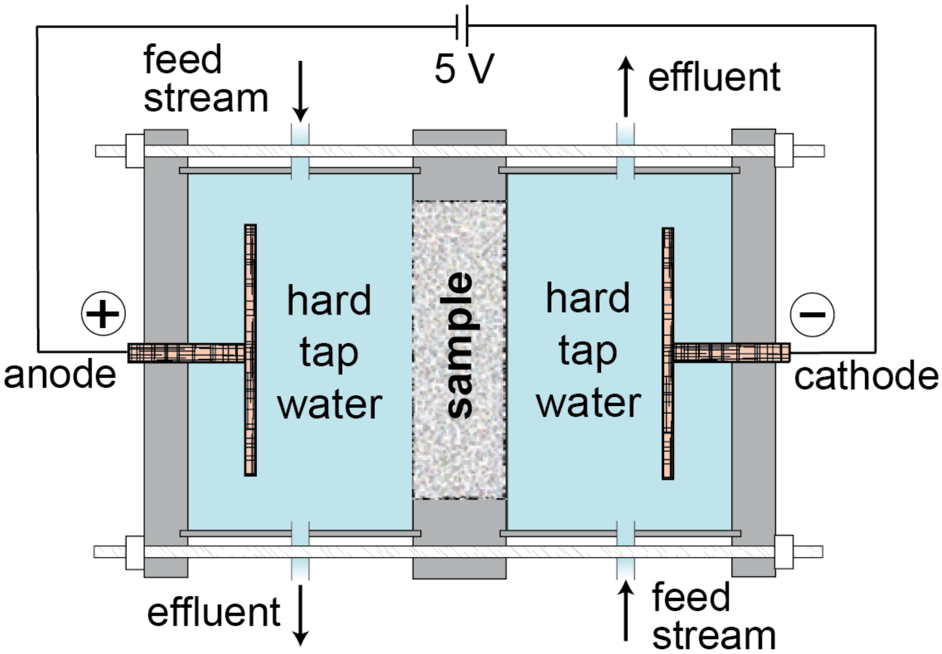

Figure 2 Schematic representation of the experimental setup

2.2. ANALYTICAL METHODS

The thermogravimetric determination of the $Ca(OH)_2$ content was performed with a TGA/SDTA 851 system from Mettler-Toledo applying a heating rate of 10°C/min under a N_2 atmosphere. The investigation of the total porosity and pore size distribution were done using Mercury intrusion porosimetry (MIP), using a combination of POROTEC Pascal 140 and Pascal 440 machines. The samples were dried for 48 hours at 50°C and measured up to a maximum pressure of 200 MPa.

3. RESULTS AND DISCUSSION

Aiming at a reduction of life-cycle costs of our water supply infrastructure, an improved durability appears to be mandatory. In particular, the recent increase of problems regarding the durability of cement-based mortar linings in tap water storage and distribution systems generates a need for action. In this context, performance oriented material developments as well as tools for quality control can contribute to a sustainable development. For this purpose, a reliable assessment of the performance of cement-based materials is essential. As the hydrolytic corrosion is causes by reactive transport processes, an accelerated degradation triggered by the impact of electrical fields represents a plausible approach for the evaluation the resilience of cement-based systems [11], in particular as the presence of electrical fields is supposedly associated with the evolution of the damage in practise [2, 4, 12]. However, this concept was mainly applied to characterize leaching processes in demineralized water as reported in [13]. Thus, in view of a performance testing, the impact of the operational environment has to be addressed by a customized experimental setup. Therefore, the exposure tests have been performed with hard tap water, creating a chemical scenario in which the hydrolytic corrosion was mostly observed in practise. The results of the determination of the $Ca(OH)_2$ content as a function of depth after 28 and 70 days exposure to hard tap water in the electrical-field-test-cells are shown in Figure 3. In the test setup without the impact of an electrical field (0 V), almost all measurements show no significant difference compared to the reference (Figure 3a and 3c). Only the mortar with the high w/c ratio showed after 70 days a slight decrease of the $Ca(OH)_2$ content (Figure 3c). In contrast to this, the exposure to 5 V leads to an extensive decrease of the $Ca(OH)_2$ content for both mortar samples. This illustrates clearly, that the impact of the reactive transport triggered by the electrical field is advancing over time from the material surface into deeper areas. The test reveals clearly, that the mortar with the lower w/c ratio appears definitely more robust against reactive transport processes due to a less extensive depletion of $Ca(OH)_2$ over time.

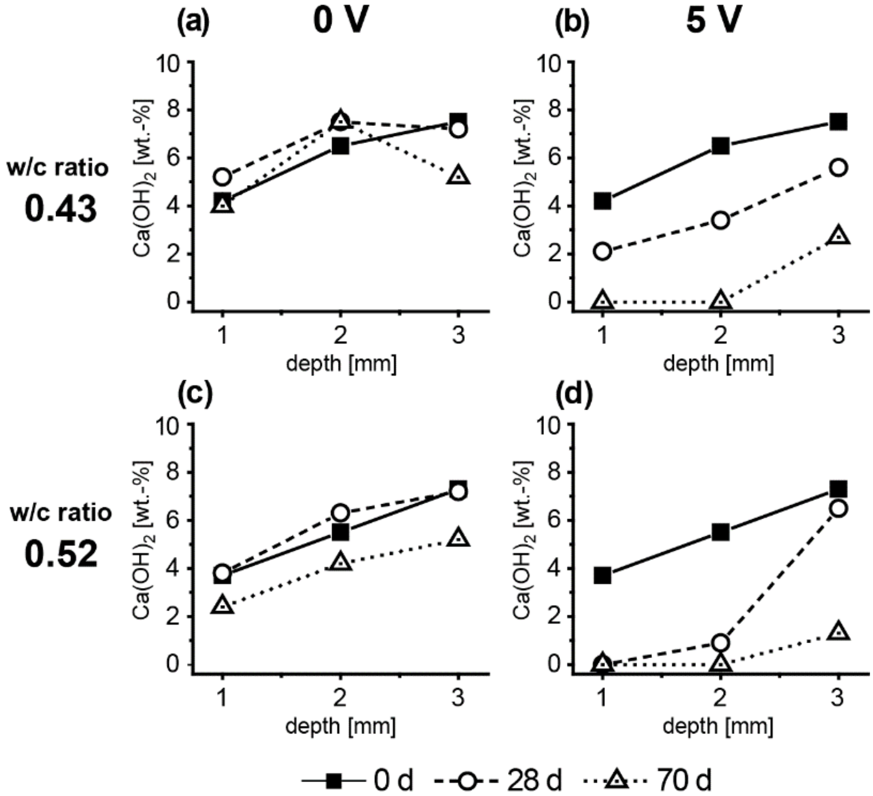

Figure 3 $Ca(OH)_2$ content after 28 and 70 days as a function of depth for the mortar samples prepared with a w/c ratio of 0.43 and 0.52, respectively; without the impact of an electrical field (left) and with 5 V (right)

The investigation of the pore structure over time underpins these observations. Table 1 compiles the results of the determination of the total porosity of both mortar samples. As expected, the values for the total porosity of the mortar with a w/c ratio of 0.43 is significantly lower than the porosity of the mortar with w/c ratio of 0.52. The exposure in the testing cells without an applied tension (0 V) shows only a slight increase of the total porosity. In contrast to this, the exposure to hard tap water under the influence of 5 V causes a distinct increase of porosity, concomitant to the extensive depletion of $Ca(OH)_2$. This process proceeds significantly faster in the less dense material prepared with a w/c ratio of 0.52.

Table 1 Results of the determination of the total porosity based on MIP measurements

w/c ratio	depth [mm]	**reference** (0 days) porosity [vol.-%]	**0 V** (70 days) porosity [vol.-%]	**5 V** (70 days) porosity [vol.-%]
0.43	1	10.7	13.9	24.9
	2	12	9.4	16.4
	3	10.4	13.2	11.6
0.52	1	8.1	12.3	27.4
	2	14.5	15.8	20.4
	3	16.3	14.1	15.2

This is confirmed by the examination of the related pore size distributions (Figure 4). Confronting the results of the reference (Figure 4a and b) with the 70-day-results without an applied voltage (Figure 4b and e), it appears that pore size distribution remains comparable for both mortars. However, the results for pore size distributions of the experiment with an applied voltage of 5 V (70 days) reveal a significant increase of capillary pores, that must be attributed to the disappearance of $Ca(OH)_2$ as stated in literature [14]. Furthermore, a significant impact on the gel pore system (pores<0,03 µm) became apparent (Figure 4c and f). This is supposed to be the result of an attack on the C-S-H gel decreasing the Ca/Si ratio, as suggested in literature [15]. Again, it can be seen that the process for the material prepared with a w/c ratio of 0.52 has advanced much further compared to the other material (w/c ratio 0.43) after a test duration of 0 days. The impact on the µ-structure in the experiment performed with the denser mortar (w/c ratio 0.43) after 70 days only the first mm was affected (Figure 4c), whereas the mortar with the w/c ratio of 0.52 shows already significant changes in the second mm (Figure 4f).

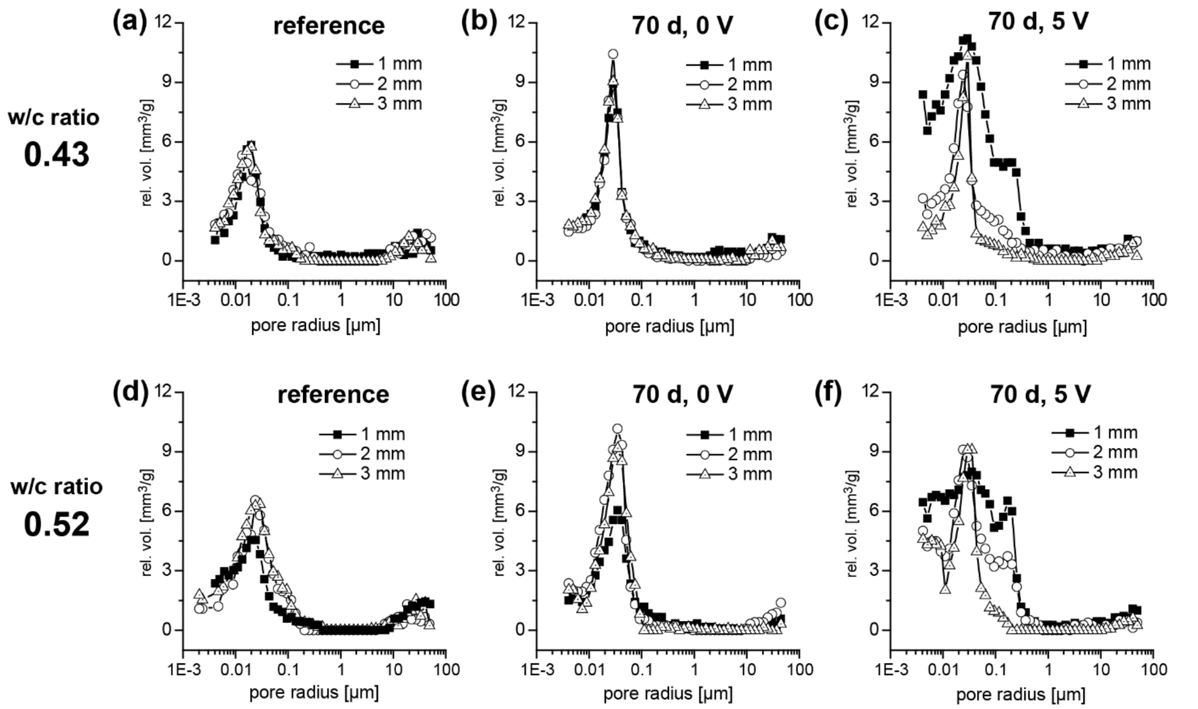

Figure 4 Depth profile of the pore size distributions for the mortar samples with a w/c ratio of 0.43 and 0.52 of the reference sample (a) and (d), exposed for 70 days without the impact of an electrical field (b) and (e), and exposed to a potential difference of 5 V (c) and (f)

Thus, the results of this study show, that an accelerated degradation of cement-based materials by the application of electrical fields allows a comparison between different cement-based materials, subjected to the impact of tap water, regarding their resilience against reactive transport processes. Therefore, an accelerated degradation test, as described in this study, appears as a promising tool for the performance assessment in particular for operational load scenarios, as present in the water supply infrastructure.

4. CONCLUSIONS

In order to contribute to a sustainable development in construction, a reduction of the total life cycle cost by means of an increased durability is mandatory. Indeed, a sophisticated requirement analysis for construction materials, addressing all the relevant load scenarios in detail, defines the destination route for performance-oriented innovations. However, the counterpart in this context is a reliable test procedure to confirm the performance of a material, e.g. in terms of resilience against chemical attacks by reactive transport processes. The results of this study show that an accelerated degradation test by means of electrical fields provides a valuable tool to perform a comparative assessment of the resilience of cement-based materials against reactive transport processes, in particular regarding the specific load scenarios that cement-based materials have to withstand during their use in tap water supply infrastructure. For an evaluation of the performance of materials with different properties, it is essential to investigate the impact of aggressive environments as a function of depth over time. Moreover, as the properties of the cement-based materials, and thus their resilience against chemical attacks, mostly develop after the application on the construction site, appropriate quality control concepts are needed in practise. Also in this context, an accelerated degradation tests may represent promising approaches.

REFERENCES

[1] DIN 4030-1:2008-06, Assessment of water, soil and gases for their aggressiveness to concrete - Part 1: Principles and limiting values, *in German*, (2008)

[2] Gerdes, A. & Wittmann, F. H.: Electrochemical Degradation of Cementitious Materials, Proceedings of the 9th International Congress on the Chemistry of Cement, New Delhi, (1992)

[3] Schwotzer, M. & Gerdes, A.: Durability of cement based materials in contact with drinking water, RILEM Proceedings PRO 60, Concrete in Aggressive Aqueous Environments - Performance, Testing, and Modeling, Alexander, M. G. & Bertron, A. (Eds.), Toulouse, France, pp. 125–132, 2009

[4] Wittmann, F. H.: Corrosion of Cement-Based Materials under the Influence of an Electric Field, *Mater. Sci. Forum,* Vol. 247, pp. 107–126, (1997)

[5] Schwotzer, M. et al.: Protective or damage promoting effect of calcium carbonate layers on the surface of cement based materials in aqueous environments, *Cem. Concr. Res.*,Vol. 40, No. 9, pp. 1410-1418, (2010)

[6] Moranville, M. et al.: Physicochemical equilibria of cement-based materials in aggressive environments -experiment and modeling, *Cem. Concr. Res.*, Vol. 34, No. 9, pp. 1569-1578, (2004)

[7] Herb, S.: Biofilmbildung auf mineralischen Oberflächen in Trinkwasserbehältern, *Berichte aus Wassergüte- und Abfallwirtschaft*, Vol. 149, Technical University Munich, Germany, PhD thesis, *in German*, (1999)

[8] Castellote, M. et al.: Synchrotron Radiation Diffraction Study of the Microstructure Changes in Cement Paste due to Accelerated Leaching by Application of Electrical Fields, *J. Am. Ceram. Soc.*, Vol. 85, No. 3, pp. 631-635, (2002)

[9] Faucon, P. et al.: Water attack of a cement paste: towards an improved accelerated test?, *Adv. Cem. Res.*, Vol. 10, No. 2, pp. 67-73, (1998)

[10] Saito, H. & Deguchi, A.: Leaching tests on different mortars using accelerated electrochemical method, *Cem. Concr. Res.*, Vol. 30. No. 11, pp. 1815-1825, (2000)

[11] Castellote, M. et al.: Accelerated leaching of ultra high performance concretes by application of electrical fields to simulate their natural degradation. *Mater. Struct.*, Vol. 36, No. 2, pp. 81-90, (2003)

[12] Wittmann, F. H. & Gerdes, A.: Beständigkeit zementgebundener Beschichtungen unter dem Einfluss elektrischer Felder, *Int. Z. Bauinstandsetzen*, Vol. 1, pp. 73-86, *in German*, (1995)

[13] Castellote, M.: Tests for Leaching and Degradation in Soft or Carbonated Waters. Performance of Cement-Based Materials in Aggressive Aqueous Environments, Alexander, M., Bertron, A. and Belie, N. D., (Eds.), RILEM State-of-the-Art Reports; Springer Netherlands, pp. 235-250, (2013)

[14] Haga, K. et al.: Change in pore structure and composition of hardened cement paste during the process of dissolution, *Cem. Concr. Res.*, Vol. 35, No. 5, pp. 943-950 (2005)

[15] Thomas, J. J. et al.: Effects of decalcification on the microstructure and surface area of cement and tricalcium silicate pastes, *Cem. Concr. Res.*, Vol. 34, No. 12, pp. 2297-2307, (2004)

MASONRY STRUCTURE OF CHURCH IN RUMA - PART 1: THE ASSESSMENT

Vlastimir Radonjanin[1], Mirjana Malesev[1], Ivan Lukic[1], Slobodan Supic[1], Suzana Draganic[1]

[1] University of Novi Sad Faculty of Technical Sciences, Department of Civil Engineering and Geodesy, Sime Miloševića 12, 21 000 Novi Sad, Serbia, email: radonv@uns.ac.rs, miram@uns.ac.rs, lookic@uns.ac.rs, ssupic@uns.ac.rs, suzanav@uns.ac.rs

SUMMARY: Repair of church buildings could be a complicated task, as historic structures were often built using quite different building materials and techniques comparing to modern construction. The paper presents the assessment of masonry structure of the church in Ruma (Serbia), built in the first half of the XIX century. Based on a detailed visual inspection of the church, identification and classification of all defects and damages of the structure, and taking into account the long-term monitoring of cracks development and behaviour of the building, it was concluded that the global and local stability of the structure are jeopardized, as well as its load-bearing capacity. Durability of the building is particularly jeopardized, especially considering the importance of the protection of cultural treasures and ornaments, whose further deterioration should be prevented. In order to prevent further progression of damages, it is necessary to take appropriate repair measures. The urgency of performing repair measures is even greater, as the church represents the building of a great cultural significance, since the interior was painted by Uros Predic, one of the most important Serbian painters.

ZIDANA KONSTRUKCIJA CRKVE U RUMI - PRVI DIO: OCJENJIVANJE STANJA

SAŽETAK: Popravak crkvenih zgrada može biti složen zadatak jer su povijesne konstrukcije često građene upotrebom vrlo različitih građevnih materijala i tehnika u usporedbi sa suvremenim građevinama. U radu se prikazuje ocjenjivanje stanja zidane konstrukcije crkve u Rumi (Srbija) građene u prvoj polovini 19. stoljeća. Na osnovi detaljnog vizualnog pregleda crkve, prepoznavanja i razredbe svih nedostataka i oštećenja konstrukcije, uzimajući u obzir dugoročno opažanje razvoja pukotina i ponašanja zgrade zaključeno je da je ugrožena globalna i lokalna stabilnost konstrukcije i njezina nosivost. Posebno je ugrožena trajnost zgrade naročito uzimajući u obzir važnost zaštite kulturnoga blaga i ornamenata čiju daljnju degradaciju treba spriječiti. Kako bi se spriječilo daljnje napredovanje oštećenja nužno je poduzeti odgovarajuće mjere popravka. Hitnost provedbe mjera popravka tim je veća što zgrada crkve ima veliko kulturno značenje jer je unutrašnjost oslikao Uroš Predić, jedan od najvažnijih srpskih slikara.

1. INTRODUCTION

Church buildings are invaluable historical resources, with some standing as the best examples of our architectural achievements. The rich and varied contribution that churches make to society, from offering counselling and training for vulnerable social groups, to providing opportunities for volunteer work and employment, means ensuring their survival is of real importance [1].

Historic churches were often built using quite different building materials and techniques to modern construction. This has implications for the way that the building works and how the maintenance needs to be carried out. Most historic buildings have changed over time. Understanding the different stages in development can help to explain why some problems arise, like cracking at the joint between old and new building segments.

This paper presents the assessment of masonry structure of the church in Ruma (Serbia), built in the first half of the XIX century. Within the assessment, a detailed visual inspection of the church was carried out, long-term monitoring of cracks development and the behaviour of the building was conducted and the conclusion about condition of the structure, in terms of load-bearing capacity, stability, durability and functionality, was provided.

2. BASIC DATA ON THE BUILDING

The Church of the Descent of the Holy Spirit in Ruma (also known as the Greek Church), was built in the first half of the XIX century. It was built as a one-nave building with a semi-circular altar apse on the east and the tall, dominant bell tower on the west side. Below the altar, there is a circular tomb that was subsequently built, and the entrance to the tomb is constructed as a separate building with a semi-circular wall. The rich facade decoration is made up of shallow pilasters that emphasize the vertical division, stepped recessed semi-circular niche and emphasized zone of attic wreath along the whole Church. A representative western facade is highlighted by massive doubled columns surmounted by a tympanum, a high gables wall and the Art Nouveau hat shaped bell tower (designed by Herman Bole). Plan view and cross section of the church structure are presented in Figures 1 and 2. Appearances of the church are shown in Figures 3-5.

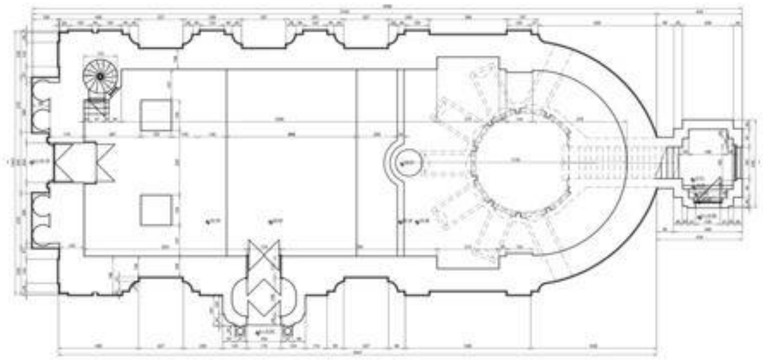

Figure 1 Plan view of the church structure

Figure 2 Cross section of the church structure

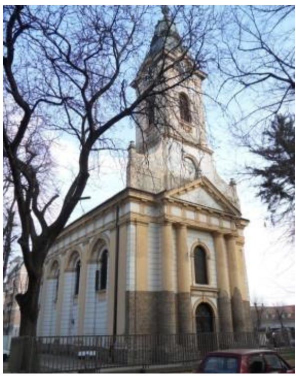

Figure 3 Western and northern façade of the church

Figure 4 The entrance to the tomb on the east side of the church

Figure 5 Southern façade of the church

The church was constructed as rectangular shape masonry structure with dimensions 14x36m in basis. The ceiling height of the ceiling structure is 12m, while the height of the bell tower is 39m. The vault is supported on arches with a width of 120 cm and variable height. Original tie-rods system was constructed with angled tie-rods where roof structure took on horizontal thrust of the arches. During the previous works on the repair (50-ies of the last century), this system was replaced by a similar one, whereby, instead of the roof structure, ties were hanging on a steel hot rolled "I" beam (Figure 6). The walls are of varying thickness. At the place of pilasters, thickness is 196cm, in parts between the pilasters 100cm, while the walls under the windows in part of the altar (which were removed during the construction of the crypt and later rebuilt) have a thickness of 45cm. The crypt extends to a depth of 3.5m below the ground surface [3].

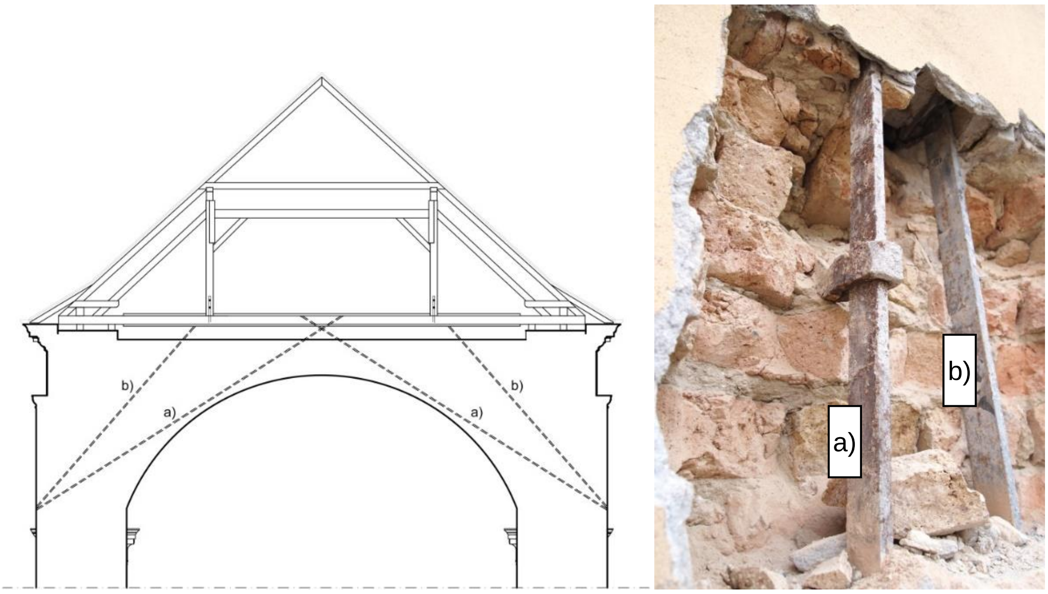

a) original tie system
b) second tie system (around 1950's)
Figure 6 Tie-rod system: a) original; b) “New” system, added around 1950’s

3. VISUAL INSPECTION

Detailed visual inspection of the church structure was carried out on several occasions in 2012 and 2013. Visual inspection revealed typical damages for this type of massive buildings. Along the entire buildings perimeter, 15 years ago, mortar was removed of the facades for the purpose of faster drying of the building after the winter. This measure was meant to be short term, however, the building is bare and exposed up to today. This has significantly contributed to the deterioration of the church, as the exposure to weathering of external facade was increased. Moisture and frost primarily affected the reduction of mechanical properties of materials. Inadequate performance of drip channel, as well as the drainage of precipitation from the building have also contributed to this building's condition. Figure 7 provides an overview of typical damages of the church facade.

The characteristic damages, registered on the inner surfaces of the walls are: spalling and falling of mortar, crumbling of damaged bricks, cracks and fissures in mortar and walls (especially in the areas of arches and openings), settlement of foundations under the pillars of the tower, mechanical damages and traces of soot. Some of the damages are presented in Figures 8-11. Registered defects include: stone crumbling, inadequately executed drip channel and inadequately executed vertical construction joints.

Substantial damages were noticed on the structural elements in the interior of the crypt: spalling and falling of mortar off the ventilation window walls due to moisture (Figure 12), de-levelling of floor slabs in the zone along the wall, as a result of settlement of the foundation (Figure 13), spalling and falling of layers of colour (Figure 14).

Table 1 provides data on the percentage assessment of the damages and defects of the church facades.

Table 1 Percentage assessment of the damages and defects of church facades

Description of defects	Affectred surface [%]			
	W	S	E	N
Stone crumbling	-	-	2	-
Inadequately executed drip channel	10	10	10	10
Inadequately executed vertical construction joints	-	5	-	10
Description of damages	Affectred surface [%]			
Colour change of the final layer	50	5	15	40
Traces of chatchment	20	15	30	20
Spalling and falling of coating - colour	10	10	10	10
Spalling and falling of mortar	10	20	10	10
Deterioration and crumbling of the surface layer of bricks	15	40	20	5
Loss of materials (brick, binder from the joints)	5	5	5	5
Cracks and fissures	-	15	1	5
Corrosion of steel beam	-	-	1	-
Net-like fissures	20	5	5	10

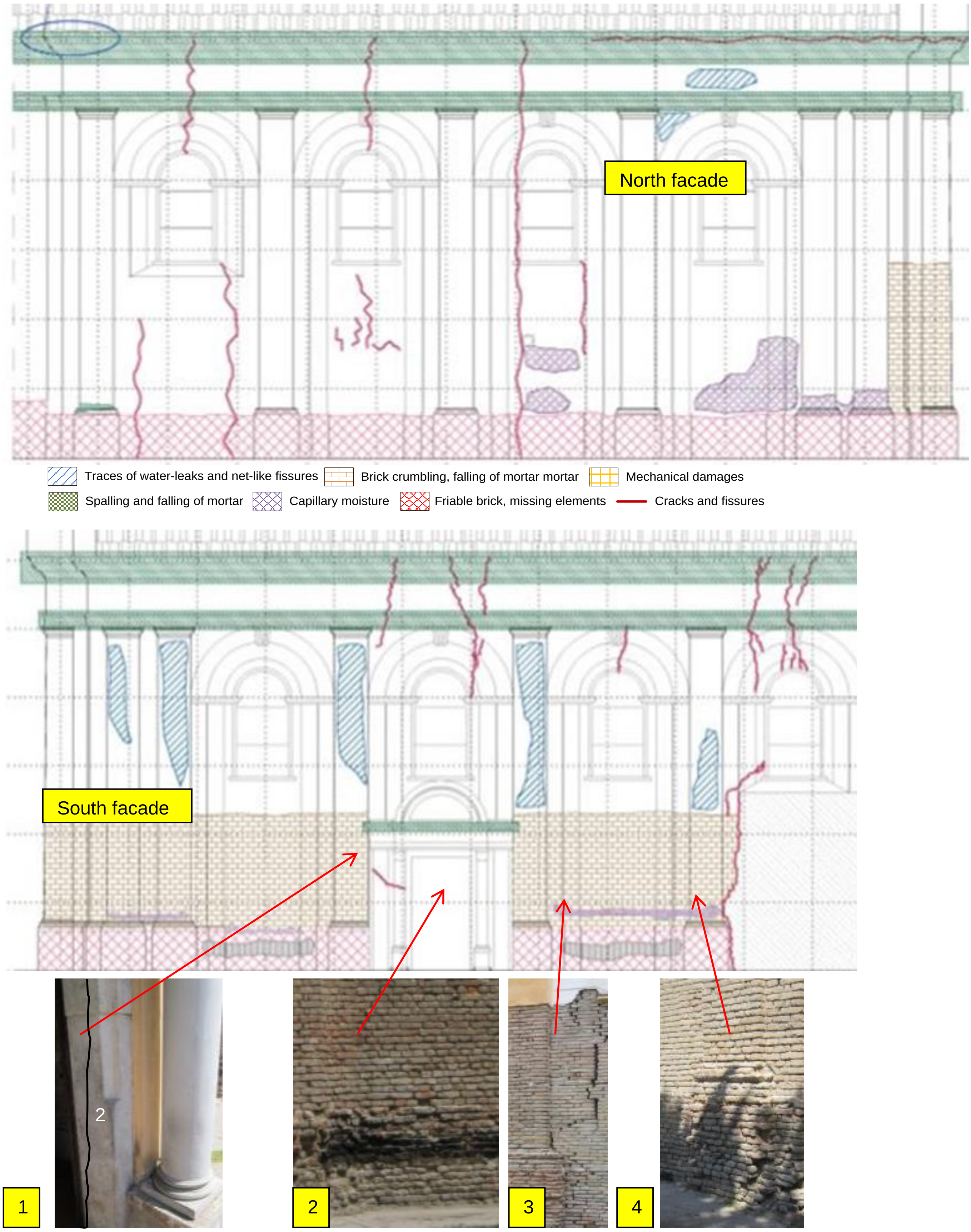

Figure 7 Schematic view of damages of north and south façade, details: 1) Vertical crack throughout the height of pillars due to incompatibility of materials, 2) traces of soot as a result of burning candles, 3) vertical crack widths of up to 3cm caused

by improper construction joints between the old building and the new wall, 4) friability of materials, spalling of the surface layer of bricks, missing brick elements, crumbling of mortar from the joints

Figure 8 Position of characteristic cracks on the external surface of north façade, after chiselling

Figure 9 Position of characteristic cracks on the internal surface of north façade, after chiselling

Figure 10 Settlement of foundations under the pillars of the tower

Figure 11 Cracks in the areas of arches and openings

Visual inspection of the roof structure revealed significant deformation of the roof laths, rafters, as well as the individual purlins, which is the result of a large axial distance between the rafters (90-110cm) and a space between the roof trusses that are larger than usual for this type of roof structure. Also, cracking was observed due to material drying on most of rafters and purlins, as well as the decay of certain elements due to poorly executed roof flashings (Figures 15-17).

Figure 12: Spalling of mortar due to moisture penetration

Figure 13: De-leveling of floor slab due to soil settlement

Figure 14: Spalling and falling of layers of colour

Figure 15: Supporting zone - visible deformation of the roof laths, decayed and fractured rafter

Figure 16: Detail of node binder: cracked roof structure

Figure 17: Detail of the connection of the central post of hangers to the ceiling joist, original tie-rods in the vault of the apse and the new "I" profile of "new" tie-rods

4. CONCLUSIONS

Based on a detailed visual inspection of the church, identification and classification of all defects and damages of the structure, and taking into account the long-term monitoring of cracks development and behaviour of the building, it was concluded that the global and local stability of the structure are jeopardized, as well as its load-bearing capacity. Durability of the building is particularly jeopardized, especially considering the importance of the protection of cultural treasures and ornaments, whose further deterioration should be prevented.

Uneven settlement is the main reason for opening of cracks and fissures in the vault and arches, around the openings and in the walls, and there were three reasons for it. Primarily, main cause is the subsequent construction of the underground crypt, for whose construction it was necessary to excavate part of the soil beneath the eastern part of the church. The second reason are missing vertical gutters, stolen from the building (after the repair of the roof structure in the seventies of the last century), hence the soil under the foundation was directly exposed to soaking by atmospheric rainfall. The third reason for unequal settlement is the difference in the weight of different parts of the building hence the pillars of the tower have sunk for a few centimetres into the ground in relation to the load-bearing walls of the church.

One of the positive indicators, when it comes to analysing the stability of the structure is the crack development and settlement. For a longer period of time (2012-2016), expansion of existing cracks and settlement was not registered.

As addition, effectiveness of used tie-rod system is an additional factor contributing to the endangerment of the buildings stability.

Most noticeable damages are the friability and deterioration of the material, especially in the area of direct exposure to the effects of weathering. Chiselling of the walls to a height of five meters for the purpose of faster drying was meant to be a short-term repair measure, but, after more than fifteen years, it has only caused more damages of the structure. Moisture and frost primarily contributed to the reduction of mechanical properties of materials. Inadequate performance of drip channel, as well as the drainage of precipitation from the building, has also contributed to this building's condition.

A visual inspection of the roof structure revealed large numbers of damages and defects on the structural elements. Cracks were registered along the large number of elements as a result of material drying. As these elements are primarily flexural loaded, the appearance of cracks significantly had reduced load capacity of the cross-section, which led to an increase in deformation, distortion of the continuity of the roof cover and, consequently, leakage and further degradation of wooden materials.

Other defects and damages, listed in the study, have local character and are not critical, although they influence durability of the building.

Therefore, a series of urgent repair measures is proposed in order to remove the causes of damages and, thus, prevent their further progress. After the repair works on structural elements and exterior, it is necessary to repair the iconostasis and the entire interior of the church.

ACKNOWLEDGMENTS

The paper presents the part of research realized within the project "Improvement of educational process and theoretical and applied research in civil engineering" conducted by the Department of Civil Engineering and Geodesy, Faculty of Technical Sciences, University of Novi Sad.

REFERENCES

[1] Edwards A.: The case for church buildings, *The Guardian* article, Available from https://www.theguardian.com/commentisfree/belief/2010/nov/24/church-buildings, Accessed: 2016-11-02

[2] Radonjanin, V. et al.: Elaboration on the assessment of the church in Ruma (in serbian), Deparment of Civil Engineering and Geodesy, Novi Sad, 2013

[3] Radonjanin V., Malešev M.: Material from lectures in the subject: "Durability and Assessment of Damaged Masonry Structures", Deparment of Civil Engineering and Geodesy, Novi Sad

LIFE CYCLE ASSESSMENT FOR SUSTAINABLE SOLUTIONS OF INFRASTRUCTURE PROJECTS

Ioanna Papayianni[1], Alexandros Liapis[1], Michalis Papachristoforou[1]

[1] Aristotle University of Thessaloniki, Department of Civil Engineering in the Faculty of Engineering, Laboratory of Building Materials, email: papayian@civil.auth.gr, aliapisk@civil.auth.gr, papchr@civil.auth.gr

SUMMARY: The importance of infrastructural works for the economical growth of a country is undeniable. However this growth should not be allowed at the expense of environmental protection. Thus, there is a worldwide interest for the promotion of sustainable growth in construction. A valuable tool for the sustainable planning of constructions is the methodology of Life Cycle Assessment (LCA). This paper evaluates five different infrastructural concrete applications (a RCC dam, a road pavement, a lean concrete embankment, self-compacting concrete and shotcrete), where parts of the binder and/or aggregates are replaced by local byproducts or materials such as fly ash (lignite combustion byproduct) and steel slag (steel industry byproduct). This strategy aims at natural resources' efficiency and reduction of waste that would otherwise be deposited into landfill, as well as reduction of transportation costs. The evaluation is conducted with the LCA methodology, but also considering the multilevel technical and economical benefits that arise from the byproducts utilization. The results show that there is a great potential in by-products' and locally available materials' utilization in infrastructure applications. In reality, these sustainable solutions are not often followed since they are not promoted by European funds and usually additional research is required to prove equivalent performance of local byproducts and raw materials for which there are not adequate regulative frames.

OCJENJIVANJE ŽIVOTNOGA CIKLUSA ODRŽIVIH RJEŠENJA INFRASTRUKTURNIH PROJEKATA

SAŽETAK: Neosporna je važnost infrastrukturnih građevina na gospodarski rast zemlje. Taj rast, međutim, ne treba dopustiti na račun zaštite okoliša. Stoga postoji svjetski interes promidžbe održivog razvoja pri građenju. Vrijedan alat održivoga planiranja građevina metodologija je ocjenjivanja životnoga ciklusa. U radu je prikazano vrednovanje pet različitih infrastrukturnih primjena za beton (armiranobetonska brana, kolnik ceste, tanki betonski pokos, samozbijajući beton i prskani beton) gdje su dijelovi veziva i/ili agregata zamijenjeni lokalnim nusproizvodima ili materijalima kao leteći pepeo (nusproizvod pri izgaranju lignita) i zgura iz visoke peći (nusproizvod iz industrije čelika). Cilj je takve strategije učinkovita upotreba prirodnih izvora i smanjenje otpada koji bi se inače odložio na odlagalištu te smanjenje prijevoznih troškova. Vrednovanje je provedeno metodologijom ocjenjivanja životnoga ciklusa uz razmatranje višerazinskih tehničkih i gospodarskih koristi koje proizlaze iz upotrebe nusproizvoda. Rezultati pokazuju da upotreba nusproizvoda i lokalno dostupnih materijala ima velik potencijal za infrastrukturne primjene. U stvarnosti ta održiva rješenja ne provode se često jer ih ne promiču europski fondovi, a obično se za dokazivanje istovrijednih svojstava lokalnih nusproizvoda i sirovina zahtijevaju dodatna istraživanja za koja nema prikladnih propisanih okvira.

1. INTRODUCTION

Infrastructural works are major contributors to global economy growth. However, they are also responsible for a great deal of environmental issues. Natural resources' overexploitation [1], extended land usage and increasing release of emissions [2] are some of the impacts related to primary building materials' as well as concrete production and implementation. On the other hand, a great deal of by-products in several production lines (with direct or indirect relation to the construction industry), are being disposed, contributing to environmental degradation. Hence, there is a common ground between the need for efficient resource usage and reduction of the construction related emissions, and the sustainable utilization of industrial by-products. The Laboratory of Building Materials, of the Aristotle University of Thessaloniki, Greece, having a previous experience in the field of by-products' utilization in the building sector [3], [4], [5] has been involved over the years in many infrastructural projects as scientific advisor, related to the use of industrial by-products in great scale constructions.

In this paper, five of these projects are presented: a concrete dam constructed with the methodology of Roller-Compaction (RCC) which uses the same principles as the asphalt road making, the construction of a RCC road section, the construction of a lean-concrete embankment, a reinforced concrete reservoir constructed with self-compacted concrete and the application of sprayed concrete (shotcrete) in a tunnel. The by-products of mainly two local industries are being used: fly ash, which is the by-product of lignite-fired power plants with 8-10 million tons of output production per year, and steel slags which are the by-products of the steel making industry, using the Electric Arc Furnace (EAF) process of production. Steelmaking by-products can be divided into two main categories, the EAF steel slag, which is produced in granulated form during the first stage of steel production, used mainly as aggregate and Ladle Furnace Slag (LFS), which is a fine material produced at the second stage of steel production and is used either as binder or filler.

For the environmental assessment of the applications, the Life Cycle Assessment (LCA) methodology was used, as it has previously proved to apply in building materials and construction applications [6], [7]. The data for the environmental assessment were taken mainly from Greek industries. The required detail in data together with the lack of recorded measurements by some industries made necessary the use of additional data by the libraries of LCA software SimaPro. For the cost estimation the data refer to mean values of the Greek market as it was formed in the second half of 2014 and the first half of 2015.

2. METHODOLOGY

The Life Cycle Assessment (LCA) methodology is being used since the late 1960's, gaining constantly momentum in industrial applications, where the environmental burden of a production line was under study. In late 1990's and early 2000's the International Organization for Standardization published the standards 14040 [8] - 14044 [9], where the LCA methodology is summarized into four main steps: goal and scope definition, inventory analysis, impact assessment and finally interpretation of the results. Although the first and the fourth steps' names are pretty much self-explanatory, the second and third one need some further elaboration.

The step of inventory analysis includes the detailed recording of all the inputs (e.g. materials, energy, transportation, labor, land occupation etc.) and outputs (products, by-products, emissions to air/water/soil) that participate in the production phase of the studied product. In construction applications, the product could be either a (concrete) mixture, a building element or an entire construction, depending on the temporal and spatial boundaries that are determined. For this study the boundaries are characterized as "cradle to gate", which means that the stages of use and disposal (or recycle) of the studied applications are not considered. The stage of construction is also not considered for the study, because it is common for all the compared scenarios for each application, and also due to lack of detailed data that would result into increased uncertainty on the results. However it should be noted that for all the applications, the utilization of by-products led to benefit throughout the use phase, due to high durability and mechanical properties, which also reduces the required maintenance works and extends the service life of the construction.

The impact assessment step is the very heart of the LCA. It is the stage where all the recorded inputs and outputs are related to certain categories of environmental issues. The correlation is accomplished by multiplying the inventory analysis results with factors (Characterization factors) according to each one's contribution to the environmental issue that is under study. For this paper, the impact of the construction applications to the climate change effect is studied, through the assessment of the carbon footprint of each application scenario, expressed in kg of equivalent CO_2 per m^3 of concrete mixture (kg CO_2 eq/m^3). The assessment is based on the Characterization factors that are proposed by the Intergovernmental Panel on Climate Change (IPCC), for a 100 year time frame.

3. RESULTS

3.1. ROLLER-COMPACTED CONCRETE DAM

The first application refers to the construction of the main body (core) of a concrete dam, with the Roller Compaction methodology. The dam was constructed near Platanovrisi, in North-East Greece, in order to control the flow of Nestos river. The dam was constructed during the period 1995-1999 and was a pioneering project for the time, combining the Roller Compaction methodology with the large replacement of cement binder with processed fly ash. Although the project was finished in 1997, the economical data that are used for this paper are projected to present values. Two concrete mixtures are to be assessed, the one is the actual mixture for the construction of the main body, containing a high percentage of fly ash as replacement for cement content, and the other is a theoretical composition for reference purpose, containing only cement as a binder.

As the results indicate, the replacement of cement with fly ash, leads to a major environmental and economical efficiency. Despite the slight increase in emissions and costs due to transportation, the overall benefit of fly ash utilization is evident. Strength-wise, the applied mixture was tested and found in complete agreement with the project's requirements.

3.1. ROLLER-COMPACTED CONCRETE PAVEMENT

The second application is the construction of a concrete road pavement using the Roller Compaction methodology. The pilot construction of the RCC road pavement was implemented in a rural road next to the National Road of Thessaloniki-Serres (E65), near Liti, again in the area of Northern Greece. The total length of the pavement was 1000 m, 500 m of which with EAF slag based concrete and 500 m with limestone concrete. A mixed type binding system based on fly ash was used instead of Portland cement in order to reduce environmental and economical costs. A reference mixture is also presented for this study, containing only cement as binder and limestone aggregates, which is the usual practice for rigid pavements in Greece.

Table 1 Composition, environmental and economical assessment of the RCC dam application

	Scenario	RD1	RD2
Composition	unit	kg/m^3	kg/m^3
	CEM I 42.5	275	50
	Fly ash	-	225
	Water	128	128
	Limestone aggregates (fine)	607	607
	Limestone aggregates (coarse)	1350	1350
Environmental footprint	unit	kg CO_2 eq/m^3	kg CO_2 eq/m^3
	Materials	272.39	68.32
	Transportation	20.28	25.15
	Production	2.33	2.33
	Total	295.00	95.80
Cost estimation	unit	€/m^3	€/m^3
	Materials	34.90	18.00
	Transportation	7.20	9.21
	Production	0.36	0.36
	Total	42.46	27.57

Table 2 Composition, environmental and economical assessment of the RCC pavement application

	Scenario	RP1	RP2	RP3
Composition	unit	kg/m^3	kg/m^3	kg/m^3
	CEM I 42.5		-	-
	Hydraulic Road Binder	280	280	280
	Water	148.2	148.4	162.2
	Limestone aggregates (fine)	985	985	1111
	Limestone aggregates (coarse)	985	985	-
	EAF Slag aggregates (coarse)	-	-	1090
	Superplasticizer (%wt. of binder)	0.60%	0.60%	0.60%
Environmental footprint	unit	kg CO_2 eq/m^3	kg CO_2 eq/m^3	kg CO_2 eq/m^3
	Materials	278.96	88.06	83.43
	Transportation	0.711	0.71	5.14
	Production	2.33	2.33	2.33
	Total	282.00	91.10	90.90
Cost estimation	unit	€/m^3	€/m^3	€/m^3
	Materials	38.7	34.90	36.30
	Transportation	0.29	0.29	2.82
	Production	0.36	0.36	0.36
	Total	39.36	35.56	39.48

In terms of costs, the mixture with the hydraulic binder and the limestone aggregates (RP2) seems the most efficient. The reason for this, despite the slight increase in materials' cost, is the transportation cost of the EAF steel slag aggregates, which is greater due to greater distance, comparing to the limestone quarry that, for this particular application, happens to be really close to the project site. However environmentally-wise, the steel slag aggregates' scenario (RP3) is slightly more beneficial than the limestone aggregates' one (both with hydraulic road binder), and both of them are much more efficient than the reference (cement binder) one. The compressive strength development of the two alternative mixtures was satisfying, reaching a level of approximately 32 MPa, and as for their abrasion resistance, RP3 mixture more resistant than RP2 by a rate of 33%.

3.2. LEAN CONCRETE EMBANKMENT

This application considers the construction of a lean concrete embankment for a reservoir, in the area of Amfiloxia, in Central-Western Greece. The project is scheduled to begin construction within 2017, and its main target is to use psammite (sandstone) which is highly available in the area, replacing limestone aggregates. For this study we considered four different mixtures, one with cement binder and limestone aggregates and one with both cement and fly ash as binders and lime stone aggregates (as reference mixtures) and their counterparts with sandstone aggregates.

Table 3 Composition, environmental and economical assessment of the lean concrete embankment application

	Scenario	LD1	LD2	LD3	LD4
Composition	unit	kg/m^3	kg/m^3	kg/m^3	kg/m^3
	CEM II 32.5	100	100	60	60
	Fly ash	-	-	60	60
	Water	176.5	176.5	197	197
	Limestone aggregates	1988	-	1953	-
	Sandstone	-	1988		1953
Environmental footprint	unit	kg CO_2 eq/m^3	kg CO_2 eq/m^3	kg CO_2 eq/m^3	kg CO_2 eq/m^3
	Materials	101.31	101.75	66.42	67.08
	Transportation	2.36	1.92	5.85	5.39
	Production	2.33	2.33	2.33	2.33
	Total	106.00	106.00	74.60	74.80
Cost estimation	unit	€/m^3	€/m^3	€/m^3	€/m^3
	Materials	19.3	9.33	16.50	6.69
	Transportation	0.93	0.79	2.37	2.23
	Production	0.36	0.36	0.36	0.36
	Total	20.59	10.48	19.23	9.28

Regarding the environmental burden, the mixtures with fly ash utilization (LD3, LD4) are by far the most beneficial, due to cement replacement. For the economical assessment, both mixtures that incorporate sandstone are clearly more efficient, with the one with fly ash utilization being slightly cheaper. The difference is so small because of the greater transportation distance (which translates into greater cost) of fly ash, as compared to cement. Regarding the strength requirements of the project (4 MPa compressive strength), both LD2 and LD4 mixtures are found satisfactory.

3.3. SELF-COMPACTING CONCRETE

The construction of a concrete reservoir for a hybrid energy production (wind-power and hydroelectric power) project in the island of Icaria in Greece, is the subject of the next application. The heavily reinforced concrete of the reservoir demanded of consolidation of the concrete without vibration, making self-compacting concrete a viable solution. The mixtures presented here are the studied laboratory mixtures for the project, a reference mixture with local limestone aggregates and limestone filler, in order to achieve the desired workability, and the actual mixture considered for the reservoir, where the limestone filler was replaced by Ladle Furnace Slag (LFS).

Table 4 Composition, environmental and economical assessment of the self-compacting concrete application

	Scenario	SC1	SC2
Composition	unit	kg/m^3	kg/m^3
	CEM I 42.5	350	370
	Water	203	214.6
	Limestone aggregates (fine)	923.4	924.4
	Limestone aggregates (coarse)	610.9	599.6
	Limestone filler	200	-
	LFS	-	180
	Superplasticizer (%wt. of binder)	2.2	2
Environmental footprint	unit	kg CO_2 eq/m^3	kg CO_2 eq/m^3
	Materials	298.54	312.24
	Transportation	8.13	9.43
	Production	2.33	2.33
	Total	309.00	324.00
Cost estimation	unit	€/m^3	€/m^3
	Materials	56.50	57.30
	Transportation	1.89	1.80
	Production	0.36	0.36
	Total	58.75	59.46

The increased environmental and economical burden of the SC2 mixture is mainly an outcome of the slightly increased quantity of cement and the additional transportation that corresponds to LFS. However this increase seems insignificant (especially in terms of costs) considering the enhancement in strength development (up to 43% in early compressive strength and 9.5% in 28-day strength) by the LFS utilization in the mixture. Furthermore, the cohesiveness and robustness of the fresh mixture were significant benefits for the construction's durability.

3.4. SHOTCRETE

The final application is referring to 3 different concrete mixtures for the implementation of sprayed concrete (shotcrete) in a tunnel, at the national road network of Northern Greece (Egnatia Odos), near the city of Grevena. The first mixture contains only cement as binder, being the deafault mixture for shotcrete applications for the contractor of the project. The other two utilize LFS as a 20% and 30% replacement of the cement, respectively. All three mixtures were implemented in different parts of the tunnel as a pilot construction.

Table 5 Composition, environmental and economical assessment of the shotcrete application

	Scenario	SH1	SH2	SH3
Composition	unit	kg/m³	kg/m³	kg/m³
	CEM I 42.5	440	352	308
	LFS	-	88	132
	Water	250	250	250
	Limestone aggregates (fine)	1540	1540	1540
	Superplasticizer (%wt. Of binder)	1%	1.60%	1%
	Accelerator (%wt. Of binder)	5-6%	5-6%	5-6%
Environmental footprint	unit	kg CO_2 eq/m³	kg CO_2 eq/m³	kg CO_2 eq/m³
	Materials	437.47	354.54	307.65
	Transportation	32.2	32.13	32.02
	Production	2.33	2.33	2.33
	Total	472.00	389.00	342.00
Cost estimation	unit	€/m³	€/m³	€/m³
	Materials	56.6	54.40	45.40
	Transportation	11.50	11.80	11.90
	Production	0.36	0.36	0.36
	Total	68.46	66.56	57.66

The replacement of cement with LFS gives to the corresponding mixtures a clear advantage in terms of both environmental and economical assessment. Moreover, it should also be noticed that this advantage is not accomplished at the expense of physical and mechanical properties; on the contrary, during the implementation there was a reduction on the rebound material (and therefore cost reduction) due to increased cohesiveness in fresh state. Also in terms of strength, the alternative mixtures developed up to 93% of the control mixture's compressive strength.

4. CONCLUSIONS

The utilization of industrial by-products in infrastructural concrete applications can be a sustainable alternative for all decision-makers. As it is shown in the presented projects, most of which have already completed a long time service life, environmental and economical efficiency can be achieved along with good strength and durability performance. Although in some applications there are small fluctuations between the most efficient scenario, the overall assessment is strongly supportive of the vital role that these (amongst many other) by-products have in the sustainable character of infrastructural works.

ACKNOWLEDGMENTS

This research work was developed in the frame of the TEFRODOS Project 2011-2014 and the SLAGPROD Project 2011-2015, both funded by the General Secretary of Research and Technology in Greece.

REFERENCES

[1] Zabalza, B. I., Valero, C. A., & Aranda, U. A.: Life cycle assessment of building materials: Comparative analysis of energy and environmental impacts and evaluation of the eco-efficiency improvement potential. *Building and Environment*, (2011), 46, 5, 1133-1140.

[2] Malhotra, V. M.: Global warming, and role of supplementary cementing materials and superplasticisers in reducing greenhouse gas emissions from the manufacturing of portland cement. *International Journal of Structural Engineering*, (2010), 1, 2, 116-130.

[3] Papayianni,I.: Use of a high calcium fly ash in blended type cement production. *Cement and Concrete Composites*, (1993), 15, 231-235.

[4] Papayianni, I., & Anastasiou, E.: Production of high-strength concrete using high volume of industrial by-products. *Construction and Building Materials*, (2010), 24, 8, 1412-1417.

[5] Papayianni, I., & Anastasiou, E.: Concrete incorporating highcalcium fly ash and EAF slag aggregates. Magazine of Concrete Research, (2011), 63, 8, 597-604.

[6] Huntzinger, D. N., & Eatmon, T. D.: A life-cycle assessment of Portland cement manufacturing: comparing the traditional process with alternative technologies. *Journal of Cleaner Production*, (2009), 17, 7, 668-675.

[7] Anastasiou, E. K., Liapis, A., & Papayianni, I.: Comparative life cycle assessment of concrete road pavements using industrial by-products as alternative materials. *Resources, Conservation & Recycling*, (2015), 101, 1-8.

[8] International Organization for Standardization: ISO 14040: Environmental management – life cycle assessment – principles and framework. CEN (European Committee for Standardization),1997, Brussels.

[9] International Organization for Standardization: ISO 14044: Environmental management – life cycle assessment – requirements and guidelines. CEN (European Committee for Standardization), 2006, Brussels

FROM MEASUREMENTS TO PREDICTION OF MOMENT OF INTERVENTION DURING THE (REMAINING) LIFETIME

Henk Voogt1, Piet Louwen1, Vincent Langelaan[1]

[1] Port of Rotterdam / Rotterdam Port Authority, Asset Management, Rotterdam Netherlands,
email: h.voogt@portofrotterdam.com, ap.louwen@portofrotterdam.com, vam.langelaan@portofrotterdam.com

SUMMARY: The Port of Rotterdam has put considerable investment into the development of models that can identify the best moment to initiate remedial intervention to ensure maximum longevity for steel-concrete quay infrastructures that are in constant use.

OD MJERENJA DO PREDVIĐANJA TRENUTKA ZAHVATA TIJEKOM (PREOSTALOG) ŽIVOTNOG VIJEKA

SAŽETAK: Luka Roterdam uložila je znatna sredstva u razvoj modela koji može prepoznati najbolji trenutak započinjanja popravnog zahvata kako bi se osigurala dugovječnost infrastrukture armiranobetonskih kejeva koji su u stalnoj upotrebi.

1. INTRODUCTION

Much research has been done worldwide to find the causes and effects of accelerated (low water) corrosion. In the Port of Rotterdam this research has been extended to find a correlation between the lab / in situ coupon tests and the actual loss of material on the substructures of the quay walls. By validating the test results, it was possible to draw up a model that is capable to predict the safety factor on both strength of structure and soil retention over the remaining lifetime of a quay wall and if needed to present the ultimate moment to start maintenance. As most of the substructures of quay walls are made of steel structure and superstructures are made of concrete, a similar method is being used to predict the aging of concrete. The results of these simulations are used in the Port of Rotterdam's new asset management tool KMS, which gives the asset manager the possibility to prioritize maintenance measures. Apart from the simulations a risk assessment is implemented in KMS to identify and rank the risks on the structures. After that the business value of an asset is being used to make the final prioritisation and the remaining risks after maintenance are made visible.

2. GENERAL SPECIFICATIONS

The port of Rotterdam is the largest port in Europe and one of the largest ports in the world. It's currently one of the first port authority's with an ISO 55001 certificate for asset management for port- and maritime structures. The maritime assets add enormous value to ports, but due to the function these structures serve as well as their location in the marine environment these assets are relatively costly to construct and maintain.

2.1. THE BACKGROUND

The Port of Rotterdam owns around 75 kilometres of quay walls with a total replacement value of around 1.45 billion euros. More than two-third of these quay walls are under attack of the accelerated low water corrosion because the substructure is made of steel sheet piling or steel combi walls (combination of tubular piles and sheet piles). The concrete top structures are under attack of chlorides in the water.

The capital invested in such maritime civil engineering structures is quite substantial too. The typical service life for these port- and maritime structures is approximately 50 years. A large proportion of these assets will be nearing the end of their service life span in the coming decades. In order to effectively and efficiently manage these assets it is critical to have a system in place to track the yearly required maintenance as well as forecast the near and distant costs of keeping these structures in service. Finally the consequences of the recent economic recession and the subsequent credit crisis also play a role: port- and maritime organizations are being forced to think – from an integrated approach – more about which assets they put their money into.

2.2. RESEARCH

A lot of research has been done worldwide to find the causes and effects of accelerated (low water) corrosion. At the Port of Rotterdam, this research has been extended to find a correlation between the lab / in situ coupon tests and the actual loss of material on the substructures of the quay walls.

Fig 1. Typical example of ALWC

Prior to the year 2000, the strategy for handling the corrosion consisted of:

- applying the EAU standard
- avoiding steel construction parts in the splash zone and
- adding an extra 1-2mm to the steel's thickness.

In 2000, the first damage caused by accelerated corrosion was discovered at a quay wall in the Maasvlakte area. This showed holes in the sheet piles, followed by soil loss – a potentially dangerous situation.

Repair works were carried out and cathodic protection was applied to the damaged quay wall. In the meantime, research into the cause was immediately started and resulted in a long list of 23 probable causes; of those, microbiologically influenced corrosion seemed to be the most important.

In order to determine the degree of influence of each cause on the corrosion rate of steel structures, an investigative action plan was drawn up. This consisted of:

- several fluorescence intensity tests on bacteria in laboratories
- in situ tests with coupons mounted on a ladder and exposed to the water conditions of different areas
- ultrasonic thickness measurements carried out on all the steel structures in the Port of Rotterdam.

This inspection resulted in more than 500,000 measurements which were statistically processed and we were then able to extract representative values for the corrosion rate.

Despite the Port of Rotterdam having quay walls with a lifespan from 0-100 years, differing types of structures, and an estuary that ranges from salt to freshwater, it was possible to identify several contributory causes to the corrosion rate.

Rotterdam's maximum corrosion rate has been determined as 27 mm in 50 years, with an average rate of 9 mm in 50 years.

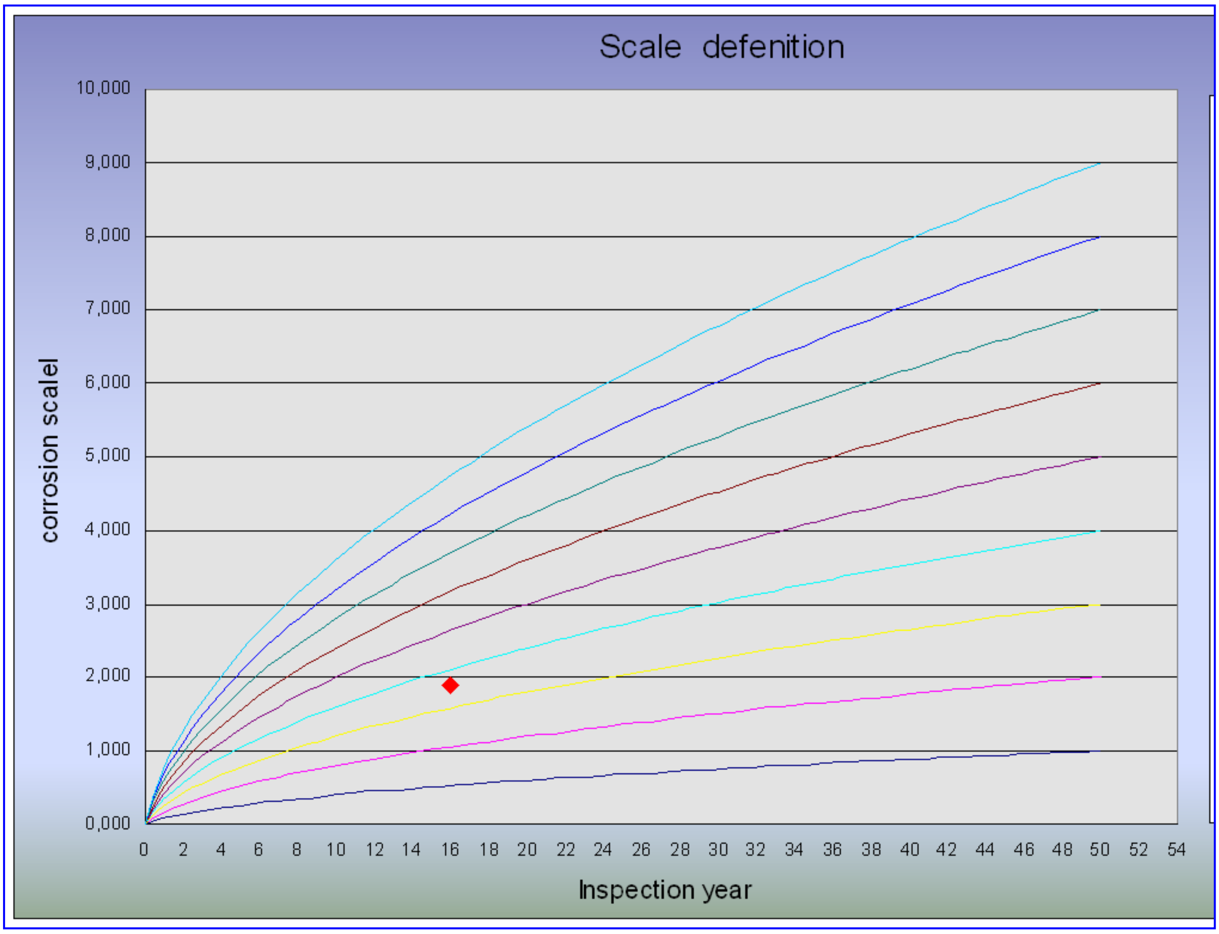

Fig 2. Standard corrosion scales Port of Rotterdam

These figures led to the development of standard corrosion scales for the Port of Rotterdam. This makes it possible to predict the moment in a structure's lifetime when it reaches the minimum safety level and needs maintenance. So the asset manager can put this in the maintenance plan.

Knowing the corrosion rate is one thing, but connecting that to asset management is another.

By validating the test results, it is possible to draw up a model capable of predicting the safety factors on both structure strength and soil retention over the remaining lifetime of a quay wall and, if needed, suggest the optimum moment to start maintenance. As most quay wall substructures are made up of a steel structure and concrete superstructure, a similar method is being used to predict the aging of concrete.

The Port of Rotterdam's new asset management tool KMS uses the results of these simulations to allow the asset manager to prioritise maintenance measures. In addition, a risk assessment is implemented within KMS to identify and rank the structure's risks. Then the asset's business value is used to clarify the final maintenance prioritisation, which makes the remaining post-maintenance risks more visible.

This makes it possible to predict the moment in a structure's lifetime when it reaches the minimum safety level and needs maintenance. So the asset manager can put this in the maintenance plan.

- What does it mean for the port's tenants?
- How safe is the structure?
- Will it reach the end of its lifetime?
- What / when is the best moment to invest in maintenance work?
- With finite budget, where do I put the money first?

2.3. THE START OF KMS

To answer these and other questions, the Port of Rotterdam Authority's invested in the development of KMS (the Dutch abbreviation for 'quay wall modelling system') delivered at the end of 2012.

This unique asset management tool for the port- and maritime market sector:

- Provides a tool for the asset owners and managers to efficiently manage a portfolio of quay walls or other maritime civil engineering structures
- Objectively supports decisions, with respect to the budget and schedule, for the required maintenance of quay walls
- Clarifies the risks and consequences, both short and long term, of postponing maintenance
- Aims to improve the prediction, simulation, analysis, prioritisation, budgeting and required maintenance planning for maritime structures, such as quay walls
- Predicts which maintenance tasks must be executed, when they should be done and how frequently, based on deterioration of materials (concrete, steel, anodes and, in future, rubber fenders too).

Quay wall modelling system in detail

The KMS (the Dutch abbreviation for Quay wall Modelling System) is a unique asset management tool for the port- and maritime market sector. It provides the asset owner and asset manager a tool to efficiently manage a portfolio of quay walls or other maritime civil engineering structures. The KMS is a system that objectively supports decisions, with respect to the budget and schedule, for the required maintenance of quay walls. In addition, it clarifies the risks and consequences, both short and long term, in case this required maintenance is postponed. The KMS aims to improve at predicting, simulating, analysing, prioritising, budgeting and planning the required maintenance to quay walls.

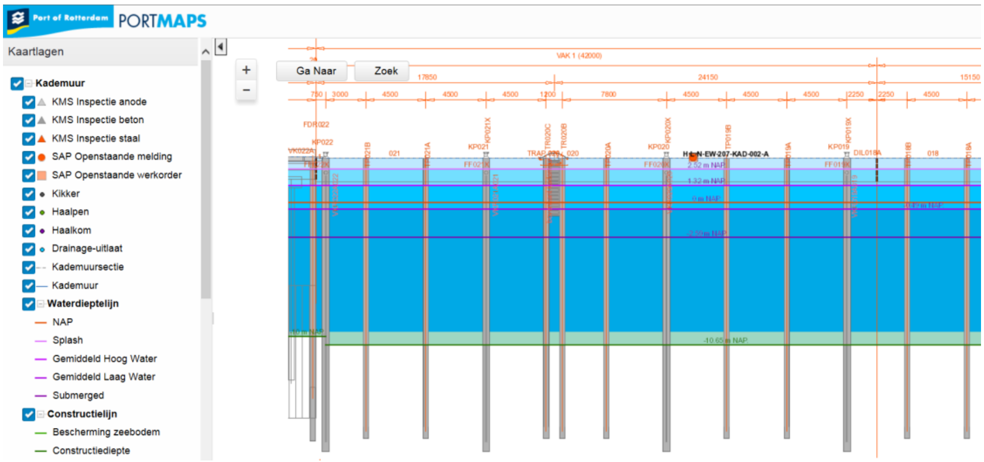

Fig 3: Front view of a quay wall with the different tidal zones

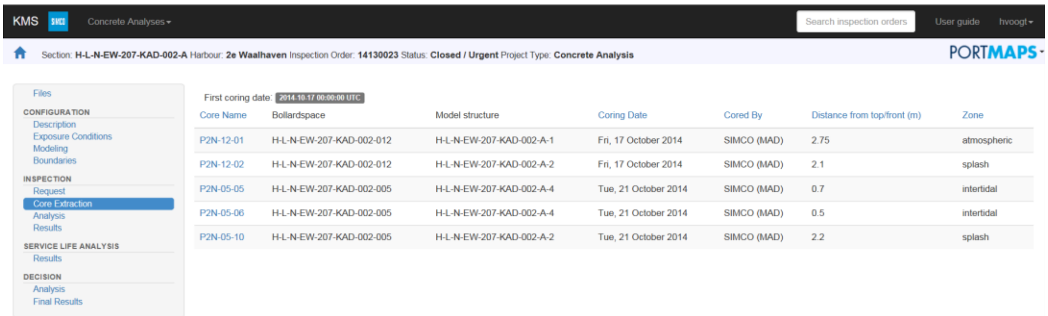

Fig 4: The extraction of concrete cores in the different zones (Atmospheric, intertidal, Splash)

2.4. PREDICTING

A quay wall's remaining lifetime is mainly determined by the quality of the sub- and superstructure. With the aid of its highly advanced deterioration models, KMS can predict when the lower safety limit for a quay wall will be reached, how the inspection regime must then be detailed and what maintenance measures must be done in order to meet the asset owner's required functionalities (such as availability for use, or asset lifetime). The KMS predicts on the basis of the deterioration of materials (concrete, steel, anodes and in the future also rubber for fenders and timber) which maintenance tasks must be executed, when these tasks should be executed and what the frequency of inspections should be for a quay wall.

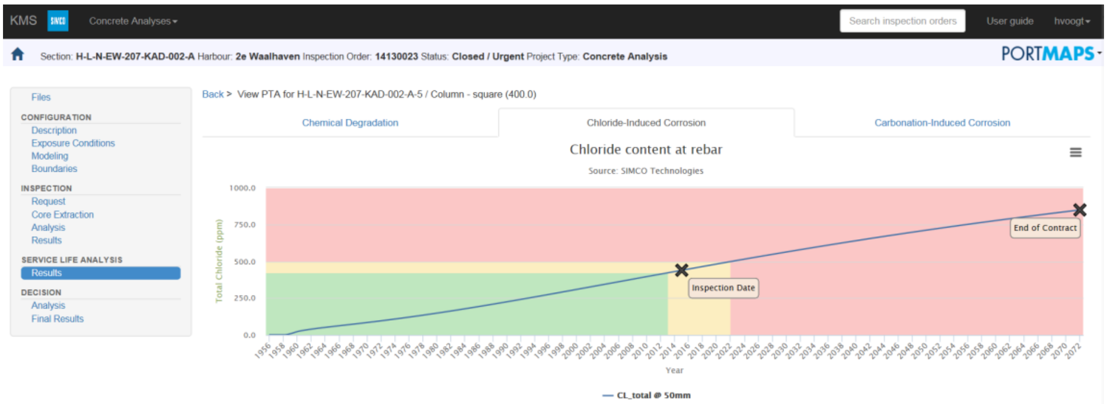

Figure 5 Concrete core analyses to determine the chloride content at the rebar. In this example we cannot get to the "end of contract" date without concrete repairs.

2.5. SIMULATING

KMS simulates various maintenance strategies, on the basis of the inspection results, so that the most efficient and cost-effective inspection regime and maintenance scenario for the quay wall in question can be selected and applied.

It will also provide insight into the consequences – such as reduction in remaining service life or availability of the structure – of postponing specific maintenance measurements. Furthermore, it will determine the consequences or advantages of different alternative maintenance measures.

2.6. RISK ASSESSMENT

The system contains the possible risks and causes that endanger the quay wall (or parts of it) relating to availability, structure safety, sustainability and aesthetics so it ranks the risks associated with retaining the desired functionality, then presents the financial consequences of postponing required maintenance for budgetary or economic reasons.

2.7. PRIORITISING

KMS prioritises the maintenance tasks to be carried out, on a multi-criteria basis. Required maintenance tasks are ranked by a quality mark: this is made up of various factors – commercial importance, availability requirement and end of contract term.

By using this quality-marking system in conjunction with the level of risk to be covered, it's possible to create a prioritised list of all maintenance measures to be executed over the next 12 months. A high quality mark combined with a top-ranked risk gives a maintenance action the highest priority. A low quality mark with a bottom-ranked risk gives it the lowest priority.

2.8. BUDGETING

KMS also creates an overall budget for a structure's prioritised work, based on the sum of individual maintenance actions. The system performs this task for the upcoming calendar year and also for the prescribed maintenance period of the structure, which for the Port of Rotterdam Authority, is when the commercial contract on the quay wall ends.

If the next calendar year's necessary maintenance work is delayed (for example, due to budgetary constraints), KMS will translate the consequences of this directly into the maintenance budget for subsequent years. In effect, it translates the risks of not performing a certain maintenance task into a budgetary dollar-cost for the coming years.

2.9. PLANNING

Once the asset manager finalizes the prioritised required maintenance on each structure, KMS can create an efficient, effective work schedule. Compiling work packages for multiple structures containing similar tasks means these packages can then be procured under one contract, in order to reduce installation time and cut costs.

So this prioritization of maintenance tasks, based on multi-criteria analysis, ensures that expenditure and maintenance is performed on those structures that are the most economically important to the Port of Rotterdam Authority – and where the safety risks are highest.

2.10. BENEFITS OF KMS

On short term the benefits of KMS are found in the transparency in annual budget for maintenance. The most important measure will be on top of list and will have priority above the other maintenance measures.

On (Mid)Long term KMS will bring insight in rest-life-time and maintenance costs per individual quay wall and in costs of concrete and steel maintenance works (total port)

The necessary inspections will be just in time, not too early and not too late. This will give a reduction of the inspection costs and/or needed manpower.

With KMS the asset management of quay walls will be proactive, prioritised and risk-based. KMS is a unique system for quay walls and maritime constructions in the world.

With KMS the Port of Rotterdam has a unique tool that can predict the degradation of quay walls, whether they are built of concrete, steel or a combination of both. This Quay Wall Modelling System(in Dutch - KMS) provides a good indication about when preventative maintenance has to be done, the costs that are involved and the safety of the object

3. CONCLUSION

The Port of Rotterdam succeeded in developing an asset management tool that can help the asset manager to make the right decision where to put the maintenance budget. Not only based on life time prediction of the most vulnerable parts, but also on business value of the quay wall and the risks involved.

ON THE DEVELOPMENT OF A DURABLE GRAPHENE-BASED SENSOR FOR CONCRETE PERFORMANCE MONITORING

Sotirios Grammatikos[1], Ingemar Löfgren[1,2], Tang Luping[1], Lilei Ye[3], Johan Liu[4,5]

[1] Chalmers University of Technology, Department of Civil & Environmental Engineering, Göteborg,
email: sotirios.grammatikos@chalmers.se, tang.luping@chalmers.se
[2] Thomas Concrete Group AB, Gothenburg, Sweden, email: ingemar.lofgren@thomasconcretegroup.com
[3] SHT Smart High Tech AB, Gothenburg, Sweden, email: lilei@sht-tek.com
[4] Chalmers University of Technology, Department of Microtechnology and Nanoscience, Gothenburg, Sweden
[5] Key Laboratory of New Displays and System Applications, SMIT Center, School of Mechanical Engineering and Automation,
email: johan.liu@chalmers.se

SUMMARY: This paper presents the procedure towards the development of a durable structural sensor based on graphene and other carbon fillers, for the monitoring of structural performance of concrete. The ultimate goal of the sensor is to capture electrical resistivity as a strength development and durability index during the whole service life of concrete. To date, performance monitoring systems usually fail in the long-run before the failure of the actual structure. The proposed sensor is embedded in the interrogated structure and ensures sustainable consolidation via appropriate physico-chemical adherence and mechanical interlocking. This allows for an efficient performance monitoring 'build-up' expected to surpass the service life of the parent concrete structure. Within this preliminary work, the effects of different concentrations of graphene and other fillers on the electrical properties of concrete were studied. After an initial investigation to select the appropriate synthesis, the ability of the sensor to monitor the development of resistivity during setting and hardening was tested and the results are presented herein.

O RAZVOJU TRAJNOG SENZORA NA OSNOVI GRAFENA ZA PRAĆENJE SVOJSTAVA BETONA

SAŽETAK: U radu je prikazan postupak razvoja trajnog senzora za konstrukcije na osnovi grafena i drugih ugljičnih ispuna za praćenje svojstava betonskih konstrukcija. Krajnji je cilj senzora mjerenje električne otpornosti (impedancije) kao mjere razvoja čvrstoće i indeksa trajnosti tijekom cijelog uporabnog vijeka betona. Dosad se, dugoročno promatrano, sustavi praćenje svojstava obično pokvare prije kvara stvarne konstrukcije. Predloženi je senzor ugrađen u promatranu konstrukciju i osigurava održivo stanje prikladnom fizičko-kemijskom prionjivošću i mehaničkim zahvaćanjem. To omogućuje stvaranje učinkovitog motrenja svojstva koje nadilazi uporabni vijek betonske konstrukcije. U ovom preliminarnom radu proučavani su učinci različitih koncentracija grafena i drugih ispuna na električna svojstva betona. Nakon početnih istraživanja radi odabira prikladnog sastava ispitana je sposobnost senzora za praćenje razvoja otpornosti (impedancije) tijekom vezivanja i očvršćivanja, a rezultati su ovdje prikazani..

1. INTRODUCTION

Cement-based composites are the most widely-employed materials on planet in a range of civil engineering applications. Concrete structures are typically designed for a working life of more than 100 years often with minimal maintenance. It is well understandable that efficient and dependable long-term performance monitoring is of primary importance in order to secure for safe infrastructure [1]. Many property monitoring systems have been proposed in years which often fail in the long-run mainly due to the insufficient life time of sensors or the failure in the interface between sensor material and concrete due to the tough alkaline environment in concrete [2]. Moreover, very few can actually monitor the porosity development and the initial curing [3]. Actually, most monitoring systems for the construction stage are purely based on the temperature development and models for maturity and strength development which do not provide any information about the properties influencing durability [4].

Cement composite itself contains a pore solution with highly conductive hydroxide ions but due to its tortuous pore structure the apparent conductivity is relatively low. Electrically conductive carbon nano-fillers (graphene, carbon nanotubes, carbon nanocaps) dispersed in the cement composite can effectively 'short-cut' the tortuous pores due to their high conductive specific surfaces so as to increase the electrical conductivity of concrete. That said, the combination of carbon nano-fillers with graphite and chopped carbon fibres is expected to increase the electrical conductivity of nano-modified concrete to a higher degree.

For the purposes of the study, metallic electrodes were embedded in a highly conductive carbon nano-modified cementitious mortar (CCM). Different combinations of carbon nano-fillers, graphite and fractions of chopped carbon fibres were examined as fillers, in order to pin-point the optimum synthesis of a cementitious blend having optimum electrical conductivity. The

CCMs were then purposely embedded in mortars made of ordinary cement (parent material), functioning as a transition phase between the metallic electrodes and the cementitious mortars under investigation. The metallic electrodes were continuously connected to a multi-meter, in order to follow electrical resistivity measurements during the setting and hardening of mortars for a total period of 28 days. At the same time, compressive strength development of the interrogated mortars was evaluated after 1, 3, 7 and 28 days, respectively. Compressive strength values were plotted against the electrical resistivity changes and presented herein.

2. EXPERIMENTAL

Figure 1 depicts a schematic representation of the developed sensor. The primary task towards the development of the structural sensor started with the realization of highly electrically conductive cementitious mortars (CCM). As aforementioned, the conductive mortars are to be used as the transition phase between the metallic electrodes and the parent cementitious structure (here is a mortar). As it is shown in Figure 1, the sensor consists of 4 metallic electrodes embedded in 4 cylindrically-shaped CCMs, each of which is formed in a PVC holder. The CCMs are equally positioned in concrete so as to be able to measure resistivity by the Wenner method for curing as well as performance monitoring.

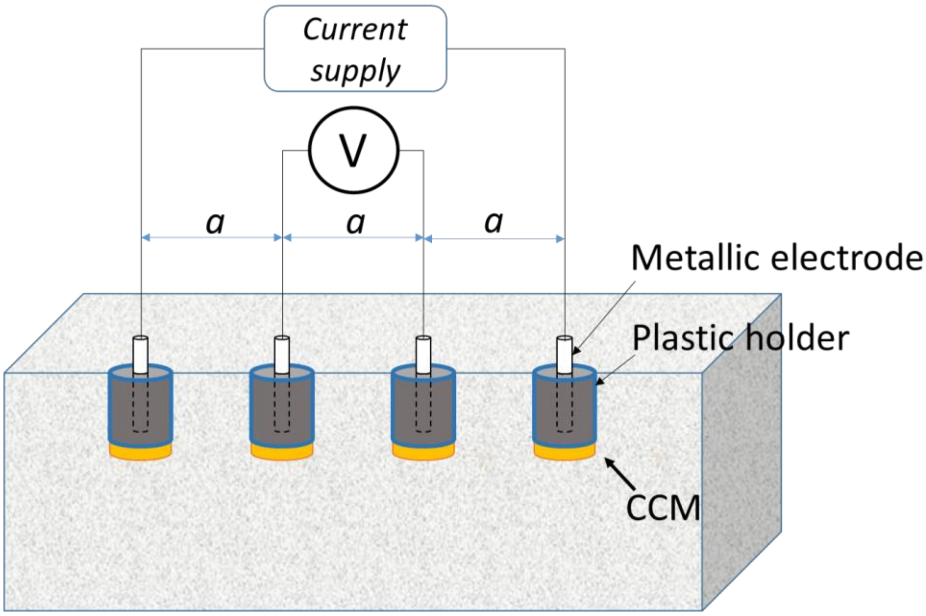

Figure 1 Schematic representation of the sensor.

Different combinations of carbon nano-fillers, graphite and chopped carbon fibres were studied as conductive fillers in order to reveal the optimum synthesis that provides highly conductive cementitious mortars. For the manufacturing of the CCMs, a graphene-based water suspension was provided by SHT Smart High Tech AB (all rights reserved). The employed suspension was in a concentration of 1.5 g graphene and other nano-fillers per 1lt of distilled water. Together with that, small fractions of graphite (150 μm) and 3 mm long carbon fibres were also blended in the conductive mix. In order to evaluate the electrical conductivity values of each mix, a set of 5 CCM specimens was manufactured and their electrical resistivity, was recorded for a period of 28 days or until stabilization. Electrical resistivity in this case was recorded by making use of the 2-wire method as shown in Figure 2. After the 'screening' process, the optimum synthesis of CCM was selected to develop the sensor shown in Figure 1. The sensor was then cast in cement mortars (parent structure) in order to capture setting and hardening through electrical resistivity measurements. Electrical resistivity by the sensor, was recorded by making use of a Keithley (2750 series) multi-meter on 4-wire resistance mode. Electrical resistivity was then estimated using Wenner's simplified approach:

$$\rho = 2\pi a R \quad (1)$$

where ρ is the electrical resistivity, a is the distance between the centers of the cylindrically-shaped CCMs (here 25 mm) and R the recorded electrical resistance measured as V/I by the multi-meter.

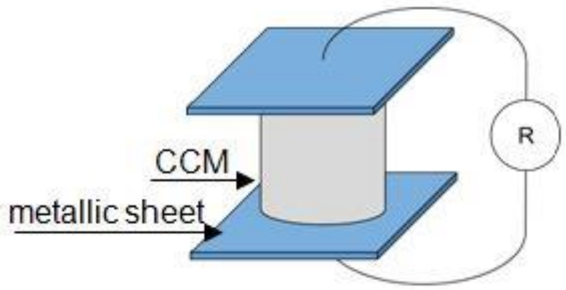

Figure 2 Two-wire electrical resistivity measurement of CCMs

With respect to the compressive strength, 100x100x100 mm^3 mortar samples were manufactured and tested on a 3000kN capacity compression testing machine (Toni Technik, 2040 series), according to the IS:10086-1982 standard for testing.

2.1. MANUFACTURING

Table 1 depicts some of the investigated mortar syntheses that were attempted in order to pin-point the optimum CCM synthesis. For CCMs fabrication, CEM I 42.5N-SR3 MH/LA Portland cement (Cementa, Sweden) was chosen. With respect to the parent mortars, a standard 450g (cement), 1350 g (sand), 225 g (water) mix was employed. Standard cement CEM II/A-V 52.5 N Portland-fly ash cement was used (Cementa, Sweden) together with 0/2 mm sand so as to facilitate the mixing procedure. After manufacturing, all samples were stored in lime-water to prevent carbonation.

Table 1 Investigated CCM recipes

CCM type	Cement [g]	Sand (0.125-0.5mm) [g]	Graphite (100mesh) [g]	Graphene suspension [g]	Carbon fibres (3mm) [g]	Superplasticizer (Glenium51) [g]
CCM1	100	80	20	50	1.2	1
CCM2	100	80	-	50	1.2	1

2.2. ELECTRICAL MEASUREMENTS

Electrical measurements with the sensor were recorded in 4-wire resistance mode. The sensor was employed to acquire measurements on fresh concrete with a view to capturing the setting and hardening caused by the cement hydration. In essence, this is expected to allow for the study of the effectiveness of the methodology to monitor the hydration process and porosity development. The latter is key for the speeding-up of the manufacturing/ casting process of concrete structures and is one step closer towards the realization of efficient 3-dimensional (3D) printing of concrete structures as well as maintenance-free and hence safe developments.

3. RESULTS

Figure 3 depicts the variation of electrical resistivity values throughout a period of approximately a month. In particular, Figure 3a illustrates the development of resistivity of a reference sample (plain mortar – control sample) as well as 2 CCMs over the course of a month. As can be seen, the addition of carbon nano-fillers and carbon fibres significantly suppresses the electrical resistivity values of about an order of magnitude difference. Figure 3b, plots the resistivity changes over time for the 2 CCM samples. It is worth mentioning that the addition of 20 g graphite in the mix (CCM1) induced a small increase in the electrical resistivity values, however, having very high experimental scatter. This may be attributed to the extra porosity, due to potential agglomeration, developed by the presence of the extra carbon phase (Figure 3b).

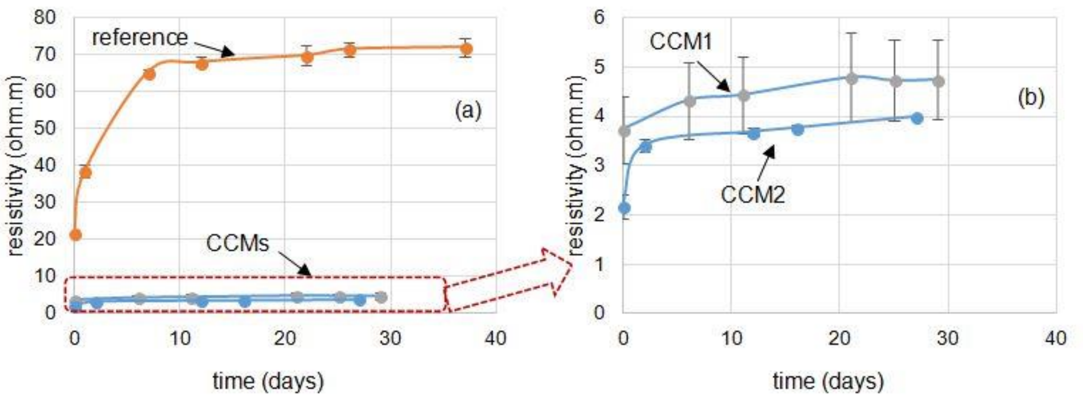

Figure 3 (a) Resistivity of CCMs and reference samples for a period of a month and (b) resistivity of CCMs for a period of month.

On the other hand, electrical resistivity of CCM2 was found to be marginally lower that its counterpart. The experimental scatter of CCM2 resistivity was noticeably lower and hence was qualified as the optimum synthesis to develop the graphene-based sensor.

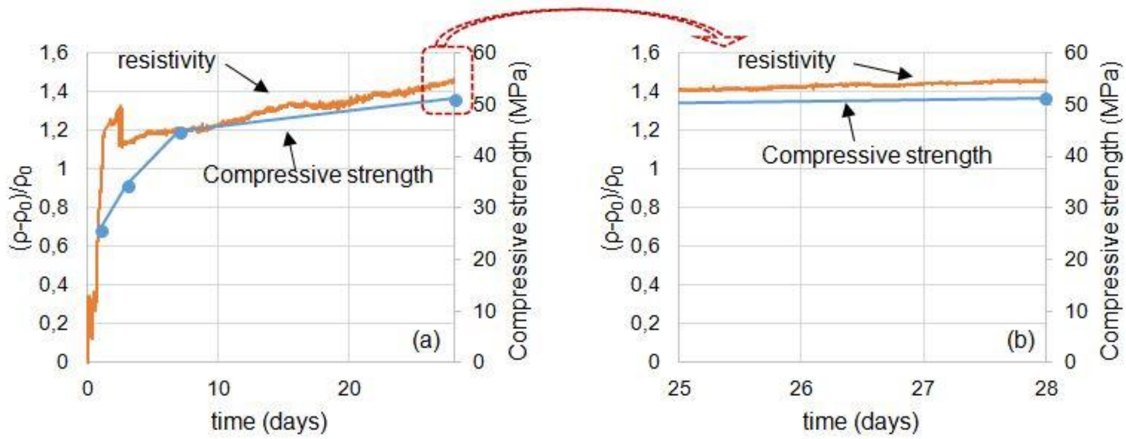

Figure 4 Strength development and electrical resistivity (graphene sensor in 4-wire mode) of mortar (parent material) for a period of a month: (a) 28days time-frame, (b) last 3days time-frame (day 25 to day 28).

Figure 4 depicts the development of electrical resistivity calculated by making use of Equation 1, for a period of approximately one month. As can be seen, the electrical resistivity curve, follows a characteristic incremental trend. Electrical resistivity initially increases after some variations recorded during the very first 2-3 days, then increases significantly until a certain value. After a slight but abrupt drop, resistivity increases steadily revealing the changes in the porosity of the material, until it finally reaches an equilibrium state. Electrical resistivity values then oscillate around a constant value exhibiting the termination of hydration. Similarly to electrical resistivity, the compressive strength of the cementitious mortar develops in a similar manner. Compressive strength follows a steady increasing behaviour until it reaches 51.2 MPa which corresponds to the recorded strength after 28 days of curing.

4. CONCLUSIONS

In conclusion, this study presents the development of a durable sensor based on graphene for the monitoring of structural performance of concrete. The developed sensor is designed to record electrical resistivity as a durability integrity index during both setting and hardening as well as the whole service life of concrete. In this work, setting and hardening of concrete as well as the development of mortar strength was followed by recording inherent electrical resistivity. The proposed sensor was appropriately embedded in the interrogated structure so as to ensure sustainable consolidation via appropriate physico-chemical adherence and mechanical interlocking with the structure under investigation. This is expected to lead to an efficient performance monitoring system that is designed to surpass the service life of the parent concrete structure. The effects of different concentrations of graphene and other fillers on the electrical properties of concrete were studied and presented. After an initial investigation to select the appropriate synthesis, the ability of the sensor to monitor the development of resistivity during setting and hardening was tested and the results were presented. It was found that the employed graphene suspension in addition with carbon fibres significantly increased the electrical conductivity of the cement paste. This highly conductive cement paste was then capable of being used as a sensing element embedded in the parent structure under monitoring.

The novelty of the study is based on the fact that the electrical signals are now led by the CCMs which possess significantly higher electrical conductivity than the surrounding parent material (mortar) and at the same time are chemically bound with the parent material so as to secure the strongest contact possible between sensor and parent mortar. Therefore, the whole sensing system is expected to be durable in the long-term (currently under investigation), and the unique properties of graphene will make it stable in the alkaline environment. Finally, the sensor is expected to ideally be connected to a data logging system to capture resistivity signals at distinct time frames, thus enabling the monitoring of the setting, pore structure development and durability of mortars/ concrete in real time.

ACKNOWLEDGMENTS

This study was part of the project DuraSens (Vinnova Strategiska Innovationsprogrammet för Grafen [DuraSens - Ref: 2016-01636]). Authors are grateful to Mr. M. Machowski for the excellent support within the experimental part of the study.

REFERENCES

[1] Rajabipour F. Insitu electrical sensing and material health monitoring in concrete structures: Purdue University

[2] Developments in Performance Monitoring of Concrete Exposed to Extreme Environments. Journal of Infrastructure Systems. 2012;18.

[3] McCarter WJ, Afshar AB. Monitoring the early hydration mechanisms of hydraulic cement. Journal of Materials Science. 1988;23:488-96.

[4] McCarter WJ, Chrisp TM, Starrs G, Blewett J. Characterization and monitoring of cement-based systems using intrinsic electrical property measurements. Cement and Concrete Research. 2003;33:197-206.

EXPERIENCE WITH CORROSION MONITORING USING EMBEDDED SENSORS IN THREE BRIDGES ON THE ADRIATIC COAST

Dalibor Sekulic1, Marijana Serdar[2]

[1] Institut IGH, Janka Rakuse 11, 10 000 Zagreb, Croatia, email: dalibor.sekulic@igh.hr
[2] University of Zagreb Faculty of Civil Engineering, Department of Materials, Fra Andrije Kacica Miosica 26, 10 000 Zagreb, Croatia, email: mserdar@grad.hr

SUMMARY: The main aim of the corrosion monitoring in advanced bridge monitoring is to enable early detection of possible failure and contribute to early detection and reliable repair in order to prolong service life as well as lower the costs of the maintenance. This paper presents overview of the results obtained on anode ladder sensors installed in large Croatian bridges exposed to aggressive marine environment for a timescale of 20 years. Data from three large Croatian bridges are presented: Maslenica Bridge (1997), Krka Bridge (2005) and Cetina Bridge (2007), which all had sensors for corrosion monitoring installed in their elements in the execution phase. The sensors have ability to measure macrocell current, half-cell potential and resistivity of concrete through different depths of concrete cover. Measurements of different parameters enable more accurate corrosion state assessment. The results of electrical quantities measured by the sensors are compared with the actual state of reinforcement and concrete observed on the site. Finally the measured corrosion parameters were transformed into damage severity categories according to obtained correlations between measured and actual corrosion states and according to the existing criteria from the literature.

ISKUSTVO U PRAĆENJU KOROZIJE S POMOĆU UGRAĐENIH SENZORA NA TRIMA MOSTOVIMA NA JADRANSKOJ OBALI

SAŽETAK: Glavna je svrha praćenja korozije pri naprednom praćenju mostova omogućiti rano otkrivanje mogućeg otkazivanja i doprinijeti ranom otkrivanju i pouzdanom popravku radi produljenja uporabnog vijeka i smanjenja troškova održavanja. U radu je prikazan pregled rezultata dobivenih anodnim ljestvičastim senzorima ugrađenim u velike hrvatske mostove izložene agresivnom morskom okolišu za razdoblje od narednih dvadeset godina. Prikazani su rezultati triju velikih hrvatskih mostova: mosta Maslenica (1997.), mosta Krka (2005.) i mosta Cetina (2007.) u koje su u njihove elemente tijekom izvedbe ugrađeni senzori za praćenje korozije. Senzori imaju sposobnost mjerenja struje makroćelije, potencijala polućelije i otpornosti (impedancije) betona na različitim dubinama zaštitnoga sloja. Mjerenja različitih parametara omogućuju točnije ocjenjivanje stanja korozije. Rezultati električnih veličina izmjereni senzorima uspoređeni su sa stvarnim stanjem armature i betona opaženim na terenu. Na kraju su izmjereni parametri korozije pretvoreni u kategorije jačine (ozbiljnosti) oštećenja u skladu s korelacijama dobivenim između mjerenih i stvarnih stanja korozije i u skladu s postojećim kriterijima iz literature.

1. INTRODUCTION

Corrosion of steel reinforcement in concrete may cause serious damage and degradation of structures. Nowadays, use of modern materials in combination to smart design and execution of details could delay or even prevent corrosion processes of reinforced concrete structures. However, since expected life time of structures is several decades, maintenance actions cannot be avoided. These actions can be made unplanned and only once the degradation of structure is such that it endangers its serviceability. That is reactive maintenance, which is more costly than the proactive ones. Proactive maintenance implies that the maintenance works are done before a significant damage of the structure occurs; their cost and impact on the structure is optimised. To be able to perform proactive maintenance of corroding structures, continuous corrosion monitoring is essential.

Techniques for corrosion monitoring should be accurate, cost effective, immune to aggressive substances, and should provide long term measurement stability. Corrosion of steel can be measured directly or indirectly by measuring parameters correlated with corrosion such as moisture, pH value, Cl- ion content, and cracks in concrete due to the corrosion process [1]. Many monitoring techniques have been developed for these purposes, of which most widely used are the electrochemical ones, such as half-cell potential measurements, macrocell current measuring, electrochemical noise, galvanostatic pulse method, etc. Different measuring configurations for in-situ testing exist, but anode ladders developed by Schiessel and Raupach [2] are one of the most used ones. In the scope of European project TRIMM "*Tomorrow's road infrastructure monitoring & management*" [3] corrosion monitoring was performed on three large Croatian bridges, Maslenica Bridge, Krka Bridge and Cetina Bridge, which all have sensors for corrosion monitoring installed in their elements in the execution phase. Sensors installed in all three bridges are anode ladders [4].

In the present paper experience from the existing corrosion monitoring systems installed in bridges is presented. Measurements from the sensors were collected and analysed. Results of electrical quantities measured by the sensors are compared with the actual state of reinforcement and concrete observed on the site. Finally the measured corrosion parameters were transformed into damage severity categories according to obtained correlations between measured and actual corrosion states and according to the existing criteria from the literature.

2. MONITORING SYSTEMS AND BRIDGES

2.1. CORROSION MONITORING SYSTEM

Anode ladder are composed of 6 rebars of black steel (A1 to A6) that act as anodes and one rebar made of titanium oxide acting as a cathode as shown in Figure 1. Additional to anodes there is a direct connection to reinforcement. Ladders are installed between the reinforcement and the formwork, under the angle, so to cover the full depth of the concrete cover. Potential and current are measured between each of the anodes versus the cathode. Concrete electrical resistivity is measured between the each pair of adjacent anodes. Therefore, with these sensors it is possible to detect corrosion through different depths of concrete cover and at the end to evaluate corrosion on the level of reinforcement.

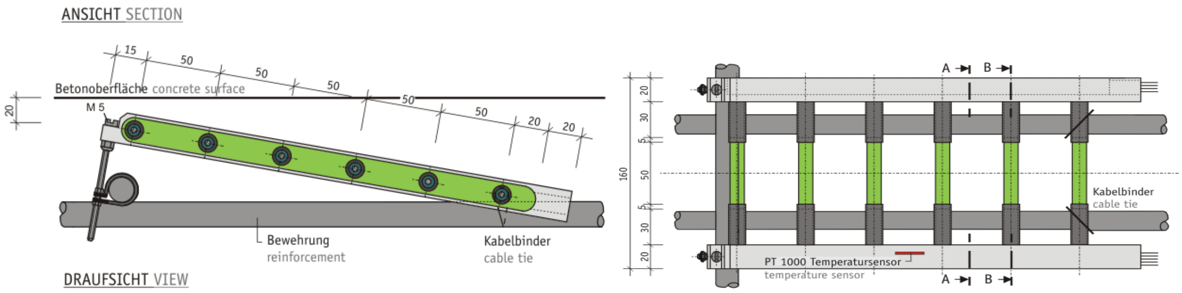

Figure 1 Anode ladder sensors installed in the bridges [4]

2.2. BRIDGES WITH INSTALLED MONITORING SYSTEMS

Maslenica Bridge is a 377.6 m long reinforced concrete arch bridge spanning Maslenica Strait of the Adriatic Sea, north of Zadar, Croatia, carrying the Croatian A1 motorway, Figure 2 a). The bridge comprises a 200 m span reinforced concrete arch, with an arch rise of 65 m. The arch comprises a box cross section, a double cell of constant depth. The superstructure is continuous across 12 spans, consisting of prestressed girders made monolithic with the in situ cast deck slab and transverse girders. Bridge was built during 1996 and 1997. It is situated close to the sea, with strong winds coming from Velebit side (North-West), bringing salt water to bigger heights if the column and arch. During the execution of the bridge 21 corrosion sensors were installed in different parts of the bridge structure, Figure 2 b).

Krka Bridge is located between the Skradin and Šibenik interchanges, Figure 2 c). It is a 391 m long concrete arch bridge spanning the Krka River at a height of 65 m. It carries the A1 motorway route south of Skradin, in immediate vicinity of Krka National Park. The Krka River canyon is spanned by 204 m reinforced concrete arch, with arch rise of 52 m. The bridge was built during 2004 and was opened to traffic in 2005. Krka Bridge is oriented from north-west to south-east, and is exposed to mixture of salt and river water on its south-west side, and to river water on its north-east side. During the execution of the bridge 6 corrosion sensors were installed in different parts of the bridge structure. Sensors K1, K3 and K5 are oriented towards the sea side, while the sensors K2, K4 and K6 are located away from the sea side, Figure 2 d).

Cetina Bridge is an arch bridge with 140.3 m span, constructed across the Cetina River canyon near the town of Trilj, Figure 2 e). The arch is of span 140 m with a rise of 21.5 m, giving rise-to-span ratio of 1/6.5. The construction of the bridge across the Cetina River canyon commenced in the year 2005 and it the bridge was opened for traffic in June 2007. Cetina Bridge is crossing the canyon over river Cetina from west to east and is not directly exposed to chlorides from sea water. During the construction of the bridge 6 corrosion sensors, anode ladder type, were installed in different location of the bridge, Figure 2 f).

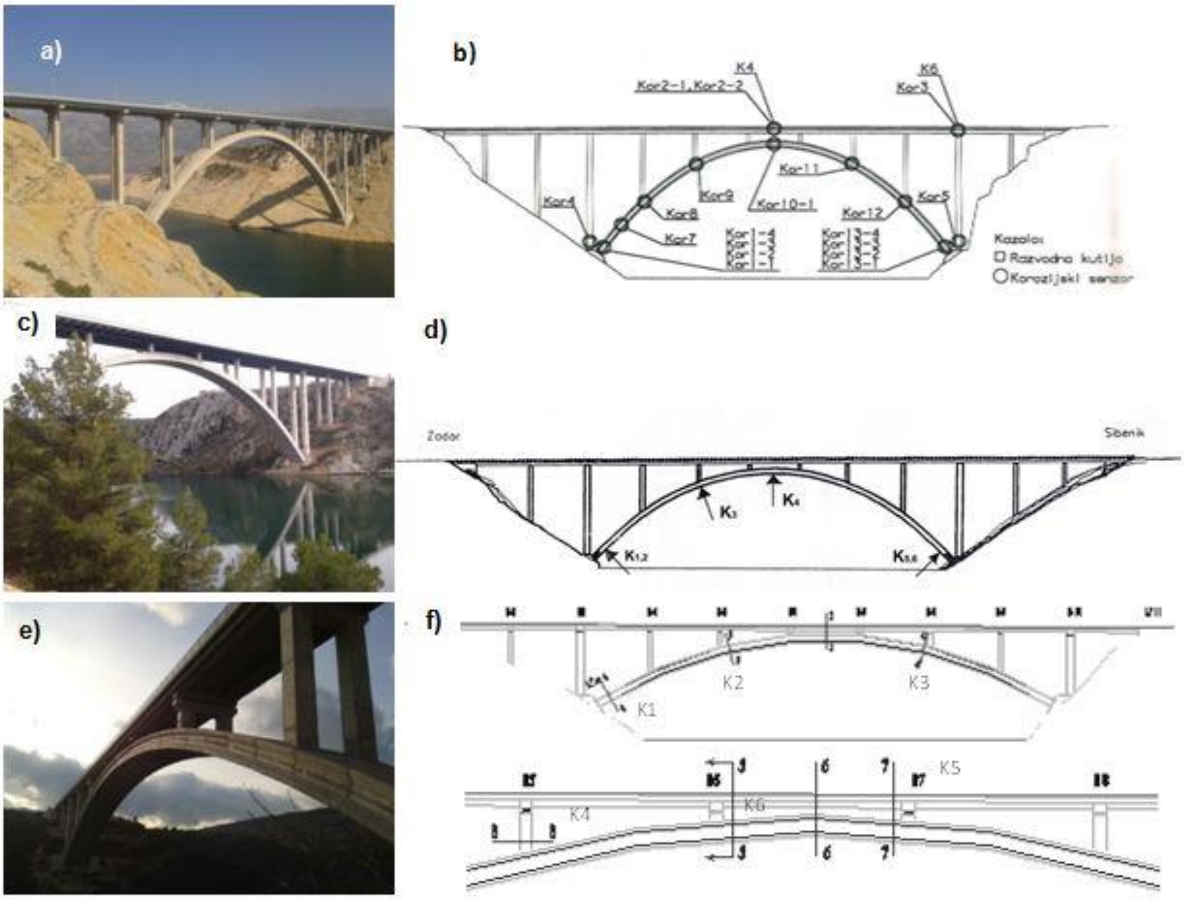

Figure 2 Bridges and location of sensors: a)-b) Maslenica Bridge, c)-d) Krka Bridge, e)-f) Cetina Bridge

3. RESULTS AND DISCUSSION

3.1. MASLENICA BRIDGE

Maslenica Bridge is situated next to the sea, with extremely strong winds. Column that is closest to the sea is severely damaged by corrosion, with visible reinforcement and concrete spalling, Figure 3 a). Localised corrosion attacks are formed on the places where low concrete cover was achieved. No zero measurements on corrosion sensors were performed. Some of the measuring boxes of sensors were destroyed by the action of wind and salt, Figure 3 b), and had to be repaired in order to perform measurement, Figure 3 c).

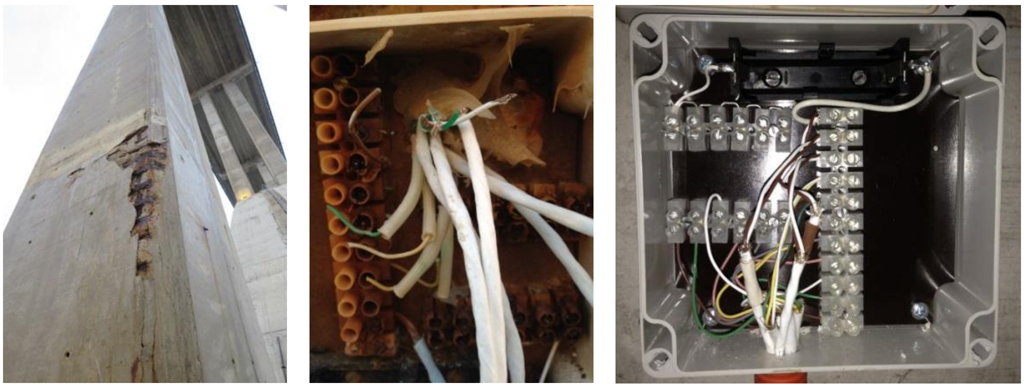

Figure 3 a) Corrosion observed on the site of Maslenica Bridge, b) Ruined measuring boxes of sensors before measurement and c) replaced boxes during measurement

In the scope of the project, 19 of 21 sensors were located, fixed and measurements were performed in 2014, 17 years after construction of the bridge and sensor installation. Beside corrosion monitoring, information on chloride levels and concrete properties are available from 2007 and 2012. Measurements of potential and current performed after 17 years of service life are presented in Figure 4.

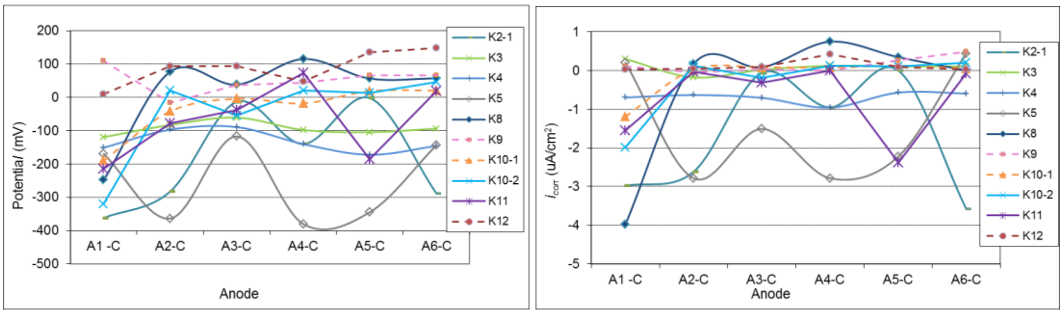

Figure 4 Measurement of potential and current on Maslenica Bridge after 17 years of exposure

Each of sensors consists of six anodes (A1 to A6), where A1 is near the surface and A6 at the same depth as reinforcement. Values of potential are between 100 and -400 mV, depending on the position of the sensor. Sensors that are embedded in columns close to the sea (K5, K4) have low values of potential (between -300 and -400 mV) even deeper within concrete, indicating that the corrosion induced throughout the concrete cover and reached reinforcement. The same can be seen from values of current density, which are high and reach -4 μA/cm^2. It is noticed that if second electrode start to corrode, first anode become cathode and its potential increase, electrode become passive. This is observed for other anodes according to depth (alternating lower and higher potentials).

4. KRKA BRIDGE

Readings from corrosion monitoring installed in Krka Bridge were performed four times during the 10 years of service life. Values of potential and current of anode ladders after 10 years of exposure are shown on Figure 5. It can be seen that the values of potential are slightly negative, with maximum negative value of -60 mV, while currents are low, both indicating that the anodes of the sensors and reinforcement inside the concrete are still passive. The lowest potential obtained on the reinforcement is -88 mV, still indicating a passive reinforcement inside the concrete. The highest negative current density on anode near the reinforcement after 10 years is -0.05 μA/cm^2, which is above the corrosion initiation limit (-0.1 μA/cm^2). From the values of corrosion sensors and based on the visual assessment of elements, it can be concluded that there is no corrosion on the structural elements of Krka Bridge.

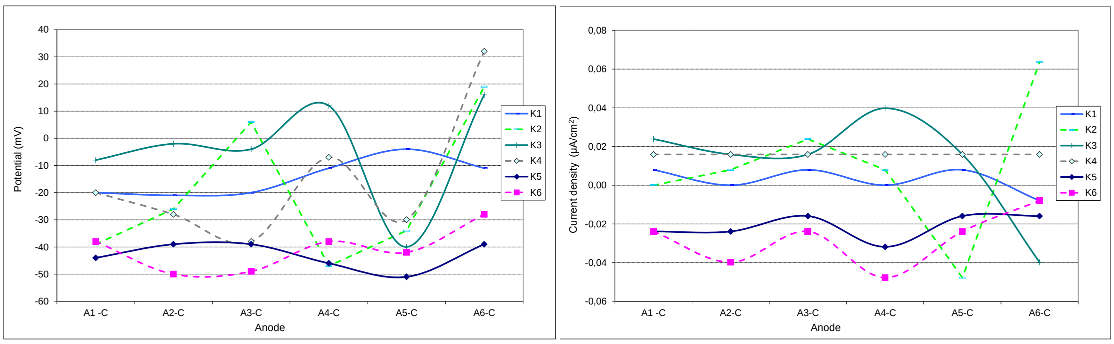

Figure 5 Measurement of potential and current on Krka Bridge after 10 years of exposure

4.1. CETINA BRIDGE

Measurements of potential and current performed after approximately 7 years of service life are presented in Figure 6. It can be seen that the values of potential are between – 50 mV and + 100 mV. The most positive values are obtained on the slab of the bridge and higher parts of the arch, while the negative values are obtained on the bottom of the arch. All the obtained values indicate a passive behaviour of anode ladders, throughout the concrete cover. The values of current density are between -0.1 and +1.64 μA/cm^2. Positive current densities are indicating that the anode is protected from corrosion and that it actually acts as a micro cathode compared to another anode close by. This can clearly be observed in the case of sensor K3, where the current density of anode A4 is higher than the current density of anode A2 and A3. It could be possible that a macro-cell formed between the anodes. No corrosion process was detected in the case of Cetina Bridge, except on the arch foot, where corrosion current density is at the limit value for corrosion initiation.

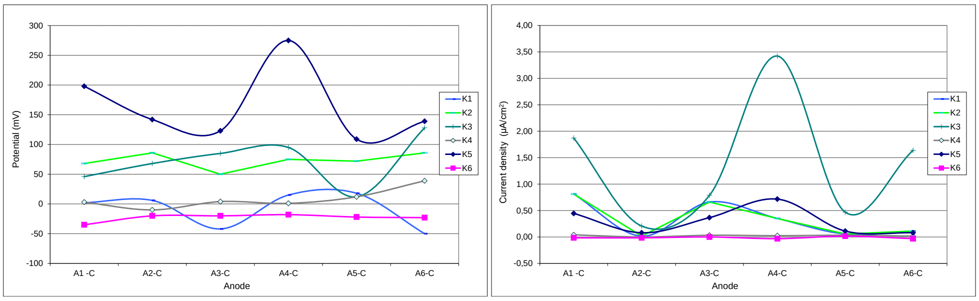

Figure 6 Measurement of potential and current on Cetina Bridge after 7 years of exposure

5. DISCUSSION

Comparison of potentials measured between steel reinforcement and cathode for all three tested bridges, according to sensor positions on arches is shown in Figure 7, on which potentials for different positions on arches are compared. For protected arch plates (oriented toward coast, or top arch plates) in all cases potentials are positive or slightly negative, which indicate that there are no reinforcement corrosion. For unprotected arch plates (oriented toward sea, or bottom arch plates) for all three bridges potentials are slightly negative, up to -50 mV which indicate that there are no severe reinforcement corrosion. For arch foots for all three bridges potentials are more negative (-60 to -150 mV) which indicate possible corrosion activity.

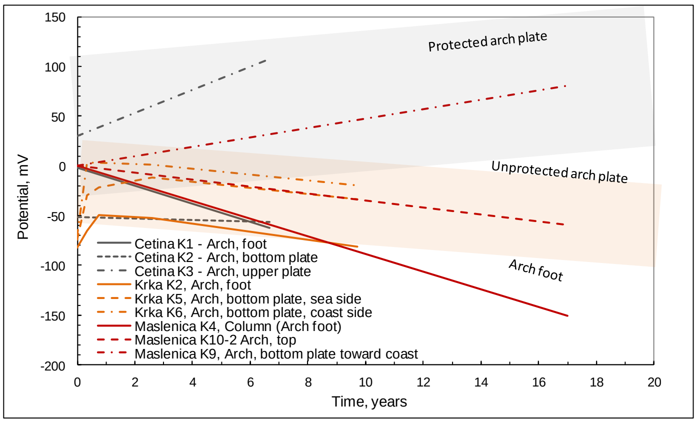

Figure 7 Comparison of measured potentials for different sensor positions on arches

Figure 8 shows comparison of measurement results of corrosion rates and potentials, where measurements on all anodes for sensors on Maslenica Bridge, for CR > 0 are considered. Criteria for potentials obtained from this correlation, considered 95 % probability confidence intervals are shown in Table 1. As potential criteria for given corrosion rates overlapping, it can be concluded that potential measurements can give only indication about corrosion activity. This table leads to criteria similar as given in ASTM 876 test standard - for positive potentials there are no corrosion activity, and for potentials lower than -200 mV corrosion activity is almost sure, and for potentials lower than -390 mV there are severe corrosion. For potentials between 0 mV and -200 mV corrosion is uncertain (50 % probability for corrosion).

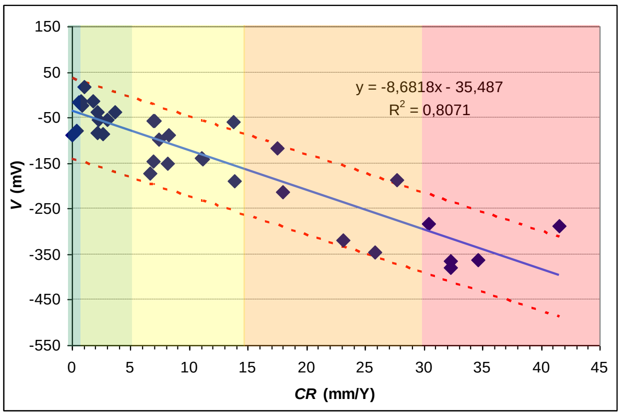

Table 1 Criteria for potentials from CR considered 95 % confidence limits

CR (µm/year)	V $_{MnO2}$ (mV)
0	36 to -140
1	28 to -148
5	-6 to -181
15	-90 to -265
30	-215 to -390

Figure 8 Correlation between Corrosion rate and potential

Figure 9 shows comparison of in-situ measurement results of corrosion rates and electrical resistivity of concrete. It is evident that for electrical resistivity of concrete higher than 1500 Ωm in all cases there are no corrosion activity (measured corrosion rates is zero). For resistivity lower than 1500 Ωm corrosion rate is uncertain - it may be either low of high. This may be connected with oxygen access, because for water saturated concrete there are low resistivity, but there are no oxygen to allow corrosion process. For corrosion rates upper than 30 mm/year, concrete resistivity is always lower than 500 Ωm. These considerations can be described by Table 2. Obtained results are in agreement with a RILEM TC 154 technical recommendation [6], which gives similar criteria for electrical resistivity for concrete with cement with slag addition.

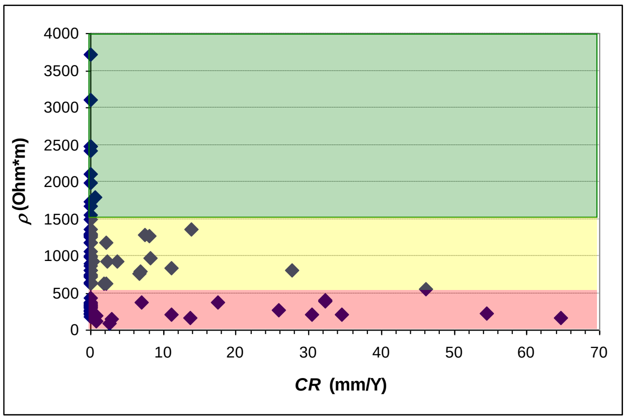

Table 2 Criteria for resistivity of concrete obtained from in-situ measurements

Concrete resistivity (Ωm)	Likely corrosion rate
<500	High
500-1500	Moderate
>1500	Low

Figure 9 Correlation between corrosion rate and electrical resistivity of concrete

Figure 10 a) shows diameter decrease of steel reinforcement bars obtained from CR test results at different ages. Figure 10 b) shows chloride content measured by chemical analysis of drilled powder from same or similar positions, also at different ages of bridges. It is noticed that for age of 10 years diameter decrease is about 3 µm which corresponds to chloride content of 0.05 % per mass of concrete. Diameter decrease of 50 µm corresponds to chloride content of 0.26 % per mass of concrete.

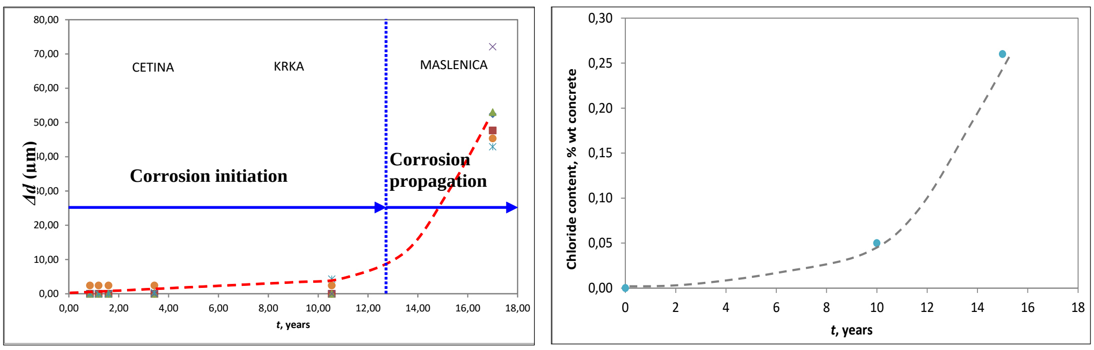

Figure 10 a) Reinforcement diameter decrease for bridges of different ages, b) Cl- ion concentrations for different ages

6. CONCLUSIONS

Data obtained from corrosion monitoring systems on three bridges on the Adriatic coast show that anodic ladders are appropriate techniques for direct assessment of corrosion activity in real structures. Based on the analysis of results from measuring campaign, criteria for translating the output of this corrosion monitoring system into values which can be implemented in the maintenance and asset management for cost-effective operation are given. The main advantage of presented corrosion monitoring system for bridge monitoring is the ability to reliably detect early corrosion processes taking place on reinforced steel as well as to monitor the evolution of corrosion. Early detection of possible corrosion failure, including the data of location, type and extent of damage, enables repair in time and thus leads to prolonged service life as well as lower overall maintenance costs during service life of reinforced structure.

ACKNOWLEDGMENTS

Corrosion monitoring in year 2014 was performed in the framework of EU project TRIMM "Tomorrow's road infrastructure monitoring & management", funded under the EC 7th Framework programme.

REFERENCES

[1] Bjegović, D., Mikulić, D., Sekulić, D, (2000), Non-destructive corrosion rate monitoring for reinforced concrete structures, 15th World Conference on Non-Destructive Testing, Rome, 15-21 October 2000, Proceedings, Paper 642.

[2] Raupach, M., Schießel, P., 2001. Macrocell sensor systems for monitoring of the corrosion risk of the reinforcement in concrete structures. Materials and Structures, 31, pp. 435-441.

[3] http://trimm.fehrl.org/

[4] Bleiziffer, J., Radić, J., 2010, Monitoring performance of large Croatian bridges ARCH'10 / Chen, Baochun ; Wei, Jiangang (ed.). Zagreb: SECON , 2010. 875-882 (ISBN: 978-953-7621-10-0). 6th International Conference on Arch Bridges, Fuzhou, Kina, 11-13.10.2010

[5] http://www.sensortec.de/

[6] Polder, R.B., 2001. Test methods for on-site measurement of resistivity of concrete — a RILEM TC-154 technical recommendation Construction and Building Materials Volume 15, Issues 2–3, March–April 2001, Pages 125–131

EXTRACTING PERFORMANCE INDICATORS FOR ARCH BRIDGE ASSESSMENT

Ana Mandic Ivankovic[1], Alfred Strauss[2], Marija Kuster Maric[1]

[1] University of Zagreb Faculty of Civil Engineering, Department of Structural Engineering, Fra Andrije Kacica Miosica 26, 10 000 Zagreb, Croatia, email: mandicka@grad.hr, marijak@grad.hr
2 University of Natural Resources and Life Sciences, Department of Civil Engineering and Natural Hazards, Institute of Structural Engineering, Peter Jordan Straße 82, 1190 Wien, Austria, email: alfred.strauss@boku.ac.at

SUMMARY: In this paper and following further research, key indicators to be monitored, for achieving efficient and effective performance of existing concrete arch bridge, through their design lifetime, will be revealed. Namely, on one hand, under the auspices of undergoing COST Actions TU 1406 (Quality specifications for roadway bridges, standardization at a European level) with a support of the COST Action TU 1402 (Quantifying the Value of Structural Health Monitoring), bridge performance aspects for achieving goals crucial for optimal bridge management are analysed. Categorisation process of operational based performance indicators is under progress, aiming further extension of operational database with the research- based one, particularly in the area of monitoring based performance indicators. On the other hand, research on development of assessment procedures for existing arch bridges is developing through several years in Croatia as a part of an extensive project to develop their appropriate maintenance strategy. To define a correct structural model of the existing structure and to perform adequate structural analysis, in order to properly assess the existing bridge, it is necessary to identify desired knowledge level of the existing structure based on the bridge importance. In order to get a valuable link between a certain indicator measurement (performance indicator) and corresponding property of structure (structural performance type or performance goal) of interest at the desired knowledge level, it is of a great importance to establish adequate data collection using appropriate monitoring methods for arch bridges. Therefore, this paper will show how the experience with Adriatic arch bridges serves as a base to extend the national project to the European level in order to prepare comprehensive guidelines for data collection to reach required knowledge level and to properly assess performance abilities of arch bridges in general.

IZDVAJANJE POKAZATELJA PONAŠANJA ZA OCJENJIVANJE LUČNOGA MOSTA

SAŽETAK: U ovom radu i u slijedećim istraživanjima dat će se pregled opažanih ključnih pokazatelja za određivanje učinkovitog i uspješnog ponašanja postojećeg betonskog lučnog mosta razmatranjem njegova proračunskog vijeka. S jedne su strane analizirani, u okviru postojećeg programa COST Actions TU 1406 (Specifikacije kvalitete cestovnih mostova, normizacija na europskoj razini) uz podršku programa COST Action TU 1402 (Kvantifikacija vrijednosti opažanja stanja konstrukcije) aspekti svojstava mosta za postizanje ciljeva važnih za optimalno upravljanje mostom. Proces kategorizacije pokazatelja svojstava osnovanih na funkcioniranju sada je u tijeku s ciljem daljnjeg proširenja operativne baze podataka istraživačkom bazom, posebno u području pokazatelja osnovanih na opažanjima. S druge strane, istraživanje razvoja postupaka ocjenjivanja za postojeće lučne mostove, u Hrvatskoj je razvoju već nekoliko godina kao dio opsežnog projekta razvoja prikladne strategije njihova održavanja. Da bi se definirao ispravan model konstrukcije postojeće građevine i proveo odgovarajući proračun konstrukcije s ciljem pravilne ocjene postojećega mosta nužno je identificirati poželjnu razinu znanja postojeće konstrukcije osnovanu na važnosti mosta. Kako bi se ostvarila vrijedna povezanost nekih pokazatelja mjerenja (pokazatelja ponašanja) i odgovarajućeg svojstva konstrukcije (vrsta ponašanja konstrukcije ili cilj ponašanja) koji nas zanima na željenoj razni znanja, od velike je važnosti ustanovljenje odgovarajuće zbirke podataka upotrebom prikladnih metoda opažanja lučnih mostova. Stoga se u radu pokazuje kako iskustvo s jadranskim lučnim mostovima služi kao baza za proširenje nacionalnog projekta na europsku razinu kako bi se pripremile sveobuhvatne smjernice za prikupljanje podataka da bi se postigla zahtijevana razina znanja i sposobnost pravilne ocjene ponašanja lučnih mostova općenito.

1. INTRODUCTION

The main objective of the COST Action TU1406 is to develop a guideline for the establishment of QC plans in roadway bridges, by integrating the most recent knowledge on performance assessment procedures with the adoption of specific goals [1]. On the other hand, the main objective of the COST Action TU1402 [2] is to develop efficient approaches to quantify, assess and optimize the benefit of SHM, in order to convince infrastructure owners and operators to invest in SHM systems. By developing new approaches to quantify and assess bridge performance, with acknowledging optimal benefit of SHM even before its implementation, bridge management strategies will be significantly improved, enhancing asset management of ageing structures in Europe.

In addition, research on development of assessment procedures for existing arch bridges is developing through last few years in Croatia as a part of an extensive project to develop their appropriate maintenance strategy. There are six major reinforced concrete arch bridges in Croatia located on Adriatic coastline, with spans ranging from 200 m to almost 400 m. Four arch bridges, the Šibenik Bridge, the Pag Bridge and the Krk Bridges (two arches) were built during the sixties and the seventies of the 20th century. They are usually referred to as the first generation of Croatian Adriatic arches. Two major bridge structures Maslenica and Skradin Bridges were constructed on Croatian motorways more recently, Maslenica Bridge in 1997, and Skradin Bridge in 2005, and Cetina bridge was designed for the inland state road in 2007. One of the causes for rapid structural degradation of the first generation of Croatian Adriatic arches was underestimation of maintenance role in the past, mainly due to lack of funding for regular maintenance activities. More recently constructed arch bridges of second generation are designed taking into account the experience from in-service performance of older arch bridges and are equipped with a range of sensors for long-term monitoring, but again due to lack of founding those are not exploited appropriately. To eliminate the errors of the past and ensure efficient and effective performance of existing but also the future concrete arch bridges, the appropriate management strategy should be further developed [3].

Having all this in mind, and inspired with the work in above mentioned European actions and Croatian national project, authors of this paper aim to present the background, current findings and plans for further research with the main objective of crating novel procedure for arch bridge assessment in order to improve their management at the European level.

2. DEVELOPMENT OF EUROPEAN PI DATABASE FOR ROAD BRIDGES

The determination of performance indicators for bridge structures from European countries and its harmonization on a European level is complex, extensive, and time consuming process. Through the activities of the Working Group 1: Performance Indicators of the Cost Action TU 1406, operators' database was created by surveying documents related to bridge maintenance, assessment and management from different European countries. The core of the survey process was structured as a user interface in Excel by storing information in four main groups [4]: Performance level, Damage, Performance indicator/index and Performance assessment. The background for this structure comes from screening of the Austrian national document [5] and two documents from United Kingdom [6]. In order to support on the interface in the screening process, a Glossary of key terms is required to store the information and terminology related to Performance Indicators, Performance Goals, Performance Thresholds and Performance Method. It has been prepared on the basis of the information from German and Austrian documents [7].

After collecting the input from different countries, heterogeneous data on bridge performance aspects were systemized through clustering and homogenization of performance related terms. Example of homogenisation within the Croatian database is shown at the Figure 1. For each available cluster of performance indicators, one example for converting terms from original database into a homogenised one is given. Upon homogenisation from all countries the number of indicators was significantly reduced.

In order to move on with the reduction of the list of Performance Indicators, an Expert Group was asked to specify PIs (YES/NO) according to the following points: Measurable?; Quantifiable?; Target value available?; Valid for ranking?; Allow decision with economic implications?.

A) Performance Level				B) Damage		C) Performance Indicator/Index		D) Performance Assessment		
level	system	Compo-nent	material	type	characteristic	indicator	detection	threshold	goal	
Sub_ System	All bridge types	Super Structure	Concrete	Damage_ State	Cracks	Damage degree	Direct_ Measurement	crack width (mm)	Damage Assessment	DEFECTS Crack width
Sub_ System	All bridge types	Super Structure	Concrete	Damage_ State	Honeycombing	Damage degree	Direct_ Measurement	affected area (m2)	Damage Assessment	MATERIAL PROPERTIES bad concrete compaction
Sub_ System	All bridge types	Super Structure		Damage_ State	Freeze-thaw	Damage degree	Direct_ Measurement	affected area (m2)	Damage Assessment	ENVIRONMENTAL BASED freeze-thaw
Sub_ System	All bridge types	Super Structure	Brick	Damage_ State	Disintegration of mortar	Damage	Visual_ Inspection		Damage Assessment	STRUCTURAL INTEGRITY & JOINTS disintegration of mortar
Sub_ System	All bridge types	Railings	Steel	Damage_ State	Missing parts	Damage degree	Visual_ Inspection		Damage Assessment	EQUIPMENT AND PROTECTION absence of equipment component
System	All bridge types			Damage_ State	Buckling	Damage degree	Visual_ Inspection		Damage Assessment	GEOMETRY CHANGES Buckling
System	All bridge types		Concrete	Damage_ State	Execution defects	Damage degree	Direct_ Measurement	affected area (m2)	Damage Assessment	ORIGINAL CONSTRUC-TION & DESIGN execution/construction defects
Element				Damaging_ Process	low demage degree (first phase)	Damage degree	Visual_ Inspection	Upper limit + Duration of damage phase	Damage Assessment	RATING damage degree +damage evolution
Element						importance of bridge element		Quantitative scale of values	Element importance assessment	COST & IMPORTANCE importance of bridge element

Figure 1 Example of homogenization of terms within the Croatian database

Safety, Reliability, Security						
PI	**Level**	**Performance indicator PI if**	**PI belongs to the Key Peformance**	**Assessment**	**rating (1-5)**	**weighting**
	Component Level (CL) System Level (SL) Network Level (NL)	Measurable? {Quantifiable? Target value available? Valid for ranking purposes? Allow decision with economic implications?} (YES/No) Technical (Tech), Socio Economical (SoEc), Sustainable (Sust)	Reliability (R), Availability (A), Maintainability (M), Safety (S), Security (Se), Environment (E), Costs (C), Health (H), Politics (P), Rating/Inspection (I)	Threshold (T = ...) Goal (G = ...) Rating (R = ...)		
concrete cover (insufficient)	CL	Yes, Tech, Sust	R, A, (C, I)	T= thickness (mm), G= assessment of damage and affected area (m2), R=important for durability	2	0,8
origin (e.g. due to loading, due to settlement, due to crumbling of concrete,...	CL, SL		R, A, S, (C, I)	T=width (mm), G=understand origin through the correlation of the observed thickness (mm), length (cm), location/orientation and spacing/pattern, R=key PI to access reliability	3	0,5
fatigue cracking	CL, SL	Yes, Tech	R, A, S, (C, I)	T= number of cracks and affected components; G= local or generalized situation and importance of affected components; R= Key for reliability.	5	0,3
settlement	SL	Yes, Tech	R, A, S, (C, I)	T= dimension (mm) and orientation (º), G= Affected components, stable/evolving, R=key for structural equilibrium	2	1
.....	....	....	...	...	...	...
					total rating	n_{SRS}

Figure 2 Cut out of the categorization of PI at different levels, taking into account different aspects

At the end, approximately 100 extricated PIs are further related with one or more Key Performance Indicators (KPI): Reliability (R), Availability (A), Maintainability (M), Safety (S), Security (Se), Environment (E), Costs (C), Health (H), Politics (P), Rating/Inspection (I). Further the process required the categorization of Performance Indicators in relation to Performance Goals (PG) and Performance Thresholds (PT) at different levels: component (CL), system (SL), network (NL); taking into account different aspects: technical (Tech), sustainability (Sust) and socio-economic (SoEc). Each expert's feedback was systemized as shown in the cut out example at the Figure 2.

Categorization process is still undergoing, aiming final overall rating of each of the five most important groups of Key Performance Indicators (with rating factors r_{SRS}, r_{AM}, r_C, r_E and r_{HP}) required to define quality specifications and control plans of road bridges at the European level. Example is presented with the Figure 3. Green areas represent the most favourable rate and the red areas should alarm the bridge operator and require immediate intervention.

KPI	
Safety, Reliability, Security	r_{SRS}
Availability, Maintainability	r_{AM}
Costs	r_C
Environment	r_E
Health, Politics	r_{HP}

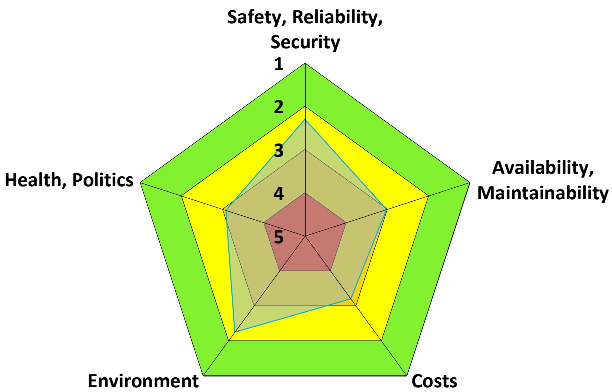

Figure 3 Overall rating example of each of the five most important KPIs groups

3. MAIN FINDINGS FROM ASESSMENT OF CROATIAN ARCH BRIDGE

Structural health monitoring as a wider term, comprise standard inspection techniques performed periodically but following regular maintenance plan and continuous or periodic but long-term measurements of time variant measures. Examples of standard inspection and investigation methods that are used in particular time at the Croatian arch bridges together with advices on future action are shown at the Figure 4.

Assessment of existing reinforced concrete arch bridges, as a part of their efficient and effective maintenance strategy, comprises assessing bridge serviceability, its capacity for traffic, seismic performance and performance due to wind load. To define a correct structural model of the existing structure and to perform adequate structural analysis, it is crucial to capture all the indicators that affect certain structural performance. Additionally it is necessary to identify desired knowledge level of the existing structure based on the bridge importance and consequences of its failure. Although the interaction of various indicators that affect certain structural performance is inevitable, they need to be segregated in order to more easily identify methods for their quantification. Categorization of performance indicators and their interaction are elaborated through the experience gathered during assessment of several Croatian arch bridges in following papers [8, 9, 10]. In this paper, the main findings on indicators related to performance assessment of arch bridges are systemized in the Table 1

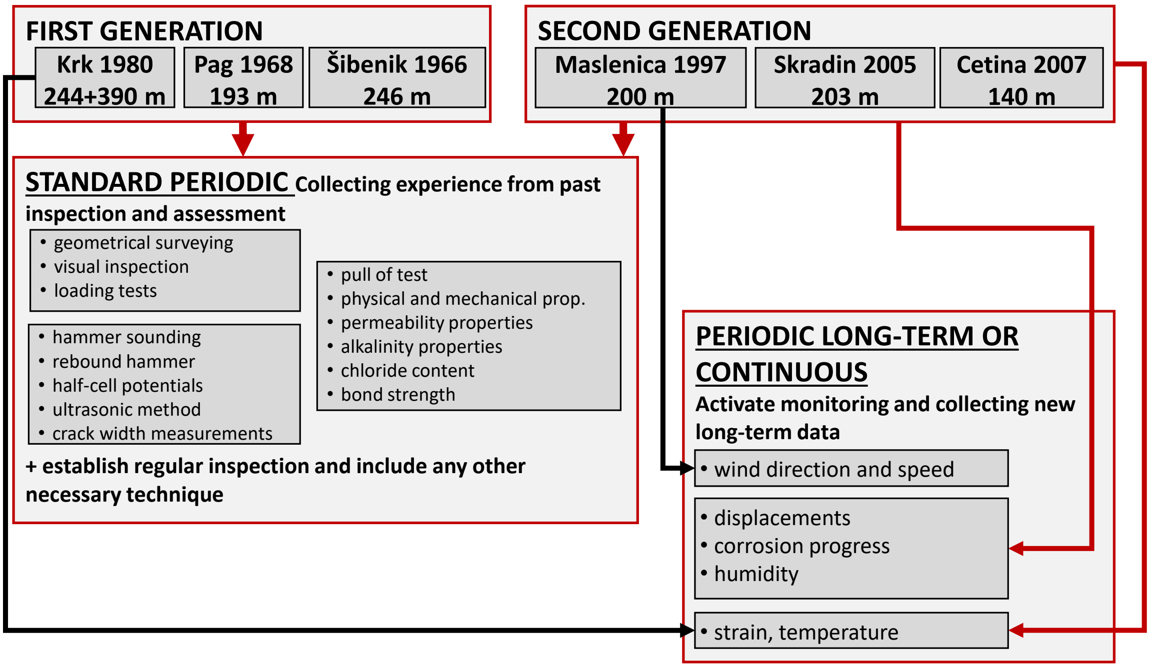

Figure 4 Monitoring methods used and available at Croatian arch bridges

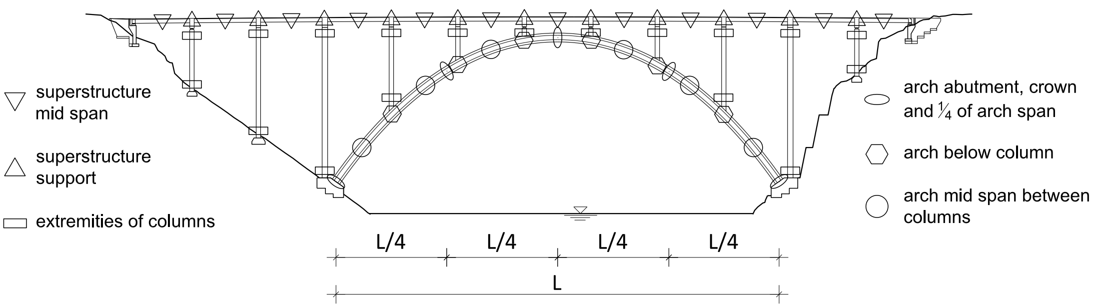

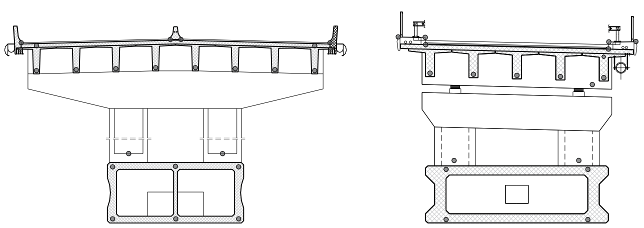

Knowledge level	Documen-tation	Percentage of critical cross section		Confidence factor
		Details inspection	Material testing	
KL2	Available incomplete	20%	20%	1.2
	Not existing	40%	40%	
KL3	Available complete	20%	20%	1.0
	Not existing	60%	60%	

Figure 5 Data collection and minimum requirements of in-situ inspection and testing in critical cross sections and critical points at the cross section of arch bridges

Table 1 Indicators related to performance assessment of arch bridges

Structural indicators
Geometry
arch axis (deformations)
pier axis (inclinations/deformations)
geometrical coefficient of columns
scale factor for columns
column global stiffness
slenderness of elements
bridge width (pavement width)
superstructure span
deformations
Cross section details
outer dimensions
depth of concrete cover (inadequate)
amount and dtailing of longitudinal reinforcement
amount and detailing of shear reinforcement
amount, spacing and detailing of confining reinforcement (piers)
design ultimate moment of the plastic hinge section
yield curvature of the plastic hinge section
effective stiffness of cross section
Materials
concrete strength
confined concrete strength
steel yield strength
steel ultimate strength and ultimate strain
modulus of elasticity
specific weight of cornices, curbs, barriers, pavement density
Integrity and structural details
arch-pier connection (level of restrain)
pier-superstructure connection
arch-superstructure connection
superstructure system (level of continuity)
support conditions (free and fixed translations and rotations)
allowable displacement at abutments
Dynamic properties/behaviour
confining reinforcement detailing
behaviour factor
chord rotation capacity
distribution of masses at the structure
stiffness distribution of cross sections
equipment properties (elastomeric bearings, dampers, shock transmitters)
dominant mode shapes and effective masses
position of reference points
target displacements

Environmental indicators
Damage degree or deterioration processes influencing structural degradation
chloride ingress (concentration in concrete cover)
carbonation depth
corrosion process
alkalinity properties
delamination of concrete cover
cracks width and spacing
area of de-bonded concrete
reinforcement corrosion
remaining cross section
Exposure parameters
height of sea- water splashing (wind influence)
height of tides influence
depth of de-icing agents influence
humidity
temperature drops
Seismic activity
peak ground acceleration
terrain category
Traffic load
heaviest national traffic load
localised traffic load
axle load and axle distances
overload
Wind influence
Wind velocity
dominant wind direction and gust
terrain roughness
Socio-Economic indicators
reference return period
remaining lifetime of a bridge
reduced value of peak ground acceleration
bridge importance / consequence class
traffic density
number of critical cross sections
number of critical points in each cross section
extent of documentation and previous inspections and test reports
knowledge level / confidence factor
cost of different inspection, testing, monitoring methods
previous maintenance activities (underestimation, lack of founding)
costs of different retrofit measures

Interaction of environmental indicators and structural ones is obvious. Structural parameters such are cross section dimensions or effective reinforcement might be changed due to deterioration processes from combined exposure to the sea and wind or on the other hand because of applied repair activities. This may result in reducing or improving a certain structural performance ability. Economic parameters will depend on the proper maintenance program offered and adequate activities performed previously at the existing bridge. Underestimation of maintenance role in the past, will cause deficiencies and deterioration and will require technically demanding, very difficult to perform and expensive repair works. Additionally higher knowledge level for a bridge of critical importance will require more extensive inspection works and comprehensive bridge monitoring which are economic indicators. For the bridges of the average importance that are not critical for communications, knowledge level KL2 is to be required. For bridges of critical importance for maintaining communications, especially in the immediate post-earthquake period and for major bridges where longer design life is required the knowledge level KL3 would be more appropriate. Due to limited budget, very often the engineer will need to assess the bridge condition based on a limited data collection. Therefore, it is of a great importance to establish appropriate collection of data including location (critical cross sections and critical point in each cross section) and extension of inspection, testing or monitoring methods. Additionally the most critical structural cross sections are the ones evaluated as damaged in the visual inspection.

4. OBJECTIVES AND TASKS FOR FURTHER RESEARCH

Main aim of the further research is to develop a guideline for performance assessment of large scale reinforced concrete arch bridges in order to achieve more effective management of large scale bridges within European road bridge network. Through the research, four specific objectives are to be reached:

- reveal the key performance indicators related to structural, environmental and economic aspects;
- define monitoring method (technique) to be used for measure certain quantity in order to define adequate performance indicator, and establish appropriate collection of data including location (critical cross sections and critical point in each cross section), type and extension of inspection, testing or monitoring methods;
- develop applicable procedures for assessment of existing reinforced concrete arch bridges, comprising assessing bridge serviceability, its capacity for traffic, seismic performance and performance due to wind load;
- identify key performance criteria for raising from the single arch bridge level to the network level for optimal priority repair ranking within the group of bridges of higher importance in a certain country,
- through following tasks and methodology
- an overview of inspections, repair, monitoring and assessment of large Adriatic arch bridges;
- update of the case study bridges database with arch bridges from several European countries (Portugal, i.e. Infante D. Henrique, Arrabida, Rio Zezere, Spain, i.e. Los Tilos, Tercer Milenio, Esla, Italy, i.e. Fiumarella, France, i.e. Chateaubriand, Morbihan, Germany, i.e. Wilde Gera, Kyll Valley);
- surveying, clustering, harmonising and categorisation of database;
- revealing key structural performance indicators (related to geometry, materials, details, integrity, dynamic properties), key environmental performance indicators (related to exposure parameters, local traffic, terrain category, seismic activity, wind influence), key economic performance indicators (related to founding for different inspections methods, required knowledge level, costs of different retrofit measures, optimum durability)
- establish appropriate collection of data for the required knowledge level;
- allocate performance indicators with appropriate weights – importance levels;
- develop procedures for assess different types of structural performances: corrosion progress, serviceability, traffic capacity, seismic performance, performance due to wind load.

5. CONCLUSIONS & FUTURE PROGRESS

The tradition in construction of reinforced concrete arch bridges in Croatia and experiences gained through their assessment will serve as the basis for improvement of assessment procedure for this type of bridges and optimal management of large scale bridges in general. Upon overviewing Croatian database, it will be expanded with the data on arch bridges from different European countries. By surveying, clustering, harmonising and categorisation of database on reinforced concrete arch bridges under the guidance of leading experts in the field, and by following procedures developed within the Working group 1 of the COST Action TU 1406, key performance indicators will be extracted. Their interactions and importance levels for assessing bridge serviceability, capacity for traffic, seismic performance and performance due to wind load will be integrated in the novel procedure for arch bridge assessment. Finally, criteria for raising from the single arch bridge level to the group of large scale arch bridges for optimal priority repair ranking will be established.

ACKNOWLEDGMENTS

This article is based upon work from COST Action TU 1406 and COST Action TU 1402 both supported by European Cooperation in Science and Technology and Croatian national project Performance indicators for assessment of existing bridges supported by Zagreb University.

REFERENCES

[1] Matos, J.C., Casas, J.R., Fernandes, S. 2016. COST Action TU1406 Quality Specifications for Roadway Bridges (BridgeSpec). Proceedings 8th international conference on Bridge Maintenance, Safety and Management, Foz do Iguaçu (Brazil), 26-30 June 2016. London: Taylor and Francis.

[2] European Cooperation in the field of Scientific and Technical Research – COST 2014 Memorandum of Understanding for COST Action TU1402

[3] Mandić Ivanković, A, Radić, J., Srbić M.: Finding a link between measured indicators and structural performance of concrete arch bridges, Proceedings of the 1st Workshop, COST Action TU1402: Quantifying the Value of Structural Health Monitoring, May 2015, DTU, Denmark, published September 2015, 102-116

[4] Strauss A. and Mandić Ivanković A. 2016. Performance Indicators for Roadway Bridges, Technical report of the Working group 1: Performance indicators of Cost Action TU1406

[5] Bundesministeriumfür Verkher, Innovation und Technologie, 2011. Quality Assurance for Structural Maintenance; Surveillance, Checking and Assessment of Bridges and Tunnels; Road Bridges, Vienna, Austria (in German)

[6] County Surveyors Society CSS, 2004. Addendum to: CSS Guidance Note On Bridge Condition Indicators. Volume 2: Bridge Inspection Reporting, Lincoln, United Kingdom

[7] Berichte der Bundesanstalt für Straßenwesen (BASt), 2015. Intelligente Brücke – Schädigungsrelevante Einwirkungen und Schädigungspotenziale von Brückenbauwerken aus Beton, Schünemann Verlag, Germany (in German)

[8] Mandić Ivanković, A., Srbić, M., Radić, J.: Performance indicators in assessment of concrete arch bridges (2016), Proceedings of the (th international conference on bridge maintenance, safety and management (IABMAS 2016), Foz do Iguaçu, Brazil 26-30 June 2016, pg 301+ cd

[9] Mandić Ivanković, A., Srbić, M., Franetović, M.: Performance of existing concrete arch bridges, Report of the IABSE Conference - Structural Engineering: Providing Solutions to Global Challenges, Geneva, Switzerland, September 23-25, 2015, 1033-1040

[10] Mandić Ivanković, A., Srbić, M., Radić, J.: Seismic performance of concrete arch bridges, fib Symposiuma 2016, Cape Town, South Africa, 21-23 November 2016., pg + cd

SERVICE LIFE PREDICTION OF CONCRETE STRUCTURES IN MARITIME ENVIRONMENT – CASE STUDY: MASLENICA MOTORWAY BRIDGE

Marija Kuster Maric[1], Josko Ozbolt[2], Gojko Balabanic[3], Ana Mandic Ivankovic[1], Dajana Zaric[1]

[1] University of Zagreb Faculty of Civil Engineering, Department of Structures, Fra Andrije Kacica Miosica 26, 10 000 Zagreb, Croatia, email: marijak@grad.hr, mandicka@grad.hr, zaricdajana1@gmail.com
2 University of Stuttgart, Institute of construction materials in civil engineering, Pfaffenwaldring 4, 70569 Stuttgart, Germany, email: ozbolt@iwb.uni-stuttgart.de
[3] University of Rijeka Faculty of Civil Engineering, Department for computational modeling of materials and structures, Radmile Matejcic 3, 51000 Rijeka, Croatia, email: gojko.balabanic@gradri.uniri.hr

SUMMARY: The paper provides a brief overview of recently developed fully coupled 3D chemo-hygro-thermo-mechanical model for simulation of chloride induced corrosion, before and after depassivation of steel as well as its consequences on degradation of reinforced concrete structures. Emphasis of this paper is given on the initiation phase of corrosion in order to analyse the influence of crack width and depth on the transport processes in concrete before depassivation of the steel rebar. The application of the model is illustrated on analysis of the reinforced concrete beam exposed to the cracking due to 4 point bending and influence of seawater. The numerical results of chloride content in concrete are compared with the results obtained on the Maslenica Motorway Bridge after 13 years of exposure to maritime conditions. Good agreement of numerical results and data obtained on the bridge is basis to predict remaining service life of the bridge. According to the assumption of the numerical analysis, depassivation of the reinforcement bar in un-cracked concrete is achieved after 100 years of exposure, while threshold chloride concentration on the level of the rebar in cracked concrete is reached within 1 year after crack opening. The service life will be shorter if the cracks in concrete are wider and deeper.

PREDVIĐANJE UPORABNOG VIJEKA BETONSKIH KONSTRUKCIJA U MORSKOM OKOLIŠU NA PRIMJERU AUTOCESTOVNOG MOSTA MASLENICA

SAŽETAK: U radu je dan kratak pregled u novije vrijeme razvijenih u potponosti kombiniranih 3D kemijsko – higro – toplinskomehaničkih modela simulacije korozije pruzročene kloridima, prije i nakon depasivizacije čelika i njegove posljedice na degradaciju armiranobetonskih konstrukcija. U radu je dan naglasak na početnu fazu korozije kako bi se analizirao utjecaj širine pukotina i procesa transporta u dubinu betona prije depasivizacije čeličnih šipki. Primjena modela objašnjena je analizom armiranobetonske grede izložene raspucavanju pri savijanju u četiri točke i utjecaju morske vode. Numerički rezultati sadržaja klorida u betonu uspoređeni su s rezultatima dobivenim na autocestovnom mostu Maslenica nakon 13 godina izloženosti morskim uvjetima. Dobro slaganje numeričkih rezultata i podataka dobivenih na mostu osnova su predviđanja njegova preostalog uporabnog vijeka. U skladu s pretpostavkama numeričke analize depasivizacija aramaturnih šipki u neraspucalom betonu nastupa nakon 100 godina izloženosti dok se prag koncentracije klorida na razini šipke u raspucalom betonu dostiže unutar jedne godine nakon otvaranja pukotine. Uporabni će vijek biti kraći ako su pukotine u betonu šire i dublje.

1. INTRODUCTION

The older Adriatic large concrete arch bridges (Šibenik Bridge, Pag Bridge and Krk Bridge) suffered greatly over decades of service, due to combination of aggressive maritime conditions such as high winds, chloride ingress, freeze/thaw and thermal action and inadequate attention to durability issues. Serious deterioration of structural members with reinforcement corrosion as the major degradation mechanism, led to many complex and expensive repairs [1]. Lessons learned from the first generation of arch bridges have been incorporated into design of the Maslenica Motorway Bridge in order to assure durability and reliability of structure in aggressive maritime environment [2]. However, beginning stage of chloride-induced corrosion on few elements of the Maslenica Bridge was noticed during the last visual inspection in 2010 [3].

The extensive cost of structure repair highlights the importance of developing a numerical model which is able to realistically simulate corrosion processes before and after depassivation of steel in concrete and the consequences for the structure. Moreover, by employing such a model, it is possible to formulate simple engineering models and design rules in order to increase the durability of structure and reduce its maintenance costs. In this purpose the coupled 3D chemo- hygro-thermo mechanical (CHTM) model is developed and implemented into a finite element code in order to enable a realistic prediction of service life of reinforced concrete structures exposed to chlorides and mechanical damage [4-8].

2. 3D CHEMO-HYGRO-THERMO-MECHANICAL MODEL FOR CONCRETE

Generally, numerical models for simulation of corrosion of steel in concrete assume that the service life of the structure consists of two phases: initiation and propagation [9]. The initiation phase is characterized by transport processes in concrete before depassivation of steel rebar. The propagation phase starts when the surface film of ferric oxide is broken or depassivated by reaching the threshold concentration of chloride ions in concrete pore solution in contact with steel surface. Corrosion of steel in concrete is an electrochemical process including dissolution of iron and formation of corrosion products (rust). The volume of corrosion products is 2 to 7 times greater than the volume of reactants, which results in local concrete cracking [10].

The coupled 3D CHTM model for transient analysis of transport and corrosion processes before and after depassivation of steel reinforcement in concrete includes the following physical, electrochemical and mechanical processes [4-8]: (i) transport of capillary water, heat, oxygen and chloride through the concrete cover; (ii) immobilization of chloride in the concrete; (iii) cathodic and anodic polarization; (iv) transport of OH- ions through electrolyte in concrete pores; (v) mass sinks of oxygen on steel surface due to cathodic and anodic reaction; (vi) distribution of electrical potential and current density; (vii) transport of corrosion products in concrete and cracks; and (viii) concrete cracking due to mechanical and non-mechanical actions. The corrosion current density is the relevant parameter to estimate reduction of the cross-section of the rebar and to predict the increase of the corrosion product volume, while realistically simulation of the corrosion induced cracking and spalling of the concrete cover enables to estimate reduction of the concrete cross-section area. Reduced areas of the concrete and rebar cross-sections lead to reduced load-bearing capacity of the structural element. The service life of the structure is achieved when the load- bearing capacity of a structural element is decreased to the threshold value.

Emphasis of this paper is given on the initiation phase of corrosion in order to analyse the influence of crack width and depth on the transport processes in concrete before depassivation of the steel rebar, while detailed discussion about the mathematical formulations of the processes after the depassivation of reinforcement bar and their implementation into a 3D finite element code can be found in reference [5-8].

2.1. INITIATION PHASE

In the model the transport of capillary water is described in terms of volume fraction of pore water in concrete by Richard's equation [11], based on the assumption that transport processes take place in aged concrete, i.e., the hydration of cement paste is completed:

$$\frac{\partial \theta_w}{\partial t} = \nabla \cdot \left[D_w(\theta_w) \nabla \theta_w \right] \tag{1}$$

where θ_w is volume fraction of pore water (m^3 of water / m^3 of concrete) and $D_w(\theta_w)$ is capillary water diffusion coefficient (m^2/s) described as a strongly non-linear function of moisture content [12]. Transport of chloride ions through a non-saturated concrete occurs as a result of convection, diffusion and physically and chemically binding by cement hydration product [11]:

$$\theta_w \frac{\partial C_c}{\partial t} = \nabla \cdot \left[\theta_w D_c(\theta_w, T) \nabla C_c \right] + D_w(\theta_w) \nabla \theta_w \nabla C_c - \frac{\partial C_{cb}}{\partial t} \tag{2a}$$

$$\frac{\partial C_{cb}}{\partial t} = k_r \left(\alpha C_c - C_{cb} \right) \tag{2b}$$

where C_c is concentration of free chloride dissolved in pore water (kg$_{Cl^-}$/m^3 pore solution), $D_c(\theta_w, T)$ is the effective chloride diffusion coefficient (m^2/s) expressed as a function of water content θ_w and concrete temperature T, C_{cb} is concentration of bound chloride (kg$_{Cl^-}$/m^3 of concrete), k_r is binding rate coefficient, α = 0.7 is constant [3].

Assuming that oxygen does not participate in any chemical reaction before depassivation of steel, transport of oxygen through concrete is considered as a convective diffusion problem [11]:

$$\theta_w \frac{\partial C_o}{\partial t} = \nabla \cdot \left[\theta_w D_o(\theta_w) \nabla C_o \right] + D_w(\theta_w) \nabla \theta_w \nabla C_o \tag{3}$$

where C_o is oxygen concentration in pore solution (kg of oxygen / m^3 of pore solution) and $D_o(\theta_w)$ is the effective oxygen diffusion coefficient [4], dependent on concrete porosity p_{con} and water saturation of concrete S_w.

Based on the constitutive law for heat flow and conservation of energy, the equation which describes temperature distribution in continuum reads [4]:

$$\lambda \Delta T + W(T) - c\rho \frac{\partial T}{\partial t} = 0 \tag{4}$$

where λ is thermal conductivity (W/(m K)), c is heat capacity per unit mass of concrete (J/(K kg)), ρ is mass density of concrete (kg/m^3) and W is internal source of heating (W/m^3).

More detailed discussion about the mathematical formulations of the processes before the depassivation of reinforcement bar and their implementation into a 3D finite element code can be found in reference [4].

2.2. HYGRO-THERMO-MECHANICAL COUPLING

The mechanical part of the model is based on the micro-plane model for concrete with relaxed kinematic constraint [14]. In the finite element analysis cracks are treated in a smeared way, i.e. smeared crack approach is employed. To assure the objectivity of the results with respect to the size of the finite elements, the crack band method is used [15]. In the mechanical part of the model the total strain tensor is decomposed as mechanical strain, thermal strain, hygro strain (swelling-shrinking) and strain due to expansion of corrosion product [4-8].

The transport processes in concrete depend on the damages of the concrete. Hence, the water diffusivity, as the relevant parameter that controls transport processes, is employed in the model as function of crack width based on the experimental results for permeability in cracked and fully saturated concrete (Figure 1, left) [4]. Algorithm of the 3D CHTM model is shown on Figure 1, right.

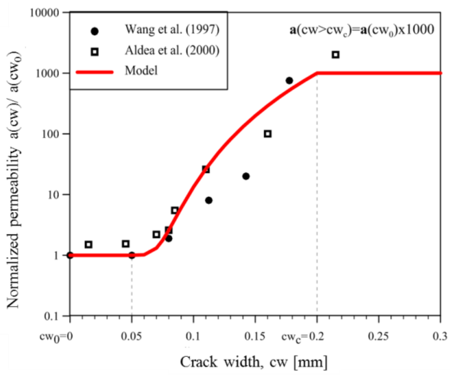

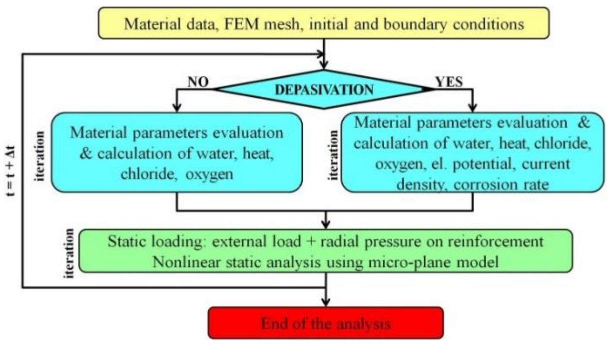

Figure 1 Figure caption Normalized concrete permeability as a function of a crack width (left) and 3D CHTM model algorithm (right)

3. APPLICATION OF THE 3D CHEMO-HYGRO-THERMO-MECHANICAL MODEL

The application of the 3D CHTM model is illustrated on a simply supported reinforced concrete beam, which was first damaged by external load and subsequently exposed to aggressive influence of seawater on the bottom side in order to analyse transport processes in cracked and un-cracked concrete before depassivation of the steel reinforcement. Moreover, the parameters are based on the designed and measured values for the concrete used for the Maslenica Bridge, in order to compare chloride profiles of the numerical analyses and the data obtained on the bridge.

3.1. NUMERICAL ANALYSIS

The geometry of the beam is shown in Figure 2. The thickness of the concrete cover is 50 mm. In order to reduce computational time only the symmetric part of the cross-section is modelled using 3D eight-node solid finite elements. At first the beam is exposed to 4-point bending causing yielding of reinforcement and concrete cracking on the bottom side, which is, subsequently, exposed to the influence of seawater. The materials parameters used in the analysis are summarized in Table 1, while initial and boundary conditions are shown in Table 2.

The crack development due to the 4-point bending and the distribution of free chlorides in concrete after 13 years exposed to exposure classes XS1 and XS3 are shown on Figure 3 (a) and (b). It can be seen that large penetration depths of free chlorides coincide with the position of cracks. The distribution of free chloride over the concrete depth for cracked (cross-section 7) and un-cracked (cross-section 1) concrete and exposure class XS3 in time sequences between 1 and 100 years is shown in Figure 3 (c) and (d), respectively.

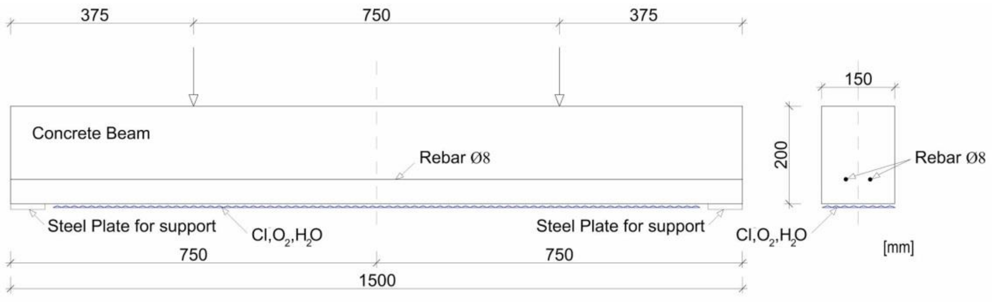

Figure 2 Geometry of numerical model

Table 1 Summary of material parameters

Modulus of elasticity of concrete, Ec (MPa)	32000.0
Modulus of elasticity of steel, Es (MPa)	210000.0
Poisson's ratio of concrete, υ	0.18
Tensile strength of concrete, f_t (MPa)	2.00
Uniaxial compressive strength of concrete, f_c (MPa)	30.0
Fracture energy of concrete, G_F (J/m^2) *	80.0
Water/Cement ratio, w/c	0.40
Amount of cement gel in concrete, W_{gel} (kg/m^3)	400.00
Chloride diffusion coefficient in un-cracked concrete, $D_{c,0}$ (m^2/s) *	5.50x10^{-12}
Capillary water diffusion coefficient in un-cracked concrete, $D_{w,0}$ (m^2/s) *	2.20x10^{-10}
* assumed values	

Table 2 Initial and boundary conditions

	Initial condition	Boundary condition
Capillary water, θ_{wi}	0.010	0.060
Oxygen concentration in pore solution, C_o (kg/m^3)	0.0050	0.0085
Temperature, T (ºC)	20.00	20.00
Concentration of free chloride dissolved in pore solution, C_c (kg/m^3) for exposure class XS1	0.00	8.50
Concentration of free chloride dissolved in pore solution, C_c (kg/m^3) for exposure class XS3	0.00	20.00

The depassivation of reinforcement is assumed to start in numerical analysis for the threshold free chloride concentration of 7 kg/m^3 of pore solution. Based on the assumptions that material parameters, mechanical damages and boundary conditions will not change during the service life of the element, depassivation of reinforcement in the cracked zone happens within 1 year after the crack formation. This is in good agreement with experimental observation [16, 17], which shows that immediately after crack opening free chlorides penetrate into the crack. Contrary to this, for the un-cracked part of the beam depassivation of reinforcement is reached after 100 years. According to the assumption of the numerical analysis, it can be concluded that the initiation phase, and consequently also service life, is shorter if the cracks in concrete are wider and deeper.

Comparing the distribution of chlorides at different times in cracked concrete (Figure 3c), it can be seen that the chloride concentration after 1 year is the highest, than it decreases and after 25 years starts to increase again. Namely, chlorides penetrate along the crack immediately after crack opening and cracks act as free, exposed surface. Hence, chlorides penetrate in the horizontal direction, in the region between the cracks. Therefore, there is a slight decrease of their concentration in the crack, i.e. with increase of time chlorides tend to be smeared-out into the horizontal direction. Contrary to cracked concrete, the chloride concentration in un-cracked concrete cover increases gradually by time (Figure 3d).

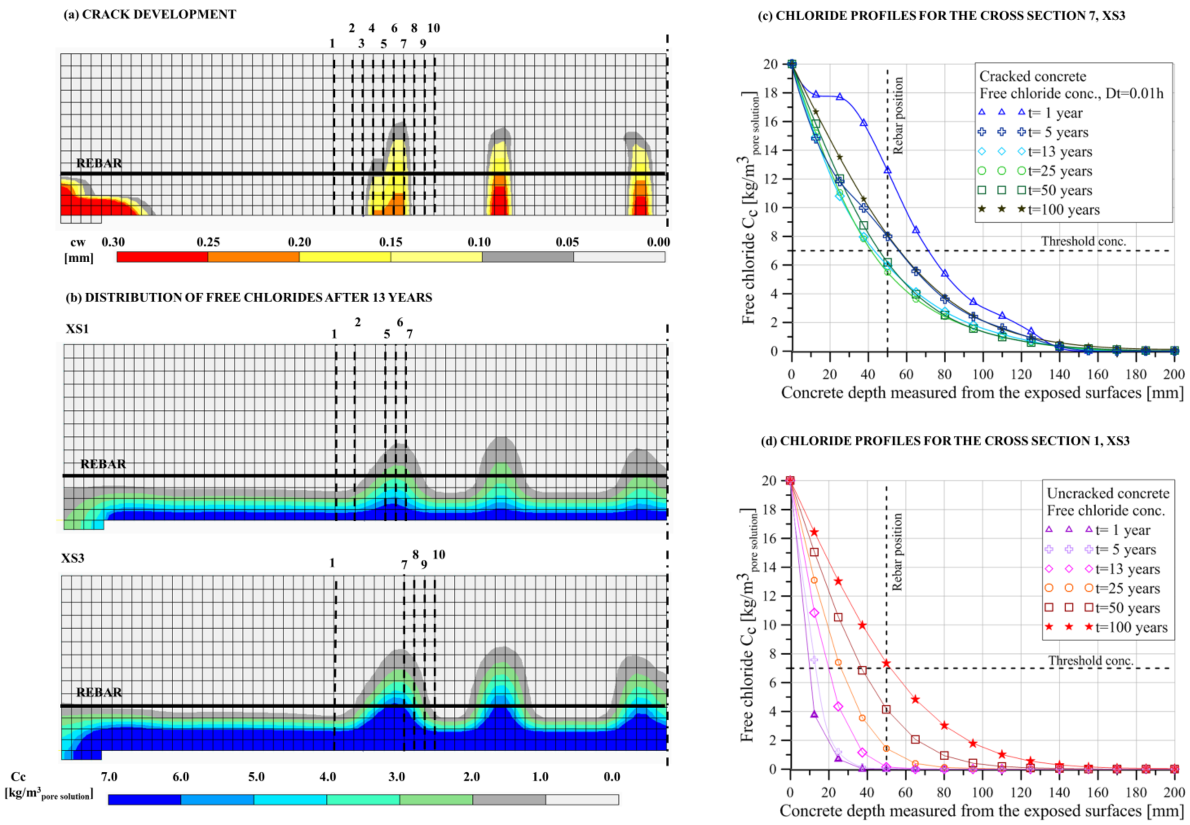

Figure 3 (a) Crack development due to the 4-point bending; (b) the distribution of free chlorides in concrete after 13 years exposed to exposure classes XS1 and XS3; distribution of free chloride over the concrete depth for (c) cracked and (d) un-cracked concrete

3.2. COMPARISON OF NUMERICAL RESULTS AND DATA OBTAINED ON THE MASLENICA MOTORWAY BRIDGE

The Maslenica Motorway Bridge is reinforced concrete arch bridge built in 1997 on Croatian Adriatic coast (Figure 4). Special attention was given to durability issue during its design and construction [2]: (i) structural details and cross section were simplified to minimise execution problems; (ii) all structural dimensions were increased, compared to previously built concrete arch bridges in the Adriatic coast area; (iii) the low permeability concrete, with water-cement ratio w/c less than 0.40, has been used; (iv) the minimum concrete cover for all the bridge structural elements was set at 5.0 cm and for the arch abutments nearest to the sea at 10.0 cm; (v) the number of structural joints has been reduced to a minimum, with most of the columns fixed to the superstructure and the expansion joints placed at the abutments only; (vi) the monitoring system was used to record relative strains and accelerations at various construction stages and under load-testing prior to opening the bridge to the trafic.

Investigation works on the Maslenica Bridge conducted in October 2010 comprised visual inspection of all structural members and determination of the chloride content in concrete according to Croatian (European) standard HRN EN 14629:2007 [3, 18]. The conclusion is following [3]: (i) the bridge is generally in good condition; (ii) localized damage in term of concrete cover cracking and spalling are more frequent on the columns S3 and S10, (iii) on the columns S3 and S10 there are areas of exposed corroded reinforcement and concrete cover is at some places only 3 cm thick, (iv) the chloride penetration in concrete cover is uneven, and depends on location - higher concentration and deeper penetration are in concrete elements facing Velebit mountain (north); (v) protective system should be applied to the entire bridge structure in order to mitigate the future repair costs.

Chloride concentration and penetration depth in concrete cover depends on the surface chloride concentration, chloride diffusivity and relative humidity. Surface chloride concentration depends on the height above sea level, longitudinal position and direction of surface according to the dominant wind direction [19]. For the structures in the Adriatic region the highest surface concentration is found on the elements exposed to the Bora winds, which blows from north and north-east causing salt spray, depositing chlorides on all structural elements [19]. The Bora is a dry wind, occurring without precipitation. Therefore, there is no flushing of chloride from the concrete surfaces during rain, while the layer of salt on the exposed surface of the concrete structures is constantly being renewed. This is in good agreement with the results of chloride content obtained on the Maslenica Bridge. On the other hand, chloride diffusivity, among many parameters, primarily depends on the concrete quality (permeability, w/c, etc.) and crack width [4, 19]. Since the relative humidity and concrete quality are uniform for all structural elements of the bridge, it can be concluded that significantly higher concentration and deeper penetration of chlorides on the columns S3 and S10 is consequences of the cracks in concrete cover.

According to the static and dynamic analyses of the structure, it can be assumed that first cracks on this columns appeared during the arch construction by free cantilevering (Figure 4, right). The arch was constructed

Figure 4 Maslenica Motorway Bridge: bridge layout (left), Bora wind at the bridge location (middle) and construction (right)

on travelling formwork carriages with the weight of 55 t each, in 5.26 m long segments, starting symmetrically from the arch abutments. Columns at the arch abutments (S3 and S10) were extended by auxiliary steel staying pylons 23 m high to facilitate successive cantilevering. The arch was supported during construction by stays radiating from two levels of the arch abutment columns and from tops of auxiliary staying pylons, where they were equilibrated by anchor stays, connected to rock anchors. With careful planning, on the basis of 24 h working days, the arch construction was finished in 11 months. The actual duration of the arch construction was only nine months, because high winds forced work stoppages for the two months period [2].

Concrete specimens for measuring chloride content at the column S3 were taken on northern column at 0.00 and 45.00 m above the sea level and on two surfaces directed to north (S3V-0-V and S3V-45-V) and east (S3V-0-Z and S3V-45-Z). Determination of the chloride content was carried out according to Croatian (European) standard HRN EN 14629:2007. Chloride concentration of the column S3 is compared with the numerical results after 13 years of exposure (Fig. 5). Although, compared structural elements do not have the same geometry and external loading, they can be compared in quality way because the relevant parameters for the numerical analyses (concrete quality, crack width and surface chloride concentration) are chosen to meet the conditions of the bridge. The total amount of chlorides in numerical simulation is for this purpose expressed as percentage of concrete mass:

$$\frac{m_{free+bound\ chlorides}}{m_{concrete}} = \frac{C_c \cdot p \cdot S + C_{cb}}{\rho} \qquad (5)$$

where p=0.10 is porosity, S=0.6 is saturation and ρ=2400 kg/m^3 is density of concrete.

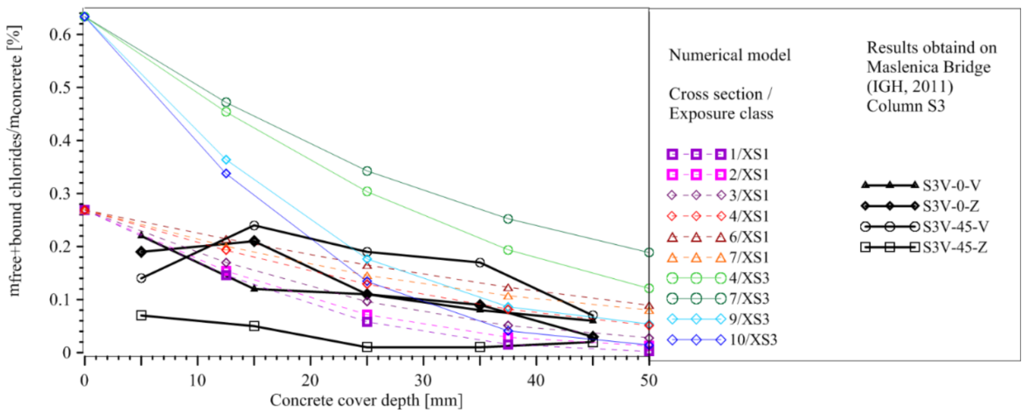

Figure 5 Chlorides profiles after 13 years of exposure – comparison of the numerical results and results obtained on the column S3 of the Maslenica Bridge

Results obtained on the bridge are within the range of numerical values at the reinforcement level (at the concrete cover depth from 25 to 45 mm) leading to the conclusion that boundary conditions for the numerical model (exposure classes XS1 and XS3) are well assumed and presents minimum and maximum chlorides loads on the structure.

Column surface facing to north - Velebit Mountain, are the most exposed to chlorides because of the Bora wind and chlorides concentrations measured at 0.00 m and 45.0 m (S3V-0-V and S3V-45-V) above sea level are high. On the east side (towards Zadar town) of the bridge chloride concentration significantly varies according to height above sea level (S3V-0-Z and S3V-45-Z). Hence, the position of the exposed surface is not the only impact on the distribution of chlorides in concrete, but also damages in concrete. Two phenomena indicate presence of cracks in the concrete cover on the column S3: (i) slight slope of measured chloride profiles and (ii) signs of advanced corrosion - brown patches of rust on all sides of the column, although the threshold chloride concentration of 0.07 % mass of concrete has been reached at the reinforcement level only on some position of the column after 13 years. The second phenomenon can be explained by above described penetration of chlorides in open crack: initially chlorides penetrate in the direction of the crack axis following by penetrating in a direction perpendicular to the crack axis.

That leads to the conclusion that the numerical model assumptions are valid and accordingly can predict remaining service life of the structure. Concrete quality and designed thickness of concrete cover provide sufficient protection of steel rebar against chloride induced corrosion on the Maslenica Bridge. Namely, according to the assumptions of numerical analysis depassivation of steel rebar in un-cracked concrete will occur after 100 years of exposure to chlorides from the sea. On the other hand, cracks in concrete, with the width of 0.2 mm or larger significantly reduce depassivation time, and consequently service life of the structure.

4. CONCLUSIONS

In order to develop consistent maintenance policy that would provide efficient and effective management of bridges in maritime environment, it is necessary to determine remaining service life of the structures. In this purpose the fully coupled 3D CHTM model for transient analysis of corrosion processes before and after depassivation of steel reinforcement in concrete is developed and implemented into 3D FE code. Emphasis of this paper is given on the initiation phase of corrosion in order to analyse the influence of crack width and depth on the transport processes in concrete before depassivation of the steel rebar. The numerical results of chloride content in concrete are compared with the results obtained on the Maslenica Motorway Bridge after 13 years of exposure to maritime conditions. Good agreement of numerical results and data obtained on the bridge is basis to predict remaining service life of the bridge. Investigation works on the Maslenica Bridge shown and numerical analysis confirmed that cracks in concrete cover, with width of $cw \geq 0.20$ mm, significantly reduce depassivation time of reinforcement bar.

Further development of the 3D CHTM model is in progress, with special attention on the application of the model to real structures exposed to sea and de-icing salts.

ACKNOWLEDGMENTS

This research was carried out in the framework of the Croatian national project “Performance indicators for assessment of existing bridges” supported by Zagreb University and DFG project Nr. 601984 supported by Deutsche Forschungsgemeinschaft.

REFERENCES

[1] Kušter Marić, M. et al.; Analysis on durability of reinforced concrete bridges in maritime environment, In Annual 2015 of the Croatian Academy of Engineering, Croatian Academy of Engineering, ISBN 0-1332-3482-00, Zagreb (2016), pp. 57-78

[2] Radić, J. et al.; Two Notable Arch Bridges on The Croatian Adriatic Highway, Structural engineering international, 20 (2010) 1, pp. 36-40

[3] Bleiziffer, J. et al.; Condition Assessment of the Maslenica Highway Bridge. In: Sustainable Arch Bridges Radić, J., Chen, B.C. (eds), Zagreb, Secon HDGK, pp. 309-316

[4] Ožbolt, J. et al.; Modelling the effect of damage on transport processes in concrete. Constr Build Mater 24(9) 2010, pp. 1638–1648.

[5] Ožbolt, J. et al.; 3D Numerical modelling of steel corrosion in concrete structures. Corros Sci 53(12) 2011, pp. 4166–4177.

[6] Ožbolt, J. et al.; Modeling damage in concrete caused by corrosion of reinforcement: coupled 3D FE model, Int J Fract 178(1-2): 2012, pp. 233–244.

[7] Ožbolt, J. et al.; Modeling pull-out resistance of corroded reinforcement in concrete: Coupled three-dimensional finite element model, Cement and Concrete Composites, (46) 2014, pp. 41-55

[8] Ožbolt, J. et al.; Modeling influence of hysteretic moisture behavior on distribution of chlorides in concrete, Cement and Concrete Composites, (67) 2016, pp. 73-84

[9] Tuutti, K. Corrosion of steel in concrete: Report No. 4. Stockholm: Swedish Cement and Concrete Research Institute, 1982
[10] Rosenberg A. et al.; Mechanism of corrosion of steel in concrete, Materials Science of Concrete, , American Ceramic Society (1) 1989, pp. 285-313
[11] Bear, J. & Bachmat, Y. Introduction to Modelling of Transport Phenomena in Porous Media. Kluwer Academic Publishers: Dordrecth, 1991
[12] Leech, C. et al.; Unsaturated Diffusivity Functions for Concrete Derived from NMR Images, Materials and Structures, (36) 2003, pp. 413-418
[13] Saetta, A. et al.; (1993) Analysis of Chloride Diffusion into Partially Saturated Concrete. ACI Materials Journal, 90 (5), 1993, pp. 441-451
[14] Ožbolt, J. et al.; Microplane model for concrete with relaxed kinematic constraint, Int J Solids Struct, 38 (16) 2001, pp. 2683–2711
[15] Bažant, Z. P. & Oh, B. H. Crack band theory for fracture of concrete. Rilem, 93 (16), 1983, pp. 155-177
[16] Marsavina, L. et al.; Experimental and numerical determination of the chloride penetration in cracked concrete, Construction and Building Materials, (23) 2008, pp. 264-274
[17] Wittmann, F.W. et al.; Eindringen von Wasser und darin gelöster Verbindungen in Beton: Visualisierung mit Hilfe der Neutronenradiographie. In: Erhaltung von Bauwerken: 1. Colloquium, Raupach, M. (ed.),. Ostfildern: Technische Akademie Esslingen (TAE), 2009, pp. 249-253.
[18] IGH; Report on main inspection of Maslenica Bridge on Motorway A1. 2011. Zagreb: Institut IGH, (in Croatian)
[19] Kušter Marić, M.; Service life prediction of reinforced concrete bridges exposed to chlorides, PhD thesis, University of Zagreb, Croatia, 2013 (in Croatian)
[20] Bamforth, P. B.; Price, W.F. & Emerson, M., An International Review of Chloride Ingress Into Structural Concrete, Volume 359 of Contractor report, Thomas Telford, 1997, ISBN 0727729284, 9780727729286

TOPIC 5.

Protection, preservation and repair of structures

Zaštita, očuvanje i popravak konstrukcija

FIRE DAMAGES OF REINFORCED CONCRETE STRUCTURES AND REPAIR POSSIBILITIES

Mirjana Malesev[1], Vlastimir Radonjanin[1]

[1] University of Novi Sad, Faculty of Technical Sciences, Department of Civil Engineering and Geodesy, Sime Miloševića 12, 21 000 Novi Sad, Serbia, email: miram@uns.ac.rs, radonv@uns.ac.rs

SUMMARY: This paper discusses causes and appearance of characteristic damages and repair methods of RC structures exposed to fire. Complexity of behavior of reinforced concrete at elevated temperature is pointed out through theoretical description and consideration of different damage mechanisms. Characteristic fire damages of concrete and steel are described, illustrated and classified with respect to affected part of cross-section of the RC structural elements. Depending on the extent of damage, several methods for concrete removal are suggested. Basic repair principles are classified regarding affected part of the cross-section and state of the reinforcement. Proposed recommendations for repair of fire damaged RC structures are based on the analyzed literature and on authors' professional experience. This paper may help engineers in practice to choose possible repair solutions related to extent and type of fire damages of RC structures.

POŽARNA OŠTEĆENJA ARMIRANOBETONSKIH KONSTRUKCIJA I MOGUĆNOSTI POPRAVKA

SAŽETAK: U radu su raspravljeni uzroci i pojave karakterističnih oštećenja i metode popravka armiranobetonskih konstrukcija izloženih požaru. Složenost ponašanja armiranoga betona pri povišenoj temperaturi istaknuta je teorijskim opisom i razmatranjem različitih mehanizama oštećenja. Opisana su karakteristična oštećenja betona i čelika prouzročena požarom, ilustrirana i razvrstana s obzirom na pogođeni dio poprečnoga presjeka armiranobetonskih konstrukcijskih elemenata. Ovisno o opsegu štete predloženo je više metoda uklanjanja betona. Osnovna načela popravka razvrstana su s obzirom na pogođeni dio poprečnoga presjeka i stanje armature. Predložene preporuke za popravak požarom oštećenih armiranobetonskih konstrukcija temelje se na proučenoj literaturi i stručnom iskustvu autora. Ovaj rad može pomoći inženjerima u praksi pri odabiru mogućih rješenja za popravak ovisnih o opsegu i vrsti požarnih oštećenja armiranobetonskih konstrukcija.

1. INTRODUCTION

Properly designed and successful execution of repair work of RC structure damaged in fire can only be provided if a detailed in-situ and laboratory investigation and correct assessment of residual structural capacity have been made. Recommendations available from various sources (books, codes, articles etc.) could help to choose appropriate solution from a wide range of available repair methods and repair materials, but in practice every single fire damaged structure is unique [20]. For realistic assessment of the structure after a fire it is necessary to know behaviour of concrete and reinforcing steel at high temperature, to be able to recognize the type and degree of damage due to the fire and to separate them from similar damages that result from other causes. Reinforced concrete is considered a material that shows an acceptable resistance to high temperatures, which allows using concrete elements without the need of any additional protection. The main reason for this statement are the following properties of the concrete: incombustibility, small thermal conductivity, small strains at rising temperatures and therefore concrete core remains intact inside the section of element and continues transmit load. On the other hand, reinforcement is sensitive to high temperatures and needs to be protected. In RC structures concrete cover plays that role. The relatively low thermal conductivity of concrete leads to a slow propagation of chemical transformations of the components of concrete, which also need time for fully developing conversions at each specific temperature. On the other hand, low thermal conductivity of concrete causes strong thermal gradient that induce internal stresses in concrete mass and development of inner cracks [1]. However, long period of exposition of reinforced concrete to high temperatures introduce physical-chemical changes in its properties that lead to mechanical strength decay which produces losses in the bearing capacity and safety of the structure.

2. DAMAGE MECHANISMS OF CONCRETE UNDER FIRE

Concrete is a composite material that consists mainly of mineral aggregates bound by a matrix of hydrated cement paste. The matrix is highly porous and contains a relatively large amount of free water. When subjected to heat, concrete responds not just in instantaneous physical changes, such as expansion, but by undergoing various chemical changes. This response is especially complex due to the non-uniformity of the material. Concrete contains both cement and aggregate elements, and these may react to heating in a variety of ways [7]. The main changes occur primarily in the hardened cement paste. With the increase of temperature in concrete to 100⁰C free water from the capillary pore system of hardened cement paste will be evaporated. In the range of 100⁰C - 400⁰C the cement paste loses physically bond water, while at temperatures above 400⁰C chemically bound water will be lost. The following chemical transformations can be observed by increase of temperature: the decomposition of ettringite between 50⁰C and 110⁰C, endothermic dehydration of $Ca(OH)_2$ at the temperatures 450⁰C-550⁰C and dehydration of calcium-silicate-hydrates at the temperature of 700⁰C [2]. The loss of pore water and chemical transformations are accompanied by shrinkage of cement stone. On the other hand, due to rising temperatures, coarse aggregate increases its volume and disruption of adhesion between the cement paste and coarse aggregate appeared. In the case of reinforced concrete, the same mechanism leads to impaired adhesion between the reinforcement and concrete [20].

Aggregate normally occupy 65 to 75% of the concrete volume, and that is why the behavior of concrete at elevated temperature is strongly influenced by the aggregate type. Commonly used aggregate materials are thermally stable up to 300⁰C–350⁰C. Aggregate used in concrete can be classified into three types: carbonate, siliceous and lightweight aggregate (LWA). Carbonate aggregates include limestone and dolomite. Siliceous aggregate include materials consisting of silica and include granite and sandstone. LWA are usually manufactured by heating shale, slate, or clay. Compressive strength of concrete containing siliceous aggregate begins to drop off at about 400⁰C and is reduced to about 55% at 650⁰C because of change of crystal structure of quartz α formation → β formation [2]. Concrete containing LWA and carbonate aggregates retain most of their compressive strength up to about 650⁰C. Lightweight concrete has better insulating properties, and transmits heat at a slower rate than normal weight concrete with the same thickness, and therefore generally provides increased fire resistance. The modulus of elasticity for concretes manufactured of all three types of aggregates is reduced with the increase in temperature. Also, at high temperatures, creep and relaxation of concrete increase significantly. The colour of concrete generally changes at increasing temperature from normal to pink or red (300-600⁰C), whitish grey (600-900⁰C) and buff (900-1000⁰C). If the concrete temperature exceeds 1300⁰C, the softening and melting of surface layer will be occur [20]. Described physical and chemical changes in concrete will have the effect on reduction of the compressive strength of the material. Generally, concrete will maintain its compressive strength until a critical temperature is reached, above which point it will rapidly drop off. This generally occurs at around 600⁰C [7].

Reinforcing steel is much more sensitive to high temperatures than concrete. Both materials are incombustible but concrete has protective i.e. insulating role. Hot-rolled steels (reinforcing bars) retain much of their yield strength up to about 400⁰C, but at temperatures >600ºC hot-rolled steel loses residual strength. Cold-drawn steels (prestressing strands) shows considerable loss of strength at 200-400ºC. Cold-worked steel loses residual strength at temperature >450ºC. Reducing the strength of reinforcement at high temperatures is usually the cause of the large permanent deflection of the structure.

When concrete is exposed to high temperature, as in the case of fire, the basic visible damages are thermal spalling and cracking, but other changes take place also, like a drop of strength and modulus of elasticity and change of colour. In most cases, a combination of these fire effects is registered.

Spalling is an umbrella term, covering different damage phenomena that may occur to a concrete structure during fire [4]. Spalling could be defined as violent or non-violent breaking off of layers or fragments of concrete from the surface of a structural element during or after it is exposed to high and rapidly rising temperatures as experienced in fires [13]. These phenomena are caused by different mechanisms [4]:

- Pore pressure rises due to evaporating water when the temperature rises;
- Compression of the heated surface due to a thermal gradient in the cross section;
- Internal cracking due to difference in thermal expansion between aggregate and cement paste;
- Strength loss due to chemical transitions during heating.

There are several main theories explaining the spalling mechanisms [11, 12]:

- **Thermal stress theory:** Thermal stresses are caused by a non-uniform temperature distribution through the structure/element or by thermal expansion of an externally restrained section. In the high temperature zone (on the surface) concrete expands more than in the low temperature zone (the interior part). As a self-equilibrating thermal stress state develops, a thin layer near the surface is in compression while the interior part is in tension. Because of the high temperature gradient, the compressive stress in the thin surface layer can be very high, which causes buckling and delamination of the outer layer, observed in the form of spalling.
- **Pore pressure theory:** When a concrete is heated, the steam pressure in the pores rises close to the surface. The pressure gradient then drives moisture in two opposite directions: to surface and towards the inner colder regions. When the steam meets a neighbouring colder layer it will condense. The condensation of vapour increases the moisture content of the concrete in that layer and thus reduces the

permeability of the concrete, which results in the formation of a barrier in the interior, the so-called "moisture clog". The interior water vapor is blocked by the clog, and the vapour pressure starts to build up rapidly. As soon as the pressure exceeds the tensile strength, then spalling takes place.

- Combined pore pressure and thermal stress spalling: In most cases, a combination of the two mechanisms takes place. Explosive spalling generally occurs under the combined effect of pore pressure, and compression in the exposed surface region induced by thermal stress and external loading and internal cracking.
- During last few decades several specific theories were developed [11]:
- The fully saturated pore pressure theory: If a saturated pore in cement paste without drainage is heated during a fire event, very high pressure, well beyond the tensile strength of concrete, occurs. If more than 32% of a closed pore is initially filled with water, the water will expand during heating and force the trapped air into solution resulting in a fully saturated pore at elevated temperatures. The hydraulic pressure development is a probable explanation for fire spalling.
- The BLEVE theory (Boiling Liquid Expanding Vapour Explosion): This mechanism is characteristic for the spalling process of high strength concrete. The walls between closed pores with super-heated water and open pores with lower pressure can be destroyed by the pressure difference and this can lead to the progressive breakdown of the microstructure.
- The frictional forces from vapour flow theory: This theory includes frictional stresses originating from vapour flow during fire exposure and probable cause spalling.

All of these theories are based on the phenomena of "the movement of heat and / or movement of moisture" that cause stresses. Unfortunately, mentioned theories have not been entirely confirmed by a number of experiments. The same conclusion can be derived for numerical modelling that attempt to explain and predict the occurrence of spalling.

Cracking of concrete exposed to fire occurs due to exceeding of concrete tensile strength. Cracks and fissures are caused by thermal expansion and dehydration of the concrete due to heating.

3. TYPES AND CLASSIFICATION OF DAMAGES

3.1. TYPES OF DAMAGES

Term "spalling" encompasses large number of damage types. The first types of spalling were described in the beginning of the 20th century (explosive, surface, aggregate and corner spalling). Over the next decades two new types were added (sloughing off spalling and post cooling spalling) [4, 13]. They are:

- Explosive spalling: Violent breaking off of concrete fragments at high temperatures generally occurs in the first 30 minutes of a fire. Explosive spalling is usually caused by: insufficient release of high pore pressure, high thermal stresses and combination of both. This type of spalling is especially likely to occur on structural members heated from more than one side, such as columns and beams. When moisture clogs are advancing into the concrete from all heated sides, at some point in time the moisture clogs will meet in the centre of the cross-section, giving a sudden rise in pore pressure which may cause large parts of the cross-section to explode.
- Surface spalling: Violent separation of small or larger pieces of concrete from the cross section at high temperatures, during which energy is released in the form of popping off of the pieces and small slices with a certain speed. Usually occurs in the first 30 minutes of a fire.
- Aggregate spalling: Splitting of aggregates due to their decomposition or changes at high temperatures. Usually occurs in the first 30 minutes of a fire (Fig. 1).
- Corner spalling: Removal of concrete cover from corners at high temperature due to the temperature impact from two sides. This type of spalling is usually connected with splitting cracks due to difference in thermal deformation between concrete and reinforcement and occurs in the first 90 minutes (Fig. 2).
- Sloughing off spalling: Sloughing off is the form of progressive gradual spalling, that is caused by strength loss due to internal cracking and chemical deterioration of the cement paste. This type of spalling is non-violent breaking off of concrete fragments after longer exposure to high temperatures, when concrete loses its strength (Fig. 3 and 4).
- Post-cooling spalling: Non-violent breaking off of concrete fragments during cooling from high temperature. This type of spalling was observed with concrete types containing calcareous aggregate. An explanation is the rehydration of CaO to $Ca(OH)_2$ after cooling, when moisture is again present on the concrete surface. The expansion due to rehydration causes severe internal cracking and thus complete

strength loss of the concrete. Pieces of concrete keep falling down as long as there is water to rehydrate the CaO in the dehydrated zone (Fig. 5).


Figure 1 Aggregate spalling


Figure 2 Corner spalling and corner cracks along main reinforcement


Figure 3 Sloughing off spalling (beam)


Figure 4 Sloughing off spalling (slab)

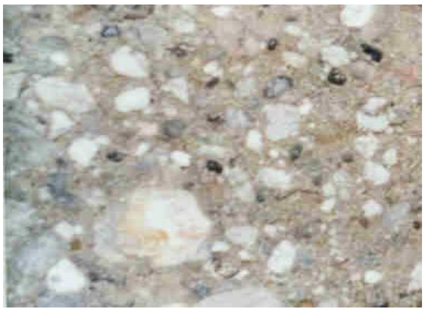
Figure 5 Post-cooling spalling


Figure 6 Crazing – mesh like cracks

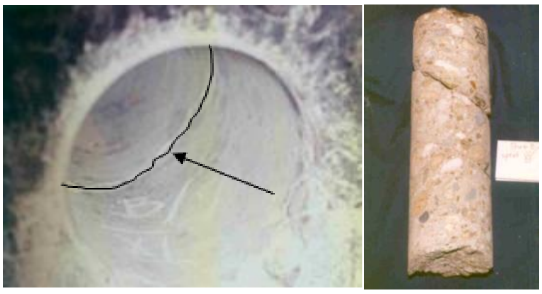
Figure 7
Inner delamination of concrete in the column


Figure 8
Plastic deformations and breaking off of bars

The term “cracking” covers the following types of damage:

- Crazing: Mesh like fissures and cracks on the surface of the concrete elements (Fig. 6), caused by additional shrinkage of hardened cement paste during drying due to high temperature.
- Corner cracks along main reinforcement: Cracking due to difference in thermal expansion/deformation between concrete and reinforcement bars. These cracks are usually located along the edge of columns and beams, especially in the direction of the main reinforcement. Also, they are associated with the separation and falling off of pieces of concrete (corner spalling) and with visible reinforcement bars (Fig. 2).
- Inner delamination of concrete: Is manifested as internal crack parallel to the fire-affected surface (Fig. 7). The main cause of this damage is high temperature gradient that induces high tensile stresses between the heated surface layer and colder inner zone of concrete. This phenomenon is typical for the columns. Since the internal cracks cannot register visually, their existence must be checked by extracting concrete cores.

Concrete surface cracking may provide pathways for direct and faster heating of the reinforcement bars and inner concrete, possibly bringing about more thermal stress and further cracking.

Loss of strength and ductility of reinforcement are usually consequences of high temperatures during fire. Visible characteristic fire damages of reinforcement are:

- Plastic deformations due to restrained elongation (Fig. 8).
- Breaking of bars (Fig. 8) due to loss of ductility of the steel or local reduction of bar cross section because of melting of steel.

Reinforced concrete elements during fire are subjected to additional stresses due to restrained deformations. In a case of slender beams and slabs buckling associated with deflection may occur. Under fire conditions, axially restrained beam/slab develops large deflections in post-buckling states [23].

Extent and type of described fire damages of RC structures depends on numerous parameters, among which the most important are: size and distribution of fire load, fire duration, fire maximum temperature, the shape and dimensions of structural elements, the existence and type of finishing layer - cover of the RC elements, the presence of defects and/or prior damage, construction details and the actual quality of concrete.

3.2. CLASSIFICATION OF DAMAGES

Among a numerous available classification of concrete fire damages authors of this paper chose the classification proposed by Ingham and Tarada [10] and modified it in relation to the degree of affected part of RC element cross section. Figure 9 illustrates parts of cross section of typical RC element that have to be considered during selection of appropriate repair method. Proposed classification is given in Table 1.

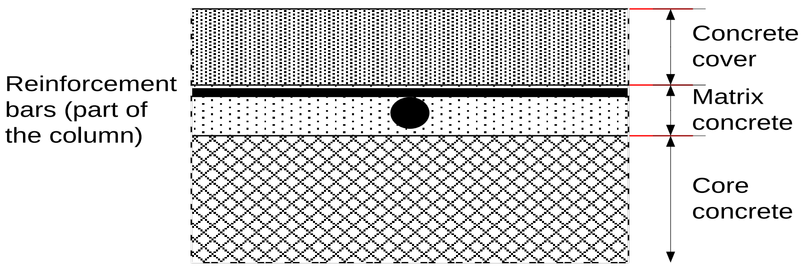

Figure 9 Characteristic parts of cross section of RC element

Table 1 Classification of fire damages with illustration of affected part of cross-section

Damage degree	Affected part of cross-section	Illustration	Features observed
1	Surface thin layer	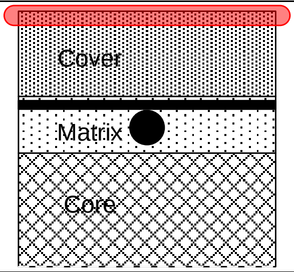	Minor crazing – mesh like fissures with normal concrete colour Spalling is non-visible Rebars are non-visible
2	Concrete cover	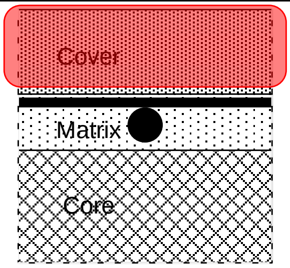	Moderate crazing - mesh like cracks Surface spalling Aggregate spalling Change of concrete colour (pink or red) Rebars are non-visible or locally visible at places with insufficient cover (up to 25%)
3	Concrete matrix		Extensive crazing Corner spalling and cracks along rebars Sloughing off spalling Change of concrete colour (pink/red/whitish grey) Up to 50% of rebars are visible Loss of concrete strength Minor deflection of RC elements
4	Concrete core	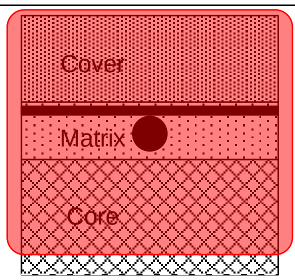	Deep extensive spalling More than 50% of rebars are visible Change of concrete colour (whitish grey/buff) Possible melting of concrete (long-lasting fires) Inner delamination of concrete Impaired bond between concrete and rebars Increase of deflection of RC elements Reduction of reinforcement mechanical properties Possible buckling and breaking off of rebars

4. METHODS FOR CONCRETE REMOVAL

Before beginning the repair and strengthening of the structure it is necessary to remove all additional loads and to support the structure. Besides preserving the stability of the structure during repair works, these activities are important in cases of structural repair where the new concrete is expected to carry its share of the load in the repaired elements. In the scope of repair very important role play proper selection of a method for concrete removal. Since there are a number of methods for concrete removal which differ in possibilities and limitations of application, it is not easy to select appropriate method. Depending on the damaged part of cross-section, authors of this paper propose following methods for concrete removal (Fig. 10).

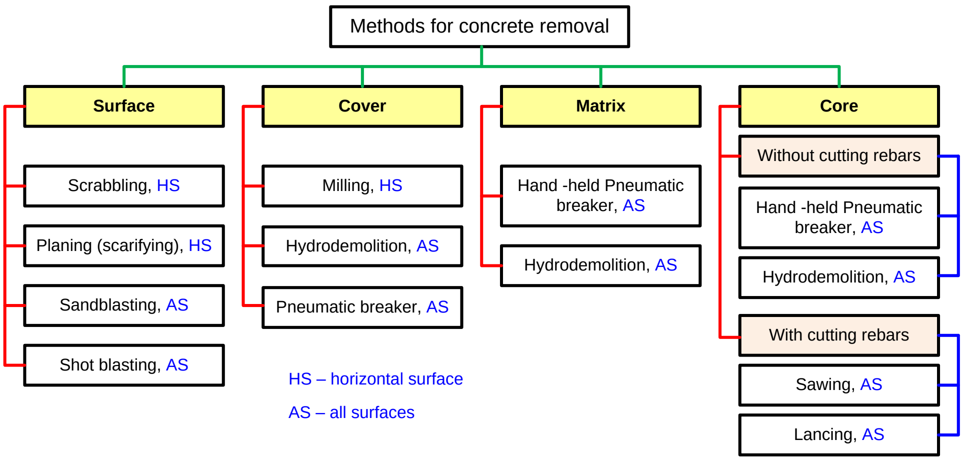

Figure 10 Suggested methods for concrete removal

5. SELECTION OF REPAIR METHOD AND MATERIAL

Based on the recommendations for repair of fire damaged RC structures in analysed literature [6, 21, 22, 24] and on authors professional experience [14, 16, 20] decision about general repair strategy (structural or non-structural repair) mainly depends on affected part of the cross-section and state of the reinforcement. Non-structural repair is proper choice if rebars are not or locally visible. In all other cases structural repair is required, when: reinforcement is visible, bond is destroyed, rebars have plastic deformations, structural elements have excessive deflections etc. Structural repair is also mandatory in situation when all pointed out features are not accented but inner delamination of concrete exists. In some cases main reasons for structural repair is doubt regarding remaining structural capacity and intention to provide additional structural safety during future exploitation. For easier decision about type of repair method, Table 2 could be useful.

Table 2 Suggested repair methods and materials

Damage degree	Affected part of cross-section	General repair method	Short description
1	Surface thin layer	Minor surface repair	Non-structural repair mortar (by hand)
2	Concrete cover	New concrete cover with/without light mesh	Structural mortar (applied by hand or spraying) Sprayed concrete with mesh
3	Concrete matrix	Structural repair and/or minor strengthening	Reinstatement of concrete cross-section with or without partial replacement of damaged rebars (flowable or sprayed concrete with mesh) Enlargement of cross-section and addition of new rebars (flowable or sprayed concrete)
4	Concrete core	Major strengthening or RC element replacement	Enlargement of cross-section and addition of new rebars (flowable or sprayed concrete) New RC element

An example of structural repair solution for damaged RC beam is shown on Fig. 11.

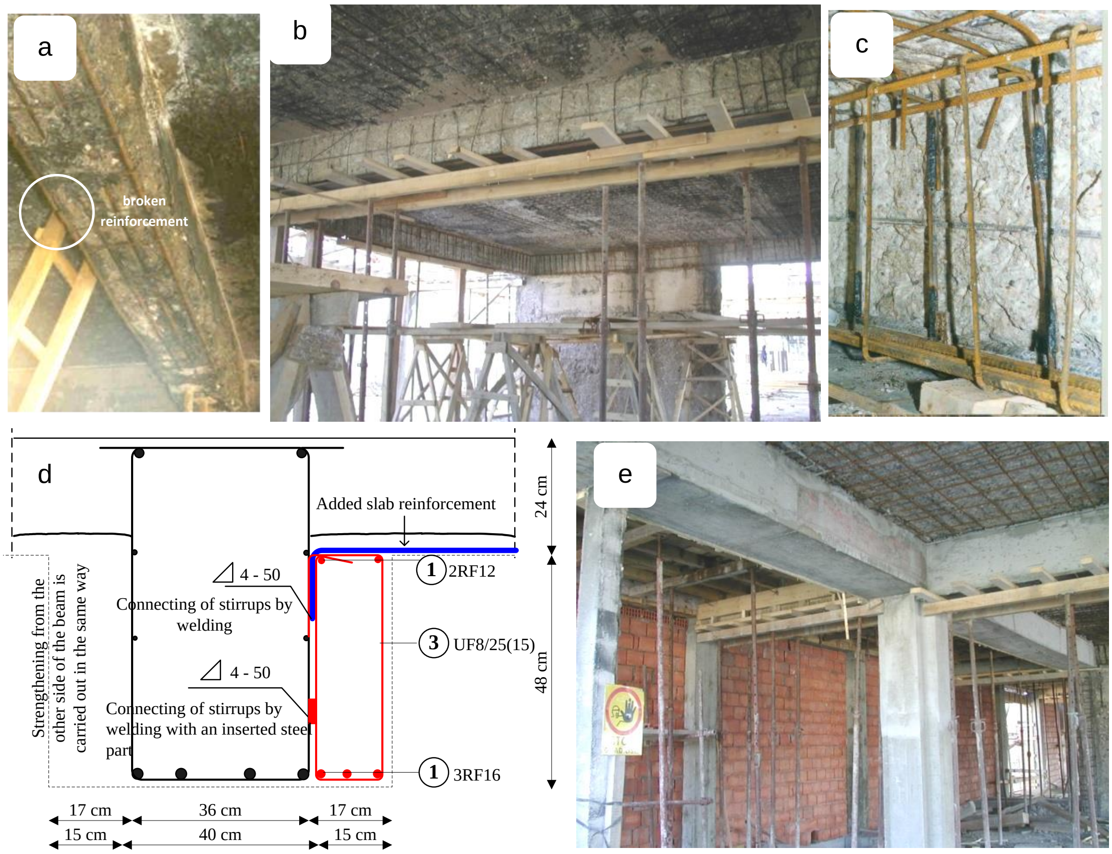

Figure 11 Strengthening process: **a)** View of RC beam damaged in fire **b)** Supporting of the beam and removal of damaged concrete **c)** Instalment of new reinforcement **d)** Detail of enlargement of existing cross section and arrangement of reinforcement **e)** View of the beam after strengthening

6. CONCLUSIONS

The authors of this paper, through brief theoretical consideration of damage mechanisms of concrete and steel, classification of fire damages of RC structures and possible repair methods with respect to affected part of cross-section, tried to assist engineers in practice to understand complex behavior of reinforced concrete at elevated temperatures and to make decision about possible repair solution.

ACKNOWLEDGMENTS

The paper presents the part of research realized within the project "Improvement of educational process and theoretical and applied research in civil engineering" conducted by the Department of Civil Engineering and Geodesy, Faculty of Technical Sciences, University of Novi Sad.

REFERENCES

[1] Alonso, C.: Assessment of post-fire reinforced concrete structures: Determination of depth of temperature penetration and associated damage" Concrete Repair, Rehabilitation and Retrofitting II – Tailor & Francis Group, London, 2009, pp.471-477

[2] Balázs, G. L., Lublóy, E.: Fire reinforced concrete structures in and after fire, Concrete Structures, 2012, pp. 73-80.

[3] Bodnárová, L., Válek, J., Sitek, L., Foldyna, J.: Effect of High Temperatures on Cement Composite Materials in Concrete Structures, Acta Geo. Geom., Vol. 10, No. 2 (170), 2013, pp.173–180.

[4] Breunese, A., Fellinger, J.: Spalling of Concrete–An Overview of Ongoing Research in the Netherlands, Proceedings of the Third International Workshop: Structures in Fire, Ottawa, Canada, 2004, pp. 249–258,

[5] Buchanan. A. H.: Structural design for fire safety, John Wiley&Sons LTD, London, UK, 2002.

[6] Concrete Repair Manual, ACI, Volume 2, 2003, pp. 1837-1910.

[7] Fletcher, I. et al.: Performance of concrete in fire: a review of the state of the art, with a case study of the Windsor tower fire, Proceedings of the 4th International Workshop in Structures in Fire, Portugal, 2006, pp. 779-790.
[8] Folić, R., Radonjanin, V., Malešev, M.: Evaluation and repair of reinforced concrete multi-story frame structures subjected to high temperatures, Workshop "Extreme Loadings, Aging and Durability of Concrete Structures", Hydro-Quebec, McGill University and Laboratoire de Beton, Montreal, 2004.
[9] Folić, R., Radonjanin, V., Malešev, M.: The assessment of the structure of Novi Sad open University damaged in fire, J. Construction and Building Materials, No.16, 2002, pp.427- 440.
[10] Ingham, I., Tarada, F.: Turning Up the Heat – Full service fire safety engineering for concrete structures, Proceedings “Concrete structures in fire”, 2007, pp.27-30.
[11] Jansson, R.: Fire spalling of concrete – Theoretical and Experimental studies, Doctoral Thesis in Concrete Structures, KTH Royal Institute of Technology, Stockholm, Sweden, 2013, pp. 154.
[12] Keun Lee: Behaviour of concrete Cylinder under elevated temperature - Focused on surface spalling, University of Colorado, Boulder.
[13] Klingsch, E. W. H.: Explosive spalling of concrete in fire, Doctoral Thesis, ETH, Zurich, 2014.
[14] Malešev, M., Radonjanin, V., Folić, R.: Assessment of Bearing Structure of Culture Center in Gradiška After Fire, 12th Int. Con. "Structural Faults & Repair - 2008", Edinburgh, UK, 10.
[15] Malešev, M., Radonjanin, V., Folić, R., Lukić, I.: Karakteristična oštećenja AB konstrukcija zahvaćenih požarom, Simpozijum DGKS, Zlatibor, Zbornik radova, pp. 365-372.
[16] Radonjanin, V., Folić, R., Malešev, M.: Investigation, Evaluation and Repair of Reinforced Concrete Structures Damaged in Fire, Workshop "Extreme Loadings, Aging and Durability of Concrete Structures", Hydro-Quebec, McGill University and Laboratoire de Beton, Montreal, 2004.
[17] Radonjanin, V., Malešev, M.: Repair of concrete structures in the light of new European standards", Introductory report, Conference, Society of structural engineers of Serbia, Zlatibor, Proceedings, 2008, pp. 147-158.
[18] Radonjanin, V. et all: Repair of the Bearing Structure of the Culture Center in Gradiška After a Fire, 12th International Conference "Structural Faults & Repair - 2008", Edinburgh, UK, 10.
[19] Radonjanin, V. et all: The Assessment of a warehouse RC structure damaged in an explosion, Int. Con. Structural faults & Repair, Editor M. Forde, London, 2003.
[20] Radonjanin, V., Malešev, M., Folić, R.: Repair of fire damaged RC structures, Congress of Structural Engineers of Macedonia, Ohrid, Macedonia, 2013.
[21] Raupach, M.: Concrete repair according to the new European standard EN 1504", Concrete repair, rehabilitation and retrofitting, Taylor & Francis Group, London, 2006, pp.1-10.
[22] Repairability of fire damaged structures, CIB W 14 Report, May 1989.
[23] Rotter, J.M. et al.: Structural performance of redundant structures under local fires, Proceedings of Interflam 99, Edinburgh, 1999, pp. 12.
[24] Technical report 68: Assessment, design and repair of fire-damaged concrete structures". Publisher Concrete Society Camberley, UK, 2008.
[25] Wagner, P.: Fire world statistic", Centre of Fire Statistics of CTIF, 2006.

SUSTAINABILITY OF ALUMINIUM IN CONSTRUCTION PRACTICE – RECENT FIRE RELATED RESEARCH

Neno Toric[1], Ivana Uzelac Glavinic[1], Ivica Boko[1]

[1] University of Split, Faculty of Civil Engineering, Architecture and Geodesy, Department of Metal and Timber Structures, Matice hrvatske 15, 21 000 Split, Croatia, email: neno.toric@gradst.hr, ivana.uzelac@gradst.hr, ivica.boko@gradst.hr

SUMMARY: The positive attributes of aluminium as a modern building material in construction practice have been used as background for a more intense application of this material type throughout the 21st century. Favourable properties of aluminium include most of the aspects of sustainability within the period of exploitation of the structure. One of the major problems with the application of aluminium in construction industry is the inherent fire resistance, which needs further research if aluminium is to be more widely applied in construction practice. This paper describes research activities of an ongoing research project examining the mechanical and creep properties of aluminium alloy EN6082AW T6 exposed to fire. The research presented here is part of a joint research programme (the Croatian Science Foundation project No. UIP-2014-09-5711) conducted by the Universities of Split and Sheffield, whose aim is to explore the influence of creep on the behaviour of steel and aluminium columns in fire, as well as to develop new creep models for structurally relevant steel and aluminium alloys. The output of this research can be used to assess the level of sustainability of aluminium in construction practice with respect to fire resistance requirements.

ODRŽIVOST ALUMINIJA U GRAĐEVINSKOJ PRAKSI – NOVA ISTRAŽIVANJA POVEZANA S POŽAROM

SAŽETAK: Pozitivna svojstva aluminija kao modernog građevnog materijala u građevinskoj praksi bila su podloga intenzivnije primjene toga materijala tijekom 21. stoljeća. Povoljna svojstva aluminija obuhvaćaju većinu aspekata održivosti u tijeku uporabe konstrukcije. Jedan od većih problema u njegovoj primjeni u građevinskoj industriji njegova je požarna otpornost koju treba i dalje istraživati ako ga se želi šire upotrebljavati u građevinskoj praksi. U radu se prikazuju istraživanja u projektu koji je u tijeku o ispitivanju mehaničkih svojstava i svojstava puzanja aluminijske legure EN6082AW T6 izložene požaru. Ovdje prikazano istraživanje dio je zajedničkog istraživačkog projekta (Hrvatska zaklada za znanost, projekt broj UIP-2014-09-5711) Sveučilita u Splitu i Sheffieldu čija je svrha istražiti utjecaj puzanja na ponašanje čeličnih i aluminijskih stupova izloženih požaru i razviti nove modele puzanja za odgovarajuće čelične i aluminijske konstrukcijske legure. Rezultati ovog istraživanja mogu se upotrijebiti za ocjenjivanje razine održivosti aluminija u građevinskoj praksi s obzirom na zahtjeve požarne otpornosti.

1. INTRODUCTION

Within the last seven decades aluminium has taken its position in civil engineering as a material for both, structural and non structural applications. Late application of this material can be explained trough high initial costs and great amount of energy consumption during production [1], which also resulted in later development of the design codes [2, 3]. Competitive features of aluminium in construction practice include good mechanical behaviour paired with low weight, corrosion resistance, high reflectivity and various design possibilities [4, 5]. Consequently, aluminium structures are most likely to be used in not easily accessible areas where erection and maintenance phases need to be simplified, or in highly corrosive environments (roof trusses, transmission line towers, window frames, cladding systems, bridges, etc.).

Despite the mentioned shortcomings in the initial stage, when considering its overall lifecycle, aluminium produces a significant reach in the framework of sustainability. Its advantages make it an ideal fit for building energy efficient building envelopes, or for improving energy efficiency of existing buildings. Aluminium also has a very long life cycle (30-50 years) paired with low maintenance costs [1]. Moreover, aluminium has an excellent recyclability, with its life cycle being almost indefinite and the energy required for recycling being only 5% of the energy required for its original manufacture [6]. As a consequence, the majority of the aluminium in the EU today is made out of the recycled materials [6], and the amount of aluminium produced today creates new reserves. It should be also noted that aluminium has a wide family of alloys. The ones we refer here are heat treatable wrought alloys of 6xxx series, as they are the most commonly used in the construction industry today. In general, mechanical properties of aluminium are the key parameter in quantifying the response of aluminium structures in fire conditions. This represents the main motivation for exploring the mechanical and creep properties of alloy 6082AW T6 with the aim of further exploring its sustainability aspects. The paper presents a description of tests conducted at University of Split and University of Rijeka, including some test results.

2. TEST SETUP AND METHODOLOGY FOR DETERMINING HIGH-TEMPERATURE PROPERTIES

In metals, three different strain components exist when exposed to high temperature. Each of these components requires a specific test methodology for quantifying its values. Testing within the research project is planned in such a way as to obtain the stress-related strain and creep strain separately at different temperatures, according to the total temperature-dependent strain relationship [7]:

$$\varepsilon_{tot} = \varepsilon_{th}(T) + \varepsilon_{\sigma}(\sigma, T) + \varepsilon_{cr}(\sigma, T, t) \quad (1)$$

where: ε_{tot} – total strain, $\varepsilon_{th}(T)$ – thermal strain (function of temperature T), $\varepsilon_{\sigma}(\sigma,T)$ – stress related strain (functions of both the applied stress σ and temperature T) and $\varepsilon_{cr}(\sigma,T,t)$ – time-dependent creep strain (function of stress, temperature and time). It can be seen from Equation (1) that creep strain is dependent on all three variables, which makes it the most complex of the strain components.

Generally, there are three main creep phases during exposure to a constant stress and temperature, as seen in Figure 1. In the primary creep stage, the creep strain rate is relatively high, but decreases with time. During the secondary creep phase, creep strain rate gradually becomes constant. This is also known as steady-state creep. During the tertiary creep phase, creep strain rate increases exponentially with time until steel rupture occurs. It can be observed from Figure 1 that, at higher temperatures and stress levels, the boundaries between the three stages is not as evident as in it is the case of lower temperature and stress exposure. Consequently, only the primary and secondary creep phases are usually taken into account in most structural fire resistance analyses.

Material parameters represent an important factor in the creep analysis, since the metallurgical composition of an alloy has a significant effect on the creep strain development at different temperature levels. Subsequently, a new study within the project for deriving material parameters for steel and aluminium creep analysis is planned.

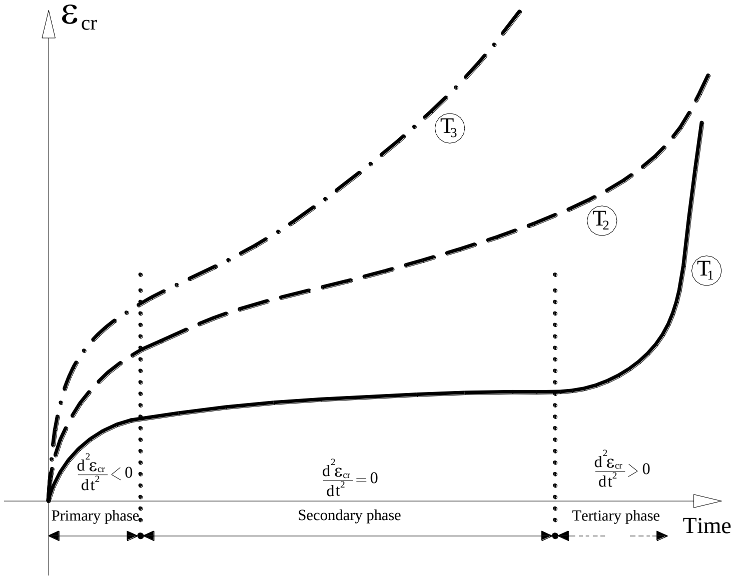

Figure 1. Creep phases at high temperature (T1< T2< T3)

wo different types of test within the research project were conducted in order to obtain stress-related and creep strains. The first is a constant stress-rate test which is used to determine the stress-related strain. The test procedure consists of a pre-heating phase (heating rate of approximately 15°C/min), soaking phase (approximately 30 min) during which the coupon achieves uniform temperature distribution, and the loading phase (uniform stress rate of10 MPa/s). This test type induces a negligible amount of creep strain during the test since it represents a fast test.

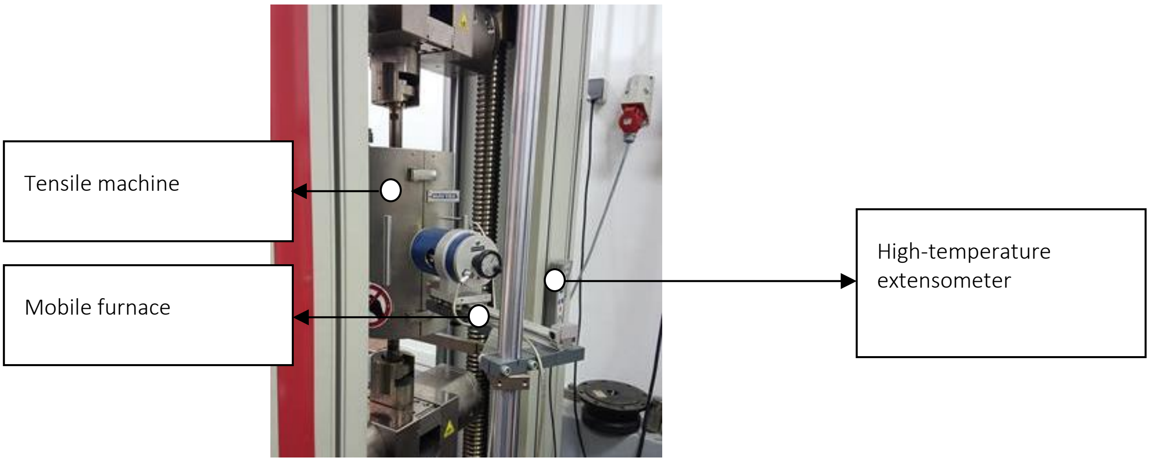

Figure 2: Test setup at University of Rijeka, Faculty of Engineering

The second test type, used mainly to determine creep strain evolution, is based on the stationary creep test. The test procedure for a stationary creep test consists of a pre-heating phase (heating rate of approximately 15°C/min), soaking phase (approximately 60 min) and the loading phase (during which the coupon is exposed to a constant stress level at the constant target temperature). The loading phase can last up to 20 hours depending on the temperature level which is being studied. The standards used for definition of coupon geometry, heating and loading are ASTM:E8M-11 for the ambient-temperature tests [8], and ASTM:E21-09 for the high-temperature tests [9]. Figure 2 presents the test setup for determining mechanical and creep properties at University of Rijeka, Faculty of Engineering.

3. COLUMN TEST SETUP

The research within the project is also planned on quantifying the creep influence on a larger scale, which includes column tests, both steel and aluminium. The testing methodology for the aluminium columns will rely on the stationary testing method where columns are heated to a predetermined temperature and subsequently loaded up to the failure point. Some of the columns will be tested using a transient testing methodology which relies on heating a column at a constant rate while being continually kept under load. Both test methodology will cover most temperature-mechanical boundary conditions that occur in a structure during fire.

The temperature ranges for the stationary tests are planned to be 100-400°C varying different load levels expressed as a percentage of the column load capacity at ambient temperature, which amount to: 20,40,60 and 80%. These tests are planned within the period of 2017/2018. Figure 3 presents the column test facility at Faculty of Civil Engineering, Architecture and Geodesy.

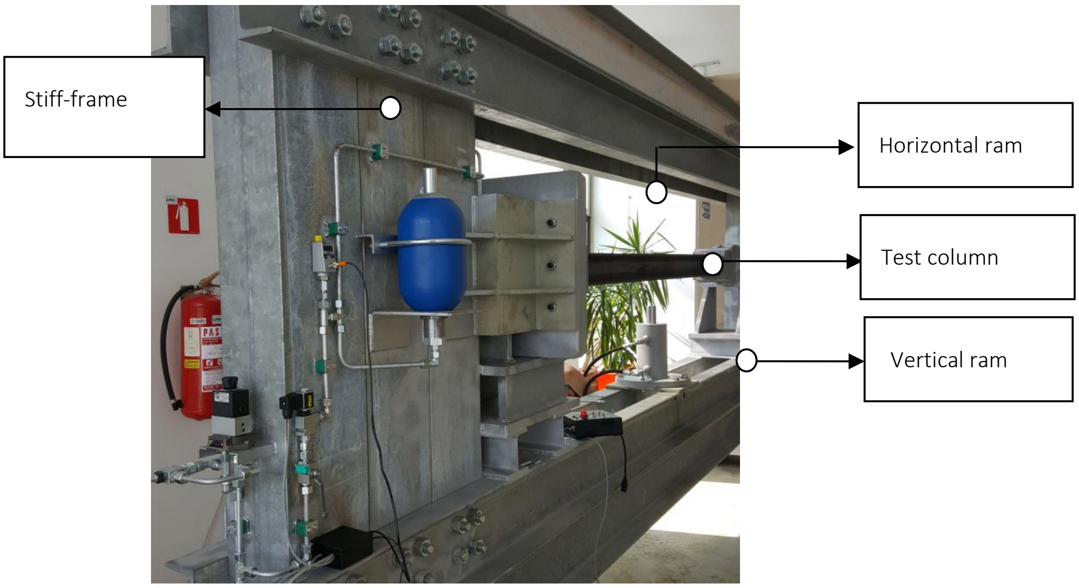

Figure 3: Column test facility at University of Split, Faculty of Civil Engineering, Architecture and Geodesy

4. TEST RESULTS

Figure 4 presents a photograph of the microstructure of a virgin specimen of aluminium obtained by optical microscope at 1000x normal magnification. As can be seen on the figure, the structure consists mostly of aluminium together with visible large rounded particles of Mg2Si and angular particles of (Fe,Mn) 3SiAl12.

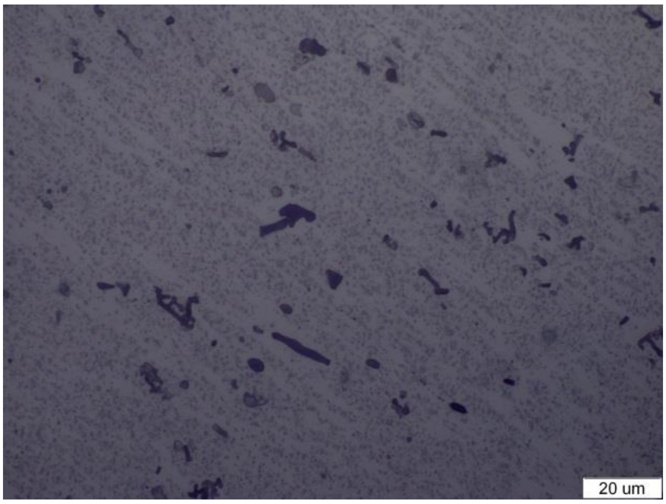

Figure 4: Microstructure of aluminium alloy EN 6082AW T6

Figure 5 presents test results of mechanical properties of the analysed alloy up to 350°C, where: $k_{E,\theta}$ - reduction factor for modulus of elasticity at temperature θ and $k_{0,\theta}$ - reduction factor for stress at 0.2% strain at temperature θ. Additionally, a comparison is given to the proposed reduction factors from Eurocode 9, part 1-2 [10].

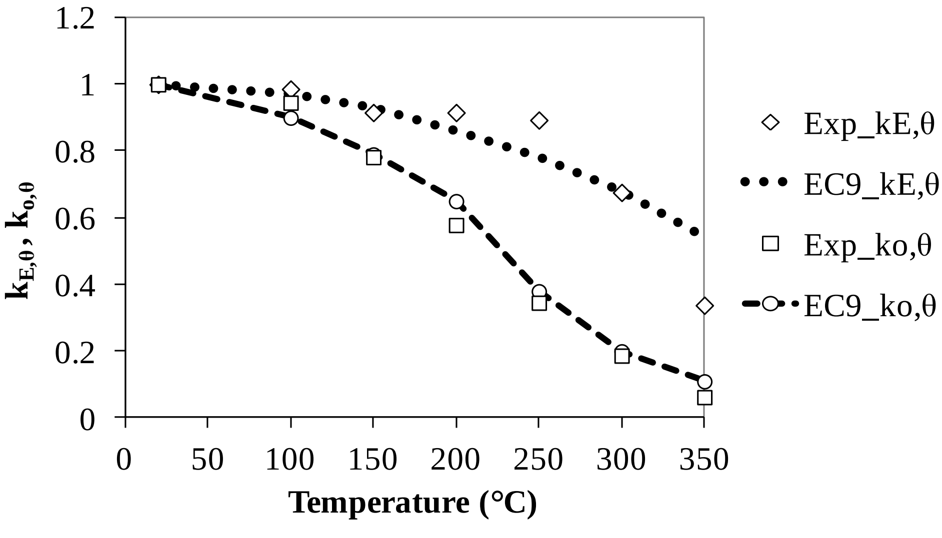

Figure 5: Reduction of mechanical properties of alloy EN 6082AW T6 – constant stress tests

It can be seen from Figure 5 that the temperature interval at which the alloy retains its mechanical properties is up to 350˘C, which is generally lower than the interval for steel (approximately 600°C). Although this interval is significantly less than steels', an addition of fire protective material can be used to increase the fire resistance rating of aluminium. Additionally, if aluminium is used as a large span roof structure, it is more likely that the fire temperature will not be so high in the far-field temperature region.

5. CONCLUSIONS

The paper presents current research activities concerning mechanical and creep properties of aluminium alloy EN 6082AW T6 at high temperature. The presented test results point out that the temperature interval for reduction of the mechanical properties of alloy EN6082AW T6 is up to 350°C, which is significantly less than steels' temperature interval. Although the temperature interval is smaller if compared to steels', the aluminium can be used regardless as a part of structure if it is not located near the fire origin. Passive fire protection can also be used to increase its fire resistance time and therefore add more value to aluminium's level of sustainability. Further research within the project will be focused on deriving an adequate creep strain model for the analysed alloy.

ACKNOWLEDGMENTS

This work has been fully supported by The Croatian Science Foundation as part of the project Influence of creep strain on the load capacity of steel and aluminium columns exposed to fire (UIP-2014-09-5711).

REFERENCES

[1] Efthymiou, E. & Baniotopoulos, C.C.: Structural Aluminium and Sustainability, 6th Hellenic National Conference of Steel Structures: Proceedings, 2nd to the 4th of October 2008, Available from http://eeme.ntua.gr/proceedings/6th/1A_3.pdf, Accessed: 2017-02-22

[2] EN1999 Eurocode 9: Design of aluminium structures, European Committee for Standardisation, Brussels, Belgium (2007)

[3] Sunday, S. et al.: *Aluminum Design Manual 2015*, Aluminum Association, ISBN-10: 0986363103, ISBN-13: 978-0986363108 (2015)

[4] Skejić, D., Boko, I., Torić, N.: Aluminium as a material for modern structures, Građevinar 67 (11), (2015) pp 1075-1085

[5] Peko, J., Torić, N., Boko, I.: Comparative analysis of steel and aluminum structures, e-GFOS (13), (2016) pp 50-61

[6] European Aluminium Association: Sustainability of aluminium in buildings, Available from http://www.european-aluminium.eu/media/1311/en-sustainability-of-aluminium-in-buildings.pdf, Accessed: 2017-02-22

[7] Anderberg, Y. : Modelling Steel Behaviour, Fire Safety Journal, 13 (1), (1988) pp 17-26.

[8] ASTM E8 / E8M-11, *Standard Test Methods for Tension Testing of Metallic Materials*, ASTM International, West Conshohocken, PA (2011)

[9] ASTM E21-09, Standard Test Methods for Elevated Temperature Tension Tests of Metallic Materials, ASTM International, West Conshohocken, PA (2009)

[10] EN1999-1-2 Eurocode 9 - Design of Aluminium Structures - Part 1-2: General Rules - Structural Fire Design, European Committee for Standardization, Brussels, Belgium (2007)

PROTECTED AND UNPROTECTED TIMBER BEAMS IN FIRE ENVIRONMENT

Cvetanka Chifliganec[1], Meri Cvetkovska[1], Ana Trombeva-Gavrilovska[2], Milica Jovanoska[1]

[1] Ss. Cyril and Methodius University in Skopje, Faculty of Civil Engineering, Partizanski odredi 24, 1 000 Skopje, Macedonia, email: c.chifliganec@gf.ukim.edu.mk, cvetkovska@gf.ukim.edu.mk, m.jovanoska@gf.ukim.edu.mk
[2] Ss. Cyril and Methodius University in Skopje, Faculty of Architecture, Partizanski odredi 24, 1 000 Skopje, Macedonia, email: agavrilovska@arh.ukim.edu.mk

SUMMARY: Timber buildings are economical, energy efficient, renewable and sustainable but, by the opinion of many engineers, prone to burning and have low fire resistance. Nowadays, ensuring the fire safety of timber buildings is a requirement in the design codes and a necessity in the design process. For the required duration of fire exposure, the fire safety can be achieved through proper fire design of the structural timber members, done either by ensuring sufficient residual cross-section to sustain the design loads during fire or by protecting the cross-sections with fire protection materials. In order to determine the fire resistance and the behaviour of unprotected and protected simply supported timber beams exposed to standard fire on three sides of their cross-sections, three different examples are analyzed. The nonlinear numerical analyses are performed with the specialized program for analysis of structures in fire – SAFIR. The results of the thermal and the structural analysis are graphically presented and comparison of the results is made. The rock wool insulated timber beam showed best thermal and structural fire performance.

ZAŠTIĆENE I NEZAŠTIĆENE DRVENE GREDE PRI DJELOVANJU POŽARA

SAŽETAK: Drvene su zgrade gospodarski i energetski učinkovite, obnovljive i održive, ali prema mišljenju mnogih inženjera sklone gorenju i imaju malu požarnu otpornost. Danas je osiguravanje požarne sigurnosti drvenih zgrada zahtjev u normama za projektiranje i nužnost u procesu projektiranja. Za zahtijevano vrijeme izloženosti požaru požarna se sigurnost može postići prikladnim projektom konstrukcijskih drvenih elemenata na požar bilo osiguravanjem dovoljnoga preostalog poprečnog presjeka za preuzimanje proračunskih opterećenja tijekom požara, bilo zaštitom poprečnih presjeka materijalima za zaštitu od požara. U radu su analizirana tri različita primjera s ciljem određivanja požarne otpornosti i ponašanja nezaštićenih i zaštićenih slobodno oslonjenih drvenih greda izloženih normiranom požaru s tri strane poprečnog presjeka. Posebnim programom za proračun konstrukcija na požar (SAFIR) proveden je nelinearni numerički proračun. Grafički su prikazani rezultati toplinskoga i konstrukcijskog proračuna, a rezultati su uspoređeni. Najbolje toplinsko i konstrukcijsko ponašanje u požaru pokazala je drvena greda izolirana kamenom vunom.

1. INTRODUCTION

Sustainability is one of the leading principles in the modern building design. The main objectives of sustainable design are: to reduce or completely avoid depletion of critical resources like energy, water and raw materials; prevent environmental degradation caused by facilities and infrastructure during their life cycle; and create built environment which is liveable, comfortable and safe. With growing pressure to reduce the carbon footprint of the built environment, building designers need to balance between costs and performance of buildings [1].

Wood is considered as renewable and sustainable construction material because: absorbs carbon dioxide while growing; it`s production is low energy and low impact process; it can be recycled or used as a bio fuel; the construction work is efficient and economical; it is characterized by durability and excellent thermal performance; etc.

Despite the fact that timber satisfies many of the contemporary building requirements, it has a disadvantage of being combustible when exposed to high temperatures and fire. Consequently wood structures are seen by many as creating an environment less safe than structures built of non-combustible materials, such as concrete and masonry. In order to prevent serious consequences fire, as an accidental action, have to be taken under consideration in timber structural design. Special parts of the Eurocodes are dedicated to the fire safety of structures and the passive fire protection. In these parts the following essential requirements are defined: load bearing resistance, structural integrity and insulation. The fire resistance of an element, of a part, or of a whole structure is ability to fulfil the above mentioned requirements for a specified load level, for a specified fire exposure and for a specified period of time [2]. Ensuring the required fire resistance of a building structure, leads us a step closure to ensuring its fire safety. Nowadays, the fire safety of a building is considered as an essential part of the Declaration of performance [3].

As building technologies and science evolve, the timber fire protection measures are improved and upgraded. The process of making wood more fire resistant usually involves application of surface coatings or impregnation with chemical treatments. The use of rock wool, gypsum plasterboards or other fireboards, as fire-resistant linings, are also common in practice.

Nowadays, as a result of the rigorous environmental and economical requirements, as well as ensured fire resistance through appropriate design, the industries in many countries are trying to shift more public sector construction to timber.

2. BEHAVIOUR OF WOOD, ROCK WOOL AND GYPSUM PLASTER BOARD IN FIRE

2.1. TIMBER IN FIRE

Wood is a complex composite of natural polymers and is generally anisotropic, heterogeneous and porous material. The properties of wood are affected by the moisture content, which, in case of fire, evaporates and diffuses. This leads to changes of material properties [4]. When exposed to the heat of a fire, the wood goes through a process of thermal breakdown into combustible gases. The pyrolysis is a thermochemical decomposition of a wood at elevated temperatures in the absence of oxygen (or any halogen). It involves the simultaneous change of chemical composition and physical phase, and is irreversible. It usually starts at temperatures of 280 °C to 300 °C. The key contributing factor in timber's fire resistance is the layer of charcoal that is formed on the burning surface during the pyrolysis process. This charred layer acts as an insulator protecting the inner core of the timber, making it resist to heat penetration and thus burn more slowly [1]. The inner uncharred core remains cold and keeps its initial properties, enabling to continue to carry its load. The progressive conversion of the fire-exposed surfaces to ever-deepening char occurs at definable rates. Since charcoal is produced at a constant rate, the time to failure of timber construction elements can be easily predicted. The rate of conversion to char decreases with increasing of moisture content and density of the timber used. The charring rate is also affected by the permeability of the timber to gaseous or vapor flow. Charring normal to the grain of timber is one-half of that parallel to the grain. As long as the residual section is large with respect to the depth of char development, the rate is unaffected by the dimension of the section exposed [5].

2.2. ROCK WOOL IN FIRE

In normal temperature environment, rock wool thermal insulation prevents convection by holding air still in the matrix of the wool. Still air is a good insulator. It also stops radiation and limits the conduction of heat through the body of the insulation. The effectiveness of rock wool in reducing heat transfer depends upon its structural properties such as density, thickness, composition and the fineness of the wool as well as the temperature at which it is used. Due to its non-combustibility rock wool insulation does not spread fire by releasing heat, smoke, or burning droplets. In fire environment it retains integrity and hampers the fire process. The maximum working temperature is about 750 °C and melting occurs at 1000 °C. Rock wool is used to: protect the flammable constructions or those susceptible to the effects of fire; to increase the structural elements resistance to fire; and to slow down the heat transfer in case of high temperatures.

2.3. GYPSUM PLASTERBOARD IN FIRE

Gypsum plasterboards are widely used in building construction. They consist of a gypsum core sandwiched between two layers of paper and can also contain other materials in small quantities such as glass fibre and vermiculite within the various proprietary products to improve their durability and performance when exposed to high temperatures.

There are three types of gypsum boards: Regular boards, Type X and Type C boards. Regular plasterboards are used as non-fire resistant partitions, while the Type X boards and Type C are used in fire-rated applications.

Gypsum is porous and non-homogeneous material which contains chemically combined water (approximately 50% by volume). When gypsum panels are exposed to fire, dehydration reaction occurs at 100ºC to 120ºC [6]. Heat is absorbed as portion of the combined water is driven off as steam i.e. calcination occurs. Thermal energy that converts the water to steam is thus diverted and absorbed, keeping the opposite side of the gypsum panels cool as long as there is crystalline water left to be converted into steam or until the gypsum panel is breached i.e. heat transmission is effectively retarded. In the case of regular gypsum board, as the crystalline water is driven off, the reduction of volume within the gypsum core causes large cracks to form, eventually causing the panel to fail due to structural integrity [7].

In Type X gypsum boards, special glass fibers are intermixed with the gypsum to reinforce the core of the panels. These fibers have the effect of reducing the size of the cracks that form as the water is driven off, thereby extending the length of time the gypsum panels resist fire without failure. Also, there are Type C gypsum boards whose core also contains glass fibers, only in a much higher percent by weight. In addition to the greater amount of glass fiber, the core of the Type C panels can also contain vermiculite, which acts as a shrinkage-compensating additive that expands when exposed to elevated temperatures of a fire. This expansion occurs at roughly the same temperature as the calcination of the gypsum in the core. It allows the core of the Type C panels to remain dimensionally stable in the presence of fire, which in turn allows the panels to remain in place for a longer period of time even after the combined water has been driven off [7].

3. NUMERICAL EXAMPLES

3.1. DESCRIPTION OF THE PROBLEM

Aiming to determine the impact of fire on protected and unprotected timber beams and their behaviour in fire environment, three numerical examples were analyzed using the program SAFIR [8]. The evolution of fire temperatures over time is defined with the standard fire curve ISO 834. In all examples, the simply supported beam is fire exposed on three sides (Figure 1). In Case study 1 an unprotected timber beam is analyzed, Case study 2 analyses the same timber beam but protected on three sides with rock wool and Case study 3 analyses the timber beam protected with rock wool on the sides and X type gypsum board at the bottom. The cross-sections of the beams used in the examples are presented in Figure 2.

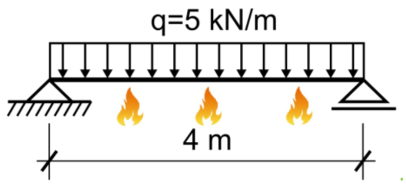

Figure 1 Geometry, support conditions and loads on a simply supported beam

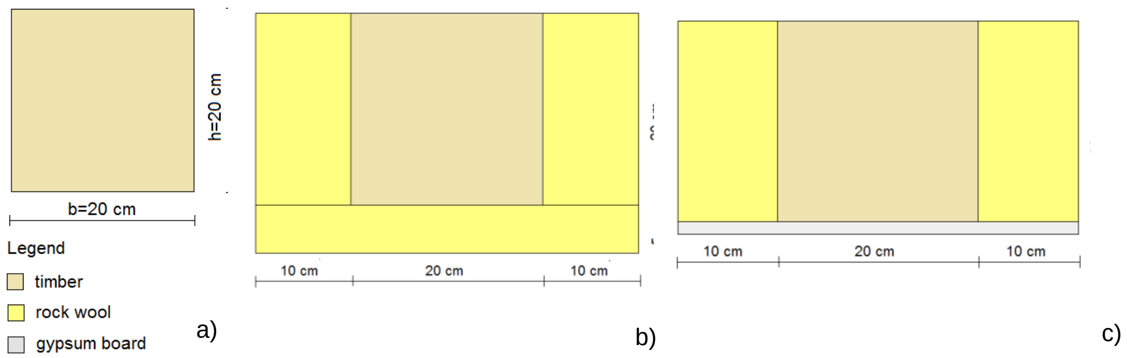

Figure 2 Cross sections of the beams, a) Case study 1, b) Case study 2, c) Case study 3

3.2. THERMAL AND MECHANICAL PROPERTIES OF MATERIALS USED IN THE NUMERICAL ANALYSIS

The characteristic values of the strength, stiffness and density of the timber beam, strength class C30, is taken in accordance with the EN 388 [9]. The material was considered with 12% moisture content.

The X type gypsum board has a density of 648 kg/m^3 and the rock wool has a density of 160 kg/m^3.

All thermal properties for the materials used in the analysis are given in Table 1. Temperature dependant thermal conductivity and specific heat for the materials are taken in accordance with the appropriate EC parts for the materials.

Table 1 Thermal properties used in the numerical analysis

Thermal property	Unit	Timber	Type X gypsum board	Rock wool
λ (20 °C)	[W/mK]	0.12	0.40	0.037
c (20 °C)	[J/kgK]	1530	960	880
ρ (20 °C)	Kg/m^3	425	648	160
α_c	[W/m^{2}K]	25	25	25
$\alpha_{c,\ cold}$	[W/m^{2}K]	4	/	/
ε		0.8	0.9	0.75

3.3. THERMAL ANALYSIS

As expected, significant differences in the time-dependant temperature fields in the cross-sections of the unprotected and the protected beams were noticed. The temperature distributions in the cross-sections of all analyzed case studies, for the specific time moments or for the usually required fire resistances, given in the regulations, are shown in Figure 3, Figure 4 and Figure 5.

In Case study 1 (Figure 3), the unprotected timber beam reaches high temperatures in relatively short time period and at the moment of failure (t_f=37 min) the charring depth in the horizontal direction is d_{char}=30.2 mm and in the vertical direction h_{char}=30.1 mm. This implies that the charring rates (the ratio of the charring depth to the time of fire exposure) are β_b=0.82 mm/min and β_h=0.81 mm/min, respectively. Charring depth is the distance between the outer surface of the original cross section and the position of the char-line (see Figure 6). The position of the char-line is taken as the position of the 300-degree isotherm.

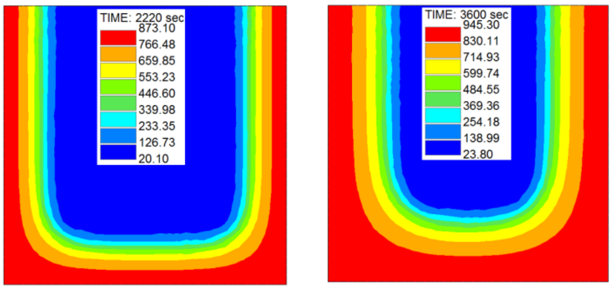

a) b)

Figure 3 Temperature distribution in the cross-section of Case study 1, a) $t_{failure}$=37 min b) t=60 min

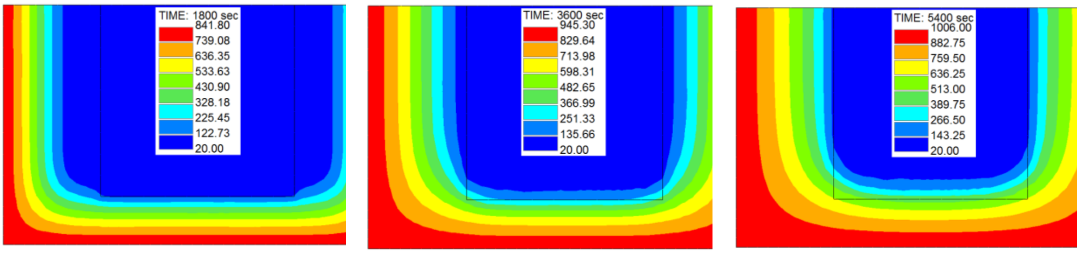

a) b) c)

Figure 4 Temperature distribution in the cross-section of Case study 2, a) t=30 min b) t=60 min 2 c) t=90 min

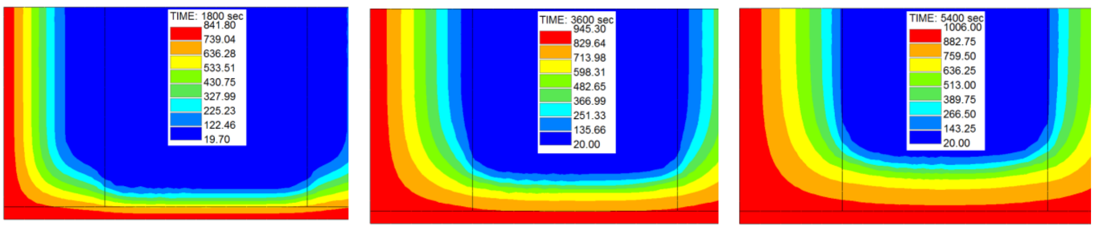

a) b) c)

Figure 5 Temperature distribution in the cross-section of Case study 3 a) t=30 min b) t=60 min 2 c) t=90 min

According to the simplified analytical reduced cross-section method given in Eurocode 5-1-2 [10], the effective charring depth in the cross-section of the unprotected timber beam in Case study 1 can be calculated by using the following relations:

$d_{ef}=\beta_n*t+k_0*d_0$=36.6 mm

$b_{fi}=b-2*d_{ef}=126.8$ mm

$h_{fi}=h-d_{ef}=163.4$ mm

$A_r= b_{fi} * h_{fi} =0.020719$ m²

A_r*(%A)=51.8%*

where: β_n *=0.8 mm/min* is the design notional charing rate under Standard fire exposure.

t=37 min is the time of fire exposure

k_0*=1* is for fire exposure t>20 min

d_0*=7 mm* is the zero strength layer

A_r is the area of the reduced cross section

It can be see that the charring rates calculated analytically and numerically match.

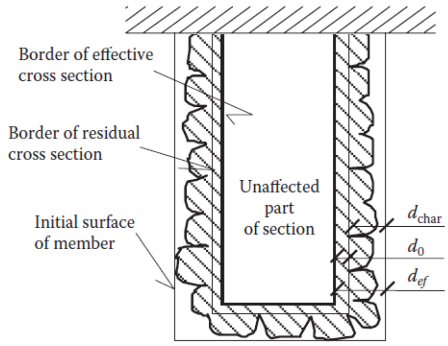

Figure 6 Definition of the residual and the effective cross-section

In case of protected timber beams, i.e. Case study 2 and Case study 3, the moment when charring process starts is delayed (Figure 4 c and Figure 5 a) and only the numerical results are presented.

At 30 minutes of fire exposure, the whole cross-section of the timber beam in Case study 2 is cold (Figure 4 a). At the same time, the timber beam in Case study 3 has 10 mm charring depth in the vertical direction of the cross-section while the sides of the section remain unheated because of the positive influence of the rock wool insulation (Figure 5 a). At time t=37 min the cross-section of Case study 1 is significantly heated and has charring depths of 30 mm in both directions (Figure 3 a).

The rock wool insulation shows far better results in the fire protection of the timber beam, in comparison to the Type X gypsum board. After one hour of fire exposure the cross-section of the beam in Case study 2 remains cold, that is not a case with the beam in Case study 3 which has a charring depth of 30 mm in the vertical direction (Figure 4 b and Figure 5 b). Figure 3 b shows that after one hour of fire exposure the unprotected beam has a highly reduced cross-section.

3.4. STRUCTURAL ANALYSIS

The timber beam protected with rock wool (Case study 2) has reached higher fire resistance (time to failure) in comparison to the timber beam protected with Type X gypsum boards (Case study 3). Both beams satisfy the required fire resistance of 60 minutes, but the beam in Case study 2 has by far favourable cross-section temperature distribution compared to the one in Case study 3 (Figure 4 b and Figure 5 b). The unprotected timber beam has a fire resistance of tf=37 min. Besides the benefit to the thermal distribution in the timber cross-section, the contribution of the rock wool to the structural fire performance of the beam is confirmed too. The cold cross-section in Case study 2 results with prolongation of the load-bearing resistance of the beam and smaller mid-span vertical displacements (Figure 7). The vertical mid-span displacements of the analysed beams (Δy) are presented in Table 2.

Table 2 Vertical displacements at mid-span of the beams, for different case studies

Type of cross section	Δy [cm]	Time [min]
Case study 1	3.72	37
Case study 2	1.37	60
Case study 3	2.15	60

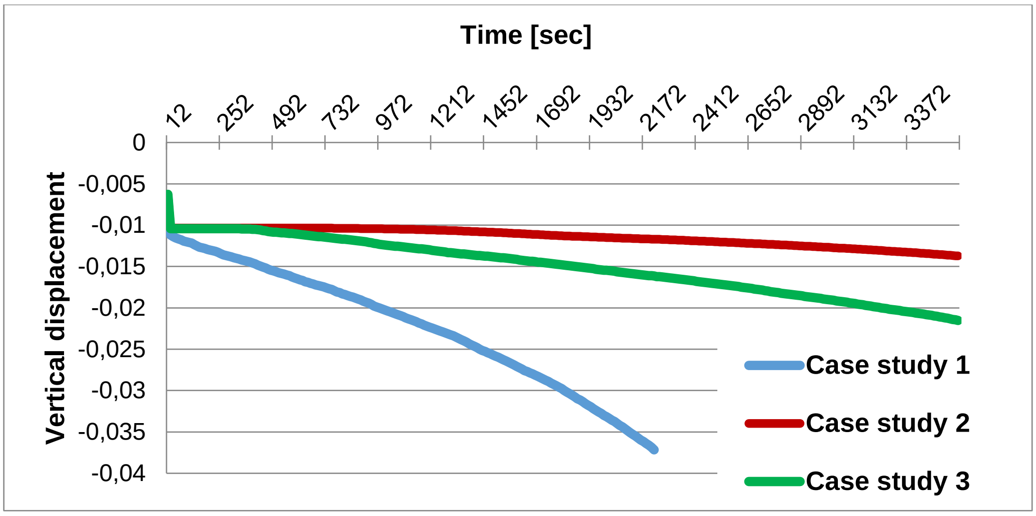

Figure 7 Time and temperature dependent vertical displacements at beams mid-span

4. CONCLUSIONS

The acceptable fire performance of unprotected timber elements should be attributed to the charring effect of the wood. The char layer acts as an insulator and protects the core of the wood section. For the required duration of fire exposure, unprotected beams may withstand the design loads only if proper dimensions of the cross-section are used. Fire exposed beams protected with gypsum fireboards at the bottom show improved fire resistance, but best results are achieved when the protection material from bottom side is rock wool. The improved fire resistance and the reduced deflections of the fire protected beams should be attributed to the positive effect of the insulation materials on the temperature distribution in the cross-sections of the beams.

In practice, if there are no architectural requirements for visibility of timber elements, floor and roof structures are constructed as in Case study 3 and the rock wool is used only for satisfying the energy efficiency requirements. The results obtained in this study show that a layer of rock wool from the bottom side of the structure (not only as an infill) will significantly improve the fire resistance of the whole structure.

REFERENCES

[1] https://www.woodsolutions.com.au, Accessed: 2016-09-12
[2] Committee of European Normalisation (CEN), EN-1991-1-2-2002, *Eurocode 1: Actions on Structures, Part 1-2: General actions - Actions on Structures Exposed to Fire*. CEN, Brussels, (1991-2002).
[3] Canadian wood council, *Fire Safety in Residential Buildings*, Building Performance No. 2
[4] Tabaddor M., *Modelling The Thermal and Structural Behaviour of Wood Beams in a Fire Environment*, Underwriters Laboratories Inc, (2013)
[5] Schaffer, E. L. *Structural fire design: Wood*, Forest Products Laboratory, Madison, (1984).
[6] Keerthan P., Mahendran M., Numerical studies of gypsum plasterboard panels under standard fire conditions. *Fire Safety Journal*, 53(Oct) (2012), pp. 105-119.
[7] https://www.usg.com, Accessed: 2016-09-15
[8] Franssen J.-M, SAFIR: A Thermal/Structural Program Modelling Structures under Fire, *Engineering Journal*, A.I.S.C., Vol. 42 No. 3 (2005), pp. 143-158.
[9] Committee of European Normalisation (CEN), *CSN EN 338 Structural timber - Strength classes*, CEN, (2009).
[10] Committee of European Normalisation (CEN), EN 1995-1-2 (2004): *Eurocode 5: Design of timber structures - Part 1-2: General - Structural fire design*, CEN, Brussels, (2004).

ASSESSMENT AND STRUCTURAL HEALTH MONITORING OF HERITAGE TIMBER STRUCTURES

Vlatka Rajcic[1], Mislav Stepinac[1], Jure Barbalic[1]

[1] University of Zagreb, Faculty of Civil Engineering, Department for Structures, Fra Andrije Kacica Miosica 26, 10 000 Zagreb, Croatia, email: vrajcic@grad.hr, mstepinac@grad.hr, jbarbalic@grad.hr

SUMMARY: Assessment and health monitoring of existing timber structures has experienced huge interest in last decades. The main reasons are protection and conservation of the heritage buildings built in timber and assessment and collection of crucial data for relatively new large-span timber structures. In this paper several assessment methods and wireless monitoring systems will be explained. The main focus of the paper is to present non-destructive and semi-destructive test methods for the assessment of old and under protection heritage buildings as well as to present possible systems and principles of their health monitoring.

OCJENJIVANJE I PRAĆENJE STANJA DRVENIH KONSTRUKCIJA BAŠTINE

SAŽETAK: Posljednjih godina znatno je narastao interes za ocjenjivanje i praćenje stanja postojećih drvenih konstrukcija. Glavni su razlozi zaštita i konzervacija zgrada baštine izgrađene od drva i ocjenjivanje i prikupljanje važnih podataka za relativno nove drvene konstrukcije velikih raspona. U radu je objašnjeno nekoliko metoda ocjenjivanja i sustava za bežično praćenje. Glavni je cilj rada pokazati nerazorne i polurazorne ispitne metode koje se mnogo upotrebljavaju za ocjenjivanje starih građevina i zaštićenih građevina baštine te moguće sustave i načela praćenja njihova stanja.

1. INTRODUCTION

Structural health monitoring (SHM) is important topic for preservation of both old and new structures, thus, SHM within the context of timber structures is not adequately represented in strategic documents. Timber is often recognized as less durable material and timber structures as short-time lasting structures. Nevertheless, there are numerous examples of timber structures which are defying time and which are still standing despite aggressive climate and/or frequent and no adequate use. In the last decade more and more papers were produced to point out the problems of monitoring the timber structures.

While monitoring helps to continuously survey the condition of structures, non-destructive (NDT) methods aim to describe the existing condition of relevant areas of the structure [1]. There are two main areas of assessment and monitoring of timber structures: monitoring & assessment of historical timber structures and monitoring & assessment of relatively new structures erected recently as a result of significant advances and development with the field of new timber materials, timber structures and timber construction in general. The assessment of the structural health of old timber structures is different than the assessment of the new timber structures, e.g. large-span structures. Therefore, advantages in technology with requirements for preservation of both historical objects and new timber structures provoked an increased interest in scientific and professional community in assessment methods for timber structures.

The need for an assessment of an existing structure can be based upon a multitude of reasons. Among the most typical are given in [2]: if errors in the planning or construction period become known, on the occasion of change of use of the building, in case of doubts about the structural safety, caused by visual damage, due to apparently inadequate serviceability an usability; because of exceptional incidents or accidental loads which might have damaged the structure; in the case of arising suspicion due to material-, construction- or system-inherent impairment of the structural safety, if a simple, initially unfounded suspicions shall be eliminated, when the remaining lifetime , determined during a previous assessment, has expired. The time and cost of structural assessment are justified by ensuring the safety, protecting of capital investments and cultural heritage.

The last decades were marked by a significant widening in the range of application of timber in structures and consequently a growing importance of the assessment of these structures. A wide variety of methods exist to assess timber structures, however, their frequency and scope, the decision making approach concerning safety and the necessary interventions are far from being agreed upon. The COST Action FP1101 which ended in year 2015 was dealing with the main problems of existing timber structures; assessment, reinforcement and monitoring of such structures. Lot of the information about the mentioned topic can be found on the website of the Action (http://www.costfp1101.eu) and the main benefit of the Action is comprehensive and gathered knowledge regarding the assessment, reinforcement and monitoring of timber structures, specifically through: benefiting from innovative methods and technologies that are available for other building materials worldwide but are not being adapted to timber structures; maximising and coordinating research and innovation, and broadening the knowledge for the assessment, reinforcement and monitoring of timber structures; disseminating the harmonized knowledge by developing guidelines for assessing, reinforcing and monitoring timber structures [3].

The main purpose of this paper is to summarize the most important assessment methods for existing timber structures and to show systems and principles for SHM.

2. STRUCTURES AND GUIDELINES

Over the past years, a multitude of guidelines on how to approach the inspection and maintenance of existing timber structures have been published, however, only a few countries have published applicable code-type documents for the assessment of existing structures [2]. There is a large number of methods and guidelines for the assessment of existing timber structures but some of them are applicable only for a certain types of structures.

Historical timber structures represent an important part of the World Cultural Heritage and many of them are still in function: they must be preserved in order to guarantee their functionality and conserved for their historical value [1]. The most common method of assessment of historical timber structures is a combination of on-site inspection and non-destructive tests. Visual inspection is giving an idea about the condition of the structure in whole, identifies weak and critical zones and allows the information about the state of the structural stability and state of timber members, and respectively critical elements and joints in timber structures. Many NDT tests and models can be used in order to assess the state of conservation and the mechanical-physical properties of old timber members and joints: all the NDT tests, offer the same limits of the on-site inspection, because the data are referred to the time of realization [1]. Design standard for the existing timber structures still don't exist but several guidelines are already published. Systematic review of criteria to be used in the assessment of load-bearing timber structures in heritage buildings is presented by document issued by CEN TC 346 *Conservation of Cultural Heritage WG10 Heritage timber* and Cruz et al. [4]. When assessing the timber structure complete assessment covers the preliminary assessment (desk survey, preliminary visual survey, measured survey, structural analysis and preliminary report), as well as the detailed survey of timbers (with a special emphasis on visual strength grading on site) and carpentry joints.

3. ASSESSMENT METHODS

In this chapter the majority of the NDT and semi-destructive methods to assess existing timber structures are listed, and the most common ones are briefly explained. Very broad overview is given by Colla et al. [5], in the reports of the FP7 European project SMooHS (www.smoohs.eu). Dietsch and Kreuzinger [2] summarized the most common methods: visual (hands-on) inspection, tapping (sounding), mapping of cracks, measurement of environmental conditions, measurement of timber moisture content, endoscopy, penetration resistance, pull-out resistance, drill resistance, core drilling, shear tests on core samples, stress waves, X-ray, dynamic response, load tests (proof loading), strain measurement, microscopic and chemical laboratory methods, macroscopic laboratory methods—testing of specimen. Tannert et al. in [6] explained also several new techniques such as infrared thermography, glue line test, screw withdrawal, radial cores to determine compressive strength, pin pushing and surface hardness. Detailed explanations of every method can be found in [7-16].

The last step in assessment of timber structure is to incorporate assessed data incorporated into probabilistic models which will be used to calculate remaining load-bearing capacity and reliability of the structure.

3.1. VISUAL INSPECTION

The simplest and most common NDT technique is visual inspection and it should be first step in assessing timber members in structure and whole structure itself. Obvious damages can be easily identified, including external damage, decay, crushed fibres, creep, or presence of severe cracks. The most common examples of damages and deterioration in structural timber elements which can be identified by visual inspection are:

a) Poor construction details in structural timber elements, due to: Bad drainage of rainfalls from the outside; Bad connection of timber elements to the foundation which causes capillary raising of the humidity and salts in timber elements; Use of too thin elements which are prone to deterioration; Use of too thin elements in combination with large diameter steel fasteners – splitting of timber elements; Lack of insolation materials which avoid condensation of water…

b) Mistakes during execution of the structure: building the structure with too moist timber can result in swelling and shrinkage of timber members, bad choice of connectors which can change static scheme of structure in a whole, miss gluing or gluing with incompatible glues can lead to insufficient load-bearing capacity…

c) Inadequate modifications to the original project: removal of structural elements, removal or alteration of structures aligned with support structures, modification in the foundations can lead to damage and instability of a structure in a whole…

d) Lack of maintenance and monitoring: cracks, rotten parts, instability of members

e) Physical-chemical-biological weathering reactions due to environmental parameters: degradation of timber properties…

Both natural defects and deterioration of wood have a detrimental effect on the mechanical properties of the material. Deterioration caused by biotic attack causes a decrement of the original quality of wood, not only because of the general decrease of density but also because of the chemical alteration of the wood substance, as in the case of decay caused by rot [17]. Visual inspection has definite limitations: variability stems from differences in visual acuity and training/experience of personnel, problems with access, knowledge is limited to the exterior surface of the wood.

3.2. ULTRASONIC ECHO TECHNIQUE

Stress wave and ultrasound methods for investigating wood are based on the propagation of compression waves through wood. The performed tests are based on the time-of-flight measurement to determine wave propagation speed. In these measurement systems, a mechanical or ultrasonic impact is used to impart a wave into a member. Piezoelectric sensors at two points on the member are used to sense passing of the wave (Figure 1a). The time it takes for the wave to travel between sensors is measured and used to compute wave propagation speed. Longer propagation times are generally indicative of the presence of defects, deteriorated wood or wood with lower stiffness or density. Stress wave techniques are also, however, affected by other factors, including MC, wood species and growth-ring orientation [17]. The speed of propagation is directly correlated to the modulus of elasticity (MoE), but primary is correlated to the local singularities (knots, grain direction, degradation area...). The energy damping of the waves is directly dependant of local singularities. The maximal value of the peak of energy represents thus a measurement of the acoustic response of the wood which translates faithfully the damping function. Method enables to measure and manage two ultrasonic variables, allows working in the wood natural axis: longitudinal, radial and transversal. When propagation velocity of the longitudinal stress wave is gained it is easy to achieve value of MOE if density of member is known. Therefore, density is an important variable that must be measured if a stress wave technique is used to estimate dynamic MoE.

3.3. MEASUREMENT OF TIMBER MOISTURE CONTENT

One of the most important factors affecting the performance and properties of wood is its moisture content. The amount of water present in wood can affect its weight, strength, workability, susceptibility to biological attack and dimensional stability in a particular end use. Moisture content is simply the mass of moisture present in wood divided by the mass of the wood with no moisture in it, expressed as a percentage. The dimensional changes of wood due to changes in moisture content (shrinkage, swelling) are different in the three material axes (longitudinal, tangential or radial). Shrinkage and swelling are significantly more pronounced in radial and tangential direction than in longitudinal direction. It is estimated that over 80% of the in-service problems associated with wood are in some way related to its moisture content.

Two general approaches to determine wood moisture content can be distinguished. In direct measurements (Figure 1b), the moisture content is determined by oven-drying or water extraction, whereby both are destructive methods with respect to timber members in-situ. Indirect measurement methods use physical properties of wood which are correlated to the wood moisture content [18]. The most common moisture meters are electrical resistance meters which work on the principle that, as the moisture content of a piece timber increases, its electrical resistance decreases. Electrical resistance meters measure the conductivity between more pin electrodes that are pushed into the timber element and are calibrated to provide the user with a corresponding moisture content reading.

3.4. DRILL RESISTANCE

To detect the quality of cross-sections, decay in timber elements and to determine density of timber elements drill/penetration techniques are used. Drilling resistance is classified as quasi-non-destructive because a small diameter (1.5mm – 3 mm) hole remains in the specimen after testing. Drill resistance devices operate under the premise that resistance to penetration is correlated with material density. Drill resistance is determined by measuring the power required to cut through the material (Figure 1c). Plotting drill resistance versus drill tip depth results in a drill-resistance profile that can be used to evaluate the internal condition of timber member and identify locations of various stages of decay.

Figure 1 a) Ultrasound testing, b) Measurement of moisture content, c) drill resistance

3.5. INFRARED THERMOGRAPHY

Infrared thermography (IRT) is a non-destructive investigation technique, which is becoming more frequently employed in civil and architectural inspections, in the diagnostic phase, in preventive maintenance or to verify the outcome of interventions. On historic structures, it allows investigating details of construction (e.g. hidden structure or masonry texture behind the plaster), damage and material decay (e.g. moisture, plaster detachment from a wall, cracks pattern evolution, temperature pattern evolution, microclimatic conditions mapping). The presence of a subsurface defect modifies the diffusion rate of thermal propagation. Infrared thermography is a contactless NDT technique able to record the distribution of surface temperatures and thus to unveil details of what is under the surface, within shallow depths, or its thermal behaviour.

4. STRUCTURAL HEALTH MONITORING OF TIMBER STRUCTURES

The authors of the article participated in the project under FP7 Collaborative Project "Smart Monitoring of Historic Structures" (SMooHS) from 2009-2012, financed by EU, altogether with 13 partners from European Union and one partner from Palestinian-administered areas. One of the principal achievements of the SMooHS project was the development of smart monitoring systems using wireless networks of miniature, robust sensors for minimally invasive installation to monitor a plethora of physical quantities. Smart data processing is provided based on the built-in material deterioration models which would inform owners and conservation professionals about changes in the object status and the environmental conditions, as well as produce warnings and recommendations for action. Finally, user-friendly, modular and open source software was developed that can be continuously updated and broadened to handle specific questions arising at the object, steer various combinations of sensors, be open for extensions, also from researchers using it in the future.

It is common today to use wireless systems since compared to wired systems, they are easy to install, cost-effective and perfectly suited to monitor historic structures due to minimal aesthetic impact. They are capable of long-term, autonomous operation under remote control and programming. They can be customized for acquiring and analyzing sophisticated physical parameters like stress, strain, inclination, salt and moisture content inside materials, vibration or even acoustic emission caused by fracture processes which is all very interesting in evaluation of old timber structures.

Two systems were developed in the project: self-contained "Smartbrick®" devices and wireless sensor networks like the "Smartmote" system [19]. The monitoring can be made intelligent by designing task-tailored methods and algorithms for data reduction incorporating material and deterioration models. The data analysis strategies allow obtaining comprehensive information on environmental influences, deterioration rates or accumulated doses, triggering alarms like sound, light, automatic SMS or initiating actions like window opening/closing, or switching ventilation/heating on and off. However, it should be kept in mind that wireless monitoring must be configured, tested and calibrated with great care to assure reliable and useful results. Continuous instrumented monitoring will never replace expert knowledge like that of restorers, but it is a powerful tool to gather more detailed information on deterioration processes and its influences and to better understand these processes. It is expected that by combining instrumented monitoring with conventional test methods and also more sophisticated non-destructive test methods as well as with simulation and modelling tools knowledge of the historic structures and sufficient measures to preserve them for future generations could be significantly increased.

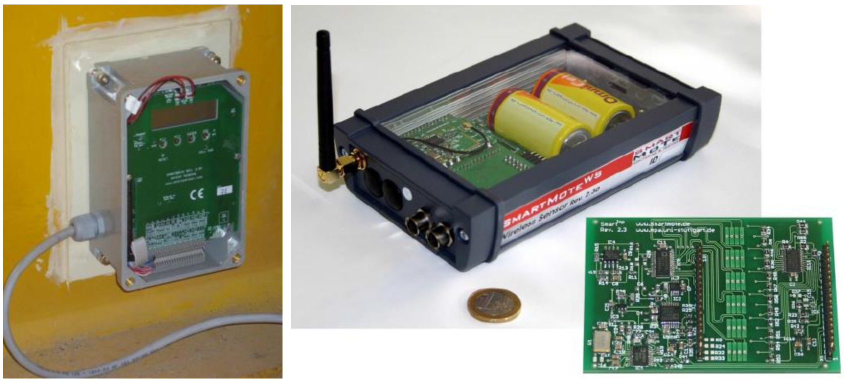

Figure 2 a) The Smartbrick® wireless sensor platform installed on a structure, b) Robust wireless sensor node (opened for demonstration) for multiple sensing and an exemplary sensor board to be used for monitoring salts and moisture.

Two monitoring systems were tested on the site for various problems and set of data on the case studies: Museum Island, Berlin, Holy Cross Minster, Schwäbisch Gmünd, The Palazzo Malvezzi de' Medici in Bologna, Old building in Hebron, Schönbrunn castle in Vienna and the Johanniskirche (St. John's) in Schwäbish Gmünd [20-22].

5. CONCLUSION

At the moment lot of different assessment techniques exists and are representing promising methods for a quantitative description of the current condition of timber members in timber structure. This concerns material properties like modulus of elasticity, moisture content and density as well as structural properties like dynamic characteristics, localization of inhomogeneities, cracks, and biological attack [1]. The lack of standardised assessment methods results in lack of reconstruction and reinforcement of timber structures. Reinforcement of new and existing timber structures has been the subject of considerable research and development in recent years. New materials and methods for reinforcement have been developed and used in practise. However, there is currently a lack of harmonised European standards governing this field [23]. Systematic review of criteria to be used in the assessment of load-bearing timber structures in heritage buildings is presented by document issued by CEN TC 346 Conservation of Cultural Heritage WG10 Heritage timber. When assessing the timber structure complete assessment covers the preliminary assessment (desk survey, preliminary visual survey, measured survey, structural analysis and preliminary report), as well as the detailed survey of timbers (with a special emphasis on visual strength grading on site) and carpentry joints. The main focus of the paper was to present non-destructive and semi-destructive test methods which are highly in use because of the assessment of old and under protection heritage objects and systems used for SHM.

REFERENCES

[1] Krause, M. et al.: Needs for further developing monitoring and NDT-methods fir timber structures, Proceedings of the International Conference on Structural Health Assessment of Timber Structures, Jasienko, J. & Nowak, T. (Ed.), pp. 89-99, ISBN 978-83-7125-255-6, Wroclaw, Poland, 2015

[2] Dietsch, P. & Kreuzinger H.: Guideline on the assessment of timber structures: Summary, Engineering Structures, Vol. 33 (2011), No. 11, pp. 2983-2986, ISSN: 0141-0296

[3] D'Ayala, D. et al.: Interdisciplinary knowledge transfer and technological applications for assessment, strengthening and monitoring of timber structures, Proceedings of the International Conference on Structural Health Assessment of Timber Structures, Jasienko, J. & Nowak, T. (Ed.), pp. 49-60, ISBN 978-83-7125-255-6, Wroclaw, Poland, 2015

[4] Cruz, H. et al.: Guidelines for On-Site Assessment of Historic Timber Structures, International Journal of Architectural Heritage, Vol. 9 (2015), pp. 277-289, ISSN: 1558-3058

[5] Colla, C. et al.: Laboratory and on-site testing activities part 3 - Historical timber elements, Report of SMooHS European FP7 project, available from

[6] http://www.smoohs.eu/tiki-index.php?page=project%20results: 2012-02-14

[7] Tannert, T. et al.; In situ assessment of structural timber using semi-destructive techniques, Materials and Structures, Vol. 47 (2014) No. 5, pp. 767-785, ISSN: 1359-5997

[8] Kasal, B.; Lear, G. & Anthony, R.: Radiography, In In Situ Assessment of Structural Timber. State of the art of the RILEM, Springer, ISBN 978-94-007-0560-9, 2011, pp. 39-50

[9] Pošta, J.; Dolejš J. & Vitek L.: In Situ Non-Destructive Examination of Timber elements, Advanced material Research, Vol. 778 (2013), pp. 250-257, ISSN: 1662-8985
[10] Kuklik, P. & Kuklikova, A.: Methods of evaluation of timber elements, Wood Research, Vol. 46 (2001) No. 1, pp. 1-10, ISSN 1336-4561
[11] Kasal, B. & Anthony, R.: Advances in in situ evaluation of timber structures. Progress in Structural Engineering and materials, Vol. 6 (2004) No. 2, pp. 94-103, ISSN 1528-2716
[12] Carpentier, O. et al.: Active and quantitative infrared thermography using frequential analysis applied to the monitoring of historic timber structures, Proceedings of the International Conference on Structural Health Assessment of Timber Structures, Jasienko, J. & Nowak, T. (Ed.), pp. 61-70, ISBN 978-83-7125-255-6, Wroclaw, Poland, 2015
[13] Hasnikova, H.; Vidensky J. & Kuklik P.: Influence of the device structure on the outputs ofsemi-destructive testing of wood by Pilodyn 6J, Proceedings of the International Conference on Structural Health Assessment of Timber Structures, Jasienko, J. & Nowak, T. (Ed.), pp. 504-513, ISBN 978-83-7125-255-6, Wroclaw, Poland, 2015
[14] Nowak, T.; Hamrol-Bielecka K. & Jasienko J.: Experimental testing of glued laminated timber members using ultrasonic and stress wave techniques. Proceedings of the International Conference on Structural Health Assessment of Timber Structures, Jasienko, J. & Nowak, T. (Ed.), pp. 523-534, ISBN 978-83-7125-255-6, Wroclaw, Poland, 2015
[15] Sandak, J. et al.: An alternative way of determing mechanical properties of wood my measuring cutting forces. Proceedings of the International Conference on Structural Health Assessment of Timber Structures, Jasienko, J. & Nowak, T. (Ed.), pp. 543-552, ISBN 978-83-7125-255-6, Wroclaw, Poland, 2015
[16] Yamaguchi, N. & Nakao M.: In-situ Assessment method for timber based on shear strength predicted with screw withdrawals, Proceedings of the International Conference on Structural Health Assessment of Timber Structures, Jasienko, J. & Nowak, T. (Ed.), pp. 569-578, ISBN 978-83-7125-255-6, Wroclaw, Poland, 2015
[17] Tannert, T.; Kasal B. & Anthony R.: RILEM TC 215 In-situ assessment of structural timber: Report on activities and application of assessment methods, Proceedings of the World Conference on Timber Engineering, Ceccotti, A. (Ed.), pp. 642-648, ISBN: 978-1-62276-175-3, Trentino, Italy, 2010
[18] Piazza, M. & Riggio M.: Visual strength-grading and NDT of timber in traditional structures, Journal of Building Appraisal, Vol. 3 (2008) No. 4, pp. 267-296, ISSN: 1744-9545
[19] Franke, B. et al.: Assessment and monitoring of the moisture content of timber bridges, Available from http://www.woodcenter.org/docs/ICTB2013/technical/papers/ID_116_Franke.pdf: 2013-09-30
[20] Rajčić, V. et al.: User friendly modular open source software for data evaluation and interpretation, Report of SMooHS European FP7 project, available from
[21] http://www.smoohs.eu/tiki-index.php?page=project%20results: 2012-02-14
[22] Pamplona, M. et al.: Case Study 1: Museum Island, Berlin, Report of SMooHS European FP7 project, available from http://www.smoohs.eu/tiki-index.php?page=project%20results: 2012-02-14
[23] Rajčić, V. et al.: Monitoring of Monitoring of Historic Structures Case study 4: Zahdeh Building, Hebron, Palestine, Report of SMooHS European FP7 project, available from http://www.smoohs.eu/tiki-index.php?page=project%20results: 2012-02-14
[24] Rajčić, V. et al.: Smart Monitoring of Historic Structures Case study 3: Palazzo Malvezzi, Report of SMooHS European FP7 project, available from http://www.smoohs.eu/tiki-index.php?page=project%20results: 2012-02-14
[25] Harte et al.: Reinforcement of timber structures – the route to standardisation, Proceedings of the International Conference on Structural Health Assessment of Timber Structures, Jasienko, J. & Nowak, T. (Ed.), pp. 78-89, ISBN 978-83-7125-255-6, Wroclaw, Poland, 2015

REPAIR OF BRIDGES IN SEISMIC AREAS FOR EARTHQUAKE RESILIENT SOCIETY

Mehmed Causevic[1], Mladen Bulic[1]

[1] University of Rijeka Faculty of Civil Engineering, Department of Structural Engineering, Radmile Matejcic 3, 51 000 Rijeka, Croatia, email: mcausevic@gradri.uniri.hr, mbulic@gradri.uniri.hr

SUMMARY: Emergency functionality and rapid recovery of road networks after a strong intensity earthquake that has triggered additional hazards such as post-earthquake fires, landslides, tsunamis, bridge collapses and a series of large aftershocks is a vital requirement for the sustainability of any modern society, which, in the light of recent earthquake events, has not yet been properly addressed. In most national codes and provisions durability of bridges is supposed to be at least 50 years. Design codes must be based on functionality criteria rather than safety. Some bridges which were built before 1970s which are still in use in either Europe or Japan or the U.S. have been designed with little or with no any consideration for seismic demand. Majority of these bridges lack the ductility and strength to resist earthquakes. Meanwhile strong motion earthquakes have revealed all vulnerable places and wrong detailing on almost all bridges built in seismically active regions more than fifty years ago. After the 1971 San Fernando earthquake the U.S. for the first time in the world started seismic retrofit programs for bridges. Japan also started similar programs, especially after the 1995 Kobe earthquake. European Union may not be out of this global problem and must have own retrofit programs for bridges. Thousands of existing bridges built more than fifty years ago in earthquake zones of EU are still in operation waiting to be retrofitting in order to withstand loading of strong intensity earthquakes. In this sense the first part of this paper is devoted to the latest knowledge concerning earthquake loading and methods of seismic analysis of bridges. Some solutions, recommendations and comments for retrofitting of supports and joints of steel and concrete bridges made by authors using new added materials and the latest concepts for structural upgrading will be presented as the main goal to contribute to earthquake resilient society.

POPRAVAK MOSTOVA U POTRESNIM PODRUČJIMA ZA DRUŠTVO OTPORNO NA POTRESE

SAŽETAK: Održavanje funkcija u hitnim situacijama i brza obnova cestovne mreže nakon jakih potresa koji su pokrenuli i dodatne opasnosti kao što su požari nakon potresa, klizanja terena, tsunamiji, rušenja mostova i nizovi naknadnih jakih udara životni su zahtjev održivosti svakog modernog društva što u svjetlu suvremenih potresa nije prikladno riješeno. U većini nacionalnih propisa i odredaba trajnost mostova pretpostavljena je najmanje 50 godina. Propisi za projektiranje moraju se zasnivati na kriterijima funkcionalnosti više nego na sigurnosti. Neki mostovi izgrađeni prije 1970-tih koji su još uvijek u upotrebi u Europi, Japanu ili Sjedinjenim Državama projektirani su uz malo ili nikakvo razmatranje seizmičkih zahtjeva. Većini tih mostova za suprotstavljanje potresima nedostaje duktilnosti i čvrstoće. U međuvremenu jaki su potresi pokazali sva oštetljiva mjesta i pogrešne detalje na gotovo svim mostovima izgrađenim u potresnim područjima prije više od pedeset godina. Nakon potresa San Fernando 1971. Sjedinjene su Države prve u svijetu pokrenule programe potresne obnove mostova. Slične je programe pokrenuo i Japan, posebno nakon potresa u Kobeu 1995. Europska unija nije izvan tog svjetskog problema i mora imati vlastite programe obnove mostova. Tisuće postojećih mostova izgrađenih prije više od pedeset godina u potresnim područjima Europske unije još su uvijek u upotrebi i čekaju svoju obnovu kako bi se oduprli opterećenjima pri jakim potresima. Prvi dio ovoga rada obuhvaća najnovija znanja povezana s potresnim opterećenjem i metodama proračuna mostova na djelovanje potresa. Prikazana su neka rješenja, preporuke i komentari o obnovi oslonaca i spojeva čeličnih i betonskih mostova uz primjenu novododanih materijala i najnovijih ideja konstrukcijskog pojačanja kao glavni cilj doprinosa društvu otpornom na potrese..

1. INTRODUCTION

Society needs bridges in assessing the transportation needs after an extreme seismic event and during the time of recovery, and how this may lead to the identification of the most critical components and the definition of bridges performance beyond their design limit (robustness). Innovative structural concepts in designing for new and rehabilitation of existing bridges as well as introduction of structural control systems that are capable of providing the required robustness has to be a main goal of a modern society.

Due to the infrastructure increasing decay, frequently combined with the need for structural upgrading to meet more stringent requirements against seismic loads, structural retrofitting is becoming more and more important and is given today considerable emphasis throughout the world. In response to this need, permanent theoretical and experimental research in seismic design of bridges (literature, authors …) as well as studies on the consequences on bridges after strong earthquakes in order to understand better retrofitting of bridges is more like a process. The important event on this issue in the US was the Annual Meeting in February 2004 in Los Angeles (theme: ten years after Northridge earthquake) organized by the US Earthquake Engineering Research Institute.

After the 1971 San Fernando earthquake the U.S. started several seismic retrofit programs. Retrofit programs in the 1980s included the first use of isolators on bridges and a program to retrofit single-column bents. These programs were greatly accelerated after the 1989 Santa Cruz (Loma Prieta) and 1994 Northridge earthquakes. **After the 1994 Northridge earthquake it was observed that no serious damage would have occurred if the previous retrofit program had already been implemented.** Japan also started similar programs, especially after the 1995 Kobe earthquake. Europe may not be out of this global problem and must have own retrofit programs not only for buildings (partly given in Eurocode 8, Part 3: Assessment and retrofitting of buildings, EN 1998-3:2005) but for bridges as well. Design codes must be based on functionality criteria rather than safety. In this sense the coming European research frame HORIZON 2020 is the opportunity for creating mutual research project among European countries especially among south European countries with the main goal to establish seismic retrofit programs for bridges older than fifty years in order to fulfil needs for earthquake resilient society. Road and rail resilience under multiple hazards in EU is recognized through recently announced competition for financing research project: Resilience to extreme (natural and man-made) events (MG-7-1-2017) under HORIZON 2020.

2. LOADING ON STRUCTURES CAUSED BY EARTHQUAKE (SEISMIC DEMAND)

Bridge engineering uses nowadays modern scientifically based codes for design and construction of bridges in comparison with the situation about 40 or more years ago. The main novelty is knowledge in the field of earthquake loading on bridges. After extensive research in the last decade loading on structures caused by earthquake has been defined as seismic demand. This seismic demand is usually the result of some real (Figure 1) or artificial (Figure 2) time history accelerations or the earthquake response spectra (Figure 3).

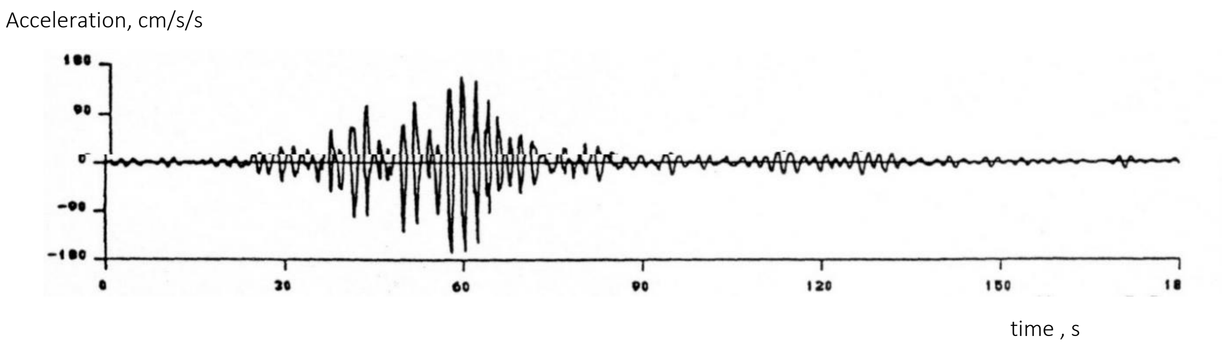

Figure 1 Time-*history* accelerations, Mexico City earthquake, September 19, 1985 (Peck acceleration 167.9 cm/s/s)

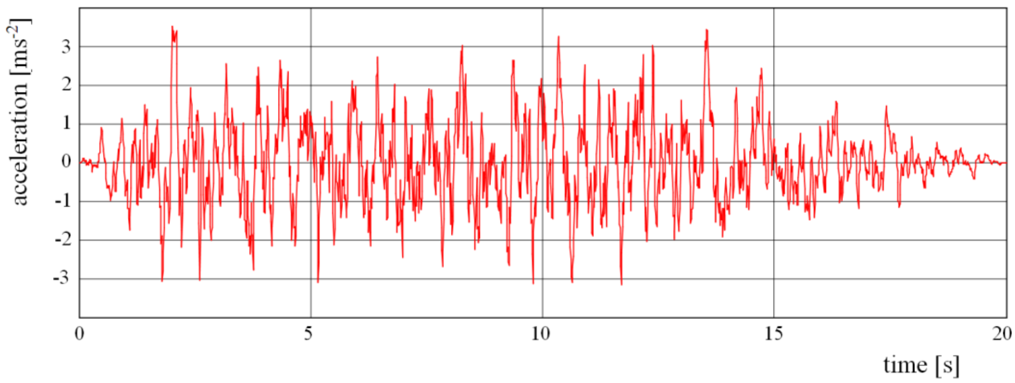

Figure 2 Artificial digitalized time-history record

In accordance to the basic condition of structural Eurocodes that the effect of loading E_d must be lower than resistance of the structure R_d, it is:

$$\gamma_{dem} \cdot (Seismic\ demand) \leq \frac{1}{\gamma_{cap}} \cdot (Capacity)$$

Seismic demand represents the effects of loading on the structure which is given with the spectrum for particular earthquake (Imperial Vally, Ulcinj, Mexico City ...) or with the spectrum given in Eurocode for common structures, Figure 3.

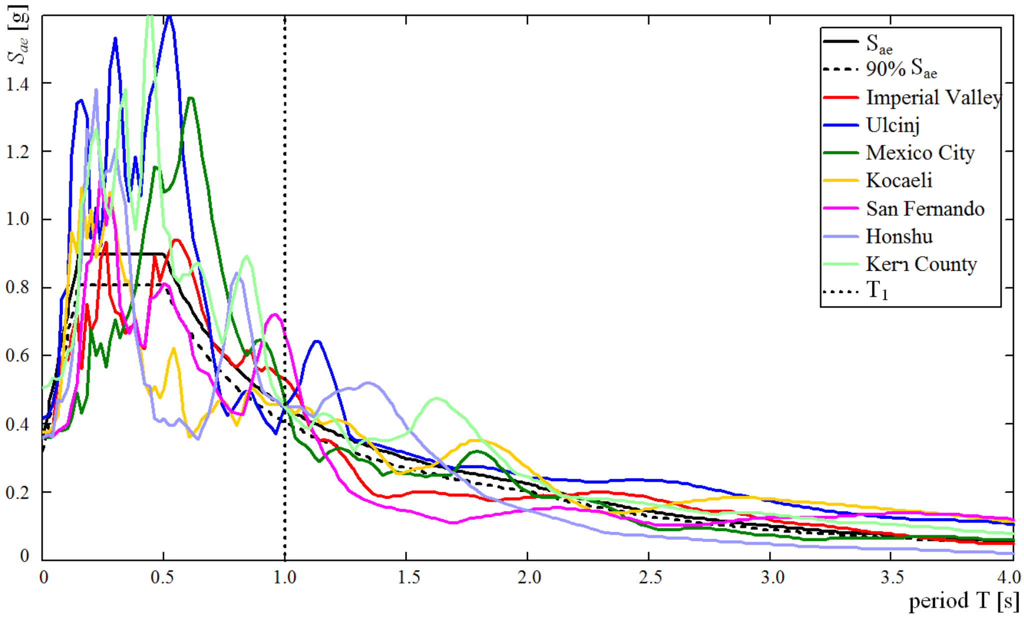

Figure 3 Acceleration response spectrum of the selected real earthquakes together with the required response spectrum obtained from Eurocode and its 90% value

There are linear and non-linear methods for seismic analysis of bridges and buildings defined in Eurocodes [1], [2], [3]. One simple static non-linear (pushover) method [4], [5] is also introduced in Eurocodes. Loading on bridges is defined through combinations of the seismic action with other actions. The design value E_d of the effects of actions shall be determined in ***the seismic design situation:***

$$E_d = G_k \text{ "+" } P_k \text{ "+" } A_{Ed} \text{ "+" } \psi_{2,1} \cdot Q_{k,1} \text{ "+" } Q_2$$

where

"+" implies "to be combined with",

G_k are the permanent actions with their characteristic values,

P_k is the characteristic value of prestressing after all losses,

A_{Ed} is the design seismic action,

$Q_{k,1}$ is the characteristic value of the traffic load,

$\psi_{2,1}$ is the combination factor for traffic loads,

Q_2 is the quasi-permanent value of actions of long duration (e. g. earth pressure, buoyancy, currents etc).

Detailed analysis of the behaviour of viaduct subjected to seismic action accordance to Eurocode [2] is presented in [6]. The analysed viaduct is selected in such a way that it covers most possibilities that can be encountered in practice: slender, moderately stiff ad stiff piers, piers founded on piles, slender piers with shallow foundations, steep and moderately inclined slopes of the obstacle to be crossed by the structure. These pier types are modelled, which includes analysis of seismic load on piers for the longitudinal and transverse direction of the viaduct and dimensioning.

3. RETROFITTING OF SUPPORTS AND JOINTS OF STEEL AND CONCRETE BRIDGES

Some solutions, recommendations and comments for retrofitting the abutment, bent and column of concrete bridges was previously presented by the authors of this paper [7]. Additionally, the retrofitting of connections and bearings of steel bridges bill be here presented. In this presentation the Eurocodes for steel buildings and steel bridges are applied [8], [9], and [10].

3.1. CONNECTIONS

In a non-composite deck, the concrete slab is not connected to the girders, and it can form a sliding surface during a strong earthquake, particularly when steel girders are used. The relative movement dissipates seismic energy [11]. When a connection is not in compression and deemed necessary to transfer inertial forces, anchor bolts can be attached on each side of the flange to stich the girder to the slab, Figure 4.

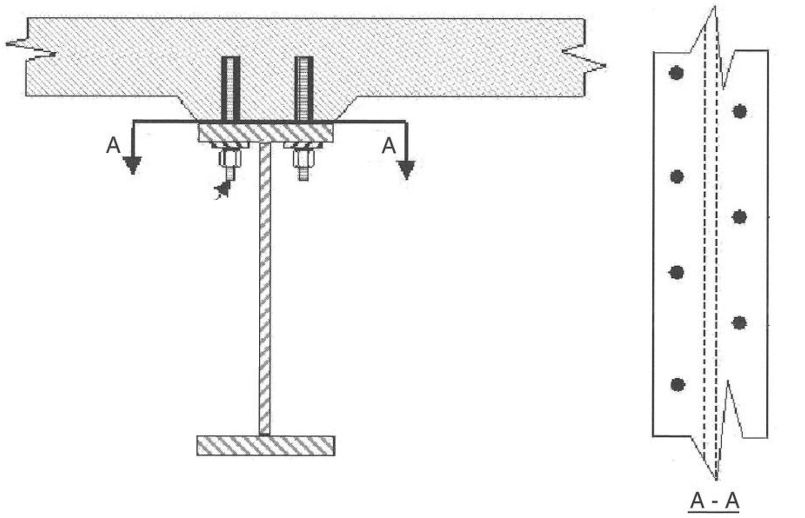

Figure 4 Beam-slab connection

Steel diaphragms (stringers) are vulnerable to transverse seismic forces near the supports. Where the transverse diaphragm over a support does not extend to the full depth of the girder, the girder web will be subjected to out-of-plane bending during an earthquake. Figure 5 shows a knee-brace strengthening detail that may be used to prevent out-of-plane bending of web plates.

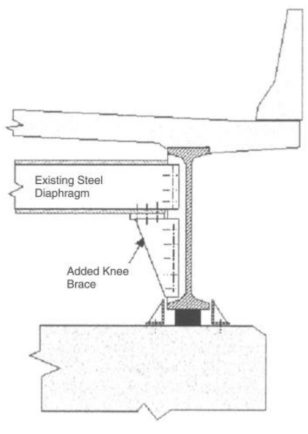

Figure 5 Steel I-girder retrofit over the support

3.2. BEARINGS

During past earthquakes, excessive transverse movement of bridge superstructure caused loss of support on a number of bridges. To transfer lateral seismic forces and prevent excessive displacements, transverse restrainers are sometimes used at the bearings [12]. Figure 6 presents steel angles as restrainers used with an elastomeric bearing that has sliding surface (a) and with a regular elastomeric bearing (b).

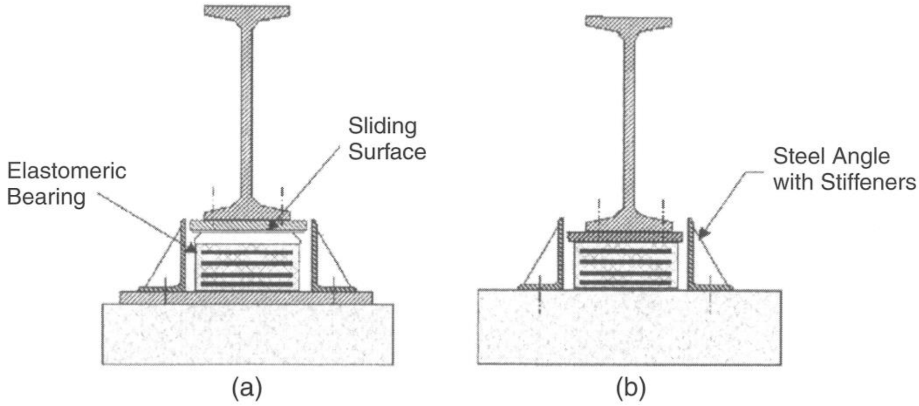

Figure 6 Transverse restrainer angles

Figure 7 presents an anchor bolt restrainer for an elastomeric bearing that has a sliding surface. The sliding surface and the bearing both accommodate longitudinal thermal movement over a rigid support. The slotted holes in the top plate allow longitudinal movement of the superstructure but resist transverse movement to the flexural deformation of the bolts. Transverse restraints should be designed to remain elastic and resist the lateral forces corresponding to plastic hinges of the columns.

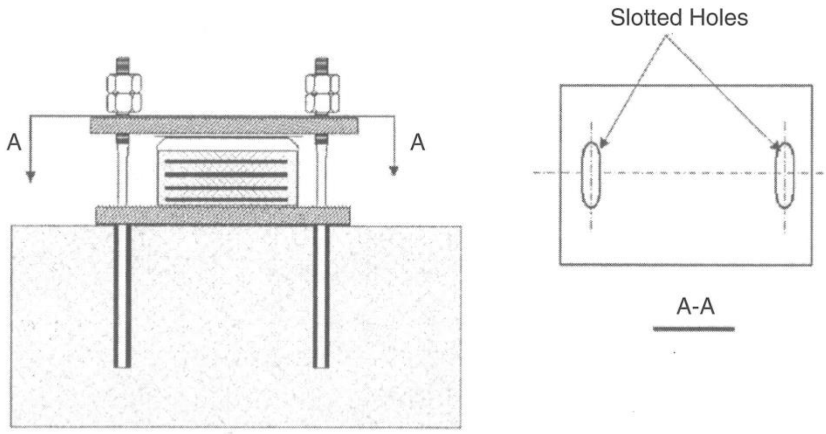

Figure 7 Restrainer anchor bolts

A type of bearing commonly used on existing bridges is high-profile rocking or fixed bearing that is vulnerable to toppling during earthquakes [12]. This toppling may be prevented by welding wedge-shaped steel plates to bearing [13] as shown in Figure 8. The increase in the longitudinal resisting force F_h developed by the wedge plates can be estimated from the equation:

$$F_h = G \tan \alpha \qquad (1)$$

where

G is dead load reaction of the bearing;α is slope angle of the added wedge plate.

Another deficiency is the bolted or welded connections between the bearing and the substructure or superstructure. Replacing the bolts with larger, stronger, or additional anchor bolts may be considered to strengthen a bolted connection. A welded connection can also be strengthened by adding bolts or additional welds. Figure 9 presents additional keeper plates at the top of the bearing and base plate extensions and additional plates and anchor bolts at the bottom to restrain the transverse movement [12].

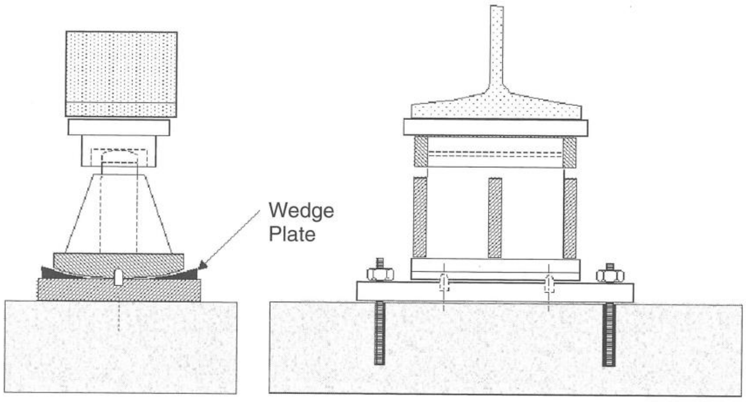

Figure 8 Tack-welded retrofit

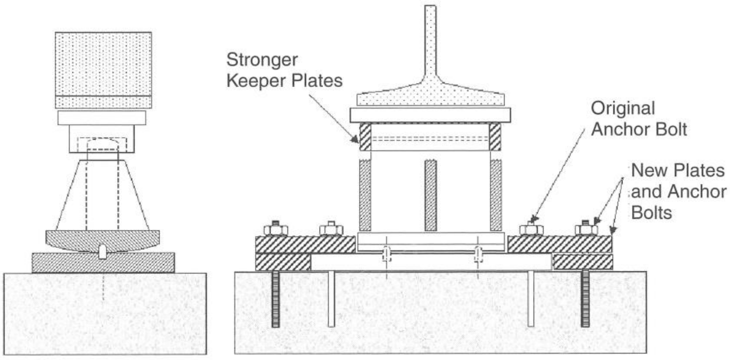

Figure 9 Transverse restrainer and connection retrofit

4. CONCLUSIONS

To provide adequate resilience, functionality requirements for bridges must be defined for three states of network operation: (1) during an extreme intensity earthquake (2) immediately after, especially with respect to search, rescue and evacuation and (3) to ensure recovery of complete functionality within an acceptable time. The knowledge about earthquake loading on bridges which were built 40 or more years ago was low in comparison with the nowadays knowledge. As the consequence many of old bridges are vulnerable and must be retrofitted for the next event. Understanding of earthquake loading on bridges and finding new methods for recovery of bridges are here presented in the segment of connections and bearings rapid recovery which also should be implemented on existing bridges identifying their remaining structural capacity before the next extreme event occurs. It is the main task of our community to avoid zero functionality for old bridges and a speedy recovery of old bridges even for extreme events. Still, we have tools to predict the seismic response of individual highway bridge but we lack methods to predict response of the entire regional highway system to a disaster, and methods to design a process of highway system recovery after disaster. This is the great task for the community in the future.

ACKNOWLEDGMENTS

Research presented in this paper was partly sponsored by the University of Rijeka, Croatia, within Research Project: "Development of structures with increased reliability with regard to earthquakes" No. 402-01/14-01/11.

REFERENCES

[1] Eurocode 0 – Basis of structural design, CEN European Committee for Standardization, Brussels, EN 1990: 2002.

[2] Eurocode 8 – Design of structures for earthquake resistance – Part 2: Bridges, European Committee for Standardization, CEN, Brussels, EN 1998-2:2005.
[3] Eurocode 8 – Design of structures for earthquake resistance – Part 1: General rules, seismic actions and rules for buildings, European Committee for Standardization, CEN, Brussels, EN 1998-1: 2004.
[4] Fajfar, P., A Nonlinear Analysis Method for Performance Based Seismic Design, Earthquake Spectra 16, No. 3, 2000, pp 573-592.
[5] Causevic, M., Mitrovic, S., Comparison between non-linear dynamic and static seismic analysis of structures according to European and US provisions, Bulletin of Earthquake Engineering, Volume 9, Issue 2, 2011), pp 467-489.
[6] Čaušević, M., Fajfar, P., Fischinger, M., Isaković, T., Seismic Analysis of viaduct according to Eurocode 8/2, GRAĐEVINAR 55, 3, Zagreb, 2003, pp 143-153.
[7] Causevic, M., Bulic, M., Retrofitting of Short-to-Medium-Span Bridges in Seismic Zones: Experiences & Recommendations, Proceedings of the 3rd Conference on Smart Monitoring, Assessment and Rehabilitation of Civil Structures (SMAR 2015) Conference; Ilki, Alper ; Motavalli, Masoud ; Inci, Pinar ; Koehli, Michele (editors), Antalya, Turkey, 2015.
[8] Eurocode 3 – Design of steel structures, Part 1-1: General rules and rules for buildings, European Committee for Standardization, EN 1993-1-1:2005.
[9] Eurocode 3 – Design of steel structures, Part 1-8: Design of Joints, European Committee for Standardization, EN 1993-1-8:2005.
[10] Eurocode 3 – Design of steel structures, Part 2: Steel Bridges, European Committee for Standardization, EN 1993-2:2006.
[11] Astaneh-Asl, A., Kanada, M., Seismic behaviour of steel bridges during the 1994 Northridge and the 1995 Hanshin earthquakes, Proceedings of the National Seismic Conference on Bridges and Highways: Progress in Research and Practice, San Diego, CA, 1995.
[12] Yashinsky, M., Karshenas, M. J., Fundamentals of Seismic Protection for Bridges, Earthquake Engineering Research Institute, Oakland, CA, MNO-9, 2003.
[13] Mander, J. B., Kim, D. K., Buckle, I, G., Seismic vulnerability analysis of steel bridge bearings, Proceedings of the Third U. S. – Japan Workshop on Seismic Retrofit of Bridges, Public Works Research Institute, Tsukuba-shi, Japan, December 10-11, 1997.

REDESIGN AND RECONSTRUCTION OF PARTIALLY COLLAPSED WASTE WATER TREATMENT PLANT

Predrag Blagojevic[1], Darko Zivkovic[1], Aleksandar Sutanovac[1]

[1] Faculty of Civil Engineering and Architecture, University of Nis, Aleksandra Medvedeva bb, 18000 Nis, Serbia, email: predragb@eunet.rs, darko.zivkovic@gaf.ni.ac.rs, aleksandar.sutanovac@gaf.ni.ac.rs

SUMMARY: The paper describes the causes of collapse and later reconstruction of the waste water treatment plant in the complex of factory „JEANCI" in Leskovac, Serbia. The collapse occurred after the first filling of the aeration tank. The entire content of the tank was spilled and 40 cm thick, 4.0 m high reinforced concrete wall collapsed. Detailed analysis identified error in calculation of all reinforced concrete walls and majority of other elements of the plant structures. Structural redesign and reconstruction were implemented in order to prevent the demolition of the entire facility. After the application of reconstruction measures, the plant became functional in a short time period.

PONOVNO PROJEKTIRANJE I REKONSTRUKCIJA DJELOMIČNO SRUŠENOG POGONA ZA OBRADU OTPADNE VODE

SAŽETAK: U radu se prikazuju uzroci rušenja i rekonstrukcije pogona za obradu otpadne vode u sklopu tvornice Jeanci u Leskovcu, Srbija. Do rušenja je došlo nakon prvog punjenja spremnika za aeraciju. Cijeli je sadržaj spremnika iscurio a armiranobetonski zid debljine 40 cm visine 4,0 m bio je srušen. Detaljnom analizom utvrđena je pogreška u proračunu svih armiranobetonskih zidova i većine drugih elemenata konstrukcije pogona. Kako bi se spriječilo rušenje cijele građevine provedeno je ponovno projektiranje i rekonstrukcija. Nakon provedbe tih mjera i nakon kratka vremena pogon je ponovno stavljen u funkciju.

1. INTRODUCTION

The waste water treatment plant (WWTP) and utility water storage tank located within factory complex of "JEANCI SERBIA" d.o.o. company in Leskovac were designed in 2013 and built during 2014. The WWTP was designed for treatment of the industrial waste water generated in several jeans production process steps.

The collapse of reinforced concrete (RC) wall of the WWTP aeration tank and content spill occurred immediately after the plant has been put into operation in 2014 [1]. The paper shows errors made during the design and consequently construction of the WWTP, redesign and reconstruction approach and realization details. The WWTP reconstruction was completed in 2014, short time after the collapse.

The WWTP consists of the following structures: equalization tank, final clarifier, sludge tank, mixer tank, flocculation tank, primary clarifier, and aeration tank. Adjacent to the plant, utility water storage tank (UWST) is situated, serving as a pure water reserve in the case of utility water shortage.

2. CAUSES OF COLLAPSE

The technical design documentation review [1] has revealed the following major causes of WWTP aeration tank structural collapse:

- Analysis of water load on RC walls was carried out incorrectly. Intensity of water load was ten times less that the real value (Figure 1).

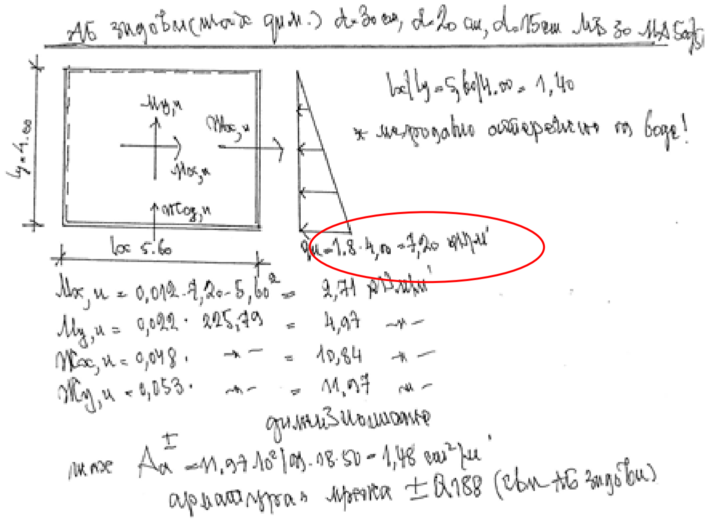

Figure 1 Excerpt from calculation with the error in terms of water load intensity

Figure 2 Collapsed reinforced concrete wall of the aeration tank

- Intensities of limit bending moments were, on average, ten times less than necessary. Based on these underestimated intensities RC cross-sections were designed and reinforcement quantity adopted.
- Loads on RC structural elements relevant for design (concrete shrinkage, temperature load, seismic load) were not taken into consideration.
- Conducted calculation of specific structural elements was a rough approximation of structural system, which resulted in unrealistic cross-section influences.

3. FACILITY RECONSTRUCTION

Reconstruction of the collapsed aeration tank wall could not be performed without thorough analysis of all structural elements of the plant.

Partial facility reconstruction referred to aeration tank would only imply the construction of all four new walls and new foundation slab within the existing layout. New structural elements would be calculated including all loads relevant for design: concrete shrinkage, temperature load, seismic load. However, there was a suspicion raised towards all WWTP structures design in the terms of water load. Therefore, the operation of the factory was stopped, the tanks were emptied, recalculation of all structural elements was carried out and measures for WWTP reconstruction were proposed [1,2].

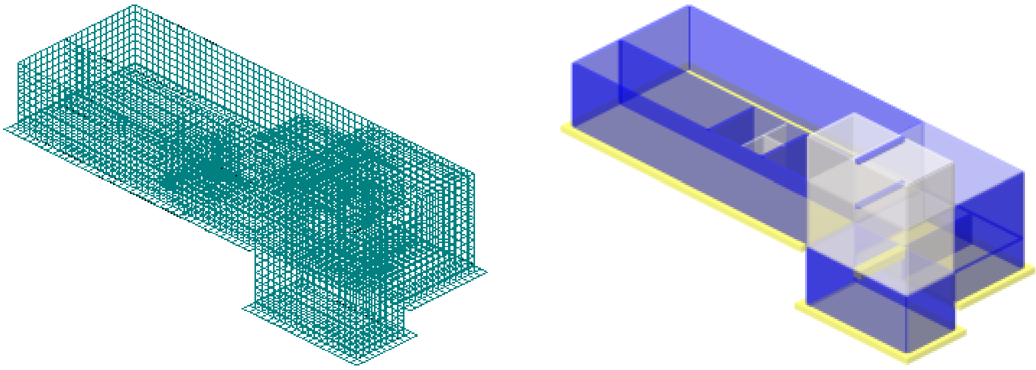

Figure 3 New calculation model of WWTP

3.1. NEW CALCULATION MODEL OF WASTE WATER TREATMENT PLANT

In the new calculation model (Figure 3 - 6) WWTP is treated as spatial system with surface elements not able to transfer moments. Structural calculation was carried out by the software package for static and dynamical analysis of spatial structures “Tower 7”© “Radimpex” – Belgrade. Influences in cross-sections were obtained by simulation of load in accordance to regulations for this type of facility and location of the plant [4]. Aside from water load, concrete shrinkage, temperature loads (summer and winter conditions) and seismic loads were analyzed in the new design calculation [2].

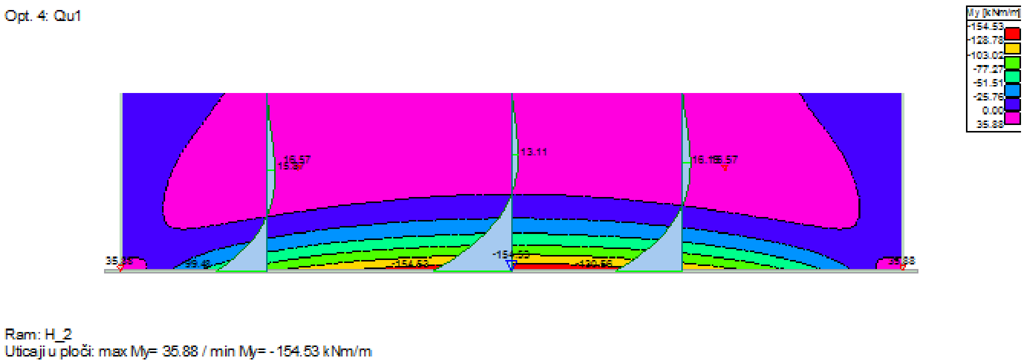

Figure 4 New calculation model of WWTP with influences for bending moment *My* shown for collapsed wall

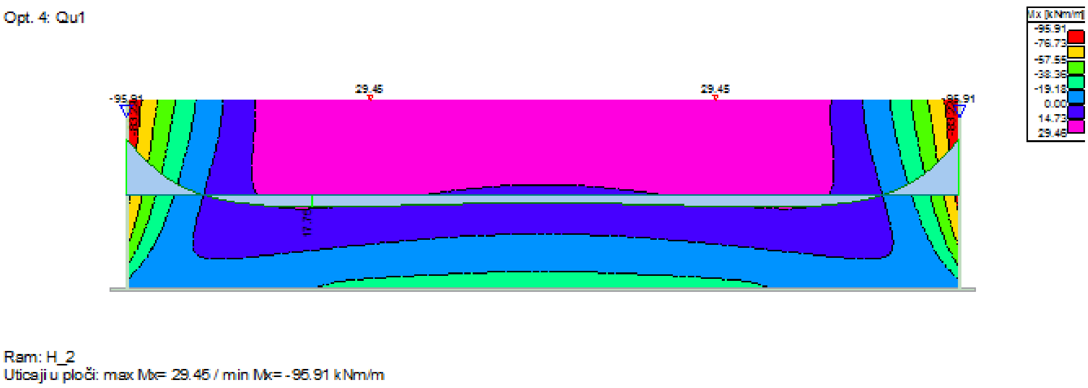

Figure 5 New calculation model of WWTP with influences for bending moment *Mx* shown for collapsed wall

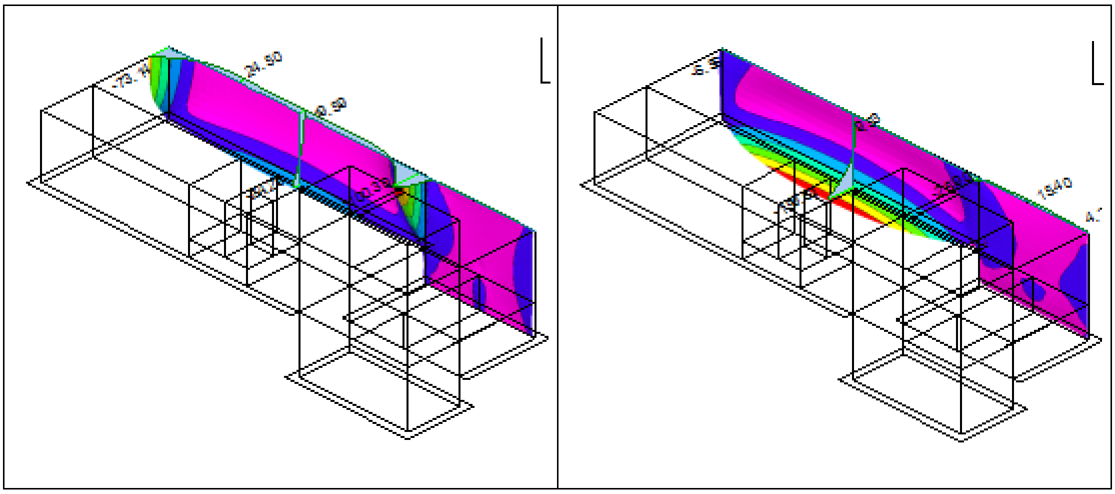

Figure 6 New calculation model of WWTP with influences for bending moment Mx (left) and My (right) shown for collapsed wall in 3D

Combinations of loads during exploitation and reconstruction stages were analyzed. Calculation of foundation structure was carried out by simulation of soil as elastic base via modulus of soil reaction for vertical direction, all in accordance with geotechnical conditions foundation survey findings.

3.2. WASTE WATER TREATMENT PLANT RECONSTRUCTION

The adopted reconstruction plan focused on new aeration tank (Figure 7) designed and constructed within the partially collapsed tank. For redistribution of loads in the whole WWTP newly constructed aeration tank has been designed as a central structure. Girders which served as edge supporters with two horizontal rods were installed on the top of newly designed walls for improving load redistribution.

Figure 7 New aeration tank in the construction stage

New aeration tank served as a support for all reinforcements designed on smaller tanks. All other tanks were reinforced by girders along the upper edge of the walls (Figure 8). This resulted in changed contour support conditions and improved load redistribution. It was shown that the existing reinforcement was satisfactory [2,3].

Figure 8 New aeration tank with beams for reinforcing smaller tanks

Figure 9 Crack injection of the existing walls

New calculation model included secondary concrete. This was the only way to avoid the demolition of the entire WWTP, as all structural elements in contact with water were designed and reinforced incorrectly in the previous design [1]. All existing cracks were injected (Figure 9) and the inner sides of RC walls were treated by penetrate coating. Outer sides of all WWTP tanks were subsequently thermally insulated.

3.3. NEW CALCULATION MODEL FOR UTILITY WATER STORAGE RESERVOIR

Disposition of the UWSR is shown in the Figure 10. New calculation model treated UWSR as a spatial system. The model included all loads defined for this type of structure and the plant location [4]. Lack of reinforcement in RC wall adjacent to the service road was identified. The underground UWSR consisting of three chambers is situated along the service road designed for 60t vehicle (V600). The initial design did not analyze vehicle load on RC walls, which consequently led to insufficient reinforcement of RS wall. Upper RC slab on ground elevation was designed without water and thermal insulation.

Figure 10 Location of utility water storage reservoir (UWSR) and waste water treatment plant (WWTP)

3.4. UTILITY WATER STORAGE RESERVOIR RECONSTRUCTION

UWSR walls parallel to the service road (Southwest-Northeast – Figure 10) and directly exposed to V600 vehicle load were reinforced on the inner side by steel stripes (Figure 11). Initial wall reconstruction works by steel stripes included removing ceramic tile cover, drying the walls, smoothing RC wall surface and testing concrete quality by the “pull off” test (Figure 12). The wall reconstruction steel was of the same quality as steel for RC wall reinforcement. The water and thermal insulation of upper RC slab was planned along with RC wall reconstruction. Green roof was designed over thermal insulation for eliminating temperature influence on the structure.

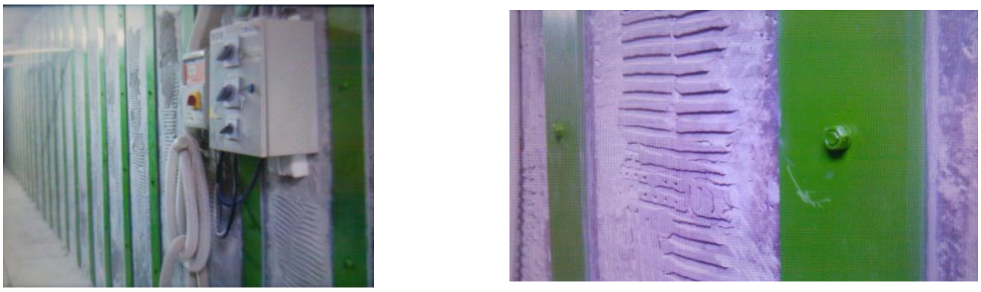

Figure 11 Reinforcement of RC walls by steel stripes.

Figure 12 Measuring moisture and “pull off” test on RC wall before steel stripe treatment.

CONCLUSION

The change of contour support conditions, introduction of new structural elements and activation of secondary concrete have resulted in system influence redistribution and preservation of original, insufficiently reinforced WWTP structural elements. The demolition of the entire WWTP was prevented by the adopted reconstruction plan. This resulted in shortening the period of production stoppage and generated significant savings for the Investor. Reconstructed WWTP has been in operation since 2014. No changes, leakages or damages on RC structure have been reported. Thermal insulation of the WWTP has proved to be purposeful at all structural elements above the ground level as well as the one designed for UWSR.

REFERENCES:

[1] Blagojević, P.; Videnović, D.: *Expertise on damage assessment in JEANCI SERBIA DOO Leskovac (Veštačenje - Utvrđivanje procene nastale štete pucanjem i urušavanjem bazena za biološki tretman tehnoloških voda koji je u vlasnoštvu privrednog društva JEANCI SERBIA DOO Leskovac, na adresi Industrijska bb Leskovac, kao i utvrđivanje uzroka urušavanja tog bazena i davanje predloga za sanaciju objekta*) Leskovac, (2014)

[2] Blagojević, P.: *Final redesign of the WWTP reinforced concrete structure in the JEANCI Leskovac factory* (*Glavni projekat sanacije armiranobetonske konstrukcije Postrojenja za prečišćavanje otpadne vode fabrike ,,JEANCI,, u Leskovcu)*, Agencija za projektovanje K168, Niš, (2014)

[3] Blagojević, P.; Živković, D.: *Detailed redesign of the WWTP reinforced concrete structure in the JEANCI Leskovac factory* (Izvođački *projekat sanacije armiranobetonske konstrukcije Postrojenja za prečišćavanje otpadne vode fabrike ,,JEANCI,, u Leskovcu)*, Agencija za projektovanje K168, Niš, (2014)

[4] -The collection of Yugoslav regulations and standards for building construction. Book 1. Structural loads (*Zbirka jugoslovenskih pravilnika i standarda za građevinske konstrukcije. Knjiga 1. Dejstva na konstrukcije)*, Građevinski fakultet Univerziteta u Beogradu, ISBN 86-80049-20-4, ISBN 86-80049-23-9, Beograd (1995)

APPLICATION OF GEOSYNTHETICS AS HYDRAULIC BARRIERS IN FLOOD PROTECTION EMBANKMENTS

Mario Bacic[1], Lovorka Libric[1], Meho Sasa Kovacevic[1]

[1] University of Zagreb Faculty of Civil Engineering, Department of Geotechnics, Fra Andrije Kacica Miosica 26, 10 000 Zagreb, Croatia, email: mbacic@grad.hr, llibric@grad.hr, msk@grad.hr

SUMMARY: Using geosynthetics as a substitution for natural low permeability materials such as clays and silts have come to fore in last few decades. Numerous advantages in their performance and installation procedure make them popular for use inside flood protection embankments. Geomembrane and geosynthetic clay liner (GCL) are commonly used as hydraulic barriers. However, some limitations of these materials need to be stressed out both from hydraulic stability and shear strength point of view. An example of application of GCL for reconstruction of embankment Virje - Otok Brezje, Varaždin county, has been demonstrated in this paper. The installation of GCL with carefully chosen characteristics proved that man-made materials such as geosynthetics can be successfully applied for ensuring stability of flood protection embankments.

PRIMJENA GEOSINTETIKE KAO HIDRAULIČKE PREPREKE U NASIPIMA ZA ZAŠTITU OD POPLAVA

SAŽETAK: Upotreba geosintetike kao zamjene prirodnih materijala male propusnosti kao što su gline i prahovi posljednjih je desetljeća sve vidljivija. Brojne prednosti njihovih svojstava i postupak ugradnje čine ju popularnom za upotrebu unutar nasipa za zaštitu od poplava. Kao hidrauličke barijere obično se upotrebljavaju geomembrane i geosintetičke obloge gline. Međutim, potrebno je istaknuti neka ograničenja tih materijala s gledišta hidrauličke stabilnosti i posmične čvrstoće. U radu je prikazan primjer primjene geosintetičke obloge gline u rekonstrukciji nasipa Virje – Otok Brezje u Varaždinskoj županiji. Ugradnja geosintetičke obloge gline uz brižljivo odabrane značajke potvrđuje da se proizvedeni materijali kao geosintetike mogu uspješno primijeniti za osiguravanje stabilnosti nasipa za zaštitu od poplava.

1. INTRODUCTION

A large number of flood protection embankments in Croatia were constructed many decades ago and their deterioration is inevitable. A lack of investment funding is a world-wide problem in infrastructure management which leads to the absence of routine maintenance efforts and has resulted in many problems in past few years, such as large-scale flooding events. Further, existing embankments are now subjected to loads for which they were not primarily constructed (higher water levels due to climate change, etc.). Stricter design procedures which came with implementation of Eurocode 7, along with investor's constant aspiration to keep the remediation costs as low as possible, brought to fore geosynthetics which offer a large range of solutions providing fulfilment of basically all requirements set in front of a designer. The 'revolution' of using geosynthetics in flood protection embankments dates back to 60's when they were used for construction of series of embankments in Netherlands after devastating flood a decade before. Since then, these materials are extensively used in flood protection embankments – from reinforcement to filtration, separation and drainage. However, one of most effective application of geosynthetics is as a hydraulic barrier whose main purpose is to secure the embankment's downstream side by controlling water seepage. A classical solution for this task includes application of materials with relatively low permeability such as clays, whose permeability coefficient ranges from 10^{-10} to 10^{-11} m/s in the compacted state [1]. However, as stated by Mulabdic et al. [2], working with cohesive materials in conditions where the moisture content level is either too high or too low and working in periods with high rainfall, can aggravate the construction procedure, with significant delays in the construction schedule as a result. Also, if the available borrow pits are made comprised of only cohesionless materials (sands and gravels), a hydraulic stability of flood protection embankment won't be achieved due to higher permeability of such materials.

The hydraulic stability of flood protection embankments is covered by Eurocode 7 standard [3] by dealing mostly with general principles of hydraulic failure. This is not unusual since Eurocode standards define principles of design (which are mandatory) as well as rules of application which satisfy principles, but which are non-mandatory. As a result of the latter limitation designers need to adapt by using some other, more straightforward, standards or relevant literature. A critical aim of these standards being that hydraulic gradients must be controlled, as well as overall seepage, and that the stability of the hydraulic structure can be achieved by considering structural measures to control or to block the groundwater flow. Further, in the chapter on embankments it is advised to prevent eventual flow problems by ensuring that *'permeability of the fill material in dams is as low as required'* while in same time geosynthetics are mentioned only in relation to the aspect *'filter criteria fulfilment'* which can be done with geotextiles. Even in the report published by CIRIA [4] on the application of EC7 to the design of flood embankments there is relatively little information on measures for securing the hydraulic stability, and the report is mostly oriented towards design situations which must be considered. The question arising, regarding remarks from Eurocode 7, is 'what if low permeability material is not readily available for construction of the embankment core?'. The German standard DIN 19712:2013-01 [5] goes step forward and gives some recommendations on securing hydraulic stability of embankments if their body is constructed of high permeability materials, see Fig 1.

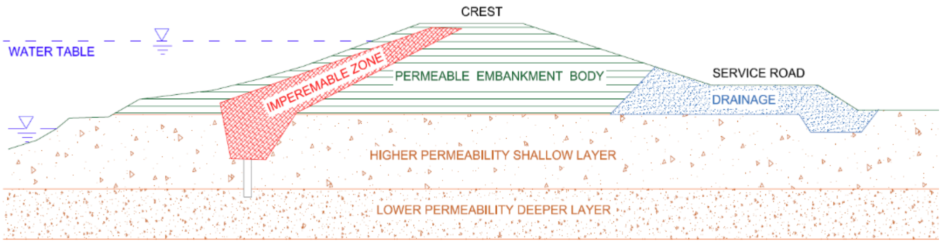

Figure 1 Zonation of flood protection embankment according to DIN standard

This paper deals with geosynthetic materials which are commonly used as hydraulic barriers in flood protection embankments and which can effectively substitute natural materials of low permeability.

2. MATERIALS USED AS GEOSYNTHETIC HYDRAULIC BARRIERS

From a wide range of geosynthetic materials, two can be used as hydraulic barriers – geomembrane and geosynthetic clay liners. While a geomembrane is synthetic component responsible for ensuring impermeability, geosynthetic clay liner is a composite formed out of mineral and synthetic components forming a compact matrix for ensuring impermeability.

2.1. GEOMEMBRANE

A geomembrane is a low permeability liner formed into thin sheets whose primary function is to control migration of fluids and its permeability is less than 10^{-13} m/s, Figure 2a. These materials can be manufactured using one of three most common ways - extrusion, calendaring or spread coating. While extrusion is used for HDPE (High Density Polyethylene), LLDPE (Linear Low Density Polyethylene) or PP (Polypropylene) geomebranes, calendaring is used for PVC (Polyvinil Chloride) or CSPE (Chlorosulphonated Polyethylene) while spread coating is used for geomembranes reinforced with geotextiles which secure non damaging of geomebrane during installation and exploitation. US Bureau of Reclamation [6] gives an extensive overview of such materials stressing out their advantages when used within flood protection embankments and dams. They can be installed on surface (without any protection layer) or deeper inside in upstream shell, following the slope of embankment (with protection layer). Even though these are the most common type of installation in embankment, they can be installed in variety of ways such as in embankment's centre, replacing clay core. The geomembrane surface layers can be rough or smooth what is conditioned by the purpose and application of geomembranes. Rough surface membranes will yield higher shear strength on interface with other materials [7]. Proper anchoring of geomembrane has a crucial role during installation where geomembrane is anchored in trenches on top of embankment as well as on its bottom. Since it is delivered on site in rolls it should be installed perpendicular to embankment's axis with overlapping whereas the overlapping surface is thermally treated.

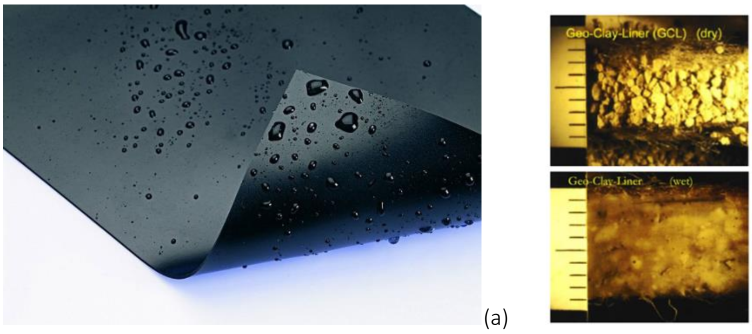

(a) (b)

Figure 2 Geomembrane (a) and hydration of geosynthetic clay liner (b) (taken from [2])

2.2. GEOSYNTHETIC CLAY LINERS

Geosynthetic clay liners GCL are barriers formed as geocomposite, where a clayey core is a mineral component of GCL - a bentonite (montomorilonite of volcanic origin), which is set between two layers of geotextile by gluing (bonded with an adhesive), needle punching or stitching. The mechanism of securing the low permeability is achieved when powdered form (or granular) which are delivered in dry condition swells (mostly due to presence on natrium cations) with presence of water, Figure 2b, leading to its volume increase and permeability of $2x10^{-10}$ to $2x10^{-12}$ m/s [2]. A variation of the GCL that also includes a bentonite glued to geomembrane is not often used in practice. As with geomembranes, it has to be anchored adequately, while the overlapping section should be covered with a bentonite powder. Unlike geomembranes, GCL are always covered with at least 50 cm of top soil which has role in providing additional weight thus preventing sliding of material, but it also prevents wrinkling of GCL due to increased moisture content.

3. ADVANTANGES AND LIMITATIONS FOR USAGE

The application of geosynthetics as hydraulic barriers has been in practice for some time now, but rapid increases in their use in the last 20 years has resulted in significant research effort and a large number of scientific and professional papers. Most of these point out to numerous advantages in comparison with natural materials, but also present some limitations when geosynthetics are installed in flood protection embankments. When it comes to the service life of these materials there is no straightforward answer mainly due to fact that they are relatively new and geosynthetics installed until now rarely show any sign of significant degradation. Reinhart et al. [8] state that a service life of less than 20 years is acceptable while the US Bureau of Reclamation [6] mentions that for uncovered geomebranes the service life should be around 30 years. Some reports even suggest that covered geomebranes (safe from puncture or UV rays) can have a service life up to even 950 years, but a more realistic estimation of 40 to 60 years is given by Swihart et al. [9]. Fleischer et al. [10] have conducted excavation of GCL's in use to check their condition after 3 to 10 years of service where the results confirmed that GCL are an appropriate solution. Some authors [2] stress out that geosynthetic clay liners are much more effective than geomembranes when used within flood protection embankments, mainly due to fact that latter has to be thermally treated on overlapping parts, it can be easily damaged with coarser grain and it is somewhat more difficult to manipulate in comparison with GCL.

The most important parameter, permeability, can be easily defined in controlled conditions. For geomembranes, it depends on the material used and the manufacturing procedure, while for GCL, besides manufacturing procedure, more bentonite per area unit will lead to lower permeability [11]. Also, by adding chemicals, its performance can be enhanced. Other geosynthetic advantages include puncture resistance, tensile strength, resistance to different impacts etc. The GCL's self-healing potential makes them ideal in case of damage with plant roots or by smaller animal. A very good seal can be achieved around various objects interfering with GCLs so no change of hydraulic conductivity can be expected. Nevertheless, a protection layer is constructed on top of GCL, which reduces potential damage event to minimum and it reduces potential moisture content coming from surface, which could affect its performance. A chemical compatibility of soil is required were higher contents of calcium should be avoided. Further, non-proper installation of GCL can lead to bentonite loss endangering its functionality.

Bozzara [12] states that by using GCLs a larger long term flux can be expected due to lowering of bentonite thickness because of normal stress and, when hydrated with some types of leachates instead of pure water, bentonite will show a minor swelling that will result in reduced efficiency of the hydraulic barrier. Other authors deal with behaviour of GCL during wetting - drying cycles, primary through assessment of its hydraulic conductivity. Lin [13] showed that there is a change in hydraulic conductivity with increase of wetting cycle with significant increase after fifth to seventh cycle of wetting. He concludes that larger increase values of hydraulic conductivity were caused by preferential flow through desiccation cracks that did not heal on rehydration in case when water had a higher concentration of divalent cations and warns that results imply that GCLs must be used with great care in environments where they may undergo wetting - drying cycles in the presence of natural pore water.

One of main limitations of geomembrane and GCL is in their contact (interface) shear strength where stability of system as whole should be checked upon sliding of soil along these relatively smooth interfaces. In addition to these interface shear strength issues, GCL could have an issue regarding internal shear strength, particularly after hydration occurs. This can be solved by connecting boundary geotextiles with stiches, leading to increased internal shear strength.

4. EXAMPLE OF GCL APPLICATION

The existing flood protection embankment Virje – Otok Brezje was constructed in 1968. The structure is located in Varaždin County, and with total length of 3 711 m it has the function of preventing flooding from the river Drava. By protecting more than 450 ha of area, this embankment generally protects all settlements from Virje Otok to Varaždin. In November 2012, the largest recorded water wave on Drava River occurred leading to water overtopping the embankment's crest over a length exceeding 1000 m (Fig 3a) followed by breaching of embankment in length of 50 m (Fig 3b). The damage was estimated at around 28 million kn (3.7 million EUR).

(a) 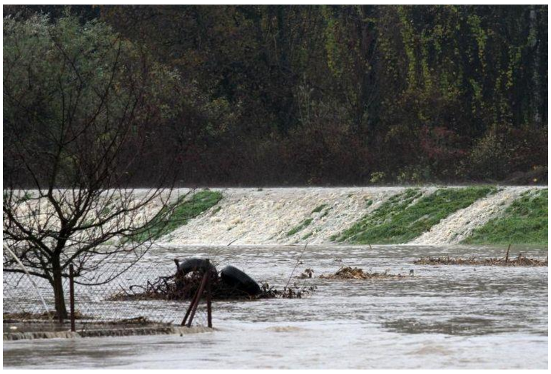

(b) 

Figure 3 Overtopping (a) and breaching (b) of Virje – Otok Brezje flood protection embankment [14]

Considering that the existing embankment does not have satisfactory dimensions in terms of expected high water, but also due to fact that it has significantly deteriorated during the decades, it was decided to reconstruct the embankment [15] with the new crest being half a meter higher than the water table for 3100 m^3/s flux (statistical water table for 100 years return period is 3015 m^3/s). However, due to fact that embankment's body will be constructed out of well graded cohesionless material (GW), as decided by Investor, it was necessary to install additional measures which will serve as hydraulic barrier. As an optimal solution, it was decided that geosynthetic clay liner (GCL) will be installed. It will be protected by 60 cm of protection layer using material excavated for foundations of embankment. On protection layer a 'sandwich' structure will be constructed consisting of protection net, humus layer and hydroseeding, as shown on Fig 4.

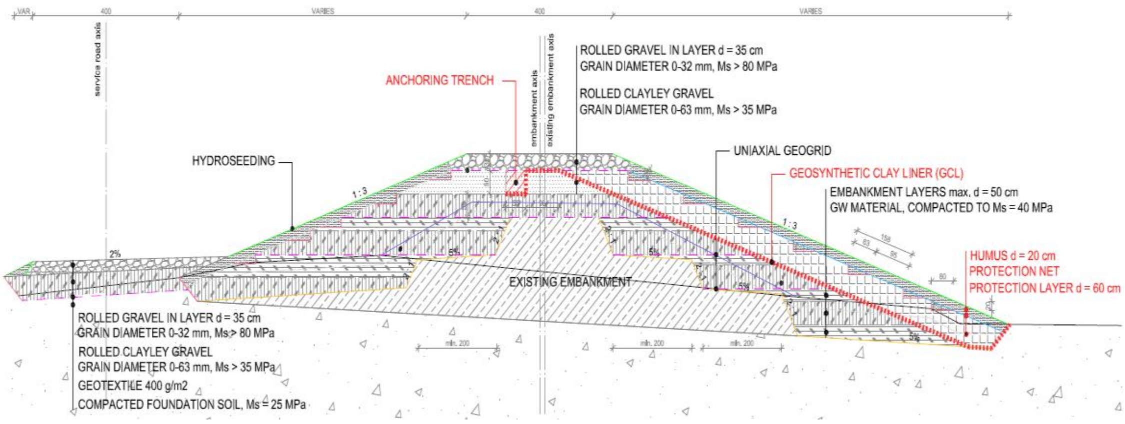

Figure 4 A cross section of reconstructed Virje – Otok Brezje embankment [15]

Detailed analyses were conducted consisting of hydraulic, stability and settlement calculations. Figure 5 shows some results of hydraulic analysis where it can be seen that the overall piezometric line (water table surface) with application of GCL is lowered more than 1 m in comparison with the case without GCL installation, Figure 6. Also, the exit hydraulic gradient was lowered from 1.6 to 0.4 which can be considered as acceptable value. This lowered value is the result of the change in total head distribution as it can be seen on Figures 5 and 6. Characteristics of installed GCL are defined as min. 24 mL / 2g for swell index, min 4.8 kg/m^2 for a mass of bentonite per unit area, 200 g/m^2 for a mass of geotextile per unit area, with a tensile strength of 8 kN/m and overall permeability coefficient of 10^{-11} m/s.

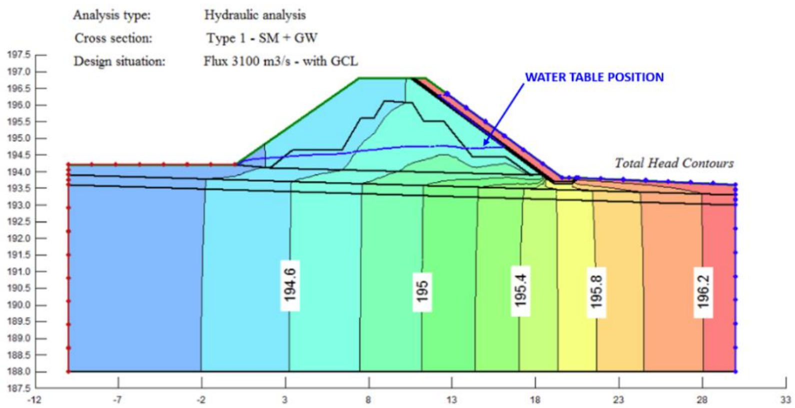

Figure 5 Total head contours and water table position with application of GCL

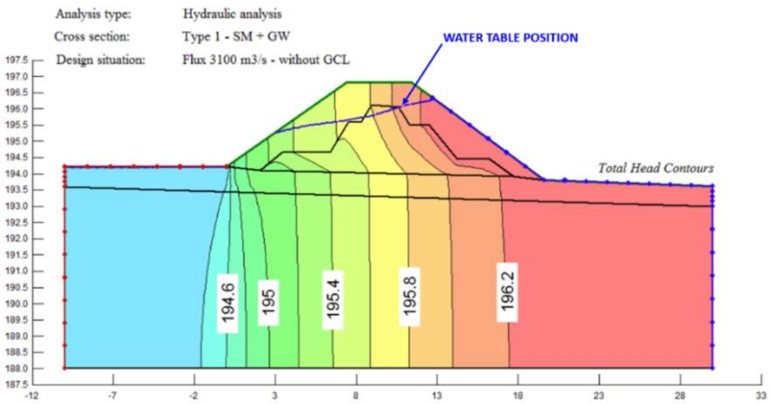

Figure 6 Total head contours and water table position without application of GCL

Stability calculations were conducted for both circular slip surfaces as well as for slip surfaces which have planar nature due to possibility of sliding of material on contact with geosynthetic clay liner. Recommendations for contact friction angle between geotextile and sand/gravel soil varied between 25° and 34° [2]. A sensitivity stability analysis was conducted including variation of contact friction angle in mentioned range, while choosing custom defined slip surface on contact between GCL and soil to obtain relevant factor of safety against sliding. One case of these analyses, for static conditions, is shown on Figure 7 while results of related sensitivity analysis are shown on Figure 8. With lower boundary friction angle a factor of safety is 1.4, while with upper boundary friction angle it goes up to 2.1. These values are satisfactory taking in consideration that Eurocode 7 design approach 3 was used which requires factor of safety minimal value of 1.0. To increase internal shear force, a GCL composite must be stitched.

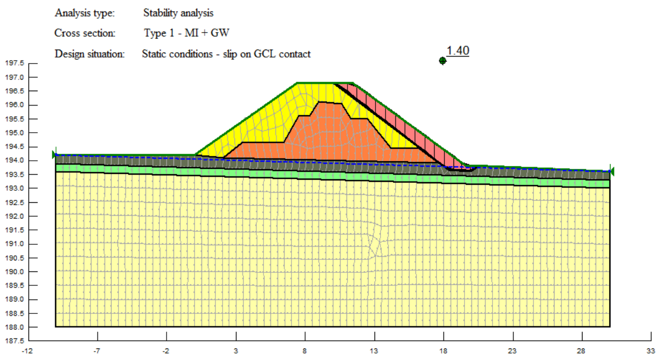

Figure 7 Stability analysis with factory of safety shown for sliding on GCL – soil interface

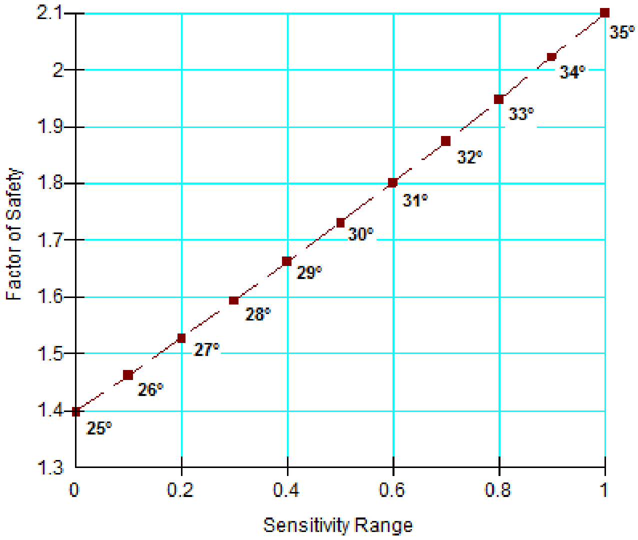

Figure 8 Sensitivity data of stability analysis for different values of contact friction angle

The installation of a GCL with the given characteristics proved that man-made materials such as geosynthetics can be successfully applied for ensuring hydraulic stability of flood protection embankments.

5. CONCLUSIONS

The low permeability of flood protection embankments is crucial for their proper functioning. This can effectively be achieved by using man-made materials called geosynthetics, where a geomembrane (synthetic material) or GCL - geosynthetic clay liner (a mineral – synthetic composite) can be employed. Despite some limitations which users need to be aware of during both design and installation phase, rapid expansion in their application can be noticed in last 20 years resulting in large number of scientific and professional papers. GCL was used for reconstruction of existing flood protection embankment Virje – Otok Brezje due to fact that embankment's body will be constructed out of well graded cohesionless material. During the design phase, hydraulic stability had to be checked, resulting in overall piezometric line (water table surface) lowered by more than 1 m when the GCL was employed. Importantly, the exit hydraulic gradient was lowered from 1.6 to 0.4 as a results of change in total head distribution. A sensitivity stability analysis was conducted including variation of contact friction angle, while choosing custom defined slip surface on contact between GCL and soil to obtain relevant factor of safety against sliding and it was shown that increase of friction angle will lead to increase of factor of safety.

REFERENCES

[1] Benson, C.H.; Trast, J.M.: Hydraulic conductivity of thirteen compacted clays, *Clays and Clay Minerals*, Vol. 43 (1995) No. 6, pp. 669-681, ISSN 0009-8604

[2] Mulabdić M.: *Priručnik – upute za primjenu geosintetika u nasipima za obranu od poplava* (In Croatian), Hrvatske Vode, Zagreb, (2016)

[3] HRN EN 1997-1:2012: *Eurocode 7: Geotechnical design – Part 1: General rules*, (2012)

[4] Pickles, A.; Sandham, R.: *Application of Eurocode 7 to the design of flood protection embankments*, CIRIA C749, London, (2014)

[5] DIN 19712:2013-01 *Hochwasserschutzanlagen an Fließgewässern, Flood protection works on rivers*, (2013)

[6] US Department of the Interior, Bureau of Reclamation: Chapter 20: Geomembranes, in *Embankment Dams – design standard No. 13,* (2014)

[7] Mulabdić M.; Bošnjaković, M: *Pojmovnik geosintetika* (In Croatian), Faculty of Civil Engineering, Osijek, (2011)

[8] Reinhart, D.R.; Townsend, T.; McCreanor, P.: Florida Bioreactor Demonstration Project Update, Proceedings WasteTech 2002, SWANA, on CD, 5 p., (2002)

[9] Swihart, J.; Haynes, J.: *Canal-lining demonstration project - Year 10*, Final report, U.S. Bureau of Reclamation, R-02-03, (2002)

[10] Fleischer, P.; Heibaum, M.: Installation of clay geosynthetic barriers under water – three years of experience. In: Zanzinger, Koerner & Gartung (Eds.): Clay Geosynthetic Barriers. Lisse (NL): Swets & Zeitlinger, p. 41-48, (2002)

[11] The United States Environmental Protection Agency: *Geosynthetic Clay Liners Used in Municipal Solid Waste Landfills*, United States Environmental Protection Agency, 5306W, Washington, (2001)

[12] Bouazza, A.: Geosynthetic clay liners, *Geotextiles and Geomembranes*, Vol. 20 (2002), pp. 3–17, ISSN: 0266-1144

[13] Lin, L.C.; Benson, C.H.: Effect of Wet-Dry Cycling on Swelling and Hydraulic Conductivity of GCLs, *Journal of Geotechnical and Geoenvironmental Engineering*, Vol. 126 (2000), No. 1, pp. 40-49, ISSN: 1090-0241

[14] URL: www.srk-cestica.hr, Accessed: 2016-12-02

[15] Faculty of Civil Engineering, University of Zagreb: *Reconstruction of embankment Virje Otok – Brezje – main design*, GLP-110-044/2015, Zagreb, (2015)

PROTECTION OF HIGHWAY OVERPASS USING MCI® – INHIBITORS

Boris Miksic[1], Ivan Rogan[2]

[1] Cortec Corporation, St. Paul Minnesota USA, email: boris@cortevci.com
[2] CorteCros d.o.o., Nova Ves 57 1000 Zagreb Crotia, email: ivan.rogan@cortecros.hr

SUMMARY: Until the middle of last century, professional public opinion was that concrete and concrete structures are "eternal". Damage of concrete structures and building damages have warned that concrete and concrete structures still are not "eternal" – that was the beginning of systematic research into the causes and mechanisms of the damage process: credit for that have building physics, chemistry and thermodynamics. According to statistical indicators, damages of the reinforced concrete structures caused by the corrosion of the reinforcing steel make more than 80 % of all damages of the reinforced concrete structures. Reinforcement corrosion and damage caused by the concrete structures are primarily economic issue and make a significant item in the budget of each country. In this paper the protection of reinforcing steel in new and existing reinforced concrete structures by using migration corrosion inhibitors (MCI) and corrosion protective materials (CM) which contain MCI is presented using example from highway overpass in Croatia.

ZAŠTITA KONSTRUKCIJE AUTOCESTOVNOG NADVOŽNJAKA PRIMJENOM MCI®–INHIBITORA

SAŽETAK: Do polovice prošlog stoljeća mišljenje stručne javnosti bilo je da su beton i armiranobetonske konstrukcije "vječni". Pojave oštećenja armiranobetonskih konstrukcija i građevinske štete upozorili su da beton i armiranobetonske konstrukcije ipak nisu "vječni" pa su počela sustavna istraživanja uzroka i mehanizama procesa oštećivanja. Zasluge za to ima građevinska fizika, kemija i termodinamika. Prema statističkim pokazateljima oštećenja armiranobetonskih konstrukcija uzrokovana korozijom armature čine više od 80 % svih oštećenja tih konstrukcija. Korozija armature i štete koje ona uzrokuje prvenstveno su gospodarsko pitanje i čine znatnu stavku u proračunu svake zemlje. U radu se razmatra zaštita armature od korozije u armiranobetonskim konstrukcijama primjenom MCI®-inhibitora (migracijskih korozijskih inhibitora) i AK-materijala (antikorozijskih materijala) sa sadržajem MCI inhibitora korozije. Prikazuje se sastav i kriteriji kvalitete AK-materijala i sustava za zaštitu novih armiranobetonskih konstrukcija nadvožnjaka na primjeru nadvožnjaka autoceste u Hrvatskoj.

1. UVOD

Rezultati dosadašnjih istraživanja doveli su do razvoja novih materijala i postupaka za zaštitu i sanaciju armiranobetonskih (AB) konstrukcija, a u funkciji poboljšanih svojstava zaštitnog sloja betona zbog njihove fluido(ne)propusnost (za vodu, vodenu paru, plinopropusnost/CO_2, $SO_{2/3}$, N_xO_y, O_2, difuzija topivih soli posebice klorida, itd.) i/ili dodatna zaštita površine betona premazima, običnim i hidrofobnim impregnacijama. Ostale aktivne metode uključuju katodnu zaštitu armature, površinsku zaštitu armature EP-smolama, primjenu nehrđajuće i armature iz drugih korozijskih postojanih materijala, itd. Istovremeno se istražuju mehanizmi i procesi korozije armature te uloga i način utjecaja agresivnih tvari kod čega su kloridi nezaobilazni predmet istraživanja.

Danas je posve normalno da se u projektima i troškovnicima radova nalaze i projekti zaštite armature od korozije novih odnosno sanacije starih AB-konstrukcija. Zaštita armature od korozije i zaštita novih i sanacija starih AB-konstrukcija MCI®-inhibitorima (migracijskih korozijskih inhibitora) korozije i antikorozijskim materijalima i sustavima sa sadržajem ovih inhibitora predstavlja bitan doprinos i veliki iskorak u produžetku trajnosti životnog vijeka AB-konstrukcija a time istovremeno značajnom smanjenju troškova održavanja i efikasnosti korištenja objekta. Ovu vrstu materijala i sustava se počelo istraživati pred nekoliko desetljeća, a uspješno se primjenjuje u svijetu već preko 20 godina. Bogata literatura vezano za istraživanja i primjenu može se naći na [1]. Prema navedenim istraživanjima migrirajući inhibitori korozije armature jednako su djelotvorni kao i opće poznati inhibitori na bazi kalcijevog nitrita i djeluju na način da usporavaju inicijaciju koroziju armature i tako produžuju životni vijek AB-konstrukcija [2].

2. MCI – INHIBITORI

Migracijski korozijski inhibitori su kemijski spojevi na bazi amina [3] (npr. aminokarboksilati, aminoalkoholi, i dr.) koji se procesom kemijske adorpcije tzv. kemisorpcije »vežu»/adsorbiraju na površinu armature (i drugih metala) tvoreći na površini postojan film rezistentan na mnoge agresivne tvari iz okoliša, prvenstveno na utjecaj u prirodi sveprisutnih kloridnih iona, a istovremeno vrlo agresivnog utjecaja za okside željeza. MCI inhibitori korozije štite armaturu od korozije u oba oksidacijska područja: katodnom i anodnom za razliku od nekih drugih tipova inhibitora korozije kao npr. nitrita [3].

MCI inhibitori korozije na bazi aminskih spojeva [4] spadaju u grupu katodno-anodnih inhibitora koji se adsorbiraju na površini armature sprječavajući difuziju reaktanata korozije (O_2, H_2O) do armature i time je štite od oksidacijskih procesa za razliku od anodnih inhibitora na bazi nitrita i/ili kromata koji štite armaturu od korozije anodnom pasivizacijom tako što sami sudjeluju u anodnom procesu tj. oksidiraju umjesto osnovnog metala.

Prema istraživanjima mnogih autora inhibitori na bazi nitrita su djelotvorni inhibitori, no pri njihovoj primjeni u obliku dodatka betonu treba ih primjenjivati s oprezom. Naime, njihova djelotvornost značajno ovisi o količini prisutnih klorida u betonu, koja se u slučaju primjene kod betoniranja novih konstrukcija mora unaprijed pretpostaviti. Također oprez se zahtijeva i kod homogenizacije betona na betonari, jer ukoliko se inhitbitor na bazi nitrita ne homogenizira dovoljno dobro u mješavini, različite koncentracije mogu djelovati negativno [5]. Pri primjeni MCI inhibitora nema takovih efekata upravo zato što su oni mješoviti inhibitori i njihova koncentracija je samo bitno da dođe do armature jer tada djeluje po cijeloj armaturi. Također ukoliko se MCI inhibitori primjenjuju kao dodatak betonu, kompatibilni su s do sada primjenjivanim plastifikatorima i/ili superplastifikatorima većine svjetskih proizvođača dodataka i veoma dobro se homogeniziraju u betonskoj mješavini i kako je već rečeno, privlačnim silama prianjaju na površinu armature na potencijalna kako katodna tako i anodna područja.

3. NAČIN DJELOVANJA I PRIMJENE MCI®-INHIBITORA

MCI®-inhibitori korozije difundiraju [6] u obliku tekuće i parne faze kroz strukturu betona do armature s kojom fizikalno- kemijski reagiraju tvoreći na njenoj površini vrlo gusti, za agresivne supstancije i reaktante korozije, nepropusni i rezistentni mikrosloj debljine cca 20 µm štiteći armaturu od korozije, slika 1. Za zaštitu armature od korozije bilo kod novih ili sanacije starih AB-konstrukcija primjenjuju se na dva načina: direktnim i/ili indirektnim dodavanjem MCI®-inhibitora. U prvom slučaju, inhibitor se nanosi u obliku premaza na armaturu ili dodaje u beton i/ili mort, ovisno radi li se o gradnji novih ili sanaciji starih AB konstrukcija. U drugom slučaju, zaštita se ostvaruje primjenom industrijskih proizvedenih materijala (koji već sadrže MCI® inhibitore) za zaštitne i sanacijske radove AB-konstrukcija, kao što su gotovi reparaturni mortovi, premazi ili hibrofobne impregnacije.

Prije nanošenja novog materijala treba se osigurati dovoljna hrapavost podloge. Podloga mora biti čista, slobodna od prašine, nevezanih zrna te nečistoća i materijala koji smanjuju prionjivost. Nakon uklanjanja betona armatura se čisti pri čemu je potrebno: ukloniti koroziju, oljuštene dijelove, mort, prašinu i ostale materijale koji smanjuju prionjivost i pridonose koroziji. Korodiranu armaturu treba čistiti do zdravog kontakta s betonom i do stupnja čistoće Sa 2 1/5. Očišćena i ohrapavljena podloga impregnira MCI®-inhibitorom (slika 1a). Reprofilacija se provodi reparaturnim mortom sa sadržajem MCI®-inhibitora (slika 1b). Završna obrada površine provodi se zaštitno-ukrasnim premazom ili hidrofobnom impregnacijom, oba sa dodatkom MCI®-inhibitora (slika 1c i 1 d).

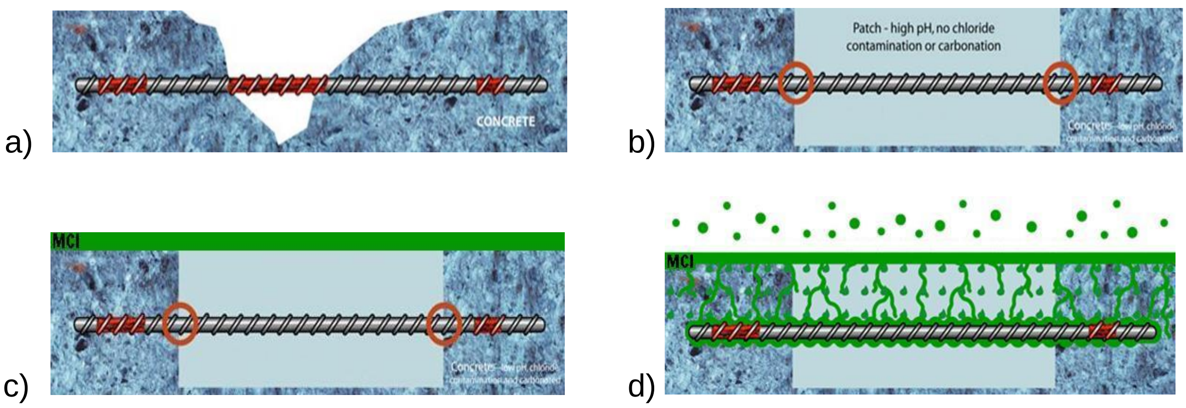

Slika 1 Način djelovanja MCI®-inhibitora

Bitno je naglasiti da zaštitu armature od korozije i zaštitu novih odnosno sanaciju starih AB-konstrukcija treba izvršiti cjelovitim zaštitnim sustavom, tj. ugraditi materijale za sve tri navedene faze, a ne samo parcijalno jer jedino puni zaštitni sustav dugotrajno i efikasno štiti armaturu od korozije i AB-konstrukciju od degradacije/oštećenja.

4. PRIMJENA MCI®-INHIBITORA NA NADVOŽNJACIMA ATOCESTE SLAVONIKA

U gradnji autocesta, brzih cesta, obilaznica i sl. često se kao manje građevine pojavljuju nadvožnjaci. Prema definiciji, nadvožnjaci su građevine za vođenje drugih prometnica preko prometnice (autoceste ili željeznice) koju projektiramo [7]. Od svih građevina na autocestama najviše je nadvožnjaka. Nadvožnjaci [8] su izloženi utjecaju atmosferilija sa svih strana te su tijekom zime češće izloženi posoljavanju zbog sigurnosti prometa, što ih stvara pogodne uvjete za inicijaciju i propagaciju korozije armature.

Zaštita od korozije novo izgrađenih nadvožnjaka na autocesti Slavonika prema zahtjevu investitora provedena je primjenom MCI®-inhibitora u cilju odgode trenutka inicijacije korozije i osiguranja produljenog vijeka građevine.

4.1. ZAŠTITA ARMATURE PRIMJENOM MCI®-INHIBITORA

Zaštita AB konstrukcije provedena je u dva koraka primjenom topivog migrirajućeg korozijskog inhibitora na bazi amina u vidu impregnacije (i zaštitno-ukrasnog premaz na bazi 1-k akrilatnog veziva u vodenoj disperziji sa dodatkom MCI®-inhibitora.

Praškasti, u vodi topivi migrirajući korozijski inhibitor na bazi amina, formuliran je tako da migrira kroz betonske uključivo i najgušće strukture do čelične armature gdje formira vrlo gusti pasivni sloj otporan prema kloridima i drugim agresivnim supstancijama tj. štiti čeličnu armaturu od korozije uključivo galvanizirani čelik i aluminij. Jedinstvena karakteristika MCI®-inhibitora je sposobnost migracije kroz beton tako da štiti ugrađenu armaturu na znatnoj udaljenosti od površine tj. nije početno u direktnom kontaktu sa armaturom [9 - 12]

Zaštitno-ukrasni premaz je brzosušeći tiksotropni premaz koji formira otpornu nezapaljivu zaštitnu barijeru koja je tijekom očvršćivanja/sušenja temperaturno stabilna (od –40^{o}C do +200^{o}C). Otporan je na UV-zračenje, a djeluje kao impregnacija sprječavajući penetraciju vode i klorida te karbonatizaciju betona.

Prije nanošenja provedeno je visokotlačno čišćenje betona kao priprema za izvedbu zaštitnih slojeva na vidljivim betonskim površinama. Pranje površine provedeno je roto mlaznicom pod takom od 800 bara sa udaljenosti ne veće od 2 m. Na taj način se osiguralo uklanjanje svih površinskih nečistoća i nanesenih slojeva bez uklanjanja samog betona (cementne površinske skramice). Na tako pripremljenoj podlozi pristupilo se impregnaciji sa primjenom topivog migrirajućeg korozijskog inhibitora na bazi amina i to premazivanjem betonske površine, slika 2. Završna obrada provedena je nakon sušenja impregnacije u trajanju od 15-24 sata.

U cilju dodatne zaštite armature od korozije i smanjenja atmosferskih utjecaja na svojstva betona provedena je završna obrada betonske površine zaštitno-ukrasnim premazom, slika 3.

Slika 2 Nanošenje impregnacije s dodatkom migrirajućeg korozijskog inhibitora na bazi amina

Slika 3 Nanošenje zaštitno-ukrasnog premaz na bazi 1-k akrilatnog veziva u vodenoj disperziji sa dodatkom MCI®-inhibitora

5. ZAKLJUČAK

Autocesta Slavonika je u prometu od 2007. godine. Investitor kod zahtijeva zaštite nadvožnjaka MCI®-inhibitorima nije zahtijevao monitoring koji bi nam dao precizne tehničke informacije o djelovanju primijenjenih MCI®-inhibitora za protekli period od 9 godina. Međutim proizvođač MCI®-inhibitora svake godine provodi vizualnu kontrolu AB-konstrukcije nadvožnjaka te na osnovu tih kontrola može se zaključiti da:

- na AB-konstrukciji nadvožnjaka nema vidljivih pojava ljuštenja betonske površine, te nema pojava žuto-smeđih pjega na površini betona koje ukazuju na pojavu korozije armature, te
- nije primijećeno ljuštenje zaštitno-ukrasnog premaza, iz čega se može zaključiti da je zaštitno-ukrasni premaz postojan i bez tragova oštećenja/bljedila izazvanog UV zračenjem.
- Kako je MCI tehnologija zasnovana na principu migriranja/difundiranja inhibitora treba imati na umu da će koncentracija inhibitora s vremenom slabiti, pa se preporuča obavljati monitoring ne samo vizualno već i mjerenjem stanja armature u betonu. Na taj način se ujedno može ustanoviti kada je potrebno ponovno obnoviti premazivanje površine betona migrirajućim inhibitorima, što znači djelovati preventivno i ne dozvoliti inicijaciju korozije na armaturi.

LITERATURA

[1] Product papers relating to MCI® http://www.cortecvci.com/Publications/Papers/mciproducts.php.

[2] Yongmo, X., Hailong, S., Miksic B.A.: Comparison of Inhibitors MCI and NaN02 in Carbonation-Induced Corrosion, Materials Performance, Vol. (43) No 1, str. 42-46, (2004), ISSN 0094-1492.

[3] Francišković J.: Zaštita armature od korozije u armiranobetonskim konstrukcijama, Građevinar, Vol. (56), No. 12, str. 743 – 748, (2004).

[4] Bjegović, D.; Mikšić, B.; Ukrainczyk, V.: Zaštita armature od korozije migracijskim inhibitorima, Građevinar. Vol. (50), No. 4, str. 193-202, (1998).

[5] Bjegovic, D., Stirmer, N.: Teorija i tehnologija betona, Sveučilitše u Zagrebu Građevinski fakultet, str. 999, (2015), ISBN 978-953-6272-77-8.

[6] Technology that Extends the Service Life of Concrete Structures, CORTEC Corporation, Minnesota, USA, (2013).

[7] Pržulj, M. Nadvožnjaci na autocestama, GRAĐEVINAR, Vol. (55), No. 2, str. 63-69, (2003).

[8] Bjegović, D.: Bjegović, D.: Projektiranje životnog vijeka armiranobetonskih objekata na prometnicama, znanstveno-istraživački projekt, ugovor br. 345-03-03-8044/94 između Javnog poduzeća Hrvatske ceste i Odjela za materijale Građevinskog fakulteta Sveučilišta u Zagrebu, listopad 1994., str. 137, (1994).

[9] Bavarian, B. & Reiner, L.: Corrosion Protection of Steel Rebar in Concrete by Migrating Corrosion Inhibitors, Corrosion 2003, NACE, (2003)

[10] Bjegovic, D. & Miksic, B.: Migrating Corrosion Inhibitor Protection of Concrete, Materials Performance. Vol. (38), No. 11, str. 52-56, (1999).

[11] Shen, M., Christianson, M., Domin, M., Merkert, E. F.: Detecting Corrosion Inhibitor Migration Depth in Topically Treated Concrete Using Mass Spectrometry, Corrosion 2016, NACE, paper No. 7235, (2016).

[12] MCI-2020 Long Term Corrosion Test; General Building Research Corporation of Japan; (1999).

BIOBASED AND SUSTAINABLE MULTIFUNCTIONAL CORROSION INHIBITING ADMIXTURE USED IN THE WORLD'S TALLEST BUILDING – BURJ KHALIFA

Usama Jacir[1], Mohamad Nagi[2], Nizar Marjaba[1]

[1] Cortec Middle East, Sidra Tower 1307, Sheikh Zayed Road, Dubai, United Arab Emirates, email: ujacir@cortec-me.com, nmarjaba@cortec-me.com
[2] American University in Dubai, Infrastructure and Sustainability Assessment Center, Sheikh Zayed Road, Dubai, United Arab Emirates, email: mnagi@aud.edu

SUMMARY: Chloride-induced corrosion of reinforcing steel in concrete is the dominant durability factor controlling the service life of concrete structures in the Middle East, which is considered one of the most corrosive places in the world. An organic amine-carboxylate, biobased and sustainable multifunctional corrosion inhibiting admixture was selected for use in the concrete mix design for the podium structure of Burj Khalifa – the world's tallest building. The building sits on a steel-reinforced concrete podium with 192 piles descending to a depth of 50meters in highly saline soil with a high-water table. The incorporation of this corrosion inhibitor was part of the strategy to achieve 100 year design life for this iconic structure. A comprehensive long-term study managed by the Middle East Durability Research Consortium (MEDRC) was initiated in March of 2010 to evaluate the service life of reinforced concrete structures in the unique environments of the Middle East, and to correlate these findings to standard testing methodology and service life prediction modelling. Seventeen concrete mix designs currently used in the region were included in the study. The mixes included different levels of supplementary cementing materials (ground granulated blast furnace slag, fly ash and silica fume) with and without corrosion inhibitors. The study consisted of laboratory testing and service life prediction. ASTM G109 is the main laboratory test considered in the study. Three specimens were prepared in accordance with ASTM G109 for each of the seventeen selected mixes and being monitored at the American University in Dubai Laboratory. In addition, for each mix the standard durability tests currently used in the Middle East, namely water permeability, Water Absorption and Rapid Chloride Penetration were conducted on every mix. For service life prediction, the chloride migration and diffusion coefficients were measured for each mix at three different ages (28, 56 and 90 days). These parameters will be used to verify the service life of each concrete mix using the currently available models. Also these data will be used to establish correlation between the rapid migration test and the effective chloride diffusion coefficient. After collecting corrosion data for three years of exposure to wetting and drying cycles, destructive testing was conducted to gain a better understanding of the electrochemical results.

ODRŽIVI I BIOLOŠKI VIŠEFUNKCIONALNI DODATAK ZA SPREČAVANJE KOROZIJE UPOTRIJEBLJEN NA NAJVIŠOJ ZGRADI NA SVIJETU – BURJ KHALIFI

SAŽETAK: Korozija čelika za armiranje u betonu prouzročena kloridima prevladavajući je faktor trajnosti koji djeluje na uporabni vijek betonskih konstrukcija na Bliskom istoku, područjem koje se smatra jednim od mjesta na svijetu najviše izloženih koroziji. Za projektiranje mješavine betona temeljne konstrukcije najviše zgrade na svijetu – Burj Khalifa odabran je organski, održivi i biološki višefunkcionalni dodatak za sprečavanje korozije – amin-karboksilat. Zgrada je temeljena na ploči od armiranoga betona s 192 pilota koji se protežu do dubine od 50 metara u tlu velike zasoljenosti uz visoku razinu podzemne vode. Upotreba tog sredstva za sprečavanje korozije bila je dio strategije postizanja 100-godišnjeg projektiranog vijeka te ikonske konstrukcije. Da bi se odredio uporabni vijek armiranobetonskih konstrukcija u jedinstvenom bliskoistočnom okolišu i nalazi doveli u korelaciju s normiranom metodologijom ispitivanja i modeliranjem predvidivog uporabnog vijeka u ožujku 2010. započela je sveobuhvatna dugoročna studija kojom je upravljao Middle East Durability Research Consortium, MEDRC. U studiju je uključeno sedamnaest mješavina betona koje su se tada upotrebljavale u regiji. Mješavine su sadržavale različite količine dodanih cementnih materijala (mljevenu granuliranu zguru visokih peći, leteći pepeo i silicijski prašinu) sa sredstvima za sprečavanje korozije i bez njih. Studija je obuhvatila laboratorijska ispitivanja i prognozu uporabnoga vijeka. Glavna norma za laboratorijsko ispitivanje bila je ASTM G109. Za svaku od sedamnaest odabranih mješavina pripremljena su po tri ispitna uzorka sukladno normi ASTM G109 te su oni promatrani u laboratoriju Američkog sveučilišta u Dubaiju. Za svaku su mješavinu provedena normirana ispitivanja trajnosti koja se danas provode na Srednjem istoku, tj. vodopropusnost, vodoupojnost i difuzija klorida. Za prognozu uporabnog vijeka mjereni su migracija klorida i koeficijenti difuzije za svaku mješavinu pri starostima od 28, 56 i 90 dana. Ti će se parametri upotrijebiti za provjeru uporabnoga vijeka svake mješavine upotrebom danas dostupnih modela. Isti će se podatci upotrijebiti za određivanje korelacije ispitivanja brze migracije i efektivnog koeficijenta difuzije klorida. Nakon prikupljanja podataka o koroziji tijekom tri godine izloženosti ciklusima močenja i sušenja provedena su razorna ispitivanja kako bi se bolje shvatili rezultati elektrokemijskih ispitivanja.

1. INTRODUCTION

During the first construction boom in the Gulf and Arabian Peninsula in the early 1970's, many concrete structures were built based on foreign codes without paying attention to the unique environment in the region. As a result, the high temperature and harsh environment have led to a major durability-related deterioration in some of the structures within 10 to 15 years [1, 2].

Currently, the Gulf and Arabian Peninsula region is on the top of the world's list in concrete construction and the daily consumption of concrete is one of the highest rates in the world. From super tall towers to marine, industrial, and highway structures, reinforced concrete (RC) stands as the material of choice used in construction in the region. In the last decade, Supplementary Cementing Materials (SCM) such as fly ash, silica fume, and ground granulated blast furnace slag (GGBFS) made their way to the Gulf and are commonly used.

Considering the high initial construction cost, developers and authorities are demanding much longer service life for their structures (75 to 100 years or more) with minimum maintenance and life cycle cost. Due to the harsh and severe environment in the Gulf region, durability characteristics of concrete control its service life. Production of durable and quality concrete is the key to extending the service life of the structures. Designers are now looking into durability modeling to assess the service life of the designed facilities.

In general, service life is the period of time during which a structure meets or exceeds the minimum requirements set for it. The requirements limiting the service life can be technical, functional or economical [3]. The technical service life is the time in service until a defined unacceptable state is reached, such as cracking, spalling of concrete or failure of elements. Service life methodologies have application in the design phase of a structure and in the operation phase where inspection and maintenance strategies can be developed in support of life-cycle cost analysis [4].

The main deterioration factors affecting the service life of concrete structures are durability related ones. Durability by definition is the ability of concrete to resist weathering action, chemical attack, and abrasion while maintaining its desired engineering properties. Concrete ingredients and their proportions, and interaction among ingredients, curing and placing of concrete control its ultimate durability [5]. In the Gulf region, while other factors exist, corrosion of reinforcing steel is the main factor controlling the service life of RC structures. The corrosion mechanism is well covered and understood. Steel reinforcement is usually protected in concrete as long as the passive layer (protective iron oxide film) is formed in the high-alkali concrete environment [6, 7]. Whenever this layer is damaged, either due to carbonation (reduction in concrete alkalinity) or due to the presence of chloride ions, and in the presence of oxygen, corrosion will start. The chloride-induced corrosion is the common form of corrosion in the region. The Gulf area is predominantly ex-seabed sand. Salt content of the soil can be several times that of the seawater, and when combined with the high ambient temperature and high humidity, the Gulf becomes one of the most corrosive locations in the world.

Burj Khalifa is an iconic structure built to be the tallest tower in the world at 828m and 163 floors. After the commencement of construction, the client requested the structure to be designed with a service life of 100 years. Of particular challenge were the soil conditions with a shallow water table saturated with salts. Chloride levels were as high as 4.5% and sulphates as high as 0.6%. Such levels are higher than concentrations found in seawater, necessitating special precautions. The design philosophy incorporated a combination of impressed current cathodic protection system for the piles and foundations with the use of a biobased, sustainable corrosion inhibitor for the podium structure. These were durability enhancement techniques used in addition to the high-performance self-consolidating concrete specification.

With the goal of improving understanding of service life prediction and design of concrete structures in the Middle East, a long-term study was initiated by the Middle East Durability Research Consortium (MEDRC). The objectives of the program, description of the experimental program, and the preliminary results collected so far are the focus of this paper.

2. EXPERIMENTAL PROGRAM

The experimental program presented in this paper focuses on assessing the concrete technology in the Middle East and developing guidelines for consultants and concrete designers to select the optimum mixtures which achieve the designed service life of reinforced concrete structures.

The program was developed by the Middle East Durability Research Consortium (MEDRC), a group of experts representing government authorities, consultants, industry, and academic centers in the region. Based on the experience of MEDRC members, a series of typical concrete mix designs currently used in the Middle East, mainly in the Gulf region were selected. The mixes were carefully selected to represent the majority of the concrete mixes used in all construction sectors in the region.

The selected mixes (Table 1) contain a control mix using Ordinary Portland Cement (OPC) with 0.4 water-to-cement ratio. Other mixes contain Fly ash, Micro silica, GGBFS and sulfate resistance cement (SRC). In addition to the mixes shown in Table 1, similar mixes were prepared using the biobased corrosion inhibitor.

Table 1. Typical concrete mix designs used in the study (kg/m^3)

	OPC	GGBS	SRC	PFA	SF	GGBS/ SF	PFA/SF	PFA/ GGBS
Date	8/5/10	12/5/10	17/5/10	19/5/10	22/5/10	25/5/10	1/6/10	3/6/10
OPC	400	136		280	368	116	260	140
SRC			400					
GGBS		264				264		180
SF					32	20	20	
PFA				120			120	80
Cement	400	400	400	400	400	400	400	400
Water	0.4	0.4	0.4	0.4	0.4	0.4	0.4	0.4
w/c (free)								

The experimental program focused on assessing the corrosion preventing characteristics of the selected mixes. Slightly modified ASTM G109 test [8] was used in the study. ASTM G109 is a laboratory test used to assess the corrosion resistance of concrete system based on macroscopic corrosion cell. In the test, two reinforcing steel layers are placed in a concrete prism. One bar is placed at the top near the surface and two bars at the bottom of the prism. The top surface of the prism is subjected to wetting and drying cycles using salt water (3% NaCl). As the chloride ions reach the top bar and exceed the corrosion threshold, the passivated layer around the bar will be destroyed (depassivated) and becomes anodic [9]. A corrosion cell is formed, which produces an electrical potential difference between the top bar and the bottom bars, which remain cathodic (chloride free concrete). This potential difference produces a flow of an electrical (corrosion) current. The top and bottom bars are externally connected through a 100-ohm resistor used to measure the macrocell corrosion current. The measured current is related to the corrosion activity at the top bar. The modification in the test from the ASTM G109 is the use of variety of mixes and reduction of the concrete cover from 25 mm to 20 mm. In addition, to the corrosion current measurement, half-cell potential using copper-copper sulfate electrode is measured as specified in ASTM G 109 to be used as indicator of corrosion activity.

For each concrete mix selected, including the corrosion inhibiting mixes, three specimens were prepared and currently being tested. For each mix, the main durability parameters are measured. Water absorption (BS 1881 Part 122) [10], effective water permeability (BS EN 12390, DIN 1048) [11], and rapid chloride permeability test (ASTM C 1202) [12] were conducted on specimens cured for 28, 56 and 90 days. One of the objectives of the study is to evaluate the current service life models used in the literature and to correlate the findings with the experimental study. The rapid chloride migration coefficient (NT BUILD 492) [13] and the chloride diffusion coefficient (Effective Chloride Transport Coefficient-NT BUILD 443) [14] were measured at the age of approximately 28, 56 and 90 days.

Rapid chloride permeability (RCP), migration and diffusion coefficients tests were developed to assess the chloride permeability and diffusivity of concrete. RCP test is based on forcing chloride ions into concrete specimen by electrical current. One side of the specimen is exposed to sodium chloride solution and the other side is exposed to sodium hydroxide solution. The specimen is subjected to potential difference of 60 V. It was found that the total charge passes the specimen in column is related to concrete chloride penetration.

The migration coefficient test is similar in concept to RCP. However, at the end of test, the specimen is split open, and the chloride penetration depth is measured. Average of measured depth value is used to calculate the migration coefficient.

In the case of diffusion coefficient test, the specimen is sealed, except the finished surface and placed in sodium chloride solution for a minimum of 35 days. Thin layers are grounded from the finished surface to measure chloride concentration in these layers. The chloride profile is used in Ficks second law of diffusion to calculate the apparent chloride diffusion.

While diffusion coefficient test requires 35 to 45 days to perform, the migration coefficient and RCP can be conducted in less than 24 hours. The reason behind conducting the diffusion and the migration coefficient tests is to establish a correlation between the two values. One benefit of this correlation is to use the rapid migration test results at the trial stage of mix development to assess the service life of a given mix, based on the preliminary design concrete cover.

The main criteria for selecting the optimum mixture will be based on ASTM G109 test findings. For each mix, the chloride content at the level of the top steel bar will be measured (corrosion threshold) for the first specimen which reaches a macrocell current of 10 micro Ampere (µA) and integrated current of 150 Coulombs. The other two specimens in the set will remain under testing until cracking. The mixes will be evaluated based on threshold values and time of cracking. The measured corrosion threshold values will be utilized in the service life computer models for predicting the service life of a given mix.

In order to correlate the laboratory findings with field performance, testing stations on the Gulf, Dead Sea and Mediterranean Sea shores are planned to be installed for conducting field studies. Relatively large scale reinforced concrete specimens using selected mixes from the laboratory study program will be placed in these field testing stations. Performance of these specimens will be monitored and compared with lab findings.

3. RESULTS

For each mix, workability of the concrete was assessed using the slump test immediately after mixing and after 30 minutes (Table 2). Forty six standard cubes were prepared for each mix. The cubes were used for compressive strength and durability testing. Compressive strength was measured at 1, 3, 7, 28, 56 and 90 days (Table 2). The data show clearly the difference in strength development between the control mixes and mixes with fly ash and GGBFS, as the hydration of the SCM's such as fly ash is slower than that of Portland cement.

Table 2. Slump and Compressive Strength Test Results

	OPC	GGBS	SRC	PFA	SF	GGBS/SF	PFA/SF	PFA/GGBS
Slump								
- Initial	150	160	160	180	150	140	160	220
30min	110	110	110	140	120	120	135	200
Strength								
1 day	23.1	7.1	21.1	11.8	23.2	6.5	16.0	7.9
3 days	37.4	33.9	37.7	24.9	39.5	27.7	27.4	25.2
7 days	47.5	38.7	50.5	33.8	49.1	43.3	36.0	39.7
28 days	57.1	46.3	60.5	52.2	68.8	54.5	50.2	51.6
56 days	63.8	54.3	69.5	63.0	75.8	56.3	60.2	55.5
90 days	69.6	55.4	69.8	68.0	78.4	59.3	59.5	58.9

Water absorption, water permeability, and rapid chloride permeability (RCP) test results are shown in Table 3. As shown in Table 3, for all SCM mixes the RCP values were less than 1000 coulombs indicating low permeability. Chloride migration coefficient (NTB 492) and diffusion coefficient (NTB 443) data for all mixes are presented in Table 3. Figures 1, 2 and 3 show comparison between the two tests for the SCM mixes at 28, 56 and 90 days, respectively. Figures 4-a, 4-b, and 4-c show correlation curves between the diffusion and migration coefficients at the three test ages. The correlation equations shown in the figures can be used to predict the diffusion coefficient of given mix based on the rapid migration coefficient test. Tang, L. and Sorenusen indicated in their paper published in 2001 [15] that both tests are fairly comparable.

The up-to-date measured corrosion currents (70-cylce) of the on-going experimental corrosion study were low for the SCM mixes (integrated current less than 20 Coulombs) indicating that no corrosion activity in the top bars has initiated yet in all of the specimens. However, mix (OPC+ PFA + MS) showed slightly higher current started at Cycle 17 as shown in Figure 5.

Powder samples were collected from one specimen of each set of specimens at the level of the steel bars. Samples were collected at the end of the 36th cycle and acid soluble chloride content was measured. Average chloride content of all SCM specimens was 0.03 to 0.06% by weight of concrete, close to corrosion threshold of normal concrete. One cycle after collecting the samples for chloride analysis and core holes in the specimens were grouted, misleading results were obtained on some of the specimens, most likely due to damage occurred in the specimens, therefore, such specimens readings were removed from data analysis of the program. The relatively high readings in the (OPC+PFA + MS) mix is most likely due to the properties of concrete of this specific mix.

In corrosion testing, the control mix containing SRC and OPC showed relatively high corrosion current starting at cycles 11 and cycle 17, respectively. At cycle 63, the integrated current of SRC control mix reached 150 Coulombs. Figure 6 shows total integrated macrocell current (Coulombs) vs. number of cycles for the control mixes with and without corrosion inhibitor (MCI). Half-cell potentials of both mixes are shown in Figure 7. The half-cell potential test was conducted using copper-copper sulfate electrode according to ASTM C 876. The potentials were within -180 to + 180 mV. Potentials of SRC mix were close to -180 mV at between cycles 10 and 15.

As stated in ASTM G 109, when the integrated current reached 150 Coulombs or higher, specimens should be broken and reinforcing steel bars examined in accordance with ASTM G 33 and ASTM G 46. SRC (control) and SRC with MCI mixes specimens were broken and reinforcing steel specimens. It should be mentioned that one specimen was tested of each tests. The other two specimens were removed from data analysis, as indicated above, due to coring at cycle 36. Photos of the reinforcing steel bars of both specimens are shown in Figures 11 and 12. As shown in Figure 9, steel bar was subjected to uniform corrosion and pitting as well, while the bar of SRC-MCI was in a good shape with no pitting or uniform corrosion observed (Figure 10). The mass loss of control bar was close to 1% and the pitting is rated 3 (size in the range of 8.0 m^2 and depth of close to 1.6 mm) in accordance of ASTM G 46. Acid soluble chloride contents measured in the vicinity of the bars were 0.11% by weight of concrete of SRC-MCI and 0.16% for the control specimens.

The service life of the tested SRC and SRC + MCI specimens were assessed using ACI Life 365 and compared with laboratory findings. Life 365 model is a software designed to estimate the service life and life cycle costs of alternative concrete mix designs proportions and corrosion protection systems. It follows research-based methodology developed by Life-365 Consortium I and II groups of companies, that gives estimates on the effects of design, chloride exposure, environmental temperature and high performance concrete mixture proportions. The main parameters considered in the model are concrete mix design, specifically diffusion coefficient and diffusion decay index, concrete cover, surface chloride content, and corrosion threshold. The average surface chloride content was 0.30%. The threshold for the control mixes used in the analysis was 0.05% by weight of concrete while for concrete with MCI a value of 0.18% was used. For a cover of 20 mm and diffusion coefficient of 8.3 x 10^{-12} m^2/sec (Table 3) were considered in the model. Findings of the predicted service life are shown in Table 4.

Table 3. Durability Parameter Test Results

	OPC	GGBS	SRC	PFA	SF	GGBS/SF	PFA/SF	PFA/GGBS
Water Absorption								
60 days	2.1	1.6	1.9	1.6	1.8	1.4	1.6	1.4
94 days	2.0	1.6	1.9	1.5	1.7	1.3	1.6	1.3
RCPT								
57 days	3345	713	2609	465	1086	279	665	472
91 days	3127	707	2206	605	815	316	627	452
Chloride Migration								
58 days	10.1	3.3	9.8	2.0	4.8	1.3	4.0	2.5
91 days	12.8	2.6	9.0	1.9	4.0	0.8	3.6	1.2
Chloride Transport								
56 days	23.3	4.9	8.3	4.1	7.8	2.0	3.3	2.7
90 days	10.9	2.6	8.2	4.1	2.5	1.7	3.8	2.8
Cl^- Content	0.007	0.007	0.007	0.007	0.007	0.007	0.007	0.007
pH	12.6	12.6	12.6	12.5	12.6	11.9	12.6	12.5

Table 4. Predicted Service Life and Observed Time of Corrosion Initiation

Mix	Diffusion Coefficient	GGBS	SRC
SRC	8.50 x 10^{-12} m^2/sec	7.2	10
SRC / MCI	8.50 x 10^{-12} m^2/sec	58.8	Not initiated at 63 months

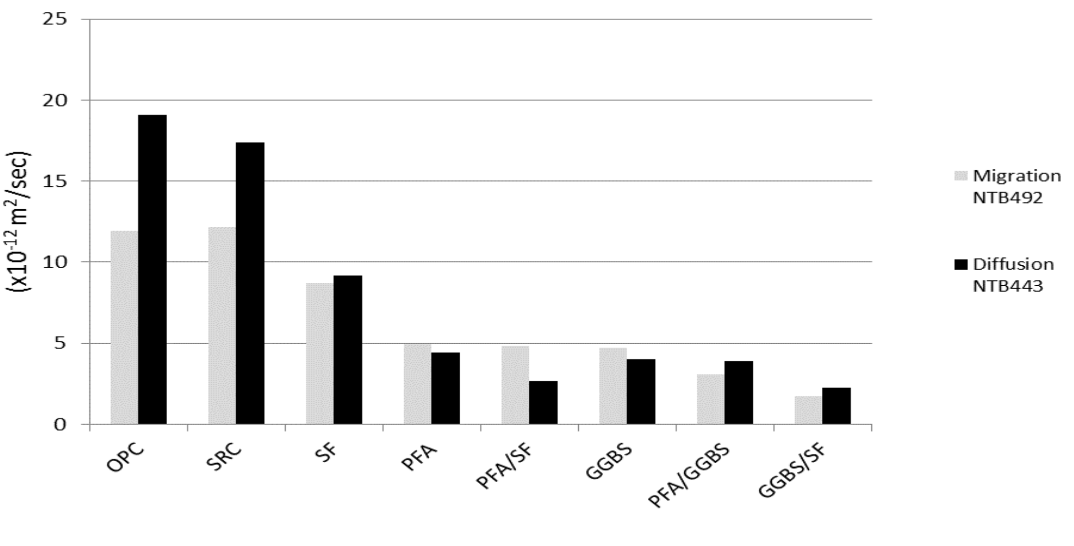

Figure 1. Comparison between Chloride Diffusion and Migration Coefficients at 28 days

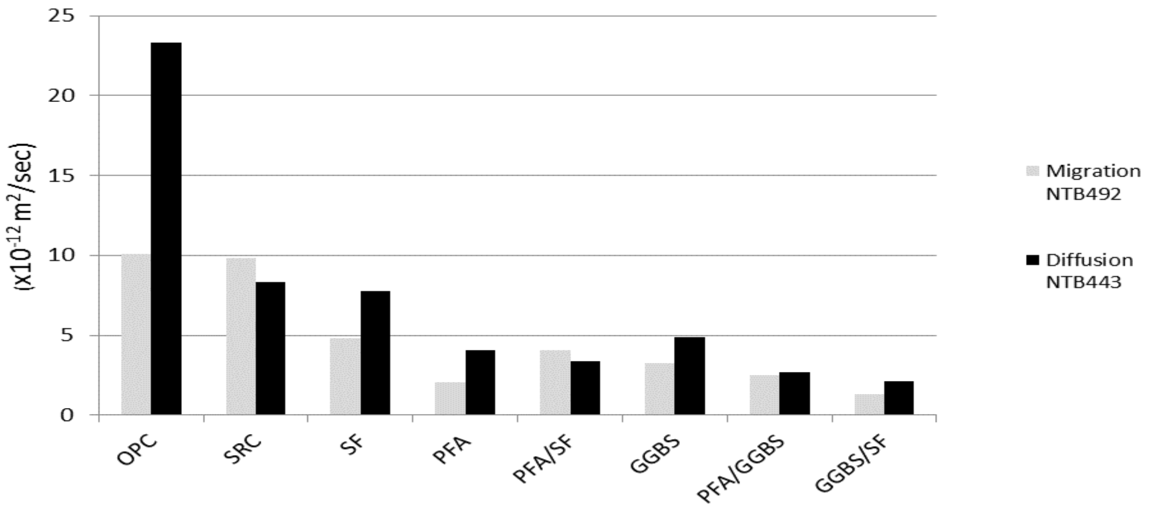

Figure 2. Comparison between Chloride Diffusion and Migration Coefficients at 56 days

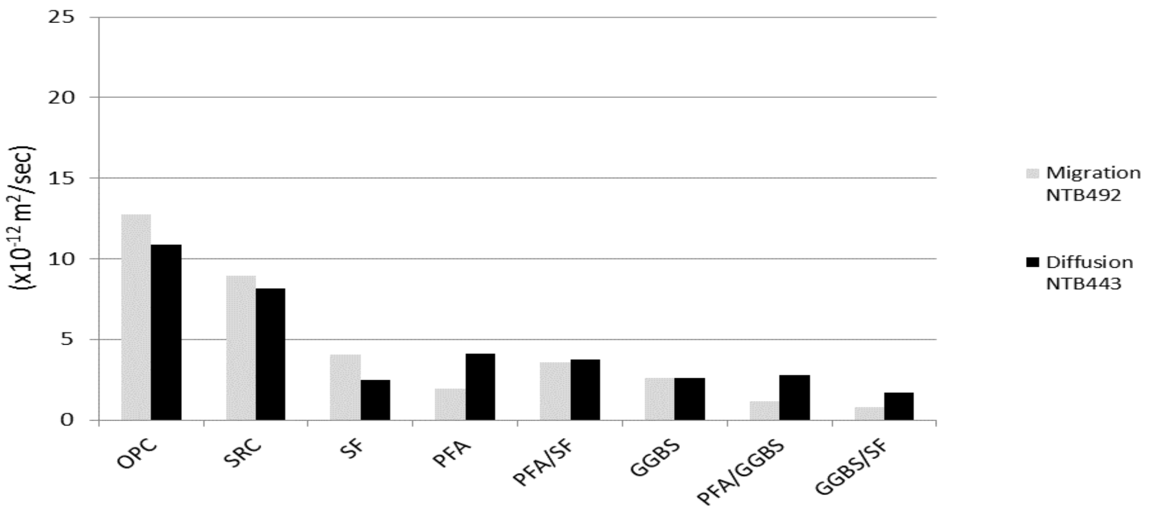

Figure 3. Comparison between Chloride Diffusion and Migration Coefficients at 90 days

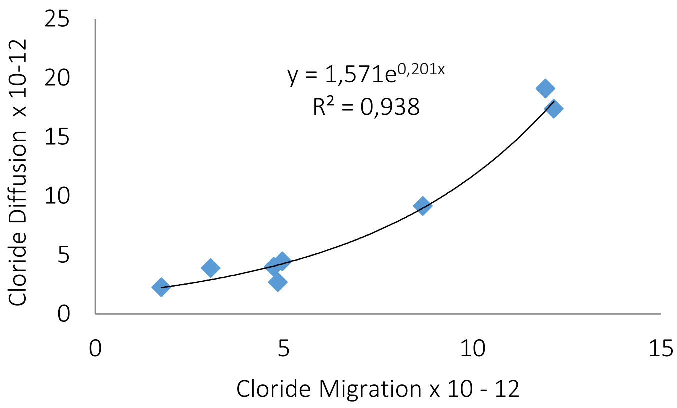

Figure 4-a 28 Days Cloride Diffusion Vs Cloride Migration

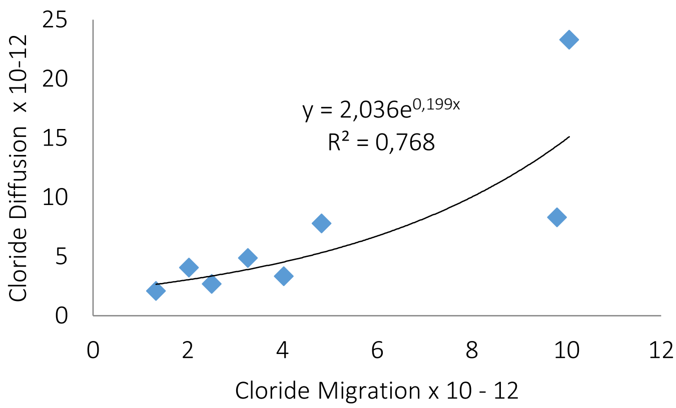

Figure 4-b 56 Days Cloride Diffusion Vs Cloride Migration

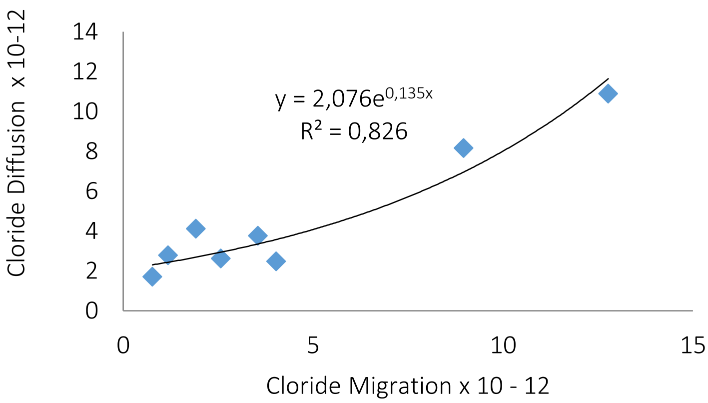

Figure 4-c 90 Days Cloride Diffusion Vs Cloride Migration

Figure 4. Correlation curves between diffusion and migration coefficient at 28, 56 and 90 days

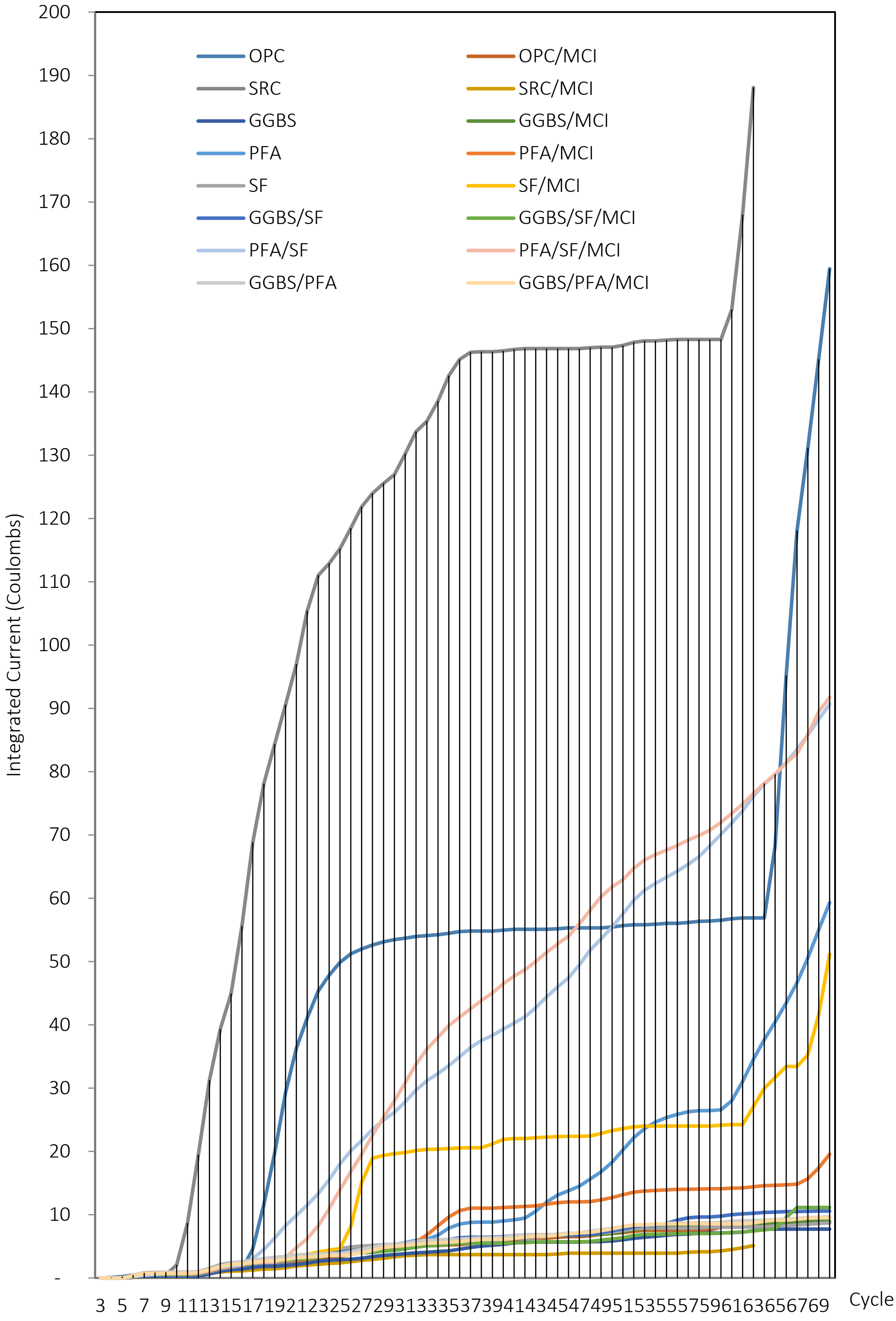

Figure 5. Integrated current (Coulombs) vs. number of cycles for all mixes

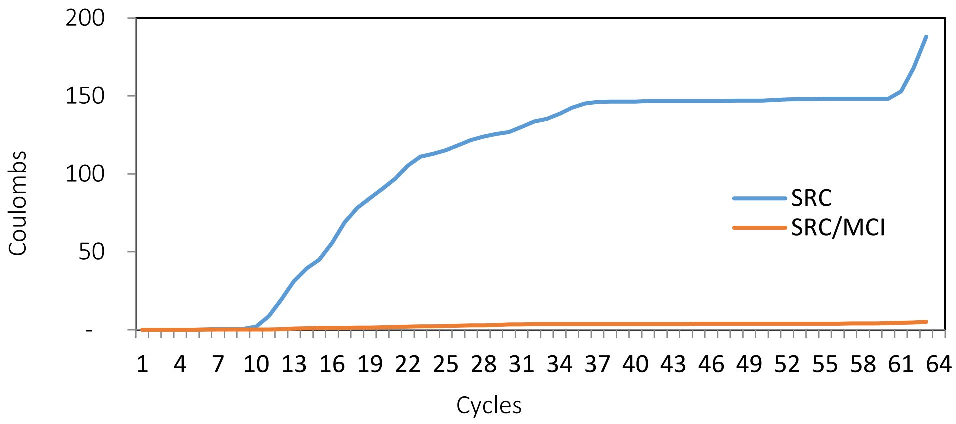

Figure 6. Integrated current (Coulombs) vs. number of cycles for SRC mixes

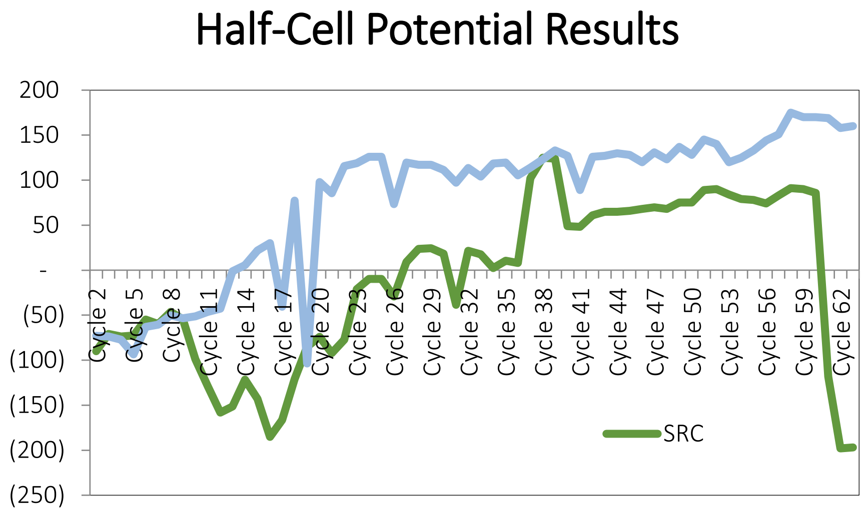

Figure 7. Half-cell Potential vs. number of cycles for SRC mixes

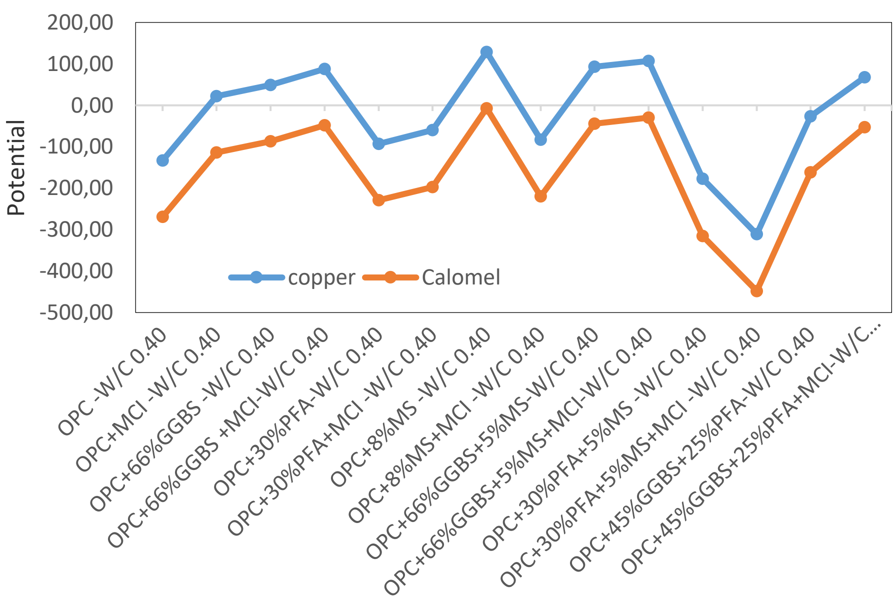

Figure 8. Half-cell Potential vs. number of cycles for SRC and OPC mixes

Figure 9. Reinforcing steel removed from SRC control mix

Figure 10. Reinforcing steel bar removed from SRC-MCI mix

4. CONCLUSIONS

A comprehensive research study is currently being conducted under the supervision of MEDRC in order to evaluate the effectiveness of the majority of concrete mixes used in the Middle East in reducing corrosion of reinforcing steel. Durability parameters and diffusion coefficients were measured for all mixes at the age of 28, 56 and 90 days. Correlation was established between the rapid chloride migration coefficient test (NTB 492) and normal chloride diffusion test (NTB 443).Long-term G109 corrosion test is being conducted for the mixes given in Table 1 with and without corrosion inhibiting admixtures.

Up-to-date results of G109 test indicated that there is no corrosion activity in the main SCM mixes. Corrosion activities were observed in the Control mixes specimens prepared with SRC. Laboratory inspection of such mixes showed that the use of MCI enhance the service life of such mixes compared to control ones. While the SRC mix showed corrosion activities exceeding the ASTM G 109 critiera, no sign of corrosion was observed in the SRC+ MCI specimen.

ACI Life 365 model was used to predict the service life of SRC mixes. Data showed good agreement between the predicted service life (corrosion initiation) and actual corrosion activities.

Half-cell potential measurements in laboratory testing can be only used as indicator of corrosion.

REFERENCES

[1] Concrete Society, *Guide to the Maintenance and Repair of Reinforced Concrete Structures in the Arabian Peninsula,* Bahrain 6th International Conference, (2000)

[2] Rasheeduzzafar et al.: Deterioration of Concrete Structures in the Environment of the Middle East, ACI Journal proceedings, Vol. 81, No. 1, pp. 13-20, (1984)

[3] Vesikari, E: Service Life of Concrete Structures with regard to Corrosion of Reinforcement, Technical Research Centre of Finland, ESPOO (1988)
[4] American Concrete Institute, ACI 365 "Service-Life Prediction," ACI, Detroit, MI, USA
[5] Kosmatka et.al, Design and Control of Concrete Mixtures, Fourteenth Edition, Portland Cement Association, Skokie, IL, U.S.A.
[6] Nagi, M. and Whiting, D, Corrosion of Prestressed Reinforcing Steel in Concrete Bridges, State-of-the-Art, Concrete Bridges Aggressive Environments Symposium, SP 151, American Concrete Institute, Detroit, Michigan, U.S.A. (1994)
[7] Broomfield, J., Corrosion of Steel in Concrete, 1997 E & FNSpon, U.K
[8] American Standard and Testing Materials, ASTM G109, Standard Test Method for Determining Effects of Chemical Admixtures on Corrosion of Embedded Reinforcement in Concrete Exposed to Chloride Environment, West Conshohocken, PA, U.S.A.
[9] Virmani, Y.P, Time-to-Corrosion of Reinforcing Steel in Concrete Slabs, Vol. VI, Federal Highway Administration, FHWA-RD-88-165, (1980-1987)
[10] British Standards Institute, BS 1881-Part 122, Testing Concrete Method for Determination of Water Absorption, London, UK.
[11] British Standards Institute, BS EN 12390-8, DIN 1048, Testing Hardened Concrete Depth of Penetration of Water under Pressure, London, UK.
[12] American Standard and Testing Materials, ASTM C 1202. Standard Test Method for Electrical Indication of Concrete's Ability to Resist Chloride Ion Penetration. West Conshohocken, PA, U.S.A.
[13] NT Build 492, Concrete, Mortar and Cement-based materials: Chloride Migration Coefficient from non-steady-state migration experiments, Nordtest, Espoo Finland, (1999)

WATERPROOF CONCRETE STRUCTURES – WHITE TUBS

Donka Würth[1], Caslav Dunovic[1], Ivan Barukcic[2]

[1] Zagreb University of Applied Science, Vrbik 8, 10 000 Zagreb, Croatia, email: dwurth2@tvz.hr, cdunovic@tvz.hr
[2] ALFA STAN d.o.o., Vrisnička 16, 10 000 Zagreb, Croatia, email: ivan.barukcic@alfastan.hr

SUMMARY: In recent years it is becoming more and more common to construct buildings without waterproofing systems by using the method of so called „white tubs" (german weiße Wanne). Term ''white tubs'' implies external walls that besides load-bearing function have to fulfill the one of beeing waterproof without using additional waterproofing materials and systems. This can be achieved by using the sealants in concrete element connections. When constructing such buildings, it is necesarry to pay attention to their purpose and the level of groundwater. Some of parameters that have to be taken into account are the type of concrete, dimensions of elements, amount of reinforcement, duration of working operations, quality of construction works and method of sealing. Construction of waterproof reinforced concrete elements in underground levels of building has its advantages compared to using the traditional waterproofing systems due to lower financial costs and higher speed of construction, as well as the lower influence of weather conditions on construction process.

BIJELE KADE – GRAĐEVINE BEZ HIDROIZOLACIJE

SAŽETAK: Posljednjih godina sve je češća izgradnja građevina bez hidroizolacije jer se primjenjuje metoda „bijele kade" (njem. weiße Wanne), što podrazumijeva da vanjski tj. obodni zidovi osim nosive funkcije imaju i funkciju hidroizolacije. Dakle, zidovi građevine moraju biti vodonepropusni bez upotrebe dodatne hidroizolacije pa je u spojevima armiranobetonskih elemenata konstrukcije potrebno primijeniti sredstva za brtvljenje. Pri izvedbi takvih građevina potrebno je obratiti pozornost na njihovu namjenu i na razinu podzemnih voda. Da bi građevina bila vodonepropusna važni su odabir vrste betona, dimenzije elemenata, količine armature, duljine radnih koraka te izvedba i način brtvljenja. Izvedba vodonepropusne armiranobetonske konstrukcije u podzemnim dijelovima građevine, čija namjena to dopušta, ima prednosti u odnosu na klasičnu izvedbu hidroizolacije zbog financijski povoljnijeg i bržeg izvođenja te manjeg utjecaja vremenskih prilika na gradnju.

1. UVOD

Hidroizolacijom štitimo konstrukciju i unutarnje prostore od prodora vode, odnosno, vlage. Važan je odabir odgovarajućeg materijala, odnosno proizvoda, pravilna ugradnja i rješenje detalja. Hidroizolacija podzemnih dijelova građevine sastavni je dio građevinske konstrukcije, a odlikuje se specifičnim zahtjevima sa stajališta hidroizolacijske zaštite. Zadnjih godina sve je češća izgradnja objekata bez hidroizolacije, na način da se primjenjuje metoda „bijele kade" (njem. weiße wanne), što podrazumijeva da vanjski to jest obodni zidovi osim nosive funkcije imaju i funkciju hidroizolacije. Dakle zidovi objekta moraju biti vodonepropusni bez upotrebe dodatne hidroizolacije, te se primjenjuju brtveće ili bubreće trake.

Hidroizolacije se dijele na dvije skupine: u obliku filma (klasična hidroizolacija) i krute hidroizolacije (vodonepropusni elementi).

Vrste klasičnih hidroizolacija su [1]:

- bitumenske trake za zavarivanje
- bitumenske emulzije
- sintetičke folije
- hidroizolacijske cementne mase
- čepičaste folije
- bentonit.

Objekti bez hidroizolacije – s krutom hidroizolacijom izvode se od vodonepropusnih betonskih elemenata, koji na mjestima spojeva vertikalnih i horizontalnih elemenata, dilatacijskim i radnim reškama imaju brtve i gume kako bi se spriječio ulazak vode u konstrukciju. U Hrvatskoj je dosta objekata projektirano i izvedeno prema principu „bijele kade" međutim ne postoje smjernice niti hrvatske norme koje vode projektante, izvoditelje i nadzor kako da se izvedu, već se primjenjuju Austrijske smjernice [2] koje nisu svima dostupne i nisu važeće za naše područje.

2. IZVEDBA OBJEKATA S VODONEPROPUSNIM BETONSKIM ELEMENTIMA

Vodonepropusne betonske objekte nazivamo i kruta hidroizolacija. Lohmeyer u svojoj knjizi "Bijele kade – jednostavno i sigurno" krute hidroizolacije dijeli na sljedeće kategorije [3]:

- žbuke ili estrisi od cementnog morta
- slojevi mlaznog morta ili mlaznog betona
- konstruktivni elementi od azbestnog cementa i mikroarmiranog betona
- konstrukcije od ferocementa
- sustavi premaza s izolacijskim muljem
- konstruktivni elementi od vodonepropusnog betona

Najvažnija od prethodno nabrojanih vrsta krute hidroizolacije je hidroizolacija vodonepropusnim betonom, koje se često naziva „bijelim kadama", te se ne izvodi se zasebna vanjska hidroizolacija, a neobrađena površina betona vertikalnih zidova je vidljiva.

Izvedba vodonepropusnih betonskih objekata temelji se na opsežnom konceptu koji se može zajednički realizirati samo u uzajamnoj suradnji investitora, projektanta i izvođača.

Radi sigurne izvedbe vodonepropusnih betonskih objekata bitno je posvetiti veliku pažnju projektiranju ab elemenata, proizvodnji betona, raspodjeli armature, izvedbi detalja s brtvama i bubrećim trakama.

Usporedbom vodonepropusnog betonskog objekta s objektom s klasičnom hidroizolacijom u obliku filma Lohmeyer navodi sljedeće prednosti [3]:

- sam beton preuzima istovremeno nosivu i izolacijsku funkciju
- idejni projekt objekta se može izvesti prema pojednostavljenim statičkim i konstruktivnim principima
- za izvedbu potrebno je manje radnih koraka budući da se mogu izostaviti zaštitni slojevi koji štite hidroizolaciju obloženu filmom od mehaničkih oštećenja
- neovisno o vremenskim prilikama, za razliku od izvedbe bitumenskog zaštitnog sloja gdje okolina mora biti suha i mora se održati minimalna temperatura zraka
- eventualne propusnosti brzo se lokaliziraju i jednostavno otklanjaju budući da na mjestu pogrešno izvedenog mjesta dolazi do eventualnog propuštanja vode, u samoj ab konstrukciji, dok kod objekata s hidroizolacijom u obliku filma bilo bi radi učinkovitog otklanjanja pogrešno izvedenog mjesta potrebno provesti mjere na samoj hidroizolaciji što je teško dostupno, odnosno apsolutno nemoguće kod podnih ploča (hidroizolacija je s vanjske strane objekta)

2.1. PODJELA VODONEPROPUSNIH ELEMENATA

Zahtjevi za vodonepropusnosi objekta različiti su ovisno o vrsti i namjeni objekta [2], što se detaljno razradilo u Austrijskim smjernicama. Kako bi se dobili podaci za izvedbu i projektiranje, potrebno je odrediti razrede zahtjeva za vodonepropušnošću (tablica 1), konstrukcijske razrede i razrede tlaka vode.

Tablica 1 Razred zahtjeva za vodonepropusnošću vanjskih ab elemenata [2]

Razred zahtjeva	Kratki opis	Opis površine betona	Primjeri primjene
As poseban razred	potpuno suho	vizualno vidljiva vlažna mjesta neprepoznatljiva (tamnija mjesta)	skladišta za robu izuzetno osjetljivu na vlagu
A1	pretežno suho	vizualno vidljiva pojedina vlažna mjesta (max. tamnija mjesta bez sjaja)	prometni objekti s visokim zahtjevima. društveni prostori, skladišta, podrumi kuća (spremišta), prostori kućne tehnike s posebnim zahtjevima
A2	lagano vlažno	vizualno i ručno vidljiva pojedina sjajna vlažna mjesta	garaže, prostori kućne tehnike (npr. kotlovnice, kolektori), prometni objekti
A3	vlažno	pojava vode u kapljicama sa stvaranjem vodenih tragova	garaže (s dodatnim mjerama, npr. odvodnim kanalima)
A4	mokro	pojedinačna mjesta prodora vode na podnim pločama, zidovima i dijafragmama	vanjska obloga načina izvedbe s dvije obloge

Prema austrijskim smjernicama [2] definirano je pet razreda zahtjeva prema namjeni objekta, te očekivanom stanju površine objekta, te uzimaju se u obzir tri konstrukcijska razreda (tablica 2) i 5 razreda tlaka vode prema tablici 3.

Tablica 2 Konstrukcijski razredi za armiranobetonske elemente izvedene u oplati [2]

Konstrukcijski razred	Debljina elementa (m)	Dimenzioniranje na opterećenje	Standard betona	Ostali konstrukcijskii zahtjevi* (* nije sve navedeno iz smjernica)
Kon_s poseban razred	$\geq$ 0,45 $\geq$ 0,60 za W_2	ograničenje širine pukotine na $\leq$ 0,15 mm	BS 1	max. duljina elementa: razmaci - dilatacijskih, prostornih reški: $\leq$ 0,15m radnih reški u zidovima: $\leq$ 0,10 m
Kon_1	$\geq$ 0,35 $\geq$ 0,60 za W_4	ograničenje širine pukotine na $\leq$ 0,20 mm	BS 1	preporučene duljine elementa: razmaci - dilatacijskih, prostornih reški: 15 do 30 m radnih reški u zidovima $\leq$ 15 m
Kon_2	$\geq$ 0,30	ograničenje širine pukotine na $\leq$ 0,25 mm	BS 2	preporučene duljine elementa: razmaci - dilatacijskih, prostornih reški: 30 do 60 m radnih reški u zidovima: $\leq$ 15 m

Tablica 3 Razred tlaka vode [2]

Razred tlaka vode [1)]	Opis	
W_0	Tlak vode	0,0 – 1,0 m
W_1	Tlak vode	> 1,0 – 5,0 m
W_2	Tlak vode	> 5,0 – 10,0 m
W_3	Tlak vode	> 10,0 – 20,0 m
W_4	Tlak vode	> 20,0

Kada se definiraju sva tri razreda u kojima se nalazi budući objekt, određuje se područje u kojem se nalazi zadana konstrukcija. (vidi sliku 1), te zahtjevi za načinom brtvljenja, zahtjevima za beton. Razred zahtjeva mora odrediti investitor u suradnji s projektantom, ovisno o predviđenoj eksploataciji. Dimenzionirana razina vode definira se na temelju mjerenja vodostaja ili poznatim podacima za to područje, a razred konstrukcije određuje sam projektant. Treba poštivati aspekte ekonomičnosti i tehničke izvedivosti.

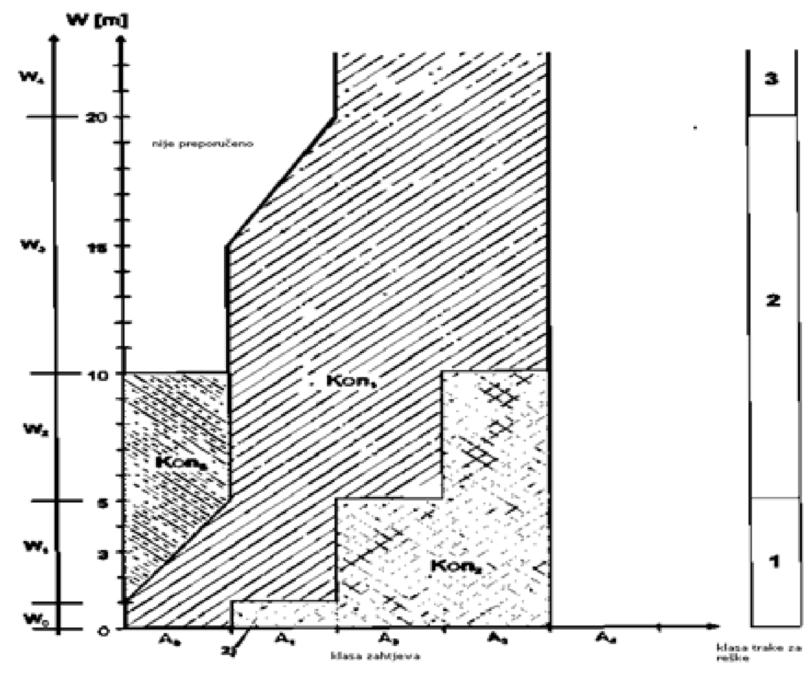

Slika 1. Povezanost razreda zahtjeva: tlak vode, konstrukcijskih razreda i razredi traka za brtvljenje [2]

2.2. NAČIN IZVEDBE OBJEKATA OD VODONEPROPUSNIH AB ELEMENATA

Osnovna pitanja za odabir načina izvedbe za izvedbu vodonepropusnog betonskog objekta (bez vanjske hidroizolacije) moraju se odrediti što ranije tijekom faze projektiranja i to na osnovi povezanosti razreda zahtjeva, konstrukcijskih razreda i razred traka za brtvljenje, uzevši u obzir postojeće zemljište te prilike koje vladaju u podlozi i podzemnim vodama. Također treba procijeniti prednosti i nedostatke kod provedbe radova, te uzeti u obzir kasnije korištenje (održavanje, rad) u konstrukcijskom, izvedbenom i gospodarskom pogledu. Postoji nekoliko načina izvedbe [3]

Zatrpani objekt - izvodi se u građevnoj jami zaštićenoj neovisno od objekta, sa ili bez snižavanja razine podzemnih voda te se nakon dovršetka zatrpava odnosno nasipava. Stjenke građevne jame izvode se ovisno o raspoloživom prostoru kao široki iskop u pokosu ili kao privremena zaštita građevne jame (bušeni piloti, dijafragme itd.) (slika 2). Na ovom principu izveden je stambeno – poslovni objekt u Laništu. [4]

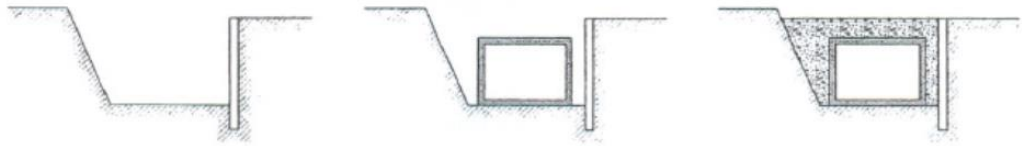

Slika 2 Zatrpani objekt [2]

Objekt s integriranim stjenkama građevne jame - stjenke građevne jame za fazu izvedbe (zidovi od bušenih pilota ili dijafragme) izvode se kao sastavni dio objekta. Treba razlikovati način izvedbe s jednom ili dvije obloge.

- način izvedbe s jednom oblogom (slika 3)

Slika 3 Objekt s integralnim stjenkama građene jame – jedna obloga [2]

Ovim načinom izvedena su dva objekta Cvjetni prolaz i Ban centar u Zagrebu

- način izvedbe s dvije obloge (slika 4)

Slika 4 Objekt s integralnim stjenkama građene jame – dvije obloge [2]
Ovim načinom izveden je objekt podzemne garaže zgrade Hrvatske elektroprivrede u Zagrebu [5]

3. ZAHTJEVI ZA PROIZVODNJOM, UGRADNJOM I NJEGOVANJEM BETONA

3.1. PROIZVODNJA BETONA

Beton vodonepropusnih betonskih objekata treba imati dovoljno zbijenu strukturu tako da u što većoj mjeri nema proslojke ili pukotine koje propuštaju vodu. U svrhu postizanja tog cilja koriste se posebne mjere izvođenja betonskih elemenata kao recimo izbjegavanjem krutog ležaja ili upetosti (primjerice klizne plohe i klizne folije, ograničene dimenzije konstruktivnih elemenata) ili raspoređivanjem (projektiranjem) armature. Posljednjom mjerom pukotine se ograničavaju smanjenjem temperaturnih razlika prilikom topline hidratacije cementa i smanjenim skupljanjem betona. Prilikom faze projektiranja potrebno je obratiti pozornost na nekoliko zadataka koje mora zadovoljiti beton, poput vrste i kvalitete betona, ujednačenosti temeljnih sastojaka za proizvodnju betona, granične vrijednosti za sastav betona, zahtjeve prema betonari, proizvodnji i ugradnji betona, rokove za demontažu oplate i njegu te sve mjere za osiguranje kvalitete pri čemu se mora izvršiti optimiziranje iz zahtjeva za obradljivošću betona, demontažom oplate, uporabnim svojstvima i izbjegavanje nastanka pukotina.

Kod same proizvodnje beton mora biti obradljiv, bez izdvajanja vode, segregacije, kako ne bi došlo do pojave „gnijezda“ ili pukotina. Kako bi se smanjila pojava pukotina uslijed hidratacije cementa, preporuka je koristiti cemente niske topline hidratacije, sa što manje portlandskog cementa, a po mogućnosti primijeniti mineralne dodatke (leteći pepeo, zgura). Također preporuka je koristiti što veće zrno agregata, kako bi se smanjila količina cementa, te na taj način smanjila toplina hidratacije. Austrijske smjernice upućuju na što manji v/c omjer, međutim sa što manjom količinom vode, te upotrebom superplastifikatora. Na pojavu pukotina u betonu veliki utjecaj imaju dvije temperature, a to su temperatura betona i temperatura okoliša. Za objekte koji se izvode kao „bijele kade“ preporuča se izgradnja u hladnije zimsko doba, a ne za vrijeme velikih vrućina, te isto tako poželjno je da se temperatura betona kreće od 10 °C – 20 °C. [2]

3.2. UGRADNJA BETONA

Prije ugradnje potrebno je paziti na to da su brtvene trake odgovarajuće prema projektu, te pravilno pričvršćene na oplatu ili betonski element. (slika 5).

Slika 5. Pričvršćenje brtve za oplatu

Beton namijenjen za ugradnju mora biti dobro homogeniziran, te obradljiv, te ne smije doći do segregacije. Ugradnja betona mora se načelno provesti kontinuirano bez prekida za jedan takt betoniranja. Tijekom same ugradnje beton ne smije imati slobodan pad veći od 1,0 m. Kod većih visina slobodnog pada treba koristiti nasipne cijevi odnosno otvore koji završavaju neposredno iznad stvarne razine ugradnje[2]. Beton se mora ugrađivati u slojevima. Visina slojeva orijentira se prema konzistenciji betona, dimenzijama konstrukcijskog elementa i postupku zbijanja, ali kod betona slabe plastične konzistencije mora biti između 30 i 50 cm. Kod visokih zidova kod kojih je između vanjske i unutrašnje zone armature tek mali razmak može biti korisno ugraditi beton u oplatu kroz prozore.

Rok za demontažu oplate i njega konstrukcijskih elemenata vodonepropusnog betonskog objekta moraju biti usklađeni s time da se beton nakon betoniranja štiti minimalno 3 dana od brzog hlađenja i 7 dana od jakog isušivanja. [2] To se najbolje postiže za površine u oplati ako konstrukcijski elementi ostaju što duže u oplati. U tom pogledu treba dati prednost drvenoj oplati u odnosu na čeličnu oplatu. Čelična oplata treba kod očekivane temperature zraka < +5 °C imati toplinsku izolaciju. U tipičnom slučaju kod konstrukcijskih elemenata na otvorenom rok za demontažu oplate je od minimalno 36 sati. Kod temperatura zraka manjih od 0 °C treba poštivati rok za demontažu oplate od minimalno 72 sata.

3.3. NJEGA BETONA

Na površine betona bez oplate (stropne i podne ploče) odmah nakon betoniranja na betonsku površinu potrebno je nanijeti sredstvo za njegu i čim je postignuta prohodnost podloge treba nanijeti pokrov. Na površine u oplati odmah nakon demontaže oplate potrebno je pokriti pokrovom koji treba spriječiti gibanje zraka (propuh) uzduž površine betona. Austrijske smjernice također preporučuju i neke konkretne zahtjeve, recimo da kod temperature zraka manje od -3 °C tijekom minimalno 3 dana potrebno je zajamčiti temperaturu betona od minimalno +10 °C. Završna faza, a to je njega također ima veliki utjecaj na smanjenje pojave pukotina, naročito ljeti.

4. ZAHTJEVI ZA REŠKAMA I BRTVAMA

Prema direktivi „bijele kade“ Austrijskog udruženja za beton, ukoliko objekti iz armiranog betona prekoračuju maksimalne duljine konstrukcijskih elemenata, potrebno ih je podijeliti u pojedinačne taktove uz pomoć dilatacijskih reški. U skladu s tim razlikujemo radne reške i reške za prihvat gibanja (tzv. prostorne reške). [2]

- Radne reške (fuge) (slika 6) su reške uvjetovane izvedbom, a njihova nepropusnost zajamčena je trakama za brtvljenje, pri čemu se prednost daje unutrašnjim trakama za brtvljenje. Raspored reški određen je radnim taktovima (oplata, armatura) i opterećenjem konstrukcijskog elementa. Između taktova objekta gibanja nisu dozvoljena te se zahtjeva da susjedni konstrukcijski elementi budu što više spojeni mehaničkim silama. Prije nastavka betoniranja radne reške potrebno je očistiti i dovoljno ovlažiti, a kod teško izvedivih radnih reški preporučuje se injektirati u kontaktnim površinama.

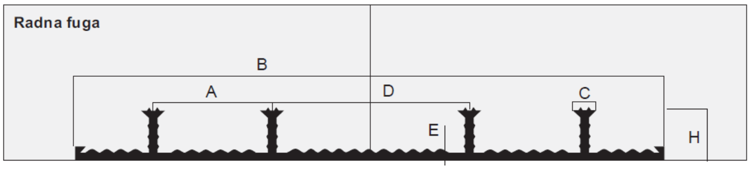

Slika 6 Radna fuga [6]

- Reške za prihvat gibanja (dilatacijske fuge) (slika 7) - razlikujemo tri vrste prostornih reški; reške za prihvat gibanja, reške kod slijeganja, dilatacijske reške. Prilikom određivanja reške, između pojedinih taktova potrebno je dovoljno prostora za vlastito gibanje bez prisile, te se u pravilu koriste kontinuirane reške za prihvat gibanja. Dilatacijske reške izvode se s mekanim uloškom ili bez mekanog uloška, a kod teško izvedivih reški za prihvat gibanja preporučuje se injektirati u području kraka trake za brtvljenje.

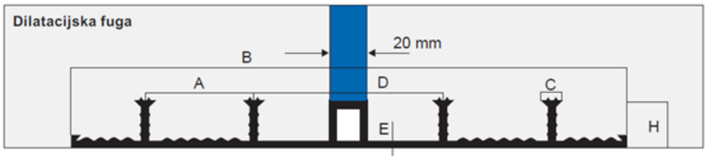

Slika 7 Dilatacijska fuga [6]

Posebnu pažnju je potrebno posvetiti fazi projektiranja i fazi izvedbe traka za brtvljenje. Prilikom projektiranja trake za brtvljenje u izvedbenim nacrtima treba naznačiti položaj, vrstu i vođenje reški, odnosno trake. Dimenzioniranje i položaj traka primjenjuje se u skladu sa nekoliko čimbenika, poput betonske konstrukcije, armature, tlak vode i korištene oplate. Prilikom polaganja traka za brtvljenje potrebni su precizni nacrti iz kojih je jasan njihov položaj i sve dimenzije. Ako je potrebno, treba izraditi zasebne nacrte za vođenje radnih reški. Transport, skladištenje i ugradnja traka za brtvljenje mora biti stručna prema uputama proizvođača. Trake za brtvljenje moraju se očistiti prije betoniranja i prekontrolirati u pogledu oštećenja [2].

Ekspandirajuće trake ugrađuju se prema uputama proizvođača tako da su u svježem betonu zaštite od uzgona, a fiksiranje ekspandirajućih traka ne smije negativno utjecati na strukturu podloge (npr. poremećaji strukture uslijed mehaničkog pričvršćivanja). Također treba spriječiti prijevremeno bubrenje ekspandirajućih traka prije betoniranja. Ekspandirajuće trake moraju se u pravilu montirati u sredini presjeka betona, ako to nije moguće treba poštivati bočni minimalni razmak od 10 cm.

5. ZAKLJUČAK

Izgradnja objekata bez hidroizolacije naziva se „bijela kada“ (njem. weiße wanne), što podrazumijeva da vanjski, obodni zidovi osim nosive funkcije imaju i funkciju hidroizolacije. Kod izvedbe ove vrste objekta potrebno je obratiti pozornost na namjenu objekta, konstruktivne zahtjeve i visinu podzemnih voda. Kako bi građevina bila vodonepropusna važan je odabir vrste betona, dimenzije ab elemenata, duljina radnih taktova, izvedba i način brtvljenja, te njegovanje betona. Izvedba vodonepropusne armiranobetonske konstrukcije u podzemnim dijelovima građevine, čija namjena to dopušta ima prednosti u odnosu na klasičnu izvedbu hidroizolacije zbog same izvedbe s manje radnika (nema hidroizolaterskih radova), te vrijeme izvedbe nema utjecaja, kao kod klasične izvedbe s hidroizolacijom (potrebno je suho vrijeme). Međutim ova metoda ima i nedostatke, a to je veći broj reški, mogućnost je da zbog lošeg izvedenog detalja dođe do prodora vode. Dimenzije konstrukcijskih elemenata te taktovi betoniranja su ograničeni što usporava zamjenu oplate, te sporije izvođenje.

Izvedba vodonepropusnih betonskih objekata temelji se na opsežnim radovima koji se mogu zajednički realizirati samo u uzajamnoj suradnji investitora, projektanta i izvođača, uz pripadajuće norme ili smjernice za projektiranje i izvođenje vodonepropusnih betonskih elemenata.

LITERATURA

[1] http://www.mapei.com/public/HR/documents/1163/attach/Hidroizolacija%20podzemnih%20dijelova%20konstrukcija.pdf

[2] Österreichische Bautechnik Vereinigung; Richtlinie "Wasserundurchlässige Betonbauwerke - Weiße Wannen" (1999)

[3] Lohmeyer G., Ebeling K., Konstruktion und Ausführung wasserundurchlässiger Bauwerke aus Beton Gebundene Ausgabe – 11. Juni 2013.

[4] Barukčić I., Izvedba podzemnog dijela stambeno – poslovne građevine na Laništu bez hidroizolacije, Diplomski rad, 2015

[5] Starčević F., Izvedba vodonepropusnih podzemnih objekata, Diplomski rad, 2015

[6] Fugaplast; Dilatacijske trake, http://fugaplast.hr/category/ponuda/dilatacijske-trake/, veljača 2015

SPECIFIC RECONSTRUCTION ASPECTS OF BELGRADE BUSINESS CENTER USCE

Predrag Blagojevic[1], Slobodan Grkovic[2], Milan Romanic[2]

[1] University of Nis, Faculty of Civil Engineering and Architecture, Aleksandra Medvedeva bb, 18000 Nis, Serbia, email: predragb@eunet.rs
[2] University of Novi Sad, Faculty of Civil Engineering, Kozaracka 2a, 24000 Subotica, Serbia, email: slobodan.grkovic@gf.uns.ac.rs, milan.romanic@gf.uns.ac.rs

SUMMARY: The reconstruction and reinforcement of 23-story office building „Ušće" structural elements severely damaged in 1999 bombing is shown in this paper. The paper reveals several methods implemented in reconstruction and structural reinforcement, including floor slabs reconstruction, collapsed and fire damaged walls recovery, steel bar reinforced concrete girders reconstruction, newly constructed openings, and supporter rehabilitation. Special focus is on the reconstruction of cylindrical supporters filled with quartz sand, used for building settlement and verticality correction. At the time of the design and construction (1960s), the supporters represented a unique solution for the high-rise building foundation. It is estimated that the applied reconstructive interventions resulted in EUR 14 million savings compared to the price for the damaged building demolition and construction of an entirely new building.

POSEBNI ASPEKTI REKONSTRUKCIJE POSLOVNOG CENTRA UŠĆE U BEOGRADU

SAŽETAK: U radu je prikazana rekonstrukcija i pojačanje 23-katne poslovne zgrade Ušće čiji su konstrukcijski elementi teško oštećeni u bombardiranju 1999. Prikazano je nekoliko metoda primijenjenih u obnovi i pojačanju konstrukcije uključujući obnovu ploča, obnovu srušenih i požarom oštećenih zidova, armiranobetonskih greda, novokonstruiranih otvora i obnovu oslonaca. Posebna pozornost usmjerena je obnovi valjkastih oslonaca/ležajeva ispunjenih kvarcnim pijeskom upotrijebljenih za provjeru slijeganja zgrade i ispravljanje vertikalnosti. U vrijeme projektiranja i gradnje (1960-tih godina) oslonci/ležajevi predstavljali su jedinstveno rješenje temelja visokih zgrada. Procijenjeno je da je primijenjenim mjerama rekonstrukcije ušteđeno 14 milijuna eura u usporedbi s cijenom rušenja oštećene zgrade i gradnje potpuno nove.

1. INTRODUCTION

Basic structural system of the office building 'Ušće' consisted of central reinforced concrete (RC) core and RC columns which, along with the system of primary and secondary RC beams, made skeleton system. At the time of the structural design, RC core was calculated only for horizontal wind load, while the structure was not tested on seismic load, as there were no regulations to calculate seismic load. This was prior to 1963 Skoplje earthquake. Building façade had thin RC columns (dimensions 20x60cm from I to V floor and 20x50cm from V floor to the building top) at 1,80m distance along the longer, and 1,90m along the shorter side of the building. Floor slab structure with RC ribs (dimension 20/33cm), span 7,40m at each module (1,80m), with a monolithic RC slab, thickness 7cm over it, was between the columns and the core [1]. On the level above the ground floor, façade columns were supported by massive continuous RC beams, span 5,40m which transfer load to ground floor columns. Foundation was carried out on RC slab, thickness of 10cm which transferred vertical load to the ground, while horizontal wind force was transferred via special base with four groups of piles activated by building settling. Special devices for regulating reactions in pile supporters and compensation of consolidation influence were planned for this purpose.

2. STRUCTURAL DAMAGE

The building had been severely damaged by 10-12 projectiles in the spring of 1999. After conducting visual inspection in the year 2002, specification and classification of structural damage has been made. Upon completion of static and seismic calculation, it was concluded that global stability of the building was not endangered [2]. However, local stability of some damaged elements could have been endangered. Therefore, strict technical measures were proposed and carried out before and during the debris clear up procedure. It consisted of special dynamic plan with instructions for necessary temporary support of the structure and its elements.

Due to the lack of relevant data, Final Design could not be carried out immediately. Structural condition could be precisely determined only after completion of the debris clear up (Figure 1). Preliminary works before the clear up implied establishing or renewing the existing measuring points at the level of foundation slab and in the zone of pile group in the basement, characteristic points at perimeter columns and RC core. Geodetic survey was conducted before the clear up to register potential vertical movement of foundation structure and building during the load relief. The measurement points for monitoring total consolidation during the works, and in the latter stage of exploitation were defined simultaneously with building clear up. Special programs for testing the features of concrete, reinforcement and reconstructed structure under test load were designed.

a) b) c)

Figure 1 Building damage: a) Southwest façade; b) Walls and floor slabs; c) Floor slabs, columns and beams.

3. CLEARING UP THE DEBRIS AND RELIEVING THE STRUCTURAL LOAD

Removal of unusable external and internal covering of structural surface, installation and parts of demolished or damaged structural elements was carried out prior to reconstruction commencement. Demolition and removal of the parts of the building were done in accordance with the dynamic plan. Support of the part of RC roof canopy structure and removal of TV tower steel structure were also conducted before the other works. At that time, it was not allowed to perform other works on the building. After the works had been completed, part of roof canopy above XXIV floor and part of floor slab structure above XXIII floor which collapsed after the fall of roof canopy part were removed. Undemolished part of roof canopy above XXIV floor was demolished and removed, as well as RC core of XXV and XXIV floor and the remaining part of the structure above XXIII floor. Demolition of partition walls from XXII floor downwards to IV floor and removal of RC core of XXIII floor were done simultaneously with the above stated works. The IV floor walls were demolished, and then I, II and III floor walls. Due to an unexpected load redistribution, parts of the structure were temporary supported during the demolition and removal of structural parts [3].

The most attractive part of removing debris was the removal of façade cover carried out by alpinist teams. By removing demolished parts of the structure, partition walls, surface coating and installation, the structure was load relieved for approximately 14500 t. This reduced the stress of elements and parts of the structure subjected to stress from demolished or damaged structural elements. Wooden braces were used for relieving façade columns. After being removed, braces returned the designed force. Wooden braces and slope supporters secured stability of façade structure.

a) b) c)

Figure 2 Reconstruction of floor slab structure and beams: a) supporting floor slabs; b) sheathing for slab and beam; c) reinforcement.

The Final Design of structural reconstruction included detailed diagnostics, static and seismic calculation, as well as details of reconstruction interventions. It was elaborated prior, during and after the clear up of the demolished part of the building. Static and seismic calculation of the structure was conducted on spatial calculation model, indicated the necessity for maximum load relief of the structure at all floors, carried out by removing heavy partition walls (>1,5kN/m^2), cement screed, the existing floor (>1,0kN/m^2) and heavy ceilings. Total structure load relief was approximately 18%. Additionally, significant mass of roof canopy (cca. 2000 t at more than 90m height) caused extremely unfavorable influences on seismic force load. Consequently, roof canopy was not reconstructed [4].

The load relief proved favorable, having in mind that during the construction stage the seismic load, the largest among all other horizontal loads, has not been analyzed. The static-dynamic analysis results showed that global stability of the building was not endangered even under the assumption that standard floor was built on XXIV floor instead of demolished roof canopy. Due to the demolition of specific number of structural elements, load was spontaneously redistributed to adjacent elements, which resulted in element overload. This was the case with part of façade columns on I, II and III floor where the remaining load, considered as damaged system, was still present after the clear up. The load, interfered with new influences in reconstructed structure, resulted in increased stress in two columns (one at I and one at II floor). Their stability was not endangered, thus they were not reconstructed.

4. RECONSTRUCTION OF STRUCTURAL ELEMENTS

Having in mind that, depending on the floor, the same types of structural elements were exposed to various influences, from direct impact to fire load, the damage degree and types were different. Various measures, procedures and materials were used for reconstructing the same type of structural elements, depending on their position in the structure, type and degree of damage, as well as the condition of adjacent elements [4].

Demolished floor slab structures (Figure 2) were replaced with new ones of the same type, but with special treatment of the base of façade walls and RC core. In some cases, the existing ribs of floor slab structure were kept, i.e. part of the ribs was constructed again, and the other part was reconstructed. Damaged slabs were removed and new slabs were constructed. Undamaged reinforcement was used for this purpose. Whenever necessary, new reinforcement welded to the existing one, was added. Injecting procedure was used for smaller damages of floor slab structure.

a) b) c)

Figure 3 Reconstruction: a) walls, b) stairs c) façade column.

In terms of damaged façade columns, damaged concrete was removed and reinforcement was returned to design position. New reinforcement was added whenever necessary. Several types of reconstruction procedures were carried out at damaged walls of RC core (Figure 3). Collapsed walls were removed and replaced with new ones. Walls with smaller damages were reinforced (in terms of increasing thickness and additional reinforcement) along several floors. All cracks were injected. Fire damaged walls were reinforced by adding two new walls, thickness of 10cm, on both sides of the existing wall. Such walls were connected by anchoring. Girders in ground floor were reconstructed and reinforced on both sides by RC beams. The existing beam was joined with new girders by means of high-strength bolts (Figure 4). Reinforcement of newly cut openings was shown in Figure 5.

a) b) c)

Figure 4 Reconstruction of RC beam girders: a) concrete-concrete; b) concrete-steel; c) new concrete casting.

a) b) c)

Figure 5 Reinforcement of newly cut openings in RC walls: a) edge - 20 cm; b) edge - 40 cm; c) center - 30 cm.

Special technology for reconstructing XXIII floor included the application of "concrete on concrete composite" in accordance with several variations of architectural functional solutions for reconstructing XXIV and XXV floor. Specificity of structural reconstruction was in the fact that works on debris clear up, detailed diagnostics of structure condition, elaboration of reconstruction project and reconstruction itself were conducted simultaneously under constant professional and designer supervision. Additionally, the function of XXIV and XXV floor was not defined at the time of reconstruction, thus the reconstruction had been completed before the adoption of the final design of XXIV and XXV floor structure. Audit of the Final Design was carried out by the Faculty of Civil Engineering Belgrade and special team of experts from England and Germany.

5. REHABILITATION OF SUPPORTERS

The supporters represented a unique solution for the high-rise building foundation at the time of the design (1960) and construction (1960-1964). The author of the foundation solution is Academician Milan Krstić, Civ. Eng. [5]. In the initial period (1964-1968) 31 cm building settlement has been recorded, while in the period after 1968 to the beginning of reconstruction in 2002, 11cm was observed. Since the reconstruction completion in 2005, any further settlement is not recorded [5].

The final rehabilitation design included replacement of hydraulic installations, hydraulic oil, installation of new valves, and installation of new glycerin manometers on hydraulic pillow blocks above the sand pots in the basement. The rehabilitation works were performed according to the special program. This extremely delicate operation required a full load relief of the existing hydraulic pillow blocks. The forces they receive were temporary accepted by a system of hydraulic presses placed on the foreheads of RC pot walls. The same pressure condition in all four hydraulic pillow blocks has been controlled by precisely measuring gauges, sensitivity of 0.01mm, and glycerin manometers. In this way, the recorded 5cm inclination measured at the structure top, has been eliminated, and the structure was brought back to the vertical position.

The complex supporter rehabilitation intervention was carried out before the construction of XXIV and XXV floor, and commencement of installation and other required indoor works. Such a sequence of rehabilitation and reconstruction works provided for recording growth in total weight of the building structure.


a)


b)


c)

Figure 6 Reconstruction of supporters: a) Structure lifting; b) Hydraulic oil change; c) New glycerine manometers on hydraulic pillow blocks above the sand pots.

6. CONCLUSION

Several aspects of damaged structural parts reconstruction, and returning the high-rise building 'Ušće' in Belgrade in its initial state are shown in the paper. The initial aim of the Investor was the demolition and construction of the new building structure. The reconstruction and rehabilitation alternative resulted in significant savings: reduction of the new RC structure costs, demolition and transportation of debris costs. According to the prices valid at the time, the savings were approximately EUR 14 million. Additionally, the interventions provided structural system ability to accept seismic load up to VIII level of seismicity by MCS scale.

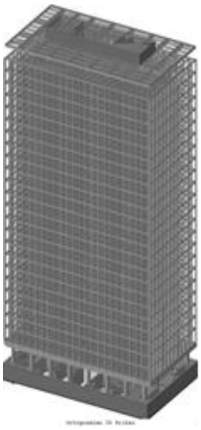
a)

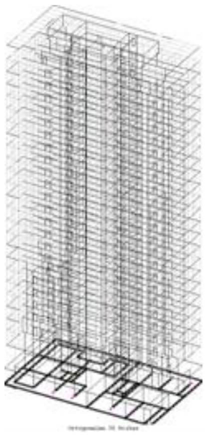
b)

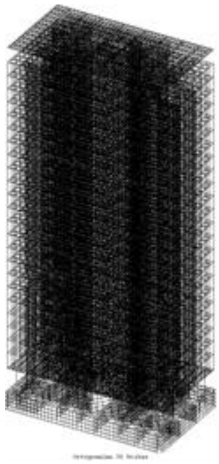
c)

Figure 7 Calculation model of the existing building, isometric schemes: a) Full rendered model; b) Wire model; c) Finite elements model.


a)


b)

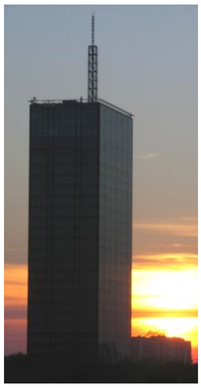
c)

Figure 8 a) Final calculation model; b) Completed building after the reconstruction – Southwest façade; c) Completed building after the reconstruction – Northeast façade

The introduction of modern, light materials reduced the building weight, thus construction of two more floors on the building top was enabled. The elements-supporters with specific foundation solution were returned to their initial state and equipped for monitoring eventual uneven settlement. The building is brought back in its vertical position during the supporter rehabilitation intervention. The building has been under constant monitoring since the reconstruction completion in 2005, and has not shown any new damage or further settlement.

ACKNOWLEDGEMENT

The authors are members of Belgrade business center 'Ušće' rehabilitation, reconstruction, adaptation and rebuilding design team, led by the late Prof. dr Ljubomir Vlajić. In the year 2006, the team received biannual prize for the best structural solution in 2004/2005 awarded by Yugoslav association of constructors.

REFERENCES:

[1] Vlajić, Lj.; Srećković, G.; Blagojević, P.: Selected characteristic structural rehabilitation problems of Business Center ''Ušće'' (Odabrani karakteristični problemi sanacije konstrukcije PC ''Ušće''), Simposia dedicated to life and work of the Academician Đorđe Lazarević, Proceedings, Surdulica 2003. Materials and Structures, pg. 203-213.

[2] Vlajić, Lj.; Blagojević, P; Grković, S.: Rehabilitation, reconstruction, adaptation and rebuilding of Belgrade Business Center "UŠĆE" after 1999 bombing (Sanacija rekonstrukcija, adaptacija i dogradnja konstrukcije poslovnog centra "UŠĆE" na Novom Beogradu posle bombardovanja 1999), Uvodna izlaganja. Knjiga 1, JDGK 12. Kongres, Vrnjacka Banja, 27-29. Septembar 2006. Str. 15-28

[3] Vlajić, Lj.; Blagojević, P.; Grković, S.; Romanić, M.: Rehabilitation, reconstruction, adaptation and rebuilding of Belgrade Business Center "UŠĆE" (Sanacija rekonstrukcija, adaptacija i dogradnja konstrukcije poslovnog centra "UŠĆE" na Novom Beogradu), Faculty of Civil Engineering in Subotica proceedings No. 13/2005., pg. 191-203.

[4] Vlajić, Lj.; Blagojević, P.; Grković, S.; Romanić, M.: Reconstruction of the business Center 'UŠĆE' reinforced concrete structure (Sanacija armiranobetonske konstrukcije poslovnog centra "UŠĆE" na Novom Beogradu), Nauka i praksa 8/2005, Faculty of Civil Engineering and Architecture in Niš, Niš. 2005

[5] Vlajić, Lj.; Grković, S.; Blagojević, P.; Romanić, M.: *Business Center 'UŠĆE' from ruin to the palace (Poslovni centar ''UŠĆE'' od ruševine do palate),* IV naučno-stručni skup Contemporary Achievement in Civil Engineering, Banja Luka, April 2008, pg. 221-239.

REHABILITATION PROJECT OF ATELIER MESTROVIC

Dean Cizmar[1], Drazen Arbutina1, Dalibor Mackic[2], Helena Alfirevic Arbutina[3]

[1] Zagreb University of Applied Sciences, Study in Civil Engineering, Vrbik 8, 10 000 Zagreb, Croatia,
e-mail: dcizmar@tvz.hr, darbutina@tvz.hr
[2] Darma usluge d.o.o., Vlaska 125, 10000 Zagreb, Croatia, e-mail: darmausluge@gmail.com
[3] HD Spatium d.o.o., Kasinci 17, 10257 Zagreb, Croatia, e-mail: hdspatium@gmail.com

SUMMARY: Paper will present basic elements within historical development of Atelier Meštrović and present procedures for architectural survey, architectural project and structural project. The presentation will describe architectural, structural and conservation procedures of design for conversion and adaptation of existing non-functional attic. Details of structural project (new steel story structure above existing timber structure and structural design of timber roof structure) are presented. In the end of article, conclusion about special demands and challenges present during design of cultural heritage structures is given.

SANACIJA KONSTRUKCIJE ATELIERA MEŠTROVIĆ

SAŽETAK: U radu će se ukratko opisati povijest današnjeg muzeja Atelier Meštrović i niz učinjenih ili potrebnih rekonstrukcija te način izrade arhitektonske snimke, arhitektonski projekt te projekt sanacije konstrukcije. U radu se prezentiraju zahvati planirani za potrebe prenamjene i adaptacije postojećih nefunkcionalnih tavanskih prostora, za potrebe kojih je izrađeno idejno arhitektonsko rješenje. Detalji projekta konstrukcije (nova čelična međukatna konstrukcija iznad postojeće drvene konstrukcije te proračun drvene krovne konstrukcije) su prikazani. Na kraju rada dan je zaključak vezan uz osobitosti te izazove koji su prisutni prilikom projektiranja objekata kulturne baštine.

1. UVOD

Povijest današnjeg muzeja Atelier Meštović započinje dvadesetih godina prošlog stoljeća, tj. od 1920. godine, kad poznati kipar Ivan Meštrović kupuje tri čestice u Mletačkoj 6, 8 i 10 u Zagrebu. Na kupljenim česticama zatiče postojeće građevine, od kojih je neke uklonio, dok su neke integrirane u sklop koji i danas u nešto promijenjenom obliku postoji i kao muzejska institucija djeluje na jednoj polovici nekadašnjeg inicijalnog zahvata. Prve urudžbene projekte buduće rezidencije i atelijera Ivana Meštrovića u Zagrebu potpisuje arhitekt Viktor Kovačić i u njima su zacrtani ključni elementi buduće dispozicije cijeloga sklopa, dok se na kasnijim nalaze potpisi graditelja Josipa Žanka (1923.) i ing. Josipa Aljinovića (1924.), dok je prilikom realizacije na poslu angažiran i graditelj Stjepan Uršić. Prve značajnije zahvate na rekonstrukciji inicijalne ideje sklop je pretrpio tijekom izvođenja samih radova, kada se nakon razvoda Ivana Meštrovića od njegove prve supruge dio sklopa i fizički odvaja, te se ostatak reorganizira sukladno novonastaloj situaciji, gdje je jedna od prilagodbi bila i izvođenje ulaznog portala iz Mletačke ulice po projektu Drage Iblera (1925.). Ta je dispozicija u načelu danas sačuvana i ona prati glavni ulaz preko atrija iz Mletačke ulice, te zid u vrtu kojim je pregrađen zahvat i u vanjskom dijelu svoga obuhvata. Naredni izniman impuls promjenama na sklopu predstavlja ugovor o darivanju potpisan 31. siječnja 1952. godine hrvatskom narodu uz brojne umjetnine daruje kuće i atelijere u Zagrebu i Splitu, te kompleks Kaštelet-Crikvine u Splitu i mauzolej u Otavicama. Nakon toga darovnog ugovora 1961. godine započinju radovi na izradi projekta rekonstrukcije i prilagodbe prostora u Zagrebu za budući muzejski postav. Inicijalni projektni tim na uređenju same zgrade atelijera i vrta uključio je uz arhitekta Miroslava Begovića i arhitekticu Melitu Viličić, gdje je temeljem Begovićeva projekta (iz 1961. godine) izvedena od 1962. do 1963. rekonstrukcija zgrade atelijera i vrta unutar sklopa, kojom je značajno promijenjena autentičnost nekadašnjeg Meštrovićeva radnog i životnog prostora. Projektom je zatvorena direktna veza kuće i atelijera, promijenjen karakter prozorskih otvora i vrata prema vrtu, a u interijer atelijera je interpolirana konstruktivno specifična galerija na armiranobetonskoj i/ili čeličnoj konstrukciji, te sagrađeno stubište prema galeriji i prostoru tavana. Radovi na sklopu nastavljeni su rekonstrukcijom stambenog dijela prema projektima arhitekta Vojtjeha Delfina i realizirani tijekom 1968 i 1969. godine. Raketiranje Banskih dvora i tada i dijelova sklopa atelijera Meštrović 07. listopada 1991. godine, tj. tijekom Domovinskog rata, iniciralo je narednu značajnu intervenciju na sklopu koja je obnovom oštećenih dijelova i uličnih pročelja završila 1992. godine [2]. Tijekom 2013. godine uređen je podrumski depo ispod ateliera, kao zadnja značajnija aktivnost na cijelom sklopu. Rad će prikazati način izrade arhitektonske snimke, arhitektonski projekt te projekt sanacije konstrukcije iz prosinaca 2015. godine koju su izradili stručnjaci s Tehničkog veleučilišta u Zagrebu. Sukladno zahtjevima investitora napravljen je proračun krovne te međukatne konstrukcije. Rad će na primjeru specifičnog zaštićenog kulturnog dobra prezentirati zahvat karakteriziran primjenom konzervatorskih principa koji uvjetuju precizno dokumentiranje, prilagodbu projektnog zadatka, analizu temeljnih zahvata i mogućnost njihova ispunjavanja, te posebice princip reverzibilnosti ili repetitivnosti odabrane metode za intervenciju na graditeljskoj baštini.

2. KONZERVATORSKI PRINCIPI I IDEJNO RJEŠENJE ZAHVATA

Tijekom zadnjih desetljeća razvoj muzeološke djelatnosti i specifične potrebe rada Muzeja Ivana Meštrovića utjecali su na iniciranje nužnih aktivnosti na planiranju i projektiranju potencijalnih zahvata rekonstrukcije sklopa ateliera Meštrović i njegove prilagodbe suvremenim potrebama. Kao inicijalna stavka svake od projektnih aktivnosti na rekonstrukciji postojećih građevina je i konzultacija postojećih projekata kao dokumentacije koja jest jedan od uvjeta zaštite kulturnih dobara, posebice nepokretnih dobara, tj. graditeljskog naslijeđa. Nažalost, u arhivima i u samom Muzeju nije sačuvana izvorna dokumentacija zadnjih zahvata (čak niti onih iz devedesetih godina XX. stoljeća, tako da se uz prikupljanje arhivskih listova pojedinih urudžbenih projekta iz dvadesetih godina XX. stoljeća, te skica zahvata iz šezdesetih godina XX. stoljeća, trebalo kao bazičnoj aktivnosti pristupiti dokumentiranju zatečenog stanja. Zahvata na izradi arhitektonske snimke tako je inicijalni posao koji je prethodio izradi idejnih rješenja arhitekture i konstrukcije, a proveden je klasičnim analognim metodama uz provjeru pojedinačnih mjera triangulacijom na višebrojnim uzorcima geometrije snimanog sklopa. Priređene podloge tako su postale osnova za izradu arhitektonskog idejnog rješenja rekonstrukcije prostora unutar atelijera i provjere mogućnosti da se unutar zatečene strukture implementiraju određene funkcije, tj. interpoliraju dijelovi konstruktivnih elemenata koji bi te funkcije trebali omogućiti. Principi kojima su bile vođene sve aktivnosti trebaju osigurati zaštitu i produljenje egzistencije oblika, tj. forme, ali i supstance, tj. materijala i konstrukcija u obliku koji je izvorni ili se od izvornoga najmanje razlikuje [1]. Pri tome se treba voditi za idejom zaštite percepcije sklopa kao cjeline koja ima svoje izvorne karakteristike i koje se trebaju čuvati, tj. ne mijenjati ako je to ikako moguće. Prilikom planiranja i projektiranja aktivnosti na baštini, tj atelijeru Meštrović u ovome slučaju, stoga se vodilo brigu o djelovanju sukladno smjernicama koje uključuju precizno i detaljno dokumentiranje, suzdržavanje od prekomjernih intervencija, te primjenu zahvata koji trebaju osigurati poštivanje estetskog, povijesnog i materijalnog integriteta baštine primjenom minimalnih reverzibilnih ili repetitivnih zahvata [1]. Prva smjernica nalaže da se stanje zgrade ili sklopa mora detaljno snimiti prije početka bilo kakove intervencije, gdje je arhitektonska snimka u ovome slučaju ne samo dokument o stanju kulturnog dobra, već i realna podloga za projektiranje, te da bez nje arhitektonski projekt i projekt konstrukcije nije moguće kvalitetno realizirati. Druga smjernica govori o tome da se materijali i postupci korišteni prilikom zahvata zaštite moraju također dokumentirati, gdje je detaljan projekt jedan od načina, no prema istom se tada mora u potpunosti i izvesti radove, ili iste naknadno dokumentirati. Prilikom projektiranja zahvata vodilo se načelom da povijesni slojevi ili elementi ne smiju biti uništeni ili uklonjeni, tj. demontirani, promijenjeni i u konačnici falsificirani, što je uvjetovalo da se prilikom izrade projekata vodilo računa o zadržavanju postojećih materijala i konstrukcija u maksimalnoj mjeri. No zahvat je trebao osigurati ispunjavanje i suvremenih temeljenih zahtjeva za građevinu, gdje njihovi uvjeti predstavljaju polazno rješenje prema kojemu se određuje projektantski pristup. Unatoč takvoj zadaći projekt je trebao osigurati i da da svaka intervencija bude minimalno potrebna, kako se izvorna struktura ne bi mijenjala u značajnijom mjeri, a ako se i mijenja tada zahvati na promjeni trebaju biti reverzibilni ili barem repetitivni. Projektirani zahvat tako treba uključiti materijale, konstrukcije, tehniku i tehnologiju koja se eventualno u budućnosti može ukloniti bez većih i značajnijih posljedica za izvornu građevinu, tj. da se građevina može reverzibilnim postupkom vratiti u stanje prije pokretanja zahvata. Isto je potrebno osigurati i ako se koriste materijali, konstrukcije, tehnike ili tehnologije koji da bi osigurali ispunjenje potrebnih minimalnih temeljenih zahtjeva trebaju biti repetitivnom aplicirani na zgradu koja je predmetom zahvata. Tako je inicijalnim projektom predviđena interpolacija novih sadržaja u prostor potkrovlja muzeja, gdje bi se izmjestile radne prostorije i biblioteka nužna za djelovanje muzejskih kustosa, no tako da se zadržava postojeća konstrukcija krovišta, gdje se između pojedinih krovnih nosača organiziraju pojedinačni radni prostori, a biblioteka uređuje iznad nosivog zabatnog zida i sve položeno na novu nosivu stropnu konstrukciju koja u potpunosti preuzima opterećenja novih funkcija unutar prostora. Nosiva stropna konstrukcija projektirana je tako da se može implementirati kao reverzibilna čelična struktura, kao interpolacija između postojećih drvenih nosivih elemenata, a na koju bi se aplicirale sve ostale nužne tehničke mjere koje zahtjeva zaštita od požara kao jedan od temeljenih zahtjeva.

3. MEĐUKATNA KONSTRUKCIJA

Za potrebe korištenja tavanskog prostora izvest će se nova čelična međukatna konstrukcija iznad postojeće drvene konstrukcije koja je pretrpjela znatne deformacije nosivih elemenata i ne zadovoljava uvjete nosivosti i uporabljivosti prema važećim normama. Tlocrtne dimenzije su 9,70x8,70m [3,4]. Nosiva konstrukcija predviđena je od glavnih i sekundarnih nosača; glavne nosače čine rešetkasti nosači a sekundarne horizontalni profili postavljeni poprečno na glavne nosače. Sukladno zahtjevu konzervatora potrebno je uklopiti novu međukatnu konstrukciju u postojeću drvenu odnosno projektni zadatak je izvesti konstrukciju maksimalne visine h=30cm. Nosiva konstrukcija odnosno glavni nosači, oslanjat će se na postojeće zidane zidove preko armiranobetonskog „oslonca“; sekundarni nosači se izvode poprečno na glavne (poravnate gornje pojasnice) prema proračunu. Navedenim oslanjanjem su preuzete sve horizontalne sile i dodatno je ukrućena drvena uzdužna greda klasične jednostrešne krovne konstrukcije. Rešetkasti nosači se postavljaju obostrano uz drvene uzdužne grede u polju, dok se uz rubne drvene grede postavlja po jedan rešetkasti nosač. Rešetkasti nosači postavljeni obostrano međusobno su povezani (gornja i donja pojasnica) s vijcima čime se povećava stabilnost nosača i nove prostorne konstrukcije. Ovim rješenjem se također dodatno bočno ukrućuju drvene grede krovišta jer im je onemogućeno bočno izvijanje [3].

Slika 1 Vizualizacija idejnog rješenja arhitektonskog projekta, kao moguće organizacije novog radnog prostora u tavanu atelijera. Vidljiva je podjela na tri radne zone i organizaciju biblioteke na južnom zabatnom zidu (prema zgradi Ustavnog suda)
[4].

Slika 2 Pogled na glavni nosač u polju međukatne drvene konstrukcije

Slika 3 Pogled na glavni nosač uz ležaj međukatne drvene konstrukcije

Čelične elemente glavnog rešetkastog nosača čine profili SH 80x80x4mm - gornja pojasnica, SH 60x60x4mm - ispuna i SH 100x100x8mm. Ukupno je predviđeno 6 glavnih nosača. Nosači su postavljeni na osnom razmaku e=2.90-3.00m (polje). Čelične elemente sekundarnih nosača čine UPN 140 profili, postavljeni na međusobnom razmaku e=1.00m. Čelični elementi se spajaju varenjem; sidrenje glavnih nosača će se izvesti preko čeličnih podložnih ploča koje će se ankerirati u novi armiranobetonski oslonac (ukupno će se izvesti 12 novih AB oslonaca lokalno na vrhu nosive zidane vertikalne konstrukcije). Čelična međukatna konstrukcija će se postaviti s gornje strane postojeće drvene konstrukcije i statički odvojena od iste. Nova međukatna konstrukcija će biti vizualno skrivena prema zahtjevu konzervatora odnosno ista se neće moći vidjeti u podgledu. Na predmetnu konstrukciju postavit će se slojevi poda prema arhitektonskom rješenju.

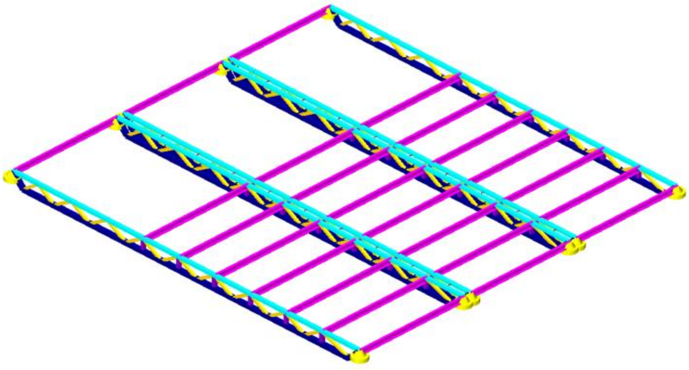

Slika 4 3D prikaz nove čelične međukatne konstrukcije

4. KROVNA KONSTRUKCIJA

Za potrebe povećanja toplinske zaštite i uporabe tavanskog prostora proveden je proračun drvene krovne konstrukcija, jednostrešno krovište s visuljom, tlocrtnih dimenzija cca 11,90x11,00m maksimalne visine 5,65m. Nosivu konstrukciju čine rogovi koji se preko podrožnica oslanjaju na konstrukciju visulje s kosnicima dimenzija. Podrožnice su dodatno ojačane rukama; a prostorno je sustav ukrućen dvostrukim pajantama. Proračunom je dokazano kako određeni elementi krovne konstrukcije ne zadovoljavaju i iste je potrebno zamijeniti s novim.

Slika 5 Pogled na kosnik drvene krovne konstrukcije

Slika 6 Pogled na uvalu krovne konstrukcije

Slika 7 Pogled na rogove

Slika 8 Krovna stabilizacija rogova i stupova

Slika 9 Visulja i uzdužne grede krovne konstrukcije

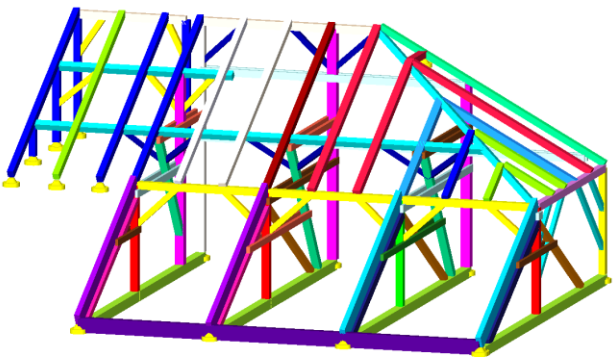

Slika 10 3D model krovne konstrukcije

5. ZAKLJUČAK

Prilikom projektiranja izazov dokumentiranja i prilagodbe novoj funkciji nije samo manifestacija principa, već i demonstracija inženjerskih mogućnosti koje su u ovom slučaju uvjetovane lokacijom, stupnjem zaštite, ali i principima i potrebama očuvanja kulturnog dobra s jedne strane, te temeljenih zahtjeva za građevine s druge strane. Cilj ovog rada je pokazati da se s minimalnim i relativno neinvazivnim zahvatom mogu osigurati moderni zahtjevi investitora a s druge strane u potpunosti zadovoljiti stroge norme u građevinarstvu. Inicijalni projekt arhitekture postavio je zadaće, a konzervatorski principi ograničenja, dok su dodatne uvjete naložili smještaj i mogućnosti realizacije potencijalnog zahvata. Stoga su projektom predviđena rješenja konstrukcije odgovorila na potrebe osiguranja mehaničke otpornosti i stabilnosti, ali i reverzibilnosti nakon eventualne odluke da navedena funkcija i poradi njena ugrađena konstrukcija neće više biti zadovoljavajuće rješenje.

LITERATURA

[1] Arbutina, D.; Dunović, Č.; Alfirević Arbutina, H.: Modern Materials in the Protection of Building Heritage, Proceedings of 11th International Conference Organization, Technology and Management in Construction; Burcar Dunović, I.; Mlinarić, V.; Završki, I. (ur.), pp. 008-018; ISBN 9789537686048 9537686043; 28-30 September, 2013.; Dubrovnik, University of Zagreb, Faculty of Civil Engineering/ Croatian Association for Organization in Construction , Zagreb (2013.)

[2] Plazibat, D.; Od doma do muzeja = From home to museum : Ivan Meštrović u Zagrebu = Ivan Meštrović in Zagreb, Fundacija Ivana Meštrovića, ISBN 9539695678, Zagreb (2004.)

[3] Čizmar, D.; Arbutina, D., Mačkić, D., Arbutina, H.: Projekt sanacije konstrukcija Ateliera Meštrović, 11 Dani ovlaštenih inženjera građevinarstva, Opatija, 2016.

[4] Arbutina, D., Arbutina, H., Arhitektonsk idejno o ješenje rekonstrukcije ateliera Meštrović, Zagreb, 2015.

RECONSTRUCTION OF THE MUNICIPAL COURT, NATIONAL MONUMENT BUILDING IN MOSTAR

Merima Sahinagic-Isovic[1], Marko Cecez[1]

[1] Dzemal Bijedic, University of Mostar, Faculty of Civil Engineering, Sjeverni logor bb, 88 000 Mostar, Bosnia and Hezegovina, email: merima.sahinagic@unmo.ba, marko.cecez@unmo.ba

SUMMARY: The reconstruction of cultural-historical buildings and national monument buildings devastated during the war is still a current issue in Bosnia and Herzegovina. Majority of these buildings are masonry constructions, whose reconstruction should be given special attention. The devastation of these buildings is deepened by weathering in the last 25 years. The range and type of intervention must be balanced in order to achieve the required level of security. The building of the Municipal Court in Mostar is located in central part of Mostar and it was built in 1909. Due to its significance it was declared as a national monument building. During the war, the building was damaged, and in 2012 project documentation for its reconstruction was prepared. In the paper assessment of buildings' current condition, as well as proposed measures of reconstruction will be presented.

REKONSTRUKCIJA OPĆINSKOGA SUDA, NACIONALNOG SPOMENIKA U MOSTARU

SAŽETAK: U Bosni i Hercegovini još je uvijek aktualno pitanje rekonstrukcije kulturno-povijesnih zgrada i zgrada nacionalne baštine opustošenih tijekom rata. Većina tih zgrada su zidane gradnje čijoj rekonstrukciji treba posvetiti posebnu pažnju. Devastacija tih zgrada produbila se posljednjih 25 godina djelovanjem atmosferilija. Da bi se postigla zahtijevana razina sigurnosti, moraju biti uravnoteženi obujam i vrsta zahvata. Zgrada Općinskoga suda u Mostaru nalazi se u središnjem dijelu Mostara, a izgrađena je 1909. Zbog svojeg značenja proglašena je zgradom nacionalne baštine. Tijekom rata zgrada je oštećena, a 2012. izrađen je projekt njezine rekonstrukcije. U radu je prikazana ocjena sadašnjega stanja zgrade, a predložene su i mjere rekonstrukcije.

1. INTRODUCTION

The building of Municipal Court in Mostar was originally built as Primary school during the Austro-Hungarian administration in Bosnia and Herzegovina. It is located in the central part of Mostar. Construction was finished in 1909, and first it was used as Serbian Primary school, and after 1938 it was known as 4th Primary school in Mostar [1]. During the war in 1992-1995, the building suffered severe damage, and it remained in that condition, unprotected for weathering actions, until its reconstruction in 2014. By the decision of Commission for Preservation of National Monuments in Bosnia and Herzegovina, related to historic urban area of Mostar, the building of Serbian Primary school was declared a national monument building and it was prescribed the first level of protection [1].

Figure 1 The building of Primary school in Mostar (1938)

2. ARCHITECTURE AND ORIGINAL CONDITION

The building is consisted of two parts (Figure 2). The first part (dio I) is facing north and east, and it is original building from 1909. The second part (dio 2) was added in the south part of the building in 1938 and it is facing east. In total east façade is 52,50 m, and north façade is 32,00 m, with average width of first part 12,50 m and second part 17,50 m. Parts are separated by 5 cm dilatation [1].

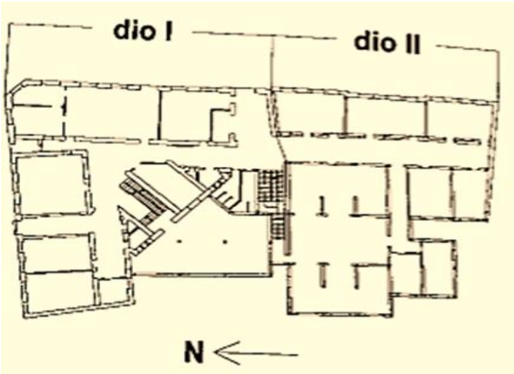

Figure 2 Layout of the building [1]

Both parts of the building have basement, ground floor, first floor and attic. The facades were richly ornamented by friezes with stone ornaments, and windows had characteristic Austro-Hungarian motifs.

First part of the building (Figure 3) is construction with stone block walls. Floor constructions were built with steel beams and shallow concrete arches, and reinforced concrete beams and slabs in the basement and ground floor, and wooden beams and boards on the first floor.

Second part of the building (Figure 3) has reinforced concrete walls in the basement and stone walls in the rest of the building on east and south side, while west side had semi-prefabricated concrete and slag-concrete walls, with reinforced concrete slabs in the basement and ground floor, and wooden beams and boards on the first floor. Vertical communication is achieved with two inner stairways located in the first part, which are composed of steel beams and stone marble stairs. The roof was wooden construction with ordinary tiles.

Figure 3 First part (left) and the second part (right) of the building [1]

3. BUILDING DIAGNOSTICS

Proper and accurate assessment is a vital basis for successful repair of construction exposed to destruction and degradation processes. Within assessment of the current construction it is necessary to respect the general methodology that includes [2]:

- Gathering the existing project documentation
- Inspection, tests and calculations
- The decision on further actions

The simplest way to gather information about any building is to inspect existing project documentation. But, usually for national monument and cultural-historical buildings, project documentation does not exist. For this building project documentation was completely destroyed during the war. Thus, new drawings were made based on measurement and geometry of the structure.

3.1. VISUAL INSPECTION

Visual inspection is usually used for detail inspection of the construction in terms of crack formations, moisture occurrence, construction deformations etc. [2]. But, when construction is totally devastated, visual inspection should provide data for condition of remaining parts of the construction.

3.1.1. GEOMETRY OF THE CONSTRUCTION

Dimensions of the first part of the building are cca 27,00 m east side, cca 32,00 m north side, with average width of 12,50 m. Total height of the building is 15,50 m. All bearing walls are made of stone blocks, 65 cm thick. Two types of stone were used, both local, miljevina and tenelija. Stone tenelija is known as the stone used for construction of famous Old Bridge in Mostar. Both type of stones were used for all the walls.

Second part of the building has average width of 17,50 m, dimension of the east side is 25,50 m and west side 26,50 m with the same height as the first part. Bearing walls in the basement are reinforced concrete walls, 35 cm thick. On the ground floor and first floor west bearing walls are semi-prefabricated concrete and slag-concrete walls 35 cm thick, but east and south walls are stone block walls, 65 cm thick. Building has stone foundations, 60 cm thick, with average depth of 60 cm.

3.1.2. DESCRIPTION OF CONSTRUCTION DAMAGE

Stone walls in both parts of the building on the ground and first floor were relatively in good condition, except the obvious damage from the shrapnel and some local damages. Stones covered with mortar had significantly less damage. Due to long term exposure to weathering actions, stone blocks at the top of the building suffered more serious damage and they need to be replaced (Figure 4). Noticeable was surface wear, cracks, flaking and chipping on some stones. Fugues are very good filled with mortar, with no obvious gaps. On all walls biological damage was noticed in the form of plants. Also black and brown stains were visible, which indicate algae growth and fire residue. In the second part, semi-prefabricated walls had notable damage, in form of detached parts and gaps.

Floor slabs of wooden beams and boards were completely destroyed. In the places where the wooden beams were settled were dents in the walls. In every third dent, steel anchor was visible and all of them were corroded. Floor slabs of steel beams and shallow concrete arches in the first part of the building are not damaged directly, but steel beams are corroded and need to be rehabilitated. In the second part, reinforced concrete slabs did not suffered notable damage.

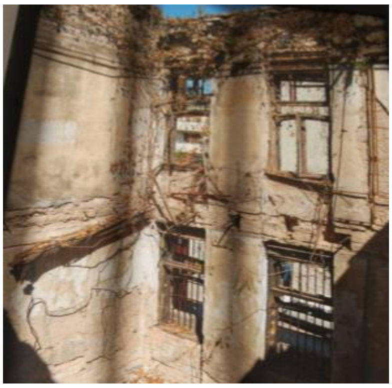

Figure 4 Condition of bearing stone walls

Both stairways were damaged in some degree (Figure 5). One stairway was completely destroyed, and other had corroded steel beams and some stone stairs damaged. Wooden roof construction was completely destroyed, as well as most of the attic and cornice. All windows were destroyed, and practically all façade ornaments and they all need to be replaced.

Figure 5 Damaged stairway in the first part of the building

3.2. TESTING OF MATERIALS AND CONSTRUCTION

Before any decision on further reconstruction measures, used stone tenelija and miljevina needed to be examined, as well as walls itself and foundations.

Both type of stones were used for the walls and they were “mixed up” inside the wall, so decision on stone type had to be made in situ by close inspection. They are limstones according to the origin. Stone miljevina is a bit "finer" and "smoother grain", while stone tenelija is "rougher" and "coarse grain", and slightly lighter than miljevina. The following laboratory tests were performed: density and specific gravity, compressive strength (in dry and water saturated state), water absorption, porosity. In total 30 samples of each type of stone was taken. Samples were cut down from irregular shape to cubes 5x5x5 cm. 15 samples were used for compressive strength in dry state, and 15 for compressive strength in water saturated state for both types of stones. Laboratory tests were performed in accordance to JUS standards [3, 4]. Results are presented in Table 1.

Table 1 Results of laboratory test for stones temelija and miljevina

Stone type	Density (kg/m^3)	Specific gravity (kg/m^3)	Compressive strength (dry) (MPa)	Compressive strength (saturated) (MPa)	Porosity (%)	Water absorption (%)
Tenelija	1965	2620	24,6	18,5	26,6	11,8
Miljevina	1792	2415	17,5	12,5	24,4	17,4

Both stone types were also subjected to frost, and they are not resistant to frost action. After the laboratory tests, some conclusions can be made. Both type of stones has high percentage of porosity which means high water absorption. That was expected for this type of limestones. Results of compressive strength are slightly lower than expected. For tenelija dry compressive strength is expected about 30 MPa, and for miljevina about 20 MPa [5].

Within geotechnical survey investigative work was conducted. Two drill holes were made in the buildings' courtyard in the south of the first part of the building, and two drill holes were made on the east edge of the second part. Laboratory tests have shown that soil beneath the building is mostly sandy gravel and low to mid-bound conglomerate. After the initial calculation with assumed static and dynamic loads, results indicate only 1 cm of foundation deflection, and 10 times greater allowable load. In conclusion the soil and existing foundations have sufficient load capacity for buildings' reconstruction.

4. FEEDBACK AND DECISION ON FURTHER ACTION

When the reconstruction of the building for the Municipal court was planned, it was obvious that first and second part needed to be considered as separate. New purpose of the building requires different layout of the rooms, which needs to be considered. For the first part of the building following actions are recommended [6]:

- Existing stone walls are recommended to be kept in original condition, except the walls in the attic. These walls will be dismantled and re-built. Damaged and deteriorated stone blocks will be discarded, and others will be cleaned and re-used. All newly acquired stones needs to be of the same type and quality as existing stones. This step is important due to significance of the building in terms of National monument title. Where needed, reinforced concrete cerclage can be built.
- Due to diverse weathering and physical damage, all stone walls will be rehabilitated with shotcrete and reinforcement bar and anchors (4 anchors per m2). For that reason, all fugues of the existing walls will be detail cleaned and deepen to a depth of 5 cm. Minimum thickness of shotcrete is recommended 4 cm.
- All slabs will be re-built. For the floor construction of steel beams and shallow concrete arches, concrete arches will be demolished, and new arches will be built, but steel beams can be kept with rehabilitation, with addition of new steel beams where needed. All other slabs will be demolished and new reinforced concrete slabs will be built. For the floor construction of attic, steel beams and semi-prefabricated floor structure is recommended.
- In the place of demolished stairway, new reinforced concrete stairway is recommended. The existing damaged stairway will be strengthen with steel beams, and damaged steps will be replaced with stone of the same quality.

For the second part of the building following actions are recommended:

- Stone walls will be treated as in the first part of the building.
- Semi-prefabricated wall on the west side will be demolished and replaced with new brick wall 30 cm thick.
- All slabs, except the floor construction of the ground floor will be demolished and replaced with reinforced concrete slabs. Slab on the ground floor is kept due to possible disturbance of stone wall stability, if demolished. Ground floor construction will be strengthened with steel beams.

As the roof construction was completely destroyed, new roof needs to be constructed regarding the buildings' new application.

5. CONCLUSIONS

A large number of devastated and partly destroyed buildings during the war, from the Ottoman and Austro-Hungarian period still exist in the Bosnia and Herzegovina. They all are mostly masonry buildings, built with local types of stones. For the region of Mostar, most used types were tenelija and miljevina. All these buildings are going to be rehabilitated one way or another in the future. Thus, it would be very useful to create data base that would contain information about previously rehabilitated buildings in terms of laboratory tests of stone, damage extent, the condition of walls etc.

As it can be seen, stone blocks used for this type of buildings, left unprotected to weathering actions for more than 20 years, they will show decrease in physical and mechanical properties. Regarding that fact, every building needs to be carefully examined, and reconstruction is to be planned individually for every building.

REFERENCES

[1] Tufek, A.: Methodology of restoration of masonry structures after the war, Master thesis, "Džemal Bijedić" University of Mostar, Faculty of Civil Engineering, (2016).

[2] Radić, J.: Trajnost konstrukcija I (Construction durability I), University of Zagreb, ISBN 978-953-169-213-7, Zagreb, (2010).

[3] JUS B.B8.002 - Natural stone - Tests for frost action - The indirect method with a solution of sodium sulfate

[4] JUS B.B8.012 - Natural stone. Testing of compressive strength

[5] Bilopavlović, V., Pekić, S., Šaravanja, K.: Petrographic and physical and mechanical properties testing of tenelija and miljevina stones, e-Proceedings of University of Mostar, Vol 6, (2013), pp 104 – 111.

[6] Čaušević A., Rustempašić N.: Reconstruction of masonry buildings (Rekonstrukcije zidanih objekata visokogradnje), University of Sarajevo, Faculty of Architecture, ISBN 978-9958-691-33-1, Sarajevo (2014).

CEMENT-FREE MORTAR FOR REFURBISHMENT OF OLD AND HISTORICAL BUILDINGS - ADVANCED TECHNOLOGY FOR SUSTAINABLE CONSTRUCTION

Andrea Nicoletti[1], Alessandro Dal Bo[1]

[1] BASF CC ITALIA, Via Vicinale delle Corti, 21 - 31100 TREVISO, Italy,
email: andrea.nicoletti@basf.com, alessandro.dal-bo@basf.com

SUMMARY: The restoration of masonry structures, both residential and heritage buildings, is always related to the problem of the techniques and materials to be used to improve from one side the mechanical/structural behavior of the structure respecting the original way of building, on the other side to reach an higher quality of living. Moreover, in particular in the last decade, the request of improving the seismic behavior of masonry is a frequent request. It appears clear that masonry's restoration is an interdisciplinary field, which involves engineers, architects, expert of art/heritage, chemists and materials experts. As part of the refurbishment's approach, and based on the millennial traditions of our territories, BASF CC offers MasterEmaco product's line (formerly know as ALBARIA), which includes all products lime based and cement free, in order to ensure the maximum compatibility with the existing structures. Lime has many properties which have made it a green material, and it do not contain nor release toxic or hazardous substances (and often it reacts to extract them from the environment). Furthermore our products ensure the highest breathability of the walls and comfortable and salubrious conditions; they are also durable materials with excellent adhesion and compatibility with the substrate. From the ecological point of view, in our MasterEmaco products for masonry, the use of traditional binders (metakaolin, natural hydraulic lime) combined with recycled raw materials and natural sand, ensure a low energy consumption and CO2 emissions. In other words with MasterEmaco products, it is possible to repair masonry with cement free products, with high performances and durability in a really sustainable way.

MORT BEZ CEMENTA ZA OBNOVU STARIH I POVIJESNIH ZGRADA – NAPREDNA TEHNOLOGIJA ZA ODRŽIVU GRADNJU

SAŽETAK: Restauracija zidanih konstrukcija, stambenih zgrada i zgrada baštine uvijek je povezana s problemom tehnika i materijala koje treba upotrijebiti za poboljšanje mehaničko-konstrukcijskog ponašanja konstrukcije poštujući izvorni način gradnje i postignuće više kvaliteta življenja. Štoviše, posebno u posljednjem desetljeću, čest je zahtjev za poboljšanjem seizmičkoga ponašanja ziđa. Jasno je da je restauracija ziđa interdisciplinarna zadaća koja uključuje inženjere, arhitekte, stručnjake za umjetnost i baštinu, kemičare i stručnjake za materijale. Kao dio svog obnoviteljskog pristupa i na osnovi tisućljetne tradicije na našem teritoriju, BASF CC nudi liniju proizvoda MasterEmaco (ranije poznatu pod nazivom ALBARIA) koja obuhvaća sve proizvode na osnovi vapna i bez cementa kako bi se osigurala maksimalna spojivost s postojećim konstrukcijama. Vapno ima mnoga svojstva koja ga čine zelenim materijalom i ne sadržava ni otpušta otrovne ili opasne tvari (a često reagira tako da ih oduzima iz okoliša). Nadalje, naši proizvodi osiguravaju najviši stupanj disanja zidova i ugodne i zdrave uvjete. To su ujedno i trajni materijali s odličnom prionjivošću i spojivošću s podlogom. S ekološkog stajališta u našim proizvodima linije MasterEmaco za ziđe upotreba tradicijskih veziva (metakaolina, prirodnog hidrauličkog vapna) u kombinaciji s oporabljenim sirovinama i prirodnim pijeskom osigurava malu potrošnju energije i emisiju CO2. Drugim riječima s proizvodima MasterEmaco moguće je popraviti ziđe s proizvodima bez cementa uz visoka svojstva i trajnost na doista održiv način.

1. INTRODUCTION

The restoration of masonry structures, in both normal residential and heritage buildings, is always related to the problem of the techniques and materials to be used, on the one hand to improve the mechanical/structural behaviour of the structure whilst respecting the building method and, on the other hand to reach an higher quality of living.

Moreover, in particular in the last decade, the request to improve the seismic behaviour of masonry is an increasingly common request.

2. SUSTAINABLE SOLUTIONS IN THE REFURBISHMENT OF MASONRY

2.1. HISTORICAL INTRODUCTION

Over the centuries, the incredible durability and technical excellence of Roman materials have been admired and emulated by scientists and builders.

The original sources of this knowledge have always been traced back to three great ancient authors, Vitruvius in the first place, but also Pliny and Cato.

The translation and re-interpretation of texts by these authors produced, over the centuries, the perpetuation of a myth that continues to this day.

The metaphor of a chain, in its succession of rings, is a good idea to describe the passage of certain experiences and ideas from those who precede to those who follow, typical of the ancient tradition, especially in the field of the art “edificatoria”. This transmission of knowledge from teacher to student, from generation to generation allows for a continuous and slow evolution of knowledge in the Neolithic age, which reaches its peak in Roman times.

However, the decline of this tradition is registered according to many authors during the Humanism, leading to major and progressive changes of techniques and ways of production. Characteristic of the new science is the rational and analytical approach free from dogmas and superstitions that characterised the medieval world.

These two different views of reality are still present today in the world of historical restoration.

By restorers there is a request to refer to the materials and construction methods of the past because they are more suited to the historical truth of the factory. On the other hand, there is the propensity to use modern materials and technologies because the old construction methods are no longer acceptable for the extinction of the traditional arts and crafts and the lack, in modern industrial production, of the basic ingredients of the ancient recipes.

Both these approaches can be disastrous. There is a large series on the unsatisfactory behaviour of restorative materials, especially since the diffusion, in this century, of the use of Portland cement. The poor compatibility of the cement-based mortar with the materials in the masonry has been the cause of many failures in the old cities.

On the other hand, it is often not appropriate to use mortars that are a faithful reproduction of ancient materials, because the current situation of the ancient buildings and the environmental context in which they are located is very different from the one present at the time they have been built.

The failure of so many works shows how a restoration is not something easy, but it is an operation involving knowledge of all the elements involved.

2.2. A “SUSTAINABLE” REFURBISHMENT APPROACH

From this introduction, it appears clear that masonry restoration is an interdisciplinary field, which involves a variety of persons, including engineers, architects, art/heritage experts, chemists and materials experts.

Following our tradition of supplying technical support in addition to our products, BASF CC has set up this guide to provide a simple introduction to restoration, divided as follows:

- recognition of the typical situations to be found in masonry constructions;
- definition of a method for recognizing phenomena, the nature and quality of the existing materials;
- definition of a refurbishment technique;
- choice of the most suitable materials for the intended use;
- definition of the material’s requirements;
- performance specifications to be in compliance with the performances required and evaluated through specific methods.

As part of this process, and based on the millennial traditions of our territories, BASF CC offers MasterEmaco product line (formerly known as ALBARIA), which includes all lime-based products and without cement, in order to ensure maximum compatibility with the structures.

Lime has many properties which have made it a green material, produced by simply heating limestone, which do not contain nor release toxic or hazardous substances, as well as having a low environmental impact.

Furthermore, in restoration lime:

- ensures the highest breathability of the walls;
- ensures comfortable, healthy conditions due to its hygroscopic and antiseptic properties;
- it is a resistant material;

- has excellent adhesion and compatibility with the substrate;
- is highly workable, i.e. maintains its cohesion and plasticity, even when applied on very porous materials, thus making it easy to use in practice;
- makes mortar long-lasting, due to the absence of potentially damaging chemical components, and renders it immune to the action of salt and alkali/silica reactions;
- enabling them to store heating/cooling energy.

In this context, the idea that is the basis of the birth of MasterEmaco product's line is the attempt to preserve and recover the ancient experience enriching and renewing it, thanks to modern scientific knowledge and in accordance with environmental and ecological compatibility.

Figure 1 typical masonry refurbishment works

2.3. CHARACTERIZATION OF MORTARS AND TEST METHODS

In the construction industry there are still some areas difficult to copying, despite the increasing use of standards, test methods and specifications.

One of these areas is the mortar used as plasters, finishes and consolidation injections, in particular in the building restoration sector.

Talking about repair mortars, we have to take in consideration, in recent decades, the progressive increase in environmental pollution, the use of modern materials, the lack of skilled workers and the absence of adequate design of the restoration.

A first attempt to formulate correctly the problem of restoration can be traced referring to the International Congress: Mortars, Cements and Grouts used in the Conservation of Historical Buildings organised by ICCROM in Rome in 1981. In this context and Peroni. 2 proposed the following preliminary requirements for a mortar-perfect restoration:

- Good workability;
- Low shrinkage during setting;
- Values of porosity, mechanical strength and thermal expansion coefficient similar to those of the materials forming the wall;
- Content of soluble salts as low as possible.

Subsequently, a number of researchers and institutions contributed to the definition of test procedures, control and specific recommendations for restorative mortars.

The following are, by way of example, the performance requirements for restoration mortars indicated recently by L. Fontaine :

- Compressive strength: 1-8 MPa
- Brazilian / compressive strength ratio: > = 10%
- Elastic modulus: 1-8000 MPa
- Slant shear strength adhesion: > = 0.3 MPa
- Freeze-thaw expansion <= 0.04%

A complete and comprehensive guide to all the proposals that have emerged in recent years would require a much larger space of this article.

The BASF CC approach to restoration tries to consider the contributions and experiences of many aforementioned scholars and guidelines of the various committees.

The BASF CC Analytical, Mortar and Technological laboratories constantly update their test methods in the light of the latest regulatory guidelines.

According to BASF CC, the philosophy that should guide the design of a restoration consists of various aspects in stages.

In the preliminary phase of the investigation is crucial to make it possible to know the condition of the building in terms of degradation, environmental exposure, load, etc. Once familiar with these conditions, it will be possible to decide how to proceed (suitable materials to ensure maximum compatibility, the application methods, surface preparation, etc.).

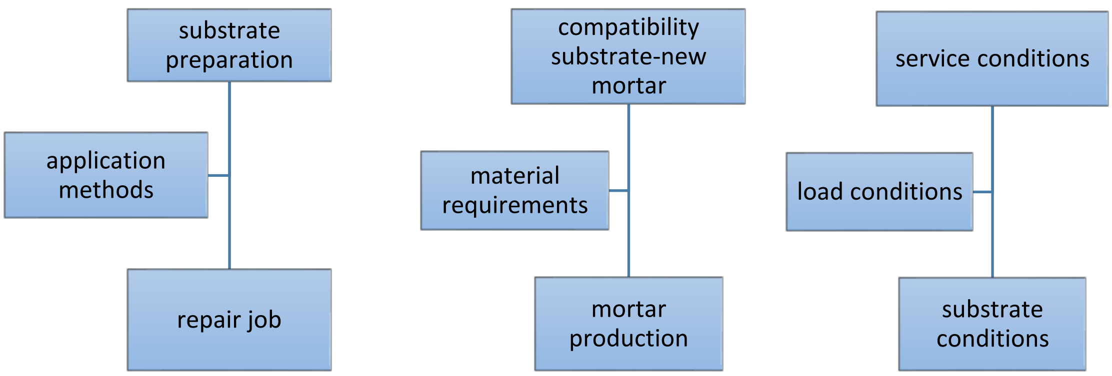

Figure 2 some of the factors that affect the durability of a restoration action

It must be also considered that the exposure and operating conditions can be different in the same building. For example, foundations in soil rich of aggressive ionic species (sea water, nitrates on agricultural land, sulphate soils

...) may require a mortar resistant to those salts, while the outer part of the same building exposed to cycles of wetting and drying or freezing and thawing cycles require specific mortars having an adequate pore distribution.

2.3.1. COMPATIBILITY BETWEEN MORTARS AND SUBSTRATE

The fundamental criteria to be considered in the development of mortars is their compatibility with the substrate and the whole building structure in the specific exposure conditions, to ensure the maximum durability.

A synthetic representation of the compatibility concept is shown in Figure 3.

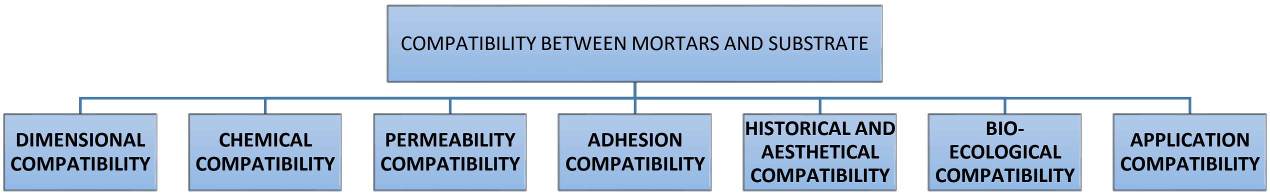

Figure 3 - Compatibility Concept

2.3.2. CHEMICAL COMPATIBILITY

It means not to introduce any substances which can interact adversely with the masonry materials.

For example, a masonry under normal storage conditions has a pH slightly above neutrality (about 7.2). If a lime-based mortar having a very basic pH (about 13) is applied, we create on the walls an increase of the ions mobility until the complete carbonation of lime (on average after 90 days) and the consequent lowering of pH.

On the contrary, a cement mortar continues to produce calcium hydroxide for several months due to the cement hydration reaction. In this way it maintains the high pH conditions and higher ionic mobility for longer periods compared to the lime based mortar.

Among the potentially harmful substances there are various types of salts which, in the presence of moisture, can produce various degradations.

For example nitrates, chlorides, sulphates and the corresponding cations (sodium, potassium, calcium, magnesium) can produce pressures of crystallisation and hydration as a result of the cycles of evaporation and crystallization into the pores.

The MasterEmaco mortars are developed with the objective of minimising the period of disequilibrium resulting from the presence of lime and the resulting high pH, and not to introduce any potentially harmful chemicals.

2.3.3. PERMEABILITY COMPATIBILITY

It is relates to the capability of the restoration material to protect the masonry from aggressive substances from the external environment, such as salts, civil and industrial gases (SO_2 - SO_3 - NOx) and at the same time to ensure a correct permeability and breathability to the masonry.

The permeability characteristics are generally related to the number and distribution of the pores of the material.

A correct microstructure will ensure a correct moisture migration, adequate breathability, a good resistance to freeze-thaw cycles and to crystallization of the salts.

2.3.4. DIMENSIONAL COMPATIBILITY

It can be related to at least four important parameters:

- the modulus of elasticity which is a measure of the stiffness of the mortar;
- the coefficient of creep given by the deformation by load;
- and the coefficient of thermal expansion that expresses the dimensional changes by temperature;
- the shrinkage leading to volumetric contractions of the mortar in the plastic phase (plastic shrinkage) and in the hardened phase (drying shrinkage).

The action of these parameters is highlighted in Figure 4.

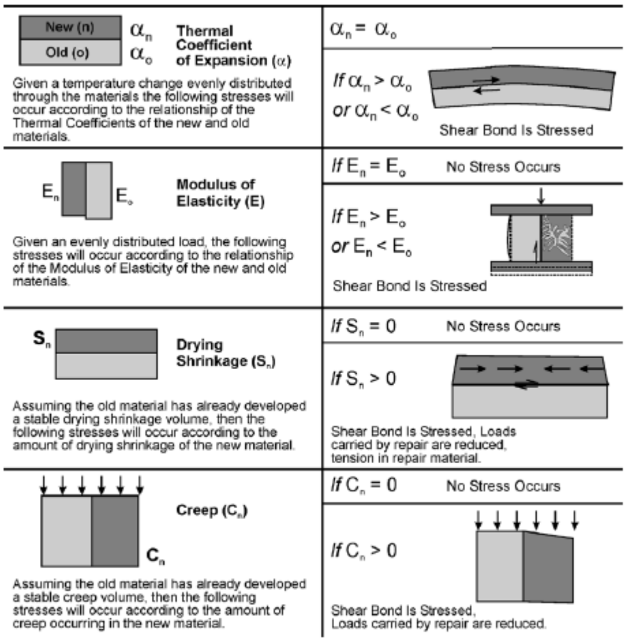

Figure 4 Some mechanisms related to the dimensional compatibility

These parameters are interconnected between them, an example is shown in Figure 5.

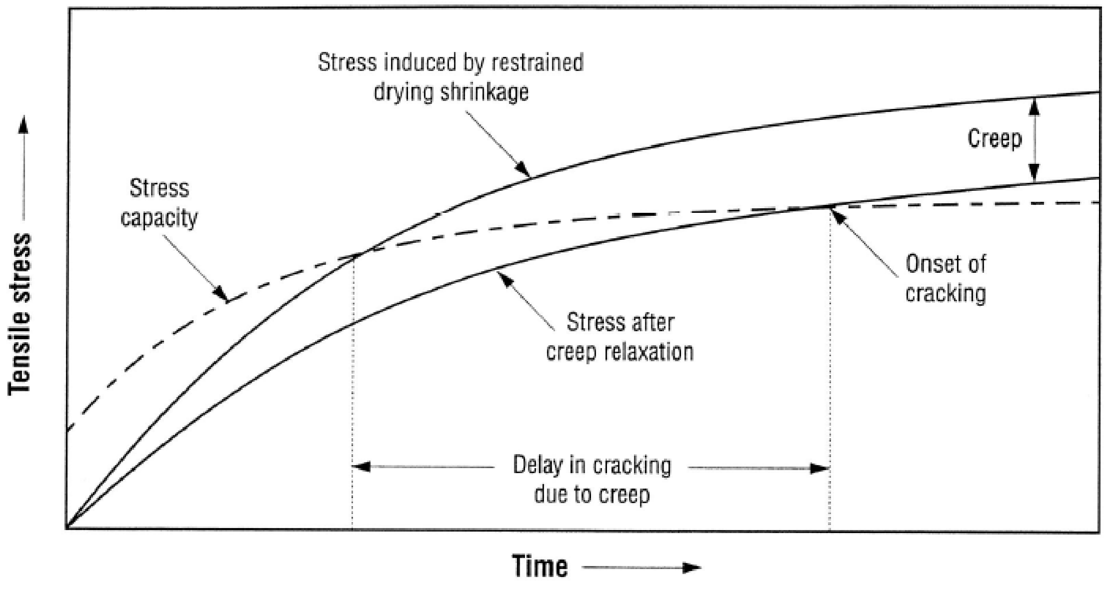

Figure 5 Interaction between shrinkage, creep and tensile strength of a mortar

Each type of hydraulic mortar shrinks volumetrically as a result of the drying shrinkage that occurs over time. Most of this shrinkage takes place in the first 30 days.

If this shrinkage is prevented by the adhesion to the substrate (masonry), it will produce stress directly proportional to the elastic modulus of the mortar according to the Hooke equation.

The shrinkage tensile stress is relieved by creep phenomenon that actually reduces the shrinkage stress.

When the stress induced by the shrinkage and reduced by the creep exceeds the tensile strength of the material you have cracking.

In the MasterEmaco products line we use various strategies to minimise the problem connected to the dimensional variations of the materials:

- Mineral expansive agents to compensate the shrinkage;

- Inorganic fibres with a high ratio aspect (length / diameter) to reinforce the mortar and to increase the tensile strength;
- New generation of superplasticisers to reduce the mixing water, improving the workability;
- Appropriate selection of binders and sands;
- Low modulus of elasticity and coefficient of thermal expansion similar to that of the masonry

2.3.5. ADHESION COMPATIBILITY

A key aspect to be considered in restoration is the adhesion that occurs between the mortar and the masonry substrate. An increase of adhesion leads to a better cooperation between the mortar and the substrate and, accordingly, an increase in performance of the system mortar-masonry, provided there is sufficient compatibility between the materials used.
If the bond strength is too low you can have the detachment of the mortar as a result of the mortar's shrinkage or caused by the pressure exerted by the crystallization of salts.
The conditions that determine an optimal interaction between mortar and support are:

1 - Proper substrate preparation;
2 – Good workability and easy application of the mortar;
3 - Good wettability of the substrate by the mortar;
4 - Sufficient retention of water by the mortar
5 - Use of pozzolanic substances to reinforce the interface area between the mortar and the substrate.

2.3.6. HISTORICAL AND AESTHETICAL COMPATIBILITY

It follows the need for adequate sensitivity to the authentic aesthetic, psychological and symbolic values of the ancient constructions. Sensitivity that should lead to a research and formulations having a final effect similar to original ancient mortars. This objective can be obtained for example by re-proposing local sands, similar to those have been used for centuries.

The historical and aesthetic compatibility is a problem to be recognised, because the urban colour constitutes the first element of identification. The use of not suitable colours as often happens, flattens and homogenizes the facades, making them stiff and unnatural.

2.3.7. BIO-ECOLOGICAL COMPATIBILITY

There are various aspects that contribute to define the ecological profile of a material, essentially:

- source of the raw materials: MasterEmaco products employ traditional binder like lime (calcium hydroxide), metakaolin, natural hydraulic lime, recycled raw materials having pozzolanic behaviour and natural sand.
- Some of greenhouse gas emissions (mainly CO2) are recovered during the hardening of lime.
- production process: Lime is produced at a much lower kiln temperature (< 1000°C vs 1450°C of Portland cement). This implies low energy use and lower CO2 emissions. Lime does not require grinding after calcination.
- Metakaolin is calcined at even lower temperature than lime.
- the impact on the environment and human of the final product: These raw materials do not cause the release of toxic or harmful residues for leaching. irradiation or emission into the atmosphere.
- durability of the material: Traditional mixtures of lime and pozzolanic minerals have proven over the centuries to be more durable and long-lasting of the modern materials based on cement

2.3.8. APPLICATION COMPATIBILITY

All these compatibility requirements may be useless if the resulting mortar does not have good application characteristics. If the mortar can be easily applied according to the data sheet requirements, you can have a complete reversal of its characteristics. For example, the need of using more water than prescribed may cause an higher shrinkage, lower resistance, less durability and impermeability.
The basic application requirements that are attributed to Masteremaco products are the following:

- Easy Mixing without lumps;
- Thixotropy or little tendency to sag;
- Good workability in terms of plasticity and cohesion;
- Good stability without formation of bleeding or segregation;
- Sufficient open time to allow the application and finishing of the mortar;
- Setting times not too long nor too short;
- Good water retention;
- Harden without cracking even when applied in a thin layer;
- Highly fluidity for grouting mortars.

2.3.9. THE DEVELOPMENT OF THE MASTEREMACO PROJECT

The development and definition of MasterEmaco project can be summarized in the following way:

- historical-bibliographical survey;
- Selection and analysis of raw materials to be used;
- Formulation and physical characterization in the laboratory;
- Chemical analytical characterization at the laboratory formulations;
- Technological evaluation and durability tests at the Technological Laboratory;
- Extensive application tests in various exposure conditions by Technical Assistance;
- Verification and certification at universities, institutes of restoration and recognised laboratories;
- Sending samples of the materials to selected users in various parts of Italy. Collection and examination of the opinions obtained;
- There is a technical support to end-users, which provides the technical visit to the building site, chemical-physical investigations on materials and types of degradation, designing customized solutions, especially where there are severe conditions of exposure or service. This process of development in sequential stages, allows to highlight with the contribution of specialists in different fields, the positive and negative aspects of the material.

Our approach thus tends to be as holistic and multidisciplinary as possible for the multiplicity of experiences that contribute to the project: historians, physicists, geologists, chemists, technologists, expert applicators.

3. CONCLUSIONS

The refurbishment and renovation of the old structures is a complicated and tricky process, based on an interdisciplinary approach which involves a variety of competences, including engineers, architects, expert of art/heritage, chemists and materials experts.

Moving from the compatibility mortar/structures from the chemical and structural point of view, to the environmental compatibility, passing through the complete and correct characterisation of the materials to be applied, we can highlight that is needed to follow a clear path moving from chemistry, engineering, architectural and historical aspects. We, as BASF CC ITALIA wants to provide such expertise, in order to merge different competencies, and different needs, with the scope of renovate masonry buildings respecting all the traditions but at the same time proving the modern technologies to the constructions industry.

REFERENCES

[1] B.P. Torsello "Tradizione e restauro" da Le ricette del restauro - Saggi Marsilio 1998
[2] S. Peroni, C. Tersigni, G. Torraca, S. Cerea, M.Forti, F. Guidobaldi, P. Rossi-Daria, A. De Rege, D. Picchi, F.J. Pietrafitta, G. Benedetti "Lime basedmortars for the repair of ancient masonry and possible substitutes" ICCROM 1981
[3] P. R. Rossi-Daria "Le malte da restauro" da Le malte nell'evoluzione del processo costruttivo:passato, presente, futuro - RILEM 1987
[4] Faller, E. Karotke, E. Althaus "Salzschaden an historichenBauwerken" ErhaltenhistorischBauwerke, Sonderforschungsbereich 315 - ISBN 1990
[5] G.B.A. Williams "Pointing stone and brick walling" Technical Pamphlet5 SPAB 1994
[6] D. Knofel, M. Huesmann" Morte) zurfegeninstandsetzung an historischebauwerken" Bautenschutz + Bausanierung 16 1993
[7] J.D. Rodrigues "In the search for tentative recommendations regarding compatible restoration mortars"
[8] F.M.A. Henriques, E. Charola" Comparative study of standard procedures for mortars" Intemational congress on deterioration and conservation of stone - Berlin 1996
[9] E. Charola, F.M.A. Henriques "Lime mortars: some considerations on testing standardization" ASTM STP 1999
[10] M. Thomson, C. Groot "Rilem TC characterization of old mortars with respect to their repair" ASTM STP 1999
[11] L.Fontaine, M. Thomson, G.T. Suter "Practice and research: the need for standards for historic mortars" ASTM STP 1999
A. Dal Bò, L. Cimitan "Un approccio olistico all'intervento di restauro" Progetto Cee - Raphael "COMARECH" Bressanone 2000
[12] M. Zerbinati "Malte con sabbie locali. Soluzioni per interventi conservativi" Arkos - Scienza e restauro 1/2000
[13] L.Cimitan, A. Dal Bò, G. Fortunati, M.Grigol etto, I.Torresan "Utilizzo della porosimetria a mercurio nell'analisi di malte storiche e di nuova formulazione: microstruttura, degrado, prestazioni" su Porosità e porosimetria - Importanza, implicazioni e sviluppo nel settore dei beni culturali ICCROM - Roma 2000
[14] T. Mannoni "Ricerche sulle malte genovesi alla porcellana" 1986

[15] D.di G. Martini "Trattati di architettura, ingegneria e arte militare" 1456-1502 Il Polifilo, Milano 1967
[16] P. Cataneo "L'architettura" Manuzio - Venezia 1567
[17] G. Branca "Manuale d'Architettura, breve, risoluta e pratica, diviso in sei libri" 1629
[18] V. Scamozzi "L' idea dell' architettura universale" 1615
[19] J. Rondelet "Traitéthéorique et pratique de l'art de batir" Paris 1802-1817
[20] L.J. Vicat "Mortars and cements, artificial and natural" London 1837
[21] G. Gallo "Studio microscopico sulle malte aeree e delle malte a pozzolana" 1908
[22] Le Chatelier " Recherchesperim. sur la constit. des mortiershydrauliques" 1904
[23] G. Quarneti "I quaderni di Giacomo Querini da Venezia 1889 - Delle calcine, dei mattoni e degl'Intonachi"
[24] Arcolao "Le ricette del restauro" Saggi Marsilio 1998

MASONRY STRUCTURE OF CHURCH IN RUMA - PART 2: THE REPAIR

Ivan Lukic[1], Mirjana Malesev[1], Vlastimir Radonjanin[1], Slobodan Supic[1], Vesna Bulatovic[1]

[1] University of Novi Sad Faculty of Technical Sciences, Department of Civil Engineering and Geodesy, Sime Milosevica 12, 21 000 Novi Sad, Serbia, email: lookic@uns.ac.rs, miram@uns.ac.rs, radonv@uns.ac.rs, ssupic@uns.ac.rs, vesnam@uns.ac.rs

SUMMARY: Based on the assessment of the masonry structure of the church in Ruma (Serbia), given in Part 1, it was concluded that the global and local stability, as well as load-bearing capacity of the structure are jeopardized. In order to remove the causes of damages and, thus, prevent their further progress, a series of urgent repair measures is proposed. Detailed visual inspection revealed that that the biggest cause of the damages of the structure is unbalanced settlement. Settlement led to opening and development of the cracks and fissures, especially in the arches, around the openings and in the walls. Low efficiency of the existing tie-rods is an additional factor contributing to the endangerment of the buildings stability. Among the other damages, the most noticeable are the dilapidation and deterioration of the material, especially in the area of direct exposure to the effects of weathering. In this paper are presented following repair solutions: sealing and routing or injection of the cracks, new tie-rods, horizontal hydro-insulation in the walls and pillars and strengthening of the roof structure.

ZIDANA KONSTRUKCIJA CRKVE U RUMI – DRUGI DIO: POPRAVAK

SAŽETAK: Na osnovi ocjenjivanja stanja zidane konstrukcije crkve u Rumi (Srbija) prikazanog u prethodnom radu zaključeno je da je ugrožena globalna i lokalna stabilnost te nosivost konstrukcije. Da bi se uklonili uzroci i oštećenja i tako spriječilo njihovo daljnje napredovanje predložen je niz hitnih popravnih mjera. Detaljnim vizualnim pregledom utvrđeno je da je najveći uzrok oštećenja konstrukcije nejednolično slijeganje. Ono je dovelo do otvaranja i širenja pukotina, posebno na lukovima, oko otvora i u zidovima. Dodatni je čimbenik koji doprinosi ugrožavanju stabilnosti zgrade mala učinkovitost postojećih zatega. Osim drugih oštećenja najprimjetnije je propadanje i degradacija materijala, posebno u području izravne izloženost atmosferilijama. U radu su prikazana sljedeća rješenja za popravak: brtvljenje i injektiranje pukotina, ugradnja novih zatega, horizontalna hidroizolacija zidova i stupova i ojačanje krovne konstrukcije.

1. INTRODUCTION

This study presents the repair solution for the masonry structure of the church in Ruma (Serbia). Based on a detailed visual inspection of the church (Part 1) [1], identification and classification of all defects and damages of the structure, and taking into account the long-term monitoring of cracks development and behaviour of the building, it was necessary to take appropriate repair measures.

It was concluded that the global and local stability of the structure are jeopardized, as well as its load-bearing capacity. Durability of the building is particularly jeopardized, especially considering the importance of the protection of cultural treasures and ornaments, whose further deterioration should be prevented. The functionality of the object is being maintained, since it is a building with religious purposes. However, it is compromised because of reduced safety of a large number of people who can be found inside the building at any time [1].

In this paper are presented repair solutions for cracks in construction joints, cracks in vaults, introduction of new tie-rods, roof structure repair.

2. REPAIR OF THE CHURCH

2.1. REBUILDING OF WALL CONSTRUCTION JOINTS

During the subsequent construction of the crypt, parts of the walls were demolished and later, after the completion of construction works, re-built, but the continuity between the new wall and the existing structure was not achieved. This resulted in the opening of cracks due to the settlement of the building. According to the terms for the execution of works issued by the Institute for Protection of Cultural Monuments, the use of materials based on limestone, "MapeWall Inject & Consolidate" and "Mapewall Render & Strengthen" (MAPEI) have been chosen as injection material and repair mortar. As a repair solution, stiching method has been chosen, where steel rods are inserted in the bed joints. The procedure and repair details of execution of works on connecting the wall with pilasters are shown in Figures 1 and 2.

a)

b)

c)

d)

e)

f)

Figure 1 Rebuilding of construction joints: cut bed joints and drill anchor holes in pilaster (a); cleaning and wetting joints and anchor holes (b); inserting reinforcement in anchor hole and grouted joint (c, d); injection of anchor hole in pilaster (c); final view of "stitched" wall (e)

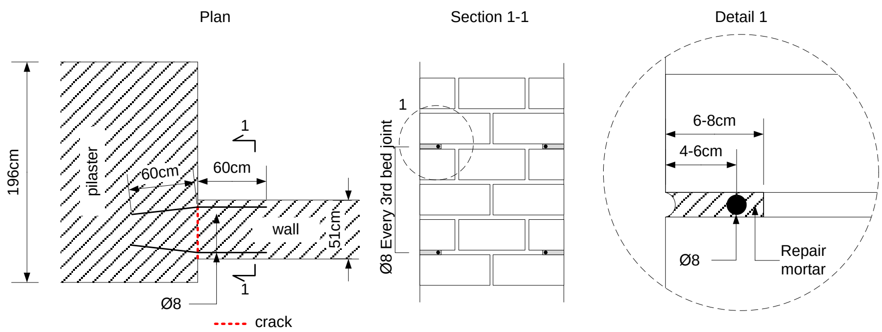

Figure 2 Construction joint rebuilding design

After the "stiching", cracks are injected with injection mass under low pressure. Injection procedure consists of the following operations:

- Drilling the hole, diameter 20mm (diameter should be adjusted to the selected type of injection nozzle). The depth of the holes is equal to 2/3 of the wall thickness (about 35 cm) and drilled along the crack at the distance of 30-50cm. The holes are usually drilled in the place of headl joints or in the place of cracks in bricks.
- Setting the casting nozzles (metal or plastic) and fixing with the epoxy mass.
- Surface sealing of cracks.
- Cleaning of the injection holes and cracks and water saturation of masonry with water.
- Injection with the pumps with low pressure (0.5 - 2 bar).

Test injection has shown that, due to the high porosity of the masonry, wetting with water is needed immediately prior to injection. During injection, due to a lack of mortar in the joints, injection mass leakage occurred in places outside crack zone (up to 50cm distant), hence injection on a single casting nozzle was performed in stages, while the time between stages was the time required for injection mass to harden. After the appearance of injection mass in casting tube and hardening, it was possible to continue with injection on next, upper nozzle. This action was possible due to the extremely fluid consistency of the mass that allowed pouring injection.

2.2. CRACKS IN VAULTS

During visual inspection, two types of cracks in the vaults in wall openings have been observed. Cracks in vaults below windows spread from base voussoirs to lower corner of window, while in vaults above windows, cracks are located in crown zone. Since all these cracks are caused by uneven settlement, and there are no signs of further settlement, selected the repair solution was designed only to restore the integrity of the masonry in the zones of cracks. These works are not yet conducted, so here is presented only designed repair solution.

Repair of cracks below window include drilling Ø30mm holes for anchoring 2Ø12 reinforcement bars bended and welded to form “T” shape. Holes are drilled at an angle of 60-90 degrees to the crack, cleaned and filled with anchorage material (ADESILEX PG1 – Mapei). After preparation, “T” shape anchors are inserted in anchorage holes (Figure 3).

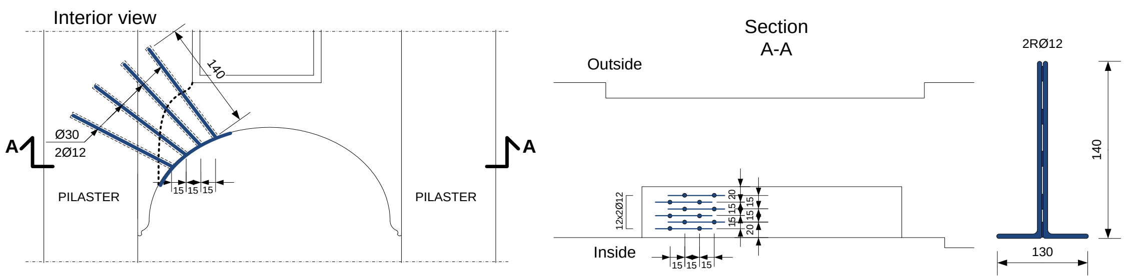

Figure 3 Repair solution for cracks in vault below window

For the repair of cracks in vaults above window was applied similar solutions, in combination with „stitching“ techique (Figure 4). First phase include placing of reinforcement bars in two rows with spacing of 15cm. The bars’ length is 85cm in inner and 130cm in outer row. The reinforcement were supposed to be inserted symmetrically on both sides of the crack at the angle of 60° relative to a plane tangent to the highest point of the vault (Figure 4).

In second phase, „stitching“ techique is applied, but unlike previous repair solution, here is also introduced reinforcement of full depth of bed joints. Reinforcement bars are placed in the bed joint at the angle of 30 degrees to the wall surface. Minimum length od bars is 120cm in first line and 200cm in second line. Bars are alternately placed symmetrically on both sides of the crack in every 8th bed joint. Surface reinforcement bars are placed in every 4th bed joint extending 50cm on the either side of the crack. Details of reinforcement of the wall is presented in Figure 5.

After execution of the reinforcement of the cracked vaults, final phase is injection of existing cracks. For the injection was recomended same material and procedure as for all injection works.

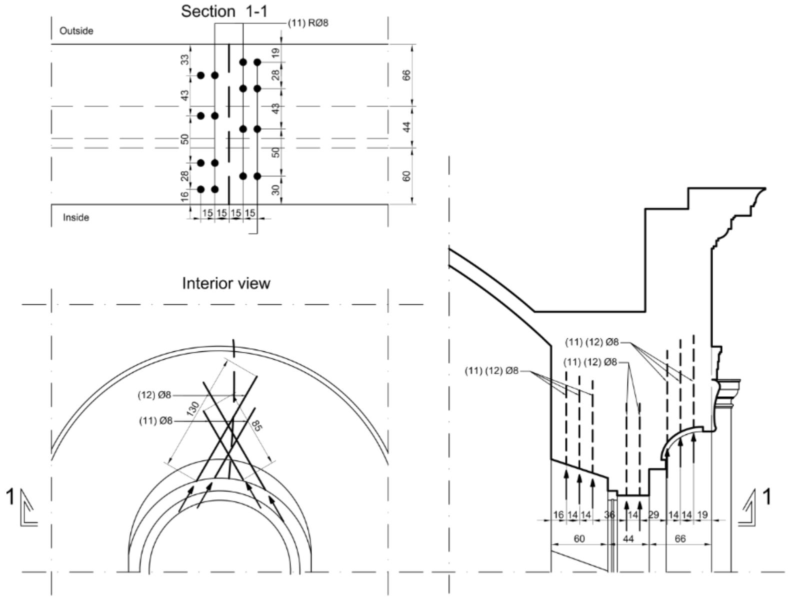

Figure 4 Repair of cracks in vault above window: Phase 1

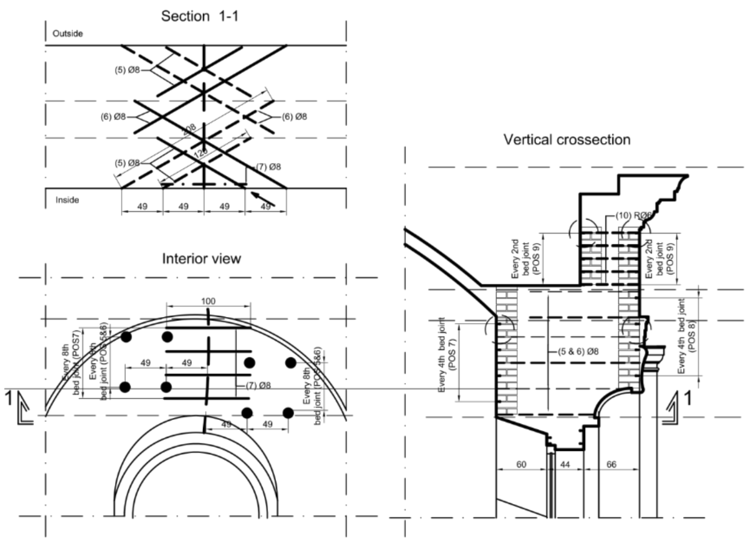

Figure 5 Repair of cracks in vault above window: Phase 2

2.3. DESIGN OF NEW TIE-RODS

Ceiling of the church was constructed as a masonry domical rib vault with the ribs on the extrados side. Initially, for balancing lateral thrust in arches, inclined ties anchored in base of arch and hung on the roof tie were used. After roof renovation in the 1950's, new ties were added (old were left but without connection to roof tie), with same structural concept, but this time, instead of hanging new ties on roof structure, new "I" beam was introduces. Since this solution is not very effective, it was decided to balance lateral thrusts with standard tie rods (Figure 6).

Design of new tie-rods includes the following operations:

- Drilling Ø30mm hole throughout the entire thickness of the walls (Figure 7a).
- Cleaning hole with compressed air.
- Cutting and profiling the surface around newly created hole, dimensions approximately 50x40cm from the outside, depth of 15cm (Figure 7b). During this procedure, old anchors were revealed.
- Leveling of substrate with repair mortar in a layer 3-4cm.
- Placing of steel plates dimensions of 400x260x15mm (Figure 8a).

- Installing the tie rod, with threads at the ends, fixing one side and tightening using turnbuckle to achieve the desired stress (Figure 8b).
- Injection of a hole in the wall with the injection mass, in order to achieve contact between the bars and the wall.
- Application of repair mortar in order to protect the anchor plate and the alignment with the surrounding wall.

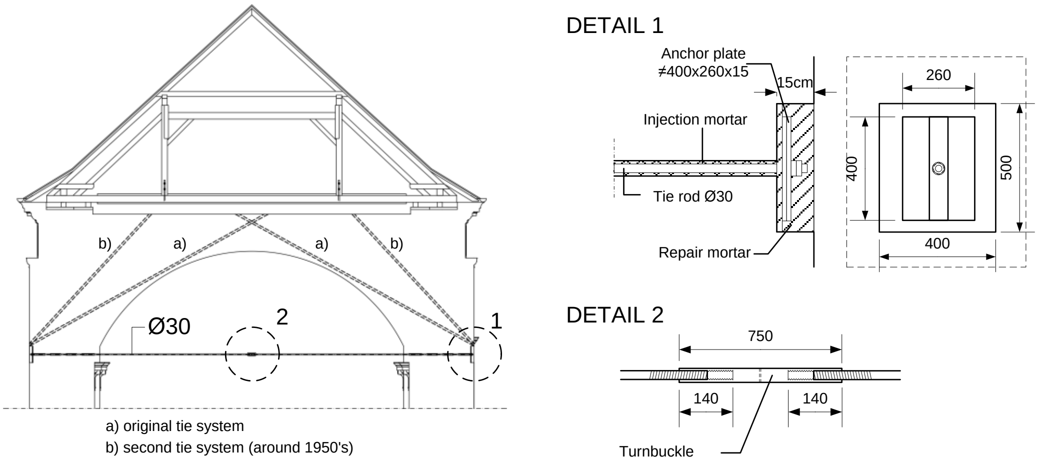

Figure 6 Design of new tie-rods

a)

b)

Figure 7 New tie-rods: drilling Ø30mm holes for new tie-rods (a); cutting and profiling wall for new anchor plate (b)

a)

b)

Figure 8 New tie-rods: Anchor plate (a); Tie rod with turnbuckle in the middle of the span (b)

2.4. ROOF STRUCTURE REPAIR

Repair works of the roof structure included the following operations:

- Removal of the roof covering;
- Removal of existing dilapidated wooden substructure and the rafters;
- Strengthening of the cross ties;
- Repair of local damage;
- Setting the new rafters, substructure and roof covering.

Static calculation is made in accordance with current regulations; some of the elements of the roof structure did not meet the criteria of capacity and/or usability, as determined by the visual inspection. The most vulnerable elements were the cross ties and, as one of the conditions issued by the Institute for Protection of Monuments of Culture was that the main elements of the roof structure cannot be removed, a following solution is adopted: reinforcing cross ties by increasing the cross section by adding new elements dimensions 16/10cm and their mutual connecting with steel stirrups (Figure 9 left). In this way, the problem of setting and leveling of new rafters is solved. The deformation of the existing structure was such that, in certain fields between the main trusses, the deflection of the cross tie was 5-10cm. By adding a new element, the leveling of the cross tie was carried out, as well.

Another problem that has been observed with cross-ties includes large deformation in the horizontal plane, occurred as a result of the large horizontal load of rafters and large range, unusual for this type of roof structure. To minimize horizontal load of rafters, each pair of rafters is interconnected with collar beam (Figure 9 right).

The appearance of the roof structure, after the repair, is shown in Figure 10.

Figure 9 Strengthening of the cross-tie: projected (left) and performed (right)

Figure 10 The appearance of the repaired roof structure

2.5. HORIZONTAL HYDRO-ISOLATION IN THE WALLS

Adopted solution for hydro-isolation is HIO Technology [3]. By using diamond saws, with no vibrations, the wall is cut in segments with width of 30-50cm and the rails are inserted in the cuts and a special polymer based compound is injected (Figure 11). Injected mass fills segment and the whole rail profile so that the rail creates an unbreakable link with a wall - new bed joint.

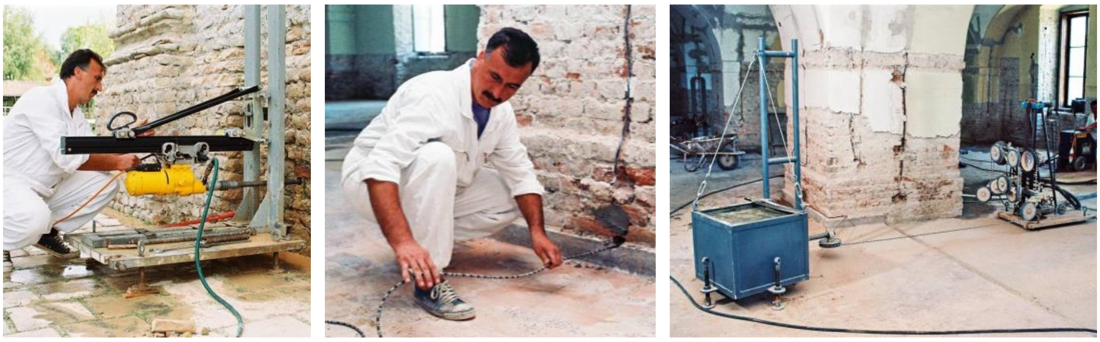

a) b) c)

d) e)

Figure 11 HIO Technology – Wall cutting and hydro-isolation procedure [5]: a) drilling initial hole in wall; b) placing diamond wire; c) cutting of wall/pillar; d-e) placing of HIO rails and injection of polymer based compound

In order to permanently and effectively solve the problem of capillary moisture, execution of horizontal hydro-insulation is proposed in the walls and pillars along the whole perimeter of the church (Figure 12). In this way, the movement of capillary moisture in the walls, and, consequentially, further deterioration of masonry and interior painting is prevented.

Figure 12 The appearance of pillar and the wall after installation of hydro-isolation membrane

3. CONCLUSIONS

Repair work on historical buildings, especially one that is considered as a cultural heritage, is extremely complex task that must be conducted taking into account both the regulations relating to the protection of monuments, as well as the technical aspects of the structure. Particular attention should be paid to the performance parameters of the built-in materials, the nature of construction work and possible interactions that may occur [4].

With this type of work, despite a visual inspection, assessment and development of detailed repair procedures, changes of repair solutions in-situ are usual. The reasons for this are mostly the lack of project documentation and subsequent interventions that were not filed. This is not a surprise, as the building is constructed more than a century ago, but it also emphasizes importance of designer's experience and knowledge of the design and construction of this type of object.

Through this case-study, several techniques of repair and strengthening of masonry and wood structure are shown. Some of presented repair works are already successfully executed, such as repair of the roof structure (finished in summer 2013), rebuilding of wall construction joints, new tie-rods and horizontal hydro-isolation of walls (finished in autumn/winter 2016). Due to inappropriate climate conditions, repair works on cracks in vaults and domes, façade and interior works are postponed for first half of year 2017.

ACKNOWLEDGMENTS

The paper presents the part of research realized within the project “Improvement of educational process and theoretical and applied research in civil engineering” conducted by the Department of Civil Engineering and Geodesy, Faculty of Technical Sciences, University of Novi Sad.

REFERENCES

[1] Radonjanin, V et al: Masonry structure of the church in Ruma - Part 1 - The assessment, Proceedings of 1st International Conference on Construction Materials for Sustainable Future, 19-21 April, 2017, Zadar, Croatia

[2] Radonjanin, V et al: Elaboration on the repair of the church in Ruma (in serbian), Deparment of Civil Engineering and Geodesy, Novi Sad, 2013

[3] Available from http://www.hio-technology.com/index_sr.html, Accessed: 2017-02-19

[4] Chmielewski, R., Kruszka, L.: Application of selected modern technology systems to strengthen the damaged masonry dome of historical St. Anna’s Church in Wilanów (Poland), *Case Studies in Construction Materials*, Vol. (3) No., pp. 92-101, 2214-5095

[5] Radonjanin, V., Malešev, M.: Material from lectures in the subject: "Durability and Assessment of Damaged Masonry Structures", Deparment of Civil Engineering and Geodesy, Novi Sad

FLEXURAL STRENGTHENING TECHNIQUES IN HISTORIC MASONRY STRUCTURES – THREE CASE STUDIES

Juraj Pojatina[1], David Andic[1]

[1] Studio Arhing d.o.o. Cire Truhelke 49, 10 000 Zagreb, Croatia, email: juraj.pojatina@gmail.com, david.andjic@yahoo.com

SUMMARY: The paper presents three cases of different masonry strengthening techniques. After inspection and field - and laboratory testing, each structure has been assessed. In the following design phase, structural analysis for seismic loading has been performed using different structural models and analytic approaches. According to the performed analysis, several different strengthening solutions for each flexural out-of-plane masonry wall are being presented with commentary. In the final stage, decisive criteria for selecting strengthening solution is shown. Presented case studies of flexural strengthening techniques in historic masonry structures with the diversity of possible solutions and selecting criteria demonstrate the complexity and interdisciplinary nature of this subject.

TEHNIKE POJAČANJA NA SAVIJANJE U POVIJESNIM ZIDANIM KONSTRUKCIJAMA – TRI PRIMJERA

SAŽETAK: U radu su prikazana tri slučaja različitih tehnika pojačanja ziđa. Nakon pregleda i terenskog i laboratorijskog ispitivanja svaka je konstrukcija ocijenjena. U narednoj fazi projekta proveden je proračun konstrukcija za potresno opterećenje primjenom različitih modela konstrukcije i analitičkih pristupa. Nakon tih proračuna u radu je prikazano više različitih rješenja pojačanja za svaki zid izložen savijanju izvan ravnine uz komentar. Na kraju su pokazani kriteriji za odlučivanje pri odabiru rješenja za pojačanje. Prikazani primjeri tehnika pojačanja na savijanje za povijesne zidane zgrade s različitim mogućim rješenjima i odabirom kriterija pokazuju složenost i interdisciplinarnu prirodu ovog zadatka.

1. INTRODUCTION

Often structural engineers with assignments in old urban areas with masonry building tradition have the challenge to find the best possible solution for out-of-plane wall strengthening. So, the main hypothesis for this paper is to show the diversity of possible solutions and general selecting criteria for out-of-plane bending resistance strengthening techniques of masonry walls, following three case studies which represent three different techniques and approaches in repair and retrofit of the existing structures. Walls as structural elements are suitable for withstanding seismic loads in plane, but problems arise when walls are loaded out of their plane. Current standards are strict when use of masonry walls as out-of-plane bending elements are discussed. Brief description of three existing masonry structures follows.

The first case structure is an art gallery in Zagreb, originally built as horse-riding hall in 1908 during Austro-Hungarian reign. The hall is around 60 m long and 25 m wide with a maximum height of 11,2 m. Masonry walls are built during Austro-Hungarian reign with traditional clay bricks (dimensions 290x140x65 mm). Walls are 59 cm thick with column widening every 5 m longitudinally. Columns are 104 x 119 cm. Gable walls are widened in thirds of their length with columns 70 cm thick and 90 cm wide (Figure 1). Concrete foundations are without reinforcement and are 2.2 (2.5) m deep with the same width as the walls above them. Visual examination of the structure as a whole was performed and overall wall out-of-plane stability was marked as questionable. New bracing system in roof plane is placed, providing lateral support at the top of the wall. However, gable wall remained unrestrained in its full height.

The second case structure is old cinema hall in Biograd na Moru, built shortly after the World War II. It is a single storey masonry structure with length of approximately 36 m and width of 12 m with maximum height around 11 m (Figure 2). Masonry wall is a combination of masonry units of different shapes and sizes made of various materials (concrete, stone, clay) and low quality mortar. After inspection, field- and laboratory testing, wall stability was marked as insufficient. Considering the age of the building, low quality of masonry, lack of confining elements, absence of tie beams and tie columns, large wall surfaces without lateral restraints and high importance category (γ =1.2), the walls were fitted suitable for out-of-plane strengthening. Again, new bracing system in roof plane is placed, providing lateral support at the top of the wall. Also, as in the previous case, the wall remained unrestrained in its full height.

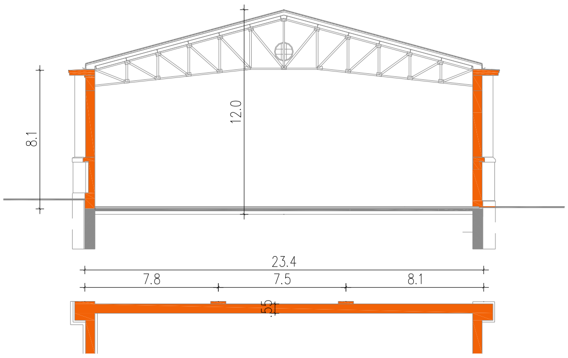

Figure 1 Cross-section of art gallery

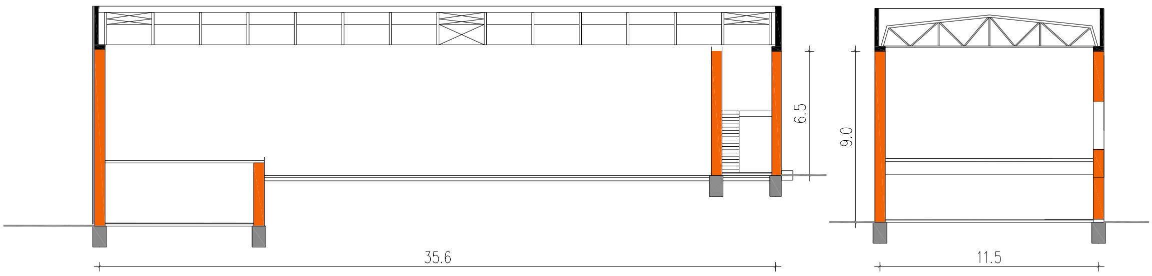

Figure 2 Cinema hall - longitudinal and cross views

The third case is a museum entrance portal in Zagreb, built around 1880. The entrance is mainly used for vehicles and it is spanned by a horizontal brick arch. Overall length of the wall containing portal is around 14,0 m with height of 7.0 m. Portal opening is 3.5 m wide and 4.0 m high (Figure 3). The primary concern with the structure were cracks and deformations of masonry portal which occurred due to deep excavation on neighboring building site. After the initial inspection, apart from the observed damage, basic structural system of the wall is marked as insufficient due to out-of-plane horizontal resistance, since the global static system of the wall is cantilever.

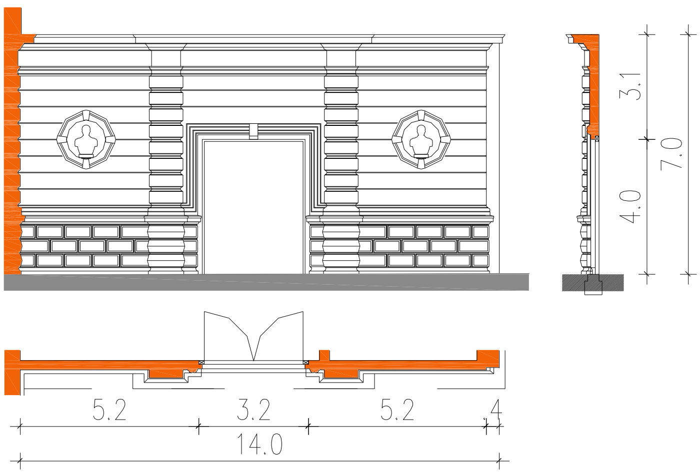

Figure 3 Museum entrance portal

2. METHODS AND RESULTS

As previously presented, three walls with out-of-plane instability problem were introduced. General approach to the problem was to calculate out-of-plane resistance in order to compare it with relevant horizontal forces. The calculations were executed using FEA modelling software with design procedures according to Eurocode.

Method one: Wall strengthening with steel structure (Art gallery in Zagreb).

As a new interior element, two storey reinforced concrete gallery is placed in front of the wall and it serves as lateral support for smaller part of the wall. The remaining area of the gable wall is strengthened and supported with new steel structure which consists of two horizontal beams and two columns. All steel elements are HEB200 profiles, anchored to foundations, tie beam on top, gallery slabs on one side and masonry wall on other with continuous connection to wall – steel anchorage M16 on 100 cm distance. Steel columns and beams are dominantly bending elements and in specific situation they stiffen an otherwise very 'soft' brick wall (Figure 4). New steel structure members represent line support for masonry gable wall. With this new flexural structure, out-of-plane bending moments and main stresses in primary brick wall are reduced to a minimum. Before strengthening, wall was unrestrained and it's out-of-plane stiffness was negligible. After the strengthening, existing masonry is divided into smaller segments which had sufficient bending capacity to withstand seismic lateral forces.

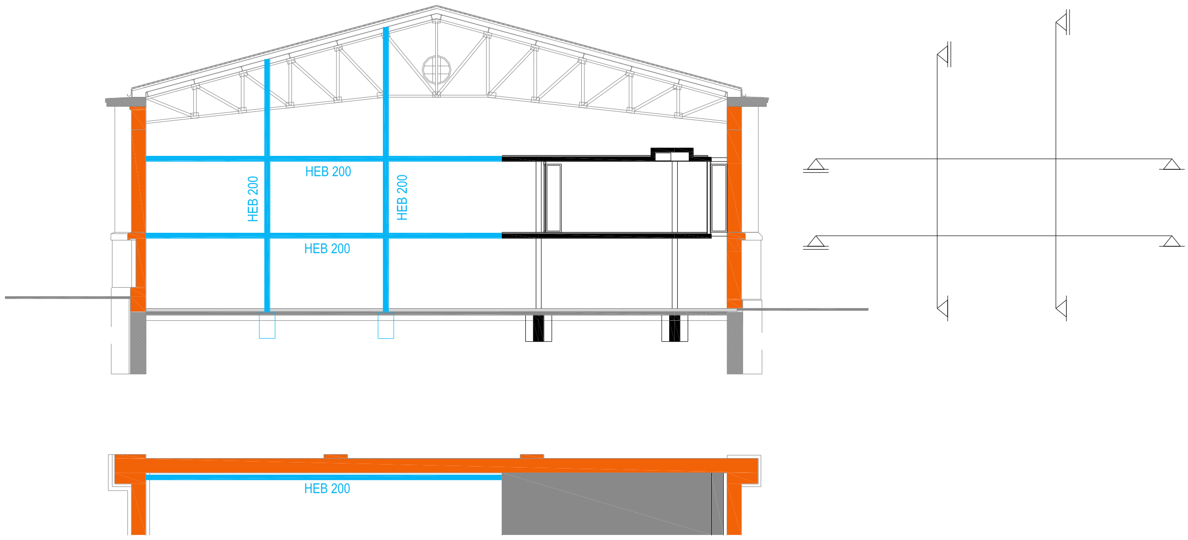

Figure 4 Cross-section of art gallery with strengthening elements

During the design phase several techniques as alternate solutions were also analyzed. Fiber-reinforced polymer (FRP) bands have difficulties in installation on moist masonry elements and reinforced shotcrete as another alternate solution was declined by the local conservation department due to its incompatibility with previously given conservation directives. Steel structure was an aesthetically and functionally acceptable solution for all participants involved: architects, conservators and structural engineers.

Method two: Wall strengthening with fiber-reinforced polymer FRP (Cinema Hall in Biograd Na Moru)

Several possibilities of flexural strengthening were analyzed with the following input factors included in the decision making process: dry wall elements (mostly stone), large unrestrained wall areas, accessibility of specific technology in this region. Other than previously stated, the most important criteria which has to be emphasized is predicted wall collapse mechanism. Very low quality of the wall due to the low quality of mortar and partial absence of it demand confining structure as tensile 'cape' around the wall surface. This kind of confining element keep wall from inner collapse, which is very often collapse mechanism of low quality stone masonry during earthquakes. Since shotcrete is not accessible in this region and steel confining elements are not suitable for large areas due to its slow mounting process, fibre-reinforced polymer (FRP) bands were selected as the most appropriate solution. Applicated diagonal grid of FRP bands creates confined 3.0 x 3.0 m areas (Figure 5). As a very important part of the installation, proper band anchorage was selected according to technical allowances as well as surface preparation which also had strict geometric tolerances.

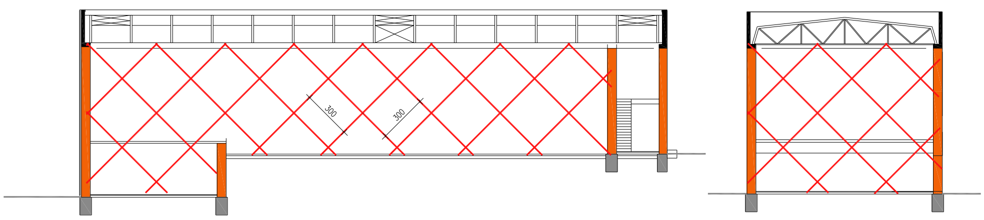

Figure 5 Cinema hall - FRP wall strengthening

Figure 6 Art gallery – construction phase

Figure 7 Cinema hall – construction phase

Method three: Wall strengthening with reinforced concrete (Museum entrance portal in Zagreb)

Insufficient out-of-plane stability of the cantilever wall is solved by strengthening with new reinforced concrete elements. New RC columns, horizontal beams and shotcreting were used in this strengthening method. New columns function as fixed cantilevers with their new foundations for entire structure. Tie beam on top of the wall is a flexural member supporting top of the wall, and shotcrete is an areal bracing that prevents masonry elements from falling out. When shotcreting the surface, reinforcement is placed on the existing surface and anchored in masonry. Aforementioned reinforcement functions as tension zone when wall is subjected to horizontal actions. Shotcrete is framed with columns and beams to ensure desired force distribution from shotcrete to edge elements. Also, new columns are connected to masonry structure by adequate anchorage elements (Figure 8). As a result of the strengthening, lateral out-of-plane deflection was successfully limited and kept under appropriate value.

Also, alternate strengthening methods were analyzed. Fiber-reinforced polymer (FRP) is not suitable because of its inability to be installed on moist brick elements and steel structure was not suitable because of corrosion hazard (outside element).

3. CONCLUSIONS

Various solutions arise during the designing process of masonry wall strengthening. As structural engineers, our job is to inspect, assess and find the optimal solution to the given problem. The more input information are gathered the solution is easier to find. Decisive criteria for selection of the strengthening solution depends from case to case and there is no uniform way to apply in every situation. The recommended steps for optimal strengthening method selection are:

- Visual inspection
- Field and laboratory testings
- Structural analysis
- Strengthening method selection

Selection criteria here presented for the case studies can apply as general criteria in similar situations:

- Structural design criteria
- Preservation directives
- Architectural (aesthetic) criteria
- Technology accessibility
- Existing structure conditions
- Functionality and maintenance criteria

Presented case studies of flexural strengthening techniques in historic masonry structures with the diversity of possible solutions and selecting criteria demonstrate the complexity and interdisciplinary nature of this subject. With the performed recommendable steps for proper assessment of the structure, specific experience and knowledge of traditional historic masonry execution, optimal strengthening method can be selected.

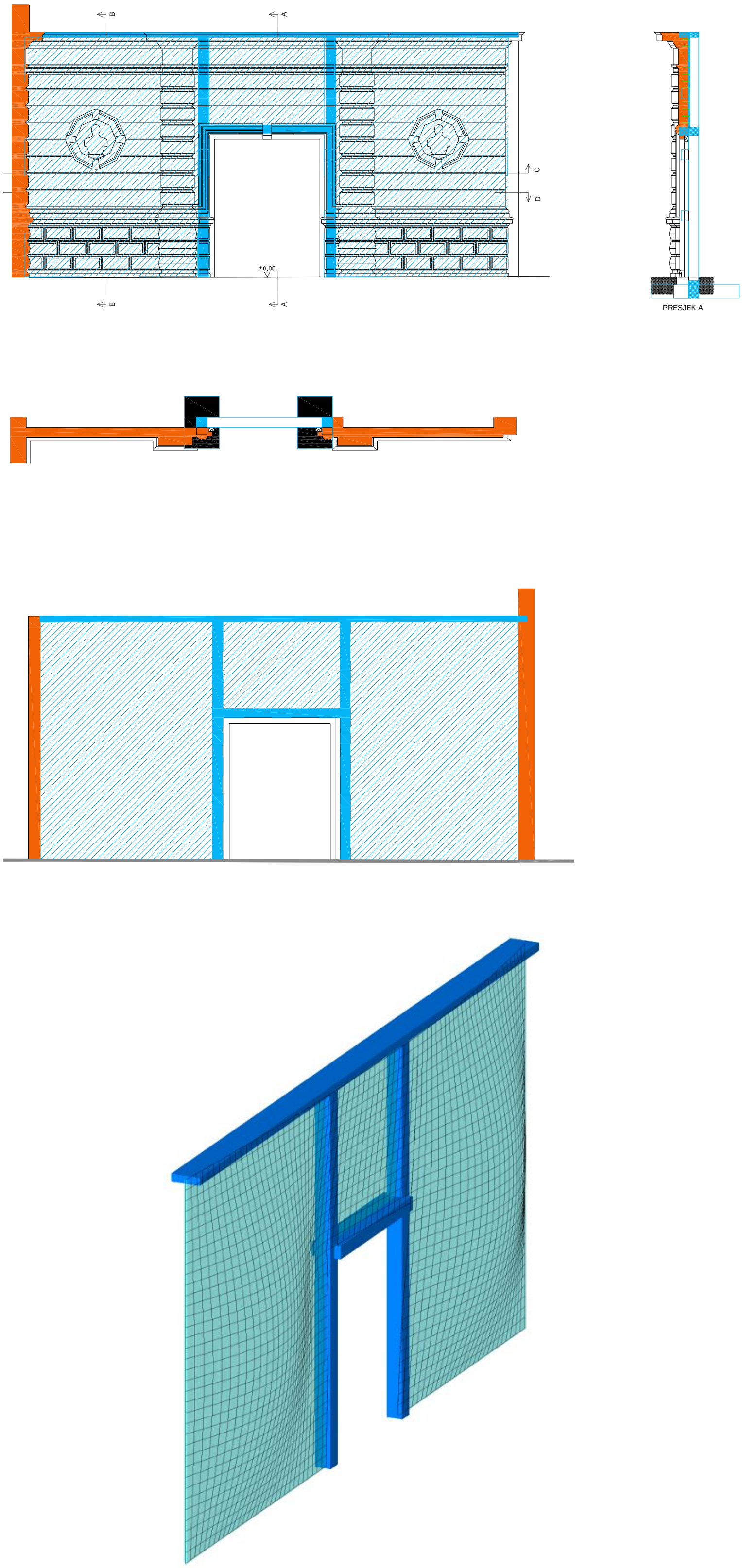

Figure 8 Portal wall strengthening plan with new concrete elements (blue) and FEA model

REFERENCES

[1] Pojatina, J. et al.: *Rekonstrukcija zgrade jašione - izložbeni prostor,* Studio Arhing d.o.o., Zagreb, (2008)
[2] Pojatina, J. et al.: Dogradnja gradske knjižnice, rekonstrukcija i adaptacija kina i zgrade pučkog učilišta, Studio Arhing d.o.o., Zagreb, (2007)
[3] Pojatina, J. et al.: S*tatička sanacija kolnog portala,* Studio Arhing d.o.o., Zagreb, (2016)

MASONRY WALLS REINFORCEMENT OF EX MARASKA BULIDING IN ZADAR

Davor Uglesic[1], Ante Uglesic[1]

[1] D&Z doo Jerolima Vidulića 7, 23 000 Zadar, Croatia, email: dz-zadar@zd.t-com.hr, ante.uglesic@gmail.com

SUMMARY: The project of existing masonry building reinforcement with carbon fibers will be presented in this paper. The building was erected in 1911. Its façade is protected as cultural heritage. We will show that applied solutions meet the basic conservation - restoration requirements: less is more, reversibility and compatibility; and the structural designers: rationality, simplicity and security; compatible with the principles of green building and minimal production of CO2. Due to the conversion of the building into a hotel, all the floor structures must be replaced with new reinforced concrete slabs, which significantly increases the weight of the building, and thus the seismic forces. The project was preceded by different on site structural tests, which will also be presented and which were performed for the structural assessment of the project. Very detailed 3D FEM model with solid elements was created on which the analysis of the structure was carried out. We will show the results of pushover analysis which proves an increase in the carrying capacity of the stone masonry walls after reinforcement with carbon fiber reinforced polymerscombined with the masonry walls grouting.

POJAČANJE ZIĐA U ZGRADI BIVŠE MARASKE U ZADRU

SAŽETAK: U radu se prikazuje projekt ojačanja postojeće zidane zgrade s pomoću traka izrađenih od ugljičnih vlakana. Zgrada je izgrađena 1911. Njezino je pročelje zaštićeno kao spomenik kulture. Pokazat će se da primijenjeno rješenje zadovoljava temeljne konzervatorsko-restauratorske zahtjeve: manje je više, reverzibilnost i kompatibilnost – i konstrukcijske zahtjeve: racionalnost, jednostavnost i sigurnost; spojivost s načelima zelene gradnje i minimalne proizvodnje CO_2. Zbog pretvorbe zgrade u hotel sve su stropne konstrukcije morale biti zamijenjene novim armiranobetonskim pločama koje znatno povećavaju težinu zgrade, a stoga i potresne sile. Prije izrade projekta provedena su različita terenska ispitivanja s ciljem ocjene konstrukcije. Ona su prikazana u radu. Proračun konstrukcije proveden je s pomoću vrlo detaljnog 3D modela metodom konačnih elemenata s krutim elementima. Prikazuju se rezultati proračuna s postupnim guranjem kojim je dokazano povećanje nosivosti kamenog ziđa nakon pojačanja trakama s ugljičnim vlaknima uz kombinaciju s injektiranjem ziđa.

1. INTRODUCTION

The former Maraska building was erected in 1911 by Michelangelo Luxardo according to the project of engineer Ludovico Pividori. Its façade is protected as cultural heritage (Figure 1). It was, for many years, the factory of the world-famous maraschino liqueur. The building has a main central section and two side asymmetrical wings. The plan dimensions are 60.5 * 10 m, west wing 15.7 * 6 m and the east wing of 12.5 * 17 m. The height of the building to the ridge is 20 m. There are the ground floor, two floors and an attic (Figure 2). According to then-custom, the structure was made up of several different materials. The walls are of roughly dressed stone with two faces and infill of stone fragments in the lime mortar. The foundations are concrete, while the lintels and pillars with beams on the second floor were made of reinforced concrete. Rigid reinforcement was embedded in the lintels on the ground floor. The window and door frames and other decorative elements on the facades and balconies were made of prefabricated concrete and reinforced concrete also. The ceiling structure above the ground floor is a shallow Prussian vault. Other inter-floor structures are wooden as well as the roof structure. The cover is of double interlocking tiles on the laths. Over time, there were interventions with concrete and reinforced concrete on the structure. Cracks are visible on the walls, lintels and cornices. The timber is decayed by fungi and woodworm. The floors and ceilings are damaged. The steel elements, especially in the walls, are corroded. The consoles and balustrade on the balconies are also damaged.

Figure 1 Main façade

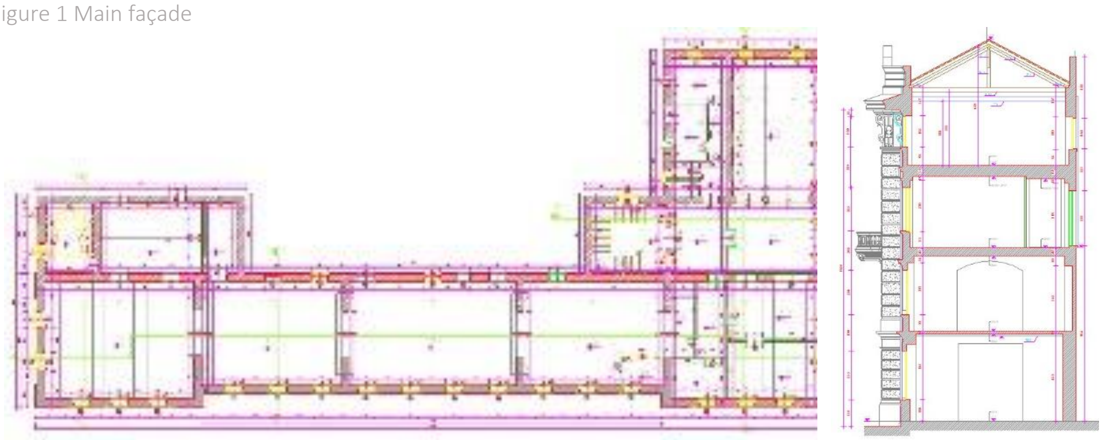

Floor plan

cross section

Figure 2 Existing state

The drafting of the hotel reconstruction project is in progress. Therefore, all the inter-floor structures will be replaced with new reinforced concrete slabs, some openings on the ground floor will be enhanced and a dozen rooms and engine rooms will be built in the attic. Several walls in the wings will be disassembled. The new roof structure will be steel. All this will significantly increase not only the vertical force but earthquake force also.

2. STRUCTURAL ASSESSMENT

Before the start of the project, extensive tests of structure and foundation soil were conducted. Soil mechanics and geophysical investigations of wider the area and foundation testing include: 17 investigation pits, 16 exploratory drillings, 8 MASW, 3 GPR profiles and 1 RF profile. Structural assessments consist of: reinforced concrete tests, stone masonry tests and structural dynamic characteristics assessment. Reinforced concrete tests include: determining the amount and position of embedded reinforcement in lintels, testing compressive strength of concrete cores (Figure 3a) and testing compressive strength of concrete by rebound hammer. Stone masonry tests: testing the shear strength of walls on 24 points (Figure 3b), testing compressive strains (Figure 3c) and the strength of masonry on 5 points and video endoscopy on 32 points (Figure 3d). Stone masonry cohesion and angle of internal friction were estimated based on the data of shear strength and compressive stresses in the masonry. Large and numerous cavities in the walls were found by endoscopy examination, which confirmed the necessity of wall grouting. We performed measurements for assessment of natural frequencies and damping on 32 points in 8 verticals using the TROMINO device (Figure 3e). We needed this data for calibrating 3D FEM model of existing structure.

Core drilling | Shear test | flat jack test | endoscopy | TROMINO

Figure 3 Structural assessments

3. DESIGN SOLUTIONS

Guided by the fundamental principles of conservation and restoration: less is more, reversibility and compatibility [1]; and structural: rationality, simplicity and security; a priori we opted for the following. The existing masonry was strengthened by grouting and deep mechanical repointing with mortars based on hydraulic lime. It is thus possible to raise the capacity of the walls for more than 50%, the rest needs to be compensated with carbon fibers. Carbon fibers are applied in the following manner: a one direction canvas (GV 160 UN TFX) in two orthogonal layers in the lime mortar based on hydraulic lime, vertical and horizontal strips (TCU 800/100) in epoxy adhesive, and ropes (G FIOCCO Ø12.0 mm) in epoxy adhesive for ensuring the continuity of the strips and interconnecting wythes. Tensile strength of carbon fibers is 4.900 MPa, Young's modulus 240 GPa and rupture elongation 2%. Hydraulic lime mortar for fixing canvas has tensile strength 3,1 MPa, compressive strength 10,6 MPa, Young's modulus 6,8 GPa and adhesion 1,2 MPa. Epoxy bond has following characteristics: tensile strength 30 MPa, bond strength >4 MPa; E-Modulus flexural 3,8 GPa and tensile 4,5 GPa, with elongation at break 0,9%. Laboratory tests have shown that the lack of connection between wythes caused the splitting breakdown of the wall in core [2] [3]. This can be prevented by wrapping walls around the range, which in our case is not possible, therefore, we decided to connect the wythes with anchors. The biggest challenge was to activate the carbon fiber to participate in the takeover of horizontal forces in the 3D FEM model. During the analysis of the model the necessity to trim enhanced openings with RC frames was shown (Figure 4).

Mortars based on hydraulic lime are compatible with the existing masonry, and do not generate harmful minerals ettringite and thaumasite which are incurred in enforcing the cement mortar. Carbon fibers in lime mortar can be easily removed from the wall, as well as fibers in epoxy adhesive remover using industrial fans. Reversibility is thus ensured.

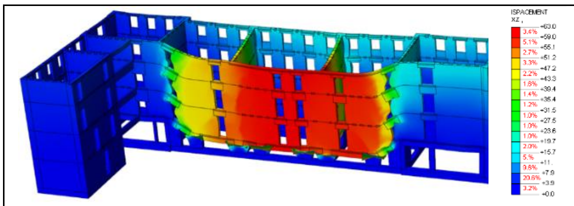	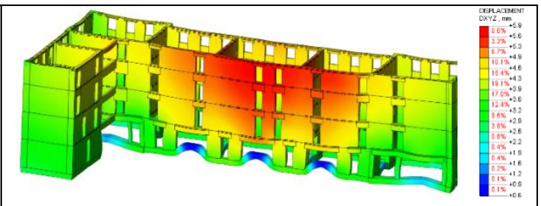
without RC frames	with RC frames

Figure 4 Axis 2 (rear façade) - Deformations of the vertical load

4. A 3D FEM MODEL AND COMPUTATIONS

Contact between structure and foundation soil are modeled as a surface spring elements. Stone walls and RC parts of the structure (beams, columns, floor structure plugs and foundations) are modeled as solid (tetrahedron) elements. New reinforced concrete slabs were modeled as plate elements as well as the steel roof structure with beam elements. Reinforcement in the existing and new parts RC structure is modeled as grid reinforcement sets, in the same way as carbon fibers walls reinforcement is modeled.

Details on which we pay attention while making numerical models are: eccentricity of masonry walls per floors (the walls are asymmetrically thinner on the upper floors); the existing lintel concrete beams with embedded existing reinforcements; lintel cross section is modeled like original "L" shape above ground, first and second floors; lintels at ground floor are modeled with embedded INP steel profile (without reinforcement) as in the existing state; masonry parapet walls are thinner than the wall, with its eccentricity in relation to walls; RC plugs through which the floor slabs are lining on walls; steel roof structure with its eccentricity in relation to walls; steel reinforcement (longitudinal and stirrups) of new RC elements (foundations, columns, beams); existing concrete and stone masonry foundation structure and new RC side foundation strip strengthens.

In the Midas FEA we made the next type of analyzes: nonlinear for vertical loads (self-weight, dead load, live load); modal (eigenvalue analyze), response spectrum and push-over (nonlinear construction stage analyze "sequence analyze"). Using this method of push over analysis we activate carbon fiber for the absorption of horizontal loads. For push over analyze inertial forces are used and obtained from response spectrum load case for modes (eigenvalues) which participated with more than 1.0% of the total mass. Acceleration on location peak ground (AgR) is: 0.185g for design spectrum Tp = 475 years and 0.091g for elastic spectrum Tp = 95 years.

Concerning the different types of materials, we used different nonlinear material behavior laws: Von-misses nonlinear behavior model for new and existing concrete reinforcement and existing steel profiles embedded in the beams above the ground floor (in axis "01"); elastic material behavior for new RC floor slabs and associated RC plugs; and "TSC" total strain crack nonlinear behavior model for concrete and stone masonry. Total strain crack "TSC" is smeared crack defined with the next parameters: crack model – fixed; stiffness – secant; lateral crack effect - Vecchio and Collins; confinement effect – none, tension function – Hordijk; compression function – parabolic; and shear function – none.

Reinforcement with carbon fibers has drastically reduced horizontal shifts and increased the carrying capacity of the walls. Overall displacements on the 10 controlled points on top of the building were reduced from an average of 84.9 mm to 9.7 so for 75.3 mm or 89% (Figure 5). Inter-story drifts have also been reduced by an average of 75% (Figure 6).

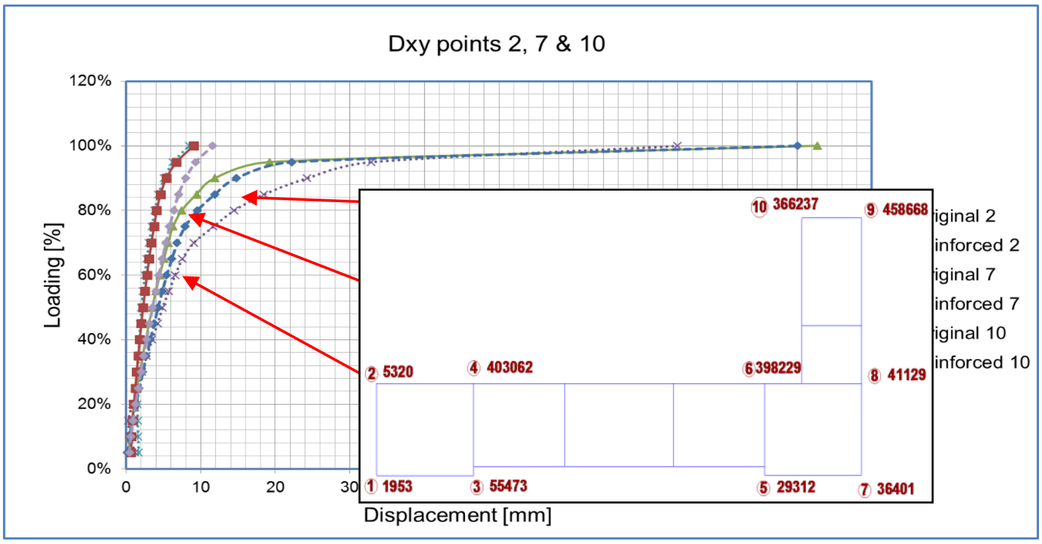

Figure 5 Overall horizontal displacements for earthquake -1Y-0,3X in points 2, 7 and 10

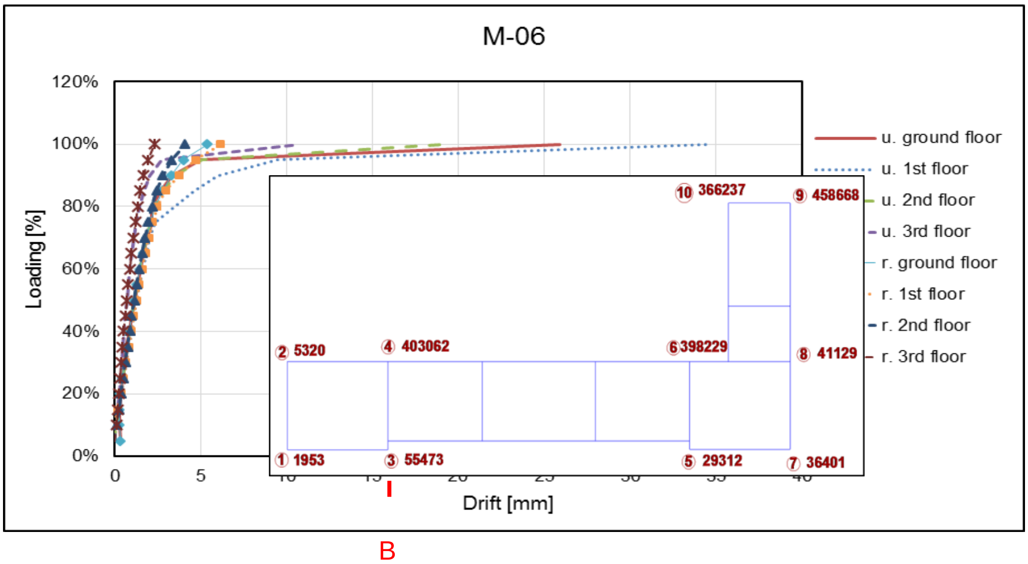

Figure 6 Drifts for earthquake -1Y-0,3X in corner M-06

Comparing the fissured state, before and after reinforcement structure with carbon fibers, shows a significantly reduced number and size of cracks. Efficiency is more pronounced on the walls which are reinforced on both sides with carbon fibers (Figure 7), compared to those that are unilaterally strengthened (Figure 8).

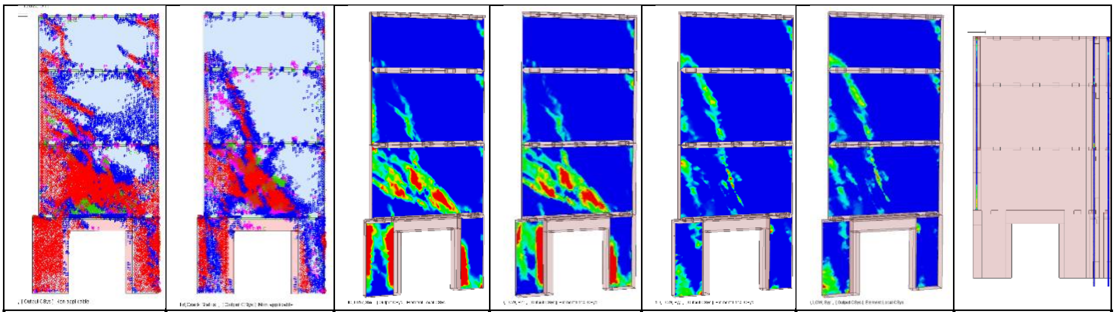

Cracks before reinforcement	Cracks after reinforcement	Tensile stresses in carbon fabrics horizontal direction side A	Tensile stresses in carbon fabrics horizontal direction side B	Tensile stresses in carbon fabrics vertical direction side A	Tensile stresses in carbon fabrics vertical direction side B	Tensile stresses in carbon tapes

Figure 7 Line B (as shown on Figure 6) - Cracks in wall and stresses in carbon fibers

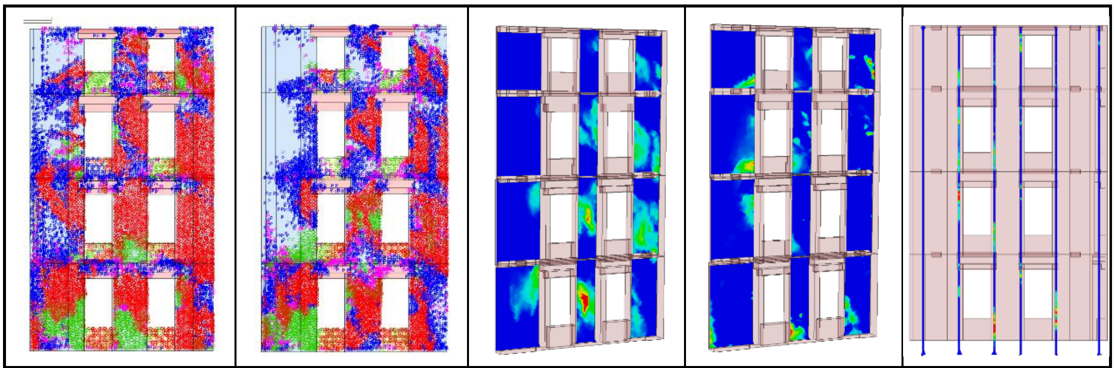

Cracks before reinforcement	Cracks after reinforcement	Tensile stresses in carbon fabrics horizontal direction	Tensile stresses in carbon fabrics vertical direction	Tensile stresses in carbon tapes

Figure 8 Line A (west façade) - Cracks in wall and stresses in carbon fibers

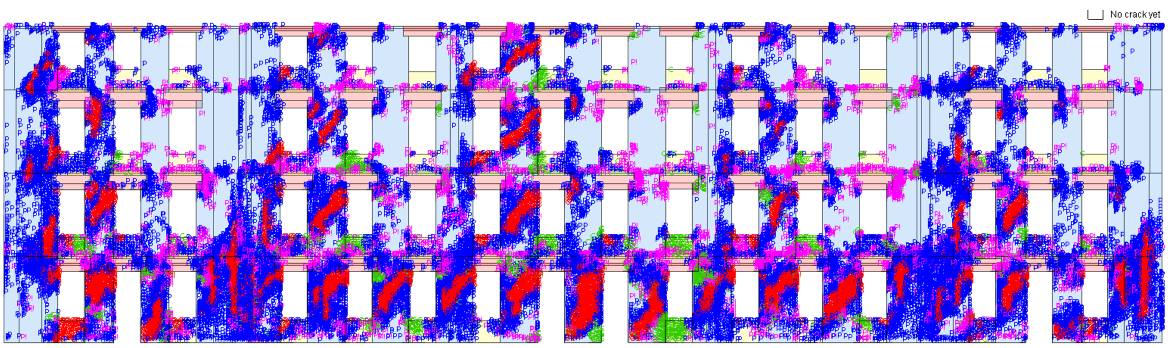

Figure 9 Axis 1 (main façade) - Cracks before reinforcement for earthquake -1Y-0.3X

The effect of reinforcing transverse walls on the longitudinal walls is reflected by the difference in the image of the cracks on the wall in axis 1 before (Figure 9) and after (Figure 10) reinforcement. Although the tapes of carbon fiber, by stress state, have not been fully utilized, we decided to install them to ensure the effect of bounded walls.

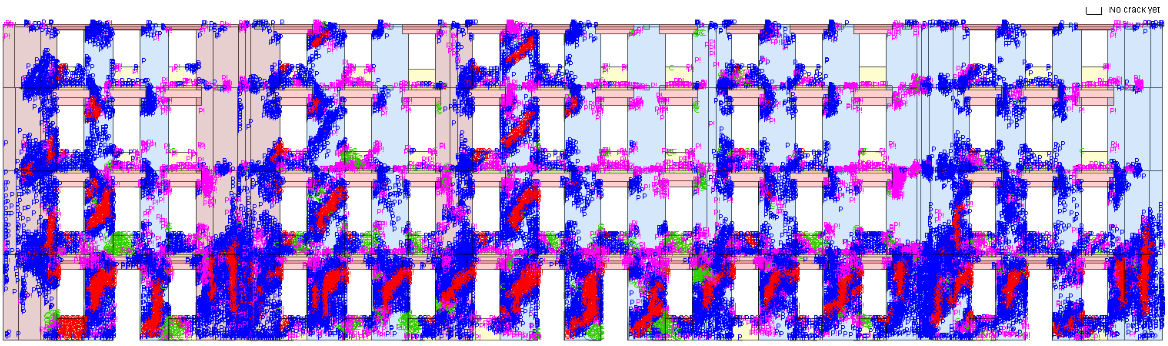

Figure 10 Axis 1 (main façade) - Cracks after reinforcement for earthquake -1Y-0,3X

5. ALTERNATIVE DESIGN SOLUTIONS

Driven by the general theme of this conference, I wanted to check if our solutions which meet the fundamental conservation - restoration and structural requirements are compatible with the principles of sustainable construction and minimal production of CO_2. The alternative was to build a new RC structure within the existing stone walls which will take over all the new vertical and horizontal loads as well as part of the horizontal forces of the existing walls. Sub-variants of this solution were shotcreting the walls with installing mesh reinforcement, construction RC frames or RC walls within the perimeter the existing stone walls. Shotcreting is unacceptable because it is irreversible and incompatible with stone masonry. It also increases the stiffness of the structure that generates higher seismic forces which, besides the shotcrete, are to take over by the existing walls. Young's modulus of masonry and shotcrete are different, rheology of materials is different which ultimately results as damages on the structure not only from horizontal loads but also from vertical loads. The flaw variant with RC framework is that RC frames do not have sufficient rigidity that cannot assume the horizontal loads without the participation of the existing walls. An absurd situation therefore arises where the existing walls must take horizontal loads with reduced vertical loads, which further reduces their bearing capacity. RC walls may be adopted as an acceptable solution, if you ignore the irreversibility and the problems of RC wall foundation within an existing building and if the separation of RC walls from the existing masonry is provided with appropriate insulation. We thus compare our and alternative solution regarding the CO_2 footprint, starting with the assumption of the RC walls being built 20 cm thick in the one-sided formwork, insulation is lost formwork supported on existing walls. The assumed amount of steel is 150 kg / m^3.

6. CO_2 FOOTPRINTS

According to the manufacturer of carbon fiber for production of 1 kg of fibers emitted from 9.7 to 23.4 kg of CO_2, on average 16.55 kg [4]. We took the highest value. We will take the same CO_2 emission for the plaster as well as for the concrete. The production of 1 kg portland cement clinker emits 0.85 kg of CO_2 [5]. To produce 1 kg of concrete emits 0.11 kg of CO_2 and for 1 kg of reinforcing steel 0.91 kg of CO_2 [6].

7. COMPARISON OF CO_2 FOOTPRINTS FOR THE DESIGN AND ALTERNATIVE SOLUTION

For the simplicity and transparency of comparison, data will be presented in following table.

Table 1 Comparison of CO2 footprints

DESIGN SOLUTION	carbon fiber	plaster	ALTERNATIVE SOLUTION	concrete C25/30	steel reinforcement
designed amount [kg]	1,440	50,000	estimated amount [kg]	2,512,500	150,750
CO_2 emission [kg/kg]	23.4	0.11	CO_2 emission [kg/kg]	0.11	0.91
CO_2 emission [kg]	33,696	5,500	CO_2 emission [kg]	276,375	137,183
total CO_2 emission [kg]		39,196	total CO_2 emission [kg]		413,558

The ratio between the total CO_2 emissions of the alternative solution and designed solution is 10.55 which undoubtedly proves that the chosen solution is more acceptable than the alternative. The total area within the existing stone walls is 2344 m2, with the construction of RC walls it would be reduced to 2164 m2, which decreases the area by 170 m2, or 7.7%.

8. INSTEAD OF CONCLUSION

Remembering professor Tonković's motto, from one of his scripts, "The numbers are sometimes only consolation to the structural engineer" we have no choice but to wait for an earthquake and see how the structure will really behave.

REFERENCES

[1] ICOMOS/ISCARSAH Committee: Recommendations for the analysis, conservation and structural restoration of architectural heritage (2005) http://www.icomos.org/ Accessed: 2012-06-23

[2] Lutman, M. et al: In situ tests for the assessment of seismic strengthening of historic brick masonry walls with carbon fiber fabric, 15 WCEE, Lisbon, (2012)

[3] Tomaževič, M. et al: Strengthening of stone masonry walls with composite reinforced coatings, *Bulletin of Earthquake Engineering*, pp. 2003-2027, ISBN, 1570-761X, July 2015, Springer

[4] Processing Advancements Within Reach for Achieving Significant Reductions in Carbon Fiber Cost of Manufacturing, *JEC Europe 2013, Paris ICS Carbon Conference* http://www.harperintl.com/wp-content/uploads/2011/09/JEC.pdf Accessed: 2016-06-18

[5] Štirmer N.: Utjecaj građevnog materijala na okoliš, *Radovi Zavoda za znanstveni i umjetnički rad u Požegi*, 1(2012), pp. 293-311

[6] Leung S.: Carbon Dioxide (CO2) Emissions of Concrete, Arup Materials Technology. SCCT 2009. https://www.devb.gov.hk/.../6_mr_stephen_leung_carbon_dioxid Accessed: 2016-06-18

STRENGTHENING OF REINFORCED CONCRETE STRUCTURES WITH TEXTILE REINFORCED MORTARS

Tomislav Kisicek[1], Martina Caric[1]

[1] University of Zagreb Faculty of Civil Engineering, Department of Structural Engineering, Fra Andrije Kacica Miosica 26, 10 000 Zagreb, Croatia, email: kisha@grad.hr, mcaric@grad.hr

SUMMARY: In the last years, textile reinforced mortars (TRM) has been investigated for strengthening reinforced concrete and masonry structures, along with fibre reinforced polymers (FRP). TRM are composites made of fibres embedded in cementitious matrix, which has better performance than epoxy one – cementitious matrix is not degraded at service temperature above the glass transition temperature and tensile behaviour is not linear elastic to failure. Fibre rovings create open-mesh geometry (fabric grids) because the bond between the fabric and the mortar is achieved by mechanical interlock. This paper presents a review of the former researches in strengthening or reinforced concrete elements subjected to bending, shear, and compression. The parameters that affect the behaviour of reinforced elements are analysed and advantages compared to FRP are presented.

POJAČANJA ARMIRANOBETONSKIH KONSTRUKCIJA POMOĆU TKANINOM ARMIRANIH MORTOVA

SAŽETAK: Uz polimere armirane vlaknima, kao materijal za pojačanja armiranobetonskih i zidanih konstrukcija, posljednjih godina istražuju se mortovi armirani tkaninom. To su kompoziti vlakana i anorganske (cementne) matrice koja se odlikuje boljim svojstvima od epoksidne matrice – ne događa se degradacija pri temperaturi višoj od temperature staklastog prijelaza i ponašanje vlačno opterećenog elementa nije linearno elastično do sloma. Snopovi vlakana formirani su u mreže kako bi se ostvarila mehanička veza s matricom. U radu je prikazan pregled dosadašnjih istraživanja pojačanja betonskih elemenata opterećenih na savijanje, poprečnu silu i tlačno opterećenih elemenata. Analizirani su parametri koji utječu na ponašanje pojačanih elemenata i prikazane prednosti u usporedbi s polimerima armiranih vlaknima.

1. UVOD

Posljednjih godina sve je veća potreba za pojačanjima ili popravcima postojećih konstrukcija kako bi im se produljio životni vijek. Uz mnoge metode pojačanja konstrukcija jedna od najčešćih je pojačanje upotrebom kompozitnih materijala - vlaknima armiranih polimera (engl. fiber reinforced polymer, FRP). FRP kompoziti sastoje se od polimerne matrice (najčešće epoksidne smole) i armaturnih vlakana od kojih su najčešća staklena (engl. glass, G), ugljična (engl. carbon, C) ili aramidna (engl. aramid, A). FRP sustavi privlače sve veću pozornost zbog svojih povoljnih svojstava kao što su: otpornost na koroziju, visoka vlačna čvrstoća, iznimno velik omjer čvrstoće i težine, dobro ponašanje pod dinamičkim djelovanjem te jednostavnost i brzina primjene [1]. Osim brojnih prednosti, FRP pojačanja imaju i nedostatke koji se pripisuju smolama koje se koriste za vezanje ili impregnaciju vlakana, kao što su: loše ponašanje epoksidnih smola na temperaturama većim od temperature staklastog prijelaza, relativno visoka cijena epoksidnih smola, nemogućnost nanošenja na mokre podloge i pri niskim temperaturama, nekompatibilnost epoksidnih smola i materijala podloga, manjak paropropusnosti koji može dovesti do oštećenja betonskih konstrukcija te teža procjena štete na njima nakon potresa, iza neoštećenog FRP pojačanja [2]. Osim toga glavni nedostatak FRP-a je njegovo linearno-elastično ponašanje do sloma, tj. njegovo neduktilno ponašanje.

Kao jedno od rješenja navedenih problema kod FRP kompozita je zamjena organskog veziva s anorganskim, primjerice cementnim mortom kao matrice kod takvog kompozitnog materijala. To dovodi do upotrebe tkaninom armiranih mortova, u stranoj literaturi poznatih kao fabric-reinforced cementitious matrix (FRCM) systems, textile-reinforced mortar (TRM), mineral-based composite (MBC) ili textile-reinforced concrete (TRC) systems. Ovi materijali sastoje se od mreže (tkanine) izrađene od snopova vlakana (staklenih, ugljičnih, bazaltnih ili PBO vlakana) u najmanje dva (najčešće ortogonalna) smjera i anorganske matrice (slika 1), pa se tako razlikuju GTRM, CTRM, BTRM ili PBOTRM. Vlakna preuzimaju vlačna naprezanja, dok matrica štiti vlakna i prenosi naprezanja s betona ili ziđa, koje se pojačava, do vlakana. Gustoća mreže, odnosno količina snopova vlakana i njihov razmak može se u svakom smjeru kontrolirati neovisno, čime se utječe na mehanička svojstva tekstila i stupanj prodiranja u mort preko mreže. TRM u kojem su vlakna formirana u trake nisu povoljno rješenje jer matrica ne može dovoljno dobro impregnirati vlakna. Prianjanje između tkanine i morta je postignuto mehaničkim uklinjavanjem kao rezultatom prodiranja morta u razmake mreže. Anorganska matrica ima veći toplinski kapacitet i kompatibilnija je s betonom za razliku od epoksidne.

Za pojačanja konstrukcija, TRM kompoziti postavljaju se na isti način kao i FRP kompoziti, najčešće „hand lay-up“ metodom. Najprije se nanosi sloj morta, zatim sloj mreže pa opet sloj morta i postupak se ponavlja ovisno o broju slojeva koji se želi postići. Važno je da se svaki sloj morta nanese dok je prethodni još svjež [3].

a)

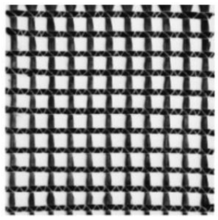

b)

Slika 1 a) cementna matrica b) ugljična vlakna

U prošlom desetljeću provedeno je više istraživanja pojačanja armiranobetonskih elemenata opterećenih savijanjem, poprečnim silama, te tlačno opterećenih elemenata. Isto tako istražuje se i seizmička obnova armiranobetonskih stupova, armiranobetonskih okvira s ispunom te obnova zidanih konstrukcija. U ovom radu dan je pregled nekih dosadašnjih istraživanja vezanih za svojstva TRM kompozita i njihovu primjenu pri pojačavanju armiranobetonskih elemenata opterećenih na savijanje, poprečnu silu ili tlačno opterećenih elemenata. Dane su i neke smjernice za buduća istraživanja.

2. PRIONJIVOST TRM KOMPOZITA

Ponašanje i učinkovitost pojačanja TRM-om ovisi o vlačnoj čvrstoći i karakteristikama prianjanja kompozitnog materijala [3-9].

Ponašanje vlačno opterećenog TRM-a sastoji se od 3 faze (slika 2a)). U prvoj fazi, do pojave prve pukotine, TRM se ponaša linearno elastično i vlačna naprezanja primarno preuzima matrica. Nakon pojave prve pukotine krutost kompozita se smanjuje. Nastavkom razvoja pukotina, s povećanjem njihovog broja, TRM prelazi u drugu fazu u kojoj se relativne deformacije povećavaju uz mali prirast vlačnih naprezanja. Duljina trajanja te faze ovisi o mehaničkim karakteristikama i matrice i tkanine te kvaliteti veze tkanina –matrica. U trećoj fazi, u kojoj ne nastaju nove pukotine nego se prethodne proširuju, TRM ima reduciranu krutost s obzirom na neraspucano stanje tako da je linearni nagib dijagrama manji u odnosu na prvu fazu. Treća faza traje do otkazivanja progresivnim slomom vlakana, koji se razvija od manjeg broja vanjskih vlakana i širi prema unutarnjim. Konačno naprezanje i modul elastičnosti u zadnjoj fazi najviše ovisi o svojstvima tkanine. slika 2b) prikazuje pojednostavljenje dijagrama sa slike 2a) u obliku bilinearnog dijagrama [9]. Za razliku od TRM-a, FRP se ponaša linearno elastično do sloma. Krajnja relativna deformacija TRM-a ograničena je krajnjom relativnom deformacijom vlakana. Kod FRP-a prianjanje između matrice i vlakana je veliko pa nema proklizavanja na spoju vlakana i matrice, što je suprotno od ponašanja TRM-a gdje proklizavanje postoji.

Za prijenos sila s podloge na TRM, važno je prianjanje između starog betona i matrice, prianjanje između vlakana i matrice te prianjanje među vlaknima. Na prianjanje između starog betona i matrice utječu vlačna i posmična čvrstoća betona i matrice, na prianjanje između vlakana utječe trenje između njih, dok na prianjanje između vlakana i matrice utječe adhezija i trenje.

S obzirom na složeno kompozitno djelovanje, postoji više modova otkazivanja TRM-a,od kojih je najčešći odvajanje na površini tkanina – matrica, karakteriziran poprečnim pukotinama koje se javljaju na opterećenom kraju uzorka i šire, s povećanjem sile prema neopterećenom kraju. Poprečne pukotine nastaju iz horizontalne koja se formira na površini tkanina – matrica. Ovaj mod sloma praćen je proklizavanjem i deformacijom uzdužnih snopova vlakana [6]. Drugi mod je proklizavanje tkanine unutar matrice koje se javlja u nekim uzorcima sa 1 slojem tkanine [7]. Treći mod otkazivanja je odvajanje TRM-a od betonske podloge, zbog čega je važna priprema podloge prije nanošenja pojačanja i kompatibilnost matrice s betonom [7]. Kao četvrti mod otkazivanja je slom tkanine u matrici koji se može dogoditi zbog loše prionjivosti vlakana i matrice.

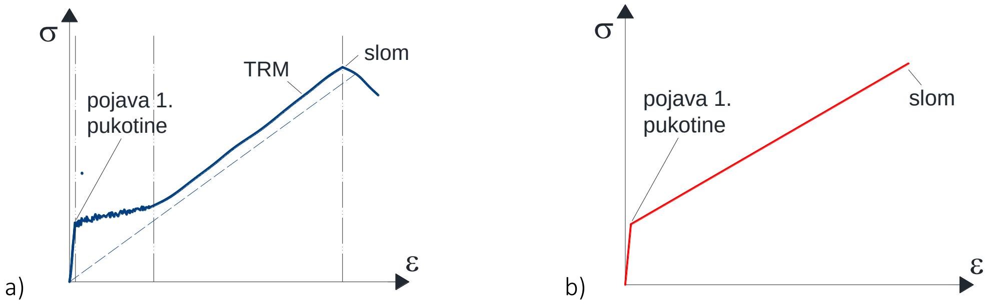

Slika 2 a) stvarni dijagram TRM-a u vlaku, b) bilinearni dijagram TRM-a u vlaku

Mnogo čimbenika i njihovo međudjelovanje utječe na prionjivost vlakana unutar kompozita i kompozita i podloge te na modove otkazivanja. Snopovi vlakana raspoređeni u mreže učinkovitiji su i do 30% od snopova u trakama zbog razmaka u mreži kroz koje prodire matrica i omogućuje bolju vezu vlakana i matrice [5]. Snopovi mogu biti obloženi smolom kako bi se poboljšala njihova prionjivost s matricom i prijenos sila među vlaknima. Na prionjivost između vlakana i matrice, kao i prionjivost između betona podloge i matrice, utječu i svojstva matrice. Mort koji čini matricu mora imati dobru obradivost, otpornost na skupljanje i viskoznost kako bi se mogao primjenjivati na vertikalnim površinama. Sitni agregat pomaže impregnaciji morta u tkaninu. Jedan od dosta ispitivanih parametara je i broj slojeva pojačanja. Povećanjem broja slojeva prionjivost se neproporcionalno povećava, a povećanje je značajnije kod promjene broja slojeva sa jednog na dva, nego pri većem broju slojeva. Broj slojeva utječe i na promjenu moda otkazivanja sa proklizavanja tkanine u matrici kod uzoraka s jednim i 2 sloja pojačanja na odvajanje TRM-a od betona kod uzoraka sa 3 i 4 sloja [8]. Drugi, u prethodnoj literaturi dosta proučavan parametar je duljina sidrenja TRM kompozita za podlogu. Zaključeno je da se prionjivost neproporcionalno povećava sve do određene duljine sidrenja koja se naziva efektivna duljina sidrenja, iznad koje je povećanje prianjanja neznatno. Ova duljina varira u literaturi, ali je u granicama 150-350 mm [6,7]. Kako bi prianjanje između starog i novog betona bilo bolje, površina starog betona mora biti obrađena brušenjem i pjeskarenjem [8]. Sidrenje se može još poboljšati ovijanjem duljine sidrenja promatranog TRM-a ili ugradnjom posebnih sidrenih sustava. Kod ispitivanja utjecaja sidrenja kroz omatanje na uzorcima sa 3 i 4 sloja pojačanja, zabilježeno je povećanje čvrstoće od 28 % i 45 % i poboljšanje prionjivosti s betonom u odnosu na neusidrena pojačanja, odnosno sprječavanje odvajanja TRM-a od betonske podloge [8]. Tlačna čvrstoća betona nema značajan utjecaj na prianjanje betona i TRM-a. Kod tlačnih čvrstoća betona od 30 MPa i 15 Mpa, niža tlačna čvrstoća uzrokovala je redukciju prionjivosti od 7,5 % [8]. Jedna od glavnih prednosti pred FRP-om je ponašanje TRM-a pri visokim temperaturama. Kao i kod većine materijala, povećanjem temperature, smanjuju se krutost i sila sloma te je moguća i promjena oblika sloma. Kod uzoraka s 2 sloja zagrijanih na 50°C i 100°C, sila sloma se smanjila 28 % i 38 %, dok se kod uzoraka s jednim slojem nije smanjila ili se smanjila 36 % [7].

3. POJAČANJA ARMIRANOG BETONA

3.1. POJAČANJE NA SAVIJANJE

Kako bi se povećala nosivost greda, odnosno ploča na savijanje, TRM pojačanja postavljaju se na njihovo vlačno područje (slika 3). Gustoća mreže može varirati ovisno o smjerovima u kojima je pojačanje potrebno. U [2,5,10-13] proučavano je ponašanje TRM-om pojačanih greda na savijanje

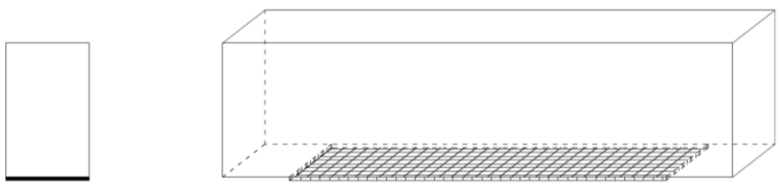

slika 3 pojačanje greda na na savijanje

Rezultati spomenutih istraživanja pokazali su da svaki tip vlakana ima različita mehanička svojstva koja utječu na kapacitet nosivosti. PBO tkanine su pokazale bolje ponašanje od ugljičnih, zbog bolje veze tkanine i matrice. Grede pojačane s CTRM otkazale su proklizavanjem tkanine u matrici i s povećanjem nosivosti 16 %, a grede pojačane sa PBO-TRM otkazale su odvajanjem na površini beton-matrica, sa povećanjem nosivosti 30 % u odnosu na nepojačanu gredu [10]. Za primjereno ponašanje kompozita, osim pravilnog odabira vrste vlakana važna je i vrsta matrice. Vlakna dodana matrici omogućuju bolju vezu između slojeva TRM-a, bolju duktilnost, odnosno povećavaju učinkovitost pojačanja [2]. Uzorci sa matricom od standardnog cementnog morta otkazali su odvajanjem TRM-a sa povećanjem nosivosti od 82 %, a s matricom od polimerom modificiranog morta slomom tkanine i povećanjem nosivosti od 91 %. Nadalje, nakon odabira vrste kompozita važna je konfiguracija pojačanja i broj slojeva pojačanja. Uzorci s 2 sloja pojačanja na donjoj površini otkazali su odvajanjem na površini matrica – beton i sa klizanjem tkanine i povećanjem čvrstoće od 9 %, dok su uzorci pojačani s jednim slojem na donjoj površini i omotani jednim „U“ slojem (slika 3) otkazali klizanjem tkanine i povećanjem čvrstoće 18 %, što znači da „U“ pojačanja imaju veću učinkovitost od pojačanja samo na donjoj površini [10]. Povećanjem broja slojeva kapacitet nosivosti neproporcionalno raste što su pokazala mnoga ispitivanja. U [12] za broj slojeva 1,2 i 3, kapacitet nosivosti se povećao 16 %, 33 % i 40 %. Broj slojeva utječe i na mod sloma. U [13] uzorci s jednim i 2 sloja lomili su se klizanjem tkanine u matrici, a uzorci s 3 sloja pojačanja, odvajanjem TRM-a od betona. Učinak sidrenja na krajevima, tj. „U“ pojačanja postavljena kao dodatan sloj na krajevima uzorka mogu povećati kapacitet ako se odvajanje TRM-a od betonske podloge odvija upravo u tim područjima. Učinak takvog sidrenja nije značajan za odvajanja pojačanja van područja sidrenja [10]. Čvrstoća betona nema značajan utjecaj na ponašanje pojačanih elemenata. S obzirom na to da se pojačavaju armiranobetonske grede, potrebno je ispitati utjecaj vlačne armature na učinkovitost pojačanja. Pri većem koeficijentu armiranja vlačnom armaturom (ρ), povećanje nosivosti je niže upravo zbog doprinosa armature otpornosti na savijanje. Kod uzoraka sa omjerima armature 0,72 % i 1,27%, povećanje nosivosti nakon pojačanja kod koeficijenta armiranja vlačnom armaturom bilo je 23 – 78 %, a kod višeg 14 – 47 % [13].

U [2, 10, 14] analizirana su TRM i FRP pojačanja na savijanje u svrhu odabiranja najpovoljnijih rješenja. Iz dobivenih rezultata pokazano je da je u usporedbi s FRP-om, TRM nešto manje učinkovit u smislu poboljšanja nosivosti na savijanje, ali učinkovitiji u smislu duktilnosti. Na temelju eksperimenata, za razliku od FRP-a, u najviše slučajeva kod pojačanja TRM-om odvajanje se događa na površini tkanina – matrica i ne uključuje beton. Pri povišenim temperaturama (50°C i 80°C), sustavima s FRP-om čvrstoća se smanjila 10 – 52 % i 64 – 74 % ovisno o gustoći vlakana, a čvrstoća TRM-a se smanjila za 6 % i 28 %, s time da je i vlačna čvrstoća betona smanjena na ovoj temperaturi izloženosti. Pri povišenim temperaturama uzorci pojačani FRP-om lomili su se odvajanjem zbog omekšavanja ljepila i smanjenja čvrstoće spoja, a uzorci s TRM-om otkazali su posmično pa smanjenje čvrstoće više predstavlja smanjenje čvrstoće betona nego oštećenje sustava pojačanja.

3.2. POJAČANJE NA POPREČNU SILU

Za povećanje nosivosti greda na poprečnu silu pojačanja se postavljaju kao na slici 5. Usvojeni nazivi za različite tipove pojačanja su SB (engl. Side-bonding), UW (U-wrapping) i FW (full-wrapping). U [15-21] proučavano je ponašanje TRM-om pojačanih greda na poprečnu silu.

Dosta je parametara kompozita koji imaju utjecaj na posmičnu nosivost. Tip tkanina ovisno o njihovim svojstvima ima veliku ulogu u pojačanjima. Mnoga ispitivanja proučavala su utjecaje različitih tipova tkanina, naročito uporabu novijih vrsta, primjerice tkanina od PBO vlakana. U ispitivanju greda pojačanih GTRM-om, CTRM-om, PBOTRM-om i BTRM-om, najučinkovitiji tip vlakana u povećanju kapaciteta nosivosti na poprečne sile je PBOTRM, dok je CTRM pokazao nekonzistentno ponašanje zbog slabe veze betona i matrice [17]. Geometrija tkanine, odnosno gustoća mreže također ima utjecaj na nosivost. U [16] je manji razmak u mreži uzrokovao veću silu pri pojavi prve pukotine zbog bolje veze na površini tkanina – matrica. Također, veća količina vlakana u tkanini povećava čvrstoću, jer na konačnu čvrstoću kompozita najviše utječu vlakna. Vlakna se mogu dodati i mortu, kako bi se povećala učinkovitost kompozita. Povećanje čvrstoće u uzorcima s polimerom modificiranim mortom u [18] je 62 % u usporedbi sa standardnim cementnim mortom. Postavljanje tkanine za pojačanje na poprečnu silu važan je parametar. Konvencionalna konfiguracija podrazumijeva pozicioniranje tkanine u smjeru okomitom na uzdužnu os grede, dok je spiralna pod kutom u odnosu na os. U [19] nije dobivena velika razlika s obzirom na konfiguraciju, dok u [18] sa većim brojem TRM slojeva spiralna konfiguracija ima 1,5 puta veću čvrstoću. Povećanjem broja slojeva neproporcionalno se povećavaju čvrstoće i progibi zbog gušće tkanine koja vodi boljem mehaničkom uklinjavanju i štiti od preranog sloma tkanine [15,18]. Utjecaj čvrstoće betona je potrebno još istražiti jer je u [16] povećanje čvrstoće sustava manje s povećanom čvrstoćom betona, dok je u [20] povećanje čvrstoće betona uzrokovalo veće povećanje čvrstoće sustava. Mehaničko sidrenje može doprinijeti poboljšanju pojačanja. U ispitivanju greda T – presjeka usidrenim sa zakrivljenim čeličnim presjecima i vijcima pod kutom od 45° u pojasnicu, sidrenje je povećalo čvrstoću uzorka, tim više što je razmak vijaka bio manji (126 % i 104 % sa vijcima na razmaku 10 cm i 15 cm). Poboljšanje ponašanja očituje se i u promjeni moda sloma [10]. Također, i doprinos postojeće čelične armature utječe na ponašanje pojačanja. Tako je u [21] povećanje čvrstoće u uzorcima s 2 sloja bez spona je 145 %, sa sponama na razmaku 15 cm 67 %, a sponama na razmaku od 7,5 cm 55 %. Veći omjer spona znači i veću otpornost prije pojačanja, pa je sam doprinos pojačanja manji.

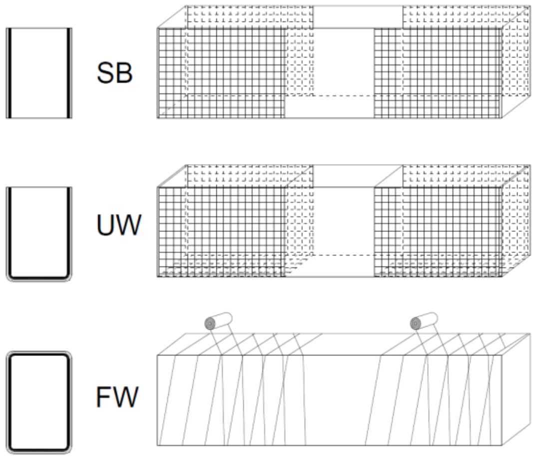

Slika 4 pojačanja pravokutnih greda na poprečnu silu

U [15, 21, 23] analizirana su pojačanja na poprečne sile FRP-om i TRM-om. TRM je generalno manje učinkovit u povećanju nosivosti na poprečnu silu od FRP-a, ali učinkovitost ovisi o konfiguraciji i broju slojeva. Učinkovitost TRM-a naspram FRP-a varira od 0,09 za 1 sloj SB pojačanja do 0,92 sa 2 sloja UW. UW pojačanje je mnogo učinkovitije nego SB kod TRM sustava u odnosu na FRP sustave. FW je za oba sustava najučinkovitiji. Glavna razlika je u povećanju broja slojeva s 1 na 2 pri čemu TRM ima mnogo veće povećanje učinkovitosti, a i mijenja se mod sloma te nema lokalnih oštećenja koja su prisutna pri 1 sloju pojačanja. TRM pojačanja imaju veću deformaciju pri slomu. Sidrenje TRM-a znatno poboljšava njegovu učinkovitost. Neusidrena FRP pojačanja su otprilike dvostruko više učinkovita od TRM-a, dok su usidrena TRM pojačanja malo manje učinkovita od FRP-a. Pri visokim temperaturama TRM je učinkovitiji u povećanju nosivosti od FRP-a, ali na povećanje znatno utječe konfiguracija pojačanja. I za TRM i FRP najučinkovitije je FW pojačanje, zatim UW, i onda SB. Modovi sloma pri visokim temperaturama SB i UW TRM-a ovise o broju slojeva tako da su pri povećanju broja slojeva s 2 na 3 spriječena lokalna oštećenja pojačanja, dok za FRP povećanje broja slojeva nema velikog učinka. Izloženost uzoraka TRM-a sa 3 sloja neznatno utječe na promjenu učinkovitosti pri temperaturama od 100°C do 250°C, dok kod FRP-a učinkovitost drastično pada pri povećanju temperature sa 100°C na 150°C.

3.3. POJAČANJE STUPOVA

U cilju povećanja nosivosti stupovi opterećeni uzdužno, a i savijanjem ovijaju se TRM-om [24-30].

Kao i kod pojačanja greda i ploča potrebno je analizirati parametre stupova i TRM-a koji utječu na nosivost. Tip tkanine i tip morta pri odabiru pojačanja imaju bitnu ulogu. U ispitivanju pravokutnih stupova ovijenih CTRM-om i GTRM-om, učinkovitost oba tipa bila je dosta slična u povećanju nosivosti na uzdužnu silu i deformacije pri slomu. Ipak, uzorci ojačani GTRM-om otkazali su lomom pojačanja kojem prethodi izvijanje čelične armature i deformiranje betona, dok je CTRM ostao neoštećen, vjerojatno zbog veće vlačne čvrstoće ugljičnih od staklenih vlakana [24]. Nadalje, uzorci čija je matrica bila mort tlačne čvrstoće 8,6 Mpa otkazali su odvajanjem TRM-a od betona na krajevima, a uzorci sa matricom od morta tlačne čvrstoće 30,6 Mpa otkazivali su lomom tkanine. Zaključuje se da na promjenu moda otkazivanja utječe promjena svojstava morta. U istom istraživanju drugi tip uzorka imao je veću nosivost na uzdužnu tlačnu silu [25]. Različiti su načini ovijanja stupova (slika 5). Konvencionalna metoda podrazumijeva omotavanje vlakana u smjeru okomito na uzdužnu od stupa, a spiralna pod nekim kutom u odnosu na os. U [26] pokazano je da je spiralno omotavanje manje učinkovito od konvencionalnog. Također, spiralno omotavanje pod kutom od 45° u odnosu na uzdužnu os stupa manje je učinkovito od onog pod kutom od 30°. U [27] razmatrana su spiralno omatana TRM pojačanja, lijepljena cijelom svojom duljinom ili samo na krajevima. Pojačanja lijepljena na krajevima imala su jednak mod otkazivanja kao i lijepljena cijelom svojom duljinom jer se slom dogodio daleko od mjesta sidrenja. Što se tiče učinkovitosti pojačanja, ono je manje kad su primijenjena 2 sloja ojačanja, a gotovo je jednako za 4 sloja ojačanja. U mnogim istraživanjima potvrđeno je povećanje čvrstoće i konačne deformacije s povećanjem broja slojeva. U [28] je pokazano da je učinak povećavanja broja slojeva manje izražen kod uzoraka s većim poprečnim presjekom. Povećanje čvrstoće stupova promjera 15 cm kod povećanja broja slojeva s 2 na 3 bilo je s 29 % na 51 %, a kod stupova promjera 20 cm s 28 % na 37 %. Oblik stupova koji se ovijaju važan je za učinkovitost pojačanja [30]. TRM je najučinkovitiji kod kružnog presjeka jer je pritisak u kružnim presjecima jednolik, a u prizmatičnim poprečnim presjecima, učinkovitiji je kod kvadratnog nego kod pravokutnog. Za učinkovitije ovijanje pravokutnih stupova, preporuča se zaobljenje njihovih uglova. Povećanje radijusa zaobljenja prizmatičnih stupova sa 15 mm na 30 mm nema velikog utjecaja na povećanje čvrstoće, ali povećanje konačne deformacije je 70 % [30]. Utjecaj tlačne čvrstoće betona na čvrstoću pojačanog uzorka treba još istražiti jer je pokazano da se za konvencionalno ojačane stupove čvrstoća uzoraka smanjila povećanjem čvrstoće betona, a za spiralno omotane stupove povećanjem čvrstoće betona povećavala se i čvrstoća uzorka [26]. Postojeća uzdužna i poprečna armatura u stupovima, također utječe na učinkovitost pojačanja. Ispitivani su uzorci sa kontinuiranom armaturom (bez preklopa), sa preklopom 20ϕ i 40ϕ. Izvijanje čelične armature u uzorku s kontinuiranom armaturom nije rezultiralo slomom. Uzorci sa kraćim preklopom imali su slom zbog gubitka prionjivosti uzdužne armature na mjestu preklopa nakon formiranja uzdužnih pukotina uslijed sila cijepanja po duljini preklopa, a u uzorcima s duljim preklopom slom je bio spriječen [24]. U [29] su uzorci ojačani sa 4 i 6 slojeva TRM-a i sponama na razmaku od 10 i 20 cm pokazali slične rezultate, pokazujući da promjena razmaka spona kod velikog broja slojeva može ostati prikrivena zbog značajne količine pojačanja.

U [24, 27, 31] analizirana su ovijanja stupova FRP-om i TRM-om. Kod kružnih stupova učinkovitost TRM-a manja je od FRP-a, a ta razlika se smanjuje povećanjem broja slojeva. Nadalje, za razliku od FRP-a, TRM ne otkazuje iznenada, nego njegov slom u obodnom smjeru počinje od malog broja snopova u trenutku kad vlačna naprezanja dosegnu vlačnu čvrstoću vlakana i onda se širi na susjedne snopove rezultirajući duktilnijim mehanizmom nego kod FRP-a. Kod pravokutnih stupova pojačanih TRM-om čvrstoća je otprilike jednaka kao kod stupova pojačanih FRP-om, ali je pojačanje TRM-om malo manje učinkovito što se tiče deformacija. Pri povećanim temperaturama TRM pokazuje bolje ponašanje. Pri promjeni temperature sa 40°C na 80°C, kapacitet nosivosti se smanjuje 5 % – 10 %, dok kod FRP-a nosivost pada otprilike 10 % za svakih 20°C povećanja, jer je iznad temperature staklastog prijelaza matrica degradirana i pojačanje gubi svoja svojstva. Pri cikličkom seizmičkom opterećenju i s kontinuiranom uzdužnom armaturom u stupu, uspoređujući čvrstoću i krutost, pojačanje TRM-om ima oko 50 % veću učinkovitost od pojačanja FRP-om. Za stupove sa preklopima uzdužne armature, kod većih preklopa pojačanja TRM-om i FRP-om imaju jednaku učinkovitost, a kod manjih preklopa FRP je nešto učinkovitiji.

4. ZAKLJUČAK

TRM sustavi imaju velik potencijal za povećanje nosivosti na moment savijanja, poprečnu i uzdužnu silu zbog čega im posljednjih godina brojni znanstvenici posvećuju pažnju. Ako se usporede s FRP sustavima, može se reći da je njihova učinkovitost pri normalnim temperaturama nešto manja, ali ne u svim slučajevima. Pri visokim temperaturama TRM kompoziti pokazuju mnogo bolje ponašanje od FRP-a. TRM kompoziti generalno su kompatibilni s betonskom podlogom i teže slomu veze na površini tkanina – matrica, dok FRP sustavi imaju uglavnom krti lom odvajanjem od betonske podloge. Veza tkanina – matrica može biti poboljšana modificiranjem gustoće mreže i pravilnim odabirom morta i vlakana. Veza tkanina – matrica a, kao i matrica – beton utječe na način otkazivanja i povećanje nosivosti pojačanih konstrukcija. Dosta parametara koji su prethodno opisani utječu na tu vezu, a time i na učinkovitost pojačanja. Potrebno je provesti još ispitivanja, kako bi se proučili i kvantificirali različiti utjecaji koji utječu na ponašanje TRM-a. Također je ispitivanja potrebno proširiti na sustave koji se češće pojavljuju u praksi, primjerice oštećeni nosači, kontinuirani i upeti. Daljnja ispitivanja su potrebna kako bi se zaključci mogli generalizirati za određeni tip kompozita. Sukladno tome bit će moguće razviti pouzdane modele i preporuke za dimenzioniranje, koji će se moći potom uvesti u smjernice i norme.

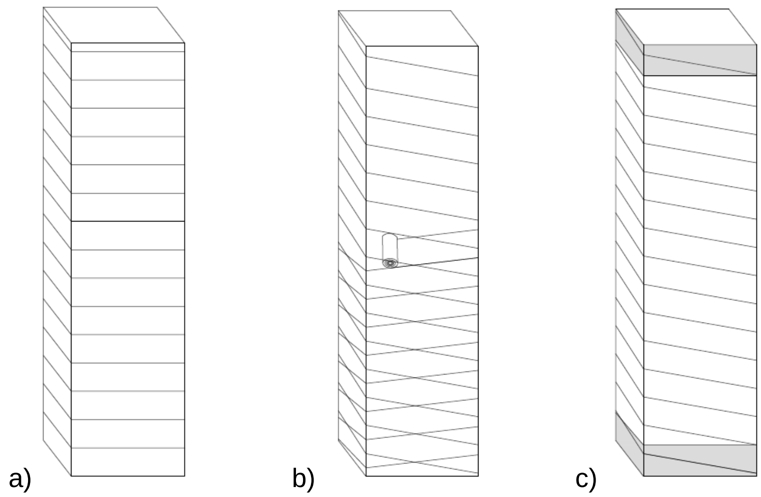

Slika 5 ovijanje stupova: a) konvencionalno, b) spiralno lijepljeno cijelom duljinom i c) spiralno lijepljeno na krajevima

ZAHVALA

Autori se zahvaljuju Ministarstvu znanosti, obrazovanja i sporta Republike Hrvatske i Sveučilištu u Zagrebu na potpori.

REFERENCES

[1] fib Bulletin 14. Externally bonded FRP reinforcement for RC structures. Technical report prepared by the working party EBR of the Task Group 9.3., International Federation for Structural Concrete, ISBN 2-88394-054-1, Lausanne, Switzerland, 2001.

[2] Elsanadedy, H.M. et al.: Flexural strengthening of RC beams using textile reinforced mortar – Experimental and numerical study, *Composite Structures*, 97 (2013), pp. 40-55, ISSN 0263-8223

[3] Awani, O., El-Maaddawy, T., Ismail, N.: Fabric-reinforced cementitious matrix: A promising strengthening technique for concrete structures, *Constr. Build. Mater.*, 132 (2017), pp. 94-111, ISSN 0950-0618

[4] Häußler-Combe, U.; Jesse, F.; Curbach, M.: Textile reinforced concrete - overview, experimental and theoretical investigations, Proceedings of the Fifth International Conference on Fracture Mechanics of Concrete Structures, Li, V. C. et al. (Ed.), pp. 749-756, ISBN 0 87031 135 2, Colorado, USA, April 2004

[5] Hashemi, S., Al-Mahaidi, R., Investigation of bond strength and flexural behaviour of FRP-strengthened reinforced concrete beams using cementbased adhesives, *Australian Journal of Structural Engineering*, 11 (2) (2010), pp. 129–139, ISSN 1328-7982

[6] Awani, O., El Refai, A., El-Maaddawy, T., Bond characteristics of carbon fabricreinforced cementitious matrix in double shear tests, *Constuction and Building Materials*, 101 (2015), pp. 39-49, ISSN 0950-0618

[7] Ombres, L., Analysis of the bond between Fabric Reinforced Cementitious Mortar (FRCM) strengthening systems and concrete, *Composites: Part B*, 69 (2015), pp. 418-426, ISSN 1359-8368

[8] Raoof S.M., Koutas L.N., Bournas D.A., Bond between textile-reinforced mortar (TRM) and concrete substrates: Experimental investigation, *Composites: Part B*, 98 (2016), pp. 350-361, ISSN 1359-8368

[9] ACI Committee 549.4R (2013), Guide to Design and Construction of Externally Bonded Fabric-Reinforced Cementitious Matrix Systems for Repair and Strengthening Concrete and Masonry Structures (ACI 549.4R-13), ISBN 0870318527, 9780870318528, ACI, Farmington Hills, Michigan, (2013)

[10] D'Ambrisi, A., Focacci, F., Flexural strengthening of RC beams with cement based composites, *Journal of Composites for Construction*, 15 (5) (2011), pp. 707–720., ISSN 1090-0268, 1943-5614

[11] Gil, L., Escrig, C., Bernat, Bending Performance of Concrete Beams Strengthened with Textile Reinforced Mortar TRM, Proceedings of the 14th Symposium on Experimental Stress Analysis and Materials Testing, Marsavina, L. (Ed.), pp.203-206, ISBN 978-3-03835-048-4,Timisoara, Romania, May 2013

[12] Ombres, L., Flexural analysis of reinforced concrete beams strengthened with a cement based high strength composite material, *Composite Structures*, 94 (1) (2011), pp. 143-155, ISSN 0263-8223

[13] Ebead, U. et al.: Effectiveness of fabric reinforced cementitious matrix in strengthening reinforced concrete beams, *Journal of Composites for Construction*, (2016) 04016084

[14] Bisby, L et al.: Comparative performance of Fibre Reinforced Polymer and Fibre Reinforced Cementitious Mortar Strengthening Systems in Elevated Temperature Service Environments, Proceedings of the international conference Structural Faults and Repair, Engineering Technics Press, Edinburgh, United Kingdom, June 2010

[15] Tzoura, E., Triantafillou, T.C., Shear strengthening of reinforced concrete T-beams under cyclic loading with TRM or FRP jackets, *Materials and Structures* 49 (1) (2016), pp 17–28, ISSN 1359-5997, 1871-6873

[16] Blanksvärd, T.,Täljsten, B., Carolin, A., Shear strengthening of concrete structures with the use of mineral-based composites, *J. of Compos. for Constr.,* 13 (1) (2009), pp. 25–34, ISSN 1090-0268, 1943-5614

[17] Escrig, C. et al.: Experimental and analytical study of reinforced concrete beams shear strengthened with different types of textile-reinforced mortar, *Construction and Building Materials*, 83 (2015),pp. 248–260, ISSN 0950-0618

[18] Al-Salloum, Y.A. et al.: Experimental and numerical study for the shear strengthening of reinforced concrete beams using textile-reinforced mortar, *Journal of Composites for Construction*, 16 (1) (2012), pp. 74–90, ISSN 1090-0268, 1943-5614

[19] Triantafillou, T.C., Papanicolaou, C.G, Shear strengthening of reinforced concrete members with textile reinforced mortar (TRM) jackets, *Materials and Structures,* 39 (1) (2006), pp. 93–103, ISSN 1359-5997, 1871-6873

[20] Contamine, R. et al.: Identifying the contributing mechanisms of textile reinforced concrete (TRC) in the case of shear repairing damaged and reinforced concrete beams, *Engineering Structures*, 46 (2013), pp. 447–458, ISSN 0141-0296

[21] Awani, O. et al.: Numerical simulation and experimental testing of concrete beams strengthened in shear with fabric-reinforced cementitious matrix, *Journal of Composites for Construction*, (2016) 04016056

[22] Tetta, Z.C., Koutas, L.N., Bournas, D.A., Textile-reinforced mortar (TRM) versus fiber-reinforced polymers (FRP) in shear strengthening of concrete beams, *Composites: Part B*, 77 (2015), pp. 338-348, ISSN 1359-8368

[23] Tetta, Z.C., Bournas, D.A., TRM vs FRP jacketing in shear strengthening of concrete members subjected to high temperatures, *Composites: Part B*, 106 (2016), pp. 190-205, ISSN 1359-8368

[24] Bournas, D.A. et al.: Textile-reinforced mortar versus FRP jacketing in seismic retrofitting of RC columns with continuous or lap-spliced deformed bars, *Journal of Composites for Construction*, 13 (5) (2009), pp. 360–371, ISSN 1090-0268, 1943-5614
[25] Triantafillou, T.C. et al.: Concrete confinement with textile-reinforced mortar jackets, *ACI Structural Journal*, 103 (1) (2006), pp. 28–37., ISSN 0889-3241
[26] Ombres, L., Concrete confinement with a cement based high strength composite material, *Composite Strucures*, 109 (2014), pp. 294–304, ISSN 0263-8223
[27] T.C. Triantafillou, T.C., Papanicolaou, C.G., Textile Reinforced Mortars (TRM) versus Fiber Reinforced Polymers (FRP) as Strengthening Materials of Concrete Structures, Proceedings of the Seventh International Symposium of the Fiber-Reinforced Polymer Reinforcement for Reinforced Concrete Structures (FRPRCS-7), Shield, C.K. (Ed.), ISBN 9780870311895, Kansas City, Missouri, November 2005
[28] Colajanni, P. et al.: Concrete columns confined with fibre reinforced cementitious mortars: experimentation and modelling, *Construction and Building Materials*, 52 (2014), pp. 375–384, ISSN 0950-0618
[29] Bournas, D.A. et al.: Textile reinforced mortar versus fiber-reinforced polymer confinement in reinforced
[30] concrete columns, , *ACI Structural Journal*, 104 (6) (2007), pp. 740–748, ISSN 0889-3241
[31] Colajanni, P., Fossetti M., Macaluso, G., Effects of confinement level, cross-section shape and corner radius on the cyclic behavior of CFRCM confined concrete columns, *Constr. Build. Mater*. 55 (2014), pp. 379–389, ISSN 0950-0618
[32] Trapko, T., The effect of high temperature on the performance of CFRP and FRCM confined concrete elements, *Composites: part*, B 54 (2013), pp. 138–145, ISSN 1359-8368

DESIGN DIAGRAMS FOR FRP FLEXURAL STRENGTHENING OF REINFORCED CONCRETE CROSS SECTION

Tomislav Kisicek[1], Martina Caric[1]

[1] University of Zagreb Faculty of Civil Engineering, Department of Structural Engineering, Fra Andrije Kacica Miosica 26, 10 000 Zagreb, Croatia, email: kisha@grad.hr, mcaric@grad.hr

SUMMARY: When calculating the required area of FRP sheet for flexural strengthening of reinforced concrete section with assumption of full composite action, depending on acting bending moment, 2 failure modes can occur: concrete crushing in the compression zone and FRP fracture in tension zone. In the first case, calculation can be carried out easily by solving quadratic formula, while in the second case the calculation must be solved iteratively using software. In order to avoid iterative calculation, analysis of parameters affecting the design was conducted and diagrams for simple calculation with sufficient accuracy were designed. A comparison of that simple calculation with more accurate iterative calculation is shown.

DIJAGRAMI ZA PRORAČUN POJAČANJA LAMELAMA OD POLIMERA ARMIRANIH VLAKNIMA ZA ARMIRANOBETONSKI PRESJEK OPTEREĆEN NA SAVIJANJE

SAŽETAK: Prilikom proračuna potrebne ploštine materijala od polimera armiranog vlaknima potrebnog za pojačanje armiranobetonskog presjeka opterećenog na savijanje, ovisno o djelujućem momentu savijanja, do sloma presjeka može doći slomom betona u tlačnom području ili slomom polimera armiranog vlaknima u vlačnom području, pod pretpostavkom pune spregnute veze između betona i polimera. Proračun se u prvom slučaju može provesti vrlo jednostavno rješavanjem kvadratne jednadžbe, dok se u drugom slučaju proračun mora riješiti iterativno s pomoću računalnog programa. Kako bi se izbjegao iterativni proračun, napravljena je analiza parametara koji utječu na proračun i izrađeni su dijagrami pomoću kojih se na jednostavan način s dovoljnom točnošću može doći do rješenja. Prikazana je i usporedba takvog proračuna s točnijim iterativnim proračunom.

1. UVOD

U nas i u svijetu postoji potreba za popravcima i pojačanjima postojećih konstrukcija kako bi im se produljio uporabni vijek. Uz mnoge metode pojačanja konstrukcija, posljednjih desetljeća primjenjuju se vlaknima armirani polimeri, tj. FRP. To su kompozitni materijali koji se sastoje od polimerne matrice i armaturnih vlakana. Za izradu matrice najviše se koriste epoksidne, nezasićene poliesterske, vinilesterske, bismelamidne i cianat esterske smole dok su vlakna najčešće staklena (G), aramidna (A) ili ugljična (C) pa se tako razlikuju proizvodi od GFRP-a, AFRP-a te CFRP-a.

Prednosti FRP-a su: otpornost na koroziju, visoka vlačna čvrstoća, dobro ponašanje pod dinamičkim djelovanjem (proizvodi od ugljičnih vlakana), otpornost na većinu lužina i kiselina, mogućnost prigušenja vibracija te izrazito dobar odnos čvrstoće i vlastite težine. Osim prednosti, proizvodi od FRP-a imaju i nedostatke kao što su: elastično ponašanje do sloma, malo istezanje pri slomu (osobito kod proizvoda od ugljičnih vlakana), te velika razlika u svojstvima uzduž i poprijeko na smjer pružanja vlakana, slom zbog popuštanja pod dugotrajnim naprezanjima (zbog smanjene čvrstoće pod dugotrajnim djelovanjem). Glavni nedostatak je da takvi proizvodi nisu duktilni.

Razvijeno je nekoliko tipova FRP pojačanja: a) „Wet lay-up" sustavi (sustavi sa mokrim polaganjem) – tkanine od FRP-a koje se lijepe na podlogu, b) Prefabricirani FRP sustavi – lijepljenje lamela od FRP-a na podlogu i c) Specijalni FRP sustavi – sustavi s automatskim ovijanjem, prednapete FRP trake , umetnute FRP trake. Isto tako postoje i šipke od FRP-a kojima se, umjesto čeličnim šipkama, mogu armirati konstrukcije.

U brojnoj literaturi [1-4] dane su preporuke za proračun takvih tipova pojačanja ovisno o vrsti elementa i djelovanju na koje se element želi pojačati. U diplomskom radu [5] i članku [6] opisan je postupak proračuna poprečnog presjeka opterećenog na savijanje pojačanog FRP lamelama. Proračun je napravljen u skladu s normom HRN EN 1992-1-1 [7] i ukazano je na problem koji se javlja prilikom proračuna jer je u jednom slučaju nemoguće proračun provesti ručno nego je potrebno provesti iterativni proračun za koji je potrebno imati praktičan računalni program.

U ovom radu izrađeni su dijagrami uz pomoć kojih je moguće izbjeći iterativni proračun te jednostavno i brzo proračunati potrebnu ploštinu FRP lamele potrebnu za pojačanje AB presjeka opterećenog na savijanje. Kako bi se dokazala opravdanost ovakvih dijagrama, napravljena je i usporedba s iterativnim, točnijim, proračunom.

2. PRORAČUN OTPORNOSTI POJAČANOG ELEMENTA NA SAVIJANJE

Prije nego se pristupi proračunu otpornosti elementa potrebno je definirati karakteristike materijala. Karakteristike betona i čelične armature definirane su normom HRN EN 1992-1-1 [7], dok se odnos naprezanja i deformacija za FRP, može pretpostaviti kao linearan te se može prikazati koristeći sljedeći izraz:

$$\sigma_{\mathrm{f}} = E_{\mathrm{fu}} \cdot \varepsilon_{\mathrm{f}} \leq f_{\mathrm{fd}} \tag{1}$$

gdje je: E_{fu} proračunski modul elastičnosti FRP-a, ε_{f} je relativna deformacija FRP-a, a f_{fd} je proračunska čvrstoća FRP-a koja se dobije dijeljenjem karakteristične vlačne čvrstoće FRP-a s koeficijentom sigurnosti.

Pri proračunu graničnog stanja nosivosti pod pretpostavkom pune spregnute veze između betona i FRP-a koriste se koeficijenti sigurnosti materijala γ_{f} navedeni u tablici 1, prema [1].

Tablica 1 Koeficijenti sigurnosti za FRP [1]

Type of FRP	Type A	Type B
CFRP	1,20	1,35
AFRP	1,25	1,45
GFRP	1,30	1,50

Pod pojmom „Tip A" podrazumijeva se predgotovljeni FRP sustav sa normalnom kontrolom kvalitete ili sustav mokrim polaganjem sa visokom kontrolom kvalitete proizvodnje i ugradnje dok „Tip B" podrazumijeva sustav s normalnom kontrolom kvalitete ili bilo koji sustav pod teškim uvjetima ugradnje.

Do sloma pojačanog poprečnog presjeka može doći zbog sloma betona u tlačnom području ili sloma FRP lamele u vlačnom području. Do sloma lamele u vlačnom području može doći pucanjem lamele, tj. dosezanjem njezine vlačne čvrstoće ili zbog gubitka njezine prionjivosti za betonsku podlogu. Poprečni presjek s raspodjelom relativnih deformacija po visini te naprezanjima i unutarnjim silama, prilikom dosezanja graničnog stanja nosivosti, prikazan je na slici 1.

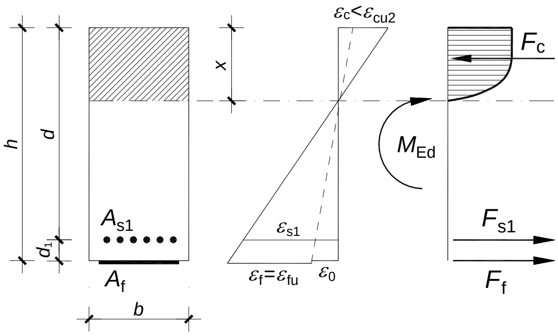

Slika 1 Poprečni presjek s raspodjelom relativnih deformacija po visini te naprezanjima i unutarnjim silama, prilikom dosezanja graničnog stanja nosivosti

Postupak proračuna potrebne ploštine FRP-a za pojačanje razlikuje se s obzirom na pretpostavljeni oblik sloma. U slučaju sloma zbog dosezanja tlačne nosivosti betona, relativna deformacija tlačnog ruba poprečnog presjeka iznosi $\varepsilon_{\mathrm{c}} = \varepsilon_{\mathrm{cu2}}$, a ukupna deformacija u razini FRP lamele je nepoznata. Postupak proračuna potrebne ploštine FRP lamele je u tom slučaju jednostavan i može se riješiti tako da se postavi izraz za sumu momenata na točku u razini FRP armature te se iz njega dobije kvadratna jednadžba čije je rješenje koeficijent položaja neutralne osi poprečnog presjeka pomoću kojeg se može odrediti ukupna relativna deformacija u razini FRP lamele. Nakon toga se iz sume horizontalnih sila dobije potrebna ploština FRP lamele. Postupak je opisan u radu [5] i članku [6].

Poteškoće nastaju ako do sloma poprečnog presjeka dolazi zbog sloma FRP lamele. U tom slučaju je relativna deformacija u razini FRP lamele poznata, a nepoznata je relativna deformacija tlačnog ruba betona. Kako koeficijent punoće proračunskog dijagrama betona α_{v} i koeficijent položaja rezultante tlačnih naprezanja u betonu k_{a}, ovise o relativnoj tlačnoj deformaciji betona, jednadžba koja se dobije iz sume momenata na točku u razini FRP lamele postaje mnogo kompliciranija pa se najlakše može riješiti iterativno, za što treba imati računalni program.

Ideja ovog rada je pojednostaviti taj proračun izradom dijagrama kojim bi se olakšalo rješavanje takve jednadžbe.

2.1. DIJAGRAMI ZA PRORAČUN

2.1.1. PRETPOSTAVKE PRORAČUNA

Tablice za proračun potrebne armature za poprečni presjek opterećen na savijanje, koje se tradicionalno koriste u praksi, izrađene su tako što su za poznate parove relativnih deformacija vlačno napregnute čelične armature i tlačno napregnutog betona, iz ravnoteže unutarnjih sila u poprečnom presjeku proračunati parametri pomoću kojih se lako može dobiti potrebna ploština armature bez rješavanja kompleksnih izraza.

U slučaju pojačanog poprečnog presjeka, za razliku od onog armiranog čeličnom armaturom, nije poznata ukupna relativna deformacija u razini FRP lamele pri slomu jer ona ovisi o početnoj relativnoj deformaciji vlačnog ruba poprečnog presjeka u trenutku pojačavanja i o relativnoj deformaciji FRP lamele pri slomu (ili pri gubitku prionjivosti za podlogu). Osim toga i ploština postojeće armature u poprečnom presjeku nije uvijek jednaka. No, uz pretpostavku ovih veličina mogu se izraditi dijagrami koji povezuju spomenute relativne deformacije i bezdimenzijski moment savijanja te mehanički koeficijent armiranja FRP lamelama. Najprije je potrebno razmotriti odnose između unutarnjih sila u pojačanom poprečnom presjeku (slika 1).

Suma momenata na točku u razini FRP lamele jest:

$$M_{Ed} = F_c \cdot \left(h - k_a \cdot \xi^* \cdot h\right) - A_{s1} \cdot f_{yd} \cdot d_1 \tag{2}$$

Sila u tlačno naprezanom dijelu betona iznosi:

$$F_c = f_{cd} \cdot \alpha_v \cdot b \cdot \left(\xi^* \cdot h\right) \tag{3}$$

dok je koeficijent položaja neutralne osi:

$$\xi^* = \frac{|\varepsilon_c|}{|\varepsilon_c| + |\varepsilon_0| + |\varepsilon_{fu}|} = \frac{|\varepsilon_c|}{|\varepsilon_c| + |\varepsilon_{f0}|} \tag{4}$$

U izrazima od (2) do (4) je: α_v – koeficijent punoće proračunskog dijagrama betona; k_a – koeficijent položaja rezultante tlačnih naprezanja; A_{s1}– ploština čelične vlačne armature; f_{yd} – proračunska granica popuštanja čelika za armiranje; d_1 – udaljenost težišta vlačne armature od donjeg ruba presjeka; f_{cd} – proračunska tlačna čvrstoća betona; M_{Ed} – proračunski moment savijanja od djelovanja na pojačani presjek.

Uvrštavanjem izraza (3) u izraz (2) i dijeljenjem tog izraza sa ($b{\cdot}h^2{\cdot}f_{cd}$), uz pretpostavku da je $d_1 = 0{,}1{\cdot}h$ dobije se izraz za bezdimenzijsku veličinu momenta savijanja $\mu_{Ed} = M_{Ed} / (b{\cdot}h^2{\cdot}f_{cd})$.

$$\mu_{Ed} = \alpha_v \cdot \xi^* \left(1 - k_a \cdot \xi^*\right) - 0{,}1 \cdot \frac{A_{s1}}{b \cdot h} \cdot \frac{f_{yd}}{f_{cd}} \tag{5}$$

U izrazu (5), dio vezan uz čeličnu vlačnu armature može se zamijeniti mehaničkim koeficijentom armiranja $\omega^* = A_{s1}{\cdot}f_{yd} / (b{\cdot}h{\cdot}f_{cd})$ pa tako izraz (5) postaje:

$$\mu_{Ed} = \alpha_v \cdot \xi^* \left(1 - k_a \cdot \xi^*\right) - 0{,}1 \cdot \omega^* \tag{6}$$

Iz sume horizontalnih sila u poprečnom presjeku $F_c - F_s - F_f = 0$ može se izraziti potrebna ploština FRP lamele:

$$A_f = \frac{\alpha_v \cdot f_{cd} \cdot b \cdot h \cdot \xi^* - \omega^* \cdot b \cdot h \cdot \frac{f_{cd}}{f_{yd}} \cdot f_{yd}}{\left(\varepsilon_{f0} - \varepsilon_0\right) \cdot E_{fu}} = b \cdot h \cdot f_{cd} \cdot \frac{\alpha_v \cdot \xi^* - \omega^*}{\left(\varepsilon_{f0} - \varepsilon_0\right) \cdot E_{fu}} = \frac{b \cdot h \cdot f_{cd}}{\left(\varepsilon_{f0} - \varepsilon_0\right) \cdot E_{fu}} \cdot \omega_f \tag{7}$$

Izraz (7) vrijedi uz pretpostavku da je vlačna armatura popustila, tj. da je $\sigma_s = f_{yd}$. Mehanički koeficijent armiranja FRP lamelom, ω_f, iz izraza (7), ovisi o relativnim deformacijama u razini FRP lamele i tlačno napregnutog betona te o mehaničkom koeficijentu armiranja čeličnom armaturom.

2.1.2. PARAMETARSKA ANALIZA

Za određene kombinacije ukupnih relativnih deformacija u razini FRP lamele ($\varepsilon_{f0} = \varepsilon_0 + \varepsilon_{fu}$) i mehaničkih koeficijenata armiranja čeličnom armaturom, ω^*, te variranjem relativne deformacije tlačno napregnutog betona između $\varepsilon_c = 0$ i $\varepsilon_c = \varepsilon_{cu2}$ mogu se izraditi dijagrami koji povezuju parove tih relativnih deformacija s bezdimenzijskim momentom savijanja, μ_{Ed}, ili mehaničkim koeficijentom armiranja FRP lamelama, ω_f. Dakle, za poznati bezdimenzijski moment savijanja, μ_{Ed}, iz takvih dijagrama bi se jednostavno mogla očitati vrijednost relativne tlačne deformacije betona, ε_c, te proračunati svi potrebni parametri i u konačnici potrebna ploština FRP lamele za pojačanje poprečnog presjeka. S obzirom na velik broj kombinacija ukupnih relativnih deformacija u razini FRP lamele i mehaničkih koeficijenata armiranja čeličnom armaturom takvi dijagrami ne bi bili prikladni jer bi se dobio velik broj različitih krivulja koje ne bi bile prikladne za grafički prikaz.

Korak dalje je dovođenje u vezu bezdimenzijskog momenta savijanja, μ_{Ed}, i mehaničkog koeficijenta armiranja FRP lamelom, ω_f, preko relativnih deformacija, ε_{f0} i ε_c, za određenu vrijednost mehaničkog koeficijenta armiranja čeličnom armaturom, ω^* i određenu vrijednost ukupne relativne deformacije u razini FRP lamele, ε_{f0}. Kod takvih dijagrama uočeno je da se za istu vrijednost ω^* krivulje ovisne o ukupnoj relativnoj deformaciji, ε_{f0}, gotovo podudaraju.

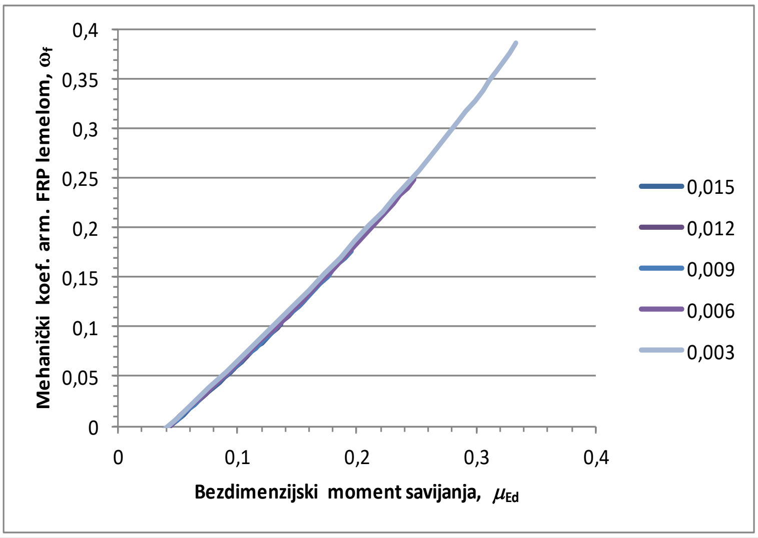

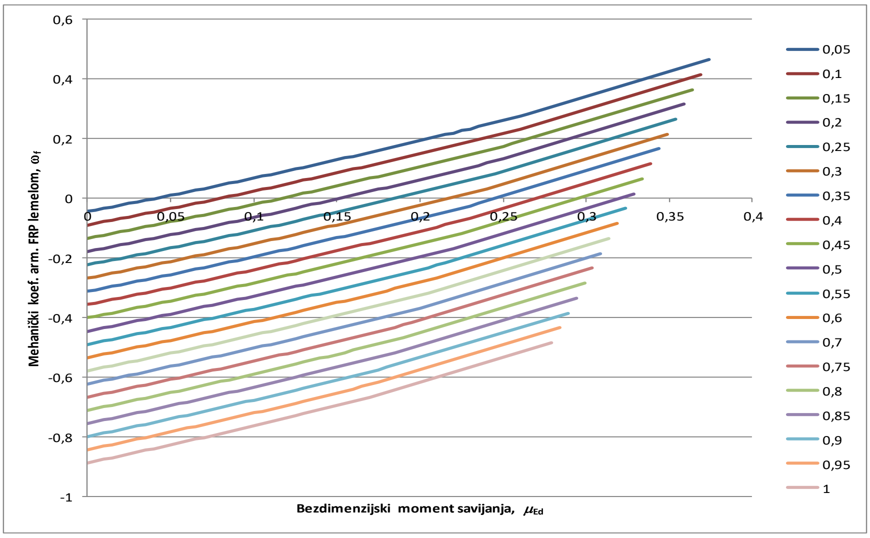

Slika 2 Dijagram ovisnosti mehaničkog koeficijenta armiranja ω_f, o bezdimenzijskom momentu savijanja μ_{Ed}: a) za ω^* = 0,05 i za vrijednosti ε_{f0} od 0,003 do 0,015, b) za vrijednosti ω^* od 0,05 do 1,0 i za ε_{f0} = 0,002

Na slici 2a) prikazani su dijagrami ovisnosti mehaničkog koeficijenta armiranja FRP lamelom, ω_f, o bezdimenzijskom momentu savijanja, μ_{Ed}, za više vrijednosti ukupnih relativnih deformacija u razini FRP lamele ($\varepsilon_{f0} = \varepsilon_0 + \varepsilon_{fu}$ = 0,003; 0,006; 0,009; 0,012 i 0,015) i za vrijednost mehaničkog koeficijenta armiranja čeličnom armaturom, ω^* = 0,05. Uočeno je da se za istu vrijednost μ_{Ed}, dobije veća vrijednost ω_f, ako se smanjuje ukupna relativna deformacija ε_{f0}. Točnim proračunom utvrđeno je da se ta razlika kreće oko 10%. S obzirom na to da bi ovakvi dijagrami služili za približni („ručni“) proračun, očitavanjem vrijednosti s takvih dijagrama radila bi se također greška tog reda veličine. Smatra se da je za praktičnu primjenu dovoljno točno dati dijagrame za neku minimalnu ukupnu relativnu deformaciju ε_{f0} i za vrijednosti mehaničkog koeficijenta armiranja čeličnom armaturom ω^* od 0,05 do 1,0. Takav dijagram prikazan je na slici 2b). Na dijagramima sa slike 2b) se vidi da s povećanjem mehaničkog koeficijenta armiranja čeličnom armaturom, ω^*, krivulje sve više padaju ispod horizontalne koordinatne osi , tj. dobivene vrijednosti mehaničkog koeficijenta armiranja FRP lamelom su negativne. To znači da se kod proračuna nosivosti pojačanog poprečnog presjeka koji ima veću količinu postojeće čelične armature, ne može dogoditi slom poprečnog presjeka preko FRP lamele, nego će se dogoditi slom preko betona. Zbog toga se za približni proračun trebaju koristiti samo dijelovi krivulje koji daju pozitivne vrijednosti koeficijenta ω_f. Takvi dijagrami prikazani su na slici 3 i oni su prikladni za praktični proračun.

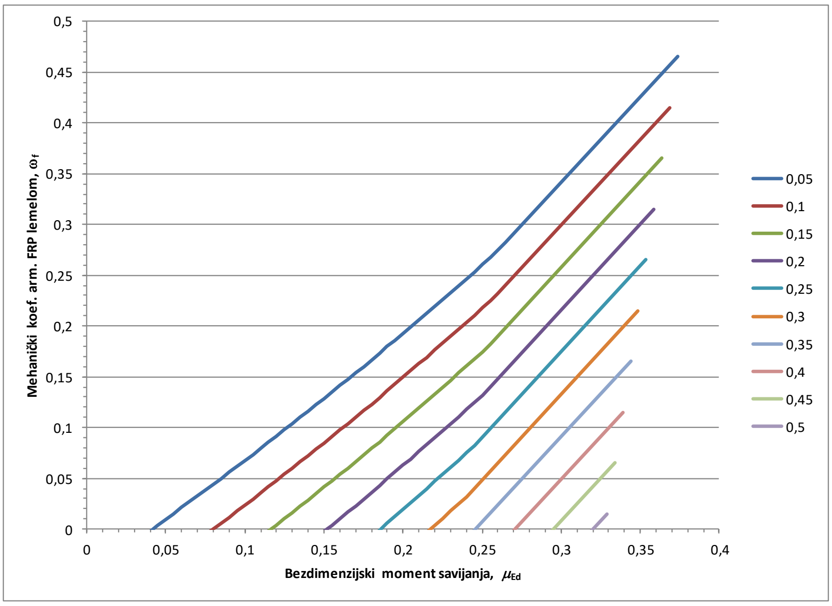

Slika 3 Dijagram ovisnosti mehaničkog koeficijenta armiranja ωf, o bezdimenzijskom momentu savijanja μEd za vrijednosti ω* od 0,05 do 0,5 i za εf0 = 0,002

2.2. PRIMJER PRORAČUNA

Potrebno je pojačati gredu poprečnog presjeka: $b/h/d$ = 30/50/45 cm izrađenu iz betona C25/30 i armiranu armaturom B500B. Za pojačanje su korištene CFRP lamele s modulom elastičnosti E_{fu} = 165000 N/mm^2 i maksimalnom relativnom deformacijom pri slomu (po preporukama proizvođača) ε_{fu} = 0,7 % = 0,007. Poprečni presjek je armiran vlačnom armaturom 3ϕ20; $A_{s1,prov}$ = 9,42 cm^2, a tlačna armatura je zanemarena u ovom proračunu. Za početno stanje prije pojačavanja uzet je moment savijanja od stalnog opterećenja i dobivena je relativna deformacija vlačnog ruba poprečnog presjeka: ε_0 = 0,00087. Presjek je potrebno pojačati tako da može preuzeti moment savijanja od 240 kNm.

Kako bi se znalo treba li proračun raditi po opisanom postupku pomoću dijagrama potrebno je proračunati granični moment savijanja za koji je relativna tlačna deformacija betona $\varepsilon_c = \varepsilon_{cu2}$ = 0,0035, dok je relativna vlačna deformacija FRP-a jednaka $\varepsilon_f = \varepsilon_{fu}$ = 0,007. Ako je moment savijanja od djelovanja manji od graničnog momenta savijanja, slom će se dogoditi preko FRP lamele i proračun je potrebno provesti po postupku uz pomoć dijagrama sa slike 3.

Relativna deformacija vlačnog ruba poprečnog presjeka u trenutku ojačavanja iznosi ε_0 = 0,00087. Uz pomoć izraza (2) može se proračunati granični moment savijanja. Iz izraza (4) dobije se koeficijent položaja neutralne osi: ξ^* = 0,0035/(0,0035 + 0,00087 + 0,007) = 0,31.

Koeficijenti α_v i k_a za $\varepsilon_c = \varepsilon_{cu2}$ = 0,0035 (za beton C25/30) iznose: α_v = 0,810 i k_a = 0,416. Prema izrazu (3) rezultanta tlačnih naprezanja u betonu (sila u betonu) iznosi: F_c = 1,667·0,810·30·(0,31·50) = 627,88 kN, a granični moment savijanja, prema izrazu (2) iznosi: $M_{Rd,gr}$ = 627,88·(50 – 0,416·0,31·50) – 9,42·43,48·5 = 25297 kNcm = 252,97 kNm.

U ovom primjeru je moment savijanja koji djeluje na ojačanom poprečnom presjeku: M_{Ed} = 240 kNm. Prema tome je $M_{Ed} < M_{Rd,gr}$ pa dolazi do sloma zbog popuštanja armature i sloma FRP lamele. Zbog toga je proračun potrebno provesti pomoću dijagrama sa slike 3.

Mehanički koeficijent armiranja poprečnog presjeka: $\omega^* = A_{s1} \cdot f_{yd} / (b \cdot h \cdot f_{cd})$ = 9,42·43,48 / (30·50·1,667) = 0,1638. Bezdimenzijski moment savijanja koji djeluje na zadani poprečni presjek je: μ_{Ed} = 24000/(30·50^2·1,667) = 0,192, pa je iz dijagrama sa slike 3, za tu vrijednost μ_{Ed}, za ω^* = 0,1638, procijenjena vrijednost ω_f = 0,082. Iz izraza (7) dobije se potrebna ploština FRP lamele: A_f = (30·50·1,667·0,082)/((0,00787 – 0,00087)·16500) = 1,78 cm^2. Točnijim, iterativnim postupkom pomoću računalnog programa dobivena je potrebna ploština A_f = 1,59 cm^2. Iz kataloga proizvođača odabrane su CFRP dvije lamele: 80×1,2 mm; A_f = 0,96 cm^2. Ukupna ploština FRP lamele iznosi A_f = 1,92 cm^2. Kada bi se odabirale lamele prema točnom proračunu tada bi trebalo odabrati CFRP lamele: 80×1,2 mm; A_f = 0,96 cm^2 i 60×1,3 mm; A_f = 0,78 cm^2. Ukupna ploština FRP lamele iznosi A_f = 1,74 cm^2. Razlika kod odabrane ploštine CFRP lamele je 10 % za ova dva slučaja.

3. ZAKLJUČAK

U radu su prikazani dijagrami za praktični proračun potrebne ploštine FRP lamele za pojačanje armiranobetonskog presjeka na savijanje u slučaju sloma presjeka preko FRP lamele. U tom slučaju, nepoznata je tlačna relativna deformacija betona i proračun se može izvršiti iterativno, tj. potrebno je koristiti računalni program. Pomoću dijagrama na slici 3 moguće je taj proračun provesti približno s dovoljnom točnošću što je i prikazano primjerom u točki 2.2 ovog rada. Osim toga tijekom izrade dijagrama napravljena analiza o veličini greške koja se radi ako se ne uzima krivulja koja bi odgovarala točnoj ukupnoj relativnoj deformaciji ε_{f0}. Utvrđeno je da je maksimalna greška reda veličine 10% što je dovoljno točno za približni proračun. Tu treba imati u vidu da prilikom odabira FRP lamele kojom će se pojačati poprečni presjek nije moguće odabrati lamelu točne proračunate ploštine, nego se uvijek odabire lamela veće ploštine te se i u tom slučaju radi neka greška. Konačno, na temelju primjera proračuna i točnijeg proračuna vidi se da je greška i veća kada se u konačnici odaberu FRP lamele.

ZAHVALA

Autori se zahvaljuju Ministarstvu znanosti, obrazovanja i sporta Republike Hrvatske i Sveučilištu u Zagrebu na potpori.

LITERATURA

[1] fib bulletin 14: *Externally bonded FRP reinforcement for RC structures*, fib, ISBN Lausanne, Switzerland, July 2001.

[2] CNR-DT 200/2004: Guide for the Design and Construction of Externally Bonded FRP Systems for Strengthening Existing Structures, Rome, 2004.

[3] Zilch, K.; Niedermeier, R.; Finckh, W.: *Strengthening of Concrete Structures with Adhesively Bonded Reinforcement*, Ernst and Sohn, ISBN 978-3-433-03086-8, Berlin, 2014.

[4] ACI Committee 440: *Guide for the Design and Construction of Externally Bonded FRP Systems for Strengthening Concrete Structures*, 440.2R-02, American Concrete Institute, Farmington Hills, MI, 2002.

[5] Pavić, K., Ojačavanje armiranobetonskih konstrukcija proizvodima od polimera armiranog vlaknima, Diplomski rad, Sveučilište u Zagrebu, Građevinski fakultet, 2012.

[6] Kišiček, T.; Pavić, K.: Proračun nosivosti pravokutnog poprečnog presjeka na savijanje ojačanog lamelom od FRP-a, Zbornik 5. Internacionalnog naučno – stručnog skupa: Građevinarstvo – nauka i praksa, Žabljak, 17.-21. veljače 2014.

[7] HRN EN 1992-1-1:2013, Eurokod 2: Projektiranje betonskih konstrukcija – Dio 1-1: Opća pravila i pravila za zgrade, Eurocode 2: Design of concrete structures – Part 1-1: General rules and rules for buildings, European Committee for Standardization, Bruxelles

[8] Sorić, Z.; Kišiček, T.: *Betonske konstrukcije 1*, Udžbenici Sveučilišta u Zagrebu, Građevinski fakultet, ISBN 978-953-6272-75-4 Zagreb, 2014.

THE RESPONSE ANALYSIS OF CONTINUOUS BEAMS WITH FRP REINFORCEMENT

Nikola Basa[1], Mladen Ulicevic[1], Radomir Zejak[1]

[1] University of Montenegro, Faculty of Civil Engineering, Cetinjski put bb, 81000 Podgorica, Montenegro,
email: nik.ma@t-com.me, mladenu@t-com.me, rzejak@t-com.me

SUMMARY: Continuous beams are often used in reinforced concrete structures which are exposed to aggressive effects of the environment, such as marine structures, bridges, overpasses, garages, reservoirs, culverts, retaining walls, foundations and others. In aggresive environments there is a reduction of alkalinity of concrete, which often results in corrosion of the steel reinforcement, and causes further damage to the concrete, which endangers the functionality and serviceability of the RC structures. Having in mind the aforementioned, in recent years FRP composites find its wider application in building construction around the world, as internal reinforcement in RC elements. Although there is currently little reliable information that describes the behaviour of continuous beams reinforced with FRP reinforcement, the necessity of research work is emphasized, especially experimental, in regard to the small database that is currently available. Since FRP reinforcement shows a linear elastic behaviour up to failure, there is a question of the ability of material, that in conjunction with concrete, redistribute internal forces in statically indeterminate structures. In this paper, the main issue associated with the redistribution of the internal forces of continuous beams with a description of the main characteristics of FRP materials and the reinforcement is stressed, and the basic characteristics of the behaviour of RC elements with the FRP reinforcement are listed. This paper presents a short review of experimental research planned on the 12 RC continuous beams with two equal span length of 1.9 m, the cross-sectional dimensions 15/25 cm, with longitudinal and transverse GFRP reinforcement. In order to determine the possibilities of the redistribution of internal forces, and the behavior of RC elements in terms of the redistribution of the internal forces, the parameters of which it depends are varied: longitudinal reinforcement ratio at the midspan and at the middle support, the percentage of the longitudinal tensioned reinforcement and concrete compressive strength. It is expected that the results of the experiment show that is, the redistribution of the internal forces at statically indeterminate structures with FRP reinforcement possible, regardless of the linear elastic behaviour of FRP reinforcement up to failure, and that has a positive effect on the load-carrying capacity and fulfill the requirements of serviceability.

ODZIV KONTINUIRANIH GREDA ARMIRANIH POLIMERNIM VLAKNIMA

SAŽETAK: Kontinuirane grede često se upotrebljavaju u armiranobetonskim konstrukcijama izloženim agresivnim djelovanjima okoliša kao što su konstrukcije na moru, mostovi, nadvožnjaci, garaže, spremnici, odvodni kanali, potporni zidovi, temelji i drugi. U agresivnom okolišu dolazi do smanjenja alkalnosti betona što često rezultira korozijom čelične armature i uzrokuje daljnja oštećenja betona čime se ugrožavaju funkcionalnost i uporabljivost armiranobetonskih konstrukcija. Imajući u vidu navedeno, posljednjih godina kompoziti od polimera armiranih vlaknima kao unutarnja armatura armiranobetonskih elemenata imaju sve širu primjenu u gradnji u svijetu. Kako danas ima malo pouzdanih podataka, a baza dostupnih podataka koji opisuju ponašanje kontinuiranih greda armiranih polimerima armiranim vlaknima je mala, naglašena je nužnost eksperimentalnih istraživanja. Kako je ponašanje armature od polimera armiranih vlaknima linearno-elastično sve do sloma upitna je sposobnost tog materijala koji u spoju s betonom raspodjeljuje unutarnje sile u statički neodeređnim konstrukcijama. U radu je stavljen naglasak na preraspodjelu unutarnjih sila kontinuiranih greda s opisom glavnih značajki polimera armiranih vlaknima i armature, a popisane su i temeljne značajke ponašanja armiranobetonskih elemenata armiranih polimerom armiranim vlaknima. Dan je kratak pregled eksperimentalnih ispitivanja planiranih za dvanaest kontinuiranih greda s dva jednaka raspona od 1,9 m, dimenzija poprečnog presjeka 15/25 cm i s uzdužnom i poprečnom armaturom od polimera armiranog staklenim vlaknima. Varirani su parametri o kojima ovise mogućnosti preraspodjele unutarnjih sila i ponašanje armiranobetonskih elemenata: omjer uzdužne armature u sredini raspona i na srednjem osloncu, postotak uzdužne vlačne armature i tlačne čvrstoće betona. Očekuje se da će rezultati eksperimenata pokazati da je moguća preraspodjela unutarnjih sila statički neodređenih konstrukcija armiranih polimerima armiranim vlaknima neovisno o linearno-elastičnom ponašanju polimera armiranog vlaknima do sloma i da ona ima pozitivan učinak na nosivost i ispunjenje zahtjeva uporabljivosti.

1. INTRODUCTION

Today, concrete reinforced with steel reinforcement is still predominantly used for the construction of the civil engineering structures, which is in aggressive environments exposed to moisture, temperature, chloride, that leads to corrosion of steel reinforcement. Corrosive process causes damages to the concrete and endangers the functionality and serviceability of reinforced concrete structures. In recent years, there are more and more researches of materials that could replace steel in reinforced concrete structures, particularly in aggressive environments. Thus, FRP composite materials (Fiber Reinforced Polymer) find their application in civil engineering structures as well as internal and external reinforcement in RC elements. Since the FRP materials are not subjected to corrosion, their use in the structure can represent significant savings in maintenance, recovery and strengthening of structures, in particular when they are in the course of its exploitation life exposed to various corrosive and destructive influences, which certainly leads to economic benefits. Today we have a significant number of structures such as bridges, retaining walls, marine structures and others, on which FRP reinforcement in structural elements is succsessfully applied. Due to different mechanical and deformation characteristics of FRP reinforcement, the behaviour of RC elements greatly vary in relation to the elements of the steel reinforcement. The behaviour of reinforced concrete structures with steel reinforcement under load is well established and parameters that relate to behavior are clearly defined. This is primarily due to the significant and extensive research conducted in recent decades on the elements with steel reinforcement. In case of structures with FRP reinforcement, which is relatively new material, despite a significant increase in research work, it is evident that a limited number of experimental results, which are certainly reflected in the lack of appropriate regulations and standards for engineering applications. The regulations and standards for the structure with the FRP reinforcement, which currently exist in the world, are largely based on the proposed models and equations that are used for structures with steel reinforcement, with the variations of the parameters and the coefficients on which depend the characteristics of the FRP reinforcements and their interaction with the concrete. All this leads to that, the civil engineers are neither familiar with the properties and characteristics of FRP reinforcement, nor with its application in reinforced concrete structures.

Research work that is currently being conducted, represents an attempt to contribute to further clarification of the behaviour of beams with FRP reinforcement. Most researchers have focused on examining the behaviour of simple supported beams with FRP reinforcement till now, whereas a very small number of tests were carried out on continuous beams. For this reason, the authors of the paper opted to study continuous beams with FRP reinforcement, taking into account the possibly significant breakthrough in the closer determination of answer of these structures to the action of the load up to failure. As a part of research an experimental program is currently being conducted, in order to provide a more reliable testing of the effect of the critical parameters on the behaviour of the continuous beams with FRP reinforcement.

As it is already mentioned, researches of FRP reinforcement have been mostly conducted on simple supported beams, so that are the provisions of certain regulations based on the conclusions reached at these elements. Although poor, database of experimental results on continuous beams with FRP reinforcement will be in any case enriched with the conducted experimental researches, that will greatly assist in the verification of accuracy and improving the results of existing experimental researches. Also, engineers and future researchers will have better insight into use and application of FRP reinforcement, a relatively new material, as internal reinforcement in elements of RC structures. In this way, contribution is given to the improvement of the guideliness and provisions of regulations and standards, applicable to designing of everyday engineering practice, especially in the area of statically indeterminate RC structures reinforced with FRP reinforcement.

2. FRP REINFORCEMENT

Development of FRP materials is intensive over the last 50 years, especially in the aero and electro industries. A major use in the building construction FRP materials have as systems for strengthening of existing RC structures with steel reinforcement, in the form of strips, and as well as an internal reinforcement in reinforced concrete structures. Such materials, as composites, may significantly vary, and their characteristics greatly depend on the constituent materials of which are composed.

FRP material is a composite material consisting a fine continuous fibers, bonded with the polymeric resins - a matrix. FRP composites are anisotropic, with mechanical characteristics and properties which are the best in the direction of the fibers, i.e. in the direction of the applied load. The polymer matrix is the material of low elastic modulus and low strength, which carries and distributes the load on the fibers which have a high modulus of elasticity and high strength. In this way, the result is a composite material of high tensile strength and a relatively high modulus of elasticity (Figure 1).

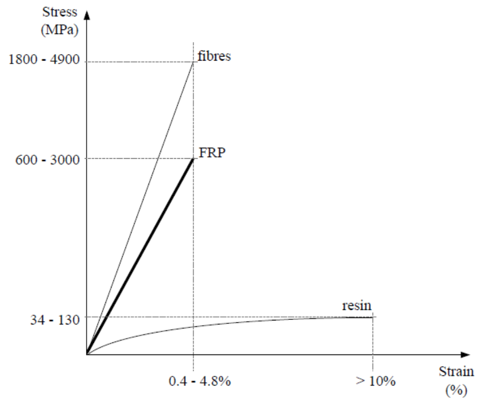

Figure 1 Samples of FRP reinforcement [7]

FRP reinforcement, as well as a steel reinforcement, may be produced in different profiles and different shapes (straight, curved, circular, spiral, etc.). Bond stresses between reinforcement and concrete depend on the workability of the surface of the bars which may be smooth, ribbed, spiral, and sand coated bars (see Figure 2). As an internal reinforcement in reinforced concrete structures, three types are mostly used: carbon (CFRP), glass (GFRP), and aramid (AFRP), and in recent years there is also basalt (BFRP) reinforcement. Mechanical and physical properties of the composite can vary depending on the type of the fiber that is used. So far the glass FRP reinforcement (GFRP) has the widest application as the cheapest, with a minimum tensile strength and the lowest modulus of elasticity in comparison to other FRP reinforcement. The most frequently used mechanical characteristics of the FRP reinforcement are shown in Table 1.

Figure 2 Samples of FRP reinforcement [1]

The main advantage of FRP reinforcement is a high tensile strength in comparison to steel reinforcement. They are not subjected to corrosion, that makes them very highly recommended in aggresive environments, but they also show the complete electrical and magnetic neutrality. They are lighter than steel, which can simplify their transport and speed building construction. In case of very reinforced sections, lower bulk density of FRP reinforcement can reduce the overall weight of the building, including static and dynamic internal forces that can negatively influence the structure itself.

Table 1 Mechanical properties of FRP reinforcement [8]

Type of reinforcement	Tensile strength (MPa)	Modulus of elasticity (GPa)	Ultimate strain (%)
GFRP	450-1600	35-60	1.2-3.7
CFRP	600-3500	100-580	0.5-1.7
AFRP	1000-2500	40-125	1.9-4.4

FRP reinforcement has certain disadvantages in comparison to steel reinforcement. FRP composites show a linear elastic behaviour in tension up to failure, and they are brittle. They are characterized by a relatively low modulus of elasticity, especially for GFRP reinforcement, which implies greater strains of reinforcement in RC elements, in comparison to RC elements with steel reinforcement. Larger strains cause wider cracks and larger deformations (deflections). However, due to the absence of possible corrosion in the RC elements with FRP reinforcement, larger width of cracks is tolerated, while the deformations are limited as in RC steel elements. Compressive strength and shear strength are significantly lower than the tensile strength.

3. MOMENT REDISTRIBUTION IN CONTINUOUS BEAMS WITH FRP REINFORCEMENT

Redistribution of internal forces in RC statically indeterminate structures throughout the literature is defined as the difference between the actual cross section forces and those resulted from the linear elastic theory for the state without cracks. Usually, this phenomenon manifests itself in two phases. The first stage is caused by the difference of uniform bending stiffness along the element, which is assumed by elastic analysis, and the actual stiffness that occurs by variation of the reinforcement along the element and the occurrence of cracks in the concrete. Redistribution of internal forces made in this way is often in literature known as an elastic redistribution (Figure 3). The second stage is the result of plastic deformations in steel reinforcement, i.e. starts after reaching the yield point of the steel, and is manifested further by changing the value of bending stiffness. This redistribution is often called plastic redistribution. Previous researches bring to the conclusion that elastic redistribution can have a significant share in the total redistribution of internal forces along the element.

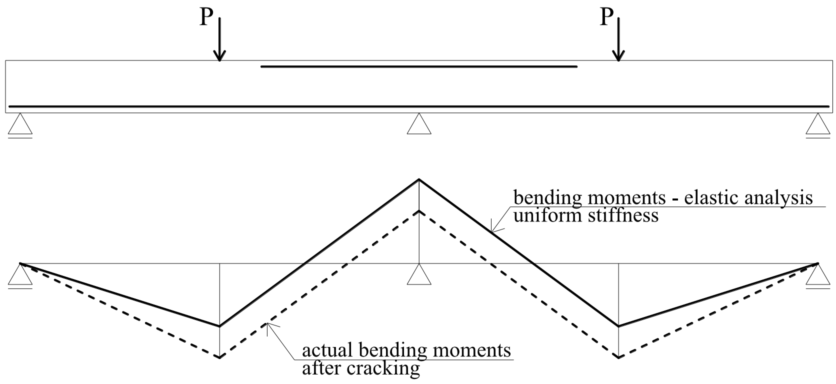

Figure 3 Moment redistribution in continuous beams

Since FRP reinforcement shows a linear elastic behaviour up to the failure, and shows a lack of material nonlinearity, there is a question of the ability of such material that in conjunction with concrete, redistribute the load in statically indeterminate structures. Taking into account the significant contribution of elastic redistribution in the total redistribution of moments in RC beams with steel reinforcement, it is expected that the continuous beam with FRP reinforcement demonstrates a certain ability to redistribution of moments, regardless of the lack of ductility at FRP reinforcement up to the failure. The redistribution of the internal forces is expected as a consequence of the difference of stiffness between the critical cross-sections, which is directly dependent on the relationship of the degree of development of cracks, and adopted reinforcement therein. In other words, one of the basic features of ductility is counted on, and that is the change of stiffness without the loss of capacity of section.

Previous research works on the continuous beams with FRP reinforcement [2], on a modest number of samples, show that the redistribution of the internal forces between the critical cross-sections is possible, especially if the reinforcement along the corresponding element is determined properly. RC continuous beam with FRP reinforcement showed significant warnings, regarding the large deformation and wide and deep cracks before failure. Increasing the bottom reinforcement at the midspan of continuous beam reinforced with reinforcement related to the cross-section at the middle support, had a positive effect on increasing the loading capacity of the beam, reducing deformation and delaying propagation of cracks in the areas of the beams, while the increase of top reinforcement over the middle support is not found as a significant contribution to increasing the load capacity and reducing deformation. This statement may be a good basis for the introduction to redistribution of moments (primarily from the middle support to the midspan of the continuous beam), to provide improved behaviour of continuous beams with FRP reinforcement for the serviceability limit state as well as for the ultimate limit state. The justification of this thinking lies in the fact, that in relation to the elastic analysis, a significant portion of bending moments from middle support displaces at the midspan, already for service load. A width of cracks that occur at the middle support of continuous beams should be controlled, and the same can be significantly increased due to the relocation of moments. However, the fact that, due to the absence of corrosion in the FRP reinforcement, with the current regulations that allow greater width of cracks in concrete beams with FRP reinforcement (even up to 0.7 mm) than it is the case with beams with steel reinforcement, encourages with a view to implementing the moment redistribution with a continuous beam with FRP reinforcement, and that current regulations are still not allowed. The ratio of bottom reinforcement at the midspan and top reinforcement at the middle support of the continuous beam with FRP reinforcement, has a major effect on the redistribution of the available moments. Percentage of longitudinal tensioned reinforcement represents also one of the important factors which directly affects the degree of redistribution moments. When it comes to over-reinforced sections with FRP reinforcement, due to inelastic deformation of the compressive concrete, there are significant deformations and wider cracks before failure, as a form of pseudo-ductile behaviour, and is expected to come to a significant redistribution of internal forces between the critical sections of the element. For this reason, most of the regulations for structures with FRP reinforcement, recommend that the sections should be over-reinforced, i.e. with the percentage of reinforcement higher than balance reinforcement ratio.

4. DESCRIPTION OF EXPERIMENTAL MODELS AND MEASURING TECHNICS

Experimental researches are being conducted currently at the Faculty of Civil Engineering University of Montenegro, within PhD theses comprising behaviour of continuous beams, primarily to bending, in the conditions of redistribution of internal forces. Experimental research comprises 12 continuous beams in total, on 2 spans of length of 1.9 m, of cross-section being 15/25 cm, with longitudinal and transverse GFRP reinforcement and one control beam with steel reinforcement. All the beams are to be examined up to failure, being loaded by concentrated forces at the middle of both spans. Dimensions and geometry of continuous beams and load disposition have been presented in Figure 4. All the beams are dimensioned in line with American standard ACI 440.1R-15 which is being used for design of elements with FRP reinforcement, while the other regulations (CSA S806-02, CSA S806-12, CNR-DT-203) have been used as control.

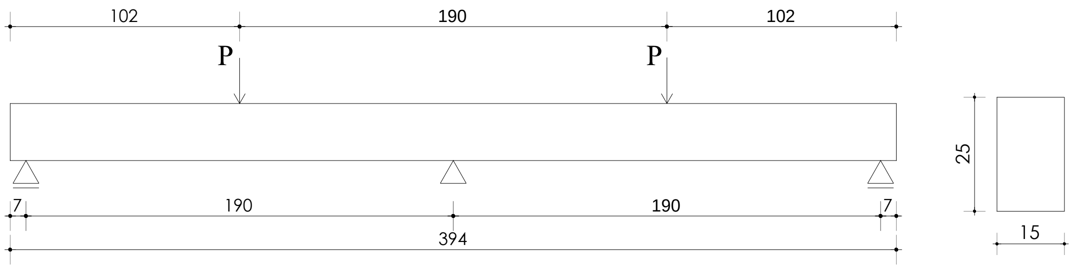

Figure 4 Geometry of the beams and the load disposition

Representative models should have enabled realisation of stated aims, therefore the following parameters have been combined: longitudinal reinforcement ratio at the midspan and at the middle support, the percentage of the longitudinal tensioned reinforcement and concrete compressive strength. All the details related to selected models with beam mark, designed failure load, designed moment redistribution from the middle support to the midspan of the beam, chosen ratio of longitudinal reinforcement ratio and balance reinforcement ratio and designed class of concrete compressive strength have been presented in Table 2. Continuous beams are reinforced by GFRP reinforcement, that having tension strength of f=1100 MPa and modulus of elasticity of E=55000 MPa.

Table 2 Details of chosen experimental models

Beam	Design failure load (kN)	Design moment redistribution (%)	Reinforcement ratio / balance reinforcement ratio		Concrete strength (MPa)
			middle support	midspan	
G-A-0-N	100	0	4.9	3.0	28
G-A-15-N	100	15	3.42	3.86	28
G-A-30-N	100	30	2.1	4.9	28
G-B-0-N	80	0	2.8	1.76	28
G-B-15-N	80	15	1.91	2.25	28
G-B-30-N	80	30	1.46	2.8	28
G-C-0-N	60	0	1.0	0.75	28
G-C-15-N	60	15	0.75	1.0	28
G-A-15-H	130	15	2.36	2.66	50
G-A-30-H	130	30	1.45	3.38	50
G-B-15-H	110	15	1.32	1.55	50
G-B-30-H	110	30	1.01	1.93	50

For the first series of beams, having A and N marks, identical failure load has been designed, hence one beam has been dimensioned to the internal forces similar to elastic analysis, while for 2 beams moment reduction above the middle support has been conducted, by 15% and 30%, and adequate moment increase at the midspan. Therefore, for the designed fixed failure load, models with 0%, 15% and 30% of designed moment redistribution from the middle support to the midspan have been obtained. Percentage of beam reinforcement at the middle support with mark 0 has been selected of cca 4.9 times higher than balance reinforcement ratio, which is in line with references of the regulations that beams with FRP reinforcement should be designed to have concrete compression failure. Even after conducted redistribution, all the cross-sections have been designed to have reinforcement ratio being higher than balance reinforcement ratio. Different profiles of FRP reinforcement in the cross-section have been selected, in order to define as precisely as possible designed moment redistribution and enable identical failure load for the beams of the same series. Mark N is adequate for the designed concrete compressive strength upon cylinder of 28 MPa. All the beams from the same series are to be constructed in the same day, in order to reduce influence of concrete strength.

For the other series of beams, having B and N marks, lower percentage of reinforcement has been selected, which above the middle support for the beam with mark 0 is adequate to the value of cca 2.5 times higher than the balance reinforcement ratio, which still results in concrete compression failure. Models with 0%, 15% and 30% of moment redistribution from the middle support to the midspan have been also adopted. Concrete compressive strength has been adopted as for the beams in the first series.

For the third series of beams, having C and N marks, reinforcement ratio have been adopted that beams have failure by reinforcing bars, and with designed moment redistribution of 0% and 15%. As failure by reinforcing bars with FRP reinforcement presents brittle failure, it was considered as unrealistic that continuous beam achieves redistribution of 30% over the middle support without reduction of failure force, hence such a beam was not even taken into consideration.

In order to examine the concrete strength onto beam behaviour, for the beams with which we have designed moment redistribution from the middle support to the midspan of 15% and 30%, with their marks being A and B, for which it was planned to have concrete compression failure, new models have been made with designed concrete strength upon cylinder of 50 MPa (beams with mark H). It is evident that the beams with adopted higher concrete compressive strength will enable achievement of significantly higher failure load, i.e. ultimate load-carrying capacity. Namely, in the case concrete compression failure, upon increase of concrete strength, it comes to increase in strains in GFRP reinforcement, which enables higher tension stresses in GFRP reinforcement, and higher load-carrying capacity of cross-section, and higher failure force accordingly.

For shear reinforcement, GFRP stirrups have been adopted, of the diameter of 8 mm and at the distance of 8 cm for all the beams, in order to enable flexural failure, i.e. to avoid shear failure. In order to fulfil the requirements, the beams have been designed in line with regulations (ACI 440.1R-15, CSA S806-02, CSA S806-12, CNR-DT-203) which show significant differences in amount of GFRP stirrups, depending on the regulation it is use. For the beams having mark N, assurance from shear failure has been enabled in line with all the regulations. For the beams having mark H, by increase in concrete strength and therefore increase in designed failure load, dimensioned onto bending, there is a possibility of shear failure. Having in mind unreliability of obtained results of dimensioning onto shear capacity upon different regulations, which significantly vary, it has been decided that these beams are not to be insured additionally to the shear capacity, but identical quantity of shear reinforcement has been adopted. Possibility that beams have shear failure has been left in this manner, and therefore the effect of redistribution of internal forces onto ultimate shear capacity to be examined.

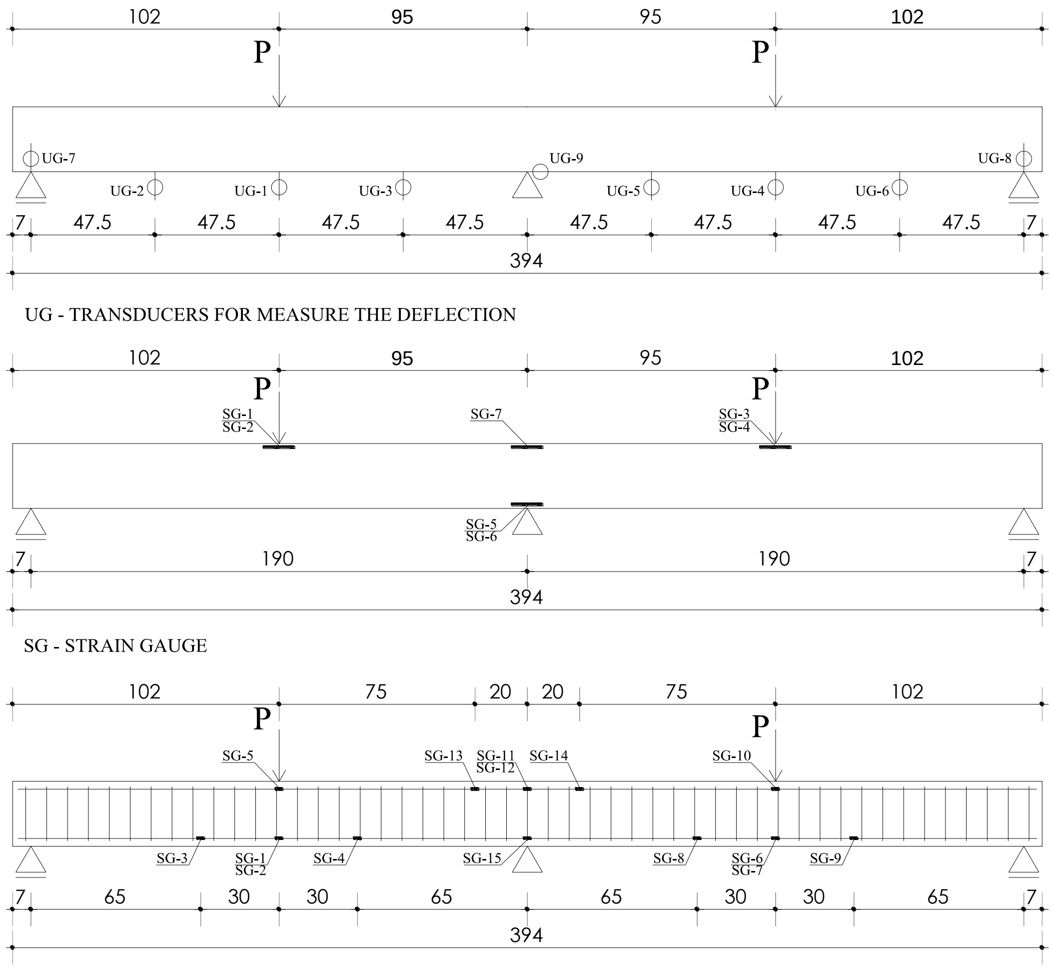

Figure 5 Disposition of measuring equipment along the beam

Upon selection of representative models, recommendations and references of actual regulations have been taken into consideration that both cross-sections at the midspan and at the middle support are to be over-reinforced, i.e. to achieve concrete compression failure, as semi-ductile, therefore more desirable in comparison to failure by reinforcing bars. Two beams have been designed to have failure by reinforcing bars in order to examine behaviour of continuous beams in the conditions of redistribution of internal forces and upon lower reinforcement percentages. While, on one hand, upon designing of beams with FRP reinforcement the quality of the same should be taken into consideration, which concrete compression failure certainly enables, on the other hand, economic aspect should be taken into account, meaning the best use of characteristics of FRP reinforcement. Namely, for reinforcement percentages being much higher than balance reinforcement ratio, strains in FRP reinforcement are low hence forces in the reinforcement remain unused (linear elastic behaviour up to failure). Therefore, such a design of FRP elements enables quality option, but is quite expensive. Failure by reinforcing bars is considered as highly undesirable, but it enables full use of tension stresses in the reinforcement, hence such a design of FRP elements is much cheaper. Therefore, reinforcement percentages for the models have been carefully selected, in order to enable their proper and quality response, but also stresses in the reinforcement not to be with low values. Such a problem is not present with the beams with steel reinforcement due to low strain at which reinforcement is yielding (higher modulus of elasticity) hence stresses in the reinforcement are used to its maximum.

The load is applied as a monotonically increasing static load in increments of zero state up to failure. At each loading level the following variables are measured: the intensity of the load, strain in the longitudinal tensioned GFRP reinforcement, strain in the concrete, deflection along the beam, the width of the cracks, and the reactions of the end supports. Measure of the reactions at the end supports are used for determining the internal forces along the beam and monitor the process of moment redistribution in which purpose two load cells are used. Transducers for deflection measuring and strain gauges for measuring the strains in the GFRP reinforcement and concrete are shown in Figure 5. For each increment photographing beam conditions is performed.

5. AIMS AND RESEARCH SIGNIFICANCE AND EXPECTED RESULTS

Main aim of this research is reviewing in behaviour of continuous beams reinforced with FRP reinforcement, loading up to failure, in the conditions of moment redistribution between critical cross-sections. Closer determination of behaviour of continuous reinforced concrete beams with FRP reinforcement is to be defined with different states as it follows: ultimate load-carrying capacity upon bending, ultimate load-carrying capacity upon shear, mode failure, state of cracks, deflection state, strains in the FRP reinforcement and compressive concrete, possibility of moment redistribution in the critical sections. Therefore, research aims have been set accordingly:

Own experimental program with the aim of examination of effect of critical parameters onto behaviour of reinforced concrete beams with FRP reinforcement, and moment redistribution alongside the beam and significant contribution in the database of experimental results.

Analysis of effect of certain parameters onto behaviour of reinforced concrete beams with FRP reinforcement, with the accent being on the effect of redistribution of internal forces onto limit state of continuous beams with FRP reinforcement.

Comparison of results of experimental researches in terms of load-carrying capacity, deflection and crack states with provisions of actual regulations for continuous beams with FRP reinforcement, and verification of correctness and reliability of certain provisions.

Research significance is especially seen in reviewing of the facts being stated below. Namely, upon literature overview it has been concluded that in the very few experiments on the beams with longitudinal FRP reinforcement, FRP reinforcement has been used for the stirrups. In the researches conducted on the beams with FRP reinforcement, steel reinforcement has been mostly used for the stirrups. Through the literature, as it was stated, corrosion was used as the main reason for implementation of FRP reinforcement instead of steel reinforcement in the RC elements, since RC elements with steel reinforcement are exposed to the same. It is therefore logical to ask the question of the purpose of use of FRP reinforcement for longitudinal reinforcement, and then use a steel one for the stirrups. Therefore, in the mentioned case, RC elements would still have the issue of corrosion, especially in the aggressive environments and bearing in mind width of cracks, being significantly wider when longitudinal FRP reinforcement is used in the beams. The problem increases with the fact that efficiency of FRP and steel stirrups is completely different, especially when the beam reaches ultimate shear load-carrying capacity. However, even when examinations with excluded reaching of ultimate shear load-carrying capacity are being done, the question still remains if the use of FRP reinforcement for the stirrups instead of steel reinforcement, would give the same effect onto behaviour of the beams where ultimate flexural load-carrying capacity is being reached. Having aforementioned in mind, it was decided that even in the experimental researches, FRP reinforcement is to be used for the stirrups, besides longitudinal FRP reinforcement.

Planned research should have shown that even statically indeterminate structures with FRP reinforcement are able to redistribute of internal forces and therefore have contributed to more quality structure response onto the action of load. It is expected that increase in ultimate load-carrying capacity is achieved by designed redistribution of internal forces in the continuous beams with FRP reinforcement, and even more important, that use conditions are achieved, i.e. reduction in deflection and cracks, which is regularly significant and relevant with these structures.

REFERENCES

[1] Baša N.: Efekti preraspodjele uticaja na granična stanja kontinualnih greda armiranih FRP armaturom, Polazna istraživanja za doktorsku disertaciju, University of Montenegro – Faculty of Civil Engineering Podgorica, oktobar 2015.

[2] El-Mogy M., El-Ragaby A., El-Salakawy E.: Flexural behavior of continuous FRP-reinforced concrete beams, J. Comp. Constr., 2010., pp. 669-680.

[3] American Concrete Institute (ACI): Guide for the design and construction of structural concrete reinforced with fiber-reinforced polymer (FRP) bars, Technical Committee Document No. 440.1R-15, 2015.

[4] CNR-DT 203/2006: Guide for the design and construction of concrete structures reinforced with fiber-reinforced polymer bars, National Research Council, Rome, Italy, 2006

[5] Canadian Standards Associations (CSA): Design and construction of building components with fibre-reinforced polymers, CSA S806-02, Rexdale, Ontario, Canada; 2002.

[6] Canadian Standards Association (CSA): Design and construction of buildings components with fiber-reinforced polymers, CSA S806-12, Toronto, 2012.
[7] ISIS Canada: Reinforcing concrete structures with fiber reinforced polymers, ISIS-M03-07, Canadian network of centers of excellence on intelligent sensing for innovative structures, Univ. of Winnipeg, Winnipeg, Man; 2007.
[8] International Federation for Structural Concrete (FIB): FRP reinforcement in RC structures, Bulletin No. 40, CEB-FIP, Lausanne, Switzerland, 2007.

EXPERIMENTAL INVESTIGATION OF BOND BETWEEN STEEL REBAR AND CONCRETE

Drago Saje[1]

[1] University of Ljubljana, Faculty of Civil and Geodetic Engineering, Jamova cesta 2, 1000 Ljubljana, Slovenia, email: drago.saje@fgg.uni-lj.si

SUMMARY: The paper shows the experimental results of the investigation of bond between concrete and steel rebar. The influence of concrete strength and/or steel fibres content on steel-to-concrete bond strength is presented. Therefore, a series of pull-out tests, based on standard EN 10080:2005, were conducted. In this study, the bond behaviour of rebars, with a diameter of 20 mm, in normal strength concrete, high strength concrete and steel fibre-reinforced concrete were tested. The results show that high strength concrete specimens indicated approximately twice as high bond strength compared to normal strength concrete specimens.

EKSPERIMENTALNO ISTRAŽIVANJE PRIONJIVOSTI ČELIČNIH ŠIPKI I BETONA

SAŽETAK: U radu su prikazani eksperimentalni rezultati istraživanja prionjivosti betona i čeličnih šipki. Prikazan je utjecaj čvrstoće betona i/ili sadržaja čeličnih vlakana na čvrstoću prianjanja čelik – beton. Proveden je niz ispitivanja izvlačenjem na osnovi norme EN 10080:2005. Ispitana je prionjivost šipki promjera 20 mm u betonu obične čvrstoće, betonu velike čvrstoće i betonu armiranom čeličnim vlaknima. Rezultati pokazuju da ispitni uzorci od betona velike čvrstoće imaju približno dvostruku čvrstoću prianjanja u usporedbi s ispitnim uzorcima od betona obične čvrstoće.

1. INTRODUCTION

Reinforced concrete is a composite material usually made of concrete and steel reinforcement. Concrete has large compressive and relatively low tensile strength. Therefore tensile force in reinforced concrete element is normally taken over by steel reinforcement, shaped as bars or welded mesh, where adequate bond between the reinforcement and the surrounding concrete should be provided. Based on adequate bond, acting at the rebar surface area, the force from the rebar is transferred into concrete and vice versa.

Several factors affect the bond behaviour between rebar and concrete, i.e.: anchoring length of the bar, bar diameter, bar position, deformation patterns and rib geometry, corrosion level of the bar, confining reinforcement around the bar, concrete quality, concrete composition, etc. [1, 2, 3]. Metelli and Plizzary [4] report that for a bar diameter increasing from 12 to 50 mm, the reduction in bond strength is about 25%. For bars anchored in normal strength concrete, bottom cast bars have better bond performance then top cast bars [3]. This is due to the increased tendency of bleeding of the concrete around top bars. However, in high strength concrete Azizinamini et al. [5] found that top cast bars have better bond performance than bottom cast bars. The improvement was in the range of 1 to 8%.

One of the tests for the determination of steel-to-concrete bond strength and bond stress-slip relationship is pull-out test, where the bar embedded into a concrete cube is pulled out of its concrete embrace. At the loaded end of the bar the tensile force is measured and at the unloaded end the relative displacement between concrete and the rebar is measured. Standard EN 10080:2005 [6] prescribes the shape and technical properties of the specimen.

2. BOND MECHANISM

During the pull-out process in reinforced concrete element the deformed bars are anchored by three bond mechanisms between reinforcement and surrounding concrete i.e. (i) chemical adhesion, (ii) friction at the interface and (iii) bearing of the ribs against the concrete surface. Chemical adhesion assures bond in the beginning, when the bond stress level is still low. After the initial slip of the bar, chemical adhesion is lost. In this moment friction forces at the surface of the bar and bearing forces at the ribs caused by the interlocking action are mobilized [1, 2, 7].

Plain bars without ribs are characterised by poor bond conditions between the bar and concrete, since forces are transferred into concrete only through mechanisms of initial chemical adhesion and friction between the bar and surrounding concrete. Both mechanisms exhibit rather small resistance to pull-out, which is why nowadays plain bars are not used in structural elements. Only ribbed bars are allowed, since ribs provide good anchoring into concrete.

The initial slip of the bar is due to transverse micro-cracks which originate at the tips of the ribs (Figure 1). As slip increases, concrete in front of the ribs starts to crush, which in turns induces a wedging action that increases the normal component of the bearing forces. This normal component is resisted by hoop stresses in the concrete, which cause splitting cracks to develop at the contact with the bar and to propagate radially. At this stage, the bond resistance is provided by an interlocking mechanism from the concrete struts confined by the undamaged outer concrete ring. In general bond can fail by the splitting of the concrete or pull-out of the bar. The split happens when splitting cracks propagate radially through the concrete towards its external surface. In the case of concrete splitting, the lower bond strengths are achieved compared to pull-out failure mode [1].

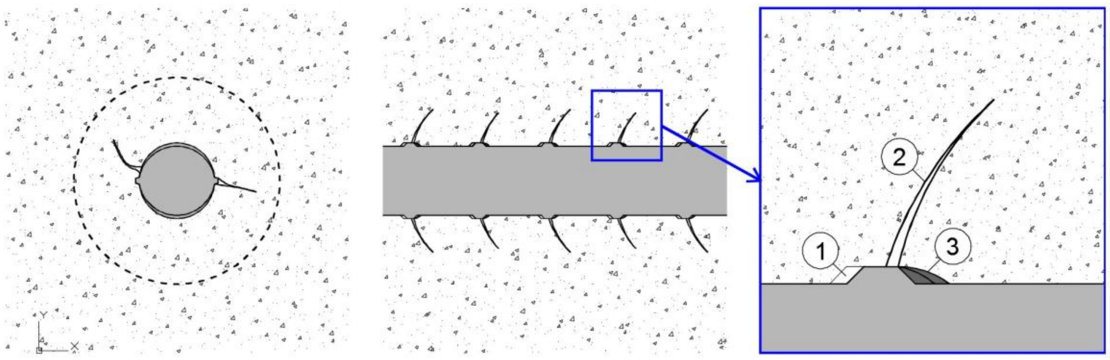

Figure 1: Schematic presentation of contact failure between ribbed rebar and concrete. (1- slip, 2-micro crack, 3-area of crushed concrete)

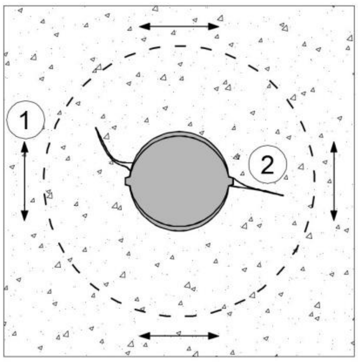

Figure 2: Cross-section, appearance of fracture cracks (2) due to transverse stresses (1)

3. EXPERIMENTAL WORK

3.1. CONCRETE MIXTURES

The test specimens were made from the mixture of normal strength concrete (NSC), high strength concrete (HSC) and of high strength fibre-reinforced concrete (HSC-SF-1.0%). The granulometric composition of the aggregate was kept the same in all four mixes. Washed crushed limestone aggregate with the maximum grain size of 16 mm and fine sand were used. To achieve higher strength and adequate workability (flow class F2) naphthalene based superplasticizer was used. Part of the cement, at high strength concrete, was replaced by silica fume, which additionally increases concrete strength.

Table 1 Composition of concrete mixes

	Mix	NSC	HSC	HSC-SF-1.0%
Aggregate [kg/m^3]	0/2 (fine sand)	264	285	281
	0/4	790	853	841
	4/8	263	284	280
	8/16	439	474	467
Cement [kg/m^3]	CEM II/A-M (LL-S) 42,5 R	400	360	360
Additives	Silica fume [kg/m^3]	0	40	40
	Steel fibres [%]	0	0	1.0
Water-binder ratio		0.52	0.36	0.36
Density [kg/m3]		2364	2449	2500

The mix proportions of high strength fibre reinforced concrete were practically the same to those of high strength concrete, except that in fibre reinforced concretes part of the aggregate were replaced by steel fibres. We used 30 mm long steel fibres IRI, with single hooks at the ends. Volume fractions of fibres used were 1.0% (Table 1).

3.2. TEST SPECIMEN

The test specimen for pull-out test was generally a concrete cube 200 mm × 200 mm × 200 mm with a bar embedded coaxially (Figure 3) [6]. Special wooden moulds were fabricated to cast nine specimens in a single batch. The rebars, with a diameter of 20 mm and yield strength of 500 MPa, were placed horizontally and concrete was cast vertically. Needle vibrator was used to compact the concrete. For each concrete mix three specimens for the pull-out test and three for the concrete compressive strength test (cubes 150 mm × 150 mm × 150 mm) were prepared. The specimens were de-moulded after one day and then cured for 28 days in water at room temperature of 22°C ± 2° till testing.

Figure 3: Mould prepared for concrete casting, bond prevention, bar deformation pattern

3.3. EXPERIMENTAL SETUP AND TESTING

The pull-out tests were carried out using the electro-hydraulic testing machine Instron 1345 with capacity ±1000 kN, according to standard EN 10080:2005 [6]. Figure 4 shows the dimensions of the the pull-out test specimen. The standard defines the specimen dimensions regarding the diameter of the used rebar. Dimensions on Figure 4 are valid for the bar with a diameter of 20 mm. The embracing with concrete is provided at a length of 10 cm (i.e. 5ϕ). At the remaining 10 cm bond is prevented by a PVC tube (8). Figure 4 also shows the schematic presentation of the test. The specimen stands on a rubber base (7) and additional steel plate (6). The rebar is clamped in the lower jaw (5) of the testing machine. In the upper jaw (1) the supporting steel cage is clamped. The lower and upper plates of the cage are connected by four steel bars. At the unloaded end of the rebar a digital dial gage with a resolution of 0.001mm (2) was used to measure the relative displacement of the bar related to the upper plane of the concrete cube. The rebar was also equipped with an extensometer (4) to monitor its strain. Loading of test samples was controlled in displacement control mode, with rate of actuator stroke 0.01mm/s. The total movement of 50 mm was set as the end value. The test continued until bond area failure or until full range displacement of the hydraulic actuator was reached – whichever occurred first.

4. RESULTS AND DISCUSSION

Using adequate measuring equipment and software for data acquisition, the values of the force and the strain at the loaded end of the embedded rebar and the relative displacement (slip) of the unloaded end were obtained. All physical properties (relative displacement, strain and force) were measured and recorded by data acquisition system Dewesoft DEWE 2500.

The notional bond stress is defined as a quotient between the applied force and the nominal surface area of the bar at the anchoring length. Thus the assumption of equal distribution of stresses along the anchoring length was considered.

The measured values of concrete compressive strength and obtained values of the bond strength are shown in Table 2. f_c denotes the average measured compressive strength of individual concrete type. τ_{max} is the obtained bond strength between concrete and rebar, τ_{mean} is the average bond strength of three specimens made of same concrete type.

Compared to normal strength concrete (NSC), high strength concrete (HSC) specimens indicated about twice as high average bond strength as well as compressive strength. When comparing HSC and its alternative with steel fibres HSC SF-1.0%, it can be seen that the values of bond strength differ by only a few MPa. The obtained values of bond strength for the HSC and NSC concretes could be compared to the research from literature [2], where a rebar with a diameter of 16 mm and concretes with a 90 day compressive strengths of 54.8 MPa and 83.2 MPa were used. Specimens from the first concrete had on average bond strength of 19.9MPa, while in specimens from the second concrete it was 29.7 MPa. Compared to our results only a small difference at normal strength concrete can be noticed.

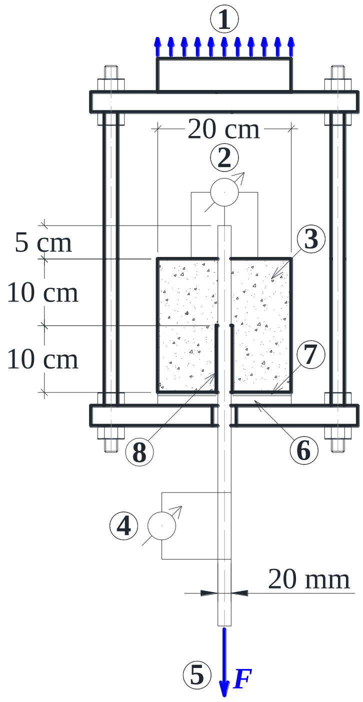

Figure 4: Scheme of pull-out test and specimen dimensions, testing apparatus

Table 2 Concrete compressive strengths and bond strengths between reinforcement and concrete

Mix	f_c [MPa]	#	τ_{max} [MPa]	τ_{mean} [MPa]	τ_{mean} / f_c
		1	15.79		
NSC	41.4	2	15.82	15.9	0.38
		3	16.19		
		1	- [1]		
HSC	79.8	2	28.49 [2]	29.3	0.37
		3	30.13 [2]		
		1	31.29 [3]		
HSC-SF-1.0%	92.9	2	31.24 [3]	31.4	0.34
		3	31.54 [4]		

Note: [1] Failed measurement, Note: [2] Splitting occur, Note: [3] Contact length between concrete and rebar in specimens amounted to 5ϕ. In the pull-out test of the rebar from concrete, yielding of the rebar appeared before bond area fails.
Note: [4] Bond area failure, steel rebar yielding and concrete specimen cracking

Bond stress-slip relationships for eight specimens are presented in Figure 5. Large influence of the concrete type on the specimen response during bar pull-out can be seen. The normal and high strength concrete specimens failed in different ways. In the beginning of the test the diagrams rise steeply. In this range the upper- free end of the bar is almost motionless. Adhesion dominates between concrete and rebar. After the initial slip, the first local cracks appear in the concrete specimen and ribs of the bar start to wedge in the concrete. At normal strength concrete the bond strength was reached at slip of approximately 1.5 mm. After reaching the ultimate bond stress, the concrete in contact area began to crush, steel-to-concrete contact was getting weaker and the rebar was pulled out. At high strength concrete, compared to normal strength concrete, twice as high bond strength was reached at approximately twice as small slip. At all specimens of HSC rebar yielding and splitting failure occurred.

At two fibre reinforced concrete specimens (HSC-SF-1.0%), the contact area between concrete and reinforcement did not fail during the test. Strains obtained from extensometer installed on the rebar showed that the steel bar yielded. The movement of the actuator of testing machine was almost the same as the rebar elongation, while the upper-free ends of the bars slipped on average only by 1.0 mm. During the pull-out test of the third fibrous high strength concrete specimen there occurred all three things: yielding of the bar, contact area failure and cracking of the concrete. Fibres in the composite retained testing specimen together. Only hairline cracks were occurred. (Figure 6)

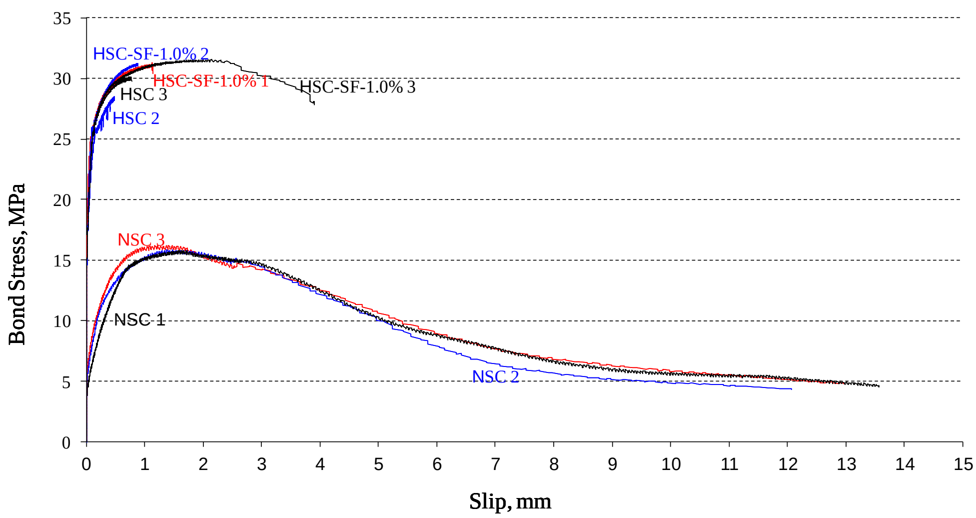

Figure 5 Bond stress-slip relationships for different concrete types

Figure 6 Failure patterns for different concrete types (left: cracking of HSC-SF-1.0%, right: splitting of HSC)

5. CONCLUSIONS

Based on the results of the test of the rebar-to-concrete bond strength of 28 days old concrete cube specimens with embedded steel rebars with a diameter of 20 mm, the following conclusions can be drawn:

The bond strengths of the high strength concrete specimens were on average about twice as high as those of normal concrete specimens. The same also applies to the compressive strength.

High strength concrete specimens and high strength fibre reinforced concrete specimens had practically the same composition, except that the latter included additional steel fibres. The values of ultimate bond stress of the fibre reinforced high strength concrete specimens with 1.0% of volume fraction of fibres are only by about 7% higher than the comparable values for high strength concrete without fibres.

Despite that rebars were anchored only by 10 cm long contact length, yielding of the bar appeared before bond failure occurred, in both high strength concrete specimens as well as in all high strength fibre reinforced concrete specimens with 1.0% of fibres. This phenomenon could not be noticed in the comparable normal strength concrete specimens.

After yielding of the reinforcement, in both types of high strength concrete specimens, the change in their behaviour was noticed. High strength fibre reinforced concrete with 1.0% of fibres preserved the steel-to-concrete contact at two concrete specimens, while at all concretes without fibres the contact failed due to splitting of the concrete. One of the specimens of fibrous high strength concrete failed due to splitting, but the test specimen did not split into two or three pieces, as it happened at the high strength concrete specimens without fibers. There was a loud bang, above and on the sides of the specimen hairline cracks width of approximately 0.1 mm were occurred.

REFERENCES

[1] Murcia-Delso, J.; Stavridis, A. & Shing, B.: Modeling the bond-slip behavior of confined large-diameter rebars, Proceedings of the III ECCOMAS Thematic Conference on Computational Methods in Structural Dynamics and Earthquake Engineering, Corfu, Greek, 2011, p 14.

[2] Barbosa, M T G.; Sánchez F S.: Investigation of bond stress in pull out specimens with high strength concrete, *Global Journal of Researches in Engineering*, Vol. 13, Iss. 3, 2013, pp 55-64.

[3] Fédération internationale du béton (fib): fib bulletin 10. Bond of reinforcement in concrete, Lausanne, 2000, p 427.

[4] Metelli G.; Plizzari, G.: Influence of the relative rib area on bond behaviour. *Magazine of Concrete Research*, Vol. 66, Iss. 6, 2014, pp 277-294.

[5] Azizinamini, A.; Stark, M.; Roller, J J.; Ghosh, S. K.: Bond performance of reinforcing bars embedded in high-strength concrete. *ACI Structural Journal*, September-October 1993, pp 554-561.

[6] EN 10080: Steel for the reinforcement of concrete – Weldable reinforcing steel – General. 2005, p 61.

[7] Appa Rao, G.; Pandurangan, K.; Sultana, F.; Eligehausen, R.: Studies on the pull-out strength of ribbed bars in high-strength concrete, IA-FraMCoS International Association of Fracture Mechanics for Concrete and Concrete Structures, Proceedings of the FraMCoS-6, Catania, Italy, 2007, p 6.

BEHAVIOR OF RC BEAMS WITH LIGHTWEIGHT BLOCKS INFILL

Wael Ibrahim[1]

[1] University of Helwan Faculty of Civil Engineering, Department of Civil Engineering, Cairo, Egypt,
email: wael.ibrahim@rwth-aachen.de

SUMMARY: In an attempt to reduce the self-weight of reinforced concrete beams, a new lightweight reinforced concrete section (LRCS) is developed with a use of lightweight block as infill material. A series of eight reinforced concrete beams with LRCS are fabricated and tested in the laboratory to examine the effects of the block infill configuration on the specimen flexural behaviour. The main goal of the tests is to find the load-carrying capacity; the test variables investigated are the influence of block infill configuration on the load-carrying capacity and failure mode. Based on the test results, the block infill configuration has an influence on stiffness, deflections, load-carrying capacity and failure mode of the beams. Results of this investigation are intended to provide information required for the design of RC beams with lightweight blocks infill.

PONAŠANJE ARMIRANOBETONSKIH GREDA S ISPUNOM OD LAGANIH BLOKOVA

SAŽETAK: Razvijen je novi lagani armiranobetonski presjek s namjerom smanjenja vlastite težine armiranobetonskih greda primjenom laganog bloka kao ispunskog materijala. Izrađena je i u laboratoriju ispitana serija od osam armiranobetonskih greda s laganim armiranobetonskim presjekom kako bi se ispitali učinci oblika ispunskog bloka na ponašanje uzoraka pri savijanju. Glavni cilj ispitivanja bio je ustanoviti nosivost. Istražene ispitne varijable su utjecaj oblika ispunskog bloka na nosivost i način sloma. Na osnovi ispitnih rezultata zaključeno je da oblik ispunskog bloka ima utjecaj na krutost, progib, nosivost i način sloma greda. Rezultati ovog istraživanja imaju za svrhu dobivanje podataka potrebnih za proračun armiranobetonskih greda s laganim ispunskim blokovima.

1. INTRODUCTION

Light weight of concrete structures is desirable particularly when designers have to deal with high rise construction. A newly developed lightweight reinforced concrete section (LRCS) has been experimentally investigated (Vimonsatit et al. 2012). The section is made up of a reinforced concrete with lightweight block infill. The LRCS can be used either as beams. The developed LRCS members are also suitable for large span construction due to the weight saving benefits. This paper is investigated LRCS section, which can be used as beams. In a reinforced concrete section design, the flexural capacity of the section is calculated from the coupling between compression in concrete and tension in reinforcing steel. The Eurocode-2 design code, permit the uses of uniform stress block to simplify the effective concrete in compression above the neutral axis. As a result the part of concrete below the neutral axis has no contribution to the flexural capacity of the section. In the following sections the details of the experimental investigation on the flexural tests of LRCS beams will be described. The results of the flexural capacities behaviour will be presented. Furthermore, the relation of the ultimate load with infill thickness and failure modes are also discussed. The results of this study will help the extension of lightweight block infill to another great potential of structural elements.

2. TEST PROGRAM

2.1. MATERIALS

The 28-day compressive strength of concrete is 30 MPa. The maximum size of aggregate is 10 mm. The steel reinforcement is Grade 360 with nominal yield and ultimate strength of 360 and 520 PMa, respectively. The strength value of AAC blocks used is 3.0 MPa.

2.2. TEST SPECIMEN

Test specimen is 3000 mm long, 250 mm wide and 500 mm deep. Each beam is singly reinforced at tension side by 2 No. 16 deformed steel bars with a concrete clear cover 25 mm. Eight beams are manufactured for three series of four-point flexural test. The distance between the two point loads is 600 for the flexural test. The flexural test is to compare the flexural capacity between the solid and LSRC beams. Eight beams are prepared, one solid (CB1) and seven with AAC blocks (LB1 to LB7). The standard dimensions of the AAC blocks used are 600 mm long, 100, 200 and 300 mm wide and 150 mm thick. The test matrix is used in the study, is given in Table 1. The specimens are as seen in Figure 1.

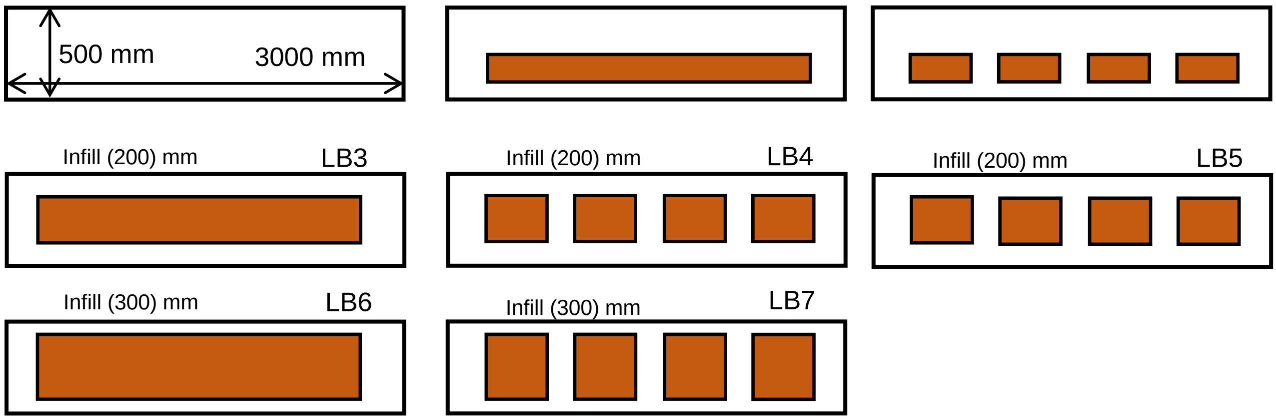

Figure 1 Front view

Table 1 Test matrix

Series	Specimen	AAC blocks dimension (mm)
Control beam	CB1	---
Group (1)	LB1	600 x 150 x 100
	LB2	
Group (2)	LB3	600 x 150 x 200
	LB4	
	LB5	
Group (3)	LB6	600 x 150 x 300
	LB7	

2.3. TEST SET-UP

The beams are simply supported and are subjected to two point loads. The distance between the two point loads is 600 mm. the typical test set up is as shown in Figure 2. The beams are loaded to failure using a 50 tonne capacity hydraulic jack to apply each of the two point loads. The jacks are attached to a reaction frame. Two supporting frames with 300 mm long × 50 mm diameter steel rollers are used as the end support. The test set up is as seen in Figure 2.

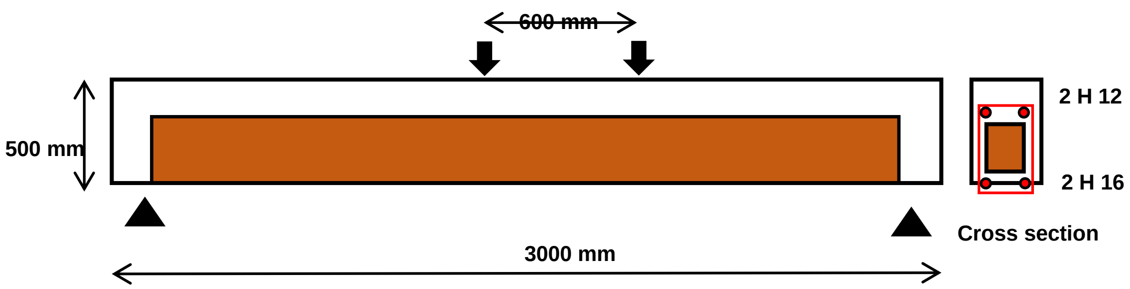

Figure 2 Front view

2.4. INSTRUMENTATION

The vertical deflections of the test beams are measured using three (LVDTs) which are placed at the mid-span and under the two point loads. During the initial set up of the LVDTs, the instruments are calibrated before the test commenced. An automated data acquisition system with a Nicolet data logger system is used to record the load-deformation from the jacks and the LVDTs.

3. EXPERIMENTAL RESULTS

The failure loads of the control beam and LSRC beams under the flexure test are found to be of insignificantly different. It is found that beams LB1 and LB2, which have the AAC blocks with 100 mm height, are failed at an average load of 168 kN, and CB1 beam failed at 165 kN, respectively. These load values are taken from the average of the loads applied from the two hydraulic jacks.

3.1. EFFECT OF INFILL THICKNESS

The relation between the thickness of block concrete infill and the ultimate load is depicted in Table 2. The relation is not linear through the infill thickness. The results showed that the average ultimate load of LSRC beam with infill thickness of 100 mm is 169 kN. It is proved that the concrete volume under the neutral axis can be considered ineffective and only acts as passive volume. While, the average ultimate load of LSRC beams with infill thickness of 200 mm and 300 mm are 163 kN and 152 kN, respectively. It is found that when the depth of infill increases, the ultimate load decreases. An insignificant 8% reduction in the ultimate load capacity of LSRC beam with infill thickness of 300 mm compared to the equivalent control beam.

3.2. FAILURE MODES

The LSRC beams under four-point bending test predominantly experience flexural-tension cracks. The cracks in LSRC beams propagate as tension crack from the bottom zone that led to the flexural cracks at the ultimate load.

Table 2 Test results

Series	Specimen	Infill thickness (mm)	P_u (kN)	Δ_u (mm)
Control beam	CB1	---	165	15
Group (1)	LB1	100	166	18
	LB2	100	172	22
Group (2)	LB3	200	168	18
	LB4	200	162	14
	LB5	200	160	18
Group (3)	LB6	300	150	15
	LB7	300	154	22

4. CONCLUSIONS

An experimental study is conducted on the structural behaviour of reinforced concrete beams with lightweight blocks infill. Based on the test results, the following conclusions can be drawn:

Under the flexure test, there is insignificant difference in the flexural capacity between the control beam and the LRCS beams filled with AAC blocks. These results show that the proposed LRCS beams seem to perform well under flexure. It is found that when the depth of lightweight blocks infill increases, the ultimate load decreases. Since the structural behaviour of the beam involves phenomena that not yet well understood, thus extensive investigations are required in both experimental and numerical studies. General a significant issue of LRCS beams lies with the behaviour at service loading. Moreover, the stiffness, the beam deflection, and the cracking behaviour of LRCS beam with discontinuous infill slightly lower than LRCS beam with continuous infill. Thus, need to be further investigated and compared with solid beams.

REFERENCES

[1] Aldrige, D. (2000). Foamed concrete: properties, applications and potential. One Day Awareness on Foamed Concrete, Dundee, United Kingdom.

[2] British Cement Association. (1994). Foamed concrete: composition and properties. Report 46.042, Slough, United Kingdom.

[3] Eurocode 2. (2004). Design of concrete structures- Part 1-1: General rules and rules for building. British Standards: London, United Kingdom.

[4] Hegger J, Roggendorf T (2008). Shear capacity of prestressed hollow core slabs in slim floor constructions. Eng. Struct. 31(2):551-559.

[5] Kayali O, Haque MN, Zhu B (2003). Some characteristics of high strength fiber reinforced lightweight aggregate concrete. Cement Concr. Compos. 25: 207-213.
[6] Memon NA, Sumadi SR, Ramli M (2007). Ferrocement Encased Lightweight Aerated Concrete: A Novel Approach to Produce Sandwich Composite. Mater. Lett. 61:4035-4038.
[7] Russo A, Zuccarello B (2007). Experimental and Numerical of the Mechanical Behaviour of GFRP Sandwich Panels. Compos. Struct. 81:575-586.
[8] Vimonsatit, V., Wahyuni, A.S. and Nikraz, H. (2012). Reinforced concrete beams with lightweight concrete infill. Scientific Research and Essay, 7(27), pp. 2370-2379.

TOPIC 6.

Modelling at material and structural level

Modeliranje materijala i konstrukcija

CALCULATION OF SHRINKAGE STRESS IN CONCRETE STRUCTURES

Jun Zhang[1], Jiahe Wang[1], Xiaoping Ding[1]

[1] Tsinghua University, Department of Civil Engineering, Beijing, 100084, China, email: junz@tsinghua.edu.cn, wangjiahe13@mails.tsinghua.edu.cn, dxp15@mails.tsinghua.edu.cn

SUMMARY: This paper reports the recent advances in simulation of shrinkage stress in concrete structures. In the modeling, an integrative model for autogenous and drying shrinkage predictions of concrete under drying environments is introduced first. Second, a model taking both cement hydration and moisture diffusion into account synchronously is used to calculate the distribution of internal relative humidity in concrete. Using the above two models, the distribution of shrinkage stress in steel ring restraint concrete ring made by normal and high strength concrete respectively under drying is calculated. The effects of concrete strength and internal curing with pre-wetted lightweight aggregates on the development of shrinkage stress are presented and discussed.

PRORAČUN NAPREZANJA PRI SKUPLJANJU U BETONSKIM KONSTRUKCIJAMA

SAŽETAK: U radu se prikazuje sadašnji napredak u simulaciji naprezanja pri skupljanju u betonskim konstrukcijama. Na početku je pri modeliranju uveden zajednički model predviđanja autogenog skupljanja i skupljanja pri sušenju u okolišu. Zatim je načinjen model kojim se sinkrono u obzir uzima hidratacija cementa i difuzija vlage za proračun raspodjele unutarnje relativne vlage u betonu. S pomoću tih dvaju modela proračunana je raspodjela naprezanja pri sušenju za skupljanje betona omeđenog čeličnim prstenom za obični beton i beton velike čvrstoće. Prikazani su i raspravljeni utjecaji čvrstoće betona i unutrašnje njege s prethodno namočenim laganim agregatom na razvoj naprezanja pri skupljanju.

1. INTRODUCTION

Concrete shrinks as moisture is lost to the environment or by self-desiccation. As concrete shrinks, tensile stresses will be developed in the structure due to restraints from adjunct materials or connected members. The stresses may exceed the tensile strength and cause concrete to crack. Cracking in concrete members reduces the load capacity of the structure. Moreover, cracks allow water and other chemical agents, such as deicing salt, to go through the cover layer to come into contact with the reinforcements, leading to reinforcement corrosion and rupture in steel reinforced concrete. The magnitude of the shrinkage strain is normally proportional to the amount of moisture lost [1-3]. Generally, there are two manners leading the moisture loss in early-age concrete. As environmental humidity is lower than the humidity inside of concrete, water in concrete evaporates and shrinkage of concrete arises, which is conventionally called drying shrinkage. Another manner of moisture loss is through cement hydration, which causes concrete to shrink also and ordinarily is called autogenous shrinkage. In practice, more water loss may happen at the places where are close to surfaces of concrete elements. Thus, shrinkage gradient should exist in concrete structures and corresponding nonlinear shrinkage stresses should be resulted. However, the effects of shrinkage gradient occurred in concrete structures have not properly been taken into account in the analyses of shrinkage stress in the structures due to the lack of an appropriate model to relate the shrinkage strain and the amount of local moisture loss.

This article focuses on the simulation of the distribution of shrinkage strain and stress in early-age concrete structures in which the shrinkage gradient is seriously taken into account. In the modelling, an integrative model for autogenous and drying shrinkage prediction of concrete at early-age is introduced first. Second, a model taking both cement hydration and moisture diffusion into account synchronously is used to calculate the distribution of internal relative humidity in concrete. Using the above two models, the distribution of shrinkage strain and stress in concrete structures made by normal and high strength concrete respectively under normal drying are calculated. With the developed model, the effects of concrete strength and internal curing with pre-wetted lightweight aggregates, as well as the use of pre-fabricated fiber reinforced engineered cementitious composite permanent formwork on shrinkage stress in concrete structures are discussed.

2. MODELING ON MOISTURE VARIATION INDUCED STRAIN

The progress of moisture inside of concrete since casting had been investigated by Zhang et al. [4,5] through measuring internal relative humidity of concrete. The variation of moisture content in concrete, represented by internal relative humidity (*RH*) can be described as follow [4,5]. After mixing of all consists of concrete, the solid cementitious particles are covered with a relative thicker layer of water to form flowable cement paste that endues fresh concrete with fluidity. Within an initial short period after concrete casting, the voids of the solid skeleton are filled with liquid water and cement particles are connected to each other through the surface water layer. In such situation, a continuous liquid network is existed in this period, and that results in the relative humidity inside of concrete is equal or close to 1 theoretically, even the salt content in concrete may lead the internal relative humidity dropping little from 1. Due to the process of water consuming is so slow that the moisture saturation period, which is defined as stage I in the present paper, can last quite long time. On the other hand, with development of cement hydration, the cement particles in the skeleton are gradually enlarged and the neighbouring cement particles gradually contact each other through breaking part of the surface water layer. Thus, as long as the connection area between solid particles is sufficient to support the self-weight of concrete, setting of concrete occurs, which represents accomplishment of the transformation from liquid state to solid state of concrete. It should be noted that the cement particle partial connection at concrete set does not mean the continuity of liquid water is already broken down. A continuous liquid network is still existed in concrete at this moment. Therefore, the time of concrete set is normally ahead of the point of relative humidity starting to drop from 1. In this stage, the water loss is governed by cement hydration and water evaporation at a constant rate. Cement hydration resulted chemical shrinkage takes place continuingly and this should partially transform to macro shrinkage of concrete due to the self-restraint of hardened concrete. Therefore, the magnitude of shrinkage strain of concrete in this stage should be controlled by both chemical shrinkage and stiffness of concrete.

With persistent hydration of cement, the continuity of the pore water is finally broken down and the pore water is isolated into some individual pocket lakes without direct connection between each others. Meanwhile, cement hydration resulted chemical shrinkage and moisture diffusion resulted water loss takes place continuously. If consumption of liquid from the pores were to expose the solid phase, a solid/liquid interface would be replaced by a more energetic solid/vapor interface. To prevent such an increase in the energy of the system, liquid water tends to spread from the interior of the body to cover that interface. Therefore, some capillary pores with curved liquid/vapor interface are finally formed within the pore water to compensate for the total volume reduction. The formation of concave liquid/vapor interface should lead the decrease of internal relative humidity of concrete. Thus, the moment when the formation of capillary pore is the time when the internal relative humidity of concrete starts to drop from 1. It should be noted that the reduction of internal relative humidity in this case is due to the decrease of saturated water vapor pressure after the formation of capillary pores. After this moment, the advance of internal relative humidity goes into the humidity reduction stage (Stage II).

Based on above analyses, shrinkage of concrete developed in moisture progressing stage I and stage II may correlate with chemical shrinkage and internal relative humidity respectively as [6]:

$$\varepsilon_w = \begin{cases} \dfrac{\phi_P}{(K+K_0)^\eta}\left[1-\sqrt[3]{1-(V_{cs}-V_{cs0})}\right] \quad \text{for RH} = 1 \\ \dfrac{\phi_P}{(K+K_0)^\eta}\left[1-\sqrt[3]{1-(V_{cs1}-V_{cs0})}\right] + \dfrac{\nu_p \rho_w R_g T}{3M}\left(\dfrac{1}{K_s}-\dfrac{1}{K}\right)\ln(RH) \quad \text{for RH} < 1 \end{cases} \tag{1}$$

Where ϕ_P is the volume fraction of cement paste in concrete that can be calculated directly from the concrete mixture proportion. K_0 and η are both constants that can be determined by fitting the model and test data. V_{cs} and V_{cs0} are the chemical shrinkage (in volume) at a given cement hydration degree and at the point of concrete set. V_{cs1} is chemical shrinkage when internal humidity of concrete starts to drop from 1. K is bulk modulus of the whole porous body and K_s is bulk modulus of the solid material. The correction factor $\phi_P/(K+K_0)^\eta$ involves volume fraction of cement paste and bulk modulus of concrete, which may be more relative comprehensively reflect the effect of mix proportion and stiffness of concrete on shrinkage developed in this stage. M is the molar weight of water (0.01802 kg/mol), ρ_w is density of water and R_g is ideal gas constant (8.314 J/molK). ν_p is water saturation related parameter that can be obtained by introducing a parameter k_0 in the accumulate pore volume as:

$$\nu_\mathrm{p} = 1-\exp(-k_0\beta r) \tag{2}$$

where β is a parameter reflecting the impact of concrete age (reflected by cement hydration degree, α on pore volume and may be simulated as $\beta=\alpha_0 e^{\lambda\alpha}$, α_0 and λ are experimental determined constants. Parameter k_0 is obtained by comparing model and experimental results [6]. The shrinkage model developed above is based on chemical shrinkage and formation of capillary pores. Therefore, the model can be used for water loss resulting shrinkage prediction regardless if the water loss is caused by cement hydration or by environmental drying. By applying the present model, calculation of shrinkage distribution in concrete structures in the case of humidity gradient existing becomes possible. In addition, the influences of curing conditions, including environmental humidity and temperature on concrete shrinkages should also be reflected in the model by cement hydration degree and internal relative humidity, which are both core parameters controlling the macro shrinkage of concrete.

The chemical shrinkage (in volume) at a given cement hydration degree can be estimated through Powers' volumetric models [7]. Assuming the hydration degree of cement is α and the total volume of cement particles and water is 1, the chemical shrinkage, V_{cs} of a hardening Portland cement paste without silica fume addition can be calculated by:

$$V_{cs} = 0.2(1-p)\alpha \tag{3}$$

Where $p=(w/c)/(w/c+\rho_w/\rho_c)$. w and c are the weight of water and cement respectively in concrete mixture. ρ_w and ρ_c are the density of water and cement respectively. The above equations can be utilized only in the shrinkage calculation for concrete without silica fume application. It should be noted that for fly ash added concrete, the effect of fly ash on chemical shrinkage in this stage is negligible because the contribution of fly ash on cement hydration in early-age is very small. Therefore, equation (3) can be used for fly ash concrete as well. For concrete with silica fume addition, according to Jensen's results [8], the chemical shrinkage Vcs can be estimated as:

$$V_{cs} = k(0.2+0.7s/c)(1-p)\alpha \tag{4}$$

Where s, c are the weight of silica fume and cement respectively. $p=(w/c)/(w/c+\rho_w/\rho_c+(\rho_w/\rho_c)(s/c)$, $k=1/(1+1.4(s/c))$.The cement hydration degree, α can be calculated from isothermal tests. By measuring the adiabatic temperature rise of concrete at different time, the cement hydration degree is estimated by [6]:

$$\alpha = \frac{T_{ad}(t)}{T_{ad}(\infty)}\alpha_u \tag{5}$$

Where $T_{ad}(t)$ is the adiabatic temperature rising at time t, $T_{ad}(\infty)$ is the ultimate adiabatic temperature rising. α_u is the ultimate degree of hydration and is a function of water to cement ratio (w/c) as [9]:

$$\alpha_u = \frac{1.031w/c}{0.194+w/c} \tag{6}$$

For concrete with fly ash or silica fume addition, the ultimate cement hydration degree need to be revised due to their filling action and pozzolanic activity. Schindler et al.[13] investigated the effect of fly ash on the ultimate degree of cement hydration by experiments. Their results show that the effect of fly ash on α_u may behave as the reduction on the thickness of the water layer formed at the surface of cement particles on one hand, which should reduce cement hydration degree, and increasing long term cement hydration degree due to its pozzolanic activity on the other hand. Therefore, concrete with fly ash addition, the cement hydration degree α_u is revised as [10]:

$$\alpha_u = \frac{1.031w/(c+f)}{0.194+w/(c+f)} + 0.50f/(c+f) \leq 1.0 \tag{7}$$

Where f is mass content of fly ash. For concrete with silica fume addition, such as C80 series in the present study, the effect of silica fume on the ultimate degree of cement hydration is preliminary displayed as the action of reducing the thickness of the water layer at surface of cement particles due to its extremely high fineness. For example, experimental results of Luzio et al. [11] show that the addition of silica fume reduces the ultimate cement hydration degree of cement. Therefore, for silica fume added concrete (mass of silica fume less than 10% of the total mass of cementitious materials), the ultimate cement hydration degree α_u is revised as:

$$\alpha_u = \frac{1.031w/(c+s)}{0.194+w/(c+s)} \tag{8}$$

To calculate the hydration degree under different temperature history, the equivalent age is used [9]. The equivalent age concept assumes that samples of a concrete mixture of the same equivalent age will have the same mechanical properties or cement hydration degree, regardless of the combination of time and temperature yielding the equivalent age. Based on the above definition, the equivalent age t_e can be expressed as

$$t_e = \int_0^t e^{\frac{1}{R}\left(\frac{U_{ar}}{293} - \frac{U_{aT}}{273+T}\right)} dt \tag{9}$$

Where t_e is the equivalent age at the reference temperature (here the reference temperature is equal to 20°C is assumed). U_{ar} and U_{aT} are the apparent activation energy (J/mol) at reference and actual temperature respectively. R is the universal gas constant, 8.314J/molk. T is temperature in Celsius (°C). Regarding apparent activation energy, a number of researchers have concluded that it could not be considered as a constant independent of time except during the beginning of cement hydration [12,13]. Based on these findings, the apparent activation energy of concrete is expressed as a function of temperature and curing time as [14]:

$$U_a = (42830 - 43T)e^{(-0.00017T)t} \tag{10}$$

Where T is curing temperature (°C) and t is curing time in days. Due to the actual temperature T inside of concrete is varied with time, it is convenient to solve t_{eq} in matrix form instead of integrating. If the curing time is divided into n sections and the temperature in each time interval is assumed to be a constant, then we have

$$t_e = \sum_{i=1}^{n} e^{\frac{1}{R}\left(\frac{U_{ar}}{293} - \frac{U_{aT_i}}{273+T_i}\right)} (t_i - t_{i-1}) \tag{11}$$

The section number n may depend on the required accuracy and normally can be equal to the time intervals for temperature measurement. Based on the equivalent age, the hydration degree of cement defined in (6) can be simulated by [15,16]:

$$\alpha = \alpha_u \exp\left(-(A/t_e)^B\right) \tag{12}$$

Where A and B are two empirical constants which can be determined by fitting isothermal experimental results and equation (12).

Under drying condition, the moisture content in concrete will be less than that under sealed state and this moisture reduction will reduce the cement hydration degree. The effect of moisture content on cement hydration should be taken into consideration in the model by [17]:

$$\frac{\mathrm{d}\alpha}{\mathrm{d}t_e} = \left(\alpha_c \cdot \frac{B}{A} \left(\ln\left(\frac{\alpha_u}{\alpha}\right)\right)^{\frac{B+1}{B}} - P \right)(RH)^n + P \tag{13}$$

Constants n and P can be determined from internal humidity measurements and isothermal tests. Thus for different drying process, the effect of interior humidity variation on cement hydration can be estimated by (13). The cement hydration degree at a given time t_e can be obtained by integrating (13) from 0 to t_e. As showed in (1), elastic modulus of concrete is also an important parameter for shrinkage calculation. After setting the elastic modulus of concrete starts to grow from zero. Based on the equivalent age, the development of the elastic modulus of concrete with age under varied temperature and drying status can be estimated by [17]:

$$E(\alpha) = 1.05E_{28}\left(\frac{\alpha-\alpha_0}{\alpha_u-\alpha_0}\right)^b \qquad (14)$$

Where α_0 is the hydration degree at concrete set. b is a constant that can be determined by fitting (14) with test data.

The shrinkage model is verified by experiments [6]. Fig.1 displays two examples of cement hydration degree and equilibrium age diagrams, C30 and C80 concretes with compressive strength at 28 days of 34.1MPa and 88.7MPa respectively. Fig.2 presents the comparisons between model predictions and experimental results for the two concretes in terms of shrinkage-age diagrams starting from concrete set to 28 days under both sealing and drying curing conditions. The related material parameters used in the model are listed in Table 2. From the figure, we can observe that the model can well catch the characteristics of the development of shrinkage of concrete starting from set. Under drying condition, a high shrinkage is obtained in the experiments and in model prediction as well. Because the model combines the effect of age and position into a single physical parameter, *RH*, the model can predict shrinkage strain in concrete structures not only for discrete time, but also for different positions. Certainly, in order to do so, the moisture distribution, represented by relative humidity inside of concrete is required prior to use the model.

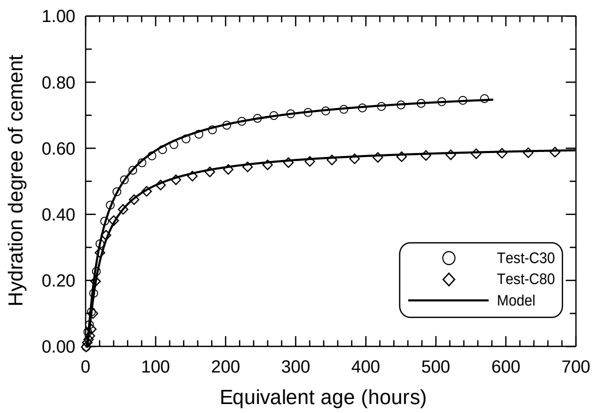

Figure 1 Relationship of cement hydration degree and equivalent age

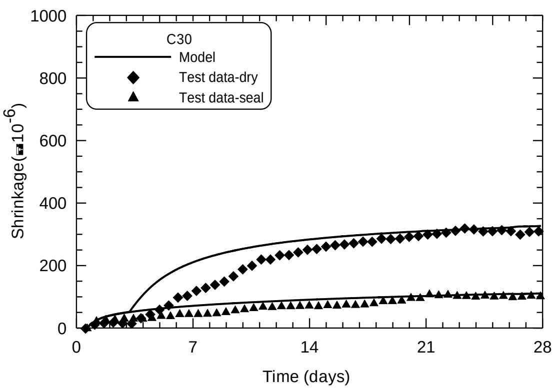

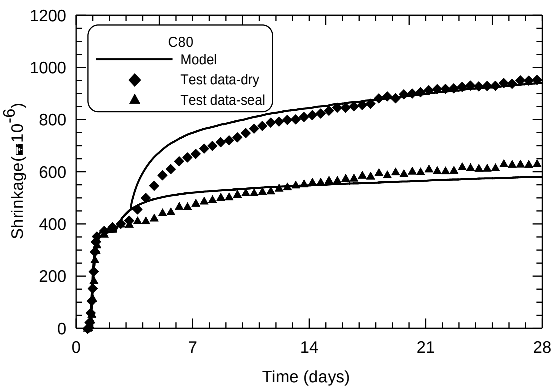

Figure 2 Comparison between model and test results on shrinkage of C30 (a) and C80 (b) concretes

3. MODELING ON THE MOISTURE DISTRIBUTION IN EARLY-AGE CONCRETE

The loss of water in early-age concrete is normally caused by either cement hydration or water diffusion. At the initial period after the concrete cast, the water in concrete pores are connected with each others and the relative humidity in concrete is almost equal to 1 (stage I). With persistent hydration of cement, the continuity of the pore water is finally broken down. The chemical shrinkage of cement hydration and diffusion of water will lead the formation of capillary pores, and simultaneously lead the decrease of internal relative humidity of concrete (stage II). The diffusion of water vapor through continuous vapor space becomes the dominant mechanism for moisture transfer in this stage in concrete. In stage II, the total variation of water content (ΔW) within a certain period (Δt) is resulted from both cement hydration (ΔW_s) and water diffusion to environment

(ΔW_d). Thus the total variation rate of water content can then be expressed as the sum of cement hydration and moisture diffusion [5,15], i.e.:

$$\frac{\partial W}{\partial t} = \frac{\partial W_d}{\partial t} + \frac{\partial W_s}{\partial t} \tag{15}$$

In this stage, the moisture is transport through the water vapor and the liquid in pores acts mainly as a source for water vapor generation. Thus, the driving force of water diffusion in concrete should be capillary potential that can directly relate to local relative humidity of concrete [5]. If one-dimensional water diffusion is considered (along the coordinate direction *x*), according to the second Fick's law, the moisture content balance requires:

$$\frac{\partial (W - W_s)}{\partial t} = \frac{\partial}{\partial x}\left(D \frac{\partial (H - H_s)}{\partial x} \right) \tag{16}$$

Where, *D* is the moisture diffusion coefficient depending on the pore humidity and on the composition of concrete. H_s is the humidity reduction due to cement hydration. Both cement hydration and diffusion through concrete is so slow that various phases of water in each pore (vapor, capillary water and absorbed water) remain almost in thermodynamic equilibrium at any time [6]. Therefore, the relationship between humidity *H* and water content *W* can be related by the well-know desorption or sorption isotherms [5,18]. Thus, equation (16) can be rewritten as

$$\frac{\partial (H - H_s)}{\partial t} = \frac{\partial (H - H_s)}{\partial (W - W_s)} \frac{\partial}{\partial x}\left(D \frac{\partial (H - H_s)}{\partial x} \right) + k \frac{\partial T}{\partial t} \tag{17}$$

The third item reflects the effect of temperature variation on the humidity. *k* is the change in *H* due to one degree change in temperature *T* at constant *W* and a fixed degree of cement hydration. Experimental results have indicated that the change in *H* due to temperature variation in early-age concrete is rather small (i.e. $k \approx 0$) that can be neglected [15]. Then, equation (17) becomes

$$\frac{\partial (H - H_s)}{\partial t} = \frac{\partial (H - H_s)}{\partial (W - W_s)} \frac{\partial}{\partial x}\left(D \frac{\partial (H - H_s)}{\partial x} \right) \tag{18}$$

Using $H_d = H - H_s$, $W_d = W - W_s$, the above partial differential equation becomes

$$\frac{\partial H_d}{\partial t} = \frac{\partial H_d}{\partial W_d} \frac{\partial}{\partial x}\left(D \frac{\partial H_d}{\partial x} \right) \tag{19}$$

For calculating the moisture distribution in concrete exposed to a given atmosphere with an initial moisture condition of *H*=1, equation (19) must be solved taking adequate boundary and initial moisture conditions into consideration. However, it is known that the relative humidity is a function of time and location in concrete and the moisture diffusivity *D* is also a function of pore humidity. Thus, the distribution of relative humidity along *x* direction cannot be solved from equation (19) directly. In order to overcome this difficulty, we define parameter *S* as [15]

$$S = \int_{H_m}^{H_d} D dH_0 \tag{20}$$

Here, H_m is a relative humidity that can be selected arbitrarily, normally is equal to the minimum humidity that may occur in concrete. From (20), we have

$$\frac{\partial S}{\partial H_d} = D\,,\ \frac{\partial S}{\partial t} = D\frac{\partial H_d}{\partial t} \tag{21}$$

Using above equations in (19), we obtain

$$\frac{\partial S}{\partial t} = \frac{\partial H_d}{\partial W_d} D \frac{\partial^2 S}{\partial x^2} \tag{22}$$

Thus, the problem for solving H_d under give time and location becomes solving S from (11) instead. In the present work, finite differential method was used to solve equation (11) numerically.

A cement hydration degree based model describing the humidity reduction due to cement hydration was proposed by Oh et al.[21]. In the present work, a modified cement hydration degree based model, which takes the initial liquid-water saturated stage (stage I) into account, is used to describe the humidity reduction in stage II due to cement hydration as indicated in equation (23) [15].

$$H_s = \begin{cases} 0 \quad for \quad \alpha \le \alpha_c \\ \left(1 - H_{s,u}\right)\left(\dfrac{\alpha - \alpha_c}{\alpha_u - \alpha_c}\right)^{\beta} \quad for \quad \alpha > \alpha_c \end{cases} \tag{23}$$

Where $H_{s,u}$ is the relative humidity considering self-desiccation at ultimate degree hydration, which is a function of *w/c* and can be determined from experiments. α_c is a hydration parameter called critical hydration degree at which the humidity inside of concrete starts to decrease from 1, which can be calculated by applying the experimental determined critical time t_c when the internal relative humidity starts to decrease, in equation (12). It should be noted that the effect of temperature inside of concrete is taken into account using the concept that equilibrant age. The parameter β is a constant that can be obtained by fitting the test data under sealing condition and equation (23).

Another required parameter to solve equation (22) is the derivative value of $\partial H_d/\partial W_d$. The relationship between moisture content in pores (W_d) and its relative humidity (H_d), and value of $\partial H_d/\partial W_d$, or called moisture capacity can be determined from sorption isotherm of concrete. A modified Brunauer-Emmett-Teller (BET) model [19], called BSB model, or three-parameter model [20], which agree well with test results of sorption isotherm of cementitious materials within a range of relative humidity of 0.05 to 1.0, will be used to solve $\partial H/\partial W$ in this paper, i.e.:

$$W_d = \frac{V_m C k H_d}{(1 - kH_d)[1 + (C-1)kH_d]} \tag{24}$$

and:

$$\frac{\partial H_d}{\partial W_d} = \frac{(1 - kH_d)[1 + (C-1)kH_d]}{CkV_m + W_d k[1 + (C-1)kH_d] - W_d k(1 - kH_d)(C-1)} \tag{25}$$

Here water content W_d is in gram in per gram cement paste. For type I and II cement, which are similar to Chinese normal Portland cement used in the present paper, the three parameters of above model are given as [21]

$$V_m = (0.068 - \frac{0.22}{t})(0.85 + 0.45\frac{w}{c})$$
$$C = \exp(\frac{855}{T}) \tag{26}$$
$$k = \frac{(1-\frac{1}{n})C - 1}{C-1}, \; n = (2.5 + \frac{15}{t_e})(0.33 + 2.2\frac{w}{c})$$

For the case of t>5 days and 0.3<w/c<0.7. t is age in days, w/c is water to cement ratio, T is absolute temperature. For t≤5 days, set t=5 days; for w/c≤0.3, set w/c=0.3 and for w/c≥0.7, set w/c=0.7. Thus, for giving H_d and the related parameters used in (26), the corresponding values of W_d and $\partial H_d/\partial W_d$ can be obtained by using (24) and (25).

Using the developed model, we are able to obtain the complete humidity distribution field in early age concrete according to the following algorithm by step-by-step integration in time. For given time increment (Δt), the humidity reduction due to cement hydration, H_s is calculated using (23). Then using (H–H_s) as initial humidity condition, the humidity variation produced by moisture diffusion after the same time interval Δt is calculated using finite differential method for solving partial differential equation (22). The above procedure goes continuously until approaching the expected concrete age. To verify the model, the progress of the humidity inside of concrete is experimentally determined. In the experiments, one dimensional heat and moisture transportation in concrete are made. Waterproof plywood mold with inner dimensions of 200×200×800 mm was used. To allow heat and moisture movement only along the specimen thickness direction, the inner surfaces of the mold were covered with a plastic sheet to prevent moisture loss and the five outer surfaces was covered with polystyrene board to prevent heat loss. Only the casting face was kept to contact with air directly. In the tests, a digital humidity and temperature combined sensor was used to measure the humidity and temperature. Detailed specimen preparation and test procedures can be found in [15]. Meanwhile, humidity distributions of the concrete slabs are calculated using the developed model.

A number of experimental studies [5, 21] have shown that the magnitude of moisture diffusivity strongly depends on the pore humidity. Based on author's previous work [5], typical moisture dependent diffusivity of normal and high strength concretes is displayed in Fig.3. From the figure, we can see that the moisture diffusivity first fast decreasing with the decrease of internal relative humidity from 100% to 80%. After that, it goes into a relatively stable stage with a small decreasing rate with decrease of internal relative humidity. The higher the concrete strength, the lower the moisture diffusivity presents. In order to use the moisture dependent diffusivity conveniently, the following empirical formula proposed by Xi et al. [21] is used to fit the moisture diffusivity:

$$D = D_1 + D_2\left[1 - 2^{-10^{\gamma(H-1)}}\right] \tag{27}$$

where D_1, D_2 and γ are fit coefficients, which are listed in Table 3 for the concrete used in the calculation. The other related parameters used in the model are listed in Table 3, in which the surface factor, a_m was obtained by measuring the weight of concrete sample under drying [5]. Fig.4 displays comparisons between predicted humidity profiles and test results at some typical ages.

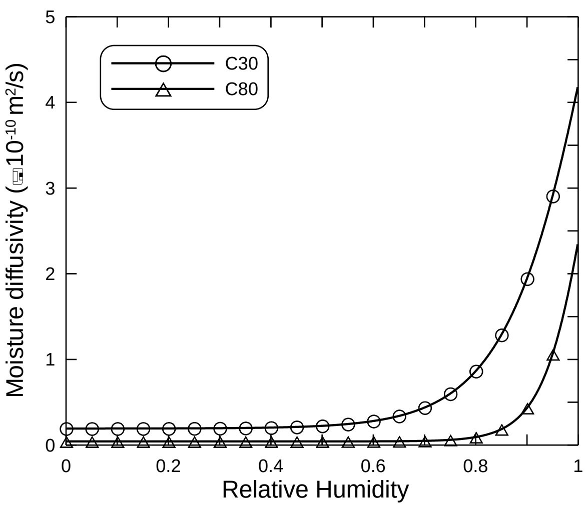

Figure 3 Water diffusion coefficient of different concrete

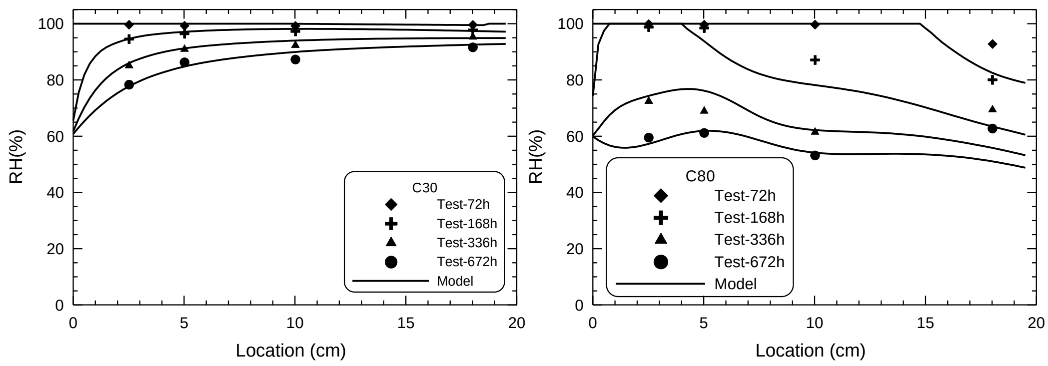

(a) (b)

Figure 4 Comparisons between predicted humidity profile and test results of concrete slabs

4. CALCULATION EXAMPLE: SHRINKAGE STRESS IN STEEL RING RESTAINT CONCRETE RING

As an example of application of above models, the distribution of shrinkage stress and its development with age in a steel ring restraint concrete ring made by C30 and C80 concrete respectively is calculated. The restrained ring test of concrete is a common test used for evaluation of shrinkage induced cracking performance of concrete that has been used for several decades [22,23]. In present paper, the restrained ring test is utilized to verify the shrinkage stress model.

The restrained ring test consists of a concrete annulus that is cast around a steel ring. As the concrete shrinks, the steel ring limits the shrinkage resulting in tensile stresses in the concrete ring and surface pressure stresses on the outer surface of the steel ring. The following section begins with a stress analysis of steel-concrete composite ring under surface pressure, as showed in Fig.5. First, we consider a thin circular ring suffers external and internal surface pressure stress, q_1 and q_2, see Fig.6. E and μ are the elastic modulus and Poisson's ratio of the material. a and b are the inner and outer radius of the ring. Now assumes the material undergoes shrinkage strain ε_{sh}. In polar coordinate, the stress-strain relations for plane stress can be expressed as:

$$\sigma_r = \frac{E}{1-\mu^2}\left[\varepsilon_r + \mu\varepsilon_\theta - (1+\mu)\varepsilon_{sh}\right]$$
$$\sigma_\theta = \frac{E}{1-\mu^2}\left[\varepsilon_\theta + \mu\varepsilon_r - (1+\mu)\varepsilon_{sh}\right] \qquad (28)$$

In addition, σ_r and σ_θ satisfy the equation of equilibrium

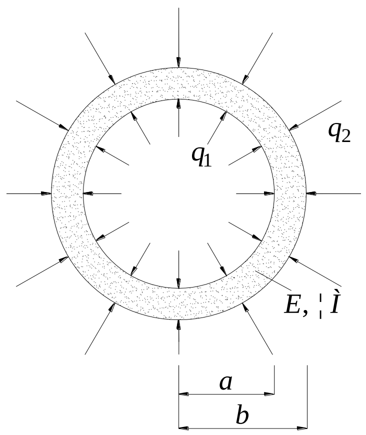

Figure 5 Circular ring under surface pressure

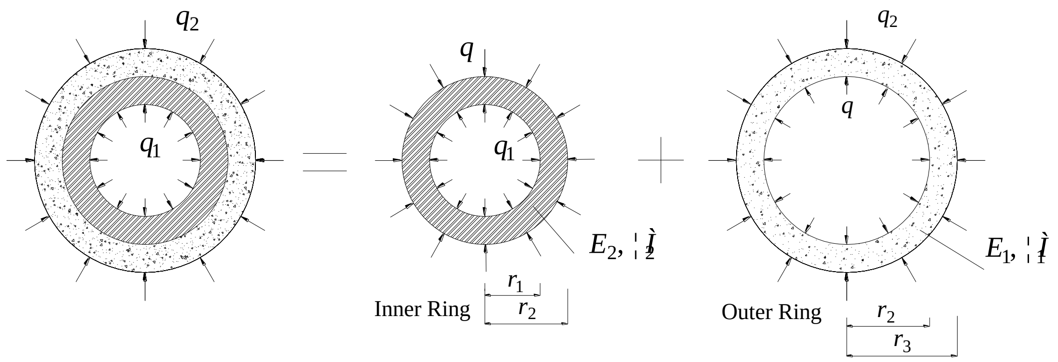

Figure.6 Decomposing of concrete-steel composite ring

$$\frac{\mathrm{d}\sigma_r}{\mathrm{d}r}+\frac{\sigma_r-\sigma_\theta}{r}=0 \tag{29}$$

If u is radial displacement, we have

$$\varepsilon_r=\frac{\mathrm{d}u}{\mathrm{d}r},\ \varepsilon_\theta=\frac{u}{r} \tag{30}$$

Using Eqs. (30) (28) in Eq. (29), we have

$$\frac{\mathrm{d}}{\mathrm{d}r}\left[\frac{1}{r}\frac{\mathrm{d}}{\mathrm{d}r}(ru)\right]=(1+\mu)\frac{\mathrm{d}}{\mathrm{d}r}\varepsilon_{sh} \tag{31}$$

Integrating this equation yields

$$u(r)=(1+\mu)\frac{1}{r}\int_a^r \varepsilon_{sh} r\mathrm{d}r+\frac{C_1}{2}r+\frac{C_2}{r} \tag{32}$$

where C_1 and C_2 are constants that can be determined by the boundary conditions. From Eqs. (32), (30) and (28), we have:

$$\begin{aligned}\sigma_r&=-\frac{E}{r^2}\int_a^r \varepsilon_{sh} r dr+\frac{EC_1}{2(1-\mu)}-\frac{EC_2}{1+\mu}\frac{1}{r^2}\\ \sigma_\theta&=\frac{E}{r^2}\int_a^r \varepsilon_{sh} r dr-E\varepsilon_{sh}+\frac{EC_1}{2(1-\mu)}+\frac{EC_2}{1+\mu}\frac{1}{r^2}\end{aligned} \tag{33}$$

From boundary condition that $\sigma_r=q_1$ at $r=a$ and $\sigma_r=q_2$ at $r=b$, we obtain:

$$C_1 = \frac{2(1-\mu)}{E}\frac{1}{b^2-a^2}\left(b^2q_2 - a^2q_1 + E\int_a^b \varepsilon_{sh} r dr\right)$$
$$C_2 = \frac{1+\mu}{E}\frac{a^2b^2}{b^2-a^2}\left(q_2 - q_1 + \frac{E}{b^2}\int_a^b \varepsilon_{sh} r dr\right) \tag{34}$$

Now let us look back at the ring test of concrete. Two layer concrete-steel composite ring can be separated into a steel ring and a concrete ring with an external interfacial pressure stress and an internal interfacial pressure stress acted on the concrete and steel interface respectively, as showed in Fig.6. For concrete ring, we have q2=0 and q1=q. For steel ring, we have q2=q, q1=0 and εsh=0. Using above conditions in Eq. (34) and noting the displacement u at the interface of concrete and steel calculated from concrete and steel rings respectively are equal, we obtain the constants of C1 and C2 for concrete and steel rings respectively as:

$$C_{11} = \frac{2(1-\mu_1)}{E_1}\frac{1}{r_3^{\,2}-r_2^{\,2}}\left(r_2^{\,2}q + E_1\int_{r_2}^{r_3} \varepsilon_{sh} r dr\right)$$
$$C_{12} = \frac{1+\mu_1}{E_1}\frac{r_2^{\,2}r_3^{\,2}}{r_3^{\,2}-r_2^{\,2}}\left(q + \frac{E_1}{r_2^{\,2}}\int_{r_2}^{r_3} \varepsilon_{sh} r dr\right) \tag{35}$$

And

$$C_{21} = -\frac{2(1-\mu_2)}{E_2}\frac{r_2^{\,2}q}{r_2^{\,2}-r_1^{\,2}}$$
$$C_{22} = -\frac{1+\mu_2}{E_2}\frac{r_1^{\,2}r_2^{\,2}}{r_2^{\,2}-r_1^{\,2}}q \tag{36}$$

The interfacial stress *q* can be expressed as:

$$q = \frac{-\dfrac{2}{r_3^{\,2}-r_2^{\,2}}\displaystyle\int_{r_2}^{r_3} \varepsilon_{sh} r dr}{\dfrac{1}{E_1}\dfrac{(1-\mu_1)r_2^{\,2}+(1+\mu_1)r_3^{\,2}}{r_3^{\,2}-r_2^{\,2}} + \dfrac{1}{E_2}\dfrac{(1-\mu_2)r_1^{\,2}+(1+\mu_2)r_2^{\,2}}{r_2^{\,2}-r_1^{\,2}}} \tag{37}$$

Clearly, the interfacial pressure is generated from volume change of concrete layer and is a function of ε_{sh} as displayed in Eq. (37). Using Eqs. (34) (35) and (37) in Eq. (33), we can easily obtain the stresses of σ_r and σ_θ in concrete and steel rings respectively as concrete undergoes shrinkage.

In concrete-steel rings, as long as the shrinkage of concrete is restraint by the steel ring, tensile stress is created immediately in the concrete. Creep of concrete then immediately takes place also as concrete is loaded in tension. Then part of the shrinkage strain is counteracted by the creep strain, behaving as the shrinkage stress decreasing with age. Such stress relation also reflects as the reduction of the interfacial stress with age in the ring test. If we define an effective shrinkage strain that actually be used for generation of shrinkage stress in the concrete ring as ε_{sh-e}, then we have:

$$\varepsilon_{sh-e}(t) = \varepsilon_{sh}(t_0) - \varepsilon_{creep}(t, t_0) \tag{38}$$

Where t and t_0 are the time of loading end and the load starts respectively. ε_{creep} is the creep strain after loading period of (t-t_0). The creep strain may relate with the effective shrinkage strain by a so-called creep coefficient factor φ as

$$\varphi(t,t_0)=\frac{\varepsilon_{creep}(t,t_0)}{\varepsilon_{sh}(t_0)} \tag{39}$$

φ is a function of load time and loading period also, and can be simulated by [25]:

$$\varphi(t,t_0)=\varphi_1 t_0^{-d}(t-t_0)^p \tag{40}$$

Where φ_1, d and p are material parameters, which should be determined directly or indirectly from experiments. Thus, using Eq. (40) in Eq. (39), we have

$$\varepsilon_{sh-e}(t)=\varepsilon_{sh}(t_0)\left[1-\varphi(t,t_0)\right] \tag{41}$$

Above discussion may well suit the situation where the strain or deformation is fixed. However, shrinkage of concrete is normally growth with age from zero. To deal with stress relaxation under varied restrained strain, a method used for prediction of stress relaxation under varied loading stress [26] was used in the present paper. Assume the initial strain without considering the effect of creep at time t_0 is $\varepsilon_{sh\text{-}0}$. After period ($t$-$t_0$), the strain becomes $\varepsilon_{sh\text{-}t}$. Now assume the time interval (t-t_0) is divided into n sections, $\triangle t_1$, $\triangle t_2$, $\triangle t_3$,…$\triangle t_i$,…$\triangle t_n$, and the strain increment in each time interval is $\triangle\varepsilon_{sh1}$, $\triangle\varepsilon_{sh2}$, $\triangle\varepsilon_{sh3}$,…$\triangle\varepsilon_{shi}$,…$\triangle\varepsilon_{shn}$. From Eq. (40), after considering the creep, the effective strain at time t_i can then be given by:

$$\varepsilon_{sh-e}(t,t_i)=\varepsilon_{sh-0}(t_0)\left[1-\varphi(t,t_0)\right]+\sum_{i=1}^{n}\Delta\varepsilon_{sh-i}(t_i)\left[1-\varphi(t,t_i)\right] \tag{42}$$

It should be noted that the time t in the above equations should be transferred into the corresponded equilibrant time if varied temperature history is experienced. Present work is focused on the calculation of shrinkage stresses starting from concrete set, therefore $\varepsilon_{sh\text{-}0}$ given in (42) should be equal to zero. Replace ε_{sh} with $\varepsilon_{sh\text{-}e}$ given by Eq. (42) in Eqs. (33) and (37), we can then obtain the shrinkage of concrete induced stresses in concrete ring. Apparently, after the creep of concrete is thought, the stresses generated from concrete shrinkage should be reduced. As long as the development of shrinkage resulted tensile stress and the corresponded cracking or tensile strength of concrete is known, the cracking tendency can thus be evaluated.

5. RESULTS AND DISCUSSIONS

As calculation example, four types of concretes, normal strength concrete, without and with internal curing with pre-wetted lightweight aggregate (PSLWA), named C30-OC and C30-IC, and high strength concrete, named C80-OC and C80-IC were used. Mix proportions and all the parameters needed for shrinkage stress calculations are listed in Tables 1 to 3. Details regarding properties of above concretes can be found in authors previous publications [27,28]. The creep parameters used in Eq. (40) of four concretes are listed in Table 2 as well, which taken the effect of moisture content into account and were determined by [24].

In the calculation, the follow seal-dry regime is used. That is first 14 and 3 days curing with plastic film sealing after concrete casting for C30 and C80 concrete respectively, which is corresponding to the time when the internal relative humidity starts to drop from I in concrete under sealing status, then the circumference of concrete ring suffers drying in air until 30 days. Using above models, the development of shrinkage stress at three typical places in the concrete ring, i.e. outer surface, middle place and inner surface, since concrete cast is calculated. The model results are present in Figs.7 and 8 respectively for C30 and C80 concretes.

Table 1 Mix proportions of concrete / (kg/m3)

No.	Water/binder ratio	Cement	Water	Sand	Stone	Fly ash	Silica Fume	PSLWA	Compressive strength at 28d (MPa)
C30-OC	0.62	240	186	750	1150	60	-	-	34.1
C30-IC	0.57	252	181	473	867	63	-	348.7	34.3
C80-OC	0.30	450	150	580	1140	-	50	-	84.3
C80-IC	0.24	494	134	309	864	-	55	340.3	93.5

Table 2 Parameters used in shrinkage strain and stress calculations

Concrete			C30-OC	C30-IC	C80-OC	C80-IC
ϕ_p			0.264	0.264	0.317	0.317
Hydration degree parameter	α_u		0.8853	0.9222	0.6014	0.6298
	A		19.730	40.4936	17.512	30.7593
	B		0.6841	0.7689	0.7980	0.9598
	α_0		0.0190	0.0180	0.0410	0.0470
	α_c		0.8150	0.8590	0.4124	0.4669
Elastic modulus parameter	K_0		6.0	3.5	4.5	4.5
	η		1.35	1.11	0.79	1.02
	E_{28}(GPa)		34.3	30.6	48.1	38.7
	E_s(GPa)		72.9	72.9	72.9	72.9
	b		1.14	1.39	0.78	0.66
Pore structure parameter	k_0		28.25	28.25	64.29	64.29
	a_0		0.0007	0.0007	0.0112	0.0112
	λ		4.375	4.375	2.224	2.224
Creep parameter	RH=1	ϕ_1	1.04	1.04	1.58	1.58
		d	0.11	0.11	0.11	0.11
		p	0.08	0.08	0.09	0.09
	RH<1	ϕ_1	38.7	38.7	28.7	28.7
		d	2.1	2.1	3.4	3.4
		p	0.053	0.053	0.070	0.070

Table 3 Input parameters used for humidity field calculation

Concrete	$H_{s,u}$	β	α_c	a_m (cm/day)	D		
					D_1(m^2/s)	D_2(m^2/s)	γ
C30-OC	0.9501	10.0734	0.8150	0.42	1.93×10^{-11}	8.03×10^{-10}	4.5
C30-IC	0.9635	15.3716	0.8590	0.42	1.82×10^{-11}	2.31×10^{-10}	5.5
C80-OC	0.8365	6.1080	0.4124	0.42	4.28×10^{-12}	4.67×10^{-10}	9.0
C80-IC	0.8559	8.1123	0.4669	0.42	4.28×10^{-12}	1.74×10^{-10}	8.0

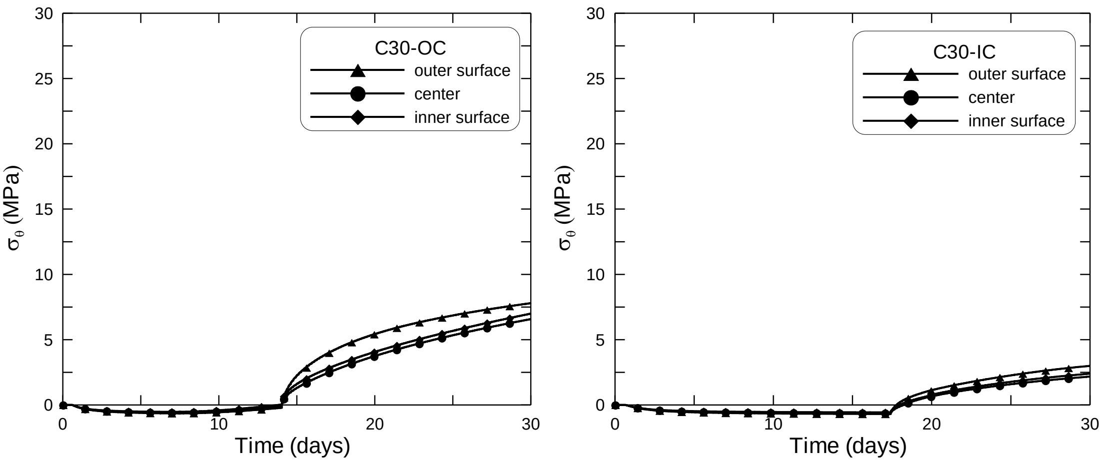

(a) (b)

Figure 7 Development of shrinkage stress at three places in normal strength concrete ring, (a) C30-OC, (b) C30-IC

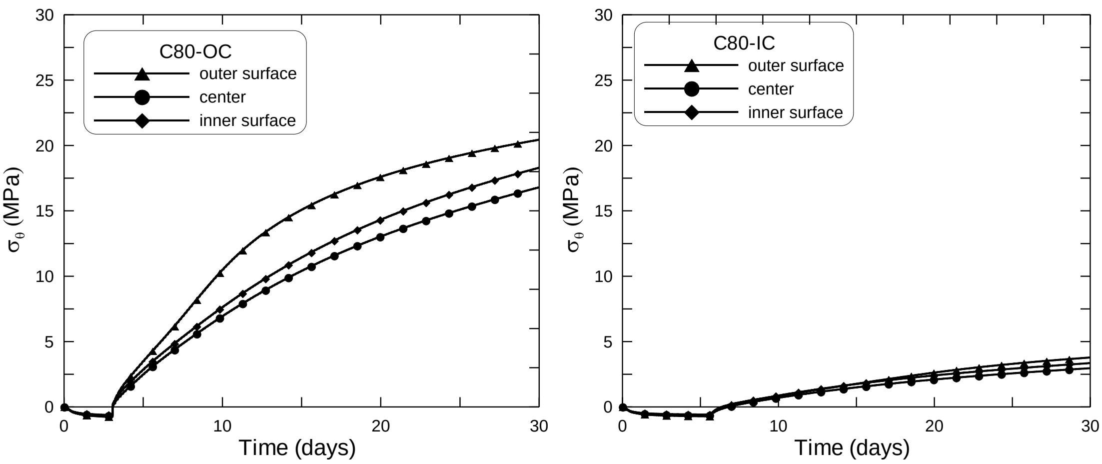

(a) (b)

Figure 8 Development of shrinkage stress at three places in normal strength concrete ring, (a) C80-OC, (b) C80-IC

From these results, first we can observe that the development of shrinkage stress in the concrete ring obeys two-stage mode, a small stress developing stage within the vapor saturated period (stage I) and a gradual increasing stage with the relative humidity gradually decreasing in the concrete (stage II). As the outer surface of concrete ring undergoes drying, the shrinkage stress starts to increase immediately with age. As expected, the closer to the drying face, the higher the shrinkage stress. Before drying, a uniform shrinkage stress is experienced throughout the ring. After drying, the shrinkage stress gradient along the radial direction gradually develops. Second, for high strength concrete (C80), shrinkage stress is much higher than that of normal strength concrete (C30). This is understandable that much higher shrinkage strain is expected for high strength concrete comparing with normal strength concrete, as displayed in Fig.2. Third, as internal curing with pre-wetted light weight aggregate is used, the shrinkage stress is obviously reduced. The benefits of internal curing on shrinkage stress reduction may be due to both of shrinkage reduction and high stress relaxation due to its high moisture content. Certainly, more detailed study on the impact of water content on stress relaxation of concrete is needed. As expected, shrinkage resulted cracking in C30-OC and C80-OC concrete ring was observed and no cracking was observed on the rings made by C30-IC and C80-IC. These experimental observations may in turn verify the shrinkage stress model.

6. CONCLUSIONS

In this paper, an integrative model for autogenous and drying shrinkage predictions of concrete is introduced first. Second, a model taking both cement hydration and moisture diffusion into account synchronously is used to calculate the distribution of internal relative humidity in concrete. Using the above two models, the distribution of shrinkage stress in steel ring restraint concrete ring is calculated. In the calculation, normal strength concrete (C30) and high strength concrete (C80) are used as examples. Meanwhile, the effect of internal curing with pre-wetted light weight aggregate on shrinkage stress is included in the calculation.

The model results show that before drying, a uniform shrinkage stress along radial direction of a concrete ring is expected. As surface drying starts, shrinkage gradient along radial direction from the center to the outer surface is gradually increased with age. The closer to the drying face, the higher the shrinkage stress. The shrinkage stress is much higher in high strength concrete ring than that in normal strength concrete ring. As internal curing with pre-wetted light weight aggregate is used, the shrinkage stress is obviously reduced. The benefits of internal curing on shrinkage stress reduction may be due to both of shrinkage reduction and high stress relaxation due to its high moisture content.

ACKNOWLEDGMENTS

This work has been supported by grants from the National Science Foundation of China (No. 50978143, 51178248) and a grant from the National Basic Research Program of China (No. 2009CB623200) to Tsinghua University.

REFERENCES

[1] Akita, H., Fujiwara, T. and Ozaka, Y., 1997. A practical procedure for the analysis of moisture transfer within concrete due to drying. Magazine of Concrete Research, 49(179), 129-137.
[2] Andrade, C., Sarria, J. Alonso, C., 1999. Relative humidity in the interior of concrete exposed to natural and artificial weathering. Cement and Concrete Research, 29(8), 1249-1259.
[3] Ayano, T., Wittmann, F.H., 2002. Drying, moisture distribution, and shrinkage of cement-based materials. *Materials and Structures*, 35(247), 134-140.
[4] Zhang, J., Hou, D. and Sun, W., 2010. Experimental study on the relationship between shrinkage and interior humidity of concrete at early age. Magazine of Concrete Research, 62(3), 191-199.
[5] Zhang, J., Wang, J., Gao, Y., Moisture movement in early-age concrete under cement hydration and environmental drying. Magazine of Concrete Research, 2015, 68(8): 391-408.
[6] Zhang, J., Hou, D. and Han, Y., 2012. Micromechanical modeling on autogenous and drying shrinkages of concrete. Construction and Building Materials, 29(3), 230-240.
[7] Powers, T.C., Brownyard, T.L., 1946. Studies of the physical properties of hardened Portland cement paste, J. Am. Concr. Inst. 43 (Oct. 1946– April 1947), Bulletin 22, Research Laboratories of the Portland Cement Association, Chicago.
[8] Jensen, O.M. and Hansen, P.F., 2001. Water-entrained cement-based materials: I. Principles and theoretical background, Cement and Concrete Research, 31(5), 647-654.
[9] Rastrup, E., 1954. Heat of Hydration. Magazine of Concrete Research, 6(17), 127-140.
[10] Schindler, A. K., and Folliard, K.J., 2005. Heat of hydration models for cementitious materials. ACI Materials Journal, 102(1), 24-33.
[11] Luzio, G. D. and Cusatis, G.,1993. Hygro-thermo-chemical modeling of high performance concrete. I: Theory. Cement and Concrete Composites, 31, 301-308.
[12] Kjellsen, K. and Detwiler, R.J., 1993. Later-age strength prediction by a modified maturity model. ACI Materials Journal, 220-227.
[13] Chanvillard, G. and Daloia, L.,1997. Concrete strength estimation at early age: Modification of the method of equivalent age. ACI Materials Journal, 94(6), 220-227.
[14] Kim, J.K., 2001. Estimation of compressive strength by a new apparent activation energy function. Cement and Concrete Research, 31(2), 217-225.
[15] Zhang, J., Qi, K. and Huang, Y., 2009. Calculation of Moisture Distribution in Early-Age Concrete. ASCE Journal of Engineering Mechanics, 135(8), 871-880.
[16] Pane, I. and Hansen, W., 2002. Concrete hydration and mechanical properties under nonisothermal conditions. ACI Materials Journal, 99(6), 534-542.
[17] Zhang, J., Han, Y. and Han, J., 2014. Cement hydration based model to predict mechanical properties of precast concrete. Magazine of Concrete Research, 66(12), 603-617.
[18] Bazant, Z.P., and Najjar, L.J., 1972. Nonlinear water diffusion in nonsaturated concrete. Materials and Structures, 5(25), 3-20.
[19] Brunauer, S. and Emmett, P.T., 1938. Adsorption of gases in multimolecular layers. Journal of the American Chemistry Society, 60, 309-319.
[20] Brunauer, S., Skalny,. 1969. Adsorption on nonporous solids. Journal of Colloid and Interface Science, 30, 546-552.
[21] Xi, Y., Bažant, Z.P. and Jennings, H.M., 1994. Moisture diffusion in cementitious materials-Adsorption isotherms. Advanced Cement Based Materials, 1(6): 248–257.
[22] Grzybowski, M. and Shah, S.P., 1990. Shrinkage Cracking of Fiber Reinforced Concrete. ACI Materials Journal, 87(2), 138-148.
[23] Hossain, A.B. and Weiss, J., 2004. Assessing residual stress development and stress relaxation in restrained concrete ring specimens. Cement and Concrete Composites, 26(5), 531–540.
[24] Zhang, J., Wang, J. and Wang, Q., 2016. Stress relaxation and water content in concrete, Submitted.

[25] Bazant Z P, and Panula, L., 1978. Practical prediction of time dependent deformation of concrete: II Basic creep. Materials and Structures, 11(65), 317-328.
[26] Zhu, B.F., 1999. Thermal Stress and Temperature Control in Mass Concrete. Beijing: China Electric Power Publishing House, in Chinese.
[27] Zhang, J., Han, Y., Zhang, J. and Gao, Y., 2016. Evaluation of Shrinkage Induced Cracking in Concrete with Impact of Internal Curing and Water to Cement Ratio. Journal of Advanced Concrete Technology, 14(7), 324-334.
[28] Zhang, J., Wang, J. and Han, Y., 2015. Simulation of Moisture Field of Concrete with Pre-soaked Lightweight Aggregate Addition, Construction and Building Materials, 96, 599-614.

A MATHEMATICAL MODEL IN CHARACTERING CHLORIDE DIFFUSIVITY IN UNSATURATED CEMENTITIOUS MATERIALS

Yong Zhang[1], Guang Ye[1]

[1] Delft University of Technology Faculty of Civil Engineering and Geosience, Department of Structural Engineering, Microlab, Stevinweg 1, 2628 CN Delft, The Netherlands, email: y.zhang-1@tudelft.nl, g.ye@tudelft.nl

SUMMARY: In this paper, a new analytic model for predicting chloride diffusivity in unsaturated cementitious materials is developed based on conductivity theory and Nernst-Einstein equation. The model specifies that chloride diffusivity in unsaturated cementitious materials can be mathematically described as a function of chloride diffusivity in saturated state, water saturation and average pore diameter of the material. A series of experiments were conducted in order to validate the model. Mortar samples with varying cementitious mixtures were cast and cured for one year, followed by oven drying at 50 °C until desired water saturation levels (18 to 100 %) and homogeneous moisture distribution were obtained. The electrical conductivities of mortar specimens at various water saturations were measured and then converted into chloride diffusivities by using Nernst-Einstein equation. It is found that the experimental results can be well described by the analytic model proposed in this work.

MATEMATIČKI MODEL PRIKAZA DIFUZIJE KLORIDA U NEZASIĆENIM CEMENTNIM MATERIJALIMA

SAŽETAK: U radu je prikazan novi analitički model predviđanja difuzije klorida u nezasićenim cementnim materijalima na osnovi teorije vodljivosti i Nernst-Einsteinove jednadžbe. Model prikazuje da se difuzija klorida u nezasićenim cementnim materijalima može matematički opisati kao funkcija difuzije klorida u zasićenom stanju, funkcija zasićenosti vodom i funkcija prosječnoga promjera pora u materijalu. Radi vrednovanja modela proveden je niz pokusa. Izrađeni su uzorci morta s različitim cementnim mješavinama i njegovani jednu godinu. Zatim su osušeni u sušioniku na 50 °C sve dok nisu postignute željene razine zasićenja vodom (od 18 % do 100 %) i homogena raspodjela vlage. Izmjerena je električna vodljivost uzoraka morta pri različitim zasićenjima vodom što je potom pretvoreno u difuziju klorida primjenom Nernst-Einsteinove jednadžbe. Utvrđeno je da se eksperimentalni rezultati mogu dobro opisati analitičkim modelom predloženim u ovom radu..

1. INTRODUCTION

The resistance to chloride diffusion is a major concern for the durability of reinforced concrete in cases of structures being exposed to seawater or deicing salts. Current durability design, e.g. DuraCrete, usually relies on measuring chloride diffusivity in saturated concrete. However, on-site concrete is seldom saturated due to long term self-desiccation or drying-wetting cycles. To effectively design new reinforced concrete structures, a reliable model for describing the relationship between saturated and non-saturated chloride diffusivity should be used.

In cementitious materials, the parameter relative chloride diffusivity (D_{rc}) is defined as the ratio between chloride diffusivity at a particular moisture condition and that at saturated condition. In the past decades, a few models have been reported for the determination of D_{rc} [1-3]. By fitting experimental results, Saetta et al. [1] proposed an S-shaped relationship that the D_{rc} was the first time expressed as a function of interior relative humidity. Buchwald [2] estimated the ionic diffusivity by impedance spectroscopy measurement and proposed a power equation which relates D_{rc} to the degree of water saturation (S_w). Zhang et al. [2012] simulated the ionic diffusivity in unsaturated cement pastes with w/c ratios of 0.4, 0.5 and 0.6 by using lattice Boltzmann method; a quadratic polynomial equation was used to describe the D_{rc} at various water saturation S_w levels.

It is noteworthy that these existing models for the determination of D_{rc} are all empirical-based. Up to date there is no consensus on the reliable description of D_{rc}. The aim of this paper is trying to, from scientific point of view, develop a new analytic model to describe the D_{rc}-S_w relation. To this end, the conductivity theory and Nernst-Einstein equation are applied and linked to microstructural parameters. A series of conductivity experiments are performed on mortar specimens at various S_w levels. The experimental results are used to validate the proposed analytic model.

2. MATHEMATICAL MODEL OF NON-SATURATED CHLORIDE DIFFUSIVITY

In porous media, diffusion of chloride ions is driven by the concentration gradient of chloride ions. Electrical conduction of chloride ions results from electrical potential differences. In principle, the two types of ionic movements are inherently correlated by Nernst-Einstein equation. In this study, a combined application of Nernst-Einstein equation and conductivity theory is used to characterize the non-saturated chloride diffusivity in cementitious materials.

2.1. NERNST-EINSTEIN EQUATION

Nernst-Einstein equation, i.e. Eq. (1), gives that the ratio of the bulk conductivity of pore solution σ_p to the conductivity of cementitious material σ_{mat} [S/m] is equal to the ratio of chloride diffusivity in the pore solution D_p to the effective chloride diffusivity in cementitious material D_{mat} [m^2/s]. This ratio is defined as formation factor F_0, which is a global factor representing the microstructure of cementitious material. D_p depends on the chloride concentration and is around 1.5×10^{-9} m^2/s at room temperature when the chloride concentration is in the range of 0.1~1.0 mol/l [4]. After obtaining σ_p and σ_{mat}, the effective chloride diffusivity in cementitious material D_{mat} can be calculated. Note that the calculated D_{mat} excludes the chloride binding effect.

$$F_0 = \frac{\sigma_p}{\sigma_{mat}} = \frac{D_p}{D_{mat}} \tag{1}$$

2.2. CONDUCTIVITY OF CEMENTITIOUS MATERIAL $\boldsymbol{\sigma_{mat}}$

The conductivity of cementitious material σ_{mat} is the inverse of its resistivity ρ_{mat} [Ω·m], which is a function of geometry *m* (*m=1* for cylinder sample), length *L* [m], cross sectional area *A* [m^2] and electrical resistance R_{mat} [Ω], as Eq. (2). For a direct current, the electrical resistance of cementitious material (R_{mat}) is determined by Ohm's law and equal to the ratio between applied voltage (U) and direct current (I), as $\mathrm{R}_{mat} = \mathrm{U/I}$.

$$\sigma_{mat} = \frac{1}{\rho_{mat}} = \frac{mL}{A} \cdot \frac{1}{R_{mat}} \tag{2}$$

In general, cementitious material is a three-phase system consisting of solid phase, pore solution phase and vapour phase. Figure 1 illustrates a simple model of cementitious material made of different phases in parallel layers. The parameters R_s (A_s), R_p (A_p) and R_v (A_v) are noted as the electrical resistances (cross sectional areas) of the solid phase, the pore solution phase and the vapour phase layers, respectively. The total resistance of cementitious material (R_{mat}) is related to the resistance of each phase layer, i.e. Eq. (3). Incorporating Eq. (2) into Eq. (3) gives the expression of conductivity, i.e. Eq. (4). Parameters σ_s, σ_p and σ_v are conductivities of the solid phase, the pore solution phase and the vapour phase layers, respectively. σ_{mat} and A_{mat} are the total conductivity and the total exposure surface area of the material. A_{mat} is the summation of the cross sectional area of all layers, i.e. $A_{mat} = A_s + A_p + A_v$.

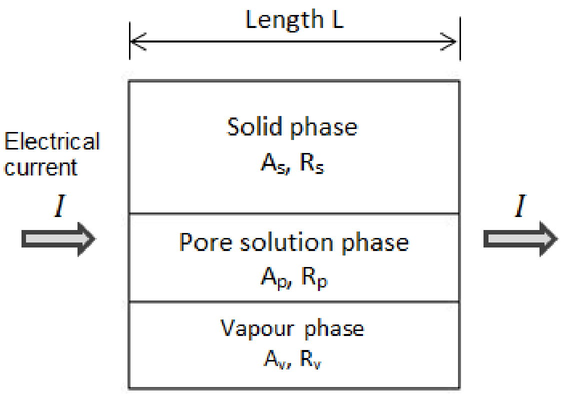

Figure 1 Cementitious material composed of different phases in parallel layers. R_i and A_i respectively represent electrical resistance and cross sectional area of each phase layer

Multiplying both sides of Eq. (4) with material length *L* produces Eq. (5). If the volume fraction of each phase is defined as $\phi_i = V_i/V_{mat}$, then Eq. (6) is deduced. Given the fact that the different phases in cementitious material are not completely in parallel layers [5], a structure factor β_i is introduced that indicates the connectivity of each phase layer and thus Eq. (7) is written. Since the conductivity of pore solution σ_p (1~20 S/m) is usually several orders of magnitudes higher than that of solid phase σ_s (10^{-9} S/m) and vapor phase σ_v (10^{-15} S/m) [4], the total conductivity of cementitious material σ_{mat} is almost equal to the conductivity of pore solution phase layer, i.e. Eq. (8).

$$\frac{1}{\mathrm{R}_{mat}} = \frac{1}{R_s} + \frac{1}{R_p} + \frac{1}{R_v} \tag{3}$$

$$\sigma_{mat}A_{mat} = \sigma_s A_s + \sigma_p A_p + \sigma_v A_v \tag{4}$$

$$\sigma_{mat}V_{mat} = \sigma_s V_s + \sigma_p V_p + \sigma_v V_v \quad (5)$$

$$\sigma_{mat} = \sigma_s \phi_s + \sigma_p \phi_p + \sigma_v \phi_v \quad (6)$$

$$\sigma_{mat} = \sigma_s \phi_s \beta_s + \sigma_p \phi_p \beta_p + \sigma_v \phi_v \beta_v \quad (7)$$

$$\sigma_{mat} \approx \sigma_p \phi_p \beta_p \quad (8)$$

At saturated condition (S_w=*100%*), the volume fraction of pore solution phase ϕ_p is equal to total porosity of the cementitious material ϕ_t (i.e. $\phi_p = \phi_t$). The structure factor of pore solution phase β_p can be indicated by the connectivity of pores present in the material (η_p). Then Eq. (8) is rewritten as Eq. (9). Here, $\sigma_{mat,Sat}$ is the conductivity of saturated cementitious material and $\sigma_{p,Sat}$ is the conductivity of saturated capillary pore solution.

$$\sigma_{mat,Sat} \approx \sigma_{p,Sat} \cdot \phi_t \cdot \eta_p \quad (9)$$

At unsaturated condition (S_w<*100%*), the volume fraction of pore solution phase ϕ_p is ($\phi_t S_w$). The structure factor β_p depends upon continuously water-filled pore channels, which are not only related to pore connectivity (η_p) but also affected by water continuity (η_{w,S_w}). Herein water continuity (η_{w,S_w}) is introduced to indicate the connectivity of pore solution phase present in the pore structure ($\eta_{w,S_w} = 0 \sim 1$) and it can be calculated as the ratio between the number of transport pore channels available for ionic diffusion at particular S_w and that at saturated state. Then Eq. (8) is replaced by Eq. (10). Here σ_{mat,S_w} and σ_{p,S_w} are non-saturated conductivities for cementitious material and pore solution, respectively.

$$\sigma_{mat,S_w} \approx \sigma_{p,S_w} \cdot \phi_t S_w \cdot \eta_p \eta_{w,S_w} \quad (10)$$

In unsaturated state, moisture tends to occupy the pores from small size to large size. Therefore, η_{w,S_w} is intimately related to the fineness of pore size distribution. According to Mercury Intrusion Porosimetry (MIP) technique, pore size in hydrated cementitious materials is usually towards to Gaussian distribution [6]. Then η_{w,S_w} and pore structure can be approximately correlated by Gaussian function as shown in Eq. (11), where a parameter c is introduced which is determined by fineness of pore size distribution. If the fineness of pore size distribution is simply indicated by the average pore diameter $d_a = 4V_t/S_t$, where V_t (m^3) and S_t (m^2) are the total volume and total surface area of the pores present in the pore structure, then parameter c shall be a function of d_a, as c= $f(d_a)$. The specific expression of $f(d_a)$ will be further determined afterwards in this paper.

$$\eta_{w,S_w} = e^{-\frac{(1-S_w)^2}{2 \cdot c^2}} \quad (11)$$

2.3. RELATIVE CHLORIDE DIFFUSIVITY IN UNSATURATED CEMENTITIOUS MATERIALS

As defined, the relative chloride diffusivity of cementitious material, D_{rc}, is calculated as the ratio of chloride diffusivity at a given S_w level (D_{mat,S_w}) over that at saturated condition ($D_{mat,Sat}$). By using Nernst-Einstein equation, i.e. Eq. (1), the D_{rc} can be calculated based on conductivity measurements (Eq. (12)). Meanwhile, once combining Eq. (1) with Eqs (9)-(11), D_{rc} can be also deduced from analytic model as shown in Eq. (13).

$$D_{rc} = \frac{D_{mat,S_w}}{D_{mat,Sat}} = \frac{\sigma_{mat,S_w}}{\sigma_{mat,Sat}} \cdot \frac{\sigma_{p,Sat}}{\sigma_{p,S_w}} \quad (12)$$

$$D_{rc} = \frac{D_{mat,S_w}}{D_{mat,Sat}} = S_w \cdot \eta_{w,S_w} = S_w \cdot e^{-\frac{(1-S_w)^2}{2 \cdot c^2}} \quad (13)$$

In Eq. (12), σ_{mat,S_w} and $\sigma_{mat,Sat}$ are measured directly from conductivity test. σ_{p,S_w} and $\sigma_{p,Sat}$ are related to the pore solution chemistry which may differ with varying S_w. They will be discussed in section 5.1. The measured D_{rc}-S_w relation from Eq. (12) will be fitted by Eq. (13) in order to examine the efficiency of analytic model; at the meantime, parameter c for various mixtures can be obtained.

3. EXPERIMENTAL PROGRAM: MATERIALS, SAMPLES AND TESTS

The raw materials for this study were ordinary Portland cement (OPC) and supplementary cementitious materials (SCMs) such as fly ash (FA), ground granulated blast furnace slag (GGBFS) and limestone powder (LP). Six different binders were designed. The mixture proportions are shown in TSlic

able 1. Both cement pastes and mortars were cast. One-year cured paste samples were prepared for pore structure measurement, which was performed by MIP technique [6]. One-year cured mortar samples were prepared for conductivity test and pore solution chemistry test.

Cylindrical mortars (ϕ100×800 mm) were cast for conductivity test. After one-year curing, both the top and bottom surfaces of mortar slices with 15 mm thick were cut off. The middle part (50 mm thick) was preconditioned to reach target S_w (ranging 18-100%) and homogeneous moisture distribution. Conductivity test was conducted on all the well-prepared mortar specimens with S_w in the range of 18-100%. Details of sample preconditioning procedures in obtaining well-prepared unsaturated mortar samples and details of conductivity test can be found in previous work [7]. For pore solution chemistry test, one-year moist-cured cylinder mortars (ϕ50×100 mm) were compressed under oil pressure machine (max. capacity 2000 MPa). The compressed pore solutions were collected and stored in plastic bottles, which were considered as the pore solutions of mortar specimens at saturated condition. The concentrations of alkalis (e.g. Na^+, K^+) were tested by means of inductively coupled plasma optical emission spectrometers (ICP-OES).

Table 1 Mixture proportions (weight percentage) used for binders

Mixtures	Type of cement and replacement by weight				Water/binder ratio
	OPC	FA	GGBFS	LP	
P4	100%	-	-	-	0.4
P5	100%	-	-	-	0.5
P6	100%	-	-	-	0.6
PF5	70%	30%	-	-	0.5
PB5	30%	-	70%	-	0.5
PBL5	25%	-	70%	5%	0.5

4. EXPERIMENTAL RESULTS

Based on measured conductivity, the relative chloride diffusivities (D_{rc}) at various water saturations (S_w) were derived following Eq. (12). Figure 2a plots the results of D_{rc}-S_w relation in OPC mortar specimens with water-cement (w/c) ratio of 0.4, 0.5 and 0.6. For a comparative study, the data from previous literature [4] are also present which exhibit consistency to the results obtained in this work. As indicated, D_{rc} decreases as S_w reduces. The most significant drop in D_{rc} is observed when S_w decreases from 90% to 60%. When S_w is below 60%, the D_{rc} is less than 10 % regardless of w/c. The D_{rc} is approaching to zero when the values of S_w are 37%, 28% and 22% for the specimens with w/c increasing from 0.4 to 0.6, respectively.

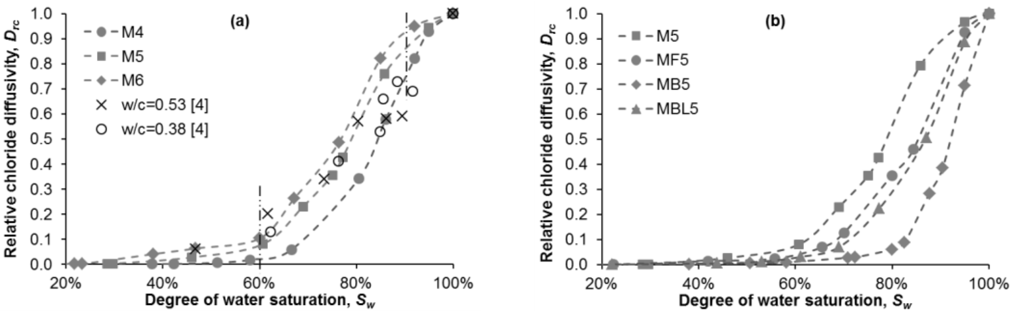

Figure 2 Experimental relationships between D_{rc} and S_w in OPC (a) and blended (b) mortars

Figure 2b shows the effect of SCMs, i.e. FA, GGBFS and LP, on the relationship between D_{rc} and S_w. As indicated, at a given S_w the mortars containing FA or GGBFS exhibit much lower D_{rc} compared to the reference OPC mortar M5. For example at S_w=80%, the D_{rc} is approximately 10% for MB5, 30% for MBL5 and 35% for MF5, while D_{rc} is as high as 60% for the reference sample M5. It is thus deduced from Eq. (13) that the addition of SCMs has great potential in affecting the water continuity in cementitious systems. According to cementing type, the capability in reducing water continuity presents a descending order as GGBFS, FA and OPC.

5. DISCUSSIONS

5.1. CONDUCTIVITY OF PORE SOLUTION $\boldsymbol{\sigma_p}$

In cementitious materials, conductivity of pore solution σ_p is mainly related to the concentrations of alkalis (Na^+, K^+) and hydroxide (OH^-). In this work, the pore solutions of various mortar specimens at *S_w=100%* were squeezed and collected. The concentrations of alkalis (Na^+, K^+) were tested by ICP-OES. The concentration of OH^- was calculated as the sum of alkali concentrations [8]. In general, the released alkalis during cement hydration are either bound by hydrates (mainly C-S-H) or freely present in pore solution. Chen and Brouwers [9] proposed an updated method that can be used to determine the relationship between bound and free alkalis content. The method was applied in this work to predict the alkalis concentrations at different S_w levels, i.e. Eqs (14) and (15). Herein, C_{Na} and C_K are concentrations of Na^+ and K^+ at particular saturation S_w in [mol/L]; V_w is the volume [L] of pore solution which linearly relates to S_w and total porosity ϕ_t; m_{C-S-H} is the mass of hydrate C-S-H [kg]; n_{Na}^r and n_K^r are the moles of alkalis released by cement hydration.

$$C_{Na} = \frac{n_{Na}^r}{V_w + 0.45 \cdot m_{C-S-H}} \tag{14}$$

$$C_K \cdot V_w + 0.2 \cdot (C_K)^{0.24} \cdot m_{C-S-H} = n_K^r \tag{15}$$

After obtaining the concentrations of Na^+, K^+ and OH^-, synthetic solutions were prepared by mixing solids (NaOH, KOH) and distilled water in proper proportions according to the calculated C_{Na} and C_K at each S_w level. The conductivities σ_p at various S_w levels were measured on these synthetic solutions. Figure 3 presents the σ_p-S_w relations for various mortar mixtures. It appears that σ_p is nearly two times larger at S_w=30% than that at saturated condition S_w=100%.

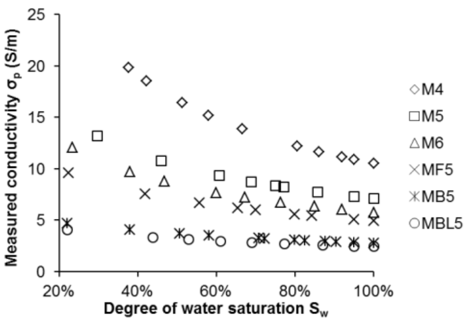

Figure 3 Conductivity of pore solution σ_p against water saturation S_w in mortars made of various cements

5.2. VALIDATION OF ANALYTIC MODEL

In order to examine the efficiency of the analytic model proposed, Eq. (13) is used to fit the measured data as presented in Figure 2b. The fitting curves are given in Figure 4a. It is observed that the Eq. (13) shows good fitness to the experimental results. For further comparison, the proposed model is compared with the current main existing models by examining the fitting goodness on the measured data in this work. Figure 4b shows the curves of three different models by fitting data set of mortar MF5, where the power model is from Buchwald [2] and polynomial model is from de Vera et al. [3]. Amongst the three models, polynomial model yields the poorest fitting that D_{rc} is zero at S_w=57% and thus D_{rc} cannot be fitted at low S_w level (S_w<57%). For power model, the fitting curve deviates greatly from the measured data at high S_w level (S_w>85%). In contrast, the proposed model, i.e. Eq. (13), agrees well with experiments.

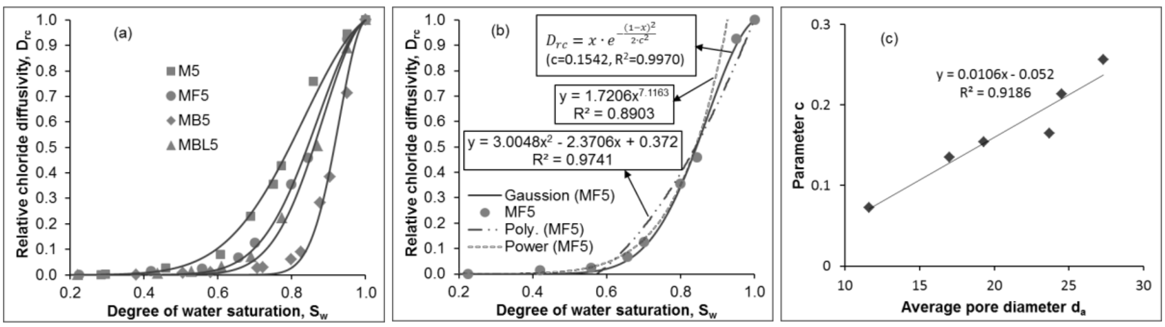

Figure 4 (a) Relationship D_{rc} vs. S_w in various mortar mixtures fitted by Eq. (13); (b) Comparison of various models by fitting plots D_{rc} vs. S_w in mixture MF5; (c) Relationship c vs. d_a for all the tested mixtures

By applying Eq. (13), the values of parameter c for various mortar mixtures are also obtained. According to MIP test, the average pore diameters d_a of corresponding paste mixtures are obtained as well. The relationship between c and d_a is plotted in Figure 4c, which exhibits a linear expression. Accordingly, the water continuity η_{w,S_w} (Eq. (11)) as well as relative chloride diffusivity D_{rc} (Eq. (13)) can be quantified directly in relation to the pore structure. On the other hand, it appears from Figure 4c that at $d_a \approx 5\ nm$, c is approaching to zero, which implies that both η_{w,S_w} and D_{rc} would be predicted as zero when $d_a < 5\ nm$. Conceivably, at $d_a > 5\ nm$, the microstructure contains both capillary pores (> 10 nm) and gel pores (< 10 nm); while at $d_a \leq 5\ nm$, there may be no capillary pores but only gel pores present in the microstructure, in this case the chloride diffusion is negligible [10].

Consequently, the effective chloride diffusivity in unsaturated cementitious material D_{mat,S_w} can be described as:

$$D_{mat,S_w} = D_{mat,Sat} \cdot S_w \cdot e^{-\frac{(1-S_w)^2}{2\cdot(0.0106 d_a - 0.052)^2}} \quad (d_a > 5\ nm) \tag{16}$$

$$D_{mat,S_w} = 0 \quad (d_a \leq 5\ nm) \tag{17}$$

where, $D_{mat,Sat}$ is effective chloride diffusivity at saturated state, S_w is water saturation and d_a is average pore diameter of the cementitious material.

6. CONCLUSIONS

In this paper, a new analytic model that characterizes the chloride diffusivity in unsaturated cementitious materials is developed based on the conductivity theory and Nernst-Einstein equation. This model specifies that the effective chloride diffusivity in unsaturated cementitious materials is a function of effective chloride diffusivity in saturated state, water saturation and average pore diameter of the material. The analytic model shows good agreement with the experimental results. Improvement to this analytic model, such as using a more accurate expression correlating the parameter c and pore structure information, is possible.

ACKNOWLEDGMENTS

The financial support from China Scholarship Council is highly appreciated.

REFERENCES

[1] Saetta A.V., Scotta R.V. & Vitaliani R.V.: Analysis of chloride diffusion into partially saturated concrete, ACI Material Journal, 90 (1993), pp. 441-451
[2] Buchwald A.: Determination of the ion diffusion coefficient in moisture and salt loaded masonry materials by impedance spectroscopy, 3rd international PhD symposium, Vienna, Austria, 2000
[3] De Vera G., Climent M.A., Viqueira E., Antón C. & Andrade C.: A test method for measuring chloride diffusion coefficients through partially saturated concrete. Part II. The instantaneous plane source diffusion case with chloride binding consideration. Cement and Concrete Research, 37 (2007), pp. 714–724
[4] Olsson N. et al.: Non-saturated ion diffusion in concrete – A new approach to evaluate conductivity measurements. Cement and Concrete Composite, 40 (2013), pp. 40-47
[5] Christensen B.J.: Microstructure studies of hydrating Portland cement-based materials using impedance spectroscopy. Dissertation, Northwestern University, 1993
[6] Aligizaki K.K.: Pore Structure of Cement-Based Materials: Testing, Interpretation and Requirements. CRC Press, Taylor & Francis, 2006
[7] Zhang Y. & Ye G.: Chloride transport in partially saturated mortar made of blended cement, Conference: 14th International Congress on the Chemistry of Cement, 13~16 October 2015, Beijing, China.
[8] Taylor H.F.W.: A method for predicting alkali ion concentrations in cement pore solutions. Advances in Cement Research, 1 (1987), pp. 5-16
[9] Chen W. & Brouwers H.J.H. Alkali binding in hydrated Portland cement paste. Cement and Concrete Research, 40 (2010), pp. 716-722
[10] Mindess S. & Young J.F.: Concrete. Prentice-Hall, Englewood Cliffs, New York, 1981

GREEN ROOFS – HYGROTHERMAL SIMULATION OF MOISTURE AND ENERGY PERFORMANCE

Daniel Zirkelbach[1]

[1] Fraunhofer Institute for Building Physics (IBP) Holzkirchen, Department Hygrothermics, Fraunhoferstr. 10, 83626 Valley, Germany, email: daniel.zirkelbach@ibp.fraunhofer.de

SUMMARY: Based on laboratory and field tests at the Fraunhofer IBP field test site a hygrothermal green roof model was developed, which allows to model the performance of extensive green roofs in hygrothermal simulation software. A comparison of the measured and simulated temperatures beneath the greenery shows, that the model well reproduces the real conditions. Also the moisture conditions in timber roof constructions as well as the heat flows through the roof assembly are compared once with the measured conditions from the field tests and once with the new simulation model. Main focus of the model is the evaluation of the moisture performance of roof assemblies which is of special importance in case of moisture sensitive timber roofs. But also a prediction of the energetic behaviour and the cooling effects of the roof as well as an evaluation of the comfort conditions in the room beneath the green roof becomes possible and is shown exemplarily for the warm Mediterranean climate of the South Croatian city Split in comparison to flat roof with a white and a black roof surface.

ZELENI KROVOVI – MODELIRANJE HIGROTERMALNOG PONAŠANJA

SAŽETAK: Na osnovi laboratorijskih i terenskih ispitivanja na terenskom ispitnom polju Instituta Fraunhofer razvijen je higrotoplinski model zelenoga krova koji omogućuje modeliranje svojstava velikih zelenih krovova u softveru za higrotoplinsku simulaciju. Usporedba mjerenja i simuliranih temperatura ispod zelenila pokazuje da model dobro reproducira stvarne uvjete. Uvjeti vlage u drvenim krovnim konstrukcijama i prolazak topline kroz sklop krova prvo su uspoređeni s mjerenim uvjetima pri terenskim ispitivanjima, a potom s novim modelom simulacije. Glavna pozornost u modelu vrednovanje je ponašanja krovnoga sklopa pri vlazi koja ima posebnu važnost kod drvenih krovova osjetljivih na vlagu. No moguće je i predviđanje energetskog ponašanja i učinaka hlađenja krova te vrednovanje uvjeta udobnosti u prostoriji ispod zelenoga krova što je kao primjer pokazano za toplu mediteransku klimu južnohrvatskog grada Splita u usporedbi s ravnim krovom s bijelom i crnom površinom.

1. INTRODUCTION

Many people regard greeneries as a rather winsome roof type. Apart from that they provide some benefits like a higher durability due to the protection of the sealing by the soil layer, energy savings and better comfort especially in summer time due to evaporation cooling, retention of precipitation water as well as reduction of heat island effects and improvement of air quality. Therefore more and more green roofs are built in many countries worldwide. However, in Central Europe there have been reported some problems and damage cases related to green roofs applied on moisture sensitive timber roofs. As the hygrothermal performance of a green roof can hardly be evaluated by means of dew point calculations like [1] or [2], a hygrothermal evaluation [6] of such assemblies is necessary. Within a project, funded by the German Federal Ministry of Transport, Building and Urban Affairs, a hygrothermal green roof model could be developed [4] which can be used together with the hygrothermal simulation software WUFI® [4]. The main focus of the model development was the evaluation of the roof construction's moisture performance. But comparison with measurements showed, that also the thermal behaviour and the energetic consequences can be well reproduced.

2. MODELING THE CONDITIONS IN THE GREEN ROOF LAYERS

The conditions beneath a green roof clearly differ from the ones on a normal roof top. This is due to the effects of the plants which cover and shade the roof from long and short wave radiation influences, the high thermal inertia of the soil layer, the stored water and its heat enthalpy including fusion and evaporation effects. Modelling these effects is rather difficult, especially under real weather conditions [7][8].

Most previous models were developed to consider the thermal performance of the roofs and handled the influences of the plant canopy in great detail, often based on the research of Perrier [9] or Frankenstein and Koenig [10]. Models are for example available from del Barrio [11], Theodosiou [12], Kumar und Kaushik [13], Lazzarin et al. [14] Alexandri und Jones [15], Sailor [8], Ouldboukhitine [16], Olivieri et. al [16] and Tabares-Velasco et al.. The detailed calculation of the plants requires input parameters which are difficult to measure and hardly available in practice. In many cases they were even not known for the greenery, used for the models validation. On the other hand, the moisture processes in the soil, with drainage, liquid water transport due to capillary forces, local moisture level and its influence on the heat capacity and the thermal conductivity as well as on the evaporation rate at the soil surface, are modeled only in a simplified way or even neglected. Also, the effect of rain water absorption and redistribution due to capillary forces and heat of fusion is not considered in most of the available models. As the evaporation rate depends on the moisture content directly at the surface and not on the average content over the whole thickness of the soil, this seems to be a crucial point. Furthermore a whole year simulation under natural weathering, which is required to reliably predict the hygrothermal performance of a roof construction, is hardly possible without considering ice formation and fusion.

3. HYGROTHERMAL GREEN ROOF MODEL

An alternative approach based on the hygrothermal simulation model WUFI® [4] was developed, which considers the moisture balance of the soil more in detail, as this is a standard application of this software. However, some effects like drainage, shading by the plants, reduced surface transfer etc. were not directly available in the software. Therefore the multidimensional effects in drainage layer, soil and plant canopy were complemented in a way, that accounts for the greenery together with the normal building component.

3.1. GENERIC AND OPTIMIZED MODEL

A first version of the hygrothermal green roof model, based on field tests at four different Central European locations, was presented in [19]. This was limited to climate conditions similar to Central European, as no sky radiation influence was considered and only a combined model for drainage and plant soil can be handled, while today mainly separate drainage boards are used. Therefore the model was further optimized to become applicable for extensive green roofs in all climates [3] [20]. Figure 1 shows the four transfer phenomena which are used to implement the greenery to hygrothermal simulation software.

This comprises the handling of precipitation including drainage transport through the soil and storage in the drainage boards, effective surface transfer and insulating properties of the plant canopy, effective hygrothermal material properties of the different layers of the greenery as well as the effective solar and sky radiation exchange of the planted surface. Thus the model requires measured properties of the used soil and drainage layers and outdoor climate data including sky radiation and precipitation. Compared to the previous models the plant canopy is just considered by its effective heat transfer, additional insulation due to the rather stagnant air in-between the plants as well as the self-shading and thus reduced long- and shortwave radiation exchange.

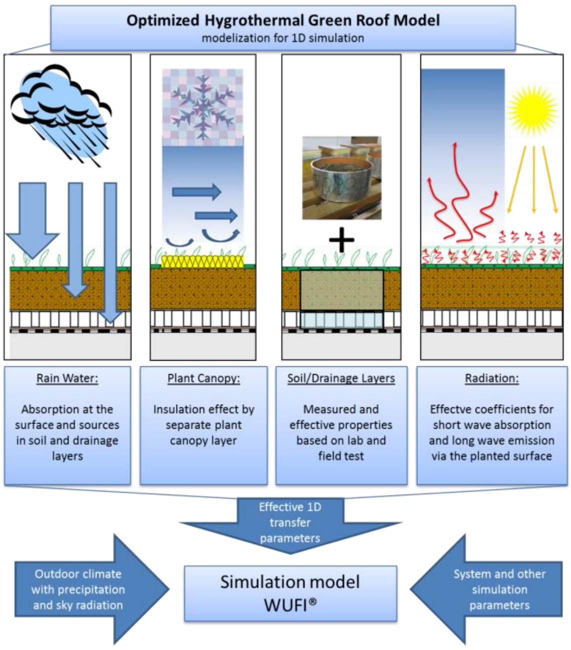

Figure 1 Input and transfer parameters of the optimized hygrothermal green roof model

3.2. VALIDATION

This approach seems rather simple – however, it leads to a good correlation with both, the measured temperatures beneath the greenery as well as the hygrothermal conditions in the roof assembly when simulating it once with the measured temperatures from the field test and once with the new model. Figure 2 shows exemplarily for roof 1 the comparison between the measured (two measurement axes in the test field) and the simulated temperature conditions.

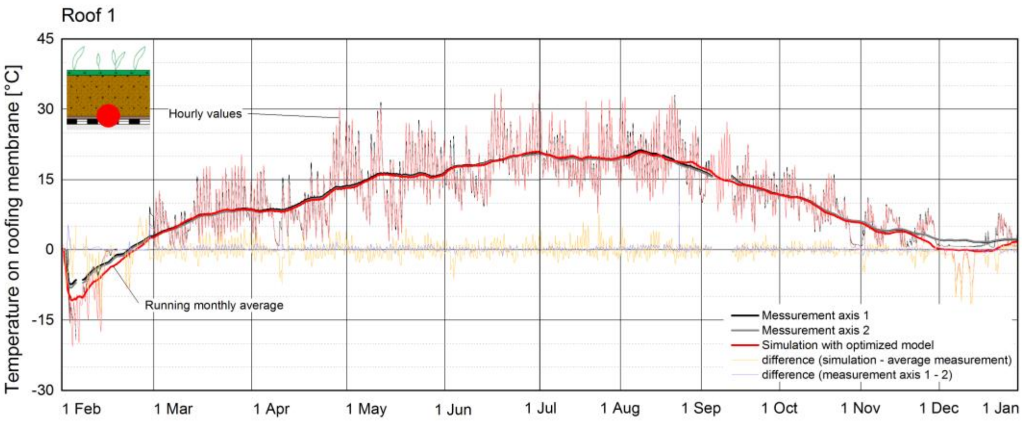

Figure 2 Comparison of the measured and simulated temperatures beneath green roof 1

The agreement is very good from spring to autumn while certain deviations can occur in winter during periods with snow cover, which cannot be accounted for in the simulation. The average annual temperature difference is -0,4 K which means, that the model remains colder and thus slightly on the save side. As the snow reduces the short wave radiation influence due to the white surface as well as the long wave radiation influence, the temperature beneath the snow remains mostly around 0 °C. As, during winter, long wave losses dominate over short wave gains neglecting the snow in the simulation leads to colder conditions than the measured ones. Thus the model remains on the safe side. More details concerning the thermal and hygrothermal evaluation can be found in [5] and [20].

To check the applicability for energy and comfort simulations, a single test room was simulated, using the hygrothermal whole building simulation tool WUFI® Plus [21]. The test room represents one room at the top floor (beneath the green roof) of a bigger residential building and is shown in **Error! Reference source not found.**. The size is 5 m by 5 m and 2.8 m height. The side and back walls as well as the bottom ceiling are assumed to be adiabatic, as the neighbour rooms feature the same operation. The influence of the thermal mass is minimized by using timber constructions. The U-value of the external wall is very low with 0,15 W/(m²K) again to minimize that side influence. The roof construction has the same U-value like the test roof from the field test – this is necessary to be able to compare the results of a simulation with the green roof model and with the measured temperatures beneath the green roof. For comparison also a simulation with a conventional black roofing membrane is performed. The room has two North oriented windows with an U_w-value of 0,8 W/(m²K), a SGHC value of 0,5 and an area of 3,6 m² (without shading devices). The internal heat load is assumed to be rather low (20 W for 24 h), the air change rate is 0,3 h^{-1}. The acceptable temperatures in the room range from 20 to 23 °C. As outdoor climate the measured data at the IBP field test at Holzkirchen (South Germany) are use.

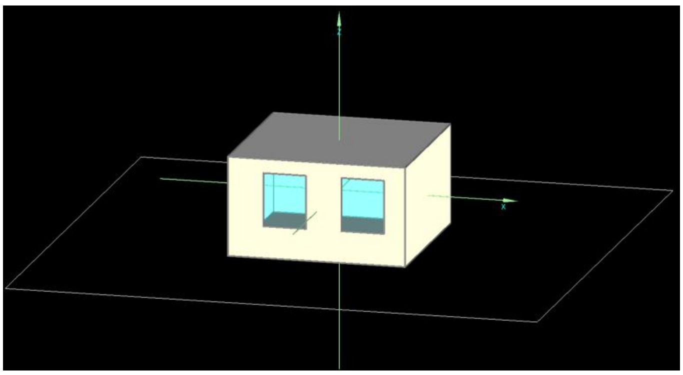

Figure 3 Test room for validation of energy performance of the green roof model
with hygrothermal whole building simulation

The results of the simulation are shown in Figure 4 as heat fluxes through the roof during winter and summer time. The overall agreement between the green roof heat fluxes with measured temperature and the new green roof model are quite good – especially in the summer months. In winter again some deviations can be observed when snow is on the roof from second half of January until last week of February. However, evaluating the hourly curves (figures on the right), the small differences between model and measured values compared to the big differences to the heat fluxes of the black roofing membrane become obvious. Looking on the energy demand for heating and cooling of the test room with measured and modelled green roof, also these values are very close to each other. The heating energy demand differs only by 0,4 % (1334 kWh with measured temperatures compared to 1329 kWh with the model). Also the black roof case needs only 1.5 % more heating energy with 1349 kWh. In summer time the cooling demand with the model with 126,3 kWh again is only 0,4 % higher than with the measured data (125,9 kWh). But now, with 255 kWh, the cooling energy demand of the room with the black roofing membrane exceeds the ones of the green roofs by 50 %.

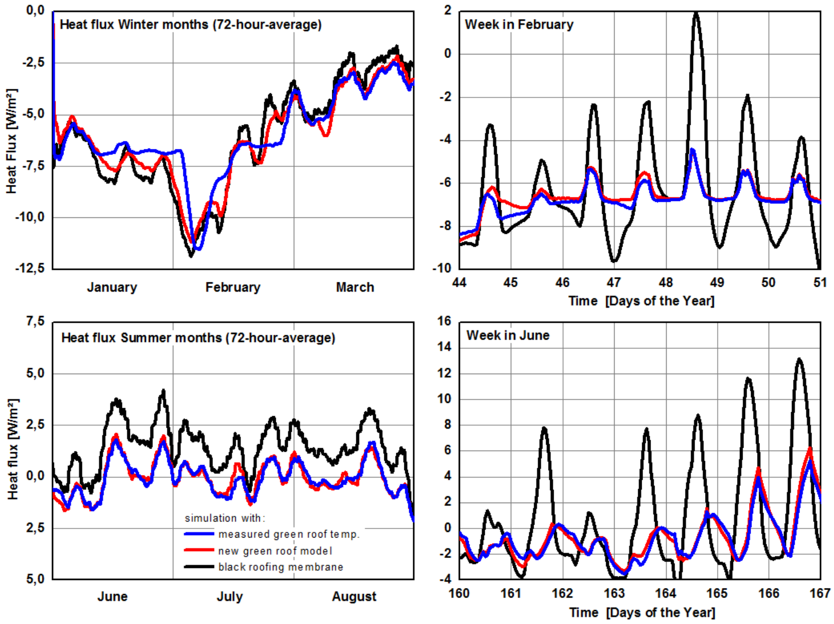

Figure 4 Heat fluxes through the roof in summer and winter simulated based on the measured temperatures beneath the green roof (blue) and the new green roof model (red) compared to the heat fluxes of a black membrane roof (black).

4. APPLICATION EXAMPLE

As application example, a residential building under the climatic conditions of Split in the South of Croatia is simulated. The climate file with hourly data including precipitation and long wave radiation data was created by the help of METEONORM. Focus is on the energy demand of the top floor when using a green roof in comparison to a white and black roofing membrane. The exemplary building, plotted in Figure 5, has an unheated basement and two heated and air-conditioned floors. The building is 9 m by 11 m and 6 m height plus 2.5 m for the basement. Walls, ceilings and flat roof are made of masonry or concrete. The 24 cm thick clay brick walls feature an U-value of 0,5 W/(m²K) and the flat roof with 15 cm concrete and 8 cm EPS insulation has an U-value of 0,44 W/(m²K). The total area of the seven windows in the second floor is 15,4 m² with an U_w-value of 2,7 W/(m²K) and a SGHC of 0,7. The windows are temporarily shaded by 75 % to limit the solar radiation gains during summer and avoid overheating. The indoor loads represent a typical operation as residential building with living room and kitchen in the first and sleeping rooms in the second floor. In the simulation different zones are used for each floor – thus the second floor with the green roof influence can be evaluated separately. The design conditions require heating, when indoor air temperature falls below 20 °C and cooling when temperatures exceed 25 °C.

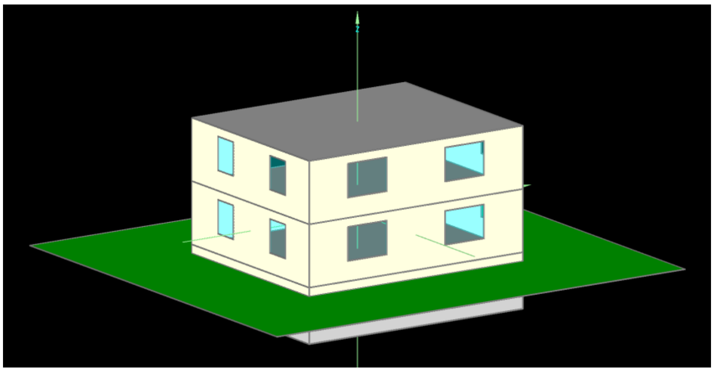

Figure 5 Exemplary residential building with two floors and basement with green roof, compared to a black or white roofing membrane.

As result, the total heat gains or losses during the summer and winter months are plotted in Figure 6. In summer the differences are obvious: the black roof shows the worst performance with gains of 1550 kWh, compared to only 590 when using a white roofing membrane instead. The green roof shows similar values as the white roof. Without irrigation the gains are a bit higher with 660 kWh. However, to ensure a good growth of the plants also during the summer months, some additional irrigation will be required anyway.

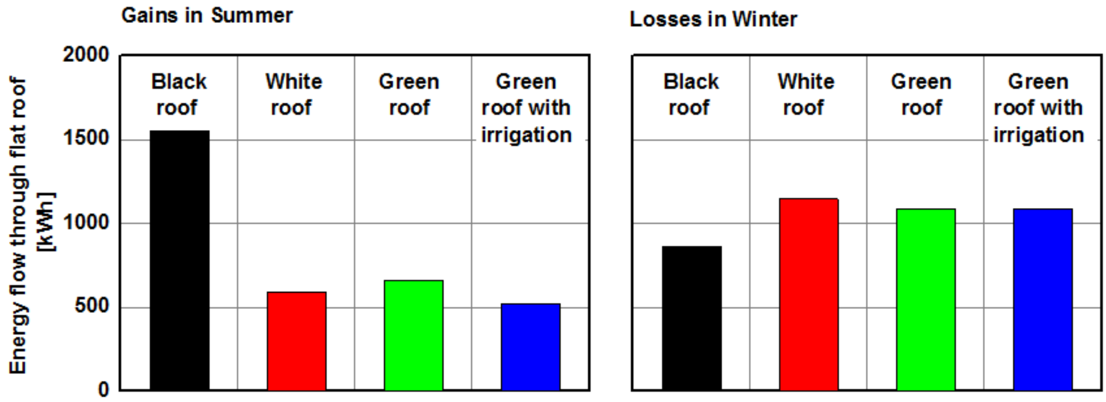

Figure 6 Energy gains and losses through the flat roof with black or white roofing membrane or greenery.

The cooling energy demand to condition the whole 2nd floor is 2073 kWh per year for the irrigated green roof compared to 3100 kWh for the black and 2156 kWh for the white roof. As expected, the heating energy behaves contrary: here the black roof requires 3318 kWh compared to 3542 for the green and 3665 kWh for the white roof. That means, green and white roofs have advantages in summer and black roofs in winter time which compensate each other to a certain extent. However, the total energy demand throughout the year is lowest for the green roof with 5615 kWh, followed by the white roof with 5820 kWh (+3,7 %) and highest for the black roof with 6418 kWh (+14,3 %).

5. CONCLUSIONS

The validations show, that the new green roof model can be used with good accuracy for both, the hygrothermal building component as well as the whole building energy simulation featuring a good agreement between measured and simulated data all year round. The simulation of the whole year is essential especially for the moisture performance of building assemblies, as both, humidification in winter and drying in summer influence the hygrothermal behaviour. Compared to other green roof models, the more detailed simulation of the moisture balance in the soil, allows consideration of the influence of the natural weather conditions with precipitation in summer and winter. The more simplified handling of the plant canopy doesn’t seem to have relevant negative effects.

The evaluation of the example case results in Split shows, like the measurements in Germany, clear advantages concerning the summer overheating protection of the green roof with a reduction of the cooling energy demand by about 25 % compared to a black roofing membrane. However, a white roofing membrane behaves rather similar - only with irrigation a slight improvement by about 4 % can be reached with a green roof. In winter the black roof provides additional solar heat gains, while the white roof still features the highest losses. While under German conditions black and green roof show a similar performance in winter, the higher solar radiation gains of the black roof and the additional evaporation cooling effects of the green roof in Split led to certain advantages of the black roof in winter time. Clear advantages of the greenery concerning energy savings during the winter month, like mentioned in different other publications, cannot be confirmed. Over the whole year period a green roof solution still provides the best energy performance – in combination with the advantages mentioned in the introduction, a high durability of the roof, but also higher costs for building and irrigation.

ACKNOWLEDGMENTS

The research results presented in this paper were funded by the German Federal Ministry of Transport, Building and Urban Affairs within the research initiative “Zukunft Bau” under the project number F 2863. For application of the model a guideline with detailed settings and input parameters as well as the required material properties are available on the IBP homepage [23].

REFERENCES

[1] EN ISO 13788 Hygrothermal performance of building components and building elements -- Internal surface temperature to avoid critical surface humidity and interstitial condensation -- Calculation methods. (2012).

[2] DIN 4108-3: Wärmeschutz und Energie-Einsparung in Gebäuden. Klimabedingter Feuchteschutz. Anforderungen, Berechnungsverfahren und Hinweise für Planung und Ausführung. Juli 2001.

[3] Schafaczek, B. und Zirkelbach D.: Ermittlung von Materialeigenschaften und effektiven Übergangsparametern von Dachbegrünungen zur zuverlässigen Simulation der hygrothermischen Verhältnisse in und unter Gründächern bei beliebigen Nutzungen und unterschiedlichen Standorten. Forschungsinitiative Zukunft Bau, Band F 2863, Fraunhofer IRB Verlag 2013.

[4] Künzel, H. M.: Verfahren zur ein- und zweidimensionalen Berechnung des gekoppelten Wärme- und Feuchtetransports in Bauteilen mit einfachen Kennwerten. Dissertation Universität Stuttgart (1994).

[5] Zirkelbach, D.: Wärme- und Feuchteverhalten von begrünten Dachkonstruktionen. Dissertation Universität Stuttgart (2016).

[6] EN 15026:2007-07: Hygrothermal performance of building components and building elements. Assessment of moisture transfer by numerical simulation (2007).

[7] Liu, K. K. Y.: Sustainable building envelope - garden roof system performance, RCI building Envelope Symposium, New Orleans, USA (2004) S. 1-14.

[8] Sailor, D.J.: A green roof model for building energy simulation programs. Energy and Buildings 40 (2008), S. 1466-1478.

[9] Perrier A.: Étude et essai de modelisation des echanges de mass et d'energie au niveau des couverts vegetaux: profils microclimatiques, evapotranspiration et photosynthese Nette. Doctorat d'Etat, Universität Pierre et Marie Curie, Paris, Frankreich (1976).

[10] Frankenstein, S. und Koenig, G.: FASST Vegetation Models. U.S. Army Engineer Research and Development Center (ERDC), Cold Regions Research and Engineering Laboratory (CRREL), Technical Report TR-04-25 (2004).

[11] Barrio, E. P. del: Analysis of the green roofs cooling potential in buildings. Energy and Buildings 27 (1998), S. 179-193.

[12] Theodosiou, T. G.: Summer period analysis of the performance of a planted roof as a passive cooling technique. Energy and Buildings 35 (2003) H. 9, S. 909-917.

[13] Kumar, R. und Kaushik, S. C.: Performance evaluation of green roof and shading for thermal protection of buildings. Energy and Buildings 40 (2005), S. 1505-1511.

[14] Lazzarin, R., Castellotti, F. und Busato, F.: Experimental measurements and numerical modelling of a green roof. Energy and Buildings 37 (2005), S. 1260-1267.

[15] Alexandri, E. und Jones, P.: Developing a one-dimensional heat and mass transfer algorithm for describing the effect of green roofs on the built environment: Comparison with experimental results. Building and Environment 42 (2007), S. 2835–2849.

[16] Ouldboukhitine, S.-E., Belarbi, R., Jaffal, I. und Trabelsi, A.: Assessment of green roof thermal behavior - A coupled heat and mass transfer model. Building and Environment 46 (2011), S. 2624-2631.

[17] Tabares-Velasco, P. C. und Srebric, J.: A heat transfer model for assessment of plant based roofing systems in summer conditions. Building and Environment 49 (2012), S. 310-323.

[18] Olivieri, F., Di Perna, C., D'Orazio, M., Olivieri, L. und Neila, J.: Experimental measurements and numerical model for the summer performance assessment of extensive green roofs in a mediterranean coastal climate. Energy and Buildings 63 (2013), S. 1-14.

[19] Zirkelbach, D.; Schafaczek, B; Künzel, H.M.: Longterm hygrothermal performance of green roofs. In: American Society of Heating, Refrigerating and Air-Conditioning Engineers, Inc. ASHRAE. Buildings XI - Thermal Performance of the Exterior Envelopes of Whole Buildings: Proceedings, Paper 105. Atlanta, USA (2010).

[20] Zirkelbach, D.; Mehra, S.-R.; Sedlbauer, K.-P.; Künzel, H.-M.; Stöckl, B.: A Hygrothermal Green Roof Model to Simulate the Moisture Performance of Building Components. Energy and Buildings - Special Issue on The effect of indoor and outdoor vegetation on the building performance (2017).

[21] Antretter, F.; Sauer, F.; Schöpfer, T.; Holm, A: Validation of a hygrothermal whole building simulation software. Proceedings 12th Building Simulation 2011 (2011) p. 1694-1702.

[22] Meteonorm V. 6.1. Software from Meteotest. www.meteonorm.com

[23] Guideline for the calculation of extensive green roofs on WUFI®-Homepage:

[24] https://wufi.de/de/wp-content/uploads/sites/9/2014/09/Guideline_green_roof_150923.pdf

ESTIMATION OF RECYCLING CAPACITY OF MULTI-STOREY BUILDING STRUCTURES USING SUPPORT VECTOR MACHINES

Aleksandra Vujkov[1], Dragana Bibic[1], Igor Pesko[1], Vladimir Mucenski[1], Goran Cirovic[2]

[1] University of Novi Sad Faculty of Technical Sciences, Department of Civil Engineering and Geodesy, Trg Dositeja Obradovica 6, 21000 Novi Sad, Republic of Serbia, email: vujkova@uns.ac.rs, draganabibic@uns.ac.rs, igorbp@uns.ac.rs, mucenskiv@uns.ac.rs
[2] University of Belgrade Belgrade University College of Applied Studies in Civil Engineering and Geodesy,
Department of Civil Engineering, Hajduk Stankova 2, 11000 Belgrade, Republic of Serbia,
e-mail: cirovic@sezampro.rs

SUMMARY: Artificial Intelligence in construction can be applied at all stages of the construction project, from the earliest stages of planning and design up to recycling of building materials during the demolition of buildings. This paper presents evaluation of amount of concrete for residential buildings constructed in skeleton structure. To estimate the amount of this material the model based on artificial intelligence using the method of Support Vector Machines (SVMs) was formed. Analyzed in detail and well prepared database is one of the most important aspects in the forming process of the SVMs model. In order to obtain more accurate prediction of the amount of material the method for data normalization, z-score normalization was applied. During the research different models of SVMs were tested and the model which has provided satisfactory accuracy prediction of the amount of concrete to the real value of the buildings was chosen.

PROCJENA RECIKLABILNOSTI KONSTRUKCIJA VIŠEKATNIH ZGRADA UPOTREBOM ALGORITMA VEKTORA POTPORE

SAŽETAK: Umjetna se inteligencija u gradnji može primijeniti u svim fazama građevinskog projekta, od najranijih faza planiranja i projektiranja do recikliranja građevnih materijala tijekom rušenja zgrada. U radu se prikazuje vrednovanje količine betona stambenih zgrada okvirne konstrukcije. Za procjenu količine toga materijala oblikovan je model zasnovan na umjetnoj inteligenciji primjenom metode algoritma vektora potpore (engl. support vector machine, SVM). Jedan od najvažnijih aspekata oblikovanja procesa modela SVM-a detaljna je analiza i dobro pripremljena baza podataka. Za dobivanje točnije prognoze količine materijala primijenjena je metoda normalizacije podataka i to normalizacija po z-rezultatu. Tijekom istraživanja ispitani su različiti modeli SVM-a a odabran je model koji je dao zadovoljavajuću točnost prognoze količine betona u odnosu na stvarnu vrijednost zgrada.

1. INTRODUCTION

Civil engineering is a specific branch of industry, and one of the main reasons for this is that in the process of realization of the construction projects there is a large number of stakeholders with different roles involved. The investor has the main role, the one who initiates the project, whose goal is to achieve the highest profit with minimum costs of project. Under the construction project we can consider construction of a new facility, as well as reconstruction and repairment of the existing one. Building construction, as a result of the construction project, has its own lifetime that begins with the emergence of the need for it until the end of that need and the impossibility of its change, that is, until its demolition. Removal of buildings whose lifetime is completed, more precisely their demolition, produces large amounts of materials that still have more or less usability. Defining the ways for easy and simple use of materials produced in the process of demolition of buildings decreases or completely eliminates the cost of transportation and landfilling. Increasing costs of transportation and landfilling products of demolition of buildings, as well as the increasing emphasis of the need for attentive attitude towards the environment, led to the fact that the utilization of recycled materials is increasingly used in construction. Depending on the materialization of buildings predicted for demolition, there are various types of materials that will be the product of demolition process, and the subject of potential recycling after the process of demolition. Bearing in mind that in the territory of SFRY from the 60s to the 80s last century, buildings were predominantly built of reinforced concrete, we can easily conclude that in the future one of the basic materials for recycling will be precisely concrete. This is supported by the fact that today the dominant building material is concrete.

Reusability of the materials obtained in the process of demolition of the existing reinforced concrete structures, with adequate preparation and processing, largely eliminates the need for lagering large amounts of materials. The use of material obtained from the recycling of concrete can lead to a reduction in the total cost of building constructions and other elements made of concrete by reducing the utilization of new materials, or by reducing the costs of depositing materials as products of demolition. For this reason, evaluation of the amount of material suitable for recycling, in the specific case concrete and its uses in the construction of new facilities is very important information. However, the evaluation of the amount of concrete for recycling resulting from the demolition of existing buildings is not always an easy process. The reason for this is often a lack of project documentation, which complicates determination of the quantity of concrete. The development of simple models for the evaluation of the recycling capacity of old buildings leads to the easy, fast and sufficiently accurate estimation of the amount of material for recycling, i.e. in the specific case concrete. The more frequent use of artificial intelligence in the construction industry certainly has great importance in the formation of a model for quick and easy estimation. Artificial Intelligence in construction can be applied at all stages of the construction project, from the earliest stages of planning and design up to recycling of building materials during the demolition of existing objects.

The basic prerequisite for the formation of a model based on artificial intelligence is an adequate database, on which the accuracy of the estimation of the model depends. This paper presents the analysis of the database and the application of SVMs (Support Vector Machines) for the purposes of estimating the recycling capacity of residential buildings which potentially can be the subject of demolition in the future due to the expiration of their lifetime. Example assessment is given for the evaluation of the amount of concrete.

2. ARTIFICIAL INTELLIGENCE - USE IN CIVIL ENGINEERING

In the field of information technology, the application of artificial intelligence has experienced greatest expansion in recent decades, in particular its application in solving practical problems. The expectations are growing alongside the development of artificial intelligence. As many of the computation fields are considered to be defined and that there will be no greater progress, so for the artificial intelligence the results are only expected in the future. In the area of research of soft computing models at the end of the 80s, SVMs and Fuzzy logic (FL) experienced an expansion. Using the above mentioned tools for modelling has significantly increased with the definition of new algorithms and the fundamental principles. These two tools complement each other and represent an example of learning tools. They basically define the relationship between the inputs and outputs using datasets for training. SVMs and FL are mathematical models that were created experimentally [1].

Today, SVMs is the tool that has the largest application for solving the problem of regression and classification by changing the parameters that control their learning, based on the training data. SVMs was introduced by Vladimir V. Vapnik [2] in 1995 and the method was primarily used for solving problems of classification, but lately, the method has spread to the domain of solving problems of regression. SVM is method for training and defining the function of separation in classification problems, or making a prediction in regression problems, respectively. This approach comes from SLT (statistical learning theory) developed by Vapnik and Chervonenkis [3] at the end of the twentieth century. SVMs are models that do not use predefined parameters, but the number of parameters depends on the training data. The above mentioned parameters are determined on the basis of data for training and they have a role to define the ability of model to interpolate data i.e. in the case of regression after training the estimation error is zero. SVMs is a method where the algorithms use kernel function to transform the nonlinear problem into a linear, which is achieved by mapping the input space into a multidimensional space.

Research conducted in this paper refers to the estimation of the amount of materials, concrete, using SVMs method. Application of SVMs is well represented and is used in all areas of human activity and in different areas of science, from medicine, information technology, and architecture up to the construction industry.

Wang et al. [4] by applying a set of neural networks (NNs) and method of SVMs have made a prediction of the cost of construction and also the time schedule of construction, i.e. they explored how the early planning of construction affects the success of the project. The database includes 92 valid samples (of the project) collected in the period from 2007 to 2010, representing a total construction cost of about $1.1 billion. The collected information was used for the construction and for testing the set of neural networks and SVMs prediction models. The data were divided into two groups: 67 sets of training and 25 sets for testing. By comparing the obtained results, the authors concluded that SVMs model provides a cost prediction accuracy of 92%; while for predicting successfulness of dynamic plan the use of NNs (Adaptive Boosting NNS) provides the accuracy of prediction of 80%.

Cheng et al. [5] by applying ESIM (Evolutionary support vector machine inference model) made a prediction of success of the project. ESIM is a method that integrates the two methods: SVMs and fmGA (fast messy genetic algorithm). The research also includes the application of CAPP (Continuous Assessment of Project Performance) in order to select the factors that influence the success of the project. The database includes 46 construction projects. The authors concluded that ESIM method provides good results in predicting the success of the project.

Zhang et al. [6] made a prediction of profitability of construction companies in China using the method of PCA (Principal Component Analysis) and SVMs. Based on PCA method, the authors attained the index (''composite index''), and then applied the technique to predict the profitability of SVMs with this index. The results showed that well 'trained' SVM model can give the prediction of profitability with over 80% of accuracy.

Cheng and Wu [7] linked two approaches to artificial intelligence (fast genetic algorithm-fmGa and SVMs) for the purpose of solving the problems in construction management. The name of the new model is ESIM (evolutionary support vector machine inference model). The aim of developing a new model was to obtain the minimum prediction error, and to find the optimal parameters C i Y simultaneously. Based on analysis and on the results obtained, the authors concluded that ESIM model can be applied for the purposes of solving the various problems in construction management.

Strobbe et al. [8] investigated whether it is possible to learn the architectural style from the set of the cases, and whether there is a possibility to classify new styles as similar or different styles (designs) from observed cases. Two methods were applied (SVMs and graph kernels). Also, the authors demonstrated the feasibility of the proposed method of detection in the case of ''Malagueira houses''. They concluded that their model with an accuracy of 87.5% is able to generalize styles that were not taken into account during training.

Cheng et al. [9] proposed a model EFSIMT (Evolutionary Fuzzy Support Vector Machine Model Inference for Time Series Data) for the prediction of high-strength concrete pressure (HPC - High Performance Concrete). EFSIMT model is obtained by joining the multiple methods FL (Fuzzy Logic), wSVMs (weighted Support Vector Machines) and fmGA (fast messy genetic algorithms). The database includes 1030 samples of concrete, and the data were divided into two groups (1) data for training; 90% or 927 samples and (2) data for testing; 10% or 103 samples. The results of the model EFSIMT by authors were compared with SVM and BNP results, which were previously explored by other authors. Comparing the results, better results are obtained from EFSIMT model for prediction of high-performance compared to the SVM and BPN. It follows that EFSIMT provides a good tool for HPC strength of concrete.

Peško [10] by applying the SVM and neural networks (NNs) proposed a model for the evaluation of cost and time of construction of urban roads. The database includes 166 contracted and realized building constructions/reconstruction projects of urban roads. The data was divided into two groups: the data for training and data for testing, by applying the method of pseudo random sample. Normalization of data was performed using the min-max and z-score normalization. By comparing the results, the method SVM gives better results.

In addition to mentioned authors, Deng and Yeh [11] also used the SVM method to estimate the costs, as well as many others. The review of the relevant literature has not given any researches that refer to the application of SVM for the purposes of evaluating the quantity of construction materials required for the construction, recycling etc.

3. DATABASE FOR SVM MODEL

For the purpose of forming the evaluation model of amount of concrete embedded in existing structures i.e. for estimation of amount of concrete that could be the subject of recycling (fundamental structures, columns, stiffening walls, beams and floor structures), the database was based on the characteristics and quantities of concrete for 100 projects (residential buildings). All buildings are located on the territory of Novi Sad. The data used in this paper was taken directly from the project documentation.

The database used for the research in this paper was based on the assumption that for prediction of the required amount of concrete, there are several key elements of data that are directly related i.e. directly affect the quantity of concrete. Based on the text above, the data within the database for the formation of SVMs model are divided into input and output. Input data are related primarily to building characteristics which are in correlation with the amount of concrete such as: the total gross area of the building, the average gross floor area, the height of the building, the number of stiffening walls, the longitudinal and transverse raster of the construction, the type of floor structure and the type of floor support structure. Output data, or a parameter that is the subject of estimation, is the amount of concrete. All structures lean on the foundation slab, so it considers that it is a constant for all buildings, and the characteristics of foundation are not analyzed as input data. Although a small number of buildings lean on other types of foundations, it is not advisable to consider those data due to lack of data, and distortion of SVMs. Also, the database includes only buildings with one or without dilatation.

For the purpose of forming the SVM model based on artificial intelligence, in this case the application of SVMs, it is necessary to divide the entire database into two subsets, the data for training and data for validation. When divided into two subsets, it is necessary to include extreme values (min and max) of all parameters (input and output) in the subset of training. The reason for this is to expand the scope of the new established model which increases the accuracy of the estimation. Also, it is necessary that all projects that fall outside the scope of the database, i.e. have a great extreme value of some of the data compared to most of data, are eliminated from further analysis. For this reason, the building with the largest area (9.500m^2), the most exceptional data, is eliminated from further analysis.

Defining data which belong to a set of training model and to a set of model validation is not performed completely by random selection. Namely, in the context of database composed of 99 buildings (after the ejection of the project with the largest surface area) the value of the output parameter (the amount of concrete) is divided into 8 intervals (from 0 to 499, from 500 to 999, from 1,000 to 1,499, from 1,500 to 1,999, from 2,000 to 2,499, from 2,500 to 2,999, from 3,000 to 3,499, and from 3,500 to 3,999). Based on the defined intervals, the counting of projects by intervals was carried out. After counting, distribution of database on training and validation data was carried out, but under the condition that the percentage for both sets of projects by intervals is equal. As described above, 10 projects were selected and they form a subset of validation. In other words, a subset of training data consists of the remaining 89 projects.

When choosing the data, it was considered that the data related to materials are harmonized, i.e. that selected projects with the amount of concrete fit right into intervals with the highest number of repetitions. In the selection of samples, it was taken into account that minimum and maximum extremes were not taken due to more accurate prediction of the amount of material. From the new created database consisting of 99 buildings, 10 samples for validation and 89 samples for training model were selected.

Bearing in mind the above input data, their characteristics and their differences in order of magnitude, it is necessary to execute their adequate preparation before their use. For the purpose of formation of the model, in this research normalization of the data due to their reduction to the same order of magnitude was carried out. "Z score" normalization was carried out for input and output data within a subset of training, as well as for input data from a subset of validation. After defining the model, it is necessary to reverse data (to return normalized data into original value) generated from the model in order to carry out comparative analysis with expected values.

4. BUILDING THE SVM MODEL

The first step for the formation of SVMs model is the consideration of database and the division of data on input and output, as explained above. After adequate database preparation, it can be accessed to formatting the model. For the purpose of forming the model software package, Statistica 8 [12] was applied, which offers the possibility of data processing by using the SVMs method.

After defining the subset of training and validation, the software offers a choice of error function. Using this software, two types of error functions were varied, where for the type 1 function the defined parameters were C (capacity) and ε (insensitivity zone), and for the type 2 function the defined parameters were C (capacity) and Nu (μ). Also, the Kernel function was defined, the RBF function in which the parameter γ was varied. Based on the entered data and selection of the above mentioned parameters, the training model was carried out and a subsequent validation of the model was formed. More precisely the accuracy of the generated and reversed data was tested i.e. deviations generated from expected values were checked. A comparative analysis was based on APE (absolute percentage error) and MAPE (mean absolute percentage error).

Five models in total were formed for estimating the amount of material (the amount of concrete). For all models the input data were identical, i.e. previously mentioned parameters for the total gross area of the building, the average gross floor area, the height of the building, the number of stiffening walls, the longitudinal and transverse raster of the construction, the type of floor structure and the type of floor support structure, while the amount of concrete is the output value. Table 1 presents the selected parameters in the process of forming the SVM model.

Table 1 Selected parameters in the process of forming the SVM model

Model No.	Type of error function	C	ε	μ	RBF kernel γ
Model 1	type 1	10	0,10	-	0,10
Model 2	type 1	10	0,10	-	0,05
Model 3	type 1	10	0,10	-	0,07
Model 4	type 2	10	-	0,50	0,01
Model 5	type 2	20	-	0,70	0,01

5. RESULTS

Out of 5 SVMs models formed on the z-score normalization for the evaluation of amount of concrete, model 1 gives the most accurate results. This model has the lowest absolute percentage error, 9.28% with parameters C = 10, e = 0.1 and $\gamma = 1/[(2\sigma)]^{\wedge 2}$ =0.1. Figure 1 represents the mean absolute percentage error (MAPE) for prediction the required amount of concrete for all five models SVMs.

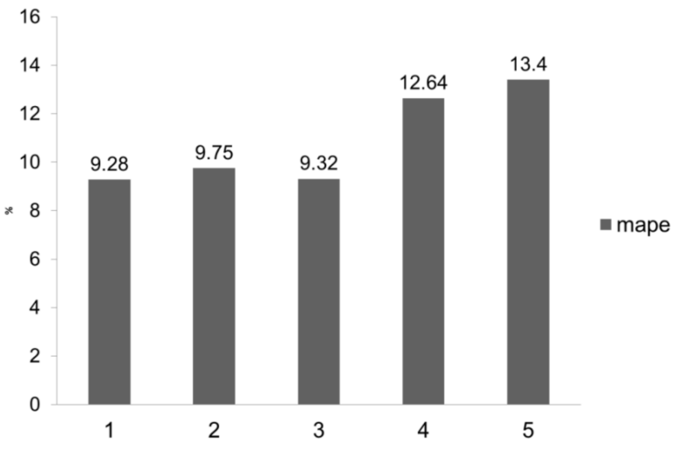

Figure 1 Mean absolute percentage error of prediction of the required amount of concrete for normalized values

Analyzing all models, it can be concluded that there is no big percentage difference between the value of the absolute percentage error between models that are formed by entering the normalized values in the software Statistics 8. Also, from the graph in Figure 1 it can be concluded that for specific cases the error function 2 gives lower accuracy of predicting the amount of concrete suitable for recycling.

6. CONCLUSIONS

In the paper, it is shown how the SVMs method can be applied for prediction of the required amount of concrete, for the database of 100 projects. Five models with different parameters were formed in total, and the model that presented the most accurate results was selected. In the case of evaluation of required amount of concrete based on historical data, the model with the lowest mean absolute prediction error provided the best results. After the analysis it was concluded that all models had a mean absolute error below 20%.

Future research should focus on analysis of the structure of the database in detail, as well as increasing the number of parameters for the database. Adding new parameters will significantly affect the increase of accuracy of the results for the amount of concrete. Also, it is possible to analyze the significance of the input data for the accuracy of prediction of the models formed, which may enable reduction in the number of input data with the potential increase in accuracy for the same amount for the used database.

In addition, it is possible to deepen the analysis with the application of other types of normalization on historical data, which can significantly affect the accuracy of results. This paper analyzes the reinforced concrete skeleton systems, which does not exclude the possibility of applying other types of systems such as load bearing masonry wall construction and prefabricated construction systems as well as structures made of steel or wood.

ACKNOWLEDGMENTS

The work reported in this paper is a part of the investigation within the research project TR 36017 ''Utilization of by-products and recycled waste materials in concrete composites in the scope of sustainable construction development in Serbia: investigation and environmental assessment of possible applications''. The project is supported by the ministry for Science and Technology, Republic of Serbia. This support is gratefully acknowledged.

REFERENCES

[1] Kecman, V.: *Learning and Soft Computing*, *Support Vector Machines, Neural Networks and Fuzzy Logic Models*, Massachusetts Institute of Technology (MIT), USA, 2001.

[2] Vapnik V., Golowich S., and Smola A.: *Support vector method for function approximation*, regression estimation, and signal processing. In M. Mozer, M. Jordan, and T. Petsche, editors, Advances in Neural Information Processing Systems 9, pages 281– 287, Cambridge, MA, 1997. MIT Press.

[3] Vapnik, V.: *The Nature of Statistical learning Theory*, 2nd ed., Springer, New York, USA, 1999

[4] Wang Y., Yu Ch., Chan H.: *Predicting construction cost and schedule success using artificial neural networks ensemble and support vector machines classification models*, International Journal of Project Management 30 (2012), pp. 470–478

[5] Cheng M., Wu Y., Wu Ch.: *Project success prediction using an evolutionary support vector machine inference model*, Automation in Construction 19 (2010), pp. 302–307

[6] Zhang H. et al: *Predicting profitability of listed construction companies based on principal component analysis and support vector machine—Evidence from China*, Automation in Construction 53 (2015), pp. 22–28

[7] Cheng M., Wu Y.: *Evolutionary support vector machine inference system for construction management*, Automation in Construction 18 (2009), pp. 597-604

[8] Strobbe T. et al: *Automatic architectural style detection using one-class support vector machines and graph kernels*, Automation in Construction 69 (2016), pp. 1–10

[9] Cheng M. et al: *High-performance concrete compressive strength prediction using time-weighted evolutionary fuzzy support vector machines inference model*, Automation in Construction 28 (2012), pp. 106-115

[10] Peško I.: *Model za procenu troškova i vremena izgradnje gradskih saobraćajnica*, doktorska disertacija, Univerzitet u Novom Sadu, Građevinski fakultet, Srbija, 2013.

[11] Deng S., Yeh T.: *Using least squares support vector machines for the airframe structures manufacturing cost estimation*, Int. J. Production Economics 131 (2011), pp. 701–708

[12] Dell Statistica, http://en.community.dell.com/techcenter/information-management/statistica

ANALYSIS OF REINFORCED CONCRETE SHEAR WALL STRENGHTENED WITH EXTERNALLY BONDED FIBER REINFORCED POLYMERS SUBJECTED TO CYCLIC LOADING USING CUSTOM MATERIAL MODEL

Vladimir V. Vitanov[1]

[1] Ss.Cyril and Methodius University – Skopje, Faculty of Civil Engineering, Partizanski odredi 24, 1 000 Skopje, Macedonia, email: v.vitanov@gf.ukim.edu.mk

SUMMARY: The use of FRP materials for structural strengthening purposes is continually expanding mainly due to their specific properties which give them a decisive advantage over the other strengthening techniques in many applications. As one of the newest materials in the structural industry, their behaviour as structural materials is still under intensive scientific investigation. However, further research is still needed. Since experimental investigations are quite expensive it would be beneficial if they could be supplemented, if not replaced, by numerical investigations which could successfully simulate the behaviour of RC members strengthened with FRP. A custom material model has been formulated for just this purpose. The model uses a well-known inelastic model for RC in plane stress as it basis, and adds additional material, the FRP, to it. In order to investigate its correctness, it was implemented into the commercial FEM software ANSYS and used for analysis of RC members for which experimental investigations have been carried out and the results published in the relevant literature. The results from the numerical analysis using the custom model were then compared with those of the experimental investigation. The obtained results show that, while showing some deficiencies which should be addressed in the further iterations and improvements, the formulated material model can successfully predict the behaviour of RC members strengthened with externally bonded FRP.

PRORAČUN ARMIRANOBETONSKOG NOSIVOG ZIDA POJAČANOG LIJEPLJENIM POLIMERIMA ARMIRANIH VLAKNIMA IZLOŽENOG CIKLIČKOM OPTEREĆENJU

SAŽETAK: Upotreba polimera armiranih vlaknima za pojačanje konstrukcija sve je veća uglavnom zbog njihovih posebnih svojstava koja im osiguravaju odlučnu prednost pred drugim postupcima pojačanja u mnogim primjenama. Kako je to jedan od najnovijih materijala u građevnoj industriji, njegovo ponašanje kao konstrukcijskog materijala još se uvijek intenzivno znanstveno istražuje. Međutim, potrebna su i daljnja istraživanja. S obzirom da su eksperimentalna istraživanja poprilično skupa bilo bi povoljno kad bi se ona mogla nadomjestiti ili čak zamijeniti računalnim istraživanjima koja bi uspješno mogla oponašati ponašanje armiranobetonskih elemenata pojačanih polimerima armiranih vlaknima. U tu je svrhu formuliran uobičajeni model materijala. U modelu je kao osnova uzet dobro poznati neelastični model za armirani beton pri ravninskom naprezanju kojemu je dodan dodatni materijal tj. polimer armiran vlaknima. Za istraživanje ispravnosti taj je model primjenjen u komercijalno dostupnom softveru ANSYS s metodom konačnih elemenata za proračun armiranobetonskih elemenata za koja su provedena eksperimentalna ispitivanja, a rezultati objavljeni u odgovarajućoj literaturi. Rezultati proračuna pokazuju, unatoč nekim nedostatcima koje treba riješiti u daljnjim iteracijama i poboljšanjima, da se formuliranim modelom materijala može uspješno prognozirati ponašanje armiranobetonskih elemenata pojačanih lijepljenim polimerima armiranih vlaknima.

1. INTRODUCTION

Among the most promising techniques for strengthening and retrofit of reinforced concrete structures in the recent years is the use fibre reinforces polymers (FRP) composites. Their specific properties such as strength, lightness, chemical resistance, ease of application, fast execution, low labour costs etc., give them comparative advantage over the classical strengthening and retrofit methods.

The usage expansion of these materials was closely followed by their extensive research expressed by the rapid expansion of numerous experimental investigations performed all over the world. This experimental research was not however adequately matched by appropriate numerical modelling work in terms of developing suitable numerical material models for the simulation of the behaviour of the FRP strengthened reinforced concrete. The majority of the used numerical models included numerical modelling of FRP strengthened RC members with FEM use element overlaying, where solid or layered that represent the FRP material are superimposed over the concrete elements, either with or without interface elements that represent the influence of the adhesive material or the bond between the FRP and the concrete.

The following sections present an attempt to formulate a material model for FRP strengthened reinforced concrete in plane stress state. The formulated model was implemented into the general purpose finite element software ANSYS as a user material model and used to create a numerical model of FRP strengthened reinforced concrete wall subjected to cyclic horizontal force for which an experimental data was available in the relevant literature. The results of the numerical analysis are compared with the experimental data in order to verify the correctness of the developed material model.

2. MODEL DESCRIPTION

The developed material model [1] for simulation of FRP strengthened cyclically loaded reinforced concrete is based on the widely used inelastic model for cyclic biaxial loading of RC concrete proposed by Darwin and Pecknold [2]. The RC model of Darwin and Pecknold uses the “equivalent uniaxial stress” approach with compressive loading curve proposed by Saenz [3] to model the biaxial material loading state, and the concrete failure surface proposed by Kupfer and Gerstle [4] based on the experimental data of Kupfer et al. [5]. Although comparably simple, it has been shown that this model is still capable of simulating the cycling behaviour of reinforced concrete members in plane stress state. The proposed model further extends the RC model by introducing the FRP, as an additional, third, component of the composite constitutive matrix which then becomes:

$$D' = D'_C + \sum_{i=1}^{n} D'_{S,i} + \sum_{i=1}^{m} D'_{F,i} \tag{1}$$

where:

D' is the constitutive matrix of the composite material in global coordinates,

D'_C is the constitutive matrix of the concrete in global coordinates,

$D'_{S,i}$ is the constitutive matrix of the steel in global coordinates,

$D'_{F,i}$ is the constitutive matrix of the FRP in global coordinates,

n is the number of different steel reinforcement,

m is the number of different FRPs.

These matrices in global coordinates are obtained by rotating their local coordinate representation using:

$$D' = T^T D T \tag{2}$$

where:

T is the transformation matrix,

$$T = \begin{bmatrix} cos^2\theta & sin^2\theta & sin\,\theta\,cos\,\theta \\ sin^2\theta & cos^2\theta & -sin\,\theta\,cos\,\theta \\ -2sin\,\theta\,cos\,\theta & 2sin\,\theta\,cos\,\theta & cos^2\theta - sin^2\theta \end{bmatrix} \tag{3}$$

where:

θ is the rotation angle between the two coordinate systems.

2.1. CONCRETE MATERIAL MODEL

The concrete is considered as incrementally linear elastic material (it is assumed that it behaves elastically during each load increment). It is also considered to be isotropic before, and orthotropic after a crack occurs at a point, exhibiting different properties in two orthogonal directions, described with two different elasticity parameter sets in the two directions. Its constitutive matrix in material coordinates is [2]:

$$D_C = \frac{1}{1-\nu^2} \begin{bmatrix} E_1 & \nu\sqrt{E_1 E_2} & 0 \\ \nu\sqrt{E_1 E_2} & E_2 & 0 \\ 0 & 0 & (1-\nu^2)G \end{bmatrix} \tag{4}$$

where:

E_1, E_2 are the elasticity moduli at the two orthogonal directions

$\nu = \nu_1 \cdot \nu_2$ is the equivalent Poisson's ratio

$G = \frac{1}{4(1-\nu^2)}(E_1 + E_2 - 2\nu\sqrt{E_1 E_2})$ is the shear modulus

The development of the cracks in the concrete is considered as the main non-linearity inducing phenomenon in the concrete. If a crack occurs in the first principle direction, it is simulated by reducing the elasticity modulus in that direction to 0 and the constitutive matrix becomes:

$$D_C = \begin{bmatrix} 0 & 0 & 0 \\ 0 & E_2 & 0 \\ 0 & 0 & \frac{E_2}{4} \end{bmatrix} \qquad (5)$$

If then a crack occurs in the other principle direction, the concrete constitutive matrix is reduced to 0. This approach in crack modelling also means that cracks in the concrete are not considered as distinct material discontinuities, but rather as and occurrence of many small cracks in the vicinity of the point considered, which is known as a "smeared" crack approach. Six different crack states can occur (Figure 1).

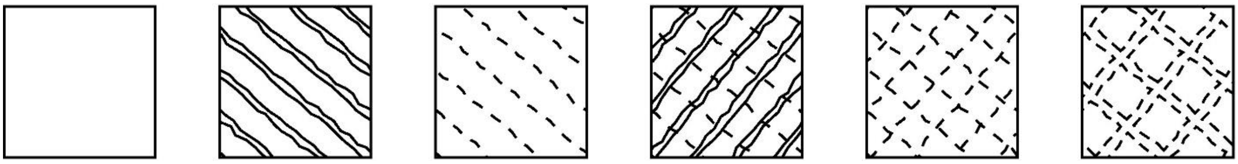

Figure 1 6 possible crack configurations: uncracked, opened crack in the first principle direction, closed crack in the first principle direction, closed crack in the first principle direction and opened crack in the second principle direction, closed cracks in both principle direction and opened cracks in both principle directions.

2.2. REINFORCING STEEL MATERIAL MODEL

Much simpler material models are adopted for the simulation of the behaviour of the other two constitutive materials. Bilinear elastic material model is adopted for the simulation of the reinforcing steel, whose constitute matrix in local coordinates is:

$$D_S = p_S \begin{bmatrix} E_{Steel} & 0 & 0 \\ 0 & 0 & 0 \\ 0 & 0 & 0 \end{bmatrix} \qquad (6)$$

where:

p_S is the reinforcing ratio

E_{Steel} is the steel elasticity modulus, which is reduced by the strain hardening stiffness ratio δ when the stress level in the steel exceeds its yield strength

2.3. FRP MATERIAL MODEL

Linear elastic material model with a brittle failure point is adopted for the simulation of the FRP, with constitute matrix in local coordinates:

$$D_F = p_F \begin{bmatrix} E_F & 0 & 0 \\ 0 & 0 & 0 \\ 0 & 0 & 0 \end{bmatrix} \qquad (7)$$

where:

p_F is the "strengthening" ratio (the ratio between the cross-section areas of the FRP and the concrete)

E_F is the FRP elasticity modulus

This adopted approach in the modelling of the steel and the FRP is known as "smeared" approach which means that the materials are considered as uniformly distributed, or smeared, throughout the element. This modelling approach implies that perfect bond between the constitutive materials exists.

This modelling approach is compatible with and suitable for the finite element method for structural multi-step analysis. The load on the structure can be divided in several steps and gradually applied. In each load step the constitutive matrix of Eq.1 can be updated by assembling the constitutive matrices of each of the materials (Eq.4, Eq.6 and Eq.7) after they are all rotated to global coordinates using the Eq.2. This procedure was coded and implemented into the FEA software ANSYS [6].

3. VERIFICATION EXAMPLE

In order to verify the mathematical model, it was implemented as a custom material model into the commercial FEA software ANSYS, and used in the simulation of the behaviour of cyclically loaded RC wall strengthened with FRP after which the results from the experimental investigation [7] and the numerical simulation were compared.

3.1. MODEL SETUP

A series of reinforced concrete shear wall specimens (Figure 2) were tested in cyclic loading conditions [7]. The walls were constructed using 40 MPa concrete with identical reinforcement of 400 MPa, 10 mm reinforcing bars. The height of the walls from the base of the panel to the centre of the cap beam is 2 m, the length is 1.5 m and the thickness is 10 cm. The vertical reinforcement consists of five pairs of 10 mm bars, spaced at 40 cm for a reinforcement ratio of 0.8%. The horizontal steel consisted of five pairs of 10 mm bars, spaced at 40 cm for a reinforcement ratio of 0.5%. Three of the test specimens included a control wall and two strengthened walls. The control wall was tested in its original state which provided a baseline for the evaluation of the repair and strengthening techniques. The two strengthened shear walls were strengthened by applying 0.11 mm carbon fibre sheets to the walls without pre-damage. The carbon fibre sheets had an elastic tensile modulus of 230 GPa and failure strain of 1.5%. The first specimen was strengthened with one vertical layer of FRP externally bonded to each face of the wall (Wall 1). The second specimen had one horizontal and two vertical FRP layers on each face of the wall (Wall 2). Both specimens were not loaded until the strengthening was applied.

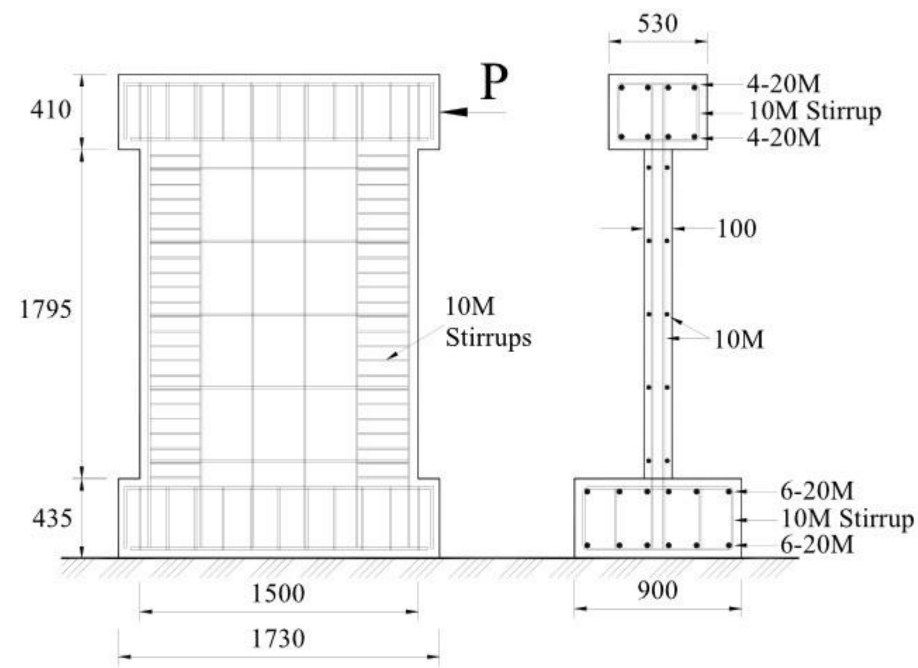

Figure 2 Measures and Reinforcement Details of the RC Wall

This paper presents the results of the analysis of the specimen Wall 2, i.e. the RC wall strengthened with a two layers of FRP with fibres in vertical direction and a single layer of FRP with fibres in the horizontal direction, on each face of the wall. For the FEM model in this case triangular as well as quadrilateral meshes were tested (Figure 3). The preliminary analyses showed that using triangular mesh generally led to better solutions. A mesh of triangular, 6-node Plane183 elements with average size of 25 cm was used for the final results.

Five different sections of the wall with different properties were defined: top and bottom beam, two side section ('columns') and a middle section ('panel'). Since the top and the bottom beam are significantly stiffer that the wall and their actual purpose is to provide the load transfer and anchorage for the tested wall, they were modelled as linear-elastic with very high elasticity modulus. The confining effect of the stirrups in the 'columns' was approximately accounted for by slightly increasing the concrete compressive strength in those regions, taking it to be 46 MPa in the 'columns', and 40 MPa in the 'panel'. The other concrete parameters were taken as: tensile strength of 4 MPA, initial elasticity modulus of 35 GPa, equivalent uniaxial strain of 0.35% and equivalent Poisson's ratio of 0.2. The steel material parameters were taken as: yield strength of 400 GPa, elasticity modulus of 200 GPa and strain hardening stiffness ratio of 1.8. The reinforcement ratio in vertical direction is 0.8%, and in horizontal direction 3% (in the 'columns') and 0.5% (in the 'panel'). The FRP material parameters were taken as: elasticity modulus of 230 GPA, ultimate strain at failure 1.5% and "strengthening" ratio of 0.22 for both the 'columns' and the 'panel'.

The cyclic load was applied at the middle of the top beam as a series of small displacements. The force and displacement at the same point were taken as results of the performed analyses. These were compared with the available experimental data.

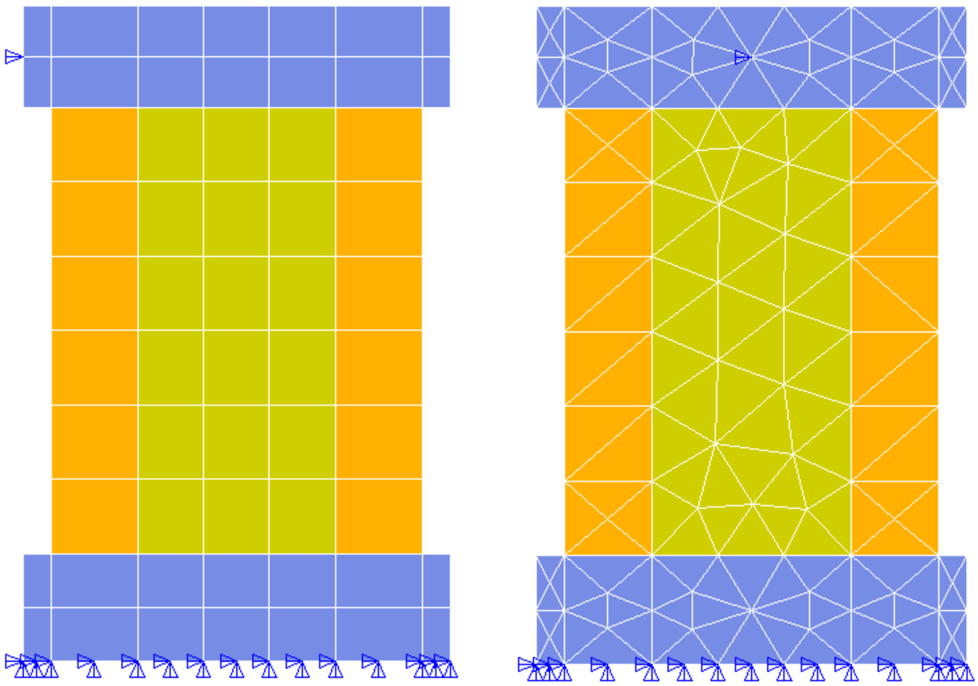

Figure 3 Quadrilateral and Triangular Element Mesh of the FEM Model

3.2. RESULTS

The resulting hysteretic loops developed at greater deflections where the model shows distinct inelastic behaviour are shown Figure 4. To measure how the numerical results compare to the experimental data the energy dissipated at each cycle (which corresponds to the area of the hysteretic loop) was calculated. The calculated energy dissipation is given in Table 1. The results indicate quite good correspondence with the experimentally acquired data.

It should also be noted that although for the cyclic loading analyses yielded good results, the solution showed significant sensitivity on the input parameters (element type and size, load step sizes, material data). Non-convergent load-step solutions frequently occurred leading to premature failure of the model. To obtain good and stable solution the model needed to be calibrated by performing several parametric analyses which would yield the most appropriate set of input parameters. As the final results show, once stable solution is reached, the simulation shows satisfactory correspondence to the test results.

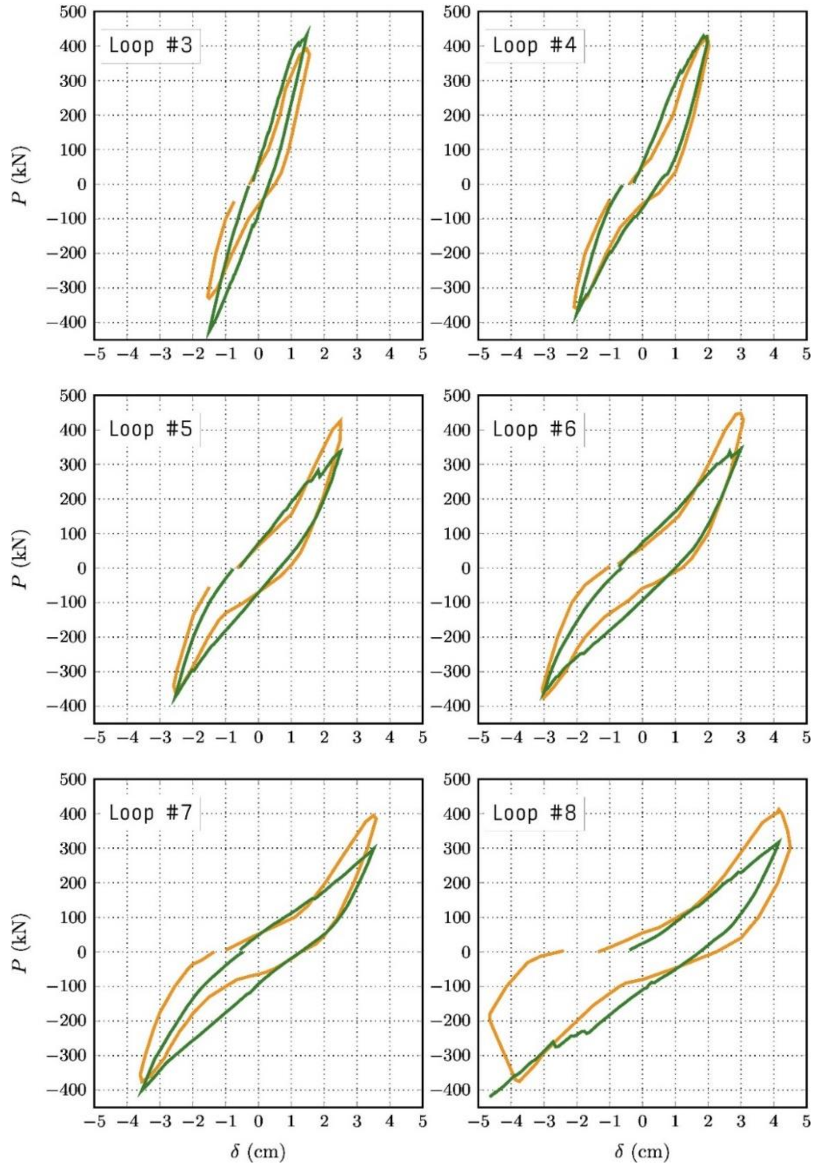

Figure 4 Load-Deflection Curves for Test Wall 2- cycles #3 to #8, Orange Line – Experimental Results, Green Line – Numerical Results

Table 1 Comparison of Energy Dissipation per Cycle (in Nm)

Loop #	Experimental	FEM	Ratio	Difference
3	3880.50	3477.32	0.90	10%
4	5327.65	5194.67	0.98	2%
5	6527.80	6000.68	0.92	8%
6	8649.65	7623.38	0.88	12%
7	8718.05	7681.69	0.88	12%
8	17520.80	7279.18	0.42	58%

4. DISCUSSION AND CONCLUSION

The results shown in Table 1 indicate that the numerical model underestimates the energy dissipation for about 8.8% on average (excluding the erroneous result of the loop #8 where the numerical analysis did not reach convergence before completing the full cycle) compared to the experimental results. Considering the highly inelastic nature of the simulated processes, this can be considered as a good result. The model also predicts the ultimate forces and displacement as well as stiffness degradation in each cycle quite favourably (Figure 4). However, it must also be pointed out that during the extensive testing of the proposed model, some drawbacks could be identified. Mostly that the model showed significant sensitivity to the values of the input parameters, while the simulation times were very high. This issues must be addressed before the model can be applied and used in real world applications. Regardless of that, the presented results seem to indicate that the adopted approach in simulation of RC strengthened with FRP is promising and could lead to simpler and faster modelling which can facilitate the design and research activities in this area. The results from the performed analysis show that the presented material model can successfully simulate the behaviour of cyclically loaded RC wall strengthened with FRP.

REFERENCES

[1] Vitanov V.: Numerical Model of FRP Strengthened Reinforced Concrete, PhD Thesis, Skopje, Macedonia, (2012)
[2] Darwin D., Pecknold D: Inelastic Model for Cyclic Biaxial Loading of Reinforced Concrete, Technical report, University of Illinois at Urbana-Champaign, Illinois, USA, (1974)
[3] Saenz L.P: Discussion of ``Equation for the Stress-Strain Curve of Concrete'', by Desayi and Krishman, ACI Journal 61.9, (1964) 1229—1235
[4] Kupfer H.B., Gerstle K.H: Behavior of Concrete under Biaxial Stresses, Journal of the Engineering Mechanics Division, (1973), 852--866.
[5] Kupfer H., Hilsdorf H. K., Rusch, H.: Behavior of concrete under biaxial stresses, Journal Proceedings, (1969), 656-666.
[6] ANSYS Inc.: ANSYS Multiphysics, Manual, Canonsburg USA, (2004)
[7] Lombard J.: Seismic strengthening and Repair of Reinforced Concrete Shear Walls Using Externally Bonded Carbon Fibre Tow Sheets, Master Thesis, Ontario, Canada, (1999)

TOPIC 7.

Social, economic and health aspects of the built environment

Društveni, gospodarski i zdravstveni aspekti izgrađenoga okoliša

POTENTIALS FOR SUSTAINABLE CEMENT AND CONCRETE TECHNOLOGIES – COMPARISON BETWEEN AFRICA AND EUROPE

Wolfram Schmidt[1]

[1] BAM Federal Institute for Materials Research and Testing, Department Safety of Structures, Unter den Eichen-87, 12205 Berlin, Germany, email: wolfram.schmidt@bam.de

SUMMARY: The fundamental knowledge about cement and concrete has made enormous progress over the last decades, and today it would be possible to find optimised sustainable concrete solutions tailored for every given boundary framework and raw material supply. However, this knowledge barely finds implementation into practice despite the urgent global need to minimise carbon emissions and energy consumption. A major reason is that most concrete developments were historically made in the northern hemisphere, where today over-regulations and stagnating market perspectives slow down innovation drive towards higher sustainability. In most African countries, however, sustainable building is simply an urgent real-life problem. The demand for building is enormous, standard solutions are not an option, and the pool of innovative local raw materials and concrete concepts is enormous. The paper provides a comprehensive comparison between the boundary frameworks of Europe and Africa, and it is explained why local African solutions shall be given priority over imported solutions. Examples of local African concrete solutions are given, and ideas for a rapid implementation are developed. Most of the potentially useful materials such as agricultural ashes, natural and calcined pozzolans, polysaccharides, etc. have not yet been subject to intensive research to date. Therefore, it is not unlikely to assume that with an open mind for non-standard solutions, combined with creativity and particularly knowledge and awareness, the next generation of innovative and sustainable concretes will be developed and applied on the African continent. Therefore, the conclusion is that particularly the African continent provides the best starting position to develop better and more sustainable concrete solutions than anywhere else in the world. Hence, Africa can become a global pioneer in green cement and concrete technology with impact to the entire world.

POTENCIJALI TEHNOLOGIJA ODRŽIVOG CEMENTA I BETONA – USPOREDBA AFRIKE I EUROPE

SAŽETAK: Posljednih desetljeća načinjen je golem napredak u temeljnim znanjima o cementu i betonu. Danas bi bilo moguće naći rješenja za optimalni održivi beton primjeren svakom danom okviru i dobavi sirovina. Međutim, takvo znanje jedva da se primjenjuje u praksi unatoč hitnoj globalnoj potrebi smanjenja na najmanju mjeru emisija ugljika i potrošnje energije. Glavni je razlog što je većina razvoja u području betona tijekom povijesti načinjena u sjevernoj hemisferi gdje danas preregulacija i perspektiva stagnirajućeg tržišta usporavaju inovacije ka većoj održivosti. Međutim, u većini afričkih zemalja održiva gradnja jednostavno je hitni problem svakodnevice. Zahtjevi za gradnjom su golemi, obična rješenja nisu opcija, rezerve inovativnih lokalnih sirovina i mogućnosti primjene betona su golemi. U radu se daje sveobuhvatna usporedba graničnih okosnica Europe i Afrike, a objašnjeno je zašto se lokalnim afričkim rješenjima mora dati prioritet pred uvezenim rješenjima. Većina potencijalno korisnih materijala kao što su pepeli iz poljoprivrede, prirodni i kalcinirani pucolani, polisaharidi itd. do danas nisu bili predmetom intenzivnih istraživanja. Stoga nije nevjerojatno pretpostaviti da će se nova generacija inovativnih i održivih betona razviti i primijeniti na afričkom kontinentu uz otvorenost prema nestandardnim rješenjima i u kombinaciji s kreativnošću i posebno znanjem i sviješću. Stoga je zaključeno da naročito afrički kontinent osigurava najbolju početnu poziciju za razvoj boljih i održivijih betona nego bilo gdje u svijetu. Prema tome Afrika može postati svjetski pionir u tehnologiji zelenoga cementa i betona s utjecajem na cijeli svijet.

1. INTRODUCTION

The perception of concrete in the public is often negative, since concrete is falsely considered as sufficiently understood today compared to allegedly newer materials. It is typically overlooked that the last two decades brought dramatic changes to the technology. The binders of today are no more the same binders as used before, and concrete mixture compositions of today diverge quite significantly from compositions in the past. In the broadly found opinion that concrete is old-fashioned and ugly, it is ignored that architectural sins are not inherent to the material. Actually concrete is extremely versatile and CO2-friendly compared to all other construction materials available [1]. In addition, it is the only reasonable solution for mass application due to its raw material sources and accessibility [2]. It will therefore be an illusion that completely new solutions will come up and develop regions and infrastructures in less developed areas in the world.

For betterment in Africa, the infrastructural development should have highest priority, since poor connections between settlements are responsible for enormous price increases [3], and urban traffic congestion is responsible for an incredible loss of productivity. Besides infrastructure, housing should have the other priority to ensure adequate living conditions to the populace. Most African countries go through a change process recently. In order to strengthen the positive perspectives, mobility and adequate urban living conditions are key to a prosperous future. This cannot be achieved without cement and concrete. Due to the high demand for construction, compared to many other regions in the world, cement and concrete technologies have a significantly higher relevance in Africa.

2. ENVIRONMENTAL IMPACT OF CEMENT AND CONCRETE

The decomposition of limestone during the production of cement clinker is responsible for about 60% of the carbon emissions of cement. Hence, the cement production process inherits by nature a high carbon emission, which cannot be improved by better technologies. Today, owed to the fact that it makes up about 50% of everything the world produces [4], cement production is responsible for about 5%-10% of the global anthropogenic CO2 [3]. Nevertheless, cement makes out only a part of concrete. Therefore, the embodied carbon of concrete is outstandingly low compared to other common construction materials [1, 5, 6]. However, despite the relatively low CO2 emission rate of the material itself, the global cement production is predicted to dramatically increase in the future so that in 2050 the cement production can be responsible for one third or more of the global CO2 emissions in case of business as usual [1, 7-9]. A variety of possibilities for the reduction of carbon emissions in cement and concrete production exist, many of which related to the cement processing technology. From a civil engineering point of view, the most efficient ways to minimise the carbon emissions are more efficient use of cement in concrete, maximum possible reduction of the clinker factor.

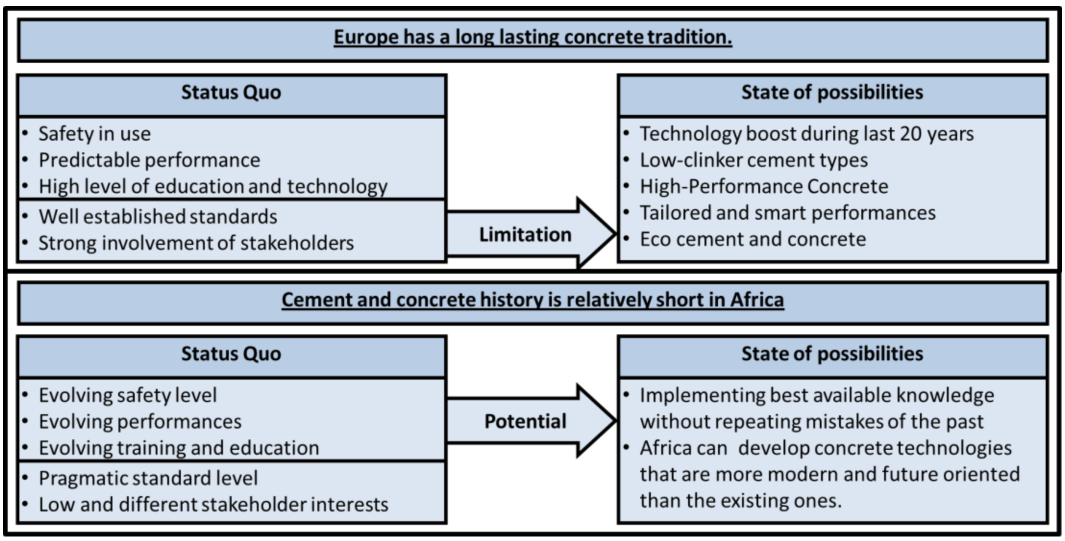

Figure 1 Comparison of innovation potentials between Europe and Africa

However, this automatically means, engineers will have to have much more awareness of how concrete's constituents interact with each other, and more knowledge is required about the performances, supply chains and potentials of raw materials. Furthermore, a significantly higher level of interdisciplinary cooperation is required between all involved parties, including cement and binder producers, admixture producers, concrete technologists, materials scientists, and architects. Also the society, industry, decision makers and politics have to identify the inevitability of sustainable concrete. Concrete has to be perceived as a global issue, and therefore general purpose solutions as in the past are dead end. Since concrete technology has been well established in most developed countries, the required change of mind-set from standard towards more sustainable is difficult to achieve. In developing countries and particularly in Africa cement and concrete have usually not been anchored in standards and regulations in the same way as they are in Europe. Therefore, the degrees of freedom and potentials to implement innovative and sustainable, knowledge based concrete approaches are enormous (Figure 1).

3. TRADITIONAL CONCRETE VS CONCRETE OF THE FUTURE

Ordinary Portland cement (OPC) has ever has been the standard binder for concrete. Today, this picture has changed all over the world. OPC is more and more reduced to the benefit of cement types blended with supplementary cementitious materials (SCMs) or inert materials. Alternative binder concepts with reduced or without need for limestone decomposition (e.g. geopolymers) are investigated and brought into practice. Since today's established SCMs are not available in the required amounts to meet the global cement demand, blended cements seem to be the most reasonable future solution. This is emphasised by the fact that SCMs typically enhance the performance giving opportunity for further reduction of the clinker factor. Hence, their use for a purely SCM based binder with performance equal to OPC seems to be waste of potential. However, eventually, the decision about the most sustainable binder concept depends upon a huge number of local boundary limitations as well as supply chains that need to be considered by concrete engineers in the future.

The higher level of complexity also holds true for the further components in concrete. The use of admixtures has dramatically changed the possibilities of engineers. Admixtures allow to tailor the flow properties as well as the medium and long term performance independent of the w/c [10, 11]. Admixtures are often petrol based but can also be based on natural sources, such as many polysaccharides [12, 13]. However, most admixtures show a complex interaction with the hydration of cement, causing that the admixtures have to be adjusted to the concrete, and in particular to the cement and filler components [14-16]. Also for aggregates, fibres, and admixtures, it is important to understand, that the use of non-traditional constituents with possibly less familiar performances, does not change the fact that eventually the result will be concrete. However, in order to convert the higher variety of constituents and performances into more sustainable concrete technologies, understanding of the raw materials as well as awareness about the potentials needs to be increased globally. Mostly, this will include locally adapted solutions.

4. POTENTIALS FOR ALTERNATIVE CEMENT AND CONCRETE TYPES IN AFRICA

A most promising approach to minimise OPC clinker in cement is using natural pozzolans or calcined clay [17-19]. However, while clay materials will assumedly have an enormous global impact, alternative solutions might have a high potential locally. Africa has a huge and growing agricultural sector [20], which creates a large number of by products that are not adequately used to date [3]. Therefore, a high potential for the reduction of the CO2-emissions in the binder lies in the replacement of cement by bio-based ashes. Due to its high amorphous silica content that can be achieved under good burning conditions, rice husk ashes (RHA) point out to be excellent cementitious materials that can outperform OPC [3, 13, 21-25]. Since for most cement types extra strength is not required, there is high potential for further replacement of OPC [4], and thus even small amounts of available RHA can have a significant potential for clinker reduction. Positive effects of pozzolanic agricultural ashes were also reported about bagasse [23, 26, 27], cassava peels [28], groundnut shells, locust beans, bamboo leafs [27].

Today, the use of polycarboxylate ether superplasticizers has become quite common in concrete technology due to their versatility [10, 29]. However, their uncomplicated and cost efficient availability is limited in most countries in Africa [13, 21]. However, alternatives are available, which can be found in many regions. Lignosulphonates are a by-product of the cellulose industry and they can be a reasonable choice to enhance the concrete properties [6, 13]. Furthermore, it was found that Acacia gum from the Karoo as well as Arabic gum from Sudan can have positive influence on set retardation as well as flow performance enhancement [6, 30, 31]. Hence, a number of alternatives to enhance the workability of concrete can be found, which do not need significant processing to become ready to use. Furthermore, a number of fibres can be used to enhance the ductility. For structural applications, typically steel fibres are used. Alternative fibres can be found again from bio-based sources such as sisal an coconut fibres [12]. Both fibre types have shown to change their performance to more brittle behaviour due to ageing. However, their deterioration can be reduced by immersion in silica fume slurry [32, 33]. Since this may not be the most cost efficient treatment, in the future, it might be interesting to observe whether a solution in RHA silica can have a similar effect.

5. CASE DISCUSSION: CASSAVA PLANT

The cassava plant is an excellent example how agricultural waste materials can be converted to valuable concrete constituents. Cassava – also known as manioc, yuca or tapioca - is a widely used edible plant all over Africa [12, 28, 34, 35]. The peels plus the attached starch, which make out 20-35% of the plant, are often dumped away with no further use [28]. Cassava peel ashes have pozzolanic properties [28, 34, 36]. However, before the peels are burnt there lies additional potential in the starch that is attached to the peels. The starch of cassava is very similar to the starch of potato. Starch can have various ways to modify the rheology, depending upon the modification [14, 15, 37-41]. Therefore, a most reasonable approach to make use of the entire plant would be to process the cassava for food processing as usual, but to obtain the waste starch at first that is attached to the peels for possible admixture productions, and to use the remaining peels for fuelling of processes and eventually to use the ashes as pozzolanic SCM to replace OPC clinker (see Figure 2).

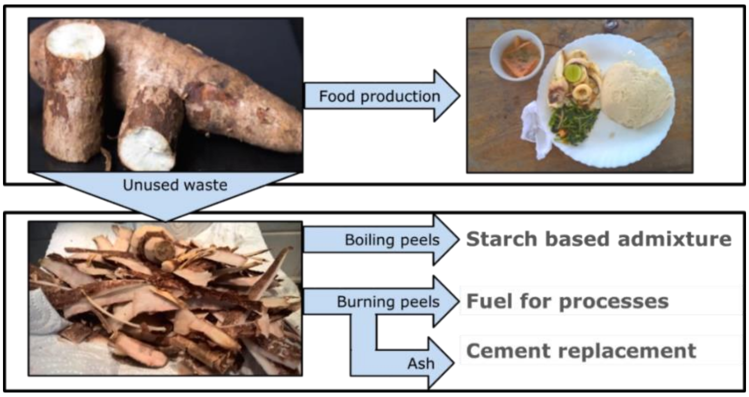

Figure 2 Optimum use of cassava wastes

6. LIMITED INNOVATION POSSIBILITIES IN EUROPE VS. GROWING POTENTIALS IN AFRICA

Differing from Europe, the boundary framework for innovative and sustainable cement and concrete technologies in Africa are highly promising:

While in other regions in the world, most relevant structures and infrastructures are already built, and building takes place rather within the built environment, in Africa the enormous need for new structures is a massive driving force for innovation.

In Europe the cement production is stagnating at approximately 250 Mt of cement. In this situation, a change towards radically new products would be an enormous risk for the producers. According to the International Energy Agency, in Africa and Middle East, the cement production is projected to increase from approximately 200 Mt to 600-800 Mt of cement. Newly built plants can directly operate at highest level of technology, and innovative products are a market advantage.

The European building regulations might have reached a level at which standards cannot cope with the velocity of new developments. In most African countries the regulative framework is less dense and more pragmatic than in most European countries. Despite the fact that a better established framework might still be required, this means that there are many degrees of freedom, which are a potential chance to adjust regulations and policies to the highest level of technology [42].

Due to the globally limited availability of ground granulated blast furnace slag (GGBS) and fly ash (FA), it is unavoidable to make use of all kinds of alternative materials. Due to the long tradition with FA and GGBS in Europe as well as the current price situation, the use of alternative materials is difficult to implement. In Africa, however, GGBS and FA do not occur at high volumes, and thus alternative binder solutions, e.g. based on natural pozzolans, calcined clays or agricultural by-products are mandatory to meet the demand.

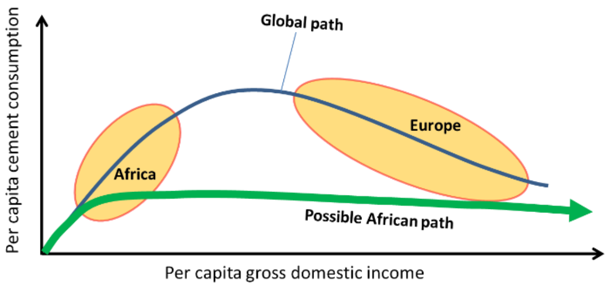

Figure 3 Qualitative correlation between per capita cement consumption based on the assumption that cement content and concrete quality are related as well as under consideration of modern concrete potentials

An increasing per-capita cement consumption has often been linked to increased economic power, while a slightly decreasing per capita cement consumption above a maximum is supposed to indicate a high level of technology again [43, 44]. Figure 3 indicates the regions on these curves, where most countries of Africa and Europe can be found. However, today there is no causality between cement consumption and good concrete technology anymore [45, 46]. Hence the correlation between economic growth and cement consumption does not hold true. The per-capita cement consumption in most African countries today is significantly lower than in most European countries

[47], which is an ideal starting point to develop more engineered concrete concepts that are performing good and durable without significantly increased cement content, as shown in Figure 3

7. CONCLUSIONS

In most African countries, sustainable building is simply an urgent real-life problem. The demand for building is enormous, standard solutions are not an option, and the pool of innovative local raw materials and concrete concepts is enormous. Most of the potentially useful materials have not yet been subject to intensive research. Therefore, it is not unlikely to assume that with an open mind for non-standard solutions, combined with creativity and particularly knowledge and awareness, the next generation of innovative and sustainable concretes will be developed and applied on the African continent.

The lesson learnt from the dramatic changes of concrete technology in the past decades, is that today general purpose solutions for concrete technology are no viable option for sustainable construction. New technology based on knowledge and interdisciplinary research has to be established. The framework of actions is limited in Europe due to a variety of parameters and implications summarised in Figure 4 These limitations do not exist in the same quality for Africa. Therefore, the potential for more sustainable concrete types is enormous. Experiences with more environmentally friendly technologies originating from Africa, can be adopted and adapted also in Europe, so that eventually they can be implemented in Europe as well.

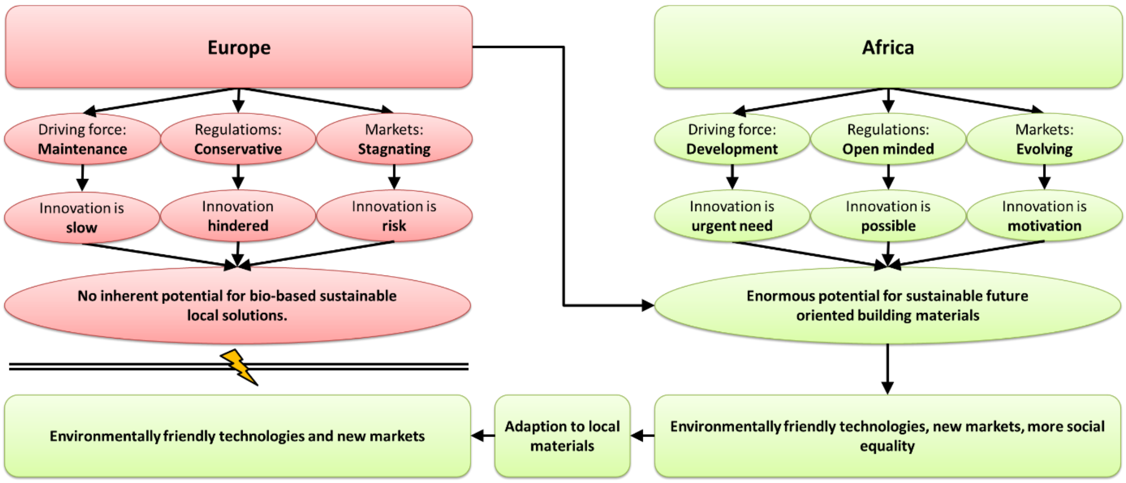

Figure 4 Comparison of possible innovation paths between Europe and Africa

REFERENCES

[1] K. Scrivener, V. M. John, and E. M. Gartner, "Eco-effcient cements: Potential, economically viable solutions for a low-CO2, cement-based materials industry," United Nations Environment Programme 2016.

[2] P. Wray and K. Scrivener, "Straight talk with Karen Scrivener on cements, CO2 and sustainable development," *American Ceramic Society Bulletin,* vol. 91, pp. 47-50, Jun-Jul 2012.

[3] N. Msinjili, W. Schmidt, A. Rogge, H.-C. Kühne, "Optimising available resources for production of good concrete properties," *Adv. in Cement and Concrete Technology in Africa*, Dar es Salaam, Tanzania, 2016, pp. 323-332.

[4] K. Scrivener, "Realistic options to meet the challenge of increasing concrete demand in Africa (Presentation)," pres. at the 2nd Intl. Conf. on Adv. in Cement and Concrete Technology in Africa, Dar es Salaam, Tanzania, 2016.

[5] L. Barcelo, J. Kline, G. Walenta, and E. Gartner, "Cement and carbon emissions," *Materials and Structures,* vol. 47, pp. 1055-1065, 2014.

[6] W. Schmidt, "Why Africa can spearhead innovative and sustainable cement and concrete technologies globally," in *KEYS Knowledge Exhcange for Young Scientists: Valorisation of Industrial By-products for Sustainable Cement and Concrete Construction*, N. S. Msinjili and W. Schmidt, Eds., ed Accra, Ghana: BAM, 2016, pp. 7-19.

[7] K. Carstensen and O. Rapf, "A blueprint for a climate friendly cement industry," WWF, Nürnberg, Germany2008.

[8] CEMBUREAU, "Cement & concrete: key facts & figures," t. E. c. association, Ed., ed, 2015.

[9] P. Edwards. (2016). *The Rise and Potential Peak of Cement Demand in the Urbanized World*. Available: http://cornerstonemag.net/the-rise-and-potential-peak-of-cement-demand-in-the-urbanized-world/

[10] W. Schmidt, M. Sonebi, H. J. H. Brouwers, H.-C. Kühne, and B. Meng, "Rheology modifying admixtures: The key to innovation in concrete technology - a general overview and implications for Africa," *Chemistry and Materials Research,* vol. 5, pp. 115-120, 2013.

[11] W. Schmidt, "Design Concepts for the Robustness Improvement of Self-Compacting Concrete - Effects of Admixtures and Mixture Components on the Rheology and Early Hydration at Varying Temperatures," PhD, Department of the Built Environment, Eindhoven University of Technology, Eindhoven, Netherlands, 2014.

[12] W. Schmidt, N. S. Msinjili, S. Pirskawetz, and H. C. Kühne, "Efficiency of high performance concrete types incorporating bio-materials like rice husk ashes, cassava starch, lignosulfonate, and sisal fibres," in *First International Conference on Bio-based Building Materials*, Clermont-Ferrand, France, 2015.

[13] W. Schmidt, N. S. Msinjili, H. C. Uzoegbo, and J. K. Makunza, "Admixture Concepts for the Sub-Saharan African Environment with Indigenous Raw Materials," in *SP-302 Eleventh International Conference on Superplasticizers and Other Chemical Admixtures in Concrete*, V. M. Malhotra, Ed., ed, 2015, pp. 491-505.

[14] J. Stroh, M. C. Schlegel, W. Schmidt, et al., "Time-resolved in situ investigation of Portland cement hydration influenced by chemical admixtures," *Construction and Building Materials,* vol. 106, pp. 18-26, Mar 1 2016.

[15] W. Schmidt, S. Peters, and H.-C. Kühne, "Effects of Particle Volume Fraction and Size on Polysaccharide Stabilizing Agents," in *SP-302 Eleventh International Conference on Superplasticizers and Other Chemical Admixtures in Concrete*, V. M. Malhotra, Ed., ed, 2015, pp. 39-52.

[16] F. Avet, R. Snellings, A. Alujas, M. Ben Haha, and K. Scrivener, "Investigation of the reactivity of various grades of kaolinitic calcined clays used as partial clinker substitute," in *Advances in Cement and Concrete Technology in Africa*, Dar es Salaam, Tanzania, 2016, pp. 137-142.

[17] L. M. Vizcaino-Andres, S. Sanchez-Berriel, S. Damas-Carrera, et al., "Industrial trial to produce a low clinker, low carbon cement," *Materiales De Construccion,* vol. 65, 2015.

[18] A. Alujas, R. Fernandez, R. Quintana, K. L. Scrivener, and F. Martirena, "Pozzolanic reactivity of low grade kaolinitic clays: Influence of calcination temperature and impact of calcination products on OPC hydration," *Applied Clay Science,* vol. 108, pp. 94-101, May 2015.

[19] A. Perry, *The Rift: A New Africa Breaks Free*: Little, Brown and Company 2015.

[20] W. Schmidt and N. S. Msinjili, "SCC: a solution to the challenges of concrete construction in Africa," *Concrete trends - Journal of the African cement and concrete industry,* pp. 16-20, 2014.

[21] J. L. Akasaki, A. R. B. Vasconcelos, J. Payá, D. R. O. Assi, M. V. Borrachero, M. M. Tashima, J. L. Melges, and C. F. Fioriti, "Durability Of High-Performance Concrete With Addition Of Rice Husk Ash And Rubber Tire," in *13th International Congress on the Chemistry of Cement*, Madrid, Spain, 2011.

[22] G. C. Cordeiro, R. D. Toledo Filho, and E. M. R. Fairbairn, "Influence of Rice Husk and Sugar Cane Bagasse Ultrafine Ashes on Hydration Characteristics of Cement Based Pastes," in *13th International Congress on the Chemistry of Cement*, Madrid, Spain, 2011.

[23] G. Rodríguez de Sensale, C. Romay, and F. Costa, "Waste Valorization From the Burning of Rice Husk," in *13th International Congress on the Chemistry of Cement*, Madrid, Spain, 2011.

[24] W. Wilson and A. Tagnit-Hamou, "Workability and Hydration of Superplasticized Cementitious Mixtures with Rice Husk Ash," *Aci Materials Journal,* vol. 111, pp. 491-500, Sep-Oct 2014.

[25] W. Schmidt, N. S. Msinjili, and H.-C. Kühne, "Rheological Optimisation for Flowable Mixture Compositions Specified for African Boundary Conditions," in *International Conference on Advances in Cement and Concrete Technology in Africa*, Johannesburg, South Africa, 2013, pp. 359-366.

[26] I. C. Mayowa, "Making Durable Concrete Through Inhibition of Chloride Ion Penetration by Pozzolanic Reaction," in *1st Symp. on Knowledge Exchange for Young Scientists (KEYS),* Dar es Salaam, Tanzania, 2015, pp. 145-150.

[27] K. A. Olonade, "Cassava Peel Ash: An Emerging Pozzolanic Material," in *1st Symposium on Knowledge Exchange for Young Scientists (KEYS) - Sub-Saharan African Standards for Cement and Concrete Research and Raw Materials, Quality Control and Maintenance of Cementitious Products*, Dar es Salaam, Tanzania, 2015, pp. 77-81.

[28] W. Schmidt, H. J. H. Brouwers, H. C. Kuehne, and B. Meng, "Influence of Env. Temperatures on the Performance of Polymeric Stabilising Agent in Fresh Cementitious Materials," *Polymers in Concrete,* vol. 466, pp. 97-104, 2011.

[29] R. Mbugua, R. Salim, and J. Ndambuki, "Effect of Gum Arabic karroo as a Water-Reducing Admixture in Concrete," *Materials,* vol. 9, Feb 2016.

[30] R. Mbugua, R. Salim, and J. Ndambuki, "Utilisation of Gum Acacia Karoo as Set-retarding Water-reducing Admixture in Cement Mortar and Concrete at Optimum Dosage," in *1st Symposium on Knowledge Exchange for Young Scientists (KEYS),* Dar es Salaam, Tanzania, 2015, pp. 97-101.

[31] R. D. Toledo, K. Ghavami, G. L. England, and K. Scrivener, "Development of vegetable fibre-mortar composites of improved durability," *Cement & Concrete Composites,* vol. 25, pp. 185-196, Feb 2003.
[32] R. D. Toledo, K. Scrivener, G. L. England, and K. Ghavami, "Durability of alkali-sensitive sisal and coconut fibres in cement mortar composites," *Cement & Concrete Composites,* vol. 22, pp. 127-143, Apr 2000.
[33] K. Olonade, A. M. Olajumoke, A. O. Omotosho, and F. A. Oyekunle, "Effects of sulphuric acid on the compressive strength of blended cement-cassava peel ash concrete," *Construction Materials and Structures,* pp. 764-771, 2014.
[34] A. A. Akindahunsi, H. C. Uzoegbo, S. E. Iyuke, and W. Schmidt, "Technological Advances in the Potential Uses of Cassava Starch in Concrete," in *The 6th International Conference of the Africa Materials Research Society*, Victoria Falls, Zimbabwe, 2011.
[35] K. A. Olonade, M. B. Jaji, and O. A. Adekitan, "Experimental Comparison of Selected Pozzolanic Materials," in *Advances in Cement and Concrete Technology in Africa*, Dar es Salaam, Tanzania, 2016, pp. 309-314.
[36] W. Schmidt, H. J. H. Brouwers, H. C. Kuhne, and B. Meng, "The Working Mechanism of Starch and Diutan Gum in Cementitious and Limestone Dispersions in Presence of Polycarboxylate Ether Superplasticizers," *Applied Rheology,* vol. 23, p. 12, 2013.
[37] A. A. Akindahunsi, W. Schmidt, H. C. Uzoegbo, and S. E. Iyuke, "The Influence of Starches on some Properties of Concrete," in *Intl. Conf. on Advances in Cement and Concrete Technology in Africa*, Johannesburg, South Africa, 2013, pp. 637-646.
[38] A. Izaguirre, J. Lanas, and J. I. Ã�lvarez, "Behaviour of a starch as a viscosity modifier for aerial lime-based mortars," *Carbohydrate Polymers,* vol. 80, pp. 222-228, 2010.
[39] H. Simonides and J. Terpstra, "Use of innovative starch ethers for paving blocks and other concrete products," *Concrete Plant + Precast Technology,* pp. 38-45, 2007.
[40] J. Terpstra, "Stabilizing self-levelling concrete with polysaccharide additive," in *SCC'2005-China: 1st International Symposium on Design, Performance and Use of Self-Consolidating Concrete*, 2005, pp. 207-213.
[41] W. Schmidt, A. Radlińska, C. Nmai, A. Buregyeya, W. L. Lai, and S. Kou, "Why does Africa need African concrete? An observation of concrete in Europe, America, and Asia – and conclusions for Africa," in *Intl. Conf. on Advances in Cement and Concrete Technology in Africa*, Johannesburg, South Africa, 2013, pp. 1139-1148.
[42] G. Nganga, M. Alexander, and H. Beushausen, "The Effect of a Reduction in Clinker Content on Concrete Properties," in *2nd Intl. Conf. on Adv. in Cement and Concrete. Technology in Africa*, Dar es Salaam, Tanzania, 2016, pp. 315-322.
[43] W. Schmidt, "Potentials for Savings in the Production of Self-Compacting and High Strength Concrete for Precast Concrete Elements," *Concrete Plant International,* pp. 76-79, 2016.
[44] W. Schmidt, N. N. M. Hirya, D. Bjegovic, H. C. Uzoegbo, and S. G. Kumaran, "Cement technology in sub-Saharan Africa—Practical and scientific experiences," *American Ceramic Society Bulletin* vol. 91, p. 82, 2012.

IMPLEMENTATION OF GOVERNMENT SUBSIDIZED LOW-COST HOUSING PROJECTS IN DOLOMITIC REGIONS OF SOUTH AFRICA

Michael Pavlakis[1], Antun Medic[2]

[1] Michael Pavlakis and Associates cc, 257 Barry Herzog Avenue, Emmerentia, 2195, Johannesburg, South Africa, email: mpavlaki@iafrica.com
[2] LTE Civil and Structural (Pty) Ltd, Belvedere Place, Building No.1,5 Eglin Road, Sunninghill, 2157, Johannesburg, South Africa, email: antun.medic@lteconsulting.com

SUMMARY: The objective of this paper is to share South African experience in implementing government subsidised low-cost housing projects in geologically unfavourable areas - more particularly sites underlain by weathered and karstified 2.5 billion year old dolomites, which are prone to sinkholes and subsidence and would otherwise be considered as unfavourable due to perceived high risks and costs. As a practical example, the Sethokga Housing Development near Johannesburg, which is underlain by dolomites, is discussed. By applying due diligence during investigation, design and implementation, including application of appropriate risk management strategies it is shown that sustainable development is possible in areas underlain by dolomites.

PRIMJENA NISKOBUDŽETNIH STAMBENIH PROJEKATA U DOLOMITSKIM PODRUČJIMA JUŽNE AFRIKE UZ DRŽAVNU POTPORU

SAŽETAK: U radu se prikazuje južnoafričko iskustvo u primjeni niskobudžetnih stambenih projekata uz državnu potporu u geološki nepovoljnim područjima. Više takvih lokacija leži na trošnim i kraškim dolomitnim podlogama starim 2,5 milijarde godina koje sadržavaju šupljine i slijeganja terena te se inače smatraju nepovoljnim jer mogu dovesti do velikih rizika i troškova. Kao praktičan primjer raspravljen je stambeni projekt Sethokga blizu Johanesburga koji se nalazi na dolomitnoj podlozi. Primjenom dubinske analize tijekom istraživanja, projektiranja i provedbe, uključujući primjenu odgovarajućih strategija upravljanja rizikom pokazano je da je u područjima lociranim na dolomitnim podlogama moguć održiv razvoj.

1. INTRODUCTION

1.1. SOUTH AFRICA – BRIEF SOCIAL OVERVIEW AND BACKLOG

South Africa is considered as the most advanced economy on the African continent. It is a leader and a competitive producer of raw commodity exports and high value-added goods and boasts a highly developed modern infrastructure. There has, however, been a large housing backlog, which increased greatly with the ever increasing influx of people into the urban areas. After South Africa's first democratic elections in 1994, the new government set a target of building 1 million houses for the lower income group by 1999. Parallel to formal (5%), informal houses in urban areas increased drastically since 1995 (142% between 1995 and 1999). In total, since 1994 until 2016, formal housing has grown by 50%, translating to 5.6 million formal houses.

1.2. HOUSING NEEDS

A total of 1.13 million houses were constructed over the period 1994-2000 at US$ 2 billion. About 1.32 million subsidies were awarded, enabling nearly five million people to have secure dwellings at the cost of US$ 3.7 billion. However, in 2001 still more than 7.3 million people lived in 1.6 million informal urban housing units. The numbers can be attributed to the continuous migration to urban areas in search of jobs.

For the period 2015-2019 the Government of Human Settlements stakeholders committed to deliver 1.5 million houses, such stakeholders being banks, mining companies, developers and large employers. Through this partnership some US$ 17.8 billion (i.e. 250 billion SA Rand) has been planned to be invested.

2. LEGISLATIVE PROCESSES

South Africa is technically well regulated. Compilation and practical implementation of building codes of practices, standards and regulations are administered by the South African Bureau of Standards (SABS). All engineering design must be executed or supervised by professionals, registered with their relevant registering councils and associations.

The National Home Builders Registration Council (NHBRC) prescribes procedures to be adhered to in both, design and implementation of the residential buildings. When a site is underlain by dolomitic formations, extensive dolomitic stability investigations have to be carried out in order to prove the suitability of the site for the proposed development. The results of these are peer reviewed by other state institutions. Only after the site has been declared suitable for development, can the normal geotechnical investigation for foundation design purposes be carried out.

3. DOLOMITE INVESTIGATIONS IN SOUTH AFRICA

3.1. PROBLEMS IN DOLOMITE LAND

Dolomites cover large parts of South Africa, especially the Gauteng Province. These were formed in a shallow epeiric sea some 2.3 – 2.5 billion years ago (Brink, 1985) and comprise calcium and magnesium carbonates. Apart from general weathering that has occurred over the extensive period since its formation, weak carbonic acid contained in the rainwater slowly dissolves preferentially the rock along fissures, fractures and other discontinuities to form random underground solution cavities and channels. These present serious challenges to the stability of buildings constructed over them.

Problems associated with dolomites include the formation of sinkholes and ground subsidence with associated total collapse or severe damage to structures constructed over and the possibility of loss of life and/or serious injury to occupants. Factors triggering instability are mostly anthropogenic and include the lowering of the ground water table and the ingress of water from leaking water bearing services or from areas with inadequate stormwater drainage, into the underlying unstable formations.

3.2. DOLOMITE STABILITY INVESTIGATIONS

Construction in dolomite land in South Africa is controlled by National Standard SANS 1936:2012. No development can occur unless extensive geotechnical/dolomitic stability investigations prove the land to be suitable for development for the intended purpose. Dolomitic stability investigations are generally expensive and a staged approach is normally adopted. Should the first investigation phase reveal highly incompetent conditions, the exploratory work is discontinued and development within the land is prohibited or restricted. Geophysical methods involving mostly gravimetric surveys, are employed to obtain a preliminary assessment of the underlying dolomites. These are carried out on a square grid covering the site. Rotary percussion borehole drilling is subsequently used to check gravity anomalies observed on the resulting Bouguer gravity map thus produced. The drilling results are used to construct a residual gravity map, such as the one shown in Figure 1, which assists in the evaluation of the stability of the site.

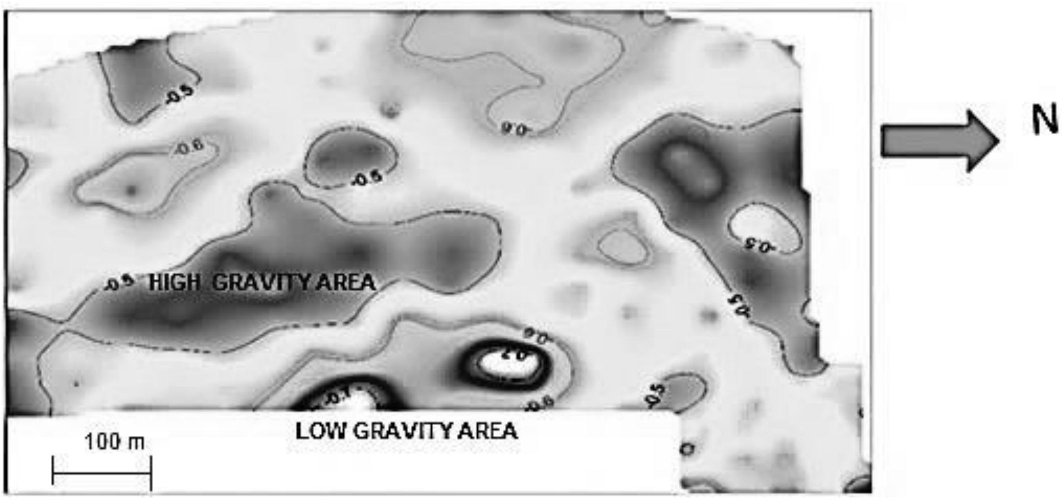

Figure 1 Residual Gravity Map – Sethokga Hostel Complex

On the basis of the results of these investigations the site is zoned into different risk classes, each associated with a different inherent hazard of sinkhole and subsidence occurring under two different scenarios, namely: that of continuous water ingress, as well as water table drawdown. Inherent hazard classes vary from IHC.1(best possible outcome), which implies a low risk of any size sinkhole or subsidence occurring under both conditions of continuous water ingress and water table drawdown through to IHC.8 (worst possible outcome), associated with a high risk of very large sinkholes (>15m diameter) occurring under the same conditions.

4. SETHOKGA HOUSING DEVELOPMENT - PHASE 1A

4.1. PROJECT HISTORY AND BRIEF

Influx of workers into urban areas resulted in necessity for accommodation of such workforce in communal developments, so called hostels, which were predominantly funded by businesses and strategically positioned close to the work place and/or urban edges. This type of accommodation provided single living units (dormitories).

One such hostel is Sethokga, built in the township of Tembisa at north-eastern outskirts of Johannesburg, which now belongs to the City of Ekurhuleni Metropolitan Municipality which is underlain by dolomites. Due to the deteriorated state of the buildings, and risks associated with dolomites, the decision was made to demolish them and proceed with the design and construction of new buildings incorporating mostly family units. The buildings needed to be suited to dolomitic conditions with implementation of all necessary mitigation measures to make them safe and habitable.

Sethokga hostel originally consisted of 29 building blocks, each incorporating 3 mostly double storey "U" shaped load bearing brick structures, built on 22 ha of land during the early 1970s. The new design for Phase 1A of the project consists of 19 mostly three storey loadbearing brickwork buildings, accommodating a mixture of single and family units. The project is being implemented through three phases.

4.2. GEOTECHNICAL INVESTIGATION

Following the evaluation of the Bouguer gravity anomaly map the Phase 1A site, covering approximately 15% of the total Sethokga site, was investigated by some 35 rotary percussion boreholes, drilled in various stages, to depths ranging within the 30-50 m. Large (800 mm) diameter auger holes were also drilled to depths up to 16m.These were profiled and sampled *in-situ* mainly for the purpose of recovering undisturbed block samples of soft and firm/medium dense dolomite residuum (wad), which is interbedded with more competent chert, for laboratory testing. A typical geological section through the site is shown in Figure 2(a).

Within this section of the site, the dolomite bedrock was found to be present at the depth range of mostly 30-40m. In certain areas the bedrock comprised very hard rock syenite. The overlying soils comprise a variable transported sandy horizon, hillwash, which is potentially collapsible, followed by more competent residual chert and by dolomite residuum (wad). The wad is, in this case, underlain by a sheet of weathered syenite, which has intruded into the dolomitic horizons and extends close to the dolomite bedrock. Additional wad was encountered in places between the underside of the syenite and the dolomite rockhead. The ground water table varies mostly within the 15-25m depth range. Laboratory oedometer compression tests indicated that the dolomite residuum is a brown clayey/sandy silt to silty clay, of generally very low to low dry density, which varies from 535 – 1400 kg/m^3 , and of high compressibility. These also indicate that it behaves as a normally consolidated or slightly overconsolidated soil with virgin compression index values varying from 0.5 -3.0, with initial void ratios of 1.5-4.1. A compression curve for the soft section of wad is shown in Figure 2(b).

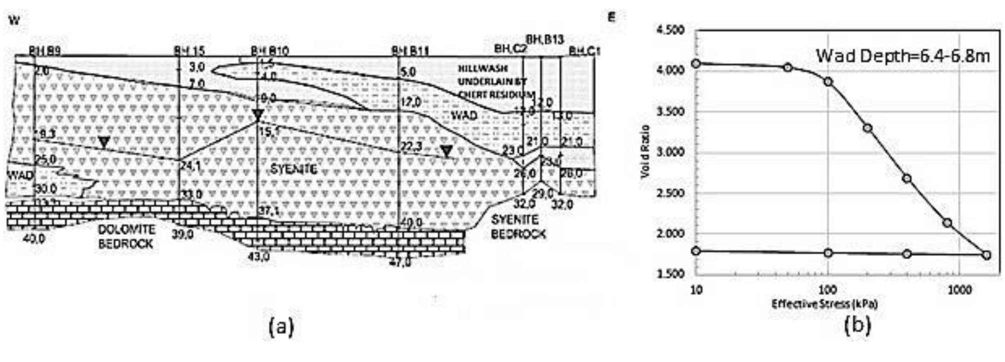

Figure 2 (a) Idealised Geological Section (b) Oedometer compression test results for wad.

Due to mostly the stabilising influence of the thick stable syenite sill the site was classified to be associated with an inherent hazard class IHC.2, which implies a medium risk of a small sinkhole (less than 2 m diameter) or subsidence occuring under both conditions of continous water ingress and water table drawdown. Within certain areas, however, the syenite was thin or absent and was underlain by thick dolomite and chert residuum, associated with total air loss and sample loss over a significant depth range, indicating the presence of small deseminated voids. Such areas were assigned an inherent hazard class of IHC.4 indicating a medium hazard of large sinkhole (5-15 m diameter) or subsidence occurring. Furthermore, within this area, certain sections contained some 2-4 m thick zones where the drilling hammer met virtually no resistance, which were interpreted as cavities. These were proposed to be stabilised by grouting in order to justify the above-mentioned hazard classification.

4.3. EVALUATION AND FOUNDATION TREATMENT

4.3.1. DOLOMITE DESIGNATION OF THE SITE

Some of the site classified as IHC.2 which belongs to the D2 dolomitic designation category. A D2 designation indicates that no special precautions are necessary, other than ensuring adequate stormwater drainage and general monitoring of the site for possible distress. Most of the site, however, was assigned a D3 status indicating that its development is permitted only on condition that: (a) stringent precautions are taken to prevent leakage of stormwater and of water bearing services into the dolomitic formations and in the design of the foundations and (b) a risk management strategy is prepared and implemented for the life of the development. Precautions include the use of high density polyethylene pipes and manholes for the construction of all water bearing servicess.

4.3.2. FOUNDATION DESIGN

Foundation design needed to take into account the presence of the near-surface collapsibe sandy soils, which extended down to the depths of up to 2,5 m in places, the presence of the thick dolomite residuum at depth, which is mostly of high compressibility and relatively low shear strength, and the fact that the site was situated mostly in a D3 dolomitic terrain. Stiffened concrete raft foundations were employed to support the 3-4 storey buildings. These were constructed at elevations, just above natural ground level after the foundation treatments referred to in Sections 4.3.3 and 4.3.4 were carried out.The rafts had to be designed to be of adequate stiffness to limit differential settlements to acceptable levels and to possess sufficient structural capacity to be stable enough to allow evacuation of people in the event of a 5 m diameter sinkhole occurring anywhere under or adjacent to the buildings. Account also had to be taken of the non uniform subsoil conditions with the thickness of the problem soils varying widely. The building rafts were required to be designed for total and differential settlements of 30-40 mm and 10-20 mm, respectively.

4.3.3. ENGINEERED EARTH MATTRESS

A 2,0-2,5 m thick earth mattress was constructed under each building by excavating the *in-situ* soils, mixing them with fine sandy gravel, when necessary, and compacting in thin layers to form a stiff soil mattress. This solved the problem of the near surface potentially collapsible soils which, if left untreated, would tend to undergo large total and differential settlements on saturation. The mattress also served to reduce differential settlements from the deep compressible layers, and to provide a uniform relatively impermeable barrier under the building.

4.3.4. REINFORCED EARTH MATTRESS

In areas where the compressible dolomite residuum was very thick,the above-mentioned soil mattress was reinforced with a geogrid placed at 300 mm depth intervals. Its primary purpose was to even out settlements and reduce further potential differential settlements of the buildings.

4.3.5. CAVITY GROUTING

Within certain areas it was evident that the weathered dolimite contained small interconnected voids and, occasionaly, 2-4 m thick suspected cavities (associated with no resistance to penetration of the drill bit) which increased significantly the risk of sinkhole or subsidence occurring. In order to reduce such a risk, a cavity grouting programme was implemented. This comprised grouting under the footprint of each building a series of boreholes placed on a 5 m square grid, using a specially designed grout mixture. Grout takes were generally very small, but occasionally up to 3-5 m^3 of grout was accepted within some boreholes.

4.4. RISK MANAGEMENT STRATEGY

A detailed risk management strategey is required to be prepared and implemented and applied stictly over the life of the development. Such a plan includes the periodical inspection of the buildings and services for distress, testing of water bearing services at set time intervals, depending on the nature of the development and dolomitic conditions at depth, and monitoring ground water levels.

Figure 3 Typical new three-storey buildings at Sethokga

5. STRUCTURAL DESIGN MODELLING

5.1. STRUCTURAL SYSTEM - SUPERSTRUCTURE

The structures consist of loadbearing 215mm thick brickwork, prefabricated reinforced concrete hollow blocks slabs (ECHO system) of 170 and 255mm thickness, without structural topping but with levelling screed 50mm thick. The roofs are made of light steel frame systems. Movement joints have been provided on buildings at distances not exceeding 30m.

5.2. FOUNDATIONS – STIFFENED RAFT

After completion of geotechnical investigation stiffened RC raft was adopted as the founding system, placed on engineered mattresses as elaborated in the previous sections. Figure 4 shows layout of one of the rafts analysed.

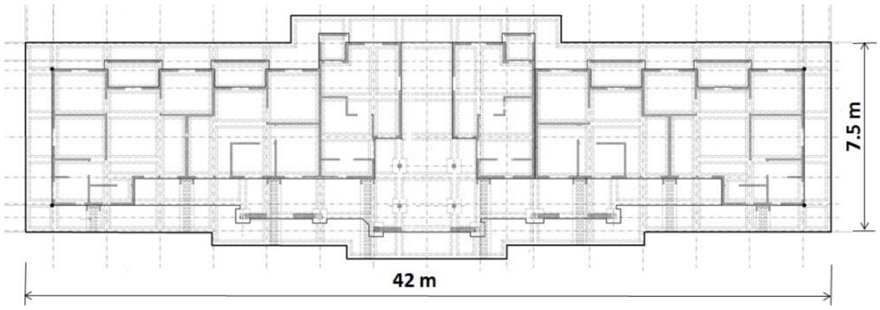

Figure 4 Typical concrete raft – plan layout

5.2.1. DESIGN ANALYSIS AND LOAD COMBINATIONS

The raft, consisting of ground beams (ribs) and slab panels in between, was analysed on prescribed combination of loading actions for both: ultimate limit state (ULS) and serviceability limit state (SLS).The raft presented in this paper has plan dimensions of 7.5x42m, with permanent (building self-weight) loading and imposed (1.5 KN/m² per floor and 0.35KN/m² on roof) loading transferred onto it. The slab was initially determined to be 175mm thick with ground beams 250x475mm deep, spaced at max 6m centre to centre (all 30MPa concrete). Following completion of geotechnical investigation and determination of site class, expected range of total and differential settlements were specified in the report. The second model was then ran as slab and beam system on elastic supports, where *spring stiffness* "ks*i*" were calculated based on modulus of subgrade reaction ranging between 1MPa/m to 3MPa/m.

Spring stiffness values were calculated using equation: **ks*i* = msr x A*i*,** where ks*i* is spring stiffness at node ***i*,** msr is *modulus of subgrade reaction* and A*i* is the *influence area* at node *i.* The analysis was carried out using ***Staad pro v8i*** computer software, adopting msr as 1MPa/m and 3MPa/m in two separate models and assuming full uniformity of strata below the entire footprint of the raft. A third model was adopted with assumption of non-uniform conditions, with msr varying between two different halves of the raft's footprint. Confirmation of the site class and data obtained from the geotechnical investigation indicated that preliminary designed raft (carried out using rigid method) would not be capable of accommodating additional stresses and deflections induced by differential settlements, thus necessitating the raft to be stiffer. The slab thickness was increased to 200mm and ground beams to 500mm deep (internal beams) and 600mm deep (edge beams), with spacing of beams reduced to 3m centre to centre. The results of the analyses showed that, with the final raft geometry, total and differential raft settlements would be limited to 40mm and 23mm respectively. The latter is associated with a deflection ratio of 1:1820, which is deemed acceptable to the load bearing brick structure

5.2.2. DESIGN ANALYSIS PERTAINING TO 5M DIAMETER SINKHOLE FORMATION.

Because of the hazard class that the site is associated it was necessary to design each concrete raft supporting the buildings in such a manner as to be capable of spanning a 5m diameter sinkhole that could occur anywhere under or next to them. Under these conditions the raft had to be provided with enough structural capacity and integrity to allow safe evacuation of residents.

A fourth model was then analysed for loss of supports, where two cases were taken into account: Case 1 assumed sinkhole formation completely encompassed within the footprint of the building, and Case 2 assumed sinkhole formation at any corner of the building. Case 1 basically means that the slab and beams will have to be capable of acting as suspended structural elements, with field tension being in the bottom zone, while Case 2 means that corner sections of the raft would be cantilevering over the sinkhole, thus tensile zone being at the top. Slab corner condition was modelled using yield line theory, while the beams were designed as suspended over the sinkhole, as well as cantilevering over it at the building's corners. This analysis indicated that the raft had to be provided with additional reinforcement with increase of slab and beams dimensions as stated above.

6. CONCLUSIONS

Highly weathered karstified ancient 2.3-2.5 billion year old dolomite formations cover a large part of South Africa and present serious challenges to the stability of buildings and other developments constructed in areas underlain by them. South African national standard SANS 1936:2012 provides methods assisting to the assessment of the stability of each dolomitic site. Geotechnical/dolomitic stability investigations within such sites assist in ensuring that only the sites where the sinkhole and subsidence hazards are tolerable to society are utilised for development. Such risks are further ameliorated by implementing stringent precautions in the design and construction of the buildings and associated infrastructure. High risk sites whereby the sinkhole/subsidence hazard cannot be reduced to acceptable levels, are rejected.

The Sethokga hostel redevelopment project has been briefly described and some of the results of geotechnical/dolomitic stability investigations and structural solutions, presented. Various methods of foundation treatment were used, including the use of stiffened concrete raff foundations, earth mattresses, reinforced earth mattresses and cavity filling. Sustainable developments are, therefore, possible on challenging dolomitic sites, as long as due diligence is followed in the investigation and selection of areas associated with acceptable risk, and in the subsequent design and implementation - with relatively small additional cost to what would otherwise be the case in areas with more favourable geological conditions. Some 3 years after construction, all buildings are performing well and there is no evidence of any significant differential settlement taking place. The risk management plan will still be implemented in perpetuity to ameliorate the ever present hazard of sinkhole and or subsidence occurring.

ACKNOWLEDGMENTS

The authors express sincere thanks to the Gauteng Department of Human Settlements, the City of Ekurhuleni Metropolitan Municipality for permission to publish this paper and the Managements of LTE Holdings and Michael Pavlakis and Associates cc.

REFERENCES

[1] Brink, A B A., Engineering Geology of Southern Africa, Volume 1, Building Publications, (1985)
[2] SANS 1936:2012, Development of Dolomite Land Part 1 to 4, (2012)
[3] Joint Structural Division of the South African Institution of Civil Engineers and the Institution of Structural Engineers: Code of Practice for Foundations and Superstructures for Single Storey residential Buildings of Masonry Construction, ISBN 0-620-19317-4 (1995)
[4] South African Government website: www.gov.za

SUSTAINABLE BUILDING: SCIENCE OR FASHION?

Kajo Feric[1]

[1] CEMEX Hrvatska d.d., F. Tuđmana 45, 21212 Kastel Sucurac, Croatia, email: kferic@gradst.hr

SUMMARY: This paper analysis how much sustainable building relays on science and how much science principles, methods, researches and it's results influence on development of sustainable building. Short analysis in this paper indicates whether or not science is already presented in the area of sustainable building and, if yes, how much science defines the term "Sustainable Building" by itself. Mentioned analysis is based on searching three globally reputable scientific papers databases by different predetermined phrases and in compliance with the given searching parameters. Author also analyzed the very nature of science discipline Sustainable building as it should be and opens discussion on how should scientists focus their scientific efforts to better connect science with practical applications in the area of sustainable building today and in the future. This paper offers motivation for all who wants to do scientific researches in the field of Sustainable building.

ODRŽIVA GRADNJA: ZNANOST ILI MODA?

SAŽETAK: U ovom radu analizira se u kojoj mjeri je održiva gradnja oslonjena na znanost i u kolikoj mjeri znanstveni principi, metode, istraživanja i njihovi rezultati utječu na razvoj održive gradnje. U radu se kratkom analizom nastoji utvrditi koliko je znanost već prisutna u području održive gradnje odnosno u kojoj mjeri sama znanost određuje pojam „održiva gradnja". S druge strane želi se utvrditi u kojoj mjeri se one aktivnosti sudionika u gradnji koje se tiču održive gradnje temelje na nalazima znanosti odnosno na rezultatima znanstvenoistraživačkog rada. Navedena analiza temelji se na provedenom pretraživanju nekoliko globalno poznatih baza podataka znanstvenih radova uz unaprijed zadane fraze i parametre pretraživanja. Autor ovim radom nudi motivaciju svima koji se na bilo koji način žele baviti znanstvenim pristupom održivoj gradnji. Pri tome također otvara diskusiju o tome na koji se način znanstveni pristup održivoj gradnji može još bolje povezati s praktičnom primjenom principa održive gradnje danas i u budućnosti.

1. UVOD

Pojam „održivi razvoj" je ušao u širu primjenu nakon izdavanja i razmatranja tzv. Bruntlandovog izvještaja [1] (WCED, 1987) na 42. zasjedanju Opće Skupštine Ujedinjenih Naroda 1987. godine. Izvještaj postavlja definiciju održivog razvoja kao razvoja koji će osigurati da današnje generacije zadovolje svoje potrebe ne ugrožavajući pri tome sposobnost budućih generacija da zadovolje svoje potrebe. Nakon toga se početkom 90-ih godina 20. stoljeća koncept održivog razvoja ozbiljno razmatra u većini znanstvenih i industrijskih grana [2] (Zeinal Hamedani, Huber, 2012.). Ta razmatranja su dovela i još dovode do razvoja postojećih i nastanka brojnih novih tehnologija čiji se razvoj temelji upravo na težnji da se njima zadovolje zahtjevi održivog razvoja. Danas gotovo da i nema privredne grane koja nema svoj ogranak kojem je pridodan predznak održivosti. Neki primjeri su održivi transport, održiva ekonomija, održivi turizam, održiva poljoprivreda, održiva energija, održiva proizvodnja hrane, održiva nabava, itd. Svim primjerima je zajedničko da označavaju onaj dio osnovne privredne grane ili tehnologije koji se može izdvojiti i koji se teži uskladiti s konceptom održivog razvoja. Slično kao u drugim privrednim granama, u građevinarstvu, ali i arhitekturi je uspostavljen pojam održive gradnje ili zelene gradnje. Na engleskom jeziku se izraz „green building" počeo koristiti u posljednjem desetljeću prošlog stoljeća. Prva sustavna nastojanja na usklađivanju procesa projektiranja, izgradnje i uporabe građevina s principima održivog razvoja se mogu pripisati sustavima certifikacije „zelene gradnje". Prvi je takav sustav predstavljen od strane BREEAM 1990. godine u Velikoj Britaniji [3], a drugi 1998. godine LEED sustav osmišljen od strane USGBC [4] u SAD-u. Nakon toga su razvijeni brojni sustavi certificiranja u drugim zemljama kao što su primjerice Australija, Japan, Francuska, Njemačka, Singapur, Španjolska, itd. U zemljama u kojima nije došlo do razvoja novih sustava certificiranja održive gradnje svoju primjenu nalaze ranije razvijeni sustavi iz drugih zemalja. Tako je primjerice BREEAM sustav do 2014. godine primijenjen u najmanje 34 različite zemlje (The Digest of BREEAM Assessment Statistics Volume 01, 2014).

2. UČESTALOST OPĆE UPOTREBE IZRAZA VEZANIH UZ ODRŽIVU GRADNJU

Pojam „održiva gradnja" (eng. „Sustainable Building") se danas svakodnevno koristi unutar stručne zajednice ali i šire. Također se pored pojma „održiva gradnja" još češće koristi sličan pojam „zelena gradnja" (eng. Green Building), a sličan pojam predstavljaju i izrazi „održiva izgradnja" ili „održivo građenje" (eng. „Sustainable Construction"). U tablici 1 su prikazani rezultati pretraživanja ovih pojmova (fraza) na hrvatskom i engleskom jeziku upotrebom internetskog pretraživača Google (datum pretrage: 12.12.2016.). Iako se navedeni izrazi razlikuju, može se reći da svi pripadaju jednoj zajedničkoj privrednoj grani koja se bavi svim procesima vezanim uz izgrađeni ljudski okoliš (planiranjem, projektiranjem, izgradnjom, opremanjem, upravljanjem, itd.) na način da se što je više moguće usklade s principima održivog razvoja. Ovi izrazi su međusobno različiti zbog različitog pristupa problematici, a s druge strane njihovo značenje i smisao se u velikoj mjeri preklapaju. U ovom radu se koristi izraz održiva gradnja kao jedinstveni izraz na hrvatskom jeziku koji objedinjuje sve navedene izraze, a koji se može smatrati sveobuhvatnim i najopćenitijim. Izuzetak su oni dijelovi rada u kojima se istražuje učestalost i zastupljenost baš određenog izraza odnosno fraze, pa tako i fraze „održiva gradnja“. Kada se u radu bilo koji izraz promatra kao fraza on je u navodnicima.

Tablica 1 Rezultati pretraživanja fraza pomoću Google pretraživača na dan 12.12.2016

Pretraživana fraza	Domena pretraživača	Broj rezultata pretrage
„održiva gradnja“	www.google.hr	63,200
„održivo građenje“	www.google.hr	1,310
„održiva izgradnja“	www.google.hr	1,130
„zelena gradnja“	www.google.hr	58,700
„sustainable building“	www.google.com	577,000
„sustainable construction“	www.google.com	560,000
„green building“	www.google.com	16,100,000

Nedvojbeno je dakle da su ove fraze široko rasprostranjene među dokumentima koji se objavljuju na internetu. Ova analiza se može produbiti filtriranjem pretrage prema datumu ažuriranja (prema nekim izvorima datum zadnjeg indeksiranja) mrežnih stranica na internetu. Rezultati filtriranog pretraživanja pomoću pretraživačkog servisa Google prema različitim godinama (2000.; 2005.; 2010. i 2015.) su prikazani u tablici 2. Na temelju rezultata se može utvrditi kako se mrežne stranice na kojima se spominju pretraživane fraze redovito ažuriraju, a pri tome i ukupni broj takvih mrežnih stranica stalno raste. Tako broj ažuriranih mrežnih stranica na kojima se spominju tražene fraze raste za približno 3.5 do 9 puta svakih 5 godina počevši od 2000. godine. Vidljiv je, također vrlo veliki skok (više od 50 puta) pojavljivanja fraze na hrvatskom jeziku „zelena gradnja“ u razdoblju od 2010. do 2015. godine.

Tablica 2 Rezultati filtriranog pretraživanja fraza pomoću Google pretraživača po godinama za po dvije najučestalije fraze na hrvatskom i engleskom jeziku

Pretraživana fraza	Broj ažuriranih mrežnih stranica u danoj godini koje sadržavaju pretraživanu frazu			
	2000.	2005.	2010.	2015.
„održiva gradnja“	0	11	38	311
„zelena gradnja“	2	12	63	3,400
„sustainable building“	416	3,790	24,500	106,000
„green building“	4,420	26,400	159,000	984,000

Iz navedenog se može zaključiti da na Hrvatskoj razini i na svjetskoj razini postoje interesne skupine koje se svakodnevno bave i promišljaju o održivoj gradnji. Može se pretpostaviti da postoji velik broj ljudi koji se na određeni način bave navedenim pojmovima te da postoji i populacija kojoj ti pojmovi ulaze u područje interesa bilo koje vrste, bilo da su potencijalni kupci tehničkih rješenja odnosno proizvoda vezanih uz održivu gradnju, bilo da su donosioci odluka ili možda samo dio zainteresirane javnosti.

3. UČESTALOST UPOTREBE IZRAZA VEZANIH UZ ODRŽIVU GRADNJU U STRUČNO ZNANSTVENOJ LITERATURI

Broj objavljenih znanstvenih radova u nekom području može poslužiti kao mjerilo utjecaja znanosti na to područje odnosno kao mjerilo utemeljenosti tog područja na znanstvenim spoznajama. Pri tome je potrebno voditi računa o ograničenjima takvog mjerila. U ovom radu se prikazuje analiza rezultata pretraživanja objavljenih znanstvenih odnosno stručnih radova u tri različite međunarodne baze podataka. To su dvije citatne baze podataka: Scopus (Elsevier B.V.) i Web of Science Core Collection (Thomson Reuters): Treća analizirana baza je Google Scholar koja obuhvaća širu bazu znanstvenih, stručnih i edukacijskih materijala te tako u pravilu daje više rezultata pretraživanja za iste tražene fraze i slične kriterije pretraživanja. Navedene baze podataka ne nude u potpunosti jednake mogućnosti podešavanja kriterija pretraživanja te rezultate nije moguće međusobno uspoređivati. Analizom su istraženi trendovi pojavnosti fraza vezanih uz održivu gradnju u razdoblju od 2000. do 2015. godine. Sličnost ili različitost pojedinih trendova uočenih u različitim bazama podataka ukazuje na postojanje ili nepostojanje određenih zakonitosti koje eventualno mogu vladati u objavljivanju stručno znanstvene literature vezano uz održivu gradnju.

3.1. POJAVNOST FRAZA VEZANIH UZ ODRŽIVU GRADNJU U RAZDOBLJU OD 2000. DO 2015. GODINE

Pretraživani su pojmovi odnosno fraze na engleskom jeziku. Odabrane su tri karakteristične fraze za održivu gradnju. To su: „sustainable building“, „sustainable construction“ i „green building“. Pretraživanje je izvršeno u 49. tjednu 2016. godine. Fraze su tražene u naslovu objavljenog rada, zatim u među ključnim riječima i u sažetku te u cijelom radu. Točni kriteriji pretraživanja za svaku pojedinu bazu podataka su dani u opisu slika. Na slijedećim slikama (slika 1 do slika 3) su prikazani rezultati pretraživanja.

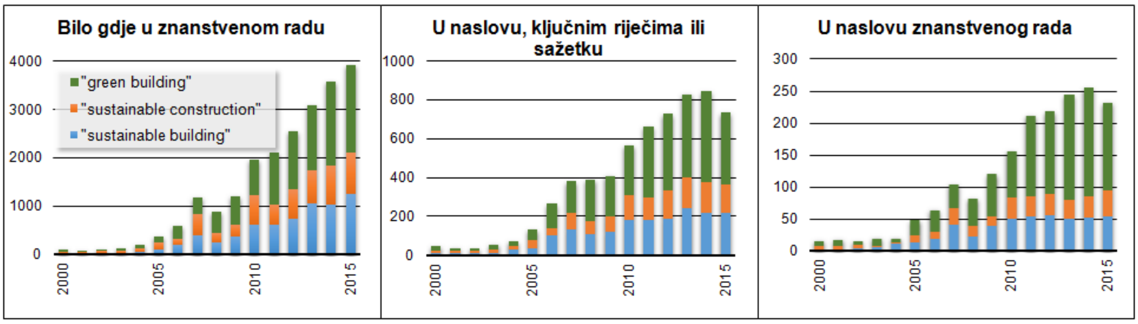

Slika 1 Broj rezultata pretraživanja odabranih fraza u bazi podataka Scopus prema godini objave dokumenta za razdoblje od 2000. do 2015. godine. Fraze su tražene među dokumentima tipa: „Article or Conference Paper“

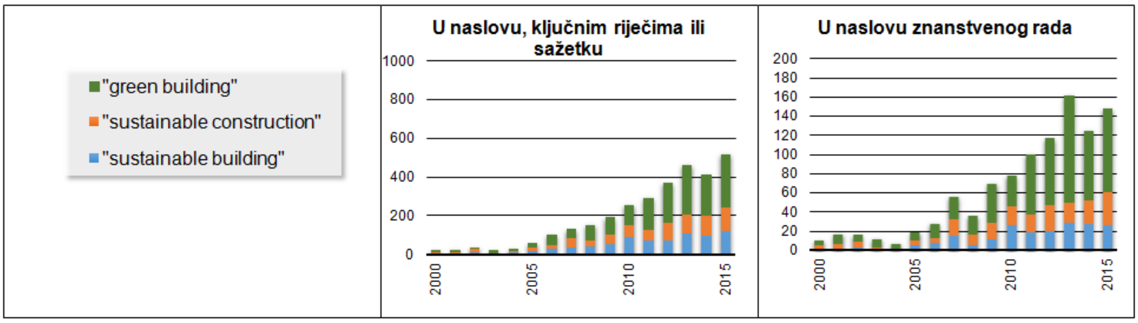

Slika 2 Broj rezultata pretraživanja odabranih fraza u bazi podataka Web of Science Core Collection prema godini objave dokumenta za razdoblje od 2000. do 2015. godine. Fraze su tražene među svim dokumentima koji su obuhvaćeni bazom. Naslov, ključne riječi ili sažetak odgovaraju polju pretrage „Topic“, a naslov znanstvenog rada odgovara polju pretrage „Title“.

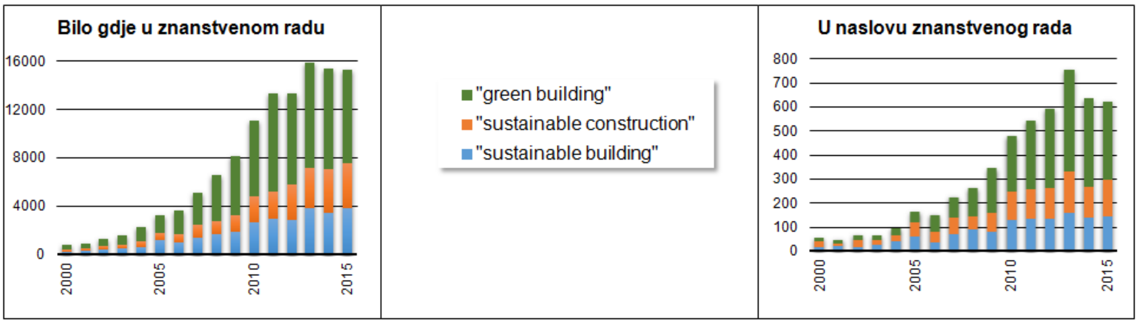

Slika 3 Broj rezultata pretraživanja odabranih fraza u bazi podataka Google Scholar prema godini objave dokumenta za razdoblje od 2000. do 2015. godine. Fraze su tražene među svim dokumentima koji su obuhvaćeni bazom.

Iz prikazanih grafova se vidi da je učestalost pojave fraza vezanih uz održivu gradnju u promatranom razdoblju značajno porasla. Učestalost pojave traženih fraza je od 2000. do 2004. godine bila vrlo niska i bez značajnog rasta, a od 2005. godine nadalje je počela rasti gotovo kontinuirano za sve tri ispitane baze podataka. Blagi pad učestalosti pojave traženih fraza u posljednjim ispitanim godinama se možda može pripisat inertnosti sustava prikupljanja i uvrštavanja znanstvenih radova u analizirane baze. Ova pretpostavka se može provjeriti ponavljanjem pretraživanja uz iste parametre u razmaku od 1, 2, 3… godine. Nejednoliki rast u pojedinim godinama se može pripisati raznim utjecajima kao što su: periodično održavanje značajnih znanstvenih konferencija u periodima većim od jedne godine, politička previranja, prirodne nepogode i katastrofe, ekonomske krize i slično.

3.2. USPOREDBA POJAVNOSTI FRAZA ODRŽIVE GRADNJE S POJAVNOŠĆU FRAZA VEZANIH UZ TRADICIONALNA I OPĆA MJERILA GRADNJE

Za usporedbu je ispitan porast učestalost pojave nekih drugih fraza koje su vezane uz procese izgradnje ljudskog okoliša. Usporedba je provedena na pojavnosti fraza u naslovima objavljenih radova. Pet fraza (structural engineering“, „construction engineering“, earthquake engineering“, „hydraulic engineering“ i „geotechnical engineering“) je odabrano tako da predstavljaju sektore građevinarstva koji su u prvom redu povezani uz tradicionalna mjerila građevina. Dvije fraze („civil engineering“ i „building materials“) su odabrane tako da predstavljaju šire pojmove vezane uz građevinarstvo. Analiziran je porast učestalosti pojave traženih fraza i to ukupna pojavnost od 2011. do 2015. godine u odnosu na ukupnu pojavnost od 2006. do 2010. godine. Razdoblje od 2000. do 2005. godine nije razmatrano jer je pojavnost fraza održive gradnje u tom razdoblju mali i bez značajnog rasta. Tradicionalne i opće fraze koje su u pojedinoj bazi podataka imale najmanje dvostruko veću pojavnost od fraze održive gradnje s najvećom pojavnošću za cijelo promatrano razdoblje su odbačene. Analogno tome su odbačene i fraze s premalom pojavnošću. Među odbačene fraze spadaju „architecture engineering“, „municipal and structural engineering“ i „transport engineering“. Ove fraze su odabrane tako da zajedno sa frazama „civil engineering“ i construction engineering“ obuhvaćaju cijelu kategoriju 2.1. Civil engineering iz dokumenta „Revised field of science and technology (FOS) classification in the Frascati manual“ [5]. U tablici 3 je dan pregled rezultata opisane analize.

Tablica 3 Porast učestalosti pojave traženih fraza u naslovima znanstvenih radova. WoS = Web of Science Core Collection, GS = Google sholar Pretraživanja fraza su provedena 20.2.2017.

Tražena fraza u naslovu znanstvenog rada	Ukupna pojavnost fraze od 2006. do 2010. godine			Ukupna pojavnost fraze od 2011. do 2015. godine			Ukupna pojavnost fraze od 2006. do 2015. godine		
	Scopus	WoS	GS	Scopus	WoS	GS	Scopus	WoS	GS
„green building“	251	130	694	723	404	1732	974	534	2426
„sustainable construction“	103	71	365	168	126	710	271	197	1075
„sustainable building“	172	67	408	270	122	711	442	189	1119
„building materials“	660	439	1163	1230	715	2067	1890	1154[1]	3230
„civil engineering“	784	398	1830	983	735	2828	1767	1133[1]	4658
„structural engineering“	252	93	359	224	154	501	476	247	860
„construction engineering“	118	72	568	154	136	774	272	208	1342
„earthquake engineering“	218	85	347	176	113	426	394	198	773
„hydraulic engineering“	78	49	252	116	72	254	194	121	506[2]
„geotechnical engineering“	245	98	490	269	120	625	514	218	1115

[1] Ukupna pojavnost fraza „building materials“ i „civil engineering“ u razdoblju od 2006. do 2015. godine u WoS bazi premašuje za više od dvostruko pojavnost najučestalije fraze koja se tiče održivosti („green building“ 534 rada). To znači da su fraze „building materials“ i „civil engineering“ značajno češće korištene u radovima koji su obuhvaćeni WoS bazom. Obzirom da ovakav nalaz nije nađen u ostale dvije baze ovi rezultati su svejedno uzeti u obzir.

[2] Ukupna pojavnost fraze „hydraulic engineering“ u razdoblju od 2006. do 2015. godine u GS bazi je za više od dvostruko manja od pojavnosti najmanje učestale fraze koja se tiče održivosti („sustainable construction“ 1075 radova). To znači da je fraza „hydraulic engineering“ značajno manje korištena u radovima koji su obuhvaćeni GS bazom. Obzirom da ovakav nalaz nije nađen u ostale dvije baze ovaj rezultat je ipak uzet u obzir.

Na temelju rezultata prikazanih u tablici 3 je izračunat postotni rast pojavnosti svake ispitane fraze u razdoblju od 2011. do 2015. godine u odnosu na pojavnost iste fraze u razdoblju od 2006. do 2010. godine (vidi Sliku 4). Cilj ove analize bio utvrditi koliko je u promatranom razdoblju narasla upotreba pojedinih fraza u naslovima radova. Eventualno preklapanje dvije ili više ispitanih fraza u pojedinom radu ovdje nije uzeto obzir.

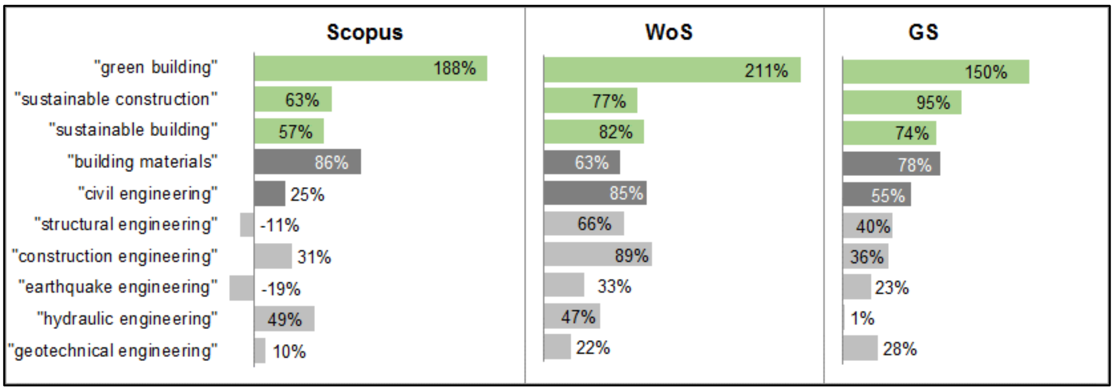

Slika 4 Rast pojavnosti pretraženih fraza u naslovima radova u razdoblju od 2011. do 2015. godinu u odnosu na pojavnost pretraženih fraza u razdoblju od 2006. do 2010. godine

Iz prikazanih rezultata se vidi da je porast pojavnosti fraza karakterističnih za održivu gradnju u promatranom razdoblju značajno veći od porasta pojavnosti fraza koje se u većoj mjeri mogu povezati s tradicionalnim mjerilima građevina. Izuzeci od ovog zaključka su: porast fraze "building materials" u radovima obuhvaćenim bazom Scopus, porast fraza "civil engineering" I construction engineering" u radovima obuhvaćenim WoS bazom i porast fraze "building materials" u radovima obuhvaćenim bazom Google Scholar.

3.3. POJAVNOST FRAZA ODRŽIVE GRADNJE U RADOVIMA ČIJI NASLOVI SADRŽE OPĆE I TRADICIONALNE FRAZE GRADITELJSTVA

Nastavljajući analize iz prethodna dva poglavlja je uočeno da se fraze vezane uz održivu gradnju pojavljuju u određenom broju radova koji u naslovu sadrže neku od općih ili tradicionalnih fraza. Ovdje je prikazana analiza za tri opće ili tradicionalne fraze u kojima se najčešće pojavljuju fraze karakteristične za održivu gradnju. To su „building materials", „civil engineering" i „construction engineering". Istraženo je koliko se često pojavljuje barem jedna od fraza održivosti bilo gdje u radu. Citatna baza WoS ne nudi mogućnost pretraživanja bilo gdje u radu pa je korišteno najšire moguće polje „Topic" koji obuhvaća naslov, sažetak, autorove ključne riječi, i ključne riječi određene WoS algoritmom (Keywords Plus®). Pretraživanje je provedeno u sve tri ranije obuhvaćene baze podataka te posebno za razdoblja od 2006. do 2010. odnosno 2011. do 2015. godine. Rezultati analize su prikazani na slici 5.

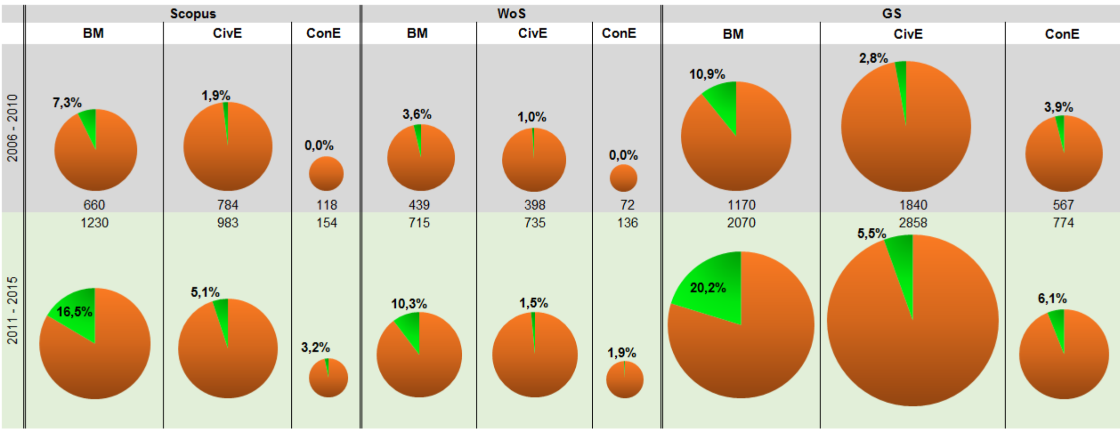

Slika 5 Učestalost pojave barem jedne fraze održive gradnje u radovima čiji naslovi sadrže fraze „building materials" - BM, „civil engineering" - CivE i „construction engineering" - ConE. Površine krugova su razmjerne broju radova koji u naslovu sadrže određenu tradicionalnu ili opću frazu (cijeli brojevi ispod odnosno iznad kruga). Pretraživanje je provedeno između 20. i 26. veljače 2017.

Iz rezultata je vidljivo da je učestalost pojave fraza održive gradnje u radovima koji u naslovu sadrže frazu "building materials" porasla: sa 7,3% na 16,5% (Scopus); sa 3,6% na 10,3% (WoS) te sa 10,9% na 20,2% (GS). Učestalost pojave fraza održive gradnje u radovima koji u naslovu sadrže frazu "civil engineering" je porasla: sa 1,9% na 5,1% (Scopus); sa 1% na 1,5% (WoS) te sa 2,8% na 5,5% (GS). Učestalost pojave fraza održive gradnje u radovima koji u naslovu sadrže frazu "construction engineering" je porasla: sa 0% na 3,2% (Scopus); sa 0% na 0,7% (WoS) te sa 3,9% na 6,1% (GS).

Ispitana je i učestalost fraza održive gradnje u radovima koji u naslovu sadrže ostale tradicionalne i opće fraze („structural engineering", „earthquake engineering", „hydraulic engineering" i „geotechnical engineering"). Međutim, tu je učestalost zanemariva te iznosi oko 1% ili manje uz dva izuzetka koji su pronađeni u GS bazi podataka i odnose se na radove s frazama „structural engineering" i „geotechnical engineering". Ovdje je učestalost pojave fraza održive gradnje porasla sa 2,8% na 3,2% odnosno sa 1,2% na 3,5%.

3.4. UDIO FRAZA ODRŽIVE GRADNJE U RAZLIČITIM TEMATSKIM PODRUČJIMA

U Kopenhaškoj deklaraciji [6] donesenoj na Svjetskom sastanku na vrhu održanom 1995. godine između ostaloga stoji: „Gospodarski rast, društveni razvoj i zaštita okoliša su međusobno ovisne i nadopunjujuće komponente održivog razvoja što zatvaraju okvir nastojanja za postizanjem bolje kvalitete života svih ljudi". Tu se prvi put izravno navode tri osnovne komponente ili stupa održivog razvoja: gospodarstvo, društvo i ekologija. Vrlo jednostavno i općenito se može reći da je održiva gradnja ona gradnja koja je usklađena s održivim razvojem. Iz toga proizlazi da navedene tri komponente (društveni razvoj, gospodarski rast i zaštita okoliša) moraju biti sastavni dio razmatranja odnosno istraživanja vezanih uz održivu gradnju te se razvoj održive gradnje mora oslanjati na razvoj tih triju komponenti. Drugim riječima, istraživanja u održivoj gradnji trebaju biti snažno isprepletena s istraživanjima u gospodarstvu, sociologiji i zaštiti okoliša. Stoga je zanimljivo vidjeti koliko objavljeni radovi vezani uz održivu gradnju, a koji su obuhvaćeni citatnim bazama,prate ova tri znanstvena područja. U ovu svrhu je razmotrena analiza rezultata pretraživanja u WoS bazi podataka. Analize provedene u prethodnim poglavljima ne ukazuju na suštinske razlike među tri korištene baze podataka. Rezultati pretraživanja odstupaju između tri baze, međutim ta odstupanja su unutar očekivanih okvira. Metodologija svrstavanja radova u znanstvena područja odnosno discipline se značajno razlikuje među korištenim bazama. Google scholar ne daje mogućnost pregledavanja radova prema znanstvenom području, Scopus i WoS daju tu mogućnost, međutim tematska odnosno znanstvena područja u ove dvije baze nisu ista. Stoga se u ovom poglavlju razmatra samo WoS baza te se smatra da rezultati te baze podataka sami mogu ukazati na traženi zaključak – u kojoj mjeri su objavljeni radovi usklađeni s trojnim temeljem održivog razvoja i održive gradnje.

Tablica 4 Komponente održivog razvoja, pripadajuća znanstvena OECD pod-područja i pripadajuće WoS znanstvene kategorije

Komponenta održivog razvoja	Pripadajuća pod-područja prema OECD klasifikaciji znanosti i tehnologije	Pripadajuće WoS kategorije
Gospodarstvo (Ekonomija) Economy (Economics)	5.2 Economics and Business	Business; Business, Finance; Economics; Industrial Relations & Labor; Management; Operations Research & Management Science
Društvo (Sociologija) Society (Sociology)	5.4 Sociology	Anthropology; Demography; Ethnic Studies; Family Studies; Social Issues; Social Sciences, Mathematical Methods; Social Work; Sociology; Women's Studies
	5.7 Social and economic geography	Planning & Development; Transportation; Urban Studies
Zaštita okoliša (Ekologija) Environment protection (Ecology)	1.5 Earth and related environmental sciences	Environmental Sciences; Geochemistry & Geophysics; Geography, Physical; Geology; Geosciences, Multidisciplinary; Meteorology & Atmospheric Sciences; Mineralogy; Oceanography; Paleontology; Water Resources; Green & Sustainable Science & Technology
	1.6 Biological sciences (Ecology)	Ecology
	2.7 Environmental engineering	Energy & Fuels; Engineering, Environmental; Engineering, Geological; Engineering, Marine; Engineering, Ocean; Engineering, Petroleum; Mining & Mineral Processing; Remote Sensing; Green & Sustainable Science & Technology

Web of Science Category Mapping [7] pridružuje znanstvene kategorije WoS baze (Web of Science Categories) OECD znanstvenim područjima i pod-područjima [5]. U tablici 4 su prikazana znanstvena pod-područja koja pripadaju pojedinoj komponenti održivog razvoja te WoS kategorije koji su pridijeljene pojedinom pod-području.

Tablica 5 WoS kategorije koje pripadaju znanstveno istraživačkim područjima koja se izravno bave izgrađenim ljudskim okolišem

Komponenta održivog razvoja	Pripadajuća pod-područja prema OECD klasifikaciji znanosti i tehnologije	Pripadajuće WoS kategorije
Graditeljstvo Civil Engineering	2.1 Civil Engineering	Construction & Building Technology; Engineering, Civil; Transportation Science & Technology
	6.4 Arts	Architecture

U tablici 5 su prikazane WoS kategorije koje su pridružene znanstveno istraživačkim područjima izravno povezanim s problemima izgrađenog ljudskog okoliša. Ovdje treba napomenuti da se arhitektura u OECD klasifikaciji navodi na dva mjesta, i to kao „Architecture engineering“ u pod-području 2.1. Civil engineering te kao „Architectural design“ u pod-području 6.4 Arts. S druge strane je u Web of Science bazi arhitekturi posvećena jedna WoS kategorija.

Također je vrlo zanimljivo sa stajališta ovog rada primijetiti da je 2016. godine uspostavljena WoS kategorija „Green & Sustainable Science & Technology“ koja je pridružena čak trima pod-područjima iz OECD klasifikacije kako slijedi: 1.4 Chemical engineering; 1.5 Earth and related environmental sciences i 2.7 Environmental engineering. Osim toga ova tri područja pripadaju u dva različita područja znanosti. To su Prirodne znanosti (Natural sciences – 1.4 i 1.5) i Tehničke znanosti (Engineering and technology – 2.7). Pridruženost ove WoS kategorije trima pod-područjima (što nije još uspostavljeno za niti jednu drugu WoS kategoriju) ukazuje na izraženu multidisciplinarnost i interdisciplinarnost zelenih i održivih znanosti i tehnologija. Radovi su retroaktivno kategorizirani u kategoriju „Green & Sustainable Science & Technology“ tako da sada najstariji rad koji je kategoriziran u ovu kategoriju potječe iz 1996. godine.

U WoS bazi su pretraženi svi radovi od 2000. godine do danas kod kojih se u pretraženom polju „Topic“ spominje barem jedna od tri fraze karakteristične za održivu gradnju: „green building“ ili „sustainable building“ ili „sustainable construction“. Zatim je analizirano koliko radova je svrstano u koju kategoriju (svaki rad može biti svrstan u nekoliko kategorija). Prema pripadnosti svake WoS kategorije, a u skladu s tablicama 4 i 5 je dan udio radova koji su na taj način posredno svrstani u jednu od komponenti održivog razvoja ili u inženjersko područje koje se bavi izgrađenim ljudskim okolišem. Na slici 6 su prikazani rezultati ove analize.

Ukupan broj obuhvaćenih radova od 2000. godine do dana pretraživanja (5.3.2017.) u kojima se u polju „Topic“ spominje barem jedna od fraza održive gradnje iznosi 3529. Ukupan broj WoS kategorija u koje su svrstani ovi radovi iznosi 7970, što znači da je svaki rad u prosjeku svrstan u 2,26 WoS kategorije. Od ukupno 253 WoS kategorije u njih 140 je barem 1 put svrstan neki rad. Po 10 i više radova je svrstano u 61 različitu kategoriju.

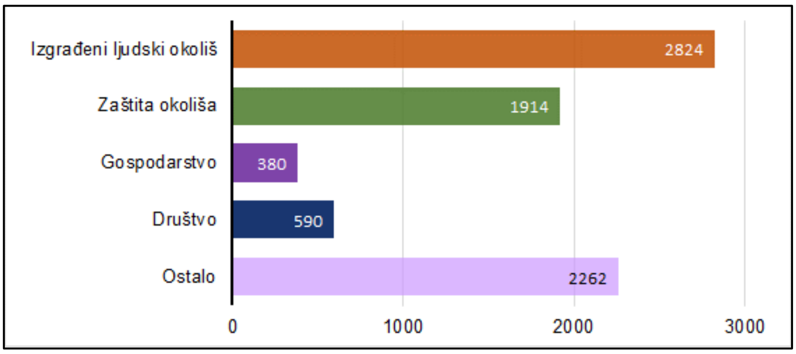

Slika 6 Broj svrstavanja radova objavljenih od 2000. godine do 5.3.2017. kod kojih se u polju „Topic“ spominje barem jedna od tri fraze karakteristične za održivu gradnju. Broj označava koliko puta je neki od radova svrstan u neku od kategorija iz pripadajuće grupe

Ukupan broj radova svrstanih u pojedinu grupu kategorija je manji jer ovom analizom nije određen broj članaka koji su svrstani u dvije, tri ili više kategorija unutar jedne grupe kategorija koje su karakteristične za pojedinu komponentu održivog razvoja ili izgrađeni ljudski okoliš.

Iz rezultata analize je vidljivo da se najčešće radovi vezani uz održivu gradnju svrstavaju u znanstveno istraživačka područja koja se bave izgrađenim ljudskim okolišem – „Civil engineering“ i „Arts“ (samo „Architecture“). Među komponentama održivog razvoja je vidljivo da se radovi približno 3 do 5 puta češće svrstavaju u neku od kategorija koja se bavi okolišem nego u neku od kategorija svojstvenih za društvo ili gospodarstvo. Također je vidljivo da se radovi vezani uz održivu gradnju često svrstavaju u znanstveno istraživačke kategorije koje nisu usko vezane niti s izgrađenim ljudskim okolišem niti sa komponentama održivog razvoja. To ukazuje na izraženu multidisciplinarnost i interdisciplinarnost znanstvenih istraživanja u području održive gradnje.

4. ZAKLJUČAK

Broj znanstvenih radova (analizama su djelomično obuhvaćeni i stručni radovi) koji se na određeni način bave održivom gradnjom uz manje oscilacije kontinuirano raste od 2005. godine nadalje.

Rast broja tih radova je brži od rasta broja radova koji se bave tradicionalnim mjerilima gradnje. Među radovima koji se prvenstveno bave općim ili tradicionalnim mjerilima gradnje se povećava udio radova u kojima se spominju fraze održive gradnje.

Analize ukazuju na izraženu multidisciplinarnost i interdisciplinarnost održive gradnje. Međutim, uočava se manja zastupljenost održive granje u znanstvenim radovima koji se bave temama vezanim uz razvoj gospodarstva i društva, a koji su važne komponente održivog razvoja pa time i održive gradnje.

5. DISKUSIJA

Počeci sustavnog usklađivanja gradnje s principima održivog razvoja su započeli 90-tih godina prošlog stoljeća, a prva kategorizacija znanosti koja jasno definira kategoriju koja se bavi zelenom i održivom znanošću i tehnologijama je uvedena u praksu 2016. godine. Široko priznata klasifikacija znanstvenih polja od strane OECD-a je zadnji put ažurirana 2007. godine, a svjedoci smo ubrzanog rasta znanstveno istraživačkog rada diljem svijeta. Trebali se i može li se stoga očekivati pojavljivanje znanstvenih područja, disciplina i grana posvećenih održivom razvoju i održivoj gradnji i u drugim institucijama i bazama podataka? Je li presudno za daljnji razvoj održive gradnje da postoje znanstvena područja, discipline i grane koja u svom nazivu sadrže pojmove vezane uz održivu gradnju? Postoje li drugi i bolji načini za poticanje multidisciplinarnog i interdisciplinarnog pristupa problematici održive gradnje? Periodične i dublje analize znanstvenih radova u citatnim i sličnim bazama podataka (npr. mapiranje citiranosti među znanstvenim područjima, istraživanje koautorstva autora iz različitih znanstvenih područja i sl.) mogu doprinijeti da se dođe do kvalitetnih odgovora na neka od ovih pitanja.

Također, promatrajući održivu gradnju kao mladu znanstvenu interdisciplinarnu granu ili ogranak može se razmatrati njen razvoj. Prema Zeleniki [8] svaka znanost prolazi kroz tri temeljne faze razvoja, a to su: 1. opisna faza; 2. logičko-analitička i sintetička faza; 3. faza usklađivanja sadržajnih i kvantitativnih metoda znanstvene spoznaje. Iako se ne daju točni kriteriji za egzaktnu procjenu faza pojedine grane ili ogranka znanosti, može se pretpostaviti da je opisna faza održive gradnje trajala od objave Brundtlovog izvještaja 1968. godine pa do 90-tih godina prošlog stoljeća. Nadalje se može reći da je tada otpočela 2. faza razvoja znanstvenog pristupa održivoj gradnji i da ta faza zasigurno još traje. Istovremeno se, međutim, već sada može zamijetiti da postoji velika potreba za globalnim usklađivanjem sadržajnih i kvantitativnih metoda znanstvene spoznaje održive gradnje, što pak pripada 3. fazi razvoja.

LITERATURA

[1] [1]United Nations World Commission on Environment and Development, *Our Common Future [Brundtland Report]*, Oxford, Oxford University Press, (1987)

[2] [2]Zeinal Hamedani, A., Huber F., *A comparative study of DGNB, LEED and BREEAM certificate systems in urban sustainability*. *WIT Transactions on Ecology and the Environment*, 155, pp. 121-132, ISSN 1743-3541

[3] [3]*The Digest of BREEAM Assessment Statistics*, Volume 01, BRE Global Ltd, (2014)

[4] [4]Kibert, C. J., , *Sustainable Construction Green Building Design and Delivery*, *Fourth Edition,* John Wiley & Sons Inc., ISBN 9781119055174, Hoboken, New Jersey, (2016)

[5] [5]Committee for Scientific And Technological Policy, *Revised Field Of Science And Technology (FOS) Classification In The Frascati Manual*, OECD, 2007

[6] [6]Unatide Nations, *The Copenhagen Declaration and Programme of Action: World Summit for Social Development, Copenhagen*, United Nations, (1995)

[7] [7]*Web of Science Category Mapping*, Dostupno na http://ipscience-help.thomsonreuters.com/inCites2Live/5305-TRS.html, Pristupljeno 2017-02-26

[8] [8]Zelenika, R., *Metodologija i tehnologija izrade znanstvenog i stručnog djela*, Ekonomski fakultet u Rijeci, ISBN 953-614-810-2, Rijeka, (2000)

SUSTAINABLE MATERIALS FOR SUSTAINABLE CONSTRUCTION

Borka Bobovec[1], Ivana Banjad Pecur[2]

[1] Ministry of Construction and Physical Planning, RepublikeAustrije 20, 10000 Zagreb, Croatia,
email: borka.bobovec@mgipu.hr
[2] University of Zagreb, Faculty of Civil Engineering, Department of Materials, Fra Andrije Kacica Miosica 26,
10 000 Zagreb, Croatia, email: banjadi@grad.hr

SUMMARY: Research into the production of construction materials and energy saving products is constantly conducted in the world today. The goal is to reduce the amount of natural raw materials and to produce new materials from the recycled waste or from the waste of other industries. Research is essential for the reduction of negative impact on the environment which is not sufficient in terms of the construction process and the sustainability of buildings. The sustainability requirements should be taken into account during urban planning, then during the design and construction, definitely during use and maintenance of a building and finally after its life cycle ends. Such attitude is required by the seventh basic requirement for a construction works. The paper examines the importance of the implementation of the sustainability concept from the stage of urban planning to the choice of construction materials. Some contemporary concepts of "measuring" project sustainability are examined. In the conclusion the paper presents the possibilities of introducing the parameters for evaluating different versions of a project in terms of sustainability.

ODRŽIVI MATERIJALI ZA ODRŽIVU GRADNJU

SAŽETAK: Danas se u svijetu svakodnevno provode istraživanja proizvodnje građevinskih materijala i proizvoda koji troše što manje energije. Cilj je pri proizvodnji građevinskih materijala smanjiti udio sirovina iz prirodnih izvora odnosno izraditi nove materijale od prerađenog otpada ili otpada iz drugih industrija. Sva su ta istraživanja neophodna kako bi se smanjio negativan utjecaj na okoliš što nije dovoljno sa aspekta zahtjeva da sam proces građenja i građevine moraju biti održive. Na zahtjev održivosti treba misliti već kod prostornog planiranja i urbanizma, zatim u fazi projektiranja i građenja, a svakako i tijekom upotrebe i održavanja građevine i na kraju nakon završetka njezina životnog vijeka. Na takvo ponašanje obavezuje nas sedmi temeljni zahtjev za građevinu. U radu se razmatra važnost implementacije koncepta održivosti već pri prostornom oblikovanju pa sve do izbora materijala za gradnju. Obrađeni su neki od danas prisutnih koncepata „mjerenja" održivosti pojedinog projekta. Na kraju su prikazane mogućnosti uvođenja parametara kojima se mogu ocjenjivati različite varijante projekata s aspekta održivosti.

1. UVOD

Umjetnost prostornog oblikovanja i uporabe materijala kojima to činimo – od prostornog planiranja do oblikovanja predmeta za uporabu, okružuje nas na svim razinama postojanja, kao pojedinca, i kao društvo, pa se ponekad i shvaća kao nešto što se samo po sebi razumije. Oblikovani okoliš u kome živimo predstavlja dragocjenost tog života, stoga onima koji oblikuju prostor valja omogućiti širenje znanja i svijesti o mjerilima koja vrijede za oblikovanje prostora i dobru arhitekturu uporabom materijala koji će naglasiti održivost i na taj način osigurati da kroz programiranje, projektiranje i izgradnju pridonosimo smanjivanju negativnih učinaka na okoliš. U kontekstu održivog razvoja mora se osigurati trajnost, kvaliteta, kao i ekonomska, energetska i ekološka prihvatljivost, što je prioritet suvremenog graditeljstva.

Jasno određenje prema arhitektonskoj izvrsnosti, odnosno njezina uloga u stvaranju kvalitete izgrađenog okoliša koji značajno pridonosi uravnoteženom održivom razvoju gradova i drugih naselja je u konačnici odgovornost za prirodni i izgrađeni okoliš kao resurs kvalitete života. Gradovi i naselja imaju ključnu ulogu u razvitku svake zemlje, budući u sebi sadrže težnju za socijalnim i kulturnim napretkom, razvitkom znanja i gospodarskim rastom. [1] Daljnje jačanje svih elemenata cjelovitog urbanog razvoja koji vodi očuvanju vrijednosti krhkog urbanog prostora je u činjenici da on ima svoje granice, stoga svaka intervencija u njemu mora biti suštinski promišljena. Da bi se ta smislenost, odnosno kvaliteta ostvarila potrebno je rabiti oporabu građevinskih materijala kroz zbrinjavanje i recikliranje koje temelj treba imati u planiranju i projektiranju. Graditi na taj način znači primijeniti idejna rješenja, arhitektonske oblike, primjenu graditeljskih materijala i tehnologija gradnje koje od svog nastanka do trenutka primjene svojom biti pronose ideju održivog razvoja i skladnog odnosa s prirodnim okolišem. [[2]

Važnost kulture građenja očituje se i u tome što je život neminovno kvalitetniji u zdravim, sigurnim i funkcionalnim prostorima. Uz poboljšanje energetske učinkovitosti i ekološki pristup u tom kontekstu nužno je osvrnuti se i na mijenjanje standarda u koji se uključuje zaštita i principi održivog okoliša, kao i instrumenti za odabir najprikladnijeg rješenja te sve značajniji aspekti postizanja održivosti u gradnji kroz zbrinjavanje i recikliranje građevinskog otpada. Ako se uzme u obzir da svaki oblik izgradnje i svaki građevni sklop postaje u određenom trenutku potencijalni otpad, otvara se izuzetno široko polje djelovanja kroz koja se može na posredan i neposredan način povezati kultura građenja i oporaba građevinskih materijala.[3] Uzroci nastanka građevinskog otpada najčešće su u procesu same proizvodnje građevinskih proizvoda, nadalje građenju, korištenju i na kraju životnog ciklusa zgrade ili drugog izgrađenog elementa u prostoru kroz rekonstrukciju i rušenje.

2. REGULATIVA KOJA NAS OBVEZUJE NA ODRŽIVOST U GRADITELJSTVU

Europska Uredba o građevnim proizvodima broj 301/2011 (Construction Products Regulation-CPR) definira sedam temeljnih zahtjeva za građevne proizvode a koji se moraju obavezno implementirati u nacionalnu regulativu. U Republici Hrvatskoj to je implementirano u Zakon o gradnji. U članku 7. Zakona o gradnji (NN 153/13) u prvom stavku navodi se: *„Svaka građevina, ovisno o svojoj namjeni, mora biti projektirana i izgrađena na način da tijekom svog trajanja ispunjava temeljne zahtjeve za građevinu te druge zahtjeve, odnosno uvjete propisane ovim Zakonom i posebnim propisima koji utječu na ispunjavanje temeljnog zahtjeva za građevinu ili na drugi način uvjetuju gradnju građevina ili utječu na građevne i druge proizvode koji se ugrađuju u građevinu.“* [5] Nadalje, u članku 8. sedmi temeljni zahtjev za građevinu je održiva uporaba prirodnih izvora koja je opisana u članku 15. na način da: *„Građevine moraju biti projektirane, izgrađene i uklonjene tako da je uporaba prirodnih izvora održiva, a posebno moraju zajamčiti sljedeće: 1. ponovnu uporabu ili mogućnost reciklaže građevine, njezinih materijala i dijelova nakon uklanjanja; 2. trajnost građevine; 3. uporabu okolišu prihvatljivih sirovina i sekundarnih materijala u građevinama.“* [5]

Zahtjevi za recikliranje građevinskog otpada proizlaze iz Strategije Europa 2020. kroz cilj „Održiv rast – promicanje zelenijeg, konkurentnijeg gospodarstva temeljenog na učinkovitom korištenju resursa“ [6] i Direktive 2008/98/EZ Europskog parlamenta i Vijeća od 19. studenoga 2008. o otpadu i stavljanju izvan snage određenih direktiva, koja je u hrvatsko zakonodavstvo prenesena kroz Zakon o održivom gospodarenju otpadom (NN 94/13) koji je u nadležnosti Ministarstva zaštite okoliša i energetike. U članku 11. navedene Direktive propisana je količina: *„Do 2020. godine, pripremu za ponovnu uporabu, recikliranje i druge načine materijalne oporabe, uključujući postupke nasipavanja u kojima se otpad koristi kao zamjena za druge materijale, neopasnog građevinskog otpada, isključujući materijal iz prirode utvrđen ključnim brojem 17 05 04 na listi otpada, treba povećati na minimalno 70 % mase otpada.“* [7] Isto je implementirano u čl. 55. st.2. Zakona o održivom gospodarenju otpadom (NN 94/13): *„Do 1. siječnja 2020. Republika Hrvatska će putem nadležnih tijela osigurati pripremu za ponovnu uporabu, recikliranje i druge načine materijalne oporabe, uključujući postupke zatrpavanja i nasipavanja, u kojima se otpad koristi kao zamjena za druge materijale, neopasnog građevnog otpada, isključujući materijal iz prirode utvrđen ključnim brojem 17 05 04 – zemlja i kamenje koji nisu navedeni pod 17 05 03, u minimalnom udjelu od 70% mase otpada.“* [8] Na slici 1 prikazana je hijerarhija poželjnosti ponašanja s otpadom.

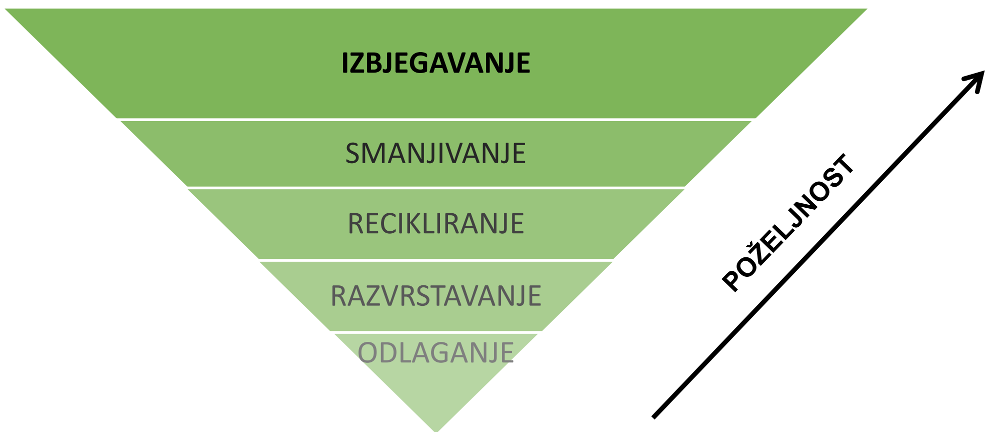

Slika 1 Hijerarhija postupanja s otpadom [2]

3. PREDNOST ODRŽIVE GRADNJE

Osiguranje urbane održivosti i održive arhitekture nužno je promatrati u kontekstu neprekinutog dijaloga i suradnje svih dionika uključenih u sve procese, od programiranja do uporabe pojedinačne zgrade ili izgrađenog prostora.

Održiva gradnja alatima koji nam stoje na raspolaganju uz aktivno djelovanje kroz podizanje ne samo znanja sudionika u gradnji, već društva u cjelini, bez obzira radi li se o urbanim ili ruralnim područjima, može pridonijeti stvaranju novih radnih mjesta i podizanju općeg ekonomskog statusa države. Poticanje programiranja i projektiranja na način da se smanji ukupna razina opterećenja koje građenje u cjelini ima na izgrađeni okoliš doprinijeti će izgradnji kroz rješenja koja će smanjiti količinu otpada, kako u proizvodnji građevinskih materijala, samom građenju i kasnijoj razgradnji, tako i u mogućnosti oporabe građevinskih materijala kroz izgradnju nove građevine na istoj građevinskoj parceli ili u neposrednoj blizini. Aktivnosti je nužno usmjeravati na razne ciljane skupine – od općih korisnika, odnosno najšire javnosti, strukovne javnosti pa sve do političke javnosti. Primjereno osviješteno društvo od vitalnog je značenja za postizanje kvalitetno izgrađenoga okoliša te je stoga potrebno provoditi stalne aktivnosti na razini cijele populacije. [1]

Neophodno je provesti edukaciju stručne javnosti (arhitekte i inženjere u graditeljstvu) o prednostima i mogućnostima održive gradnje kroz radionice u okviru cjeloživotnog učenja, jer veliki dio te javnosti nije imao priliku saznati što sve znači održiva gradnja i koje su to obaveze koje se postavljaju na stručnu javnost kako bi se implementirali zahtjevi održivosti. Održiva gradnja je multidisciplinarno područje i u edukaciji o održivosti trebaju sudjelovati različite struke iz različitih sektora.

3.1.1. ODRŽIVI PROIZVOD ECO-SANDWICH®

Problem zbrinjavanja građevinskog otpada u RH još uvijek nije riješen na zadovoljavajući način iako je prvi pravilnik o građevinskom otpadu donesen još početkom 2008. godine. Još uvijek nema dovoljno reciklažnih dvorišta koja prihvaćaju građevinski otpad i koja će taj otpad preraditi kako bi dobio novu uporabnu ulogu. Zapravo većina građevinskog otpada ne završava na za to predviđenom mjestu. Kada bi se tom otpadu dala neka nova dodatna vrijednost vjerojatno bi se i tok građevinskog otpada promijenio.

Slika 2 ECO-SANDWICH® panel

Udruživanjem akademske zajednice i Hrvatske industrije razvijen je novi inovativni održivi proizvod ECO-SANDWICH® (slika 2). ECO-SANDWICH® je predgotovljeni ventilirani fasadni sendvič panel izrađen od unutarnjeg i vanjskog sloja betona koji u svom sastavu imaju 50 % agregata od recikliranog materijala (opeke i betona). Unutar dva sloja betona nalazi se sloj toplinske izolacije od mineralne vune proizvedene po ECOSE tehnologiji (bez umjetnih ljepila). Na taj način je smanjena eksploatacija prirodnog kamena, smanjene su količine građevinskog otpada koji treba zbrinuti, osmišljen je i proizveden novi inovativni proizvod koji se u potpunosti uklapa u zadatke kružne ekonomije i što je isto tako vrlo bitno, pokazano je da suradnja između domaće akademske zajednice i domaće industrije može dovesti do rezultata koji su priznati i van granica Hrvatske.

4. METODE ZA PROCJENU ODRŽIVOSTI GRAĐEVINE

Još 1990. godine je BRE (The Building Research Establishment) prvi predložio i opisao metodu za procjenu utjecaja zgrade na okoliš s aspekta upotrjebljenih materijal i tehnologije gradnje BREEAM (The Building Research Establishment Environmental Assessment Method) [9]. Nakon BREEAMa mnogi istraživači u svijetu su razvijali vlastite metode za procjenu održivosti građevine i procjenu kroz cijeli životni ciklus. [10]

Većinu metoda su razvijali privatni istraživači ili organizacije kao npr. LEED, HKBEAM, GHEM, GreenStar i drugi. Neke od metoda su razvijale pojedine države: EMBG (Tajvan), NABERS i BASIX (Australija), gdje su onda te metode i obavezne za pojedine kategorije gradnje. Velika prednost kod primjene bilo koje od metode za procjenu održivosti građevine je ta što vas potiče da postignete što bolji rezultat, što znači da će te paziti na više detalja tijekom gradnje, kao npr. izbor građevinskog materijala ovisno o tehnologiji proizvodnje, mjestu proizvodnje i duljini transporta, njegovoj trajnosti i mogućosti recikliranja.

Upotreba ovih metoda procijene održivosti od faze projektiranja utječe na minimizaciju mogućih štetnih utjecaja na okoliš. Još se bolji rezultati postižu ako se metode počnu primjenjivati od razrade konceptnih rješenja, gdje ove metode utječu i na projektiranje. Također neke metode ne uzimaju u obzir financijski aspekt gradnje čime mogu znatno poskupiti gradnju pa želja za troškovno optimalnim rješenjem nije zadovoljena. [10]

4.1.1. JEDNOPARAMETARSKE ILI VIŠEPARAMETARSKE METODE PROCJENE ODRŽIVOSTI

Većina metoda za procjenu održivosti je bila jednoparametarska, ali takav pristup nije mogao zadovoljiti zahtjeve složenih projekata, pa su istraživači razvijali višeparametarske modela. Model od autora Dinga i Langstona [11] bazira se na četiri indeksa održivosti koji su primjenjivi i za nove projekte ali i za rekonstrukcije. Po njihovom modelu, četiri indeksa održivosti su: povećanje prihoda, povećanje korisnosti, mnimiziranje resursa i smanjenje utjecaja. Cijeli koncept ovakvog višeparametarskog indeksa održivosti shematski je prikazan na slici 3.

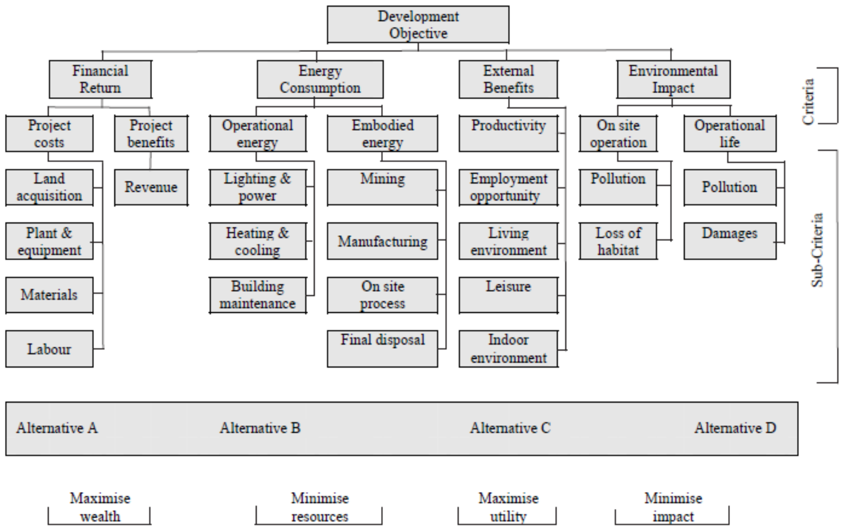

Slika 3 Koncept Modela indeksa održivosti [10]

5. IZJAVA O UTJECAJU PROIZVODA NA OKOLIŠ (ENVIRONMENTAL PRODUCT DECLARATION - EPD)

Danas se u procesu građenja koriste razne vrste građevnih proizvoda, ali i građevni proizvodi iste vrste ali različitih proizvođača. Postavlja se pitanje kako odabrati građevni proizvod koji najmanje negativno utječe na okoliš. Jedna od mogućnosti je da se uspoređuju EPD za te građevne proizvode. EPD za neki proizvod nam kaže koliko je energije utrošeno za proizvodnju tog proizvoda, od svih sastavnih komponenti do tehnološkog procesa. Također navodi se još puno drugih detalj (emisije plinova, utjecaj varijacija sastavnih komponenti …). Uspoređujući građevinu izvedenu od različitih građevnih proizvoda i njihovih EPD-ova moguće je utvrditi optimalnu kombinaciju proizvoda za specifičnu građevinu. To je jedan od načina kako izabrati koje proizvode ugraditi ali i koje izvođače odabrati za izvođenje radova.

Izvođenje javnih radova (radovi koje financiraju javni naručitelji) mora se ugovarati putem javne nabave. Kako za dobivanje posla putem javnog natječaja više ne smije biti kriterij „najniža cijena“ nego „ekonomski najpovoljnija ponuda“, jedan od načina da se odabere izvođač radova je da se projekti ocjenjuju preko modela procjene održivosti i preko EPDa za svaki građevni proizvod.

6. ZAKLJUČAK

Prioritet koji nam se danas nameće u puno aspekata života je održivost. Isto tako pitanje održivosti u svijetu u sektoru graditeljstva je top tema i evidentno je da tvrtke koje u svojim strategijama uvažavaju principe održivosti imaju bolje poslovne rezultate od ostalih. U graditeljstvu se o održivosti treba razmišljati od razrade varijanti nekog projekta, pa preko projektiranja odabrane varijante, do izvođenja i kasnije održavanja građevine. Također u tom procesu od početka trebaju sudjelovati stručnjaci iz više struka.

Razvijeno je više različitih metoda za procjenu održivosti neke građevine, od jednostavnih do kompleksnih za koje treba imati specifična znanja iz tog područja.

Kako nas i regulativa obvezuje da u projektima na neki način procijenimo održivost građevine, neophodno je da se donese nacionalni model za takvu procjenu.

LITERATURA

[1] Arhitektonske politike Republike Hrvatske 2013-2020, ApolitikA, Nacionalne smjernice za vrsnoću i kulturu građenja, [ur. Knifić Schaps, H.], Hrvatska komora arhitekata i Ministarstvo graditeljstva i prostornoga uređenja, Zagreb, 2013.
[2] Bobovec, B.: Zeleni uredi - zdravlje, dobrobit i produktivnost u uredima, 11. Dani ovlaštenih inženjera građevinarstva, Zagreb : Hrvatska komora inženjera građevinarstva, 2016: 150-151
[3] Motik, B.; Šimleša, D.: Zeleni alati za održivu revoluciju, Održivo graditeljstvo, Što čitaš i ZMAG, Zagreb, 2007: 132
[4] Hijerarhija postupanja sa otpadom, Izvor: Vodič kroz zeleni ured, 8. Otpad, MGIPU, APN i SGE, Zagreb, 2016: 27
[5] Zakon o gradnji (NN 153/13)
[6] Strategija Europa 2020., Europska strategija za pametan, održiv i uključiv rast, 3.3.2010., Brisel, file:///C:/Users/bbobovec/Downloads/europa-2020.pdf
[7] Direktiva 2008/98/EZ Europskog parlamenta i Vijeća od 19. studenoga 2008. o otpadu i stavljanju izvan snage određenih direktiva
[8] Zakon o održivom gospodarenju otpadom (NN 94/13)
[9] Larsson, N.: Building Research and Information, Green Building challenge '98: international strategic considerations, 26 (2), 1998., 118–121.
[10] Ding, G. K. C.: Sustainable construction – the role of environmental assessment tools, Journal of Environmental Management, Volume 86, Issue 3, February 2008, Pages 451–464
[11] Ding, G.K.C.; Langston, C.: A methodology for assessing the sustainability of construction projects and facilities. Proceedings of Environmental & Economic Sustainability–Cost Engineering Down Under, ICEC Melbourne 2002

GREEN SENSE CONCRETE

Juergen Huber[1]

[1] BASF Construction Solutions GmbH, Salzachstrasse 2-12, 68199 Mannheim, Germany,
email: juergen.a.huber@basf.com

SUMMARY: A significant proportion of global CO2 emissions and primary energy consumption are attributed to construction industry. Due to its large mass within a structure, concrete has a big impact on the technical and ecological performance of a building. Typically concrete has to meet requirements on workability and strength, but – due to the lack of standards and experience - not for sustainability. With Green Sense Concrete, BASF offers a concrete proportioning service, which is based on the know-how to utilise environmentally beneficial concrete constituents with specially designed admixtures. A life cycle analysis (LCA) quantifies environmental impacts and costs over the entire lifecycle (from raw materials and manufacturing to transportation and disposal). The tool-report contains all relevant results for building certifications (DGNB, LEED, BREEAM, etc.) and is the basis for an Environmental Product Declaration (EPD). By the use of adapted superplasticisers (e.g. low-viscosity concrete for less power consumption when pumping, higher amount of SCM), hardening accelerators (e.g. replacement for heating, faster demoulding), etc. conventional concretes can be compared and improved – economically, technically and ecologically. Green Sense Concrete is the perfect method to use existing solutions more efficiently.

ZELENI BETON

SAŽETAK: Građevinskoj industriji pripisuje se znatan udjel u globalnoj emisiji CO2 i potrošnji primarne energije. Zbog svoje velike mase u konstrukciji beton ima velik učinak na tehnička i ekološka svojstva zgrade. Tipični beton mora ispuniti zahtjeve obradivosti i čvrstoće, ali, zbog nedostatka norma i iskustva, ne i zahtjeve održivosti. Sa zelenim betonom BASF nudi uslugu određivanja sastava betona osnovanu na know-how upotrebe sastojaka betona korisnih za okoliš u posebno projektiranim mješavinama. Analizom životnoga ciklusa kvantificiraju se okolišna opterećenja i troškovi za cijeli životni ciklus (od sirovina i proizvodnje do prijevoza i odlaganja). Izvještaj o tome sadržava sve mjerodavne rezultate certificiranja zgrade (DGNB, LEED, BREEAM itd.) i osnova je Izjave o okolišu za proizvod. Upotrebom prilagođenih superplastifikatora (npr. betona male viskoznosti radi manje upotrebe energije pri pumpanju, većeg sadržaja materijala iz upravljanja opskrbnim lancem (engl. supply chain management, SCM) ubrzivača za vezivanje (npr. kao zamjene za zagrijavanje i brže uklanjanje oplate) uobičajeni betoni mogu se uspoređivati i poboljšati – ekonomski, tehnički i s obzirom na okoliš. Zeleni beton savršena je metoda učinkovitije upotrebe postojećih rješenja..

1. INTRODUCTION

The building sector contributes up to 30% of global annual greenhouse gas emissions and consumes up to 40% of all energy – largely due to the use of fossil fuels during their operational phase [1]. Ongoing efforts and developments, like thermal insulations, adapted constructions or modern energy systems continuously lead to a specific reduction of energy consumption during usage-phase, ideally ending in zero or plus-energy housing. At the same time greenhouse gas (GHG) emissions resulting from construction and particularly materials become more important. Especially reinforced concrete plays a significant role due to its high mass percentage in the supporting structure combined with ecologically unfriendly materials like cement.

2. APPROACH

Concrete is a technically and economically widely established building material, which cannot easily be replaced without jeopardising economic and environmental aims. So the basic question is how the existing system, mainly bound to local resources, can be modified and optimized in order to reduce its environmental footprint. A system only can be tweaked with the target of improvement if the main parameters can be measured and benchmarked. Relating to concrete a life cycle assessment for an “ecological mix design” has to be carried out. But also the technical and economical requirements have to be met or exceeded.

3. GREEN SENSE CONCRETE

3.1. GENERAL

As mentioned before Green Sense Concrete is an approach to ecologically, economically and technically optimize concrete for a specific building project, see Figure 1 Although being basically a sophisticated and at the same time pragmatic approach, using highly developed but already existing chemistry or supplementary cementitious materials (SCM), considering all parameters is challenging. So global as well as local support for sourcing, calculating and testing is necessary and given.

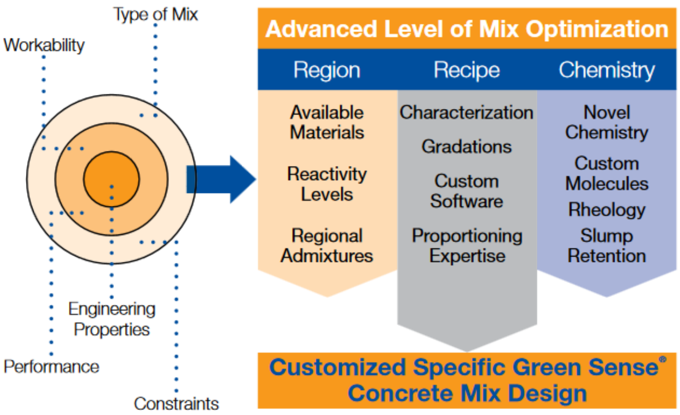

Figure 1 BASF Green Sense Concrete - concept

3.2. LIFE CYCLE ASSESSMENT

In order to carry out a life cycle assessment for concrete, a tailor-made solution is used, the BASF Life Cycle Analyzer. It is compliant to DIN EN 15804, based on the GABI-system and database and externally certified by DEKRA. All relevant data for concrete (cements, concrete additives and admixtures, steel, etc. – also standard values for mixing energy or truck loads, etc.) are already contained in the database or can be added if specific values (e.g. EPD data) are available. The database itself is updated on a regular basis.

In a calculation all relevant parameters (materials, energies, transport distances, etc.) for a specific building project can be taken into account from production to construction to use and end of life including reuse / recovery or recycling. As a result, all relevant environmental impacts are calculated. The primary energy demand is split in renewable and non-renewable, for the emissions e.g. GWP (Global Warming Potential), AP (Acidification Potential), EP (Eutrophication Potential), ODP (Ozone Depletion Potential) and POCP (Photochemical Ozone Creation Potential) are calculated, see Figure 2

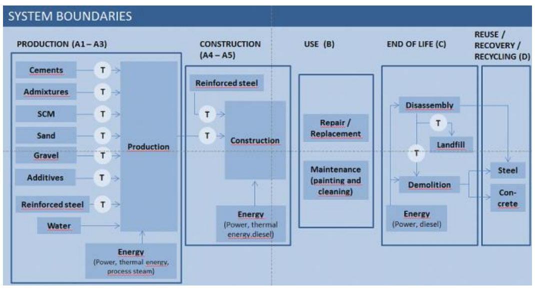

Environmental Indicator	Abbreviation	Unit	Description
Primary energy demand (fossil/ non renewable)	PENRT	MJ	Calorific value / energy content and the effort for provision of energy carriers and raw materials which results from non renewable resources
Primary energy demand (renewable)	PERT	MJ	Calorific value / energy content and the effort for provision of energy carriers and raw materials which results from renewable resources
Global warming potential	GWP	kg CO_2-eq.	Climate change
Acidification potential	AP	kg SO_2-eq.	Acid rain / forest dieback
Eutrophication potential	EP	kg PO_4^{3-}-eq.	Over-fertilization of soil and water
Ozone Depletion Potential	ODP	kg CFC-11 eq.	Ozone depletion in higher atmosphere leading to thinning of ozone layer
Photochemical Ozone Creation Potential	POCP	kg Ethene-eq.	Ozone creation in lower atmosphere

Figure 2 BASF Life Cycle Analyzer - system boundaries and environmental parameters

For demonstration purpose, a random but representative project is shown below. Besides the exact numbers, the results are displayed in charts for simple but effective analysis, see Figure 3

The mix design and other parameters for 1 m³ of concrete:

- C30/37, 350 kg CEM II/B-LL 32,5 R, w/b= 0.47, natural aggregates
- local materials (< 150 km), transported to and mixed on-site

	Total	A1-A3	A5	C1	C2	C4	D
PENRT [MJ]	1.81E03	1.41E03	1.76E02	2.41E02	1.51E01	6.09E01	-9.17E01
PERT [MJ]	1.17E02	9.27E01	1.43E01	1.14E01	5.92E-01	5.02E00	-7.35E00
GWP [kg CO2-Equiv.]	2.83E02	2.55E02	1.44E01	1.48E01	1.09E00	4.43E00	-7.38E00
AP [kg SO2-Equiv.]	6.16E-01	4.99E-01	5.51E-02	6.92E-02	3.36E-03	2.81E-02	-3.89E-02
EP [kg Phosphate-Equiv.]	1.00E-01	8.00E-02	5.72E-03	1.53E-02	7.12E-04	3.86E-03	-5.31E-03
ODP [kg R11-Equiv.]	1.39E-08	1.45E-08	3.05E-10	1.25E-10	5.21E-12	5.55E-11	-1.12E-09
POCP [kg Ethene-Equiv.]	3.87E-02	3.48E-02	6.45E-03	4.16E-04	-9.59E-04	2.64E-03	-4.66E-03

A1-A3: manufacturing (incl. raw materials), A4: transport to site, A5: installation, B2: maintenance (painting and cleaning), B4: replacement, C1: disassembly/ demolition, C2: transport to landfill, C4: landfill, D: reuse/ recovery/ recycling

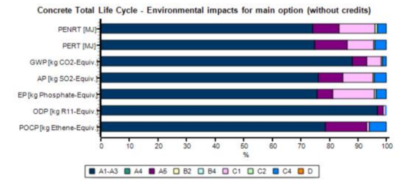

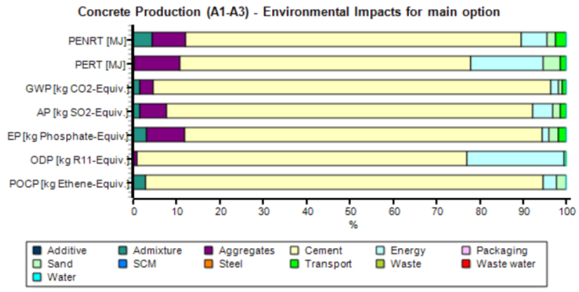

Figure 3 BASF Life Cycle Analyzer – Demo calculation

In this given example, the production / materials stage (A1-3) is responsible for at least 80% of the primary energy use and environmental emissions. A closer look into that process shows, that cement here is the most influencing factor, with a share of 80% with that stage.

Based on that information and knowledge about local resources like cement (e.g. type, amount), concrete additives (e.g. fly ash, limestone power) or aggregates (e.g. natural, crushed, recycled) an ecological and technical optimization can be done. Same applies for a comparison e.g. between fibers and ordinary reinforcement or natural and recycled aggregates. Transportation has to be adjusted accordingly.

Depending on materials and performance now an optimal mix design can be found. In this example the substitution of cement by SCM will improve the material's performance, but will downgrade the transportation part.

In a separate section, all materials can be assigned with their (purchase) prices, so the cost of a defined unit (normally 1 m³) can be calculated.

All data (input, methods, calculation, results, etc.) are compiled into a comprehensive report, so the BASF Life Cycle Analyzer is an easy tool to assess concrete of its lifespan. Additionally, the tool report is the basis for an individual EPD for the specific concrete mix. Hence Green Sense Concrete offers the user a convenient and affordable way to provide EPDs for his concrete or his concrete based products.

3.3. MIX DESIGN OPTIMIZATION

In order to meet the technical specifications (workability and compressive strength), the mix design (w/b-ratio, fines content, paste volume, admixture type, etc.) has to be adjusted. BASF uses an internal tool for the evaluation, extended lab tests (incl. rheological measurements) have to be carried out to prove the performance.

Beyond ordinary values like slump flow, rheological parameters are taken into account to characterize and optimize fresh concrete's behaviour regarding flowability, pumpability and stability. Very often classical mix-designs are replaced by flowable or self-consolidating concretes with higher performance on site.

3.4. CONCRETE ADMIXTURES

Concrete with an enhanced ecological footprint often have special behaviour. Due to their higher fines, higher additives and lower clicker content compared to ordinary concrete their fresh state and hardening behaviour is different. So special concrete admixtures are used to counteract and enhance that behaviour.

Inert, pozzolanic and latent-hydraulic materials as a replacement for clinker slow down hydration significantly and delay demoulding time in a precast plants or on-site and so the construction process itself. Special hardening accelerators on C-S-H-basis are used to (over-)compensate this issue, eliminating additional heating processes with significant higher energy demand. The Crystal Seeding Technology boosts the natural hydration of the clinker and reduces hardening time in the first 48 hours while leaving working time of the fresh concrete unchanged.

High fines volumes often lead to sticky concrete. New types of admixtures like PAE-based superplasticisers (Poly-Aryl-Ether), an advancement to those on PCE-base (Poly-Carboxylate-Ether), offering lower viscosity while maintaining the desired yield stress of the concrete. So sedimentation resistance is unchanged, flowing and pumping behaviour improved. In practice pumping pressure reduction up to 20% is achievable, depending on the concrete type, see Figure 4

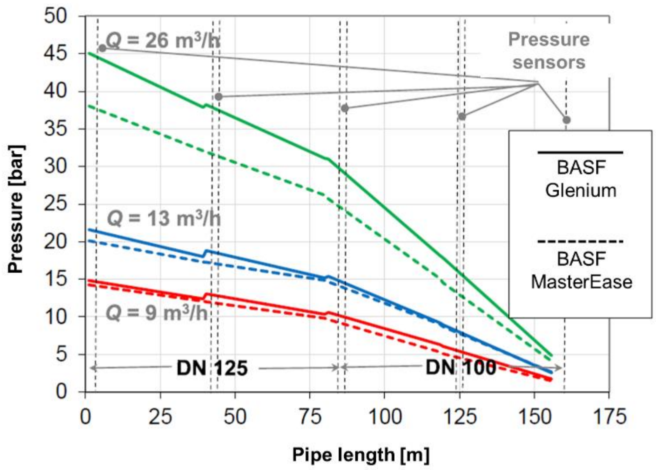

Figure 4 Pumping pressure tests – [cont.] with PCE, [dotted] with PAE

3.5. REFERENCES

Ongoing projects all over the world show the performance and effectiveness of this approach. Table 1 shows as an example savings for outstanding buildings in the US.

Table 1 Reference projects - savings

Name	Green Sense Concrete [m³]	GHG [t CO2-Eq.]	Energy [GJ]	Water [Ml]	Solid waste [t]
432 Park Ave.	69000	9579	2959	724	274
One World Trade Center	110900	15785	91440	19862	780
Virginia Tech	3820	442	2325	n/a	9

The savings refer to standard mixes, which would have come to use for this projects.

In Table 2 the technical requirements for the One World Trade Center (lower 40 floors) are shown:

Table 2 One World Trade Center – Requirements

Type	Value	Requirements
Compressive strength	83 MPa	Engineering
Over-design satfety	13 MPa	Engineering
Modulus of elasticity	48 GPa	Engineering
Max. Heat of hydration	70 °C	Engineering
Others	No air entraining	Engineering
Slump flow	610-710 mm	Contractor
Pumpability	40 floors	Contractor

The optimized mix replaced 71% of the cement by recycled materials, non-cementitious fillers and specialized admixtures in order to reach the results given in Table 1 and 2.

A comparison of different contents of fly ash on different environmental categories for the Virginia Tech project is shown in Figure 5 It can clearly be seen that for this project a replacement of cement by fly ash has got a positive ecological effect (50% was the requirement here).

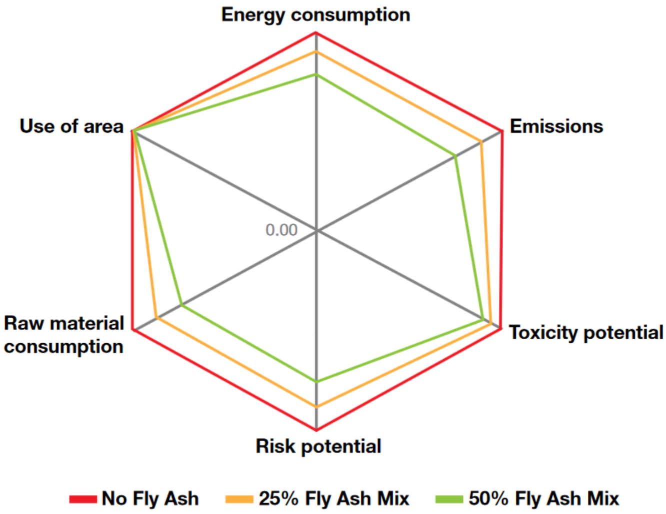

Figure 5 Effects of fly ash on environmental properties

4. CONCLUSION

Green Sense Concrete is basically both a pragmatic and sophisticated approach, working with already existing products and solutions enhanced by a comprehensive life cycle analysis. Results depend on the variety of parameters which are relevant for a specific project on site. An optimized mix design always has to meet technical, economical and ecological requirements and so is always unique.

Altogether Green Sense Concrete is a comprehensive and ready to use service for all building projects and offers all building owners and planners the possibility to ecologically, economically and technically optimise a common but important building material with high impact. Bringing environmental aspects into consideration this approach prepares concrete as a building material for the future.

REFERENCES

[1] United Nations Environment Programme – Sustainable Buildings and Climate Initiative: Buildings and Climate Change - Summary for Decision Makers, 2009

CONTRIBUTING TO A CIRCULAR ECONOMY BY PUTTING RECYCLED CONTENT & SCARCITY OF THE PRIMARY RAW MATERIALS, ZERO WASTE AND RECYCLABILITY IN THE FOCUS

Georg Schöner[1], Agnes Schuurmans[1]

[1] ROCKWOOL International A/S, Hedehusene, Denmark, email: georg.schoner@rockwool.com, agnes.schuurmans@rockwool.com

SUMMARY: Circular economy and resource efficiency in the construction sector are in the focus of European policies. The ROCKWOOL Group supports the life cycle thinking that can lead to a circular economy. The company does so by focusing on the goals of zero wool waste and recyclability of the product at the end of a buildings lifetime. When working towards these two goals, the whole life cycle and therefore for example high resource efficiency and the recyclability of the product being produced needs to be considered, next to the secondary/recycled materials it contains. This presentation will use the mineral wool industry as an example and start of by looking at the need to ensure a good building performance, as building assessment schemes, such as LEED, BREEAM, HQE and DGNB are trying to assess. This is followed by assessing the need to reduce the waste of buildings and consequently the recyclability of its components and their recycled content. Conclusions on what is needed to achieve a circular economy and how Life Cycle Management needs to contribute are presented and serve as basis of discussion.

DOPRINOS KRUŽNOM GOSPODARSTVU STAVLJANJEM U ŽARIŠTE RECIKLIRANI SADRŽAJ I NESTAŠICU PRIMARNIH SIROVINA

SAŽETAK: U žarištu su europskih politika kružno gospodarstvo i učinkovitost resursa u građevinskom sektoru. Grupa ROCKWOOL podržava razmišljanje o životnom ciklusu koje može dovesti do kružnoga gospodarstva. Kompanija to čini usredotočenošću na postignuće nultoga otpada od mineralne vune i reciklabilnosti proizvoda na kraju životnoga vijeka zgrade. Radeći u smjeru tih dvaju ciljeva treba razmotriti cijeli životni ciklus, a onda i, primjerice, veliku učinkovitost resursa i obnovljivost proizvoda uz sekundarne/reciklirane materijale koje proizvod sadržava. U radu se prikazuje industrija mineralne vune kao primjer i razmatra potreba osiguravanja dobrih svojstava zgrade putem shema za ocjenjivanje zgrada kao što su LEED, BREEAM, HQE i DGNB. Nakon toga slijedi ocjenjivanje potrebe smanjenja otpada od zgrade i potom ocjenjivanje recikliranih njezinih dijelova i recikliranog sadržaja. Kao osnova za raspravu služe zaključci o tome što je potrebno postići kružnim gospodarstvom i upravljanjem životnim ciklusom.

1. RESOURCE EFFICIENCY VERSUS RECYCLED CONTENT

Circular economy as a concept has been suggested by environmental economists from the 1990s to better connect economy and environment. Circular economy models are designed to avoid major disadvantages of linear models, particularly intensive resource use and waste creation. More recently a wide-spread illustration for circular economy has been published by the Ellen MacArthur Foundation; it shows the model of an industrial system that is restorative by design.

These models are also applicable for the construction sector. A construction products performance in its application in a building is key, in order for the building to operate as designed. This optimal operation is the best resource efficiency measure in the construction sector. The durability of a product but also the right properties with regard to 'social' sustainability indicators of buildings according to EN16309, are also positively contributing parameters to consider. For the product itself, higher resource efficiency means using less scarce resources and using more secondary materials that cannot be used elsewhere. This can be assessed through LCA impacts such as resource depletion.

When assessing the resource hierarchy in Figure 1 from most to least preferable. Unextracted natural capital reserves are the most preferable, but abundant available versus scarce resources need to be differentiated. After the extraction took place, the Conversion of extracted resources into products and services via manufacture happens. This is followed by the use and reuse before products undergo RE-pair, -furbishment or –manufacture. Products Recycled (closed) loop stay within the original manufacturing facility or sector and fulfil the same purpose. Products Recycled (cascade) are resources used after their 'end-of-life' in different value streams. When resources cascade (are being 'down-cycled') their value or recyclability declines. Recovery of energy could be limited to resources from which all further cascade recycling opportunities have been exhausted. The recovery minimizes the nutrient leakage into the biosphere. If the zero waste goal is achieved this is one indicator of a functioning circular economy because then Landfilling of waste does not exist.

As Figure 1 indicates there are a lot of circumstances and differences to consider when looking at a single indicator such as recycled content. Comparing sums of recycled content can be misleading for obtaining a resource efficient built environment.

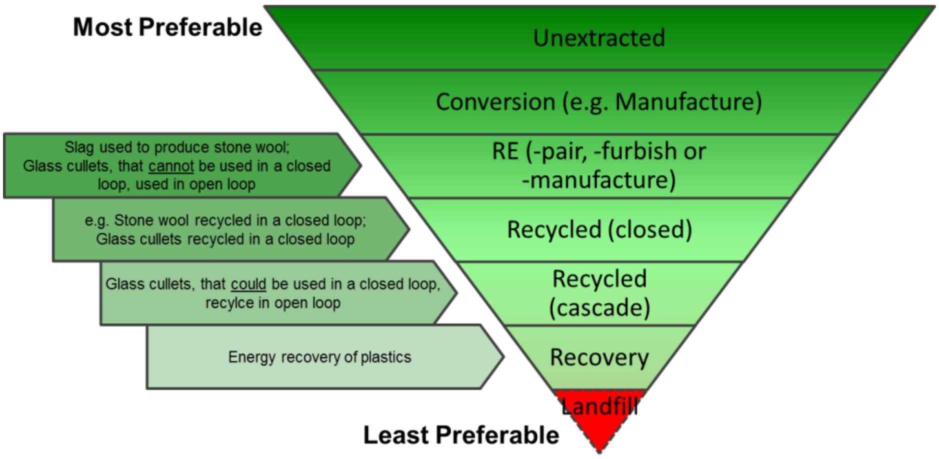

Figure 1 European resource hierarchy [adapted from McLanaghan, 2015

Table 1 Table of terms [4]

Resource hierarchy	Description
Unextracted	Virgin resources in the biosphere; unextracted natural capital reserves (e.g. minerals and ores) whether proven, or otherwise.
Conversion*	Conversion of extracted resources into products and services via manufacture.
RE (-pair or –furbish or -manufacture)	Products that undergo repair, refurbishment or remanufacture, resulting in their retained use within the productive economy.
Recycled (closed)	Closed-loop recycling within the original manufacturing facility or sector, for the same or similar purpose.
Recycled (cascade)	‘Cascade recycling’ or ‘down-cycling’: resources recycled after product ‘end-of-life’ in different value streams. As resources descend the cascade their value declines (entropy increases.)
Recovery	Nutrient leakage into the biosphere is minimised by restricting energy recovery to resources from which all further cascade recycling opportunities have been exhausted. The arrow to RECYCLECASCADE from RECOVERY represents subsequent use in manufacture (e.g. inert ash used as in secondary aggregates.)
Landfill	In a functioning circular economy waste does not exist and no resources would be landfilled, other than for subsequent storage/ mining. Transitionally, some landfill will be required, but only when all cascade recycling opportunities have been exhausted.

* In practice, additional interim steps exist: ‘extraction’ takes place before conversion and ‘use’ and ‘reuse’ before RE (-pair or -furbish or -manufacture); these are not shown above.

2. THERMAL INSULATION PRODUCTS AND THE CIRCULAR ECONOMY

Stone wool uses, next to the abundantly available natural rock materials, a significant amount of ashes, slag or dust as raw materials. These materials are considered pre-consumer recycled material. If for example slags are used to produce stone wool, then these low quality by-products of other industries are not disposed into landfills or used in applications such as road fillings.

Here up-cyclin[1]g takes place because ashes/slag/dust is turned into stone wool and the stone wool can later be recycled back into stone wool in a closed loop. Using such secondary materials for stone wool production has

[1] Note: ROCKWOOL Group understands up-cycling as the process of converting materials into new materials with higher reusability and recyclability options and/or higher quality of a material and/or a higher value over time.

sustainability benefits[2] as the stone wool product will improve the building performance, such as acoustics, long term facade cladding or thermal insulation, which is not the case when the waste material is disposed into landfills. For example, the insulation of buildings can save hundredfold the environmental impacts associated with the production of the stone wool used for insulation.

Glass wool uses a significant amount of glass cullet as raw material. The use of glass cullet for glass wool production reduces the use of primary raw materials, such as sand and boron. The use of glass cullet also enables a reduced energy use and therefore a reduction of fossil resources.

Depending on the market environment the use of glass cullet to produce glass wool, can lead that it is taken out of the closed recycling loop of glass bottle glass cullet production and more virgin raw materials may be necessary to produce glass bottles because glass cullet has a constrained market[3] . Glass wool cannot be turned into glass bottles at the end of life of the wool which can be a limitation to the reuse possibilities. But glass wool can be recycled in a closed loop ore used as blowing wool or in bricks.

Under a different market environment glass cullet from different purposes bottles is available as the demand for the original purpose is decreasing. An illustrative example are CRT displays used for computers and TVs, for which the last production in Europe was closed in 2012. Though the techniques for disassembly and closed loop recycling are established, there is no longer a demand and the use in glass wool eliminates landfilling.

3. CONCLUSIONS

Policies and private sector activities aim to encourage the development towards circular economies that reduce resource use and waste streams. Instruments that are used in this context need to apply reliable indicators that consistently and comprehensively express several aspects. The use of (scarce) resources is relevant as well as options to safely treat residues in a viable process to produce materials that can be used "again and again".

An assessment of products can be based on their function, the necessary resources for producing them and the resources to treat them at the end of their useful service life. To ensure that different aspects are addressed, an indicator needs to be comprehensive.

Recyclability, recycled content and scarcity of the primary raw materials of the product under study need to be analysed together in the context of moving towards a circular economy.

- Comparing products on recycled content figures as requested in LEED or BREEAM is often not meaningful. A differentiation of recycled material into pre- and post-consumer material does not indicate if the use of the recycled material is more or less environmental beneficial.
- The system (for example closed loop) in which a recycled material exists and other reuse options of a recycled material need to be analysed in order to choose the application that supports the zero waste goal the most.
- Using non-scarce raw materials combined with secondary material that would otherwise be landfilled, can be environmentally preferable over using 100% secondary material that would be reused anyhow.
- Recycled content is one indicator, not a goal in itself and not an environmental impact such as climate change or resource scarcity.
- Meaningful life cycle assessment based calculations are necessary to reduce environmental impacts.

REFERENCES

[1] European Commission to the European Parliament – Towards a circular economy: A zero waste programme for Europe [online]. EC, 2008 [cit. 2015-08-21]. www: < http://eur-lex.europa.eu/legal-content/EN/TXT/?qid=1415352499863&uri=CELEX:52014DC0398R%2801%29>.

[2] Note: the environmental benefits have to be established by Life Cycle Assessment. As secondary materials replace natural rock with usually low environmental impact, the benefits for some impact categories could be limited, but benefits will be gained in others.

[3] Note: A constrained market is a market where all or part of a change in demand is not reflected in a corresponding change in supply, but instead in a change in consumption elsewhere (Source: http://www.ecoinvent.org/support/faq/methodology-of-ecoinvent-v3/#irfaq_7_1fa6c). For example, glass cullet is produced exclusively as an output from the glass (bottle) recycling steam. Although there is a high demand for glass cullet, there will not be more supply, under the current market conditions, where the demand for glass cullet would not be enough to drive the glass collection mechanisms for recycling.

[2] European Commission to the European Parliament – Communication on resource efficiency opportunities in the building sector [online]. EC, 2008 [cit. 2015-08-21]. www: < http://ec.europa.eu/environment/eussd/pdf/SustainableBuildingsCommunication.pdf.>.

[3] World's leading sustainability assessment methods for buildings; American LEED (Leadership in Energy and Environmental Design), British BREEAM (BRE Environmental Assessment Method), French HQE (Haute Qualité Environnementale), German DGNB (Deutsche Gesellscahft fur Nachhaltiges Council)

[4] Ellen MacArthur Foundation – "System diagram" [online]. [cit. 2015-08-21]. WWW: < by the http://www.ellenmacarthurfoundation.org/circular-economy/circular-economy/interactive-system-diagram>.

[5] MCLANAGHAN, S. – European Resource Strategy and supporting Resource Hierarchy. Discussion Paper [online]. 2015-05-10 (Version 1.08). www: <http://www.eden21.co.uk/>.

KNOWLEDGE ENGINEERING APPROACHES FOR BUILDING MATERIALS DOMAIN

Andrej Tibaut[1], Branko Kaucic[2], Daniela Dvornik Perhavec[1], Hervé Panetto[3], Piero Tiano[4]

[1] University of Maribor, Faculty of Civil Engineering, Transportation Engineering and Architecture, Smetanova ulica 17, Maribor, Slovenia, email: andrej.tibaut@um.si, daniela.perhavec@um.si
[2] Initut, Institute of Information Technology Ltd, Ljubljanska ulica 93, 2000 Maribor, Slovenia, email:branko.kaucic@initut.com
[3] University of Lorraine, CRAN, CNRS, Nancy, France, e-mail: herve.panetto@univ-lorraine.fr
[4] National Research Council, Institute for the Conservation and Valorization of Cultural Heritage, Florence, Italy, e-mail: piero.tiano@gmail.com

SUMMARY: Architecture, Engineering, Construction, Ownership and Operation (AECOO) industry collects Big Data during the entire lifecycle of a building or infrastructure. First phases in the lifecycle account for majority of static design data (i.e. architecture, constructive elements, equipment) while later phases contribute more dynamic data (cons truction site, operation). The industry efficiently utilizes common information engineering approaches for storing, updating and processing of the data. However, the traditional information management approaches (i.e. SQL databases and queries) are not efficient enough in the digital construction era where a growing amount of semantic content is available as Linked Open Data. The AECOO projects will have to upgrade traditional databases to knowledge bases. This will enable semantic reasoning about project data beyond the capacity of an expert (i.e. construction foreman) in situations where project documentation is incomplete. In the paper, an overview of existing research in knowledge engineering technologies appropriate for AECOO projects with focus on building materials domain is given. In the second part, usage of knowledge base for building materials is demonstrated with a use case from the heritage building domain.

INŽENJERSTVO ZNANJA ZA PODRUČJE GRAĐEVNIH MATERIJALA

SAŽETAK: Industrija arhitekture, inženjerstva, građenja, vlasništva i upravljanja (engl. AECOO) prikuplja goleme količine podataka tijekom cijelog životnog ciklusa zgrade ili infrastrukture. U prvim fazama životnoga ciklusa nastaje većina statičkih podataka o projektu (tj. o arhitekturi, konstrukcijskim elementima, opremi) dok se u kasnijim fazama prikuplja više dinamičkih podataka (građenje, funkcioniranje). Industrija učinkovito koristi opće informatičke inženjerske pristupe za spremanje, noveliranje i procesiranje podataka. Međutim, tradicijski pristupi informatičkoga upravljanja (tj. SQL baze podataka i upitnici) nisu dovoljno učinkoviti u digitalnom dobu u kojemu je narasla količina semantičkog sadržaja dostupna u vidu povezanih otvorenih podataka (engl. linked open data). Projekti iz područja AECOO morat će pretvoriti tradicijske baze podataka u baze znanja. To će omogućiti semantičko razmatranje projektnih podataka koje nadilazi sposobnost stručnjaka (tj. građevinskog poslovođe) u situacijama kad je projektna dokumentacija nepotpuna. U radu je dan pregled postojećeg istraživanja tehnologija inženjerstva znanja primjeren projektima AECOO s težištem na područje građevnih materijala. U drugom dijelu rada pokazana je primjena baze znanja za građevne materijale na primjeru zgrade koja pripada baštini.

1. INTRODUCTION

1.1. MOTIVATION

In reality, documentation for AECOO projects (i.e. Technical Data Book) is often incomplete, not available or non-existent. Also, information that is exchanged between stakeholders throughout the lifecycle of a construction project does not necessarily have an understood meaning [1]. In such situations, additional steps are needed outside the project's information system to search for specific technical information. Additionally, such additional searches are costly. There is also a cost for not finding information. Although it's impossible to measure the exact cost of employees not finding information on a company's intranet, the Intranet Cost Analyzer [2] gives a ballpark figure of over 17.000 EUR for a company with 50 employees (50 page visits per day per employee, 20 confusion seconds and average employee annual salary of 50.000 EUR). This is huge cost for not finding information.

It is known that traditional information management approaches correspond to the concept of "closed world assumption" where failed data search assumes that data does not exist. For example, consider the task [3] of designing a minimal concrete cover for a reinforced concrete beam placed outside a residential building situated close to the coast. To obtain an adequate concrete durability for the exposure class XS1, an information system is required to query the Eurocode 2 table for appropriate concrete strength class (i.e. C30/37). If the table is not part of the system, the information is considered non-existent. But, the information does exist outside of the information system.

Another explanatory example has happened on construction site where workers were in charge to connect new reinforcement to existing cured concrete using specific (Hilti) injection adhesives in drilled holes as designed by structural engineer (Post-installed rebar connections [4]). The workers replaced the planned system with (cheaper) alternative adhesive. At that moment, depth of the drilled hole had to be checked against the requirements of the alternative adhesive material. This is an unpredictable event and the information about the required depth of the hole for the rebar was not available. The goal is to transform such unpredictable events into predictable ones because, again, the information does exist outside of the information system.

1.2. BUILDING MATERIALS

For any construction project to succeed, it is very important to select the materials accurately during the project's initial stage. Trying to choose the best-performing materials is a crucial task for the successful completion of a construction project [5].

Building materials can be standard, alternative, composite, and smart materials. The availability of 4000 different types of the metallic alloy and 5000 varieties of plastic, ceramics, and glass reveals that building materials data are highly diverse [6]. Furthermore, these materials possess thousands of unique properties of their physical, mechanical, thermal, chemical, optical, acoustical, and physiochemical characteristics [7]. Apart from the challenging task of capturing the semantics of large and complex properties of the building materials, another major challenge is associated with the strenuous data management issues related to the storage and maintenance of building data [8].

The materials industry is highly innovative and produces materials with different properties over the period to meet the current design, production and construction needs [5]. Because of the continuous development distributed across multiple producers, data about any materials used in AECOO projects could be integrated directly from the producers' data sources [9].

1.3. KNOWLEDGE BASES

In an organization, knowledge exists in tacit, explicit and implicit form [10]. Tacit knowledge refers the personal knowledge of an individual which is gathered through experience, personal belief, instinct and values. It is a dynamic form constantly updating and changing. Tacit knowledge is difficult to extract for an organisation and is an extremely valuable asset. Explicit knowledge is ideally what tacit knowledge needs to become. Explicit knowledge takes the form of structured language and is easily transferred to others through IT techniques. Implicit knowledge on the other hand is unstructured and difficult to explain and share with others. Knowledge can be described in terms of "know what", "know how" and "know why". In Figure 1 [11] the creation of knowledge is shown as a pyramid beginning as data gathered from experience and organised into information which can be shared and analysed to become knowledge used in decision making.

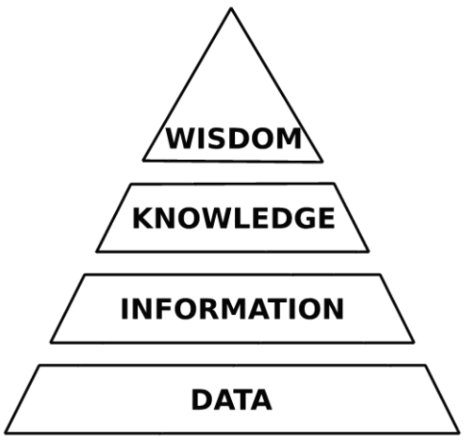

Figure 1 The pyramid of knowledge [11]

The two motivation examples above demonstrate the need for move from the concept of "closed world assumption" (information management) to the concept of "open world assumption" (knowledge management) for building materials domain. The change of concept technically corresponds to the migration from traditional databases (DB) to knowledge bases (KB) [12]. The advantages of KBs are:

- distributed KBs can be integrated by design,
- data stored in KBs can be used in reasoning mechanisms,

- in KBs data is converted to semantic information (i.e. C30/37 is minimal concrete strength class for exposure class XS1)
- Big Data [13] collected during building lifecycle can be stored in KB

Knowledge bases are intrinsic part of Semantic Web (or Web of Data technologies (RDF, OWL)) where a growing amount of semantic content is available as Linked Open Data (LOD) [14]. LOD enables linking of entity mentions in text (i.e. inside Technical report or Data Book) with their corresponding entities in a knowledge base [12]. Generally, there is a manifest lack of AECOO projects leverage to utilize knowledge engineering approaches. But, there is a growing research community for LOD for Building Information Modeling (BIM) [15].

1.4. CONTRIBUTION

Contribution of the paper is a short overview of the literature related to research and application of knowledge engineering technologies in the context of building materials. The overview is complemented with real use case as an example of knowledge engineering for building materials domain.

Therefore, in the first part of the paper, we shortly overview existing research in knowledge engineering technologies appropriate for AECOO projects with focus on building materials domain. In the second part of the paper, usage of knowledge bases for building materials is demonstrated with a use case from the heritage building domain.

2. LITERATURE REVIEW

2.1. KNOWLEDGE ENGINEERING FOR BUILDING MATERIALS DOMAIN

From a construction engineer's point of view proper identification of building materials knowledge assets and their modelling is very important for correct elements design and construction details, because together with a proper maintenance schedule, materials can reach levels of nominal life of the structure prescribed by the regulations [16].

From the knowledge engineer's point of view availability of the computer-readable building materials data and their specific properties is fundamental to performing different engineering analysis [9]. Another important feature is possibility for linking data. Linked data approach means that a knowledge base (i.e. ontology) can reference (integrate thru linking) complementary remote knowledge bases specializing in specific building materials (i.e. only insulation).

In the use case [5] authors demostrated the use of support vector machine model for selection of suitable materials in a construction project in South Korea. They reported about 87.5% accuracy against highly experienced decision maker. This case study indicates that the support vector machine model appears feasible to be the decision support model for selecting construction methods.

In [7] authors had similar overall goal as in [5] but used different, more knowledge enginering oriented approach (semantic inference, ontology). They developed material name matching system to find a standardized material name and its associated material properties from BIM model in IFCXML format. One of the results was a knowledge base (ontology) for building materials. The system was applied for building energy analysis domain. Using the proposed system, engineers will be able to increase their efficiency in entering required data into building energy analysis tools and to reduce the possibility of erroneous data input.

In [9] authors demonstrated use of ontologies for developing building material database capturing highly accurate and semantically conflicting data of building materials. Authors see the database as the first step to the development of a simulation tool for the building waste analysis. The proposed system provides syntactical homogeneity while accessing the diverse and distributed data of building materials. Following knowledge enginering technologies were used: knowledge engineering technologies: Resource Description Framework (RDF), Web Ontology Language (OWL), Protégé and Oracle RDF Graph database.

With the advance of BIM-centric approaches, semantics contained in BIM-models [17] is subject to knowledge engineering tasks. One such task is verification of objects from a BIM-model against semantical rules. In such cases knowledge engineering technologies are needed (i.e. knowledge base referring to the concept of "open world assumption"), which basically introduce general knowledge (i.e. meta description) about domain (i.e. building materials). Another ITC concept that supports interoperability and upgrades the concept of a knowledge-base is linked data (LD). Linked data utilizes Semantic Web standards and technologies [18] so that knowledge-bases from diverse domains can be interlinked [19].

New and innovative semantic applications (i.e. Semantic MediaWiki [20]) can utilize knowledge-bases with the advanced searching and querying mechanisms provided by SPARQL [19]. One such SPARQL example is to query knowledge-base for historical buildings where specific type and dimension of brick was used for walls. Since masonry brick is found on nearly every continental historic building, the query results can be used during a restoration project to learn from another previously completed restoration projects.

In addition to that, semantic applications can also employ reasoning mechanisms to infer logical consequences from asserted facts in knowledge-base. Semantic reasoning is an advancement to what was previously referred to as case-based reasoning approach [21]. For semantic reasoning a knowledge base composed of ontology (or many interlinked ontologies) and semantic rules [22][23] is needed.

In consequence, proper knowledge engineering in construction projects [24] results in knowledge-based system (KBS) acting as a consultation system [25], which supports more effective management of projects and application of building materials.

3. RESEARCH EXAMPLE: KNOWLEDGE BASE FOR CONCRETE PRODUCTION

Our research was focused to concrete production process. Figure 2 shows a process diagram (notation is IDEF) of concrete production which we developed as part of our research.

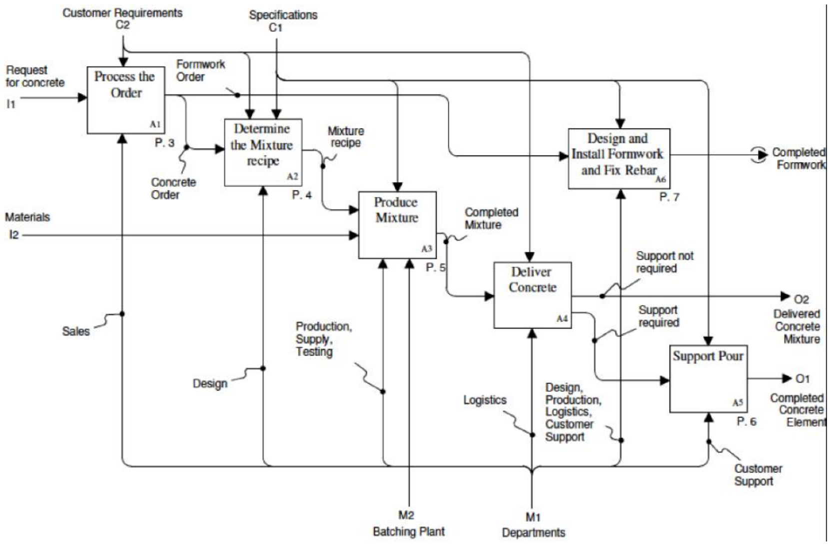

Figure 2 Concrete production process diagram (IDEF)

The process diagram shows following activities in concrete production:

- Order processing
- Specification of mixture recipe
- Mixture production
- Concrete delivery, and
- Pour support

For the process a knowledge base (Figure 2, left) with 49 concepts, 15 object properties and 15 data properties (Figure 2, right) was designed. The knowledge base was implemented as an ontology in Protégé. The ontology also contains SWLR rules that infer fine aggregates, coarse aggregates, Mortar, MediumSand, CoarseSand, FineSand, Pebble, Pebble, Cobble. Some of the rules are deined in Table 1.

Table 1 Rules for concrete production ontology

Rule for	SWLR rule
Coarse aggregate	Aggregate(?a1), hasSize(?a1, ?dm), greaterThan(?dm, 4.0) -> CoarseAggregate(?a1)
Fine Aggregate	Aggregate(?a1), hasSize(?a1, ?dm), greaterThan(?dm, 0.063), lessThan(?dm, 4.0) -> FineAggregate(?a1)
Mortar	hasConcreteMixProportions(?c, ?x) ^ Concrete(?c) ^ hasSize(?a, ?sz) ^ lessThan(?sz, "4.0"^^xsd:double) ^ hasAggregate(?x, ?a) -> Mortar(?c)
Fine sand	Sand(?sd), hasSize(?sd, ?sz), greaterThanOrEqual(?sz, 0.063), lessThanOrEqual(?sz, 0.2) -> FineSand(?sd)

The concrete production ontology is an open and therefore scalable repository of knowledge, which server as a basis for development of further semantic applications for construction domain.

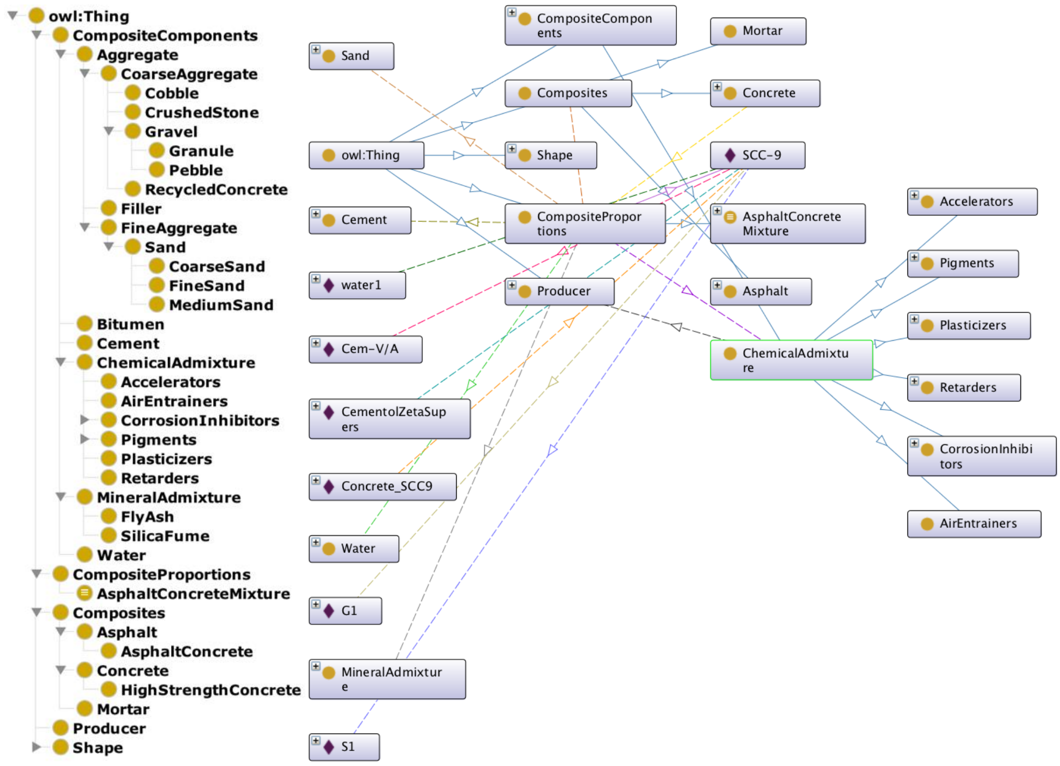

Figure 3 Hierarchy of concepts (left) and their relations (right) for concrete production ontology

4. CONCLUSIONS

In the paper, we reviewed research and application of knowledge engineering technologies in the context of building materials.

There is only little research literature published at the crossroad of building materials and knowledge engineering (keywords: linked data, semantic web, knowledge bases). One of the reasons for this is that, generally, application of knowledge engineering to building materials domain is out-of-scope for AEC researchers while IT researchers are more interested in basic IT research than applicative research. Luckily, construction informatics has growing interest in knowledge engineering in AEC.

Pioneering applications of knowledge engineering technologies for building materials can be found where linked data approach is utilized thru a knowledge base (i.e. ontology) that can link complementary remote knowledge bases specializing in specific building materials (i.e. concrete).

Research activities are most active in the following domains:

- building energy analysis,
- building waste analysis,
- building material catalogues,
- material name matching from BIM models,
- ontologies for verification of objects from a BIM-model against semantical rules
- concrete production.

Our research in concrete production ontology proved the usefulness and efficiency knowledge engineering.

Future research will include integration of different complementary ontologies from the AECOO domain.

REFERENCES

[1] A. Tibaut and D. Jakoša, *Development of knowledge model for construction projects*, vol. 224. 2015.

[2] Dack.com, 'The excellent intranet cost analyzer'. [Online]. Available: http://www.dack.com/web/cost_analyzer.html. [Accessed: 15-Feb-2017].

[3] J. Walraven, P. Chana, and R. S. Narayanan, 'Eurocode 2 Worked Examples', p. 120, 2008.
[4] Hilti, 'Post installed rebar connections (white paper)', 2011.
[5] hr022165@reading. ac. u. Jungseop Kim1, rd026992@reading. ac. u. Sangyong Kim2, and L. Tang L.Tang@reading.ac.u, 'Case Study on the Determination of Building Materials Using a Support Vector Machine.', *Journal of Computing in Civil Engineering*, vol. 28, no. 2. pp. 315–326, 2014.
[6] M. M. Farag, 'Quantitative methods of materials selection', in *Handbook of material selection*, 2006, pp. 466–488.
[7] K. Kim, G. Kim, D. Yoo, and J. Yu, 'Semantic material name matching system for building energy analysis', *Autom. Constr.*, vol. 30, pp. 242–255, 2013.
[8] [A. Radinger, B. Rodriguez-Castro, A. Stolz, and M. Hepp, 'BauDataWeb: the Austrian building and construction materials market as linked data', in *Proceedings of the 9th International Conference on Semantic Systems - I-SEMANTICS '13*, 2013, p. 25.
[9] M. Bilal, L. O. Oyedele, K. Munir, S. O. Ajayi, O. O. Akinade, H. A. Owolabi, and H. A. Alaka, 'The application of web of data technologies in building materials information modelling for construction waste analytics', *Sustain. Mater. Technol.*, 2017.
[10] O. K. Creation, I. Nonaka, T. Knowledge, and E. Knowledge, 'Nonaka ' s Four Modes of Knowledge Conversion', *Organization*, vol. 5, pp. 14–37, 1997.
[11] R. L. Ackoff, 'From data to wisdom', *J. Appl. Syst. Anal.*, vol. 16, no. 1, pp. 3–9, 1989.
[12] W. Shen, J. Wang, and J. Han, 'Entity linking with a knowledge base: Issues, techniques, and solutions', *IEEE Trans. Knowl. Data Eng.*, vol. 27, no. 2, pp. 443–460, 2015.
[13] M. Bilal, L. O. Oyedele, J. Qadir, K. Munir, S. O. Ajayi, O. O. Akinade, H. A. Owolabi, H. A. Alaka, and M. Pasha, 'Big Data in the construction industry: A review of present status, opportunities, and future trends', *Adv. Eng. Informatics*, vol. 30, no. 3, pp. 500–521, 2016.
[14] P. Pauwels, S. Törmä, J. Beetz, M. Weise, and T. Liebich, 'Linked Data in Architecture and Construction', *Autom. Constr.*, vol. 57, pp. 175–177, 2015.
[15] C. Eastman, P. Teicholz, R. Sacks, and K. Liston, *BIM Handbook: A Guide to Building Information Modeling for Owners, Managers, Designers, Engineers and Contractors*, vol. 2. 2011.
[16] F. Asdrubali, B. Ferracuti, L. Lombardi, C. Guattari, L. Evangelisti, and G. Grazieschi, 'A review of structural, thermo-physical, acoustical, and environmental properties of wooden materials for building applications', *Build. Environ.*, vol. 114, pp. 307–332, 2017.
[17] H. Liu, M. Lu, and M. Al-Hussein, 'Ontology-based semantic approach for construction-oriented quantity take-off from BIM models in the light-frame building industry', *Adv. Eng. Informatics*, vol. 30, no. 2, pp. 190–207, 2016.
[18] J. H. M. Tah and H. F. Abanda, 'Sustainable building technology knowledge representation: Using Semantic Web techniques', *Adv. Eng. Informatics*, vol. 25, no. 3, pp. 547–558, 2011.
[19] R. Meymandpour and J. G. Davis, 'A semantic similarity measure for linked data: An information content-based approach', *Knowledge-Based Syst.*, vol. 109, pp. 276–293, 2016.
[20] A. Tibaut and D. Jakoša, 'Development of Knowledge Model for Construction Projects', in *Lecture Notes in Business Information Processing*, vol. 224, 2015, pp. 248–259.
[21] H.-J. Wang, C.-W. Chiou, and Y.-K. Juan, 'Decision support model based on case-based reasoning approach for estimating the restoration budget of historical buildings', *Expert Syst. Appl.*, vol. 35, no. 4, pp. 1601–1610, 2008.
[22] M. Slota, J. Leite, and T. Swift, 'On updates of hybrid knowledge bases composed of ontologies and rules', *Artif. Intell.*, vol. 229, pp. 33–104, 2015.
[23] P. Pauwels, D. Van Deursen, R. Verstraeten, J. De Roo, R. De Meyer, R. Van de Walle, and J. Van Campenhout, 'A semantic rule checking environment for building performance checking', *Autom. Constr.*, vol. 20, no. 5, pp. 506–518, 2011.
[24] M. Belsky, R. Sacks, and I. Brilakis, 'Semantic Enrichment for Building Information Modeling', *Comput. Civ. Infrastruct. Eng.*, vol. 31, no. 4, 2016.
[25] Y.-L. Chi, T.-Y. Chen, and W.-T. Tsai, 'A chronic disease dietary consultation system using OWL-based ontologies and semantic rules', *J. Biomed. Inform.*, vol. 53, pp. 208–219, 2015.

THE DEVELOPMENT OF THE REGULATIONS IN THE AREAS OF ENERGY EFFICIENCY FOR BUILDINGS IN THE REPUBLIC OF CROATIA

Nada Mardetko Skoro[1], Toni Borkovic[2]

[1] Ministry of Construction and Physical Planning, Republike Austrije 20, 10 000 Zagreb, Croatia, email: nada.mardjetko@mgipu.hr
[2] Energy Institute Hrvoje Pozar, Savska cesta 163, 10 000 Zagreb, Croatia, email: tborkovic@eihp.hr

SUMMARY: Energy efficiency is an imperative for long-term economic development. Reducing energy needs in buildings sector contributes significantly to the achievement of the overall goals of reducing energy consumption and reducing emissions of carbon dioxide. Building sector consumes about 40% of final energy consumption and in total emissions of carbon dioxide participates with around 36%. Due to great potential of energy savings in the building sector, requirements are set on the reduction of energy consumption for new buildings and for existing buildings undergoing renovation and a compulsory share of renewable sources of energy. In addition, requirements on the quality of indoor air are set, the use of systems of automation and management as well as the use of individual measure of energy and water consumption. The long-term goals of the energy savings in the building sector as well as the commitment of a significant reduction in carbon dioxide emissions from this sector, resulted with a set of strict conditions on the buildings which are constantly increasing in accordance with the techniques and technologies development. National legislation in the field of energy savings and thermal protection are being developed since 1970, when the basic requirements are prescribed related to the fulfilment of the maximum allowed transmittance coefficients of elements of the building envelope. Since then, all of the requirements of the European policy in this area are continuously transposed into national legislation.

RAZVOJ REGULATIVE U PODRUČJU ENERGETSKE UČINKOVITOSTI ZGRADA U REPUBLICI HRVATSKOJ

SAŽETAK: Energetska činkovitost imperativ je dugoročnog gospodarskog razvoja. Smanjenje potreba za energijom u zgradarstvu znatno doprinosi postizanju općih ciljeva smanjenja potrošnje energije i smanjenju emisije ugljičnoga dioksida. Zgrade troše oko 40 % ukupne potrošnje energije, a u ukupnoj emisiji ugljičnoga dioksida sudjeluju s oko 36 %. Zbog velikog potencijala za uštede energije u zgradarstvu utvrđeni su zahtjevi za smanjenje potrošnje energije u novim zgradama i postojećim zgradama koje se obnavljaju. Određen je i obvezni udio obnovljivih izvora energije. Osim toga utvrđeni su zahtjevi za kvalitetu unutarnjeg zraka, upotrebu sustava automatizacije i upravljanja te mjere za individualnu potrošnju energije i vode. Dugoročni ciljevi uštede energije u zgradarstvu i željeno znatno smanjenje emisije ugljičnoga dioksida doveli su do skupa strogih uvjeta za zgrade koji se stalno povećavaju sukladno razvoju tehnike i tehnologije. Nacionalna regulativa u području uštede energije i toplinske zaštite razvija se od 1970. kad su propisani osnovni zahtjevi za ispunjenje najvećih dopuštenih koeficijenata prolaska topline za elemente ovojnice zgrada. Otada se svi zahtjevi europske politike u tom području neprekidno preuzimaju u nacionalno zakonodavstvo.

1. INTRODUCTION

One of the objectives of energy policy is to reduce energy needs in all sectors in order to reduce the dependence on energy and the impact on the environment. Buildings are recognized as the sector with the largest potential savings. The need of reducing energy consumption in this sector finds its place in the European Union policies and directives. Requirements on energy consumption, the share of renewable sources of energy, carbon dioxide emissions and quality assurance of internal climate are placed on buildings.

The first regulation which refers to a thermal protection of buildings-the Regulation on technical measures and conditions for thermal protection of buildings has been passed in 1970 and is related to the appearance of the first norms that have been developed in Europe. The regulation related to the heat transmission and on the air permeability of building construction. Consequently the first conditions are to be set up on the building envelope, and in the 1980s this conditions were followed by the modifications and include solar radiation. In the early 1990s the building is treated as a whole in the European Union policies which deal with setting conditions on the energy consumption.

1.1. EUROPEAN POLITICS

With the aim of Member States to reduce carbon dioxide emissions by increasing energy efficiency, the obligation of drawing and implementation programes on thermal insulation of new buildings, energy certification of buildings and on the regular inspection of boilers and heating installations and energy surveys of large energy consumers is recorded in "SAVE" directive in 1993 [1].

Directive 2002/91/EC [2] set out four requirements: the obligation of making the national General methodology for the calculation of the energy performance of the building, which must include all the aspects which determine the energy efficiency: thermal insulation, installations of heating and cooling, lighting, and other aspects such as the orientation of the building, etc., the minimum energy performance requirements for new buildings, necessary measures to ensure that buildings undergoing major renovation upgrade their energy performance, energy certification of buildings, regular inspections of boilers and air conditioning systems.

Directive 2010/31/EU [3] set out the conditions of introduction of nearly zero-energy buildings: by 31 December 2020 all new buildings in the EU have to be nearly zero energy buildings, and after 31 December 2018, new buildings occupied and owned by public authorities have to be nearly zero energy buildings.

Minimum energy performance requirements for buildings or building units are set with a view to achieving cost-optimal levels, a more detailed procedure for issuing energy certificate is required, as well as independent control systems by the Member States to check the conformity with the requirements and obligation of introducing penalties. A comparative methodology framework was established to be used by Member States for calculating cost-optimal levels of minimum energy performance requirement for new and existing buildings and building elements [4]. In addition, in order to ensure that, by 31 December 2020, all new buildings are nearly zero – energy buildings, Member States should follow Commission Recommendation of 29 July 2016 [5].

2. THERMAL PROTECTION AND ENERGY CONSUMPTION IN NATIONAL REGULATIONS IN THE REPUBLIC OF CROATIA

2.1. DEVELOPMENT OF THE REGULATION REGARDING ENERGY ECONOMY AND THERMAL PROTECTION

The first regulation relating to thermal protection for buildings was adopted in 1970 [6]. The former Yugoslavia was divided into three climatic zones, and for each zone, the maximum transmittance coefficients for individual building elements of the buildings envelope were prescribed.

First improvement of requirements for thermal protection was in 1980, and after that in 1987 with adoption of national standard JUS U.J5. 600 - Technical requirements for the design and construction of buildings. Requirements of this standard are equally applied when designing, building and renovation of existing buildings heated or air – conditioned at an indoor temperature above 12° C.

In order to reduce the energy consumption of the building sector it was necessary to change the regulations in favor of increasing the thermal protection. Better thermal protection in the buildings sector will contribute in reduction of greenhouse gas emission. Greater modification of national legislation is related to the obligation of harmonization with the European.

Technical regulation on energy economy and heat retention in buildings from 2005 [7] prescribes maximum permitted annual energy use for heating per m^2 of usable floor area of a building for residential and non-residential buildings. Regulation refers to Croatian standard HRN EN 832:2000 and HRN 832/AC:2004 for calculation of annual energy need for heating. Minimum heat retention was insured by maximum allowed heat transmission coefficients of building elements.

A Certificate of energy need for heating and cooling of a building was introduced to be an integral part of the main design. It contained calculated need for heating and cooling of a building and must be signed by the project engineer for a main design section relating to energy economy and heat protection and the main building project engineer. This certificate was also an integral part of the documentation relating to the maintenance and improvement of the essential requirements of a building.

In order to determine the expected benefit of energy savings by applying this regulation, analysis and calculations on several buildings of different purposes were carried out. The results of the calculation of the residential-business building in Slavonski Brod and the office building in Zagreb showed that the results depend on the orientation of the building and the heat gains. The regulation has allowed greater freedom in the design. Tests and analysis which were carried out (limited number analysis) confirmed the savings on energy for heating about 23%, and the need to reduce the transmission heat transfer coefficient [8].

Technical regulation on rational energy consumption and thermal protection in buildings from 2008 [9] prescribed the tougher conditions for the minimum thermal protection for the elements of the building envelope and introduced measures for the elements of the heating system in the building. For buildings with a surface area of a usable floor area exceeding 1000 m^2, the application for building permit or the main design approval respectively should be accompanied by a study of technical, environmental and economic feasibility of alternative systems for electricity supply, cogeneration systems, long – distance or block heating and systems containing heat pumps and fuel cells.

By modifying this regulation in 2013, maximum annual primary energy consumption was prescribed for single family houses 90-160 kWh/m^2 depending on the climatic conditions.

Annual energy need for heating and cooling of a building, $Q_{H,nd}$ (kWh/a) and $Q_{C,nd}$ (kWh/a) should be calculated according to the HRN EN ISO 13790:2008.

Technical regulation on rational energy consumption and thermal protection in buildings from 2014 [10] prescribed the requirements on the energy performance of new buildings and in case of reconstruction of existing buildings. Requirements were prescribed regarding maximum allowed heat transmission coefficients, maximum allowed annual primary energy consumption and maximum allowed annual energy need for heating depending on the reference climate, reduction of the effects of thermal bridges (for this purpose a catalogue of good solutions has been developed), the efficiency of technical solutions, the efficiency class of the building automation and control system, the airtightness of buildings, and the shares of renewable energy sources. Provision of indoor comfort (air quality, thermal comfort, lighting and acoustics) was ensured through microclimate parameters for which the values recommended in HRN EN 15251:2008 were used.

Pursuant to the Technical regulation, reference climate is the climate for meteorological stations taken over as characteristic for the area of continental and littoral Croatia. Continental Croatia includes all places where the mean monthly outdoor temperature of the coldest month on location of the building for the closest meteorological station that is relevant in terms of climate amounts to Θ_{mm} is ≤ 3 °C. Littoral Croatia includes all places where the mean monthly outdoor temperature of the coldest month on location of the building for the closest meteorological station that is relevant in terms of climate amounts to Θ_{mm} is > 3 °C.

Based on the cost-optimal analyses that were carried out in 2013 and 2014, requirements regarding primary energy consumption were set on individual types of buildings. Rounded values of requirements were included in the Technical regulation [10], [11]: maximum annual primary energy for single family houses, multifamily houses, offices, educational buildings, hospitals, hotels and restaurants, sport facilities, wholesale and retail trade services buildings and other types of energy-consuming buildings. Special conditions for maximum annual energy need for heating and maximum annual primary energy consumption are laid down for non-residential buildings of other purpose with height of the floor larger than 4.20 meters (Table 5).

In 2015 new regulation [12] brought new requirements and among others prescribed maximum allowed specific annual: primary energy consumption, energy need for heating and delivered energy; reduction of the effects of thermal bridges; maximum allowed heat transmission; energy efficiency of technical system for heating, cooling, ventilation, air conditioning and hot water, maximum allowed annual energy need for lighting of a building, energy efficiency class of automation system, requirements on nearly zero energy buildings and share of renewable energy in total consumption of primary energy.

- Table 1 gives the comparison of some transmittance coefficients (external wall, floor on the ground, flat and sloping roof and window) in the regulations of 1970, 1987, 2005, 2008 and 2015. In Tables 2, 3 and 4 values of maximum allowed specific thermal energy need for heating of residential and non-residential buildings before and after cost-optimal study are presented according to regulations adopted in 2008, 2014 and 2015.

Compliance with the requirements of airtightness should be proven by testing the new or renovated existing building according to HRN EN 13829:2002 method A (HRN EN 9972:2015), before the technical inspection of the building. Testing is mandatory for nearly zero-energy (nZEB) buildings and for buildings which maximum annual energy need for heating should be less than 50 kWh/(m^2a) or less than 25 kWh/(m^2a) depending on the climatic conditions.

Table 1 Comparison of some transmittance coefficients in the regulations of 1970, 1987, 2005, 2008 and 2015

Building element	Maximum permitted thermal transmittance value U [(W/m^{2}K)] of building elements Climatic zones (conditions) III -							
	Year/Indoor temperature							
	1970	1987	2005 $\Theta_{int,set,H}$>12°C		2008		2015	
	$\Theta_{int,set,H}$ >12°C	$\Theta_{int,set,H}$ >12°C	$\Theta_{int,set,H}$ ≥18°C	12°C<$\Theta_{int,set,H}$ <18°C	$\Theta_{int,set,H}$ ≥18°C	12°C<$\Theta_{int,set,H}$ <18°C	$\Theta_{int,set,H}$ ≥18°C	12°C<$\Theta_{int,set,H}$<18°C
External wall	1,28	0,80-1,20	0,80-1,00		0,45-0,60	0,75	0,30-0,45	0,50-0,60
Floor on the ground	0,93	0,65-0,90	0,65-0,80		0,50	0,65-0,80	0,40-0,50	0,65-0,80
Flat and sloping roof	0,93	0,55-0,75	0,55-0,70		0,30-0,40	0,40-0,50	0,25-0,30	0,40-0,50
Window		1,60-3,70	1,80	3,00	1,80	3,00-3,00	1,60-1,80	2,50-2,80

$\Theta_{int,set,H}$- indoor temperature

Table 2 Maximum allowed specific thermal energy need for heating of residential and non-residential buildings heated to a temperature of 18°C and more according to the Technical regulation on rational use of energy and heat retention in buildings (OG 110/2008, 89/2009, 79/2013, 90/2013) before cost-optimal study

Building type/ Energy need for heating	Climate	Shape factor f_0 = A/Ve (m^{-1})		
		f_0≤0,20	0,20<f_0<1,05	f_0≥1,05
Residential $Q''_{H,nd}$ kWh/(m^2•year)	Continental & Littoral	51,31	41,03 + 51,41·f_0	95,01
Non-residential $Q'_{H,nd}$ kWh/(m^3•year)	Continental & Littoral	16,42	13,13 + 16,45·f_0	30,40

Table 3 Maximum allowed specific thermal energy need for heating of residential and non-residential buildings heated to a temperature of 18°C and more according to the Technical regulation on rational use of energy and thermal protection in buildings (OG 97/2014, 130/2014) after cost-optimal study

Building type/ Energy need for heating	Climate	Shape factor f_0 = A/Ve (m^{-1})		
		f_0≤0,20	0,20<f_0<1,05	f_0≥1,05
Building ≤80 m^2 $Q''_{H,nd}$ kWh/(m^2•year)	Continental & littoral	51,31	41,03 + 51,41·f_0	95,01
Single family house $Q''_{H,nd}$ kWh/(m^2•year)	Continental	40,50	33,62 + 34,4·f_0	69,74
	Littoral	21,60	17,73 + 19,33·f_0	38,03
Other residential & non-residential high ≤4,20m $Q''_{H,nd}$ kWh/(m^2•year)	Continental	40,50	32,39 + 40,58·f_0	75,00
	Littoral	21,60	17,27 + 21,65·f_0	40,00
Other residential & non-residential high >4,20m $Q'_{H,nd}$ kWh/(m^3•year)	Continental	10,13	8,10 + 10,15·f_0	18,75
	Littoral	5,40	4,32 + 5,41·f_0	10,00

Table 4 Maximum allowed specific thermal energy need for heating of residential and non-residential buildings heated to a temperature of 18ºC and more according to the Technical regulation on rational use of energy and thermal protection in buildings (OG 128/2015)

Building type/ Energy need for heating $Q''_{H,nd}$ kWh/(m²•year)	Climate	Shape factor f_0 = A/Ve (m^{-1})		
		$f_0 \le 0,20$	$0,20 < f_0 < 1,05$	$f_0 \ge 1,05$
Single family house	Continental	40,50	$32,39 + 40,58 \cdot f_0$	75,00
	Littoral	24,84	$17,16 + 38,42 \cdot f_0$	57,50
Other non-residential	Continental	40,50	$32,39 + 40,58 \cdot f_0$	75,00
	Littoral	24,84	$19,86 + 24,89 \cdot f_0$	45,99

Table 5 Maximum primary energy for new buildings and for nearly zero-energy buildings by building type

Requirements for new buildings	E_{prim} new buildings/nearly zero-energy buildings [kWh/(m²·a)]					
	Technical regulation (OG 97/2014)		Technical regulation (OG 130/2014)		Technical regulation (OG 128/2015)	
Building categories	θ_{mm} ≤3°C	θ_{mm} >3°C	θ_{mm} ≤3°C	θ_{mm} >3°C	θ_{mm} ≤3°C	θ_{mm} >3°C
Apartment blocks	-	-	120/80	90/50	120/80	90/50
Single-family houses	100/40	60/30	100/40	60/30	115/45	70/35
Offices	-	-	65/30	65/25	70/35	70/25
Educational buildings	-	-	60/55	55/50	65/55	60/55
Hospitals	-	-	280/200	280/190	300/250	300/250
Hotels and restaurants	-	-	120/80	70/65	130/90	80/70
Sports facilities	-	-	400/190	170/100	400/210	170/150
Wholesale and retail trade services buildings	-	-	450/170	280/140	450/170	280/150
Other types of energy-consuming buildings	-	-	150/-	80/-	150/-	100/150
Other types of energy-consuming buildings high>4,2m	-	-	225/-	120/-	-/-	-/-

2.2. COST-OPTIMAL LEVELS OF MINIMUM ENERGY PERFORMANCE REQUIREMENTS

According to Article 4 of the EPBD, "Cost optimal levels shall be calculated in accordance with the comparative methodology framework referred to in Article 5 once the framework is in place".

Minimum performance requirements must be set for new and existing buildings and building elements. The use of the cost-optimal framework methodology is obligatory and it prescribes calculation of cost optimal levels for the macroeconomic and financial viewpoints. Discrepancies should not exceed 15% between the calculated cost optimal levels of minimum energy performance requirements and the minimum energy performance requirements in force.

Cost optimal levels of minimum energy performance requirements for Croatia were calculated in two consecutive steps – first the analysis of single family buildings followed by the analysis for the apartment blocks buildings, office buildings, buildings for education, retail buildings, sports buildings, hotels, and hospitals.

Reference single family houses were defined as virtual buildings, with technical characteristics based on statistical data and research on energy consumption for building in three time bins – before 1971, 1971-1987 and after 1987

– following the major milestones in legislation on thermal protection of buildings in Croatia. Separately, as average single family building deviates from optimal geometry regarding form factor and passive solar gains, optimized schematic design for new building was adopted in order to investigate cost optimal level of building envelope and technical systems for nearly zero energy building (as Directive 2010/31/EC isn't explicit on nZEB requirements for building refurbishment). This approach set the theoretical highest energy performance as the nZEB requirements for new buildings. First primary energy requirement for the single family homes has been adopted concurrently to the cost optimal analysis through the amendments of Technical regulation on rational use of energy and thermal protection in buildings [9], but based on simplifies assessment of primary energy through useful heating energy requirements for the buildings.

Subsequent analysis for apartment block buildings, office buildings, buildings for education, retail buildings, hotels and restaurants, hospitals and sports halls followed the same approach, but with modified time bins to reflect legislation changes in 2005. Definition of reference buildings was based on registry of energy performance certificates, which had approximately 15.000 entries at the moment of analysis and was used as most reliable source of information on basic building geometry, thermal characteristics of external envelope and energy performance. Data on actual energy consumption of public buildings was obtained from EMIS system, in order to check reliability of virtual reference buildings models based on average values from registry of energy performance certificates for all building types except hotels (where median values were used due to large range of actual buildings).

Cost optimal levels were calculated using cost optimal methodology defined in CDR 244/2012 [4]. Selection of packages of measures was in order for the analysis to be cost effective based on four different energy performance levels of external envelope (regarded as single envelope package), most common energy carriers – electricity, natural gas, LPG, fuel oil, pellets, district heating, and use of renewable energy sources by solar thermal collectors and photovoltaics. For the purpose of definition of reference buildings and cost optimal calculation, total of 450 preliminary architectural designs of buildings corresponding the statistical input parameters were generated, followed by 560 useful heating energy calculation, 450 cost estimates for external envelope reconstruction, 2000 preliminary designs and cost estimates of building technical systems, 400 cost estimates of lighting systems and separate modular photovoltaic systems with cost estimates for use in off grid mode on the buildings (as regulation on grid connection of the PV systems in the buildings to the network was restrictive, and use of the temporary export of the energy to the grid was seldom feasible).

The Report from the Commission to the European Parliament and the Council from 2016 [13] showed a significant potential for cost –effective energy saving. The result of the comparison of the cost optimal levels and minimum requirements showed that around half Member States have minimum performance requirements within the 15% threshold. Minimum performance requirements for new buildings as well for major renovations in Croatia according to the Report were set about 50% above the threshold Gap in Croatia was reported based on the results for single family homes for which, at the time when cost-optimal calculations were performed, primary energy requirements were set at approximate level using average system efficiencies and values based on calculations not fully compliant to the national calculation algorithm. As cost-optimal level was expressed as the range of values rather than single value due to the low number of packages of measures, evaluation of reported gap was based on calculation of equally weighted average gaps per reference case [14]. This gap has been later addressed in new requirements set by Technical regulation on rational use of energy and thermal protection in buildings (OG 128/2015) [12]. For other building types (apartment block, office, education, retail, sports buildings, hotels and hospitals) reference primary energy requirements haven't been set at the time of the definition of cost optimal levels in legislation – results of the cost optimal analysis were actually used to define primary energy requirements for the apartment blocks and non-residential buildings, annulling the gap between actual requirements and cost optimal levels.

Final report on Technical assessment of national/regional calculation methodologies for the energy performance of buildings [15] states that 54% of methodologies used by Member States comply to CEN standards, and only 43% are deemed fully reliable for the calculation of the primary energy demand, indicating that further training of the Member States experts is needed. Assessment of cost optimal calculations in the context of the EPBD [14] gives more insight into the conformity issues regarding scope, definition of reference buildings, measures and packages, calculation of primary energy, global costs, sensitivity analysis, derivation of cost-optimal levels and plans to reduce the gap between the minimum requirements and cost optimal levels.

3. CONCLUSION

Cost optimal levels of energy performance requirements for the buildings and building elements in Croatia are set according to the national calculation algorithm, national primary energy factor and cost optimal calculation. Gap which was recognized in single family homes has been addressed in Technical regulation on rational use of energy and thermal protection in buildings (OG 128/2015) [12] providing the new primary energy requirement within 15% deviation from cost optimal level until new iteration of cost optimal calculations. Remaining issue are cost optimal requirements on building elements, which have to be resolved in new cost optimal calculations.

Cost optimal performance levels need to be monitored and adjusted every 5 years, with regards to introduction of nearly zero energy buildings from 2019 onwards, introduction of NZEB refurbished buildings and environmental targets for the entire sector. Report [14] gives best practice examples in current cost optimal analysis, where Croatian sensitivity analysis has been recognized as best practice (driven by uncertain input values of the simulations due to negative economic trends). At the present moment, before new cost optimal calculations, current requirements set in legislation regarding primary energy, delivered and useful energy and building elements should be monitored, and primary energy factors confirmed for their effect on entire energy sector.

Other requirements that are now set out in current regulations, it is necessary to develop and improve and particularly those that improve indoor climatic conditions and microclimate inside and around buildings.

REFERENCES

[1] Council Directive 93/76/EEC of 13 September 1993 to limit carbon dioxide emissions by improving energy efficiency (SAVE)

[2] Directive 2002/91/EC [2] of the European Parliament and of the Council of 16 December 2002 on the energy performance of buildings

[3] [3] Directive 2010/31/EU of the European Parliament and of the Council of 19 May 2010 on the energy performance of buildings (recast)

[4] Commission Delegated Regulation (EU) No 244/2012 of 16 January 2012 supplementing Directive 2010/31/EU of the European Parliament and of the Council on the energy performance of buildings by establishing a comparative methodology framework for calculating cost-optimal levels of minimum energy performance requirements for buildings and building elements (Text with EEA relevance)

[5] Commission Recommendation (EU) 2016/1318 of 29 July 2016 on guidelines for the promotion of nearly zero-energy buildings and best practices to ensure that, by 2020, all new buildings are nearly zero-energy buildings

[6] Regulation on technical measures and conditions for thermal protection of buildings (OG 35/70)

[7] Technical regulation on energy economy and heat retention in buildings from 2005 (OG 79/2005, 155/2005, 74/2006)

[8] Marđetko-Škoro, N., Fučić, L., Bertol-Vrček, J.: Technical regulation on energy consumption and thermal protection in buildings, GRAĐEVINAR 57 (2005) 7

[9] Technical regulation on rational use of energy and thermal protection in buildings (OG 110/2008, 89/2009, 79/2013 and 90/2013)

[10] Technical regulation on rational use of energy and thermal protection in buildings (OG 97/2014., 130/2014.)

[11] Marđetko Škoro, N.: Implementation of the EPBD in Croatia, status in December 2014

[12] Technical regulation on rational use of energy and thermal protection in buildings (OG 128/2015)

[13] Report from the Commission to the European Parliament and the Council Progress by Member States in reaching cost-optimal levels of minimum energy performance requirements, COM(2016) 464 final

[14] Assessment of cost optimal calculations in the context of the EPBD (ENER/C3/2013-414) Final report 19 November 2015; Ecofys 2015 by order of: European Commission

[15] Technical assessment of national/regional calculation methodologies for the energy performance of buildings - Service contract number: ENER/C3/2013-425/SI2.679523 -Final report (2015-01-30)

HEALTH ASPECTS IN BUILDING CERTIFICATION SYSTEMS

Tajda Potrc[1], Roman Kunic[2], Andraz Legat[1], Mateja Dovjak[2]

[1] Slovenian National Building and Civil Engineering Institute, Dimiceva ulica 12, 1000 Ljubljana, Slovenia,
email: tajda.potrc@zag.si, andraz.legat@zag.si
[2] Faculty of Civil and Geodetic Engineering, Jamova 2, 1000 Ljubljana, Slovenia,
email: Roman.Kunic@fgg.uni-lj.si, mateja.dovjak@fgg.uni-lj.si

SUMMARY: Human of the developed countries are spending 90% of their time indoors. The quality of the indoor environment plays an important role for the health status of the residents. The health effects may occur due to the exposure to various health risks in the indoor environment. The paper studies which health related topics are present in the selected sustainable building certification schemes LEED, BREEAM, DGBN. The schemes are compared to a health and wellbeing certification scheme WELL. Air quality and visual comfort are represented and evaluated in all studied schemes. The water quality is present in all certification schemes, but most of the sustainable building certification schemes are dealing with efficient water use and potential water saving opportunities, less with the quality of the water regarding health and wellbeing of the occupants. The sustainable building certification schemes incorporate some aspects connected with fitness, comfort and mind. The topics connected to nourishment are almost not present in the studied sustainable building certification schemes. The essential topics connected with health are generally present also in the sustainable building certification schemes. The health and wellbeing certification schemes offer a more comprehensive view on health related topics but often exceed the scope of the building and include other, non-building-related aspects.

ZDRAVLJE I DOBROBIT U SADAŠNJIM PROGRAMIMA CERTIFICIRANJA

SAŽETAK: Ljudi u razvijenim zemljama provode 90 % svoga vremena u zatvorenom prostoru. Kvaliteta unutarnjega okoliša ima važnu ulogu za zdravstveno stanje stanovnika. Učinci na zdravlje mogu biti posljedica izloženosti različitim zdravstvenim rizicima unutarnjeg okoliša. U radu se proučava koja pitanja povezana sa zdravljem postoje u odabranim (shemama certificiranja održivih zgrada poput LEED-a, BREEAM-a i DGBN-a. Te su sheme uspoređene sa certifikacijskom shemomom za zdravlje i dobrobit WELL. U svim proučenim shemama nalaze se i vrednovani su kvaliteta zraka i vizualna udobnost. Kvaliteta vode postoji u svim certifikacijskim shemama, ali većina shema certifikacije održivih zgrada obrađuju učinkovitu upotrebu vode i mogućnosti uštede vode, a manje se bave kvalitetom vode s obzirom na zdravlje i dobrobit korisnika. Programi certificiranja održivih zgrada uključuju neka pitanja povezana s tjelesnom kondicijom, udobnošću i raspoloženjem. U tim programima gotovo nema pitanja povezanih s prehranom. Bitna pitanja povezana sa zdravljem postoje općenito. Sheme certificiranja s obzirom na zdravlje i dobrobit nude opsežnija razmatranja o pitanjima povezanim sa zdravljem, ali ona često premašuju pitanja povezana sa zgradom, a uključuju druge aspekte koji sa zgradom nisu povezani.

1. INTRODUCTION

Human of the developed countries are spending 90% of their time indoors [1]. The quality of the indoor environment plays an important role for the health status of the residents. The health effects may occur due to the exposure to various health risks in the indoor environment (living and working environment). Many health problems are related to the indoor building conditions, either to the construction materials and equipment, to the size or design of the building. Health issues in buildings are connected with environmental hazards (radiological, chemical, biological, physical), building design (ventilation, pressurization, filtration, lighting, acoustics), social factors (location, safety), behavioral factors (curriculum, work activities, wellness programs), adjacent land use (chemical releases, walkability, noise sources, green spaces), architectural design (physical activity promotion, eating spaces, material selection, bio phallic design and access to natural lighting) and operations and maintenance (preventative maintenance)[2].

An exposure to unhealthy building conditions may result in the occurrence of Sick Building Syndrome (SBS) or Building Related Illnesses (BRI). US Environmental Protection Agency describes SBS as situations in which building occupants experience acute health and comfort effects that appear to be linked to time spent in a building, but no specific illness or cause can be identified[3]. The complaints may be localized in a particular room or zone, or may be widespread throughout the building. The characteristic symptoms of SBS that may occur singly or in combination with each other are headache, eye, nose, or throat irritation, dry cough, dry or itchy skin, dizziness and nausea, difficulty in concentrating, fatigue and sensitivity to odours [4]. In contrast, the term Building Related Illness (BRI) is used when symptoms of diagnosable illness are identified and can be attributed directly to airborne building contaminants[3]. Existing technologies and procedures are able to improve indoor environments in a manner that significantly increases productivity and health of the occupants [5]. Additionally, a healthier indoor environment quality (IEQ) for working environment is beneficial for the employees since they are more productive and decreased absenteeism [6].

The European Union released the Energy Performance of Buildings Directive [7] to make buildings more energy efficient. This decrease on energy is indirectly also contributing to less air pollution thus to less energy production and environmental pollution connected with it. Another step forward is to make buildings sustainable. Sustainable buildings should fulfill environmental, social and economic as well as functional and technical aspects. The environmental and the economical aspect relating buildings are often being valued and are familiar to the people related to the building industry, while social aspect of building are gaining more importance in the recent times. The health aspects of building are often a part of social aspects of buildings; in some cases they are also overlooked.

For assessing and measuring sustainability in buildings special schemes were developed. Certification schemes are tools for evaluating the objectives and strategies for the development of buildings. Existing certification schemes like LEED, BREEAM, DGNB and etc. are developed as a tool to measure the sustainability of the buildings[8]. These tools are often based on auditing of buildings, putting a score to each investigated parameter that result in a final score for the buildings. Parameters are either quantitative using a physical life cycle approach with quantitative inputs and outputs of material and energy, or qualitative based on scores and criteria [9]. While some aspects of sustainability can be measured, a lot of aspects connected with health and social factors are qualitative and are not easy to quantify. Most of the sustainability certification schemes are also focusing on the IEQ in some part, but there are also certification schemes that are dealing only with one aspect of the sustainability. With the growing attention of the occupant wellbeing in building special rating schemes were developed that in most cases are complementing the existing green building certification schemes. The International Well Building Institute has launched it certification scheme in 2014 and is focused on the assessment of health and well-being related questions in the built environment [10]. A similar certification program is Living Building Challenge, created by the International Living Future Institute in 2006 [11]. We have also noticed other tools to measure health and well-being as for example Health, Wellbeing and Productivity in Offices published by World Green Building Council [12] or Fit well launched by the Center for Active design [13].

Some of the aspects assessed in the certification schemes are already regulated with standards. In Europe there are standards that are applied Europe wide (standardization initiatives, Construction Products Directive, REACH, Biocides Directives, etc.), while some standards are valid only in certain countries. The European standard organization (CEN) is working on the development of horizontal standards under Construction Products Directive (CPD) aimed at removing barriers to trade in construction products. One of the essential requirements of the CPD is hygiene, health and the environment. The standard will be used for CE marking of construction products and attestation of conformity [14]. The existing standard in the EU are mainly focused on products and their performance in the indoor environment, less with the impact of the wellbeing of the occupants. Certification schemes are more qualitatively orientated and less dependent on standards although certain aspects are underlined with standards. Depending on the origin of the certification schemes there are also different standards and regulations used in the certification scheme.

The purpose of this research was to analyze the existing sustainable building certification schemes and compare them with existing certification systems that focus on the health aspects of buildings. This study is offering insights which topics are already covered in the sustainable building certification schemes and where are the possibilities for improvement.

2. METHODS

In the following study we have compared different schemes for certifying building on their aspect regarding health and wellbeing of the occupants in the buildings. Three sustainable building certification schemes, namely LEED BD+C: new Constructions v4[15] , DGNB New Construction Residential[16] and BREEAM New Construction 2016[17], are compared with WELL certification scheme[10], which is a scheme to assess only aspects of buildings connected with health and wellbeing of the occupants. The comparison is divided to different topics, following the example of the WELL certification; namely Air, Water, Nourishment, Light, Fitness, Comfort and Mind. Firstly, it is analyzed which sections of the studied scheme are dealing with certain topics. Further, the topics are described and compared. The tables are in the Appendix.

3. RESULTS AND DISCUSSION

3.1. AIR

Indoor air quality (IAQ) is one of the aspects of indoor environment quality. The World Health Organization estimates that 1.6 million excess deaths are associated to exposure to indoor air pollutants. The major sources for the indoor air pollution are including the consumption of solid fuels indoors, tobacco smoking, and outdoor air pollutants, emissions for construction materials and furnishings and improper maintenance of ventilation and air conditioning systems. This sources cause the emittance of fine particles, carbon monoxide, polyclinic aromatic hydrocarbons, nitrogen dioxides, sulfur oxides, arsenic and fluorine, volatile and semi-volatile organic compounds, aldehydes, pesticides, asbestos, leas, biological pollutants, radon, free chemicals, etc. The improvements of airtightness of the buildings is resulting in raising indoor pollutant levels [18].

A recent research found out that the average contribution of the IAQ to the certification schemes surveyed was 7.5%. In general, America certification schemes are placing more emphasis on IAQ. The most often considered air pollutants were volatile organic compounds (VOC), formaldehyde and carbon dioxide (CO_2). Emission source control, ventilation and indoor air measurement were discovered to be the main pathways used in green building schemes [19]. Some certification schemes introduced mandatory requirements for addressing IAQ. For example, in the 2009 LEED certification ASHRAE 62.1 ventilation standard and apply of environmental tobacco smoke control have to be followed to obtain the certification. In DGNB each category has to meet minimum number of credits to be certified, although there are no rules which of the criteria should be addressed in each category.

The IAQ is related to the occurrence of the sick building syndrome (SBS). A survey conducted in three different buildings where the IAQ parameters temperature, relative humidity, carbon monoxide CO, carbon dioxide CO_2, air velocity and the presence of fungi were measured. In general, a person is considered of having SBS if two or more symptoms occur once or twice weekly. It was shown that in the three selected buildings had the same prevalence of SBS. The study concluded that the important parameters of IAQ in relation to the occurrence of SBS are ventilation and accumulation of possible contaminants within the indoor environment [20].

In the Table 1 there is a comparison of the categories in the studied assessment schemes, which cover the topic IAQ. In the sustainable building certification schemes health and wellbeing is often addressed as a separate category. For example LEED has a section IEQ where obligatory rules are defined as the minimum IEQ and smoking prohibition and credits are given for enhanced IAQ strategies, low-emitting materials, construction IAQ plan and IAQ assessment. In the DGNB scheme IAQ is a category in the section Health, comfort and user-friendliness. In BREEAM IAQ is a category in the section Health and Wellbeing. WELL certification scheme has a section Air with 29 subsections.

LEED standard provides information about minimum air quality standards that should be fulfilled. In and around the building smoking should be prohibited. Effective air ventilation, air filtration and VOC reduction is rewarded. During the construction it is necessary that there is no air pollution. It is advised that the air quality is being monitored. DGND certification scheme has requirement for the air quality, about VOC reduction and effective ventilation. BREEAM evaluates air quality, smoking prohibition, ventilation effectiveness, VOC reduction and air filtration. Additionally, the management of air infiltration, the air quality monitoring and operable windows are evaluated. The WELL standard evaluates all of the mentioned topics, as well as microbe and mold control, cleaning protocol influencing the air quality, pesticide and moisture management. The topics in the well standard are extensive and require a lot of information to make and adequate evaluation..

The 29 subsections of the WELL certificate are listed in Table 2 and are compared with the requirement in the scheme LEED, DGNB and BREEAM. The compares certification schemes all have some standards that the building should fulfill to score in a category although these are not obligatory to obtain the certification. Generally most of the certification schemes require a smoking ban except DGNB and are dealing with ventilation and VOC reduction. The LEED certification covers also topics related to entering of the building, air pollution during the construction and monitoring the air quality while in operation. BREEAM additionally covers aspect related to air infiltration, air monitoring and operable windows. The comparison is made in Table 2 (Appendix).

3.2. WATER

An average person consumes 1,5 l of water per day. Access to safe drinking water is essential to health. World Health Organization has published Guidelines for drinking water quality. The general framework developed to ensure safety of drinking water with an approach that entails systematic assessment of risks from catchment to the consumer and identification of ways in which the associated risks can be managed. It includes strategies how to deal with everyday water quality management, provides supporting information related to microbial, chemical, radiological and acceptability aspects. They are also applicable to buildings. Drinking water systems in buildings can be a source of contamination if not maintained well. The water quality in building is ensured by management practices, maintenance protocols, regular cleaning and flow management [21].

The building certification systems are often dealing only with aspects related reducing water use. In the case of LEED as special section is devoted to water efficiency. The aim of this chapter is to evaluate the measures taken to reduce indoor and outdoor water use. For example how much water do we need for irrigation, for the supply of sanitary rooms and in kitchens, are there measures for water metering indoor and outdoor, etc. A similar case is with the DGNB certification in the section Drinking water use and waste water. Maximum flow rates for toilets, showers, baths, and some home appliances are also provided. The BREEAM certification system has a special section dedicated to reduce the water use but also provides requirements for the water quality in buildings in the chapter Health and Wellbeing. The sections and categories are listed in Table 3 (Appendix).

The Well Standard evaluates if there are any sediments or microorganism present in the water that comes in contact with humans. Also the maximum concentration of inorganic contaminants is set for the following dissolved metals: lead, arsenic, antimony, mercury, nickel and copper. The maximum concertation for organic contaminants is set for styrene, benzene, ethylbenzene, polychlorinated biphenyls, vinyl chloride, toluene, xylenes and tetrachloroethylene. A special emphasis is on the presence of pesticides, herbicides and fertilizers since they are often present in the water. Also the chemicals intentionally added should remain in certain concentrations because in larger quantities they can have a negative impact on human health. The WELL standard proposes periodic water quality testing and monitoring. Beneficial is also the use of diverse water filters, for example for organic compound, sediments or microbes or other water treatments. Beneficially rated is also the promotion of drinking water by improving its taste.

To demonstrate the compliance with BREEAM certification the risk of water contamination should be minimized and in commercial and education buildings fresh drinking water should be provided for the occupants. All water systems in the building should be in compliance with the relevant national health and safety best practice guides or regulations to minimize the risk of contamination and also in the cases where humidification is required, a failsafe humidification system should be provided. The appropriate guides for own country should be followed or a compliance with the local standardization. For the promotion of drinking water coolers and access to drinking water in kitchenette or in suitable locations should be provided.

DGNB and BREEAM certification do not pay special attention on the quality of water. The comparison is presented in Table 4 (Appendix).

3.3. NOURISHMENT

The WELL standard requires the availability of fresh, wholesome food, limits unhealthy ingredients and encourages better eating habits and food culture. The surrounding is affecting the dietary patterns. Distance and access to stores, farmers markets, the availability to fresh and healthy food, reduced access and raised awareness about unhealthy food and similar strategies do affect the choice of food and dietary patterns.

The LEED certification system does not cover any topics related to the nourishment, while DGNB and BREAM incorporate topics connected with the proximity to amenities like restaurants. Also, the DGNB certification scheme evaluates the inside and outside quality and one criterion is the possibility of roof and terrace gardening. No of the certification systems deals with the topic nourishment so detailed as the WELL certification scheme.

In the WELL certification requirements are applicable to projects that provide food service or vending. Offering and promoting fruit and vegetables and refining ingredient restriction for processed foods and banning trans-fat are required. Also adequate food allergy and artificial ingredients labeling and information about the nutritional value of food is required. It should be encouraged to consume whole, natural food and cuisines and food from sustainable and humane agriculture. There should be enough space and adequate temperature conditions to store the food, but also the facilities for hand washing and safe food preparation (cooking materials and appropriate cutting surfaces) are being evaluated. There serving sizes and the dinnerware sizes are also determined. Optional and welcome is also to cover special diets. The only topics, directly connected to the building, and not to services, are rewarding on site food production and providing areas for eating. The results are presented in Table 6 (Appendix).

3.4. LIGHT

It is generally known that light influences physical, physiological and psychological behavior of people. Good lightning conditions provide the needed visual performance, determine the spatial appearance and contribute to the wellbeing of the occupants. Various studies confirmed, that insufficient or inappropriate light exposure can disrupt standard human rhythm and may have consequences for performance, safety and health[22].

Buildings create an artificial environment with restricted access to daylight. To compensate natural lightning artificial lightning sources are installed in the building. Artificial lightning can compensate the visual performance of daylight but does not take into account the non-visual effects of light like sleeping patterns, daily patterns of hormone secretion, body temperature cycles, etc. It is suggested that light optimal for vision is not necessarily effective for non-visual effects [23]. In a review, made by Galasiu and Veitch it was found out that there is a strong preference for daylight in buildings, especially offices and that in general larger windows with wide lateral views are preferred. The shading of the windows is often used by the occupants but they tend not to readjust the shading due to changing outdoor conditions. Automated lightning and shading systems are also acceptable if a certain degree of manual control is provided. It is stated, that discomfort glare form windows and daylight glare are variable from one person to another but also depend on the outside view[24].

The aspects related to light are also present in sustainable building certification schemes. The LEED certification scheme has three categories in the section Indoor Environmental Quality dedicated to light, namely Interior lightning, Daylight and Quality Views. The DGNB includes the category Visual comfort in the section Health, comfort and user-friendliness. BREEAM has the category Visual comfort in the section Health and well-being dealing with issues connected to light. The health and wellbeing certification scheme WELL includes the section Light.

The LEED certification is evaluating Interior lightning, Daylighting and Quality Views. The aim of the first category is to promote people productivity, comfort and well-being by providing high quality lightning. The ability of the occupants to adjust their lightning condition and the lightning quality is evaluated. The occupants have to have at least three stages to adjust the lightning conditions, in case of presentations lights must be controlled separately and the person has to have direct line of sight for the controlled luminaries. The lights have to be positioned between 90 and 45 degrees form nadir and have an illuminance less than 2500 cd/m^2, the lights have to provide a color rendering index higher than 80 and the majority of light has to have a rated life higher than 24000 hours. The surfaces and furnishing should meet certain surface reflectance. Also the appropriate ratio between work plane and wall or celling illuminance is suggested.

The DGNB standard is evaluating the availability of daylight in the building and in the working area, the connection to outside, the avoidance of glare, the quality of artificial light, the color rendering and the illuminance.

The BREEAM standard evaluates glare minimization, minimum daylight factors and illuminance, views outside, internal and external lightning. The glare control should be avoided through building form or building design measures such as shading. For the daylighting tables with appropriate daylight factors and illuminance values are provided. The distance from window to workplace should determine the window-to-wall ratio so that the windows are big enough to provide an adequate view.

Internal lightning is designed to provide an appropriate illuminance to the undertaken tasks and to avoid potential glare. External lightning should enable users to perform outdoor visual tasks efficiently and accurately. The lightning control should be zoned to allow adequate occupant control.

The WELL standard offers the most complete evaluation of lightning conditions. The lights should be able to maintain an average light intensity of 215 lux and maintain luminance balance between spaces and support the circadian system. The electric light glare should be minimized with the correct positioning of light or with lamp shielding while for the solar glare control manageable window shading. Glare should also be avoided in workstations. The color rendering index should be higher than 80 and the light reflectance values for surfaces like walls, ceilings, floors and furniture are suggested. Additional points can be gathered with the automated shading and dimming control, modeling daylight conditions and right size a fenestration types. While BREEAM and LEED are emphasizing views to outside, in WELL certification the view to outside have less meaning and are briefly mentioned in the subsection Right to light where it evaluated if the majority of the workstation or occupied spaces are within a certain distance from the window. The results are illustrated in Table 8 (Appendix).

3.5. FITNESS

The absence of physical activity is leading to an increase of diseases like diabetes, metabolic problems, obesity, heart diseases and other chronic conditions. The World Health Organization has identified physical inactivity as the forth leading risk factor for global mortality. The Global Recommendations on Physical Activity for Health has set out recommendations for different age groups. For children the recommended daily physical activity is 60 minutes per day with exercises strengthening the muscles and bones at least three times a week. For adults the recommended time for exercising is 150 minutes of moderate-intensity physical activity per week with muscle strengthening at least 2 times a week[25].

Sustainable building certification schemes are not dealing directly with fitness and physical activity of the occupants. The studied certification schemes are all promoting quality access to the building and the enhancement of bicycle use, but are not directly dealing with promotion of fitness in the building. The LEED certification system is evaluating active transport means in the chapters Access to Quality Transit, Bicycle Facilities. The access to remote sport facilities is evaluated in the chapter Surrounding density and diverse uses. DGNB evaluates active means of transport in chapters Indoor and outdoor quality, Mobility Structure and Access to Transport. BREEAM is dealing with fitness promotion in sections Accessibility, Proximity to amenities, Private Space and Alternative modes of transport (Table 9).

LEED certification rewards the location within existing infrastructure that promotes walkability and reduces the vehicle miles travelled. For school buildings the possibility to reach the facility by foot is rewarded, while generally it is beneficial for al building to be connected to bicycle paths and to provide storage and additional showers for occupants arriving by bike. DGNB is rewarding the access to bicycle pathways and also the proximity of parks and open spaces for possible outdoor activities, the outdoor deign to promote going outside as well as the proximity to sport facilities. BREEAM is additionally also rewarding bicycle storage. The outdoor private spaces should be furnished to promote that the occupants spend time outside. The WELL standard is the most complex about promoting fitness in buildings. It is evaluated if the use of stair in the building is promoted by the right design, accessibility and also aesthetic elements appealing for the users like music, artwork, interesting views, etc. Incentives encouraging greater levels of physical activity like subsidy for gyms or bicycle share or access to fitness classes are being promoted. Also exercise spaces and fitness equipment inside the building are promoting daily physical activity of the occupants. Pedestrian amenities and pedestrian promotion through attractive outdoor design is optional and beneficial. The promotion of bicycle transportation is evaluated through providing storage and post commute and workout facilities. Active furnishing, like for example standing desks or bicycle desks is promoted (see Table 10).

3.6. COMFORT

The indoor space should provide comfort for the occupants. Acoustic, thermal, ergonomic and olfactory comfort provides a pleasant indoor environment that prevents stress and increases productivity.

The WELL certification systems has a section devoted to Comfort, covering ergonomics, thermal, acoustic and olfactory comfort. In other sustainable building certification systems the comfort issues mainly covered are thermal and acoustic comforts. Ergonomic and olfactory comforts are not covered in the studied certification systems. The LEED system covers thermal and acoustic comfort in the section Indoor air Quality. In the DGNB certification system the comfort related themes are mainly located in the section Health, comfort and user friendliness and Functionality, partly in the section Site Quality. BREEAM covers most of the comfort related themes in the section Health and wellbeing, some also in the section Pollution (Table 11).

LEED certification evaluates the thermal comfort design via existing standards. One option is to fulfill the requirements of the ASHREE Standard 55-2010 for the HVAC design and Thermal Comfort Conditions or the requirements of ISO 7730:2005 and CEN 15251:2007. ISO 7730:2005 covers ergonomics of the thermal environment, analytical determination and interpretation of thermal comfort, using calculation of the PMV and PPD indices and local thermal comfort criteria. The CEN 15251:2007 covers indoor environmental input parameters for design and assessment of energy performance of buildings, addressing indoor air quality, thermal environment, lighting, and acoustics. A special part is evaluating the possibility for the occupants to regulate the thermal conditions. Individual thermal comfort should be provided for at least 50% of the occupants. For the acoustic comfort the noise from HVAC systems should be kept low according to ASHRAE standards, the maximum sound transmission class ratings between spaces and the reverberation time requirements are determined. If sound reinforcement or sound masking systems are installed, they should meet certain criteria to be positively evaluated.

DGNB is evaluating the operative temperature, the airflow, the maximal temperatures of the heat or cooling emitting surfaces and the air moisture for the heating and the cooling temperature. The values should comply with the DIN EN and ISO standards. The occupants should also be able to regulate the temperatures according to their individual needs. For choosing the location also the exterior noise is an evaluation criterion. Generally the acoustic comfort is evaluated in the category Soundproof. The indoor acoustic performance should comply with DIN 4109. Also the wheelchair accessibility is a criterion. To get a good score, buildings should have wheelchair friendly access to public areas. The apartments should be accessible indoor and outdoor, have adequate parking facilities and space to store the wheelchair.

BREEAM certification evaluates thermal comfort and acoustic performance. In the category Thermal comfort three aspects are evaluated, namely Thermal modelling, Adaptability and Thermal zoning and control. The building should be compliant in accordance with ISO 7730:2005, similar as LEED certification. The system should be adaptable to possible future changes due to climate changes and have a strategy how to be adjusted to different situations, user needs and be capable of interacting with other systems. For the acoustic performance the building should be inspected by a suitably qualified acoustician to provide early stage design on external sources of noise, good site layout and zoning, acoustic treatment of different zones and facades and acoustic requirements for users with special hearing and communication needs. All spaces should comply with the ambient noise level target levels and provide an adequate sound insulation between acoustically sensitive rooms and other occupied areas. The reverberation times should achieve the targeted levels and for residential buildings it is important to reduce airborne and impact sound insulation values and it is advisable pre-completion testing should be carried out. The building should also not contribute to noise pollution. Also the access for disabled people should be provided.

The WELL certification evaluates the accessibility for disabled people. The building furniture should ensure visual ergonomics, desk and heat flexibility. This is especially important for offices. To provide acoustic comfort the average sound pressure level from outside should stay below dB in average. For internally generated noise it is beneficial if the space is divided into quiet and loud zones and the maximum noise criteria are given. The reverberation time for conference rooms should not exceed 0.6 seconds, for open workspaces 0.5 seconds. Optional and beneficial are also measurements for sound masking, implementations of sound reducing surfaces and installations of sound barriers. The thermal comfort criteria should comply with ASHRAE Standard 55-2013. The users should be able to personally control their thermal environment. A special comfort criterion in WELL certification is also olfactory comfort that is evaluating the occurrence of unpleasant smells. The spaces where the smells are generated, like restrooms, kitchens, etc., should be separate from other spaces. The comparison of the criterion between the standards is presented in Table 12 (Appendix).

3.7. MIND

The mind and the physical health are inextricably connected. Environment that supports a healthy mental state can have significant psychological and physical benefits. Some features of the build environmental and also workplace policies are able to positively impact mood, sleep, stress levels and psychosocial status.

In the WELL certification system a special section is devoted to the state of mind. Other certification systems studied have some aspects incorporated in other sections, but generally fewer criterions are evaluated by other certification schemes studied. The sections and categories dealing with the state of mind are presented in Table 13 (Appendix).

LEED certifications do not incorporate a lot of topics connected with the state of mind. For the materials the material ingredients should be reported, either in the form of Manufacturer Inventory, Health Product Declaration or with similar documents. It is especially important that information about health hazards is reported. The connection to outdoors and nature should be provided by enabling quality views.

DGNB evaluates indoor and outdoor quality. Important is providing community spaces, offering additional activities for the occupants, family friendliness, the quality of the communication spaces, the possible future scenarios, the design concept for outdoors, possible terraces, loggias or balconies, etc. One aspect is also the quality of the outdoor space by providing sitting opportunities, protection from sun and rain, etc. One aspect that is not covered by any other of the studied certification schemes is safety. The building should offer the occupants the feeling of safety by limiting the possibility to see in the building, lighting the main accesses, technical security systems and preventive measures. The building should be located in an adequate environment and contribute to a better surrounding. Occupants should also be involved in the design process to ensure maximum satisfaction.

BREEAM also do not incorporate a lot of topics connected with the state of mind. One, connected to the state to mind in providing private spaces for occupants, especially outdoor spaces with sitting opportunities.

The WELL certification offers a broad spectrum of building features that contribute to the state of mind, but also work policies that enable a better working environment. First of all, the occupants should be aware what is beneficial for their health and wellbeing and also be able to be integrated in the design process. Once the building is standing, the wellbeing of the occupants should be monitored via surveys. The project should contribute integrate aesthetically pleasant details and spaces should be dimensioned to an adequate heights. Also the connection to the nature and outdoor spaces should be provided. Spaces should be adaptable, provide privacy and support also sleeping at workplace if needed. Policies regarding healthy sleeping, business travelling, health and family support are advisable. Also enabling users the means to monitor their health state, like weighting, measuring activity and so on are welcome. It is advisable that the occupants are informed about the build in materials and the organizational scheme. One aspect is also charitable activities and contributions.

3.8. INNOVATION

The innovation section is a part of WELL, LEED and BREEAM certification. Generally point can be given, if measures are taken that contribute to some aspect related to buildings (BREEAM, LEED) or health and well-being, that are not covered within the exiting scheme.

4. CONCLUSION

The comparison of the WELL certification with existing sustainability certification schemes revealed that some topics are of great importance all of the studied scheme. Air quality and visual comfort are well represented and evaluated. The water quality is generally present in all certification schemes, but most of the certification schemes are dealing with efficient water use and potential water saving opportunities, less with the quality of the water regarding health and wellbeing of the occupants. All the certification schemes incorporate some aspects connected with fitness, comfort and mind. The category, present only in the WELL certification scheme is the category Nourishment.

In the WELL standard, the studied topics are evaluated in detail and sometimes the level exceeds the limits of the building and includes also other strategies as for example food advertising or stimulating physical activity via various subventions. Generally, the building should be design in compliance with the basic requirement regarding the health of the occupants, but also the social environment should contribute to health and wellbeing of the occupants

Such strategies are not covered by any other of the studies schemes. Some of the topics present in the WELL certification scheme are also covered by law of the specific country.

Generally, the WELL certification schemes can be seen as a complementary scheme for evaluating buildings. It does only cover specific health related themes. A lot of these topics can also be found in sustainable building certification schemes, but in the WELL certification schemes these topics are more detailed and highlighted from the health perspective. In the well certification there are also a lot of topics, which are not directly connected with the building, but also with working environment or living conditions.

REFERENCES

[1] G. Evans, J. McCoy, WHEN BUILDINGS DON'T WORK: THE ROLE OF ARCHITECTURE IN HUMAN HEALTH, J. Environ. Psychol. (1998) 85–94.
[2] J.G. Allen, P. Macnaughton, J. Guillermo, C. Laurent, S.S. Flanigan, E.S. Eitland, et al., Green Buildings and Health, (2015) 250–258. doi:10.1007/s40572-015-0063-y.
[3] E.U.E.P. Agency, Indoor Air Facts No. 4 (revised). Sick Building Syndrome. Air and Radiation, 1991. http://www.epa.gov/iaq/pdfs/sick_building_factsheet.pdf.
[4] A. Kukec, M. Dovjak, Prevention and control of Sick Building Syndrome (SBS). Part 1 : Identification of risk factors, 8 (2014).
[5] W.J. Fisk, H EALTH AND P RODUCTIVITY G AINS FROM B ETTER I NDOOR E NVIRONMENTS AND THEIR R ELATIONSHIP WITH B UILDING E NERGY E FFICIENCY 1, (2000).
[6] A. Singh, M. Syal, Effects of Green Buildings on Employee Health and Productivity, 100 (2010) 1665–1669. doi:10.2105/AJPH.2009.180687.
[7] European Union, Directive 2010/31/EU of the European Parliament and of theCouncil of 19 May 2010 on the Energy Performance of Buildings (recast), Off. J.Eur. Union L 153, Strasbourg, France, 2010.
[8] G.K.C. Ding, Sustainable construction—The role of environmental assessment tools, J. Environ. Manage. 86 (2008) 451–464. doi:10.1016/j.jenvman.2006.12.025.
[9] A. Forsberg, F. von Malmborg, Tools for environmental assessment of the built environment, Build. Environ. 39 (2004) 223–228. doi:10.1016/j.buildenv.2003.09.004.
[10] WELL, (n.d.). https://www.wellcertified.com/ (accessed November 4, 2016).
[11] Living Builing Challange, (n.d.). http://living-future.org/lbc (accessed November 4, 2016).
[12] Health, Wellbeing and Productivity in Offices, (2014). http://www.worldgbc.org/files/9714/3401/7431/WorldGBC_Health_Wellbeing__Productivity_Full_Report_Dbl_Med_Res_Feb_2015.pdf (accessed November 4, 2016).
[13] fitwel, (n.d.). https://fitwel.org/assets/pdf/brochure.pdf (accessed November 4, 2016).
[14] C. Yu, Indoor and B uilt Indoor Environmental Quality – Standards for Protection of Occupants ' Safety , Health and Environment, 44 (2016) 499–502. doi:10.1177/1420326X10381106.
[15] US Green Building Council, LEED BD+C: New Construction v4, (2014). http://www.usgbc.org/credits/homes?page=1 (accessed November 10, 2016).
[16] DGNB, DGNB New Construction Residential, 2015. (n.d.).
[17] BRE Global, BREEAM New Construction 2016, (2016). http://www.breeam.com/new-construction (accessed November 10, 2016).

[18] [G. Update, Air Quality Guidelines, (2005).
[19] W. Wei, O. Ramalho, C. Mandin, Indoor air quality requirements in green building certi fi cations, Build. Environ. 92 (2015) 10–19. doi:10.1016/j.buildenv.2015.03.035.
[20] [A. Norhidayah, L. Chia-kuang, M.K. Azhar, S. Nurulwahida, Indoor Air Quality and Sick Building Syndrome in Three Selected Buildings, Procedia Eng. 53 (2013) 93–98. doi:10.1016/j.proeng.2013.02.014.
[21] F. Edition, Guidelines for Drinking-water Quality, (n.d.).
[22] L. Bellia, F. Bisegna, G. Spada, Lighting in indoor environments : Visual and non-visual effects of light sources with different spectral power distributions, Build. Environ. 46 (2011) 1984–1992. doi:10.1016/j.buildenv.2011.04.007.
[23] A.R. Webb, Considerations for lighting in the built environment : Non-visual effects of light, 38 (2006) 721–727. doi:10.1016/j.enbuild.2006.03.004.
[24] A.D. Galasiu, J.A. Veitch, Occupant preferences and satisfaction with the luminous environment and control systems in daylit offices : a literature review, 38 (2006) 728–742. doi:10.1016/j.enbuild.2006.03.001.
[25] [WHO, Global recommendations on physical activity for health, (n.d.). http://apps.who.int/iris/bitstream/10665/44399/1/9789241599979_eng.pdf (accessed December 2, 2016).

APPENDIX

Table 1 Section and categories covering health and wellbeing aspects related to air

	LEED	DGNB	BREEAM	WELL
Section	Indoor Environmental Quality(EQ)	Health, comfort and user-friendliness	Health and Wellbeing	Air
Categories	EQ prerequisite Minimum Indoor Air quality Performance Environmental Tobacco Smoke Control EQ Credits Enhanced indoor Air Quality strategies Low-Emitting Materials Construction Indoor Air Quality Plan Indoor air Quality Assessment	Indoor Air Quality	Indoor air Quality	

Table 2 Health and wellbeing topics connected to air

	LEED	DGNB	BREEAM	WELL
Air quality standards	x	x	x	X
Smoking ban	x		x	X
Ventilation effectiveness	x	x	x	X
VOC reduction	x	x	x	X
Air filtration	x		x	X
Microbe and mold control				X
Construction pollution management	x			X
Healthy entrance	x			X
Cleaning protocol				X
Pesticide management				X
Fundamental material safe				X
Moisture management				X
Air flush				X
Air infiltration management			x	X
Increased ventilation	x			X
Humidity control				X
Direct source ventilation				X
Air quality monitoring and feedback	x		x	X
Operable windows			x	X
Outdoor air systems				X
Displacement ventilation				X
Pest control				X
Advanced air purification				X
Combustion minimization				X
Toxic material reduction				X
Enhanced material safety				X
Antimicrobial activity for surfaces				X
Cleanable environment				X
Cleaning equipment				x

Table 3 Section and categories covering health and wellbeing aspects related to water

	LEED	DGNB	BREEAM	WELL
Section	Water Efficiency	Resource use and waste	Health and Wellbeing	Water
Categories	/	Drinking water use and waste water	Water Quality	

Table 4 Health and wellbeing topics connected to water

	LEED	DGNB	BREEAM	WELL
Fundamental water quality			x	x
Inorganic contaminants				x
Organic contaminants				x
Agricultural contaminants				x
Public water additives				x
Periodic water quality testing				x
Water treatment				x

Table 5 Section and categories covering health and wellbeing aspects related to nourishment

	LEED	DGNB	BREEAM	WELL
Section	/	Site quality	Transport	Nourishment
Categories	/	Proximity to relevant objects and structures Inside/outside quality	Proximity to amenities	

Table 6 Health and wellbeing topics connected to nourishment

	LEED	DGNB	BREEAM	WELL
Fruits and vegetables				X
Processed foods				X
Food allergies				X
Food contamination				X
Artificial ingredients				X
Nutritional information				X
Food advertising				X
Safe food preparation materials				X
Serving sizes				X
Special diets				X
Responsible food production				X
Food storage				X
Food production		x		X
Mindful eating				X

Table 7 Section and categories covering health and wellbeing aspects related to light

	LEED	DGNB	BREEAM	WELL
Section	Indoor environmental quality	Health, comfort and user-friendliness	Health and wellbeing	Light
Categories	Interior lightning Daylight Quality Views	Visual comfort	Visual comfort	

Table 8 Health and wellbeing topics connected to light

	LEED	DGNB	BREEAM	WELL
Visual lighting design	x	x	x	X
Circadian lighting design				X
Electric light glare control			x	X
Solar glare control		x	x	X
Low-glare workstation design				X
Color quality	x	x		X
Surface design	x			X
Automated shading and dimming controls				X
Right to light			x	X
Daylight modeling				X
Daylighting fenestration				x

Table 9 Section and categories covering health and wellbeing aspects related to fitness

	LEED	DGNB	BREEAM	WELL
Section	Location and transportation	Technical Quality Site Quality	Health and wellbeing Transport	Fitness
Categories	Access to Quality Transit, Bicycle Facilities Surrounding density and diverse uses	Mobility Structure Access to Transport Inside/outside quality	Accessibility, proximity to amenities, Alternative modes of transport Private space	

Table 10 Health and wellbeing topics connected to fitness

	LEED	DGNB	BREEAM	WELL
Interior fitness circulation		x		X
Activity incentive programs				X
Structured fitness opportunities				X
Exterior active design	x	x		X
Physical activity spaces				X
Active transport support	x	x	x	X
Fitness equipment				X
Active furnishing				X

Table 11 Section and categories covering health and wellbeing aspects related to comfort

	LEED	DGNB	BREEAM	WELL
Section	Indoor Environment Quality	Health, comfort and user-friendliness Functionality Site Quality	Health and wellbeing Pollution	
Categories	Thermal Comfort Acoustic Performance	Thermal comfort Wheelchair Accessibility Soundproof Control of the occupants Micro location	Thermal comfort Acoustic performance Noise pollution Private space	Comfort

Table 12 Health and wellbeing topics connected to comfort

	LEED	DGNB	BREEAM	WELL
ADA Accessible design standards		x		X
Ergonomics: Visual and Physical				X
Exterior noise intrusion		x	X	X
Internally generated noise	x		x	X
Thermal comfort	x	x	x	X
Olfactory comfort				X
Reverberation time	x		x	X
Sound masking	x			X
Sound reducing surfaces				X
Sound barriers				X
Individual thermal control	x	x	x	X
Radiant thermal control				X

Table 13 Section and categories covering health and wellbeing aspects related to the state of mind

	LEED	DGNB	BREEAM	WELL
Section	Materials and resources Indoor Environment Quality	Health, comfort and user-friendliness Planning Quality Site Quality	Health and wellbeing Materials	

Categories	Building disclosure and optimization Quality views	Indoor and outdoor quality Safety State of site and Block Project preparation and planning Inside/outside quality	Private space	Mind

Table 2 Health and wellbeing topics connected to state of mind

	LEED	DGNB	BREEAM	WELL
Health and wellness awareness				X
Integrative design		x		X
Post-occupancy survey				X
Beauty and design I		x		X
Biophiliy I-Qualitative	x			X
Adaptable spaces		x		X
Healthy sleep policy				X
Business travel				X
Building health policy				X
Workplace family support		x		X
Self-monitoring				X
Stress and addiction treatment				X
Altruism				X
Material transparency	x			X
Organizational transparency				X
Beauty and design II				X
Bio philia II-Quantitative				X

HEALTH, SAFETY AND WELL-BEING: A CORE PART OF SUSTAINABLE BUILDINGS

Georg Schöner1, Agnes Schuurmans[1]

1 ROCKWOOL International A/S, Hedehusene, Denmark, email: georg.schoner@rockwool.com, agnes.schuurmans@rockwool.com

SUMMARY: There is a growing awareness that health, safety and well-being aspects are integral elements of sustainable buildings. Resilient buildings with a good indoor climate, good acoustic performance, thermal comfort in winter and summer and sufficient daylight are essential to obtain a resource-efficient housing stock with durable buildings that are not demolished prematurely. Relevant 'social' aspects for sustainable buildings are listed in the CEN TC 350 standards for sustainable construction, providing assessment methods for the environmental, social and economic performance of buildings. Whilst the environmental pillar is well implemented, with Environmental Product Declarations (EPD) available all over Europe and used by the important building rating schemes, the social performance assessment is less well known and not systematically implemented. The upcoming EU framework of core indicators for sustainable buildings may include some health and well-being indicators.

ZDRAVLJE, SIGURNOST I DOBROBIT: SREDIŠNJI DIO ODRŽIVIH ZGRADA

SAŽETAK: Sve je veća svijest o tome da su zdravlje, sigurnost i dobrobit sastavni elementi održivih zgrada. Otporne zgrade s dobrom unutarnjom klimom, dobrim akustičkim svojstvima, toplinskim komforom zimi i ljeti i s dovoljno dnevnog svjetla bitne su za ostvarenje trajnih i s obzirom na resurse učinkovitih stambenih zgrada. Odgovarajuća društena pitanja održivih zgrada popisana su u normama tehničkog odbora CEN TC 350 za održivu gradnju, a sadržavaju metode ocjenjivanja okoliša, društvena i gospodarska svojstva zgrada. Dok su okolišna pitanja dobro primijenjena uz Izjavu o okolišu za proizvod (engl. Environmental Product Declaration, EDP) koja je dostupna širom Europe i koja se upotrebljava u važnim programima vrednovanja zgrada, ocjenjivanje društvenih svojstava manje je poznato i nije sustavno primijenjeno. Predstojeći okvirni program Europske unije za središnje pokazatelje održivih zgrada može obuhvatiti neke zdravstvene pokazatelje i pokazatelje dobrobiti.

1. INTRODUCTION

Whereas the TC350 standards for sustainable construction implemented health, safety and well-being aspects in assessment methods, the World Green Building Council's healthy building's campaign put it in the spotlights. The WGBC's well-received global report on Health, Wellbeing and Productivity in Offices: The Next Chapter for Green Building raised awareness on important issues for sustainable buildings, such as good indoor climate and acoustic performance [2]. The evident importance of health, safety and well-being has set the scene for taking the social building performance as an integral part of European policies. The proposed European Commission's common EU framework of indicators for the environmental performance of buildings [3] include indicators for indoor air quality and thermal summer comfort next to traditional ones such as energy consumption and carbon. The own-initiative report of the European parliament on Circular Economy also urges to take this into account [4].

The next challenge is action and implementation. An example is the Dutch tool "AQSI" for assessing the social building performance according to EN16309. AQSI is developed by building consultancy Nieman with support of NGOs and industry. It is the first tool that applies the standard for sustainable construction in a systematic way and makes it easy to use in practice. The systematic overall performance asssments function as a plug-in to the broader sustainable building rating schemes. The purpose of this paper is to show that such as tool is available, and how results can be used to gain more insight in the building performance on social issues.

2. ASSESSING AND QUALIFYING ON SOCIAL IMPACT OF BUILDINGS

The 2014 WGBC's report showed that staff cost often account for up to 90% of business operating costs, meaning that even a modest improvement in employee health or productivity can be much larger than any other financial savings associated with an efficiently designed and operated building. It shows the importance of buildings that offer people a healthy environment to work and live in. Office noise for example decreases the employee performance by 66% [6, 7]. The importance of sound is often not given much thought, but science shows that it significantly affects our well-being, our relationships and our productivity [8]. Costs for the Dutch society by noise nuisance are estimated to be € 2.5 million [7]. The value of real estate decreases with 1.6% per dB at a level >55 dB. which clearly shows the business case of good acoustics.

Concerning safety issues there is a similar story: It has been calculated that the costs of fires for society in the Netherlands are about € 1 billion a year, € 120 million due to people dying in fires [7]. Many of these people are elderly people and it is expected that the number of fire victims over 65 years of age will increase with 60% by 2030. In Belgium the societal costs are slightly lower than in the Netherlands, but the number of deadly victims is higher and older; in 2014 27 out of 69 victims were over 60 years. The average age of the buildings lost in fires was appr. 25 years old … Fires do not just occur randomly, but happen on a regular basis. Most people are not aware that building codes only have minimum requirements for how long people are allowed to escape burning buildings. But buildings should perform better than just meeting minimum compliance standards to be considered sustainable [9].

The motivation behind developing the AQSI (Assessing and Qualifying on Social Impact of buildings) Social Impact Tool [5] is that buildings are built for people to use them. This tool supports stakeholders (architects, investors, insurers, developers etc.) to assess their building according to their social performance. Today's issues on energy-efficiency and the preferred construction materials are already in the picture, but taking the 'people' aspect into account is the key issue to have a solid business case with sustainable buildings.

AQSI is based on the European Standard EN 16309, 2014; 'Sustainability of construction works – Assessment of social performance of buildings – Calculation methodology'. Although the title suggests it to be a calculation method, it is in the first place a very well-structured assessment method. Consequently the standard is rather conceptional.

Although the title suggests it to be a calculation method, it is in the first place an very well-structured assessment method. Consequently the standard is rather conceptional. The methodology is to assess the building performance as far as it exceeds the minimum legal level of performance that is required. Having a higher performance level will contribute to the sustainability of the building.

EN 16309:2014 (E)

Table 1 — Building-fabric-related aspects, user- and control-system-related aspects

Building life cycle – Use Stage	
Building-related characteristics	**User-and control-system-related characteristics for interaction with the building**
Accessibility, see 7.2	Health and comfort
1) Accessibility for people with additional needs (see 7.2.2)	18) Thermal comfort, see 7.4.2.2
2) Access to building services (see 7.2.3)	19) Indoor air quality, see 7.4.3.2
Adaptability	20) Visual comfort, see 7.4.5.2
3) ease of potential for adapting to other use (see 7.3)	Impacts on neighbourhood
Health and comfort, see 7.4	21) Emissions, see 7.5.3
4) Thermal characteristics, see 7.4.2	Safety and security
5) Characteristics of indoor air quality, see 7.4.3	22) Security against intruders and vandalism, see 7.7.4.3
6) Acoustic characteristics, see 7.4.4	
7) Characteristics of visual comfort, see 7.4.5	
8) Spatial characteristics, see 7.4.6	
Impacts on neighbourhood, see 7.5	
9) Noise, see 7.5.2	
10) Emissions, see 7.5.3	
11) Glare/overshadowing, see 7.5.4	
12) Shocks/vibrations, see 7.5.5	
Maintenance and Maintainability, see 7.6	
13) Maintenance operations, 7.6	
Safety and security, see 7.7	
14) Resistance to climate change, see 7.7.2	
15) Accidental actions (earthquake, explosions, fire and traffic impacts), see 7.7.3	
16) Personal safety and security against intruders and vandalism, see 7.7.4	
17) Security against interruptions of utility supply, see 7.7.5	

Figure 1 Table with social performance aspects of EN16309

Figure 2 Aspects assessed in AQSI: safety and security; health and comfort; maintenance; adaptability; accessibility; impacts on neighborhood

In this contribution the stepwise approach in AQSI will be shown as well as examples on how AQSI is applied to several building types and how the results contribute to improving the sustainable performance.

Step-wise approach:

An assessment in AQSI consists of a number of logical steps based on a similar approach as in EN16309 (Figure 3):

1. Characteristic space through a brief description of the building and the capture of basic data. Then a number of characteristic areas is requested. That are areas that are characteristic for the building and its use. In an office that are for instance a common workplace, a meeting room, etc. and in a dwelling it most likely will be the living, sleeping room and perhaps the outdoor area.

2. A Scenario for the future of the building is defined. The review based on a future scenario is a characteristic part of EN16309. A number of example scenarios is included in AQSI, in addition one can define a project-specific scenario.

3. The Materialisation of the building and the characteristic areas are registered by a choice of pull-down menus. AQSI has a database with a large number of specific data of building parts and construction products. It is always possible to choose for more generic materials or constructions. The database is composed of data from public sources and with detailed information of affiliated companies.

4. The Assessment generates a number of aspects of social quality from EN 16309 that can be assessed. AQSI generates at each line a number of quality aspects associated with the chosen materialization. The assessor writes a summary per topic, based on his own knowledge and perception of the project.

5. A Report is automatically generated and the assessor completes the report with his final conclusion based on the assessmentFigure 3 Screenshot of AQSI Report showing the structure: project description – short description and assessment on each aspect – summary evaluation

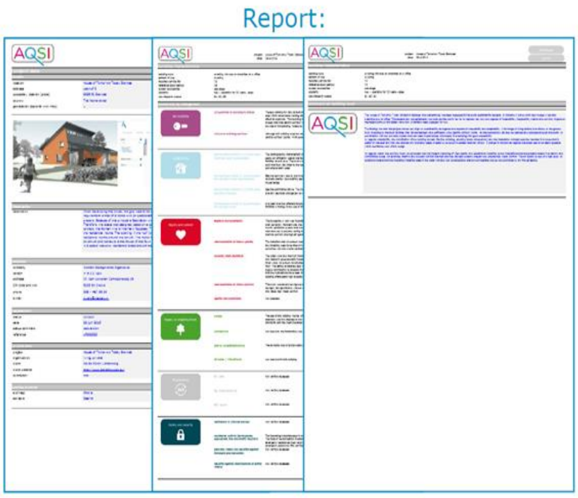

Figure 3 Logical steps of the assessment in AQSI

3. EXAMPLES

In this contribution examples[4] will be provided on how AQSI is applied to several building types and how the results contribute to creating awareness as a basis for improving the sustainable performance. The tool is referred as one of the instruments to be used as possible plug-in for BREEAM-NL [10].

[4] The AQSI format is in English but the reporting in Dutch. The contribution in the conference will translate the summary of the report in order to show the type of results

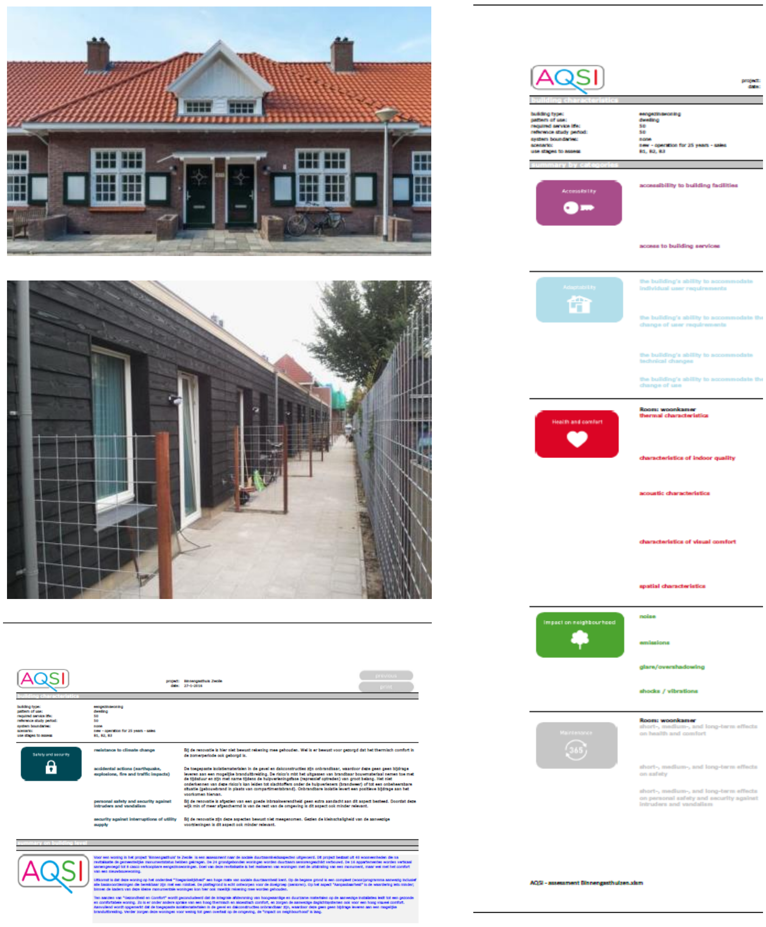

Figure 4 Example of applying AQSI to a project in Zwolle (NL) – report is in Dutch (not for reading purpose; just to show the structure)

4. COMMON EU FRAMEWORK OF CORE INDICATORS FOR THE ENVIRONMENTAL PERFORMANCE OF BUILDINGS

In September 2016, the European Commission launched a stakeholder consultation on their proposal of core indicators for building performance [6]. One of the so-called macro-objectives to achieve in Europe is healthy and comfortable spaces. Buildings can contribute to that in many ways. So far, the Commission proposal includes only some of the relevant issues.

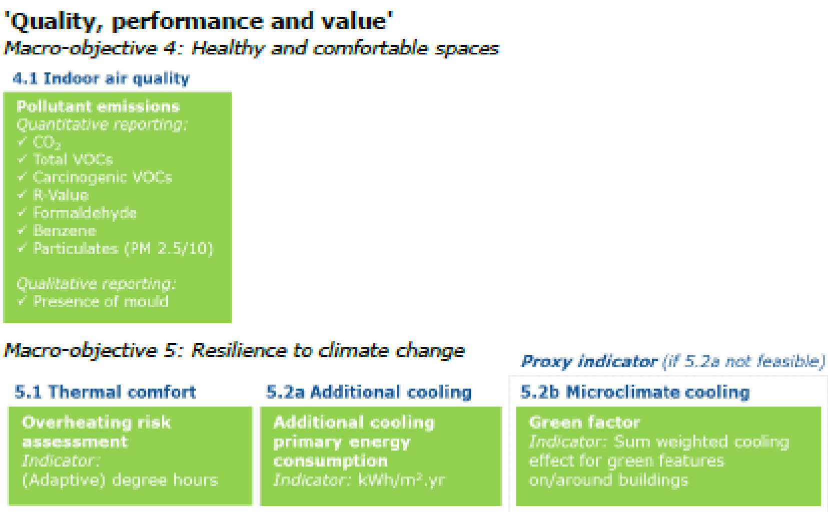

Figure 5 Aspects of health and well-being and comfort in the draft proposal of the common EU framework of core indicators for the environmental performance of buildings

5. CONCLUSIONS

Buildings have a huge impact on our sense of comfort, our health, the awareness of safety and security and on our environment. Buildings affect our well-being. That's what we call social impact. That impact is hidden to a large extent and should be taken more explicitly into consideration when designing and retrofitting our homes, offices, schools and hospitals. By using tools such a AQSI as an assessment-tool during design, realisation and usage, social impact of buildings becomes visible and tangible and therefor manageable. Further integration into sustainable building rating schemes is underway, as well as the first steps towards integration in the EU context of sustainable buildings.

REFERENCES

[1] ANDERSON, J. – There are over 2000 Verified Environmental Product Declarations (EPD) to EN 15804 for construction products registered globally. What do we know about them? [online]. 2015-11-16

[2] WWW: < https://infogr.am/constructionlcas_guide_to_epd>.

[3] World Green Building Council – Health, Wellbeing and Productivity in Offices: The Next Chapter for Green Building [online]. WorldGBC, 09-2014 [cit. 2015-08-21].

[4] WWW: < http://www.worldgbc.org/files/9714/3401/7431/WorldGBC_Health_Wellbeing__Productivity_Full_Report_Dbl_Med_Res_Feb_2015.pdf.>.

[5] European Commission to the European Parliament – Call for interest: Stakeholder group for a study on resource efficient buildings [online]. EC, 2015 [cit. 2015-08-21].

[6] WWW: < http://ec.europa.eu/growth/tools-databases/newsroom/cf/itemdetail.cfm?item_id=8251&lang=en&title=Call-for-interest%3A-Stakeholder-group-for-a-study-on-resource-efficient-buildings >.

[7] European Parliament resolution of 9 July 2015 on resource efficiency: moving towards a circular economy (2014/2208(INI)), P8_TA-PROV(2015)0266

[8] AQSI (Assessing and Qualifying on Social Impact of buildings) Social Impact Tool –Assessment with AQSI [online]. WWW: http://www.aqsi.nl/nl/hoe/

[9] Banbury SP and Berry DC (1998), Disruption of office-related tasks by speech and office noise. Britisch Journal of Psychology 89:3, pp. 499-517 and

[10] Banbury SP and Berry DC (2005), office noise and employee concentration: identifying causes of disruption and potential improvements. Ergonomics 48:1, pp 25-37

[11] As cited in [7]

[12] (Re-) building the future, CSR report 2014 ROCKWOOL Benelux Holding, pp 52-53

[13] WSB14 Barcelona, session 19, Acoustic comfort: Is invisible architecture the secret to productive and healthy buildings?

[14] WSB14 Barcelona, session 1, Fire safety as sustainability parameter - Are buildings that burn down sustainable?

[15] Announcement DGBC of Dutch publication of [2] on https://www.dgbc.nl/gezondheid / Dutch publication p.61 http://www.verosol.com/media/55827/dgbc-health-welbeing-rapport-def-2015lr.pdf

TOPIC 8.

Innovative reuse of all tyre components in concrete – Anagennisi

Inovativna uporaba svih produkata reciklaže otpadnih guma u betonu

PROPERTIES OF CONCRETE REINFORCED WITH RECYCLED TYRE POLYMER FIBERS

Ana Baricevic[1], Marija Jelcic Rukavina[1], Martina Pezer[1], Nina Stirmer[1], Marijana Serdar[1], Dubravka Bjegovic[1], Matea Dzaja[1], Marija Held[1], Petra Ruzic[1]

[1] University of Zagreb Faculty of Civil Engineering, Department of Materials, Fra Andrije Kacica Miosica 26, 10000 Zagreb, Croatia, email:abaricevic@grad.hr, jmarija@grad.hr, mpezer@grad.hr, ninab@grad.hr, mserdar@grad.hr, dubravka@grad.hr

SUMMARY: The aim of the study presented in this paper is to research the possibility of replacing polypropylene fibres (PP) in concrete with recycled polymer fibres obtained from end-of-life tyres (RTPF). Therefore, reinforced concretes with RTPF mixed with rubber particles, as received from the factory, (in amounts of 5, 10 and 15 kg/m^3) and mechanically cleaned RTPF (in amounts of 1, 2 and 5 kg/m^3) were tested in compare with plain ordinary concrete and concrete with 1 kg/m^3 of polypropylene (PP) fibres. Study comprised testing of fresh concrete properties (workability, air content and density), mechanical properties (compressive strength and modulus of elasticity) and early age deformations. Obtained results showed significant reduction in early age deformations within concrete mixes utilising RTPF compared to reference mixes with negligible difference in mechanical properties, in the same time.

SVOJSTVA BETONA ARMIRANOG POLIMERNIM VLAKNIMA IZ RECIKLIRANIH AUTOMOBILSKIH GUMA

SAŽETAK: Svrha studije prikazane u radu istraživanje je mogućnosti zamjene polipropilenskih vlakana u betonu recikliranim polimernim vlaknima dobivenim iz starih guma (engl. recycled polymer fibres obtained from end-of-life tyres, RTPF). Ispitani su betoni armirani takvim vlaknima koja su onečišćena česticama gume (u količini 5, 10 i 15 kg/m^3) i mehaničkih očišćenih RTPF-a (u količinama od 1, 2 i 5 kg/m^3) te uspoređeni s običnim nearmiranim betonom i betonom s 1 kg/m^3 polipropilenskih vlakana. Obuhvaćeno je ispitivanje svojstava svježega betona (obradivost, sadržaj zraka i gustoća), mehanička svojstva (tlačna čvrstoća i modul elastičnosti) i određena veličina deformacije u ranoj starosti. Dobiveni rezultati pokazuju znatno smanjenje vrijednosti deformacija mladog betona za mješavine betona u kojima je upotrijebljen RTPF u usporedbi s referentnim mješavinama uz istodobno zanemarivu razliku u mehaničkim svojstvima.

1. INTRODUCTION

Tyre recycling belongs to the field of sustainable development as the recycling of used products results in valuable raw materials that can be used for manufacturing products with a new value [1]. Three raw materials can be obtained by waste tyre recycling: a) rubber granules, b) steel fibres, and c) polymer fibres. Only 5% of recycled waste tyres are currently used in construction industry. Apart from rubber granules and steel fibres, recycled tyre polymer fibres (RTPF) have not so far found their use in construction industry. The aim of Anagennisi project [2] is to develop innovative solutions to reuse all tyre components in high value innovative concrete applications with reduced environmental impact.

Since the dimensions and composition of RTPF obtained from waste tyre recycling are similar to dimensions of polypropylene (PP) fibres, a concept involving replacement of industrial fibres with fibres obtained by waste tire recycling has been developed. Previous research state that micro PP fibres are activated during early age cracking, meaning that low modulus of fibres are to be effective only during first 24 hours of hardening while stress are transferred through the cement matrix [3-5].

In study presented in this paper, as part of Anagennisi project, experimental study conducted on the influence of RTPF addition on properties of ordinary concrete in fresh and hardened state. Obtained properties were compared with those obtained on plain mix and mix with 1 kg/m^3 of monofilament polypropylene fibres. The main goal was to define behaviour of this type of concretes in the exploitation.

2. EXPERIMENTAL PROGRAM

Experimental programme was based on the research of 8 different mixes divided into three groups according to type of added fibres, as follows:

- Group I - 2 reference concrete mixes: plain concrete mix and mix with 1 kg of monofilament PP fibres,

- Group II – 3 mixes with 5, 10 and 15 kg/m3 of mixed RTPF,
- Group III - 3 mixes with 1, 2 and 5 kg/m3 of mechanically sorted RTPF.

2.1. MIX DESIGN AND PREPARATION

All concrete mixes were prepared with CEM II/B-M (S, V) 42.5 N, crushed limestone as aggregate (0/4 mm, 4/8 mm and 8/16 mm) and superplasticiser (polycarboxylic ether hyperplasticiser). Following, maximum aggregate size was selected to be 16 mm and reference grading curve according Fuller`s equation was used [6, 7]. Properties of used types of PP fibres, as declared by the producer, used for reference mix is presented in Table 1 and Figure 1a.

Table 1: Properties of PP fibres

Type	Length, mm	Density, g/cm^3	Tensile strength, MPa
monofilament	6 mm	0.91	> 270

Properties of used RTPF are presented in Table 2, where mixed type is related to RTPF as received from the factory (Figure 1b), while sorted type of RTPF (Figure 1c) were obtained with cleaning procedure described in [8].

a) b) c)

Figure 1. a) Polypropylene fibres b) Mixed RTPF c) Sorted RTPF

Table 2. Properties of RTPF used in study

Quality parameter	Mixed RTPF		Sorted RTPF
Length, mm		8.4 ± 3.8	9.5 ± 4.6
Fineness, µm (Diameter)	type 1	30.9 ± 2.5	30.1 ± 2.0
	type 2	20.7 ± 1.8	20.2 ± 1.7
	type 3	13.2 ± 1.8	12.4 ± 1.8

Concrete mix designs are presented in Table 3 where mixes are designed to satisfy consistency class S4 (160 – 210 mm) in fresh state.

All constituting materials were kept for at least 24 hours in the laboratory at a temperature of 20 ± 2°C before mixing. The mixing procedure was as followed: First, the aggregates and the recycled tyre polymer or polypropylene fibres were mixed together to ensure a good dispersion of fibres. Mixing was then proceeded for two minutes after adding half of the water. To allow the aggregates to absorb the needed amount of water, the mixing was stopped for about two minutes. The cement was then added and mixing started again with continuous addition of the residual water and superplasticiser. After the insertion of all materials, the mixing continued for another two minutes. The mixing procedure for the plain reference concrete excluded first stage and was the same from the second stage, as described previously.

Table 3. Concrete mix design

Group of mixes	I		II			III		
Components (kg/m³)	OC	$1PP_m$	$5RTPF_m$	$10RTPF_m$	$15RTPF_m$	$1RTPF_s$	$2RTPF_s$	$5RTPF_s$
Cement	370	370	370	370	370	370	370	370
Water	170	170	170	170	170	170	170	170
Superplasticizer	2.22	2.05	2.22	3.21	3.54	1.29	1.67	2.67
w/c	0.46	0.46	0.46	0.46	0.46	0.46	0.46	0.46
Fibres								
Monofilament PP	-	1	-	-	-	-	-	-
Mixed RTPF	-	-	5	10	15	-	-	-
Sorted RTPF	-	-	-	-	-	1	2	5
Aggregates								
0-4	822	880	816	810	801	880	878	875
4-8	383	344	380	378	366	344	344	342
8-16	680	603	675	670	645	603	602	599

2.2. TESTING METHODS

Testing of concrete properties in fresh and hardened state was performed according to the standards listed in tables 4. As can be seen from the tables, all methods for testing concrete properties (for both fresh and hardened) are standardised except method for autogenous deformation. Detailed description of this testing method can be found in [9].

Table 4 Tests on fresh and hardened concrete

Property	Standard
Density	HRN EN 12350-6:2009
Slump-test	HRN EN 12350-2:2009
Air content -- Pressure method	HRN EN 12350-7:2009
Autogenous deformation	-
Compressive strength	HRN EN 12390-3:2009
Modulus of elasticity	HRN EN 12390-13:2013

Fresh concrete properties in terms of density, workability and air content were obtained immediately after mixing. Autogenous deformations were tested after the mixing, as well. For mechanical property testing, concrete was, after mixing, cast in cube moulds with dimensions 150x150x150 mm for compressive strength and cylinder of ⌀/L = 100/200 mm for modulus of elasticity testing. After casting, the specimens were kept covered in the laboratory condition for 24 hours until demoulding, to prevent evaporation of water. After demoulding, the specimens were kept in the moist room at 20 ± 2°C and RH ≥ 95%, until testing at the age of 28 days.

3. RESULTS AND DISCUSSIONS

3.1. PROPERTIES OF CONCRETE IN FRESH STATE

Table 5 shows the results of fresh concrete properties, namely: consistency, density and air content. As seen from table, slump values of all tested mixes were in the range of 170 – 190 mm indicating that all mixes can be classified into target consistency class S4 (160-210 mm).

From mix design presented in Table 3 and values presented in Table 5, comparing concrete mixes with RTPF within the same group (both mixed and sorted types - group II and III), amount of superplasticizer was increased with increased amount of fibres. Higher demands for superplasticizer was especially highlighted in group comprising mixed RTPF where for mix $15RTPF_m$, addition of superplasticizer was about 40% higher compared to plain reference mix. The need for an increased amount of superplasticiser indicated that the consistency of fresh concrete mixes was decreased with the addition of mixed RTPF fibres, as previously demonstrated in the available literature [10, 11].

Density of the studied mixes was between 2.32 kg/dm^3 (for mix 5RTPF$_s$) and 2.40 kg/dm^3 (for reference plain mix, OC). The differences in density between mixes are up to 3.3 %, which leads to the conclusion that recycled tyre polymer fibres do not have significant influence on concrete density in its fresh state. Although fibres have a low specific gravity, if added in the studied amount, it represents replacement for a maximum of 1% aggregates by weight, which, in turn, cannot affect the density of concrete mix.

Obtained results of air content testing showed that all mixes with fibres (1PP$_m$ and all mixes with RTPF) had higher values (ranging 2.07 – 3.56 %) compared to plain concrete mix, OC, (1.83%). The air content is increased with increased amount of fibres in each group. Furthermore, groups of mixes containing mixed types of RTPF (group II) generally have higher values of air content indicating that residual rubber in fibres additionally entrap air during mixing of fresh concrete. Particularly, mix with 15 kg of mixed RTPF showed 1.9 times higher air content compared to plain concrete reference mix.

Table 5 Results of fresh concrete properties

Property		Slump (mm)	Density (kg/m^3)	Air content (%)
Mix	Group			
OC	I	190	2.40	1.83
1PP$_m$		180	2.36	2.87
5RTPF$_m$	II	180	2.38	2.13
10RTPF$_m$		180	2.36	3.40
15RTPF$_m$		180	2.33	3.56
1RTPF$_s$	III	180	2.37	2.07
2RTPF$_s$		180	2.37	2.23
5RTPF$_s$		170	2.32	3.13

3.2. COMPRESSIVE STRENGTH

Results of compressive strength testing at the age of 28 days are presented in Figure 2 with average and absolute deviation values based on testing of minimum 6 specimens per mix.

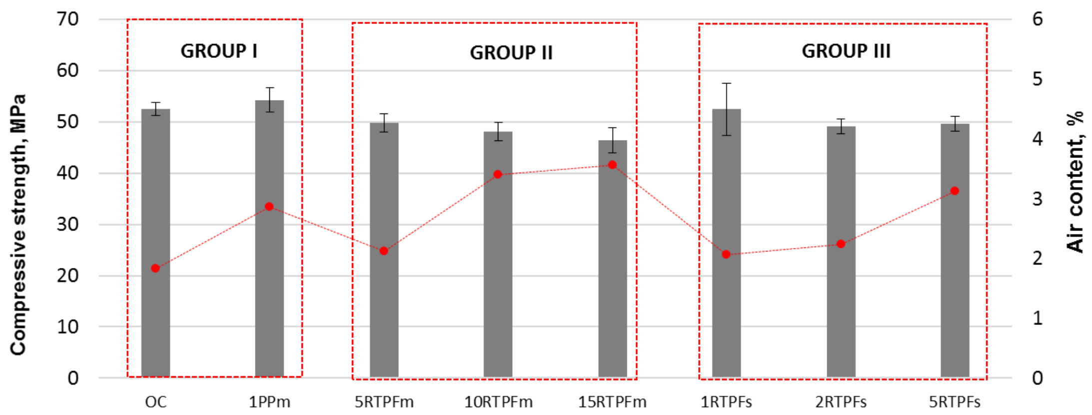

Figure 2 28-days compressive strength and air content of tested concrete mixes

Compared to plain concrete mix, addition of 1 kg of fibres (PP and sorted RTPF) did not affect compressive strength significantly because the differences in the results are within 3%. Higher amounts of sorted RTPF (2 and 5 kg/m^3), in group III, further decreased compressive strength up to 6.5%. Addition of mixed RTPF, resulted in decreased compressive strength up to 12% compared to plain reference mix. The latest obtained results could be explained with increased air content of mixes with mixed RTPF fibres (see Figure 2) which was, in turn, entrapped by the presence of high amount of residual rubber in this types of fibres.

3.3. MODULUS OF ELASTICITY

The results of modulus of elasticity at the age of 28 days are presented in Figure 3 with average and absolute deviation values based on testing of 3 specimens per mix.

The obtained values ranged from 34.7 GPa for a concrete mix $15RTPF_m$ to 37.6 GPa for mix $1PP_m$. Results of modulus elasticity followed almost the same trend as per compressive strength results. Addition of PPm and sorted RTPF in amounts up to 5 kg/m^3 resulted in negligible differences up to 4% compared to reference plain concrete. Modulus of elasticity was decreased with higher amounts of mixed RTPF fibres (up to 7.7 % for mix 15RTPFm compared to plain reference mix OC). The obtained results were in a good agreement with available literature data [12].

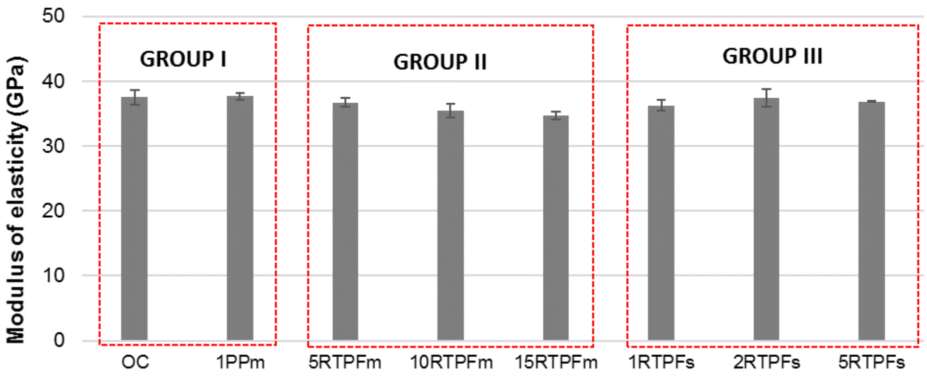

Figure 3 Modulus of elasticity of tested concrete mixes

3.4. AUTOGENOUS DEFORMATIONS

Figure 4 presents results of early age deformations and temperature profiles of studied concrete mixes as average values based on testing of three specimens per mix. These results are concerned only mixes with sorted fibres (group III) in compare to mix with PP_m fibres. Results of early age deformations for other mixes concerned in this study can be found in [13] where positive effect of added mixed RTPF on autogenous deformations are observed.

Deformations concerned here are sum of the autogenous and thermal deformations, where later are caused by the temperature increase of fresh concrete mix. Thermal deformations are not separated from autogenous shrinkage, because the thermal coefficients of studied mixes were not determined and their influence on total deformations is negligible after 24 hours. Therefore, early age deformation is considered here as an autogenous deformation.

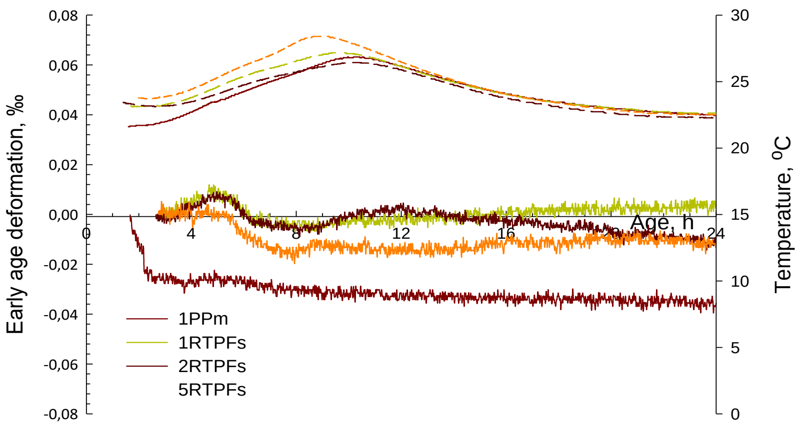

Figure 4 Results of the autogenous deformations measurements for the second stage of testing

All specimens could not be prepared at the same time. This is the reason why the initial temperatures presented in Figure 4 at the beginning of the measurement are not the same for all mixes. The greatest difference amounted up to 3°C. In accordance to Saje et al. [14] the initial temperature has the negligible influence on the size of the autogenous deformations. In accordance to Tazawa et al. [15] start of the autogenous deformations can be taken as the time of cement setting which approximately coincides with the start of temperature rise in the specimens put in the environment with constant temperature. Therefore, ˝time zero˝ or start of autogenous deformation was determined from the moment when cooling of the concrete becomes influenced by the liberated heat of hydration.

In Figure 4, autogenous deformations are presented from the ˝time zero˝ as defined before. These results also show positive influence of added sorted RTPF on autogenous deformations compared to addition of monofilament PP fibres. At the end of measuring period, autogenous shrinkage of mix with PP fibres were 0.035 ‰, while for mixes with 2 and 5 kg/m^3 of sorted fibres, autogenous shrinkage were 0.009 and 0.013 ‰, respectively. In the same time, mix with 1 kg/m^3 of sorted RTPF had swelling in the range of 0.004 ‰. Although, there were not consistent link regarding amount of added fibres and magnitude of autogenous deformation, this testing showed that, compared to mix with monofilament PP, there were decrease in total deformation in the range from 62.8 to 77.9 %.

4. CONCLUSIONS

In the framework of this study, 6 mixes of fibre reinforced concrete made with RTPF (mixed and sorted types) were prepared and tested for fresh (density, workability and air content), hardened properties (compressive strength and static modulus of elasticity) and early age deformation. For comparison purposes, plain concrete mix and mix with 1 kg/m^3 of monofilament polypropylene fibers were prepared and tested as well. The obtained results of fresh concrete indicate that there is no significant difference in concrete densities between tested mixes. Increased amount of superplasticizer with increased amount of RTPF fibres, for the same workability class (S4 in this case), indicate that amount of added fibres decrease workability of fresh concrete. Furthermore, air content in fresh concrete was increased with increased amount of fibres, especially in mixes with mixed RTPF indicating that rubber, resided in fibres, entraps additional air in the fresh mix. Results of mechanical properties showed that studied amount of RTPF fibres (especially sorted) do not have significant influence those properties. In compare to plain mix, within mixes comprising sorted fibres the obtained differences are up to 6.4% and 3.5% for compressive strength and modulus of elasticity, while within group comprising mixed RTPF the differences are up to 11.7% and 7.4%, respectively. The main expected influence of the addition of mixed RTPF is on deformation properties. There was not consistent link regarding amount of added fibres and magnitude of autogenous deformation. Nevertheless, this testing showed that, compared to mix with monofilament PP, there were decrease in total deformation in the range from 62.8 to 77.9% with mixes using sorted RTPF.

ACKNOWLEDGMENTS

The research presented in this paper are conducted within the project "Anagennisi - Innovative Reuse of all Tyre Components in Concrete" funded by the European Commission under the 7th Framework Programme Environment topic. Authors would also like to thank Prof. Edita Vujasinovic, PhD and Marijana Pavunc Samarzija, mag. ing. techn.text, Faculty of textile technology, Department of Materials, Fibres and Textile Testing, Centre for Development and Transfer of Textile and Clothing Technologies and Fashion Design, for their contribution for geometrical characterization of RTPF fibres. Authors would like to thank GUMIIMPEX for their support and students Kristina Vujnović, Ivana Vladić and Anita Mihaljević for their contribution during experimental work.

REFERENCES

[1] Serdar, M. et al: Possibilities of use of products from waste tyre recycling in concrete industry, *Journal of Applied Engineering Science*, 12 (2014) 1, 89–93, ISSN 2284-7197
[2] Anagennisi Project. 2015. Retrieved from http://www.anagennisi.org/
[3] Swamy, R.N., Stavrides, H. 1979, Influence of Fiber Reinforcement on Restrained Shrinkage and Cracking. ACI Journal Proceedings, 76, 3, 443-460.
[4] Saje, D., Bandelj, B., Sustersic, J., Lopatic, J., Saje, F., 2012, Autogenous and Drying Shrinkage of Fibre Reinforced High-Performance Concrete, Journal of Advanced Concrete Technology, 10, 59 – 73.
[5] ACI 544.5R-10, 2010, Report on the Physical Properties and Durability of Fiber-Reinforced Concrete, Reported by ACI Committee 544. 5R-10.
[6] Fuller, W. B., Thompson, S. E., 1907, The laws of proportioning concrete.Trans. ASCE, 59(2), 67–143.
[7] Collepardi, M., 2010, The new concrete. Grafiche Tintoretto, Second edition, Italy.
[8] Pezer, M., Pavunc Samaržija, M., Baričević, A., Vujasinović, E., Jelčić Rukavina, M., Štirmer, N., 2016, Textile Fibres from Recycled Tyres , Dragčević, Z., Hursa Šajatović, A., Vujasinović, E, editors, Book of Proceedings of the 8th International Textile, Clothing & Design Conference 2016 – Magic World of Textiles, Zagreb: University of Zagreb, Faculty of Textile Technology, 474-479.
[9] Gabrijel I., Jelcic Rukavina M. and Bjegovic, D., 2014, Autogenous deformations of dolomite based self-compacting concretes with different mineral, Bjegovic, D.; Beushausen, H. and Serdar, M., editors, Proceedings of the RILEM International workshop on Performance-based specification and control of concrete durability, Zagreb, Croatia, RILEM Publications S.A.R.L., 507-514.
[10] Mavridou S., 2011, Utilization of Textile Fibres from Worn Automobile Tires in Cement based mortars, Global Nest Journal, 13(2), 176–181.
[11] Serdar M, Baricevic A, Bjegovic D, Lakusic S., 2014, Possibilities of use of products from waste tyre recycling in concrete industry, Journal of Applied Engineering Science, 12(1), 89-93.

[12] Baricevic, A., Pezer, M., Stirmer, N, 2015, Utilization of polypropylene fibre reinforced cement composites as a repair material: a review. Concrete Repair, Rehabilitation and Retrofitting IV - Proceedings of the 4th International Conference on Concrete Repair, Rehabilitation and Retrofitting (ICCRRR-4), Leipzig, Germany, October 5-7, 2015, Dehn, F., Beushausen, H. - D., Alexander, M. G., Moyo, P. (eds.), Taylor & Francis Group, 465-472.

[13] Serdar, M., Baricevic, A., Jelcic Rukavina, M., Pezer, M., Bjegović, D., Stirmer, N., 2015, "Shrinkage Behaviour of Fibre Reinforced Concrete with Recycled Tyre Polymer Fibres," International Journal of Polymer Science, International Journal of Polymer Science. http://dx.doi.org/10.1155/2015/145918.

[14] Tazawa, E., 1999, Autogenous shrinkage of concrete. E&FN Spon, London.

[15] Saje, D., Bandelj, B., Šušteršič, J., Lopatić F., 2011, Shrinkage of polypropylene fibre reinforced high performance concrete, ASCE Journal of Materials Civil Engineering, 23, 941–952.

FLEXURAL PERFORMANCE OF STEEL FIBRE REINFORCED CONCRETE WITH MANUFACTURED AND RECYCLED TYRE STEEL FIBRES

Hang Hu[1], Panos Papastergiou1, Harris Angelakopoulos[2], Maurizio Guadagnini1, Kypros Pilakoutas[1]

[1] The University of Sheffield, Faculty of engineering, Department of Civil and Structural Engineering, Sir Frederick Mappin Building, Mappin Street, Sheffield, S1 3JD, UK, email: hhu6@sheffield.ac.uk, p.papastergiou@sheffield.ac.uk, m.guadagnini@sheffield.ac.uk, k.pilakoutas@sheffield.ac.uk
[2] Twincon Ltd, 40 Leavygreave road, Sheffield, South Yorkshire, S3 7RD, UK, email: h.angelakopoulos@gmail.com

SUMMARY: Cleaned and sorted fibres recycled from end-of-life tyres called “Recycled Tyre Steel Fibres” (RTSF) can be used as concrete reinforcement, but understanding their performance requires extensive testing work. This paper investigates the flexural performance of various SFRC mixes using RTSF and two types of Manufactured Steel Fibres (MSF). The post-cracking flexural strengths of these mixes are obtained using 3-point notched prism tests. A simplified equation is proposed to determine the relationship between the post-cracking flexural tensile strength and required SFRC ground-supported slabs thicknesses. It is found that the required slab thicknesses largely depend on f, a single coefficient obtained from the post-cracking flexural strengths of SFRC. In all SFRC mixes, the lowest required slab thickness is obtained when using hybrid fibre reinforcement containing 10 kg/m3 of RTSF. It is concluded that hybrid fibres using RTSF can be a competitive and environmentally-friendly alternative for industrial concrete flooring applications.

PONAŠANJE PRI SAVIJANJU BETONA ARMIRANOG PROIZVEDENIM ČELIČNIM VLAKNIMA I RECIKLIRANIH ČELIČNIM VLAKANIMA IZ AUTOMOBILSKIH GUMA

SAŽETAK: Za armiranje betona mogu se upotrijebiti očišćena i sortirana vlakna iz starih guma zvana reciklirana čelična vlakna iz guma, ali razumijevanje njihovih svojstava zahtijeva opsežna ispitivanja. U radu su istražena svojstva pri savijanju različitih mješavina betona armiranog čeličnim vlaknima iz oporabljenih guma i betona armiranog proizvedenim čeličnim vlaknima. Ponašanje tih mješavina pri savijanju nakon raspucavanja određeno je opterećivanjem prizmi sa zarezom u tri točke. Za određivanje odnosa vlačne čvrstoće pri savijanju nakon raspucavanja i zahtijevane debljine betonske ploče armirane čeličnim vlaknima oslonjene na tlo predložena je pojednostavnjena jednadžba. Utvrđeno je da zahtijevana debljina ploče znatno ovisi o koeficijentu f dobivenom iz čvrstoće pri savijanju nakon raspucavanja betona armiranog čeličnim vlaknima. U svim mješavinama najmanja zahtijevana debljina ploče dobivena je pri upotrebi hibridnog armiranja u količini od 10 kg/m^3 oporabljenih vlakana iz guma. Zaključeno je da hibridna čelična vlakna iz oporabljenih guma mogu biti konkurentna i po okoliš prijateljska alternativa u primjenama za industrijske betonske podove.

1. INTRODUCTION

According to ETRA [1], approximately 1.5 billion tyres are produced annually and around 1 billion tyres (17 million tonnes) [2] reach the end of their life worldwide. To minimise the environmental impact of end-of-life tyres, the tyre recycling industry has developed various processes to extract and recycle all tyre constituents (steel and polymer fibres, rubber) [3]. The most commonly used and financially viable tyre recycling techniques adopt mechanical shredding at some stage, which produces tyre wire of irregular shapes, lengths and diameters. However, these fibres are often heavily contaminated with rubber (up to 10% by mass) and agglomeration (balling) can be caused with their irregular shapes and geometries. Further processing is thus required to: (1) minimise rubber contamination to less than 0.5% by mass, (2) limit the fibre length distribution and diameters to those that are effective in concrete (3) avoid agglomeration. After processing, the cleaned and sorted fibres are called as “Reused Tyre Steel Fibres” (RTSF) and can be used in concrete as reinforcement. Since 1999, a number of studies have been conducted at The University of Sheffield to investigate the mechanical properties of RTSF [3][4][5] and their possible applications [4][6], and a patent application was filed in 2001 [7].

Currently manufactured steel fibres (MSF) are commonly used as reinforcement in concrete applications such as industrial flooring [3][4]. Steel fibre reinforced concrete (SFRC) can provide high resistance to concentrated loads and impact loading, minimising the number of joints and overall thickness of slabs [4]. Under loading or other actions (e.g. shrinkage), stresses in a SFRC slab are transferred across cracks through the fibres [8]. Multiple distributed cracks with relatively small openings subsequently tend to occur instead of large through cracks, with a global enhancement of flexural toughness and serviceability. Nevertheless, only single-type fibre reinforced concrete (i.e. Manufactured Steel Fibres (MSF)) is now currently used in the majority of SFRC applications [9][10]. This requires a substantial amount of raw materials and energy input for the production of MSF. Moreover, Using a single type of fibre may only be effective in arresting and bridging cracks for a limited range of deformations, and some researchers [6][9][10] have suggested that the fracture process of SFRC matrix is multi-scale and gradual. Multiple types of fibres with different length-to-diameter ratios (called as “fibre hybridisation” [9]) in concrete may optimise crack control across a broader range of crack widths [10]. Limited studies on hybrid FRC [9][10][11][12] have demonstrated that fibre hybridisation leads to a better flexural performance of concrete, although these have not always been observed in previous studies due to fibre balling or issues with the concrete mix design [9][10]. Extensive studies on the mechanical properties of various hybrid fibre mixes using RTSF, are being conducted under a FP7 European Commission sponsored project “Anagennisi” [13] since 2014.

Different tests are being used to quantify the flexural performance of SFRC. Compared with other tests, the advantages of the popular 3-point notched prism tests are simplicity and reliability; and this test method has been adopted by several design guidelines [14][15][16]. Residual flexural tensile strengths (i.e. f_R values) are used in these guidelines to estimate the post-cracking flexural behaviour of SFRC in design.

No universally-accepted design guidelines exist for the various SFRC applications. Design guidelines for SFRC industrial ground floors are only provided by The Concrete Society TR 34, ACI 544 and RILEM TC162 [17]. These guidelines, however, can be difficult to follow accurately and efficiently. Thus simplified and designer-friendly design methods and equations are required for the design of typical SFRC structures under certain critical loads, particularly when new construction materials are utilised.

Based on all above considerations, the flexural performance of various SFRC mixes using RTSF and two types of MSF have been investigated in this study. The post-cracking flexural strengths of these mixes were obtained by means of 3-point notched prism tests. A simplified equation has been proposed to furnish a clearer relationship between the post-cracking flexural tensile strength of SFRC and required ground-supported slabs thicknesses.

2. MECHANICAL CHARACTERISTICS OF FIBRES USED

RTSF (Figure 1 (a)) and two types of manufactured undulated steel fibres, MSF1 and MSF 2 (Figure 1 (b)) were used in the study. For quality control, the RTSF length distribution analysis was undertaken using a specially developed photogrammetry system, and the length distribution was found to be 70% by mass between 15-40 mm. Table 1 summarises the geometrical and mechanical characteristics of all three fibre types.

(a) (b)

Figure 1 (a) RTSF, (b) manufactured undulated fibre

Table 1 Specification of RTSF, MSF1 and MSF2

Fibre type	Length (mm)	Diameter (mm)	Tensile strength (MPa)	Elastic modulus (GPa)
a - RTSF	15-40	0.1	2000	200
b - MSF1	60	1.0	1450	200
c - MSF2	55	0.8	1000	200

3. SFRC MIXES TESTED AND MIX DESIGN

Table 2 shows details of the mixes tested including the number of specimens, fibre type as well as fibre dosage. Two fibre dosages, typical of industrial flooring applications, were mainly investigated in this study: 30 kg/m^3 and 45 kg/m^3. An extra mix of 35 kg/m3 (mix F) was used to evaluate the performance of the higher strength MSF1 fibre at a lower dosage than the typical dosage of 45 kg/m3. Average compressive cube strength and standard deviation for these mixes in this table are discussed later.

For mixes A, B, F, G, and H, twelve prisms and six cubes were cast per mix to comply with BS EN 14651: 2007 [14] in order to obtain the flexural and compressive properties of SFRC, respectively. For the rest of the mixes, C, D, E, I and J, only 6 prisms and 3 cubes were cast to examine how small variations of fibre dosages can affect the mechanical properties of concrete.

Table 2 Tested SFRC mixes

Total dosage (kg/m^3)	Mix	Batch no.	No. of cubes	No. of SFRC prisms	Fibre type 1	Dosage 1 (kg/m^3)	Fibre type 2	Dosage 2 (kg/m^3)	Avg. f_{cu} (MPa)	Std. deviation (MPa)
30	A	3	6	12	MSF2	30	-	-	43.9 (42.0)	1.8 (0.9)
	B	4	6	12	MSF2	20	RTSF	10	42.6 (46.1)	2.2 (2.0)
	C	1	3	6	MSF2	15	RTSF	15	44.3 (47.5)	1.9 (1.1)
	D	1	3	6	MSF2	10	RTSF	20	44.6 (47.5)	1.9 (1.1)
	E	5	3	6	MSF2	-	RTSF	30	41.8 (37.6)	1.9 (3.7)
35	F	3	6	12	MSF1	35	-	-	42.9 (42.0)	1.9 (0.9)
45	G	3	6	12	MSF1	45	-	-	41.9 (42.0)	1.0 (0.9)
	H	4	6	12	MSF1	35	RTSF	10	42.8 (46.1)	0.2 (2.0)
	I	1	3	6	MSF1	22.5	RTSF	22.5	50.3 (47.5)	2.4 (1.1)
	J	2	3	6	MSF1	10	RTSF	35	44.5 (39.9)	0.7 (1.0)

Note: The values in brackets are average compressive cube strength and standard deviation of plain concrete for each batch.

Due to the large volume of concrete (together with the prisms, large concrete slabs were also cast, for comparison purposes – these results will be presented in a separate paper), the SFRC mixes were cast in 5 separate batches of ready mixed concrete. For each batch, 6 plain concrete prisms and 3 cubes were also cast and then tested as control specimens.

The initial slump of the concrete mixes ranged from 20 to 100 mm. Additional water was added to the concrete mix if the measured slump was less than 100 mm. After the addition of the water, the slump was checked again to confirm that it was 70 mm or more. Superplasticiser was then added which increased the slump to more than 200 mm. After the addition of fibres, the slump reduced to roughly the same levels after the addition of the water (70-100 mm). No major balling issues were observed during all 5 concrete castings; the target concrete compressive strength, f_{cu}, was 40 MPa. The concrete mix design was: 150 kg/m^3 of cement, 1097 kg/m^3 of coarse aggregates (4-20 mm), 804 kg/m^3 of coarse aggregates (0-4 mm), 150 kg/m^3 of GGBS and 2.25 L/m^3 of Plasticiser. The water cement ratio (w/c) was 0.55.

4. MECHANICAL PROPERTIES OF SFRC

4.1. COMPRESSIVE CUBE TESTS

In this study, the SFRC cubes were tested under uniaxial compressive loading on the same dates as prism testing. Six SFRC cubes for each mix and another three plain concrete cubes for each casting were tested according to BS EN 12390-3: 2009 [18].

For all 5 castings, the SFRC cube compressive strength ranged from 41.8 to 50.3 MPa whilst the plain concrete compressive strength ranged from 37.6 to 47.5 MPa (Table 2). The variability found is considered natural for ready mixed concrete. Overall, the compressive strength of concrete was not affected dramatically either negatively or positively by adding steel fibres.

4.2. FLEXURAL PRISM TESTS

The flexural testing was performed according to BS EN 14651:2007 [14]. The prisms were tested under 3-point flexural testing (Figure 2), in a 300 kN electromagnetic universal testing machine. An aluminium yoke, based on the Japanese Society of Civil Engineers standard [19], was mounted on the specimens to eliminate common experimental errors (due to spurious support displacements, machine stiffness, or concrete crushing) and to accommodate the effect of torsion on the deflection measurements [20] . Two LVDTs were mounted on the yoke. The tests were controlled by Crack Mouth Opening Displacement (CMOD) measured at the centre of the prism axis with a clip gauge (mounted under the prism). Two central deflections were measured on either side of the specimen using Linear Variable Differential Transformers (LVDTs) placed in the vertical direction

4.2.1. RESIDUAL FLEXURAL TENSILE STRENGTH, f_R

The British standard BS EN 14651:2007 [14] follows a methodology first adopted by RILEM [15], to characterise the residual flexural tensile behaviour of SFRC prisms. Four flexural stresses (f_{R1}, f_{R2}, f_{R3} and f_{R4}) are taken at 0.5, 1.5, 2.5 and 3.5 mm of CMOD, respectively. The coefficients of variation for the residual flexural tensile strengths for all mixes (except for mix A of 27% -35%) were within the range of 30%. This is in agreement with literature [21]. Among the four values, f_{R1} and f_{R4} are usually used in several design guidelines to estimate the residual flexural tensile strength of SFRC in design[15][16]. The f_{R1} and f_{R4} values for 30 kg/m^3, 35 kg/m^3 and 45 kg/m^3 of SFRC mixes and their variability are presented in Figure 3. It is shown that generally the residual strengths f_{R1} and f_{R4} enhanced with the total fibre dosage, from 30 kg/m^3 to 45 kg/m^3. For design of ground-supported slabs, f_{R1} and f_{R4} are used to calculate the ultimate positive moment capacity M_p of SFRC, as discussed later.

Figure 2 Flexural prism test arrangements

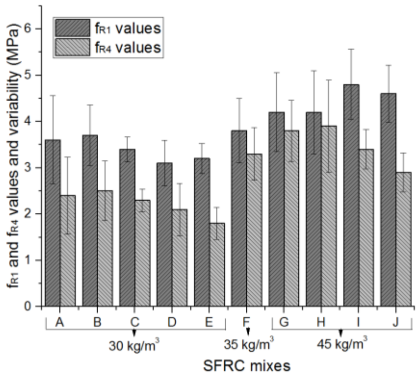

Figure 3 f_{R1} and f_{R4} values and variability (MPa)

5. SFRC GROUND-SUPPORTED SLABS THICKNESSES

TR 34 [16] provides a guidance on the structural design of ground-supported slabs. The slab is assumed as fully supported, and two typical failure modes of the ground-supported slabs are considered flexure and punching shear. At the Ultimate Limit State (ULS), the design for flexure under point load is based on the yield line theory, where a sufficient rotation capacity along sagging and hogging yield lines is required. Adequate ductility of a SFRC slab section along sagging yield lines is therefore required to mobilise the hogging moment capacity [16][17]. The ultimate positive moment capacity M_p can be obtained by assuming the limiting compressive strain ($\varepsilon_{cu} = 0.0035$) is reached simultaneously with the ultimate tensile strain of the SFRC ($\varepsilon_t = 0.025$) [15][16]. The calculation of M_p is given as

$$M_p = \frac{h^2}{\gamma_m}(0.16\sigma_{r1} + 0.29\sigma_{r4}) \tag{1}$$

At the ULS, σ_{r1} represents the axial tensile strength at the crack tip, while the strength at the bottom crack opening is represented by σ_{r4} [16]. The equations are given by:

$$\sigma_{r1} = 0.45 f_{R1} \tag{2}$$

$$\sigma_{r4} = 0.37 f_{R4} \tag{3}$$

Equation 1 can be rearranged as,

$$M_p = \frac{(0.072 f_{R1} + 0.107 f_{R4}) h^2}{\gamma_m} = \frac{f h^2}{\gamma_m} \tag{4}$$

Where h is the slab thickness and $\gamma_m = 1.5$ is the partial safety factor for fibre reinforced concrete. $f = 0.072 f_{R1} + 0.107 f_{R4}$ is defined as a coefficient characterising the general post-cracking flexural behaviour of SFRC, from micro-cracking to macro-cracking. $Re_{,3}$ value was adopted in an older version of TR 34 [22], given by the ratio of the average load up to a deflection of 3mm of a SFRC prism to the first crack load of a plain concrete prism. Compared with $Re_{,3}$ value, the use of f value can reduce the effect of ambiguous definition of first crack load, and the related plain concrete prisms are unnecessary to be tested. From Table 3, it can be seen that f increases with the total fibre dosage, from 30 kg/m^3, to 35 kg/m^3 and 45 kg/m^3. Among mixes at 30 kg/m^3 and 35 or 45 kg/m^3, the highest f values were obtained from hybrid mixes B [MSF2 (20) + RTSF (10)] and H [MSF1 (35) + RTSF (10)], respectively.

To quantify the enhancement of post-cracking performance for hybrid SFRC mixes comparing to MSF-only reinforced concrete at the same total dosage, a ratio e (in terms of coefficient f) was therefore introduced. e is caculated as,

$$e = \left(\frac{f_{hybrid}}{f_{MSF}} - 1\right) \times 100 \tag{5}$$

Where f_{hybrid} is the f value for a hybrid mix and f_{MSF} is the f value for a MSF-only mix at the same total fibre dosage as the hybrid. An enhanced post-cracking performance is obtained if e is positive.

Table 3 f and e values

Fibre dosage	Mix	f (MPa)	e (%)
30 kg/m^3	A – MSF2 (30)	0.51	-
	B – MSF2 (20) + RTSF (10)	0.54	5.2
	C – MSF2 (15) + RTSF (15)	0.50	-3.1
	D – MSF2 (10) + RTSF (20)	0.46	-11.0
	E – RTSF (30)	0.42	-
35 kg/m^3 or 45 kg/m^3	F – MSF1 (35)	0.62	-
	G – MSF1 (45)	0.71	-
	H – MSF1 (35) + RTSF (10)	0.73	2.9
	I – MSF1 (22.5) + RTSF (22.5)	0.72	1.7
	J – MSF1 (10) + RTSF (35)	0.64	-9.3

Hybrid mixes B [MSF2 (20) + RTSF (10)], H [MSF1 (35) + RTSF (10)] and I [MSF1 (22.5) + RTSF (22.5)] exhibited positive e values. This demonstrates that improved post-cracking flexural performance and therefore the increased ultimate positive moment capacity M_p can be obtained from hybrid mixes containing RTSF. The ultimate hogging moment capacity M_n (limited to the cracking moment of plain concrete) is not generally affected by adding fibres [16].

$$M_n = f_{ctd,fl} \left(\frac{h^2}{6}\right) \tag{6}$$

Where $f_{ctd,fl}$ is the design concrete flexural tensile strength.

Soutsos et al. [17] proposed a simplified method to calculate the ground slab thickness of FRC slabs under a back-to-back racking load applied internally, and the assumption of zero contact area of the load was made. However, in practical applications, TR 34 [16] suggests a typical minimum spacing between dual loads as 250mm -300mm. Also, the contact area is calculated as the sum of the contact area of the two independent loads and the area between them (Figure 4) [16].

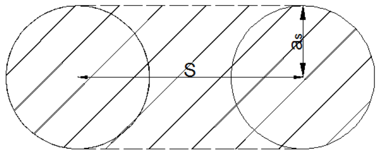

Figure 4 The equivalent contact area of closely spaced dual point loads ($s \leq 2h$)

The onset of the top surface cracking needs to be avoided for the Serviceability Limit State (SLS) requirement, so this is assumed as the criterion for flexural design. When ground-supported slabs are designed for sustaining back-to-back racking loads, a critical case for flexure is considered as two adjacent point loads applied near an edge. TR 34 [16] suggests that the dual point loads near an edge can be obtained from the multiple of the internal load and the ratio between the edge load to internal load for a single point load. The collapse load for dual adjacent point loads at an edge, $P_{u,de}$ is given as,

$$P_{u,de} = P_{u,di}\left(\frac{P_{u,se}}{P_{u,si}}\right) = P_{u,di} \times k \tag{7}$$

Where $P_{u,di}$ is for dual point loads applied internally, $P_{u,se}$ is for single point load at an edge and $P_{u,si}$ is for single point load applied internally. k is the ratio between $P_{\mathrm{u},se}$ and $P_{u,si}$.

The dual point loads considered were induced by back-to-back racking legs, with the design maximum load of 78 kN and a typical contact area of $100\ \mathrm{mm} \times 100\ \mathrm{mm}$ for each leg was assumed. The radius of relative stiffness l was considered as 650mm. The spacing between two racking legs s was considered as 300 mm, which is less than twice as the slab thickness (the minimum slab thickness 150 mm was recommended by TR 34 [16]). $f_{ctd,fl}$ for all mixes was considered as 3 MPa, $\frac{M_p}{M_n} = \frac{4}{3}f$ was thus obtained from Equations 4 and 6. When single racking leg was applied, $P_{u,si} = 3.03\pi M_n(1 + \frac{4}{3}f)$ was obtained by interpolation, for $\frac{a_s}{l} = 0.09$. a_s is the equivalent radius of a racking leg. $P_{u,se} = \pi M_n(1.72 + f)$ was for an edge load. The ratio k was thus calculated as,

$$k = \frac{1.72+f}{3.03+4.04f}. \tag{8}$$

For dual point loads, $\frac{a_d}{l} = 0.18$, where a_d is the equivalent radius for the dual point loads. $P_{u,di}$ was given as,

$$P_{u,di} = 4.06\pi(M_p + M_n) \tag{9}$$

From equations 4, 5, 6, 7 and 8, the collapse load for closely-spaced dual point loads at an edge, $P_{u,de}$ was calculated as,

$$P_{u,de} = \pi(\frac{4f+3}{1478})(\frac{1.72+f}{3.03+4.04f})h^2 \tag{10}$$

For the design dual point loads of 156 kN induced by adjacent back-to-back racking, an equation can be derived as below,

$$156 \leq \pi(\frac{4f+3}{1478})(\frac{1.72+f}{3.03+4.04f})h^2 \tag{11}$$

Therefore the relationship between required SFRC slab thicknesses and the coefficient f can be expressed as,

$$h \geq \sqrt{\frac{72655}{f+1.72}} \tag{12}$$

It is found that the required slab thickness is largely dependent on f, when the same M_n is assumed for all SFRC mixes. From Equation 12, it can be seen that SFRC with higher f can result in a lower slab thickness. The slab thicknesses obtained from Equation 12 are presented in Figure 5. Other checks were also found to be satisfactory using the thicknesses obtained, according to [16]. These checks are: (1) Ultimate flexural capacity under single point load (racking leg or a forklift truck wheel) applied internally, at an edge or corners. (2) Ultimate flexural capacity under multiple point loads (dual or quadruple point loads) applied internally, at an edge or corners. (3) Ultimate flexural capacity under line loads. (4) Ultimate flexural capacity under Uniformly Distributed Loads (UDL) (5) Shear capacity under punching shear at the face of the loaded area and on the critical perimeter. (6) Deflection and cracking checks at the SLS.

The required slab thicknesses ranged from 172 mm to 184 mm. As the total fibre dosage increased from 30 kg/m3 to 35 and 45 kg/m3, the required slab thicknesses deceased as expected. However, the required slab thicknesses did not vary considerably at the same dosage, and hybrid mixes showed the lowest required thicknesses. This shows that RTSF is a competitive substitute to MSF. In all SFRC mixes, it was noted that the lowest required slab thicknesses were obtained from the hybrids containing 10 kg/m3 of RTSF, and a higher dosage than that of RTSF can lead to an increase of required thicknesses.

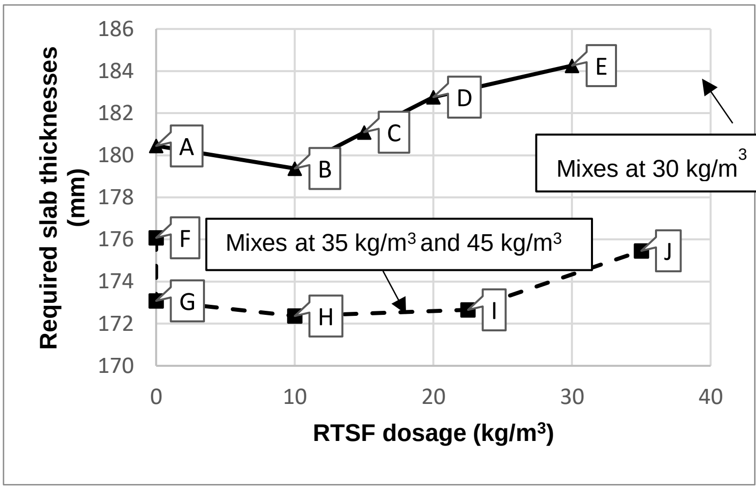

Figure 5 The relationship between RTSF dosage and required slab thicknesses

6. CONCLUSIONS

In this study, the mechanical properties of different SFRC mixes using manufactured and recycled tyre steel fibres have been investigated. From compressive cube tests, very similar compressive strength with small variability were obtained from all SFRC and plain concrete mixes. Adding steel fibres did not affect the compressive strength of concrete considerably. From flexural prism tests, f_R values were used to characterise the post-cracking performance of SFRC. It was found that the coefficients of variation for the f_R values for all mixes tested (except for mix A of 27% -35%) were within the range of 30%. f_{R1} and f_{R4} enhanced with the total fibre dosage, from 30 kg/m^3 to 45 kg/m^3.

A SFRC ground-supported slabs thickness analysis was made based on f and e values, where f characterises the post-cracking strength of a SFRC floor section, and e represents the post-cracking strength enhancement of a hybrid mix compared to a MSF-only reinforced mix at the same total dosage. From the slab thickness analysis, it was found that the required slab thicknesses were largely dependent on f. As the total fibre dosage increased from 30 kg/m^3 to 35 and 45 kg/m^3, the required slab thicknesses decreased. However, the required slab thicknesses did not vary considerably at the same dosage. This shows that RTSF is a competitive substitute to MSF, partially or possibly even entirely. In all SFRC mixes, it was found that the lowest required slab thicknesses were obtained from the hybrids containing 10 kg/m^3 of RTSF.

It is therefore concluded that hybrid fibres using RTSF can be a competitive alternative to MSF-only solutions for industrial concrete flooring applications. A simple equation is derived that can allow engineers to optimise slab depth based on the value of f.

ACKNOWLEDGMENTS

The authors would like to acknowledge the support from EC collaborative FP7-ENV-2013-two-stage project "ANAGENNISI— Innovative Reuse of All Tyre Components in Concrete" (Project number: 603722).and The China Scholarship Council (CSC number: 201508060086).

REFERENCES

[1] The European Tyre Recycling Association (ETRA): Introduction to tyre recycling: 2013, Available from http://www.etra-eu.org/joomla/libraries/articles/ETRA Introduction001.pdf. Accessed: 2016-12-06.

[2] World Business Council for Sustainable Development (WBCSD): End-of-Life Tires: A Framework for Effective Management Systems, Available from http://www.etrma.org/uploads/Modules/Documentsmanager/a-framework-for-effective-elt-management-systems-final-25.6.10.pdf. Accessed: 2016-12-06.

[3] Pilakoutas, K., Neocleous, K. & Tlemat, H.: Reuse of steel fibres as concrete reinforcement, Engineering Sustainability, 157(ES3), (2004), pp. 131-138.

[4] Tlemat H.: Steel fibres from waste tyres to concrete: testing, modelling and design, PhD thesis, The University of Sheffield, Sheffield, UK, (2004).

[5] Jafarifar N.: Shrinkage behaviour of steel fibre reinfoced concrete pavements, PhD thesis, The University of Sheffield, Sheffield, UK, (2012).

[6] Graeff, A. G. et al.: Fatigue resistance and cracking mechanism of concrete pavements reinforced with recycled steel fibres recovered from post-consumer tyres, Engineering Structures, 45, pp. 385-395.

[7] TWRC: Thin wire reinforcement for concrete. British patent application no 130852.7 filed by the University of Sheffield on 24/12/01, 2001.

[8] Brandt, A. M.: Fibre reinforced cement-based (FRC) composites after over 40 years of development in building and civil engineering, Composite structures, 86(1), (2008), pp. 3-9.

[9] Banthia, N.; Sappakittipakorn, M.: Toughness enhancement in steel fiber reinforced concrete through fiber hybridization, Cement and Concrete Research, 37(9), (2007), pp. 1366-1372.

[10] Banthia, N.; Soleimani, S. M.: Flexural response of hybrid fiber-reinforced cementitious composites, ACI Materials Journal, 102(6), (2005), pp. 382-389.

[11] Bjegovic, D. et al.: Positive interaction of industrial and recycled steel fibres in fibre reinforced concrete, Journal of Civil Engineering and Management, 19(sup1), (2013), pp. S50-S60.

[12] Sorelli, L. G., Meda, A., & Plizzari, G. A.: Bending and uniaxial tensile tests on concrete reinforced with hybrid steel fibers, Journal of materials in civil engineering, 17(5), (2005), pp. 519-527.

[13] Anagennisi: Innovative Use of all Tyre Components in Concrete, Available from http://anagennisi.org/wordpress/ Accessed: 2016-12-06.

[14] BS EN 14651: Test Method for Metallic Fibered Concrete - Measuring the Flexural Tensile Strength (Limit of Proportionality (LOP), Residual, British Standards Institution, London, UK, (2005).

[15] RILEM Technical Committee: TC 162-TDF: Test and design methods for steel fiber reinforced concrete, Materials and Structures, 36, (2003), pp. 560-567.

[16] The Concrete Society: Technical Report 34: Concrete Industrial Ground Floors - A guide to Design and Construction, The Concrete Society, Surrey, UK, (2013).

[17] Soutsos, M. N., Le, T. T. & Lampropoulos, A. P.: Flexural performance of fibre reinforced concrete made with steel and synthetic fibres, Construction and building materials, 36, (2012), pp. 704-710.

[18] BS EN 12390-3: Testing Hardened Concrete Part 3: Compressive Strength of Test Specimens, British Standards Institution, London, UK, (2002).

[19] JSCE-SF4: Standard for flexural strength and flexural toughness, method of tests for steel fiber reinforced concrete, Concrete Library of JSCE, Japan Concrete Institute (JCI), Japan, (1984).

[20] Banthia, N.; Sheng, J.: Fracture toughness of micro-fiber reinforced cement composites, Cement and Concrete Composites, 18(4), (1996), pp. 251-269.

[21] Oikonomou-mpegetis S: Behaviour and Design of Steel Fibre Reinforced Concrete Slabs, PhD thesis, Imperial College London, London, UK, (2013).

[22] The Concrete Society: Technical Report 34: Concrete Industrial Ground Floors - A guide to Design and Construction, The Concrete Society, Berkshire, UK, (2003).

FATIGUE BEHAVIOUR OF STEEL FIBRES REINFORCED CONCRETE ELEMENTS

Marina Francic Smrkic1, Domagoj Damjanovic[1], Ana Baricevic[2]

[1] University of Zagreb Faculty of Civil Engineering, Department of Engineering Mechanics, Fra Andrije Kacica Miosica 26, 10 000 Zagreb, Croatia, e-mail: mfrancic@grad.hr, ddomagoj@grad.hr
[2] University of Zagreb Faculty of Civil Engineering, Department of Materials, Fra Andrije Kacica Miosica 26, 10 000 Zagreb, Croatia, email: abaricevic@grad.hr

SUMMARY: Steel fibres can be used as reinforcement in concrete elements to enhance their post cracking flexural behaviour. The inclusion of fibres can also benefit the fatigue performance of concrete elements. This paper presents a study on the fatigue flexural strength of steel fibre reinforced concrete elements containing 0.5% volume fraction of fibres with hooked ends, 35 mm long and 0.55 mm in diameter. An experimental programme was conducted to obtain fatigue lives of SFRC elements at various stress levels. Twenty four prism specimens of size 150 mm x 150 mm x 600 mm were tested under four point flexural fatigue loading. Six static flexural tests were conducted prior to fatigue test to obtain static LOP (limit of proportionality) load. The load obtained from the static test was multiplied by 4 different stress levels (0.3, 0.5, 0.7 and 0.9) to calculate the load for the fatigue test. Load was applied following a sinusoidal wave pattern, at a frequency of 15 Hz until specimen failed or until it reached the maximum number of 2 million cycles. The results are presented as S – N relationship, with fatigue stress expressed as a percentage of the strength under static load and number of loading cycles to failure. Maximum and minimum displacements versus number of cycles for each specimen during testing are also presented. Fatigue strength of SFRC elements was compared to plain concrete elements.

PONAŠANJE BETONSKIH ELEMENATA ARMIRANIH ČELIČNIM VLAKNIMA NA ZAMOR

SAŽETAK: Za armiranje betonskih elemenata mogu se upotrijebiti čelična vlakna kako bi se poboljšalo njihovo ponašanje pri savijanju nakon raspucavanja. Ugradnja vlakana može poboljšati i ponašanje betonskih elemenata na zamor. U radu se prikazuje istraživanje čvrstoće na savijanje pri zamoru betonskih elemenata armiranih čeličnim vlaknima u količini od 0,5 % volumena sa zakrivljenim krajevima, duljine 35 mm i promjera 0,55 mm. Da bi se odredila čvrstoća na zamor takvih elemenata pri različitim razinama naprezanja proveden je eksperimentalni program. Ispitana su dvadesetčetiri ispitna uzorka veličine 150 mm x 150 mm x 600 mm opterećenjem u četiri točke na zamor pri savijanju. Prije ispitivanja na zamor provedeno je šest statičkih ispitivanja na savijanje da se odredi statičko opterećenje na granici proporcionalnosti. Opterećenje određeno statičkim ispitivanjem pomnoženo je s četiri različite razine naprezanja (0,3, 0,5, 0,7 i 0,9) pa je tako određeno opterećenje pri ispitivanju zamora. Opterećenje je nanošeno u obliku sinusnoga vala s frekvencijom od 15 Hz sve dok nije došlo do sloma ispitnog uzorka ili dok nije postignut maksimalni broj od 2 milijuna ciklusa. Rezultati su prikazani kao odnos S – N pri čemu je naprezanje pri zamoru izraženo postotkom čvrstoće pri statičkom opterećenju i brojem ciklusa opterećenja do sloma. Prikazani su i maksimalni i minimalni progibi tijekom ispitivanja u odnosu na broj ciklusa za svaki ispitni uzorak. Čvrstoća pri zamoru elemenata armiranih čeličnim vlaknima uspoređena je s elementima od nearmiranog betona.

1. INTRODUCTION

Industrially produced fibres can be added to concrete to improve its post cracking flexural strength and a fatigue resistance. The use of fibres can lead to a reduction of reinforcement and speeding up the on-site process [1]. Many structures are often subjected to repetitive cyclic loads (e.g. traffic, wind action, sea waves, machine vibration). An exposure to repeated loading may result in a decrease in stiffness of a structure, which may lead to the fatigue failure. Fatigue is defined as a process of progressive, permanent internal structural changes in a material subjected to repeated loading [2]. In concrete, these changes are mainly associated with the progressive growth of internal microcracks. At the macrolevel this manifests as changes in the material's mechanical properties. In well designed steel fibre reinforced concrete (SFRC), fibres can control a crack propagation and increase an endurance life of a material and provide a more ductile behaviour [3][4]. This paper presents materials and methods used in an experimental programme carried out to test concrete prism elements subjected to cyclic flexural loads. The results are presented in terms of S – N curves, or Whöler curves, where S represents the stress level and N the number of cycles. A discussion is focused on a crack mechanism and a displacement rate during testing.

2. EXPERIMENTAL PROGRAMME

SFRC mix with 0.5% volume fraction of fibres (40 kg/m^3) was tested and compared to a plain concrete mix. Fibres used in this experiment were straight with hooked end, with a length of 35 mm and a diameter of 0.55 mm. The nominal tensile strength was around 1200 MPa.

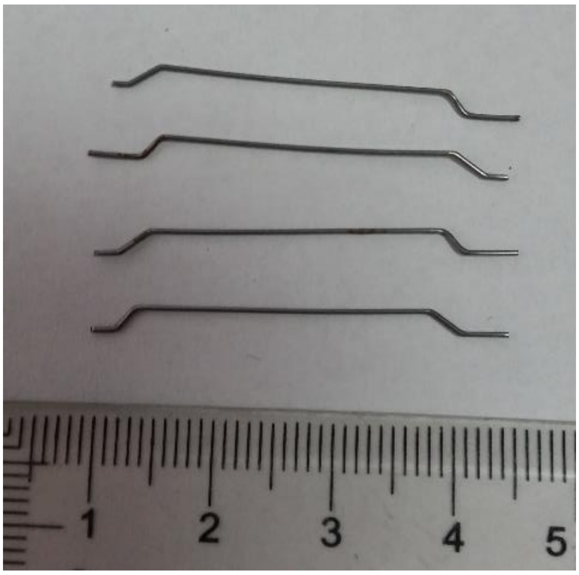

Figure 1 Appearance of industrial fibres

Portland cement type CEM II (42.5 N), river stone aggregate with maximum size 16 mm and polycarboxylic superplasticizer were used. Details are given in Table 1. A mixing was conducted in a rotary mixture and fibres were manually added into a drum. The concrete was placed in moulds in two layers and an each layer was vibrated 15 to 20 seconds. Cube specimens of size 150 x 150 x 150 mm were used to determine 28 days compressive strength of concrete, while cylinder specimens of size 150 x 300 mm were used for a modulus of elasticity and a tensile splitting strength determination. The specimens used for flexural test, as well as a flexural fatigue test, were prisms of size 150 x 150 x 600 mm.

Table 1 A description of a mix proportion

Component [kg/m^3]	PCA	SFRC
Aggregate (all sizes)	1840	1825
Cement	370	370
Water	170	170
w/c ratio	0.46	0.46
Superplasticizer	2.22	2.22
Steel fibres	0	40

Fatigue tests are usually very time consuming. To minimise testing time, a special frame was manufactured which could accommodate three specimens simultaneously. Yokes were placed at the mid-height of the each specimen and LVDT (*Linear Variable Differential Transformer)* sensors were mounted on them to measure vertical displacements. A static flexural test was conducted prior to fatigue tests to define LOP (*Limit of Proportionality*) static load, i.e. a load at which the first crack appers. For each mix, the load obtained from the static test was multiplied by 4 different stress levels (0.3, 0.5, 0.7 and 0.9) to calculate the load for the fatigue test. During dynamic test, a minimum of 0.1 of the load was continuously applied to the specimens and the maximum load was 0.3, 0.5, 0.7 and 0.9 of the static load. Load was applied following a sinusoidal wave pattern, at a frequency of 15 Hz until any of the three specimens failed or reached the maximum number of 2 million cycles, a limit commonly used in the literature for concrete fatigue testing [5] [6] [7] . Machine was set to stop every time the system reached displacement higher than 10 mm, i.e. when one specimen failed. After one specimen failed, test rig was not capable to continue testing with only two remaining specimens. For this purpose so called „dummy“ specimens were used to ensure load transaction on remaining specimens. Failed specimen was replaced by a dummy and the test was then continued until the last specimen failed or reached 2 million cycles. Testing machines involved were static-dynamic hydraulic Zwick/Roell machine for dynamic test and static electro-hydraulic Zwick/Roell machine for static flexural test. Both of these machines have nominal load capacity of 600 kN. A typical setup of the specimens is shown in following figures.

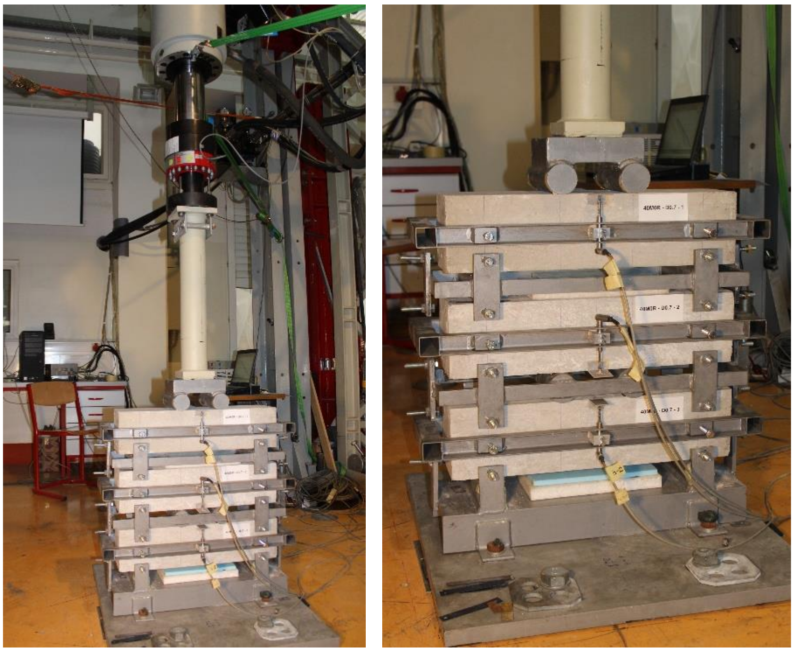

Figure 2 Fatigue test setup

The main output was the number of cycles until failure. Two LVDT sensors were used per specimen, one on each side, from which average value of deflection was determined. In order to obtain the points that form the sinusoidal wave pattern of displacements in each cycle of loading the sampling frequency of displacement measurement was 300 Hz. Other information provided are the machine displacement and the minimum and maximum load applied in each cycle.

3. ANAYSIS OF TEST RESULTS

3.1. MECHANICAL PROPERTIES

The mechanical properties of specimens are summarized in Table 2. All results are average value of 3 tests.

Table 2 Mechanical properties of mixtures

Mix	Compressive strength ± stand. deviation (MPa)	Modulus of elasticity ± stand. deviation (GPa)	Tensile splitting strength ± stand. deviation (MPa)
PC	48.1 ± 0.9	32.9 ± 1.1	3.1 ± 0.2
SFRC	46.8 ± 0.7	30.1 ± 0.7	4.1 ± 0.1

Flexural tensile strength was evaluated from experimentally obtained load-deflection curves during three point bending test performed on notched prisms. Deflection was measured by two LVDT sensors, from which the average value of deflection was determined, Figure 3.

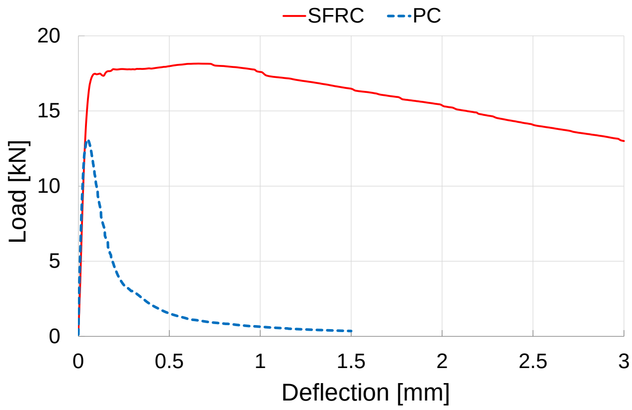

Figure 3 Average load – deflection curves

Flexural strength at limit of proportionality is determined, results are expressed as average values of all tested specimens for plain concrete and SFRC. Results of residual flexural strengths at four characteristic points, $CMOD_1$ to $CMOD_4$ (*Crack Mouth Opening Displacement*) are shown in Table 3**Error! Reference source not found.**.

Table 3 Flexural strength of PC and SFRC specimens

Mix	Flexural strength at LOP (MPa)	Residual flexural strength at $CMOD_1$ (MPa)	Residual flexural strength at $CMOD_2$ (MPa)	Residual flexural strength at $CMOD_3$ (MPa)	Residual flexural strength at $CMOD_4$ (MPa)
PC	4.26	0.54	0.14	0	0
SFRC	5.57	5.74	5.39	4.78	4.16

3.2. FATIGUE TEST

To determine the load level for each stress level, three specimens for each mix were subjected to four point static flexural test. The values obtained in static test are shown in Table 4.

Table 4 Static load and fatigue load for different stress levels

STATIC TEST			FATIGUE TEST		
Prism specimen	Static load [kN]	Average value of static load [kN]	Stress level S	Max. fatigue load [kN]	Number of specimens for fatigue testing
PC-S1 PC-S2 PC-S3	33.8 33.1 32.2	33.0	0.3 0.5 0.7 0.9	9.9 16.5 23.1 29.7	2 3 3 3
SFRC-S1 SFRC -S2 SFRC -S3	41.7 39.3 39.2	40.1	0.3 0.5 0.7 0.9	12.0 20.1 28.1 36.1	2 3 3 3

In the following figures results of fatigue tests are presented at stress levels 0.7 and 0.9, in maximum and minimum displacement *versus* number of cycles for each specimen during testing. At lower stress levels (0.3 and 0.5) all specimens reached 2 million cycles. Two straight lines in charts represent static displacements, which are shown for comparison purposes. High deviations in the results are usually expected in fatigue test of SFRC, mainly because of the random orientation of fibres [8][9] and also because the specimens tested against fatigue are not the same tested to determine the static flexural load.

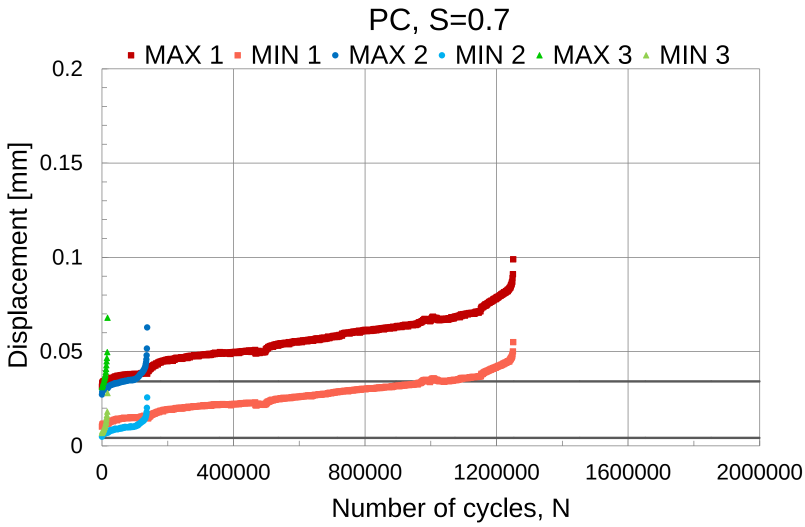

Figure 4 Displacements – number of cycles curve for PC at S = 0.7

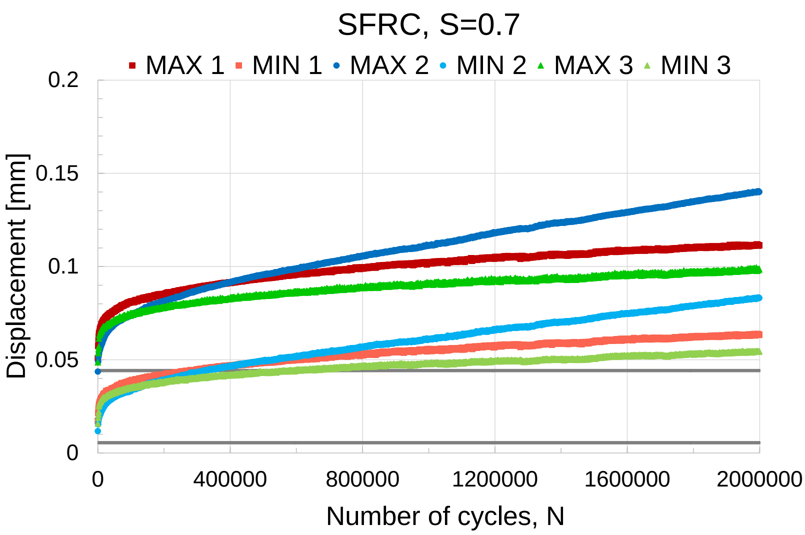

Figure 5 Displacements – number of cycles curve for SFRC at S = 0.7

Table 5 Number of cycles until failure (or 2 million cycles) for all specimens

PC				SFRC			
S=0.3	S=0.5	S=0.7	S=0.9	S=0.3	S=0.5	S=0.7	S=0.9
2 000 000 2 000 000	2 000 000 2 000 000 2 000 000	1 250 500 137 670 16 990	1 170 3 380 27 900	2 000 000 2 000 000	2 000 000 2 000 000 2 000 000	2 000 000 2 000 000 2 000 000	394 050 77 440 975 600

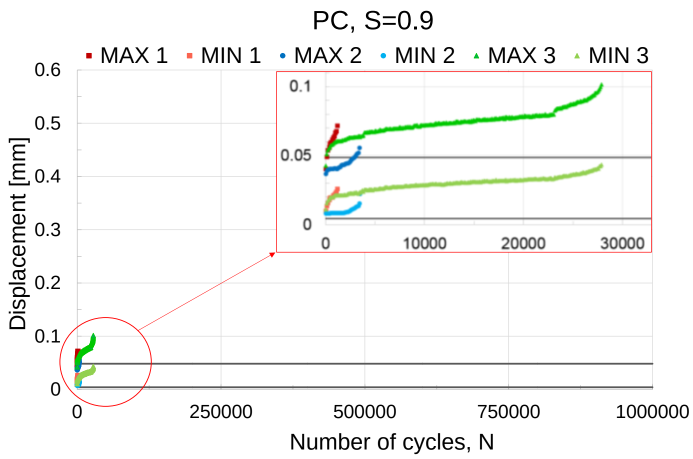

Figure 6 Displacements – number of cycles curve for PC at S = 0.9

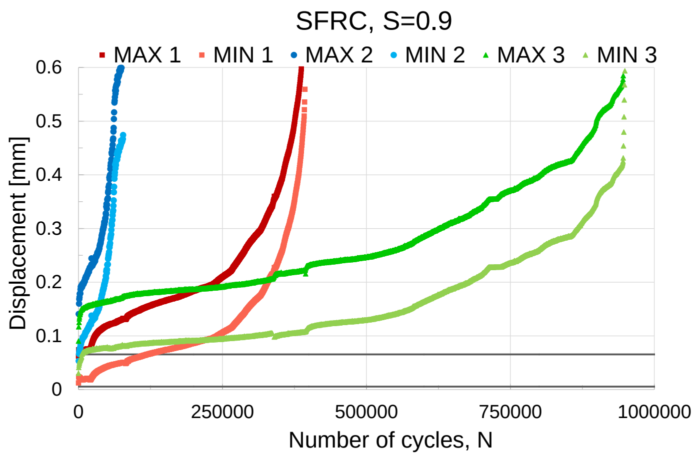

Figure 7 Displacements – number of cycles curve for SFRC at S = 0.9

In Figure 8, results are presented in S – logN diagram. LogN was used instead of number of cycles N to comply with the common procedure regarding fatigue testing.

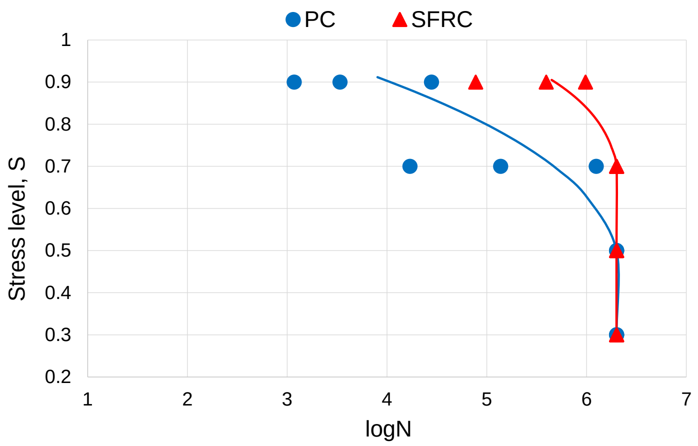

Figure 8 S – logN diagram for all specimens

4. CONCLUSIONS

All tested specimens reached 2 million cycles at stress level 0.3 and 0.5 (there was no signs of cracks or deterioration) while SFRC specimens reached 2 million cycles even at stress level 0.7. Number of cycles reduced drastically when the stress level increased from 0.7 to 0.9. Variability in the results was expected due to inhomogeneity of concrete itself and additionally because of random distribution of the fibres in SFRC specimens. SFRC specimens didn't break in two, as fibres kept two half of specimen together. After examining the break surface it was noted that fibres didn't break but were pulled out (no yielding was observed). SFRC specimens resisted much higher displacements then PC at higher stress levels.

The addition of fibres in quantity of 40 kg/m^3 reduced vertical displacements, enhanced ductility and durability of concrete.

ACKNOWLEDGMENTS

The research presented in this paper was conducted in the scope of FP7 European founded project Anagennisi - Innovative Use of all Tyre Components in Concrete. The authors extend their thanks to participants in the project as without them the scientific research presented herein would not have been implemented.

REFERENCES

[1] ACI, Report on fibre reinforced concrete, ACI 544 1R-96, American Concrete Institute, 1996.

[2] Lee, M. K.; Barr, B. I. G.: An overview of the fatigue behaviour of plain and fibre reinforced concrete, *Cement and Concrete Composites,* vol. 26, no. 4, pp. 299–305, 2004.

[3] Li, V. C.; Matsumoto, T.: Fatigue Crack Growth Analysis of Fiber Reinforced Concrete with Effect of Interfacial Bond Degradation, *Cement and Concrete Composites* vol. 20, pp. 339–351, 1998.

[4] Rossi, P.; Parant, E.: Damage mechanisms analysis of a multi-scale fibre reinforced cement-based composite subjected to impact and fatigue loading conditions, *Cement and Concrete Research*, vol. 38, no. 3, pp. 413–421, 2008.

[5] Johnston, C. D.; Zemp, R. W.: Flexural Fatigue Performance of Steel Fibre Reinforced Concrete - Influence of Fibre Content, Aspect Ratio and Type, *ACI Materials Journal*, vol. 88, no. 4, pp. 374–383, 1991.

[6] Chang, D.; Chai, W.: Flexural fracture and fatigue behavior of steel-fiber-reinforced concrete structures, *Nuclear Engineering and Design*, vol. 156, pp. 201–207, 1995.

[7] Graeff, A. G. et al.: Fatigue resistance and cracking mechanism of concrete pavements reinforced with recycled steel fibres recovered from post-consumer tyres, *Engineering Structures*, vol. 45, pp. 385–395, 2012.

[8] [Singh, B. et al.: Probability of fatigue failure of steel fibrous concrete, *Mag. Concr. Res.*, vol. 57, no. 2, pp. 65–72, 2005.

[9] Singh, S. P.; Ambedkar, B. R.: Flexural fatigue strength prediction of steel fibre reinforced concrete beams, *Electronic Journal of Structural Engineering*, no. 8, pp. 46–54, 2008.

SHEAR BEHAVIOUR OF CONFINED AND UNCONFINED RUBBERIZED CONCRETE

Zhao Wang[1], David Escolano Margarit1, Maurizio Guadagnini[1], Kypros Pilakoutas[1]

[1] The University of Sheffield, Faculty of engineering, Department of Civil and Structural Engineering, Sir Frederick Mappin Building, Mappin Street, Sheffield S1 3JD, UK, email: zwang88@sheffield.ac.uk, d.escolano@sheffield.ac.uk, m.guadagnini@sheffield.ac.uk, k.pilakoutas@sheffield.ac.uk

SUMMARY: This article presents the experimental results of an ongoing investigation aiming to develop high-strength high-deformability confined rubberised concrete (CRuC) suitable for structural applications. The Rubberised Concrete (RuC) utilises recycled rubber particles as replacement for both fine and coarse aggregates. The inclusion of rubber in concrete can lead to significant reductions in compressive strength and stiffness thus limiting the application of RuC for structural purposes. However, confining RuC with fibre reinforced polymer jackets recovers the strength and allows the development of the high deformability, ductility and energy dissipation capacity of RuC. Although recent research mainly focuses on the axial performance of RuC, there is still a lack of understanding of the behaviour of this novel material under shear conditions. The aim of this paper is to investigate experimentally the shear behaviour of unconfined and confined rubberised concrete. Four prisms with reduced width in the mid-span and 12 prisms with different shear-span-to-depth ratios were tested under axisymmetric four point bending test. In this test set-up, the stress state in the mid-span section approaches pure shear, with uniformly distributed shear stress and low normal stress. Test results indicate that FRP confinement is extremely effective at enhancing the shear strength of rubberised concrete, whilst developing a high level of shear deformability. This supports the idea that CRuC can be effectively used to develop highly ductile RC structural components for structures located in high seismicity regions. This study is part of the ongoing EU-funded collaborative research project Anagennisi.

POSMIČNO PONAŠANJE BETONA S GUMOM SA I BEZ OJAČANJA

SAŽETAK: U radu se prikazuju eksperimentalni rezultati istraživanja koje je u tijeku o razvoju betona s gumom, velike čvrstoće i velike deformabilnosti, prikladnog za konstrukcijske primjene. U betonu s gumom upotrebljavaju se čestice reciklirane gume kao zamjena za sitni i krupni agregat. Uključivanje gume u beton može dovesti do znatnog smanjenja tlačne čvrstoće i krutosti što ograničava njegovu upotrebu za konstrukcijske svrhe. Međutim, ojačanje betona s gumom oblogama od polimera armiranog vlaknima daje betonu čvrstoću i omogućuje postizanje velike deformabilnosti, duktilnosti i sposobnosti raspršivanja energije takvog betona. Iako su suvremena istraživanja uglavnom usmjerena na svojstva betona s gumom pri osnom tlaku još uvijek nema razumijevanja ponašanja tog novog materijala pri posmiku. Svrha je rada eksperimentalno istražiti posmično ponašanje ojačanog betona s gumom i onong bez ojačanja. Ispitane su četiri prizme širine smanjenje u sredini raspona i 12 prizama različitih omjera posmičnog raspona i visine prizme pri osnosimetričnom ispitivanju na savijanje opterećenjem u četiri točke. U takvoj postavci ispitivanja stanje naprezanja u presjeku u sredini raspona približava se čistom posmiku uz jednoličnu raspodjelu posmičnog naprezanja i malo normalno naprezanje. Rezultati ispitivanja pokazuju da je ovijanje polimerima armiranim vlaknima izuzetno učinkovito za poboljšanje posmične čvrstoće betona s gumom uz veliku posmičnu deformabilnost. To podržava ideju da se ojačani beton s gumom može učinkovito upotrijebiti za stvaranje vrlo duktilnih armiranobetonskih konstrukcijskih dijelova konstrukcija u područjima jake seizmičnosti. Ovo istraživanje dio je zajedničkog istraživačkog projekta Anagennisi koji podupire Europska unija.

1. INTRODUCTION

In EU countries, more than 3M tyres reach their end of life each year according to ETRA 2013 [1]. Given these indicative numbers it is clear that disposal of used tyres constitutes a growing worldwide problem that is regulated by environmental legislation in developing countries. In Europe, the directives 1991/31/EC and 2008/98/EC favour reusing or recycling scrap tyre components over the disposal in landfills or the lesser preferable option of burning tyres for energy recovery. In this environmental context, there has been an increasing effort in industry and research institutions for creating novel applications for waste tyre components. Among these, the inclusion of rubber particles in materials for construction, such as concrete, is receiving the attention of researchers.

Tyres are made of high quality vulcanised rubber, placed in layers, many of which are structurally reinforced with corded steel wire or polymer textiles. The rubber crumb can be extracted from tyres through a varieties of chemical and mechanical means (shredding and granulating). Rubber extracted from tyres is a highly durable material, it has good strength, flexibility and a remarkable ability to maintain its volume under stress. This makes it an ideal candidate as aggregate for concrete and can be used in high-value applications in the construction industry.

Significant research work has been carried out to replace part of the concrete aggregates with recycled tyre rubber [2, 3]. These studies reported that the ductility of concrete was found to increase with a relatively modest addition of rubber (1% by weight of aggregates). However, the inclusion of large amounts of rubber affects negatively both the fresh and hardened properties of concrete, limiting its applications to low level non-structural components as pedestrian blocks or lightweight fills [4-6].

Recent research proved that confining Rubberised Concrete (RuC) with Fibre Reinforced Polymers (FRP's) recovers the losses in the strength of RuC while maintaining its large deformation capacity [7, 8]. Recent studies at the University of Sheffield within Anagenissi project (http://www.anagennisi.org/) developed a Confined Rubberised Concrete (CRuC) able to withstand large level of stress (up to 80 MPa) at large levels of deformation (up to 5%). These results show that if appropriate confinement is provided, RuC can be used for structural applications while exploiting its excellent deformation capacity. However, there is still a lack of understanding of the behaviour of this new material under shear conditions. Therefore, this study focuses on the shear behaviour of unconfined and confined RuC and its possible structural applications in components where large ductility or large deformability is required, such as coupling beams or bridge bearings.

2. OPTIMISED MIX

An optimised mix developed by Rafoul [7] is adopted in this work. The original mix, designed for bridge piers, was optimised to enable large replacements of aggregate with rubber, yet minimising the effects on both fresh and hardened properties of the concrete. The final mix adopted for the tests replaces 60% by volume of fine and coarse aggregates with rubber. Table 1 shows the optimised mix components and proportions.

Table 1 The components and proportions of optimized mix (60C/F)

Material	Water	CEM II – 52.5MPa	Fine Aggregate - 0/5mm	Coarse Aggregate - 5/10 and 10/20mm	Fine Rubber - 0/5mm	Coarse Rubber - 5/10 and 10/20mm	Plasticizer	Superplasticizer
Quantity/m^3	180 L	425kg	328.0kg	400.4kg	148.5kg	181.3kg	2.5L	5.1L

3. EXPERIMENTAL PROGRAMME

The axisymmetric four point bending test was adopted in this experimental programme. The test was conducted on rectangular concrete prisms in which the central part -where the maximum shear forces are expected- was cast with RuC, whereas the sides were cast with regular concrete. Two different geometries were considered for the specimens: (a) Prisms shown in Fig 1 with reduced width in the mid-span. In this group of prisms the sides were reinforced with 6mm steel bars, while the central part was left unreinforced. The shear-span-to-depth ratio fixed on 0.7. Four samples were produced. Two were tested unconfined while the other two were tested after confining the mid-span with one layer of CFRP, (b) Prisms with different shear-span-to-depth ratios shown in Fig 2. This group of prisms were reinforced with 4 basalt FRP bars along the length of the prism (see Fig 2). For this group of specimens, three different aspect ratios (1, 1.5 and 2) were considered.

1. INSTRUMENTATION

The tests were carried out on a 300 kN electromagnetic universal testing machine. The load was applied monotonically in displacement control until failure at a rate of 0.1 mm/min. 2 LVDT and 4 potentiometers were used to measure the deflections during the tests: LVDT1 & 2 were mounted on an aluminium yoke (fixed at the middle height of the prism) to measure the relative deflection at mid-span on each side of the prism. POT 3 measures the deflection at mid-span externally. POT 1 measures the deflection at the free end of the prism. POT 2 & 4 measure the deformations at the supports. Two 10mm 120 ohms strain gauges were placed at mid-span and inclined 45 degrees to the longitudinal axial of the prisms, to measure the shear strains. Fig 3 and Fig 4 show a sketch and a picture of the instrumentation and the experimental setup respectively.

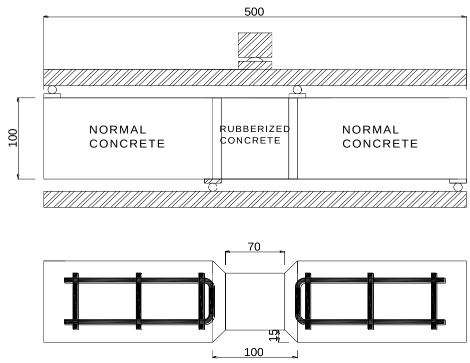

Figure 1 Prisms with reduced width in the mid-span

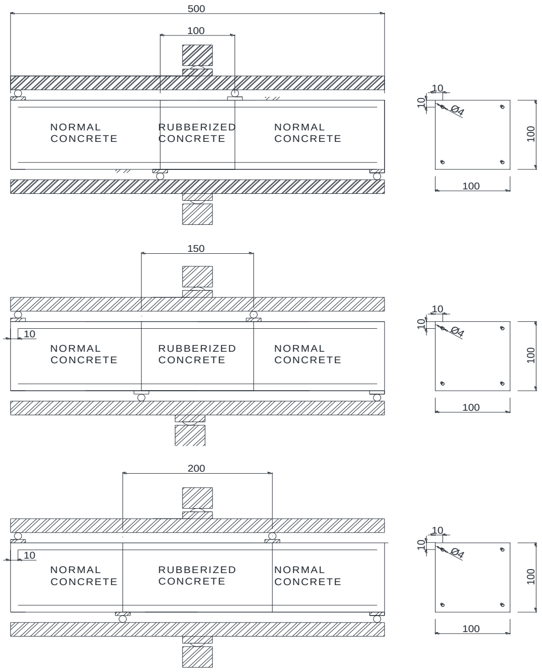

Figure 2 Prisms with different shear-span-to-depth ratio

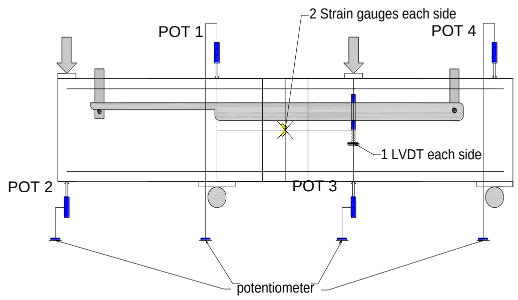

Figure 3 Instrumentation

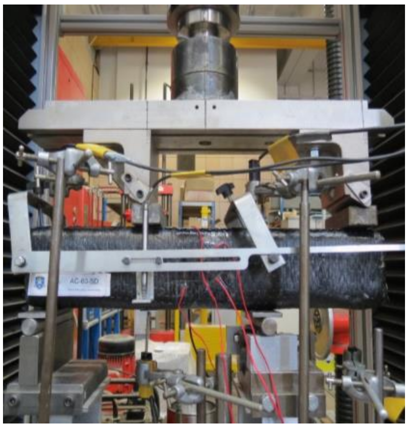

Figure 4 Set-up overview

2. TEST RESULTS AND DISCUSSION

2.1. FAILURE MODES

For unconfined rubberised concrete, the prisms with reduced width in the mid-span and prisms with shear-span-to-depth ratio 1 and 1.5, as expected, showed a 45 degree shear crack (see Fig 5a-c). The shear crack formed near the mid-point of the shear-span-to-depth at around 60 to 70% of the ultimate capacity and developed towards the load points with increasing load. After the maximum load, conversely to what happens on regular concrete, the shear crack gradually increases in both width and length avoiding a sudden failure. For the prisms with shear-span-to-depth ratio 2, the first flexural crack appeared at 55% of the ultimate capacity, followed by first shear crack in the shear span. More cracks appeared with increasing load. At load descending stage, several flexural cracks and shear cracks formed (see Fig 5d).

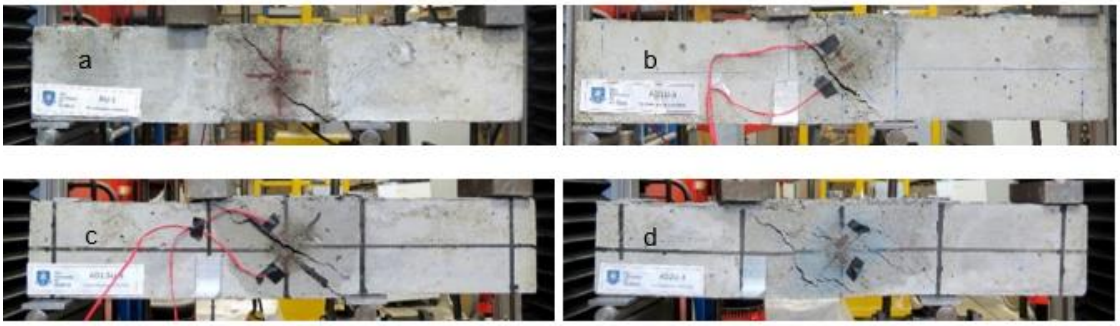

Figure 5 Crack patterns of RuC

For confined rubberised concrete, there different failure modes were observed: i) rupture of the FRP jacket (see Fig 6a); ii) concrete crushing; and iii) flexural failure. FRP rupture was observed in the case of prisms with enough flexural reinforcement and with the FRP-overlap area situated at the top of the beam. Concrete crushing was observed in the specimens with shear-span-to-depth ratio 1 and low confinement (see Fig 6b). Flexural failure (see Fig 6c), occurred mainly in specimens with shear-span-to-depth ratio 1.5 and 2, and was caused by lack of adequate flexural reinforcement.

Figure 6 Failure modes of CRuC

2.2. MECHANICAL PROPERTIES OF RUC AND CRUC

Along with the 16 prisms, 6 cubes and 6 cylinders were used to determine the compressive and tensile strength of RuC and CRuC. The detail experiment results are presented in Table 2. The summary is shown in Table 3.

The tensile strength was estimated from the splitting tensile strength,$f_{ct,sp}$, according to EN 1992-1-1:2004(E) [9], and taken as:$f_{ct} = 0.9f_{ct,sp}$. Hence, the axial tensile strength of RuC is considered to be 1.17 MPa.

Approximate values for the initial modulus of elasticity (E_0) and initial shear modulus (G_0) of RuC can be estimated by dividing the compressive stress (σ_{LOP}) by the axial strain (ε_{LOP}), and the shear stress (τ_{LOP}) by the shear strain (γ_{LOP}), at limit of proportionality (LOP, which corresponds to the onset of microcracking). Hence, according to the stress – strain curve of uniaxial compression tests on cylinders and axisymmetric shear tests, the initial modulus of elasticity (E_0) of RuC is 7.8GPa, while the initial shear modulus (G_0) is 1.48GPa.

2.1. LOAD DEFLECTION PERFORMANCE

Fig 7 shows the experimental Load-deflection curves of the prisms with reduced width in the mid-span. It can be seen that all specimens with FRP-confinement (RC-1, RC-2) have higher shear capacity and exhibited higher ductility than the unconfined specimens (RU-3, RU-4). This can be explained by the fact that the confinement pressure provided by the CFRP jacket maintains the integrity of the concrete and enhance its ability to carry loads.

Fig 8 shows the shear stress-strain curves obtained from the experimental results. As can be seen in Fig 8 (b-c) large variability was observed in the prisms with shear-span-to-depth ratios 1.5 and 2 in terms of stress and strain. This can be explained by the high variability in the material [7] and possibly because of the manufacturing quality of the FRP jackets. The average shear stress τ_{avg} was determined by dividing the shear force (V) by the cross section area (A) of the mid-span. The shear strain was estimated using the measurements given by 2 strain gauges placed at 45 degree on the surface of the beam or the CFRP jacket. Due to the pure shear state in mid-span, it is expected that $\sigma_1 = -\sigma_2 = \tau$. Therefore, the shear strain is taken as the sum of the two 45 degree strain gauge readings, $\gamma = \varepsilon_1 + \varepsilon_2$. In comparison to RuC, the ultimate strain of CRuC was enhanced about 20 to 40 times, whilst the ultimate shear capacity increased twice.

Table 2 The geometry and strength of tested specimens

Specimen	Shear Capacity (kN)	Height (mm)	Width (mm)	Ultimate shear stress (MPa)
RC-1	15.67	101.5	73.2	2.11
RC-2	18.90	104.7	74.7	2.41
AD1C-1	20.97	101.2	100.0	2.07
AD1C-2	21.40	101.9	100.1	2.10
AD1.5C-1	28.62	106.9	100.0	2.68
AD1.5C-2	23.43	102.3	100.3	2.29
AD2C-1	18.68	100.8	100.0	1.85
AD2C-2	21.80	104.1	100.0	2.09
RU-3	4.95	100.1	68.2	0.73
RU-4	6.05	102.2	70.7	0.83
AD1U-3	12.34	104.4	100.1	1.18
AD1U-4	15.33	107.1	100.1	1.42
AD1.5U-3	12.00	103.6	100.0	1.16
AD1.5U-4	12.36	104.1	100.3	1.19
AD2U-3	14.49	106.5	100.0	1.36
AD2U-4	11.53	101.4	100.0	1.14

*Note: R = reduced width in mid-span, AD = the shear-span-to-depth ratio, C = FRP-confined specimen, U= unconfined specimen

Table 3 Test results

	Cube compressive strength	Cylinder compressive strength	Splitting tensile strength	Average shear stress (RuC)	Average shear stress (CRuC)
	MPa				
Average Value	11.5	7.2	1.3	1.12	2.2
Standard deviation	1.05	1.21	0.18	0.93	1.06

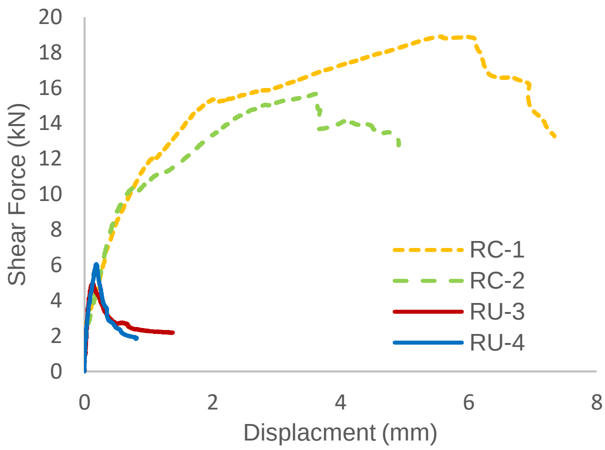

Figure 7 Load-Deflection curves of the prisms with reduced width

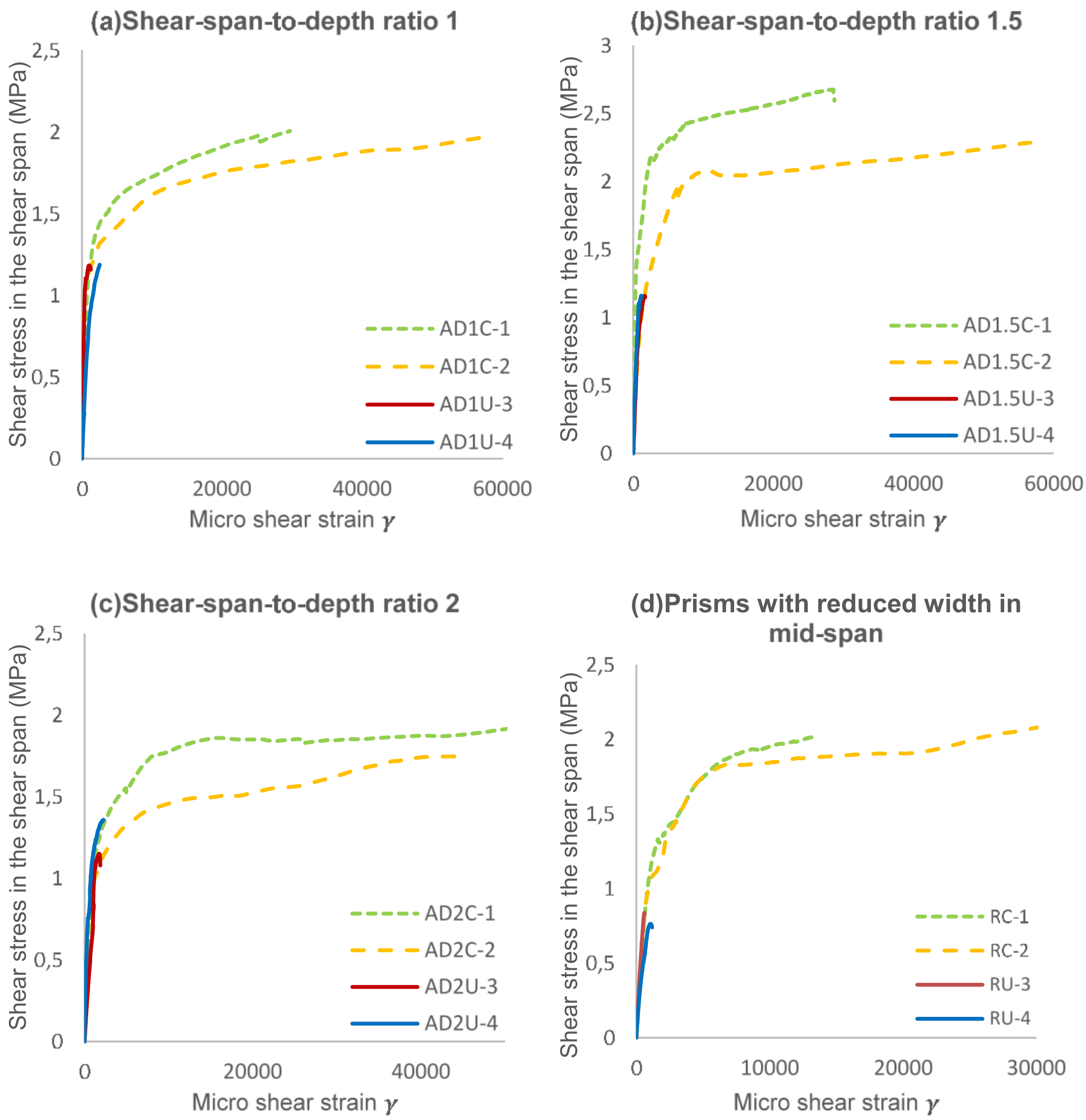

Figure 8 Comparison of the shear stress-strain curve of prims with different shear-span-to-depth ratios

2.2. CONSTITUTIVE LAW FOR UNCONFINED RUBBERISED CONCRETE

Based on the experimental results discussed above, a constitute law for shear stress-strain of RuC is proposed.

2.2.1. SHEAR STRENGTH OF RUC

The shear strength of concrete (τ_p) monotonically increases with the cube compressive strength (f_{cu}). Guo [10] suggested a formulation to predict the shear stress of conventional concrete (Eq.1). This formula was adapted empirically to fit the results of RuC as shown in Eq.2.

$$\tau_p = 0.39 \times f_{cu}^{0.57} \tag{1}$$

$$\tau_p = 0.36 \times f_{cu}^{0.57} \tag{2}$$

2.2.2. SHEAR STRAIN AND MODULUS OF RUC

The shear strain (γ_p) and the principle tensile and compressive strain$(\varepsilon_{1p}, \varepsilon_{2p})$ at peak point (failure of concrete), monotonically increases with shear strength (τ_p) (see Fig 9). The regression formulas of the peak strains are:

$$\varepsilon_{1p} = (1160.2\tau_p\text{-}448.5) \times 10^6 \tag{3}$$

$$\varepsilon_{2p} = (999.8\tau_p\text{-}318.11) \times 10^6 \tag{4}$$

$$\gamma_p = (2160\tau_p\text{-}766.61) \times 10^6 \tag{5}$$

Where $\tau_p$is the shear strength of RuC in N/mm^2.

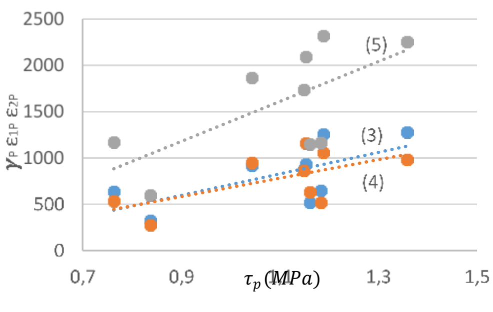

Figure 9 Principle tensile/compressive strain and shear strain at peak load

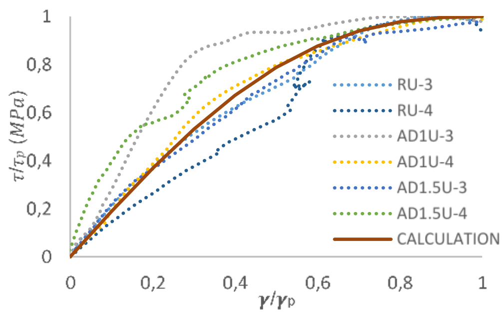

Figure 10 Normalised stress-strain curve

By normalising the shear stress-stain curves ($x = \frac{\gamma}{\gamma_p}, y = \frac{\tau}{\tau_p}$) and assuming a cubic function($y = Ax + Bx^2 + Cx^3$), which satisfies the following boundary conditions: (1) $x = 0, y = 0$, (2) $0 \leq x < 1, \frac{d^2y}{dx^2} < 0$. $\frac{dy}{dx}$ is decreasing, No inflexion point, (3)$x = 1, y = 1, \frac{dy}{dx} = 0$, a shear stress-strain curve can be determined as shown in Eq.6 below. Fig 10 shows the normalised shear stress-stain curve of RuC. The red bold line shows the regression of the experimental data and can be derived from the following expressions:

Normalised shear stress strain

$$\frac{\tau}{\tau_p} = 2.5 \times \frac{\gamma}{\gamma_p} - 2 \times (\frac{\gamma}{\gamma_p})^2 + 0.5 \times (\frac{\gamma}{\gamma_p})^3 \tag{6}$$

Secant shear modulus:

$$G_s = \frac{\tau}{\gamma} = \frac{\tau_p}{\gamma_p}[2.5 - 2 \times \frac{\gamma}{\gamma_p} + 0.5 \times (\frac{\gamma}{\gamma_p})^2] \tag{7}$$

Tangent shear modulus:

$$G_t = \frac{d\tau}{d\gamma} = \frac{\tau_p}{\gamma_p}[2.5 - 4 \times \frac{\gamma}{\gamma_p} + 1.5 \times (\frac{\gamma}{\gamma_p})^2] \tag{8}$$

Secant shear modulus at peak point is:

$$G_{sp} = \frac{\tau_p}{\gamma_p} = \frac{10^3}{2160 - 766.61/\tau_p} = \frac{10^3}{2160 - 2129/f_{cu}^{0.57}} \tag{9}$$

Initial tangent shear modulus is

$$G_{t0} = 2.5G_{sp} \tag{10}$$

The average cube compressive strength of RuC is 11.5MPa, according to Eq.9 and Eq.10, $G_{sp} = 0.6$ MPa, $G_{t0} =$1.5 MPa, which have good agreement with the experiment results.

3. CONCLUSIONS

The main goal of this study was to examine experimentally the shear behaviour of confined and unconfined rubberised concrete.16 small scale prisms, unconfined and confined with CFRP jackets in the mid-span and different aspect ratios were tested under pure shear using the axisymmetric four point bending test. Based on the experimental results the following conclusions can be drawn:

The shear strength of RuC is close to its direct tensile strength.

Confining RuC with CFRP jacket prevents shear failure of the RuC and changes its brittle and softening behaviour into a significantly more ductile and stable performance.

Confining RuC with one layer of CFRP increases the ultimate shear stress up to two times, while enhancing the shear strain up to 40 times.

Empirical expressions are derived from the experimental results for the stress- strain curve $(\tau - \gamma)$, and the secant and tangent shear moduli G_s and G_t.

The test results confirm that confining RuC with CFRP jackets can lead to highly deformable elements under shear conditions and increase the strength of RuC to levels required from structural elements, hence opening the possibility of using CRuC in applications where large strength and shear deformation are required.

ACKNOWLEDGMENTS

The research leading to these results has received funding from the European Union Seventh Framework Programme [FP7/2007- 2013] under grant agreement n° 603722 and EU H2020 Marie Skłodowska-Curie Programme grant agreement n° 658248 (SHDS project). The first author is supported by the scholarship from China Scholarship Council (CSC) under Grant CSC n° 201608060059.

REFERENCES

[1] ETRA, The European Tyre Recycling Association. Available from http://www.etra-eu.org Accessed: 2014-06-10.

[2] Freakley, P.K. & A.R. Payne.: Theory and practice of engineering with rubber, Applied Science Publishers, 9780853347729, London, (1978).

[3] Sienkiewicz, M.; Kucinska-Lipka, J.; Janik, H. & Balas, A.: Progress in used tyres management in the European Union: a review, Waste Management, 2012. 32(10): pp.1742-1751.

[4] Zhu, H.; N. Thong-On. & X. Zhang.: Adding crumb rubber into exterior wall materials, Waste management & research, 2002. 20(5): pp. 407-413.

[5] Pierce, C. & M. Blackwell.: Potential of scrap tire rubber as lightweight aggregate in flowable fill, Waste Management, 2003. 23(3): pp. 197-208.

[6] Sukontasukkul, P.: Use of crumb rubber to improve thermal and sound properties of pre-cast concrete panel, Construction and Building Materials, 2009. 23(2): pp. 1084-1092.

[7] Raffoul, S., et al.: Optimisation of rubberised concrete with high rubber content: An experimental investigation. Construction and Building Materials, 2016. 124: pp. 391-404.

[8] Papastergiou, P.: 2010. A confinement model for concrete wrapped of pretensioned with frp. Doctoral dissertation, The University of Sheffield.

[9] Comité Européen de Normalization (CEN). "Design of concrete structures—Part 1-1: General rules and rules for buildings." Eurocode 2, EN 1992-1-1: 2004: E (2004).

[10] Z.H. Guo.: Principles of reinforced concrete, Tsinghua University Press, 9780128008591, Beijing, (1999).

SELF-COMPACTING CONCRETE REINFORCED WITH TYRE RECYCLED STEEL FIBRES

Andreas Christofe[1], Kyriacos Neocleous[1], Thomaida Polydorou[1], Andreas Kkolos[1], Diofantos Hadjimitsis[1]

[1] Cyprus University of Technology, Department of Civil Engineering and Geomatics, 2-8 Saripolou Street, Lemesos, Cyprus, email: andreas.christofe@cut.ac.cy, kyriacos.neocleous@cut.ac.cy, thomaida.polydorou@cut.ac.cy, andreas.kkolos@cut.ac.cy, d.hadjimitsis@cut.ac.cy

SUMMARY: An experimental study is presented on the development of steel fibre-reinforced concrete mixes, that are suitable for thin overlays in new and damaged concrete surfaces. To minimise the effort required for casting and compacting, the study aimed at developing concrete mixes that can be classified as self-compacting. Thus, a range of fresh concrete properties were examined to assess the workability of these mixes; the compressive and flexural strength was also examined experimentally. In total, six mixes were examined including a plain concrete mix; five types of short steel fibres were trialled: Recycled Tyre Steel Fibres with a dominant length range of 5 to 15 mm, and four types of Tyre Steel Cord Filaments, each type cut to a specific length. Three fibre contents were trialled (25, 50 and 100 kg of fibres per m^3 of concrete), but preliminary results indicated that the self-compacting properties (i.e. filling and passing ability, viscosity as well as segregation resistance) are diversely affected for concrete mixes with fibre contents greater than 25 kg/m^3. The main conclusion of this study was that screed mixes containing short Tyre Steel Cord Filaments can be classified as self-compacting. While, the mix containing Recycled Tyre Steel Fibres did not fulfil the acceptance criteria set for passing ability. However, this does not imply that this fibre type should not be used in fibre-reinforced overlays of concrete surfaces, since conventional rebars are not expected to be used in such applications and, thus, passing ability is not considered crucial for this type of application. The bending test results indicated that the longer Tyre Steel Cord Filaments as well as the Recycled Tyre Steel Fibres are effective in providing crack bridging at high crack-openings.

SAMOZBIJAJUĆI BETON ARMIRAN ČELIČNIM VLAKNIMA IZ OTPADNIH GUMA

SAŽETAK: Prikazuje se eksperimentalno istraživanje razvoja betonskih mješavina armiranih čeličnim vlaknima prikladnim za tanke prekrivne slojeve novih i oštećenih betonskih površina. Kako bi se napori pri ugradnji i zbijanju betona sveli na najmanju mjeru istraživanje je usmjereno na razvoj betonskih mješavina koje se mogu svrstati u samozbijajuće. Stoga je, radi ocjene obradivosti tih mješavina, ispitano više svojstava svježega betona. Ispitana je i tlačna čvrstoća i čvrstoća na savijanje. Ukupno je ispitano šest mješavina uključujući običan beton. Ispitano je pet vrsta s kratkim čeličnim vlaknima: čelična vlakna iz oporabljenih guma s prevladavajućim duljinama od 5 do 15 mm, četiri vrste s ispunom od čeličnih žica iz užadi pri čemu je svaka vrsta bila isječena na određenu duljinu. Ispitane su mješavine s tri količine vlakana (25, 50 i 100 kg/m3 betona). Preliminarni rezultati pokazuju da su svojstva vezana za samozbijanje (tj. sposobnost punjenja i prolaska, viskoznost i otpornost na segregaciju) sve nepovoljnija za betonske mješavine sa sadržajima vlakana većim od 25 kg/m3. Glavni je zaključak istraživanja da se mješavine koje sadržavaju kratke čelične žice iz užadi iz guma mogu svrstati u samozbijajuće. Istovremno, mješavina s pojedinačnim recikliranim čeličnim vlaknima iz oporabljenih guma nije zadovoljila zahtjeve za sposobnost prolaska. To međutim ne znači da se takva vlakna ne mogu upotrijebiti za završne slojeve jer se ne očekuje da će se u takvim primjenama upotrijebiti uobičajene čelične šipke pa se sposobnost prolaska ne smatra bitnom u takvoj primjeni. Rezultati ispitivanja na savijanje pokazuju da su dulje čelične žice iz užadi i pojedinačna reciklirana čelična vlakna iz oporabljenih guma učinkoviti za premoštenje pukotina pri velikim širinama pukotina.

1. INTRODUCTION

The implementation of a number of European Union (EU) environmental directives and policies, including the recent EU action plan on Circular Economy [1], is actively promoting the reuse and recycling of products and materials that otherwise would have been either disposed of to landfill or incinerated for energy recovery.

A typical example of such material is End-of-Life (EoL) tyres that are increasingly recycled to recover valuable materials, mainly rubber and steel wires. The recycled rubber is used in a diverse range of high-added value applications and products; while the recycled steel wires are mainly used as scrap feed in steel manufacturing. This is despite the fact that these steel wires are highly engineered material with exceptional strength characteristics (e.g. tensile strength over 1000 MPa). To this end, extensive research activities, carried out since the early 2000s, have successfully demonstrated that tyre-recycled steel wires can be used as fibre reinforcement in concrete, provided that they are clean of rubber and their length ranges between 15 to 25 mm [2-7]. To achieve these specifications, the tyre-recycled steel wires normally require further processing, which often yields large quantities of relatively shorter steel wires (length less than 15mm) that are not considered effective in bridging concrete cracks. Hence, these short wires (Figure 1a) are sent to steel kilns instead of being used in high-added value applications.

Another example of reused/recycled material is tyre-cord steel filaments, which arise as "surplus material" of tyre manufacturing, and in fact are the same material as the tyre-recycled steel wires. The only difference between the two material is their length and the fact that the filament surface is not contaminated with rubber dust. To use effectively the tyre-cord steel filaments in concrete, it is necessary to cut them to specific lengths, for instance 15 mm (e.g. Figure 1b).

(a) 

(b) 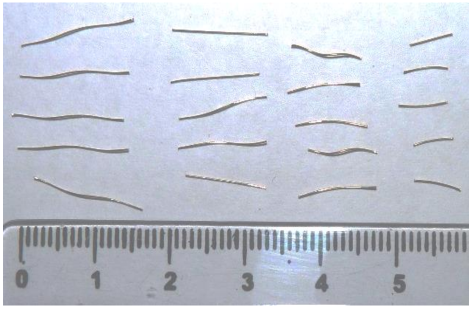

Figure 1 Short steel fibres used in the study: (a) tyre-recycled steel wires and (b) tyre-cord steel filaments

The experimental study, reported in this paper, aimed at developing steel fibre reinforced concrete (SFRC) mixes that are suitable for thin overlays in new and damaged concrete surfaces; to this end, the study examined the suitability of the short steel fibres, described above. To minimise the effort required for casting and compacting the concrete, the study aimed at developing concrete mixes that can be classified as self-compacting. Thus, a range of fresh concrete properties were examined to assess the workability of these mixes; the compressive and flexural strength was also examined experimentally.

The reported research is undertaken as part of the European research project "Anagennisi", funded by the EC's 7th Framework Programme and aims at promoting material recycling of EoL tyres through the development of innovative and high-added value applications in concrete construction for all the tyre components.

2. EXPERIMENTAL PROGRAMME

In total, six concrete mixes were examined including a plain concrete mix. The experimental study aimed at examining three fibre contents per mix (i.e. 25, 50 and 100 kg of fibres per m^3 of concrete), but preliminary results of a pilot mix (containing tyre steel-cord filaments, 15 mm long) indicated that only mixes with 25 kg of fibres (per m^3 of concrete) can be classified as self-compacting according to EN 206-9 [8] and EFNARC [9]. Figure 2 shows the reduced filling and passing ability of SFRC containing 100 kg of fibres per m^3 of concrete. Thus, the study considered only the fibre content of 25 kg of fibres per m^3 of concrete.

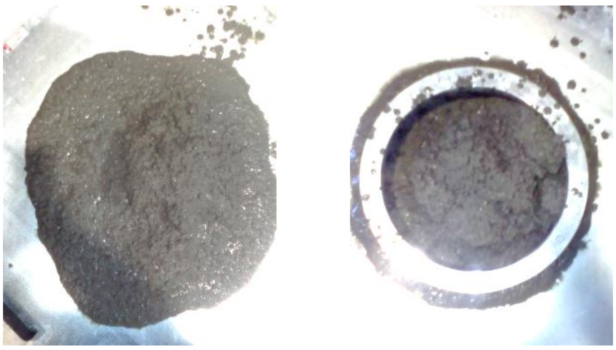

Figure 2 Slump-flow (left) and J-ring (right) testing of SFRC with 100 kg of TCF-15 per m3 of concrete

2.1. MATERIALS, MIXING AND CURING

Five types of steel fibres were used (Table 1): tyre-recycled steel fibres (RTSF) with a dominant length range of 5 to 15 mm, and tyre-cord steel filaments (TCF) with four different lengths (i.e. 6, 9, 12 and 15 mm). The study used cement CEM II /A-L 42.5 N, manufactured locally. Furthermore, imported silica fume and pulverised fuel ash were used as supplementary cementitious materials. To achieve the desired self-compacting properties, the study used a commercial superplasticizer, based on modified polycarboxylates. The aggregate used in this study were crushed limestone aggregates (0/4, 4/10 mm) as well as crushed calcareous sandstone (0/4 mm). The aggregate were manufactured at local quarries and Figure 3 shows their gradation.

Table 1 Geometrical and mechanical properties of steel fibres

Fibre type	Length (mm)	Diameter (mm)	Aspect ratio (l/d)	Tensile strength (N/mm^2)	Shape
Sorted RTSF	5 - 15 (85% of fibres)	0.1-0.2	varied	~2000	Irregular (wavy)
TCF-6	6	0.2	30	~2000	Straight
TCF-9	9	0.2	45	~2000	Straight
TCF-12	12	0.2	60	~2000	Straight
TCF-15	15	0.2	75	~2000	Straight

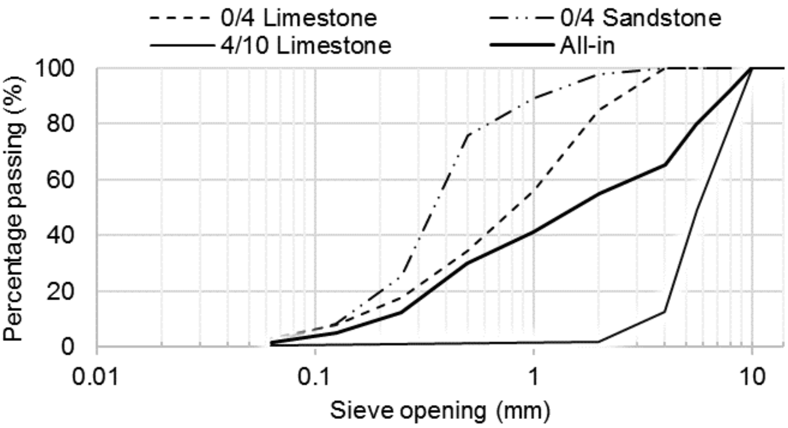

Figure 3 Gradation curves of fine and coarse aggregate

The absolute volume method (as elaborated by Gambhir [10]) was utilised for the derivation of the design mix for plain-concrete, which was also used as the basis for the five SFRC mixes (Table 2).

Table 2 Mix proportions of plain and SFRC mixes (based on SSD condition of aggregate)

Material type	Plain Concrete mix (kg/m^3)		RTSF (kg/m^3)		TCF-6 (kg/m^3)		TCF-9 (kg/m^3)		TCF-12 (kg/m^3)		TCF-15 (kg/m^3)	
	SSD	Actual	SSD	Actual	SSD	Actual	SSD	Actual	SSD	Actual	SSD	Actual
Crushed limestone 10 mm	580	569	580	598	580	586	580	588	580	588	580	586
Crushed limestone 0/4 mm	565	596	565	576	565	576	565	583	565	583	565	559
Crushed calcareous sandstone 0/4 mm	320	345	320	336	320	327	320	334	320	334	320	337
CEM II /A-L 42.5 N	315	315	315	315	315	315	315	315	315	315	315	315
Pulverised Fly Ash	70	70	70	70	70	70	70	70	70	70	70	70
Densified Silica fume	70	70	70	70	70	70	70	70	70	70	70	70
Superplasticizer	6	6	7	7	7	7	7	7	7	7	7	7
Potable water	256	212	256	211	256	231	256	216	256	216	256	239

The six concrete mixes were prepared in the laboratory at room temperature of 20° C. A drum concrete mixer (60 litre capacity) was used for the mixing. A conventional mixing sequence was applied to produce the mixes; the steel fibres were (manually) added last with continuous operation of the mixer. The specimens were not compacted to assess the effect of the added superplasticizer on the self-compacting properties.

The preparation of each mix was followed by a series of fresh concrete tests (slump-flow [11], V-funnel [12], L-box [13], J-ring [14] and sieve segregation [15]). The L-box and J-ring tests were undertaken to evaluate the passing ability of the concrete, while the slump flow and V-funnel tests were carried out to assess the filling ability of the mixes. The sieve segregation test was undertaken to assess the segregation resistance.

For each mix, nine cubes (150 mm) and three prisms (150x150x600mm) were also cast for compressive and flexural testing, respectively. A day after casting, all specimens were immersed in water (at room temperature). The cubes for compressive testing were removed a day prior to testing, while the prisms were removed at an age of 28 days and stored at controlled conditions until the day of testing. The flexural tests (CMOD controlled) were carried out according to EN 14651 [16], with the only modification that a 4-point testing arrangement was applied.

3. EXPERIMENTAL RESULTS

3.1. FRESH CONCRETE PROPERTIES

Table 3 outlines the results of the fresh concrete tests undertaken to assess the filling and passing ability, viscosity and segregation resistance of the six mixes.

The L-box results indicate that only the RTSF mix did not fulfil the acceptance criteria of EN 206-9 and EFNARC [2] for the passing ability. This could be attributed to the irregular shape of RTSF. Furthermore, the mix with TCF-9 fibres satisfied marginally the PL2 class of EN 206-9 and the minimum criterion of EFNARC. While, the J-ring test results indicate that only the mixes with TCF-9 and TCF-12 fibres satisfied the criteria of EN206-9 and EFNAC; the mix with TFC-6 fibres satisfied marginally these criteria.

The slump-flow of the six concrete mixes fulfilled the acceptance criteria of EN206-9 and EFNARC for the filling ability of self-compacting concrete. However, the V-funnel time fulfilled only the EN 206-9 viscosity criteria.

The sieve segregation results indicate that the EN 206-9 classes for segregation resistance were clearly satisfied by the plain concrete mix and the SFRC mixes with TFC-6 and TFC-15 fibres. While the remaining mixes marginally satisfied the SR1 class.

Table 3 Results of fresh concrete properties

Concrete Mix	Passing ability ratio PL (L-box)	Passing ability ratio PJ (mm) (J-ring)	Slump-flow (mm)	Viscosity (V-funnel) t=10 s	Viscosity (V-funnel) t=5 minutes	Segregation portion (%)
Plain	1.01	14	785	2.3	2.6	14.4
RTSF	0.69	16	740	2.5	2.7	20.6
TCF-6	0.82	11	745	2.5	3.2	19.7
TCF-9	0.78	10	740	2.4	2.7	21.2
TCF-12	0.85	10	720	2.8	3.1	20.9
TCF-15	0.94	21.3	710	2.6	3.3	17.5
EN206-class	PL2 ≥ 0.8 (3 bars)	PJ2 ≤ 10 (16 bars)	0.66m ≤SF2≤0.75m 0.76m≤SF3≤0.85m	VF1<9s	VF1	SR1 ≤ 20 SR2 ≤ 16
EFNARC criterion	0.8 ≤ PL ≤ 1.0	0 ≤ PJ ≤ 10	0.65 m ≤ SF ≤ 0.8 m	6s ≤ t ≤ 12s	6s ≤ t ≤ 15	-

3.2. HARDENED CONCRETE PROPERTIES

Figure 4 outlines the results obtained from the compressive cube tests at an early age, 7 and 28 days. The results demonstrated that there was a steady strength development with time; at the age of 28 days, the cube-strength class of 40 MPa was achieved by the four SFRC mixes with TCFs. The SFRC mix with RTSF reached a cube-strength of 45 MPa, and this was more than double the early age strength. Furthermore, the results indicate that the compressive cube strength was marginally improved by fibre addition (in the range of 8 to 17%). At this fibre content, the concrete density was not adversely affected (apart from the case of the mix with RTSF), and this indicates the beneficial effect of the chemical additive on the concrete's void content [17] (as observed during the casting of the specimens). Air-content tests of fresh concrete prisms indicated that the void content ranged from 3.5% to 4.9% (TCF-6: 4.5%, TCF-9: 4.9%, TCF-12: 4.7%, TCF-15: 4.6% and RTSF: 3.7%).

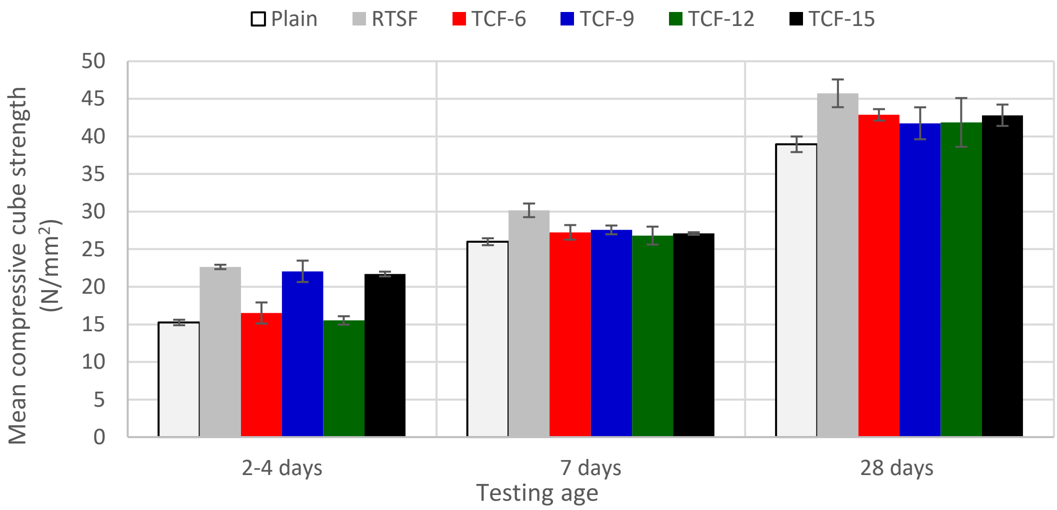

Figure 4 Compressive cube strength for the six concrete mixes at different ages

Figure 5 outlines the results of the flexural tests for the 5 SFRC mixes. The effect of fibre length is clearly demonstrated, where the mix with the longest fibres (i.e. TCF-15) exhibited the highest flexural strength amongst the 5 mixes. The RTSF mix exhibited a similar behaviour with the TCF-12 mix, but failed at a much lower crack-mouth-opening displacement. This is because the length of the RTSF fibres is variable (ranged from 5-15 mm). Furthermore, the TCF-15 and TCF-12 fibres satisfy the conformity criteria of EN 14889-1 for steel fibres (i.e. achieve a flexural tensile stress of 1.5 and 1 MPa at a CMOD of 0.5 and 3.5 mm, respectively) [18]. The test results also indicated that the prisms failed without exhibiting an extended tail in their post-peak response, as normally expected for concrete [19].

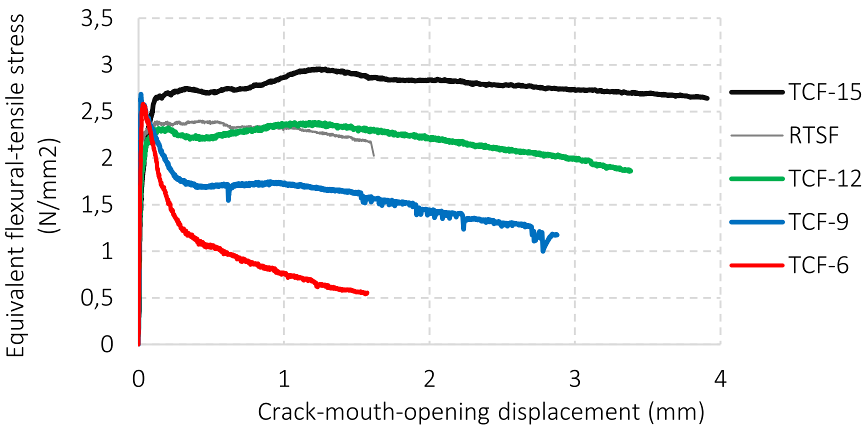

Figure 5 Results of the flexural tests of SFRC prisms

4. DISCUSSION AND CONCLUSIONS

This paper examined the development of self-compacting SFRC mixes for use as thin overlays in new and damaged concrete surfaces. The use of short tyre-recycled steel wires as well as tyre-cord steel filaments was trialled in the study, aiming to promote the reuse of these fibrous materials in high-added value applications in concrete construction.

Preliminary results of the fresh concrete tests indicated that SFRC mixes with high fibre contents (i.e. 50 and 100 kg of fibres per m³ of concrete) have reduced passing and filling ability. Furthermore, some fibre agglomeration was also observed for these fibre contents. Thus, the study focused on the fibre content of 25 kg of fibres per m³ of concrete.

The mixes reinforced with the tyre-cord steel filaments fulfilled the consistency criteria, set for the passing activity of self-compacting concrete. While the mix containing tyre-recycled steel wires did not satisfy these acceptance criteria. Furthermore, the test results showed that the six concrete mixes fulfilled the consistency criteria adopted for the filling ability of self-compacting concrete; while only three mixes fulfilled the consistency criteria for the segregation resistance of self-compacting concrete. However, the other three mixes have the potential to pass this criterion with marginal changes in their mix design.

The 28-day compressive (cube) strength class of 40 MPa was achieved by the four steel fibre-reinforced concrete mixes containing tyre-cord steel filaments; while the strength class of 45 MPa was attained by the mix containing tyre-recycled steel wires. As expected, fibre addition improved marginally the compressive strength of the mixes (in the range up to 17%). It is worth noticing that similar densities were obtained for the plain-concrete and the fibre-reinforced mixes, and this is an indication that fibre addition did not adversely affect the concrete's void content.

The bending test results demonstrated the effect of fibre length on the post-peak flexural characteristics of concrete; the mix with the 15mm tyre-cord steel filaments exhibited the best flexural behaviour while the mix with 6mm tyre-cord steel filaments exhibited the worst behaviour. Furthermore, the results indicated that concrete reinforced with relatively short steel fibres (e.g. 6mm and 9mm tyre-cord filaments) does not exhibit an extended tail in their post-peak response.

Conventional steel rebars are not expected to be used together with steel fibre-reinforced concrete screeds and, hence, the mixes developed in this study are suitable for use as overlays of concrete surfaces. This is despite the fact that the developed mixes did not pass all the criteria set for self-compacting concrete, especially the passing ability which relates directly to steel rebar reinforcement.

ACKNOWLEDGMENTS

This research has been funded by the EC collaborative FP7-ENV-2013-two-stage project "ANAGENNISI— Innovative Reuse of All Tyre Components in Concrete", Project number: 603722.

REFERENCES

[1] COMMUNICATION FROM THE COMMISSION TO THE EUROPEAN PARLIAMENT TC, THE EUROPEAN ECONOMIC AND SOCIAL COMMITTEE AND THE COMMITTEE OF THE REGIONS,. Closing the loop - An EU action plan for the Circular Economy. In: Commission E, editor. COM/2015/0614 final. Brussels: European Commission; 2015.

[2] Pilakoutas K, Neocleous K, Tlemat H. Reuse of Tyre Steel Fibres as Concrete Reinforcement. Proceedings of the Institution of Civil Engineers, Engineering Sustainability 157. 2004;ES3:131 - 8.

[3] Neocleous K, Angelakopoulos H, Pilakoutas K, Guadagnini M. Fibre-reinforced roller-compacted concrete transport pavements. PROCEEDINGS OF THE INSTITUTION OF CIVIL ENGINEERS-TRANSPORT. 2011;164:97-109.

[4] Graeff AG, Pilakoutas K, Neocleous K, Peres MVNN. Fatigue resistance and cracking mechanism of concrete pavements reinforced with recycled steel fibres recovered from post-consumer tyres. Eng Struct. 2012;45:385-95.

[5] Jafarifar N, Pilakoutas K, Bennett T. The effect of shrinkage cracks on the load bearing capacity of steel-fibre-reinforced roller-compacted-concrete pavements. Materials and Structures. 2016;49:2329-47.

[6] Bjegovic D, Baricevic A, Lakusic S, Damjanovic D, Duvnjak I. Positive interaction of industrial and recycled steel fibres in fibre reinforced concrete. Journal of Civil Engineering and Management. 2013;19:S50-S60.

[7] Younis KH, Pilakoutas K. Strength prediction model and methods for improving recycled aggregate concrete. Constr Build Mater. 2013;49:688-701.

[8] European Committee for Standardization. CYS EN 206-9, Concrete - Part 9: Additional rules for self-compacting concrete (SCC). Brussels: CEN; 2010. p. 31.

[9] EFNARC. Specification and guidelines for self-compacting concrete UK: EFNARC; 2002. p. 32.

[10] Gambhir ML. Concrete Techology: Tata McGraw-Hill Education; 2004.

[11] European Committee for Standardization. CYS EN 12350-8, Testing fresh concrete - Part 8: Self-compacting concete - Slump-flow test. Brussels: CEN; 2010. p. 13.

[12] European Committee for Standardization. CYS EN 12350-9, Testing fresh concrete - Part 9: Self-compacting concrete - V-funnel test. Brussels: CEN; 2010. p. 12.

[13] European Committee for Standardization. CYS EN 12350-10, Testing fresh concrete - Part 10: Self-compacting concrete - L box test. Brussels: CEN; 2010. p. 14.

[14] European Committee for Standardization. CYS EN 12350-12, Testing fresh concrete - Part 12: Self-compacting concrete - J-ring test. Brussels: CEN; 2010. p. 14.

[15] European Committee for Standardization. CYS EN 12350-11, Testing fresh concrete - Part 12: Self-compacting concrete - Sieve segregation test. Brussels: CEN; 2010. p. 13.

[16] European Committee for Standardization. CYS EN 14651+A1, Test method for metallic fibre concrete - Mesuring the flexural tensile strength limit of proportionality (LOP), residual). Brussels: CEN; 2007. p. 21.
[17] Final report of RILEM TC 205-DSC: durability of self-compacting concrete. Materials and Structures. 2008;41:225-33.
[18] European Committee for Standardization. EN 14889-1 Fibres for concrete - Part 1: Steel fibres - Definitions, specifications and conformity. Brussels: European Committee for Standardisation; 2006. p. 30.
[19] Elices M, Guinea GV, Planas J. Measurement of the fracture energy using three-point bend tests: Part 3—influence of cutting the P-δ tail. Materials and Structures. 1992;25:327-34.

A NEW WAY TO SUSTAINABILITY: DESIGNING MORE SLENDER BUILDING STRUCTURES BY USING RECYCLED STEEL FIBRES

Alejandro Perez Caldentey[1], Carlos Mestre García[1], Javier Mendoza Cembranos[1]

[1] FHECOR Consulting Engineers, Technical University of Madrid (UPM), Barquillo, 23, 28004 Madrid, Spain, email: apc@fhecor.es, cmg@fhecor.es, jmc@fhecor.es

SUMMARY: Control of deflections determines the depth needed for slabs in building structures. Deflections are influenced by load distribution, load history, reinforcement ratio, time-dependent material properties, concrete strength and support conditions. Given values for these parameters it is possible to determine the minimum depth necessary to comply with the required deflection limits. Concrete is a major contributor to CO_2 emissions and minimising concrete consumption can help mitigate the effects of the construction industry on climate change. One way of doing this is to design more slender structures. For slabs, that are mostly elements with low reinforcement ratios, this can be achieved without compromising serviceability by increasing tension stiffening effects and this can be efficiently done by using recycled steel fibres (RSF) in concrete. This approach is being investigated in FP7 project Anagenesis (rebirth) aimed at recycling all components of end-of-life tyres in structural concrete applications. In this paper, a parametric study is presented taking into account the main parameters affecting deflections and how the slenderness limits of traditional designs can be boosted by adding steel fibres obtained from recycled tyres. The paper provides a comparison for different load compositions, for different concrete classes and different steel ratios.

NOVI PUT KA ODRŽIVOSTI: PRORAČUN VITKIJIH KONSTRUKCIJA ZGRADA UPOTREBOM RECIKLIRANIH ČELIČNIH VLAKANA

SAŽETAK: Potrebnu debljinu ploča u konstrukcijama zgrada određuje kontrola progiba. Na progibe utječe raspodjela opterećenja, povijest opterećenja, omjer armiranja, svojstva materijala ovisna o vremenu, čvrstoća betona i uvjeti oslanjanja. Ako su vrijednosti tih parametara poznate moguće je odrediti minimalnu debljinu nužnu za ispunjenje zahtjeva ograničenih progiba. Beton najviše doprinosi emisiji CO2 pa smanjenje upotrebe betona na najmanju moguću mjeru može pomoći ublažavanju učinaka građevinske industrije na klimatske promjene. Jedan je od načina da se to postigne proračun vitkijih konstrukcija. Kod ploča koje su većinom elementi s malim omjerima armiranja to se može postići bez ugrožavanja uporabljivosti primjenom oporabljenih čeličnih vlakana u betonu. Taj je pristup istraživan u projektu FP7 Anagenesis (ponovno rođenje) u kojem su oporabljeni svi dijelovi starih guma i upotrijebljeni u konstrukcijskom betonu. U ovom je radu prikazana parametarska studija u kojoj su u obzir uzeti svi glavni parametri koji utječu na progibe te kako se ograničenja vitkosti u tradicijskom proračunu mogu poboljšati dodavanjem čeličnih vlakana dobivenih iz oporabljenih guma. U radu je dana usporedba različitih rasporeda opterećenja, različitih razreda betona i različitih omjera armiranja..

1. INTRODUCTION

As is well known by building designers, deflections determine the depth of concrete floors, which have to be optimized in order to maximize the available free space. It very important to have good tools to determine for each case the required minimum depth at an early stage of the project and this topic has been addressed in several papers ([2][3][4][5]), and incorporated, with more or less success into major design codes ([6][7][8]).

On the other hand, improving the sustainability of the construction industry, as one of the main contributors to global climate change has become a pressing task. One of the ways to achieve this is to reduce the use of materials. For reinforced concrete structures, this can be done in structures that are governed by serviceability conditions by improving the contribution of concrete in tension, that is, by enhancing tension stiffening effects. This type of strategy is effective in elements with low reinforcement ratios, which are typically slab-type structures. The authors [5] showed that this can be done in water-retaining structures, whose design is determined by the maximum crack width opening, by replacing conventional steel by steel fibres. If this can be done by using recycled steel fibres [10],[11] and [12], then sustainability can be further enhanced since the Carbon footprint of Recycled Steel Fibres (RSF) is negligible with respect to that of manufactured steel fibres.

This paper looks at a new application of this technique aimed at increasing the slenderness of concrete floors. The potential of this application is illustrated by computing the slenderness limits for Recycled Steel Fibre Reinforced Concrete (RSFRC) floors taking into account the reinforcement ratio, the load composition and concrete strength, and comparing them to traditional reinforced concrete solutions.

2. ANALYSIS OF FRC SECTIONS IN SLS, INCLUDING SOME SIMPLIFICATIONS

One of the major difficulties in determining the deflections of SFRC elements is that non-linearity is further complicated by the addition of fibres. This is also made more complex by the need to take into account the load history and the time-dependent behaviour of concrete.

For this study the following assumptions have been made regarding the load history:

- The full characteristic load is applied at t_0=7 days thereby producing the most severe cracking effects at an early age. The load in excess of self-weight is assumed to be removed shortly afterwards. This hypothesis is meant to model the often applied technique of supporting the self-weight of upper floors on the two or three lower floors, previously built.
- The flooring and partitions (superimposed dead load - SDL) are assumed to be applied at an age of t_1=60 days
- The quasi-permanent live load, which is taken as ψ_2=30% of the characteristic value, is assumed to be applied at an age of t_2=365 days.

For a given reinforcement ratio, slenderness limits are determined by calculating the deflection of a simply supported beam subjected to service loads derived from the section capacity. Assuming a certain depth, the maximum span is derived by limiting the maximum deflection to a maximum l/d ratio, usually of 250. This procedure is normally iterative. The deflections are determined by integrating curvatures derived by sectional analysis for a number of sections, assuming a certain discretization of the simply supported beam (for the case of this study, 20 sections have been used).

The sectional analysis has been carried by adapting the software developed by Pérez Caldentey [13], which derives from the original software of Corres Peiretti et al [14]. The strategy followed by this software to determine the strain plane is based on the original formulation of Marín [15], which allows to integrate a polynomial law over a polygonal surface. The software allows the use of any constitutive laws, as long as they are defined by a series of straight segments.

The analysis performed is divided into short term and long term analyses. In the short term analysis the strain plane is determined for the characteristic load. The result of this analysis is the strain at the reference fibre of the cross section ε_0, and its curvature, *1/r*. By integrating curvatures the maximum instantaneous deflection for characteristic loads is determined. The quasi-permanent instantaneous deflection is determined by multiplying this value by the ratio of the quasi-permanent load to the characteristic load. In this way, the deterioration of stiffness due to high early loads is accounted for.

For the determination of the time-dependent effects, a generalization of the aging coefficient method, first proposed by Trost [16], developed by Bazant [18] and formulated more generally by Ghali et al [19], is applied. In order to get fairly accurate results, this analysis must account for the existing pre-strain. This is done by introducing a tensional pre-strain $(\varepsilon_0,1/r)$ in the different parts of the cross section (concrete, tension reinforcement, and compression reinforcement, where applicable) by using the generalization of the software described in [13]. When these pre-strains are introduced, the cross section subjected to no forces has strain and stress planes which are the same as those derived from instantaneous analysis. However, since to allow for relaxation of stresses due to creep, the aging coefficient method is based on reducing the concrete stiffness by a factor of $(1+\chi\varphi)$ – where χ is the aging coefficient ~0.8 and φ is the creep coefficient – in order to maintain equilibrium with the instantaneous applied forces, the tensional pre-strains of concrete must be multiplied by this same value, while the strains of the constitutive law of concrete also multiplied by $(1+\chi\varphi)$. Then, non-tensional pre-strains, are introduced in the concrete. For this, a strain equal to $\varphi\times\varepsilon_0+\varepsilon_{cs}$ is introduced at the reference fibre and a curvature of $\varphi\times 1/r$ is introduced on the concrete subsection. It is relevant to point out here that the stresses derived from non-tensional imposed strains result from the difference between the final strain and the imposed non-tensional strain. A sectional analysis is then carried out for the long-term section which results in a change in the strain at the reference fibre $\Delta\varepsilon_0$ and an increase of curvature $\Delta 1/r$. Long term deflections are then determined by integrating the increases in curvature obtained at the different sections into which the beam has been divided.

Since the above analysis is already complex, the load history is simplified by using a mean value of the creep coefficient, as shown in eq. 0, where q_{DL} is the uniform load due to self-weight, q_{SDL} is the superimposed dead load (flooring+partitions) and q_{LL} is the live load.

$$\varphi_{mean} = \frac{\varphi(\infty,t_0)q_{DL} + \varphi(\infty,t_1)q_{SDL} + \varphi(\infty,t_2)\psi_2 q_{LL}}{q_{DL} + q_{SDL} + \psi_2 q_{LL}}$$

It must be pointed out that the analysis methodology described above is safe-sided, since it does not take into account conventional tension-stiffening effects. These effects are neglected because they are not significant with respect to the increased tensile behaviour due to the addition of fibres. However, for large reinforcement ratios the contribution of fibres is less relevant, and it can occur that slightly lower values of the slenderness limit would be provided by this methodology with respect to that of EN 1991-1-1 for RC structures.

It is also worthy to remark that before evaluation it seemed that for low reinforcement ratios the effect of shrinkage could be neglected. However analysis has shown that slenderness ratios are sensitive to shrinkage even for low steel ratios.

3. ADOPTED VALUES OF PARAMETERS AND RESULTS

In order to make the calculations some further data are necessary. The first is the definition of the constitutive law of fibre-reinforced concrete. To demonstrate the potential of this technology for deflection control, a lower bound-type constitutive law – one that could easily be obtained using recycled steel fibres – has been considered. The assumption here is that the residual stress at serviceability, that is for a crack mouth opening of 0.5 mm in the three point bending test, is equal to half the mean tensile resistance of concrete (i.e. $f_{Fts}=0.5f_{ctm}$) and that the residual tensile resistance at ULS, that is for a crack of 2.5 mm in the three point bending test, is equal to ¼ of the mean tensile resistance of concrete (i.e. $f_{Ftu}=0.25f_{ctm}$). Figure 1 shows the resulting law for a concrete of class C30/37. The shape of the constitutive law is taken from MC 2010 [8]. Table 1 shows the values of the residual strengths adopted for concrete classes C30/37 and C60/75.

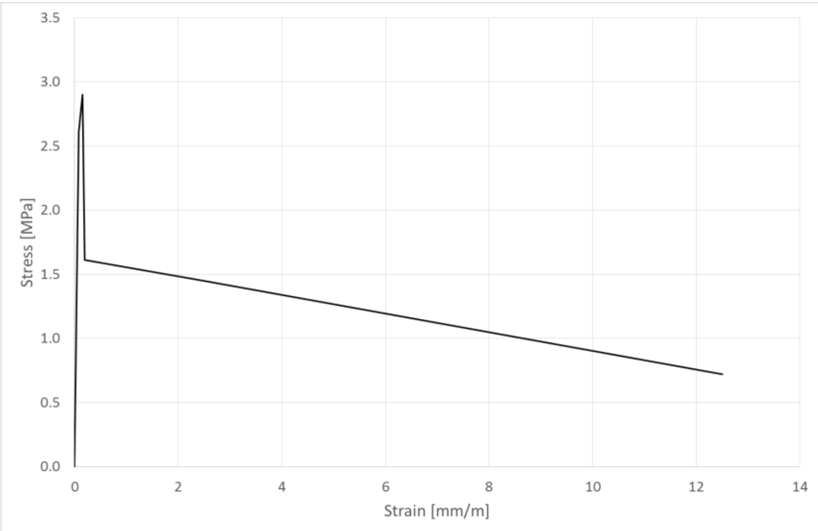

Figure 1 Assumed tensile behaviour for FRC of class C30/37

Table 1 Assumed residual strengths for concrete classes C30/37 and C60/75

f_{ck} [MPa]	f_{ctm} [MPa]	f_{Fts} [MPa]	f_{Ftu} [MPa]
30	2.90	1.45	0.72
60	4.35	2.18	1.09

Other important values for analysis are those pertaining to time dependent behaviour. For this, the rheological models of EN 1992-1-1 [7] have been adopted. The base values for the different loading ages of the creep coefficient as well as the shrinkage strain are given in Table 2.

Table 2 Rheological parameters adopted (in accordance with EN 1992-1-1)

RH=70%		
f_{ck} [MPa]	30	60
$\varphi(\infty,7)$	2.48	1.47
$\varphi(\infty,60)$	1.65	0.98
$\varphi(\infty,365)$	1.16	0.69
ε_{cs} [mm/m]	0.345	0.351

By applying expression 0 the mean values of the creep coefficient shown in Table 3 are obtained depending on the type of concrete and the assumed ratio of permanent load (qG) to total load (qTot), which here has been varied between 0.5 and 0.75. Additionally it has been assumed that the superimposed dead load (qSDL) is 20% of the self-weight (qSW)

Table 3 Mean creep coefficient considered depending on the concrete class and the permanent load to total load ratio.

	q_G/q_{Tot} =50% ; ψ_2=0.30		q_G/q_{Tot} =75% ; ψ_2=0.30	
	q_{SW}/q_{Tot}	q_{SdL}/q_{Tot}	q_{SW}/q_{Tot}	q_{SdL}/q_{Tot}
	0.417	0.083	0.667	0.133
f_{ck} [MPa]	30	60	30	60
	φ_{mean}			
	2.069	1.227	2.259	1.340

With the above values, and using the methodology described in paragraph 2, the slenderness limits were determined for the four combinations of permanent load to total load ratios and concrete classes and compared to those obtained according to the methodology described in Section 7 of EN 1992-1-1. The results are presented in Figures 2 to 5.

In these figures, normal geometrical reinforcement ratios for slabs (taken as 0.5%) and beams (taken as 2%) are singled out (in the last case only for C60/75), from the values corresponding to the mechanical ratio. Table 4 summarizes the improvement of allowable slenderness for a typical reinforcement ratio of a slab. As can be seen, the difference is considerable and can be used to improve design.

Table 4 Slenderness limit (L/d) for a geometric steel ratio of ρ=0.5%

		Conventional concrete	RSFRC
C30/37	q_G/Q_{Tot}=0.50	20.90	27.98
	q_G/Q_{Tot}=0.75	16.68	22.45
C60/75	q_G/Q_{Tot}=0.50	29.86	52.29
	q_G/Q_{Tot}=0.75	23.26	41.15

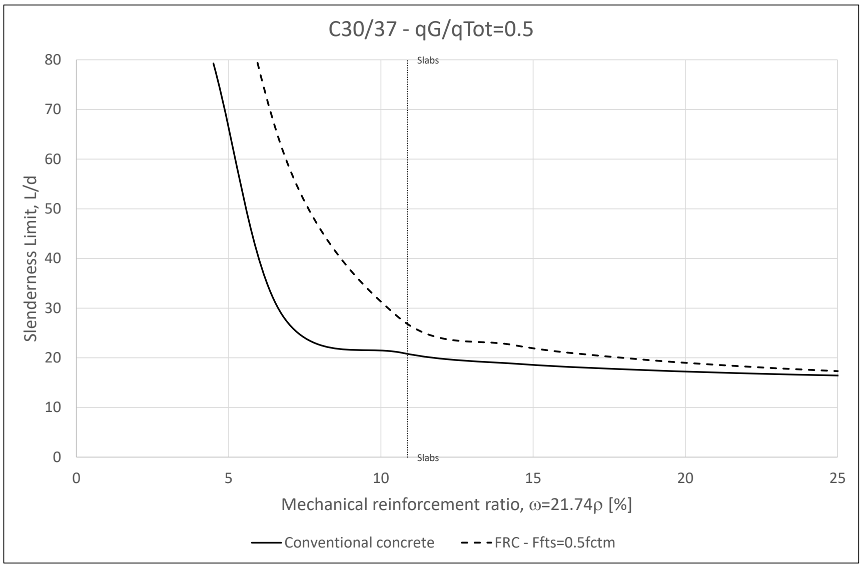

Figure 2 Slenderness limits for concrete class C30/37 and q_G/q_{Tot}=0.50

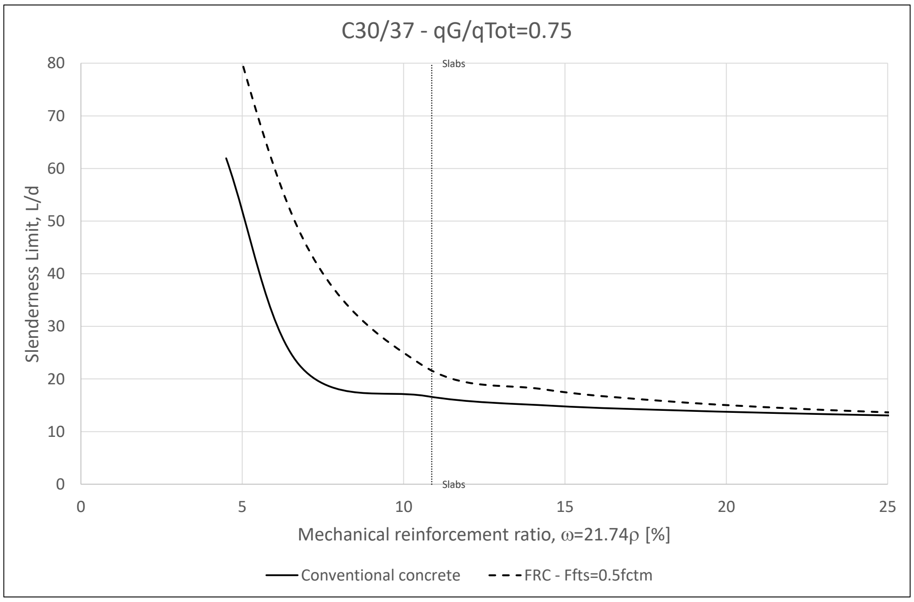

Figure 3 Slenderness limits for concrete class C30/37 and q_G/q_{Tot}=0.75

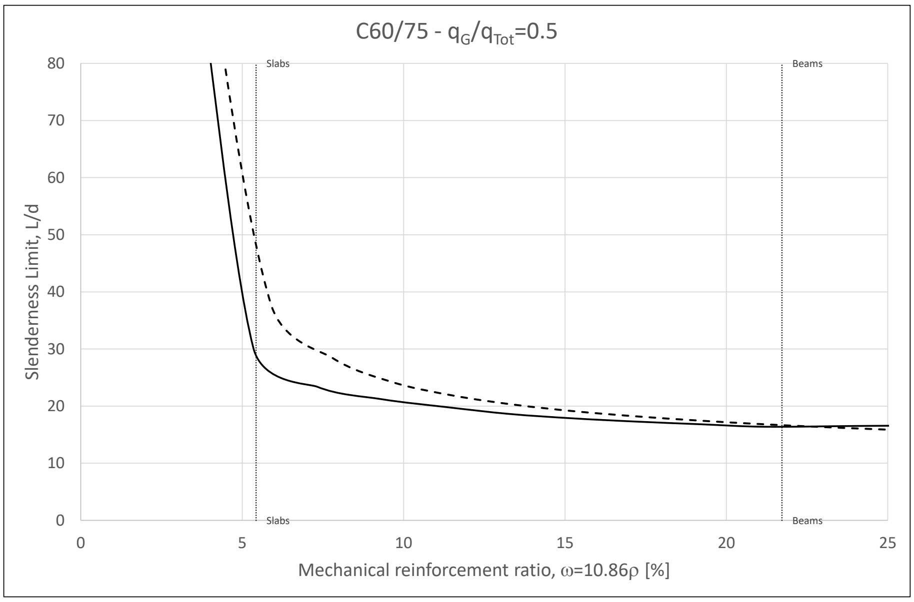

Figure 4 Slenderness limits for concrete class C60/75 and q_G/q_{Tot}=0.50

In order to better illustrate the meaning of the potential increase in slenderness in Table 5, the minimum effective depth (d) and minimum total depth (h) are given for different span lengths and support conditions for conventional RC solutions and RSTFC solutions. As can be seen, the floor depths can be significantly reduced, so much in some cases, that instead of a reduction of depth this type of solution would lead to an increase in span.

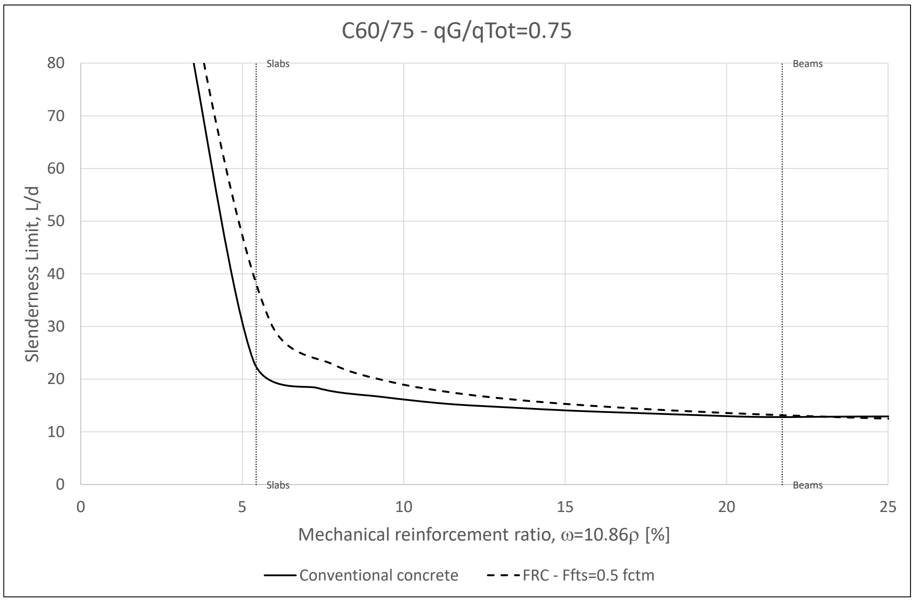

Figure 5 Slenderness limits for concrete class C60/75 and q_G/q_{Tot}=0.75

Table 5 Determination of minimum depths for different support conditions and typical span lengths (ρ=0.5%).

			L [m]	d_{RC} [m]	d_{FRC} [m]	**h_{RC} [m]**	**h_{FRC} [m]**
C30/37	q_G/Q_{Tot}=0.5	Simply supported	6	0.29	0.21	**0.34**	**0.26**
			8	0.38	0.29	**0.43**	**0.34**
		Continuous	6	0.19	0.14	**0.24**	**0.19**
			8	0.26	0.19	**0.31**	**0.24**
	q_G/Q_{Tot}=0.75	Simply supported	6	0.36	0.27	**0.41**	**0.32**
			8	0.48	0.36	**0.53**	**0.41**
		Continuous	6	0.24	0.18	**0.29**	**0.23**
			8	0.32	0.24	**0.37**	**0.29**
C60/75	q_G/Q_{Tot}=0.5	Simply supported	6	0.20	0.11	**0.25**	**0.16**
			8	0.27	0.15	**0.32**	**0.20**
		Continuous	6	0.13	0.08	**0.18**	**0.13**
			8	0.18	0.10	**0.23**	**0.15**
	q_G/Q_{Tot}=0.75	Simply supported	6	0.26	0.15	**0.31**	**0.20**
			8	0.34	0.19	**0.39**	**0.24**
		Continuous	6	0.17	0.10	**0.22**	**0.15**
			8	0.23	0.13	**0.28**	**0.18**

4. CONCLUSIONS

From the above discussion, the following conclusions can be drawn:

- There is significant potential for the use of RTFRC for the improvement of deflections of building slabs. This technique can be effectively used to improve sustainability of concrete structures.
- When combined with high strength concrete, RSFRC can make deflection a non-critical verification
- For shorter spans the depths may become too low to be buildable, but this type of solution opens the door to increasing normal spans in buildings, up from the usual values of 6 or 8 meters.
- For beams (large reinforcement ratios), no significant improvement is to be expected by the use of RTSFRC.

ACKNOWLEDGMENTS

This work has been carried out within the framework of European FP7 project, Anagennisi (Rebirth/Renaissance) [1], focused on the recycling of all components of end-of-life tyres into concrete (www.Anagennisi.org).

REFERENCES

[1] Pilakoutas, K., Raffoul, S., Papastergiou, P., Garcia, R., Guadagnini, M. and Hajirasouliha I.: Innovative reuse of all tyre components in concrete: the Anagennisi project, in Proc. of the International Conference on Sustainable Structural Concrete 2015, La Plata, Argentina, September 15-18, (2015).

[2] Branson, D.E.: Deformations of concrete structures. McGraw-Hill, New York (1977)

[3] Gilbert, R.I. Deflection Calculation for Reinforced Concrete Structures—Why We Sometimes Get It Wrong. ACI Structural Journal. Vol 96, No. 6, pp 1027-1032, Nov. 1999.

[4] Bischoff, P.H., Scanlon, A. Effective Moment of Inertia for Calculating Deflections of Concrete Members Containing Steel Reinforcement and Fiber-Reinforced Polymer Reinforcement. ACI Structural Journal. Vol. 104, No. 1, pp. 68-75, Jan-Feb, 2007.

[5] Pérez Caldentey, A., Mendoza Cembranos, J., Corres Peiretti, H.: Slenderness Limits for deflection control: a new formulation for flexural RC elements. Structural Concrete (2016). DOI: 10.1002/suco.201600062

[6] ACI Committee 318: Building Code Requirements for Structural Concrete (ACI 318-08) and commentary (318R-08), American Concrete Institute, Farmington Hills, Mich., (2008), 430 p.

[7] CEN: EN-1992-1-1. Eurocode 2. Design of concrete structures – Part 1-1. General rules and rules for buildings, (2004).

[8] fib: fib Model Code for Concrete Structures 2010. Ernst & Sohn. ISBN 978-2-88394-105-2 and ISBN 978-2-88394-106-9.

[9] Pérez Caldentey, A., Gimenez Vila, J., Ortolano González J.M., Rodríguez F.: Contributing to sustainability of concrete by using steel fibres from recycled tyres in water retaining structures. II International Conference on Concrete Sustainability (ICCS16), (2016).

[10] Groli, G.: Crack width control in RC elements with recycled steel fibres and applications to integral structures: theoretical and experimental study. PhD Thesis. Technical University of Madrid (2014)

[11] Groli, G., Pérez Caldentey, A., Giraldo Soto, A.: Cracking performance of SCC reinforced with recycled fibres–an experimental study. Structural Concrete, Vol 15, nº2, 136-153 (2014).

[12] Groli, G., Pérez Caldentey, A.: Improving cracking behaviour with Recycled Steel Fibres, targeting specific applications. Analysis according to MC2010. Structural Concrete. 10.1002/suco.201500170 (2016).

[13] Pérez Caldentey, A., Fernández-Espartero Rodríguez-Barbero, I.: Prontuario Informático de las estructuras metálicas y mixtas. Asociación para la Promoción Técnica del Acero (APTA) (2009)

[14] Corres Peiretti, H., Martínez Martínez, J.L., Pérez Caldentey, A., López Agüí, J.C.: Prontuario Informático del Hormigón Estructural 3.0. IECA. (2015)

[15] Marín J.: El cálculo de integrales dobles con momentos de área. Boletín Técnico nº76 del Instituto de Materiales y Modelos Estructurales. Universidad de Venezuela. Caracas, (1988).

[16] Trost, H., "Implications of the Superposition Principle in Creep and Relaxation Problems for Concrete and

[17] Prestressed Concrete," Beton-und Stahlbetonbau (Berlin-Wilmersdorf), No. 10, 1967, pp. 230-238, 261-269. (in German)

[18] Bazant, Z.P.: Prediction of Concrete Creep Effects Using Age-Adjusted Effective Modulus Method. Journal of the American Concrete Institute April 1972, Vol. 69, p. 212-217.

[19] Ghali, A., Favre, R., Elbadry, M.: Concrete Structures: Stresses and Deformations: Analysis and Design for Sustainability, Fourth Edition. CRC Press , September 20, 2011.646 pages.

ENVIRONMENTAL LCA OF INNOVATIVE REUSE OF ALL END-OF-LIFE TYRE COMPONENTS IN CONCRETE

Sebastian George Maxineasa[1], Kyriacos Neocleous[2], Laura Dumitrescu1, Kyriacos Themistocleous[2], Nicolae Taranu[1], Diofantos Hadjimitsis[2]

[1] "Gheorghe Asachi" Technical University of Iassi, Faculty of Civil Engineering and Building Services, Department of Civil and Industrial Engineering, 1 Prof. Dr. docent Dimitrie Mangeron Street, Iasi 700050, Romania, email: sebastian.maxineasa@gmail.com, laura.dumitrescu@gmail.com, nicutara@yahoo.com
[2] Cyprus University of Technology, Department of Civil Engineering and Geomatics,2-8 Saripolou Street, Lemesos, Cyprus, email: kyriacos.neocleous@cut.ac.cy, kyriacos.themistocleous@cut.ac.cy, d.hadjimitsis@cut.ac.cy

SUMMARY: This paper presents the environmental life-cycle assessment of concrete mixtures containing materials recycled from End-of-Life tyres, i.e. rubber particles, sorted steel wires and polymer/textile cord fibres. This life-cycle assessment is based on ILCD and the ISO standards and considers "cradle to grave", i.e. from extraction of raw materials, tyre-recycling and up to concrete production in ready mixture concrete plants. In total, 21 different concrete mixtures were analysed, including rubberised concrete and fibre reinforced concrete; mixtures with hybrid fibres were also considered (i.e. reinforced with both recycled and manufactured fibres). The results of this LCA show that, for a functional unit of 1 m^3 of concrete, cement is the main parameter contributing to the inventory of the examined concrete mixtures; this indicates the need of utilising "low energy" and low calcination cements to minimise their environmental impact. When performance-based functional units are considered in the LCA, the results highlight the importance of using these recycled materials in structural concrete applications that fully utilise the specific mechanical characteristics of each material, as demonstrated for rubberised concrete and steel fibre-reinforced concrete mixtures.

ANALIZA ŽIVOTNOG CIKLUSA S OBZIROM NA OKOLIŠ INOVATIVNE UPORABE SVIH PRODUKATA RECIKLAŽE OTPADNIH GUMA U BETONU

SAŽETAK: U radu se prikazuje ocjenjivanje životnog ciklusa s obzirom na okoliš betonskih mješavina koje sadržavaju reciklirane materijale iz starih guma, tj. čestice gume, sortirane čelične žice i vlakna užadi od polimera/tekstila. Ocjenjivanje životnoga ciklusa zasniva se na ILCD-u (engl. International Life Data Cycle System) i na normama ISO-a te obuhvaća faze od kolijevke do groba tj. od vađenja sirovina, recikliranja guma do proizvodnje betona u tvornicama betona. Ukupno je analizirana 21 različita mješavina betona uključujući beton s gumom i beton armiran vlaknima. Razmotrene su i mješavine s hibridnim vlaknima (tj. armirane oporabljenim i proizvedenim vlaknima). Rezultati takvog ocjenjivanja životnoga ciklusa pokazuju da je za 1 m^3 betona cement glavni parametar koji doprinosi skupu ispitanih betonskih mješavina. To znači da za najmanje opterećenje za okoliš postoji potreba upotrebe niskoenergetskih cemenata i cemenata s malom kalcinacijom. Pri razmatranju svojstava pri ocjenjivanju životnoga ciklusa rezultati pokazuju važnost upotrebe tih oporabljenih materijala u konstrukcijskom betonu koji u potpunosti ima posebne mehaničke značajke svakoga materijala kako je to dokazano za mješavine betona s gumom i betona armiranog čeličnim vlaknima.

1. INTRODUCTION

An estimated one billion tyres are produced each year and a similar number reach the end of their life. In the EU alone, it is estimated that 3,400,000 tonnes of End-of-Life (EoL) tyres arise per year. Following the introduction of EU legislation on waste management, the majority of EoL tyres are either incinerated for energy recovery or mechanically treated to produce recycled rubber, steel wires and textile cord. The recycled rubber is used in a wide range of applications, while there are limited applications for the recycled steel wires and recycled textile cord [1].

To promote material recycling of EoL tyres, it is desired that innovative and high-added value applications are developed for all tyre components. This is the focus of the FP7 collaborative project "Anagennisi, which aims to innovatively reuse all tyre components in concrete construction. The recycled rubber can be used as a full/partial replacement of aggregate [2] with the aim of developing high deformability concrete. The recycled steel wires (provided they are cleaned and sorted to specific lengths [1]) can be used as fibre concrete reinforcement, to replace fully/partially manufactured steel fibres, as demonstrated by other research activities [3, 4]. The use of the recycled polymer/textile cord, recovered in the form of very fine and short fibres, has been mainly demonstrated in thermal insulation building applications, while current research activities are focused on shrinkage [5] and fire-spalling mitigation [6] of concrete elements.

To promote the reuse of all tyre components in concrete, the research activities of Anagennisis also involve environmental life cycle assessment (LCA), and this paper presents the “cradle to gate” LCA undertaken as part of the preparatory concrete mixture development of the project. In total, 21 different concrete mixtures were analysed, including rubberised concrete and fibre reinforced concrete; mixtures with hybrid fibres were also considered (i.e. reinforced with both recycled and manufactured fibres).

2. METHODOLOGY

The LCA utilised provisions of the ILCD [7] and the ISO standards [8, 9]; the software GABI-6 was used to undertake the study. The LCA system boundary considered all processes from extraction of raw materials and up to concrete production in ready mix concrete plants (Figure 1), obtaining a comprehensive energetic and environmental picture of the materials and concrete mixtures developed by the preparatory concrete mixture study.

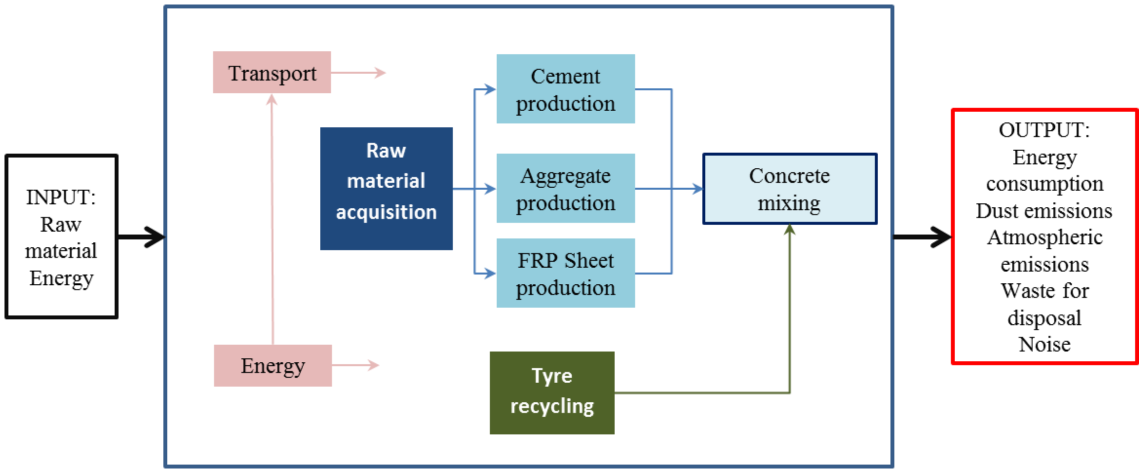

Figure 1 System boundary for the analysis

The LCA was implemented into four phases: goal definition, scope definition, inventory analysis and impact assessment. The intended goal of the LCA study was to evaluate and interpret the environmental impact of the following:

- recycled materials derived from EoL tyre recycling (rubber, steel wires and polymer/textile fibres),
- rubberised concrete mixtures (obtained by replacing a partial volume of coarse and fine aggregate with recycled tyre rubber in the modified concrete mixtures),
- fibre reinforced concrete mixtures (obtained by using tyre-recycled steel wires – RTSF - and polymer/textile fibres – RTPF - in concrete mixtures).

The LCA examined 21 concrete mixtures that were considered suitable for a range of applications, including precast elements, pavements and reinforced concrete building frames. The main functional unit was the production of 1 m^3 of concrete containing recycled materials from EoL tyres and, thus, three reference flows were considered: 1 m^3 of plain concrete mixture, 1 m^3 of fibre reinforced concrete, 1 m^3 of rubberised concrete. To account for the specific performance characteristics of concrete containing tyre-recycled materials, additional performance-based functional units were also considered for the rubberised concrete and steel fibre-reinforced concrete mixtures.

3. INVENTORY ANALYSIS

The Life Cycle Inventory analysis was based on “Situation A: Micro-level support”, i.e. attributional. In this case, the input and output processes of the system (Figure 1) were modelled as they occurred. Furthermore, the ILCD provision for subdivision and virtual subdivision for black box unit processed was followed. “Open loop - different primary route” and “Allocation with determining Physical Causality” were considered to solve the multi-functionality of tyre recycling. In addition, a Euro 4 diesel truck with 5t payload capacity was considered for material transportation. It is noted that the feedstock energy of the recycled materials was not accounted in the analysis.

3.1. CONCRETE MIXTURES

Table 1 outlines the materials used in the concrete mixtures examined by the LCA study. The concrete mixtures included 3 plain concrete mixtures (used as the basis for comparison), 2 rubberised concrete mixtures, 10 steel fibre-reinforced concrete mixtures and 6 polymer/textile reinforced concrete mixtures.

Table 1 Material details and proportions of concrete mixtures

Constituent materials	Rubberised concrete	Steel fibre reinforced concrete	Polymer fibre reinforced concrete
Fine Aggregate (kg/m^3)	Natural sand (820)	Natural sand (804)	Crushed limestone (219)
Coarse Aggregate (kg/m^3)	Round gravel (1001)	Round gravel (1097)	Crushed limestone (1417)
Water (l/m^3)	Potable (150)	Potable (150)	Potable (215)
Cement (kg/m^3)	CEM II / A-LL 52.5N (42)	CEM I 52.N (150)	CEM II/BM SV 42.5 N (470)
Cement replacement (kg/m^3)	PFA (42.5)	GGBS (150)	-
Chemical additive (l/m^3)	Superplasticizer (5.1)	Superplasticizer (2.3)	Superplasticizer (3.1)
EoL Tyre secondary goods (kg/m^3)	Rubber (volume replacement: 10% = 24.75 & 40% = 99)	Sorted steel wires (30)	Polymer/textile fibres (1, 2, 3, 15, 30)

The two rubberised concrete mixtures contained recycled rubber particles (sieve sizes: 0-4 mm, 4-10 mm and 10-20 mm) which were used as partial aggregate replacement (at 10% and 40% volume replacement). The steel fibre-reinforced concrete mixtures contained sorted recycled and manufactured fibres at different contents. One mixture contained only sorted recycled steel wires (at 30 kg/m^3), three mixtures were reinforced only with manufactured steel fibres (at 30, 35 & 45 kg/m^3), while six mixtures contained both sorted recycled steel wires (R) and manufactured (M) steel fibres, since the effectiveness of hybrid steel fibres has already been demonstrated, e.g. [4]. The hybrid fibre contents were 20M10R,15M15R, 10M20R, 35M10R, 22.5M22.5R and 10M35R. The diameter of the sorted recycled steel wires was less than 0.3 mm while their length ranged between 15 to 25 mm; two types of manufactured steel fibres were used: their diameter/length was 08/55 & 1/60. Three of the polymer reinforced concrete mixtures contained only manufactured polymer fibres (at 1, 2, 3 kg/m^3), while the remaining three mixtures contained recycled polymer/textile fibres (at 1, 15 and 30 kg/m^3).

3.2. TYRE RECYCLING DATA

A data survey was undertaken amongst the tyre recyclers participating in Anagennisi in order to gather data on the energy consumption of the ambient-temperature mechanical-treatment of EoL tyres. The collected data was analysed and the multi-functionality of EoL tyre recycling was solved according to the ILCD recommendations where the inventory of the recycling process was shared between the two co-functions of the tyres (as per §14.1 of the ILCD handbook). It is noted that a gate fee is normally paid to the recycling plant in order to accept the EoL tyres for recycling and, hence, the EoL tyres were assumed to have a negative value up to the gate of the recycling plant. For this reason, the inventory of the waste management processes up to the gate of the recycling plant (i.e. collection and transportation of the tyres) was fully allocated to the first co-function of the tyre.

Based on the collected data, a typical recycling plant (which uses ambient-temperature mechanical-treatment technology) consumes on average 430 kWh to treat one tonne of EoL tyres. On the absence of detailed data on the processes and equipment used to treat the EoL tyres, it was decided to provisionally share 50% of this energy consumption (215kWh) to the first co-function and the other 50% (215kWh) to the second co-function of the tyres (i.e. provide secondary goods for use in other systems). The 215 kWh per tonne was allocated by mass to each secondary good produced by the mechanical treatment of EoL tyres (Table 2).

Table 2 Allocation of energy consumed during the ELT recycling process

EoL Tyre secondary goods	Mass per tonne of EoL Tyres (kg)	Allocated energy consumption (kWh/ kg)	Total allocated energy consumption (KWh)
Steel wires	150	0.215	32.25
Polymer (textile) fibres	50	0.215	10.75
Rubber	800	0.215	172
Total	1000	-	215

4. IMPACT ASSESSMENT & INTERPRETATION

Figure 2 outlines the results for the ILCD impact category "Climate change midpoint" obtained for the two rubberised concrete mixtures as well as for the plain concrete mixture, used as a basis of comparison. It is clear that, for the specific functional unit of 1 m^3 concrete, there is only a marginal increase on the amount of CO2-Equiv. as a result of the partial replacement of natural aggregate with recycled rubber particles. In this case, cement is the main factor contributing to the LCA inventory of these mixtures, since the mechanical behaviour of the mixes is not accounted in the analysis. However, a different outcome is obtained by changing the functional unit of these concrete mixes, e.g. to provide a 100 kN axial load capacity for a concrete column. As shown in Figure 3, the partial replacement of aggregate with rubber leads to an increase to the expected amount of CO2-Equiv, since the compressive strength of concrete decreases due to replacement of aggregate with recycled rubber particles. Hence, a bigger cross-section is required to provide the 100kN axial load capacity. To arrive at environmentally friendly applications for rubberised concrete, it is important that this material is used in structural applications that fully utilise the mechanical characteristics of the material. One possibility, it is to use rubberised concrete in structural applications which require high-deformability; and this is one of the main applications currently being developed for rubberised concrete by the Anagennisis project [2].

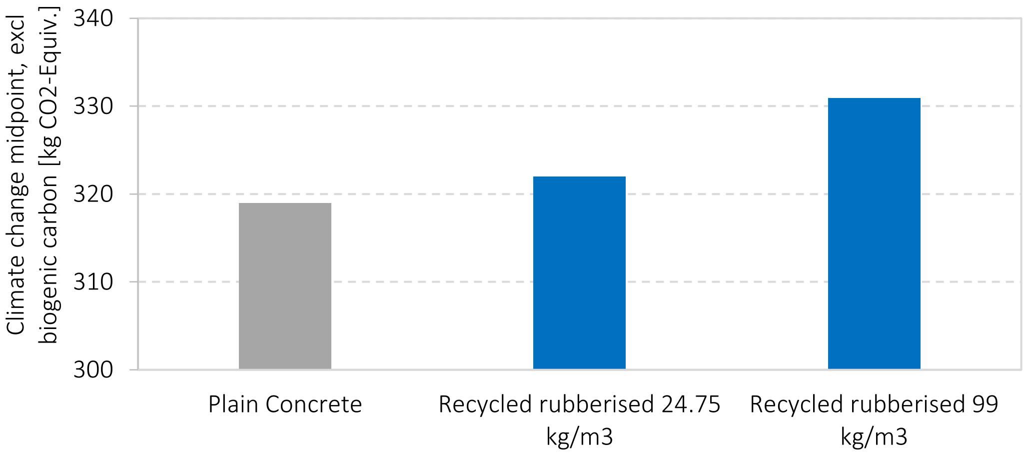

Figure 2 Rubberised concrete mixtures – Climate change midpoint, excl. biogenic carbon

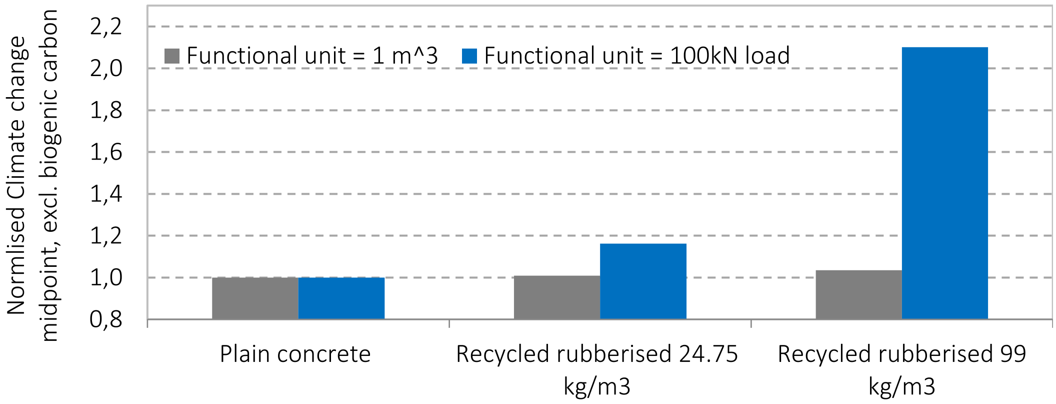

Figure 3 Rubberised concrete mixtures – Functional unit comparison

Figure 4 shows the results for the ILCD impact category "Climate change midpoint" obtained for the steel fibre-reinforced concrete mixtures. As expected for a functional unit of 1 m^3 of concrete, the amount of CO2-Equiv increases with the fibre content. By comparing mixtures with similar fibre contents (e.g. 30 kg / m^3), it is clear that the inventory of mixtures with manufactured fibres is much higher than that for mixtures with hybrid or recycled steel wires. When the content of manufactured fibres equals to 45 kg / m^3, the amount of CO2-Equiv associated with fibre addition is almost the same as the amount attributed to the cement and GGBS (i.e. 99 kg CO2-Equiv). By considering a performance-based functional unit (e.g. design criteria for industrial ground floors [10]), the LCA results for "Climate change midpoint" indicate that the use of recycled steel wires or hybrid fibres (with at least an equal amount of recycled fibres, e.g. mixtures C and I) can provide an environmentally friendlier solution than plain concrete or a mixture containing only manufactured steel fibres (Figure 5). This demonstrates the high-performance obtained by the synergy of recycled wires and manufactured fibres [4].

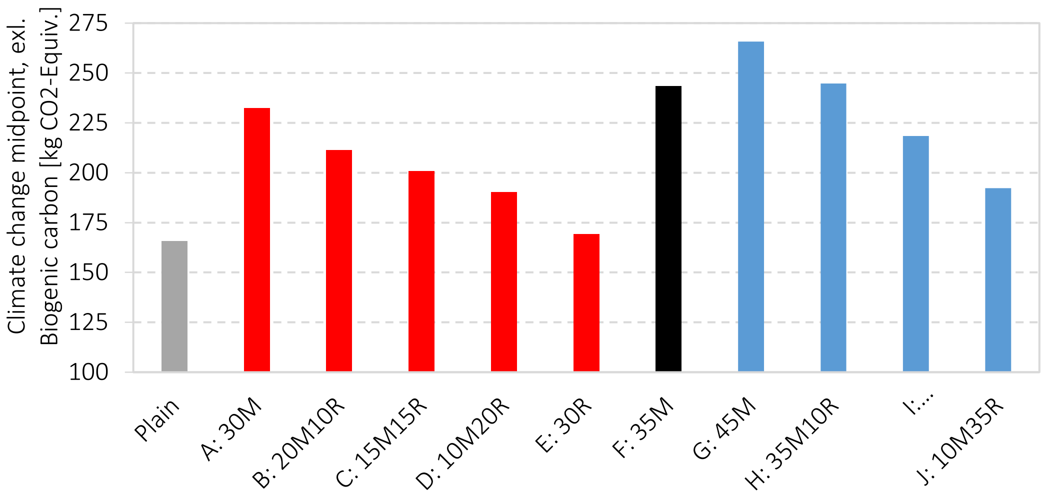

Figure 4 Steel fibre-reinforced concrete mixtures – Climate change midpoint, excl. biogenic carbon

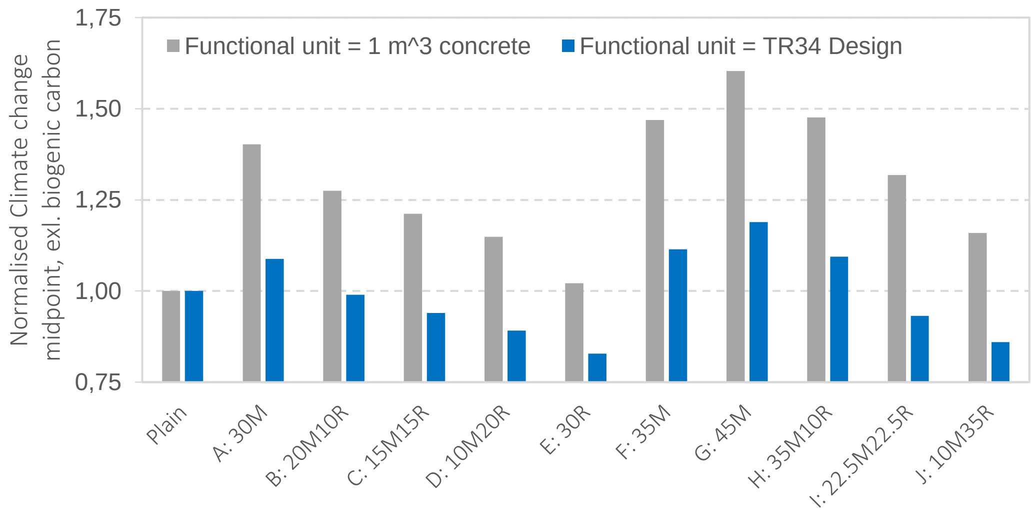

Figure 5 Steel fibre-reinforced concrete mixtures – Functional unit comparison

Figure 6 shows the LCA results for the ILCD impact category "Climate change midpoint" obtained for the polymer reinforced concrete mixes. Similarly, to steel fibre reinforced concrete mixes, the amount of CO2-Equiv increases with the amount of polymer/textiles fibres added to the concrete mixture. However, the results indicate that the use of recycled polymer/textile fibres leads to marginal increase of the amount of CO2-Equiv; thus, demonstrating the environmental benefits of using recycled materials. However, this claim should be further elaborated with performance-based functional units, which are currently under development by the Anagennisis project.

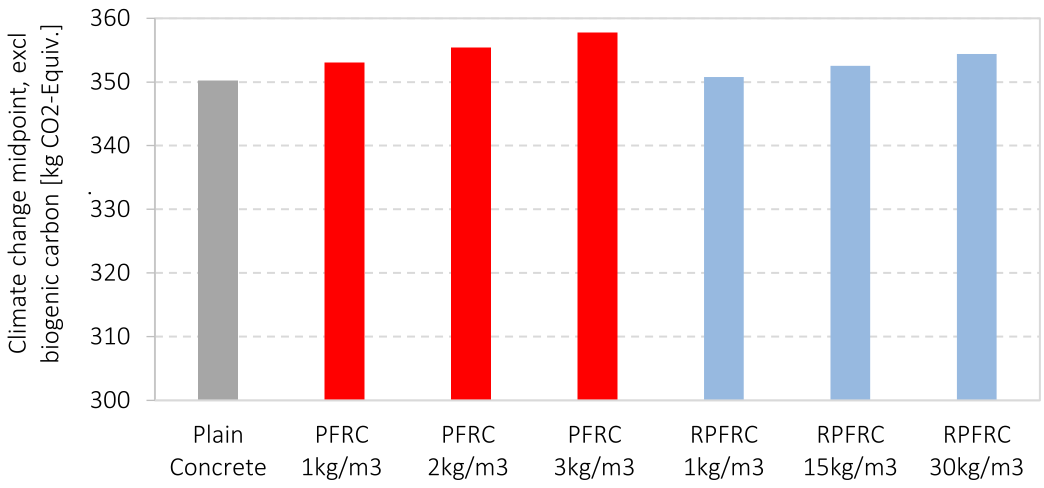

Figure 6 Polymer fibre-reinforced concrete mixes – Climate change midpoint, excl. biogenic carbon

5. CONCLUSIONS

This paper presented a “cradle to gate” environmental life-cycle assessment undertaken for concrete mixtures containing materials recycled from End-of-Life tyres, such as rubber particles, sorted steel wires and polymer/textile fibres.

Results of the ILCD impact category “Climate change midpoint” indicate that, for a functional unit of 1 m^3 of concrete, cement is the main factor contributing to the amount of CO2-Equiv; and this highlights the importance of using less-polluting cements, such as “low energy” and low calcination cements. Furthermore, for this functional unit, the results showed that the amount of CO2-Equiv increases marginally by the addition of tyre-recycled materials.

When performance-based functional units are considered in the LCA, the results highlight the importance of using these recycled materials in structural concrete applications that fully utilise the specific mechanical characteristics of each material.

ACKNOWLEDGMENTS

This research has been funded by the EC collaborative FP7-ENV-2013-two-stage project "ANAGENNISI—Innovative Reuse of All Tyre Components in Concrete", Project number: 603722.

REFERENCES

[1] Pilakoutas K, Neocleous K, Tlemat H. Reuse of Tyre Steel Fibres as Concrete Reinforcement. Proceedings of the Institution of Civil Engineers, Engineering Sustainability 157. 2004;ES3:131 - 8.
[2] Raffoul S, Garcia R, Pilakoutas K, Guadagnini M, Medina NF. Optimisation of rubberised concrete with high rubber content: An experimental investigation. Constr Build Mater. 2016;124:391-404.
[3] Neocleous K, Angelakopoulos H, Pilakoutas K, Guadagnini M. Fibre-reinforced roller-compacted concrete transport pavements. PROCEEDINGS OF THE INSTITUTION OF CIVIL ENGINEERS-TRANSPORT. 2011;164:97-109.
[4] Bjegovic D, Baricevic A, Lakusic S, Damjanovic D, Duvnjak I. Positive interaction of industrial and recycled steel fibres in fibre reinforced concrete. Journal of Civil Engineering and Management. 2013;19:S50-S60.
[5] Serdar M, Baricevic A, Jelcic Rukaniva M, Pezer M, Bjegovic D, Stirmer N. Shrinkage Behaviour of Fibre Reinforced Concrete with Recycled Tyre Polymer Fibres. International Journal of Polymer Science. 2015;2015:9.
[6] Huang S, Angelakopoulos H, Pilakoutas K, Burgess I. Reused tyre polymer fibre for fire-spalling mitigation. 4th International conference on Applications of Structural Fire Engineering ASFE'1. Dubrovnik Croatia2015. p. 6.
[7] European Commission - Joint Research Centre - Institute for Environment and Sustainability. International Reference Life Cycle Data System (ILCD) Handbook - General Guide for Life Cycle Assessment - Detailed guidance. Ispra, Italy: European Union; 2010. p. 394.
[8] European Committe for Standardization. EN ISO 14044 Environmental management - Life cycle assessment - Requirements and guidelines. Brussels: CEN; 2006. p. 58.

[9] European Committe for Standardization. EN ISO 14040 Environmental management - Life cycle assessment - Principles and framework. Brussels: CEN; 2006. p. 32.
[10] Concrete Society. Technical Report 34 Concrete industrial ground floors, a guide to design and construction. Oxford UK: Concrete Society; 2013. p. 87.

SU STAI NABI LITY

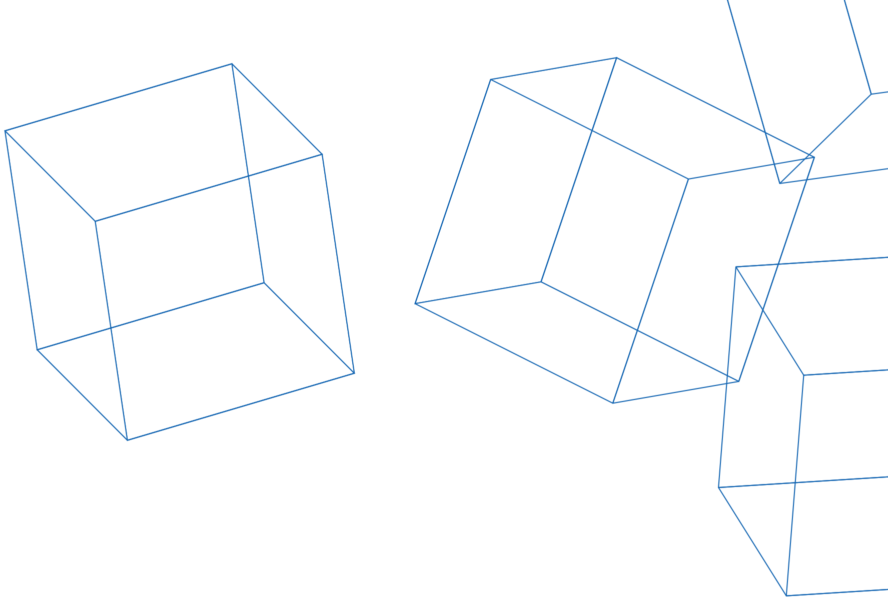

MAPEI AND THE ENVIRONMENTAL IMPACTS OF THEIR PRODUCTS

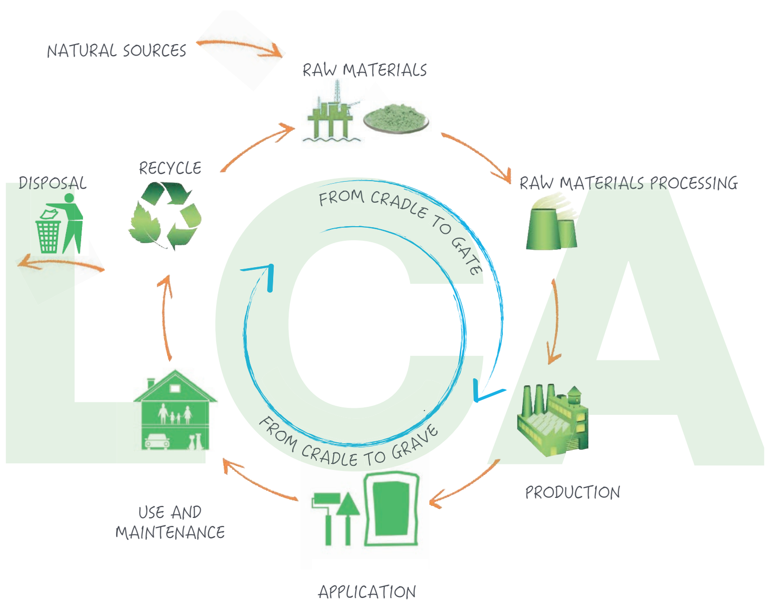

EPD®

THE INTERNATIONAL EPD® SYSTEM

ENVIRONMENTAL PRODUCT DECLARATION

Mapei prove the environmental credentials of their products using the Environmental Product Declarations (EPD).
An EPD is a transparent document, verified and certified by a third party body, which describes all the environmental impacts of a product during its whole life cycle, measuring all impacts by the LCA (Life Cycle Assessment) standardized methodology.
Typically an EPD will include information about a product's impact on categories such as the global warming, caused by greenhouse gas emissions, the ozone depletion, the natural resources depletion, the eutrophication (abnormal growth of aquatic organisms, such as algae, which causes the depletion of aquatic fauna), the acidification due to pollutants, which causes acid rains.

Mapei EPDs are developed according to ISO 14025, EN 15804 and PCR Environdec (Version 2.01) and are published on the EPD International Platform.

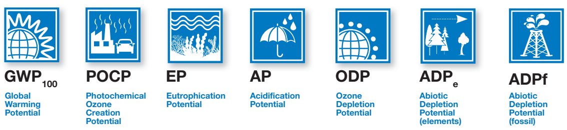

The International EPD® System
www.environdec.com


Gradimo održive kolnike!
Betonski kolnici odlikuju se iznimnom trajnošću i niskim troškovima održavanja. Njihovo korištenje predstavlja značajan napredak u pogledu održive gradnje. Utjecaji betonskog kolnika na okoliš tijekom njegovog životnog vijeka značajno su manji u usporedbi s drugim vrstama kolnika. Štoviše, veća refleksija sunčevih zračenja te utjecaj na smanjenu potrošnju goriva vozila predstavljaju pozitivan učinak na okoliš.
CEMEX

INFRASTRUCTURE INDUSTRY

BE SURE. BUILD SURE.

Sustavi za pitku i otpadne vode

Zaštita vodospremnika premazima protiv korozije.

Industrijski podovi

Rješenja za industrijske podove s posebnim zahtjevima.

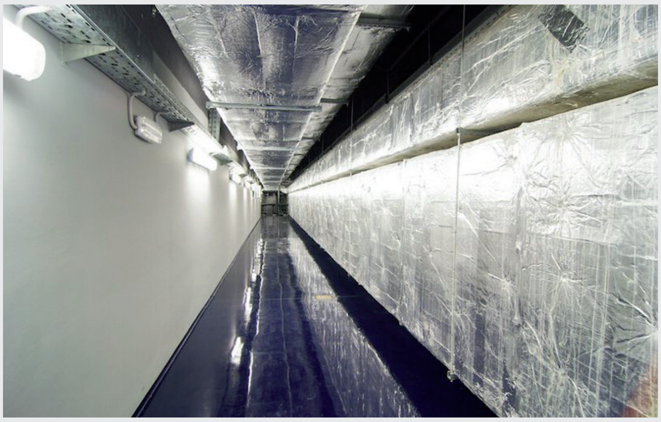

Proizvodi za sanaciju i zaštitu betona

Rješenja za objekte vezane uz VODU i obnavljanje te produljenje životnog vijeka građevine.

Tehnologija i materijali za injektiranje

Rješenja kod ojačavanja konstrukcija, brtvljenje pukotina i zaustavljanje prodora vode.

MC Building Chemicals d.o.o.

Kovinska 4A, 10090 Zagreb Tel: 01 5587 797 Fax: 01 5587 378

www.mc-bauchemie.hr e-mail: infocro@mc-bauchemie.com

BE SURE. BUILD SURE.


Građevinska kemija
za profesionalce
TKK
SINCE1947
TKK DODACI ZA BETONE,
MORTOVI I ZAŠTITNI PREMAZI
CEMENTOL
dodaci za proizvodnju trajnog i kvalitetnog betona
SILIFOB
vodootporne i druge zaštite mineralnih i drugih
građevinskih materijala
TEKAMAL
mort za popravak betonskih konstrukcija
CEMENTOL®
HIDROIZOL
N
www.tkk.si


nexe
CEMENT
GRADIMO POVJERENJE
STANDARD
NAMAL
SPECIJAL
50 kg
45 kg
25 kg
www.nexe.hr

UNDER THE AUSPICES OF / POD POKROVITELJSTVOM:

Ministry of Construction and Physical Planning
MINISTARSTVO GRADITELJSTVA I PROSTORNOGA UREĐENJA

Croatian Chamber
of Civil Engineers

rilem

GENERAL SPONSOR / GENERALNI SPONZOR:

MAPEI
ADHESIVES · SEALANTS · CHEMICAL PRODUCTS FOR BUILDING

GOLDEN SPONSORS / ZLATNI SPONZOR:

Holcim

CEMEX

MC
BE SURE. BUILD SURE.

SILVER SPONZORS / SREBRNI SPONZOR:

KNAUF INSULATION
vrijeme je za štednju energije

nexe
GRADIMO POVJERENJE

Toni Technik

TKK

ROCKWOOL
FIRESAFE INSULATION

proceq

BASF
We create chemistry

Labtim Adria d.o.o.

Beton Lučko

instrumentalia

Wienerberger

BRONZE SPONZORS / BRONČANI SPONZOR:

ARKADA d.o.o.
47250 DUGA RESA, Kolodvorska 1A

NAF
UPRAVLJANJE PROJEKTIMA d.o.o.

COLAS
Hrvatska

INSPEKTING d.o.o.
NADZOR, PROJEKTIRANJE, VJEŠTAČENJE

CTPPROJEKT

TEHNIKA

EURCO

ADING
ingredient of each construction

MEDIA PARTNERS / MEDIJSKI POKROVITELJ:

gradimozadar.hr
WEB PORTAL I MAGAZIN

KORAK u prostor
www.korak.com.hr

GREEN PARTNER /
ZELENI PARTNER:

HRVATSKI SAVJET ZA ZELENU GRADNJU
CROATIA GREEN BUILDING COUNCIL

GALA DINNER SPONSORED BY /
SPONZOR VEČERE

FIRE SAFE EUROPE